June 5-8, 2018
Rome, Italy

International Conference on Deep Foundations and Ground Improvement

Urbanization and Infrastructure Development: Future Challenges



www.dfi-effc2018.org

Lectures

John Mitchell Lecture: Geophysics for Geotechnical Design

Michele Jamiolkowski Emeritus Professor and Andrea Masella, Project Manager……...1

Keynote Lecture: Specification, Procurement, Quality Control and Certification of Bottom-Feed Stone Columns

Giovanni Vaciago..……18

Contracts and Geotechnical Investigation

Bearing Behaviour of Dubai Standstone and Dubai Siltstone Due to High-Rise Structures

Rolf Katzenbach, Prof., Steffen Leppla, Ingenieursozietät Professor Dr.-Ing and Marwan Alzaylaie..……30

Civil Engineering Feasibility Study for CERN's Future Circular Collider

John Andrew Osborne Senior Civil Engineer at CERN and Joanna Louise Stanyard, Civil Engineering Consultant……...40

Correlation between Axial Capacity of Driven Pile and Standard Penetration Test Blowcount

Jinyuan Liu Associate Professor and Markus Jesswein, Civil Engineering……..48

Delivering Added Value via Advanced Ground Investigations for Deep Shaft Design in Urban Areas

Anthony S. O'Brien, Global Practice Leader-Geotechnics and Hock L. Liew……..…….58

Evaluation of Seepage Barrier Wall Performance Using Instrumentation

Georgette Hlepas, PhD, PE and Vanessa Bateman, PG……71

Geotechnical Baseline to Manage Contractual Risk Caused by Unforeseen Ground Conditions

Andrea Antiga…….81

Impact from the Construction of a Working Platform and Girder Lifting Operation on Bridge Pile Foundation in Soft Soil

Bosco Poon, Principal Geotechnical Engineer and Kim Chan, Senior Principal and Service Line Leader……90

Sampling of Stabilized Clay by Use of Kiso-Jiban GP-Tr Sampler

Bjorn Kristian Fiskvik Bache and Alf Kristian Lund……...100

Working Platforms for Tracked Plant - Experience from 13 Years of Best Practice

Derek Egan, Managing Director……..106

Deep Foundations Behavior and Testing

A Study of the Augmenting Effect of Equipping Piles with an Expander Body

Bengt H. Fellenius, Dr.Tech., P.Eng., K. Rainer Massarsch, Dr. Tech., Mario Terceros H., Eng. and Mario Terceros A……114

Controlling Ground Movements Due to Pile Installation Adjacent to London Underground Tunnels for the Southbank Place Project

Stuart Hardy, Associate Director, Thomas Beales Ferguson, Geotechnical Engineer, Duncan Nicholson, Fellow, Jonathan Ly, Senior Design Manager and Laurent Olivier, Project Manager……..124

Design, Construction and Performance of Single Bore Multiple Anchored Diaphragm Wall in Izmir, Turkey

R. Düzceer, General Manager, D. Mothersille, Managing Director, A. Gökalp, Deputy General Manager and S. Adatepe, Technical Manager……135

Drilled Pier Load Tests on Dulles Metrorail Project - Overview, Results and Discussions

Sujan K. Bhattacharya, Senior Geotechnical Engineer, Lloyd W. Young, Senior Principal Geotechnical Engineer and Jeongbok Seo, Project Tunnel Engineer……149

Experimental Comparison on Different Pile Load Testing Methods

Gianpiero Russo and Gabriella Marone ……159

Experimental Investigations on the Lateral Bearing Behaviour of Vibratory-Driven Open Steel Pipe Piles

Johannes Labenski, M.Sc. and Christian Moormann, Univ.-Prof. Dr.-Ing. Habil……170

Experimental Studies on the Lateral Load Carrying Capacity of Pier Foundations for Bridges

Sukhmander Singh, Professor of Civil Engineering……180

Group Effects for Pile Rows under Passive Lateral Loading

Johannes Aschrafi, Shreyas Giridharan and Christian Moormann, Univ. Prof. Dr.-Ing……189

Investigating the Development of Pile Capacity over Time

Jeffrey R. Barrow, President / Geotechnical Engineer, Tumal J. Karunaratne, Project Engineer and Katie E. Persons, Project Engineer……199

Laboratory Evaluation of a Proposed Nondestructive Testing System for Detecting Anomalies below Drilled Shaft Excavations

Alireza Kordjazi, Joseph T. Coe, Assistant Professor and Trumer Wagner……211

Numerical and Experimental Study of Axially Loaded Non-Displacement Piles in Sand

Fei Han, Rodrigo Salgado and Monica Prezzi……221

Performance of Foundations in the Kanto Plain North of Tokyo during the MW=9.0 Tohoku Earthquake of March 2011

Daniel Pradel, PE GE DGE, Joseph Wartman, Prof. and Binod Tiwari, Prof……230

Quick, Efficient & Safe Preloading of High Capacity Hydraulic Modular Props

Peter Richardson, B.Eng.(Hons.), C.Eng., FICE, Vp PLC……..240

Recent Experience with Tremie Concrete Properties and Testing

Aidan Thorp, Christopher Wilkes, Duncan Nicholson and Bryan Marsh……244

Static Load Tests by Bi-Directional Method in the Brazilian Context

Felipe V. A. de Souza Cruz, Civil/Geotechnical Engineer, Marco A. G. Conte, Civil/Geotechnical Engineer, Renan Basso, Civil Engineer and Alessandra C. de Freitas, Professor of Civil/Geotechnical Engine……...254

Study of Effects of Construction Methods on Performance of Drilled Shafts

Sohail Kibria Vice President and Sajid Iqbal Senior Geotechnical Engineer…….262

Study on the Bearing Capacity of Bored Piles with Improvement Techniques

Ana B. A. N. Dias, Leonardo B. D. Brandão and Juliane A. F. Marques……270

Study on the Resistance of Bored Piles with Rings

Leonardo B. D. Brandão, Ana B. A. N. Dias and Juliane A. F. Marques……280

The Application of Fibre Optic Sensor Technology in the Integrity Testing of Deep Foundations

Anthony N. Fisher Testing and Instrumentation Manager and Andrew G. Bell Chief Engineer…….289

The Case of a Building Design Review Requiring a Full Foundation Redesign

Brendan Atarigiya, Geotechnical Engineer, Philip Amankwah, Structural Engineer, Isaac Osei, Structural Engineer, Nii K. Allotey, Geo-Structural Earthquake Engineer, Josesph Oddei, Geotechnical Engineer and William Albert-Viala, Structural Engineer……...299

The Influence of a Thin Weak Soil Layer on the Pile Bearing Capacity

Shilton Rica, PhD student and Stefan Van Baars, Professor……...308

Diaphragm Walls

Application of Long-Chain Polymer Slurry as Soil Stabilization in Reverse Circulation Drilling System

Goncalo António de Araújo Costa and Sri Ram Ramankutty I.R……....318

Challenges Faced in the Construction of 60M Deep Diaphragm Walls, with Hydraulic Grabs in Central London, England

Paul Wiltcher, Operations Director and Peter Handley……..324

Doha Metro's Flagship Triple Line Interchange Station

Christina Mavrommati, Principal Geotechnical Engineer, Cremona Makaginsar, Chartered Engineer and Carlos Posso, Senior Project Manager……334

EFFC/DFI Guide to Tremie Concrete for Deep Foundations

Karsten Beckhaus Ph.D. and Chris Harnan……344

Good Reasons to Swap from Trench Cutter to Hydraulic Grab; Liebherr and Saos, Actual Cases from Florence, Rome and Milan

S. Bechter, G. Franco, F. Rossi and M. Bringiotti……...360

Positive Cut-Off Wall in Indian Dam - ANew Technique for Difficult Geology

Steni Stefani, Consulting Engineer and Sanjay Dave, Civil Engineer Vice President & Sector Head……370

Recommended Junctions between Diaphragm Wall Panels for Deep Excavations

Paul Vidil, Deputy Design Manager……389

Suez Canal Underpass: 260.000 M² of Deep Diagraphram Wall Excavation Experienced with LWN at Almost 360°

M. Bringiotti, G. Bringiotti, D. Nicastro and G. Fumagalli……399

The Gaasperdammertunnel - Geotechnical Challenges in Amsterdam

D. Grotegoed, Geotechnical Engineer and N. Goedhart, Deep Foundation Specialist……...409

TTMJ - The New System for Slurry (Diaphragm) Wall Joints

Julian Crawley, John Coupland, Maurizio Siepi and Paul van Horn……..416

Unveiling the Vision of Soil Stabilization Fluids: The Future

Eonio Trindade, Technical Team Leader (Eng.)……..426

X10 Concept to Improve Quality and Durability of Diaphragm Walls

M. M. R. Boutz, B. J. Admiraal, R. van Berkel and P. R. B. van der Werff ……434

New Developments and Innovative Techniques

Advances in Resonant Pile Driving and Applications

Matthew Janes, M.E.Sc., P.Eng. ……..444

Annular Monoblock Bridge Foundations

Francesco Alessandrini, Nicola De Biaggio, Dario Fedrigo, Civil Engineer and Diego Valusso……..455

Conventional Excavation of Connecting Tunnels in C13 Metro Station (Poland - Warsaw - Line 2)

Marco Aurelio Piangatelli, Massimiliano Bringiotti and Ferdinando De Angelis……..464

Innovative Pile Extraction Technique of CFA Piles for the New Harbor Bridge Project

Tracy Brettmann, P.E., D.GE, Vice President……474

Job Site Reports Related to Deep FDP, Big Diameter CSP and Ring Vibrator Executed at the Limits by the Same LWN Drill Rig

M. Bringiotti and S. Bechter……484

Slope Stabilization with Multiple Anchors Monitored by Glass Fibre Technique

Dominik Gächter, Dipl. Ing., Reinhard Kulmer and Vaclav Racanský……494

Suggestion for Controlling the Implementation of Root Piles Partially Embedded in Bedrock

Marilia D. Silva, Civil Engineering, Roberto Q. Coutinho, University Professor and Myckelle M. S. Ferreira, Civil Engineering……504

The Field Investigation of Tension Cracks on a Cement Grouted Slender Column during the Thermal Response Test

Yue Ouyang, Project Manager, Loizos Pelecanos, Lecturer, Kenichi Soga, Chancellor's Professor and Duncan Nicholson, Director……514

Ventilation Shafts and Drifts for the Metro Line 6 Project in Naples, Italy

Vittorio Manassero, Giorgio Mormone and Federico Moccia……523

Why Using an Air-Entrainer to Increase Workability Is Not a Great Idea for Deep Foundations

Dimitri Feys……..533

Pile Construction

A Major Infrastructure Project and the Formation of the UK's Largest Rotary Pile under Polymer Support Fluid

Yue Ouyang, Project Manager, Stephan Jefferis, Director, Paul Wiltcher, Operations Director and Tony Suckling, Director……541

Brunnholen Bridge: Norway - Design and Supervision of Foundation Works

Arne Schram Simonsen and Vetle Kolberg Stene ……551

Cast-in-Place Piles Using Toe-Grouting Cell: Application in Bolivian Rivers

Tomás Murillo Pérez, Geotechnical engineer……..561

Current Practice of CFA Piling in Australia and New Zealand

Martin D. Larisch, PhD ……...572

Design and Construction of a 130.000 SQM Logistic Platform in Trieste's Port, ICOP & LWN: An Organization, Logistic and Powerful Rigs Winning Combination

M. Bringiotti, L. Grillo, S. Vitalini and R. Grisolia……..581

Extraction of Precast Piles and Secant Piles up to 27m

Thomas George Design Manager and Chris Price……..591

Micropiling in Urban Infrastructure: Advantages, Experience and Challenges

Freddy Lopez, MSc.-Ing. and Giorgio Severi, Dott. Ing……...601

New York City Landmark Structures - Reconstructing from the Inside Out

Michael J. Chow, PE, Senior Consultant…….611

Performance of Pile Foundations with Internal Diaphragm in the Red Sea Formations

Salwa Yassin, MICE, CENG, Ph.D,……621

Recent Innovations to Facilitate the Construction of Large Diameter Piles in London

Yue Ouyang Project Manager and Paul Wiltcher Operations Director……630

Steel Sheet Piling in Liquefiable Soils in Maasvlakte, Rotterdam

Bruno Pasqualini, Maria Carmela Romano and Mauro Tommasini……...640

Threaded Rotary Bored Piles at Paddington New Yard

David A. Hard and Ana T. Carvalho……655

Deep Foundations Executed with Excavation

A Call for Code Revisions for High Capacity Micropiles in Rock

Anthony C. Barila, P. E., Lawrence F. Johnsen, P. E. and John McKinnon, Project Manager……..663

An Approach for Optimization of Drilled Shaft Design in Dubai

Emad Y. Sharif, B. Sc - M. Sc GTC Lab Director and Hardev Sidhu, Lab Manager……..678

Behavior of Large Diameter Bored Piles in Calcareous Cemented Sand in Kuwait

Mohamed M. Al-Deab and Nabil F. Ismael……692

Cost-Benefit Analysis of Foundations with Revit-Assisted: Case Study

Mateus N. Farina, Student and Alexandre D. Gusmão, Professor ……..702

Diaphragm Walls and Ground Improvement on the Open-Cut Excavation of Bologna HS Railway Station

Luca Utzeri, Stefano Ciufegni and Francesco Sacchi……..716

Estimation of the Load Bearing Capacity of Root Piles Partially Embedded in Rock Mass Rhyolite, Using Empirical and Semi-Empirical Methods

Myckelle M. S. Ferreira, Engineer and Roberto Q. Coutinho, Teacher……..730

Innovative Design and Quality Control of Single Stage High Pressure Injection Micropiles, Waal-Compact-Piles

Floris Schokking Director and Jan van der Wiel……741

Performance and Analysis of Braced Secant Pile Wall for a Multi-Story Building in Manhattan, NY

James D. Maniscalco, P. E. and Evangelia S. Ieronymaki, Ph.D.……752

Pile Foundations of Trieste's New Logistic Platform

Francesco Alessandrini, Civil Engineer, Dario Fedrigo, Luca Grillo, Federica Pedrini, Civil Engineer and Diego Valusso……...762

Pile Load Test: Analytical Methods for Bearing Capacity, Including Brazilian Methods

Denise I. S. Gomes Venturi and Roberto Quental Coutinho, DSc……...771

Deep Foundations Executed without Excavation

A New Method of Quality Control for Jet Grouting Online Vibration Monitoring

Nikolaus Schneider, General Manager / Dipl.-Ing. and Silke Appel……...781

A Non Linear and Plastic-Hardening Modelling of Vertically Loaded Piles

Maurizio Lenzi, Professional Engineer and Paola Campana, Professional Engineer……791

About the Influence of Time on the Bearing Characteristics of Precast Driven Piles

L. Vavrina, Project Manager, U. Plohmann, C. Moormann, Univ.-Prof. Dr.-Ing. habil. Christian Mo and P. Wardinghus……801

Design and Load Testing Program of Large Diameter Open-Ended Piles for a Bridge Construction Project in Louisiana

Murad Y. Abu-Farsakh, Ph.D., P.E., Md. Nafiul Haque, Ph.D. and Chris Nickel, P.E.……...811

Evaluation of Effectiveness of Slope Stabilization Using Monitoring Techniques: An Application in Northern Italy

Alessandro Micheli, Maurizio Martino, Enrico Mittiga and Giorgio Ricci……823

Laterally Loaded Piles in an Embankment of Dry Sand

J. W. R. Brouwer, Principal Consultant……...830

Modeling the Effect of Excess Pore-Water Pressure on the Bearing Capacity of Full Displacement Piles in Group: A Case-Study in Parma (Italy)

F. Simone, Engineer, G. Guadagnini, G. Marchi, C. Cremonini and M. Marchi……839

The Importance of Energy Evaluation on an Individual Pile Basis

Julian P. Seidel, Technical Director……849

The Mechanism of Grouting Action under the Base of Bored Pile

Adam Krasinski, Dr Hab. Eng. and Mateusz Wiszniewski, MSc. Eng……858

The Normalized Bearing Graph and Dynamic Reduction Function Concepts in Pile Acceptance

Julian P. Seidel, Technical Director……868

Design and Modeling Criteria: Other Techniques

Keynote Lecture: The Sochi Case: The First Real Comparison Between NATM and A.DE.CO-RS**

G. Lunardi, CEO, G. Cassini, Technical Director, A. Bellocchio, Technical Manager……1372

Anchor Head Models : Classification, Adaptability & Design

M. Ansriou, Studies Engineer, T. Wulleman, C. Rabeux and A. Ouaar……878

Damaging of the St. Benedetto Tunnel after the Quake of October 30, 2017: Study and Repair

Alessandro Micheli, Luca Cedrone, Geotechnical Engineer and Maurizio Martino……888

Finite Element Numerical Analysis to Evaluate the Lateral Behavior of Three Pile Group Configurations

Murad Abu Farsakh, Research Professor, Ahmad Souri, Research Associate and George Voyiadjis, Boyd Professor……901

Influence of the Loading Duration on Undrained Shear Resistance of Soft Clays Observed during the Construction of a Roadway

Giana Laport Alves de Souza, M.Sc., Marcus Peigas Pacheco, PhD and Rubenei Novais Souza, PhD…….913

Method for Assessing Damage Induced in Utilities Due to Ground Movements from Major Infrastructure Projects

Francesc Mirada, Geotechnical Engineer, Riccardo Impiumi, Geotechnical Engineer and Zeena Farook, Geotechnical Engineer……925

Pile Groups with Negative Skin Friction

Francesco Basile, PhD, MEng……934

Seismic Performance of a Piled Raft Foundation with Grid-Form DMWS Considering Softening of Stabilized Soil

Yoshimasa Shigeno, Kiyoshi Yamashita and Junji Hamada……948

Soil Improvement by Expanding Polyurethane Resins

Andrea Dominijanni, Assistant Professor, Nicolò Guarena, PhD Candidate and Mario Manassero, Professor……958

Grouting

Keynote Lecture: Challenges in the Design of Jet Grouted Structures

Alessandro Flora, Ph.D., Giuseppe Modoni, Stefania Lirer and Valeria Nappa……968

A Ground Improvement Treatment for Two Raise Bored Elevator Shafts in a Historical Site of Central Italy

Massimo Grisolia, Ignazio P. Marzano, Giuseppe Iorio, P.E., Giuseppe Panetta, P.E., Ferruccio Cribari and Giuseppe Trovato……..989

Cement and Superabsorbent Polymer to Solidify Slurry

Jinyuan Liu, Associate Professor and Ali Ahmad, Civil Engineering……..999

Foundation Shaft Executed with Jet Grouting

G. Modoni, M. Ochmañski, E. Salvatore, Ahn Dan, L. Q. A. D. and P. Croce……1007

Compaction Grouting Intervention for the Mitigation of Soil Liquefaction Risk within the Earthquake-Stricken Area of Emilia in 2012

Claudio Asioli, Eng., Federico Fanti, Eng. and Paolo Zuffi, Geol……1019

Deep Jet Grouting for the Construction of MRT Blue Line Extension in Bangkok

Bruno Vingiani, Technical Manager and Maurizio Siepi……..1028

Intervention for Improving Characteristics in Fault Zone in Tunnel Alignment - Consolidation Using Chemical Grouting with Mono and Bi-Component Resins

Pasquale Petrocelli, Aldo Bellone, Francesca Rossano and Marco Aurelio Piangatelli……..1039

Lattice-Shaped Jet Grouting Configuration to Prevent Soil Induced Liquefaction at Christchurch Town Hall – New Zealand

Antonio Cristovao, David Brito and Abilio Nogueira……1050

Study on the Quality of Multifan Shaped Jet Grouting

Takashi Shinsaka, Dr.Eng, P.E.jp, Sen.Pro.C.E, Junichi Yamazaki, P.E.jp, Yasuharu Nakanishi and Kazuhito Komiya, Prof……1061

The Multi-Purpose Bottom Plug (MPBP): An Innovative Solution for the Galataport Project in Istanbul, Turkey

Salvatore Miranda, Claudio Asioli and Claudio Nastasi……...1071

Ground Modification Technologies: Other Techniques

Assessing the Effectiveness of RIC/RDC Technique for Deep Fill Compaction Application

Aymen Brik, Technical Manager and Emmanouil Spyropoulos, Geotechnical Engineer……..1082

Case Studies of Ground Improvement Using Rammed Aggregate Piers in Problematic Soils Allowing for Conventional Foundation

Roberto Avendano, B.Eng. P.Eng. and Matt J. Kokan, M.A.Sc. P.Eng……..1092

Dynamic Compaction of Rockfill on Land and under Water at Stockholm Norvik Port

Sölve Hov, Håkan Eriksson and Carl Wersäll……...1100

Effect of Steel Fibres on the Behaviour of a Chemically Stabilised Soil

A. A. S. Correia, Oliveira P. J. Venda , PhD and J. M. N. P. C. Teles, MSc…….1110

Ground Improvement by Inclusions in Unstable Slopes

Carlos S. Oteo, Ing. C. C. y P., Javier Oteo, Ing. C. C. and P. and Pedro Sola, Ing. C. C. and P..……1118

Ground Improvement Instead of Piling - Effective Design Solutions for Heavily Loaded Structures

Michal Topolnicki, Prof. PhD. DSc..……1128

Innovations in Ground Improvement: Creating Composite Ground with Drill Displacement Column™ and Auger Cast Column™

Tom Farrell, M.S., G.E., John Ho, Ph.D., G.E., Neville Su, G.E. and Sam Warren, P.E..……..1138

Long Term Mechanical Property of Cement Treated Loam Used in Road Embankment

Yukika Miyashita and Genki Inoue…….1151

Mega Soil Improvement Case Study: Improvement of Soft Soil Using Prefabricated Vertical Drains

Robert Thurner, Technical Director ME and Mohamed Ayeldeen, Senior Engineer……1160

Performance of a New Driven Battered Micropiles System in Sand

Amirhassan Mehdizadeh, Mahdi M. Disfani, Dr., Chin F. Tsang, Guillermo A. Narsilio, Robert Evans and Emad Gad……...1169

Properties of Ground Improvement Using Low CO2 Emission Cement

Takao Kono and Masamichi Aoki, Executive Manager…….1179

Secant Piles Shafts and Directional Drilling (SPPD) for a Modular Drainage System

Marco Angelici ……..1189

Underground Car Park in the Ancient "Morelli" Cavern in Naples

M. Bringiotti, A. Bellone and F. Rossano……...1200

Vacuum Preloading with Drain to Drain Method for the New International Airport of Mexico City

Vito Nicola Ghionna, Prof., Luiz Guilherme de Mello, Prof., Valeriano Pastore, Managing Director, Roberto Andrighetto and Luca Pereira Cammarota……..1210

Soil Mixing

A Deep Soil Mixing Application for a Road Slip Fast Repair

Massimo Grisolia, Ignazio P. Marzano, Giuseppe Iorio, Raffaele Papa and Giuseppe Panetta……..1222

A New Quantitative Approach in the Evaluation of Homogeneity in Deep Mixing

Diego Bellato, Ph.D., M.Sc., P.E., Paolo Fania, M.Sc., P.E. and Ulli Wiedenmann, Dipl.-Eng. (FH)……1232

An Innovative Soil Mixing Treatment to Underpin Existing Buildings

Massimo Grisolia, Ignazio P. Marzano, Giuseppe Iorio, Raffaele Papa and Giuseppe Panetta……..1242

Applications of Cement Stabilization for Mitigating Earthquake Disaster

Masaki Kitazume, Prof. ……1251

Cutter Soil Mixing as Ground Improvement Technology in Under-Consolidated Clays

Sandro Gomes, Joao Nunes, Franz-Werner Gerressen and Thomas Vohs ……..1261

Liquefaction Countermeasures Using Floating Grid-Form Soil Improvement for the Container Yard Located in Harbor Area

Shoichi Tsukuni, Takahiro Sugano, Takahiko Masumoto, Kazuhiro Kaneda and Yoshio Hirai……...1271

Strength Design of Cement-Treated Piles Subjected to Lateral Flow of Liquefied Ground

H. Takahashi, Head of Group, W. Tsuda, N. Takahashi, M. Fuchiyama, Y. Morikawa and I. Towhata…...1281

Testing and Evaluation of Residues as a Binder Component for Deep Mixing and Jet Grouting

Per Lindh Ph.D. and Håkan Eriksson Ph.D..……...1290

Unconfined Compression Tests of Cement-Treated Soil Containing Unmixed Soil

Tsutomu Namikawa Civil Engineering and Sae Suzuki……..1300

Project Information Management Systems (PIMS) and BIM

BIM - A UK Foundation Sub-Contractors Perspective

Mark Pennington Technical Director and Tracey Fitch Principal Technician…….1306

Data Management, Analysis, and Reporting for Small Foundations

Jamey Rosen and Andrew Higgins…….1316

Deep Foundation Job Sites of the Future: Digitization and Networking as Major Strategic Factors for Information Management Systems

Arno Halbeisen, MA, MA……...1325

Electronic Support in Installation of Special Foundation Products - Ensuring Safe Production and Increasing Quality Control

Franz-Werner Gerressen……1336

Evaluation of Spatial Variability for Site Characterization Based on Standard Penetration Test Results

Salwa Yassin, MICE, CENG, Ph.D..……1345

Mosul Dam - Building 2D & 3D Project Information Systems for Construction Monitoring and Risk Assessments

Vanessa C. Bateman, Baron M. Worsham, Laurel E. Blackman, Nathan D. Williams and Bobby S. Sells……1355

Recent Advances in Bim in Geotechnics

Jim De Waele……..1365

****PLEASE NOTE: This is out of page sequence**

FOREWORD

Following the tradition established over the last three decades, DFI organizes in Europe, since 2000 jointly with EFFC, international conferences on piling and deep foundations generally focused on specific themes.

In this international conference, we opened a window on the megaprojects that are quickly transforming the world, changing our way of travel and communication, and constituting related opportunities for the geotechnical industry.

In this context, the conference showed how advanced geotechnical machines and technologies and the use of special materials support and also challenge designers and contractors to jointly develop new designing approaches that reflect new codes and contractual rules.

For these purposes, in a not so usual manner, DFI and EFFC invited all the different stakeholders in the geotechnical industry - academics, designers, clients, contractors, suppliers and owners - to gather and work together to discuss problems and propose new solutions for bigger, faster, more specialized and complex works.

The conference was organized in the prestigious Engineering Facility of the Sapienza University in my splendid and magical Rome.

Over 150 papers from all over the world were submitted from which 70 were chosen for verbal presentation in 12 technical sessions and 38 selected for poster presentation.

Supplementing keynote lectures and paper presentations by speakers from various countries, as usual, the conference attracted students and enthusiastic young engineers. An active plenary session panel discussion structured with technical video presentations was specifically dedicated to young professionals.

This conference would not have been possible without the support of our partner sponsors and the cooperating organizations. I would like to express my gratitude to all members of the organizing committee, to the technical committee - Maurice Bottiau, Daniele Vanni, Gianfranco Di Cicco, Frank Haehnig and Paolo Marzano – and especially to the conference manager, Theresa Engler, Executive Director of DFI, Mary Ellen Large, DFI Director of Technical Activities and the DFI event team.

Thanks to international advisory board, too, and lastly, to our Italian colleagues who helped throughout the planning and hosted DFI, EFFC and the conference attendees in a great, unforgettable way.

Massimo Grisolia, Conference Chair



GEOPHYSICS FOR GEOTECHNICAL DESIGN

Michele Jamiolkowski, Emeritus Professor, Tech. University, Torino, Italy,
m.jamiolkowski@studiogeotecnico.it
Andrea Masella, M. Sc. Project Manager, Studio Geotecnico Italiano, Milano, Italy,
a.masella@studiogeotecnico.it

ABSTRACT

The paper presents some selected topics related to the role of in-hole geophysical tests in the design and construction of the Zelazny Most depository, one of the world's largest copper tailings disposal, in South-West Poland, owned by KGHM (Polish acronym for Copper Mine and Mill Company). Considering the dimension of the object dealt with and the volume of the tailings already stored, presently ~ $618 \times 10^6 m^3$, one of the most demanding challenges to geotechnical engineers involved with its design and construction concentrates on its safety with respect to the hazard of flow failure. To ensure the overall security of the surrounding area, the safe development of the disposal is overseen by an International Board of Experts (IBE) by applying the R. Peck (1969, 1980) observational method. After mentioning the role of geophysical in-hole tests in geotechnical design, this paper focuses on the use of seismic waves, P-wave and S-wave, in combination with dedicated consolidated undrained triaxial tests to evaluate the susceptibility of tailings to liquefaction in fully and partly saturated state. The following selected topics, oriented towards practitioners interests, are discussed: brief description of Zelazny Most tailings depository; characterization of propagation of S-waves in down-hole mode to determine the shear wave velocity V_s ; mapping the state of the tailings with depth by propagation P-waves from 16 cross-hole station, to distinguish between fully from near to saturated tailings and the greater increase of the liquefaction resistance of partly saturated with respect to fully saturated tailings.

Keywords: Copper tailings, tailings disposal, in-hole geophysical tests, partly saturated tailings, gel-push sampler

INTRODUCTORY REMARKS

In the last two decades the role of in situ and laboratory geophysical tests has grown and becoming increasingly important in the characterization of the soil properties and the geotechnical design.
The broad spectrum of geophysical in situ and laboratory tests, applied to solve various geotechnical boundary value problems are thoroughly documented in recent geotechnical literature, as partly summarized in Table 1.
This paper focus on the role of seismic shear (V_s) and compression (V_p) in-hole body waves velocity measurements in the design and construction of the copper tailings at the Zelazny Most Storage Facility (ZMSF), the world second-largest disposal facility of this kind, see Fig.1.

Table 1. Seismic shear and compression body waves velocities-aid in geotechnical design in situ and in-hole laboratory tests.

Difference between fully and partly saturated soils	→ V_P
Evaluation of undisturbed samples quality †	→ V_S
Assessment of porosity in situ †	→ $V_P + V_S$
Soil stiffness at small strain, 10^{-3}	→ V_S
In situ lateral stress coefficient K_0 †	→ V_S
Settlements of shallow foundations on sands †	→ V_S

(*) See list of selected references †.

© 2018 Deep Foundations Institute

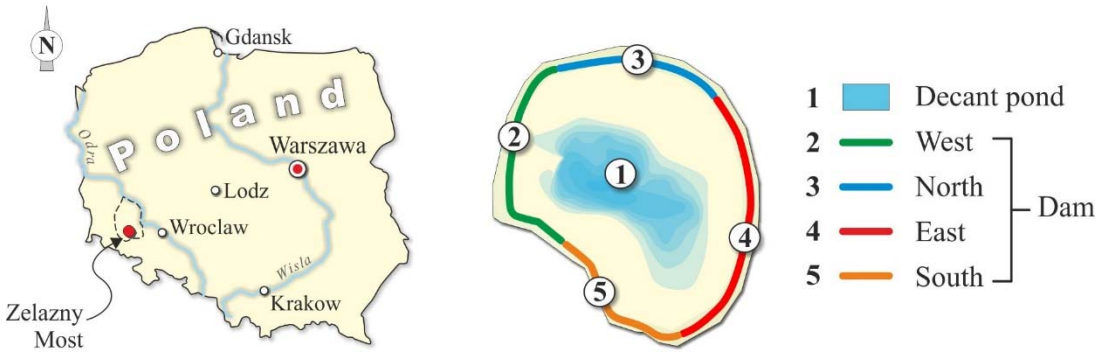


Fig. 1. Plan of depository

The aerial view of the ZMSF is shown in Fig.2 and displays updated information as to its current dimensions.

As with all the tailings dams, the ZMSF poses several challenges to the geotechnical engineers involved with its design and construction. In the examined case, the risk of static liquefaction and the considerable influence of the various Pleistocene glaciations represent the key issues for a safe design and construction of the object.

Considering the above background, the dimension of the object dealt with, given its strategic role to ensure the safety of the surrounding area and taking also into account that it is an on-going project, whose overall period of operation will exceed 70 years, in 1992, KGHM appointed a four-member International Board of Experts (IBE) [Dr. David Carrier (USA), Prof. R. Chandler (UK, resigned in 2016), Prof. K. Hoeg (Norway), Prof. M. Jamiolkowski (Italy), and Prof. J. Standing (UK)], to oversee the safe development of the ring dam confining the tailings, by applying the R. Peck's observational method. [Peck (1969), Peck (1980)].
IBE task is supported by the state-of-the-art monitoring system which is constantly upgraded and is managed by the highly skilled team of the Mine Hydrotechnical Division.

TAILINGS DISPOSAL

The Zelazny Most dam that surrounds the tailings disposal, hereafter will be referred as the *ring dam*. Fig.3, reports the present elevation and the height of the ring dam crest.
The Zelazny Most ring dam is being raised adopting the upstream construction method, see Fig.4. The shell of the dam is built using the coarser tailings, see Fig.5, which are fine sands and low plasticity silts, separated from the remainder of the tailings by spigotting. The overall range of the tailings grading encountered at ZMSF is shown in Fig.6.



Maximum dam height:	71 m
Tailings volume stored:	618×10^6 m^3
Storage rate:	17×10^6 m^3/annum
Ring Dam's length:	~ 15 km
Total Area:	~ 14 km^2
Beach Area:	~ 7 km^2
Pond Area:	~ 5 km^2
Water volume:	~ 8×10^6 m^3
Operation time:	1977 throughout 2050

Fig. 2. Zelazny Most Tailings Disposal, updated as of March 2018.

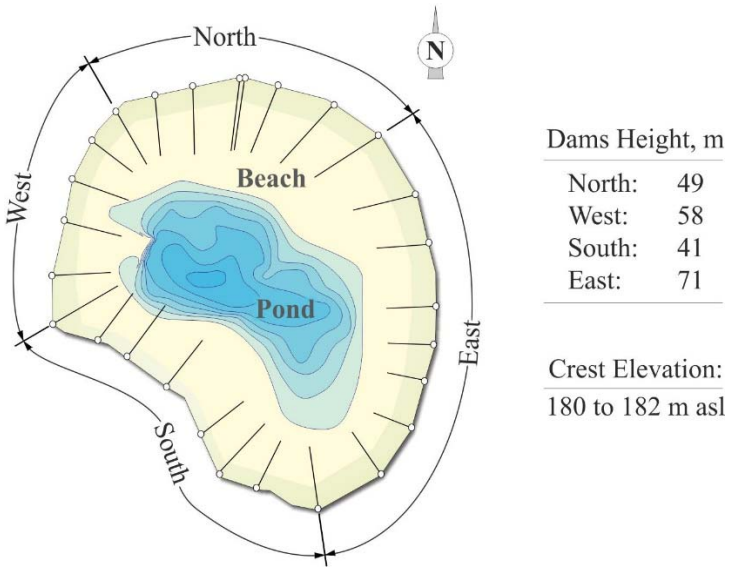


Fig. 3. Dam height and crest elevation, updated at March 2018.

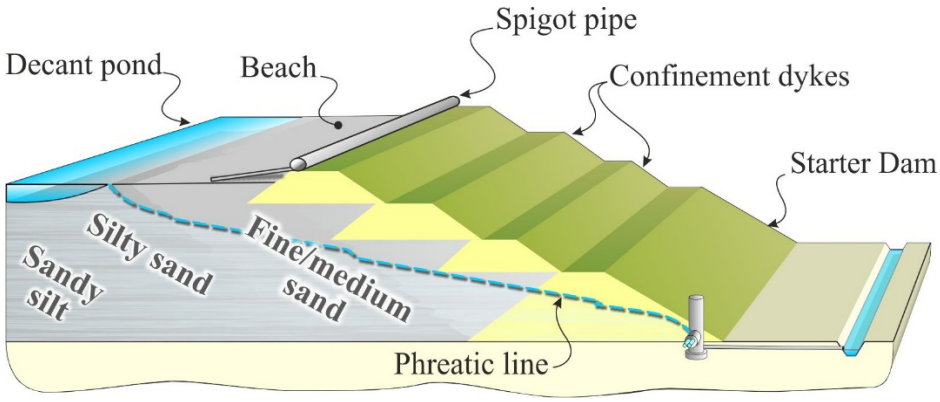


Fig. 4. Ring Dam - Schematic Cross-section.

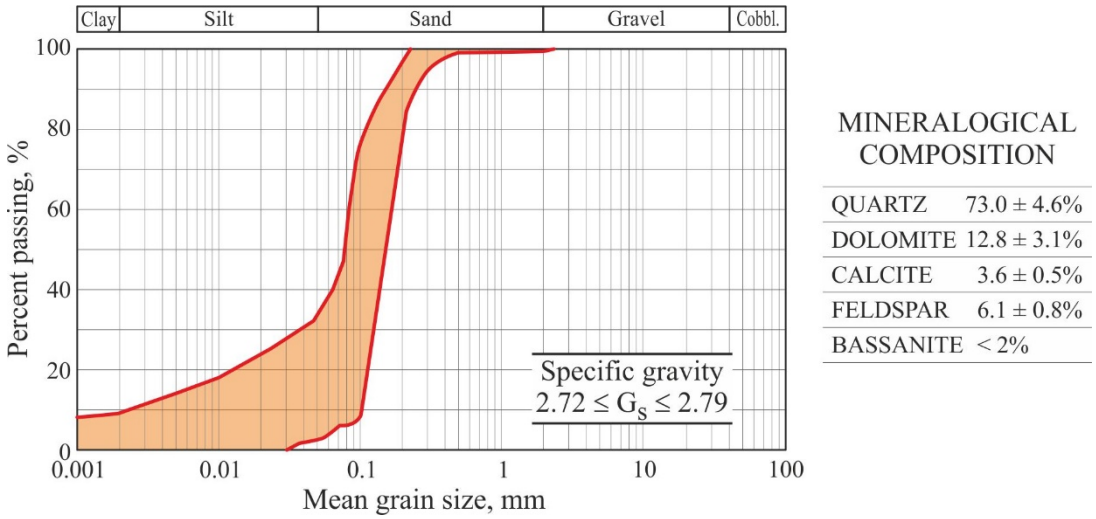


Fig. 5. Coarse tailings used to build the ring dam - Lipinski (2000, 2012).

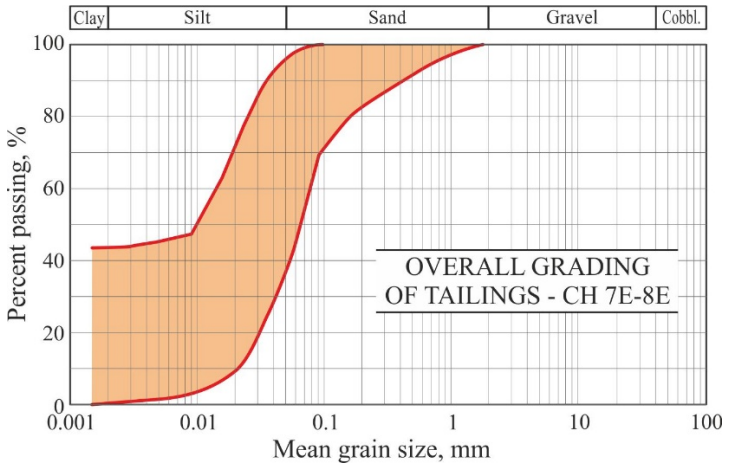


Fig. 6. Overall grading of tailings.

The dam crest has been risen overall at a rate of approximately 1.5 to 2.0 m/year and constructed with an average downstream slope of 3.5 horizontal to 1 vertical. Furthermore, the beach (i.e. the distance from the dam crest to the pond edge) is maintained with a length of not less than 200m, to keep the phreatic surface in the ring dam shell depressed. In addition to the toe drain, four levels of circumferential drains have been installed as the dam was raised and a fifth level is now under construction, see fig.7. This drainage system, has proven to be very efficient, see Fig.8, allowing to keep the phreatic surface well below the beach, thus reducing the risk of the tailings flow failure.

More detailed information on ZMSF features can be obtained from Chandler et al. (2011), Lipinski (2000, 2012), Jamiolkowski et al. (2010), and Jamiolkowski (2014) of this latter reference, this work is an updated excerpt.

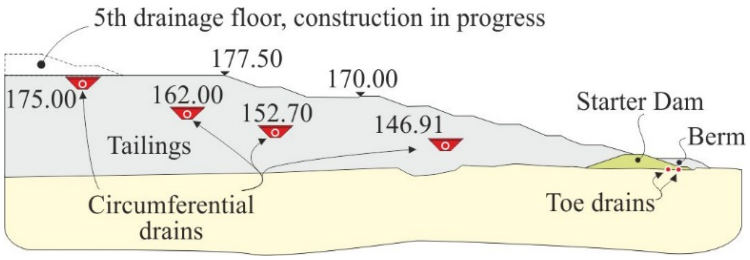


Fig. 7. Ring Dam - Circumferential drains.

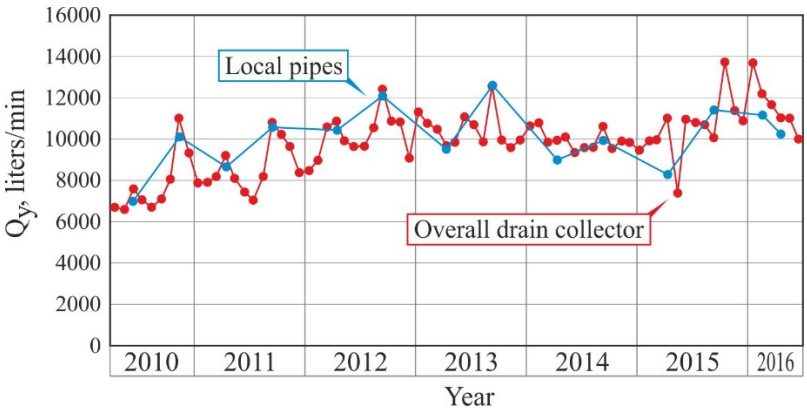


Fig. 8. Circumferential drains yield.

GEOTECHNICAL CHARACTERIZATION OF TAILINGS

The tailings characterization was mostly supported by the results of situ penetration tests: CPTU, DMT, S-CPTU and S-DMT, allowing, during the execution of the latter two tests, to measure V_s in a down-hole mode.
This limitation was overcome in 2003 with the use of the Gel-Push sampler. This tool, that will be illustrated next, allows to retrieve the tailings undisturbed samples.

In 1997, on an experimental basis, on the dam beach were installed some cross-holes (CH) to allow the propagation of horizontal (P-wave) and (S-wave) at different distances from the dam crest.

The addition of extra cross-holes in the existing monitoring system has further enhanced the value of the information yielded by the geophysical tests. In particularly they allow to:

- check the reliability of the measured shear wave velocity V_s using different in-hole geophysical methods (S-CPTU, S-DMT and CH), see Fig.9
- Verify feasibility and reliability of the measured compression wave velocity V_p, as a very sensitive tool to map the depth of the phreatic surface below the beach, distinguishing the fully (S_r=1) from the partly (S_r<1) saturated tailings. As an example, Figs. 10 and 11, display the profiles of V_p and V_s determined by means of CH tests, respectively carried out in tailings (CH-XIXE) from the ZMSF beach and from the original ground level (CH-KP), in heavily OC Pliocene clay outside the dam imprint (CH-KP). Both figures allow locating unequivocally the depth of the phreatic surface based on measured V_p values.

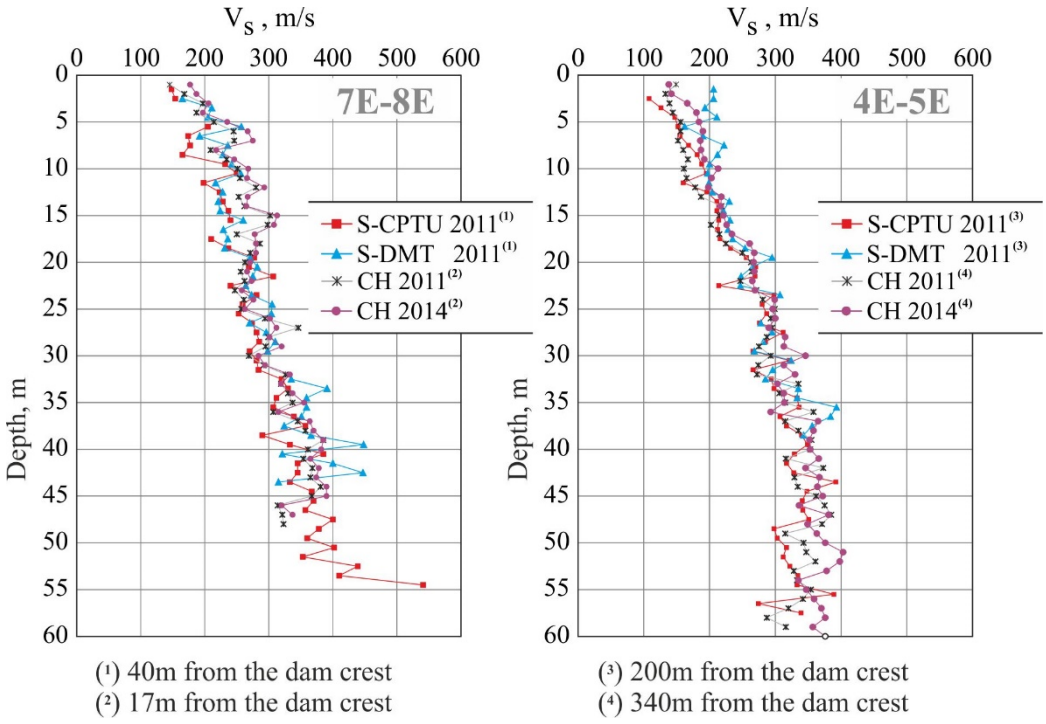


Fig. 9. Shear wave velocity tailings profiles from CH 4E-5E and CH 7E-8E, S-DMT and S-CPTU after Tschuschke et al. (2014).

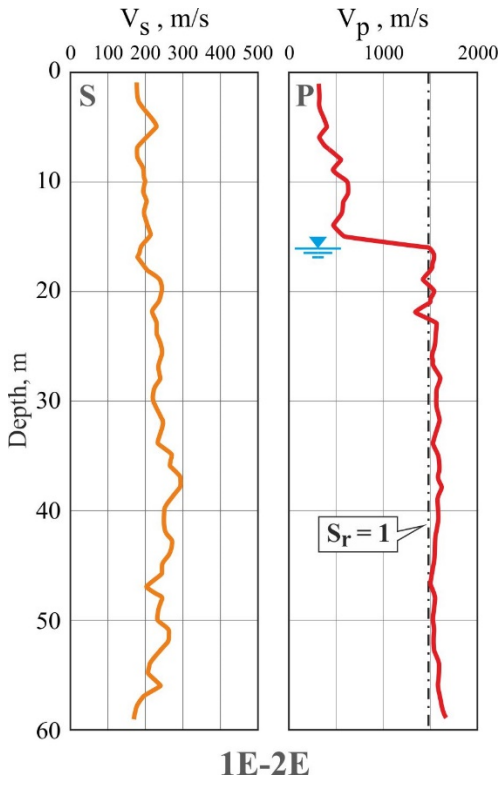


Fig. 10. CH-XIX-E Copper tailings.

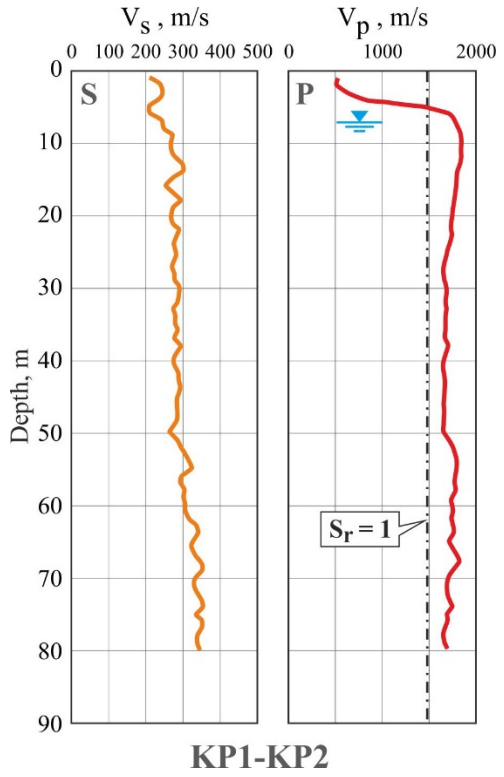


Fig. 11. CH-KP Copper tailings; Highly OC Pliocene Clay.

STATE OF TAILINGS DEPOSITED AT ZELAZNY MOST

This chapter recaps the steps undertaken by KGHM to obtain a deeper insight into the susceptibility of the tailings to flow failure.
With reference to the state-of-art enhancement of Geotechnical Engineering in the area in question, in the following are examined the most relevant features, pertinent to the safety of the ZMSF.

Location of Phreatic Surface in Tailing

As well documented in geotechnical literature [Ishihara, et al. (1998), Nakagawa, et al. (1997), Yoshimi et al. (1989).], the susceptibility of the tailings to liquefaction strongly depends on their, although small, deviation from the state of full saturation.
Consequently, KGHM decided to monitor, roughly every second year, the spatial distribution of partly saturated tailings, with reference to the P-wave velocity V_p measured in CH.
Currently this activity is supported by 18 CH stations installed along the selected geodetic cross-sections on East, West and North Dams, see Fig.12.

Each geodetic cross-section has been equipped with three CH stations located at 162m to 485m from the starter dam.
Every CH station consists of two boreholes spaced about 4m to 5m and reaching a depth ranging from 42m to 62m.

By using two boreholes to ensure the reliability of the measured seismic waves velocities, the trigger delay has been calibrated in laboratory, separately for P and S waves, employing appropriate electrical power unit.

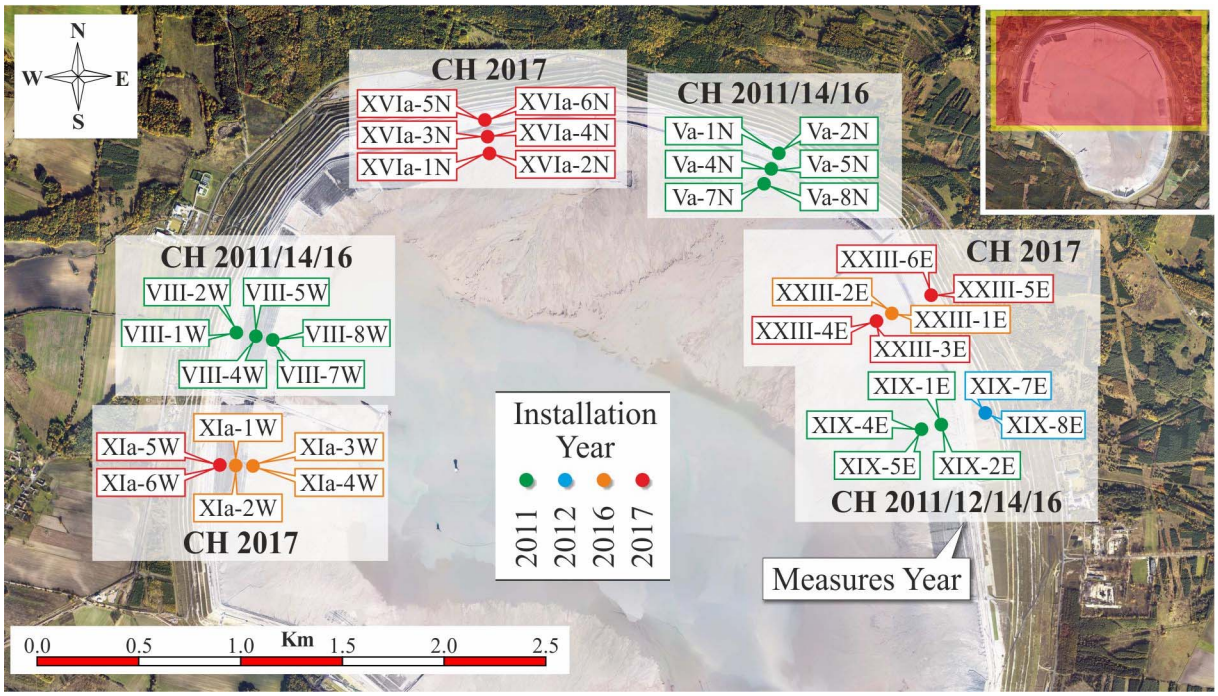


Fig. 12. Cross-holes at Zelazny Most tailings depository - Locations and installation date.

In Fig.12, the white rectangle reports the years when the P-wave and S-wave velocities were measured on the CH stations of the three mentioned dam segments. The colored dots indicate the locations of CH stations operating on different geodetic cross-sections, marked by Roman numbers.

In the following are illustrated two examples of the use of the compression wave velocity propagated from CH, aimed at delineating the spatial distribution of the partly saturated tailings within the body of ZMSF.

The boundary between partly and fully saturated tailings has been identified as the depth below the beach, beyond which the compression wave velocity $V_p \geq 1550$m/s, remains constant or increases with depth.

The first example presented in Fig. 13, summarizes the results of the tests carried out on CH1-2 station, of the North dam, located 185m away from the starter dam, during the period 2011-2017, see Fig.12. Fig.13 shows that, despite the time elapsed between the first V_p measurements campaign (2011), and the last one (2017) and the dam crest has been risen by 9 to 12 meters, the depth of the phreatic surface has remained stable

This testify the crucial role played by the circumferential drainage system (Figs. 7 and 8) to keep the phreatic surface depressed in the ring dam shell and under a large part of the beach, thus reducing the risk of flow failure of the tailings.

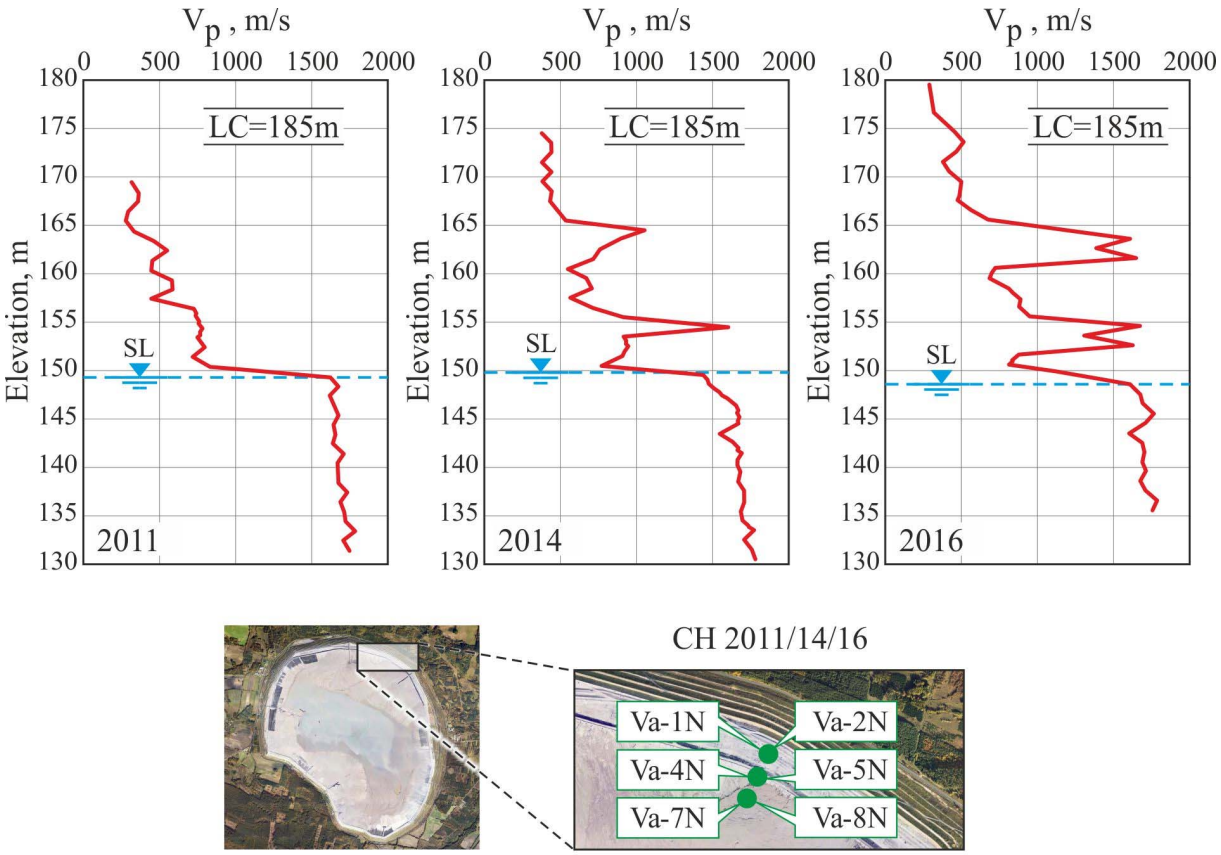


Fig. 13. North dam, CH1-2N, depth of the saturation line.

To make the readers acquainted with the overall picture emerging from mapping the depth of partly saturated tailings below the beach based on the measured V_p , Tab.2, presents a resumé of the depth of the phreatic surface measured in all the 18 CHs, located at different distance (LC) from the starter dam updated as of March 2017. The data shown confirm the idea that overall, in all the CHs operating at ZMSF, the depth of the phreatic surface depends on the distance from the pond, and except minor oscillations +/- 3m, stays constant, while the ring dam is risen. This clearly implies that the Mine will continue to complement the dam height increase with the installation of circumferential drains, as it has been done so far.

The second example, shown in Fig.14, refers to three cross-hole stations (CH1-2, CH4-5 and CH7-8), installed along the geodetic cross-section VIII of the West dam, and respectively located at the distance of 210m, 295m and 380m from the starter dam. The measurement of $V_{p,}$ carried out at the end of 2016 in three cross-holes offered the opportunity to explore how the elevation of the phreatic surface changes when it decreases the cross-hole station distance from the pond.

The above examples prove the reliability of P-waves velocity as a mean to identify fully from partial saturated tailings even when the latter is very close to a fully saturated state, i.e. up to $S_r \geq 0.98$.

Figs.13 and 14 show that the operational drainage system keep the phreatic surface considerably depressed, close in the shell of the confining dam, but significantly under the beach, up to 350 to 400 from the dam crest.

This indicate *qualitatively* the efficiency of the drainage system in question which reduces appreciably the risk of tailings flow failure.
However, to *quantify* the beneficial effects of the partial saturation of the tailings with respect to the hazard of flow failure, it is crucial to supplement the value of P-wave velocity measured in the field with laboratory tests.
The issue is summarized in the following section.

Table 2. Depth to saturation line, A. Callerio, Studio Geotecnico Italiano (2017).

Geodetic	Distance from	Dam Elevation	Phreatic Surface
XIX E	145	164	36
	365	179	26
	465	178	13
XXIII E	150	170	37
	365	180	29
	450	178	21
Va N	185	171	31
	265	183	36
	345	180	32
XVIa N	190	174	>44
	265	183	46
	340	178	42
VIII W	210	183	42
	295	179	29
	380	178	19
XIa W	200	183	37
	300	179	32
	380	178	28

Updated as of March 2017

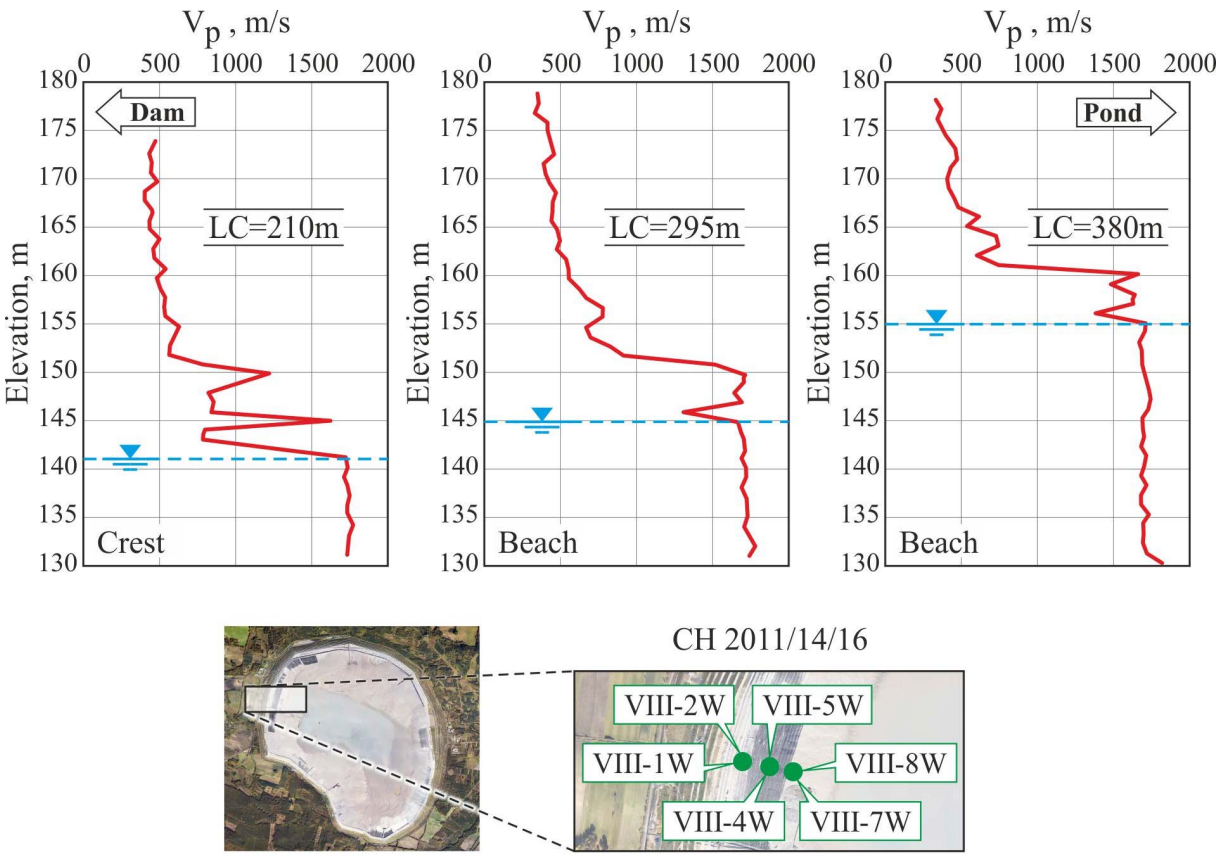


Fig. 14. West dam, section VIIIW, CH's Survey 2016.

Degree of Saturation versus Liquefaction Resistance

Since late nineties, many renowned geotechnical research centres have invested massive research efforts to investigate the behaviour of partly saturated sands and low plasticity silts, whose pore fluid contains air or gas, e.g.: Huang et al. (1999), Kokusho (2000), Ishihara et al. (2001), Okamura and Soga (2006), Tamura et al. (2002, Tsukamoto et al. (2002), Emerson and Foray (2006) and many others. Their works have been focused at investigating the increase of the liquefaction resistance, both under cyclic and monotonic loading, as function of the saturation degree S_r. In the examined case, the liquefaction of the tailings under monotonic shearing is of prominent interest.

To achieve this goal the routine procedure consists in carrying out laboratory consolidated undrained triaxial tests on fully and on partly saturated specimens of the same soil for which the P-wave velocity V_p has been measured in the field. The above tests are usually carried out on specimens reconstituted in laboratory and more seldom on undisturbed specimens.

To be representative of the soil conditions in the field, the specimens used in this case, should replicate, as close as possible, the soil in situ state and its relevant material properties.
In laboratory, for specimens tested in fully saturated state, the proof of their complete saturation, requires that the measured Skempton's (1954) pore pressure parameter B at failure attains a value ≥ 0.95.

As to the partly saturated specimens, they are reconstituted to the desired combinations of the unsaturated soil stress and state variables and then subject to consolidated undrained triaxial tests at different degrees of saturation and confining pressure.

Considering that the resistance of the tailings to liquefaction increases as the values of B and of S_r decrease and that their values cannot be directly monitored in the field, it is worthy to mention a comment quoted in the paper by Ishihara et al. (2001):

"P-wave velocity can be measured both in the field deposits and in the laboratory samples while other index properties such as B-value and ***saturation ratio*** *cannot be monitored by any means in the field. Therefore, the P-wave velocity V_p may be used as a parameter to identify conditions of laboratory specimen and that in-situ soil deposits in relation to the degree of saturation"*

With reference to the above, Fig.15a reports the results of cyclic undrained stress ratio of Niigata sand causing D.A. strain of 5% in 20 cycles as function of the saturation degree, see Ishihara et al. (2001). In this case, even a minor deviation from the full saturation, S_r=99.3% determines an increase of the cyclic stress ratio by ~16%, which in case of S_r=95.5% attains a value of ~ 47% and for the S_r =90% approaches the value of above 85%.

Whereas Fig.15b presents the results of a series of cyclic undrained triaxial tests carried out by Ishihara et al. (2001) on different coarse grading geomaterials as function of V_p, illustrating the effect of partial saturation on the cyclic undrained strength normalized with respect to that of fully saturated coarse grained soils, in the following called Liquefaction Resistance Ratio (LRR), applicable both to cyclic and monotonic loading conditions, He et al. (2014).

To corroborate the above picture, Fig.16 displays a set of data collected by Okamura and Soga (2006) from different case records in Japan and Taiwan, including the mentioned data by Ishihara et al. (2001).

It is worthy to notice that the normalized LRR, here expressed in terms of the ratio of partly saturated soil liquefaction resistance versus the liquefaction resistance of fully saturated soil, exhibits quite a consistent trend with respect to the S_r, quoted by the five referenced authors.

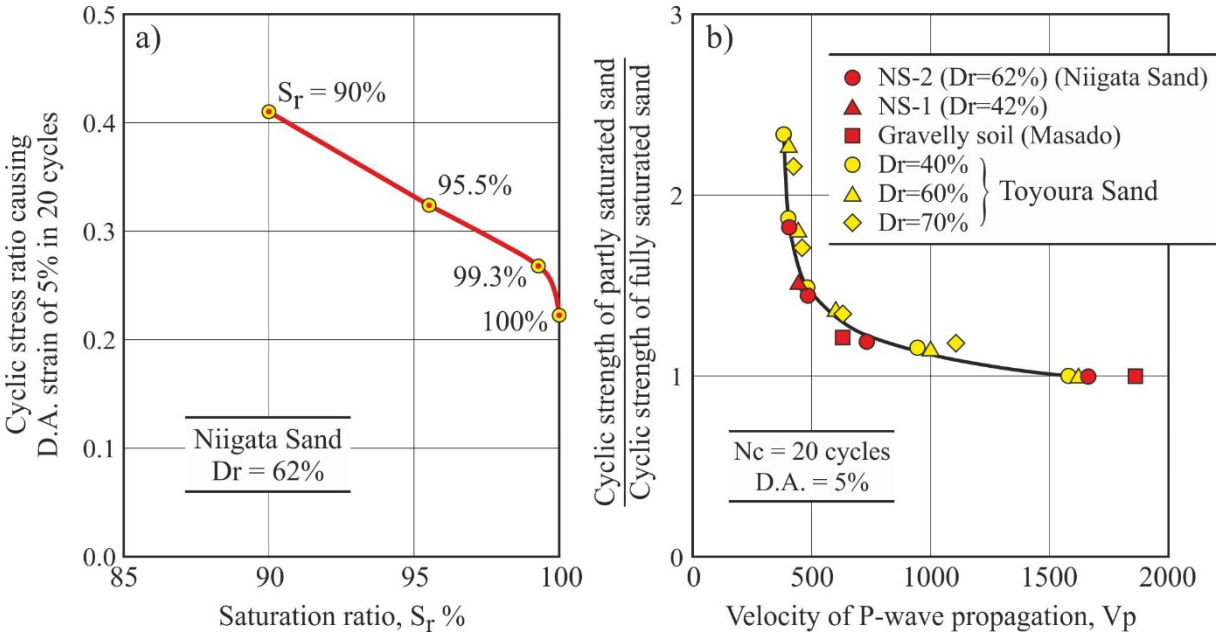


Fig. 15. Effect of partial saturation on cyclic strength - K. Ishihara et al. (2001)

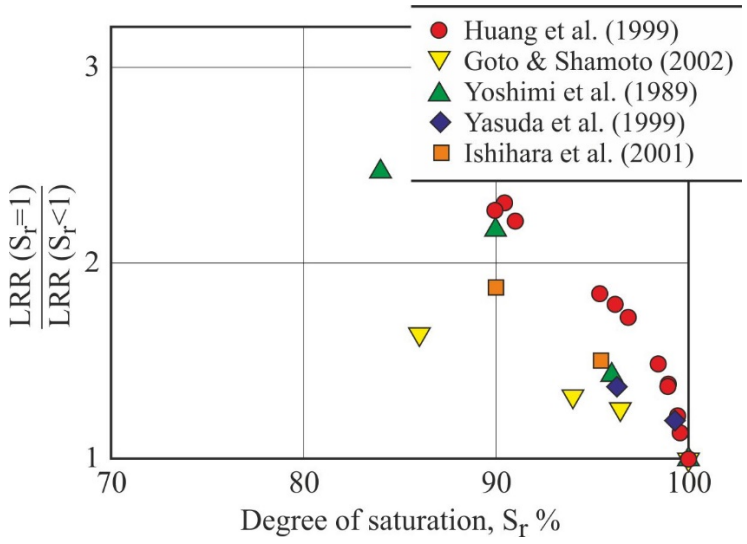


Fig. 16. Effect of saturation degree on liquefaction strength - M. Okamura and Y. Soga (2006)

Some further enhancements of the above experimental procedure can be found in the works by Enseller-Bayat et al. , Part 1 (2013) and Leong and Cheng (2013) whose valuable contributions to the problem in hands can be summarised as follows:

- Limitations of Skempton's pore pressure coefficient B as index of soil saturation, suggesting V_p as its better proxy (both authors).
- Use of Bender Elements and Bender Disks Elements to measure respectively S-wave velocity V_s , and P-wave velocity V_p , on soil specimens in laboratory (both authors).
- Experimental setup and procedures aimed at preparation quality, of uniform density, partly saturated soil specimens, (both authors).

Moreover, Enseller-Bayat et al. (2013) in Part 2 of their work have presented an empirical model estimating the susceptibility of the tested soil to liquefaction based on the magnitude of the maximum pore pressure ratio r_u caused by cyclic loading inducing the shear strain.

The findings and the scenario emerged as to the difficulties to assess the gain in liquefaction strength of the partly saturated tailings using P-wave, see literature cited in this section, have led to a semi-empirical procedure summarized here below.

In situ tests

- Measure of V_p velocity, mapping depth and spatial variability of the phreatic surface, making distinction between fully and partly saturated soils to which P-wave is extremely sensitive.

Laboratory tests

- Carry out consolidated undrained triaxial test, checking its full saturation (FS) by propagating P-waves through the specimen.
- Carry out consolidated undrained triaxial tests on a series of uniformly desaturated specimens having approximately Sr respectively equal to: 0.97%, 0.95% and 0.90%.
- On each of these specimens, propagate P-wave during the shearing stage to measure the V_p velocity.

The data interpretation

- Compare V_p (Field) vs V_p (Lab) of fully saturated specimens to verify to what extent the laboratory specimens are representative of the field condition.
- As to laboratory tests results, the ratio of the liquefaction resistance of partly saturated specimen vs. liquefaction resistance of the fully saturation specimen, provides the LRR, from which the liquefaction strength of the near to saturated soil in the field can be estimated at first glance.

Moreover, the magnitude V_p (Field) of partly saturated soil allows to estimate the reliability of the LRR inferred from the results of laboratory tests. Last not least, the procedure dealing with the determination of the liquefaction resistance of sandy and silty like soils described in this section, can now significantly benefit from the new Gel-Push sampler, a tool developed jointly by Japan and Taiwan under Prof. Ishihara guidance and manufactured by Kiso-Jiban Consultants Co. Ltd. Tokyo.

This technology has been used extensively in Asia [Huang et al. (2007, 2008)], New Zealand [Taylor and Cubrinovski (2012), Taylor (2014)], Italy [Manassero and Dominijanni (2016)], Poland [Swidzinski et al. (2013)] and since 2013 has been employed to retrieve undisturbed samples of tailings at Zelazny Most. The essential feature of the Gel-Push sampler, see Fig.17, consists in supplying, during sampling, a gel that reduces the friction between the soil and the internal lining, forming a thin gel around the soil core. This polymer soluble gel is removable after the sample extrusion.

Fig. 18 presents two specimens of tailings sitting on the pedestal of the triaxial cell to be tested. The figure displays also the outcome of the specimen quality assessments estimated according to Sasitharan et al. (1994) relying on the comparison between the normalized S-wave velocity V_{s1} propagated respectively in the field (F) and through the specimen in the laboratory.

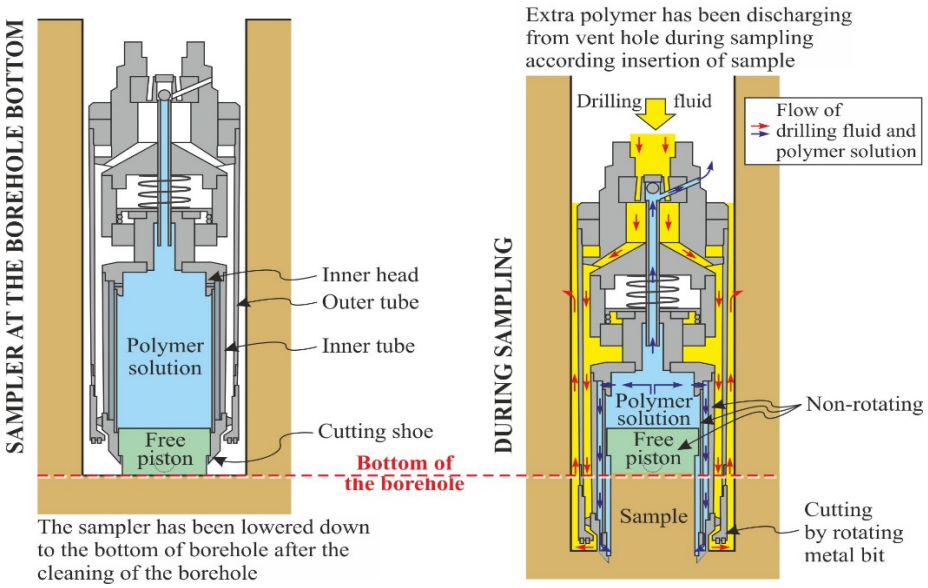
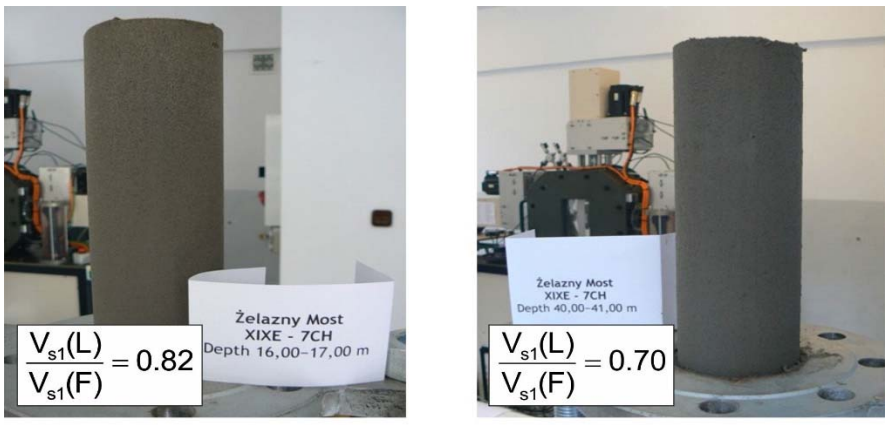


Fig. 17. Illustration of gel push TR-sampler.



XIXE - 7CH Sample, depth 16-17m XIXE - 7CH Sample, depth 40-41m

Fig. 18. Specimens for TX-CIU and TX-CK$_0$U tests, Geoteko (2014).

CONCLUSIONS

Based on the experience gained in more than two decades in the use of in-hole geophysical tests, and thoroughly benefitting of the current state of the art of their application in the geotechnical characterization of sand-like and silt-like soils, the following tentative conclusions can be drawn as the Zelazny Most tailings storage facility is concerned.

- The extensive use of different in-hole geophysical tests (SCPT, SDMT, CHT) plays a relevant role in a comprehensive and consistent assessment of the shear wave velocity Vs of the Zelazny Most tailings, despite three different testing methods used for their measurement and the intrinsic variability of the tailings in situ.

- The propagation of P-waves from CHT's stations have revealed to be crucial for mapping the depth and the spatial distribution of the phreatic surface within the ZMSF body, aimed at distinguishing the partly from the fully saturated tailings.

- The almost steady depth of the phreatic surface locations, monitored by the propagation of the P-waves from 18 CH stations, in the period 2011-2017, when the dam had been risen from 9 to 12 meters, testifies the importance of the circumferential drains system in keeping the phreatic surface well depressed in the shell of the confining ring dam.

- Section 3.2 of this paper, shows that the ZMSF design and construction is carried out making remarkable efforts to assess the susceptibility of the tailings with respect to liquefaction hazard. Efforts are focused on the combined interpretation of the P-waves and S-waves velocities measured in situ and on the results of the consolidated undrained triaxial tests carried out in laboratory on fully saturated tailings, retrieved by means of the Gel push sampler.
  This approach proves to be suitable for evaluating the liquefaction strength and the fully saturated tailings, though does not allow quantifying the gain in the liquefaction strength when dealing with partly saturated tailings.

- Based on numerous references, e.g. Ishihara (2001), Okamura and Soga (2002), Tamura et al. (2002), Enseller-Bayat (2013), Leong and Cheng (2013) and many others, it can be concluded that it is not feasible to assess S_r directly from the results of seismic wave propagation in partly saturated soils. As an alternative, in the partly saturated soils, the related geotechnical literature suggests coupling the seismic wave propagation in situ and in laboratory with the dedicated consolidated undrained triaxial tests. This approach allows to assess the liquefaction strength for both fully and partly saturated soils and express the opinion about their susceptibility with respect to flow failure.

ACKNOWLEDGEMENTS

The Authors are grateful to the Mine (KGHM) for making available the Zelazny Most information and data. Special thanks and recognition to the Colleagues of the International Board of Experts (IBE): Dr. D. Carrier (Argila Enterprises), Prof K. Hoeg (NG) and Prof. J. Standing (Imperial College), whose expertise and team work have been crucial for the demanding effort to characterize the tailings. Much appreciation also to Prof. Wolski and to his Geoteko team for the high-quality laboratory testing on Zelazny Most tailings.

REFERENCES

†Cai, G., Liriu, S., Puppala, A., & Tong, L. (2011) Assessment of the Coefficient of Lateral Earth Pressure at Rest (K_0) from In Situ Seismic Tests. ASTM Geotechnical Testing Journal 34(4). p 11.

Callerio, A. (2017), Studio Geotecnico Italiano, Milano, Italy. Personal communication.

Chandler, R. J., Jamiolkowski, M., Faiella, D., Ridley, A. M. & Rocchi, G. (2011) Suction measurements on undisturbed samples of heavily overconsolidated clays. Proceedings, of the. XXIV Convegno Nazionale di Geotecnica, Napoli. Patron Editore vol. 1 pp 361-374.

Emerson, M. & Foray, P. (2006) Laboratory P-wave measurements in dry and saturated sand. Acta Geotechnica, 1(3) 167-177.

Eseller-Bayat, E., Yegian, M., Alshawabkeh, A. & Gokyer, S. (2013) Liquefaction response of partially saturated sands. I: experimental results. ASCE Journal of Geotechnical & Geoenvironmental Engineering 139(6) 863-871.

Eseller-Bayat, E., Yegian, M., Alshawabkeh, A. & Gokyer, S. (2013) Liquefaction Response of Partially Saturated Sands. II: Empirical Model. ASCE Journal of Geotechnical & Geoenvironmental Engineering 139(6) 872-879.

†Fioravante, V., Jamiolkowski, M., Lo Presti, D. C. F., Manfredini, G., & Pedroni, S. (1998) Assessment of the coefficient of the earth pressure at rest from shear wave velocity measurements. Geotechnique 48(5), 657-666 Rest (K_0) from In Situ Seismic Tests. ASTM Geotechnical Testing Journal 34(4).p 11.

†Foti, S., Lai, C. G., & Lancellotta, R. (2002) Porosity of fluid-saturated porous media from measured seismic wave velocities. Geotechnique 52(5), 359-373.

†Foti, S. & Passeri, F. (2016) Reliability of soil porosity estimation from seismic wave velocities. Proceedings, ISC5 5th International Conference on Geotechnical and Geophysical Site Characterisation Queensland Australia (Brisbane) Vol 1, pp 425-430 B.M. Lehane H. E. Acosta Martinez & R. Kelly Editors AGS, Australian Geomechanics Society Sydney Australia.

Geoteko (2014), Geotechnical Consulting and Design Ltd. Warsaw, Poland. Personal communication.

He, J., Chu, J. & Liu, H. (2014) Undrained shear strength of desaturated loose sand under monotonic shearing. Soils and Foundations 54(4) 910 – 916.

Huang, A. B. & Huang, Y. T. (2007) Undisturbed Sampling and Laboratory Shearing Tests on a Sand with Various Fines Contents. Soils and Foundations 47(4), 771-782.

Huang, A. B., Tai, Y. Y., Lee, W. F. & Ishihara, K. (2008) Sampling and field characterization of the silty sand in central and southern Taiwan. Proceedings, ISC'3 3rd International Conference on Geotechnical and Geophysical Site Characterization, Taipei, Taiwan A.B. Huang & P.W. Mayne Editors, Taylor and Francis. Pp 1457-1463.

Ishihara, K., Huang, Y. And Tsuchiya, H. (1998) Liquefaction resistance of nearly saturated sands as correlated with longitudinal wave velocity. Proceedings, 1st Conference on Poromechanics: A tribute to Maurice A. Biot, Louvain-la-Neuve, Belgium. Editor CRC Press, Leiden, pp 583-586.

Ishihara, K., Tsuchiya, H., Huang, Y. & Kamada, K. (2001) Recent Studies on Liquefaction Resistance of Sand - Effect of Saturation. Proc. 4th International Conference on Recent Advances in Geotechnical Earthquake Engineering and Soil Dynamics. Symposium in Honor of Professor W. D. Liam Finn, San Diego California, S. Prakash Editor, University of Missouri-Rolla 4.28.

Jamiolkowski, M., Carrier, W. D., Chandler, R. J., Hoeg, K., Swierczynski, W., & Wolski, W. (2010) The geotechnical problems of the second world largest copper tailings pond at Zelazny Most, Poland, Za-Chieh Moh Distinguished Lecture Proc. of the XVII Southeast Asian Geotechnical Conference. Geo-Engineering for Natural Hazard Mitigation and Sustainable Development, Taipei Taiwan, J.C.C. Li & .M.L. Lin Editors, Taiwan Geotechnical Publishers Society Taipei Taiwan Vol 2 pp 12-27.

Jamiolkowski, M. (2014) Soil mechanics and the observational method: challenges at the Zelazny Most copper tailings disposal facility 53rd Rankine Lecture. Geotechnique 64(8) 590-619.

†Kacar, O. (2014) Building a Framework for Predicting the Settlements of shallow foundations on Granular Soils using Dynamically Measured Soil Properties PhD thesis. University of Texas, at Austin, Texas.

Kokusho, T**.** (2000) Correlation of Pore-Pressure *B*-value with *P*-wave Velocity and Poisson's Ratio for Imperfectly Saturated Sand or Gravel. Soils and Foundations 40(4) 95-102.

†Kulhawy, F. H., Mayne, P. W., & Longo, V. J. (1990) Manual on Estimating soil properties for foundation design. EPRI El-6800. EPRI, Electric Power Research Institute. Cornell University Ithaca.

Leong, E. & Cheng, Z. (2013) Effects of Confining Pressure and Degree of Saturation on Wave Velocities of Soils. International Journal of Geomechanics 16(6) 10 p.

Lipinski, M. J. (2012) Laboratory Tests on Undisturbed Samples of Tailings from Zelazny Most Tailings Pond. Report 144/2645/10, Geoteko Geotechnical Consultants Ltd. Warsaw, Poland.

Lipinski, M. J. (2000) Undrained response of cohesionless soils to monotonic loading. PhD thesis. Technical University of Gdansk, Poland.

Manassero, M. and Dominijanni, A. (2016) La qualità delle indagini geotecniche in campo ambientale a Pieve Borgone. Personal Communication.

†Mayne, P. W. & Kulhawy, F. H. (1982) K (0) - OCR relationships in soil. Journal of Geotechnical & Geoenvironmental Engineering, ASCE 108(6), 851-872.

Nakagawa, K., Soga, K. and Mitchell, J. K. (1997) Observation of Biot compressional wave of the second kind in granular soils, Geotechnique, 4(4), 143-147.

Okamura, M. & Soga, Y. (2006) Effects of Pore Fluid Compressibility on Liquefaction Resistance of Partially Saturated Sand. Soils and Foundations 46(5), 695-700.

Peck, R. B. (1980) Where has all the judgment gone? The fifth Laurits Bjerrum memorial lecture. Canadian Geotechnical Journal 17(4) 584-590.

Peck, R. B. (1969) Advantages and limitations of the observational method in applied soil mechanics Ninth Rankine Lecture. Geotechnique 19(2), 171-187.

†Sasitharan, S., Robertson, P.K. & Sego, D.C. (1994) Sample disturbance from shear wave velocity measurements. Canadian Geotechnical Journal, 31(1), 119-124.

Skempton, A. W. (1954) The Pore-pressure coefficients A and B. Geotechnique 4(4) 143-147.

Swidzinski, W., Mierczynski, J. and Milkos, A. (2017) Response of Partially Saturated on-cohesive Soils. Archives of Hydro-Engineering and Environmental Mechanics, Vol.64, No.3-4.

Tamura, S., Tokimatsu, K., Abe, A., & Sato, M. (2002) Effects of Air Bubbles on B-Value and P-Wave Velocity of a Partly Saturated Sand. Soils and Foundations 42(1) 121-130.

Taylor, M. L. & Cubrinovski, M. (2012) Application of new 'Gel-Push' sampling procedure to obtain high quality laboratory test data for advanced geotechnical analyses. Proceedings, NZSEE Annual Technical Conference & AGM, 13-15 April, Christchurch. Christchurch, NZ. New Zealand Society for Earthquake Engineering pp 123-131.

Taylor, M. L. (2014) The geotechnical characterization of Christchurch sands for advanced soil modelling PhD thesis University of Canterbury UK.

Tschuschke, W. (2014) Personal Communication.

Tsukamoto, Y., Ishihara, K., Nakazawa, H., Kamada, K. & Huang, Y. (2002) Resistance of Partly Saturated Sand to Liquefaction with Reference to Longitudinal and Shear Wave Velocities. Soils and Foundations 42(6) 93-104.

Tyminski, K. (2015), Geoteko Company, Warsaw, Poland, Personal communication.

Yoshimi, Y., Tanaka, K, and Tokimatsu, K. (1989) Liquefaction resistance of a partially saturated sand. Soils and Foundations 29(3) 157-162.

SPECIFICATION, PROCUREMENT, QUALITY CONTROL AND CERTIFICATION OF BOTTOM-FEED STONE COLUMNS

Giovanni Vaciago, Studio Geotecnico Italiano, via G. Ripamonti 89, Milan, Italy, +39025220141, g.vaciago@studiogeotecnico.it

ABSTRACT

The paper presents recommendations for specification, technical assistance to procurement, quality control and certification of ground improvement works. Roles and responsibilities of the various parties may vary from case to case, depending on the specific requirements of each project, and must be clarified at an early stage. The key question is to what extent it is appropriate and beneficial to transfer responsibility for design and certification of performance of the completed works to the specialist contractor performing the works, especially when the design is governed by exceptional conditions (such as mitigation of seismic liquefaction hazard) which may not materialize in practice except well after works completion. These subjects are discussed with special reference to stone columns installed by the dry, bottom-feed method, drawing on the Author's experience.

Keyword: specification, certification, ground improvement, stone columns

1 INTRODUCTION

The technical and commercial success of any project depends on many factors. Defining success, identifying Critical Success Factors CSF, a concept first introduced by Rubin and Seeling (1976), and success criteria for construction projects have been the subject of academic research for many years.

Extensive literature reviews have been published by many authors. In a review of literature related to CSF in seven major management journals involving a total of 43 articles, Chan et al. (2004) grouped CSF in five main categories: project-related factors, procurement-related factors, project management factors, project participants-related factors and external factors, as summarized in Fig. 1. Whilst those factors which depend in whole or in part on environmental conditions need to be considered, but cannot be controlled proactively, many others can be influenced by decisions taken by the stakeholders and the project team as the project develops.

External factors, such as economic, social, political, physical and industrial relations environments, technological advances and generally the capability of the supply chain, cannot be influenced, at least in the short term of a single project, but need to be considered when defining the type, nature and complexity of the project. Whilst necessity is the mother of invention and it is more than legitimate to try to always take capabilities a step further, an excessive mismatch between environmental conditions and the scope of the project can be highly detrimental to its success. Proportionate scoping must be addressed at strategic planning level early on and continuously reviewed as more information becomes available and more diverse capabilities are brought into the project team. Too many are the examples of projects which are stillborn or abandoned before completion simply because they are too ambitious and unsustainable in the first place.

Particularly significant for the subject addressed here are factors classified among "project management actions", such as implementing effective communication systems, control mechanisms, organization, safety program, quality assurance program, control of subcontractors' works, and "project procedures", such as procurement and tendering method. Specification, procurement, quality control and certification of any construction work need to be managed in a structured and consistent manner to balance risks and opportunities and to maximize the project benefits and the likelihood of success for the various stakeholders. This is particularly true when dealing with highly specialized categories of work, such as specialist geotechnical works in general and ground improvement in particular, which typically fall outside the technical capability and previous experience of most clients, program managers and project teams.

 © 2018 Deep Foundations Institute

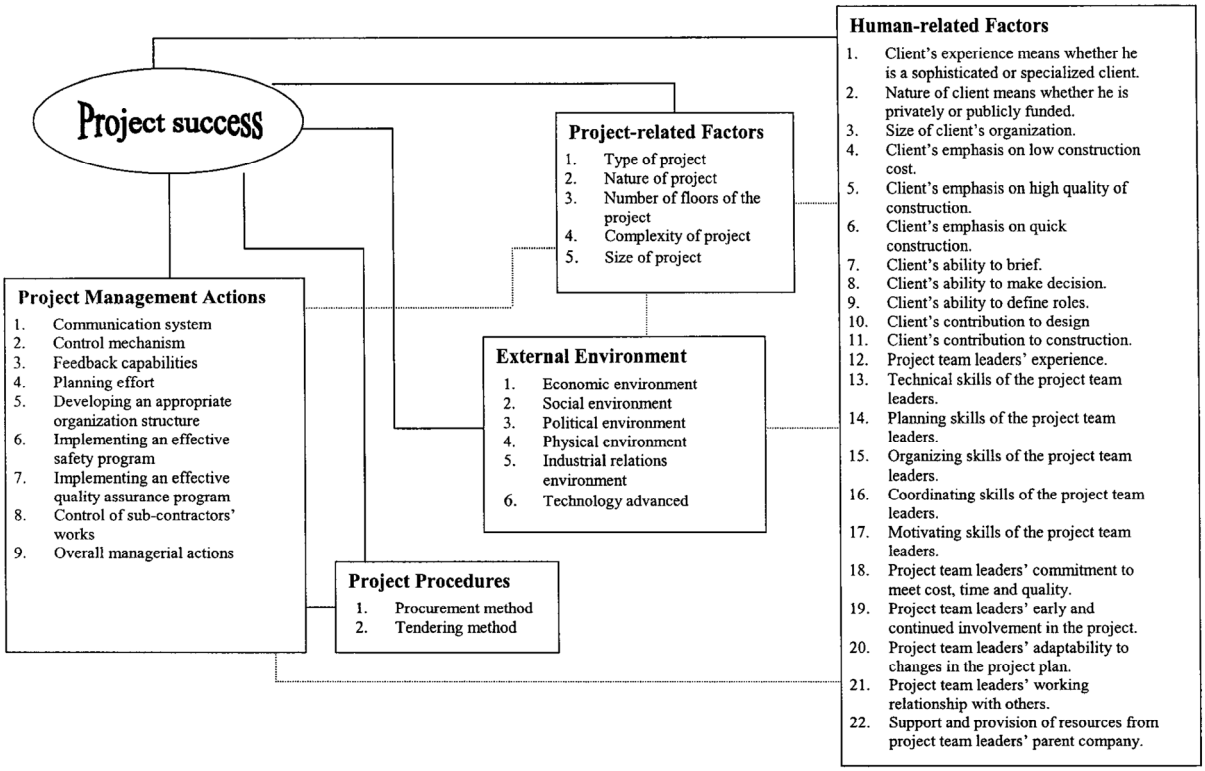


Fig. 1. Factors affecting project success according to Chan et al. (2004)

Elaborating on these general concepts, this contribution presents the author's personal reflections on and provides recommendations for specification, technical assistance to procurement, quality control and certification of ground improvement works. The key question is to what extent it is appropriate and beneficial to transfer responsibility for design and certification of performance of the completed works to the specialist contractor performing the works, especially when the design is governed by exceptional conditions (such as mitigation of seismic liquefaction hazard) which may not materialize in practice except well after works completion.

The subject is addressed based primarily on personal experience. Accordingly, this contribution does not pretend to be an exhaustive or definitive treatise on the subject. It is hoped, however, that it will stimulate discussion and provide food for thought to personnel from clients, designers, main contractors and specialist contractors involved in their respective roles in planning, implementing and certifying specialist geotechnical works.

The general principles discussed in the paper are applicable to most types of ground improvement. They are illustrated here with special reference to stone columns installed by the dry, bottom-feed method, which are formed by inserting a heavy vibrator (vibroflot) in the ground to the required depth and by withdrawing it slowly with alternate upward and downward movements while feeding gravel through a delivery pipe directly to the tip of the vibrator (bottom feed) using only compressed air to aid penetration of the vibroflot and gravel delivery (dry method) (Fig. 2).

The alternate upward and downward movements and the horizontal vibration of the vibroflot compact the gravel and expand it into the surrounding soil. Besides forming an inclusion of highly compacted gravel, the combined effects of vibration and expansion of the stone columns also induce compaction of the surrounding soil and increase the horizontal stress and thus the overall stiffness. The degree of compaction that can be achieved and the relative contribution of vibration and expansion depend on the nature of the native soil, being greater for relatively clean sands having less than 10 – 12% non-plastic fines (silt and clay) and decreasing rapidly as the proportion and plasticity of the fines increase.



(a)



(b)



(c)

Fig. 2. Stone columns installed by the dry, bottom-feed method:
(a) installation process (source: www.vibroflotation-ng.org)
(b) detail of vibroflot and gravel delivery pipe (source: SGI project files)
(c) general arrangement of equipment – note skip to replenish the gravel supply and air lock chamber at the top of the delivery pipe (source: SGI project files)

2 SPECIFICATIONS

As used in the construction industry, the term Specification is defined in the Shorter Oxford English Dictionary on Historical Principles (1973) as "*a detailed description of the particulars of some projected work in building, engineering, or the like, giving the dimensions, materials, quantities, etc., of the work, together with the directions to be followed by the builder or constructor*".

Strictly speaking, this definition encompasses and refers to all the documents and models that collectively define the scope and nature of the work to be performed, which once used to include drawings and schedules, now supplemented and possibly one day to be replaced in whole or in part by BIM models. In practice, the term specification refers to a (mainly text) document which includes a description of systems or products and how these systems or products should be installed, finished and tested, providing technical information that supplements the information conveyed by drawings and models (Hamil, 2017).

Specifications are normally produced at technical design stage and are included in tender packages and contract documents to provide clear instructions on the intent, performance and construction of the project and to define applicable quality standards, materials and products, as well as requirements for installation testing and handover (Pringle, 2017).

Depending on project requirements, specifications can be:

- performance-based, describing the desired performance level or performance target to be achieved, without making specific demands on how that level/target is reached;
- prescriptive, providing detailed descriptions of what specific materials must be used as well as the installation instructions;

- proprietary, requiring that only specific products be used for a given installation (this is often not allowed in public tenders, on the grounds that it is contrary to the overriding requirement to allow open competition); or
- a combination of the above.

The specification for ground improvement by stone columns should clarify as a minimum, with reference to other contract documents if appropriate, the scope and objectives of the work to be carried out, applicable reference standards and project documents (including a geotechnical baseline report or equivalent), roles and responsibilities of the various parties with particular reference to detailed design and final evaluation and acceptance of the works, quality control and certification, checking and maintenance of working platform, setting out, supply and handling of materials, equipment, preliminary trials, management of spoil, vibration monitoring and mitigation and dealing with obstructions, as well as specific requirements for phasing of the works, equipment and calibrations, materials, preliminary trials, main works, records and control tests and tolerances.

Advocates of performance-based specifications often cite the main benefits of this approach as fostering innovation, forcing the procuring authority to conduct in-depth need analysis, increasing the possibility of identifying (or, conversely, reducing the risk of neglecting) the "best option" in the market, facilitating the implementation of sustainable procurement practices aimed at providing value for money and environmental, societal and overall economic benefit, as well as allowing changes in ownership patterns, such as leasing instead of purchase, thus creating incentives for the supplier to make their product more efficient, longer lasting and easer to reuse and recycle (Turley et al., 2014).

Performance-based specifications can be subdivided in two sub-categories: performance-based specifications sensu strictu, which define requirements in terms of broad objectives, and specifications which use specific measurable parameters as a proxy of performance, which are more properly referred to as end-product specifications and fall somewhere between performance-based and prescriptive specifications.

The performance criteria used in performance-based specifications depend on the scope of the procurement. At macro-scale, performance criteria may relate to availability and service level of the complete project or service as a whole. For example, at global level, performance for road projects may be expressed in terms of lane availability (obstacle free) and mobility (flow speed at or over specified value), as done for example in some projects in the Netherlands (Turley et al., 2014). Other examples are tolls on privately-operated motorways in Italy, which are set taking into account, inter alia, a composite performance indicator which measures the service level in terms of pavement condition and traffic safety, and lane rental schemes in highway maintenance contracts, widely used in the UK, which exploit the same principle.

Performance criteria may be defined also at the level of specific sub-systems. For geotechnical works, performance-based specifications may define criteria directly related to overall geotechnical performance of the completed works, such as resistance to static, dynamic and/or earthquake loads, limits on allowable settlement of foundations, maximum transmissivity of a barrier system, and so on. Classic examples are the limits on track settlement and distortion (absolute or in any given planned maintenance period) specified by the client for the high-speed railways in Italy or resistance to seismic liquefaction for a given design event and bearing capacity and maximum settlement of foundations of specified dimensions for reclamation fill in artificial islands in the Arabian/Persian Gulf.

Such global system or sub-system performance may be difficult to define and especially difficult to evaluate at tender stage and/or to monitor in practice. It is often the case that such global performance criteria are accompanied or replaced by nominally more easily verifiable proxy indicators, such as dry density of compacted fill specified to be not less than a certain percentage of the maximum dry density as determined in a standard compaction test. This approach often allows simple quality control protocols to be established and implemented, but all too often the selected proxy and the specified value bear little or no direct relation with the required global performance of the geotechnical system.

In certain cases, inappropriate proxies are selected, which are not as easily verified as originally intended, thus becoming an additional problem, rather than a solution.

The use of performance-based specifications is especially attractive when dealing with specialist geotechnical works and in particular with ground improvement works, since what can be achieved in practice and how it can be achieved depend to a significant extent on the particulars of the equipment used for the works, which for any given combination of ground and groundwater conditions may vary depending on the specific contractor performing the works, without necessarily adversely affecting the end result, provided the working methods are adjusted to suit.

For this reason, it is good practice, widely used in the industry, for project specifications to require the specialist contractor to provide at the start of the work, prove by trial and abide by detailed method statements in which the specialist contractor provides a detailed description of equipment, materials and methods that will be applied to perform the task in hand. It cannot be overemphasized that, contrary to widespread malpractice, method statements produced by specialist contractors should not be used as a covert way to modify the project specification without a formal variation, but only to clarify how the requirement detailed in the specification will be satisfied.

3 PROCUREMENT

What type of specification is best suited to a particular project depends on several factors. Particularly relevant in this respect is the procurement strategy that will be adopted.

Detailed prescriptive specifications which leave little or no space for technical innovation or optimization of design are intended to and will induce bidders to compete mainly on price, based only on their own efficiency and effective procurement from the supply chain. This may be a desirable scenario for a procuring authority particularly concerned with accountability.

Technical bid evaluation will only need to focus on relatively simple questions about compliance, however proven, without the need to express any value-judgement and the associated responsibility. Technical clarifications from bidders may need to be sought only as necessary to confirm compliance in the face of ambiguous or insufficient information.

Some authorities request express confirmation of compliance and disqualify automatically all bids which fail to provide such confirmation. Bids are then evaluated mainly on price and commercial terms, on the sometime misplaced assumption that adequate policing will be sufficient to enforce compliance.

In order to simplify verification of compliance and at the same time prompt the Bidder to examine the specification in detail and take note of project specific requirements, it may be useful, if somewhat pedantic, to include in the bid documents a “bid evaluation form” which lists all specification requirements for each bidder to expressly confirm compliance and how it will be achieved, or highlight possible deviations in his proposal, if any are admitted. A similar document can be used by the procuring authority for bid evaluation purposes and/or as a basis for seeking clarifications, even if not included in the bid package.

Reducing technical bid evaluation to a compliance checklist is a simplistic and typically unrealistic approach in practice, especially for geotechnical works. It is necessary to verify that the bidder has understood the scope of work and all general and project specific requirements and that he has the resources to honor his commitments. Requesting the bidder to provide a preliminary method statement detailing resources and procedures that will be used in the works and verifying, preferably by direct inspection, that the stated resources are indeed available is of great assistance in making a realistic evaluation, especially for one-off projects where there is no consolidated track record for similar work. Well organized, competent contractors should be only too happy to have the opportunity to demonstrate their capability.

Bidders will typically qualify their bids and/or rely on the possibility to introduce variations at a later stage, especially if the design and associated prescriptive specification are not supported by a detailed and reliable ground investigation and a thorough geotechnical baseline report to minimize the risk of unforeseen ground conditions and to suppress spurious claims.

Performance-based specifications and the (partial) transfer of responsibility for design to the contractor will tend to shift the focus of competition from optimizing the unit cost of each specific work item to optimizing the design, trying to demonstrate that indeed more can be achieved for less.

This is obviously attractive in principle, but it puts the procuring authority in the unenviable position of having to compare and rank bids which may be based on very different technical grounds. Finally, the procuring authority will need to introduce value-judgement in the evaluation process, putting a greater degree of responsibility on those involved.

A detailed analysis of the validity of the different technical proposals and associated residual risks will typically prove a demanding task in itself, as each bidder will put forward apparently irresistible arguments to demonstrate that their and only their proposal merits attention. In this context, the concept of compliance blurs, unless the performance targets and evaluation criteria are set so tightly that the specification risks to become a prescriptive specification in disguise.

When electing to base the process on a performance-based specification, the procuring authority should take into account that the technical evaluation will most likely require a series of technical clarifications, supported by specialist technical advice to verify and comment on the validity of the technical claims made by the bidders. Also in this case it may prove advantageous to include in the bid package or otherwise prepare a “bid evaluation form” and to request preliminary method statements as described previously.

Comments and clarifications may be exchanged by correspondence, at least initially, but face to face meetings are most likely to be necessary at some point to avoid stalling the process. It is important that face to face meetings are attended by personnel having both the technical know-how and authority to conduct such meetings to clear conclusions, with full appreciation on both parts of the implications of the clarifications requested and provided. Face to face technical meetings with selected bidders before final award may also allow both parties to assess non-technical aspects of the prospective relationship, although it must be borne in mind that all too often those attending these meetings will not be involved directly in performing the works.

Using performance-based specifications does not prevent Bidders qualifying their bids and it does not protect the procuring authority from more or less legitimate subsequent claims for unforeseen ground conditions. Hence it is in all cases necessary to support the process with a detailed and reliable ground investigation and a thorough geotechnical baseline report.

One particular variation on the theme is alternative proposals. To overcome the limitations imposed by prescriptive specifications on the possibility to mobilize the bidders’ expertise and at the same time limit the difficulties associated with comparative evaluation of bids based on performance-based specifications, one strategy adopted by some procuring authorities is to allow or even encourage alternative proposals, subject to bidders also submitting a conforming proposal based on a prescriptive specification.

This approach allows bidders to be compared on a level ground (the conforming proposals), while at the same time providing direct evidence of the potential benefits, in terms of time, cost and/or performance, of alternative proposals optimized to suit the bidders’ specific capabilities and expertise.

The procurement strategy will depend on the role of the procuring authority within the project team. Many large and complex projects are commissioned to a main (or general) contractor, often on a

design & build basis, in which case typically the design and procurement of specialist geotechnical works will be performed by the main contractor, rather than the final client.

In these cases, the procuring authority (i.e.: the main contractor) will attempt to transfer to the specialist contractor the same requirements and obligations which are detailed in the main contract, plus all such additional requirements and obligations that he consider necessary. The work performed by the specialist contractor may be subjected to scrutiny by the final client, besides the main contractor.

Requirements imposed on specialist subcontractors detailed in specifications issued by a main contractor having design responsibility can become at the same time self-imposed obligations that the main contractor will need to satisfy with respect to the client.

4 QUALITY CONTROL AND CERTIFICATION

Irrespective of type, it is essential that specifications provide a clear statement of the methods, metrics and criteria used to confirm compliance with the stated requirements. Adequate systems must be in place to ensure that compliance is indeed verified, primarily to assure that the intended objectives are indeed achieved but also to guarantee a fair marketplace, in which conscientious contractors are not penalized at tender stage compared to others who rely on requirements being waived at a later stage.

Once performance requirements have been identified by in-depth need analysis, writing a performance-based specification to be included in a tender package may seem much easier for the procuring authority than preparing a detailed prescriptive technical specification. However, the use of such type of specification might just shift the work of the purchaser away from the specification/bid-writing stage into the evaluation and monitoring stage (Turley et al., 2014). This approach implies a strong requirement for adequate monitoring and enforcement, which is made more difficult by the fact that performance criteria and metrics tend to be more prone to relative and subjective judgements (Knight et al., 2007).

It is essential to recognize that specifications are a key contract document, with potential fall-out which may go well beyond the intended technical scope. In particular, difficulties in demonstrating compliance of the Works with the specified requirements will almost invariably lead to delayed acceptance and payment, increased risk of claims and, possibly, litigation. It is therefore very important that the methods of testing and acceptance criteria defined in the specification are clear, unambiguous and relatively simple to verify in practice.

Even in the simplest cases, as is the case with proof testing of working piles under axial loads, final testing measuring directly the performance of the completed works is typically carried out on a relatively small percentage of items. Proof load testing of piles in axial compression is typically carried out on only 0.5% to 2% of all piles. For acceptance testing, the density of compacted fill is typically verified by direct testing on only 0.001 to 0.005% of the total volume. Clearly, it is necessary to have in place reliable rational procedures to extrapolate the results of such limited testing to the entire population.

In many cases, it is technically impossible or disproportionately onerous to verify the satisfactory performance of geotechnical woks by direct testing. A classic example is the requirement to compact reclamation fill placed below sea level in artificial islands to achieve a particular density. Direct determination of the post-compaction density of high permeability granular fill placed below sea level is clearly not feasible or, at best, very expensive and time consuming and thus not applicable in practice for routine control testing.

In this and similar cases, it is necessary to perform indirect tests, for example, in the case in point, geotechnical tests such as SPT, CPT, pressuremeter tests and/or geophysical tests, either from the surface (SASW, MASW) or in hole (down-hole or cross-hole seismic, suspension logging, acoustic).

Each of these techniques introduces its own uncertainty and variability, which is superimposed on the intrinsic variability of the parameter(s) measured in the test. The main source of uncertainty is the correlation between the parameter actually measured in the test (number of blows, electric current in a load cell behind the tip in cone penetration testing, time related accelerations or displacements in geophysical tests), the physical parameter measured indirectly in the test (load on the cone tip during penetration, wave velocity in geophysical seismic tests), which is governed by instrument calibration, and the physical parameter effectively of interest (density), derived by empirical correlations, such as correlations between cone tip resistance and soil density like for example the correlation proposed by Jamiolkowski et al. (2001).

Even greater uncertainty is introduced in the evaluation when the performance criterion to be verified is an engineering performance, rather than a physical parameter, albeit determined indirectly. In some cases, the engineering performance may be verified by direct testing, as is the case with zone load testing or load testing on large rigid plates simulating real foundations. However, the cost and time required to perform such tests make this approach unsustainable for routine testing. In this case, and even more so in those cases when direct testing is simply technically not feasible, verification of compliance with the target engineering performance is based on calculations, which in turn may be based on derived parameters (e.g.: soil stiffness derived from the results of penetration tests or geophysical tests), or on empirical correlations, as is the case for resistance to seismic liquefaction.

Last, but not least, failure of control tests to demonstrate compliance of completed works with the specification requirements will typically result in the need for rework or other, more complex, remedial action, which may be difficult or physically impossible in some cases. It is therefore necessary for the work to be "right first time, every time". In accordance with the principles and practice of quality assurance, ideally final acceptance testing should be performed only to prove compliance, whereas reasonable assurance that the final outcome will prove satisfactory will result from ensuring that appropriate resources (equipment, material, personnel) and methods are used in the works.

In order to address the several challenges mentioned above, it is good practice to perform full scale preliminary trials in advance of or at the start of the main works. The main objective of preliminary trials is to demonstrate that the equipment, methods and materials used are suitable to complete the works in accordance with the specification requirements, with particular reference to determining/confirming suitable operating procedures and operating parameters as necessary to obtain specified/design performance.

Such preliminary trials form part of an overall strategy for quality control and certification which must be clear to all parties from the outset. Since it will be impossible to test the completed work with any great intensity, the preliminary trials must be a full-scale prototype of the works as will be performed. The operating parameters must be set in advance and automatically recorded, so that the outcome of the trial, to be determined by the necessary testing, can be uniquely associated with a combination of initial ground and groundwater conditions on one side and a unique and well controlled set of operating parameters on the other. Subsequent work must then replicate in the production works the work as performed in the trial, as demonstrated by mandatory automatic recording of operating parameters for 100% of the operations.

Automatic recording and subsequent analysis of operating parameters is essential in those types of work, such as stone columns, which do not lend themselves to post construction testing and dimensional control. In those applications where it is important to achieve a predetermined minimum dimension throughout the element, as in the case of stone columns used to mitigate the risk of seismic liquefaction, the accurate recording of operating parameters associated with techniques which allow to control the volume and point of delivery of the material provides the most effective way, albeit indirect, to estimate finished geometry.

In line with this approach, preliminary trials must be performed using the same equipment, methods and materials that will be used in the main works, including all quality control and data recording procedures, preferably by the same specialist contractor who will perform the main works. Since the effectiveness of many ground improvement techniques depends on the cumulative effect of repeated application over a wide zone of influence, to be representative, preliminary trials must involve an adequate volume of soil. However, before investing in such trial, it is useful to perform preliminary tests on isolated work items to fine tune operational aspects.

In order to evaluate the representativeness and effectiveness of the preliminary trial(s), the area of the trial must be thoroughly investigated before any ground improvement is carried out and again after completion of the works portion of the trial. Post-trial investigation must focus on those characteristics of the improved soil which are relevant for the specific objective(s) of the work carried out. Where the works result in a composite mass consisting of improved soil and inclusions, ideally the post-trial investigation should extend to verifying the as-built characteristics and performance of the inclusions and of the composite. Since direct verification of stone columns is generally not practical, in this specific case the attention will be focused on testing the performance of the composite mass.

Once the preliminary trials are proven satisfactory, by direct testing and/or, more often, by interpretation of indirect tests and calculations, the preliminary method statement can be confirmed and the main works proceed accordingly. If instead it proves necessary to modify some aspects of the procedure, the preliminary trials must be repeated using the revised procedure. In the interest of saving time, it may be expedient to perform several trials in parallel to explore a plausible range of operating parameters at once. However, each preliminary trial must be internally consistent, to avoid unnecessary additional uncertainty in the interpretation of results.

As main works proceed, records of operating parameters and control tests must be collected and analyzed systematically to identify promptly possible deviations from defined procedures and/or expected outcome. On large projects, systematic and timely management of this information is a full-time job and requires adequate staffing. Backlogs cannot be allowed to build up, on pain of losing control. On completion, all “as-built” drawings, records and test results should be collated to form the basis for final acceptance and certification of the works. The whole process is summarized in Fig. 3.

Different strategies may be adopted for quality control and certification. One approach that works well in practice is to make the specialist contractor responsible for implementing systematic quality control and self-certification of all its activities, including all monitoring, tests and inspections, to be performed in accordance with a predetermined Quality Plan which must provide a clear and detailed definition of activities and responsibilities.

For each treatment point and each phase of work, summary and detailed construction records should be submitted daily, including automatic records of selected operating parameters. These records should be signed by the specialist contractor, which signature shall constitute a certificate of proper and satisfactory construction. Non-conformities should be highlighted promptly by the specialist subcontractor, together with proposals for corrective action. Systematic checking of installation records as described here allows to quickly identify operators who fail to apply the procedures correctly and/or equipment defects, allowing the specialist contractor to implement corrective action at source before these defects propagated through the works to the extent that reworking become necessary.

Depending on the circumstances of the project, the main contractor or the Engineer must verify the correct implementation of the system, with systematic checks on the completeness of the documentation produced by the specialist contractor and spot checks on its accuracy. This approach relies on mutual trust; records or test results certified as satisfactory which are found on subsequent checking by the main contractor or the Engineer to be non-conforming are cause for serious concern and require strong corrective action.

For the system to be reliable, it must be based on reliable records and measurements. All instruments must be calibrated before the start of the preliminary trials and at regular intervals. Simple checks are often sufficient to identify potentially critical issues. On one occasion, comparing penetration depth measured by the automatic system and by depth markers painted on the vibroflot and followers allowed to identify discrepancies of over 5%.

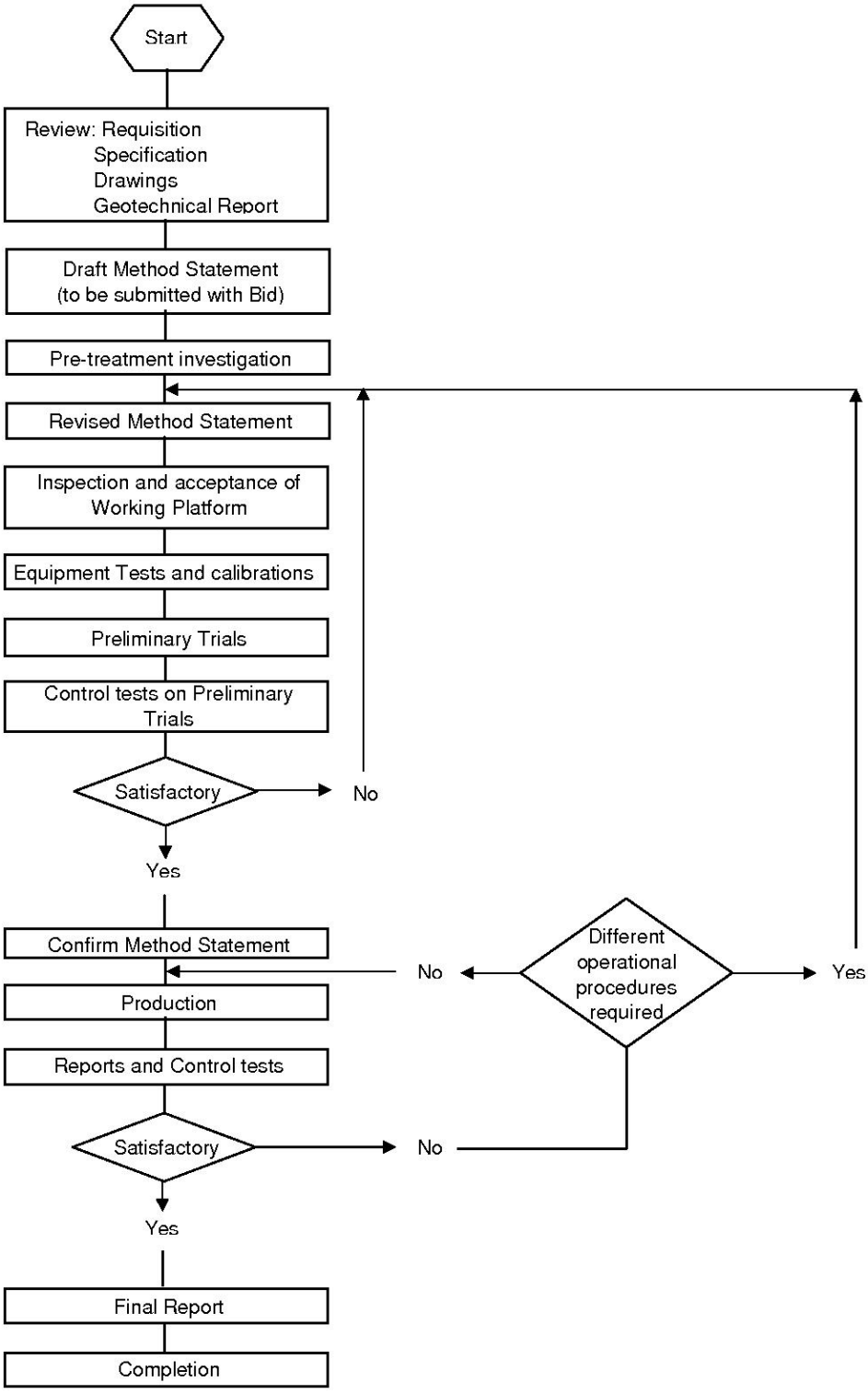


Fig. 3. Implementation, verification and certification of ground improvement

5 ALLOCATING RESPONSIBILITY FOR DESIGN AND CERTIFICATION OF PERFORMANCE

It is evident from the above discussion that a strategic decision has to be made at an early stage in the whole process, regarding the allocation of responsibility for design and certification of performance of ground improvement works.

On one hand, it is tempting to transfer this responsibility entirely to the specialist subcontractor, on the basis that he is best placed to identify the most efficient technical solution that satisfies the project objectives. He has the necessary equipment and experience … in short, surely he knows best!

On the other hand, as made clear by the discussion on procurement and quality control and certification, it would be irresponsible for the procuring authority not to consider that technical expertise is in any case necessary to evaluate alternative proposals and to monitor compliance of the works with the commitments made at bidding stage. Leaving quality control, final appraisal and certification to the specialist contractor alone would result in an unsustainable conflict of interest.

This may be acceptable when the objective of the ground improvement is to satisfy an immediate requirement that can be readily verified by representative full-scale testing requiring only data reduction but no interpretation, making final acceptance conditional on satisfactory results of such testing. Typical examples would be the design and construction of a grout bottom plug for a temporary excavation below the groundwater level, with acceptance conditional on maximum flow during pumping tests from within the volume confined by the impervious barrier, or foundation piles with acceptance conditional on the piles sustaining a specified load with corresponding pile head displacements within specified limits.

In most cases, direct full-scale proof testing of ground improvement works is not practical and can be technically not feasible. The procuring authority and the specialist contractor may feel satisfied and agree that the works are covered by latent defects liability and guarantees whereby the specialist contractor will make good any defects, even if they manifest themselves well after completion and acceptance. However, if any such defects do arise at a later stage during a major project they will certainly have an immediate significant deleterious effect on the main contractor, while it may prove very difficult if not impossible to establish with the necessary degree of certainty the liability of the specialist contractor.

This concern is even more poignant when the design is governed by exceptional conditions which may not materialize in practice except well after works completion. This is commonly the case when ground improvement is carried out primarily if not exclusively to mitigate seismic liquefaction hazard. There have been attempts to evaluate the effectiveness of ground improvement as a means of mitigating seismic liquefaction by performing full-scale tests in which pseudo-seismic actions are generated artificially by controlled blasting, but this approach cannot be considered for routine acceptance testing, hence the final evaluation is typically performed by a combination of indirect testing and calculation.

Predefining evaluation and acceptance criteria involves necessarily specifying in great detail the methods of investigation, data reduction, interpretation and calculation that must be applied to perform the evaluation. The technical expertise involved in this task is at least as demanding as performing the evaluation itself. Furthermore, in so far as it will govern final acceptance and payment, any such system of evaluation must be applied rigorously, with little or no tolerance for possible local exceptions which might otherwise prove acceptable when judged on technical merit alone.

On balance, considering that the procuring authority must in any case mobilize specialist technical expertise to evaluate technical proposals, in these cases it is preferable for the entity commissioning the work to retain authority and responsibility for technical monitoring and final evaluation of the works.

6 SUMMARY AND CONCLUSIONS

Project success depends on many factors. Selecting and implementing an appropriate strategy for specification, procurement, quality control and certification of the works is certainly one of them and one which calls for well-considered strategic decisions early in the process. They form part of a continuous process, which must be designed to deliver effective solutions which can be certified to satisfy the project objectives.

Effective quality control and final evaluation and certification of ground improvement works require 100% monitoring and timely review of operating parameters and evaluation of the results of control tests, implementing a quality plan which suits the specifics of the project.

When dealing with ground improvement works, it is tempting to delegate responsibility for design and certification to the specialist contractor, on the basis that he is best placed to identify the most efficient technical solution that satisfies the project objectives, while the administration often lacks the necessary specialist expertise in house. However, for the very same reasons it is advisable for the procuring authority to mobilize specialist support to provide independent advice throughout the process, from drafting an appropriate specification which reflects the selected procurement strategy through monitoring the technical performance of the specialist contractor during the works, to final evaluation and acceptance.

7 ACKNOWLEDGMENTS

I take full responsibility for the opinions expressed in this paper. However, it goes without saying that they are the result of many years of discussion with colleagues, clients and contractors encountered along the way. They are too many to acknowledge individually. I must however give special credit to Prof. Jamiolkowski, whose vision and determination created and sustained Studio Geotecnico Italiano, providing the environment where these discussions could come to fruition, and to Ing. Gianfrancesco Rocchi, a close friend and valued mentor.

REFERENCES

Chan, A.P.C., Scott, D., and Chan, A.P.L., 2004. Factors affecting the success of a construction project. Journal of Construction Engineering and Management, ASCE, Vol. 130, pp. 153-155.

Hamil, S., 2017. The alternative to last-minute specification writing. Specification Report 2017, NBS, Newcastle upon Tyne, pp. 8-11.

Knight, L., Harland, C., Telgen, J., Thai, K. V., Callender, G. and McKen, K., 2012. Public procurement: International cases and commentary. Routledge, London, 372 p.

Jamiolkowski, M., Lo Presti, D.C.F., and Manassero, M., 2001. Evaluation of relative density and shear strength of sands from CPT and DMT. Soil Behavior and Soft Ground Construction: ASCE Geotechnical Special Publication No. 119, 201-238

Pringle, T., 2017. The alternative to last-minute specification writing. Specification Report 2017, NBS, Newcastle upon Tyne, pp. 4-7.

Rubin, I.M., and Seeling, W., 1976. Experience as a factor in the selection and performance of project managers. IEEE Transactions on Engineering Management, Vol. 14(3), pp. 131-135.

Turley, L., Hug Silva, M., Benson S. and Dominguez C., 2014. Performance-based specifications: exploring when they work and why. International Institute for Sustainable Development, Winnipeg, Manitoba, Canada, 54 p.

BEARING BEHAVIOUR OF DUBAI SANDSTONE AND DUBAI SILTSTONE DUE TO HIGH-RISE STRUCTURES

Rolf Katzenbach, Technische Universität Darmstadt, Institute and Laboratory of Geotechnics, Germany, +49 6151 16 22 810, katzenbach@geotechnik.tu-darmstadt.de
Steffen Leppla, Ingenieursozietät Professor Dr.-Ing. Katzenbach GmbH, Darmstadt · Weinheim · Frankfurt am Main · Bensheim · Kiev, +49 6151 130 13 64, leppla@katzenbach-ingenieure.de
Marwan Alzaylaie, Dubai Creative Clusters Authority, UAE, +971 4 36 93 680, marwan.alzaylaie@dcca.gov.ae

ABSTRACT

Safety, optimisation and the sustainability are the most important aspects for the design of any foundation system. An optimised and safe design of foundation systems for high-rise structures in difficult soil and groundwater conditions is based on a reduction of construction material used, construction time spent, energy consumed and the adequate consideration of the soil-structure interaction. This is also important for the high-rise structures like skyscrapers and bridge piers in Dubai, UAE. Due to the large loads most of these structures are founded in the Dubai Sandstone and Dubai Siltstone. Up to now the rock mechanical parameters for these rock layers have been defined on the very conservative side which led to over-dimensioned foundations in many cases. In a large research program the bearing behaviour of Dubai Sandstone and Dubai Siltstone has been investigated by field and laboratory tests, by in-situ pile load tests and the numerical back-analysis using the Finite-Element-Method (FEM). The comprehensive research investigations show, that the stiffness of Dubai Sandstone and Dubai Siltstone is more than 20 times higher as it is assumed up to now. The paper presents the scope of research, the epoch-making results and the significance for the engineering practice.

Keywords: Dubai Sandstone, Dubai Siltstone

INTRODUCTION

Dubai in the United Arab Emirates (UAE) is one of the cities with the biggest density of high-rise buildings in the world (Fig. 1). All these high-rise buildings are founded on conventional deep foundation in the Dubai Sandstone and the Dubai Siltstone. The load of the high-rise structures into the subsoil is transferred by bored piles or barrettes.



Fig. 1. Skyline of Dubai, UAE

© 2018 Deep Foundations Institute

In the scope of a large research program the bearing behavior of the Dubai Sandstone and the Dubai Siltstone due to high-rise structures has been analyzed at the Institute and Laboratory of Geotechnics of Technische Universitaet Darmstadt (TU Darmstadt), Germany. This research program included a high amount of field and laboratory tests. The area for the research program was the Business Bay District of Dubai (Fig. 2). This area is about 3.5 km long and about 2 km wide. The subsoil conditions in the Business Bay District are representative for whole Dubai.



Fig. 2. Business Bay District, Dubai (UAE)

At the moment the highest high-rise building of the world, the Burj Khalifa, is located in this area (Fig. 3). The Burj Khalifa has 163 floors and a height of 828 m. This impressive high-rise building is surrounded by a water basin where every 30 minutes fountains accompanied with music enthuse the inhabitants and the many guests and tourists (Fig. 4). In a few years the Burj Khalifa will be only the second highest high-rise building in the world. The Jeddah Tower in Saudi Arabia will be 1,007 m high. The Business Bay District is located about 2.5 km landwards of the coast line (Fig. 5).



Fig. 3. Burj Khalifa, Dubai (UAE), h = 828 m



Fig. 4. Fountains at Burj Khalifa in Business Bay District, Dubai (UAE)



Fig. 5. Palm Island and Business Bay District, Dubai (UAE)

SUBSOIL AND GROUNDWATER CONDITONS IN DUBAI

The subsoil and groundwater conditions in Business Bay District in Dubai have been investigated by 166 core drillings. The results can be summarized as follows:

Under the surface middle dense sands and partly gravels can be detected unto a depth of about 15 m. Below the sands and gravels follows the Dubai Sandstone with a thickness of 15 m to 40 m. Under the Dubai Sandstone follows the Dubai Siltstone. The two rock layers are also named as "Weak Sandstone" and "Weak Siltstone" (Sharif & Ahmed 2010, Stipho 1984). The groundwater level is similar to the sea water level. That means that the groundwater level is about 3 m to 4 m below the surface. The subsoil and groundwater conditions are shown in Figure 6.

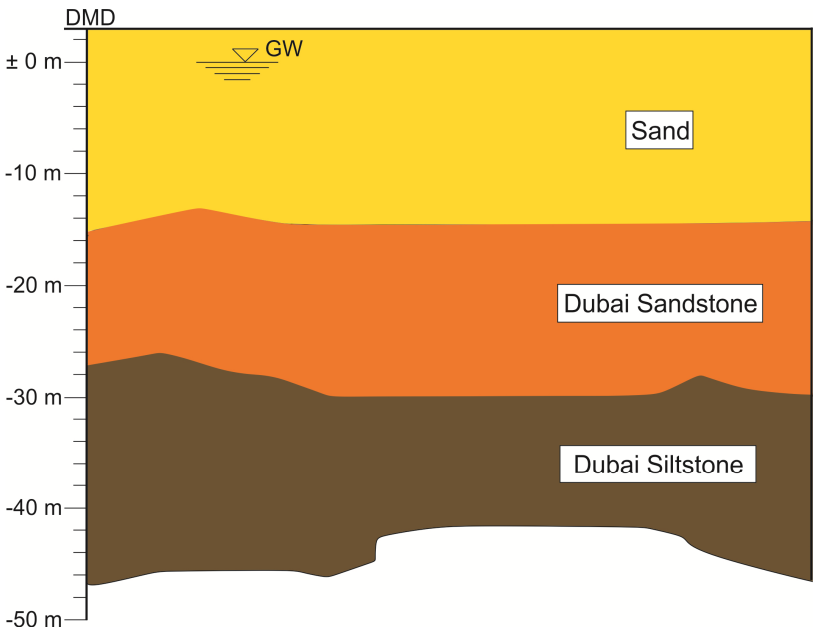


Fig. 6. Subsoil and groundwater conditions in Dubai (UAE)

The subsoil reports are normally developed by geotechnical consulting engineers from UAE, UK, USA and Australia. In these reports the following shear parameters and deformation parameters are given:

- angle of friction φ'
  - Dubai Sandstone: 30-45 °
  - Dubai Siltstone: 38-45 °
- cohesion c'
  - Dubai Sandstone: 20-105 kN/m^2
  - Dubai Siltstone: 50-155 kN/m^2
- Young´s Modulus E
  - Dubai Sandstone: 24-120 MN/m^2
  - Dubai Siltstone: 60-180 MN/m^2

PILE LOAD TESTS

The scientific research of the authors covers 28 large construction projects with more than 40 high-rise buildings. For these large construction projects 116 static pile load tests have been carried out, which have been analyzed scientifically by the authors.

108 of the static pile load tests have been carried out on the final building piles. 8 of the static pile load tests have been carried out on separated piles that have not been used for the load transfer. Only 3 of the test piles have been instrumented with strain gauges, extensometers or load cells. Due to this fact for the most static pile load tests only the load and the pile head settlement have been recorded. A typical example of the pile load tests is shown in Figure 7.

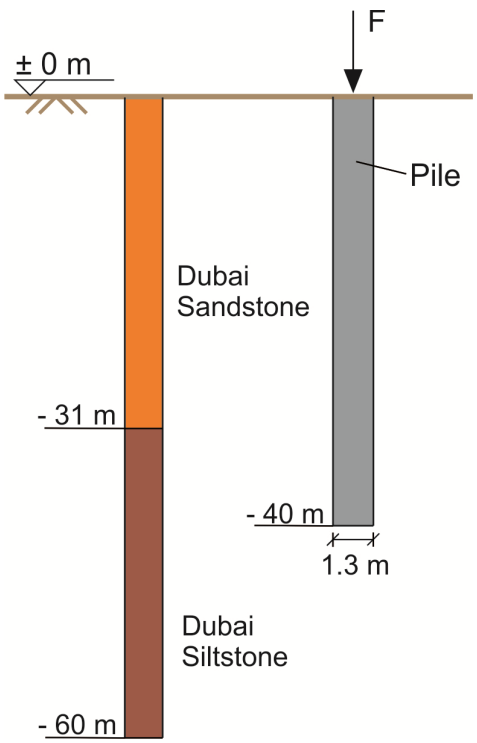


Fig. 7. Pile load test at pile No. 73

The test pile No. 73 is 1.3 m thick and 40 m long. The pile goes through the Dubai Sandstone and ends in the Dubai Siltstone. The maximum load was about 32 MN. The measured settlement at the pile head was only 0.7 cm.

The pile load test No. 73 was back-analyzed with numerical simulations using the Finite-Element-Method (FEM). For the first back-analysis the mechanical parameters of the soil reports have used. The comparison of the first back-analysis (grey line in Fig. 8) and the measurement data (red line in Fig. 8) shows no good accordance. Based on this insight additional numerical simulations have been carried out to calibrate the mechanical parameters (green line in Fig. 8). As a result of the calibration the stiffness of the Dubai Sandstone respectively of the Dubai Siltstone is about E = 5,500 MN/m^2. Using the information of the existing soil reports, the stiffness of the rocky subsoil is definitely under estimated. Based on this follow a totally wrong estimation of the bearing capacity and the load deformation behavior of the pile.

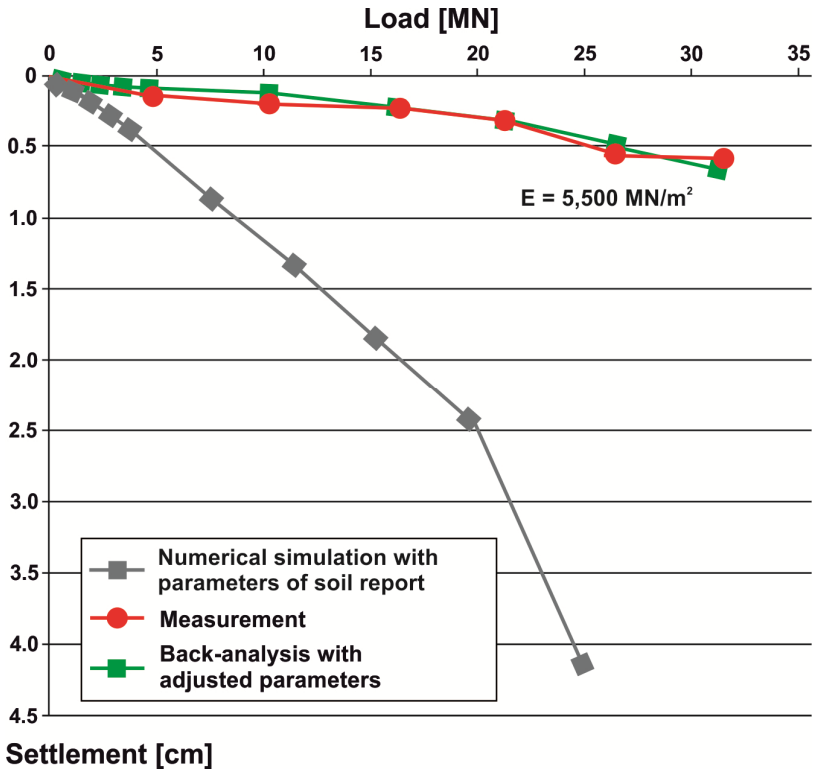


Fig. 8. Measured and calculated load-settlement curves of pile No. 73

To proof the research results of Figure No. 8 a simple calculation of the necessary shaft area of the pile for the maximum load was carried out using two simplifications:

- the settlement of the pile head is only due to the compression of the concrete
- the shaft resistance creates no settlements

With these simplifications the elastic relationship between stress and stiffness can be used which is given by Hooke´s Law in Equation 1.

$$\sigma = E \cdot \varepsilon \qquad [1]$$

The requirement for this simple calculation is that the calculated length L is smaller than the length of the test pile and the bearing capacity of the test pile is not reached. If the pile load is reduced by the shaft resistance linearly with the depth Equation 3 can be used which is a transformation of Equation 2.

$$s = \frac{F/2 \cdot L}{E \cdot A} \qquad [2]$$

$$L = \frac{s \cdot E \cdot A}{0.5 \cdot F} \qquad [3]$$

In these Equations are:

s	=	settlement at pile head [m]
E	=	Young´s Modulus of the concrete [MN/m²]
F	=	load at pile head [MN]

With a maximum load at the pile head of 32 MN and a maximum settlement at the pile head of 0.7 cm Equation 3 gives a length of the pile of about 18 m, which is necessary for the load transfer via shaft resistance. The result is visualized in Figure 9.

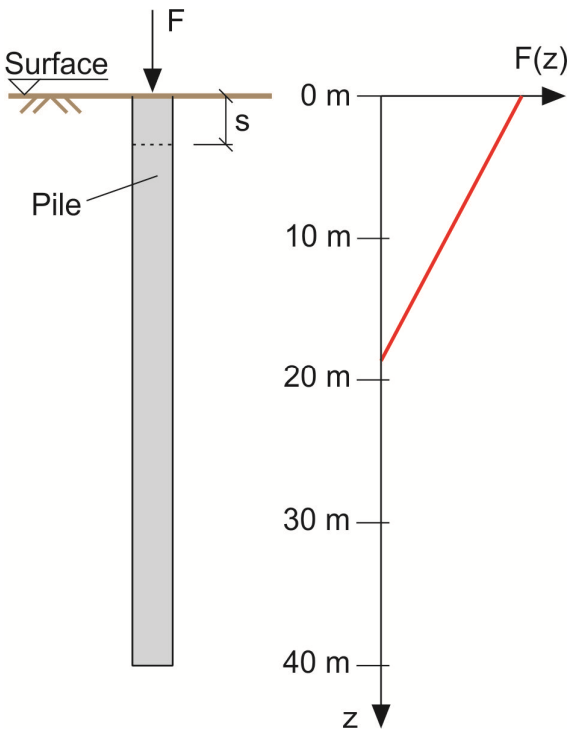


Fig. 9. Calculation of the necessary length L based on the maximum load and the measured settlement at the pile head

The scientific research for test pile No. 73 was carried out for all of the 116 test pile in Business Bay District. Some more data about the results of the pile load tests, the numerical simulations using the mechanical parameters of the soil reports and the numerical calibrations of the mechanical parameters are shown in the Figure 10, 11 and 12. For the Dubai Sandstone and the Dubai Siltstone the stiffness of E = 1,500 - 2,700 MN/m² gives a good accordance between the measurement data and the numerical results.

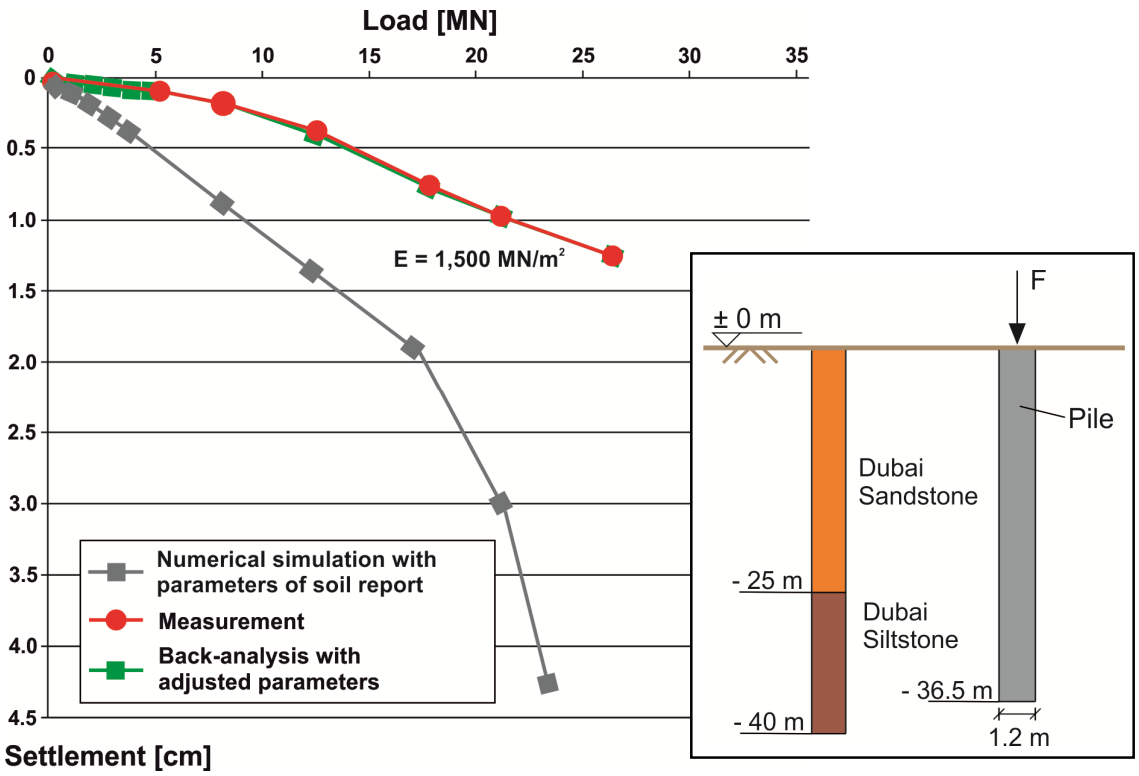


Fig. 10. Measured and calculated load-settlement curves of pile No. 67

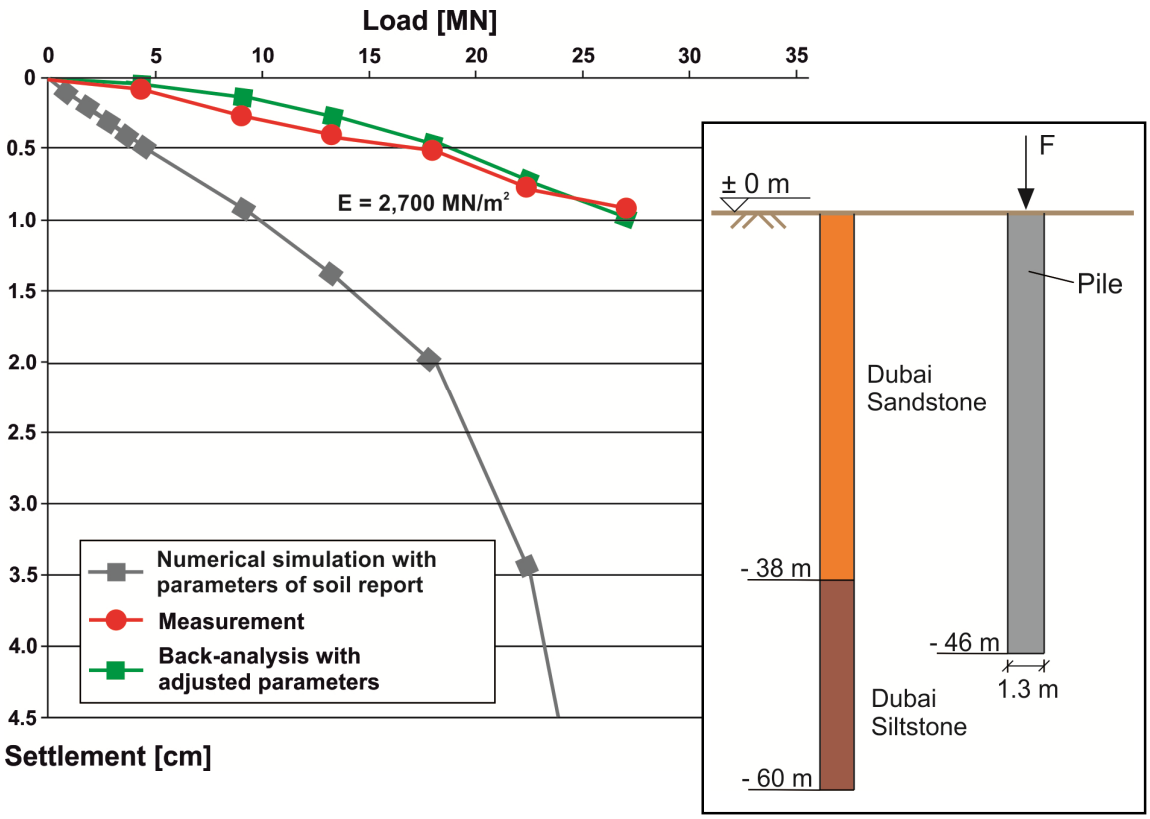


Fig. 11. Measured and calculated load-settlement curves of pile No. 74

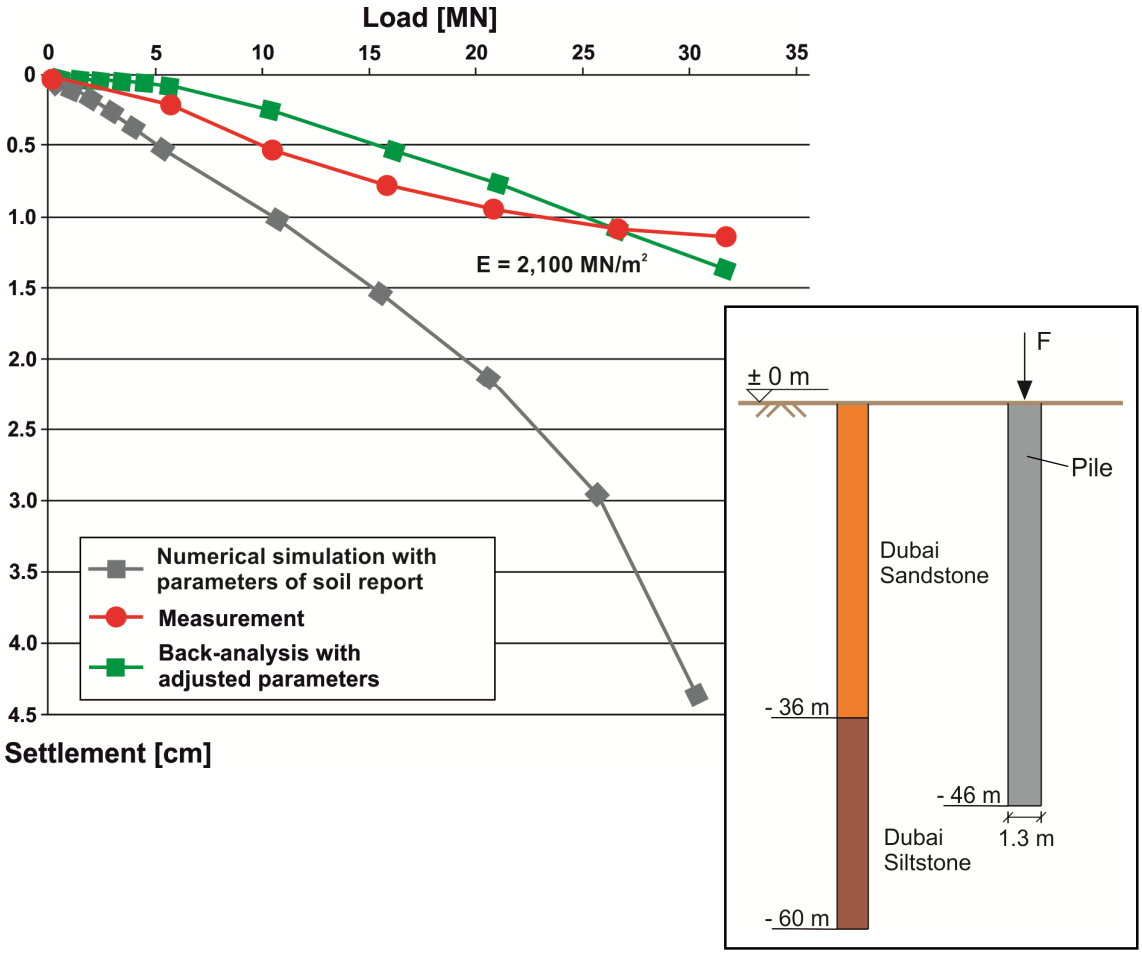


Fig. 12. Measured and calculated load-settlement curves of pile No. 76

Another possibility to proof these research results is the simplified back-analysis of the settlements of the Burj Khalifa (Figure 3). The measures settlements are about 5 cm, caused by an average load of the total building of about 8.000 MN. Neglecting the fact that the Burj Khalifa is founded on a large pile group, the stiffness of the subsoil can be calculated to E = 1,600 MN/m^2 using the equations of the classic settlement analysis. This result is in the range of the stiffness that is determined by the scientific research of the authors.

SUMMARY OF THE SCIENTIFIC RESEARCH

The results of the scientific research show, that the stiffness of the Dubai Sandstone and the Dubai Siltstone is much higher than estimated in the soil report. The stiffness of the rocky subsoil of Dubai given in the soil report is about 70-80 MN/m^2. The detected stiffness of the scientific research is more than 1,500 MN/m^2. The relation factor is between 21 and 70. A summary is given in Table 1.

Table 1. Comparison of the estimation and of the back-analysis of the stiffness of Dubai Sandstone and Dubai Siltstone

pile No.	Young´s Modulus E [MN/m²]		factor
	estimation $E_{soil\ report}$	back-analysis $E_{back\text{-}analysis}$	$E_{back\text{-}analysis}/E_{soil\ report}$
67	72	1,500	21
73	78	5,500	70
74	75	2,700	36
76	78	2,100	27

This totally new knowledge is proofed scientifically and will lead to an optimized planning and design of the foundations of large construction projects in Dubai and the whole UAE. This optimized planning and design lead to massive reduction of construction material, money and time and reduces the CO_2 output significantly.

This optimization can be increased in combination with the hybrid foundation system Combined Pile-Raft Foundation (CPRF). The design principles and the application of a CPRF are explained in the CPRF Guideline (ISSMGE 2013) and in Katzenbach et al. (2016).

Regarding the necessary safety and quality assurance including the observational method practical information is given in Katzenbach et al. (2010) and Katzenbach et al. (2013).

REFERENCES

ISSMGE International Society of Soil Mechanics and Geotechnical Engineering (2013). Combined Pile-Raft Foundation Guideline.

Katzenbach, R., Bachmann, G., Leppla, S., Ramm, H. 2010. Chances and limitations of the observational method in geotechnical monitoring. 14th Danube-European Conference on Geotechnical Engineering, 2.-4. June, Bratislava, Slovakia, 13 p.

Katzenbach, R., Leppla, S., Weidle, A., Choudhury, D. 2013. Aspects regarding management of soil risk. 4th International Seminar on Forensic Geotechnical Engineering, 10.-12. January, Bengaluru, India, 12 p.

Katzenbach, R., Leppla, S., Choudhury, D. 2016. Foundation systems for high-rise structures. CRC Press Taylor & Francis Group, New York, USA.

Sharif, E.Y., Ahmed, M.J., 2010. Engineering Geology of Dubai. Arab Centre for Engineering Studies (ACES).

Stipho, A.S., 1984. Soil conditions and foundation problems in the dessert regions of the Middle East. First International Conference on Case Histories in Geotechnical Engineering, St. Louis, Missouri, USA, 21-25.

CIVIL ENGINEERING FEASIBLITY STUDY FOR CERN'S FUTURE CIRCULAR COLLIDER

John Andrew Osborne, CERN, Geneva, Switzerland, john.andrew.osborne@cern.ch
Joanna Louise Stanyard, CERN, Geneva, Switzerland, joanna.louise.stanyard@cern.ch

Keywords
CERN. Tunnelling. Feasibility. Technology. Geographic Information System.

Abstract

The European Organization for Nuclear Research (CERN) is currently investigating the feasibility of the "Future Circular Collider" (FCC) as a potential successor to the Large Hadron Collider (LHC). The civil engineering team at CERN have employed a bespoke, interactive, geological tool to consider the suitability of multiple layout options for the FCC, situated in the Geneva Basin, in particular quasi-circular options with circumferences in the order of 100 km. The tool has been used to provide feedback on potential lattice designs that are assessed based on criteria such as geological risk, shaft depth and the environmental sensitivities of access and experimental sites. This paper describes the impact the tool has had on optimising the design and location of the FCC and also the key construction challenges, in particular deep shafts and large span caverns.

Introduction

In 2014 a major study was launched to investigate the feasibility of a circular collider to succeed the Large Hadron Collider at CERN. The emphasis of the study is on a hadron collider with a centre-of-mass energy of the order of 100 TeV in a new 80 km – 100 km tunnel. The design study includes a 90-350 GeV lepton collider, seen as a potential intermediate step. A lepton-hadron collider option is also being examined.

By the end of its construction in 2008, civil engineering accounted for around one third of the consolidated project cost of the LHC. Therefore, significant importance is placed on the civil engineering design when investigating the feasibility of the FCC. The earliest stages of any construction project offer the most opportunity for maximising quality and reducing total project costs. With this in mind, CERN is working in partnership with world leading engineering consultancies to utilise the latest methods and technology in order to ensure the best possible outcome from the first stages of design.

This paper describes the geological features of the region and how a web-based, three-dimensional, interactive geological tool has been utilised to assess the feasibility of a tunnel of the required dimensions. In addition, the paper will explore the remaining challenges for the early planning stages of this project, including the required future geological investigations and the key construction challenges to be face.

Geology of the Region

CERN is located in the Geneva basin, the existing infrastructure for the LHC and its injector chain sits on the border of Switzerland and France. In terms of geology, the region consists of the sedimentary rock of the Leman Basin known as "molasse", which is bounded by the significant limestone structures of the Jura, Vuache and Salève mountains. Shallow glacial deposits, referred to as moraines, make up the uppermost layer of geology.

© 2018 Deep Foundations Institute

The molasse comprises an alternating sequence of marls and sandstones (and formations of intermediate compositions) (Fern et al., 2017). The layers exhibit a wide range of geotechnical properties ranging from strong sandstone to very weak marls, but even so, it is considered good, stable conditions for tunnelling; the main risk is swelling of the marls (GIBB et al, 1996).

The limestone formations in the region, however, are considered higher risk environments for tunnelling due to the existence of water-filled karsts. Significant issues were encountered by CERN engineers whilst excavating a portion of the Large Electron Positron (LEP) tunnel in the Jura limestone (Schopper, 2009).

Tunnel Optimisation Tool Development

The very first stages of a construction project offer the highest opportunity for overall reduction of cost, schedule and environmental impact (see Fig. 1). A digital approach to the FCC feasibility study has enabled CERN to extract the maximum value from the large amount of available data relating to the terrain, geology, hydrology, environment and built-environment of the Geneva basin, including man-made hazards such as geothermal boreholes. Locating the optimal position for any given design of the FCC tunnel requires all elements of this data to be analysed simultaneously.

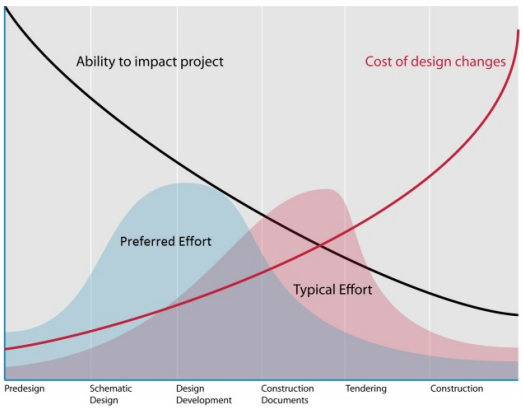


Figure 1: Macleamy's Curve (2004) from the Construction Users Roundtable

The Tunnel Optimisation Tool (TOT), developed specifically for the FCC study in collaboration with Consultants Arup, is based on an open source Geographical Information System (GIS) driven technology stack. GIS computer systems enable multiple sets of data to be arranged spatially, usually together with a physical or topographical map, all of which can then be manipulated, managed and analysed concurrently. For TOT, this means the user is able to input any size, shape and position of tunnel and to instantly see how this interacts with the geology, terrain, the environment and the build-environment in the study area.

The basis of the tool is existing geological data from the Geneva basin region; this is made up of boreholes, geological maps, and reports, which have been interpreted to create rockhead maps of the limestone and the molasse. In addition CERN has extensive geotechnical reports from the construction of the Large Electron Positron (LEP) and LHC, from which the geotechnical parameters for FCC can be approximated.

Placement

A range of machine shapes for the FCC were developed, with variations in the lengths of the straight sections and arcs. Figure 2 shows a sample of these shapes within the study boundary. These files were uploaded onto TOT and assessed. Within the tool, the machine shape can be moved laterally and

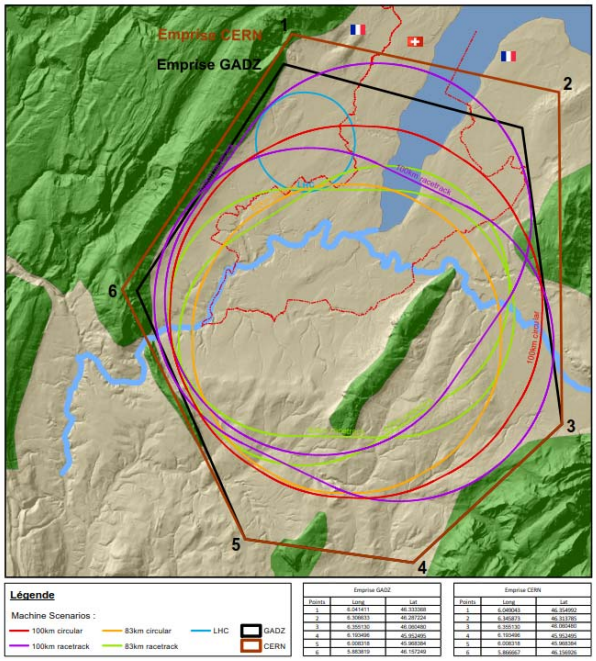


Fig. 2. Early Stage FCC options

rotated in the x,y plane, and the depth at the centre of the shape can be adjusted in the z direction. The angle of the slope of the tunnel is also adjustable; it is necessary for the tunnel to be positioned with a small gradient in order for a gravity drainage system to be utilised.

The position of the tunnel layouts are adjusted into an optimal position and evaluated on the following criteria:

Geology along the Tunnel Alignment

The initial assessment of the tunnel alignment is based on the geology along the length of the tunnel. Figure 3 shows the graphical output from TOT illustrating the geological conditions along the profile of an example layout. It is the aim of the civil engineers to maintain the tunnel in the molasse, for as much of the length as possible. This strategy has been implemented based on previous experience at CERN, where the molasse has provided favourable conditions for the Tunnel Boring Machine (TBM) (GIBB, 1996); in comparison, significant issues with water ingress and damage to the tunnel due to a build-up of water pressure have arisen in the sectors of the LEP tunnel excavated in the Jura limestone. Tunnelling in the fluvio-glacial deposits, known as moraines, is also considered a risk, especially water bearing moraines under the lake, as the conditions are soft and inconsistent. However, it is possible to excavate in the soft ground using a multi-mode TBM with an earth or slurry pressured system (Amberg, 2016).

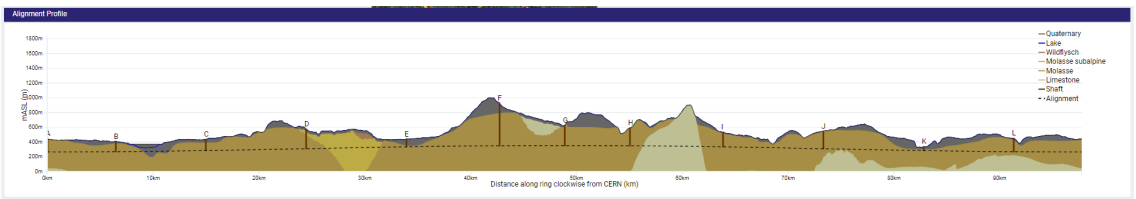


Fig.3 Geological profile of FCC

Overburden

During excavation there is a risk of rock squeezing at the face of the excavation, leading to the TBM potentially becoming immobilized (Anagnostou, 2018), which would have significant repercussions on the schedule; this risk is exacerbated by a large overburden. It has therefore been a strategy to try to limit the depth of the overburden in order to mitigate this risk, the result of this is that wherever possible the tunnel has been kept out of the Pre-Alps and Vuache regions, where the depth of ground cover becomes excessive.

Shaft Depth

Shaft depth is also a major consideration when locating the machine tunnel; it is important to consider both total shaft depth and individual cases of very deep shafts. There are significant cost and schedule benefits of reducing the total shaft depth, as vertical construction is notably more expensive and time consuming than the horizontal construction of the tunnel. Reducing the depth of the shafts also has the secondary benefit of reducing lengths of the services required for the operation of the accelerator. It is also intended to avoid having any individual very deep shafts, as this introduces additional construction and schedule constraints.

Surface Locations

As the feasibility study progresses, further consideration is being given to the location of the surface sites. TOT is able to automatically identify clashes with buildings and protected areas, but there are further constraints to be considered in addition, such as access and gradient of the particular site.

Selected Alignment

These are a sample of the key parameters that are considered when evaluating potential machine layouts and positions. This analysis is undertaken using a combination of quantitative and qualitative methods. Figure 4 shows a proposed position of a layout following assessment based on the discussed criteria.

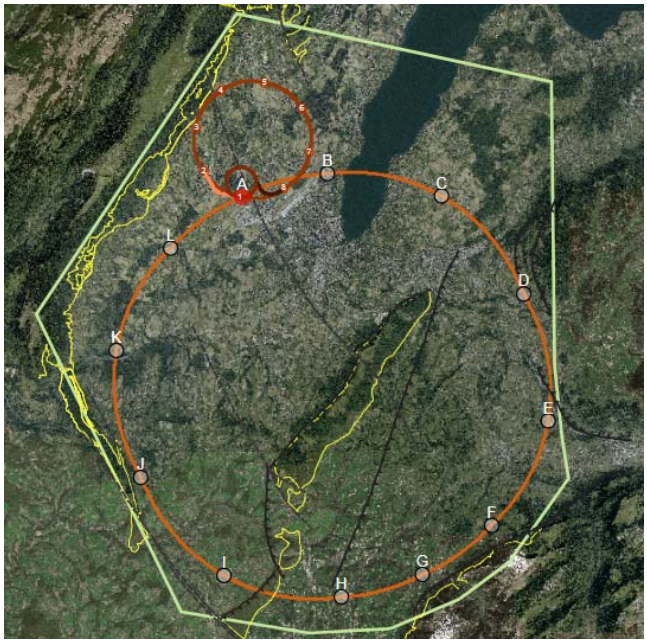


Fig. 4. Plan View shown in TOT

The results from the assessment of the different layout options indicate that, even when the total

circumferences of the lattice files are the same, the different configurations of lengths of straight sections and arc lengths create significant differences in terms of risk and feasibility. This is due to the 100 km quasi-circular design fitting tightly within the natural boundaries of the Jura Mountains to the north-west, the Vuache Mountain to the south-west and the Pre-Alps to the south-east and east, meaning small differences between layout designs can easily lead to notable differences in the output. The favoured layouts avoid the Jura and Pre-alps limestone whilst also avoiding exceptionally deep shafts at Points H, G and F, however it has proved difficult to simultaneously fulfil these criteria. The surface site locations of point A and B have also proven to be critical, as B is in close proximity of Lac Leman and in certain siting solutions it is possible to place Point A on CERN land close to the Meyrin site; this is an attractive option for the study as Point A will house one of the main experiments. It is likely that some shafts will be shifted along the length of the tunnel from their original positions to avoid difficult surface locations such as protected water sources and built-up areas; it has been deemed acceptable for the shafts located at points that do not house experiments or the beam dumps to be adjustable.

There have been extensive studies regarding the depth at which the tunnel passes below Lac Leman. An early strategy involved avoiding the moraines, as these soft and inconsistent conditions are considered a risk. However, this strategy had a large negative influence on the total shaft depth as this was the critical feature defining the depth of the tunnel. Positions are now under consideration that include the tunnel passing through the fluvial deposits under the lake. It is acknowledged that the moraines under the lake improve with depth, therefore a minimum depth of 80 m below the lake bed has been defined such that at worst the tunnel traverses a layer of impermeable, well-compacted moraines.

The assessment process has indicated that it is very difficult to position the tunnel in such a way that avoids having at least one undesirably deep shaft; inclined access tunnels are therefore being considered as an alternative or complementary structure. Adding inclined tunnels could facilitate an accelerated programme for the construction of the tunnel as the additional access points can potentially bisect the longer arc lengths to allow two construction fronts.

Structures Required

The principal structure required for the collider is a 6 m internal diameter 97.75 km long tunnel, which is a combination of straight sections and arcs. In addition, a large span experimental cavern is required at each of the four experimental points L, A, B and G; these caverns have a clear span of 35 m, which is considered to be at the limit of what is possible to construct in the presented ground conditions. At each of the access points around the ring, a service cavern is required with a span of 25 m. Auxiliary structures are required in the form of by-pass tunnels, alcoves for housing electrical equipment and connection tunnels. Figure 5 shows a schematic of the required underground structures.

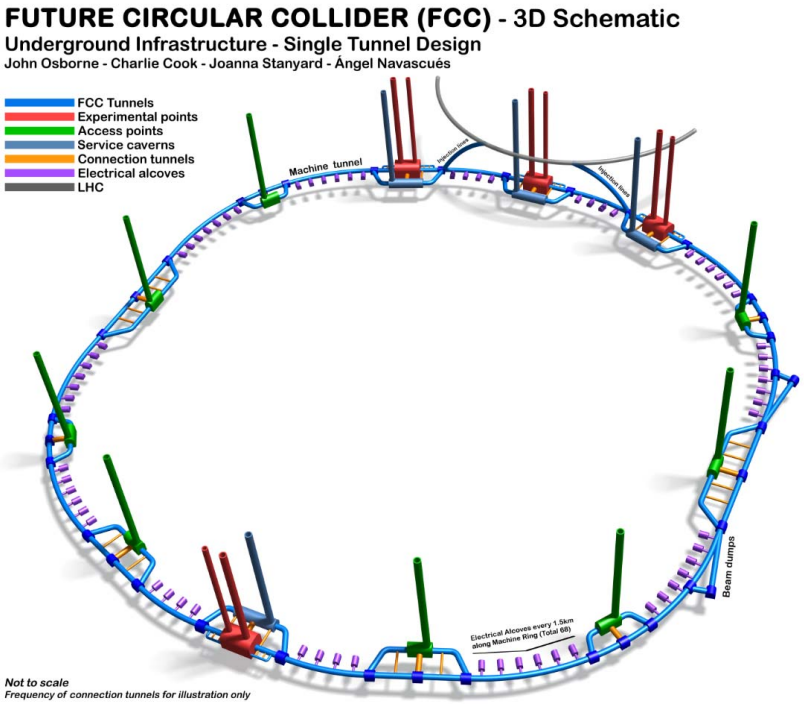


Fig. 5. 3D schematic of underground structures

Key Construction challenges

Apart from the magnitude of the project and the associated cost, schedule and environmental impact issues, the key construction challenges are the deep shafts and large span caverns at depth. A total of 20 shafts are required around the ring at 12 different locations. At each point an access shaft with a diameter of 12 m is required, and then an additional 2 shafts are required at each of the 4 experimental points, with internal diameters of 10 m and 15 m.

The initial excavation for the shafts is through the moraine layer, this layer varies in depth between access points from 10 to 90 m. Due to the poor ground conditions and presence of water in this layer, the shaft needs to be pre-supported prior to excavation. At this stage of the feasibility study we are assuming this will be achieved via diaphragm walls. However, ground-freezing has previously been required for the construction of shafts at CERN due to high water flow rates (see Fig. 7). Other techniques are also under consideration such as secant pile walls and vertical sinking machines (VSM), these will be assessed on a site specific basis once conditions are better understood.

The VSM, as shown in Figure 6, developed by Herenknecht, consists of main components: the shaft boring machine and the lowering units. A modified road-header, in the form of a rotating cutter drum is attached to a telescopic boom, this breaks the ground. The shaft is flooded with slurry water and so the excavated material can be removed via a submersible pump. The shaft rings are lowered continuously until the desired depth is reached. The VSM is a good option for the constructing shafts in the moraine as it functions well in soft ground, and the presence of water would not be a significant issue. It is an attractive option due to high excavation rates and improved safety conditions.

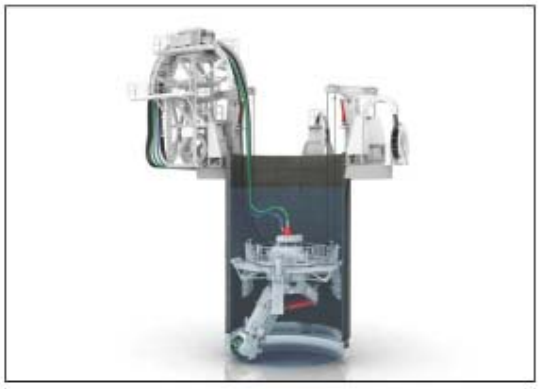


Fig. 6. Vertical Sinking Machine (Herrenknecht)



Fig. 7. Ground Freezing during CMS construction

The remainder of the excavation through the molasse is anticipated to be mined using rock-breakers and roadheaders. Rock-bolts and a shotcrete lining will provide the primary support, followed by a waterproof membrane and a permanent, slip-formed, inner lining.

The deepest access point is located at approximately 550 m below the surface with at least 100 m of moraines at the surface, and requires a 12 m diameter access shaft for personnel and services. This is deemed to be unacceptably deep for scheduling reasons and also introduces challenges for the lift system to be installed for transportation of personnel. It is therefore planned to off-set this shaft from the alignment, allowing it to be sited at a significantly lower elevation, combined with an inclined tunnel to connect into the necessary cavern. The shaft will be approximately 300 m deep followed by a 1 km inclined tunnel.

The large span caverns also pose a construction challenge, especially as at the experimental points the 35 m span experimental caverns are required to be as close as possible to the 25 m span service cavern. It is therefore planned for the caverns to be separated by a 10 m wide concrete pillar; this pillar will be excavated first and then filled with reinforced concrete, the adjacent caverns will then be excavated.

Conclusion

The results of the study so far provide a solid basis for early decision making for the FCC project in terms of design, cost and planning. The TOT tool has allowed CERN to find a location for the underground infrastructure, which based on the current available information, is technically feasible. The conclusions of the FCC study, for all disciplines, are to be presented to the European Strategy for

Particle Physics at the end of 2018, following which a decision on the continuation of the project will be made.

References

Amberg Engineering, 2016, Comparison of 100 km FCC options from an engineering perspective, Unpublished.

Anagnostou M.R.G, 2008, TBM drives in squeezing ground – shield-rock interaction, in AFTES Congrès Internationale, Paris, 2008.

Fern E.J ,Di Murro V, Soga K, Li Z, Scibile L, Osborne J.A, 2017 Geotechnical characterisation of a weak sedimentary rock mass at CERN. Geneva. Engineering Geology manuscript no.

Gibbs, SGI Ingeniere, Geoconsult, 1996, LHC civil engineering consultancy services Package 02, Getechnical Interpretive report – LHC-DZ-1399-0130. Unpublished.

MacLeamy, P. 2004, Collaboration, integrated information and the project lifecycle in building design, construction and operation, Construction Users Roundtable

Schopper H., 2009, LEP – The lord of the collider rings at CERN 1980-2000. 211

Acknowledgements

Arup

Amberg Engineering

GADZ

ILF Consulting Engineers

CORRELATION BETWEEN AXIAL CAPACITY OF DRIVEN PILE AND STANDARD PENETRATION TEST BLOWCOUNT

Jinyuan Liu and Markus Jesswein
Department of Civil Engineering, Ryerson University, Toronto, Ontario, Canada

ABSTRACT

This paper presents a correlation study between the axial capacity of a single pile and standard penetration test blowcount (SPT N-value). Piles have been commonly used to support structures for many centuries. However, the uncertainties and variabilities from the soil conditions still lead to conservative or unsafe designs to date. One challenging ground condition for designers is glacial deposit. These deposits are known for their unsorted grain sizes and varying geotechnical properties. The Ministry of Transportation of Ontario in Canada accumulated a database with more than 100 pile load tests in various ground conditions over the course of four decades. Most of these piles were driven H piles or pipe piles. This study selected a total of 23 piles with both compression and extraction tests. From the test results, the relationships were calculated between the skin resistance and tip resistance of driven piles and SPT N-values. The coefficients to estimate the pile capacity are presented at the end of this paper.

Keywords: Pile Capacity, SPT, Correlation, Side Resistance, Tip Resistance

INTRODUCTION

The axial capacity of a pile involves many influential factors, including the pile installation method and soil conditions. Glacial deposits covering Ontario, Canada are known for their inconsistent material properties, which create difficulties for engineers to achieve accurate evaluations (Barnett 1992). Over the last few decades, several approaches were proposed to predict the ultimate capacity of a pile for either fine-grained or coarse-grained soils. However, there is still a lot of variation between the predicted and measured pile capacities in the field. In order to evaluate the design assumptions and verify the pile capacity in the field, time-consuming and expensive load tests were applied in Ontario over a period of four decades from 1952 to 1994. A database of over 100 pile load tests was accumulated by the Ministry of Transportation of Ontario (MTO 1993). In this database, several piles were subjected to both compression and extraction tests. The difference between the applied compression and extraction loads can be related to the tip resistance, and the applied extraction loads can be related to skin resistance. A similar approach was used by Boostra (1936). In addition, the standard penetration test (SPT) is the most popular geotechnical investigation method in Ontario due to the restraints by many other investigation methods to be applied in gravel or cobble rich glacial deposits. Many correlation studies have been conducted internationally between the skin and tip resistances and SPT blowcounts (N-values), such as Meyerhof (1956); Decourt (1982); and Brown (2001). However, the proposed correlations largely differ due to the soil conditions, and the soil characteristics can also easily change within local regions. For glacial deposits in Ontario, a limited number of studies have been performed with driven piles.

This research involves a total of 23 piles with both compression and extraction load tests and correlates the pile resistances with SPT N-values. These correlations with the SPT N-values will help to improve the design of driven piles in Ontario.

© 2018 Deep Foundations Institute

RESEARCH BACKGROUND

Current pile design methods

As a compressive load is applied to a pile, the ultimate axial capacity (Q_u) is composed of two mechanisms: the skin resistance and tip resistance. The skin resistance, also called the side resistance, is the friction between the soil and pile walls. The tip resistance is generated by the strength of the soil at the pile tip. If the weight the pile, *Wp*, is included, the axial capacity can be expressed below:

$$Q_u = q_s A_s + q_p A_p - W_p \quad [1]$$

Where A_s is the outside skin area of the pile where fully plugged is assumed in the study, A_p is the area of a fully-plugged pile tip, and q_s and q_p are respectively called the unit skin resistance and the unit tip resistance of the pile.

Generally, design methods that correlate the unit resistance factors with soil parameters are divided into total stress methods and effective stress methods. The total stress methods, or α methods, are intended for the short-term conditions of fine-grained soils (Kulhawy and Jackson 1989; Karlsrud et al. 2005). The effective stress methods are usually called β methods and are for coarse-grained soils or the long-term conditions of fine-grained soils (Meyerhof 1976; Vesic 1977).

Standard penetration test (SPT)

The SPT method is a rapid, simple, and economical test that is widely adopted to assess the properties of most soil types. The test is performed after advancing a boring to a desired depth. The drilling crew first slowly removes a string of drill rods and cleans out the hole to the desired depth of testing. After the drilling tools are removed, a standard thick-walled split-spoon sampler is attached to drill rods and is lowered to the bottom of the hole. With the sampler resting at the bottom of the hole, a slide hammer with a standard weight of 63.6 kg (140 lb) is allowed to fall freely 762 mm (30 in) onto a collar that is attached to the top of the sampler. The hammer is raised and dropped by a string until 457 mm (18 in) of penetration has been achieved by the sampler. The number of blows are recorded to penetrate three 152 mm (6 in) intervals. The first interval is generally considered to be a seating drive, and the number of blows for the final 305 mm (12 in) is reported as the SPT blowcount (SPT N-value).

SPT has many limitations. For example, it has poor repeatability and provides erroneous recording for soils containing coarse gravel and cobbles, and it is inapplicable for sensitive clays (Kulhawy and Mayne 1990). However, the SPT test is still the most popular field investigation method in Ontario.

Since many different forms of SPT are used worldwide, standardization is essential in order to facilitate the comparison of results from different investigations, even at the same site. The practice now in the United States is to express the SPT N-value measured to an average energy ratio of 60 %. Correction factors are applied for variations in hammer energy, borehole diameters, sample methods, and rod lengths (Skempton 1986).

Literature research on correlations between SPT-N and pile capacity

Many correlations have been observed between resistance factors and field test values, such as the cone penetration test (CPT) tip resistance. In particular, Meyerhof (1956) conducted a correlation between SPT N-values and pile capacity, and he concluded the following formulas for driven displacement piles:

$Q_u = q_s A_s + q_p\, A_p$ [2]

$Q_u = \overline{N}/50\, A_s\ + 4N_p\, A_p\ (tons)$ [2a] for displacement piles

$Q_u = \overline{N}/100\, A_s + 4N_p\, A_p\ (tons)$ [2b] for small displacement piles, like steel H piles

Where N_p is the SPT N-value at the pile tip and $\overline{N}$ is the average SPT N-value over the pile length. The upper limit of unit skin friction is 1 ton per square foot (95.76 kPa). Meyerhof (1956) studied a limited number of piles, and most of them were from published cases around the world. In addition, these parameters were proposed for general soil conditions. Refinements can be made for Ontario soils based on data from pile load tests by MTO.

RESEARCH METHODS

Glacial deposits covering Ontario

Since glaciers once covered most of North America, glacial deposits will be heavily encountered within Ontario. Glacial till is sediment that was eroded, transported, and deposited by glacial ice and usually contains an inconsistent mixture of particle sizes, mineral types, and weathered rock types. According to Barnett (1992), tills are often compact or overconsolidated (OC) due to the weight of the previously overlying glaciers. In Ontario, normally consolidated (NC) or lightly overconsolidated tills can also be found, but they would exist by areas where drainage of meltwater occurred, such as the shores of the Great Lakes (Barnett 1992). The different origins and processes that created tills lead to a variety of soil characteristics and contents.

The formation of till in Ontario can vary the soil content. Precambrian igneous and metamorphic rocks composed a large portion of the Canadian Shield. If these igneous and metamorphic rocks eroded to form the till, the till can contain over 70 % sand and less than 5 % clay (Barnett 1992). Tills likely range from non-plastic, especially from eroded Precambrian rocks (Barnett 1992), to low plasticities due to the low silt content. However, tills from carbonate rocks, limestones, and dolostones can have a content of 40 to 50 % silt and 15 to 30 % clay. Well graded sediments from carbonate rocks leads to compact to very compact tills. Tills located deeper into the ground are expected to be more compact, and layers overlying bedrock are typically thin and contain a fair amount of boulders and gravels (Barnett 1992). Fine-grained tills were likely formed by the addition of glaciolacustrine deposits and are composed of clay to a maximum of approximately 55 % (Barnett 1992). Observing these formations show that tills generally range in fine- and coarse-grained contents.

Pile load tests and the database from MTO

Pile load tests are costly and time-consuming, but full-scale tests are reliable and are commonly applied to verify designs in local ground conditions. A database of more than 100 piles was obtained over four decades by MTO (1993). This database contains the results from tests with static axial loads. Piles were tested as recommended by ASTM D 1143, titled the "Standard Test Method for Piles Under Static Axial Compressive Load." Axial loads were applied to piles by hydraulic jacks that acted against an anchored reaction frame, weighted box, or weighted platform. These pile load tests are invaluable to provide local or regional geotechnical parameters and can be used to develop design methods for piles in Ontario. For example, McVay et al. (2000) achieved reliable design methods for regions in Florida after analysing results from local pile load tests.

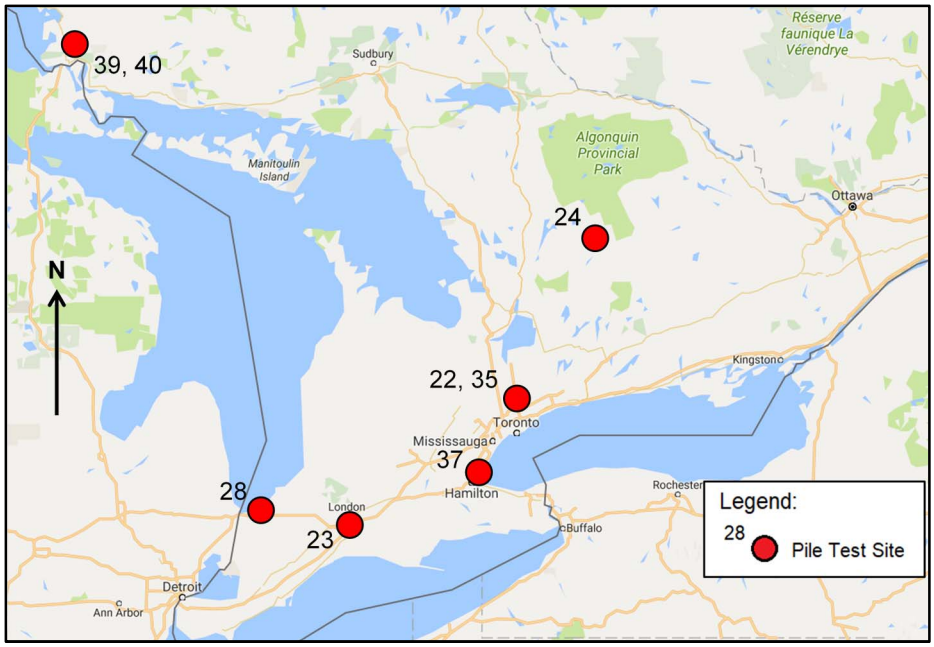


Fig. 1. Location of the Sites of Studied Pile Load Tests

From the pile tests by MTO, a number of piles were subjected to both compression and extraction tests. The difference between the applied compression and extraction loads was related to the tip resistance of the pile, and the applied extraction loads was related to skin resistance. Boostra (1936) applied a similar approach. The selected piles and the test sites are shown in Table 1 and Figure 1. Both closed-ended pipe piles and H piles driven into fine- and coarse-grained soils were selected in this study. The procedure of this study included extracting the measured capacity from test results; evaluating the unit skin resistance and tip resistances; correlating these resistances with SPT N-values; and conducting a statistical analysis with the findings.

RESEARCH METHODOLOGY AND RESULTS

Overview of the methodology

The ultimate goal is to develop an accurate and reliable design method for pile foundations in Ontario. The methods applied in this study will involve four steps: 1) Pile load tests and soil conditions were collected from the database by MTO; 2) The measured ultimate capacities for both compression and extraction tests were obtained; 3) The skin resistance and tip resistance in terms of the SPT N-values were calculated; 4) A brief statistical analysis was conducted with these resistances and impacts from various parameters, such as the pile type, pile length, and soil conditions.

Testing sites and pile information

The focus in this paper was on steel H or concrete-filled driven piles that were tested with both a static axial compression test and extraction test. In Table 1, most piles ranged in length from 12 m to 30 m, but a few were as short as 3 m. As shown in Figure 1, tests occurred in various regions of Ontario, but a majority of piles were located in Southern Ontario.

All the soil measurements and pile test results were conducted by MTO, and the results were extracted for this study. Site 39 is used here as an example to illustrate the study method. At Site 39, two of the three

tested piles (Pile No. 2 and 3) were tested with both compression and extraction tests and were selected for this correlation study.

Soil conditions at tested sites

Borehole logs were collected from each test site, which showed both the physical properties and geotechnical properties of the soils at various sampling depths. This includes the soil descriptions and classifications and shear strength values from unconfined compressive strength, triaxial, and field vane shear tests. At some sites, the percentages of clay, silt, sand, and gravel were also included in the borehole log along with the unit weight and the Atterberg limits. Every site varied in the extent and diversity of the site investigations. Specifically, SPT N-values were commonly found, especially for sites with coarse-grained soils. The distribution of SPT N-values along the depth is shown in Figure 2 for Site 39.

Table 1. Details information on selected piles and load tests

Site	Pile	Pile Type[1]	Length[2] (m)	Embedded Soil Type[3]	Q_u (kN)	Q_s (kN)	Q_p (kN)	Notes
22	3	324 OD Pipe	15.30	Clayey Silt	192	179	13	343 mm Ø shoe
22	4	324 OD Pipe	30.15	Clayey Silt	996	462	534	343 mm Ø shoe
22	5	324 OD Pipe	15.28	Clayey Silt	233	193	39	324 mm Ø shoe
23	2	324 OD Pipe	3.02	Silty Clay	449	224	225	343 mm Ø shoe
23	3	HP 310x110	3.05	Silty Clay	429	244	185	
24	2	324 OD Pipe	15.39	Sand	638	434	204	343 mm Ø shoe
24	3	324 OD Pipe	22.40	Sand	709	488	221	343 mm Ø shoe
24	4	HP 310x79	22.40	Sand	1389	438	951	
24	5	HP 310x79	15.39	Sand	715	288	426	
28	2	HP 310x79	18.29	Clayey Silt	486	345	141	
28	7	324 OD Pipe	6.10	Clayey Silt	671	582	88	343 mm Ø shoe
28	8	324 OD Pipe	18.29	Clayey Silt	695	479	216	343 mm Ø shoe
28	9	324 OD Pipe	12.04	Clayey Silt	615	608	8	343 mm Ø shoe
35	1	HP 310x110	14.69	Layered Clayey Silt and Silty Sand	1609	539	1069	
35	4	324 OD Pipe	14.69	Layered Clayey Silt and Silty Sand	1537	790	747	343 mm Ø shoe
35	5	HP 310x110	27.58	Layered Clayey Silt and Silty Sand	2744	1554	1190	
37	3	HP 310x79	14.48	Sand to Silty Sand	1054	357	697	
37	5	HP 310x79	31.24	Sand to Sandy Silt	1633	469	1164	
37	6	HP 310x110	14.48	Sand to Silty Sand	798	416	381	
39	2	HP 310x110	25.50	Silty Sand; Layered Clay and Silt	1307	670	637	
39	3	324 OD Pipe	25.40	Silty Sand; Layered Clay and Silt	1170	582	588	343 mm Ø shoe
40	2	HP 310x110	24.50	Layered Sand and Silty Clay	1232	652	580	
40	3	324 OD Pipe	17.20	Sandy Silt to Sand	1167	583	583	343 mm Ø shoe

Notes: [1] Steel H pile designations are size (mm) by weight (kg/m). Steel pipe piles were filled with concrete before testing, and OD is the outside diameter (mm); [2] Embedment Length; [3] Classifications according to MTO standards.

Compression and extraction tests

A few special cases were excluded from this analysis, such as timber piles and pile load tests in organic soils. The pile tests were conducted with loads in static axial compression or extraction. Normally, the duration between conducting compression and extraction tests was about 10 days. A dial gauge measured displacements on the pile butt, and the load-settlement from the pile top were available for all the pile load tests. The difference between compression and extraction tests was considered to be the tip resistance. The load-settlement curves are shown in Figure 2 for Site 39, and the failure loads for compression, extraction, and tip resistance are also shown at corresponding points on the curves. The failure loads were evaluated using the De Beer failure criteria (Fellenius 1980). For this criteria, both axes on of load-settlement curves are plotted with a log-scale, and the failure load corresponds to the load with the greatest change in slope (Fellenius 1980).

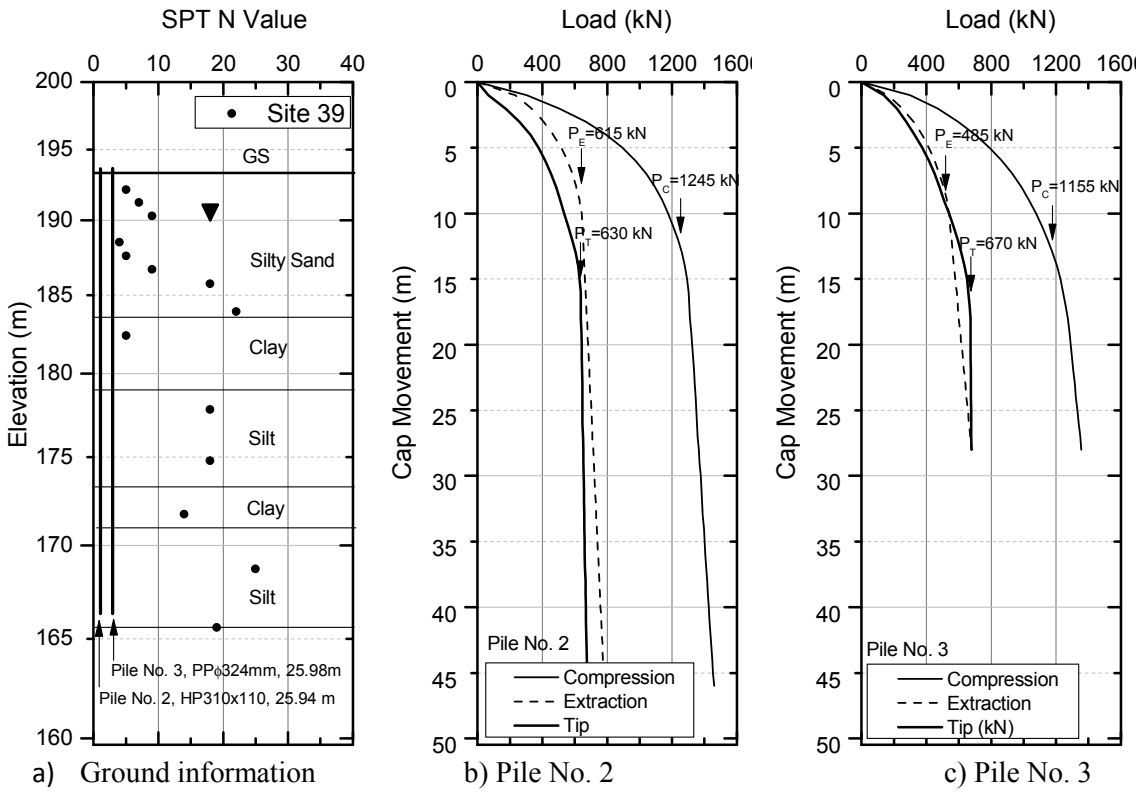


Fig. 2. Two load tested piles at Site 39

STATISTICAL ANALYSIS OF CORRELATION COEFFICIENTS

Unit side resistance

The side resistance was analysed based on the average uncorrected SPT N-value along the pile length as shown in Figure 3. A general linear relationship can be obtained for both H piles and pipe piles. The wide scatter for N-values in the range between 15 and 30 is due to the fact that these are the typical SPT N-values encountered in various sites.

$q_s = 0.56\,\bar{N}$ $(R^2 = 0.555)$ [3a] for driven H piles in Ontario

$q_s = 1.77\ \bar{N}\ (R^2 = 0.705)$ [3b] for driven pipe piles in Ontario

While the same set of data was plotted against the pile length (L) in Figure 4, it was found that the unit skin resistance tends to decrease with the increasing pile length. It is believed that the larger scatter with the shorter piles was due to the influence of seasonal variation or desiccation of soils at shallow depths. In this study, most of the short piles were driven in fine-grained soils, which may vary in cohesion and plasticity.

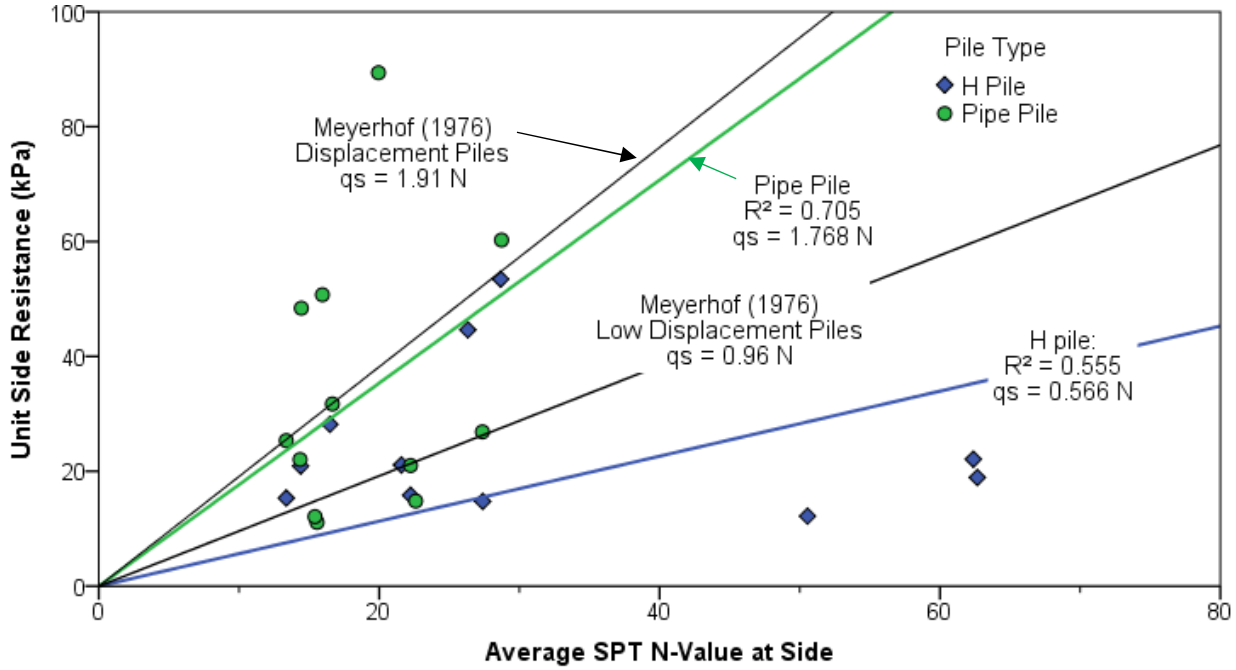


Fig. 3. The relationship between the unit side resistance and average uncorrected SPT N-value

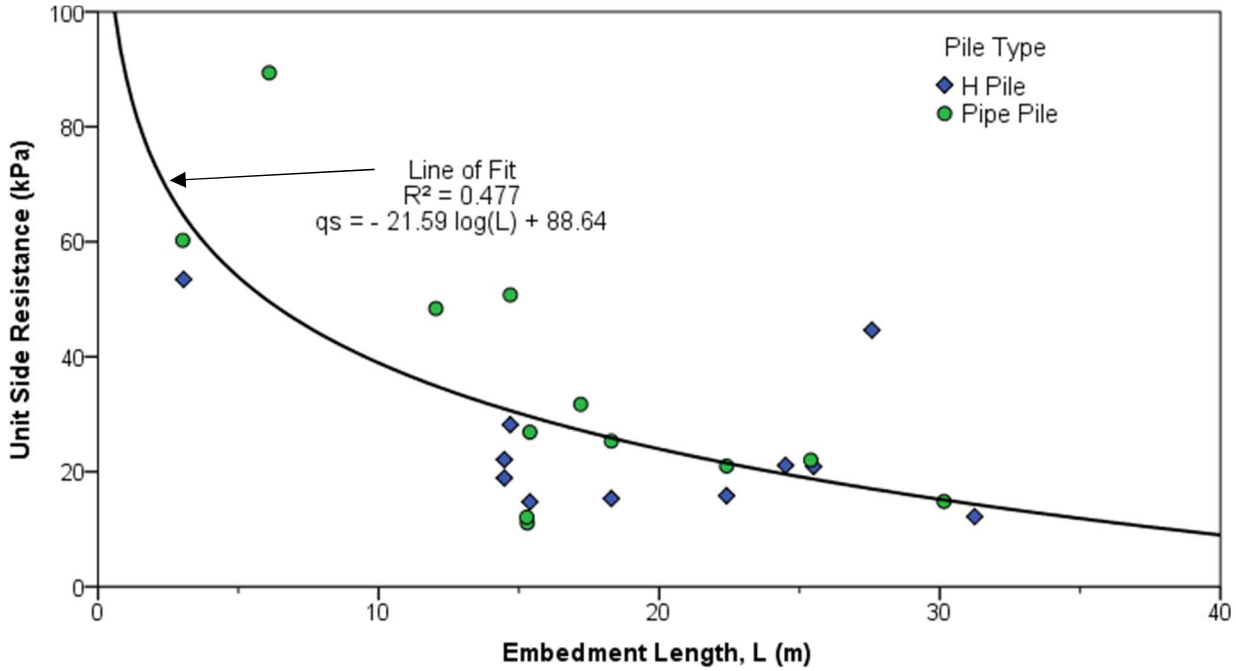


Fig. 4. The relationship between the unit side resistance and pile length

If more than two thirds of the pile length was covered by fine-grained soils, the pile belongs to the "mainly fines" group, and the same criteria is applicable for "mainly coarse-grained soil". Otherwise, the pile had a "mixed ground" soil profile. In Table 2, the most consistent unit side resistance was obtained with mainly coarse-grained soils, while the mainly fine-grained soil had the least accuracy.

Table 2. The influence of soil type on the unit side resistance

Dominating Soil Type along Pile Length	No of Piles (-)	Mean Unit Side Resistance (kPa)	Standard Deviation of Unit Side Resistance (kPa)
Mainly Fine-grained soil	11	34.8	25.1
Mixed ground	5	33.3	13.6
Mainly Coarse-grained soil	7	18.8	5.0
Total	23	29.6	19.5

Unit tip resistance

The unit tip resistance is plotted against the uncorrected SPT N-values at the tip of each pile in Figure 5. A slight higher unit tip resistance is obtained for H piles compared to pipe piles. It is believed this is due to the difference in geometry. Based on this study, a linear relationship can be proposed for the driven H piles or pipe piles in Ontario.

$q_p = 163\ N_p\ (R^2 = 0.897)$ [4] for driven H or pipe piles in Ontario

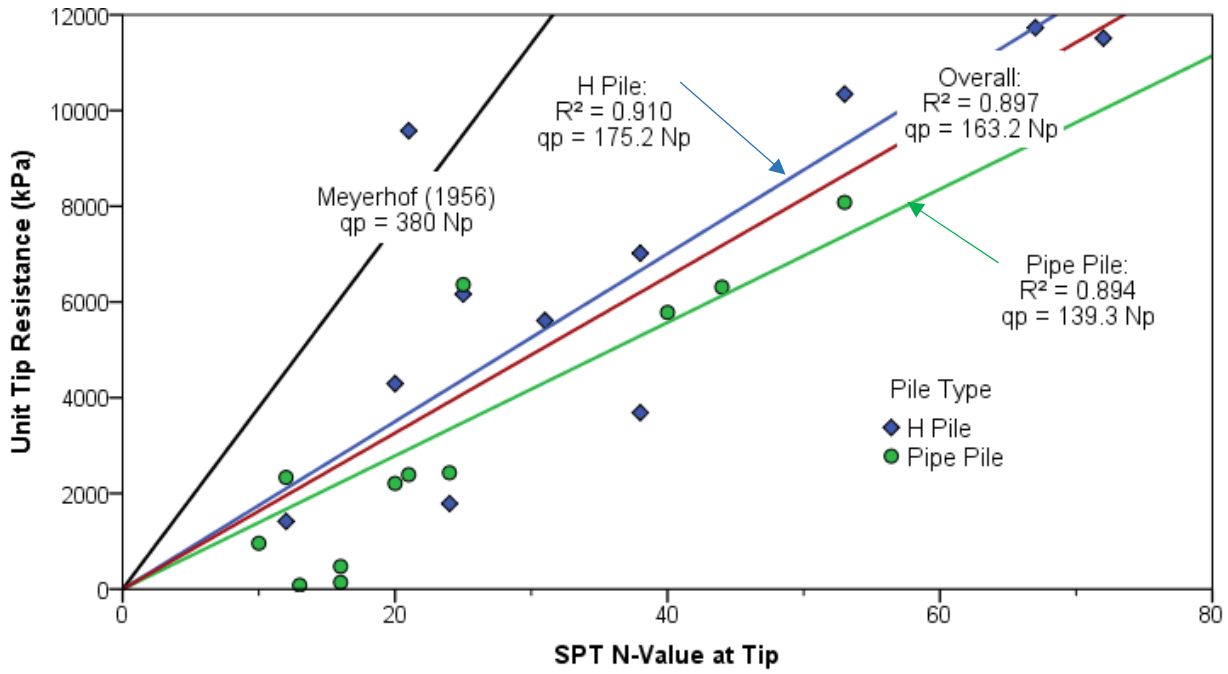


Fig. 5. The relationship between the unit tip resistance and uncorrected SPT N-value

CONCLUSIONS AND DISCUSSIONS

In this study, a total of 23 piles were collected since they were tested with both compression and extraction loads in Ontario. Based on the correlation study with SPT N-values, two general linear relationships can be obtained for estimating the average pile resistances with SPT N-values in Ontario soils.

$$Q_u = 0.56\,\overline{N}\,A_s + 163\,N_p\,A_p \qquad \text{[5a] for driven H piles in Ontario}$$

$$Q_u = 1.77\,\overline{N}\,A_s + 163\,N_p\,A_p \qquad \text{[5b] for driven pipe piles in Ontario}$$

The relationship for the tip resistance may be influenced by the pile type, but the soil type is not very impactful. However, Table 2 showed that the soil type can influence the side resistance, especially at shallow depths and for fine-grained soils. From the selected sample of pile tests, more pipe piles were installed in fine-grained soils than H piles. Due to the inconsistency of the soil conditions, especially for mixed grounds and varying N-values, the relationship with the side resistance can be further refined with numerical approaches, such as artificial neural networks.

The axial capacity of a pile foundation is a complex system. Although variability is commonly found, a statistical analysis can bring greater insight towards the performance of design methods and measurement techniques. A few improvements can be applied and will require further study:

1. Uncorrected SPT N-Value: In this study, the field SPT N-values are directly applied in the correlation. The field SPT N-values are required to be corrected to consider the variations on energy level along with the development of SPT practice over a four-decade period of time.
2. Ground Condition: Currently, a typical borehole log was given in the MTO report for each site and occasionally missed the SPT N-value at the pile tip. In the next stage, the influence of spatial variation with the SPT N-value will be evaluated with a detailed geotechnical investigation at each project site.
3. The Ultimate Pile Load Capacity: In this study, the De Beer failure criteria was applied to estimate the side and tip resistance at failure. However, for load-settlement curves with gradual slopes, this method requires judgement to estimate the exact failure load. Other failure criteria are based on different assumptions, such as the Davisson method, and may offer different results. The consistency of various failure methods shall be investigated to minimize the inaccuracies.
4. Pile Geometry: In this study, H piles were assumed to be plugged. This condition may be applicable for long piles, but it is arguable for short piles.
5. Pile Tip Deformation: Currently, the loads and deflections were collected only at the top of the piles. More pile load test data will be sought from other sources for fully instrumented piles to get a better evaluation of the deformation along the whole pile length.

ACKNOWLEDGEMENTS

The presented research was made possible with funding from the National Sciences and Engineering Research Council of Canada and support and resources provided by Arup Canada Inc. and the Ministry of Transportation of Ontario. In addition, the authors appreciate Ms. Mei Cheong and Mr. Colin McCreath of Arup Canada Inc. for their assistance and advice; Mr. David Staseff and Ms. Minkyung Kwak from MTO for sharing the data of pile load tests; and Mr. Andy Lai, Mr. Filipe Batista, Ms. Chantel Yung, Ms. Maeeda Khan, and Ms. Maribel Castro for their help with the collection of data.

REFERENCES

Barnett, P. J., 1992. Chapter 21: quaternary geology of Ontario. In: P. C. Thurston et al. eds. Geology of Ontario: Ontario Geological Survey. Sudbury, ON: Ontario Ministry of Northern Development and Mines, Special Vol. 4, Part 2, 1011-1088.

Boonstra, G.C. 1936. Pile loading tests at Zwijndrcht, Hollad. Proc. of the 1st International Conference on Soil Mechanics and Foundation Engineering, Vol. 1, 185-191.

Brown, R. P. 2001. Predicting the ultimate axial resistance of single driven piles. PhD Dissertation, The University of Texas at Austin.

Decourt, L. 1982. Prediction of bearing capacity of piles based exclusively on N values of the SPT. Proc. of the 2nd European Symposium on Penetration Testing, Amsterdam, 1 29-34.

Fellenius, B. H. 1980. The analysis of results from routine pile load tests. Ground Engineering, Foundation Publishing Ltd., London, 13(6), 19-31.

Karlsrud, K., Clausen, C. J. F., and Aas, P. M. 2005. Bearing capacity of driven piles in clay, the NGI approach, In Proceedings of the International Symposium on Frontiers in Offshore Geotechnics, 775-782.

Kulhawy, F. H. and Jackson, C. S. 1989. Some observations on undrained side resistance of drilled shafts. In Foundation Engineering: Current Principles and Practices, Edited by F. H. Kulhawy, ASCE, New York, NY, USA, 2, pp. 1011-1025.

Kulhawy, F. H. and Mayne, P. W. 1990. Manual on estimating soil properties for foundation design: report EL-6800, Electric Power Research Institute, Palo Alto, California, USA.

McVay, M. C., Birgisson, B., Zhang, L. M., Perez, A., and Putcha, S. 2000. Load and resistance factor design (LRFD) for driven piles using dynamic methods – a Florida perspective, Geotechnical Testing Journal, 23(1) 55-66.

Meyerhof, G. G. 1956. Bearing capacity and bearing capacity of cohesionless soils. ASCE, Journal of the Soil Mechanics and Foundations Division, 82(1), 1-19.

Meyerhof, G. G. 1976. Bearing capacity and settlement of pile foundations, ASCE, Journal of the Geotechnical Engineering Division, 102(3), 197-228.

Ministry of Transportation of Ontario (MTO). (1993). Pile load and extraction tests: 1954 – 1992 (Rev. 1993). Toronto, ON: MTO.

Skempton, A.W. 1986. Standard penetration test procedures and the effects in sands of overburden pressure, relative density, particle size, ageing and overconsolidation, Geotechnique, 36(3),425-447.

Vesic, A. S. 1977. Design of pile foundations, synthesis of highway practice 42, Transportation Research Board, Washington, DC, USA.

DELIVERING ADDED VALUE VIA ADVANCED GROUND INVESTIGATIONS FOR DEEP SHAFT DESIGN IN URBAN AREAS

Anthony S. O'Brien, Mott MacDonald Ltd, Croydon, Surrey, UK, 0208 774 2547, Anthony.obrien@mottmac.com

Hock L. Liew, Mott MacDonald Ltd, Croydon, Surrey, UK, HockLiong.Liew@mottmac.com

ABSTRACT

For the Crossrail project the Moorgate shaft, at depth of 42m, was the deepest shaft on the project and was also located within one of the most confined areas, with surface and subsurface structure located with a few metres of the shaft perimeter. The start of the shaft construction was delayed due to difficulties in removal of old foundation piles that had previously occupied the site. A major constraint was limiting the movement of an adjacent existing tunnel, which meant that the original design required a series of closely spaced props close to the base of the excavation. The paper describes the practical application of an advanced soil stress-strain model, which directly uses field geophysics measures of shear modulus at very small strain (Go). The advanced soil model also facilitates stiffness anisotropy to be considered, based on field or laboratory geophysical tests. The shaft construction programme was shortened by 14 weeks (which meant that the Crossrail TBM drive was not delayed) by implementing the advanced soil model, within a 3D numerical model, together with a carefully controlled verification process (which included detailed field observations of actual shaft deformation). The modelling predictions were sufficiently accurate to reassure external stakeholders that internal propping could be significantly reduced, without causing adverse movements of adjacent buildings or tunnels. The paper outlines the ground investigations and the way in which the advanced soil model input can be measured directly.

(keywords need to be in bold, font size 10 – times new roman)

1.0 INTRODUCTION

The design of deep shafts and retaining walls in densely populated areas is largely governed by the need to predict and control ground movements, and minimise the risks of adverse impacts on existing buildings and infrastructure. Clayton, 2011, has clearly described the need to directly measure ground stiffness, especially at small strain. Conventional ground investigations focus on the measurement of basic index and strength properties. Hence, the term "advanced" ground investigation is used in the context of deriving non-linear ground stiffness parameters. Clayton also outlines some of the difficulties in measuring ground stiffness, data interpretation and subsequent practical applications; especially for heavily overconsolidated soils, which are typically both anisotropic (horizontal stiffness higher than vertical) and highly non-linear (with mobilised stiffness more than 5 times higher at very small strain than at large strain). This paper describes how these challenges were overcome by the application of a new soil stiffness interpretation framework, known as A*. A case history is described which demonstrates the value of both the advanced ground investigation data and the new interpretative framework.

2.0 CROSSRAIL'S MOORGATE SHAFT

The construction of the Moorgate shaft was on the critical path for the completion of Crossrail's central tunnelled section. The shaft is geometrically highly constrained due to numerous existing underground structures and surface buildings., Figure 1. Existing London Underground Ltd (LUL) tube tunnels lie to the North and to the East (the Northern Line tunnel is only 4m away from the shaft), a listed building lies to the south and the existing Moorgate station ticket hall to the west of the shaft. The shaft was

© 2018 Deep Foundations Institute

designed as an irregular polygon in plan, roughly 35m by 35m, formed by 1.2m thick diaphragm walls, 55m deep. The shaft is 42m deep, the deepest on Crossrail. The geometrical complexity of the new Crossrail SCL tunnels which enter the shaft are illustrated in Figure 2. The majority of these new tunnels were excavated concurrently with the shaft excavation, together with shallow permeation grouting on the east side of the shaft.



Figure 1a: Moorgate Shaft – Site Plan

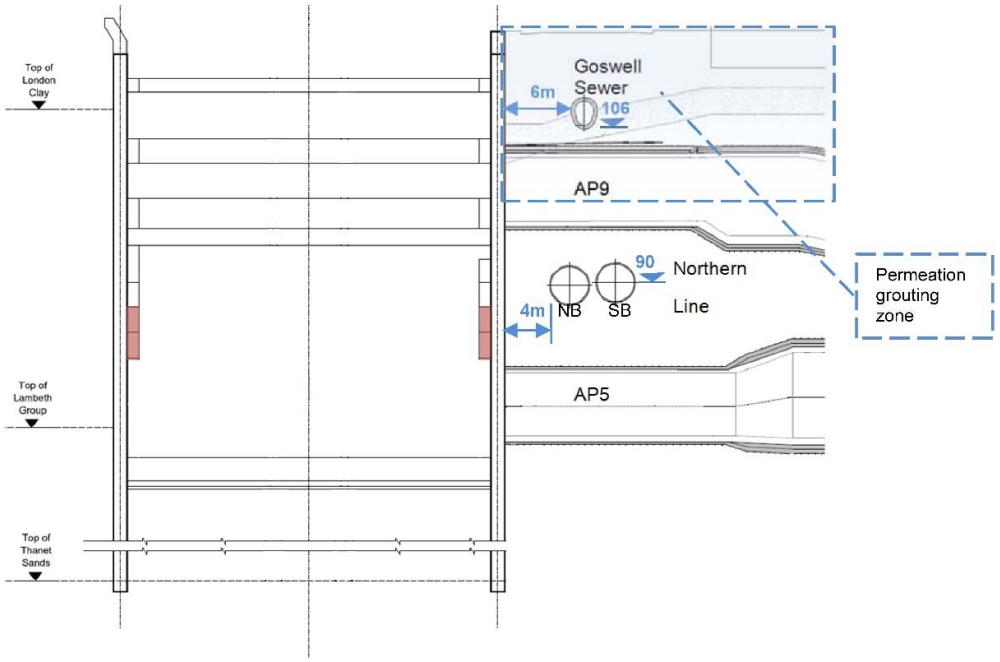


Figure 1b: Moorgate Shaft – Cross-Section

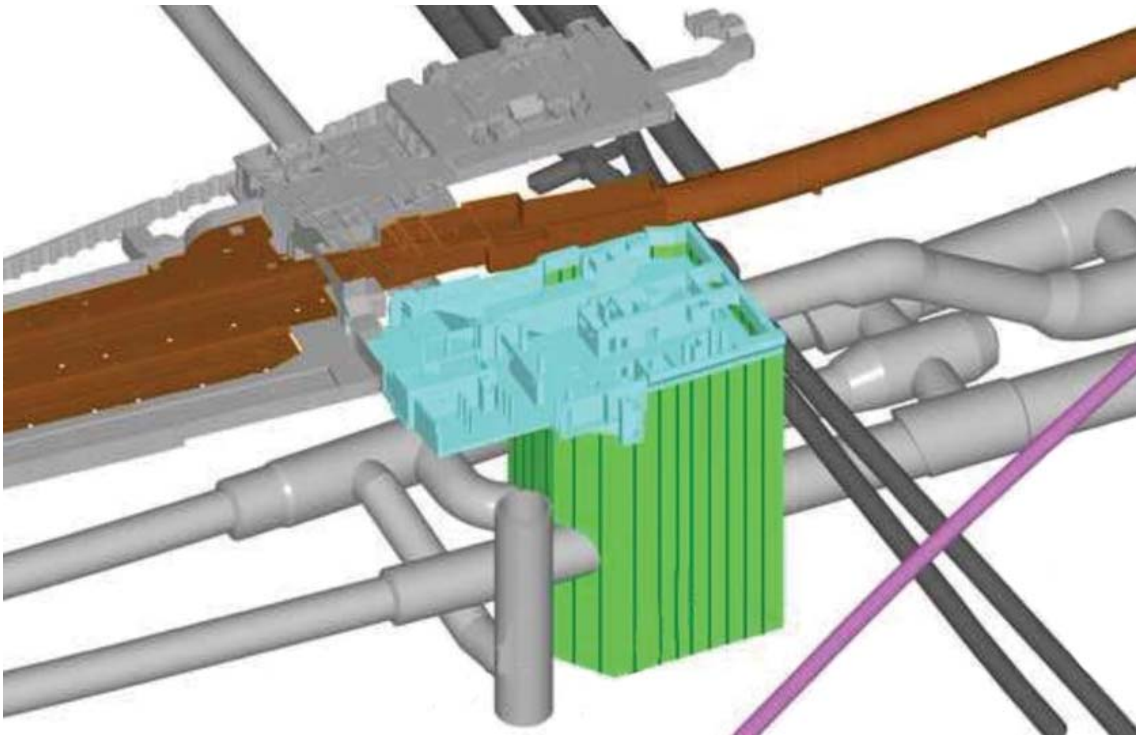


Figure 2: 3D CAD Model of Moorgate Shaft and adjacent tunnels

3.0 GROUND CONDITIONS

Figure 3 shows a geological section across the shaft location. The large variation in thickness of the River Terrace Deposits (between 3m and 13m) and corresponding variation in London Clay thickness is due to a scour feature ("drift filled hollow"), thought to be associated with a historic river channel. This raised some concerns about local variations in London Clay properties, especially in the upper zones of London Clay. However, index properties (Table 1) and penetration test data, Figure 4 appeared to be unaffected. Unusually, for central London, the shaft is deep enough to penetrate about 5m into the Lambeth Group. Hence the characterisation of the Lambeth Group and lower unit (A2) of the London Clay was important for predicting the shaft wall deflection, as the base of the excavation was approached. These lower layers tend to be more silty and less plastic than the more commonly encountered upper units (A3) of the London Clay. Table 2 summarises the undrained shear strength profile assumed for analysis, for the London Clay and Upper Mottled Beds of the Lambeth Group.

Table 1: Summary of index parameters

Unit	Moisture Content(%)	Liquid Limit (%)	Plasticity Index (%)	Clay Fraction (%)
London Clay A3	24-30	65-80(2)	40-55(2)	45-65(2)
London Clay A2	22-28	72-60(3)	52-36(3)	50-32(3)
Lambeth Group Upper Mottled Beds	15-25	30-65	20-40	30-40

Notes: (1) unless stated otherwise values fluctuate within stated range
(2) values increase with depth, values are median values at top and base of layer
(3) values reduce with depth, values are median values at top and base of layer

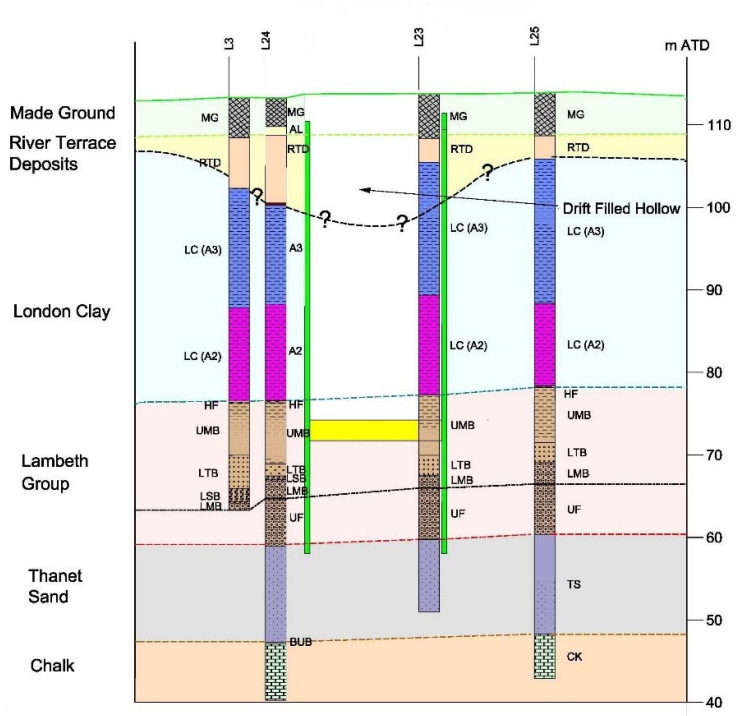
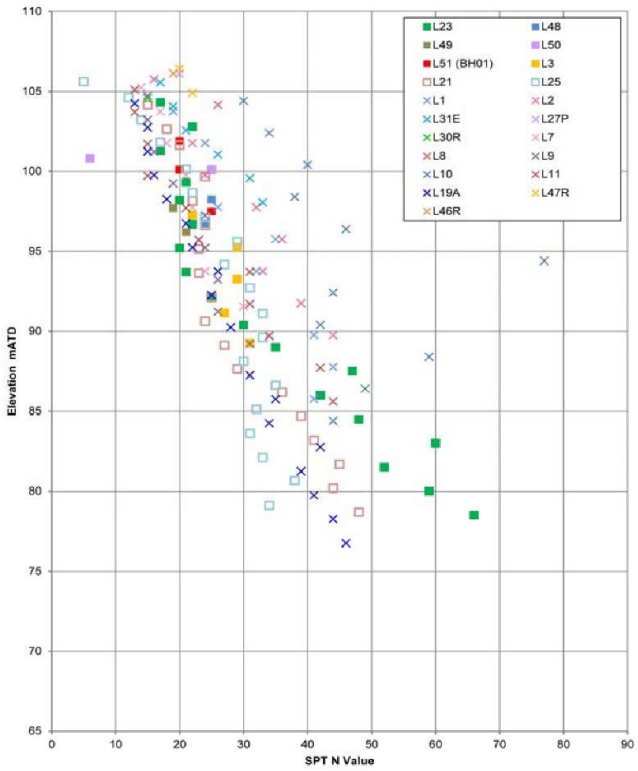


Figure 3: Moorgate Shaft – Geological section



Notes:

Shaded data points are obtained from boreholes in the hollow; L21 and L25 are potentially in the hollow; other data points are from boreholes away from the hollow.

Figure 4: SPT "N" data, beneath and remote from scour hollow

4.0 ADVANCED GROUND INVESTIGATIONS

For the Crossrail project, a suite of advanced in-situ and laboratory testing was carried out, including:

i) Seismic cone, cross-hole and down-hole geophysics for G_o (shear modulus at very small strain);
ii) Self boring pressuremeter, SBP, measuring in-situ lateral stress, and shear modulus, G_{SBP} (at intermediate strain amplitudes);
iii) Laboratory stress path triaxial tests, locally instrumented (for accurate strain measurement), to measure non-linear variation of undrained Young's modulus with strain amplitude from small to large strain.
iv) Bender element measurement, in laboratory, to measure G_o

A common approach for interpreting small strain stiffness is to combine normalised stiffness (e.g. shear modulus divided by mean effective stress) from advanced laboratory testing with estimates of insitu mean effective stress (from SBP and laboratory suction measurements). Table 3 summarises the normalised shear modulus data from triaxial stress path tests. Also, shown are K_o (horizontal effective stress divided by vertical effective stress) values, derived from SBP tests, and normalised shear moduli from SBP tests. Normalised shear moduli, both at 0.1% and 0.01% shear strain, vary by a factor of two for the laboratory and SBP data. The K_o values also vary by more than a factor of two. Laboratory initial effective stress measurements, probably adversely affected by sample disturbance, recorded a wide scatter in mean effective stress, typically these implied low, sometimes very low ($K_o << 1.0$) values of K_o. This means that there is a significant level of uncertainty in deriving any shear modulus profile, based on mean effective stress as a normalising parameter. Insitu and laboratory geophysics data for G_o are summarised on Figure 5. The sampling techniques used for laboratory specimens were of the highest quality (triple tube wire line rotary coring with mud flush). Despite these efforts, sampling disturbance appears to be problematic, with G_o insitu typically 50% larger than G_o lab. Comparing the normalised stiffness data, Table 3, the SBP G/p'_o values are relatively high at depth, compared with the laboratory data (SBP values are 20% higher for A3 London Clay, but more than 60% higher for the UMB, Lambeth Group). It is considered that sample disturbance is the main reason for this difference, sample disturbance becomes progressively worse as depth increases. Both the A2 London Clay and Lambeth Group Clays often contain silt and sand lenses, and this would exacerbate sample disturbance. Figure 6, plots insitu G_o measurements versus depth, for vertical (G_{vh} and G_{hv}) and horizontal (G_{hh}) oriented shear waves with G_{hh} typically 1.5 to 2 times larger than G_{vh}/G_{hv}. Stiffness anisotropy was also measured in laboratory bender element tests which also confirmed that G_{hh} is consistently higher than G_{vh} for these heavily overconsolidated clays. These observations are consistent with those reported in the literature (e.g. Clayton, 2011). As indicated in Table 3, stiffness non-linearity is also significant with normalised stiffness at 0.01% strain between about 2.5 and 3 times higher than at 0.1% strain.

Table 2: Design profile for Undrained Shear Strength, and Failure Strain

Unit	Undrained Shear Strength, Su (kN/m^2)	Failure Strain, ε_f (%)
London Clay A3	65 to 180	3.5 to 2.5
London Clay A2	210 to 290	2.4 to 2.0
Lambeth Group Upper Mottled Beds	290 to 330	2.0 to 1.0

Notes: (1) S_u increases with depth for each layer;
(2) ε_f reduces with depth for each layer.

Table 3: of Normalised Shear Moduli and K_o from triaxial stress path and SBP testing

Unit	Normalised Shear Modulus G/p'$_o$			At Rest Earth Pressure, K_o
	Laboratory Triaxial		Insitu - SBP	
	Shear Strain (%)		Shear Strain (%)	
	0.1	0.01	0.1	
London Clay A3	81-161, 124	195-430, 320	85-210, 150	1.1 – 1.7
London Clay A2	80-133, 110	190-400, 300	100-200,160	2.0 - <1.0
Lambeth Group Upper Mottled Beds	61-132, 108	150-350, 290	120-225,180	1.0 – 2.5

Notes: (1) Lab triaxial comprise triaxial compression and extension, consolidated anisotropically, then sheared undrained. All tests use local instrumentation.
(2) Insitu SBP – self boring pressuremeter tests.
(3) Values quoted, e.g "85-210, 150": are the range in measured values, followed by the average
(4) K_o is derived from SBP, and based on range of interpretive methods
(5) G is secant shear modulus (= Eu/3 for triaxial); p'$_o$ is mean effective stress.

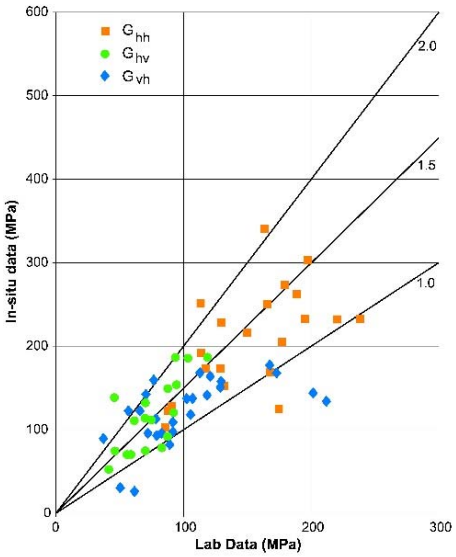


Figure 5: Insitu vs Lab Shear Modulus, G_o, data

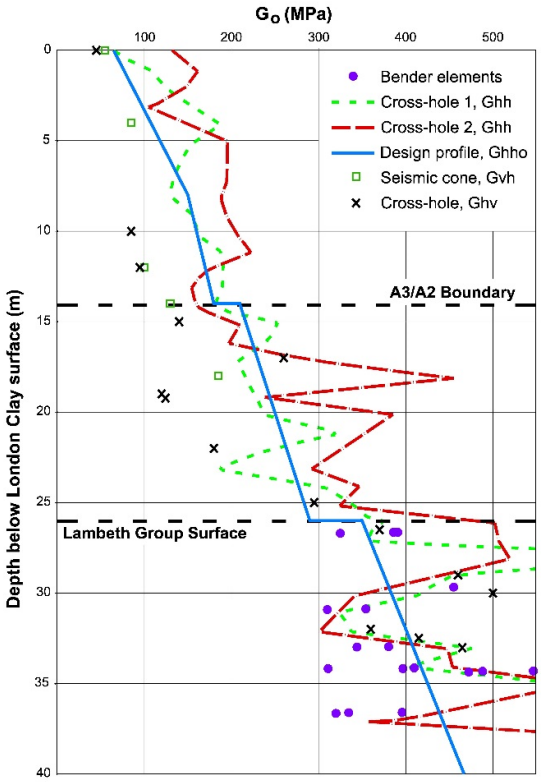


Figure 6: Insitu Shear Modulus, G_o, profile (horizontal and vertical)

5.0 ESTIMATING AN IN-SITU NON-LINEAR STIFFNESS CURVE, A* MODEL

Hence, data interpretation is challenging due to several inter-related factors: sample disturbance; different strain amplitudes measured by different tests; stiffness non-linearity and anisotropy. Some of the practical challenges associated with advanced laboratory tests are summarised in Table 4. In order to derive an insitu non-linear stiffness curve, Ishihara (1996) proposed:

$$\text{Insitu } G_s = C_r \left(\frac{Lab\ Gs}{Lab\ Go}\right) \text{Insitu } G_o$$

Where insitu G_s and Lab Gs = secant G at any given shear strain, based upon insitu and lab measurements respectively; with insitu G_o and Lab G_o measured from insitu and laboratory geophysics. If the stiffness degradation curves have the same shape insitu and in laboratory, then Cr = 1.0. This is illustrated in Figure 7. A practical problem is the gap in non-linear stiffness data between geophysics data (at shear strains of 0.001% or less) and laboratory axial strain measurements (for commercial tests, data becomes increasingly inaccurate at strains of less than 0.01%), similarly SBP test data loses precision at strains of less than 0.05%. Atkinson, 2000, describes a simple method for describing soil non-linearity (independently of mean effective stress), which depends upon 4 parameters: G_o; S_u; failure strain, ε_f; linear elastic strain limit, ε_o. The Ishihara and Atkinson methods have been combined into an overall conceptual framework (within MM this is known as A*), and the data sources for the A* model inputs are summarised in Table 5. The main practical advantage of this framework is that multiple data sources can be used, and the 3 main inputs (G_o, S_u, E_f) are directly measurable, and can be readily cross-checked (using theoretical, empirical methods and from technical literature). The influence of stiffness anisotropy can be taken into account by using: initial horizontal stiffness, G_{hh}; vertical stiffness, G_{vh}; or

assuming an average "isotropic" value (taking average of G_{vh} and G_{hh}). Insitu geophysics data is used as the "anchor" point for subsequent stiffness degradation. Stiffness non-linearity is derived from undrained shear strength, failure strain and the elastic strain limit, which together define the area under the tangent shear stiffness-strain curve. Eadington and O'Brien, 2011, have discussed how the framework provides realistic stiffness degradation curves when compared with advanced laboratory tests on hand cut block samples of low and high plasticity overconsolidated clays.

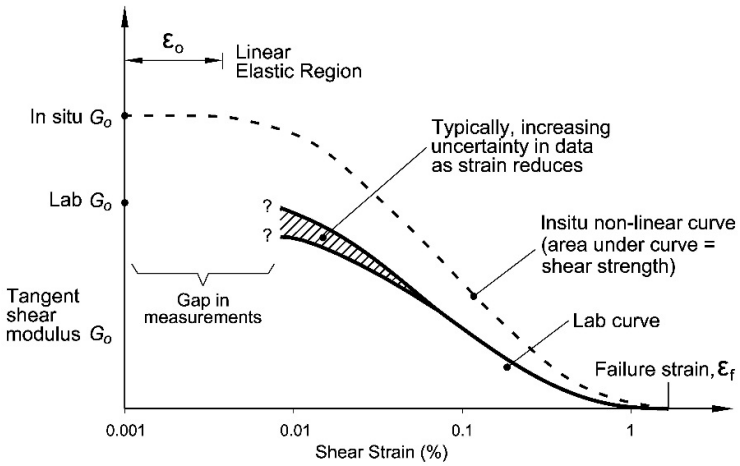


Figure 7: Estimating an Insitu non-linear stiffness curve

Table 4: Advanced Laboratory testing – practical challenges

Sample Disturbance	Even high quality wireline triple tube rotary cored samples are prone to disturbance. More significant with increasing depths; and in strata with sand/silt laminations, local hard bands etc.
Representative Data	Influence of geological variations, such as changes in plasticity index, bonding/cementation, difficult to quantify. Typically, only a small number of stress path tests available, which exacerbates challenges.
Slow	Each test typically requires one to two months to carry out, hence expensive.
Complex	Tests are complex to set up and run, and vulnerable to several potential source of error. Due to long durations, leakages are a common problem.

Table 5: Data Sources for A* model inputs

A* model Inputs	Insitu Measurements	Laboratory Measurements	Empirical/Theoretical checks
Shear Modulus at very small strain, G_o (1)	Downhole/Crosshole geophysics. Seismic Cone.	Bender Element	Viggiani and Atkinson, 1995
Undrained Shear Strength, S_u (2)	SBP; SPT; CPT	Triaxial tests (from routine UU, to advanced)	Skempton, 1961 Hight et al, 1993
Failure Strain, ε_f (3)	NA	Triaxial tests (more weight given to C. U. P. data)	Technical Literature
Linear Elastic Strain Limits, ε_o (4)	NA	NA	Technical Literature

Notes: For Moorgate Shaft, site specific A* model inputs: (1) refer to Figure 6; (2) refer to Table 2; (3) refer to Table 2; (4) ε_o assumed equal to 0.005%

Figures 8 and 9 show the insitu non-linear stiffness curves derived from the A* model, for two elevations at the Moorgate shaft, for the upper A3 London Clay and the Upper Mottled Beds of the Lambeth Group. The design profile for initial horizontal stiffness G_{hh} is shown on Figure 6, and was a cautious estimate based on the relevant insitu geophysics data. Also shown on Figures 8 and 9 are the derived shear moduli from advanced laboratory and insitu SBP tests based on normalised moduli (G/p'_o) and estimates of mean effective stress insitu. For the shallow A3 London Clay the laboratory moduli (at 0.01% and 0.01%) are about 80% of the A* isotropic moduli. For the deeper UMB Lambeth Group, the equivalent laboratory moduli are only about 65% of the A* isotropic moduli. The SBP derived moduli are closer to the A* moduli with the mean value similar to the isotropic A* stiffness curve, and the upper bound SBP moduli similar to the horizontal A* stiffness curve. However, it should be noted that the stiffness non-linearity of the A* model (characterised by the reduction in secant shear modulus between 0.01% and 0.1% strain) is the same as that measured in the laboratory (consistent with Ishihara's proposal). The initial stiffness of the A* model is larger, since it is based on insitu geophysics data.

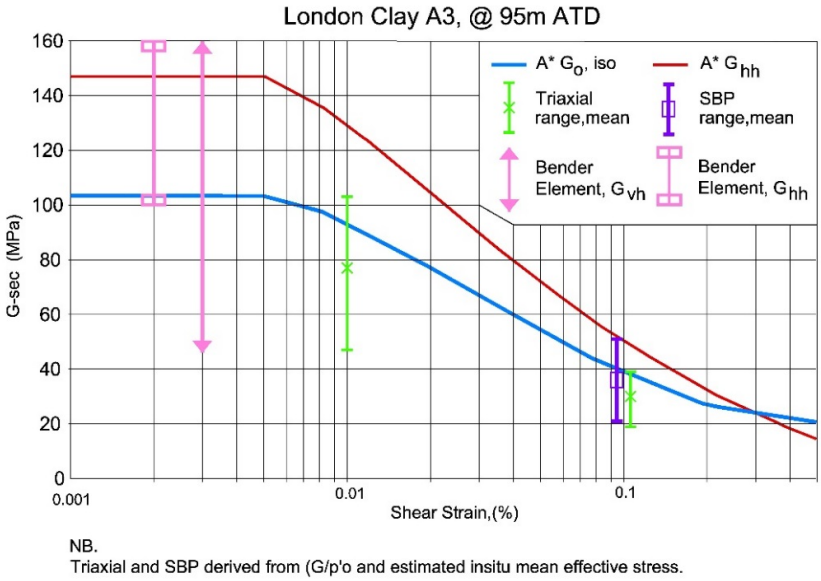


Figure 8: A* model Insitu non-linear stiffness curves vs lab and insitu measurements, London Clay at 95mATD

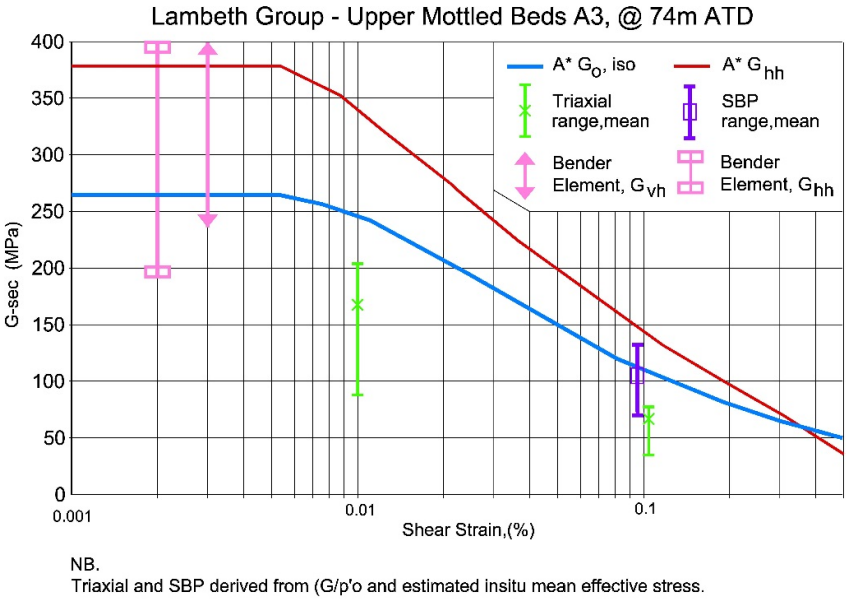


Figure 9: A* model Insitu non-linear stiffness curves vs lab and insitu measurements, London Clay at 74mATD

6.0 PREDICTED AND OBSERVED SHAFT DISPLACEMENT

The shaft design was initially based on a linear elastic, perfectly plastic soil model, with the elastic stiffness based on the SBP derived moduli at 0.1% strain. The shaft was designed to be constructed top down, and supported by 7 levels of reinforced concrete ring beams (between 107.5 and 83.1 ATD). To minimise ground movements in the vicinity of the Northern Line tunnels, two temporary reinforced concrete props (3m wide and 1.5m deep), "slab strips" on Figure 12. were planned to be built at 83mATD, orientated east-west across the shaft in addition to two levels of temporary steel props at 80.5mATD and 76mATD. The shaft was constructed within a basement of a demolished building. Prior to installation of the shaft's diaphragm walls, the old building foundations had to be removed. However, removal of these foundations took longer than anticipated, and the commencement of diaphragm wall construction was delayed by 11 months. To mitigate the delay Mott MacDonald proposed a variation of the Observational Method by progressive modification (Powderham, 1998), referred to as the "Verification Process", Farooq et al, 2015. The instrumentation and real time monitoring is discussed by Liew et al, 2016. It was hoped that the Verification Process would facilitate a reduction of the shaft temporary support measures, in order to speed up shaft construction. However, because of the nearby buildings and infrastructure, including the busy LUL Northern Line tunnel only 4m from the shaft, it was essential to have accurate predictions of shaft and sub-surface ground movements. It was also essential to be able to demonstrate the accuracy of the predictions before excavation began below the lowest ring beam. Three verification points were set at 19, 26 and 30.5m depth (known as VP1, VP2, and VP3). A FLAC3D model was constructed of the shaft, and adjacent tunnels. The A* model was used to define the non-linear stiffness of the London Clay and Lambeth Group. Initially the isotropic model was used, Figures 8 and 9. At VP1 it was observed that the isotropic A* model generally resulted in predictions of shaft displacement that were higher than observed displacements. At VP2 this trend was confirmed, and it was decided to modify the A* stiffness model, so that initial stiffness was based on G_{hh} only, Figures 8 and 9, (it was considered that horizontal stiffness was likely to dominate the response of the walls during shaft excavation). Figure 10 compares the predictions from the 3 different soil stiffness models (initial non-linear elastic-plastic; A* isotropic; A* horizontal) with the observed displacement of the south wall. It can be seen that the linear elastic model significantly overpredicts maximum wall displacement (about a factor of two) and the deflected shape is also incorrect (toe

displacement is excessively high). The isotropic A* model provides a better prediction of the deflected shape, although maximum displacement is about 40 to 50% too high. The A* horizontal model provides a close match of both the deflected shape and maximum wall displacement. Figure 11 provides predictions and observations of the north and east walls, using the A* horizontal model, for the final 23m of shaft excavation. The east wall predictions are very close to observed maximum wall displacements, with the north wall predictions being slightly conservative.

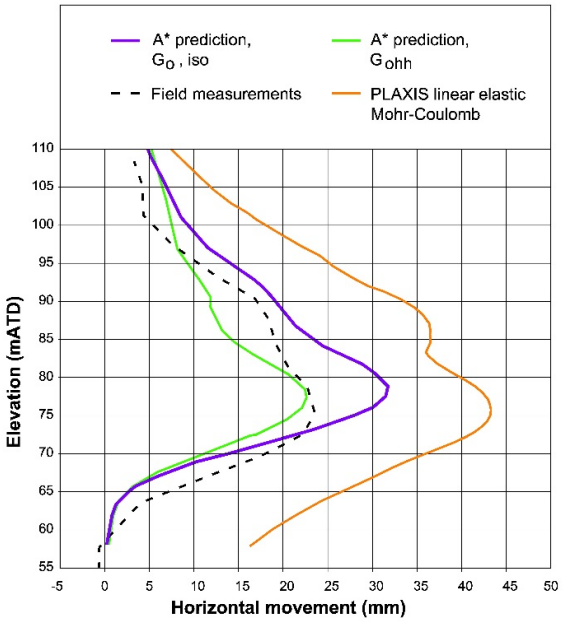


Figure 10: Shaft Wall displacements, south wall. Predictions vs observations

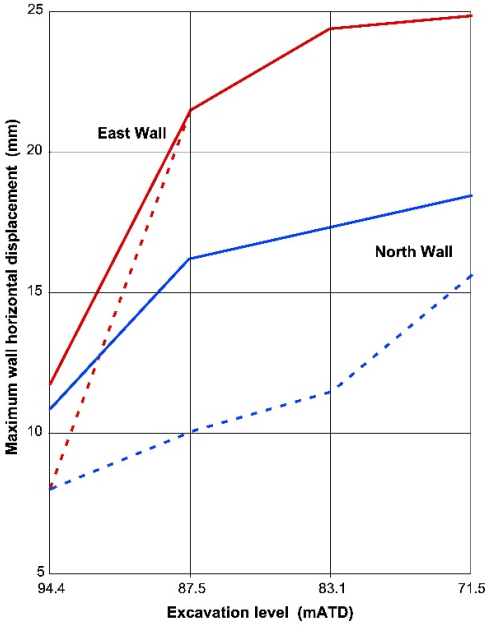


Figure 11: Shaft Wall displacements. Predictions vs observations

7.0 PRACTICAL BENEFITS OF THE ADVANCED CHARACTERISATION

As the works progressed through VP1 to VP3, there was increased confidence in the reliability of the shaft wall and ground movement predictions. Because of the sensitive existing infrastructure it was essential to be able to demonstrate the accuracy of the predictions, and provide reassurance to key external stake holders. This enabled all the temporary props between 83.1mATD and the final excavation level of 71.4mATD (a vertical span of nearly 12m) to be omitted, and the number of construction stages for the final 4 levels of ring beams to be halved. Blinding layers (200mm thick unreinforced concrete) were cast at 4 levels, to reduce clay softening. At the base of the excavation, at 71mATD, a 300mm thick, 20N/mm^2, unreinforced concrete slab was cast to both minimise clay softening and provide temporary structural support (through diaphragm action), while the 2m thick reinforced concrete base slab was constructed. These modifications are summarised in Figure 12 and enabled the construction programme to be accelerated substantially. The shaft was completed early, avoiding delay to the TBM which had to traverse through the shaft, and the potential 11 month delay was avoided. The movement of the adjacent LUL tunnels were consistent with predictions and were acceptably small.

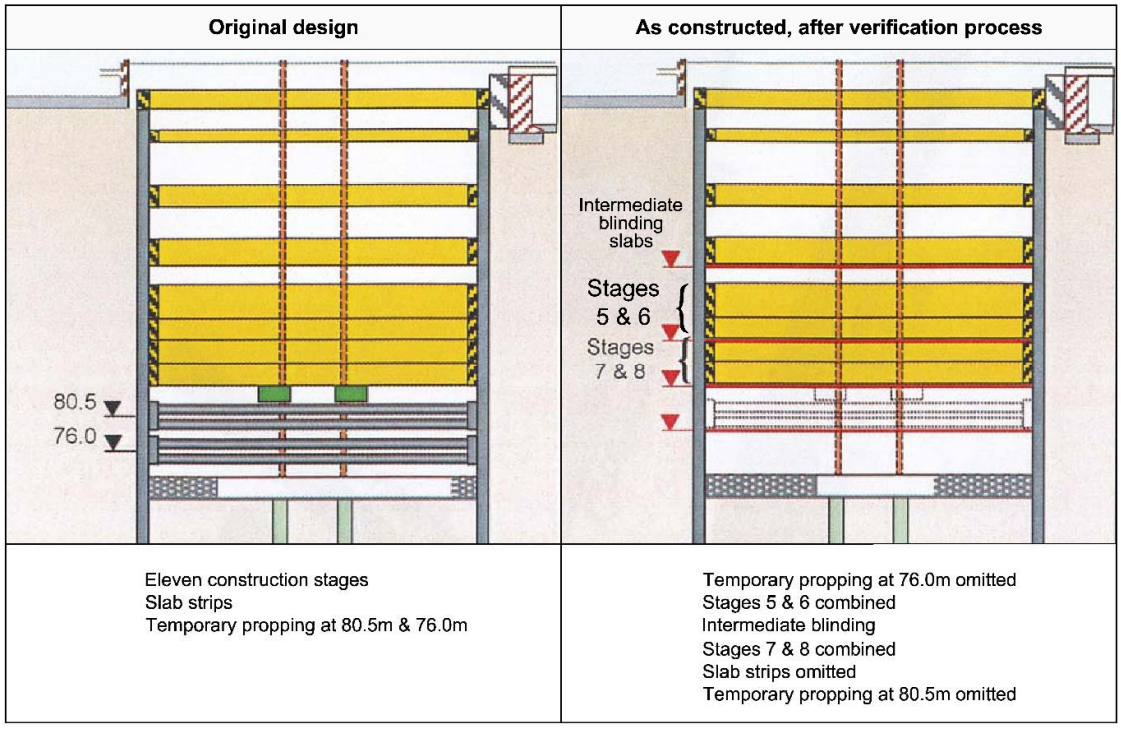


Figure 12: Changes to the Construction sequence and temporary support measures

8.0 CONCLUSIONS

The design of deep shafts and retaining walls in urban areas is often controlled by the need to minimise the movement of adjacent infrastructure. Advanced ground investigation techniques with direct measurements of ground stiffness, at a range of different strain amplitudes, are required if reliable predictions of ground movements are to be made. Nevertheless, data interpretation is challenging, due

to several practical challenges (including intrinsic equipment limitations, and sample disturbance) and the complexity of soil stiffness behaviour (including stiffness non-linearity and anisotropy). A novel soil stiffness characterisation framework (A* model) has been discussed, and a practical application for the deepest shaft on Crossrail has been described. The advanced test data, used within the A* model framework, facilitated improved predictions of shaft displacement; which enabled the temporary works to be reduced and the construction programme to be accelerated on a critical component of the Crossrail project.

9.0 REFERENCES

ATKINSON, J.H. 2000. Non-linear soil stiffness in routine design. Geotechnique, 50, p.487-508

CLAYTON, C. R. I., 2001. Stiffness at small strain, research and practice. 50th Rankine Lecture. Geotechnique, 61, p. 5-37

EADINGTON J. and O'BRIEN A. S. 2011. Stiffness parameters for a deep tunnel – developing a robust parameter selection framework, Proc. Of the 15th European Conference on Soil Mechanics and Geotechnical Engineering. P. 531-536

FAROOQ. I., PLACE, D. and STEELE, B. 2015. Verification process speeds Crossrail's Moorgate Shaft, Proc. Instn. Civ. Engrs. Civ. Engng. Under review.

HIGHT, D. W. and JARDINE, R. J., 1993. Small strain stiffness and strength characteristics of hard Lonodn Tertiary clays. Proc. Int. Symp. On Hard Soils – Soft Rocks, Athens, Greece, Vol. 1, Balkema, Rotterdam, 533-522.

ISHIHARA, K. 1996. Soil behaviour in earthquake Geotech-nics. Clarendon Press, Oxford.

LIEW, H. L, FAROOQ, I. and O'BRIEN, A. S. 2016. Performance based design for the Crossrail Liverpool Street Station. Proc. Of the Int. Conf. on Smart Infrastructure and Construction. Pg. 505-510

POWDERHAM, A. J. 1998. The observation method – application through progressive modification. Proceedings of Journal ASCE/BSCE 13, 87-110

SKEMPTON, A. W. 1961. Horizontal stresses in an overconsolidated Eocene clay. Proc. 5th Int. Conf. Soil Mechanics and Foundation Engineering, Paris, 1, 72-78

VIGGIANI, and ATKINSON, J.H. 1995. Stiffness of fine grained soil at very small strains, Geotechnique, 45, No.2, p.249-265.

EVALUATION OF SEEPAGE BARRIER WALL PERFORMANCE USING INSTRUMENTATION

Georgette Hlepas, Dam Safety Modification and Mandatory Center of Expertise, United States Army Corps of Engineers. Georgette.Hlepas@usace.army.mil
Vanessa Bateman, Nashville District, United States Army Corps of Engineers.
Vanessa.C.Bateman@usace.army.mil

ABSTRACT

Evaluations of the effectiveness of seepage barrier walls and foundation grouting programs requires multifaceted analysis at the US Army Corps of Engineers. During construction, on site quality control measures are put into place to carefully monitor and ensure that seepage barriers are constructed as per specification. However, the evaluation of the design intent and long term performance of the barrier wall installation is still required. Each project is required to be assessed as part of a Post Implementation Evaluation (PIE) after construction is complete. This process examines whether the design intent of the wall was achieved and evaluates whether the project achieved potential failure mode risk reduction. After the risk evaluations are complete, monitoring is still needed to continue to verify that the wall continues to achieve the designers' intent and continues to successfully reduce the risks at the project. A well designed monitoring program is used to verify project performance for both pre- and post-construction. For seepage barrier projects, one of the most useful instruments for performance monitoring are piezometers. These installations provide the basis for understanding of the influence of the constructed works on the groundwater beneath the dam and are used to evaluate the effectiveness of grouting program and barrier wall installations. Common methods include the use of traditional time series plots. However, use of net head dissipation calculations, correlation plots, multi-variable statistical analysis, contour plots and other analysis methods can also be used to understand the behavior of the project performance over time. Methods of analysis used to monitor the barrier wall and foundation grouting performance with key consideration using examples from Center Hill Dam and Mosul Dam are presented herein.

Keywords: seepage barrier walls, piezometer, instrumentation

INTRODUCTION

Any properly maintained and operated dam requires an appropriate level instrumentation and monitoring program to verify project performance. Piezometers, combined with other instrumentation and visual monitoring information, provide baseline information on the groundwater and piezometric conditions needed to evaluate project performance. The need for the installation of a seepage barrier, such as a grout curtain or a cutoff wall, are typically evaluated based on the project performance evaluation combined with the project site characterization. When a decision is made to install a seepage barrier wall, there is a need to establish piezometric baseline conditions prior to barrier wall installation. This baseline condition sets the stage for the design and for future post-construction evaluation. The expected piezometric conditions both during and post barrier installation are thus required to determine if the barrier wall installation has met the design intent. For these purposes, appropriate methods of analyses need to be employed. This paper discusses the evaluation methods used to evaluate the piezometer data for two seepage barrier projects, Center Hill Dam and Mosul Dam, both earthen embankments built on top of a karst foundation. For ease of use, the term seepage barrier is used for both grouting programs meant to fill open void space in the rocks of the foundation and for a barrier wall installation that involves complete excavation of the rock within specified limits and replacement with concrete. Both installations have the same design intent, a reduction in seepage across the barrier sufficient to prevent internal erosion issues from developing within the dam.

© 2018 Deep Foundations Institute

Center Hill Dam is combination concrete and earthen embankment dam that required the installation of a concrete cutoff wall to address potential internal erosion issues. The project, located in Central Tennessee was put into service in 1951 and the earthen embankment was placed on a poorly treated karst foundation. Most of the earthen embankment was built directly on the alluvial soils overlaying the karst foundation rock and only the core trench area was excavated to rock and treated. Unfortunately, this was not an uncommon design at the time and it did not take into account the realities of the geology. The limestones present at the site have extensive vertical karst development and the risk assessment of the project concluded that the initial construction of the project lead to an unacceptable internal erosion risk. While a significant grouting program was conducted in 1982-84 and in 1993, by the 2000s the effectiveness of the programs was being called into question (Adcock & Brimm, 2008). With the Corps standup of the Risk Management Center, the project was re-evaluated and judged to have an immediate need for further protection. Thus another grouting program was conducted in 2008-2009 along the crest with both an upstream and downstream line of grouting. A concrete barrier wall was then installed between these two lines through the dam and up to 330 feet into the karst foundation from 2012-2015. While the site had numerous manual piezometers and inclinometers installed before these efforts, at the initiation of the grouting program USACE added a significant number of instruments to the site to monitor the effects of the dam safety modifications being constructed as well as the long-term project performance. Numerous vibrating wire sensors were installed, in both fully grouted and retrofit open-pipe installations to increase the data collection frequency (every 3 minutes during 2008-2009; every 15 minutes post-2009). An automated data acquisition system (ADAS) was implemented on site on to both store and transmit data in near real time.

Mosul Dam, located north of Mosul, Iraq, also required the installation of a seepage barrier, in the form of a double row grout curtain. Mosul Dam is a unique seepage barrier installation in that the design of the dam included the continual maintenance of this grout curtain throughout the life of the project (Washington International/Black and Veatch, 2004). A grouting gallery was installed directly on top of the rock foundation along the centerline of the dam, beneath the earthen embankment. This unique design feature was due to the nature of the foundation material which is comprised of beds of gypsum, gypsum-breccia, anhydrite, limestones and marls. This complex geology is prone to solutioning on a much faster time scale than is typical for a limestone karst foundation. As per the original designer's intent, and throughout the life of the project, continual monitoring of the piezometric pressures is one of the many parameters needed evaluate the project performance and most especially the solutioning of the foundation. In 2015 the US Army Corps of Engineers, at the request of the Government of Iraq, initiated an upgrade of some of the instrumentation at the site. An automated data acquisition system, with vibrating wire transducers were installed in existing manual piezometer installations. This permitted a higher frequency of data and remote monitoring of the project. A current grouting effort is currently underway at the project, additional automated instrumentation is being installed, and all monitoring data are being continually assessed through the use of the ADAS installation.

GENERAL CONSIDERATIONS

Any appropriate level analysis of piezometer data must take into consideration basic principles of instrument location, frequency of data collection, and influencing variables. Understanding the zone that the piezometer is monitoring and its position (horizontal and vertical) in relation to the dam and project features is critical before embarking on evaluation of the data being collected. For example, an instrument located in a downstream filter zone of the dam verses the foundation material are typically expected to react differently. The baseline behavior of that instrument in relationship to its' influencing variables, typically reservoir, tailwater and/or rainfall, must also be understood in order to properly evaluate changes during and after construction or project modification. Other variables that can influence piezometric response include barometric pressure (in some cases), and construction activities.

The frequency of data collection also plays a critical role in understanding the piezometric responses. In projects where there is relatively frequent variation in reservoir or tailwater elevation, the frequency of the data collection should be sufficient to capture both piezometric fluctuations and driving variable changes. Data that are collected too infrequently may not capture responses to critical loading events. This can be particularly true during grouting operations or barrier wall installations where transient pressure spikes may not be recorded. An example of this can be seen from the Center Hill project where instrument C-68R, located on the downstream side of the grouting alignment was highly reactive to the grouting program (Figure 1) (USACE, 2017).

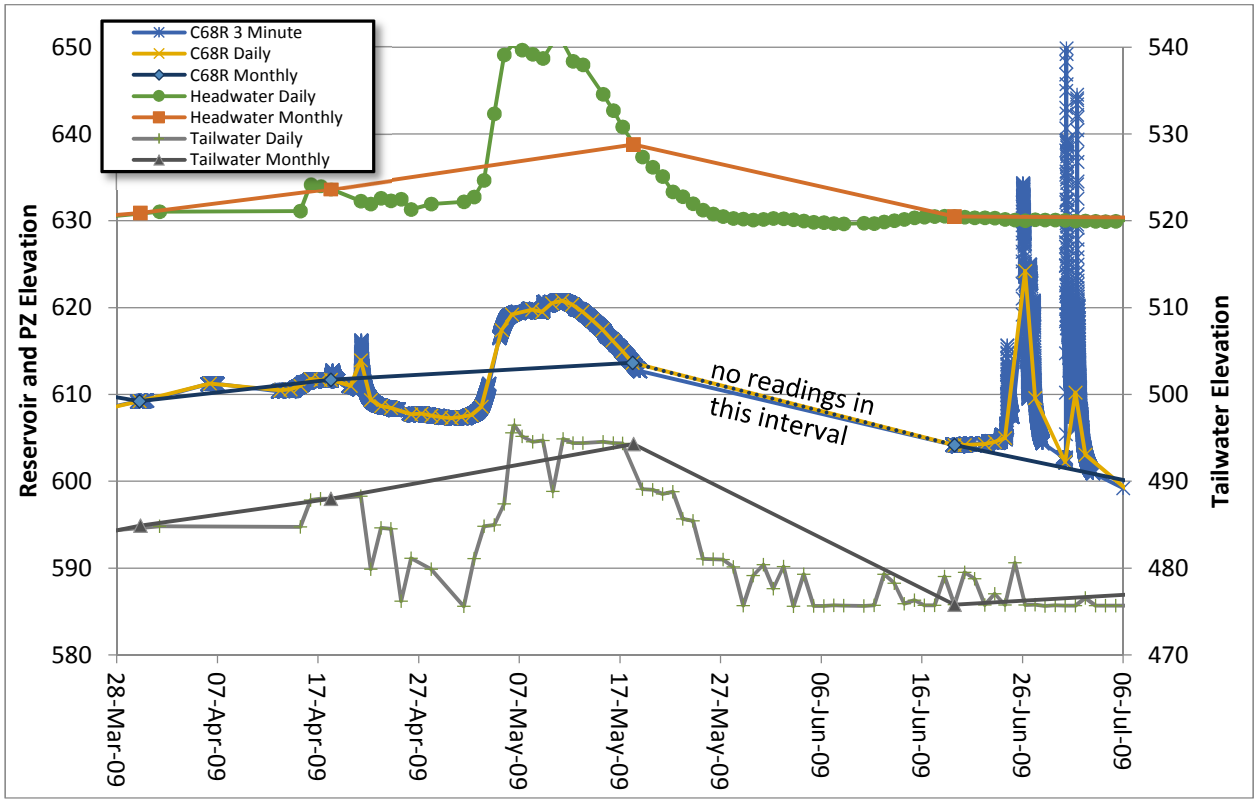


Figure 1. Comparison of Piezometer, Reservoir and Tailwater on Various Reading Frequencies

The instrument C-68R was chosen for this illustration as it has a long monitoring history at the project. Before the grouting program, this instrument was monitored on a monthly basis. As can be seen in Figure 1, around May 2009, monthly readings did not capture the variability of the instrument between data points. The daily reading interval, which is typically the practical limit of manual piezometer readings due to manpower issues, better captures the baseline reactivity of the instrument. In the May 2009 timeframe, Figure 1 clearly shows the instrument reacting to reservoir. The June 2009 readings show pressure spike responses in C-68R that are typical of a response to pressure grouting operations. The monthly reading frequency, of course, cannot capture this transient pressure situation. Even daily readings do not capture the extent of the pressure spike. Thus, when monitoring invasive procedures such as drilling and grouting, where automated data gathering can be used, higher frequency data collection will provide a more complete picture of how the ground is reacting to the construction operations. Experience at Center Hill showed that a 15-minute reading frequency was sufficient to correlate drilling/grouting and barrier wall installation efforts with piezometer response. However, this type of monitoring frequency is only practically possible with automated instruments (Bomar & Bateman, Monitoring frequency matters: A case study from Wolf

Creek Dam, 2012) and USACE Engineering Manual EM110-2-1908 Instrumentation and Monitoring of Embankment Dams and Levees (Draft Pending)).

Further, when evaluating seepage barrier wall performance, both local and global scale performance should be considered. Evaluating instrumentation on an individual basis will give an indication of the piezometric behavior at the local instrument location. However, there is a need to look at groupings of instruments and their behavior as a whole to aid in the understanding of the project performance. Instrument groupings should take into consideration zones being monitored, parameters being monitored, and relationship of responses in the system. Where there are different geological units that may have different groundwater responses, it may be useful to group instruments into which formations they are monitoring.

CONVENTIONAL TIME SERIES ANALYSIS

Time series plots are typically used to determine the overall trending behavior of piezometric pressures over time. This is the most common method of analysis, however there are some key factors to take into consideration during analysis: time frame, appropriate plot scales and appropriate grouping of instruments that measure similar subsurface conditions. The time frame should consider both short term and long term trends. Data can appear to have a correlation that is not correct if the time frame is too compressed in the plot. For this reason, lifetime plots, which are very useful for seeing long term trends in an instrument, should be used along with shorter time scale (1 year or less) such that the engineer/geologist has sufficient resolution of data to be able to recognize instrument reactivity. Critical variables, such as headwater, tailwater and precipitation should be included at the same time scale. When analyzing a seepage barrier wall project, short term plots such as monthly or yearly may provide insight into piezometric behavior for one reservoir operation cycle, but may not provide a long enough extent to determine if there is a subtle trending behavior over time. The following is an example of a set of instruments from Mosul Dam using time series plot method of analysis considering both short term and long term data (Figure ***2*** 2 & Figure 3).

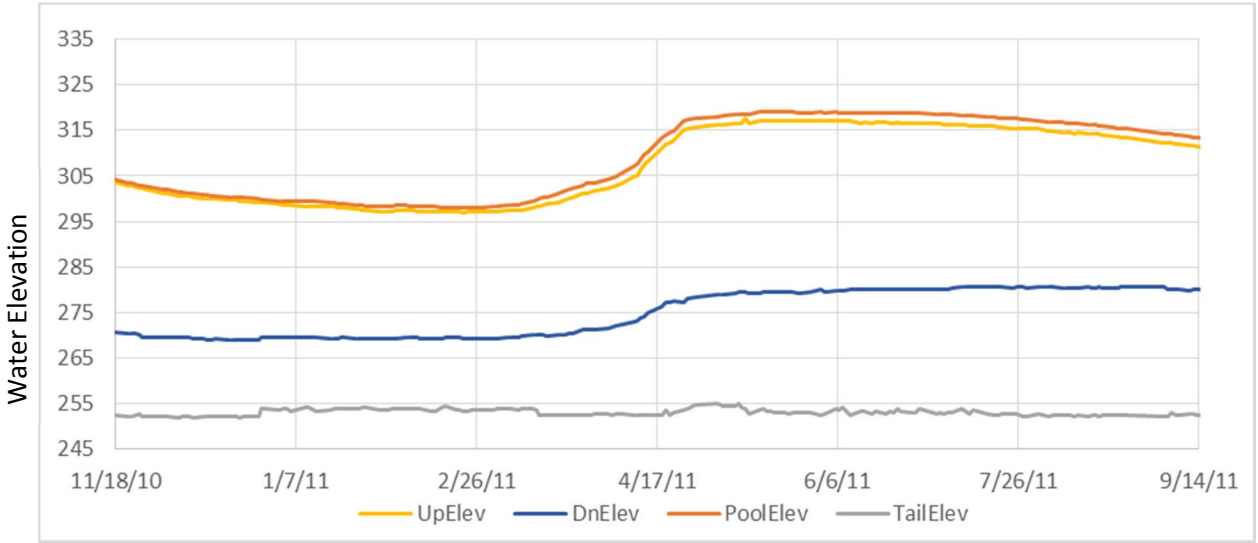


Figure 2. Example Time Series Plot with Relatively Shorter Time Frame (less than 1 year)

Figure 2 is a time series plot of the reservoir elevation (PoolElev), Tailwater Elevation (TailELev), and paired piezometers, one on the upstream (UpElev) and one on the downstream (DnElev), of the grout curtain. The time frame shown is less than 1 year. This relatively short time frame makes the trending behaviors of the two piezometer responses appear correlated with reservoir elevation. There is head loss between the paired piezometers, but the overall trend does not appear to correlate with tailwater fluctuations. However, when using a relatively short time scale, an important trend in the instrument

response may be missed. Thus, as is shown in Figure 3 for the same instrument, there is a need to look at both the short and the long time scales to properly evaluate the instrumentation response and trends.

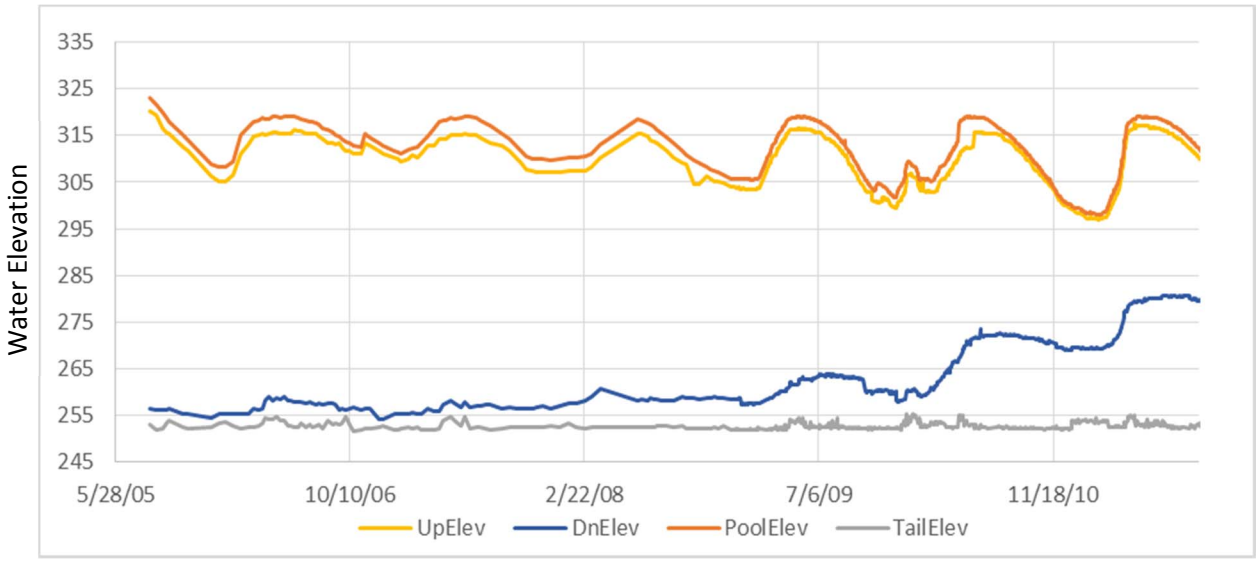


Figure 3. Example Time Series Plot with Relatively Longer Time Frame

Figure 3 shows the same set of variables shown in Figure 2 and also ends in 2011, but in this plot the readings are plotted from 2005 through 2011 and after a previous grouting program was completed in the area where these parired instruments are installed. The longer time history shows a trending increasing behavior in the DnElev piezometer starting in approximately 2008. In addition to the overall increase in water elevation, DnElev demonstrates an increasing correlation to reservoir over time. Since this instrument is located downstream of the existing grout curtain, a trending behavior such as this is very important to recognize when assessing the efficacy of the grouting program over time.

PIEZOMETRIC PROFILES

It is always important to assess a piezometer, or piezometer grouping, with respect to the 3D details of the monitored zone and surrounding impacts such as local geology and neighboring construction activities. This can be clearly seen in an example from Center Hill Dam (USACE, 2016). In Figure 4, the piezometers installed in the Hermitage Epikarst group, located within 10 feet of the top of rock and along the new Barrier Wall Installation at Center Hill are plotted. Figure 5 shows the tip elevation of the instruments plotted in Figure 4 in plan and profile views. All of the instruments are located on the downstream side of the barrier wall and within the same geologic zone, the Hermitage Epikarst and all were installed after the 2009 grouting program. Figure 4 clearly shows that these instruments were highly reactive to the barrier wall installation activities. Several instruments were destroyed during the barrier wall installation, but four survived. These four remaining instruments indicate a significant head difference between pre- and post-barrier wall installation. Piezometer MD-32D, which was responsive to reservoir prior to barrier wall installation, starts being reactive to tailwater post-barrier wall construction which was not the case before the barrier wall was completed.

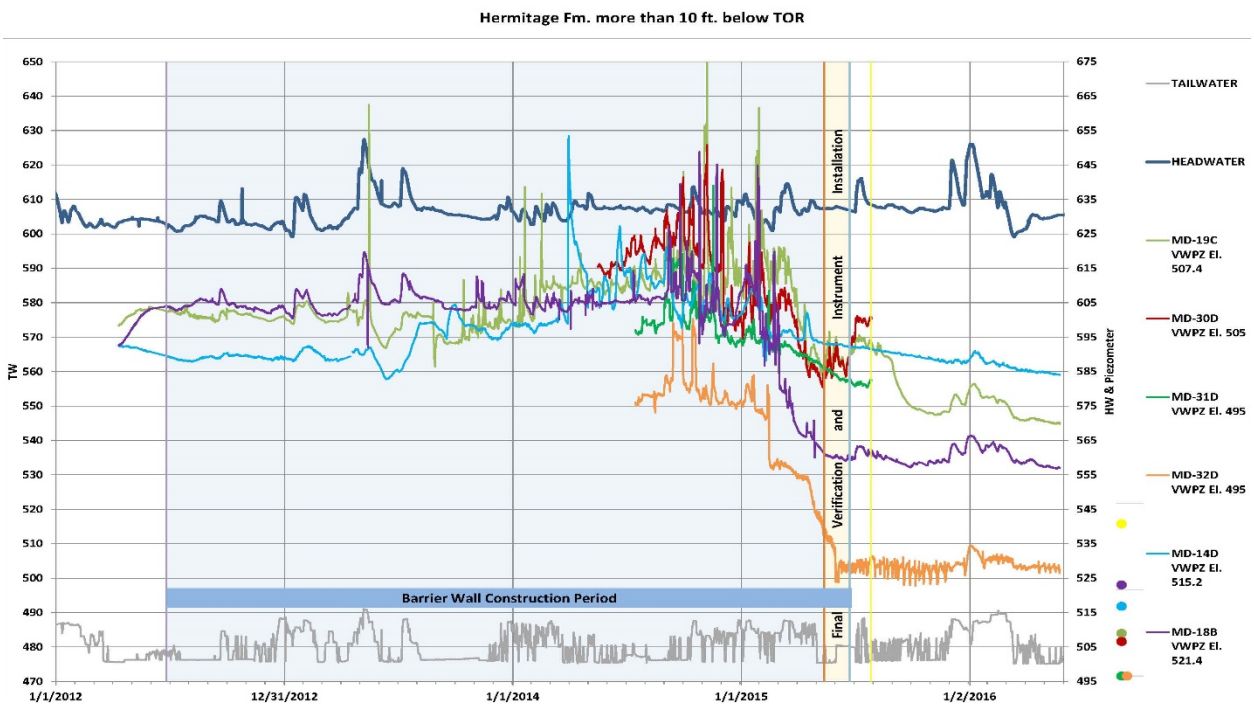


Figure 4. Center Hill Dam – Hermitage Formation Epikarst Grouping during and post Barrier Wall Construction

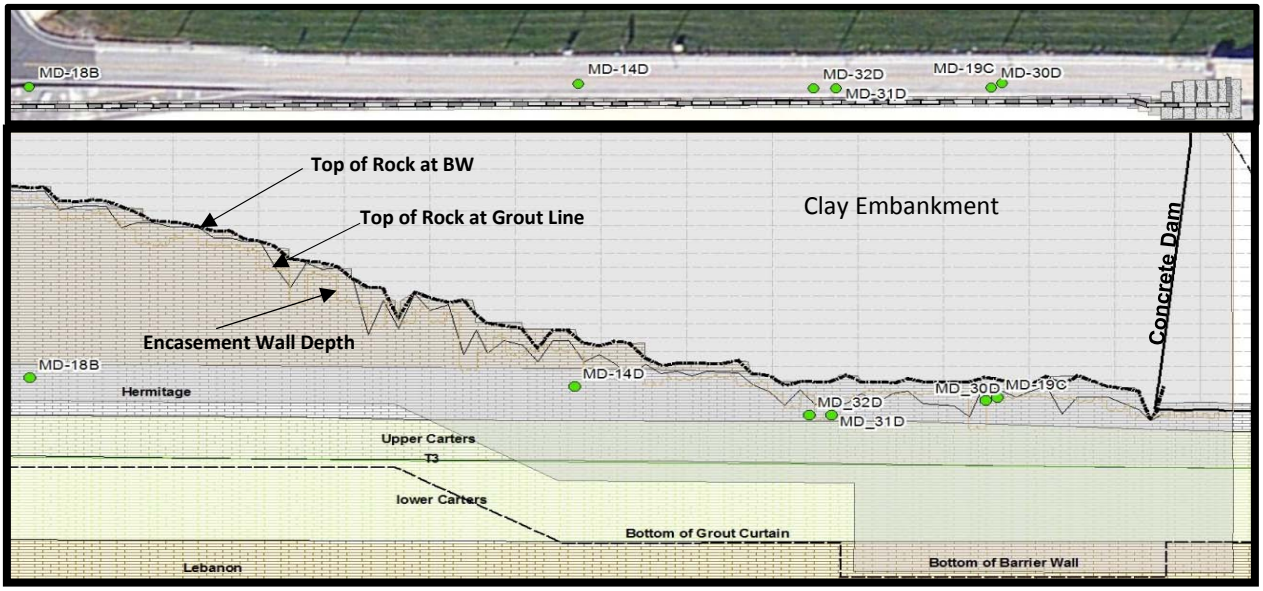


Figure 5. Location of Instruments in Figure 4 with respect to the Geology, Grout Curtain and Barrier Wall

NET HEAD DISSIPATION

The percent efficacy of a seepage barrier wall can be determined through use of a Net Head Dissipation (NHD) calculation. In this method of evaluation, the difference in head between the upstream and downstream side of the barrier wall is evaluated over the difference in head between the reservoir and tail

water elevation. While this may not be the most appropriate method in most karst foundations, it has been a useful tool at Mosul Dam. The calculation is as follows:

$$NHD = \frac{U_{PZ} - D_{PZ}}{\text{Reservoir Elevation} - \text{Tailwater Elevation}} * 100 \quad [1]$$

Where U_{PZ} = upstream piezometer water elevation readings and D_{PZ} = downstream piezometer water elevation reading. The upstream and downstream piezometers used in the NHD calculation should be monitoring the same geologic zone as a pair. Where there is no upstream piezometer, the water elevation of the reservoir may be used. This latter method may not account for head losses due to the upstream embankment.

Figure 6 is a schematic of an example cross section at the Mosul Dam. The grout curtain is installed vertically from the grouting gallery. Piezometers are installed on angles on both the upstream and downstream side of the grout curtain in targeted geologic units. The upstream and downstream instruments are typically installed in monitoring pairs.

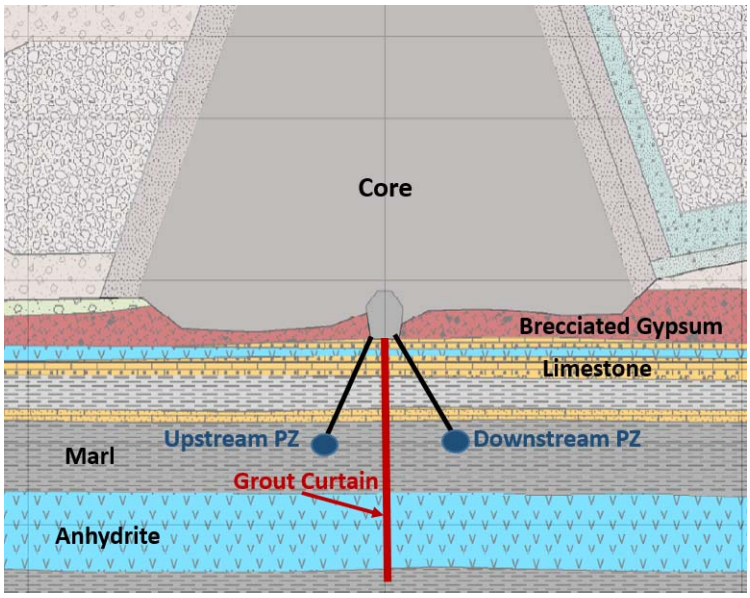


Figure 6. Example Cross Section of Mosul Dam showing piezometer pairs on the upstream and downstream of the seepage barrier wall

The NHD calculation provides the efficacy of the seepage barrier at the specific monitored zones and locations along the seepage barrier at a specific point in time. The NHD calculation can be used in a variety of analyses such as i) change in NHD over time or ii) NHD values across the length of the seepage barrier. The change in NHD over time is simply the plot of the calculated NHD for a given monitored zone over a specified time history. As with time series plots, the frequency of data collection will have an effect on the understanding of the data. The following is an example of the NHD calculation for a given pair of instruments where the NHD value is plotted on the y-axis and the time is on the x-axis. From the plot, it can be determined if the efficacy of the seepage barrier wall has improved (higher NHD) or deteriorated (lower NHD) with time.

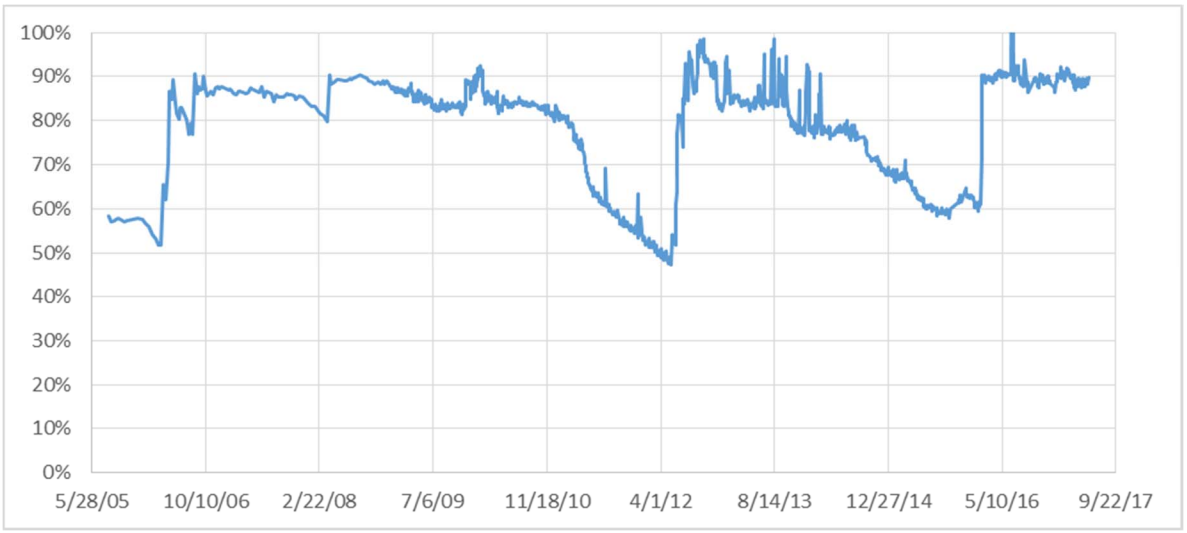


Figure 7. Example NHD Plot indicating grout curtain efficacy at a specific monitored zone over time

In Figure 7, it can be seen that there were periods of time in the monitored zone where there was reduced efficacy of the grout curtain, most notably between 2011-2012 and 2014-2016, followed by a substantial increase. The decrease is attributed to deteriorating conditions of the foundation while the increase is attributed to successful maintenance grouting activities. However, it is not readily apparent which variable in the equation is controlling the decreases and increases. Where there is a decrease in the NHD value, it is either the upstream piezometer decreasing or the downstream piezometer increasing (or both). In order to evaluate which instrument is controlling the results, alternate methods of analysis, such as time series plots should also be employed. Figure 8 is the time series plot for the NHD calculation indicating that the downstream instrument was the main variable resulting in the decreases (and subsequent increases) seen in the NHD plot.

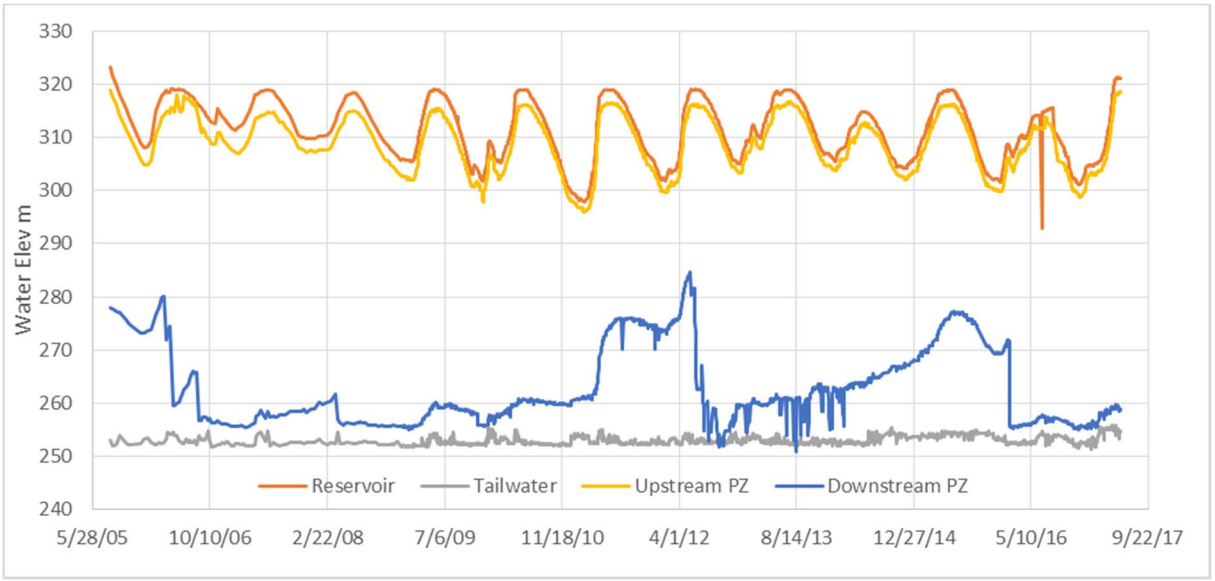


Figure 8. Time Series Plot of the Upstream, Downstream, Reservoir, and Tailwater used in the NHD calculation in Figure 7.

Plotting NHD values (y-axis) verse the location of the piezometer pair (x-axis) can aid in evaluating the NHD across the length of the seepage barrier. This may help target specific areas of interest where efficacy is low. However, this plotting method is only a "snapshot" in time. It may be useful to plot targeted time periods of interest such as before, during, and post barrier wall construction to identify if low efficacy areas have improved. It should be noted that the reservoir and tail water elevations are key variables in this analysis and can impact the efficacy results. For comparing pre- to post-barrier wall installation using NHD, the reservoir elevations and tailwater elevations used for the time periods for the before and after conditions should be similar. Also, when monitoring during construction, "windows" in the barrier wall may concentrate flow and/or pressures resulting in an area indicating a decreased efficacy. A successful closure of the "window" would be revealed by a subsequent increase in efficacy post barrier wall completion in the area.

As mentioned in the general consideration section, there should be consideration given to the location of the piezometers being considered both horizontally and vertically in relation to the barrier wall extents. The NHD calculation is only providing insight to the specific point in the geologic formation being monitored at a specific point in time. A determination as to the efficacy of the barrier wall in areas where there is limited or no instrumentation cannot be evaluated with certainty.

CORRELATION PLOTS AND STATSTICAL ANALYSIS

Correlation plots can also be of significant benefit when assessing the change in behavior of an instrument over time. A good example of this can be seen on the Center Hill Dam project where a rock piezometer shows an increasing correlation with reservoir over time. Figure 9 illustrates the value of correlation plots and single variable linear regression. The plotted instrument responses clearly shows an overall increasing head as well as an increasing correlation to reservoir over time. The coefficient of determination (R^2) is increasingly closer to 1.0 indicating that the variance in the instrument is increasingly predicted by the reservoir value. A perfect correlation between the two variables would yield an $R^2 = 1.0$. This is particularly of interest at Center Hill as this instrument maintained its' increasing correlation with reservoir even after then 1982-84 grouting program along the crest of the dam was completed. Analyses such as this can be expanded to multivariable linear regression as well (Bomar, Bateman, & Zoccola, Evaluating the Effectiveness of a Seepage Barrier in a Karst Environment: A Case Study from Wolf Creek Dam, 2014).

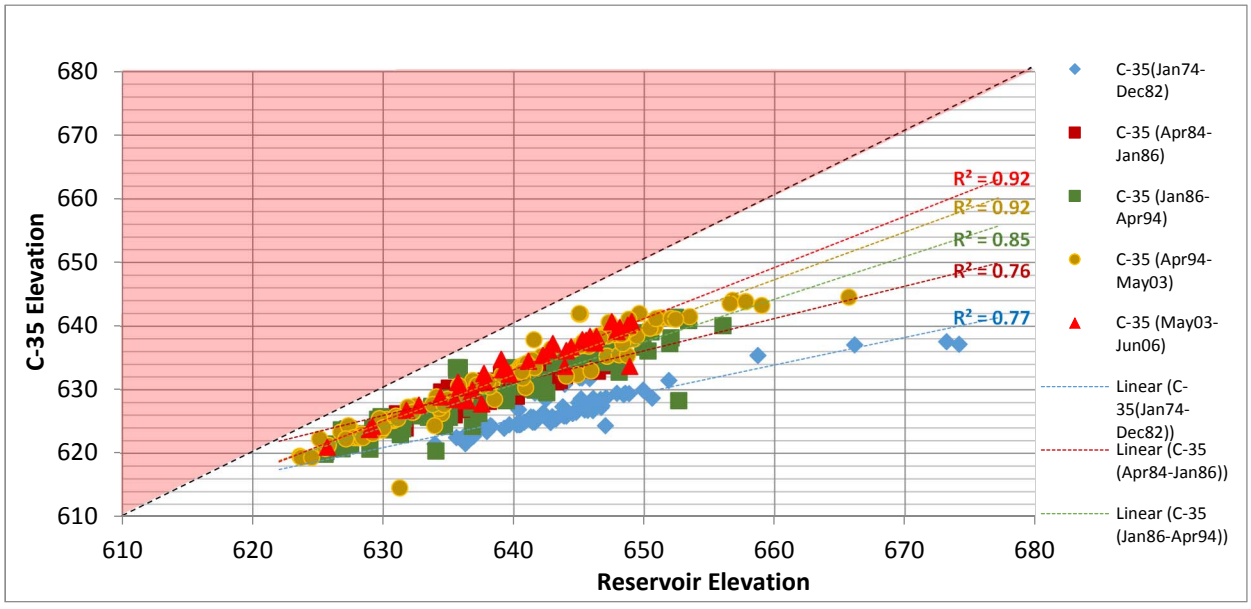


Figure 9. Correlation Plot from Center Hill Dam showing Increasing Headwater Correlation

CONCLUSION

There are many tools in the toolbox for analyzing piezometer responses and in determining the efficacy of seepage barrier installations; only a select few have been presented herein. However, the context of the instrument installation both in 3D space and in terms of construction activities that can affect the instrument, remains the most important parameters to examine. No single analysis method is sufficient for understanding the behavior of an instrument and several tools should be used when providing a thorough evaluation. Understanding both the short term and long term trends of the instrument response, the baseline behavior of the instrument, how to use a variety of data plots effectively, and the use of statistical methods such as linear regression and correlation plots, will aid the engineer or geologist evaluating the instrument response. Additionally, in order to effectively monitor the seepage barrier installation, it is not sufficient to only evaluate the instrumentation on a project before and after construction. Evaluations should be performed over the life of the project to ensure the design intent and project performance are maintained. As was illustrated from the Mosul Dam project, deterioration of the completed works can occur over time. Thus protecting dam safety requires continual reassessment of the instrumentation data over time to ensure that the works continue to provide the protection needed. Furthermore, instrumentation only provides insight into specific locations being monitored and can be somewhat limited to the locations and monitoring frequencies used. Engineering judgment and visual monitoring are also always needed for a full assessment of the project performance.

REFERENCES

Adcock, L., & Brimm, R. (2008). A history of karst seepage—Center Hill Dam rehab. *International Water Power & Dam*, http://www.waterpowermagazine.com/features/featurea-history-of-karst-seepage-center-hill-dam-rehab/.

Bomar, J., & Bateman, V. C. (2012). Monitoring frequency matters: A case study from Wolf Creek Dam. *AEG News, Volume 55, No. 4*, 23-25.

Bomar, J., Bateman, V., & Zoccola, M. (2014). Evaluating the Effectiveness of a Seepage Barrier in a Karst Environment: A Case Study from Wolf Creek Dam. *Annual Conference Proceedings - Association of State Dam Safety Officials* (pp. 1049-1060). Lexington, KY: ASDSO.

USACE. (2016). *Center Hill Dam (TN04102) Post-Implemetnation Evaluation Main Dam Barrier Wall.* Nashville, TN: US Army Corps of Engineers.

USACE. (2017). Geotechnical and concrete materials completion report for installation of Grout Curtain at Center Hill Dam.

Washington International/Black and Veatch. (2004). *Mosul Dam Library of Documents, Thirteen volumes of data and information on Mosul Dam 1984-2004.* Washington, DC: Unpublished.

GEOTECHNICAL BASELINE TO MANAGE CONTRACTUAL RISK CAUSED BY UNFORESEEN GROUND CONDITIONS

Andrea Antiga, Soil S.r.l., Milan, Italy, +393292153437, andrea.antiga@gmail.com

ABSTRACT

Geotechnical engineering is strongly associated with significant uncertainties and risks. Geotechnical issues are an essential part of the project for practically every civil construction works. Difficulties occur during the construction when the discovered conditions differ from the result of the earlier geotechnical investigations.
Contractual arrangements are often clear about which party is responsible for unforeseen ground conditions but definitions of what ground conditions will be contractually considered as unforeseen are often vague; time-consuming and expensive disputes, claims, overwhelmingly higher costs, time delay in the construction, are the consequences. All stakeholders are increasingly interested in developing contractual tools to better manage and fairly allocate the geotechnical risks.
The Geotechnical Baseline Reports (GBR) is a document which establishes contractual interpretations of expected geotechnical conditions. The main purpose of the GBR is to set clear representative "baselines" for geotechnical conditions expected to be encountered during construction, and thereby serve as a basis for administering the contract.
The use of GBR to manage "geo" risks in tunnelling has developed over the course of three decades and has become a frequently accepted practice. Extension of the GBR model to non-underground projects has the potential to be an effective and impartial means of managing geotechnical risks.

Keywords: geotechnical uncertainties, geotechnical risk, baseline, risk allocation, contract

GEOTECHNICAL RISKS

Almost all construction projects tend to change as they progress. "Change orders" may occur frequently on construction projects for various reasons: unexpected and unpredictable site conditions, inadequate site investigation, design errors, increases in project scope and other project changes.

In contrast with structural engineers, geotechnical engineers deal with subsurface materials that nature provides, and they have limited knowledge about their conditions and resistances despite time consuming and costly field and laboratory investigations they undertake. Investigations can be made only at discrete points, and most of a specific soil volume is never tested. All soils experience inherent spatial variability, which contributes to some uncertainty in the design process of a geotechnical structure. Furthermore, uncertainties also arise during testing and when design properties are inferred from these tests; and other uncertainties are ineradicable, first of all model uncertainty.

Unforeseen geological conditions are not the main source for all cost and time overruns. However, there is abundant evidence that the effects of inadequate geological data, their inappropriate interpretation and incompetence to deal with the resulting ground-related problems they often play a primary role.

The failure to predict geological conditions and related geotechnical problems are noticeable factors to cost and schedule overruns on construction projects (Hoek and Palmieri 1998).

Numerous case histories over the last century illustrate that failure to anticipate ground conditions is a main factor in construction problems (Fookes et al., 2000).

There is extensive bibliography on geotechnical uncertainties and risks.

© 2018 Deep Foundations Institute

Baynes (2010) classified the various types of geotechnical risks into the following categories:

1. Project Management Risk – caused by the poor management of the geo-engineering process due to lack of sufficient knowledge about the significance of ground conditions.
2. Contractual Risk – caused by poor management of site investigation and contract documentation due to lack of knowledge about the significance of the ground conditions.
3. Technical Risk - caused by the choice of an unreasonable analytical model, by the choice of unreasonable design values, by unforeseen ground conditions or by errors in geotechnical design.

Unforeseen ground conditions represent a source of risk that affect technical risk and contractual risk. Expensive disputes and claims often happen when ground conditions differ from the expectations of the earlier geotechnical investigations.

Risks caused by unforeseen ground conditions can be mitigated mostly by:

1. allocating appropriate technical and economic resources for obtaining extensive subsurface information
2. delivering contractual documents that accounts for the risks involved and establish where conditions encountered during construction that are materially more adverse may be considered as 'unforeseen'.

SITE INVESTIGATIONS

When we deal with ground conditions the "unknown" usually exist in inverse proportion to the amount and quality of the geotechnical investigations.

It is always important to remember that a foreseen hazard is a controlled hazard and small unforeseen hazards can be worse than big foreseen hazards and therefore an effective site investigation program is of major significance to obtain the necessary information essential for construction; we should increase our knowledge about possible hazard to be ready to treat them in a right way.

The most effective strategy to reduce geotechnical risk is to minimize the unforeseen and site investigations are the basis on which the risks associated with the project are identified; on the other side without sufficient information from site investigations the inherent risks in construction would be unacceptably high.

It would be obvious to conclude that a lot of time and economic effort need to be concentrated in site investigations. The greater the completeness of the site investigation program, the better the estimation of quantities on the plan and design stage and, the better the correspondence with actual quantities used for construction. Hence, an in-depth site investigation program would ensure that the project sees fewer change; resources dedicated to site investigations should be considered as an investment. Any apparent economy in terms of cost could result in bigger residual geotechnical risks. We should remember that residual uncertainties can lead to excessively conservative design approaches, higher provisions for risks and higher exposure to the risk of contractual claims.

Nevertheless, a balance needs to be identified in determining the extent of site investigation. Soil investigations can be carried only to the extent that is reasonably possible, compatibly with time and budget available. It is necessary to establish a balance between the resources spent through site investigations and the losses prevented by them. Considering the increasing emphasis on cost cutting measures and considering practical considerations, site investigation is bound to be an area of compromise.

Anyway, it is experienced that geotechnical residual risks tend to prevail despite robust site investigations and therefore a contract cannot specify all future possibilities. This makes it very essential to manage the risk of geotechnical surprises, with the help of contractual agreements. A contract should incorporate a mechanism to determine how to deal with residual risks. Furthermore, an undefined scope

for ground conditions that are to be expected under the contract is an open door to disputes, and the remedy is finding a way to define the parameters of what is or ought to be included in the contract price, as work or as a contingency.

CONTRACTUAL ALLOCATION OF RESIDUAL GEOTECHNICAL RISKS

Why should we allocate risk? The answer is simple: a risk that is not defined or allocated through the contract may result in disputes, moreover risk will be managed and controlled when explicitly allocated to one or more parties.

The contract should give a clear allocation of risks for the case they occur, it is a vehicle for the allocation of risks between the contracting parties. Contract negotiation is a process for the allocation of risks. At any given time in the project development cycle, there is a discrete, yet generally indeterminate, quantum of risk. For every potential hazard to the achievement of the desired results of a project, there is a risk premium, i.e. the amount of money that a party is prepared to be paid for taking on that risk.

The theoretical ideal allocation of risk in a contract is that point where the sum of the risk premiums is minimized, the point where each party takes on the risks for which it is best placed to control and manage those risks.

Speaking of risk allocation, it is important to note that a factor which tends to defeat the efficient allocation of risk in construction contracts is that the Owner may have significantly more power at the contract formation stage than does the contractor.

Actually, under most legal systems, ground conditions are treated as contractor risks; in most situations the contractor carries the risk of unforeseen ground conditions and will not get extra time or money if the work progress is affected by unexpectedly troublesome ground conditions.

At first glance one might believe that the Owner will always win. However, history shows that when projects fail, all parties are liable to be affected adversely. The attempt to transfer the total geotechnical risk to contractor does not liberate the owner of his final responsibilities. This transfer of geotechnical risk is often paid by the owner in terms of either conservative design and increased risk of contractual claims, revised design and schedule overruns. Moreover, a contractor bearing the risk of unforeseeable ground conditions is forced to adapt the project and the method of construction in line with expected economic returns. In the event of a high level of losses, the contractor will (almost certainly) look for all possible ways to terminate the contract in advance; this can impact on the total costs, quality, safety of the entire project. Experience has many times demonstrated that unreasonable risk allocation strategies will keep good bidders away and attract entities who are ready to take advantage of the situations also with pre-defined claims at the bid preparation stage.

Many construction and engineering contracts contain a clause that deals expressly with ground conditions. However, the detailed content of these clauses varies widely between the different standard forms. Some merely recommend the general position in law and confirm that the contractor is to carry the risk of unforeseen ground conditions.

How does FIDIC deal with allocating risk? Clause 4.12 of the FIDIC Red Book modifies the severity of the position under general law. It states that if the contractor meets adverse physical conditions which were 'not reasonably foreseeable by an experienced contractor by the date for submission of the tender', he shall give notice to the engineer as soon as possible and may then be entitled to an appropriate extension of time and/or payment of cost. Thus, the Red Book allows for extension of time and additional cost where the physical conditions are not reasonably foreseeable at the time of the tender by an experienced contractor. This represents a risk distribution in line with the philosophy that it is better for the employer to take on ground condition risks which cannot reasonably be ascertained or priced by an experienced contractor.

Ultimately, we can say that it is unwise to generalize and that allocation of residual geotechnical risk is a major example of an issue that must be considered on a case by case basis. Risk sharing should be fair and none of the contractual partners should carry the entire load of the residual risks.

Fair risk sharing between the client and the contractor helps to reduce potential claims and therefore the total project costs. Therefore, the first question to ask is what conditions were expressly or impliedly "foreseen" under the contract.

THE GEOTECHNICAL BASELINE REPORT (GBR)

As seen so far, it is clear that the possibility of incorporating information on ground conditions under the contract has to be viewed as a tool for defining those conditions that should be considered 'reasonably foreseeable'.

Eventually, many Owners recognized the need to present the designer's interpretations as part of the Contract Documents. Various names were given to this report through the years.

The American Society of Civil Engineers (1970, 2007) published the guideline to be used for drafting this contractual document named Geotechnical Baseline Report. This guideline focuses on subsurface projects involving tunnels, but also expands the applicability of GBR to deep foundations, open-cut pipelines, braced and tied-back excavations.

The GBR is a document where contractual statements describe the geotechnical conditions predicted (or to be assumed) to be met during construction. The contractual statements are referred to as "baselines" and they should be considered as the reference point for risk evaluation and pricing.

In fact, before executing a contract, the tenderer needs to know 'with a sufficient degree of certainty' the risk that he is going to price, while the employer needs to know what he is going to pay for. In fact, both parties have to evaluate the cost of known conditions and to estimate the contingencies that should be included either in the contract price or in the owners' budget.

The "baselines" serve as contractual references to establish where conditions encountered during construction that are significantly more adverse, onerous and time consuming, may be considered as 'unforeseen'. Then, the contract should also include a 'differing site conditions clause' that allocates the risk of such changed conditions to the employer.

Risks associated with conditions consistent with or less adverse than the "baselines" are allocated to the contractor, and those more adverse than the baselines are accepted by the owner.

The primary objectives of the GBR are to:
1. provide a summary of the ground conditions, ground behavior, groundwater, and in-ground obstructions, contamination to facilitate the understanding of the geotechnical features to be addressed during proposal preparation and during design and construction;
2. establish baselines for the anticipated geotechnical conditions, to be relied upon in the preparation of proposals, in bid submittals, and in the design and the construction;
3. assist in administering the differing site conditions clause contained in the Contract Documents by providing a basis for their evaluation.

It is important to provide clear baseline statements. It is also important to describe the possible range of property values or ground behavior. The recommended approach is to indicate the expected range of conditions and uncertainty, but then state a specific baseline (upon which bidders may rely) that has been established for contractual purposes. The baseline may be expressed as a maximum value, a minimum value, an average value, a histogram distribution of values, or a combination of them.

The contents of GBR should be balanced and realistic, since ‘overly conservative baselines can result in overly conservative and costly bids’. Cautiously drafted baselines may cause the Contractor to bear the total responsibility of the ground risk that would allocate unlimited risks on the contractor, resulting in a higher bidding price. The contrary would also be deleterious, when an over simplified baseline would absolve the contractor from otherwise foreseeable risks. A good reason to give a balanced position to GBR is that of motivating each party to resolve the difficulties that eventuate during construction, within their capability and in the interest of the project that should be completed in time and within the budget.

Baseline statements in the GBR should be interpretations expressed as contractual representations of anticipated subsurface conditions. The baselines should be meaningful, reasonable and realistic, and to the maximum extent possible should be consistent with available information contained in the other geothechnical documents. If baselines are extreme and unrealistic, the "law of unintended consequences" is likely to prevail, and the practical value of the GBR is otherwise frustrated. However, if accurate data is not available baselines may be based on other information (e.g., previous experiences in similar geology) and engineering judgment, provided the reasoning is clearly explained.
Owners should participate in and contribute to the setting of the baselines and should understand the consequences of the levels at which the baselines are set.

Many ground-related baselines can be defined using existing project information data, as provided by the previous project phases but, in the case of very critical risks and related baselines, additional, detailed and advanced ground investigation data may be required.

The Owner may decide to allocate certain risks and costs of potential differing site conditions to the Contractor through the use of more adverse baselines. This will usually result in an increased bid price. Alternatively, the Owner may choose to share the risks and costs through less adverse baselines and utilization of either alternative payment provisions or a change order process, if the more adverse conditions materialize. In this instance, such an Owner may enjoy a lower bid price but in either case, the costs associated with handling the site conditions are the Owner's responsibility. The difference is that in the latter case, the Owner will accrue certain financial benefits if the adverse conditions are not realized.

Therefore, the client has primarily to decide upon two major strategic options for the project with regard to risk and rewards:
1 to allocate part of the risk to the contractor, at an initial cost (the risk premium for the contractor) that is paid, independent whether the risk occurs or not
2 to allocate part of the risk to him- or herself and to provide a contingency budget, to pay only when the risk occurs.

In the latter option, the risk premium is, in fact, stored in a risk contingency budget, while recognizing that the risk premium and the risk contingency budget may be of different size.

In considering risk allocation, baselines should not be arbitrarily established in a manner that is intended simply to shift all subsurface risk to the contractor. Since the GBR has contractual precedence over the other geotechnical documents, unrealistic baselines not supportable by data have the affect of disclaiming the subsurface data. Such practices are likely to reduce the number and responsiveness of bids.

To be useful for risk allocation, a geotechnical baseline must clearly establish the boundaries of those conditions which are expected, and define how they are measured. For example, many geotechnical design parameters can be established by a variety of test methods. In establishing a baseline, the specific field or laboratory test method(s) which will be accepted for evaluation against the baseline must be defined. The baseline parameter must also be measurable during construction.

There are encouraging benefits of the GBR in several countries.

The British Tunnelling Society and the Association of British Insurers, which represent insurers and re-insurers on the London-based insurance market, issued their the "Code of Practice for Risk Management" and the GBR concept is entirely adopted in this code (British Tunnelling Society, 2003).

GBR FOR FOUNDATION PROJECTS

As the application of GBR has grown in acceptance within the tunneling industry, many Owners have used GBR for projects or project components involving construction operations other than tunneling. The risks and potential impacts of unforeseen subsurface conditions are just as important for other projects involving geotechnical works as deep building and bridge foundations, open-cut pipelines, braced and tied-back excavations, and highway and other types of earthworks.

It appears logical that those non-underground projects most likely to benefit from the application of GBR are projects where complex subsurface conditions or specialized geotechnical construction poses a significant risk of cost escalation or delay.

GBR should be considered for any project where complex subsurface conditions or specialized geotechnical construction pose a significant risk of cost escalation or delay. Where construction will involve geotechnical works, a set of baseline conditions can reduce uncertainty in the pricing of the work and can serve to assist Contractors and sub-contractors in evaluating the work.

In drawing up the GBR for foundation, rather than mechanically baselining every measured geotechnical property, the designer should consider the potential influence of the parameter on the design, construction and performance of the project. Since the primary purpose of the GBR is management of subsurface risk, judgments should be made regarding the contribution of parameters to risk for the specific type of construction planned.

The zone within which the parameter is to be measured must also be specifically defined. For foundation construction the specific limits should be developed considering the limits of influence of the proposed construction.

Many subsurface risks can be effectively managed contractually through the use of payment items, as are typical for the ground excavatability, the presence of boulders, the relocation of unknown utilities, and the over excavation of unsuitable soils. Inclusion of allowance quantities for such conditions constitutes a form of baselining.

The key to developing appropriate baselines is to first recognize those aspects of the project that are most dependent on a proper and realistic assessment of the subsurface conditions. As the consequences of geotechnical variations increase, the importance of clear descriptions of key properties and behaviors in the Contract also increases.
Critical factors are those that relate to:

- potential construction methods;
- schedule-related issues;
- techniques to improve or control the ground or groundwater conditions;
- environmental and public impacts; and
- design and performance parameters.

The goal of baselines is to explain the results of geotechnical investigations and previous experience into clear descriptions of anticipated subsurface conditions upon which bidders may rely. The baselines also provide the Owner with the opportunity to allocate risks associated with these conditions.

Items to be addressed in baselines include fundamentally:

- the estimated amounts and distribution of different materials on the project;
- description, strength, permeability, grain size, and mineralogy of the various intact materials;
- description, strength, and permeability of the ground mass as a whole;

- quality of rock mass and characteristics of discontinuities;
- groundwater levels and groundwater conditions anticipated;
- construction impacts on adjacent facilities;
- other geotechnical and known man-made sources of potential difficulty or hazard that could impact the construction process (boulders, abandoned piles, buried utilities and other obstructions, high or low top of bedrock, mixed face conditions, geologic contacts, contaminated ground etc…).

To the maximum extent possible, baseline statements are best described using quantitative terms that can be measured and verified during construction. Qualitative descriptions, if required, should be clearly defined using generally accepted industry definitions and recognized standards.

The baselines should focus on specific ground properties and should avoid relying on ranges or ambiguous definitions.

Baseline statements should be in terms of measurable properties or parameters that can be objectively observed and recorded during construction. The use of adjectives such as "large," "significant," "local", "many", and "minor" should either be quantified or avoided. If qualitative terms are used, they should be standardized and defined in a summary table or a glossary.

As a simple test when writing a baseline statement, ask the question: "If I encountered a site condition pertaining to this baseline would I know if it differed from the indicated conditions?" If a reasonably straightforward affirmative answer is not given, the baseline statement is not sufficiently clear.

Baselines should be relevant to the anticipated construction methods, and readily quantifiable and verifiable using methods that are clear to both the Contractor and the Owner.

SUMMARY AND CONCLUSION

Contractual geotechnical interpretive reports have sometimes several shortcomings, resulting in disputes, such as:

- descriptions of anticipated conditions are overly broad, ambiguous or qualitative;
- descriptions of assumed conditions and behaviors are much more adverse than indicated by the data, or are arbitrary and unrealistic, without adequate explanation or justification for such conservatism;
- the effects of ground conditions on means and methods of construction are not well described.

The purpose of the GBR is to establish a realistic, common basis for evaluating any contractor claims for differing site conditions that develop during construction. The GBR is the basis for equitable contractual risk sharing and risk allocation between the Owner and the Contractor.

Properly drafted GBR reduces construction costs and set clear terms between the parties in the event of unforeseen ground conditions, contributing to minimize the likelihood of expensive and time-consuming disputes and litigation.

We may conclude that the GBR is a promising means to specify the intrinsically fuzzy differing site conditions clause.

By establishing clear baselines as a part of the Contract Documents, the parties are more likely to agree on the conditions indicated in the Contract, without time consuming and costly disputes that become counter-productive to a successful project.

Contractual measures, like GBR, help in reducing the various risks involved with geotechnical work on a construction project. Through the GBR, it can be ensured that there is a complete awareness and

preparedness towards the risks associated with a project and that the result of the risks, if encountered, is not concentrated just on the owner or the contractor, but equally divided among them.

Apart from sharing risks and responsibilities, a contract document should act as a unifying force that ties both sides to a common objective, and the GBR can should be considered a mean to address that common objective.

A contract document as GBR, that undoubtedly explains and classifies all the risks associated with the project, should go a long way in preventing change orders and resulting disputes that occur during the construction phase.

BIBLIOGRAFIA

Baker E., Turrini M., 2013. The Underlying Problem: Negotiating the Ground Conditions. Meeting of Society of Construction Law, London.

BTS, ABI, 2003. The Joint Code of Practice for Risk Management of Tunnel Works in the UK. British Tunnelling Society (BTS) and the Association of British Insurers (ABI).

F.J. Baynes, 2001. Sources of geotechnical risk. Quarterly Journal of Engineering Geology and Hydrogeology, August 2010.

Dwyre E.M., Batchko Z., Castelli R.J., 2010. Geotechnical Baseline Reports for Foundation Projects. Advances in Analysis, Modeling & Design. GeoFlorida 2010.

Essex R., 2007. Geotechnical Baseline Reports for Construction: Suggested Guidelines. ASCE.

Klee L., 2015. International Construction Contract Law. Wiley & Sons.

Godwin P., Roughton D., Gilmore D., Kratochvilova E., 2011. Bearing the risk of the unexpected in the ground – Lexology, www.lexology.com.

Fookes P, Baynes F.J., Hutchinson J.N., 2001. Total Geological History: A Model Approach to the Anticipation, Observation and Understanding of Site Conditions. ISRM International Symposium, Melbourne, Australia.

Henriod E., Le Masurier J, 2002. The Contract in Successful Project Management. Centre for Advanced Engineering. University of Canterbury – New Zeland

Hoek E., 1982. Geotechnical Considerations in Tunnel Design and Contract Preparation. Transactions Institute Min. Metall.

Hoek, E., Palmieri A., 1998. Geotechnical risks on large civil engineering projects. International Association of Engineering Geologists Congress. Vancouver, Canada.

Hosie J., 2016. Red Yellow and Silver Books – The treatment of unforeseen physical conditions. Mayer, www.mayerbrown.com.

FIDIC, 1999. The Red Book: Conditions of Contract for Construction for Building and Engineering Works Designed by the Employer.

FIDIC, 1999. The Yellow Book: Conditions of Contract for Plant and Design-Build.

FIDIC, 1999. The Silver Book: Conditions of Contract for EPC/Turnkey Projects.

Powell G, 2016. Construction Contract Preparation and Management: From Concept to Completion. Palgrave

Walton J., 2008. Unforeseen ground conditions and allocation of risk. Society of Construction Law Auckland, New Zeeland.

Walton J., 2013. Allocation of Risk and Dispute Avoidance. Australasia Users Group conference, Christchurch, New Zeeland.

Zoppis E., 2016. Ground Risk, Geotechnical Baseline Reports and their contractual implications. www.kcl.academia.edu

IMPACT FROM THE CONSTRUCTION OF A WORKING PLATFORM AND GIRDER LIFTING OPERATION ON BRIDGE PILE FOUNDATION IN SOFT SOIL

Bosco Poon, Aurecon, Neutral Bay, NSW, Australia, 61 434 342 613, bosco.poon@aurecongroup.com
Kim Chan, GHD Pty. Ltd., St Leonards, NSW, Australia, 61 29462 4843, kim.chan@ghd.com

ABSTRACT

To facilitate the initial construction of the bridge pier piles on the bank of Nambucca River in NSW Australia, a working platform was constructed over 25 m thick soft alluvial deposits. Subsequent to the pile installation and the construction of columns and headstock, it was determined that the platform needed to be raised by 1.5 m in order to allow for adequate clearance between the boom and the headstock. The raising of the working platform generated sub-soil flow that caused the piles to displace horizontally of up to 50 mm towards the river. Further, the erection of each 160 tonne girder was carried out by a super-lift operation at the raised platform. This exerted enormous bearing pressure on the platform. Surveying indicated that during the first two girder lifts, the tops of the bridge columns had displaced a further 39 mm towards the river, then recovered by about 15 mm after the lifting operation. To mitigate potential further lateral displacement for the remaining two girder lifts, a 5 m wide berm was constructed on the riverside of the pier. Surveying indicated that the placement of this counterweight had effectively limited further movement of the columns to less than 10 mm. One of the concerns with the lateral displacement of the pier was that the bending moment induced in the piles may exceed the moment capacity. Numerical analysis was carried out to back-analyse the measured lateral displacement and to assess the likely future performance of the piles. This paper focuses on the geotechnical design of the working platform and the predictions of the lateral displacements of the pier piles. The comparison of the predictions and measurements, as well as the permanent effects on the pier piles are also outlined.

Keywords: working platform, girder erection, foliation, sub-soil movement induced pile forces

INTRODUCTION

The Bridge over Nambucca River consists of a single bridge structure, comprising single substructures and separate superstructures. The bridge is approximately 850m long and comprises 20 piers. Driven steel tubular piles of up to 2 m diameter were used to support abutments and piers of the bridge structure. To create the spans between each of the piers, and the abutments at either end, four prefabricated U-shaped concrete girders between 39.5m and 41.5m in length and weighing up to 153 tonnes each were lifted into place. To facilitate the initial construction of the pier pile foundations, working platforms were constructed over soft alluvial deposits of up to 25 m thickness along the alignment of the bridge. Subsequent to the piles installation and the in-situ casting of the columns and headstocks, a challenge arose when it was determined that a working platform at Pier 09 next to the river bank needed to be raised by 1.5m in order to allow for adequate clearance between the crane boom and the pier during the girder lift operation. Furthermore, the girders were erected by a super-lift operation at the raised platform with a lift radius of up to 33 m. This has increased significantly the bearing pressure of the 600 tonne crawler crane, which was positioned in close proximity of the pier. While the working platform was designed to have adequate factor of safety for stability, the existing structures such as the pier piles founded in soft soils could experience movements and induced bending moment and stresses when the surrounding ground was loaded by platform filling followed by crane loading. Such movements and stresses could potentially impact on the future performance of the installed pier pile structures if not recognised or detected. This paper reports a case study where the construction of a working platform and the crane operations caused lateral displacement of the existing pier piles.

SUBSURFACE CONDITIONS

The soil profile in the vicinity of Pier 09 comprises approximately 22 m thick soft to firm clay/ sandy clay, followed by 4.5 m thick firm to stiff sandy clay interbedded with gravels, and underlain by Phyllite bedrock. The adopted water level is at about RL 0.0m, which is approximately 0.4 m below the existing

© 2018 Deep Foundations Institute

ground surface. Figure 1a shows the adopted undrained shear strength, S_u, derived from a nearby piezocone CPTU based on the corrected cone resistance (q_t) and using a cone factor (N_{kt}) of 16. The adopted over-consolidation ratio (OCR) for the alluvial clay layer varies from 1.05 to 2.3 as shown in Figure 1b. The assessed OCR values are consistent with the adopted S_u profile through SHANSEP relationship proposed by Ladd (1991):

$$S_u = S(OCR)^m \sigma'_{v0} \quad [1]$$

where S and m are SHANSEP parameters and σ'_{v0} is the vertical effective stress. The adopted S and m values are 0.22 and 0.94, respectively, which have been back-analysed from the survey monitoring for settlement for the preload fill embankment at the bridge abutments and approaches. The back-analysed compressibility of the soils, including the compression ratio (CR= $c_c/(1+e_0)$), the recompression ratio (RR= $c_r/(1+e_0)$) and the creep strain rate ($c_\alpha/(1+e_0)$) are 0.18, 0.025 and 0.006, respectively. The symbols c_c, c_r c_α and e_0 are the compression index, recompression index, creep coefficient and initial void ratio, respectively. There are five dissipation tests undertaken at the CPTU. The assessment of soil permeability uses the evaluated dissipation time, t_{50}, derived from the dissipation test results and the relationship presented in Figure 1c.

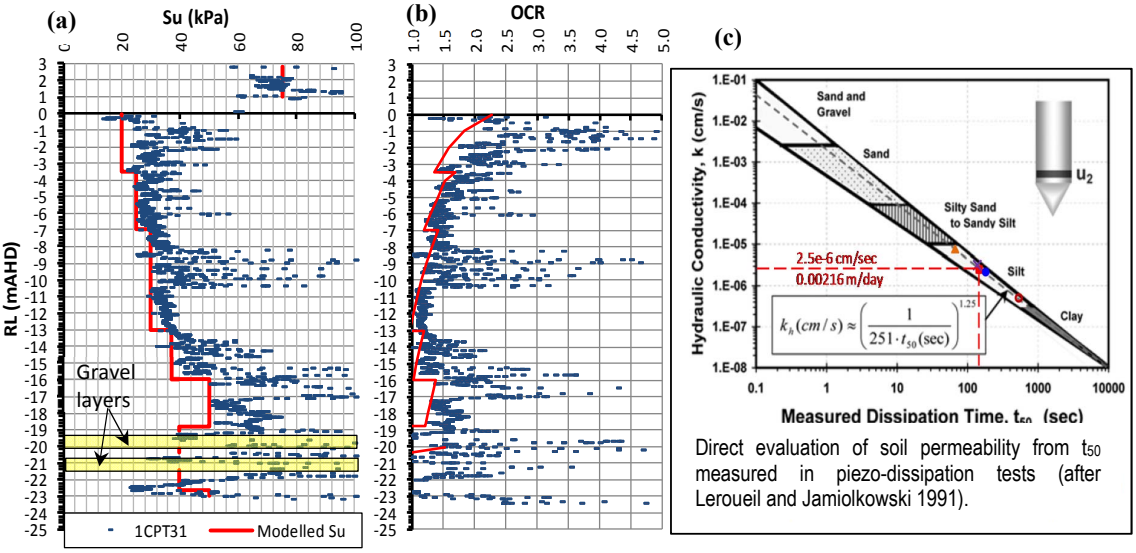


Fig. 1. (a) S_u vs. RL profile inferred from 1CPT31, (b) Inferred OCR profile from S_u via SHANSEP, (c) Permeability vs. t_{50} inferred from dissipation tests conducted at 1CPT31

BACKGROUND AND DESIGN OPTIONS

Pier 09 of the Nambucca River Bridge is located on the northern riverbank. It consists of two columns, each supported by a 2 m diameter steel tubular pile driven into medium strength or better Phyllite bedrock. To facilitate the initial construction of pier pile foundation, a 0.8 m to 1.1 m thick rockfill platform with high strength geotextile was constructed to RL 1.9 m. The high strength geotextile has a short-term characteristic tensile strength of 800 kN/m, placed perpendicularly to the pier at approximately RL1.1 m. However, it has been damaged near the piles as a result of the piling activities.

Subsequent to the piles installation and the in-situ casting of the columns and headstocks, it was determined that the working platform at Pier 9 next to the river bank needed to be raised to RL 3.0m in order to allow for adequate clearance between the boom of the crane lifting the girders and the headstock of Pier 09. Note that Pier 09 is located beneath the summit of the bridge; it has the highest bridge columns with the bearing levels setting at RL 14.65 m. The raising of the platform fill, about 1.3 m thickness, would activate renewed sub-soil flow that was likely to cause horizontal displacement of the installed piles. Further, the girders were to be erected by a 600 tonne crane positioned in close proximity to the pier, along with its super-lift counterweight of 300 tonnes. This would exert enormous bearing pressure

on the platform, further exacerbating the complexity of the design tasks for platform stability and impact assessment of the pier piles. A number of design options were considered to address the platform stability and the issue of potential pile movements. These include: (1) Incremental launching method (ILM) for bridge span installation; (2) Soft ground treatments using stone columns, deep soil mixing etc.; (3) Installation of temporary supporting piles beneath crawler crane location; (4) Installation of sheet pile walls with tie-back reinforcements at the river bank in front Pier 09; (5) Installation of stability berm in front of Pier 09; or (6) Placement of additional high strength geotextiles within the raised platform plus the use of steel mat for load spreading.

Option 1 to Option 3 were ruled out for the reasons of high mobilisation costs and delay in construction. The installation of sheet pile wall in front of the installed Pier 09 columns (Option 4) would not be possible because of space constraint. A platform built out from the shore into the river is required for sheet piling construction. In this instance, however, sheet pile wall would not be necessary since the extended platform fill in front of Pier 09 could act as a berm for platform stability (Option 5). The berm option was also considered an effective and economical method to limit the potential pile movement. The use of the river for berm construction was not unacceptable, provided that a detailed environmental management plan was set in place for the temporary work to minimise environmental impacts. Some of the controls required in the plan included the use of clean rock fill, and the application of floating barriers around the berm to contain and control the dispersion of silt in the river. The last option (Option 6) would involve the minimum construction effort, and is therefore the most economical method from the construction standpoint. Whilst this method might be able achieve a satisfactory factor of safety for platform stability, it was considered less effective in controlling the potential movements of the piles. The design prediction of the lateral pile displacement and the induced forces and bending moments in the piles had become vital in determining the feasibility of this option. Unfortunately, it is well known that, due to the non-homogenous and anisotropic nature of the soils, the horizontal pile displacement induced by the lateral soil flow is difficult to predict accurately (Poulos, 1972). The variation in the analysis results meant that an observational approach to this design option should be adopted.

Upon review of the ground conditions and in consultation with the Construction Team, a combination of design Options 5 and 6 was adopted. In this approach, a reasonable design with the minimum construction cost (i.e. Option 6) was adopted (see Figures 2a, and 4c). The performances of the crane settlement and horizontal displacements of the columns and headstock at Pier 09 were extensively and carefully monitored during the girder lift operation. A suitable remedial berm (i.e. Option 5) would be instituted should the survey measurements indicated the need (see Figure 8a).

GIRDER LIFTING PLAN AND TRACK PRESSURE LOADS

The erection of bridge girders involved a non-routine lifting operation that required detailed planning. Following the adopted design option discussed in the previous section, the rock platform was firstly raised to the required elevation at RL3.0 m (Figure 2a). The crawler crane was further raised to RL3.25 m via the placement of 250 mm thick 310UC steel mats. These crane mats were used to spread the load imparted by the crane crawler, and to add extra height to compensate for the ground settlement during the lifting operation. Further, the configuration and the movement of the crane were predetermined. Figure 2a (also shown in Figure 4c) indicates that the 1.5 m wide crawler tracks were centralised over the 4.5 m wide steel mats, which had a clear spacing of about 3.1 m from the crest of the rock fill batter over the river bank, and about 2.1m from Pier 9 column face at the closest point. As per the lifting plan outlined in Figure 2b, the 600 tonne Demag CC2800-1 crawler crane picked up the 158 tonne girder from the haul road at a lift radius of 14 m and tracked back over the steel mats to the lift position. The crane then slewed 90˚, connected the 284 tonne super-lift tray with counterweights, and lowered the lattice boom to a maximum of 33 m lift radius to place girder. This process was repeated successively for the erection of four 41.4 m long girders spanning over Pier 8 (at the river) and Pier 9 (at the riverbank).

The track bearing pressure was assessed for a range of operation and lift orientation that was carried out. To assess the performance of the raised rock platform and the impact of crane loading on the permanent

pile design, an equivalent "block" pressure was obtained. This was obtained by first identifying the track bearing pressure for the critical orientation of the crane as it lowered the 158 tonne girder into position with a maximum slew radius of 33 m. The trapezoidal/triangular distribution of this critical bearing pressure was then converted to an equivalent rectangular or "block" pressure by determining the effective length and width of the crawler crane using Meyerhof (1991) method. Note that for the plane strain analyses undertaken as part of the stability and deformation assessments to be discussed later tin this paper, the adoption of an equivalent "block" pressure was considered appropriate to reflect how the crane would impart load onto the rock platform.

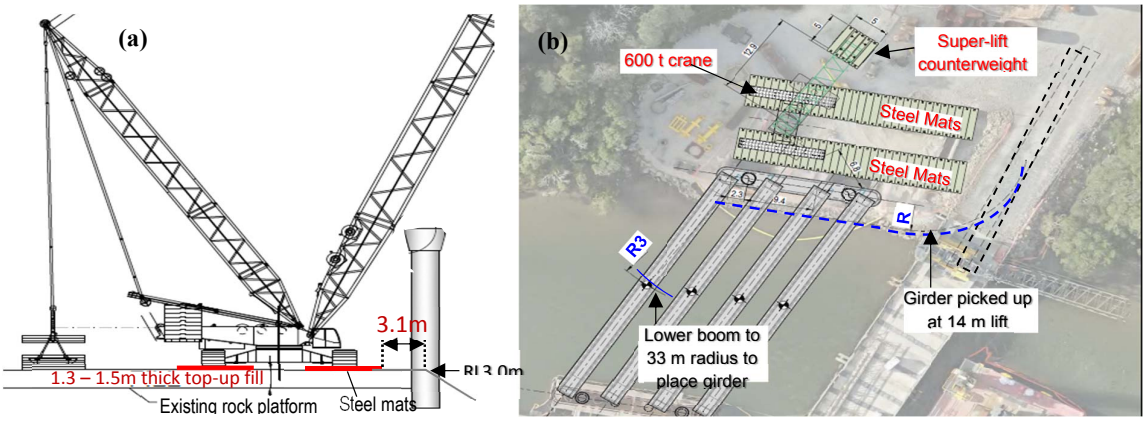


Fig. 2. (a) Position of crane relative to as-installed Pier 09 column, (b) Lifting Plan

Steel mats were placed underneath the crawler tracks in order to assist with spreading load over a larger area. Each steel mat was constructed from twelve 200UC52.2 universal columns (Figure 3a), each 4.5 m in length, which had been welded together and placed perpendicular to each crawler track. While the total width of the steel mat is 4.5 m, it is less likely that the applied crawler load would be spread over the entire mat width since the steel mat experienced some bending under loading. A 2D plain strain finite element analysis (FEA) using PLAXIS 2D (Version 2016.01) was conducted to model the steel mat and the overlying imposed equivalent block pressure of 592 kPa closest to the river (Figure 3a). More details of the FEA are discussed later in the paper. Figure 3b shows the pressure distribution at the underside of the steel mats derived from the 2D FEA. The analysis result indicates that the effective spread width can be considered to be about 3.5 m. For design purposes, in particular for the stability check of the platform using limit equilibrium method (discussed in the next section), an averaged block pressure of 254 kPa (= 592 kPa × 1.5 m / 3.5 m) could be adopted based on this assessed effective width at the underside of the steel plates closest to the river. For the other side of the crawler track away of the river, the assessed equivalent block pressures at the undersides of the track and steel plate were 425 kPa and 182 kPa, respectively, as depicted in Figure 4c.

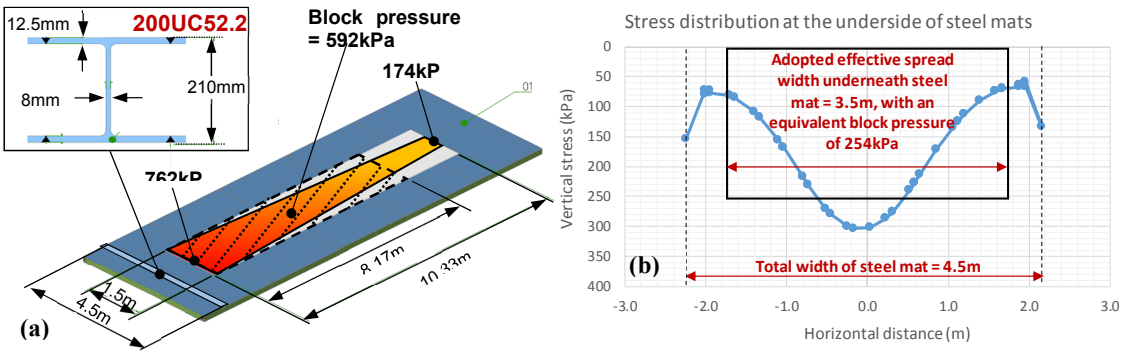


Fig. 3. (a) Track pressure over steel mat, (b) Assessed pressure distribution from PLAXIS at the underside of the steel mat for an imposed equivalent block pressure of 592kPa

PLATFORM STABILITY

The stability of the raised working platform was critical for the girder lifting operation. The consequence of platform failure or significant damage to the installed pier piles and columns was unacceptable. The working platform must be designed to have adequate factor of safety for stability against the following failure modes: (i) punching failure; (ii) slope failure; (iii) lateral sliding of fill above basal reinforcement and (iv) foundation extrusion.

Punching failure mode

For the applied equivalent block pressure of 254 kPa over an effective area of 3.5 m × 8.2 m at the underside of the steel mat closest to the river (Figure 3b), the total bearing resistance was considered to be the sum of the shear required to punch through a vertical plane of the platform and the bearing capacity of the subgrade. This simplified punching failure mechanism is outlined in the practice guide for working platforms for tracked plant produced by Building Research Development (BRE), 2004. As the effective strip width of 3.5 m was offset at a distance of about 4.3 m parallel to the crest of the batter, it was considered sufficiently far away from and not to be impacted by the adjacent batter. Further, punching failure was not considered the most critical failure mode due to the relatively think platform in place (2.1-2.6 m) and the presence of multi-layered high strength geotextiles.

Slope failure mode

The assessment of slope stability using the conventional method of slices was not able to consider load spreading through the rock fill platform. It was therefore necessary to apply a dispersed design pressure, as opposed to the bearing pressure at the underside of the steel mats, in the global stability analysis. The load spreading was assumed to follow a line with a vertical-to-horizontal slope of 2:1, all around the equivalent block pressure at the underside of the steel plate, until it intercepted the base of the working platform. Note that the adopted 2V:1H load spreading was considered conservative for the compacted rock fill. It can be demonstrated using elastic solution or more sophisticated finite element methods that the angle of load spread will increase (up to 1V:1H) as the stiffness of the soil increases.

Lateral Sliding

The stability against lateral sliding of the fill wedge above high strength geotextile was assessed in principle following clause 8.3.2.6 of *BS8006.1 2010: Code of practice for strengthened/reinforced soils and other fills* (BS8006). The determination of the minimum reinforcement bond length to resist the horizontal outward thrust of the platform fill given by BS8006 assumes that a surcharge load is applied uniformly across the top of the embankment. The situation that occurred during girder lift however did not have a uniform surcharge applied across the platform but rather two strips of crawler track loads. The resulting stress distribution within the platform fill material is shown in Figure 4a, and the minimum reinforcement bond length, L_e, was given by the following equation slightly different to that of BS8006:

$$L_e \geq \frac{\left(0.5K_a f_{fs} \gamma_{fill} H^2 + f_q \int_0^H \sigma_H d\sigma\right) f_s f_n}{\gamma_{fill} h \frac{a' \tan \phi'_{cv}}{f_{ms}}} \quad [2]$$

where the partial factors f_{fs}, f_q, f_s, f_n and f_{ms} are defined in BS8006.1 2010. The other parameters of the equation including ϕ'_{cv}, K_a, γ_{fill}, H, h, a' and σ_H are defined in Figure 4a and the legend in Figure 4. In particular, σ_H denotes the lateral pressure distribution within the platform fill caused by crawler track loadings, and was assessed based on the theory of elasticity. For design purposes, it was determined along a vertical plane immediately adjacent to the edge of the strip load closest to the crest of the rock fill batter, i.e. the dashed red line shown in Figure 4a. The σ_H was calculated as a result of the two strip loads, each applied over an effective width of 3.5m, and where q_1 = 254 kPa and q_2 = 182 kPa (offset 8.40 m from the vertical plane along which stress are to be determined), as shown in Figures 4a and 4c. From the aforementioned method outlined, it was determined that the minimum reinforcement bond length of approximately 10 m was required to resist the horizontal outward thrust of the platform fill. This was achieved by anchoring the high strength geotextiles at the batter slope via a minimum of 5.5 m wrap length as depicted in Figure 4c.

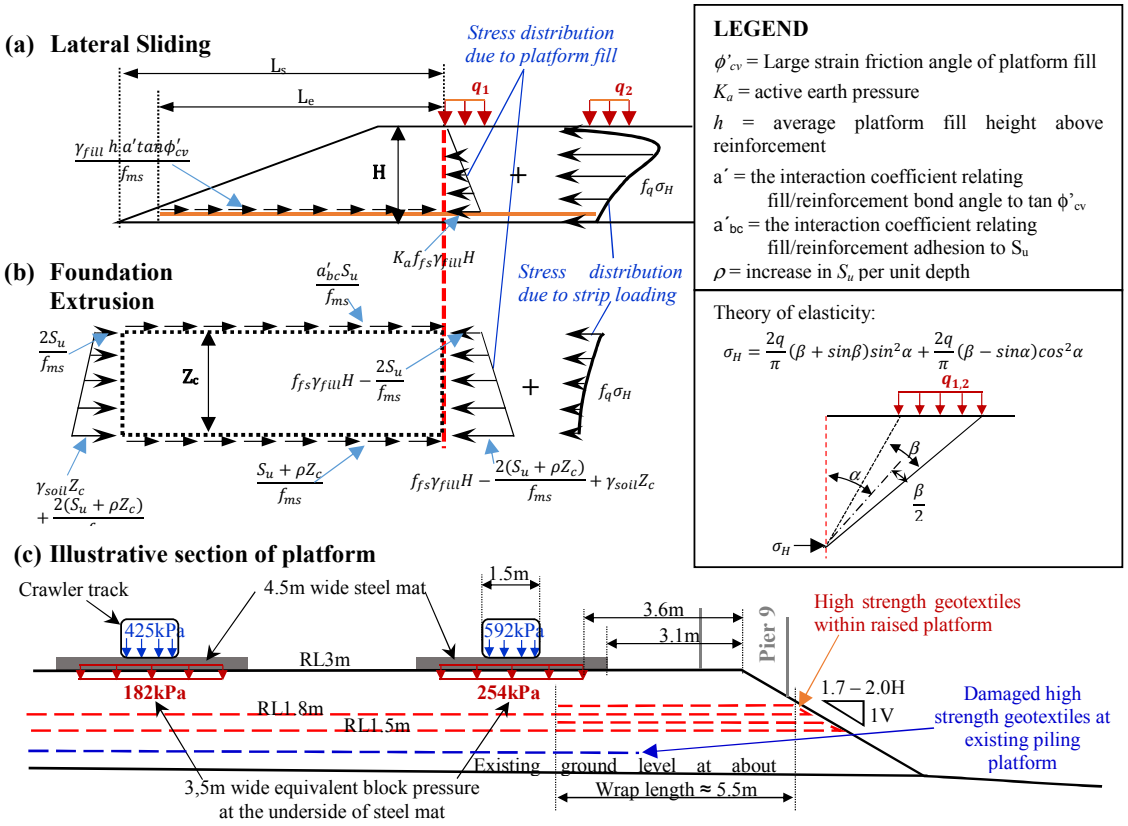


Fig. 4. (a) Force components for lateral sliding, (b) Force components for foundation extrusion, (c) Illustrative section of platform

Foundation Extrusion

An assessment of foundation extrusion, which occurs when the geometry of the embankment induces outward shear stresses within the soft foundation soil, and where the foundation soil is soft and of limited depth, was undertaken in a manner similar to that outlined in clause 8.3.2.6 of BS 8006.1:2010. Figure 4b schematically illustrates the force components in the foundation extrusion stability analysis. Two strip loads were applied, as opposed to an uniform surcharge, over the top of the working platform. The minimum side slope length, L_s, required to prevent foundation extrusion was calculated based on:

$$L_s \geq \frac{\left(\left(f_s \gamma_{fill} H - \frac{2(2S_u+\rho Z_c)}{f_{ms}}\right)Z_c + f_q \int_{-Z_c}^{0} \sigma_H d\sigma\right)}{\frac{(\alpha'_{bc}+1)S_u+\rho Z_c}{f_{ms}}} \quad [3]$$

where the engineering parameters including s_u, γ_{soil}, a'_{bc} and Z_c are defined in Figure 4b and the legend in Figure 4. The term σ_H is the lateral pressure distribution within the foundation soil. Noting the apparent change in undrained shear strength at RL -7.0m (see Figure 1a), it was considered that this would be an appropriate cut-off in respect of determining the lateral pressure within the soil that should be considered when assessing lateral extrusion. With the assessed σ_H reducing with depth, the foundation extrusion was not considered as a critical failure mode. The side slope length depicted in Figure 4c was assessed to be greater than the minimum required length L_s.

IMPACT OF PLATFORM RAISING AND CRANE LOADING ON PIER PILES

The impact of platform raising and crane loading on pier piles was assessed by the combination of a 2D finite element (FE) method and a boundary-element (BE) method. The 2D FE analysis was carried out first to generate the lateral soil movements due to the above construction activities without the presence of the pile. These generated free-field soil movements along the pile depth were then used in the BE

analysis as the applied soil movement loads to assess the pile response. The BE analysis considered the 3D nature of the pile.

The preceding FE analysis was carried out using PLAXIS 2D. In this analysis, the soft clays were modelled using Soft Soil Model in the PLAXIS programme, which resembles the Modified Cam-Clay model with a Mohr-Coulomb hexagon yield surface in the deviatoric plane. Further, the FE analysis involved coupled consolidation to assess soil movements with time. The adopted coefficient permeability, k, was related to the void ratio, e, in accordance with $e = e_0 + c_k \log (k/k_0)$, where e_0 is the initial void ratio, c_k is the permeability index and k_0 is the initial permeability value. Consistent with the laboratory results, the e_0 for the low to medium plasticity clays is 1.2. The c_k can be related to e_0 in the form of $c_k = 0.5 \times e_0$ as proposed by Tavenas *et al*. (1983), thus $c_k = 0.6$ was adopted. The adopted k_0 was 2.5×10^6 cm/sec, which is consistent with the results inferred from the dissipation tests shown in Figure 1c. The FE analysis has also considered the placement of steel mat, 4.5 m wide, centred beneath each 1.5 m wide crawler track of the crane. To assess the soil deformations as a consequence of girder lifting operations, equivalent block pressures of 425 kPa and 592 kPa were imposed across the respective width of the crawler tracks as depicted in Figure 4c. The adopted construction sequences are summarised in Figure 5a. Figure 5b shows the assessed horizontal soil displacement contour 1 day following the application of the sustained crane lifting load. Figure 5c shows the assessed horizontal soil displacement at the inferred location of Pier 09, which is 2.1 m from the edge of the steel mat, 3.15 m from the edge of the crane crawler AC. The analysis results indicate that the predicted maximum horizontal free-field soil displacement at the pile location due to platform raising plus 1 day of sustained crane loading is about 65 mm.

(a).Stage	Construction
1	Initial Stress State for in-situ ground condition prior to platform construction
2	Construct piling platform up to RL1.2m
3	Left in place for consolidation over 5 months (piling activities not modelled)
4	Reset displacement to zero
5	Raise the platform to RL3 including high strength geotextiles
6	Apply sustained crane loads over 1 day period

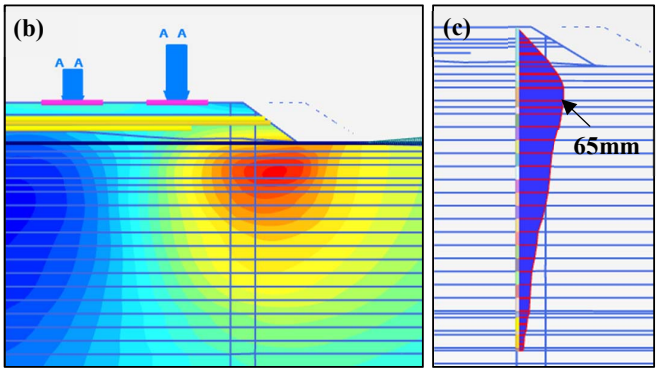


Fig. 5 (a) Construction sequence in PLAXIS analysis, (b) Contour of horizontal displacement from PLAXIS, (c) Predicted horizontal greenfield displacement from PLAXIS along the pile surface of the proposed pile location

The computed lateral soil movements from the FE analysis were then used as input into the BE program for pile response analysis. The BE program used is named PALLAS (for Piles And Lateral Loading Analysis) and has been described in Poulos *et al*. (1996). PALLAS uses a simplified form of BE analysis in which the pile is idealised as an elastic beam and the soil as an elastic continuum, but with limiting pressures, p_y, at the pile-soil interface to allow considerations of yielding of soil surrounding the pile. The program can consider a single pile or a group of non-identical piles, and take into account of the proximity of the pile to slope batter based on Poulos (1976). The input parameters for the piles consist of the bending stiffness, diameter and length of individual pile within the group. The soil model requires the specification of the Poisson's ratio and the distributions with depth of p_y and soil Young's modulus, E_h for horizontal loading. In the design, $p_y = 9S_u$ and $E_h = 225 \times S_u$ were adopted. Note that E_h was taken as 75% of E_v, where E_v is the soil Young's modulus for vertical loading and $E_v = 300 \times S_u$ was adopted. The red curve in Figure 6a shows the BE analysis input of the specified greenfield horizontal soil displacement under crane loading as obtained from PLAXIS (Figure 5c). The analysis results, as shown by the red curves in Figures 6b to 6e, include the pile horizontal displacement, rotation, shear force (normal to the pile) and bending moment and shear force with depth. The predicted lateral displacement and rotation of the pile/column at the top of the platform were about 57 mm and 0.0014 rad, respectively. The predicted horizontal displacement at the top of Pier 9 headstock, which was about 11 m above the top of the platform, was approximately 72 mm (= 57 mm + 0.0014 rad × 11000 mm).

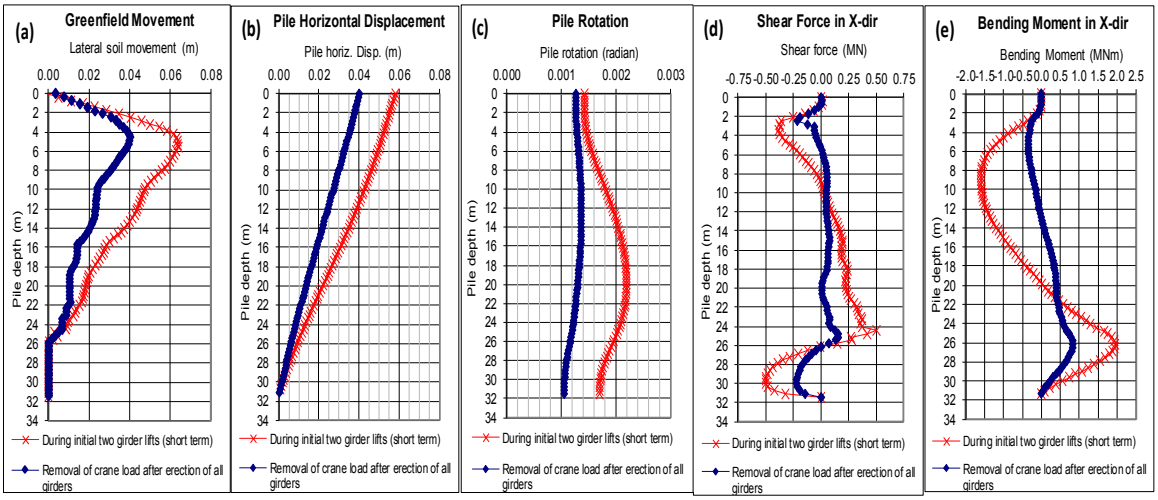


Fig. 6 (a) Predicted greenfield horizontal soil displacement from PLAXIS, (b) Predicted pile horizontal displacements, (c) Predicted pile rotations, (d) Predicted shear forces in piles, (e) Predicted bending moments in piles

MONITORING RESULTS DURING LIFTING OPERATION

Pier 09 of the Nambucca River Bridge comprises two columns, COL 9-01 and COL 9-02. Following the construction of COL 9-01 and COL 9-02 the columns were surveyed to be deviated less than 5 mm in any direction from the design location for the column. Prior to the first two girder lifts for Span 09, the Pier 09 columns were re-surveyed. This survey indicated that the tops of the columns had displaced between 25 mm and 50 mm towards Nambucca River since the as-built survey was completed. These displacements recorded prior to the Span 09 girder lifts were inferred to have occurred as a result of the platform raising from approximately RL 1.5m to RL 3.0m, with the additional rock having increased the lateral pressure acting on the Pier 09 piles since no additional rock being placed on the riverside of the piles.

There were in total four girders to be lifted at Span 09. Following the completion of the second girder lift the displacement at the top of columns COL 9-01 and COL 9-02 were surveyed again, which indicated that an additional 39 mm and 28 mm of horizontal displacement took place, respectively, towards the river. The total horizontal displacements of the column tops at this stage were between 64 and 78 mm, as shown in Figure 7. The average of these displacements has reached the design prediction of 72 mm outlined in the previous section at the end of the second girder lift, and the subsequent lifting operation was halted. There were some gradual recovery of the lateral displacements perpendicular to Pier 09 alignment, up to about 15 mm of rebound, when the columns were re-surveyed after 9 days following the second girder lift. The rock platform did not show signs of distress in the form of cracking or slumping near the platform slope. In fact, the occurrence of rebound in horizontal displacement of the columns after unloading indicated that the foundation soil was still within the elastic range, in a global sense, before developing a plastic slip plane.

As a response to the observed displacements to the Pier 09 columns as a result of the first and second girder lifts, the Construction Team has deployed the back-up plan, in which the rock platform was widened on the riverside of the Pier 09 columns by constructing a 5 m wide unreinforced berm (Figure 8a). The berm was constructed of the same rock material as the existing rock platform, had a batter slope no steeper than 1.7H:1V, and be raised to a level commensurate with the existing rock platform, i.e. RL 3.0 m. There were some minor restoring movements of the columns observed, less than 5 mm, after the installation of the rock berm (Figure 7). Further, the berm has greatly limited further displacements of the columns in the subsequent girder lifts. Survey monitoring indicated that the additional incremental horizontal displacements as a result of the third and the forth girder lifts are up to 8 mm towards Nambucca River.

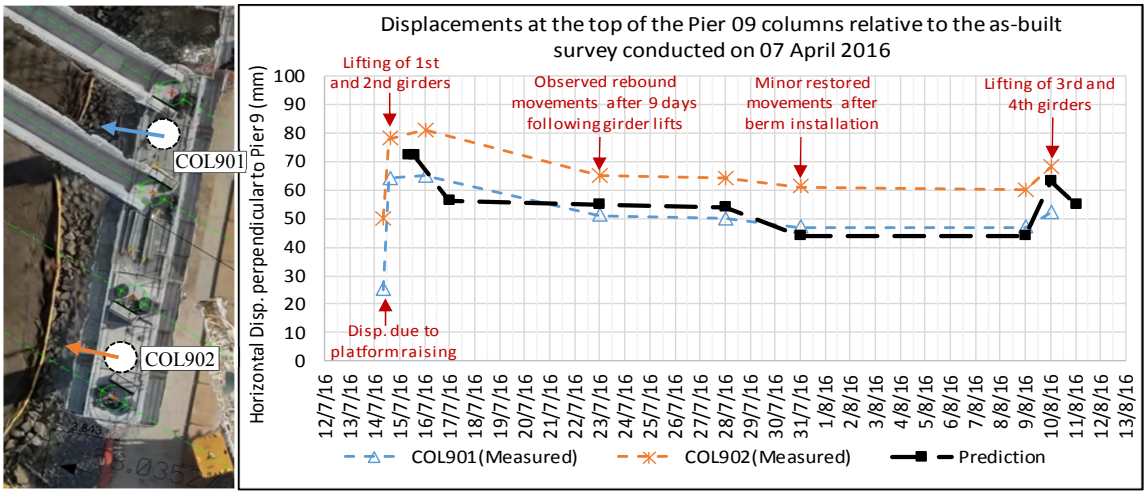


Fig. 7 Recorded horizontal longitudinal displacements at the top of Pier 09 columns

IMPACT ON PERMANENT DESIGN OF PIER PILES

The assessed bending moment of the piles during girder lifting presented by the red curve in Figure 6e was a temporary induced load caused by short term girder lift operation. After the unloading of the crane and the stripping of the working platform, there would be invariably some recovery of horizontal displacements, leading to a reduced bending moment of the piles. This is evident from the survey monitoring, which showed a rebound horizontal displacement of up to about 15 mm at the top of columns after the removal of crane load; followed by a further minor recovery of column displacements after the installation of the rock berm at the riverside of Pier 09.

To assess the impact on the permanent design of the pier piles, numerical analyses utilising the 2D FE and BE methods as outlined in the previous section were carried out to further simulate the horizontal movements of the column top and the induced pile forces corresponding the main construction activities after the initial two girder lifts. For all of the pile analyses using BE methods, in particular, the pile heads were considered free to translate and rotate without restraints. It is acknowledged that some lateral resistance could have developed progressively against longitudinal movement at the top of Pier 09 as the girders were installed, which propped the pier top back to Pier 08. However, full restraints due to full frame action of the bridge portal frame was not considered to have established since the erection of Span 09 girders were ahead of those for the adjoining Spans 08 and 10 as shown in Figure 8b.

The black dashed curve in Figure 7 shows the predicted pier top longitudinal displacements for the different construction activities in relation to girder lifts at Pier 09. The predicted displacements are in general comparable with the surveyed movements in terms of the trend. The predicted total recovery of longitudinal displacements since the initial two girder is about 25 mm, which includes the contribution of elastic rebound and the installation of rock berm. The survey measurements shows a slightly lower corresponding recovery of about 15-20 mm. There was no significant shear distortion observed at the elastomeric bearings beneath the seated girders, indicating that the recovered longitudinal displacement could have been transferred, either totally or partially, to Pier 08 at the other end of Span 09. However, we have not been able to confirm this mechanism as no survey data was available for Pier 08 movements. The blue curves in Figures 6d and 6e shows the assessed shear force and residual bending moment of the piles under SLS after the removal of crane load following the erection of the 3rd and the 4th girders. It would be anticipated that in the finished condition after the stripping of the platform, the residual pile forces and displacement would further reduce. The assessed residual bending moment in the piles is much lower than the maximum values during the application of the crane loading (loaded and un-loaded). In accordance with an assessment conducted by the design Structural Engineer, the piles and columns would have sufficient reserve capacity to accommodate the additional bending moments due to eccentricity of vertical loads and the assessed residual bending moments in the piles. Bending due to

the design eccentricity of the vertical loads was a relatively small component of the total bending moment so the additional moment from increased eccentricity was relatively small. The largest bending moments came from horizontal forces such as braking, creep and shrinkage and earthquake which were not affected by the eccentricities. Bending in the column also came from frame action of the portal frame that were similarly not affected. The residual bending moment in the pile was also relatively small and the locations of the peak values did not coincide with the locations of the peak values from other design loads and effects. Furthermore, the piles would have sufficient capacity to withstand the assessed short term maximum bending moment occurred during construction as a result of the crane loading.

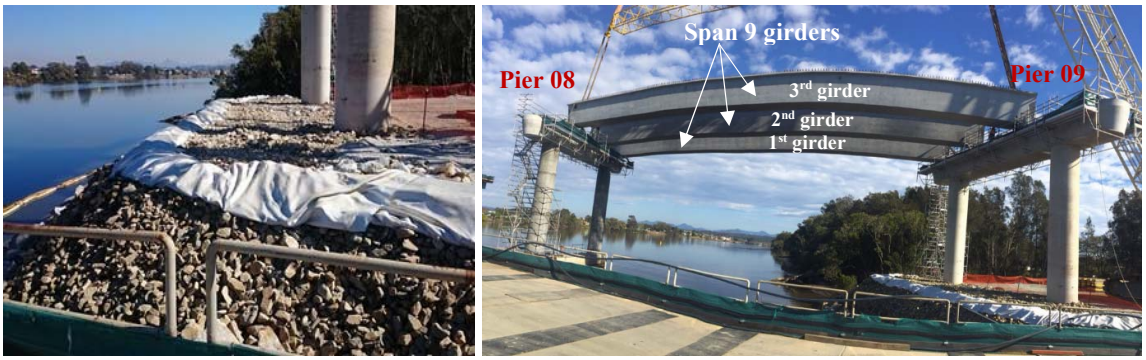


Fig. 8 (a) Installation of 5 m wide stability berm at the riverside (b) erection of the 3rd girder

CONCLUDING REMARKS

Heavy lifting is a high risk operation that must be planned and executed properly, in particular when it occurs close to a permanent structure. There are currently a number of guidelines/standards available for cranes and for working platform design (e.g. BR470 2004). These references aim at preventing lifting failure caused by supporting ground not being firm enough, highlighting the importance of having a proper lifting plan and the design of working platform for stability. For soft soil foundation, the experience with unconfined pile and pier movement at the riverbank emphasises the need for careful consideration and management of the risk of structure displacements resulting from the temporary crane loading in close proximity. Proactive approach shall be established before the temporary construction between the site Geotechnical and the Construction Teams to mitigate and avoid possible structural damages due to soft ground displacements associated with temporary construction loading such as platform construction and crane lifting operations.

REFERENCES

BR470. Working platforms for tracked plant: good practice guide to the design, installation, maintenance and repair of ground-supported working platforms. Building Research Establishment 2004.

BS 8006:-1:2010 Code of Practice for Strengthened / reinforced soils and fills, BSi London.

Leroueil, S. and M. Jamiolkowski., 1991. Exploration of Soft Soil and Determination of Design Parameters. Proceedings, GeoCoast'91, Yokohama, Japan, Vol. 2, Port and Harbour Research Institute, Hasaki, Japan, pp. 969–998.

Meyerhof, G.G. 1991. Shallow foundations. ASCE, JSMFD, SM2, pp21‑31.

Poulos, H.G. 1972. Difficulties in prediction of horizontal deformations of foundations. J. Soil Mech. Found. Div., Proc. ASCE, 98 (SM8), 843-848.

Poulos, H.G. 1976. Behaviour of laterally loaded piles near a cut or slope. Australian Geomech. J., Sydney, 6-12.

Poulos, H.G., Chen, L.T. and Hull. T.H., 1996. Tests on single model piles subjected to lateral soil movement. Soil and Foundation. 35(4), 85-92.

Tavenas, F., Leblond, P., Jean, P. and Leroueil, S., 1983. The permeability of natural soft clays, Part 2: Permeability characteristics. Canadian Geotechnical Journal, 20: 645-660.

SAMPLING OF STABILIZED CLAY BY USE OF KISO-JIBAN GP-Tr SAMPLER

Bjørn Kristian Fiskvik Bache, NGI, Trondheim, Norway, +47 92884996, bkb@ngi.no
Alf Kristian Lund, NGI, Trondheim, Norway, +47 47659532, akl@ngi.no

ABSTRACT

Ground improvement of clays by use of lime-cement stabilization is widely used in Norway and Scandinavia. However, there is great uncertainty with regards to strength and deformation characteristics of the resulting stabilized material. Sampling by traditional methods, like geotechnical piston sampling, is unsuitable due to the brittleness and high strength of the stabilized material.

This paper presents the preliminary results of samples collected within lime-cement columns using a Kiso-Jiban GP-Tr sampler to obtain undisturbed, high quality samples from the field. The sampler uses a gel-polymer to lubricate between the sample and the sampler walls to reduce the friction and disturbance of the sampling process.

The method allows for continuous high quality sampling of lime-cement stabilized clay down to great depths. High quality samples allows for determination of material parameters from advanced laboratory tests, e.g. triaxial and oedometer tests, which can be used to investigate the properties of the stabilized material, and thereby determine if the designed strength has been reached.

Keywords: Ground improvement, Kiso-Jiban GP-Tr, sampling, lime-cement

INTRODUCTION

Ground stabilization by use of lime-cement columns is the most common method applied in the Nordic countries. The method is used to increase the strength and stiffness of sensitive clay soils, and can be applied for e.g. stability improvement of natural slopes, cuts and excavations, or to increase the soil resistance in an excavation pit. Experience shows that variations in the material properties of stabilized clay can be large and that there is a need to assess those conducted stabilization works. Testing of the stabilized material can be performed *in situ* or in the laboratory on representative samples. The latter case is usually preferred as it provides direct inputs to geotechnical analyses.

A prerequisite for obtaining valuable information when testing stabilized soil in the laboratory is sample quality. The material has a brittle behavior, and is often too hard for normal piston sampling. A common approach used today is to excavate a part of the stabilized material and cut samples with a saw. Such excavations are costly, disturbs a large area, and are not suitable for sampling at large depths.

This paper present results from sampling and testing of stabilized clay material at large depths at two different test sites in Norway. The samples were obtained using Kiso-Jiban Gel Push Triple (GP-Tr) sampler (Mori and Saki; 2016). The aim of this study is to present the sampling technique, show how it can be used for sampling stabilized soils and present some preliminary results from laboratory work on the collected samples.

GEL PUSH TRIPLE SAMPLER (GP-Tr SAMPLER)

The GP-Tr sampler is based upon a conventional rotary triple tube sampler (Mori and Saki; 2016). It includes self-adjusting shoe penetration, stationary liner and inner tubes, and an outer tube tipped with a bit that rotates and drills the soil above the shoe. The sampler uses ordinary drilling fluid to remove the cuttings and to cool the drilling bit. The drilling bit is placed above the cutting shoe, which prevents the flushing from disturbing the sample material. The difference from regular triple tube samplers is that the GP-Tr sampler uses a gel polymer to lubricate the core sample as it enters the

 © 2018 Deep Foundations Institute

inner tube, significantly reducing the friction between the sample and the liner tube walls. The liner tube is made of PVC-U and has an inner diameter of 83 mm and a length of 900 mm, which also corresponds to the sample size. The sampler was mounted on a Geotech 607 drilling rig powered by a 126 kW diesel engine. Figure 1 shows a schematic illustration of the GP-Tr sampler.

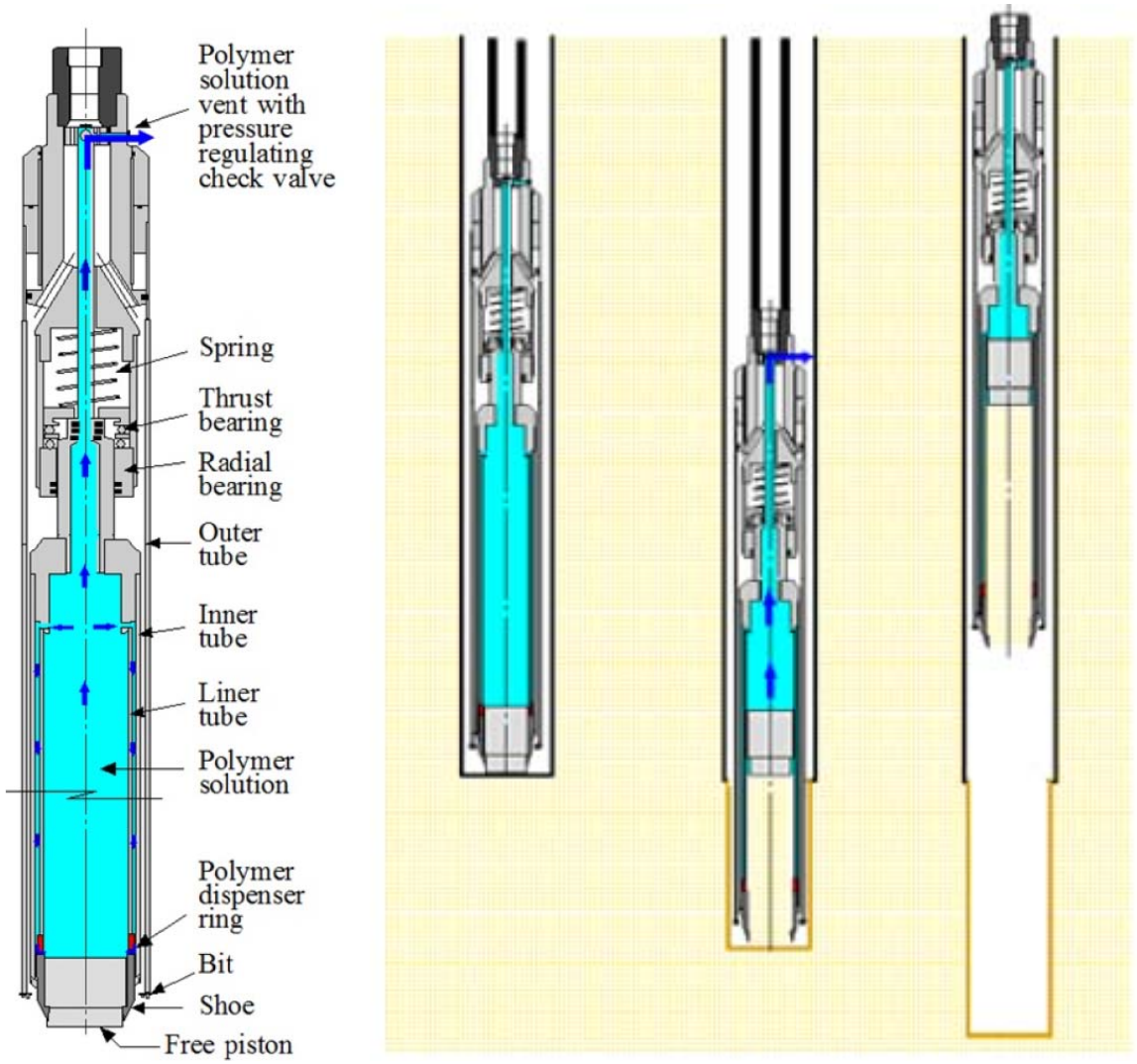


Fig. 1 Schematic illustration of the cross-section of the Kiso-Jiban GP-Tr sampler and of GP-Tr sampling. Illustration from Mori and Saki (2016).

DESCRIPTION OF THE TEST SITES AND STABILIZATION WORKS

The GP-Tr sampler was tested at two different locations in Norway. The first site at Klett is situated just south of Trondheim in central Norway, where the Norwegian Public Road Administration (NPRA) has a large road project including installation of approximately 40 000 lime-cement columns. The second site is situated in Oslo close to the Oslo central station, where the National Railway Infrastructure Company (BaneNOR) is building a new gateway to the station.

At the Klett site, the soil consists of a very sensitive clay (or quick clay) with a shear strength of 30-40 kPa and water content from 30-35%. The clay was stabilized using lime-cement columns with a diameter of 600 mm and with a 50/50 mix of lime/cement and a binder content of 90 kg/m^3. The columns were installed in a rib pattern, with an intersection between the piles of 100 mm. The curing time for the piles at the sampling date was 120 days. It took another 30 days before the tests were completed in the laboratory.

At the Oslo central station the soil consists of a non-sensitive clay with a shear strength of 45-60 kPa and water content around 35%. The clay was stabilized using 100% cement columns with a diameter of 800 mm and a binder content of 110 kg/m^3. These columns were installed in a grid pattern with an intersection between the piles of 150 mm. The curing time for the piles at the sampling date was 30 days. It took another 30-40 days before the tests were completed in the laboratory.

SAMPLING OF LIME-CEMENT COLUMNS

During installation of the lime-cement columns the upper 0,5-1 m are usually installed without binder to prevent blowout. This zone, that consists mostly of remolded soils was therefore removed before sampling to ensure collection of representative stabilized material, and to prevent the hole from collapsing. This was experienced during the first sampling campaign at Klett when the upper part of the column crumbled, causing the hole to collapse and preventing further sampling. The use of casing would have prevented this from happening, but such equipment was not available at the site at the time the sampling took place.

Sampling was carried out to retrieve stabilized material both at Klett and at Oslo central station. The columns were sampled continuously in its full length of 8 and 7 meters respectively. The sampling could easily have continued to greater depths if the columns had been longer. Figure 2 shows the drilling rig with the first lime-cement sample from the Klett site.

The sampling method is quite time consuming since it requires extra work with mixing and loading the sampler with the gel polymer. During a normal work day of c. 10 hours it was possible to collect 6 samples a day.

At Oslo central station, the sampling was performed under temperatures ranging from -8^{O}C to -3^{O}C. This caused some difficulties during sampling, as the water in the system risked freezing between the samples. This was solved by keeping the sampler warm, soaking it with heated water at regular intervals.

A total of 14 samples were collected, 7 at each site. The inner liner containing the sample was removed from the sampler and sealed off with a rubber cap, before an empty liner was inserted in the sampler for the sampling to proceed. The samples were then transported to NGIs laboratory in Oslo for testing.

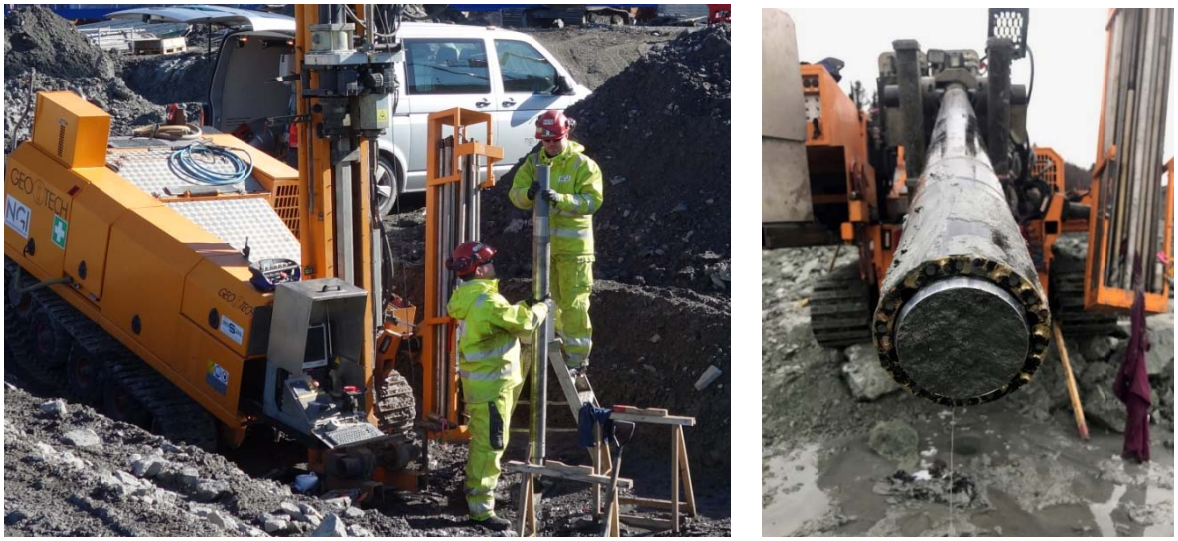


Fig. 2a and b. a) Preparation of the GP-Tr sampler. b) Picture of the drilling rig with the Kiso-Jiban Gp-Tr sampler after sampling of the first lime-cement sample at the Klett site (photo courtesy NGI).

RESULTS AND DISCUSSION

An important aspect of this study was to evaluate sample quality from samples collected with the GP-Tr sampler. An initial assessment was visually performed in the field when the first sample was extruded. The sample easily came out as a result of the low friction between the inner liner and the sample due to the gel polymer. Pictures of the extruded sample are shown in figure 3a and 3b. The sample looked very good, and no distinct signs of cracking or disturbance could be observed on the material. The surface of the sample was smooth without any dents or damages from the sampling. However, the handling of these brittle samples required great care. The first sample that was collected was directly put on the ground and broke into several pieces due to the unevenness of the ground.

Extrusion of samples in the laboratory showed that most of the samples were intact and continuous. However, some of the samples broke into several pieces during extrusion. Trimming of the samples down to 72 mm in diameter was necessary so that they could fit in the testing equipment. A picture of this is shown in figure 4b. A series of uniaxial compression tests, active and passive triaxial tests, oedometer tests and direct simple shear tests were performed in the laboratory and showed good results. Figure 4a and 5a and b shows the results of some of the tests.

The uniaxial compression tests failed at an axial strain between one and two percent. This corresponds to the failure strain of laboratory mixed samples, which indicates that the sample is of good quality. Most of the triaxial tests had a larger failure strain than the uniaxial tests. The dilative behavior of the material is considered to be the main cause of the large failure strains. The shear strength achieved from the tests varied between 60 – 310 kPa. The lowest values are caused by disturbed samples which crumbled during testing.

The stabilized soil material is very brittle in nature and easy to disturb when handling and during transportation. A few samples that were extruded in the laboratory had already broken into several pieces. The reason is difficult to pinpoint, but factors such as the sampling process itself, vibration during transport, insufficient sealing or extrusion process may all have impacted. It may also have been caused by a weakness zone in the sampled pile. The source of the disturbance should be investigated more closely.

In general most of the samples were of good quality and extruded as a whole piece. With respect to the material having a very brittle behavior, this indicates that the GP-Tr sampler is able to sample the stabilized material without much disturbance.

Even though the sampling process was time consuming, the equipment is more time efficient than regular triple tube core sampling. This is mainly because the equipment fits to a regular geotechnical drilling rig, which can start drilling as soon as the drilling rig is in place. Other triple tube core samplers takes close to a day to prepare before the sampling can start. The use of a geotechnical drilling rig also has an advantage when it comes to accessibility.

After adjusting the sample diameter by using a lathe, it was possible to perform advanced laboratory results on the samples. This is important as it enables verification and quantification of the material properties. By combining results from advanced tests to i*n-situ* field tests like CPTU and RCP, correlations may be established so that the material properties can be determined from *in situ* tests in the future.

The process for adjusting the sample is a possible source of disturbance. Ideally, the sample should be tested at its sampled diameter of 83 mm. This would have required special equipment, such as larger pistons, membranes and filters for the triaxial apparatus. If the method is applied for commercial projects in the future, laboratory equipment should be customized to fit the sample diameter.





Fig.3 a) and b). a) Photo of removing the inner lining of the sampler. b) Photo of a sample from a lime-cement column extruded in the field. No signs of cracks or sample disturbance was visible (photo courtesy NGI).

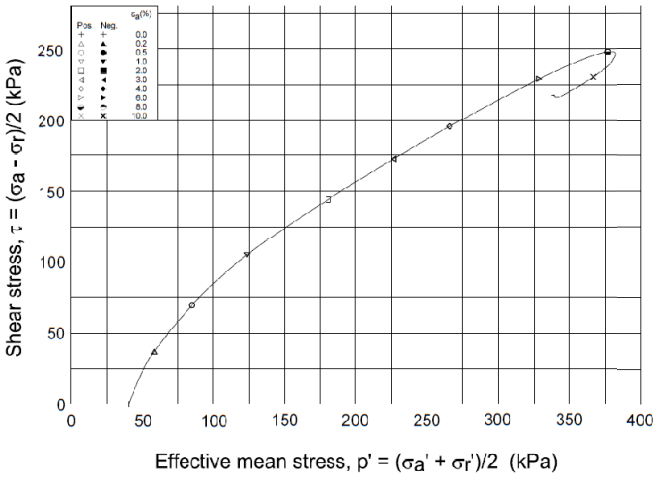




Fig. 4a and b. a) Results from an active triaxial test on stabilized material. b) Photo of sample adjustment by use of lathe (photo courtesy NGI).

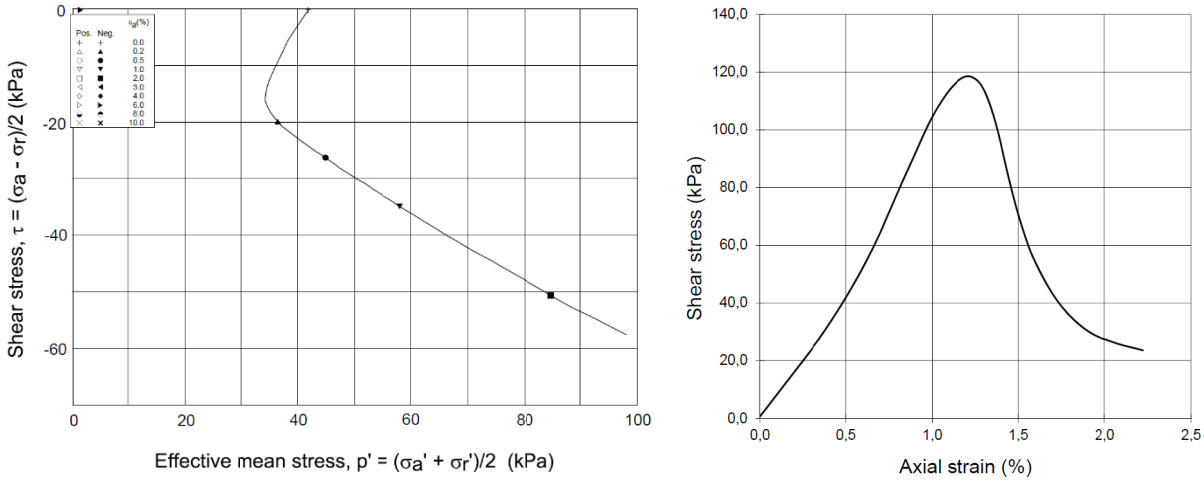


Fig. 5a and b. a) Results from a passive triaxial test on stabilized material. b) Results from a uniaxial compression test.

SUMMARY AND CONCLUSION

To sample and verify the material properties of stabilized soils at two construction sites, the NGI collected samples using the Kiso-Jiban GP-Tr sampler. High quality samples were successfully collected down to depths up to eight meters. The sampler was able to shear the stabilized soil, and bring apparently undisturbed samples to the surface.

The sampling results show that the method is suitable for sampling stabilized clays. However, some of the samples had broken into pieces before extrusion of the sample. The reason for this disturbance is unknown, but it may have been caused by transportation of the sample or by a weakness zone in the sampled pile.

ACKNOWLEDGEMENTS

The Norwegian research council has provided financial support for the tests provided in this article through the GBV project 20150117at NGI and through the infrastructure project Norwegian GeoTest Sites (NGTS). The Norwegian Public Road Administration and the National Railway Infrastructure Company are gratefully acknowledged for allowing us to test the equipment on their construction sites.

REFERENCES

Mori, K. and Saki, K., 2016. The GP-sampler: a new innovation in core sampling. Proceedings, ISC5, Sydney, September 5-9, Vol 1, pp. 99-124.

WORKING PLATFORMS FOR TRACKED PLANT – EXPERIENCE FROM 13 YEARS OF BEST PRACTICE

Derek Egan, Remedy Geotechnics Ltd., ICON Environmental Innovation Centre, Daventry, Northamptonshire, UK., +44 (0) 1788211778, derekegan@remedygeotechnics.com

ABSTRACT

The impact of piling rigs toppling over due to weak ground is significant, not only in the risk it poses to human life, but in the economic impact on the piling contractors and their clients, not to mention the reputational damage to all involved. In 2004 the UK piling industry launched its very successful piling platform initiative which changed the practice of the UK construction industry with respect to the provision of safe working platforms. This has led to a significant reduction in the number of piling rig instability incidents. This paper reviews the development and implementation of the working platform initiative and illustrates the process successfully used for evaluating the bearing pressure imposed by a working piling rig, designing and then testing of a working platform. Recognising improvements in safety usually require a culture change experience of the management process for implementing a working platform initiative is also described.

Keywords: granular working platform, tracked plant

INTRODUCTION

The publication of BRE 470 "Working platforms for tracked plant", Charles et al. (2004) was a milestone in the UK for the provision of granular working platforms for tracked plant, and piling rigs in particular. This publication was the outcome of a drive by the Federation of Piling Specialists (the UK trade body representing piling and specialist geotechnical contractors) to improve the safety of piling and associated operations. The Federation of Piling Specialists (FPS) had recognised that the incidences of piling rigs toppling over because of poor support from the ground was unacceptably high and they implemented an industry leading initiative to improve the safety of piling plant operations by tackling the issue of poor quality working platforms. The initiative had three components:-

i. The development of a methodology, backed by a spreadsheet calculation tool, to enable estimation of the ground bearing pressures exerted by a tracked piling rig onto the ground during various modes of operation (standing, travelling, handling, penetrating, extracting etc.).
ii. The development of best practice guidance on the design of granular working platforms for tracked plant, using the track bearing pressures calculated from (i) above.
iii. Implementation of a consistent approach to manage and control the process of specification, design, construction and maintenance of working platforms by the use of the Working Platform Certificate.

In practice the individual that does the calculation to estimate the rig ground bearing pressures is not the person who performs the granular working platform design for a specific site, however it is important that each have an appreciation of the whole process including its assumptions and limitations.

Where BRE 470 led the way, and established a precedent in the design and management of granular working platforms, other guidance followed. The Federation of Piling Specialists produced guidance on hydraulically bound platforms, FPS (2007). The interrelationship between granular platform thickness, angle of friction of platform material and strength of sub-grade was investigated by Corke & Gannon (2010), who examined the choice of platform material angle of friction, ϕ', and subgrade

© 2018 Deep Foundations Institute

strength noting that overly conservative selection of angle of friction, ϕ', had a significant impact on increasing the thickness of the platform. They went on to recommend that, where appropriate, plate load testing be undertaken to validate the platform sub-grade and the platform material design parameters with the intention that testing can lead to improved economy. A review of the BRE 470 design method approach, in response to criticism of the way the beneficial effect geosynthetics was being incorporated in granular platform design, was addressed by BRE (2011). The review concluded that while BRE 470 had proved satisfactory in its principle objective improving safety, and confirmed that it was able to embrace alternative approaches to the design of platforms. The BRE 470 approach was endorsed for the design of granular working platforms by the Construction Plant-hire Association (CPA, 2014). This publication sought to raise awareness of the importance of provision of safe working platforms across all sites, not just where piling was being undertaken. Alternative design methods for granular platforms, including proposals to align the design to EC7 were considered in a draft document produced by the Temporary Works Forum (Temporary Works Forum, 2015). This document could mark a useful development in the wider acceptance of alternative design methods if formally published.

Whilst developments and variation of granular platform design methods have been proposed since the publication of BRE 470 in 2004, the original design method still appears to remain the most frequently used granular platform design method in the UK.

DETERMINATION OF TRACK GROUND BEARING PRESSURES

Clearly before designing a granular working platform it is necessary to define the bearing pressures and contact area arising from the rig loading under different modes of operation.

Ground Bearing Pressures

Rudimentary guidance on the method to use to estimate track bearing pressures had been provided in BS EN 996:1996 (now withdrawn), and later slightly amplified in BS EN 16228-1:2014. The approach is to undertake a theoretical calculation using static equilibrium equations to determine the resultant force, R, and point of action perpendicular to the working surface. This requires knowledge of the mass and of the position of the various rig components and any applied winch or crowd forces relative to the centre of the tracks. Then the magnitude and position of the resulting reaction forces under each track (P_{TLH}, P_{TRH}) are found. Fig. 1 illustrates the principle.

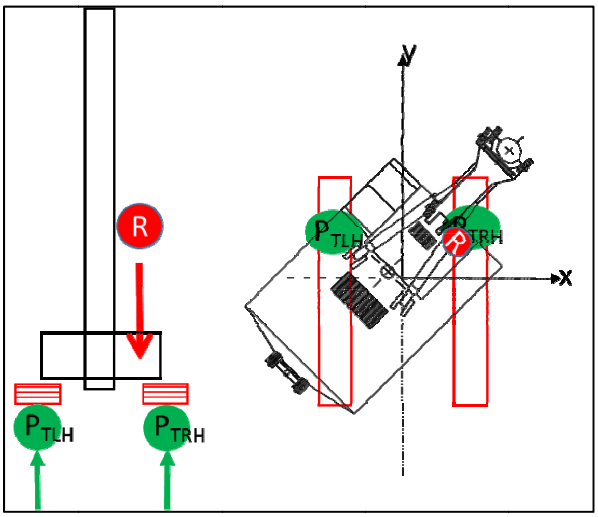


Fig. 1. Illustration of forces applied to a tracked piling rig.

Once the magnitude and point of action of P_{TLH} and P_{TRH} are known Table F1, BS EN 16228-1:2014 is used to determine the applied bearing pressure distribution under the rig tracks. The pressure distributions may be rectangular, triangular or trapezoidal, and the loading may be different under each track. For some loading conditions, the proportion of the track in contact with the ground may be less than the full track length; implying one end of the track is on the verge of lifting.

The calculations must be undertaken for all combination of slew angle and operating situations to find the most adverse situation.

The actual distribution of the applied track force, P, through a granular working platform and into the sub-grade is highly complex. In 2004 BRE 470 recommended the use of a simplified stress distribution based on the formulation by Meyerhoff (1953) to derive an effective rectangular stress, q_{eq}, over effective track length l_{eq}, an approach that continues to be used for the design granular working platforms, but may not be appropriate for other types of working platform. To accompany the publication of BRE 470 the FPS launched a spreadsheet tool to facilitate the calculation of track bearing pressures for use in the design of working platforms, the tool was modified to make it more flexible to use in 2016, as discussed in greater detail below.

Dealing With Footpads and Outriggers

Where the piling rig is only supported on its two tracks the equilibrium calculation is statically determinate. However some rigs have one (or more) foot pads or outriggers that are deployed in certain operating situations. (For example many CFA rigs have a foot pad located at the bottom of the leader mast which applies force to the ground, particularly during auger extraction). Introducing points of support in addition to the rig tracks renders the equilibrium equations statically indeterminate. This is addressed within the FPS spreadsheet tool by iterative calculation where the inputted footpad resistance force is varied until the track and foot pad bearing pressures equalise. It is crucial that it is fully understood that inputting the footpad resistance force is only a means to render the equilibrium calculations statically determinate. The actual forces applied to a footpad under operating conditions may vary from those calculated. The granular platform is designed for the maximum calculated bearing pressure, q_{max}, for the most adverse dimension of loaded area (i.e. the worst of the footpad or track area). This approach has satisfactorily been used since 2004 and remains adopted practice in the UK.

Track Bearing Pressures & Rig Stability

It is extremely important to recognise that the calculations undertaken to estimate the track ground bearing pressures **are not** the same as those required by BS EN 16228 to demonstrate a piling rig is inherently stable. The two sets of calculations, namely the track ground bearing pressure calculation and the rig stability calculation are for different purposes; the two approaches must not be confused.

Spreadsheet Tool

The FPS has made an excel spreadsheet bearing pressure calculation tool publically available via its web site (https://www.fps.org.uk/guidance/working-platform-guidance/1065/), with the important caveat that it is only used by a competent person. The operator of the tool should be intimately familiar of the operation of the rig that they are estimating the track pressures for.

The following assumptions apply to the use of the Tool:-

- The rig is operating on a flat, horizontal surface with the mast in vertical orientation (only);

- The mass and position of the various rig components are known and input as required into the spreadsheet;
- The point of rotation of the slewing component lies in the middle of the tracks;
- The Tool is restricted to uses where all loads and forces are vertical;
- The rigs are working on a flat horizontal surface;
- The rig behaves as a rigid body such that Meyerhof pressure distributions may be used;
- Foot pad resistance (where used) is entered as an input parameter to make resolution of the forces statically determinate;
- The Tool is operated by a competent person.

Extensions and add-ons to the standard spreadsheet are possible to accommodate operating conditions outside of the standard limitations, such as sloping sites, inclined mast etc.

Loading Factors

Within BRE 470 the margin of safety against the occurrence of a granular platform bearing capacity failure is covered by the use of load factors applied to the calculated track bearing pressures, with cautious selection of characteristic design parameters for the platform material and subgrade. Two loading Cases are considered:-

Case 1: Where the rig operator is **unlikely to be able to aid recovery** from an imminent platform failure. Operations such as standing, travelling, and handling are examples.

Case 2: Where the rig operator can control the load safely, to aid recovery from an imminent platform failure for example operations applying to piling rigs such as installing casing, drilling, extracting an auger. BRE 470 includes travelling or slewing with a fixed mast which has a foot or fixed load (e.g. a pile held in the leader) close to the platform surface within this category.

Table 1 shows the loading factors required by BRE 470 for determination of the thickness of the platform, where one is required.

Table 1 BRE 470 Values for loading factors where a platform is required.

Loading Condition	Loading Factor
Case 1	1.6
Case 2	1.2

At the time BRE 470 was published the Eurocodes were not in regular use in the UK and limit state design was not in routine use for geotechnical structures. Since Eurocode 7 does not provide specific guidance for the design of working platforms in general practice it is not usually used for the design of granular working platforms for piling rigs. With development of design methods and analytical ability alternative design approaches may start to gain traction in the future leading to more diversity in the form of calculation used to determine granular platform thickness.

Practical Aspects

In principle it is relatively straightforward for a competent person to carry out the static equilibrium calculations to determine the ground bearing pressures for a given piling rig, but practical and operational factors add complexity to the process.

Obtaining reliable data on rig component weights and centres of gravity has not always been easy. In 2004, when BRE 470 was published many rig manufactures did not always supply the information required for the bearing pressure calculations and for older rigs the information was simply not available. To overcome this it was occasionally necessary to go to the expense of removing and

weighing rig components to determine their mass and centre of gravity. Fortunately the provision of the necessary input data avaible from rig manufactures has improved with time.

For most applications it has not been UK practice to consider dynamic loading in the estimation of track bearing pressures for the use of granular platform design. In routine situations this may be reasonable due to the low speed of rigs when travelling, low vibration during operation, gradual lifting or release of suspended loads and the fact that dynamic bearing capacity and stiffness of soils (including the granular platform) are greater than static values. Likewise wind loading may not be significant in routine situations. However the potential for these additional forces to critically affect the applied track bearing pressures used in the granular platform design should not be overlooked, and where necessary incorporated into the bearing pressure calculation.

DESIGN OF A GRANULAR WORKING PLATFORM

Provision of Site Information

Establishing the near surface ground and groundwater conditions for the subgrade of the platform, over the whole of its plan area, is a clear prerequisite to the design process. This must include adequate topographical information and knowledge of the final reduced level of the working surface. Unfortunately, not all specifiers of ground investigation, ground investigation contractors, or others within the supply chain, appreciate the importance of providing near surface information. This may become particularly problematic on brownfield sites which usually have an abundance of heterogeneous Made Ground that exhibit lateral and vertical variability in the nature and depth of near surface soils. Ignoring shallow ground strength where the ground investigation is solely designed with deep piled foundations in mind must be recognised a potentially unsafe and costly oversight, especially on sites of large plan area. Experience indicates that the assessment of the subgrade ground conditions may be the most uncertain step in the design process.

There is significant risk associated with isolated spots of weak subgrade (including poorly backfilled excavations) which must always be considered even where there is good quality near surface ground investigation. In this regard the importance of a thorough proof rolling of the subgrade, by the platform installer, supplemented by inspection by a competent person cannot be over emphasised. Strength testing (usually using plate testing) of the subgrade is sometimes undertaken to inform the design prior to laying the platform, and can be beneficial. This does not, however, remove the risk that isolated weak spots may still exist, and this needs to be considered by the platform designer. In this regard, it is the platform installers responsibility to exercise rigorous inspection and control to ensure the strength requirements for the platform sub-grade are achieve at all points across the platform area.

BRE 470 presented a simple design calculation based on methods investigated by Meyerhof (1974), Valsangkar and Meyerhof (1979), Hanna and Meyerhof (1980) and Hanna (1981). The analysis is based on the principle of a relatively shallow thickness of platform placed on a weak sub grade. Experience has shown this to have been appropriate for the majority of piling sites, however the designer should be aware of the limitations of this method in other design situations.

In the BRE 470 analysis the bearing resistance is considered to be the sum of the shear required to punch through a vertical plane in the granular platform material and the bearing capacity of the subgrade, as shown in Fig. 2. Limitations are placed on the applicability of the method to where subgrade undrained shear strength is between 20kPa and 80kPa, and where the platform thickness is less than 1.5 times the track width, W.

Where a structural geosynthetic is incorporated within the platform material it is considered to provide increased resistance to the punching failure mechanism. The approach came in for some criticism, particularly from geosynthetic manufacturers, as being too conservative. In a follow up paper, BRE (2011), it was stated “unlikely” that a simple design method could be developed for the design of reinforced platform which would preserve safety and economy and have universal application.

Where poor subgrade strength prevails and the BRE 470 method is not appropriate more complex design methods are required, such as shown in CIRIA SP123 (Jewell, 1996), or by propriety design methods developed by geosynthetic suppliers. The specialist capability of geosynthetic suppliers can lead to efficient granular platform design particularly for very weak subgrades, but their design methods can be opaque and may be very difficult to independently verify.

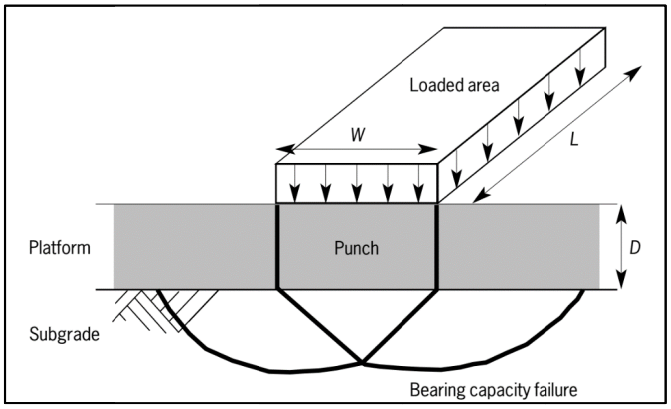


Fig. 2. Mode of punching failure.

Conclusion

Notwithstanding the limitations of the BRE470 method, it has generally proved to provide a straightforward design method for the majority of UK piling sites and has gained wide acceptance. The complexities of other methods, such as CIRIA SP123, can be a barrier to its use by all but geosynthetic design specialists and are not widely used. On the relatively small proportion of sites where poor subgrade strength prevails many contractors rely on the provision of a geosynthetic suppliers design. In the future it is probable that evolution in design methods will provide sufficient impetus for the wider adoption into main stream practice of alternative methods used to calculate granular working platform thickness.

MANAGEMENT AND DRIVING INDUSTRY CHANGE

At the launch of BRE 470 in 2004 FPS member companies undertook not to work on unless a signed Working Platform Certificate was in place. Developed by the FPS the Working Platform Certificate provides control documentation to confirm that a working platform has been designed by a competent person, constructed (and where specified tested) in accordance with the design will be regularly inspected and adequately maintained to ensure its integrity over its design life by a named organisation (usually the Principal Contractor). The FPS continues to make the Working Platform Certificate publically avaible on its web site (https://www.fps.org.uk/content/uploads/2017/01/FPS-WPC4d-June-2015.pdf).

Although generally welcomed by the wider construction industry as a step forward in the safety culture of piling operations acceptance of the Working Platform Certificate in 2004 was not universal. Two common complaints were that granular working platforms had suddenly become thicker and more expensive and that additional programme time was required to design, construct and test platforms. On the positive side the incidences of toppling piling rigs was demonstrably reduced and where problems have been encountered a better understanding of the causes of failures and the development of improved piling practice has been facilitated. At the current time due to the concerted efforts of the FPS the use of the working practice is now universal in the UK on construction sites where piling and ground improvement is undertaken.

SUMMARY AND CONCLUSIONS

In 2004 the UK piling industry launched its very successful piling platform initiative which changed the practice of the UK construction industry with respect to the provision of safe working platforms. In the 13 years since the publication of BRE 470, UK practice of systematic assessment of the bearing pressures generated by piling rigs, platform design, construction and maintenance on piling sites has improved safety and benefitted piling productivity. This improvement required some change in industry culture and management which was driven by the introduction of the Working Platform Certificate which has now achieved routine acceptance in the UK construction industry. Numerous developments in the design and testing of granular working platforms for tracked plant have been proposed, these continue to be evaluated, and with time may become more widely adopted. Notwithstanding these more recent developments, the important contribution and influence on construction industry practice relating to piling operations brought about by the FPS working platform initiative, supported by publication BRE 470, is undeniable.

REFERENCES

BRE, 2011. BR470 Working platforms for tracked plant. Use of 'structural geosynthetic reinforcement – A BRE review seven years on. Building Research Establishment. Bucknalls Lane, Watford. WD25 9XX.

BS 996:1996. Piling equipment – Safety requirements (withdrawn). BSI, London.

BS EN 16228-1:2014. Drilling and foundation equipment – Safety. Pt.1 Common Requirements. BSI, London.

Charles, A., Driscoll, R. and Skinner, H. 2004. Working platforms for tracked plant. BRE 470.Building Research Establishment, Watford.

Construction Plant-hire Association, 2014. Ground Conditions for Construction Plant. Accessed October 2017. https://www.cpa.uk.net/sfpsgpublications/#Groundconditions

Corke, D. and Gannon, J. 2010. Economic design of working platforms for tracked plant. Ground Engineering, February.

FPS, 2007. Guide to Hydraulically Bound Working Platforms. Accessed October 2017. https://www.fps.org.uk/content/uploads/2017/01/Hydraulically-Bound-Working-Platforms.pdf

Hanna, A.M. 1981. Foundations on strong sand overlying weak sand. ASCE Journal of Geotechnical Engineering Division, vol 107, no GT7, July, pp 915–927

Hanna, A.M. and Meyerhof, G.G. 1980. Design charts for ultimate bearing capacity of foundations on sand overlying soft clay. Canadian Geotechnical Journal, vol 17, no 2, pp 300–303

Jewell, R.A. 1996. Soil reinforcement with geotextiles. CIRIA Special Publication 123. Construction Industry Research and Information Association, London.

Meyerhof, G.G. 1953. The bearing capacity of foundations under eccentric and inclined loads. Proceedings of 3rd International Conference on Soil Mechanics and Foundation Engineering, Zurich, vol 1, pp 440–445.

Meyerhof, G.G. 1974. Ultimate bearing capacity of footings on sand layer overlying clay. Canadian Geotechnical Journal, vol 11, no 2, May, pp 223–-229

Temporary Works Forum, 2015. Working Platforms. Design of granular working platforms for construction plant. A guide to good practice. DRAFT. Accessed October 2017.

https://www.twforum.org.uk/media/70911/tw15_120_wg5_granular_platforms_for_plant___draft_for_discussion__final__reduced.pdf

Valsangkar, A.J. and Meyerhof, G.G. 1979. Experimental study of punching coefficients and shape factor for two-layered soils. Canadian Geotechnical Journal, vol 16, pp 802–805.

A STUDY OF THE AUGMENTING EFFECT OF EQUIPPING PILES WITH AN EXPANDER BODY

Bengt H. Fellenius[1)], K. Rainer Massarsch[2)], Mario Terceros H.[3)], and Mario Terceros A.[4)]

[1)]Consulting Engineer, 2475 Sidney, BC, Canada, V8L 2B9. <Bengt@fellnius.net>
[2)]Geo Risk & Vibration Scandinavia AB, Bromma, Sweden. <rainer.massarsch@georisk.se>
[3)]Incotec S.A., Santa Cruz de la Sierra, Bolivia <math@incotec.cc>
[4)]Incotec S.A., Santa Cruz de la Sierra, Bolivia <mta@incotec.cc>

ABSTRACT. A full-scale study is reported of the response of four pairs of piles of 150 mm through 620 mm diameter, bored piles drilled with slurry, continuing-flight auger-cast pile (CFA), and a full-displacement pile (FDP). One of each pair was equipped with an Expander Body to increase the pile-toe diameter, preload the pile axially, as well as bring about a stiffer pile toe and, thus, achieve a stiffer pile. All piles were constructed to 9.5 m depth in a loose to dense silty to dense sand. The EB-equipped piles were supplied with bidirectional cell immediately above the EB (depth 8.3 m). Static loading tests performed on all piles showed that the expansion of the EB markedly increased the pile toe stiffness. This, not just by increasing the pile toe area, but also by preloading the soil underneath the pile toe and increasing the shaft resistance acting around the 1.5 m long EB.

Keywords. Bored piles, CFA piles, Full Displacement piles, static loading test, pile-toe augment.

INTRODUCTION

The pile testing programme at the ISSMGE TC212 research site in Santa Cruz, the Bolivian Experimental Site for Testing Piles (B.E.S.T.) was organized in conjunction with the 3rd International Conference on Deep Foundations, April 27 – 29, 2017, in Santa Cruz de la Sierra, Bolivia. The programme included static loading tests on piles with and without a toe augment, an expandable device (Expander Body, EB), to increase the pile toe area and to improve the pile toe resistance. Four types of piles were constructed in pairs to 9.5 m depth in a silty to dense sand**:**

(Piles A) 620-mm diameter pile drilled with slurry
(Piles B) 450-mm diameter continuous flight auger pile
(Piles C) 450-mm diameter full displacement pile
(Piles D) 150 mm diameter gravity-grouted micro-pile

Each pair had one pile with an EB and one without. A head-down static loading test was carried out on the piles without an EB. The four EB-piles, were tested using a bidirectional test. The purpose of the here reported tests was to compare the static response of piles with and without an EB.

SOIL PROFILE

The site investigation at the B.E.S.T. site, the soil exploration, notably the CPTU sounding results, showed the soil profile to consist of essentially two soil layers: an upper 6 m thick layer of loose silt and sand on compact silty sand. The CPTU pore pressure measurements indicated a groundwater table at or near about 0.5-m depth and a hydrostatically distributed pore pressure. Figure 1 shows a diagram compiling the SPT N-indices and the CPTU cone stress, q_t. All in-situ test results at B.E.S.T., including pressuremeter and dilatometer tests, are available at the conference web site. The link to the site is: http://www.cfpbolivia.com/web/page.aspx?refid=157.

© 2018 Deep Foundations Institute

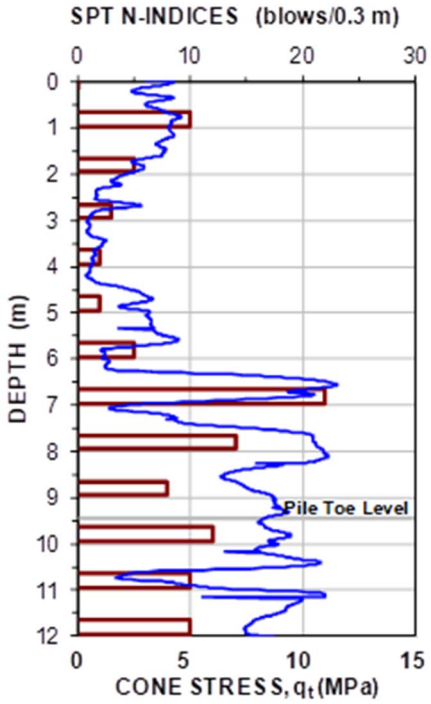


Fig. 1. SPT N-indices compiled with the CPTU q_t-stress at Pile A3.

THE EXPANDER BODY (EB)

The EB is a 1 to 2 m long folded, 120 mm wide steel tube that is expanded (inflated) by a primary-phase pressure-grouting delivered through a grouting tube placed in the reinforcing cage (Figure 2). Different models allow for expansion to 400 through 800 mm diameter width. Pressure and volume of the grout during the expansion of the EB are continuously recorded. The lateral expansion of the EB causes the length of the EB tube to shorten by about 100 mm, manifested as a lifting of the EB bottom-end or, in loose or soft soil, a pull-down of the shaft. As the EB is connected to the pile reinforcing cage, the expansion imposes tension in the pile and, potentially, a soil decompression below the expanded EB. The latter is offset by a second-phase grouting of the soil at the pile toe. The second-phase grout is delivered to the toe through a separate grout tube inside the grout tube (passing through the EB). Maximum grouting pressure below the EB is typically of the same magnitude as the EB-expansion pressure. For the here presented test piles, it was about 1.0 through 2.5 MPa. To compare, in-air tests have shown that about 100 kPa pressure is needed to expand the unconfined EB.

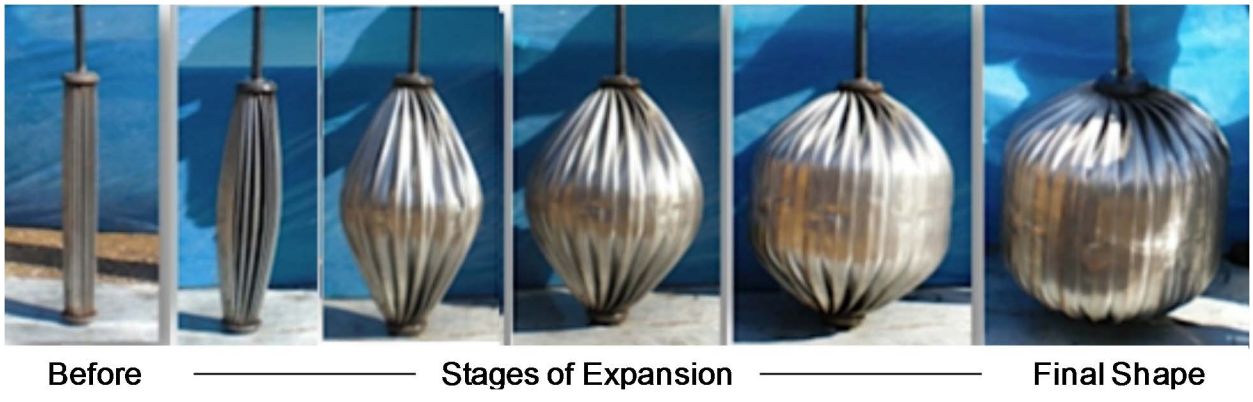


Fig. 2. In-air demonstration of EB expansion.

Figure 3 shows a sketch of the pile and EB arrangement at the B.E.S.T. site. The EB original length was 1.20 m and a bidirectional cell (hydraulic jack) jack, 300 mm high by 220 mm wide, was connected to the top of the EB and reinforcing cage.

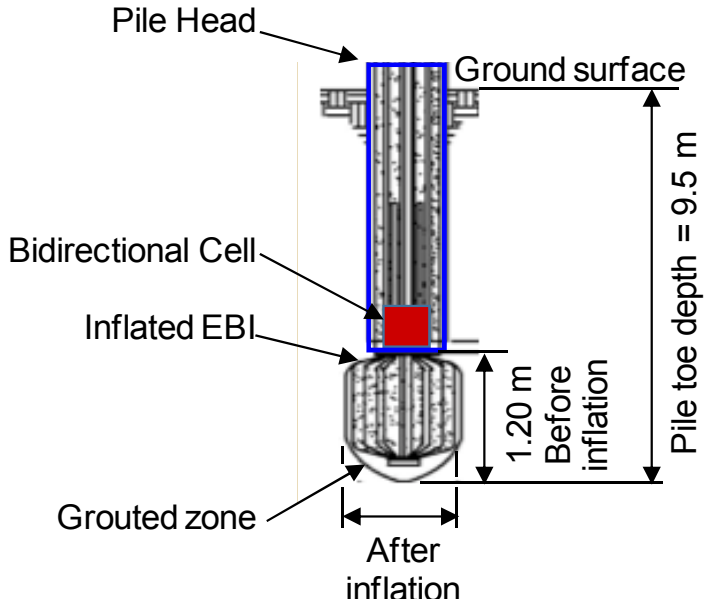


Fig. 3. Sketch showing the EB and BD arrangement (not to scale).

TEST PILES

The details of the test piles are listed in Table 1.

Table 1. Pile description.

Type		BD EB	Final EB Volume (L)	Final Pressure (MPa)	Estimated EB and TB width (mm)	Shaft Grouting Method
150-mm micro pile	D1	EB	130	1.1	400	Gravity
150-mm micro pile	D2	- - -				Gravity
450 mm CFA pile	B1	BD+EB	200	1.0	500	Pressure
450 mm CFA pile	B2	- - -				Pressure
620 mm Bored Pile	A1	BD+EB	245	2.3	600	Gravity
620 mm Bored Pile	A3	- - -				Gravity
450 mm FDP pile	C1	BD+EB	210	2.0	500	Pressure
450 mm FDP pile	C2	- - -				Pressure

BD = bidirectional jack, EB = Expander Body with post-grouting below EB (maximum pressure: 2.5 MPa).

TEST RESULTS

The static loading tests, bidirectional (BD) and head-down (HD) tests, were carried out by applying equal increments of load holding the load level constant for ten minutes. Tests on piles with BD jack and EB device started with the BD test followed by the HD test. In each static loading test—bidirectional as well as head-down—the applied load and movement along with readings of strain at three strain-gage levels (2.0, 5.0 and 7.5 m depth) were recorded.

Bored piles, Piles A and D, comparison of head-down test results

Piles A1 and A3 and D1 and D2 and were bored with slurry and gravity-grouted. Piles A1 and A3 were 620-mm diameter with a nominally 0.3019 m^2 cross section area and Piles D1 and D2 were micro piles with a nominally 0.0177 m^2 cross section area. Piles A1 and D1 were equipped with an EB at 8.3 m depth, while Piles A3 and D2 had no such augment. Strain values between the construction of the piles and start of the test were not recorded. Pile A1 was tested using a bidirectional cell placed immediately above the EB at 8.3 m depth. In Pile D2, the strains recorded during the tests were small and erratic. In contrast, the strain records in Pile A3 were consistent. Due to small strains and to the residual force in the pile (induced when the EB expanded), the strain records in Piles A1 and D1 are of limited value.

Figure 4A shows the Pile A3 (620-mm pile without an EB) pile-head load-movement curve. After assessing the load-movement curve, a "target point" (835 kN load at 30 mm movement), on the curve was chosen and the target load was matched in an effective stress analysis using proportionality coefficients (ß) for the shaft and a unit toe resistance for the toe movement (target pile-head movement minus pile compression). For the 0 to 6.0 m soil layer consisting of loose silt and sand ß = 0.40 was used. For the 6.0 to 9.5 m layer consisting of compact silty sand, ß = 0.60 was used. (N.B., the shear resistance does not occur as slippage, but as shear within a band of soil of small, but unknown, thickness). A unit pile toe stress, r_t, equal to 1.0 MPa, was used in the fit to the target point (at a 29-mm pile toe target movement). The analysis, using the UniPile software (Goudreault and Fellenius 2014), then continued by trying out different t-z and q-z functions, assuming and adjusting the function coefficients for the shaft and toe resistances until obtaining a simulated load-movement curve that fitted the measured curve. The adjustments were for the shape of the t-z and q-z curves, the resistance values that gave the fit to the at target point were not changed. (Background and mathematics of the t-z/q-z functions are presented in Fellenius 2016). The so-simulated pile-head, pile-toe, and pile-compression curves are shown along with the measured Pile A3 load-movement curve.

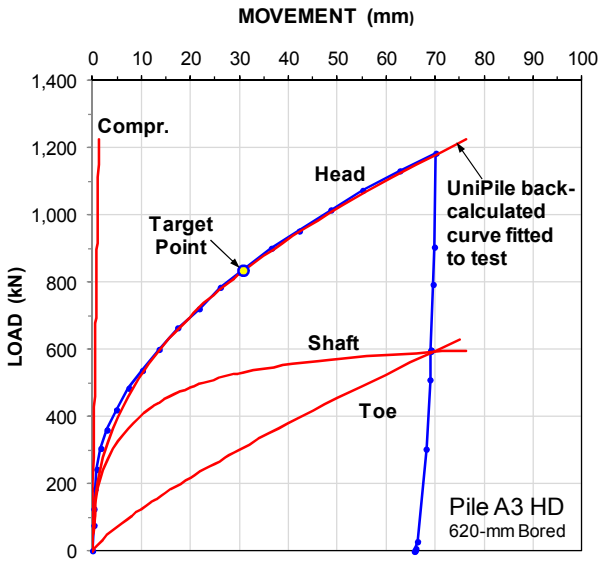


Fig. 4A Pile A3 load-movement curves.

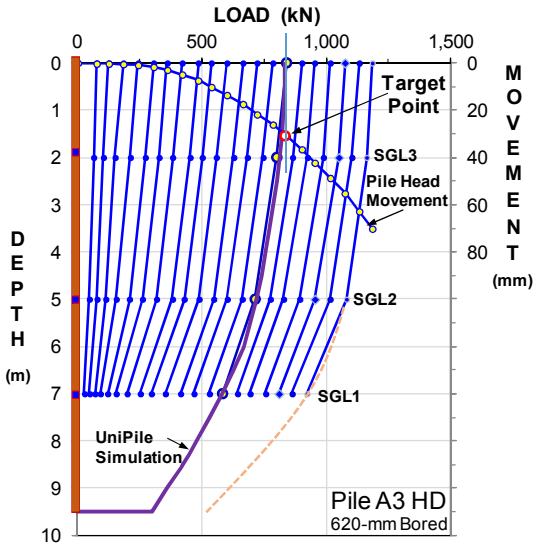


Fig. 4B Pile A3 load distribution.

Figure 5A shows the pile-head load-movement curve and the load distribution of the test on Pile D2 (150-mm micro-pile without an EB) and Figure 5B shows the simulated load distribution for the target load (144 kN at 15 mm movement) and includes also the distribution determined from the strain-gage values. The strain-gage values were too small and erratic for meaningful evaluation. The load-distribution graph is supplemented with the CPTU q_t-distribution and the load-movement curve with the target point indicated.

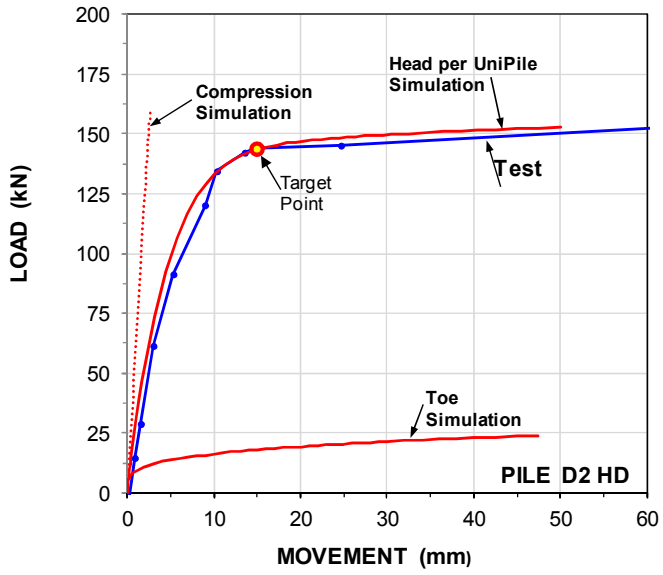


Fig. 4A. Pile D2 load-movement curves.

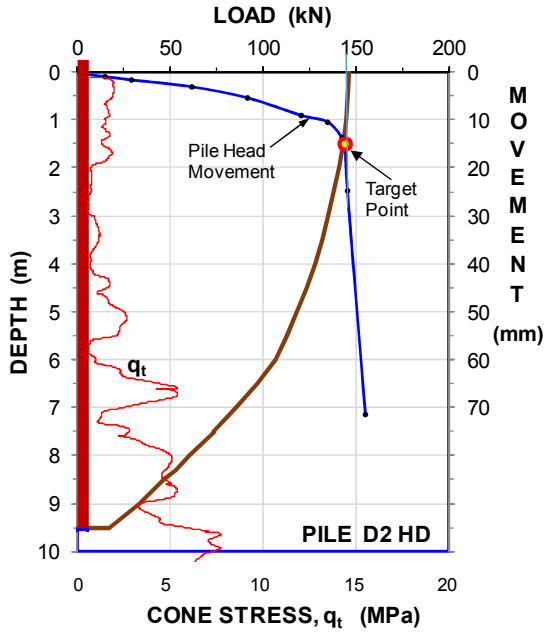


Fig. 4B. Pile D2 load distribution.

The target point for Pile D2 was chosen because it was produced with the same beta-coefficients and the same target toe stress as used for the analysis of Pile A3. However, the movement necessary for the coincidence to the target load of the beta-coefficients and the pile toe unit stress, was precisely twice for the analysis of the Pile A3 records as for the Pile D2 records. Pile A3 has a four times larger diameter and a 16 times larger toe area. The movement difference is indicated in comparing Figures 4A and 5A and in Figures 6 and 7 for the Pile A3 and D2 shaft resistance t-z functions and Figure 8 for the toe resistance q-z functions, respectively, used to obtain the load-movement fit for Piles D2 and A3. The "δ" indicates the movement for the target point and the "100 %" indicates the target resistance for the soil-pile elements. The t-z and q-z functions are quite different and the fact that the ß-coefficients and unit toe resistance values are the same is essentially a coincidence. Comparing the t-z and q-z curves shows that Piles A3 and D2 actually responded very differently to the applied load.

Figure 9A shows the simulated bidirectional-test load-movement curve of Pile A1 (identical to Pile A3, but for the EB at the pile toe). Figure 9B shows the Pile A1 simulated load distribution for the target load and includes also the calculated equivalent head-down load distribution. (the same Beta-coefficients were used above the BD, which gave 682 kN load at 5 mm upward and 1.7 mm downward movements). The strain-gage at 2.0 m depth did not function and the strain recorded by the gages at 5.0 m and 7.5 m depth were too small (<40 με) to allow conversion to load. However, the bidirectional test provides the benefit that the load applied and measured by the bidirectional device (hydraulic jack) is the true load. That is, it includes any potential residual force, unlike strain-gage instrumentation, which always requires consideration of adjustment to potential residual force in the pile. Thus, the "Target Point bidirectional load" is a true load.

Similarly, Figure 10A shows the simulated test curves head-down load-movement curve of Pile D1 (identical to Pile D2, but for the EB at the toe of Pile D1). Figure 10B shows the Pile D1 load-distributions. Again, the same beta-coefficients were used, which gave a 550 kN target point at 7 mm movement. The test records, notably, the strain-gage records, indicated that residual force had developed in the pile before the static loading test, but they were not consistent enough to warrant analysis. The dashed set of pile-head and toe load-movement curves in the figure are a speculative set of load-movement curves for the test had it been unaffected by residual force. (The procedure and decisions for establishing the distribution unaffected by residual force is beyond the scope of this paper).

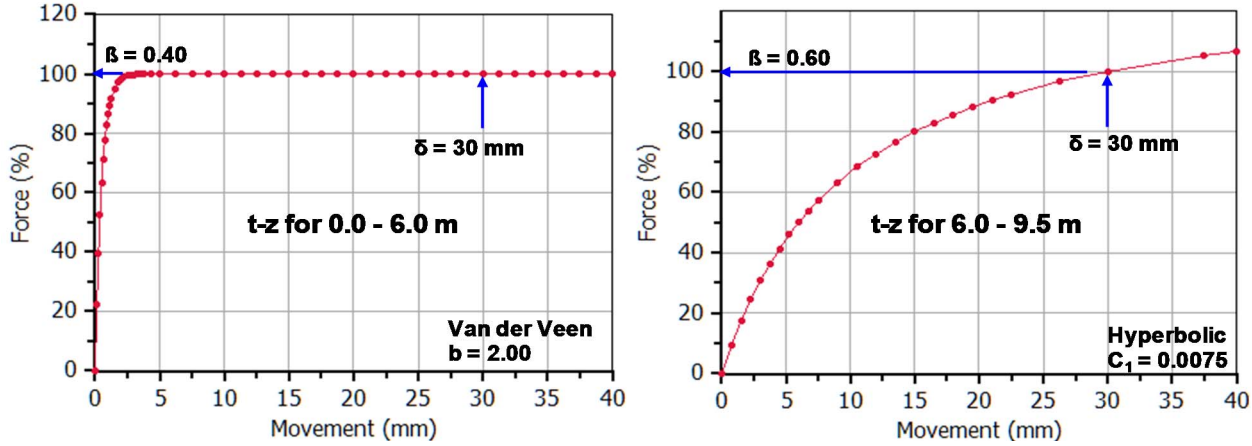


Fig. 6. Pile A3 t-z functions for the fit to the pile head load-movement curve.

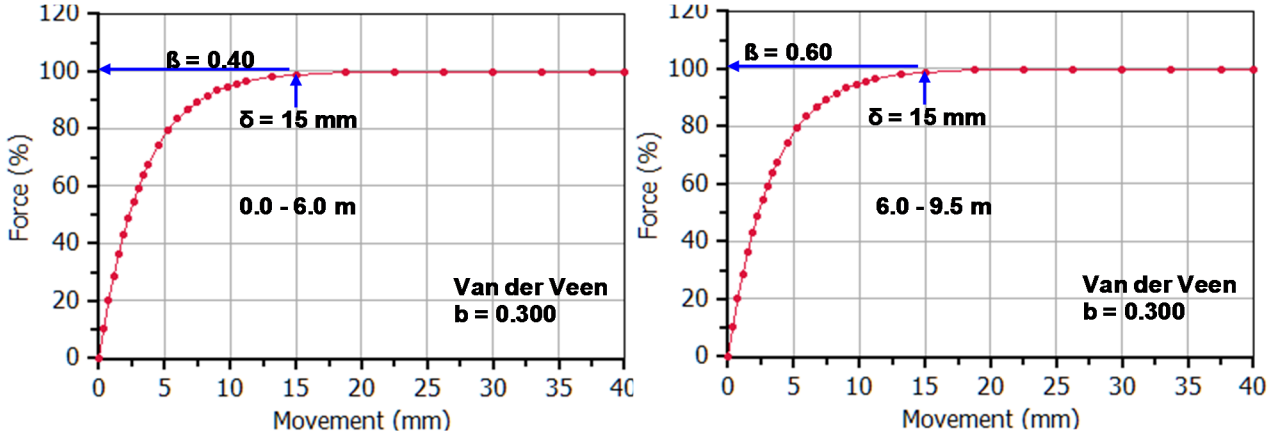


Fig. 7. Pile D2 t-z functions for the fit to the pile head load-movement curve.

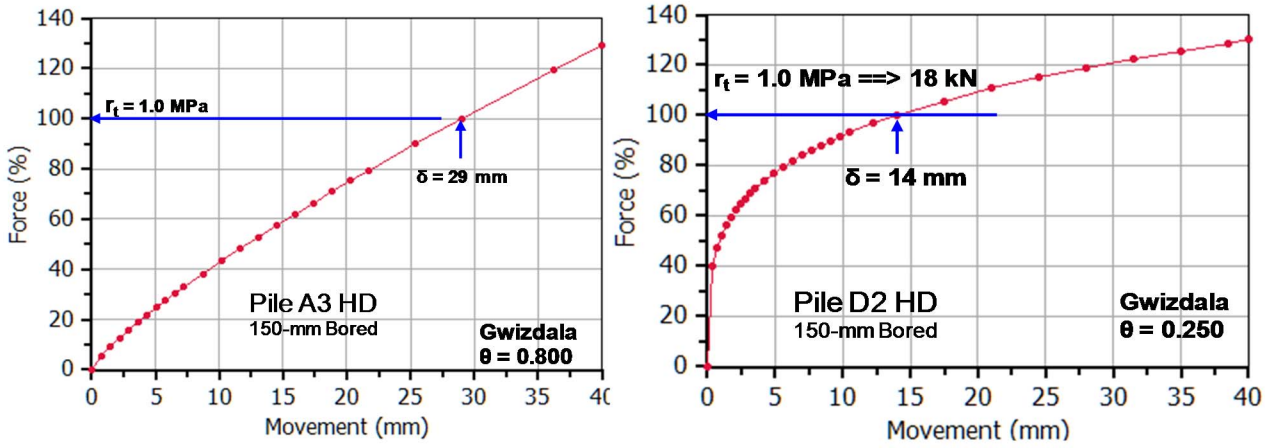


Fig. 8. Pile A3 and Pile D2 q-z functions for the fit to the pile head load-movement curve.

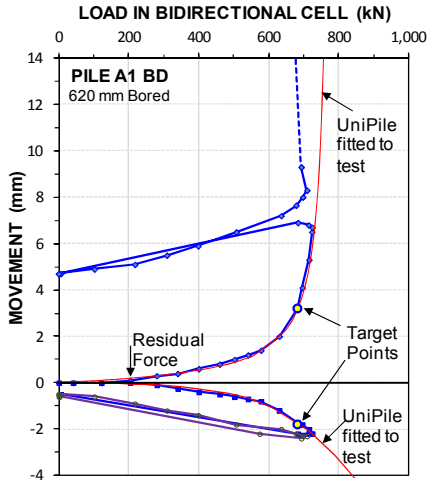


Fig. 9A. Pile A1 load-movement curves.

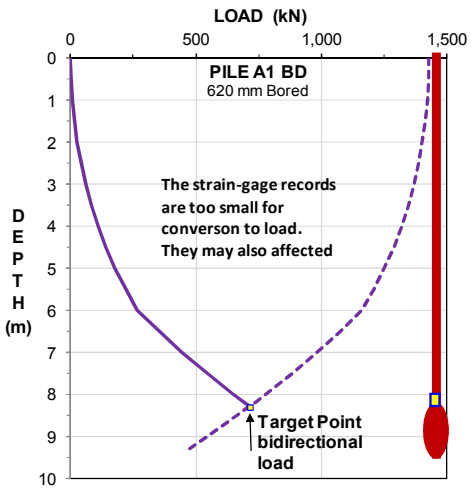


Fig. 9B. Pile A1 load distribution.

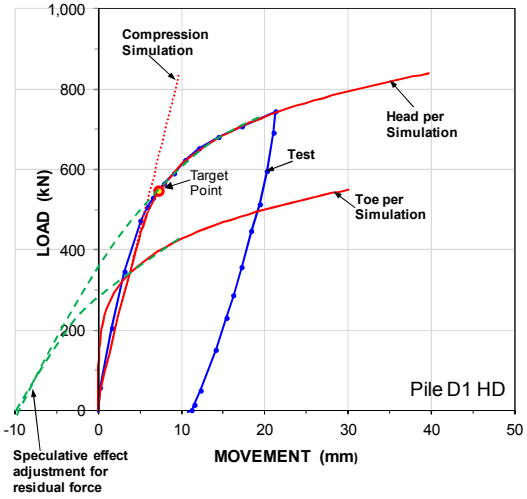


Fig. 10A. Pile D1 load-movement curves.

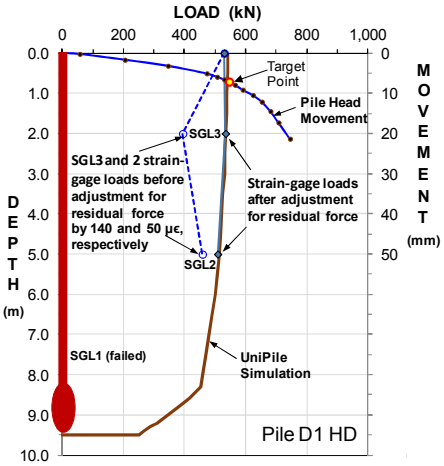


Fig. 10B. Pile D1 load distribution.

Micro piles, Piles D, with and without EB

For the micro piles, Piles D1 and D2, the beta-coefficients above the EB level (8.3 m) were the same as used for Pile D2 (and Piles A3 and A1). Below this depth, i.e., along the EB, the Pile D1 simulation fit showed ß = 1.50, i.e., more than twice that for Pile D2 along the same depth. The fitted unit toe resistance for Pile D1 was 2.0 MPa at 1 mm movement (corresponding to 3.8 MPa at 14 mm) as opposed to 1.0 MPa for Pile D2 at 14 mm movement. The t-z and q-z function produced in the fitting show that the EB had not just provided a larger resistance, it had also stiffened up the response of the pile.

The load-movement curves and load distributions for the two micro-piles bored with slurry, gravity-grouted (Piles-D) are compared in Figures 12A and 12B. The pile-head load-movement curves show that equipping the micro pile with the EB increased the total pile resistance about four times. No change in shaft resistance occurred above 8.3 m depth, while the resistance below 8.3 m depth, the EB zone, increased from 50 kN to 450 kN. Below 8.3 m depth, the unit shaft resistance along the EB and the unit toe resistance was more than about twice that of the pile with no EB. If the acceptable limit would be 5 to 10 mm movement (settlement) for an applied load, the EB-equipped micro pile would support an about three times higher load than the pile without an EB.

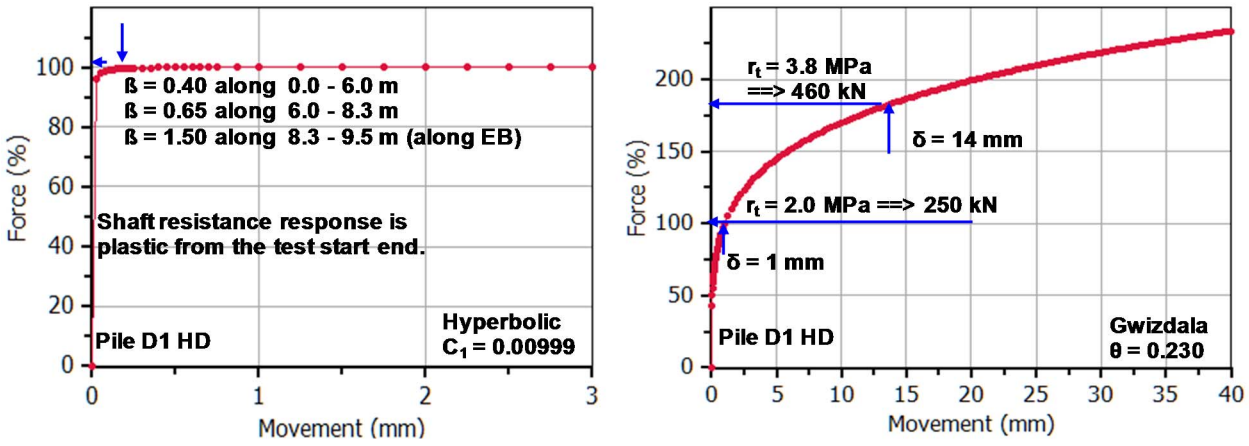


Fig. 11. Pile D1 t-z and q-z functions for the fit of the EB response.

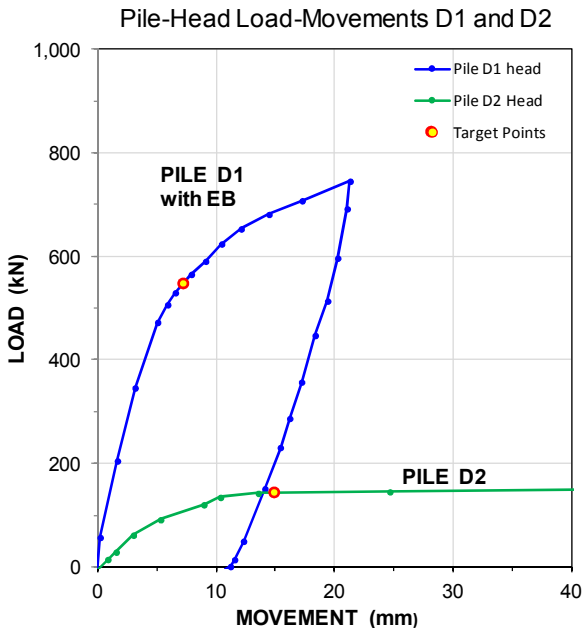


Fig. 12A. Piles D1 and D2 load-movement curves.

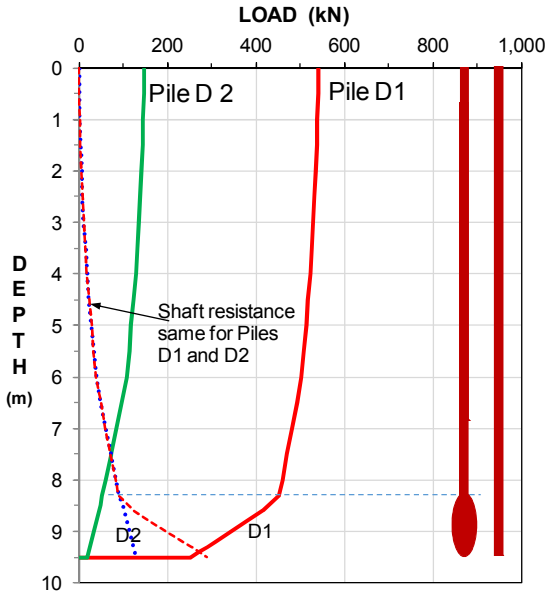


Fig. 12B. Piles D1 and D2 load distribution.

Bored piles, Piles A, with and without EB

For the 600-mm diameter bored piles, Piles A1 and A3, Figure 13A shows the Pile A1 actual downward test and the simulated downward test for Pile A3 calculated using UniPile from the conditions for the simulation by the head-down test. Similarly, Figure 13B show the Equivalent head-down test calculated from the simulation of the bidirectional test and the actual head-down test on Pile A3. Again, the comparison shows that the response of the EB-equipped pile was considerably stiffer than that of the unaugmented pile. As for Piles D, if the acceptable limit would be 5 to 10 mm movement (settlement) for an applied load, the EB-equipped Pile A1 pile would support an about three times higher load than Pile A3, the pile without an EB. To have about equal response, Pile A3 would have to be lengthened by about 6 m.

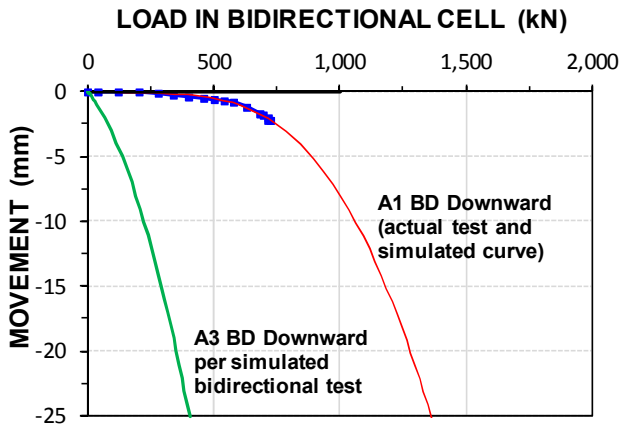


Fig. 13A. Piles A1 and A3 downward curves for a BD at 8.3 m depth.

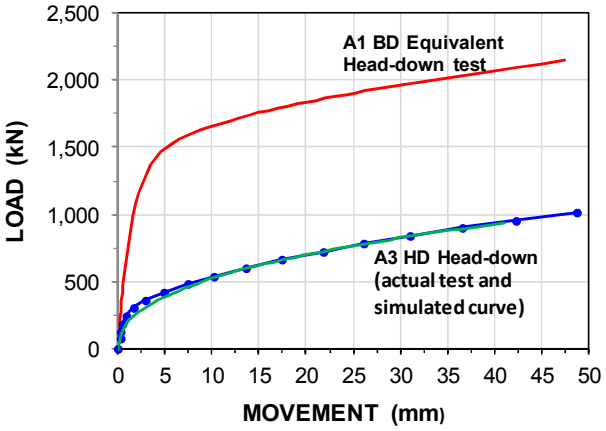


Fig. 13B. Piles A1 and A3 pile-head load-movements.

CFA piles, Piles B1 and B2, with and without EB

The 450-mm diameter CFA piles, Piles B1 and B2 were, 9.5 m long, pressure-grouted CFA piles with a nominally 0.159 m^2 cross section area. Pile B1 was equipped with an EB at 8.3 m depth, while Pile B2 was without an EB. Pile B1 was tested using a bidirectional cell placed immediately above the EB. Unfortunately, the telltale measuring the downward movement of the EB (the EB was the base of the bidirectional test) of Pile B1 test failed. That is, the test records only included the upward movements and the BD loads.

Piles B test records were analyzed similarly to the procedure used for the bored piles, Piles D and A, and showed that the unit shaft resistance along the CFA-constructed piles was stiffer than for the bored piles. In order to save space, the factual load-movement, load-distribution, and simulation results are not presented here. The can be examined at: http://www.cfpbolivia.com/web/page.aspx?refid=157. Figure14A compares the bidirectional downward curve of Pile B1 (movement measurement failed) to the similar curve simulated from the results of the head-down test on Pile B2calculated using UniPile. Similarly, Figure 14B shows the actual and simulated load-movement curves of the head-down test on Pile B2 and the equivalent head-down curve calculated from the simulation of the bidirectional test. Again, the comparison shows that the response of the EB-equipped pile, Pile B1, was considerably stiffer than that of the unaugmented pile, Pile B2. If the acceptable limit would be 5 to 10 mm movement (settlement) for an applied load, the EB-equipped pile would support about a twice higher load than the pile without an EB. To have about equal response, Pile B2 would have to be lengthened by about 3 m.

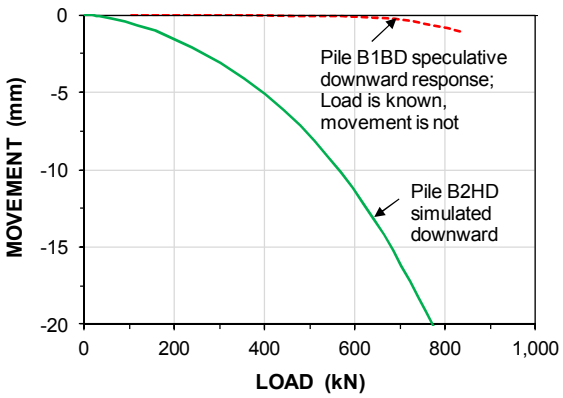


Fig. 14A. Piles B1 and B2 downward curves for a BD at 8.3 m depth.

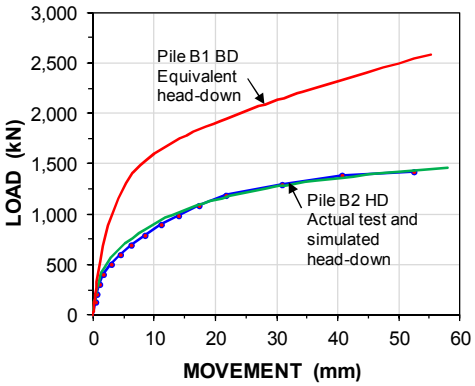


Fig. 14B. Piles B1 and B2 pile-head load-movements.

FDP piles, Piles C1 and C2, with and without EB

Piles C1 and C2 were 450-mm diameter, 9.5 m long, pressure-grouted, full-displacement (FDP) piles with a nominally 0.1590 m^2 cross section area. Pile C1 was equipped with an EB at 8.3 m depth, while Pile C2 was without an EB. Pile C1 was tested using a bidirectional cell placed immediately above the EB. Unfortunately, the records of the BD tests were lost. A head-down reloading test was carried out after first closing the 12-mm opening in the BD jack produced in the BD test. Again, in order to save space, the factual load-movement, load-distribution, and simulation results are not presented here. The results are available at: http://www.cfpbolivia.com/web/page.aspx?refid=157.

The analysis of Piles C test records showed that the unit shaft resistance was stiffer than for the bored piles. Figure 15 shows the load-movement curve of the head-down test on Pile C2 and the equivalent head-down curve calculated from the simulation of the bidirectional test. As was the case for Piles B, the comparison shows that the response of the EB-equipped Pile C1 was considerably stiffer than that of the unaugmented pile, Pile C2. If the acceptable limit would be 5 to 10 movement (settlement) for an applied load, the EB-equipped CFA-pile would support about an about 30 % higher load than the unaugmented pile. To have about equal response, Pile C2 would have to be lengthened by about 3 m. It is interesting to note that the response of the FDP pile was considerably stiffer than that of the CFA pile with or without the EB.

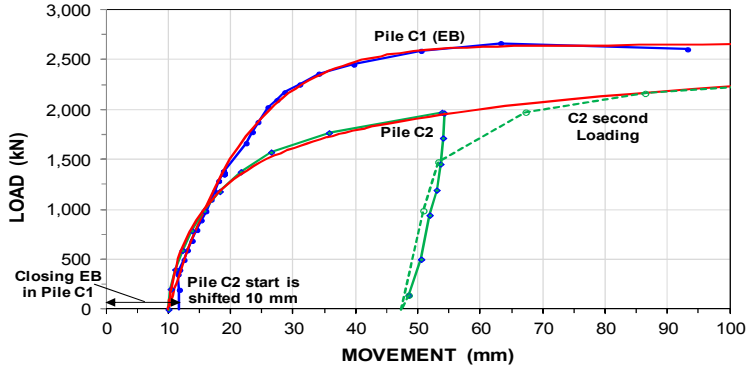


Fig. 15. Piles C1 and C2 pile-head load-movement curves.

CONCLUSIONS

For all four piles types, equipping the pile toe with the EB with post-installation grouting considerably increased the pile stiffness response to applied load. The improvement was largest for the micro-pile and the bored pile and smaller, but still significant, for the CFA and the FDP piles, as their construction methods improve the pile shaft resistance making the relative improvement of the toe less pronounced. Expansion of the EB is in a sense a loading test of the pile toe, assuring stiff pile response, enhanced capacity, and substantiation of the pile response, which also results in fewer piles and shorter construction time. The expansion of the EB resulted in imposing axial residual force in the piles further enhancing the pile stiffness. At site conditions similar to those at the subject site, the EB augment results in significant cost savings and enhanced quality control.

References

Fellenius, B.H., 2016. An Excel template cribsheet for use with UniPile and UniSettle. www.Fellenius.net.

Goudreault, P.A. and Fellenius, B.H., 2014. UniPile Version 5, User and Examples Manual. UniSoft Geotechnical Solutions Ltd. [www.UniSoftGS.com]. 120 p.

Terceros, M.H. and Massarsch, K.M, 2014. The use of the expander body with cast in-situ piles in sandy soils. Proceedings of the DFI-EFFC International Conference on Piling and Deep Foundations, Stockholm, May 21-23, pp. 347-358.

CONTROLLING GROUND MOVEMENTS DUE TO PILE INSTALLATION ADJACENT TO LONDON UNDERGROUND TUNNELS FOR THE SOUTHBANK PLACE PROJECT

Stuart Hardy, Arup, 13 Fitzroy Street, London, stuart.hardy@arup.com, Thomas Beales Ferguson, Arup, Duncan Nicholson, Arup, Jonathan Ly, Canary Wharf Contractors, One Canada Square, Canary Wharf, London, E14 5AB, Laurent Olivier, Canary Wharf Contractors

ABSTRACT

The Southbank Place project comprises the redevelopment of the Shell headquarters in the Waterloo area of London with eight new buildings and refurbishment of the existing central tower. The site is bisected by London Underground's Bakerloo Line tunnels that pass just below the existing basement. The Northern Line tunnels also pass beneath the north east corner of the site. The foundations for the tallest building comprise rotary bored piles up to 2100mm in diameter founded in the Thanet Sand layer, approximately 65m below ground level. A number of the piles were installed at a minimum offset of 1m from the extrados of the London Underground tunnels; the closest that piles have ever been installed next to live running tunnels in London. The paper describes the installation technique developed to minimise the impact of the pile installation on the tunnels, the state of the art numerical analyses used to predict the movements due to pile installation, the full scale instrumented field trial undertaken as part of the assurance procedure with London Underground's infrastructure protection team and the observed tunnel movements following the installation of all the contract piles. The observed movements demonstrate the importance in the choice of soil model when analysing pile installation effects which include complicated stress paths, stress rotations and stress reversals. The work also demonstrated that with modern analytical tools and careful controls in place, piles can safely be installed at a 1m offset from live running tunnels in London Clay.

INTRODUCTION

The Southbank Place project comprises the redevelopment of the Shell Centre office complex in the Waterloo area of London. The redevelopment includes the construction of eight new mixed use buildings within the footprint of the existing site and the refurbishment of the Shell Centre tower. The site is constrained by the Bakerloo Line running tunnels that bisect the site below the existing basement and the Northern Line tunnels that cross the corner of the site as shown in Fig. 1.

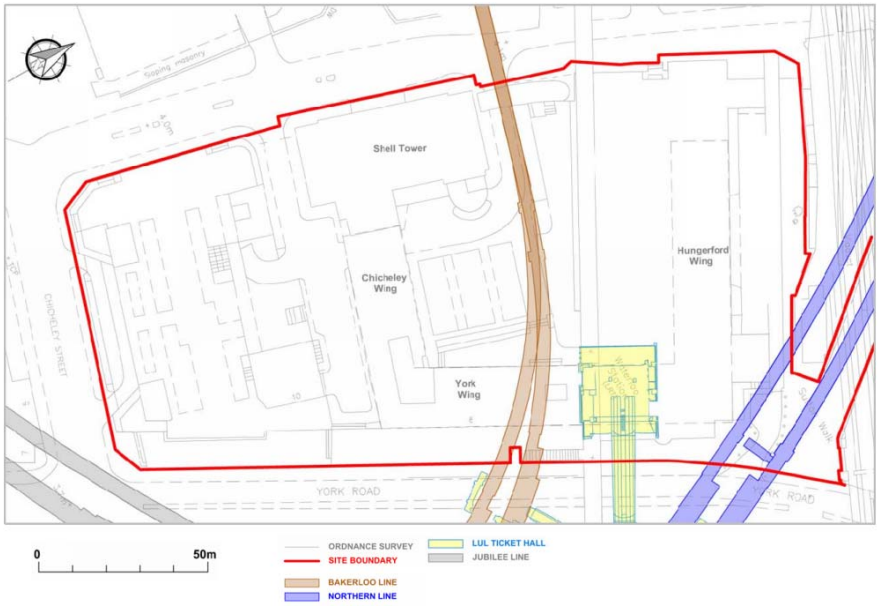


Fig. 1. Southbank Place site boundary and location of Bakerloo and Northern Line tunnels

© 2018 Deep Foundations Institute

The original design and construction of the Shell Centre in the late 1950's, and its effect on the underlying Bakerloo Line tunnels, was well documented by Williams (1957), Skempton and Henkel (1957), Ward (1961), Measor and Williams (1962), Measor and Williams (1963), Burford (1988), and Burford (1996). The net unloading of the Bakerloo Line tunnels in the central court yard area of the site due to the basement excavation has caused over 80mm of heave within the tunnels (Burford 1996) and has become a seminal reference case history for the long term behaviour of London Clay.

The proposed building masterplan for the Southbank Place project is shown in Fig. 2. Building 4a in the north east corner of the site is a 36 storey residential tower that is located directly over the northbound Northern Line tunnels.

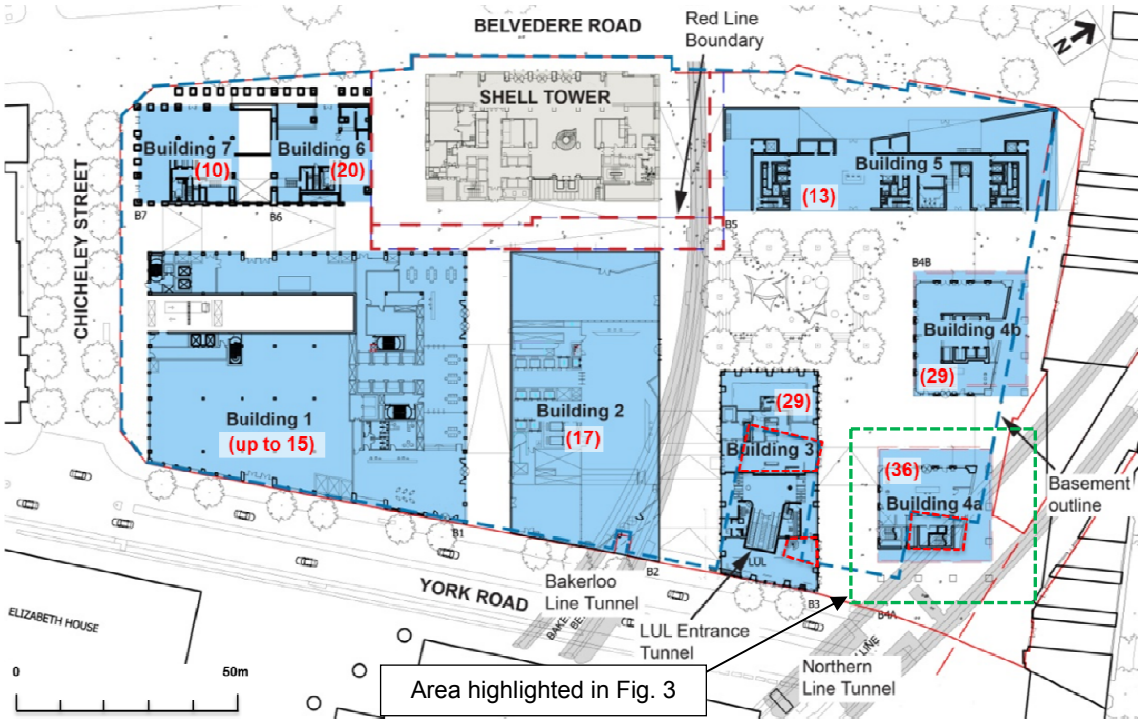


Fig. 2. Southbank Place building master plan (brackets indicate number of floors)

The construction of Building 4a required an extension to the existing Shell Centre basement to accommodate the structural core and the installation of high capacity rotary bored piles as close as 1m to the Northern Line tunnels.

The requirement to pile at a minimum lateral offset of 1m from the Northern Line running tunnels does not comply with the LUL engineering standard 1-050 which requires an exclusion zone of 3m laterally and 6m vertically. To allow the installation of the Building 4a bearing piles, a concession against this standard was required from LUL.

The outline of the original Shell Centre basement, the basement extension and the pile locations relative to the Northern Line tunnels is shown in Fig. 3.

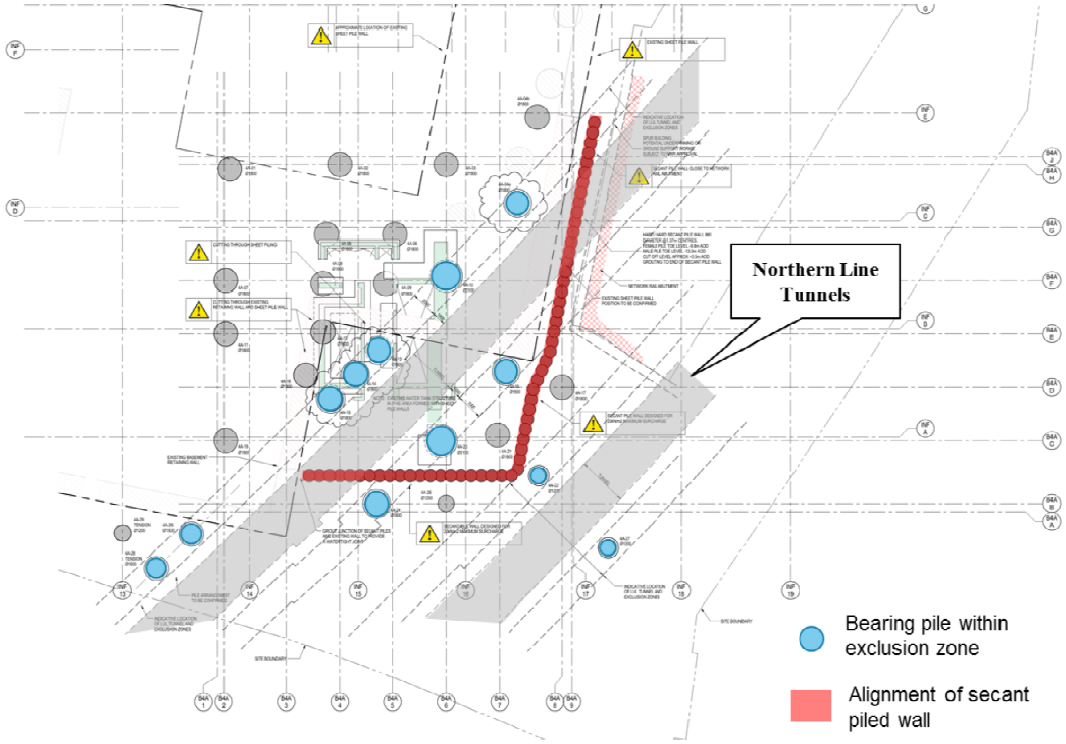


Fig. 3. Building 4a basement and bearing pile locations

This paper describes the pile installation method that was agreed with LUL for these piles, the full scale field trial that was undertaken to demonstrate the validity of the method, the numerical predictions that were undertaken for the installation effects on the tunnels and the vertical tunnel movements observed during the installation of the contract piles.

PILE INSTALLATION METHOD

The location of Building 4a directly over the Northern Line tunnels constrained the locations where deep foundations could be installed. Therefore high capacity rotary bored piles that extend to the Thanet Sand layer (approximately 65m below original ground level) were required. Pile diameters of between 1200mm and 2100mm were adopted with a fixed penetration of 2m into the Thanet Sand layer. The piles were not base grouted as is common practice for high capacity piles in London as the shaft capacity in the London Clay and Lambeth Group under bentonite support fluid was proven through a series of preliminary test piles.

The principle risks associated with installing the rotary bore piles within 1m of the Northern Line tunnels were identified as being; (1) collapse of the unsupported pile bore during “dry” excavation in the London Clay, (2) migration of bentonite support fluid towards the tunnel during “wet” excavation in the Lambeth Group and/or Thanet Sand, (3) excessive tunnel movement during the pile boring process due to stress relaxation and (4) excessive tunnel movements during construction of the superstructure due to load being shed into the ground. To mitigate the first three risks, the pile construction methodology described in Fig. 4 was developed.

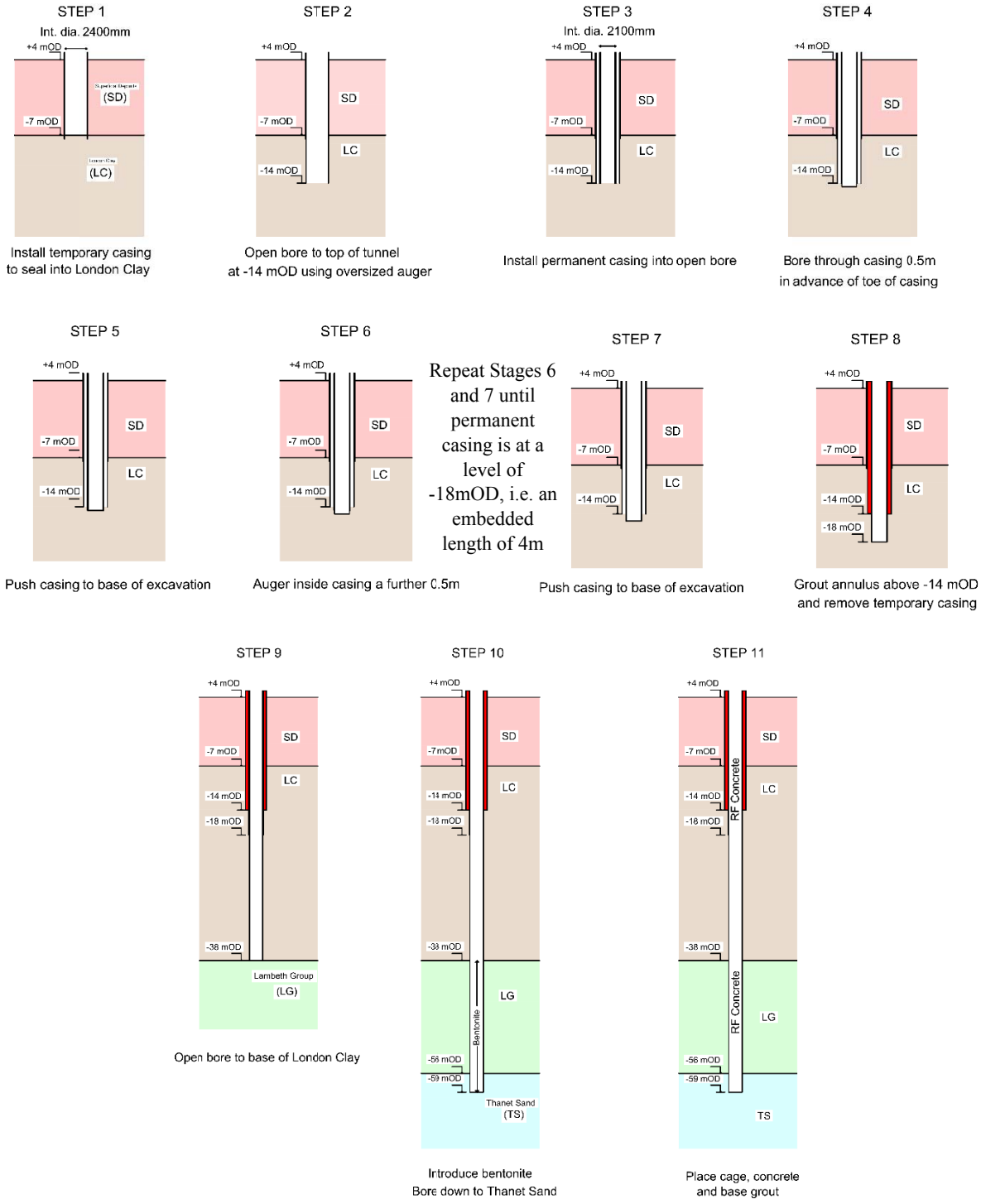


Fig. 4. Pile installation methodology

The inclusion of a permanent steel liner over the depth of the tunnel was effective in preventing any pile bore instability or the migration of any bentonite support fluid into the tunnel, and also limited the amount of stress relaxation that could occur during the pile boring process. It was chosen to not use a slip coated double casing to limit the load shed in to the ground over the depth of the tunnel as is sometimes adopted in London. The tunnel movement due to pile loading was assessed by numerical analysis and found to be acceptable. The effectiveness of a slip coating in preventing the stress being shed into the ground was also questioned and the additional risk to the tunnel posed by installing a

second casing was deemed worse than allowing the load to be shed into the ground and allowing the associated tunnels movements to occur.

NUMERICAL PREDICTIONS

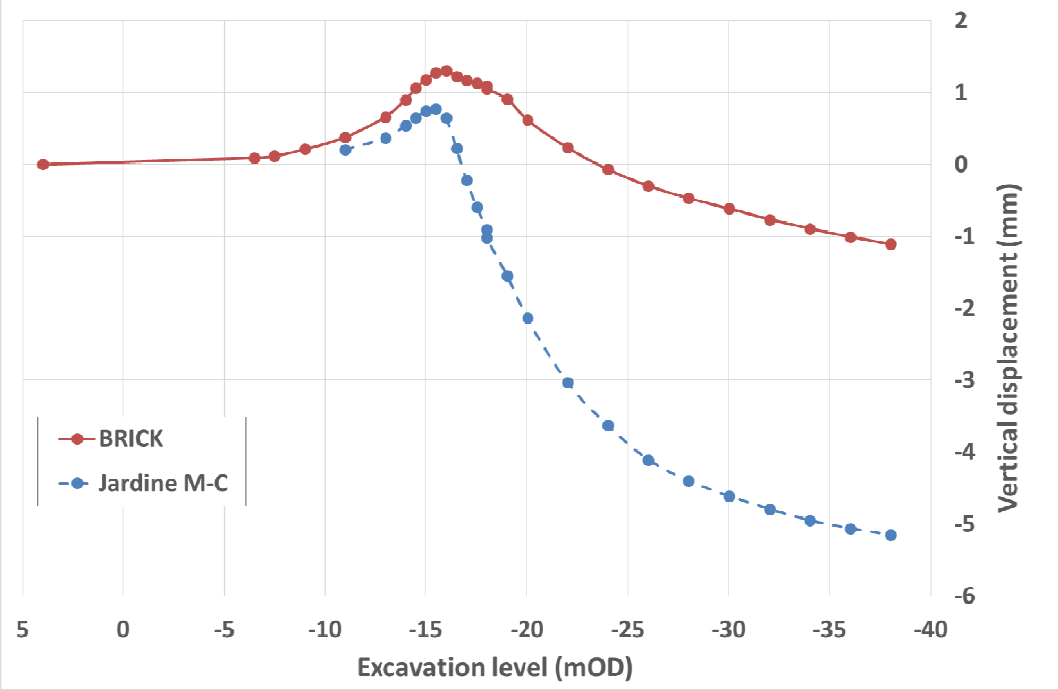
To assess the ground movements due to the installation of a single pile, a three dimensional finite element analysis was undertaken using the geotechnical software LS-DYNA. The non-linear behaviour of London Clay was modelled by the use of two constitutive models; BRICK (Simpson 1992) and an elastic-perfectly plastic Mohr-Coulomb failure criteria with the addition of a non-linear elastic stiffness model described by Jardine *et.al* (1986), referred to hereafter as the Jardine model. The soil parameters for both constitutive models was calibrated by back analysing the long term heave behaviour of the Bakerloo Line tunnels since the excavation of the existing Shell Centre basement in the late 1950's as reported by Burford (1996). .

A good correlation was found between the observed Bakerloo Line tunnel movements and the back analysed tunnel movements from the BRICK and Jardine models, giving confidence in the predicted movements due to the site redevelopment. A comparison of the normalised stiffness curves used in the analyses is included in Fig. A1 in the Appendix. The predicted movements due to the installation of a single pile was then used to assess the cumulative effect of the installation of all the piles shown in Fig. 3 using elastic superposition.

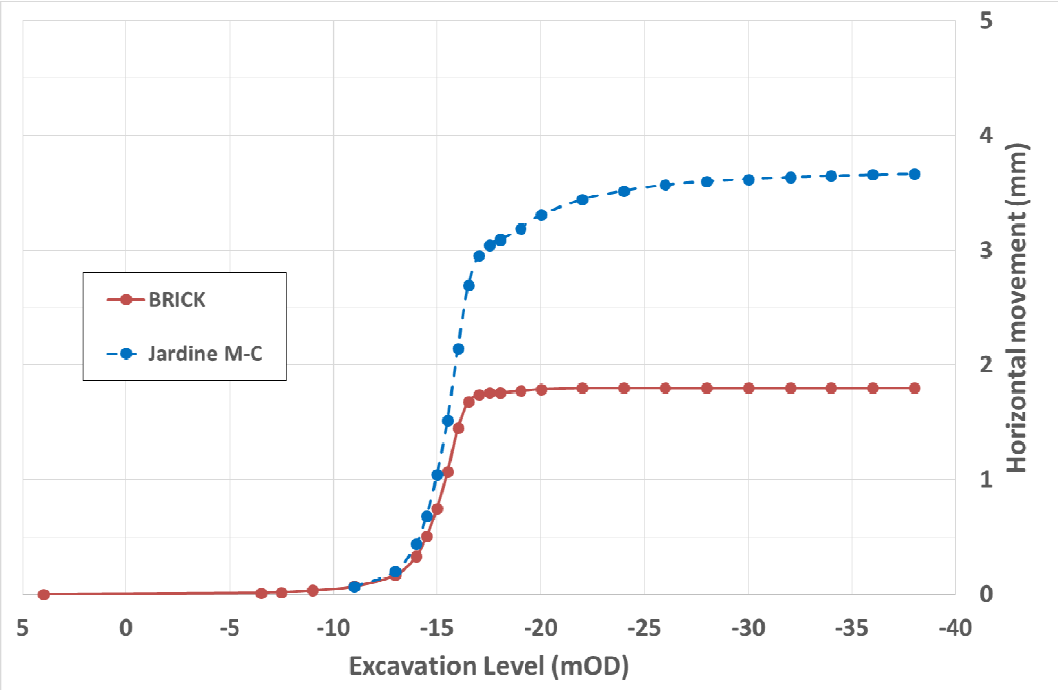
The horizontal and vertical movements predicted by the two finite element analyse at a distance of 1m from the edge of the pile bore are shown in Fig. 5. The vertical and horizontal movements are plotted against the pile bore depth to illustrate how the movements develop as the pile bore extends past the theoretical position of the Northern Line tunnel.

There is a significant difference in the predicted tunnel movement from the two analyses which had previously given similar predicted movements when back analysing the historical movement of the Bakerloo Line tunnels (the Jardine model predicting 500% more vertical movement and 100% more horizontal movement).

Due to the large discrepancy in the results of the two analyses, it was agreed with LUL that an instrumented trial pile bore would be undertaken at a location distant from the tunnels to (a) determine which of the two models predicted more accurately the ground behaviour and (b) demonstrate the feasibility of the proposed pile installation method.



(a)



(b)

Fig. 5. Predicted vertical (a) and horizontal (b) movements due to installation of a single 1800mm diameter pile

TRIAL PILE INSTALLATION

The full scale trial pile installation was undertaken in the area of Building 6 shown in Fig. 2. The instrumentation comprised rod extensometers at three levels (simulating tunnel crown, axis and invert) to measure vertical movement and Shape Accel Arrays to measure horizontal movement, both

located at a distance of 1m from the edge of the pile to replicate the movement of the tunnel. The layout of the instrumentation and the geometry of the trial pile bore is shown in Fig. 6.

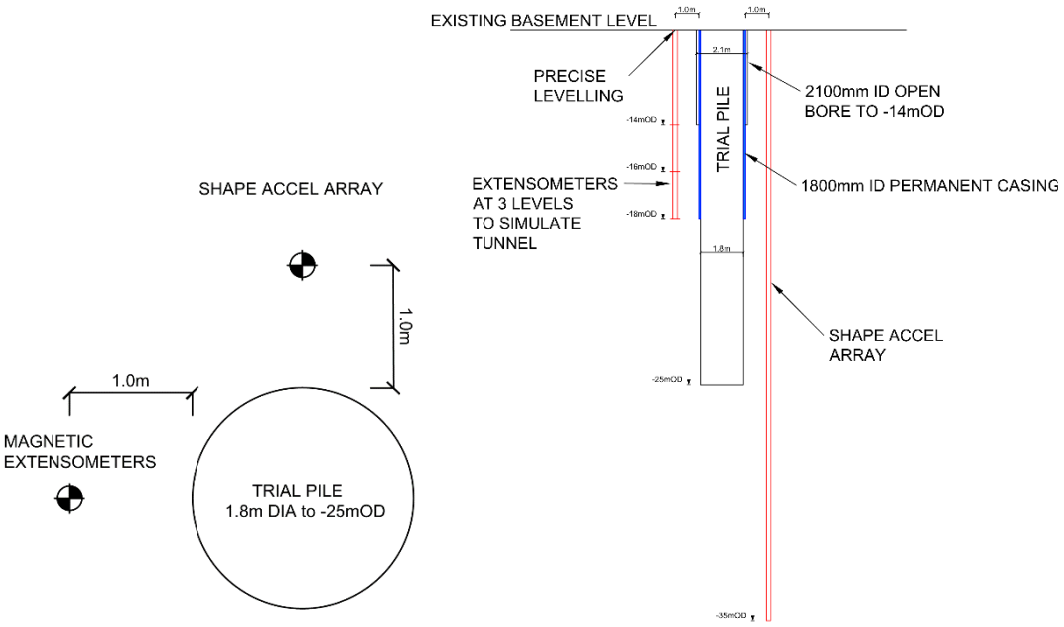
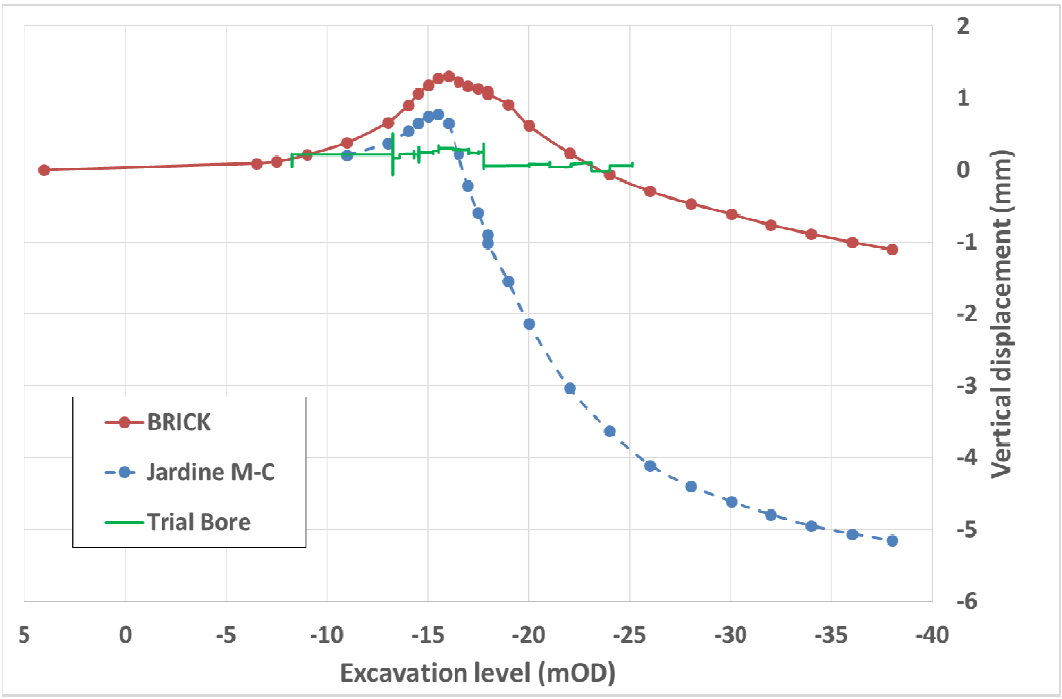
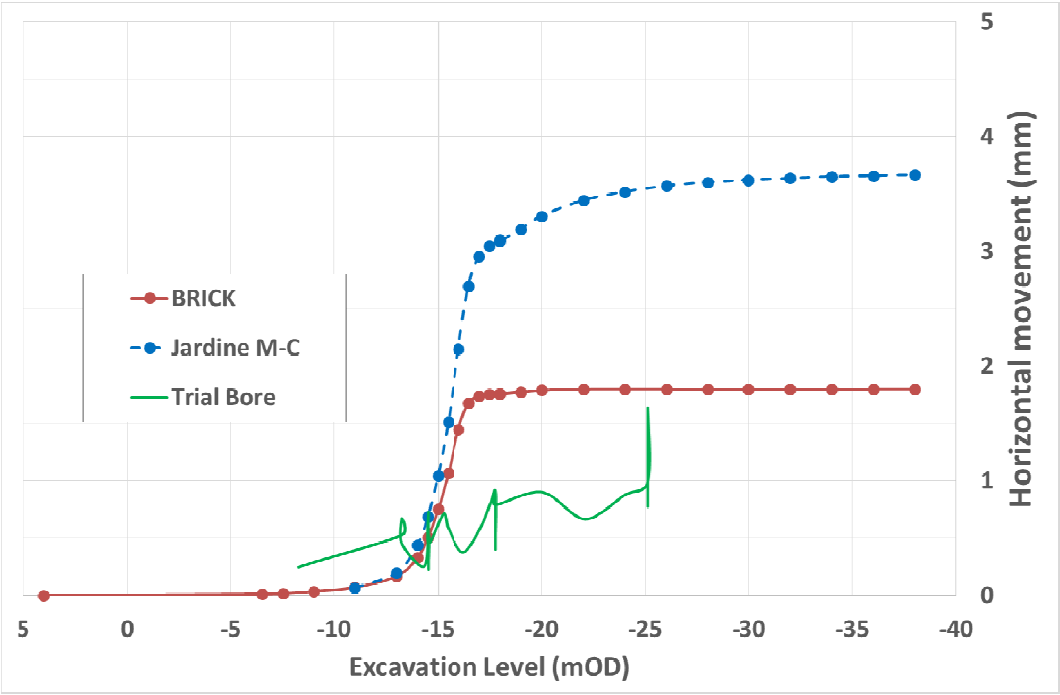


Fig. 6. Trial pile bore and instrumentation layout

The pile installation methodology described in Fig. 4 was followed and the ground movement observed by the extensometers and the Shape Accel Array. The horizontal and vertical movements recorded during the trial are compared to the two finite element analyses in Fig. 7.



(a)



(b)

Fig. 7. Ground movements observed during full scale field trial

The vertical movements were extremely small, less than 1mm, and therefore within the accuracy of the extensometer system. The horizontal movements were also small but appear to give a reasonable behaviour that compared well with the predictions from the DYNA analysis that used the BRICK constitutive model.

The pile installation methodology was proved to be feasible and effective at controlling ground movements during the pile boring process. The movements were also shown to be very small and closer in magnitude to the DYNA predictions. On the basis of the results of the trial bore, the concession against the engineering standard was granted by LUL for piling at an offset of 1m from the Northern Line tunnels.

TUNNEL MONITORING

Real time monitoring of the Northern Line tunnels was agreed as part of the assurance procedure with LUL. The narrow clearance within the running tunnels meant that an automated total station solution could not be implemented. An automatic monitoring system that used the bi-directional tiltmeters provided by Senseive and installed by Getec (giving movements at 15 minute intervals) was installed in combination with a manual monitoring system (that was surveyed on a monthly basis during the piling works). The monitoring arrangement around the tunnel rings is shown in Fig. 8. The monitoring system was repeated at 10m intervals and closed up to 5m spacings beneath the basement of Building 4a.

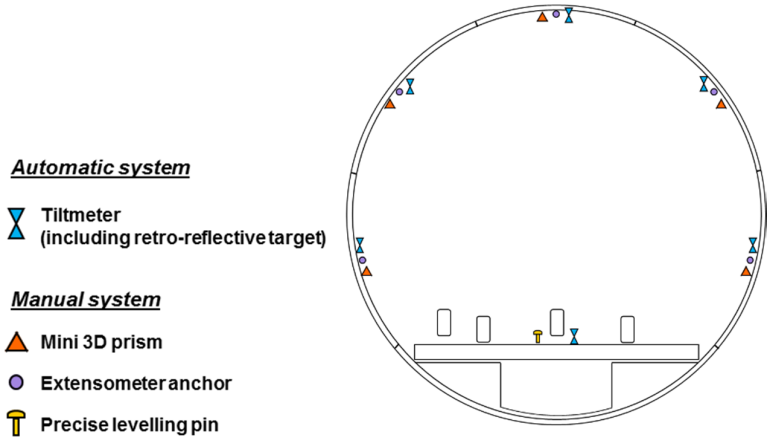


Fig. 8. Monitoring arrangement within Northern Line tunnels

The ovalisation of the tunnel ring can be calculated from the tiltmeters at each cross section and the longitudinal tunnel movement can be calculated by using the crown tiltmeters and summing the measured tilts along the tunnel length and assuming the movements are zero at each end of the tunnel (this is analogous to treating the tunnel as a horizontal inclinometer). The validity of this approach was confirmed by comparing the vertical tunnels movements derived from the tiltmeters with the manual survey.

MOVEMENTS DURING CONSTRUCTION

A total of 12 contract piles were installed around the northbound Northern Line tunnels as shown in Fig. 3 using the methodology described in Fig. 4. The incremental vertical movement of the tunnel due to the installation of each pile has been extracted from the tiltmeter data and plotted against distance from the tunnel in Fig. 9. The figure also includes the predicted vertical movement due to the installation of a single piles from the DYNA model with the BRICK constitutive model.

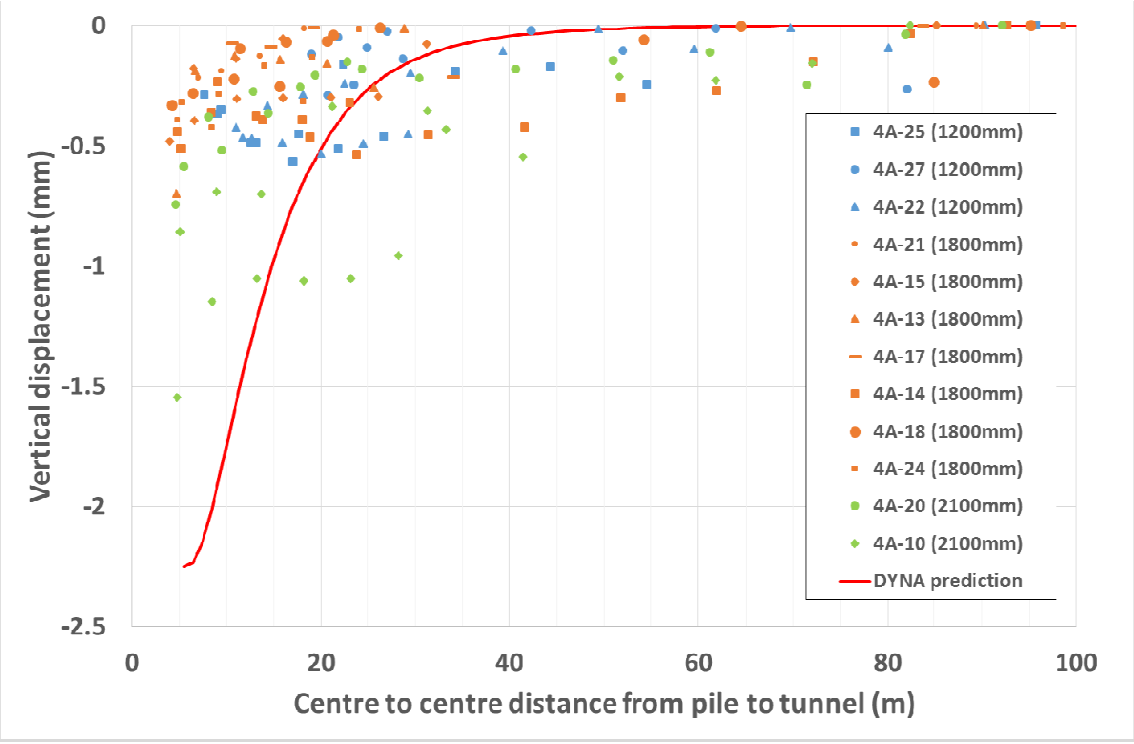


Fig. 9. Incremental tunnel movements due to the installation of each pile for Building 4a

It can be clearly seen that the installation of the 2100mm pile caused slightly more vertical movement that the 1800mm, as would be expected and that the maximum vertical movement is around 1mm to 1.5mm. The movements are very small and close to the resolution of the system, however the trends demonstrate that the data generally correlates well with the instrumented field trial and the numerical prediction from the DYNA model.

DISCUSSION ON THE RELATIVE PERFORMANCE OF THE SOIL CONSTITUTIVE MODELS

A large discrepancy was found between the two equivalent finite element analyses for predicting ground movements due to pile installation. The only difference between the analyses was the soil constitutive model used to represent the behaviour of the London Clay layer. One of the DYNA analyses used the BRICK model (Simpson 1992) and the other an elastic-perfectly plastic Mohr-Coulomb failure criterion with a non-linear elastic model proposed by Jardine *et al* (1986). The analysis with the Jardine model predicted much larger movements compared to the BRICK model. The instrumented field trial and the installation of the contract piles demonstrated that the predictions made by the BRICK model were more appropriate.

The Jardine model uses an empirical stiffness degradation curve that has been shown to produce good predictions for the behaviour of large excavations in London Clay when combined with a Mohr-Coulomb failure creation. The model however does not automatically detect stress reversals or stress rotations and therefore in practice when these are thought to occur, it is typical for the analyst to manually reset the strains to zero to re-engage the small strain stiffness behaviour. For the case of the pile installation in close proximity to the LUL tunnel, the ground strained as the pile bore progressed, and consequently the stiffness dropped. This continued until the pile bore was complete when a stress reversal was initiated as the wet concrete pressure was applied. The continued straining of the ground and reduction in stiffness caused the large predicted displacement shown in Fig. 5. On the other hand, the BRICK model automatically detected stress reversals and rotations and continually re-engaged the small strain stiffness of the London Clay giving the significantly smaller predicted displacements. The results of the field trial and the installation of the contract piles demonstrated that, in this circumstance, the BRICK model captured better the behaviour of the London Clay layer. This is in contrast to the monotonic unloading experienced by the Bakerloo Line following excavation of the Shell Centre basement which was back analysed effectively by both soil models.

CONCLUSIONS

To the authors' knowledge, the piles installed for Building 4a as part of the Southbank Place development are the closest ever installed next to a live London Underground tunnel. An effective pile installation methodology was developed which mitigated the principle risks during pile installation of: pile bore instability, migration of bentonite support fluid into the tunnel and excessive ground movements due to stress relaxation. The feasibility of the pile installation methodology was proved through a full scale instrumented trial pile bore.

The ground movements predicted by two otherwise equivalent finite element analyses demonstrated the importance of using a soil constitutive model that can replicate the stress reversals and stress rotations when considering small scale complicated stress paths that occur during pile installation.

ACKNOWLEDGEMENTS

The authors are indebted to the Southbank Place project team for the successful completion of the piling work around the Northern Line tunnel for Building 4a. The team includes piling contractor Expanded, instrumentation and monitoring contractor Getec, tiltmeter suppliers Sencieve, structural engineers WSP and most importantly the Infrastructure Protection team from London Underground

Limited. The numerical analyses presented in this paper were undertaken by Andrew Richmond of Arup.

REFERENCES

Burford D. (1988), Heave of tunnels beneath the Shell Centre, London, 1959 – 1986, Géotechnique 38, No. 1, pp 135 - 137.

Burford D. (1996), Heave of Bakerloo Line tunnels under the Shell Building, London - June 1994 and June 1995 observations, BRE note N31/96.

Jardine, R J, Potts, D M Fourie, A B, and Burland, J B (1986) Studies of the influence of non-linear stress-strain characteristics in soil-structure interaction, Géotechnique, vol 36, 3, ICE Publications, Institution of Civil Engineers, London, pp 377–396

Measor E.O. and Williams G.M.J. (1962), Features in the design and construction of the Shell Centre, London, Proc. Instn. Civ. Engrs., 21, pp 475 - 502.

Measor E.O. and Williams G.M.J. (1963), Discussion. Features in the design and construction of the Shell Centre, London, Proc. Instn. Civ. Engrs., 24 Issue 3, pages 409 –424.

Simpson, B. (1992), Development and application of a new model for prediction of ground movements. In: Proc of the Wroth memorial symposium. Predictive soil mechanics, St Catherine's College, Oxford, 27–29 July 1992, Thomas Telford, London, pp 628–643

Skempton and Henkel (1957), Tests on London Clay from Deep Borings at Paddington, Victoria and the South Bank, Proc. 4th Int. Conf. Soil Mech. Fdn. Engng., 1, pp 100 - 106.

Ward W.H. (1961), Displacements and strains in tunnels beneath a large excavation in London, Proc. 5th Int. Conf. Soil. Mech. Fdn. Engng., 2 pp 749 - 753.

Williams G.M.J. (1957), Design of the foundations of the Shell Building London, Proc. 4th Int. Conf. Soil Mech. Fdn. Engng., 1, pp 457 - 461.

APPENDIX

Figure A1 shows a comparison of the normalised stiffness curves used for the BRICK and Jardine analyses.

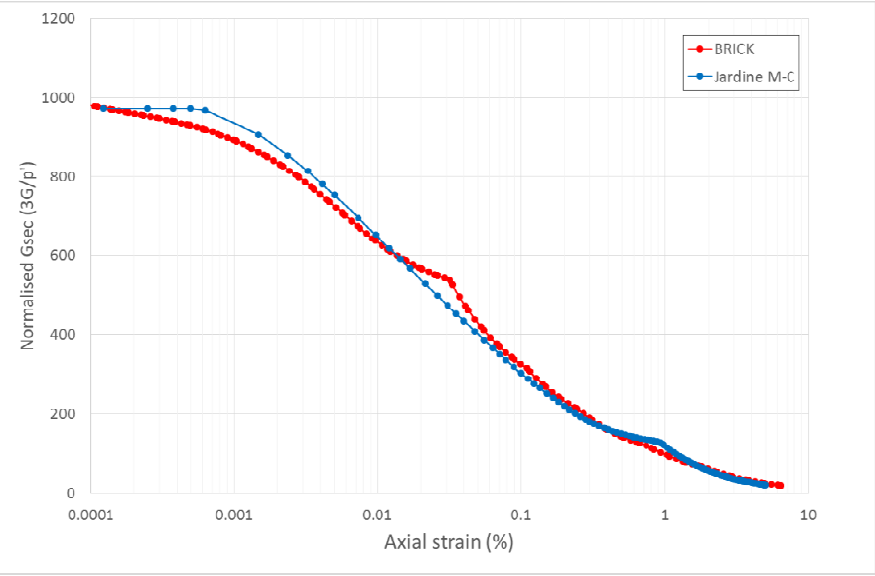


Fig. A1. Comparison of stiffness degradation curves for both soil models

DESIGN, CONSTRUCTION AND PERFORMANCE OF SINGLE BORE MULTIPLE ANCHORED DIAPHGRAM WALL IN IZMIR, TURKEY

Düzceer R, PhD. CEng, Kasktaş A.Ş., İstanbul, Turkey, rasin.duzceer@kasktas.com.tr
Mothersille D, PhD. CEng. FICE, SBMA Ltd, UK, devon.mothersille@sbmasystems.com
Gökalp A, M.Sc. CEng, Kasktaş A.Ş., İstanbul, Turkey, alp.gokalp@kasktas.com.tr
Adatepe Ş,M.Sc. CEng, Kasktaş A.Ş., İstanbul, Turkey, adatepe@kasktas.com.tr

ABSTRACT

The Mahall Bomonti Project located in Bayraklı, İzmir. It is currently under construction, and when completed, will comprise residential, office and commercial facilities covering an area of approximately 45,000 m^2. Within the scope of the project, a foundation excavation with a maximum depth of 18.5 m was proposed in the soft alluvial soil layers under a high water table. In order to ensure that the excavation was executed safely, without endangering the surrounding structures, a ground support system comprising a diaphragm wall supported by high-capacity prestressed anchors (SBMAs) was designed and constructed. The paper provides details on the calculated and observed deformations together with the design, construction phases and quality control tests applied during the implementation of the excavation support system.

Keywords: Deep Excavation, Diaphragm Wall, SBMA, Single Unit Test, Load Cell, Artesian Pressure

INTRODUCTION

The Mahall Bomonti Project comprises both residential and commercial developments and is being constructed by Türkerler İnşaat on a land of approximately 45,000 m² in the Bayraklı - İzmir region in Turkey. To improve the social welfare of the region, nine historical buildings will be restored within the scope of the project. Three new blocks will be constructed; Block-A consisting of a 15-storey podium area and a 57-storey tower , which will be the highest skyscraper in the region, and the Blocks B and C consisting of three and four storey commercial and office areas respectively (see Figure 1).

An important feature of the project was the foundation excavation to a maximum depth of 18.50 m in the soft alluvial soil layers under a high water table. In order to ensure that the planned excavation could be carried out safely, without endangering the surrounding structures, a ground support system consisting of a diaphragm wall supported by high-capacity prestressed single bore multiple anchors (SBMAs) was designed and constructed.

The general layout plan, geometric dimensions of the project and the maximum excavation depths (based on an average ground level of +2.00 m) for each block is shown in metres in Fig. 1.

For effective ground support a total of 27,500 m² of 80 cm thick diaphragm wall was constructed and 55,200 linear metres of high capacity SBMAs, with design loads of 650kN, were installed. As part of the investigation anchor test program; a number of Single Unit Anchor Tests (SUTs) and SBMA test anchors were installed and tested before the commencement of the production anchor works in order to verify and determine the design load of anchors in accordance with the limiting creep criteria. A maximum anchor load capacity of 1,850 kN was achieved on the test anchors; which were installed by using special drilling and grouting techniques. These test anchors achieved the highest anchor capacities in İzmir region; where the subsoil conditions are composed of deep and soft alluvial layers.

© 2018 Deep Foundations Institute



Fig. 1. General Layout Plan

A strict quality control program has been applied so that the registered historical structures, located within the vicinity of the ground support system, were not damaged by anchor drilling, installation and excavation works. In addition, the performance of the ground support system was continuously monitored and readings from inclinometers and anchor load cells were taken and reported on a weekly basis.

SOIL CONDITIONS

Meles delta alluviums were observed in the study area (Fig. 2) and generally contain clayey, silty sandy and locally gravelly layers. It is noteworthy that the project area lies on a tectonic depression. This depression, formed during the collapse of the Aegean Sea, was filled with alluvial materials at the next stage and thus became an alluvial plain. In addition, parts of the plain near the sea were covered with marshes and shallow lakes, indicating that these parts of the deposition have not yet been completed.

The subsoil conditions at the construction area consists of Quaternary alluvial units containing clay, silt, sand and gravel from the surface up to the depth at the maximum depth of 24.2 m in depth. These layers were composed of plastic clay, silicate clay, silt, clay sand and non-plastic silt sand units up to the first 10 m depth. Below these layers the subsoil conditions consists of plastic clay containing clayey sand, clayey gravel and silty gravel bands with clay units. The water table is 2 m below the ground level and artesian ground water was observed at the levels of 38 m below ground level in the gravel layers.

The SPT-N values obtained from 26 boreholes are shown in Fig 3. Fig. 4 shows the relationship between q_c and f_s values and depth, obtained from 6 CPT boreholes. Examination of SPT-N values show values of 30-45 in the top 30 m, where the gravel bands are located, whereas SPT-N values of 5-15 exist within the clay and silt layers. The results obtained from the CPT tests confirm the prevailing subsoil conditions and provided a sound basis for the preliminary soil anchor design.

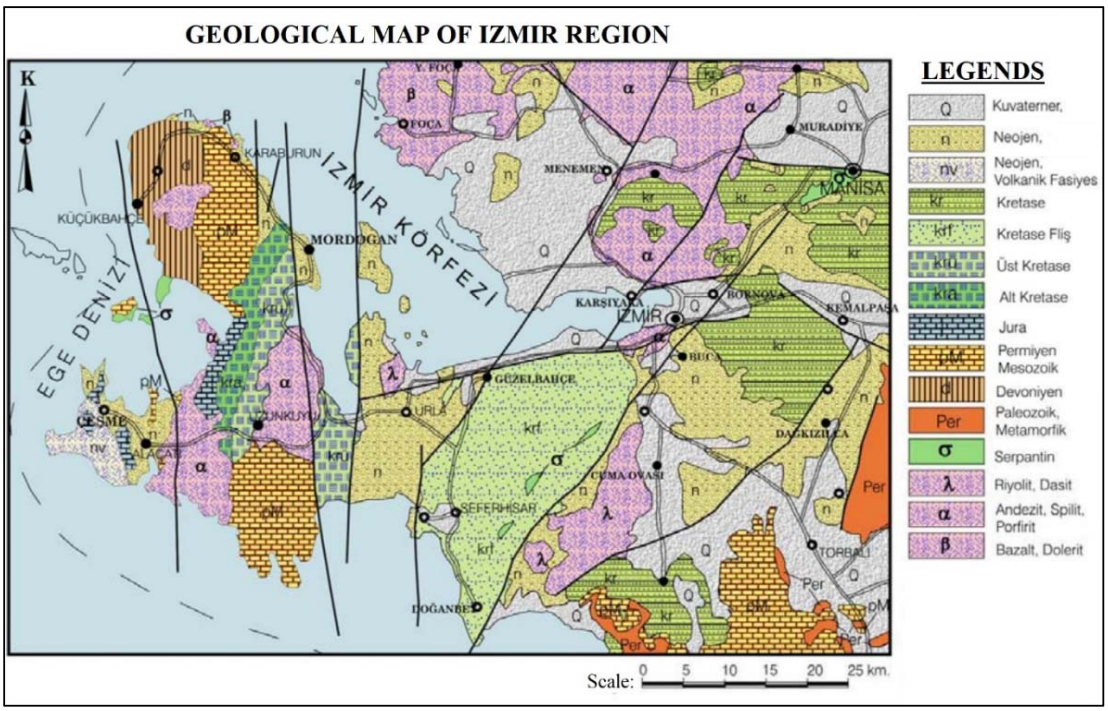


Fig. 2. Generalized Geological Map of İzmir

DESIGN OF THE GROUND SUPPORT SYSTEM

An impervious ground support system was designed to accommodate the maximum excavation depth of 18.5 m and comprised an anchored diaphragm wall. The thickness of the diaphragm wall was 80 cm and this was laterally supported by high capacity SBMAs.

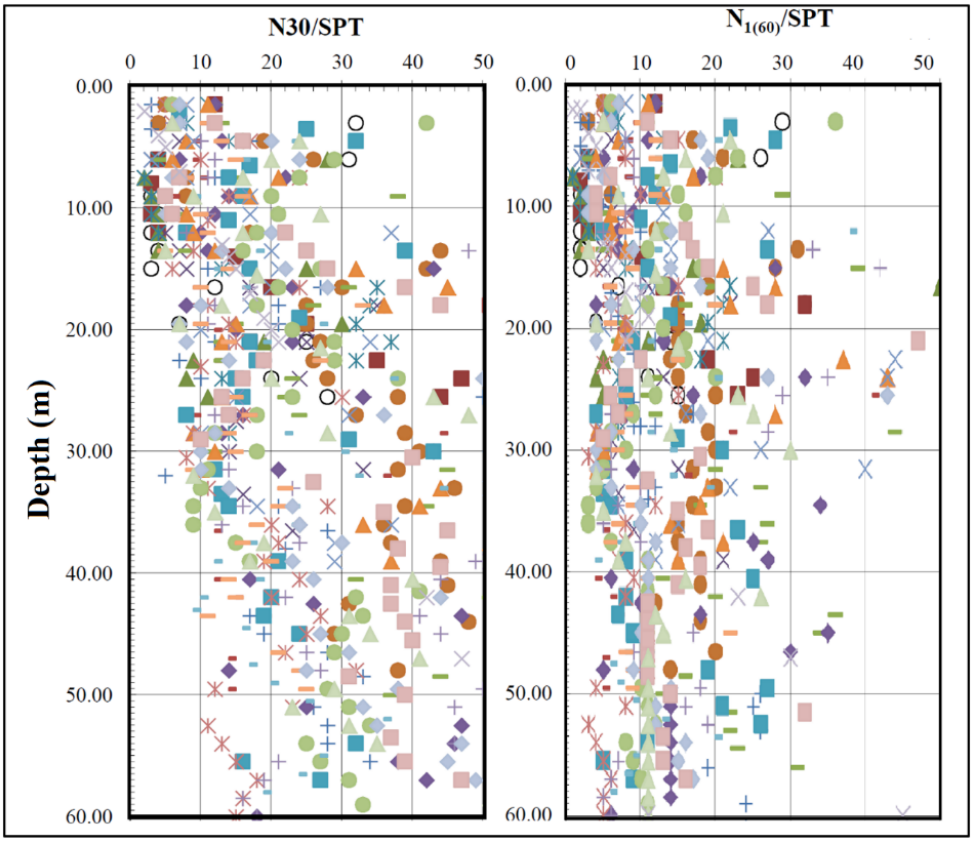


Fig. 3. Variation of SPT N30 ve N1(60) Values with Depth

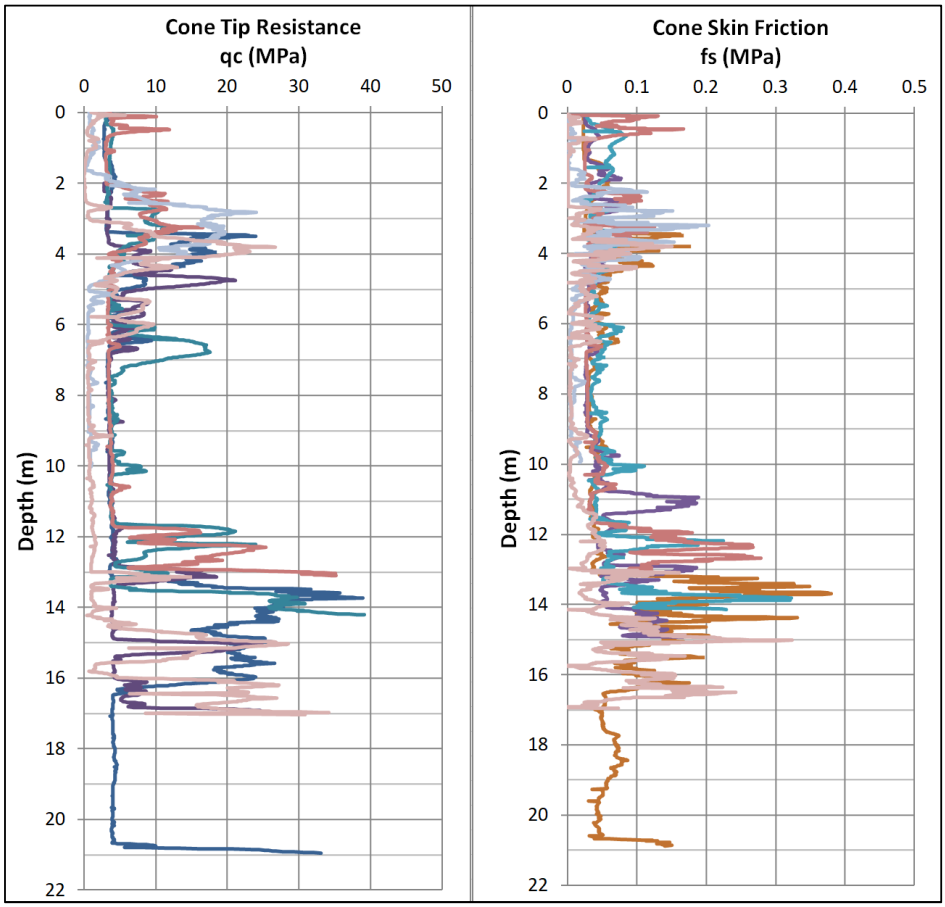


Fig. 4. Variation of q_c and f_s values from CPT tests with Depth

Initially the design load of anchors, based on desk studies, was assumed to be 550 kN, however, the results from investigation tests incorporating SUT and SBMA tests, carried out before the commencement of the anchoring works, demonstrated increased anchor capacities and the design loads were subsequently revised to 650 kN thereby facilitating a more economical design.

The ground support system was designed as "temporary" and calculations were carried out for 3 Blocks according to 4 different excavation elevations. Excavation depths and the details of the anchoring works at each Block are given in Table 1. The ground support system design was optimized using finite element analysis as shown in Fig. 5. Wall deformations, shear force and bending moment distributions of the four design sections considered are given in Fig. 6 to Fig. 9.

Table 1. Details of Ground Support System

Block Name	Excavation Depth (m)	No. of Anchor Rows (no.)	Anchor Design Load (kN)
A Block-Podium	15.3	4	650
A Block- Tower	17.8	5	650
B Block	13.8	3	650
C Block	18.5	5	650

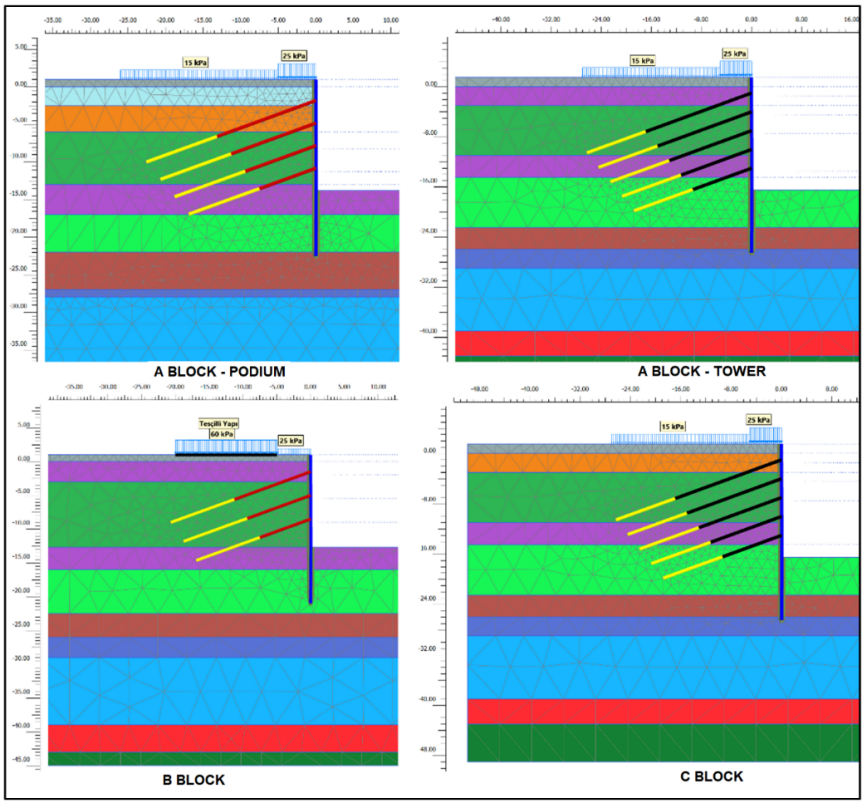


Fig. 5. Analysed sections for design of ground support system

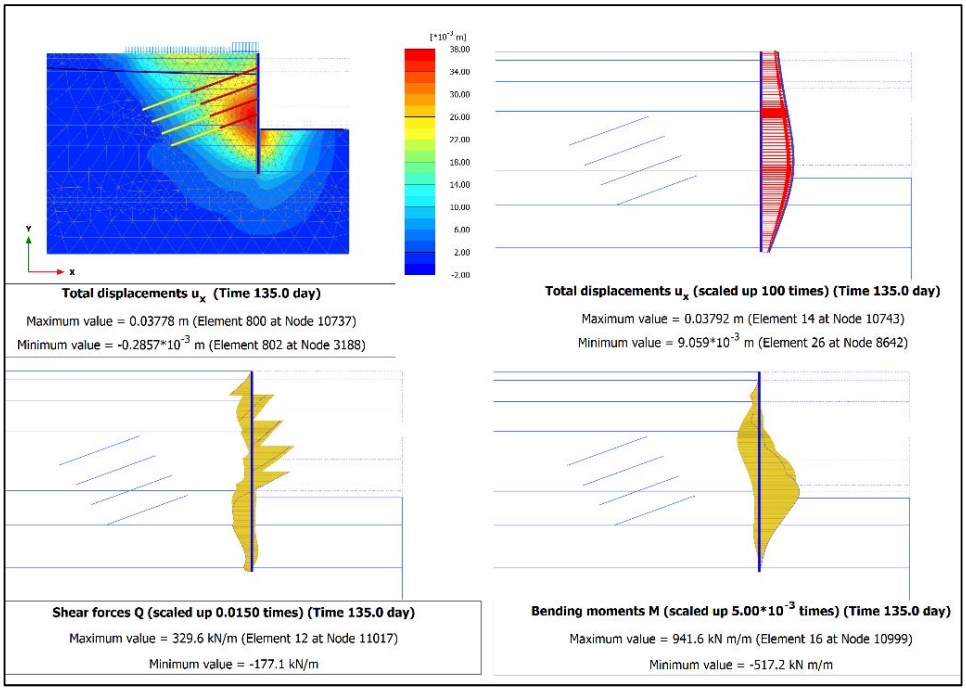


Fig. 6. Block-A Podium Area – Ground support system analysis

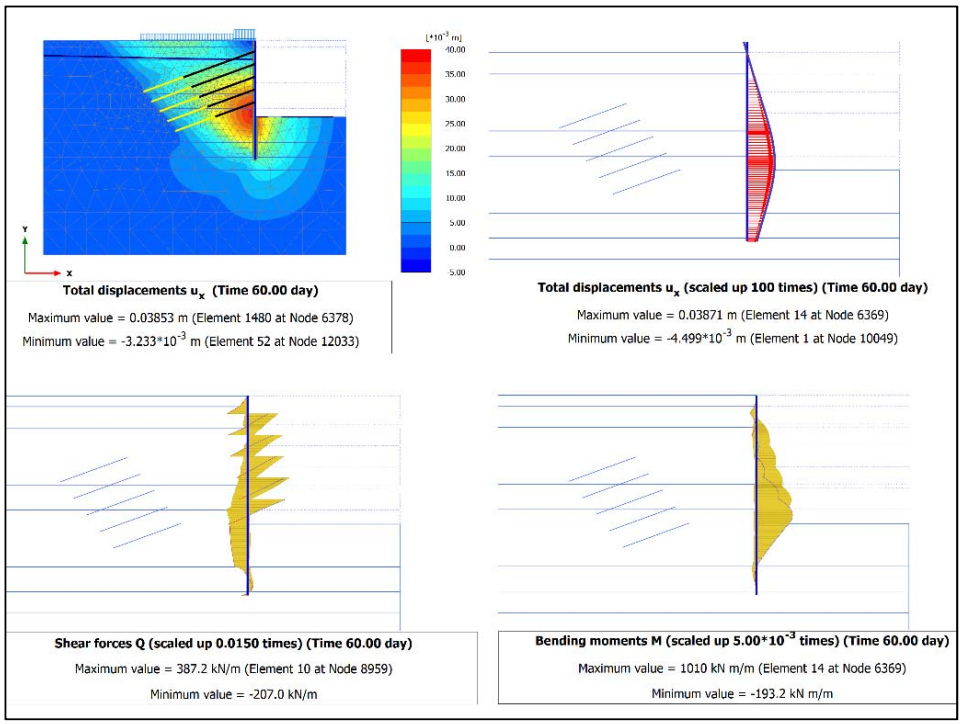


Fig. 7. Block-A Tower Area – Ground support system analysis

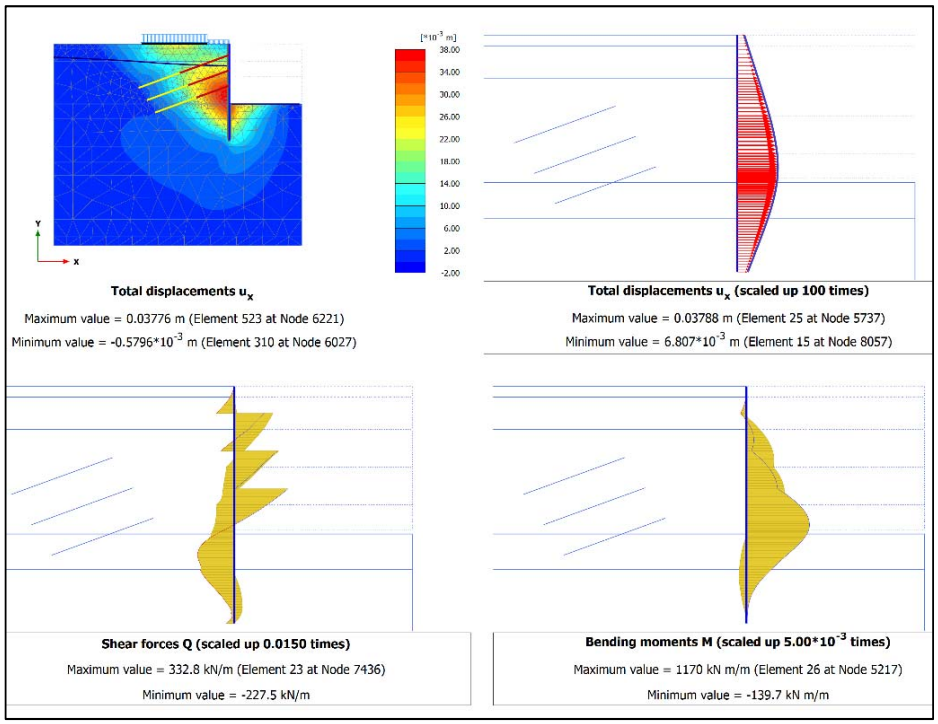


Fig. 8. Block-B Ground support system analysis

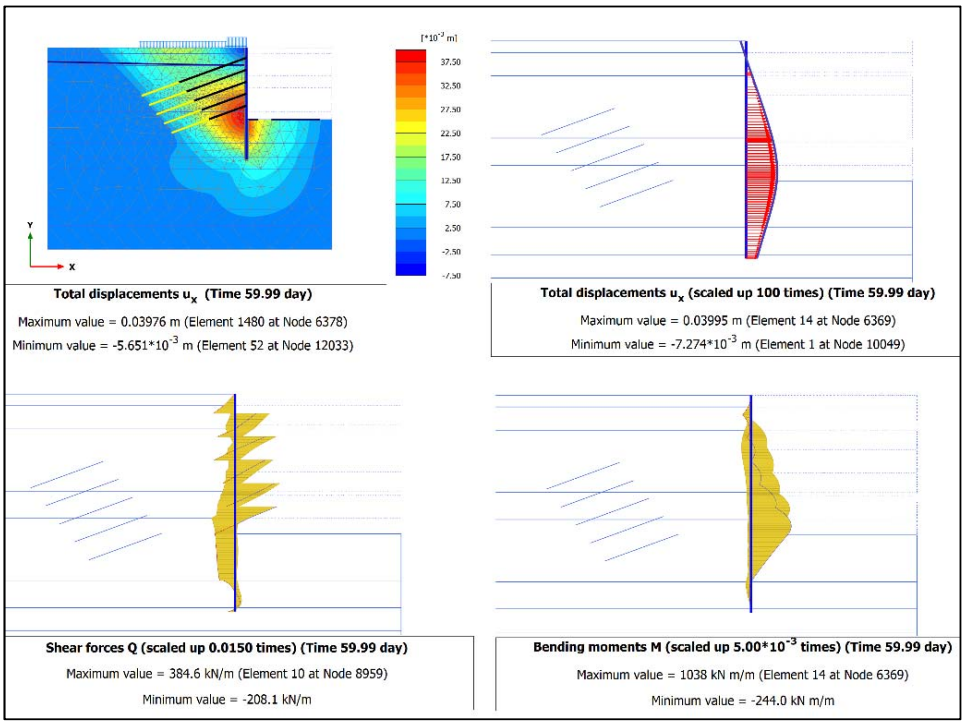


Fig. 9. Block-C Ground support system analysis

DESIGN OF SBMAs

By effectively designing the anchor bond length using a series of efficient unit lengths, the SBMA system is able to achieve higher capacities than conventional anchors in soils and weak rocks. A comparison between the bond stress distributions in a conventional anchor and a SBMA is schematically shown in Fig. 10.

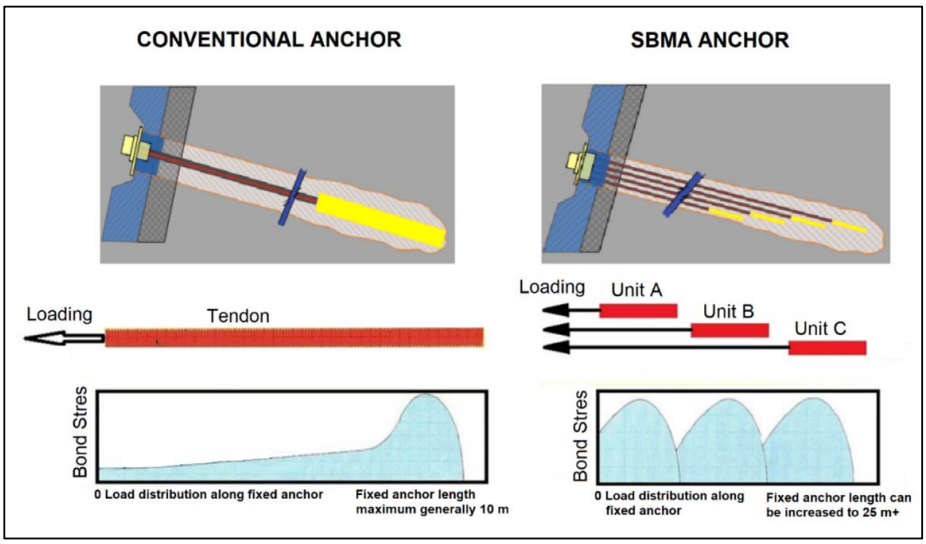


Fig. 10. Distribution of bond stress in a conventional anchor and a SBMA

It is known that the maximum load, which can be carried by anchor bond, depends on the mobilized in situ bond stress and the effective length of anchor bond. The studies carried out by Ostermayer (1974 and 1977) and later by Barley (1995) show that mobilized anchor capacity does not increase linearly with the increase in bond length. Furthermore, empirical studies have confirmed that anchors constructed with highly efficient bond lengths of 3 m operated at approximately 85% efficiency, whereas conventional anchor bond lengths of 10m were approximately 50% less efficient for similar magnitudes of applied load.

With respect to the costs of construction, it is noteworthy that although SBMAs require a more sophisticated tendon configuration, significant economies are still achieved compared to conventional anchors since the overall number of anchors required is reduced.

Prior to the design of the SBMAs, a SUT was performed at the project site to determine the maximum load that an anchor unit could achieve and the maximum unit bond stress at that load level. Different drilling and grouting techniques were applied in these single unit anchor tests. Thus, the most appropriate drilling and grouting method was selected in accordance to the ground conditions at the project site. (Fig. 11)

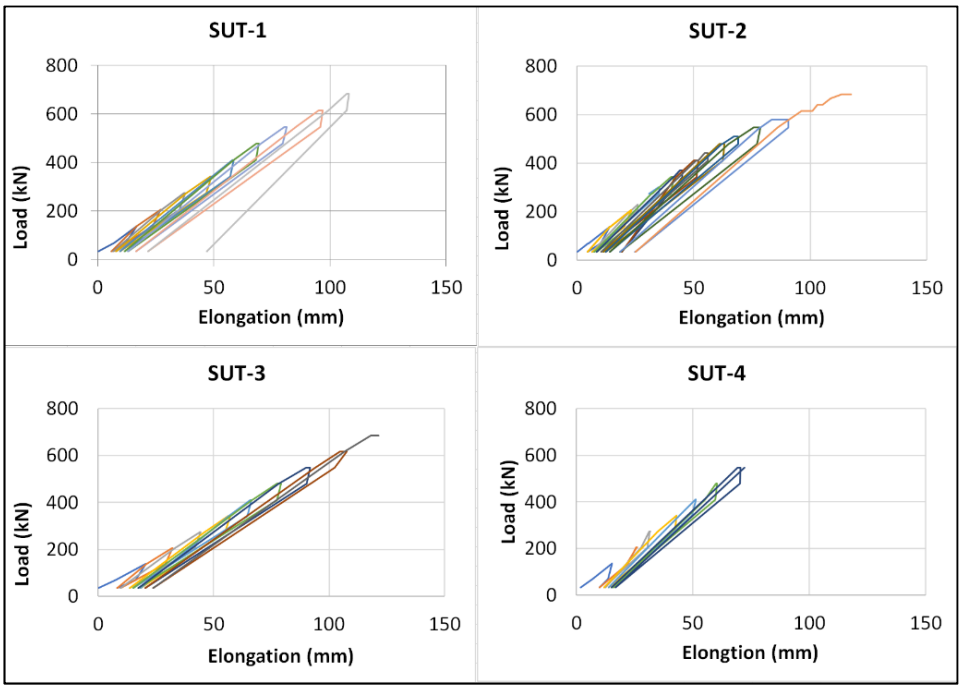


Fig. 11. Test Results of SUT

The number of anchor units and unit bond lengths of the SBMA test anchors were determined taking into account the unit bond stress obtained from the test results. Investigation tests were performed on SBMA test anchors with three and four units (Fig. 12 & Fig. 13). The SBMA test anchor which effectively achieved the target design load, whilst satisfying the creep criterion, was used to determine the configuration of the production anchors.

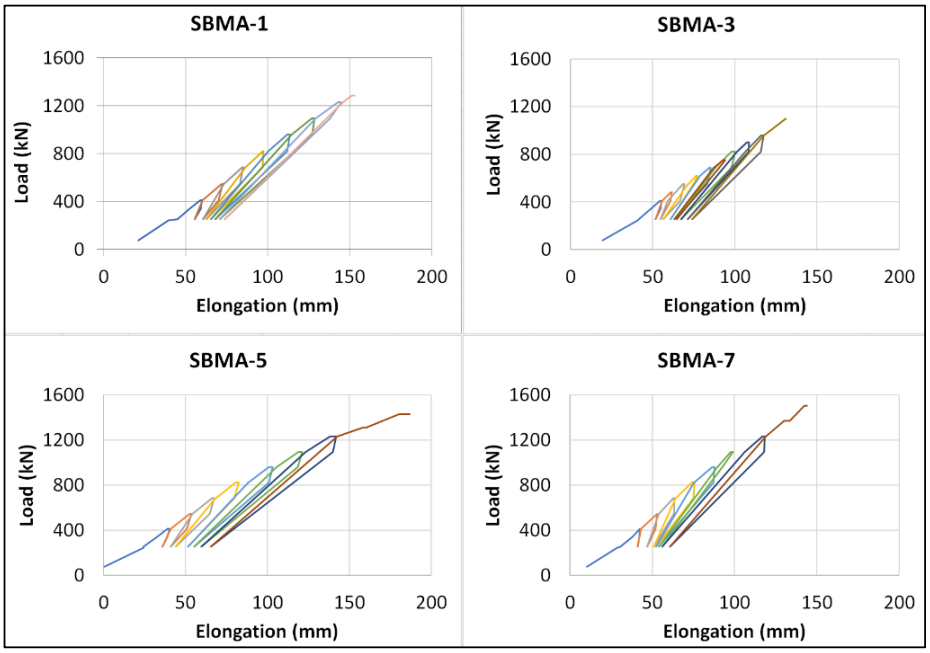


Fig. 12. Test Results of SBMA with 3 Units

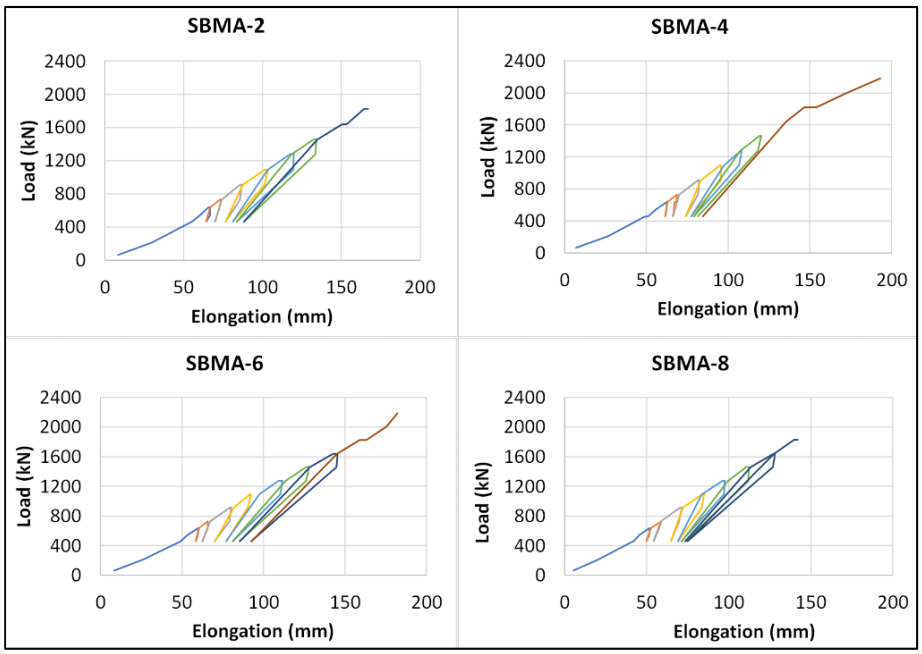


Fig. 13. Test Results of SBMA with 4 Units

A summary of the results of the tests are given in Table 2. Based on development of special installation and grouting techniques; post-grouting and end-of-casing grouting, it was possible to achieve higher anchor capacities than those reported in previous field studies (Düzceer, 2015, Mothersille et.al. 2015, Düzceer et.al. 2014). The maximum anchor capacity achieved in the research tests was specified as 1,850 kN.

Table 2. Research Test Summary Table

Test Area	Anchor No	Bond Area / Soil Type	Bond Area SPT-N	Unit No	Grouting Type
1	SUT-1	Brown clayey sandy gravel	10	1	End-of-casing
	SBMA-1	Brown clay with sand inclusions	10	3	End-of-casing
	SBMA-2	Greenish gray clay / Brown clay with sand inclusions	8-16	4	End-of-casing
2	SUT-2	Greenish brown sandy clay	8	1	Post Grouting
	SBMA-3	Greenish brown sandy clay / Brown sandy clay with gravel inclusions	8-17	3	Post Grouting
	SBMA-4	Brown sandy clay interbedded with gravel	28	4	Post Grouting
3	SUT-3	Yellowish brown sandy clay-gravel	16	1	End-of-casing
	SBMA-5	Brown sandy gravel with clay inclusions / Brown clay with sand inclusions	12-29	3	End-of-casing
	SBMA-6	Gray sandy silty clay/ Yellowish brown sandy clay-gravel / Yellowish brown clay with sand inclusions	8-26-14	4	End-of-casing
4	SUT-4	Greenish gray clay with sand inclusions	6	1	Post Grouting
	SBMA-7	Brown clay, coarse grained gravel	12-40	3	Post Grouting
	SBMA-8	Brown gravelly and sandy clay / Brown sandy gravel	14-35	4	Post Grouting

PERFORMANCE OF GROUND SUPPORT SYSTEM AND QUALITY CONTROL

Some 55,200 linear metres of SBMAs were installed within the scope of the project. All anchors were tested to 1.25 times the design load and locked to 1.10 times the design load. One in every 200 anchors of anchors was tested to 1.5 times the anchor design load and performance checked against the creep criteria. Example acceptance test results for a typical production anchor are presented in Fig. 14.

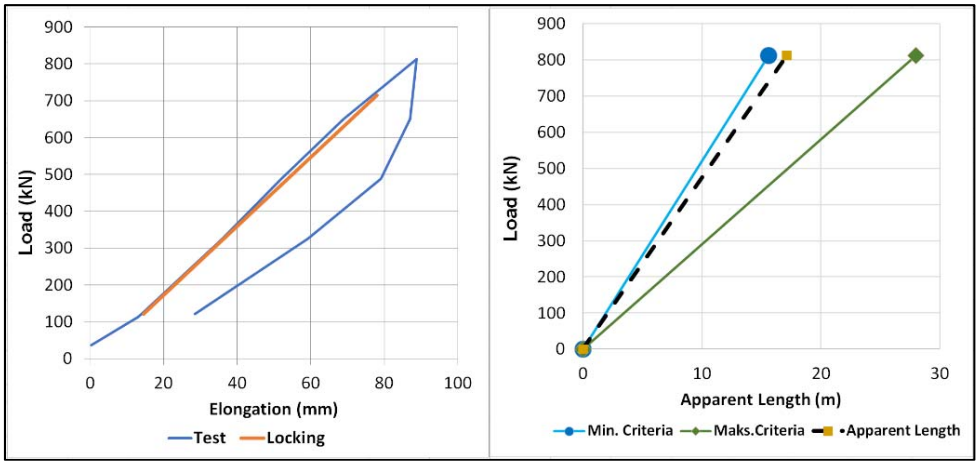


Fig. 14. Example acceptance test results for a typical production anchor

To ensure that historic adjacent structures were not adversely affected by the construction works, a strict quality control program was implemented. The behaviour of the anchored structure was checked on a weekly basis by observing the behavior of 21 inclinometers, nine 9 anchor load cells and 6 piezometer wells. In addition, the water level behind the diaphragm wall was controlled. The close corroboration between calculated and measured deformations, for four different selected sections, used in the design of the ground support system, is shown in Fig.15. The measured relationship between anchor load and time at these sections is given in Fig.16 and a general view from the project area is shown in Fig.17.

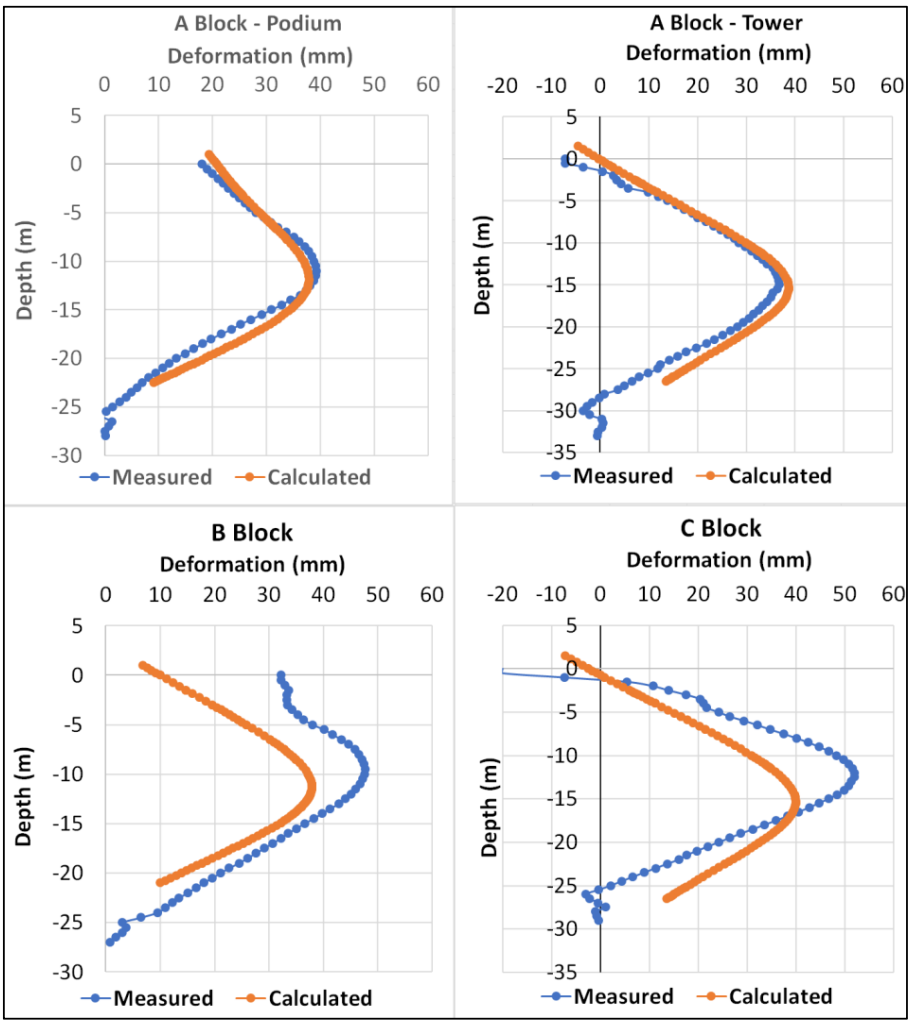


Fig. 15. Calculated and Measured Deformations

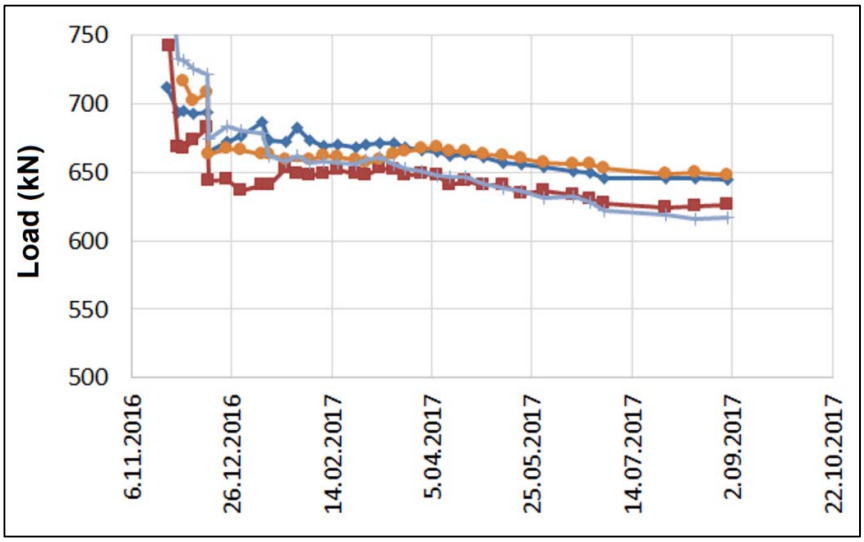


Fig. 16. Load Cell Readings

It is noteworthy that during the drilling of boreholes for the lower row anchors, high artesian water pressure was encountered in the gravel bands between the clayey layers. This challenging site condition was overcome by using special drilling and grouting techniques and this ensured that the anchors were installed satisfactorily so that target anchor loads were successfully achieved.



Fig. 17. General View of Site Area

CONCLUSION

The use of some 2400 No. SBMAs, in challenging ground conditions, as an intergral part of the ground support system for the foundations of the Mahall Bomonti Project has proven highly effective. Deformations of the diaphragm walls, used as the principal support structure, were controlled to within tolerable limits (< 55mm; established by finite element analysis) and this effectively safeguarded the integrity of historic building located in close proximity to the foundation excavation.

The success of this challenging project has largely been achieved through extensive investigation tests, including post-grouting trials. The maximum anchor load capacity of 1,850 kN is the highest anchor load, complying the creep criteria, ever achieved in Izmir Region. Significantly, the use of SBMA technology reduced the total quantity of anchoring works from 153,000 m (as specified in the original design) to 55,200 m, generating a saving up to 60% in time and %35 in the total price of the anchoring works. The effective use of geotechnical instrumentation including inclinometers, load cells and peizometers permitted regular monitoring of the anchored structure behaviour during the porcess of construction.

REFERENCES

Barley, A.D and C.R. Winsdor. (2000). Recent advances in ground anchor and ground reinforcement technology with reference to the development of the art. GeoEng2000, International Conference on Geotechnical and Geological Engineering, Melbourne.

BS 8081:2015 British Standard Code of Practice for Ground Anchorages.

Düzceer R., (2015) "Zayıf Zemin ve Kayaçlarda SBMA Tipi Ankrajların Tasarımı ve Performansı", 6. Geoteknik Sempozyumu, 26-27 Kasım, Çukurova Üniversitesi, Adana.

Düzceer R., Gökalp A., Adatepe Ş., (2014) "Tekli Delgi Çoklu Ankraj İle Desteklenen Diyafram Duvarın Tasarım, Uygulama ve Performansı", Teori ve Uygulamada Zemin-Yapı Etkileşimi Sempozyumu", 24-25 Nisan, Akdeniz Üniversitesi, Antalya.

Mothersille D., Düzceer R., Gökalp A., (2015) "Design, Construction and Performance of Single Bore Multiple Anchored Diaphragm Wall", XVI th European Conference on Soil Mechanics and Geotechnical Engineering, 13-17 Eylül, Scotland, UK.

Mothersille D., Düzceer R., Gökalp A., (2015) Okumuşoğlu B., "Support of 25 m deep excavation using ground anchors in Russia", Proceedings of the Institution of Civil Engineers, Geotechnical Engineering, Vol. 168 , pp 281-295.

DRILLED PIER LOAD TESTS ON DULLES METRORAIL PROJECT - OVERVIEW, RESULTS AND DISCUSSIONS

Sujan K. Bhattacharya, Ph.D., P.E., Special Project Manager, Intertek-PSI, 95 Chastain Rd, Suite 301, Kennesaw, Georgia, USA, sujan.bhat@psiusa.com, (678) 571-8265
Lloyd W. Young, P.E., Principal Geotechnical Engineer, Bechtel Infra. Corporation, 12011 Sunset Hills Rd, Reston, VA, USA, lwyoung@bechtel.com, (925) 628-9205
Jeongbok Seo, Ph.D., P.E., Area Manager, Bechtel Infra. Corporation, 10148-95 Street, Edmonton, Alberta, Canada, jseo@bechtel.com, (587) 532-8228

ABSTRACT

Dulles Corridor Metrorail Project (DCMP) is an extension of the existing 106-mile Washington, D.C. Metrorail system from the current Orange Line in Fairfax County, Virginia through Tysons Corner to the Washington Dulles International Airport and beyond the airport into Loudoun County. Phase I of the Project consists of approximately 11.7 miles of rapid rail transit that includes about 3 miles of aerial guideway structures supported by 725 drilled shafts. A total of 14 load tests, including ten (10) Osterberg Cell (O-Cell) Tests and four (4) Statnamic Tests, were performed to verify the axial load carrying capacity of drilled shafts at selected locations along the alignment. The capacity results of skin friction (side resistance) and end bearing (base resistance) measured by load tests are compared with values computed in accordance with the AASHTO 1999 β- Method (Beta) and the FHWA-1999 Method for cohesionless soils and Intermediate Geo-Materials (IGM), respectively. Comparisons for skin friction were made for the fill/low strength soils, high strength native soils, and for the decomposed rock of the Piedmont formation. Comparisons of end bearing were made for the decomposed rock only. According to results of these comparisons, the approach used by DTP can be considered somewhat conservative overall, which proved to be prudent later to accommodate construction conditions at some shafts.

Keywords: drilled shaft, O-Cell, side shear and end bearing

INTRODUCTION

Dulles Corridor Metrorail Project (DCMP) includes about 23 miles of metro-rail expansion in the suburban Washington DC in Northern Virginia. The new alignment (Silver Line-Phase I) begins near the East Falls Church Station and passes through the congested Tysons Corner Mall area along Route 7, merging with Dulles International Airport Access Highway (DIAAH, VA Hwy 267). The alignment of DCMP is shown in Fig. 1.

The first phase of the project (Phase I) includes construction of about 11.7-mile long metro-rail alignment up to Wiehle Avenue Station from where, the second phase (Phase II) of construction will begin for the final 11.4 miles, ending near Route 772 in eastern Loudon County via, Dulles International Airport.

The drilled shaft foundation configurations included mono-shafts, two, four, five and six shafts in groups. For the shafts or shaft groups, subsurface exploration and geotechnical engineering investigations were performed in various areas and in various phases of the project. As a part of foundation design approach recommended by AASHTO (AASHTO 1997), at least one load test was performed in each separate area of the alignment where aerial guideways are located.

© 2018 Deep Foundations Institute

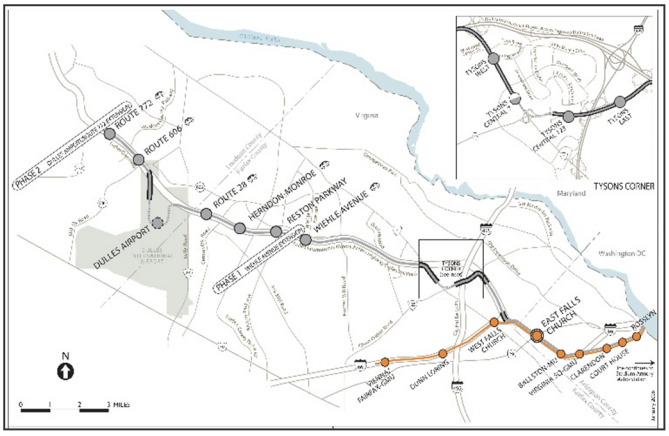


Fig. 1. Alignment of DCMP – Phase I

The purpose of this paper is to present the load test data obtained from the 14 load tests. Although most of the tests were conducted on production shafts without exceeding the limit of loading to twice the structural demand, we believe this data can be utilized for a preliminary estimation of side shear and end bearing of soils and decomposed rocks in Piedmont geology.

LOCAL GEOLOGY AND SUBSURFACE CONDITIONS

The Dulles Metrorail Project site is located within the Piedmont Physiographic Province of Northern Virginia that is underlain by metamorphic rocks with occasional igneous intrusions. These rocks are composed of crystalline structures.

Typical soil profile includes silt and clay in upper layers where weathering is predominant. Below the silt and clay layers, less weathered sand, sandy silt or, silty sand exists to depths where weathered rocks underlain by bedrock are encountered. The boundary between soil and rock is not clearly defined and a transitional zone known as, "Decomposed Rock" (Partially Weathered Rock or PWR) typically exists on top of bedrock. Groundwater in Piedmont geology is encountered within upper soil layers or, within decomposed rock layers. Generally, the groundwater flow direction mimics the topography.

For modeling the soil strata for foundation calculations, the natural soils were divided into two classes designated as S1 and S2 based on their respective N-values (Table. 1). Below S1 and S2 soils decomposed rocks D1, D2 and D3 were encountered. Decomposed rock was classified as cohesionless reddish brown to gray-brown sands with traces of rock fragments. Bedrock was encountered below the decomposed rock.

The N-values recorded for decomposed rocks exceeded 60 and often, were as high as 100 blows for 1″ of penetration. For foundation calculations, decomposed rocks were divided into three classes designated as D1, D2 and D3 based on their respective N-values: $61 \leq N \leq 100$ (D1), $101 \leq N \leq 100/6''$ (D2) and $100/5'' \leq N \leq 100/1''$ (D3). Bedrock classified as schist, phyllonite, gneiss and metagraywacke existed below decomposed rocks. Unconfined Compressive Strength (q_u) for the bedrock ranged between 740 pounds per square inches (psi) to 16,560 psi. Rock Quality Designation (RQD) in the upper layers of bedrock ranged from 0 to 25% which gradually improved to 75%+ for depths greater than about 25 feet below the Auger Refusal depth.

Table 1. Typical Soil and Rock Properties

Strata	N Value	Unit Weight (pcf)	Friction Angle (°)
S1	1≤N≤16	120	25
S2	17≤N<60	125	30
D1	61≤N≤100	130	33
D2	101<N≤100/6″	135	35
D3	100/5″<N≤100/1″	140	38
Bedrock	100/1″<N	145	40

LOAD TEST PROGRAM

According to AASHTO, the Factor of Safety (FOS) for allowable side shear and allowable end bearing is 2.0 if a load test is performed and 2.5 if no load is performed. Using a FOS 2.0 was a goal in the design approach for achieving an economic design for drilled shafts. Also, performing sufficient number of load tests using test loads equal to twice the design load was in line with the general criteria of safety and serviceability philosophy of the project.

The alignment of the Dulles Corridor Metrorail Project was divided into various construction zones. Drilled shafts were installed in those construction zones such as, O-1 guideway area, Tysons East area, etc., where, aerial structures were located. At least one load test was conducted in all major drill shaft construction zones. Table 1 below summarizes test locations, dates and test shaft numbers. A brief description of test locations and test types is included in the following paragraphs.

O-1 Guideway

Two O-Cell tests and one Statnamic test were performed in O-1 Guideway area in January 2008 during the final design of drilled piers began. During the installation of rebar cage in Test Shaft # 2, the welds supporting the O-Cell failed. The rebar cage and the welds supporting the O-Cell were repaired and lifting methods changed before a second successful lift was performed. In addition, in all cased shafts, concrete was placed to a height above the groundwater table to prevent the groundwater inflow into the casings.

Tysons East Package 1 Area

Tysons East Aerial Guideway Package 1 area was about 4200 feet long that included 29 structural piers most of which consisted of four-shafts in a group configuration. A total of six load tests were conducted within this segment.

Tysons East - Station

Tysons East Station was founded on 12 structural piers that were supported by various groups of shafts such as, 2, 4 and 5 shaft groups. The length of this segment was about 800 feet. The station structure included tracks and platforms. One O-Cell test was conducted at shaft 1 of Pier 31 (drilled shaft 31-1).

Tysons East - Package 2 Area

Tysons East Package 2 area began immediately west of Tysons East station from where, the alignment of about 2700 feet crosses over Interstate 495 (I-495) and terminated at the boundary of Tysons Central Station. Shaft 1 of Pier 46 (shaft 46-1) was located in an easily accessible location.

Tysons Central 123 Station

Tysons Central 123 Station included 10 structural piers within a stretch of about 600 feet. The station included tracks, platforms and a service room on the western section of the station. The O-Cell test was performed at drilled shaft 5 of Pier 66 (shaft 66-5).

Tysons West Package 2

The Tysons West Package 2 portion of the alignment was located within the median of Route 7, beginning from the north boundary of Tysons Central 123 Station and ending near the intersection of Spring Hill Road. This portion was about 2800 feet including 21 structural piers in a heavily congested area posing some challenges in re-routing traffic and other construction issues. One O-Cell test was performed at shaft 4-2.

Tysons West Package 1

Tysons West Package 1 area began where Tysons West Package 2 ended in the median of Route 7, near the intersection of DIAAH. This segment is about 2900 feet long including 23 structural piers and the aerial guideway leaves the median of Route 7 and lands in the median of DIAAH. The O-Cell test was performed at shaft 45-2.

Wiehle Avenue Station

Wiehle Avenue Station and Platform is about 800 feet long which included 600 feet long platform and about 200 feet long mezzanine floor. The foundation system consisted of drilled shafts in groups or mono-shafts with diameters ranging between 3 ft and 5 ft. One O-Cell test was performed at production shaft 2 of pier 15 in November 2009.

Table 2. Summary of Load Test

Test Area	Test Shaft #	Test Type	Test Date	Remark
O-1 Guideway	01	Statnamic	Jan. 2008	Test Shaft, Test completed
	02	O-Cell	Jan. 2008	Test Shaft, Test completed
	03	O-Cell	Jan. 2008	Test Shaft, Test completed
Tysons East-1	4-4	O-Cell	Nov. 2009	Production Shaft, Test completed
	18-1	Statnamic	Mar. 2010	Production Shaft, Test completed
	19-3	O-Cell & Statnamic	Nov. 2009 and Jan. 2010	Production Shaft, O-cell Test was not completed, Statnamic Test was completed.
	20-4	Statnamic	Apr. 2010	Production Shaft, Test completed.
	21-2	Statnamic	Mar. 2010	Production Shaft, Test completed
Tysons East 2	46-2	O-Cell	Mar. 2010	Production Shaft, Test completed
Tysons East Stn.	31-1	O-Cell	Mar. 2010	Production Shaft, Test completed
Wiehle Ave Stn.	15-2	O-Cell	Nov. 2009	Production Shaft, Test completed
Tysons Central Stn.	66-5	O-Cell	Apr. 2010	Production Shaft, Test completed
Tysons West-1	45-2	O-Cell	Aug. 2010	Production Shaft, Test completed
Tysons West-2	4-2	O-Cell	Sep. 2010	Production Shaft, Test completed

Load Test Methodology

<u>O-Cell Test</u>

The O-Cell test essentially consists of two sacrificial metal plates that are loaded by hydraulic pressures acting upward and downward, respectively. Strain gauges are placed at various depths along the shaft to record the relative movements. Typical charts showing upward, and downward movement of the O-cell and the loads recorded by various strain gauges at various depths are given below in Figures 2A and 2B respectively.

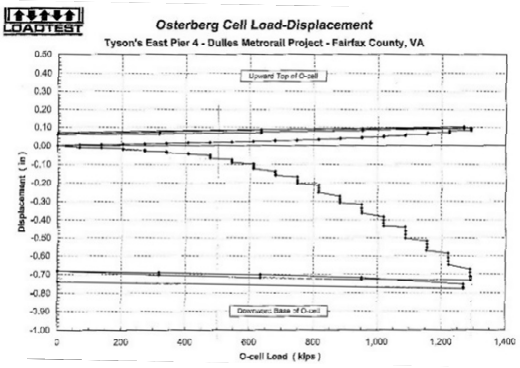


Fig. 2A. Loads versus Displacement

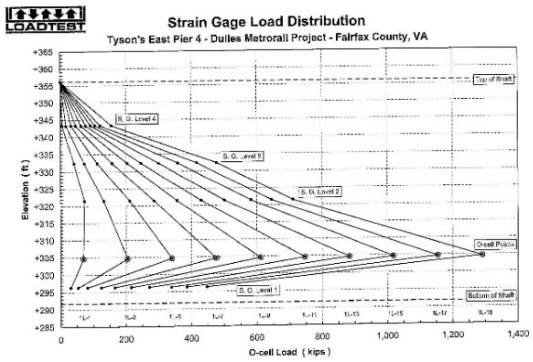


Fig. 2B. Strain Gauge Loads versus Depths

Generally, the maximum load applied depends on project specifications such as, loading until failure or, load to twice the maximum structural load which was specified in this project. From the load versus upward displacements curve, it is possible to calculate the equivalent downward displacements of the top of the shaft and then, construct a curve showing the load versus equivalent downward displacement of the top of shaft for various loadings till the maximum load or, failure load. Also, from readings obtained from various strain gauges, displacements of the shaft in various soils and decomposed rock layers can be used to estimate the side shear. End bearing capacity is calculated by subtracting computed side shear from the applied load. O-Cell test procedure is an easy and quick static load test procedure which, sometimes may be difficult to complete due to construction procedures, as described below.

O-Cell Test at Shaft 19-3

Drilled shaft 19-3 was installed between November 4 and November 5, 2009 using a full depth temporary inner casing seated with a vibratory casing hammer. Due to the placement of the O-Cell near the bottom of the shaft excavation, and the intent to place concrete in dry condition, the bottom of casing had to be sealed at the hard-decomposed rock/bedrock layer. The O-Cell Test performed after about a week was not fully completed due to the lack of side shear resistance to upward movement of the cell (See Fig. 3).

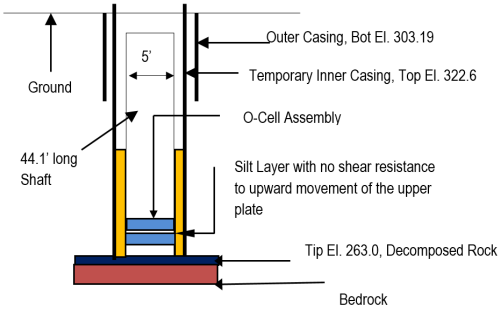


Fig. 3. O-Cell Assembly in Shaft 19-3

The reason for the lack of uplift resistance was determined to be a thin layer of silt that became disturbed by excessive vibration to achieve a water-tight seal in the bedrock as shown in Fig. 3 above.

In order to confirm the capacity of the shaft 19-3, a Statnamic Test was conducted in January 2010 two months after conducting the O-Cell test. The Test results showed a maximum top displacement of 0.96 inch under the applied load of 2274 kips which is more than twice the structural demand of 1100 kips. The top displacement estimated at 1100 kips was 0.10 inch. These results demonstrated the acceptability of shaft 19-3 in accordance with project requirement confirming the acceptability of three other shafts grouped with shaft 19-3 that were installed to the same depth and ground conditions.

Statnamic Test

Statnamic test is a very quick, static load test that can be completed within minutes. The basic principle of the Statnamic Test generally complies with Newton's third law of motion according to which, by burning explosive materials a heavy weight is lifted creating a downward pressure on the test shaft. If the shaft is a planned test shaft, strain gauges can be attached, and relative shaft movement can be measured. From the relative shaft movement, shear data can be calculated. The top displacement is also recorded using a survey instrument. All four Statnamic tests that were performed for the project, were successfully completed.

ENGINEERING PROPERTIES AND GEOTECHNICAL CAPACITY CALCULATIONS

Engineering Properties such as unit weight of soils (γ), friction angle (ϕ) and cohesion (c), etc. were determined in the laboratory. Also, Standard Penetration Resistance (N) values were recorded from about 500 Standard Penetration Test (SPT) borings. In order to use soil and rock properties readily available for axial capacity calculations, an engineering properties calculation was prepared for the project. For all axial capacity calculations, γ, and ϕ values included in Table 1 were used.

Drilled Shaft geotechnical axial capacity for resisting vertical axial load was computed in accordance with AASHTO (17th Edition) and FHWA-1999 Methods (FHWA 1999). According to AASHTO Method, side shear generated by each layer of soil/decomposed rock is averaged over its depth and computed based on the average weight multiplied by a factor β which is a function of depth to the center of gravity of the layer from the top of the ground surface. End bearing was calculated using FHWA 1999 Method that simply considers the effective stress (thickness x unit weight) of each layer above the bearing stratum.

TEST RESULTS AND DISCUSSION

The results of all fourteen load tests are given in Table 3 below. The following Sections below are included for the discussion of results.

Side shear

From above results, it can be seen that the magnitude of unit side shear in S1 and S2 soils varied between minimum 0.2 ksf (at 4-2) to maximum 4.6 ksf (66-5). According to our computations, the side shear recorded based on strain gauge movements sometimes did not fully mobilize. The minimum side shear in shaft 4-2 was recorded generally in fill soils and/or residual soils of blow count of about 10 (S1 soils). Higher side shear was recorded in deeper residual soils with blow counts greater than 10 (S2 soils). The recorded side shear in decomposed rocks ($60 \leq N \leq 100/1''$) varied between minimum 2.3 ksf and maximum 8.0 ksf. Table 3 below includes the computed side shear based on beta method and side shear recorded from load tests.

End Bearing

The end bearing values recorded from all above tests ranged between 41 ksf and 91.8 ksf corresponding to recorded downward O-Cell bottom plate movements between 0.1 inch to 2.81 inches. This magnitude of O-Cell bottom plate movements included movements within the bottom D2/D3 materials combined with the drilled shaft tip movements. The average end bearing resulted was 55.4 ksf. Average end bearing computed using FHWA 1999 Method was 58.3 ksf. These results indicated a general uniformity in strength properties of the decomposed rock.

Assessment of Movements

After reviewing the data of strain gauge data, it can be concluded:

- In all O-cell tests, Strain Gauge Level 1 (in decomposed rock) recorded the maximum upward average shear zone displacement. Maybe the highest side shear values were measured in decomposed rocks.
- The recorded end bearing and side shear values probably do not represent maximum end bearing and side shear capacity of soils and decomposed rock; the applied loads were not continued to ultimate loads because almost all tested shafts were production shafts except for the three tests in the O-1 Guideway.
- Estimated total permanent settlements including elastic settlements in eight O-cell Tests varied between 0.01-inch at shaft O-1#3 to about 0.19-inch at shaft 46-2. Recorded permanent /total settlements in Statnamic Tests at 20-4 and O-1#1 were respectively, 0.29-inch/ 0.46-inch and 0.16-inch/0.38-inch.

COMPARISON OF LOAD TEST RESULTS WITH COMPUTED RESULTS

The side shear values computed according to AASHTO β-Method seemed to result inconsistent side shear values for decomposed rocks (D2/D3) materials; hence side shear of 3.0 ksf was used for D2/D3 materials (Table 4). The computed average side shear values for soils above decomposed rock at load tested piers varied generally from 1.06 ksf in upper Fill/S1 soils to about 2.17 ksf in S2 soils and 2.5 to 3.0 ksf in D1 to D2/D3 materials. The calculated ultimate end bearing generally varied between 55 ksf and 62 ksf with an average end bearing of about 58 ksf which is consistent with tested average end bearing of 55 ksf.

Table 3. Load Test Results in Shafts

Test Location	Test Shaft No.	L x D (ft x ft)	Soil and rock conditions	Test Load Applied (kips)	Equivalent Top Deflection (in)	Side Shear Results (ksf)	End Bearing Results (ksf)
O-1 Gwy	#1	60 x 4	Upper residual soil underlain by Decomposed Rock	3,053	0.38	1-1.6 (Soil) 2.3-5.1 (DR*); upper and lower side shear probably fully mobilized	58.9
	#2	50 x 4	-	1,364	0.03	0.5-0.7 (Soil) 1.5-4.2 (DR); upper side shear not fully mobilized but lower side shear probably fully mobilized	56.0
	#3	50 x 5	-	1,420	0.01	0.4-1.7 (Soil) 5.1 (DR); upper side shear probably not fully mobilized but lower side shear probably fully mobilized	41.0
TE-1	4-4	74 x 4.5	Fill, Residual Soil underlain by Decomposed Rock	1,100	0.07	0.6 to 2.3 (Soil) 7.1 (DR); upper side shear probably not fully mobilized but lower side shear probably fully mobilized	Not Available-insufficient data
	18-1	57 x 5	Fill, Residual and BR (5 ft)	4,191	0.22	Not Available[1]	Not Available[1]
	19-3 O-cell	55 x 5	Fill, Residual				Incomplete
	19-3 Stat	-	-	2,274	0.96	Not Available[1]	Not Avaiable[1]
	20-4 Stat	48.5 x 5	Fill, Residual, Decomposed Rock	2,887	0.46	1.6 – 2.3 (Soil) 2.65 (DR); upper side shear probably fully mobilized but lower side shear probably did not fully mobilize	50.7
	21-2 Stat	54 x 5	Fill, Residual Soil and Decomposed Rock	2,367	0.50	Not Available[1]	Not Available[1]
TE-Stn	31-1	33 x 5	Decomposed Rock (D2/D3)	950	0.03	0.9 to 2.3 (Soil) 6.6 (DR); both upper and lower side shear fully mobilized	49.8
TE-2	46-2	61.5 x 5.5	Fill, Residual Soil and Decomposed Rock	1,259	0.19	1.2 – 2.4 (Soil) 2.5 (DR); probably upper side shear fully mobilized but, lower side shear did not	49.1
T-Central	66-5	39 x 4	Mainly D2/D3	826	0.04	0.4 to 4.6 (Soil) 8.0 (DR); both upper and lower side shear probably fully mobilized	91.8
TW-1	45-2	60 x 6	Fill, Residual soil and Decomposed Rock (D3)	1,539	0.12	0.6 to 1.8 (Soil) 3.9 (DR); both upper side shear probably did not fully mobilize but lower side shear probably fully mobilized	51.3
TW-2	4-2	67 x 6	Fill, Residual Soil and Decomposed Rock	1,320	0.10	0.2 to 1.9 (Soil) 2.5 (DR); none of the upper and lower side shear probably fully mobilized	50.3
Wiehle Ave	15-2	49 x 4	-	700	0.11	0.4 to 1.2 (Soils) 2.8 (DR); none of the upper and lower side shear probably fully mobilized	48.8

*Decomposed Rock, D2/D3

[1] The Statnamic Tests at shafts 18-1, 19-3 and 21-2 were production shafts without strain gauges; no side shear/bearing was recorded.

Table 4. Side Shear Values of Various Subsurface Strata

Layers	Fill/S1	S2	D1	D2	D3
Computed values (β method) (ksf)	1.06	2.17	2.5	3.00	3.00
Load test values (ksf)	0.7	1.7	2.5	4.2	4.2

Comparing the results of load tests with results of project calculations, it is understood that project calculations slightly under estimated side shear values in decomposed rocks and slightly over predicted side shear values in surficial soils (S1 and some S2 soils near surface). As β-Method makes estimates of the unit side shear values based on depth alone, it appears that the method may have tendency to over-estimate the side shear in the surficial soils typically with lower blow counts (corresponding to S1 and S2 soils) and have a tendency to under-estimate the side shear of in the deeper soils typically with higher blow counts (corresponding to D2/D3 soils). But, as a conservative but prudent approach, project calculation for ultimate geotechnical capacity ignored the contribution of skin friction from surficial soils.

Since results of both end bearing and side shear depend on movements of surrounding soils and rock, we believe a possible correlation may exist between the two materials (Osterberg 2000). After reviewing 7 O-cell test results, following plot between end bearing and side shear was prepared:

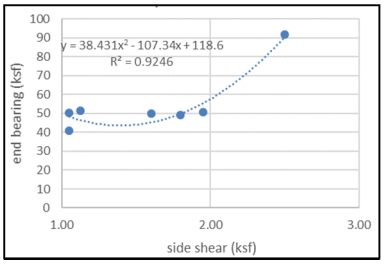


Fig. 4. End Bearing and Side Shear Relationship

Note: Only test results of piers O1-3, 20-4, 31-1, 46-2, 66-5, 45-2 and 4-2 were used for the best fit polynomial graph with R^2 above 0.9.

COMMENTS ON CONSTRUCTION AND DESIGN ISSUES - LESSONS FOR FUTURE PROJECTS

Construction Methodology - Choice of temporary Casing or Slurry

After the incomplete O-Cell Test at shaft 19-3, it was believed that excessive casing vibration duration in the silty soils was the reason for the loss of capacity during the test. In addition, casing handling was becoming increasingly difficult in the congested work area. The drilled shaft contractor made the decision to use slurry from ground support and water control for the remainder of the project.

During drilled shaft installation, many shafts were installed with tip elevations shallower than planned tip elevation due to early refusal. Therefore, both axial and lateral capacities were checked making sure enough geotechnical capacity was available to support structural loads.

Group Effects

Since soils become over stressed (shadowing effects) due to load transferred by a group of piles or drilled shafts, normal practice is to use a lower allowable end bearing capacity considering over stressing of soils due to group action. During initial design, 35% reduction in end bearing due to group effects were considered for shafts spaced at 3 times the shaft diameter. But, after performing load tests, it was believed that reduction of 35% end bearing in decomposed rock (D3) or bedrock, would be too conservative. The capacity of these materials was believed too high to be over stressed. Consequently, during installation of shafts when D3 or rock were encountered and confirmed, no group capacity reduction was considered.

AASHTO 2014 Method of Calculation for Geotechnical Axial Capacity

The computation of drilled pier capacity using FHWA 1999 and AASHTO 1997 Methods began in 2004 when the project started. We believe FHWA 2010 (FHWA 2010) and current AASHTO 2014 LRFD Method (AASHTO 2014) can result higher capacities in dense sands and IGMs matching load test data more closely.

CONCLUSION

A total of 14 load tests consisting of 9 O-Cell tests and 5 Statnamic tests were performed at Dulles Corridor Metrorail-Phase I Project. From these tests, values of side shear for soil and decomposed rock strata and values of end bearing for decomposed rock strata could be determined. We believe these results could be used as a guide for a preliminary design of drilled shafts in Piedmont geology, especially in Northern Virginia. Comparing computed results with test results, it was understood that calculations slightly over predicted surficial (Fill/S1 and S2) soils, matched closely with the test results of D1 soils and slightly under estimated D2/D3 materials (deeper layer materials). Average end bearing in D2/D3 materials resulted from these tests was about 55 ksf which was slightly lower than computed average end bearing 58 ksf. The geotechnical capacity of each pier was calculated using AASHTO-17th Edition and FHWA 1999 Method. The results show that calculated values were generally consistent with overall test results. Some construction lessons were learnt and some new computation methodologies according to AASHTO (2014) have become available; all of this information is anticipated to help design and construct drilled shafts in similar geological settings in the future.

REFERENCE

American Association of State Highway and Transportation Officials (AASHTO) Specifications for Highway Bridges, 17th Edition, 1997.

Federal Highway Administration (FHWA), Publication Number FHWA-IF-99-025, “Drilled Shafts: Construction Procedures and Design Methods”, August 1999.

Federal Highway Administration (FHWA), Publication Number FHWA-NHI-10-016, “Drilled Shafts: Construction Procedures and Design Methods”, May 2010.

American Association of State Highway and Transportation Officials (AASHTO) LRFD Bridge Design Specifications, 7th Edition, 2014.

Osterberg, Jorj, 2000. Side Shear and End Bearing in Rock Sockets for Drilled Shafts, Geo Strata, July 2000, pp 14-17.

EXPERIMENTAL COMPARISON ON DIFFERENT PILE LOAD TESTING METHODS

Gianpiero Russo, DICEA, University of Napoli Federico II, Italy, phone:+390817683475, email: pierusso@unina.it
Gabriella Marone, DICEA, University of Napoli Federico II, Italy, phone:+390817683475, email: gab.marone@gmail.com

ABSTRACT

The paper presents experimental results of two Osterberg's cell load tests (OLTs) and three conventional load tests (COLTs) in the same subsoil conditions on similar Continuous Flight Auger (CFA) piles. The instrumentation along the pile shaft in all the tests allows interesting comparisons of both global behavior and local load transfer. Significant differences in the stiffness of the pile-soil system with the different tests procedures are outlined. The main differences between the two test procedures occur at the two opposite ends of the pile while the observed behavior is similar in the middle part of the tested piles. The stiffness of the piles obtained by the two testing procedures are largely different with the OLTs providing by far the stiffest response. As many methods for the settlement predictions of pile groups rely upon the stiffness of the single pile care should be taken when considering the experimental results obtained different pile testing procedures.

Keywords: Kentledge, **Load test, Osterberg, Pile, Stiffness.**

INTRODUCTION

It is widely accepted that a static load test to failure is by far the most reliable method to determine both the bearing capacity and the load-settlement relationship of a pile. Consequently, the most significant progresses in the field of pile design have been obtained just by collecting and interpreting data from load tests. Until a few years ago, research was mainly focused on the bearing capacity; only recently, attention has been switched to settlement under live load. Two main factors have pushed the research in this direction:

- the increasing use of large-diameter bored piles and barrettes whose current design methods are settlement based;
- the development of new settlement-based design criteria for piled raft foundations.

The static load test may be very expensive and the cost is mainly related to the arrangement of the reaction system. To this aim kentledge or tension piles are alternatively used in order to find the cheapest solution out of the two. In both cases the raw data measured during the test should be corrected because of the interaction between the reaction system and the tested pile (Poulos, 1998; Mandolini et al. 2005). Osterberg's cell load test (Osterberg, 1989; Schmertmann & Hayes, 1997) is a cheaper alternative to the conventional static top-down load test, at least when the load to be applied exceeds 3-4 MN (England, 2003). The higher the load to be applied the more the saving on the total cost of the load test. To transform the experimental results of such a test in those of an equivalent top-down load test, an interpretation based on several hypotheses is needed (Russo *et al.,* 2003). The approximations induced by these hypotheses, even if generally accepted, have never been investigated neither experimentally nor theoretically.

In this paper, three CO*nventional* top-down static L*oad* T*ests* (COLTs) and two O*sterberg's* cell L*oad* T*ests* (OLTs) on the same pile type (CFA piles) in the same subsoil conditions are presented. The five tested piles were all instrumented to measure axial strains along the pile shaft. Interesting conclusions are deduced directly from the experimental data and from the observed differences.

© 2018 Deep Foundations Institute

SUBSOIL CONDITIONS AND LAYOUT OF THE TESTS

The test site is located in the plain east of Napoli where the subsoil is composed by products of the Vesuvius and Phlegrean volcanoes (Russo et al. 2012). The groundwater table is located close to the ground surface. The load tests were carried out in the framework of the design of the foundations of a new big trade centre; on the whole, five design load tests to failure and twelve proof load tests have been carried out. The design tests included three conventional, top-down, maintained stage load tests (COLTs) on piles with different lengths and diameter and two OLTs on piles with similar geometry and length.

Eleven boreholes allow to describe the soil profile on the whole area. First made ground is found in all the boreholes with thickness ranging between 1 m and 3 m. A second layer with a thickness in the range 8-11 m consists of pyroclastic sandy soil. Finally, at a depth ranging between 10 and 12 m below the ground surface, the bedrock is encountered. It is a volcanic grey tuff characterized by a rather variable degree of cementation in the upper few meters. A few deep boreholes show that the thickness of the tuff layer is rather uniform on the whole area and is equal to at least 20 m. In Fig.1 the results of CPTs and SPTs are plotted against the depth together with a schematic soil profile derived by the available boreholes.

The intermediate pyroclastic soils is a silty sand, with a gravel fraction consisting in volcanic white pumices not exceeding 10%. In the middle of the layer the silt (volcanic ashes) slightly prevails over the coarser fraction as it is confirmed by the CPT profiles.

In Fig. 2 the values of the friction angles ϕ, derived from the CPTs and SPTs results, are plotted versus the depth. The values derived by the correlations based on SPTs are slightly larger than those derived by the correlations based on CPTs even if the trend with the depth is similar: this result is quite common in pyroclastic soils.

The piles are CFA which is a widely adopted installation technology in the Italian market. In Table 1, the geometry of the tested piles, the maximum applied load and the maximum recorded displacement are summarised.

Table 1. Summary of Conventional top-down load test (COLTs) and Osterberg's load cell test (OLTs) data

Pile test	L (m)	d (m)	Applied load (MN)	Settlement (m)	Maximum stress in the pile section(MPa)
COLT1	14,40	0,80	8,00	0,008	15,9
COLT2	13,00	0,80	8,56	0,010	17,0
COLT3	13,00	0,60	6,04	0,027	21,4
OLT1	12,60	0,80	5,75	-	11,4
OLT2	13,90	0,80	7,75	-	15,4

All the piles were embedded in the tuff layer with a socket depth ranging between 2.5 and 5 diameters and were instrumented with vibrating wire gauges to measure the load transfer along the pile shaft. The three piles CO*nventionally* L*oad* T*ested* were used as pilot piles at the design stage and for this reason they had slightly different geometry. The two OLTs were carried out for research purposes and the length of the pile was slightly different because of the slightly different depth of the bedrock at the pile's location.

The reaction to the hydraulic jack used to load the pile in the COLTs was provided by a kentledge supported by two provisional rectangular foundations placed on two opposite sides relative to the pile to be tested. For the OLTs the settlement is not reported because two different values are available: one is the settlement of the tip of the pile and the other is the upwards displacement

of the head of the pile. In the case of OLTs, the hydraulic jack were linked to the bottom of the reinforcement cage, which had to be lowered down in the fresh concrete as usual for CFA piles. Care was taken in this step which was supposed to be a critical one, but, however, no special difficulties were recorded. Since the reinforcement cage was long as the pile shaft, the hydraulic jack was exactly placed at the pile base. The settlement of the pile head for the COLTs and the vertical displacement of three points for the OLTs– that is, the pile head, the top and the bottom plate of the base load cell - were measured using precision survey and adopting a benchmark sufficiently far away from the area of the test. Ordinary tell-tales were adopted to allow the measurements of the plates of the base load cell. In both cases (OLTs and COLTs), vibrating wire gauges were installed after the pile construction in a closed-end steel pipe linked to the reinforcement cage, centred in the pile section and subsequently concreted (Russo, 2004). It is to be noted that the piling machine, the construction sequence, the concrete and the reinforcement cages adopted were the same for both the groups of piles tested either conventionally or by the Osterberg's load cell.

LOAD TEST RESULTS

The five piles tested were carefully monitored in the execution stage. The piling machine had a data logger on board which registered data from the sensors and provided useful real time data to the operator.

The load settlement relationships of the three COLTs on pilot piles are represented in Fig. 3. The curves show that only in the third test, COLT3, the pile fully mobilised its shaft friction, showing a sudden increase of the settlement at about the maximum applied load. The two tests COLT1 and COLT2 were executed on piles with the same diameter but with different socket lengths: both the piles are far from failure and exhibit similar behaviour mainly governed by the shaft friction along the shaft. The end bearing mobilised at maximum load was rather small in all the tests. As summarized in table 1 at the maximum test load the average stress in the structural section was fairly high and not so far from the yielding stress of the concrete (20-25 MPa). The load tests were stopped both for this reason and for having almost equated the available weight provided by the installed kentledge.

In Fig. 4 the load displacement relationships measured in the two OLTs are plotted. In such a case, as usual for this test type, for each pile test, two separate curves for the shaft friction, S, and for the end bearing, P, are plotted. The sharp increase of the upwards displacement at the end of both tests show clearly that the limiting value of the shaft friction was nearly reached while the full end bearing in the tuff socket was still far to be mobilised as shown by the linear trend of the P-w curve. The pile in the case of the OLT1 was 12,60 m long while in the case of OLT2 was 13,90 m long. The shaft friction mobilised in the OLT1 was about 6 MN while in the OLT2, at the same upward displacement, the mobilised shaft friction was about 7 MN, the ratio between these two values being very similar to the ratio between the two different lengths as it could be expected being the piles embedded in the same subsoil.

In the same Fig. 4 the shaft and the point resistance mobilised during the COLTs 1 and 2 are also superimposed to the values obtained by the OLT2 and the OLT1 respectively. In order to compare the shaft resistance mobilised during the COLTs and the OLTs both the resistances are plotted against an upwards displacement, which in the case of the COLT is simply the observed downwards displacement changed in sign. The selection of two COLTs out of the three available has been made on the obvious basis of the geometric similarity with the piles tested with the Osterberg's load cell. All the compared piles have a diameter of 80 cm but not exactly the same length due to some variability of the bedrock local depth. First of all, a general agreement between the results obtained with the two different test procedures must be remarked. Nevertheless, some minor differences can be noted and commented. In both the compared couple of tests, the measured pile's stiffness' in the OLTs are higher than those observed in the COLTs. As shown by the same Fig. 4, the two test procedures allow to investigate the tip or point resistance in largely different ranges, the OLT being capable of investigating the mobilisation of the tip resistance at much larger displacements than the COLT's ones. Little can be said on the comparisons for the ultimate tip resistance while the comparisons show that the stiffer behaviour, if any,

is that obtained during a COLT. Of course the results of the OLTs provide valuable information on the large tip resistance available in the tuff socket for the tested piles. More details on the experimental results and on the interpretations are available elsewhere (Russo, 2013). Further to the separation between shaft and base resistance, the gauges installed along the pile shaft allowed the building of local load-transfer functions widely known as t-z or t-w curves (Kraft et al. 1981).

EQUIVALENT TOP-DOWN LOAD-SETTLEMENT CURVES

Osterberg (1989) and Schmertmann & Hayes (1997) suggested the possibility to derive an equivalent load-settlement curve of the pile head from the results of the OLT, similar to that obtained via a COLT. The suggested procedure relies upon two main hypotheses:

i) the pile is axially rigid;
ii) the load-displacement relationship for the shaft resistance is independent of the direction of the relative movement between the pile and the surrounding soil.

A third implicit and often neglected assumption is that the stress-strain field at the pile base and along the pile shaft are not mutually interacting: that is, the load-settlement relationship of the base and of the shaft are practically independent and can be considered separately.

The assumption i) could indeed easily be removed at the cost of some complexity in the process of the interpretation of the experimental results. The remaining two assumptions are mandatory, not only to work out the equivalent load-settlement relationship at the pile head, but also to use simply the results of the OLT in any design method for piles under axial top load.

The main steps of the suggested procedure, keeping the assumption of a rigid pile, are as follows:

- an arbitrary value of the settlement is selected; being the pile rigid, the settlement has a unique value along the whole shaft;
- the values of both the shaft and the end bearing resistance mobilized at the selected value of the settlement are evaluated on the appropriate load-displacement curves;
- the two forces are simply added obtaining the value of the total head load corresponding to the selected value of the settlement in the equivalent curve.

A point of the equivalent load-settlement curve of the head of the pile is thus obtained. A complete load settlement curve can be obtained by repeating the procedure, adopting different values of the tentative settlement. The equivalent curves obtained by the two available OLTs are compared with the load-settlement curves measured during the two COLTs in Fig. 5. In such a case the curves derived by the OLTs were obtained removing the hypothesis of rigid pile and using the average of the two settlement values recorded at the pile head and at the pile tip (i.e. the upward displacement of the top plate of the embedded load cell) as the tentative displacement entered in the shaft curve.

As clearly shown by the plotted curves, the initial stiffness obtained by the equivalent curves of the OLTs is much higher than the initial stiffness of the piles measured during conventional load tests. This occurs even though the piles conventionally tested were a bit longer than the corresponding ones submitted to OLTs. This result however may be not surprising because it corresponds to behavior predicted also by numerical analysis (Russo et al., 2003) and may be a straightforward consequence of the different tests procedures. Experimental comparisons as the ones reported in this paper are however very rare despite the long time the bottom-up load test has been proposed and used. The difference between the two load test procedures however mitigates at increasing load and, at least for the first comparison, at the maximum test load, with the shaft friction fully mobilized in the OLT, the two experimental curves tend to superimpose almost perfectly. For the second comparison the curve measured during the COLT stops before approaching the equivalent curve obtained by the OLT. Even in this second case, however, the differences between the two curves are clearly attenuated at larger load.

LOAD TRANSFER CURVES

The load transfer curves for each load step are plotted in Fig. 6. Each curve obviously correspond to the base load applied at that step. The values of the axial load were obtained simply multiplying the strains measured by the vibrating wire gauges times the axial stiffness of the pile E_pA. The value of E_pA was experimentally derived equating the bottom value of the axial force to the nominal load applied via the load cell at the bottom of the pile. The experimentally derived E_pA was about 20% higher than the theoretical value obtained multiplying the Young's modulus of the concrete (E_p=28GPa) adopted for the construction of the pile shaft for the area of the nominal section of the pile (d=0,80 m). This experimental finding is mainly due to the fact that the true section of the pile was a bit larger (20% increase) than the nominal one as observed by the data on the concrete volume poured along the pile shaft and logged in the computer of the piling machine.

The two piles were both socketed into the deep layer of volcanic tuff and showed similar axial load transfer. In the bottom part of the piles, below 8 m, nearly 65 % of the total load applied at the pile tip was transferred to the surrounding soil. Only the residual 35% was transferred to the upper part of the pile where the curves of the axial force N show a rather small gradient. From the curves of the axial force N the classical t-w curves can be easily deduced (Kraft et al., 1981), such curves being a local relationship between the unit friction t and the local settlement w.

In fig. 7 t-w curves derived by the OLTs and the COLTs are plotted and compared for each of the three main soil layers sketched in Fig. 1. As it could be expected the higher strength is available in the bottom layer which includes the tuff socket with limiting shaft friction mobilized at the end of the test as high as 0,4-0,45 MPa. The lowest mobilized shaft friction, in the intermediate sand layer , is in the range 0,09 – 0,12 MPa while in the upper sand the mobilized shaft friction ranges between 0,15 and 0,18 MPa. The plots of Fig. 7 allow to explore the nature and the exact location of the differences emerged between the two load test procedures; the comparison between the two test procedure in terms of strength is rather satisfactory, even being the COLTs generally far from the entire mobilization of the pile base bearing capacity. Little more can be said on the same topic looking at the local behavior represented by the t-w curves. Particularly in the upper layer of sand and made ground the COLTs approach larger values of the limiting shaft friction compared to the OLTs. This fact may be at least partially due to the beneficial influence of the weight of the kentledge used in the COLTs on the confining stress around the piles. A scattered behavior emerges from the comparison between the two test procedures in the intermediate layer whose thickness however, as shown by the CPTs profiles, is largely variable around the test site. In the tuff socket a rather brittle behavior is obtained during the OLTs and little can be said on the comparison between the two test procedures due to the early stop of the COLTs.

The comparison on the stiffness looks more interesting. In the upper layer the stiffness measured during the COLTs is higher than the one measured during the OLTs. The opposite occurs in the bottom layer. The scatter of the data in the intermediate layer allows only to state that in terms of average behavior no substantial differences arise between the two test procedures.

As it could be expected the larger differences between the two test procedures are located at the top and at the bottom of the piles, while only minor differences are detected in the middle of the piles.

CONCLUSIONS

The paper has presented and compared the experimental results obtained from two OLTs and three COLTs in the same subsoil conditions on CFA piles carefully monitored during construction stages. The three COLTs were carried out on pilot piles at the design stage which had slightly different diameter (0,6 and 0,8 m) and length. The two OLTs were carried out on piles with a diameter of 0,8 m and only minor difference in length due to the local variability of the bedrock's depth.

The vibrating wire gage installed along the pile shaft in all the tests allowed to determine local load transfer and to separate the pile's shaft and the pile's base contribution.
The stiffness of the pile-soil system measured with the two load tests procedures show significant differences. The OLTs provide a stiffer response compared to COLTs the difference being a decreasing function of the load intensity. This experimental result correspond to the expectations of already published numerical studies (Russo et al., 2003). At least within the limits of the explored range the load-settlement relationships observed with the two testing methods tends to be more more similar at high load levels. Since in recent years a number of methods for the predictions of the settlement of pile groups based on the very initial part of the load-settlement relationship of the single pile have been published (Randolph, 1994; Mandolini et al., 2005) care should be thus taken when considering the results of pile tests obtained with different testing methods.

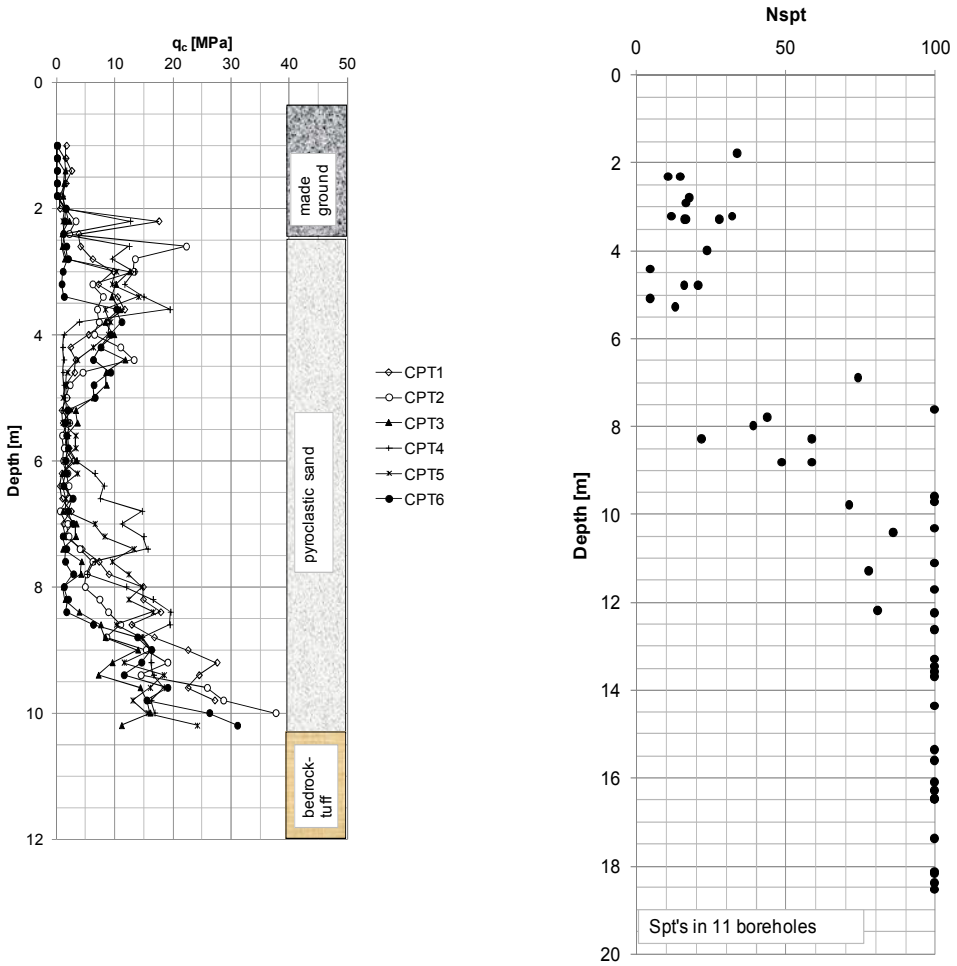


Fig. 1. Cpt, Spt, and soil layering as deduced by boreholes.

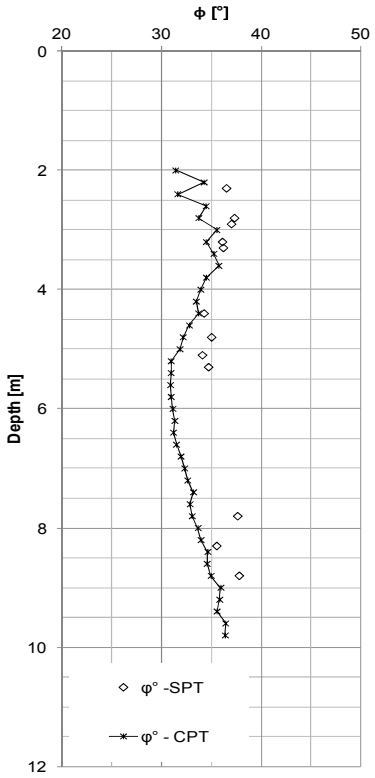


Fig. 2. Friction angle deduced by penetration tests.

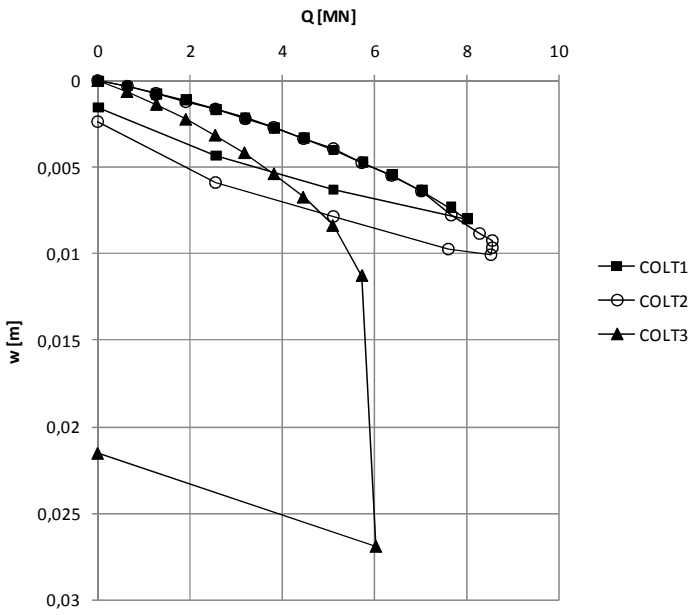


Fig. 3. Results from conventional load tests on three different piles.

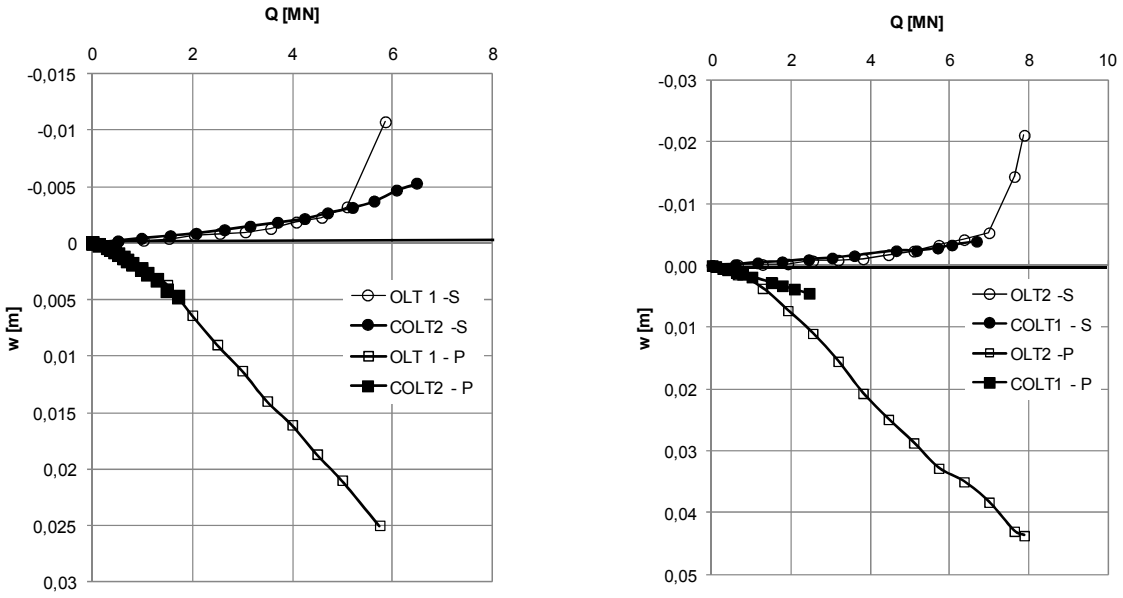


Fig. 4. Shaft and Tip load-displacement curves as mobilised in the OLTs and in the COLTs

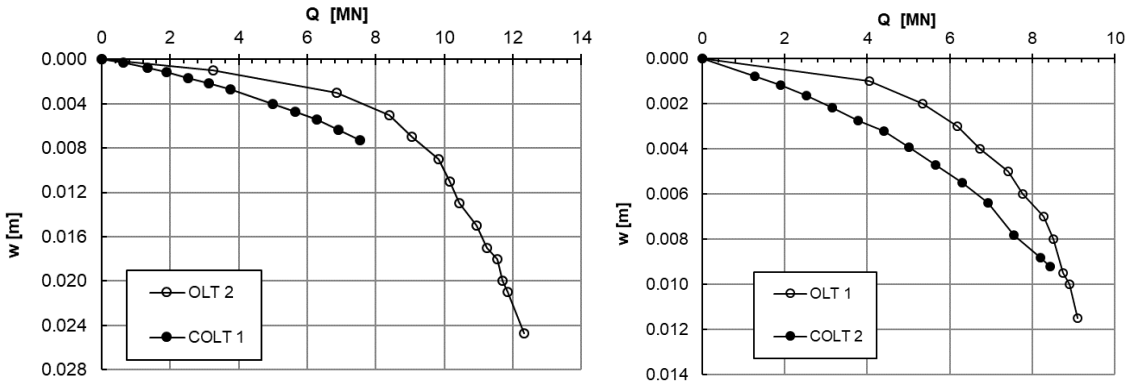
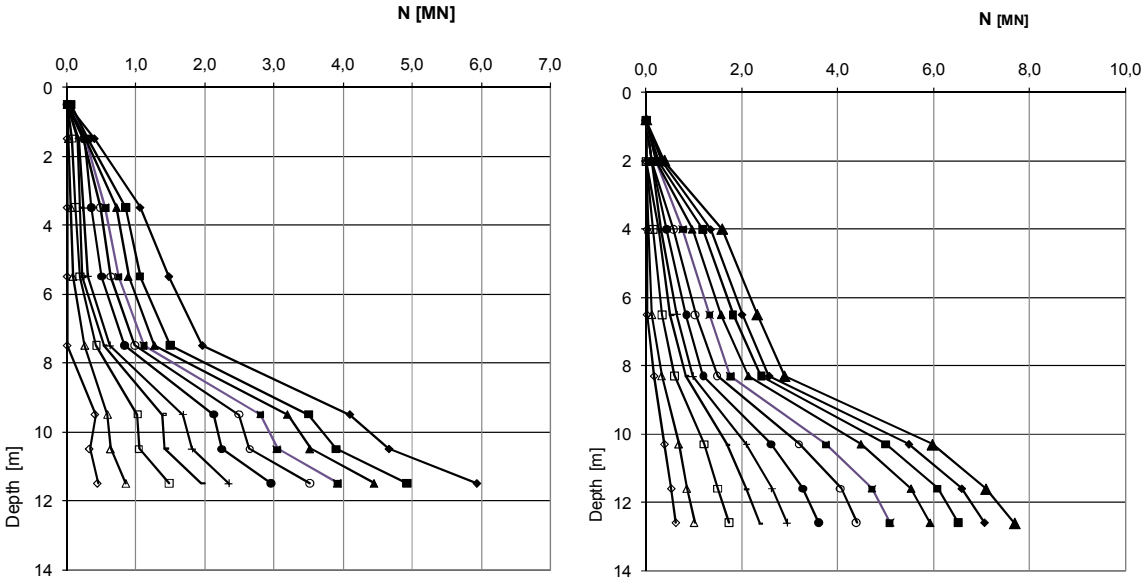


Fig. 5. Equivalent Top-Down Load-settlement curves derived by OLTs and Load-settlement derived by COLTs.



a) b)

Fig. 6. Axial load, N, transfer along the shaft at various load levels for the OLT 1 a) and OLT 2 b)

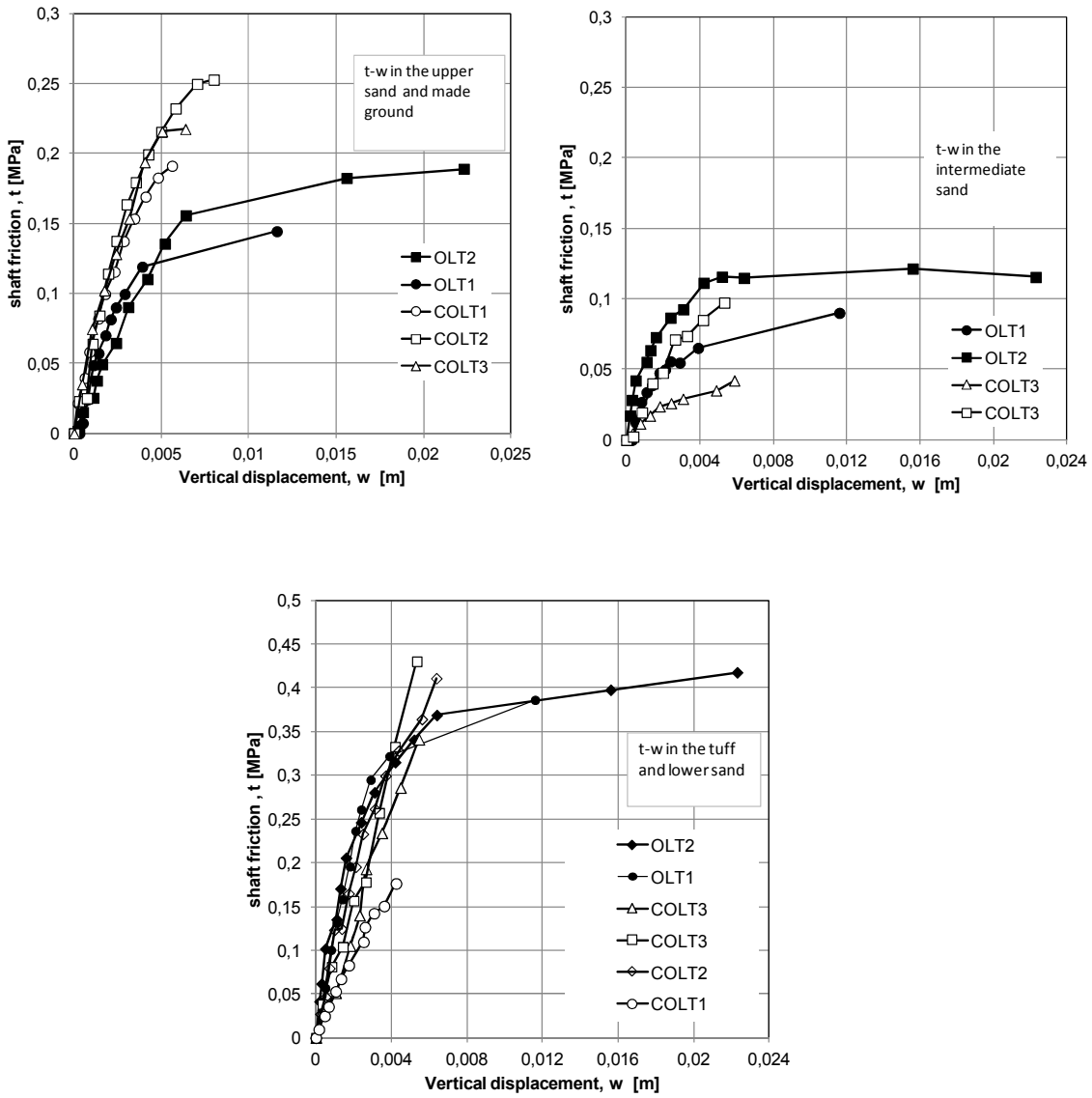


Fig. 7. Comparison among t-w curves for each soil layer derived by OLTs and COLTs

References

England M. (2003) Bi-directional static load testing – State of art. Proc. 4th Int. Geot. Seminar on Deep Foundations on BAP, Ghent, Belgium, June 2003, pp. 309-313

Kraft L., Ray R.P. and Kagawa T. (1981) Theoretical t-z curve. Journal of Geotech. Eng. Div. Asce, vol. 108 n° 11, 1981, pp. 1543-1560

Mandolini A., Russo G., Viggiani C.(2005) Pile foundations: experimental investigations, analysis and design. State of the Art Report. Proc. Of the Sixteenth International Conf. on Soil Mechanics and Geotech. Eng. Vol. I, Osaka, Japan, 2005 pp.123-168 .

Osterberg J.O. (1989) Breakthrough in load testing methodology. Foundation Drilling, Ed. ADSC., vol.28, n° 8, 1989, pp. 13Poulos H.G.(1998) Pile testing-from the designer's viewpoint. Proc. 2nd Int. Statnamic Seminar, Tokyo,1998, pp.3-22.

Poulos H.G., Carter J.P., Small J.C. (2001) Foundations and retaining structures – Research and practice. Proc.XV ICSMGE, Istanbul, 2001, vol. 4, pp. 2527-2606

Russo G. (2004) Full scale load tests on instrumented micropiles. Journal of Geotechnical Engineering proc. I.C.E. vol. 57, GE3, 2004, pp. 127-137.

Russo G., Recinto B., Viggiani C. & de Sanctis L. (2003) A contribution to the analysis of Osterberg's cell load test. Proc. 4th Int. Geot. Seminar on Deep Foundations on Bored and Auger Piles, Ghent, Belgium, June 2003, pp.331-338

Russo G., Viggiani G, Viggiani GMB (2012). Geotechnical design and construction issues for Lines 1 and 6 of the Naples Underground. Geomechanik und Tunnelbau (ISSN:1865-7362) pp. 300 - 311 Vol. 3

Russo G. (2013) Experimental investigations and analysis on different pile load testing procedures. Acta Geotechnica vol.8 pp. 17 – 31

Schmertmann J.H., Hayes J.A.(1997) The Osterberg cell and bored pile testing – A symbiosis. The third International Geotechnical Engineering Conference, Cairo, Egypt, 1997.

EXPERIMENTAL INVESTIGATIONS ON THE LATERAL BEARING BEHAVIOR OF VIBRATORY-DRIVEN OPEN STEEL PIPE PILES

Johannes Labenski, Institute for Geotechnical Engineering (IGS), University of Stuttgart, Germany, PH: +49 711 685 63779; email: johannes.labenski@igs.uni-stuttgart.de

Christian Moormann, Institute for Geotechnical Engineering (IGS), University of Stuttgart, Germany, email: christian.moormann@igs.uni-stuttgart.de

ABSTRACT

The paper describes the experimental setup used at the Institute for Geotechnical Engineering (IGS) at the University of Stuttgart to investigate the lateral load bearing behaviour of vibratory-driven steel pipe piles in dense saturated sand. The test material, the measurement devices and the experimental procedure are explained in a comprehensive manner. Afterwards the result of the pile installation and the lateral load test of one representative model test are shown and explained for one typical test in detail. The results are given in dimensionless values, i.e. a comparison with other model tests documented in literature is possible. To demonstrate the installation behaviour, the pile penetration velocity and the vertical acceleration measured at the pile head are shown. The lateral load bearing behaviour is investigated using a lateral load-displacement curve of the pile head. The experimental lateral load-displacement curve is compared with analytically determined curves using different p-y approaches. This comparison shows partially good agreement between model test and analytical solution. Nevertheless, it indicates need for further investigation, which is an ongoing process at the IGS.

Keywords: vibratory driving, steel pipe piles, monopile, lateral bearing behaviour, soil-pile-interaction

INTRODRUCTION

The lateral load bearing behaviour of open steel pipe piles depends, among others, on the pile diameter, the embedment length of the pile, the interface friction angle between the pile and the soil, the relative density of the soil and the installation method. During the vibratory-driven installation the pile is vertically excited by a dynamical force acting down- and upwards. This vertical excitation of the pile leads to an excitation of the soil grains which are moved not only vertically, but also horizontally (Hartung 1994). In accordance with findings by Hartung (1994) for piles vibratory driven with a frequency of 40 - 50 Hz, the soil around the pile shaft during installation can be divided into two different zones: a liquefaction zone close to the pile shaft and a compaction zone. Due to the dynamical excitation the soil grains in the liquefaction zone are moving with high velocities leading to a higher volume of the soil in this area. After pile driving, the relative density in the liquefaction zone is low while there is a high relative density in the compaction zone. In the area around the pile toe, the soil is behaving similarly.

Current research by e.g. Kallehave et al. (2012) or Klinkvort et al. (2013) on the lateral load bearing behaviour of monopiles focuses on the modification of current approaches, e.g. the p-y approach (DNVGL-ST-0126). In this research pile installation effects are neglected, while the influence of different lateral load situations is investigated. In literature only one large scale field test is documented investigating the lateral load bearing behaviour of vibratory-driven monopiles (cf. Moormann et al. 2016). In this field test, a slightly stiffer lateral load bearing behaviour has been observed, if the pile was impact-driven. This lack of research was motivation to conduct own experimental tests with the focus on the investigation of the influence of installation effects due to vibratory pile driving on the lateral load bearing behaviour.

© 2018 Deep Foundations Institute

EXPERIMENTAL SETUP

Test Material – Sand

The scaled model tests have been conducted with saturated Berlin Sand. The corresponding grain size distribution curve is shown in Fig. 1. The sand has a maximum density $\rho_{d,max}$ of 1.856 g/cm^3 corresponding to a minimum void ratio of 0.433, as well as a minimum density $\rho_{d,min}$ of 1.563 g/cm^3 corresponding to a maximum void ratio of 0.702. Further laboratory tests on the sand used for the tests are provided by Le (2015).

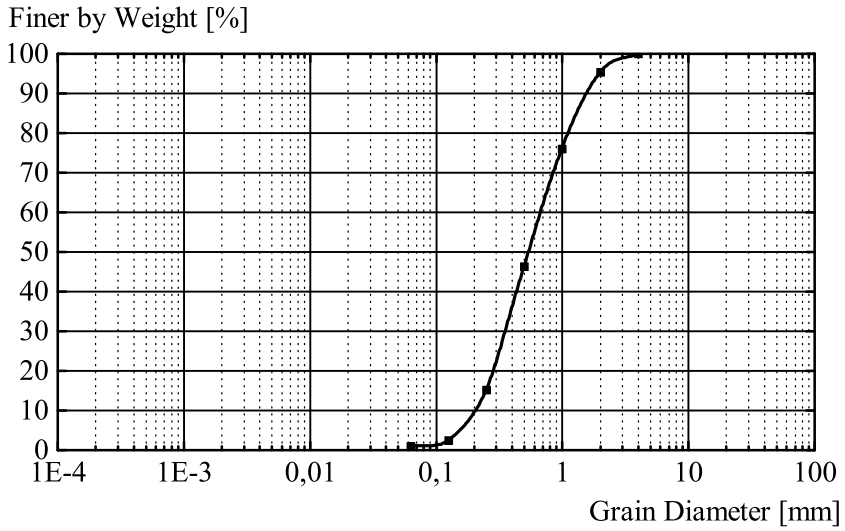


Fig. 1. Grain size distribution curve of Berlin Sand used in the scaled model tests

Test Material – Pile

The properties of the model pile are depicted in Table 1. In reality steel tube piles are used as monopiles. In the scaled model tests, a glass-fibre reinforced pile has been used instead to accurately scale down the flexural rigidity of the pile (cf. Wood 2004). A picture of the pile is shown in Fig. 2. The dimensions of the pile lead to an L/D ratio of 4.2, which is typical for monopiles.

Table 1. Properties of the model pile

Property	Unit	Value
Diameter	[m]	0.208
Length	[m]	2.00
Embedment length	[m]	0.87
Wall thickness	[m]	0.0032
Mass	[kg]	10.0
Mass incl. vibrator and vibrator mount	[kg]	75.0
Flexural rigidity EI	[kNm^2]	550

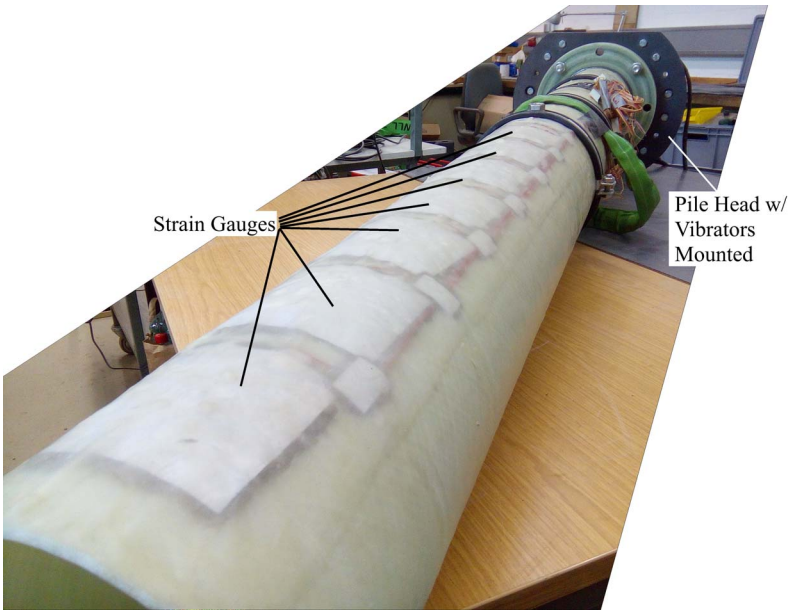


Fig. 2. Photo of the model pile

Test Container and Measurement Devices

The set-up of the 1-g model scaled tests is illustrated in Fig. 3. The scaled model tests were conducted in a cylinder shaped concrete container with a diameter of 2.0 m and a height of 2.5 m. The container was filled with a 0.3 m drainage layer followed by 2.2 m of Berlin Sand. The two layers were separated by a fleece. The whole concrete container can be flooded with water rising from the bottom, which has the advantage that the structure of the installed sand is not disturbed and remained homogeneous while being saturated (cf. Tasan 2011). The dimensions of the concrete container ensure a horizontal distance of 4.5D from the external pile shaft surface to the boundaries and a vertical distance of 7.5D from the bottom of the pile to the bottom of the concrete container.

During the pile installation, the acceleration at the pile head was measured with a triaxial accelerometer. Furthermore, a position transducer was continuously monitoring the penetration of the pile. In further tests, acceleration sensors have been placed within the soil to precisely investigate the dynamic behaviour of the sand during pile installation. During the horizontal pile load test, the bending moment of the pile was measured with strain gauges, which were placed along the part of the pile shaft that is embedded into the sand. Only one pair of strain gauges was placed at the pile head where no bending occurs, i.e. temperature effects can be compensated. In total, nine strain gauge measurement layers were placed on the pile. Furthermore, the pile head displacement was measured with three displacement sensors. With these two quantities, the bending curve of the pile could be back-calculated. Also the horizontal force was continuously monitored and recorded during the horizontal pile load test. In Table 2 the abbreviations used in Fig. 3 are documented.

Table 2. Sensors used in the scaled model test

Sensor	Shortcut
Acceleration Sensor	ACC
Position Transducer	PT
Strain Gauges	DMS 1..9
Load Cell	H_0
Displacement Transducer	W1, W2, W3

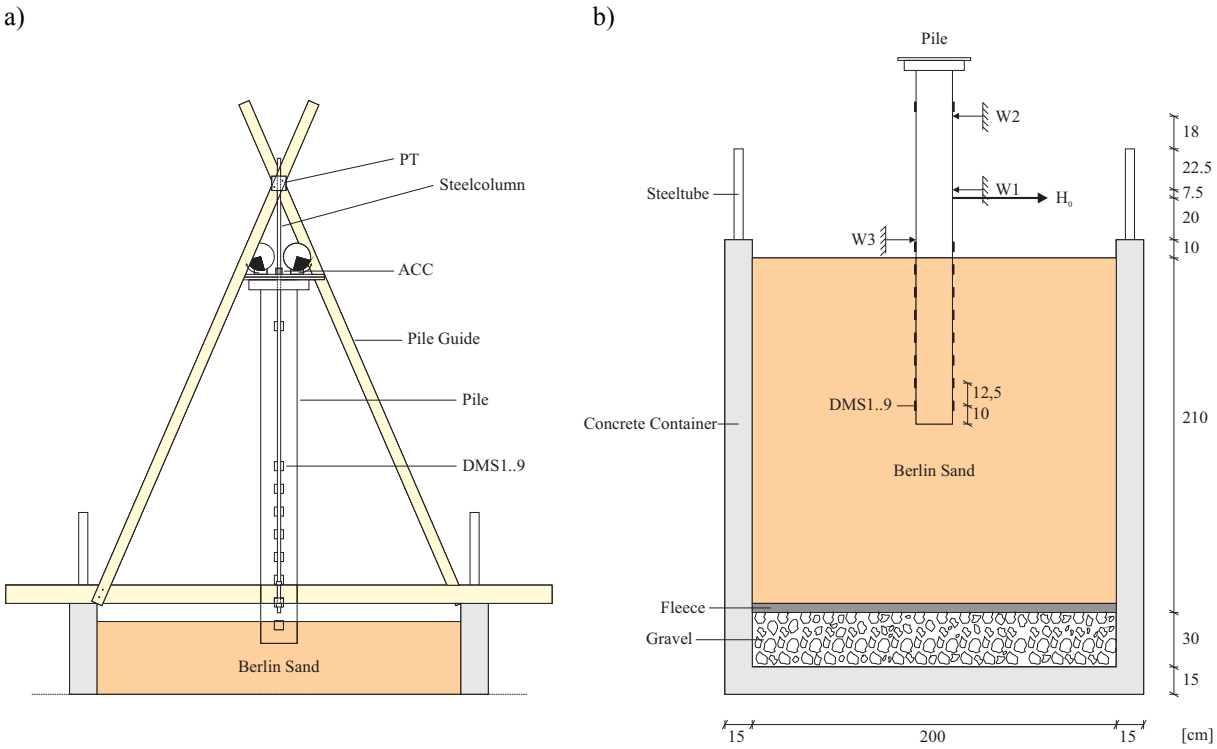


Fig. 3. Model setup a) for pile installation and b) for lateral pile load test

Experimental Procedure

The main target of the scaled model tests was to investigate the influence of different installation parameters on the lateral load bearing behaviour of vibratory-driven monopiles. Installation parameters are the frequency f and the static moment M_{stat} of the vibrators. Besides the installation parameters, also the density of the sand was varied. The scaled model tests were carried out under 1g conditions.

The scaled model tests consist of different steps. In the first step, the sand was filled homogeneously in the model container. In the second step, the pile was vibratory-driven to the desired embedment depth. In the third step, a lateral pile load test was carried out to investigate the lateral load bearing behaviour.

The tests were conducted in medium-dense, dense and very-dense sand. The sand was installed layer by layer. Trickling of the sand was not possible, because the sand could not be dried after each test, thereby remaining moist. Every layer was compacted by an electrical vibratory plate.

The pile was installed in the sand with a vibrator unit generating a maximum centrifugal force of 4.4 kN at a frequency of 25 Hz. Two WUERGES HV 6/4-18 were mounted on top of the pile via two steel plates. The frequency and harmony of the vibrators was controlled by a frequency converter.

The lateral pile load test was carried out with a pneumatic cylinder, which generates the tension force H_0. The pneumatic cylinder can be controlled by an electric function generator. This setup has the advantage that only with slight modifications a cyclic lateral force can be applied as well.

Prior to the test series with the vibratory-driven piles, a reference test was carried out by jacking a pipe pile instead of vibrating. A maximum force of 25 kN was needed to push the pile to the desired embedment depth, which exceeds the maximum centrifugal force of the vibrator by a factor of 5.5.

SELECTED RESULTS

Pile Installation

In the following section results of a representative model test are shown. Different dimensionless values are introduced to investigate the results.

The installation parameters can be expressed as a dimensionless frequency f^* and a dimensionless static moment M_s^*:

$$f^* = \frac{f_{Vibration}}{f_{Resonance}} \quad [1]$$

where $f_{Vibration}$ is the vibration frequency and $f_{Resonance}$ is the investigated resonance frequency of the vibrator-pile-soil system (cf. Massarsch et al. 2017).

$$M_s^* = \frac{M_{stat}}{M \cdot D} \quad [2]$$

where M_{stat} is the static moment of the vibrator, M is the mass of the vibrator-pile system and D is the diameter of the pile.

As depth, the relative embedment depth L^* is introduced, which is defined as follows:

$$L^* = \frac{L(t)}{L_{Vibration}} \quad [3]$$

where $L(t)$ is the measured vibration depth at time t and $L_{Vibration}$ is the total length installed by vibration.

In the presented model test the pile was vibratory driven with a $f^* = 0.82$ and a $M_s^* = 0.0075$ in dense sand. In Fig. 4 the penetration velocity over depth as well as the vertical acceleration measured at the pile head over installation time are shown. Positive accelerations are directed downwards in penetration direction. Negative accelerations are directed upwards, against penetration direction.

The velocity profile presented in Fig. 4a shows a decrease of velocity with increasing embedment depth. At the start of the installation process the penetration velocity has its maximum at 55 mm/s and already drops to 30 mm/s after 10% of pile penetration. Afterwards it is increasing and decreasing again in a pseudo sinusoidal pattern. This may be due to minor inhomogeneities during the sand preparation process. Nevertheless, in these two regions, a mean velocity can be considered. It can be noted, that these regions have the same size, i.e. $\Delta L^* = 0.3$ for both regions. In the first region between $L^* = 0.1$ and $L^* = 0.4$ a mean velocity of 25 mm/s can be considered. In the next region between $L^* = 0.4$ and $L^* = 0.7$ the mean velocity decreases to 20 mm/s. Between $L^* = 0.7$ and $L^* = 1.0$ the penetration velocity decreases drastically to a value of 2.5 mm/s just before the end of the penetration process. The large decrease of penetration velocity at the beginning of the installations emerges from the small initial embedment depth of the pile. At the beginning of the installation process, the pile can more or less move free. After 10 % of pile penetration, it is likely that the soil resistance at the pile toe and shaft increases and the penetration velocity decreases.

Pile penetration is only possible, if there are plastic deformations in the surrounding soil. If there were only elastic deformations, no (further) pile penetration could be possible. Between $L^* = 0.7$ and $L^* = 1.0$ it seems that the soil behaviour around the pile is transforming from a plastic behaviour to an elasto-plastic or almost elastic behaviour. This effect might result from a densification of the

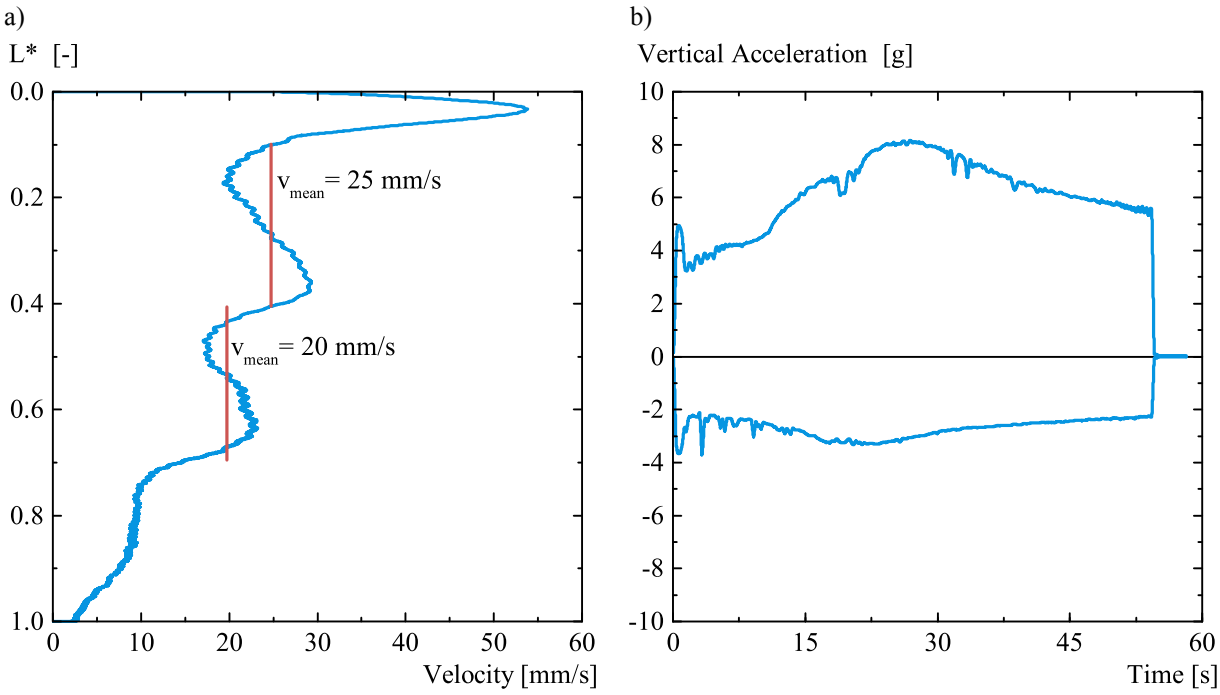


Fig. 4. a) Pile penetration velocity over relative embedment depth; b) Vertical acceleration measured at the pile head during installation

surrounding sand. If the sand is densified, the shaft resistance of the pile increases. With an increased shaft resistance, the displacement amplitude of the pile reduces and thus, also the penetration velocity.

Another possible reason might be arching of the soil within the pile and thus a higher soil resistance. This reason is supported by observations during the model test. After completion of the test, as the pile was extracted from the sand, a soil plug inside the pile was extracted too. This might be a "local" effect due to the small pile diameter in the scaled model tests, though numerical simulations on vibratory-driven piles revealed an increase of lateral stress acting on the pile shaft at the inside of the pile (cf. Labenski et al. 2016).

The acceleration profile in Fig. 4b shows a strong increase of accelerations directed downwards until a peak value of 8g is reached. After this peak value, the acceleration is decreasing. This decrease corresponds to a depth between $L^* = 0.7$ and $L^* = 1.0$, i.e. when the velocity decreases, the acceleration decreases as well. The vertical acceleration can be directly linked to the displacement amplitude of the pile, i.e. when the displacement amplitude of the pile reduces the pile penetration rate reduces as well for the reasons stated above.

Lateral Pile Load Test

In Fig. 5 the normalised lateral load-displacement curves of the model tests are shown. The horizontal force H_0 was made dimensionless according to Klinkvort et al. (2013) as follows:

$$P^* = \frac{H}{\gamma' D^3 K_p} \quad [4]$$

with

$$K_p = \tan^2(45° + 0.5\,\varphi') \quad [5]$$

$$\varphi' = 31.5° \exp\left(0.42\, I_D^{2.9}\right) \quad [6]$$

according to Le (2015) for Berlin Sand.

The lateral deflection y was made dimensionless as follows:

$$y^* = \frac{y}{D} \quad [7]$$

In the diagram the lateral load scheme can be depicted. The lateral load was increased step-wise. At different load levels, the load was decreased and increased again. The maximum lateral load applied in the model test is considered to be higher than the maximum load in reality..

It can be seen, that the lateral deformations of the vibratory-driven pile are smaller than of the jacked pile. In the mean, the lateral displacements of the jacked pile are increased by a factor of 1.75 in comparison to the vibratory-driven pile.

The load-displacement curve shown in Fig. 5 indicates, creep effects becoming more severe with increased lateral load, especially in the case of the jacked pile. These creep effects may result from a pre-failure stage in the soil. In some tests failure of the soil could be observed as a failure surface developed in the soil on the passive side of the pile.

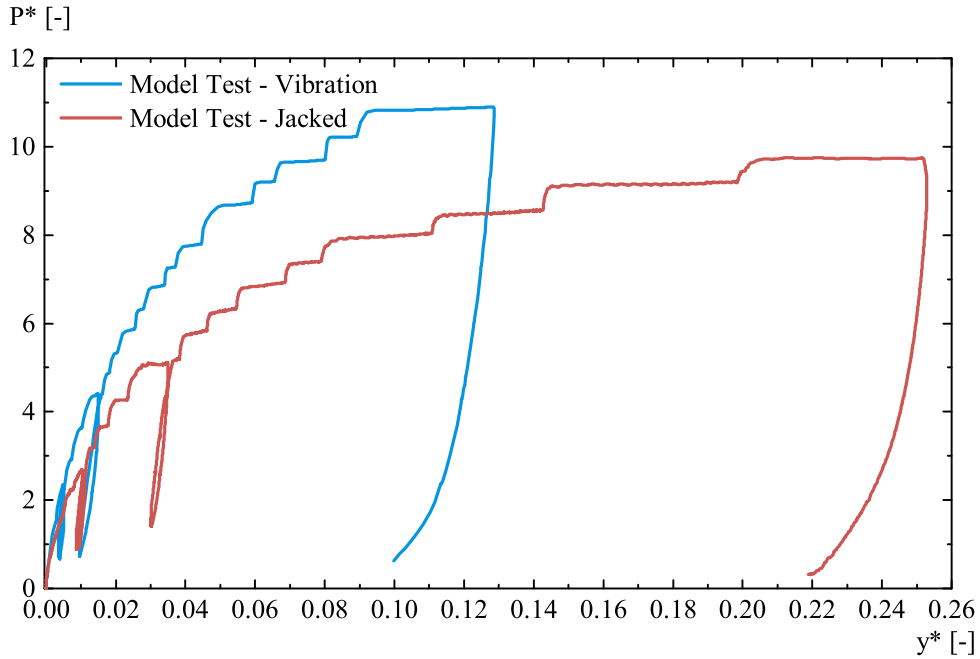


Fig. 5. Normalised lateral load-displacement diagram

COMPARISON

To evaluate the lateral load-displacement curves obtained in the scaled model tests, they are compared with analytical determined lateral load-displacement curves. The p-y approach (cf. DNVGL-ST-0126) was utilized to determine lateral soil reaction springs. In the literature different approaches exist to determine the non-linear spring stiffness in order to take different mechanical and geometrical boundary conditions into account.

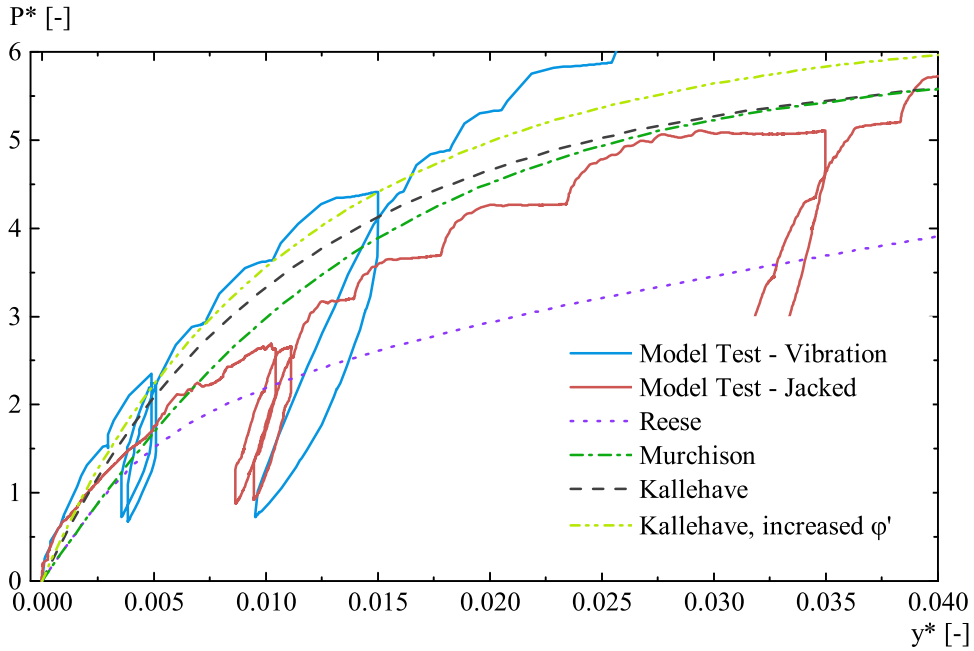


Fig. 6. Normalised lateral load-displacement diagram comparing the result of the scaled model test with the result of the analytical p-y approach

In this paper, the following p-y approaches have been utilized:

- Reese et al. (1974)
- Murchison & O'Neil (1984)
- Kallehave et al. (2012)

The results are presented in Fig. 6. Utilizing the approach by Reese et al. (1974) leads to an overestimation of the true lateral displacements of the vibratory-driven and the jacked pile. This could be expected, as the approach by Reese et al. was originally developed for long slender piles and not for short rigid piles, which are used in the scaled model tests. The approach by Murchison & O'Neil (1984), which is equivalent to the method proposed in DNVGL-ST-0126, shows results closer to the experimental curves. Though this approach is also not validated for monopiles, the characteristics of the load-displacement curve are similar to the experimental curves corresponding to a short rigid pile. This approach overestimates the lateral displacements of the vibratory-driven pile by 30% to 50% in the range of P* = 0 to 5, but underestimates the displacements of the jacked pile only slightly. Considering the modified p-y approach as proposed by Kallehave et al. (2012), even better results can be achieved. The approach by Kallehave et al. (2012) considers an increased soil stiffness at low strain in comparison to the approach by e.g. Murchison & O'Neil (1984). This can be seen in Fig. 6 as well. The initial slope of the experimental load-displacement curve is steeper in comparison to the load-displacement curve obtained with the approach by Murchison & O'Neil (1984), while the ultimate load remains the same. The lateral loading behaviour determined with the modified p-y approach by Kallehave et al. (2012) shows good agreement with the behaviour obtained in the experimental test with the vibratory-driven pile, especially concerning the curvature and slope of the curve up to a lateral load of P* = 4.5.

The comparison of the experimental results with the three analytical determined lateral load-displacement curves shows that with a current modification of the p-y approach suitable for short rigid piles, good agreement can be achieved to the load-displacement behaviour of a vibratory-driven pile in a conservative manner. All presented methods slightly overestimated the lateral displacements. The reason might be the p-y approach itself, as it was not developed for vibratory-driven piles and also current modifications of the p-y approach do not especially consider pile installation effects. As a first

workaround it seems likely to increase the stiffness of the soil springs to achieve better agreement between experiment and analytical solution. This approach was applied, i.e. the friction angle φ' was slightly increased, and is denoted as *Kallehave, increased φ'* in Fig. 6. Very good agreement between the experimental and analytical results can be achieved for the vibratory-driven pile up to a lateral load of P* = 4.5. Even though this approach is only a workaround, it still reveals that due to vibratory-driving lateral load bearing behaviour might become stiffer than analytically determined.

It should be noted, that the ultimate load determined with all the analytical approaches has a value of P* = 6 which is only half of the lateral load applied in the experiment.

CONCLUSIONS

In this paper the experimental setup as well as one representative result of scaled model tests with vibratory-driven piles carried out for 1g conditions has been presented in comparison to the result of a jacked pile. The penetration velocity and the pile head accelerations measured during vibratory-driving have shown that if the pile displacement amplitude reduces, also the penetration velocity reduces. A possible reason might be the densification of the surrounding soil as well as the soil inside of the pile. The comparison of the experimental load-displacement curves of the vibratory-driven pile with the jacked pile has revealed a stiffer lateral load bearing behaviour in case of the vibratory-driven pile. The further comparison of the experimental lateral load-displacement curves with the analytical determined curves has revealed, that with current p-y approaches the lateral load bearing behaviour of short rigid piles can be predicted within a certain range of uncertainty. In the case of a jacked pile, lateral deformations are underestimated whereas in the case of the vibratory-driven pile, lateral deformations are overestimated. The comparison further revealed that the influence of vibratory-driving of monopiles might result in a stiffer lateral load-bearing behaviour than predicted by analytical models. Though, this aspect needs further research and investigation of the test results. Especially the influence of the installation parameters 'frequency' and 'static moment' will be further investigated.

ACKNOWLEDGEMENTS

The tests presented in this paper have been conducted in the frame of the "VibroPile II" project. The authors would like to acknowledge the founding by innogy SE and the support of Ben Matlock and Volker Herwig. The calculations presented in this publication were performed with the IGtHPile software developed by the Institute of Geotechnical Engineering (IGtH), Leibnitz Universität Hannover, Germany.

REFERENCES

DNVGL-ST-0126, April 2016: Support structures for wind turbines. DNV GL Standard.

Hartung, M, 1994: Einflüsse der Herstellung auf die Pfahltragfähigkeit in Sand. Dissertation, Institut für Grundbau und Bodenmechanik, Technische Universität Braunschweig, Heft 45.

Kallehave, D., LeBlanc, C., and Liingaard, M.A., 2012: Modification of the API p-y formulation of initial stiffness of sand. Offshore Site Investigation and Geotechnics: Integrated Technologies - Present and Future, 12-14 September. Society of Underwater Technology, London. pp. 465–472.

Klinkvort, R.T., Hededal, O., and Springman, S., 2013: Centrifuge modelling of drained lateral pile - soil response: Application for offshore wind turbine support structures. Dissertation, Technical University of Denmark.

Labenski, J., Moormann, C., Aschrafi, J., and Bienen, B., 2016: Simulation of the plug inside open steel pipe piles with regards to different installation methods. Proceedings of the 13th Baltic Sea Geotechnical Conference. Vilnius Gediminas Technical University, Vilnius, Lithuania. pp. 223–230.

Le, V.H., 2015: Zum Verhalten von Sand unter zyklischer Beanspruchung mit Polarisationswechsel im Einfachscherversuch. Dissertation, Fachgebiet Grundbau und Bodenmechanik, Technische Universität Berlin, Heft 66.

Massarsch, K.R., Fellenius, B.H., and Bodare, A., 2017: Fundamentals of the vibratory driving of piles and sheet piles. geotechnik, 40(2): 126–141.

Moormann, C., Kirsch, F., and Herwig, V., 2016: Vergleich des axialen und lateralen Tragverhaltens von vibrierten und gerammten Stahlrohrpfählen. Proceedings of the 34. Baugrundtagung, DGGT. Bielefeld. pp. 73–81.

Murchison, J.M., and O'Neill, M.W., 1984: Evaluation of p-y relationships in cohesionless soils. Proceedings of the ASCE Symposium Analysis and Design of Pile Foundations, 01-05 October, San Francisco. pp. 174–191.

Reese, L.C., Cox, W.R., and Koop, F.D., 1974: Analysis of laterally loaded piles in sand. Offshore Technology Conference, 1974, Houston, Texas.

Tasan, E., 2011: Zur Dimensionierung der Monopile-Gründungen von Offshore-Windenergieanlagen. Dissertation, Fachgebiet Grundbau und Bodenmechanik, Technische Universität Berlin, Heft 52.

Wood, D.M., 2004: Geotechnical modelling. E. & F.N. Spon.

EXPERIMENTAL STUDIES ON THE LATERAL LOAD CARRYING CAPACITY OF PIER FOUNDATIONS FOR BRIDGES

Sukhmander Singh, Nicholson Family Professor of Civil Engineering, Santa Clara University, Santa Clara, CA, USA, 408-554-6869, ssingh@scu.edu

ABSTRACT

Piers are the oldest bridge foundation for bridges in countries like India and China. Shallow pier foundation is often subjected to scour by the river. It is desirable to adopt a minimum size which will meet requirements governed by the minimum obstruction to the water way, the economy, length of the pier below the maximum scour level. This length should develop sufficient passive resistance to counteract the overturning movement due to horizontal forces acting on the bridge deck, and those due to wind and water. At IIT-Delhi, a comprehensive study was undertaken on behavior of pier foundation in sandy soils which modeled the influence of the length-to-diameter ratio on the behavior of pier foundations subjected to horizontal loads in terms of the position of the center of rotation, the maximum bending stress and the mobilized lateral soil resistance. It was found that decreasing the length-to-diameter ratio of the pier lowered the location of center of rotation and mobilized higher passive soil resistance. An increase in embedded length reduces the horizontal deflection but increases the bending stresses. The center of rotation was located at a lower level than predicted by the theoretical analysis based upon rigid bulkhead and sub-grade reaction theories.

Keywords: Pier foundation, Lateral load capacity

INTRODUCTION

Pier foundation is one of the oldest types of foundation for bridges in countries like India and China. Piers that are set in the river beds to support bridges are subjected to scour by the river waters. This can adversely affect the lateral load carrying capacity of the pier.

In the construction of piers and caissons, it is desirable to adopt a minimum size which will meet requirements governed by (a) the minimum obstruction to the water way, (b) the economy, (c) length of scour and (d) the grip length. The grip length is defined as the length of the pier below the maximum scour level. This length should be adequate for developing sufficient passive resistance to counteract the overturning movement due to horizontal forces acting on the bridge deck, as well as those due to wind and water. The pier should also be taken deep enough to rest on the strata of adequate bearing capacity in relation to the load transmitted.

The grip length has a very important bearing on the economical design of a pier foundation. An accurate evaluation of the above factor and the manner in which it affects the final design has been given minimal consideration (Bowles, 1988).

The method of designing and sinking caisson foundations has been developing rather slowly from the primitive methods into a successful engineering process; with the results the scientific design of a caisson or a pier for bridges has been an open subject (Rao & Muthushwamy, 1963; Ninan & Murthy, 1964; Teng & Manuel, 1976; Yudhbir 7 Madhav, 1977; Fukuoka, 1977; Hazivar, 1981; Baker, 1985; and Bowles, 1988). More recently, experimental studies on the lateral load carrying capacity including effects of seismic leading and laterally spreading soil have been undertaken (Knappett et al., 2010; Chen et al., 2012; Muhammad et al., 2014; Hung and Yau, 2014).

A comprehensive effort to study the behavior of pier foundation in sandy soils was undertaken at the Indian Institute of Technology-Delhi. Model tests on cylindrical single and double pier foundations were carried out to study to partially explored aspects of scour, lateral earth pressure, length-to-

© 2018 Deep Foundations Institute

diameter ratio, point of rotation and maximum bending stresses. This paper presents and discusses the test results related to the lateral load carrying capacity of piers.

EXPERIMENTAL TEST PROCEDURE

A tank with inside dimensions of 3.8 ft. (width) X 8.25 ft. (length) X 4.1 ft. (height) was fabricated out of steel plates and rolled steel joists.

All model piers were of cylindrical shape. Most of them were made of galvanized iron hollow pipes; and some made of cast iron pipes. Solid wooden cylinders were inserted into these pipes flushing with their inner sides such that each formed one solid piece with the pipe and acted as bottom plug. In all, seventeen models were prepared for single pier testing and eight models for double-pier testing. Five models, each with an external diameter 'd' of 3.47" but with lengths 3d, 4d, 5d, 6d, and 7d formed the first set of models. In the second set, there were five models each with an ext. dia. 'd' of 3.375" and lengths 3d, 4d, 5d, 6d, and 7 times of diameter. And similarly the third set consists of four models each with an ext. dia. 'd' of 1.9" and lengths 3d, 4d, 5d, and 7d.

The rigidity criterion is satisfied in general when length over diameter ratio is less than 8 except in very poor soils (Teng et al. 1976).

Figure 1 shows the component part to measure the horizontal deflection of the model when it is subjected to lateral loading. The arrangement consisted of a spring, a pulleyed block and an inverted gentry girder system. It was designed to keep the vertical load vertical as the pier tilts under the influence of lateral load.

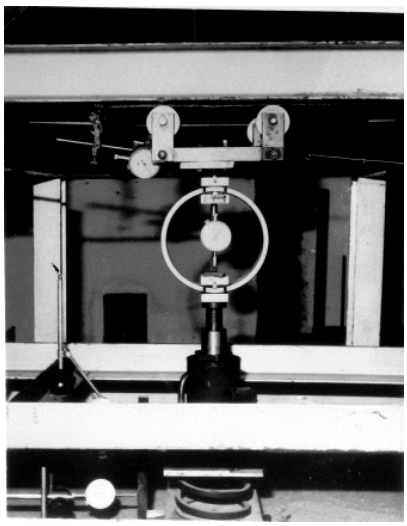


Figure 1. Component Parts to Measure Lateral Deflection

Each of the pier models were set in dry sand which was fairly uniform sand with an effective grain size of 0.2 mm. The filling of the tank was done by carefully spreading sand through a sprinkling process. The sprinkling process was carried out in such a way as to allow a uniform spreading of the sand. The same process was repeated for each test. The model was installed first and sand was deposited around it.

EXPERIMENTAL RESULTS

The experimental results and their discussions as they relate to the lateral load carrying capacity are presented first. In a subsequent section, the results and discussions as they relate to the maximum bending are presented.

Figure 2 shows a pier foundation under lateral load P. Figure 3 shows it in a deflected position. Figure 4 shows the setup for a model to simulate the above two conditions. Fourteen model tests were carried out to study the influence on length-diameter ratio on the lateral load carrying capacity of the pier foundations. Figure 5 shows plots of lateral load vs deflection at the scour level (sand level in the tank) under zero vertical loading for five typical tests. Failure load being reckoned as the load causing complete failure of the model by excessive deflection or a continuous increase in deflection without an increase in the lateral load. For a given horizontal deflection at the scour level, the change the lateral load carrying capacity of the pier model with an increase in the length-diameter ratio was plotted (Fig. 6).

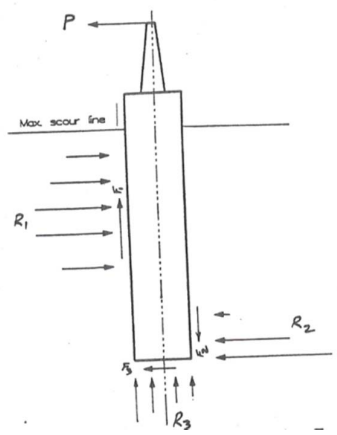


Figure 2. Contact Pressure Distribution according To Sub-Grade Reaction and bulk head theories

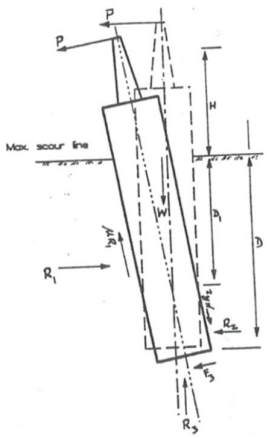


Figure 3. Pier in a Deflected Position

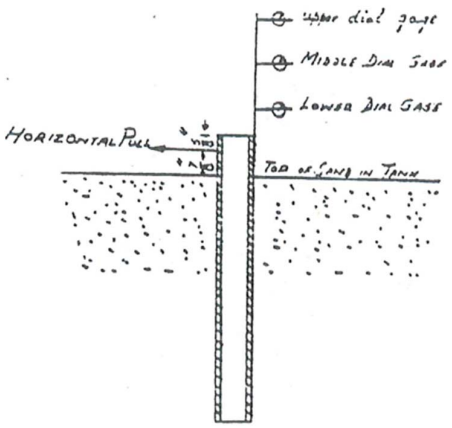


Figure 4. Set up of a Model Pier

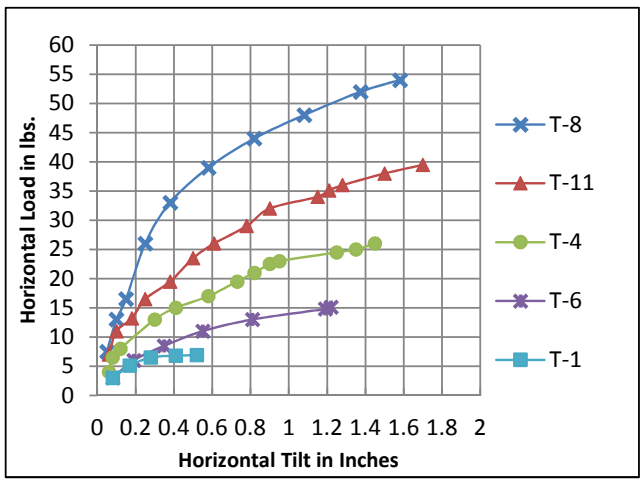


Figure 5. Horizontal Load vs. Deflection at the Top of Sand (For Zero Vertical Loading)

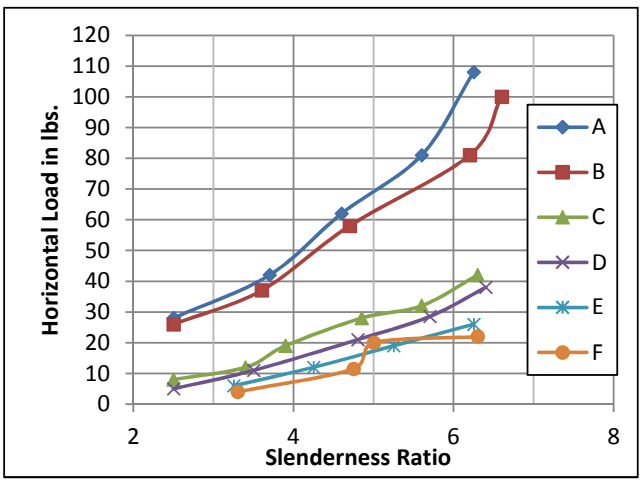


Figure 6. Horizontal Load vs. Slenderness Ratio for a Given Deflection at Top-Sand-Level

The following conclusions can be advanced.

- For a given lateral load, the deflection (tilt) at the sand level reduces as the embedded length of the pier is increased. However, an increase in bending stresses results and is discussed later in a section for maximum bending moment.
- With an increase in the embedded length-diameter ratio, the point of rotation moves up (Figure 7). This is important to note because a greater embedded length will not result in a corresponding increase in lateral load carrying capacity. Conversely:
- With a decrease in the embedded length-diameter ratio of the pier by an increase in diameter, the location of the center of rotation is lowered and higher passive soil resistance is mobilized resulting in an increase in the lateral load carrying capacity of the pier.

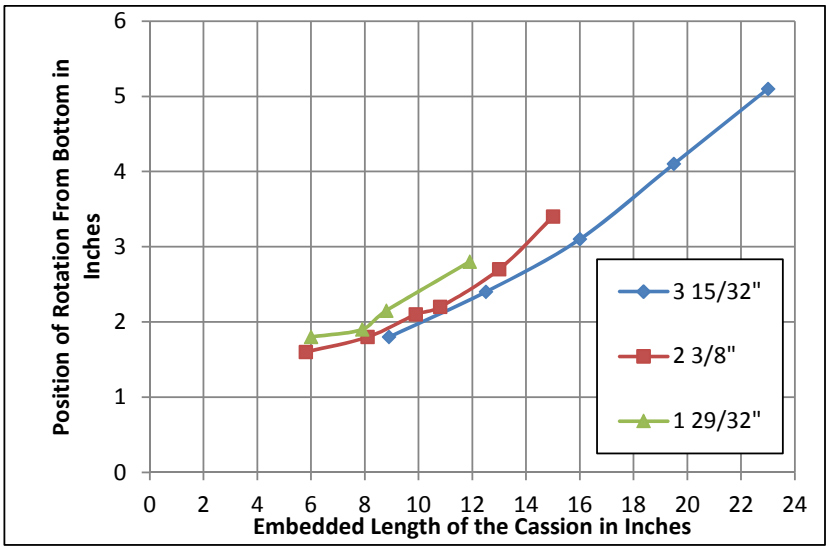


Figure 7. Change in the Position of Rotation of the Caisson with the Increase in the Embedded Length

DISCUSSION

Comparison of the Theoretical and Experimental Results on the Center of Rotation of a Pier under Lateral Loads

The principal of free rigid bulkhead and the theory of sub-grade reaction have traditionally been applied for the design of a pier and caisson foundation (Davisson and Parkash, 1963, Ninan & Murthy, 1964, Davidsson & Salley, 1969, Teng & Manuel, 1976 and Bowles, 1988). Experimental data obtained from the model tests provided the opportunity to examine the applicability of these theories for evaluating lateral earth support to the pier foundation set in sandy soils.

The simplifying assumptions upon which the theories are based are:

1. That the ratio k, between the contact pressure p and the corresponding displacement y is independent of pressure p.
2. The coefficient of vertical sub-grade reaction K_s has the same value for every point of the surface acted upon by contact-pressure.
3. If the sub-grade consists of stiff clay, the coefficient of horizontal sub-grade reaction also has the same value K_h for every point of surface contact.
4. For the cohesionless sub-grades, the value of the coefficient of horizontal sub-grade reaction is determined by the equation:

$$k_h = N_h.Z \qquad [1]$$

Where N_h is an empirical constant.

For the case of a pier set in sand (Fig. 3):

$$N_h = \frac{\frac{P+F_b-F_s}{(3D_1D^2-2D^3)Y_1}}{6D_1} \quad [2]$$

Equation 2 can be readily obtained by applying the above theory and integrating lateral stresses between the appropriate limits determined by D and D_1 the embedded length and the length to point of rotation respectively (see Figure 3). F_b and F_s represent the side friction and Y represents the tilt.

In the case of free rigid bulkhead, the development of side and base friction are of no consequence, the above expression for N_h, therefore reduces to:

$$N_h = \frac{\frac{P}{(3D_1D^2-2D^3)}}{6D_1} Y_1 \quad [3]$$

The equation 3 gives the value of N_h when the theory of sub-grade reaction is applied.

Now for a given tilt of y_1 for a cylindrical pier or caisson, the term:

$$\frac{(3D_1D^2 - 2D^3)}{6D_1}$$

is constant, and for N_h to be a constant as required by the theory of horizontal sub-grade reaction, the ratio of p/Y_1 should be constant i.e., the horizontal tilt of the pier should increase in a direct proportion to the horizontal pressure P. But as seen by the non-linear relationship between horizontal load vs horizontal tilt (Fig. 5) this is not true, i.e. the nature of P-Y curve is non-linear.

Obviously the limit for applying the evaluating the pressure distribution over the face of the pier is the elastic limit strains in the surrounding soil i.e. when the ratio p/y is essentially constant. This can yield horizontal deflections that can be grossly in error when the load P is much greater than say 1/3 to ½ of its ultimate value. As the plastic flow in soil starts, this equation is no longer applicable. Again as the pier deflection and though the soil in the top zone i.e. near the scour line (sand level in tank) and below down to a certain length, has entered into a plastic state, yet a considerable portion of the soil surrounding the pier is still in an elastic state. There can also be an elasto-plastic state where we need yet another approach different from that in the other two cases. As also noted by Teng et al. (1974), a method for predicting P-y curves has been suggested by Reese and Welch (1975), for deep foundations in stiff clays but because of the lack of results from properly instrumented full scale tests on piers subjected to lateral loads, the validation of a method is very slow. Recently lateral load tests on drilled piers have been reported by Bhushan et al. (1978), and Bhushan and Askari (1984). These tests were on short drilled piers. One can use lateral pile type analysis, Bowles (1988) has presented an analysis of laterally loaded piers using the lateral pile program.

Finally a comparison of the center of rotation as determined experimentally and as determined using theoretical approach was made. In the theoretical approach based on sub-grade reaction theories, the expressions for lateral soil reactions R_1 and R_2 (Fig. 8) are obtained by integrating the basic equation for pressure ($P = N_h Z$) between the appropriate limits.

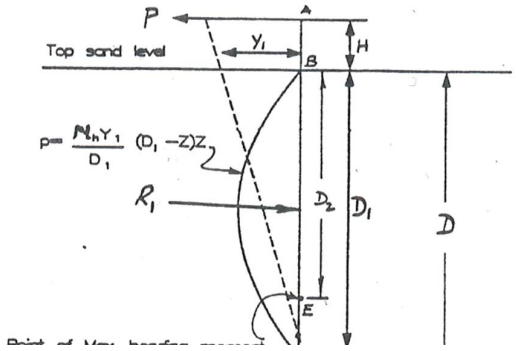


Figure 8. Lateral Soil Pressure Distribution

Then from the equilibrium condition and by taking moments about point C (Fig. 9) and finally by substituting for

$$N_h = \frac{\frac{P}{(3D_1D^2 - 2D^3)}}{6D} Y_1,$$

and expression for D_1, the position of the location of the center of rotation below the scour line, can be obtained in terms of known quantities.

The experimental determination of the point of rotation was straight-forward. For example, the line joining the three gage readings would readily establish the position of the center of rotation. The theoretical and experimental values have been plotted against the length-diameter ratio (Fig. 9).

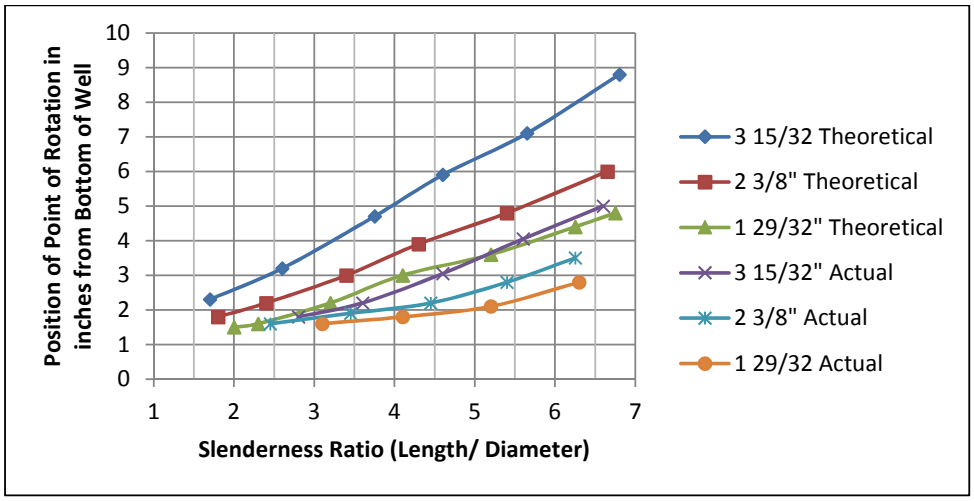


Figure 9. Change in the Position of Rotation of the Pier with the Increase in Slenderness Ratio

The considerable difference between the theoretical and experimental positions of the point of rotation emphasizes the importance of modifying the approach based upon the sub-grade reaction theories.

MAXIMUM BENDING MOMENT

To find the maximum bending moment in the piers, contact pressure diagrams were first drawn for different horizontal loadings.

The horizontal soil reaction at any length below maximum scour line (sand level in tank) is given by the expression:

$$p = N_h \frac{Y_1}{D_1}(D_1 - Z)Z$$

When X varies from 0 to D_1 and the value of P has been chosen from within the elastic state of soil.

And,

$$p = N_h \frac{t_1}{D_1}(D_1)Z \; when \; Z \; is \; greater \; than \; D_1.$$

Calculations for the contact-pressure at various lengths are then made and contact-pressure diagrams are drawn. The shape of the contact-pressure diagrams are shown in Fig. 10 for one of the models.
The pressure diagram was used to establish a general equation for bending moment and then the magnitude and the point of the maximum bending moment was determined. For a given lateral load and for a given diameter of a pier, the maximum bending moment induced in the caisson, has been plotted against the embedded length of the pier (Fig. 11).

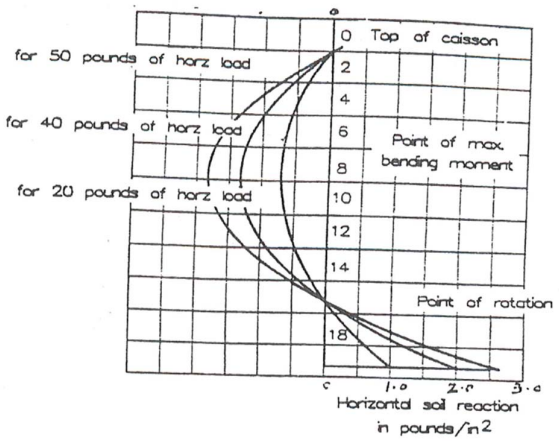


Figure 10. Horizontal Soil Reaction (Contact Pressure) Along the Embedded Length of Pier for Different Horizontal Loadings in Case of Pier No. T-9

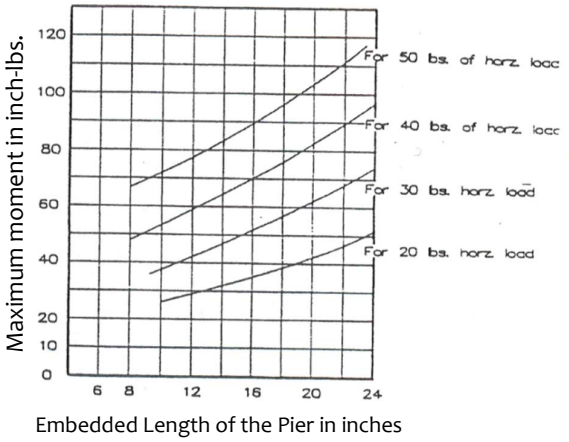


Figure 11. Maximum Bending Moment Vs. Embedded Length of the Pier For a Given Horizontal Loading

The conclusions which may be drawn from the above analysis are discussed below.

I. If the embedded length obtained from the consideration of bearing capacity requirements, is inadequate to develop enough passive resistance against lateral loads then normally the following two alternatives are considered.
   (i) To increase the grip (or the embedded) length while keeping the pier diameter unchanged.
   (ii) To increase the pier diameter while the grip length is kept unchanged.

The present investigation indicates the following results in that regard:

(a) It is better to increase the diameter than to increase the embedded length of the pier because:
   (i) For a given horizontal load, an increase in the embedded length will result in an increase in maximum bending moment, which in turn will necessitate a stronger and heavier pier and hence an uneconomical design
   (ii) The difficulty in sinking deeper lengths does not favor increasing the embedded length of the pier.
   (iii) With an increase in the embedded length, the point of rotation moves up and the capacity of the pier to take up lateral load under a given deflection is compromised.

(b) On the other hand, with an increase in the diameter of the pier, not only the object of developing adequate passive resistance against lateral load is achieved, the maximum bending moment induced for a given lateral load will also remain unchanged. With the result, a

corresponding decrease in the thickness of the large diameter pier is possible; and the pier does not become too heavy to satisfy the bearing capacity criteria.

CONCLUSION

On the basis of the model studies described above, on single cylindrical piers subjected to lateral loads, the following conclusions can be advanced.

1. It was found that with a decrease in the embedded length-to-diameter ratio of the pier, the location of the center of rotation is lowered and higher passive soil resistance is mobilized.
2. An increase in embedded length reduces the lateral deflection at scour level but increases the bending stresses.
3. The center of rotation as determined experimentally was found to be located at a lower level than predicted by the theoretical analysis based on rigid bulkhead and sub-grade reaction theories.
4. If the embedded length obtained from the consideration of bearing capacity requirement, is inadequate to develop enough passive resistance against lateral loads then with regard to the two alternatives which are usually considered viz (i) to increase the embedded length of the pier, while keeping the pier diameter same or (ii) to increase the pier diameter while the embedded length is kept unchanged; the present investigation has drawn the following conclusions:
    (a) An increase in the embedded length would result in an increase in the maximum bending moment, although the horizontal load carried by the pier under zero vertical loading remains unchanged. The increase in maximum bending moment would in turn necessitate a stronger and heavier pier.
    (b) On the other hand, by increasing the diameter of the pier, not only the object of developing adequate passive resistance against lateral load could be achieved, but, for a given lateral load, the maximum bending moment induced in the section of the pier will also remain unchanged. With the result, the wall thickness for a larger diameter pier can be reduced such that the section of the pier remains strong enough to take up the unchanged bending moment, the pier does not become too heavy for bearing capacity criteria.

ACKNOWLEDGEMENTS

I gratefully acknowledge the help given by Melanie Massie, Rachel Flores, and Gianluca Onorato.

REFERENCES

1. Baker, C. N. Jr., et al., (1989), "New Combined Footing and Drilled Shaft Foundation Design", Found. Eng. Curr. Princ. Pract. Vol. 2, Pub. By ASCE, New York, NY, pp. 1459-1472
2. Baker, C. N. Jr., (1985), "Drilled Piers and Caissons of Foundations", Proceedings, ASCE Convention, USA, Publ. ASCE, New York, USA, p. 153
3. Banarjee, A., Gangopadhaya, S. (1960), "Study on the Stability of Caisson Foundations for Major Bridges", Journal of the Indian Road Congress, Paper No. 226, Vol. XXV, Part 2.
4. Bowles, J.E. (1988), Foundation Analysis and Design. 4th Edition, McGraw Hill Book Co. New York, pp. 886-889
5. Chaturvedi, D.C., (1981), "Practical Problems in Well Foundation of Bridges", Journal of the Institution of Engineers, India, Civil Engineering Division 61: 5, p. 253-262.
6. Dawood, H., ElGawady, M., Hewes, J., (2012), "Behavior of Segmental Precast Posttensioned Bridge Piers under Lateral Loads", Journal of Bridge Engineering, Vol. 17, No. 5, pp. 735-746.

7. Fukuoka, M. (1977), “Interaction Problems of Well Foundation and Piers”, Int. Symp on Soil Struct. Interaction, Univ. of Roorkee, India, Pub. By Abhay Rastogi for Sarita Prakashan, Meerut India, p. 537-556.
8. Hazivar, W.K., (1981), “Behavior of Caisson-Like Deep Foundations”, Proc. Int. Conf. Soil Mech. Found. Eng. 10th, Pub. By A.A. Balkeme, Rotterdam Neth, and Salem, NM, USA, Vol. 2, pp. 133-140.
9. Hung, C., and Yau, W., (2014), “Behavior of scoured bridge piers subjected to flood-induced loads”, In Engineering Structures, 80:241-250.
10. Knappett, J. A., Mohammadi, S., and Griffin, C., (2010), “Lateral Spreading Forces on Bridge Piers and Pile Caps in Laterally Spreading Soil: Effect of Angle of Incidence”, Journal of Geotechnical and Geoenvironmental Engineering, Vol. 136, pp. 1589-1599.
11. Matlock, H., Reese, L, (1960), Journal of Soil Mechanics & Foundation Engineering, Division of ASCE, Vol. 86, No. SM500??
12. Muhammad, S., and Reza, (2014), “Lateral Load resistance of Bridge Piers under flexure and shear using factorial analysis”, Engineering Structure, Feb. 2014, Elsevier Ltd. 59:821-835.
13. Ninan, P.K., and Murthy, V.N.S., (1964), “Experimental Studies on Stability of Caisson Foundations for Bridges in Sand”, Journal of Ind. National Society of Soil Mechanics and Foundation Engineering.
14. Rao, B., Balwant, and Muthuswamy, C., (1963), “Consideration in the Stability of Cassion Foundations for Bridge Piers”, Journal of the Indian Road Congress, Paper No. 238, Vol. XXVII.
15. Teng, W., and Manuel, F., (1976), Cassion Foundations Subjected to Lateral Forces”, IEEE Transactions on Power Apparatus and Systems, V PAS-95 No. 4, p. 1435 – 1445.
16. Yudhbir, M.R., and Madhav, (1977), “Settlement of Large Caissons on Stratified Alluvial Deposits”, Proc. Of the Fifth Southeast Asian Conference on Soil Engineering, Thailand, p. 55 - 62.

GROUP EFFECTS FOR PILE ROWS UNDER PASSIVE LATERAL LOADING

Johannes Aschrafi, Institute for Geotechnical Engineering (IGS), University of Stuttgart, Germany,
PH (0049) 711 685-62437; Fax (0049) 711 685-62439; email: johannes.aschrafi@gmx.de
Shreyas Giridharan, Institute for Geotechnical Engineering (IGS), University of Stuttgart, Germany,
PH (0049) 711 685-63777; Fax (0049) 711 685-62439; email: shreyas.giridharan@igs.uni-stuttgart.de
Christian Moormann, Institute for Geotechnical Engineering (IGS), University of Stuttgart, Germany,
PH (0049) 711 685-62437; Fax (0049) 711 685-62439; email: christian.moormann@igs.uni-stuttgart.de

ABSTRACT

Ground movements in soft cohesive soils impose lateral pressure on piles. Among others, here the magnitude of pressure depends on the amount and speed of ground movement, the pile's bending stiffness and the geometrical boundary conditions. In recent decades, considerable effort has been devoted by many researchers to study the problem of lateral pressure on piles in soft cohesive soils, experimentally and using numerical methods. Unfortunately, these investigations have led, for example, to highly divergent calculation approaches, e.g. pile group factors.

In classical *Lagrangian* Finite Element Method, large soil displacements distort the finite element mesh which might lead to inaccurate results or the numerical analysis does not converge to a stable solution. Therefore, most numerical based research on lateral loads was done for moderate soil displacements. Numerical investigations of the problem are more challenging when large deformation respectively is involved. In continuum-based models, the traditional description of kinematics is either based on *Lagrangian* or *Eulerian* approach where each has its own advantages and disadvantages. Coupling the two descriptions in one approach by exploiting the best features of each is therefore desirable. One coupling approach, called the Material Point Method (*MPM*) will be explained in brief. The potential of the method is shown with respect to the results of a small-scale test on a single pile in soft clay. Furthermore, numerically calculated lateral pressure and group effects will be discussed.

Keywords: piles, lateral thrust, passive, soil-pile-interaction, CPDI-method

INTRODUCTION

Pile foundations are selected whenever structural loads must be transferred to deeper and less compressible soil layers (e.g., gravel, rock, etc.). Such pile foundations tend to be loaded primarily in the axial direction. On the other hand, they may experience shear forces and bending moments if the pile caps are fixed to the building and are laterally acted on by horizontally moving ground.

This can occur if piles are installed in creeping slopes or next to heavy surcharge loads, especially in soft cohesive soils with high water content, or in highly organic soils such as tidal mud or peat. Owing to the extreme loading conditions, the pile shafts may become heavily stressed, which in turn may lead to serviceability problems (*SLS*), or even pile failure (*ULS*) as the soil 'squeezes' between and around piles. Typical applications where pile systems or groups are loaded in the lateral direction, e.g. by creeping soil has been reported by Ito et al. (1982), Poulos (1995), Ausilio et al. (2001), Cai & Ugai (2011). Laterally loaded piles associated with moving ground have also been reported for one-sided surcharge loads (Bransby & Springman 1997, Jeong et al. 2004) and piled bridge abutments (e.g. Stewart et al. 1994, Ellia & Springman 2001).

Determining the magnitude of the passive lateral loads requires not only knowledge of the material properties, but also of the stress fields that develops around a pile. Predicting these stresses requires taking into account the highly nonlinear stress-strain relation of the soil, as well the complex, large non-linear deformation and contact processes between the pile and the moving ground.

© 2018 Deep Foundations Institute

Wenz (1963) was one of the first to treat the problem of passive loads on piles in soft soils in detail. Based on plasticity theory and model experiments, the limiting pressure on a single pile was determined to be between 7*cu* and 10*cu*, where, *cu* is the undrained shear strength of the soil. Broms (1964) proposed a limiting pressure of 9*cu*. This solution was largely empirical and had no theoretical background. Close to the ground surface, this value was reduced to allow a different mode of deformation. Based on a mathematical expression of viscous clay, Winter (1979) suggested that limiting pressure on a single pile is between 2*cu* and 5*cu*. In the analysis by Randolph & Houlsby (1984), it was found that the values of ultimate soil pressure ranges roughly between 9*cu* to 12*cu*. However, in the back-analysis of piles in unstable slopes conducted by Vigiani (1981), the ultimate soil resistance was found to be somewhat lower, i.e., between 2.8*cu* and 4*cu*. Poulos (1995) indicated that the limiting lateral soil pressure increases linearly from 2*cu* at the ground level to 9*cu* at a depth of about 3.5 times the diameter of the pile and remained constant below that depth. Based on two-dimensional numerical analyses adopted by Bransby et al. (1999), it was found that the ultimate soil resistance was equal to 11.75*cu*, and thus slightly smaller than the value of 12.5*cu* that is suggested by Goldscheider & Gudehus (1974). To investigate the passive load on a single pile and pile group, an analytical approach according to the 'Recommendations of the German Piling Committee - EA Pfähle' (2013) is proposed that is based on the experimental works of Wenz (1963) and Winter (1979). Figure 1 summarizes the most important approaches for different pile spacings.

Figure 1 shows the displacement field of the soil around a pile, the compressive forces of the soil along with its components, the stress field on the pile on a plane, and along the length of the pile.

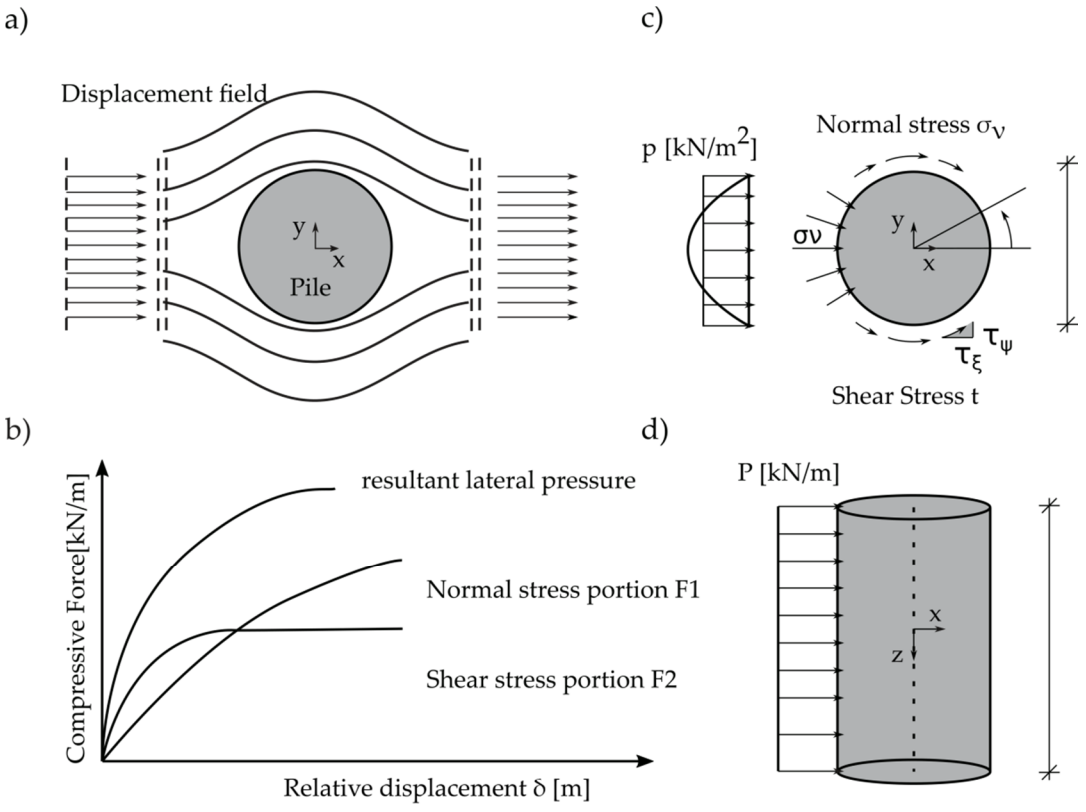


Fig. 1. General definitions for passive piles

According to Chen (1994), the distribution of transmitted passive loads varies diversely from case to case and no general rules can be specified for practical use. Furthermore, existing analytical solutions are often limited to special boundary conditions, and thus are not able to predict the soil-structure interaction correctly, as required by the Eurocode EC 7-1 (EN 1997-1:2004). In recent years this has resulted in the damage of several piled bridge abutments or piled foundations of overhead bridge cranes next to heavy loads. To overcome the shortcomings of conventional analytical approaches, many researchers have studied pile-soil interaction based on classical *Lagrangian* Finite Element Method (*FEM*). However, this method has limitations when solving geotechnical problems with large deformations; e.g. soil flowing around a pile. Difficulties with contact algorithms and large finite element mesh distortions may lead to inaccurate results or even to a non-convergent solution to the problem. For this reason, use of more sophisticated modelling techniques is being sought out.

NUMERICAL APPROACHES

The Material Point Method *(MPM)* is a particle-based method that combines both *Eulerian* and *Lagrangian* procedures to model large deformation problems. In *MPM*, the continuum is represented by *Lagrangian* points, also called as material points, which move through a fixed *Eulerian* mesh. The physical properties of the continuum such as mass, momentum, strains, stresses as well as state variables are stored in the particles, whereas the *Eulerian* mesh carries no permanent information. At the beginning of the computational time step, the information is transferred from the particles to the computational mesh. Incremental solution of governing equation is then determined in a *Lagrangian* fashion on the mesh. At the end of the computation step, the solution is mapped back to the particles from the mesh, updating the information. Figure 1. represents the sequence of events for one computational step in solution using material point method.

This approach in *MPM* combines the best aspects of both *Lagrangian* and *Eulerian* formulations, at the same time, overcoming some shortcomings in them. The problem of mesh distortion which is present in a calculation using the updated *Lagrangian* solution for large deformation is avoided. In spite of its advantages over other methods, *MPM* has shown to exhibit numerical difficulties during extreme deformation, causing oscillation in stress state. To overcome this difficulty, the classic *MPM* formulation has been improved over the years, specifically by method in which the concentrated mass of the material point is distributed over a finite subdomain.

CONVECTED PARTICLE DOMAIN INTERPOLATION METHOD (CPDI)

During large material movements of the continuum, the particles cross the computational grid, causing severe oscillations in the stresses. This occurs when linear shape functions are used, causing the gradients to be discontinuous at the interfaces, leading to unbalanced forces on the common shared nodes. This is referred to as the grid-crossing or cell-crossing error. By increasing the number of particles per cell, or by using a higher order shape function, the oscillations can be reduced. This consequently increases the computational load for the solution, and is therefore, not feasible. Instead, by using the same number of particles and linear shape functions, Bardenhagen & Kober (2004) proposed the Generalized Interpolation Material Point (*GIMP*) method, wherein the concentrated mass of the particle is spread over a finite square domain. A later improvement in *GIMP* was brought about in the form if *cpGIMP* in which the axial update of the geometry configuration was allowed. Sadeghirad et al. (2011) proposed a procedure where the domain is updated according to the particle deformation. The initial domain is parallelogram shaped, and its sides are continuously updated using the deformation gradient. This version of *MPM* was named as Convected Particle Domain Interpolation (*CPDI*). Figure 2 highlights the differences in the domains between the various versions of *MPM*. In this work, an axisymmetric CPDI procedure has been used. A more rigorous explanation for the formulation of *CPDI* is presented in the work of Hamad (2016).

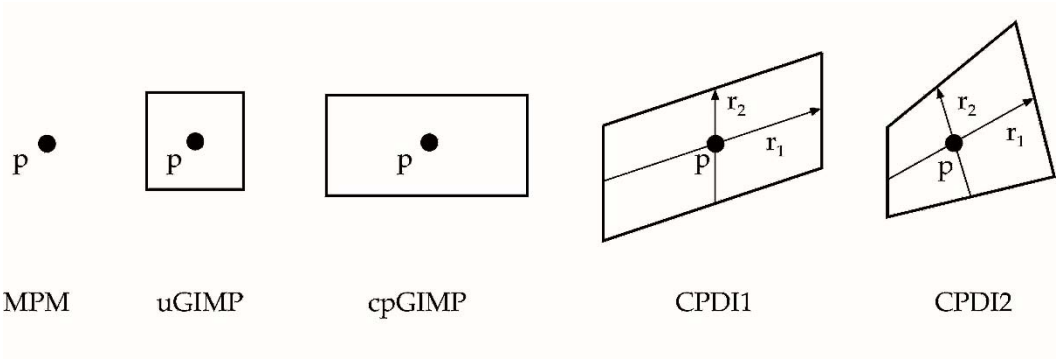


Fig. 2. Versions of Material Point Method

Standard *MPM* formulations provides an automatic no-slip condition. In the classic sense of contact in *MPM*, contact is detected when the material points of different entities contribute to the same grid node of the computational mesh. Therefore, interaction is activated before the actual contact taking place. Furthermore, a lack of smoothening function also contributes to oscillations in contact stresses. In the present implementation, a penalty function method that is often implemented in the FE analysis is introduced in *CPDI*, where the contact force is assumed proportional to the residual of the impenetrability constraints and the surface stiffness.

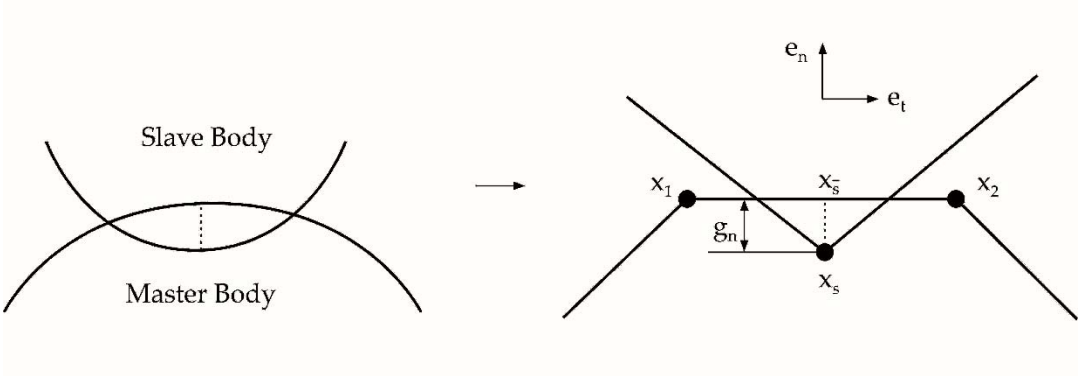


Fig. 3. Penalty contact conditions

The surface of the continuum in *MPM* is discretized separately from the volume discretisation. By setting an amount of mass to the interface, the surface nodes are able to follow the deformation of the continuum. Upon the equation of motion, the surface nodes of individual entities might interact according to the penalty function. Frictional forces are then traced back as an external contact force acting on the boundary. Early works focussed on relaxing the no-slip and no-separation condition Bardenhagen, et al. (2001). Subsequent works have been carried out to incorporate coulomb friction in the contact formulation and has been applied to geotechnical applications like pile installation successfully Hamad (2016). As an improvement to the contact algorithm, the penalty function method is introduced by Hamad et al. (2017) to evaluate the contact forces between interacting bodies. In the penalty function method, if a region Γ_c where contact violation exists, as shown in Figure 3, the potential energy is penalised proportional to the amount of constraint violation by using a penalty function P, expressed as

$$P = \frac{1}{2}\omega_n \int_{\Gamma_c} g^2{}_n d\Gamma_c + \frac{1}{2}\omega_t \int_{\Gamma_c} g^2{}_t d\Gamma_c, \qquad [1]$$

where, ω is the penalty parameter, g is the gap function, and the subscripts n and t are the normal and tangential directions, respectively.

In this method, the interface of the continuum is discretised using two-node linear segments. Normal and tangential stiffness is assigned to these elements, which are here, the penalty parameters in the formulation. A distinction between master and slave is made in the formulation for numerical convenience. Detailed formulation of the algorithm is presented in the work of Hamad et al. (2017).

BENCHMARK PROBLEM

To evaluate the methods presented, the numerical prediction of the bearing capacity of a strip footing is chosen, owing to the availability of an analytical solution. In addition to evaluating the *CPDI* method, various other methods used in *ABAQUS* is also evaluated. The analytical solution of the problem is given by

$$q = (2 + \pi)c, \qquad [2]$$

where, q represents the footing pressure at collapse, and c, the cohesion and is chosen as 100 kPa for all the calculations.

Figure 4 shows the results of *CPDI* compared with the analytical solution. Other results have been obtained from Qui (2012). It is evident that the results from *CPDI* and *CEL* simulation are closer to the analytical solution. This, therefore leads us to choose these two methods for further simulation in this work.

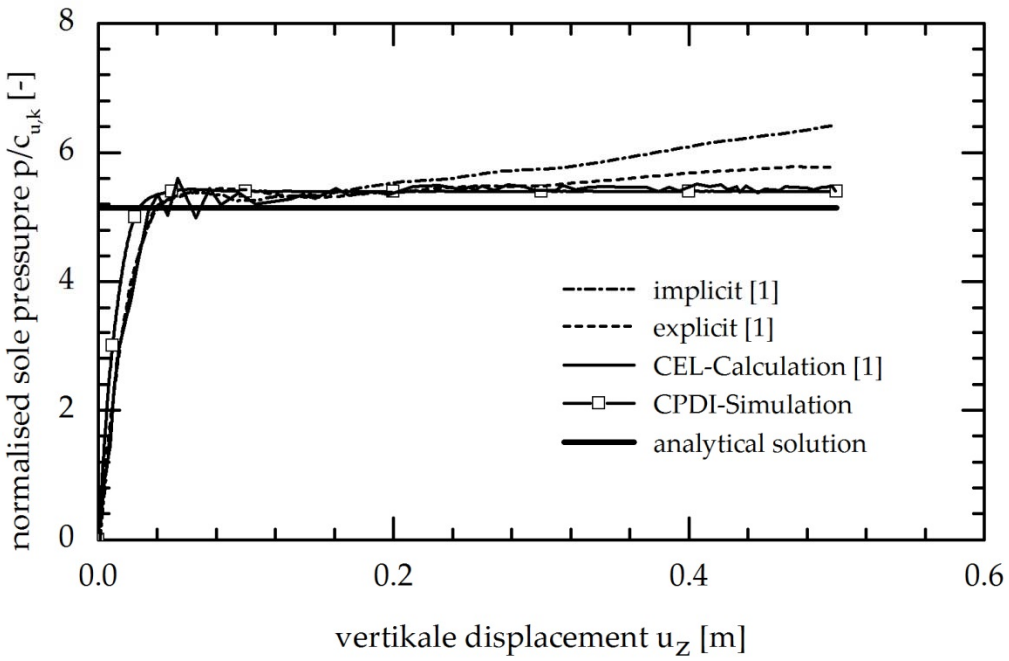


Fig. 4. Load-displacement-curves

NUMERICAL SIMULATION

The numerical simulation of the displacement of pile in soil deals with large deformations. A standard *Lagrangian* Finite Element simulation would fail, because of the high mesh distortion. To overcome this problem, a new numerical method, the Convected Particle Domain Interpolation (*CPDI*) method is used. Hamad (2016) and Hamad et al. (2016) have shown the potential of *CPDI* method for geotechnical

applications undergoing large deformations. To simulate the behaviour of the soil, a Mohr-Coulomb constitutive law is utilised.

Constitutive model

Although soil behaves rather non-linear when subjected to changes in stress and strains, and this behaviour can be replicated using advanced soil models. For this work, however, the well-known Mohr-Coulomb model, which is a linear elastic perfectly plastic model is chosen. The linear elastic part of the model is based on the Hooke's law of isotropic elasticity, and the perfectly plastic part is based on the Mohr-Coulomb criterion, formulated in a non-associated plasticity framework.

The constitutive parameters for Kaolin-clay used in this paper are listed in Table 1.

Table 1. Material parameters for Kaolin-clay (Bauer et al. 2016)

		small scale tests		
parameter	**unit**	V1	V2	V3
γ / γ	[kN/m^3]	18/18	18/18	18/18
E_u	[kN/m^2]	125	125	125
ν_u	[-]	0,495	0,495	0,495
φ	[°]	0	0	0
c_u	[kN/m^2]	2,3	2,4	2,5
ψ	[°]	0	0	0
K_0	[-]	0,685	0,685	0,685

The settlement of the pile is needed to activate the frictional and bearing resistance, and it is assumed that the resistance of the pile is fully activated after a settlement of 0.1D.

Numerical model

The geometry of the numerical model is based off of the geometry of the scaled model test. The dimensions of the model, along with the orientation of the pile groups are shown in Figure 5.

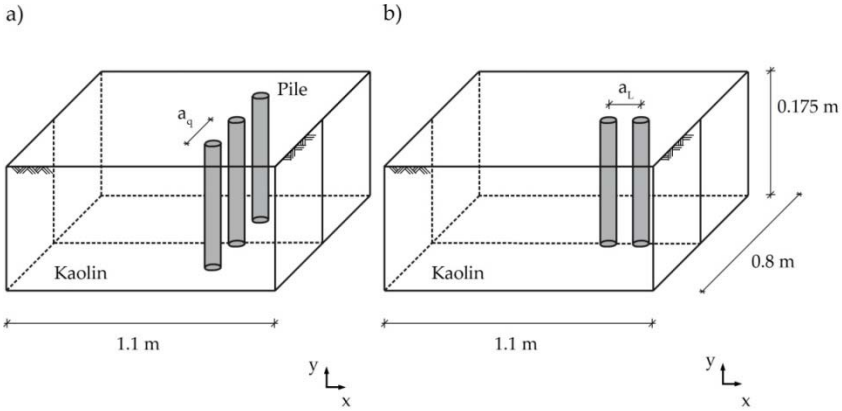


Fig. 5. Geometrical configuration: a) pile group in horizontal rows, b) pile group in transverse row

Results

Figure 6 shows the contour plot of the total horizontal deformation u_x [m] for a pile row consisting of 2 piles with varying center distances, 2D and 10D, respectively, at different soil displacement distances at $0.5d_D$and $1d_D$, respectively.

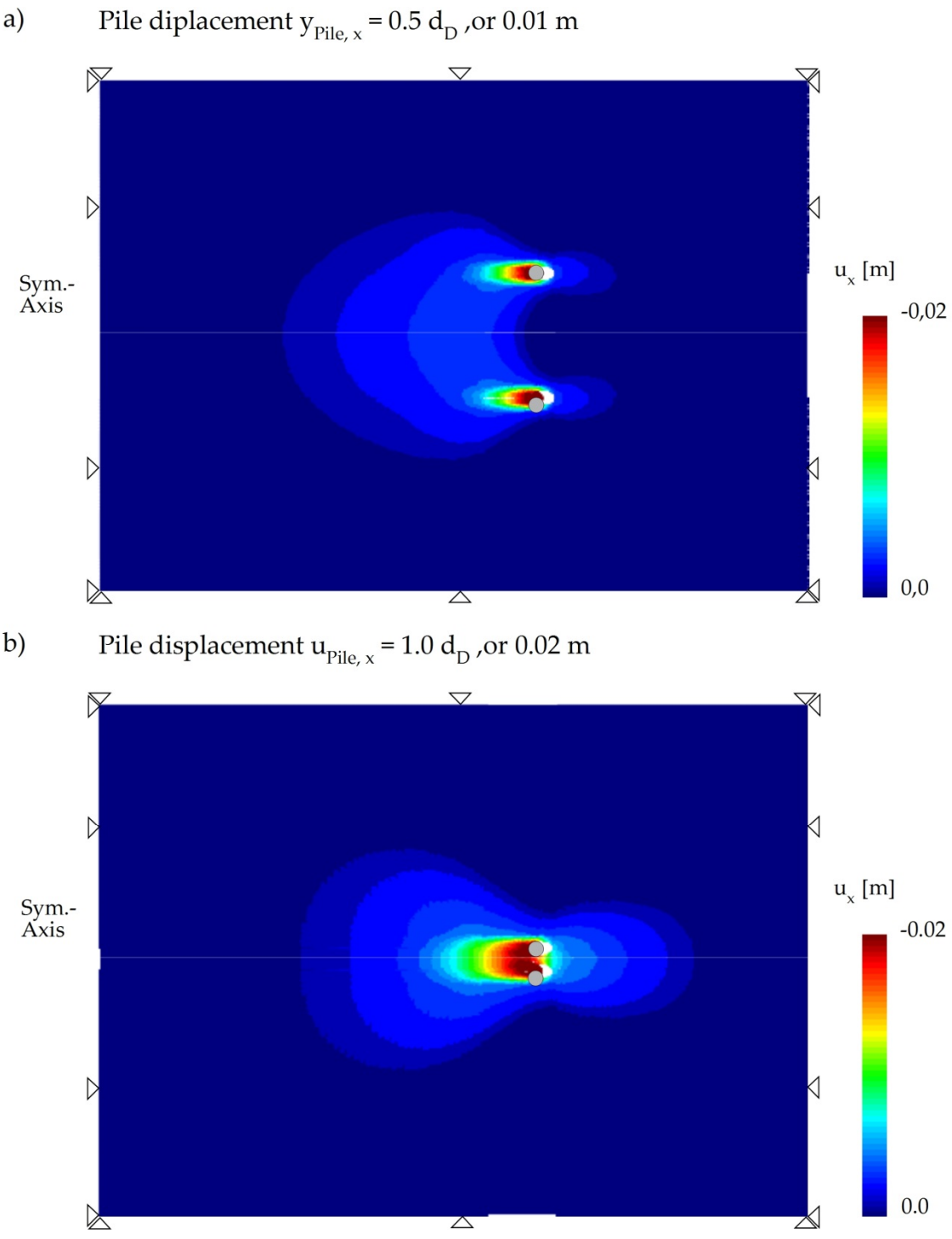


Fig. 6. Displacement of soil around pile a) center distance 10D, b) center distance 2D

Figure 6 (a) shows the horizontal displacement field for a normalised centre distance of 10D, with a normalised horizontal displacement of $0.5d_D$, i.e., 0.01 [m]. In Figure 6 (b) shows the results of displacement field for an axis distance of 2D, for a horizontal pile displacement of $1d_D$, i.e., 0.02 [m]. With the pile group for a smaller value for the axis distances, the mutual dependence of the piles on each other is clearly observable. The total displacement fields of the soil overlap in the vicinity of the individual piles. As the centre distance a_q of the pile row group increases, the mutual dependence of the piles on their displacement fields decreases significantly, as shown in Figure 6 (b) In case of widely spaced piles, i.e., for an axis distance more than 10D, the corresponding behaviour would resemble the behaviour of a single pile.

Figure 7 shows the results of the normalised force-displacement curve from the numerical simulation of a transverse pile rows, and is compared with the results from the experimental simulation. The calculations are carried out for two centre distances, 2D and 10D, respectively.

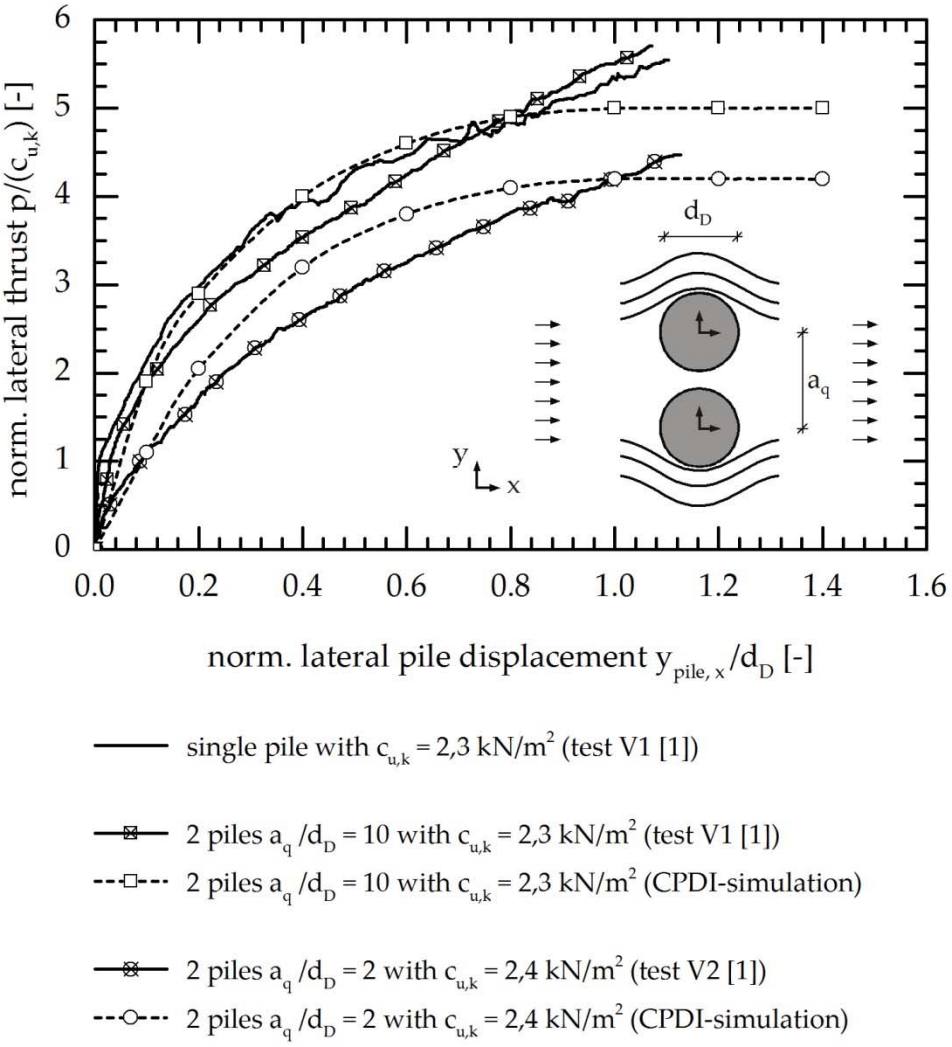


Fig. 7. Results for two piles in transverse configuration, comparison of test results and simulation

The results for the two-pile row, with varying centre distances, from numerical simulation is presented, and is compared with the experimental results for pile group, along with the result for a single pile. In this work, the normalised pressure is calculated as an average of the force measured on both the piles. It is observed that with increasingly narrower centre distances, the normalised force-displacement curve starts to resemble that of a single pile. In addition, it is observed that there is an increasingly less rigid behaviour of the experimentally measured and numerically determined load-deflection curves. For an axis distance of $a_d = 10D$, the normalised load-displacment curve of the pile group and the single pile are nearly superimposed. In this axis distance, the pile group behaves almost like a single pile. As with the single pile, a limit state is formed, due to the chosen constitutive model for the soil, for which in experiments, the soil displacement of 0.02 [m] or $1d_D$ could not be determined. For a pile displacement of more than $1d_D$, the results from experiments and the results from the numerical simulation using *CPDI* start to deviate. To conclude, it can be said that the case of transverse pile row, each consisting of two piles, there is a good agreement between the experimental results shown by Bauer et al. (2016) and the results from the numerical analysis.

CONCLUSIONS

In this paper, a novel method to investigate the displacement of the soil around a pile group is presented. To overcome the effects of mesh distortion due to large deformation of soil, a novel method, known as *CPDI* is adopted for numerical analysis. One cases of pile row with varying centre distances were chosen, and the results of the *CPDI* simulation were compared with the results of the experimental work. It is observed that the experimental and numerical results are in good agreement with each other, and is able to reproduce the behaviour of the soil around the pile accurately.

REFERENCES

Aussilio, E. & Conte, E., Dente, G. (2001). "Stability analysis of slopes reinforced with piles", *Computers and Geotechnics*, 28(2001), 591-611.

Bardenhagen, S. G., & Kober, E. M. (2004). The generalized interpolation material point method. CMES: *Computer Modeling in Engineering & Sciences*, 5, 477-495.

Bardenhagen, S. G., Guilkey, J. E., Roessig, K. M., Brackbill, J. U., Witzel, W. M., & Foster, J. C. (2001). An improved contact algorithm for the material point method and application to stress propagation in granular material. CMES: *Computer Modeling in Engineering & Sciences*, 2, 509-522.

Bauer, J., Kempfert, H. G., & Reul, O. (2016). Lateral pressure on piles due to horizontal soil movement. *International Journal of Physical Modelling in Geotechnics*, 16(4), 173-184.

Bransby, M. F. & Springman, S. (1997). "Centrifuge modelling of pile groups adjacent to surcharge loads", *Soils and Foundations*, 37(2), 39-49.

Bransby, M. F. & Springman, S. (1999). "Selection of load-transfer function for passive lateral loading of pile groups", *Computers and Geotechnics*, 24(1999), 155-184.

Broms, B. B. (1964). "Lateral resistance of piles in cohesive soils", *J. Soil Mech. Fdns Div. Am. Soc. Civ. Engrs 90*, 27-63.

Cai, F. & Ugai, K. (2011). "A subgrade reaction solution for piles to stabilise landslides", *Geotechnique* 61(2), 143-151.

Chen, L. (1994). Effect of lateral soil movements on pile foundations (*Doctoral dissertation*).

Ellia, E. A. & Springman, S. M. (2001). "Modelling of soil-structure interaction for a piled bridge abutment in plane strain FEM analyses", *Computers and Geotechnics,* 28(2001), 79-98.
Goldscheider, M. & Gudehus, G. (1974). Verbesserte Standsicherheitsnachweise, *Vorträge der Baugrundtagung 1974 in Frankfurt/Main-Höchs*t, 99-118.

Hamad, F. (2016). Formulation of the axisymmetric CPDI with application to pile driving in sand. *Computers and Geotechnics*, 74, 141-150.

Hamad, F., Giridharan, S., & Moormann, C. (2017). A Penalty Function Method for Modelling Frictional Contact in MPM. *Procedia Engineering*, 175, 116-123.

Hamad, F., Stolle, D., & Moormannm C. (2016). Material Point Modelling of releasing Geocontainers from a Barge. *Geotextiles and Geomembranes*, 44, 308-318.

Ito, T., Matsui, T. & Hong, W. P. (1982). "Extended design method for multi-row stabilizing piles against landslide", *Soils and Foundations, Japanese Society of Soil Mechanics and Foundation Engineering*, 22(11), 1-13.

Jeong, S., Seo, D., Lee, J. & Park, J. (2004). "Time-dependent behaviour of pile groups by staged construction of an adjacent embankment on soft clay", *Ca. Geotechn. J.*, 41(2004), 644-656.

Poulos, H. G. (1995). "Design of reinforcing piles to increase slope stability", *Can. Geotechn. J.,* 32(1996), 808-818.

Qiu, G. (2012). Coupled Eulerian Lagrangian Simulations of Selected Soil-Structure Problems (*Doctoral dissertation, Dissertation, Veröffentlichungen des Instituts für Geotechnik und Baubetrieb der TU Hamburg-Harburg*).

Randolph M.F. & Houlsby, G.T. (1984). "The limiting pressure on a circular pile loaded laterally in cohesive soil", *Geotechnique*, London, 34(4), 613-623.

Sadeghirad, A., Brannon, R. M., & Burghardt, J. (2011). A convected particle domain interpolation technique to extend applicability of the material point method for problems involving massive deformations. *International Journal for Numerical Methods in Engineering*, 86, 1435-1456.

Stewart, D. P., Jewell, R. J. & Randolph, M. F. (1994). "Design of piled bridge abutments on soft clay for loading from lateral soil movements", *Geotechnique*, 44(2)2, 277-296.

Vigiani, C. (1981). "Ultimate lateral load on piles used to stabilize landslides", Proceedings. *The 10th Int. Conf. of Soil Mech. and Found. Eng.*, Stockholm, Vol. 3, 555-560.

Wenz, K. P. (1963). Über die Größe des Seitendrucks auf Pfähle in bindigen Erdstoffen. Universität Karlsruhe, *Heft 12*.

Winter, H. (1979). Fließen von Tonböden. Eine mathematische Theorie und ihre Anwendung auf den Fließwiderstand von Pfählen. Universität Karlsruhe, *Heft 82*.

INVESTIGATING THE DEVELOPMENT OF PILE CAPACITY OVER TIME

Jeffrey R. Barrow, Civil Solutions Associates, Cincinnati, Ohio, USA, (513) 477-3753, jbarrow@civilsolutionsassociates.com
Tumal M. Karunaratne, Civil Solutions Associates, Cincinnati, Ohio, USA, (513) 387-9160, tumalk@civilsolutionsassociates.com
Katie E. Persons, Civil Solutions Associates, Cincinnati, Ohio, USA, (859) 801-7276, kpersons@civilsolutionsassociates.com

ABSTRACT

By implementing compounding safety factors throughout deep foundation design, the foundational elements embody excess capacity which they may never require. Current design practices which increase the safety factor include elongating drilled shafts to socket further into competent bearing material and placing inessential steel reinforcement to create a heavier and stiffer element. In addition to these intentional safety considerations, the capacity of drilled shafts increases over time as a result of soil consolidation, pore pressure dissipation and improved adhesion. These mechanisms of strength gain are not currently accounted for throughout the design phase, which further intensifies the safety factor. While we have not quantified the increased capacity with respect to time, we have investigated this concept through a case study wherein a single-level book depository was remodeled into office lofts. Renovation plans included the construction of additional stories to accommodate an evolving building use. The foundation system of the original structure was tested prior to the renovation to determine its competence in supporting the proposed lofts, which directed the notion that its capacity was enhanced over time. The importance of addressing changes in the behavior of drilled shafts is presented in this report in order to optimize the design of deep foundation systems. Through this paper, we intend to identify the processes by which foundation designs become unreasonably conservative.

Keywords: Safety Factor, Soil Relaxation, In-Situ Testing, Pile Capacity, Adhesion, Drilled Shafts, Long-Term Strength Gain, Soil Friction, Adhesion

INTRODUCTION

While constructing a deep foundation system, it is of utmost importance that the installed pile is capable of withstanding superior loads to what the overlying structure may apply. This ensures that the completed building can perform its intended purpose without jeopardizing the safety of its inhabitants and surrounding structures. Incorporating safety factors throughout the design phase confirms that the deep foundation will withstand the applied loads without compromise.

A measure of safety that is oftentimes overlooked by engineers occurs *after* the design phase and pile installation are complete. This alludes to the development of capacity within the deep foundation system over time. As a result of pile relaxation (pore pressure dissipation), growth of concrete stiffness, and long-term settlement, deep foundation systems gain capacity. Because this strength gain is unaccounted for throughout the preceding phases, the resulting foundations embody a factor of safety that surpass their expectations.

An analysis of pile relaxation, concrete setup, and long-term settlement in regards to deep foundations is presented in the following report in order to understand how a pile develops capacity over time. Thereafter, a case study is investigated to display how these elements are exemplified in the field upon installation. To conclude, a theoretical model of the case study was generated to compare the estimated and actual capacity of the deep foundation system.

© 2018 Deep Foundations Institute

A Comparison of Driven Piles and Drilled Shafts

It is important to clarify that the research presented in the following report is pertinent to drilled shafts rather than driven piles. While there have been numerous studies conducted for the long-term performance of driven piles, there is considerably less data revolving around drilled shafts. Consequently, this investigation and case study focus on the latter of the two foundation systems. Figures 1 and 2 below depict the construction variances between these two pile types.

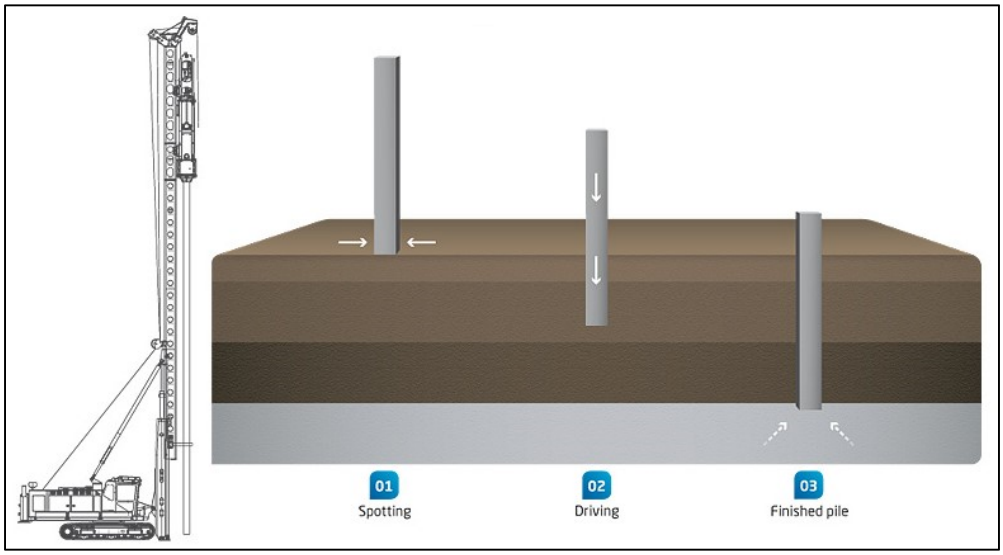


Figure 1: Driven Pile Construction Sequence

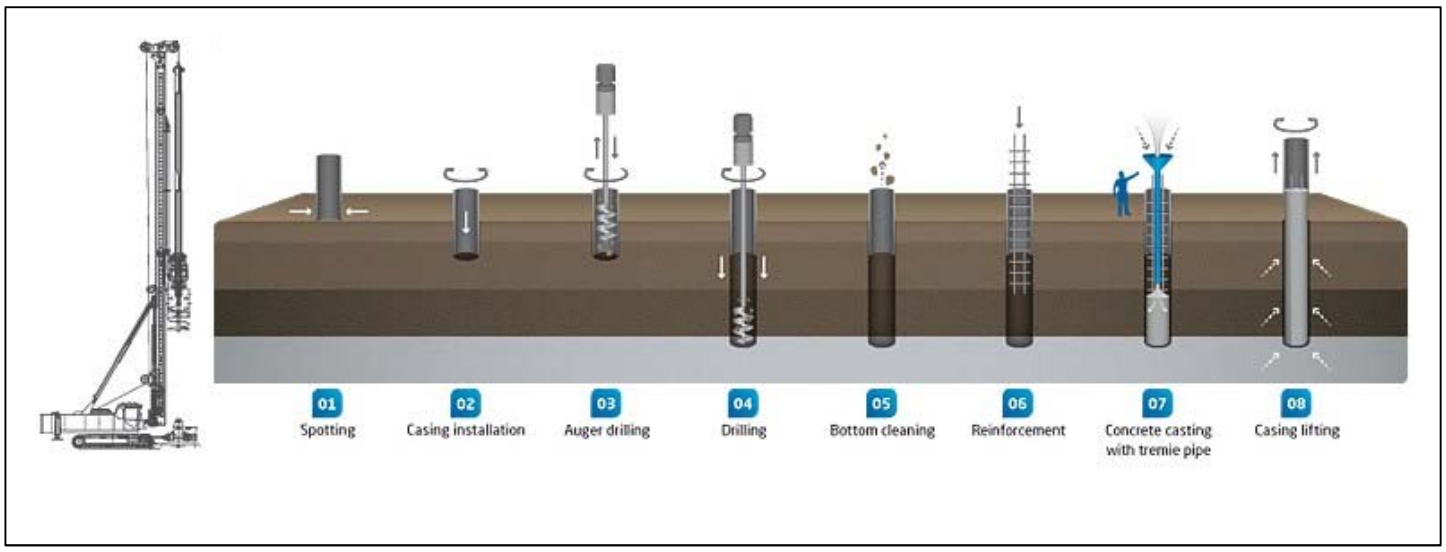


Figure 2: Drilled Shaft Construction Sequence

In short, a driven pile is a type of displacement pile in which the subsurface material is disturbed radially and vertically as a result of the structural element being driven or jacked into place. They are typically smaller and less expensive than alternative methods, but provide a lower capacity (Camp, 2013). Drilled shafts, on the contrary, are a type of non-displacement pile in which soil is removed prior to placing the pile in order to provide adequate space. As a result of this construction process, drilled shafts have the capability of supporting larger elements and providing a higher capacity (Camp, 2013). The foundation systems presented in the following research and proceeding case study are composed of drilled shafts.

MECHANISMS OF LONG-TERM STRENGTH GAIN

The following sections of this report investigate methods through which deep foundation systems gain capacity over time. Specifically, the effects of pile relaxation, concrete stiffness, and long-term settlement are analyzed with respect to in-situ drilled shafts.

Pile Relaxation

Although a drilled shaft is categorized as non-displacement, the subsurface material surrounding the excavated hole is nonetheless affected by the auger twisting into the soil and extracting material. Stress changes occur in the adjacent soil from the excavation procedure, which may be exacerbated by the subsequent construction processes, such as steel and concrete placement. Upon the completion of drilled shaft installation, however, the adjacent soils react to the structural unit and restore their previous state of stress. This restoration is referred to as pile relaxation (Li et al., 2017).

The stresses within subsurface materials induced by the installation of drilled shaft foundations are not permanent. Rather, the adjacent soils in contact with the drilled shaft experience an unloading process after the installation is complete (Li et al., 2017). During this time, the subsurface materials respond to the recently-drilled unit. The soil is provided the opportunity to consolidate beneath the drilled shaft, and excess pore water pressure can adjust to the deep foundation system. Once pile relaxation occurs, the capacity of the unit is improved because the subsurface soil and groundwater have sufficiently engaged around the concrete/soil interface.

It is important to clarify that pile relaxation is of heightened concern for driven piles because the stress changes induced by the construction mechanisms are significantly greater than those of drilled shafts. Nonetheless, stress changes are created throughout drilling and excavation operations; henceforth, drilled shafts as well are capable of experiencing pile relaxation to a degree. The process and time frame by which drilled shafts undergo pile relaxation have not been empirically quantified due to their variability and complexity (Li et al., 2017). As a result, the increase in capacity produced by pile relaxation is not currently considered by foundation engineers throughout the design process of drilled shafts. In addition, differing geologic components such as soil type and groundwater elevation may alter the effects of pile relaxation. For these reasons among others, it is conservative for geotechnical engineers to disregard the rise in capacity induced by pile relaxation until design standards have been empirically formulated.

Growth of Concrete Stiffness

Once the subsurface material has been removed for a drilled shaft, a reinforcement cage or steel beam is typically placed within the drill hole and concrete is poured to fill the drilled shaft to the desired elevation. This concrete is a secondary source of capacity development within a drilled shaft because the capacity is enhanced by the hydrophilic properties of concrete. Due to the porosity of concrete, the resulting drilled shaft contains capillary voids, joints, and cracks. Water freely travels through these crevasses and fills the voids over time. Concrete is considered hydrophilic because it does not possess the properties required to prevent the infiltration and subsequent movement of water.

Alternatively, the drilled shaft may draw in water from its surrounding subsurface materials. It absorbs moisture and humidity from the in-situ soils, which creates a denser zone of transition between the interface of the two materials (He et al., 2017). The infiltration of groundwater reduces the porosity of the bond interface between the soil and concrete pile. As a result, the frequency of micro-cracks is reduced in the concrete in direct contact with soil material. When excessive micro-cracks are present in this area, the bond between the soil and concrete is jeopardized by the creation of stress concentrations. The hydrophilic properties of concrete help to reduce these stresses while simultaneously increasing the resistance along drilled shaft. Developing the shaft resistance further contributes to the long-term growth of capacity within deep foundations.

Long-Term Settlement

A third mechanism by which drilled shafts experience long-term growth in capacity is long-term settlement beneath the foundation unit. Once drilled shafts are installed, the stress state of the subsurface material is altered by the additional load applied by the drilled shaft and overlying structure (Gabrielaitis et al., 2013). In its previous condition, the soil supported only its self-weight and occasional groundwater pressure. Introducing drilled shafts causes the underlying soil material to experience settlement. Although excessive settlement can threaten the integrity of the foundation system and accompanying structure, limited quantities of settlement enhance the capacity of the pile toe.

Through the process of settlement, the moisture content of saturated soils is decreased by the expulsion of water. Groundwater is pressed out of the soil, densifying the base upon which the drilled shaft is placed. The axial load applied by the structure through the drilled shaft causes the underlying soils to compress and decrease in volume. A benefit of this densification is the decrease of voids within the soil, which inversely increases the capacity of the pile toe. Ultimately, the long-term application of compression onto the drilled shaft causes the underlying soil material to gradually compress and strengthen with time.

CASE STUDY: CINCINNATI SKY LOFTS

In 2006, a geotechnical evaluation was completed for a 94,535-square foot, 5-story warehouse in downtown, Cincinnati, Ohio. The all-concrete structure, known as the Anderson Building, was erected in 1936 by the America Publishing Company and was originally utilized for storage as a book depository. In 2010, however, a renovation was completed which converted the space into *The Edge—a* five-story commercial loft which rents office space to local Cincinnati tenants.

Project Description

The proposed development included adding a floor between the original first and second levels, and constructing additional levels on top. It was intended that upon completion, the first three levels would be used for parking while commercial office space would occupy the overlying levels. Because the universal purpose of the space was evolving, it was of utmost importance to first consider how the new loading configurations would affect the existing structural and foundational components. In other words, would a structure that was originally designed for book storage adequately support the loads implied by vehicles parking and employees working throughout the upper levels? A geotechnical evaluation was conducted to answer this question with certainty.

The general purpose of the geotechnical evaluation was to study the subsurface conditions and to determine the existing footing depths/dimensions at several locations within the ground floor level. Overall, the goal was to understand the design of the foundations in order to judge their competency, considering both bearing failure and settlement. Since the building was erected in 1936, actual foundation and structural plans were unavailable for review. It is unknown for certain the design loads, depth, and steel reinforcement implemented within the original construction of the Anderson Building.

The following case study reviews the subsurface investigation, assesses the methods of pile testing which occurred throughout the geotechnical evaluation, and discusses the results and consequent significance of the findings.

Origin of Greater Cincinnati Soils

The overburden soils throughout the Greater Cincinnati Area include glacial deposits, water-deposited alluvium, wind-blown loess, and residuum. Glacially deposited soils are the most predominant materials and cap the majority of the ground surface in this area. Three separate continental glacial invasions caused profound drainage changes and created a variety of deposits in the valleys and hillsides. Consequently, the

depth to bedrock material in portions of the area are excessively deep. This was evidenced throughout the geotechnical evaluation, as further discussed below.

Test Borings

In order to obtain subsurface data, the geotechnical evaluation included drilling three Standard Penetration Test borings within the project site using track-mounted drill rigs. The test borings were advanced and stabilized using hollow-stem augers while sampling was accomplished using the Standard Penetration Test procedure (ASTM-D 1586).

Existing fill material, approximately 12 ft. to 17 ft. thick, was encountered at the surface at each of the test boring locations. Most of the existing fill was described as a non-cohesive material with varying amounts of black cinders, silty sand, gravel, glass fragments, clay, asphalt brick, wood and organics. Generally, the compactness of the existing fill ranged from soft to medium dense, or medium stiff when a larger percentage of clay material was present. Interpretation of the test boring results indicated the existing fill to be extremely variable in consistency and was placed with minimal compactive effort.

Lean clay and silt soils were encountered below the existing fill in two of the three of the test borings. The thickness of the encountered lean clay and silt was 7.5 ft. to 12 ft. at depths of 13.0 feet to 17.5 feet. The lean clay consisted of interbedded partings of silt that was moist and medium stiff. The silt soil was very moist and loose in consistency.

Brown and gray, varved, fat clay and silt were recovered below the lean clay and silt in all three test borings locations. The thickness of the encountered lakebed deposit was at least 25 ft. at depths of 15 to 25 ft. The soil was soft to medium stiff in consistency and very moist to moist. Refer to Table 1 below for an overview of the encountered soils within the three test borings.

Table 1: Summary of Subsurface Materials

Boring No.	Ground Elevation (ft.)	Top El. Of Existing Fill (ft.)	Existing Fill Thickness (ft.)	Top El. Of Clay and Silt (ft.)	Clay and Silt Thickness (ft.)	Top El. Of Lakebed Soil (ft.)	Lakebed Soil Thickness (ft.)
B-01	506.7	506.3	17.1	489.2	7.5	481.7	25.0
B-02	506.4	506	14.6	491.4	0	491.4	Boring Terminated
B-03	508.6	507.8	12.2	495.6	12.0	483.6	Boring Terminated

Existing Foundations

In order to determine the type of foundation system beneath the Anderson Building, three test pits were excavated within the building. In general, the test pits were performed to provide information in regards to footing depths, sizes of structures, thickness of the floor slab, and the depth and quality of fill material.

At the three test pit locations, the project engineers observed that the concrete floor slab varied in thickness from 6.0 to 7.25 inches. It contained steel mesh reinforcement at mid-depth. The slab was underlain by non-cohesive, uncontrolled fill with a varying amount of clay. The fill was loose to medium dense. The engineers noted that the encountered material was likely backfilled to compose the finished floor slab subgrade.

The excavations extended from 10 to 11 feet beneath the floor slab and exposed entirely fill material within those depths. In some locations, there were pockets of construction debris in the middle of the fill. The fill was moist and was able to maintain a vertical cut. No groundwater was encountered in the test pit excavations.

In the first test pit, the pile cap beneath the column was rectangular with the approximate dimensions of 7'-6" wide and 10'-10" long. The pedestal foundation extended to a depth of 69 inches below the bottom of the floor elevation. This foundation supported a partial bay. A pile integrity test (P.I.T.) was performed on the observed drilled shafts, which yielded a total shaft length of approximately 40 feet. The test pits also revealed the pile caps throughout the structure were supported by 16-inch diameter, cast-in-place drilled shafts. The following images display the foundational elements encountered beneath the Anderson Building.



Figure 3: Photo of Pedestal Foundation

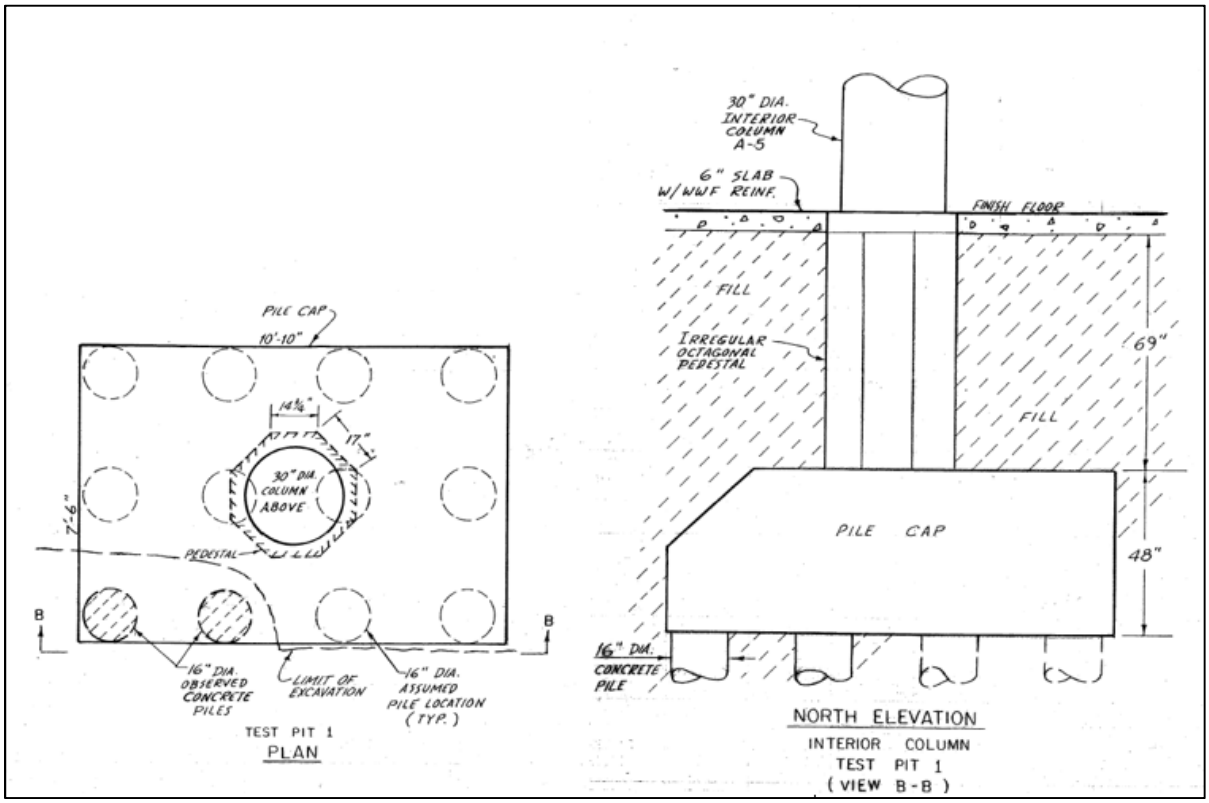


Figure 4: Findings Within Test Pit 1

Pile Load Testing

In addition to drilling three test borings and excavating three test pits, one 16-inch-diameter existing cast-in-place drilled shaft was selected to be subjected to a pile load test. The load test was performed on March 29th and 30th of 2006 and was performed in general accordance with ASTM D 1143-81, "Standard Test Method for Piles Under Static Axial Compressive Load - *Quick Method*."

The process of load testing an existing drilled shaft was an arduous and complicated procedure that involved excavating below the existing pile cap to expose the center shaft along the exterior edge. Dimensions of the pile cap and drilled shaft spacings were recorded, along with the size and the assumed number of drilled shafts. A 28-inch section of drilled shaft, displayed in Figure 5, was cut using a concrete wire saw and a capping compound was cast to create a smooth, flat surface. The removed section of drilled shaft was transported to the Cincinnati Soil Mechanics Laboratory where a concrete core was removed from the shaft. Subsequently, this core was tested in compression and ruptured at 4,660 psi. The 100-ton hydraulic ram, wobble plate, load cell and upper bearing plate were installed in the 28-inch section previously removed.

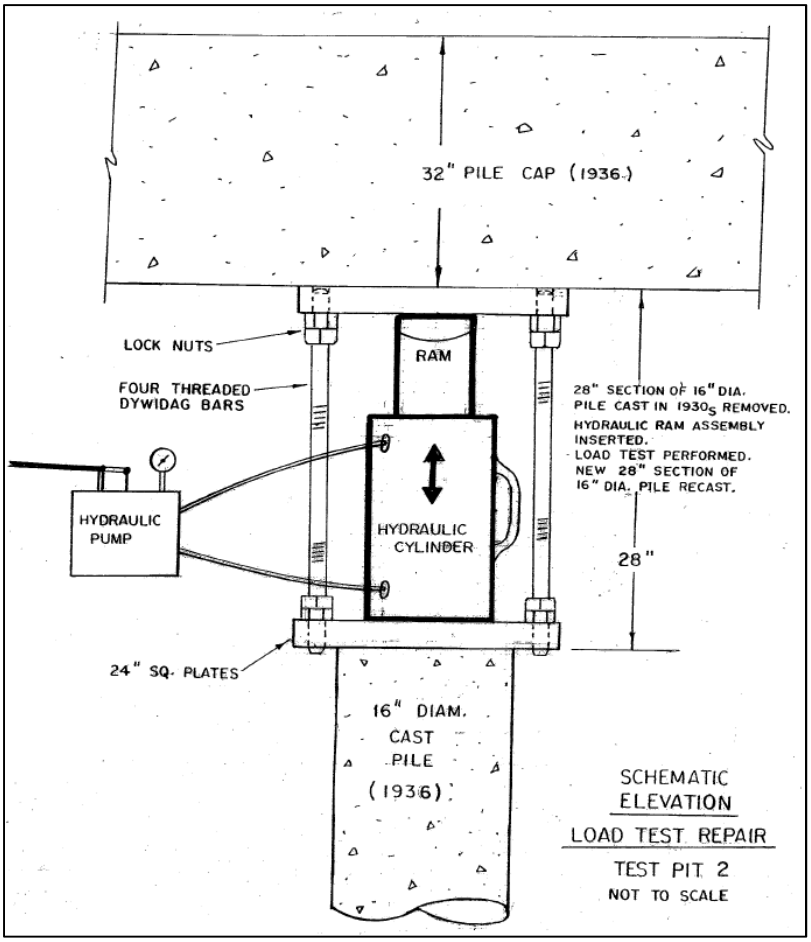


Figure 5: Configuration of Drilled Shaft and Testing Equipment

Vertical displacement at the toe of the test drilled shaft was measured by two Starrett dial indicators (Model 25-3041J, 3 in. travel, 0.001 in. accuracy), evenly spaced. These gages were mounted on a welded angle iron reference beam independent of and supported no closer than 8 ft. from the test drilled shaft. One end of each reference beam was free to expand/contract with temperature changes.

Design axial loads for the original structure were unknown because the foundation details and construction documents were unavailable. A design axial load of 28 tons was formulated by the structural engineers for the new expansion. As such, the drilled shafts were loaded and unloaded at 28 tons (100% Design Load) and 65 tons (>200% Design Load) throughout the geotechnical investigation. During the loading sequences, the load was applied in 2.5 to 5-ton increments and was reduced in four equal decrements while unloading.

When loaded to 28 tons, the load was maintained for a 45-minute duration and when loaded to 65 tons, the load was maintained for a 30-minute duration. Upon completion of the load tests, the dial indicators were monitored for 12 hours at 10 tons in order to obtain the total net displacement of the drilled shaft.

Load Test Results
After applying the 10-ton load for 12 hours, the gauges were recorded to measure how the drilled shaft had moved as a result of the testing. The gross and net displacements for the drilled shaft at 28 tons (100% Design Load) and 65 tons (>200% Design Load) load increments are summarized in the table below. For this study, the gross displacement referenced the movement which occurred while the load was applied. The net displacement was measured upon removal of the load.

Table 2: Pile Load Test Results

Test Load (ton)	Gross Displacement (in.)	Theoretical Elastic Compression (in.)	Net Displacement (in.)
28	0.02	0.030	0.000
65	0.074	0.0714	0.026

Per Section 1817.4 of the Ohio Basic Building Code (OBC, 2005) the allowable loads shall not be more than one-half of that test load which produces a permanent net settlement of not more than 0.01 inch per ton of test load, and not more than ¾ inch. Based on the OBC criteria, the drilled shaft had an allowable load capacity of at least 33.25 tons.

Settlement Analysis
Along with testing the bearing capacity, the geotechnical evaluation included assessing the potential of settlement caused by the building renovations. A settlement analysis was performed to determine the anticipated future settlement of the proposed structure. This was accomplished using the equivalent footing method. For drilled shafts supported by shaft resistance in clay, the equivalent footing method involves placing the pile group load at a depth of 2/3 the shaft length (FHWA-HI-97-013). Calculations were then performed to determine the expected settlement of the clay and silt layers below this depth.

Two loading conditions for each location were analyzed. Due to the load applied on the drilled shafts from the past several decades, partial consolidation had occurred within the foundation soils. To model this first, the calculations were performed using the full existing load and the full proposed load. Secondly, a case was performed using 66% of the existing load and the full proposed load.

The completed settlement analysis for an interior column yielded a total expected settlement in the range of 0.4 to 0.6 inches. Beneath a corner column, the settlement calculations estimated between 0.3 and 0.5 inches of total settlement. Henceforth, the differential settlement over the 28-foot span between the two columns was approximately 0.1 inches.

Geotechnical Evaluation Findings

In redeveloping the former Anderson Building, a book depository, into lofts which accommodate parking on the basement and first floor levels, certain changes had to be made in the structure of the building. Most importantly, a floor was added between the existing first and second floors and an additional five levels were added to the height of the building. From the load test analysis, it was determined that the existing foundations were capable of supporting the new proposed loads.

The data obtained from the load test suggested that the existing foundations were capable of withstanding significant additional load. The load test was stopped at approximately twice the design load, at which point the engineers observed only a fraction of the 3/4 inch allowed by the 2005 Ohio Building Code.

Settlement analyses estimated that between 0.3 and 0.6 inches of total settlement may occur as a result of the adding the proposed floors to this building; although, the total settlement observed may in fact be much less than that calculated. The difference in actual and observed settlement is a result of the previous loading conditions in the building during the past seven decades. Due to the existing building storing printing presses, paper stock, and bound materials, the foundation soils were partially consolidated. This consolidation helped prevent excessive settlement beneath the new office building.

The goal of the geotechnical study performed at this site was to analyze the subsurface materials, determine the current condition of the existing foundation system, and estimate how the foundation would respond to the proposed renovations. Through the use of test borings, test pits, and various pile tests, it was determined that the original Anderson building foundation system would sufficiently support the 5-story, office structure and parking facility.

THEORETICAL MODEL

Unfortunately, it is unfeasible to compare the aforementioned analysis to the original foundation system because initial load tests were not performed upon construction completion. Installing a drilled shaft within similar soil material and analogous foundation properties and performing a load test would assist in determining the initial capacity of the Anderson Building's foundation. Due to construction and budget limitations, however, this was not a viable option for this study. In lieu of this process, a geotechnical design program was utilized to produce a theoretical model of the drilled shafts in order to predict its initial capacity.

The available subsurface information from the case study was combined with geotechnical experience in the Cincinnati area to prepare a theoretical model in DeepFDN 2017. This computer program analyzes the soil parameters and pile type input by the user and outputs its predicted drilled shaft capacity. The purpose of testing this model was to create a comparison between the predicted initial capacity of the drilled shafts and the results of the in-situ testing performed during the geotechnical investigation 70 years later.

Soil parameters input into the program were determined from the completed test borings, subsequent soil testing and geotechnical experience in the Greater Cincinnati Area. The completed soil testing provided estimates for standard penetration resistance (N-values), triaxial failure stress (psi), dry density (pcf), specific gravity, void ratio and water content (%). These values were used to postulate appropriate measurements of total density (pcf), cohesion (psf), friction angle (degrees), and side friction (psi).

Two scenarios were analyzed to produce a range of anticipated capacity, as organized in Tables 3 and 4. Case 1 represents a conservative estimate, wherein weaker soil parameters were assigned to the subsurface materials to generate a theoretical minimum predicted load. Alternatively, Case 2 was generated using stronger soil properties to yield the maximum predicted load.

Table 3: Soil Parameters for Case 1 (Conservative Estimate)

Soil Material	Total Unit Weight (pcf)	Effective Cohesion (psf)	Effective Friction Angle (degrees)	Ultimate Side Friction (psi)
Fill	105	50	15	1.6
Lean Clay and Silt Soils	119	300	16	5.3
Lakebed Clays (Varved Fat Clay and Silt)	116	350	17	3.1

Table 4: Soil Parameters for Case 2 (Aggressive Estimate)

Soil Material	Total Unit Weight (pcf)	Effective Cohesion (psf)	Effective Friction Angle (degrees)	Ultimate Side Friction (psi)
Fill	112	120	18	3.8
Lean Clay and Silt Soils	128	500	20	8
Lakebed Clays (Varved Fat Clay and Silt)	124	550	20	7.2

The model incorporated 16-inch diameter drilled shafts, as these were encountered beneath the Anderson Building during the geotechnical investigation. The minimum required steel reinforcement was implemented, along with a 28-day compressive concrete strength of 3,000 psi. The capacities were generated utilizing the effects of side friction and neglecting any end-bearing capacity provided by the pile drilled shaft toe. The soil layers were analyzed under drained conditions to represent a long-term setting. Additionally, the model followed the Federal Highway Administration's GEC-10 Drilled Pier Guidelines. A safety factor of 2.0 was incorporated into the design.

The soil profiles, standard penetration numbers (N-values), and soil descriptions provided in the geotechnical report were used to create a model representative of what a geotechnical engineer would implement for a foundation design in the Cincinnati area for today's real-world design conditions. Based on the model, the predicted allowable capacity of the drilled shafts ranged from 19-25 tons. Table 5 further summarizes the results yielded from DeepFDN 2017.

Table 5: Results of Predicted Capacity

Condition	Shaft Length (ft)	Predicted Allowable Capacity (tons)	In-situ Allowable Capacity (tons)	Percentage Difference
Case 1	40	19	33.25	75%
Case 2	40	25	33.25	33%

Significance of Theoretical Model

The data obtained through the case study was applied to the design of a foundation system that upholds the accepted procedures of geotechnical engineers within the Cincinnati Area. It was determined that a drilled shaft subjected to analogous building loads and subsurface material would yield an allowable capacity of 19-25 tons. However, the in-situ drilled shafts provided an allowable capacity of 33.25 tons, as determined through the pile load testing conducted during the geotechnical investigation.

These calculations indicate a percent increase in drilled shaft capacity of 175%-133% over their lifespan. This gain in capacity is first attributed to the soil relaxation which commenced immediately upon installation. It is anticipated that this process occurs within the first five years of a drilled shaft's life. Capacity developed from concrete setup occurs in conjunction with soil relaxation. The hydrophilic

concrete draws in water from the soil material and fills capillary voids within the drilled shaft. Long-term settlement is the slowest method through which drilled shafts develop capacity. The subsurface material beneath the shaft toe may experience settlement up to 30 years upon installation. Due to these mechanisms, a deep foundation system develops capacity in the long-term setting, resulting in substantially over-designed drilled shafts.

SUMMARY AND CONCLUSIONS

Compounding safety factors throughout the deep foundation design process result in drilled shafts capable of withstanding heightened loads to which they may never be exposed. Drilled shafts may be lengthened to establish a guaranteed embedment within suitable bearing material to resolve axial force and settlement requirements. Although it is important to design deep foundations for the worst-case scenario, incorporating supernumerary safety factors results in excessive building material and construction costs. It is important to optimize this balance in order to create safe structures without warranting unnecessary expenses.

One item that is oftentimes overlooked throughout the design phase is how a deep foundation unit will perform over time. In theory, the capacity of drilled shafts increases as a result of pile relaxation, concrete setup, and long-term settlement. The notion of increased drilled shaft capacity was evidenced in the case study discussed, in which the foundation system of a single-level book depository was deemed structurally competent for its renovation and construction of additional stories to the concrete structure. This likely would not have been the case if the original drilled shafts had not gained capacity over the 70-year time span.

Due to the lack of research performed for drilled shafts, this increase in capacity with respect to time has not been empirically quantified and therefore is disregarded throughout the design phase. With more study, the contribution of pile relaxation, concrete setup, and long-term settlement could contribute to the calculation of capacity. Alternative methods of incorporating safety factors could then be alleviated—producing decreased construction materials and cost.

When load tests are required, these tests should be carried out to failure of the drilled shaft so that the information can be utilized to make knowledgeable decisions during construction. If the deep foundation design will not change based on the load test, the decision to perform a load test should be evaluated. Load tests to failure provide more substantial information and an opportunity to evaluate changed conditions and construction criteria.

When designing deep foundation systems, it is important to consider how the aforementioned factors will affect the drilled shaft over time. Incorporating an increase in capacity may help alleviate alternative safety measures, ultimately producing structurally competent systems while simultaneously decreasing construction costs.

REFERENCES:

Camp, Billy, "A Deep Foundation Comparison: Driven Vs Bored Piles," Pile Driving Contractors Association, Professor' Driven Pile Institute, 2013
http://www.piledrivers.org/files/222878A6-57C7-493C-8E27-6DAD34F0CEBD--3E6630CF-2786-47C9-9AC7-D9A84D93E0E9/driven-v-bored-piles.pdf

Gabrielaitis, L., Papinigis, V., Zarzojus, G., "Estimation of Settlements of Bored Piles Foundation," Procedia Engineering 57 (2013) 287-293, 2013
https://ac.els-cdn.com/S1877705813007698/1-s2.0-S1877705813007698-main.pdf?_tid=b006af40-9f26-11e7-b262-00000aacb360&acdnat=1506037597_66174e968fea5db1b6a11594eb899ec0

He, Y., Zhang, X., Hooton, R.D., Zhang, X., "Effects of Interface Roughness and Interface Adhesion on New-to-Old Concrete Bonding," Construction and Building Materials 151 (2017) 582-590, 2017
http://ac.els-cdn.com/S0950061817309418/1-s2.0-S0950061817309418-main.pdf?_tid=32da04bc-9e0f-11e7-8a09-00000aacb362&acdnat=1505917557_e6f27491097932d55f7b8812c0041d89

Li, L., Li, J., Sun, D., Zhang, L., "Time-Dependent Bearing Capacity of a Jacked Pile: An Analytical Approach Based on Effective Stress Method," Ocean Engineering 143 (2017) 177-185
https://ac.els-cdn.com/S0029801817304638/1-s2.0-S0029801817304638-main.pdf?_tid=0ebaf2b4-9f20-11e7-9b5a-00000aacb35d&acdnat=1506034749_d907fca963dd46938225b868123d36e5

LABORATORY EVALUATION OF A PROPOSED NONDESTRUCTIVE TESTING SYSTEM FOR DETECTING ANOMALIES BELOW DRILLED SHAFT EXCAVATIONS

Alireza Kordjazi, Temple University, Department of Civil and Environmental Engineering, 1947 N. 12th St., Philadelphia, PA. alireza.kordjazi@temple.edu
Joseph T. Coe, Temple University, Department of Civil and Environmental Engineering, 1947 N. 12th St., Philadelphia, PA. joseph.coe@temple.edu
Trumer Wagner, Temple University, Department of Civil and Environmental Engineering, 1947 N. 12th St., Philadelphia, PA. tuf53109@temple.edu

ABSTRACT

Anomalous conditions such as voids, soil seams, or zones of weakness beneath deep foundation elements constructed in situ (i.e., drilled shafts) can greatly affect the development of base resistance. These conditions are seen in many geological environments across the world, including in areas of karst and/or significant residuum. Current standards of practice to evaluate conditions underlying a drilled shaft can have trouble identifying the true vertical and lateral extent of anomalous conditions underlying the base once excavation is complete. Moreover, methods such as rock coring and probing are invasive and can be time intensive. A nondestructive system that can effectively identify anomalous conditions beneath drilled shaft excavations prior in a timely manner prior to concrete placement would be a welcome tool to address drilled shaft capacity in areas with significant karst and weathered bedrock. To address this concern, a nondestructive testing (NDT) system was developed in this study that utilizes seismic stress waves and a series of receivers at the base of an excavation. Elastic stress waves (P-waves and S-waves) are generated by a seismic source at the base of the excavation and the corresponding reflected are recorded and analyzed using geophysical analytical techniques. In this manner, the stiffness of the underlying earth material stiffness is estimated and the extent of anomalous conditions can be profiled. This study consisted of initial laboratory efforts in the development of this NDT system. A large cemented sand model was constructed to represent the bottom of a drilled shaft excavation in karst conditions with softer soil seams present. This paper summarizes the development of the system, including hardware components, system operation, as well as the construction of the laboratory soil model to represent field conditions. Two-dimensional seismic stress wave data was acquired for the model and analyzed to present a depth profile of the base conditions. A discussion is provided regarding data reduction, analysis, and the resulting interpretation. Finally, the paper also discusses development issues related to anticipated future applications of the system in the field.

Keywords: Nondestructive Testing, Drilled Shafts, Karst, P-waves, S-waves, Stress waves

INTRODUCTION

Given their high bearing capacity and ability to limit settlement, drilled shafts are essential foundation systems in the construction of infrastructure. They present a number of advantages over other foundation systems, including the ability to be constructed in geological environments unfavorable for pile driving and high capacity relative to costs (O'Neill and Reese 1999; Brown et al. 2010). However, construction quality has a tremendous impact on drilled shaft performance (O'Neill 2001). In fact, construction is as important to the success of a drilled shaft foundation project as the analytical techniques used for design

© 2018 Deep Foundations Institute

(Turner 2006). The design, construction and inspection of drilled shafts are consequently challenging tasks. In the case of drilled shafts constructed on rock sockets, the design may be based solely on the capacity generated from end bearing on the bedrock (O'Neill and Reese 1999). This necessitates a thorough investigation of subsurface condition to evaluate the competence of bedrock. This is particularly the case in geological environments where soluble bedrock (e.g., limestone and dolostone) is dissolved by underground water and leaves behind karst cavities filled with air or loose materials. Approximately 18% of the United States is underlain by such materials (Weary and Doctor 2014). Such features can significantly decrease the bearing capacity of drilled shafts and lead to drastic settlements, consequently posing a major threat to the safety and proper operation of the superstructure. Extensive geotechnical site investigation is certainly warranted in these circumstances (ADSC-DFI 2004, Brown et al. 2010), but the extreme variability of actual conditions for a specific drilled shaft often cannot be determined with an adequate degree of accuracy before construction (Turner 2006). Therefore quality control activities during construction and proof load testing become critical to ensure adequate drilled shaft performance.

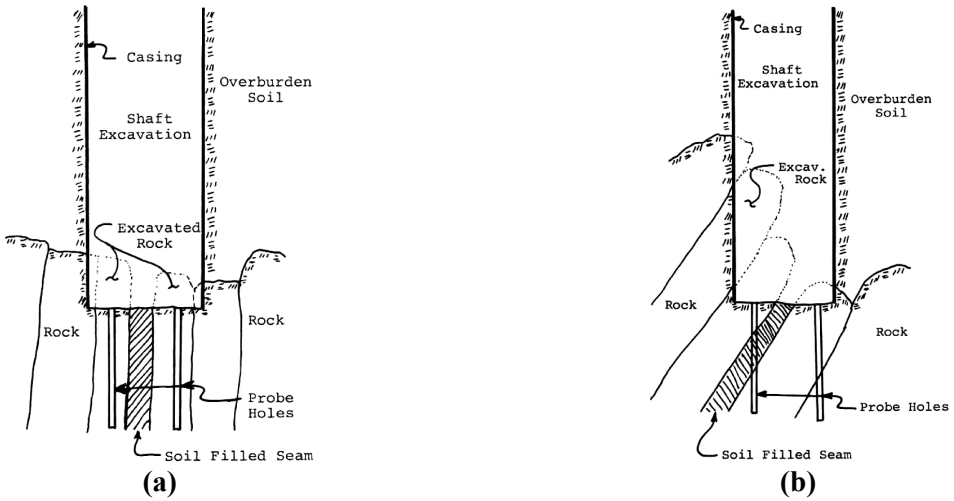


Fig. 1: Soil seams in karst terrain (Brown 1990): (a) vertical; and (b) non-vertical.

Proof load testing (e.g., conventional axial load testing, O-cell, etc.) can ensure that conditions beneath the base are capable of generating the required end bearing. However, this approach is cost prohibitive for implementation on each shaft. Therefore, current approaches inspect the bearing surface and indirectly evaluate the underlying base materials. In carbonated rock, it is very common to carry out these inspections by coring a hole and probing with a feeler rod. The presence of seams and rock quality are indirectly determined based on sound and feel. The subjective judgment of inspectors can highly influence the results using this technique. Moreover, the outcome of the inspection does not provide a continuous image of rock condition underneath the shaft base. The diameter of the probe hole is very small compared to typical diameters of drilled shafts and the point source nature of the probing may completely miss the presence of seams and loose soils (Fig. 1). There is also some evidence to suggest that the destructive nature of corings can affect shaft capacity (Vipulanandan et al. 2007). Finally, probing may necessitate downhole entry by inspectors to perform the testing, which can pose a serious safety risk. Visual inspection based on cameras [e.g., shaft inspection device (SID)] has been employed to avoid this safety issue but does not provide as much information regarding the materials underlying the shaft base. Recent advances in base inspection include more sophisticated/automated probing tools such as the Ding inspection device (DID) (Ding et al. 2015) and the Shaft Quantitative Inspection Device (SQUID) (PDI 2017). However, these devices are mainly intended to inspect the cleanliness of the shaft base and not intended to penetrate the bed rock and provide information on the underlying rock condition.

Geophysical and nondestructive testing (NDT) techniques can potentially address some of the limitations associated with the aforementioned traditional inspection methods. Geophysical site investigation techniques, especially methods based on the propagation of seismic stress waves, have become quite popular to evaluation subsurface conditions in geotechnical engineering applications (e.g., Stokoe et al. 1994; Park et al. 1999; Lee and Santamarina 2005). A very practical description of geophysical methods and their applications in civil engineering and for drilled shafts is presented in Wightman et al. (2003), Anderson et al. (2008), Turner (2006), and Brown et al. (2010). NDT methods such as sonic echo, impulse response, parallel seismic, cross-hole sonic logging, gamma-gamma logging, and thermal integrity profiling (TIP) have all been utilized to improve defect detection in completed drilled shafts to varying degrees of success (e.g., Finno and Gassman 1998; Iskander et al. 2003; Jalinoos et al. 2005; Mullins 2010). However, the focus of NDT and geophysical approaches has typically been on conditions along the length of drilled shafts after construction or on improved characterization of site conditions prior to construction. Given the lack of available literature and the continued difficulties with evaluating base conditions, there exists demand for a robust NDT system to evaluate anomalies and stiffness of the materials underlying drilled shaft excavations. This is particularly true for an NDT system that can use high resolution imaging technique with high frequency seismic waves. Only a limited number of studies have explored such systems for civil/geotechnical applications (Santamarina et al. 2001; Lee and Santamarina 2005; Coe and Brandenberg 2010; Coe and Brandenberg 2012; McGovern et al. 2013).

The goal of this study was to initiate efforts to develop a new NDT system that can image subsurface conditions underneath the base of drilled shafts. High frequency P- and S-wave transducers were used to ensure high resolution images capable of providing extensive coverage of anomalous features such as soil seams. The NDT system was used on a large scale soil model as a proof-of-concept to demonstrate its imaging capabilities. The following sections provide details regarding the laboratory model construction to mimic realistic karst conditions, a description of the hardware and software components for data acquisition, an evaluation of system performance, and a discussion on insights for future field applications.

LABORATORY TESTING

Model Preparation

The main challenges related to the laboratory model included the choice of representative materials (i.e., bedrock and soil seams), the geometry of the anomalies, and construction methodology. It was important to ensure that the laboratory model mimicked an appropriate level of stiffness mismatch between the rock material and soil seam. Based on reported acoustic impedances (i.e., the product of material density and P-wave velocity) in Santamarina et al. (2001), limestone/dolostone can be as much as twenty to forty times stiffer than saturated clay. To approximate such an impedance contrast and maintain constructability, the model was constructed using mixtures of silica sand and Portland cement with different cement contents. It was anticipated that this would primarily result in differences in wave velocity rather than density. A cement-sand mix with 20% of cement by weight was used to simulate the carbonated rock and another mix with only 1% of cement content formed the soil-filled seams of the model. The cement and sand were mixed at an optimum water content (12% by the weight of the sand/cement mix) to develop the highest wave velocities (Khan et al. 2006). Independent measurements of P- and S-wave velocities (V_p and V_s) were made on small samples of cemented sand with similar cement content and construction procedures as the model in this study. The average V_p and V_s of the 20% cement sand mix was measured as 2700 m/s and 1850 m/s, respectively. For the 1% cement-sand mix, V_p = 725 m/s and V_s = 490 m/s on average. Assuming similar density for both sand/cement mixes, the differences in velocities resulted in an impedance contrast of approximately three to four. This was much lower than the twenty to forty cited above, but still presented a large contrast for imaging purposes.

The geometry of the model was another key aspect of this study. The model needed to include features commonly encountered in karst terrains. Soil filled seams in karst rock can be encountered in both vertical and non-vertical orientations (Fig. 1). Therefore, the model contained both vertical and horizontal soil seams. The model was constructed in a 3.0 x 3.0 x 2.0 ft (approximately 0.90 x 0.90 x 0.60 m) wooden container anda schematic of the cross section is presented in Fig. 2. The anomaly illustrated in Fig. 2 is extended for 2.0 ft (0.60 m) in the direction perpendicular to the cross section of the figure. The remaining 1.0 ft (0.30 m) of the container is filled with 20% cement-sand mix as the control zone. The steps on the left side of Fig. 2 represent vertical seams located at various depths below the base of the drilled shaft when imaged in the out-of-plane direction. Additionally, the anomaly simulates an inclined seam filled with soil when data is acquired from scans across the cross section in Fig. 2. On the right side of the model, the anomaly cross section models two horizontal soil seams at different depths.

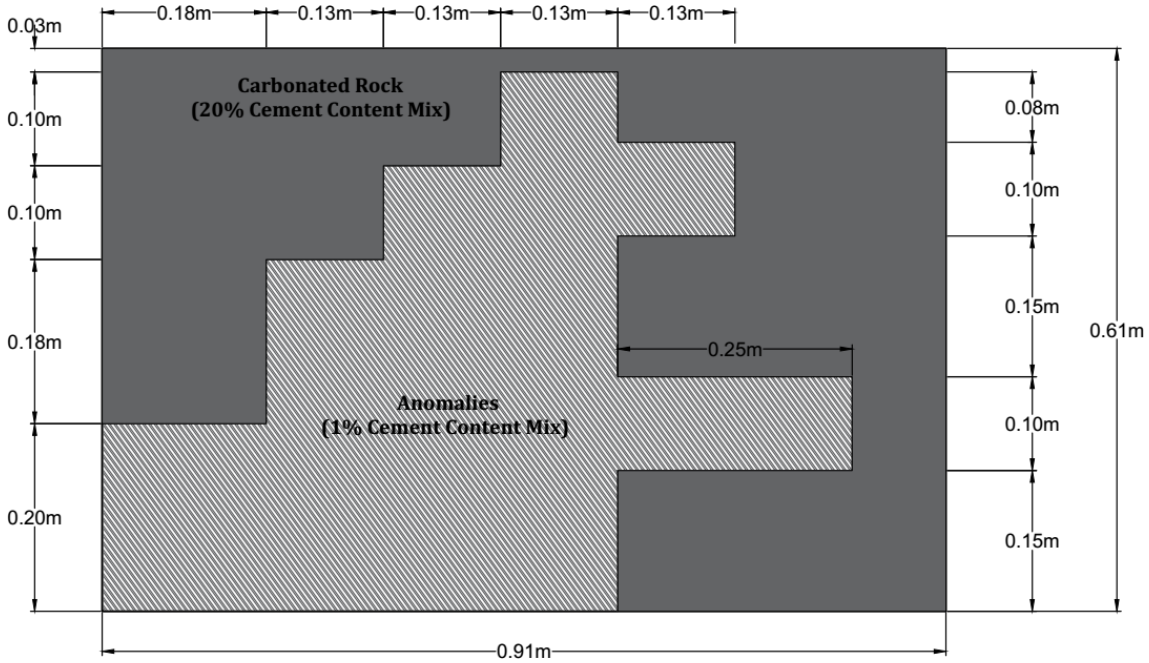


Fig. 2: Cross section of the laboratory model with geometry of the soil seams.

Regarding model construction, the sand/cement mixes were placed inside the container and compacted using 2 in thick lifts. Plywood separators were used to maintain the boundaries between sand/cement mixes and removed as construction proceeded. Each lift was placed inside the container, spread by hand and then leveled using a trowel. A 1.25 lb (0.58 kg) plastic mallet was used to strike a wooden base plate with dimensions of 18 in x 7 in x 0.75 in (45.7 cm x 17.8 cm x 1.9 cm). The baseplate was struck at consistent locations along the model surface and care was taken to strike with the same energy. After compaction of each layer, the trowel was used to gently re-level the surface. A square notch trowel was then used to scratch the surface and increase the bonding between consecutive lifts. Extra care was taken to provide as level a finish as possible to the surface of the model. A long piece of lumber was dragged across the surface of the model for this purpose. The exposed surface of the model was covered with plastic sheets to retain moisture while the model cured at room temperature for three weeks.

Instrumentation and Data Acquisition

This study focused on the propagation of seismic stress waves through the laboratory model. Generally, seismic surveys rely on the reflection and refraction of body waves (P- and S-waves) at the boundaries between materials or on the propagation of surface waves [e.g., the multichannel analysis of surface wave (MASW) method]. For proof-of-concept, it was decided that the common offset mode of the seismic

reflection technique would provide a straightforward approach to develop a high resolution image of the soil seams in the laboratory scale model.

In order to conduct the seismic reflection survey on the model, a system consisting of a pair of transducers (source and receiver), data acquisition hardware, and a personal computer was configured. Much of the instrumentation and hardware/software was utilized by the authors in previous ultrasonic imaging projects (e.g., Coe et al. 2014; Coe and Kermani 2016). The propagation of both P- and S-waves was examined separately using two different pair of transducers. The P-wave transducers (Ultran Group® model GRD-100-50) has a nominal central frequency of 100 kHz and nominal active element diameter of 2.0 in (5.1 cm). The shear wave survey was conducted with a pair of normal incident shear wave transducers (Olympus® model V150-RB), which have a nominal central frequency of 250 kHz and an active element diameter of 1.0 in (2.5 cm). A pulser (Panametrics® model 5800PR) was used to generate the negative voltage spike (275 V_{DC}) and excite the source transducer. The transducers and pulser system were interfaced with a National Instruments (NI) PXI chassis with various modules to handle signal inflow and outflow. Custom LabVIEW coding was developed to control a digitizer (NI-PXI 5620) and arbitrary function generator (NI-PXI 5412) mounted on the NI PXI chassis and to provide a user-friendly graphical user interface to acquire data. The acquired signal was amplified using a low noise amplifier (HD Communications model 25143) prior to acquisition by the digitizer. Each recorded waveform was written to an ASCII file containing a header with metadata, allowing the user to add experimental notes and remarks during the data acquisition. Figure 3 presents the model, data acquisition system, and shear wave transducers.

The survey plan consisted of three survey lines along the transverse direction of the soil seams in Fig. 2. The survey lines were located 6.0 in (15.2 cm) apart and were referenced as LT1 through LT3. P- and S-wave data was collected separately along each survey line, resulting in 6 sets of acquired waveforms. During data acquisition, the source-receiver transducer sets were displaced by 0.4 in (1 cm) along each survey line, which resulted in approximately 83 to 84 recorded reflection traces depending on size of the transducer. Petroleum jelly was placed on the face of the P-wave transducers and a shear wave couplant manufactured by Echo Ultrasonics, LLC was used on the S-wave transducers to improve coupling. Additionally, 8.8 lb (4.0 kg) weights were placed on top of the transducers to provide additional coupling pressure (Fig. 3).

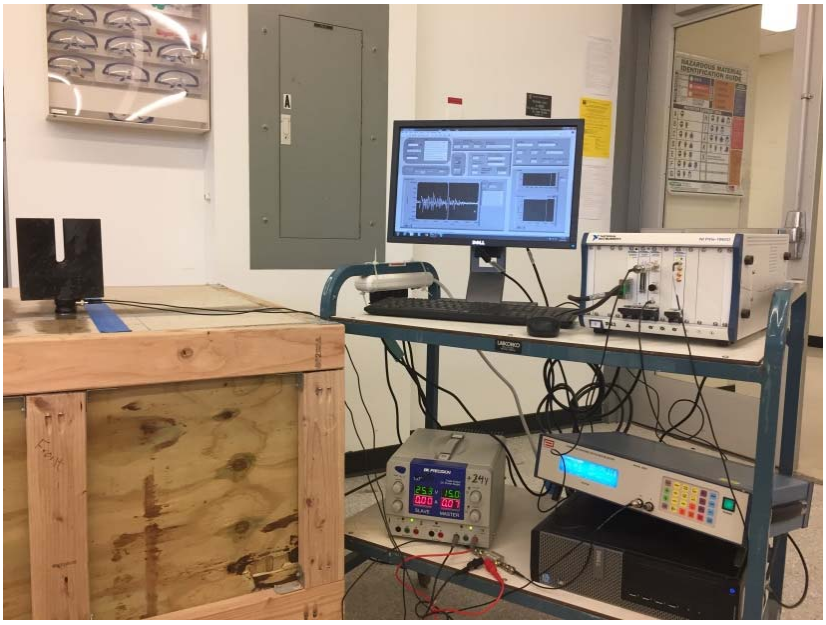


Fig. 3: Laboratory model, data acquisition system, and shear wave transducers.

RESULTS AND DISCUSSION

Common offset seismic reflection technique relies on a consistent offset between source and receiver and the acquisition of waveform data using multiple "shots" across the area of interest (Steeples and Miller 1990). Since the anomalies are much farther than the source-receiver offset, the depths of any anomalies can be estimated directly from the arrival time of the reflected waves with the known wave velocity. The acquired waveforms were preprocessed by applying a band-pass filter and non-linear gain function in order to improve the quality of the resulting image. The filter removed undesirable noise and the gain function compensated for the smaller amplitudes in deeper reflectors caused by geometric spreading. The pass band for the P-wave traces was within 20% of the central frequency of the transducers. This band pass filter was less effective on the S-wave data so lower frequencies were used in that case (50 – 160 kHz). Other studies have also exhibited similar behavior where data primarily outside the central frequency of the transducer was useful in analyzing S-wave results (e.g., McGovern et al. 2013). Data preprocessing, normalizing, and analysis were performed using a custom MATALB® script.

Figure 4 presents the P- and S-wave results as a series of two-dimensional (2D) slices. There are a number of notable features in these results. First of all, the estimated soil seam geometries generally agreed well with actual model dimensions, particularly for the vertical soil seams. Small discrepancies in predicted geometry can be attributed to the zero offset assumption used in this study and slight differences in wave velocity between the model and samples used for wave velocity testing. Additionally, it is worth mentioning that despite the tremendous care exercised during model construction, some small margin of error is expected between the schematic and what was actually constructed. However, the differences between estimated and expected anomaly geometries are generally acceptable from a practical point of view.

Clearly visible in Fig. 4 are reflections from the vertical soil seams at the shallowest three depths in the model. Generally, the P-wave results tended to overestimate the depth of these anomalies. For example, the shallowest vertical soil seam was located at approximately 0.03 m below the ground surface. The P-wave results estimated this depth at approximately 0.07 m to 0.09 m compared to estimates of 0.02 m to 0.04 m with S-waves. However, there is better agreement between P- and S-wave results for deeper targets, indicating that transducer near field effects may play a role in the discrepancies. Moreover, differences in transducer construction and damping produced "ringier" P-wave signals. This behavior combined with multiple strong reflection events from shallow anomalies may lead to constructive interference, which masks the first arrival of the initial reflected wave. Even though there is limited confidence in the predicted depth for the shallowest soil seam in the P-wave results, the system still performed well and detected its presence. Figure 4 also highlights strong reflections from the upper most horizontal soil seam. There is also limited evidence of reflections from the deepest horizontal soil seam. For example, Fig. 4(f) has some faint reflection signals located at approximately 0.35 m below the surface and from 0.73 m to 0.80 m along the scan axis that are likely attributable to the deeper horizontal soil seam. Also evident in both sets of results are a few sets of reflections that do not otherwise agree with the model geometry. For example, in all the scans there appears a set of reflections extending from approximately 0.68 m to 0.85 m at the same depth as the shallowest horizontal soil seam (i.e., approximately 0.12 m below the surface). There are reflections signals at a similar depth and location on the opposite side of the scan. In both cases, these spurious signals may be attributable to potential model boundary effects. However, additional data collection would be necessary to rule out any construction-related issues that may have developed an impedance contrast not originally planned in the model cross section.

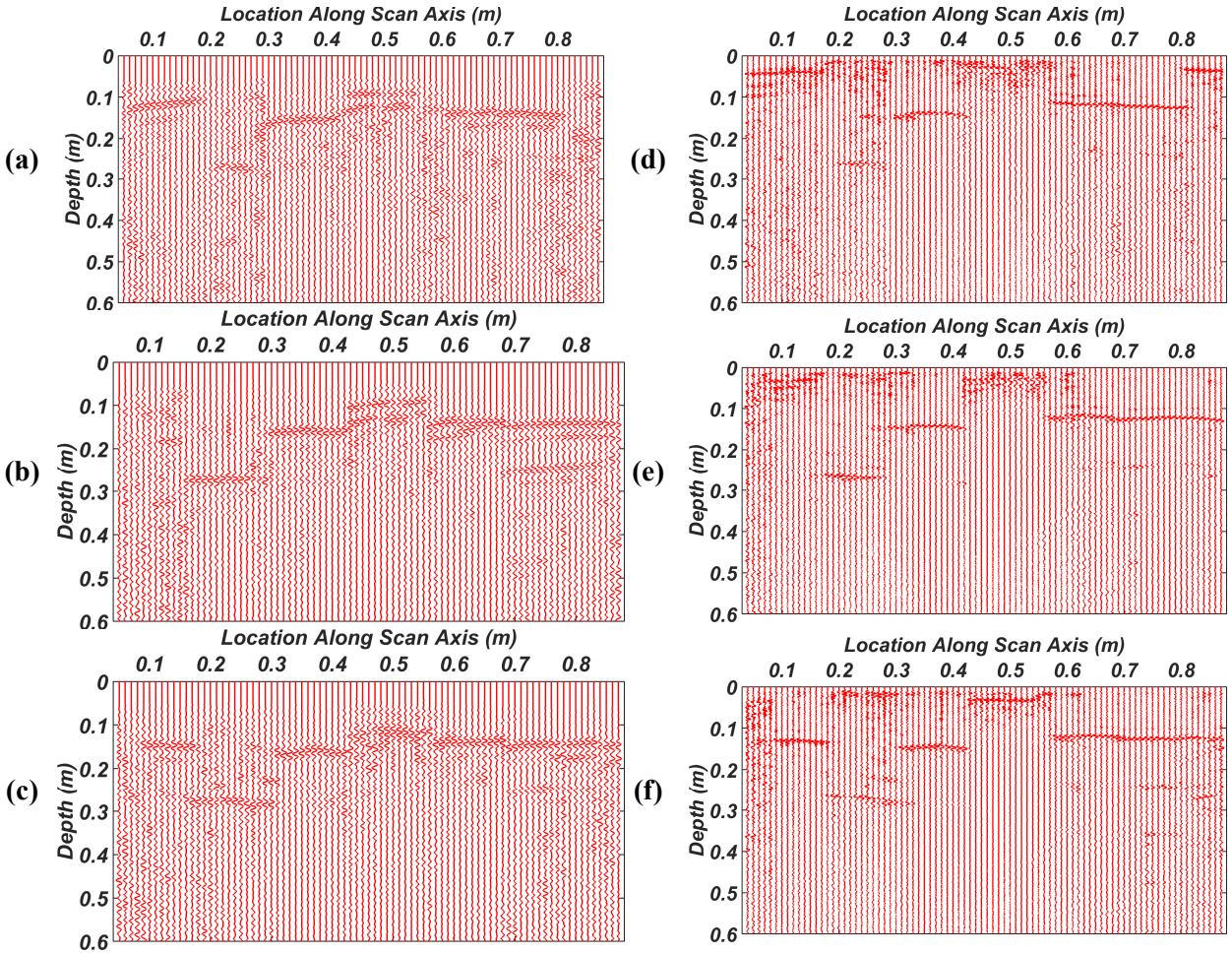


Fig. 4: Processed reflection signals: (a) P-wave TL1; (b) P-wave TL2; (c) P-wave TL3; (d) S-wave TL1; (e) S-wave TL2; and (f) S-wave TL3.

One advantage of using both P- and S-waves is that they are sensitive to different characteristics of the subsurface. For example, S-waves may be more likely to be affected by transverse anisotropy beneath the shaft base. In cases where multiple receivers are simultaneous employed and velocities can be estimated, the Poisson's ratio can be also evaluated for the underlying shaft materials. In this particular study, the S-wave results exhibited higher signal-to-noise ratio and slightly more accurate estimates for soil seam geometry. Additional testing is warranted with different source-receiver pairs and model geometries to ensure this pattern is consistent. Finally, it should be noted that the 2D scans can be arranged to develop a three-dimensional (3D) image of the soil seams (Fig. 5). The usefulness of the 3D image was relatively modest in this study largely because of the boundary effects, the limited number of 2D slices acquired, and the relatively uniform geometry in the out-of-plane direction of the model. However, in more complex settings, a 3D image can encourage better interpretation by highlighting subtle details that change between the 2D sections.

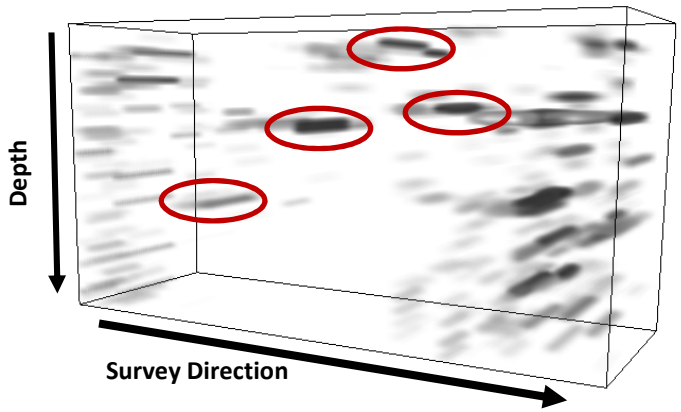


Fig. 5: 3D rendering of the shear wave data with interpreted locations of the soil seams.

CONCLUSION

The main purpose of this study was to examine the performance of a stress wave NDT technique for evaluating subsurface conditions below the base of drilled shafts. The experimental model was specifically designed to include conditions encountered in karst terrain. Given the model geometry, boundary conditions, and limitations posed by the transducers, the acquired data necessitated careful interpretation. However, the results of this study confirmed that a common-offset seismic reflection approach is a promising technique to generate high-resolution images of soil seams beneath rock sockets. The results also highlighted potential issues with scaling up the laboratory measurement system for field applications. For instance, the inability to consistently image the deepest soil seams in the model can be potentially addressed by changes in source characteristics and/or receiver properties (e.g., operating frequency). The use of a piezo-shock generator or seismic "sparker" source can potentially yield relatively high energy seismic waves with more favorable frequency content (e.g., less than 50 kHz) to address attenuation concerns. Highly sensitive accelerometers can also be considered as alternative receivers to improve signal to noise ratio. Additionally, different data acquisition schemes (e.g., body waves versus surface waves), sensor configurations (e.g., 2D versus 3D), and data post-processing techniques should be examined to evaluate their impacts on system capabilities, particularly in more complex subsurface conditions likely encountered under real field conditions. Nevertheless, the results from this study established proof-of-concept that an NDT system can evaluate conditions underlying the base of drilled shafts.

REFERENCES

ADSC-DFI (2004). *Drilled Shaft Inspector's Manual*. Prepared by the International Association of Foundation Drilling (*ADSC*) and the Deep Foundations Institute (*DFI*).

Anderson, N., Croxton, N., Hoover, R., and Sirles, P. (2008). *Geophysical Methods Commonly Employed for Geotechnical Site Characterization*, Transportation Research Circular E-C130, Transportation Research Board, Washington, D.C.

Brown, D.A. (1990). "Construction and Design of Drilled Shafts in Hard Pinnacled Limestones." *Transp. Res. Rec.*, 1277, Washington, D.C., 148-152.

Brown, D.A., Turner, J.P., Castelli, R.J., (2010). *Drilled Shafts: Construction Procedures and LRFD Design Methods*. Publication No. *FHWA-NHI-10-016*, Washington, D.C.

Coe, J.T. and Brandenberg, S.J. (2010). "p-Wave Reflection Imaging of Submerged Soil Models Using Ultrasound." *J. Geotech. Geoenviron. Eng.*, 136(10), 1358-1367.

Coe, J. T. and Brandenberg, S. J. (2012). “Cone Penetration Test-Based Ultrasonic Probe for P-wave Reflection Imaging of Embedded Objects.” *J. Bridge Eng.*, 17(6), 940-950.

Coe, J. T. and Kermani, B. (2016). “Comparison of Borehole Ultrasound and Borehole Radar in Evaluating the Length of Two Unknown Bridge Foundations.” *DFI Journal*, 10(1), 8-24.

Coe, J. T., Kermani, B., Nyquist, J. E., Berg, P. H., McInnes, S. E., and Sybrandy, L. (2014). “Use of P-wave Reflection Imaging and Other Nondestructive Testing Techniques to Evaluate Unknown Bridge Foundations.” *Proc. Geo-Congress 2014*, Atlanta, GA.

Ding, J.Z., McIntosh, K.A., and Simon, R.M. (2015). "New device for measuring drilled shaft bottom sediment thickness." *DFI Journal*, 9(1), 42-47.

Finno, R. and Gassman, S. (1998). “Impulse Response Evaluation of Drilled Shafts.” *J. Geotech. Geoenviron. Eng.*, 124(10), 965-975.

Iskander, M., Roy, D., Kelley, S., and Ealy, C. (2003). “Drilled Shaft Defects: Detection, and Effects on Capacity in Varved Clay.” *J. Geotech. Geoenviron. Eng.*, 129(12), 1128-1137.

Jalinoos, F., Mekic, N., Grimm, R.E., and Hanna, K. (2005). *Defects in Drilled Shaft Foundations: Identification, Imaging, and Characterization.* FHWA-CFL/TD-05-003, Lakewood, CO, 138 pp.

Khan Z., Majid A., Cascante G., Hutchinson D.J., and Pezeshkpour P., (2006). “Characterization of a Cemented Sand with the Pulse-Velocity Method.” *Can. Geotech. J.*, 43(3), 294-309.

Lee, J.S. and Santamarina, C.J. (2005). “P-Wave Reflection Imaging.” *Geotech. Test. J.*, 28(2), 197 – 206.

McGovern M.E., Behnia B., Buttlar W.G. and Reis H., (2013). “Characterisation of oxidative ageing in asphalt concrete –Part 1: Ultrasonic velocity and attenuation measurements and acoustic emission response under thermal cooling.” *Insight - NDT and Cond. Monitor.*, 55(11), 596-604.

Mullins, G. (2010). "Thermal integrity profiling of drilled shafts." *DFI Journal*, 4(2), 54-64.

O'Neill, M. (2001). “Side Resistance In Piles and Drilled Shafts.” *J. Geotech. Geoenviron. Eng.*, 127(1), 3-16.

O’Neill, M.W. and Reese, L.C. (1999). *Drilled Shafts: Construction Procedures and Design Methods*. FHWA-IF-99-025, Washington, D.C., 758 pp.

Park, C.B., Miller, R.D., and Xia, J., (1999). “Multichannel Analysis of Surface Waves.” *Geophysics*, 64(3), 800-808.

Pile Dynamics, Inc. (PDI) (2017). “SQUID: Shaft Quantitative Inspection Device.” Shaft Quantitative Inspection Device. http://www.pile.com/pdi/products/squid/. Accessed 01 Aug. 2017.

Santamarina, J.C., Klein, K.A., and Fam, A.M. (2001). *Soils and Waves.* John Wiley & Sons, LTD.

Steeples, D.W., and Miller, R.D. (1990). “Seismic reflection methods applied to engineering, environmental, and groundwater problems.” Soc. Explor. Geophys. Investigations in Geophysics no. 5, Stan H. Ward, ed., Volume 1: Review and Tutorial, 1-30.

Stokoe, K.H., II, Wright, S.G., Bay, J.A. and Roesset, J.M. (1994). “Characterization of Geotechnical Sites by SASW Method.” ISSMFE Technical Committee #10 for XIII ICSMFE, Geophysical Characterization of Sites, A. A. Balkema Publishers/Rotterdam & Brookfield, Netherlands, 15-25.

Turner, J.P., (2006). *Rock-Socketed Shafts for Highway Structure Foundations.* NCHRP Synthesis 360, Transportation Research Board, Washington D.C.

Vipulanandan, C., Hussain, A., and Usluogulari, O. (2007). “Parametric Study of Open Core-Hole on the Behavior of Drilled Shafts Socketed in Soft Rock.” *Proc. Geo-Denver 2007*, 1-10.

Weary, D.J., and Doctor, D.H. (2014). *Karst in the United States: A Digital Map Compilation and Database*. Open-File Report 2014-1156, U.S. Geological Survey, Reston, Virginia.

Wightman, W.E., Jalinoos, F., Sirles, P., and Hanna, K. (2003). *Application of Geophysical Methods to Highway Related Problems*. Federal Highway Administration, Central Federal Lands Highway Division, Lakewood, CO.

NUMERICAL AND EXPERIMENTAL STUDY OF AXIALLY LOADED NON-DISPLACEMENT PILES IN SAND

Fei Han, Purdue University, West Lafayette, Indiana, USA, hanfei@purdue.edu
Rodrigo Salgado, Purdue University, West Lafayette, Indiana, USA, rodrigo@ecn.purdue.edu
Monica Prezzi, Purdue University, West Lafayette, Indiana, USA, mprezzi@ecn.purdue.edu

ABSTRACT

This paper reports the results of recent studies on the response of non-displacement piles in sand using both numerical and experimental approaches. Three-dimensional Finite Element (FE) analyses were performed with an advanced, two-surface-plasticity constitutive model to investigate the response of non-displacement piles subjected to axial loads. The configuration of the mesh in the soil domain of the models was such that localization of strains and shear band development along the pile shaft and near the pile base during loading were captured properly. In addition, axial load tests were performed on model piles pre-installed in sand samples prepared in a large-scale calibration chamber with Digital Image Correlation (DIC) capabilities to obtain the displacement and strain fields in the sand during loading and to advance the understanding of resistance mobilization mechanisms in non-displacement piles. Design equations for the unit limit shaft and ultimate base resistances of non-displacement piles are proposed based on the results of the analyses.

Keywords: finite-element analysis, DIC, non-displacement piles, sand

INTRODUCTION

A non-displacement pile is installed in soils that do not require excavation support by creating a cylindrical void and filling it with concrete that is reinforced as needed. Non-displacement piles are often used as foundations of high-rise buildings, bridges, oil tanks and other structures due to their flexibility in geometry, suitability of installation in strong soils with minimal vibration and noise. In experimental or theoretical simulations, non-displacement piles are pre-installed or "wished-in-place" (Han et al. 2015, 2017a; Mascarucci et al. 2014; Pucker and Grabe 2012; Salgado et al. 2017b). This mode of pile installation in calibration chambers or centrifuges is a good approximation of the installation of drilled shafts (or bored piles) in the field when pile installation is properly performed (Brown et al. 2010; Fleming et al. 2008; Han et al. 2016; Salgado 2008; Viggiani et al. 2011).

In the last decades, considerable progress has been made on the understanding of the response of non-displacement piles subjected to axial loading using both numerical (e.g., Han et al. 2017; Lee and Salgado 1999; Loukidis and Salgado 2008; Mascarucci et al. 2014; Salgado et al. 2017a) and experimental (e.g., Brown 2002, 2012; Fioravante 2002; Ghionna et al. 1994; Mayne et al. 2010; Niazi and Mayne 2013; Tehrani et al. 2016, 2017) approaches. Nonetheless, the design of non-displacement piles (e.g., AASHTO (2014)) is mostly done using empirical equations developed based on results of pile load tests. The reason for this is that realistic numerical analyses able to capture mobilization of unit resistances require the implementation of advanced constitutive models and adequate understanding of the formation of shear bands along the shaft and near the base of the pile for proper mesh configuration in the soil domain.

In this paper, results of both advanced numerical analyses (finite-element analyses with the implementation of a two-surface-plasticity constitutive model and suitable mesh configuration) and experiments (chamber model pile tests with displacement/strain obtained from digital image correlation technique) are presented. The mechanisms for mobilization of both shaft and base resistances with increasing load are discussed. Based on the results of the analyses, design equations for both unit shaft and base resistance calculations of non-displacement piles are proposed.

© 2018 Deep Foundations Institute

SETUP FOR THE NUMERICAL AND EXPERIMENTAL STUDY

Finite-element analysis setup

Two-dimensional, axisymmetric finite-element analyses were performed using Abaqus/Explicit (ABAQUS 2012) with implementation of the two-surface-plasticity constitutive model developed by Loukidis and Salgado (2009). The constitutive relations were coded in a user-defined model subroutine VUMAT that is used to update stress state at a material point with the strain increment input in the finite-element program. Details of the constitutive formulation and the model parameters can be found in Loukidis and Salgado (2009). Fig. 1 shows the mesh configuration and the boundary conditions used in the axi-symmetric finite-element analyses performed in Abaqus/CAE 6.12-1 (ABAQUS 2012). The mesh consists of about 6400 four-noded, quadrilateral, axisymmetric elements. The mobilization of both the shaft and base resistance is very sensitive to the mesh configuration (Han et al. 2017c; Loukidis and Salgado 2008), particularly to the size of the mesh adjacent the pile shaft and near the pile base, when highly-nonlinear plasticity models are used. The drilling and any possible effects of the slurry are not explicitly modeled, with the in-situ coefficient of earth pressure at rest assumed to be K_0 initially. Following Loukidis and Salgado (2008b), the thickness (width) of the first elements adjacent to the pile shaft was taken as the shear band thickness t_s. Based on the DIC analyses of microscopic images taken in the vicinity of the pile shaft, the shear band thickness is of the order of $5D_{50}$ for non-displacement model piles (this corresponds to 2 mm for Ottawa sand and 1 mm for Toyoura sand). Based on the parametric study by Han et al. (2017b), a structured mesh (square elements) with the size of 6 mm was adopted near the pile base. Since the pile stiffness is significantly greater than that of the soil, the pile is modeled as a linear-elastic material, with Young's modulus E = 30 GPa and Poisson's ratio v = 0.2.

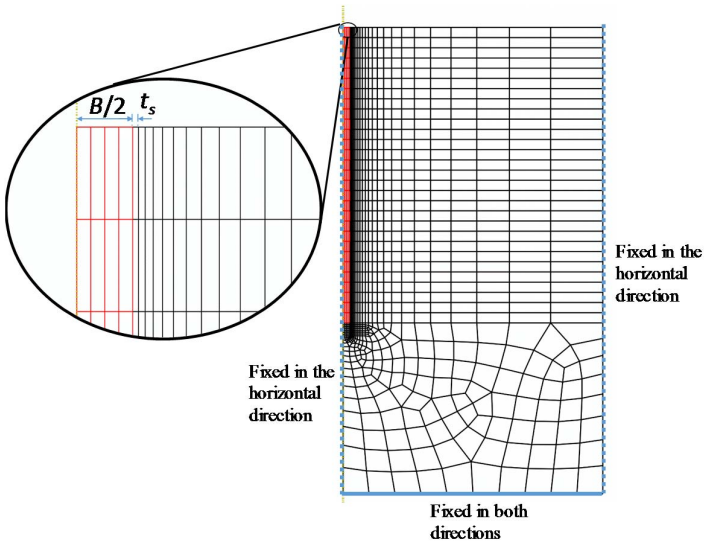


Fig. 1 Mesh configuration and boundary conditions for the axi-symmetric finite-element analysis

Experimental setup

Fig. 2 shows the DIC calibration chamber that was used for the model pile load tests. The half-cylindrical calibration chamber has three observation windows in the plane of symmetry, allowing image recording of the entire pile load testing. The DIC technique has been used for the study of many advanced geotechnical topics such as pile response to cyclic loading, setup effect for pile capacity, and shaft degradation (Arshad et al. 2014; Castro et al. 2017; Tehrani et al. 2016; Tovar et al. 2017). A 490-mm-long, half-circular steel model pile with a diameter of 31.75mm was pre-installed and load tested in medium dense (D_R = 66%) and dense (D_R = 86%) Ohio-Gold-Frac sand, a coarse-grained silica sand with sub-angular particles. A vertical surcharge pressure of 50 kPa was applied at the soil surface during

the test. The digital images during load testing were analyzed using the Digital Image Correlation (DIC) technique, producing the displacement field within the entire soil domain.

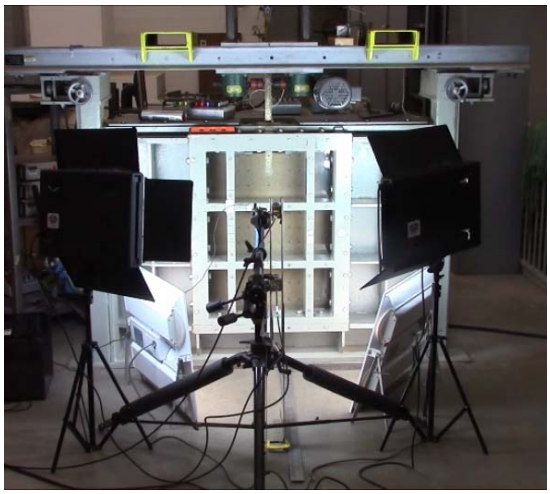


Fig. 2 Experimental setup for the calibration chamber model pile test with the digital image correlation (DIC) equipment

SHAFT RESISTANCE

Limit shaft resistance

The shaft resistance of a pile is fully mobilized on the early stages of axial loading. The limit shaft resistance Q_{sL} is mobilized at pile head settlements of the order of 1 to 2% of the pile diameter B. This is due shearing localization and formation of a shear band along the pile shaft (even small vertical movement of the pile leads to large shear strains within the shear band). The unit limit shaft resistance q_{sL} may be expressed as a function of the sand-pile interface friction angle δ and the coefficient of lateral earth pressure K (the ratio of mobilized horizontal effective stress σ'_h to the initial in-situ vertical effective stress σ'_{v0}):

$$q_{sL} = K\sigma'_{v0}\tan\delta \qquad [1]$$

The interface friction angle δ for non-displacement piles in sand can be taken as the triaxial compression critical-state friction angle $\phi_{c,TXC}$ of the sand since shearing happens within the shear band.

A series of finite-element analyses were carried out to model the response to axial loading of a 0.3-m-diameter, 10-m-long, non-displacement pile in sand considering 4 different relative densities (D_R = 30%, 50%, 80%, 90%). Fig. 3 shows the mobilized coefficient of lateral earth pressure K (at the critical state) as a function of σ'_{vo} and D_R. As σ'_{vo} increases, the value of K decreases with increasing depth due to the reduced tendency for sand dilation at greater confining stress levels.

In the chamber model pile tests, the average unit shaft resistance q_{sL} was obtained from the difference in the readings taken from the load cells placed on the head and base of the pile, from which the coefficient of lateral earth pressure K was back-calculated. The values of K obtained from the model pile tests are plotted in Fig. 3. At the same vertical effective stress level, the K value mobilized for the model pile is greater than that mobilized for a full-size pile considering similar values of relative density. The reason for this is because the radial stress build-up is greater for model piles (with smaller B), resulting in greater unit shaft resistance q_{sL}. Based on the one-dimensional FE analyses performed to study scale effects by varying the sizes of the pile used in the simulations (Loukidis and Salgado 2008), it was concluded that the value of K stabilizes when the pile diameter B exceeds $500D_{50}$ (D_{50} being the

mean particle size of the sand). If we assume a shear band thickness t_s = 2.5 mm, this criterion is equivalent to B ≥ 0.25 m.

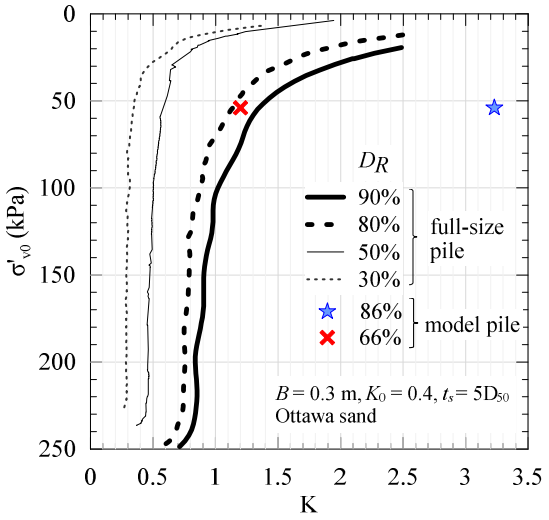


Fig. 3 The coefficient of lateral earth pressure K mobilized (at the critical state) along the shaft of non-displacement model piles (values obtained from experiments) and field-size piles (obtained from FE analyses) installed in sand with different relative densities

Design equations

Based on the finite-element analyses performed for full-size piles (as shown in Fig. 3), an equation for the coefficient of lateral earth pressure K was developed (Han et al. 2017c):

$$\frac{K}{K_0} = \frac{1}{F(K_0)} 0.67 \exp\left\{\frac{D_R}{100\%}\left[1.5 - 0.35 \ln\left(\frac{\sigma_{v0}'}{p_A}\right)\right]\right\} \quad [2]$$

where F(K_0) is

$$F(K_0) = \exp\left[0.3\sqrt{K_0 - 0.4}\right] \quad [3]$$

Note that, due to the scale effects discussed in the previous session, these design equations are only suitable for the field-scale, non-displacement piles.

BASE RESISTANCE

Load-settlement curve

Displacement near the pile base

Digital images taken during the model pile tests were analyzed using the DIC technique, producing the displacement field (in both vertical and horizontal directions) in the soil near the pile base, as shown in Fig. 4 for a dense sand sample with D_R = 87%. Finite element analysis was also performed considering the same pile geometry, sand relative density and boundary conditions as used in the model pile test. In the absence of calibrated parameters for the test sand used in the test, constitutive model parameters calibrated for Toyoura sand were used in the FE analysis because these two sands have similar particle morphology. Fig. 5 shows the displacement field obtained from the FE analyses (note that only half of

the pile-soil domain is shown for an axi-symmetric model). The finite element results closely reproduce the loading response of the model pile in sand.

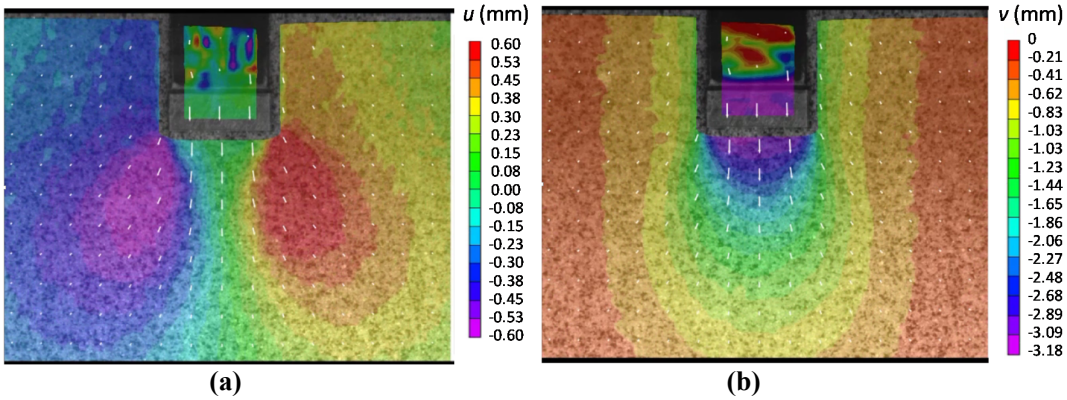


Fig. 4. Contour plots of: (a) the horizontal displacement and (b) the vertical displacement in sand near the pile base obtained using the DIC technique (after Han et al. 2017b)

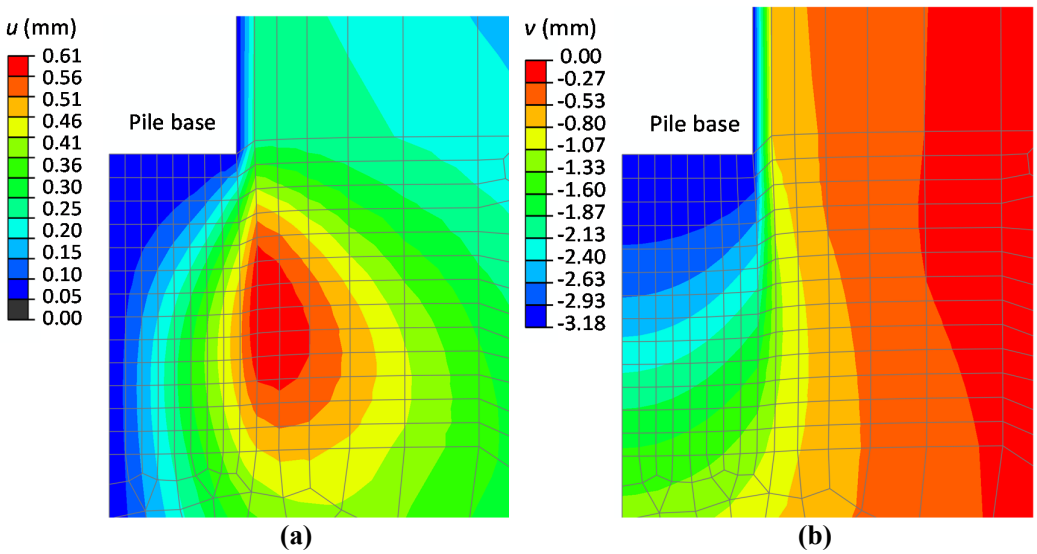


Fig. 5. Contour plots of: (a) the horizontal displacement and (b) the vertical displacement in sand near the pile base obtained from finite element analysis (after Han et al. 2017b)

Design equation for ultimate base resistance

In contrast with the process of mobilization of shaft resistance, which progresses quickly with loading and stabilizes at a critical-state value equal to Q_{sL}(see Fig. 3), a pile would need to plunge into the ground for the base resistance to reach a limit value equal to Q_{bL}. For this reason, it becomes necessary to define an ultimate base resistance criterion that produces an ultimate load that when divided by a factor of safety ensures the safety of the superstructure supported by the pile. In this paper, the ultimate base resistance is defined as the base resistance developed when the pile head settlement reaches 10% of the pile diameter B. The 10%B ultimate base resistance criterion is widely used in research and design practice (Basu and Salgado 2012, 2014; Fleming et al. 2008; Ghionna et al. 1994; Han et al. 2016, 2017b; Jardine et al. 2005; Kim et al. 2009; Mandolini et al. 2005; Paik et al. 2003; Randolph 2003; Salgado 2008; Salgado et al. 2017a; Viggiani et al. 2011). In order to study the dependency of the unit

ultimate base resistance on the pile diameter, pile length and the relative density of sand in which the pile is installed, a series of FE analyses were performed considering three pile lengths (5 m, 10 m and 15 m), two pile diameters (0.3 m and 0.6 m) and four different relative densities (D_R = 30%, 50%, 80%, 90%). The simulation results are shown in Fig. 6. The ultimate unit resistance $q_{b,ult}$ is independent of the pile diameter B and approximately proportional to $\sigma'^{0.4}_{h0}$, σ'_{h0} being the initial in-situ horizontal stress. The following equation was fitted to the results of these analyses:

$$\frac{q_{b,ult}}{p_A} = 62\left(\frac{D_R}{100\%}\right)^{1.83}\left(\frac{\sigma'_{h0}}{p_A}\right)^{0.4} \quad [4]$$

Fig. 6 shows that the $q_{b,ult}$ values normalized with respect to the horizontal effective stress for cases with the slenderness ratio L/B = 50 is smaller than the corresponding values for the cases with L/B < 50. This is because of the significant axial compression of the pile, which leads to a settlement at the pile base much smaller than that at the pile head, and consequently an insufficient mobilization of the base resistance at the ultimate load level (when w/B =10%). Therefore, Eq. [4] is only applicable to non-displacement piles with slenderness ratio L/B < 50.

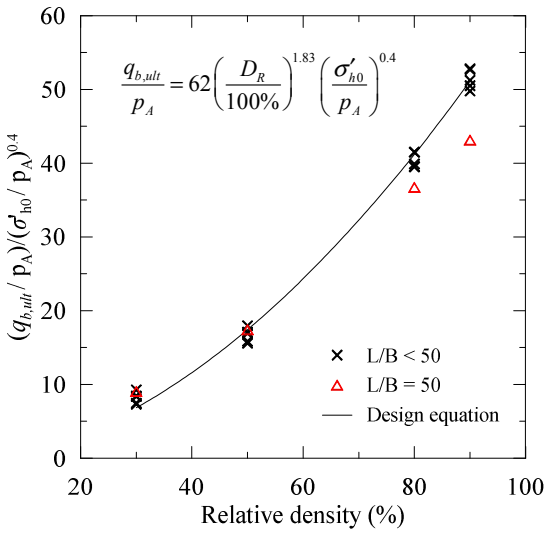


Fig. 6. Results of the FE analyses and proposed relationship between the normalized ultimate unit base resistance $(q_{b,ult} / p_A)/(\sigma'_{h0} / p_A)^{0.4}$ and the relative density of sand

CONCLUSIONS

In this paper, realistic finite-element analyses and calibration chamber model pile tests were performed to study the response of non-displacement piles to axial loading. With the use of an advanced, two-surface-plasticity constitutive model and a carefully prepared mesh that considers shear localization near the pile, the FE analyses match closely the results obtained (with the DIC technique) from the digital images taken in the chamber model pile tests. The combined use of advanced numerical and experimental technologies significantly improves our understanding of the resistance development mechanisms for non-displacement piles. Design equations for the unit limit shaft and ultimate base resistances were proposed based on the results of the FE analyses.

ACKNOWLEDGEMENTS

The work presented in this paper was partially funded by the Joint Transportation Research Program (JTRP) administered by the Indiana Department of Transportation (INDOT) and Purdue University through contract SPR-3636. The support of the Indiana Department of Transportation (INDOT) and the Federal Highway Administration (FHWA) are gratefully acknowledged.

REFERENCES

AASHTO. (2014). *AASHTO LRFD Bridge Design Specifications (7th Edition)*. Washington, DC.

ABAQUS. (2012). "ABAQUS 6.12-2." *Abaqus Analysis User's Manual (RI, USA: SIMULIA Inc)*.

Arshad, M. I. ., Tehrani, F. S. ., Prezzi, M. ., and Salgado, R. (2014). "Experimental study of cone penetration in silica sand using digital image correlation." *Géotechnique*, 64(7), 551–569.

Basu, D., and Salgado, R. (2012). "Load and resistance factor design of drilled shafts in sand." *Journal of Geotechnical and Geoenvironmental Engineering*, 138(12), 1455–1469.

Basu, D., and Salgado, R. (2014). "Closure to 'load and resistance factor design of drilled shafts in sand' by D. Basu and Rodrigo Salgado." *Journal of Geotechnical and Geoenvironmental Engineering*, 140(3), 7014002.

Boulon, M., and Foray, P. (1986). "Physical and numerical simulation of lateral shaft friction along offshore piles in sand." *3rd International Conference on Numerical Methods in Offshore piling*, Nantes, France, 127–147.

Brown, D. (2002). "Effect of construction on axial capacity of drilled foundations in piedmont soils." *Journal of Geotechnical and Geoenvironmental Engineering*, 128(12), 967–973.

Brown, D. (2012). "Factors affecting the selection and use of drilled shafts for uransportation infrastructure projects." *ADSC EXPO 2012 Geo-Construction Conference Proceedings*, San Antonio, TX, 25–35.

Brown, D. A., Turner, J. P., and Raymond J. Castelli. (2010). *Drilled shafts: Construction procedures and LRFD design methods*.

Castro, A. C. G., Tovar, R. D., Salgado, R., and Prezzi, M. (2017). "Effect of loading direction on the shaft resistance of jacked piles in dense sand." *Geotechnique*, Submitted.

Fioravante, V. (2002). "On the shaft friction modelling of non-displacement piles in sand." *Soils and foundations*, Japanese Geotechnical Society, 42(2), 23–33.

Fleming, K., Weltman, A., Randolph, M., and Elson, K. (2008). *Piling engineering*. CRC Press.

Ghionna, V., Jamiolkowski, M., Pedroni, S., and Salgado, R. (1994). "The tip displacement of drilled shafts in sands." *Vertical and Horizontal Deformations of Foundations and Embankments, Proc. Settlement '94*, New York, 1039–1057.

Han, F., Lim, J., Salgado, R., Prezzi, M., and Zaheer, M. (2016). *Load and resistance factor design of bridge foundations accounting for pile group–soil Interaction*. West Lafayette, IN.

Han, F., Prezzi, M., and Salgado, R. (2017a). "Energy-based solutions for nondisplacement piles subjected to lateral loads." *International Journal of Geomechanics*, 17(11), 4017104.

Han, F., Prezzi, M., Salgado, R., and Zaheer, M. (2017b). "Axial resistance of closed-ended steel-pipe piles driven in multilayered soil." *Journal of Geotechnical and Geoenvironmental Engineering*, 143(3), 4016102.

Han, F., Salgado, R., and Prezzi, M. (2015). "Nonlinear analyses of laterally loaded piles – A semi-analytical approach." *Computers and Geotechnics*, Elsevier Ltd, 70, 116–129.

Han, F., Salgado, R., Prezzi, M., and Lim, J. (2017c). "Shaft and base resistance of non-displacement

piles in sand." *Computers and Geotechnics*, Elsevier Ltd, 83, 184–197.

Jardine, R., Chow, F., Overy, R., and Standing, J. (2005). *ICP design methods for driven piles in sand and clays*. *Heron*, Thomas Telford Ltd.

Kim, D., Bica, A. V., Salgado, R., Prezzi, M., and Lee, W. (2009). "Load testing of a closed-ended pipe pile driven in multilayered soil." *Journal of Geotechnical and Geoenvironmental Engineering*, 135(4), 463–473.

Lee, J. H., and Salgado, R. (1999). "Determination of pile base resistance in sands." *Journal of Geotechnical and Geoenvironmental Engineering*, 125(8), 673–683.

Loukidis, D., and Salgado, R. (2008). "Analysis of the shaft resistance of non-displacement piles in sand." *Géotechnique*, Thomas Telford, 58(4), 283–296.

Loukidis, D., and Salgado, R. (2009). "Modeling sand response using two-surface plasticity." *Computers and Geotechnics*, 36(1–2), 166–186.

Mandolini, A., Russo, G., and Viggiani, C. (2005). "Pile foundations: Experimental investigations, analysis and design." *Proceedings of the 16th International Conference on Soil Mechanics and Geotechnical Engineering: Geotechnology in Harmony with the Global Environment*.

Mascarucci, Y., Miliziano, S., and Mandolini, A. (2014). "A numerical approach to estimate shaft friction of bored piles in sands." *Acta Geotechnica*, 9(3), 547–560.

Mayne, P. W., Niazi, F., and Woeller, D. (2010). "Drilled Shaft Response in Piedmont Residuum Using Elastic Continuum Analysis and Seismic Piezocone Tests." *Deep Foundations and Geotechnical In Situ Testing*, American Society of Civil Engineers, Reston, VA, 200–205.

Niazi, F. S., and Mayne, P. W. (2013). "A Review of the Design Formulations for Static Axial Response of Deep Foundations from CPT Data (DFI 2013 Student Paper Competition Runner-Up)." *DFI Journal: The Journal of the Deep Foundations Institute*, 7(2), 58–78.

Paik, K., Salgado, R., Lee, J., and Kim, B. (2003). "Behavior of open- and closed-ended piles driven into sands." *Journal of Geotechnical and Geoenvironmental Engineering*, 129(4), 296–306.

Pucker, T., and Grabe, J. (2012). "Numerical simulation of the installation process of full displacement piles." *Computers and Geotechnics*, Elsevier Ltd, 45, 93–106.

Randolph, M. F. (2003). "Science and empiricism in pile foundation design." *Géotechnique*, 53(10), 847–875.

Salgado, R. (2008). *The Engineering of Foundations*. McGraw-Hills.

Salgado, R., Han, F., and Prezzi, M. (2017a). "Axial resistance of non-displacement piles and pile groups in sand." *Rivista Italiana di geotecnica*.

Salgado, R., Zhang, Y., Abou-Jaoude, G., Loukidis, D., and Bisht, V. (2017b). "Pile driving formulas based on pile wave equation analyses." *Computers and Geotechnics*, Elsevier Ltd, 81, 307–321.

Tehrani, F. S., Han, F., Salgado, R., and Prezzi, M. (2017). "Laboratory study of the effect of pile surface roughness on the response of soil and non-displacement piles." *Geotechnical Frontiers 2017*, American Society of Civil Engineers, Reston, VA, 256–264.

Tehrani, F. S., Han, F., Salgado, R., Prezzi, M., Tovar, R. D., and Castro, A. G. (2016). "Effect of surface roughness on the shaft resistance of non-displacement piles embedded in sand."

Géotechnique, 66(5), 386–400.

Tovar, R. D., Galvis-Castro, A. C., Salgado, R., Prezzi, M., Galvis, A., Salgado, R., and Prezzi, M. (2017). "Effect of surface roughness on the shaft resistance of displacement model piles in sand." *Journal of Geotechnical and Geoenviromental Engineering*, Accepted.

Viggiani, C., Mandolini, A., and Russo, G. (2011). *Piles and pile foundations*. Spon Press, London and New York.

PERFORMANCE OF FOUNDATIONS IN THE KANTO PLAIN NORTH OF TOKYO DURING THE MW=9.0 TOHOKU EARTHQUAKE OF MARCH 2011

Dr. Daniel Pradel, PE GE DGE, The Ohio State University, Columbus, Ohio, USA, pradel.1@osu.edu
Dr. Joseph Wartman, University of Washington, Seattle, Washington, USA, wartman@uw.edu
Dr. Binod Tiwari, California State University, Fullerton, California, USA, btiwari@fullerton.edu

ABSTRACT

The Tohoku Earthquake caused widespread geotechnical damage in the towns of Fusa and Katori, two towns situated immediately north of Tokyo. The damage to structures and foundations in these towns was mainly the result of ground liquefaction, and surprising since they are located at an epicentral distance of about 300 km. The authors investigated the performance of foundations and liquefaction-induced damage during a post-earthquake engineering field reconnaissance in April 2011. In areas where the ground liquefied, they observed that structures constructed on deep foundations generally behaved very well, as opposed to those constructed on shallow foundations, which settled and tilted considerably. The performance of small residential and commercial buildings supported by deep foundations consisting of closely spaced small diameter piles that extended below the liquefied layer was also excellent. Numerical modeling shows that the flexibility of small diameter piles, such as the ones typically used in Japan, makes deep foundations particular resilient when liquefaction occurs in laterally confined areas.

Keywords: driven piles, drilled shafts, earthquake, seismic performance, soil liquefaction,

INTRODUCTION

In seismic regions, deep foundations are often used to mitigate the adverse potential effects of soil liquefaction on large structures such as buildings and bridges. Because liquefaction affects the depth at which lateral resistance develops, to design piles and drilled shafts engineers must often consider both large seismic inertial loads and lengthy moment arms; a condition that can result in exceptionally large bending moments. The Great Hyogoken-Nambu earthquake of January 17, 1995 damaged the foundations of many structures built on piles in the city of Kobe and its harbor (Tokimatsu and Asaka, 1998). Following this devastating earthquake, a major effort to understand the behavior of piles during earthquakes and improve their designs was conducted by researchers in Japan. These efforts which included large shake table experiments (e.g., Cubrinovski et al., 2006) were used to validate and/or modify previous simplified pseudostatic models (e.g., Ishihara, 1997), and have resulted in new and revised design standards for the modern (i.e., post Kobe earthquake) analysis and construction of deep foundations in liquefaction prone areas.

The March 11th, 2011, Tohoku Earthquake (magnitude M_w=9.0) is one of the largest recorded earthquakes in history. Throughout the east coast of northern Japan, it caused wide spread liquefaction, lateral spreading, landslides, dynamically induced settlements, and a destructive tsunami. Shortly after the earthquake, the authors conducted a post-earthquake engineering field reconnaissance in some of the most geotechnically-affected areas (e.g., Pradel et al., 2011). This paper addresses some of the authors' observations of buildings and foundations in the town on Fusa and in the Sawara neighborhood of Katori, which are situated in the Kanto plains, about 20 km north of Tokyo. Damage resulting from ground liquefaction in these towns was extensive and surprising based on epicentral distance (Figure 1). Modern buildings built on small diameter piles in these localities performed exceptionally well (e.g., Figure 2) and numerical modeling was performed to better understand their performance and verify the observed resilience of these deep foundation systems at sites were the strata prone to ground liquefaction was laterally confined.

© 2018 Deep Foundations Institute

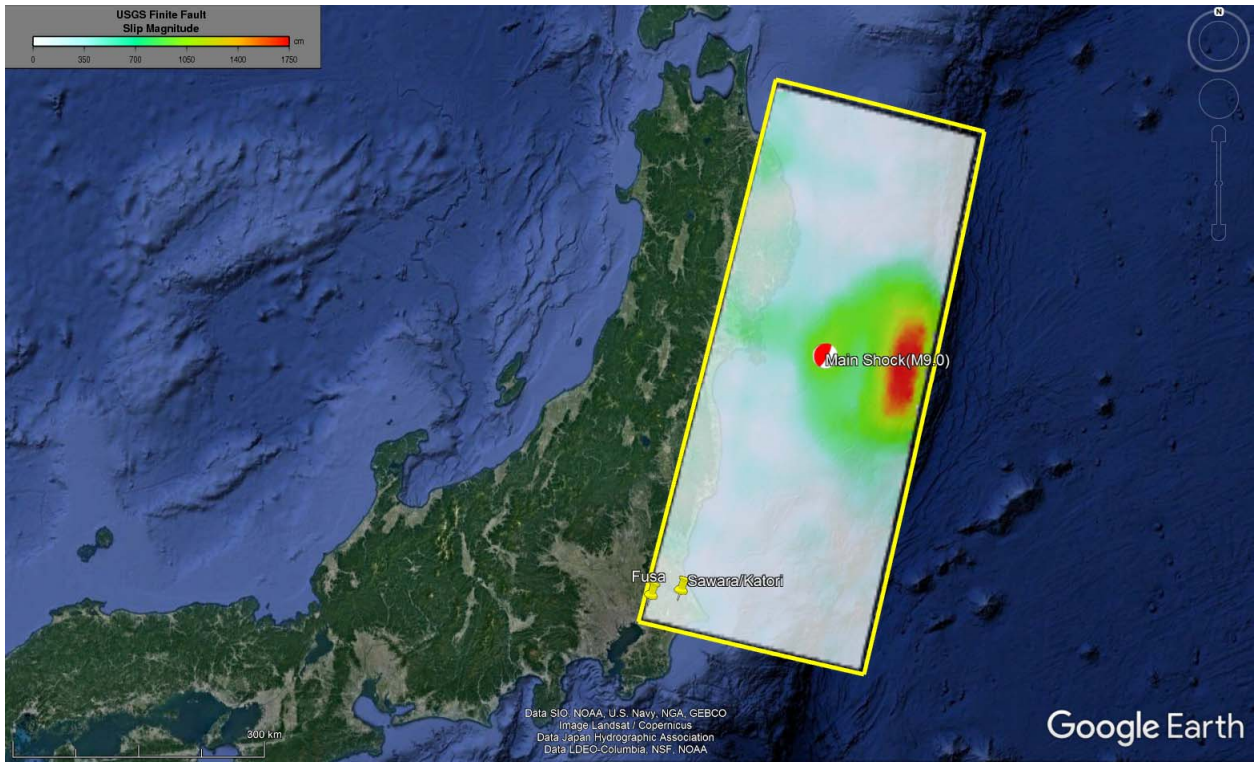


Figure 1. Location of Fusa and Sawara/Katori and fault rupture plane according to USGS



Figure 2. Liquefaction related settlement (~45 cm) in front of government building supported by piles in Sawara/Katori

GEOTECHNICAL SETTING

The Kanto plain covers a total area of 17,000 km^2 and is the largest plain in Japan. It was created by alluvial deposition from several large rivers, including the Tone, Watarase, Kinu, Kokai and Sagami rivers, as well as by ashes from surrounding volcanoes, including Mounts Asama, Akagi and Fuji. Its rivers and fertile lands attracted dwellers, which later built large cities, such as Saitama, Chiba and Tokyo.

Today, the Tone River runs in an easterly direction about 20 km north of Tokyo. This is not the river's natural alignment, but the result of four hundred years of anthropogenic changes to facilitate fluvial transportation, land development and agricultural changes to the land. As explained in Pradel et al. (2014), these man-made changes have resulted in the presence of recent alluvial deposits (less than 500 years old) and poorly compacted fills within numerous urban areas in cities located along the Tone River. As indicated in Youd and Perkins (1977), young natural deposits and loose fills are highly prone to soil liquefaction; hence, their presence strongly affects the performance of deep foundations during earthquakes. Such deposits were present in the town of Fusa and in the Sawara neighborhood of Katori (Figure 1); thus the presence of liquefaction and lateral spread prone deposits in this localities is not surprising.

SEISMOLOGIC CONDITIONS AND TOHOKU EARTHQUAKE

The Tohoku Earthquake was an undersea mega-thrust earthquake, which occurred on March 11, 2011. The earthquake was caused by the Pacific Plate moving westward under the island of Japan (subduction) at the exceptional rate of ~9 cm per year. The fault rupture plane was estimated by the USGS to be about 500 km long and 200 km wide and have permanent fault displacements of up to 40 meters (Figure 1).

The Tohoku Earthquake is most comparable to the Sanriku Earthquake of July 9, 869 (estimated magnitude M_w=8.6), which is recorded in both historical documents, as well as in the geologic record (e.g., many inland tsunami deposits have been discovered that indicate flooding similar to 2011, i.e., with similar inundation areas and run-up heights of up to 40 m). The earthquakes post-Sanriku are many, but of much lesser magnitude; they include the 1703 Genroku Earthquake (~M_w=8.2), the 1855 Ansei Earthquake (~M_w=7.2), and the famous Great Kanto earthquake of 1923 (~M_w=8.2).

The Tohoku Earthquake triggered in excess of 6000 seismic station belonging to various agencies, including almost 500 equipped with vertical arrays. Stations located along the Tone River, near Fusa and Katori (Figure 1), typically recorded PGAs between 0.2 and 0.4g and PGVs between 20 and 40 cm/s; noteworthy, was the roughly 300 seconds duration of the earthquake in these localities .

JAPANESE MODERN FOUNDATION PRACTICES

In areas susceptible to ground liquefaction (e.g., in reclaimed land areas along the shores of Tokyo Bay such as Urayasu City) new skyscrapers, shopping centers, industrial buildings and pedestrian bridges are, in our experience, generally supported on deep foundations that are considerably rigid (e.g., Figure 3). The piers of modern bridges in Japan also utilize rigid deep foundations (e.g., drilled shafts) to support their large loads, but also to avoid the effects of lateral spreading from liquefaction along river banks (e.g., Figure 4).

In our experience, small residential and commercial buildings in Japan are most often supported by shallow and continuous footings, mats, and occasionally by long and closely spaced small diameter piles (Figures 2 and 5). The areas around buildings, including streets and sidewalks, are rarely improved and therefore susceptible to major to seismically induced settlements in areas prone to liquefaction. In 2011, this practice resulted in significant damage to lifelines and the inability to use structurally sound buildings due to lack of water, sewer and gas services; hence, causing major relocation of populations in areas affected by widespread liquefaction, such as Urayasu City (in Tokyo Bay).



Figure 3. Installation of prestressed concrete piles for skyscraper in Tokyo bay.



Figure 4. Upper photos: sand boils from soil liquefaction under a bridge near the town of Fusa; Lower photo: ground cracking from lateral spread in excess of 100 cm near the Tone river.



Figure 5. Building pad ready for construction of residence near Tokyo to be supported on closely spaced small diameter steel piles filled with concrete, and close-up view of a pile.

PERFORMANCE OF SHALLOW AND DEEP FOUNDATIONS

In the most affected areas of Fusa and Sawara (a neighborhood of Katori), the authors measured post-liquefaction induced settlements often exceeding 50 cm (e.g., Figures 2 and 6). Although settlement around modern buildings built on piles was considerable, we did not observe structural damage, severe distortions or adverse tilting in these buildings (Figures 2 and 6), i.e., they generally performed very well.

Buildings supported by conventional shallow footings and/or mat foundations in areas of Fusa and Sawara that experienced ground liquefaction performed, in contrast, very poorly, i.e., sinking significantly and/or tilting severely (e.g., Figures 7 and 8).

The difference in performance, between structures on deep and shallow foundations was particularly clear in areas where hydraulic fill had been placed in 1954 in the town of Fusa. The small three-story commercial building in Figure 7, which was built over the hydraulic fill, sank on the order of 100 cm into the ground; in contrast a nearby three-story apartment building built on piles which extended into the alluvium below the hydraulic fill did not suffer any structural or geotechnically related damage.

The overall excellent structural performance of buildings constructed on deep foundations was also observed in Tokyo and other areas of Japan, and is reported in the "Summary of Geotechnical Engineering Problems associated with the Tohoku Earthquake" by Tokimatsu et al. (2012).



Figure 6. Temporary ramp to access Katori Hospital (built on piles) as a result of ~60 cm of post-liquefaction settlement in the front driveway and parking area.



Figure 7. Sinking of a commercial building (upper photo) in the town of Fusa at the location where a pond was hydraulically filled in 1954.



Figure 8. Sinking of a residence (lower photo) in the town of Fusa at the location where a pond was reclaimed using hydraulic fill in 1954.

NUMERICAL MODELLING

To better understand how small diameter deep foundations supporting small buildings behaved during the Tohoku Earthquake, we performed a series of simplified Geomechanical Numerical Analyses using the program FLAC version 8.0 (Itasca, 2016). The analyses are qualitative in nature since ejecta was not modeled and the geometry as well as soil properties have considerable variability. We opted to model a small building in the subject area, since their weight, as well as the rigidity of their deep foundations had lesser uncertainty. Similar analyses for bridges and tall buildings would have had to be tailored to those specific structures and model predictions analyzed on a case-by-case basis. The analyses performed for this paper are for conditions in the middle of Fusa, where several small buildings of similar size where constructed on both deep and shallow foundations over a pond that was reclaimed in 1954 using hydraulic fill. The geometry of the old pond was inferred from local borings (which showed alluvium starting at a depth of ~11 m) and aerial photographs taken immediately after WWII by the U.S. Air Force (Figure 9).

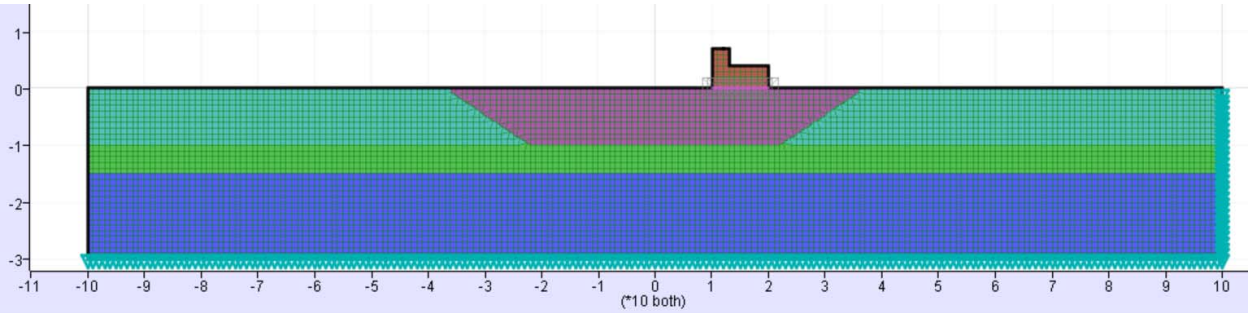


Figure 9. Mesh (1 m x 1 m) used in FLAC for the modeling of the commercial building in Figure 7.

The modeling procedure is similar to the one used for the modeling of the Fujinuma Dam failure in Pradel et al. (2013). Profiles of shear wave velocities and SPT blow counts, provided to us by Japanese scholars, were used to obtain soil properties. The maximum shear modulus G_{max} at various depths was calculated from the shear wave velocities, and hysteretic damping was implemented using as backbone the "upper range" shear moduli curve in Seed & Idriss (1970), thus allowing damping variation during the earthquake. A minor amount of Rayleigh damping (0.1%) was also included for numerical stability, and pore pressure generation was predicted using the Finn-Byrne model and calibrated with SPT blow counts (Itasca, 2016). Blow counts ranged from "push" to N=4 in the hydraulic fill, and in the alluvial soils below the fill increased from about N=15 (immediately below the fill) to N=40 (at depths deeper than 15 m). To facilitate convergence we adopted N=4 in the hydraulic fill, since our analyses were qualitative in nature. To model the large distortions associated with soil liquefaction, we regularly remeshed the grid in FLAC to prevent numerical instabilities associated with large-strains. Structural elements were used to model piles, and the soil mesh was connected to the piles by elastic-perfectly plastic springs. Ground motions from the Tohoku earthquake were used in our analyses.

Without piles, our FLAC model predicted sinking of the building in Figure 7, on the order of 30 cm, as well as large settlements (~10 cm) near the middle of the old pond (Figure 10). The position of the structure as well as the slope of the contact, between alluvial soils and hydraulic fill, resulted in lateral displacements; however, little permanent displacements were calculated in the areas outside of the old pond (Figure 10).

Analyses were conducted using the same soil properties (described above) and building loads, but with the building supported on 10 cm diameter concrete filled steel piles that are embedded 3 m into the alluvium (similar to those shown in Figure 5). As expected, the FLAC model predicted a complete transfer of the building loads to the piles as well as some downdrag forces. Nevertheless, very modest seismically induced bending moments were generated, which we attribute the high flexibility (small EI/L^3 ratio) of the piles, as well as the ability of the liquefied soil to flow between the small diameter piles. Therefore, the numerical predictions are consistent with our observations in Fusa where a nearby residential apartment, that was also built over hydraulic fill, did not experience structural damage nor adverse tilting (Figure 12).

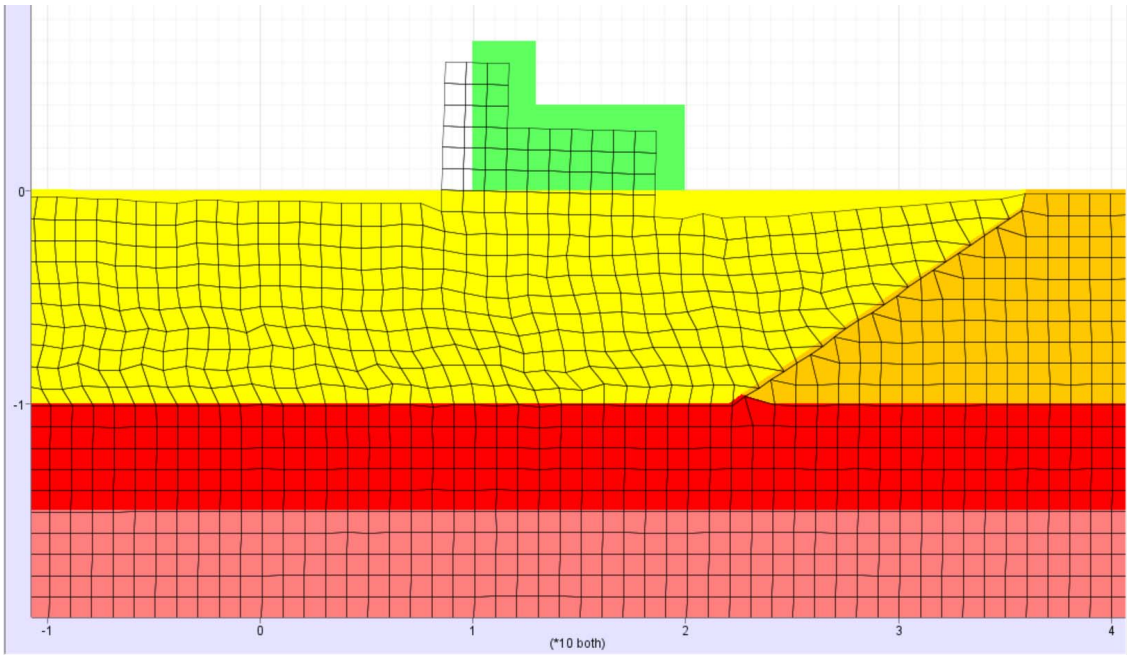


Figure 10. FLAC prediction for the building in Figure 7 (exaggerated deformed mesh shown, the original mesh size was 1 m x 1m).

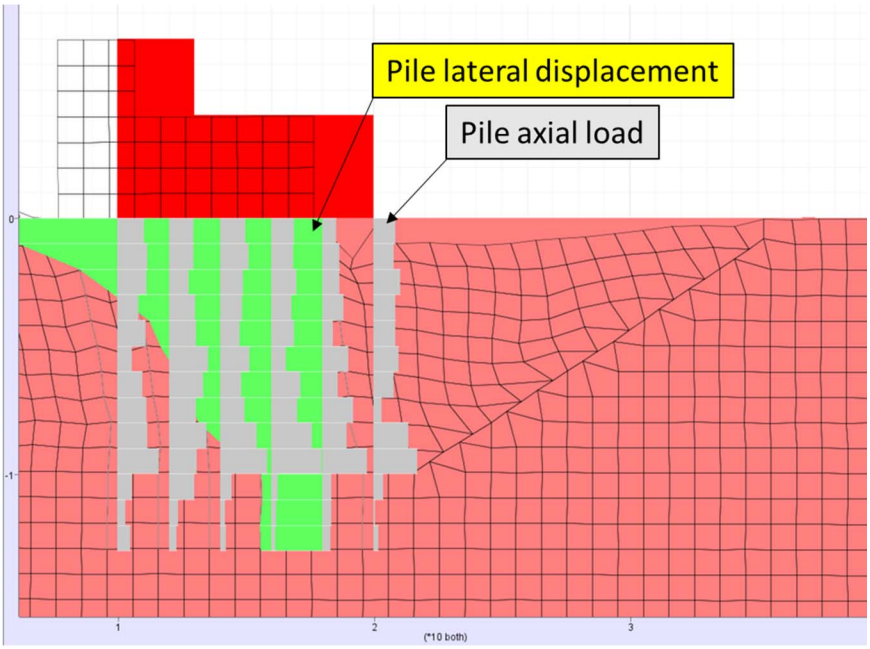


Figure 11. FLAC prediction for the building in Figure 7, if supported on piles (exaggerated deformed mesh shown, the original mesh size was 1 m x 1m).



Figure 11. Residential building constructed on piles that did not suffer structural damage, with building in Figure 7 shown in background.

SUMMARY AND CONCLUSIONS

Although the M_w=9.0 Tohoku Earthquake is one of the largest recorded earthquake in history, and soil liquefaction affected many sites in the Kanto plains surrounding Tokyo, the performance of modern (post Kobe Earthquake) deep foundations was excellent and structural damage to buildings on deep foundations was extremely limited.

In the town of Fusa and in the Sawara neighborhood of Katori, anthropogenic changes resulted in widespread soil liquefaction. Traditional small buildings (2 to 3 stories in height) built on shallow foundations performed very poorly in areas were the soil liquefied, and resulted in considerable sinking and tilting of structures. Although the surrounding ground often settled in excess of 50 cm, modern buildings supported on small diameter piles, generally did not suffer structural damage, i.e., behaved very well. Nevertheless, their driveways, walkways and lifelines were often damaged by differential post-liquefaction induced settlements from the earthquake.

Simplified and qualitative numerical modeling, using the Finn-Byrne model in FLAC, predicts well the overall effect of the type of foundation and the benefits of using small diameter piles in areas where liquefaction prone soils are laterally confined; more specifically, the model predicts the poor performance of structures on shallow foundations and the adequate performance of buildings supported by highly flexible small diameter piles. Our field observations as well the numerical model show the high resiliency during seismic events of closely spaced small diameter piles in laterally confined areas prone to liquefaction.

REFERENCES

Cubrinovski M., Kokusho T. and Ishihara K. (2006). Interpretation from large-scale shake table tests on piles undergoing lateral spreading in liquefied soils, Soil Dynamics and Earthquake Engineering, Vol.26, pp.275-286

Ishihara, K. (1997). Terzaghi oration: geotechnical aspects of the 1995 Kobe earthquake. Proceedings of 14th International Conference on Soil Mechanics and Foundation Engineering, Hamburg, 4, 2047–2073.

Itasca (2016). FLAC Fast Lagrangian Analysis of Continua, Version 8.0," Minneapolis, USA, www.itascacg.com.

Pradel D., Tiwari B., and Wartman J. (2011). Landslides Triggered by 2011 Tohoku Pacific Earthquake: Preliminary Observations, ASCE Geo□Strata, Sept. /Oct. 2011, 28□32.

Pradel D., Wartman J., and Tiwari B. (2013). Failure of the Fujinuma Dams during the 2011 Tohoku Earthquake, ASCE Geo□Congress 2013: Stability and Performance of Slopes and Embankments III, GSP 231, 1566□1580.

Pradel D., Wartman J., and Tiwari B. (2014). Impact of anthropogenic changes on liquefaction along the Tone River during the 2011 Tohoku Earthquake, ASCE Natural Hazards Review. Vol.15, 13□26.

Seed H.B. and Idriss I. M. (1970). Soil Moduli and Damping Factors for Dynamic Response Analyses, Report No. UCB/EERC 70/10, Earthquake Engineering Research Center, University of California, Berkeley.

Tokimatsu K. and Asaka Y. (1998). Effects of Liquefaction-Induced Ground Displacements on Pile Performance in the 1995 Hyogoken-Nambu Earthquake, Soils and Foundations, Vol.38, pp.163-177.

Tokimatsu K., Tamura S., Suzuki H. and Katsumata K. (2012). Geotechnical Problems in the 2011 Tohoku Pacific Earthquake, 9th Int. Conf. on Urban Earthquake Engineering and 4th Asia Conference on Earthquake Engineering, March 6-8, 2012, Tokyo Institute of Technology, Tokyo, Japan

Youd T. L. and Perkins D. M. (1987). Mapping of Liquefaction Severity Index, J.GED, ASCE, Vol.113, No.11, pp.1374-1392.

QUICK, EFFICIENT & SAFE PRELOADING OF HIGH CAPACITY HYDRAULIC MODULAR PROPS

Peter Richardson B.Eng.(Hons.), C.Eng., FICE, Vp PLC
Uithoorn, The Netherlands +31 650 991862, peter.richardson@vpplc.com

ABSTRACT

Preloading of wall support systems is a standard, yet oft misunderstood procedure common to most support systems. Maximising the efficiency and safety of this procedure is paramount to successful preloading.

KEYWORDS: Preloading, Hybrid props, Safety

Preloading of wall support systems is a standard, yet oft misunderstood procedure common to most support systems. Preloading of the support system is a means of anticipating the loads which will occur during excavation by which actual movement or perhaps more correctly deflection of the wall can in practice be reduced.

With anchored walls it is necessary to differentiate between strand anchors and bar anchors. With strand anchors pre-stressing of the anchor tendons initially reduces the risk of extension in the free anchor length at the time of installation and is an essential procedure to allow the anchor to work as required by the wall stability calculations. . With bar anchors the rigidity of the bar in comparison with strands reduces the extension of the free length and permits significant post-tensioning which effectively preloads the wall.

With standard steel props, flat jacks are often used to enable preloading, these can be loaded and permanently locked off or they can be applied externally and the gap between the end of the prop and the wall or waling packed with steel plates. More modern complex heavier duty systems allow the flat jack to remain in place and permit adjustment of the preload during the life time of the support system.

With prefabricated modular hydraulic props the integral hydraulic ram is used to speed up the installation and removal process however also provides an immediate preloading option without the need to use additional materials or systems. The hydraulic element is integral to the concept and remains continuously in place throughout the duration of the work.

Hydraulic props, with working load capacities up to 250tonnes, have been available for many years. In current terminology a Groundforce MP250 prop would provide a maximum design resistance of 3380kN.

In 2008 Groundforce were required by the Bouygues / Bachy Soletanche JV to produce a prop capable of withstanding a working load of 500t. The availability, of or lack thereof, of 500tonne hydraulic rams with 1m extensions excluded a purely hydraulic solution and led to the introduction of the world's first hybrid mechanical/hydraulic prop.
This was achieved by mounting 2 heavy duty 160mm diameter screws either side of the standard 250 tonne hydraulic cylinder with the intention that the hydraulic system would be used for speed of installation and initial preload. As the job progressed and the excavation continued the movement of the ground/retaining wall would impose loads beyond the capacity of the hydraulic unit but well within the capacity of the twin screws.

When the job ended it was apparent that not all props demonstrated the expected loss of load which should naturally occur as a result of construction of the permanent works and various techniques, some very traditional were used to reduce the load or loosen the nuts. Where this was not possible and as a last resort 2 props were actually cut out, at no small inconvenience and cost.

© 2018 Deep Foundations Institute

The system required improving and tapered sacrificial washers were incorporated which improved to a degree the reliability of prop removal but did not guarantee its success.

After Groundforce developed the external pre-load jacking system for the Crossrail Paddington job (see fig 1),



Figure 1: The remote jacking system in operation

the spin- off bonus from the adoption of external jacks meant that they could be re-used at the end of the job to re-pressure the system to relieve the load on the load holding screws, thus allowing them to be unscrewed without resorting to brute force methods to get units out of the ground.

However, there are few issues with the remote jacking system:

1. It is a
    a. relatively complex process
    b. time consuming operation
    c. skilled operation to fit and remove the jacks and ancillary bracketry to the MP500 unit
2. The system requires
    a. a dedicated complex high pressure hydraulic system.
    b. a good working area or platform to fit the units
3. The jacking forces occur some way off the centre line of the screws see fig 2. hence applying significant eccentric loading meaning that additional force in the rams is required in order to relieve load on the nuts. Rams have been damaged by over-pressurisation during release operations necessitating expensive repair bills.

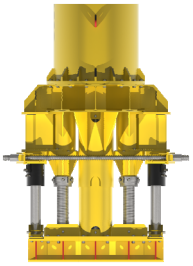


Figure 2: schematic of the supplementary jacking rams

Proposal

To solve this issue all Groundforce have developed a hydraulic nut release system that operates directly under each nut head as shown in fig 3.



Figure 3: A pair of hydraulic nuts as fitted to a MP500 unit

The hydraulic nuts offer the ability to safely, quickly and efficiently

a. pre-stress on installation
b. adjust within a specific load range load during the life span of a project
c. do not apply damaging eccentric loading to the unit

Operation

Installation & preload

1. Initially the central 250t hydraulic cylinder is extended until the required length and some initial force / limited preload is achieved.
2. The locking screws are now tightened to maintain the initial prop length /initial force
3. The central hydraulic cylinder can now be depressurised.
4. The hydraulic nuts are now pressurised using the dedicated manifold/ intensifier unit illustrated in figure 4.



Figure 4: the hydraulic manifold unit

5. Pressurisation takes place in standard increments on alternative nuts.
6. The hydraulic manifold is shown in figure 4. The centre lever is designed to facilitate initial extension / preload of the central hydraulic cylinder, the left and right hand levers serve respectively the left and right hand nuts. This avoids variation in pressure due to the manifold and allows more controlled pressurisation / loading of the nuts
7. The final locking nut is now tightened and the hydraulic hoses depressurised and removed
8. Although a pressure / load chart is available, variations in mechanical conditions, conversion of hydraulic pressure into torque and torque into axial load give too much scope for inaccuracy. It is advisable therefore to use a load monitoring pin mounted at the opposite end of the prop to accurately monitor the preloading operation. See figure 5.



Figure 5: Load monitoring

9. It is worth remembering that with every incremental increase in pre-load in each prop, redistribution of load will occur throughout the support system. Continuous monitoring of each prop therefore ensures the correct amount of pre-load is left in each prop at the end of the pre-loading operation.

Removal

Removal involves reversing the installation procedure

Major advantages

1. The preload is applied directly to the structural elements, i.e. the 160mm Ø bolts avoiding eccentric loads
2. The load is applied hydraulically without the need for brute force
3. The applied load can be introduced in phases without handling heavy external jacks and ancillary structures
4. Access platforms are required only to actually connect and disconnect the hydraulic hoses rather than to permit heavy lifting and manual tightening / loosening of nuts
5. Continuous measurement of load ensures accuracy throughout the process
6. Reducing the manual element of the work not only increases safety during the operation but also reduces the access requirements.
7. Guaranteed success on removal

Conclusion

Groundforce's hydraulic nuts provide a safe, controlled means of both pre-loading and de-loading heavily loaded hybrid props without substantial manual effort and with a significantly improved ability to remove the hybrid props without resorting to cutting them out. This provides both safety improvements and time and cost benefits to projects where heavy duty propping is required.

RECENT EXPERIENCE OF TREMIE CONCRETE PROPERTIES AND TESTING

Aidan Thorp, Ove Arup and Partners Limited, London, UK, +44 20 755 3352, Aidan.thorp@arup.com
Christopher Wilkes, Cambridge University, Cambridge, UK, cw646@cam.ac.uk
Duncan Nicholson, Ove Arup and Partners Limited, London, UK
Bryan Marsh, Ove Arup and Partners Limited, London, UK

ABSTRACT

The EFFC/DFI Best Practice Guide to Tremie Concrete for Deep Foundations published in 2016 has highlighted the complexity of modern tremie concrete. Concrete additions and admixtures are increasingly used to adapt tremie concrete to the particular requirements of deep foundations. Despite these advancements, issues arising during the concreting process can occur. This paper discusses these issues and shares recent experience of static segregation of tremie concrete in bored piles. The paper outlines recent industry guidance on tremie concrete behaviour and testing in the 3rd Edition of the ICE Specification for Piles and Embedded Retaining Walls, 2017. This details fresh concrete tests that can be used for site acceptance of concrete batches, and provides guidance on more detailed concrete testing at laboratory mix design, initial batching stages and during the project. The paper also summarises the results of detailed testing carried out during a recent project in London, and compares the results with suggested test acceptance limits. The benefits of carrying out these tests are listed along with recommendations for future research to refine acceptance limits.

Keywords: tremie concrete, workability, stability, static segregation, case studies, test acceptance criteria.

INTRODUCTION

For over 50 years reinforced concrete deep foundation piles and diaphragm walls have been constructed by placement of concrete through a tremie pipe. However, the behaviour of the fresh concrete once it leaves the tremie pipe is not well understood. Recently a number of projects in the UK and worldwide have suffered defects incurring significant cost and programme delays. The types of defects range from mattressing and shadowing, to inclusions and channels; all of which have implications on the durability of the pile and in severe cases the structural performance.

Deep foundations demand concrete with sufficient workability to be self-compacting and to flow homogeneously around reinforcing cages submerged in a support fluid. The workability must be maintained long enough to allow for the transport of the concrete to site and pouring of the concrete in the deep foundation. Concrete technological advances have enabled deep foundations to be constructed larger and deeper than previously possible. However, it is still uncertain whether the continuously embedded tremie pipe means that the initial batches of concrete rise with the top of the pile concrete and form a plug of old concrete at the pile head. Applications such as plunging steel column sections in this old concrete highlight the need for workability retention for many hours.

These technological advances have been achieved by development of chemical admixtures and additions, such as Ground Granulated Blast Furnace Slag, abbreviated as GGBS. The resulting concretes are complex and have different properties compared to the more traditional mixes. Workmanship guidance and concrete testing has not followed at the same pace as the advances in concrete technology. This has resulted in risks to the deep foundation industry.

DEFINITIONS

This paper mainly follows the definitions set out in the EFFC/DFI Guide, which focus on workability issues during placement.

Some additional definitions are given below which mainly relate to concrete stability issues:

© 2018 Deep Foundations Institute

Interface layer: This layer develops during concreting at the interface between the concrete and support fluid. Typically, it comprises of a mixture of excavated material, segregated concrete and support fluid, see Fig. 1. This material can form the material encountered in mattressing and inclusion defects as defined in the EFFC/DFI guide.



Fig. 1. Interface material exposed at the top of a diaphragm wall.

Stability: Resistance of concrete to segregation, filtration and bleed.

Dynamic segregation: The segregation that occurs while the fresh concrete is in motion, or when it hits reinforcement in dry piles. This segregation may occur during concrete pumping, or when concrete is flowing around obstacles such as a reinforcing cage.

Static segregation: Segregation that occurs while the fresh concrete is stationary. Exhibited by a change in distribution of the aggregate particles, which tend to sink and result in the concrete paste tending to rise to the top of the fluid concrete.

Filtration: Mechanism by which fluid (water or cement paste) from concrete which has not set tends to flow from a higher hydraulic pressure in the fluid concrete out into a surrounding area with a lower hydraulic pressure. For example, horizontal flow of fluid from concrete into the surrounding permeable ground and the filter cake is acting as a filter.

RECENT INDUSTRY GUIDANCE ON TREMIE CONCRETE:

In 2012, the Concrete Institute of Australia published Recommended Practice (CIA, 2012) on the use of tremie concrete for deep foundations. This provided guidance on tremie concrete properties, constituent materials and proportions, mix design. Test methods were introduced which were not normal practice. These tests included the L-Box test and Bauer Filtration Test and this helped to provide a more complete assessment of the concrete properties in terms of workability and stability.

In 2016, the European Federation of Foundation Contractors and the Deep Foundations Institute published a Best Practice Guide to Tremie Concrete for Deep Foundations, abbreviated herein as the EFFC/DFI Tremie Guide. The interface and responsibilities between the designer, the constructor, the concrete specifier and the concrete supplier was addressed. The guide also provided guidance on tremie concrete properties, constituent materials and proportions, mix design and testing. The guide recognised the importance of the execution of the works and provided guidance on workmanship and quality control. The suite of recommended tests on fresh concrete properties was expanded from the CIA guide.

The guide recommended acceptance criteria for these tests, but highlighted that further research was needed to refine these criteria.

In 2017, the Institute of Civil Engineers (ICE) of the United Kingdom published the third edition of the ICE Specification for Piling and Embedded Retaining Walls, abbreviated herein as the SPERW. This incorporated information on the detailed test methods suggested by the EFFC/DFI Tremie Guide.

The EFFC and DFI are currently compiling an update to the EFFC/DFI Tremie Guide to incorporate the results of research projects on detailed test methods, concrete properties and numerical modelling of the concrete flow. This is expected to be issued in 2018.

OBSERVED ISSUES WITH STATIC SEGREGATION IN BORED PILES

Static segregation in a large station excavation in London

In 2013 a large station box was constructed using the top down method in London. The work included 51 internal piles of 1800mm diameter with a depth of 58m. The cut-off level for the piles was approximately 20m below the piling platform level. Forty-nine of these piles had steel H section columns plunged to 3.6m below the cut off level of the pile. The plunge columns carried a large vertical load and had shear studs installed on the web to transmit the vertical load into the piles. The piles were bored through 9m long temporary casings. Below these casings the piles were dry bored through the London Clay and into the Upper Lambeth Group stratum. Following this, the full length cage was installed and the pile concreted without support fluid using a tremie pipe. The base of the pipe was kept no more than 10m above the top of the concrete level when free falling concrete, and embedded no more than 6m into the concrete when the concrete level rose above the tremie pipe. The piles were integrity tested using sonic logging and no significant anomalies were recorded.

The concrete mix was specified as C35/45 strength class (cube compressive strength of 45MPa) and a consistency of F5 (560-620mm flow table test results). The concrete supplied contained 490kg/m^3 cementitious content with 70% comprising GGBS, and a water/cement ratio of 0.36. The aggregate was coarse gravel and natural sand. The fine aggregate content was 45.2%. Admixtures were a combination of a Polycarboxylate Ether (PCE) superplasticiser, and a non PCE superplasticiser.

Following excavation, the majority of these piles were observed to contain a sequence of grout above mortar on top of concrete, see Figs. 2-3. The mortar extended up to 4.5m below the cut-off level. In some piles large bleed channels were observed in the cover zone which still comprised concrete.

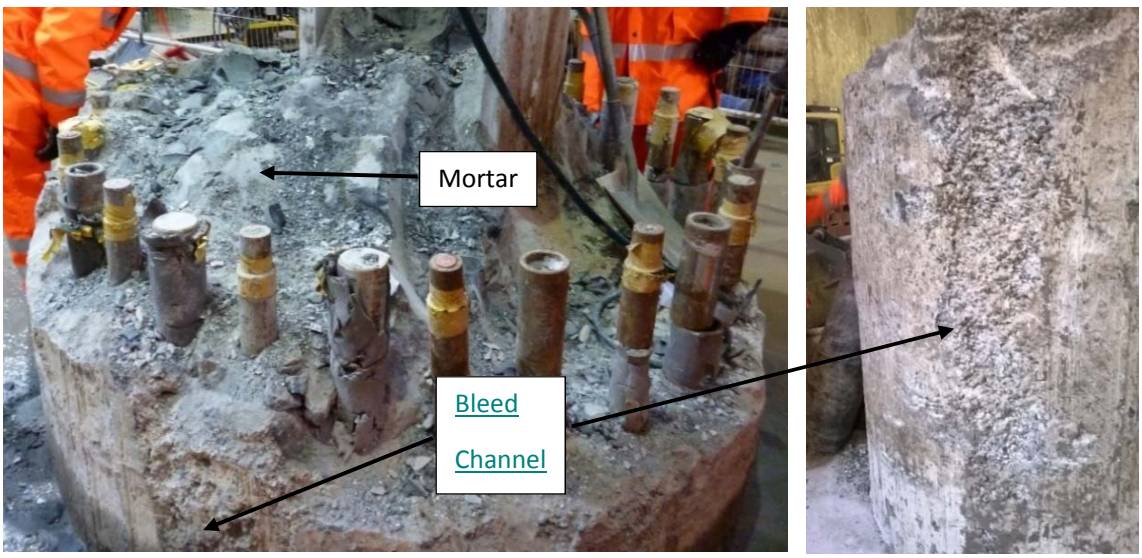


Fig. 2. Mortar exposed in the top of a pile (left) and a large bleed channel (right)

Following these observations, cores were drilled from the top of the piles to investigate the depth and properties of the anomalous concrete. Fig. 3 shows the distribution of grout, mortar and concrete in the tops of the piles below cut off level.

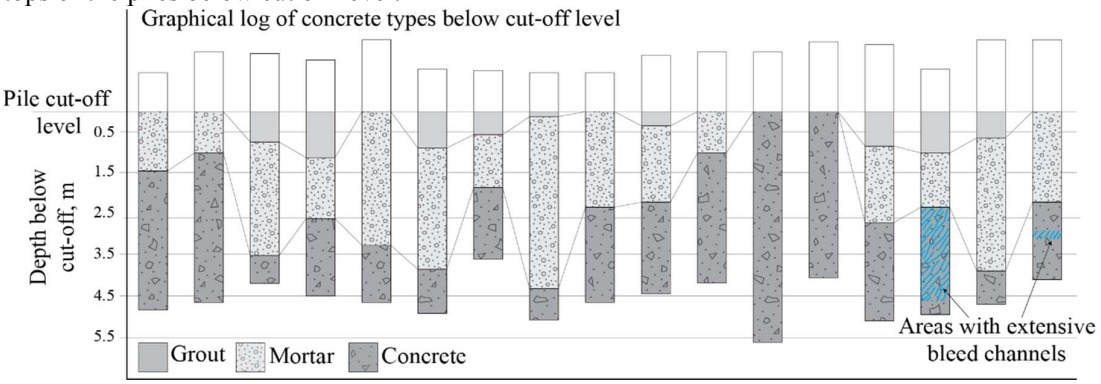


Fig. 3. Graphical log showing the distribution of grout, mortar and concrete in the tops of the piles

Samples were prepared for compressive strength testing at approximately 200mm centres and an example of the results is shown below in Fig. 4. It can be seen that the density and strength is lower in the first metre below cut off level.

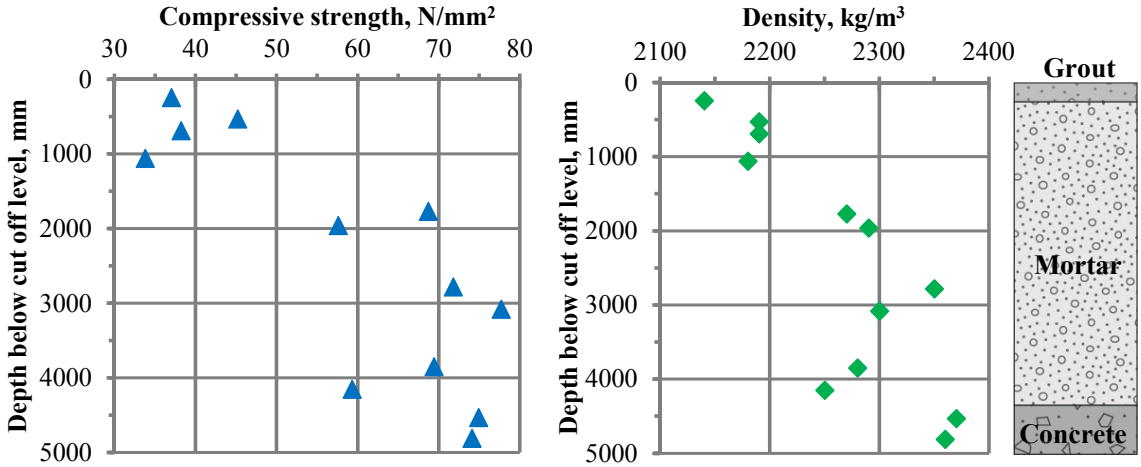


Fig. 4. Strength and density versus depth below cut off level

The investigation concluded that the observed anomalies in aggregate distribution in the core of the pile were due to static segregation, whereby the concrete had segregated by density into grout above mortar above concrete at some time after concrete placement. The concrete mix chosen resulted in concrete with a cement paste fraction with a combination of low yield stress (essential for compaction under self-weight), low plastic viscosity and severely extended setting time. This resulted in the aggregate particles being able to sink through the cement paste.

There was concern that the properties of the concrete in the upper section of the pile did not conform to design expectations and this could have affected the ability of the plunge columns to transmit load to the piles. There was particular concern in the depth of the grout zone where intact core samples could not be obtained because of the fracturing due to the laminar nature of the grout layer. A design check was carried out concluding that if the top of the pile contained mortar or concrete it was able to transfer the plunged column loads. However, the inability to obtain suitable specimens for grout strength testing mean that the grout was broken down and replaced with new concrete. Petrographic testing of the grout and mortar showed that while the segregated concrete had a higher water/cement ratio compared to the original mix design, it was still expected to achieve the required durability

Static segregation in a secant pile wall in Central London

In 2014 a secant pile wall with 1200mm diameter piles was constructed at a site in central London. Piles were dry bored in London Clay to depths of 13 to 25m using segmental casings. The secondary secant pile concrete was C32/40, high GGBS replacement and S4 consistency class (160-210mm slump).

For some of the piles it was observed that at 10 to 30 minutes after placing the concrete, the cement grout rose to the surface of the concrete in what was termed a 'grout volcano', see Fig. 5. Following excavation to expose the pile tops, a number of piles were observed to contain layers of grout and mortar overlying sound concrete. As this extended to below the cut off level of the piles, there were concerns about the adequacy of the concrete strength and durability. A review of the concrete batching records and slump test results indicated that the concrete placed was within the original mix specification.

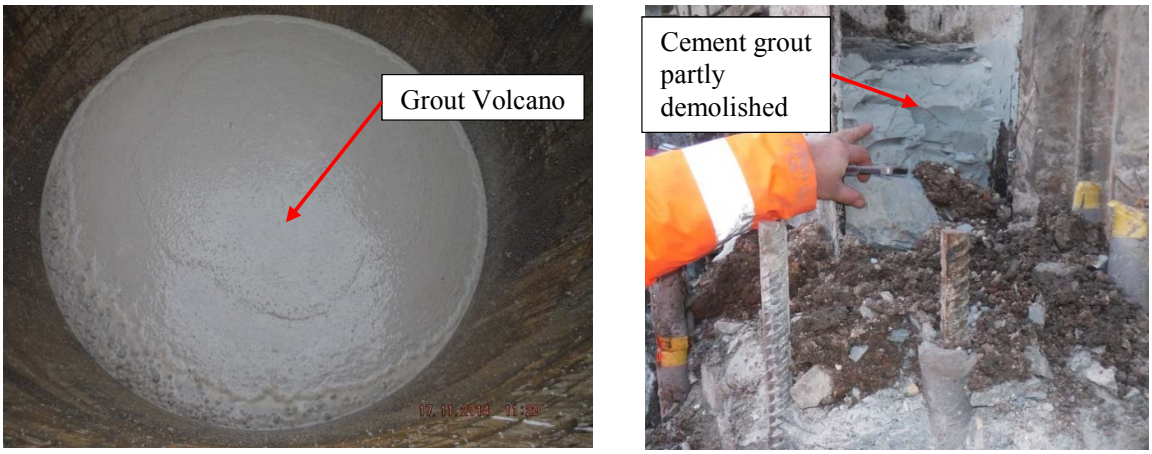


Fig. 5. Grout rising to surface of pile without evidence of bleed water (left) and aggregate-deficient zone at top of pile (right)

In the most severe instance, a core hole was drilled from cut-off level to investigate the concrete with depth. The strength of the concrete was approx. 14N/mm^2 at cut off level, approx. 25N/mm^2 at 300mm below cut off level, approx. 29N/mm^2 at 700mm below cut off level, and approx. 38N/mm^2 at 1.4m below cut off level. A design review was carried out which indicated that for this pile a lower design strength of 26N/mm^2 could be accepted. Consequently, it was decided to demolish the pile to 700mm below cut off level where the measured strength was above 26N/mm^2. Petrographic analysis indicated that the water/cement ratio at this depth would provide the required durability. It was concluded that the piles had exhibited static segregation. Subsequently, a new concrete mix was trialled which contained addition of fly ash to reduce the risk of static segregation. This was successful with no further significant issues of static segregation occurring.

RECENT INDUSTRY GUIDANCE ON FRESH CONCRETE TESTING METHODS

The EFFC/DFI Tremie Guide and the SPERW recommend tests for assessing fresh tremie concrete behaviour, each test measuring a different aspect of concrete workability and stability. Table 1 lists for each concreting stage, construction issues, what concrete behaviour affects the construction issues and what concrete test recommended in the SPERW is most applicable.

Section 1.2 of the EFFC/DFI Tremie Guide explains that tremie concreting involves inputs from the client, designer, constructor, concrete mix specifier, and concrete supplier. The designer must consider detailing and crack width requirements as outlined in Appendix F of the EFFC/DFI Tremie Guide. There is a trade-off between reducing a foundation section size and increasing reinforcement congestion and resulting difficulty of concrete flow. Setting more comprehensive concrete test standards reduces the risks. However, the workmanship of the constructor is also important in preventing construction issues.

Table 1. Concreting stages, construction issues, concrete behaviour and available tests

A) During concrete placement stages where workability is important

Concreting stage	Construction issues	Concrete behaviour	Applicable tests and workmanship
Initial charging of tremie pipe filled with support fluid	Concrete segregates when it mixes with support fluid in tremie pipe	Determined by effectiveness of separator	Review separator size and type
Tremie pipe placed on base of pile during charging	Potential for blocking the tremie pipe with stiffened concrete	Filtration Resistance	Bauer Filtration Test to assess risk of water loss, tremie placement technique
Free falling concrete down the tremie pipe	Concrete segregates while flowing down the hopper and tremie pipe or when flowing across pile base	Dynamic Segregation Resistance	Visual Stability Index
Concrete allowed to free fall through a reinforcing cage in a dry bored pile	Coarse aggregate segregated from cement paste as it impacts the reinforcing cage	Dynamic Segregation Resistance	Visual Stability Index, ensure tremie is centralised
Flow of concrete across the pile base	Debris present on pile base and support fluid becomes mixed with concrete or debris becomes left on the pile base	Determined by cleanliness of base and dynamic segregation resistance	Base cleanliness and Visual Stability Index
Flow of concrete from bottom of tremie pipe	Tremie concrete flow patterns lead to concrete flow up the side of the tremie and outward radial flow at the concrete surface	Workability, Workability retention, Continuity of concrete supply	Slump, Flow table, Slump flow and retention test, continuity of concrete supply
Concrete flow around obstacles, e.g. reinforcing, instrumentation, void formers	Concrete does not fully combine after flowing around an obstacle leading to an entrapment of interface layer forming mattressing, shadowing and inclusions	Workability, Passing ability, Density and viscosity of interface layer materials	L Box test, Workability and retention tests, Full scale trials at project start

B) Post concrete placement where stability is important

Concreting stage	Construction issue	Concrete behaviour	Applicable tests and workmanship
Cage placement within CFA piles and plunging columns within piles	Difficult to install cage or column in stiffened concrete. Concrete stiffened from water loss due to lateral filtration of concrete water into surrounding permeable ground	Filtration resistance. Concrete thixotropy and stiffening.	Bauer Filtration Test, Workability retention test.
Vertical flow of concrete fluids	Bleed water builds up on concrete surface. Small mounds of fine sand and cement at top of bleed channels. May lead to loss of cover and reinforcement bond	Water retention ability.	Bleed test. Monitor concrete surface post placement.
Static segregation	Concrete segregated by density profile of grout, mortar, concrete	Static Segregation Resistance.	HVSI test, Column Segregation test

CASE STUDY AT EAST LONDON SITE

Following the static segregation experience a more rigorous approach was adopted at this East London site which comprises several buildings and a deck structure. The foundations comprised bored piles from 900mm to 1500mm diameter constructed under either bentonite or polymer support fluid. The concrete was C32/40 or C40/50 concrete strength class, high GGBS cement replacement, F5 flow class (560-620mm). Continuous flight auger (CFA) piles up to 900mm diameter were also constructed. The project specification included detailed concrete tests based on the recommendations of the CIA, (2012) guide which have subsequently been recommended in the SPERW and are listed in Table 2.

Table 2. Concrete test methods conducted and applicable concrete property

Concrete Test Method	EFFC/DFI Tremie guide reference	Workability	Stability
Flow Table Test	Appendix A 2.1	✓	
Flow Retention Test	Appendix A 3.1	✓	
L-Box Test	Appendix A 2.4	✓	
ASTM Bleed Test	Appendix A 4.4		✓
Bauer Filtration Test	Appendix A 4.6		✓
Hardened Visual Stability Index (HVSI)	Appendix A 4.3		✓

These tests were required at the initial laboratory mix design stage, on the first day of piling to confirm that the ready mix plant produced concrete conformed to the laboratory tests, and at weekly intervals to identify any changes in the behaviour of the delivered concrete. The weekly testing was carried out independently of the contractors' acceptance testing typically at 2 hours after batching due to the time taken for transport to site and site practicalities.

Workability test results

The independent weekly testing showed the concrete generally complied with the F5 flow class, refer Fig. 6, but was often close to the upper limit and in some instances was outside the specified limits. It is understood that it is standard practice for the concrete supplier to target the workability of the concrete to be in the upper range of the specified class as this allows more flexibility for the contractor if the concrete lorry is delayed by traffic or the concrete pour is delayed due to a site complication.

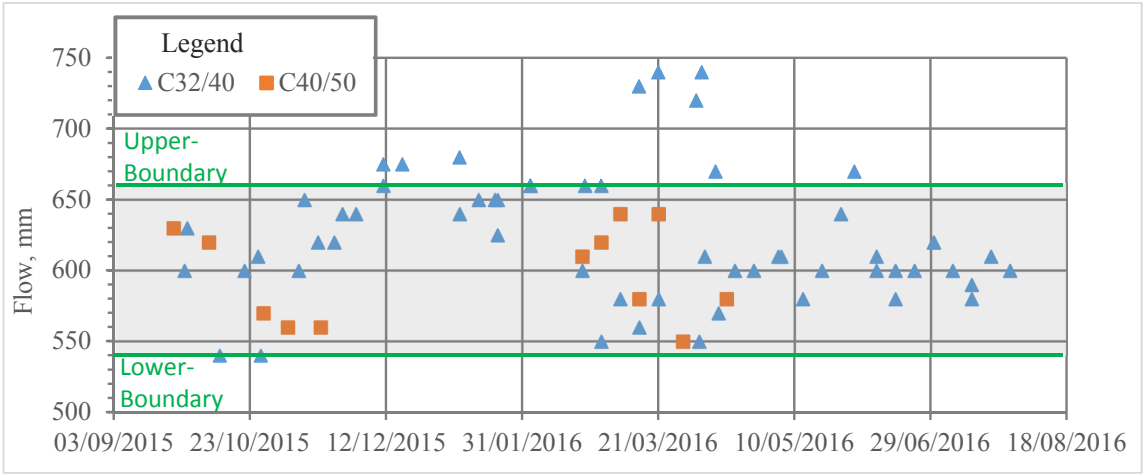


Fig. 6. Independent weekly flow table test results

For the East London project, the field flow table results occasionally fell outside the upper limits applied to the initial flow result (Fig. 6). Consideration then needs to be given to whether flows that fall out of specification are indicative of poor concrete performance with an increased risk of segregation and/or

bleed. Site engineers did not report any significant instances of bleed or segregation at the tops of the piles following pile construction. No significant anomalies were recorded in the pile quality from integrity testing. This might suggest that in certain cases, relaxing the upper limit of workability may be reasonable, provided results from the other tests are satisfactory for concrete of this higher workability.

The L-Box T_{end} results were within the recommended limits defined in the SPERW (Fig. 7). The L-Box results were relatively sensitive and were able to distinguish a change in behaviour of the concrete due to a small change in the mix composition. In contrast, the flow table testing did not clearly show this change. Typically, when an L-box result (T_{end}) fell outside of the 3-7 seconds range there was a resulting investigation into why a sudden change in workability had occurred.

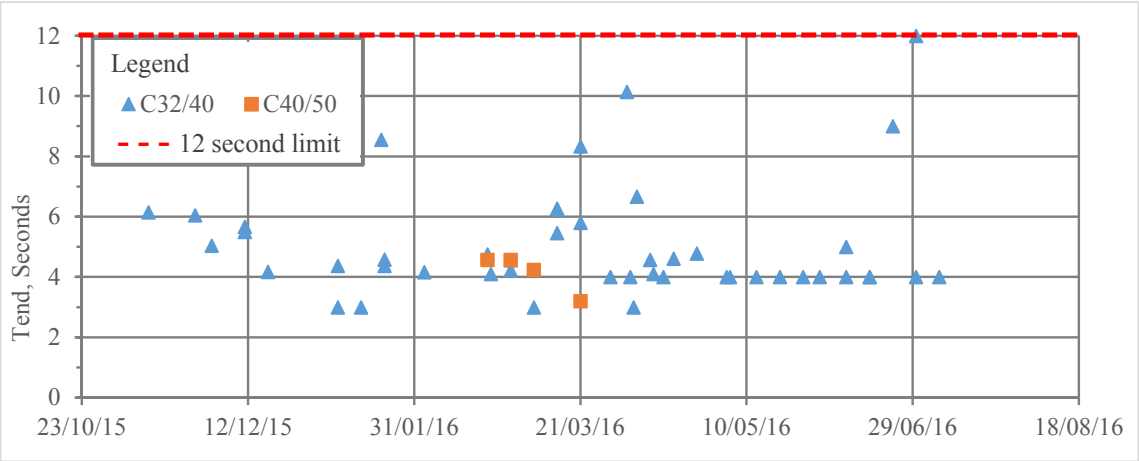


Fig. 7. L box test results

The SPERW does not recommend criteria for flow retention and suggests contractors specify a limit based on the particular site and foundation requirements. One contractor advised a 4-hour flow limit of 450mm, which was met for 73% of the test results. Understanding the flow retention of a concrete is important when considering how the concrete will behave inside the foundation when a fresh load is placed in a pile containing concrete that is now several hours old. If concrete is placed in a pile where the old concrete at the pile head has begun to stiffen, the risk of pile defects is increased.

Stability test results

The HVSI results were consistently within the stable range (Index 0-1), indicating the concrete was not susceptible to static segregation. Guidelines on grading are based on an individual's interpretation of the criteria and illustrations in the test standard, and therefore there is an element of uncertainty in the results.

The Bauer Filtration Test results indicate all results are within the SPERW recommendations (Fig. 8) and display a good correlation with bleed test results. For Bauer Filtration Tests, a limit of 15 l/m^3 appears to be readily met by the concrete used at the East London site. However, the test data appeared to be constrained to 4-12 l/m^3. Taking the approach that typically the concrete would have a test result between 4-12 l/m^3, a test result outside of this range would be considered anomalous and may warrant further investigation.

The ASTM Bleed Test results are repeatedly close to the recommended limits (Fig. 8). This suggests that the recommended ASTM Bleed Test limits may be more onerous than the Bauer Filtration Test limits. Note that the bleed rate was assessed at 2 hours after the start of the test and not the average rate from 0 to 2 hours. This is because the bleed rate can be slower at the start of the test.

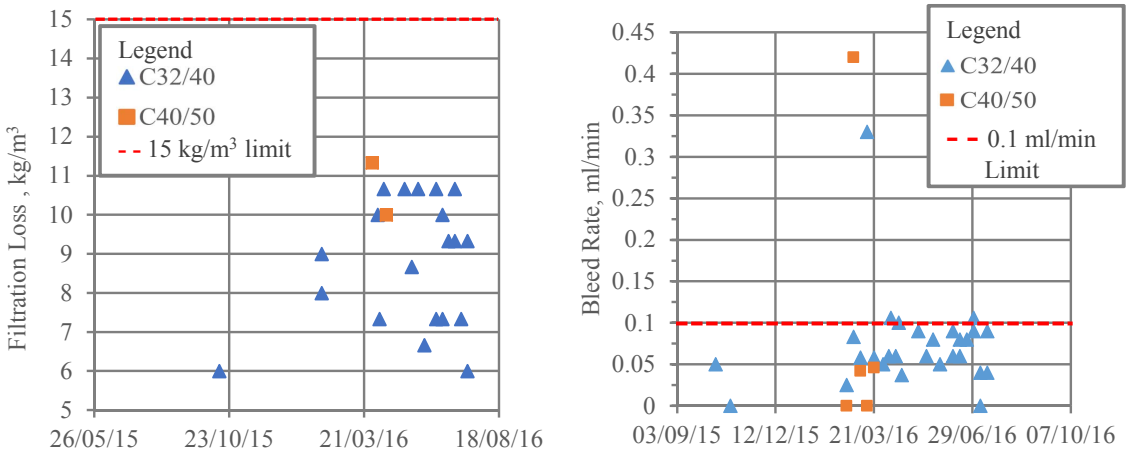


Fig. 8. Bauer Filtration and ASTM Bleed test results

The lack of exceedances of the suggested acceptance criteria for the tests relating to stability indicates that the concrete used was not susceptible to significant bleed or segregation. This was corroborated with site observations. The tops of the piles were routinely observed and no significant instances of bleed or static segregation was noted. The integrity of the piles was verified with cross hole sonic logging which did not identify any significant defects due to bleed or segregation.

DISCUSSION ON THE TESTING REGIME RECOMMENDED BY THE SPERW

This section discusses the benefits of carrying out detailed testing as recommended by the SPERW.

Detailed concrete testing at mix design stage

The detailed concrete testing at the mix design stage as recommended by the SPERW enables the project team to confirm that the behaviour of the concrete conforms to the expected behaviour based on the test criteria set out in the EFFC/DFI Tremie Guide and subsequently adopted in the SPERW. This enables the project team to assess the suitability of the concrete for the particular application, which reduces the risk that the concrete will not perform.

Detailed concrete testing during the project

The SPERW recommended detailed concrete testing during the project. This testing enables the project team to confirm that the behaviour of the concrete supplied by the batching plant conforms to the expected behaviour. Variations in behaviour during the contract may be due to changes in aggregate supply or aggregate moisture content, sources of additions (e.g. GGBS) or changes in the mix design. This empowers the project team to investigate significant changes and form a basis to adapt the mix if required.

Full scale trials

The most robust method to assess the applicability of the concrete for the chosen application is to carry out a Full Scale Trial. These would typically comprise the preliminary foundation elements constructed for load testing prior to the working pile construction. These offer an opportunity to review concrete behaviour and refine the construction methodology, including demonstrating that the concrete can be placed as expected. It is suggested that the full scale trial replicate as close as possible the working foundations, including installing any box outs or void formers used for connections to the foundation. These can be included in the reaction piles at shallow levels for subsequent excavation. The foundation construction should be as slow as anticipated on site to replicate delays. Following load testing, the reaction piles can be excavated to inspect the concrete quality. Techniques such as cross hole sonic

logging or thermal integrity profiling may be used to assess the concrete quality in these foundation elements.

Recommended further research

It is noted that recommended test acceptance criteria in the SPERW are based on limited test data. More research is needed to understand whether the acceptance criteria can be refined by studying projects where concrete issues occurred and whether the concrete used complied with the recommended acceptance criteria. A research programme by the Technical University of Munich, funded by the EFFC and DFI is being carried out to visit deep foundation sites, carry out detailed concrete testing. This research will be reported in the next revision of the EFFC/DFI Tremie Guide. It is suggested that industry bodies, such as the EFFC and the DFI continue this research and data collection from other projects as was described above for the East London Site. This is important to allow refinements to the test acceptance criteria and to determine their applicability for different concrete types.

It is noted that the presence of an interface layer between the support fluid and the rising body of concrete is the material that becomes trapped in the pile concrete in defects such as mattressing and inclusions. Further testing both in the field and numerically using computer modelling is required to understand the role the interface layer has in the formation of these defects. Research could focus on identifying the properties of the layer, how it affects concrete to flow and how to minimise the formation of the layer.

CONCLUSIONS

Tremie concrete is a complex material with additions and admixtures being used to tailor a mix to a particular application. There is a need for a more detailed concrete testing regime to control the workability and stability of tremie concrete. The risk of static segregation of concrete is not assessed by traditional concrete acceptance tests. Recent problems with static segregation highlights the need to control concrete by carrying out detailed concrete testing.

The EFFC/DFI Tremie Guide explains that the tremie concreting process involves the client, designer, constructor, concrete mix specifier, and concrete supplier. The designer must consider code detailing requirements. There is a trade-off between reducing a foundation section size and increasing reinforcement congestion and resulting difficulty of concrete flow. Setting more comprehensive concrete test standards reduces the risks. However, the workmanship of the constructor is also important.

The concreting process requires the fresh concrete to have sufficient workability and stability throughout the concreting process or construction issues may arise as listed in Table 1. Detailed concrete testing enables the project team to assess whether the concrete is conforming to expected behaviour which reduces the risk of construction issues occurring. The execution method can also influence the foundation quality as well as the concrete quality.

The EFFC/DFI Tremie Guide and the SPERW set out detailed concrete tests and acceptance limits. These limits were met for the East London Site during construction with good concrete results in the completed foundations. More case history data is needed to assess the acceptance limits to see if they can be refined. It is noted that the test acceptance criteria may not be appropriate for certain low strength mixes such as those used for firm primary secant piles.

REFERENCES

Recommended Practice Tremie Concrete for Deep Foundations, Concrete Institute of Australia, CIA, 2012

EFFC/DFI Best Practice Guide to Tremie Concrete for Deep Foundations, EFFC/DFI, 2016

ICE Specification for Piling and Embedded Retaining Walls, 3rd Edition, ICE, 2017

STATIC LOAD TESTS BY BI-DIRECTIONAL METHOD IN THE BRAZILIAN CONTEXT

Felipe V. A. de Souza Cruz, GeoEstática Engineering, Rio de Janeiro/RJ, Brazil, felipe@geoestatica.com.br
Marco A. G. Conte, COPPE/UFRJ, Rio de Janeiro/RJ, Brazil, marco.conte@hotmail.com
Renan Basso, RB Consulting Engineer, São Paulo/SP, Brazil, renan.basso@hotmail.com
Alessandra C. de Freitas, POLI/UFRJ, Rio de Janeiro/RJ, Brazil, alessandracfreitas@poli.ufrj.br

ABSTRACT

Bidirectional tests are an option for pile static load tests that have been growing significantly in Brazil in the last years. This work presents the procedures used in the interpretation of this test. In the bidirectional method generally one Expendable Static Cell (ESC) is installed near the pile toe (about 1/3 of pile length). The cell is pressurized by fluid (generally water), thus generating a load that is applied to the two parts of the pile. The test provides directly two load x displacement graphs, corresponding to the upper and lower parts of the pile. The load x settlement curve which the pile would present under a load applied to its top has to be constructed from these graphs. Different methods can be used to construct the top load x settlement curve, and the proposals of Silva (1983) and Massad (2015) are the most used in Brazil. In the interpretation of the test, a key parameter is the elastic shortening of the pile. If the pile is rigid, the method proposed by Silva (1983, 1986) can be used, but, if the pile is compressible, it is of the utmost importance to measure the elastic shortening.

Keywords: Bi-Directional Load Test, Static Load Test, Foundations Performance Control

INTRODUCTION

Static load tests in cast in place piles by the bidirectional method have been carried out since the 1980's in Brazil. Historical records indicate that the bidirectional test was first designed by Silva (1983). Afterwards a very similar system was proposed by Osterberg (1989), known as "O-Cell Test". Schmmertmann and Hayes (1997) have mentioned that bidirectional tests using O-Cell was first performed experimentally in 1984 and commercially in 1987. According to them, until 1996 more than 200 tests had been carried out in United States and Southeast Asia. Nowadays, it has already been conducted more than 6000 static load tests by the bidirectional method around the world, and 2000 just in Brazil. Despite the brazilian pioneering in bidirectional tests, unfortunately there are few studies related to the behavior of cast in place piles using this method.

STATIC LOAD TESTS IN BRAZIL

Conventional static load test

Static load tests can be used to study the soil-pile behavior. They verify important features like bearing capacity of the foundation, displacements and stresses along the pile shaft. Furthermore they can be employed to evaluate the structural integrity (indirect way).

The test is done by applying a static load on the pile cap. Thus it is necessary a reaction frame to cause axial compression in the tested pile (Fig. 1).

© 2018 Deep Foundations Institute

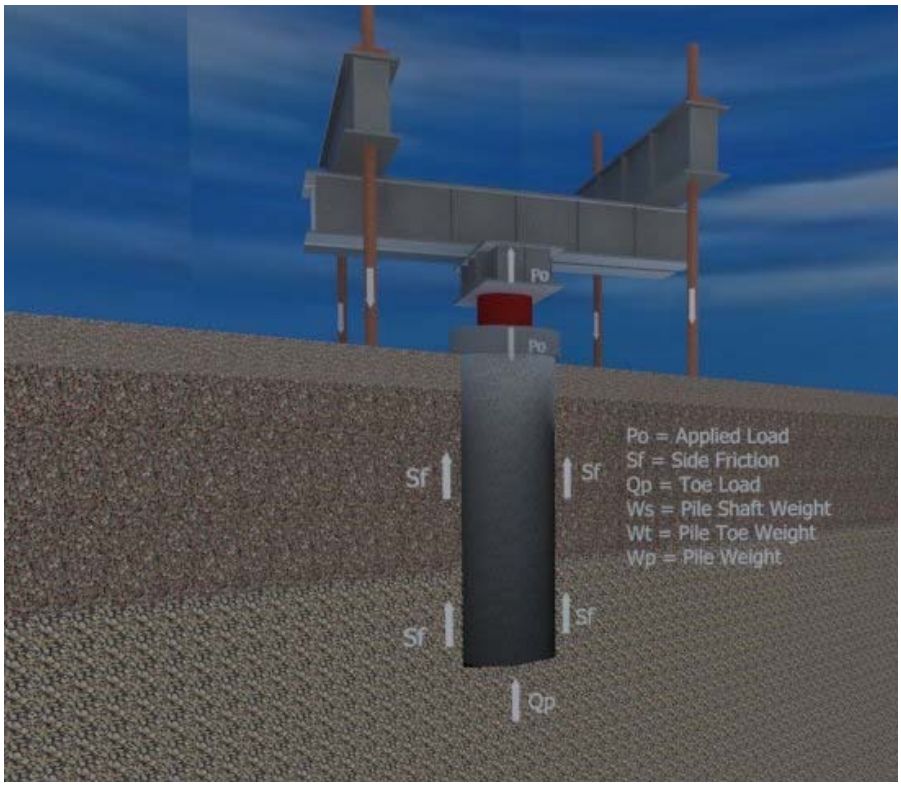


Figure 1. Conventional static load test (Souza Cruz at al., 2017)

Succesive loads are applied to the pile and the respective settlements are measured. To apply the load is necessary to install a properly reaction frame system. Reaction piles, anchors and a loader generally compose this system (Fig. 2). Depending on the loading system, the test can be considered low, fast or mixed, according to the brazilian current standard (NBR 12131, 2006).

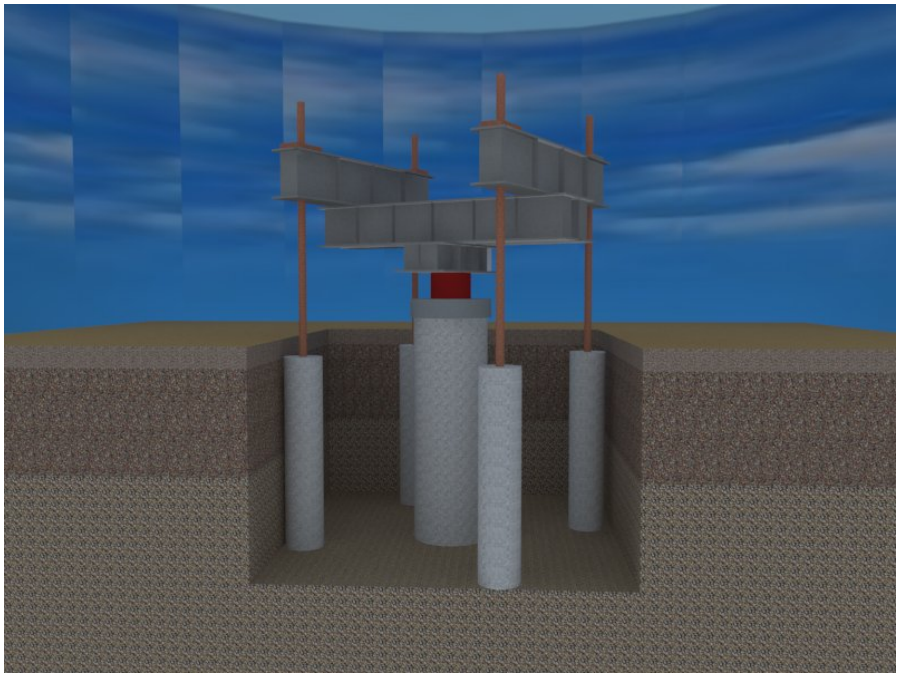


Figure 2. Reaction frame system employed in the conventional static load test (Souza Cruz at al., 2017)

Bidirectional test

One or more Expendable Static Cell's (ESC) are generally placed near the pile toe and a load is applied in opposite directions. The acting stresses in the pile shaft will seek for equilibrium.

The bidirectional test was first idealized by Silva (1983; 1986). According to him, often builders had a great reluctance to carry out conventional static load tests (high value and extended execution time). So he realized the need to create a tool that could evaluate the behavior of soil and foundations simultaneously. This methodology should be fast and should please builders and designers. Also it should have a small impact on the project cost and its schedule, as well as provide relevant and reliable results.

Obviously any attempt in this way would have to eliminate the factor that most impact costs and deadlines in the conventional static load tests: the reaction frame system. The first logical solution was to employ the pile shaft itself as a reaction system. However that would only be possible in cast in place piles and/or in some excavated belled caissons. So it would be necessary to install an hydraulic jack inside the pile shaft, in such a position that would get the maximum side friction (force equilibrium).

The bidirectional test is performed basically in 4 stages (Fig. 3), which are listed below:

1st stage – Installation
The Expendable Static Cell's (ESC) are installed coupled together with the pile cage. The ESC position is designed in order to reach an equilibrium region (the side friction of the pile shaft above the ESC should be equal to the side friction of the shaft pile below the ESC plus the toe resistance).

2nd stage – Concreting
After installing the ESC, concrete pouring should be verified to confirm whether the measurement system is in accordance with the project or not. This is an important stage since if there is any problem with the measurement system the test will be lost.

3rd stage – Testing
A static load is applied through the loading system (which uses injection tubes) and monitored by a dial gauge or a LVDT.

4th stage – Pile recovery
After unloading, pressurized grout (cement slurry) is injected in order to recover the pile (make it usable), since it was fissured during the test. The recovery process generally causes an enlargement of the pile cross section, once the grout is under higher pressures than the soil stresses. As the cells employ water instead of oil for the pressurizing system, the fissures generated during the test can be filled.

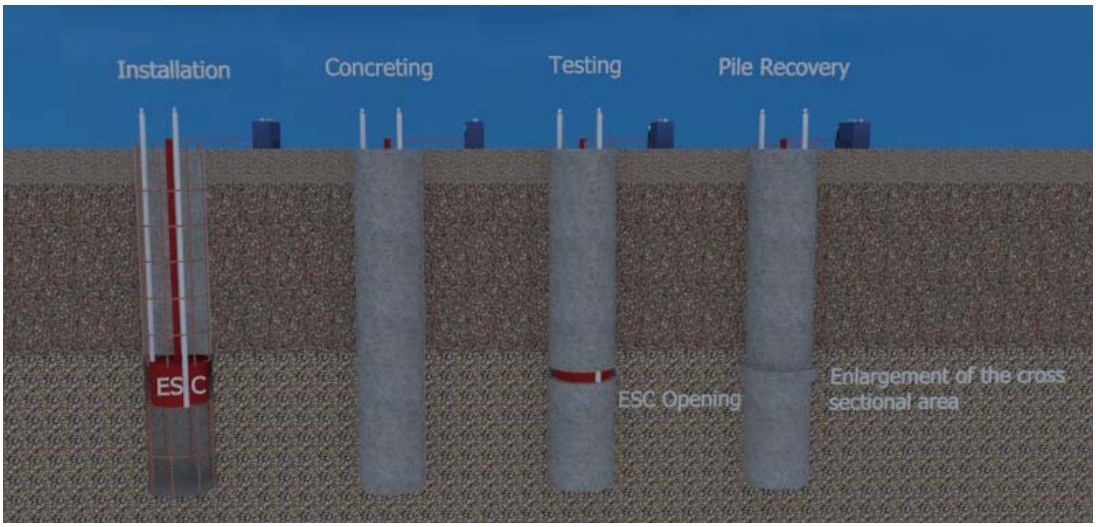


Figure 3. Stages of a bidirectional test (Souza Cruz et al., 2017)

ANALYSIS AND INTERPRETATION OF THE BIDIRECTIONAL TEST

According to Silva (1983; 1986) the bidirectional test provides three different curves:

i) the load - displacement curve of the ESC top (Fig. 4);
ii) the load - displacement curve of the ESC base (Fig. 4);
iii) the adjusted load - displacement curve of the whole pile, considering causes and effects (Fig. 5).

Nowadays it is possible to obtain one more curve than those proposed initially by Silva (1983; 1986):

iv) the load - displacement curve of the pile top.

This curve is correlated with the measurement of the upward elastic shortening, which will be better developed in this paper. Commonly the downward elastic shortening is not measured because the segment below the ESC is much shorter than the one above; it means there is no significant elastic shortening.

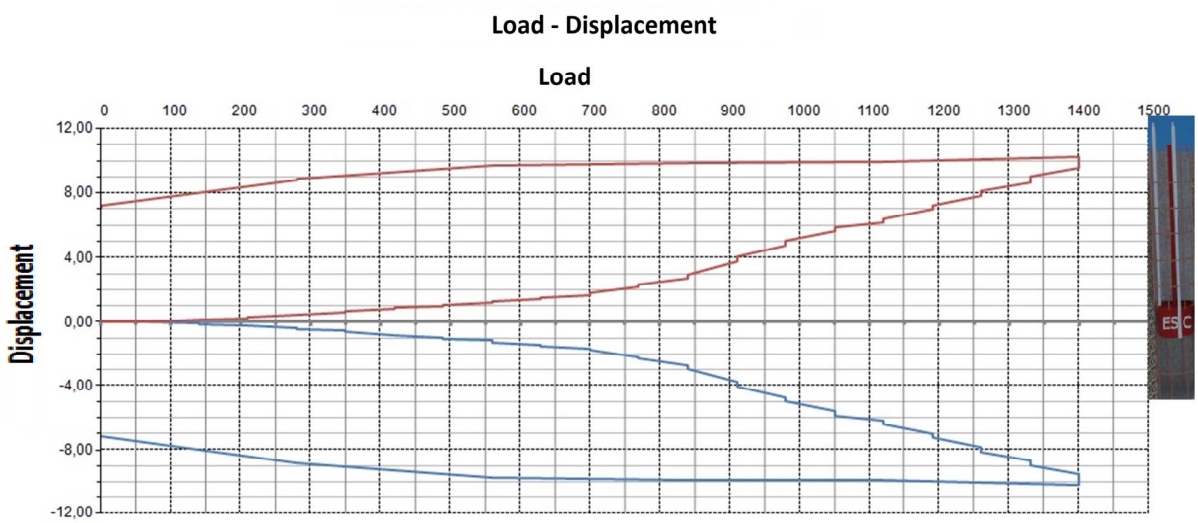


Figure 4. Load - displacement curves of the ESC top and base (Souza Cruz et al., 2017)

As the test is based on Newton's Third Law (action and reaction), the values obtained range from zero up to two times the load applied.

According to Silva (1983; 1986) to convert the load - displacement curves obtained (Fig. 4) into a single one (Fig. 5), it is necessary to take the following steps:

a) in the load - displacement curve of the ESC top verify which load corresponds to the displacement "ρ" (any value);
b) in the load - displacement curve of the ESC base look for the load that has caused the same displacement "ρ";
c) plot the load - displacement adjusted curve by summing the loads which has caused the same displacement to the ESC base and top.

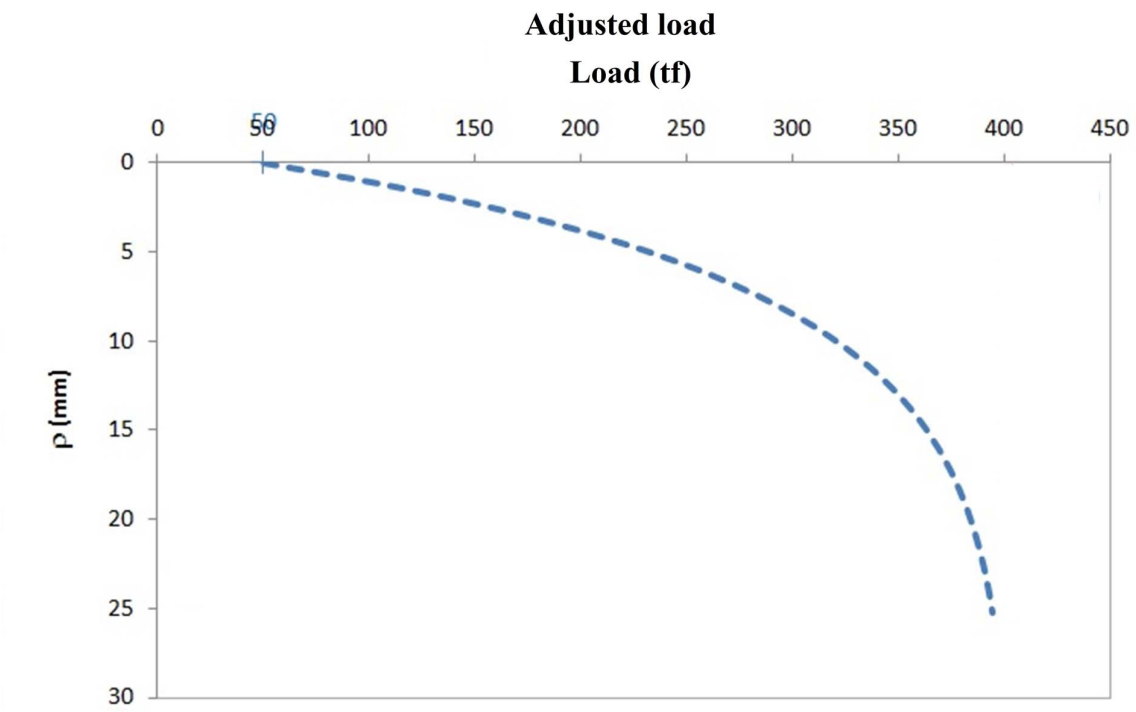


Figure 5. Adjusted load - displacement curve of the whole pile (Souza Cruz et al., 2017)

It is not always possible to obtain the same displacements in the ESC top and base curves. In these cases extrapolation methods (e. g. Van der Veen, 1953) are used to reach the same settlements so that the resulting loads may be summed.

Silva's (1983; 1986) adjusted curve is the transposition of bidirectional test results to the conventional load test. That is necessary so that all experience gathered along the years about conventional load tests may be kept. The adjusted curve is considered conservative because it is understood that only one of the pile segments reaches the ultimate load.

In order to plot the adjusted curve by Silva's (1983; 1986) method the pile must be rigid or the elastic pile shortening should be measured or calculated.

ELASTIC PILE SHORTENING

Conventional load test

According to Massad (2015) to evaluate the elastic shortening (Δe) of a vertical pile under axial compression at the top, the following expressions can be used:

$$\Delta e = \frac{Q_p}{K_r} + c.\frac{A_l}{K_r} \qquad [1]$$

Where Q_p is the the toe load and A_l is the shaft load. K_r is the pile stiffiness (height *h*, cross sectional area *S*, and elastic modulus *E)*, given by the expression:

$$K_r = \frac{E.S}{h} \qquad [2]$$

According to Lovell (1979), the ratio (c) between the mean value of the shaft load transferred ($\overline{A_l}$, shaded area of Fig. 6a) and the total shaft load (A_l), is given by the expression:

$$c = \frac{A_l - \overline{A_l}}{A_l} \qquad [3]$$

The coefficient c depends on the skin friction distribution (f). Values of c to simple f distributions can be obtained easily by the abacus developed by Leonards and Lovell (1979), or the equation proposed by Fellenius (1980).

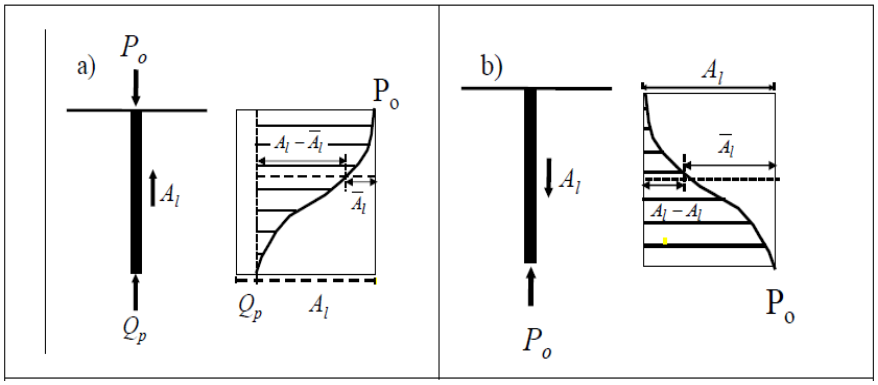


Figure 6. (a) Conventional load test: load distribution (b) Bidirectional test: upward load distribution (adapted from Massad, 2015)

Bidirectional test

According to Massad (2015) for loadings carried out by bidirectional test, considering only the upward elastic shortening, equation [1] changes to:

$$\Delta e = c' . \frac{A_l}{K_r} \qquad [4]$$

It should be noted that the coefficient c is related to downward loadings (conventional load test and bidirectional load test under the ESC), meanwhile the coefficient c' is related to upward loadings (Fig. 6b). Thus the following expression can be written:

$$1 = c + c' \qquad [5]$$

Mathematical modelling of the bidirectional test

For the simulation of a bidirectional test, a mathematical model developed by Massad (1995) for conventional load tests is used. It is based on Modified Cambefort relations, which take into account some mechanisms of load transfer, such as progressive failure. Residual stresses due to driving have been ignored. A coefficient that measures relative stiffness of the pile-soil (shaft) is introduced and defined as follows:

$$k = \frac{A_{lr}}{K_r . \gamma_l} \qquad [6]$$

Where A_{lr} is the ultimate shaft load and γ_l is the pile displacement required to mobilize the full shaft resistance. The model has given some light on the pile behavior, resulting in a new classification concerning k values: "short" or rigid ($k \leq 2$); intermediate ($2 \leq k \leq 8$); and "long" or compressible ($k \geq 8$).

In order to simulate the bidirectional test, this model has been modified incorporating a soft top layer (fu_2) over a more resistant one (fu_1).

For both layers has been assumed the same $\gamma 1$ value, so that k (Eq. 6) may be associated to the whole subsoil along the shaft pile. It should be noticed that K_r refers to the pile lenght over the ESC.

Massad (2015) presented some simulations of bidirectional tests changing the relations fu_1/fu_2 and h_2/h_1. They were carried out in Brazil and United States (Figs. 9-10). In each case the soil under the ESC was the same and the following expression may be written:

$$\frac{R'.S_p}{K_r.K} = 0{,}80 \qquad [7]$$

where Sp is the cross sectional area of the pile toe and R' is the soil stiffness at the pile toe according to the Cambefort relations. The results presented in Fig. 7 point out that the top curves, normalized for bidirectional test, are approximately invariant with respect to the product $c'.k$, regardless the distribution of shaft resistances (Massad, 2015).

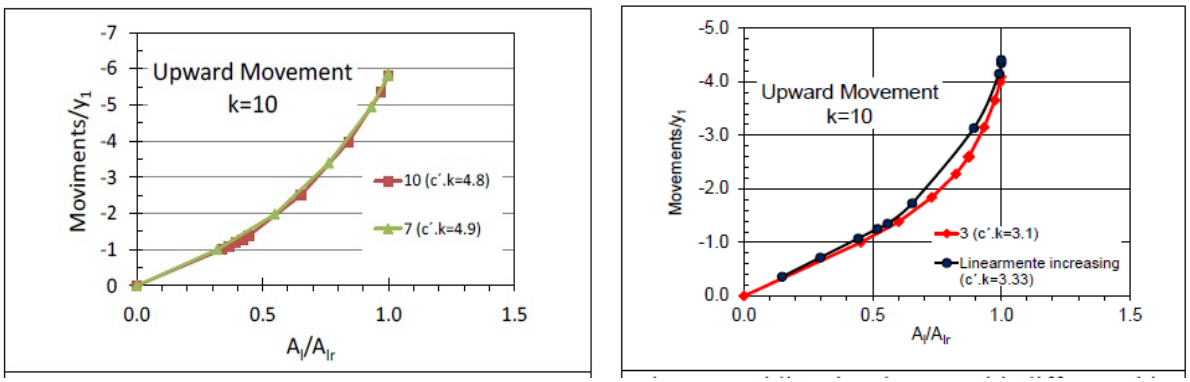


Figura 7. Bidirectional tests with different side friction distributions (adapted from Massad, 2015)

Analytical determination of the equivalent curve

In order to derive formulas to find an equivalent curve, let us assume that the upward displacement was measured at the ESC top. In the ascending curve of a bidirectional test the coordinates of point P are γf and Al (Fig. 8).

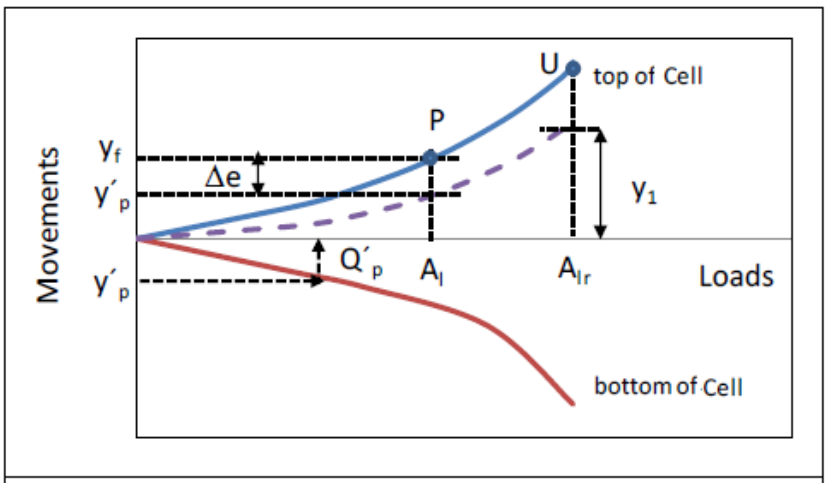


Figure 8. Apward displacements of a bidirectional test (adapted from Massad, 2015)

The elastic shortening of the shaft may be calculated according to Eq. 4. An aproximate measure of the displacement of the pile top (γ'_p) is given by Massad (2015):

$$\gamma'_p = \gamma_t - \Delta e \geq 0 \quad [8]$$

To simulate the conventional load test γ'_p corresponds to Q_p (Fig. 8). Finally points γ_o and P_o of the equivalent curve are determined by the equation:

$$\gamma_0 = \gamma'_p + \Delta e \cdot \frac{c}{c'} + \frac{Q_p}{K_r} \quad [9]$$

If pile head displacements may be measured, instead the ESC displacement, the process is similar. Finally if both displacements of the pile head and the ESC top may be measured, Silva's (1983; 1986) method should be used.

CONCLUSIONS

Static load tests by the bidirectional method has had Brazilian pioneering, although it has been widely diffused and studied in the United States.

The bidirectional method, although little known and disclosed in Brazil, is easily correlated to the conventional method with high convergence rates.

The different side friction distributions provided by bidirectional and conventional static load tests lead to the same elastic shortening, that is, the same equivalent curve. Thus the key factor is the measuring of the elastic pile shortening.

If the pile is considered rigid $\left(K_r \to \infty, \gamma_0 = \gamma'_f\right)$, the methodology proposed by Silva (1983; 1986) is valid. But if the pile is considered compressible, it is of utmost importance to measure the elastic shortening.

REFERENCES

Fellenius, B. H., 1980. The analysis of results from routine pile loading tests. Ground Engineering, Foundation Publishing Ltd., London, 13(6) 19-31.

Leonards, G. A. and Lovell, D., 1979. Interpretation of Load Tests in High Capacity Driven Piles. Behavior of Deep Foundations, ASTM STP 670, Raymond Lundgren, Ed., ASTM, pp. 388-415.

Massad, F., 1995. Pile analysis taking into account soil rigidity and residual stresses. Proceedings, X Pan-American Conference on Soil Mechanics and Foundation Engineering, Mexico, Vol. 1, pp. 1199-1210.

Massad, F., 2015. Bidirectional Test With Use Of Hydrodynamic Cell - Testing And Its Interpretation. Proceedings, 8th Seminar on Special Foundations, São Paulo, Brazil, Vol. 2, pp. 1199-1210.

Osterberg, J., 1989. New Load Cell Testing Device. Proceedings, 14th Annual Conference, Deep Foundations Institute. pp. 17-28.

Schmertmann, J. H. and Hayes, J. A., 1997. The Osterberg cell and bored pile testing – a symbiosis. Proceedings, 3rd IGEC, Cairo, Egypt.

Silva, P. E. C. A F. da, 1983. Hydrodynamic expansive cell – a new way to perform loading tests. Arcos – Architecture, Constructions Ltda, Belo Horizonte, Brazil, 106pp. (In Portuguese)

Silva, P. E. C. A F. da, 1986. Hydrodynamic expansive cell – a new way to perform loading tests. Proceedings, 8th Brazilian Conference on Soil Mechanics and Foudation Engineering, Porto A1egre, Brazil, pp.223-241. (In Portuguese)

Souza Cruz, F. V. A., Basso, R. and Bottino, C., 2017. Analysis and interpretation of the bidirectional test. Foundations and Geotechnical Works, Brazil, Vol. 77, pp. 56-64. (In Portuguese)

Van der Veen, C., 1953. The bearing capacity of a pile. Proceedings, 3rd ICSMFE, Zurich, Vol. 2, pp. 84-90.

STUDY OF EFFECTS OF CONSTRUCTION METHODS ON PERFORMANCE OF DRILLED SHAFTS

Sohail Kibria, Vice President, National Engineering Services Pakistan (NESPAK), Lahore, Pakistan, +92-332-4498837, sohailkibria18@yahoo.com
Sajid Iqbal, Senior Geotechnical Engineer, National Engineering Services Pakistan (NESPAK), Lahore, Pakistan, +92-306-0648010, sajid_gunjial@yahoo.com

ABSTRACT

Different methods of boring are in vogue for the construction of drilled shafts in the world. The most commonly used methods include rotary drilling, rotary bucket auger, percussion, continuous flight auger etc. It is widely reported in the literature as well as supported by some design codes that the load carrying capacity of drilled shafts depends a lot on the local construction practices in addition to the soil parameters. In Pakistan, recently about twenty thousand drilled shafts have been constructed for the first ever Metro Electric Train and RLNG power projects. A host of boring methods have been used in different contract packages, for drilling in the wet as well as in the dry conditions. The subsequent performance of full-scale static load tests on the selected drilled shafts has divulged variable load carrying capacities of drilled shafts constructed by different techniques. This paper is based on a study of different factors involved during the construction of drilled shafts by different methods and their effect on load carrying capacity as ascertained from pile load tests. Practical conclusions have been drawn and recommendations have been made for the sound construction of drilled shafts in alluvial conditions as in Punjab Province, Pakistan.

Keywords: Drilled shafts performance, rotary bucket auger, reverse rotary, pile load tests

INTRODUCTION

The improvement in bored pile construction practices in Pakistan has led to an increased reliance on different methods of boring for the construction of drilled shafts. The most commonly used methods include rotary drilling, rotary bucket auger, percussion and continuous flight auger. Pile load testing is a part of the design process in piling practice in the world. These tests provide valuable information regarding load-deformation behaviour of the prototype pile foundations. It is widely reported in the literature as well as supported by some design codes that the load carrying capacity of drilled shafts depends a lot on the local construction practices in addition to soil parameters (Brown 2002; Camp et al. 2002; Seavey and Ashford 2004; and Brown 2004). About twenty thousand drilled shafts have been constructed for first ever Metro Electric Train and RLNG power projects in Punjab Province, Pakistan using a host of different boring methods, for drilling in wet as well as in dry conditions.

Metro Electric Train is the first mass transit project of its kind which is being constructed in the metropolis of Lahore. The elevated portion of metro route is supported on pile foundations in alluvium. Besides, three RLNG Power projects have been recently constructed in alluvial soils at three different sites including Bhikki, Balloki and Jhang where pile foundations were suggested as optimum foundation system for heavily loaded power plant structures in addition to mat foundation.

In order to verify the load carrying capacity of drilled shafts, before construction of actual working drilled shafts, ultimate pile load tests were carried out. The results of these load tests were used to finalize the drilled shafts design capacities. From experience of review of design and load testing of piles in alluvial soil conditions as in Punjab Province, Pakistan, the authors have attempted to study different factors involved during the construction of drilled shafts by different methods and their effect on load carrying capacity as ascertained from pile load tests. This paper tends to compare theoretically predicted loads and interpreted loads from pile load tests to describe the influence of methods of construction on the load carrying capacity of drilled shafts and provides recommendations

© 2018 Deep Foundations Institute

for sound construction of drilled shafts in similar ground conditions.

GROUND CONDITIONS

Subsurface conditions from Metro Electric Train and RLNG power projects sites have been selected for this study. Soil parameters have been adopted for test pile design based upon the analysis of field data, laboratory tests results, engineering judgement and experience in similar soil conditions. The bored piles/drilled shafts in the strata of Lahore derive their major part of load carrying capacity from shaft friction. The design value of Phi (φ) represents the peak value of friction angle.

Metro Electric Train Project Site (NESPAK 2015)

Subsoil conditions enroute, consist of alluvial deposits comprising 5-7 m thick top layer of firm to medium-stiff silty clay followed by medium-dense to dense silty sand/sand with silt stratum. Groundwater table depth varies from 15–22 m in general below existing ground level. The subsoil parameters provided in Table 1 were used for evaluation of pile capacities.

Table 1: Soil parameters for design of project test piles

Depth (m)	Material Type	Selected Parameters
0-3	Fill	-
3-5	Silty Clay	Undrained shear strength (s_u) = 30 kPa, N_{avg} = 8 Bulk Density γ_b= 17.0 kN/m^3
5-33	Silty Sand	Phi (φ) = 30^o, N_{avg} = 19, N'$_{70}$ = 12 Bulk Density (γ_b)=17.5 kN/m^3
33-50	Sand with Silt	Phi (φ) = 32^o, N_{avg} = 40, N'$_{70}$ = 20 Bulk Density (γ_b)=18.5 kN/m^3

Balloki RLNG Power Project Site (Berkeley Associates 2015a)

Subsoil conditions consist of alluvial deposits comprising top layer of firm to stiff silty clay/lean clay up to thickness of 8 m. This stratum is followed by dense silty sand/ poorly graded sand with silt. Groundwater table depth varies from 3.3 to 4.4 m below existing ground level. Table 2 shows the subsoil parameters for evaluation of pile capacities.

Table 2: Soil parameters for design of project test piles

Depth (m)	Material Type	Selected Parameters
0-4	Silty Clay/Lean Clay	Undrained shear strength (s_u) = 15 kPa, N_{avg} = 3 Bulk Density γ_b= 19.0 kN/m^3
4-8	Silty Clay/Lean Clay	Undrained shear strength (s_u) = 25 kPa, N_{avg} = 9 Bulk Density γ_b= 19.0 kN/m^3
8-13	Silty Clay/Lean Clay	Undrained shear strength (s_u) = 50 kPa, N_{avg} = 16 Bulk Density γ_b= 19.5 kN/m^3
13-40	Silty Sand/Sand with Silt	Phi (φ) = 34^o, N_{avg} = 41, N'$_{70}$ = 26 Bulk Density (γ_b)=18.5 kN/m^3

Bhikki RLNG Power Project Site (Berkeley Associates 2016a)

Subsoil conditions consist of alluvial deposits comprising top layer of firm silty clay/lean clay up to thickness of 5 m followed by medium-dense silty sand stratum. This stratum is followed by very stiff silty clay/lean clay. This clay stratum is underlain by dense to very dense silty sand/sand with silt. Groundwater table depth varies from 1.9 to 3.15 m below existing ground level. Table 3 shows the subsoil parameters for evaluation of pile capacities.

Table 3: Soil parameters for design of project test piles

Depth (m)	Material Type	Selected Parameters
0-5	Silty Clay/Lean Clay	Undrained shear strength (s_u) = 25 kPa, N_{avg} = 5 Bulk Density γ_b= 19.0 kN/m^3
5-18.5	Silty Sand/Sand with Silt	Phi (φ) = 32^o, N_{avg} = 19, N'_{70} = 15 Density (γ_b)=18.0 kN/m^3
18.5-25.5	Silty Clay/Lean Clay	Undrained shear strength (s_u) = 75 kPa, N_{avg} = 33 Bulk Density γ_b= 19.0 kN/m^3
25.5-45	Silty Sand/Sand with Silt	Phi (φ) = 34^o, N_{avg} = 47, N'_{70} = 24 Bulk Density (γ_b)=18.5 kN/m^3

Jhang RLNG Power Project Site (Power Construction Corporation China 2016a)

Subsoil conditions consist of alluvial deposits comprising 2 m thick top layer of very soft silty clay/silt followed by medium dense to very dense silty sand stratum. Groundwater table depth varies from 2 to 4.6 m below existing ground level. Table 4 shows the subsoil parameters for evaluation of pile capacities.

Table 4: Soil parameters for design of project test piles

Depth (m)	Material Type	Selected Parameters
0-2	Silty Clay/Silt	Undrained shear strength (s_u) = 5 kPa, N_{avg} = 6 Bulk Density γ_b= 17.5 kN/m^3
2-5.5	Silty Sand	Phi (φ) = 28^o, N_{avg} = 10, N'_{70} = 8 Density (γ_b)=16.8 kN/m^3
5.5-19.25	Silty Sand	Phi (φ) = 31^o, N_{avg} = 20, N'_{70} = 14 Bulk Density (γ_b)=17.3 kN/m^3
19.25-29.25	Silty Sand	Phi (φ) = 32^o, N_{avg} = 40, N'_{70} = 20 Bulk Density (γ_b)=17.5 kN/m^3
29.25-40	Silty Sand	Phi (φ) = 34^o, N_{avg} = 63, N'_{70} = 28 Bulk Density (γ_b)=18.5 kN/m^3

PILE CONSTRUCTION METHODS USED

Dry Method of Construction

The dry method of drilled shaft construction is usually employed in those types of soils that will not cave-in during and after drilling. Soils of this nature include stiff clays, soft and hard rock, and some sands with silt, cementation, aging effects etc. The wet ground conditions or presence of groundwater table at shallow depth prevented the use of dry boring. Rotary Bucket Auger (RBA) is an example of this method that has been used for test piles construction in dry conditions at Metro Electric Train project sites. This type of boring in the strata of Lahore, has been the first ever experience for drilled shafts construction in bulk. RBA provides a good control over verticality of the borehole and allows an almost vibration-free operation. This method results into a rather smooth shaft.

Wet Method of Construction

When caving soils exist below the water table or are too deep, wet method is used for drilling. Plain water, bentonite or other polymeric compounds are used for fluid circulation. Based on local experience, presence of some cementation, aging of deposits, presence of higher silt content and absence of seepage from the ground will generally be the conditions favouring use of water only. Reverse Rotary with water and bentonite have been used for boring in wet conditions for test piles construction for Metro Electric Train project. Whereas, both the Rotary Bucket Auger (RBA) with bentonite without circulation and Reverse Rotary (RR) with water/bentonite circulation have been used as boring methods for test piles construction at power projects sites. RR method generally results

into somewhat irregular shaft, and some times the overconsumption of the concrete becomes excessive.

PREDICTION VS. PERFORMANCE IN LOAD TESTS

Table 5 provides summary of interpretation of all pile load tests carried out, under this study.

Table 5: Summary of pile load test interpretation results (NESPAK and Berkeley Associates 2015; Berkeley Associates 2015b, 2016b; Power Construction Corporation China 2016b)

Location	Test Pile No.	Test Load (kN)	Pile Geometry		Settlement (mm)		Interpreted Allowable Load, Q_a (FOS=2) in kN					
			Length (m)	Dia. (m)	Gross	Net	Tangent Method	Davisson Limit Value Method	Chin Method	80%, Hansen Method	90%, Hansen Method	Avg. Load
Lahore	TP-1	10000	30	1.2	89.1	85.6	4750	2500	2500	-	-	3250
	TP-2	8000	22	1.2	8.0	5.2	NA	NA	NA	-	-	4000
	TP-3	8000	22	1.2	9.0	5.9	NA	NA	NA	-	-	4000
	TP-4	10000	40	1	31.7	22.8	4750	4630	5000	-	-	4790
	TP-5	10000	30	1.2	7.6	1.4	NA	NA	NA	-	-	5000
	TP-6	10000	30	1.2	46.6	38.7	4900	3750	4560	-	-	4400
	TP-8	10000	30	1.2	76.5	71	4750	3850	4350	-	-	4320
	TP-9	10000	30	1.2	14.8	9.9	NA	NA	NA	-	-	5000
	TP-10	10000	40	1	91.8	79.1	4700	3400	3770	-	-	3960
	TP-11	10000	22	1.2	25.0	17.3	4900	4700	5000	-	-	4870
	TP-12	12000	35	1.2	71.4	62.3	5750	4400	4950	-	-	5030
	TP-13	10000	30	1.2	124.4	116.2	3880	2750	3170	-	-	3270
	TP-14	8000	22	1.2	11.8	4.7	NA	NA	NA	-	-	4000
	TP-15	7000	22.4	1.2	82.6	78.9	1325	980	-	-	-	1153
Balloki	TP-1	5970	30	0.76	11.1	3.3	NA	NA	NA	NA	NA	2985
	TP-2	10200	30	0.76	74.5	56.7	4950	3875	5100	NA	NA	4640
	TP-3	6120	20	0.76	42.1	30.6	2950	2675	NA	3095	NA	2910
	TP-4	6120	20	0.76	114.7	104.9	2300	1725	2935	2600	NA	2390
	TP-5	10200	30	0.76	99.9	74.1	4800	3400	NA	NA	NA	4100
	TP-9	10200	30	0.76	92.1	77.9	4875	3000	NA	NA	NA	3940
	TP-10	6690	30	0.76	117.7	109.6	3000	2150	NA	NA	NA	2575
	TP-11	10200	30	0.76	81.4	66.7	4900	2800	NA	NA	NA	3850
	TP-12	6120	20	0.76	112.7	104.2	2300	1600	2895	2615	NA	2353
Bhikki	TP-1	4500	30	0.76	4.8	1.2	2250	2250	2250	2180	2250	2240
	TP-2	4850	26.5	0.76	9.3	2.4	NA	NA	NA	NA	NA	2425
	TP-3	4500	26.5	0.76	9.0	2.1	NA	NA	NA	NA	NA	2250
	TP-6	4780	26.5	0.6	13.2	5.3	NA	NA	NA	NA	NA	2390
	TP-7	5210	26.5	0.6	23.4	9.6	NA	NA	NA	NA	NA	2605
Jhang	TP1-3	6250	30	0.76	116.9	107.3	2850	1500	-	-	3250	2530
	TP1-4	4800	30	0.76	119.6	112.3	2000	1150	-	-	2400	1850
	TP1-5	6250	30	0.76	115.3	107.9	2575	1750	-	-	3100	2480
	TP2-1	2140	20	0.6	90.5	84.9	800	400	-	1420	1100	930
	TP2-2	2400	20	0.6	93.9	89.2	900	550	-	-	1250	900
	TP2-3	3980	20	0.6	96.2	84.5	1700	875	-	-	2000	1525

Drilled shaft capacities in compression were predicted by the use of static method, as specified by NAVFAC Design Manual 7.02 (Navy 1982). Ultimate pile load tests were performed to determine the ultimate load carrying capacity of test piles. Most of these tests carried were taken to the yielding stage to determine the load vs. settlement behaviour before failure. Load tests on all the test piles of the projects under current study were carried out according to the ASTM D1143 M-07 standard procedure. Tangent method, Chin Method, Davisson Limit Value Method, 80% and 90% Hansen Methods were used for interpretation of pile load test results (Chin 1972; ASCE 1993). Table 6 shows a comparison of predicted allowable loads and interpreted loads with estimate of over/under prediction.

Table 6: Comparative Values of Predicted Allowable and Interpreted Loads (NESPAK and Berkeley Associates 2015; Berkeley Associates 2015b, 2016b; Power Construction Corporation China 2016b)

Location	Test pile No.	Drilling Method	Drilling Fluid	Predicted Allowable Load (kN)	Test Load (kN)	Test/Predicted Load Ratio	Interpreted Allowable Load (kN)	Over /Under Prediction (-/+) %
Lahore	TP-1	RR[a]	water	4000	10000	2.5	3250	-19
	TP-2	RBA[b]	-	2830	8000	2.8	[d] Not Yielded(>4000)	>40
	TP-3	RBA	-	2830	8000	2.8	Not Yielded(>4000)	>40
	TP-4	RR	water	4000	10000	2.5	4790	+20
	TP-5	RR	water	4000	10000	2.5	Not yielded(>5000)	>25
	TP-6	RR	water	4000	10000	2.5	4400	+10
	TP-8	RR	water	4000	10000	2.5	4320	+8
	TP-9	RR	water	4000	10000	2.5	Not yielded(>5000)	>25
	TP-10	RR	water	4000	10000	2.5	3960	-1
	TP-11	RBA	-	2830	10000	3.5	4870	+72
	TP-12	RR	water	4750	12000	2.5	5030	+6
	TP-13	RR	water	4000	10000	2.5	3270	-18
	TP-14	RBA	-	2830	8000	2.8	Not yielded(>4000)	>40
	TP-15[c]	RR	Bentonite[c]	2850	7000	2.6	1153	-60
Balloki	TP-1	RBA	Bentonite	1990	5970	3.0	Not yielded (>2985)	>50
	TP-2	RBA	Bentonite	1990	10200	5.1	4640	+133
	TP-3	RBA	Bentonite	1630	6120	3.8	2910	+78.5
	TP-4	RBA	Bentonite	1630	6120	3.8	2390	+47
	TP-5	RBA	Bentonite	1990	10200	5.1	4100	+101
	TP-9	RR	Water	1990	10200	5.1	3940	+98
	TP-10	RR	Water	1990	6690	3.4	2575	+29
	TP-11	RR	Water	1990	10200	5.1	3850	+93
	TP-12	RR	Water	1630	6120	3.8	2352.5	+44
Bhikki	TP-1	RR	Water	1500	4500	3.0	2240	+49
	TP-2	RR	Water	1500	4850	3.2	Not yielded (>2425)	>62
	TP-3	RR	Water	1500	4500	3.0	Not yielded (>2250)	>50
	TP-6	RR	Water	1500	4780	3.2	Not yielded (>2390)	>59
	TP-7	RR	Water	1500	5210	3.5	Not yielded (>2605)	>74
Jhang	TP1-3	RBA	Bentonite	2500	6250	2.5	2530	+1
	TP1-4	RBA	Bentonite	2500	4800	1.9	1850	-35
	TP1-5	RBA	Bentonite	2500	6250	2.5	2480	-0.8
	TP2-1	RBA	Bentonite	1150	2140	1.9	930	-19
	TP2-2	RBA	Bentonite	1150	2400	2.1	900	-22
	TP2-3	RBA	Bentonite	1150	3980	3.5	1525	+33

[a] RR: Reverse Rotary, [b] RBA: Rotary Bucket Auger, [c] Use of uncontrolled bentonite in Lahore/TP-15 only
[d] Not yielded: could result into more allowable load

COMMENTARY ON PILE BEHAVIOUR AND REASONS FOR DISCREPANCIES

The results as shown in Table 6 have indicated that drilled shaft constructed with the RR method using plain water as the drilling fluid indicate that six piles do not exhibit significant settlements so that ultimate loads could be determined. It is therefore expected that had other these six load tests been loaded to more than the current test load, they would have resulted into determination of a higher value of allowable load. Referring to Table 6 and Fig. 1, for 16% of the data for RR drilled shafts (using water as drilling fluid, where yielding has taken place), allowable load has been overpredicted ranging from 18% to 19% whereas for the remaining 84% data allowable load has been underpredicted ranging from 6% to 98%.

Drilled shafts constructed with RR method using bentonite (in uncontrolled conditions) was not able to carry the test load and yielded at 1153 kN, thus making the overestimation of predicted load by 60%.

The load tests carried out on RBA drilled shafts constructed in dry condition have revealed that the three out of four load tests have not shown yielding even under 2.8 times the design load. The fourth load test was loaded to 3.5 times the design load and has shown the interpreted allowable load to be 70% higher than the predicted load. It is therefore expected that had other three load tests been loaded to more than 8000 kN, they would have yielded the allowable load of much more than 4000 kN. Therefore the load carrying capacity of RBA drilled shafts in dry condition is expected to be far greater than that of RR drilled shafts in wet condition using water for the same length and diameter.

RBA drilled shafts using bentonite as the drilling fluid are showing that one drilled shaft has not shown significant settlement and has not yielded. It is therefore expected that had this been loaded to more than the current test load, this would have resulted into increased allowable load. About 30% data indicates overestimation of predicted load by 19% to 35% and 60% data indicates underestimation of predicted load by 33% to 133% for drilled shafts constructed with RBA method using bentonite.

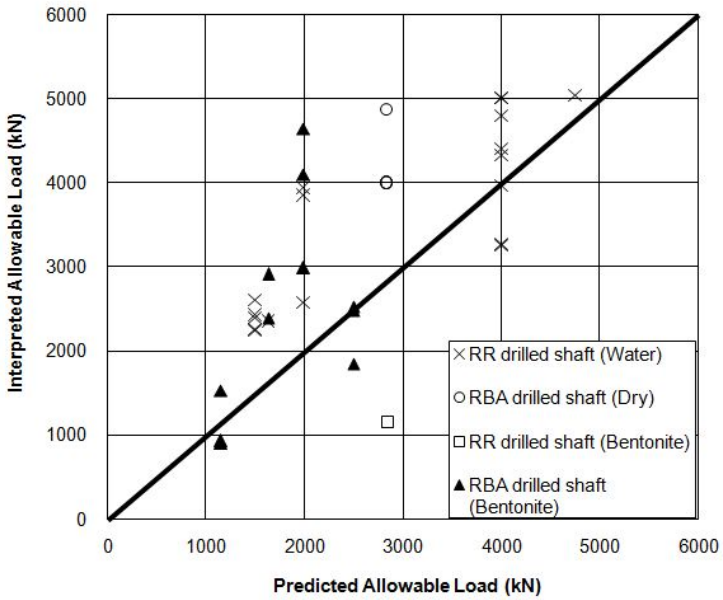


Fig. 1: Predicted vs. Interpreted Allowable Loads

The results also depict that there is not much difference in the load vs. Settlement behaviour of piles bored by RR using plain water and by RBA using bentonite., provided good control is exercised on the consistency of bentonite. It reveals that assumption of using the same pile capacities for dry RAB and RR were not correct. The test results have indicated the wide variation of pile load capacity by the all four methods of construction.

It is considered that bentonite slurry gets removed from the bore walls with the rising concrete column, if construction is done within 4-5 hrs. If slurry remains in the hole for too long, the bentonite cake can become stiff and thick, which is difficult to be removed with the rising concrete. The thicker the slurry layer, the more likely is that the slurry will not get properly removed. Slurry remains on the bore wall excessively reduce the side resistance of a drilled shaft. Besides, use of desander to maintain the sand content below 4% in the slurry ensures effective cleaning at the pile tip (Brown et al. 2010; Lam et al. 2014).

CONCLUSIONS AND RECOMMENDATIONS

Following are the major conclusions and recommendations:

1. Drilled shafts construction using RBA method has the least disturbance effect on the soil. Besides, RBA provides a good control over verticality of the borehole.

2. RBA drilled shafts in dry condition yield higher load bearing capacity than those obtained by RR drilled shafts.

3. In RR method, when bentonite is used, if slurry remains in the hole for too long, the bentonite cake can become stiff and thick. The thicker the slurry cake, the more likely is that the slurry will not get properly removed during concreting. Slurry remains on the bore wall excessively reduce the side resistance, leading to reduced load bearing capacity. Therefore, the use of bentonite slurry should be with very strict control over its specific gravity and time for construction, after completion of bore.

4. The load carrying capacity of RR drilled shafts with bentonite slurry/water and RBA drilled shafts may be of same order of magnitude, provided control over consistency and time of construction is being exercised.

5. Pile load test must be a mandatory requirement for finalizing the design of drilled shaft for the boring methods to be employed for the project.

6. It is recommended to adjust parameters including k, N_q, $L_{critical}$ by back-calculation as per load test results for designing drilled shafts to be constructed by all four boring methods for ground conditions, similar to those indicated in the paper.

REFERENCES

ASCE, 1993. *Bearing Capacity of Soils*. American Society of Civil Engineers Press, New York.

Brown, D.A., 2002. Effect of construction on axial capacity of drilled foundations in piedmont soils. Journal of Geotechnical and Geoenvironmental Engg., 128(12) 967-973.

Brown, D.A., 2004. The effect of construction techniques on axial capacity of drilled foundations. Auburn University, Alabama, Report B-424.

Brown, D.A., Turner, J.P., and Catelli, R.J., 2010. Drilled shafts: Construction procedure and LRFD design procedures. U.S. Department of Transportation, Federal Highway Administration, Report FHWA-NHI-10-016.

Berkeley Associates, 2015. Geotechnical Investigation Report of Balloki RLNG Power Project. Berkeley Associates (EPC contractor of NESPAK), Lahore, Pakistan.

Berkeley Associates, 2015. Pile Load Tests Report of Bhikki RLNG Power Project. Berkeley Associates (EPC contractor of NESPAK), Lahore, Pakistan.

Berkeley Associates, 2016. Geotechnical Investigation Report of Bhikki RLNG Power Project. Berkeley Associates (EPC contractor of NESPAK), Lahore, Pakistan.

Berkeley Associates, 2016. Pile Load Tests Report of Balloki RLNG Power Project. Berkeley Associates (EPC contractor of NESPAK), Lahore, Pakistan.

Chin, F.K., 1972. The inverse slope as a prediction of ultimate bearing capacity of piles. Proceedings of the 3rd SE Asian Conference on Soil Engineering, Hong Kong, pp. 83-91.

Camp, W.M., Brown, D.A., and Mayne, P.W., 2002. Construction methods effect on drilled shafts axial performance. *Deep Foundations*, Reston, Virginia, ASCE Geotechnical Special Publication No. 116, pp. 193-208.

Lam, C., Jefferis, S.A., and Martin, C.M., 2014. Effect of polymer and bentonite support fluids on concrete-sand interface shear strength. Geotechnique, 64(1) 28-39.

Navy, U.S., 1982. *Foundation and Earth Retaining Structures* 7.02, Naval Facilities Engineering Command, Washington D.C.

NESPAK, 2015. Geotechnical Investigation Report of Lahore Orange Line Electric Metro Train Project. NESPAK Geotechnical and Geoenvironmental Engineering Division, Lahore, Pakistan.

NESPAK and Berkeley Associates, 2015. Pile Load Tests Report of Lahore Orange Line Electric Metro Train Project. NESPAK Geotechnical and Geo-environmental Engineering Division and Berkeley Associates (EPC Contractor of NESPAK), Lahore, Pakistan.

Power Construction Corporation China, 2016. Geotechnical Investigation Report of Jhang RLNG Power Project. Power Construction Corporation China (EPC contractor of NESPAK), Lahore, Pakistan.

Power Construction Corporation China, 2016. Pile Load Tests Report of Jhang RLNG Power Project. Power Construction Corporation China (EPC contractor of NESPAK), Lahore, Pakistan.

Seavey, D.A. and Ashford, S.A., 2004. Effect of construction methods on axial capacity of drilled shafts. University of California, San Diego, Rep. SSRP-04/17.

STUDY ON THE BEARING CAPACITY OF BORED PILES WITH IMPROVEMENT TECHNIQUES

Ana B. A. N. Dias, Universidade de Brasília, Brasília, Brazil, anabeatriznobre@outlook.com
Leonardo B. D. Brandão, Universidade Federal de Alagoas, Maceió, Brazil, leodantasbrandao@gmail.com
Juliane A. F. Marques, Universidade Federal de Alagoas, Maceió, Brazil, julianemarques@hotmail.com

ABSTRACT

The upper part of the city of Maceió began to develop rapidly in recent years. Because of its characteristics, the use of bored piles became very popular in the area, demanding new techniques that could increase the load bearing capacity of the piles. To meet these demands, a local geotechnical company developed two solutions: the execution of rings along the shaft and the consolidation of the pile toe, being the combination of them the subject of this paper. To determine the contribution of the toe consolidation two semi-empirical methods were used: the Aoki-Velloso and the Décourt-Quaresma methods; and two methods based on the extrapolation of the curve "load vs. settlement": the Van der Veen and the Décourt methods. As a result, the Décourt-Quaresma method was the one that showed the most representative values of the contribution of the pile toe consolidation, when executed simultaneously with rings along the shaft.

Keywords: bored piles, toe consolidation, load bearing capacity.

INTRODUCTION

Das (2007) defines foundation as the inferior part of a structure, with the function of transfer loads to the soil in which it is being supported without overloading it. The type of foundation depends on several factors, such as, the structural material, the soil type, the surrounding buildings, the available foundation companies, among others. Foundations can be classified as shallow and deep. Deep foundations transfer load to the soil using its base, along its shaft or by a combination of both.

Dry bored piles are executed with a mechanical auger with or without stabilizing fluid. Some of the advantages of using this type of foundation are its high productivity (15 to 20 piles can be executed per day) and the use of less manpower. However its length is limited by the water level. Also, the capacity of this type of pile is lower than other pile types because in its drilling process there is an accumulation of loose soil in the base, caused not by any negligence in the execution process, but because it is inevitable that when the auger is removed from the hole, the slightest vibration presented by the machine, will drop the soil accumulated in the screw of the auger at the bottom of the hole. Because of that, designers do not consider toe resistance values in order to determine the load bearing capacity.

The execution of rings along the shaft and the toe consolidation are improvement techniques used in bored piles, but, since the techniques are relatively new, the contribution of them to the ultimate resistance is still being studied.

The execution process of piles with improvements is identical to the conventional bored piles until the project drilling depth is achieved. After that, a piece called "pointer" is coupled and it enlarges the shaft diameter in determined depths along the perforation.

© 2018 Deep Foundations Institute

After the drilling process, concrete is put in the end of the hole. Currently the volume of concrete varies accordingly to the pile diameter: for piles with diameters of 300 mm and 400 mm, it is added 50 liters (or 0,05 m^3); for larger diameters, the volume is doubled. To finalize the toe consolidation process, the auger mixes concrete with loose soil in the bottom of the drilling hole. The toe consolidation and the pile concreting should be done one after the other immediately to guarantee the quality of the pile and avoid changes in the hole geometry and the concrete characteristics. Figure 1 shows a representation of dry bored pile with rings and toe consolidation.

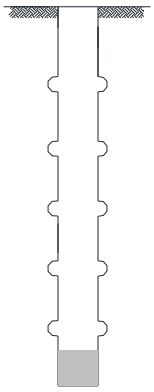


Fig. 1. Dry bored piles with rings and toe consolidation

To analyze the ultimate resistance, it is commonly used the extrapolation of the load vs settlement curve methods, obtained by loading tests, described in Brazil by the standard NBR 12131 (2006); theoretical methods and semi-empirical method.

The rings work by enlarging the diameter of the pile in some points along the shaft without the need of a larger auger or hole. Even though it is known that this alone does increase the lateral resistance of the pile (BRANDÃO, 2016), the focus of this paper is not to quantify how much each of the improved techniques contribute to the overall bearing capacity, but to take into account the increase caused by them working together.

The geomorphological region in which the piles were tested is one of the three main regions in the city of Maceió, capital of the state Alagoas in Brazil. This region has been the target of the construction sector in the last couple of years, increasing the interest in its natural geology. Two major information about this soil formation is that the water ground table is deep, usually below 30 meters; and the soil profile is composed of sandy and silty clay, and/or, silty and clayey sand, favoring the use of dry bored piles with rings along the shaft and the toe consolidation. This paper aims to determine the contribution of the toe consolidation when it is executed with the rings along the shaft. For that, two semi-empirical methods (the Aoki-Velloso and the Décourt-Quaresma methods) and two extrapolation methods (the Van der Veen and the Décourt methods) were chosen to be used in the analyses.

GENERAL INFORMATION

Sixteen piles with toe consolidation and rings along the shaft (E1 to E16) were selected to be analyzed in this paper. General characteristics, such as pile length, pile diameter, maximum settlement and maximum applied load in loading tests, for each of them are provided in Table 1.

ANALYSIS USING THE EXTRAPOLATION OF THE LOAD-MOVEMENT CURVE METHODS

To interpret the load-movement curves obtained by loading tests, it is necessary to use mathematic methods that determine the ultimate resistance of the piles. For this objective, two methods were chosen: the Van der Veen method (1953) and the Décourt method (1998).

The Van der Veen method (1953)

The Van der Veen method (1953) extrapolates the load-movement curve considering its resembles to an exponential curve, governed by the Equation:

$$\alpha^{VDV} * \rho + \ln\left(1 - \frac{P}{Q^{VDV}}\right) = 0 \quad [1]$$

In which P represents the load applied on the pile head, Q^{VDV} is the ultimate resistance, α^{VDV} is a coefficient of the curve and ρ is the settlement.

Table 1. Piles data given by the load test

Pile	Pile		Maximum load (kN)	Maximum settlement (mm)
	Diameter (mm)	Length (m)		
E1	600	8,50	2750	72,61
E2	600	8,50	2250	69,97
E3	700	6,50	3000	95,23
E4	600	7,50	2800	125,99
E5	600	7,00	2340	68,85
E6	500	7,00	2400	7,60
E7	600	8,00	2200	48,08
E8	600	7,00	2600	24,07
E9	600	10,00	2600	66,89
E10	600	11,30	2600	5,10
E11	600	11,30	2600	2,32
E12	600	11,30	2500	2,62
E13	900	7,20	3600	11,94
E14	800	7,20	3000	19,44
E15	500	9,30	3000	21,22
E16	500	9,30	3000	12,71

To find the best linear regression, with settlement and applied loads values measured, the values of the ultimate resistance are arbitrated (Cintra, 2013).

$$P = Q^{VDV} * \left(1 - e^{-\alpha^{VDV} * \rho}\right) \quad [2]$$

With the assistance of spreadsheets, which receives as input data the values obtained in the loading test of the pile, the ultimate resistances of all piles were determined. The adjustment generates a coefficient R^2 and a^{VDV}. A good fit is found, when its values are closer to 1 and 0, respectively.

The Décourt method (1998)

The Décourt method (1998) proposes an approximation of the curve to a hyperbole. Initially, it is necessary to determine the stiffness values and draw the stress-stiffness curve. Then, a linear regression of the points is made to obtain first iteration. The aim is to find the best line that adjusts these points and the linear Equation. The objective is obtained when R^2 values are as close to 1.00. If the goal is not reached in the first iteration, a second one must be executed, excluding the first point, and so on. The ultimate resistance is the load value for when the stiffness is zero.

ANALYSIS USING THE SEMI-EMPIRICAL METHODS

Among the several methods available in literature to calculate the load bearing capacity, two were chosen: the Aoki-Velloso method (1975) and the Décourt-Quaresma method (1978). These methods were chosen mainly for two reasons: (1) due to the fact that they allow the calculation of the shaft resistance and the toe resistance separately, allowing the analysis of the toe resistance; and (2) because they are the most used semi-empirical methods in Brazil. Although the formulation of these methods are based on SPT results, being more applicable to driven piles, factors of conversion were developed to adapt them to other types of piles, such as the bored piles.

The Aoki-Velloso method (1975)

The method uses the cone penetration test (CPT) results, resistance (q_c) and lateral friction in the glove (f_s), to determine the unit toe resistance (r_p) and the unit shaft resistance (r_L). Since, in Brazil, CPT is not as well used as the standard penetration test (SPT), its Equations were adapted, as shown in Equations 3 and 4.

$$r_p = \frac{K * N_p}{F_1} \quad [3]$$

$$r_L = \frac{\alpha * K * N_L}{F_2} \quad [4]$$

In which F_1 and F_2 are factors of conversion, K and α^{AV} are constants that depends on the soil type, N_p and N_L are, respectively, the SPT values at the toe and the mean of each layer with thickness ΔL along the shaft. The values for F_1, F_2, K e α^{AV} can be observed in Tables 2 and 3.

Table 2. Conversion factors F_1e F_2 for each type of pile

Type of Pile	F1	F2
Franki	2,50	2F1
Steel	1,75	2F1
Precast concrete	1+D/0,80	2F1
Bored	3,00	2F1
Root and Helical	2,00	2F1

Table 3. K e α^{AV} values for the Aoki-Velloso method

Soil	K (MPa)	α^{AV} (%)
Sand	1,00	1,4
Silty Sand	0,80	2,0
Silty Clayey Sand	0,70	2,4
Clayey Sand	0,60	3,0
Clayey Silty Sand	0,50	2,8
Silt	0,40	3,0
Sandy Silt	0,55	2,2
Sandy Clayey Silt	0,45	2,8
Clayey Silt	0,23	3,4
Clayey Sandy Silt	0,25	3,0
Clay	0,20	6,0
Sandy Clay	0,35	2,4
Sandy Silty Clay	0,30	2,8
Silty Clay	0,22	4,0
Silty Sandy Clay	0,33	3,0

The load bearing capacity (R) is obtained by adding the toe resistance to the shaft resistance to each layer of soil, as shown in Equation 5. In which A_p is the toe cross sectional area of the pile, and A_L is the lateral area of the pile, considering each layer of the soil.

$$R = r_p * A_p + r_L * A_L = \frac{K*N_p}{F_1} A_p + \sum \frac{\alpha^{AV}*K*N_L}{F_2} A_L \quad [5]$$

Two simulations were established for each of the piles in order to obtain more realistically values of the ultimate loads, they were: (I) all the piles without any improvements (rings or toe consolidation); and (II) with a 25% increase in capacity. The 25% value was found comparing previously the calculated load bearing capacity with no increase to the values of ultimate resistance found in the extrapolation methods.

The Décourt-Quaresma method (1978)

The Décourt-Quaresma method uses the values obtained by the SPT investigation to calculate the load bearing capacity, in which the shaft resistance (Equation 6) is associated to the mean of SPT values along the shaft (N_L), and the toe resistance (Equation 7) depends on a C coefficient that varies with the soil type (Table 2) and the mean of SPT values at the toe, the immediately preceding and the posterior one.

$$r_L = 10 * \left(\frac{N_L}{3} + 1\right) \quad [6]$$

$$r_p = C * N_p \quad [7]$$

Table 1 . C coeficiente values

Soil Type	C (kPa)
Clay	100
Clayey Silt	120
Sandy Silt	140
Sand	200

Equation 8 represents the load bearing capacity, in which α^{DQ} and β^{DQ} are coefficients empirically defined by Décourt (1998), that varies accordingly to the type of pile and soil, as shown in Table 4.

$$R = \alpha^{DQ} * C * N_p * A_p + \beta^{DQ} * 10 * \left(\frac{N_L}{3} + 1\right) * A_L \quad [8]$$

Table 4. α^{DQ} and β^{DQ} values.

Soil type	Bored pile α^{DQ}/β^{DQ}	Bored pile (bentonite) α^{DQ}/β^{DQ}	Helical pile α^{DQ}/β^{DQ}	Root pile α^{DQ}/β^{DQ}
Clay	0,85/0,80	0,85/0,90	0,30/1,00	0,85/1,50
Clay and sand	0,60/0,65	0,60/0,75	0,30/1,00	0,60/1,50
Sand	0,50/0,50	0,50/0,60	0,30/1,00	0,50/1,50

Simulations were made in order to find the most representative values for the Décourt-Quaresma methods: (I) all the piles without any improvements (rings or toe consolidation); (II) 50% increase (III) and 60% increase. Comparing the values of capacity for the piles without improvements with the ones found by extrapolation methods, is was observed that the average increase was between 50% and 60%.

RESULTS

Ultimate resistance obtained by the extrapolation of the load-movement curve methods

The Van der Veen method does not separate toe and shaft resistances, the only data given by the method is the ultimate resistance (Q^{VDV}). On the other hand, the Décourt method provides ultimate (Q^{VDV}), shaft (R_L^{RIG}) and toe (R_P^{RIG}) resistances. The values found for each of the piles are shown in Table 5.

Table 5. Ultimate bearing load for the extrapolation methods

		Décourt		Van der Veen
Pile	Q^{RIG} (kN)	R_L^{RIG} (kN)	R_P^{RIG} (kN)	Q^{VDV} (kN)
E1	3012	1750	1262	2835
E2	2888	1500	1388	2385
E3	3660	2100	1560	3070
E4	3628	1680	1948	2920
E5	2880	1560	1320	2444
E6	2153	960	1193	2430
E7	2248	1320	928	2240
E8	*	*	*	2610
E9	2747	1820	927	2620
E10	3569	1040	2529	2830
E11	*	*	*	3310
E12	*	*	*	3000
E13	*	*	*	3630
E14	3214	2100	1114	3030
E15	3337	1800	1537	3030
E16	*	*	*	3070

The asterisks indicate that the toe resistance was not solicited until the end of the pile loading test, which made impossible the application of the method.

Load bearing capacity obtained by the semi-empirical methods

The load bearing capacity obtained using the Aoki-Velloso method (Q^{AV}), considering the simulations mentioned before, are shown in Table 6, as well as the shaft ($R_L{}^{AV}$) and toe ($R_P{}^{AV}$) resistances. In Table 7, the values found using the Décourt-Quaresma method (Q^{DEC}, $R_L{}^{DEC}$ and $R_P{}^{DEC}$) are presented.

Table 6. Ultimate bearing load using Aoki-Velloso - Simulations (I) and (II)

Pile	No increase			25% increase		
	Q^{AV} (kN)	$R_L{}^{AV}$ (kN)	$R_P{}^{AV}$ (kN)	Q^{AV} (kN)	$R_L{}^{AV}$ (kN)	$R_P{}^{AV}$ (kN)
E1	3757,1	560,2	3196,9	4696,4	700,3	3996,1
E2	1753,8	478,6	1275,2	2192,3	598,3	1594,0
E3	2996,8	751,9	2244,9	3746,0	939,9	2806,1
E4	1352,7	317,0	1035,7	1690,9	396,3	1294,6
E5	766,9	207,1	559,8	958,6	258,9	699,8
E6	1093,5	614,0	479,5	1366,9	767,5	599,4
E7	1595,2	558,5	1036,7	1994,0	698,1	1295,9
E8	657,2	263,2	394,0	821,5	329,0	492,5
E9	1404,3	305,8	1098,5	1755,4	382,3	1373,1
E10	3238,5	658,9	2579,6	4048,1	823,6	3224,5
E11	1680,1	560,4	1119,7	2100,1	700,5	1399,6
E12	1979,5	763,4	1216,1	2474,4	954,3	1520,1
E13	2719,0	806,2	1912,8	3398,8	1007,8	2391,0
E14	2639,3	796,2	1843,1	3299,1	995,3	2303,9
E15	2289,3	497,9	1791,4	2861,6	622,4	2239,3
E16	2665,3	603,6	2061,7	3331,6	754,5	2577,1

It is possible to observe that the values of load bearing capacity found for piles E4, E5 and E8, for both semi-empirical methods, are dispersed comparing to the ones found in the extrapolation of the load-movement curve. This is probably caused by a mistake made in determining the SPT values. To avoid misinterpretations, it was chosen not to use them in the following analyses. It is worth to highlight that as shown before in Table 5, it was impossible to determine the load bearing capacity of E8, E11, E12, E13 and E16 with the Décourt method, so they will also not be evaluated.

Comparison involving the semi-empirical and the extrapolation of the load-movement curve methods

Based on the simulations results presented before, Table 8 shows the percentages between the semi-empirical and the extrapolation methods.

The Brazilian Standard NBR 6122/2010 specifies a factor of safety of 25% in the ratio involving the values of capacity estimated by semi-empirical methods and by extrapolation methods. Then, it is reasonable to consider, as the safety limit, load bearing capacity values (from semi-empirical methods) up until 25% higher than the ones found ultimate resistance (from extrapolation methods).

It is also reasonable to establish an inferior limit, since oversizing the pile length and diameter is not economical. Local foundation designers consider that values down until 60% of the load bearing capacity would be practical. Table 9 shows the percentage of piles attending these two limits, in other words, the percentage of piles which have load bearing capacity values between 40% and 125% of the ultimate resistance determined by the extrapolation methods.

Table 7. Ultimate bearing load using Décourt-Quaresma method - Simulations (I), (II) e (III)

	No increase			50% increase			60% increase		
Pile	Q^{DEC} (kN)	$R_L{}^{DEC}$ (kN)	$R_P{}^{DEC}$ (kN)	Q^{DEC} (kN)	$R_L{}^{DEC}$ (kN)	$R_P{}^{DEC}$ (kN)	Q^{DEC} (kN)	$R_L{}^{DEC}$ (kN)	$R_P{}^{DEC}$ (kN)
E1	1892,7	582,0	1310,7	2839,1	873,0	1966,1	3028,3	931,2	2097,1
E2	1202,7	551,3	651,4	1804,1	827,0	977,1	1924,3	882,1	1042,2
E3	2220,3	1065,8	1154,5	3330,5	1598,7	1731,8	3552,5	1705,3	1847,2
E4	976,4	433,5	542,9	1464,6	650,3	814,4	1562,2	693,6	868,6
E5	723,4	265,4	458,0	1085,1	398,1	687,0	1157,4	424,6	732,8
E6	1090,9	632,6	458,3	1636,4	948,9	687,5	1745,4	1012,2	733,3
E7	1510,0	763,6	746,4	2265,0	1145,4	1119,6	2416,0	1221,8	1194,2
E8	779,7	457,4	322,3	1169,6	686,1	483,5	1247,5	731,8	515,7
E9	988,8	420,5	568,3	1483,2	630,8	852,5	1582,1	672,8	909,3
E10	1414,6	753,0	661,6	2121,9	1129,5	992,4	2263,4	1204,8	1058,6
E11	1359,4	765,6	593,8	2039,1	1148,4	890,7	2175,0	1225,0	950,1
E12	1733,3	1041,1	692,2	2600,0	1561,7	1038,3	2773,3	1665,8	1107,5
E13	2586,3	1101,5	1484,8	3879,5	1652,3	2227,2	4138,1	1762,4	2375,7
E14	2943,0	1012,8	1930,2	4414,5	1519,2	2895,3	4708,8	1620,5	3088,3
E15	1485,1	603,9	881,2	2227,7	905,9	1321,8	2376,2	966,2	1409,9
E16	1873,9	695,8	1178,1	2810,9	1043,7	1767,2	2998,2	1113,3	1885,0

Table 8. Comparison involving the semi-empirical and the extrapolation of the load-movement curve methods.

	Semi-empirical / Décourt			Semi-empirical / Van der Veen		
Pile	Q^{AV} (II)/Q^{RIG}	Q^{DQ} (II)/Q^{RIG}	Q^{DQ} (III)/Q^{RIG}	Q^{AV} (II)/Q^{VDV}	Q^{DQ} (II)/Q^{VDV}	Q^{DQ} (III)/Q^{VDV}
E1	156%	94%	101%	166%	100%	107%
E2	76%	62%	67%	92%	76%	81%
E3	102%	91%	97%	122%	108%	116%
E6	63%	76%	81%	56%	67%	72%
E7	89%	101%	107%	89%	101%	108%
E9	64%	54%	58%	67%	57%	60%
E10	113%	59%	63%	143%	75%	80%
E14	103%	137%	147%	109%	146%	155%
E15	86%	67%	71%	94%	74%	78%

Table 9. Percentages of piles with load bearing capacity values obtained by semi-empirical methods between 40% and 125% of the ultimate resistance methods values.

	Aoki-Velloso (II)	Décourt-Quaresma (II)	Décourt-Quaresma (III)
Van der Veen	77%	85%	92%
Décourt	89%	67%	78%

CONCLUSIONS

From the comparison between the two extrapolations of the load-movement curve methods, it was noticed that the Décourt's Stiffness method presented less conservative results, in most cases, with values higher than those from Van der Veen method. As for the consideration of the base resistance itself, with the same method, the values did not point to a tendency line or behavior, which made it hard to apply the method. Despite the differences among the results, in terms of contribution from the base and the shaft to the ultimate bearing capacity of the piles, one can verify that piles with rings along the shaft and toe consolidation presented both the shaft and the base working under similar load levels.

To draw a comparison between the predicted values of loads and those obtained from the extrapolation of the curve, more attention was given to the Van der Veen method. This fact is justified by the number of piles considered. Assuming the load bearing capacities given by semi empirical methods could reach values 25% higher and even 40% lower than the ultimate bearing capacity, the Décourt-Quaresma method for simulation III presented the best results with 92% of the piles in compliance with the assumption adopted. By that, such method can be considered the most representative for the execution of piles with rings along the shaft and toe consolidation.

Thus, the research showed that the contribution obtained from the use of toe consolidation in bored piles with rings along the shaft can be better calculated by the Décourt-Quaresma method, presenting a growth of 60% in the value of the bearing capacity. This percentage is higher than the one currently used by designers (between 30% and 40%), being in favor of the structural safety. By using this increase, the load bearing capacity must be calculated simply dividing it for the factor of safety of 2, not being necessary to adopt a higher coefficient for the contribution of base.

As for the continuation of studies, the authors suggest: the use of a larger sample and an analysis of the soil/concrete relation for the execution of the toe consolidation; analysis of piles executed with only the toe consolidation; the instrumentations of piles; the execution of more pile load tests and application of new methods, especially the extrapolation of the load-movement curve methods that take into account the contribution of both the shaft and base resistance.

REFERENCES

Associação Brasileira de Normas Técnicas - ABNT. Estacas. Prova de Carga Estática: NBR 12131/06. Rio de Janeiro, 2006.

Brandão, L. B. D. Estudo da Capacidade de Carga de Estacas Escavadas a Seco com Anéis. Senior Thesis (Bachelor's degree in Civil Engineering) – Universidade Federal de Alagoas, Maceió, 2016.

Das, B. M.. Fundamentos de Engenharia Geotécnica. 6 ed. São Paulo: Thomson Learning. 488 p. 2007.

Décourt, L.; Albiero, J. H.; Cintra, J. C. A. Análise e projeto de fundações profundas: Estacas. In: Hachich, W.; Falconi, F. F.; Saes, J. L.; Frota, R. G. Q.; Carvalho, C.S.; Niyama, S. (Org.). Fundações: teoria e prática. 2. ed. São Paulo: Pini. p. 265-301. 1998.

Décourt, L. & Quaresma, A R. (1978). Capacidade de Carga em Estacas a Partir de Valores de SPT. In: VI COBRAMSEF. vol. 1. p.45-53.

Lessa, V. A. Análise da capacidade de carga de estacas escavadas a seco com anéis e consolidação da ponta. Trabalho de Conclusão de Curso (Graduação – Bacharelado em Engenharia Civil) – Universidade Federal de Alagoas, Maceió, 2014.

Marques, J. A. F.; Marques, R.F.; Marques, A.G.. Estacas Escavadas com Trado Mecanizado, com Anéis ao Longo do Fuste. In: XVI Congresso Brasileiro de Mecânica dos Solos e Engenharia Geotécnica - COBRAMSEG, 2012, Porto de Galinhas - PE. COBRAMSEG 2012, 2012.

Van der Veen. The Bearing Capacity of a Pile. In: 3 rd ICSMFE. vol. 2. p.84-90. 1953.

Velloso, D.A., Aoki, N., Lopes, F.R., Salomon, J.A. Instrumentação Simples para Provas de Carga em Tubulões e Estacas Escavadas. In: Simpósio sobre Instrumentação de Campo em Engenharia de Solos e Fundações. Rio de Janeiro/RJ. Anais... Rio de Janeiro: COOPE-UFRJ, vol.1. 1975.

STUDY ON THE RESISTANCE OF BORED PILES WITH RINGS

Leonardo B. D. Brandão, Universidade Federal de Alagoas, Maceió, Brasil, +5582993258080, leodantasbrandao@gmail.com
Ana B. A. N. Dias, Universidade de Brasília, Brasília, Brasil, anabeatriznobre@outlook.com
Juliane A. F. Marques, Universidade Federal de Alagoas, Maceió, Brasil, julianemarques@hotmail.com

ABSTRACT

Dry bored piles with rings were developed to increase the capacity of regular dry bored piles, reduce settlements and generate savings. The objective of this paper is to study the load-bearing capacity of this type of foundation by comparing the results of semi-empirical methods to stress-settlement methods applied to field, loading test results. The capacity values presented in this paper were obtained from the semi-empirical methods of Aoki-Velloso (1975) and Décourt-Quaresma (1978). The method of Van der Veen (1953) and Décourt (1996) were the methods based on the extrapolation of the "load-movement" curve used in the analysis. The comparisons indicate that bored piles with rings provide a viable, economically-attractive, deep-foundation alternative for use in the Maceio-AL region of Brazil.

Keywords: bored piles, rings, semi-empirical, extrapolation, capacity.

INTRODUCTION

The demand of large buildings in the uptown area of Maceió-AL, in Brazil, made necessary the development of new techniques to execute deep foundations in its particular type of soil, composed of sediments from Formação Barreiras. Dry bored piles, commonly used in other regions of Brazil, such as the southeast and midwest, have high productivity (about 15 to 20 piles can be executed per day), its execution uses less manpower and the equipment have high mobility. However, there are negative characteristics, which deserve attention, such as low load bearing capacity, because generally foundation designers do not consider the toe resistance in its determination, and the impossibility of execution when water is present.

To increase the load bearing capacity of this type of foundation, in addition to reducing settlements and providing greater savings, the bored pile with rings (Figure 1) was developed. The rings are executed with a part called "pointer" coupled to the auger. The "pointer" enlarges the shaft diameter along the perforation in determined depths, aiming to increase the resistance of the pile (MARQUES, 2012).



Fig. 1. Bored piles with rings.

© 2018 Deep Foundations Institute

The load bearing capacity prediction methods commonly used in projects are semi-empirical and it is necessary to validate the predictions with loading tests on piles. The result of this test is the construction of a load-movement curve, in which the values for the applied loads are represented on the abscissa axis and settlements are arranged on the vertical axis, facing down (CINTRA, 2013).

The load bearing capacity of a pile can be estimated by theoretical methods, according to Velloso &Lopes (2002). Cintra & Aoki (2010) mention the existence of several methods in the literature, mainly due to the difficulty in determining an ideal model for the rupture. The authors also emphasize that most of them are ineffective.

The objective of this paper is to study the load bearing capacity of bored piles with rings. The methods used was the Van der Veen Method (1953), the Décourt Method (1996), the Aoki-Velloso Method (1975) and the Décourt-Quaresma Method (1978).

GENERAL INFORMATION ABOUT THE PILES

The preliminary stage of the study was characterized by sorting the data referring to the bored piles with rings executed in the city of Maceió/AL, as shown in Table 1 below. It is also necessary to know the maximum load resistance obtained by loading test for each pile and their respective settlement (Table 2).

Table 1 – General characteristics of the piles.

Pile ref.	Shaft		Rings			
	Diameter (mm)	Length (m)	Quantity	Diameter (mm)	Distance between rings (m)	Height (m)
E1	400	13,00	7	640	1,50	0,10
E2	500	10,80	6	740	1,50	0,10
E3	500	10,50	6	740	1,50	0,10
E4	400	7,60	4	640	1,50	0,10
E5	600	7,60	4	840	1,50	0,10
E6	600	9,10	5	840	1,50	0,10
E7	600	9,10	5	840	1,50	0,10
E8	600	8,00	4	840	1,50	0,10
E9	600	8,00	4	840	1,50	0,10
E10	600	11,50	6	840	1,50	0,10

Table 2 – Maximum load bearing capacity and settlement values.

Pile ref.	Maximum Load (kN)	Maximum Settlement (mm)
E1	1200,00	3,84
E2	1750,00	36,07
E3	1800,00	6,55
E4	1500,00	29,73
E5	2200,00	51,85
E6	2200,00	3,99
E7	2200,00	3,39
E8	1960,00	39,22
E9	2200,00	67,94
E10	2340,00	74,18

ANALYSIS USING THE SEMI-EMPIRICAL METHODS

The Décourt-Quaresma Method (1978)

The Décourt-Quaresma method uses values obtained by the standard penetration test (SPT) to obtain the load bearing capacity (Q). It associates the total shaft resistance with a mean of the SPT values along the pile shaft and the toe resistance to a C coefficient, which depends on the type of soil, whose values are presented in Table 3, and a mean of the SPT values at the toe, the immediately preceding and the posterior. To determine the lateral area (Al), the pile length (L) and the pile diameter (∅) are required. Equation 1 shows the calculation of this area. The toe cross sectional area calculation uses Equation 2. The general formula to determine the load bearing capacity of the pile is shown in the Equation 3.

$$A_l = \pi * \emptyset * (L - 1) \quad [1]$$

$$A_p = \frac{\pi * \emptyset^2}{4} \quad [2]$$

Table 1 – coefficient C values.

Type of soil	C (kPa)
Clay	100
Clayey silt	120
Sandy silt	140
Sand	200

$$Q = \alpha^{DQ} * C * N_p * A_p + \beta^{DQ} * 10 * \left(\frac{N_L}{3} + 1\right) * A_l \quad [3]$$

α^{DQ} and β^{DQ} are coefficients related to the type of soil and the type of pile, their values are in Table 4.

Table 4 – α^{DQ} and β^{DQ} values.

	Bored pile α^{DQ}/ β^{DQ}	Bored pile (Betonite) α^{DQ}/ β^{DQ}	Helical pile α^{DQ}/ β^{DQ}	Root pile α^{DQ}/ β^{DQ}
Clay	0,85/0,80	0,85/0,90	0,30/1,00	0,85/1,50
Clay and sand	0,60/0,65	0,60/0,75	0,30/1,00	0,60/1,50
Sand	0,50/0,50	0,50/0,60	0,30/1,00	0,50/1,50

In order to obtain load bearing capacity values by the Décourt-Quaresma method, five simulations were performed for the ten bored piles with rings, in order to find the most representative values by this method. We considered the following simulations: (I) All the piles without the rings; (II) 50% increase in the total shaft resistance; (III) 60% increase in the total shaft resistance; (IV) The rings working together, as a cylinder; (V) The rings working separately, as "multiple bases".

In the first simulation, the influences of the rings were ignored, adopting the piles as regular bored piles, as shown in Figure 2 a. In the second case, the total shaft resistance was increased by 50%, as this is the practical consideration usually made by the designers to determine the load bearing capacity. The third case, in which there was a 60% increase in the total shaft resistance, was performed in order to verify the possibility of increasing the work load of this type of pile.

In the fourth simulation, it was imposed that the rings worked together, forming a cylinder in the shaft with a diameter 24 cm larger than the nominal one (Figure 2 b). Finally, the last simulation analyzed the rings working separately, each acting as a sort of "intermediate base", as shown in Figure 2 c.

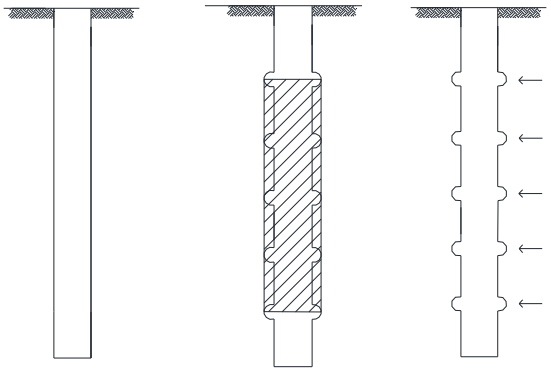


Fig. 2. a) Pile without rings; b) Pile with a "cylinder" in the shaft; c) Pile with isolated bases.

The Aoki-Velloso Method (1975)

The Aoki-Velloso method uses the following Equation to determine the load bearing capacity. The same five simulations, using in the Décourt-Quaresma method, were performed in the Aoki-Velloso method.

$$Q = \frac{K \cdot N_p}{F_1} A_p + \sum \frac{\alpha^{AV} \cdot K \cdot N_L}{F_2} A_l \quad [4]$$

In which K and α^{AV} are soil coefficients. Np and NL are respectively the SPT values at the toe and the mean of each layer (ΔL) of soil. Tables 5 and 6 show the values for the coefficients F1, F2, α^{AV} and K. Ap is the toe cross sectional area and Al is the lateral area of the shaft in each layer (Equation 5).

$$A_l = \pi * \emptyset * \Delta L \quad [5]$$

Table 5 – *K* and α^{AV} values.

Type of soil	K (MPa)	α^{AV} (%)
Sand	1,00	1,40
Silty sand	0,80	2,00
Silty clayey sand	0,70	2,40
Clayey sand	0,60	3,00
Clayey silty sand	0,50	2,80
Silt	0,40	3,00
Sandy silt	0,55	2,20
Sandy clayey silt	0,45	2,80
Clayey silt	0,23	3,40
Clayey sandy silt	0,25	3,00
Clay	0,20	6,00
Sandy clay	0,35	2,40
Sandy silty clay	0,30	2,80
Silty clay	0,22	4,00
Silty sandy clay	0,33	3,00

Table 6 – F_1 and F_2 values.

Type of pile	F1	F2
Franki	2,5	2 F1
Steel	1,75	2 F1
Precast concrete	1+D/0,80	2 F1
Bored	3	2 F1
Root and Helical	2	2 F1

ANALYSIS USING THE EXTRAPOLATION OF THE LOAD-MOVEMENT CURVE METHODS

The Van der Veen Method (1953)

The Van der Veen method estimates the load bearing capacity from the extrapolation of the load-movement curve. The method predicts when the curve becomes asymptotic. This load value represents the ultimate resistance.

A spreadsheet was created in *Microsoft Excel software* to determine the values with the stress and settlements values obtained by the loading test. With these data, the spreadsheet performs the necessary adjustment and returns the load bearing capacity values, the coefficient of determination (R^2) values and the parameters of the representative Equation of the method ($R = Q^{VDV} * \left(1 - e^{-a^{VDV} * \rho}\right)$).

The Décourt Method (1996)

The Décourt method determines the ultimate resistance of the pile from the extrapolation of the curve. First, it is necessary to determine the stiffness values and plot the stress x stiffness curve. The next step is to do a linear regression of the points to obtain first iteration. The objective here is to find the Equation of the line that best adjusts these points. This happens when R^2 values are as close as possible to 1.00. If the value is not reached in the first iteration, a second one must be performed, excluding the first point, and so on. The value of the ultimate resistance is the value of the load for when the rigidity is zero.

RESULTS

Load bearing capacity obtained by the Semi-empirical methods

The values obtained for the load bearing capacity by the Décourt-Quaresma (method for all the simulations are shown in Table 7. The values for Aoki-Velloso are shown in Table 8.

Table 7 – Results of the Décourt-Quaresma Method (in kN).

Pile ref.	(I) Without rings	(II) 50% of increase	(III) 60% of increase	(IV) "Cylinder"	(V) "Multiple Bases"
E1	845,5	1008,8	1041,5	992,5	1695,6
E2	909,2	1109,3	1149,3	1056,2	2894,3
E3	1274,2	1549,0	1604,0	1482,5	3212,6
E4	739,8	892,5	923,1	864,8	1741,0
E5	1582,4	1852,0	1905,9	1729,4	3409,6
E6	1267,3	1565,0	1624,5	1443,7	2849,3
E7	1801,6	2066,3	2119,2	1958,5	3164,7
E8	1035,7	1278,7	1327,3	1160,6	2234,2
E9	1755,8	2241,8	2339,0	2005,7	4491,6
E10	1796,3	2246,5	2336,6	2053,6	3985,8

Table 8 – Results of the Aoki-Velloso Method (in kN).

Pile ref.	(I) Without rings	(II) 50% of increase	(III) 60% of increase	(IV) "Cylinder"	(V) "Multiple Bases"
E1	1216,3	1328,9	1354,7	1288,3	1782,1
E2	1273,4	1575,3	1635,7	1477,3	2705,3
E3	1486,0	1818,6	1885,1	1724,6	3407,6
E4	672,8	801,9	827,7	770,5	1204,8
E5	1686,5	1886,4	1926,4	1793,1	2903,4
E6	1498,9	1735,1	1782,4	1627,0	2659,9
E7	2086,7	2305,4	2349,2	2186,8	3062,6
E8	1270,0	1469,6	1509,5	1354,2	2086,4
E9	1642,0	2037,9	2117,1	1846,1	3500,8
E10	1891,8	2231,2	2299,1	2046,8	3331,4

The values from the Aoki-Velloso method were higher than the Décourt-Quaresma values for almost all the piles in the first four simulations. The last one showed very divergent results. The most interesting data for further analysis were provide by the 50% and 60% increase simulations because they have less dispersed results.

Ultimate resistance obtained by the extrapolation of the load-movement curve methods

The ultimate resistance values for each pile were obtained by the Van der Veen and Décourt methods. These values are represented in the Table 9, including the coefficients of determinations (R^2) and maximum load values.

Table 9 – Results of the Van der Veen and the Décourt Methods.

Pile ref.	Maximum Load Applied (kN)	The Van der Veen Method		The Décourt Method	
		Q^{VDV} (kN)	R^2	Q^{RIG} (kN)	R^2
E1	1200,00	1400,0	0,99835	1874,0	0,9902
E2	1750,00	1755,0	0,96616	1779,2	0,9631
E3	1800,00	1860,0	0,99299	2264,8	0,9981
E4	1500,00	1530,0	0,98468	1793,3	0,9968
E5	2200,00	2250,0	0,96231	2444,0	0,9332
E6	2200,00	2290,0	0,99682	2764,6	0,9963
E7	2200,00	2330,0	0,99746	2941,8	0,9977
E8	1960,00	1966,0	0,98033	2065,5	0,9944
E9	2200,00	2230,0	0,95206	2391,7	0,9092
E10	2340,00	2364,0	0,96445	2504,7	0,9000

The values found by the Décourt method were superior to those found using the Van der Veen method, in all the piles. The most discrepant values were found on piles E1, E3, E6 and E7. The small settlements observed, less than 10% of the pile diameter, might have interfered in the prediction of the ultimate resistance of these piles. Load values at E2 pile are practically the same.

Analysis of the semi-empirical methods vs the extrapolation methods

We selected the values obtained by simulations (II) and (III), for both Aoki-Velloso and Décourt-Quaresma methods, to do a comparison between the semi-empirical and each of the extrapolation methods (Tables 11 and 12). Table 10 shows all values needed for the analysis.

Table 10 – Décourt-Quaresma, Aoki-Velloso, Van der Veen and Décourt values (in kN).

Pile ref.	Décourt-Quaresma (II)	Décourt-Quaresma (III)	Aoki-Velloso (II)	Aoki-Velloso (III)	Van der Veen	Décourt
E1	1008,8	1041,5	1328,9	1354,7	1400,0	1874,40
E2	1109,3	1149,3	1575,3	1635,7	1755,0	1779,92
E3	1549,0	1604,0	1818,6	1885,1	1860,0	2264,8
E4	892,5	923,1	801,9	827,7	1530,0	1793,3
E5	1852,0	1905,9	1886,4	1926,4	2250,0	2444,0
E6	1565,0	1624,5	1735,1	1782,4	2290,0	2764,6
E7	2066,3	2119,2	2305,4	2349,2	2330,0	2941,8
E8	1278,7	1327,3	1469,6	1509,5	1966,0	2065,5
E9	2241,8	2339,0	2037,9	2117,1	2230,0	2391,7
E10	2246,5	2336,6	2231,2	2299,1	2364,0	2504,7

Table 11 – Percentage comparison between the Semi-empirical methods and the Van der Veen method values.

Pile ref.	Décourt-Quaresma (II) / Van der Veen	Décourt-Quaresma (III) / Van der Veen	Aoki-Velloso (II) / Van der Veen	Aoki-Velloso (III) / Van der Veen
E1	72%	74%	95%	97%
E2	63%	65%	90%	93%
E3	83%	86%	98%	101%
E4	58%	60%	52%	54%
E5	82%	85%	84%	86%
E6	68%	71%	76%	78%
E7	89%	91%	99%	101%
E8	65%	68%	75%	77%
E9	101%	105%	91%	95%
E10	95%	99%	94%	97%

Table 12 – Percentage comparison between the Semi-empirical methods values and the Décourt values.

Pile ref.	Décourt-Quaresma (II) / Décourt	Décourt-Quaresma (III) / Décourt	Aoki-Velloso (II) / Décourt	Aoki-Velloso (III) / Décourt
E1	54%	56%	71%	72%
E2	62%	65%	89%	92%
E3	68%	71%	80%	83%
E4	50%	51%	45%	46%
E5	76%	78%	77%	79%
E6	57%	59%	63%	64%
E7	70%	72%	78%	80%
E8	62%	64%	71%	73%
E9	94%	98%	85%	89%
E10	90%	93%	89%	92%

Based on the results shown in Tables 11 and 12, we can conclude that the Aoki-Velloso values, in both simulations, presented better values, since these are closer to the load bearing capacity values obtained by extrapolations, especially the Van der Veen ones. Also, the 60% increase in the total shaft resistance was quite satisfactory when it was compared to the 50%, which is currently used to determine the word load of this type of pile.

The E4 pile showed very low values for the load bearing capacity, resulting in a large discrepancy with the other piles and the extrapolation methods values. A possible explanation for these incompatible values may be a misunderstanding in the classification of the soil where the pile was executed. For the posterior calculation and analysis, this pile was excluded.

It is known from the designers' experiences that values lower than 0,25 in the coefficient of variation are considered good. Table 13 shows the values for the mean, the standard deviation and the coefficient of variation for the set of piles analyzed, with the exclusion of the E4 pile.

Table 13 – Mean, standard deviation and coefficient of variation values.

	Décourt-Quaresma (II)	Décourt-Quaresma (III)	Aoki-Velloso (II)	Aoki-Velloso (III)
Mean (kN)	1657,5	1716,4	1820,9	1873,2
Standard Deviation (kN)	444,5	461,9	314,1	322,5
Coefficient of Variation	0,27	0,27	0,17	0,17

As observed in Table 13, for both situations (50% and 60% increases), the Aoki-Velloso method presented a value of 0,17 for the coefficient of variation. This is another useful information in ratifying the method as the best one for this type of pile.

Schulze (2013) states that for a satisfactory comparative analysis between a semi-empirical method and an extrapolation method, the uncertainty should be at most 20%. Table 14 shows the percentages between the means of the bearing capacity values of the semi-empirical methods and the means of the extrapolation methods.

Table 14 – Percentage between means.

Décourt-Quaresma		Aoki-Velloso	
50% / VDV	**60% / VDV**	**50% / VDV**	**60% / VDV**
81%	84%	89%	91%
50% / RIG	**60% / RIG**	**50% / RIG**	**60% / RIG**
71%	73%	78%	80%

Based on the values presented in Table 14, we can conclude that both the Décourt-Quaresma (50% and 60% increases) and the Aoki-Velloso simulations presented results within the limit of 20% when they were compared to the Van der Veen means. The Aoki-Velloso second simulation (60% of increase) was the only one within this range when compared to the Décourt (or RIG) method, and it presented the highest percentage values in comparisons with Van der Veen (91%) and Décourt (80%).

CONCLUSIONS

In this paper, ten bored piles with rings were analyzed. The semi-empirical methods of Décourt-Quaresma and Aoki-Velloso were used to predict the load bearing capacity of the piles. To obtain the ultimate resistance, from the extrapolation of the load-movement curve, the Van der Veen Method (1953) and the Décourt Method (1996) were used.

To find the best capacity values by the semi-empirical methods, five simulations were performed due to the non-specificity of these methods for this particular type of pile. The simulations were: (I) All the piles without the rings; (II) 50% increase in the total shaft resistance; (III) 60% increase in the total shaft resistance; (IV) The rings working together, as a cylinder; (V) The rings working separately, as "multiple bases".

It was possible to conclude that the Aoki-Velloso method presented load bearing capacity values higher than those provided by the Décourt-Quaresma method for almost all the piles. In addition, we could notice that the less dispersed results were those referring to simulations that considered increases of 50% and 60% in the total shaft resistance. When the methods of extrapolation of the curve were compared, we could observe that the values found by the Décourt method were higher than those of Van der Veen in all the piles.

We could observe that the Aoki-Velloso (with 50% and 60% increase in the total shaft resistance) method presented values closer to the values found by the extrapolation methods, especially the Van der Veen ones. The 60% increase in the total shaft resistance was also the most satisfactory. In general, we could affirm that the Aoki-Velloso method proved to be the most satisfactory in the load bearing capacity predictions for bored piles with rings.

REFERENCES

ASSOCIAÇÃO BRASILEIRA DE NORMAS TÉCNICAS - ABNT (2010). Projeto e Execução de Fundações: NBR 6122/10. Rio de Janeiro.

CINTRA, J. C. A.; AOKI, N.; TSUHA, C. H. C.; GIACHETI, H. L. (2013). Fundações: ensaios estáticos e dinâmicos. 1 ed. São Paulo: Oficina de Textos. 144 p.

CINTRA, J. C. A.; AOKI, N. (2010). Fundações por estacas: projeto geotécnico. 1 ed. São Paulo: Oficina de Textos. 96 p.

DAS, B. M. (2007). Fundamentos de Engenharia Geotécnica. 6 ed. São Paulo: Thomson Learning. 561 p.

DÉCOURT, L. (1996) Análise e Projeto de Fundações Profundas. Estacas. In: HACHICH W.,FALCONI, F.F., SAES, J.L., FROTA, R.G.Q., CARVALHO, C.S., NIYAAMA, S. Fundações Teoria e Prática. 1. ed. São Paulo: Editora Pini.

MARQUES, J.A.F.. MARQUES, A.G.; MARQUES, R.F. (2012). Estacas Escavadas com Trado Mecanizado, com Anéis ao Longo do Fuste. In: XVI Congresso Brasileiro de Mecânica dos Solos e Engenharia Geotécnica (XVI COBRAMSEG), Porto de Galinhas/PE.

SCHULZE, T. (2013) Análise da capacidade de carga de estaca escavada instrumentada de pequeno diâmetro por meio de métodos semi-empíricos. Dissertação (Mestrado). Curso de Engenharia Civil. Faculdade de Engenharia Civil, Arquitetura e Urbanismo. Universidade Estadual de Campinas. Campinas.

VAN DER VEEN (1953). The Bearing Capacity of a Pile. In: 3 rd ICSMFE. vol. 2. p.84-90.

VELLOSO, D.A., AOKI, N., LOPES, F.R., SALOMON, J.A. (1975). Instrumentação Simples para Provas de Carga em Tubulões e Estacas Escavadas. In: Simpósio sobre Instrumentação de Campo em Engenharia de Solos e Fundações. Rio de Janeiro/RJ. Anais... Rio de Janeiro: COOPE-UFRJ, vol.1, p.269-280.

VELLOSO, D. A.; LOPES, F. R. (2002). Fundações Profundas. Rio de Janeiro: COPPE/UFRJ, Vol. 2, 472 p.

THE APPLICATION OF FIBRE OPTIC SENSOR TECHNOLOGY IN THE INTEGRITY TESTING OF DEEP FOUNDATIONS

Anthony N. Fisher, Testing and Instrumentation Manager, Cementation Skanska, UK. +44 (0) 3301 050168, anthony.fisher@skanska.co.uk
Andrew G. Bell, Chief Engineer, Cementation Skanska, UK. +44 (0) 3301 050142, andrew.bell@skanska.co.uk

ABSTRACT

Thermal integrity profiling is a recognised technique for assessing the integrity of concrete foundation structures. This paper describes CemOptics, a new method for obtaining the temperature measurements required for this technique which makes use of distributed fibre optic sensing to collect temperature data. CemOptics has been used on a variety of foundation projects in the UK including the construction of Battersea Junction Station, part of the Northern Line extension project. As well as providing the details of this project, this paper also presents data on the measured temperature changes following completion of concreting operations. Known defects are evaluated to establish the optimal monitoring periods for identifying significant anomalies. Finally, temperature measurements taken during the construction process are presented which provide an insight into the flow pattern of tremied concrete within a diaphragm wall panel.

Keywords: distributed fibre optic sensing, thermal integrity profiling, concrete

INTRODUCTION

Deep foundations are a vital part of the built environment in which we live, however, unlike the above ground structures which they support, they remain hidden from view. Furthermore, the varied and complex nature of the ground into which deep foundations are placed and the methods used in their construction give rise to a number of hazards which, if not managed properly, can cause defects which will degrade their performance and durability. It is essential, therefore, that methods are employed to ensure that the quality of these foundations is of the required standard and that they will perform acceptably for the life of the structure.

The primary focus of these methods must be preventing the formation of defects rather than purely on identifying their presence. The role of testing is, therefore, not solely to identify the presence of potential defects but also to provide as much information as possible about why they have formed and so aid in preventing their formation in the future.

Thermal Integrity Profiling (TIP) is one technique for investigating the integrity of cast in place concrete foundations. Although it can no longer be regarded as new, having been in commercial use since 2007 (Mullins and Piscsalko, 2012), it is still a relatively recent development and is gaining acceptance as more case studies and data are being documented. Most recently in the UK, TIP has been proposed by the Institution of Civil Engineers (2017) in their Specification for Piling and Embedded Retaining Walls (SPREW) as one of the techniques best suited to the assessment of foundation integrity. This document is a model project specification to which many UK construction projects adhere.

To date, published example of the use of TIP such as Piscsalko et al (2014) have almost exclusively been based on the use of either thermal probes lowered into cast in reservation tubes or Thermal Wire, manufactured by Pile Dynamics Inc. The latter of these is currently the most common approach in the UK and it consists of a string of sacrificial temperature sensors, embedded within the concrete.

© 2018 Deep Foundations Institute

Each system for measuring the temperature of buried concrete has its own strengths and weaknesses, however, in the last few years a new system, CemOptics, has been developed by Cementation Skanska Ltd, working closely with the University of Cambridge and ARUP. This system is well suited to TIP on large construction projects. The approach uses distributed fibre optic sensing (DFOS) technology to measure the concrete temperatures from which the TIP can be carried out. The ease of deployment of this system has also facilitated the acquisition of a large amount of temperature data, including measurements during the construction stages of deep foundations.

SYSTEM DESCRIPTION

The use of DFOS within the geotechnical sector has been increasing over the last 15 years and, according to Ouyang et al (2015), has now reached the point where the technology involved can be considered mature. A number of excellent publications (Kechavarzi, C. 2017, and Soga, K. 2015) give detailed descriptions of how these systems work and the range of applications they have.

The important distinction between a DFOS system and one reliant on embedded point sensors is that the fibre optic cable itself is the sensor rather than a means to transmit data from a network of sensors. As light propagates along these optical fibres, some is reflected back. This reflected light, often referred to as back scatter, can be measured and analysed through a process known as Optical Time Domain Reflectometery (OTDR). The amplitude and frequency of certain components of this back scatter can be directly related to both the strain and temperature of the fibre at the point from which the reflections came.

For the purposes of temperature sensing, CemOptics uses standard grades of fibre optic cables which are manufactured in large quantities for the telecommunications industry. These are deployed in reinforced concrete by attaching the cables to embedded reinforcement with cable ties. A typical example of installed cables is shown in figure 1.

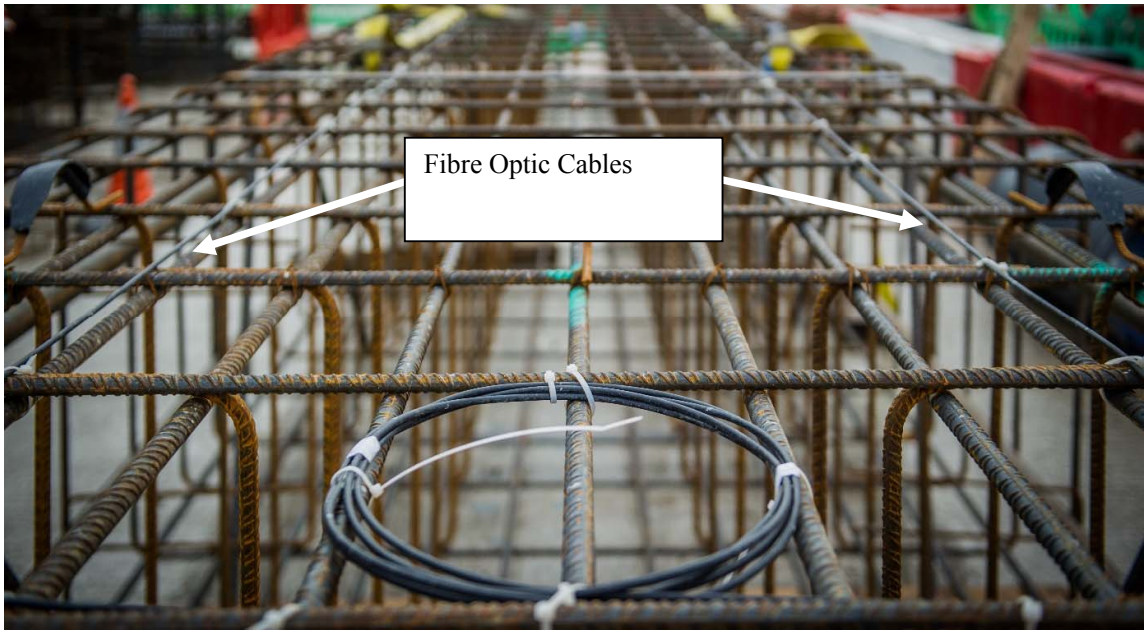


Fig 1. Photograph of a diaphragm wall reinforcement cage with a loop of fibre optic cable attached.

The embedded fibres are connected to an analyser which is able to convert the measured changes in backscattered light into measurements of temperature. Each analyser can, when attached to a multiplexer, sequentially carry out measurements on a number of different fibres, allowing multiple installations to be monitored at the same time.

DFOS systems are sensitive to changes in both temperature and strain. For the purposes of measuring temperature only, loose tube fibre optic cables are employed. In these cables, the individual optical fibres (typically 4 core cables are used for CemOptics) are encased within a gel filled tube, isolating the fibres from the effects of strain. This tube is then protected by braided tensile reinforcement and a durable PVC sheath.

The results returned by CemOptics are described as a distributed measurement, one in which the temperature is known at every point along an individual fibre. However, these values are resolved into discreet measurements, averaged at regular intervals along the fibre. This interval is known as the sampling interval. At each sampling point, the measurements are an average value for a set length of fibre. This distance is know as the spatial resolution. These parameters, and others, can be varied to affect the speed, precision and accuracy of the measurement. In SPREW, a maximum sampling interval of 0.25m and maximum spatial resolution of 1.0m are prescribed. Although higher resolution measurement are possible, for TIP, these settings have been found to be an appropriate balance of speed and accuracy.

Fibres are attached to the reinforcement cages as a series of loops with each loop equivalent to 2 strings of conventional instrumentation. Once the reinforcement has been installed, the separate loops are then connected together at ground level by the process of fusion splicing. Installing fibres in multiple loops makes them convenient to attach to the reinforcement. Fusion splicing ensures that the optical losses at the connections, which could otherwise reduce the reliability of the measurements are minimised.

For the purposes of TIP, fibres are run vertically along reinforcement cages and the spacing between fibres has generally followed the accepted rules for the deployment of cross hole sonic logging (CSL) tubes. It is worth highlighting that the low cost of the telecoms fibre used allow it to be deployed more densely with relative ease. It is also possible to deploy fibre in different configurations to increase the measurement resolution in the desired direction.

SYSTEM ADVANTAGES

The development of CemOptics has been greatly aided by the availability of fibre optic technology and expertise in the telecommunications industry. As a result, much of the materials and equipment necessary to install and connect the cables is readily available and sufficiently robust for use on construction sites. That these technologies have not been developed specifically for the construction industry has not been a hindrance and, in fact, has been beneficial.

In addition to the potential technical benefits of TIP described by Mullins and Piscsalko (2012), much of the drive towards the use of TIP in the UK has come from the need to reduce the risk to site operatives from installing reinforcement cages. When cages are spliced together, connecting the steel tubes required for carrying out CSL has lead to many incidents and near misses, particularly involving crushing or trapping of fingers, hands and arms. Attaching fibre optic cables to reinforcement as the cage is lowered into the bore has proved to be much safer and, after installing over 75km of fibre to date, has not lead to any injuries or near misses. There are also savings in time and productivity compared to conventional splicing operations, particularly because it removes the risk of tube sections not fitting together.

In general, the fibre optic cables are very durable. If installed correctly, avoiding any kinks or pinch points, all the loops can be connected together and measured as a single length of fibre. However, in the challenging construction environment any embedded instrumentation is vulnerable to damage during the installation process. In the event of some damage-, a benefit of a fibre optic system is that a measurement can be made from either end of a fibre. In the event of a breakage, data can be obtained from either side of the damaged area and then the results spliced together.

ANALYSIS METHOD

The data from CemOptics can be analysed using the same principals as any other TIP system. This approach is outlined as follows.

It is first necessary to associate the various points in the data set with their level within the foundation to form a temperature profile from each length of fibre. This allows the measurement to be compared to one another and to known conditions at each level. Good quality records are essential to ensure that the full potential of the data can be realised.

Once this has been carried out, it is first important to review the amount of heat generated at each level over the period immediately following the completion of concreting operations. This can be compared to the known trends for the particular concrete mix and site conditions. Localised reductions in the change in temperature can be identified and recorded as potential anomalies.

Secondly, the variation between the temperature changes measured at each level can be quantified. Although small variations are to be expected, more notable variations should be identified and recorded as potential anomalies.

Finally, the potential anomalies can be reviewed with reference to the construction information, ground conditions and, if possible, previous data measured in similar conditions. This can determine whether the anomalies identified are an expected feature of the temperature profiles or an anomaly which need to be investigated further.

The approach described above is purely an observational method. It relies on the identification of anomalies based on variation from observed normal values for temperature change. The theoretical normal values for temperature may be evaluated from a solution of the conduction equation which, according to Kreith and Bohn (2001), for a control volume within the body of concrete can be described as,

Rate of heat conduction into control volume	+	Rate of heat generation inside control volume	=	Rate of heat conduction out of control volume	+	Rate of energy storage inside control volume	[1]

Kreith and Bohn (2001) give examples of a number of numerical solutions to the idealised problem, however, for the case of heat transfer in concrete, a detailed knowledge of the governing parameters of heat generation, storage and conduction for the materials involved is required if the model is to be accurate. If sufficient information is available, a theoretical model of the expected heat distribution can be compared to the observed temperatures to assist with assessing the significance of any defects encountered. However, in most cases, the observational approach outlined above has proven sufficient for both the identification of anomalies and the assessment of their significance.

In order to develop an observation based model for the normal temperatures within a foundation, analysis of different concrete mixes and observed defects has been carried out. The data for this study has been obtained from real projects around the UK on which CemOptics has been installed. To illustrate the potential difference between concrete types, figure 2 presents measured temperature values and rates of temperature rise within similar foundation elements but with different concrete mixes. As can be seen from this figure, there is significant variation in the rate, duration and magnitude of the temperature changes leading up to the peak temperature. Similar variations and patterns are observed by Schindler and Folliard (2005) in adiabatic conditions, however, the variations are more pronounced in the foundation mixes due to the impact of admixtures such as retarders. These compounds are routinely added to concrete mixes for foundations in order to prolong and improve their workability. The details of the concrete mixes studied are presented in table 1.

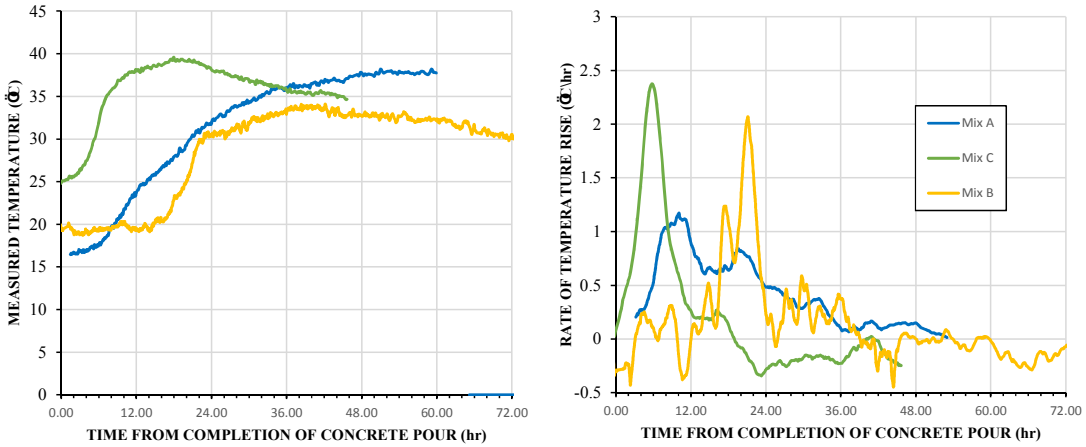


Fig 2. DFOS measurements of concrete temperature and rates of temperature change during the hydration of different pile concrete mixes.

Table 1. Concrete mix details for the results shown in figure 2.

Mix	Concrete Grade	Cement Type	Additives
Mix A	C32/40	CEM1 190kg, GGBS 230kg	Retarder and Plasticiser
Mix B	C50/60	CEM1 294kg, GGBS 196kg	Retarder and super plasticiser
Mix C	C32/40	CEM II/B-V +SR (21-35% Fly Ash)	Water reducing agent

An important consideration for the collection and analysis of thermal data is the duration of monitoring required to sufficiently understand the integrity of the concrete. To assist with the correct identification of this period, a number of known defects, both artificial and real, have been compared to establish when they are most visible.

By comparing the measured temperature at the location of the defect to the measured temperature at a similar location, it is possible to quantify the variation as a percentage of the normal value. Normalising the time at which this occurs with respect to the time of the peak temperature allows for comparison of different defects. This analysis is presented in figure 3. Defects 2 and 3 were artificial inclusions within the cover zone of a diaphragm wall panel. Both were 60mm thick and constructed from plywood. Defect 2 was 1.2m deep in the vertical plane and defect 3 was 0.67m deep and an example of these defects is shown in figure 4. Defect 1 was a 1.0m thick zone of poor quality concrete within the shaft of a 1.2m diameter pile. In this case, the absolute dimensions of the defect were not proven.

These figures show that the defects are at their most observable after the peak rate of temperature change and close to, or slightly before the peak measured temperature. Smaller defects are most apparent earlier than larger ones. In these cases, an optimum period for carrying out the analysis was when the measured concrete temperature was between 60 and 90% of it peak value.

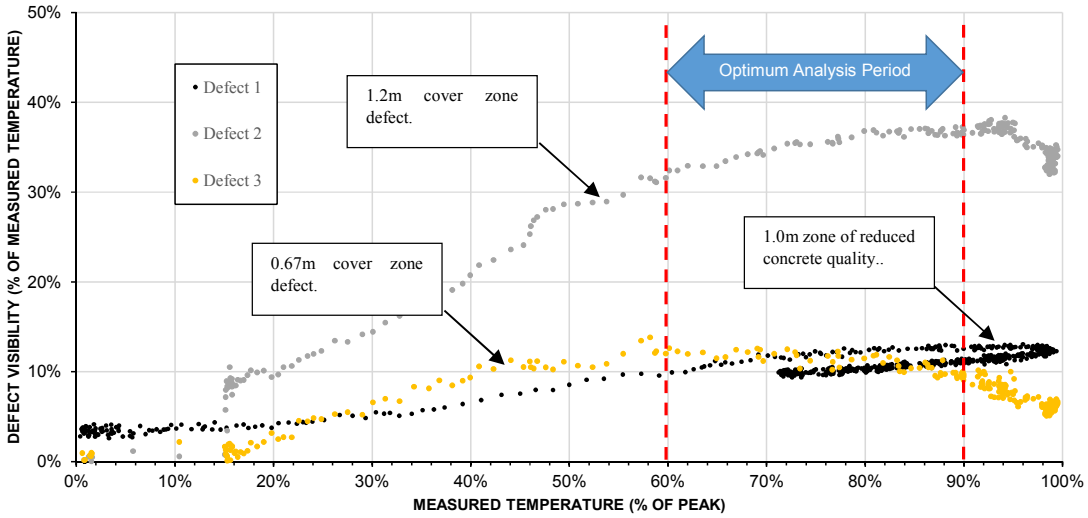
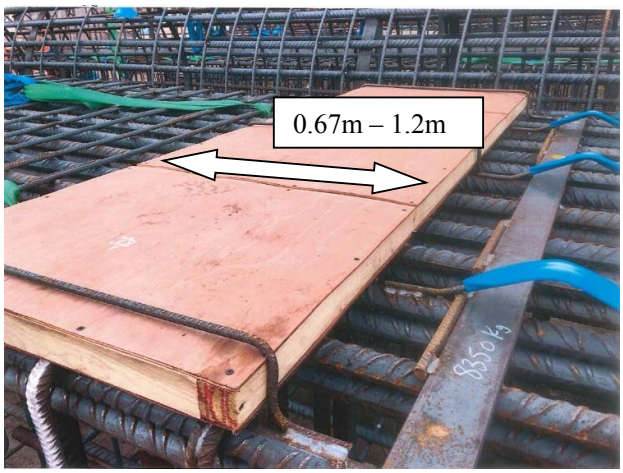


Fig 3. Graph of defect visibility as a % difference from normal temperature.



The analysis presented in figure 2 and figure 3 demonstrates that monitoring must be carried out from the completion of concreting to the point of measured peak temperature. Experience of the concrete mix and ground conditions may be sufficient for this to be determined in advance, however, for most projects, it will be necessary to initially monitor the temperatures for at least 48 hours before an assessment of the appropriate period can be made.

Fig 4. An artificial cover zone defect.

An initial assessment of concrete integrity can be made at a set number of hours from completion of the concrete pour. This approach ensures consistency in the analysis and allows one structure to be compared to another. This time chosen should be within the optimum analysis period presented in figure 3. If a more detailed assessment of potential anomalies is required, a dynamic approach should be adopted which also considers the persistence of the anomalies throughout the monitoring period. Further understanding and modelling of defect visibility will improve the quality and consistency of TIP and analysis.

CONSTRUCTION PROCESS OBSERVATIONS

In addition to quantifying concrete integrity, thermal data, measured during the concreting process can yield valuable information about the flow of concrete within the bore. With the flexibility and low cost deployment of the CemOptics system, a large number of sensing fibre can be deployed on a reinforcement cage without a proportionate increase in cost or effort. This permits high resolution measurements of the concreting process.

Figure 5 shows four temperature measurements from the front of a 2.6m wide, 1.2m thick diaphragm wall, constructed in December 2016. These measurements come from two lengths of fibre, positioned 0.8m apart on the rear face of the reinforcement cage. In figure 5A, shortly after concreting of the panel had commenced, the difference between the temperature of the bentonite support fluid and the freshly placed concrete can be clearly seen. After this time, there was a delay in the concreting operations and, as a result, the next loads of concrete had to wait for several hours to be poured. During this period they cooled down. Figure 5B shows that this cooled concrete entered the panel at a lower temperature than the earlier deliveries. Figure 5C, measured once fresh, warm concrete was again being placed, shows that this concrete flows over the colder concrete seen in 5B. From a review of the tremie embedment, also presented within figure 5, it is apparent that the fresh concrete did not displace the cooler mixes but rather flowed up through and over it. This is consistent with the experience of Schindler and Brown (2006) who used coloured concrete in a sacrificial trial pile. In their study it was found that the concrete flow from the discharge point of a tremie was confined to a central portion of the pile shaft.

This finding demonstrate the potential of CemOptics to yield information about the flow of concrete within a foundation structure. Although this information can also be obtained by the use of coloured concrete, in many cases the technique has proven to be prohibitively expensive due to both the challenges of obtaining coloured concrete and the costs of coring through it. CemOptics provides a potential means to obtain valuable knowledge on this subject with minimal additional cost and effort.

CASE STUDY – BATTERSEA JUNCTION STATION

The largest deployment of CemOptics to date has been for checking the integrity of diaphragm walls and piles associated with the construction of Battersea Junction, a new underground station in London which has been built as part of the Northern Line extension. Working closely with the client, CemOptics was selected as the preferred method for integrity testing due to the improvements in safety, increased productivity and cost savings it offered over other techniques. An initial validation exercise was carried out with CemOptics and CSL installed on the same panel. This study demonstrated that CemOptics was able to pick up cover zone information which could not be identified using CSL alone.

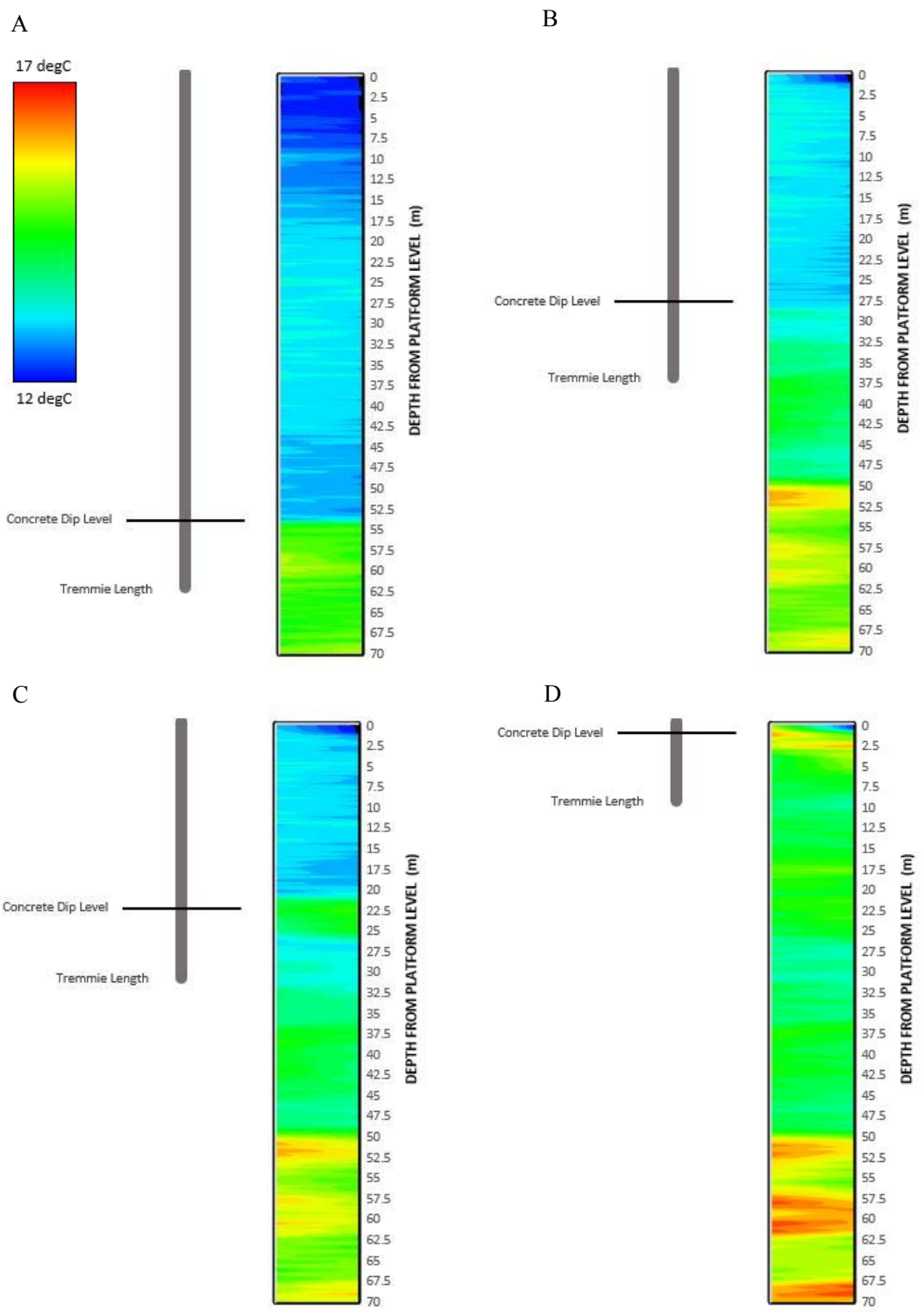


Fig 5. Measured temperatures, tremie lengths and concrete levels on the face of a diaphragm wall panel at four points during the construction process.

The diaphragm walls were dug between 30m and 60m deep using hydraulic grabs, digging under bentonite through London Clay, the Lambeth Group and Thanet sands. The majority of the instrumented panels were 1.2m thick and 2.6m wide and were installed with 2 loops of fibre optic cable. Corner panels and T shaped panels were also instrumented using different configurations of up to 10 loops of fibre. 50% of all panels were instrumented.

CemOptics was also used on the 60m deep bearing piles which extending through the same strata and were constructed using a polymer based drilling fluid. two loops of fibre were placed in piles of 1.5m and 1.8m diameter and three loops in 2.1m and 2.6m diameter piles. The piles were constructed with a low cut off level and plunge columns so careful consideration of sequencing was required to ensure that the fibre optic cables were protected from damage at the head of the pile. All of the piles were instrumented.

The CemOptics works on this project involved 116 diaphragm wall panels and 74 bearing piles, requiring a total of more than 50km of fibre to be installed. Up to 6 elements were monitored at any one time by a single analyser, located centrally on the site and with fibre optic lead cables routed around the site perimeter to the different monitoring positions.

The thermal profiling results from the project were positively received and yielded some valuable information about the installation processes and the ground conditions. A typical result from this project is presented in figure 6. From these results the variation in temperature due to the ground conditions can be clearly seen as well as the location and impact of the box outs, similar to those shown in figure 4.

From this project, and others around the UK, a data set of temperature measurements from concrete foundations in different ground conditions and with different concrete mixes has been built up.

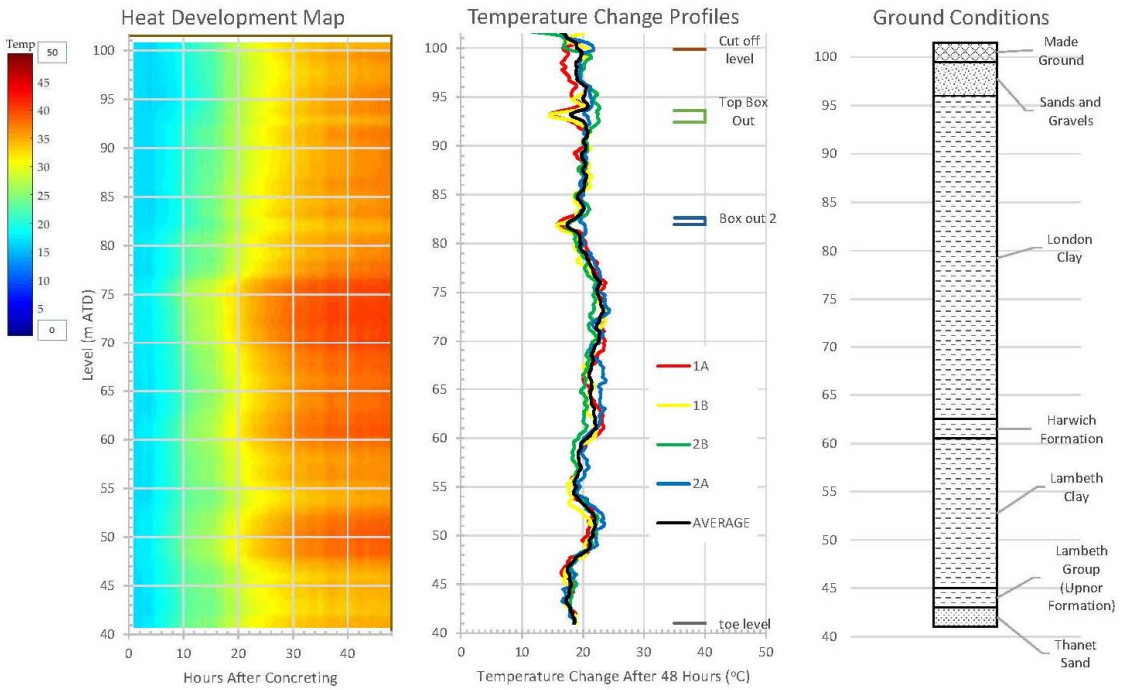


Fig 6. CemOptics results from a 2.6m wide, 1.2m thick diaphragm wall panel.

CONCLUSION

The use of CemOptics for TIP has demonstrated that it is a valid approach which can yield valuable information about both the integrity of a concrete foundation and how it has been constructed. Its development has demonstrated the benefits of cross industry co-operation and the importance of bringing new technologies from other industries into construction.

Through an observational approach, potential defects in concrete foundations can be identified if monitored at the correct time. The relatively early identification of defects, often within 48 hours, can be invaluable, allowing corrective actions to be adopted earlier. This places a requirement on construction works to ensure that the monitoring is in place and maintained through the optimum analysis period.

Measurement of temperature can also provide information about the construction process which is important for an understanding of how to prevent defects. The flexibility and affordability of the CemOptics system makes it ideal for capturing this data.

As more data is collected and shared, the use and reliability of TIP will continue to improve. The combination of a consistent observational approach and a developed theoretical model will provide a greater understanding of the significance of the anomalies encountered.

REFERENCES

Institution of Civil Engineers, 2017, ICE specification for piling and embedded retaining walls, third edition, ICE Publishing, London, 230p.

Kechavarzi, C., Soga, K.,De Battista, N., Pelecanos, N., Elshafie, M. and Mair, R.J., 2017. Distributed Fibre Optic Strain Sensing for Monitoring Civil Infrastructure: A Practical Guide. ICE, London.

Kreith, K. and Bohn, M.S., 2001. Principles of heat transfer, sixth edition. Brookes/Cole, California, 700p.

Mullins, G.and Piscsalko, G., 2012. Thermal integrity profiling: and innovative technique for drilled shafts. Deep Foundations Magazine, May/June 2012, pp51-54.

Piscsalko, G., Alvarez, C., Belardo, D.S. and Galvan, M., 2014. Using thermal integrity profiling to evaluate the structural integrity of soil nails. Deep Foundations Institute, pp195-202

Schindler, A.K. and Folliard, K.J., 2005. Heat of Hydration Models for Cementitious Materials. ACI Materials Journal Technical Paper, January/February 2006, 102-M04,pp24-33.

Schindler, A.K. and Brown, D.A., 2006. Evaluation of self-consolidating concrete for drilled shaft applications at the lumber river bridge project, South Carolina. Highway Research Center Project 4-20793, Research Report No. 2.

Soga, K., Kwan, V., Pelecanos, L., Rui, Y., Schwamb, T., Seo, H., and Wilcock, M, 2015. The role of distributed sensing in understanding the engineering performance of geotechnical structures. Proceedings of the XVI ECSMGE Geotechnical Engineering for Infrastructure and Developoment, Edinburgh, September, pp13-48

Ouyang, Y., Bell, A., Elshafie, M., Kechavarzi, C., Soga, K., Fernie, R. and Mair, R., 2015. The history of UK experience in the use of fibre optic monitoring of geotechnically associated installations. Proceedings of the XVI ECSMGE Geotechnical Engineering for Infrastructure and Development, Edinburgh, September, pp637-642

THE CASE OF A BUILDING DESIGN REVIEW REQUIRING A FULL FOUNDATION REDESIGN

Brendan Atarigiya, University of Ghana, Accra, Ghana, brendanatarigiya@live.com.
Philip Amankwah, ESPCo Ltd., Accra, Ghana, pamankwah@espco-gh.com
Isaac. Osei, ESPCo Ltd., Accra, Ghana, iosei@ espco-gh.com
Nii. K. Allotey, ESPCo Ltd., Accra, Ghana, nkallotey@espco-gh.com
Joseph. Oddei, Architectural and Engineering Service Limited, Accra, Ghana, joddei@outlook.com
William Albert-Viala, ESPCo Ltd., Accra, Ghana wdalbertviala@espco-gh.com

ABSTRACT

In light of the recent collapse of buildings in Ghana, and also the protection of professional integrity, it has become more imperative for local engineers to exercise greater caution in the design and review of engineering works, especially when dealing as a third party consultant. This paper narrates the story of the design review of a 9-storey building design that ended up in a total overhaul of the whole design; i.e., from the architectural concept to the entire structural and MEP design of the building. The paper, however, mainly focusses on the geotechnical design of the building foundation since this was a critical part of the redesign.

Keywords: piles, collapsible soil, raft, foundation

© 2018 Deep Foundations Institute

INTRODUCTION

The recent collapse of various structures in Ghana, notably the Achimota Melcom disaster in 2012 has resulted in loss of property, and most importantly, the loss of human lives. The reasons for these collapses are varied, including, poor building design, use of inferior construction materials, ignorance, poor regulatory oversight, unethical behaviour, and also poor/wrong design by built environment professionals. The story of this hotel building rests greatly on the latter two factors.

The story about this design project started when the building owner wanted to secure a building permit to start construction of the proposed hotel. When our office was asked to review the drawings, we noticed many inconsistencies in the drawings and design reports including:

- Inadequately sized columns
- Foundation designs not addressing the geotechnical findings of low bearing capacity
- Lack of any form of ground improvement measures in the foundation drawings
- No sign of seismic ductile detailing
- Poorly designed beams spanning long lengths with limited supports at the roof level
- etc.

These inconsistencies prompted the call for a thorough review of all other designs, and also the need for a reconnaissance field visit. Upon the field visit, it was noted that the proposed hotel (9-storey) with a basement was to be placed in a confined area, with 3-storey buildings already constructed on the adjacent sides of the facility. The space between the existing walls of the adjacent buildings and the plan area of the proposed building was noted to very be small, with some sides even being less than the required width of 3 m. Considering the findings from the geotechnical investigation report, the presence of collapsible soils was noted in the upper 5 - 6 m with an associated high groundwater level. This pointed to the possibility of the instability of excavated unprotected slopes below the ground level. At this point, it was clear that the problem being faced was bigger than rectifying inconsistencies in the structural drawings. Apart from the identified structural and geotechnical issues, later on, while setting out, the contractor noted that location of the building on the provided area was also wrong. Furthermore, the mechanical and electrical services designs were noted to be totally flawed. In short, the whole saga led to the need for a total architectural, structural, geotechnical, mechanical and electrical redesign of the entire structure.

In regards to the geotechnical design of the building foundation, the original geotechnical report recommended shallow foundations below the basement level, i.e., greater than 4 m. The report noted weak soils composed of collapsible soils with low SPT to about 6 m, and underlain by medium dense decomposed schist. Furthermore, the report stated that the SPT-N values at 9 m from the two boreholes were 40 and 60, respectively, and showed a sharp increasing trend pointing to the change from a weathered intermediate geomaterial type of ground medium to that of firm rock.

PRELIMINARIES

Raft Foundation with Basement

The initial foundation choice provided for the building was a raft foundation at about 4 m below the ground level, with a one-storey basement. Taking into account the adjacent structures and the collapsible soil to a depth of 6 m, it was decided that there was the need to conduct slope stability analyses to determine the stability of the proposed excavations. Slope/W GeoSlope Inc (2008), a commercial slope stability analysis programme was used to perform a short-term stability analysis. It showed that the excavations were going to be very unstable. Figure 1 shows the output results from Slope/W, showing a factor of safety (FoS) of as low as 0.391, which is less than the limiting acceptable value of between 1.2 – 2 WSDOT (2005).

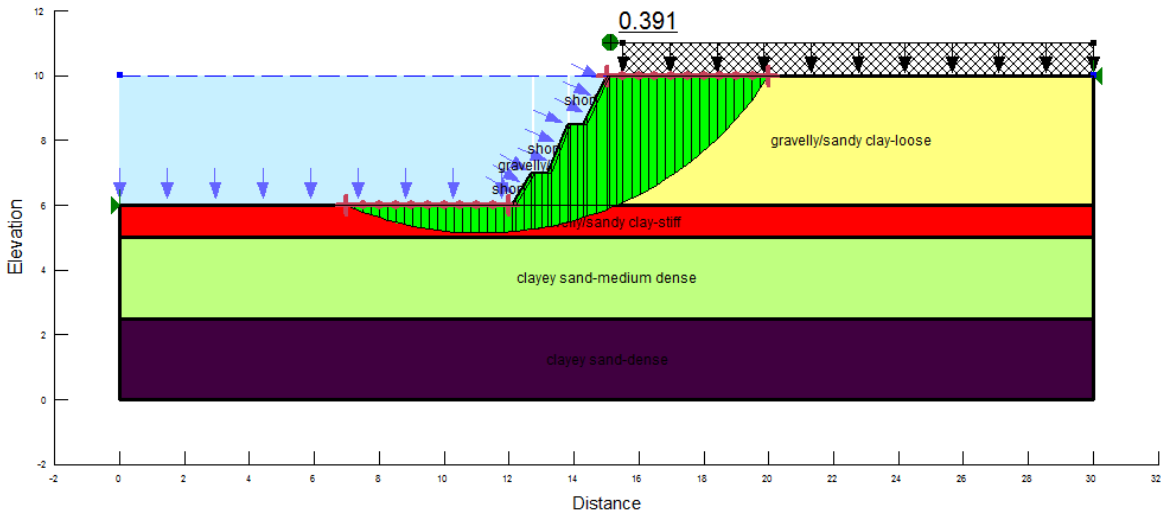


Fig. 1. Slope Stability Analysis

Considered Solutions

Due to slope instability the initial proposed raft foundation with the basement foundation options was considered not viable. The option of a raft foundation without a basement, with the provision of shoring and side bracing was thus considered. This option was, however, discontinued since it required ground improvement to a significant depth, which was considered not cost-effective. The only option available was thus to consider the use of deep foundations. Two options were examined.

- The use of micropiles. This was investigated to quite an extent, but was not continued since the limited load carrying capacity, rendered the number and length of piles to be on the high side, thus making the option not cost-effective.
- The final option was thus the use of conventional bored concrete piles. This was to be combined with a raft foundation. The cost-benefit analysis for this option was the best; its constructability was also satisfactory.

PILED RAFT FOUNDATION DESIGN

General

Based on availability and costing, 600 mm augured concrete piles were selected for the project. From the initial geotechnical report (SPT-N values), an initial pile length of 10 m was chosen The structure take-down gravity and seismic loads showed this length to be insufficient. The initial geotechnical drilling ended at 10 m; two confirmatory percussion boreholes were thus ordered to confirm the soil/rock medium below 10 m.
The confirmatory tests showed the upper 6 m to be consistent with the initial geotechnical report. However, whereas, the initial geotechnical investigation pointed to the presence of increasingly dense weathered rock material from 8 m onwards, the confirmatory tests showed the ground condition at this level to be medium dense silty sand. This new revelation raised eyebrows since the new subsurface conditions could not support the structure, and as such, there was a need sink the piles far deeper. This resulted in a lot of disagreement between the geotechnical engineer who performed the confirmatory tests, our firm, the piling contractor, the general contractor, and the building owner.

A compromise was later reached between all parties that a third confirmatory percussion borehole be ordered. Drilling of this borehole was to be witnessed by all the parties. It was also agreed that this percussion borehole be sunk until there was strong resistance to penetration, signifying the presence of hard/strong ground conditions. The results of this third borehole confirmed that results obtained by the additional two confirmatory boreholes. In summary, it became clear to the entire team that the results of the initial geotechnical investigation were inaccurate, and most probably the result of unethical engineering practice. This reinforces the need to proceed with a lot of caution when adapting third party data/information for one's own work!

Pile Raft Design Overview

Based on the second confirmatory geotechnical investigation, 15 m piles were initially investigated. This was, however, increased to 17.5 m. A pile cap of 1 m depth was also adopted for the pile raft design.

The undrained cohesive strength parameters for the different soil layers were estimated based on SPT – C_u correlations obtained from the Canadian Foundation Engineering Manual (CFEM) (2006). The values of unconfined compressive strength (q_u) for the weak decomposed rock (intermediate geomaterial) were obtained from the result of q_u tests conducted on similar rocks from two other project sites within the Airport area. For these sites, they showed the weathered rock material to have very low RQDs (between 10 – 30) representing poor rock, with an associated q_u of between 7 - 9 MPa. The pile input parameters for both the axial and lateral responses were computed using the approach provided by the API guideline (2014).

These values were used to estimate the required pile axial and lateral load-deformation parameters and also associated pile capacity parameters. The axial and lateral pile analyses were conducted with commercial program, ALLPILE, CivilTech (2011). The program ALLPILE analyses provide both the axial and lateral pile load-deformation response and also provides the respective pile capacities. The program is able to consider different types of piles,

including: drilled shafts, driven piles auger-cast pile, steel H and pipe piles, tapered piles, etc. Figure 2 below shows an interface of the ALLPILE program.

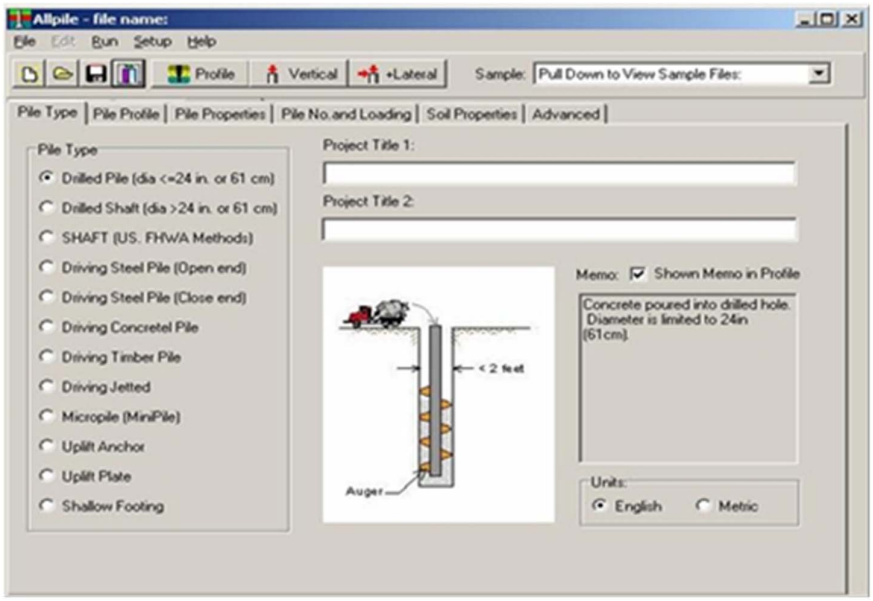


Fig. 2. ALLPILE Interface
Source: AllPile (2011)

Axial & Lateral Pile Analysis

The axial response of the pile was computed assuming the pile to mobilize strength through both side friction and end-bearing. The top 3 m of the pile was not accounted for in the side friction computations.

In the axial direction, under gravity loading, the factor of safety (FS) for compression loading was taken as 2.5 for both side friction and tip resistance. Under seismic loading a FS of 2 was used for both components.

For the horizontal direction, the piles were assumed to be fixed at the pile head due to the rigid nature of the pile cap. Based on IBC (2012) recommendations, the lateral load was taken as the load at 25 mm deflection. It is important to note that the computed deflections, moments and shears take into account the 2nd order P-delta effects due to the supported axial loads being part of the pile analysis. Also, the pile capacities include an increased pile resistance contribution due to the presence of the pile cap.

Some summary plots from the ultimate analysis of the pile are shown in the Figs. 3 and 4 below. In addition, Table 1 provides a summary of the results obtained from analysis.

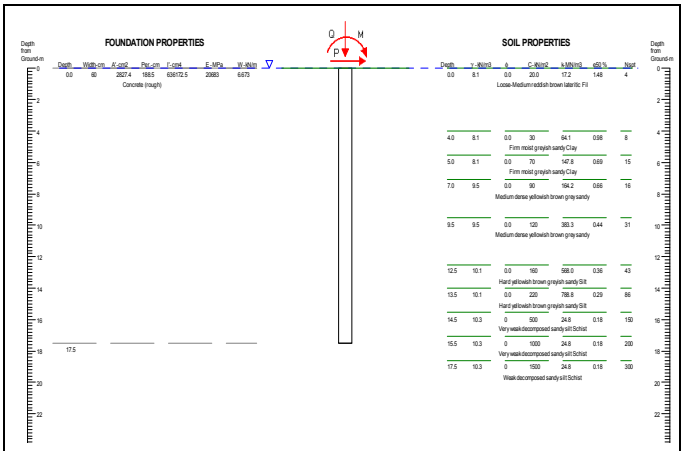


Fig. 3a. Soil Layering and Side Friction Characteristics

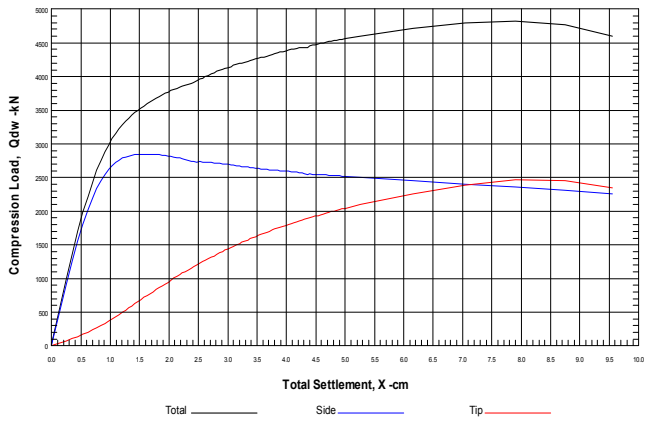


Fig. 3b. Vertical Load Deformation Curves

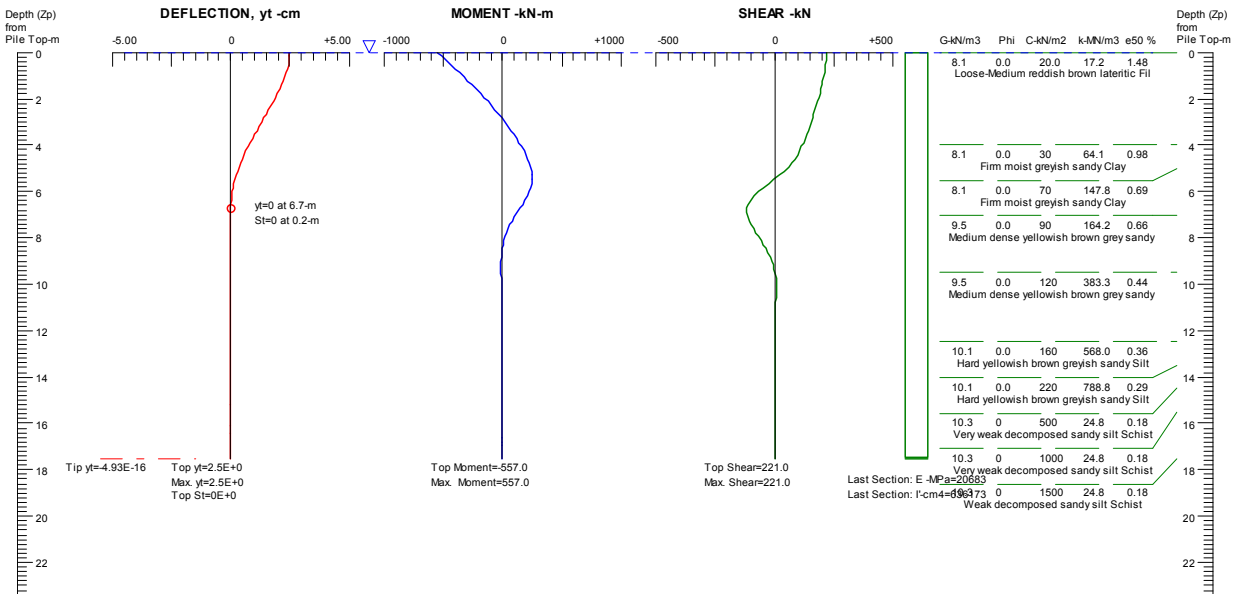


Fig. 4. Summary of Ultimate Lateral Load Analysis Plots

Table 1. Summary of Axial & Lateral Pile Loading Results

Axial Load Results	**Value (kN)**
Ultimate Compression load	5300
Allowable Compression load - Gravity	2000
Allowable Compression load – Seismic	3000
Ultimate Uplift load	3000
Allowable Uplift load - Gravity	1200
Allowable Uplift load - Seismic	1700
Lateral Load Results	**Value (kN)**
Ultimate Lateral load (at 25 mm deflection)	370
Allowable Lateral load (half ultimate – IBC 2012)	240

Structure-Pile-Soil-Interaction Analysis

Based on the axial and lateral load-deformation responses, the effective vertical and horizontal pile stiffnesses were computed. These were then entered into the CSI SAFE analysis program to conduct the structure-pile-soil interaction analyses. The foundation action forces (i.e. gravity and seismic action forces), raft pile cap geometry, load cases and combinations were exported from CSI ETABS building analysis program to SAFE. Additional overburden soil surcharge was applied to the model where required, and modulus of subgrade reaction springs were also placed under the raft foundation, in addition to the lateral and axial pile springs computed from the ALLPILE analysis. Pile group effect was considered in the analysis in an overall manner by reducing the axial and laterally computed pile stiffnesses.

From the various analyses, it was noted that the gravity load case impacted considerably piles within the vicinity of the highly loaded columns. On the other hand, the seismic load combinations were observed to highly impact the columns within the vicinity of the core walls. In fact, the seismic load cases were the cases in which it was very difficult to satisfy the required maximum pile load limits. From the optimization analysis conducted, a total number of 103 – 600 mm augured concrete bored piles were observed to be required.

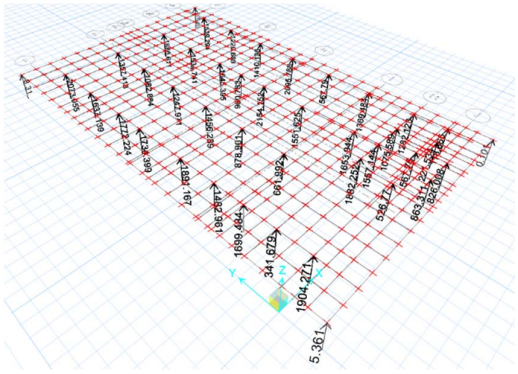


Fig. 5a. Vertical Pile Forces for Building Portion A under Gravity Loading

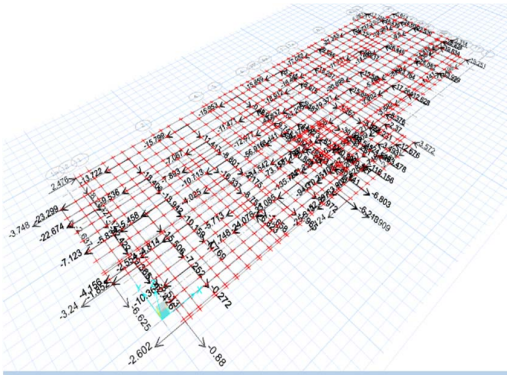


Fig. 5b. Horizontal Pile Forces for Building Portion B under Seismic Loading

CONCLUSIONS

This paper has provided a summary of the design of a piled raft foundation for a 9-storey hotel building in the Airport area of Accra. The design had been provided by a team of earlier professionals. A preliminary review of the design showed a number of flaws in virtually all the required disciplines that needed to be rectified. Particularly significant was the foundation design that needed to redesigned. Among the options considered, a piled raft foundation with concrete bored piles was chosen.

The initial design of the piled raft foundation had to be redone since the initial geotechnical investigation was found to be incorrect. This led to some level of mistrust developing between the various project team members. Upon carrying out a second confirmatory field boring, it became clear that the initial geotechnical results had been cooked. This unethical behaviour was both surprising and astonishing, and could have led to a totally wrong foundation design, that would have resulted in the hotel building experiencing overly large settlements. The following lessons have been learnt by our engineering firm from this experience:

- It is important (even crucial) to undertake a confirmatory geotechnical assessment when in doubt about any findings from a third-party consultant.
- Pragmatic stakeholder discussions are critical in projects of this nature, especially when project cost can be significantly affected.
- The review of a third party consultant's project documents is very critical in order to achieve project goals and to avert any discrepancies, so as to safeguard the Client's investments.
- No matter the rules governing engineering practice, there would certainly be some criminal elements who would flout the ethical requirements of the profession.
- The Ghana Institution of Engineers us strengthening its ethical enforcement functions so such issues are now reported to the Institution for investigations and punishment if found guilty.

REFERENCES

API RP-WSD (2014). Recommended practice for planning design and construction of fixed offshore platforms, working stress design, American Petroleum Institute, Houston, TX, US.

CFEM (2006) Canadian Foundation Engineering Manual. Second Edition, Canadian Geotechnical Society, Bitech Publishers, Vancouver, BC, Canada, 503 p.

CivilTech (2011). AllPile Version 7, Pile Design and Analysis Software, CivilTech Software, US, 100 p.

CSI ETABS (2015). Structural software for building analysis and design, 2015 Version, Computers & Structures International, Berkeley, CA.

CSI SAFE (2012). Concrete slab and foundation design software, 2012 Version, Computers & Structures International, Berkeley, CA.

GeoSlope Inc, (2008). Slope Stability Modeling with Slope/W 2007 Version, An Engineering Methodology, 3rd Edition, Geo-Slope International Ltd., Calgary, AB, Canada, 355 p.

WSDOT (2005). Chapter 10 - Slope cut design, Geotechnical Design Manual, M46-03, Washington State Department of Transportation, Seattle, Washington, US.

THE INFLUENCE OF A THIN WEAK SOIL LAYER ON THE PILE BEARING CAPACITY

Shilton Rica, PhD student, University of Luxembourg, Luxembourg, 00352-4666445304, shilton.rica@uni.lu
Stefan Van Baars, Professor, University of Luxembourg, Luxembourg, Stefan.VanBaars@uni.lu

ABSTRACT

Most pile design methods for estimating the pile bearing capacity, are based on data from the cone penetration tests (CPT), such as the Dutch (Koppejan) method, the Belgium (De Beer) method or the French (Bustamante & Gianeselli) method. In all these methods, the unit cone resistance of the CPT has to be averaged within an influence zone around the pile tip, in order to be able to calculate the pile tip bearing capacity. The influence zone is defined as the zone in which the parameters of the soil have an influence on the pile tip bearing capacity. For the French method this zone is between 1.5 times the pile diameter, D, above and below the pile tip; while for the Dutch method this zone is between 8 D above to a maximum of 4 D below the pile tip. Numerical simulations on piles installed in homogeneous sandy soil, show that these definitions of the influence zone are not accurate. The simulations show an influence zone from 1 or 2 D above, to 5 or 6 D below the pile tip, depending on the soil parameters. In this research, also the influence of a weak thin soil layer on the pile bearing capacity has been studied. All simulations are made for two different thicknesses of the thin soil layer. Also the soil strength parameters and soil stiffness parameters have been varied, in order to show the influence of this thin soil layer. This influence zone has been confirmed by laboratory tests.

Keywords: Piles, Numerical simulations, bearing capacity, influence zone

INTRODUCTION

The pile design methods based on CPT data include the assumption that the CPT was carried out under the same conditions as the pile driving, meaning that no sand fill or excavation work was carried out in the time between the CPT field test and the pile driving. Boonstra (1940) was the first author who used the CPT data to estimate the pile bearing capacity, but he was not focused on an influence zone around the pile tip. In 1951, Huizinga was the first who looked at a certain influence zone around the pile tip, although no specific averaging procedure was detailed. A definition of this influence zone was proposed by Meyerhof (1951) and Van Mierlo and Koppejan (1952) who based the failure mechanism around a pile tip on the logarithmic spiral of the Prandtl's wedge, which was developed for shallow strip foundations (Prandtl, 1920). This influence zone was presented to be from 8 D above down to 4 D below the pile tip.

Begemann (1963) noted that the pile tip bearing capacity, q_t, is approximately equal to the averaged CPT measurement below and above the pile tip, q_c. He concluded that the soil above and below the pile tip contributed almost equally to the pile tip bearing capacity, q_t. Based on the theory of Van Mierlo and Koppejan, he developed the method by applying the minimum path for the values of q_c, while averaging q_c , as shown in Figure 1. The procedure is the same for pile tips embedded in either sand, clay or mixed soils.

© 2018 Deep Foundations Institute

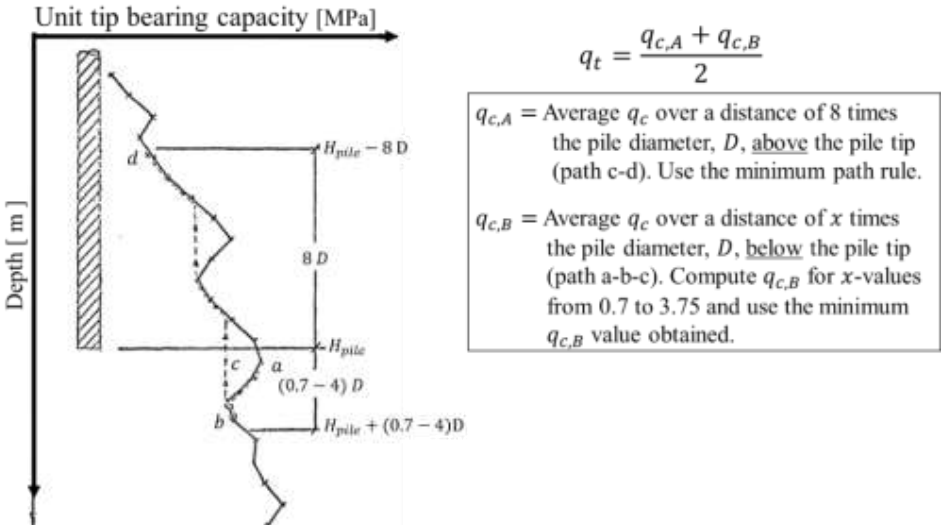


Fig. 1. Begemann procedure for predicting the pile tip bearing capacity. (Adapted from Schmertmann, 1978)

The so-called Dutch CPT-based method is mainly based on:

The Koppejan method, which proposes the influence area from 0.7 to 4 D below the pile tip up to 8 D above the pile tip.

The Begemann method, which proposes to use the method of the minimum path for the values of the CPT measurement, q_c, while averaging, procedure.

Figure 2 shows an example of a pile tip bearing capacity calculation based on the Dutch method.

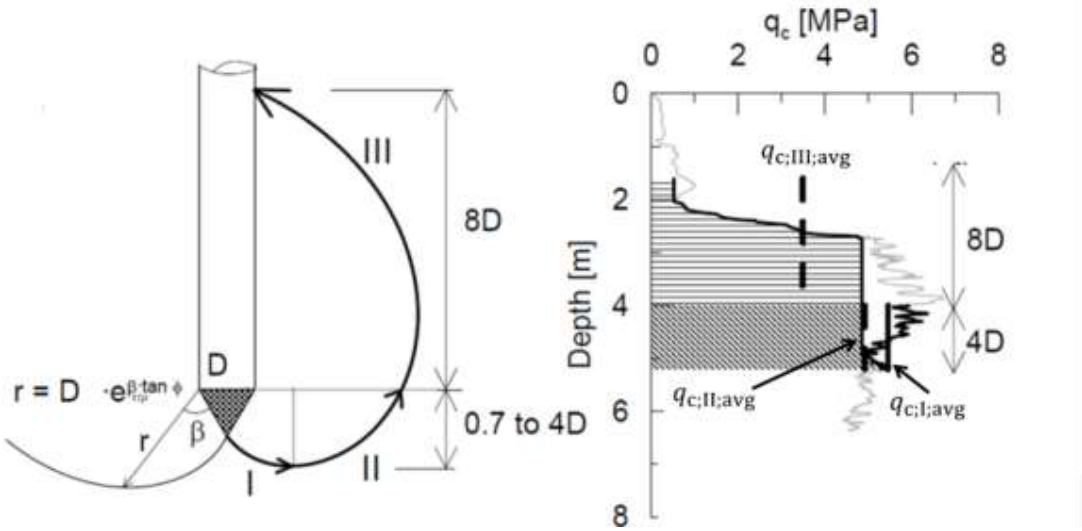


Fig. 2. Dutch, Koppejan's, method (adapted from Kort, 2008).

This leads to the following equation:

$$q_t = \frac{1}{2}\alpha_{tp}\beta_t \, s\left(\frac{q_{c;I;avg} + q_{c;II;avg}}{2} + q_{c;III;avg}\right) \quad \textbf{(1)}$$

where:

q_t	the pile tip resistance
$q_{c;I;avg}$	the average value of q_c in Zone I, from the level of the pile tip of at least 0.7 D and at most 4 D below the pile tip, depending on which level leads to the lowest possible average value. This means that if the cone resistance progressively increases below the pile point, the influence zone is limited to 0.7 D
$q_{c;II;avg}$	the average value of the cone resistance in Zone II, where the cone resistance to be taken into account, shall never increase in relation to the q_c-values below
$q_{c;III;avg}$	the average value of the cone resistance in Zone III where the cone resistance to be taken into account, shall never increase in relation to the q_c-values below, starting from the end-value of $q_{c;II}$
α_{tp}	the pile type factor (e.g., 1.0 for driven piles, or 0.5 to 0.6 for bored piles). In the Netherlands these values have been reduced with 30% since 2017.
β_t	the pile tip factor (β_t = 1.0 for concrete piles and decreases for piles with an increased pile tip area)
s	the shape factor of the pile tip (1.0 for square and circular pile tips and lower for more rectangular or elliptical elements)

De Beer (1963) provided significant insight into the scale effect problem on the evaluation of the pile tip bearing capacity, q_t. He used penetrometers of different sizes and showed that at some depths all penetrometers registered the same tip resistance as the cone resistance, q_c. If a layer is penetrated by a cone penetrometer of small diameter ($d_{CPT} = 3.57$ cm), the depth of embedment effect is minimal and the cone resistance, q_c, ideally follows the profile of the dashed curve. However, if a large diameter pile would be pushed into the second layer, the pile tip bearing capacity, q_t, would not equal the cone resistance until the pile tip reaches a critical depth, H_{crit}, see Figure 3. De Beer showed that the curve of pile tip bearing capacity, q_t, varies linearly over H_{crit} (solid curve); thus, the pile tip bearing capacity at any intermediate depth can be determined if the cone resistance, q_c, and h_{crit} are known.

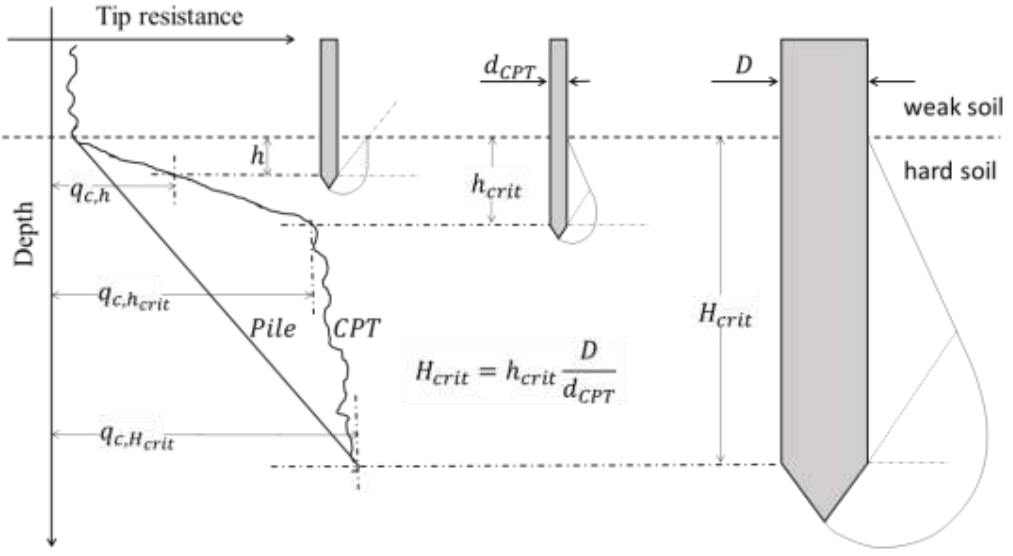


Fig. 3. Belgian method (adapted from De Beer, 1971).

The symbols used in Figure 3:

D the pile tip diameter

d_{CPT} the CPT diameter

$q_{c,i}$ the cone tip resistance at the depth " i " from the bottom level of the weak soil layer, where: $i = \{h, h_{crit}, H_{crit}\}$

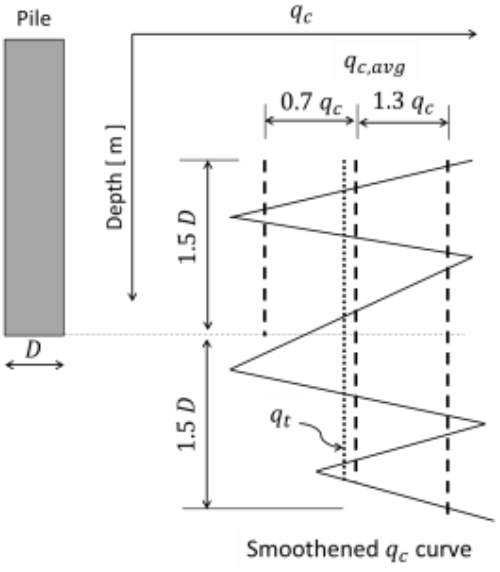
h the depth from the bottom level of the weak soil layer

h_{crit} the critical depth, the depth from which the foundation is considered as a deep foundation (this is the case when the pile tip has a diameter equal to d_{CPT}).

H_{crit} the critical depth, the depth from which the foundation is considered as a deep foundation (this is the case when the pile tip has a diameter equal to D).

Bustamante and Gianeselli (1982) proposed a new method for the averaging procedure, $q_{c,avg}$. Figure 4 shows that their averaging procedure involves the cone resistance, q_c, for a zone from 1.5 D above the pile tip to 1.5 D below the pile tip. This method is nowadays called the French CPT-method for foundation piles. The Menard-penetrometer method is also often called the French method, but the Menard method does not use the CPT, but the Pressiometer.

The influence zone for the pile tip of both the Dutch and the Belgian method is bigger above than below the pile tip. For the French method, this zone has the same size below and above the pile tip. However, the numerical simulations reveal that the influence zone should be bigger below the pile tip. This means that, the measured cone tip resistance below the pile tip level, is more important for the calculation of the pile tip bearing capacity.



Calculation procedure of the pile tip bearing capacity:

Step 1: Smoothen the raw q_c curve to control the local irregularities.

Step 2: From the smoothened curve, calculate the average value ($q_{c,avg}$) of q_c within the zone 1.5 D above and below the pile tip.

Step 3: From the smoothened curve, remove peak values bigger than 1.3 times q_c below the pile tip and 0.7 times $q_{c,avg}$ above the pile tip.

Step 4: Take the average of the values found at step 3 as a representative value of the pile tip bearing capacity (q_t).

Fig. 4. French Method (adapted from Niazi and Mayne, 2013).

Over the years, a lot of people have presented improved CPT-based design methods for estimating the pile bearing capacity, such as Kolk et al. (2005) who presented the Furgo-05 method, Jardine et al. (2005) who presented the ICP-05 method, and Lehane et al. (2005) who presented the UWA-05 method.

NUMERICAL SIMULATION

In order to validate the position of the influence zone, pile load tests have been numerically simulated with PLAXIS. Each numerical simulation is considered to be an axial symmetrical calculation with standard 15-nodes elements. The disadvantage of simulations with Plaxis, like any other Finite Element Model, is that there are no continuous large deformations, so the pile installation process cannot be taken into account. Therefore, in this calculation, a large w = 25 % D displacement was used to model as good as possible failure of the pile foundation. The modelled pile is a reinforced prefabricated concrete pile with a diameter of 0.4 m and a length of 10 m (L/D = 25). The groundwater level is at ground level. The soil is homogeneous sand, which is modelled with a Mohr-Coulomb material model. The geometry of the calculation and all parameters are shown in Figure 5. The pile has already been installed in the soil from the beginning, which means that no installation effects (e.g. soil densification or installation method) could be included in the calculation.

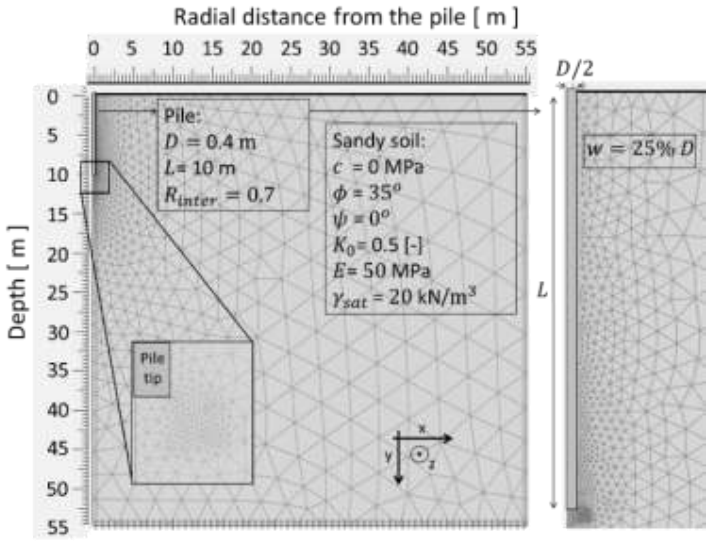


Fig. 5. Plaxis simulation: Geometry and parameters.

The numerical simulations show a plastic zone from 2 D above, down to 5 D below the pile tip, see Figure 6. It is assumed that the influence zone and plastic zone are roughly the same. This zone depends, besides on the pile head displacement w, also a bit on the soil and pile parameters. This zone also depends on the ground pressure, which follows from Figure 7, which shows the results of seven different pile lengths, from 2 to 45 m. All piles were subjected to the same pile head displacement. If one compares the size of the zone for the pile which is10 m deep, with the pile which is 45 m deep, the zone is roughly twice smaller.

In Figure 7, the deeper the pile, the smaller the plastic zone, because the stresses in the soil get higher with depth. Figure 7(b) shows that at the same time, the total pile bearing capacity increases. This is mainly because the area of the shaft, and therefore the friction along the shaft is increasing. The pile tip bearing capacity increases only slowly and only until a pile length of about 15 m. This last point is unexpected since, from a theoretical point of view, a deeper pile tip should have a higher tip resistance due to the higher vertical stresses in the soil (based on the analytical solution from Meyerhof, 1951). This will have to be checked with laboratory tests in the future.

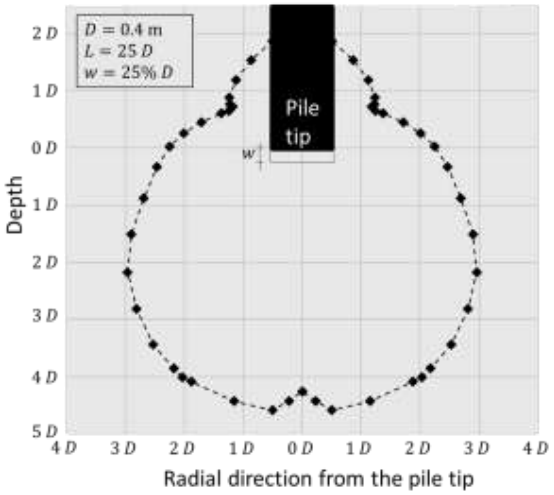


Fig. 6. The plastic, influence, zone around the pile tip.

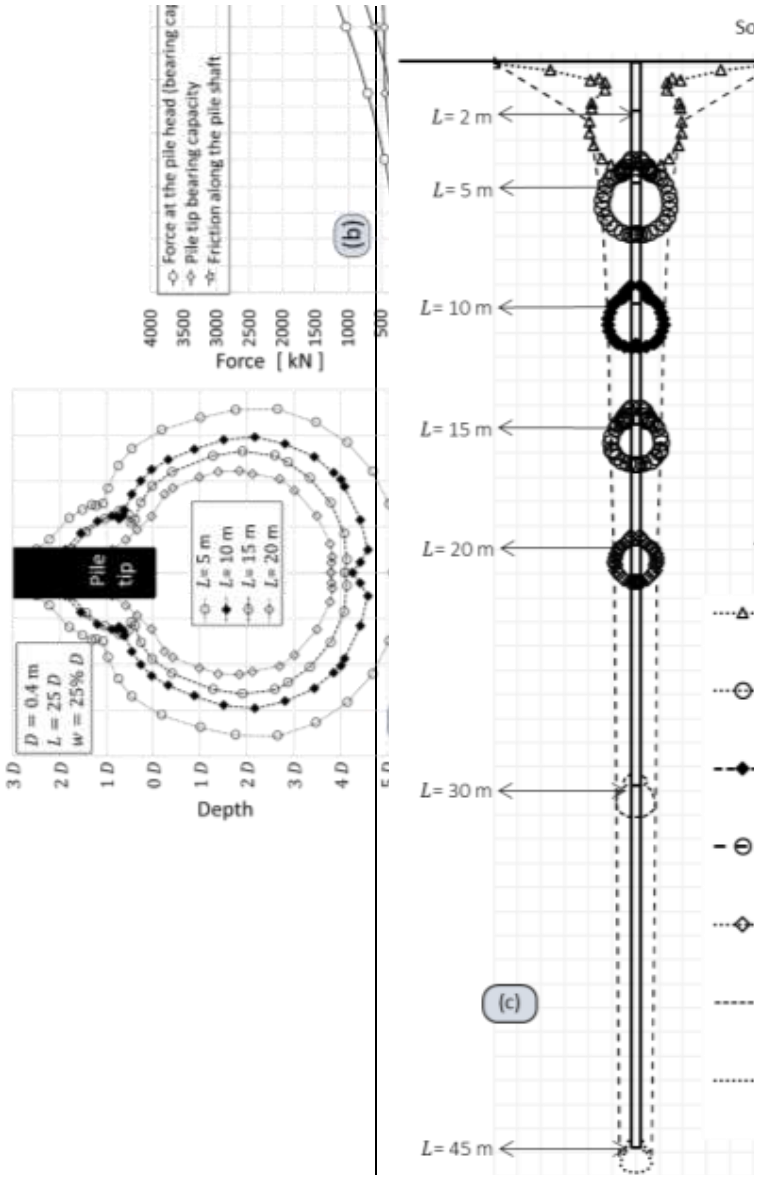


Fig. 7. The influence zone around the pile tip as a function of the pile length.

THIN SOIL LAYER INFLUENCE

The influence of a thin weak soil layer on the pile bearing capacity has been studied as well, because it indicates the position of the influence tone and also the amount of influence. The soil and the pile remain the same parameters as the simulations of the previous section. The term "weak" means that, or the strength (friction angle), or the stiffness (Young's modulus) of the thin layer is weaker than the respective parameter for the homogeneous soil in the previous simulation. Only one parameter is changed at a time in order to study the pure influence of the given parameter. The depth of the thin soil layer changes from 5 D above down to 10 D below the pile tip during one simulation, see Figure 8. The abovementioned soil parameters are studied for 2 different thicknesses of the thin soil layer; 0.5 D and 1 D, therefore, one simulation includes respectively 31 and 30 calculation phases. The first phase represents the simulation made for a pile installed in a homogenous soil, so there is no influence of the weak soil layer. This influence is studied from the second phase, until the thirty-one phase, regarding the depth of the thin soil layer.

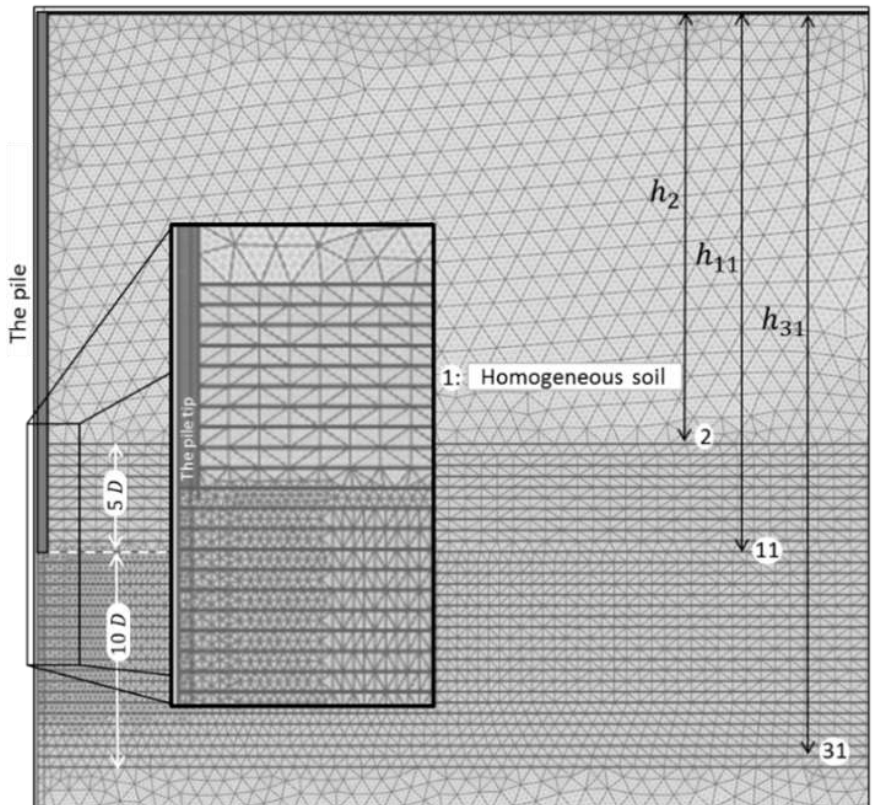


Fig. 8. Plaxis simulation for the influence of the weaker thin soil layer: Geometry.

Figure 9 shows the results of the simulation for a lower Young's modulus of the thin soil layer, which is taken equal to 50 % of the Young's modulus of the homogeneous soil. The results reveal that the pile bearing capacity depends on the Young's modulus of the soil, therefore, on the soil stiffness. The thin weak soil layer influences the pile bearing capacity when the soil layer is found to be from 2 D above the pile tip down to 6 D below the pile tip. This influence zone is in accordance with the plastic zone found in the simulation of Figure 5.

Almost the same influence zone can be found from the laboratory results of Van der Linden (2016), who performed model tests in a steel tank in which the soil stress were increased by pressure cushions. A CPT- cone was acting as a pile, penetrating weak layers of clay in the sand, more or less similar as in the numerical simulations.

The bearing capacity decreases with a maximum influence of 10.8 %, and 6 %, for the weak soil layer with a thickness of respectively 1 D, and 0.5 D. Therefore, the pile bearing capacity depends almost linearly with the thickness of the weak soil layer. The maximum influence is found to be around 1 D below the pile tip and not immediately at the pile tip, and this influence is negligible when the soft soil layer is found outside the influence zone. For this reason, there must be a weighted average value of the q_c-values of CPT in order to estimate accurately the pile tip bearing capacity.

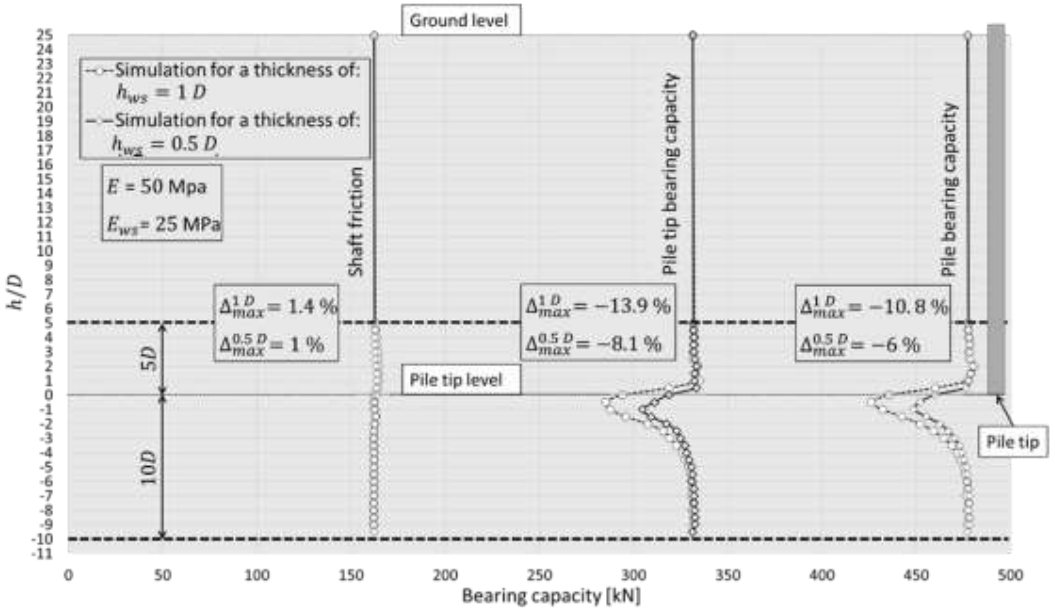


Fig. 9. Weak soil layer influence on the pile bearing capacity [Young's modulus is lower]

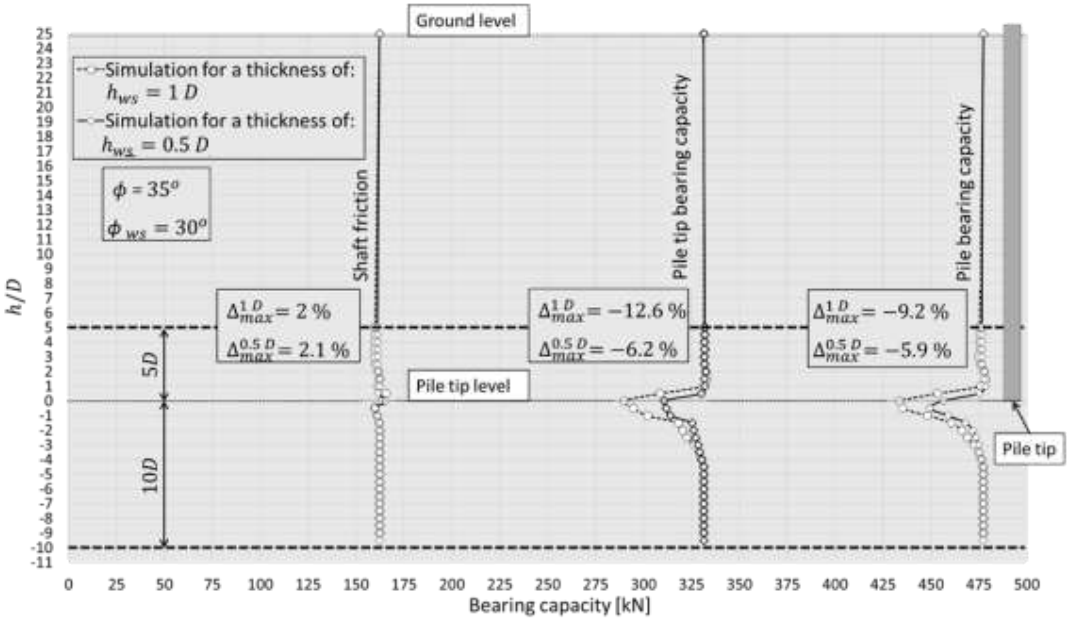


Fig. 10. Weak soil layer influence on the pile bearing capacity [Friction angle is lower]

The same conclusion can be drawn from Figure 10 for the case of the reduced friction angle. The friction angle of the weak soil layer is just 5° less than the friction angle of the homogenous soil layer. The results show that the pile bearing capacity depends on the strength parameter of the soil, as expected from existed

analytical solutions (Meyerhof, 1951). The influence of the friction angle is negligible if the weak thin soil layer is more than 5 D below the pile tip.

For both cases, the pile shaft is almost not influenced by the weak thin soil layer, only when this soil layer is found to be above the pile tip (as far as the soil layer is in contact with the pile shaft). However, this influence is very small and can be neglected.

The following symbols are used in figures above:

D	the pile diameter
h	the position of the weak soil layer regarding each phase of the simulation
h_{ws}	the thickness of the weak soil layer
E, E_{ws}	the Young modulus of the homogeneous soil, of the weak soil layer
ϕ, ϕ_{ws}	the friction angle of the homogeneous soil, of the weak soil layer
$\Delta_{max}^{1\,D}$	the change of the pile bearing capacity in % for a thickness of the thin layer of 1 D
$\Delta_{max}^{0.5\,D}$	the change of the pile bearing capacity in % for a thickness of the thin layer of 0.5 D

Based on Figures 9 and 10, and the laboratory results of Van der Linden (2016), the authors conclude that there is far more evidence for an influence zone which is mostly below the pile tip, as for the currently used influence zones, which means that these have to be adapted. An aditional option could be that the averaging procedure of the q_c values within the influence zone will be presented as a weighted average value of all the CPT values within this influence zone, see equations (2) and (3). In order to do so, a new set of weighting parameters must be defined, I_i. This set of parameters may be found from numerical or laboratory tests.

$$q_{c,avg} = \frac{I_1 * q_{c,1} + I_2 * q_{c,2} + \ldots + I_i * q_{c,i} + \ldots + I_n * q_{c,n}}{I_1 + I_2 + \ldots + I_i + \ldots + I_n} \tag{2}$$

$$q_{c,avg} = \frac{\sum_1^n I_i * q_{c,i}}{\sum_1^n I_i} \tag{3}$$

where:

$q_{c,avg}$	is the average value of the cone tip resistance within the influence zone
$q_{c,i}$	is the cone tip resistance at the i-th depth
I_i	is a set of weighting parameters for the $q_{c,i}$ value of the cone resistance

CONCLUSIONS

The rather simple numerical simulations made in this article deal about a pile already installed in a homogeneous sand layer which is described by a Mohr-Coulomb constitutive soil model. The results show that the plastic zone and the influence zone around the pile tip have almost the same size which is found to be from 2 D above down to 5 D below the pile tip. This zone has been confirmed by laboratory scale tests performed and published by Van der Linden. This reveals that the CPT values should be averaged more from the values below the pile tip than for the CPT values above the pile tip (unlike the existing methods propose).The plastic zone around the pile tip depends on the depth (and its higher stresses) near the pile tip. Since the plastic zone and the influence zone are in accordance, it is obvious that the influence zone is influenced by the depth of the pile tip, just as for the plastic zone.

Finally, the simulations show that the pile bearing capacity depends on the stiffness of the soil, something that is not taken into account by the existed pile design methods. The influence of the strength of the soil (friction angle) is, as expected, also observed in the numerical simulations.

REFERENCES

Begemann, H. P. (1963). The use of the static soil penetrometer in Holland. *New Zealand Engineering.* Vol. 18, No. 2, Feb. 1963, p. 41.

Boonstra, G. C. (1940). Eenige Beschouwingen over den Puntweerstand van Palen. *De Ingenieur*, 55, Feb. 1940, p. 33-45.

Bustamante, M. and Gianeselli, L. (1982). Pile bearing capacity prediction by means of static penetrometer CPT. *Proc. of the 2-nd European Symposium on Penetration Testing,* Amsterdam, May 1982, p. 493-500.

De Beer, E. (1963). The scale effect in the transposition of the results of deep-sounding tests on the ultimate bearing capacity of piles and caisson foundations. *Geotechnique.* Vol. 13, No. 1, Mar. 1963, p. 39-75.

De Beer, E. (1971). Application of the De Beer algorithm. Méthodes de déduction de la capacité portante d'un pieu à partir des résultats des essais de pénétration. *Annales des Travaux Publiques de Belgique/Tijdschrift der openbare werken van België*, No. 5, p. 321-353, Bruxelles 1971.

Jardine, R., Chow, F., Overy, R. and Standing, J. (2005) *ICP design methods for driven piles in sands and clays*. Marine Technology Directorate (MTD), London, Jan. 2005

Kolk, H. J., Baaijens, A. E. and Senders, M. (2005) Design criteria for pipe piles in silica sands. *Proc. of the 1st Int.Symposium on Frontiers in Offshore Geotechnics*. Perth. 2005, p.711-716.

Kort, A. (2008). Going Dutch with Geoengineering in Norway. *The 15th Nordic Geotechnical Meeting*. Norway, Sept. 2008.

Lehane, B. M., Schneider, J. A. and Xu, X. (2005) The UWA-05 method for prediction of axial capacity of driven piles in sand. *Proc. of the 1st Int. Symposium on Frontiers in Offshore Geotechnics*. Perth. 2005, p. 683-689.

Meyerhof, G. G. (1951). The ultimate bearing capacity of foundations. *Géotechnique*, Vol. 2 No. 4, Synopsis, p. 301-332.

Niazi, F. S. and Mayne, P. W. (2013). Cone penetration test based direct methods for evaluating static axial capacity of single piles. *Geotechnical and Geological Engineering. Vol. 31, No.4,* Atlanta, Jun. 2013, p. 979-1009.

Prandtl, L. (1920). Über die härte plastischer körper. *Nachrichten von der Gesellschaft der Wissenschaften zu Göttingen, Mathematisch-Physikalische Klasse,* Feb. 1920, p. 74-85.

Schmertmann, J. H. (1978). *Guidelines for cone penetration test, performance and design*. Monograph, Washington DC, Jul. 1978.

Van der Linden, T.I. (2016) *Influence of multiple thin soft layers on the cone resistance in intermediate soils*, Master thesis, Delft University of Technology, Feb 2016, p. G-29, G-62.

Van Mierlo, W. C. and Koppejan, A.W. (1952). Lengte en draagvermogen van heipalen. Vaststelling hiervan en enige daarbij verkregen ervaringen. *Bouw*, nr.3, Jan. 1952.

APPLICATION OF LONG-CHAIN POLYMER SLURRY AS SOIL STABILIZATION IN REVERSE CIRCULATION DRILLING SYSTEM

Gonçalo António de Araújo Costa
GEO Ground Engineering Operations Malaysia Sdn. Bhd, Kuala Lumpur, Malaysia.
E-mail: goncalo.costa@geosoil.com

Sri Ram Ramankutty
GEO Ground Engineering Operations Malaysia Sdn. Bhd, Kuala Lumpur, Malaysia.
E-mail: sriram.ramankutty@geosoil.com

Keywords: Polymer slurry, long-chain polymer, soil stabilization, reverse circulation drilling, pile foundation

ABSTRACT: Polymer based slurries are becoming increasingly popular among foundation contractors as a choice of soil stabilizer. Being environmental friendly, improving the structural capacity of the foundation element and optimizing the production rate of work progress and cost makes polymer-based slurries an ideal replacement for conventional Bentonite slurries as soil stabilizer. Reverse circulation drilling (RCD), is a dynamic drilling system, widely used in installation of bored piles and diaphragm walls due to its ability to reach deeper excavations. This method of drilling is compatible with the usage of the long chain polymer slurries with exceptional results.

1. INTRODUCTION

Since middle of the XX century drilling fluids have been used in civil engineering. In the last decades there was an increase of breakthroughs and improvements that continue until today. For years bentonite-based slurries were commonly used in the foundations industry, but the improvements made on polymer-based slurries make them increasingly popular amongst foundation contractors.

Now with these improvements polymer-based slurries are replacing Bentonite slurries as the choice for the soil stabilization due to their ability to increase the structural capacity of the foundation elements, production rates of the projects while still leaving a low footprint in the surrounding environment.

Polymer based slurries have improved along the years not only in their properties but also in their molecular level. Structurally polymer can classify as linear, ramified, short chain or long chain Polymers and their composition can be natural, semi-synthetic or synthetic.

1.1 Long Chain Polymers

Polymers, such G3 System Polymer, have a high molecular weight with long carbon chains acting as a primary structure; this is dually charge with their positive charge being responsible for soil binding and their negative charge responsible for the hydration.

These chains also have cross linkers that establish a three-dimensional web making this solution to develop a higher hydration rate and develop a higher viscosity than compared to bentonite slurries and short chain polymers.

The ability to mix with salt waters maintaining the slurry properties is also an improvement and an advantage when compared with other solutions. Being carbon based and biodegradable is also one

© 2018 Deep Foundations Institute

advantage that polymers can bring when compared with bentonite slurries.

1.2 Reverse circulation drilling – RCD

In a world that has seen breakthroughs in the structural engineering, buildings and landmarks are increasing their complexity which also leads to a higher standard of quality in the foundations work, deeper foundations and bigger diameters. One of the methods that is widely used is static drilling system, in which the drilling rig extracts lumps of soil in a bucket from the borehole and the slurry is pump to the borehole to replace the extracted soil. Current ongoing projects have projected depths of 116m to be drilled in Bukit Bintang City Centre, Kuala Lumpur with 2200mm and 2500mm diameters

The dynamic drilling system with reverse circulation drilling (RCD) consists in continuous drilling of the soil while the rig pumps the cuttings together with the polymer slurry out from the borehole into a series of sedimentation tanks or sedimentations ponds. This continuous process only halts during each section extension.

This method is used either to go through hard rock or achieving deeper target depths that cannot be reached with the static method, due to limitations of the rig's Kelly bar. Until today the maximum depth verified by the author with this method was 90m in a pile of 1800mm, still this can be an indicator that there isn´t virtually any depth limitation, which is a strong point for the higher demands of the engineering world. Still until

1.3 Continuous boring with RCD using Polymer

When drilling using reverse circulation process it is important to keep the slurry cycle on a continuous loop ongoing without letting it stop the drilling process. This means that no stoppages can occur until the element is complete to maximize the production rate.

Before the start of the drilling the tanks/pond and the pre-bored hole must be filled with slurry up to the platform level. When the drilling starts, the slurry is supplied from the sedimentation tanks into the excavation the slurry is sucked by the RCD pump position at the tip of the excavation together with the soil cuttings, is pumped back out through the rig outlet into the sedimentation tanks where the soil particles will settle.

The particles settle by gravity and are removed out of the tanks to keep the slurry density low.

After the slurry complete a full cycle through the tanks it is necessary to increase the volume of slurry in circulation to keep it at the platform level. In this stage either polymer slurry, previously prepared and stored in silos, or water is added to keep a stable running slurry volume. This occasion is also key to adjust slurry parameters to the target values.

When the parameters of the slurry are within the expected range, the slurry is supplied to the borehole. This process is continuous until the end of the drilling process.

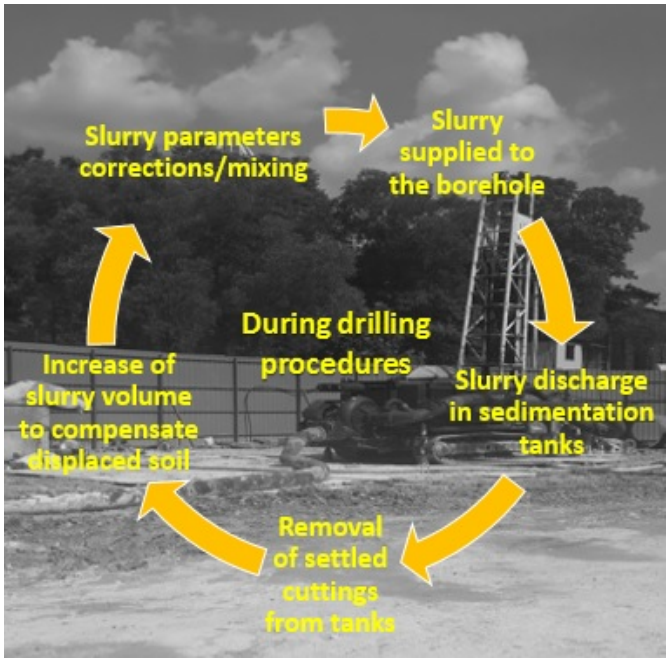


Figure 1. Slurry cycle during drilling procedures

2. PROJECT

2.1 Brief Project summary

The project PJ Sentral was in Petaling Jaya, Malaysia as a part of the PJ Sentral development area. The total piles excavated with PolyMud® using the static system were 354 bored piles another 88 bored piles were completed using the dynamic system Reverse Circulation Drilling (RCD) machine.

The excavation works with the long chain polymer slurry were done as an alternative to bentonite slurry for soil stabilization. The project started on the 13th of February 2014 and was completed on the 6th of October 2015.

Bored piles diameters ranged from 1050mm up to 2000mm and with a maximum depth of 90m resulting in an average of 62m depth for the 88

piles drilled with this method. The metallic guiding casing used was 3m in length.

2.2 Geological Conditions

The soil conditions encountered during this project with the usage of long chain polymer and RCD in PJ Sentral were as per Table 1

Table 1 SI Report for PJ Sentral

Depth (m)	Description	SPT (N)
0 - 9.0	Brownish whitish slightly gravelly sandy Silt of low plasticity	8
10.0 - 21.0	Very stiff, brownish red gravelly sandy Silt	18
22.0 - 48.0	Hard yellowish brown gravelly sandy Silt	30
49.0 - 69.0	Very dense, yellowish dark brown gravelly sandy Silt	45
70.0 - 90.0	Hard, dark brown grey gravelly sandy Silt	50

The ground water level was at 8.40m deep.

2.3 Targets

The targets to achieve during the foundation work progress with the encountered soil conditions were:

- Achieve a concrete overbreak inside the range of 2% - 15% of wastage to guarantee the structural capacity of the foundation elements;
- Guarantee quality of the slurry at the pile toe and mid column during drilling and before concrete pour with:
  - Viscosity above 40 seconds in Marsh Funnel API
  - Density inferior to 1,20g/cm^3
  - pH within the range 7 -12
  - Sand content below 3%
- Have the lowest carbon environmental footprint possible with nowadays technology during and after the project was completed

3. RESULTS

3.1 Quality

The control of the slurry quality parameters has a direct impact on the outcome of the foundation elements. For this to happen the borehole must be clean before the concrete pouring to avoid structural abnormalities.

If the cuttings from the drilling process settle between the time elapsed from the moment final depth was achieved until the first concrete lorry discharge we could have had a “soft toe” in the element and therefore the quality could be compromised.

The final average values for the 88 elements drilled before concrete were:

- Viscosity: 44.6 seconds
- Density: 1.062g/cm^3
- pH: 9.2
- Sand content: 0.48%

All the values were inside the range for the project targets.

3.1.1 Viscosity

On the static drilling system, the viscosity values usually are kept above 50 seconds in Marsh Funnel API. On the dynamic system of reverse circulation drilling the polymer slurry is responsible of ensuring the borehole stability and at the same time increase the cutting settlement time so that the borehole was kept clean. For this reason, the recommended viscosity for this project was to keep the viscosity between 40 and 50 seconds.

One of the advantages of using polymer slurry is in the mixing which can be done by the addition of the powder to a flow of existing water or slurry to perform viscosity adjustment at any stage anywhere in the batching plant and without the need of specific equipment. The slurry parameters check at any point of the slurry cycle. Sampling is collect inside the borehole with the aid of a bottom sampler or at the discharging inlet of the first sedimentation tank. To perform these slurry adjustments direct mixing is done either at the mouth of the excavation or at the outlet of the last sedimentation tank. All the viscosity readings are performed with an API Marsh Funnel.



Figure 2. Viscosity testing in Marsh Funnel API

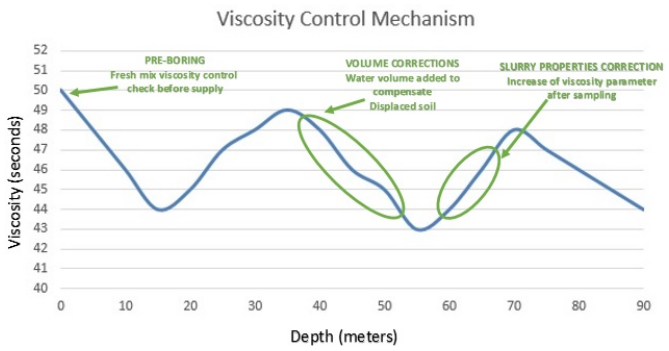


Figure 3. Viscosity control mechanism

3.1.2 Density

Density in foundations element is directly associated with the capability to increase or decrease the the specific weight of the slurry and therefore convey additional pressure to the sidewalls of the excavation soil preventing it from collapsing. The challenge present within reverse circulation is to monitor and control the slurry density and keep it in a desirable range necessary to stabilize the borehole without settling soil cuttings during drilling process.

Since this process is continuous, from the start until the reach of the final depth of the foundation element, the density of the slurry needs to be adjusted in the sedimentation tanks. The cuttings in suspension settled by gravity as it passes from each compartment to the next one in self-settlement, and subsequently removed with the assistance of a backhoe. As the slurry flows, back into the borehole the number of particles in suspension is adjusted to transport to surface additional mass of excavated soil.

Another method used in combination with the mechanical means to control the slurry density is the usage of MicroBond®, a chemical agent specifically designed to increase the settlement rate of the suspended particles out of the slurry. This chemical agent is applied directly in the sedimentation tanks and ponds and inside the boreholes as well. Figure 3. shows the density development and its control mechanisms working as the excavation of the borehole progresses. The graph highlights the slurry density varying as depth increases.

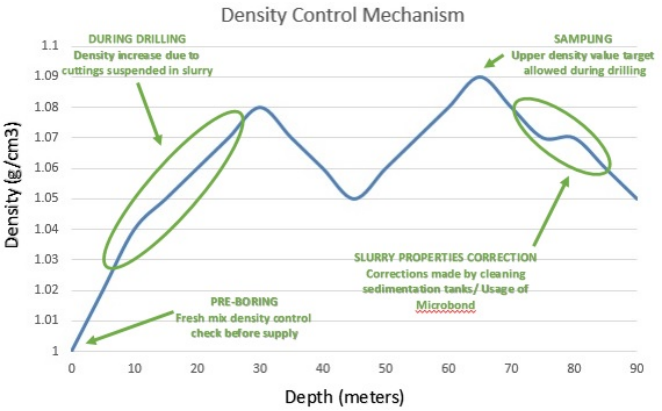


Figure 4. Density control mechanism

To keep a tight control on the progression of the slurry density it was necessary to check the slurry density in a calibrated mud balance after collecting a sample from the borehole. Additionally, a sample from the sedimentation tank closest to the discharge borehole point is also collected and values are recorded.



Figure 5. Density mud balance testing

3.2 Stability

The importance of the stability affects the foundation elements on cost and production levels. A high overbreak on the foundation element reflects itself on increasing the volume of concrete poured and this corresponds to a higher cost for the foundation contractor.

Having a high overbreak means that the foundation element maintains a larger geometry function of a deficient stability control during the drilling process. This higher overbreak also means that

there is more soil to excavate hence more time is required to complete the borehole. Higher concrete overbreak results in lower production rates as more time is allocated to finish each borehole. This leads to a higher cost associated with the rig given the operational costs associated such staff, consumables and maintenance cost increasing the rig downtimes.

Having this in mind, a strict control of the slurry parameters is necessary to maintain stability of the foundation element.

The upper limit target of 15% is the indicator that stability of the pile is not compromised from the start of drilling until it is cast with concrete. The lower limit of 2% indicates the volume of concrete poured is above the theoretical volume of the pile. The calculation of the overbreak follows the equation below:

$$\frac{(Actual\ Volume\ of\ concrete\ poured - telescopic\ theoretical\ volume)}{telescopic\ theoretical\ volume}$$

The average overbreak for the 88 elements drilled during the project is 11.6% which represents an excellent result. This value is checked on every concrete lorry discharge by measuring the level where the concrete is inside the borehole and compare it with a theoretical value of where it should be to occupy a theoretical perfect cylindrical volume. Both plots are drawn on a graph of concrete versus depth and results are analyzed for all piles.

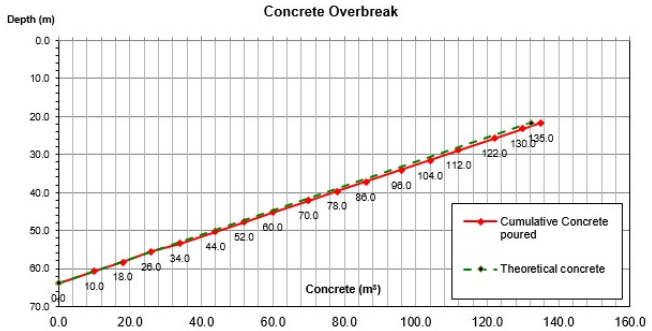


Figure 6. Concrete overbreak control graph

3.3 Production

For every project it is important to have production above a target value to ensure project profitability. The choice of the soil stabilization fluid becomes vital to achieve the desired production.

Compared to bentonite slurries, that require a minimum period of hydration of 8 hours of before use, the polymer slurry is ready to supply to the borehole immediately after mixing and it can even be mix, directly at the mouth of borehole reducing the downtime of the production cycle. For every batch of 1m3 of bentonite slurry mix takes 5 minutes meaning that 100 m3 takes 500 minutes and subsequent hydration of a minimum of 8h. On the other hand, a batch of 100m3 of polymer takes less than 30minutes to mix and hydrate. The readiness of polymer slurry to use boosts the production uptime and decreases the size of the batching plant making the production increase and the costs associated with it decrease.

Another big difference between the applications of these two types of slurries rely on the de-sanding time required. When we investigate the bentonite slurry cycle and compare it to the polymer cycle there is a huge difference in terms of equipment required, time consumed and slurry life time. The polymer slurry recovered for the borehole transporting the excavated soil into surface discharges in the sedimentation tanks for particles settlement, properties checking and readjustment before going back into the borehole. The cycle repeats itself until the end of the project without the need to dispose of the slurry keeping its life span indefinite until project completion. The sedimentation tanks need to hold a fraction of the entire volume of the excavation. Space and equipment required is minimum as not much more than 1 to 3 tanks. The polymer slurries do not require having to pass one single time through a de-sanding unit to remove all the fines out of suspension.

On the other hand, bentonite requires a mixing unit, a large desanding unit with the capacity to process large volumes of slurry per hour and at the same time remove out of suspension: small, medium and large size soil particles. These desanding unit have great deal of trouble to remove a minimum amount of silt or clay particles of suspension generally requiring several passes to remove 30 to 60% of cuttings. This leads to a progressive density increase of the slurry as pile depth increases. With repetitive cycles bentonite eventually needs to be disposed and fresh mixes are made to replace the original volume. The life span of bentonite in RCD is very limited and extremely costly. To keep up with excavation progress the batching plant storage volume set in place needs to be more than 3-fold the size of an excavation. Additionally, continuous disposal of bentonite is ongoing as its life span is short. All this sum up increases the time that the slurry needs to reach the storage and return to the borehole.

For a comparison of production rates, the project Da:Men USJ in Subang Jaya can be used as a reference since in that said project bentonite-based slurry was used prior to a polymer-based slurry replaced the system. The project started on 22-May-2012 and used bentonite-based slurry until 21-December-2012. In table 2 the rate of production is presented:

Table 2 Production rates with bentonite slurry

Production with Bentonite
2,5 piles per day with 7 boring rigs
0,357 piles/day/Boring rigs

A polymer-based slurry started with a trial pile on 6-December-2012 replacing step by step the number of rigs using bentonite-based slurry on 22-December-2012 completing the project on 6-March 2013.

Table 3 Production rates with polymer slurry

Production with polymer
2.93 piles per day with 7 boring rigs
0,418 piles/day/Boring rigs

For PJ Sentral, by using long chain polymer slurry from start to end of project and considering the example of the production rates achieved on Da:Men project, we can consider that the increase of 17% of production would have been achieved, when compared with a common bentonite slurry production, which translated on the time saving means that 128 working days were saved with the correspondent reduction in the production costs.

3.4 Environment

The environmental impact and carbon footprint is increasingly becoming a factor when time comes to choose the stabilization fluid. It is important to keep the project surrounding areas without influencing the normal environment cycle. Having undisturbed and unaltered surroundings like roads, drains, lakes or rivers due to the slurry used to stabilize the soil in a project is an indispensable factor to keep the population, fauna and flora untainted. The carbon footprint for its manufacturing and mainly transportation required for its large quantities applied on each site make it unique when it comes to damage the planet

The G3 System polymer, unlike bentonite, is biodegradable and carbon based. Since carbon is one of the most common existing elements in the environment the associated costs with slurry treatment and disposal are eliminated.

The slurry can be disposed either by direct discharge to a sewage system, after simply lowering the viscosity, and pH to the range values encountered in water (viscosity 26.5 seconds and pH 7), the resulting fluid is environmentally safe to dispose with no harmful effect at all.

On this project the disposal was performed with the following parameters:

- Viscosity: 28 seconds
- Density: 1.00g/cm^3
- pH: 7
- Sand content: 0%

4. CONCLUSIONS

The implementation of new innovations and technologies in the drilling stratus plays a significant role on how the foundation contractors are becoming more aware each day of the increasing demands of their scope of work. Implementing new products and procedures are a fundamental advantage when quality and environment are becoming a top priority.

The results achieved in PJ Sentral case study lead to the fact that long-chain polymer slurries like G3 system can be used with the dynamic system of drilling of reverse circulation drilling.

This combination can reduce the costs that are directly associated with stability and production therefore having a solution that can guarantee the expected results or even surpass them.

Stability, production and quality were achieved in all 88 elements due to the product capabilities and the strict control of the drilling method and slurry management.

5. REFERENCES

American Petroleum Institute. Recommended Practice for Field Testing Water-based Drilling Fluids, December 2003.

European Committee for Standardization. Eurocode 7: Geotechnical Design, January 2004.

European Committee for Standardization. Execution of special geotechnical work – Bored piles, September 2010.

British Standards Institute. Code of practice for Foundations, September 1986.

CHALLENGES FACED IN THE CONSTRUCTION OF 60M DEEP DIAPHRAGM WALLS, WITH HYDRAULIC GRABS IN CENTRAL LONDON, ENGLAND

Paul Wiltcher, Skanska, Denham Way, Maple Cross, Rickmansworth, Hertfordshire WD3 9SW, United Kingdom, paul.wiltcher@skanska.co.uk.

Peter Handley, Skanska, Bentley Works, Pipering Lane, Bentley, Doncaster, South Yorkshire DN5 9NB, United Kingdom, peter.handley@skanska.co.uk

ABSTRACT

This paper will discuss how utilising standard hydraulic grab technology, the Northern Line Extension (NLE) Project Team tackled the geotechnical challenges of constructing 1.2m thick, 60m deep diaphragm walls through highly variable London strata and overcame the significant impact that the ground conditions had on grab productivity, excavation rates, wear and tear of the equipment and delivered a high quality diaphragm wall, with zero lost time accidents, on programme and on budget. In addition to overcoming the difficult ground conditions, one third of the Station Box was constructed from within a three sided, 3m deep sheet piled cofferdam. The paper will present how the Project Team overcame the difficulties this presented to the management of the works together with the procedures and innovations developed to successfully install structural steel plunge columns into diaphragm wall panels with cut off levels up to 10m below the working platform.

Keywords: Northern Line Extension, Diaphragm Walls, London Clay, Harwich Beds, Lambeth Group, Thanet Sands, excavation rates, damage to grabs, BIM, plunge columns

INTRODUCTION

The Northern Line Extension (NLE) connects the Northern Underground Line from the existing "Kennington Loop" to the Battersea Power Station redevelopment. Although relatively short at 3.2km, the route includes the construction of two new in-line stations, one at Nine Elms and one at Battersea Power Station (refer to Figure 01). When completed the extended underground line will bring much needed public transport infrastructure into the wider Nine Elms and Battersea redevelopment areas of the Borough of Wandsworth. This paper focuses on the Battersea station development.



Figure 01: Overview of the Northern Line Extension route from the existing Kennington Loop to Battersea Station and a computer generated photograph and the Battersea and Nine Elms Developments.

© 2018 Deep Foundations Institute

The Battersea Station Box was divided into two discreet sections, the Crossover Box and the Station Box. The diaphragm walls for the Crossover Box, also the launch chamber for the Tunnel Boring Machine (TBM), were constructed first and from within a 3m deep, three sided sheet pile cofferdam. The Station Box diaphragm walls were constructed second. The Station Box will form the main public areas of the Station and are designed to provide step free access to the ticket halls, platforms and retail outlets.

Construction of the diaphragm walls commenced in November 2015 and was completed in March 2017.



Figure 02: Photographs showing panel excavation in the Crossover Box from within the 3m deep cofferdam.

GROUND CONDITIONS AND DIAPHRAGM WALL PANEL LAYOUT

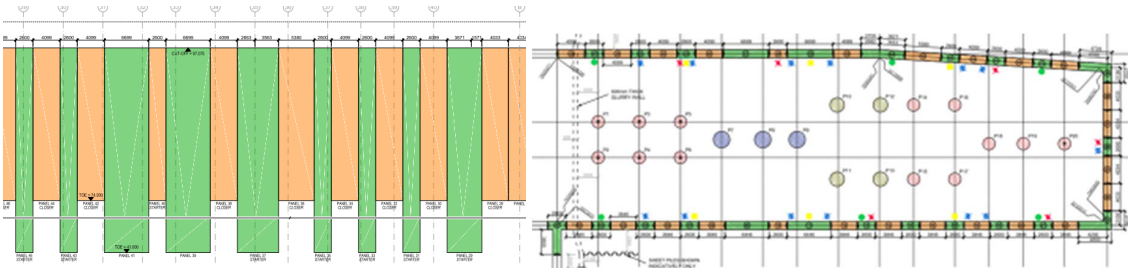
The London Clay formation, prevalent within the London basin, provides ideal conditions for the construction of diaphragm walls. It is uncommon however, for walls to extend beyond this strata, through the hard and variable Harwich Beds and Lambeth Group to found in the dense Thanet Sands some 60m plus below ground level (refer to Table 1).

Table 1: Summary of Ground Conditions

Soil strata	Thickness
Made Ground & River Terrace Deposits	0m - 5m
London Clay	5m – 38m
Harwich Beds (London Clay Formation)	38m – 42m
Lambeth Group	42 m – 54m
Thanet Sand	54m – 60m ++

The diaphragm walls were designed for two conditions. In the first instance, to provide lateral stability of the station box structure itself and to satisfy this design requirement, the depth of the walls extended approx. 27m from existing ground level, with each panel founding within the London Clay.

Secondly, the diaphragm walls were designed to accommodate the loads imposed by the future Battersea Power Station Phase 3 (BPS Ph3) development. This design requirement necessitated that alternate diaphragm wall panels be extended to a depth of 60m below existing ground level. To achieve this depth, excavation through Harwich Beds and Lambeth Group was required before founding each panel into the dense Thanet Sands (refer to Figure 03).



(i) (ii)

Figure 03: (i) Typical diaphragm wall elevation showing the alternate deep (green) and shallow (orange) diaphragm wall panels. The horizontal length of the deep panels was determined by the load draw down and bearing capacity required by the proposed BPS Ph 3 structure (ii) The actual plan view of the Crossover Box diaphragm wall panel layout.

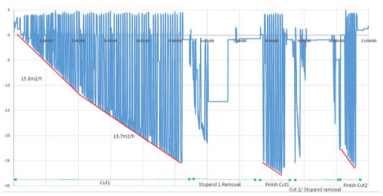
PANEL EXCAVATION

Panel lengths varied between single bite, 2.8m long panels; ~1.5 bite, 5.6m long panels and multi bite, 7m long panels. Target excavation rates varied through each of the strata encountered but as an average, each 2.8m long, 60m deep panel was scheduled to take approx. 3 days to excavate. However, actual excavation rates achieved on the first two panels were approximately 50% slower than the target excavation rates.

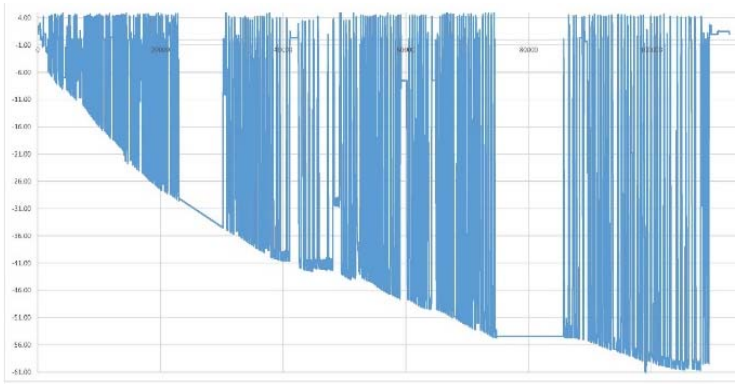
Excavation through the uniform London Clay proceeded as expected, excavation through the Harwich Beds and Lambeth Group was significantly more difficult but also considerably variable. Excavation rates into the Thanet Sands to form the panel toe, were largely as expected. With 50% of the panels extending through the Harwich and Lambeth formations to the Thanet Sand, subsequently panel sequencing was extremely difficult. With individual panel concrete volumes ranging between ~90m3 and ~500m3, planning for the large concrete pours was also extremely difficult because very little sequencing could be determined with any degree of confidence until productivity had settled.

In order to understand the problems faced it was important to determine the variability of the ground conditions and relate this back to the changes in strata levels. By logging the excavated spoil as accurately as possible and utilising basic “time and motion” techniques combined with an analysis of the on board grab instrumentation (refer to Figure 04), an as-built geotechnical long section (refer to Figure 05) through the site was developed to determine the worst case, baseline scenario. In the first instance, this enabled “time windows” to be set for delivery of the reinforcement cages and target dates for concreting to be organised with the ready mix concrete supplier, bringing back some degree of normality to the planning and sequencing of the works.

Secondly, this enabled the success of each small change to the excavation strategy to be measured against the baseline. After trialling a number of modifications to the grab teeth with mixed success, a strategy for pre-drilling of each of the 60m deep panels over their full depth was developed.



(i) Typical 24m deep panel



(ii) Typical 60m deep panel

Figure 04: Typical time verses excavated depth plots taken from the on board Jean Lutz rig instrumentation. When overlaid with the strata profiles, the plots were used to determine excavation rates (m2/hr) through the different soil layers.

A number of different pre-drilled configurations were considered before opting for a single pre-drill in the geometrical centre of each panel (refer to Figure 06). The Project Specification allowed for a maximum verticality of 1:200 over the exposed face of the diaphragm wall and so there was a risk that any pilot hole, pre-drilled with a verticality less than 1:200, may cause problems with grab verticality during subsequent diaphragm wall excavation.

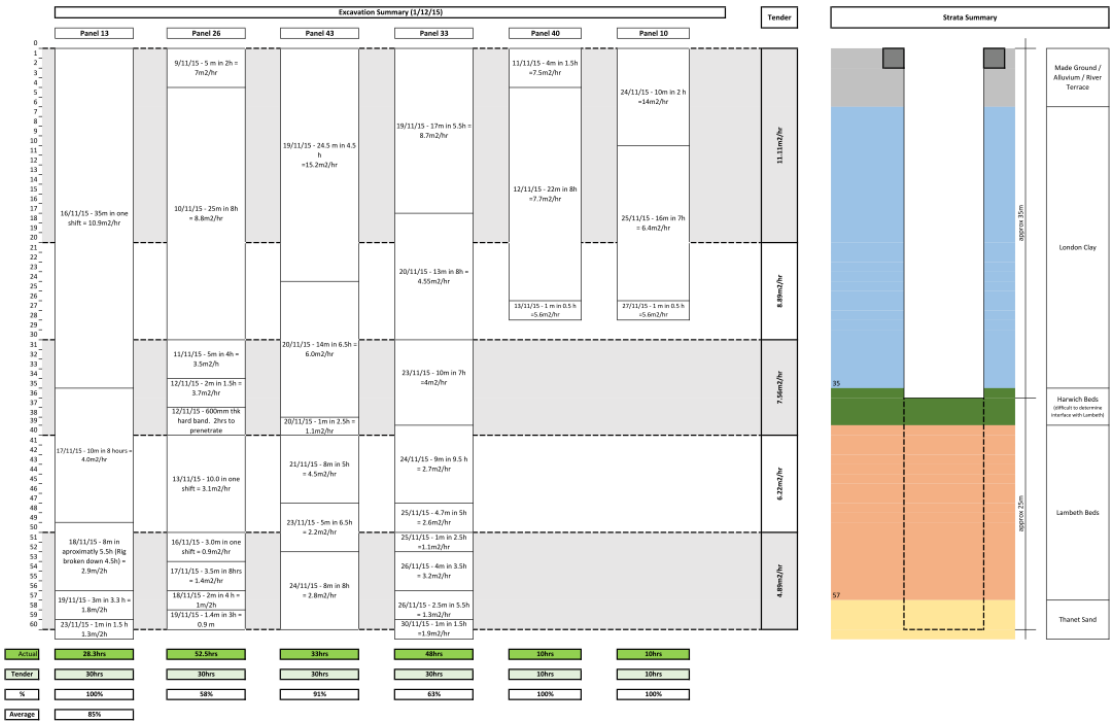


Figure 05: Extract from the "as-excavated geotechnical long section"

It was decided that an 880mm temporary cased, 800mm diameter pilot hole, drilled centrally within the 1200mm thick diaphragm wall would offer sufficient improvement to grab excavation rates and with a [target] tolerance of 1:125, provided sufficient mitigation to the risk that the pilot hole would not adversely impact the verticality of the later diaphragm wall excavation.

The Geotechnical Baseline Report for the site, stated that the Harwich Beds contained bands (up to 100mm) of hard strata with a maximum unconfined compressive strength of 100MPa. Our construction records showed that grab excavation rates reduced to as little as 0.3m2/hr and that the band ranged in thickness from 0.6m to 3.5m. In its in-situ state the grabs simply could not penetrate the strata. However, experience of piling through the same strata presented no significant difficulty to conventional piling techniques. It was therefore considered that a central pre-drill through this hard band would create a weak spot that would assist the grabs in breaking up the material.

A similar theory was developed for the Lambeth Group. Excavation rates through this strata varied from between 1.9m2/hr and 3.0m2/hr. The strata consists of an unpredictable make up of hard clays, silty clays and sands. In its confined in-situ state, a 27 tonne grab could at best only scrape across the excavation face and in turn achieve very little penetration. However, traditional piling techniques had again no significant difficulty excavating through the same strata. It was considered that the single central pre-drill would put the strata into an "unconfined" state and provide a pathway into which the material could fail into with each bite of the grab. Refer to Figure 06.

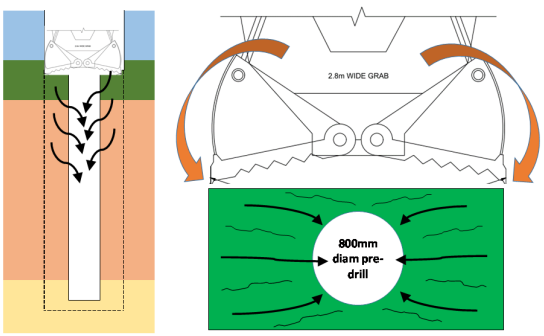


Figure 06: Schematic showing the location of the centrally drilled pre-drill in each of the 60m deep panels.

The success of the pre-drilling was immediate and is presented in Figure 07. Excavation rates through the Harwich Beds increased to an average of 2.9m2/hr and through the Lambeth Group, increased to an average of 5.1m2/hr.

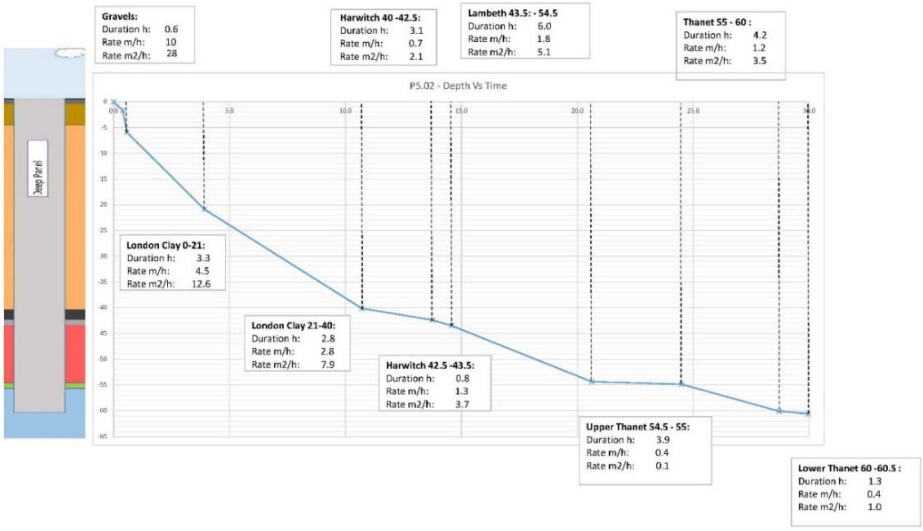
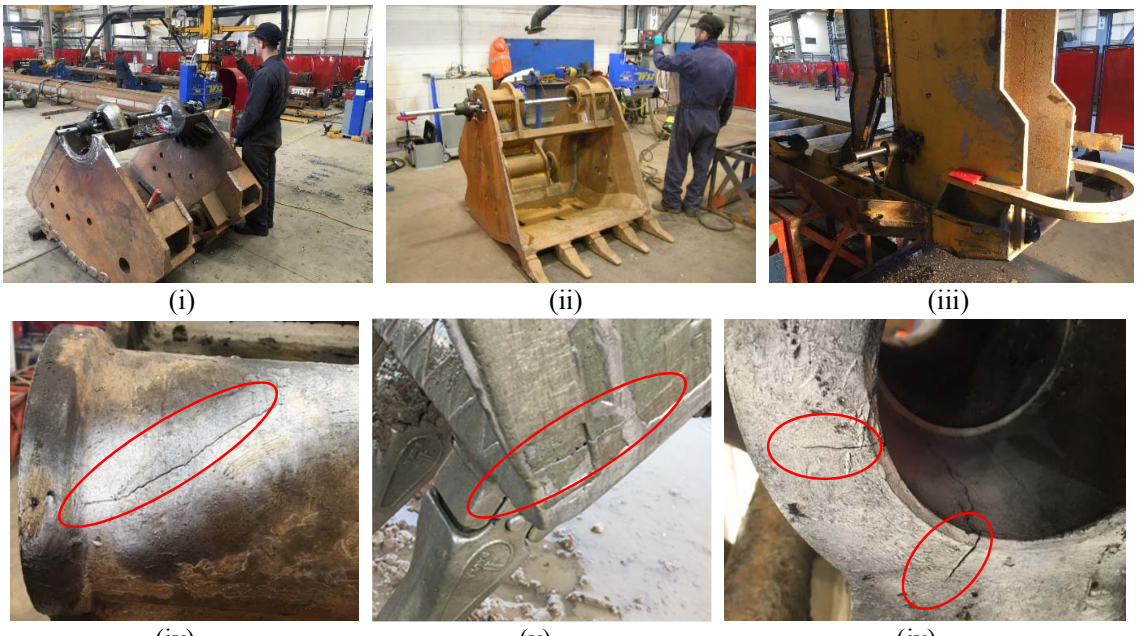


Figure 07: Typical plot of grab excavation rates against depth verses time against strata

DAMAGE TO THE GRABS

The hard excavation through the Harwich and Lambeth formations had a significant impact on wear and tear of the grabs. After completion of the Crossover Box, where the grabs had been working continuously for 20 weeks, both grabs required significant repair not only to the jaws and other typical wear parts of the grab but also to the main structural body (refer Figure 08)

All repairs to the grabs was carried by our own Specialist Plant Department in Doncaster, England.



(i) (ii) (iii)

(iv) (v) (iv)

Figure 08: Clockwise (i) Replacement of spring bushes (ii) In line boring of grab jaw (iii) Replacement pivot bosses (iv) Structural cracking to grab body (v) Structural cracking to the jaws of the grab (vi) Structural cracking to the jaw pivot, repaired by speacialist welding techniques.

The occurance of major breakdowns was of significant concern and detailed record keeping of productive verses non-productive time identified that there was a re-occuring pattern to the major breakdowns. From the graph presented in Figure 09, it can be seen that cumulatively and approximately every 10 to 11 weeks, the grabs experienced some kind of significant breakdown. A programme of preventative maintenance, over and above what would normally be considered as routine preventative maintenance was introduced. This included the strip down and structural checking and testing of all major welds on the body of each grab.

The maintenance programme proved successful in limiting the amount of non-productive time as can be seen from Figure 09, where during the last 18 weeks of the Project grab productivity reached its highest levels and grab break down time was minimised.

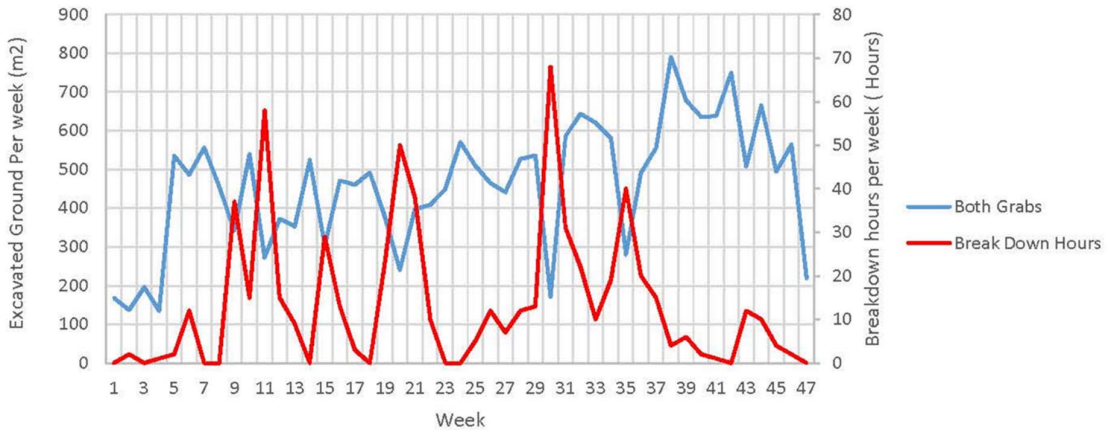


Figure 09: Graphical representation of the 10-11 week cycle of major grab breakdown (Note: the impact of each breakdown can be seen in the corresponding reduction in excavated m2).

CONCRETE DISCHARGE CHUTES

Constructing the Crossover Box diaphragm walls from within a three sided sheet piled cofferdam presented a number of logistical and health & safety challenges. Access for excavated spoil, reinforcement cages and concrete into the box was restricted to a single entry and exit ramp. In real terms a standard 60m deep x 2.8m long panel produced ~200m3 of excavated spoil, required 5 reinforcement cages sections and ~200m3 of concrete to complete the panel. The excavation sequence and programme necessitated concurrent excavation and concrete operations and truck logistics therefore required careful planning and coordination not only to ensure that activities did not grind to a halt, but also to ensure the safety of operatives working within the box.

A number of options were considered to try and negate the need for any trucks to enter into the Crossover Box. The use of concrete pumps from the high level was considered as an expensive but viable option. With planned production requiring an average of three panels per week to be concreted, the use of pumps would eliminate approximately 80 concrete truck deliveries from the site logistics plan (~160 truck movements when considering entry and exit from the box).

However, the use of concrete boom pumps was an expensive solution. Following the principle idea of delivering and discharging concrete from the higher level to the lower level, the Project designed and fabricated a simple but effective concrete discharge chute. A fully articulated lower chute section provided flexibility in the system to allow for variances in site constraints and panel lengths and enabled a “one type fits all” chute to be developed (refer to Figure 10).

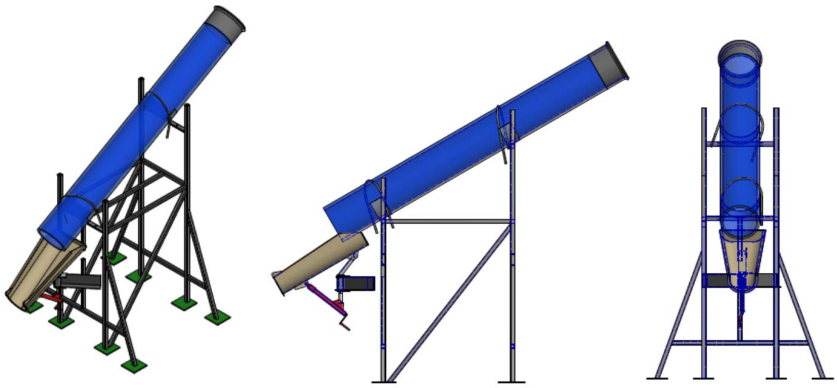


Figure 10: Schematics of the concrete discharge chute used in the Crossover Box.

Designed and fabricated by Cementation Skanska and costing a fraction of the equivalent concrete boom pump costs, the system was extremely successful and was a key factor in maintaining the high levels of health & safety management required on the Project and was a significant factor that contributed to final zero lost time accident statistics achieved by the Team.

DIAPHRAGM WALL PLUNGE COLUMNS

The construction of plunge columns, installed to structural steelwork tolerances in rotary bored piles using long plunging frames to facilitate top down construction techniques, is common practice and the methodology is well defined. However, the construction of plunge columns in low cut off diaphragm wall panels where the ability of a plunging frame to obtain reaction from a pile casing to accurately move and position the plunge column does not exist, had not been done before as far as the author is aware.

The Station Box design called for the installation of 12 plunge columns within the low cut off, internal diaphragm wall running longitudinally along the length of the box. In order to construct these columns, a bespoke frame for placing and positioning the columns was designed and fabricated by Cementation Skanska (refer to Figure 11).

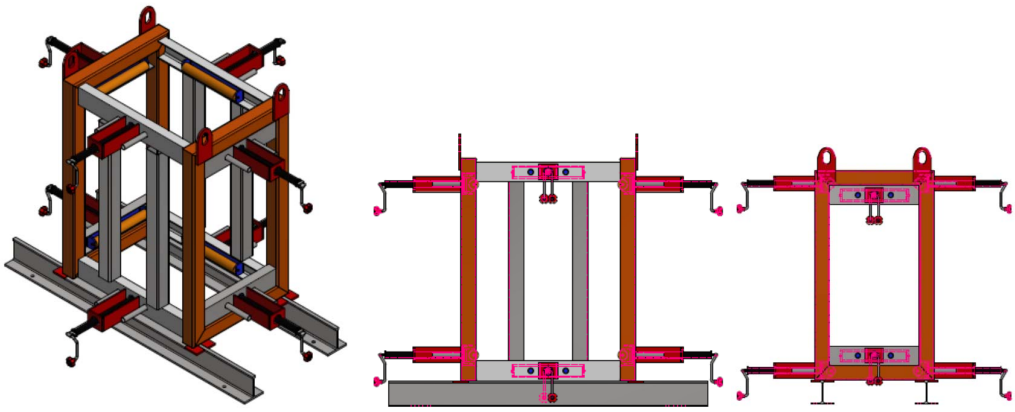


Figure 11: Extracts from the diaphragm wall plunge column frame fabrication drawings.

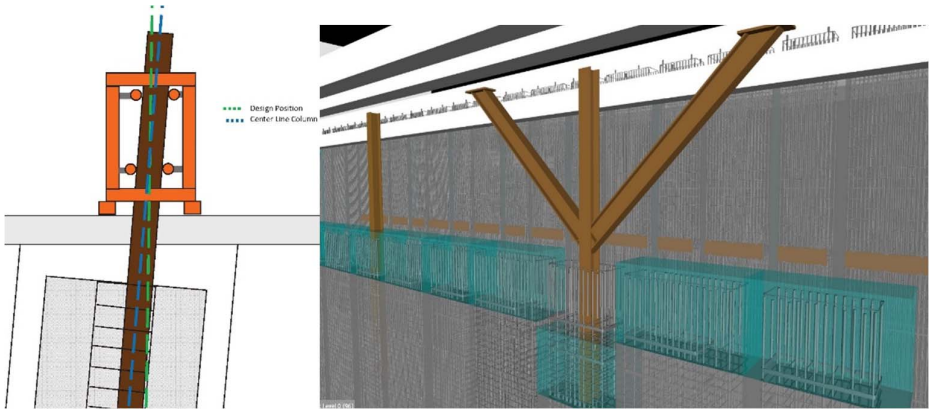
In their final working condition, each plunge column section was designed to be encased in concrete. However in the short term, each column was designed to carry the temporary construction loads

imposed as the ground within the station box was excavated and the roof support structure was constructed. Therefore, in both conditions, installation tolerances were critical, 1:300 verticality, +/-10mm in plan and +/-5mm in level.

The installation frame was based on the same principles as a typical plunging frame (but inverted) and needed to be sufficiently robust to (i) carry the self-weight of each column (ii) be sufficiently stable and rigid so as to provide adequate reaction to move and position each column into its final design position and (iii) to be able to have a mechanism suitable to make fine adjustments to the column position.

The successful installation of each plunge column relied upon a number of elements of the panel construction being within acceptable limits of deviation, most importantly the final position of the reinforcement cage, through which each column need to be placed. During the construction of Panel 8.20, verticality of the panel excavation, the final position of the reinforcement cage and the position of the internal shear links within the reinforcement cage were all at the limit of their tolerances and the combined effect resulted in the reinforcement cage clashing with the position of the plunge column (refer Figure 12(i)).

Consequently, the plunge column was installed with a verticality tolerance 1:104. Unfortunately, this column was designed as the main support for a temporary bridge over the Station Box and back analysis of the design demonstrated that the column now failed in the temporary condition. Due to the accuracy of the construction records, the as-built details were fed into the Project's BIM model and remedial works to strengthen the column were designed and fabricated in advance of bulk excavation by the main contractor. This is a good example of pro-active use of the BIM model to assist in the timely resolution of a construction issue that resulted in minimal cost and programme impact to the follow on works (refer Figure 12(ii)).



(i) (ii)

Figure 12: (i) Schematic (exaggerated) sketch of the as-built position of the plunge column in panel 8.20 and (ii) an extract from the BIM model showing the remedial works solution to the out of verticality plunge column in Panel 8.20.

CONCLUSION

The difficulties encountered during the excavation of 60m deep diaphragm wall panels through what is generally considered to be well known, well understood and typical of the strata of the London Basin, demonstrated that the relationship and understanding between ground conditions and excavation technique can never be taken to be mutually exclusive. This diaphragm wall is the deepest ever

constructed by Cementation Skanska and one of the deepest constructed in the UK with hydraulic grab technology.

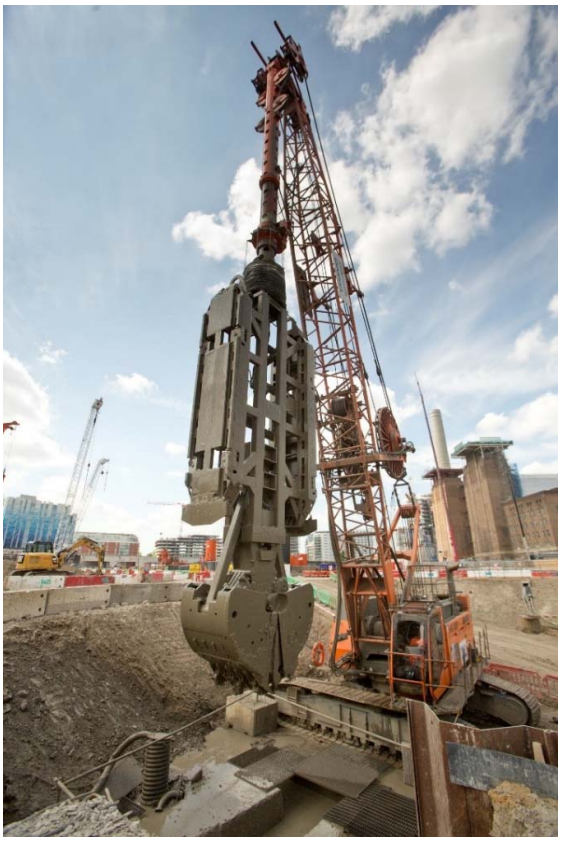
In addition to resolving the unforeseen difficulties presented by the ground conditions, the Project Team also demonstrated the positive impact that BIM and 3D modelling can have on a projects costs and programme by informing and changing construction strategies as the project works continue.

Many of the successes of the Project were made possible by the accuracy of the as-built records collected by the Project Engineers out in the field who were managing and supervising the construction activities. Although the benefit of this level of data collection is often questioned, the data collected and the often real-time data analysis undertaken on this Project demonstrated that with the right focused approach, data can be a powerful tool.

The design and fabrication of the bespoke and innovative Concrete Discharge Chutes not only mitigated hundreds of concrete delivery truck journeys into a restricted work area, reducing congestion and improving productivity but more importantly set the tone for the Project that Safety was important, a message and theme that continued throughout the Project and was rewarded with a zero lost time accident achievement record for the Project Team.

ACKNOWLEDGEMENT

The Authors would like to thank the Ferrovial Laing O'Rourke JV Northern Line Extension Project Team, Mott MacDonald, London Underground and many other colleagues within Cementation Skanska Ltd for their support and professionalism throughout the construction of diaphragm walls for the Battersea Station Box.



DOHA METRO'S FLAGSHIP TRIPLE LINE INTERCHANGE STATION

Christina Mavrommati, Mott MacDonald Ltd, Croydon, UK, 020 8774 2679,
christina.mavrommati@mottmac.com
Cremona Makaginsar, Mott MacDonald Ltd, Croydon, UK, 020 8774 2248,
cremona.makaginsar@mottmac.com
Carlos Posso, Mott MacDonald Ltd, Croydon, UK, 020 8774 2591, carlos.posso@mottmac.com

ABSTRACT

The paper describes the design of Msheireb station, part of the Doha Metro, which required complex structural and geotechnical interactions with numerous interfaces, including 25-storey oversite development. Solutions to suit site constraints and fast-track construction were chosen to deliver significant sustainable benefits. Robust anchored diaphragm walls minimised the potential ground movements that could have an adverse impact on adjacent structures, reduced the overall volume of excavation and provided unobstructed excavation areas allowing multiple construction activities to be undertaken in parallel and in safety. Where spatial constraints allowed it, open cut excavations provided cost, time, energy and construction material savings balanced against the added excavation. The project was delivered by an extremely diverse team through a fully integrated design and construction process, aided by the use of Building Information Modelling (BIM) and rigorous document management. The complexity of design and construction coordination is reflected in the successful synchronization of an unprecedented 12 Tunnel Boring Machine (TBM) breakthroughs for a single station. The experience gained from the design and the monitored and observed response of the earthworks and retaining structures allowed the optimisation of subsequent contract packages of work across the Doha Metro project.

Keywords: metro, diaphragm wall, anchor, depressurisation, crack width

INTRODUCTION

In 2013, Qatar Railways Company (QRC) awarded contracts to various international firms to construct sections of Phase 1 of the Doha Metro. Msheireb station is considered to be the Doha Metro's jewel in the crown, situated in the heart of Doha (Figure 1). It will act as the hub not only for the Metro but for the entire Qatar Rail network. With an X-shape footprint, measuring 350m by 175m at its widest and at a maximum depth of 37m, Msheireb station is one of the most complex and largest below-ground metro stations in the world.

Mott MacDonald provided multidisciplinary detailed design for Msheireb station, including ground engineering disciplines comprising civil, structural and geotechnical design of both main temporary and permanent works, engineering geology and hydrogeology, potential damage assessments, as well as instrumentation and monitoring plans.

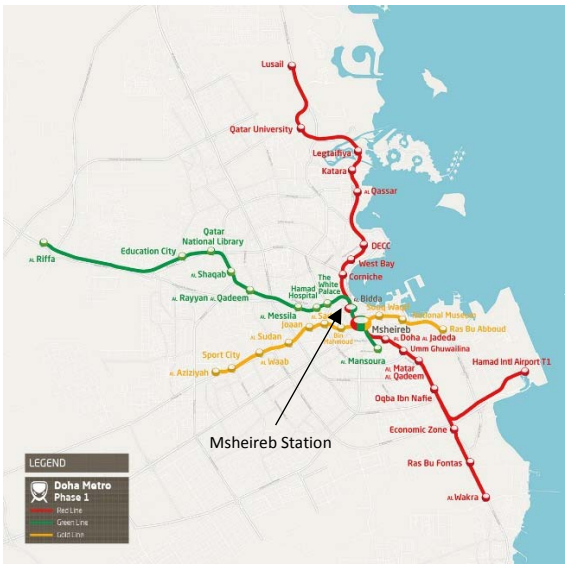


Figure 1. The Doha Metro Map

© 2018 Deep Foundations Institute

MSHEIREB STATION

Msheireb Station, being the only interchange station between the Red, Green and Gold lines and the largest station in the network has a crucifix shape. It is 350m long and 55m wide in one direction (including the Cross Over box) and 175m long and 35m wide in the other direction. The deepest section, at the Gold Box is 37m deep and it is one of the deepest stations of the Doha Metro. Along the Red/Green line box the typical depth is 28m. It will have five entrances at ground level and large open spaces at Mezzanine and Concourse levels. The six platforms are housed over two levels and passenger flow will be facilitated through 63 escalators and 6 travelators. Isometric 3D views of each level can be seen in Figure 2. Adding to the complexity, the station serves as a foundation for several buildings up to 25-storeys part of the regeneration development of *Msheireb Properties* (MP) *Downtown Doha*.



Figure 2. Isometric view of Msheireb Station split in levels

SITE AND CONSTRAINTS

The station is located in the heart of Doha, which is a busy, densely populated city with heavy traffic volume creating logistical nightmare for a construction of this size. The spatial constraints resulted in very tight working site boundaries limiting the available options for optimisation of the temporary works solutions. In addition, the program constraints and coordination with the design and construction activities of adjacent developments required that the temporary works had to start onsite before the design of the permanent works was completed.

With the station serving as a foundation to the huge MP Over Site Development (OSD), the interfaces, planning and phasing of works were a challenge to the design and construction of the station. The extent of the interface with MP is shown in Figure 3. The OSD above ground level are directly over the Red/Green and Cross Over Boxes, with basements extending to the sides of the Station Box in areas 4D and 4A.

The key connection details as agreed, included a full pinned structural connection between the station's Red/Green Box (Area 1) and any adjacent MP's basements and no structural connection (full movement joint) at any level between the Gold Box (Area 2.2) and any adjacent MP's basement. All these created large out of balance lateral loads causing the station box to sway, which required large diameter bored piles and thick walls and slabs to be designed. These are discussed further in the *Permanent Works* section of this paper.

All geotechnical and structural designs were based on Eurocodes considering local Qatari Construction Standards and any requirements set out in the Project Specifications.

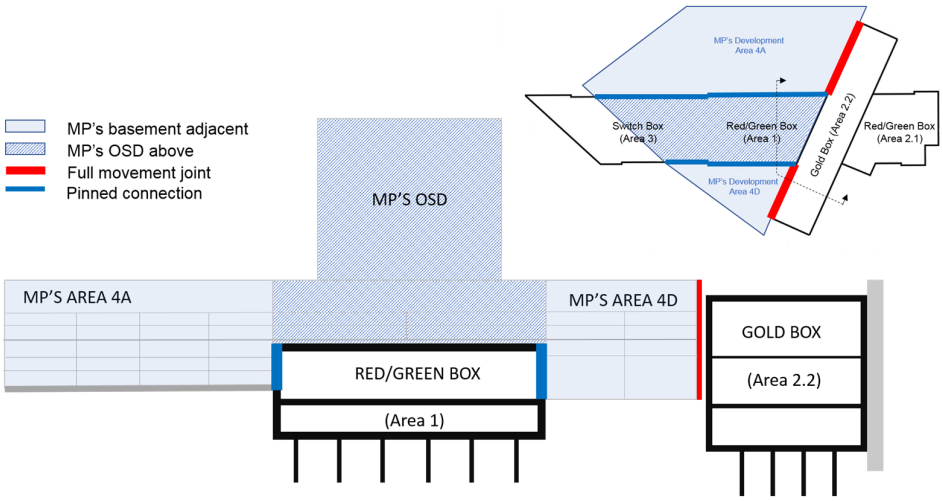


Figure 3. *Msheireb Properties Downtown Doha Development* interface with Msheireb Station

GROUND AND GROUNDWATER CONDITIONS

The stratigraphy of the Msheireb station site comprises approximately 2m of made ground/residual soils followed by 14m to 17m thick Simsima Limestone and 4-5m thick Midra Shale underlain by the Rus formation with thickness in excess of 30m.

The Simsima Limestone forms most of the land surface in Qatar. A feature of the Simsima Limestone, which was a main geotechnical risk for this project is the presence of voids and cavities. The size of these features varies considerably from small solution, pockets to large cavities filled with silt/sand. The upper portion is generally found to be weak, fractured and highly weathered. The lower Simsima Limestone is found to be weak to moderately weak and is generally more uniform with fewer fractures and small clay filled pockets.

The Midra Shale and the associated Fahahil Velates Limestone and Alveolina Limestone are relatively thin deposits mostly consisting of attapulgite rich shale which locally may be described more as a weathered siltstone. The Rus Formation is usually described as weak to very weak, whitish or yellowish chalky dolomitic limestone. The limestone varies in thickness, and is underlain by either siltstone or gypsum deposits. In Doha, the Rus formation had never been exposed in the past to such extents.

The estimation of Mohr-Coulomb rock mass strength parameters, which were used in diaphragm wall design and slope stability analyses, was undertaken using the software Roclab, utilising the Generalised Hoek Brown Rock Failure Criterion and Geological Strength Index (GSI). Several tests were carried out to estimate rock stiffness however, it was concluded that with the exception of the crosshole seismic velocity profiling, none of the tests could help evaluate rock mass stiffness at a large scale and conversions would be needed to account for scale, strain level and direction of loading.

The main means to directly evaluate rock mass stiffness are zone load tests and case history data, such as foundation settlements and movement of ground around retaining walls, but there is a general lack of these kind of data for the main rock types of Doha. The various sources of stiffness test data, in terms of mobilised strain range, were compared and conservative lines representing the Young's Modulus versus shear strain relationship of intact rock (red line) and rock mass (dashed black line) were defined as shown in Figure 4. By comparing the two trend lines, it was deduced that intact, E_{intact}, is approximately twice rock mass, E_{mass}, for any constant level of shear strain.

With regards to ground water conditions, the station site is underlain by the two aquifers of the Simsima Limestone and Rus Formation, separated by the Midra Shale. The water table is very high, at a few meters below the ground surface and the water is also saline, i.e. very aggressive containing both

sulphates and chlorides, the combination of which lead to challenging designs for durability both for the Temporary and Permanent Works.

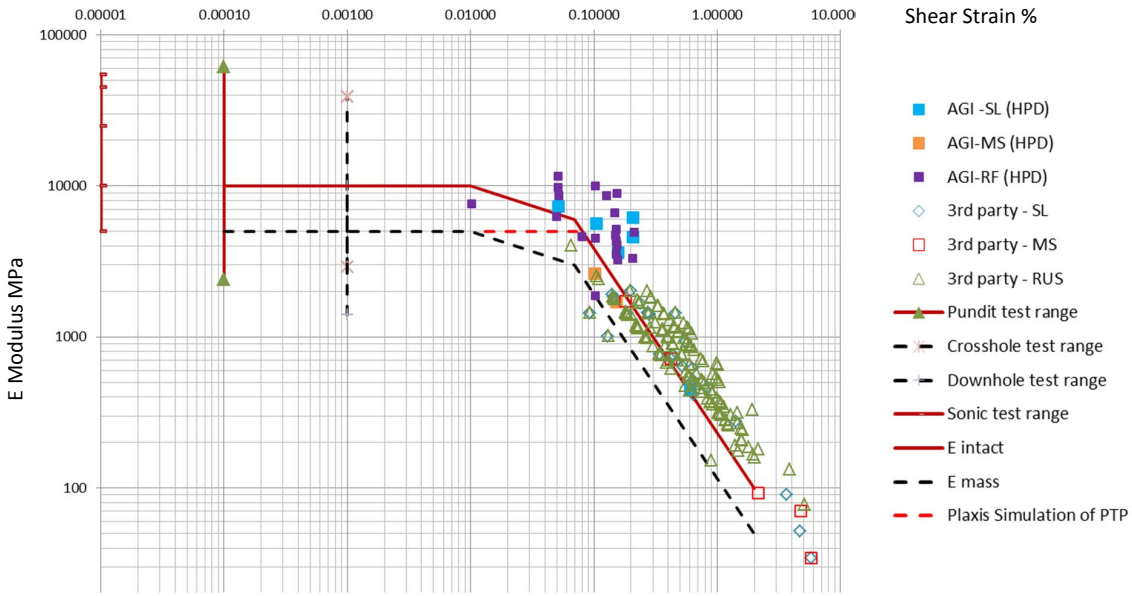


Figure 4. E vs strain relationship for the rock formations at Msheireb station

TEMPORARY WORKS

At tender stage, the construction methodology for the station box included the construction of temporary and permanent diaphragm walls along the whole perimeter of the station as well as secondary (internal) layer of diaphragm walls where excavation levels within the station footprint varied significantly. The permanent box was envisaged to be built using top down construction. As the design of the temporary works progressed construction sequencing, spatial and programme related restrictions lead to the adoption of alternative solutions and opportunities were identified that would lead to the optimisation of the temporary works.

By the end of the design period, the construction for the station box comprised (a) temporary diaphragm walls with props or with tie-back anchors, (b) temporary contiguous pile walls cantilevered and with tie-back anchors, (c) open cut excavations up to 27m deep (including rock bolts and interim berms) and (d) open cut excavations up to 8m deep combined with sections of temporary cantilever diaphragm walls up to 7m high.

The excavation resulted in approximately 1.3Million m^3 of excavated material. The complete design development of the temporary works excavation encompassed:

- Groundwater controls in the form of a dewatering scheme designed and operated by the specialist Dewatering Subcontractor. Depressurisation was fundamental to the temporary diaphragm wall design and basal stability requirements.
- Design verification by the Contractor i.e. mapping of encountered rock mass conditions; recording of representative discontinuity data to facilitate kinematic analysis (in order to identify any localised or global probable modes of failure; identify additional control methods e.g. rock bolting, hand scaling, reinforcement).
- Monitoring of instrumentation by the Contractor during and following the excavation works, including piezometers, ground surface movement markers and inclinometers.

Diaphragm Walls

The Station and Cross Over Boxes were constructed from the bottom up with anchors and props being progressively destressed and removed as the permanent walls were built. The diaphragm walls are 1.0m wide and the required embedment were generally 4.5m. There were 14 different designs of anchored or cantilevered diaphragm wall and they were all structurally independent from the permanent structure. The diaphragm wall layout can be seen in Figure 5. As part of the design process, they were considered sacrificial upon completion of the permanent station walls and all anchors had to be destressed. The diaphragm wall design considered total permissible wall movements up to 50mm and for most cases the critical construction stage which governed the structural design was the moment when anchors were destressed prior to construction of the next permanent slab mainly due to the large spans (more than 7m) between consecutive slabs.

To ensure wall durability the concrete was designed to satisfy 0.3mm flexural crack width for concrete faces exposed to the ground and 0.5mm flexural crack width for excavated concrete faces. This design crack width value was selected to provide the diaphragm wall structure with adequate durability for the specified 5 year design life.

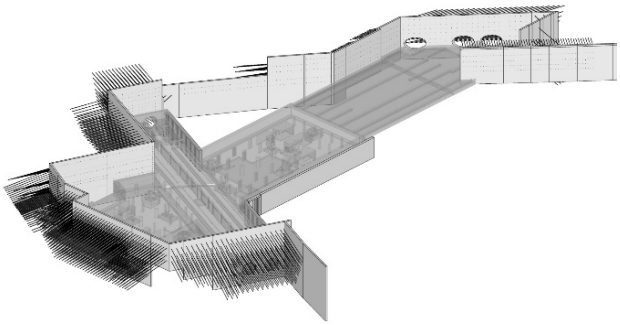


Figure 5. 3D view of the diaphragm wall layout and anchors

Anchors

Ground anchors were the primary support mechanism for the diaphragm and contiguous walls and resisted the load behind the walls during excavation and bottom up construction activities. The ground anchors had to provide continuity of support for the diaphragm and contiguous walls and they were pre-stressed prior to undertaking excavation activities to the next excavation level. According to the Project Specifications, a minimum design life of 10 years was required for temporary anchors.

Based on global stability analyses, a sliding wedge failure surface behind the diaphragm wall was found to be the critical failure surface. Based on various assessments and sensitivity checks, a two-part wedge failure mechanism was adopted to determine the anchor free lengths. Anchors were also extended at least 1.5m behind the failure surface and the minimum free length was specified as 4.5m. The failure surface considered in order to define the anchor free (unbonded) length is shown in Figure 6.

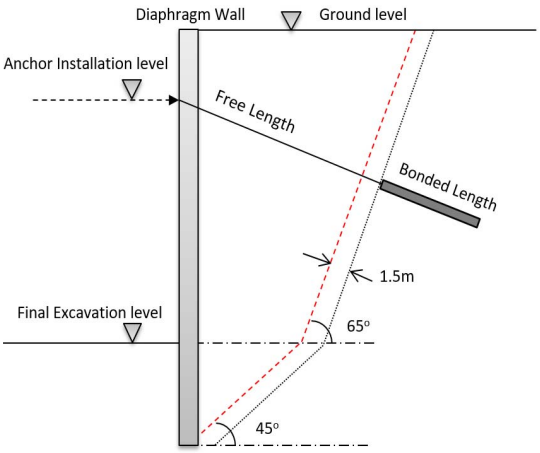


Figure 6. Sketch illustrating the failure surface considered in order to define the anchor free (unbonded) length

The anchor bonded lengths were initially estimated based on empirical relationships and were subsequently determined by the subcontractor based on preliminary anchor tests carried out on vertical and inclined anchors. The characteristic pullout resistance for the anchors was defined as approximately 1000kPa for anchors installed in the Midra Shale and between 500kPa and 700kPa for anchors installed in the Rus Formation. Carbon Fibre Reinforced Polymer anchors were specified where ground anchors would clash with the Tunnel Boring Machine and 10° declination angles were adopted for the anchors above the tunnel eye to avoid clashes with the TBM route. For all other anchors 20^0 declination angles were typically adopted. Where diaphragm walls formed re-entrant corners, anchors were also skewed.

Groundwater Control

Due to the favorable ground conditions for retaining wall design (the ground consisted of rock and therefore the earth pressures were somewhat limited), ground water pressure behind the diaphragm wall was always the governing design factor. Consequently, a key assumption which evolved into a requirement, in the temporary diaphragm wall design, was the groundwater pressure profile behind the diaphragm walls and below the base of the excavation.
In the absence of early site-specific hydraulic test information, as well as design program constraints, the initial diaphragm wall design assumed full hydrostatic pressures acting at the back of the diaphragm walls. However, considering the particular ground conditions and the fact that the diaphragm walls were not going to be providing a ground water cut-off, seepage modelling was undertaken part way through the design to develop more effective target groundwater pressure profiles considering the beneficial effects of natural ground water flow and depressurisation.

It was demonstrated with appropriate modelling, that pumping water collected in sump pits from within the excavation would not provide the optimum reduction in groundwater pressures. But the required pressure profile could be achieved by means of active deep well dewatering. Therefore, the dewatering design evolved to active diaphragm wall depressurization including deep dewatering wells outside the perimeter of the walls, instead of simple sump pumps within the excavation as originally planned.

As part of the design and upon completion of the additional ground investigation, after undertaking a thorough review of available permeability information including the invaluable in situ pumping test results, a series of target groundwater pressure profiles were developed through seepage modelling for the different stages of excavation and diaphragm wall configurations. A typical set of target groundwater pressure profiles are shown in Figure 7. It was required that dewatering enabled the gradually reduced pore water pressure profile behind each wall to be effective at each specific construction stage before excavation was advanced until reaching formation level. The final reduced pore pressure profile had to be achieved prior to de-stressing any of the diaphragm wall ground anchors in the bottom-up construction process and maintained until completion of construction of the permanent structure.

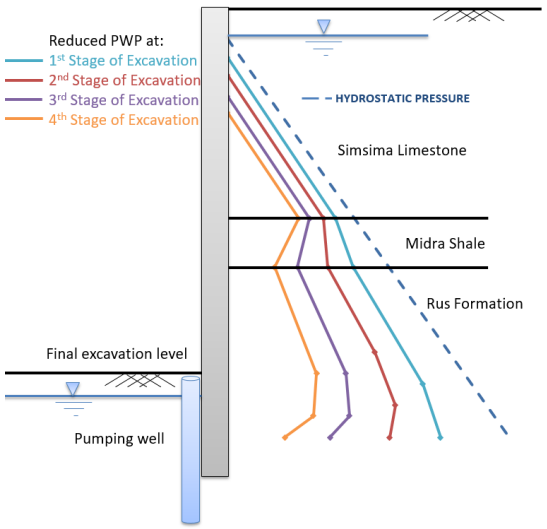


Figure 7. Diagram illustrating a typical set of target groundwater pressure profiles

Reduction in groundwater pressures behind the diaphragm walls also resulted in shallower potential failure surfaces. As a result, significant reduction in the number and length of anchors, from that initially determined, was achieved resulting in significant savings both in terms of construction time as well as in materials and resources. Appropriately placed piezometers, inclinometers and load cells were the key tools employed to ensure the target groundwater pressures profiles behind the temporary diaphragm walls were continuously verified and all design assumptions were validated on a regular basis.

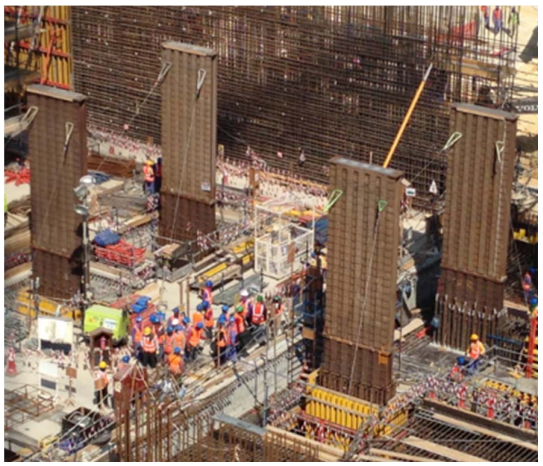
PERMANENT WORKS

Design life of 120 years in highly aggressive ground conditions resulted in the specification of high concrete density (C40/50 typical) and large concrete cover (up to 75mm nominal) to ensure durable structures. Flexural crack width limit of 0.3mm internally and 0.15mm externally were also specified in the original design, the latter relaxed to 0.25mm following an optimisation exercise on the durability requirements. The design requirements for durability and the large out of balance ground lateral loads due to the presence of the MP basements resulted in thick heavily reinforced walls and slabs.

Structural elements

The design of the structural elements was carried out using a comprehensive 3D structural STAAD model comprising more than 40,000 elements and 75 load cases to account for all temporary and permanent loading combinations. A global analysis model was constructed using plate and beam elements in order to generate design forces for use with Eurocode design methods for slabs, walls and columns. Localised models were also created using solid elements to map the stress distribution within a section's thickness. The reinforcement for the elements was optimised by adopting minimum steel area to control Early Age Thermal (EAT) and shrinkage cracking and specifying additional Serviceability Limit State (SLS) flexural reinforcement where that was required to control the crack width to the limit identified in the Project Specifications and from the durability assessments.

The large open spaces designed in accordance with the Architectural Branding resulted in large beam spans, of up to 30m and very slender columns (0.85 x 2.85m) having to take heavy OSD loads of up to 120MN per column. These columns, as illustrated in Figure 8, were designed with 6 Nos. 356 x 368 x 202 Universal Columns (UC) sections welded to 10 Nos. 250 x 50mm steel plates and additional 40 NoB40 rebars, all encased in self-compacting high-grade C50/60 concrete.



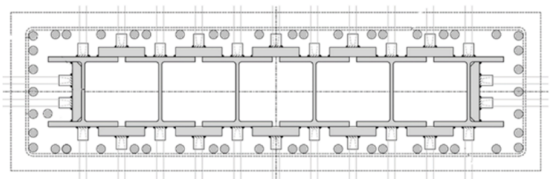


Figure 8. Composite columns being erected and their typical cross section to take OSD loading

Bored Piles

A worst case scenario of groundwater conditions, where ground water table is at ground level and no overburden pressure exists on top of the roof slab, required the design and construction of bored piles working in tension to keep the structures from floating. The uplift resistance had to be provided by the self-weight of the concrete structural elements while disregarding any overburden and the weight of the MP's development above, considering that it could be demolished in the future. At locations where the MP's development is located directly on top of the station box, the piles also act as integral part of the foundation system for the OSD.

The piles were also designed to resist large lateral forces. Asymmetric boundary conditions (as shown in Figure 3), where there is no structural connection between the Gold Box and the adjacent MP's basement developments and a full pinned connection to the Red/Green Box, resulted in very large lateral loads. The piles, being very stiff elements connected to the base slab, attracted a significant proportion of the lateral loads and therefore they had to be designed to resist large shear forces. These conditions resulted in 342 heavily reinforced, 1.5m diameter bored piles, working in bending, in compression and/or in tension designed for a 0.2mm crack width limit.

The reaction of the rock subgrade and the lateral reaction of the rock adjacent to the station box were modelled in the structural model as uni-directional compression only springs. The vertical, and lateral reaction and rotational stiffness of the piles was applied as bi-directional springs at the pile head with the spring stiffness magnitude dependent on the load or moment applied to the pile. Lateral support from the adjacent MP basement slabs was also applied as bi-directional springs at the assumed levels of the basements slabs to represent a pinned connection. The values of the subgrade springs to represent the Rus formation beneath the metro station box have been derived using the settlement software Pdisp.

Preliminary pile load tests were carried out using Osterberg cells. Calibration of the tests was based on Fleming's method using the in-house software "Cemset". This helped determine the non-linearity of the shaft response i.e. the vertical load-settlement response of the pile. The ultimate shaft friction derived from the back analysis of the pile tests for the various segments varied between 1200kPa and 1900kPa however, it was considered that peak skin friction may not have been mobilised. Considering the general form for the correlation between ultimate unit skin friction and UCS as $f_{ult}=K(UCS)^{0.5}$, it was deduced that 'K' may be around 0.35 and 0.45 for a rock mass UCS for the Rus formation between 10MPa and 15MPa.

The load settlement response of the piles was then used to derive the tangent spring stiffness values for the anticipated loads on the piles as calculated from the 3D STAAD model. For piles acting in tension the spring stiffness value was reduced to allow for the relaxation of radial stress around the pile and cracking of the pile concrete. The lateral spring stiffness of the piles was derived using the software Repute and an iterative process. The iterated load response from STAAD was then used to design each pile structurally, limiting the crack width to 0.2mm in flexure and tension. The length of the piles was determined such that enough skin friction, as determined from preliminary pile load tests, would be mobilised to counteract the uplift forces.



Figure 9. (a) diagram of amended reinforcement; (b) installed piles (c) piles at the Gold Line box

Due to large number of bars from the pile, the reinforcement interaction at the pile to base slab interface had to be validated by preparing a full-size mock-up at Msheireb station. As per the design intent, not all the base slab reinforcement could pass through the vertical pile reinforcement. As a result, some areas at this interface could end up under-reinforced, with the risk of localised cracking greater than the limit being able to form. Several methods of inserting additional reinforcement were assessed and an alternative solution was proposed with bundled straight bars provided on both sides of the pile with additional L-bars to cover the unreinforced area as shown on Figure 9 resulting in sufficient reinforcement at those locations and crack widths within acceptable limits.

Tunnel Boring Machine (TBM) Arrivals

The complexity of design and construction was also reflected in the successful coordination of an unprecedented 12 TBM breakthroughs at Msheireb Station. It is especially unique, that at each end of the station the TBMs were received in different ways as described in the paragraphs that follow.

At the Cross Over Box end of the station, due to spatial constraints, the external wall through which the TBMs had to breakthrough is skewed. This is impractical for the TBM cutter head as, normally, it must cut through uniform materials during breakthrough operations. The original design included Sprayed Concrete Lining (SCL) stubs through which the TBMs would enter the station, but due to cost and programme constraints these could not be constructed. The alternative solution involved a tailored external permanent wall combined with concrete 'plugs' of similar stiffness to the rock. These concrete plugs were built between the temporary diaphragm wall and the newly squared permanent wall, as illustrated in Figure 10.

At the Gold Box and Red/Green box the TBMs broke through tunnel eyes reinforced with Glass Fibre Reinforced Polymers (GFRP) and were received onto the base slab (Figure 11a) and onto an elevated platform, 7m above ground (Figure 11b), respectively. The GFRP tunnel eyes were designed in collaboration with the supplier, considering a strain limit of the material limited to 0.82% and limiting the yield stress to that of steel reinforcement.

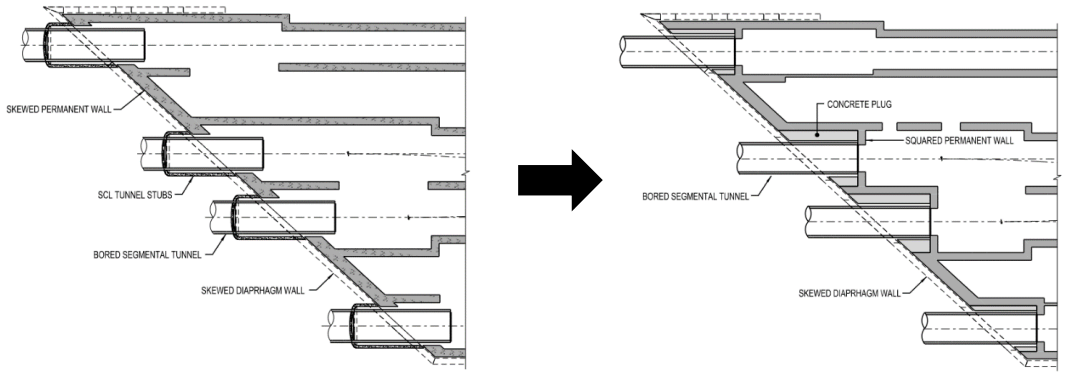


Figure 10. Switchbox Retrieving chambers for Red and Green Line TBM's



Figure 11a. Permanent Gold Box Headwall for TBM retrieval



Figure 11b. Elevated platform in front of the Red/Green line headwall for TBM retrieval

INNOVATION AND TECHNOLOGY

The project was delivered through a fully integrated design and construction process by an extremely diverse team of designers and contractors. This was heavily aided by the utilisation of Building Information Modelling (BIM). BIM Level 2 was utilised in the project where each discipline (Architectural, Structural and MEP) produces models which are then clash detected and resolved through Inter Disciplinary Coordination meetings. A snapshot of the combined BIM model can be seen in Figure 12. The use of BIM in this project allowed the team to virtually investigate different construction options which then enabled them to choose the optimum solution. Clashes and changes to the structure made by the various disciplines could be easily identified at any moment during the design process.

SUSTAINABILITY

The construction of the Doha Metro system, will not only allow easy public movement across the city, but it will also fulfil Qatar National Vision 2030 which aims to transform Qatar into a more sustainable society by improving mobility and delivery mechanisms of public services. Msheireb Station is the first development to receive a 5-star rating in the final certification stage of the Global Sustainability Assessment System (GSAS). QRC has set a goal to also receive 4-star rating for the Gold Leadership in

Energy & Environmental Design (LEED) which relates mainly to the Mechanical Engineering and Public Health design and installation of equipment. With regards to Civil and Structural design the focus is in material usage and procurement. At the time of writing, the predicted energy saving is 29%.

As part of the Doha Metro scheme, the project for Msheireb Station alone, delivered significant sustainable benefits. Robust diaphragm walls minimised the potential ground movements that could have an adverse impact on adjacent structures, reduced the overall volume of excavation. This provided clear excavation areas giving the Contractor independence from the adjacent developments thus allowing multiple construction activities to be undertaken in parallel and in safety free of obstructions. Where spatial constraints allowed it, open cut excavations provided cost, time, energy and construction material savings balanced against the added excavation.

A well planned and controlled groundwater pumping scheme backed up by pumping tests, additional investigation and monitoring, geotechnical modelling and analyses allowed more realistic ground water pressure profiles to be used in design optimisation leading to a 20km reduction of total anchor length. A further major cost saving was the application of measured concrete pour temperature data, allowing a reduction of the amount of early-age thermal crack control reinforcement by 20,000 tonnes.

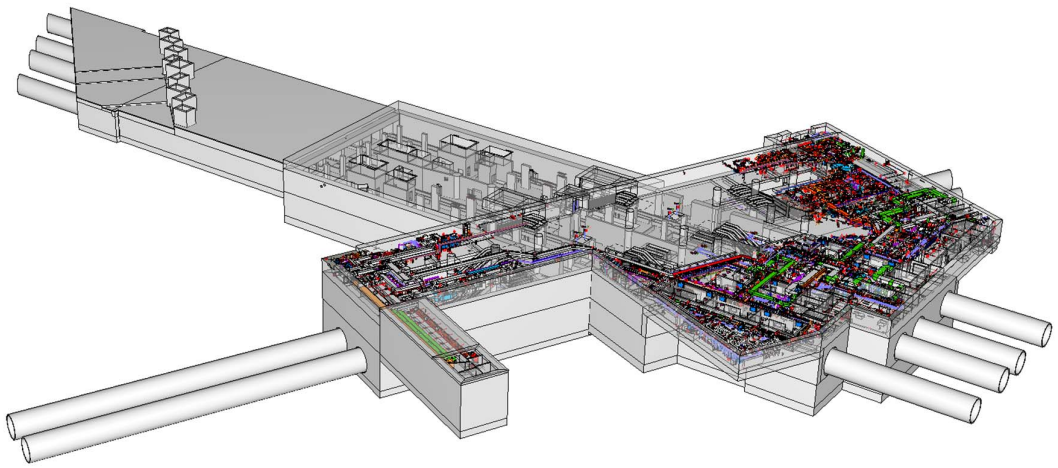


Figure 12. Combined BIM model of Msheireb Station

HEALTH AND SAFETY

The design and construction of the station had a strong focus on safety. Buildability and maintainability of the structure were always paramount in the design of the station. 3D modelling of congested elements and regular discussions with the Employer, the Contractor and Subcontractors were carried out to ensure safety during construction. Risk registers were also kept updated to ensure any residual risks are transferred into the Operation and Maintenance manual of the station. Throughout the construction of the station, where 2000 construction workers are working on site each day for over 4 years, there has been zero fatality.

EPILOGUE

Msheireb Station is one of the largest underground station ever built, mobilising 2000 construction workers on site each day. Over the 4 years design period of the station, more than 6000 drawings and over 500 reports and calculations have been produced by Mott MacDonald, engaging more than 500 staff in total across the globe. At the time of writing, permanent works construction is 95% complete with completion of all works including Architectural finishes planned for 2019. The station opening will take place in 2020.

EFFC/DFI Guide to Tremie Concrete for Deep Foundations

Karsten Beckhaus, Ph.D., BAUER Spezialtiefbau GmbH, Germany, +49 8252 97-1174, Karsten.Beckhaus@bauer.de
Chris Harnan, Ceecom Consult Limited, United Kingdom, chris.harnan@e-ceecom.com

ABSTRACT

The European Federation of Foundation Contractors (EFFC) and the Deep Foundations Institute (DFI) published the 1st Edition of the EFFC/DFI Guide to Tremie Concrete for Deep Foundations in 2016. A research and development project, funded by the Sponsors of the Guide, and carried out by the Technical University of Munich in conjunction with the Missouri University of Science and Technology was completed in 2018. The 2nd Edition of the Guide was published in June 2018 and this includes results from the research and development program including numerical modelling studies of concrete flow. Numerical modelling gives a better understanding of the interaction between design, concrete properties and execution methods.

The 2nd Edition of the Guide presents a review of concrete rheology, its dependence on raw materials and composition, applicable testing methods and recommended target values, as well as providing recommendations on specific design and execution details. It is intended as a practical addition to existing standards, although it is hoped that after implementation and review in practice, the principles contained in the Guide will be adopted in future revisions of Standards. Recommendations on support fluids have been removed from the 2nd Edition as these are now covered by the EFFC/DFI Support Fluid Guide which is due for publication in 2019.

GENERAL

In addition to strength and durability requirements, both of which have become more stringent within the last decades, concrete must be suitable for being cast in deep or extremely deep excavations. Today's specialist foundation engineering equipment makes it possible to drill or cut down to a depth in excess of 100 m (see Figure 1).

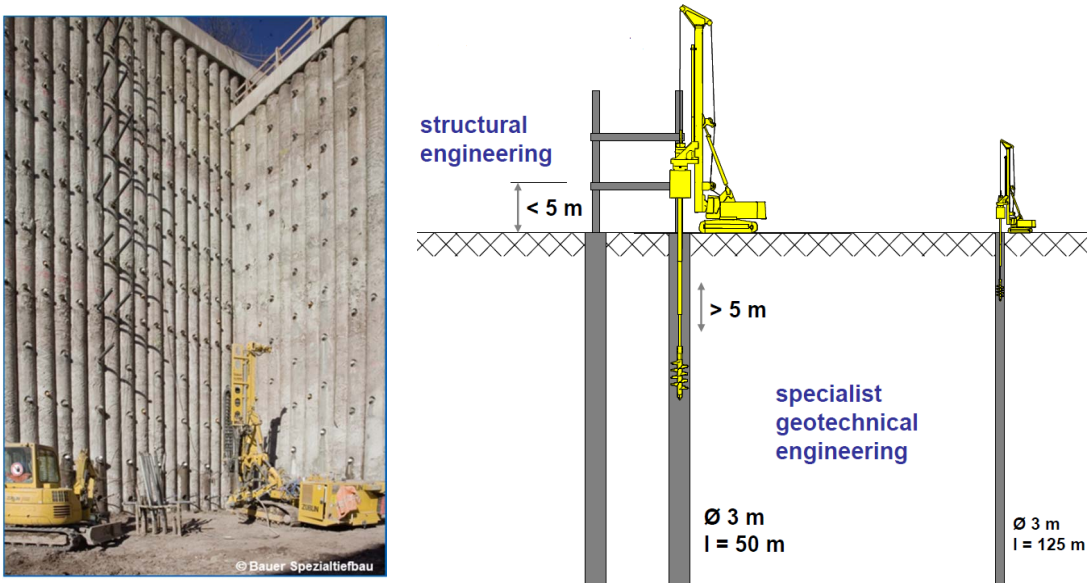


Fig. 1: Exposed secant pile wall and schematic showing execution of bored piles and their dimensions (Beckhaus, 2014)

© 2018 Deep Foundations Institute

In deep foundations, the excavation is usually “wet” i.e. filled partly or fully with water or support fluid (slurry), and concrete must be placed with a tremie pipe as shown in Figure 2. The rising concrete must displace the fluid upwards. If casing is used, in both the dry or wet process, the concrete must still be sufficiently workable at the time of subsequent extraction of the temporary casings.

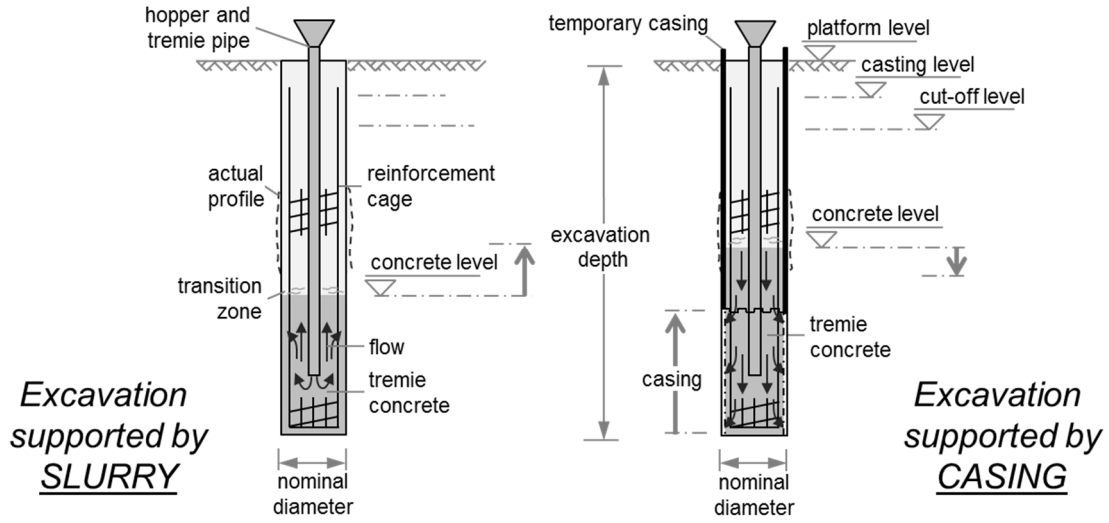


Fig. 2: Tremie Concrete (TC) placement; excavation supported by slurry or casing (Beckhaus, 2014)

It is obvious that tremie concrete for such special geotechnical works needs special properties in its fresh stage (during the casting process) to completely fill the excavation and embed any reinforcement or box-outs, to allow self-levelling and self-consolidation, all without undergoing excessive segregation, bleeding, or filtration of water or cement paste to the surrounding soil, until the concrete has been finally placed and starts to set.

Considering the concrete flow and, in particular, the resistance to flow, i.e. the reinforcement and the excavation surface inside and outside of the concrete cover zone, it should also be self-evident, that the structural design of deep piles or diaphragm walls needs to consider the constraints originating from usual and inevitable execution tolerances and imperfections, and of the limitations of concrete workability, the latter being dependent on the complex rheology of modern concrete.

REGULATIONS IN EUROPEAN NORMS

Eurocodes EC2 and EC7 comprise general rules for geotechnical design and for design of concrete structures, but no specific regulations for concrete in terms of its placement. Both assume concrete or reinforced concrete elements of adequate quality and integrity, i.e. with limited imperfections, and EC2 sets requirements only for durability after execution, e.g. minimum concrete cover to protect the reinforcement. For further regulations EC2 refers to the concrete standard EN 206.

EN 206 comprises general regulations for the composition and quality of fresh concrete, and, in Annex D of its recent Edition EN 206:2013, particular rules for deep foundation concrete used in bored piles and diaphragm walls, taken from EN 1536:2010 and EN 1538:2010. Besides the demand for principal suitability of fresh concrete and the required measure for consistence, there are additional important regulations on the raw materials, and on the composition of the concrete e.g. minimum cement content, minimum fines content, and maximum water-cement ratio.

Specific restrictions for deep foundations for composition and consistence, according to Annex D, depend on the placement procedure (see Table 1 for bored piles). It is understood that maximum consistency has been standardized on the basis of experiences at the time, to reduce the risk of

segregation and associated negative effects. The upper consistency limits appear to disregard the frequent need for higher values corresponding to a sufficient flowability e.g. in order to flow freely around and through the reinforcement.

Accordingly, in terms of pile or wall integrity and quality, it is also important to consider requirements for concrete cover and clearance between reinforcement bars. In this context, the maximum coarse aggregate size is correctly regulated in the European standards, for deep foundations to a maximum of ¼ of the clear space between bars, in order to ease the flow through and around reinforcement.

Table 1. Requirements for Bored Piles, in accordance with Annex D of EN 206:2013

Placement condition	Cement content [kg/m³]	Water-cement ratio [-]	Slump [mm]	Flow diameter [mm]
Dry	≥ 325	≤ 0.60 and in compliance with provisions valid for specified exposure classes	150 ± 30	500 ± 30
submerged under water,	≥ 375		180 ± 30	560 ± 30
under a stabilizing fluid			200 ± 30	600 ± 30

In total, with regulations on consistency, concrete composition, cover and clear space, an integral control system has been established to achieve high quality end products. This has been done empirically, by experiences which are now old. In other words, for the time being there are fixed values, but these could be insufficient to fulfil the basic principles for concrete like the requirement to flow properly. Such conflicts can easily be missed by the parties involved as this requires expertise and experience in both deep foundations and concrete technology.

MODERN CONCRETE TECHNOLOGY

Modern design of structures reflects the possibilities of making economic use of building materials. It has become very common for the industry to supply or use concrete with low water-cement ratios, nevertheless highly flowable and set-retarded for several hours if needed. Dense reinforcement in high-load substructures may already demand special requirements on the passing ability of fresh concrete. It usually demands well graded aggregates and a stable paste to avoid blocking. Stable paste is mainly driven by a low water-cement ratio which is typical also for concrete of higher strength classes or for specific durability classes, i.e. for a very low porosity which is required for a long service life in aggressive conditions (e.g. chlorides).

Today's concretes consist of comparatively low water contents and low water-cement ratios, often below 0.45. Therefore, modern mix designs clearly deviate from those of "classic concrete" which can also be named "water type concrete".

Even if fly ash or other additions can partly advantageously replace cement, such concretes need the assistance of chemical admixtures, often as a cocktail of superplasticizers and retarders, sometimes even topped by stabilizers. It is clear that such modern concretes behave differently from the classic types used 15 or even 30 years ago, when today's standards and regulations were established.

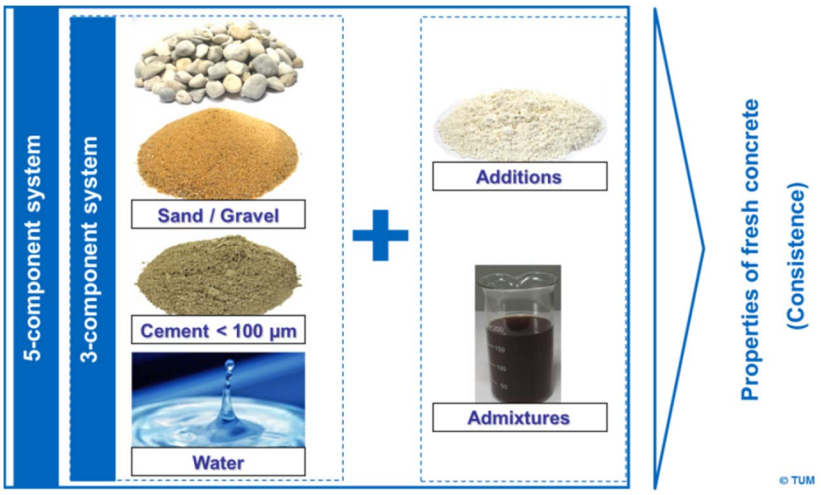


Fig. 3. Modern five-component substitutes the old three-component concrete technology

PERFORMANCE BASED QA/QC

As long as the concrete design was rather 'one-dimensional', using only the three components of cement, water and aggregates, and changing its strength class or durability mainly by adapting the water-cement ratio, the concrete workability was reliably described by its consistence, usually measured by slump or flow table test according to EN 12350-2 and -5. However, an individual practical test for consistence cannot fully describe today's fresh concrete workability and stability features, simply because the available tests give only one integral value for the concrete's rheology and cannot differentiate between the key rheological parameters (EFFC/DFI, 2018).

With modern, five-component concrete the options to individually design the concrete for specific properties are multi-dimensional, i.e. the characterisation of fresh concrete has become more complex and needs at least two rheological parameters to be sufficiently described. One is viscosity and the other is yield stress. Figures 4 and 5 illustrate the characterisation of fresh concrete by its generic rheology and it is obvious that the present normative regulations do not, and cannot, capture the actual fresh concrete performance.

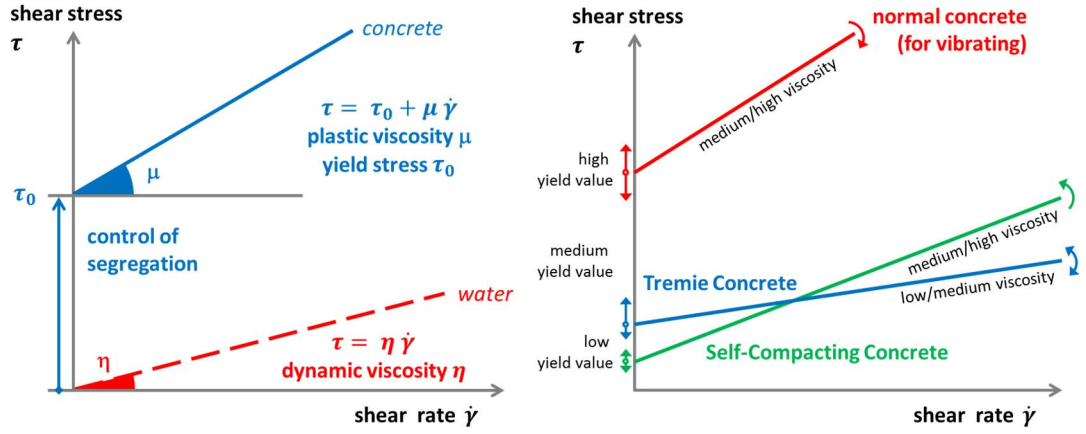


Fig. 4. Plastic behaviour of a Bingham fluid (e.g. concrete) versus a Newtonian fluid (e.g. water), and comparison of concrete types by rheology (EFFC/DFI, 2018)

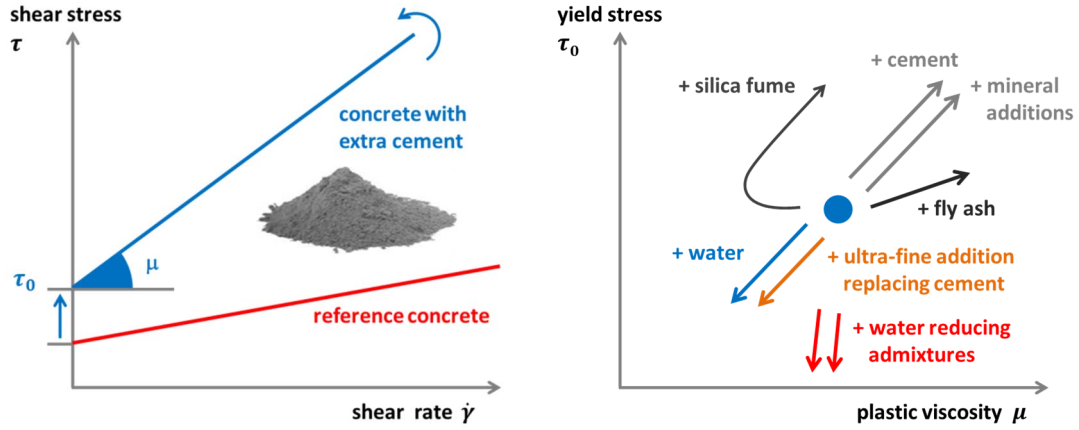


Fig. 5. Effect of concrete mix design on rheological behaviour acc. to Wallevik (2003), from (EFFC/DFI, 2018)

The left graph in Figure 4 describes in a simplified way "that concrete requires a certain amount of energy to start moving (the yield stress) and, thereafter, it resists this movement (by viscosity)" (EFFC/DFI, 2018). However, the typical behaviour of deep foundation concrete might be easier understood if compared to other concrete types for different applications, see the right graph in Figure 4. "Normal concrete, compacted using mechanical means, has a relatively high yield stress whereas self-compacting concrete requires very low yield stress to achieve the requirement for self-levelling and compacting by self-weight alone. The yield stress of tremie concrete lies between the two and needs to be balanced between the relatively low yield stress required for a good filling ability, and the higher stress required to displace the support fluid and control segregation in deep foundations. The large concrete head, which exists during placement in deep foundations, assists in compaction and makes it unnecessary to work with very low yield stress values which might result in sensitive concrete mixes." (EFFC/DFI, 2018)

In order to control the stability of a fresh concrete it was commonly understood within the Concrete Task Group that further advice on concrete stability is needed within the Guide. However, due to the fact that concrete technology measures to stabilise concrete are often reducing its workability, "the need to control stability should be balanced against requirements for workability" (EFFC/DFI, 2018).

Typical concrete mix designs for deep foundations will always contain excess water and paste which in general allows segregation, bleeding and filtration. In more detail for one of these "the extent to which bleeding will occur in deep foundations depends on many factors including, but not limited to, the water to fines content, the aggregate particle size distribution, the total concrete height and the time when the concrete reaches final consolidation" (EFFC/DFI, 2018). As shown in Figure 6, the present understanding from scientific studies is presented by dividing the bleeding into three stages and emphasising the benefit of stiffening which would lead to an early cessation of bleeding but must not happen before final placement which shows the above-mentioned balancing issue.

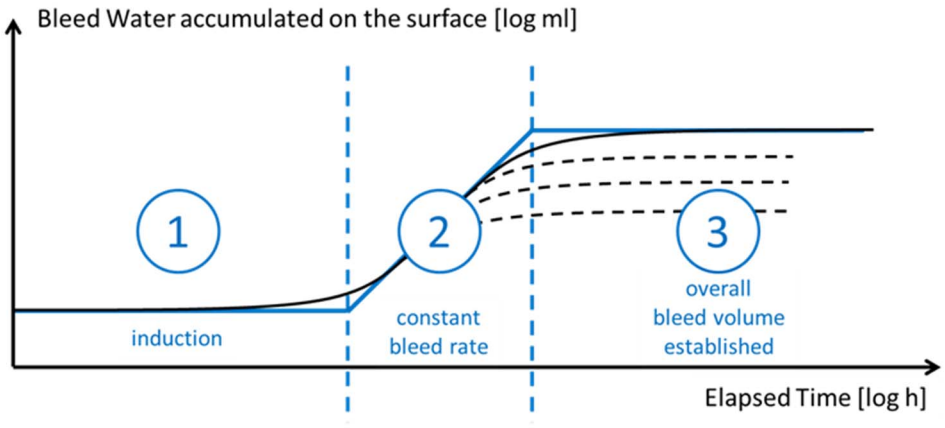


Fig. 6. Conceptual diagram on the bleeding process in cement pastes (based on Massoussi et al, 2017), with possible interruption of bleeding due to stiffening (EFFC/DFI, 2018)

A Research and Development Project was carried out by the Technical University of Munich together with the Missouri University of Science and Technology. This project included desk studies, laboratory testing, and onsite testing at worksites in Europe and the US (Kraenkel et al., 2018).

The research work was funded and supported by many sponsors from all stakeholder parties (named in the Guide (EFFC/DFI, 2018)). Further research work being carried out on fresh concrete performance and also on numerical modelling of concrete flow was discussed in detail at six Concrete Task Group meetings, starting on 19 January 2017 in Munich, plus three specific workshops on numerical modelling. In accordance with mandatory practice for norms and standards a review process was undertaken and comments from all stakeholders were debated within the final task group meeting on 10 April 2018 in Boston. Subsequently, the "Guide to Tremie Concrete for Deep Foundations" by joint EFFC/DFI Concrete Task Group (EFFC/DFI Tremie Guide) represents a broad and common understanding of all parties involved. The 2nd Edition (2018) replaces the 1st Edition from 2016.

EFFC/DFI TREMIE GUIDE

The EFFC/DFI Tremie Guide is aimed at those involved in the procurement, design, and construction of bored piles (drilled shafts) and diaphragm walls including Owners/Clients, Designers, General Contractors, Specialist Contractors and Concrete Suppliers. It is intended as a practical addition to existing standards, not a substitute.

The primary purpose of the Guide is to give guidance on the characteristic performance of fresh concrete and its method of placement using tremie methods in bored piles and diaphragm walls, and on specific detailing issues, all together allowing construction of high quality elements. Getting the mix right can best be achieved in a joint approach by the Specialist Contractor (to achieve the execution requirements), the Designer (to meet the durability and structural needs), and the Supplier (to produce an economic and practical mix).

In particular, the Guide helps understanding of the concrete's rheology, as shown above in section 4, which is necessary to properly appreciate the main placement characteristics of workability and stability, where:

- workability is simply defined as that "property of freshly mixed concrete which determines the ease with which it can be mixed, poured, compacted, and finished" (EFFC/DFI, 2018), and
- stability is simply defined as the "resistance of a concrete to segregation, bleeding and filtration" (EFFC/DFI, 2018).

Figure 6 explains how the composition determines the concrete rheology as a generic property which subsequently defines its practical characteristics, and controls the principal requirements allowing high quality placement.

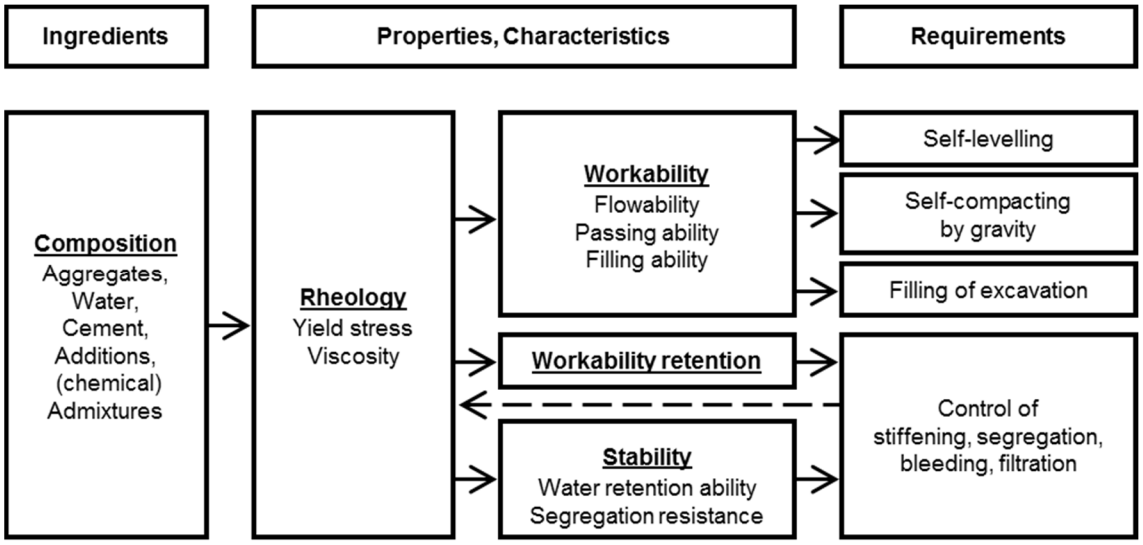


Fig. 6. Dependencies between composition, rheology and related characteristics, and overall requirements (EFFC/DFI, 2018)

The EFFC/DFI Tremie Guide (EFFC/DFI, 2018) proposes additional requirements for the fresh tremie concrete.

The Guide also addresses design considerations including concrete rheology, mix design, reinforcement detailing and concrete cover as well as good practice rules for placement. A review of methods to test the as-built elements is presented together with advice on the identification and interpretation of results. An optional use of numerical simulations is presented and discussed including current limitations. Numerical parameter studies help to better understand dependencies between design, concrete and execution, as well as assessing sensitivities.

As the concrete cover zone is potentially critical to concrete flow, and because the structural design and the execution standards set specific requirements which may seem to be conflicting, the Guide clarifies that "for both requirements, the designer should specify a nominal cover, c_{nom}, based on a minimum cover, c_{min}, plus an allowance for construction tolerances, Δc_{dev}", as shown in Figure 7.

$$c_{nom} = c_{min} + \Delta c_{dev} \quad \text{with} \quad c_{min} \geq \max \begin{bmatrix} c_{min,structural} \\ c_{min,execution} \end{bmatrix}$$

"For execution, a nominal concrete cover of at least 75 mm [3 in] is recommended, which takes into account a minimum cover of 50 mm [2 in] and an allowance for construction tolerances of 25 mm [1 in]. In most cases, the minimum nominal cover for execution will exceed those derived from structural and durability requirements" (EFFC/DFI, 2018). It is further emphasised that the designer should consider an extra allowance Δd_c for the installation of the reinforcement cage, see Figure 7, and more specific rules are listed in the Appendix of the Guide.

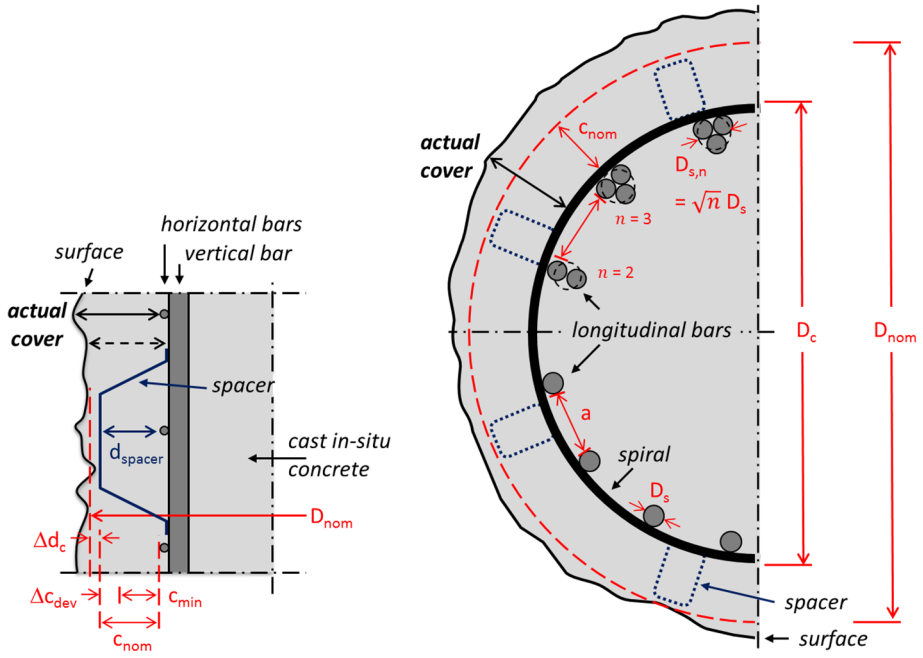


Fig. 7. Concrete cover and bar spacing in deep foundations (EFFC/DFI, 2018)

Appendix E of the Guide summarises International Standard requirements for minimum reinforcement and spacing for bored piles and diaphragm walls. One common requirement is that a clear reinforcement spacing of four times the maximum aggregate size is essential to prevent concrete blocking. In addition the Guide recommends an absolute minimum, min a, for clear spacing for vertical bars of 100 mm (including lap zones).

It is not within the scope of the Guide to discuss the general principles of mix design and proportioning of materials. It does however give limited guidance on typical steps to develop a concrete mix design and specific considerations on initial selection of constituents and tentative proportioning. The influence of materials on rheology is shown in Figure 5, which explains the overall role of specific constituents and how they affect workability and stability. The following is an excerpt from Section 4.3:-

"In order to obtain a more workable concrete mix i.e. to decrease the viscosity and/or the yield stress, some suitable measures could be:

- Replacing the cement partly with ultra-fine additions (significantly finer than the cement).
- Adjusting the aggregate particle size distribution
- Adding water reducing admixtures (plasticiser or super-plasticiser).
- Increasing the water quantity or paste volume.

Note: It is good practice to limit the percentage of water reducing admixtures in order to avoid excessive sensitivity to small variations in water content or other constituents e.g. sand, which in turn may lead to insufficient robustness of the concrete mix.

In order to obtain a more stable concrete mix i.e. to increase the viscosity and/or yield stress which would reduce a concrete's tendency to static segregation and bleeding, suitable measures can include:-

- Adding fly ash, which generally has greater influence on viscosity than on yield stress.
- Adjusting the aggregate particle size distribution
- Adding a viscosity modifying admixture.
- Reducing water quantity and/or adding cement or filler, e.g. limestone powder.

Note: Silica fume can play a special role in that it is sometimes specified to achieve high performance such as extra durability. Up to a small percentage, silica fume may have a positive effect on workability (like ultra-fine filler) but the concrete will become more viscous and reach a higher yield stress at higher percentages i.e. silica fume can also have an adverse effect and reduce workability."

The aggregate plays a key role in the concrete properties. The aggregate particle size distribution curves of the tremie concrete used in the R&D program (Kraenkel et al., 2018) varied widely. For example, lower and upper bounds with a preferable curve in between representing a "medium grained grading" is shown for an aggregate of 16 mm maximum particle size in the Guide and the following number of factors is mentioned to be balanced (EFFC/DFI, 2018) "in developing an appropriate aggregate particle size distribution (grading)…:-

- The shape of the aggregate: (naturally) round shape supports the production of flowing concretes better than the more angular shape of crushed aggregate.

Note: At the same grading and volume, the blocking resistance at reinforcement is considered higher for concrete with crushed aggregate, so that usually more (stable) paste is required for concrete using crushed aggregate.

- The size of the aggregate: a coarser grading (i.e. a higher proportion of larger aggregates) can give better workability but will also be more prone to segregation.
- The proportion of fine material: a higher proportion of fine material will give a more cohesive concrete mix.

Note: An excessive amount of fines might compromise workability due to its high water demand and may lead to higher required admixture dosages."

The Tremie Guide discusses the approach of using acknowledged concepts according to which materials such as cement can be partially replaced, and on the necessity of carrying out field trials to prove acceptability of a concrete mix design. The latter is considered essential to recognise potential problems e.g. due to improper dosages of (chemical) admixtures which "for some combinations of cements and admixtures can cause a lack of robustness in fresh Concrete" (EFFC/DFI, 2018). The overall aim should be to produce robust concrete mixes meeting the varied requirements of the specification for the properties of fresh and hardened concrete. This is a complex task where suitable test methods are necessary.

The R&D program (Kraenkel et al., 2018) has shown that, for tremie concrete, additional requirements for the concrete should be specified in terms of single target values, test methods and acceptance criteria. It was further shown that "the fundamental properties characterising concrete workability are yield stress and viscosity. As there are currently no practical field tests to measure these properties directly, indirect measurements are required".

The slump flow test (in accordance with EN 12350-8 and ASTM C1611) was found suitable to reliably measure the yield value of tremie concrete (see Figure 8).

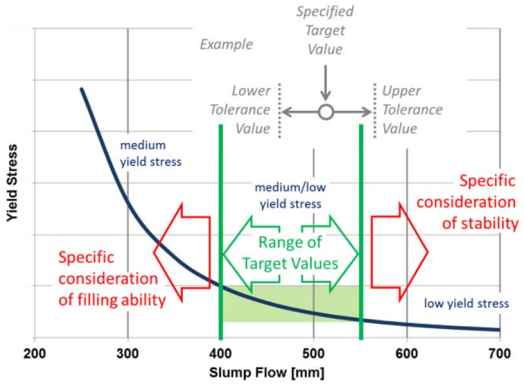


Fig. 8. Slump Flow Curve related to yield stress and recommended range for tremie concrete (EFFC/DFI, 2018)

The recommended range of a "medium/low yield stress" represents the majority of yield stresses of real tremie concrete mixes used in the R&D program in the laboratory as well as in the field, acknowledged as favourable mixes and with no defects or other issues recorded. The Tremie Guide (EFFC/DFI, 2018) states that the "chosen target value must be determined by the Specifier after an engineering assessment (by the Structural Designer and/or Constructor) of the specific details of the deep foundation element. The most important factors include the clear spacing of the vertical and horizontal reinforcement bars, the volume of the element, the estimated pouring time, and the depth." Some further factors which could be considered in a risk analysis are listed in another Appendix.

In order to reflect the practice of using "flowable" or "sticky" mixes (of low or high yield stress) and to allow values outside the recommended range, specific considerations are advised. The user should be aware that even with a specified target value at the lower or upper bound of the recommended range of slump flow, values of -50 mm or +50 mm shall be accepted to cover allowable measurement tolerances. Furthermore, if "the detailed assessment results in a requirement for high workability (e.g. slump flow target of 550 mm [22 in]), then this may require additional testing to ensure that there are no stability issues. Conversely, where a low workability is deemed appropriate (e.g. slump flow target of 400 mm [16 in]), then this may require additional testing to ensure filling ability with time i.e. workability retention" (EFFC/DFI, 2018). For rather "sticky" mixes with slump flow values below 400 mm the sufficient filling ability could be proven by full scale trials or by comparative studies proving that an extraordinary wide clear spacing of the reinforcement bars, maybe combined with increased cover can make up for a lesser workability (if this situation is the case). For "wet" mixes with slump flow values above 550 mm sufficient stability can also be proven by full scale trials. An engineering assessment could also result in the conclusion that a limited stability might not lead to problems and therefore be acceptable.

The viscosity is considered a secondary rheological property of fresh tremie concrete. It is well known from practical experiences that the viscosity has a considerable influence on the time needed for the concrete placement in a deep foundation. A high viscosity may lead to excessive pouring times which in turn could have negative effects on the concrete flow over several hours as previously poured concrete may change its properties over time but still has to flow through the reinforcement. As the viscosity is usually hard to adjust independently from the yield stress, no discrete range is recommended in the Tremie Guide. Nevertheless, a medium viscosity as shown in Figure 9 is still considered preferable for tremie concrete. Instead of a direct measurement of viscosity by an outflow test, which can also be found in the Tremie Guide, a rough measure can be derived from the slump flow test by simply recording the time the concrete needs to its final spread, by dividing the average travel distance of the concrete ((slump flow in mm – 200 mm)/2) to the time required (in seconds).

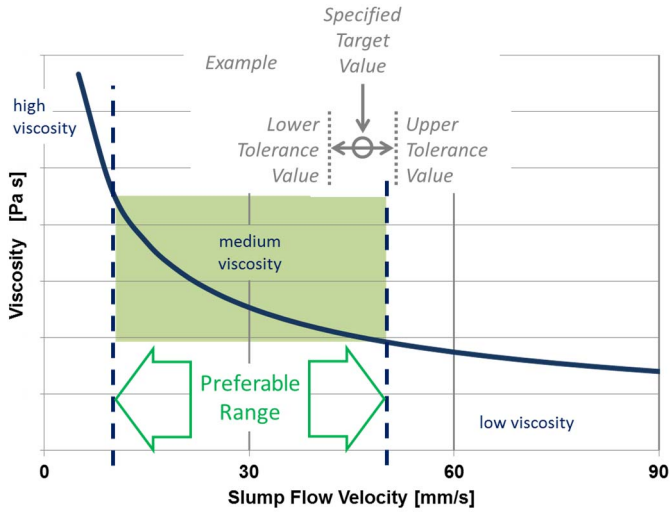


Fig. 9. Slump Flow Velocity Curve related to viscosity showing the recommended range of medium viscosity for tremie concrete (EFFC/DFI, 2018)

The stability of concrete is harder to assess. One of the simpler tests for stability is the Visual Stability Index (VSI) test which can be conducted as part of the slump flow test. It allows the concrete to be visually checked. After slumping, a visual check is made to look for segregation or bleeding i.e. no wet sheen on the surface, no mortar halo or aggregate pile in the centre of the mass (see Figure 10).



Fig. 10. Examples of Visual Stability Index Classes (EFFC/DFI, 2018), photo courtesy of BASF Corporation

Suitable test methods are given in Table 1 of the Guide. These are all described in detail in Appendix A of the Guide (EFFC/DFI, 2018).

Table 1. Suitable tests for tremie concrete (EFFC/DFI, 2018)

TEST No		determining Workability	Thixotropy	Stability
A1.1	Slump Flow	✓	✓*	-
A1.2	Slump Flow Velocity	✓	-	-
A1.3	VSI	-	-	✓
A2	Slump	✓	✓*	-
A3	Flow Table	✓	✓*	-
A4	Modified Cone Outflow**	✓	-	-
A5	Manual Vane Shear**	✓	✓*	-
A6	Workability Retention**	✓	-	-
A7	Static Segregation**	-	-	✓
A8	Sieve Segregation**	-	-	✓
A9	Bleeding**	-	-	✓
A10	Filtration**	-	-	✓

* *Note: Information on thixotropy can be obtained as outlined in the related Appendix A.6.*

** *Note: These tests are not covered by European Standards or US Standards (except A7 Static Segregation with ASTM C1610) and not all Concrete Suppliers will be familiar with the properties specified and might need specific agreement with the Supplier on a case by case basis. Optional test methods are listed and described in Appendix A (EFFC/DFI, 2018).*

Depending on the complexity of the deep foundation, the set of test methods specified may be extended at design stage and target values should be specified in accordance with the engineering assessment. When it comes to the execution on site, provided the concrete is produced with the same raw materials according to the approved composition, a minimum testing should be sufficient to identify individual load conformity. If other values have shown the concrete mix to be reliably stable, the correct slump flow and the VSI class 0 are sufficient to demonstrate acceptability (see Table 2).

Table 2. Recommendations for testing tremie concrete (EFFC/DFI, 2018)

No	TEST	Recommended RANGE for TARGET VALUES	TOLERANCE on specified Target Value	RELEVANCE for SUITABILITY & CONFORMITY	FREQUENCY * * of specified ACCEPTANCE testing
A1.1	Slump Flow	400 – 550 mm	± 50 mm	M	Each load
A1.2	Slump Flow Velocity	10 – 50 mm/s	± 5 mm/s	M	At least 1/week
A1.3	VSI	0	-	M	Each load
A4	Modified Cone Outflow	3 – 6 s	± 1 s	R	As required
A6	Workability Retention	to be specified	- 50mm	R/M*	As required
A7	Static Segregation	≤ 10%	+ 2%	R/M*	As required
A9	Bleeding	≤0.1ml/min	+ 0.02 ml/min	R/M*	As required
A10	Bauer Filtration	≤ 22 ml***	+ 3 ml	R/M*	As required

M = Mandatory; R = Recommended

* *Note: Based on detailed engineering assessment.*

** *Note: Testing frequency may be reviewed once target values have been reliably and consistently achieved.*

*** *Note: Higher filtration values may be acceptable based on previous experiences with similar mixes*

The Workability Retention test (A6 according to above tables) considers the particular requirement for tremie concrete for long duration pours in deep foundations. The standard case is that concrete needs to be workable until the end of the pour. The Tremie Guide recommends that a minimum slump flow should be specified for the project as assessed sufficient for filling ability at that time. It may be difficult to achieve extremely extended workability time and this may not be required not if the early concrete batches can be proven to be finally placed at lower elevations when still younger concrete is poured. A compulsory condition for this "consumption" of older concrete over the height during the pour is the so called "Bulging Flow", as shown in figure 11 below.

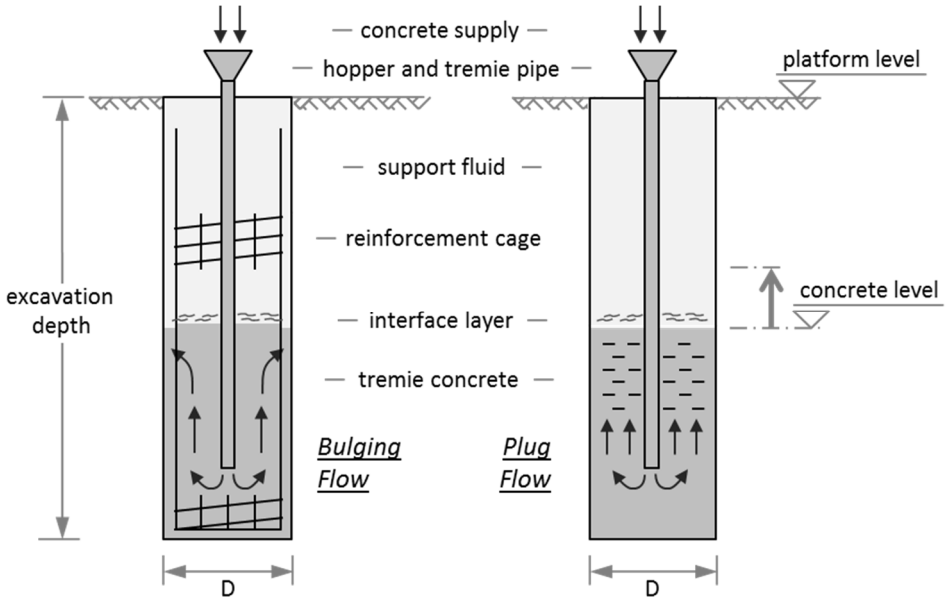


Fig. 11. Schematic of Bulging and Plug Flow (EFFC/DFI, 2018)

For discrete site conditions a full-scale trial with dyed concrete could prove such flow patterns but more generally numerical models may be used to explain the relevant dependencies on concrete flow. To cater for this and to prepare for the future opportunities given by modern computational tools a new Section 9 Numerical Modelling of Concrete Flow has been introduced in the new Tremie Guide (EFFC/DFI, 2018). Figure 12 indicates how numerical studies can help to understand the flow path of freshly poured concrete and its general consumption over height and time.

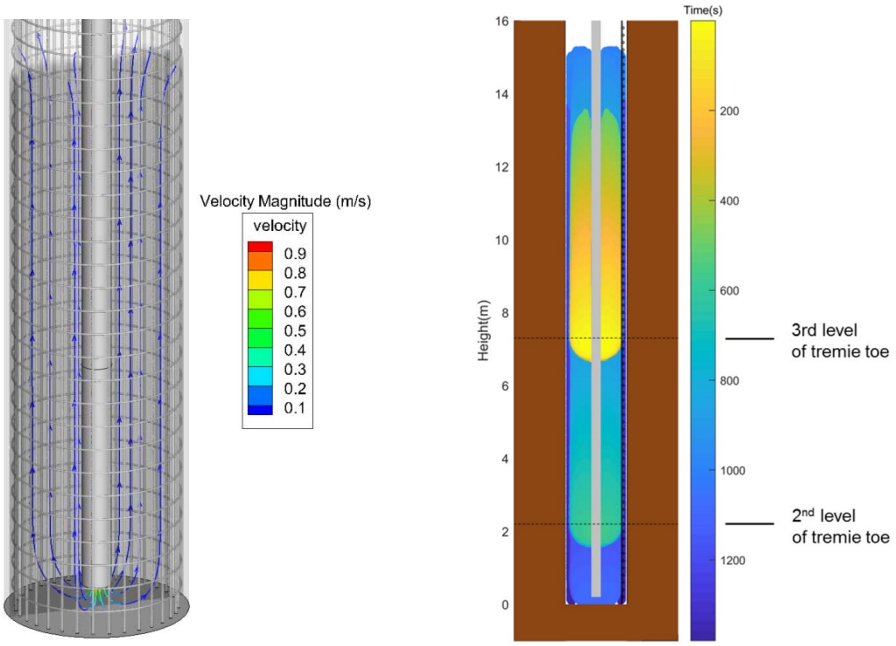


Fig. 12. Simulations presenting bulging flow of bulk concrete by velocity streamlines (left), and by dyed concrete following a staged lifting of the tremie pipe (EFFC/DFI, 2018; Li et al, 2018)

It should be noted that processing time for numerical modelling studies is dependent on the degree of detail as well as the applicability of the underlying physical model (e.g. the Bingham Fluid model)

which is also the basis for the rheology model used in Figure 12. Further work is planned using full scale trials to validate the findings from models.

SUMMARY AND NEXT STEPS

Testing methods to determine the true rheological properties of tremie mixes have not developed at the same rate as concrete mixes. The Guide presents new methods to test the concrete with the primary goal of preventing defects and anomalies in deep foundation elements. The EFFC/DFI Guide to Tremie Concrete for Deep Foundations, with its specific recommendations, should assist all stakeholders in this objective.

The 2nd Edition (2018) presents supplementary fresh concrete test methods together with actual criteria which will better characterise concrete properties which cannot be easily assessed from the commonly used current test methods. The relevance of these extended recommendations should be backed up by numerical studies of concrete flow explaining the main interdependencies of design, concrete and execution.

A limited set of criteria characterising different properties quantitatively could substitute present specifications, or at least lead to a revision of present recommendations which may be inappropriate or ineffective. Such a new performance based approach to test and assess tremie concrete workability, also with respect to stability, is overdue. Inclusion of the recommendations in the Guide should be considered in the next generation of European standards.

MEMBERS OF THE EFFC/DFI CONCRETE TASK GROUP

Karsten Beckhaus (Chairman), Bauer Spezialtiefbau, Contractor
Bartho Admiraal, Volker Staal en Funderingen, Contractor
Andrew Bell, Skanska, Contractor
Björn Böhle, Keller Grundbau, Contractor
Michel Boutz, SGS-Intron, Consultant
Dan Brown, Dan Brown & Associates, Consultant
Sabine Darson-Balleur, Soletanche Bachy, Contractor
Peter Faust, Malcolm Drilling, Contractor
Raffaella Granata, Trevi, Contractor
Chris Harnan, Ceecom Consult, Consultant
Duncan Moore, Implenia, Contractor
Duncan Nicholson, ARUP, Consultant
Alexander Rostert, Züblin, Contractor

REFERENCES

EFFC/DFI, 2018: Guide to Tremie Concrete for Deep Foundations, 2nd edition. European Federation of Foundation Contractors, UK, and Deep Foundation Institute, USA

Beckhaus, K., 2014: Are Specifications for Deep Foundation Concrete up-to-date? DFI/EFFC Proceedings of the 11th International Conference on Piling and Deep Foundations in Stockholm, Sweden

Kraenkel T., Gehlen C., 2018: Rheology and Workability Testing of Deep Foundation Concrete in Europe and the US. Research Report No. 20-F-0107, Chair of Materials Science and Testing, Centre for Building Materials, Technical University of Munich

Li C., et al, 2018: Numerical simulation of fresh concrete flow in deep foundations, Engineering Computations*, UK*

Massoussi N. et al. (2017). The heterogeneous nature of bleeding in cement pastes. Cement and Concrete Research 95, pp. 108-116.

GOOD REASONS TO SWAP FROM TRENCH CUTTER TO HYDRAULIC GRAB; LIEBHERR AND SAOS, ACTUAL CASES FROM FLORENCE, ROME AND MILAN

Bechter S., Liebherr-Werk Nenzing GmbH, Sascha.Bechter@liebherr.com
Franco G., SAOS S.r.l., g.franco@saossrl.it
Rossi F., SAOS S.r.l., f.rossi@saossrl.it
Bringiotti M., GeoTunnel S.r.l. - LWN Agent, Genoa, Italy, info@geotunnel.it

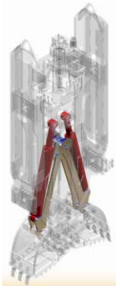
Keywords: foundation equipment, grab, lifting, Saos, Florence, Rome, Milan, LWN, Liebherr

ABSTRACT



Worldwide it may notice a relevant increase of Metro Projects; as a matter of fact in most of the cases new lines have to cross their path with existing ones. Due to these reasons, combined with the frequent need to encounter better geological conditions and, especially in Italy, having to solve the issue related to the preservation of the archeological heritages, tunnels, stations and technological shafts are often designed to be realized at deeper depth.
Another topic is related to the very frequent limited construction space available; this is occurring especially in ancient towns, where station's design need to take into consideration the space constraint, interferences with existing buildings and infrastructures.
What the market has recognized in the last 2 decades is that trench cutter technology evolution has been quite and as a matter of fact the world is looking for something new since a long time (which probably will arrive very soon by LWN). What has been really, technologically speaking, evolving in the last decade is the "marriage" between heavy duty crawler crane and both mechanical and hydraulic grab. The well-known traditional diagraphram wall excavation has experienced new applications also in metro projects; deeper depth, higher accuracy, top joint quality, easy and fast mob & demob phases, limited site spaces available.
Liebherr Werk Nenzing GmbH and Saos S.r.l. report of urban successful job site executed in Italy.

1 INTRODUCTION



For the construction of diaphragm walls, grabs, both mechanical or hydraulic in function of the jaws closing system, are frequently used. It can be named that it is more and more an international practice for the construction of very deep walls (and not only) to use combined systems: crawler excavator and hydraulic grab in its different technical declinations; this combination represents a real modern evolution for the excavation of diaphragms walls. A lifting and excavating equipment, such as a crawler crane class LWN HD-HS, powerful, silent, with generous, redundant and fast winches, with integrated controls coupled to a hydraulic grab (there are some types worth to mention) may really make a difference in a project that foresees high depths, cutting precision, work in urban environment, minimum pollution (also acoustic) and optimal management of the excavation materials.

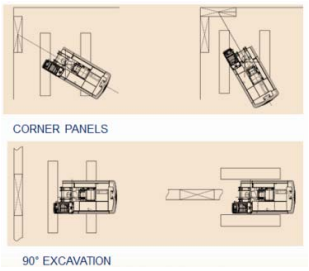
2 HYDRAULIC GRABS

In general, the diaphragm excavation grab may be of two different types: mechanical and hydraulic. The mechanical grab is the easiest to be manufactured and requires a crawler excavator equipped with 2 winches; the first able to lift the grab body and the second able to operate the mechanical kinematic of opening and closing the grab jaws. The mechanical grab, with freefall winch, although in certain situations can be slightly faster than the hydraulic one and may be efficiently used for repeated chiselling works (particularly resistant materials):

1. Of course requires a heavy duty type crane
2. The grab is particularly mechanically stressed
3. Definitely requires a very experienced operator
4. The operator must always be very concentrated during the entire working phase
5. It can rotate only by using the winding direction of the ropes by manually using the winches
6. It is not equipped with deviation correction systems

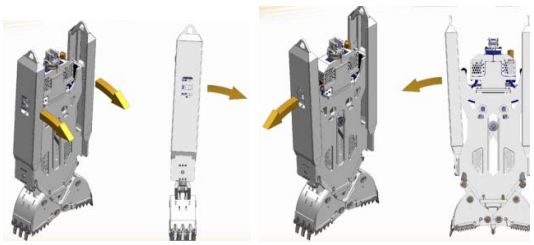
© 2018 Deep Foundations Institute

7. It cannot manage for high depths deviations
8. It cause excessive ropes consumption



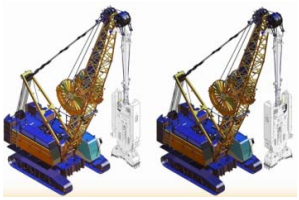
The hydraulic grab, besides, has a whole series of undoubted advantages due to its management through suitable hydraulic circuits that allow it to tighten the excavations jaws, rotate, divert ... with safe, controlled, precise and "smooth" manoeuvres. For example, the grab model used for the excavation of some diaphragms walls in the Milan Metro has been equipped with a patented grab rotation device that allows the structure to be swing at 180° on the longitudinal axis. This system can also reduce the excavation deviation and, especially in the case of hard soils, considerably improves the production performance; the device allows to realize panels in narrow spaces or corners where the carrier cannot be perfectly positioned in front of the excavation.

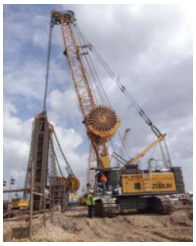
The asymmetry of the excavation teeth between the two jaws is compensated by the 180° rotation device. This equipment may be supplied with special thrust systems placed in various areas of the grab frame, used for the correction of the grab deviation during the excavation thus in order to allow a constant verticality. Usually grabs are equipped with two sets of steering plates (flaps, pushing cylinders, …), which may be operated independently. This operation and the effect on the deviation is controlled and monitored by an inclinometer installed on the grab itself and displayed in the operator's cab. It may be directly linked to the crane through different connection systems, depending on the type of carrier, the type of hoses reeling and the size of the panel to be realized. The control system is usually designed to continuously monitor the verticality of the grab during the excavation. The position of the grab is displayed on the operators monitor in real time; an inclinometer is installed in the frame in order to measure the inclination along two orthogonal axes (x and y). The data transfer from the inclinometer to the operator's cabin is carried out via a particularly resistant power cable, which to follow the grab movements automatically winded or unwinded by a dedicated hydraulic reeler. There are interesting variants that involve the information transfer through batteries properly installed on the digging body but which have the drawback of returning the information only at the end of each working cycle. Naturally data are displayed in a touch screen and can be stored and printed.



2.1 Dragon White

For some of the M4 Stations (Metro Milan), for example, it has been used an hydraulic grab called Dragon White (design and manufactured by Negrini S.r.l.) specifically configured according to the operational requirements, handled by a new Liebherr crane type HS 8100 HD in order to primarily excavate 2,8 x 1 m diaphragms wall. It is a modular hydraulic grab integrated with the operating machine without having to modify its support structure or having to re-certify the crane boom and neither the boom head. It may be manufactured with several optional accessories to increase its performance and it is mainly composed by a central body and an excavation set divided into: jaws, ejector, jaw supports (by simply replacing jaw supports it may be possible to achieve a wide range of excavation dimensions: from a minimum of about 500 x 2.500 mm up to a maximum one of about 1.800 x 3.600 mm) and hulls. By fitting a special hull handling device, it may be possible to adjust the excavation verticality using the guided hulls. The hulls may be remotely managed (therefore not using electrical cables) directly from the operator's cabin; without getting out of the crane's cabin, by means of a transmitter integrated in the "machine system" and the supplied joysticks, it may be possible to handle all the excavation operations. The receiver is integrated into a suitable enclosure fitted inside the top frame of the grab. All accessories are interchangeable between hydraulic and mechanical grab; a significant economic advantage because different excavation set may be used on both type. A specific extension can increases the grab height, allowing greater verticality of the excavation at high depths. In hard soils or particularly high depths, finally, it may be possible to apply additional counterweights, adding weight and lowering the center of gravity of the grab, resulting – as for the Milan Metro – in an effective and versatile device.





3 THE CRAWLED EXCAVATOR LWN HS 8100 HD



The crane subject of this brief description is part of a range of machines specifically designed for special foundations application. The HS 8100 HD crawler excavator, which for example has been used for the works of the M4 (Metro Milan), has been designed to perform various foundations works such as: trench cutter, dynamic compaction, drag line, several kinds of seaport works, with the help of appropriate "leader": pile, CFA, vibropiling, vibrofloatation, bored piles grab and casing oscillator, application frequently used for the construction of deep piles of large diameter, ...

3.1 Operating Weight: 115 ton

This parameter has a significant importance since the stability of the entire working group has a close connection with the mass of the undercarriage and all the components = > greater weight, greater stiffness, less vibrations and consequently less deviations (in addition to minor possible breakages for fatigue).

3.2 Motor power and consumption: 390 kW

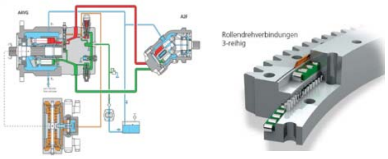
The engine power is a feature that clearly links all the machine hydraulic functions; having more power means not only be faster in all functions but also to generate spare power in potential critical situations i.e., for example, at high depths. Moreover, the greater power can be useful to manage different kind of works (trench cuter, vibrators, …). The Liebherr engine is of the latest generation Tier 4i; it is provided with DPF regenerative particle filters, which greatly reduce the environmental impact of machines and allow them to be used in sites particularly environmentally sensitive.

The abundant power available means having an engine that works at a lower rpm, despite having spare power available. LWN has developed low-consumption engine, integrated through the electronics with the hydraulic system, having an innovative concept called ECO-Mode able to limit the fuel consumption; summarizing, it is a new generation 8 cylinders engine with an electronic system that optimizes or disconnects all the hydraulic services when not used. Moreover, thanks to the automatic thermoregulation of the fan system (which allows to work in any climate) helps to reduce fuel consumption. It is reasonable to say that the hourly consumption of the Liebherr combination (Engine-Electronic-Hydraulic) is lower at least of about 20% lower compared to the consumption of comparable machines employed for similar kind of works, per linear meter of excavated panel. For instance, for the Port Said Project, the average consumptions for 100 h of work has been equal to 16,2 l/h!

3.3 Noise emissions

With regards to noise emission, it has been developed a specific system called ECO.SILENT-Mode; it is a function that when activated by the operator limits the number of rpm of the engine as well as of the cooling fan, ensuring a significant reduction of noise emission, with a negligent loss of power. This is a very important feature especially in urban areas operation. (i.e. construction works of diaphragms wall for metro stations, such lastly Milan, Rome, Paris, London or Warsaw). In a construction site, it is clearly perceived the difference between HS 8100 HD and all any other machine available on the same site.

3.5 Hydraulic system and swing ring



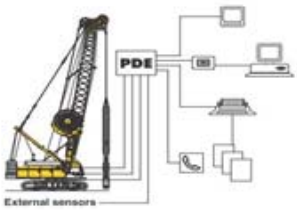
LWN machines are equipped with hydraulic pumps operated by a distributor gearbox; axial piston displacement pumps work in close and open circuits supplying oil only when needed (flow control on demand), thus to minimize peak pressure, and an automatically working pressure cut-off is integrated, which again entails a considerable energy savings. The hydraulic oil is cleaned by means of electronically controlled valves and return filters, any potential circuit contamination is reported in the operator's cabin. LWN has also designed a special swing ring (consisting in a hydraulic motor, spring loaded and hydraulically released multi–disc holding brake, planetary gearbox and pinion) able to guarantee precision handling and long service life; The speed is continuously variable 0-4,6 rpm with a 3-speed selector to increase the precision and the rotation automatism

3.6 Winches and depth



The winches are outstanding in their compact design and easy assembly. Clutch and braking functions on the free-fall system are provided by a compact designed, low wear and maintenance-free multi–disc brake.
The drag and hoist winches use pressure controlled and variable flow hydraulic motors. This system features sensors that automatically adjust oil flow in order to provide max. winch speed depending on load. The rated speed of the 2 synchronized winches (stnd. 25 ton capacity) is equal to 88 m/min with approx. 40 m of rope in the first layer. It is reasonable to be said that the pure speed of the LWN HS 8100 HD is at least 20-30% higher when compared to similar machines and the winch speed is one of the key points for excavation productivity! The depth achievable in standard configuration is equal to 120 m.

3.7 Telematics System for assistance



The integrated Li-Tronic + PDE system allows not only the transmission of operational data but also the remote assistance from the manufacturer headquarter; this "architecture" apart from being a modern feature is also an important operational advantage in the construction sites and a great savings in case of problem occurrence, easing a fast assistance service knowing in advance the cause of any problem, frequently been able to remotely fix it.

3.8 Crane's boom and compatibility with any kind of grab

The duty cycle crane's boom, which is mainly used with grab and other multifunction tool for deep foundation works, shall be able to withstand significantly higher loads of a standard crane boom. The loads are generated essentially by the horizontal forces due to the lateral grab acceleration, by the potential lateral flexion forces, by the dynamic forces connected to the operation of the grab itself and by the auxiliary tools applied to the boom; the lateral stresses components are also added to the axial forces generally stressing the boom. The structure is therefore dimensioned for heavy loads thus in order to absorb all these actions. For the record, it is worth to mention that the LWN system is compatible with any kind of grab: mechanical, hydraulic, kelly and semi-kelly.



4 INTEGRATION OF DUTY CYCLE CRANE AND GRAB

It should be noted that there is an important integration between the excavator and the excavator tool (the grab, in this case); in short, there is a hydraulic and electronic dialogue platform that transfers information, commands, data returns (in visual, graphic and system format) and can transmit them to the User and to the Mother House with the other potential related analysis and active interventions, such as maintenance, if needed.

4.1 Integration, control and data management



The crane / grab system can be integrated with the LWN electronic system called Li-Tronic. The crane management system is the centerpiece for precise and reliable crane operation. Li-Tronic is a unique one-system-solution which unites the best technologies available for reliable crane control; it is the one-level interface between crane and driver. Various analysis tools provide relevant information on the operation. The system empowers the driver to efficiently control the crane and to optimize turnover.

4.2 Grab chiseling

Chiseling with an hydraulic grab is not really a usual practice, nevertheless LWN system provides a specific integrated function allowing to perform chiseling with grab operating in freefall at a certain height. This option

can be used in various scenario, for instance: breaking through supporting slabs, excavating lenses of compact material at variable depths, headings in the bed rock ....

4.3 Grab safety and double winch availability

The fact that these machines work with 2 synchronized winches and consequently with 2 ropes simultaneously guarantees a redundant system not only for the loads lifting but also providing a high degree of safety for the grab itself. It has occurred more than once, having a single grab lifting block (i.e. crane equipped with a sole winch only) that rope got broken subject to excessive fatigue or wearing, particularly in the area of the return pulley on top of the grab lifting block (the lower pulley, very delicate zone!). Moreover, these types of machines are first of all cranes; their system, manufactured considering the strict referred design standards, takes care of monitoring the lifting loads as well as the position of the boom, putting them in closed relation. There are excavation machines suitably designed for such operations (lifting), which may not be provided with any load safe indicator when used just as excavators (it's also an accuracy and integrated stress calculation problem) and not as lifting equipment, a clear limit and a safety issue handling extraordinary unbalanced loads at high depths.

4.4 Ropes tensioning and wearing

The load indicator device is also used to calibrate the pressures of the winches in order to keep the rope in tension (without affecting the grab) during the excavation phase; this ensures no loosening, unloading of the pulleys, irregular wear, offload operation of the winches, tears, undesired turbulence along the panel walls, …. This specific function aims to reduce the deviation tendency during the operational phase, a further factor minimizing the danger of deviation from the design verticality. A further consideration on the ropes wearing shall be made on the geometry of the reeling drums of the winches; the greater is the drum length or the diameter, the greater will be the reeling length in the first layer of the rope, the less will be the wearing. Therefore, it is essential, in order to optimize the useful ropes lifetime, to provide larger winches (as well as powerful and reliable). The useful life of a lifting rope is in direct function of the type of material to be excavated (presence of stones hanging on the pulleys, anomalous wearing cause by friction, …) and of the excavation depth (numbers of reeling cycles and multi-layer reeling, …). Considering the mechanical grab, the technology foresees 2 ropes having 2 different tasks: the first winch bears the full weight of the grab (while with the hydraulic version the weight is equally distributed on both ropes), being this element particularly stressed. The second rope is engaged for the excavation jaws opening and closing procedure; it passes through a series of suitably dimensioned pulleys and through a numbers of referral mechanism (with short curvature radii) as well as the presence (quite frequent) of soil between the groove of the pulley and the rope itself, resulting in a reduced useful life. Moreover, the ropes consumption is not symmetrical, being subjected to anomalous strains. It is reasonable to say that the ratio of the ropes lifetime for the mechanical grab vs the hydraulic grab is 1:5 (indicatively 500 h : 2.500 h); steel ropes not only have a cost and are related to operational safety, but also provide long stop for their replacement ... at the expense of production.

5 THE FLORENCE HIGH SPEED RAILWAY LINK PROJECT

The works related to the Florence High Speed Railway Link and the realization of the new high speed train station represents a kind of urban revolution of the famous city; it provides for a vertically distributed development (a "negative" skyscraper), more like a large metro stop than a railway station. The new structure has been designed by Norman Foster & Partners; the platform level in the new station is located 25 meters below ground. The station chamber consists of a single volume, 454 meters long and 52 meters wide, built using cut-and-cover techniques similar to those deployed at Canary Wharf Station in London. The station will be linked to the existing Santa Maria Novella station, 2 km to the south, with the aim of realizing a multimodal hub sensitive to its historic location, but looking forward in its use of energy and other resources, offering a model for contemporary rail travel.



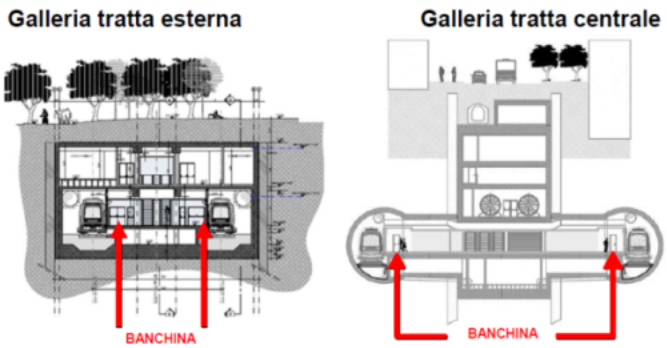
The diaphragms walling has been realized providing complex reinforcement having the slab rebars directly link to the bulkheads, the latter working in the entire structure and, by virtue of that choice, no longer having the need to build a foundation supporting wall, but more likely a make-up lining of the existing one.

For the realization of the diaphragm walls n. 5 duty cycle cranes, LWN HS-HD class, have been deployed, owned and operated by SAOS S.r.l., a well-known company specialized in deep foundation works; three working crews has been arranged for the excavation of 40 m deep diaphragm walls handled by two HS 855 HD (450 kW power) and one HS 845 HD both equipped with hydraulic grab, while a HS 833 and a HS835 cranes have been employed as service cranes, handling the 36 ton rebar cages. The site manager, Geom. Fabio Rossi, reported: “Negrini has provided us with special bucket jaws and grab shoulders for the existing grabs and with Liebherr we have designed and implemented a new software solutions with the aim to increase the effectiveness of the diaphragm slurry walls realization. We may say that it has been possible to pursue a wide range of experimentation benefitting of the unlimited horizons provide by Liebherr’s research and development on the heavy cycle machines. Without this assumption, we could not have been able to give such a decisive impetus to the planned intervention times of this works."

6 METRO LINE 4 IN MILANO AND SAOS COMPANY



For some years, the city of Milan is increasingly projected into a European scenario, particularly from the point of view of services designed to ensure the best sustainable mobility. One of the latest improvements involving the city infrastructure is Metro 4 (M4 or "Blue Line"), which will allow the Lombard capital to compete with other European capitals in terms of transport as well. Among the stated goals of M4 S.p.A. - the company that manages the works and which was set up in 2014 by the Milan City Council as a majority shareholder - is the decline in wheeled traffic for the benefit of public transport, with a forecast of 30 million moves in less annually and reducing pollutant emissions by 2%, about 16 million ton less fuel (figures which, however, also include the contribution provided by the new M5 service).
Line 4 crosses the city transversely by connecting the east and west boundaries and passing through the historic center along the Cerchia dei Navigli; by importance of the connected and crossed areas can be compared to Line 1. Given its track and intersections with the other lines and the Passive Railroad will be of fundamental development at the metropolitan and regional TPL. By 2022 the metro network in Milan will be the sixth in Europe; with M4, the metro of Milan will have a total of 118 km of line, 136 stations and an increase in the network in 10 years by 34%, a pace of development among the highest in Europe.
The main features of the M4 are: 15 km of extension, 21 stations, 86 million passengers a year, 6 interchange points (Sant'Ambrogio M2, San Babila M1, Crocetta / Policlinico Sforza M3, Bypass Dateo, St. Christopher FS, Forlanini FS), 1 workshop in San Cristoforo; frequency in peak/hours 90 seconds, maximum speed 80 km / h, automated without driver.
The features of the “center” stations are:
- Central Stations are defined as "deep typological stations" (about 30 m in depth).
- Located in the city center, in the oldest and most urbanized part, these stations have greater constraints than those of the outer trails.
- The solution adopted combines the small spaces on the surface with the necessary distance of the galleries where the trains run, through the creation of a deep central shaft between the two tunnels.
- Inside the tunnels they find the train travel routes and the related platforms



To carry out this kind of intervention, the Contractor has entrusted an important number of foundational works to S.A.O.S. (Società Appalti Opere Specializzate) S.r.l. - a company specialized in foundations and which plays a role as interlocutor of large general construction companies for the creation of special foundations.
SAOS used its existing LWN diaphragms crane fleet and also purchased a new HS 8100 HD crawler excavator and a special hydraulic grab from Negrini.

7 DIAPHRAGM WALLS AND JOINTS FOR THE BLU LINE

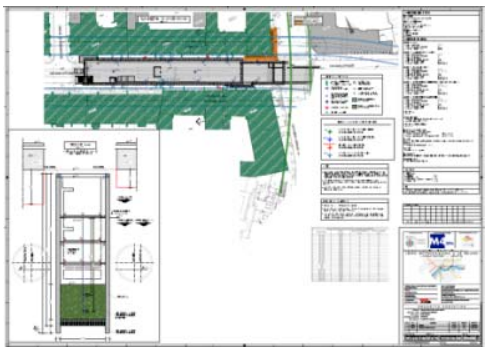
The project of the Metro Milan Line foresees the construction of reinforced concrete diaphragms walls, side by side eventually bonded by struts and tie back rods, as supports structures for the excavations of deep shaft stations and line tunnels, or in any case, in general, for underground works. The drilling technique is normally based on the use of bentonite slurry. "Dry" excavation, without the use of stabilization slurry, is not allowed. Excavation shall not, in any case, compromise or worsen the mechanical characteristics of the ground surrounding the diaphragm; therefore, it shall be avoided or at least minimized: any possible variations of the groundwater levels, the reduction of the relative density of the incoherent layers, the decrease of the effective horizontal tensions of the natural soil state and the adhesion reduction between the diaphragm and surrounded ground due to an improper use of the bentonite slurry. Realizing diaphragms slurry walls in urban area, means operating: in presence of road traffic, close to existing buildings and their foundations, balconies, canopies and any other protruding structures, street lighting, electric overhead lines, sewer pipeline and any other subservice, it is therefore required to conduct such a works by using proper equipment taking care of ensuring the full functionality of these services, constantly monitoring them during the whole the duration of the works. The employed equipment shall also comply with the stringent regulation and standards related to noise emission and vibration transmission to the surrounding environment.

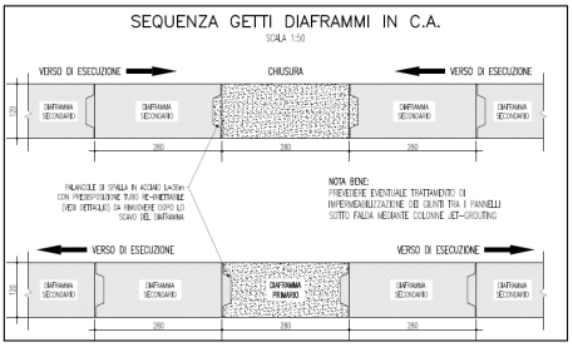
Diaphragm walls shall be realized bearing into consideration their precise geo-localization and in compliance to the parameters and tolerances given by the designer (with exception of stricter limitations indicated in particular situations) such as:



- Floor plan: ± 3cm
- Diaphragm head: ± 5cm
- Depth: ± 25cm
- Verticality: ± 0,5% and, in any case, not to involve, by the work performed, an off-axis of the internal line of the plane in relation to the vertical one through the path of the track exceeding 10 cm (for total diaphragm length ≤ 20 m)
- Joints complanarity: ± 1% which implies a restriction in the permissible tolerance for the absolute verticality of the panels; if a panel vertical offset is equal to 1%, the adjacent panel shall bear the same vertical offset following the same direction, or it shall be perfectly vertical.

During the excavation of the diaphragm panels, the machine systems and operators shall be able to monitor and record verticality, stratigraphy, the actual depth reached by the excavation tool, bentonite slurry consumption (thus in order to record any slurry loss due to anomalous ground condition) and as well as any other relevant information. The excavation technology could be chosen by the Client and the Contractor between the various types of grabs or trench cutter; of course, with high depths (> 50 m), potential presence of resistant hard materials, proximity to existing (historical) buildings, space and environmental constraints as well as the need to comply and guarantee high construction tolerances, it could have driven Everybody to the trench cutter technology; this has not happened!





The typical phases for the realization of diaphragm walls are as follows:

- Preparation of the ground surface
- Topographic alignment
- Realization of guide walls

- Consolidation injections where required
- Preparation of the stabilizing fluid (bentonite slurry)
- Excavation with grab in bentonite slurry
- Installation of the rebars cages;
- Concrete placing and retrieval of the bentonite slurry
- Diaphragm wall top level cropping
- Head concrete beam construction

The diaphragms walls shall be realized assuring a perfect hydraulic seal (in Milan the spring line is everywhere at very low level); all its elements shall be perfectly in contact and seamlessly compenetrating. Therefore, realizing a waterproof diaphragm to ensure a perfect hydraulic joint, before the casting at both ends of the primary panel, a stop-end shall be placed, which usually consists in a:

- Form pipe (stop hand) with diameter equal to the diaphragm thickness
- Suitable shaped elements (semicircular, sheet pile, etc.)

Project's specification requires that these elements are to be removed after the pouring (after concrete setting), leaving in the casted element their semi-circular footprint, interfacing groove. During the excavation of the secondary panels, it is necessary to clean the groove of both panel ends, thus is order to produce a rectangular shaped groove in order to have a perfectly matching joint during the casting of the secondary panel.

Alternatively, different types of joints may be realized, i.e. by fitting tubes or plastic formwork panels. In this case, during the excavation of the secondary panels, the plastic material of the formwork needs to be taken out by the grab; this will result in a concave impression similar to that described above.

Diaphragm wall cannot be realized continually for a very long section due to various limitations; the wall is usually constructed in alternative section. Two stop end tubes will be placed at the ends of the excavated trench before concreting; the designed technology foreseen that the tubes are withdrawn at the same time of concreting so that a semi-circular end section is formed. Wall sections are formed alternatively leaving an intermediate section in between. The in-between sections are built similarly afterward but without the end tube. At the end a continual diaphragm wall is realized with the panel sections tightly joined by the semi-circular groove.

7.1 MM Line 4: Usage of GFRP Rebar Cages for Tunnel Boring Machine "Soft-eye" openings



Metro Line 4 will be serving the densely populated areas in city center of Milan. In order to minimize disruption caused by construction activities, it has been designed to be compatible with other modes of transport and maintain sufficient groundwater level. Metro Line 4 will have twin tunnels with single tracks in each direction. Extensive use of tunnel boring machines (TBM) will be required. Metro Line 4 will have a total of 21 stations, including interchange stations on Lines 1, 2 and 3. The 21 stations, including the terminal, are San Cristoforo FS, Segneri, Gelsomini, Frattini, Tolstoi, Washington-Bolivar, Foppa, Parco Solari, S. Ambrogio, De Amicis, Vetra, S. Sofia, Sforza-Policlinico, San Babila, Tricolore, Dateo, Susa, Argonne, Forlanini FS, Q.re Forlanini and Linate Airport. The future stations will be built in open construction pits: An open central shaft and blind-hole side tunnel technique will be implemented to facilitate passage of the TBM and minimise excavation. TBMs cannot cut through steel-reinforced concrete drilled shaft walls as the steel bars get caught in the shovels of their shield. In addition, the steel bars cannot be cut into pieces small enough to allow their transport by the TBM's conveyor belt system. As a result, the conventional construction method with steel-reinforced drilled shaft walls needs the manual removal of the steel reinforcement in the path of the TBM. Not only is this time-consuming and expensive in itself, it also required the stoppage and retraction of the TBM in front of each shaft wall. Finally, to ensure that neither the soil nor potential groundwater outside the shaft wall would collapse into the opened hole, complex and expensive soil stabilization measures are required outside the wall. All these time-consuming and costly measures are not required when the areas of the launch shaft head walls to be penetrated by the TBM are reinforced with glass fibre-reinforced polymer (GFRP). Even though these bars have a much higher tensile strength than steel rebars, they are easily machined and can be broken down into small bar segments by the cutter head of the TBM. These segments can then be transported by the machine's conveyor sy-



stem together with the excavated soil. The TBM does not have to be stopped, and soil stabilization measures are not required, as the soil is always stabilized by the TBM. The resulting savings in the overall construction time and cost are substantial. Construction of the first two shafts for the project, at Argonne and Frattini Stations, was opened for bids in January 2015. In both cases, GFRP reinforcement was specified in the bid documents. In early July 2015, MAPLAD was awarded the contract to deliver the soft-eyes GFRP rebar cages.

8 THE ROME METRO PROJECT EXPERIENCE AND THE JOINTS MODIFICATION FOR THE MILAN METRO PROJECT: GRAB VS HYDROMILL



After a careful analysis of the excavation methodology and process specifications for the construction of the " Lot T4 - Line 4 Milan Metro" and been familiar with the Milan's ground morphology, SAOS has proposed an alternative construction method stated, keeping the same quality standards, beneficial time and economically wise. SAOS with a consolidated experience particularly in the construction of diaphragms walls at considerable depths, proposed a solution, which has been accepted, able to ensure a successful result; this technology was already used by SAOS for the "WHSD" in St. Petersburg. The equipment indicated for the excavation of the diaphragms wall is an hydraulic operated grab manufactured with a special long frame; this device allows to reach high depths (over 60 m), guaranteeing speed and verticality comparable to a trench cutter.

The willing of using a grab in place of a cutter was referred to the previous experience in Rome where, for the construction of Metro Line C San Giovanni Station (diaphragms 2,8x1,2 m, depth 56 m), in order to avoid leakages of bentonite slurry and ground collapses (such as the one occurred during the construction with the trench cutter of the neighbor Lodi Station), it has been successfully chosen the grab option. Here following the report draft prepared in collaboration with Metro C Roma Metropolitane: "... the choice of using an *intelligent grab* have been taken after the experience gained during the construction of the slurry wall central panels of Lodi station. As reported, during the excavation with cutter, a rapid loss of bentonite slurry occurred within a layer of sands and gravel. This phenomenon is attributable to the presence of confined groundwater with reduced hydrostatic pressure within the gravelly layer not sufficient to counter balance the vertical pressure of the bentonite. To make the situation worse the use of the cutter it has been required a continuous recirculation of slurry not properly mixed with correct amount of bentonite affecting the chiseling capability of the cutter. The diaphragms, of the new San Giovanni Station, has a height of about 56 m and crossing entirely a sand and gravel layer with a thickness of about 13 m, heading for about 10 m in a layer of Pliocene's Clays. Given the geometry of the diaphragm walls and the geological nature of the ground, the phenomenon, observed at Lodi's jobsite, would be amplified in San Giovanni jobsite. The design choice pursued involves the use of an "intelligent hydraulic grab" to replace the trench cutter, in order to limit the bentonite slurry recirculation therefore reducing the risk of leakages of the excavation stabilizing fluids, having the benefit of using thicker slurry mix without affecting the excavation capability ...".



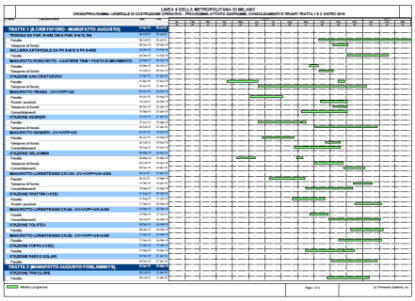
Excavation verticality is guaranteed by the considerable length of the grab, approx. 10 m, and the ability to rotate by 180 degrees, while the speed control is given by the crane's lifting configuration. A key feature of this type of equipment is the heavy weight (in configuration 2,8x1,2 m it is about 20 tons), easing the excavation at high depth. The verticality of the diaphragm, in this case, has been constantly monitored in the operator's cab also by means of a dedicated Jean Lutz monitoring device. At the end of each excavation cycle, it has been possible to print reports, having most of the time excavation verticality in a good range minor of 0,5%.

Experience in the long story of Metro of Roma Linea C has therefore foreseen 4 different technologies; panels excavated with trench cutter, primary panels with grab and secondary with cutter and then diaphragms solely excavated with grab, mechanical first, hydraulic afterwards. In terms of precision, productivity, cost and time the experience has slowly indicated the hydraulic grab excavation methodology as the most reliable one.

8.1 Operational methodology for the joints realization

Given the considerable height of the diaphragms walls to be constructed in Milan (50 m depth) and the need to realize a water tight joint, it has proposed the "virgin-interlocking" methodology with sheet pile stop-end. This methodology consists in realizing "virgin" or "primary" panels by installing at both ends trapezoidal 36 m long sheet pile in one go. Two cranes of suitable capacity have been used to lift them. The first one, supporting vertically the sheet pile placed on end and the second, which acting as a support, placed at about 2/3 of the sheet pile length. The sheet pile head is equipped with a dedicated lifting anchor, while the second crane is using omega shaped clamp. Once the two cranes are in position, the lifting operations are carried out; the tail of the sheet pile acts as a fixed point resting on the ground and the second crane holds the sheet pile in position, in order to avoid the bending. The first crane moves forward lifting the sheet pile by keeping its position perpendicular to the lifting point until it is fully lifted in a vertical position. When the lifting operations are finished, the sheet-pile is then lifted into the borehole. Once two adjacent primary panels have been completed, the "interlocking" or "secondary" panel are excavated. After the excavation phase, the two sheet piles previously installed are removed with the help of a vibrator. The demolding operation is very fast (ca. 4 minutes per sheet pile) without causing any damage to the realized structure. The advantage of this operation is to guarantee the absolute cleanliness and integrity of the hydraulic coupling, result not easily obtained by using extraction type sheet or pipe stop ends.





8.2 Compliance with the project schedule

The works part of SAOS subcontract for the M4 Metro Line foreseen the realization of various size of diaphragm walls having thicknesses ranging from 600 up to 1.500 mm, at a depths up to ca. 50 m. Given the variety of works to be realized, versatile and modular/adaptive equipment has been required; the collaboration between Liebherr LWN & Negrini has shown its strength. The time schedule of the contractualized foundation works has been successfully achieved: technological Building San Vittore: 56 days, Station San Ambrogio: 60 days, Technological building de Amicis: 73 days, Station de Amicis: 120 days, technological building Ticinese: 76 days, station Vetra: 116 days, technological Building Vettabia: 68 days, Stazione Santa Sofia: 60 days, technological building San Calimero: 70 days, station Sforza Policlinico: 125 days, technological building Augusto: 57 days, station San Babila: 78 days and technological building San Damiano: 18 days. The synthetic schedule of the previous lot is reported, just to give a picture of the working phases complexity, especially from the organizational point of view and of simultaneous workings activities to be conducted with suitable equipment in a cost effective and punctual manner.



SUMMARY AND CONCLUSIONS

The first SAOS experience in the Metro of Rome line C has taught us that in many of the Italian soil, at even high depths (> 50 m), diaphragms walls may be realized with hydraulic grab with excellent results in terms of cutting precision, productivity and costs; the Florence Railway link and the Metro of Milan are the clear successful evidence. Nevertheless, it is pretty clear that in order to achieve such a result Contractors shall be equipped with state of the art machineries and tools as well as supported by experienced technical operators.

REFERENCES

Bringiotti M., 2003, Consolidamenti e Fondazioni, Edizioni PEI, Parma, I
Bringiotti M., 2010, Geotecnica & Macchine da perforazione, Edizioni PEI, Parma, I
Comune di Milano, 2010, Capitolato speciale opere strutturali, N. M4-0730
Finotto A., Set-Ott 2011, Dal cantiere Liebherr – squadra ad Alta Velocità, PF, SCI Editrice, RA, I
M4 La linea Blu, 2016, Cerchia dei Navigli, Pubblicazione interna
SAOS, 2016, Tratta T4 Linea4, Proposta migliorativa diaframmi
Vitali S., Settembre 2017, On Site Construction, Capoverso Editrice, RA, Italy

POSITIVE CUT-OFF WALL IN INDIAN DAM – A NEW TECHNIQUE FOR DIFFICULT GEOLOGY

Steni Stefani, Consulting Engineer and President (Proprietor), Ricerca e Sviluppo – Cantieri e Gestioni of Lodi, Italy. Tel. +39 0371 68788; steni.stefani@gmail.com
Sanjay Dave, Civil Engineer, Vice President & Sector Head - Engineering Management (CEMG), Hindustan Construction Company Limited, Mumbai, India. Tel. +91 22 2575 1144; sanjay.dave@hccindia.com

ABSTRACT

This paper describes an innovative method, used for the first time in India, for the construction of a 1.0metre-thick positive plastic concrete cut-off wall (CoW) at the upstream toe of the dam at the Kishanganga Hydro-Electric Project in Jammu & Kashmir - India. The extremely difficult bouldery geology with an overburden laden with very hard Panjal Volcanics (quartz, feldspar, muscovite and chlorite minerals) boulders of up to 0.8m by 1.8 metres in size having UCS of up to 265 MPa and the requirement of socketing the CoW into the underlying hard bedrock (UCS 265 MPa) for 1.50m, made the choice for the excavation methodology critically difficult. After having evaluated several other existing methods – including hydromill trenchers – the Civil Contractor, Hindustan Construction Company, in agreement with its Foundations Engineering Consultant (Ricerca e Sviluppo – Cantieri e Gestioni) opted for a two-stage construction method: firstly, preliminary full-depth drilling and "surgical" blasting with full-length inclinometer checking of borehole verticality to ensure the exact location of rock fracturing and fragmentation coincided with the required position and that it was vertical, notwithstanding efficient trenching into the bedrock of a nominal 1m by 1.5m section; and, secondly, excavation by using heavy duty mechanical rope grabs made locally and developed by the Consultant in collaboration with the Contractor. The details of the methodology and the salient construction data is presented and commented for the 33-metre deep CoW installed at a working platform elevation of 2364.50 m above sea level in a very remote mountainous area.

Keywords: Positive Cut-off wall, Surgical Blasting, Kishanganga HEP, Difficult Geology

BACKGROUND

The Kishanganga Hydro Electric Project (KGHEP) is a ROR (run-of-the-river) 330MW capacity project located on the Kishanganga River some 140kms North-West of Srinagar, capital of the Jammu & Kashmir State of India. It is designed for generating 1350MUs of power annually in a 90% dependable year. The key components of the project are: Concrete Face Rockfill Dam (CFRD), Chute Spillway, Plastic Concrete Cut-off Wall (CoW), Head Race Tunnel (HRT), Surge Shaft (SS), Inclined Pressure Shaft (PS), underground Power House and Transformer Hall, Tail Race Tunnel (TRT).

The Power House Site is accessible throughout the year from Srinagar while the remote Dam Site, with its tortuous road climbing up to the Rajdhan Pass at 3556m (11,667 ft) above sea level and several 20-tonne capacity Bailey bridges which are removed prior to snowfall, remains inaccessible for around 5 months between mid-November and mid-May due to winter and heavy snowfall - the only access is by helicopter, weather permitting. With temperatures at the Dam Site reaching minus 27degrees Celsius during winter, careful planning from the beginning was most essential for the successful delivery of the Project.

This paper deals with the construction of the dam's panel-type plastic concrete cut-off wall which was performed, for the first time in India, adopting accurate pin-point blasting termed "Drilling and Surgical Blasting"; a method which allowed excavation of the panel trenches in very difficult geology with

© 2018 Deep Foundations Institute

clamshell rope grabs. However, this technology is not new and diaphragm wall excavation with the aid of drilling and blasting has already been implemented in some other projects globally; namely:

- Montalto di Castro Nuclear Power Station, Italy.
- San Lorenzo Dam, El Salvador.
- Pehuenche Dam, Chile.

The construction of the KGHEP dam involved foundation treatment work to ensure both stability and impermeability (water tightness) of the underlying overburden and foundation rock to avoid unacceptable under-dam seepage. A key element of the design is the installation of a cut-off wall (or diaphragm wall) under the dam to stem such seepage through any natural water passages such as joints and cleavage planes in the rock massif; through passages between ground constituents such as boulders and cobbles and through existing granular material such as sands and gravels. A 1.0 m thick cut-off wall had to be installed in bouldery ground in the river bed which, in turn, is underlain by bedrock and into which the cut-off had to be keyed at its base for a depth of 1.0 metre. Not being structural, the cut-off had to be a "flexible" plastic concrete wall without any steel reinforcement.

GEOLOGY

Overburden: The depth of the overburden along the dam axis varied from 12m to 33.55m. Permeability of the overburden ranged from 2.1 x 10^{-5} m/s to 98 x 10^{-5} m/s.

Bedrock: In general, greenish, hard, compact, medium strong to very strong, but jointed. Panjal volcanics composed of quartz, feldspar, muscovite and chlorite minerals were exposed in the dam area on both river banks around the dam axis. Greenish grey colored, fine-grained, hard, and strong to very strong, massive to jointed rock of basalt and andesite. Permeability of the bedrock ranges from 12 to 50 Lugeons. The rock quality, based on deformability considerations, can be considered from good to very good.

River Bed Geology: At the dam site, the width of the river is about 90 m (295 ft) with a nearly 30 m (100ft) wide main channel being confined to the right bank, defined by expanses of slope wash material and low-level fluviatile terrace deposit on the left bank comprising river-borne material. The river-borne material (RBM) generally consisted of boulders and cobbles ranging in size from 15cm-50cm (6"–20") and pebbles of volcanics, granite and gneiss embedded in a silty sand matrix. The larger-sized boulders were also present in the riverine deposits. The depth of the overburden in the riverbed section ranges between 18m and 29m, according to interpretation and projection of cored boreholes. Below the riverine overburden lies the bedrock. The RBM is like a series of stacked boulders and cobbles held in place by a loose sandy gravelly matrix and proved quite difficult to excavate and avoid large cave-ins.

CONSTRUCTION METHOD REVIEW AND CHOICE

In consideration of the difficult geology existing in the project area, with rock hardness ranging from 95 to 265 MPa (UCS), but particularly the bouldery nature of the subsoil overlying the bedrock, several methods of cut-off wall construction were examined.

Among these were:

- Reverse circulation drilling with large diameter borings.
- Large diameter down the hole hammer for constructing a secant pile cut-off wall.
- Using a Hydromill to carry out the trenching.
- Use of grabs and chisels aided by a preliminary drilling and blasting campaign.

Having elaborated the data and the thoughts gathered, it was felt that the only way risk was mitigated to allow a vertical continuous cut-off wall to be autonomously constructed in an acceptable technical manner was to revert to drilling and blasting as an excavation aid. Excavation would then proceed with traditional clamshell grab diaphragm wall techniques adopting a limited amount of chiseling wherever required.

PLASTIC CONCRETE CUT-OFF WALL

Construction of the 120m long and approximately 33m deep Cut-Off Wall was started by Hindustan Construction Company Ltd. in August 2012 (drilling and blasting) and was wholly completed in January 2016. The final CoW length executed was actually 134m (440 ft). Excavation of the 1.0m-thick cut-off wall to a maximum depth of 35m was done by excavating the trench by grab and chisel. The trench area was first subjected to tightly-controlled blasting to shatter the boulders in order to facilitate the excavation by grabbing. The drilling and blasting also provided the socket trench in the bedrock to key the base of the CoW into it. The excavation was then done by mechanical grab. Chisels were used to break any occasional boulders still left unbroken or just fractured, but not fragmented, which obstructed the progress of the grabbing, to remove any corners of external boulders protruding into the trench and to remove any burrs of rock in the CoW key within the bedrock.

The 1m-thick wall was constructed in an alternating sequence of primary and secondary panels. Originally, it was envisaged that, using a 2.5m wide grab, primary panels would be a 3-bite trench making up a maximum combined total length of 7m. Using 1m diameter tubular end-stops, this would yield a primary panel of 5m. The secondary panels were to be excavated once the adjacent primary panels were complete and end-stops removed. Hence, the secondary panels were to be a 2.5m single-bite yielding a 4m long trench (1m shafts at each end left by end-stops). Later, in the “Construction” paragraph, the actual panel configuration used is explained. The walls of the excavated trench were supported by bentonite slurry during excavation. Upon completion of the excavation of a panel, trench verticality was checked with a Koden DM-604 ultrasonic profiler and, then, low-strength plastic concrete was poured into the trench using the tremie pipe. The displaced bentonite slurry coming out of the trench while concreting was pumped back to the bentonite slurry plant for treatment and re-use. A general view of the project layout is shown in Fig.1.



Fig.1. Layout of CoW operations – position of wall shown in red.

INITIAL PLANNING

From the initial stages of the project, HCC's core planning team was on the lookout for the method to construct the cut-off wall. Before selection of the methodology, risks associated with construction of the CoW were chalked out to be taken into account while finalizing the best possible construction method as per the requirements. A lot of time and effort was spent to identify the risks, which included:

- Complex geological conditions.
- Expertise, competency and experience required for construction of Cut-Off Wall.
- Delivery schedule of Cut-Off Wall with required quality and budgeted cost.

The mitigation measures to overcome above risks are detailed below.

Geological conditions

Information of three cored boreholes done during the DPR stage of Kishanganga Hydro Electric Project was already with HCC; those borehole logs were carefully studied and different geological sections with approximate depth, hardness and properties were located.

Expertise, competency and experience

To ensure the best and most favorable manner for installing the cut-off wall required to prevent under-dam seepage at the Kishanganga main dam, Hindustan Construction Company (HCC) of Mumbai, India, called for a diaphragm wall expert to help define a solution and formulate the methodology for the construction of a Cut-off Wall designed by HCC and Halcrow Consulting, UK.

Delivery schedule

A team of HCC engineers worked with the CoW expert consultant to determine the best possible solution as per the contractual deliverables and concluded that, from a work schedule viewpoint and remaining within the budgeted cost and quality standards, the method to be adopted which gives the most assurances was conventional diaphragm wall grabbing and chiseling preceded by accurate "surgical" blasting.
The methodology was submitted to and approved by the Client/Owner, Messrs. NHPC.

CONSTRUCTION PLANNING

Risks associated during construction were found out which included:

- Selection of equipment for drilling of holes and excavation (grabs and chisels)
- Piping
- Bentonite losses within a trench panel leading to collapse of the trench.
- The connection of the wall joints including panel alignment, overlap and concrete joint integrity.
- Integrity of wall itself with ingress of groundwater from upstream.
- Financial risks involved due to geological variations.

Selection of equipment

The location where the cut-off wall was to be constructed is very remote and politically sensitive. There was a weight limitation of several bridges which limited the size of the cranes for cut-off excavation and there was considerable risk in terms of getting special parts on site and effecting competent maintenance

that the mobilized equipment could not perform continuously as per Work Schedule requirement. That would lead to significant impact in terms of time and cost. Thus, before mobilizing the equipment due consideration was given with respect to following available information:

- The results of the geological borehole logs.
- The design requirements for the Cut-Off Wall.
- De-rating of engine output deriving from a near 3000 m (9850 ft) above sea level workplace.
- Spare Parts Requirement Plan for critical equipment and drilling tools for an on-site inventory.

From the above information, the following were the major equipment deployed:

- 2 nos. EGT make MD1500/MD515 hydraulic crawler drilling rigs with DTH Hammers were purchased and deployed for drilling of holes after ascertaining the performance from the vendor.
- 2 nos. Silenced XRH1100 diesel air compressors, 520 l/s free air delivery (1100 ft^3/min) and 17 bar (250 psi) operating pressure were purchased.
- 2 nos. 80-ton Kobelco 7080 Crawler cranes were used from inventory for operating mechanical grabs and chisels (larger cranes not possible because of road and bridge load limitations).
- 1 no. TATA-P&H-955A 40-ton lattice boom crawler crane for chiseling & concrete placement.
- 3 nos. Mechanical Rope Grabs and 6 nos. chisels from inventory were additionally strengthened and modified as per suggestion by the Cut-Off Wall expert.
- 1 no 100m^3/h desanding unit.

Piping

Piping risk was mitigated by a grout curtain installed through and under the full extent of the upstream (u/s) cofferdam. The u/s cofferdam axis was situated about 50m (165 ft) u/s of the cut-off wall axis. A trench and pump sump were also made at the d/s toe of the cofferdam to collect any residual seepage through piping and the water was pumped back into the river just u/s of the cofferdam. Manned batteries of diesel dewatering pumps were deployed to ensure a water-free area for the CoW activities.

Bentonite losses

The stability of the trench was maintained by keeping the bentonite slurry fluid within 0.5 m (20 in) from the top of the guide walls and at 0.3m (1 ft) with the grab within the trench. Normal bentonite loss for "cake" formation is controlled by preparing bentonite of sufficient density and, above all, ensuring it had been hydrated for at least 24 hours.
Rapid bentonite slurry loss can occur due to highly permeable material zones, defects in the foundation or piping from upstream river water. Apparent anomalous bentonite fluid loss can lead to a collapse of the panel trench, thus whenever such a case was encountered during excavation and or chiseling, slurry pumping into the trench was increased while excavation was temporarily suspended, in order to maintain the constant slurry level inside the trench and allow a determination of the rate of efflux. In some cases, the panel trench was backfilled with granular material (sand and pebbles) that could enter and plug the mud loss channels. After waiting for the bentonite slurry to gel, resumption of excavation within the panel could take place. This occurrence was experienced on five occasions. A sand stockpile of 50 cubic metres (65 cu. yd) was kept on the work platform ready for any instant remedial action required.

Integrity of wall

Misalignment of panels and sediment at its base can trigger piping resulting in failure of the CFRD and the project. This risk was minimized by constructing reinforced concrete guide walls below work

platform level. During blast hole drilling, a DAT data logger fitted to the drill rig was used to log the hole to determine the position of boulders and the bedrock as well as for monitoring the verticality of the drill hole so that blasting impact is restricted only to within trench limit.

The explosive charge distribution was derived from the drilling data and a mining specialist was assigned to create the controlled blasting pattern according to the borehole logs. The essential things were avoidance of over break and of any damage to the bedrock. Blasting was done well ahead of any cut-off wall trenching to ensure the integrity of any panel was not jeopardized.

The use of a Koden ultrasonic trench profiler also contributed to assessing the deviations and torsional twist of excavated trenches and allow HCC to effect any necessary rectification that may be required, prior to approving the casting of concrete. This QC/QA panel trench verification removed any doubt as to the continuity of the cut-off wall and its correct embedment into the underlying bedrock.

CONSTRUCTION

With reference to the original plan of using tubular stop-ends and multi-bite primary panels, the method envisaged for initial Start-up and Learning Curve phases foresaw using only 2.5m panels, but primarily because of logistics, this approach was maintained throughout the entire cut-off wall construction. This simplified procedure -without the use of end-stops - involved setting the 2.5m (8.20 ft) wide primary trenches 1.75m (5.74 ft) apart; subsequently, the 2.5m (8.20 ft) wide secondary panel trench was excavated between the two completed primary panels and, therefore, with a 375 mm (15 in) overlap at both ends any bentonite accumulated in the sides during primary panel concreting was removed thus ensuring a watertight joint between the primary and secondary panel and meeting the requirement of cut-off wall continuity. With this methodology the excavation of the secondary panels could suffer the hardened plastic concrete at both ends if their excavation is excessively delayed, an occurrence incurred at the beginning of each new season. The advantage is that each panel bite is excavated and promptly filled with concrete and this reduces the instability of the trench and the likelihood of cave-ins.

This choice – approved by the Client-Owner – was to be the only method compatible with the unexpected restricted space available and with the almost daily demobilization and remobilization of drilling and blasting and cut-off construction equipment because of blasting by others. Nonetheless, even with protective barriers in place, flyrock damage was experienced several times by cranes, drill rigs, welding machines and other items such as casings, with considerable time loss. On three occasions the bentonite storage shed had to be rebuilt.

Drilling of holes

The drilling system used was dual-tube down the hole hammer (DTHH) drilling; i.e., dthh drilling with simultaneous casing of the hole. This method ensured minimal disturbance to the overburden strata by the drill exhaust air, which returns to the surface within the annular space between the drill pipe and the casing. The drilling system consists of a concentric drill bit design that is credited with “incomparable” hole straightness and deep drilling capability. The drilling principle is based on a pilot bit and a concentric ring bit, which together drill a hole slightly larger than the external diameter of steel casing which is advanced downwards by percussion on its shoe by the pilot bit. The ring bit was then disengaged from the pilot bit to allow the retrieval of the internal drillstring, thus leaving an open fully-cased hole.
The drilling machines used were an EGT MD1500 and an EGT MD 515 hydraulic crawler-mounted machine. Typical drilling activity in progress is shown in Fig. 2.



Fig.2. Drilling with EGT crawler drill.

Drilling sizes

Drilling was performed using two gauges: Ø115mm (4.5 in) and Ø250mm (10 in.). Typically the blastholes were Ø115mm and the relief holes were Ø250mm. However, some additional central blastholes along the cut-off axis were also Ø 250mm. Blast hole drilling was performed to create blasting modules consisting of 4 nos. blastholes and one central relief hole as seen in Fig.3.
The Ø115mm drill string consisted in Ø 76mm (3 in) drill rods by 3m (10 ft) length and Ø114mm x 3m (4.50 in. O.D. x 10 ft) casing. The Ø250mm drill string had Ø114mm (4.5 in) drill rods by 3m (10 ft) length and the casing was Ø245mm x 3m (9.63 in. O.D. x 10 ft).
The use of stabilizers on the drilling rods and drill collars favored drilling verticality in truly adverse conditions, especially prior to the completion of the u/s cofferdam grout curtain when copious amounts of ground water were drill-pumped.



Fig. 3. Drilled 4-Hole Module Ready for Charging (left) and charged (right).

Drilling problems

Initially, during drilling, the manufacturer factory-supplied welded casing drive shoe at the leading edge would break off because of fatigue induced by the impact load of the down-the-hole hammer drill. This was overcome by introducing additional button welds and adopting a pre-heat and stress-relieving post-weld heat cycle when fitting new shoes in replacement of worn out ones. This improved service life of the shoe assembly more than fourfold.

Although the drill casing was a passive (non-rotated) component, dragged down by the dth hammer impacting the shoe element, the withdrawal of the casings after installing the PVC blasthole casing, evidenced problems with the threaded joints and the casing steel for the Ø115mm (4.5 in) blasthole drilling, This was overcome by introducing higher quality steel (API Spec 5CT – N80) and effecting heat treatment of the mating threads. In the deeper CoW section, i.e., in the over 30m (100 ft) part, some of the external row blastholes were drilled using the Ø250mm (10 in) diameter to avoid casing retrieval problems and casing loss.
Throughout the job, there was no availability of good-quality zinc-based or copper-based dope thread, a fact that exacerbated the casing tool joint failures.

Drilling pattern and sequence

The drilling pattern prepared, based on past experience, both in diaphragm wall trenching through rock in bouldery strata and general drilling and blasting practice, is as shown in Fig.4.
The drilling pattern represents a 7-metre (23 ft) stretch consisting of just over three 4-hole modules:

- 14No. x Ø115mm (4.5 in) holes
- 06No. x Ø250mm (10 in) holes

To avoid damaging blastholes being drilled, a gap of 20 m (65 ft) was maintained between simultaneous drilling and blasting work on any two modules. Once two successive 4-hole modules were completed (drilled and blasted), the drill rig could then return to the 1metre gap left between these and drill a central Ø250mm secondary blast hole to be charged and fired according to the lithology encountered. It is important to underline the fact that the intensive blast hole drilling acts as a detailed "depth to top of bedrock" survey, thus allowing the definition of the depth of the cut-off wall panels and to define bottom blast-hole cushion to avoid damage to the bedrock.
All drilling was done at least 2m (6.5 ft) into bedrock – typically 3m - to avoid any judgemental error of being in a large block or boulder (maximum 800mm to 1200mm in size) instead of in bedrock.

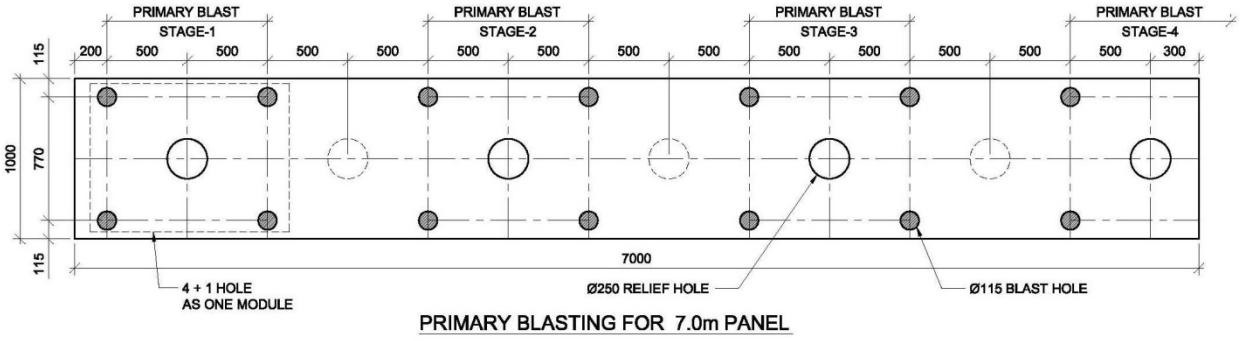


Fig. 4. Drilling pattern and layout of blastholes.

Logging of boreholes

The bore holes were logged from a lithological viewpoint so as to determine size and the position of the explosive charges. This charge distribution along the blast hole to achieve the desired result of rock shattering, without damaging the overburden stratum, was based on the rock hardness as evidenced by the drilling: the rate of advance and the sound produced. This constant full-time monitoring of the blast hole drilling by a geologist was to record and log the lithology traversed by the drilling from top to bottom and the penetration rate achieved in boulders and in bedrock.

Drilling Instrumentation

The instrumentation used as a drilling aid was an accurate digital X-Y inclinometer with which the drill rig mast is equipped. This instrument has a digital display mounted on the drill operator's control stand with a warning buzzer should there be any deviation of the mast from vertical. This allows the operator to intervene immediately as required and have an objective instrumental definition of vertical. Subsequent to completion of drilling a hole, an inclinometer test was performed on selected holes (initially on all holes) to accurately measure the verticality and the straightness. On-board DAT instrumentation output was used to check the verticality of the drill holes and, also, interpret the hardness along the borehole and define the nature of the strata drilled - see Fig. 5. This was then compared to the previously described "manual" method.



Fig. 5. DAT datalogger instrumentation on drill rig.

Checking Blast Holes

Blastholes were checked for continuity and verticality using the precision inclinometer before loading. Quality Control personnel checked that the bore holes were of proper depth by using a steel measuring tape with a bullet-shaped plummet at the bottom. If the hole was deeper than planned, an extended sand cushion followed by drill cuttings or other stemming material was introduced within the charge tube to bring the bottom charge up to the proper level. While checking the hole for proper depth, a check for water in the hole was made using a reed switch with cable reel. The ground water level was noted as a reference to be considered during loading. Whenever a blast-hole was found to be deviated and unacceptable, it was charged only to the depth which was within tolerance and the remainder back-

filled beforehand with granular material. A new conforming hole was then drilled at a 200 mm (8 in) distance, verified, logged and, if totally within the CoW footprint, approved for charging to full depth.

The gyroscopic borehole inclinometer deployed to check blast-hole verticality and its downward trajectory along its entire length had the following features and specifications: the inclinometer probe was a Ø40mm x 1000mm brass body unit weighing 4kg (1½"dia. x 40"x18lbs) connected to a recording unit via a data transmission/suspension cable with special IP69 connectors for working in up to 200bar (2900 psi) pressure environs. the probe featured a 360° Orientation range about all axes (orientation angles); inclination, azimuth, GTF, MTF, Dip Angle. A 24-bit accelerometer and a16-bit magnetometer. The angle resolution was 0.02° and its accuracy was ± 0.2° inclination and ± 0.5° azimuth and the angle measurement repeatability was 0.1°

Charging and firing the hole

For charging of drilled blast-holes, long delay Nonels (175, 200, 250, 300, 350, 400 and 450ms intervals) at multiple intervals were used. The Initiation system was from bottom to top; which is known as BOS or Bottom Initiation System. The charge density in the blast-holes was in the range of 0.7 to1.5 kg/m. Holes were not charged in the upper 5m, but this depth was later reduced to 3m. As shown in Fig. 3, the group of four nos. Ø115mm blastholes with a Ø250mm relief hole at the centre of the module were blasted all at once. This module of 4+1holes repeats itself every 1m (39 in) interval. In the rock socket the first charge was placed in position with a nominal 300 mm cushion below the charge to avoid any damage to the underlying bedrock. Depending on the depth of the cut-off, there may be 6 or more charges placed within the hole at those locations, dictated by adverse soil conditions (e.g., large boulders and blocks). The blast holes were cased with 3"dia. socket-jointed PVC pipes having a 75mm O.D. and 70.4mm I.D.

Each charge was pre-packed on the ground in a 2½" dia. PVC charge tube (63mm O.D. with 57mm I.D.) under QC (Quality Control) supervision (see Fig. 6) and the charge tube was then lowered down the hole to the designated depth defined during drilling. Multiple charges were lowered down the hole, one at a time, only after adequate stemming had been performed for the previous charge. After completing the charging and blasting for one primary panel length of 7m, the secondary Ø250mm hole, only one in between the two earlier blasted 4-hole modules, was then drilled, charged and fired.



Fig.6 –Loading Explosive Charges into Tubes.

Handling Misfires

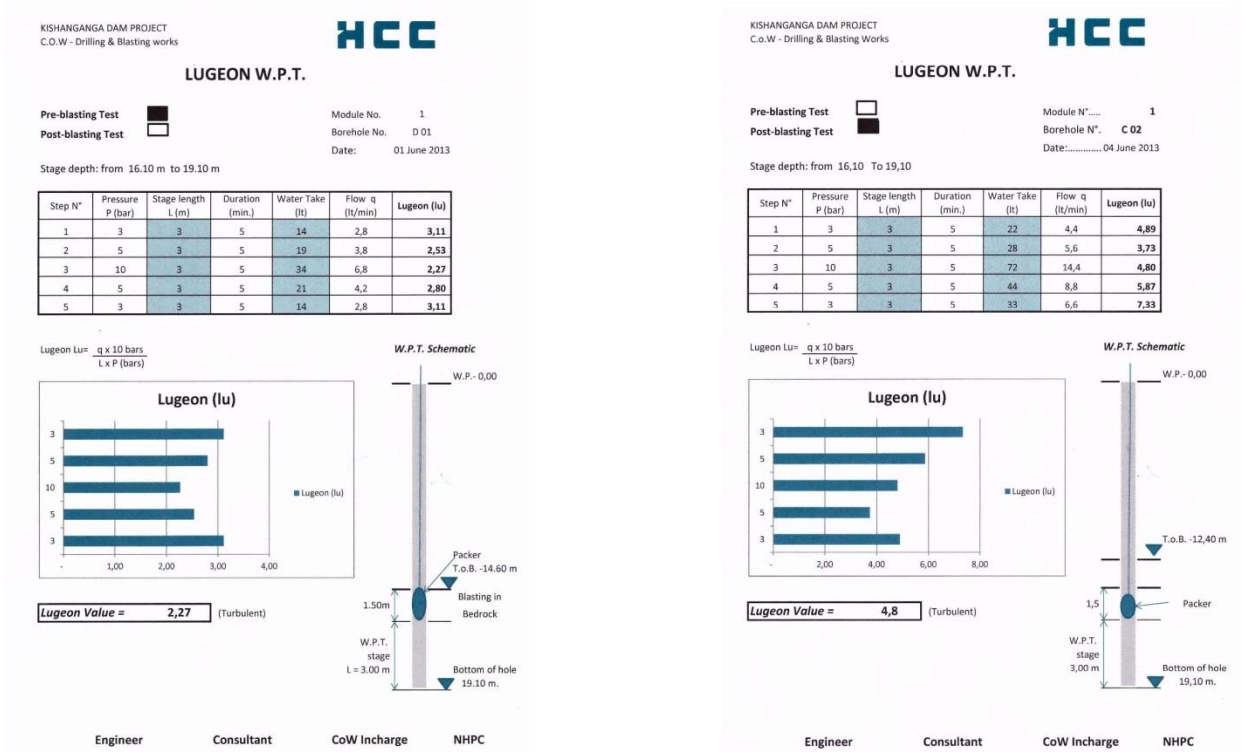
To avoid misfires the explosive cartridges were primed with two numbers of Nonel detonators of a premium manufacturing company. In fact, the number of misfires of charges experienced was truly insignificant.

Drilling and Firing Secondary Holes

After completing the blasting in one primary panel for the first set of the (4+1) holes sequences, drilling of the intermediate or secondary Ø 250 mm hole took place. One of the major concerns of secondary drilling was the danger of intercepting an undetonated explosive column, with a high risk of detonation while operating so close in unstable rock. However, no such inconvenience occurred. Hence, the secondary blasting safely contributed to the fracturing of the rock, thereby favoring the subsequent excavation.

Bedrock investigation and protection

During drilling of the blast holes, one hole in the first (4+1) module was extended 2m to 3m (6 – 9 ft) beyond the required depth to allow conducting a water pressure test to ascertain the soundness and the permeability of the bedrock (before blasting). This was done for every third panel, corresponding to approximately every 20m along the CoW alignment. In the post-blasting secondary drilling with Ø 250 mm holes, the first such hole in each panel was also be progressed 2m to 3m (6 ft to 9 ft) beyond the required blasting depth to allow a water pressure test to be conducted in the Ø115mm x 3m pocket drilled at the base. The observations for the second stage water pressure testing were also recorded and compared to those of the primary water pressure testing to understand the impact of blasting on the bedrock.


KISHANGANGA DAM PROJECT
C.O.W - Drilling & Blasting works

LUGEON W.P.T.

Pre-blasting Test ■
Post-blasting Test □

Module No. 1
Borehole No. D 01
Date: 01 June 2013

Stage depth: from 16.10 m to 19.10 m

Step N°	Pressure P (bar)	Stage length L (m)	Duration (min.)	Water Take (lt)	Flow q (lt/min)	Lugeon (lu)
1	3	3	5	14	2,8	3,11
2	5	3	5	19	3,8	2,53
3	10	3	5	34	6,8	2,27
4	5	3	5	21	4,2	2,80
5	3	3	5	14	2,8	3,11

Lugeon Lu= q x 10 bars / L x P (bars)

Lugeon (lu)

Lugeon Value = 2,27 (Turbulent)

W.P.T. Schematic

W.P.- 0,00
Packer
T.o.B. -14.60 m
Blasting in Bedrock
1.50m
W.P.T. stage L = 3.00 m
Bottom of hole 19.10 m.

Engineer Consultant CoW Incharge NHPC

KISHANGANGA DAM PROJECT
C.o.W - Drilling & Blasting Works

LUGEON W.P.T.

Pre-blasting Test □
Post-blasting Test ■

Module N°..... 1
Borehole N°. C 02
Date:..... 04 June 2013

Stage depth: from 16,10 To 19,10

Step N°	Pressure P (bar)	Stage length L (m)	Duration (min.)	Water Take (lt)	Flow q (lt/min)	Lugeon (lu)
1	3	3	5	22	4,4	4,89
2	5	3	5	28	5,6	3,73
3	10	3	5	72	14,4	4,80
4	5	3	5	44	8,8	5,87
5	3	3	5	33	6,6	7,33

Lugeon Lu= q x 10 bars / L x P (bars)

Lugeon (lu)

Lugeon Value = 4,8 (Turbulent)

W.P.T. Schematic

W.P.- 0,00
T.o.B. -12,40 m
Packer
1,5
W.P.T. stage 3,00 m
Bottom of hole 19,10 m.

Engineer Consultant CoW Incharge NHPC

Fig. 7. WPT Reports from KGHEP CoW – Tests performed on June 1 & 4, 2013

The two Water Pressure Test Reports of Fig.7 above refer to two holes in the same module (No.1), a blasthole before blasting, the other a Ø 250mm (10" dia.) central hole after the blast indicate there was no damage to the bedrock caused by the blasting.

Trench and Guide wall

Guide Walls, 1.5m (5 ft) high with a 1.15m internal distance (45 inches) were constructed after blasting and prior to the diaphragm wall construction. Their purpose is to provide guidance to ensure the correct alignment of the excavation and accurate location with panel number and extent markings upon them. During panel excavation guidewalls afford protection against the instability of the uppermost soil layers caused by surging (washing induced by fluctuating levels of bentonite slurry) caused by the grab during excavation. The top of the guidewall is used as the excavation depth reference for trenching.
Also, they provide prevention to the collapse of the top of the trench due to equipment loads close to the excavation, especially transit mixer traffic during concrete placement; and, had the end-stops been used, they would have had to provide support for the vertical loads imposed by the extraction of the end-stops.

The 0.3m-thick guide walls were constructed in sections as a cast in-situ reinforced concrete unit having an "L"-shaped cross-section with 1.5m wings equidistant from the CoW axis.

Bentonite Slurry

Bentonite slurry (or mud) was prepared in 1000-litre batches (250 US gallons) using a high-speed colloidal mixer at the CoW site. The concrete storage tanks for the bentonite slurry were as shown in Table 1:

Table 1: Bentonite Slurry Plant Storage Tanks.

Bentonite Slurry Tank	**Volumetric Capacity (m^3)**
Fresh Mud	420
In hydration (for 24 hours)	450
Regenerated Mud – ready for use	450
Return from trench	420
Hydrated Mud for plastic concrete	40

The bentonite/water ratio (B/W) usually adopted in diaphragm walls ranges between 2% and 8% by weight, according to the quality of the bentonite and of the water, as well as the type of soil excavated. The weight of the fresh mud, a function of the W/B ratio, should be within 9.91×10^3 N/m^3 and 10.60×10^3 N/m^3 (63.05 lb/ft^3 – 67.5 lb/ft^3) and the Marsh viscosity generally within 35 and 45 seconds.
The bentonite slurry typically used at Kishanganga was a 70 kg/1000 liters of water (6.5% by weight and S.G. = 1.044) with 41 seconds Marsh.
The slurry level within the trench was maintained at all times ≤500mm below the top of the guide walls (typically 150mm to 300mm max., with the grab submerged in the trench); and, in any case, not less than 1.50 m above the existing water table. Towards the left abutment, where the RBM was predominant and the sandy soil with subterranean water flow created some trench problems, the work platform was raised about 1.0m above the guide walls to increase the hydrostatic load and mud with 80 kg/1000 l of water was used.

An on-site laboratory with a Mud Balance for checking slurry density, a Marsh Funnel and graduated cylinder for measuring mud viscosity (with beaker and stopwatch) and a Baroid sand content kit was used for daily slurry tests, with sampling from the panel trench during grabbing and prior to approving concrete placement to cast a panel after final clean-up.

Pumping the slurry to the trench

The slurry has to be pumped into the trench at the same rate at which the soil and slurry are removed by the excavating equipment. During normal trenching operations, the slurry circulates in a circuit between the de-sanding unit and the panel being excavated. A view of the bentonite slurry storage plant is shown in Fig. 8. A submersible dredging pump with a 30m (100 ft) Head and 1.5 m^3/min (400 US gpm) Discharge was used to transfer the bentonite slurry from the panel trench to the specific slurry tank under the desander. Five submersible pumps installed at the slurry plant transferred slurry from one tank to another (recirculation or transfer) and pumped mud to the trench as required.



Fig. 8. Bentonite mixing plant with anti-dilution covers and paddle agitators.

Construction of CoW panels

Diaphragm wall construction begins with the trench being excavated in discontinuous sections or "panels" using heavy grabs or trenching mills. Typically, primary single or multiple bite panels are constructed first, followed by the construction of intermediate secondary or closing panels – see Fig.9 below.
At Kishanganga the 2.5m wide single-bite panels were adopted for the cut-off Start-up and Learning Curve, but were retained throughout thereafter, as explained earlier. Hence, the KGHEP Cut-off Wall is a 2.50m (8.2 ft) panel bite wall: i.e., 1.75m effective primary panels and 2.50m effective secondary panels.

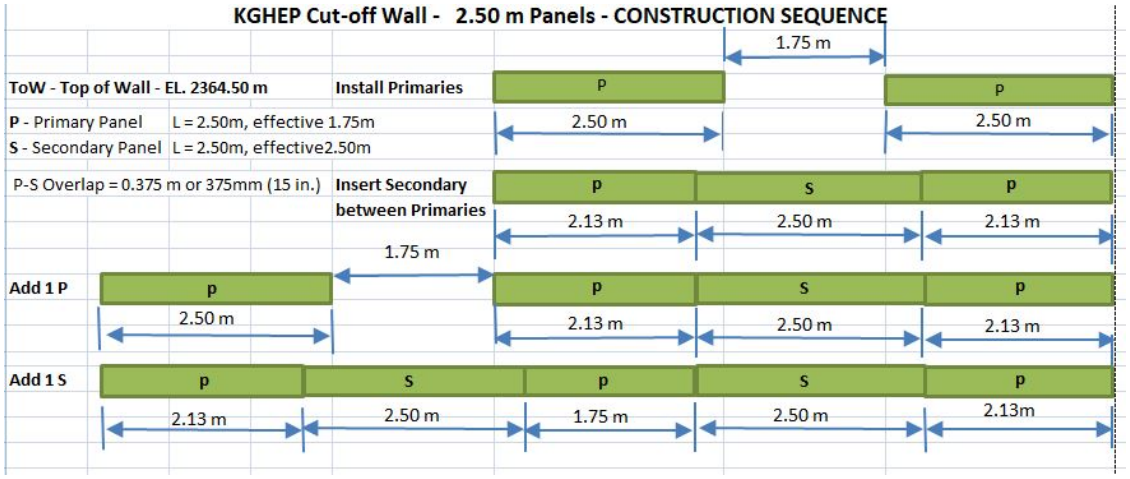


Fig. 9. Layout and sequence of 2.50m Primary and Secondary panels without using end-stops.

The minimum width of any one panel was 2.50 m (8.2 ft), as determined by the bite width of the grab. The originally proposed option of multiple 'bite' primary panels was kept open, but never implemented.
Typical grab excavation with clamshell rope grab is shown in Fig. 10 and Fig. 11.



Fig. 10. Grabbing operation in progress within guide walls.



Fig. 11. Grab hoisted full of boulders (left) and with blast fragmentation of boulders in spoil (right) in same panel.

At Kishanganga, the excavation tool was a heavy wire rope-suspended mechanical clamshell grab operated by using the two hoists on a lattice boom hydraulic crawler crane (80-ton Kobelco 7080). Initially, the grabs with a 2500mm x 1000mm nominal bite dimension, were approx. 4.8 m tall (16 ft) with the jaws opened and weighed 7 ton (1unit) and 9 ton (2 units). Their jaw capacity was nominally 1.0m^3. Following modifications executed on site, the grabs had the following features: overall height with open jaws, 6.40 m (21 ft); weight 13.5 metric tons. The main modifications are indicated in Table 2.

The modifications to the original grabs, to render them suitable for the hard work in excavating a cut-off in very difficult bouldery ground, were both structural and mechanical. The grabs, in their original form, were too weak, too light and too short for the work at hand. The clamshell jaws were particularly inadequate from

a design viewpoint with their 20mm (¾ in.) low-strength steel plate and the added 10mm (⅜ in.) plate where the steel stub "teeth" were weld-attached. One grab had been used in the test plot a few kilometers upstream and had suffered considerable damage in performing just one panel.

Table 2: Comparison of Clamshell Grabs Before and After Modification

Item Description	**Before Modification**	**After Modification**
Weight	7 tonnes (1No.)/ 9 tonnes (2Nos.)	12 tonnes (1) / 13.5 tonnes (2)
Height (with jaws open)	4.8m	6.10m (1) / 6.4m (2)
Grab Body Plate Thickness	20mm (1) / 30mm (2)	40mm (1) / 50mm (2) bottom half
Teeth Type	Hard-faced EN-9 Steel stumps	Komatsu Rock, KM15RC
Tooth Adaptor	Inexistent	Komatsu KM 16.1/2/3
No. of Teeth on Jaws	2T, 3T	3T, 4T
Tooth support Jaw plate	20mm IS2062GR A/B	45mm Hardox 500
Jaw Curved Plate Thkness - Material	20mm + 10mm IS2062GR A/B	40mm Weldox
Jaw Faceplates - Material	25mm - IS2062 GR A/B	Single 35 mm Hardox 400
Jaw Sidecutter Plate	25mm - IS2062 GR A/B – HF	25mm Hardox 400 hard-faced
Rope Operating Reeving	4-Pulley – 4-part line	5-Pulley – 6-part line
Jaw Closing Force	30 tonnes ca.	55 tonnes
Reeving Wire Rope	6 x 19 Ø28mm R.L. Parallel Lay	6 x 37 Ø 28mm E.I.P.S. L.L Parall.
Jaw Hinge Pins	Ø 100mm x 742mm EN9 Steel	Ø 100mm x 850mm EN16 Steel
Jaw Actuating Links – 4 No	2900mm x 175 mm x 50mm Thk	3000mm x 175mm x 80mm Thk
Jaw-Link Connecting Pins (2 No)	Ø 80mm x 770mm EN9 Steel	Ø 80mm x 770mm EN16 Steel

Apart from strength and weight considerations, it is important to underline that the longer grab, along with the much lowered center of gravity obtained, worked in the desired pendulum mode which favors trench verticality and linearity. Clamshell weight (excavating jaws) underwent a more than threefold increment.





Fig.12. Original jaws with bent 2-tooth carrier plate. Fig.13 Modified jaws with 45mm Hardox plate.

Excavation of Primary Panel Trenches

Panel excavation was a 2.5m x 1.0m bite performed with the modified heavy duty grabs.
Whenever any stubborn obstacle was met that delayed the advancement of excavation for more than 20-30 minutes, or if there was need to correct any unacceptable deviation, heavy chisels were available – both box and cross/star types – to chisel through the rock or to further break up any boulder not fully fragmented by the preceding blasting operations. The types of chisels used for this are shown in Figs. 14 and 15.



Fig. 14. A 12-ton box chisel used in CoW excavation.



Fig. 15. A 10-ton cross chisel for CoW.

For Upstream-Downstream verticality correction and/or rectification of inner and outer face of the panel, a crane operated scraper chisel shown in Fig. 16 was provided and was used as required.



Fig. 16. Face Rectifying Scraper Chisel.

After reaching final depth and following a bentonite slurry substitution (desanding) and trench base clean-up, the Koden test was immediately performed - as shown in Fig. 17 & Fig.18 - to verify both the verticality of the trench and the panel profile to enable an estimation of the plastic concrete requirement.

The main specifications of the Koden DM-604 Ultrasonic Monitor are given in Table 3.:



Fig. 17. Koden DM-604 Recorder unit at Panel location.



Fig.18. Koden Profiler Winch set up on trench.

Table 3. Specifications of Koden DM-604 Ultrasonic Monitor

Recorder unit

Measuring system	Ultrasonic echo sensing system
Recording system	Direct recording using the belt
Recording paper	Electro-sensitive recording paper 250 mm x 20 m
Measuring range (radius)	0.5 m, 1.0 m, 2.0 m, 4.0 m
Measuring accuracy	±2% at full scale
Power supply	100/110/120/220/240/440 VAC, 50/60 Hz
Operating temperature	-10°C to +50°C (14°F to 122°F)

Winch unit

Up/down speed (Continuously controllable)	0 to 20 m/min
Up/down movable distance	100 m maximum
Bottom and trench and casing sensing system	Automatic sensing by limit switch
Operating temperature	-10°C to +50°C (14°F to 122°F)

Concrete Placement

The tremie pipe was a Ø 250mm (10-inch id) thread-coupled assembly and was set at the centre of the panel trench with the base shoe about 300mm (1 ft) off the bottom.. The concrete was delivered in 6 m^3 transit mixers loaded with 5 m^3 (6.5 cu. yd) to avoid spillage on steep hills and was discharged into the tremie pipe hopper. The tremie was supported by a crane and, when necessary, subjected to jerk to promote the outflow of the concrete from the submerged bottom (shoe) of the tremie – see Fig.19.

At the start of concrete placement, a tightly balled up cement bag or other suitable "go-devil" was placed at the bottom of the tremie hopper, protected by a shovel until the 1.5m^3 hopper was full of concrete. The shovel was then removed and the concrete flowed down the tremie, pushing the "go-devil" ahead of it, thus keeping the concrete from mixing with the bentonite slurry. Except at the very beginning, the tremie immersion depth in concrete was not less than 2.0m, but typically 4m. Except for suspension to remove tremie elements, concrete placement proceeded without interruption until the concrete reached the required height, coincident with the top of the guide walls. The level of the concrete was measured at frequent intervals by soundings and, at a minimum, upon complete discharge of each truckload.



Fig. 19 Concrete Placement – Transit mixer discharging into tremie funnel.

During placement, tremie pipe elements (2m lengths) were removed from the panel to avoid exceeding a 7m (23 ft) submerged depth; these were placed in the tremie pipe rack and washed. Threads were inspected these for thread and tube damage and replaced if necessary. As soon as placement was completed with a minimal overfill, any scum accumulated on the surface of the concrete was removed.
A concrete placement time log of the actual concrete volume poured per truckload and the corresponding depth to concrete were recorded along with the length of the tremie pipe at the time. These data provided a direct "readout" not only of how much, but more importantly, of where any concrete shortage or overrun occurred within the panel (any cave-in or interconnection) and if any immediate remedial action was required.

Concrete Placement report

For each Cut-off Wall panel, a Concrete Placement Report was prepared in which the following data is recorded: Panel No.; Date of concreting; Dam Reference Chainage; whether it is a Primary or Secondary panel; date of start of and of completion of excavation; Crane used (Model and S/N); Depth of panel trench; Composition and overall length of the tremie pipe; Tabular record of data from the concrete placement log; slump tests and temperature of the concrete at both the batchplant and at the panel for every second truckload,
In the report a graph of Actual and Theoretical concrete volumes were plotted against depth. The laboratory personnel took samples at the site to make cubes for 7, 14 and 28-day unconfined compressive strength tests.

Excavation of Secondary Panel Trenches and formation of joints

The 2.5m (8.2 ft) wide secondary panels were excavated straddling two successive primary panels which were previously constructed 1.75m (5.74 ft) apart, as indicated in the schematic of Fig.9. This gives a nominal overlap of 375mm (15 in) at both ends, thereby ensuring a good watertight joint between successive panels.
The final clean-up and verification with the Koden instrument and concreting is as per the primary panel.

PLASTIC CONCRETE

Following technical requirements were to be met by the plastic concrete

- Maximum grain size 30 mm
- Unconfined compressive strength (28days) >1.5 MPa
- Confined compressive strength >2.5 MPa
- Strain at failure >5%
- Permeability $<10^{-8}$ m/s

Based on the above requirements, Trial mixes were prepared in Laboratory for the design of plastic concrete and tests were conducted on the trial mix producing the following results:

- Unconfined compressive strength 1.59 MPa
- Slump 180mm
- Initial / Final Setting time 26min / 49min.

Mix design with two types of cement was approved after satisfying the requirement as per the technical specifications. The mix design adopted at site is given in Table 4.

Table 4. Mix design of Plastic Concrete for Cut-off Wall at KGHEP.

Material	**Unit**	**Quantity (m^3)**
Cement	kg	150
Bentonite	kg	80
Aggregate <10mm	kg	551
Crushed Sand	kg	1023
Water	kg	350
Admixture	kg	0.98

The bentonite was introduced into the transit mixer as slurry. The truck then drove to the batchplant to load the concrete mix that had been prepared with the remainder of the components and the complete blending of the two took place at the plant and during the 8 km drive back to the CoW site. A series of rapid drum revolutions of the transit mixer were effected at the panel location prior to discharge.

CONCLUSION

It is concluded that a plastic concrete cut-off wall or a structural concrete diaphragm wall can be constructed in difficult geology by using accurate preliminary pin-point blasting termed “Surgical Blasting” throughout, followed by excavation with conventional chisel and clamshell grabbing methods.

The blasting effected for cut-off wall produced no flyrock, so demobilization of equipment was not required, just the personnel was gathered in dedicated safe areas on site during firing of the charges.

It has also been demonstrated that the drilling and blasting methodology adopted caused no damage to the underlying bedrock, as evidenced by the water pressure tests (WPT) conducted.

RECOMMENDED JUNCTIONS BETWEEN DIAPHRAGM WALL PANELS FOR DEEP EXCAVATIONS

Paul Vidil, Soletanche Bachy, Rueil-Malmaison, France, +33(0)147764262, paul.vidil@soletanche-bachy.com

ABSTRACT

Diaphragm walls are often used for permanent retaining walls and shafts; they are particularly suitable for deep projects under high water head. The work sequence of diaphragm walls leads to different adjoining panels. In this way, junctions between diaphragm wall panels are key points, whether it be for formwork, guidance or waterproofing.
This hereby document concerns the watertightness aspect and first provides positive and negative backgrounds of several junction types (stop end tubes, double or triple blade system, addition of pipe for aquareactive resin injection, watertight seals, milling) depending on the excavation tools' type (hydrofraise, hydraulic or mechanic grabs).
This paper also lists the different junctions nowadays used for deep excavations, and gives a compendium of good practices, based on recent experience.
Finally, it deals with the subject of the joint depth compared to the panel depth, and ends with the special case of diaphragm walls carried out under low clearance.

Keywords: diaphragm wall, panel, joint, watertightness, deep excavation, feedback, good practice

INTRODUCTION

It has been more than 60 years since diaphragm walls are carried out around the world, and of course the methods have improved. Diaphragm walls become more and more necessary in dense urban environments (whether it be above or under surface), and especially under high water head. The progresses in terms of depth and watertightness now enable to consider projects at very high depth, such as deep buried railway stations.
Junctions between diaphragm wall panels are key points. In general, they don't have any structural purpose, but they are very often used as a hydraulic bar. The aim of this document is not to describe in detail the different stages to implement those joints: this hereby note rather lists the different junctions nowadays used for deep excavations, and that have proved to be the most efficient at depth. Some recent experiences are also given.

DRILLING MACHINES

A state of the art of structural diaphragm walls has been undertaken long ago by Puller (1994). Although it has been more than 20 years ago, two drilling machine categories still remain to achieve a diaphragm wall:

- on one hand, the rop/cable operated grab (mechanical clamshell) and the hydraulic grab (Kelly bar mounted),
- and on the other hand, hydraulic cutter machine, also called hydromill or hydrofraise.

The latest evolution relates to high depth, large thickness, progress in a verticality tolerance, electric excavation machine, and the hydrofraise with grippers for hard soil.

There are several ways to ensure watertightness between diaphragm wall panels: waterstop joints and milled joints.

© 2018 Deep Foundations Institute

WATERSTOP JOINTS

Description

Decades of feedbacks have allowed to find the best shape and method to assure watertightness at the panels' butt joints.
Anecdotal techniques will be put aside, such as soldier beam stop ends, v-shape polystyrene blocs, tubes with fins, joints with cotters…

At the beginning, stop end tubes were used (Fig. 1); they lead to a semi-circular concreting surface.

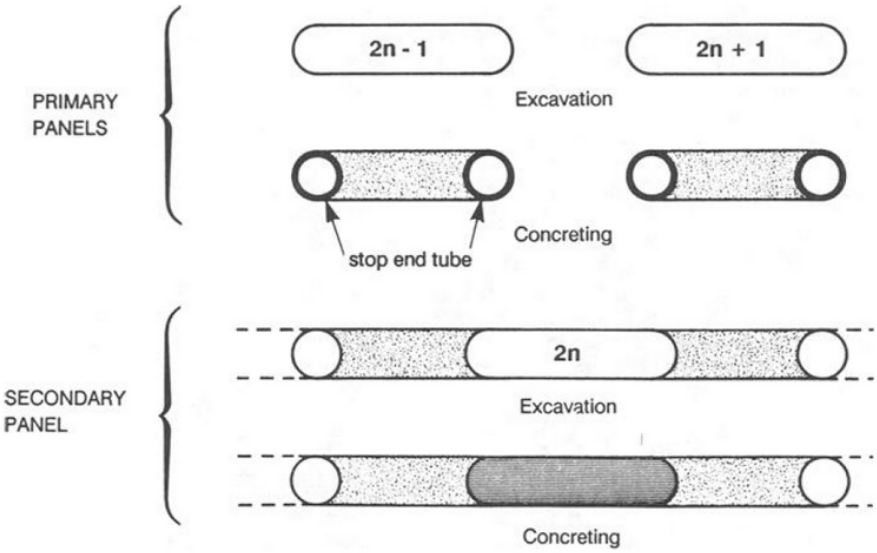


Fig. 1. Construction scheme with stop end tube (Vanel, 1992)

It soon became clear that these stop ends were not the solution, mainly because of waterproof issues. The CETMEF (2002) points out that, by its nature, a joint implemented by juxtaposition of fresh concrete on indurated concrete is not waterproof. During its hardening, the concrete endures shrinkage that leads to the joint detachment; and during the excavation a thin layer of bentonite stands still at the previously cast panel. Moreover, this type of joint increase the risk of concrete by-pass and problem during the tube removal.

Then, flat stop end joints were experimented: the ones proposed by Fleming (Cementation), the Stopsol proposed by Vial (Solétanche) and the Bachy's patented CWS (Complete WaterStop) Stop End. The incorporation of a waterbar ensures maximum watertightness between adjoining panels.
The principle is that a temporary metal formwork is supporting the waterstop sealing strip (Fig. 2)

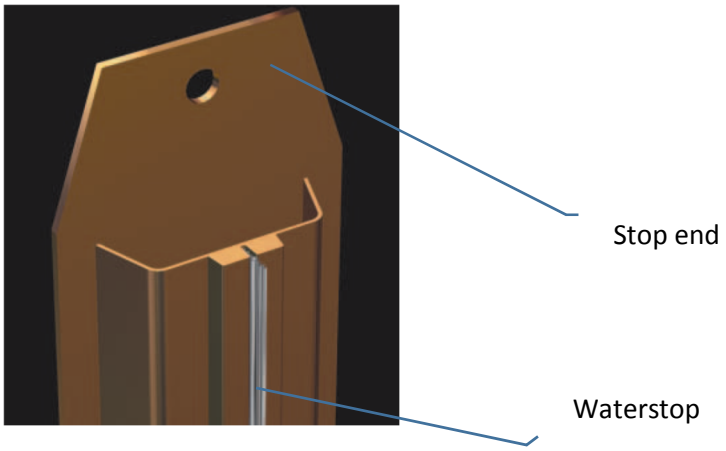
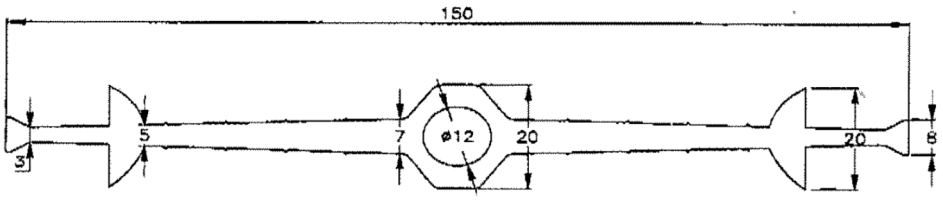


Fig. 2. Joint with a waterbar

The typical dimensions of the PVC (polyvinyl chloride) waterstop joint (Fig. 3) are the following (in mm):



- tolérance +- 5%

Fig. 3. Waterstop typical dimensions

Another advantage of the waterbar is that it has a high breaking elongation.

Several other shapes have been tried (Fig. 4), but the single blade (15 to 20 cm long) turns out to be the best shape.

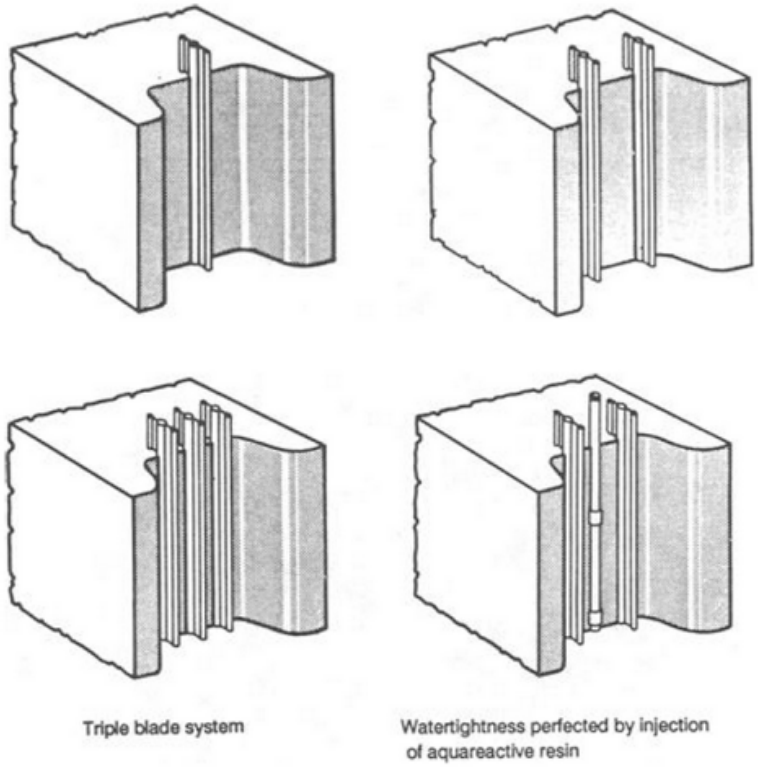


Fig. 4. Different blade systems (Vanel, 1992)

As a matter of fact, the multiple blade system presents a risk of pollution between the blades (mud pocket, pebble nest) and it is very hard to clean. It finally leads to more pathologies that the single blade.

Full-scale watertightness tests have been carried out on site (Fig. 5) that confirms the single blade efficiency.

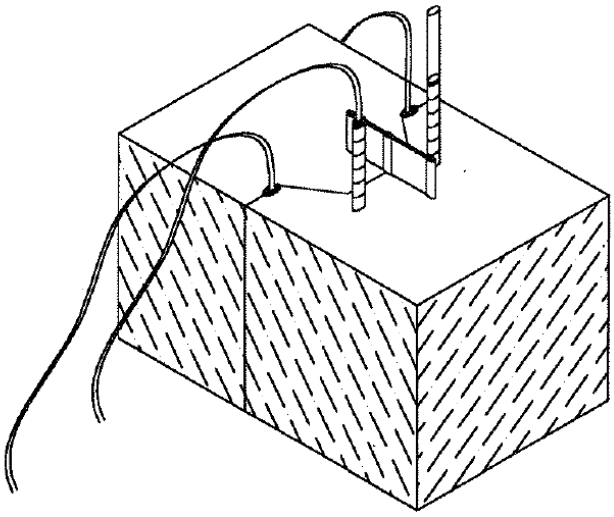


Fig. 5. Watertightness test in 2002 (Le HAVRE – Port 2000)

Moreover, the French National Standard DTU 14.1 (NF P 11-221) only mentions one watertight blade.

Finally, tests with longer blade (up to 25 cm) didn't bring improvement, and quite the opposite in fact: the concrete put in place through hoppers produces high energy with a fall under mud that can bend longer blade.
The consequence of years of practice therefore comes to the withdrawal of the stop end tubes, the multiple blade system, and grouting tube.
The waterstop joint is particularly recommended when the water head is high for deep structures (shafts, railways stations….), and also for quay walls. The stop end is also used to guide the excavation and allows better deviation controls of the excavation device.
Waterstop can be used for an excavation with a grab or a hydrofraise.

When there is an angle between two panels in the diaphragm wall lay out (Fig. 6), a wedge (plasterboard and polystyrene) can be used to put the stop end in place.

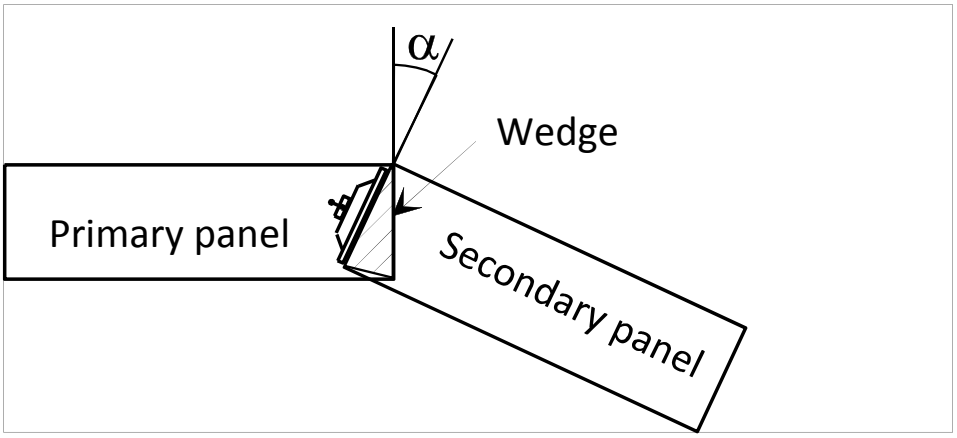


Fig. 6. Extract of a panel lay out with a wedge

Implementation

This formwork is positioned at each end of the primary panels. The formwork is removed laterally after excavating the adjacent secondary panels (Fig. 7).

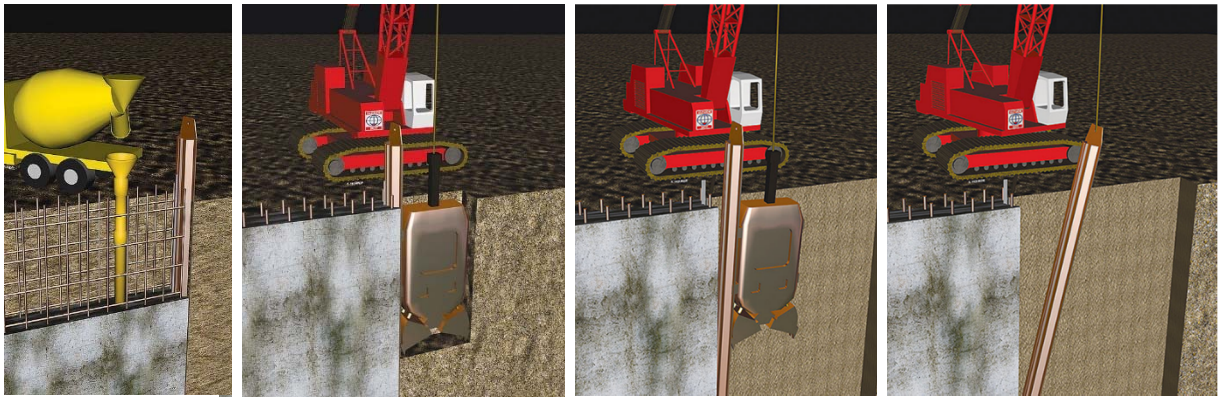


Fig. 7. Work sequence of diaphragm wall construction

The stop end formwork elements are put together by means of splines/pins at the edge (Figs. 8-9).

Depth of the waterstop joint with respect to the base of the excavation

There was no need so far to put in place a waterstop joint beyond 55 m. Deepening is of course feasible, providing one could guarantee an almost perfect verticality while the diaphragm wall completion. Anyway it remains a delicate operation: it requires a risk management of bypassing during concreting, obstruction of the formwork withdrawal, and blade tearing.
The latest evolutions of excavation machine enable to reach this high standard of performance.

It is not compulsory to take the waterstop down systematically to the diaphragm wall toe. It depends on what type of soil is the embedment. It is nevertheless recommended to take it down at least to the final excavation level.



Fig. 8. Stop end assembly



Fig. 9 Stop end lifting

Between two panels, the upper part is therefore with a waterstop sealing strip, and the lower part is made up of a “dry” joint, that is to say a contact with two concreted surfaces.

In order to decide of the waterstop depth, two subjects should be studied: the absence of waterstop sealing strip from a certain depth may lead to

1. an increase of the water flow through the diaphragm wall,
2. and a washing out of fines.

It depends on the permeability and the layer distributions.

It is also possible to drill a hole in the ground behind the butt joint, and to equip it with a sleeved pipe on the height of junction without waterstop. Thereby, a cement/silicate grout can limit the potential leakage through the joint.

The waterstop depth should be decided on a case-by-case basis: weigh up the pros and the cons with respect to the related risks.

Recent experience

Vidil et al. (2015) describe a pumping station and an access shaft that have been carried out during the Liquefied Natural Gas terminal construction in Dunkirk (France). The access shaft diaphragm wall is 65 m high (Fig. 10), with waterstop joints up to 55 m deep. The embedment is in the Flanders clay, and the water head is 45 m. The final 10 m of diaphragm wall panels are connected by “dry” joints.

Besides, as part of the construction of the new metro system in Paris, Société du Grand Paris recently awarded a civil engineering contract for the works for Line 15 South on the section between Villejuif-Louis-Aragon (excluded) and Créteil-l’Échat (included). This operation is ongoing (Fig. 11), and in a few months, waterstop joints will be taken down to the diaphragm toe, for some stations.
The objective is clearly to go beyond the present references on this new metro system.

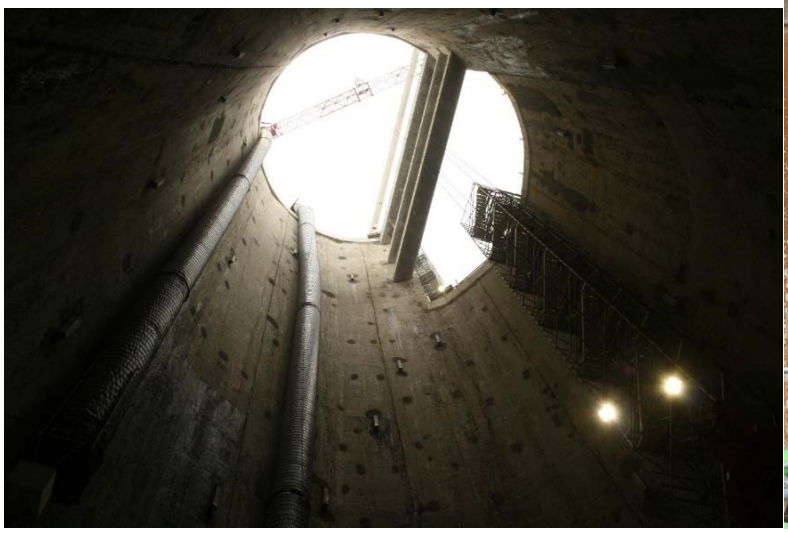


Fig. 10. View from the bottom of excavation (access shaft - Dunkirk)



Fig. 11. Sticking out formworks, in a primary panel (Line 15 south- Paris)

MILLED JOINTS

Description

There is another solution that avoid waterstop joints, while assuring watertightness; the joints between panels are realized by milling/grinding the hardened concrete at the edge of primary panels (Fig. 12): the closure panel consists in a single pass, also called unitary pass, and the joints are milled on both sides by the cutter.
Of course, this type of joint can only be used for an excavation with a hydrofraise.

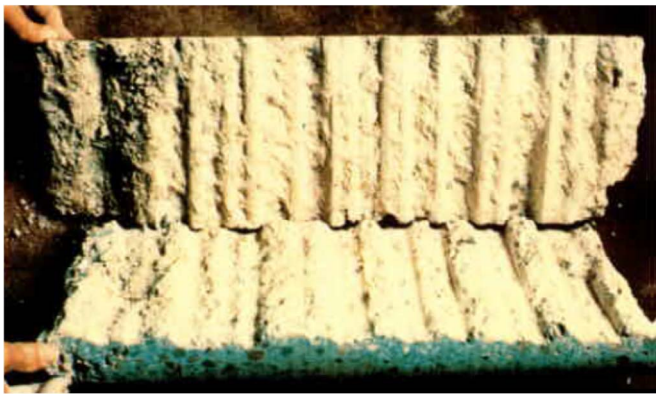


Fig. 12. Milled concrete

When it comes to circular enclosures, the milling can be facilitated by adding polystyrene or plastic castellated tubes at the edge of primary panels.

Recent experience

In 2006, a Hydrofraise rig with alignment correction was used to construct the Carrousel circular shaft in Versailles (France) up to a depth of 65 m, which achieved a verticality tolerance of less than 0.1 % (Fig. 13).

Recently, a diaphragm wall forming the enclosure of the Beckton overflow shaft (Fig. 14) has been completed: this is the first of the four shafts being constructed on Thames Water's Lee Tunnel project (England). The 90 meters' deep shaft, with 1.5 meter thick walls, was the first to be constructed. Then it was the turn of the construction of the 98 meters deep, 1.8 meters' thick diaphragm wall of the Beckton pumping shaft, with a water pressure at the chalk base around eight bars.

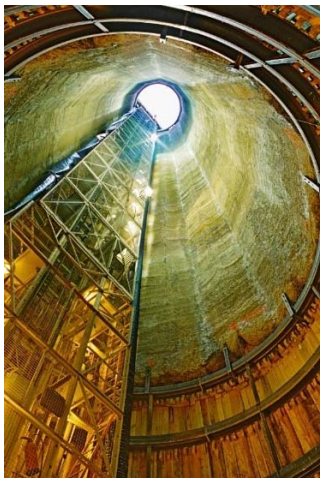


Fig. 13. Carrousel shaft (Versailles)



Fig. 14. Overflow Shaft – Excavation 73.6m deep

EXPANSION JOINTS

Description

It deals with combining the diaphragm wall carrying out by milling the hardened concrete at the edge (see previous chapter), with the placing of expansion joints that are pressed against adjacent primary panels' facings (Fig. 15).

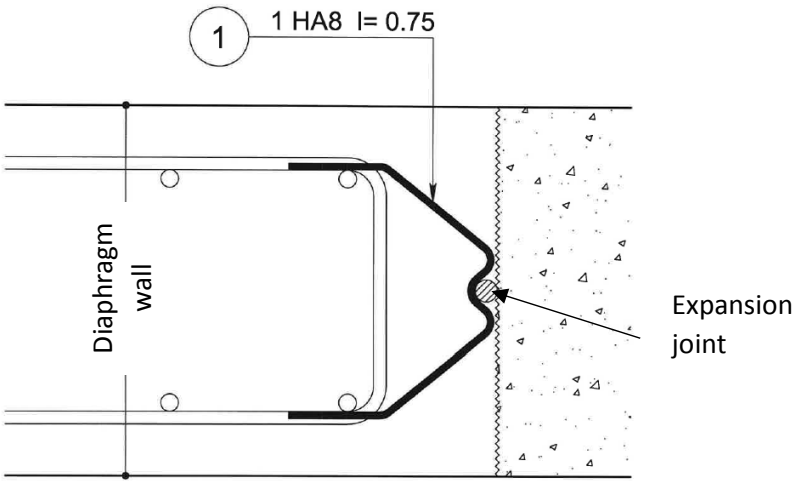


Fig. 15. Expansion joint principle

Thus this technique enables to put a physical bar between panels.

Expansion joints can be added in specific cases, for example when diaphragm walls are carried out under low clearance, preventing from putting stop ends in place.

There are two main systems to press joints against adjacent panels:

- an iron frame is fastened on the reinforcing cage; then this frame needs to be laid out, in order to put the joint against the adjacent panels. However, this system might have limitations when applied to cages made of multiple elements.
- a jacking system is installed in the steel reinforcement bearing water-swelling joints on light steel plates. The steel reinforcement and the joints are then installed at the same time into the excavated panel. A flexible water system simply controls the cylinder's movement. The pistons go out under water pressure. The support plate is pushed until it reaches the adjacent panel on full height.

These systems have been implemented on hydrofraise excavation; a similar system for grabs or KS works is under discussion.

This technique can be combined with under pressure cement/silicate grouting in the ground behind the joint. In that case, grouting can be carried out by means of sleeved pipes putting in place in boreholes just behind the diaphragm wall.

Recent experience

This system (Fig. 16) was first installed on 3 panels on the works site of Saint Tropez (France).

Another application appeared when Société du Grand Paris awarded in 2016 a Contract for the works on the Fort d'Issy Vanves Clamart station (Line 15 South).

In the central area of this project, single bite panels were executed under a metallic railway bridge (Fig. 17). Junctions between panels were realized by concrete milling. Expansion joints were put in place in the reinforcing cages to increase watertightness.



Fig. 16. Piston attached on the earth side (Saint Tropez)



Fig. 17. Excavation under low clearance (Fort d'Issy Vanves Clamart)

For the moment, the technique of expansion joints only has been carried out for work sites under a low to medium water head.

AVERAGE PERMEABILITY

The diaphragm wall is considered as a relatively waterproof structure, according to the French National Standard DTU 14.1 (NF P 11-221).

First and foremost, it is obvious that the watertightness of the diaphragm wall is very much dependent upon the skill, experience and personnel of the specialized firm, in addition with a good quality control. In which case, the efficiency of those joint types in terms of watertightness can be estimated in Table 1.

Table 1. Rough estimate of diaphragm wall permeability

Type of joint	Diaphragm wall permeability (m/s)
Stop end tubes	10-8
Formwork with Waterstop sealing strip	10-10 to 10-9
"Dry" joint	10-8
Milling	10-10 to 10-9
Milling and expansion joint	10-10 to 10-9

The DTU 14.1 gives limitations for the flow of seepage and leaks through the wall.

The hereafter values do not separate joints and walls; values are for the complete diaphragm wall:

- 0.5 l/m² per day on yearly average;
- 1 l/m² per day on weekly average;

Moreover, no area of 10 m² is allowed with more than 2 l/m² per day on weekly average.
It means, that above those values, that is to say as soon as there is a noticeable leak, joints between panels should be treated (aquareactive resin injection in general).
In practice, those limitations are only applicable on the diaphragm wall height above final excavation level.

CONCLUSION

Junctions between diaphragm wall panels play a key role for formwork, guidance or waterproofing.
The waterstop joint is particularly recommended when the water head is high for deep structures (shafts, railways stations….), and also for quay walls.

Their watertightness depends on the junction type; single blade waterstop or milling have proved to be the more efficient at depth. It is therefore absolutely necessary to guarantee an almost perfect verticality while the diaphragm wall completion

Expansion joints can be added in very specific cases.

The trend of the deepening of civil engineering structures makes even more essential to resort to high qualified and skilled contractors. The latest evolutions of excavation machine, and in particular the new generation of hydrofraise, enable to reach high standard of performance.

The construction of the new metro system in Paris is going to go beyond the present references of waterstop joint depth.

REFERENCES

Centre d'études techniques maritimes et fluviales (CETMEF), 2002. Fascicule 5, Surveillance, auscultation et entretien des ouvrages maritimes, Quais en parois moulées, Notice PM n° 02.02

NF P 11-221-1 alias DTU 14.1, 2000. Travaux de bâtiment - Travaux de cuvelage - Centre Scientifique et Technique du Bâtiment

Puller, M. 1994. The waterproofness of structural diaphragm walls, Geotechnical Engineering (ICE), January, 107-1

Vanel, P., 1992. Making Diaphragm wall joints watertight with the CWS system, ASTM 04-011290-38

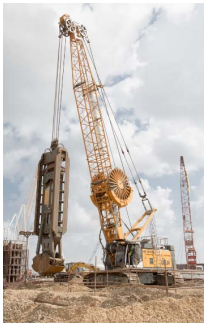
Vidil, P., Poirrier N., and Utter N., 2015. Conception et dimensionnement du puits d'accès et de la station de pompage du terminal méthanier de Dunkerque, 16th ECSMGE, Geotechnical Engineering for Infrastructure and Development, Edimbourg

SUEZ CANAL UNDERPASS: 260.000 M^2 OF DEEP DIAGRAPHRAM WALL EXCAVATION EXPERIENCED WITH LWN AT ALMOST 360°

Bringiotti M., GeoTunnel S.r.l. – LWN Agent, Genoa, Italy, info@geotunnel.it
Bringiotti G., GeoTunnel S.r.l.
Nicastro D., GeoTunnel S.r.l.
Fumagalli G., GeoTunnel S.r.l.

ABSTRACT

The present case history has been drafted with the aims to illustrate the most important features of the preparatory foundation works related to the construction of n. 2 tunnels crossing the Suez Canal, taking a pictures of the jobsites activities.
Many equipments have been employed, whose main supplier is Liebherr Werk Nenzig (LWN), a world's leading company specialized also in the design and manufacturing of special foundation and heavy duty lifting machinery.
Various job site technical topics will be described and attention will be drawn as well to the use of a new duty cycle crawler crane, HS 8100 HD, combined with an innovative hydraulic grab, used for the excavation of complex and deep diaphragm walls. Data comparison between different kind of technologies and equipment, recorded in the site, will be reported as well.



1 PORT SAID

Port Said (Egyptian Arabic: بورسعيد Borsaʿīd) is a city sited in the north east of Egypt extending about 30 km (19 mi) along the coast of the Mediterranean Sea, north of the Suez Canal, with an approximate population of 603.787 (2010). The city was established in 1859 during the building of the Suez Canal. Port Said has been ranked the second among the Egyptian cities according to the Human Development Index in 2009 and 2010; the economic base of the city is fishing and industries, like chemicals, processed food and cigarettes. Port Said is also an important harbor for export of Egyptian products like cotton and rice, but also a fueling station for ships that pass through the Suez Canal. It thrives on being a duty-free port, as well as a tourist resort especially during summer. It is home to the Lighthouse of Port Said (the first building in the world built with reinforced concrete). Port Said's twin city is Port Fuad, which lies on the eastern bank of the canal. The two cities coexist, to the extent that there is hardly any town center in Port Fuad. The cities are connected by free ferries running all through the day and together they form a metropolitan area with over a million residents that extends both on the African and the Asian sides of the Suez Canal (the only other metropolitan area in the world that also spans two continents is Istanbul). Port Said acted as a global city since its establishment and flourished particularly during the nineteenth and the first half of the twentieth century when it was inhabited by various nationalities and religions. Most of them were from Mediterranean countries and they coexisted in tolerance, forming a cosmopolitan community.



The port of Port Said is the 28th-busiest seaport for container transport, the second-busiest in the Arab world (narrowly behind the port of Salalah in Oman) and the busiest container seaport in Egypt. The port is bordered, seaward, by an imaginary line from the western breakwater boundary till the eastern breakwater end. And from the Suez Canal area, it is bordered by an imaginary line extending transversely from the southern bank of the Canal connected to Manzala Lake and the railways arcade livestock. Two breakwaters protect the port entrance channel: the western breakwater is about 3,5 miles (5,6 km) long and the eastern breakwater is approximately 1,5 miles (2,4 km).The Suez Canal dwelling area is situated between latitudes 31° 21' N and 31° 25' N and longitudes 32° 16.2' E and 32° 20.6' E, where vessels awaiting to accede Port Said port stay whether to join the North convoy to transit the Suez Canal to carry out stevedoring operations or to be supplied with provisions and bunkers. The dwelling area is divided into two sections: the northern area is allocated for vessels with deep drafts and the southern area is for all vessel types.



© 2018 Deep Foundations Institute

2 SUEZ CANAL



The Suez Canal (Arabic: قناة السويس qanāt as-suwēs) is an artificial sea-level waterway in Egypt, connecting the Mediterranean Sea to the Red Sea through the Isthmus of Suez. Constructed by the Suez Canal Company between 1859 and 1869, it was officially opened on November 17, 1869. The canal offers watercraft a shorter journey between the North Atlantic and northern Indian Oceans via the Mediterranean and Red seas by avoiding the South Atlantic and southern Indian oceans, in turn reducing the journey by approximately 7.000 km (4.300 mi). It extends from the northern terminus of Port Said to the southern terminus of Port Tewfik at the city of Suez. Its length is 193,30 km (120,11 mi), including its northern and southern access channels. In 2012, 17.225 vessels traversed the canal (47 per day).
The original canal was a single-lane waterway with passing locations in the Ballah Bypass and the Great Bitter Lake. It contains no locks system, with seawater flowing freely through it. In general, the canal north of the Bitter Lakes flows north in winter and south in summer. South of the lakes, the current changes with the tide at Suez. The canal is owned and maintained by the Suez Canal Authority (SCA) of Egypt. Under the Convention of Constantinople, it may be used "in time of war as in time of peace, by every vessel of commerce or of war, without distinction of flag". In August 2014, construction was launched to expand and widen the Ballah Bypass for 35 km (22 mi) to speed the canal's transit time. The expansion was planned to double the capacity of the Suez Canal from 49 to 97 ships a day. At a cost of $ 8,4 billion, this project was funded with interest-bearing investment certificates issued exclusively to Egyptian entities and individuals.



The "New Suez Canal", as the expansion was dubbed, was opened with great ceremony on 6 August 2015. On 24 February 2016, the Suez Canal Authority officially opened the new side channel. This side channel, located at the northern side of the east extension of the Suez Canal, serves the East Terminal for berthing and unberthing vessels from the terminal. As the East Terminal is located on the canal itself, before the construction of the new side channel it was not possible to berth or unberth vessels at the terminal while the convoy was running.

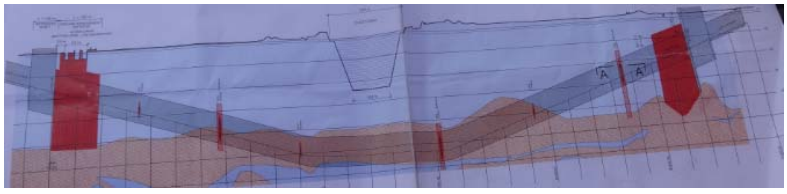
3 ACTORS AND PROJECT TIMING



Züblin AG is a company founded in 1898 by Swiss engineer Eduard Züblin in Strasbourg, Alsace. Since 2005 the majority is held by the group Strabag, colossus of the Austrian constructions. Züblin has acquired, in joint venture with an Egyptian private company, Orascom Construction Industries, the work to realize special foundations aimed at building 2 new road tunnels located below the Suez canal in Port Said; it is south, east and west shafts and related works. The shipyard also works as a JV between the Trevi and the The Arab Contractor, a company owned by the Egyptian state; this JV deals instead with the realization of the north, east and west shaft. The jobsite has been opened in May of 2015; the foundations of the East well began in July of the same year; works completion has been in the end of 2016. It was than planned a further year to move the shipyard from the other side of the canal and the realization of the work, specular to the first, for the realization of the west shaft and the roadworks exiting from the tunnels. Züblin also intervened on the parallel shaft (north) to speed up the foundational works in order to prepare in advance the launching shaft of the first TBM.

4 THE JOB AND SOME WORKING DETAILS

The Egyptian Government has long been planned a road link to the south of Port Said to sub-cross the Suez Canal in order to connect the Sinai Peninsula and the Nile Delta more effectively. The project consists of the construction of 3 tunnels, two motorway and one railway with an inner diameter of 10,8 m and an external one of 11,8 m. Underground works are parallel to 2 existing viaducts, Al-Qantarah and Al-



Fardan; the new infrastructure has been designed to provide a contribution to the expansion plan for the east coast of the Suez Canal (along with the realization of the international project of a coastal road) and the development of the Sinai peninsula. The TBM, a slurry shield, will face a journey of approx. 2,8 km, passing below the Suez Canal, deep ca. 25 m at that point, approx. 20 m below it (calculated from the extrados of the concrete lining).

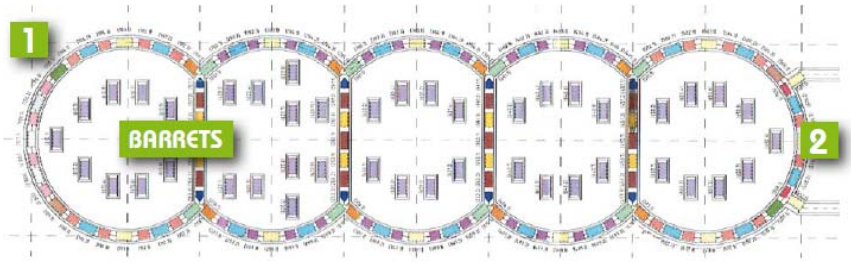
5 FOUNDATION WORKS AND DIAPHRAGM DIMENSIONS



In general, with regard to the main foundational works for the construction of the tunnels, about approx. 260.000 m^2 of diaphragms are foreseen, realized mainly with grabs capable of excavating 2,8 m long, 1,2 m thick panel, at a maximum depth of 70 m. From the geological point of view, the conformations are relatively simple to be excavated, but complex for the work to be done:

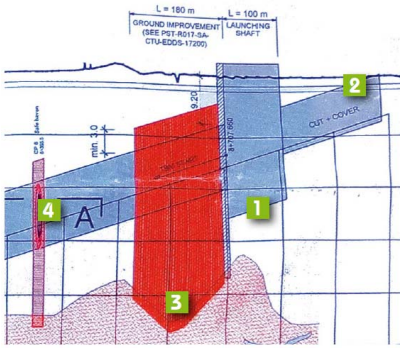
- Gravel and compacted sand for the first approx. 4 m
- Horizontal stratified clay with sand lenses
- Rock bed in sand thickened to approx. - 46 m
- No presence of boulders

Generalizing it can be said that for ~80% are found in clay and for the remaining sands.



4 major work areas may be identified as follows:

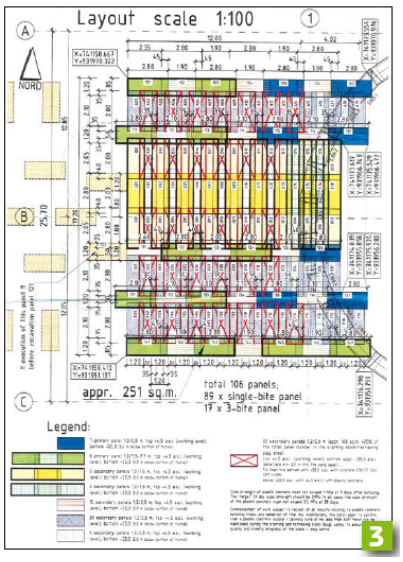
1. Main shaft, having a poly-circular section, in which the TBM will be lowered to start the mechanized tunnelling, toward East-West. Inside the shaft bottom slab support barrets are foreseen. The excavation depth is at - 21 m. A similar arrangement has been designed by Geodata S.p.A. for the São Paulo subway in Brazil; in detail it is an alternative solution compared to the classic rectangular shaft design (generally realized with struts, tie rods and over dimensioned diaphragms walls) replaced by a polycentric shaft having a similar cross section but with the benefit of hoop stress compression effect of its multi-profile; the advantage of such a solution normally generates substantial savings in execution time and building materials.



2. Diaphragms for the access road to the shaft (east-west direction).

3. Launching shaft front stabilization block, through which the TBM will have to start its run.

4. Diaphragms of consolidation and protection to the banks of the Suez Canal.



There is also an ongoing and controversial debate about the construction of a safety shaft facing the Canal, aimed at any TBM services in the event that the need arises. The pictures shown, referring to the numbering (1, 2, 3 and 4), indicate the macro intervention areas. Foundation works are provided with diaphragms walls having different shapes and depths; referring to the above numbering, the main geometric and typological information are listed here following:

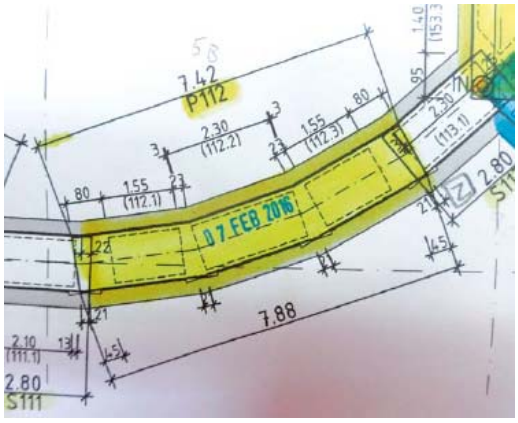
1. Shaft: diaphragms at - 53 m. The shaft has an overall dimension of approx. 22 x 100 m.

2. Access: online diaphragms from - 53 to - 21 m. The length of the road (inclined) to the shaft is approx. 400m.

3. Block: 29 m deep diaphragms walls on a rectangular area having a 16 m (12,5 m + 4 m intersection with the shaft end area) in length and 25 m width. This work is peculiar; these are TBM axis plastic panels and

orthogonal to the same axis, in a continuous solution, so that they are realized for primary and secondary inline and tangents between themselves the orthogonal ones (interlocked to the inline panles).
4. Approach to the Canal: diaphragms from - 53 to - 70 m, for a length of approx. 1 km.

6 THE EXCAVATION METHODOLOGY



Trevi and Arab Contractors have opted for a classic methodology that includes single primary panels with grabs and trench cutter for the secondaries. No multiple excavation modules were provided. Some of the online diaphragm panels have been executed with sheet piles, to realize their joints, always for excavations for single panel modules.
The Züblin project, on the other hand, provides for multiple diaphragms with a length varying from approx. 7,40 to 7.90 m, with secondary closure panels of approx. 2,1 – 2,3 m in length (hence high overlaps). Again, the primary (multiples) are carried out with a grab and the trench cutter for the closures.

7 BENTONITE SLURRY AND TREATMENT PLANT

The execution of multiple and so deep panels has been possible by studying a particular bentonite mixture of weighted stabilization slurry with barite. In fact, it has been necessary to create a special backpressure on the walls of the multiple and deep diaphragms able to guarantee their stability during the drilling phase. This operating methodology involved the commissioning of a suitable slurry mixing and treatment plant, discharging and pumping system, with considerable size and capacity. Therefore n. 2 independent slurry treatment plant with a capacity 500 m^3/h has been installed. A plant with a continuous mixer was dedicated to the online preparation of bentonite slurry; through this equipment there is no need for store bentonite slurry for its curing. Another classical mixer is used for the preparation of slurry added to the barite. Large capacity storage tanks of 800 to 2.200 m^2, for:



1. Fresh bentonite
2. Bentonite slurry with fresh barites
3. Working muds
4. Recirculation slurry

were made in situ and from these, through several km of piping, the drilling fluids is pumped in both directions along the working area.
The typical mix-design of the bentonite slurry is:

- 1.000 l of water
- 165-200 kg of nanogel bentonite (local production)
- 125 kg of barite (comes from Alexandria of Egypt)

8 CONCRETE AND REBAR CAGES

All the concrete used is produced by an "important" plant managed by the customer, facing the construction site. Structural concrete has special formulations to protect the reinforcing steel against salt water attacks and important resistances > 50 MPa. The plastic blends that are used for the stabilization block, which will be crossed by the TBM, have the following average composition:
- Cement: Cemex 170 kg/m^3
- Inert class: 1 (2-5 cm): 750 kg/m^3
- Sand: 750 kg/m^3
- Bentonite: 45 kg/m^3
- Water 365 l/m^3

The resistances are as follows:

- Air temperature: 17° C
- Concrete temperature at 60 min : 18,5° C
- Resistance to 3 days: 0,55 MPa
- 7 days resistance: 1,75 MPa
- Resistance to 14 days: 2,85 MPa



Concrete is brought to the construction site with high capacity concrete mixers, up to 12 m^3.
Rebar cages are made in a dedicated land plot, managed by the main contractor. They are carried in situ in long elements of approx. 20 m and assembled for their length during the casting phase inside the diaphragm.

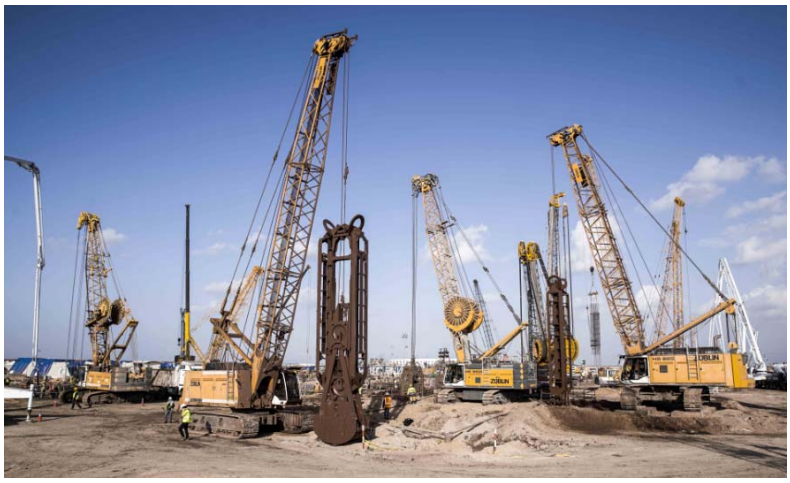
9 GUIDING WALLS



Generally driving guides are concrete made according to conventional procedures. Interestingly, the guiding walls for the block panels, both single and multiple, are performed through suitable removable steel guides. These are laid on an armored concrete made slab, with a thickness of approx. 30 cm, having sufficient strenght to bear the workloads and designed to be demolished by the grab bucket. Guiding walls are therefore:
- Fitted on the upper slab
- Geo-referenced
- Buried with filling material to stabilize them
- Repositioned after the panel completion

10 CRAWLER MOUNTED EXCAVATOR CRANES

The fleet deployed is pretty big; the following machines, manufactured by Liebherr, have been found during a site visit along the "heavy" working period:
- LR 1160, lifting cranes
- HS 885 HD + hydromill
- HS 885 HD + hydromill
- HS 845 HD + hydraulic grab
- HS 855 HD + hydraulic grab
- HS 875 HD + mechanical grab
- HS 875 HD, service crane
- HS 885 HD + mechanical grab
- HS 885 HD, service crane, ready for hydraulic grab works
- HS 8100 HD + hydraulic grab ADC Leffer XY-360 °



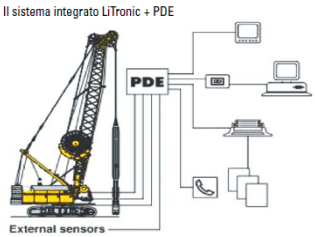
The jobsite started immediately using mostly mechanical grabs; in this case (and not just that, it happens for any diaphragm) the final vertical control for each panel is realized by Koden (with considerable time consuming).
But, right away Züblin decided to equip himself with a modern hydraulic grab with active control over verticality by purchasing a crawler excavator of the latest class (Liebherr HS 8100 HD) equipped with a special hydraulic grab, the Leffer XY-360 ° in ADC version - Active Deviation Control, also taken in order to deal with the 70 m panel excavation (the latest ones which need to be realized).

Communication	Minimise Close
Last transfer	23/02/2016 09:34:37
Time since last transfer	0 d, 3 h, 31 min
Time zone	GMT+03:00

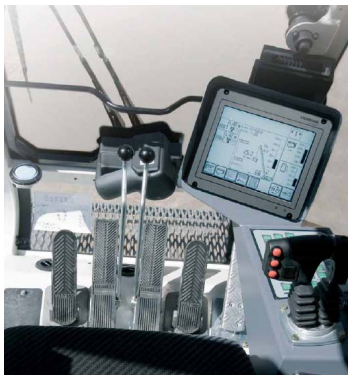
Key data	Minimise Close
Based on transfer from	23/02/2016 09:31:47
Time zone	GMT+03:00
Operating mode:	Leffer hydraulic grabber
Average daily OH	1 h, 48 min
Fuel level	77.0 % (639.1 l)
Total fuel consumption	10753.0 l
Average consumption over last 100 hours	16.2 l/h
Operating hours	602 h

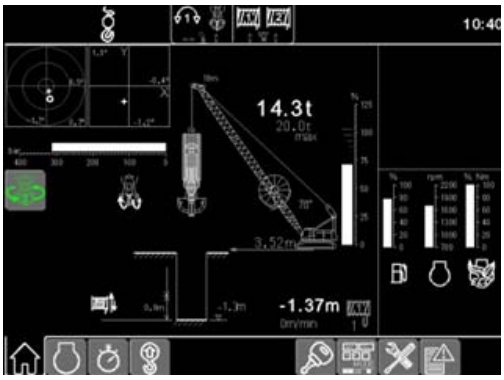
Interesting to report is the very low fuel consumption recorded in the job site especially related to the new LWN model type HS 8100 HD; we are talking of < than 20 l/hours!

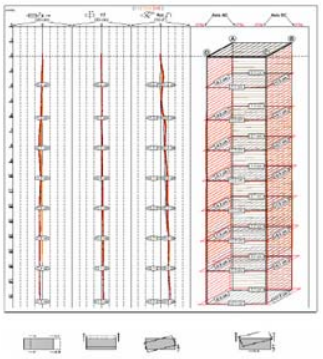
10.1 Integration between excavator and grab system, control and data restitution



It should be noted that there is an important integration between the excavator and the excavator tool (the grab); in short, there is an hydraulic and electronic dialogue platform that transfers information, commands, data returns (in visual, graphic and system format) and can transmit them to the user and to the Mother House with the additional ability for potential analysis connected and active interventions, such as maintenance, if necessary.
The Leffer ADC system is integrated with the LWN electronic system called Li-Tronic.
This function is important as the control and data analysis; the working platform is efficient, reliable and unique and can be interfaced in real time with office workstations.







10.2 Grab chiseling

Chiseling with an hydraulic grab is not really a usual practice, nevertheless LWN system provides a specific integrated function allowing to perform chiseling with grab operating in freefall at a preset height. This option can be used in various scenario, for instance:
- breaking through supporting slabs,
- excavating lenses of compact material at variable depths,
- headings on the rock beds, ...



10.3 The double winch and the grab safety

The fact that these machines work with 2 synchronized winches and consequently with 2 ropes simultaneously guarantees a redundant system not only for the load lifting but also providing a high degree of safety for the grab itself. It has occurred more than once, having a single grab lifting block (i.e. crane equipped with one winch only) that the rope got broken subject to excessive fatigue or wearing, particularly in the area of the return pulley on top of the grab lifting block (the lower pulley, very delicate zone!). Moreover, these types of machines are first of all cranes; their system, manufactured considering the strict referred design standards, takes care of monitoring the lifting loads as well as the position of the boom, putting them in closed relation. There are on the market excavation machines suitably designed for such operations (lifting), which may not be provided with any integrated load indicators while working as excavators (in difficult stress conditions to be calculated and taken automatically in consideration); this could be a clear limit and a safety issue handling extraordinary load at high depths.

10.4 Ropes tensioning and wearing

The load indicator is also used to calibrate winches pressures in order to keep the rope in tension (without affecting the grab) during the excavation phase; this ensures no loosening, unloading of the pulleys, irregular wear, offload operation of the winches, tears, undesired turbulence along the walls of the panel, ... This specific function aims to reduce the deviation tendency during the operational phase, a further factor minimizing the

danger of deviation from the design verticality. A further consideration on the ropes wearing, shall be made on the geometry of the reeling drums of the winches;
- The greater is the length or the diameter of the drum, the greater will be the reeling length in the first layer of the rope, the less will be the wearing.
- Therefore, it is essential, in order to optimize the useful life of the ropes, to provide larger winches (as well as powerful and reliable). The useful lifetime of a lifting ropes is direct function of the type of material to be excavated (presence of stones hanging on the pulleys, anomalous wearing cause by friction,…) and of the excavation depth (numbers of reeling cycles and multi-layer reeling, …).

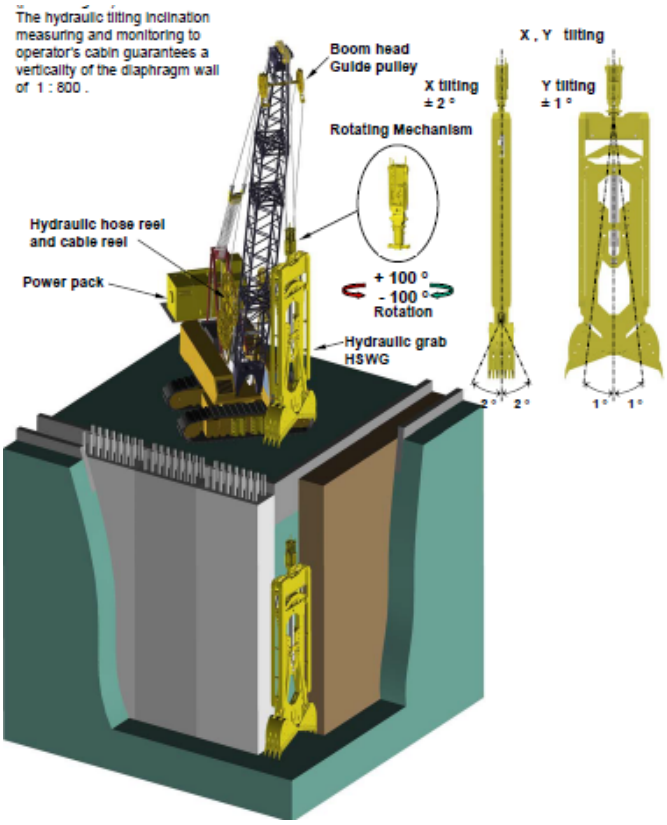


Considering the mechanical grab, the technology foresees 2 ropes having 2 different tasks:
- The first winch bears the full weight of the grab (while with the hydraulic version the weight is equally distributed on both ropes), having this element particularly stressed.
- The second rope is engaged for the opening and closing of the excavation jaws; the rope pass through a series of suitably dimensioned pulleys and through a numbers of referral mechanism (with short curvature radii) as well as the presence (quite frequent) of soil between the groove of the pulley and the rope itself, resulting in a reduced useful lifetime.

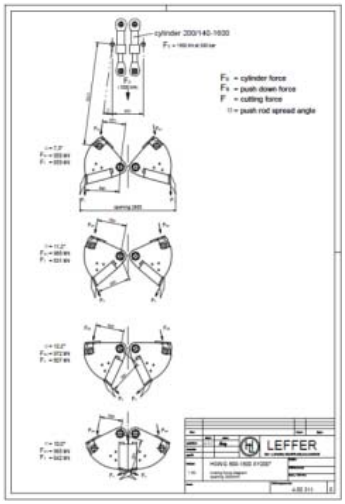
Moreover, the consumption of the ropes is not symmetrical, being subjected to anomalous strains. This has led to a build in statistics of useful life for mechanical grab ropes very variable; in the job site it has been communicate replacement situations of the same at 65, 250 and 500 h and maybe it can be stated that medium useful life (in absence of particular issues) is between 400 and 500 h. Interestingly, it has been verified that the useful life of ropes on hydraulic excavators with pure hydraulic grab had a range between 2.000 and 3.000 h, 4/5 times greater than that of mechanical grab. One last comment: the steel ropes not only have a cost right not negligible but above all they expect yardsticks for their replacement at the expense of production.

11 THE GRAB HSWG A-B XY 360° ADC

For the record it may be mentioned a further type of hydraulic grab, similar to the above mentioned one manufactured by Negrini; this is a new system manufactured by Leffer, called HSWG "(A)-(B)" XY 360°. The standard width configurations range from 500 up to 1.800 mm, with a length from 2,5 up to 3,2 m, designed in an extensible modular configuration. In Port Said, the wall panels were having a dimension of 2,8 m (A) in length by 1,2 m in width (B); the weight of the empty grab was equal to 28,4 tons, having a full loaded weight of about 32 ton. The bucket body height is about 9 m (with grab opened, from rope set, approx. 10,5 m). Knowing that verticality of excavation is related to various parameters, in particular one of them is the stiffness of the grab frame (related obviously to the type and weight of the structure); in this case the machine has been designed to be practically insensitive to potential torsions or misalignments. This consideration become more important (mechanically and from the point of view of works efficiency) even in case of "chiselling", where a possible shortage of



weight and lower rigidity of the entire structure could compromise the excavation process. High clamping forces on the jaws are guaranteed through powerful and fast acting hydraulic cylinders and obviously by a responsive and powerful hydraulic system on the crane: the open jaws cutting force is equal to 831 kN while 642 kN in closed mode. The operating speed has been measured on the site; clamping time is about 5-6 sec while the opening period is 7-8 sec. On the grab assembly is installed a device allowing the rotation at 360 ° synchronized with the other movements, required for instance during the de-mucking phase thus to offload the excavation material on the dump trucks or for cycle excavations (even vs. odd teeth). The control of verticality of the Leffer grab is guaranteed by the integration of 3 systems (ADC Active Deviation Control):



1. 2 Hydraulic cylinders placed on top allowing to displace the hook fulcrum of the grab. This system allows to adjust the deviation of 1° on the Y plane.
2. 2 Hydraulic cylinders fitted on the grab shoulders allowing the tilt of the frame body. This system allows to adjust the deviation of 2° on the X plane.
3. A deviations control system, through a dedicated HMI installed in the operator's cabin, which is allowing the operator to actively influence the verticality of the excavation on the X and Y axes, minimizing the deviations in the range of 1:800.

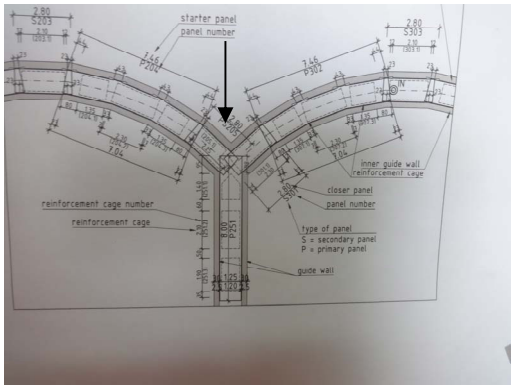
12 EXCAVATION PERFORMANCE

The jobsite, as it can be imagined, is pretty complex; it is not easy to identify representative data and, above all, perfectly comparable or duplicable.

12.1 Issues related to the trench cutter interlocking construction

It is worth to mention how hard to realize a waterproofing panels. Such a works can be very laborious for various reasons:

1. High overlap thicknesses
2. Concrete particularly resistant
3. The presence of clay clogging the cutting wheels
4. Discrete excavation depth

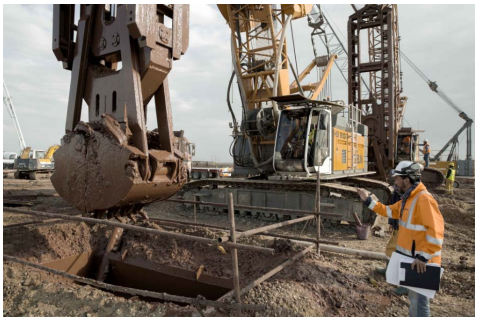




In some already casted interlocking panels sides were already hardened, especially with the triple joints such as the nodes of the shaft.

Penetrations rates have been revealed as few millimeters per minute evidenced by the need, for some interlocking panels, to cut the rebar cages of the corresponding primary panels.

13 DIAGRAPHRAM TIMING



Data was collected from different sources and reports.

1. Simple average excavation times can be summarized in:

- 53 m long grab for multiple panels: 3-4 hours for the primary and 233 h for the secondary => 8-11 h. In the site 12 h of excavation cycle is the duration time considered.
- Trench cutter at 53 m, minimum time 30-36 h up to 1 week (even 10 days) for difficult panels (high overlapping, presence of steel, plastic clay, plus Koden measurements).

2. Average excavation time for a completed diaphragm:

- Excavation, reinforcement and casting of a 53 m multiple panel: 3 shifts, 36 h.
- Excavation, reinforcement and casting of a standard non-problematic interlocking panel: 4 shifts, 48h

The casting time of a plastic panel at 23 m depth, of approx. 100 m^3, is 5-6 h. This time may increase up to 12 h because of problems related to the supply of the plastic concrete having a not standard mix design for the batching plant and due to relatively high working rate of the same.

14 MEASURED GRAB PERFORMANCE

In the jobsite, the excavation performance of 5 machine has been recorded:
- No.1 semi-kelly hydraulic grab (manufactured in Italy)
- No 2 hydraulic grab
- No.1 mechanical grab
- No.1 hydraulic grab manufactured by Leffer ADC XY-360°

It has been noticed that the working conditions were similar (panels between -2 and -14 m).

The mechanical grab operator (Polish) of the jobsite was the best of all staff. The Leffer grab was realizing an interlocking panel on a secondary panel with hardened plastic concrete at approx. 4 MPa, all the others worked on primary or interlocking of multiple primary panels.

Type of crane	Type of grab	Grab weight (approx)	Grab capacity	Penetration rate (approx)	Cycle time
Produttore AB	Hydraulic semi-kelly	15 ton	1.500 l	25 cm	5'50"
HS 845 HD	Hydraulic	18 ton	1.700 l	30 cm	4'20"
HS 885 HD	Mechanical	17 ton	1.600 l	30 cm	3'40"
HS 885 HD	Hydraulic	18 ton	1.700 l	30 cm	4'45"
HS 8100 HD	Hydraulic Leffer ADC XY-360°	28 ton	2.200 l	40 cm	4'30"



CONCLUSIONS



To report personally about this huge job site has been really an interesting experience; concepts and facts are now for the Authors very clear.
The mechanical grab, operated in free fall, although in certain situations it can be slightly faster than the hydraulic grab and can be efficiently used for repeated chiseling (with particularly resistant materials):
- Requires a heavy duty crane
- The excavator is particularly stressed mechanically
- To be operated it is required a very experienced Operator
- The operator shall always be very focused during the whole works phases
- It can only rotate by using the rope winding direction manually by means of winches
- Does not have deviation correction systems
- Can not handle deviations for high depths
- It cause a high ropes' consumption

It worth to mention that the international practice for deep shaft (and not only) is the use of combined crawler excavator & hydraulic grab system in its various technical declinations.



HS crane model, powerful and silent equipment with generous, redundant and fast winches, with integrated controls and an ADC hydraulic grab is the combination which can really make a difference. Mechanical Supervisor, Dr. Alexa Tarta, among other things, said, "*Satisfied with the limited consumption that gets even lower if you work with the system which reduce the engine RPM up to 1.500*". The Project Director, Ing. Harald Armbruster, summarized as follows: "*The future in the grab excavation is the hydraulic system due also to the issue that skilled Operators working with the mechanical grab are very hard to find. Really effective the deviation control system; we used it also to correct some over-deviated panels realized with other type of grabs. We will soon start also for Emsher project in Germany with a big Liebherr HS crane; deep panels for various shafts with a width of 2 m and extremely accurate tolerances, a big challenge*".
As for Egypt, we found good people, smiles, no discomfort and ate good fish ... the country is quiet but well-controlled at strategic points, as it should be!

REFERENCES

Bringiotti M., 2003, Consolidamenti e Fondazioni, Edizioni PEI, Parma, I
Bringiotti M., 2010, Geotecnica & Macchine da perforazione, Edizioni PEI, Parma, I

THE GAASPERDAMMERTUNNEL – GEOTECHNICAL CHALLENGES IN AMSTERDAM

D. Grotegoed, *Ballast Nedam NV*, Nieuwegein, Netherlands, d.grotegoed@ballast-nedam.nl
N. Goedhart, *Ballast Nedam NV*, Nieuwegein, Netherlands, n.goedhart@ballast-nedam.nl

For: Proceedings of the International Conference of Deep Foundations and Ground Improvement 2018

ABSTRACT

The Directorate-General for Public Works and Water Management of the Netherlands (Rijkswaterstaat) has planned to increase the capacity of the motorway corridor between Schiphol Airport, via Amsterdam to Almere. A subproject was awarded to IXAS, a consortium consisting of Fluor, Ballast Nedam, Heijmans and investment partner 3i Infrastructure in 2014. This subproject concerns the expansion of the A9 motorway in Amsterdam between the junction Holendrecht and Diemen. A large part of the new expanded road will be constructed below ground level in a three kilometre cut-and-cover tunnel, the Gaasperdammer tunnel. For the foundation design of the tunnel a large scale soil investigation was carried out with more than 800 Cone Penetration Tests (CPT's). The soil investigation was intended to reduce uncertainty in the foundation design of nearly 10,000 foundation piles. In addition, a series of CPT's was performed to identify "dump" zones. Specific areas in the existing A9 motorway appeared to be founded on landfill consisting of large concrete fragments. This was not only a problem for the foundation piles, but also for the 10,000 tonnes of sheet piling that had to be installed over a length of nearly three kilometre in the central reservation of the existing A9. Based on the results of the soil investigation, it was decided to mobilize pre-drilling rigs with bentonite and some crushers. During pile driving, another problem was encountered. The blow count of a few piles corresponded to the lower bound values of our predictions. Limit values were imposed to the operational manager on site. For piles with low blow counts the option of driving deeper was discussed immediately with the geotechnical engineer on site. In specific cases, driving deeper was not an option. For those cases, CPT's were carried out after excavation and pile installation to investigate whether the bearing capacity was reached. Some CPT's that had been performed afterwards, appeared to be even more favourable compared to CPT's before installation with a theoretical reduction for excavation. In 2015 the first pile was driven and in the spring of 2017 the foundation works were completed. This article addresses several challenges during the preparation and execution of the foundation works of the Gaasperdammer tunnel.

INTRODUCTION

The Dutch Directorate-General for Public Works and Water Management (Rijkswaterstaat) has planned to increase the capacity of the existing motorway A9 between Schiphol Airport and Almere. The capacity will be increased from three to five lanes in both directions and a middle reversible lane. A subproject concerns a specific part of the motorway in Amsterdam Southeast from the junction Holendrecht to Diemen. A large part of the new expanded road will be constructed below ground level in a three kilometre long tunnel, the Gaasperdammer tunnel. This subproject was awarded to IXAS, a consortium consisting of Fluor, Ballast Nedam, Heijmans and investment partner 3i Infrastructure in 2014.

THE WINNING DESIGN

After a thorough investigation about technical feasibility and environmental impact analyses by Rijkswaterstaat, this project became available on the market as a DBFM contract in a public tender. Contractors were challenged to not only submit a low price but also come up with an environmental-friendly construction methodology. Especially the users of the existing A9 motorway should experience as little inconvenience as possible and also a minimum capacity should be guaranteed during construction. This was an important criterion for EMVI score (a Dutch classification model for the most economically advantageous tenders including weighing factors for e.g. impact on the environment).

© 2018 Deep Foundations Institute

Therefore, a small amount of loss in traffic congestion hours meant a high fictitious reduction on the total monetary project value. IXAS came up with a staged construction. The middle reversible lane of the new tunnel is built first, parallel to the embankment of the existing motorway. Making a temporary bypass for the entire A9 motorway. The construction of the middle reversible lane, creates capacity to close off one half of the existing motorway. A part of the final structure can be used temporarily as well. The other half of the existing motorway remains available during construction. In order to create space for construction of the new tunnel, a sheet pile wall is designed over a length of nearly three kilometre in the central reservation of the existing A9 motorway. The projection of the new tunnel is positioned a little northwardly compared to the existing A9, see figure 1.

Currently, the A9 motorway divides the district of South-East Amsterdam into two separate parts. On top of the new tunnel a green zone with a large park will be created that will connect these parts. The presence of the tunnel will result in cleaner air and less traffic noise for the environment. The vertical alignment of the tunnel does not have to be very deep and is not completely horizontal. In the IXAS tender design, the ground water level dictates the zones where a concrete floor is needed. Some parts of the tunnel do not need a concrete floor because they are sufficiently high above the groundwater level. In those areas the tunnel cross section will only have a roof and walls. The foundation piles have been designed under the walls for all sections, to create extra robustness in the foundation design. When problems arise during installation of an individual pile, a large plate will act as a superstructure redistributing stresses to neighbouring piles. The middle reversible lane, however, will be built in a very early stage and has been designed with piles under the floor.

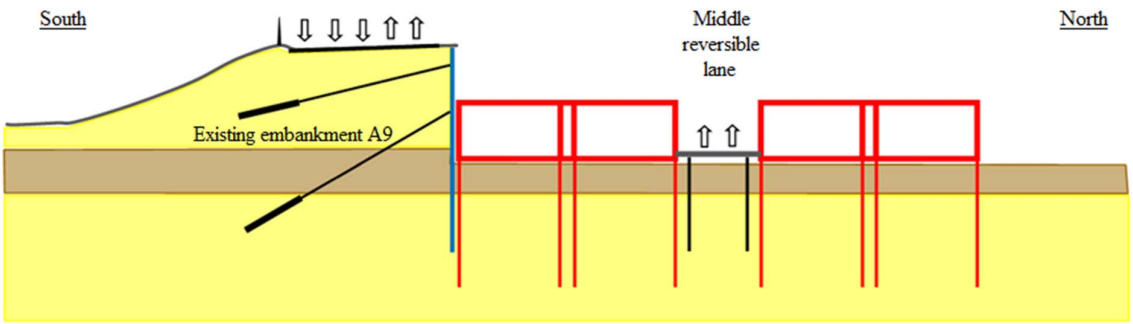


Figure 1. Principle of the winning IXAS design

SOIL PROFILE

An extensive soil investigation campaign was carried out with more than 1,000 planned CPT's. More than 800 CPT's were done for the foundation design of the tunnel. A grid of 25 x 25m was projected over the entire length of three kilometre. The remaining 20% of the soil investigation was carried out for the foundations of several bridges and earth works. Additional CPT's were performed to identify obstacles in the subsoil in specific areas (see paragraph about dump zones). Based on the results of the soil investigation, a soil profile and parameters were established, see table 1 and figure 2. Ground water level was found at NAP -4.2m

Table 1. Soil profile and characteristic properties

Soil type	Top of layer [m NAP]	γ/γ_{sat} [kN/m^3]	φ‘ (°)	c' [kPa]	δ [°]	$k_{1;hor}$ [kN/m^3]	$k_{2;hor}$ [kN/m^3]	$k_{3;hor}$ [kN/m^3]
Sand, moderate	+5.0	18/20	32.5	0	20	20,000	10,000	5,000
Peat, moderate	-5.0	11/11	15.0	5	0	2,000	800	500
Clay, weak	-7.0	15/15	22.5	5	11	4,000	2,000	800
Peat, moderate	-8.5	11/11	15.0	5	0	2,000	800	500
Sand, Pleistocene	-9.2	18/20	32.5	0	20	20,000	10,000	5,000

In longitudinal direction the soil profile at the location of the tunnel can be characterized as a top layer of sand over a soft clay/peat layer with a thickness of approximately four metre, on average. The foundation layer exists of the Pleistocene sand layer starting at about NAP -9m.

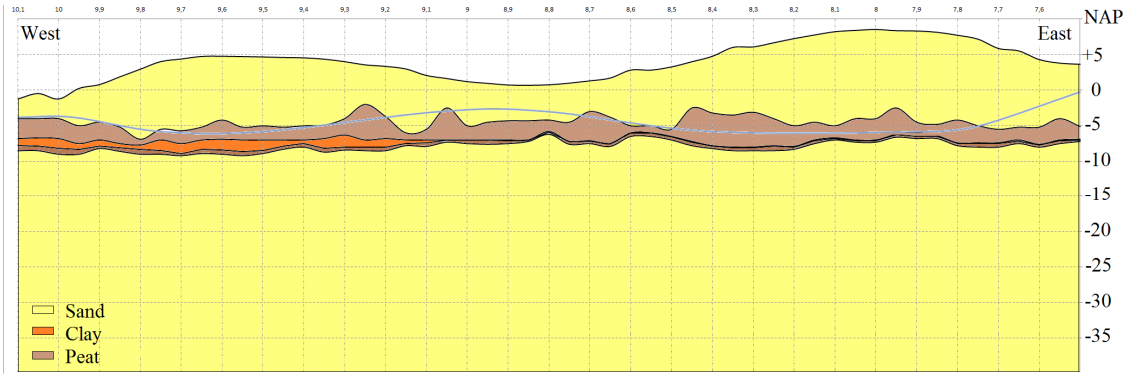


Figure 2. Soil profile in longitudinal direction along the tunnel axis

DUMP ZONES WITH LANDFILL OF CONCRETE DEBRIS IN THE SUBSOIL

In order to reduce uncertainty in the design of the 10,000 foundation piles, a large soil investigation campaign was planned. In addition to the standard soil investigation for design purposes, CPT’s were planned to identify “dump” zones. In the early 1980’s, some parts of the existing A9 motorway appeared to be founded on landfill of concrete debris (see figure 3) with fragments with a diameter up to one metre or more. These landfills with a thickness of approximately three to four metre were situated at about seven metre below ground level. The foundation piles and sheet piling had to be driven through this layer. Especially for the sheet piling this was a challenge. Sheet piling had to be installed over almost three kilometre length in the central reservation of the existing A9. Based on the results of the soil investigation, the use of pre-drilling rigs equipped with a crusher and bentonite suspension was ought to be necessary.

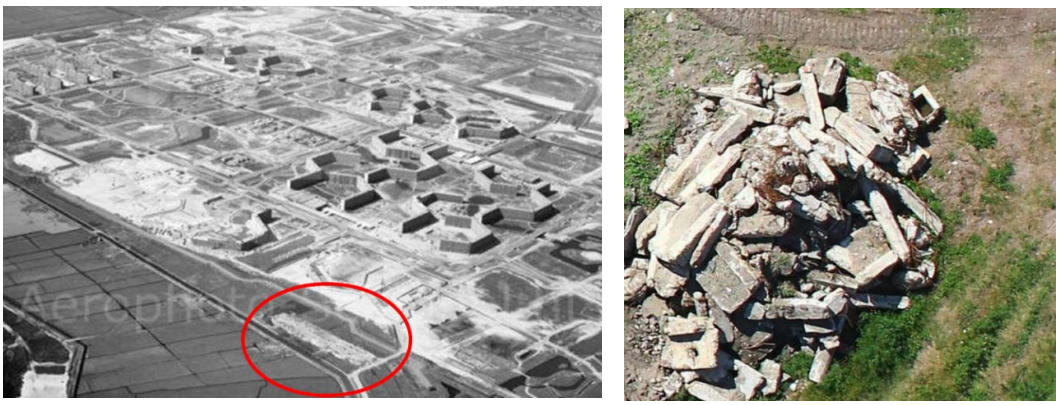


Figure 3. Aerial photo with dump site (left) and encountered fragments during excavation (right)

In order to investigate the feasibility of the approach with crushers, an extensive test was prepared on a test site close to the planned position of the sheet piling with similar conditions (see figure 4). Based on the results of the tests, the most suitable crusher type and bentonite cement mix was determined. Using this method it was possible to sufficiently crush the concrete fragments and install the sheet piling AZ28-700. A leader-guided vibrator ICE 36RF was used to install these 22.5 metre long sheets to the required depth without damage.



Figure 4. Pre-drilling rig with crusher (left) and reinforcement from concrete fragments in crusher

LOW BLOW COUNTS

The tunnel will be founded on “vibro” piles. A vibro pile is a cast-in-situ foundation pile, commonly used in the Netherlands. Piles are driven with a steel temporary casing and a steel base plate. The base plate is not welded to the casing. Immediately after installation of the reinforcement and pouring concrete in the casing, the casing is pulled back by driving. The steel base plate cannot be recovered. In the foundation design of the tunnel, a casing diameter of 457mm is used while the base plate has a diameter of 560mm. This pile type is often used for situations where e.g. the soil resistance to driving is expected to be high or highly variable. Pile loads are typically in the range from 1600 to 1900 kN SLS. In order to determine a suitable impact hammer for pile installation, several drivability analyses have been made for the most critical vibro piles. For the drivability analyses an unfavourable CPT was used for every group of piles. A CPT with high cone resistances and maximum penetration depth is unfavourable for driving resistances. A safe estimation of the maximum soil resistance to driving is essential since an impact hammer with insufficient energy can result in significant delay and cost exceedances. The program GRL WEAP was used to determine blow counts from estimated dynamic soil resistances in upper bound and lower bound values. Eventually, a relatively heavy hydraulic impact hammer IHC S-90 was used for a large number of the piles.

In general, measured blow counts are lower than predicted because an impact hammer should be chosen based on upper bound values. CPT’s with low cone resistances are of less importance for these purposes. During pile driving, the blow count of a few piles appeared to be low compared to the predictions. After comparison of the blow count of a specific pile with a prediction based on a reference CPT nearby, blow counts still appeared to be close to the lower bound values rather than expected values. See figure 5. A low blow count does not necessarily have to be a problem. Nevertheless, it does require extra attention. The piles with a low blow count have a relatively smaller pile toe resistance compared to the bearing capacity from (static) shaft friction. In addition, the chosen ratio between base plate diameter and steel casing diameter of the pile D_{base}/D_{casing} is large for this project. The reduction of the blow count due to this ratio was more than expected.

Limit values were imposed to the superintendent on site. In case of a final blow count below 15 bl./0.25m the option of driving deeper was considered immediately, in close cooperation with the geotechnical engineer on site. In specific cases driving deeper was not an option because of decreasing cone resistances with increasing depth below pile tip level or because of insufficient length of the casing due to the noise mitigation enclosure. For these cases, the blow counts were compared over the entire penetration depth with corresponding cone resistances from CPT's nearby. Blow counts that change over depth with the measured cone resistances accordingly, give an extra indication that the CPT is representative for the determination of the static bearing capacity. Moreover, if these low blow counts were encountered, an indication of the static bearing capacity was estimated from dynamic driving formulae. Note that these formulae are questionable for design purposes in the Netherlands. This is due to the large scatter of possible outcomes and should only be used as an additional verification after completion of the foundation design and after obtaining a reliable set of installation data of the piles that were installed first.

For piles where bearing capacity could not be proven with 100% reliability, additional CPT's were carried out after excavation and after pile installation. A minimum distance of four to five times the diameter from the pile was used to exclude the higher horizontal stresses due to pile installation from the measured cone resistances. The additional CPT's indicated sufficient bearing capacity in these cases.

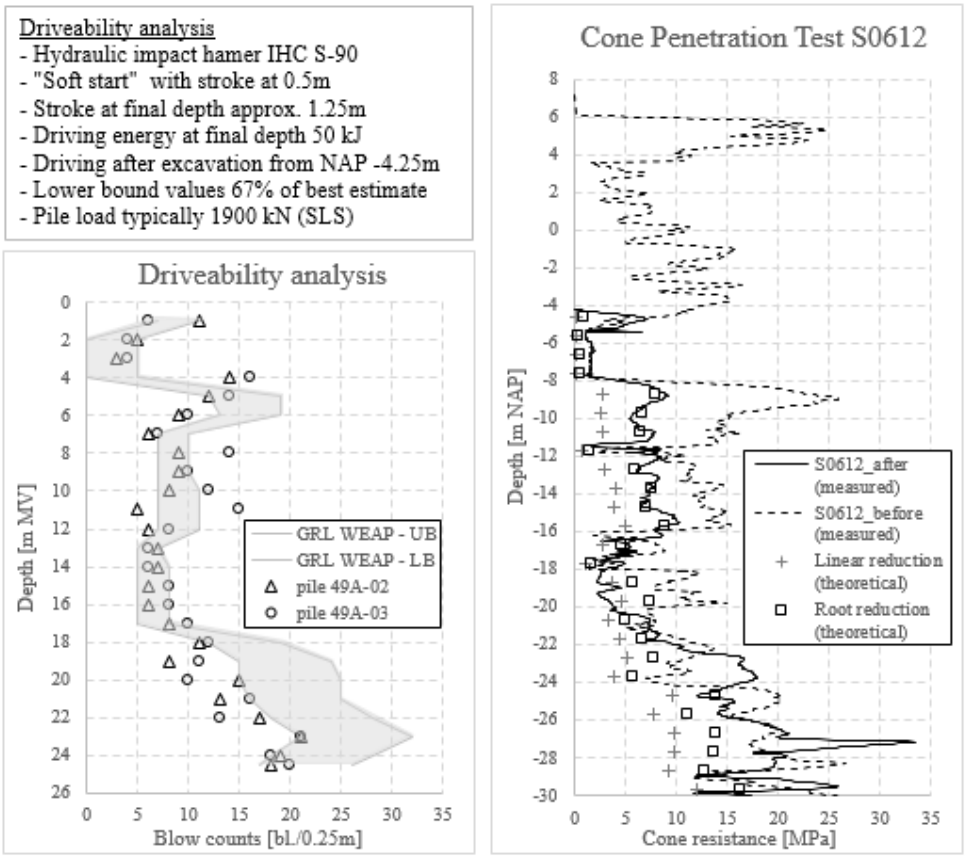


Figure 5. Measured and predicted blow counts (left) and CPT before/after excavation (right)

CPT REDUCTION FOR OVERBURDEN PRESSURE

The CPT's for the foundation design of the tunnel have been executed before excavation. The vibro piles have been installed after excavation. In the determination of the bearing capacity of the piles a theoretical reduction of the CPT's was accounted for. For driven piles with this construction sequence, cone resistances have to be reduced with a linear reduction method, according to the Eurocode,

art.7.6.2.3. This means that the ratio of overburden pressure before and after excavation determines the reduced CPT's linearly. Based on several CPT's after excavation, the actual reduction appeared to be more favourable near pile tip level. Measured cone resistances after excavation and driving correspond better to the square root reduction method (see figure 5). Recently, more authors have reported the same conclusion for specific projects (Ref. [4]). According to the Eurocode, the square root method should be used only for excavations after pile driving. With the limited number of additional CPT's after excavation, the more favourable square root reduction could not be proven with sufficient reliability for all piles within this project. Therefore, it was decided not to use the more favourable reduction method and to follow the standard design rules according to the Eurocode.

CONCLUSIONS

During the execution of the foundation works of the Gaasperdammer tunnel some specific geotechnical challenges arose. The known presence of large dump zones with concrete fragments from earlier landfills was one of them. The exact area and layer thickness, however, was not exactly known on beforehand. The consequences on the foundation work, and installation of the sheet piling in particular, were hard to predict. It can be concluded that a decent preparation of the foundation works including a test site contributed to the right choice for the crusher type and method. In this way further delay, consequences for the construction of the tunnel and inconvenience for the environment were kept to a minimum. A second challenge that popped up was a low blow count during pile driving of the vibro piles. An impact hammer was chosen based on the most severe soil conditions. For a limited number of piles this resulted in low blow counts. For these cases, pile bearing capacity was proven with additional CPT's after excavation. Moreover, these additional CPT's indicated that a theoretical reduction for piles driven after excavation corresponds better to a square root reduction method rather than to the standard linear method according to the Eurocode. The more favourable square root reduction could not be proven with sufficient reliability for all piles and for every depth in this project. It is recommended to exchange more measured data on CPT's after excavation in order to potentially update the current design guidelines.



Figure 6. Overview construction site during driving of the vibro piles (courtesy Rijkswaterstaat)

REFERENCES

Ref. [1] NEN9997-1, Geotechnical design of structures - Part 1: General rules, Delft, 2016.

Ref. [2] Pile Dynamics Inc., GRL WEAP Wave Equation Analysis software, 2010.

Ref. [3] CUR 114, Supervision of the execution of deep foundations, Gouda, 2009.

Ref. [4] Brouwer, R., Reduction of cone resistance due to excavations – new insights, 16th European Conference on Soil Mechanics and Geotechnical Engineering, 2015

TTMJ – THE NEW SYSTEM FOR SLURRY (DIAPHRAGM) WALL JOINTS

Julian Crawley, CCMJ Systems, Basingstoke, Hampshire, UK.
John Coupland, CCMJ Systems, Strathpeffer, Highlands UK. john.coupland@ccmjsystems.com
Maurizio Siepi, TREVI SpA., Cesena, Italy. msiepi@trevispa.com
Paul van Horn, Arup, Amsterdam, Netherlands. paul.van-horn@arup.com

ABSTRACT

TTMJ is the acronym for the Diaphragm Wall Tension Track Milled Joint currently in development as part of the European Union's innovative and far-reaching Horizon 2020 initiative (FTI Pilot-2015-1 720579). The TTMJ system is protected by patent in Europe and the USA and is currently under development by a consortium comprising TREVI SpA (Italy), Arup (Netherlands) and CCMJ Systems (UK).
The TTMJ System is a method of forming panel joints in diaphragm walls. The system theoretically can be used to any depth and can be used to provide a water-stop in the joint and a tension connection between adjacent panels.
This paper follows on from the one presented at the DFI New Orleans Conference in October 2017 which outlined the principles of the TTMJ System. In this paper, further details of the system are provided and the testing carried out to date reported. The intentions and scope of the proposed full-scale field trails are then described.

Keywords: Slurry Walls, Diaphragm Wall, joints, CWS,

INTRODUCTION

The average depth of Diaphragm or Slurry Walls ('D-Walls') has increased steadily over the last 50 or so years. When the technique was first developed in the 1950s, the grabs had rounded clamshells and the joints were formed by installing steel tubes at the end of the panel and extracting them immediately after the concrete had achieved an initial set.

In the second half of 1980s the "peel off" Coffrage avec Water Stop, or Complete Water-Stop (CWS) steel joint former (Fig. 1) came into use, particularly in Europe. This became a highly successful and efficient method for forming the joint between adjacent slurry wall panels. The joint could incorporate a water bar and it was no longer necessary to extract steel joint formers in the middle of the night.

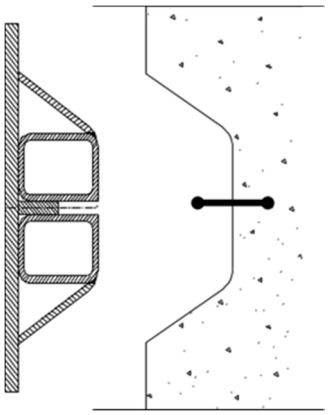


Fig. 1 – Example of a CWS

© 2018 Deep Foundations Institute

As slurry wall depths have increased, problems have arisen with the removal of the CWS joint formers. It was found that beyond 30m it was sometimes difficult, and time consuming to peel them away from the concrete of the previously constructed panel.

The TTMJ System utilises tracks cast into the ends of a diaphragm wall panel to guide a machine to trim back the concrete at the end(s) of the panel, to form a construction joint to any depth. A water-stop can be provided, and the system allows for a tension connection between adjacent panels if required.

TTMJ SYSTEM – BASIC COMPONENTS

The TTMJ Track

The TTMJ track (Fig. 2) is manufactured from pultruded GFRP and is approximately 150mm in diameter. The track has external shear strips to anchor it into the concrete and a sacrificial arc that is removed by the trimmer as it prepares the joint.



Fig. 2 - TTMJ Track

A pair of tracks, supported at the bottom of the reinforcement cage, are restrained by brackets, at 3m to 4m centres, fixed to the ends of the cage. Steel spacer straps attached to the rear of the tracks ensure that the spacing between them is constant. The restraint brackets provide some “rattle” room so that the tracks can align themselves somewhat independently from any distortion of the reinforcement cage. A typical arrangement both before and after trimming is shown below (Fig. 3).

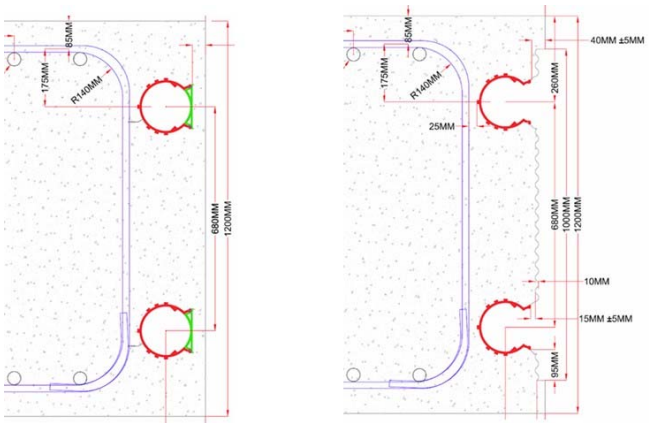


Fig. 3 - Track Cast into Panel (left) and Panel joint after trimming (right)

To maintain the reinforcement cage centrally within the excavation and ensure that there is at least 20mm concrete cover to the outside of the TTMJ track, adjustable GFRP spacers might be used. Details and a prototype of the proposed spacer are shown in Fig. 4.

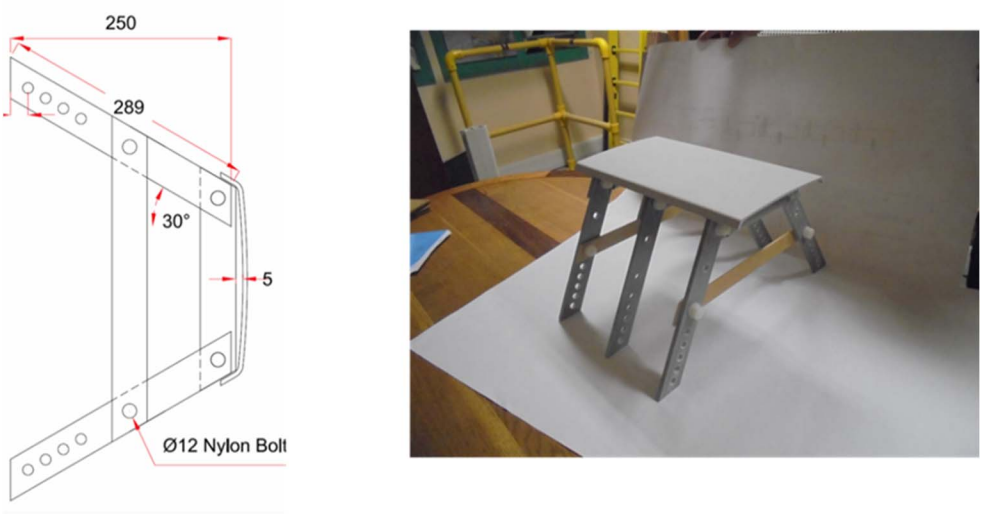


Fig. 4 - Prototype of the GFRP cage spacer

The TTMJ Trimmer

The TTMJ trimmer, currently being manufactured by TREVI, has a chain driven rotary cutting wheel. The trimmer is held in position by two pairs of guides mounted above the cutting wheel. The guides descend inside the guide tracks. The soil and concrete cuttings removed from the end of the panel drop to the base of the excavation as trimming proceeds, to be subsequently removed by grab. Air-lift or other suction systems can be used to clean the base of the panel, if preferred.

The pre-production version of the trimmer currently being manufactured has an overall height of 7.5m and a weight of 11,000kg. The cutting depth and the position of the cutting wheel relative to the guide tracks can be adjusted using the hydraulic ram located between the upper guide frame and the top of the milling machine as shown in Fig. 5.

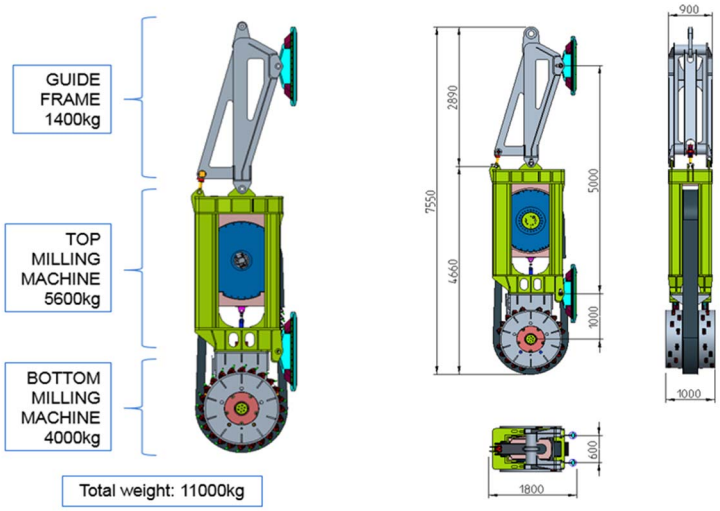


Fig. 5 - TTMJ machine dimensions and weight

For the field trials the TTMJ trimmer will be powered by and supported from a SOILMEC Hydro-Mill base machine. Later the trimmer will probably be used with either a small crane or pile rig adapted for the purpose.

The TTMJ Tension Track Arrangement

To provide a tension connection across the panel joint the standard TTMJ track described previously described is used in conjunction with friction welded headed bars. (Fig. 6).



Fig. 6 - Headed bars

Pairs of headed bars are spaced externally along the length of each track, and then a series of single headed bar fitted in the cage of secondary element is cast into the track during concreting of the adjacent panel. This arrangement forms a compression cone between the anchor heads (Fig. 7).

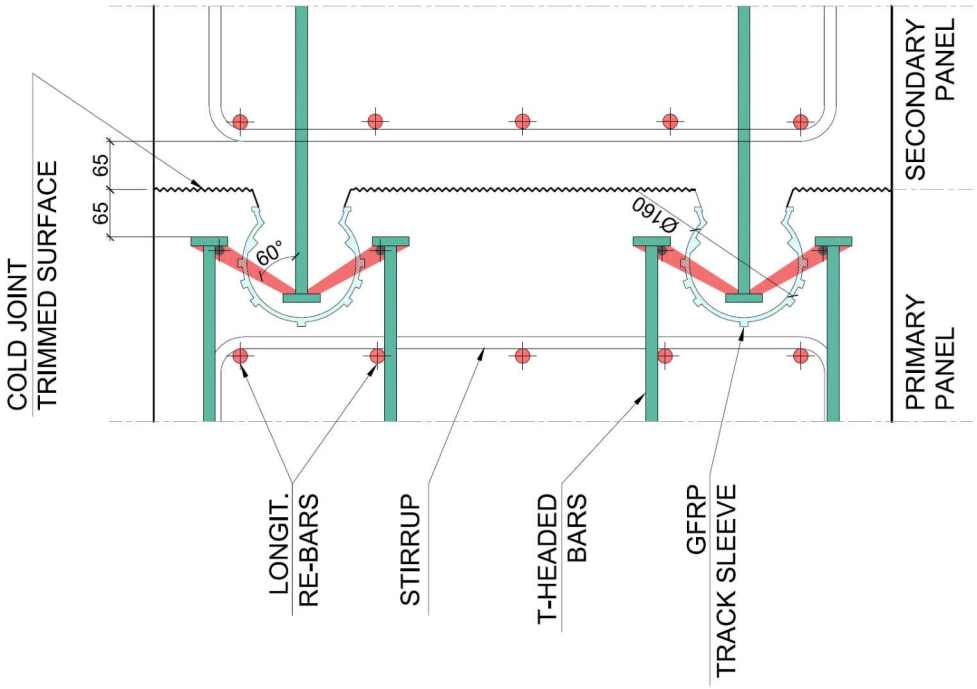


Fig. 7 - Arrangement of the headed bars for the Tension Track

The TTMJ Water Stop Arrangement

To provide an effective water stop several different arrangements were considered and evaluated. The one selected used a modified version of the TTMJ track and a PVC carrier strip to locate a hydrophilic rope in the panel joint.

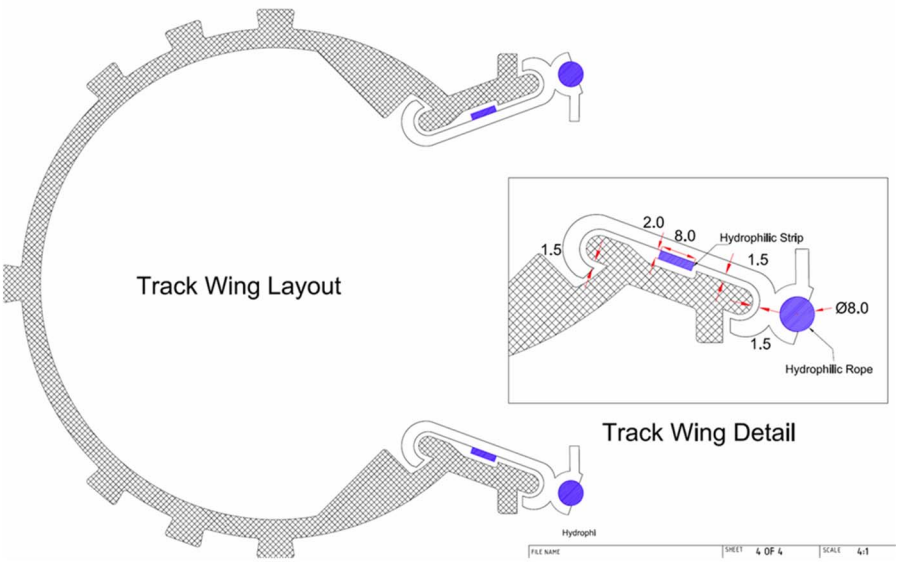


Fig. 8 - Arrangement of the water stop slipped over the track wings

Fig. 8 above shows the proposed arrangement. Sections of an extruded PVC carrier strip are slid down over the track wings. Each section will have a hydrophilic strip (shown blue in Fig. 8) glued to the rear face to prevent the possibility of water getting between the strip and the track wing. The primary component of the water stop will be a continuous hydrophilic rope (also shown blue in Fig. 8) clipped into the end of the carrier strip as it is installed into the joint. The two opposing nibs on the carrier strip are intended to act as crack inducers.

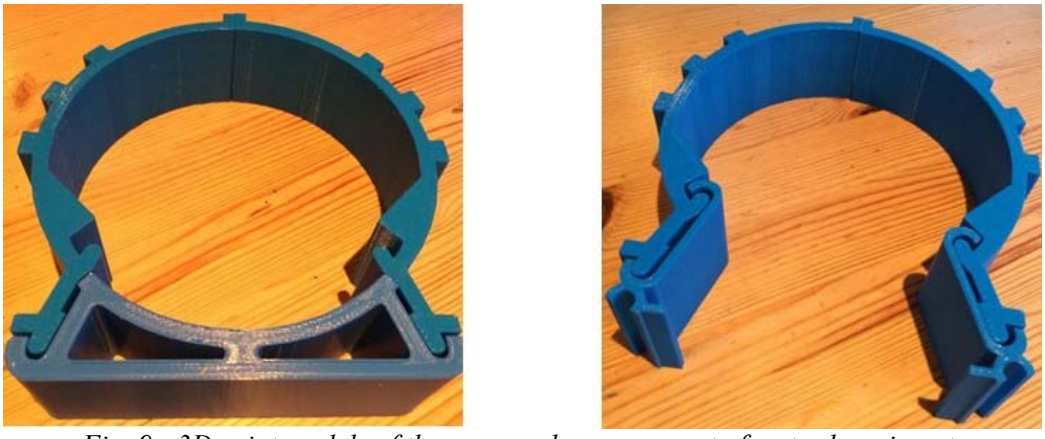


Fig. 9 - 3D print models of the proposed arrangement of water bars inserts

In Fig. 9 are 3D prints of the proposed arrangement. On the left is shown the revised TTMJ track arrangement and on the right is shown the PVC carrier strip restrained by the track wings.

TTMJ LABORATORY SCALE TRACK TESTING

The selection of the TTMJ track material and physical properties was an “educated guess”. Before field trials could be contemplated it was essential that the actual restraint likely to be provided by the track was established. It was also important to determine the actual force required to remove the sacrificial arc. Additionally, the intended arrangement of the tension connection needed to be verified and the potential tension capacity evaluated. During the latter half of 2017, over 50 blocks of concrete were cast, with various track and reinforcement arrangements, and tested to destruction. The blocks ranged in size from 400mm x 500mm x 300mm deep to 800mm x 500mm x 450mm deep. For the track pull out tests the sample were tested when the concrete had a compressive strength of ±20N/mm² and for the tension tests when the concrete had a compressive strength of ±40N/mm².
Fig. 10 below shows one of the samples for the track pull out tests and Fig. 11 shows examples of the track break out testing.



Fig. 10 - Samples of track pull out tests



Fig. 11 - Samples of track break out tests

Tension testing went through several arrangements of block size and headed bar. With the optimum arrangement using 400mm long, 500mm wide and 450mm deep blocks and a single 20mm bar inside the track, failure occurred at 140KN and 150KN for the two samples. (Fig. 12)



Fig. 12 - Samples of tension track tests

TTMJ FULL SCALE FIELD TRIALS

The field trials of the TTMJ System are due to take place later this year at TREVI's sister company SOILMEC's factory in Cesena Italy. Within the facility, SOILMEC has a steel lined shaft 1.5m wide, 3.5m long and 20m deep, that will be used to carry out the field trials. There will be six cutting trials, each using two 10m long beams coupled together. Two trials will test the trimmer on samples with a flat face, two on samples with a sloping face representative of forming the joint for a circular shaft and two on samples with a bulging face (Fig. 13).

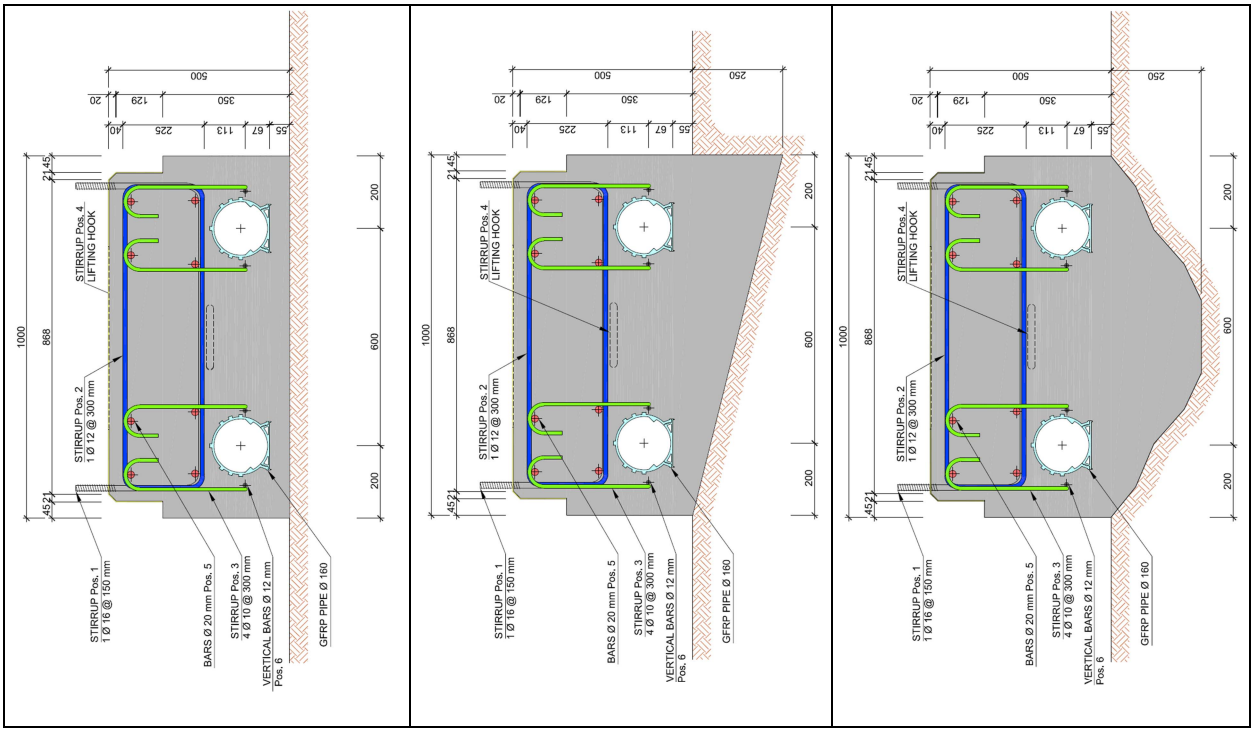


Fig. 13 - Test concrete beams - Flat face type (left), slanted face (center) and bulged (right)

The concrete beam samples are fixed to steel support beams before lifting and positioning in the test shaft, where, once the two 10m sections are jointed, a reaction frame secures them tightly within the shaft (Fig. 14).

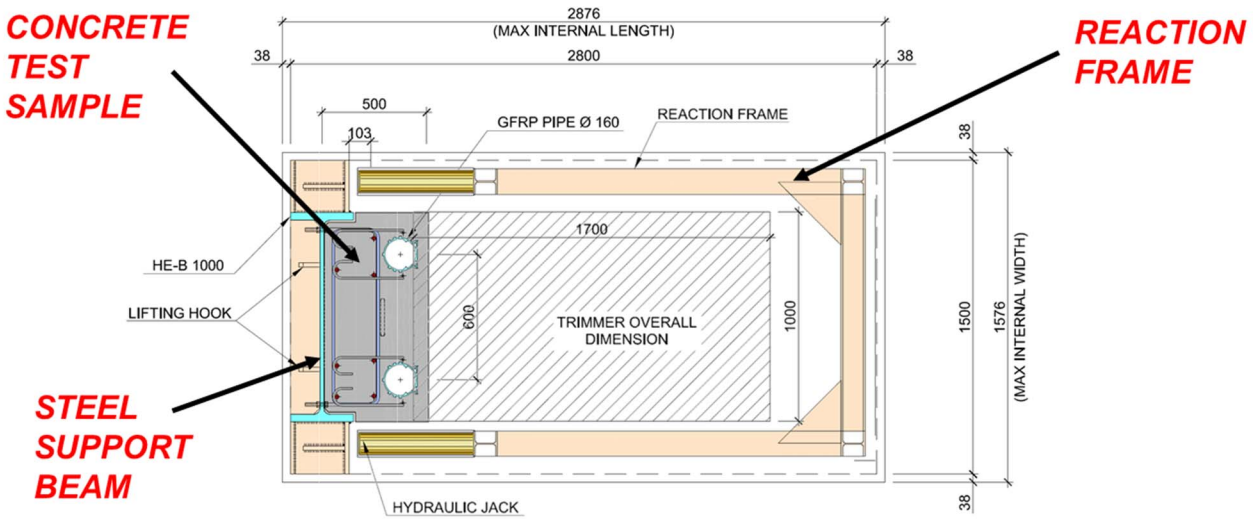


Fig. 14 - Test concrete beams – reaction frame

Once the shaft has been filled with a support fluid, to represent site conditions, the TTMJ Trimmer will be used to cut back the concrete. All control parameters will be monitored as well as rate of progress and the pull-out loads exerted on the track during the tests.

Once the sample has been trimmed, it can be removed from the shaft for inspection. At least one of the beam sections will be used to carry out a large-scale track pull out test (Fig. 15*)*. A crane equipped with a dynamoter or a hydrauic jack will be used to test the restraint capacity of the TTMJ track.

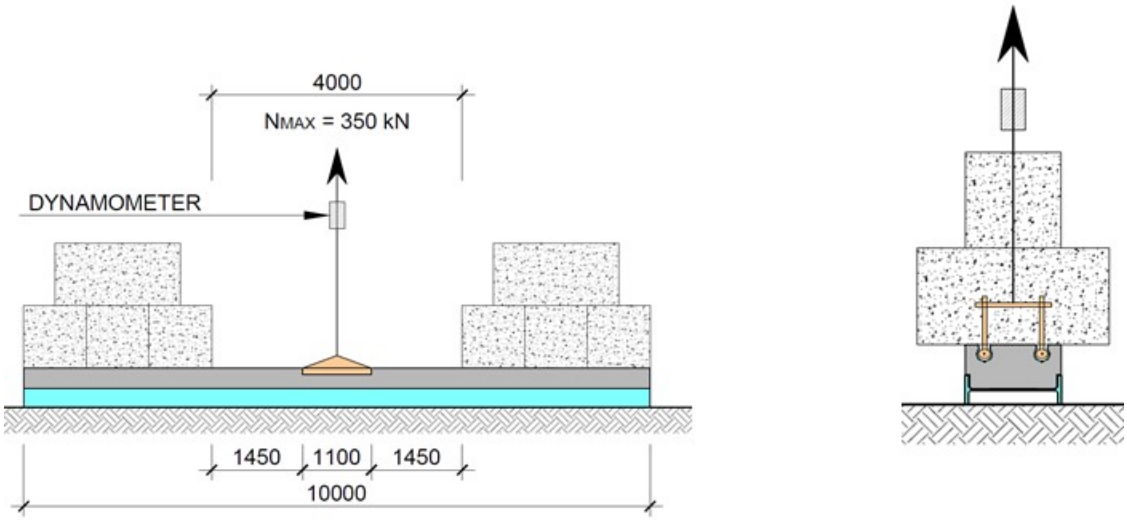


Fig. 15 - Pulling test

One more type of field trial is planned to investigate whether the tremied concrete in the adjacent panel adequately fills the TTMJ tracks cast into the first panel. A steel box will be fixed to one of the 10m long trimmed samples and then the whole assembly lowered to the base of the test shaft. Concrete will then be placed through a tremie until the steel box is filled. The position of the tremie and other arrangements will

be representative of actual site conditions (Fig. 16). Optic fibre monitoring will be carried out during and after the concrete pour to assess if there are any anomalies in the concrete.

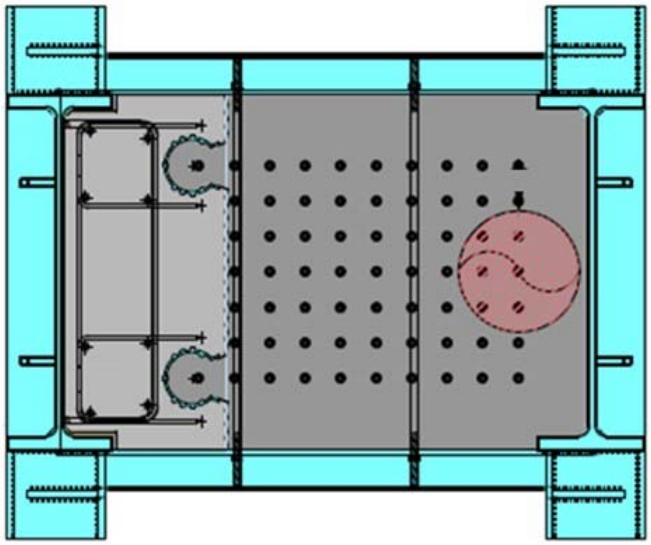


Fig. 16 - Concreting test

Once the concrete has set, the sample will be removed from the shaft and cut into sections to visually inspect the concrete and compare these observations with the data from the optic fibre monitoring.
At least one of the cut sections will be used to test the tension connection arrangement on a much larger scale than previously possible. Rock splitters will be inserted into PVC tubes cast into the concrete joint and then used to split the joint apart (Fig. 17).

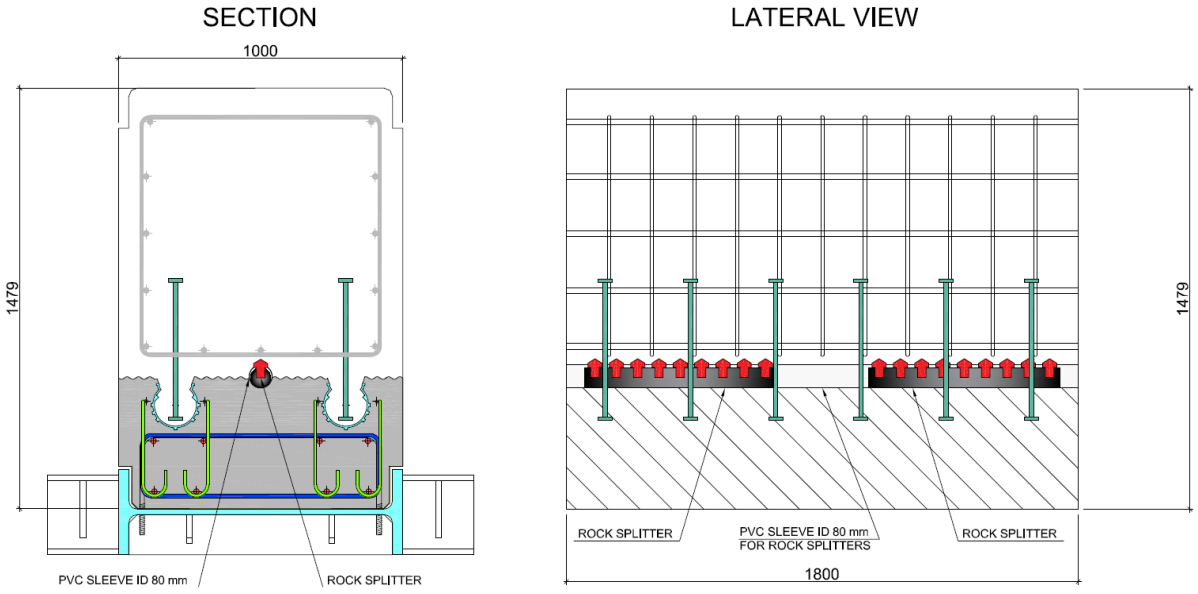


Fig. 17 - Splitting tests

CONCLUSIONS

The preliminary test conducted on the tracks demonstrated the complete suitability of the tracks to resist the anticipated traction forces exerted by the trimmer.
The design of the machine has been completed and the assembly of the components is currently ongoing.
A complete suite of several tests has been envisaged to provide a full picture of the potential of the method and to satisfy the designers.
The TTMJ System is a step change for diaphragm walling, because the system will offer:

- Technically superior panel joints to greater depths than currently achievable.
- A tension connection between adjacent diaphragm wall panels.
- An effective water-stop in the joint.
- Potential cost savings of up to 20% on diaphragm wall projects.
- Programme benefits on diaphragm wall projects.
- Improved Health & Safety control of site operations
- Improved Risk Management

ACKNOWLEDGEMENTS

Unfortunately during the period of preparation of this paper, Julian Crawley, after a long and brave battle with cancer, passed away. His love of life, enthusiasm for the TTMJ system, and dedication to its development set an example for the other members of the consortium team and provided the encouragement to solve the problems encountered along the way.

Reference List

Crawley, J., Siepi, M., van Horn, P., Coupland, J.: TTMJ – The New System For Slurry (Diaphragm) Wall Joints. Proceedings of the 42nd Annual Conference on Deep Foundations, 2017, New Orleans, LA, USA, 379 p.

UNVEILING THE VISION OF SOIL STABILIZATION FLUIDS: THE FUTURE

Trindade, Eonio; Technical Team Leader at GEO – Ground Engineering Operations; Lisbon, Portugal. eonio.trindade@geosoil.com

ABSTRACT

Obtained from the research on oilfield drilling fluids as a way to improve colloidal and rheological properties of bentonite (sodium montmorillonite) mud (slurry), the polymer based synthetic fluid reached a point that itself can work as a substitute of mineral slurry on excavations for foundations of engineering structures.

The use of this type of fluid in the geo-construction industry was born from the need to find a new solution with less environmental impact and at the same time improve the final results (improving excavation geometry, decreasing concrete consumption and allowing increase in production).

This article intends to clear old myths and old fashioned mindsets about the characteristics, how to use and in which aspects can the use of polymer slurry be more advantageous than bentonite slurry on soil stabilization. Moreover we will look into the potential that is inherent to the synthetic fluids and the future progress that is expected. The advantageous characteristics of this technology allow a reduced environmental footprint with a wider capability for problem solving. These fluids will, in the near future offer a real complete and optimized solution, for all soil conditions and project requirements, almost tailor-made to each case scenario and foundation contractor.

Keywords: drilling fluids; polymer; bentonite; composed slurries; soil stabilization; deep foundations

INTRODUCTION

Besides water itself there are two main (water based) slurries in use on the deep foundation industry: bentonite and polymers. Bentonite slurry is being used since the first approaches for deep excavations in the oilfields first and later in construction. Since its beginnings the techniques behind bentonite use have not changed much. Its properties and quality may vary according to the origin of the materials, the technological improvements on equipment have helped in the cleaning processes. But, besides the combination with polymers, there is not much else that can be done to improve and develop.

In general, all the drilling/stabilization fluids have two main functions: support the excavation by exerting hydrostatic pressure; and remain in the excavation, not flowing to any great extend into the soil. In addition, the FPS (2006) also mentions for bentonite that it should: suspend detritus and prevent sludgy layers build up; clean displacement by concrete; possibility to be cleaned of suspended detritus using screens and hydrocyclones; and be easily pumpable. When the drilling is done with a dynamic mud circulation system, the slurry needs also to: be capable of transport solid out of the bore and cool down the drilling tool.

POLYMER

Main Features

Polymers that are in general used as drilling fluids have the capacity of involve clay minerals avoiding expansibility problems due to water absorption but PHPA (Partially-Hydrolyzed Polyacrylamide) and Polyvinyl Alcohol (PVA) are known for their best results (Clark et al, 1976, in Caenn & Chillingar, 1996). Other polymers are used in slurries for drilling purposes. The NHI (2010) separates them in two main groups: natural (or semi-natural) and synthetic. The most common natural polymers are: starches, guar/xanthan gum, welan gums, scleroglucan and carboxymethyl cellulose. These polymers degrade fast as they have a very short life spam, usually not superior to 2 days, and tend to be used mainly as additives of bentonite slurries. Pure synthetic polymers are therefore the ones in broader use as soil stabilization slurries for foundation drilling today.

© 2018 Deep Foundations Institute

Taking advantage from the way PHPA works on the soil this synthetic polymer was used in the development of a fluid suitable to civil construction. In some cases, is PHPA itself that is used to get a stabilization fluid applicable to foundation excavations (e.g. Poly-Bore™; BAROID, 2008).
From the research and development of PHPA and the possibility of changing the branches of the main Carbon chain is also possible to change the way the polymer interacts. From this concept was possible to find a polymer with better properties. This polymer is also a Polyacrylamide, more specifically Sodium Polyacrylamide. All polymers known as "last generation" polymers are developed from this molecule and they have as main characteristic the high viscosity obtained in a low concentration mix of granular polymer (Fig. 1 &Fig. 2).



Fig. 1. Granular Polymer.



Fig. 2. "Fresh" colorless mixture of Polymer slurry.

In the "Construction Procedures and LRFD Design Specifications" (NHI, 2010), the most recent synthetic polymers are considered to be a totally different group. Though still having a main backbone of acrylamide molecules, they are highly engineered together with other chemicals to form new polymers with tailored properties that optimize their performance as drilling slurries.

The recent generations (3rd generation) of granular synthetic polymers:
- Are highly water soluble and designed to interact with different types of soils.
- Have high molecular weight that allows high viscosity water solutions, proper to all kinds of soil foundations stabilization and other geotechnical applications.
The standard amount of granules added to water to obtain the slurry is of 0.1% (1 kg per cubic meter) but it can vary according to the suppliers or the specific soil conditions encountered.

In opposition to the mineral slurry, polymer fluid doesn't form "cake". Due to the polymer long chains associated with hydrophobic, anionic and cationic groups its solution has a very particular behavior. The hydrophobic groups are responsible for the union between the carbon chains that originate a tridimensional net responsible for the fluid high viscosity and the covering of the excavated soil walls (Fig. 5). This covering or, more precisely, the way the tridimensional net of polymer chains wrap the soil it's also attributed to the cationic groups that by opposite electrical charge hold to the soil particles. On the other hand, the anionic groups are responsible for the hydration of the polymer thru their bonds with the water molecules.

BENTONITE

Main features

Bentonite (Fig. 3) is a clay (aluminum phyllosilicate) constituted mainly by a mineral named Montmorillonite that belongs to the Smectite group (FPS, 2006 and MURRAY, 2007). There are different types of bentonites and their names depend on the predominant chemical element present in its constitution, like Potassium (K), Sodium (Na), Calcium (Ca) and Aluminum (Al). The most important types for industrial purposes are Sodium and Calcium Bentonites. Sodium bentonite (montmorillonite) is the more commonly used as a drilling/stabilization fluid and it:

- Has the capacity of expanding when hydrated, absorbing several times its own dry weight of water;
- Works as a sealing agent;
- Has excellent coloidal and reological properties that allow its use for oil/gas drilling, mining or geotechnical exploration drilling and for the construction of foundations (piles and diaphragm walls).



Fig. 3. Dry Bentonite powder.



Fig. 4. Bentonite Slurry

Usually for bentonite concentrations equal or superior to 30 grams of bentonite powder per liter of water (3%) a homogenous solution is obtained (viscous slurry). This slurry is thick enough while at rest but also quite fluid when agitated. This effect is known as thixotropy and results from the way that the bentonite particles are organized. The particles in a solution look like small plates, with negative charge at its surface and positive charge at its ends. While at rest there is a tendency for particles to align due to electrical affinity (FPS, 2006). This electrical forces will originate a uniform structure that causes the fluid to go to a gel state. This state is responsible for the high suspension capability of bentonite slurry. When this "gel" is agitated the electrical connections are broken. The small plates are then randomly orientated and the mixture is again fluid. The gel state is also originated by water loss. When used as a drilling fluid, the contact of the fluid with the soil causes water absorption that will allow the bentonite accumulation on the bored walls originating an impermeable layer known as "cake". This "cake" is most important to soil stabilization. It's formed by the fluid penetration on the terrain and it is responsible of distributing hydrostatic pressure to the excavated walls, allowing its support.

COMPARISON

Having the same basic purpose in terms of soil stabilization (in deep foundations), the main difference between polymer and bentonite slurries is that polymer slurry does not allow the suspension of colloidal fines or sand particles (NHI, 2010). The soil particles are constantly settling down and being removed by the action of the drilling tool. A good understanding of this process is needed to allow appropriate bottom of excavation cleaning after completion.

When comparing in more detail polymer with bentonite slurry, the other differences that may be point out, are:
- Less quantity of product is required for preparation of polymer slurry. Reduced environmental footprint in transportation and small site stock.
- Fast mixing process, with less equipment required. Can be used almost immediately while bentonite should hydrate for 24h (when viscosity stabilizes).
- Does not accumulate soil particles in suspension, allowing them to settle fast. Sand can be removed using the excavation tools.

- No mechanical desanding involved – less need of equipment.
- Less total storage volume. There is no need to have double the excavated volume to proceed with slurry replacement.
- Can be recycled and re-dosed, during the full duration of the project
- Salted or brackish water do not tend to affect directly the quality of the polymer slurry meanwhile the bentonite
- Slurry polymers are biodegradable and do not accumulate in the environment, in opposition to bentonite.
- Slurry elimination can be done directly (as per local environmental laws) on site after treatment (chains breaking and pH reduction).

On the other hand, bentonite can be advantageous for:
- Traditional soil stabilization slurry that every foundation company knows how to handle.
- Prompt availability of various equipment and suppliers to manage the slurry.
- The cake formation allows to block soil porosity efficiently. In the case of polymer slurries, soils with permeability above 5.5 x 10^{-3} m/s tend to generate a drop in the fluid column that is difficult to sustain.
- Works perfectly as an impermeable layer/barrier – slurry walls.
- Is very effective in the transportation of solids ("cuttings") in slurry circulation systems (direct and reverse).

Table 1: Main comparative features between Polymer and Bentonite slurries

	Bentonite Slurry	**Polymer Slurry**
Mix	Mixing hoper or *venturi* system. Concentration: 30-60 kg/m^3. 24h maturation required	Mixing directly in a flow plate. Concentration: ≈1 kg/m^3. Water with pH adjusted
Circulation	Centrifugal pumps	Positive displacement pumps
Stability	Filtration and cake formation	Chemical interaction polymer/soil. May also include filtration
Concrete pour	After desanding/slurry replacement	After using a cleaning tool and additives (if required)
Cleaning	Mechanical desanders: Sieves and hydrocyclones.	Natural sedimentation and additives
Recycling	After cleaning ("desanded") and parameters correction (if required).	After the passage through a sedimentation tank and parameters correction (if required).
Fluid elimination	Should be transferred to a sludge treatment plant that separates liquid from solids	Polymer chains can be broken with chlorine and pH reduced before direct disposal onsite

The accumulation of bentonite is its major setback. Although being considered has non-hazardous waste, it can be highly pollutant (FPS, 2006; JEFFEREIS & LAM, 2013). When in contact with porous soils it tends to block the voids between soil granules, thus affecting strongly the local water table recharge and percolation. It basically, will influence the natural hydrological cycles of underground water. In the proximity of watercourses or waterbodies the use of synthetic fluids is also preferred over bentonite as they do not pose a risk to fish. More specifically because they don't accumulate in fish gills, causing them to suffocate (SCHUNMANN, 2004).



Figure 5 - Bentonite accumulation on topsoil

Due to its properties, bentonite slurry needs to be disposed of correctly. The cheapest method is to place it in an approved landfill. Though, recent restrictions and tougher environmental laws limit the number of landfills that are able to manage this type of waste. FPS (2006) presents alternative methods that are more reliable but also more expensive:

- Continuous belt filtration, that is meant to reduce the quantity of water and produces a clay product with approximately 65% of solids content;
- Decanting centrifuge units, that reach to similar solids contents as belt filtration;
- Bentonite flocculation, followed by the addition of cement to form clay-like product, generally with 25% of solids content.

These methods are meant to transform the slurry into a product that can be disposed of as solid waste, but the same also needs to follow strict environmental regulations.

Polymers have been commonly accepted has environmental friendly as they don't tend to accumulate in nature. The quantities involve in the slurry preparation also tend to be 50 times less when compared to bentonite. A dosing ratio of 0.1% is usually sufficient to get the slurry in the desired quality to be used.

To prove that they are non-pollutants, many projects demand the products to be tested. In Spain, a governmental authority named CEDEX preformed a thorough analysis under the Spanish and European standards to identify if there are any contaminant elements in the slurry mix. All the analysed hazardous elements that were measured did not present a concentration above the established limits. The CEDEX report concluded that the polymer could not contaminate soil nor water and could be declared as non-contaminant.

Other specific test was also performed under Brazil's environmental laws. The focus of this test was to determinate the grade of aerobic biodegradation of the synthetic polymer with time. It was executed according to the ISO 14852:1999 standard method and intended to simulate the biodegradation processes that occur in nature (aqueous medium). Fig. 6 shows the biodegradation curves that correspond to:

- Treated slurry – sample of polymer slurry that underwent previously trough a chemical treatment with Sodium Hypochlorite, that breaks the molecules chains thus reducing its viscosity;
- Polymer slurry – is the basic slurry with all required properties to be used as stabilization fluid;
- Control Sample – microcrystalline Cellulose;
- Inhibition Solution – used to validate the test.

Using this method, it was possible to confirm that polymer was biodegradable with time. The treated slurry (residual solution that is generated at the end of a project, prior to polymer disposal) had full biodegradation within 9 days. The slurry in its original state also reached 100% rate of biodegradation after 145 days.

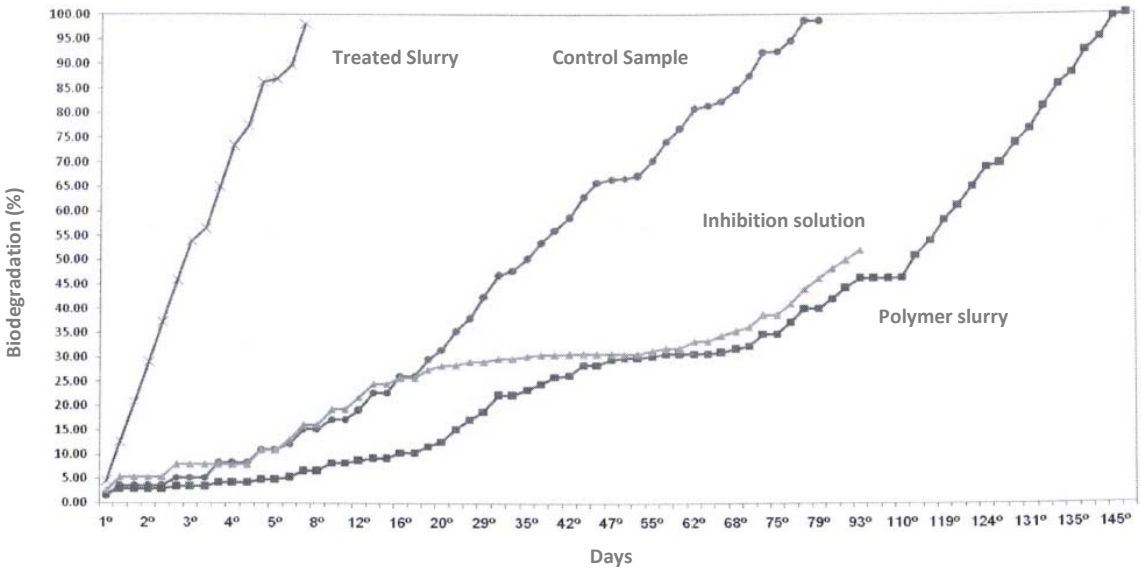


Figure 6 – Polymer slurry biodegradation curves

RECENT DEVELOPMENTS

Being a technology that is not yet well understood by the deep foundation companies, the synthetic soil stabilization fluids are not getting all the recognition they should get. Besides that, the foundation contractors rely themselves in the availability of the diverse mechanical equipment that allows bentonite to be used inside the standards that are already well known. Nevertheless, several positive experiences and studies have been documented recently, for direct comparisons in the use of both slurries, and these reveal real benefits in the use of the polymers.
Most of these experiences rely in well-educated and instructed individuals that know out to adequately use the products, implement methodologies, control parameters, collect date and report the results.

JEFFEREIS & LAM (2013), clearly indicate in their article that there are great benefits in the substitution of a bentonite slurry system with the use of a synthetic polymer:

- The operational benefits of managing a smaller batching plant, makes is more economical when working in restricted spaces and it's also more advantageous when the setup needs to be moved from site to site;
- The improved foundation performance, as in recent times many field studies were carried out to observe the effect of polymers in the load bearing capacity and it was appreciated that they significantly improved the load performance.

Furthermore, the polymer higher percolation capacity (when compared to bentonite) has recently been tackled and reduced greatly by means of controlling its suspension capabilities. Having control on the percolation allows the polymer to perform well in more permeable soils (permeability > 5.5 x 10^{-3} m/s). Usually loose sand soils with fines content lesser than 10% are a real challenge to polymer slurries as the rate of fluid loss is so high that it becomes difficult to maintain the fluid column level stable.
In the use of filler, the objective is to create a composed fluid that only incorporates inert fine particles (with more than 60% of particles with size <600mesh), e.g. powdered silica, originated from granite quarries. The fine particles that incorporate the polymer slurry will occupy the spaces between the

treads/chains, generating a homogeneous and stable mix. To help the suspension capabilities of the slurry, a suspending agent may also be used.

The main purpose of adding the filler is to block the fill soil porosity therefore allowing to maintain the slurry level stable inside the excavated trench. With that aim in mind the slurry supplied to excavation must have a density around 1.06 g/cm^3 (Sp. Gr.). This combined application of Polymer + Inert Filler is to be adjusted taking in consideration the soil investigation reports and previous site visits that have helped to access the *in situ* conditions. With the problem anticipated, fluid loss can be effectively mitigated from the start of the first excavation. The increment on slurry density maybe also essential in soil conditions where extra head pressure is required to assure stabilization.

In terms of slurry quality prior to concrete pour, the density stays homogeneous throughout the fluid column and, as in all polymer slurries, the sand contents are kept low (inside the standard limits). These values reveal the capability of the slurry to integrate the filler at the same time it avoids the accumulation of sand particles in suspension. It is also common to have the density of the slurry gradually decreasing. This drop, can be compensated if required by just mixing more filler with the polymer.

All the excavated soil can be easily disposed of without any environmental restrictions. After drying it can be reused in backfilling operations. The remaining fluid and the filler do not affect the soil natural conditions.

In these difficult soil conditions, it was proven the efficiency and adaptability of the polymer slurry that is fully capable of assuring provisional stabilization in high porosity soils. At the same time, it is safe for the surrounding environment and does not require any type of mechanical desanding.

THE FUTURE

With the growing environmental concerns and restrictions, the synthetic polymers are a trustworthy option in the future as support fluid for construction of deep foundations. Of course, they have their limitations but those might be mitigated with the adequate quality control and correct application of technical procedures. The versatility of the product will be better acknowledged if the foundation contractors start to gain more trust on its usage and follow the usage recommendations given by the suppliers.

The polymer slurry has still a long way of development ahead. Certainly, more R&D is required but, being a synthetic molecule, it can be tailored for any specific objective. Sometimes the limitation for this development is just the need of having one single product that meets most projects demands and soil conditions, being at the same time cost-effective.

A broader use of the polymers will also make possible its use as a support fluid suitable for trench cutter (hydrofraise) and reverse circulation. This means that the slurry will have specific and unique thixotropic properties, resistance to salts and adequate mechanical performance in the reverse circulation methods.

It is expected that the polymers will may, in the near future, also provide the possibility of incorporate nanotechnology. The main objective is to allow a better control of excavation stability and verticality without needing to depend on bulky equipment. Nowadays the only technology available to record vertically during the drilling is located in the sensors that are installed in the drilling tools, these are not 100% reliable and tend to have serious calibration problems. Other available option is the KODEN, but it can only be used when the excavation process is stopped or even completed thus meaning that deviation control is a time-consuming operation. Also, in case of deviation, the problem is not adequately anticipated and the only corrective measure is to proceed with excavation rectification (“trimming”) that ultimately will generate higher concrete consumption.

Meanwhile the approach for a more reliable and broad solution finds its way in the use of additives and combined application with other market products. Aiming always to environmental safe options.

SUMMARY AND CONCLUSIONS

Bentonite has serious limitations, mainly at environmental level, and there are no recent developments that may take it to a better level of acceptance. It has been used for the same physical characteristics since same were discovered. Nowadays the high-quality standards and strict environmental laws are making the use of synthetic fluids more attractive. Although this should not be the main reason for the contractors to choose this innovative and state of the art technology.

Even without having yet the diversification of solutions that would please all mindsets, the majority of fine granular soils can be stabilized using synthetic slurry as they would be with bentonite. While simplifying processes that need less equipment and quantity of bulk products.
Besides the reduction of space required to install all the setup, polymer slurry can reach higher quality standards with more effective production cycles. There are also the positive environmental characteristics and the safeguard of sensitive areas.

In the near future the foundation contractors will be able to trust more in the use of synthetic polymers. The understanding that they represent a more cost-effective solution will arrive with a more frequent use and handling of the products. Creating also better onsite quality management practices that optimize final results.

Polymer slurries nowadays can already offer a wide range of solutions that may effectively replace bentonite. Growing restrictions in bentonite slurry disposal and its high costs are a relevant factor that is already creating a transition. Hopefully also the polymer suppliers will start giving new innovative options to their products in a way they become more attractive to the deep foundation contractors.

REFERENCES

Baroid, “Poly-Bore™ - Borehole Stabilizing Dry Polymer”. Halliburton, 2008. www.baroidmud.com

Caenn, Ryan & Chillingar, George V. - “Drilling Fluids: State of the Art” - Journal of Petroleum Science and Engineering 14; Elsevier; 1996; pp: 221-230.

Clark R.K., Scheurman R.F., Rath H. & Van Laar, H.G. - “Polyacrylamide/Potassium Chloride Mud for Drilling Water Sensitive Shales”. J. Pet. Technol., 28(6), 1976. pp:642-651 (in Caenn & Chillingar, 1996).

(FPS) Federation of Piling Specialists; “Bentonite Support Fluids in Civil Engineering” (2nd Edition). January 2006. pp 1-5

Jefferis, S. A. & Lam, C. – “Polymer support fluids: use and misuse of innovative fluids in geotechnical works”. Proceedings of the 18th International Conference on Soil Mechanics and Geotechnical Engineering. Paris, 2013. pp: 3219-3222.

(NHI) National Highway Institute; Drilled Shafts: “Construction Procedures and LRFD Design Specifications”. U.S. Department of Transportation – Federal Highway Administration; Publication no. FHWA-NHI-10-016; May 2010. Chapter 7.

Murray, Haydn H - “Applied Clay Mineralogy”. Elsevier. Amsterdam, 2007. pp: 12-14, 50-59, 79-81 & 111-119.
(USGS) United States Geological Survey; on-line picture archive. www.usgs.gov

Schunmann D. – “Fisherman’s friend” – *Ground Engineering* 37 (12). pp: 17.

X10 CONCEPT TO IMPROVE QUALITY AND DURABILITY OF DIAPHRAGM WALLS

M.M.R. Boutz, SGS INTRON, Sittard, the Netherlands, michel.boutz@sgs.com
B.J. Admiraal, Volker Staal en Funderingen, Rotterdam, the Netherlands, b.admiraal@vsf.nl
R. van Berkel, BAM Infraconsult, Gouda, the Netherlands, rob.van.berkel@bam.com
P.R.B. van der Werff, Volker Staal en Funderingen, Rotterdam, the Netherlands, p.vanderwerff@vsf.nl

ABSTRACT

In recent years, an increasing number of diaphragm walls has been built in the Netherlands. Studies have shown that the quality of the concrete in these D-walls is not comparable to that of compacted concrete poured in formwork, as is often assumed. There are known incidents of bentonite inclusions and insufficient concrete cover of the reinforcement. Less well-known problems are the presence of cavities around the reinforcement and porous zones in the concrete cover. Such defects limit the suitability of D-walls for use in aggressive environmental conditions, like the tidal and splash zone of marine structures.

The problems mentioned above are either fully or partly caused by insufficient workability and/or stability of the fresh concrete. An extensive research program has been carried out to improve the properties of D-wall concrete both in the fresh and hardened phase. The introduction of a stabilizing admixture proved to be a breakthrough to obtain high flowability and excellent stability in the fresh state. Whereas conventional D-wall concrete typically has F5 consistence, the innovative concrete mix (developed under the name: X10) has a consistence in the self-compacting concrete (SCC) range (SF1, SF2). Full scale trials have shown that this high flowability results in a quite even pouring front up to relatively large distances from the tremie pipe. As a result, the risk of bentonite inclusion in D-walls is considerably reduced. Investigation on cores revealed a very dense concrete cover with nearly no defects, leading to a high durability.

In 2015 X10 has been used in D-walls for strengthening of a river embankment. At present, it is being used for construction of the walls of a large sea lock for the port of Amsterdam in IJmuiden (NL). Experiences from the research program and the projects are shared in this paper.

INTRODUCTION

D-walls are being used more and more in the Netherlands and contractors are increasingly becoming responsible for their design and service life as a result of DBFM-contracts. The quality of a D-wall regarding leakages and soil inclusions, as well as the quality of the concrete cover on the reinforcement, are extremely important. The properties of the concrete, both in the fresh and hardened state, are dominant impact factors for these quality aspects.

When building a D-wall, concrete is poured into a trench, filled with a bentonite suspension as a supporting liquid. Because of the difference in density, the concrete mix displaces the bentonite suspension along the entire cross-section. The concrete mix often must pass several layers of reinforcement before entering the cover zone. The high density of reinforcement impedes the flow through the reinforcement cage. As such, the workability of the concrete mix is very important, particularly because compaction by using vibrators is not possible in D-walls. Since the concrete cannot be vibrated, it is no wonder that the compaction in the the concrete cover is generally poor to moderate.

Concrete can also lose water by bleeding, which is aggravated by the high hydrostatic pressures in a deep D-wall panel. This problem might manifest itself as water-bearing continuous cavities along the vertical reinforcement and bleeding channels on the surface. These phenomena can have a negative effect on durability, depending on the design, the extent of the deviations and the environment in which the D-wall is located. The concrete strength is not compromised, though, since there is a high degree of compaction by

© 2018 Deep Foundations Institute

gravity within the reinforcement cage. The high cement content of D-wall mixes leads to compressive strengths that are significantly higher than the design strength (usually C28/35).

However, it is evident that a wider use of D-walls is a real option if it is possible to design concrete mixes with high flowability in combination with good water retention under pressure. Internationally, there is a growing opinion that great improvements can be achieved in this field.

Volker Staal en Funderingen (VSF) and BAM Infra, both specialist deep foundation contractors with expertise in D-walls, have formed a partnership with research institute SGS INTRON to develop such an innovative concrete mix. The research program consisted of laboratory tests, followed by a full-scale trial and finally the application in several construction projects.

PLAN OF ACTION

To achieve improvements in the stability and workability of D-wall mixes, an investigation was carried out on a series of concrete compositions. The D-wall mix, applied for several projects in the Netherlands, was used as a reference mix (Table 1) and as the basis for different variants. The strength class of this reference mix is C28/35, the exposure class XS2 and the consistence class F5. The water/binder ratio was 0.46 and maximum aggregate size 16 mm. This mix can be regarded as state of the art for D-walls in the Netherlands.

To bring about a major improvement of the fresh concrete properties, a new admixture was introduced, with which a significant better performance was achieved in the laboratory. This admixture was used for the development of the so-called X10 concept. This concept produces a highly flowable, but stable concrete mix with strong thixotropy, very suitable for application under difficult pouring conditions.

LABORATORY RESEARCH PROGRAM

The laboratory investigation was divided into two separate studies, i.e.:

- A stability study
  The parameters in the concrete composition that may influence stability, such as fine sand, other admixtures and other fillers, were investigated. The emphasis was on determining the bleeding behaviour, also under increased pressure.
- A workability study
  For this study, compositions that showed the least amount of bleeding and/or which were most similar to those that are available on the market were selected. Here, the emphasis was on determining the (retention of) workability and fluidity around the reinforcement bars.

NEN-EN 1538 was used as the basis for the composition.

Table 1 Composition of the reference mix

Constituent	Dosage (kg/m^3)
Cement (CEM III/B 42.5 N)	360
Filler (Fly ash)	40
Sand 0-1	55
Sand 0-4	751
Gravel 4-16	955
Water	169

Stability study

The study into the stability of the various D-wall mixes particularly looked at the following parameters:

- The initial workability (flow or slump flow).
- Bleeding using a PVC standpipe.

- Bleeding using an API filter press with a gas pressure of 2 bar (test method for cement-bentonite slurries).
- Bleeding using an Austrian filter press with a gas pressure of 3 bar (according to Austrian Merkblatt - Weiche Betone).

Workability study
The study into the workability of the various D-wall mixes particularly looked at the following parameters:
- Retention of workability in the first 2 h after mixing.
- Passing ability using an adapted J-ring (EN 12350-12).
- Flowability using an L-box.
- Viscosity using a V-funnel (EN 12350-9).

Since the X10 mix is highly flowable, its workability was determined using methods that are normally used for SCC (slump flow, J-ring, L-box and V-funnel).

RESULTS OF THE LABORATORY INVESTIGATION

The investigated mixes are shown in Table 2. Each mix is indicated by a code, such as 1A (see Table 2).

Table 2 Mixes investigated

Mix no.	Variable	Variants	
		A	B
0	Reference mix		
1	Higher sand percentage	+ 3%	+ 9%
2	Extra fly ash	+ 10 l	+ 30 l
3	Dosage of retarder	None	0.39%
4	Superplasticizer	0.27%	0.40%
5	X10	0 kg fly ash	+ 40 kg fly ash, - 40 kg cement

Stability
Only the most notable results are discussed here.
The stability of the X10 mix was much better than that of the reference mix and its variants. This was shown by the filter press tests.
Testing the total water loss in the small standard API filter press showed the striking result that for the X10 mixes the time required for the water loss was longer than for the other mixes by a factor of 2 to 5 with far less water loss.

The Austrian filter press test also clearly showed that the X10 mixes performed considerably better than the other mixes (Fig. 1). Another striking observation is the difference in consistency after the Austrian filter press test. The conventional mixes were drained over the full height (Fig. 2), while the X10 mix was still 'plastic' after the test (Fig. 3).

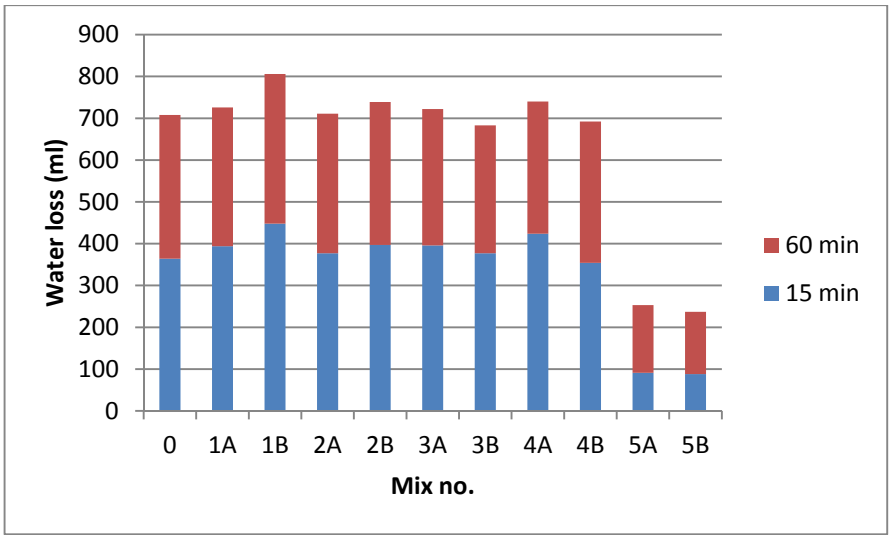


Fig. 1. Water loss after 15 min and 60 min in the Austrian filter press



Fig. 2. Conventional mixes after the Austrian filter press test



Fig. 3. X10 mix (5a) after the Austrian filter press test

Workability study

For this study, a selection of the mixes used in the stability study was made based on their performance. Flowability was investigated to make a link to the actual flow of the concrete around the reinforcement bars in a D-wall.

The following variants were tested:

1. Reference mix (360 cement + 40 fly ash)
2. Reference mix with PCE superplasticizer (360 cement + 40 fly ash)
3. Reference mix with PCE superplasticizer WP (320 cement + 80 fly ash)
4. X10-4 mix (360 kg cement + X10 + PCE)
5. X10-4 WP mix (320 kg cement + 40 fly ash + X10 + PCE), k-factor for fly ash equal to 1.0.

Numbers in kg/m^3.

Even with the addition of a third-generation superplasticiser (polycarboxylic ether, PCE), the workability of the reference mix could not be increased to more than F5 (flow 560 - 620 mm). The workability of both X10 mixes meets consistency class F6 (flow > 620 mm) and the workability had to be measured with the slump flow. Figure 4 shows the slump flow of both X10 mixes as a function of the time after production.

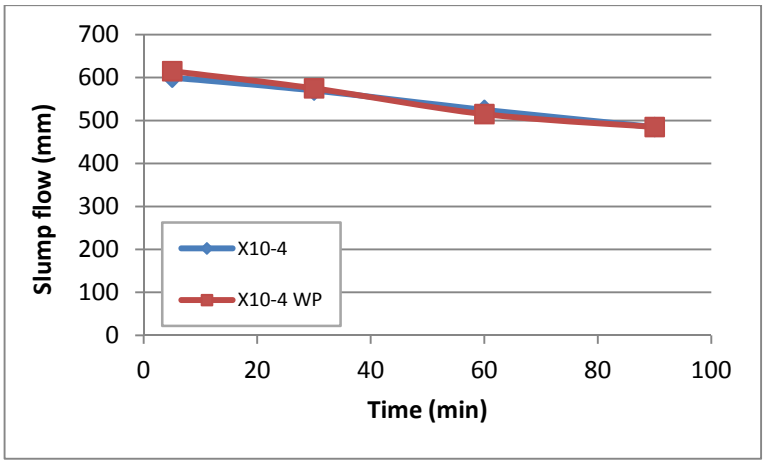


Fig. 4. Slump flow versus time for the X10 mixes

The high flowability of the X10 mixes also resulted in greatly improved passing in the J-ring (see figures 5 and 6). This results in full enclosure of the reinforcement bars when using X10, whilst this is clearly not the case when using the reference mix.



Fig. 5. Reference mix in the J-ring



Fig. 6. X10 mix in the J-ring

Based on the investigation described in this chapter, the X10-4 WP mix was selected for the full-scale trial.

Compressive strength and RCM value

The following two properties of the five mixes were also measured:

- The development of the cube compressive strength.
- The development of the resistance against chloride penetration as measured using the Rapid Chloride Migration (RCM) test in accordance with NT Build 492. The lower the RCM-value, the higher the resistance.

After 28 days and 56 days, the cube compressive strength of both X10 mixes was higher than that of the reference mix and its two variants (Fig. 7). After 28 days and after 56 days, the resistance of both X10 mixes against chloride penetration, measured by the RCM test, was higher than that of the reference mix and its two variants (Fig. 8).

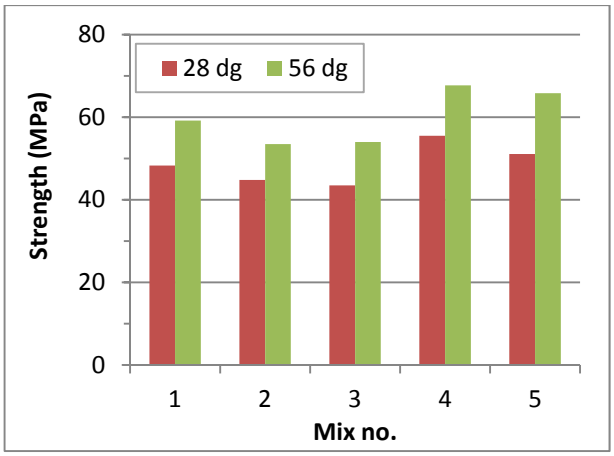


Fig. 7. Compressive strength after 28 and 56 d

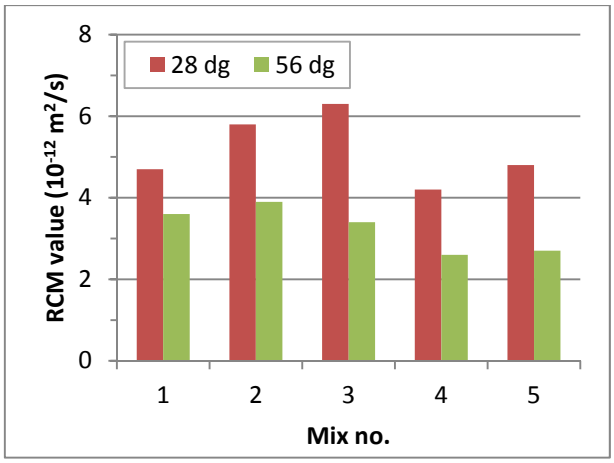


Fig. 8. RCM value after 28 and 56 d.

FULL-SCALE TRIAL

Within the scope of this investigation, it was important to use the optimised mix in a full-scale trial, both to gain experience as well to determine the quality in actual practice. The full-scale trial was performed with the reference mix and the X10 mix (X10-4 WP). The length of the reference panel was 3 m (1 pass of the excavation tool), the X10 panel approximately 7.5 m (2-pass), both panels have been 1.2 m wide and 22 m deep. Both panels were separated by a joint.

Process monitoring

While casting the concrete, different parameters were determined to monitor the process. The workability was measured both at the concrete mixing plant and at the construction site to determine the reduction in workability. The slump flow measured 570 - 640 mm after production and 590 - 655 mm on arrival at the site (30 min drive).

For the X10 panel, the tremie pipe was not placed in the middle as for the reference panel, but on the left-hand side of the panel. Therefore, the concrete in the X10-panel has to flow a larger distance to the joint than in the reference panel. This is normally disadvantageous for the concrete quality near the joint. In this way, it can be seen if the high flowability of X10 will prevent such quality issues.

The casting heights were measured at three positions along the panel (left, middle and right). There was only a small difference in casting height at the two ends of the X10-panel (0 - 40 cm). No particularities were reported in relation to the casting process of the reference panel.

Inspection of the test panels

Table 3 shows the reinforcement configuration in the excavated section (up to NAP -3 m). The reinforcement configuration was identical for both panels. Configuration 1 is present from approx. NAP -0.8 m and higher and configuration 2 from NAP -1.4 m and deeper. The concrete cover specified on the drawing is 120 mm with a tolerance of ± 50 mm.

Table 3 Reinforcement configuration of the excavated section of the test panels

Layer	**Configuration 1** Water side	**Configuration 1** Land side	**Configuration 2** Water side	**Configuration 2** Land side
1 (vertical)	15Ø40-240	15Ø25-150	15Ø40-240	15Ø20
2 (horizontal)	6Ø20-325/360	16Ø20-325/360	6Ø25-325/650	16Ø20-325/360
3 (vertical)	6Ø40-480/960 7Ø32-480		6Ø40-480/960 7Ø32-480	15Ø20
4 (horizontal)				4Ø32
5 (vertical)			14Ø32-140	15Ø20

Visual inspection
The test panels were visually inspected. A bulge on both sides of the top of the panel was removed prior to the start of the inspection (see figures below). A striking observation was that the surface of both sides of the X10 panel was much smoother than the reference panel. No defects were observed in both panels.

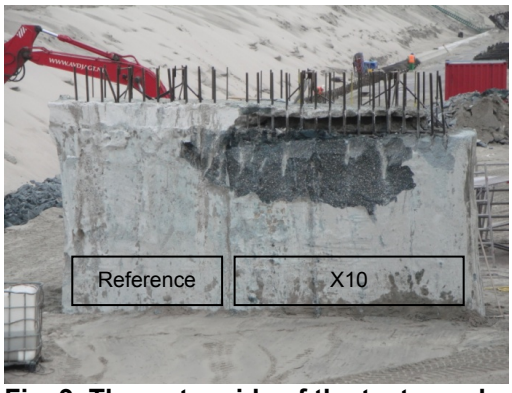


Fig. 9. The water side of the test panels



Fig. 10. The land side of the test panels

Concrete cover
The concrete cover, measured in the grooves that were cut open at approx. NAP -1 m on both sides of the panels, is given in the table below. The concrete cover on the land side of both panels is considerably greater than on the water side and falls outside of the tolerance of the specified value (120 ± 50 mm).

Table 4 Concrete cover of the outer vertical bars of the test panels

	Reference	**X10**	**Reference**	**X10**
	Land side	Land side	Water side	Water side
Average concrete cover (mm)	185	190	115	145

The generally greater concrete cover of the panel made with the X10 mix is not attributed to the mix itself, as this panel is a 2-pass panel and the reference panel is a 1-pass panel. There is a considerably greater number of bucket movements on the overlap of a multi-pass panel, particularly for the top of the panel. This results in more wear of the soil's wall surface in the open trench.

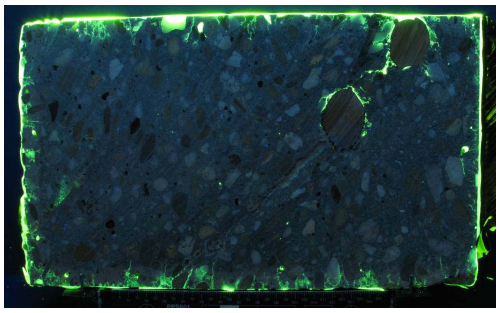
Tensile tests of the reinforcement steel
Tension bars were included in the panels to test the anchoring of the reinforcement in the concrete. These tests were performed to detect any influence of the quality of the concrete cover on the anchoring. The maximum load for the tensile tests corresponds to the yield point of the reinforcement steel and is approximately 200 kN for the tested rebars. In the reference panel, the bars could only withstand 100 - 170 kN, while in the X10 panel, the anchoring remained fully intact until reaching maximum load.

RESULTS LABORATORY INVESTIGATION CORES TEST PANELS

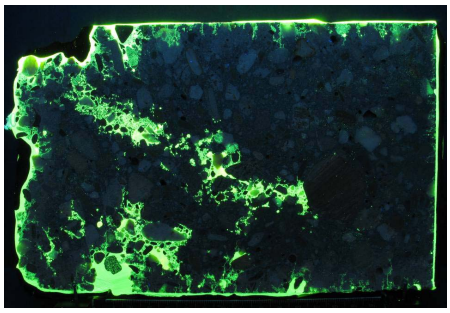
Compressive strength
The compressive strength of cores was tested at an age of 27 - 28 days. The specified strength class was C25/35. The measured compressive strengths were much higher than the specified value. The average compressive strength of both the reference and the X10 concrete was almost identical (52 – 53 MPa).

Concrete petrography
A total of 26 cores Ø145 mm were taken: 10 on the land side and 16 on the water side. All the cores were visually assessed. For 16 cores, the front part of the core was impregnated with a fluorescent resin. The resin fills any pores and defects, that are accessible from the outside. After impregnation, the impregnated cores were sectioned in longitudinal direction and photographed under normal and UV light.

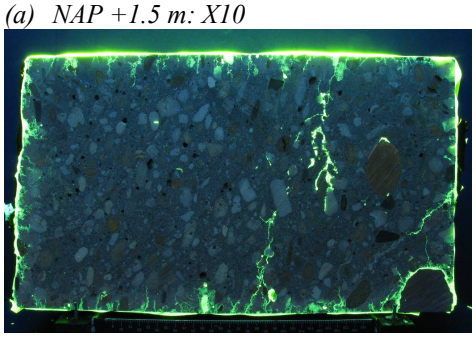
The quality of the concrete cover and the enclosure of the reinforcement in the X10 panel was considerably better than in the reference material. This is shown in two series of six UV photographs below. Cores drilled at the same height in both panels are placed next to each other. The first series of photographs is from the land side and the second series of photographs is from the water side. The left-hand side of the core is always the original surface of the D-wall in the photographs.



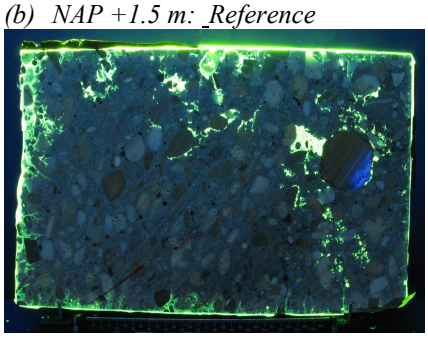
(a) NAP +1.5 m: X10



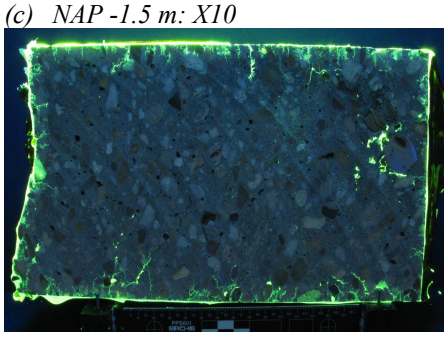
(b) NAP +1.5 m: _Reference



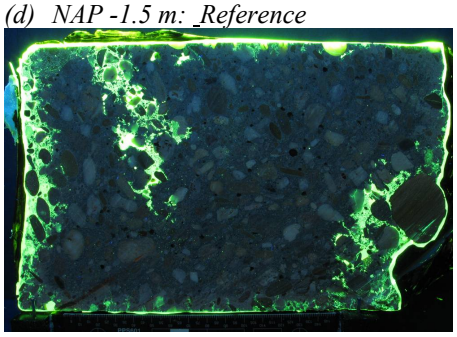
(c) NAP -1.5 m: X10



(d) NAP -1.5 m: _Reference

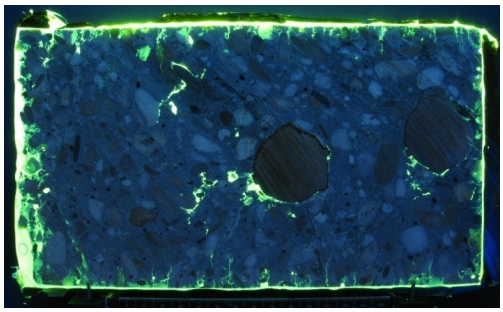


(e) NAP -2.5 m: X10

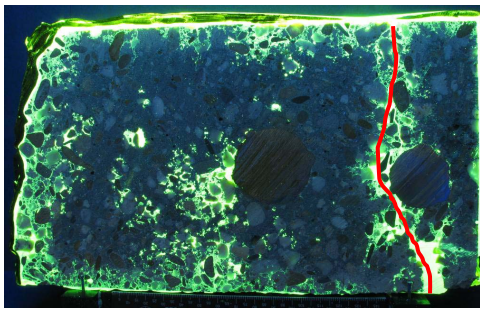


(f) NAP -2.5 m: _Reference

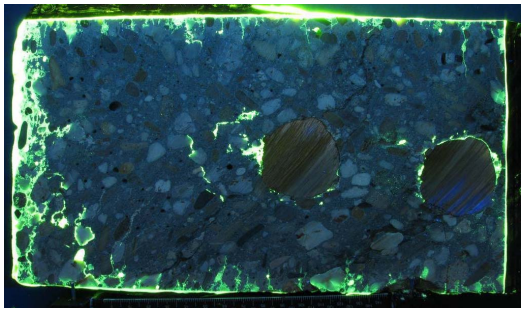
Fig. 11. Cross-sections from land side of the X10 and the reference panel at different heights.



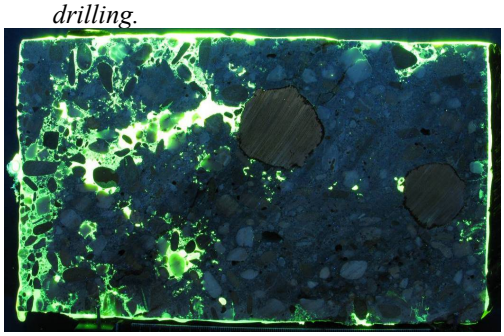
(a) X10, NAP 0 m



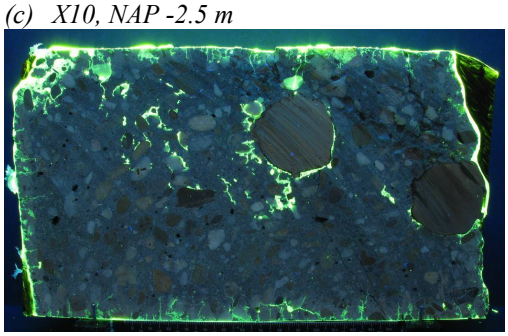
(b) Reference, NAP 0 m. Red line = crack caused by drilling.



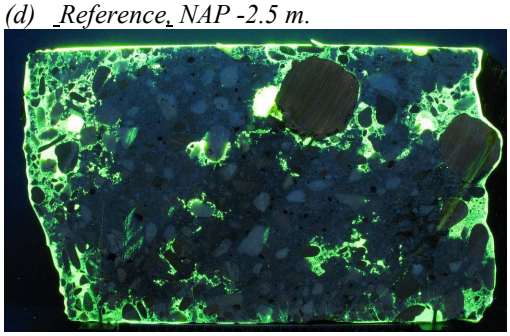
(c) X10, NAP -2.5 m



(d) Reference, NAP -2.5 m.



(e) X10, NAP -3.0 m



(f) Reference, NAP -3.0 m

Fig. 12. Cross-sections from water side of the X10 and the reference panel at different heights.

There are no UV photographs available of the core samples taken at NAP +1 m on the water side. The photographs of the cores below also clearly illustrate that the concrete cover in the X10 panel was considerably better.



(a) X10



(b) Reference

Fig. 13. Cores from the panels on the water side taken at NAP +1.0 m

The enclosure of the reinforcement bars was measured in all cores. The enclosure is the percentage of the bar's circumference, that is enclosed by concrete. The average enclosure in the X10 panel is 94%. In the reference panel, it is only 83%. Furthermore, it was determined that the cavities along the outer bar form a continuous channel in 7 of the 10 core samples taken from the reference panel. This was not the case in any of the core samples taken from the X10 panel.

Impregnated cores (taken at NAP -2.5 m) were also examined under UV to assess to what extent the quality of the concrete cover in the X10 panel reduces as the distance to the chute increases. The chute was placed on the left-hand side (when looking towards the panel on the land side). There was no clearly noticeable reduction in quality with increasing distance from the chute.

For the reference panel, the chute was placed in the middle. Cores were taken at two heights (NAP – 2.0 m and -2.5 m), at approximately the same distance to the left and right of the chute's position. The quality of the concrete cover was similar on both sides of the chute's position and was considerably poorer compared to the X10 cores at NAP -2.5 m, while the distance to the chute for cores in the X10 panel was considerably larger than for the cores taken from the reference panel.

FIRST APPLICATION IN CONSTRUCTION PROJECT

In 2015 X10 has been used for the first time in a construction project by VSF. In total 4.500 m^3 of X10 concrete was used for production of 24 m deep D-walls for strengthening of a river embankment in Krimpen aan de Lek (NL). The slump flow at the concrete plant was 680 ± 40 mm (consistence class SF2) and at the construction site (travel time 45 min) 620 ± 45 mm (consistence class SF1). The fresh concrete properties were intensively tested on site by TU Münich as part of the DFI EFFC R&D program on deep foundation concrete. Workability in the SCC-range, good retention of workability, high stability, excellent water retention under pressure and excellent flowability (L-box) were key results of this test program. Cores were drilled in one panel and the concrete quality was investigated by SGS INTRON. The concrete cover was very dense without significant defects and the enclosure of the rebars was >90%.

X10 FOR WALLS NEW SEALOCK IJMUIDEN

As demonstrated above, D-walls can be produced with X10 concrete that have very little defects and a very dense concrete cover. In this way, high service life can be reached even in aggressive environments, such as the tidal and splash zone of marine structures (environmental class XS3). At present, the joint-venture OpenIJ, with BAM and VolkerWessels as the main contractors, is constructing a new sea lock in IJmuiden (NL). The required service life equals 100 years. The heavily reinforced walls of the lock are constructed with D-walls using the X10 mix. More details on the concrete quality of these walls will be given in future publications.

CONCLUSIONS

The investigations that were carried out in the laboratory and in the full-scale test showed that application of the X10 mix leads to a strong improvement of the quality of the concrete cover. This concerns the enclosure of the reinforcement, the permeability and the number of defects (cavities, cracks) in the cover. With regard to the fresh concrete properties, the stability, i.e. the extent of bleeding under pressure, has been greatly improved. Furthermore, the fact that the X10 mix has a much higher level of workability, combined with excellent stability, while using a smaller amount of binder, is particularly striking.

The laboratory study also showed that the X10 mixes studied have a higher compressive strength and a higher resistance to chloride penetration compared to the reference mix.

The investigation of the core samples from the panels showed that the X10 mix had a compressive strength at least equal to that of the reference mix. The durability of the X10 panel is considerably better due to the large reduction in the number of defects (cavities, cracks) in the concrete cover.

Based on the current standard for D-walls, the composition does not meet the minimum binder content. However, based on the proven performance (as recorded in this document), such a mix may be used based on the Equivalent Concrete Performance concept as included in the European concrete standard EN 206.

When using the X10 mix, a higher final quality can, therefore, be achieved with less risk of bentonite inclusions. In the case of high reinforcement concentrations or environmental conditions where corrosion by, for example, salts, chemicals or varying water levels may lead to a reduction in durability, use of X10 should certainly be considered. X10 can also be of great value when using underwater concrete or standard concrete constructions with very high reinforcement densities.

ADVANCES IN RESONANT PILE DRIVING AND APPLICATIONS

AUTHOR: Mathew Janes, M.E.Sc., P.Eng., Resonance Technology International Inc.
Vancouver, BC, Canada, 604-317-6799 mj@rtii.ca

ABSTRACT:

The RD 260 Resonant Pile Driver (resonant driver) has proven to install long piles with negligible ground disturbance in urban areas. Recent projects further prove the versatility and applications possible using the RD 260 Resonant pile driver.

The resonant driver was recently used at the site of a major grade separation south of Amsterdam, at Den Haag, to install 34 m long micro piles. The micropiles are used as both compression and tension elements for the support of the structure walls and roof and to hold down the roadway base due to hydraulic uplift forces. A test program for a similar, more challenging project, with deeper anchors in harder soils was recently completed. The single pass tube was installed into soils with CPT Qc of greater than 300 Bar (30 MPa) in 11 to 15 minutes with no flushing and no spoil production. Tension load testing confirmed the anchor capacity to be 1125kN to 2160 kN, depending upon the grouting procedures.

The resonant driver was also used to install both combi sheet pile walls for Dyke stabilization and for displacement bearing piles. The combi wall required the installation of closed end 323 mm dia tubes with double AZ 18 – 700 pairs for dyke raising and stabilization. The bearing piles include closed end 273 mm and 355 mm dia mandrel driven piles (with a loss bit) which were concreted and the mandrel removed.

INTRODUCTION

The resonant pile driving method is gaining acceptance around the world as a new method to rapidly drive piles free of ground borne vibrations. The high frequency vibrator resonates the pile, essentially changing the pile into an axial spring, to excite the toe of the pile with high accelerations and low amplitude. High acceleration with low amplitude generates high penetration rates but the high frequency stress waves are quickly dissipated in the soil. Typically ground borne vibrations are measured at below 1 mm/sec within 1 to 5 m of the pile. The resonant method can drive a pile negligible next to a glass of wine, as has been demonstrated on numerous piling sites.

How Does Resonance Work?

The resonant method uses a hydraulic piston - cylinder geometry to generate high magnitude, high frequency oscillating force. This is a very different mechanism than the eccentric mass technology used in conventional sonic drills and vibrators.

A unique valve geometry achieves the high frequency flow switching necessary to oscillate the hydraulic piston at up to 180 Hz (10800 VPM). The valve rotation is controlled electronically for maximum accuracy of the desired frequency. The volume of hydraulic oil delivered through the valve (flow rate) determines the amplitude and the hydraulic pressure determines the peak force.

© 2018 Deep Foundations Institute

The main advantage of the resonant piston-cylinder method is that it allows the vibration frequency to be tuned to the natural frequency of the pile, which excites the pile like a spring. Exciting the pile like an axial spring allows the storage (build up) of vast amounts of energy available for delivery to the pile tip. In this way the pile tip is brought to a high acceleration state that penetrates through the soil. The challenge is to continuously tune the vibration frequency to the natural frequency of the pile as it is being driven into the ground. A computer algorithm has been developed for the resonant driver which automatically performs this tuning function. Through tuning the maximum driving efficiency and maximum force at the pile tip is achieved.

Deep Anchors in the Netherlands

The Netherlands are building tunnels and highway underpasses in an effort to reduce traffic congestion while avoiding conventional overpasses which suffer from long term settlements in the deep soft sediments of Holland. Below grade approaches require deep tension anchors and micropiles to counteract the hydraulic uplift loads. Conventional drilling methods require up to 3 hours to install the 34 m deep anchors using casing and flushing media.

The tunnel approaches and TBM launch portals are constructed in the wet using steel sheet piling cofferdams. The base of the cofferdams are susceptible to hydrostatic uplift forces and piping due to the high water table and weak soils. Deep tension anchors are constructed from existing grade to depths of 34-37m. The anchors are constructed in dense to very dense, saturated alluvium using high tension reinforcing bars and high strength grout placed in 'resonated' holes or conventional drilled holes. A tremmied base slab (unreinforced under water concrete) encompasses the anchor heads and is topped with a 1-1.3 m thick reinforced concrete slab.

Test Programs and Tension Load Test Results

BAM Infra BV was awarded the foundation construction for two early projects. The contractor undertook extensive test programs at each site to prove the construction methodology, productions and anchor capacity. Three methods of anchor construction were used for the first test program: conventional drilling double rotary with water flushing, the sonic drill method and Resonant mandrel driving.

Conventional rotary drilling using a casing and drill string with water flushing installed 178 mm dia segmental casing to a depth of 28 m. A 63 mm dia high strength bar was inserted and grout tremmied into the hole with incremental pressure grouting up to 20 Bar. Grout volumes were monitored during each test pile to ensure consistency between anchors and prevent a false test result due to over grouting. The second method used the Mid-sonic drill mounted on a 168 mm dia drill casing made up of two sections: the first 19 m long and the second proposed 15 m long. The casing was advanced using a loss bit with no flush. The sonic method vibrates the pipe axially at very high frequency (150Hz or 9000 VPM) in order to advance the tip. The BAM had used this method successfully on a previous anchor program and achieved very high productions for anchors driven to a depth of 30 m. However, at this site a dense layer at a depth of 16 m proved to be too tough for the sonic drill method. The Midsonic drill advanced the 19 m casing to a depth of about 17.5 m and could not advance it further or remove the casing.

The third method used the Resonator driver on the same 19 m and 15 m long casings. In this case the Resonator was used to remove the 19 m stuck casing from the sonic drill test. The casing was moved to a new location and driven to 19 m depth and the 15 m section added and welded to form a 34 m long mandrel. The mandrel (casing) was driven with a loss bit in place and no flushing to the target depth of 28 m where soils with Qc on the order of 30+ MPa were encountered. The Static Cone Penetration soil profile is provided in Figures 3a and 3b. The red line shows Qc in MPa and the blue line shows skin friction (Qf) in The casing was driven with the Resonant driver in only 14 minutes, so an attempt was made to drive the casing to the full length of 34 m. The casing was driven to full depth in another 3 to 4 minutes. Despite the ease of achieving additional anchor length, all test anchors were installed to a 28 m depth. The loss bit was fitted with an O-ring seal to prevent groundwater from entering the casing during driving. As a result the bar could be inserted into the casing in the dry and grout placed into the casing without the need for a tremmie, which improved production. The grout line was connected to the top of the casing and the Resonator clamp was fabricated with a seal to permit constant pressure grouting to 20 Bar during casing extraction.

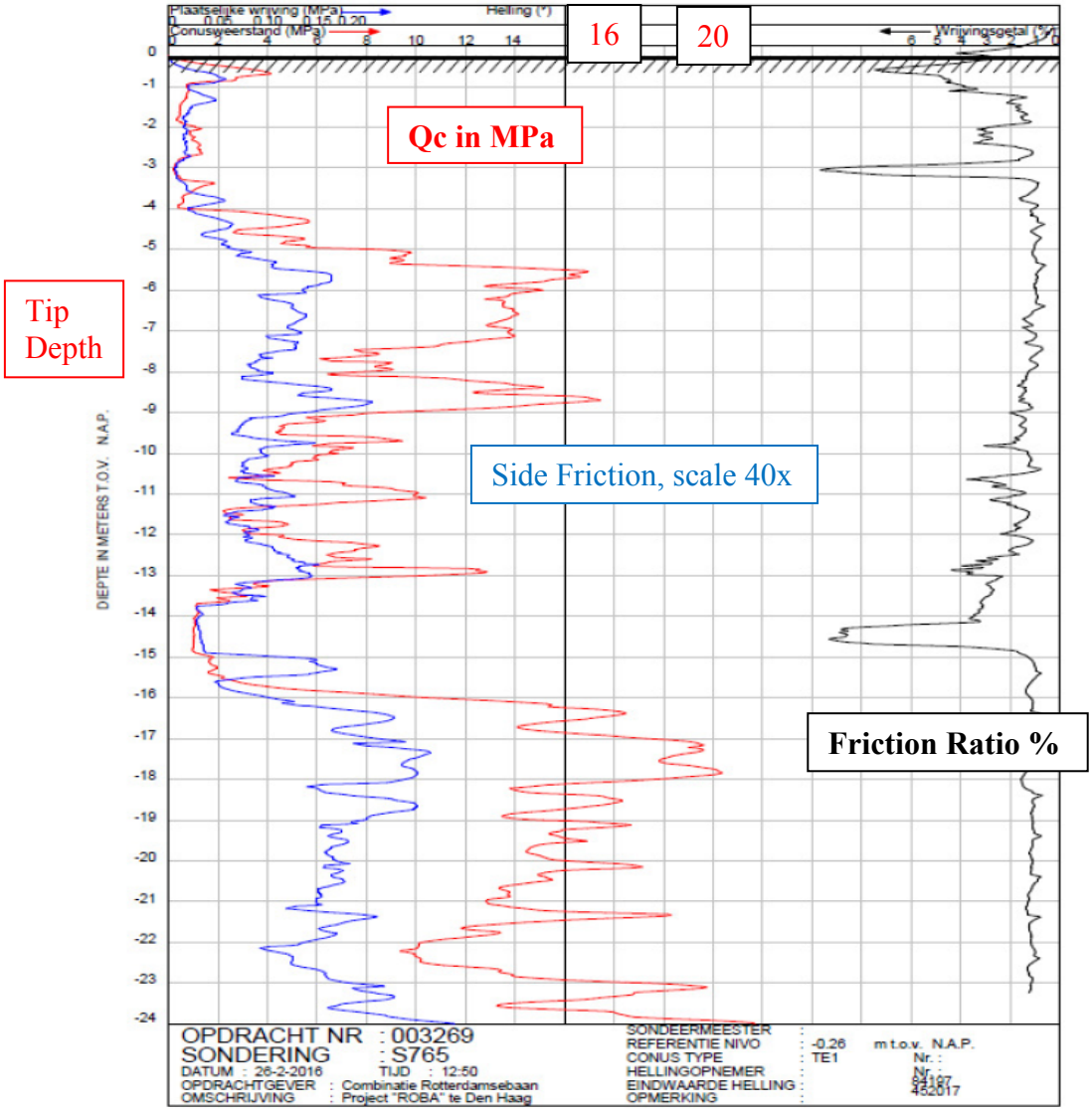


Figure 3a. Typical CPT at Rotterdamsebaan site, Den Haag, plate 1.

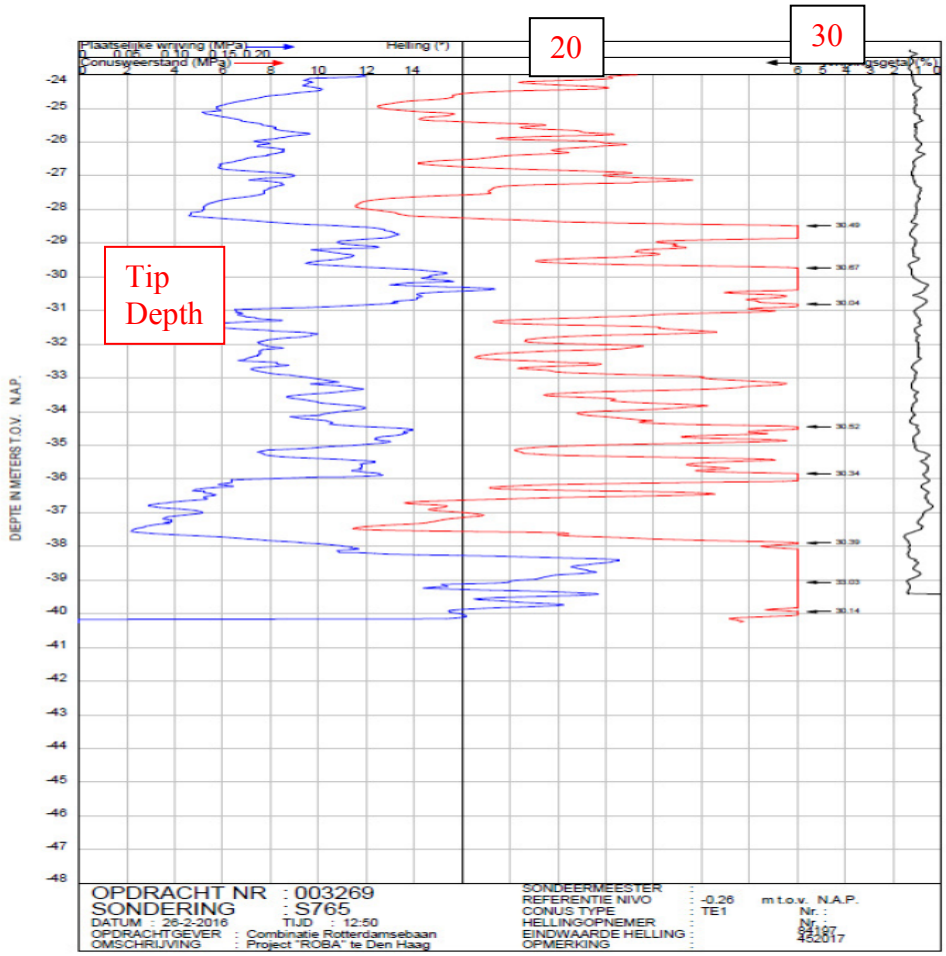


Figure 3b. Typical CPT at Rotterdamsebaan site, Den Haag, plate 2.

The test program was continued using the conventional drill method and Resonator driver for over 30 anchors to explore alternative methods and establish optimum production. On several occasions grout takes were deemed too large and the anchors abandoned. In the end a selection of 6 anchors were tension load tested.

Anchor testing was conducted on selected, representative anchors. Selection was based upon optimum production methods and what were deemed to be representative grout takes for both initial grouting and during pressure grouting. Despite the care taken during installation tension load test capacity varied greatly between anchors.

Three resonant method installed anchors were tested with bond zones of 6.5 m, 7.5 m and 8.5 m for piles P01, P02 and P18 respectively. All bond zones were developed to 28 m tip elevation. Thus the anchor bond zones started at 21.5 m, 20.5 m and 19.5 m respectively. The load test results indicated peak loads for the Resonator driven anchors varied between 1250 kN and 2200 kN (failure was by creep at 2 mm per log cycle). Pile P02, with the 7.5 m bond zone provided the highest capacity at 2200 kN, or 442 kPa bond stress while anchors P01 and P18 provided 228 kPa and 238 kPa bond stress respectively. The wide range may have been due to variance in grout takes during pressure grouting. Anchor P02 took 200% of the pressure grout volume of anchors P01 and P18. The P01 and P18 anchor capacities fell below the expected bond stress (approximately 300 kPa). Though the higher capacity bond stress was achieved with the higher grout takes under pressure grouting, it was not assumed that this could be achieved for all production anchors.

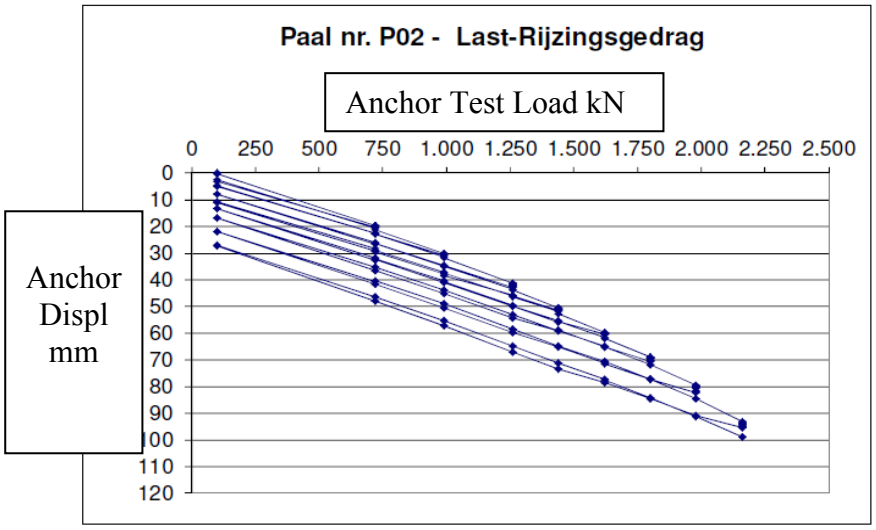


Figure 5 Test Anchor load results

Thus, the lower grout takes and lower bond stress was assumed for design purposes. The resonant driven anchors proved to have slightly lower bond strength than the conventionally installed anchors. This is thought to be due to the smoother hole the resonant method would produce. A loss bit or pipe mandrel end that generates a rougher hole is thought to be an improvement.

Production Micropiles

A total of over 1600 tension anchors were required for the two tunnel approaches to the Den Haag Twin Tunnels. The anchors were spaced at 1.8 to 2.4 m centre to centre on a rectangular grid. Low cut offs, at between 2 m and 9 m below grade, meant that bars were not proud of the working surface. However, anchor 'holes' were abundant and treacherous for equipment and workers. Given the large number of anchors two



Figure 6. The South Tunnel Approach during foundation construction

spreads of equipment were commissioned for the project. A conventional drilling spread was used which included 4 Klemm drills, 4 support excavators outfitted with drill casing and drill string handling arms, an excavator for spoil removal, a 80 tonne service crane and a grout plant. The drills andaccompanying equipment comprised a crew of 11, including a foreman. The crews worked an 11 hour day and produced up to 4 anchors per drill per day.

Figure 6 shows the conditions on site during anchor installation. The drills and service machines are seen in the foreground within the future cofferdam footprint. The 70 tonne crane handling the resonant driver is located beyond the drills. The drilling area of the site proved problematic due to the introduction of copious amounts of water and drill spoil. Spoil removal proved particularly problematic with large amounts of wet sands and grout to be handled on a crowded site with poor access.



Figure 7. Resonant driver showing the drive casing and connection detail

For production work the Resonator was installed on a 42 m vertical leader mounted on a 70 tonne base crane. The power pack (400 Hp) was mounted on a frame attached to the back of the crane. The leader was mounted with a sliding casing gate to support the 168 mm dia, 34 m long casing at its midpoint to avoid buckling. A permanent grout nipple was integrated into the top of the casing for introduction of pressurized grout during extraction. Figure 7 shows the resonant driver with clamp and sealing spigot and the top of the casing. A machined and polished centre spigot was attached to the clamp base which located and centered the clamp into the casing, but also offered a high pressure seal during pressure grouting. The clamp was connected and removed hydraulically, moved away from the centre opening of the casing during bar insertion and initial grouting and then re-introduced to form a grout seal and clamp attachment during extraction. The crew of 3 consisted of a crane operator, a front end man and the grout plant operator. The crane operator had a Resonator controller in

the cab along with grouting and crane loading readouts. Frequent site visits and support were provided by PVE staff for training and equipment support. The Resonator production averaged 14 to 17 minutes for installation of the micropile casing, 12 to 17 minutes to flush the grout lines and fill the casing with grout and 17



Figure 8. Resonant rotary loss bit detail

to 20 minutes to extract the casing during pressure grouting. As a result typical production consisted of 1 anchor per hour. Anchor driving as rapid as 4 minutes for the full 34 m length was achieved. Higher productions are achieved with accurate tuning of the driving frequency to resonance and the correct blend of vibration amplitude and downward force. A common mistake is to over crowd or push on the pile while driving. This tends to dampen the vibration and alter the natural frequency



Figure 9. Resonant rotary unit (base mounted) and swivel connection detail

of the system. Similarly on extraction, the use of too much pull can slow removal of the casing. While push and pull are required during install and extraction, the use of limited assistance results in the highest production rates.

At Driebergen, the second deep anchor site, tougher soils, higher anchor loads and deeper penetration depths required enhancement of the RD 260 Resonator with rotation. A 1.1 tonne-m rotary system was added to the resonant driver to permit simultaneous rotation and resonating of the drill pipe. This increased anchor penetration rates permitting completion of a hole in just 9 minutes. The drill pipe was fitted with slots which mated with tabs on the loss bit to permit the transfer of torque. Electrical tape around the inset portion of the loss bit created a seal and the anchor could be grouted from the top without a tremmie. Unfortunately the piles were not pressure grouted during extraction of the pipe which reduced the tested anchor capacity. In addition the smooth mandrel pipe exterior did not disrupt the bond zone soil surface upon extraction. It is probable that the smooth hole and lack of pressure grouting upon extraction lead to lower bond stress than anticipated for the anchors.

Woubrugge, NL Combi wall Dyke reinforcement

The Netherlands is suffering from a combination of raising North Sea levels, more violent North Sea storms and increasingly rapid variations (rise) in the levels of the Rhine following precipitation or spring melting in Germany. Each of these phenomenon lead to more rapid and higher water levels in the Dutch rivers and dykes. As a result the Netherlands has undertaken a long term plan to improve the strength and increase the topping levels of the dyke system. A typical solution is to install a structural barrier that deepens the toe (increases the slip circle radius by driving the failure to deeper strata) and whose top is proud of the existing crest of the dyke.



Figure 10. Resonator driving closed end pipe at Woubrugge, NL.

At Woubrugge the Resonator was used to install combi sheet pile walls for Dyke stabilization. The combi wall required the installation of closed end 323 mm dia pipe piles with double AZ 18 – 700 pairs for dyke raising and stabilization. The 16 to 17 m long 323 mm dia pipe piles penetrated 12 m below the toe elevation of the

dyke. The intermediate double paired AZ 18-700 sheet piles (four singles) were 4 to 5 m in length and served to increase the strength of the upper portion of the dyke and decrease the permeability (seepage) of the dyke core. In this case the remedial works permitted the dyke road bed to be reworked, raised and allow heavier vehicle traffic. The resonant driver installed the pipe piles in 13 to 17 minutes. In many cases houses were located within 2-3 m of the pile driving and sensitive structures such as bridges, walkways and porches were within 1 m of the pile driving. No vibration related issues or complaints were generated by local residents. Pile driving noise was within allowable construction levels of 85-88 dBa at 5 m, and for the most part was the same or less than conventional vibratory methods. Similar projects in the Netherlands have seen sheet piles and pipe piles up to 508 mm in dia installed using the resonant driver for Dyke reinforcement and support.

Breskens Waterschap, NL

At Breskens Waterschap bearing piles with a working capacity of 80 to 100 tonnes were installed for a water purification structure. The original project design called for a drilled or auger cast solution, but contaminated soils presented a problem with spoil production and disposal. Driven solutions were not permitted due to ground vibrations which would damage proximal neighbouring structures.

A solution was presented using a resonant driven and rotated mandrel pipe with a loss bit to install a concrete reinforced pile. The mandrel and loss bit displaced the dense to very dense, saturated, sand and sandy silts soils. The mandrel was 21.5 m in length. A test pile program was conducted to prove the concept and pile capacity ahead of production piling. CPT testing indicated Qc of 12 to 20 MPa in the target sandy strata where the majority of skin friction and end bearing was anticipated.

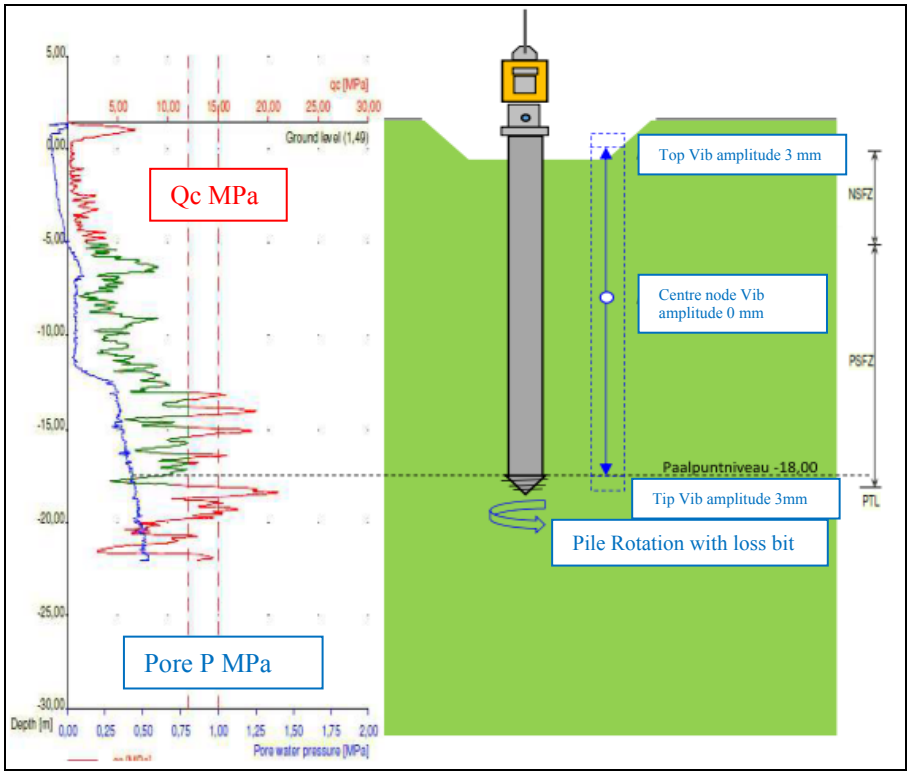


Figure 11. Mandrel drivel pile method at Breskens Waterschap, NL

Mandrel piles of 253 mm dia (initial test program) and 355 mm dia (second test program and production) were driven using the resonant driver combined with rotary. The piles were resonated at 120 Hz (7200 VPM) and approximately 10 rpm rotation. Piles were driven 19.5 m in approximately 9 minutes. The loss bit was fitted with a seal to provide a dry hole. This permitted free falling of concrete into the pipe without pumping or tremmie and ease of cage placement. Ground vibration monitoring proved less than 1 mm /sec velocities at 5 m.

The original test pile program suffered from poor loss bit and concreting procedures and resulted in very low pile side friction, with tested capacity of only 50 tonnes. A subsequent test program was conducted using a 355 mm dia mandrel with careful attention paid to the overall pile construction geometry and concreting procedures. Driving and screwing of the pile into the formation densified the soils along the side wall and at the pile toe. Increasing the soil density at the pile toe and leaving behind the loss bit ensured good pile end bearing. The mandrel was resonated



Figure 12. Resonant driver with the rotary drive on 355 mm dia mandrel

and rotated out leaving behind the reinforced concrete pile. Upsets on the exterior of the toe of the mandrel left behind a scored soil bond surface. Resonant vibration during extraction vibrated the concrete to ensure good mating of the concrete and soil surface. 12 hr static pile load tests were conducted on piles constructed with using 355 mm dia mandrel pipe and a 405 mm dia loss bit proved capacity of over 194 tonnes (the piles held the 194 tonne load with low creep). The mandrel resonated pile system proved to have high production rates for installation, high pile capacity, no ground vibration transmitted to neighbouring structures and produced virtually spoil. The porewater pressure effects appear to be simialr to conventional methods of displacement pile installation, where a high fones content will result in elevated pore pressures immediately after intallation. Pore water pressures are expected to dissipate as they would in undisturbed soils.

Conclusion

Resonant pile driving has proven to provide rapid pile installation with negligible ground borne vibrations and negligible settlement of nearby soils or structures. High frequency vibrations cause liquefaction of the soil adjacent to the pile and high pile toe accelerations which cut through soil cleanly, leaving the soil undisturbed. Numerous previous projects with vibration monitoring and published results have proven typical vibration levels of 1 to 2 mm/sec at 1 m distances from the pile. Vibration and optical survey monitoring during resonant driving of piles indicates little to no disturbance occurs. Noise levels are typically less than that of conventional pile driving but may be affected by off axis vibration modes and are noisier for lighter sheet piles. The addition of rotation to the resonant vibrator system allows for greater penetration depths and productions for round pile profiles.

This paper would not be possible without the co-operation and efforts provided by the staff of BAM Infra, Gebre de Koning and PVE – Dieseko Staff of Sliedrecht, Netherlands.

References:

Janes, Matthew, P.Eng., Resonance Pile Driving with Zero Ground Vibration, Proceedings: DFI – PFPS Piled Foundations and Ground Improvement Technology for the Modern Building and Infrastructure Sector, March, 2017, Melbourne, Australia.

Janes, Matthew, P.Eng., Deep Resonant Micro Piling for Netherlands Grade Separation, Proceedings: 13th International Workshop on Micro Piling, March, 2017 Vancouver, BC.

Janes, Matthew, P.Eng., The Resonant Pile Driver – Case Histories of Piling Free of Ground Disturbance, Proceedings DFI Superpile, Chicago, IL, 2016.

Janes, Matthew, P.Eng., The Resonant Driver – Ultra High Frequency Pile and Casing Installation, Proceedings 33rd DFI Annual Conference, 2008, New York City, NY.

ANNULAR MONOBLOCK BRIDGE FOUNDATIONS

Alessandrini eng. Francesco, Alpe Progetti s.r.l. Società di Ingegneria – Udine – Italy
De Biaggio Nicola, I.Co.P. S.p.A – Basiliano (UD) – Italy
Fedrigo eng. Dario, Alpe Progetti s.r.l. Società di Ingegneria – Udine – Italy
Valusso eng. Diego, Alpe Progetti s.r.l. Società di Ingegneria – Udine – Italy

ABSTRACT

Annular monoblock foundations are increasingly used in bridge pillar construction, where they guarantee high bearing capacities, safety, speed and ease of execution.

Here we illustrate their main design and calculation features as well as the constructive modalities from some recent examples of Italian road bridges.

The advantage of this foundational typology is evident in the realization of high and medium span bridges in water, where the cost of construction is particularly optimized. The facilitation is significant since the construction operations are all from above and dry compared to the classic foundations of piles and pile cap that require the construction of provisional sheet pilings in water or other shafts, to allow the construction of the pile cap under the water level.

These last elements generally interact negatively on hydraulic behavior around the pillar; this interaction is considerably reduced with annular monoblock foundations.

keywords: bridge foundation, drilled pile, annular monoblock foundations

INTRODUCTION

In the construction of bridges on watercourses, the construction of pillars in the riverbed always poses the problem of defining the interaction between the body of the pillar and the fluid stream, a subject widely studied as purely hydraulic matter. There is also an interaction between the ground at the feet of the pillar and the stream, whose effects are reflected in the geotechnical and structural resistances of the pillar's foundation.

The design and construction method of pillars with the annular monoblock foundation allows us to optimally address the aspects above, offering also significant constructive and economic benefits.

CLASSICAL FOUNDATIONS

The classical foundation construction typology of a pillar in a riverbed includes a reinforced concrete (RC) cap, headed on a series of piles, from which extrudes the pillar elevation. The use of deep pile foundations for this type of work is almost always necessary because, in the case of base erosion, it guarantees the maintenance of static and geotechnical functions. It is well known that the interaction between the motion of the fluid and the overall pillar can produce the phenomenon of "baring the roots", which is manifested first in the erosion of the soil in the area near the pillar shaft and, gradually, at the foundation level, once this interacts with the water flow. The size of this process can be very variable, and basically depends on the speed of water, the size of the immersed body, the shape of the pillar (according to Yarnell's classic experimental approach, 1934, the shape can affect up to 40 % in the erosion process, and a circular shape is one of the least affected) and, finally, on soil characteristics.

© 2018 Deep Foundations Institute

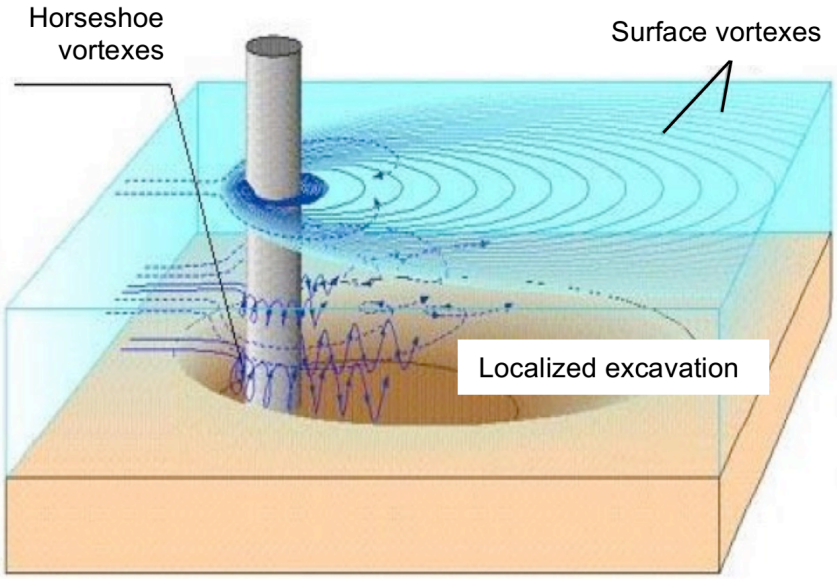


Fig. 1. Schematic representation of the movement field and local excavation process near a circular bridge pillar (Breusers & Raudkivi, 1991)

In order to contain this phenomenon, which can remove the soil to a significant depth, it is frequently chosen to place the pile cap deeper than the bottom of the expected erosion: for this purpose, large excavations must be carried out. It is necessary to build temporary earth support structures and the construction workers will have to operate below the water level, even in deep wells.

ANNULAR MONOBLOCK FOUNDATION

The technological solution analyzed in this paper involves the realization of a single pile, coaxial to the pillar shaft, both with a circular section, and with a diameter suitable for supporting vertical and horizontal loads: for large bridges with spans over 20-30m, this can require foundations with a single pile diameter of more than 2m. By neglecting the cases in which the excavation of the pile can be realized directly with a single digging and casting operation (classic monolithic pile), the method illustrated is equally applied, regardless of the diameter of the final pile. The latter is made by means of a group of deeply intersected piles aligned along a circumference of appropriate diameter and coaxial to the shaft of the pillar. Thus, an annular section pile is obtained, which is achieved by joining each small diameter pile. From a hydraulic point of view this allows one to maintain the diameter of the elevation even at the base, reducing the effects of the interaction with the water flow thanks to the geometric external continuity. From a geotechnical point of view, the execution of a single pile, although large in diameter, avoids the formation of group effects and so the performance reduction concerning both horizontal and vertical loads.

CONSTRUCTION METHODOLOGY

The construction of this type of pile is articulated as follows:

Stage 1: Creating the service area in the riverbed, protected from water and extraordinary flood events;

Stage 2: Insert into the ground the circular self-founder caisson (more easily feasible for diameters not exceeding 3-4m), coaxial to the pillar shaft and the annular pile to be realized. The caissons are generally settled down into the soil a little beyond the level of the maximum allowable erosion so

that, in case of an extreme event, the water stream behaves as a smooth flow toward the precast concrete external shape;

Stage 3: Restore the terrain inside the caisson in order to maintain the service area almost at the ground level;

Stage 4: Primary and secondary intersected piles are executed up to the design level;

Stage 5: The top connecting element is realized, which solidifies the head of all the piles and forms the lower part of the shaft of the pillar;

Stage 6: The concrete of the upper part of the pillar shaft is cast.

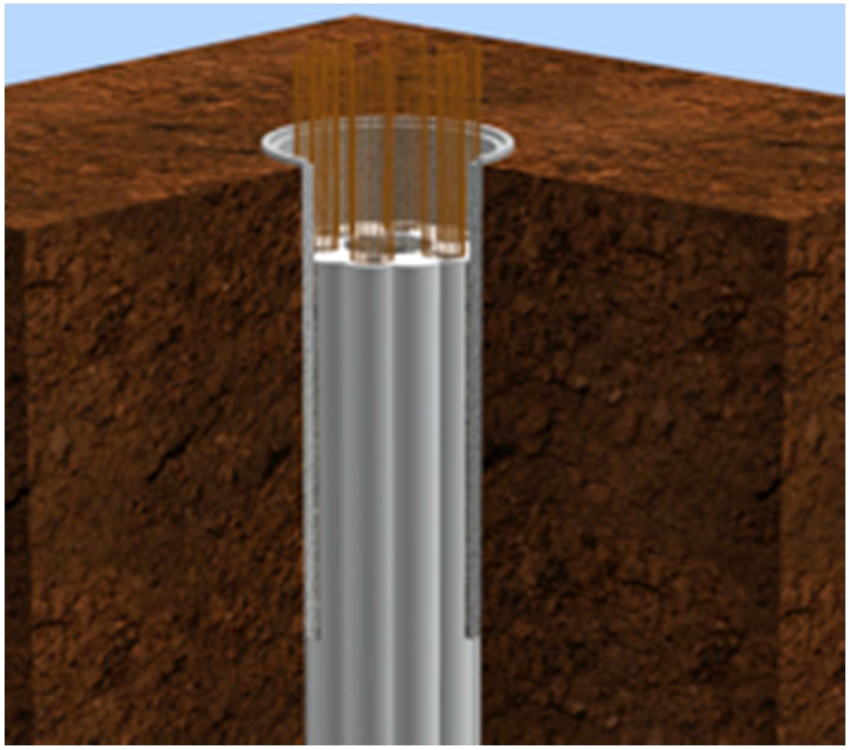


Fig. 2. Foundation structure - detail of the top of the element at the end of stage 4

During all stages, manufacturing is carried out on the ground level, without the creation of wells for staff intervention: this guarantees faster execution times and lower risks for people and machinery, especially in case of possible sudden floods.

IMPROVED ASPECTS IN THE HYDRAULIC-GEOTECHNICAL FIELD

The described construction methodology, besides the "classic" one, has some notable hydraulic and geotechnical advantages:

a. the shape and the transverse dimension of the pillar-pile assembly does not show any increments or variations, hence the hydraulic interaction between the water flow and the obstacle does not change when the depth of localized erosion changes;

b. there are no excavations or fillings in in the prior natural soil of riverbed, except those strictly necessary for pile excavation; this maintains the level of surface protection close to the pile, the so-called "armoring", leaving the original soil in place, generally less affected by erosion;

c. the presence of self-founder caissons throughout the depth potentially subject to erosion preserve the cross-section, and ensure the protection of internal piles (with structural function) from external mechanical actions of water and debris;

d. the use of "average"- diameter piles allows one to reduce risks during the execution (the machines have less power requirements), especially in dense soil with possible presence of boulders.

IMPROVED ASPECTS IN THE STATIC-CONSTRUCTION FIELD

From a static and construction point of view there are several advantages:

a. the presence of the self-founder caissons causes the "annular pile" to be secured (armored) by a high-strength and durable element inserted without causing significant disturbance to the surrounding soil;

b. the use of self-founder caissons serve as a template for the execution of the following piles, thereby giving a greater guarantee of the final geometry;

c. the use of many small diameter piles allows an easier control of the execution, which can be monitored through non-destructive techniques (S.I.T., Sonic Integrity Test, e.g.), optimized with lower casted volume elements;

d. it avoids the construction of a connection element (pile cap) between the head of the piles and the elevation, thereby saving on the quantity of material;

e. the strong intersection between the piles allows for a monolithic behavior of the system, utilizing the adhesion between the non-negligible concrete surfaces that are placed in contact;

f. the operations are all done from ground level; this allows for a greater yield-per-hour and thus shorter working times;

g. there are no significant excavations in the riverbed (except for the self-founder caissons), which is often a problematic operation due to the lack of free areas for temporary soil storage and subsequent reuse.

EVALUATION OF THE EFFECTIVENESS OF THE INTERSECTION BETWEEN PILES

Intersection between piles, even though it involves higher execution costs than a “side by side” arrangement (the greater number of elements to be constructed creates greater potential costs for the used tools and longer time required for execution), it allows one to obtain a monolithic, almost annular cross-sectional structure.

The monolithic structure allows a behavior in which the local compression peaks acting on the individual elements are damped.

Detailed analysis highlights how this function can be obtained utilizing the only shear and adhesion resistance that develops between two concrete surfaces cast in successive phases. Also considering that all the piles are connected to the top by a monolithic casting of concrete and from the following shaft of the pillar, the foundation structure can be considered as a single monolithic element consisting of a ring of reinforced concrete inserted into the ground. Calculation of the load bearing capacity is generally performed by considering lateral friction resistance on the overall outer surface to which the bottom resistance is added assuming the contact surface equal to the overall annular section of the monoblock.

Alternatively, the external lateral resistance mentioned above may be considered together with a bottom resistance calculated from the whole base section (circular section with outer annular ring diameter) reduced by a “scale effect” assessed from Meyerhof’s (1983) or Alessandrini’s et al. (1988, 2015) considerations.

Calculation of horizontal loads (shear and bending moment from pillar) can also be carried out using simple 2D software (e.g. based on the "bed constant method", using a simplified pile-ground interaction through a double wall of nonlinear Winkler's springs). This analyzes the pile behavior under horizontal loads, without necessarily resorting to more sophisticated 2D or 3D FEM software, whose results have proven to be very close to the first.

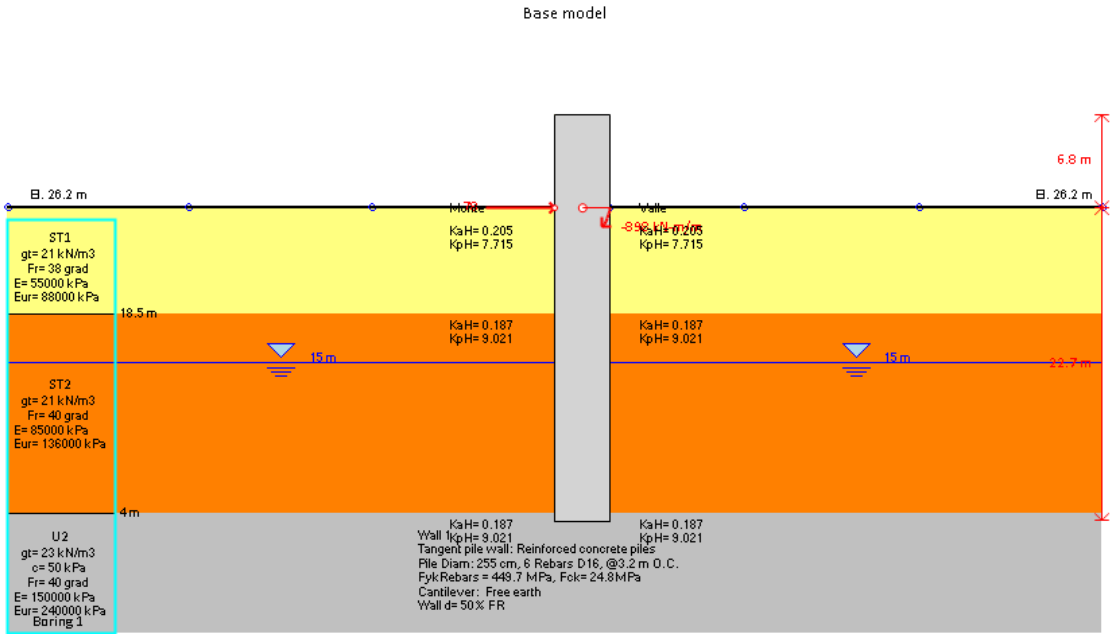


Fig. 3. Annular monoblock calculation scheme using 2D software based on the SRM (Subgrade Reaction Method)

CASE HISTORY

The annular monoblock foundation technology has been used in recent years for the realization of various bridges, including the new one over the river Torre, between the municipalities of Chiopris-Viscone and Palmanova, near Udine, Italy.

The bridge has a total length of 665 m, divided into 15 spans with a typical length of 47.5 m, allowing the river to be crossed alongside the existing bridge (demolished at the end of the work).

The bridge deck is made of a framework steel structure with overall height of 3.5m, at supports, and 2.8m, at the midpoint of the spans.

Each pillar is made up of a single cylindrical element with an outer diameter of 3.25m, which at the top of the frame extends in a transverse direction up to 7m, to allow the positioning of the support devices.

The foundation structure of the pillars consists of the annular monoblock made by 12 intersected drilled piles, with a diameter of 0.75m, nearly 30m long, carried out at constant pitch along a circumference with a radius of 0.99m: thus, the intersection of primary and secondary piles is 23.5cm.

The overall concrete section has a theoretical surface of 4.22m^2, with outer circumference of 8.23m (or a diameter of 2.62m).

The pile is inserted in a soil with good geotechnical characteristics. Low-density alluvial deposits near the surface form the hydraulic movable base of the riverbed. Progressively the coarse gravels become thicker with weak sandy filler. At about 25m depth, a stronger layer can be found, consisting of banks of conglomerates, in which the tip of the piles is based.



Fig. 4. New Torre Bridge rendering; the bridge has the pillars based on annular monoblock foundations

The realized annular monoblock has a calculated capacity at vertical loads of about 25,000 kN in compression and about 15,000 kN in tension. The breaking bending moment, with only 6 reinforced piles out of 12 constituting the annular section, has a value of about 28,000 kNm. The shear strength, estimated as the sum of individual reinforced piles strength, is approximately 2,800 kN.

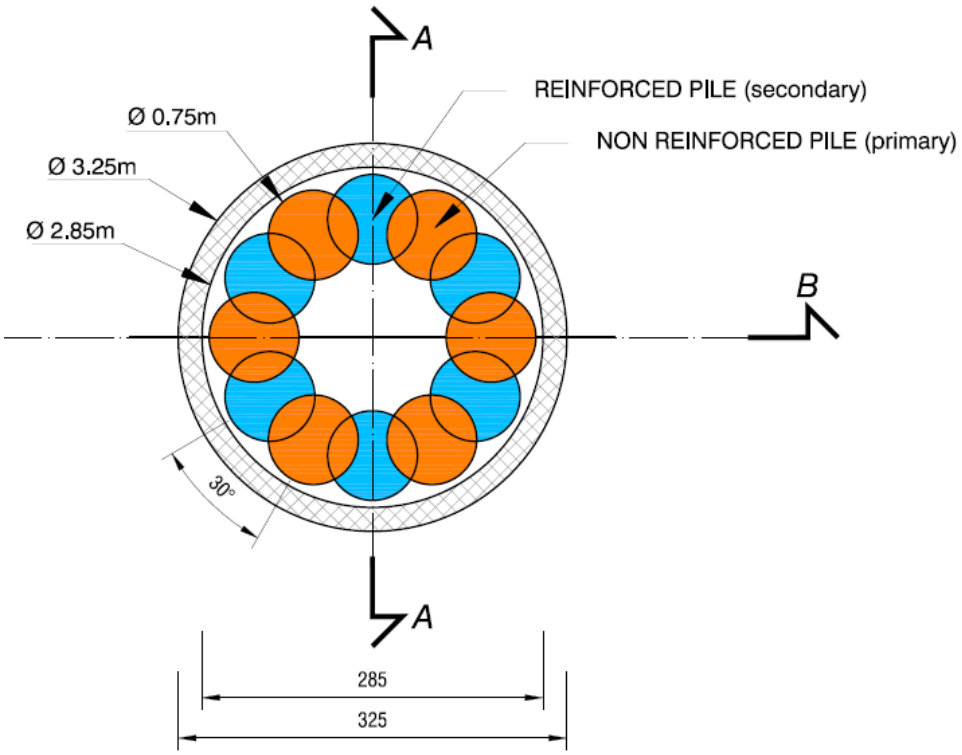


Fig. 5. Horizontal section of the annular monoblock foundation at the level protected by precast caissons

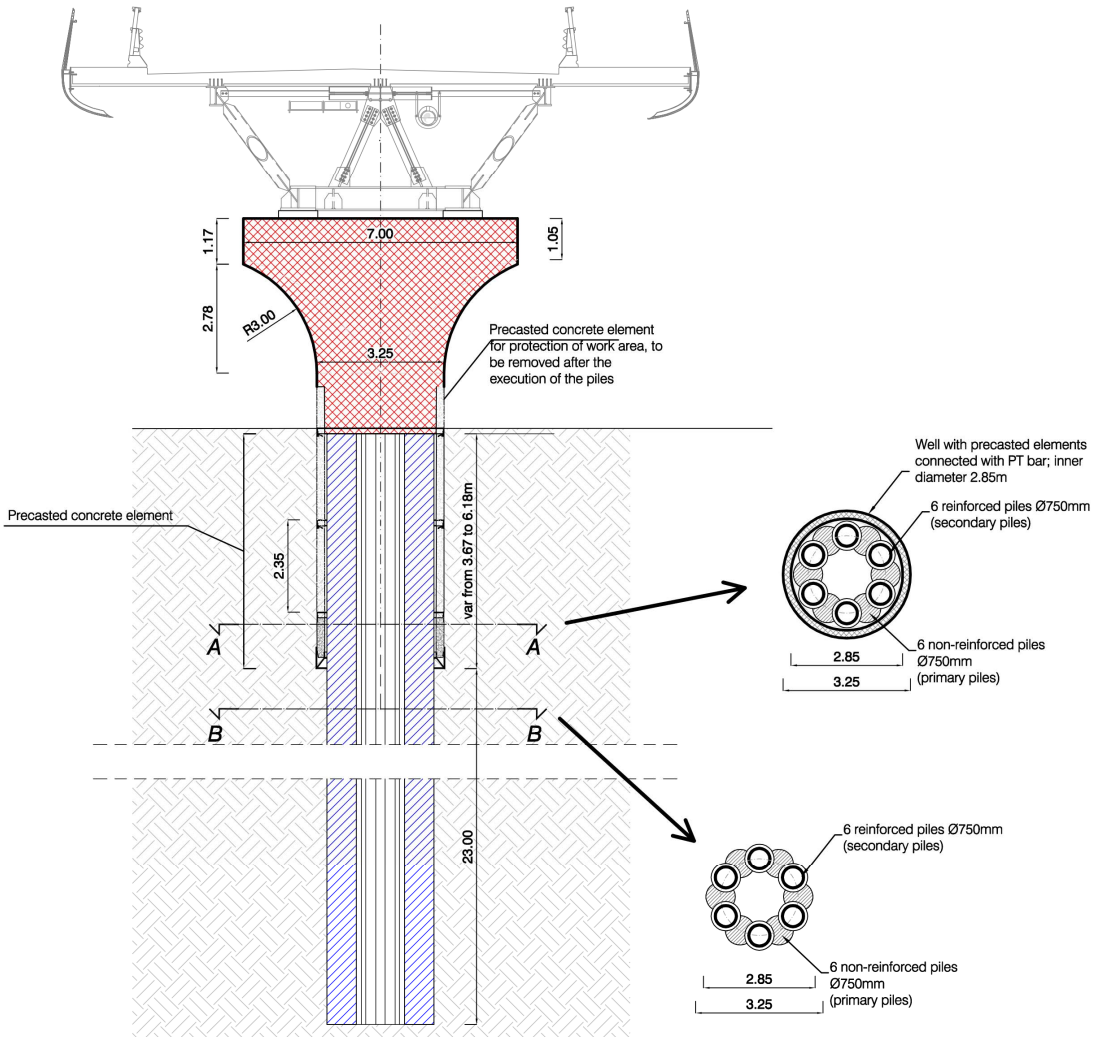


Fig. 6. Vertical section of the whole structure with highlighted annular monoblock foundation and the well with self-founder precast caissons. Above, the foundation section with linings and, below, the same made only by piles

Construction stages are shown in Fig.7:

step 1: inserting self-founder caisson;

step 2: filling the caisson;

step 3: execution of primary piles;

step 4: execution of RC secondary piles;

step 5: provisional protection element removal;

step 6: circular monolithic pillar construction

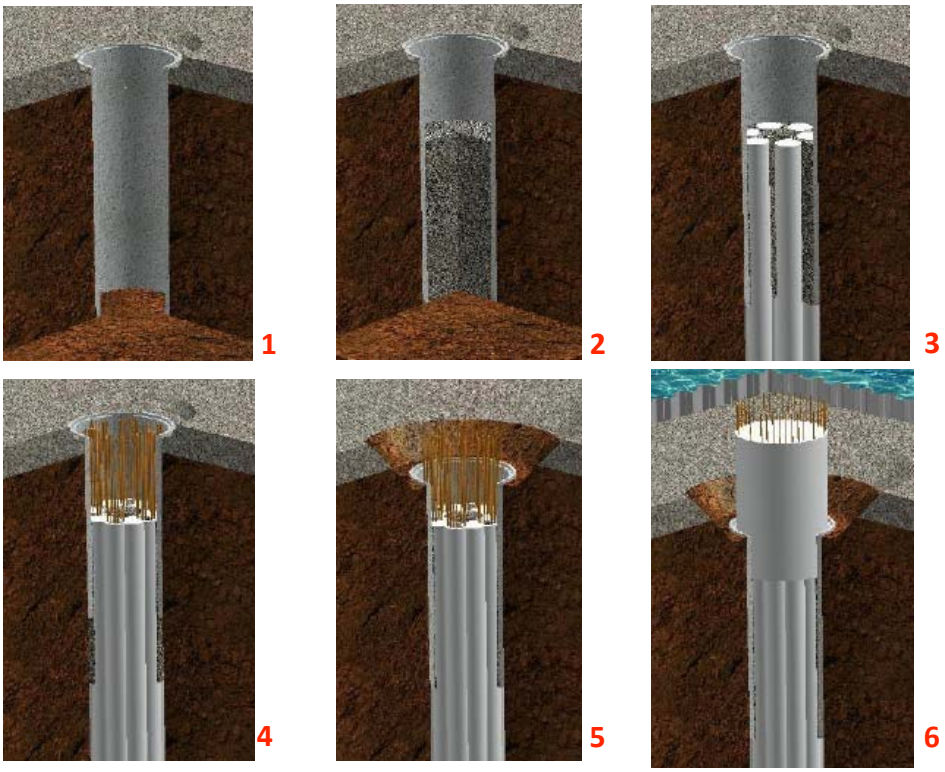


Fig. 7. Construction stages of the annular monoblock foundation. In stage 5 the upper part of the caisson is removed.

CONSTRUCTION COSTS

The foundation typology illustrated, as well as having undoubted constructive advantages, is also cheaper than a classical foundation made up of a deep cap on piles. In the illustrated case, for example, the tender project expected a foundation of this type, then modified in the annular monoblock (during the tender procedure as a technical and economic proposal). For the entire foundational structure, the annular monoblock solution has shown a construction cost about 25% lower than the tender solution with caps on piles.

Furthermore, the construction is faster than the traditional one. In the case shown the expected time to build up an annular monoblock foundation is reduced to about 33% compared to the initial solution.

CONCLUSIONS

This article illustrates the constructive method of the annular monoblocks which allows one to obtain significant technical and economic benefits in the realization of bridge pillar foundations on riverbeds.

The technology is capable of being implemented independently of the pile shaft size, and it is easy to apply in those hard soils where the realization of individual piles is still difficult.

The recent application example presented showed the advantages of the methodology, which can offer rapidity of construction, adequate structural and geotechnical strength and overall economic advantages.

Depending on the specific foundation requirement, the structure can be optimized with particular regard to the pile intersection degrees, and the global bearing capacity assessment.

REFERENCES

- Alessandrini F., Cragnolini P., Stefani E., 1988. Un dispositivo di prova su pali modello – verifica sperimentale dell'effetto scala relativo alla portata di base (A model pile tester – experimental test of the scale effect on tip resistance), Trieste University
- Alessandrini F., 2015. Corso di Tecnica delle Fondazioni (Foundation Techniques Course), Ed. Forum – Udine
- Brath A., 2006. La sicurezza idraulica degli attraversamenti fluviali (The hydraulic safety of river crossings), Bologna University
- Icop, Omba, AIstudio, Alpe progetti, Sist, 2017. Progetto esecutivo della riqualificazione S.P. 50 – Ponte sul Torre – nell'ambito del collegamento stradale veloce fra l'Autostrada A4 (Casello di Palmanova) e l'Area del Triangolo della Sedia in comune di Manzano (Final rehabilitation project of S.P. 50 - Bridge over the Torre River - Fast speed road connection between the A4 motorway (Palmanova exit) and the area of "Triangle of the Chair", Manzano municipality) – Autovie Venete – Udine
- Meyerhof G.G., 1983. Scale effects of ultimate pile capacity. American Society of Civil Engineers, ASCE Journal of the Geotechnical Engineering Division, Vol. 109, Issue 6, pp. 797-806

CONVENTIONAL EXCAVATION OF CONNECTING TUNNELS IN C13 METRO STATION (POLAND - WARSAW – LINE 2)

Marco Aurelio Piangatelli, CIPA S.P.A., Rome, Italy
Massimiliano Bringiotti, CIPA S.P.A., Rome, Italy
Aldo Bellone, CIPA S.p.A., Rome, Italy

ABSTRACT

The construction of the three connecting tunnels between the east side and the west side of station C13, adjacent to the Vistula river, has a long and complex history, as they cross beneath one of Warsaw's main road arteries (Wisłostrada). After the attempt to excavate the first tunnel, the face of the tunnel collapsed on the night of August 13, 2012, and a volume of about 10,000 cubic meters of liquid mass (water, silty soil and sand) entered and flooded the west side of the station, which was filled with more than seven meters of material. Fortunately, the workers managed to escape, but machines and equipment were lost. This is the story of how the tunnels were completed, by adopting soil improvement, jet grouting, GRP bars, ground freezing and a careful choice of work steps.

INTRODUCTION

The Centrum Nauki Kopernik station on Line II of the Warsaw Underground is located alongside the Vistula river (Fig. 1). This station hereinafter is referred to as station C13.



courtesy Image ©2015 DigitalGlobe by Google Earth)

Fig. 1. The Centrum Nauki Kopernik station and the Vistula river

The station consists of three parts: the east and west part, and three connecting tunnels 40 meters in length with a large cross section (170 m^2). It includes the rails along the sides and the platform along the centre. The reason for the underground connection of two shafts with a tunnel is due to the presence of a road tunnel (Wisłostrada, hereinafter called WS), which must be underpassed by the new metro line (Fig. 2).

The existing tunnel (Wisłostrada) was built many years before, between diaphragm walls, and some foundation structures interfere with the underground tunnel. The challenge was to build the connectors without stopping the traffic of vehicles along the highway above. All works took place in very difficult geological and groundwater conditions due to the presence of Vistula alluvial deposits with poor mechanical characteristics. The soil profile consists of relatively loose sands on top, and silts overlying

© 2018 Deep Foundations Institute

high plasticity Pliocene clays highly disturbed by the effects of the repeated over-sliding of glacial moraine deposits.

The station is located entirely on the west side bank of the Vistula River: the eastern boundary of the station shaft is less than 10 m from the river bank. The station has been constructed in top-down technology with diaphragm walls (1.40 m thick). The maximum excavation depth reaches a level of 24 metres. The two side tunnels have an internal diameter of about 7 meters and their shape is perfectly circular to allow, after their completion, the TBM's passage.

The three tunnels were to be excavated in clayey soil using conventional methods. Instead, the soil turned out to be of sandy materials below groundwater. In essence, it is as if the tunnels were excavated in the river's sub bed, in the presence of flowing water. A further major complication was due to the presence of the of WS tunnel foundations made by diaphragm walls, which would have been dismantled during tunnels excavation and in the presence of normal vehicle traffic. This paper focuses on the several attempts at excavation that were implemented to complete the connector.

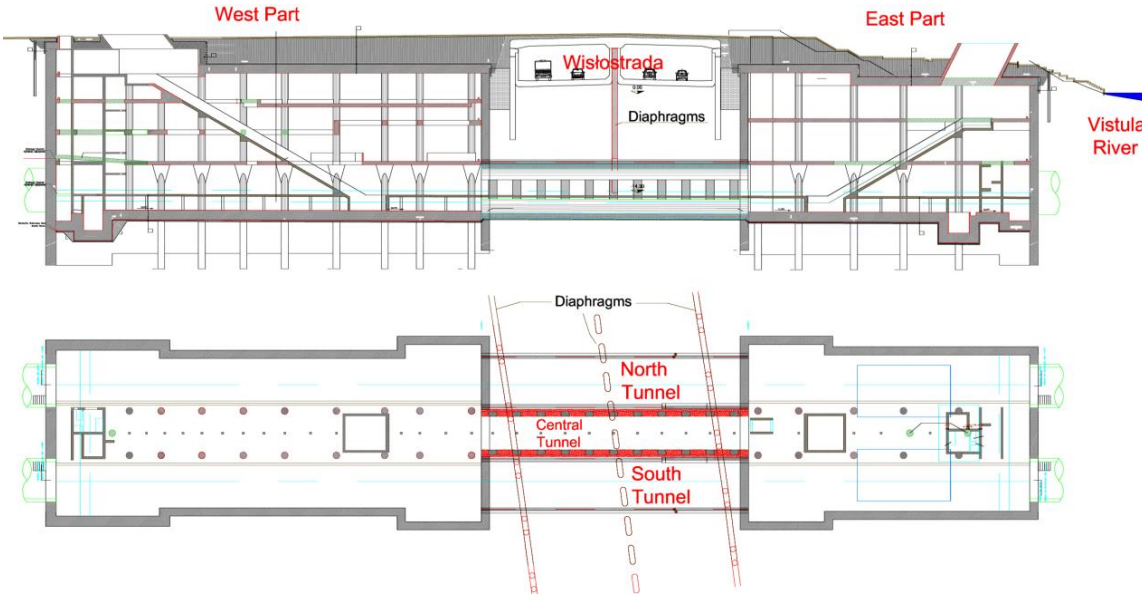


Fig. 2. The two parts of the station and the connecting tunnels.

EXCAVATION ATTEMPTS

Several attempts to construct the three tunnels were carried out. The first attempt followed the original design that was based on a geological profile that turned out to be inaccurate. Only clay was expected along the tunnel path, but this was not the case.

The First Attempt – Umbrella of Micropiles (Canopy Piles)

The original construction scheme entailed the excavation and lining of the two side tunnels (for the tracks), followed by the excavation and lining of the central tunnel (for the platform), connected to the two side tunnels by arches.

The excavation of the two side tunnels would have to be supported by umbrellas of steel micropiles except for the sides bordering the central tunnels and Fiber Reinforced Plastic tubes (hereinafter called FRP tubes) at the face. On the sides of the two tunnels bordering the central tunnel, the design required FRP tubes instead of steel ones, to allow the subsequent excavation of the central tunnel, whose final lining was to have been supported by the final lining of the two side tunnels (Fig. 3).

After the first core drilling on the diaphragm walls of the entrance of the north tunnel on the west side, on February 2, 2012, a massive flow of sand and water occurred from the hole into the shaft (Fig. 4).

There was no clay soil behind the wall, as expected, but something else. The need to proceed with geological surveys along the tunnel path became clear. Beforehand the surveys could not be executed in order not to close the WS. The hole was plugged and a new investigation campaign begun.

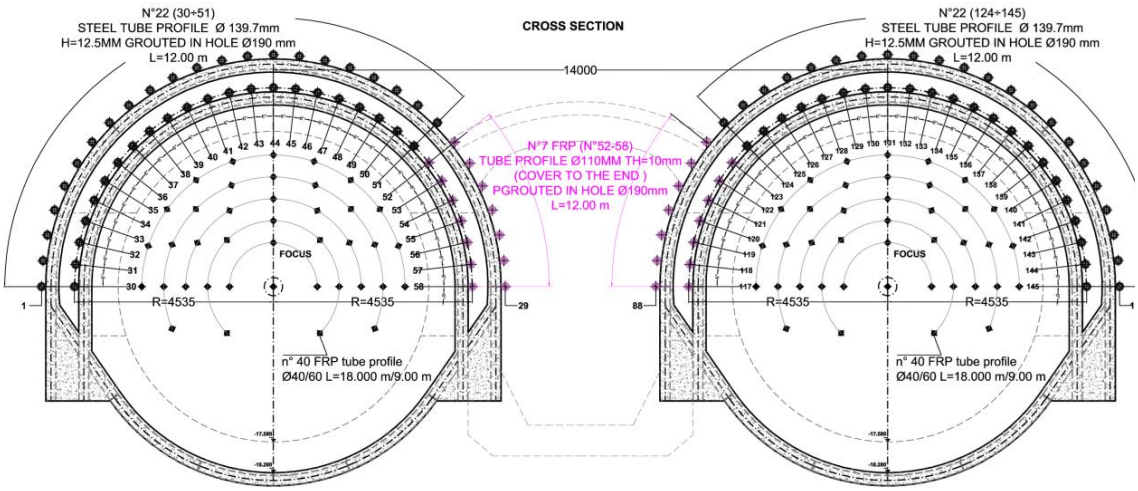


Fig. 3. Original design of the two side tunnels to be excavated.

The Geological Survey of the Path

Once the east and west parts of the station were excavated, it was possible to perform a geological survey of the tunnel path, with horizontal and sub-horizontal borings, starting from the station diaphragm walls and without having to close the busy WS tunnel above.

As a result of this survey, it appeared that the level of the clayey soil was lower than expected and that the top of the tunnel sections were in sandy material below ground water.

The decision was made to perform a soil improvement, but since the interventions could not be implemented from the WS tunnel in order not to close it, a new design including columns of jet grouting on top of the tunnel was drawn up (Fig. 5).

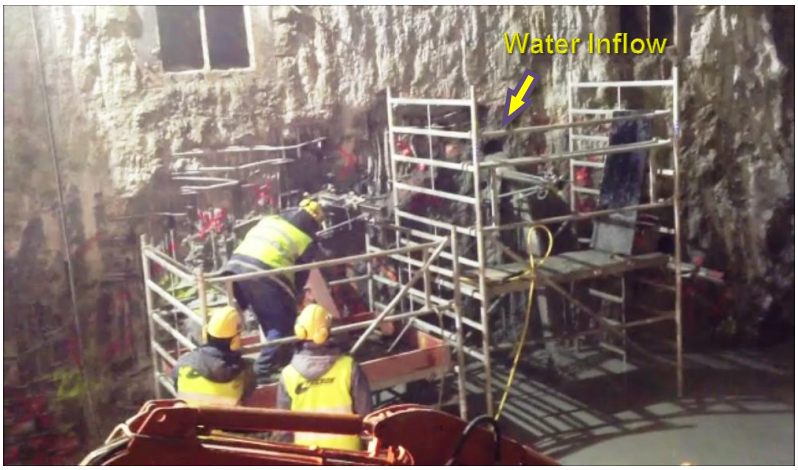


Fig. 4. Water inflow.

The Second Attempt – Jet Grouting

The new work schedule provided for excavating the north tunnel first, followed by the south tunnel. The central tunnel would have been the last one. Excavation would have been done from both the east and west heading of each tunnel, up to the central diaphragm walls supporting the WS tunnel.

Jet grouting and the micropiles umbrella started on the diaphragm walls of the north tunnel's west side with a big machine, then the big machine moved to the east side of the station, to the other face of the north tunnel, and a smaller one arrived in the west side. Afterwards, the east face of the other two tunnels was dealt with. The remaining face of the south tunnel in the east side would have been the last.

During the soil improvements carried out at the east side, the excavation of the north tunnel started from the west side, following the phases shown in Fig. 6.

After the demolition of the station's diaphragm walls, the first excavation step was finished. The diaphragm walls supporting the WS tunnel were also demolished and the primary lining was applied, consisting of steel ribs, wire mesh, struts on the invert and shotcrete.

The second excavation step began and continued without problems. Every 75 cm, a layer of shotcrete was applied to the face of the tunnel during the primary lining of the previously excavated portion of tunnel. On the evening of August 13, 2012, the excavation arrived at the fifth steel rib of the second excavation step (Fig. 6). The workers applied the shotcrete to the face of the tunnels in order to stabilize them, and went to dinner at 10:30 PM.

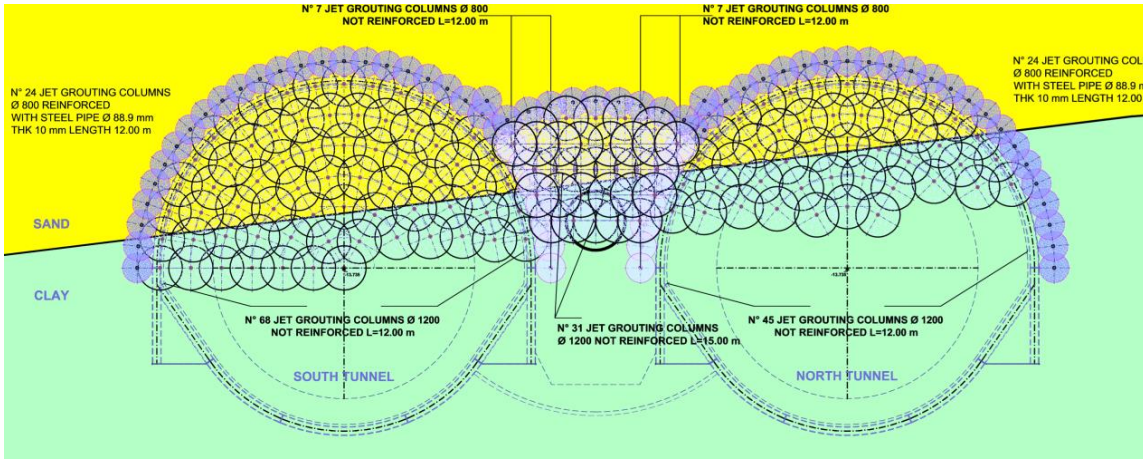


Fig. 5. Updated design with columns of jet grouting.

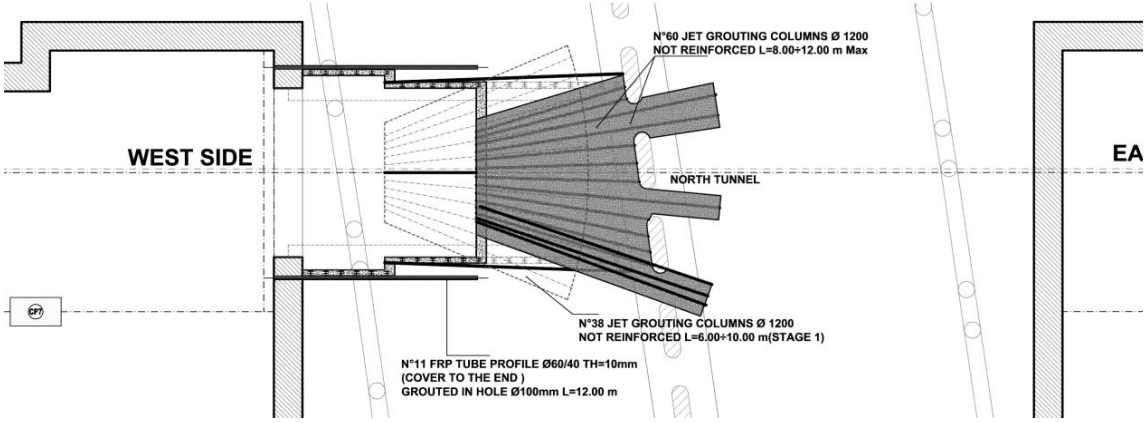


Fig. 6. Plan view of an excavation phase of North tunnel from west side.

The Collapse of the Tunnel Face

At 10:45 PM, a foreman saw that something strange was happening. Some water was inflowing from the top and from the face of the tunnel. He immediately sounded the alarm, and a team of workers ran down. At 11:00 PM they began to spray another layer of shotcrete on the face of the tunnel, but because the sprayed shotcrete was swelling and cracking in some areas on the face, the action taken was interrupted and all the workers attempted to place material against the face to contain it (Fig. 7).

At the same time, because the face was continuing to move despite the containment action, the workers also managed to save equipment and machines using the gantry crane, but were unable to finish this operation because the immediate evacuation of the station was ordered.

To avoid the feared collapse of the west side of the station, the flooding in progress was intentionally accelerated by pumping water from the Vistula river in order to balance the external pressure of the soil on the walls (Fig. 9). Access to the WS tunnel was forbidden for safety reasons.

Many machines were lost in the station (Fig.10). Fortunately, no one was injured.

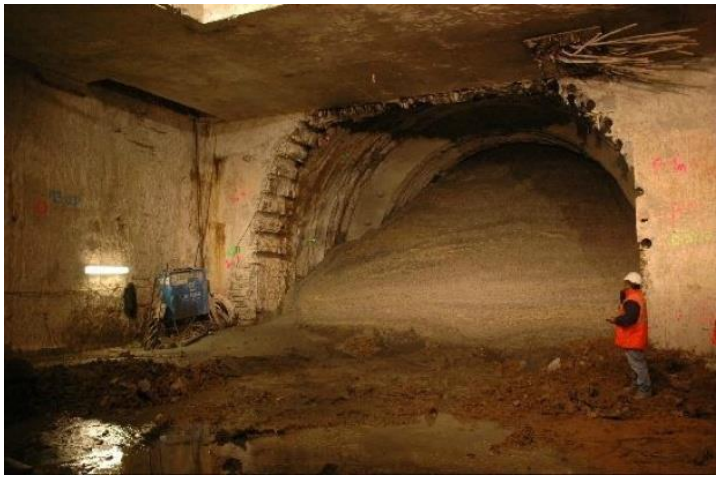


Fig. 7. The collapse of the tunnel face.



Fig. 8. Water, sand and clay inflow from the tunnel.



Fig. 9. The station before the event and after the intentional flooding.



Fig. 10. One of the buried machines.

The Concrete Filling Under the WS Tunnel

After non-destructive fact-finding surveys, it was determined that there was a deposit of solid material, mostly sand, of approx. 6,500 cubic meters inside the station, and a loss of the equivalent amount of material beneath the road slab of the Wisłostrada tunnel. The cavity underneath the WS tunnel was filled with water up to approximately 2 meters from the bottom of the slab. The road slab thus was not supported by natural subsoil, and was suspended in risky equilibrium between the lateral diaphragm walls.

In order to fill the cavity with concrete, there was an initial campaign with a massive injection of concrete, self-levelling, with mixes designed to cure underwater. The second campaign for deep consolidation was obtained with a low-pressure injection of cement mixes followed by chemical mixes, using manchette tubes.

The second campaign stopped and was not completed because the grouting lifted the road slab up to 20 cm in some points.

The Third and Final Attempt – Soil Freezing

Soil freezing was the final solution adopted to improve the soil (see Capata et al. 2015, Balossi Restelli et al. 2016).

Divers inspected the bottom of the station and found a large pile of sand which obstructed the tunnel entrance, so the station was carefully emptied of inflow material. The pile of sand was carefully removed, layer by layer, and a reinforced concrete wall was built by underpinning methodology. Horizontal and vertical freezing probes were installed. The excavation phases were quite complex.

The figure 11 shows some design phases for the north tunnel (similar to those for the south and the central tunnels).

The horizontal probes were put in place all around the tunnel section, and vertical probes were placed at the sides of the central diaphragm walls supporting the WS tunnel. The excavations were carried out from the two headings and stopped near the diaphragm walls. The two sections were lined and after the vertical probes were partially pulled up, the central section was excavated and lined.

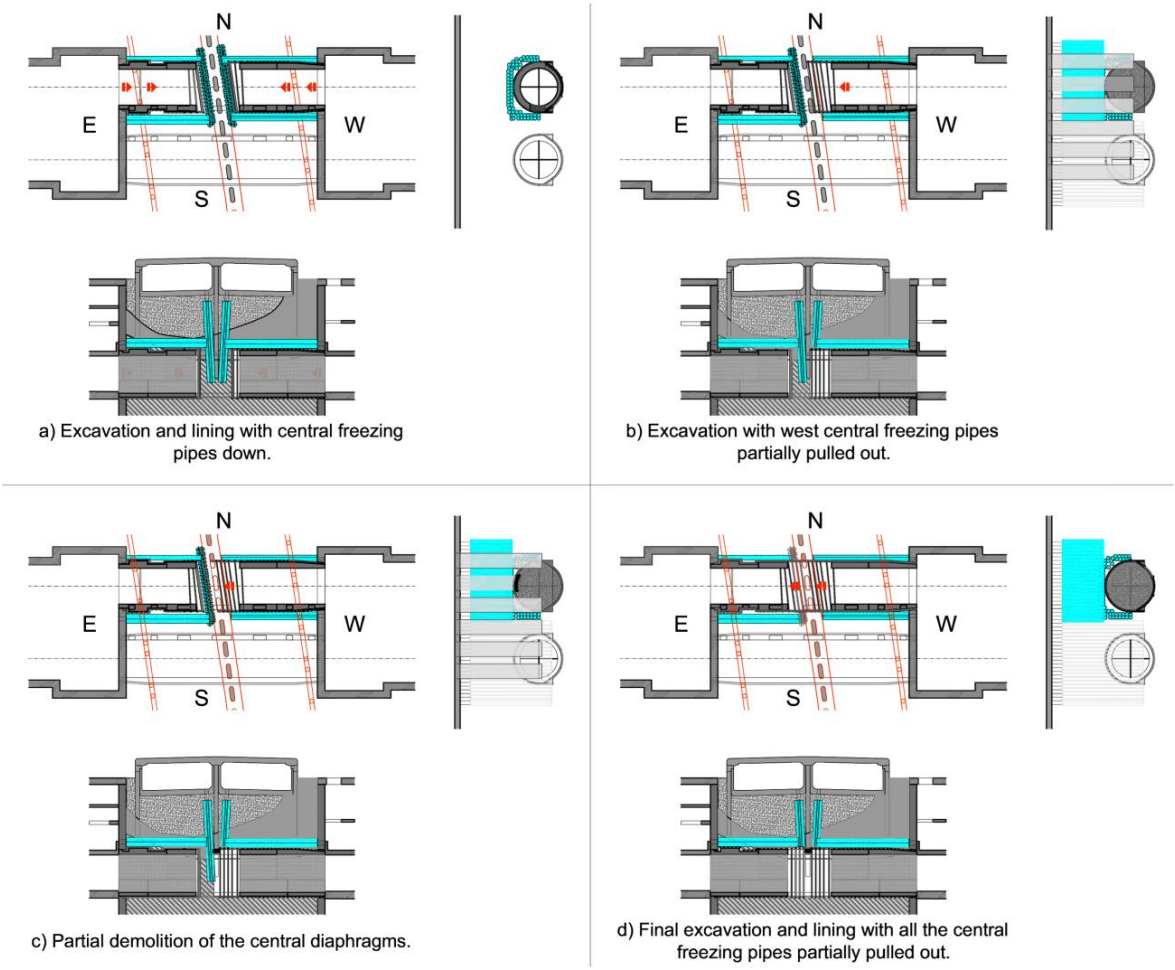


Figure 11. Excavation and lining phases.

The two side tunnels were completed and then the central tunnel was excavated adopting, in the primary lining, steel ribs bearing on the steel ribs of the side tunnels, uncovered during the excavation. The central ribs were welded on the side tunnels' ribs and, at the end of the excavation cycle, the side tunnels' piers were cut. Omega-type steel ribs (Fig. 12) were chosen to compensate for the variability of the several lengths of arc.

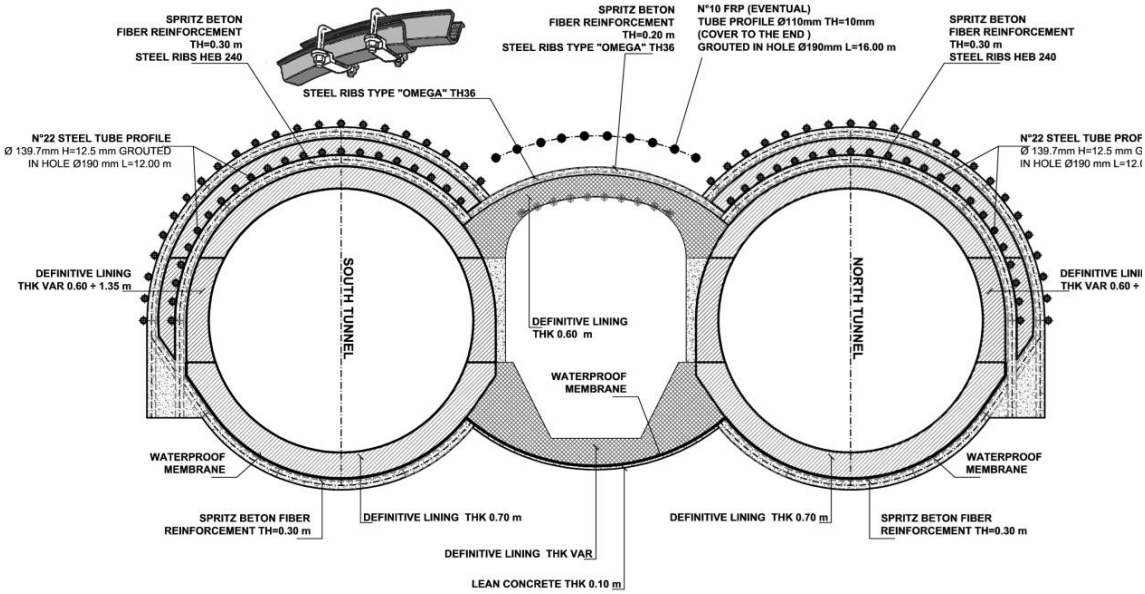


Fig. 12. Central tunnel with adjustable Omega Type steel ribs.

CONCLUSIONS

The first attempt failed due to the presence of sand and water along the excavation path. Many people believe that the second attempt probably failed because the water was in motion and washed away the injected grout. In both cases, the failures are attributable to the water that negatively affected the consistency of the soil and the consolidation attempt.

The third attempt, the freezing of the soil, worked well because the same water, whose presence was harmful in the two previous attempts, was successfully used as a support system in an ice form.

EPILOGUE

As shown in Fig. 13, it took 33 months to complete the excavation and structural works of the station:

- 9 months for flooding,
- 5 months for freezing,
- 18 months of effective works

Six of the 18 months were used for the tunnel during the 3rd attempt (Fig. 14) and the work was completed 15 days in advance of the last milestone.

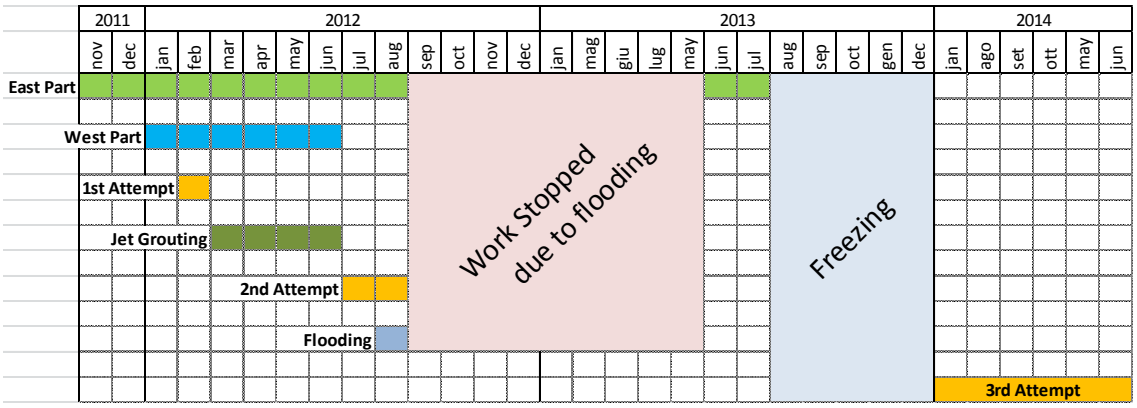


Fig. 13. Chronological of events

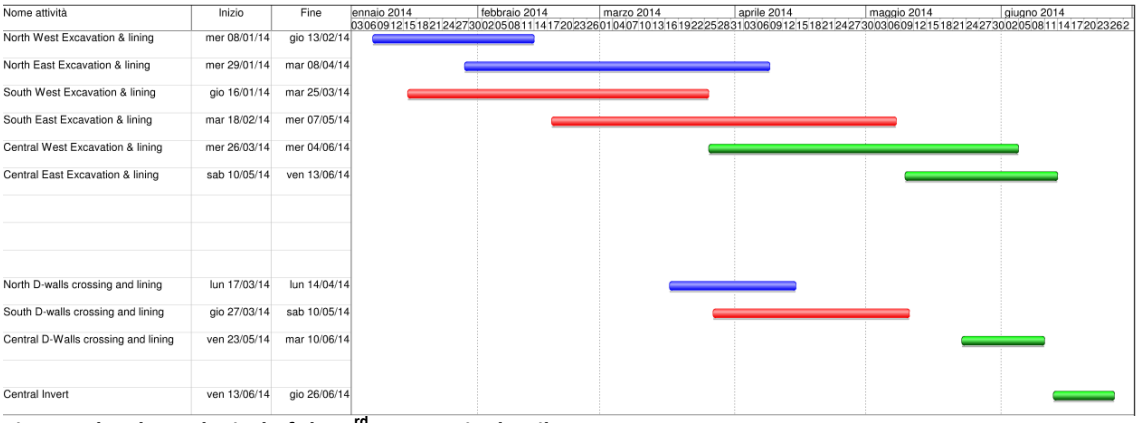


Fig. 14. The chronological of the 3rd attempt in detail

The history of the excavation of the tunnels is much more complex than what these few pages tried to describe quickly. As you can imagine, the construction of the tunnel was part of a larger and more complex work and the difficulties encountered in this construction have influenced continuously the scheduling of all the works.

It took more than two and a half years to complete the tunnels, but, thanks to the efforts of the people who worked to solve the serious issues of this work in order to safeguard people, structures and equipment as far as possible, the tunnels were finished. Fig. 15 and Fig. 16 show some pictures of the tunnels during the works and how it appears today.



Figure 15. At top, a side tunnel; at centre, the central tunnel; at bottom, a panoramic photo of the three tunnels.



Fig. 16. At left, a side tunnel; at centre, at right, the central tunnel.

REFERENCES

Capata, V., Lombardi, A., and Bizzi, F. 2015. *Line II of Warsaw Underground: the excavation of tunnel connector (Centrum Nauki Kopernik station).* Infrastructure Conference Proceedings – ICE Publishing

Balossi Restelli, A., Rovetto, E. and Pettinaroli, A. 2016. *Combined Ground Freezing Application for the Excavation of Connection Tunnels for Centrum Nauki Kopernik Station—Warsaw Underground Line II*. ITA-AITES World Tunnel Congress 2016 (WTC 2016) - Proceedings of a meeting held 22-28 April 2016, San Francisco, California, USA

INNOVATIVE PILE EXTRACTION TECHNIQUE OF CFA PILES FOR THE NEW HARBOR BRIDGE PROJECT

Tracy Brettmann, P.E., D.GE, Vice President, A. H. Beck Foundation Company, Houston, Texas, (713) 413-3800, tracy.brettmann@ahbeck.com

ABSTRACT

The nearly $900 million US 181 Harbor Bridge Project in Corpus Christi, Texas will include the development, design and construction of 10 km of combined bridge and roadway. It will include the new six-lane Harbor Bridge as well as the reconstruction of adjoining sections of two freeways. This will be the longest cable stay bridge in the United States when completed. Once the new bridge is open to the traveling public, the project will conclude with the demolition of the existing Harbor Bridge. The main towers of the bridge will be 164 m (538 ft) tall and are supported on a group of large diameter drilled shafts. Each tower is supported on twenty two 3 m (10 ft) diameter by 75 m (250 ft) deep shafts. The north tower is located where a previous industrial warehouse was sited. This warehouse was supported on closely spaced 400 mm (16 in) nominal diameter by 20 m (65 ft) long CFA piles, which required the removal of these piles where they conflicted with the new drilled shafts. The amount of steel reinforcing in the piles required that they be extracted in one piece. The actual diameter of the piles was also expected to vary significantly due to the soft layered soil conditions encountered in the upper 15 m (50 ft). An innovative wet rotary coring technique involving the combined use of both hanging lead CFA drilling equipment and a drilled shaft bentonite slurry drilling system was used to rapidly extract the large quantity of conflicting piles.

INTRODUCTION

The Harbor Bridge Project (HBP) currently under construction in Corpus Christi, Texas will replace the existing adjacent steel arch bridge. The Texas Department of Transportation (TxDOT) has determined that US 181 and the Harbor Bridge must be improved to maintain a safe and efficient transportation corridor. The existing bridge has safety issues associated with the lack of shoulders, steep grade, a reverse curve, and an accident rate that is higher than the statewide average. The current Harbor Bridge also has high maintenance costs and provides no acceptable access for those on foot or on bicycles. Furthermore, the bridge's 42 m (138 ft) of navigational clearance, which met World War II standards when it was built, makes it difficult for the Port of Corpus Christi to compete with other Gulf Coast deep water ports because of larger ship sizes today.

The new bridge will allow TxDOT to improve safety, thereby reducing accident rates; provide better opportunities for moving people and goods throughout the region; provide adequate capacity to meet future traffic demand; and provide greater economic development opportunities for the Port of Corpus Christi.

The new cable stayed bridge shown in Fig. 1 will have a main span length between the towers of 506 m (1661 ft) with main tower heights of 164 m (538 ft) making the bridge the tallest structure in south Texas. The navigational clearance of the new bridge will be 62.5 m (205 ft). The height of the top of the current steel arch bridge is 74 m (243 ft) so it would almost fit under the new bridge indicating how much taller the new bridge will be.

© 2018 Deep Foundations Institute

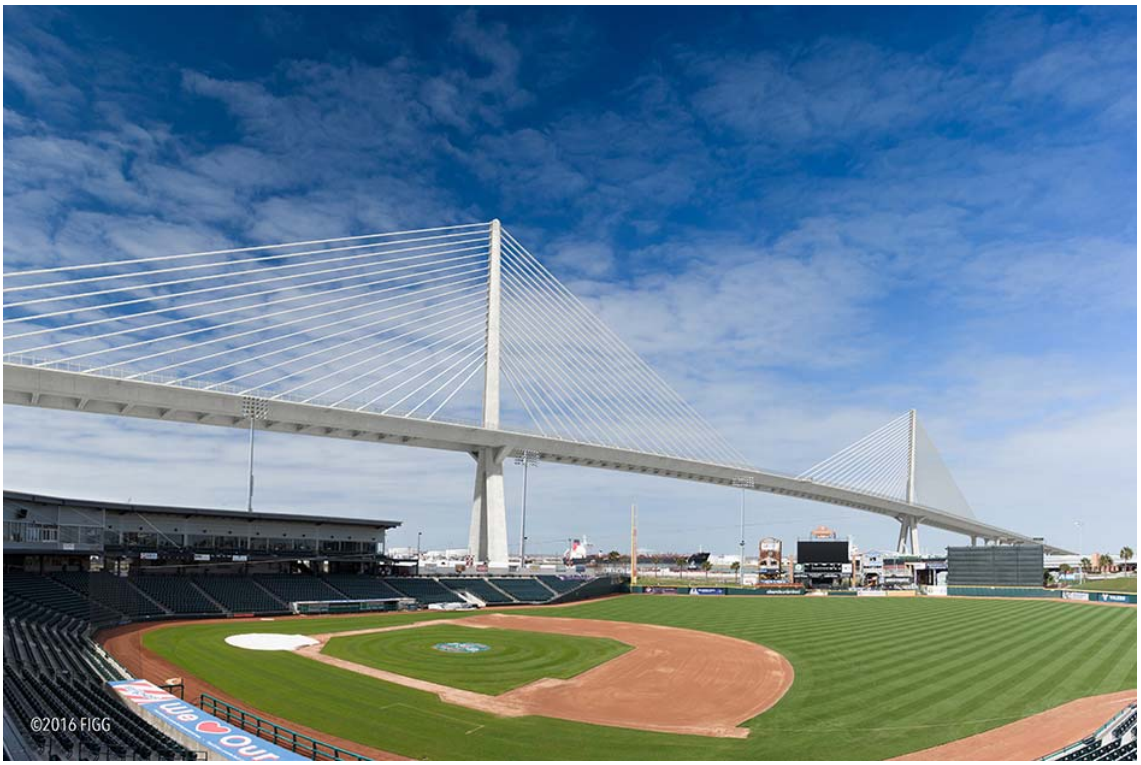


Fig. 1. Rendering of the New Harbor Bridge

NORTH TOWER FOUNDATION

The foundation for the north tower is positioned adjacent to the Corpus Christi ship channel where an industrial warehouse had been located. The warehouse was built in 1999 and is supported on 400 mm (16 in) and 450 mm (18 in) diameter Continuous Flight Auger (CFA) piles. Both pile types are 20 m (65 ft) long. CFA piles are also known as Augered Cast-in-Place (ACIP) piles in commercial and industrial markets in the US. The term CFA piles are more associated with European terminology where the piles are typically installed with fixed mast drill rigs. ACIP piles (as were installed for this warehouse) are more associated in the US with hanging lead drill rigs supported by lattice boom crawler cranes. Coincidentally, the Author was also the Regional Manager in charge of the pile installation for that original 1999 project.

The group of 3 m (10 ft) diameter drilled shafts that support the north tower conflicted with many of the existing CFA piles as shown in Fig 2. The piles would need to be removed prior to installation of the drilled shafts. The CFA piles were heavily reinforced with relatively large diameter rebar (for CFA piles). The reinforcing consisted of a 7.6 m (25 ft) long rebar cage at the top with four No. 9 (29 mm diameter) bars plus a full length No. 9 center bar. The amount of reinforcing steel in the upper portion of the piles required the piles to be removed in one piece rather than trying to drill through them. The conflicting piles all turned out to be 400 mm (16 in) diameter.

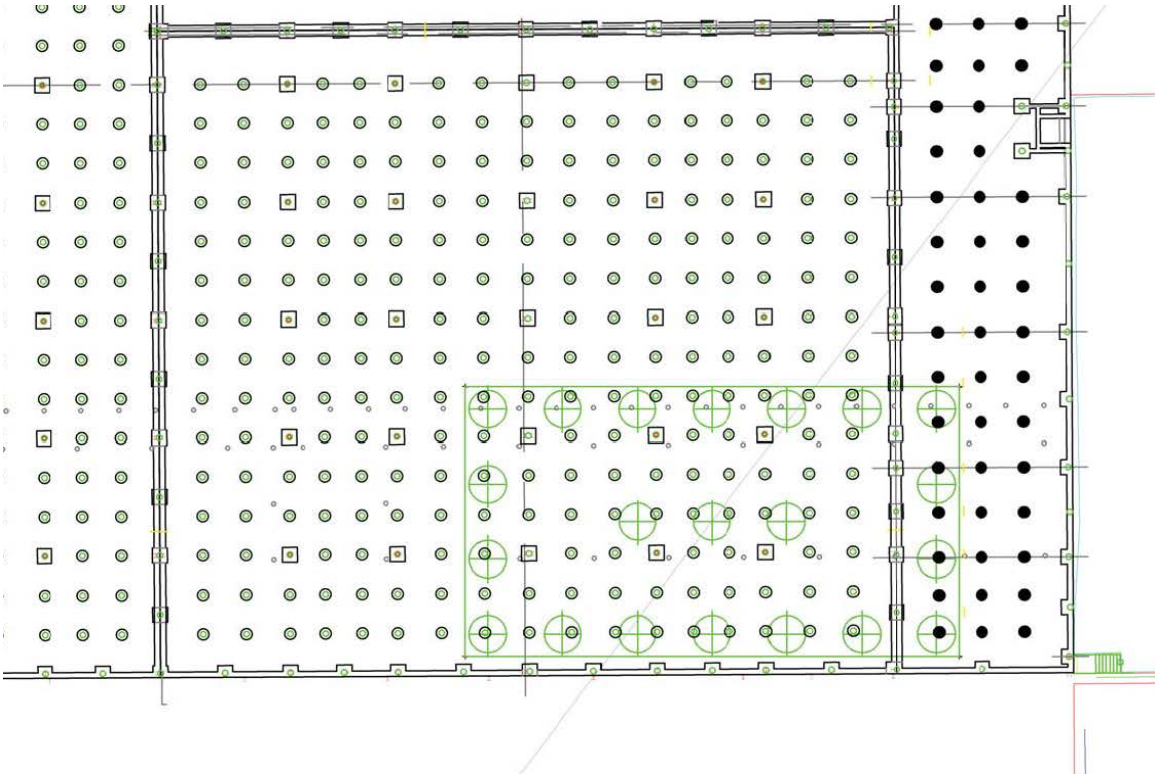


Fig. 2. CFA Pile Interaction with Drilled Shafts

SOIL CONDITIONS

The soil conditions consist of a loose to medium dense sand to a depth of 4.5 m (15 ft) which is approximately the depth to groundwater and the water level in the ship channel. Very soft clay is present to a depth of 15 m (50 ft) with SPT blow counts ranging from zero to 2. A medium dense to dense (blow counts of 15 to 31) sand layer of variable thickness ranging from 5 to 10 ft is present below the soft clay stratum. A stiff to very stiff clay is then present to a depth of 27 m (90 ft) with blow counts ranging from 12 to 18, although typically the blow count was around 12 at the pile tip depth of 20 m (65 ft). These layered soil conditions result in CFA piles with high grout takes (pumped volume) and variable diameters. There was no way to know what pile diameters would actually be encountered in the soft soil conditions at this site.

PILE EXTRACTION

A wet rotary coring technique involving the combined use of both hanging lead ACIP pile drilling equipment and a drilled shaft bentonite slurry drilling system was used to extract the conflicting piles. A large diameter core barrel was attached to a gearbox that would travel up and down the leads (Fig. 3). A hanging lead system allowed for a large reach since the area around the piles to be extracted had to be excavated down to top of pile elevation. It also allowed the core barrel to better follow the shape and verticality of the installed piles since the leads were not fixed.



Fig. 3. Wet Rotary Pile Extractor

A grout pump (Fig. 4) was used to pump bentonite slurry through the grout hose and into the core barrel similar to how grout is pumped in the ACIP pile installation process.

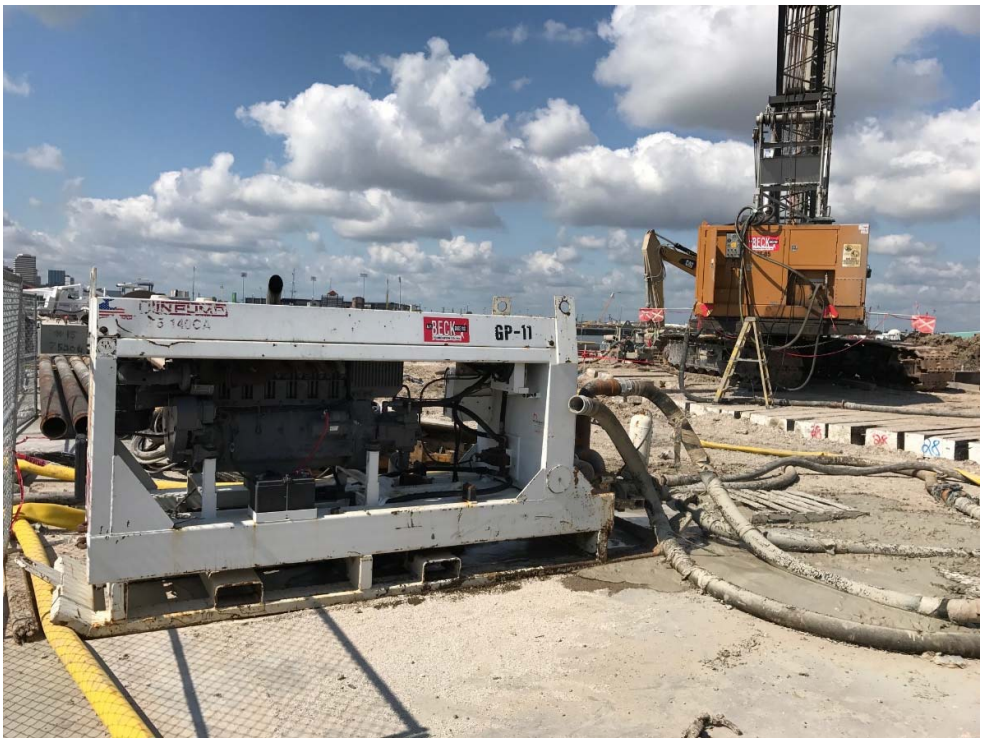


Fig. 4. Grout Pump Used to Pump Slurry

The bentonite slurry was mixed and stored in slurry tanks (Fig. 5) and directly piped into the grout pump intake bypassing the grout hopper.



Fig. 5. Slurry Tanks

The slurry was returned to the slurry tanks by pumping from a sump in the bottom of the pile excavation.

EXTRACTED PILES

The shapes of the extracted piles were measured and photographed so the variability could be documented for these soil conditions. Several key aspects were noted in the piles. Most of the piles showed a smooth and straight side as shown in Fig. 6.



Fig. 6. Typical Smooth and Relatively Straight Pile Shaft

Several of the piles also showed a bulge in the pile section that was only on one side as shown in Fig. 7. These bulges were unusual in that they were not concentric but typically off to one side of the pile. The bulge in the pile in Fig. 7 measured 56 mm (22 in) in diameter.



Fig. 7. Bulge in Side of Pile

As shown in Fig. 8 Pile 29 had a noticeable bend. This pile is hanging from the tip of a crane boom in the figure below. This pile showed the largest bend of any of the extracted piles. Most of the piles looked fairly plumb after being extracted.

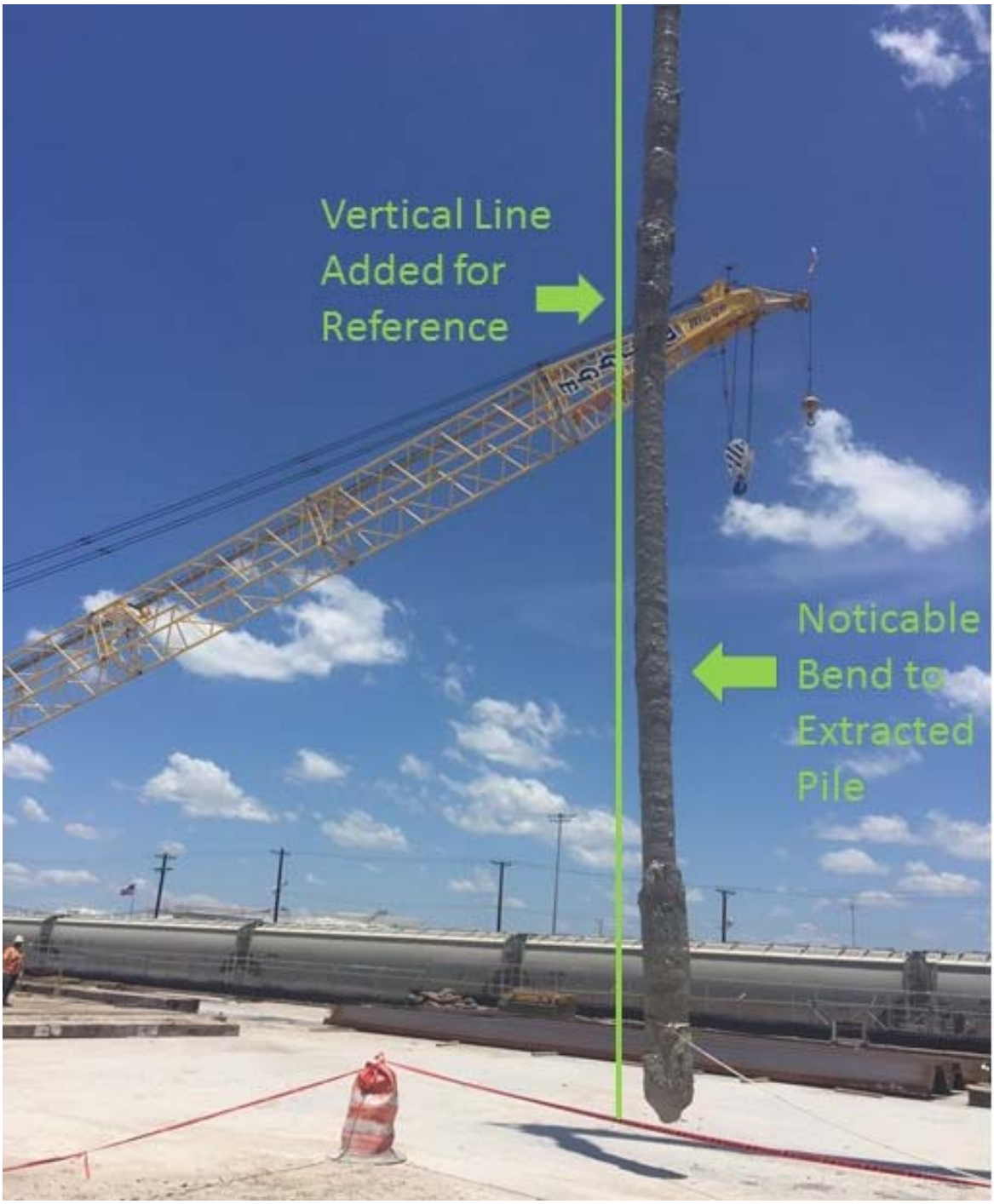


Fig. 8. Pile 29 Showing a Significant Bend

The bottom section of Pile 25 was unusually shaped for being installed in stiff clay as shown in Fig. 9. The bottom portion measured 600 mm (24 in) in diameter and the portion right above that (presumably in the sand layer) measured only 330 mm (13 in) in diameter. Pile 25 had the largest variation in diameter of all the extracted piles. The bottom section of the piles were only reinforced with a center bar so no rebar cage was present at this depth.



Fig. 9. Pile 25

The typical pile tip was the shape of the auger bit since they were tipped in stiff clay as shown in Fig. 10. These pile tips were slightly oversized relative to the pile shaft.



Fig. 10. Typical Pile Tip

SUMMARY AND CONCLUSIONS

An innovative wet rotary coring technique involving the combined use of both hanging lead CFA drilling equipment and a drilled shaft bentonite slurry drilling system was used to rapidly extract a large quantity of conflicting piles to allow for large diameter shafts to be installed. While most of the extracted piles were relatively straight, many of the piles showed unusual shapes.

The nominal piles diameter (auger diameter) was 400 mm (16 in) but the diameters measured in the extracted piles ranged between 33 mm (13 in) and 600 mm (24 in). Typically where bulges in the pile section were present, they were not concentric. The bulges tended to be on just one side of the pile.

A few of the extracted pile showed what can only be described as a seemingly continuous bend. Although the very upper section could have been straight and plumb it seems once these pile started curving they tended to follow that same curve to their full length. The piles were clearly not "dog-legged" where they showed a clear change of direction at a specific depth.

The piles were installed in 1999 before the use of automated monitoring equipment was prevalent in the industry. The results of these pile extractions in soft soil conditions demonstrate the need for good quality control and quality assurance practices to be used when installing CFA/ACIP piles. Furthermore the use of newer technology non-destructive integrity testing method of Thermal Integrity Profiling can also now be used to determine pile diameter versus depth in installed piles. This type of testing would provide better information on what the pile shapes are in these soil conditions.

PROJECT CREDITS

The Harbor Bridge Project is a design-build project being constructed by the joint venture firm Flatiron/Dragados, LLC. The bridge designer is FIGG Bridge Engineers. The Owner of the project is the Texas Department of Transportation. A.H Beck Foundation Company is installing the drilled shafts for the main tower supports.



JOB SITE REPORTS RELATED TO DEEP FDP, BIG DIAMETER CSP AND RING VIBRATOR EXECUTED AT THE LIMITS BY THE SAME LWN DRILL RIG

M. Bringiotti, GeoTunnel S.r.l. - LWN Agent, Genoa, Italy, info@geotunnel.it
S. Bechter, Liebherr-Werk Nenzing GmbH, sascha.bechter@liebherr.com

Keywords: foundation equipment, piles, FDP, CSP, ring vibrator, report, LWN, Liebherr

ABSTRACT

The present memory is intended to illustrate the main peculiar foundation technologies executed to the mechanical limits of the same drill rig. Full Displacement Pile in standard and lost bit version technique will be shortly described and an interesting experience application will be shown with single pass drilling procedure at 32 m depth for 420 mm diameter having a high industrial productivity. Also CSP will be described with some details related to the Front of Wall mode and technical hints related to the torque converter vs. double rotary technique; synthesis production data of a job site will be commented, where secant piles, 22 m depth with 920 mm diameter, in quite hard geological conditions and urban logistic difficulties have been successfully performed. The article will be concluded with a short description of a special technology named Ring Vibrator which represents a unique and interesting system able to install construction elements, naturally in function of the geologic conditions, at an almost “infinite” depth.



1. FDP, FULL DISPLACEMENT PILE, I.E. FULL COMPACTION PILE

The Full Displacement Pile (FDP) represents the optimization of the principle of the "lateral compaction pile" and can also be considered the best (and most economical) alternative to the conventional drilled piles or to the CFA piles (Continuous Flight Auger) in frequent geological conditions.

1.1 FDP standard tool



Essentially the method consists in using a special tool, with different diameters, which is inserted into the ground by rotation and pushed by a rod mounted on a special mast. The FDP tool is built with a pipe designed to withstand torsions and to deliver the concrete to the bottom of the excavation. The lower drilling element and the upper compaction element can be designed with different lengths to better adapt the tool to the ground conditions; therefore, the length may vary from a minimum of ca. 6 m to a maximum standard of ca. 30 m. Diameters may vary; from 360 to 620 mm as standard up to 800 mm as special. The drilling bits are also interchangeable and foreseen for different types of material in order to maximize the production performance.

1.2 FDP drilling tool with lost bit

The casing for the "Lost Bit" tool has a much larger diameter than the standard tool; it is designed to pour concrete by gravity and used for the insertion of the re-bar cages at the pile bottom. The inner surfaces are therefore completely smooth. The advantages of the lost bit technology vs. the standard tool are:

- Easy installation of the re-bar of any shape and also at a great depth
- Re-bar cages always centered in the pile
- Easy procedure for concrete placement
- High productivity

by the way, the disadvanges are:

- Additional costs for lost bit



© 2018 Deep Foundations Institute

- Additional torque and thrust required to drive the tool.

Also in this case, particular care shall be taken for the coupling between the drilling rods. A perfect linearity of the compaction line shall be guaranteed for use of the torque delivered by the rotary (the frictions are very high and misaligned drilling generates asymmetric stresses and potential danger for successful operation). This is the reason it has been designed male-female HD (Heavy Duty) couplings, provided with suitable conical bolt joints.

1.3 Drilling procedures

The typical drilling procedure is following:

1. Positioning of the drilling equipment.
2. Start drilling with the tool in continuous rotation and advancement. The soil is fluidized by the rotating auger and constipated around the hole by the special displacement body.
3. With the help of additional rods it is possible to extend the excavation at higher depths (it is possible to reach up to 40 m, clearly according to the machine type and type of ground).
4. Once the final depth is reached, the tool is extracted and, at the same time, the concrete is pumped through the hollow rods and injected through the nozzle fitted at edge of the cutting head.
5. Once the drilling tool is extracted, if required, re-bar cage is fitted (eventually by means of a special vibrator) or alternatively reinforcement having different geometry (pipes or beams).

Using the lost bit drilling tools, the insertion of the re-bar cage takes place before the concrete placement, through the hollow drilling rod. Once concrete is placed then the drilling tool will be removed.

1.4 Concrete pouring procedure

The concrete placing can be carried out by gravity by means of an hopper or under pressure. In the first case concrete is pumped on top of the drilling casings and by simple gravity placed through it; the operator can have a visual feedback thanks to a suitable camera installed in that zone.

In the second case, the most advance method, the concrete is poured under pressure, i.e. the pump is connected with a suitable pipe directly to the tool and the process is fully automated, managing the concrete flow and pressures. This is important not only in order to optimize the concrete quantities but also to manage the overconsumption which may occur for different reasons. Additional benefits by using such a technology are:



- Fully automated concrete procedure
- Faster concrete placing procedures
- Limitation of the obstruction phenomena of the hollow drilling rod
- Less manual operation on top of the operator's shoulders

1.5 The drilling assistant



Both during the drilling and pull-out phase as well as during the pouring phase the machine can handle all procedures in full automatic mode. During drilling, the Li-Tronic (System installed on the LRB 355) controls mainly:

− Descent speed
− Downward thrust
− Rotary head rotation speed
− Thrust
− Strokes

While during the extraction (pull-out) phase:

− Concrete pressure
− Concrete flow rate
− Pull-out speed
− Rotary head rotational speed

The system measures and stores all the values and information of the production process, being able to define various parameters singularly or through their interpolation (e.g. value λ).

1.6 Advantages



The advantages of using FDP technology, when compared to conventional ones, can be summarized as follows:

- High bearing capacity: moving the soil around the excavation creates a considerable thickening of the soil itself. The loading area (due to the volume of the compressed soil) is increased by approximately 30-40%. The lateral friction of the pile acquires, consequently, an increase of the same order of magnitude.
- Vibration-free installation process: using a tool of this type, combined with the rotational drilling technique, guarantees the absence of vibration or shock towards the adjacent structures to the work site.



- Minimum quantity of material is due to the excavation (comparing for example to drilling with CFA method). The ground is totally constipated around the pile. The system is ideal, for example, when the drilling activities are performed in contaminated areas; moreover, practically, no loading and disposal costs need to be calculated for the excavation material.
- Real time monitoring of the drilling parameter (torque, penetration, value "lambda", ...) means carry out surveys of soil consistency, optimizing in real time the drilling activities. In layman's terms, the value "Lambda" – λ – is a measure of the energy used during the drilling process; in synthesis, this data provides an indication of the consistency of the various soil layers and a relative indication of the pile bearing capacity. The value λ is interpolated to the operator's "monitor" in real time. Based on this value, it is possible to modify the depth of the pile as, by realizing sample/test pile, measuring the value λ and carrying out load tests (to evaluate the actual bearing capacity), it is possible to schedule the lengthening or shortening of the real scale piles in real time with reference to the given λ value, defined above, which is encountered during the drilling phase.

2. FDP CASE HISTORY: DOBRIN, AUSTRIA

The purpose of the work was the realization of the foundations for a fair pavilion new building.

2.1 Geology



The geological profile shows predominantly soft clay with layers of sand at 12 m depth for a thickness of about 3 m and at 28 m again sand but consolidated, where the piles lean and fit. The jobsite is located in the Rhine River valley.

2.2 Operational data

The drilling technique provides lateral displacement piles without lost bit: diameter is 420 mm and depth is constant at 32 m.



The pouring foresees "concrete under pressure" for which the concrete is directly pumped using a concrete pump, radio controlled by the operator of the drilling machine, monitoring concrete's volumes and pressures through the integrated system on the drilling machine itself. The type of aggregates includes round gravel with grain size 0-4 and 4-8 mm; the concrete is self-compacting type. As regards to the reinforcements, it has been designed a mixed element: built in cages and linear. The cage features are Φ 20 cm steel bars (without spacers) and is formed by 5 longitudinal bracing elements of 20 mm and 2 central of 30 mm with reinforcements for the first 12 m, then running bars in number of 2-3. In the last portion of the reinforcement there's a spacer that carries the finished diameter of the cage to Φ 28 cm closed by a pyramidal shaped insertion profile.

2.3 Equipment

The drilling equipment is the LBR 355, manufactured by Liebherr-Werk Nenzing GmbH, with 750 kW installed. The mast has a 26 m length with a drilling tools 8 m long extension stroke. Two rear cylinders are also fitted to stabilize the weight of the machine in case of need of additional pull-out force and a service auxiliary winch is fitted on top of the must with 360° of freedom.

The additional equipment available on the jobsite:

- Liebherr D57 crawler mounted concrete pump (it has been notably an extremely gentle pump pulsation, low noise, remarkable mobility, totally radio-controlled)
- Liebherr telescopic crane with 50 m arm for the handling of the rebar cages
- Small electric vibrator for the insertion of the rebar cages (to ease insertion 2 m below the ground)

2.4 Machine positioning via GPS



The positioning of the machine at the drilling points is carried out by a GPS in automatic mode. Machine is equipped with a system able to manage the geo position of the machine, the drilling data as well as the concrete pouring data. In fully automatic manner, the system detects the actual positioning of the machine giving then the exact drilling point pattern while during the drilling and casting activities record the related parameter.

2.5 Production records



The Times Tracking and observations were carried out by the writer:

<u>Time Tracking Pile #1</u>

9:25 Drilling start

9:34 Pile drilling stopped at 24 m depth reached, 20 seconds measured for the 8 m long drilling rods extension

9:37 Rebar cage vibration of the previously drilled pile finished (additional re-bar gravity thrust vibration for about 1 minute)

9:39 Pile drilling finished 32 m depth reached

9:42 Concrete pouring start (lost 3 minutes)

9:49 Concrete pouring stopped, no concrete available and additional concrete mixer required



9:51 Concrete pouring resumed

9:59 Pile finished

Summary of drilling activities – Pile #1

9 minutes to drill the pile at 32 m depth

15 minutes for concrete placing

Total drilling time, casting and rebar cage insertion including the time lost for additional concrete mixer: 25 minutes



<u>Time Tracking Pile #2</u>

10:05 Drilling start

10:11 Pile drilling stopped at 24 m depth reached, 20 seconds measured for the 8 m long drilling rods extension

10:10 Re-bar cage vibration of the previously drilled pile finished (additional re-bar gravity thrust vibration for about 1 minute)

10:14 Pile drilling finished at 32 m depth reached

10:15 Concrete pouring started

10:24 Pile finished

Summary of drilling activities – Pile #2



9 minutes for drilling at 32 m depth

9 minutes for concrete placing

Total drilling time, concrete placing and re-bar cage insertion: 18 minutes

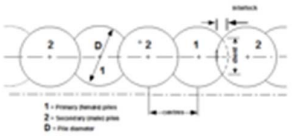
Complete pile with machine positioning (6 min): 24 min

Summarizing, we may assume that 20-30 min shall be taken per each pile of 32

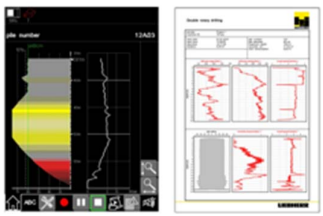
m, resulting in a production of about 80 m of finished piles per hour, meaning average 600 m per shift. Take note that the day before n. 21 piles were drilled in 9 hours shift (equal to 672 linear meter production!).

3. CSP: CASED SECANT PILE METHODOLOGY

The secant piles are used for the construction of diaphragm or more generally for the formation of support structures and consist of a series of large diameter piles drilled with various methodologies interacting with each other. All construction methods of secant piles foresee the excavation of a series of primary piles and the closure of the structure by the excavation of the secondary ones. Secant piles walls are generally a preferred solution for inner city projects. The reason is that they can be more flexible in shape and in compact operations when compared, for example, with diaphragm wall (which also requires a bentonite plant). The interlocking piles of a secant wall can also form a closed structure to act as a barrier in water bearing soils.



3.1 Secant piles advantages



The CSP system generally has the following advantages:
- Automatic drilling and pouring procedure.
- They can be built on all types of soil; their use is particularly interesting in the most resistant soils or where it is difficult to support the excavation, such as refilling soils of poor quality or loose or in the presence of boulders or particularly hard formations.
- The secondary interlocking piles are excavated when the primary ones have reached a certain consistency, avoiding any distress of adjacent buildings. The use of casing pipe (required for the excavation of the secant piles) minimizes the risk of settlements even during the excavation of the primary piles.



- The absence of drilling slurry avoids the risks associated with them, such as leakage of slurry, the need to provide for slurry mixing and treatment plants, the problem of pollution, the workability of the excavated material and the transportability of the same.
- The drilling considerably reduces vibrations compared to sheet piling and the use of kelly buckets or suspended one for diaphragms, often used with free-fall winches to "chisel" by releasing the bucket.
- The secant piles can be excavated inclined, allowing design flexibility and deviation from structures.
- The use of casings, of relevant structural inertia, allows to excavate perfectly aligned piles with negligible vertical deviations.
- In urban areas or more generally where in narrow jobsite, compact machines can be used to drill close to other constructions.
- The concrete requirement does not deviate that much from the theoretical calculated value (about 3-4% more), no concrete leakages occurs since the pouring is protected by the casing.



- Better tolerance than an uncased CFA secant wall.
- Better ultimate appearance and reduced overbreak than an uncased CFA secant wall.
- Speedier operation than the more traditional “kelly/casing” bored piles.
- Reduced risk of “flying” in poor soils than a standard CFA system.
- As it is a cased system, it reduces the risk of distress to adjacent structures in certain soils like sands or gravels.
- In general terms, whilst the CSP process has limitations with respect to diameter and depth, it will generally give the client a better assured product in terms of vertical tolerance and visual appearance

4. CSP: PECULIARITIES IN FoW DRILLING MODE

In this chapter, we survey into some of the prerogatives of the equipment already mentioned, named LRB 355, in the drilling phase of fully cased piles excavated in CSP-FoW mode.

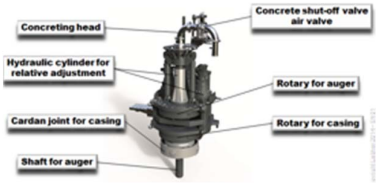
4.1 Disposal of the excavation material (muck) in CSP drilling mode



The equipment includes a concentric piping to the casing, built with a commercial spiral steel wires reinforced PVC pipe, of suitable thickness. An automatic system manages the operation of the winch that governs the lifting and the pulling of the piping itself according to the working phases; a very simple system, easy to maintain with limited operative cost for any eventual replacement may be required (for wear, it can happen ...). A suitable machine (mini excavator ...) shall be available to load the excavation material on suitably dimensioned dumper truck.

4.2 Double head drilling DBA 300

The LRB 355 operates with a simple operative philosophy; it uses the motor power delivered by the machine to generate an hydraulic power able to operate directly n. 2 rotary drives (physically coupled but totally independent from the hydraulics): the system is called DBA 300. Therefore, 2 independent rotary drives are installed, being able to run at full speed:



A. Rotary on the auger: 150 kNm torque
B. Rotary on the casing: 300 kNm torque

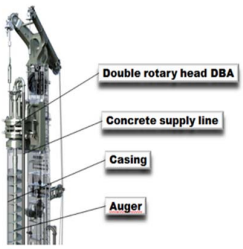
Therefore, we have 450 kNm of total torque available at the maximum available speed = > this is the reason why hydraulic power is needed, resulting in higher productivity of the machine itself and consequently of the entire drilling process.

The system also has other advantages:

A. Compact in geometry (especially for "Front of the Wall" excavations, typical of urban areas closed to existing buildings and structures).
B. Integrated in all its components (integrated intake for concrete delivery, cylinders for a relative movements of the auger vs. the casing, compressed air inlet,...).
C. Easy and quick assembly
D. Easy to maintain

4.3 Comparison between the FoW system and the torque converter

The torque converter or multiplier, therefore a mechanical "gear" = planetary gear converter, is connected between the rotary and the casing in order to increase the torsion on the casing itself resulting in speed reduction; it is a technology available on the market allowing the drilling single pass cased piles which may generates some limitations. One of the main feature of this system is the fact that the torque delivery is constant, since the connection is mechanical, so the speed is always mechanically defined. In particularly harsh situations (very resistant materials) the FoW system, with 2 separate rotating heads, works on the principle of “cutting speed” and the possibility of always expressing the maximum torque, having available 2 independent hydraulics circuits and abundance of power. In layman's terms it is like selecting the “first gear" (having only two speed available, such as these types of rotary has) and facing a climb with a standard car (let’s say with Audi 4) compared with the performances reached, on same route, with a more powerful car (let’s say Audi R6!) faced selecting the "second gear".



There’s another factor which needs to be taken into consideration: the torque multiplier cause a loss of efficiency of the system, as any mechanical device in between the endothermic engine and the driven equipment. Said loss, inside the planetary (obviously due to friction) and at the second cardan joint (due to "clearances"), may be considered generally speaking from 5 to 10% (not really negligible!). It is also important to consider that the rotation speed, usually displayed with the rotary charts, cannot be exactly parameterized because of factors which may varies in function of:

- Weight of the casing, auger, material and concrete inside the auger itself.
- Clutch with digging materials (inside and outside the casing)
- Resistance of the material to be drilled
- Grain size of the excavated material (which passes through the casing and along the auger pitches)

Bearing into account the abundant power available on the LRB 355 it may clearly be assumed the real potential of such machine. An already mentioned factor, of further importance and advantage for the FoW-DBA system, is the fact that both rotary speed may be individually controlled; by modulating the relative rotation (between auger and casing) it is possible to optimize the production (feeding the material along the auger) in function on the type soil, resulting in higher productivity in the range of ca. 20%. In double-rotary drilling technology, the ability to control the rotational speeds is a determining factor for the productivity that can be achieved (in addition to having the right tools and the correct mix design). With the torque converter, of same class, from 30 to 50% less power and torque is generated (depending on how we cross the comparisons and with which efficiencies) being able to excavate only with a constant speed ratio between the auger and the casing.

5. CSP CASE HISTORY: ST. GALLEN, SWITZERLAND



The jobsite subject of this case history is pretty much peculiar because it shows the application of fine technologies and machinery for the realization of a civil construction foundations (the extension of a school building), in Italy probably would have foreseen more simple and conventional methodologies (secant piles with the use of casing oscillator? drilled piles with jetting closure?), realized in a longer time frame, probably with lower quality, greater disturbance to the population and surely with higher operative costs.

5.1 Geology



The jobsite is located in Constance lake area, Rhine valley, so the encountered geological formation are the classic ones of such orographic configurations:
- 0-10 m, sand, gravel and clay
- 10-15 m, compact moraine deposits
- 15-22 m, sand and consolidated gravel

There is also a frequent presence of decametric boulders, perhaps even metric, in some unidentified random areas.

5.2 Operational data

It is a foundation work which includes 360 secant piles, diameter 920 mm and depth: 18, 20 and 22 m depending on the levels of the building construction.



The daily working shift is 8-10 hours (depending on the working cycles).
The shift crew is composed by 5 operators: LRB, crane, mini excavator, dumper operator and plus a steel rebar cages handler.
The pouring mode foresees "concrete under pressure" meaning direct pumping, radio controlled by the operator of the drilling rig, with automated control of concrete volumes and pressures managed by the integrated system on the machine.



With regards to the rebar cages these are designed as individual elements fitted into the borehole by gravity for approx. 1/3 of their length and then pushed till the bottom of the borehole with the use of a suitable vibrator.
The machine while drilling kept the mast foot raised, highlighting the robustness and power of the rig itself.
The operator is keeping an eye to the instruments of the machine in the meanwhile he smokes (!) while the machine performs the drilling in fully automated manner.



5.3 The equipment

Again a LRB 355 at work, with some peculiarities: mast boom 33 m, pull-out 900 kN (kelly winch with in double line, 2 x 25 ton, and pull down winch 40 ton),

synchronized winches (the operator works on a single joy stick in manual mode), 750 kW (fuel consumption 44 liters/hour).
In CFA drilling, with standard mast, it may realize 25 m in single pass, Φ 1 m, with the auger cleaner sliding along the entire mast.

5.4 Construction records and average times

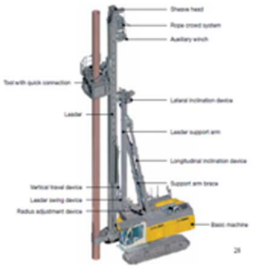


The excavation was relative to Piles Φ 920 mm at depth of about 22 m.
Time Tracking Pile #1
14:11 Drilling started
14:50 Drilling ended
14:51 Concrete placing started
14:59 Downtime waiting for Truck Mixer
15:08 Concrete pouring resumed
15:18 Concrete pouring ended
15:20 Drilling rig moves to discharges the remaining material of the casing
15:23 Discharge operation ended
15:24 Change of worn tools (n 2 peaks)
15:28 End of operation
14:21 Steel cage installation of the previously drilled pile
14:23 Steel cage is installed for 1/3 of its length but the vibration cannot be switched (electric vibrator supplied by a Gen-Set installed on the service cranes)
14:27 Vibrator start again
14:37 Steel cage is installed
39 minutes for drilling at 22 m, 27 minutes concrete placing with 9 minutes downtime waiting for the arrival of the concrete mixer, 16 minutes for steel cage installation with 3 minutes wasted for inconvenience. Total time drilling, casting and steel cages installation including downtime for worn tool replacement: 77 minutes



Time Tracking Pile #2
15:29 Drilling steel positioning
15:31 Drilling started
16:28 Concrete placing started
16:38 Concrete placing ended
16:40 Drilling rig moves to discharges the remaining material of the casing
Total drilling time, concrete placing and cage insertion: 71 minutes
The third pile has been realized in 60 minutes.
There isn't any drilling times difference between primary and secondary piles. The productivity has been slowed down just due to the presence of numbers of boulders encountered during the excavation. The average production time has been recorded as 8 finished piles per day = > 160 lm/shift.

6. VIBRATED PILES - "RING VIBRATOR": DOMDIDIER, CH



LRB class had been used in a construction site successfully employing the particular and interesting technology of the "ring vibrator".

6.1 Technology

A pipe, with a lost cap (eventually provided with a sealing gasket), is vibrated at high frequency. Once the excavation depth has been reached, the cage is placed inside the casing and then concrete is poured starting from the top side of the pipe; then the pipe is pulled out still trough vibration. Thanks to this procedure, the poured fresh concrete is compacted. In addition to this effect the concrete and the soil in the surrounding are penetrated offering a higher lateral friction and increasing the load capacity. This technology offers two important advantages vs. the usual top vibration:
1. Ability to place the steel cages and pour the pile without unplugging the vibrator
2. Possibility to vibrate casing longer than the mast (leader)

6.2 Summary of work

The working site is 650 m long and 350 m large, area designed to build loading and unloading platforms of about 128 trucks at the same time.

Objective: construction of about 7.500 piles Φ 355,6 mm at a depth of about 35 m.

Type of machine: n. 3 type LRB 355 with vibrator PVE 32 VRM



Project duration: 7 months with n. 2 daily shift (6-14/14-22)

Performance: 8-10 finished piles per shift per machine

Pile construction time: average 50 min, 25-30 min minimum

Shift crew type: 1 operator/machine attendant and 3 helpers

Fuel consumption: 48 l/h

Geology: layers of silt, clays, peat and sands with a bedrock in consolidated sandy clay

Water: abundant water flow at different levels

The basic tasks were: bearing effect (FDP), dry pile, noise reduction, exact depth reached according to the bedrock (first factor, coefficient λ!); all the target has been successfully reached.

7. LRB 355 BRIEF NOTES

The LRB 355, presently the most powerful multipurpose drilling rig on the market, is a newly designed equipment that includes various technical innovations, unique in the world. For example, in the standard configuration, it can perform, as already shown, single-stroke piles in CSP mode (Cased Secant Pile) at 23 m depth, Φ 900 mm.



7.1 Operating weight, approx. 128 ton

This parameter has its importance since the stability of the whole working group has a close connection with the tonnage of the equipment and all its components = > greater weight, greater stiffness, less vibrations therefore minor deviations and risks of interference with close piles especially when used in CSP-FoW method (besides minor possible breakages due to fatigue).

7.2 Motor power, fuel consumption and noise emissions

The motor power is a feature that clearly binds all the hydraulic functions of the machine; the rig can be equipped with a 600 or 750 kW last generation engine. Having more power means not only be faster in all functions but also having spare power in potential critical situations, for example at high depths (in double head or FDP), with strong lateral friction (potentially in soil with sandy matrix), with heavy bored columns full of material .... In addition, the greater power can be useful to manage different kind of works may be necessary (type the "Ring Vibrator") or design change in the course of work (larger diameters or higher drilling depths).

The abundant power involves the engine working at a lower rpm, despite having a spare power available. LWN has developed new low-consumption engines, integrated through the electronic with the hydraulic system, having an innovative concept called ECO-Mode able to limit the consumption of fuel; summarizing, it is a new generation engine with an electronic system that optimizes or disconnects all the hydraulic services when not used. It may be stated that the hourly consumption of the Liebherr combination (Engine-Electronic-Hydraulic) is lower at least of about 20% as pure cost per linear meter of excavated piles compared to any other competitors' combinations.

With regards to noise emission, it has been developed a specific system called ECO.SILENT-Mode; it is a function that when activated by the operator limits the number of rpm of the engine as well as of the cooling fan, ensuring a significant reduction of noise emission, with a negligent loss of power. This is clearly a very important feature especially in urban areas operation.



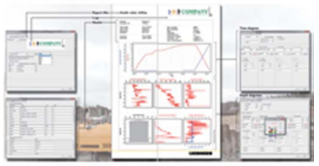
7.3 Geometry of the mast kinematics

Liebherr has designed a robust kinematic with a specifically designed H shaped pantograph, which guarantees a couple of undoubted advantages: rigidity of the system in any working position and possibility of having a relative movement between the slew ring (bearing disc) axis and the pile axis > 1 m, resulting in additional advantages:

- ability to reach work positions that are further away from the slew ring, where it is needed smaller movements or to cover complex work positions (such as corner piles or piles interfering with geometries or where obstacles are encountered for any reason in the operating area);
- ability to manage the casing without moving the machine, interesting situation for the individual cased piles excavated in kelly mode.
The above mentioned are considerations to highlight that the H shaped kinematic is particularly advantageous, especially in urban areas operations (versus the V shaped kinematic).

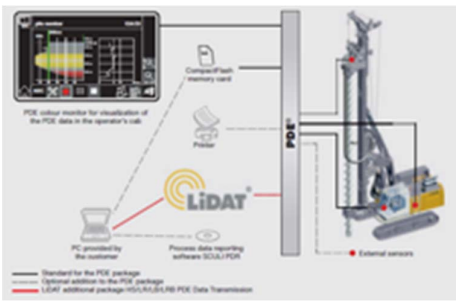
7.4 Electronic systems in standard drilling





A very reliable electronic system is installed on the machine; it is called Li-Tronic. It manages the control, operation as well as it manages the collection of an impressive number of data, involving the operator in an action no longer manual but namely of "logical control", working with features like:
- Pull down winch thrust percentage and adjustment
- Tilting data of mast and undercarriage
- Drilling and feed speed adjustment
- Drilling assistant: torque vs. pull down
- Overview of drilling activities in CFA, CCFA, FDP, SM,...
- Extraction assistant according to the concrete pouring pressure
- Display of kelly locking positions, ...

Machine is equipped as well with a process data recording system called PDE; it serves to electronically record and visualize the working data: the PDE records process data from the LiTronic control system which can be delivered to the construction site offices or to the headquarter of the manufacturer. Such management systems, nowadays more and more reliable and of proven efficiency and frequently used, called Li-Dat, is capable of managing:



- Data acquisition of the machine
- Transmission of the same via GPRS or via support
- Generating operational reports
- Generation of functional reports of the medium
- Planning and management of machines and shipyards
- Warning on machine malfunction
- Remote maintenance assistance
- Spare parts management …

SUMMARY AND CONCLUSIONS

The possibility of addressing different excavation technologies with LRB 355 in various geological condition, all at the extreme of geometrical limits, may give us a clear impression. It can be said that this rig generates undoubted advantages, when comparing, like: productivity, working accuracy, operative savings, low noise pollution, low wear and tear, remote assistance, multi-functionality ….
Coming to an end, when comparing 2 technologies and 2 different equipment, it is the cost per linear meter of finished pile the key factor that determines the real incidence of the machine and consequently guides the choice.

REFERENCES

Bringiotti M., 2003, Consolidamenti e Fondazioni, Edizioni PEI, Parma, I
Bringiotti M., 2010, Geotecnica & Macchine da perforazione, Edizioni PEI, Parma, I
Bringiotti M., Nicastro D., 2016, Palificazioni profonde realizzate con tecnologia FDP e Ring Vibrator tramite l'impiego di una macchina da perforazione multipurpose: LRB 355 – Job site reports, IAGIG Congress, Verona 20-21 May '16

SLOPE STABILIZATION WITH MULTIPLE ANCHORS MONITORED BY GLASS FIBRE TECHNIQUE

Dominik Gächter Author, Keller Grundbau GesmbH., Austria, d.gaechter@kellergrundbau.at
Reinhard Kulmer, Co-Author, Keller Grundbau GesmbH., Austria, r.kulmer@kellergrundbau.at
Vaclav Račanský, Co-Author, Keller Grundbau GesmbH., Austria, v.racansky@kellergrundbau.at

ABSTRACT

A new Refinery, with a capacity of 10 Mio. Tons of crude oil per year, is under construction on an area of about 2.300 hectare. Keller Grundbau won the contract to execute the slope stabilization for two locations of the project, with test loads for the permanent anchors up to 3700 kN. Due to the geographical location of the project, close to a tectonic fault zone and, moreover, in between 2 volcanos, highly heterogeneous soil conditions, including pressured groundwater were the main challenges for the drilling works of the permanent ground anchors. To fulfil the design requirements, multiple strand anchors with three-bond length, up to 16 strands were used, after an intensive testing program, and manufactured directly at site. The testing included two multiple anchors fully equipped with glass fibre sensors to investigate the load distribution behaviour with an outstanding resolution. The main goal was to get the full picture of the strain distribution along the whole length of the anchor, in the strand as well as in the ground – grout interface. This kind of measurement technique allows a real time monitoring with an accuracy of the measured strain of ±1.0 µm/m. In the following paper the results of the glass fibre measurement and the details of the multiple anchor design are discussed.

Keywords: glass fibre sensors, multiple strand anchor, slope stabilization, ground anchors, grout – ground interface

MOTIVATION

The use of fiber-optic technology was investigated and tested for the monitoring of anchor pull-out tests on Single Bore Multiple Anchors, which were used in the context of the slope stabilization works at the construction of a new refinery. The main reason behind these investigation is to measure and visualize the distribution of the load in the different bond lengths of the SBMA in combination with the presence of heterogeneous soil conditions at the construction site.
In the following paper the anchoring work, the characteristics of the fiber optic instrument, the design of the sensor cables and the investigations which were carried out will be discussed. Furthermore, the geological conditions as well as the critical steps regarding the installation process of the different sensor cables, which were assembled directly at the construction site, as well as some of the remarkable results from the pull-out tests are shown.

PROJECT

Keller Grundbau was awarded with the slope stabilization works (see Fig. 1) of two areas, for which permanent anchors with test loads of up to 3700 kN were used. Due to the geographic location (near to a tectonic boundary and between two volcanoes) highly heterogeneous soil conditions and the presence of groundwater under pressure were the major challenges for the anchor works at this project. Prior to the main execution of the works a major number of in-situ tests were carried out with various anchor types and different bonding lengths to find the correct drilling technique to execute the anchors and the optimal system in such difficult soil conditions. Most of the works were carried out with multiple permanent anchors each consisting of three single anchors, with a total of 14 strands and lengths of up to 50 m. With this type of retaining system, a safe distribution of the forces into the ground can be ensured in the event of an earthquake respecting the difficult geological situation at site and the required safety factors.

© 2018 Deep Foundations Institute



Fig. 1: Construction site of the slope stabilization with multiple anchors

FIBRE OPTIC SYSTEM

Following chapter is focused on the individual components of the fibre-optic system and explains in detail the characteristics and functions of the fibre-optic instruments and the structure of the sensor cables. A main part of the work was the calibration process of the fibre optic equipment prior to the installation at site. The Calibration for the accuracy of the sensors was done at the Technical University of Graz, Institute of Engineering Geodesy and Measurement Systems (IGMS). Information regarding the fibre optic sensors and measurement devices used can be found in the Literature stated at the end of this paper. A temperature compensation during the anchor testing (10 hr) at site was not executed, as the conditions in the bond length were taken into account as stable during the testing period. A zero reading of all installed sensor was done directly before starting the test which represented the reference level to all measurements during stressing of the anchor.

SENSOR CABLE

In the geotechnical application of fibre glass sensors, the working conditions at site are the main challenges for the team to protect the equipment in order not to damage the sensors during the installation process. The glass fibre of the fibre optic instrumentation is therefore protected with several different layers which are shown in Figure 2 to avoid the demolition of the cable during installation or stressing of the anchors.
The metal-coated sensor fiber has a polyimide layer, on which a special reinforcement, made of steel is applied (see FIG. 2a), hereinafter referred to as cable type # 01. This ensures a very good protection of the optical glass fiber during mounting and installation of the anchor. In addition, the texture of the metal coating ensures a reliable bond with the surrounding material (concrete mortar).

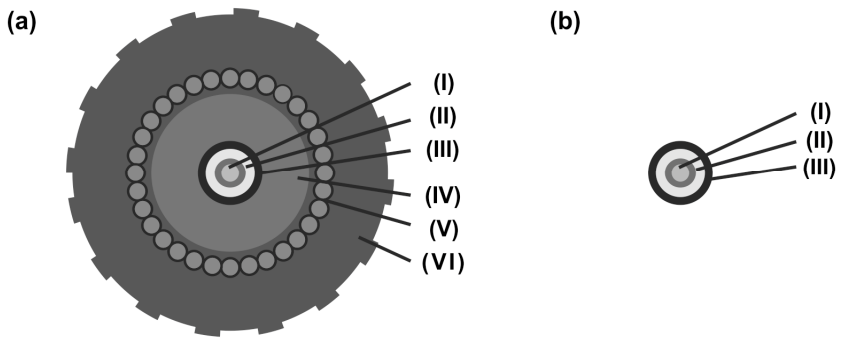


Fig. 2: Schematic presentation of the structure of the sensor cables used;(a) Type # 01 (∅ 7.2mm) and (b) Type # 02 (∅ 0.9mm) with (I) single-mode glass fibre (∅ 250 µm), (II) multiple dilatation layer, (III) metal sheathing, (IV) polyamide layer, (V) special steel reinforcement, (VI) outer structured polyamide layer

FIELD TRIALS

During the field trial carried out in April 2016, two 25m long SBMAs were instrumented with fibre optic cables directly on the construction site, where the anchors were produced for the whole project. The pull-out tests were carried out 24 days (test anchor # 01) and 25 days (test anchor # 02) after the installation of the anchor.

GEOTECHNICAL CONDITIONS

The investigation of the heterogeneous soil conditions at the construction site represented an essential component of the experiment to understand the influence on the load distribution behaviour of the anchor. Therefore, the soil conditions in proximity of the test anchors was determined by core drillings. A simplified description of the geological conditions, starting from a depth of 10 m corresponding to the beginning of the bond length of the anchors, can be found in Table 1.

Tab. 1: Geological conditions in the area of the bond length of the test anchors

Depth [m]	*Description*
10.0 – 13.3	*Tuff / mudstone (fine): gray, light to moderate weathered*
13.3 – 14.5	*Tuff (fine): light gray to gray, medium dense, stones (grain size: 5 to 8 cm)*
14.5 – 16.0	*Sand (fine to medium): dark gray, very loose*
16.0 – 16.9	*Limestone (fine): gray, medium dense*
16.9 – 18.3	*Tuff (fine) / clay (gritty): gray to dark gray, very loose, stones (grain size: 3 to 5 cm)*
18.3 – 19.5	*Sand (fine) / Sandstone (soft): dark gray, very loose*
19.5 – 23.5	*Tuff (medium grain): dark gray to gray, very loose*

Two holes were drilled to a depth of approx. 24 m with an inclination of 20 ° (test anchor # 01) and 25° (test anchor # 02) for the two test anchors. After installing the two anchors, the borehole was filled with injection grout, then the casings were extracted and the post grouting was carried out.

Both instrumented SBMAs were designed for a load of 2500 kN and have the same geometry and configuration. The most important parameters are summarized in Table 2 below.

Tab. 2: Configuration and geometry of the instrumented test anchors

	Test anchor #01			*Test anchor #02*		
	A#01	*A#02*	*A#03*	*A#01*	*A#02*	*A#03*
Free length [m]	*9.0*	*13.7*	*18.6*	*10.7*	*15.4*	*20.1*
Bonded length [m]	*4.0*	*3.9*	*3.9*	*4.0*	*4.0*	*3.9*
Over length - length between the anchor head and the stressing head for testing [m]			*2.9*			*2.2*
Number of strands	*4*	*5*	*5*	*4*	*5*	*5*
Type of strands	*Y1870 S7 (∅15.7mm)*					

INSTALLATION OF GLASS FIBRE SENSORS

The instrumentation of the test anchors were carried out directly in front of the drilling spot for the testing at the construction site, see Fig. 3. In such a way the transport distance between the instrumentation and the final installation was kept short to reduce the possibility of damaging the sensor cable during transportation to the borehole.



Fig. 3: Installation of the sensor cables at construction site for a 25m long strand anchor

The installation of the sensor cable type # 02 along the anchor strand was carried out by using an epoxy adhesive. This application was tested in the laboratory to ensure the efficacy of the bond prior to the installation. The sensor fibre was glued directly into a groove between two cables of the respective strand. The sensor fibre was bonded along the entire strand, which in addition to the good connection between the cable and the steel strand, ensured a good protection of the glass fibre during installation. However, in the evaluation process, the helix shape of the measuring fibre plays an important role. The sensor cable used for monitoring the grout ground interface (type # 01) was attached directly to the anchor corrugated pipe by means of adhesive tape. The fixation took place on a point-by-point basis, as the structured cable surface provided a sufficient bonding with the anchor grout.

For the greater robustness against possible failures (for example in the transition area between the individual sub-anchors) of the fibre-optic system, the installation of all sensor fibres has been carried

out redundantly. Each individual anchor of an SBMA was equipped with two strands, see Fig. 4b. The sensor cable positioned in the grout ground interface was installed in a loop with a 180° rotation at the anchor deepest bond length. In the case of a single fracture of a sensor fibre, a measurement of both fibre ends would nevertheless enable a complete detection of the deformations in the grout ground interface. For the redundant configuration, a sensor cable was installed in both main directions of the drilled hole. In addition to the increased fail-safety, the double configuration also made it possible to evaluate the performance of the fibre optic system.

As in Fig. 4a shown, all fibre optic sensor cables were installed alongside the anchor until reaching the measuring instrument through the anchor head and passing the stressing jack, mounted on the anchor plate which was located on a prefabricated concrete element. Due to the robust design of the fibre optic system and the corresponding protective measures during the anchor installation, damage to the sensor fibres could be avoided. As a result, by both test anchors six fibre optic sensors could be used to monitor the elongations along the anchor strands and two to register the deformations in the grout ground interface.

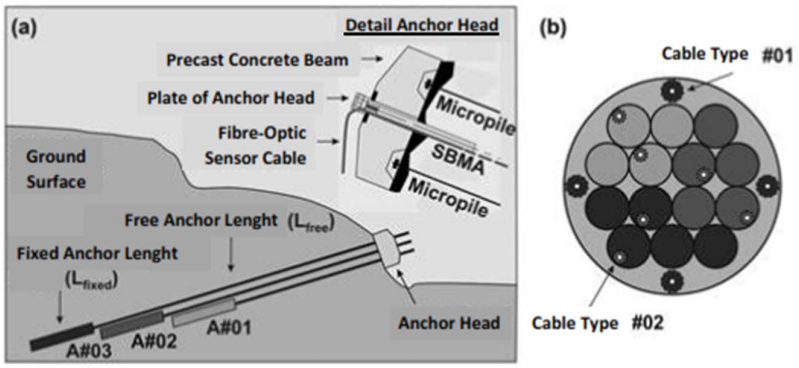


Fig.4: (a) Schematic presentation of an instrumented test anchor with bond length (Lfixed) and free length (Lfree) and (b) Arrangement of the different sensor cables (the arrangement of the strands is schematic)

TEST PROCEDURE

The setup of the testing equipment on the construction site is shown in Fig. 5a. In addition to the fibre-optic measurements, the displacements of the anchors were measured by means of a micro-meter at the anchor head (electronically and analogue), which is the standard procedure for the anchor testing but cannot provide any information about the load distribution along the bond length.

Figure 5b shows that anchors were stressed gradually to 1800 kN (600 kN on each single anchor). Afterwards the anchor has been released to 300 kN, which was followed by the next loading step of a total load of 2400 kN. The anchor was released and loaded again and blocked at 1200 kN in order to investigate permanent deformations. A higher load of the test anchor # 01 was avoided for safety reasons, since increased cracks were detected in the grout ground interface.

During the entire test period, the readings of all sensor cables were recorded continuously by the fibre-optic measuring system. The duration of a measurement took up to 12 seconds, each installed sensor fibre could be measured at a time interval of approximately 90 seconds.

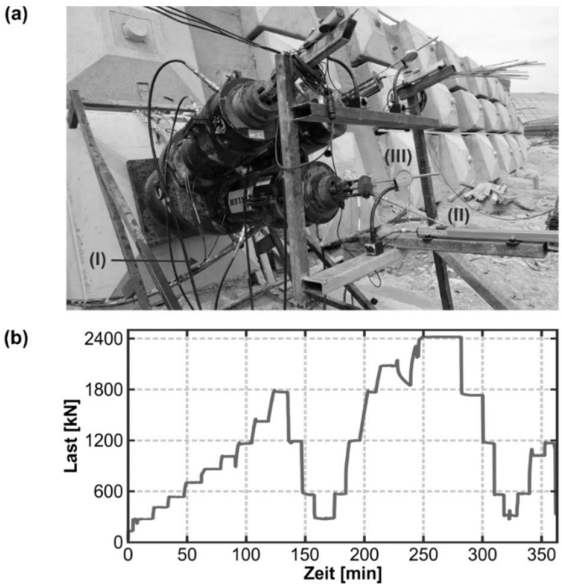


Fig. 5: (a) hydraulic stressing jack and sensors at the anchor head with (I) fibre optic sensor cables, (II) electronic micrometres and (III) analogue micrometres and (b) the sum of the test forces from the three stressing jacks

RESULTS

For a clear illustration of the results of the fiber-optic measurements, the strain along the strands as well as in the surrounding grout ground interface during different load stages are shown in Fig.6. The results are shown separately for the three separate anchors of each SBMA. As a reference level the ground level (0.00m) was chosen.

The elongation profile along the steel strands (Fig. 6a-c) confirm the assumptions made previously: In the area of the free length, all the instrumented anchor strands show a relatively constant expansion. The strains are also increasing with higher test forces. In the bond length, a decrease of the strains with the depth can be seen. Misleading values were recorded in some areas (for example at anchor # 03 at a depth of about 4.9 m in Fig. 6c). Compared to the first tests (Račanský et al., 2016), the homogeneity of the stressing procedures could be significantly increased by the optimization of the system and the improvement of the installation techniques. Furthermore, it can be noted that limited to very small deviations the measured strain values showed the same results. Due to the measurements with totally independent sensors directly mounted on the steel strands, this is an outstanding result which reflects the performance of the developed fibre optic measuring system.

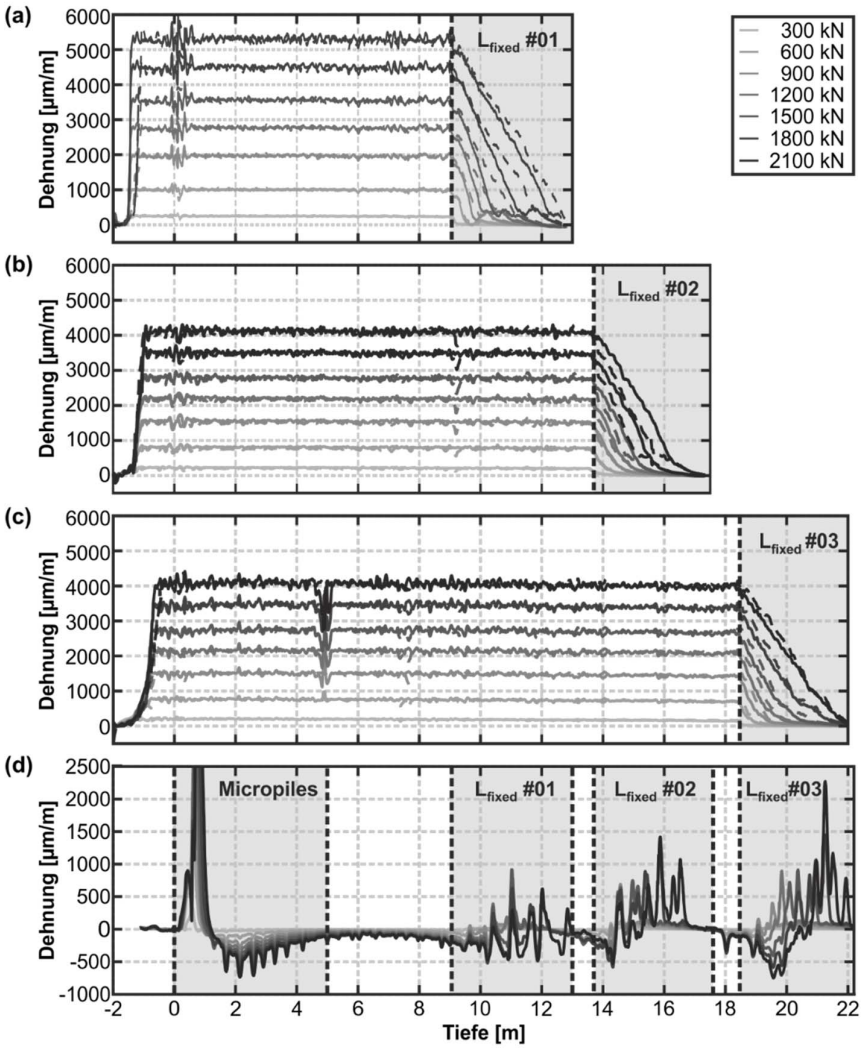


Fig. 6: Measured strain profiles on selected load steps at test anchor # 01; (a) Anchor # 01 - short, (b) Anchor # 02 - medium, (c) Anchor # 03 - long and (d) grout grout interface

To analyse the increasing numbers of cracks in the grout ground interface at a test load of 1200 kN, the load anchor was reloaded four times (see Fig. 5b). At time (t1= 100 min), the anchor is loaded with 1200 kN for the first time. After the load has been increased to 1800 kN, the anchor was released (t2 (= 142 min) to 1200 kN. Then the anchor is loaded to 2400 kN, (t3= 193 min) and released (t4= 307 min) to 1200 kN.

The measured elongation in different positions over the time shows that the number of tensile cracks in the grout material depends on the force which was previously applied to the anchor as a maximum. At the stage of t1 the cracks in the grout and herewith a reduction of the bond length of about 1.0 to 1.5m can be seen. After increasing the load to 1800 kN, the further reduction is in a range of about one meter at time t2, see Fig. 7(a). Between the time stage t2 and t3, there are hardly any changes in respect of cracking, see Fig. 7(b), since the anchor load has not changed. However, as a result of the releasing and reloading of the anchor, slight changes occur in the range of the elongations at some certain spots. At time stage t4, see Fig. 7(c) the cracks can be observed almost over the entire bond length of the anchor. As shown in the diagrams below the absence of cracks in a depth between 16.5 and 18.0 m indicates that the grouting of the anchor in that part is still solid and the anchor can still absorb additional forces.

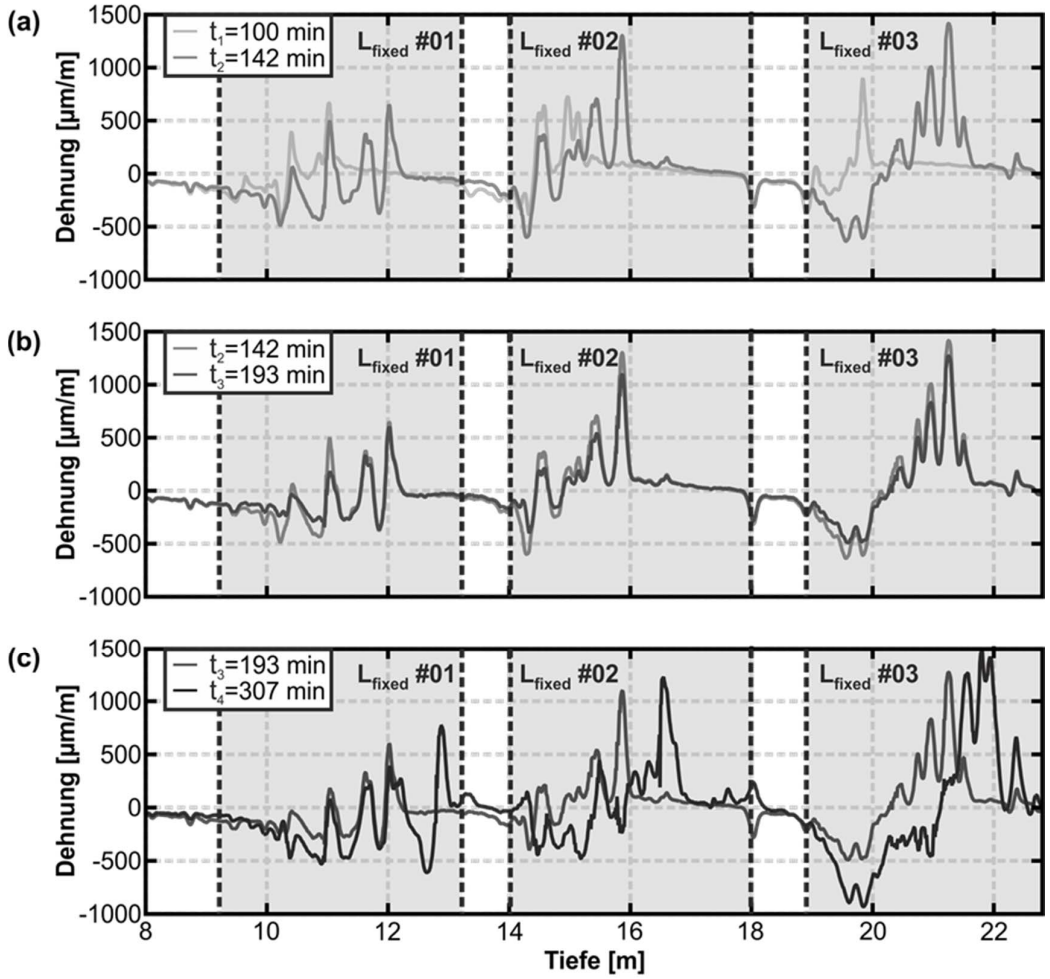


Fig. 7: Measured strain profiles along the grout ground interface at a test load of 1200 kN (a) strain before and after reaching 1200 kN, (b) strain before and after reaching 1800 kN and (c) strain before and after reaching 2400 kN

Similar to the analysis of the grout ground interface, the elongation profiles of the instrumented strands at the times t1 to t4 are shown in Fig. 8. It can be seen that the elongations due to the previous, greater load stages decrease only at a greater depth. Accordingly, an increase in the free length and a corresponding reduction in the bond length of the strands can be observed by the stepwise cracking of the grout ground interface. It is also noticeable that a local strain maximum occurs in the area of the transition between free anchor length and the respective bond length (Lfixed) during releasing of the anchor. Following this observation, further cracking in the grout appears due to the load releasing process, which occurs as a local increase in elongation and furthermore in a larger free length of the anchor.

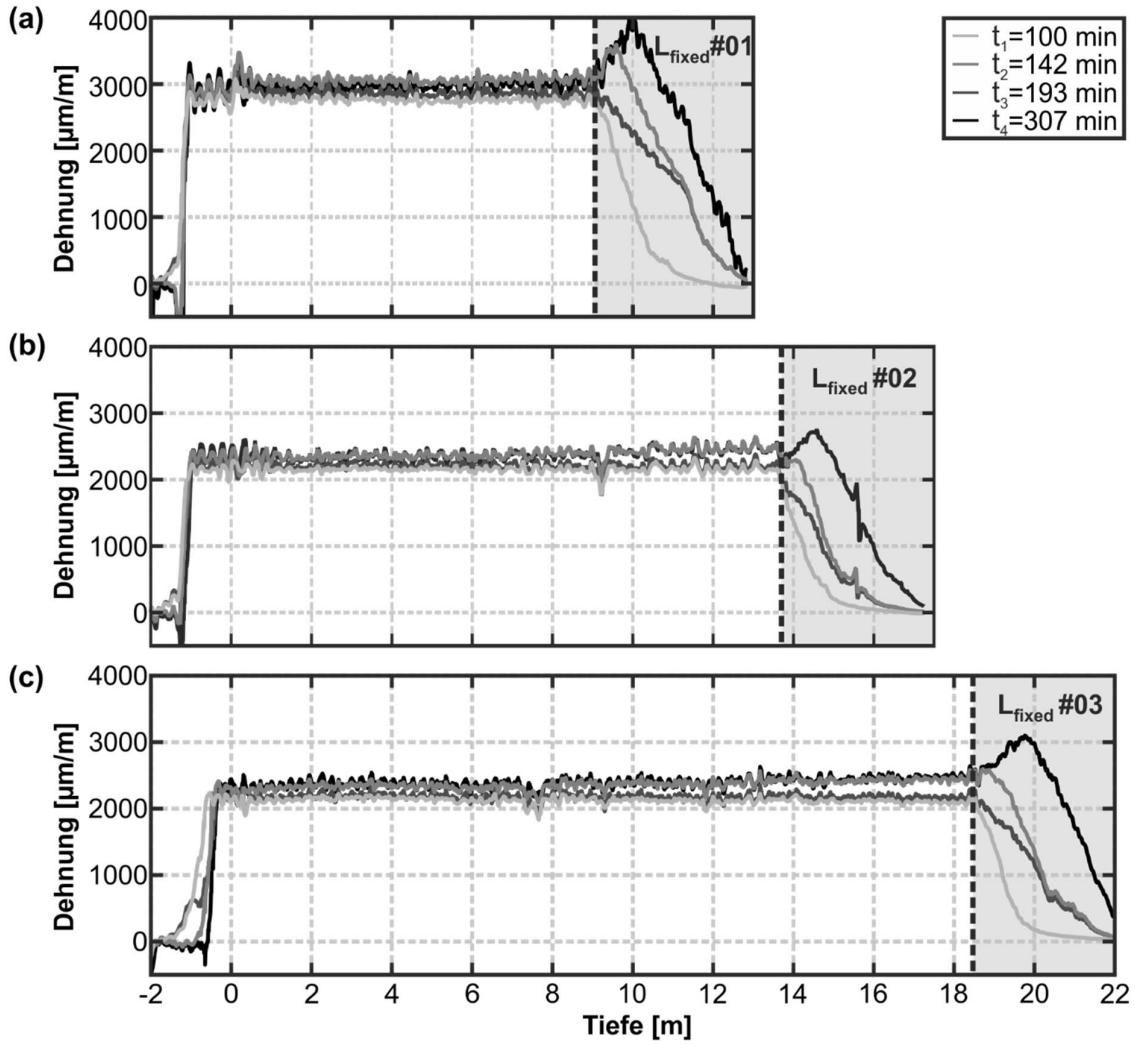


Fig. 8: Measured strain profiles along the anchor strands at a test load of 1200 kN (a) Anchor # 01 - short, (b) Anchor # 02 - medium and (c) Anchor # 03 - long

CONCLUSION AND OUTLOOK

During the pull out tests a high resolution of elongation and strain distribution along the whole length of the anchor was measured with the installed fibre optic system. The cracking of the grout ground interface with increasing anchor force was shown through the lifetime measurement of the anchor. Moreover allows the continuous strain measurement a back calculation of the grout ground behaviour of the single anchor. In the future more detailed information regarding the most effective length of the anchor bond length and distance between the single anchors will be available using the fibre optic technique. The installation of fibre optic sensors in the anchor grout as well as directly on the anchor strand was successfully tested with an outstanding resolution of the measured data. The application of the sensors in form of a loop placed in the anchor grout ensured that in case of damages during installation the fibre still can be measured during the stressing procedure. The continuous bond between steel strand and fibre sensor showed similar results of the measurements for the single anchor strands of the multiple anchor.

In the future we plan to investigate more in detail the interaction between the sensor cable, anchor strand and grouting material. Especially the grout ground interface is from the geotechnical point of view interesting. Therefore similar tests will be executed in different types of soil to have a better understanding of the load distribution along a ground anchor. This intensive testing process showed that fibre optic sensors opens a new range of detailed information for geotechnical monitoring of ground engineering applications.

LITERATUR

Barley, A D. (1995). Theory and Practice of the Single Bore Multiple Anchor System, International Symposium on ”Anchors in Theory and Practice”, Salzburg Austria

Chalmovsky, J. (2016). Behaviour of Ground Anchors. PhD Thesis, TU Brno, Tschechien, 169 S.

Kreger, S.T., Gifford, D.K., Froggatt, M.E., Soller, B.J. & Wolfe, M.S. (2006). High resolution distributed strain or temperature measurements in single-and multi-mode fiber using swept-wavelength interferometry. Optical Fiber Sensors, Optical Society of America, Washington DC, USA, ThE42 - 4 S.

Luna (2014a). Data Sheet: Optical Backscatter Reflectometer (Model OBR 4600). Ver. LTOBR4600 REV. 004 02/13/2014, Luna Technologies Inc., Roanoke, USA, 4 S.

Luna (2014b).User Guide: Optical Backscatter Reflectometer Model OBR 4600. Version User Guide 5, OBR 4600 Software 3.6, Luna Technologies Inc., Roanoke, USA, 230 S.

Mayer, A. (2008).FE – Berechnungen zum Tragverhalten von Ankern im Boden. Masterarbeit, TU Graz, 114 S.

Monsberger, C., Woschitz, H., Lienhart, W., V., Racansky, Gächter, D., Kulmer, R.,(2017). Faseroptische Überwachung von Ankerausziehversuchen im Rahmen der Hangsicherung für den Neubau einer Raffinerie, 32. Christian Veder Kolloquium, S. 173-192

Monsberger, C., Woschitz, H., Hayden, M. & Lienhart, W. (2016). Faseroptische Instrumentierung und Deformationsmessung eines duktilen Rammpfahls. Messen in der Geotechnik 2016, Stahlmann, J. (Hrsg.), Mitteilung des Instituts für Grundbau und Bodenmechanik, TU Braunschweig, Heft 101, S. 195-216

Presl, R. (2009). Entwicklung eines automatisierten Messsystems zur Charakterisierung faseroptischer Dehnungssensoren, Masterarbeit, FH Oberösterreich, Wels, Österreich, 148 S.

Račanský, V., Weidacher, R., Lienhart, W., Monsberger, C., Woschitz, H. & Schweiger, H. (2016). Überwachung eines Ankerausziehversuches mittels Glasfasersensoren. 34. Deutsche Baugrundtagung, Bielefeld, Deutschland, S. 315-322

Soller, B.J., Wolfe, M.S. & Froggatt, M.E. (2005). Polarization resolved measurement of Rayleigh backscatter in fiber-optic components. OFC Technical Digest, Los Angeles, USA, 6 S.

Woschitz, H., Klug, F. & Lienhart, W. (2015). Design and calibration of a fiber optic monitoring system for the determination of segment joint movements inside a hydro power dam. IEEE Journal of Lightwave Technology, Vol. 33, Issue 12, S. 2652-2657

Woschitz H., Monsberger C. & Hayden M. (2016). Distributed fibre optic strain measurements on a driven pile. Proc. SPIE 9916, Sixth European Workshop on Optical Fibre Sensors (EWOFS 2016), International Society for Optics and Photonics, S. 99162P - 4 S.

Wuilpart, M. (2011). Rayleigh scattering in optical fibers and applications to distributed measurements. In: Advanced Fibre Optics: Concepts and Technology, Thévanez, L. (ED.), EPFL Press, Lausanne, Schweiz, S. 207-262

SUGGESTION FOR CONTROLLING THE IMPLEMENTATION OF ROOT PILES PARTIALLY EMBEDDED IN BEDROCK

Marilia D. Silva, UFPE, Recife, Pernambuco, Brazil, 00115581992248378, mariliadantas@hotmail.com

Roberto Q. Coutinho, UFPE, Recife, Pernambuco, Brazil, 0011558121268222, rqc@ufpe.br

Myckelle M. S. Ferreira, UFPE, Recife, Pernambuco, Brazil, 0011558121268222, myckellemichely@hotmail.com

ABSTRACT

This article provides suggestions of control measures for implementing root piles embedded in bedrock. The control measures included the use of the rockdrill to check the elevations of the overburden and continuity of the resistant layer, and to determine the average drilling time to reach design lengths by separating the bedrock into equivalent regions so that the length of the pile embedded in the rock is not shorter than the design. In order to collect the data used in the evaluation of the executive stages of the piles, changes were made to the accompanying table suggested by ABEF (Brazilian Association of Foundations Engineering and Geotechnics). From assessing the obtained data, it was found that the subsoil of the project consists initially of weathered soil followed by granite bedrock, and could be divided into four different geotechnical regions. The use of the rockdrill proved to be a good control tool, ensuring greater precision with regard to the location of the overburden. The analysis of the data of 91 root piles showed that most were drilled in less than two hours, where 70% presented the equivalent of one meter of rock drilled in 20 minutes, providing greater safety in the length actually drilled in bedrock.

1. INTRODUCTION

The root pile is widely used for deep foundations on sites of high compactness or consistency, or which demonstrates the presence of unaltered or weathered rocks (DER/SP - 2006).

According to the ABEF (Brazilian Association of Foundation Engineering and Geotechnics), root piles are a type of foundation cast in loco and driven by rotary or rotary-percussion drilling, fully cased into the ground, using a metal pipe (casing pipe) to guarantee drillhole stability.

In the rock section, whether passing by boulders or being embedded in the bedrock, it is implemented by the internal drilling of the casing pipe, following up with reduction in diameter in that sequence.

Control has become increasingly important when executing deep foundations in rock, in order to guarantee safety and reliability of the work, driven by the growing need for further information regarding this type of foundation and definition of responsibilities in constructions in general.

Thus, an efficient executive control throughout the construction stages of piles drilled into bedrock is essential, because any failures could not only cause delays in the works schedule, but also result in a considerable reduction in the pile's bearing capacity, which might be identified or not during the load bearing tests, after the piles are in place.

© 2018 Deep Foundations Institute

2. IMPLEMENTING AND CONTROL OF ROOT PILES PARTIALLY EMBEDDED IN BEDROCK

2.1 Implementation stages

Implementing root piles basically comprises three executive phases:

a) Circulation water during drilling, Figure 1 (a);
b) Assembly and placement of reinforcement, Figure 1 (b);
c) Grouting, Figure 1 (c).

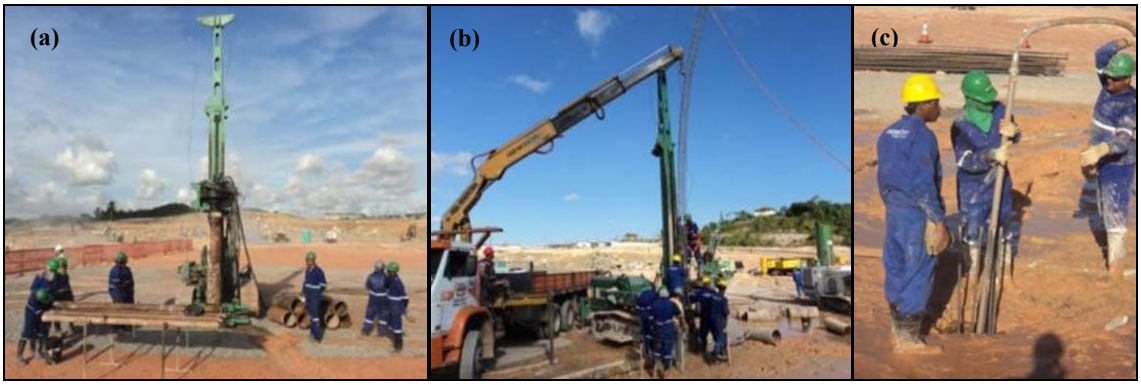


Figure 1: (a) Drilling root piles into ground (b) Reinforcement installation; (c) Grout injection pipe inside casing.

The root pile drilling process should be carefully supervised, since compliance with the standard specifications guarantees the integrity of the shaft in order to ensure perfect transmission of infrastructure loads to the soil/rock.

2.2 Implementation controls

The main control measures applied to root piles generally include the inspection of the drilling diameter, the diameter, thickness and depth of the steel pipe to be recovered, proper hole cleaning, positioning of longitudinal reinforcement and stirrups, drilling depth, injection pressures at each elevation, the volume of the grout injected at each stage and the total grout injected after completion of the pile, as well as the grout mix design and preparation method.

All this information shall be supervised by a specialist and recorded in a specific bulletin. The following are some recommendations for ensuring the executive control of the piles:

a) Boring

The execution must be verified "full time" by a specialist, in addition to the contractor's professionals involved. The specialist should also check the bored length with the full introduction of casing pipes, segmented and threaded to each other. The boring depth is checked using the number of pipes multiplied by the length of each pipe.
It is necessary to compare the measurement resulting from the sum of the lengths of the segment of the casing pipes used, with the designed measurement. The differences found must be analyzed carefully, since the root pile drilling process is itself a borehole.

b) Rock drilling

The analysis is relatively easy, since the drilling noise is differentiated as well as the material being expelled from the hole. This is when the equipment must be changed for rock drilling using pneumatic hammer drilling.

During bedrock drilling, the time required for the operation must be recorded to be able to perceive the next drillings with the same embeddedness of the pile in rock and same compressor capacity.
Rock drilling time is associated with the operator's experience, the bored material, tools used, methodology adopted, and so on.

This stage requires close attention, since the drilled length can only be checked by observing the descent of the hammer drill, and being concerned with the lengths drilled in smaller rocks than those specified in the design, since the latter must be absolutely equal to or greater than designed.

c) Reinforcement assembly and placement

The pile reinforcement must be assembled as a cage, guaranteeing the minimum covering of 2cm (NBR 6118). The splices must conform, when necessary, to ABNT (2003), ensuring their verticality.

During the installation of the reinforcement, the inside of the casing pipe must be cleaned, using the washing composition, which must be introduced as far as the pile's bottom elevation. Cleaning is completed when the return water no longer shows traces of transported material.

The total length of the drilled pile should be noted exactly, checking to see if the reinforcement has been placed to the end.

d) Grouting

During the grouting phase, it must be ensured that the PVC pipe is introduced to the end of the drilling and the grouting is performed from the bottom up until it completely fills the borehole and leaks from the top of the pipe, in order to expel all drilling impurities. Next, a cap is threaded to the top of the pipe, connected to an air compressor that blows in compressed air with pressures of 49 KPa to 392 KPa. All piles were implemented in this way and there was no problem whatsoever.

It is important to record the amount of grout used in each pile, in order to identify any possible escape of material.

3. SUGGESTED CONTROL IN ROOT PILE DRILLING

3.1. Study area

The study area is located in the West Zone of the metropolitan region of Recife, in the town of São Lourenço da Mata, Pernambuco, Brazil (Figure 2).

The entire project covers the granites of the Salgadinho Complex, located at the far eastern end of the Capibaribe River basin, and its weathered soils.



Figure 2. Location of study area

They are old lands, formed mainly by granites of various compositions, gneisses and shales, intensely deformed by several overlapping tectonic processes.

The project was divided into ten modules, where only in the southern modules, part of the southeast, southwest, northeast and west deep rock foundations were carried out. For this study herein, information was registered of 91 piles distributed through the southern, southeastern, southwestern and western stretches 1 and 2 of the project.

3.2 Use of rockdrill to confirm root piles support elevations

When drilling deep foundations embedded in bedrock, the depth to be anchored in the rock depends on the correct determination of the overburden.

Since it is a major project, the quantity of mechanical boreholes required to confirm all support elevations would be unfeasible due to the time and increased cost of geotechnical inspection.

Therefore, it was necessary to develop a faster and less costly investigation technique to confirm the overburden.

The rockdrill is a tool that drills into soil and rock, providing several boreholes in a short space of time, which allows a larger amount of data per stretch. According to the data shown by Silva and Coutinho (2012), the tool was used to verify/confirm the overburden and possible layers of soil found in a particular drilling.

Since it is a destructive survey, the use of the rockdrill requires the close attention and experience from the operator and the professional accompanying the drilling, being determined by performance versus the equipment's progress and soil classification.

Figure 3 presents a diagram of the project's subsoil profile, observed with the expedient drilling, using rockdrill equipment.

As the rockdrill advances, the two boreholes indicated the beginning of the overburden near the average elevation 28.50 m. From this elevation, the drill advanced slowly, not encountering less resistant materials.

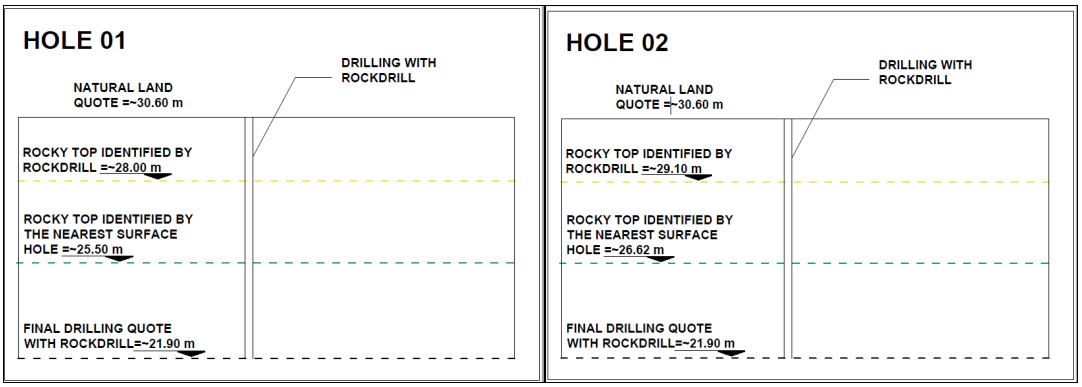


Figure 3. Holes 01 and 02 - Rocky gap measured with rockdrill

On average, they were drilled 2.50m below the settlement elevation stated in the design. The elevation of the overburden identified by the closest boreholes, average elevation 26.50, showed a difference of approximately 2.0m, emphasizing the importance of the complementary drilling using the rockdrill.

3.3 Root pile drilling controls

The ABEF monitoring chart (Figure 4) was used for the project under study, with some necessary adjustments, such as, for example, extra control of soil and rock drilling time, in order to verify the time suitable for executing the designed embedded length, thereby ensuring safety of the work done.

Executing company			Root piles execution bulletin			
Work/place:						
Location:					Nº Pile/axis:	
Natural ground quota					project support quota	
Load work (kN)					Pile type	
Drilling - field						
Start		Term		Diameter of the coating (mm)	Length	Inclination
Date	Hour	Date	Hour			
Depth				Soil classification		
Start	Term	Total (m)				
Characteristics frame						
Stretch		frame			Stirrup	number of amendme
On soil						
On Rock						
Pile depth check - release for injection						
Injeção						
Date	Schedule		injection pressure (kgf/cm3)		Amount of cement	Amont of sand
	start	Term				
Comments:						
Executing company						

Figure 4. Follow-up bulletin template. Adapted from ABEF (2010).

Figure 5 shows some data for analysis and control of execution. The purpose of presenting these data is to verify the heterogeneity of the site with field data, which are the drilling times of the piles in the rock section.

SECTION	PILE	MIXED SURVEY	DEPTH SOIL (m)	DEPTH ROCK (m)	DEPTH TOTAL (m)	DRILLING TIME IN SOIL	DRILLING TIME IN ROCK
SOUTHEAST	E2096	3002	1.00	6.50	7.50	00:29:00	02:31:00
SOUTHEAST	E2097	3002	1.00	6.50	7.50	00:45:00	03:01:00
SOUTHEAST	E2098	3002	1.00	6.50	7.50	00:54:00	02:52:00
SOUTHEAST	E2099	3002	1.00	6.50	7.50	00:21:00	01:30:00
SOUTHEAST	E2102	3002	1.00	6.50	7.50	00:15:00	01:30:00
SOUTHEAST	E2120	3002	2.50	5.00	7.50	00:13:00	01:35:00
SOUTHEAST	E2123	3002	1.60	6.00	7.60	00:25:00	02:42:00
SOUTHEAST	E2124	3002	2.50	6.50	9.00	00:28:00	03:05:00
SOUTHEAST	E2131	3002	1.60	6.00	7.60	00:20:00	02:00:00
SOUTHEAST	E2132	3002	1.50	6.00	7.50	00:20:00	02:17:00
SOUTHEAST	E2133	3002	1.50	6.00	7.50	00:34:00	02:25:00
SOUTHEAST	E2134	3002	1.50	6.00	7.50	00:14:00	01:34:00
SOUTHEAST	E2066A	3002	3.00	6.20	9.60	00:11:00	02:19:00
SOUTHEAST	E2072A	3002	2.57	6.42	9.50	00:07:00	01:31:00
SOUTHEAST	E2094A	3002	1.08	7.20	8.50	00:12:00	00:56:00
SOUTHEAST	E2118	3002	1.00	6.50	7.50	00:25:00	02:05:00
SOUTHEAST	E2059A	3002	4.43	8.53	13.33	00:13:00	01:30:00
SOUTHEAST	E2064A	3002	3.88	8.87	12.75	00:20:00	01:24:00
SOUTHEAST	E2087B	3002	2.60	5.10	8.00	00:20:00	00:51:00
SOUTHEAST	E2111	3002	4.00	5.00	9.00	00:28:00	01:21:00
SOUTHEAST	E2112	3002	3.50	5.00	8.50	00:40:00	02:58:00
SOUTHEAST	E2105	3002	1.30	6.50	7.80	00:12:00	02:52:00
SOUTHEAST	E2108A	3002	4.70	8.35	14.60	01:40:00	01:50:00
SOUTHEAST	E2023B	3002	7.10	2.83	9.93	04:20:00	01:45:00
SOUTHEAST	E2033A	3002	6.80	7.70	14.50	01:50:00	01:00:00
SOUTHEAST	E2057A	3002	7.20	7.90	15.50	00:20:00	01:35:00
SOUTHEAST	E2079A	3002	10.78	5.00	16.08	00:10:00	00:57:00
SOUTHEAST	E2127A	3002	11.60	5.00	16.90	00:40:00	00:57:00
SOUTHEAST	E2129A	3002	10.50	5.00	16.70	01:15:00	02:35:00

Figure 5. Drilling records of piles in the southeast section.

The table shows that some piles with the same inlay in bedrock or relatively close to each other have a very different drilling time. This demonstrates the existence of a more or less resistant rock depending on the drilling section, which can be confirmed later by the compressive strength tests.

The geological-geotechnical characterization established for the bedrock was based on the parameters of physical indices, uniaxial compressive strength, RQD value, recovery of the borehole test sample and petrographic analysis, presented in detail in the paper by Silva and Coutinho (2012).

In the southern section, a petrographic analysis was performed on two samples of mixed borehole 3004, in which it was found that sample 8, even being on the same vertical and with a variation of

1.58m, is shown to be pure igneous rock, while sample 7 is meta-igneous, already showing signs of metamorphization

In the characterization of the southeastern section one hole only was made, with analysis of two samples, which reveals a section of high recovery (< 80%), poor degree of fracturing (RQD =~ 40) and medium and high strengths. Porosity diminishes with depth and shows an increase in strength. The southwestern section is characterized by showing medium to high strengths, high recovery and low RQD in most of the samples. And lastly, in the western section, there is considerable increase in strength from elevation 14 to elevation 1.5, as well as an increase in the specific density of the rock the deeper it goes.

It is worth noting that drilling time records must be separated for each drilling stage (soil/rock). With the data presented, different types of foundation rocks in the project and the average times of rock drilling for each foundation rock can be analyzed.

In the southeastern section, 29 piles were analyzed, with lengths embedded in rock varying between 2.83 and 8.87 m, which in this section are all designed to be 5m into the rock. However, during drilling there were some cases where the continuity of good quality rock was not verified, and drilling was extended until completing the continuous 5m. In addition, rock drilling time for this variation in lengths ranged from 51 minutes to 3:05 hours.

Figure 6 schematically shows the frequency distribution of the times spent to drill an average of 6.20m into rock of 29 piles from the southeast section of the project.

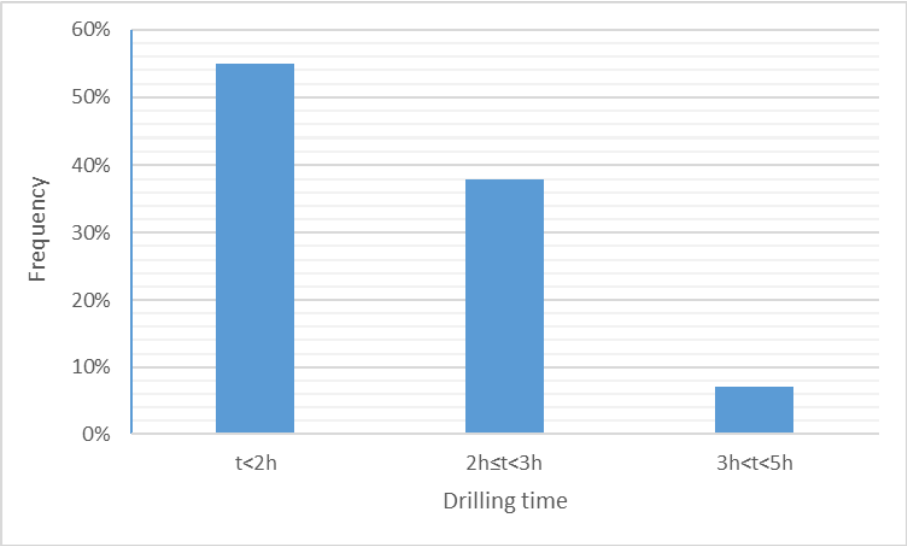


Figure 6: Rock drilling time of the piles in the southeastern section

Figure 7 schematically illustrates the frequency distribution of the time spent to drill an average of 5.5m in rock of 30 piles in the southern section of the project.

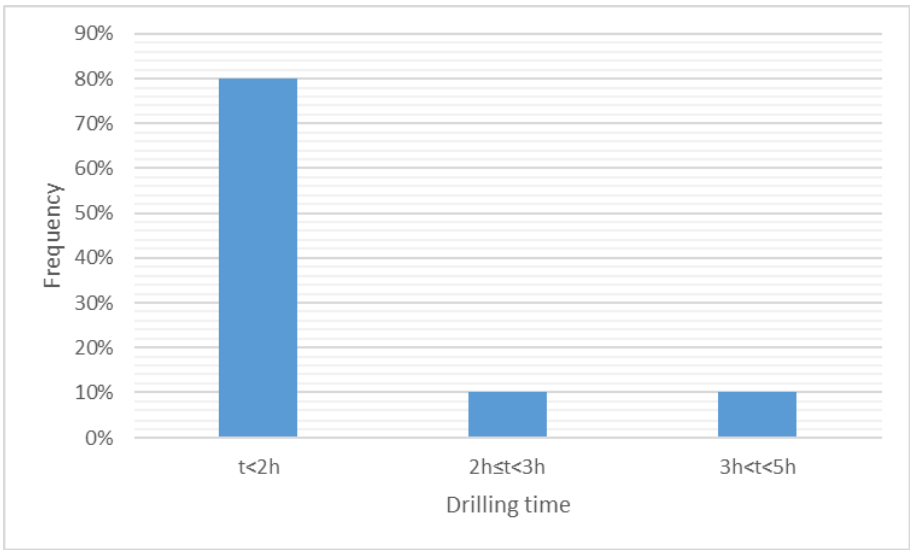


Figure 7. Rock drilling time of piles in the southern section

Figure 8 schematically shows the frequency distribution of the times spent to drill an average of 5.63m of 15 piles in the southwest section of the project.

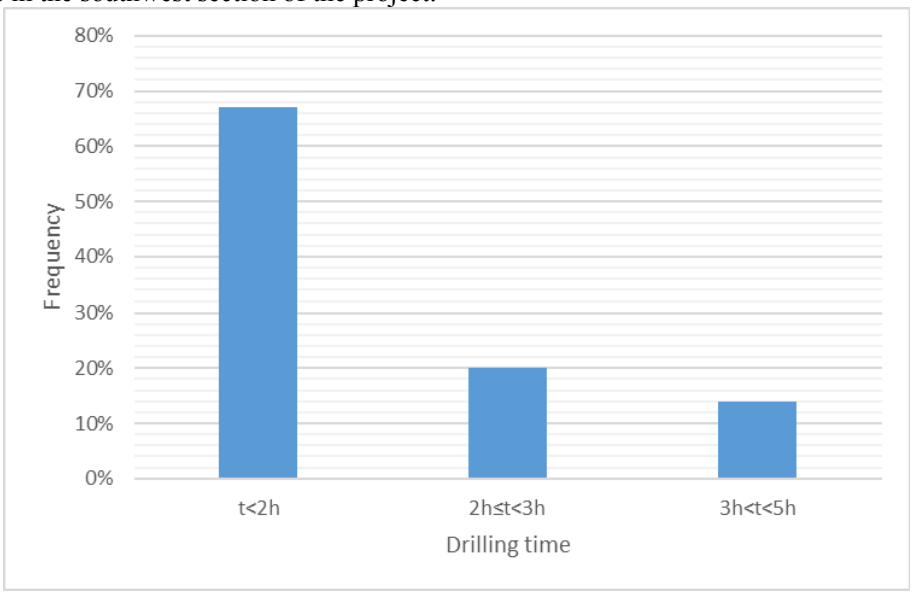


Figure 8. Rock drilling time of the piles in the southwestern section

Figure 9 schematically shows the frequency distribution of the times spent to drill an average 4.68m of 17 piles in the west section of the work.

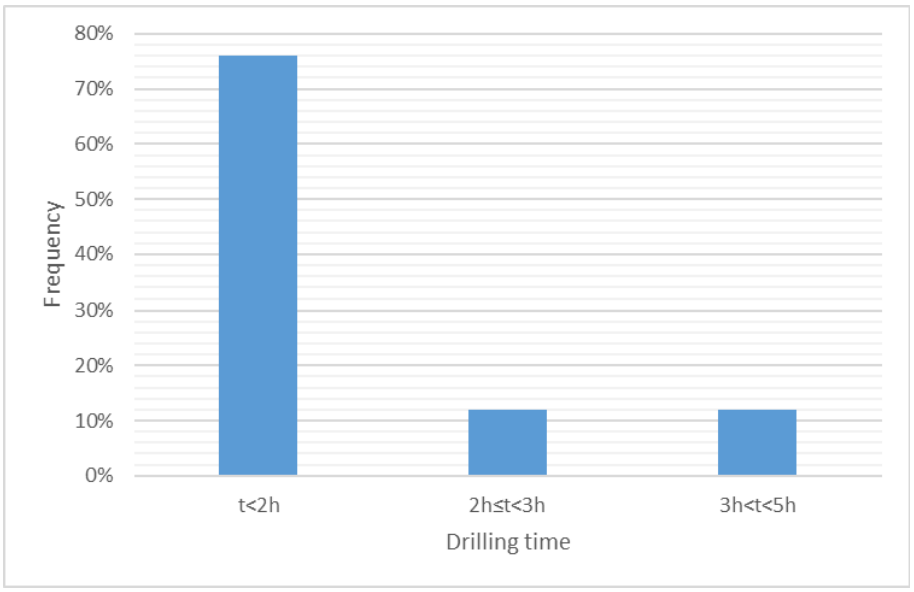


Figure 9. Rock drilling time of the piles in the western section

The graphs indicate that a significant part of the piles were drilled in times of less than two hours. Rock drilling piles take different drilling times, depending mainly on the strength of the rock, the state of the drilling equipment and especially the power of the compressor used.

The hammer's state of repair, which is part of the rock drilling equipment, is a very important factor in this time because. If it is obstructed, although it is apparently drilling a section of rock due to the characteristic noise, it actually drills almost nothing, and therefore could spend 20 min only descending 5cm; this can be confirmed by monitoring on site and by the fragments being placed outside the hole.

Accordingly, two errors may occur: the register of the beginning of the overburden and drilling time, and consequently the length embedded in the rock, could be compromised.

This is why it is important to monitor the root pile drilling process to check the suitable time, considering the characterization of the rock presented in the paper by Silva and Coutinho (2012). Furthermore, the power of the compressor used also interferes in this drilling time, and in the case of the project under study the compressors used had a minimum capacity of 20,000 KPa and maximum of 25,000 KPa.

The results were based on the characteristics of the rock sections presented and on the methodology adopted in the work under study, but the drilling parameters could be monitored manually, using routine records and related parameters, to determine the boring rate of the rock, in addition to automatic monitoring, which record in real time the parameters required to quantify the drilling capacity, as in the article by Bruce et al. (2005).

5. CONCLUSION

The rockdrill can be used as an aid to rapid investigations, confirmation of rocky terrain and less resistant layers, before or during the pile placement, simplifying the services, being faster and being less costly.

Disregarding the start of good quality rock drilling could lead to two errors: recording the beginning of the overburden and drilling time, thereby compromising the actual length embedded in the rock, hence

the designed bearing capacity. This is why it is important to monitor the root pile drilling process, using data of this process and the rockdrill.

From the data of the drilled 91 root piles, it was found that a significant part of the piles were drilled in less than two hours. The drilling time depends directly on the operator's experience, the drilled material, tools used, methodology adopted, and so on.

The analysis of the data, taking into account the characteristics of the project and conditions obtained by the work, showed that 70% of the piles for drilling in the rock section had a velocity of one meter in 20 min, with slight variations.

Thus, piles with the same characteristics drilled in generally good quality bedrock, must at least present the average time observed, otherwise they could not have been drilled with the designed length, raising serious problems in the project, which could only be identified from the results of the load tests.

REFERENCES

ABEF 2004. Manual of Product and Procedure Specifications, Foundations Engineering and Geotechnics. São Paulo, Brazil, 3rd Edition, 500 p.

ABNT 2003. Execution of Concrete Structure - NBR 6118. Brazilian Association of Technical Standards, Brazil, 154 p.

Bruce D.A., Heenan D.M. & Wilson D.B. - Quality and Quantification in Rock Drilling and Grouting. Geo-Frontiers Congress (2005).

DER/ SP- *Departamento de Estradas e Rodagens – Relatório Técnico Estaca Tipo Raiz* (2006)

Silva, M.D. & Coutinho, R.Q., 2012. Release for running rock-backed shoes with rockdrill: Case Study, Cobramseg (Brazilian Congress of Soil Mechanics and Geotechnical Engineering), Pernambuco, Brazil, September 15 -21, 10 p.

Silva, M.D. & Coutinho, R.Q., 2015. Geotechnical characterization of rock mass for pile foundations embedded in rock: case study. XV Pcsmge (Pan-American Congress of Soil Mechanics and Geotechnical Engineering), Buenos Aires, Argentina, November 15-18, 8 p.

Silva, M.D., 2013. Geotechnical characterization of rock massif and foundations in piles embedded in rocks. Master's Dissertation, Federal University of Pernambuco, 169 p.

THE FIELD INVESTIGATION OF TENSION CRACKS ON A CEMENT GROUTED SLENDER COLUMN DURING THE THERMAL RESPONSE TEST

Yue Ouyang, Project manager, Skanska, Maple Cross House, Denham Way, Maple Cross, Rickmansworth, Hertfordshire, U.K., +44 (0)330 050202, Email: Yue.Ouyang@gmail.com

Loizos Pelecanos, Lecturer, Department Architecture and Civil Engineering, University of Bath, Claverton Down, Bath. U.K., Email: l.pelecanos@bath.ac.uk

Kenichi Soga, Chancellor's Professor, University of California, Berkeley, Department of Civil and Environmental Engineering, 447 Davis Hall, Berkeley, California, USA, Email: soga@berkeley.edu

Duncan Nicholson, Director, Ove Arup, 13 Fitzroy St, Bloomsbury, London, U.K., Email: Duncan.Nicholson@arup.com

ABSTRACT

The paper reports the field thermal response test carried out on a slim column installed in London Clay. The column was enlarged from a site investigation borehole, and a bespoke supporting system was installed within the column to host geothermal pipe work and instrumentations. The column experienced several thermal cycles and the thermo-mechanical reaction of the column was captured by fibre optic strain and temperature sensors. Tension cracks were detected along the column for the first time. This paper investigates the generation of tension cracks from the field test, and discusses the subsequent modification on the thermo-mechanical behaviour of the column from the field measurement.

Keywords: Geothermal energy, energy pile, Thermo-mechanical response, Soil-Structural Interface, Distributed fibre optic sensing, tension crack, Thermal Response Test (TRT).

INTRODUCTION

Energy piles have been considered as an effective means to tap into sustainable geothermal energy resources. Research have been carried out to study the behaviour of energy structures when they are subject to thermal load. There were several full scale field tests reported by Brandl (2006), Bourne-Webb et al. (2009), Knellwolf, et al. (2011), and Rotta Loria & Laloui, (2016) which investigated thermal mechanical behaviour of a single energy pile or energy piles group. Although all field tests were carried out in relatively shorter duration than operational energy piles, there were several framework and conceptual models was proposed by Amatya, et.al. (2012) and Bourne-Webb et.al. (2011) to describe thermo-mechanical behaviour of the pile in different end-restraint conditions. These frameworks formed the basis to understand the behaviour of an energy pile, which also encouraged several thermo-mechanical numerical models, to replicate the observed behaviour of energy piles (Ouyang, 2014; 2011, and Peron, et.al., 2011).

Brandl (2006) raised the caution in case of cooling below 0^0C, which could cause freeze-thaw impacts in soil, and then affect the load-bearing capacity of the pile. The energy pile test at Lambeth College in London (Bourne-Webb et al., 2009) had an intention to freeze the ground by circulating much cooler fluid (-6^0C) over an extensive period of up to one month. The test results concluded that the pile was not sufficiently cooled to freeze at pile/soil interface. However, there were tensile strains observed at the lower third part of the pile shaft. Bourne-Webb et al. (2009) suggested that tensile strain or load which could develop depends on the magnitude of temperature change applied to the pile.

© 2018 Deep Foundations Institute

Encouraged by the field test carried out at Lambeth College, the current research was set up to understand the thermo-mechanical behaviour of a cement grouted slender column installed in London Clay. Optical Fibre Sensor (OFS) were used in the test together with Vibrating Wire Strain Gauge (VWSG) to capture the behaviour of the column. Several tension cracks were captured during the test by OFS in the first cooling phase and following thermal cycles. This paper discusses the behaviour of the column with tension crack from thermal and geotechnical aspects.

PROJECT DESCRIPTION

Site information

The site locates in Central London bounded by Belvedere Road to the west, Chicheley Street to the south, York Road to the east and the Waterloo East Charing Cross railway line to the north. The site investigation report indicates that the borehole contained 1.1 m of concrete and underlain by firm to stiff London Clay in Thames Group. The water table is found at 1.8 m below the existing basement level. The column is constructed in the basement with limited headroom and founded within the London Clay formation.

Field installation and monitoring

The column was constructed on an existing borehole, which was initially progressed to a depth of 26.8 m at a diameter of 200 mm to investigate the ground conditions. This borehole was then enlarged to 300 mm in diameter up to 24 m in depth to install instrumentation and 32mm diameter geothermal loop. The remaining section of the borehole was backfilled by cement. The borehole was grouted via galvanized pipe with site mixed C35 cement/sand/water, pump-able mortar grout mix, which can achieve a compressive strength of 35N/mm2 at 28 days.

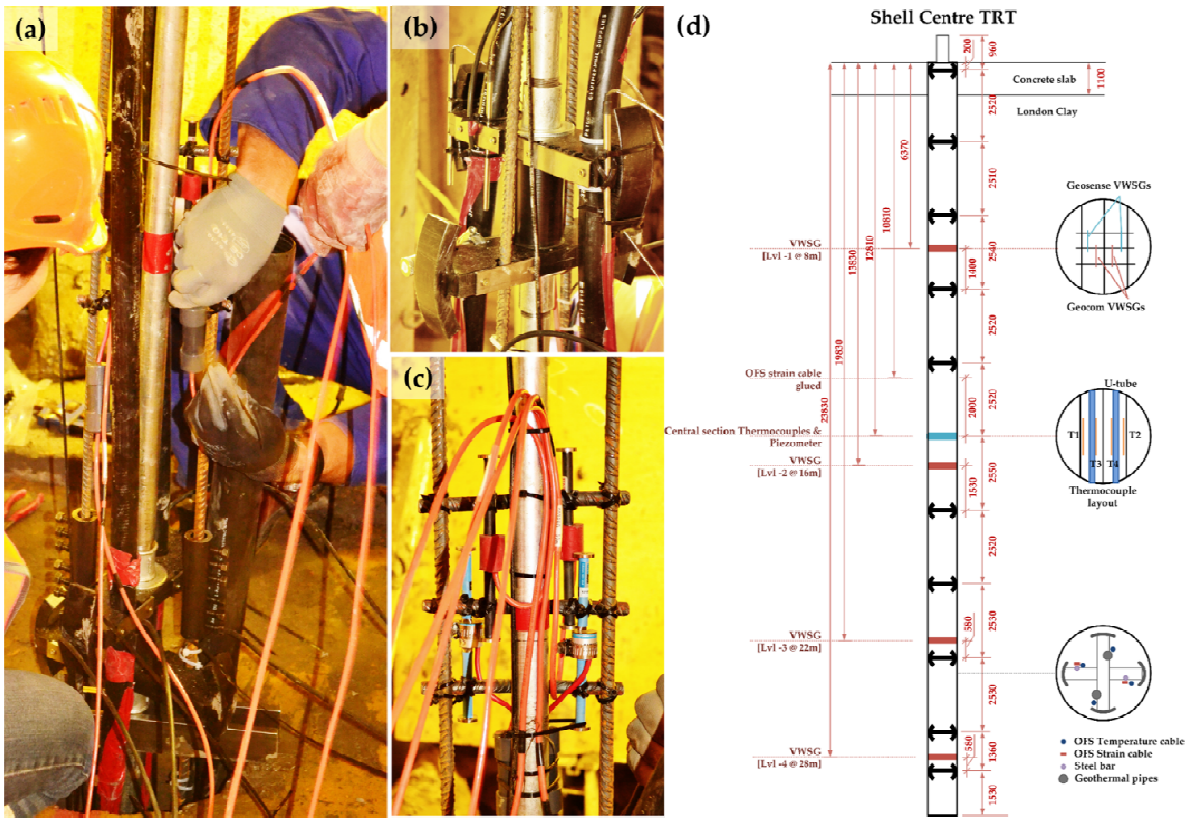


Fig. 1. Field installation. a) Installation of the bottom plate with all instrumentation as well as the HPVC geothermal pipe; b) Detailed orientation of the geothermal pipe and instrumentation; c) VWSG arrangement details; d) As-built instrumentation details of the column.

The installation of the column was carried out at the basement level in a car park with only 2 m of headroom space. Due to restrictions with the limited headroom space, a staggered supporting system was designed to host all instrumentation and geothermal pipes in Fig. 1.

The supporting system consisted of a cross-shaped spacer as shown in Fig. 1(b), which could clamp the inlet and outlet of geothermal pipe. It could also host all instrumentation on the separated 'wing' to avoid potential direct impact from dynamic temperature change from the circulating thermal fluid.

A series of these cross-shaped spacers were staggered by 1 inch perforated British Standard Pipe (BSP) galvanised pipe with 1.25 m in length in Fig. 1(c) with the installation detail of VWSGs.

The use of such a support system improved the installation efficiency by clamping the geothermal pipes and instrumentation to the spacer, where the BSP could be used later on as grouting pipe. The sketch in Fig. 1(d) shows the details of instrumentation levels and the spacer supporting sections along the column.

There are two types of Optical Fibre Sensors (OFS) employed in the current project in Fig. 2, which includes temperature and strain sensing cable. OFS in each sensing cable were the single mode OFS sensor, however, the OFS sensors are coated differently as shown in Fig. 2. Temperature sensing cable is designed not to carry any deformation so that OFS can be used to detect changes by temperature solely, therefore OFS is encapsulated in a gel filled tube as shown in Fig. 2(a) and the fibre optic cable is strengthened by an outer jacket which is flame retardant, UV stabilised and extremely resistant to the ingress of moisture. However, the OFS in Fig. 2(b) is tightly bonded by strong nylon coating in strain sensing cable which enables the deformation to be transferred to the OFS for strain sensing, and ensures that there is no creep among, the sensor, the coating material and host structure.

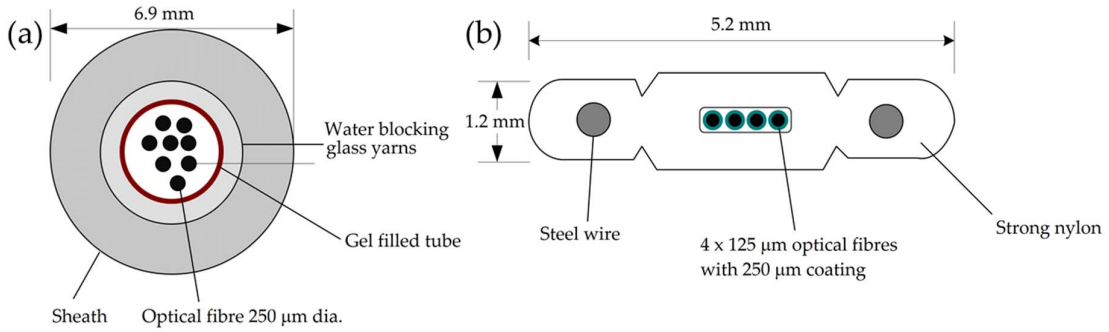


Fig. 2. Fibre optic sensing cable adopted in the project. (a) Unitube temperature sensing cable; (b) Fujikura strain sensing cable.

The OFS cable usually installed with a loop configuration to provide the access from both ends of the column. In this case a base plate was designed to host OFS cables at the bottom of the column, and both the OFS strain and temperature cables were looped and protected on the base plate as shown in Fig. 1(a). One set of OFS strain and temperature cables was attached to the rebar by cable ties and the other loop of OFS temperature cable attached to the geothermal pipe by the heavy-duty tape as shown in Fig. 1(a). Both of instrumentation and geothermal pipe work were installed simultaneously as the whole support system was being lowered down into the borehole.

The OFS strain cable was installed with approximately 2000 με of pre-tension strain along the column by Alridite2021 glue, whilst VWSGs were installed concurrently with the OFS cable at staggered levels along the column. OFS strain cable normally needs to pre-tensioned during the installation to ensure that the OFS strain cable is constantly subject to tensile strain. The benefit of applying pre-tension to the strain cable was to avoid buckling the cable. To ensure the VWSGs were secured to the

designated location along the column, two additional steel bars were added to create a bridge to align the four VWSGs in Fig. 1(c). The data logger for VWSG and fibre optic system was set up after installation. Fig. 3 summaries magnitude of input fluid temperature from each thermal cycles together with the data measurement from both types of system.

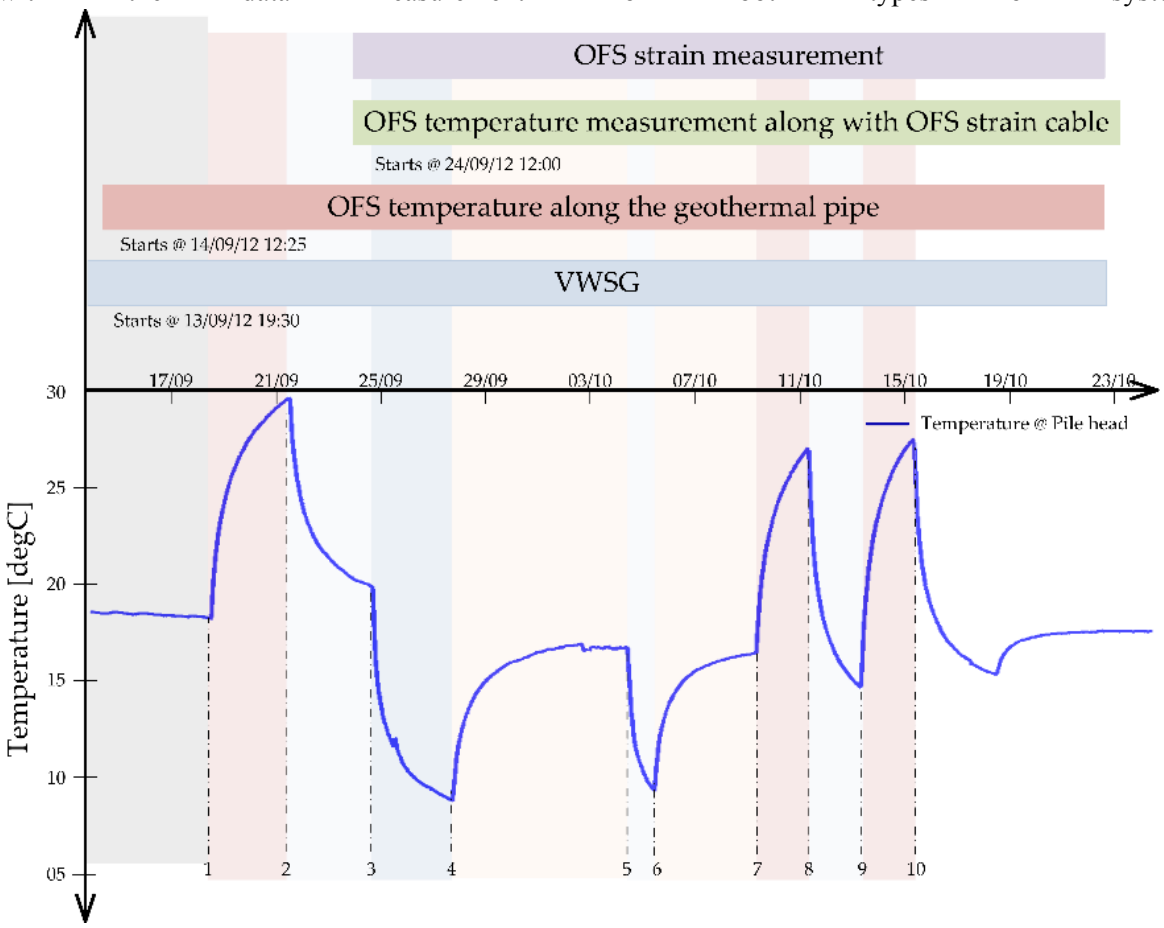


Fig. 3. Chronology of the field test.

DISSCUSSION

Discussion - 1: Calibration of thermal locked-in strain

Each sister-bar-typed VWSG has a built-in thermistor to compensate temperature. Due to the magnitude of temperature fluctuation during the TRT, it is important to highlight the importance of compensating temperature from the strain measurement. After the VWSG is embedded in the structure, the movement will be restricted by its host material due to the thermal inertia responses. The thermal locked-in strain would be a composite strain due to the relevant movement of host material and gauge due to the temperature change. Therefore to compensate for the temperature effects for a VWSG fixed in a concrete member, thermal restrained strain can be obtained by

$$\varepsilon_{th,R} = (\varepsilon_1 - \varepsilon_0) + (T_1 - T_0) * K$$

where ε_0, ε_1, T_0, T_1 are the initial and final strain and temperature recorded by VWSG, K is the difference of thermal expansion coefficients between VWSG and concrete material. In the current study the thermal expansion coefficient of VWSGs is $12.2x10^{-6}m/m/°C$ (similar to steel material) and that of the concrete is $9.65x10^{-6}m/m/°C$, which gives the composite thermal expansion coefficient K as $2.55x10^{-6}m/m/°C$. The fully restrained thermal strain profiles are calculated as the product of the temperature and the thermal expansion coefficient of the concrete.

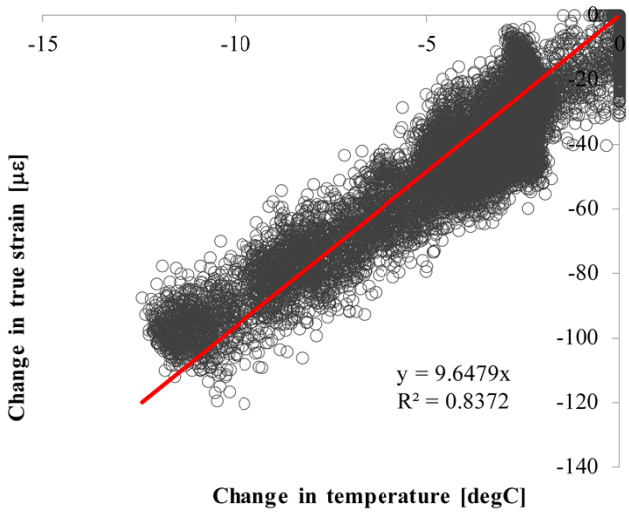


Fig. 4. The overall thermal response of the pile in the cooling phase from the top pile section.

It is often difficult to estimate the thermal expansion coefficient from the in-situ pile. As the column is thermally loaded without structural load, the top section is assumed to respond only to the thermal load, and has minimal interaction with the surrounding soil. The strain and temperature measurement reported by VWSG at the top of column shown in Fig.4 suggests that the effective thermal expansion of the concrete is approximately $9.56\ x\ 10^{-6} m/m/°C$.

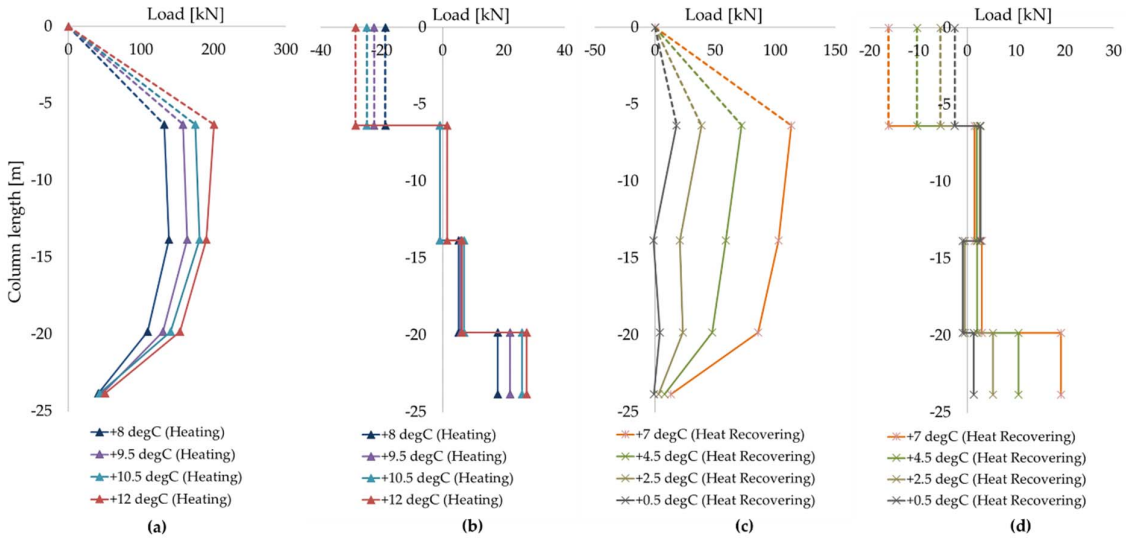


Fig. 5. Calculated thermal load profile with the mobilised skin friction from the first heating phase recorded by VWSG. (a) thermal load profiles from the column and the mobilised skin friction in (b); (c) thermal load profiles from the recovering period after heating and the associated skin friction mobilised during this period in (c).

The corresponding thermal strain generated during the first active heating and the heat recovery phases are shown in Fig. 5. The maximum thermally generated load is found at the middle of the column with no/negligible amount of thermal load generated at both ends of the column. It implies that the column is expending at the both ends in heating with small amount of restriction with increasing restriction on column movement towards the middle of the column. The movement at the middle of the column was small, therefore the mobilised skin friction in Fig. 5(b&d) was smaller than both ends. The mobilised shaft resistance at bottom of the column is found to be 30 kPa, with the equivalent amount of negative shaft resistance developed at the top of the column.

Discussion - 2: strain spikes

The OFS system is capable of providing distributed measurement at 10 cm interval, which offers advantages to examine the behaviour of the structure in significant detail. Fig. 6 presents two sets of strain profiles measured by OFS sensors at the first heating and cooling phase respectively together with the position of each plastic spacer. There are six pronounced strain spikes generated at the first cooling phase comparing with the strain profile collected at the end of the first heating phase in Fig. 6(a). Further investigation has carried out to examine the cause of these peak strain events along the column. According to the built records from site, spacers are staggered at approximately 2.5 m intervals along the column. Each spacer location are marked by the red dots in Fig. 6(b), which shows that the peak strain events with relevant locations of the spacers.

Arguably that the spacer system could potentially contribute to the fact that it disturbed the integrity of the column as there is not enough clearance space for the grout. As the spacer is made of HPVC material, and the thermal expansion of HPVC material is roughly 10 times of the grout material. Such a difference in thermal expansion coefficient between the spacer and grout material can cause a localized cracking or discontinuity between two materials at the beginning of the thermal testing period, which was the first heating sessions. But the strain measurement reported by OFS does not show any peak strain at the heating phase. It is more likely that cracks are formed during the first cooling session when the column is subject to cooling compression. This agrees with the field measurement presented by Bourne-Webb et al. (2009) that the energy pile experienced significant amount of tensile strain at the bottom of the pile after an extensive cooling period. Strain spikes generated at the end of the first cooling phase are found consistently throughout the testing period.

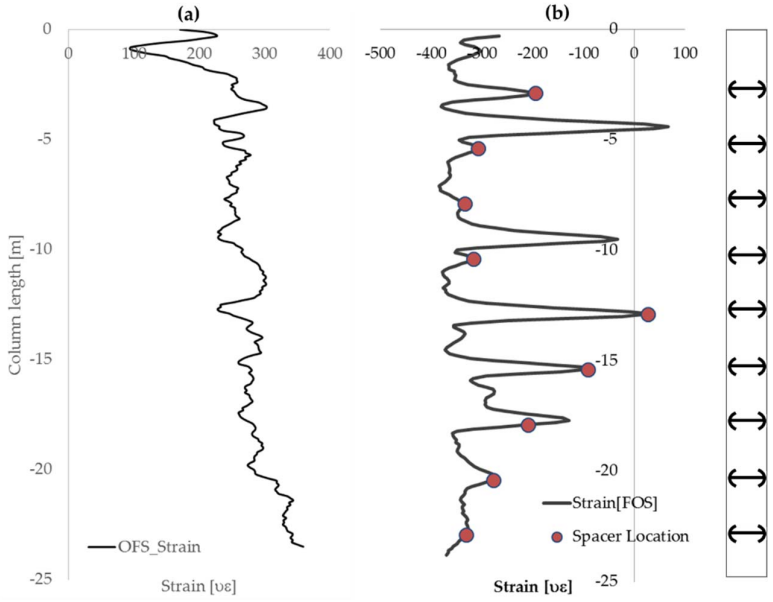


Fig. 6. Thermal cracks generation along the column shaft due to the cooling load. (a) Strain measurement at the end of the 1st heating; (b) Strain measurement at the end of the 1st cooling phase with corresponding spacer position along the column.

Discussion -3: cyclic behaviour of the column

Two sets of strain measurement reported by OFS together with VWSG and the free expansion strain from the column are presented in Fig. 7 from the cooling and heating phases. The measurement reported by OFS and VWSG sensing system shows reasonable agreement throughout the test. However, the VWSGs are unable to capture the cracks. Due to the existence of the cracks along the column, the strain profile reported by both sensing system indicates that the column contracts freely

during cooling where the strain profile shows similar magnitude to the free expansion or contraction as the temperature applied to the column in Fig. 7(a). The cracks have weakened the soil-pile interaction during the cooling phase. However, the magnitude of the cracks reduces during heating as shown in Fig. 7(b). The strain profiles reported by OFS and VWSG show that the column expands with tensile strain developing at both ends in the heating phase. The middle section of the column is restrained by the soil. The soil-pile interaction re-establishes during the heating phase as the magnitude of cracks reduces.

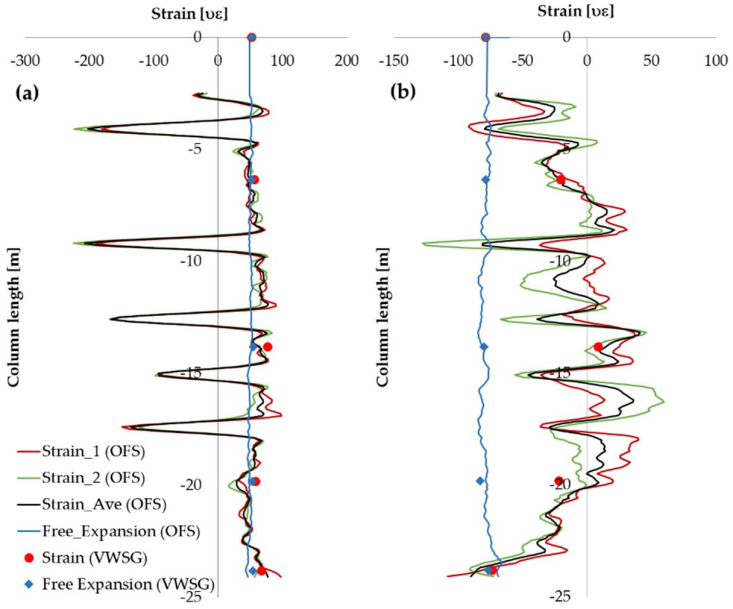


Fig. 7. Strain profiles measured from OFS and VWSG at the end of cyclic cooling and heating phases. (a) Cooling; (b) Heating.

The temperature distribution along the geothermal pipe from inlet and outlet is captured by OFS throughout the testing period in Fig.8. Temperature reported along the inlet and outlet pipes show a similar magnitude from the cooling phase, but there is an approximate -3°C difference between the inlet and outlet temperatures in the heating phase. It indicates very limited amount of thermal exchange process during cooling phase. As the column was found to contract freely in the cooling phase from the OFS strain measurement in Fig. 7(a), it confirms that the cooling generates tensile cracks along the column which leads to a reduction in soil-pile interaction. The weakened soil-pile interaction also reduces the thermal exchange process between the column and the surrounding soil in Fig. 8(a).

The soil-pile interaction re-establishes during the heating phase as shown in Fig. 7(b). The inlet fluid temperature in Fig. 8(b) at the top of the column is 13°C, and the majority of the temperature from the outlet started to reduce between – 17 to 0 m along the column. The outlet fluid temperature shows approximately 10°C at the bottom of the column. This agrees well with the physical behaviour of the column observed by the OFS strain measurement in Fig. 7(b), where the soil-pile interaction can be re-established with smaller magnitude of tensile strain. The magnitude of cracks reduces in the heating phase due to expansion of the grout material, which improves the soil-pile interaction. As the column expands at both ends, the middle section of the column is restrained by the surrounding soil. It also leads to the further improvement in thermal exchange process in Fig. 8 (b).

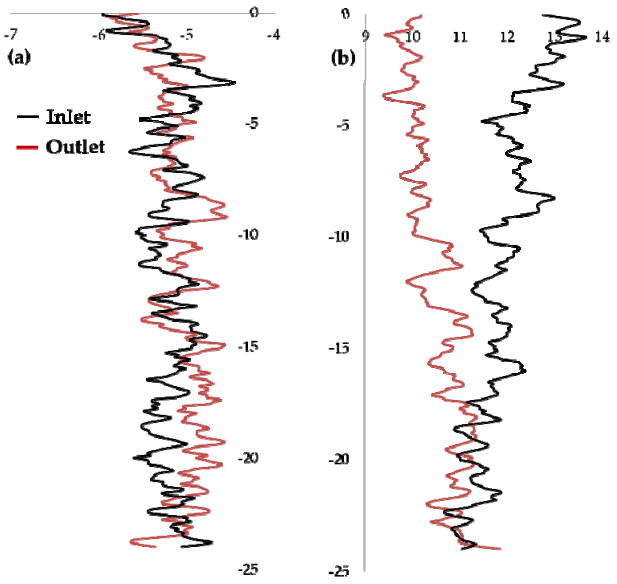


Fig. 8. Temperature measurement reported from geothermal pipe along the column from cooling and heating phases respectively. (a) Cooling; (b) Heating.

The locked-in thermally load at the end of the heating phase can be estimated by assuming that the both end of the column were not experiencing any thermally generated load as shown in Fig. 9. The difference between free expansion strain and the strain reported by OFS indicated the total amount of locked-in thermal strain along the column. The thermal load profiles from the two heating phases are summarised in Fig. 9, which implies the mobilized thermal shaft friction between 0m to 9m was +19 kPa, and -34 kPa between 19 to 24m along the column. Comparing with the mobilised friction at the first heating phase, the shaft friction between 0m to 9m reduced from +30 kPa to +19 kPa, which could be potentially caused by the cracks.

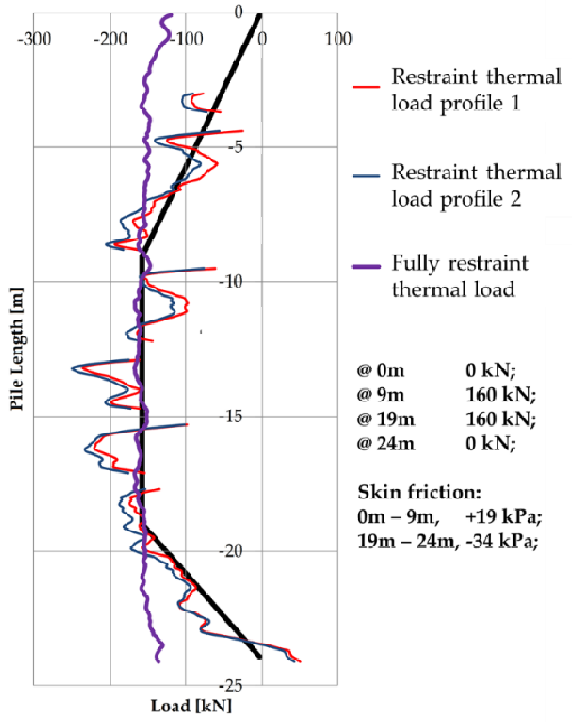


Fig. 9. Mobilised shaft friction calculated from OFS and VWSG in relevant to the temperature change during the heating phase with +13□C change in temperature.

CONCLUSIONS

The behaviour of the cement grouted column was successfully captured by VWSG and OFS at different thermal cycles. The distributed measurement reported by OFS captured the several tensile cracks generated along the column, which was missed by the VWSG. It demonstrated the advantage of using distributed sensing in monitoring geotechnical infrastructure.

Due to the tensile cracks, the thermo-mechanical behaviour of the column was modified throughout the test. The column was able to contracting freely in the cooling phases with weakened soil-pile interaction. But the soil-pile interaction was re-established in the heating phase as the magnitude of cracks reduced. The column was found to be fully restrained at the middle section during the heating phase, while both ends were expanding freely. The mobilised shaft friction was estimated to be 30kPa from the first heating phase at both ends of the column. However, it reduced to 19 kPa at the top section of the column at the end of the cyclic heating phase.

Temperature measurement from the geothermal pipes also indicated the active thermal exchange process between the column and soil in heating phase comparing the cooling phase. It corresponds well with the thermo-mehanical behaviour of the column captured by the OFS. Therefore the physical interaction between the column and soil appeared to also have influenced the thermal interaction. It provided further evidence to suggest that there were more active thermal exchange activities between the column and soil during the heating phase than the cooling phase.

ACKNOWLEDGEMENTS

The authors would like to thank Arup, Canary Wharf Group in supporting the field trial. Further acknowledgement goes to the site investigation contractor Concept for facilitating the field work, and especially Geosense Ltd for providing the field support in installing the VWSGs and fabricating the spacer supporting system for the project.

REFERENCES

Amatya, B. L., Soga, K., Bourne-Webb, P. J., Amis, T., & Laloui, L. (2012). Thermo-mechanical behaviour of energy piles. Géotechnique, 62(6), 503–519. https://doi.org/10.1680/geot.10.P.116

Bourne-Webb, P. J., Amatya, B., Soga, K., Amis, T., Davidson, C., & Payne, P. (2009). Energy pile test at Lambeth College, London: geotechnical and thermodynamic aspects of pile response to heat cycles. Geotechnique, 59(3), 237–248.

Bourne-Webb P. J., Amatya B, & Soga, K. (2011). A framework for understanding energy pile behaviour. Proceedings of the ICE - Geotechnical Engineering.

Brandl, H. (2006). Energy foundations and other thermo-active ground structures. Geotechnique, 56(2), 81–122.

Knellwolf, C., Peron, H., & Laloui, L. (2011). Geotechnical Analysis of Heat Exchanger Piles. Journal of Geotechnical and Geoenvironmental Engineering, 137(10), 890–902.

Ouyang, Y. (2014). Geotechnical behaviour of energy piles. University of Cambridge.

Ouyang, Y., Soga, K., & Leung, Y. F. (2011). Numerical back-analysis of energy pile test at Lambeth College, London. In Geotechnical Special Publication (pp. 440–449).

Peron, H., Knellwolf, C., & Laloui, L. (2011). A method for the geotechnical design of heat exchanger piles. In Geotechnical Special Publication (pp. 470–479).

Rotta Loria, A. F., & Laloui, L. (2016). The interaction factor method for energy pile groups. Computers and Geotechnics, 80, 121–137. https://doi.org/10.1016/j.compgeo.2016.07.002

VENTILATION SHAFTS AND DRIFTS FOR THE METRO LINE 6 PROJECT IN NAPLES, ITALY

Vittorio Manassero, Underground Consulting, Pavia, Italy, v.manassero@undergroundconsulting.it
Giorgio Mormone, Paolo De Luca Costruzioni Generali, Napoli, Italy, g.mormone@dlholding.com
Federico Moccia, Ansaldo STS, Napoli, Italy, Federico.Moccia@ansaldo-sts.com

ABSTRACT

The paper deals with the application of construction methods which have a low impact on the surrounding buildings and utilities, while geotechnical and underground works are being carried out. At Metro Line 6 in Naples the ventilation system entails underground chambers connected to the TBM tunnel by a vertical shaft and a horizontal drift. The shafts are constructed adopting a technologically innovative solution, the VSM (Vertical Shaft-sinking Machine) construction method. This mechanized system, as well as enabling a faster and safer excavation compared with conventional techniques, allows the whole construction to be completed without operators having to descend into the shaft and without lowering the surrounding water-table. This means a considerable increase in safety for operators and a significant reduction in the effects on the surrounding environment, particularly relevant when operating in urban areas. For the connection drifts a preliminary soil or rock improvement was designed according to the soil to be bored: penetration grouting in rock and jet grouting in loose soil. Monitoring of the effects on the surrounding buildings and utilities is in service before, during and after the site activities. The monitoring is confirming the low impact of the construction method adopted, settlements and disturbance by vibration resulting as negligible.

Keywords: shaft, VSM, tunnelling, grouting, jet grouting

INTRODUCTION

Metro Line 6 is becoming part of the integrated system of the Naples subway and represents a coastal East-West corridor for the town, connecting Fuorigrotta, Riviera di Chiaia and the Harbour (Fig. 1). Conceived at first as a tramway line, it was then converted into a metro line, adopting the architectural and functional standards already successfully tested on Line 1. (De Risi 2014).

The new metro lines in Naples are in fact now constructed adopting a new design approach, involving the architectural and functional review of all the stations, and installing numerous contemporary artworks; the by now well-known “Art Subway”. This has allowed an ever-tighter connection between the construction works and the involved land, consisting of frameworks with great urbanistic and historical value, but also with a heavy urban and social decay (De Risi 2007). Furthermore, the



Fig. 1. Layout of Metro Lines 1 and 6 in Naples

© 2018 Deep Foundations Institute

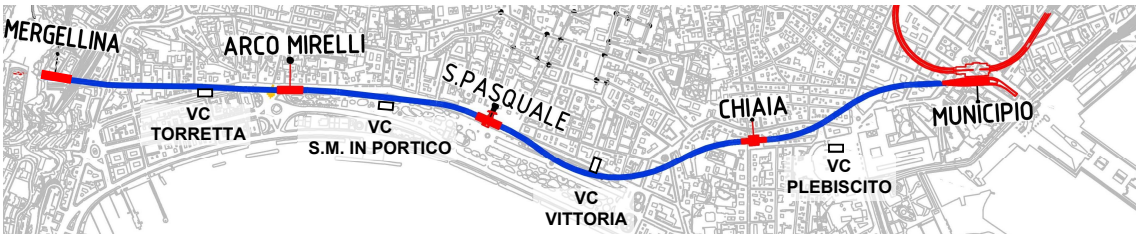


Fig. 2. Layout of the stretch under construction of Metro Line 6, from Mergellina to Municipio

important archaeological remains found, in particular along Line 1, suggested during construction design reviews at some stations to allow the housing of such finds, in this way integrating Architecture, Archaeology and Art (as an example Russo et al. 2016) and leading to the new term "3 A Subway".

Line 6 consists of a stretch already completed and in service, connecting the Fuorigrotta and Mergellina districts, and a stretch currently under construction between the Mergellina district and Piazza Municipio. The first stretch, 2.2 km long with 4 stations, reutilized and completed the works carried out for the Rapid Tramway Line (LTR), that was previously supposed to come into service for the "Italia 90" football world championship. The stretch currently under construction, 3.3 km long, is characterized by a double track TBM tunnel and 4 stations. Starting from Mergellina, the stations are: Arco Mirelli, S. Pasquale, Chiaia and Municipio (Fig. 2).

Line 6 interconnects at Mergellina station with Line 2 and at Municipio station with the Line 1 station of the same name, with which it composes a unique important hub, not only for the railway but also including the Marine Terminal and Beverello Wharf. Once in service, Line 6 will be able to transport 7.600 passengers per hour for each direction, a further contribution to reducing the surface traffic. At each tunnel segment between stations, there is a ventilation chamber (VC), 4 in total. Each ventilation chamber is connected to the TBM tunnel by a vertical shaft and a horizontal drift at the base of the shaft. The system, in addition to tunnel ventilation, provides a safety access/escape route that increases passenger safety in case of fire (De Risi 2009).

DESCRIPTION OF THE PROJECT

The ventilation chambers envisaged are at Torretta, Santa Maria in Portico, Piazza Vittoria and Piazza Plebiscito (Fig. 2). The last one at design level was originally foreseen at Piazza Carolina, then moved to Piazza Trieste e Trento, then to the Carlo Felice Theatre car park and is now at the location of Piazza Plebiscito. The design of this ventilation chamber is still under study.

The ventilation chambers are relatively shallow underground spaces used as technical rooms and each connected to the metro tunnel by a vertical shaft with a horizontal drift at its base (Fig. 3). The chambers to be used as technical rooms have a floor surface of about 200 m^2 and reach down to a depth of about 9 m. They are excavated thanks to a retaining structure made of a reinforced concrete secant pile wall, supported by appropriate internal struts. Since the excavation depth is lower than the water table, a horizontal low-permeability blanket is foreseen at the bottom, in order to avoid excessive dewatering from the excavation, which might cause a generalized lowering of the surrounding water table, with not inconsiderable consequences on the pre-existing buildings and utilities.

The ventilation shafts are 5.5 m I.D. and from 24 to 29 m deep. They were constructed by using the VSM (Vertical Shaft-sinking Machine) construction method, a recent innovation in mechanized technology for boring and simultaneously lining vertical circular shafts, with inner diameter from 4.5 to 10.0 m, down to a maximum depth of 80 m or more. The method is applicable to any type of soil and to many types of rocks, both above and below the water-table (Manassero 2012).

Boring is carried out by inverse circulation of fluid within a flooded shaft, and the permanent lining, made up of rings of precast reinforced concrete segments which are added at the surface, is sunk into

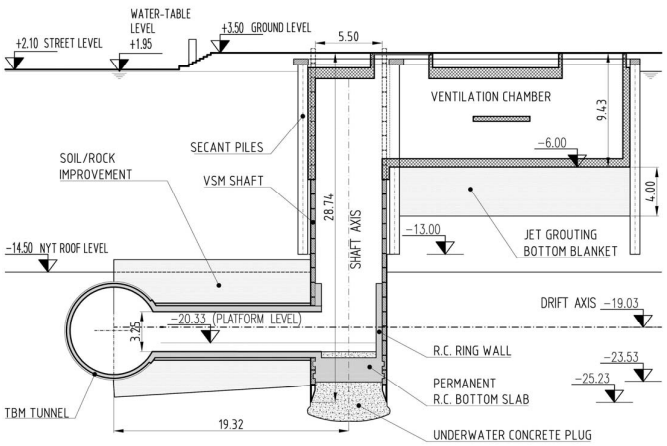


Fig. 3. Example of the construction arrangement of a ventilation chamber (S. Maria in Portico)

the shaft progressively as the excavation continues at the bottom. The permanent lining is built up of rings 1.2 m high and 35 cm thick, composed of 3 segments. The lining, fitted with rubber seals, is designed to ensure watertightness for pressures of up to 5 bar.

The connection drifts have inner size of (b x h) 3.00 x 3.25 m and they are 5 to 15 m long. For their excavation, an intervention of soil improvement was specifically designed, keeping in sight the different soils and rocks to be excavated: penetration grouting for the Neapolitan Yellow Tuff and jet grouting for the loose soils.

GEOLOGICAL AND GEOTECHNICAL BACKGROUND

The soil profiles at the ventilation chamber locations, within the depths relevant to the works, may be summarized as follows:

- Torretta we find an alternation of seaside and dune deposits made of sands (first medium-fine and deeper medium-coarse) and volcanic deposits made of cinerites down to a depth of 18 m below ground level (at about the center of the connection drift to be excavated); below this depth we find the bedrock made of Neapolitan Yellow Tuff (NYT);
- Santa Maria in Portico (SMP) we find an alternation of medium-fine sands and cinerites down to about 18 m (3 m above the connection drift crown) and below this depth NYT;
- Piazza Vittoria we find an alternation of medium-fine sands and cinerites down to the maximum depth of interest for the works;
- Piazza Plebiscito we find pyroclastic sands down to a depth of about 15 m and then NYT.

For further details please refer to L'Amante et al. 2012.

SECANT PILE WALLS AND BOTTOM BLANKETS

The secant piles are foreseen as retaining structures at the boundary of each shaft and of each chamber to be used as a technical room (Fig. 3), except for Torretta VC where it was possible to take advantage of the existing diaphragm wall installed during the '80s within the network of the LTR. The secant piles are bored by using a rotary rig and by simultaneously penetrating the soil with the temporary casing and the continuous flight auger fitted inside. The latter, further to producing the disaggregation of soil or rock at the tip, acts as screw conveyor to evacuate the debris from the borehole. Upon reaching the design depth, concreting is carried out by pumping concrete through the hollow rod of the continuous auger and simultaneously withdrawing the whole drilling string as the concrete level rises. The piles are separated into primary and secondary. Primary piles remain unreinforced, while the secondary ones are fitted with a steel cage lowered into the hole at the end of concreting, by sinking it into the fluid concrete. The concrete has fluidity and workability characteristics specific to enabling the sinking of the cage.

The low permeability bottom blankets are foreseen at both shaft pre-excavations and chambers, in order to allow digging without excessive dewatering from the excavation. The blankets are made with 1.2 m jet grouting columns located in an equilateral triangle pattern with side 0.90 m and overlapping each other. The pattern was calculated taking into account the possible and unavoidable drilling deviations from the theoretical axis, within the tolerances allowed by the technical specifications.

THE VSM TECHNOLOGY

What makes the VSM system special is the specifically designed equipment, which includes the following four main components (Manassero et al. 2016):
- a shaft boring unit,
- a hanging/lowering unit,
- a separation plant,
- a remote control unit.

A diagram of the equipment is shown in Fig. 4, while the installation of the boring unit at one of the sites is shown in Fig. 5.
The boring unit consists of a milling machine fitted with a cutter drum, driven by a telescopic swiveling and rotating boom (Fig. 4 and 5). During operation, the boring unit is tightly fixed by hydro-mechanical devices to special steel plates welded at the bottom of the shaft's permanent lining and it can be locked/unlocked as necessary by dedicated hydraulic system. The cutter drum disaggregates soil and rock and the resulting debris, in suspension within the fluid, is pumped out by a pump positioned just above the cutter drum, to the separation plant on the surface. The boring unit is connected to the surface by means of an "energy chain" made of high pressure hoses, electric cables and evacuation pipes. The machine is driven by devoted hydraulic power-pack and 1000 kVA electricity generator.

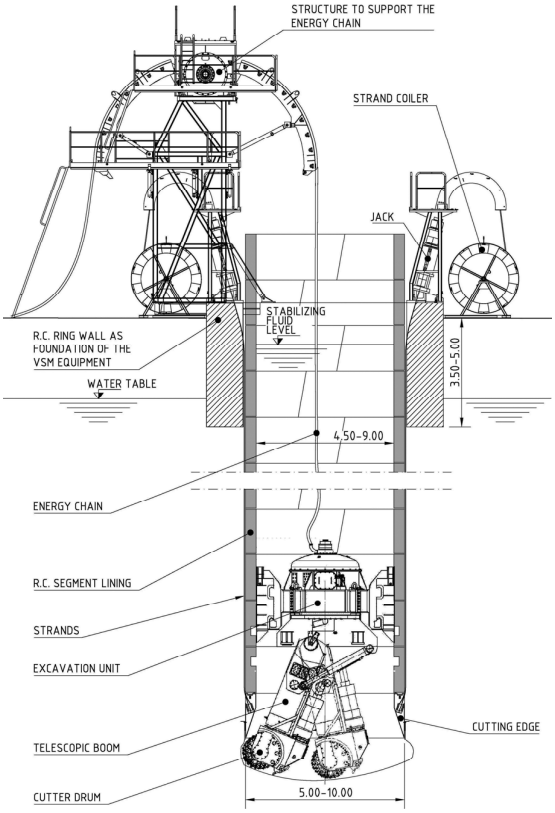


Fig. 4. Example diagram of the VSM equipment



Fig. 5. Boring unit during installation at the Santa Maria in Portico shaft

The hanging/lowering unit (Fig. 4) is located at the surface and performs the function of hanging and lowering the shaft lining as the excavation proceeds. It is fitted with a set of jacks (usually 3), bundles of strands (each one driven by a jack), a tower to support the "energy chain" and a set of three winches to recover the machine at the end of sinking or at any time when necessary. The unit is also capable of applying a downward force to the lining, should it be required, and to control and subsequently correct any boring deviation due to constant inclinometer measurements.

The separator plant (Fig. 6) is located at the surface and performs the function of regenerating the slurry coming from the shaft under excavation, by separating debris from drilling fluid. It is composed of desanders with vibro-screens to intercept the coarser particles, and cyclones to intercept the finer particles (fine sand and silt). When boring through clayey layers, it may be appropriate to integrate a centrifuge into the plant, to help the separation of clayey particles.

The remote control unit consists of a cabin located at the surface, nearby the shaft, containing all the monitors and control panels to allow the operator to drive the machine (in the same way as with the TBM driving for mechanized excavation of tunnels).

The precast segment permanent lining

The permanent lining consists usually of superposed rings made up of precast reinforced concrete segments. However, the use of cast in place permanent lining was already experienced (Schmäh 2009). The lining is assembled at the surface simultaneously to shaft sinking, by erecting on top of the shaft the segments forming each ring. The segments are mechanically connected to each other by a system of circumferential bolts and a system of vertical steel threaded bars, plates, nuts and couplers (Fig. 7). In this way, the lining becomes a monolithic hollow cylinder, capable of carrying compression stresses in both vertical and horizontal planes and, if necessary, also bending moments. The assembled lining is made watertight by rubber seals installed on all the contact surfaces between segments.

The lowest ring, also referred to as the shaft's cutting edge, is made of a ring of either box-shaped steel or concrete and steel. Bevelled at the bottom, it can cut into the soil underneath (Fig. 7 and 8). The cutting edge is fitted with an external steel ring forming an enlargement, to grind and overcut the



Fig. 6. Separator plant at the Torretta ventilation chamber

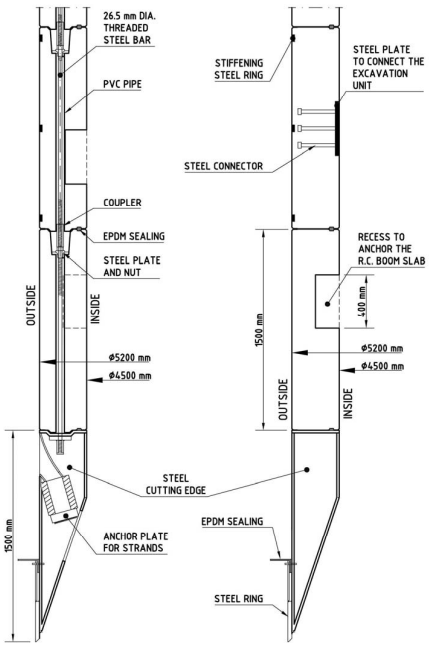


Fig. 7. Precast lining, showing connection system, lower segment and cutting edge



Fig. 8. Cutting edge and strand anchoring system for lining hanging and lowering



Fig. 9. A lower segment with bottom slab recesses and boring unit fastening plates

surrounding soil, in order to ensure a temporary annular gap between permanent lining and soil for the whole duration of sinking. The cutting edge is equipped with devices to anchor the hanging and lowering strands and with a circular L-shaped EPDM seal (Fig. 7).

On the lowest precast r.c. rings, dedicated steel plates are set up on the internal surface (Fig. 9) to fasten the boring unit. As a rule, suitable recesses to allow the subsequent interlocking of the final reinforced concrete bottom slab are installed on these rings, just above the cutting edge (Fig. 9).

Construction procedure

As a first step, a pre-excavation is carried out down to 3.5-5.0 m below ground level. This is in order to lower the first precast rings necessary to install and fasten the boring unit, and to prime the submerged evacuation pump at the beginning of boring. Without particular boundary restrictions, the pre-excavation may be carried out simply by slope digging, followed by casting in place an annular reinforced concrete wall. This wall acts as both retaining structure and equipment foundation. Alternatively, when there are restrictions that prevent this way to proceed, such as the proximity of buildings or utilities or a very shallow water table (both restrictions are present in this case study), the pre-excavation is carried out within a specific retaining structure installed in advance at the boundary. This retaining structure is usually a secant piles (technique chosen for this case study) or diaphragm wall and acts also as equipment foundation. In presence of shallow water table, a low permeability bottom blanket may be necessary.

The first rings are assembled within the pre-excavation, above the cutting edge. Once the segments fitted with the dedicated steel plates are in place, the boring unit is lowered in and fastened to them.

The boring unit operates entirely submerged within the stabilizing fluid (water or bentonite slurry). The fluid fulfils the double purpose of supporting the soil and evacuating the debris. The ring-shaped gap between permanent lining and soil is continually kept full of dense and viscous bentonite slurry, for the whole duration of sinking. This also reduces the frictional forces between shaft wall and surrounding soil. The selective filling of the external gap is made possible by two features. Firstly, the presence of special non-return valves, installed on the bottom segments at two different levels, which are fed with bentonite slurry through dedicated circuits. Secondly, the circular L-shaped EPDM seal, which keeps the stabilizing fluid flooding the shaft separate from the bentonite slurry filling the external annular gap. The level of both fluids is maintained continuously above the water table. In this way the soil supporting and the water pressure balancing functions are performed.

Soil and rock are disaggregated by the cutter drum, which covers programmed paths thanks to its ability to swivel up and down and to rotate 360°. Such programmed paths are controlled together with the on-going sinking process by the operator in the remote control unit, and they allow the drum to gradually sweep the entire cross section of the shaft below the cutting edge, plus an overcut usually of

50 to 150 mm. At each construction step, the soil disaggregation proceeds down to a predetermined depth, so as to create the necessary room for the partial sinking of the permanent lining which is carried out in uniform sized steps (usually 0.30-0.50 m). The resulting debris, in suspension within the fluid, is evacuated by a submersible pump installed just above the cutter drum and piped to the separation plant located on the surface, where they are separated from the drilling fluid. The material separated from the slurry is dumped beside the plant and then loaded by loader or backhoe and disposed of by truck. The regenerated fluid is pumped back to feed the excavation, at a rate equal to the evacuation rate, to continuously replace the evacuated fluid as boring proceeds.

Simultaneously to boring, the permanent lining is lowered (or pushed, if necessary) to replace the soil removed by the cutting drum below the cutting edge. Once the lining has been sunk for a depth equal to the height of the ring, the erection of the segments to assemble a new ring on top of the shaft can proceed. The ring assembly is completed by clamping the mechanical connections, both vertical and circumferential. Now sinking of the permanent lining may be resumed as boring proceeds. This step working process of simultaneous boring, evacuation of debris, sinking of lining, segment ring assembly, is repeated up to achieve the design depth. Once the shaft sinking has been completed, the boring unit is unlocked and withdrawn using the dedicated winches installed within the hanging/lowering unit.

Subsequently, the shaft bottom is sealed by an underwater concrete plug (shaped like an inverted champagne-cork) poured through a tremie pipe, to backfill both the specific over-excavation and the lowest portion of the shaft lining. Then, the annular gap between permanent lining and soil is filled up and sealed with cement grout, creating a frictional support locking the shaft in place to avoid the long term buoyancy. The grout, fed through the same circuits and valves already used to pump in the bentonite slurry, replaces the bentonite slurry present within the gap since the start of sinking. Finally, after suitable curing of the bottom plug concrete and gap grout, the drilling fluid is pumped off and the shaft is ready for the installation of the permanent reinforced concrete bottom slab, which is locked into the segments fitted with the dedicated recesses. The shaft is now ready for use.

CONNECTING DRIFTS

To allow a safe and dry excavation of the drifts connecting VSM shaft and TBM tunnel, interventions of preliminary soil/rock improvement were designed according to the different characteristics of the soil/rock to be bored. Therefore, as a function of the different soil profiles at the ventilation chambers, the soil improvements are carried out by the following techniques:

- at the Santa Maria in Portico drift the NYT is improved by penetration grouting (both cement and chemical mixtures) carried out through *tubes à manchettes* installed from the bottom of the shaft;
- at the Piazza Vittoria drift the loose soil is improved by jet grouting installed from the surface;
- at the Torretta drift, with an intermediate condition between the two just mentioned, a combined soil improvement treatment is applied: jet grouting from the surface within the loose soil and penetration grouting (cement and chemical) from the shaft within the NYT underneath;
- no soil improvement design is available yet at the moment for the fourth drift (piazza Plebiscito).

The preliminary soil/rock improvement entails the formation of a min. 3 m thick shell of soil/rock of a higher strength/modulus and lower permeability all around the drifts to be bored. The NYT is a soft rock with widespread presence of cracks, both vertical (scarpine) and horizontal (suoli). These cracks, formed during the cooling process of the pyroclastic matrix, are the reason for the significant secondary permeability of the tuff, which may release a huge amount of water during excavation works. The intervention of tuff improvement all around the drift to be bored is therefore necessary to reduce to the minimum the dewatering flow-rate, for increased safety and a better work environment during boring and construction of the drift and to reduce to the minimum the effects of the works on the surrounding buildings and utilities. Within the NYT the improved shell is achieved by penetration grouting, by which the grout mixtures fill and seal the system of cracks replacing the water previously present inside, without any significant change of the original soil volume and structure. The technique entails an artificial seepage of grout mixtures with penetrability characteristics enabling them to flow through the cracks in the tuff. The thinner the cracks are, the better the penetrability of the mixtures has to be.

Grouting is performed using the MPSP method (Multi Packer Sleeved Pipes). This construction method consists essentially of the installation inside a borehole of a *tube à manchettes* (TAM), which is a plastic or steel pipe fitted at regular intervals with rubber grouting sleeves, equipped with geotextile bags fastened to the pipe. These bags act as permanent packers to seal off the holes at regular intervals, between which the grouting is to be confined. The sealing action of the bag packers is obtained by expanding them against the hole walls by injection of a suitable grout into the bags. After the packer grout has hardened, an upstage grouting is performed by means of double packer.

MPSP TAMs are installed inside sub-horizontal boreholes drilled from the inside of the VSM shaft, arranged in several concentric alignments along the whole boundary of the drift. As an example, Figure 10 shows a 3-D view of the soil improvement by grouting at the Santa Maria in Portico drift.

Grouting NYT by MPSP is an already well-tested method for rock improvement, having been applied in several cases at the Naples Line 1 jobsites (as an example Manassero et al. 2008; Manassero and Di Salvo 2012). The selective grouting is performed under pressure at low delivery. Two different grout mixtures are injected: a high-penetrability cement-based grout and a silica-based chemical grout (Silacsol-S).

In loose soils the improved shell is achieved by jet grouting, with vertical overlapping columns installed from the surface. The columns are 1.50 m dia. and arranged in an equilateral triangular pattern with sides of 1.05 m. The pattern was calculated also taking into account the likely and unavoidable deviations of the boreholes from the theoretical axis, within the maximum allowed tolerance range. At Piazza Vittoria drift, where the loose soil is found down to the maximum depth of interest for the works, the jet grouting treatment is integrated at the invert by permeation grouting through conventional TAMs. This is necessary in order to reach the volume of soil to be improved which would be unreachable with jet grouting from the surface, because obstructed by the TBM tunnel already in place. Through the jet grouting columns, once installed, horizontal boreholes from the VSM shaft are drilled in order both to check the success of the jet grouting treatment and to allow the installation of MPSP TAMs. These then perform additional grouting in order to enhance the soil improvement result. As an example, Fig. 11 shows the combined soil improvement treatment at the Torretta drift.

Once the soil improvement for the drift is in place, the permanent reinforced concrete bottom slab may be constructed, locked into the segments fitted with the dedicated recesses. To allow for boring the drift, it is necessary to open a hole of at least 3.50 m dia. through the segment rings which line the shaft (by diamond wire or saw). Without taking suitable measures, this hole would cause the lining to lose its structural continuity and hence its capacity to bear horizontal thrusts. Therefore, a ring-shaped

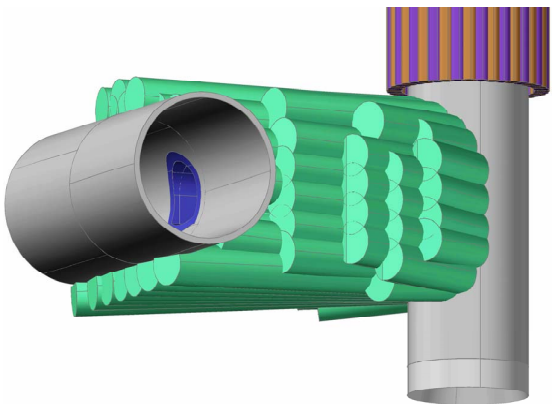


Fig. 10. 3-D view of the soil improvement at the Santa Maria in Portico drift

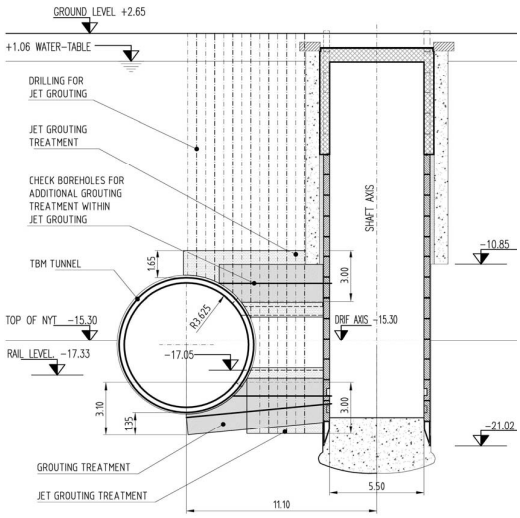


Fig. 11. Vertical section of the soil improvement at the Torretta drift



Fig. 12. View of the Santa Maria in Portico drift after boring and pre-lining with steel ribs and spritz beton

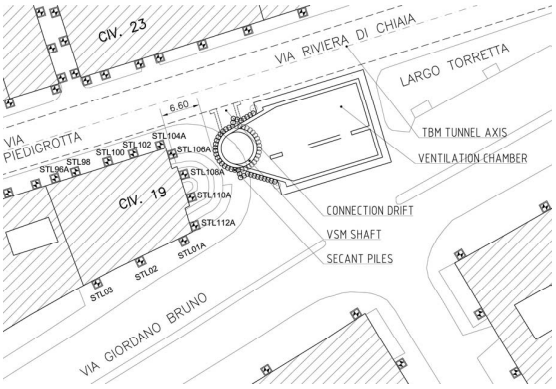


Fig. 13. Layout at Torretta VC, showing benchmark locations (numbered are those at 19 Largo Torretta)

wall made of cast-in-place reinforced concrete, 30 cm thick and 5 m high, is preliminarily constructed inside the shaft. This ring wall, already fitted with the necessary drift hole, replaces, statically speaking, the segment rings to be cut. The drift is then bored and pre-lined with steel ribs and shotcrete (Fig. 12) and then waterproofed and permanent lined.

MONITORING

The ventilation works at Line 6 are constructed in highly urbanized areas, sometime in narrow spaces and very close to surrounding buildings. At all the working areas a Displacements Monitoring System (survey monitoring) on all the surrounding buildings and utilities was operating before, during and after the construction. As an example, the results of the survey monitoring on the building at 19 Largo Torretta are shown. The building looks over the Torretta ventilation shaft and is located 6.60 m away from the nearest edge of the shaft. Figure 13 shows the layout of the area with the location of the structures and the control benchmarks, while Figure 14 shows the graph of vertical displacements vs. time for the most significant benchmarks installed on the building, over the different phases of the work. As we can observe, the vertical displacements during the whole period are fluctuating within a maximum range of ±2 mm, without any trend towards settlement. This graph is representative of vertical displacements measured on all the other buildings facing the working area. We can therefore state that displacements during and after construction on the surrounding area are negligible.

At Torretta a vibration monitoring system was installed inside the building at 23 Riviera di Chiaia street. Measurements are being taken since December 28, 2015. Figure 15 shows, as an example, a

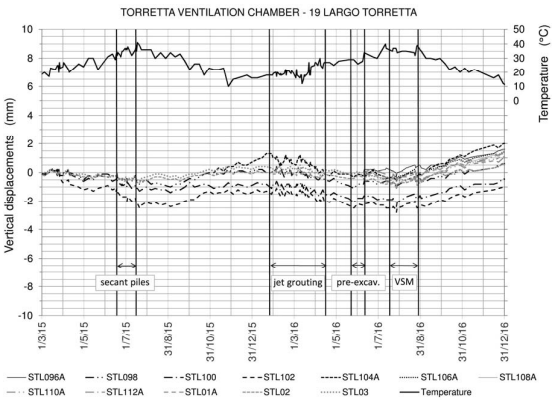


Fig. 14. Graph of the vertical displacements on the building at 19 Largo Torretta, before, during and after the works

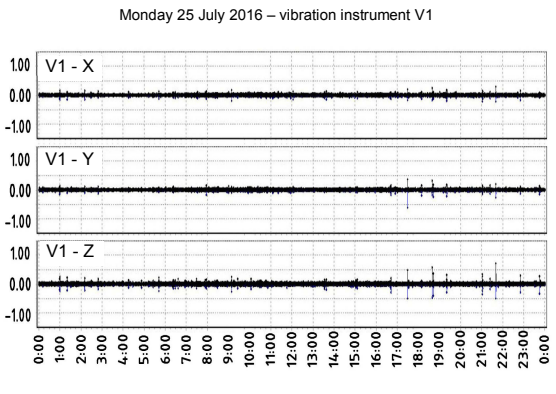


Fig. 15. Typical graph of vibration instrument installed on the building at 23 via Riviera di Chiaia, during VSM shaft sinking

typical graph of the vibration measurements during one day while shaft sinking was operating (July 25, 2016). In general, the measured velocities were fluctuating within a maximum range of ±0.5 mm/s and in all cases, as a consequence of the works, no significant increase in velocities was measured, compared to those in standard conditions.

CONCLUSIONS

This case study is a very good example of how complex underground works, below the water-table and in urban environments can be carried out with a low or zero impact on the surrounding architectural heritage. The application of a technologically innovative solution for the shaft construction; appropriate interventions of soil/rock improvement for the drift boring; low deformability retaining structures and low-permeability horizontal bottom blanket for the ventilation chambers; allowed the minimizing of settlements on the buildings surrounding the working area.

Specifically, the VSM system adopted for the shaft construction as well as enabling a faster and safer excavation compared with conventional techniques, allows the whole construction to be completed without operators having to descend into the shaft and without lowering the surrounding water-table. This means a considerable increase in safety for operators and a significant reduction in the effects on the surrounding environment, particularly relevant when operating in urban areas with an architectural and archaeological heritage.

REFERENCES

De Risi, A., 2007. Un gioiello che corre nel cuore di Napoli. Quarry and Construction, July.

De Risi, A., 2009. Il prolungamento della linea 1 della metropolitana di Napoli. Strade & Autostrade, No. 1/09.

De Risi, A., 2014. La linea 6 delle metropolitana di Napoli. Quarry and Construction, October.

L'Amante, D., Flora, G., Russo, G., Viggiani, C., 2012. Displacements induced by the installation of diaphragm panels. Acta Geotech. 7 (3), 213–218. http://dx.doi. org/10.1007/s11440-012-0164-9.

Manassero, V., 2012. Una soluzione d'avanguardia per la realizzazione di pozzi meccanizzati di grande diametro. Il Giornale dell'Ingegnere. No. 6, June, pp. 20-21.

Manassero, V., Di Salvo, G., Giannelli, F., Colombo, G., 2008. A combination of artificial ground freezing and grouting for the excavation of a large size tunnel below groundwater. Proc. of 6th Int. Conference in case Histories in Geotechnical Engineering. Arlington, VA, USA, August 11-16.

Manassero, V. and Di Salvo, G., 2012. Two difficult tunnelling problems solved by using permeation grouting: the excavation of submerged large size tunnels for Roma and Napoli metro projects. Proceedings of the 4th International Conference on Grouting and Deep Mixing. New Orleans, LA, USA, February 15-18. ASCE Geotechnical Special Publication No. 228.

Manassero, V., Cavuoto, F., De Risi, A., 2016. An advanced shaft construction method to install ten ventilation shafts, as applied in the Naples metro project. Proceedings of ITA WTC 2016. San Francisco, CA, USA, April 22-28.

Russo, G., Corbo, A., Cavuoto, F., Manassero, V., De Risi, A., Pigorini, A., 2016. Underground culture: Toledo Station in Naples, Italy. Proceedings of the Institution of Civil Engineers. November. http://dx.doi.org/10.1680/ jcien.16.00027.

Schmäh, P., 2009. Una nuova alternativa allo scavo di pozzi. Gallerie e Grandi Opere Sotterranee, No. 91, pp. 43-49.

WHY USING AN AIR-ENTRAINER TO INCREASE WORKABILITY IS NOT A GREAT IDEA FOR DEEP FOUNDATIONS

Dimitri Feys, Department of Civil, Architectural and Environmental Engineering, Missouri University of Science and Technology, Rolla, MO, United States, feysd@mst.edu

ABSTRACT

Many strategies to increase the workability of concrete either have a negative effect on performance, or come at an important cost for the concrete producer or contractor. Entraining air can be a strategy to enhance workability of concrete, but it should be kept in mind that air is compressible and the workability under pressure may be different than the workability in atmospheric conditions. This paper shows the theoretical concepts of the behavior of air bubbles under shear and under pressure, highlighting the differences between both conditions. Full-scale pumping tests on air-entrained and non-air-entrained concrete have further shown that the pressure loss in 100 mm pipes is approximately equal for both concrete mixtures, while the pressure loss was different in the 125 mm pipes. Based on these results, it is argued that a pressure of 5 bar may eliminate the positive effects of air on workability. This would correspond to a hydrostatic pressure under a concrete column of approximately 20 m, which is not exceptional for deep foundations.

Keywords: Workability, air-content, pressure

INTRODUCTION

Adequate placement of concrete is an important step in the creation of concrete elements. Generally, the ideal properties of concrete for placement more or less contradict the requirements during service life. Increasing water content affects strength and durability negatively (Neville, 2011). Increasing paste volume increases shrinkage (Neville, 2011), smooth aggregates may reduce bond between concrete and the rebars, etc. The ACI 318 design code for structural concrete specifies typically a compressive strength, maximum w/cm (water-to-cement ratio), allowable cement types (potentially in combination with SCMs), a target air content and limits on the amount of chlorides initially present in the concrete (ACI, 2015). The designer further specifies the concrete strength requirements and the configuration of the rebars to ensure that the structure does not fail. In some cases, service life requirements, based on durability parameters, and shrinkage reducing strategies are also prescribed. However, for workability, it is up to the contractor to determine what the best placement strategy would be.

Some strategies to increase workability, like adding water, are detrimental for the quality of the concrete. Unfortunately, this still occurs daily without being noticed (officially). Other strategies are available to increase workability, but they come at a price. Increasing paste volume increases the cost of the concrete and increases drying shrinkage potential. Optimizing aggregate proportions is a cost-effective tool (Goltermann et al. 1997, Esmaeilkhanian et al. 2017), but requires multiple piles of different aggregates at the ready mix company. These strategies increase the amount of free water in the concrete, which increases workability. Other strategies include the use of some supplementary cementitious materials, or the use of chemical admixtures. Water-reducing agents are beneficial for workability, without significantly affecting any other concrete property. However, using these products requires some training as small changes in quantities and adding time can have substantial consequences on workability (Flatt and Houst, 2001).

Air-entraining agents (AEA) are typically added to increase the freeze-thaw and scaling resistance of concrete. With increasing air content, the strength of the concrete is negatively affected, but the workability of concrete increases in most cases. This increase in workability can be attributed to the deformability of the air bubbles, acting as a liquid in the mixtures. However, it should be noted that air is the only compressible material in concrete, and that under pressure, the air bubbles shrink and can dissolve in the water of the concrete (Hover, 1995, Pleau et al., 1995, Yingling et al. 1992, Pigeon and

© 2018 Deep Foundations Institute

Pleau, 2010). As such, if the concrete is under pressure, the workability will be different compared to atmospheric pressure, and the difference will increase with increasing air content.

This paper discusses the effect of pressure and shear on air bubbles in concrete. The next section shows the theoretical concepts, followed by the description of full-scale pumping tests performed at the Universite de Sherbrooke (Feys et al., 2015, Feys et al., 2016). The analogy between pumping and placing concrete in deep foundations will show how effective the air is in enhancing the workability of concrete.

THEORETICAL CONCEPTS

This paragraph describes the theoretical concepts of the behavior of air under pressure. These concepts are essential to understand the behavior of air in concrete. Three concepts are discussed: the Capillary number, which is the ratio of shearing forces to surface tension forces, the Universal Gas Law which shows the dependency of air bubble size to pressure, and Henry's Law, which describes the dissolution of air into water once pressure is increased.

Capillary number

The Capillary number is a dimensionless number indicating the relative importance of shearing to surface tension (eq. 1) (Rust and Manga, 2002, Feys et al. 2009):

$$Ca = \frac{a \cdot \dot{\gamma} \cdot \eta_s}{\Gamma} \quad [1]$$

where: Ca = Capillary number (-)
a = undeformed bubble radius (m)
$\dot{\gamma}$ = shear rate (s^{-1})
η_s = apparent viscosity of the suspending medium (Pa s)
Γ = surface tension (N/m)

If Ca is much larger than 1, this means that the shearing forces dominate surface tension, and the bubble will deform. If Ca is much smaller than 1, the shearing forces are insufficient to overcome surface tension and the bubble remains spherical. If Ca >> 1, the viscosity of the material with air decreases. If Ca << 1, the viscosity of the material increases with increasing air content, as the undeformed bubbles can be considered as solid particles. For example, consider two air bubbles: one with 100 μm diameter, and one with 1 mm diameter. Assume also that during flow, the concrete undergoes a shear rate of typically 5 s^{-1} (Roussel, 2006) and that the apparent viscosity is in the range of 50 Pa s (SCC-like material) to 500 Pa s (conventional concrete). The surface tension between air and water is 0.07 N/m at 25°C, which we will assume to be valid in this case. For a 1 mm diameter bubble in conventional concrete, Ca is approximately equal to 35, meaning that the bubble will deform. In SCC though, Ca becomes 3.5, indicating it may deform, but it is not certain. For the 100 μm air bubble, Ca in conventional concrete is 3.5, while Ca = 0.35 in SCC for a 100 μm air bubble. The latter case indicates that the bubble mainly remains spherical during concrete flow, except during high shear rates (mixing and pumping). However, air-entraining agents mostly stabilize the smaller air bubbles, which remain spherical in slow flow conditions and thus increase viscosity.

Universal Gas Law

The Universal Gas Law describes the relationship between pressure, volume and temperature, according to (eq. 2):

$$p\,V = n\,R\,T \qquad [2]$$

where: p = pressure (Pa)
V = volume (m^3)
n = amount of gas (mol)
R = ideal gas constant = 8.314 J/K mol
T = temperature (K)

During concrete placement, n, R and T remain approximately constant, which means that an increase in pressure will cause a decrease in air bubble volume. As such, to reduce the air bubble diameter by a factor 2, a pressure of 8 bar is required (as 1 bar is atmospheric pressure). As discussed above, larger shearing forces are required to deform smaller air bubbles.

Henry's Law

Henry's Law states that at each pressure, a certain amount of gas can be dissolved in the surrounding fluid. Increasing pressure allows for more gas to dissolve. Reducing pressure causes supercritical gas concentration, causing the creation of air bubbles if they can nucleate somewhere. Opening a new soda bottle is the best way to visualize Henry's Law. Specifically for concrete, increasing pressure allows for more gas to be dissolved (Dyer, 1991). Although no dissolution speeds have been determined, it is estimated that gas dissolution needs a period of time in the order of seconds. With increasing pressure, air progressively leaves the air bubbles, which occurs faster in smaller air bubbles due to the larger surface area. When relieving the pressure, the air reappears, but most likely in a different place than where it dissolves.

Consequences

Air-entraining agents can be used to increase the workability, but there is no guarantee for success. The larger the stress applied to make the concrete flow, the more likely the air will deform and reduce the flow resistance. However, if the concrete flows under low stresses, such as SCC or near-SCC concrete mixtures, some part of the air will not deform and will rather act similar to a solid particle. Applying pressure reduces the air bubble size and dissolves air in the water. As such, less air is available to increase workability. In fact, the workability assessment under atmospheric pressure is not indicative for the workability of the concrete under pressure.

In the next section, experiments are described which validate the above statement that under sufficient pressure, the beneficial influence of air on workability is no longer present. The validation is provided through results of full-scale pumping tests on high-performance concrete, executed at the Universite de Sherbrooke.

FULL-SCALE PUMPING TESTS

In 2012, a series of full-scale pumping tests were executed to evaluate the influence of mix design on pumpability of high-performance concrete. This project was sponsored by an admixture company active in the Middle East, and the NSERC industrial research chair at the Universite de Sherbrooke (PI: K. Khayat), cooperating with 17 industrial partners. In particular for this paper, two mix designs will be compared: a self-consolidating concrete without AEA, and an identical mix design with AEA.

Pumping circuit

The pumping tests were performed with a Schwing BPL 900 pump. The maximum flow rate which could be reached was 25 l/s, the maximum pressure is 6000 kPa. The pump had two pumping pistons with 2 m stroke length and 200 mm diameter. The placing boom was disconnected and a horizontal loop circuit was installed behind the pump (Figure 1). The loop circuit consisted of two 11 m straight sections. The first section was built with 100 mm diameter pipes, while the second, return section was constructed with 125 mm pipes. In between both sections were two 90° bends with a reducer in between (increasing the diameter from 100 to 125 mm). The end of the circuit consisted of a portal, pumping the concrete back in the hopper of the pump, or allowing to take a sample of the concrete for characterization (Feys et al., 2015).

Each horizontal section was equipped with pressure sensors spaced approximately 10 m apart. In the vicinity of the pressure sensors, strain gauges were attached to the pipes, acting as back-up in case the pressure sensors failed. The flow rate was measured by recording the time necessary to pump a specific number of strokes. Calibration constants were determined by pumping a full stroke of concrete inside a reservoir attached to a load cell to ensure that the flow rate measurements were accurate (Feys et al., 2015)

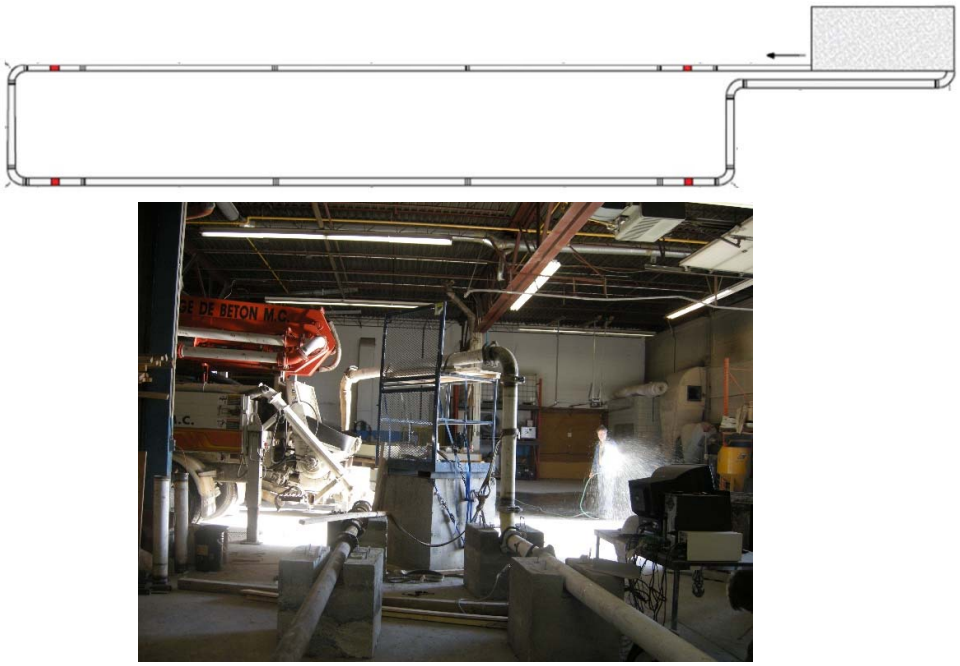


Figure 1: Top: Loop circuit. The concrete pump is at the right top corner. The concrete flows counterclockwise through the circuit. The first horizontal section is made with 100 mm diameter pipes, the return section with 125 mm pipes. The red areas indicate the locations of the pressure sensors. Figure after Feys et al., 2015. Bottom: picture of the setup, the concrete flows from the left (100 mm pipes) to the right (125 mm pipes). The portal directs the concrete back in the reservoir.

Testing procedure

Concrete was delivered to the site from a local ready mix company approximately 15 min after water-cement contact. The amount of HRWRA was adjusted on-site to achieve the desired slump flow of the mixture prior to pumping. After insertion of the concrete in the pipes, the concrete was sent through the loop at least once to eliminate the effect of thixotropy. Once the properties of the concrete from the truck were fully characterized, the concrete was subjected to a pumping cycle: it was pumped at 6 to 8 different flow rates, in decreasing order, maintaining each flow rate for either five full strokes or 45 s minimum (Figure 2) (Feys et al., 2015).

The data acquisition system registered pressure and strain at a rate of 10 Hz, providing sufficiently accurate data to identify the strokes of the pump and the changes in flow rate. From the data, for each measurement location, the pressure was averaged at each flow rate, eliminating data in the transition period of the pumping stroke (switch of the valve). For each horizontal section, an upstream and downstream pressure was derived, and the pressure loss is calculated as the difference between upstream and downstream pressure, divided by the separation distance of the pressure sensors. As such, for a pumping test, the pressure loss over a 100 mm pipe and 125 mm pipe are determined simultaneously for at least 6 different flow rates (Feys et al., 2015).

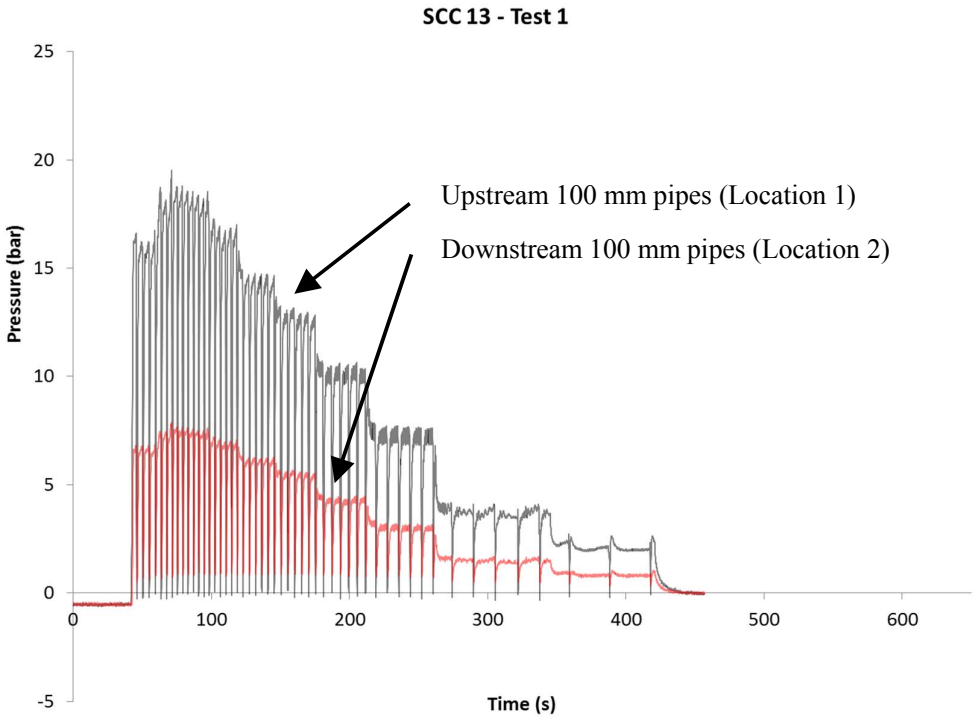


Figure 2. Example acquisition of pressure (from the strain gauges) for locations 1 and 2 over time. The flow rates were 14.0; 13.3; 11.8; 10.7; 8.7; 6.4; 3.2 and 1.6 l/s for this test.

Concrete mix design

Although a variety of concrete mixtures were evaluated (Feys et al., 2015, Feys et al., 2016), two mix designs are of particular interested for this paper. Within some variation in the balances of the ready mix plant, 1 m^3 of the mixtures contained 600 kg of GUb-SF, 180 kg of water, 830 kg of sand and 600 kg and 145 kg of coarse aggregate with 10 mm and 20 mm nominal aggregate size, respectively. The GUb-SF cement type is a blended cement available on the Canadian market, consisting of Portland cement mixed with 8% silica fume. Two HRWRA were employed: one with long workability retention added at the plant (10 kg/m^3), and a short workability retention admixture added on-site (1.5 kg/m^3 for the non-air-entrained concrete and 1.3 kg/m^3 for the air-entrained admixture). The main difference between both mixtures is the air-entrainment: none for the first and 0.67 kg/m^3 of AEA for the second mixture. The first mix design showed 670 mm slump and 1.7% air. The second mixture had 690 mm slump flow and 7.6% air after the considered test. The air contents were measured with the pressure method according to ASTM C231. As can be seen, the mixtures have similar properties, apart from the air content, and slightly lower rheological properties (yield stress = 36 Pa and plastic viscosity = 41 Pa s for the air-entrained concrete (V-Funnel 4.7 s) vs, yield stress = 41 Pa and plastic viscosity = 43 Pa s for the non-air-entrained concrete (V-Funnel 5.0 s)). All rheological properties were measured with an ICAR rheometer. More details on the measurements are described in (Feys et al. 2015).

PUMPING RESULTS

Figure 3 shows the pressure loss vs. flow rate results of both mixtures. The results are divided into small pipes (100 mm diameter) and large pipes (125 mm diameter), as well as the air content of the mixtures (evaluated after pumping). For the 125 mm diameter pipes, a clear distinction can be seen between the mixtures, as the mixture with more air shows a lower pressure loss at each flow rate, due to the beneficial effect of deforming air on viscosity (note that the shear rates during pumping are larger than those during rheometry). However, for the 100 mm diameter pipes, the beneficial effect of air has disappeared, as no distinction can be made between the lines, especially for flow rates larger than 10 l/s.

This difference in pressure loss between the smaller and larger pipes is remarkable, but can be explained by the pressure in the system. As described above, the smaller pipes are installed upstream of the larger pipes. As such, the pressure in the smaller pipes is larger than in the downstream larger pipes. Considering the point at approximately 9 l/s flow rate for the mixture with 7.6% air, the gauge pressure was 10.3 bar in sensor 1, 4.5 bar in sensor 2, 3.2 bar in sensor 3 and 0.8 bar in sensor 4. It appears thus that starting at a (gauge) pressure of around 5 bar (500 kPa), the air no longer contributes to decreasing the viscosity in concrete. Taking the theoretical concepts discussed previously in the paper into consideration, an increased pressure reduces bubble size, resulting in less deformability. In addition, a higher pressure allows for more air to be dissolved (Henry's law), which will reappear at lower pressures, potentially in pre-existing bubbles increasing the bubbles' size. A decrease of approximately 0.4% of air has been observed each time the concrete was pumped through the pipes (5 times in total). However, no hardened air void analysis was performed to confirm the change in bubble size distribution.

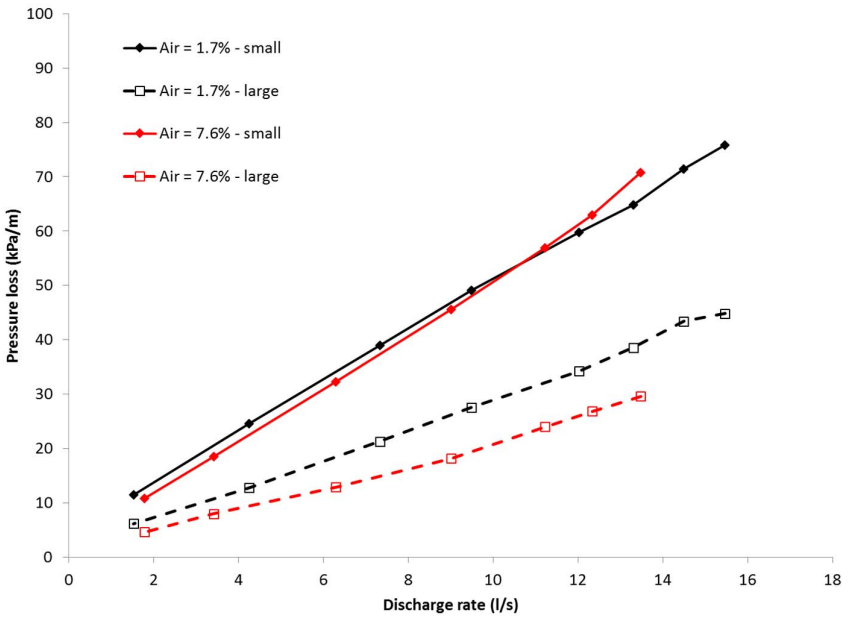


Figure 3. Pressure loss vs. flow rate for an SCC mixture without and with AEA, in both the 100 and 125 mm pipes.

CONSEQUENCE FOR CONCRETE USED IN DEEP FOUNDATIONS

For concrete in deep foundations, the pumping pressure may not be elevated, as the mixtures have relatively low viscosity and are most likely placed in wide tremie pipes (125 mm diameter or larger), so a direct application of the results above may not be valid. However, the weight of the material column

(bentonite, polymer-modified support fluid, or even concrete) above the flowing concrete may be sufficient to induce the pressure necessary to reduce the beneficial effect of air on workability of concrete. As a simplified estimation, it can be assumed that only hydrostatic pressure needs to be considered. As such, the pressure can be calculated accordingly:

$$p = \rho g h \quad [3]$$

If we assume a density of concrete equal to 2500 kg/m^3 (for simplicity), a concrete depth of 20 m delivers 500 kPa pressure. If we even assume a density of 1000 kg/m^3, again for simplicity for a polymer-modified support fluid, a depth of 50 m delivers a pressure of 500 kPa. Knowing that from the pumping experiment, the critical pressure for the positive influence of air bubbles on workability is set on a safe side, as it is likely to occur at lower pressures, and that only hydrostatic pressure is assumed (means the concrete is only flowing very slowly), deep foundations can be sufficiently deep to eliminate the positive effect of air on workability. As such, adding air to concrete for deep foundations to increase workability may not be a great idea. This will especially go unnoticed during quality control, as quality control is usually performed at atmospheric pressure.

CONCLUSIONS

Theoretical concepts show that air bubbles may, or may not, have a positive effect on the workability of concrete, depending on the shear rate, concrete type (reflected in the viscosity), and diameter of the air bubble. Applying pressure on concrete will reduce the air bubble volume proportionally to the applied pressure and will provoke the dissolution of air in the surrounding liquid.

Full-scale pumping tests carried out on an air-entrained self-consolidating concrete and an equivalent non-air-entrained SCC have revealed that in pipes with low pressure, the air-entrained concrete requires less pressure to flow. However, in the pipes with higher pressure, the pressure loss at a certain flow rate is approximately equal. This latter observation can be attributed to the disappearance of the beneficial effect of air in cases with more elevated pressure (all other parameters are expected to remain constant). As a safe estimate, the lowest flow rate at which the difference between air-entrained and non-air-entrained concrete becomes negligible is around 9 l/s for the conducted experiment. The pressure at the end of the upstream measuring section is approximately 5 bar for this flow rate and the evaluated concrete.

The beneficial effect of air on workability of concrete becomes unnoticeable at 5 bar (or 500 kPa) during pumping. No physical effects prevent applying this principle to hydrostatic pressure. As such, a 20 m long concrete tremie pipe causes a hydrostatic pressure of approximately 5 bar. In this case, the beneficial effect of air should disappear and the workability of concrete should be equivalent to that of a non-air-entrained concrete.

Workability assessment is conducted above ground, in atmospheric conditions. If a concrete must fulfill certain workability criteria before placement, the entrained air will influence this workability measure. However, under sufficiently high pressure, the air no longer contributes to the workability, increasing the yield stress and viscosity, or the stiffness and stickiness of the mixture, potentially causing the workability to be out of spec. As such, for deep foundations, entraining air to improve the workability of concrete is not such a great idea.

ACKNOWLEDGEMENTS

The author would like to acknowledge Sodamco Inc., NSERC, and all partners involved with the industrial research chair on flowable concrete with adapted rheology (U. Sherbrooke, 2008-2013, PI. K. Khayat), for the financial support of the project. All graduate students and technical staff involved in the set-up, execution, and analysis of these large scale experiments are also thanked for their substantial efforts.

REFERENCES

ACI Committee 318, 2015. Building Code Requirements for Structural Concrete (ACI 318-14) American Concrete Institute.

Dyer, R.M., 1991. An investigation of concrete pumping pressure and the effects of pressure on the air void system of concrete (Doctoral dissertation, University of Washington).

Esmaeilkhanian, B., Diederich, P., Khayat, K.H., Yahia, A. and Wallevik, Ó.H., 2017. Influence of particle lattice effect on stability of suspensions: application to self-consolidating concrete. Materials and Structures, 50(1), p.39.

Feys, D., Roussel, N., Verhoeven, R. and De Schutter, G., 2009. Influence of air bubbles size and volume fraction on rheological properties of fresh self-compacting concrete. In 3rd International RILEM symposium on Rheology of Cement Suspensions such as Fresh Concrete (pp. 113-120). RILEM Publications (August, 2009).

Feys, D., Khayat, K.H., Perez-Schell, A. and Khatib, R., 2015. Prediction of pumping pressure by means of new tribometer for highly-workable concrete. Cement and Concrete Composites, 57, pp.102-115.

Feys, D., Khayat, K.H. and Khatib, R., 2016. How do concrete rheology, tribology, flow rate and pipe radius influence pumping pressure?. Cement and Concrete Composites, 66, pp.38-46.

Flatt, R.J. and Houst, Y.F., 2001. A simplified view on chemical effects perturbing the action of superplasticizers. Cement and concrete research, 31(8), pp.1169-1176.

Goltermann, P., Johansen, V. and Palbøl, L., 1997. Packing of aggregates: an alternative tool to determine the optimal aggregate mix. ACI Materials Journal, 94(5), pp.435-443.

Hover, K., 1995. Investigating Effects of Concrete Handling on Air Content. Concrete Construction, pp.745-750.

Neville, A.M., 1995. Properties of concrete (Vol. 4). London: Longman.

Pigeon, M. and Pleau, R., 2010. Durability of concrete in cold climates – Chapter 6: Air-entrainment. CRC Press.

Pleau, R., Pigeon, M., Lamontagne, A. and Lessard, M., 1995. Influence of pumping on characteristics of air-void system of high-performance concrete. Transportation research record, pp.30-36.

Roussel, N., 2006. A thixotropy model for fresh fluid concretes: theory, validation and applications. Cement and Concrete Research, 36(10), pp.1797-1806.

Rust, A.C. and Manga, M., 2002. Effects of bubble deformation on the viscosity of dilute suspensions. Journal of non-newtonian fluid mechanics, 104(1), pp.53-63.

Yingling, J., Mullings, G.M. and Gaynor, R.D., 1992. Loss of Air Content in Pumped Concrete. Concrete International, 14(10), pp.57-61.

A MAJOR INFRASTRUCTURE PROJECT AND THE FORMATION OF THE UK'S LARGEST ROTARY PILE UNDER POLYMER SUPPORT FLUID

Yue Ouyang, Project manager, Cementation Skanska, Denham Way, Maple Cross, Rickmansworth, Hertfordshire, U.K., Phone: +44 (0) 330 050202, Email: yue.ouyang@gmail.com.

Stephan Jefferis, Director, Environmental Geotechnics Limited, St Mary's Grove, 4, Adderbury Park, Adderbury, Banbury, U.K., Email: egl@environmentalgeotechnics.com.

Paul Wiltcher, Operations Director, Cementation Skanska, Denham Way, Maple Cross, Rickmansworth, Hertfordshire, U.K., Email: Paul.wiltcher@skanska.co.uk.

Tony Suckling, Director, A-Squared Studio Engineers Ltd., One Westminster Bridge Rd, London, England, U.K., Email: contact@a2-studio.com

ABSTRACT

Polymer fluids are now widely used to support excavations for piles and boreholes and more rarely (in the UK) diaphragm walls. Despite this concerns can still be voiced by those not familiar with their behaviour. Concerns include performance of polymers from different suppliers in different grounds and more generally how to specify and manage polymer support fluids. Those who have mastered their use have found that they can offer substantial benefits over conventional bentonite slurries and yet until very recently there was limited published guidance on their use and there are still significant differences in the approaches across the World. In the interest of sharing experience across the foundation industry, this paper presents a case history of the use of a polymer fluid on a major infrastructure project. This project included the largest polymer supported rotary pile ever constructed in the UK; a pile that required 270 m^3 of support fluid. The paper highlights the technical challenges and collective operational experience derived from managing such a complex project and the developments in polymer fluid specification that have flowed from it.

Keywords: Rotary pile, drilled shaft, polymer support fluid, bentonite slurry thermal integrity testing

INTRODUCTION

Polymer fluids are now a viable and sustainable alternative to bentonite slurries as excavation support fluids. Typically the base polymers are partially hydrolysed polyacrylamides (PHPAs) with molecular weights over 10 million and long chain structures. PHPAs are synthetic polymers which behave quite differently from bentonite. For example, polymers fluids do not rely on filter cake formation to seal an excavation but on high solution viscosity at low shear rates and for some polymers, film formation. This ensures that the hydrostatic pressure of the fluid acts near the wall of the excavation and so can stabilise the excavation. Bentonites are natural materials and will vary between suppliers as a result of the different sources of the raw bentonite and differences in the processing employed by individual suppliers. It follows that specifications for bentonite slurries can vary across the World because of variations in bentonite behaviour. Polymers can and do vary much more widely than bentonite as they can be synthesised with distinct physical and chemical properties. As a result specifications may need to be specific to products but generic guidance is now available.

THE PROJECT

The Northern Line Extension (NLE) includes a station at Battersea, London, immediately adjacent to the former and iconic coal-fired Battersea power station. The station box required the construction of 650 linear metres of diaphragm walling and 74 large diameter piles. The pile diameters ranged from 1.5 to 2.4 m with depths up to 60 m.

© 2018 Deep Foundations Institute



Fig. 1. Polymer fluid being pumped to a pile bore

By way of example, Fig. 1 shows a fresh polymer fluid being pumped to a pile during excavation. It can be seen that it is a clear solution and in this instance in laminar flow. The volume of excavation support fluid required to construct the largest pile was 270 m^3. In addition to this volume, further support fluid was required for the diaphragm wall construction which was to be carried out concurrently. Concurrent operations, each with high fluid demands, bring substantial operational risks, for example, if there is any down-time on the bentonite plant. Polymer offered the opportunity of an alternative support fluid for the piling works. The use of a separate fluid in a separate plant would alleviate the issue of high fluid demand and de-risk the impact of a bentonite plant breakdown or over-load such as can occur in the soil-slurry separation plant. However, as a total of 13,260 m^3 of excavation would have be carried out under polymer fluid with the construction of large diameter piles up to 2.4 m in diameter and over 60 m deep there were challenges. These included the cost of setting up a separate polymer plant, risks associated with retro-fitting existing bentonite equipment for polymer fluids and the still evolving knowledge and experience in managing polymer fluids.

This paper discusses the detailed on-site management system put in place to control the quality of the polymer fluid in operation. As bentonite slurry was being used on site it was possible to construct a pile under bentonite so enabling a direct comparison of the construction efficiency with the two types of fluid in the same ground.

OPERATION WITH POLYMER FLUIDS

As summarised by Jefferis et al. (2017) and discussed in more detail in Lam and Jefferis (2018), PHPA based polymer fluids have the ability to sorb to soil. This inhibits the dispersion of fine soils. Thus when excavating in fine soils, the cut soil tends to remain as coherent lumps which if spilled from the excavation tool settle rapidly and are removed as excavation progresses. This prevents the build-up of fines in the fluid as happens with bentonite slurry which does not inhibit fines dispersion, indeed sodium from the bentonite can promote dispersion.

However, sorption removes polymer (PHPA), from solution as does damage from operational processes such as pumping and excavation both of which involve mechanical shear which can break down the long-chain polymer molecules. The returned polymer fluid from an excavation therefore requires rejuvenation (addition of further polymer) to replenish the polymer lost. If the polymer concentration is not rebuilt the fluid may flip from a polymer solution to a soil-water slurry with all the

problems that flow from the use of unstable soil-water slurries including inclusions in the concrete. It was in the light of these aspects of polymer behaviour that the polymer plant and excavation equipment were designed.

PLANT SET-UP AND QUALITY CONTROL FOR POLYMER FLUIDS

The project employed four 30 m^3 polymer fluid preparation tanks; a water treatment tank and three polymer mixing tanks which also could be used for rejuvenating the polymer fluid when returned from a pile after excavation and during concreting. From the preparation tanks the polymer was pumped to a tank farm. Here, there were 13 storage silos with an overall storage capacity of 500 m^3 polymer fluid. These were necessary to provide sufficient polymer fluid to meet the piling programme, noting that the largest single excavation volume was 270 m^3 and that there had to be spare fluid capacity for parallel operations and in the case of large losses to the ground. Fig. 2 presents a schematic of the plant set up showing two key components: the fluid preparation tanks and the storage silos together with their associated quality control points. The four preparation tanks were planned as mixing tanks for fresh polymer fluid and rejuvenation of the fluid returned from the pile bores. However, whilst commissioning the plant, it was found that the local mains water had sufficiently high levels of calcium and magnesium (hardness) to reduce the performance of the PHPA based polymer (Jefferis et al., 2017). To counter this, one of the mixing tanks was reserved for on-site water treatment. In this tank a small amount of sodium hydroxide was added to the mains water to raise its pH to 10.5, sufficiently alkaline for the reduction of the effects hardness and the development of the polymer properties. The pH of the treated water was checked at control point Q1.

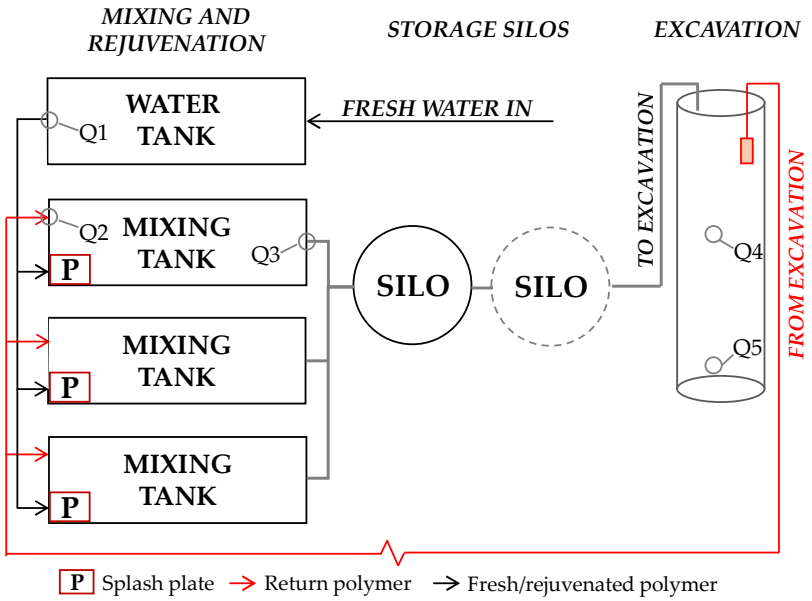


Fig. 2. Schematic diagram of polymer operations at NLE

The treated water was pumped from the treatment tank to the splash-plate mixers of the mixing tanks where polymer powder was sprinkled on to flowing water. Splash-plate mixing was appropriate as base polymer was used at 0.7 to 1 kg/m^3. This is a significantly lower concentration than for bentonite where the concentration is typically between 20 and 60 kg/m^3 (SPERW, 2017). Because of the small amount of polymer powder to be added, mechanical polymer dosing plant was not required. However, polymer mixing requires careful attention as the polymer powder tends to clump when wetted and must be sprinkled into running water. If this is not done clumps may form and remain as undissolved polymer fish-eyes in the fluid – a waste of polymer. After polymer powder addition, the fluid must be kept agitated until the polymer is fully dissolved. On-site this was achieved by aeration bars set near

the base of each of the mixer tanks. Diaphragm pumps were used for transfers of the polymer fluid between tanks and silos to limit shear damage to the polymer.

At the quality control points Q3 (for clarity Fig. 2 shows the Q2 and Q3 control points only for one tank but sampling was undertaken at all three preparation tanks), for fresh polymer, the required the minimum viscosity was 90 seconds with a maximum of 120 seconds as shown in Table 1. As experience developed on site it was found that preparing the fresh polymer at near the lower limit was sufficient to ensure satisfactory results. In use, polymer fluid management requires the blending of fresh fluid (to make up for losses to the ground and with excavated soil) and rejuvenated fluid to maintain the Marsh funnel times within the specified range. At the start of a project the polymer tended to have a relatively high viscosity as can be seen from the Marsh funnel test results in Fig. 3 (the Marsh funnel time is a surrogate for viscosity). This was mainly due to the 'viscosity surge' from a large quantity of fresh polymer in the initial production, which had been prepared towards the upper viscosity limit. This was to ensure that the polymer fluid remained within specification during the first excavations. Once the required polymer addition rate for rejuvenation had been established and a stable working practice developed, the operational viscosity was controlled to somewhat lower value within the permitted range. The main risk from low viscosity is flipping of the polymer fluid to a soil-water slurry, whereas over-high fluid viscosity can raise concerns about fluid displacement during concreting. However, for the polymer used, poor displacement would occur only at Marsh funnel times much above the maximum specified or employed on project.

Table 1 Polymer fluid testing regime and quality control

Polymer testing: parameters and test point	Test parameters			
	Marsh funnel time [Sec]	Sand content [%]	Density [g/ml]	pH
Mix water, Q1	N/A	N/A	N/A	10.5
Fresh polymer, Q3	90 – 120	0	<1.01	9-11
Rejuvenated polymer, Q2	70 – 120	2	<1.02	9-11
After excavation, middle and base of the pile, Q4, Q5	60 – 90	<5	<1.05	9-11
Before concreting, middle and base of the pile, Q4, Q5	>60	<1	<1.02	9-11

Base cleaning and concreting

At the end of excavation, there will be some suspended solids in the polymer fluid; solids dispersed into the fluid by the excavation process. To confirm that the digging fluid was within specification, two samples of the polymer fluid were taken from each pile bore, one from the middle and one from near the base. The maximum specified limit for density was 1.05 g/ml and the maximum sand content was 5%. As can be seen from Fig. 3 these requirements were readily met. It should be noted that there was a planned suspension of polymer works between May and July. During this period the fluid was held in the storage silos (open topped) with no significant loss of properties during the storage.

After excavating a bore to the design toe level, the tool would be switched to a cleaning bucket. Samples were taken from the middle and near the base to confirm the density and sand content were within the specification after excavation. A minimum wait period of 45 mins was then observed so that the majority of solids settling through the fluid had reached the pile base. Once the fluid had been confirmed as within specification, the final excavation with cleaning bucket would take an extra 100 to 200 mm of soil so that all settled soil could be removed to provide a freshly cut and clean base for concreting. After this, samples were again taken from the middle and near the base to confirm that the density and sand content were within the specification for concreting. The test results (see Fig. 3) show that the samples from test points Q4 and Q5 all had sand contents below 1% before concreting. Sampling from middle and base of the pile provided information on the settling of the solids in suspension and the required holding time after excavation and before concreting.

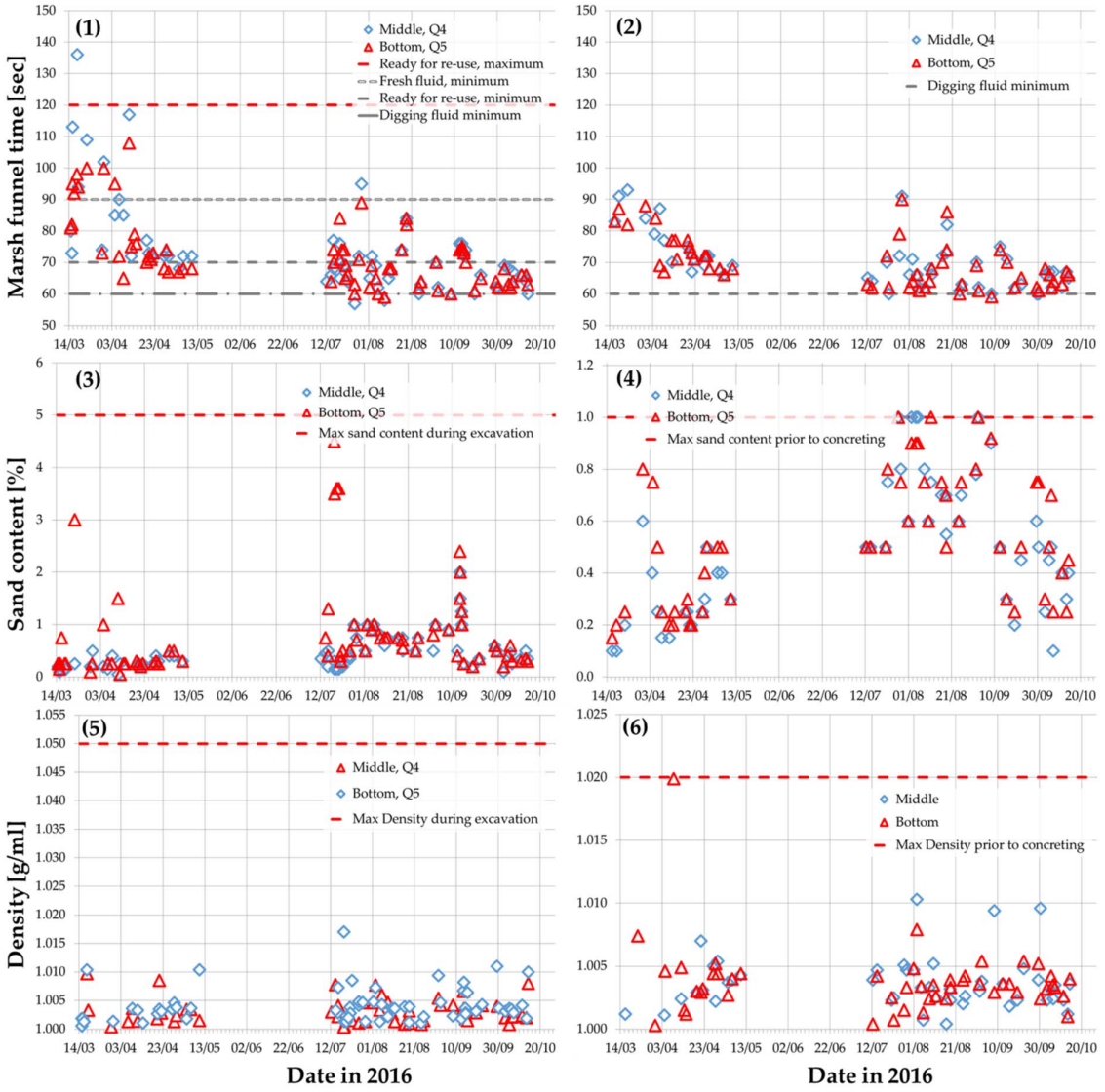


Fig. 3. Field test results for polymer samples collected from control points Q4 and Q5: (1) Marsh funnel time at the end of excavation; (2) Marsh funnel time before concreting; (3) Sand content at the end of excavation; (4) Sand content before concreting; (5) Density at the end of excavation; (6) Density before concreting.

During concreting, the displaced polymer fluid was pumped back to the mixing plant with a submersible centrifugal pump. It was necessary to use a centrifugal pump to match the concrete placement rate. The polymer molecules may have been damaged by passage through the centrifugal pump (Lam et al., 2010a) but this was redressed by rejuvenating the fluid. The amount of polymer required for the rejuvenation at the mixing tanks was determined from Marsh funnel time measurements at the quality control points Q2.

Polymer testing regime and quality control

It can be seen from Fig. 3 which shows some of the field test data collected during the project, that the fluid density after excavation was readily maintained within the specified range 1.00 to 1.05 g/ml. Prior to concreting the densities were typically less than 1.01 g/ml, the one reported result of 1.02 g/ml, at the base of the excavation, control point Q5, may have been a field measurement error as the associated sand content was 0.25%. The sand content of the fluid was carefully controlled and

managed via the tests at the end of excavation and prior to concreting as can be seen from Fig. 3. It should be noted that sand content is an indication of the volume of material coarser than 74 μm. To ensure a clean base it is important to consider the total solids content and not just the +74 μm material – especially for polymer fluids which have no, or no significant, gel strength. Total solids can be controlled by density but for this better precision is required than can be achieved with the conventional mud balance (Jefferis and Lam, 2017). A pycnometer bottle and electronic balance were used for density measurements on site.

ON SITE OPERATIONAL CHALLENGES

In order to optimise polymer fluid operations on site, a total storage volume of 480 m^3 was planned. This was assessed on the basis that the average volume required for all support fluid operations is 2.5 times the volume required to construct a single pile.

From the site investigation, ground conditions at the site consisted of approximately 5 m of river terrace gravel overlying London Clay with a thickness of 33 m. Beneath this there were Lambeth group soils with the piles founded 3 m into the Thanet sand. For excavation, the piles were cased to 1 m into the London Clay. The excavations were flooded to the piling platform level when water-bearing strata were encountered at depths of 38 to 39 m. The volumes required for the initial flooding of piles of diameter 1.5 to 2.4 m are shown in Table 2. The fluid storage capacity in the silos permitted the flooding of one pile while receiving the return polymer from another pile. The piling programme was developed to avoid, so far as possible, the consecutive construction of two 2.4 m diameter piles – the largest piles. A contingency plan was also put in place to strictly control the quality of polymer fluid should the consecutive construction of two such piles be necessary.

After a bore had been flooded, a digging bucket instead of twin-flight augers was used to complete the excavation to slightly above the design depth as suggested by Jefferis et al. (2017). This helped to minimise the risk of dispersing cut soil into the fluid. However, as a result the excavation rate was reduced by 50%. Due to the volume of excavation required for each pile, the excavation and concreting processes often could be not completed on the same shift. On occasion, pile bores therefore had to be left open overnight or longer. Lam et al. (2010b) reported a full-scale field trial which showed that the polymer fluid is capable of stabilising an open-bore for extended periods without sacrificing shaft resistance. In contrast, an equivalent long open period with bentonite slurry can lead to the development of a thickness of filter cake at the wall of the excavation sufficient to compromise the shaft resistance (Lam et al., 2014).

Table 2. Volume of polymer fluids required to support excavation throughout the construction

Polymer volume in m^3	Pile Diameter [mm]			
	2400	2100	1800	1500
Initial flooding volume when groundwater reached	180	140	100	70
Excavation to founding level	100	80	60	40
Polymer fluid returned for rejuvenation during concreting	280	220	160	110

Note: volume of hole excavated under polymer fluid requires ≈10% allowance for polymer fluid lost with the excavated soil

The average casting level of pile was 19 m below the ground level. Fig. 4 shows the quality of the concrete at the top of a pile; minimal contaminated concrete at the casting level and a fair face to the exposed shaft between the casting level and cut-off level. This confirmed that the controls on density and sand content and solids settling time in the pile bores were sufficient to ensure that, during concreting, no significant excavation soil was carried up on the top of the rising concrete.

CONSTRUCTION PERFORMANCE OF PILES SUPPORTED BY DIFFERENT FLUIDS

As diaphragm walls were being constructed under bentonite slurry on the site, there was an opportunity to construct a pile under bentonite to compare the construction performance of the piles under polymer fluid and a pile under bentonite slurry. Construction details were recorded throughout the process together with concreting details. Both of piles were subjected to thermal integrity testing using distributed fibre optic technology. The following section compares the results obtained for the two support fluids.

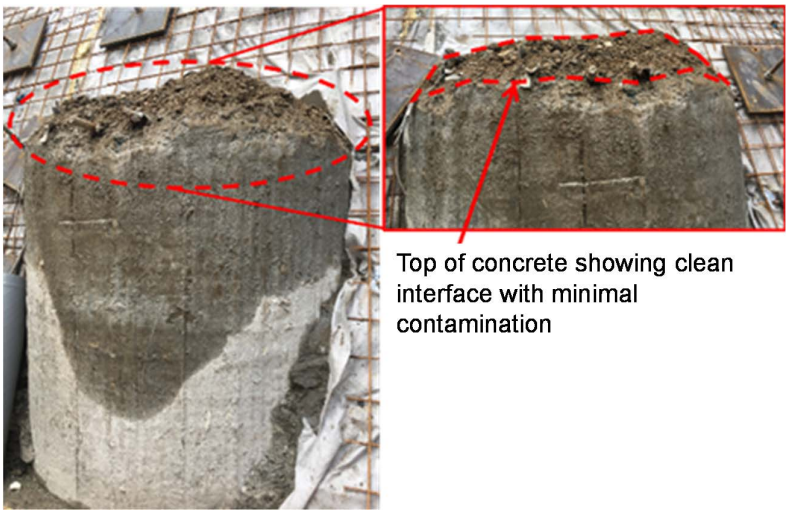


Fig. 4. Good quality of concrete exposed at casting level

Comparison of plant set-ups

Unlike the bentonite plant, the polymer plant was successfully managed without a storage facility (dry powder silo), or the need for soil-slurry separation plant (de-sander and de-silter); compare the plant layouts in Fig. 5. The soil separation plant can be eliminated for PHPA polymer fluids as they sorb soil and inhibit soil dispersion. This limits the amount of soil in suspension. At the end of excavation suspended soil can be removed by settlement after treatment, if necessary, with chemical agents. As the polymer fluid was 'cleaned' by settlement in-hole, there was no need for a soil-fluid separation plant. However, sorption onto soil and the in-hole cleaning process consumes some active polymer and so tends to reduce fluid performance. Therefore, additional rejuvenating treatment is required to restore the active polymer content of the return fluid for its re-use.

The polymer fluid operation demonstrated several advantages over bentonite slurry. For example, typically for the excavation of a 2.4 m diameter pile to a depth of 60 m it would take approximately 4 to 5 hours to de-sand and de-silt the bentonite slurry before it could be re-used. In contrast for the polymer fluid simple in-hole settlement was sufficient for solids control – though time had be allowed for this at the pile whereas desanding for bentonite slurries is done away from the pile.

There were additional diaphragm pump and air compressor requirements for polymer operations. Diaphragm pumps to move the fluid from mix tanks and to the storage silos and to the pile bores. A large capacity compressor was required for the aeration (mixing) bars in the mixing tanks and the storage silos. The smaller footprint of the polymer plant, achieved by eliminating the soil-slurry separation process, offers potential advantages when working in confined areas.

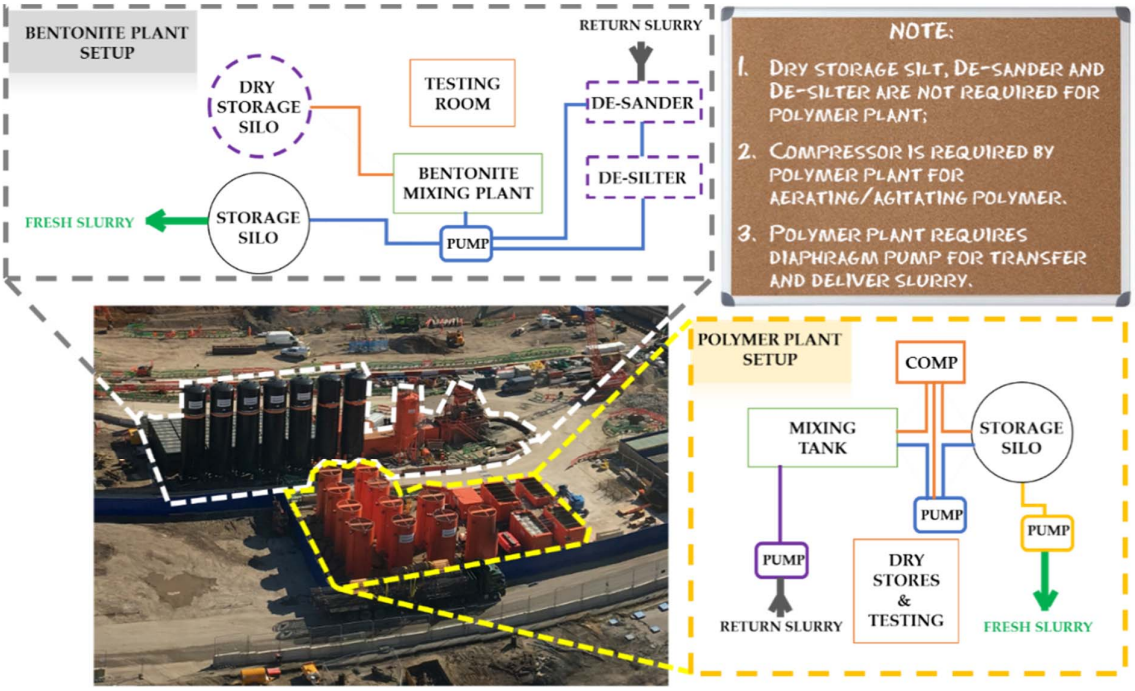


Fig. 5. Plant set ups for polymer fluid and bentonite slurry operations

COMPARISON OF OPERATIONAL EFFICIENCY AND QUALITY

Relative excavation efficiency for PHPA fluid and bentonite slurry

It was found that the rig took 1 hour extra to excavate under polymer fluid with the digging bucket. This was due mainly to the extra wait time required to allow the fluid to drain from the bucket at the top of casing before emptying the soil from it. However, the excavation efficiency is also dependent on the rig driver. Extra attention was required under polymer fluid to avoid unnecessarily agitating and so dispersing cut soil into the polymer fluid. This also contributed a slight increase in excavation time. The slurry flooding time was also compared throughout the operations for the two piles, this showed that it took less time to flood with polymer fluid. This was because for the bentonite pile, the bentonite supply was prioritised for the D-Wall operations, the delivery of bentonite slurry to flood the pile bore was thus dependent on the demands of the D-Wall operations. This demonstrated the increased operational efficiency achieved with the two separate support fluid plants Polymer and bentonite).

The support fluid control and the concreting process

Fluid test results from both piles complied with parameters set in the ITP (Inspection Testing Plan). The concrete rise level for the polymer and bentonite piles was monitored and is shown in Fig. 6 together with the predicted theoretical rise level. The concrete rise was determined with a weighted tape though this does rely on the experience of the operator. The measurements showed good agreement with the predicted levels for both the bentonite and the polymer piles. Thus in this instance the concrete overbreak was similar for both polymer fluid and bentonite slurry.

Pile integrity testing procedure and results

The thermal integrity system was adopted to assess the integrity of all piles on site including the pile constructed under bentonite slurry. The system uses the heat developed during cement hydration to assess the integrity of a pile based on the temperature development over the initial 48 hours after the concrete placement. The thermal integrity system uses the proven distributed fibre optic sensing technology (Ouyang et al., 2015) as an alternative to Cross-Hole Sonic Logging (CHSL) system.

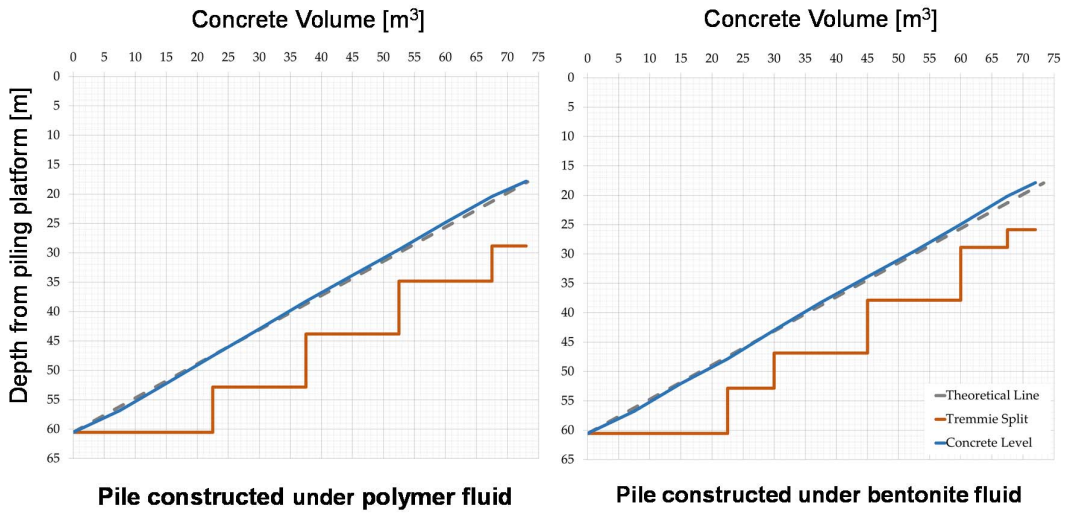


Fig. 6. Concrete levels together with the predicted theoretical levels and tremie split stages

Fibre optic sensor lines, are installed along the pile during the cage installation and are connected to an interrogator on site to continuously log the temperature development along the pile. Temperature is recorded from four lines of sensors set equidistant around the circumference of the pile. Fig. 7 shows the temperature difference, ΔT, between the temperature 48 hours after concrete placement and the initial temperature at placement at the four locations around the pile shaft for the 1.5 m diameter bentonite pile and a 1.5 m polymer pile. The integrity assessment criteria are based on the variation of ΔT between the four lines as well as the ΔT profiles in different soil layers. As the ground conditions changed from London Clay at approximately 60 m ATD (Above Tunnel Datum) to the Lambeth group, which is a water bearing layer. The recorded measurements show a consistent change of ΔT in the water-bearing strata for all four lines. For both piles, ΔT below the cut-off level, showed a similar profile for the four locations around the circumference of the piles, and thus verified the integrity of both the pile installed under bentonite slurry and that under polymer fluid.

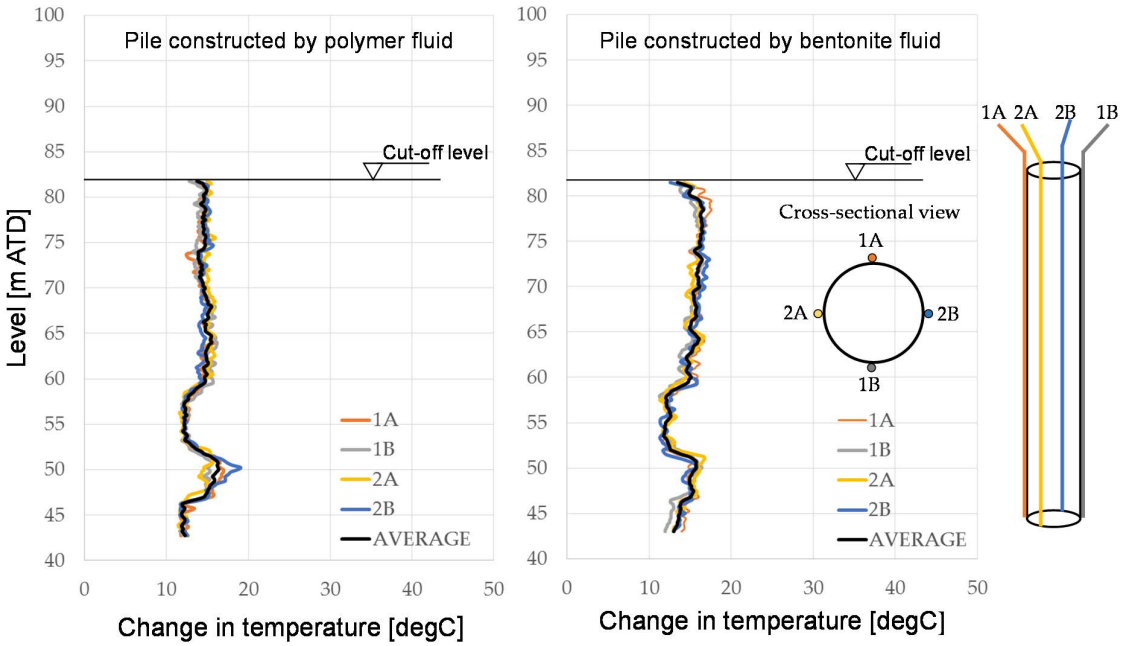


Fig. 7. Results of Thermal integrity testing: polymer fluid and under bentonite slurry

CONCLUSIONS

This project has proven the use of polymer support fluid for large diameter pile construction on a major infrastructure project. The use of polymer fluid offered several major advantages including:

- there was clean displacement of polymer fluid by concrete;
- simple plant setup with no soil-polymer separation plant or settlement tanks;
- all settlement of suspended solids was done in-hole which was straightforward given the good on-site quality control of the polymer fluid properties: Marsh funnel time, sand content and fluid density;
- the fluid was kept in a cycle of use: excavation, concreting and then rejuvenation of the fluid to make up for the reduction in polymer concentration during excavation and addition of fresh polymer fluid to make up for fluid losses;
- the polymer fluid was held in the storage silos during the planned suspension of polymer works between May and July without significant loss of properties;
- no polymer fluid at all was disposed during the works;
- at the end of the works the polymer viscosity was broken and the fluid discharged to foul sewer in compliance with a discharge consent. This eliminated the otherwise high cost of liquid waste disposal.

ACKNOWLEDGEMENTS

Authors gratefully acknowledge the contribution of KB International LLC, Mott MacDonald, and the Ferrovial Laing O'Rourke NLE Team in supporting the use of polymer fluids on the site.

REFERENCES

ICE, 2017. ICE Specification for Piling and Embedded Retaining Walls (SPERW) - Third Edition, Institution of Civil Engineers Publishing.

Jefferis, S.A. and Lam, C., 2017. Using density to determine the solids content of construction slurries, *Proceedings of the 19th International Conference on Soil Mechanics and Geotechnical Engineering*, Seoul, 1695-1698.

Jefferis, S.A., Ouyang, Y., Wiltcher, P., Sucking, T., & Lam, C., 2017. The On-Site Management of Polymer Support Fluids for the Construction of Drilled Shafts and Diaphragm Walls, 523–532.

Lam, C. and Jefferis, S.A., 2018. Polymer support fluids in Civil engineering. ICE Publishing, London, p296.

Lam, C., Jefferis, S.A., & Goodhue, K.G. Jr., 2010a. Observations of viscosity reduction of PHPA polymer support fluids. Proceedings of the Geoshanghai 2010 International Conference, Shanghai, ASCE Geotechnical Special Publication, 205, 184–191.

Lam, C., Troughton, V., Jefferis, S.A., & Sucking, T., 2010b. Effect of support fluids on pile performance – a field trial in East London. Ground Engineering, 43(10), 28–39.

Lam, C., Jefferis, S.A., & Martin, C.M., 2014. Effects of polymer and bentonite support fluids on concrete–sand interface shear strength. Géotechnique, 64(1), 28–39. https://doi.org/10.1680/geot.13.P.012

Ouyang, Y., Bell, A., Elshafie, M., Soga, K., Fernie, R., & Mair, R., 2015. The history of UK experience in the use of fibre optic monitoring of geotechnically associated installations. Geotechnical Engineering for Infrastructure and Development, 2, 637–642. https://doi.org/10.1680/ecsmge.60678.vol2.079.

BRUNNHOLEN BRIDGE – NORWAY - DESIGN AND SUPERVISION OF FOUNDATION WORKS

Arne Schram Simonsen, Multiconsult Norge AS, Oslo, Norway, +47 901 50 451, ass@multiconsult.no

Vetle Kolberg Stene, Multiconsult Norge AS, Oslo, Norway, +47 993 51 375, vks@multiconsult.no

ABSTRACT

The Brunnholen Highway Bridge in Norway is a geotechnically-challenging project. Complicating factors include ø914 mm drilled steel pipes, large lengths to solid rock and difficult soil conditions. Steel pipe piles are drilled with a full face symmetric drilling system with reversed circulation. The piles are drilled through layers of fill, sand and gravel, stiff clay, stiff moraine, soft rock and at least 1.5 m into solid rock.

The pile design is based on Eurocode 7 with use of soil-structure interaction calculations with soil springs as defined by API.

Keywords: Drilled steel pipe piles, ø914 mm, geotechnical supervision, highway bridge foundation

INTRODUCTION

Brunnholen Bridge is a 245 m long highway bridge located outside Stavanger City in Norway. The bridge is a part of the Fv 505 Skjæveland – Foss Eikeland highway project. Multiconsult Norge AS is engaged as Geotechnical Consultant for the design and supervision works.

Fig. 1 and Fig. 2 show the location of the bridge, Fig. 3 shows a model of the bridge and Fig. 4 a section drawing of the bridge. The bridge is founded on pile groups in six axes using 914 mm diameter and 14.2 mm thickness steel pipe piles filled with reinforced concrete. The axial pile design loads are in the order of 11 000 kN, the lateral pile design loads are in the order of 800 kN and the design pile moments are in the order of 2 100 kNm.

The bridge will be built using the incremental launching construction method shown in Fig. 5.

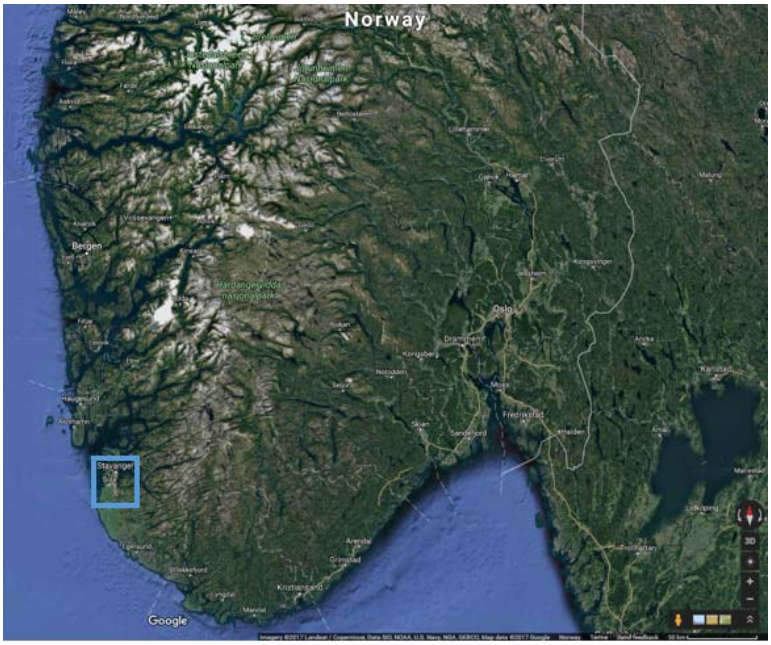


Fig. 1. Location of the Brunnholen Bridge, highlighted in blue.

© 2018 Deep Foundations Institute

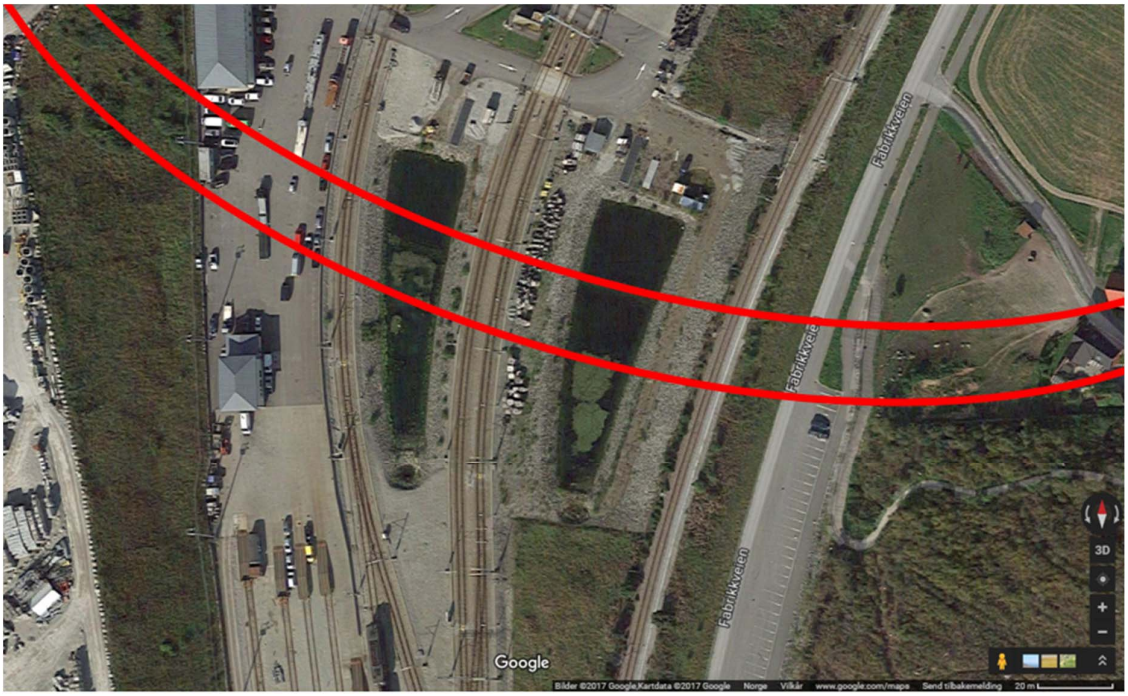


Fig. 2. Satellite picture of the area the bridge will cross (red lines represents future bridge). Note the four railway tracks

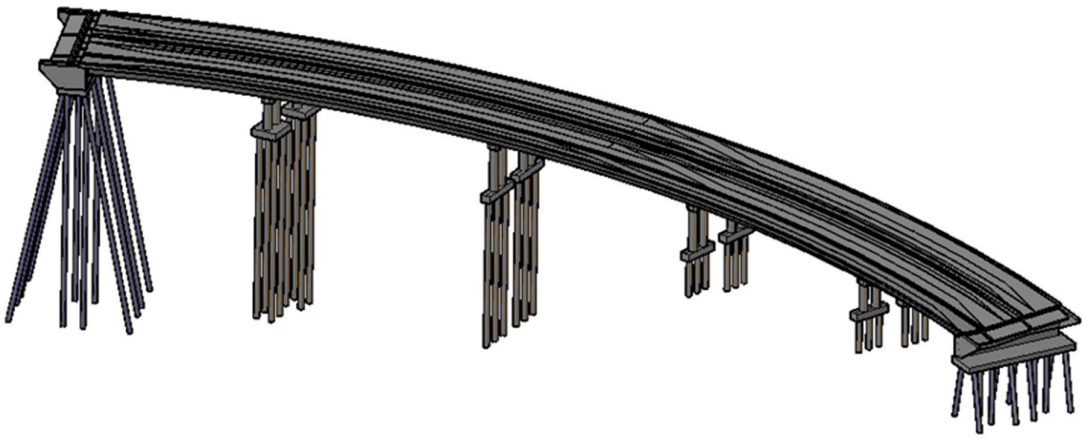


Fig. 3. Model of the Brunnholen Bridge

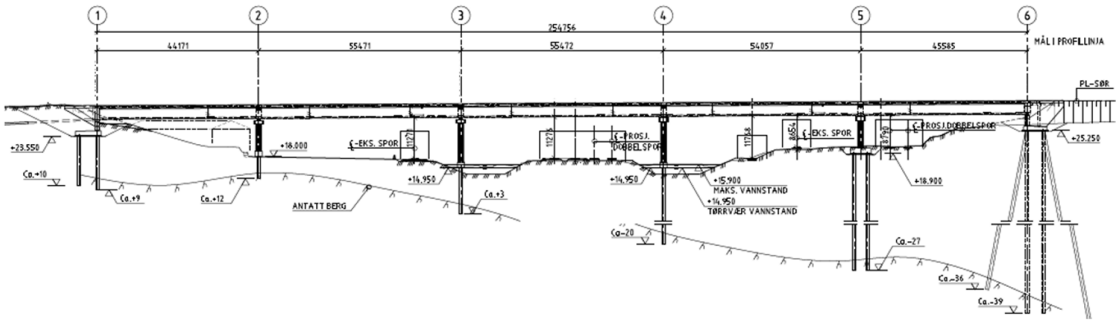


Fig. 4. Drawing of the bridge with axis one to the left and axis six to the right

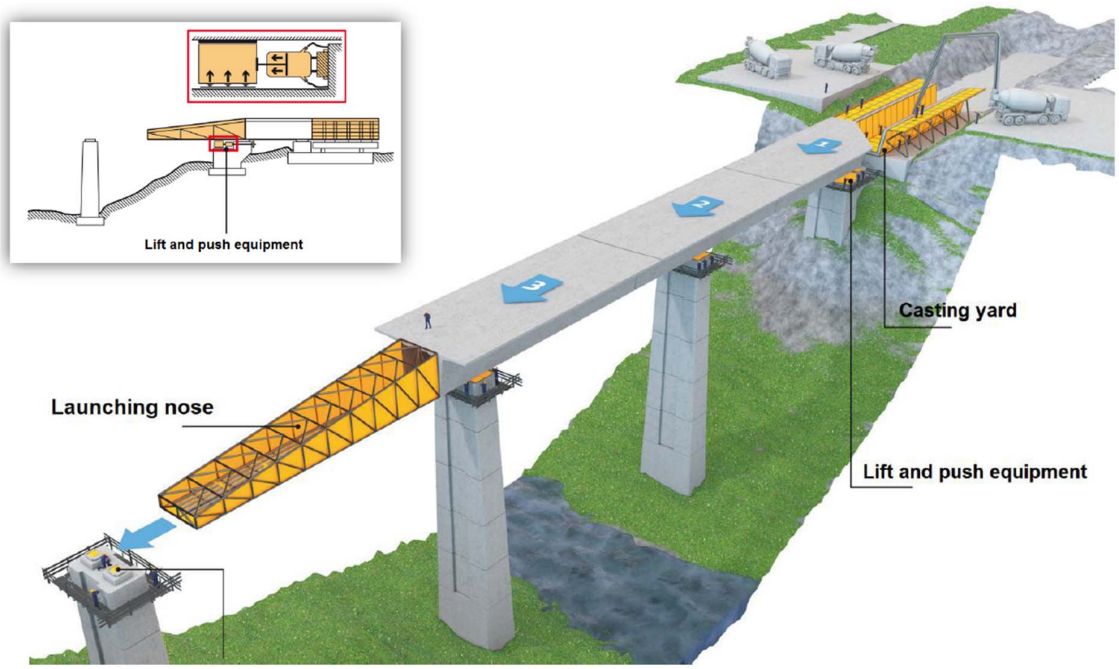


Fig. 5. Principle drawing of the incremental launching construction method (Mihal 2017)

Construction work on the pile foundations began in August 2017 and is expected to be largely completed by April 2018.

Each pile group is comprised of between 3 and 12 steel pipe piles drilled at least 1.5 m into solid rock. A full face symmetric drilling system with reversed circulation is used. In total 46 piles will be installed with lengths up to approx. 75 m. Some of the piles will be installed with inclination of 5:1. In Norway, drilled piles with this length and dimension have never been used before.

The geotechnical design of the pile groups is based on Eurocode 7 and an advanced soil structure interaction program with soil springs defined by API. The soil structure interaction program was used for two purposes; to derive stiffness matrices for structural design and to derive pile forces and moments for pile design. The experience from pile installation is also discussed.

SOIL CONDITIONS

The soil consists mainly of an upper layer of fill material over a natural deposit of sand, gravel, and silt. Below this, a layer of overconsolidated very stiff clay overlays hard moraine with boulders and rock is situated. The rock is a mixture of phyllite, mica schist and quartz. The rock layer starts with a layer, up to 5 m thick, of soft rock before transitioning to solid rock. Fig. 6 shows a 3D model with assumed soil layering under the bridge. The layering in Fig. 6 is based on performed total soundings, the locations of which are shown as white lines in soil and red lines in rock.

The depth to rock from the foundations varies from approx. 10 m in axis one to approx. 75 m in axis six.

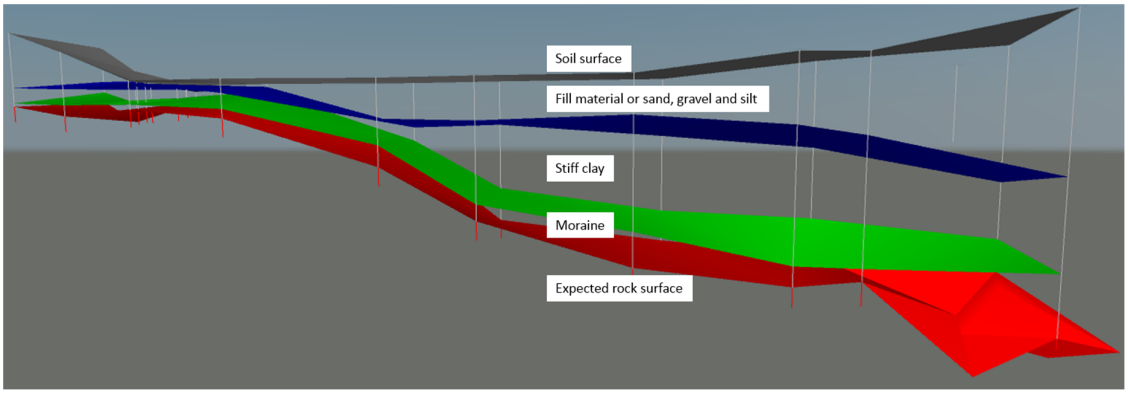


Fig. 6. 3D model with assumed soil layering beneath the bridge, axis one to the left and axis six to the right

FOUNDATION CONCEPTS

In the early phases of the project, three foundation concepts were considered:

1. Concrete caissons. Could be a good option since the soil is stiff. However, caissons need large areas and deep excavations. Thus, the risk for deformations on the train tracks close to the foundations are large.
2. Driven steel piles. Could be a good option in the axes where the depth to rock surface is great. In an early phase of the project, pile drivability analyses were performed and it was concluded that it would be hard to drive the piles to required depth, as well as to prove sufficient bearing capacity with available hammers.
3. Drilled steel pipe piles. This was selected as the most robust foundation concept. Large axial loads will be transferred to solid rock and drilling through stiff soil layers is achievable. Another advantage is that the foundation concept can be used in all the axes, i.e. the same drilling rig can be used in all the foundation work. However, in Norway, piles with diameter as big as 914 mm has never been installed to 75 m depth before. Geotechnical supervision of the piling work will be necessary throughout construction.

PILE DESIGN

The structural consultant Aas-Jakobsen AS presented the pile group loads after an iteration process between structural consultant and Geotechnical Consultant. The iteration process was needed because the piles and the surrounding soil was not included in the structural model. The iteration procedure that was followed is detailed below:

1. Structural Consultant gave estimated pile foundation loads to Geotechnical Consultant
2. Based on the estimated loads, Geotechnical Consultant calculated stiffness matrices for each pile foundation. The stiffness matrices were then given to Structural Consultant
3. Structural Consultant calculated new foundation loads based on the stiffness matrices for each pile foundation and gave updated pile foundation loads to Geotechnical Consultant
4. Based on the new loads, Geotechnical Consultant calculated stiffness matrices for each pile foundation. The stiffness matrices was then given to Structural Consultant
5. Structural Consultant calculated new foundation loads based on the new stiffness matrices for each pile foundation and gave updated pile foundation loads to Geotechnical Consultant
6. Point 4 and 5 were repeated until the effect on pile foundation loads was negligible. The iteration process stopped and Geotechnical Consultant had the correct pile foundation loads

The pile foundation loads in SLS, ULS and ALS were used to perform pile design according to Eurocode 7. Three main checks were carried out using the advanced soil structure interaction program GeoSuite PileGroup (Vianova GeoSuite AB 2017):

1. Displacements are checked with SLS loads and characteristic soil parameters.
2. Pile capacity check is performed with ULS and ALS loads.
3. Stability of the pile foundations is checked with ULS loads and design soil parameters.

Structure-Pile-Soil Interaction Calculations with GeoSuite PileGroup

The structure-pile-soil interaction analysis program is used for pile analysis. The program allows easy manipulation of pile group geometry and is particularly suited to analysis of multiple load combinations. In total 120 load combinations were analysed for each pile group. Foundation with 8, 6, 6, 6, 8 and 12 piles were selected for axis 1, 2, 3, 4, 5 and 6 respectively. The inclined piles have an inclination of 5:1.

The program is a powerful tool to perform analysis and design of 3D pile groups. It models all piles in the pile group as rigidly connected at pile top and includes soil stiffness along piles and at pile tip. The soil stiffness is included by soil springs based on American Petroleum Institute (API), i.e. the pile foundation is modelled as beams on a nonlinear Winkler foundation. The springs/soil stiffness and a pile element are illustrated in the left side of Fig. 7. The middle of Fig. 7 illustrates a section through axis six where the inclined piles are blue and the vertical piles are green. The forces Fx, Fy, Fz, Mx, My and Mz (marked with a black dot) act centrally under the foundation. The right side of Fig. 7 is a deformation plot from the piles in axis six. Based on this plot, it appears that the piles in axis six will be laterally fixed from 10 m into the soil.

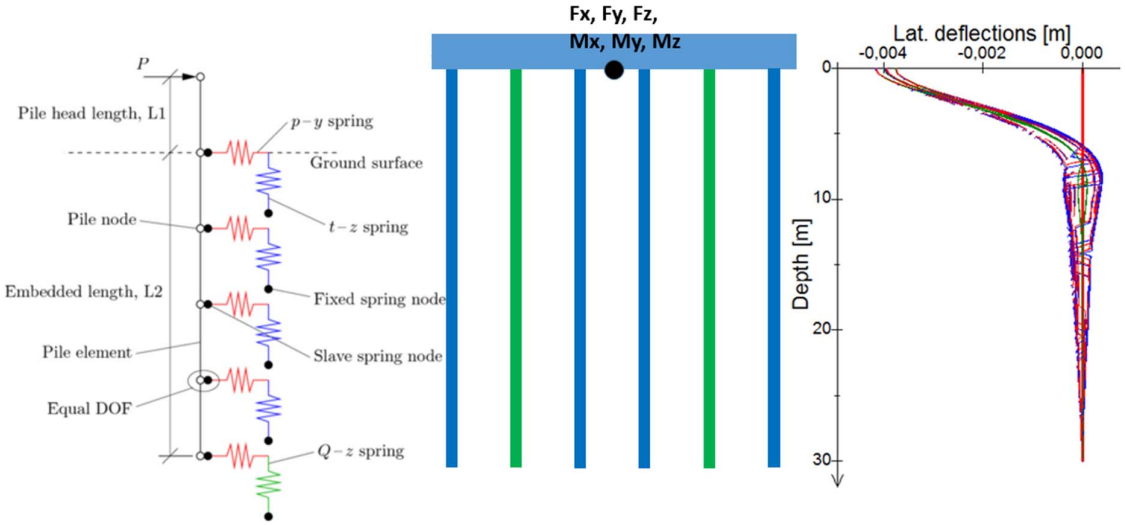


Fig. 7. Left: Sketch of a pile element represented as a beam on a nonlinear Winkler foundation (Open See 2017). Middle: A section trough axis six where the inclined piles are blue and the vertical piles are green. Right: Deformation plot from the piles in axis six

EQUIPMENT

Large pile dimensions, large pile lengths and stiff soil requires large and stable equipment using down hole hammer (DTH) and reversed circulation system. The casing used for DTH drilling is left in place after drilling, along with the reamer bit. Fig. 8 shows the drilling rig used for pile installation, Fig. 9 shows the reamer bit and the pilot bit and Fig. 10 show drawings of reversed circulation drilling.



Fig. 8. The drilling rig used for pile installation

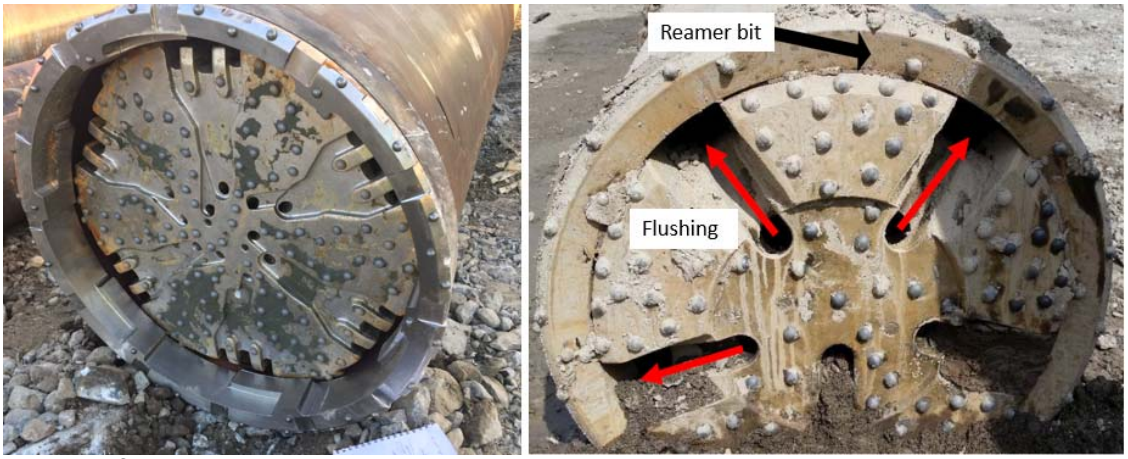


Fig. 9. Left: The reamer bit and the pilot bit used in the project (note that the pilot bit on the picture is not yet fastened to the reamer bit.) Right: Picture from (Baardvik et al. 2016), here red arrows illustrate the flushing.

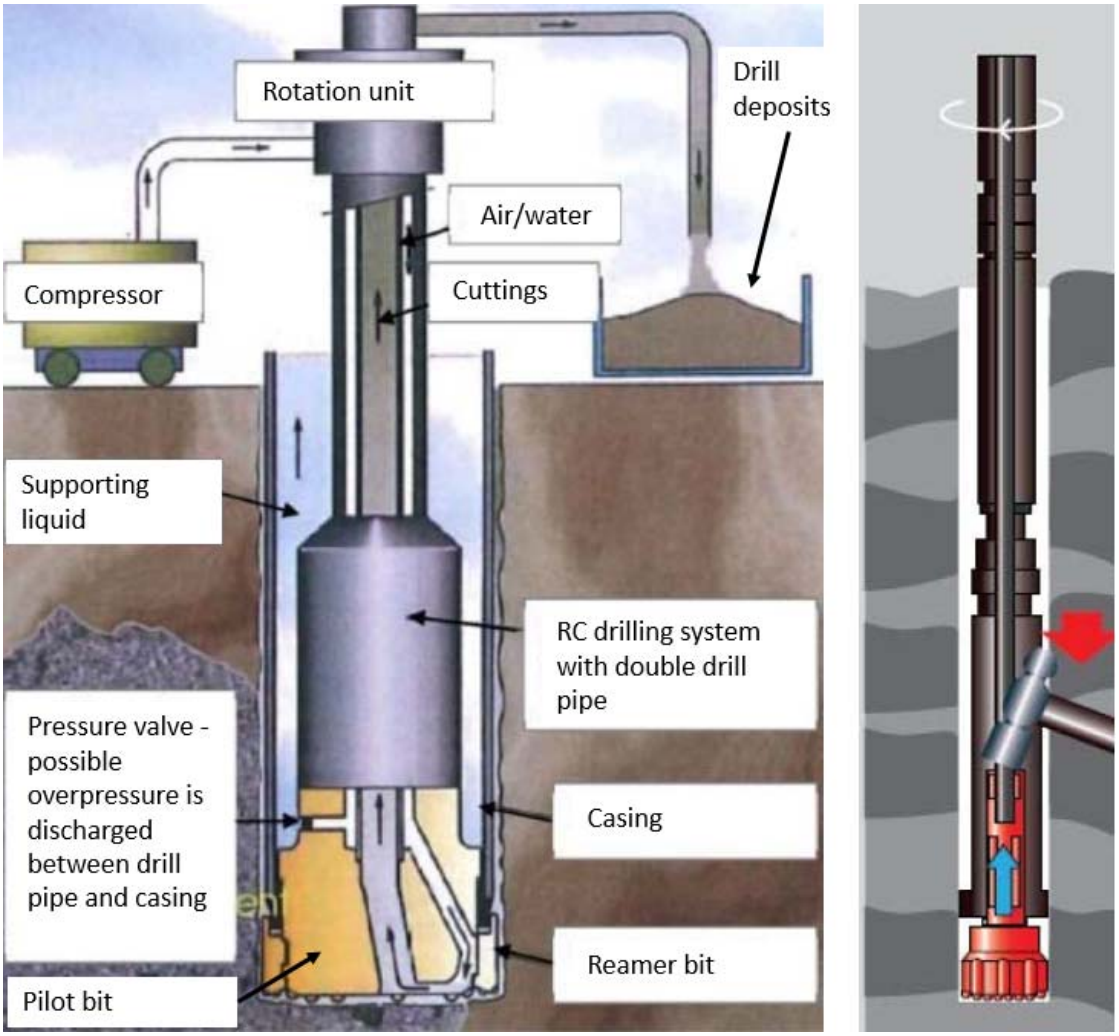


Fig. 10. Left: Principle drawing showing reverse circulation drilling, edited from (Den Norske Pelekomité 2012). Right: Principle drawing showing reverse circulation using down hole hammer (DTH) and double drill pipes where air, water and cuttings are transported through the centre of the drilling bit and drill string so that it can be accumulated (Baardvik et al. 2016).

SUPERVISION

The supervision work comprises mostly of ensuring proper drilling into solid rock, gentle drilling to minimise deformation of the surrounding soils, satisfactory cleaning of the pile feet before concreting and ensuring no gravel, cuttings or holes between the concrete and the rock after concreting.

Proper Drilling into Solid Rock

It is of vital importance that the piles are installed sufficiently into solid rock to ensure sufficient vertical bearing capacity. According to the Norwegian Public Roads Administration (Statens vegvesen 2012) drilled steel pipe piles should be drilled at least 1.5 m into solid rock. It is also required in this project, that the angle between one lower pile tip and one higher pile tip should not be steeper than 45 degrees. Fig. 11 shows the 3D-model of installed piles and assumed rock surface (the red surface). The model is used to control the “45 degree” requirement.

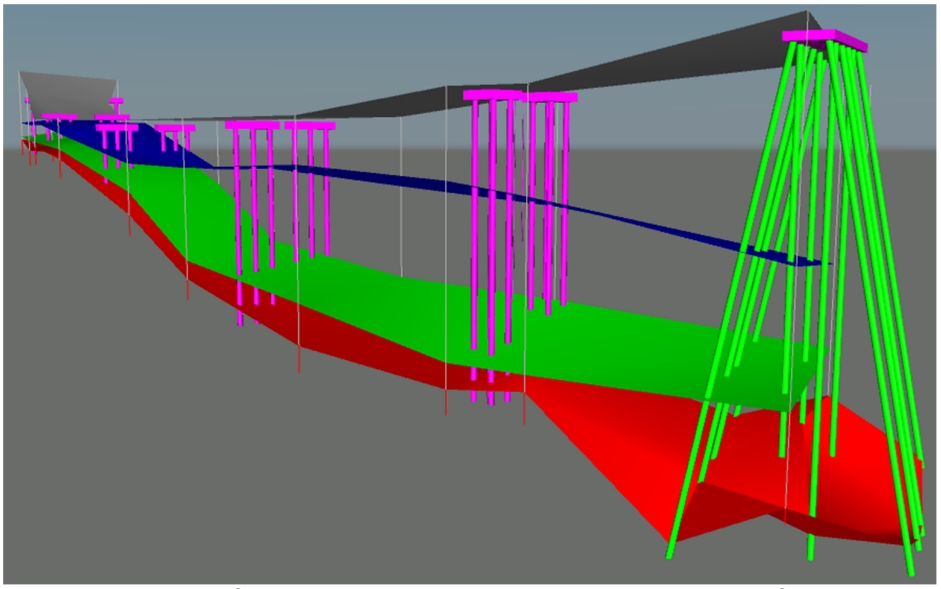


Fig. 11. 3D model of the installed piles and the assumed rock surface in red colour

The challenge with this project was to be sure of proper drilling into solid rock. With pile lengths up to approx. 75 m and hard moraine, it is difficult to "feel" when the pile starts to drill in solid rock, especially when the layer over solid rock is soft rock. Confirmation of drilling in solid rock is achieved by evaluation of the recorded drilling parameters, as well as interpretation of the cuttings. Some of the drilling parameters are as followed:

- The penetration rate in soft rock is typically 8 – 12 cm/min and in solid rock typically 2 – 8 cm/min.
- Required oil pressure to rotate the reamer and pilot bit varies based on material. In soft rock and moraine, the oil pressure has high variation and in solid rock, the oil pressure is more constant.

In addition to the drilling parameters, the drill cuttings are interpreted. Fig. 12 is a picture of the drill cuttings from one of the pile installations. Text is included to show where different cuttings have been taken from. The cuttings from solid rock will have sharp edges. When the cuttings are similar enough to the assumed solid rock, one can be sufficiently certain that the pile is drilled into solid rock.

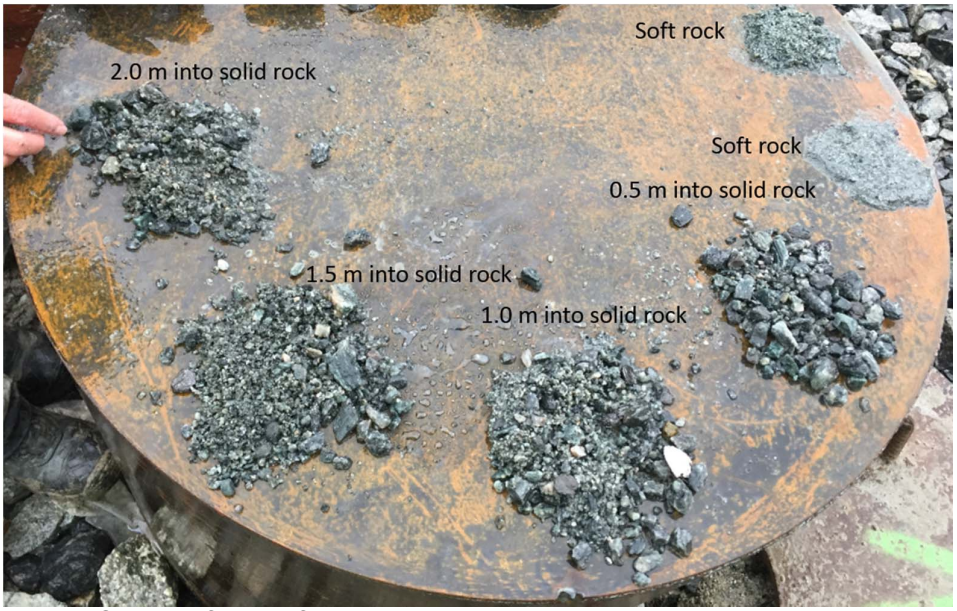


Fig. 12. Cuttings from soft and solid rock in one pile

Gentle drilling

Gentle drilling is highly important to ensure that limited deformation occurs at the surrounding soil surface due to excessive pore pressure erosion outside the casing. According to the Norwegian Public Roads Administration (Statens vegvesen 2012) the performance should be such that air pressure for the hammer die is controlled as much as possible and does not go out in the formation. High air pressure shall not be used to accelerate drilling or quickly dissolve drill bit blockages made by temporary stops or welding work. Unnecessary stopping in drilling should be avoided to prevent blockage of reamer and pilot bit.

Gentle drilling is also ensured by maximum values of flushing pressure. The flushing pressure in stiff soils should preferably not be more than 8 – 10 bar and a maximum 15 bar.

Water leakage through the pile feet is documented with water level control and water-loss measurements, with packer and, if necessary, the pile feet is injected using full face packer.

Pore Pressure

One of bridge axes is located approx. 10 m from a national railway line. To control possible settlement of the railway tracks, settlement measurements were carried out from total stations on the railway sleepers and pore pressure measurements were recorded from two piezometers between the pile foundation and the railway. Piezometer 1 was installed approx. 26 m below the soil surface in the stiff clay layer and piezometer 2 was installed approx. 35 m below the soil surface in the moraine layer directly over the rock. Fig. 13 shows the pore pressure development in the piezometers during pile installation and pile feet improvement. The pore pressure in the moraine layer shows large variations during pile drilling into the moraine and rock layer for each of the eight piles in the foundation. The figure is marked with 1 to 8, corresponding to the eight pile installations. For pile number 4 there was an error in the piezometer data sending system resulting in no data in that short time period. Pile installation 5 to 8 showed variation in the pore pressure in the stiff clay layer as well as in the moraine layer. This corresponds to the pile installations nearest to the piezometers.

After installation of all the pile casings in the pile group, the pore pressure in the moraine layer was approx. 30 kPa lower than before installation. In the stiff clay layer, the reduction was approx. 10 kPa. After pile feet improvement (injection using full face packer), the pore pressures in both the moraine and the stiff clay layer are soon back to their initial pressure.

Settlement measurement from the total station on the sleepers has not reported settlements exceeding the acceptance criteria from the Norwegian Nation Rail Administration.

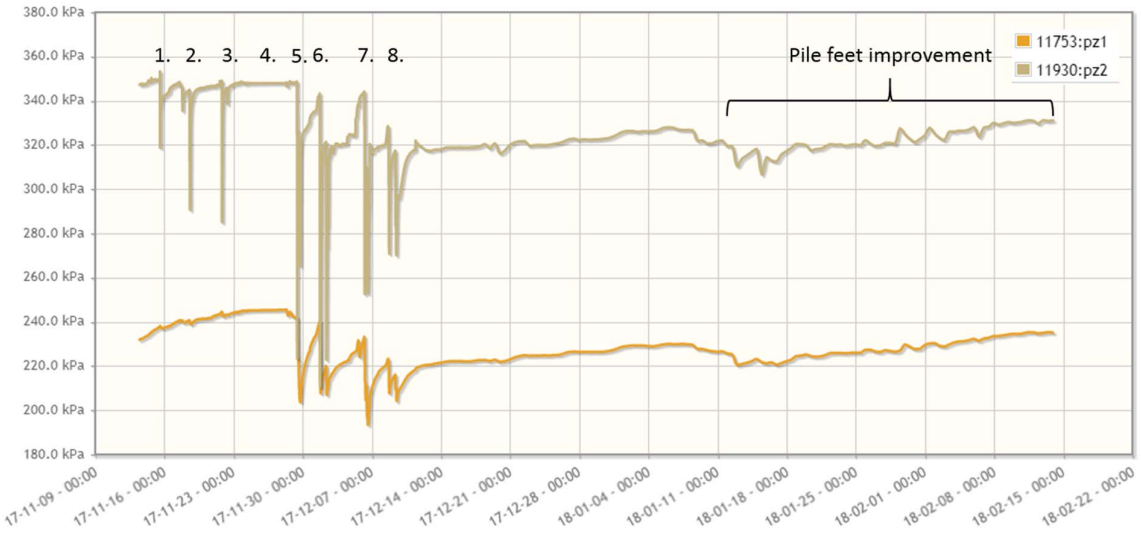


Fig. 13 Pore pressure readings from the two installed piezometers

Challenges

During the pile installation period, the contractor has faced several challenges related to the cleaning of the pile feet and underwater concreting of the piles. The challenges were found during video inspection of the pile footing before concreting, and core sampling of the concrete and the rock in the pile feet after concreting.

The biggest challenge was to ensure quality pile feet with no gravel or cuttings between the reinforced concrete and the rock. The piles where it was found gravel or cuttings at the pile feet after concreting, was injected through the core sampling casings fixed in the reinforcement cages.

SUMMARY AND CONCLUSIONS

The given iteration procedure was a good way to find foundation loads and the pile-soil interaction program is an excellent program to analyse 3D pile groups with many load combinations.

For large-scale drilled steel pipe piles, geotechnical follow-up is vital for the pile design. Deviations from planned pile foundations can then be redesigned without major influence on the progress plan.

ACKNOWLEDGMENTS

We would like to thank the contractor Norwegian Public Roads Administration for positive cooperation through the early phase of evaluations, pile design and supervision. Gratitude is also given to Structural Consultant for professional discussions during pile design. In addition, we would like to thank the piling contractor for excellent communication during pile installation works and the main contractor for their willingness to perform improvements in the cleaning and concreting procedures.

REFERENCES

Baardvik, Engen, Kalsnes, Karlsrud, Lande, Langford, Simonsen, Tvedt, Veslegard
2016 Begrensning Av Skader Som Følge Av Grunnarbeider - Sluttrapport. Begrens Skade.

Den Norske Pelekomité
2012 Peleveiledningen 2012. 2012th edition. Norsk Geoteknisk Forening (NGF).

Mihal
2017 The Formwork Experts. Fv 505 Skjæveland - Foss Eikeland / Brunnholen Bru. GEC Infrastructure.

Open See
2017 Http://Opensees.Berkeley.Edu/Wiki/Index.Php/Laterally-Loaded_Pile_Foundation.

Statens vegvesen, Vegdirektoratet
2012 Prosesskode 2. Standard beskrivelsestekster for bruer og kaier. Hovedprosess 8. Retningslinjer. Håndbok R762. Digitalt arkiv GEO, Oslo: Vegdirektoratet. www.vegvesen.no/Fag/Publikasjoner/Handboker.

Vianova GeoSuite AB
2017 Trimble Novapoint - GeoSuite Toolbox. Pile Group. Version 15.3.

CAST-IN-PLACE PILES USING TOE-GROUTING CELL: APPLICATION IN BOLIVIAN RIVERS

Tomás Murillo, Uriel&Asociados, S.A., Pozuelo de Alarcón, Spain, +34 606824957;
tomasmurillo@urielyasociados.es

ABSTRACT. The paper describes the design and construction of pile-toe, post-grouted drilled piles for bridge foundation, in sandy alluvial soils of rivers Piraí, Yapacaní, and Ichilo, in Bolivia. The grouting system is based on a grouting cell located at the pile toe, which allows distribution of the grout in a known zone underneath the pile toe. The cell's behavior is similar to a hydraulic cell that stresses the ground downward and the pile itself upward. An advantage of this system is that it measures the force that is exerted on the toe (grouting pressure times cell area). The toe force is supported by the reaction developed along the pile shaft. Thus the lower bound value of the shaft resistance is obtained. Additionally, if the upward and downward movements of the toe cell are monitored, the process is similar to that of a bi-directional loading test.

Keywords: toe-grouting, grouting cell, drilled pile on sands

PROJECT DESCRIPTION

Introduction and purpose

The proposal and subsequent construction of the post-grouted-cast-in-place piles described in this article was due to the presence of several geotechnical factors, which could be summarized in:

a) The existence of very clean sands in the alluvial soils of the Piraí, Yapacaní, and Ichilo rivers.

b) The severe toe bearing limitation in sands, according to applicable standards (AASHTO)

These technical circumstances, coupled with the search for the most economical foundation possible (in terms of both, time and cost), gave Uriel and Asociados the chance to propose to Grupo Puentes, contractors and designers of three railroad bridges, the advantages of building toe-grouted cast-in-place piles using grouting cells.

Project description

The project is located in Bolivia, in the railway line between the petrochemical plant of Bulo Bulo and Montero, close to Santa Cruz de la Sierra, and part of the *Bioceánico* Railway.

The bridges, 331, 799 and 331 m in length, cross rivers Ichilo, Yapacaní, and Piraí, tributaries to the Amazon. The spans were established at 39 meters and the designers were able to limit the foundations to 4 piles per bent. Pile diameters were established at 1,200 and 1,500 mm. Drilling used temporary casing for the whole length of the pile and no slurry was used.

The diameter was chosen based more on compatibility with the available rigs than on the loads, as these were similar for all three bridges. Most of the piles had a factored vertical load between 7,000 and 7,700 kN (un-factored loads were between 4,900 and 5,400 kN). The corresponding working stresses were 4.7 and 3.0 MPa for the 1,200 and 1,500 mm piles. The maximum un-factored tension load was 2,600 kN.
Scour depth was defined as 5, 8, and 10 meters for each of the mentioned rivers, although it did not condition the length of the piles due to the reduced safety factors associated to this extreme event. The same can be said for seismic design. The tension loads exceeded the limit only in a few cases.

© 2018 Deep Foundations Institute

Soil profile

From a geological perspective, the bridges are located in the *Chaco – Beniana* plain (as it is called in Bolivia). This is part of the Amazonian plains, at an elevation of 275 above sea level. They are quaternary soils of alluvial and flood plain origin, with thicknesses that exceed 50 meters.
The geotechnical investigation works were carried out in two phases, consisting mainly on 29 boreholes with SPT tests for the 42 bents. In some cases, these borings were drilled on top of a pontoon. Laboratory tests carried out were sieve analysis and Atterberg limits.

The alluvial soil was predominantly fine sandy and clean. At a certain depth, sand was dense or very dense, which usually coincided with past scour depth.

At varying depths, lenses of heterogenic clays and silts could be found, as well as sands with gravel (see next figure).

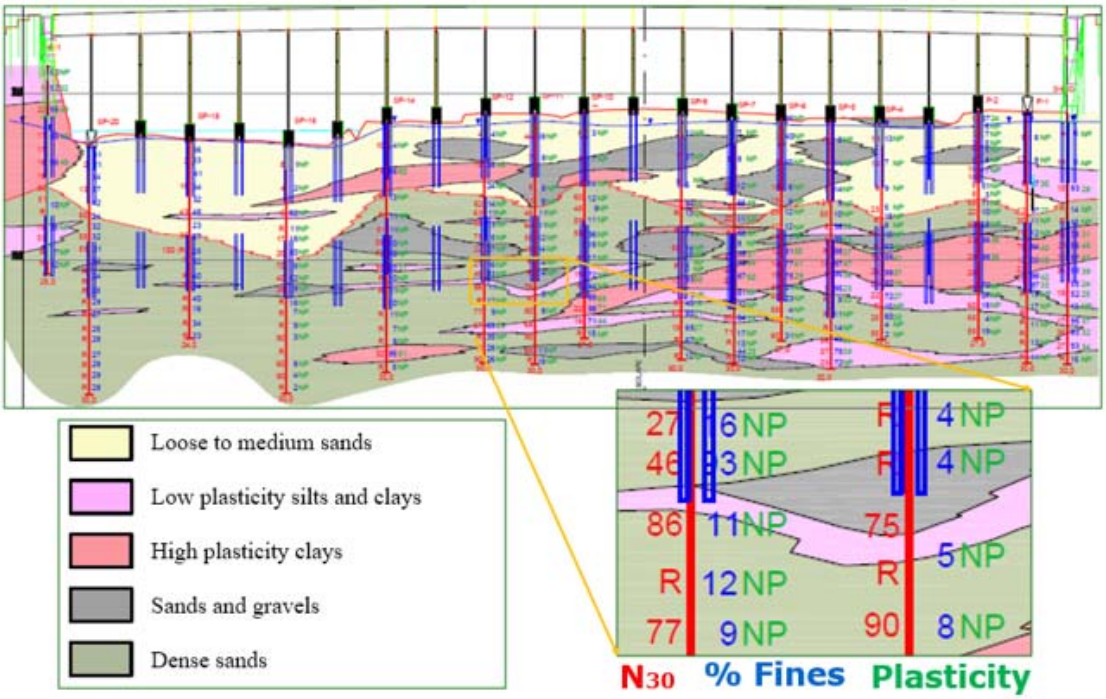


Fig 1. Section of the geological profile in Yapacaní

For the finer and looser sands, an angle of shearing resistance between 30º and 32º was chosen. For the denser and coarser sands, the values reached 34º and 36º. In clays, angles of shearing resistance of 28º-29º were chosen for the low plasticity clays and of 26º for the high plasticity clays.

TOE RESISTANCE CALCULATIONS IN SANDS

Standards

The bridges in Bolivia were designed according to US standards, specifically AASHTO LRFD Bridge Design Specifications (2012). This standard is based on the FHWA document Drilled Shafts: Construction Procedures and Design Methods (1999), written by O`Neill, M. and Reese L. C. The FHWA document has a newer version dated 2010, but it was not used in the drafting of AASHTO 2012.

Calculation method for drilled piles in sands

The FHWA's document that discusses drilled piles mentions the disturbance of the sands at the pile toe as well as the accumulation of debris as sufficient reasons to justify the use of an empirical method, based on SPT results. By other hand, ultimate toe resistance is defined in US standards as the load that causes a movement of 5% of the pile toe diameter.

It mentions, in addition, that the analytic formulations used for obtaining the capacity would give the maximum resistances reachable, but the movement needed for the mobilization of those loads would be too high for the structure.

Consequently, AASHTO's method for toe resistance in sand is limited to an SPT based method, using these equations:

$$q_p = 0.057\, N_{60} \quad ;\, N_{60} \leq 50 \quad [MPa] \tag{1}$$

$$q_p = 0.0285 \left[N_{60} \left(\frac{p_a}{\sigma'_v} \right) \right]^{0.8} \sigma'_v ;\; N_{60} > 50 \tag{2}$$

FHWA's 2010 version now only accepts the first equation; the second one was included in the 1999 version. AASHTO seems to still be based on the old FHWA document.

The maximum toe resistances estimated when using this method, based on static loading tests results, are 2.9 and 6.0 MPa for Equations 1 and 2, respectively.

Calculation method for toe-grouted piles

Mullins et. al (2004) developed an investigation program sponsored by the Florida Department of Transportation, based on full scale testing. The tests results led to a proposed calculation method for piles with grouted toe that was incorporated into the FHWA's document on cast-in-place piles (2010).

Without going into its applicability and related aspects that go beyond the scope of this paper, the method considers that the improvement obtained depends on an index (GPI), equal to the grouting pressure (pi) divided by the ultimate toe resistance without grouting (qp):

$$GPI = \frac{Pi}{qp} \tag{3}$$

The toe resistance, $q_{p\ grouted}$, after grouting is expressed using a multiplier, TCM, of the toe resistance (the ultimate capacity)

$$q_{p\ grouted} = (TCM)(qp) \tag{4}$$

The equation for this multiplier depends on the pile toe movement expressed in terms of a percentage of the pile diameter:

$$TCM = 0.713\ (GPI)(\%D^{0.364}) + \frac{\%D}{0.4(\%D)+3.0} \tag{5}$$

If we focus only on the ultimate load, defined as 5 % of the toe diameter, the relation between TCM and the GPI-index (Eq. 3) is linear (TCM = 1+1.28GPI).

With the method discussed, as well as with any other based on grouting pressures, some concerns have to be taken into account and settled before construction. The following should be considered:

- The available shaft resistance limits the maximum grouting pressure. At a certain point, attempts to increase the grouting pressure on the toe will just result in pile uplift (when grouting with a grouting cell or a flat jack).

- The design grouting pressure will have to be achieved during the construction phase, something that is not guaranteed in the design phase, since it depends on many factors.

Design methodology

With the aim of searching for the most conventional calculation procedure possible, which also had to be accepted by local standards, Mullins' method was used for estimating the grouting pressures required during construction.

It was assumed that grouting would cancel the negative effects related with the response of a bored pile on sands: disturbance of the sands and debris at the pile toe, as well as increase the stiffness of the soils at the pile toe.

The analytical method used for shaft and toe resistance calculations was based on effective stress distribution, internal angles of friction, and cohesion. An 11-MPa limit toe resistance was applied for each bent.

For the pile length of each cap, a required grouting pressure was calculated in order to obtain the toe resistance. For this, the non-grouted resistance was calculated according to the AASHTO formula, that is, 6 MPa for a sand with SPT N-indices indicating very dense conditions, instead of following the current FHWA formula. In order to reach the maximum 11 MPa toe resistance in sands, a TCM multiplier of 1.83 would be required, which could be obtained with a grouting pressure of 3.9-MPa, following the calculations presented herein.

The calculation process was completed by checking that, for each required grouting pressure, the estimated shaft resistance was sufficient for the pile not to move upwards.
The results for the bents are summarized in the following table:

Table 1. Summary of toe resistances and grouting pressures

	Ichilo	Yapacaní	Piraí
Pile length (m)	27	20-25	22-30
Nominal toe resistance (MPa)	10	5-9	9-11
Required grouting pressure (MPa)	3	1-3	2-4

Comparison of grouted and not-grouted pile lengths

Benefits of post-grouting piles are an increase in toe capacity and a higher level of confidence in the design. But in order to justify the use of these grouting techniques, these advantages must be also accompanied by a reduction in foundation costs, which has to compensate the increased construction complexity and technification they require.

In the case of cohesionless soils, if design methods based on displacement criteria are considered, toe grouting will be a very cost effective option in many cases. In this specific project of Bolivia's bridges, several prior calculations were performed in order to decide the viability of using the toe-grouting technique. The following figure shows a simple example of one of the most representative piles in the river Yapacaní, on which the factored load applied to the piles was 6,050 kN. The non-grouted toe capacity was 6.0 MPa, and the toe capacity to be achieved by grouting was established according to the analytical method. A length of 22 m was enough for a toe-grouted pile, with a toe capacity of 8.9 MPa (TCM=1.48). The length of a not-grouted pile would be approximately 10 m larger. (Fig.2).

In some cases, this lower capacity of the not-grouted piles would have required the design of bents with 6 piles, instead of the ones designed with 4 piles.

In the specific case of the bent used as an example, the necessary grouting pressure to achieve a multiplier TCM=1.48 was 2.2 MPa.

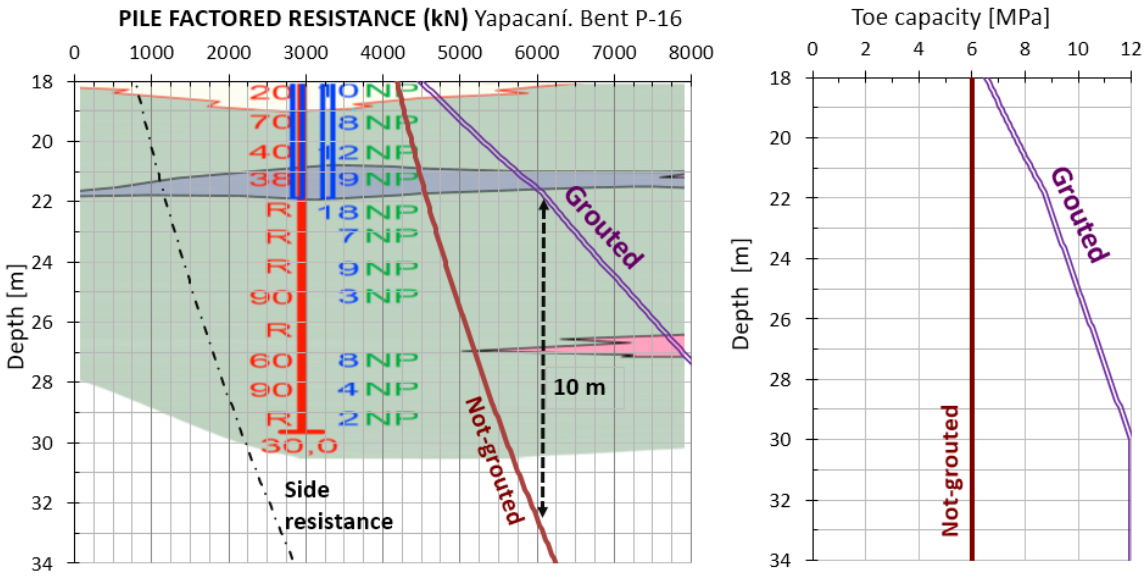


Fig 2. Comparison example between grouted and not-grouted pile resistance

GROUTING

Toe-grouting device

The grouting device used in the bridges of rivers Piraí, Yapacaní and Ichilo, subject of this article, is grouting cell or toe-box. It features two concentric steel cylinders that can shift around each other telescopically, enabling the expansion of the cell downwards as the grouting pressure increases. The cell is completed with 2 steel plates welded to the cylinders at the ends of the cell.



Fig 3. Grouting cell a) Before expansion b) Cylinders partially expanded

One or more rubber seals are placed between the cylinders to achieve better sealing during the expansion of the cell. However, when a certain pressure is exceeded the grouting mix leaks from the cell, grouting the surrounding soil. In conclusion, the cell's behaviour is initially similar to a hydraulic cell that stresses the ground downward and the pile itself upward, and then allows a conventional grouting of the soil.

The cell is also wrapped with a non-woven geotextile. This geotextile provides an additional isolation of the cell from the pile concrete, and also helps to create a grout bulb below the pile toe, minimizing hydro-fracture grout losses.



Fig 4. Grouting cell fixed to the pile reinforcement cage. a) Bottom view. b) Top view

This system allows the installation of movement-monitoring devices (tell-tale) in the grouting cell, with which the expansion reached may be controlled.

A more detailed description of this expansion-grouting cell can be found in Terceros et al (2017).

The grouting cell's behaviour is similar to a hydraulic cell/jack that stresses the ground downward and the pile itself upward. In fact, the pressured grouting bulb has a known horizontal cross-section, which is the cell's or jack's circular area, and which diameter is approximately equal to the diameter of the pile reinforcement cage, and slightly smaller than the pile's diameter. In this way, it is possible to measure the force that is exerted on the toe (grouting pressure times cell area). The toe force is supported by the reaction developed along the pile shaft and, consequently, the shaft mobilizes its shear resistance gradually as the grouting pressure increases, and a minor uplift of the pile occurs. The maximum grouting pressure is limited by the shaft's ultimate resistance.

Monitoring the movement of the pile head during the grouting operation would be sufficient to serve as an approximate loading test for shaft resistance. If the downward movement of the grout cell is also monitored, the system serves as a bi-directional loading test for each pile. (In the event that the pile does not reach the uplifting point, a lower limit for the shaft resistance would have been obtained). An advantage of this is, therefore, that applicable standards' provisions allow the use of lower resistance factors when loading tests are available.

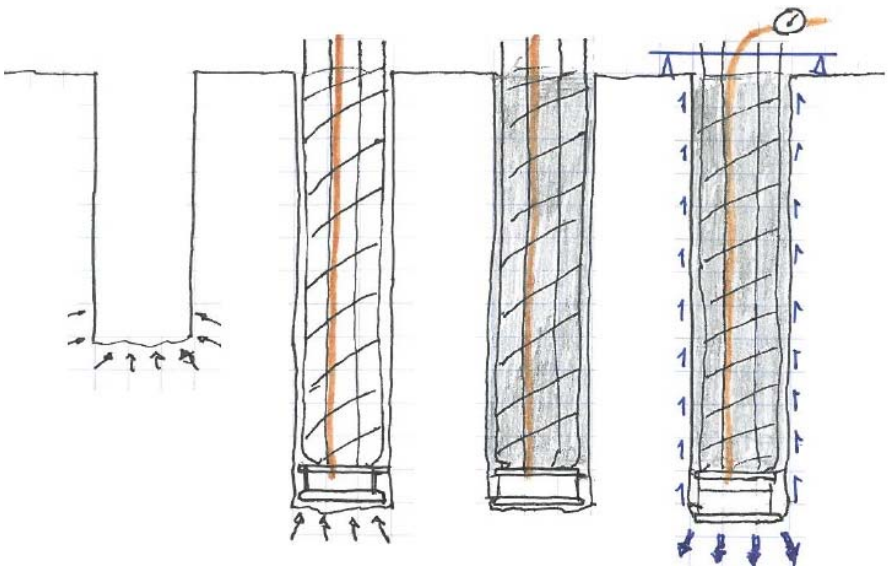


Fig 5. Construction and loading of the flat jack or grouting cell

Grouting procedure

Grouting, carried out by INCOTEC, was taken to the maximum pressure possible. The limit was given either by the pile uplift or when a certain volume was reached.

The volume was increased to a maximum of 1,000 liters, after observing that the grout could leak out between the cylinders of the cell once a certain pressure was reached (the volume of the cell is 200 liters). Grouting pressure was released during the curing of the grout.

Pressure, volume, and flow controls were performed in real time using transducers. This enabled the evaluation of each grouting for validation purposes, together with the data measuring the pile uplift and pile toe movement. Movements were measured with tell-tales (free moving rods inside a tube that is resting on the base plate of the cell). These movements were measured manually, with the inconvenience that grouting is a dynamic process and the response measured at the pile head is not instantaneous.

Pile uplift was limited to 5 mm, allowing slightly higher values if the expected grout pressure was not obtained.

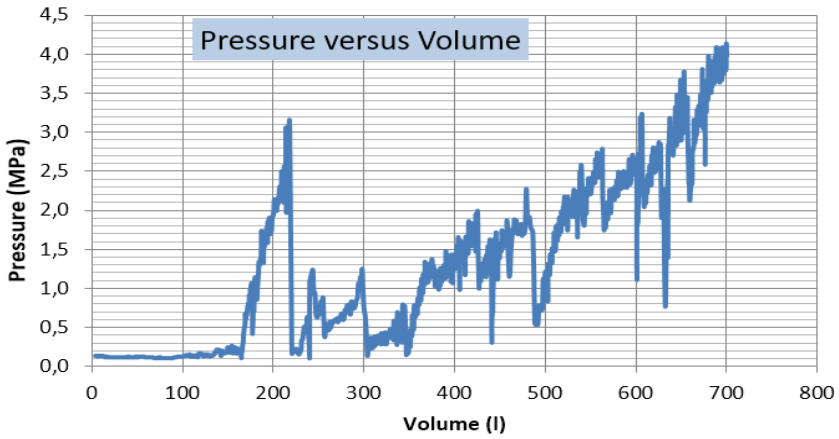


Fig 6. Grouting pressure-volume log example

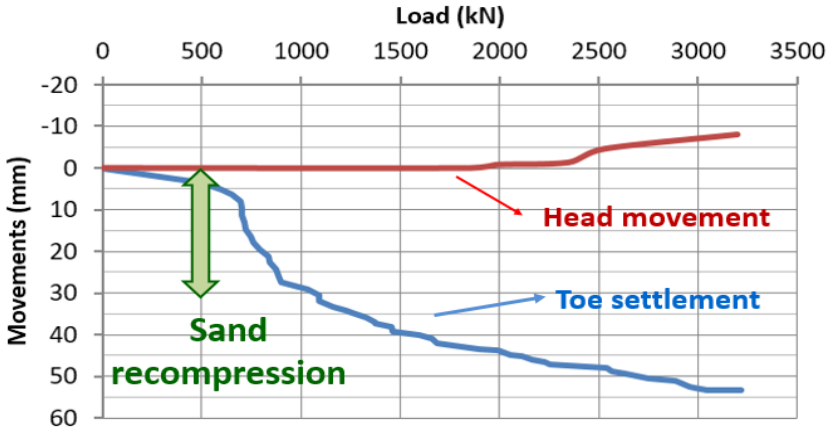


Fig 12. Measured movements example

Analysis of toe load-movement

Grouting pressures reached are quite variable, mostly due to the fact that no maximum value was established. In general, pressures were greater than the required grouting pressure (Table 1), and show figures similar to the factored toe resistances.

Figure 8 shows the pressures obtained with the cell and the movement obtained when grouting the 1,200 mm diameter piles. The heavy line at 60 mm indicates the limit value defined by FHWA and AASHTO (downward movement equal to 5 % of the diameter).

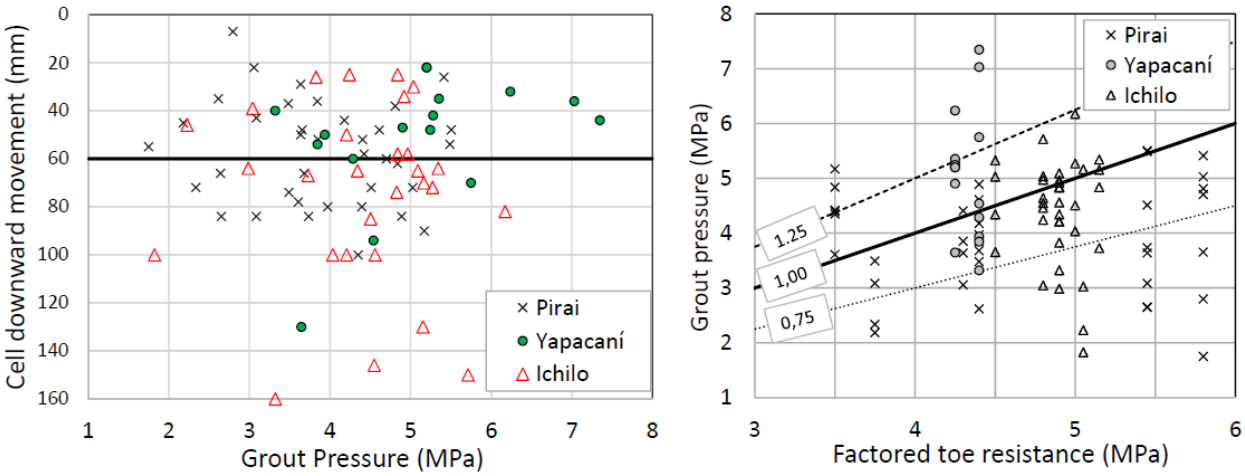


Fig 8. Grouting pressures at toe vs. movement

With regards to the movements recorded, dispersion is due to several factors. On the one hand, it can be explained by the heterogeneity of the alluvial soils, as well as by the different results obtained in the construction of each pile (for example, the effort needed to control water inflow in each of the piles was very variable, depending on the unpredictable presence of artesian sand layers). On the other hand, the grouting cell used expands until the grout seeps through, and then the expansion rate decrease.

In general, movements recorded reveal the dubious behaviour of drilled-pile toes, especially if the piles have been drilled in sandy soils and are beneath the water table. If we assume that pile toe movement during grouting is, approximately, proportional to grouting pressure, this simplification would result in an average toe resistance of 5.2 MPa for a 60-mm movement before grouting. The standard deviation is high, 3.0 MPa.

A recommended improvement for future applications would be the use of tell-tales with LVDT sensors for data collection in real time. Thus, during the grouting process it would have been possible to record a fact observed on site, namely that induced toe movements are practically irreversible and that re-loading also causes a very stiff response. This is one of the mechanisms that enhances toe performance, and is stated in several references (Mullins G. et al (2006); CALTRANS (2016)). The following diagram illustrates this concept, through the use of a conceptual sketch from California's Department of Transportation.

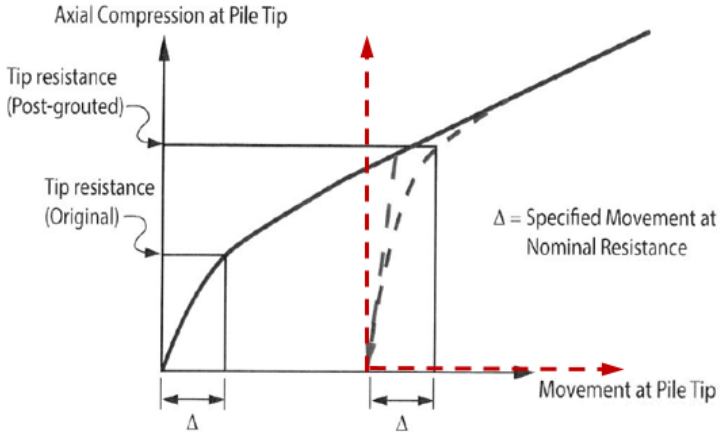


Fig 9. Effect of post-grouting on nominal toe resistance (adapted from CALTRANS)

Mobilized shaft resistance

The following graph depicts the mobilized shaft resistances, compared to calculated shaft resistance in the design phase, in piles that moved upwards during the grouting.

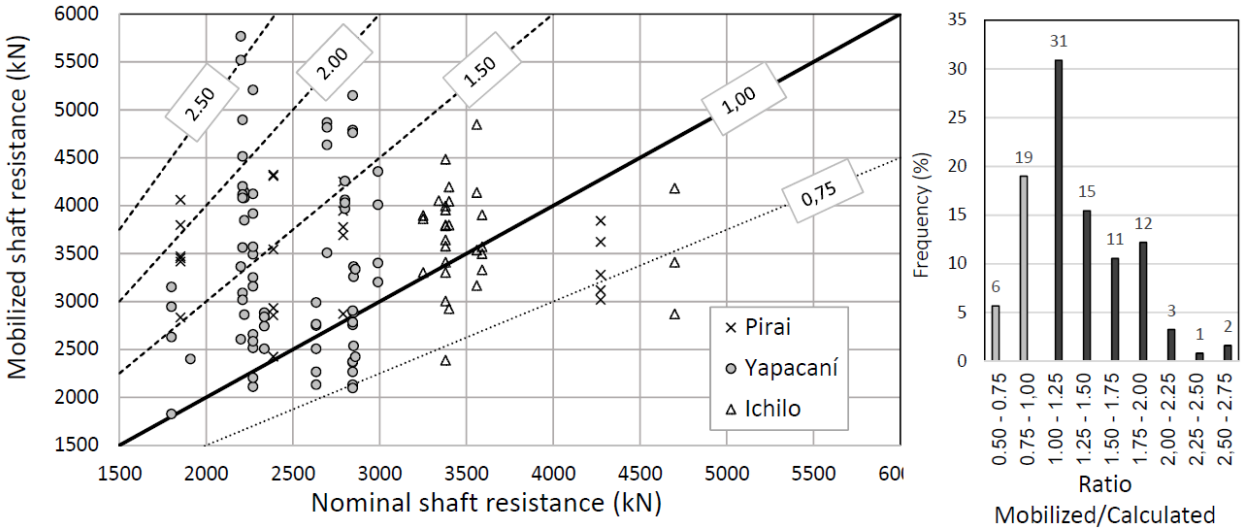


Fig 10. Mobilized shaft resistance vs. nominal shaft resistance.

Mobilized shaft resistance was larger than nominal shaft resistance for 75 % of the piles. It is worth highlighting that mobilized shaft resistance is a lower bound of the actual shaft capacity of the pile, as the pile displacement was limited to avoid reaching the maximum shaft resistance. In addition, for many piles this limitation proved unnecessary, and the grouting process was fully performed without the upward movement limit pressure having been reached (volume was the limiting variable).

Average upward measured displacement of the piles was 4, 2 and 6 mm for rivers Piraí, Yapacaní and Ichilo, respectively, values that are clearly below those usually considered necessary for fully developing ultimate shaft resistance in sandy soils (0.5 and 1.0 % of the diameter of the pile).

On average, mobilized shaft resistances were 40, 37 and 36 kPa in each river, respectively. For a group of 16 piles, the only ones with a 1200 mm diameter along the river Yapacaní, situated in 4 consecutive piles, uplifts reached significantly high figures, between 5 and 16 mm, and an average of 13 mm. On these piles, the mobilized force was between 1.2 and 1.6 times the calculated capacity, with the average multiplier being 1.8. The average mobilized resistance was 48 kPa.

As these figures became known during the piling works, they were taken into account when it came to re-evaluating the load capacity of some of the piles in which the design pressures had not been reached.

It can be concluded that the calculation method based on effective stresses has been conservative. This method is based on the beta parameter ($\beta=K_o \tan \phi$), which is not very sensitive to variations in the angle of shearing resistance. The conservative factor does not result from the representative parameters selected as much as from the method itself.

Load applied on piles by grouting

Finally, the following graph compares the total loads mobilized by grouting with the un-factored load in each pile.

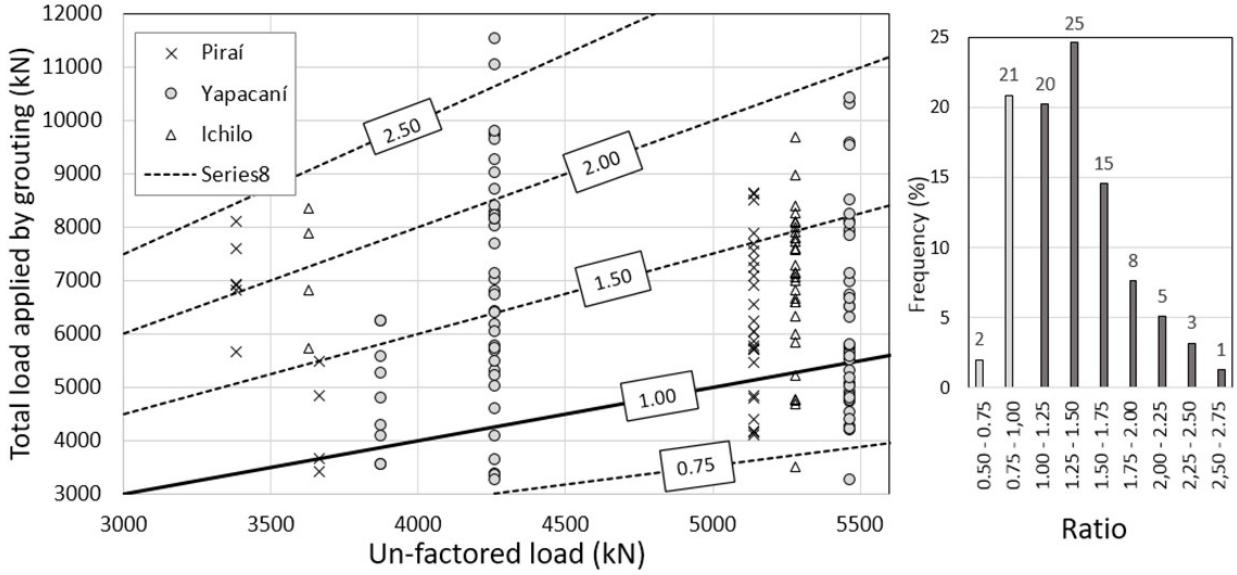


Fig 11. Mobilized load vs. un-factored load.

As it can be seen, most of the piles (76 %) were subjected to loads higher than the working loads.

Although data recorded for grouting parameters, as well as pile head and toe displacements, is not sufficient to be considered a comprehensive load test that fulfils standards, grouting is a bi-directional loading monitored process. Thus, this data contributes to increasing confidence in the design during construction, and constitutes a step forward in the execution, in comparison with not-grouted piles.

CONCLUSIONS

Excavation and concreting of a pile in soils, especially in sandy soils under the water table, can significantly affect its capacity and, especially, the proper response of the pile toe. Toe-grouting technologies can mitigate the disturbance of the soil and debris accumulation, and increase pile toe stiffness.

In this specific project of Bolivia's bridges, 1,200 and 1,500 mm diameter cast-in-place piles were post-grouted using toe-grouting cells. The calculated nominal resistances were twice what the AASHTO recommends for conventional cast-in-place piles in sands. Consequently, a substantial reduction in shaft lengths was achieved and, therefore, significant savings (both, in cost and time) on foundation works were made.

In addition, the use of toe-grouting cells, coupled with grouting parameters (pressure, volume, flow) being monitored and pile movements being controlled during grout loading, enhances the reliability of the pile's design and construction.

ACKNOWLEDGEMENTS

The author would like to thank the Grupo Puentes team, led by their Project Manager, Ángel Eiras Sánchez, and their Head of Construction, José Antonio Rodríguez Quevedo, for their trust.

References

AASHTO, 2012. LRFD Bridge Design Specifications.

Brown, D. (2012) Recent Advances in the Selection and Use of Drilled Foundations. Geotechnical Engineering State of the Art and Practice: Keynote Lectures from GeoCongress ASCE Oakland, California, pp. 519-548.

Bruce, D.A. (1986), “Enhancing the performance of large diameter piles by grouting, I and II, Ground Engineering, May and July

Bustamante M., Gianeselli L., 2008. Reglas de cálculo de la resistencia de pilotes por el método de los estados límites últimos. Método presiométrico. CEDEX. Madrid. Spain

CALTRANS, 2016. Memo to designers. 3-8 October.

CEN, 1994. Eurocode 7: Geotechnical design - Part 1: General rules, Pre-standard ENV 1997-1. European Committee for Standardization (CEN): Brussels.

CEN, 2004. Eurocode 7: Geotechnical design - Part 1: General rules, EN 1997-1:2004 (E), (F) and (G), November 2004, European Committee for Standardization (CEN): Brussels.

CEN, 2007. Eurocode 7: Geotechnical design - Part 2: Ground investigation and testing. EN 1997-2:2007 (E), March 2007, European Committee for Standardization (CEN): Brussels.

Daap S., Muchard M., Brown, M. 2006, Experiences with base grouted drilled shafts in the southeastern United States. DFI Conference. Amsterdam.

DTU 13.2, 1983. Fondations profondes pour le bâtiment, Chap 11: Calcul des fondations profondes soumise à charge axiale: 1-8.

FHWA, 1999. Drilled Shafts: Construction Procedures and Design Methods.

FHWA-NHI, 2010. Drilled Shafts: Construction Procedures and LRFD Design Methods.

Mullins G., Winters D. 2001. Post-grouted drilled shafts Tips. Phase I. University of South Florida.

Mullins G., Winters D. 2004. Post-grouted drilled shafts Tips. Phase II. University of South Florida.

Mullins G., Winters D., Dapp S. 2006. Predicting end-bearing capacity of post-grouted drilled shafts in cohesionless soils. Journal of Geotechnical and Geoenvironmental Eng. ASCE.

Terceros M, Terceros M, 2017. Expander Body and Toe-Box: Expansion Devices for Deep Foundations Enhancement. 3rd B.F.P.B Santa Cruz de la Sierra. Bolivia.

CURRENT PRACTICE OF CFA PILING IN AUSTRALIA AND NEW ZEALAND

Martin D. Larisch, Brian Perry Civil, Auckland, New Zealand, +64274055406, martinla@fcc.co.nz

Martin D. Larisch, Geotechnical Engineering Centre, School of Civil Engineering, The University of Queensland, Brisbane, QLD, Australia, +61419799701, m.larisch@uq.edu.au

ABSTRACT

Despite the introduction of Continuous Flight Auger (CFA) piles in Australia about 30 years ago, the pile type has not yet been fully accepted in the geographically 'neighbor' country of New Zealand. One of the main advantages of CFA piles is the high production rate which can be achieved with the system. This can make CFA piles very economical. Their installation is vibration free and lateral stress relief associated with bored piles can be reduced notably if construction is carried out correctly. Pile diameters and pile lengths are limited compared to rotary piling applications.

The construction of CFA piles in water saturated or unstable soils is possible without any additional measures like casings or drilling fluid to keep the excavation stable, as long as installation parameters are monitored and controlled correctly. Compared with conventional bored piles the visual verification of the pile excavation is not possible as concrete is poured whilst the auger is extracted. CFA piling is a "blind process" and advanced quality assurance is critical to construct a conforming pile. Modern piling rigs are fitted with electronic and mechanical sensors and measurement devices to monitor construction parameters during pile construction.
Pile lengths in access of 40m have been achieved in Australia with 900mm diameter CFA piles and maximum pile diameters of 1,500mm for pile depth close to 30m were achieved in Australia.
In New Zealand, 1,200mm piles with depth around 24m are the current state of practice. The main challenge in New Zealand is around the strong seismic requirements which makes full depth cages necessary.
The paper discusses the current state of practice in Australia and New Zealand with a particular focus on seismic design requirements and typical applications for ground improvement, working platforms and basic design principles for foundation piles constructed with the CFA methodology.

KEYWORDS

CFA piles, dynamic pile testing, seismic design, pile design, ground improvement

INTRODUCTION

In the last two decades the piling and deep foundation industry has dramatically changed around the world but especially in Australia and New Zealand. The author have had the privilege to work in both countries leading piling and deep foundation contractors for 12 years. Particularly in Australia CFA piling has significantly shaped and changed the deep foundation market during the last decade.

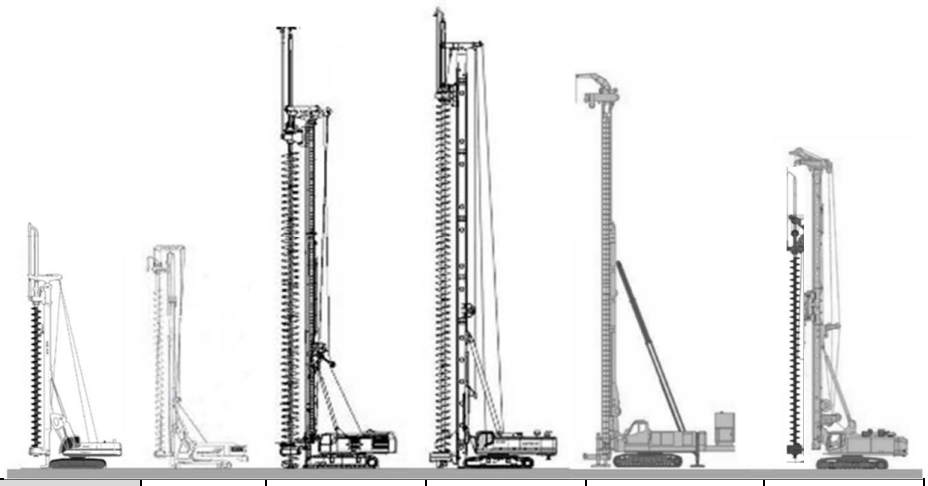
The construction and mining boom in Australia during the last two decades was a driver for commercial and residential construction projects, in urban areas but also in the densely populated cities at the East Coast of the country. The requirement for high rise building fueled innovation in deep foundation practice and a few companies have driven this transformation in recent years.

CFA piling is an efficient and cost effective method to transfer building loads into the suitable bearing layer. The method can also be used for embedded retaining walls providing better stiffness and water proofing performance than sheet piles. Especially secant pile walls are much cost efficient for 2-3 level basements and with the introduction of medium sized CFA piling rigs (40 to 60 ton operational weight) this market segment was developed with great success in Sydney, Melbourne and South East (SE) Queensland on the East coast of Australia.

© 2018 Deep Foundations Institute

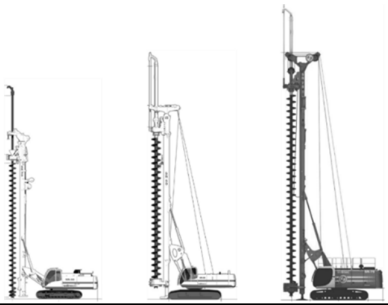
Some deep foundation contractors in Australia transformed the market by including the design risk into their scope of work for embedded retaining walls and foundation piles offering their clients highly competitive and cutting edge solutions.

Figures 1 and 2 show the different sizes of current CFA piling rigs in Australia and New Zealand. It is obvious that CFA rigs in Australia are generally larger and have the ability to drill much deeper using bigger diameter than the majority of the CFA piling rigs in New Zealand. The Soilmec SR50 is a good reference for both markets – it is considered 'medium sized' rig in New Zealand but a small scale rig in Australia.



Type	Soilmec SR50	Mait HR160	MaitHR420	Enteco E25MD	Fundex F3500	Bauer BG40
Rotary Drive Torque	180 kNm	163 kNm	420 kNm	530 kNm	450 kNm	400 kNm
Operational weight	50 T	52 T	130 T	130 T	120 T	120 T
Pile diameter	900 mm	1,000 mm	1,500 mm	1,500 mm	1,500 mm	1,200 mm
Maximum drill depth	21 m	19.5 m	35 m	38 m	45 m	26.5 m

Fig. 1. Selection of typical CFA piling rigs in Australia



Type	Soilmec SR30	Soilmec SR50	Soilmec SR75
Rotary Drive Torque	108 kNm	180 kNm	293 kNm
Operational weight	30 T	50 T	75 T
Pile diameter	750 mm	900 mm	1,200 mm
Maximum drill depth	19 m	21 m	25.5 m

Fig. 2. Selection of typical CFA piling rigs in New Zealand

The situation in New Zealand was slightly different as the country (and therefore the construction market) are much smaller and there was no construction boom until 2015. Therefore, the New Zealand construction industry didn't experience a similar boom CFA of piling as in Australia. CFA was introduced at a much smaller scale about 15 years ago and projects were generally smaller, even though the construction industry in New Zealand has successfully delivered some significant and challenging infrastructure and building projects in the last decades. However, ground conditions are generally less suited to the CFA technique than in Australia and the penetration of rock was required for most regions. For reliable rock penetration, larger rigs with higher torque and pull-down forces were required and the market didn't respond as well as in Australia. In addition, contractors didn't offer design and construction work for their clients which was mainly due to rather complex seismic design requirements and a strong influence of consultancy firms. Foundation piles for larger structures were usually built using large diameter bored piles and the required diameters and depths were usually far beyond the industry standards of CFA capabilities.

CFA PILING IN AUSTRALIA – IT IS ALL ABOUT SIZE…

CFA piling was introduced in Australia in the 1970's. The technology has been used as niche product until about 2005. With the growth of the cities on the East Coast, CFA piling became more attractive. Especially piling companies in Melbourne developed CFA piling very quickly and used this technology to design and construct deep foundations.

The driver for this change were the ground conditions in Melbourne which consists of a thick layer of soft silts (10-25m) underlain by gravels and weak rock. Usually foundation piles need to be socketed into the rock layer and therefore pile lengths are typically in the range of 40m. The gravel layer is permeable and therefore the use of drilling support fluids can be risky. Therefore deep CFA piles are an optimal solution for ground conditions in Melbourne, especially as production rates are high if the piles can be installed in a single stroke. Usually only short reinforcement cages are required as no lateral (seismic) loads are expected.



Fig. 3. Fundex CFA piling rigs transformed the CFA piling market in Australia in the last decade, advanced concrete technology was required to install reinforcement cages for CFA piles

It is reported by various authors (Tchepak 1998, Slatter 2005) that CFA piles as well as drilled displacement piles were used for the foundation of various landmark buildings in Melbourne. Slatter (2005) reported about the foundation of the Eureka Tower (291m high, 91 floors, opened in October 2006) as a milestone in CFA technology in Australia. The original foundation scheme was based on the installation of 1.2m diameter bored piles, 40m deep with 12m rock sockets and installed under drilling fluid.

As the use of polymer fluid was risky due to the high sand content of the soil, the piling contractor proposed a competitive design & construct scheme to install CFA and drilled displacement piles as a replacement for the bored piles. Dynamic pile load testing was carried out by the contractor on 3% of the foundation piles to verify pile capacities of 10-12 MN ultimate vertical loads.

Based on this extremely successful combination of in-house engineering capabilities, modern CFA technology for deep piles in the range of 40m single stroke and internal construction verification by (dynamic) load testing, the deep foundation market in Melbourne developed world class standards and innovations in the niche market of deep CFA piling. Figure 3 shows the typical Fundex CFA piling rigs which revolutionized the CFA market in Australia and were pioneers for the installation of deep CFA.

The installation of CFA piles of around 40m depth requires extremely skilled operators and site crews as well as highly developed concrete technology. The use of grout was limited as the Australian Piling Standard AS2159-1995 penalized the use of grout by applying a reduction factor for skin friction. Consequently, concrete suppliers in Melbourne developed highly workable and very stable CFA mixes which were measured using spread rather than slump testing.

The large and powerful CFA piling rigs could also be used for the installation of basement retention systems (e.g. secant piles or contagious piles) as shown in Figure 4. In combination with highly advanced tooling, CFA piles were able to penetrate rock providing an excellent transition between the pile shaft and the rock mass.



Fig. 4. The powerful CFA pilings were able to install straight CFA piles for basement retention and the tools were able to penetrate rock

PILE DESIGN

Pile designs in Australia and New Zealand are usually based on the Australian Piling Standard AS2159-2009.

Foundation piles are designed using various proven methods like the alpha-cu method, the beta method or, especially for CFA piles, the method after Bustamante and Gianeselli (1998). This method was originally based on the prediction of the bearing capacity and settlement of drilled displacement piles. The method has since been used successfully by many practitioners (including the author) for both, drilled displacement piles and CFA piles and the designs were successfully verified by load tests on site. It appears that auger shape does not have a significant influence if one design method covers a wide range of different screw auger tools.

This design method can be used in displaceable soil only (e.g. sand, gravel, silt, clay, marl and chalk) and is based on in situ soil investigation data. The design method is largely based on CPT and MPT test data and the SPT has only an indicative character.

Based on the correlations carried out between the initial design assumptions for various CFA piling jobs in Australia (especially Melbourne) and the correlating PDA and CAPWAP results, the design approach was found to be suitable for the design of CFA.

PILE LOAD TESTING

The use of dynamic pile load testing for CFA piles was a novelty in Australia prior to the first decade of the new millennium. Typically, only driven piles were tested using dynamic pile testing methods and bore piles as well as CFA piles were tested using static pile testing methods, which don't allow testing of working piles and therefore incur higher costs and program implications. However, Australian piling contractors in collaboration with some geotechnical consultants utilized external drop hammers of typically 10 ton and up to 3.0 m drop height to mobilize the CFA piles. Dynamic pile load testing of CFA piles allow designers to apply lower geotechnical reduction factors in accordance with AS2159-2008, which makes pile load testing very attractive.

Larisch et al (2013) report about the use of PDA testing for a deep foundation scheme of more than 700 CFA piles in Queensland, Australia. For the whole project twenty four working piles (each 900 mm in diameter and typically between 15 m to 22 m long) were tested dynamically using the Pile Driving Analyzer (PDA). Typically four strain gauges and four accelerometers were installed about one meter below the pile head and the tests were carried out at least fourteen days after installation to ensure sufficient concrete strength. The piling contractor used a 10 ton drop weight which operated inside a structurally certified steel frame (Figure 5) to re-strike the piles using one meter drop height. One representative blow was selected for each pile and analysed using the computer program CAPWAP.

For all dynamic load tests the ultimate geotechnical strength Pg (8 MN) of the piles was achieved, in all cases with less than the specified maximum settlements of 20 mm (ULS). A typical CAPWAP load settlement curve for a working pile is shown in Figure 5 and the load-settlement data show adequate agreement with the static load test results which were carried out prior to construction.

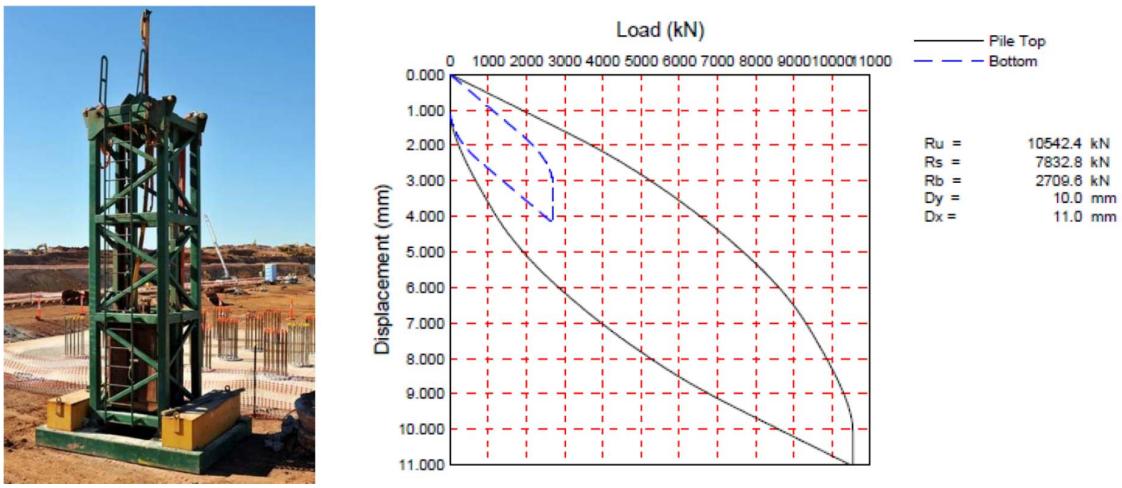


Fig. 5. Certified PDA testing frame with 10 ton drop weight (left), typical CAPWAP load displacement curve for a working pile (right) after Larisch et al (2013)

CFA PILING IN NEW ZEALAND – IT IS ALL ABOUT SEISMIC…

In New Zealand, CFA piling is a relatively new technology, which was introduced about a decade ago. It needs to be understood that the requirements of the foundation and ground engineering market are very different from those at the other side of the Tasman Sea as New Zealand is a seismic region.

Due to these seismic requirements in New Zealand, it is not uncommon, that foundation piles of 1.5m up to 3.0m in diameter are required to be able to resist the lateral loadings in an earthquake event. Such large pile diameters are typically achieved by rotary bored piles as shown in Figure 6.

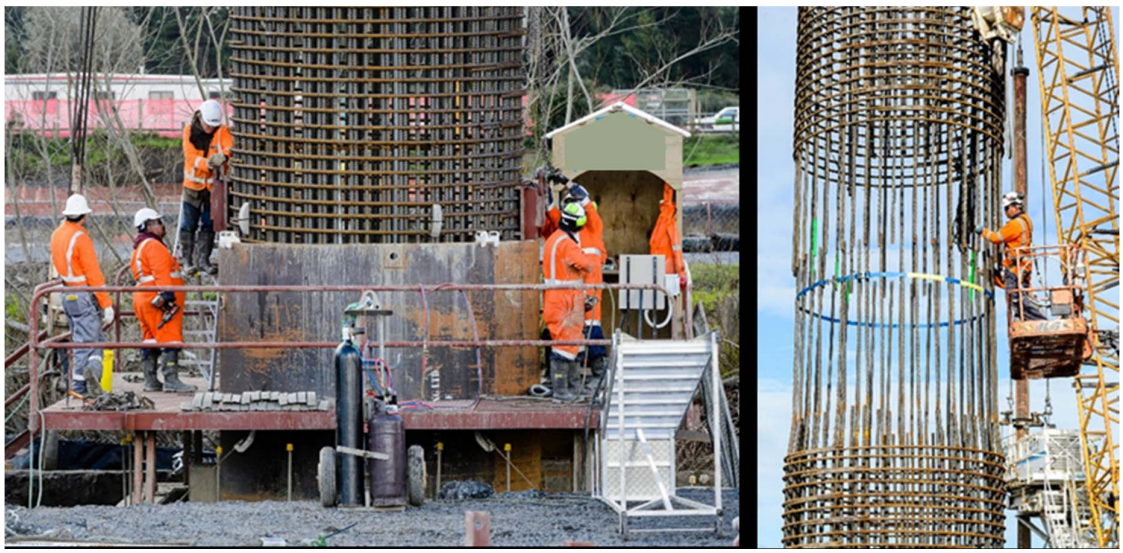


Fig. 6. Large diameter bored piles with diameters of up to 3.0m are required for many projects in New Zealand as a result of seismic design requirements

Piling and ground engineering works in New Zealand are not less challenging than in Australia, most probably the opposite is the case due to the seismic requirement in designs. However, CFA piles are slim foundation elements which are installed at a fast rate and the opportunity for this piling system lies in retaining wall structures and moderately loaded foundation piles. Recently, the largest piling rig in the country was upgraded to install 1.200mm diameter CFA piles up to 25m depth, which provides an opportunity for clients and designer alike to implement the more efficient CFA technique.

The majority of piles in New Zealand require rock sockets in low to medium strength rock. This has been a challenge for the 50 ton class of piling rigs in the past. Even basements in Auckland, which are typically only 2-3 levels deep, are usually installed using rotary techniques as the location of locally cemented soils will result in refusal of CFA techniques. Figure 7 shows a circular shaft retention system in Auckland using CFA piling.



Fig. 7. Shaft and basement retention systems in New Zealand were built using CFA technology, due to the local geology, basements are usually only 2-3 levels deep

CFA piling technology is very common in New Zealand for ground improvement works. The construction of lattice structures as liquefaction mitigation is a successful ground improvement method in loose granular soil conditions with high silt contents, which can't be improved by vibratory methods (e.g. vibro-compaction or stone columns). Based on the experience of recent infrastructure projects, CFA piles for lattice structure are rarely exceeding 10m as the liquefiable soil layers are often located close to the surface.

Based on the design of Nguyen et al. (2013), lattice boxes of about 6m x 6m are installed. Deep soil mixing (DSM) to form in-ground shear walls has been used to remediate against the potential effects of earthquake induced liquefaction on many projects. A grid pattern of soil-cement walls act as a confined shear box, which can provide additional shear stiffness and strength for sites to withstand liquefaction. Current design practice for DSM grids commonly relies on the strain compatibility assumption, where the DSM walls and confined soil are assumed to experience the same shear strain.

The walls of the boxes are made of overlapped piles constructed of low strength concrete (with typical UCS values of 1-3 Mpa). Figure 8 shows a typical lattice structure for liquefaction mitigation of a bridge abutment.



Fig. 8. Lattice structures are commonly used as liquefaction mitigation measures in silty soil conditions, the wall of the boxes are usually overlapping CFA piles installed with small rigs

The biggest challenge for concrete lattice works are typically concrete technology. In some instances, and based on the availability of local aggregates, the low concrete mixes might have difficulties in pumping.

CONCRETE TECHNOLOGY

Due to seismic events in New Zealand, foundation piles normally require full length reinforcement cages. Concrete technology in New Zealand is currently developing fast and it is expected that shortly similar standards will be achieved as in Australia. The 'Recommended Practice: Tremie for Deep Foundations' booklet (2012) is a common guideline for the design of tremie and CFA piling mixes in Australia and it has found its way to the New Zealand market as well. The current tremie concrete guideline developed by the DFI/EFFC (2016) provides very similar recommendations.

In previous years contractors used an admixture which was added to the concrete truck on site, turning stiff concrete of about 120mm slump into fluid concrete with almost grout like properties. Deep foundation contractors have started to walk away from this practice as the addition of the admixture was their own risk and there were reported incidents related to concrete quality which resulted in arguments between concrete suppliers and piling companies. As a result, concrete suppliers were asked to develop highly workable mixes in their plants so that the addition of external additives is not required anymore.

WORKING PLATFORM DESIGN

The Australian piling and deep foundation industry, in this case represented by the Piling and Foundation Specialist Federation (PFSF), has implemented the procedure which was developed by the Federation of Piling Specialist (FPS) in the UK. The guidelines to calculate bearing pressures for different piling rigs, based on different load cases as well as guidelines for a sufficient working platform design are based on the BRE 470 document (2004) for 'tracked plant'. Even though these guidelines have been in place for more than a decade and, based on the author's personal experience, all major piling companies in Australia and New Zealand strictly comply with the recommendations, a CFA piling rig toppled over in June 2017 as a result of a working platform failure Figure 9).

It is important to note that the bearing pressure of piling rigs is heavily dependent on extraction and pull-down forces applied by the piling rig. Based on the application, these forces can change and if designers only allowed for partial extraction forces due to the assumption that for shallow piles the rig operator doesn't need to activate the full force, these assumptions must be carefully checked. It should also be noted that for CFA piling rig, about 90% of the extraction force is typically transferred through the mast foot. If required load spreading devices should be installed to the piling rig to avoid peak pressures and potential failure of the working platform under the mast foot.



Fig. 9. Despite the regular use of best practice in bearing capacity calculations and working platform design for most projects, this CFA rig collapsed in Australia in June 2016 [1]

The construction and maintenance of a certified working platform is critical for the safety of the operations and for achieving specified tolerances and sufficient productivity. Maintenance of the working platform shall be ongoing and it will be optimized when rotation of the tracks can be reduced.

SUMMARY AND CONCLUSIONS

Applications for CFA piling vary greatly in Australia and New Zealand. Due to the geology in Australia, deep CFA technology has developed over the past decade which created a highly competitive deep foundation market in Australia for both, foundation piles and embedded retaining wall structures. This market has been developed and supported by strong in-house design capabilities of the majority of the major deep foundation contractors. Frequent pile load testing for design & construct projects offer good risk management for all parties involved in the project.
CFA piles for foundation piles were installed beyond 50m depths in Melbourne using 900mm diameter augers. Secant pile walls are very popular and the overall construction quality is high in most cases.

In New Zealand CFA piling is mainly used for small to medium sized deep foundation projects. Designs are usually carried out by external consultants and pile load testing is uncommon. Therefore, the market is not as dynamic as in Australia. Due to seismic requirements, full length cages are typically required

and advanced concrete technology for plunging reinforcement cages is required but not (yet) readily available outside the major cities.
CFA piling rigs are typically smaller than in Australia (50 ton class) as the ground conditions require maximum penetration depths of 20 – 25m.

Another profitable market for the CFA technology in New Zealand is ground improvement using lattice box structure for liquefaction mitigation in seismic events.

ACKNOWLEDGEMENTS

The authors thank the DFI-EFFC technical committee for the opportunity to prepare this paper and to share his personal experience during the conference in Rome.

REFERENCES

AS2159-1995 Piling - Design and Installation. Sydney, Standards Australia.

AS2159-2009 Piling - Design and Installation. Sydney, Standards Australia.

Building Research Establishment, 2004 'working platforms for tracked plant', BRE Press, Garston Watford, United Kingdom

Bustamante, M. and Gianeselli, L. 1998. Installation parameters and capacity of screwed piles. Proceedings of the 3rd Int. Geotechnical Seminar on Deep Foundations on Bored and Auger Piles, Ghent, Belgium, 19–21 October 1998, pp. 95–108

Larisch, M, Poskitt, N, Netterville, H and Dredge S 2013, 'Advanced quality assurance for piling works for the WICET project in Gladstone', AGS journal, vol. 48, no. 1, pp. 99–112.

Nguyen, T, V, Rayamajhi, D, Boulanger, R, W, Ashford, S, A, Lu, J, Elgamal, A, and Shao, L, 2013, 'Design of DSM Grids for Liquefaction Remediation', Journal of geotechnical and geoenvironmental engineering, pp. 1923-1933

Scott, JN, Suckling, TP, et al. 2006, 'Business benefits of an integrated CFA rig instrumentation system', 31st Annual Conference on Deep Foundations, D. F. Institute, Washington, DC, pp. 535–540.

Slatter, JWand Seidel, JP 2000,'A proposed model for soil/auger interaction during installation of screw piling augers', 25th Annual Members Conference and 8th International Conference and Exhibition, New York

Tchepak, S 1998,'The performance of CFA piles in residual clays', Proceedings of the 3rd International Geotechnical Seminar on Deep Foundations on Bored and Auger Piles, Ghent, Belgium, 1–4 June 1993, A. A. Balkema, Rotterdam, pp. 349–354

[1] http://www.couriermail.com.au/news/queensland/falling-crane-crushes-car-at-brisbane-building-site-at-breakfast-creek/

Tremie Concrete for Deep Foundations, 2012, 'Recommended Practice', Concrete Institute of Australia, Book

Tremie Concrete for Deep Foundations, 2016, 'EFFC / DFI Best Practice Guide', European Federation of Foundation Contractors and Deep Foundation Institute, Book

DESIGN AND CONSTRUCTION OF A 130.000 SQM LOGISTIC PLATFORM IN TRIESTE'S PORT, ICOP & LWN: AN ORGANIZATION, LOGISTIC AND POWERFUL RIGS WINNING COMBINATION

M. Bringiotti, GeoTunnel S.r.l. - LWN Agent, Genoa, Italy, info@geotunnel.it
L. Grillo, Icop S.p.A., Basiliano, Udine, Italy, luca.grillo@icop.it
S. Vitalini, Icop S.p.A., Basiliano, Udine, Italy, stefano.vitalini@icop.it
R. Grisolia, Icop S.p.A., Basiliano, Udine, Italy, roberto.grisolia@icop.it

Keywords: foundation equipment, piles, lifting, port, offshore, Icop, LWN Liebherr, LB36-410, LR1300

ABSTRACT

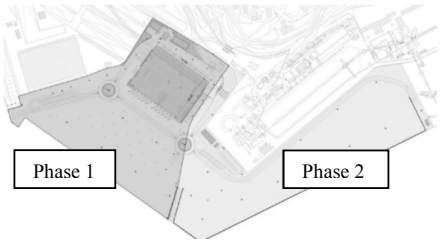
The Trieste's port is the most favorable sea connection for goods handling direction South-Est to the corridor North, Centre and Est Europe; a new logistic platform has been designed wrapping ca ¼ of one million square meters to the sea in order to load and unload Ro-Ro & container vessels and various material & good trans-ships. An approx 150.000 square meters sea suspended dock has been designed in a 2 working phase lots; foundations has been performed in flysch overlaid by alternation of arenaceous layers and marle of variable thicknesses, above clayey silts of plastic consistency. A subsea dump of ca. 500.000 cubic meter capacity is as well realized. Main works foreseen are: consolidation and foundation works for the sediment tanks (dragging and piling works), construction of water proof confinement beach diaphragm walls (mixed technique cutter soil mix and sheet piles), river diversion foundation works (secant piles), drainage trenches and heavy off shore piling works. Particular it is also the design and usage of special technologies able to realize the marine deep and large diameter piles and the peculiar lifting equipment able to erect the huge sea suspended deck.



1 FOREWORD

The intervention for the realization of the first operational phase works related to the logistic platform in the port of Trieste, consists in the development of the area enclosed between the docks timber yard, the former Sidemar/Italsider yards, including the connection between the Dock and the Sediment tank (currently under construction) and the new North-end of the dock timber-yard, the connection between the same and the area of the Serva Iron-foundry; the intervention is part of the larger project for the Trieste's logistic platform construction (Fig. 1.1).





The new logistic platform project will allow the construction of a new fully equipped pier designed for Ro-Ro ships, the construction of new piers for ships, the opportunity to use the areas for port operations and/or the combination and handling of containers and goods storage. Therefore, the realized terminals will be connected to the big junction roads nearby the new port infrastructures, thus in order to ease the goods logistic by an effective road and rail transport.

© 2018 Deep Foundations Institute

After a long tender phase the works for the design, construction and management were awarded to the special purpose company PLT, part of which are ICOP, Cosmo, Parisi, Interporto of Bologna as well as Altieri and Alpe Progetti is the designers responsible for the drafting of the detailed design. The following is a list of the main works to be carried out under the first operational phase:

1. Environmental restoration of the seabed included into the area of intervention on-shore.
2. Diaphragm walls realized with CSM technique (about 990 sqm), perimeter to the area of intervention and directly connected to the sea front sheet piling.
3. Trench for the drainage of groundwater crossing to the hydrogeological front of the diaphragm wall; the trench is completed with pump sets for the conveyance of the water to the dedicated treatment plant (including the received groundwater treatment plant called TAF).



4. Deviation and full covering of the Baiamonti river and of the emergency drainage ditch of the Acegas APS-AMGA water treatment plant by means of off-shore secant pile.
5. Completion of the docks construction works and of the Ro-Ro terminal above an off-shore area of about 8 ha; there are planned works combined with steel sheet piling (king piles Φ 1,626 mm, 18 mm thk. with overlapped AZ 17-700) by shore line of about 431 linear meters.
6. The entire functional area of the platform above the land reclamation wet area is a cantilever deck built with prefabricated and pre-compressed beams and panels foreseeing structural concrete filling in the caissons area; the whole assembling is resting on piles Φ 1.270 mm on a 10 × 10 m grid; the foundation on the perimeter is realized with drilled and casted Φ 1.100 mm piles. The deck includes the link with the mainland, the link with the existing caissons and the dock platform structures.
7. Confinement of the land reclamation caissons, at south of the intervention area consisting of a steel sheet piles wall combined and isolated king piles.
8. Waterproofing of the dock platform section related to the 13 caissons by means of sheets piling and concrete filling of the gap between the top portion of the sheet piling and the foot of the caissons.
9. Sealing of the gaps between existing adjacent caissons and the combined sheet piling placed on the continuation of the beams to the north and south by means of a double line of micro-piles casted in a geotextile sheath.
10. Commissioning of the wet dumpsite with a capacity of about 500.000 m^3; hydraulic works are included (mud pumps, pipes, fittings and gate valves) for the controlled caissons filling; in addition to this are also foreseen the hatches Φ 600 mm on mesh 40 × 40 m for the payment of the materials in close (and attached filling water treatment plant called TAC).

2 GEOLOGICAL ASPECTS

It is basically a material of anthropogenic origin used for the offshore land reclamation area toward the Trieste seaport since the early 1800's. The geological complex of the whole area is based Trieste's flysch overlaid by more recent quaternary sedimentary complexes of different origin. The Flyschoide complex is characterized by a rhythmic alternation of arenaceous layers and marly of variable thicknesses. Above the intact flysch there is an altered level with variable power known as "crostello" or "cappellaccio", in which the arenaceous lithotypes are variedly altered, while the marne are reduced to clayey silts of plastic consistency. The physical and mechanical characteristics of these materials are extremely variable, highlighted by the succession of different sedimentation environments, from continental to marine. Based on an accurate analysis of the available surveys, the reference stratigraphic schemes of the intervention areas have been updated; as per the interpretative geological profile shown with Fig. 2-1.



In general, the thicknesses of the anthropogenic landfill materials and the clayey marine silts increase from the ancient shoreline; at the south-eastern boundary of the area, smaller thicknesses of the

landfills has been found, with a power of 6/8 m, above powerful clays from 7 to 13 m. At sea, silt-clayey sediments have thicknesses of about 15/19 m and are overlapped with the end of alteration of the flysch rocky base (C1 and C2). The intact flysch (C3) has been found at a depth from 15 to 20 m from the a.s.l.. towards the southeast limit of the area of intervention, while deepening to values of -30÷-40 m a.s.l. towards the western limit of the project area.

3 GEOTECHNICAL SOIL CHARACTERIZATION

Terreno	γ (kN/m³)	c′ (kPa)	φ′ (°)	c_u (kPa)	E′ (MPa)
Coltre eluvio-colluviale C1	18.5	5	31	100	20
Flysch alterato C2	23.0	40	22	250	350
Flysch integro basale C3	24.0	150	28	-	800

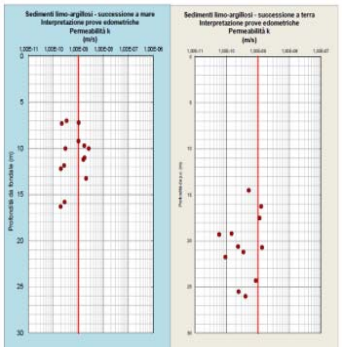
The results of the geotechnical tests carried out on the different soils samples have been systematically collected and analyzed in order to better calibrate the geotechnical behavior model to be used during the additional stability tests. Based on the interpretation of the available geotechnical data, the following benchmarks table have been draft for next geotechnical tests (tables in Fig. 3-1).

Terreno	γ (kN/m³)	c′ (kPa)	φ′ (°)	c_u (kPa)	E′ (MPa)
Successione a mare					
Limi argillosi AL_O	16.5	0	22	10	1.5
Argille limose grigio-verdi AL_C	16.5	5	23	50	2.5
Successione a terra					
Riporti R	18.0	0	25	-	3.0
Limi argillosi AL_R	17.0	20	24	80	5.0
Termini di alterazione del flysch					

3.1 Liquefaction

The reference standards require to verify that construction works sites are stable and not subject to liquefaction, intending with this term those phenomena associated with loss of shear strength or accumulation of plastic deformation in saturated soils, mainly sandy soils, stressed by cyclic and dynamic actions occurring in undrained conditions. Summarizing, based on the conducted studies, the occurrence of this phenomenon has been reasonably excluded.

3.2 Marine sediment permeability characteristics



The available data have been integrated with the results of a specific supplementary survey campaign, where it has therefore been possible to confirm that:

- There is a low permeability cohesive level below the mud layers of the seabed, which is continuous and present throughout the investigated area.
- The above cohesive level has a thickness of at least 10 m.
- For this horizon, it is possible to consider, as widely supported by the laboratory tests, a permeability value $k < 10^{-9}$ m/s.

So, the cohesive horizon assuring the bottom seal of the caissons is available and continuous with thickness and a permeability values satisfying the standard requirements (Fig. 3-2).

4 PLATFORM'S FUNCTIONAL REQUIREMENTS AND STRUCTURE STRESS ANALYSIS



The analysis of the stresses acting on the piers' structures is directly related to the average characteristics of the vessels to be moored. Given the functional requirements of the platform, designing the construction works related to first operational phase, different types of specific traffic have been taken into consideration: Ro-Ro, containers and bulk generic goods.

Given the worldwide average vessel dimensions for the said type of traffic, it has determined the size and displacement of vessels to be considered; in particular, the maximum permissible draught (13 m) at the quay and, for Ro-Ro traffic, the width of the stern lift gate (26 m).

In particular, the geometrical characteristics of the ship have been defined, as follows:

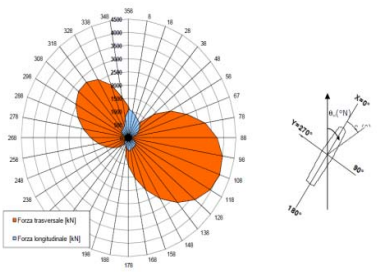
- Deadweight: DWT = 50.000 t
- Displacement: M_D = 69.900 t
- L_{OA} = 266 m maximum length

- L_{BP} = 252 m length between the perpendiculars
- B = 32,3 m keel width
- A_L = 5.810 m^2 and the side area of the ship offered to the wind
- A_T = 1.250 m^2 and the transverse area of the ship offered to the wind
- Maximum draught: D = 13 m
- freeboard: F = 8,4 m

The above features are used to size the bollards of all the moorings and the fenders of the main platform, of equal to 437 m in length; with regards the connecting platform with the timber yard, the size of the fenders has been referred to the maximum permissible dimensions for Ro-Ro vessels, considering the stern dock manoeuvre.
In view of these dimensions it has been possible to define the stresses on the dock platforms as a result of the docking manoeuvres and mooring during storms. The following shows the stress calculating method and the summary the ones arising from the functional requirements.

4.1 Bollard pull

For the evaluation of the stresses, exerted by the typical vessel on the dock platform, it has been considered the actions induced by winds during potential storms, blowing in the most unfavorable direction for the withstand of the mooring, while the actions induced by the waves motion and the sea currents, hasn't been considered significant because of the shelter provided by the project's works. The intensity of the wind has been set to 50 m/s considering the orientation of the docks thus to expose to the *bora* winds the minimum bulwark area of the ships. The force impressed by the wind on the topside of the ship has been calculated with the algorithms proposed by the "Spanish Standard ROM 0.2-90". Fig. 4-1 shows the transverse and longitudinal force values represented by a polar graph. As it may be noticed from an accurate analysis, the maximum value of the transverse force is obtained by placing θ_W = 79° (107° N), resulting in $F_{T\,WIND}$ = 4.061 kN ≈ 414 ton. The distribution of the stresses on the bollards has been determined by applying the methodology set out with the manual "Marine structures Engineering: Specialized Applications" by Gregory P. Tsinker.



By applying this relation (with n. 6 bollards on which sharing the load along the ship bulwark) it has been possible to calculate the total value of the mooring forces, thus providing on the dock platform, related to the first operational phase, 150 t bollards installed with 20 m step. According to similar analysis, it is expected to keep the installation of 150 t bollards, with a 25 m step, also along the Ro-Ro dock platforms, for the stern-on mooring.

4.2 Mooring damp force transmitted through the fender

During the ship mooring phase, the fenders are subject to a crushing contact, due to which a damp force is generated and applied to the dock platform, the value of which depends on the type of fender and the extent of its deformation. The type of fender chosen for the project is the " wrapped cylindrical fender " that turns out to be the most suitable for the ship mooring. In particular, the choice of the type of fender to be used has been made by taking into account the above-mentioned project's parameters. The kinetic energy which shall be absorbed by the elastic defenses during alongside mooring is equal to 1.400 kNm.

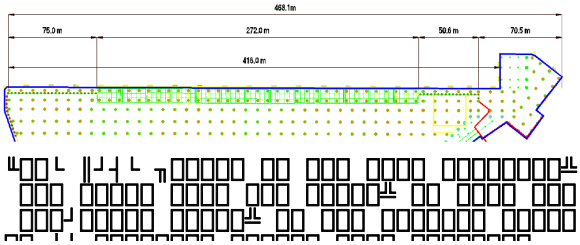
5 DESCRIPTION OF MARITIME AND STRUCTURAL WORKS

The containment of non-hazardous dredging materials used to fill up the land reclamation caissons will be ensured by the following interventions:
- Realization of a combined diaphragm wall, tubular piles and sheet piles; on the south and partially west area of intervention.
- Realization of a perimeter plastic diaphragm wall, connected to the combined diaphragm wall.

- From the existing frontline caissons, suitably waterproofed, to the realization of a sheet piling just in front/parallel of said caissons and connected to the combined diaphragm wall (west side, facing the sea).



The Intervention in numbers:
- Total concession area: ~ 12.3 ha
- Quay length: 431 m
- Ro-Ro mooring dock platform (considering the possible installation of a floating mobile dock)
- Cantilever dock platform to be realized with piles and slabs: 74.350 m^2, including approx. 3.050 m^2 corresponding to the Ro-Ro dock platform external to the perimeter of the reclaimed land
- Capacity of the containment area under the cantilever dock platform: over 500.000 m^3, about 80.000 m^3 of which filled, during the construction phase, with compatible materials resulting from the drilling of piles and from the technical dredging, functional to the construction works.



The seabed along the new dock platform has a depth which varies between 10 and 13 meters on the sea level and, only closed to the timber-yard, dredging is required to reach the project depth: about 15.700 m^3 of non-dangerous and therefore compatible excavation material will be taken out. The height of the new dock platform, along the mooring edge, is equal to 3,10 m: the height, on-shore, may varies thus to allow the collection of rainwater. Including the protruding Ro-Ro dock platform and measuring the length of the new dock platform, the sea front has a length of about 468 m; starting from north and for about 70 m, the front is occupied by free drilled piles, for approx. 50 m the cantilever dock platform is sitting on a combined wall, for about 272 m the cantilever platform is sitting on 13 previously installed closed cell caissons and the remaining 75 m on a combined wall (Fig. 5-1).

5.1 Drilled piles

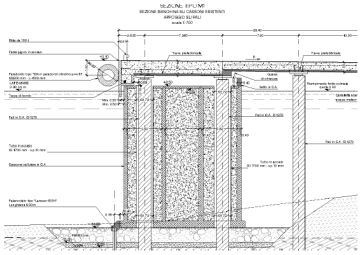


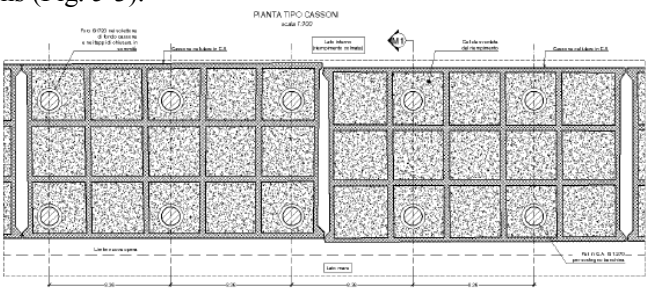
The slab of the logistic platform, as part of the works related to the first operation phase, is sitting on 864 drilled piles about which 793 are with a Φ 1.270 mm and 71 are with a Φ 1.100, all headed on the unaltered flysch.
In addition to this there are also other 55 spiral steel piles for the realization of the combined walls (king piles Φ 1.626, thk. 18 mm with a variable length between 18 and 39 m with interposed AZ 17-700 extended at least until the embedment on the cohesive top). Ro-ro dock platform is also sitting on secant piles (Φ 880 mm) of variable length 16÷23 m, thus in order to realize the drainage area of the Baiamonti river. The same technology is used in place of the CSM diaphragm walling in some sections of the shoreline where the presence of boulders and the narrow spaces available is not applicable. With the Φ 1.270 m piles drilled will be realized a main grid 10×10 m then top up with a deck realized with a monolithic post-tensioned concrete slab. Low profile ribs (main beams), 1,0 m thickness (including the loose formwork), is sitting on the system of piles. Among these the slab has a thickness of 0,75 m (considering as well the loose formwork). In shoreline area, in order to absorb the damp forces generated by ship impact of the fender, the thickness of the beams changes to 1,56 m and the one of the slab to 1,36 m.

5.2 Existing closed cell caissons

The previously installed closed cell caissons are occupying a length of 272,18 m, will form part of the containment area acting at the same time as waterproofing elements of the reclaimed area itself, integrated with injections of the gaps between the caissons, and carrying out sheet piling able to reach the deepest in front to impermeable layers. The rearward sheet piling is then connected to the bottom

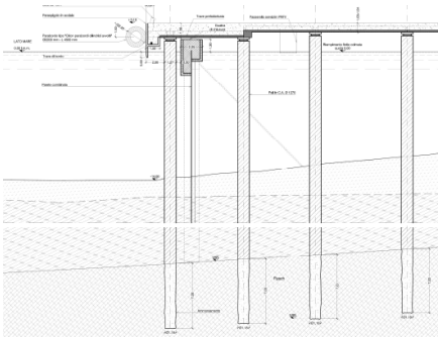
of the caissons with concrete. The whole of these elements will also offer the guarantee against a possible erosion of the seabed, where are sitting the caissons, eventually caused by the turbulence generated by the ships propellers, thus preserving the stability of the whole structure. The support of the deck over the existing caissons is also assured by the realization of a series of piles, inside the closed cell caisson and not linked to the caisson itself, thus in order to guarantee a completely independent behavior of the two structures. Particular attention has been paid to the static and seismic deformations of the two structures in order to avoid contact between the structures of the two elements in all the assumed most severe conditions (Fig. 5-3).





[illegible]

5.3 Combined wall

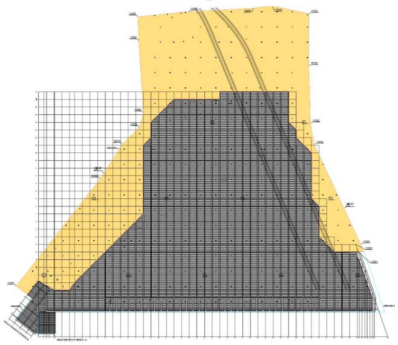


With regard to the completion of the containment area (reclaimed area), this is realized with a combined wall to the fitten to right hand side and to left hand side of the caissons. The combined wall consists of steel piles with a diameter of 1.626 mm (king piles) and between them steel sheet pile type AZ17-700. The spacing between the piles is about 309 cm. The pile casing will reach the flysch surface, on which will be supported. The piles length of the combined wall varies between 18 and 39 m. On top of the combined wall there is a reinforced concrete capping beam, realized with a loose formwork, able to connect the elements of the wall and to protect the top portion of the same from the aggressive agents (Fig. 5-4).

[illegible]

5.4 The dock platform

The cantilever dock platform is made of a posttensioned concrete slab, sitting on the already mentioned piling forming a 10×10 m grid, throughout the whole central section, having irregular edges which are closing the perimeter of the dock platform (Fig. 5-5).





[illegible]

The slab consists on a series main beams, 1,40 m wide and 0,8 m height (measures taken not considering the prefabrication formwork), sitting on a series of piles, and a cushion between them, with a thickness of 0,50 m (measure taken as well not considering the prefabrication formwork). From an executive point of view, prior of anything it is envisaged the positioning of the prefabricated formwork, which is independent and able to support the weight of the fluid concrete during the casting phase (those of the beams are made up with a 20 cm thickness concrete caseback, with n. 2 pretension embedded steel profiles, generally IPE 600. On top of this element are laid a series of prefabricated pre-compressed alveolar panels, 25 cm thickness, acting like a disposable slab formwork in the area between the beams. Therefore, the slab has a footprint of 75 cm and the beams of 1,00 m. Facing the shoreline the thickness of the structural elements is increased of about 0,50 m (Fig. 5-6).
In general, high performance materials are used: piles and deck are casted in situ with reinforced concrete with a resistance class Rck 45N/mm^2 (XS3 exposure Class) and B450C steel reinforcing bars; the pre-compression steel and lubricated strands $f_{p(1)k}/f_{ptk}$ 1.670/1.860 N/mm^2.
The piles are sitting on the layers of unaltered flysch, which guarantees an adequate bearing capacity; the upper stem area, which crosses the water and the soft soil layers, is protected by a metal sheet protection. The deck's extrados is used as a finished surface for the road: a chemical additive is used to treat the superficial layer, to guaranty a perfect cortical hardening.

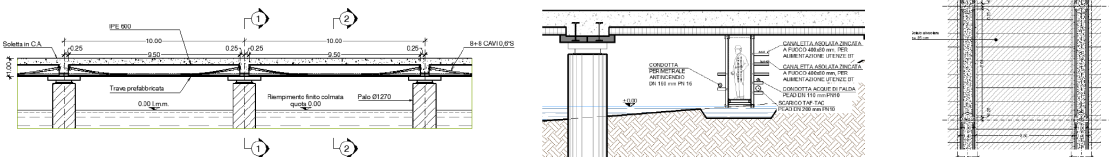


Figure 5-6 Typical cross section of the dock platform

5.5 Flood defense works
In correspondence of the dock platform deck interfacing the drainage area of the Baiamonti river, an excavation is carried out to reach the project mooring height of -14.0 a.s.l.. The area is located in correspondence with the stern propellers of the Ro-Ro ships, requiring an adequate flood defence works. The sizing of the flood defense work is in function of erosion caused by the action of the ships propellers and foresees the use of geotextiles mats filled with concrete in place of loose reef. The reef remains for the sole protection of the outer end of the mat. For the portion affected by the breaking of the waves the mat is windowed and laid on a non-woven geotextile and has a thickness of 165 mm; the mat in the submerged area affected by the action of the propellers of the ships is instead continuous and has a constant thickness of 150 mm. The side link between the geotextiles is given by double-height zips (in correspondence with the sides in direct contact with the reef to be protected and with the one towards the water): this guarantees a perfect sealing mat and an homogenous performance to the encountered hydrodynamics (Fig. 5-7)

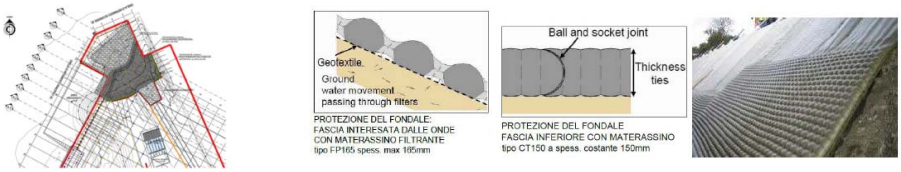


Figure 5-7 Typical cross section of the dock platform

6 CONTAINMENT RESERVOR (RECLAIMED AREA)

The containment reservoir (reclaimed area) is realized in the surface below the project dock platform, providing for the required definition of the perimeter of the actual reservoir already consisting in a level of natural soil, clayey silt with reduced permeability, and constituting the bottom seal of the containment area. The water filled containment reservoir cover an area of approximately 6,0 ha with average depth of about 8,3 m and maximum depth of over 13,0 m; the capacity is approximately

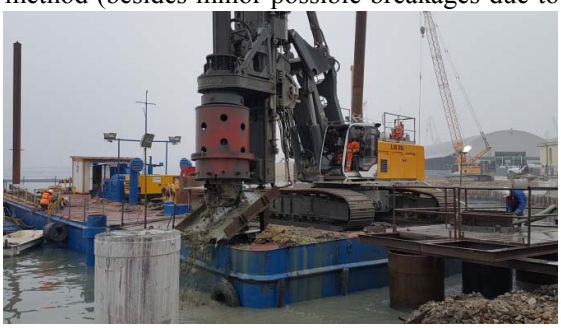
500.000 m^3. Along the off-shore perimeter the containment reservoir is closed by an alignment of steel sheet piles in hydraulic continuity with the 13 caissons already positioned and by a combined wall external to the caissons. On-shore the seal is guaranteed by a 65 cm thick CSM diaphragm wall. On the seabed, the seal is guaranteed by the powerful layer of natural cohesive benches. The intervention includes the realization of the site, the management of sediments backflow and the waste water management as well as of the management of all the sanitary aspects, here following listed:

- Definition of containment area perimeter
- Sediments backflow
- Water management
- Air treatment.

The sizing of the perimetral structures has been carried out taking into consideration the thrust provided by the filling materials of the containment reservoir at a maximum height of + 0,5 m a.s.l.. Filling of containment reservoir volumes will be done in "sediment conoids"; the material is normally pumped.

7 POONTON MOUNTED DRILLING RIG: LIEBHERR LB36-410

Icop S.p.A. for the pontoon driven off-shore drilling activities has decided, the first in Italy with this model, to rely on a Liebherr LB36-410 drilling rig.
The main technical feature of this machine are:
- Operating weight: 115 ton. This parameter has its importance since the stability of the whole working group has a close connection with the tonnage of the equipment and all its components = > greater weight, greater stiffness, less vibrations therefore minor deviations and risks of interference with close piles especially when used in CSP-FoW method (besides minor possible breakages due to fatigue).



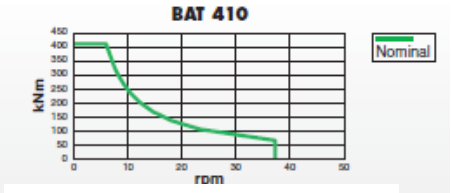
- Motor power: 390 kW. The motor power is a feature that clearly binds all the hydraulic functions of the machine; having more power means not only be faster in all functions but also having spare power in potential critical situations i.e., for example, at high depths (in double head or FDP), with strong lateral friction (potentially in soil with sandy matrix), with heavy bored columns full of material .... In addition, the greater power can be useful to manage different kind of works may be necessary (type the "ring vibrator") or design change in the course of work (larger diameters or drilling depths).
- Consumption: the abundant power involves an engine that works at a lower rpm, despite having a spare power available. LWN has developed low-consumption engines, integrated through the electronics with the hydraulic system, having an innovative concept called ECO-Mode able to limit the consumption of fuel; summarizing, it is a new generation engine with an electronic system that optimizes or disconnects all the hydraulic services when not used. Moreover, thanks to the automatic thermoregulation of the fan system (which allows to work in any climate) helps to reduce fuel consumption. It may be stated that the hourly consumption of the Liebherr combination (Engine-Electronic-Hydraulic) is lower at least of about 20% as pure cost per linear meter of excavated piles compared to any other competitors' combination.
- Acoustic emissions: with regards to noise emission, it has been developed a specific system called ECO.SILENT-Mode; it is a function that, when activated by the operator, limits the number of rpm of the engine as well as of the cooling fan, ensuring a significant reduction of noise emission, with a negligent loss of power. This is a very important feature especially for urban areas operation.
- Maximum torque: 410 kNm. This data is the most significant for a piling rig, it normally defines the class; LWN has developed, unique in the world, a class of continuous gear exchange rotary, which mainly translates into a much smoother operation, without stalling dangers, which is more performance-critical with significant benefits from the user's point of view (absence of separate

lubrication, lower wear parts, ...). In Fig. 7-1, the rotary BAT 410 curve is provided with the LB 36-410, with a nominal torque of 410 kNm (41 ton/meter).
- Liebherr has designed a robust kinematic with a specifically designed H shaped pantograph, which guarantees a couple of undoubted advantages (Fig. 7-2):
- Rigidity of the system in any working position
- Possibility of having a relative movement from the swing bearing wheel axis / pile axis > 1 m, resulting in additional advantages:

a. Ability to reach work positions that are further away from swing bearing gear and ability to cover complex work positions (such as corner piles or piles interfering with geometries or where obstacles are encountered for any reason in the operating area).

b. Ability to manage the casing without moving the machine, interesting situation for the individual cased piles excavated in kelly mode.

The above mentioned are considerations to highlight that the H shaped kinematics is particularly advantageous, especially in urban areas operations (e.g. vs. the V shaped kinematics).

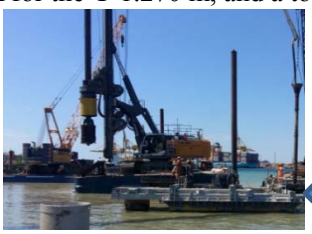






7.1 Logistics and productivity

The LB36-410 was installed on a suitable pontoon, from which it worked efficiently. Special templates, hydraulically adjustable, have been designed and used to position the piles in the right spots. As far as productivity is concerned, the average production was about 12 off-shore piles per week for the Φ 1.270 m, and a total drilled pile average production of about 150 m /day (Fig. 7-3).





8 LIFTING EQUIPMENT: LIEBHERR LR1300

Two types of cranes have been used for the material handling. The classic HS855, crawler crane "heavy duty" with 120 ton lifting capacity, 114 ton operating weight and 450 kW installed power. It is used for various works from the lifting of the pile casing, to the handling of powerful vibrators for the driving of pile casing or sheet piles.





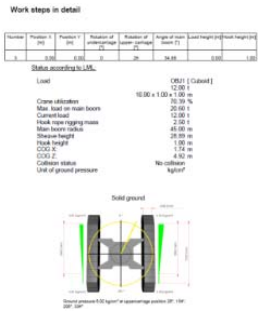
But the real queen of the job-site was the new LR1300, 290 ton crawler crane, with 300 ton lifting capacity and 390 kW engine. The machine, despite its considerable dimensions, is easy to transport and is designed to be assembled autonomously (Fig. 8-1).

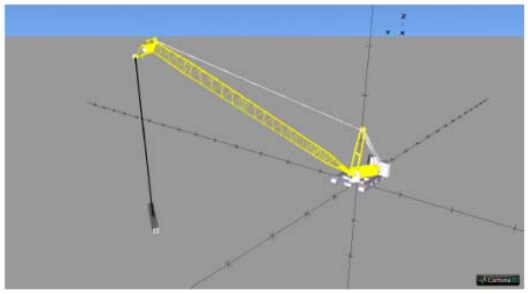
It is used for the handling of the cantilever deck. In layman's terms only with such equipment you can get the following features needed in Trieste:



- Boom length: 50 m
- Working weight: 12 ton
- Boom working angle: 34.88 °
- Max reachable distance: approx. 40 m
- Maximum load discharge in the heaviest position (Fig. 8-2): 6 kg/cm^2

Based on the above-mentioned features, it has been specifically sized and designed the deck platform and above it has have been designed the geometries of the slabs to be laid, optimizing the dimensions and consequently minimizing the handling time and the related costs.





[illegible]

SUMMARY AND CONCLUSIONS

A complex job requires precise planning and a careful analysis of operational logistics; the "smart" Entrepreneur is the one who, in the pre-executive phase, dares to change decisions already taken. LB36-410 is one example of “open mind for a different view” … and for instance, always in this case, the decision to use a single high capacity mobile crane (LR1300) in place of n. 3 tower cranes sliding on rails for the prefabricated elements installation (system which was foreseen in the tender phase) has been for sure a winning decision.



REFERENCES

Bringiotti M., 2003, Consolidamenti e Fondazioni, Edizioni PEI, Parma, I
Bringiotti M., 2010, Geotecnica & Macchine da perforazione, Edizioni PEI, Parma, I
PLT, 16/12/2015, Progetto esecutivo primo stralcio, Relazione Generale

EXTRACTION OF PRECAST PILES AND SECANT PILES UP TO 27m
Tom George / Chris Price (Wagstaff Piling, Melbourne Australia)

Introduction

HY-Tech Concrete Pty Ltd had leased a parcel of land from the Victorian Government in the suburb of North Melbourne approximately 1.5km northwest of Melbourne CBD. The site comprised a concrete batching plant that was originally built in 2002. The batching plant (Refer Fig 1 and 2 below) consisted of an office building, silo tower, aggregate bin pit (6m wide x 30m long x 6m deep) and a waste tank pit (3m diameter x 3m deep). The pits were constructed using 600mm diameter secant piles and all structures were supported on 275mm and 300mm square precast piles driven to practical refusal on the siltstone rock which ranged between 23m to 27m below working level. The stirrer tank and the bin pit were excavated within secant pile walls. The secant pile walls were approximately 9m deep for the 3m dia. circular stirrer pit and 12m deep for the 30m long x 6m wide aggregate bin pit.

Adelaide Brighton Cement purchased the HyTech Concrete Company and little did they realise that the conditions on the lease were to return the land to its original condition. No one had expected this would mean extraction of all the driven and secant piles installed on the site as an underground rail tunnel is now to be built beneath the site. The Melbourne Metro Authority was concerned that a tunnel boring machine set up for the soft ground conditions expected could not bore through reinforced concrete piles. Removal of the piles was a critical path activity for this major infrastructure project and it could not fail. Severe consequences and liquidated damages would be applied if the piles were not removed in time. The requirement to extract these piles that have been buried for 15 years has provided us with an opportunity to inspect the structural steel splices and the state of the concrete exposed to the soil profile.

The geotechnical profile consisted of fill over a marine silt (Coode Island Silt CIS) with a typical undrained shear strength of up to 15kPa, overlying Fishermans Bend Silt (FBS) which is an over-consolidated clay with a shear strength in the order of 75kPa which overlays the Silurian Melbourne Siltstone at 23 to 25m below the existing ground level.

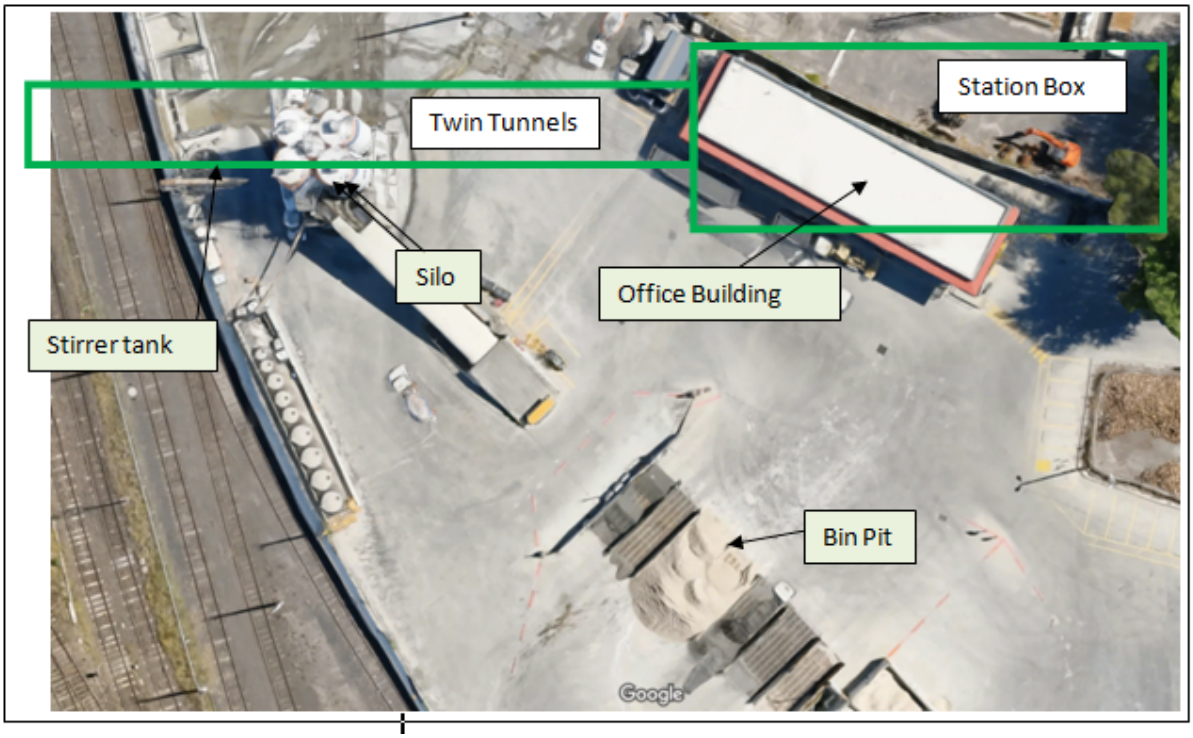


Figure 1: An aerial shot of the Hy-Tech Batching Plant with an overlay of the future station box and twin tunnels

© 2018 Deep Foundations Institute

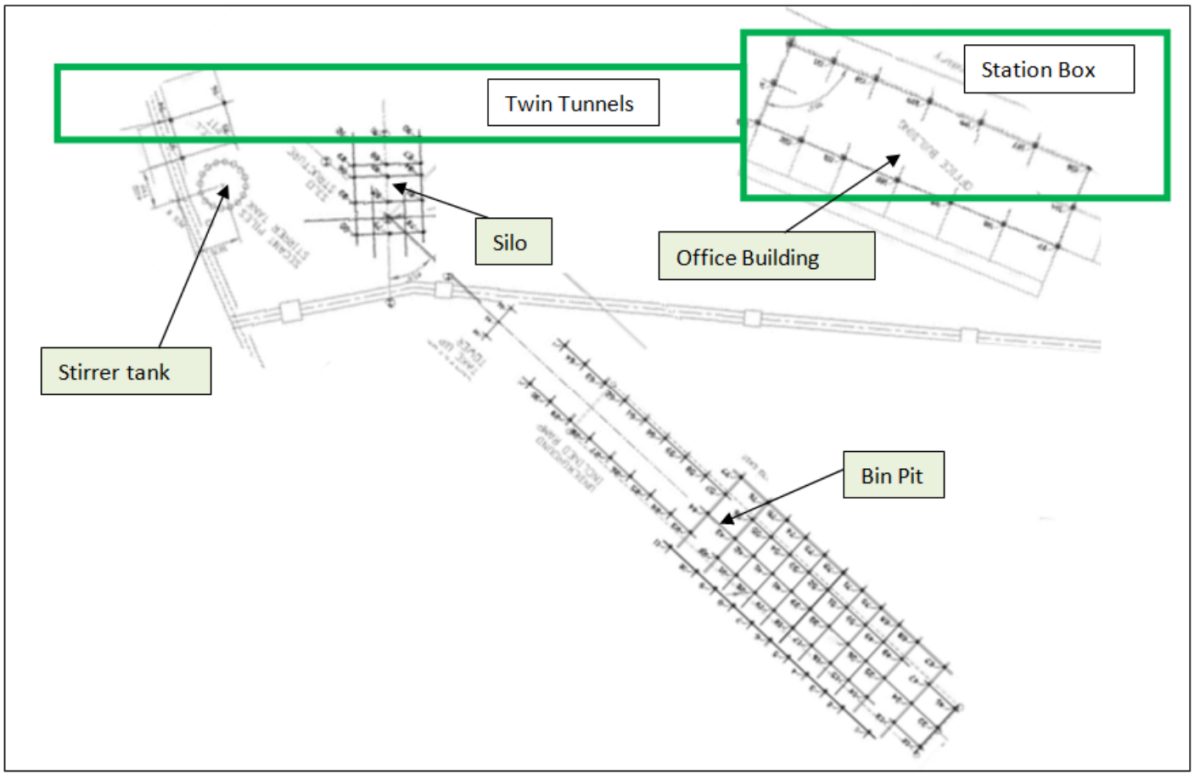


Figure 2: Overall piling plan layout for Concrete Batching Plant with tunnel and station pit overlay.

TEST PILES

The driven piles were jointed 275mm and 300mm square precast driven piles. The piles were typically 28m long segmental precast piles reinforced with 4N20 longitudinal bars driven to practical refusal up to 2m into the siltstone resulting in extremely high skin friction at depth.

From the PDA records the typical skin friction profile / pile resistance was estimated as follows.

Table 1: Pile Shaft Friction Estimated from CAPWAP

Depth	Shaft Friction (kPa)	Shaft Resistance 275mm
2 to 10m	15kPa (5 to 20kPa)	100kN
10 to 21m	70kPa (40kPa-90kPa)	900kN
21 to 25m	150kPa (100 to 200kPa)	800kN
Base Resistance	12 to 16MPa	600kN
Total Capacity compression	2400kN (275mmsq)	2,400kN

The tension capacity of the joints was governed by the joint starter bars and the longitudinal steel in the pile. The tension capacity was calculated to be approximately 500kN (50 tonne), hence extraction forces needed to be limited to 500kN to avoid structural failure during extraction. Given there was in the order of 1,800kN of shaft friction on an individual pile and the extraction force was limited to 500kN it was essential that the shaft friction was reduced before extraction forces could be applied to the pile. Based on the lifting capacity of

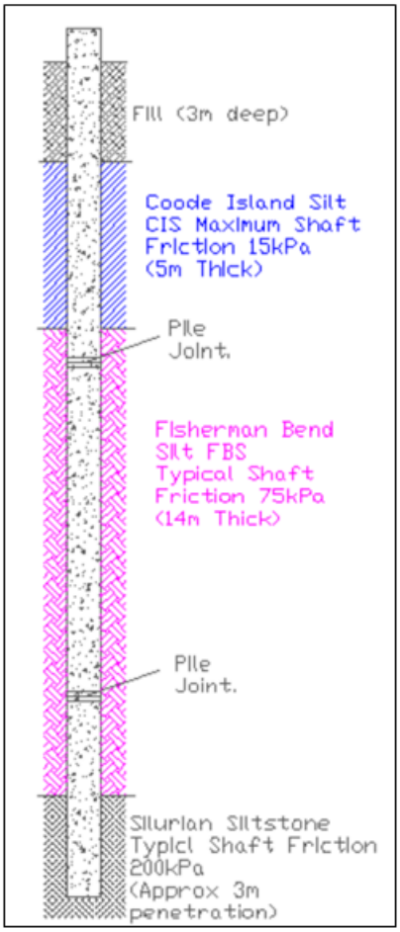


Figure 3 Summary of Geotech profile and precast pile schematic

500kN less the weight of the pile the average skin friction needed to be reduced to an average of 15kPa to enable extraction without risking ripping the pile apart.

If a pile separated during extraction then removal of the lower section would be difficult. Hence non-critical piles were to be removed first to demonstrate the effectiveness of the process.

Original Proposal

A Llamada P-240TT CFA piling rig was established on site with a 30m long string of 600mm diameter auger, refer Figure 3. While it was imperative that the piles be removed some economical common sense needed to be adopted. Given the cost to remove and dispose of the CIS (Acid Sulphate Potential Soil) it was proposed to drill only down the side of the piles on all four sides to 2m past the recorded pile toe penetration depth and then reverse screw the auger out. Given the high skin frictions in the Siltstone it was required to drill into the siltstone with the aim to break up/relieve the shaft adhesion within siltstone layer. Extraction of the first non-critical pile was attempted by only pre-drilling 2 sides of the square precast piles. This trial proved to be unsuccessful as it was unable to reduce the skin friction to a level where the pile could be extracted successfully. The second attempt was to pre-drill the remaining 2 sides of the pile and repeat the extraction process. This method also proved unsuccessful; refer Figure 4 for the pre-drilling arrangement.



Figure 4 Llamada P-240TT with 30m string of auger

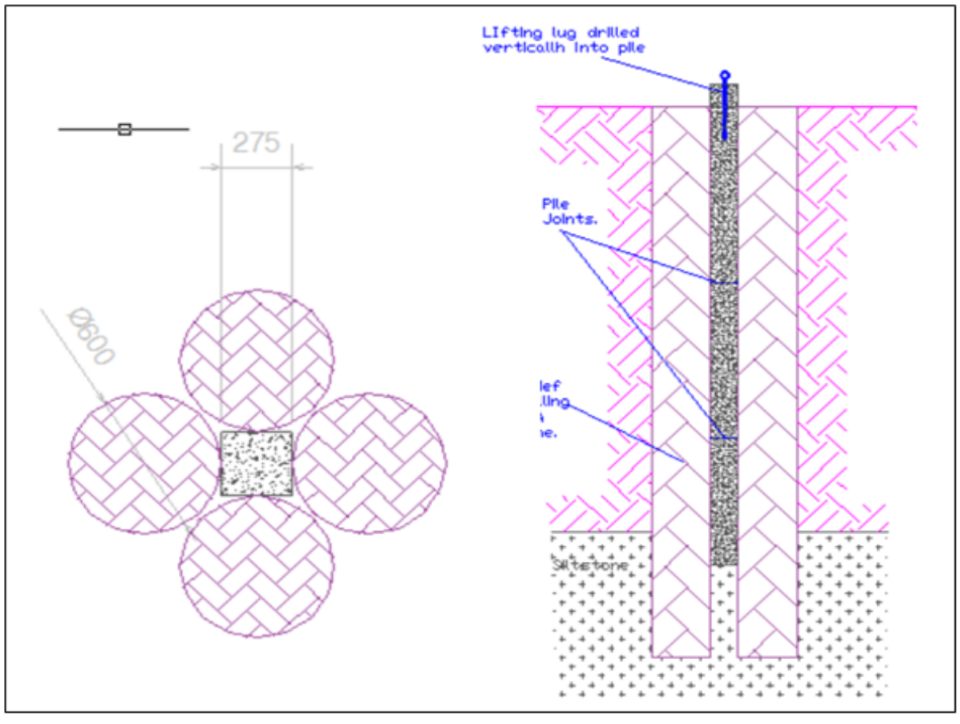


Figure 5: Schematic showing pre-drill pattern around pile

As the first 2 trial methods were unsuccessful it was then decided to trial a vibrated jetting pipe. A 30m 610mm diameter x 20mm wall thick tube was fabricated with four small diameter external jetting pipes feeding to the toe of the tube to allow the feed of fluid at high pressure through the four x 3.5mm diameter jet nozzles at the toe of the steel tube. A manifold system was constructed with a series of valves which allowed the flexibility to turn individual jet nozzles on and off when required.

An Oberman High Pressure Grouting pump was used to pump bentonite slurry at 60bar (6MPa). The Bentonite slurry was intended to surround the pile annulus and lubricate the pile as well as cut the soil and aide the installation of the tube. The tube and the vibrator were handled by a 150-tonne pin jib tracked crane.

An ICE4450 hydraulic vibrator was used to handle the tube between the "rat hole" and pile locations. Once on pile location the tube was vibrated to refusal. The tube was then extracted and placed back in the "rat hole". The crane would then connect to the top of the pile via the engineered lifting lugs which had been previously welded to the top of the pile. Given this was unchartered territory various options for each of the above steps were considered and tried on non-critical piles to ensure that the best method was selected while also being relatively economical. The first tube was damaged during the extraction process and a second reinforced tube was built to finish the project.



Figure 6 Initial jacking trials



Figure 7 Lifting plates welded to longitudinal bar ready for connection to crane.



Figure 8 Above left, pile extracted with soil adhering to the sides. Above right top steel extraction tube being lowered over pile to be removed. Above right left toe of steel tube with jets turned on ready for insertion into ground.

Observations

The soil profile was matched with the existing logs, the PDA and CAPWAP analyses to provide an overlay of all the information. Although there is expected to be some variation in the level of the CIS across the site, for this paper the CIS has been modelled at one level. Some piles were unable to be extracted due to obstructions, pile breaking during extraction and the tube not being able to penetrate to full depth of pile. However, enough piles were extracted to enable construction of the station pit. The majority of piles which were unsuccessfully extracted were located within the office building. It has been proposed to move the station pit slightly west in order to include the piles that could not be extracted to ensure the TBM does not have to drill through these piles.

The piles are fabricated in steel moulds with three sides having formed finishes and the fourth side having a steel float rough finish. When the piles were extracted it was interesting to note how much soil had "caked" onto the rough face of the pile. From this activity it could not be determined if this increased the skin friction. Further research studies could look at casting a pile with four smooth sides and drive the piles adjacent to a standard pile and compare the skin friction profiles from a CAPWAP analyses. Although it could not be conclusively stated, an observation was that the piles tended to curl towards the rougher face when driven which would appear reasonable when you consider it is a rougher boundary with more friction.



Figure 9 Shows stack of extracted piles, note the "clagging" of soil to the side without the formed finish.

All in all there were forty piles extracted. Of all these piles there were 68 Joints that had been located in the ground for 15 years. The extracted joints that were located within the marine silt appeared as clean as the day they were installed. As soon as they were exposed to oxygen "Flash" surface rust appeared. This is understood to be a microbiological process.

While in the ground the theory suggests the lower temperature makes the aerobic bacteria dormant and the lack of oxygen prevents any bacterial oxidation. Sulphate reducing bacteria (SRB) are anaerobic when provided with acidic environments pH 5 to 5.9 , access to a food source (Organic carbon), trace minerals, sulphate and water, can be responsible for localised corrosion of steel and stainless steel.

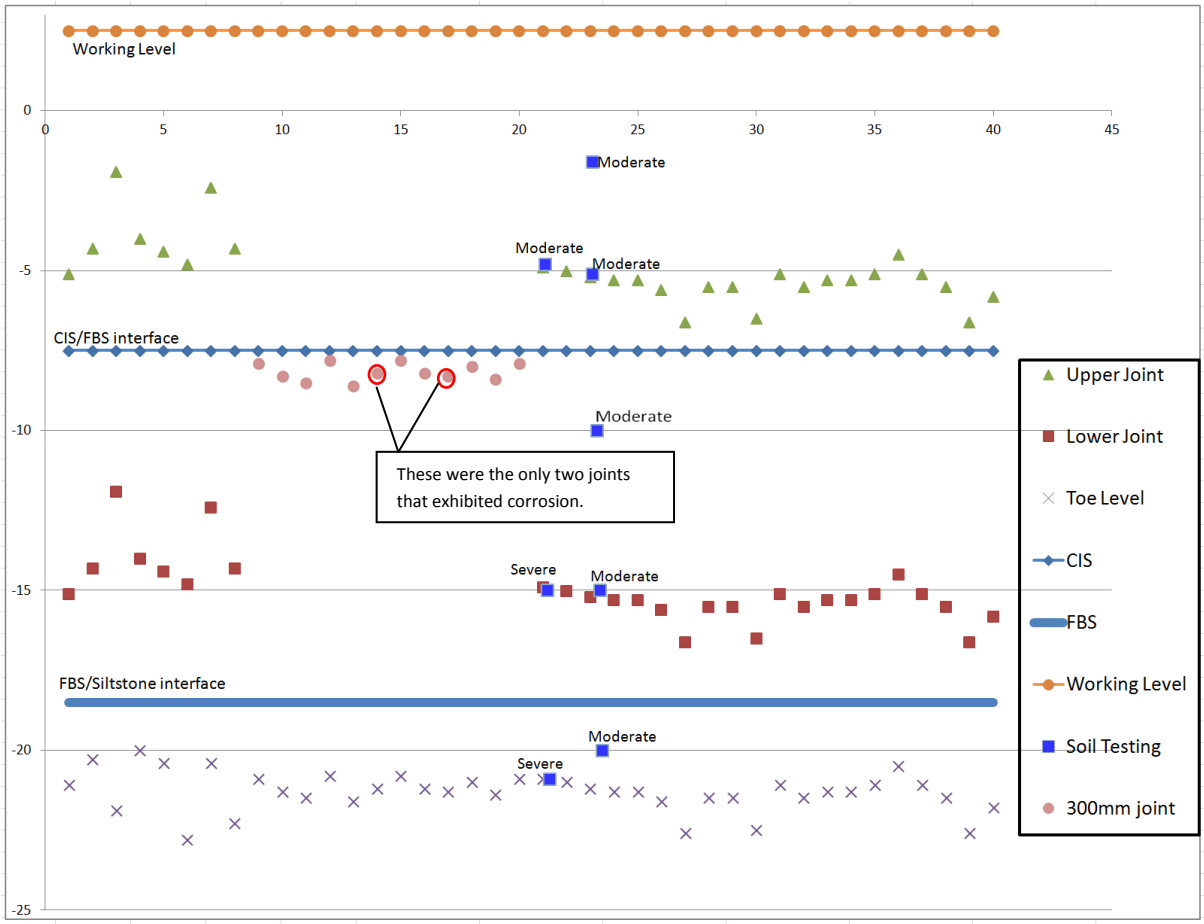


Figure 10 Graph summarising joint locations, soil type and Soil Testing locations

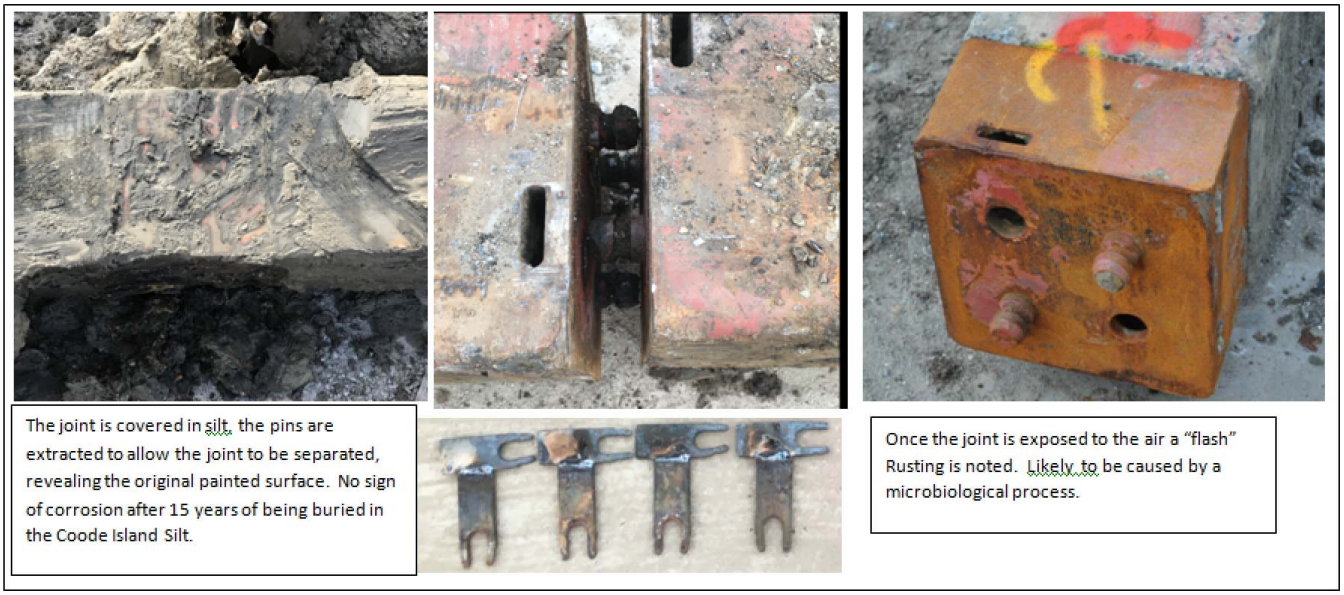


Figure 11 Typical condition of joint with pins extracted, shows flash rusting (orange) appearing on fresh metal

Of the 68 joints extracted there were two joints that exhibited some heavy corrosion on the skirt (Non-structural) plate around the outside of the joint. The remainder of the joints were generally described as shiny steel and much of the steel still had the original painted coating. Limited to negligible corrosion was observed. The wedges were extracted and the pile joints inspected. Only two joints exhibited a higher level of corrosion, the skirts/collars around the outside of the pile which are non-structural/sacrificial had experienced severe corrosion to the point where one of the collars fell apart on extraction, the pins experienced localised corrosion only of up to 2mm on the worst pins. The wedges exhibited corrosion of 0.5 to 1mm max corrosion. This type of corrosion is associated with microbiological corrosion, given the low levels of organic matter this is not considered sufficient to

provide a food source and it is believed these joints were located within a random zone high in organic matter where the SRB bacteria were able to be provided a food source.

From extracted piles No 93 and 95, eight soil samples were taken by an independent consultant from the soil fixed to the sides of two piles. Of these samples 6 No. were classified as "Moderate" and the remaining two classified as "Severe" as determined by the AS2159 Piling Code. Although all samples exhibited the potential for SRB (Sulphate Reducing Bacteria) to be present, the two "severe" samples were classified as severe due to their higher permeability i.e. being more sandy. The soil permeability affects the mobility of the aggressive species and food source of the bacteria. SRB can be a source of localised corrosion as witnessed on two of the joints, the independent corrosion report suggests that a small zone of peat (organic) material could have been encountered around these joints , corrosion on all the other joints was negligible.

It was noted that when many of the joints were first exposed they exhibited a shiny surface when first extracted and then flash corrosion was observed. The very shiny surface appearance and flash corrosion is suggestive of the bacteria that influence corrosion or access to free oxygen in the air.



Figure 12 300mm square joint exhibiting up to 2mm corrosion on the skit pate and an isolated <2mm pitting (Point) corrosion on one of the pins. This was considered to be the highest level of corrosion identified on the two joint in one area.

Table 2: Estimated expected levels of corrosion based on AS2159-2009 Piling Code.

Exposure Classification	Corrosion Rate (mm/yr)	Corrosion for 15 years (mm)
Non Aggressive	< 0.01	0.15
Mild	0.01 to 0.02	0.225
Moderate	0.02 to 0.04	0.45
Severe	.04 to 0.1	1.05
Very Severe	>0.1	1.5

The maximum estimated corrosion of 2mm was based on the independent consultant review at an isolated point, note that this was a point corrosion, the average corrosion would be less than 1.0mm which is within the guidelines of the piling code above.

Along the length of piles that were extracted several piles were cored through the piles and carbonation testing was undertaken again by an independent consultant at both faces of the pile at each of the depths below, the results are summarised in the table below. The piles were constructed with 40mm cover and 60MPa concrete and a w/c ratio<0.22. The depth of carbonation was negligible at all depths and no corrosion of any reinforcing steel could be seen within the concrete as reported by and independent concrete technologist. Although more concrete cores were taken the carbonation testing was discontinued as there was no evidence on any pile extracted showing any signs of concrete deterioration.

It should be noted that precast pile concrete mix design is driven by the requirement for high early strength, the low water cement ratio and high cement content result in an extremely durable mix which at 56 day often attains a strength of 80-90MPa.

Table 3: Minimum concrete cover required in accordance with AS2159-2009 Piling Code.

Exposure Classification	Required Cover for 50 years precast piles	Required Cover for 100 years precast piles
Non-Aggressive	20	25
Mild	20	30
Moderate	25	40
Severe	40	50
Very Severe	40	50

Table 4: Depth of Carbonation Results measured from extracted piles.

Sample Number	Pile No	Depth Sample (m)	Depth of Carbonation Face 1	Depth of Carbonation Face 2
1	88	2.5	<1mm	<1mm
2	88	5	<1mm	<1mm
3	88	8	<1mm	<1mm
4	88	10.5	<1mm	<1mm
5	88	11.5	<1mm	<1mm
6	88	14.5	<1mm	<1mm
7	88	17	<1mm	<1mm
8	88	19	<1mm	<1mm
9	88	21	<1mm	<1mm
10	98	9	<1mm	<1mm
11	98	11	<1mm	<1mm
	98	14	<1mm	<1mm



Figure 12 Extracted pile showing tube damage during installation of the sleeve



Figure 14 Demolition jaws were used to assist in laying down the long piles.

In Figure 14 you can see the bentonite fluid within the tube has created a slippery surface lowering the overall friction to allow the annulus of soil around the pile to slip within the tube and stay with the pile during extraction.

The soil is still tightly bound onto the pile. The soil particularly binds to the roughened surface.

Another interesting observation was the "straightness" the piles drove. The tube being 610mm diameter x 20mm wall thickness provided a theoretical clearance to the corner of the piles of 90mm. Upon reviewing the extracted piles it was noted that the tube tended to collect the corner of the piles at around 15 to 18m chipping the corner off the piles. This suggests the piles have verticality within the ground of around 0.6% or less which for a 275mm sq pile seems quite good.



Figure 15 Shows extracted pile and curvature indicating that the pile has driven towards the roughened side.

Secant Pile Wall

For the secant pile wall a Casagrande B400 was used with a casing to core over the top of the secant piles and core out the hard piles. During this process the high torques applied resulted in shearing of the hard secant piles from the lower sections which were held by the "soft" piles. These piles had to be cored out in several sections. The wall could not be excavated out as it was in close proximity to a rail line.



Figure 16 During coring out of the Secant wall the applied torque completely sheared the piles.

Conclusion

It is very rare to be provided with an opportunity to extract piles driven into the ground to observe and investigate physical and chemical effects of the installation and contact with the soil. It would appear that the guidelines in the AS Piling Code for corrosion and concrete cover are conservative.

It would also be reasonable to assume that the dense 60MPa concrete mix design used for precast piles provides a very high level of durability against carbonation attack in PASS (potentially Acid Sulphate Soil)

Other observations including the following:
Piles tend to curve towards the rougher side when driven.
Pile verticality tolerance of 1% is reasonable for a driven pile provided there are no significant obstructions.

Predrilling on all four sides to past the pile toe level combined with vibrating and simultaneously jetting with a bentonite fluid proved to be a successful way of extracting segmental precast piles by reducing the skin friction to allow extraction of piles.

MICROPILING IN URBAN INFRASTRUCTURE: ADVANTAGES, EXPERIENCE AND CHALLENGES

Freddy Lopez, Friedr. Ischebeck GmbH, Ennepetal, GERMANY, lopez@ischebeck.de
Giorgio Severi, Friedr. Ischebeck GmbH, Ennepetal, GERMANY, severi@ischebeck.de

ABSTRACT

The ongoing urban development is a global phenomenon which has high demands on urban infrastructure (housing, public services, transportation, telecommunications, etc.). This a very dynamic process, that requires not only the design and construction of new infrastructure, but also to increase the capacity and to extend the serviceability of the existing facilities. Intra-urban interventions are frequently carried out in densely populated and built-up areas, and they have to be implemented in short time frames, causing the less possible disturbance to the daily activities of the population.

The implementation of worldwide well known technologies and construction methods, such as micropiling, has enabled designers to come up with optimal solutions in order to satisfy the challenging requirements of the urban development.

The following paper presents an overview of different intervention projects, where self-drilling micropiles were designed and implemented to provide a geotechnical solution for infrastructure in four relevant areas in the urban development: public services (health care and schools), transportation, telecommunications and conservation of patrimonial heritage.

The special requirements of the projects will be briefly described, and the adopted solutions, with their correspondent design considerations and execution process will be presented.

Finally, a review of the advantages, gained experience and future challenges for micropiling will be presented.

Keywords: Micropiling, urban development, design and construction, retrofitting, new and existing infrastructure

INTRODUCTION

According to the World Bank (2017), 54% of the population lives in urban areas today, and by 2045, the number of people living in cities will increase by 1.5 times to 6 billion, adding more urban residents.

The ongoing worldwide urbanization brings challenges to urban infrastructure (housing, public services, transportation, telecommunications, etc.). This a very dynamic process, that demands not only the design and construction of new infrastructure, but also requires to increase the capacity and to extend the serviceability of the existing facilities.

Micropiling is one of the most successfully implemented deep foundation technologies in intra-urban interventions, which are often carried out in densely populated and built-up areas. The use of micropiles enabled the implementation of several solutions within short time frames, causing the less possible disturbance to the daily activities of the population.

Among the different micropile typologies, self-drilling micropiles have been proven to be a very versatile solution and are increasingly used in urban intervention projects, both for the construction of new infrastructure and as reinforcement to retrofit existing structures. The use of self-drilling micropiles allows a flexible use of the drilling equipment, enabling the installation of long micropiles even in confined spaces, obtaining high drilling performances associated to very low vibrations.

Self-drilling micropiles consist of continuously threaded hollow bars, made out of seamless steel pipes, installed via rotary percussive drilling. During the drilling process, the micropiles are continuously grouted

© 2018 Deep Foundations Institute

(dynamic injection), building a rough interlocking at the interface grout-soil, increasing the skin friction (Fig. 1).

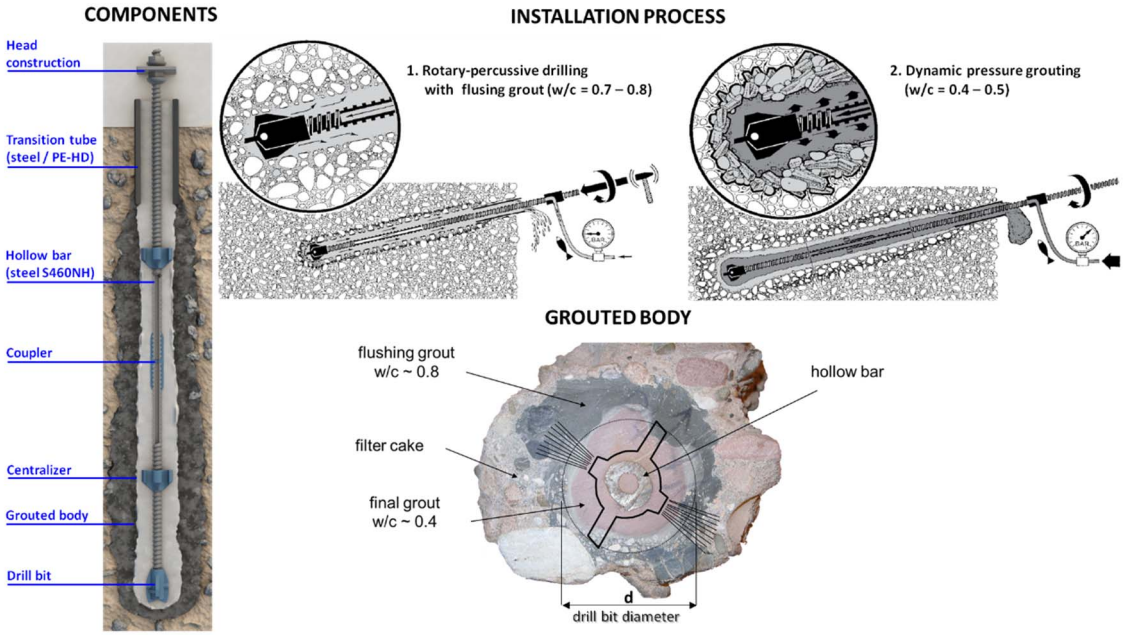


Fig. 1 Self-drilling micropiles: components, installation and grouted body (Friedr. Ischebeck GmbH, 2016)

As a composite material, the permanent use is limited by the corrosion protection of the steel elements. According to the European Standards that regulate the use of composite materials for geotechnical applications, such as micropiles (EN 14199) and soil nails (EN 14490), the corrosion protection can be provided, among other measures, by an efficient encapsulation in grout. Research has shown that crack widths controlled to less than 0.1mm can be considered to be self-healing, therefore, cement grout is considered acceptable as an impermeable protective encapsulation, provided that the crack width within the grout body can be demonstrated not to exceed 0.1mm (EN14490, 2010). In Germany, this requirement has been adopted by the German Institute of Building Technology to assess the structural behavior of self-drilling micropiles, as highlighted for example in the National Technical Approval Z.34.14-209 (DIBt, 2014).

PUBLIC SERVICES INFRASTRUCTURE

Health care infrastructure - The Bolivarian University Clinic in Medellin, Colombia

The Bolivarian University Clinic (*Clínica Universitaria Bolivariana*) belongs to the social and academic project of the Bolivarian Pontifical University of Medellin, Colombia.

The clinic is located in northwestern Medellin (Department of Antioquia), in the area of Robledo. It was originally built in 1995 and buildings were founded on caissons. The increasing demand on health care, mainly in the field of neonatology, led the administration to increase the attention capacity, with the correspondent extension of its facilities. Furthermore, in order to fulfil the structural requirements of the updated Colombian Earthquake Resistant Design Code (NSR-10), the foundation of the existing and the new buildings should be provided with structural reinforcement.

In 2016, the retrofitting works were carried out by Ischebeck Colombia S.A.S. The use of portable drilling equipment minimized the effect of the installation works (noise and dust pollution, vibrations, etc.), reducing disturbances (i.e. relocation of patients or medical personal) to the absolute minimum, affecting the least possible the operative capacity of the clinic. The micropiles were installed both outside (Fig. 2) and inside the existing facilities (Fig. 3). Table 1 presents a summary of the installed micropiles.

The constructive measures implemented have enabled the Bolivarian University Clinic to increase its capacity, and it is able to attend up to 25% of the births in the metropolitan area of Medellin (Clínica Universitaria Bolivariana, 2017).

Table 1. Summary of the installed micropiles (Ischebeck Colombia S.A.S, 2016)

Micropiles	120
Length	12 m
Type	Self-drilling micropiles (TITAN 52/26)
Application	Permanent
Design Resistance	500 kN
Drill bit / Diameter	Carbide button / 130 mm
Ground conditions	Alluvial deposits / presence of boulders (>1.0m) from 7.0m below ground level



Fig. 2 Installation of reinforcement micropiles outside the facilities (Ischebeck Colombia S.A.S., 2016)

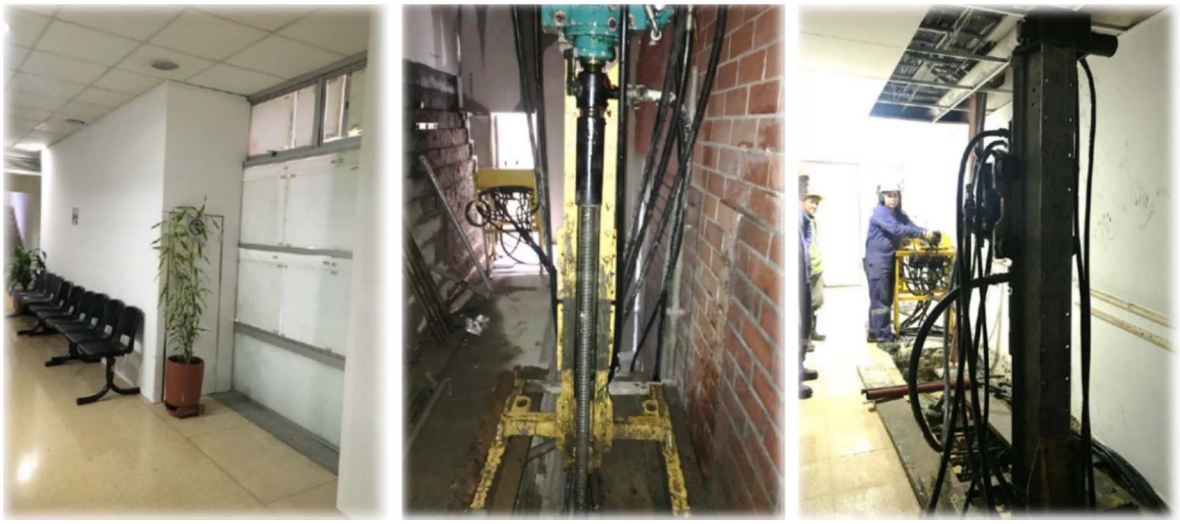


Fig. 3 Installation of reinforcement micropiles inside the facilities (Ischebeck Colombia S.A.S., 2016)

School infrastructure – The Professional School "Sandro Pertini" in Monfalcone, Italy

The professional school (*Istituto Statale Di Istruzione Superiore "Sandro Pertini"*) is located in eastern Monfalcone, Province of Gorizia – Autonomic Region of Friuli Venezia Giulia. The school hosts students

attending the Technical Institute of Transportation and Logistics, and the Professional Institute of Maintenance and Technical Assistance.

The school was built in the decade of the sixties. After a structural evaluation, the Technical Department of the Province Gorizia designed several measures to adjust the existing building to the updated Italian Technical Building Code (NTC 2008), which adopted a new structural verification philosophy and introduced the concept of the local seismic risk (Balliana, 2015).

Among other measures, the seismic adjustment of the school facilities contemplated the retrofitting of the existing foundations. In 2015, the retrofitting works were carried out by Di Betta Giannino SRL. The micropiles were installed inside the existing facilities (Fig. 4), under restrictive space conditions: ceiling height approx. 2.4m (Severi, 2017).



Fig. 4 Micropile installation (Severi, 2017)

On October 24th 2015, the Regional Administration Office re-inaugurated the school building. Table 2 presents a summary of the installed micropiles.

Table 2. Summary of the installed micropiles (Severi, 2017)

Micropiles	145
Length	11 m
Type	Self-drilling micropiles (TITAN 52/26)
Application	Permanent
Design Resistance	565 kN
Drill bit / Diameter	Cross-cut / 130 mm
Ground conditions	Alluvial deposits / silty gravels and silty sands up to depth of 7.5m, clayey sands below

TRANSPORTATION

The Funicular Network in La Paz, Bolivia

On May 29th 2014, the Bolivian public company *Mi Teleférico* began operating the worldwide largest and highest funicular (cable car) network. Operating at about 4000m above sea level and with a transportation rate of 3000 passengers/ hour, its implementation has a mayor influence in the public transportation in the metropolitan area of the neighboring cities of La Paz and El Alto, with an estimated population of 1.8 Million inhabitants. According to official information (Mi Teleférico, 2017), to June 2017 more than 82 Million passengers have used the cable transportation system. Five lines are currently operative (*Red, Yellow, Green, Blue and Orange lines*), while the rest (six lines) is either under construction or in the final design stage (Fig. 5).



Fig. 5 Metropolitan Funicular (cable car) Integration Network of La Paz and El Alto (Mi Teleférico, 2017)

The Blue Line is the longest in the network (4.98 km) and has five stations and 40 towers. The typical shallow foundation solution for the towers of the line is presented in Fig. 6a.

Along the line, the towers 14 to 17 are located above an existing canalization vault, making the standard solution inapplicable. A deep foundation solution using a group of eight self-drilling micropiles was designed and implemented by the company Pilotes Terratest Bolivia S.A. for each of the four affected towers (Fig. 6b and Fig. 6c).

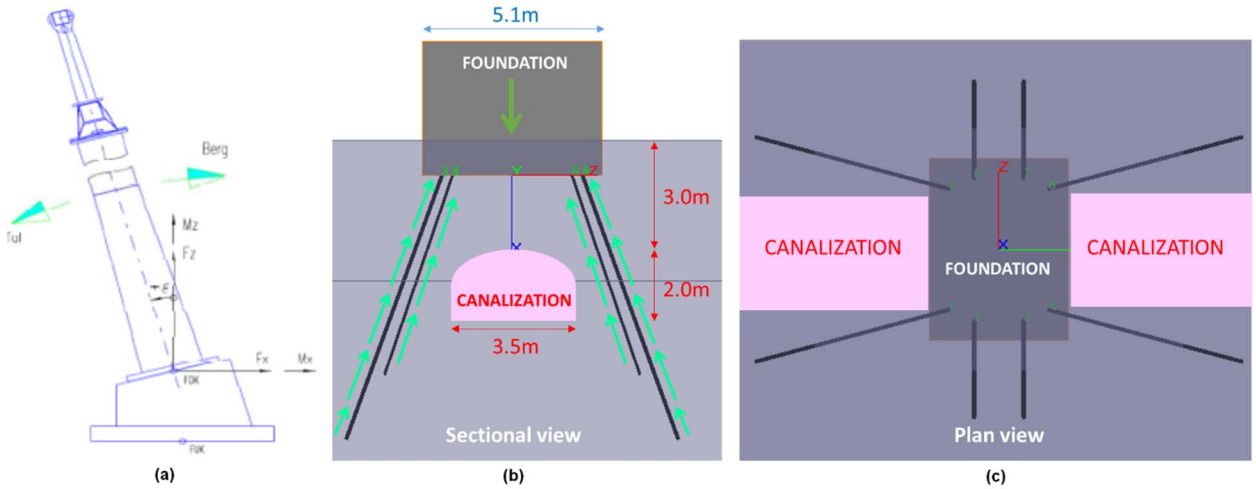


Fig. 6 a) Typical shallow foundation b) Sectional viewmicropiles c) Plan view micropiles (Pilotes Terratest, 2015)

Early 2016, the micropiles were installed (Fig. 7, Pilotes Terratest Bolivia, 2016). Table 3 presents a summary of the installed micropiles. The Blue Line began its operations officially on November 21st 2016 and was opened for the public on March 3th 2017 (Mi Teleférico, 2017). Approximately 770'000 passengers have been transported in the first month of operations.



Fig. 7 a) Self-drilling micropiles b) Micropile installation c) Head connection to the foundation (Saucedo, 2016)

Table 3. Summary of the installed micropiles (Pilotes Terratest Bolivia, 2016)

Foundations	4
Micropiles	32 (8 for each foundation)
Length	9.0 – 10.5 m
Type	Self-drilling micropiles (TITAN 52/26)
Application	Permanent
Design Resistance	520 kN
Drill bit / Diameter	Carbide button / 130 mm
Ground conditions	Alluvial deposits (gravels in a cohesive matrix)

TELECOMUNICATIONS

The 4G Network in India

Since 2014, several providers are expanding the coverage areas of their mobile networks throughout India, to satisfy the increasing demand of their customers. Ongoing projects contemplate the erection of more than 50´000 telecommunication towers for the new 4G (or LTE) network. Evaluation reports (OpenSignal, 2017) present the 4G coverage maps of the 3 largest mobile data providers in India (Fig. 8).

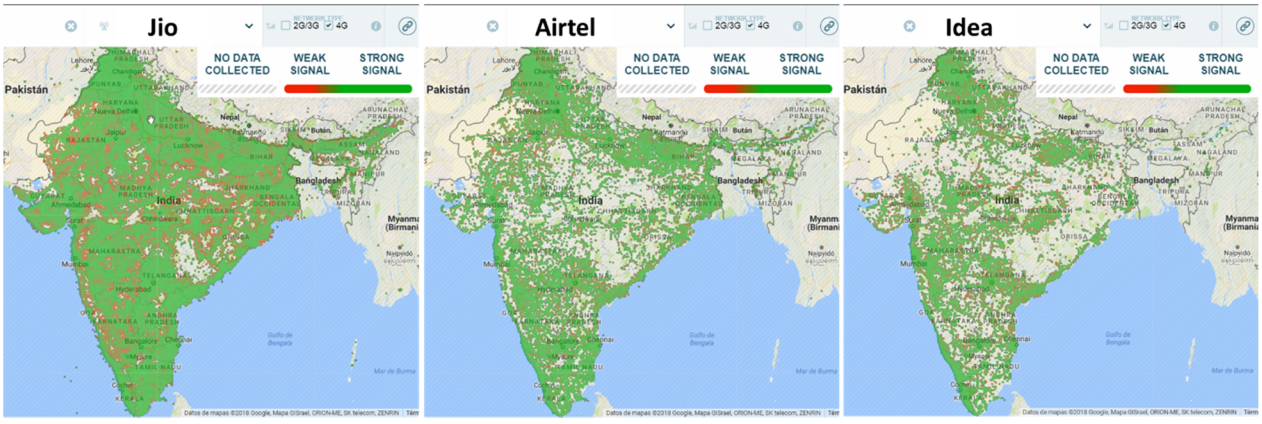


Fig. 8 4G-Coverage map of the 3 largest mobile data providers in India (OpenSignal, 2017)

About 830 tower foundations were designed to transfer the loads using micropiles. The design considered four foundations micropiles, with an average length of 15.0m. The structural response of the foundation under different load conditions was evaluated (Fig. 9).

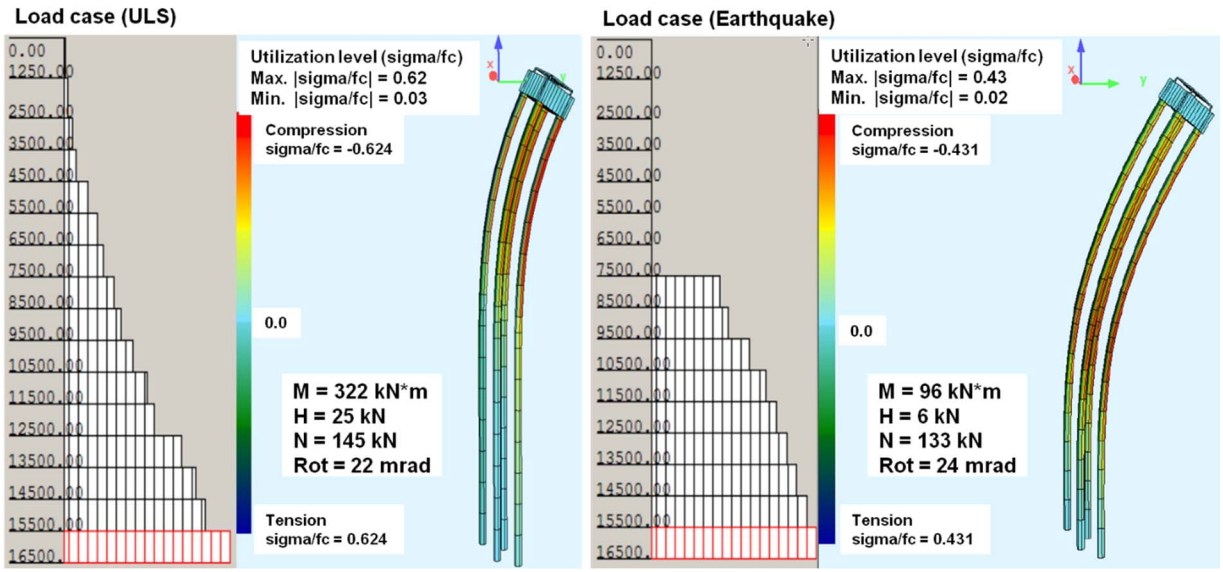


Fig. 9 FEM-analysis of a typical micropile foundation for 4G towers (Eberlein, 2013). Left: Ultimate Load State (ULS). Right: Earthquake, with no lateral bedding in the upper 6.2m (liquefaction)

The micropiled foundation reduced considerably the dimensions of the originally planned shallow foundations, with the correspondent reduction of the concrete and reinforcement steel. Furthermore, the use of self-drilling micropiles increased the efficiency of the installation process, since it was possible to work with compact drilling rigs, facilitating the transport between installation sites. Table 4 presents a summary of the installed micropiles.

Table 4. Summary of the installed micropiles (Ischebeck, 2016)

Foundations	Approx. 830
Micropiles	Approx. 3300
Length	12 – 18 m
Type	Self-drilling micropiles (TITAN 40/16 and 52/26)
Application	Permanent
Design Resistance	400 - 500 kN
Drill bit / Diameter	Hardened clay / 150mm and 170mm, and cross-cut / 130mm
Ground conditions	Silty, sandy and gravely soils. Liquefaction potential in the upper 6.0m

An overview of the construction stages is presented in the following Figure.



Fig. 10 a) Micropile installation b) Load testing (compression) c) Assembly of the tower d) finished tower

PATRIMONIAL CONSERVATION

The City Hall in Monfalcone, Italy

Monfalcone´s City Hall was first built in 1860 and over the years it was object of successive extensions and modifications.

Several structural problems have been observed in the building (i.e., differential settlements and cracking, Fig. 11) and in order to reestablish its structural functionality, as well to increase the safety against seismic actions, different engineering measures have been implemented since 2015.

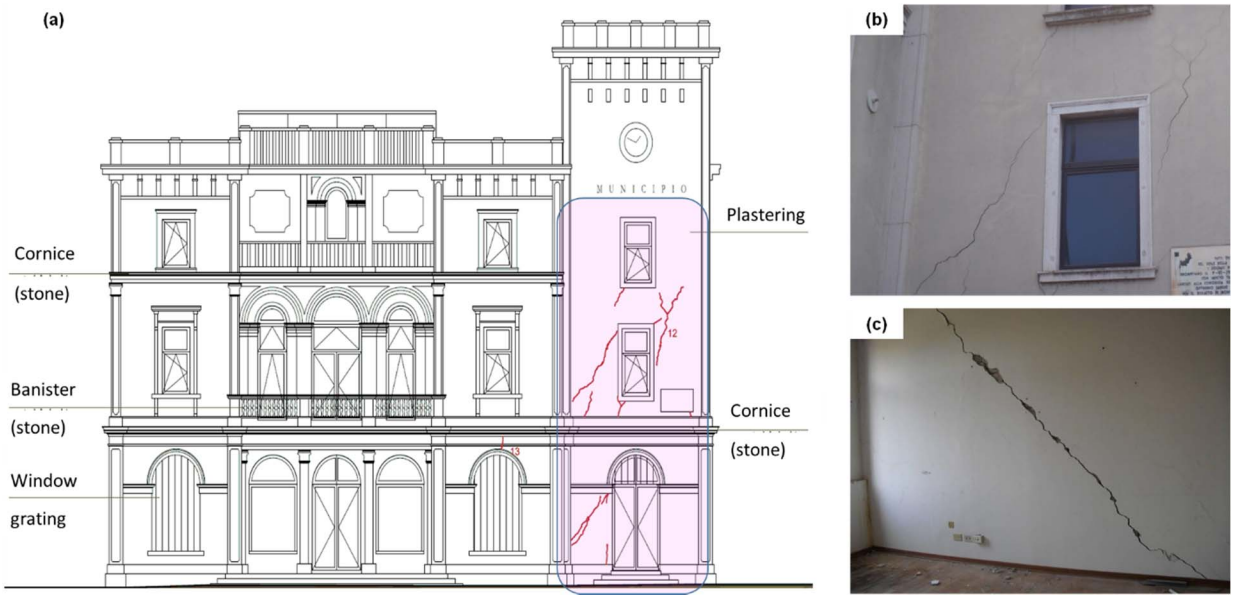


Fig. 11 a) Registered damages b) Cracking at the facade c) Cracking in the inner rooms (Cooprogetti, 2013)

A relevant part of the reinforcement concept consisted in underpinning the original foundations with self-drilling micropiles, and in order to provide additional stiffness, the foundations were linked to each other with connection beams and a 0.5m-thick foundation slab (Fig. 12).

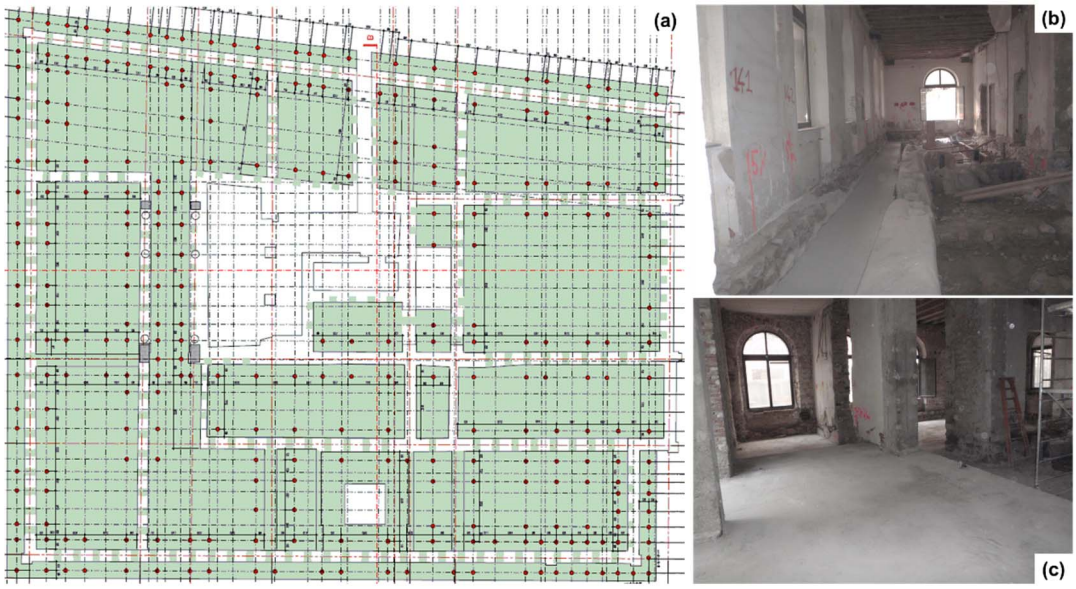


Fig. 12 a) Disposition of the micropiles b) Connection beam b) Foundation slab (Severi, 2017)

The retrofitting works were carried out in 2015 by ICI Soc. Coop. A.R.L. The micropiles were installed both inside and outside the building (Fig. 13). Table 5 presents a summary of the installed micropiles.



Fig. 13 Installation of reinforcement micropiles a) inside the building b) outside the building c) connection to the structure (Severi, 2017)

Table 5. Summary of the installed micropiles (Severi, 2017)

Micropiles	294
Length	9.5 – 11.7m
Type	Self-drilling micropiles (TITAN 73/53)
Application	Permanent
Design Resistance	635 kN
Drill bit / Diameter	Cross-cut / 175mm
Ground conditions	Alluvial deposits: Silty, clayey gravels and sands up to depth of 9-10m, Limestone below

SUMMARY AND CONCLUSIONS

The present document described the implementation of self-drilling micropile solutions in specific projects, related to urban interventions in different countries.

Civil Engineers are confronted with the challenging demands of the present and future urban development, which requires flexible and fast solutions, with the least possible affection to the functionality of both the new and the existing infrastructure.

The use of self-drilling micropiles is a very suitable and cost effective solution for different kind of projects, due to the flexibility and velocity of the installation. The availability of adequate equipment enables to carry out interventions even in areas with restricted space (i.e. retrofitting, underpinning of existing foundations, etc.), causing only small affection to the surrounding work environment (reduced noise and air pollution, reduced vibrations, etc.). The use of micropiles also makes possible to reduce the dimensions of the foundation structures (i.e. for slender elements, such as communication, railway and power masts), reducing the footprint of the intervention area, correspondingly.

Urban interventions do not only have an exclusive functional character, they can also be conceived to preserve the cultural and architectural identity of the cities. To this effect, micropiles have been also successfully used in the preservation of patrimonial structures.

Finally, since urban interventions usually represent a very important investment and have an economic impact, special attention should be paid to the serviceability of the urban infrastructure in the middle and long term. For permanent applications, the design loadbearing capacity of the used structural elements needs to be guaranteed during the planned life time of the structures. In the case of micropiles, it must be ensured that the steel load bearing elements are effectively protected against corrosion.

REFERENCES

Balliana, F., 2015. Evoluzione normative sismica. Website: http://www.ingballiana.it/Normativa.html

Clínica Universitaria Boliviariana, 2017. Website: http://virtual.upb.edu.co/clinica/

Cooprogetti, Politecnica, Iconia, 2013. Lavori di ristrutturazione del Palazzo Comunale di Monfalcone – Progetto esecutivo Lotto 1

Deutsches Institut für Bautechnik (DIBt), 2014. Allgemeine bauabsichtliche Zulassung Z-34.14-209: Mikropfähle TITAN

Eberlein, M., 2013. Report: Self-drilling micropile foundation of GSM tower in India / Review of foundation design (EGT GmbH, Germany)

European Norm: Execution of special geotechnical works – Micropiles (EN 14199), 2015.

European Norm: Execution of special geotechnical works – Soil Nailing (EN 14490), 2010.

Friedr. Ischebeck GmbH, 2016. Technical Brochures

Ischebeck Colombia S.A.S., 2016. Revista Clinica Boliviariana

Lopez, F., Fernandez, J.M., 2017. Edificio Piedra Real – Concepcion, Chile. Case study of an uplift reinforcement project. Proceedings of the 13th International Workshop on Micropiles, Vancouver, March 29-April 1.

Mi Teleférico, 2017. Los Números de Mi Teleférico. Website: http://www.miteleferico.bo/

Norme Tecniche delle Costruzioni del 2008 (NTC 2008)

OpenSignal Inc., 2017. Report: State of Mobile Networks: India

Pilotes Terratest S.A., 2015. Design Report for the Foundation Reinforcement for the Blue Line

Reglamento Colombiano de Construcción Sismo Resistente (NSR-10), 2010.

Saucedo, M. (Pilotes Terratest Bolivia), 2016. Micropiles Design Seminar - CADECO, La Paz, November 16.

Severi, G., 2017. Consolidamento delle Fondazioni e Adeguamento Sismico delle Costruzioni con Micropali Iniettati Tubolari Compositi a Perforazione Diretta. XXVI Convegno Nazionale di Geotecnica "La geotecnica nella conservazione e tutela del patrimonio costruito" (AGI), Rome, June 20 - 22.

World Bank, 2017. Website: http://www.worldbank.org/en/topic/urbandevelopment/overview

NEW YORK CITY LANDMARK STRUCTURES - RECONSTRUCTING FROM THE INSIDE OUT

Michael J. Chow, PE, Senior Consultant, GZA GeoEnvironmental of New York, 104 West 29th Street, 10th Floor, New York, NY; 212-594-8140, michael.chow@gza.com

Amber T. Vail, PE, Senior Consultant, GZA GeoEnvironmental, Inc. 372 West Street, Suite 100, Keene, NH; 603-232-8797, amber.vail@gza.com

ABSTRACT

Booming NYC Real Estate development includes private owners purchasing property(ies) within designated Landmark Historic districts desiring entirely replaced interiors, joining multiple properties together, and/or extending properties downward (since they often cannot build up). Like other major cities around the world, Government/Historic Landmark Preservation Commissions (LPCs) are tasked with preserving these historic districts with strict rules on preserving facades, future building profiles affecting public site lines, and required precautions during construction that may impact adjacent structures.

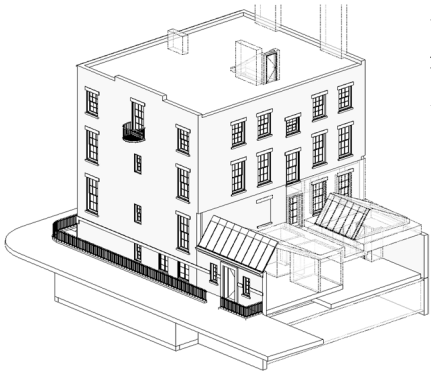
One such project in NYC's Greenwich Village joined three 120-year-old properties together utilizing a complex coordination, sequencing, and construction of intricate underpinning/wall extensions, lateral and vertical supports and bracing, and positive load transfer within tight clearances between existing floors prior to a complete interior demolition and multi sub-cellar excavation and included suspending the west wall above grade for access to below grade construction. These systems included deep foundations consisting of rock socketed drilled-in caissons (micropiles) which were a key element in transferring both vertical and lateral forces to suitable bearing stratum. In this manner the historic façade, adjacent properties, and workers were protected and allowed above grade renovations including removing interior walls, floors. Also, it allowed removal of an existing shared load bearing and shear wall (party wall) between townhouses.

The sub-cellar needed to be extended 24 feet (7.30 meters) below grade in these tight urban landmarked structures and the neighbor's refusal to allow underpinning presented geotechnical challenges. A real-time instrumentation monitoring program was implemented to protect and document movement of the building under construction as well as those directly abutting.

This paper describes the project parameters, challenges, design approach, monitoring, and lessons learned for this Historic District property requiring intricate vertical and lateral support systems to be in place prior to gut demolition, party wall removal, and below grade access.







Figures 1 and 2 (East Façade and West Carriage House; Northwest Isometric)

© 2018 Deep Foundations Institute

INTRODUCTION

Real Estate development has been booming in NYC. Many of these are private owners whom have purchased property within designated Landmark Historic Districts and now desire to entirely replace the interiors, join multiple properties together, and/or extend the properties downward (since they often cannot build up).

Similar to other major cities around the world, NYC's Landmark Preservation Commission (LPC) is tasked with preserving these historic districts with strict rules on preservations of façades, future building profiles affecting public lines of site, and precautions which must be taken during construction.

One such project in Greenwich Village consists of joining three four-story townhouses with a partial 8 feet (2.4 meter) cellar located in the Historic West Village ***(Figures 1 to 3)***. Due to the historic significance of the location and Historic District requirements, overseen by the LPC, outside appearances of the building could not be changed. A few of the project key elements were the preservation of the historic façade without any damage, protection of adjacent properties, and ability of workers to perform their jobs safely.

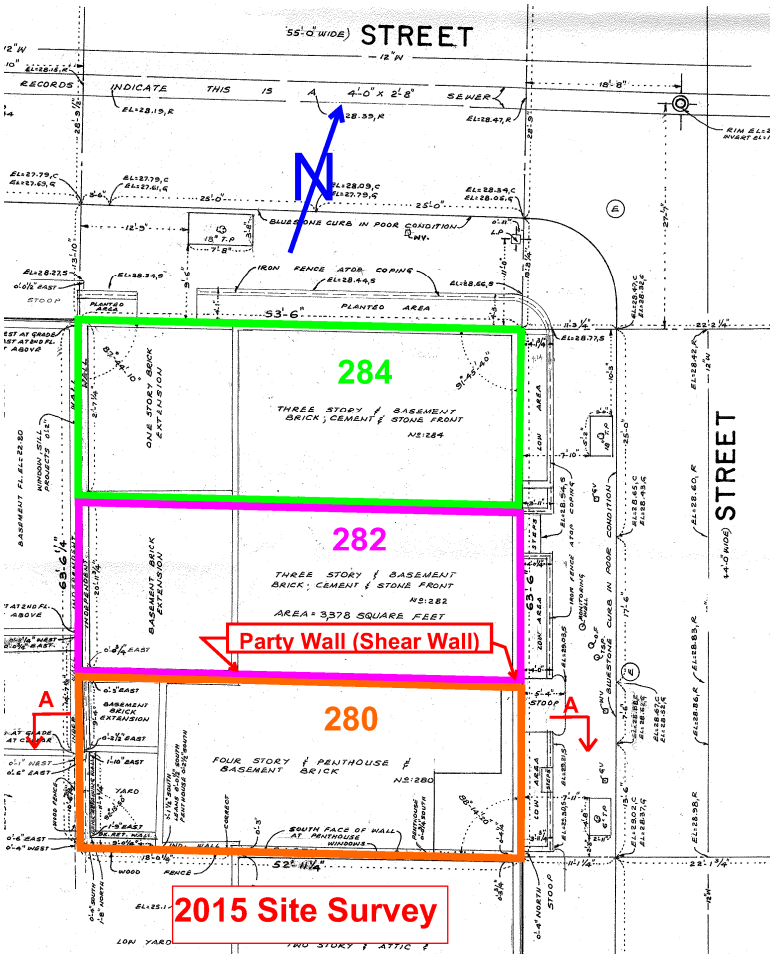


Figure 3 – 2015 Site Survey

The buildings were completely gutted and renovated with all existing interior walls, floors, and roof diaphragms removed. In addition, since the new floor levels matched the original floor levels, upon floor removal, an 35 feet to 40 feet (10.7m -12.2m) high unsupported brick shell would exist unless proper precautions were implemented (***Figure 4***). Further complications included the removal of an existing load

bearing and shear wall (party wall) shared by two of the townhouses and partial removal of the west (rear) wall to gain access to the interior and below grade portion of the project. Accordingly, temporary vertical and horizontal support of the remaining structural elements was essential to achieve this ambitious scheme.

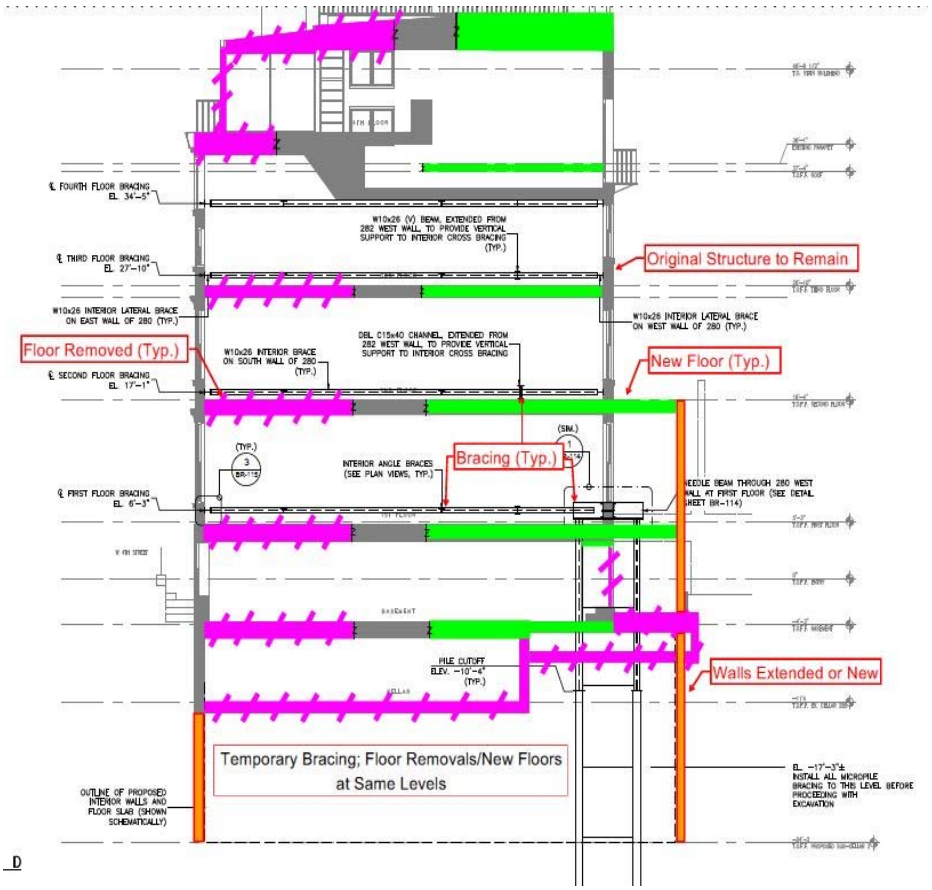


Figure 4– Section A-A

The project's geotechnical scope included the downward extension of the existing partial cellar to create two full footprint sub-cellars. The excavation would extend up to 24 feet (7.30 meters) below the sidewalk throughout the development's combined footprint. For this special situation, underpinning/support of excavation would be required to satisfy the New York City Building Code requirements. Since the construction would involve not only the project's footprint, but also, a structural modification of the neighbor's foundation, an agreement between parties would need to be formalized. Moreover, a real-time monitoring program was implemented to protect adjacent structures and minimize damage.

The neighbor's refusal to allow underpinning, the site-wide downward extension of the existing cellar, challenging intricate coordination, sequencing, complex underpinning/wall extensions, select demolition, lateral and vertical supports and bracing, and positive load transfer presented significant geotechnical, structural, construction and management challenges./.

LATERAL WALL SUPPORT

To preserve the historic façade, protect adjacent properties, and provide worker safety to allow gut renovation above grade, a temporary multi-tiered support system was constructed to stabilize the perimeter brick shell (avoiding 35 to 40 feet [10.7m -12.2m] high unbraced walls). A horizontal steel truss/frame near each of the existing floor levels provided temporary diaphragms, prior to the beginning of demolition (***Figures 4 and 5***). Temporary diaphragms were supported vertically by the exterior brick walls, which

mimicked the existing floor diaphragms that were to be demolished. These temporary diaphragms were designed to transfer lateral forces due to wind forces into the existing shear walls or into vertical temporary shear frames in cases where existing shear walls were removed. Horizontal diaphragms consisting of bracing frame with perimeter steel wales, struts and corner bracing was chosen in lieu of perimeter truss towers due to ease of construction and better construction access as well as the ability to provide rigidity similar to the existing floor system. This system resulted in less engineering effort as well because a full analysis of the existing building was not required. This was because the temporary bracing was functionally equivalent to the existing floor system. Our analyses included:

- First modeling the internal horizontal diaphragm (***Figures 5, 8, and 15***).
- Then modeling the temporary vertical shear frame (***Figures 6, 9, and 10***) to ensure a continuous load path of lateral loads to the ground, which allowed for the removal of the existing party wall (described in more detail in the next section).
- A total of 5 load cases were developed (based on wind load on the exterior walls ***(Figure 7)***
- Maximum reaction envelopes were generated to determine the loads put on the internal shear frame (***Figure 5***).
- Lateral loads from the internal bracing frame reaction envelope are entered into the GT STRUDL model (***Figure 6***).
- Steel framing was selected and the AISC code check capability in GT STRUDL was used to check stresses and design members.
- Vertical support members included drilled-in rock socketed small diameter caissons (micropiles)
- The controlling connection forces from the analyses was tabulated and provided to the steel fabricator for connection design.

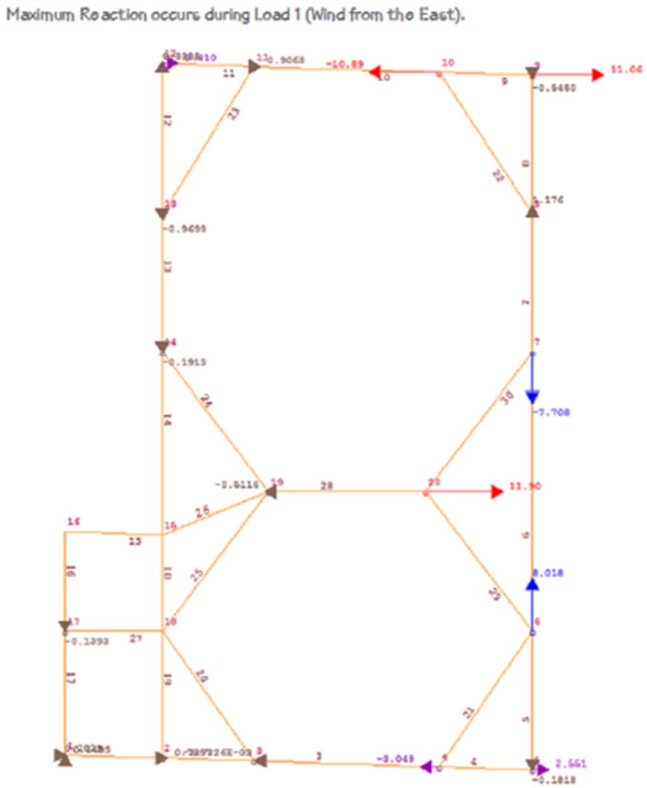




Figure 5 – Diaphragm (Envelope – Horizontal) **Figure 6- Shear Frame (Envelope – Shear Wall)**

Note: Reactions at exterior wales. Wales are assumed supported in their axial direction by the brick shear walls. Max Reaction = 11.9 kips (52.9 KN)

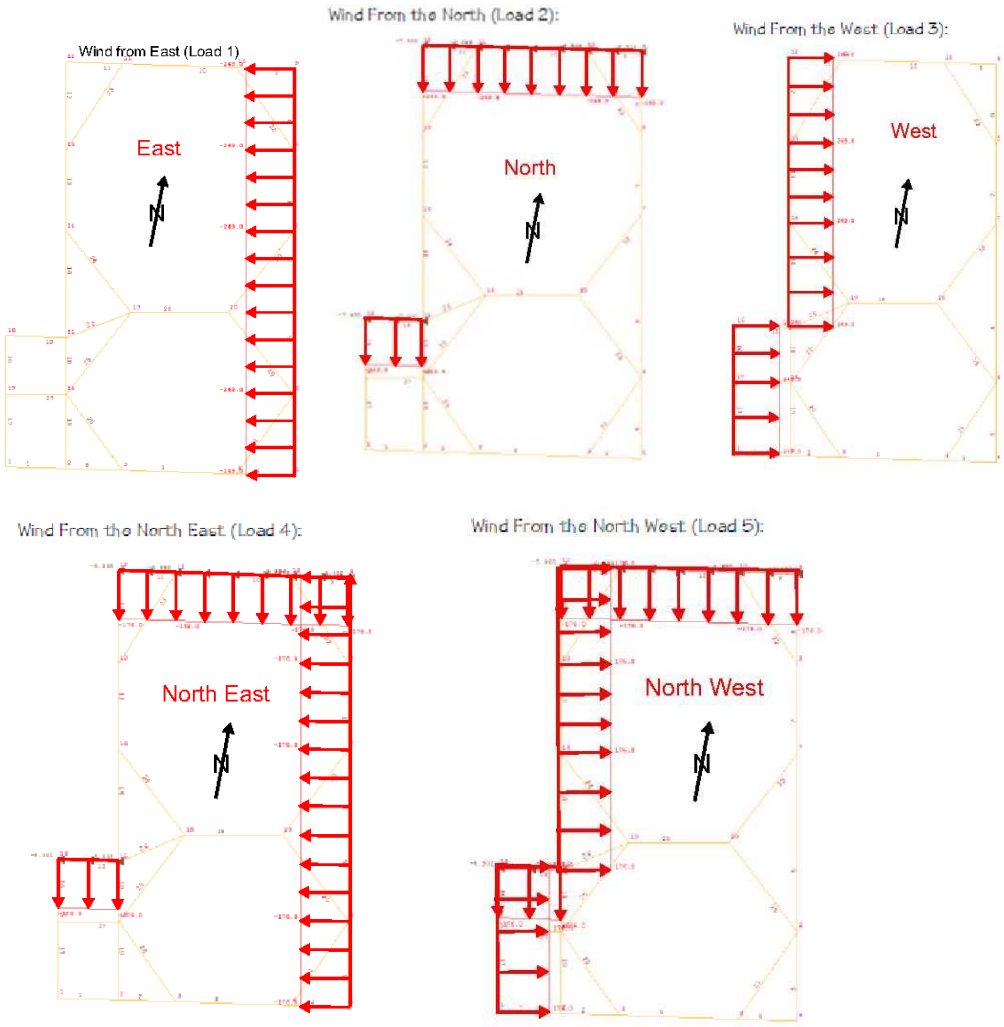


Figure 7 – Wind Load Cases



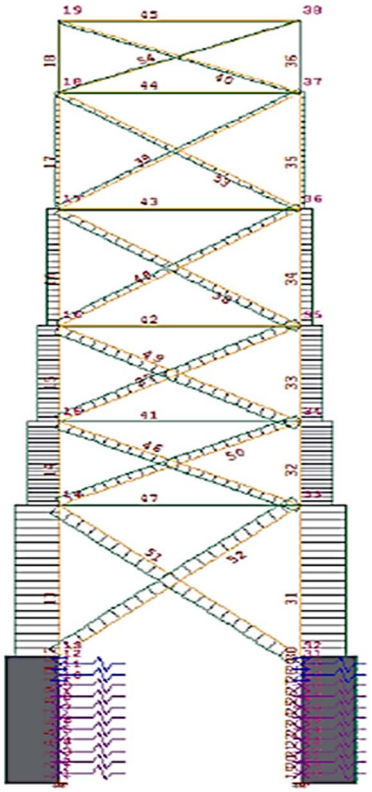
Figure 8 – Horizontal Truss/Frame (Temporary Diaphragm)

PARTY WALL/SHEAR WALL REMOVAL

To allow removal of the party wall between townhouses temporary vertical braced frame systems integrated with the horizontal trusses at each floor level were utilized to create an alternative load path to transfer lateral forces to the ground. The temporary frame needed to replace support from the original party wall by providing similar or higher rigidity in order to provide stability during the demolition and construction of the new shear wall. An east-west braced vertical shear frame was modeled which resisted the lateral diaphragm forces and is supported by micropiles.

The frame was modeled in GT STRUDL, which generated the maximum reaction envelopes to determine the loads on the shear frame, controlling connection forces, axial uplift, and compression reactions at the base to be supported by the micropiles ***(Figures 9, 10, and 11)***. The controlling connection forces from the analyses was tabulated and provided to the steel fabricator for connection design.

Overall, the forces generated by the different envelopes resulted in very large axial loads on the micropiles with a maximum axial reaction of 111.5 k (496 KN). Micropiles consist of 9-⅝" (244mm) O.D. x 0.545" (13.8mm) wall casing (Fy=80ksi (552MPa), 4000psi (27.6MPa) grout, #18 (57mm) centerbar (Fy=75ksi (517MPa)), and 10ft (3.0m) min. rock socket.



Uplift **Compression**

Figure 9 - Shear Frame- Axial Reactions/Lateral Springs



Figure 10- Shear Frame Bracing



Figure 11- Micropile-Column Connection

WEST WALL SUPPORT / BELOW GRADE ACCESS

The final building design required the removal of portions of the west (rear) wall. The Contractor utilized the openings in the wall for equipment and material access during construction of the proposed horizontal diaphragms at each floor, shear wall braced frame installation, and below grade construction. The removal of the lower portion of the wall created a discontinuous load path for lateral loads acting on the building.



Figure 12- West Wall Framing – Brick Removal Limits

The design of the west wall support was the most complicated part of the design because not only did it need to support the weight of the entire structure above it, but it also needed to resist lateral forces acting on it from the temporary diaphragm system (***Figures 12 and 15)***. To help preserve the building's historical appearance, the removed brick was stockpiled offsite for re-use in the new west façade.

AutoCAD sketches were first developed of the two support systems and then the geometry was input to create GT STRUDL models ***(Figure 13)***. AISC code checking was used, innate to the program, so the design process was much faster than by hand or MathCAD. A clamping mechanism was developed to "grab" onto the base of the wall which framed into needle/transfer beams supported by micropiles ***(Figure 14)***. The micropiles were modeled as steel members supported by linear elastic springs below grade and fixed at bedrock. Similar to the lateral trusses and shear wall, controlling connection forces were tabulated and provided to the steel fabricator for connection design.

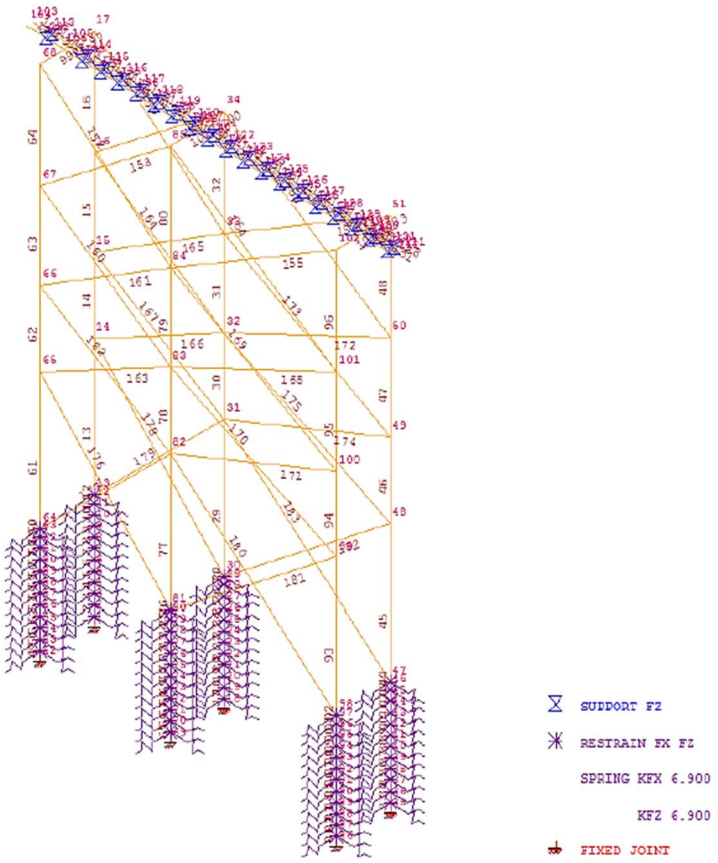


Figure 13 – West Wall Support Frame (North)

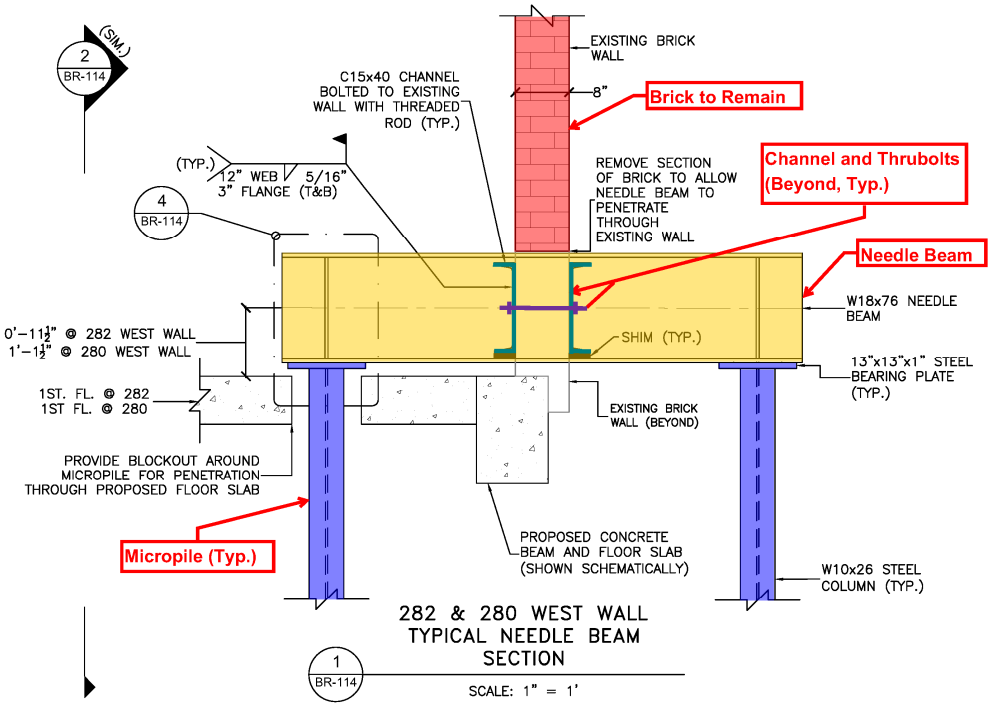


Figure 14 – Needle Beam and Channel "Clamp"



Figure 15 - Horizontal Diaphragms and West Wall Support (Post Demo)

SUPPORT OF EXCAVATION AND UNDERPINNING

Although not the focus of this paper, underpinning and support of excavation in order to construct the two cellar levels required up to 24 feet (7.30 meters) site-wide downward extension below grade required relatively deep braced underpinning of existing foundation walls, up to approximately 18 feet (5.50 meters) depth below the existing cellar floor. Due to the neighbor's refusal to allow underpinning an off-set support of excavation wall consisting of drilled-in micropile soldier piles and timber lagging was used along one side of the site to keep the excavation outside of the zone of influence of this challenging neighbor's foundation.

MONITORING

The Instrumentation monitoring program consisted of one Automated Motorized Total Station (AMTS) to monitor existing above ground structures and adjacent structures. The AMTS monitored up to 30 prisms that were affixed to the adjacent structures and structures being underpinned. Liquid level sensors were utilized to supplement the optical monitoring. Monitoring data was collected every hour on a 24/7 basis during the excavation and foundation installation process over an 18-month period. Settlement of the buildings being underpinned and adjacent structures within the zone of influence of the SOE was mostly negligible, with up to ½-inch maximum settlement in an isolated area.

SUMMARY AND LESSONS LEARNED

- This was a very complex project involving multiple teams (Architectural; Structural Geotechnical; Mechanical, Electrical, Plumbing; Code consultants; Contractors).
- This project had many design challenges associated with it:
  - Changes by architect / structural engineer
  - Changes due to legal issues (adjacent property owners)
  - Contractor proposed changes to design
  - Conflicts with other systems.
- Of significant consequence were the severe site limitations in constructing the horizontal diaphragms, vertical shear wall, and west wall support: Each member of portion of a member could not be more than 10 feet (3.05 meters) long, could not weigh more than 500 lbs. (226.8 kgs.), and needed to be intricately field measure (length, angle, orientation) by the steel fabricator on site prior to fabrication and delivery to the site (***Figures 8, 10, and 15***).
- Early and frequent coordination with steel fabricator to anticipate as many changes required and evaluate alternatives in a timely manner thereby reducing project delays.
- Contractor often stored material and miscellaneous items on the horizontal diaphragms (e.g. convenient shelf each 10 feet (3.05 meters) height). Accordingly, future designs include a higher vertical live load allowance.
- Due to potential for bolt misalignments and other unforeseen field conditions, more alternative welded connections were proactively prepared upfront to reduce delays.
- Due to observed misalignment for framing and micropiles, where possible, connections and members with increased capacity/tolerance for misalignment were designed (within reason).
- Coordination with other trades was crucial. There were bracing conflicts with other work which could have been noticed earlier if 3D modeling software such as Revit were used. The building industry is apparently moving toward Revit and other BIM technologies, so the various trades can coordinate permanent work to avoid conflicts. This modeling is costly and time consuming but depending on a cost benefits/time saving evaluation, we believe there is justification for using this technology in temporary works as well.

PERFORMANCE OF PILE FOUNDATIONS WITH INTERNAL DIAPHRAGM IN THE RED SEA FORMATIONS

Salwa Yassin, MICE, CENG, Ph.D, Geotechnical Consultant and Senior Geotechnical Engineer, Dar group Company, Cairo, Egypt, Salwa.Yassin@dar.com

ABSTRACT

The heterogeneous nature and characteristics of coral formations and carbonate deposits in the Red Sea present engineers with a unique challenge when designing pile foundations. Recorded pile load test results indicate that pile capacity tends to be overestimated when adopting the common soil mechanics and foundation design methods. This is mainly due to the inherent uncertainty and high variability in the engineering properties of such formations and their particular characteristics behavior. Consequently, adopting the appropriate type of deep foundations with limiting values for skin friction and end bearing based on pile load test results are the choice for more realistic and economic design. This paper presents a comparison between driving records for two open-ended test piles driven offshore, with an internal diaphragm, and their correspondence theoretical driving resistances estimated by GRLWEAP program.

Keywords: red sea, driven open-ended, internal diaphragm, inherent uncertainty

INTRODUCTION

Coral formations are typically found between 30^{o} N latitude and 30^{o}S latitude (Murff 1987), scattered in tropical seas, such as the Red Sea, northeast of Australia, the island of West Pacific Ocean and the Caribbean (Bermet and Ormond 1981). Based on their mechanical behavior, coral formations could be grouped under the carbonate formations (Harry 1999), and characterized by complex physical, chemical and engineering properties due to compositional and depositional characteristics (Tirant and Nauroy 1994). Although they differ significantly from one place to another, they share some common features (Semple 1988) such as compressibility which is attributed to a combination of porosity, irregularity and brittleness of particles, and could be changed erratically over short distances whether vertical or lateral. Such nature and variability presents serious difficulties in obtaining representative samples and complications in site investigation, and hence site characterization to an acceptable level of accuracy, which affect predictions of pile driveability and foundation behavior in general (Chaney et al. 1982, Datta et al. 1979, Nauroy and Titan 1983, Angemeer and Macmillan, 1982, Tirant and Nauroy 1994)

Different types of deep foundation have been adopted for the offshore structures such as bored, grouted, and driven (closed-ended and open-ended pipe piles). In general, pile driving in calcareous soils, particularly coral formations, presents a special problem and could be exceptionally costly if pile type is not well selected (Rausche and Hussein 1999). The current practice is to install driven open-ended piles which are easier to install than the closed-ended piles. For the projects reviewed by karlowskis (2014), the average driving time for open-ended piles was 9 minutes versus 26 minutes for closed-ended piles. Open-ended piles displace less soils, especially in granular formation where an end bearing is likely to be high and soil plug (if formed) could slide inside the pile (Carter et al. 1980).

Generally, driven open-ended piles provide about one fifth the geotechnical resistance as a similarly-sized bored pile. This is primarily due to crushing of soil particles (Murff 1987), which leads to lower unit skin friction along the pile shaft, and lower end bearing capacity due to incomplete plug formation.

The theoretical end bearing capacity of the soil at the pile toe level can be determined using the known procedures and soil mechanics theories, except that lower values of limiting strength along the shaft

© 2018 Deep Foundations Institute

and base are recommended. However, the actual end-bearing capacity of a pile will depend on the extent to which the available capacity is mobilized. If the available capacity is fully mobilized, then the actual end-bearing capacity of an open-ended pile will be substantially equivalent to that of a closed-ended pile having the same diameter (Vijayvergiva 1980).

Typical methods to ensure full plug formation are to drill out the soil column and set a grout plug, or to place a grout plug on top of the soil column inside the pile. However, these methods are time consuming and particularly expensive for offshore foundations. Alternatively, an internal diaphragm can be used to ensure the formation of a complete soil plug and, hence, full mobilization of end bearing capacity.

This paper presents a comparison between an in-situ driving records of two test offshore open-ended pipe piles with an internal diaphragm, located near the west coast of the Red Sea, and the theoretical driving resistance which was estimated using GRLWEAP program for drivability analyses.

PLUG FORMATION

When an open-ended pipe pile is driven, it could penetrate the soil in an unplugged or plugged manner (David et al. 2000). During driving, a soil column will be formed within the pile and upon loading, vertical stresses within the soil column will increase at an exponential rate, creating an increased lateral stresses on the pile wall, which in turn increases the inside skin friction at the pile wall. Once the inside skin friction becomes equal to or more than the vertical stresses developed during driving or pile loading, the soil column inside the pile will stop moving upward and the soil column will come to plug or lock-up (Vijayvergiva 1980 and Krlowskis 2014).

The formation of the soil plug and its behavior are influenced by many factors among which are: the pile installation method, applied load, rate of loading, the arching level inside the soil column, and the permeability of the soil column. All of these factors are difficult to determine, and the effects of each on plug formation or behavior are not satisfactorily captured by the existing design guidelines (Vijayvergiva 1980, Randolph 1985, Carter et al. 1980, Brucy *et al* 1991, De Nicola & Randolph 1997, Karlowskis 2014).

As suggested by Randolph (1985), when an open-ended pile is loaded and the soil column inside the pile is plugged or locked-up, the available capacity at the pile tip will most likely be fully mobilized in a full drained conditions. Drained conditions exist when pore water pressure within the soil column approaches the hydrostatic pressure level or alternatively, dissipates quickly. Accordingly, permeable soils are more likely to develop low pore pressure and, consequently, more prone to plug or lock-up and hence, the available capacity at the pile toe level will more likely to be fully mobilized during driving or in a short-term.

In undrained or partially drained condition, shear loads affecting the soil column will be carried partially or totally by water within the pores. The soil column tends to develop low vertical intergranular stress, which leads to low lateral stress on the pile wall. At this stage, the skin friction between the soil column and the pile wall may not increase enough to mobilize a soil plug, and the soil column may slip rather than plug.

SITE CONDITIONS

The two open-ended pipe piles considered in this paper are located in a close proximity to latitude 22.648083^{o} and longitude of 39.027743^{o}, near the west coast of the Red Sea. Site investigation comprised several offshore boreholes with drilling depth of up to 60 m below sea bed level. The recovered formations comprised random sequence laterally and vertically, of the following layers:

- Cohesionless coral detritus in the form of loose to very dense sand or silty sand,
- Clayey sand and silty gravel including various amounts of coral fragments.
- Very stiff to hard lean silty clay (very rare),
- Lean sandy clay and silt with occasional coral fragments.
- Coralline limestone recovered as fragments in the form of coralline sand and gravel.

The above random sequence of the recovered formations was a clear evidence of the heterogeneity of the coral formations in addition to the random variation of the recorded Standard Penetration Test (SPT) values. The recorded SPT blow counts ranged between practically zero and refusal in random sequence within the same borehole as well as in neighboring locations.

STATIC CAPACITY OF DRIVEN PILES IN CORAL FORMATIONS

There is a tendency towards a conservative design of pile foundation in coral formations due to the lack of a common design procedure for such formations and the poor foundation's performance recorded in several case histories (API 2005). However, the most common approaches used for pile design in coral formations are: (1) the beta method for friction and bearing factor for end bearing with limiting values suggested by Hangenaar (1982), (2) The beta method for friction and bearing factor with limiting values recommended in ARGEMA by Tirant et al. (1994), and (3) finally and most reliable, site specific load test results.

For ARGEMA approach (Tirant et al. 1994), the suggested limiting values for skin friction and end bearing are evaluated through a correlation with compressibility limit, which was not covered in the site investigation programme. Therefore, method 1 was cautiously applied for the theoretical assessment of the pile capacity. It should be mentioned that the theoretical pile capacity was assessed mainly for drivability analyses and not for pile toe level determination.

The recorded SPT (i.e. zero to refusal) gave high variability coefficient as anticipated. However, a characteristic SPT value of 30 (medium dense sand with silt) was adopted in the design. According to Hangenaar (1982 and 1984), a limiting skin friction of 20 kPa, bearing capacity factor (Nq) of 12, and an averaged limiting end bearing of 4 MPa was adopted to determine the static capacity of the two open-ended piles. Accordingly, a penetration depth of 18.0 m into coral formations was initially suggested for the tested piles, with an internal diaphragm to be installed at that height measured from the pile toe level. However, an allowance for additional penetration depth of 5.0 m was made to ensure an adequate quantity of granular soils for the development and engagement of the soil plug. The final penetration into the coral formations becomes 23 m, and the full pile length (free height, water, sea formation) was approximately 34 m long as shown in Fig. 1.

Using the above design parameters, limiting strength values, penetration length and submerged unit weight of 8 kN/m^3 for coral formation, an ultimate pile capacity of approximately 2600 kN was calculated for a pipe pile with a diameter of 914 mm and wall thickness of 19 mm.

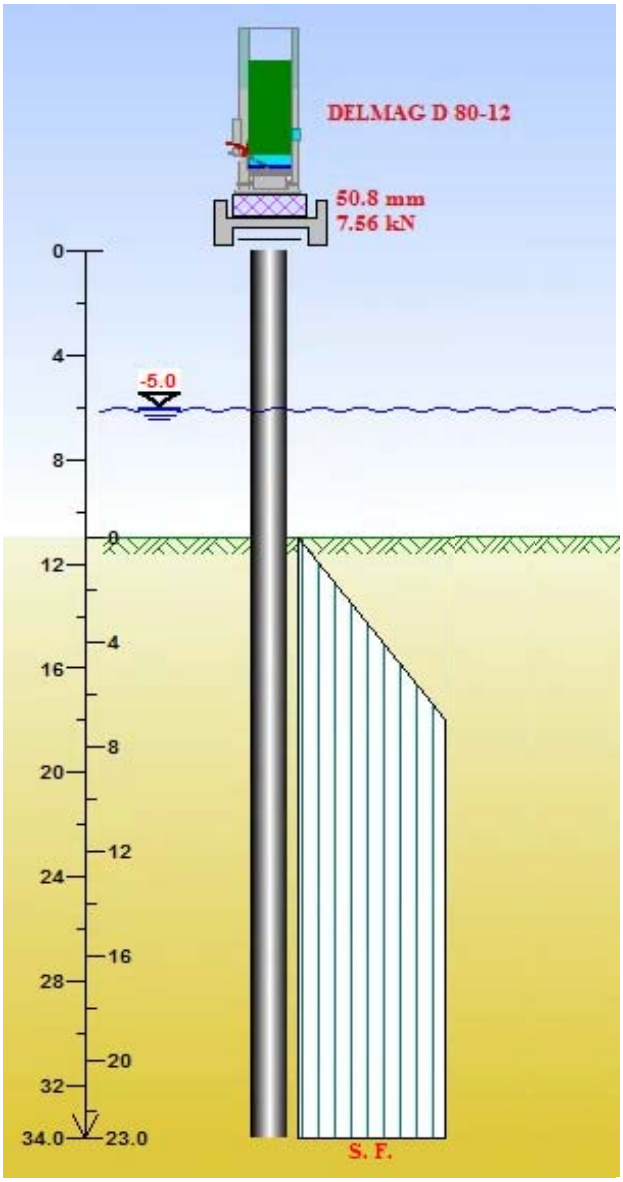


Fig. 1. Pile driving system and penetration depth

DRIVABILITY ANALYSES

Drivability analysis was performed based on the wave equation concept developed by Smith (1960), which is often used to determine the driving stresses, not predicting pile capacity (Bowles 1997). The analyses were carried out using GRLWEAP program version 10 (Goble et al. 1997), which models the pile driving system (hammer, helmet, and cushion), pile (series of masses, springs and dashpots) and soil (series of elastic-plastic springs and linear dashpots).

The configurations of the driving system are shown in Fig. 1, with the properties of the use hammer on site (Delmag D 80-12). The outputs of the analyses represented in a bearing graph and a drivability analyses–ultimate capacity graph are shown in Figs. 2 and 3, respectively.

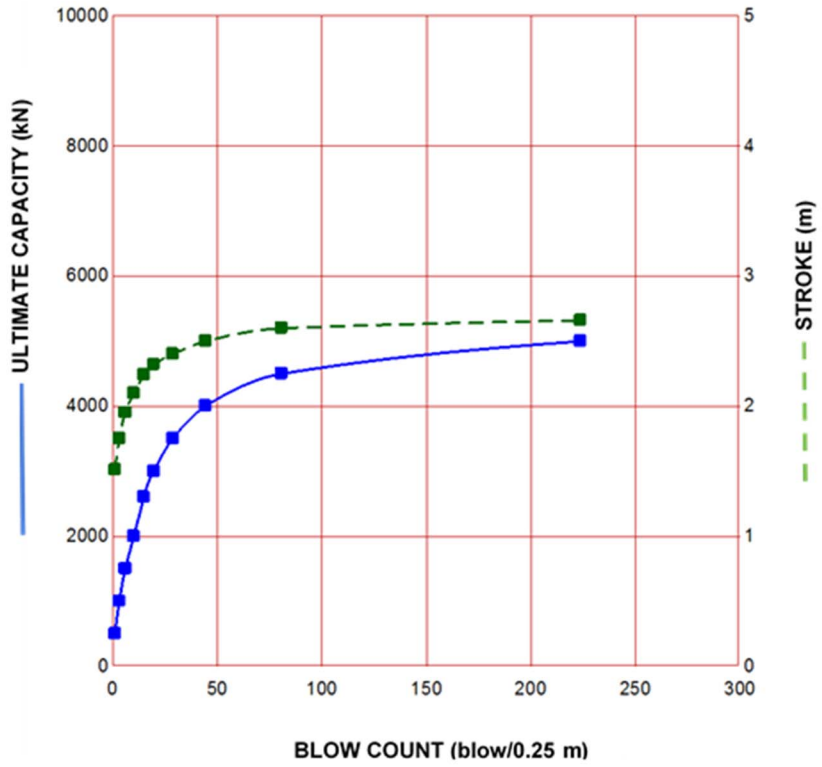


Fig. 2. Bearing graph (ultimate capacity/blow count)

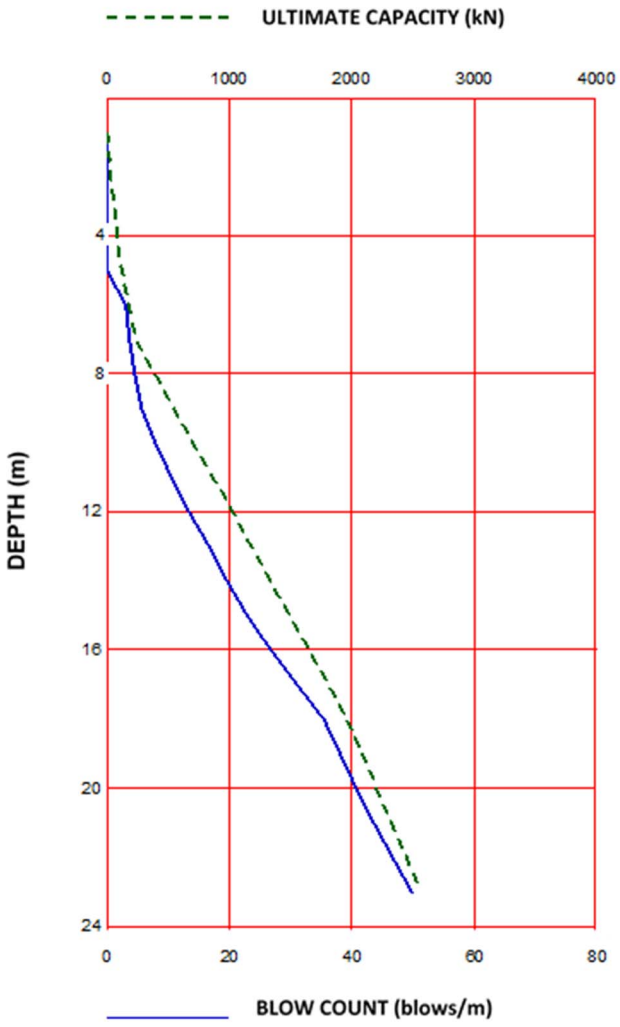
Bearing graph is normally used to identify a pile capacity for a certain blow count or vice versa (Goble et al. 1980). However, using the bearing graph to relate between the pile capacity and the blow counts should be exercised with a reasonable amount of caution. This is due to the fact that, its accuracy is a function of the accurate representation of field conditions and soil strength that have been modeled during analysis (Hussein et al. 2003).

According to Fig. 2, the corresponding blow counts to the calculated ultimate bearing capacity of the pile is 15/0.25 m. As per Fig. 3, blow count of 12.5/0.25m (with total blow counts of 422) corresponds to approximately the same ultimate bearing capacity. However, this difference between the two figures in blow counts was accepted by the author, especially for drivability purposes.

IN-SITU DRIVING RECORD

The two test piles considered in this paper, were driven almost 10 m apart with a difference in the sea bed level of approximately 0.4 m and actual penetration depths of 23 and 22.8 m respectively. The refusal criteria for pile driving were set to a minimum penetration of 23 m into the coral formation and a minimum blow count of 50/1 m penetration. The in-situ driving records for the two piles are shown in Figs. 4 - 5 for test pile 1 and 2, respectively.

Figures 4 - 5, show clear increasing rate in the driving blow count starting from 18 m depth onwards for both piles (i.e. With the engagement of the internal diaphragm).



Depth m	Ultimate Capacity kN	Friction kN	End Bearing kN	Blow Count blows/m
1.0	9.2	4.1	5.1	0.0
2.0	26.7	16.4	10.3	0.0
3.0	52.3	36.9	15.4	0.0
4.0	86.1	65.6	20.5	0.0
5.0	128.2	102.5	25.6	0.0
6.0	178.4	147.7	30.8	3.2
7.0	236.9	201.0	35.9	3.7
8.0	394.1	258.4	135.7	4.5
9.0	551.3	315.8	235.5	5.8
10.0	708.5	373.2	335.3	8.0
11.0	865.8	430.6	435.1	10.7
12.0	1023.0	488.1	534.9	13.5
13.0	1180.2	545.5	634.7	16.7
14.0	1337.4	602.9	734.5	19.8
15.0	1494.7	660.3	834.3	23.0
16.0	1651.9	717.8	934.1	26.8
17.0	1809.1	775.2	1033.9	31.1
18.0	1966.3	832.6	1133.7	35.6
19.0	2086.7	890.0	1196.7	38.1
20.0	2207.1	947.4	1259.7	40.8
21.0	2327.5	1004.8	1322.7	43.6
22.0	2448.0	1062.3	1385.7	46.6
23.0	2568.4	1119.7	1448.7	50.0

Fig. 3. Driveability analyses- ultimate capacity

The figures also show an increase in the actual recorded blow counts for both piles than theoretically calculated for both piles. This increase, however, in addition to confirming a full mobilization of base resistance, was credited to the following reasons:

- The initial value of the end bearing factor was considered as 20 corresponding to the medium dense condition. However, with the advancement of the open-ended pile, less disturbance of the soil was anticipated until the engagement of the internal diaphragm and full formation of soil plug. From that point onward, densification in the soil formation around and beneath the pile toe level should have been anticipated and an allowance for a higher end bearing factor should have been considered in the design.
- An allowance, for a higher value of coefficient of lateral earth pressure (i.e. Ks to be 1 instead of 0.8) should have been made when calculate the initial theoretical shaft resistance, at least along the lower part of the pile shaft, i.e. with the commencement of the internal diaphragm engagement at a depth of 18.0 m.

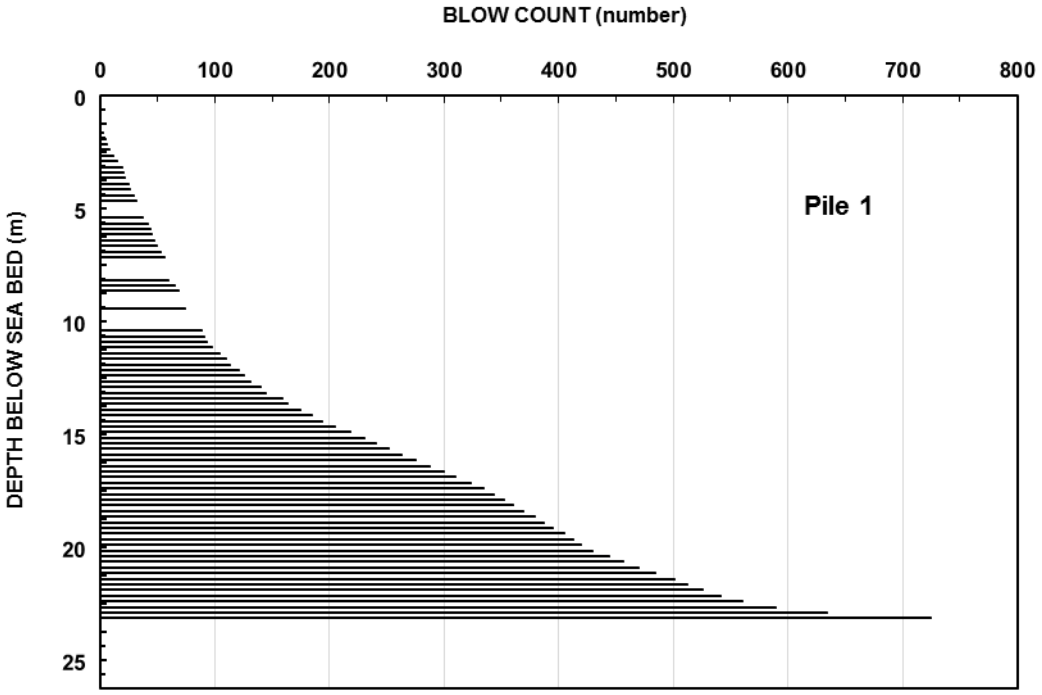


Fig. 4. Recorded blow counts for Pile 1

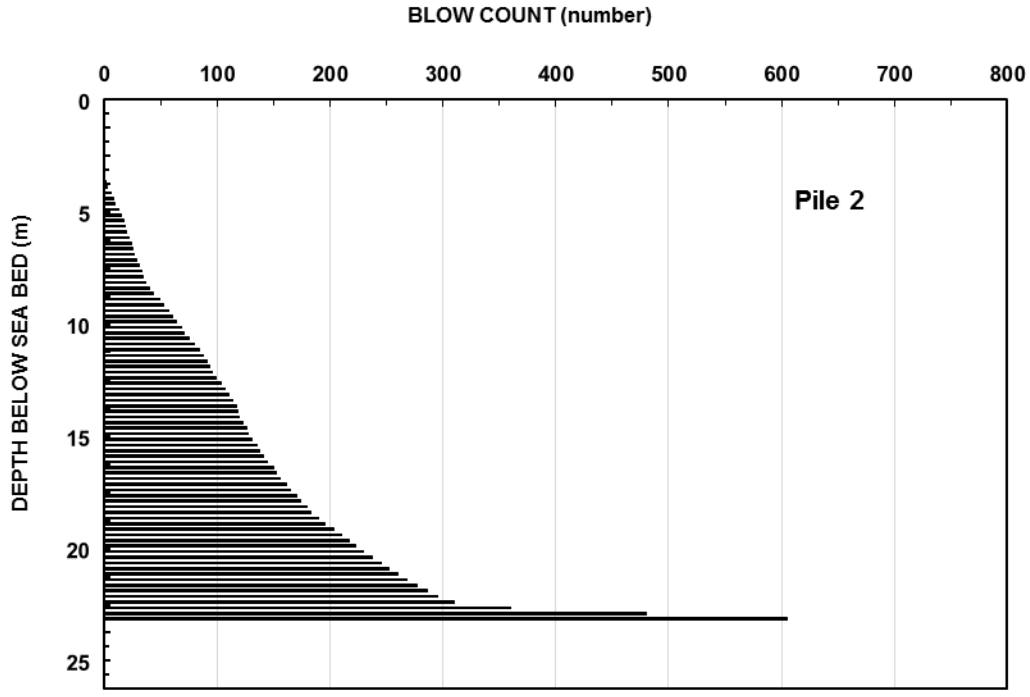


Fig. 5. Recorded blow counts for Pile 2

CONCLUSIONS

This paper presents the actual driving record of two open-ended test piles with internal diaphragm, driven offshore in the coral formations near the west cost of the Red Sea. A comparison between the actual driving records and the drivability analyses was also made.

Theoretical bearing capacity of the open-ended piles was evaluated using the limiting values published by Hangenaar (1982 and 1984) for end bearing and skin friction. The internal diaphragm was used to ensure the formation of the soil plug and hence full mobilization of the end bearing component, while benefiting the easiest installation of an open-ended pile. An internal opening of 100 mm was introduced in the middle of the internal diaphragm to ensure and expedite the drained condition for the inside soil column during pile driving (especially for cohesion-less and permeable formation) or static loading.

The actual driving records for the two piles revealed a higher blow counts than estimated during drivability analyses due to the reasons discussed earlier. Accordingly, effect of construction process on formations behavior and design parameters, whether softening or densification as in the current case, should be carefully investigated and considered from the initial design stage,

Based on the results presented here, it can be fairly concluded that by adopting the appropriate foundation type and design method in coral formations, significant improvement in the project budget and construction time took place by eliminating the need to drive longer or additional piles. However, in general, it is worth mentioning that, an adequate and comprehensive site investigation programme, mainly, with compressibility index measurement, should be adopted in coral formation. This would increase the understanding of coral formation behavior and enhance the accuracy of site characterization. More importantly, it would allow trying different design methods, for comparison, before deciding on the most suitable method and design parameter.

REFERENCES

Angemeer, J., and McNeilan, T.W., 1982. Surface variability- the key to investigation of a coral atoll. Symposium of Geotechnical Properties, Behavior and Performance of Calcareous Soils, ASTM, Special Technical Publication STP 777, ASTM, Philadelphia: 36-52.

American Petroleum institute, API, 2005. Recommended practice for planning, designing, and constructing fixed offshore platforms-working stress design.

Bowles, J.E. 1997. Foundation analysis and design. 5th edition, McGraw Hill International editions.

Brucy, F., Meunier, J., and Nauroy, J.F., 1991. Behaviour of a pile plug in sandy soils during and after driving, Proceedings of the Offshore Technology Conference, Houston, Texas, OTC6514:145-154.

Carter, J.P., Randolph, M.F. and Wroth, C.P. 1980. Some Aspects of Performance of Open- And Closed-Ended Piles, Proceedings of the conference on numerical methods in offshore piling, Institution of Civil Engineers. Numerical, ICE, London, pp. 165- 170.

Chaney, R.C., Slonim, S.M., and Slonim, S.S.1982. Determination of calcium carbonate content in soils. Symposium of Geotechnical Properties, Behavior and Performance of Calcareous Soils, ASTM, Special Technical Publication STP 777: 3-15.

Datta, M, Gulhati, S.K., and Rao, G.V., l979. Crushing of calcareous sands during shear. Proceedings, Eleventh Annual Offshore Technology Conference, Houston, Texas, pp. 1459-1467.

David, j.W., Haramrita. K.S., Tim, c.R., Malcolm, d.B., and Teruo, N., 2000. Press-in piling, the influence of plugging on driveability. 8th international conference of the deep foundations institute, New York, pp. 299-310.

De Nicola, A. and Randolph, M. F., 1997. The plugging behaviour of driven and jacked piles in sand, Geotechnique, 47(4), pp. 841-856.

Hangenaar, J. 1982. The used and interpretation of spt results for the determination of axial bearing capacities of piles driven into carbonate soils and coral. Proceeding of 2nd Euro Symposium on Penetration Testing, Amsterdam.

Hangenaar, J. Sijtsma, H. and A. Wolseger, A. 1984. Selection and use of piles for marine structures in coral formations and carbonate sediments. Piling and Ground Treatment Journal, pp. 77-86.

Harry J.k., 1999. Deep foundation in calcareous sediments. Proceeding of The Second International Conference on Engineering For Calcareous Sediments, Bahrain.

Hussein, M.H. Bixler, M. and Rausche, F., 2003. Pile driving resistance and load bearing capacity (Resistencia Al Hincado y Capacidad Portante en Pilotes). 12th Pan-American Conference on Soil Mechanics and Geotechnical Engineering, Cambridge, MA, pp. 1817-1823.

Murff, J.D. 1987. Pile Capacity In Calcareous Sand: State of The Art, Journal of the geotechnical Engineering Division, ASCE, Vol. 113 (7), pp. 490-507.

Nauroy, J.F. and Le Tirant, P. l983. Model tests of piles in calcareous sands. Proceedings ASCE Conference on Geotechnical Practice in Offshore Engineering, University of Texas, Austin, pp. 83-91.

Tirant, P.L and Nauroy, J.F. 1994. Design guides for offshore structures- foundations in carbonate soils, club des actions de recherché sur les ouvrages en mer (CLAROM) or Club for Research activities on offshore structure and Association de Researche en Geotechnique marine (ARGEMA).

Randolph, M.F., 1985. Capacity of piles driven into dense sand. Presentation to the XI International Conference of Soil Mechanics and Foundation Engineering, San Francisco.

Rausche, F. and Hussein, M., 1999. Pile driving in calcareous sediments. Proceeding of the Second International Conference on Engineering For Calcareous Sediments, Bahrain.

Semple, R.M., 1988. The mechanical properties of carbonate soils. Proceeding International conference on calcareous sediments, Perth, Vol. 2, pp.807-836.

Smith, E.A.L., 1960. Pile-driving analysis by the wave equation. Journal of the Soil Mechanics and Foundations Division, ASCE, 86 (1), pp. 35-61.

Karlowskis, V., 2014. Soil plugging of open-ended piles during impact driving in cohesion-less soil. Master of Science Thesis, Stockholm, Sweden,14/13, royal institute of technology (kth), department of civil and architectural engineering, division of soil and rock mechanics.

Vijayvergiva, V.N., 1980. Soil response during driving. Proceedings of The Conference on Numerical Methods In Offshore Piling, Institution of Civil Engineers, ICE, London, pp. 53- 58.

RECENT INNOVATIONS TO FACILITATE THE CONSTRUCTION OF LARGE DIAMETER PILES IN LONDON

Yue Ouyang, Project manager, Cementation Skanska, Denham Way, Maple Cross, Rickmansworth, Hertfordshire, U. K., Phone: +44 (0)330 050202, Email: Yue.Ouyang@gmail.com.

Paul Wiltcher, Operations Director, Cementation Skanska, Denham Way, Maple Cross, Rickmansworth, Hertfordshire, U. K., Email: Paul.Wiltcher@skanska.co.uk.

ABSTRACT

The economic regeneration of London South Bank area requires a better transportation network for local business and residential communities. As a part of the transformation plan, London Underground's Northern Line was proposed to extend into Nine Elms and Battersea with the requirement for two additional stations. This paper discuss the recent innovations adopted in foundation construction for Battersea station, to manage challenges in delivering the project. A trial pile, supported by polymer slurry, was constructed prior to the main piling work. This helped to build up the knowledge and confidence to construct the largest piles to be supported by polymer fluids in the UK. The paper also includes the successful use of Distributed Temperature Sensing (DTS) technology in assessing the integrity of the pile as well as capturing the dynamic tremie concrete rise.

Keywords: Large Diameter Rotary Pile, Polymer Support Fluid, Distributed Fibre Optic Sensor, Distributed Temperature Sensing

INTRODUCTION

Northern Line Extension to Battersea station is one of major construction projects for extending London Northern Line from Kennington to Battersea. There are two underground stations to be built at Battersea Power Station and Nine Elms which will serve a new embassy district for US and Dutch Embassies, the local community as well as the new commercial and residential redevelopment at Battersea Power Station (Fig. 1). The project will generate up to 25,000 jobs and 20,000 new homes within the local communities. This will reduce the journey time from Nine Elms or Battersea to the City to less than 15 mins, which means that it could generate substantial benefits to the area.

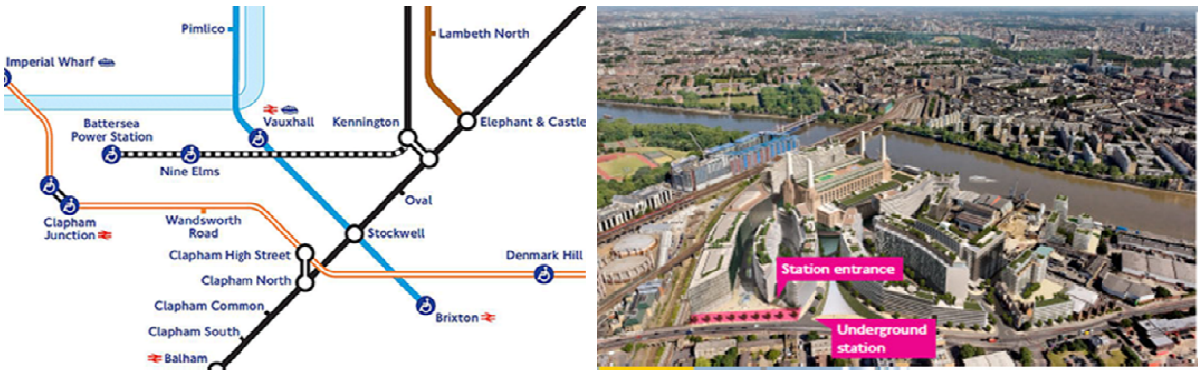


Fig. 1. The Overview of Northern Line Extension Project and Battersea Power Station.

Battersea station as a part of the Northern Line Extension project is formed by two separate but connected diaphragm walled box structures as shown in Fig. 2. The station box contains the station entrance, ticket hall, platforms and premises and services or tunnel ventilation. The cross-over box contains a track crossover at the entry point to the station platform, an LU substation, and tunnel ventilation shaft serving the eastern end of the station and running tunnels.

© 2018 Deep Foundations Institute

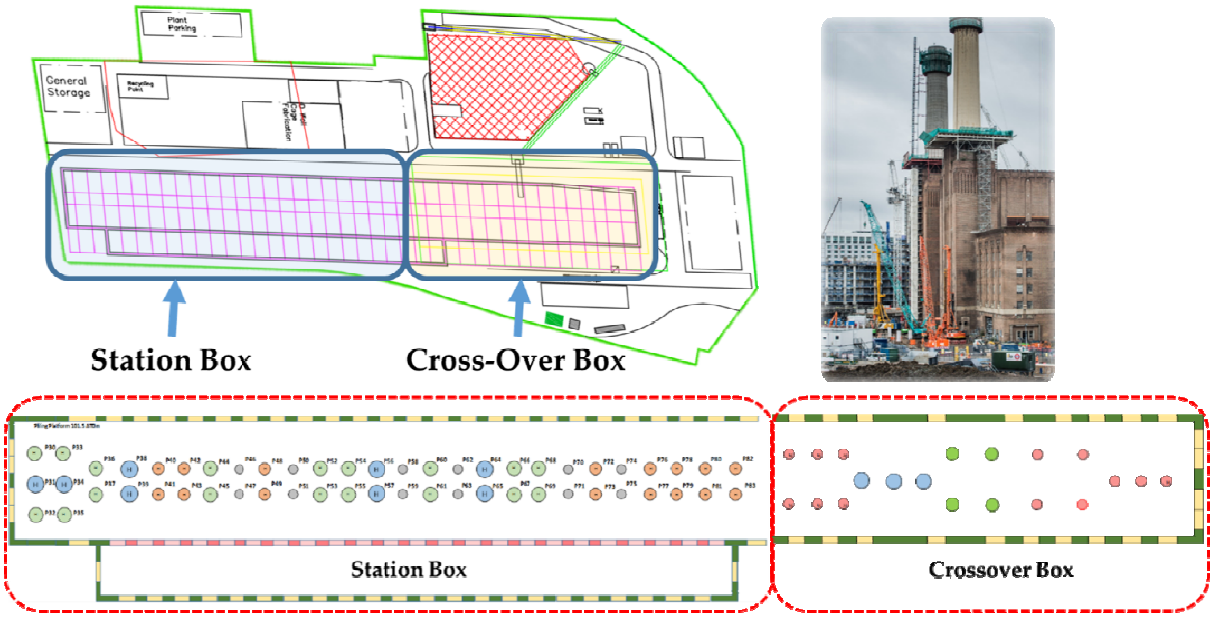


Fig. 2. The site layout with detailed construction elements.

The scope of work includes the construction of Large Diameter Piles (LDP) under the polymer support fluid, plunge columns were installed as well to enable top-down construction. As the piling project was carried out concurrently with the Diaphragm wall (D-Wall) panel construction, it posed huge challenge in operating piling work independently, however, also dependent on all site activities. This paper is going to provide a different perspective of managing the LDP project by adopting several innovative approaches.

PILING SCHEME.

SITE LAYOUT AND SCOPE OF WORK

The site layout of NLE project shown in Fig. 2 shows the main construction work was split into two phases for construction the Cross-Over box as well as the Station Box at different stages. The main scope of LDP piling included:

- 74 no. bearing piles, 1500 mm to 2400 mm in diameter installed from crossover box and station box area in two phases.
- 49 no. piles with plunge columns. These piles contain 'H' steel beams which were accurately plunged and cast into the pile in order to allow the 'top-down' construction of the basement simultaneously with the construction of the superstructure.
- The use of CemOptics for thermal integrity testing of all pile elements as an alternative to conventional Cross-Hole Sonic Logging (CHSL) system.
- The use of polymer support fluid as an alternative to bentonite.

GEOLOGY

The site investigation shows that the underlying geology on site consists of River Terrace Deposit overlying London Clay. The site encountered a hard band of approximately 4 m of Swanscombe group from Hardwick Formation above the Lambeth Group, and the piles are found in Thanet Sand as shown in Table 1.

Table 1. Site investigation the details of ground condition

Soil strata	*Thickness*
River Terrace Gravel	*0m - 5m*
London Clay	*5m – 38m*
Swanscome (Hardwick Formation)	*38m – 42m*
Lambeth Group	*42 m – 54m*
Thanet Sand	*54m – 60m*

PILE CONSTRUCTION

Although the construction of D-wall governed the critical path of the project, the piling construction sequence was required to optimise the use of the piling rig on site in assisting excavation for D-Wall panel construction. Therefore it was important to understand the sequence/time required to construction a LDP on site. The LDP construction sequence for piles with different diameter is summarised in Fig. 3, which accounts for the excavation and the polymer slurry flooding time required for each pile type. Typically the casing would often be installed in advance of excavation to support the open-bore. It allows the further excavation using flight auger in stiff clay material, then the digging bucket and cleaning bucket were used after the bored hole is flooded by polymer slurry. This sequence also reflected the averaged excavation performance on site that the concreting process needed to start within 12 hours after excavating the final 1 m of Thanet sand.

	1.5 m in Dia. Pile Construction Time	1.8 m in Dia. Pile Construction Time	2.1 m in Dia. Pile Construction Time	2.4 m in Dia. Pile Construction Time
Inadvance of Day 1	Install casing	Install casing	Install casing	Install casing
Day 1	Bore pile from underside of casing to 42 mATD	Bore pile from underside of casing to 42 mATD	Bore pile from underside of casing to 42 mATD	Bore pile from underside of casing to 42 mATD
Day 2 (Overnight or Over a weekend)	Final 1 m Install Cage Concrete the pile	Final 1 m Install Cage Concrete the pile	Excavate pile to 1m above pile toe	Excavate pile to 1m above pile toe
Day 3 (Overnight or Over a weekend)			Final 1 m Install Cage Concrete the pile Install plunge column	Final 1 m Install Cage Concrete the pile Install plunge column

Fig. 3. Construction sequence of piles with different diameters.

POLYMER SUPPORT FLUIDS

One of challenges was the selection of support fluid. Bentonite slurry was used on site to support the excavation of D-Wall panels. The use of bentonite for LDP construction would potentially increase the maximum storage capacity of bentonite to approximately 1700m^3 in order to ensure the concurrent operation of both activities on site. It also impose risks of managing the bentonite plant on site in balancing the potential plant break-down and the operational demand. After initial technical review about polymer slurry, the project proposed to use polymer slurry as an alternative to bentonite slurry. This can alleviate the demand from bentonite plant, and increase the operational efficiency. In order to confirm the proposal for polymer fluids, a trial pile was proposed to verify the performance of polymer slurry in supporting the excavation of a 60m long pile.

TRIAL PILE SUPPORTED BY POLYMER SLURRY

As the original LDP design was based on the bentonite fluid, there are potential risks of using a polymer fluid due to the lack of operational experience as well as understanding the operational requirements. These two types of fluids operate under different principles:

- bentonite fluid would act as a heavy fluid in the borehole to stop the ingression of ground water in simple terms,
- polymer fluids are designed to form a surface film to reduce the fluid loss (SPERW, 2017).
- There are potential technical benefit in using polymer slurry as Lam, et al. (2014) found that polymer fluids improved the pile performance by increasing shaft resistance.

This trial pile was only planned to verify its operational performance and confirm the testing regime for quality control and management throughout the project. This construction of the trial pile took three days in total which represented the scenario of constructing the largest pile with an extended slurry supporting period (typically over weekend supporting period or unforeseeable events on site). The key learning points can be summarized as follows:

- Mixing of polymer slurry.

It is important to test the local water supply at the beginning of the project. Whilst commissioning the plant at the trial pile phase, it was found that the local mains water had sufficiently high levels of calcium and magnesium (hardness) to reduce the performance of the PHPA based polymer (Jefferis, et.al., 2017). Polymer molecules were unable to achieve the targeted viscosity as required with the prescribed ‘recipe’ by the supplier, where the viscosity is the main indicator of active polymer in the fresh polymer. In the water treatment tank, a small amount of sodium hydroxide was added to the mains water to raise its pH to 10.5, a sufficiently alkaline environment for the development of the polymer properties. One of mixing tanks on site was then fully dedicated to pre-treat the local water with pH value to 10.5 prior to the mixing process. It also brought potential saving which reduced the requirement of main polymer products by 50%.

- Testing regime for polymer slurry on site

There were four types of tests were carried out on site to monitor the quality of polymer fluids similarly to bentonite fluids as shown in Fig. 4, however, the density test was replaced by a bespoke digital weight scale and pycnometer. Typically the concentration of polymer required to produce the competent support fluid is around 0.5 to 2 kg/m3, whereas the concentration required for bentonite fluids would be 20 to 60 kg/m3. The conventional mud balance which were commonly used for measuring bentonite fluids would not be able to provide accurate measurement to assess the density of polymer fluids as discussed by Jefferis, et.al., (2017). It was challenging to find the correct type of pycnometer to ensure the correct quantity of polymer as it was very challenging to sample the exact

quantity of viscous ‘long-chain’ type of PHPA polymer slurry in site environment. The use of digital weight scale and pycnometer has been a success to measure quality of polymer throughout the project.

The full sets of tests were carried out at the end of the first day after excavating the pile to 1m above the pile toe. Three polymer samples were collected from the pile base, middle and top in order to understand the stratification of sand content and fluid density, where the viscosity and pH of the fluids would likely to be consistent. It was found that there were slight variation between samples collected from pile base and middle section, but samples collected from top and middle sections of the pile showed similar results. On the second day, polymer samples were collected and tested from three positions along the pile, and the full sets of tests repeated after the pile was excavated to the full depth, these results will be discussed in (Ouyang, et al., 2018). The trial pile construction provided the opportunity to confirm the testing regime in managing the quality of polymer fluid, and the testing scheme were later incorporated in SPERW (2017).

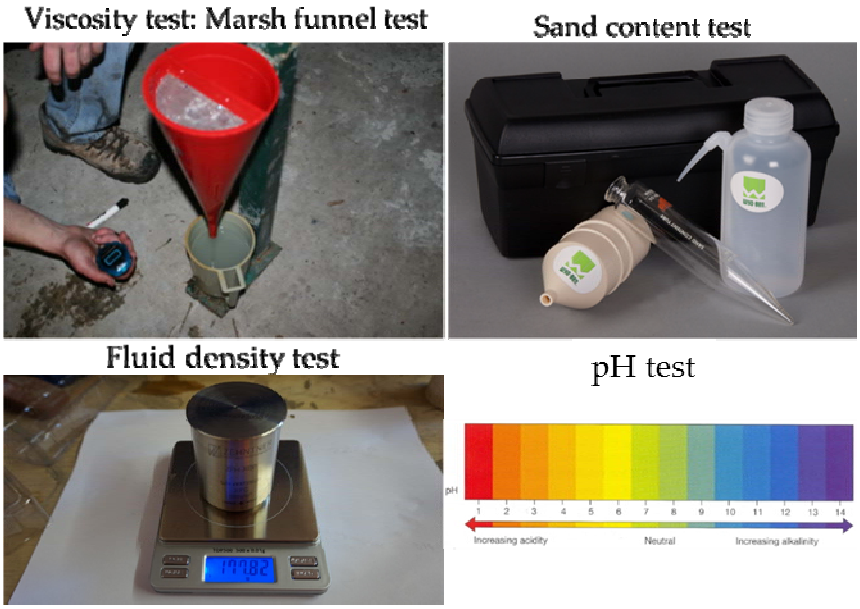


Fig. 4. On-site polymer test

- Operation experience

In addition to confirming the performance of polymer fluids, the trial pile also offered the opportunity for the rig operator to gain confidence in excavation. As high viscosity fluid under low shear conditions tends to slow the settlement of cuttings in suspension, the physical excavation with different digging tools and rate would directly impact in introducing cuttings into the slurry system with high sand density. It requires the rig operator to understand the difference between two types of fluids, and collectively helping in controlling the quality of polymer fluid throughout the operation process.

THE USE OF THERMAL INTEGRITY TESTING SYSTEM

The use of distributed fibre optic sensing technology has gain wider acceptance in the past decades for monitoring embedded structure elements, as summarised by Ouyang et al., (2015). The concept of using temperature development during cement hydration period for assessing the integrity of the cast-in-place infrastructures was developed in early 2000s in the US by G. Mullins & Kranc, (2007) & Gray Mullins, (2010). The main advantages of using the distributed fibre optic sensor can be summarised as,

1. Distributed fibre optic measurement can be obtained along the pile shaft, which covers the 'blind-zone' comparing with the conventional 'point-wise' sensing system,
2. Easier to install on site with no manual handling at the connections between two cage sections,
3. Improving the health and safety standards during installation by attaching the fibre cable to outside reinforcement cage,
4. Providing further understanding about the concrete flow patterns during concreting phase.
5. Providing the effective assessment of integrity within 48 hrs.

Distributed Temperature Sensing (DTS) system has been widely used in the industry for detecting temperature change over long distance in oil and gas industry for detecting the long term temperature change along pipeline, power cables (Glisic, et al., 2000; O'Donnell et.al., 2015; Ouyang, et al., 2017). The DTS utilises back-scattered signal to detect localised changes in temperature along the sensing cable. The backscattered signal often include three main components as: Rayleigh, Raman and Brillouin with stokes and anti-stokes. The stoke and anti-stoke components for Raman and Brillouin spectrum lies on two sides from Rayleigh spectrum and the relative change in the stoke and anti-stoke components from Raman and Brillouin spectra forms the assessment for change in strain and temperature reported from a point along the sensing cable. Raman spectra differ from Brillouin spectra by having a fixed frequency but variable intensity, where the assessment of change in temperature can be quantified. The system employed for thermal integrity assessment for the current application adopts the Raman back-scatter sensing principle. The DTS system can be used to measure spatial and temporal variability at a high resolution along one sensing cable over long distance, which provides huge advancement to most conventional point sensor.

The system contains one data collecting unit, Opthermo FTR3000X from Sumitomo electric industries. It offers the maximum optimum sensing range of 5 km together with an 8 channel optical switch to increase the logistic capacity of monitoring multiple panels and piles on site and avoid any possibility to lose data. The system was placed on site throughout the testing duration and fibre optic cable were connected immediately after the reinforcement cage installed to capture the concrete flow patterns as well as assessing the thermal integrity of the pile.

CONCRETE FLOW DURING TREMIE PROCESS

In the case of a pile is excavated under the support fluids, the typical construction technique is to use the tremie technique placing the concrete from bottom of the pile. The tremie would extend to the bottom of the pile. Vermiculite will then be poured down the tremie to create a plug and form a separation barrier between the concrete and the polymer. After filling the hopper with concrete the whole tremie pipe was charged by slightly raising it, allowing the concrete to flow down the hopper at a controlled and continuous rate, and the tremie would be kept topped up with concrete during the discharging process.

EFFC/DFI (2016) explains that it is still a challenging issue in understanding the upward flow pattern of concrete from the downward flow through the tremie into a large diameter hole together with the pattern of displacing the supporting fluid. Generally, after the initial spreading of concrete over the area of the bore, the upward force of the flow will gradually reduce from centre to the periphery. As a result, a heap of concrete will be created centrally around the tremie pipe. This cone diminishes gradually based on various parameters such as the embedded tremie depth in concrete, concrete height, the concrete mix design, etc. This paper is not intended to reveal these details, but offers a possible solution to review the dynamic rise of concrete head captured by DTS system.

As the fibre optic cable was connected prior to the start of concreting process as shown in Fig. 5. The average temperature of polymer fluid in the bored hole was close the ambient temperature at approximately 18 ^{0}C, the concrete placed in the bored hole varies between 22 ^{0}C to 25 ^{0}C. This provides the opportunity to capture the dynamic concrete head rise from six locations where the fibre

optic cables were attached to the reinforcement cage. Fig. 5(1) shows the averaged heat development together with the field recorded concrete head rise as shown in the black line at the end of each concrete pour. The steps shown in the black line indicate the duration of each concrete pour process, however, the DTS measurement indicates more accurate concrete head rise. The recorded concrete rise by fibre optic cable shows the agreeable match with the recorded measurement from the weighting tape shown in the black line in Fig.5 (1).

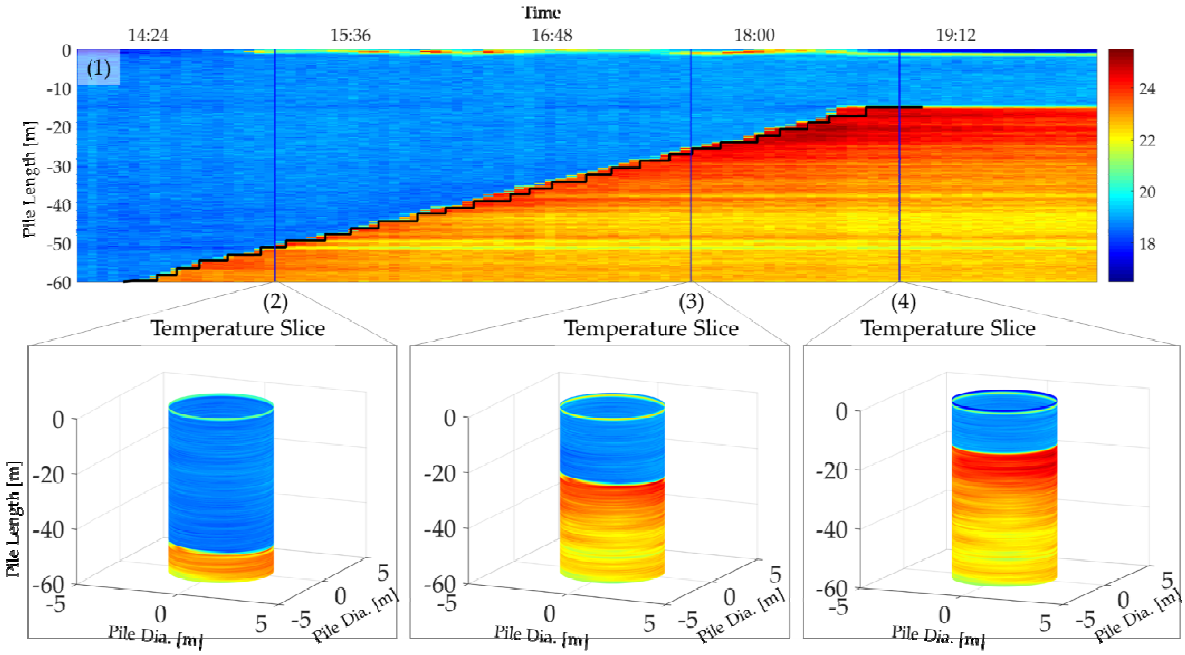


Fig. 5. The temperature development during concrete pouring process with three temperature slices from selected time. (1) The average temperature measurement taken at six locations around circumference of the pile, (2-4) Temperature slices at different concrete stages.

The temperature was measured at six positions with equal distance around the circumference of the pile as indicated in Fig. 7. We are able to interpret temperature around the circumference of the 2.4 m diameter pile are shown in Fig. 5 (2-4) at three selected phases, where the concrete head between concrete and polymer are highlighted by the temperature between these two types of fluid. The concrete head were found to rise at similar level throughout the concreting process, Fig. 5 (3&4) indicates that there are slight temperature variation between different batches of concrete, where recorded temperature shows slightly higher temperature in the top 7 m than the concrete placed in the pile. As the minimum and maximum required embedded tremie length was between 3.0 m and 6.0 m, it is likely that the fresh concrete was placed at the top. The concrete temperature experiences a slight reduction after being placed in the hole before the temperature rises caused by the cement hydration, which indicates that heat dissipate to the ground after being placed.

CHARACTERISTIC OF TEMPERATURE DEVELOPMENT

The temperature development over the initial 60 hrs is shown in Fig. 6 with highlighted monitoring period of 24 hours and 48 hours. The cement hydration process started at approximately 6 hours after the concrete placement. Temperature increased from 23^{0}C to 40^{0}C within the first 24 hours, where the rate of temperature decreases before achieving the maximum temperature at 44^{0}C. Temperature measurement indicates that the majority of the heat is developed in the initial 24 hours and the rate of heat development reduced between 24 hrs and 48 hrs, where the maximum temperature was achieved after 48 hrs as shown in Fig. 6. As the integrity assessment was based on the heat generating period during the cement hydration process, Fig. 6 demonstrated that the majority of the heat has been generated during the initial 48 hrs period with the maximum temperature change along the pile shaft.

Baran & Pichniarczyk, (2017) suggested the correlation factor between heat of hydration and compressive strength based on 200 samples from industry commonly used cements produced in different manufacturing plants. As the change in temperature correlated proportional with the heat generated during the cement hydration process, the in-situ temperature measurement from the 2.4 m diameter pile reported similar a group of samples collected which accumulated 80% of the strength which equivalent to 44% of concrete cube strength from the 28 hrs data as reported by Baran & Pichniarczyk, (2017). It highlight the potential for further research to correlate the in-situ temperature measurement with the concrete strength.

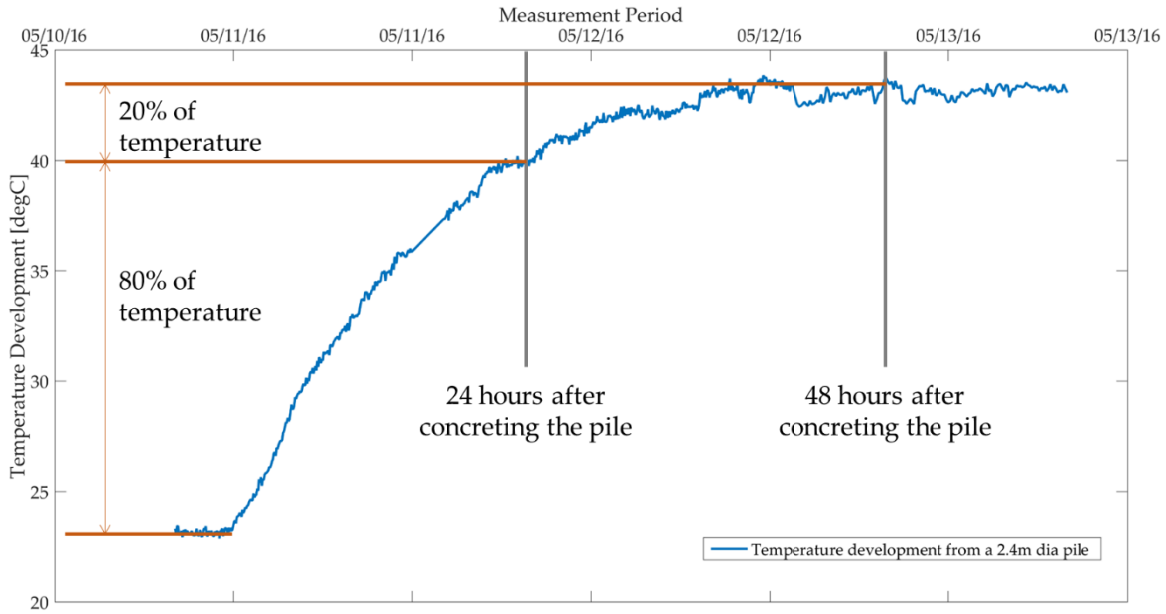


Fig. 6. Temperature development of a 2.4 m diameter pile from the initial 60 hours.

THERMAL INTEGRITY ASSESSMENT

Temperature measurement along the pile shaft from six positions are reported in Fig. 7 with the change in temperature by offsetting with the initial concrete temperature prior to the commencement of cement hydration. The temperature profile is also compared with the geology condition recorded during the pile excavation, which agrees in general with the Table 1. The temperature reported from six positions agrees along the pile shaft with the average temperature highlighted in black line.

The change of temperature profile along the pile shaft was highlighted in different sections in Fig. 7 along with the corresponding strata. As suggested by Mullins, (2010) that the temperature varies mainly within different soil strata, temperature reported within London clay has shown there is an temperature increase of 18^0C for a 2.4 m diameter pile in London Clay within the initial 48 hrs in Fig. 7(1). As the soil strata changes to the water bearing layer through Harwick formation into Lambeth Group, the change in temperature reduces to 15.5^0C as shown in Fig. 7 (1-3). As the sensing principle of a typical DTS system, each temperature measurement was recorded based on an average temperature over a typical spatial resolution range, i.e. 1m. As the temperature of pile reported a transition of temperature reduction between Fig. 7 (1-2, 3-4, 5-6), this does not reflect the transitional gradient of temperature change along the pile between two different soil strata. The temperature change among 6 measurement indicated the similar reduction rate.

As the medium sand layer within Lambeth Group overlaying by a band of very stiff sandy clay, the change of temperature increases to 19^0C in Fig. 7(4-5). As the pile was found in water-bearing layer in Thanet Sand, change of temperature reduces to 16^0C in Fig. 7(6-7), where Fig. 7(7-8) reflects the boundary effect at the bottom of the pile in temperature with a slight temperature decrease.

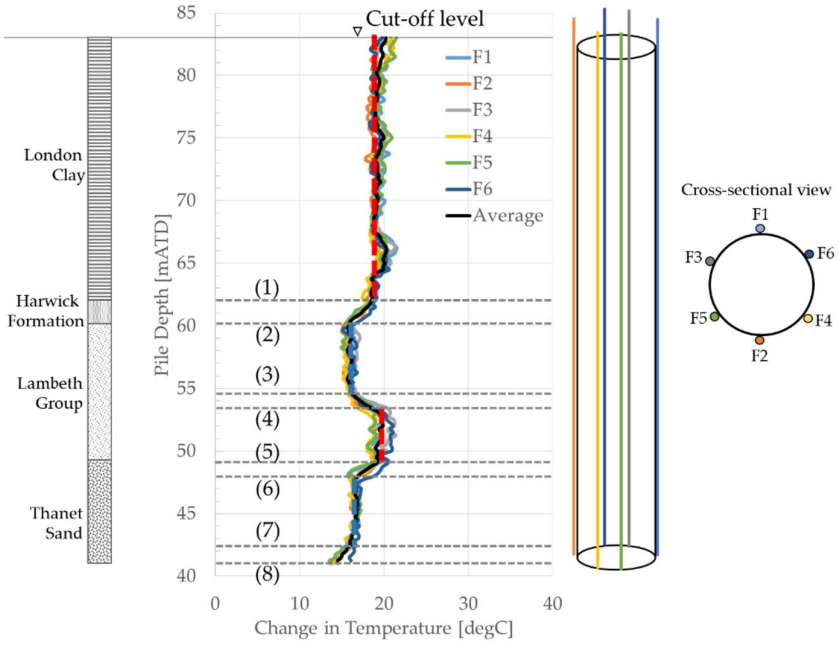


Fig. 7. Temperature developed from a 2.4 m diameter pile after 48 hrs.

The average temperature profile shown in Fig. 7 has also been found consistently from all piles constructed on site, with different magnitude of temperature development according to the diameter of the pile. It has fully demonstrated the applicability of using the temperature development during concrete hydration process to assess the integrity of embedded element.

CONCLUSIONS

The innovative approaches adopted in the constructing large diameter piles to bring further benefits to the project. The use of polymer slurry alleviated the potential demand for bentonite plant to allow the concurrent construction of Diaphragm wall as well as pile on site. To mitigate the risk before confirming the scheme to construct the largest pile supported by polymer fluid, the trial pile was proposed to replicate the construction process. The trial was extremely informative in verifying the polymer mix design, the polymer mixing procedure as well as polymer testing scheme which was later being incorporated in the ICE SPERW in providing guidance for the use of polymer slurry. The other innovative approach is the use of distributed fibre optic sensing technology to assess the integrity of the pile by registering the early temperature change during concrete hydration. The characteristic of temperature development within concrete suggests that the first 48 hrs was the optimum period in assessing the integrity of the pile and suggested potential works to correlate the concrete strength with the characteristic of temperature development. In addition the characteristics of concrete flow behaviour during tremie process were captured by the dynamic temperature measurement along pile shaft. It highlight the potential of using dynamic temperature measurement as a direct measurement to record sufficiency of tremie process.

ACKNOWLEDGEMENTS

Authors would like to thank Northern Line Extension Team from Ferrovial Laing O'Rourke JV and Mott MacDonald, London Underground in supporting the use of innovative approaches in this project. Furthermore, acknowledgement goes to Stephan Jefferis, Tony Suckling, and the other Cementation Skanska staff who provided assistance for the project, and Professor Kenichi Soga, University of Cambridge, Centre for Smart Infrastructure and Construction in supporting the use of fibre optic sensing technology in the project.

REFERENCES

Baran, T., & Pichniarczyk, P. (2017). Correlation factor between heat of hydration and compressive strength of common cement. *Construction and Building Materials*, *150*, 321–332.

EFFC/DFI. (2016). *EFFC/DFI Best practic guid to tremie concrete for deep foundations*.

Glisic, B., Inaudi, D., Vurpillot, S., Bu, E., & Chen, C. (2000). Piles monitoring using topologies of long-gage fiber optic sensors.

ICE. (2017). *ICE Specification for Piling and Embedded Retaining Walls - Third Edition*. *Institution of Civil Engineers Publishing* (3rd ed.).

Jefferis, S. A., Ouyang, Y., Wiltcher, P., Sucking, T., & Lam, C. (2017). The On-Site Management of Polymer Support Fluids for the Construction of Drilled Shafts and Diaphragm Walls, 523–532.

Lam, C., Jefferis, S. A., & Martin, C. M. (2014). Effects of polymer and bentonite support fluids on concrete–sand interface shear strength. *Géotechnique*, *64*(1), 28–39.

Mullins, G. (2010). Thermal Integrity Profiling of Drilled Shafts. *DFI Journal - The Journal of the Deep Foundations Institute*, *4*(2), 54–64.

Mullins, G., & Kranc, S. (2007). *Thermal integrity profilling of drilled shafts*.

O'Donnell Meininger, T., & Selker, J. S. (2015). Bed conduction impact on fiber optic distributed temperature sensing water temperature measurements. *Geoscientific Instrumentation, Methods and Data Systems*, *4*(1), 19–22.

Ouyang, Y., Bell, A., Elshafie, M., Soga, K., Fernie, R., & Mair, R. (2015). The history of UK experience in the use of fibre optic monitoring of geotechnically associated installations. *Geotechnical Engineering for Infrastructure and Development*, *2*, 637–642.

Ouyang, Y., Hird, R., & Bolton, M. (2017). The use of fibre optic distributed sensing technology to detect changes in sediment overburden. *Underwater Technology*, *34*(2), 63–74.

Ouyang, Y., Jefferis, S. A., Wiltcher, P., & Suckling, T. (2018). A major infrastructure project and the formation of the UK's largest rotary pile under polymer support fluid. *DFI-EFFC International Conference on Deep Foundations and Ground Improvement: Urbanization and Infrastructure Development-Future Challenges*, (Submitted).

STEEL SHEET PILING IN LIQUEFIABLE SOILS IN MAASVLAKTE, ROTTERDAM.

Bruno Pasqualini, TechnipFMC, Rome, Italy, +390665985737,
bruno.pasqualini@technipfmc.com
Maria Carmela Romano, TechnipFMC, Rome, Italy, +390665983637,
mariacarmela.romano@technipfmc.com
Mauro Tommasini, MOST CND, Rome, Italy, +390697247253, tom@mostsrl.eu

ABSTRACT

Despite the sands of reclaimed Maasvlakte peninsula in the port of Rotterdam are potentially prone to liquefaction induced by vibration loads, driven steel sheet piles are a typical method of construction used for their relatively low cost compared to other solutions. Sheet piles were installed at the base of a sloping shore to allow construction of an industrial plant jetty, with plant structures in proximity of the top of the slope. Construction experiences gained will be illustrated with relevant risk analysis, soil, and plant structures monitoring plan, implemented during the construction, that allowed for the successful completion of the works.

Keywords: steel sheet piles, monitoring, risk, liquefaction

INTRODUCTION

During the EPCm contract execution by Technip Italy of Neste Oil "Rotterdam NExBLT Plant", the design and construction of the loading Jetty for the plant was added to the scope of work with the plant already in advanced status of construction.
This addition was to be built in a very tight schedule, without modifications to the schedule of execution of the adjacent plant and according to a basic design performed by others with a building permit already in place.

Main works engineered and built are: 285m long and 23m deep anchored steel sheet piles, with a maximum depth of excavation of around 9m, dredging of sea bottom, scour protection, piles for jetty foundations, jetty structures, jetty installations such as loading arms, sleeper ways, etc., whilst the main adjacent facilities under construction for the on-shore plant are: Harbor control room, Tank Farm Substation, and Interconnecting pipe rack (see Figures 1 and 2).

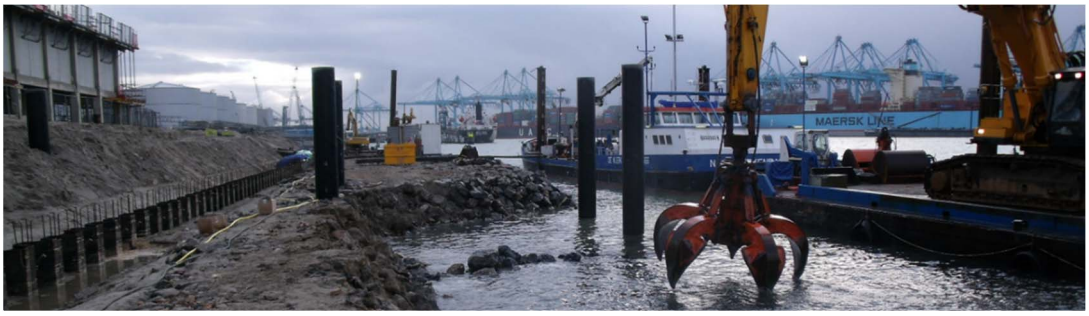


Fig. 1. Picture of the dredging of the "temporary dam" showing the sheet piles and the Tank Farm Substation.

© 2018 Deep Foundations Institute

From the analysis of the basic design documents, it resulted that the effects on the adjacent structures due to the construction of the sheet piles and the dredging had not been studied and addressed during basic design. The TechnipFMC design team had to introduce mitigation measures within the constraints of the already approved project.

A monitoring system was set up during sheet piling and dredging allowing direct live control of the construction and resulting in a safe work. Settlements induced by construction of the adjacent industrial facilities were maintained within allowable limits, with no consequences on the facilities performance, as approved by Client.

PROJECT GEOMETRY

According to the basic design, the new sheet piles had to be installed at a distance of around 6.5m from existing (or under construction) installations.
The detail design introduced as mitigation for potential settlements induced damages on the onshore plant installations a local longer distance between the sheet piles and the installations, bringing it to around 16m.
As illustrated in Figure 3 below, the industrial plant rests at 5.2m NAP (local sea level reference elevation) and the head of the sheet piles at 2m NAP.
The depth of excavation is variable with a maximum value of 9m. The sheet piles maximum depth is -26m NAP; sheet piles have the same steel quality S335 but different lengths and cross sections.
.



Fig. 2. Picture of the sheet piles and the Harbor Control Room.

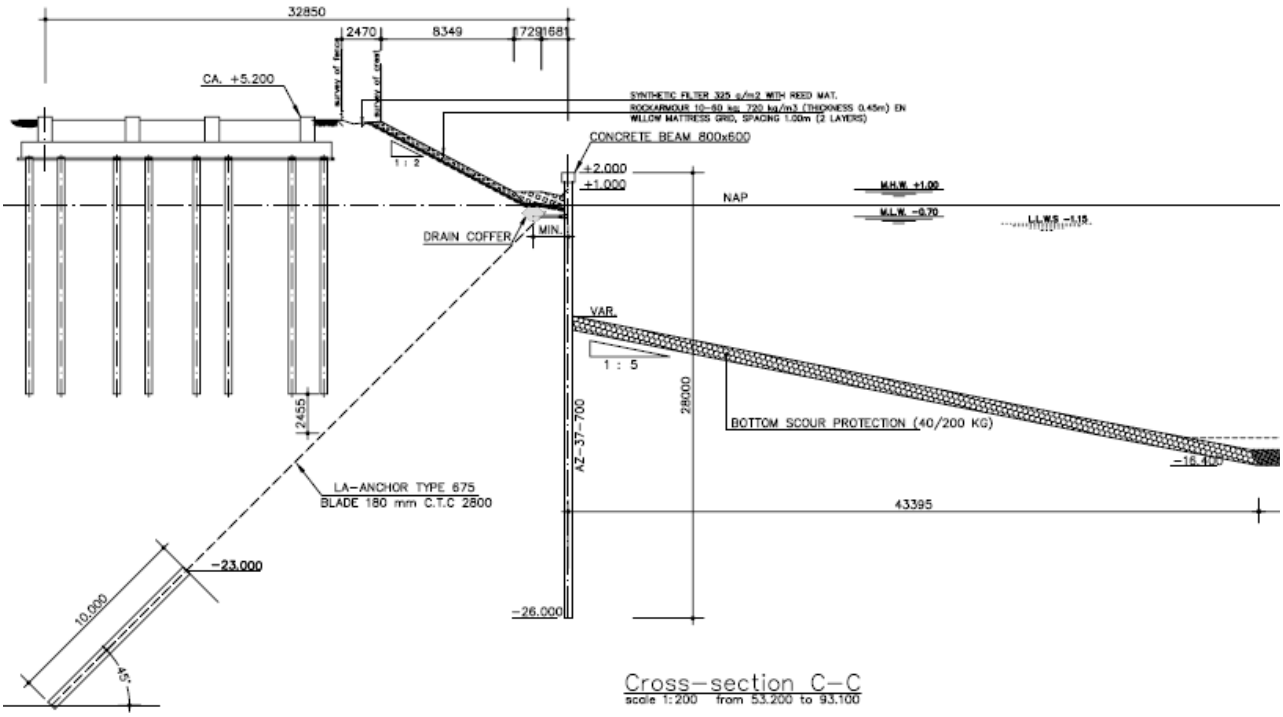


Fig. 3. Section showing the anchored sheet piles and the adjacent onshore facilities.

STRATIGRAPHY

Site characterization was mainly based on CPTs test results. The main soils types encountered are described below and typical profiles and section are summarized in Table 1 and Figure 4.

Recent sand unit consists of Holocene deposits.
Found up to a depth of about -22 m NAP: the site is an artificial peninsula built with material dredged in the adjacent Holocene sand deposits. This fill is above the Holocene sand deposits and the two have been considered as a single unit for the purposes of the geotechnical characterization; the qc of the first say 10 meters range between 3 and 15 MPa, growing then to say 7 to >30MPa in a scattered way.

Clay to clayey silt lenses of variable thickness (generally modest) within the above deposits.
These lenses are found frequently at about -15.5mm NAP, with a maximum registered thickness of about 1 to 1.5 m, and locally at about -20m NAP, with a maximum registered thickness of about 2 m. CPT readings for this layer range between 1-2MPa

Pleistocene sands, medium to coarse, densely packed.
Placed generally beneath -21 to -22 m NAP, but locally the top of this layer deepens up to -30 to -35 m NAP. The available CPTs generally refuse in the first few meters of this layer, where the qc is greater than 30 MPa.

CPT	Soil Layers	Depth [m NAP]
DKM01	Sand (elevation)	5,20
	Sand loose	-0.50
	Clay, Silt, Sand	-15,50
	Sand loose	-17,50
	Sand, Clay with Peat deposits	-20,00
	Sand dense	-22,00
DKM06	Sand (elevation)	5,00
	Sand loose	-0,50
	Clay, Silt, Sand	-15,50
	Sand loose	-17,50
	Sand, Clay with Peat deposits	-19,50
	Sand dense	-21,50
DKM10	Sand (elevation)	5,00
	Sand loose	0,50
	Sand and Clay deposits	-27,00
	Sand dense	-33,50

Tab.1 Soil Profiles.

The representative water levels, based on the Hydro Meteo nr. 3 (Port of Rotterdam-HbR) adopted for the detailed design of the sheet pile wall are as follow:

- ground water level (GWL) of NAP +0,20m;
- the mean highwater level (MHW) of NAP +1,0m;
- the mean low water level (MLW) of NAP -0,70m;
- the mean low water spring (MLWS) of NAP -1,15m;

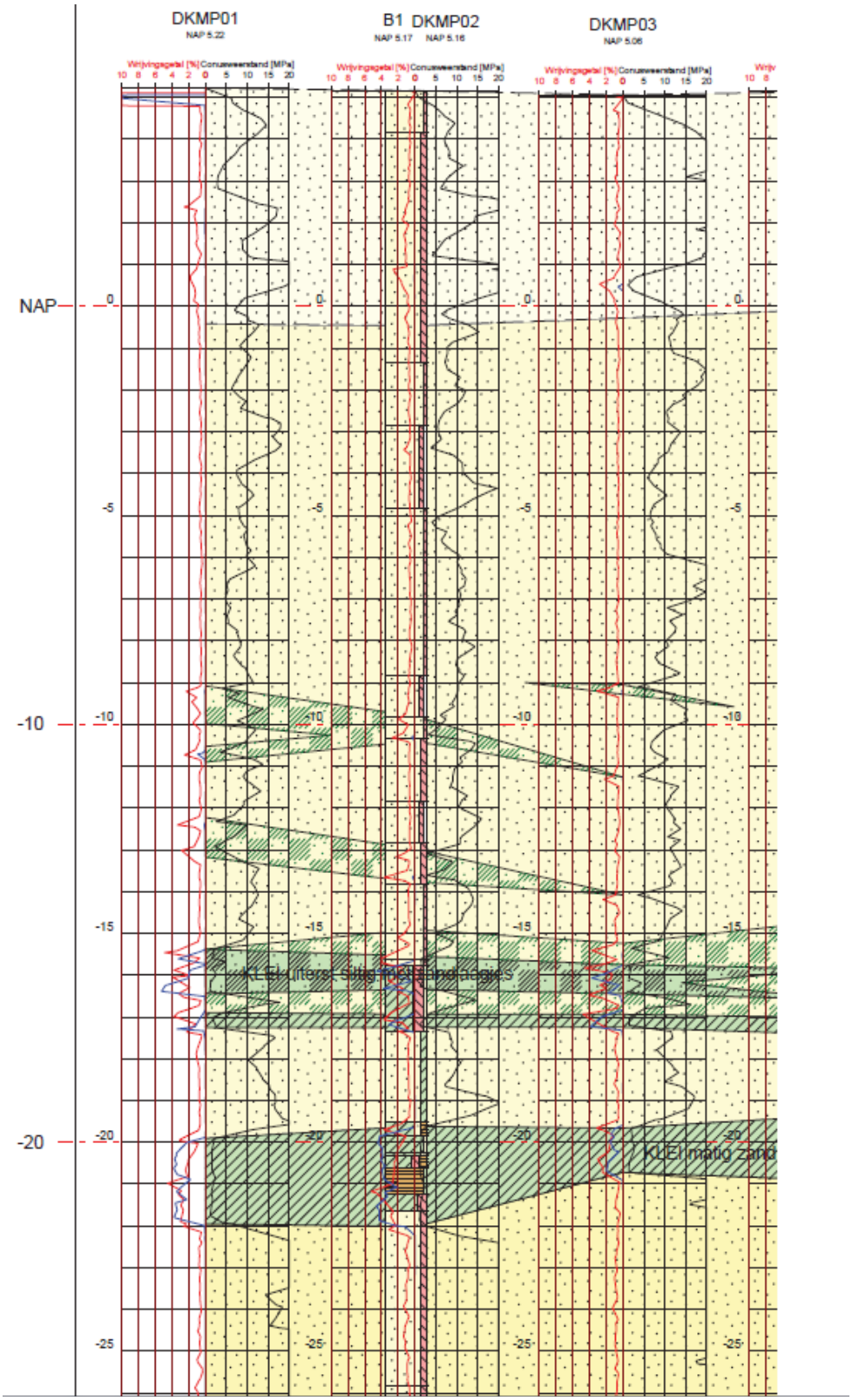


Fig. 4. Typical soil profile section based on CPT results.

GEOTECHNICAL RISKS

During the sheet pile construction, there are three main source of soil and structure settlements to be monitored:

1. Settlements induced by deformation of the sheet pile during dredging activities.
2. Settlements induced by construction activities itself: unknown unexpected events such as incorrect profiling of the slope, or extra loads imposed by cranes and rigs.
3. Settlement induced by vibrations during driving activities.

The first source of settlements has been calculated and addressed modifying the geometry where required.

The second source of settlements was avoided intrinsically in the method statement for the installation: a temporary dam (see Figure 1) was built for the rigs to operate from the sea in proximity of the onshore installations and the slope between those and the dam was profiled as gently as possible. This solution was also used to mitigate the eventual "lateral spreading" induced by vibration during construction.

The additional mitigation measures for the risks related to vibrations are addressed in the following sections.

LIQUEFACTION AND LATERAL SPREADING

Vibrations in saturated soils can cause water pressure to increase to the point where the soil particles can readily move with respect to each other. This phenomenon, called liquefaction, is extensively described in literature and in technical norms and standards with particular reference to earthquakes.

Liquefaction prediction due to earthquakes is elaborated in Youd et al. (2001), Idriss and Boulanger (2014) and addressed (for example) in Eurocode EN-1998-5.

Liquefaction prediction due to blasting is described by Charlie (1992), Al-Qasimi (2005) and under study by Baille (2017).

Liquefaction induced by pile driving is described by Massarsch (2004) and also settlements induced by pile driving is elaborated. Vibrations during sheet piles driving are discussed by Deckner et al. (2012).

Liquefaction of sloping, saturated soil deposits might generate a finite, lateral movement called lateral spreading as described for example by Bartlett and Youd (1995).
Lateral spreading is usually studied in earthquake engineering but, as will be documented in the following, may be caused by liquefaction of any origin.

Indeed, Rotterdam NExBLT Plant sheet piles geometry (sheet piles driving in the middle of a slope) and the nature of site deposit (saturated sands with sometimes relatively low qc, furthermore somewhere with trapped interbedded clay lenses) presented an high risk of liquefaction and lateral spreading induced by sheet piles driving.

TRIAL FIELD

As reported by Deckner et al. (2012), the problem cannot be studied completely unless the entire chain of vibration transmission (fig. 5) is considered.

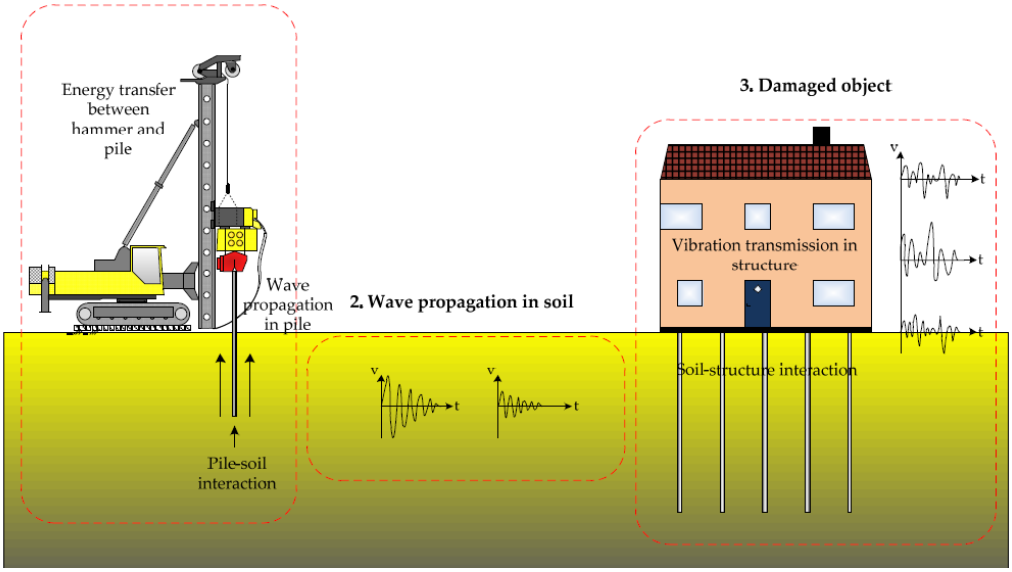


Fig. 5. Schematic illustration of the vibration transfer during driving, after Deckner et al. (2012).

Considering that, and furthermore the effects of foreseen lateral spreading due to the geometry of the site, it was evaluated that performing a reliable calculation of the expected settlements in the limited time frame of the project could not be feasible without introducing excessive conservativism.

Project strategies to mitigate liquefaction and lateral spreading risks induced by sheet pile installation were based on two main steps:

1. Execution of a sheet pile drivability trial field with the main scope of:
    a. Confirming drivability design prediction and driving methodology
    b. Monitoring driving associated induced slope settlements and vibrations.
    c. Set up a driving methodology and parameters to reduce such vibrations.
    d. Set up threshold values of monitoring parameters and associated actions to be followed during driving.
2. Implement an active monitoring system during construction based on the information gained during the trial field.

The trial field location was chosen far from existing installations (to avoid posing any risk on them) at the west end side of the sheet piles where geotechnical characterization was still representative of the site conditions.

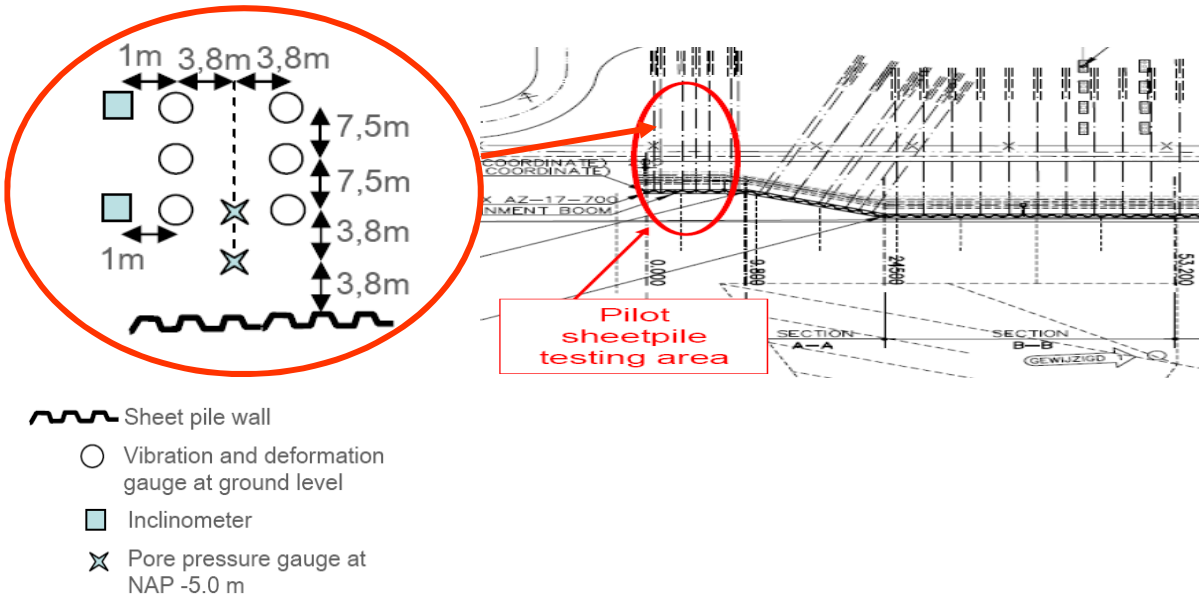


Fig. 6. Trial field plan and legend.

As per the scheme shown in Figure 6, the pilot sheet piling geotechnical monitoring system was constituted as follows.

- N. 2 standpipe piezometers
- N. 2 inclinometer
- N. 6 accelerometers
- N. 6 surface survey points on the ground

Piezometers and accelerometers were installed with continuous recording devices; inclinometer needed manual reading, similarly to the survey points where manual measurements were required.

As a general criterion, a baseline reading was made at every change of equipment set; i.e. switching from vibro to hammer or when hammer energy was changed during driving.

Pilot sheet piles have been installed with the following main equipment: Crane THW-A 1200 HC, Vibratory block ICE 1412 C; Vibratory block PVE 2335 VM; Hammer Delmag 62-22.

The Stichting Bouwresearch (SBR[1]) directive A provides guidelines, widely used in the Netherlands, regarding the level of vibrations allowed for existing buildings and surroundings and it was used (in its 2008 edition) to fix preliminary threshold alarm values.

The following tentative criteria were adopted during the trial field:

[1] SBR was a Dutch knowledge institute established in 1963 in the field of construction and civil engineering, merged since 2013 with another similar Dutch institute, the CURnet, into the SBRCURnet which operated till 2017 in publishing guidelines and data reports about site activities (http://www.sbrcurnet.nl/).

- The sheet pile installation rate with vibrating machine, should not be lower than 1m/min. In case this value is reached the installation by vibration shall be suspended and the installation method shall be by hammering for the remaining part of the sheet pile;
- The vibrator should operate with a frequency around 25Hz; hence amplitude of velocity of vibration limits are set at around 10mm/sec according to SBR-A
- Pore pressure at -5m NAP should not exceed 50kPa;

In order to check the compliance with these criteria's, a visual alarm was connected with the instruments, allowing to stop the works if the limits were exceeded.

The first three sheet piles were installed entirely by vibrator and the following three sheet piles were commenced by vibrator and completed by hammer. Additionally, the hammer was only used by applying 25% to 50% of its total capacity.

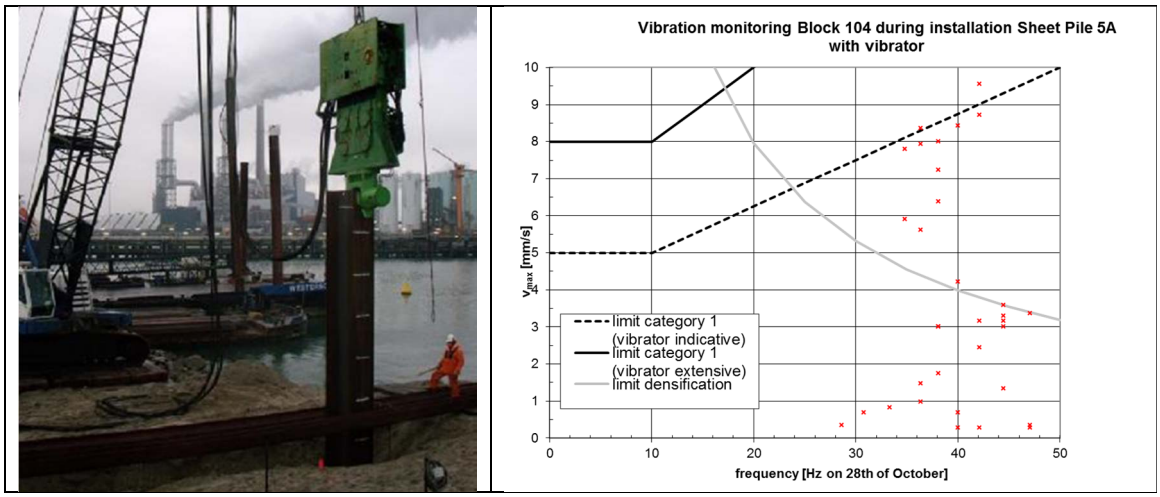
As visual inspections, the following was observed:

a) sheet pile driving was disturbing the slope, inducing settlements and horizontal displacements (see Figure 7);
b) slope disturbance increased with depth, that is, vibration recorded by accelerometers generally was growing with sheet pile depth;



Fig. 7. Trial field (far from the project installations): lateral spreading cracks.

Vibration recorded by accelerometers nearby for both vibrator and hammer often proved to be higher than recommended values (see Figures 8a and 8b for vibrator and hammer installation respectively).



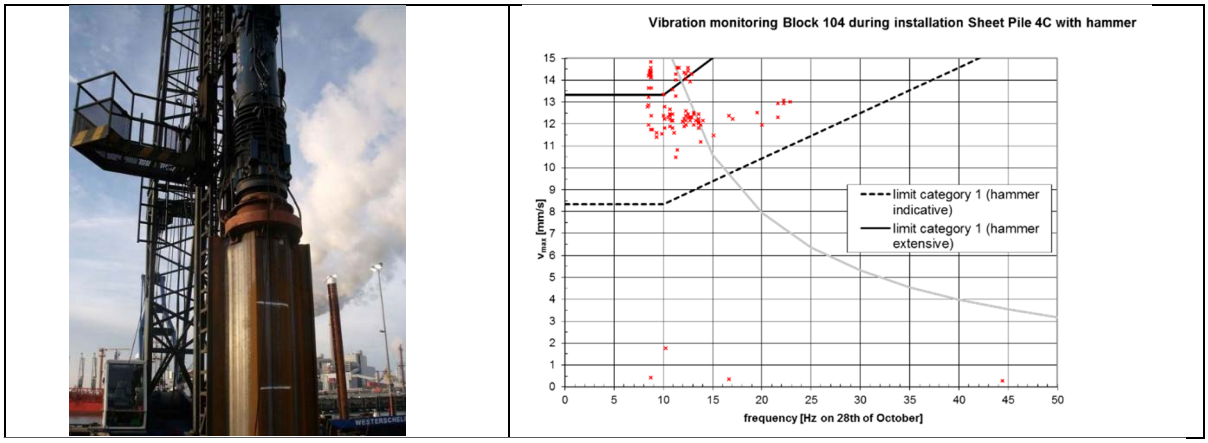


Fig. 8a and 8b. Trial field (far from the project installations): Amplitude of velocities of vibrations vs. frequency reported in the SBR directive A limiting spectra for concrete structures.

Water pressure measured in the piezometers increased from 46 to 52kPa.

Inclination up to 15mm in 25m were recorded in the inclinometers.

Based on outcomes of the trial field monitoring, the following execution criteria was established: driving the sheet piles initially by vibrator and then by hammer switching the installation method at around 7m depth.

MONITORING PLAN

The trial field provided a valid indication on how to limit the level of vibrations and their effects. However, it was clearly showed that it would not be possible to limit the vibration to a safe established value “a priori”.

Then a monitoring plan was put in place to allow to control the installations effects and instruct the execution accordingly.

The design of this monitoring plan is based on twenty years of experience in similar cases for recently built or historical-artistic heritage adjacent to sheet piling or deep foundation structures near to groundwater.

As it is well known, the vibrations induced by these kind of works, particularly in concomitance with groundwater, can have dramatic consequences in the case of poor observation of causes and effects.
As an example and memento (in a different part of the world and not pertinent to TechnipFMC activities), Figure 9 shows a catastrophic effect of ground water infiltration that in the writers opinion could be anticipated if an adequate monitoring system were in place.



Fig. 9. Recent disaster in Rome, Italy caused by the infiltration of ground water during infrastructural construction work in absence of monitoring system – Feb. 2018.

The additional data provided by a monitoring system in these critical conditions prevent emergency situations that may occur during and immediately after construction works (Il’ichev et al., 1999). Moreover, monitoring provides useful data for quantitative assessment and review of the design under construction and improving the existing technology (Elnahhas, 1992).

In critical geotechnical conditions (such as the presence of a high amount of water in the foundation soil) it is a well-established practice to base the causes-effects monitoring on the following measurement technique (Tommasini et al., 2014):

- high precision topographical levelling system with digital self-leveling, invar stadia and fixed benchmarks (periodic manually measurements);
- geodetic measurements based on automatic total station and optical miniprisms (periodic manually/automatic measurements);
- electronic crack-meters (continuous automatic measurements);
- electronic inclinometers (continuous automatic measurements);
- thermometers (continuous automatic measurements);

- piezometers (continuous automatic measurements).

Furthermore, vibration monitoring (UNI 9916 and 9614), continuous or spot, can be very useful during processing to verify the compatibility with the safety of structures and comfort for people (Boscato et al., 2012).

The alarm thresholds must be selected based on multiparametric criteria.
A preliminary observation period, typically of at least six months of monitoring before the works start, should be planned to establish the normal conditions, identify significant events and avoid false alarms during the works.
A post-works observation period shall also be planned that should typically last at least one year after the completion.

The monitoring instruments for the Rotterdam NExBLT Plant sheet piles foresaw:

- Piezometers with continuous recording devices;
- Vibration monitoring geophones installed on soils and structure with visual light alarm in case allowed thresholds were reached;
- A network of 32 mini prisms and an automatic total station, installed on soil and structures;
- Inclinometers installed on soil and buildings;
- Monitoring of the main potential cracks of the adjacent buildings, near to the structural joints between panels and between panels and columns, by means of 6+6 LVDT displacement transducers connected to an automatic data logger.

Unfortunately, the time schedule of the works did not allow for the preliminary observation period. To overcome this difficulty, the thresholds were chosen based on the trial field observations and it was planned to review them cyclically during the works based on the updated data recorded to that moment.

A decision flowchart was prepared to give guidance to the TechnipFMC Field Engineer who, with continuous observation during the works, instructed the Subcontractor according to the outcomes of the monitoring system.

This is illustrated in figure 10:

- The driving starts with the vibrator monitoring vibration driving velocity, driving time and pore pressure; in case driving time of delta pore pressure thresholds are reached, then the driving would be interrupted until the delta pore pressure is dissipated; in case vibration diving is too slow, then method is switched to hammering.
- Whilst hammering, blow count and piezometers are monitored, eventually reducing energy if penetration is too high or holding the works is pore pressure rises too much.
- During both hammering or vibrating, the geophones are under control: a visual alarm would alert the Engineer on two threshold values: the Alert level and the Alarm level.
- The Alert level will hold the works until the check of the instruments on the existing installations is completed and successful.
- Whether this latest check is unsatisfactory or the Alarm level is reached, a desk analysis shall be run prior to restart the works and the thresholds levels eventually revised.
- At the end of each day, the whole set of readings is analyzed and the full

topographic survey is run, thus to control that the criteria are followed and the consequences of driving are under control and acceptable.

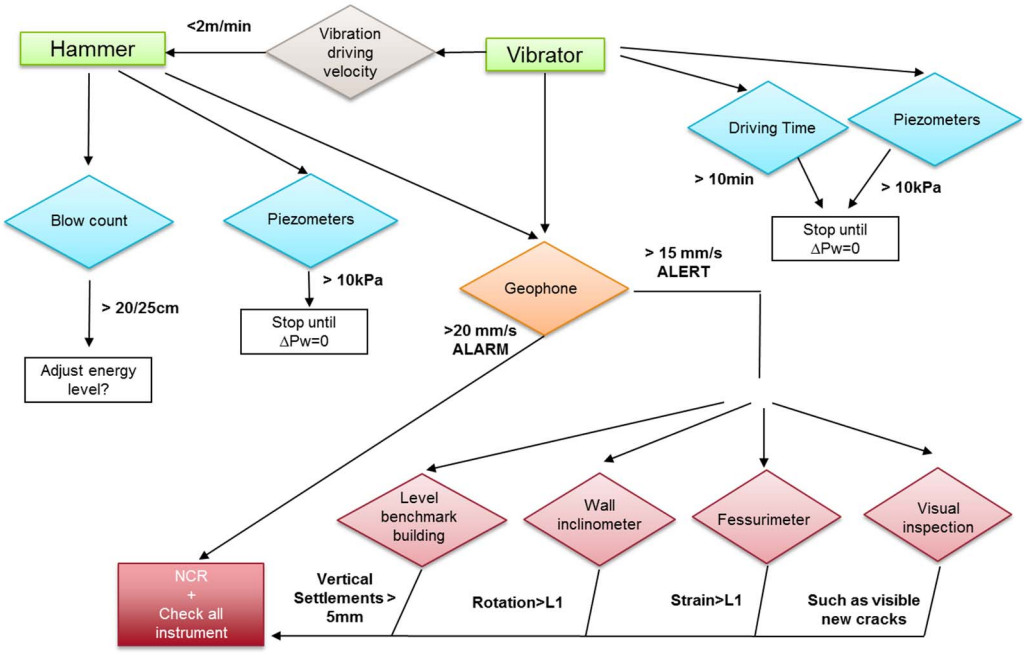


Fig. 10. Monitoring decision flowchart.

WORKS EXECUTION

The works proceeded quite smoothly: usually keeping control of the pore pressure was enough to achieve the purpose without consequences but occasionally the threshold values were exceeded to allow penetrating in harder portions of the Holocene sand.



Fig. 11. Soil cracks that occasionally appeared during the works, without affecting the adjacent installations.

In these cases, the analysis of the data acquired with the geodetic measurements, the crack-meters and electronic inclinometer, synchronized with the recoding of piezometers and vibration, was paramount to establish that the installation procedure was still allowable in terms of consequences for the buildings and other on-shore installations, notwithstanding that some of those cases created visible (though much smaller than in the trial field) cracks in the slope (see Figure 11).

SUMMARY AND CONCLUSIONS

The risk analysis, consequent trial field and subsequent monitoring system of the sheet piles installation allowed for the safe sheet piles driving in liquefiable sands prone to lateral spreading even in presence of very near existing buildings and on shore plant facilities.

ACKNOWLEDGMENTS

The Authors wish to thank Neste Oil for the trust and collaboration given during the execution of the works.

REFERENCES

Al-Qasimi, E., Charlie, W., and Woeller, D. "Canadian Liquefaction Experiment (CANLEX): Blast-Induced Ground Motion and Pore Pressure Experiments," Geotechnical Testing Journal, Vol. 28, No. 1, 2005, pp. 9-21, https://doi.org/10.1520/GTJ11848. ISSN 0149-6115

Baille W., Rahemi N., Schanz T., "Liquefaction Potential of Sands Containing Fines: From Critical States Soil Mechanics to Engineering Applications" Presentation held at Studio Geotecnico Italiano, Milan, Italy 26/5/2017.

Bartlett S.F., Youd T. L., "Empirical Prediction of Liquefaction-Induced Lateral Spread", Journal of Geotechnical Engineering, Vol. 121, Issue 4 (April 1995), https://doi.org/10.1061/(ASCE)0733-9410(1995)121:4(316)

Boscato G., Dal Cin A., Rocchi D., Russo S., Sciarretta F., Sperotto E., Tommasini M. (2012.) "Structural identification of damaged Anime Sante Church using ambient vibration, forced vibration and earthquake action". SAHC2012, Structural Analysis of Historical Constructions, Centennial Hall, Wroclaw, Poland

Boulanger R. W., Idriss I. M., "CPT and SPT based liquefaction triggering procedures", Report No. UCD/CGM-14/01, Center for Geotechnical Modeling, Department of Civil and Environmental Engineering, University of California, Davis, California, April 2014

Charlie, W., Jacobs, P., and Doehring, D. "Blast-Induced Liquefaction of an Alluvial Sand Deposit," Geotechnical Testing Journal, Vol. 15, No. 1, 1992, pp. 14-23, https://doi.org/10.1520/GTJ10220J. ISSN 0149-6115

Deckner, F., Viking, K. and Hintze, S. (2012). Ground vibrations due to pile and sheet pile driving – prediction models of today. In Proceedings of the European Young Geotechnical Engineers Conference (Wood, T. and Swahn, V. (eds)). Swedish Geotechnical Society, Gothenburg, Sweden, pp. 107-112.

Elnahhas, F. 1992. Construction monitoring of urban tunnels and subway stations. Tunneling and Underground Space Technology, Volume 7, Issue 4, p. 425-439

Eurocode 8: Design of structures for earthquake resistance - Part 5: Foundations, retaining structures and geotechnical aspects.

Il'ichev, V.A., Konovalov, P.A., Nikiforova, N.S. (1999). "Characteristic features of geomonitoring during the installation of underground structures in a dense urban setting". Soil Mechanics and Foundation Engineering. Volume 36, Issue 4, p. 140-147.

Massarsch, K.R. (2004) "Vibrations Caused by Pile Driving" (two parts), Deep foundations Part 1: Summer Edition pp 41-44, Part 2: Fall Edition pp 39-42.

Tommasini M., Virgilio L. (2014). "Monitoring and Structural Testing of the Papal Basilica of Saint Peter in the Vatican City From the Origins to our Days". UARC International Journal of Architectural Heritage.

Youd, T. L., et al. (2001). "Liquefaction resistance of soils: Summary report from the 1996 NCEER and 1998 NCEER/NSF workshops on evaluation of liquefaction resistance of soils." J. Geotech. Geoenviron. Eng., 127(10), 817–833, doi:10.1061/(ASCE)1090-0241(2001)127:10(817).

THREADED ROTARY BORED PILES AT PADDINGTON NEW YARD

David A. Hard, Bachy Soletanche, Camberley, UK, +44 (0)7870246916, david.hard@bacsol.co.uk
Ana T. Carvalho, Bachy Soletanche, Camberley, UK, +44 (0)7771718127, ana.carvalho@bacsol.co.uk

ABSTRACT

This paper addresses a technique that has been developed to improve the pile efficiency through the modification of existing rotary bored pile techniques. This is achieved by the creation of a thread around the main straight shaft of the pile, enhancing the interface with the ground. This mechanism allows a greater load to be carried than the equivalent full concreted section, whilst reducing the volume of concrete and volume of pile spoil. Following ten years of development, SolThread was delivered by Bachy Soletanche for the first time in 2014 on the Crossrail site at Paddington New Yard, as a sustainable alternative to conventional piles. Remote access inspection techniques were used to demonstrate the effectiveness of the threading process, combined with static load tests to validate the design assumptions. The paper presents the construction methodology and discusses the advantages and drawbacks of this technique based on lessons learned from this project. The successful implementation of the pile method at Paddington New Yard has allowed the verification of the technique as a practical alternative to traditional rotary bored piles. Static load tests have been used to verify the design parameters and predicted 40% enhancement in shaft friction produced through the creation of the threads.

Keywords: bored pile, pile test, clay, SolThread

INTRODUCTION

The materials used in constructing piles form a significant part of the cost of the construction and have high environmental impact through a large amount of embedded carbon. The largest part of this is the concrete, which typically forms around a third of the cost. It is not normally the case however that pile sections work to their structural maximum as the pile design is controlled by the amount of load that can be transferred into the ground.

The use of open bore rotary bore piles has long been a viable solution for deep foundations in stable ground conditions such as London Clay. The load that can be carried on such piles however is limited not by the structural capacity of the section, but rather by the geotechnical capacity. These piles are at their most efficient when relatively long and slim and working predominantly in shaft friction.

The shaft friction is a function of the adhesion between the pile and the clay and is controlled by the condition of the interface. There are several factors that affect this, including but not limited to, the relaxation of the bore with time, the possible softening due to seepages and ratio of length to depth.

The use of a thread on the pile helps counter act these and improve the interaction between the pile and the surrounding clay. This is due to the interface being improved mechanically by the thread which causes the two to be interlocked. The result of this is that the failure plane is pushed out to be in undisturbed ground away from the initial bored shaft and so the possible softening and relaxation effects are reduced. The effective geotechnical diameter of the pile is also increased through this process.

The potential of using threads on the shaft of such piles, as a method of increasing capacity, had been recognised by the industry but it had proven difficult to implement such a technique. This has in part been possibly due to a reluctance from Clients to deviate from tried and tested methods, and in part by a belief within the industry that the process of creating the threads added complication to a construction process that relies on efficiency to return profit.

As part of an in house R&D programme, Bachy Soletanche Ltd (BSL) spent time developing a tool and process that would allow them to produce a threaded rotary bored pile. This was taken to sites and pile

© 2018 Deep Foundations Institute

tests carried out to determine the degree of enhancement that could be expected. At the end of this process a patented threaded pile type, called SolThread for marketing purposes, had been brought to the point of being ready for industrial implementation.

CONSTRUCTION METHODOLOGY

The aim of the development of SolThread was to increase the efficiency of the pile section so as to minimise the amount of concrete required, or to increase the load carried for the same pile size. At the same time, in order for the new technique to gain acceptance it needs to have similar or better levels of productivity when compared to existing traditional methods.

The process is based upon the normal construction technique for an open bore rotary bored pile, where a conventional 750 mm diameter pile is constructed using a Kelly bar and auger to excavate the pile to the required depth. The SolThread tool is then placed inside the open bore and lowered to the bottom of the pile shaft. Once the pile threading process is ready to commence, the teeth are mechanically extended outwards to give a thread cutting diameter of 900 mm diameter and the thread forming process is initiated (Fig. 1). The thread forming procedure inside the pile shaft wall is performed by rotating the tool and at the same time extracting the tool from the pile bore at a given rate to produce a pre-defined thread pitch.

The design incorporates a so called crumb bucket (Fig. 2) beneath the cutting tool to catch the spoil produced by the thread formation, and hence reduce the amount of cleaning required at the end of the pile threading. This bucket minimises the amount of times tools are required to be placed within the shaft after thread formation and so minimises the chance of any damage to the thread prior to concreting of the pile.

Remote access inspection techniques, based upon those for inspection of under ream piles, are used to allow a visual inspection of the completed bore prior to moving to the next stage of cage installation. This forms an important part of the quality control process as it gives the opportunity to demonstrate the effectiveness of the threading process.

A secondary and immediate check on the effectiveness of the threading process can be made during construction when the tool is withdrawn to empty the crumb bucket. If the contents at this point do not match the amount of pile that has been threaded then it is an instant indicator of a potential problem.

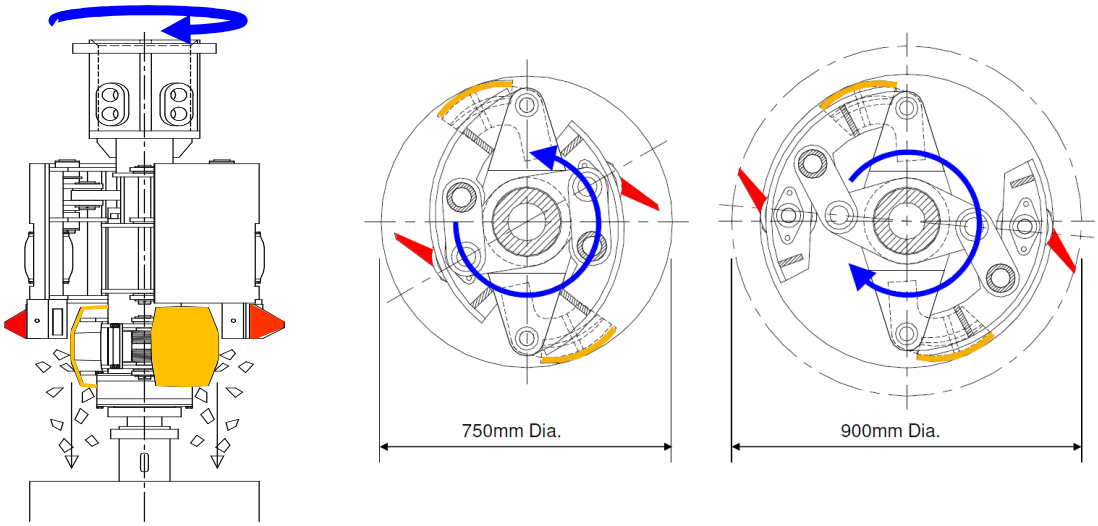


Fig. 1. From left to right: Threading Tool and Opening and Closing of Tool.



Fig. 2. From left to right: CCTV Unit, Portable Generator, Crumb Bucket, Threading Tool on Stand, Traditional Auger and Cleaning Bucket.

IMPLEMENTATION AT PADDINGTON NEW YARD

The project works involved the construction of a new elevated bus deck alongside the existing "Westway" and a new batching plant for Tarmac Lafarge which needed to be relocated in order for this structure to be built. The project is adjacent to Paddington Station in the Westbourne Park area, on Crossrail land designated as contract C336. BSL was appointed to design and construct the bored piles to support the proposed structures.

The proposed piling for the new structures at Paddington New Yard offered a potential location to use the SolThread technique at full industrial scale on a live contract. The ground conditions were suitable, with a short depth of superficial materials overlying the London Clay, and the Engineer's choice on diameters already meant that traditional open bore rotary piles were the preferred solution.

Just as importantly however was the contractual arrangement that allowed the Main Contractor to put forward alternatives to the Client, Crossrail, through the use of an OCI period. This reflected the approach of an open minded Client who was keen to investigate value engineering options, plus support the use of innovative methods to the benefit of the project.

During the tender period BSL had identified to the Main Contractor, Costain, the potential for savings through the use of threaded piles. Upon award of the contract this option was further investigated and the decision made to present it to Crossrail for their consideration. This entailed technical presentations to both the Crossrail site team and their technical team in order to explain the benefits being put forward, and to give them the confidence in the new system.

Working alongside contractor Costain, BSL installed 162 CSP secant piles, 106 Batching Plant LDA piles, 122 Derailment LDA piles, 77 low headroom LDA piles, 74 SolThread piles and 51 restricted access minipiles, the latter operating in a head room of 5 m.

The first five works piles were checked after threading using this technique to give confidence to the Crossrail site team (Fig. 3-4). Based on the positive results that were seen in these it was deemed acceptable to relax the inspection regime and the rate was dropped to one in every twelve piles.

The proposal for preliminary static load tests to be carried out, combined with the historical information from previous tests carried out by BSL, allowed sufficient confidence for the scheme to be taken to construction. Final approval of the scheme was dependant on the results of the pile tests.



Fig. 3. Rotary Bored Solthread



Fig. 4. Remote Inspection of Pile Threads

BENEFITS TO THE PROJECT

The use of threaded piles meant that less concrete was required to carry the same load, compared to the conforming scheme. This of course then also meant a reduced volume of spoil to be removed from site. Both of these reductions in volumes lead to a reduction in the amount of truck movements that would be needed on the site. This had potential benefits both to the project and to the surrounding community.

The site is long and narrow in shape with the access route running from end to end. This arrangement created a long potential interface between site workers and traffic. A solution that reduced the risk on this through less traffic had safety benefits for site operatives in addition to any environmental improvements.

A similar benefit was to be gained for the local community. The site entrance was immediately adjacent to both a bus station and a tube station as well as busy roads. This combination meant a significant number of potentially vulnerable pedestrians would be interacting with the site traffic. The reduction in the number of trucks that needed to traffic through this area would therefore reduce the potential risk to these individuals, plus through reduced emissions aid in improving local air quality. As the concrete plant used for the project was local this also produced an indirect improvement to local air quality through the use of less concrete meaning that there is less CO_2 produced by the plant. These benefits encouraged Crossrail to proceed with the SolThread alternative, in addition to the technical and commercial benefits.

PILES DESIGN

Soil Model

The soil model was based upon the relevant information for the site contained within the ground investigation reports and in agreement with Crossrail Geotechnical Design Summary Report. All the piles were founded within the depth of the site investigation.

Across the site the London Clay Formation was identified underlying a thin layer of made ground, in general between 1 to 2 m. The upper part of the formation is weathered and shows reduced shear strength. In depth occurs a stiff to very stiff fissured clay, typical of the unweathered London Clay formation.

The SPT blow counts were used to estimate the shear strength of the soil, applying a simple direct correlation that was calibrated with the results from undrained triaxial tests. A factor f1 of 4.25 was applied to SPT results to obtain London Clay undrained shear strength. The distribution of SPT “N” (uncorrected) values along the depth can be seen in Fig. 5. Figure 6 shows the undrained shear strength from the correlation with SPT values, triaxial tests results and the assumed design line.

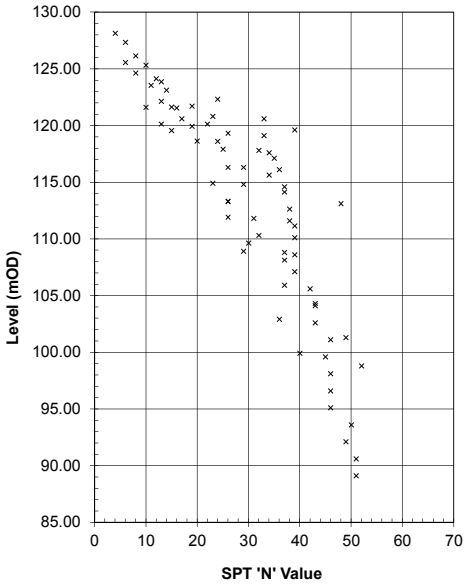


Fig. 5. SPT Tests blow counts

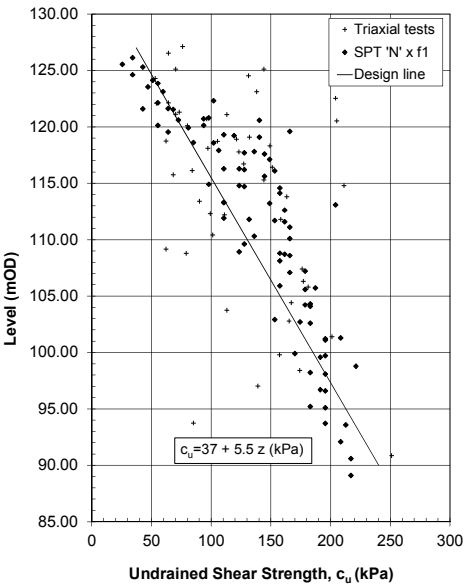


Fig. 6. Undrained shear strength from triaxial tests and from correlation with SPT "N" values

Design Method

The piles design was according to the Eurocodes (BS EN 1997-1:2004), applying the Design Approach 1, combinations 1 and 2. The partial factors for the shaft, base resistance and model factor were as per UK National Annex of Eurocode 7, for piles designed with both working and preliminary test piles.

The shaft friction in the London Clay was assumed to be a direct relation with c_u ($\alpha \times c_u$). Following LDSA (1999) recommendation an adhesion factor α of 0.5 was applied on the rotary bored piles design. For the SolThread piles, based on the effective area of the shaft and previous experience, a value of α of 0.8 was assumed for design purposes.

For the base resistance a bearing capacity factor N_c of 9 was considered suitable for pile design (Tomlinson and Woodward 2008).

Pile Ultimate Resistance

The anticipated ultimate shaft resistance and end bearing resistance for the test piles can be found in Table 1.

Table 1. Predicted pile Ultimate Resistance

Pile Reference	Pile Diameter (mm)	Ultimate Shaft Resistance Q_{us} (kN)	Ultimate End Bearing Q_{ub} (kN)
PTP1	750	2955	725
STP1	750/900	4715	725
PTP2	750	2850	715
STP2	750/900	2940	595

PILE TESTS RESULTS

A critical part of getting the alternative foundation solution accepted was the proposal to carry out sacrificial pile tests to verify the design assumptions. Due to the site geometry it was proposed to carry out tests in two locations at either end of the site. At each set up both SolThread and traditional piles would be installed and load tested. The tests were carried out in accordance with the ICE (2007) specification.

The pile loads and characteristics can be found in Table 2, corresponding the PTP designation to straight shafted rotary piles and STP to threaded piles. The graphs presented in Fig. 7 compare the performance of the straight shafted rotary piles with that of the associated threaded piles.

Table 2. Pile Tests Loads

Pile Ref	Pile Dia (mm)	Pile Toe Level (mOD)	Pile Length (m)	Safe Working Load (kN)	Design Verification Load (kN)	Peak Test Load (kN)
PTP1	750	100.50	21.50	2000	2050	5050
STP1	750/900	100.50	21.50	3150	3175	6955
PTP2	750	101.00	21.00	2000	2050	5050
STP2	750/900	106.50	15.50	2000	2050	5050

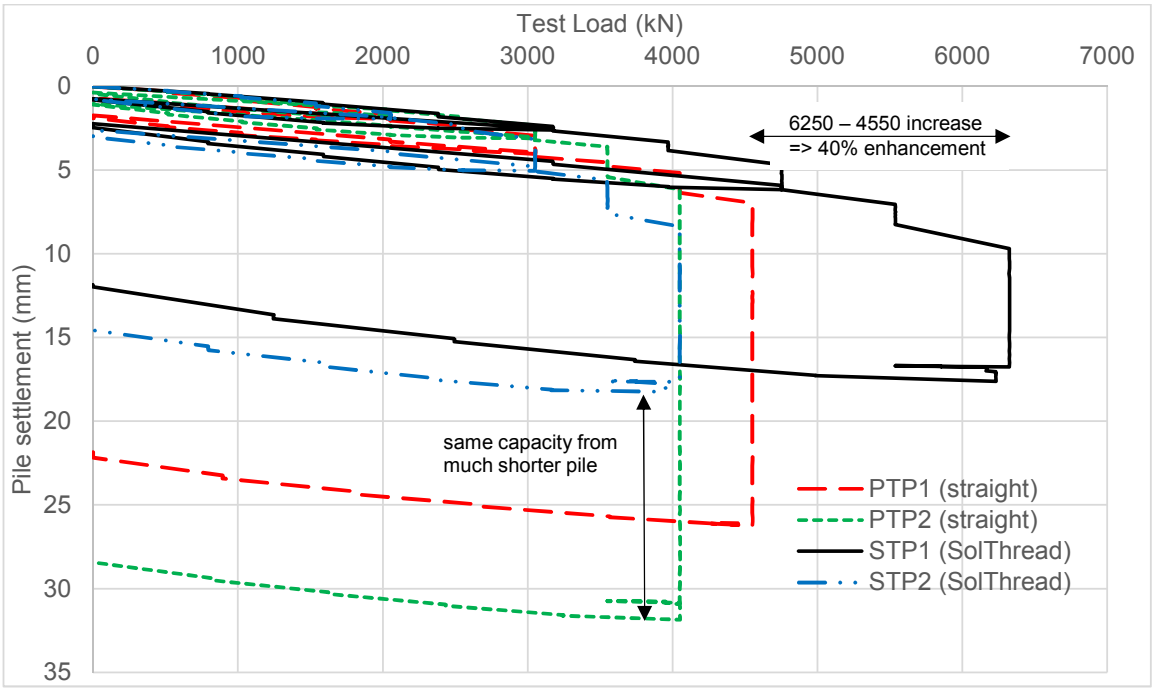


Fig. 7. Load versus settlement plots for preliminary test piles

The results show that where the threaded pile is the same length as the straight pile (PTP1 vs STP1), there is a significant increase in load carried. The shorter SolThread pile, which was designed to have the same capacity as the longer traditional pile (PTP2 vs STP2) has shown very similar performance but on a significantly shorter pile.

The design of shaft friction of a pile in clay is a function of the undrained shear strength of the clay and the interface between the pile and the ground, represented by an adhesion factor (α). The creation of the

thread around the pile shaft meant that the traditional values were no longer valid and new ones had to be determined through the testing process. The results from previous testing carried out by BSL meant that the design principles had already been established but needed to be refined for this particular project.

The testing carried out has proved that the shaft adhesion factor can be increased from the usual value of 0.5 up to 0.8 through the use of the thread. This results in an increase in shaft capacity of 40%. The volume of concrete used in the thread is around 10 to 15% above the volume of the core of the pile, depending on the exact diameter used. The current tool used at Paddington New Yard was based on a 750 mm diameter central core, threaded out to 900 mm diameter. Table 3 compares the volumes of 1.0 metre depth of pile for standard 750 mm diameter pile against a standard 900 mm diameter pile and a 750/900 mm diameter SolThread pile.

Table 3. Pile tests loads

Pile Diameter	Volume	% increase (volume)	% increase (shaft capacity)
750	0.442	0	0
900	0.636	44	20
750/900 SolThread	0.508	15	40

The design of the pile has to make an allowance however, for the proportion of the pile which is threaded, and that which is not, to reflect the fact that the bottom 3 meters over the depth of the crumb bucket cannot be threaded. The upper portion of the pile above the top of the clay which is supported by a temporary casing is also not threaded, although this may not be load bearing depending on the ground conditions. Due to the bottom of the pile not being threaded, the base capacity is calculated on the basis of the smaller core diameter and not the larger threaded diameter.

On the Paddington project the increased capacity of the SolThread pile resulted in the piles being shortened from 21.0 m for standard 750 mm diameter piles to 15.5 m for the 750/900 mm SolThread, a saving of 27% on length, and 15% on volume.

An assessment of the carbon savings using the EFFC "Carbon Calculator" indicates that this corresponds to a reduction of 10% for the SolThread pile compared to an equivalent straight shafted pile.

LESSONS LEARNT

The first lesson, and probably the most important, to be learnt from the project is that the use of an OCI period allowed the time for alternatives to be fully investigated by the Contractor and then presented and discussed with the Client. This meant that the benefits and reasoning could be thoroughly examined without time pressures cutting the process short before the full potential could be established.

This process still required both the Client and their Engineer to be open to the proposal for a new technique to be used on the project. It also required the site representatives from these organisations to be educated in how the new technique varied from the processes they were more familiar with.

The enhancement in skin friction of threaded piles over straight shafted have been verified through the use of pile tests. These tests also allowed the use of lower design factors in the pile design with additional savings resulting on pile length.

The initial construction process had a significant amount of check points to verify the threading had been carried out successfully, most notably through the use of the CCTV to allow Crossrail site staff to satisfy themselves as to the end result. Initial dialogue had identified however a willingness to allow this to be relaxed to a regime of occasional spot checks if the site team could be convinced of the consistency and quality of the process. A process for managing expectations on both sides ensured that the necessary

requirement to prove the process and quality did not result in an unwieldy system of checks that would negate the benefits of the reduced volumes through the increase in time spent on construction.

SUMMARY AND CONCLUSIONS

The SolThread pile technique consists of a central core, with a helical thread formed around this, increasing the effective geotechnical diameter of the pile by 150 mm. The use of threaded piles offers improved geotechnical capacity for the use of fewer materials compared to traditional straight shafted piles to carry the same load.

This paper presents the construction methodology and discusses the advantages and drawbacks of this technique based on lessons learned. The pile design is discussed, referring the method and the approach according the Eurocodes. The results from preliminary pile tests, which were carried out to provide information on the ultimate geotechnical resistance of both the straight shaft piles and the alternative threaded piles, are reported and analysed.

The degree of enhancement in alpha value has been demonstrated through tests. As the degree of enhancement taken in the design is significant it was important that the piles performed in line with predictions for the credibility of the alternative.

It is clear however that following this successful implementation there is now scope for this technique to be used on other projects. This will be both in the current diameter and also potentially in other larger ones as well.

The savings in materials used and subsequent sustainability benefits are real and of a level that allows Clients to consider the environmental benefits to their project as well as the commercial ones. This covers not just the material coming into site but also the spoil to be removed, with the associated knock on benefits that this produces.

The ability to carry the same load on shorter pile through the use of the threading means that there will be sites where the toe level of the piles will no longer penetrate into strata requiring the use of support fluid. This is a situation commonly seen in the London area where the penetration of piles into the potentially water bearing Lambeth Group beneath the London Clay can have a significant impact on the pile construction technique. If the piles can be kept up in the “dry” strata then the whole process will be quicker and the environmental impact of having to dispose of spoil classified by the use of support fluid as “contaminated” is removed.

The construction process is neutral in terms of time as the increased time on the threading process is offset against time saved on the initial shorter pile bore. This is important as confirms that there is no negative impact on the programme.

REFERENCES

BS EN 1997-1:2004 Eurocode 7: Geotechnical Design – Part 1: General Rules

BS EN 1997-1:2004 UK National Annex for Eurocode 7: Geotechnical Design – Part 1: General rules

ICE. 2007. Specification for Piling and Embedded Retaining Walls 2nd Edition. Thomas Telford, London.

LDSA. 1999. Guidance notes for the design of straight shafted bored piles in London Clay. London District Surveyor’s Association Publications, Note N°1.

Tomlinson, M.J. and Woodward, J. 2008. Pile Design and Construction Practice. Taylor & Francis.

A CALL FOR CODE REVISIONS FOR HIGH CAPACITY MICROPILES IN ROCK

Anthony C. Barila, P.E., Lawrence F. Johnsen, P.E. and John McKinnon

ABSTRACT

Today's micropiles are not the pali radici of Dr. Lizzi. The availability of relatively inexpensive but high strength pipe manufactured for the oil drilling industry has revolutionized the design of high capacity rock-socketed micropiles. However, the growth of this sector of the micropile market is constrained by the governing codes which unnecessarily limit design stresses, do not account for the difference in material properties of grout and concrete, and are silent on issues particular to rock socketed micropiles.

Hub Foundation has performed numerous pile load tests of rock-socketed micropiles in compression (up to 1010 tons or 8.9 MN) and tension (up to 458 tons or 4.1 MN). This paper will present several of these test results with plots of movement at the top of pile versus load and plots of load distribution within the rock sockets using data from strain gauges. These test results along with several publications from other authors will provide the basis to reevaluate the various codes used in the U.S. and Europe in regards to the issues of design stresses, grout cover, bar spacing, strain compatibility, video inspection and load shedding.

This evaluation process was initiated by Barila and McKinnon at the 2017 ISM in Vancouver with the presentation of "33 Congress Square – A Case Study". This was followed with a publication in the May/June 2017 edition of Foundation Drilling, "33 Congress Square – A Case Study and Call for Code Revisions".

REVIEW OF CURRENT CODE PROVISIONS FOR MICROPILES

In the U.S. the primary Codes used for design of micropiles are the International Building Code (IBC) for buildings and AASHTO LRFD Bridge Design Specifications (AASHTO) for bridges. AREMA is used for railroad structures. Most local jurisdictions provide local amendments to the IBC. The 2014 New York City Building Code and the 2014 Massachusetts State Building Code provide specific requirements for micropiles. The IBC and local codes use allowable stress design methods. AASHTO uses LRFD. Some bridge projects specify allowable stress design in accordance with "Micropile Design and Construction, FHWA NHI-05-039", December 2005, although this document is a design guideline and not a code.

European pile design follows Euro Code and national annexes. The Eurocode uses partial safety factors in a manner somewhat similar to the AASHTO LRFD method. The Eurocode is divided into sections. Those relevant to pile design include Eurocode 7 - Geotechnical Design, Eurocode 2 - Design of Concrete Structures and Eurocode 3 – Design of Steel Structures.

The IBC 2015 limits the allowable stress on grout to 0.33 fc when cast-in-a pipe, tube, permanent casing or rock, and 0.3 fc when cast-in-place without a permanent casing. The allowable stresses on nonprestressed reinforcement are 04.fy, not to exceed 30 ksi (207 mPa), in compression and 0.6 fy for tension. The allowable stress for pipes or tubes in micropiles is 0.4 Fy, not to exceed 32 ksi (220.6 mPa).

© 2018 Deep Foundations Institute

Micropiles grouted inside temporary or permanent casing inside a hole drilled in bedrock must be designed for the steel reinforcement to carry at least 40% of the design compression load. Micropiles grouted open hole without casing and without suitable means of verifying hole diameter must be designed for the steel reinforcement to carry the entire compression load.

Massachusetts State Building Code amendments to the IBC for micropiles are limited to a maximum usable allowable grout stress of 1600 psi (11.0 mPa).

New York City Building Code 2014 classifies rock socketed micropiles as small diameter caissons. The NYCBC allows the use of an allowable bond stress of 200 psi (1.4 mPa) for competent bedrock. The Code also requires all rock sockets to either be tested or inspected. The common method for inspecting small diameter caissons is by video camera.

FHWA provides design guidelines in FHWA NHI-05-039, Micropile Design and Construction, December 2005. The FHWA ASD design method uses strength reduction factors of 0.40 for grout and 0.47 for steel, with an upper limit of 87 ksi (600 mPa) for usable fy. The document is intended for bridges and highway structures.

The AASHTO LRFD Bridge Design Specification provides structural resistance factors of 0.75 for compression and 0.80 for tension, geotechnical resistance factors of 0.5 for tip resistance with no load test, 0.55 for side resistance with no load test and 0.70 for combined tip and side resistances with a load test. The verification load test is typically taken to a maximum load equal to the factored design load divided by 0.7. The usable yield stress is limited to 0.003 strain. AASHTO Table C10.9.3.5.2-1 provides typical nominal grout-to-ground bond values that are used for preliminary micropile design. The table provides bond values for various soil and bedrock types and five types of installation methods.

AREMA limits grout stress to 0.3 f'c not to exceed 1.6 ksi (11.0 mPa) and steel stress to 12.6 ksi (86.9 mPa) for cast-in-place concrete piles.

Eurocode 2 (concrete design) provides load factors of 1.4 for dead load, 1.6 for adverse imposed load. Eurocode 2 reduces ultimate limit state material strengths with partial safety factors of 1.05 for reinforcement and 1.5 for concrete under axial load. Eurocode 7 (geotechnical design) requires design for both ultimate strength and serviceability. Eurocode 7 requires that geotechnical design of piles be based on one of the following, given in order of increased factor of safety: (1) results of static load tests, (2) empirical or analytical calculation methods, (3) dynamic load tests, and (4) observed performance of a comparable pile foundation that includes subsurface testing.

COMPARISON OF ALLOWABLE STRUCTURAL LOADS

The following table provides allowable loads for rock sockets designed by various codes and guidelines. The pile consists of a Grade 80 12"x0.5" (305 mm x 12.7 mm) casing seated into bedrock, two full length Grade 75 #28 bars, 6 ksi (41.4 mPa) grout and a 11" (279 mm) diameter rock socket formed in competent metamorphic bedrock. For AASHTO and Eurocode, the LRFD factors were divided by an assumed load factor of 1.5 to estimate allowable loads.

Code	Grout Factor	Grout Load Kips	kN	Steel Factor	Steel Load Kips	kN	Total Load Kips	kN
IBC 2016	0.33	150.1	667.7	0.4 (2)	576.6	2565	726.7	3232
MBC 2014	0.33 (1)	121.3	539.5	0.4 (2)	576.6	2565	697.9	3104
NYCBC 2014	0.33	150.1	667.7	0.4 (2)	576.6	2565	726.7	3232
AREMA	0.30 (1)	121.3	539.5	0.35 (3)	363.3	1077	484.6	1617
FHWA	0.40	181.9	809.3	0.47 (4)	677.5	3013	859.4	3823
AASHTO	0.36	163.8	728.4	0.425	612.6	2725	776.4	3453
Eurocode 2	0.32	145.6	647.4	0.54	778.4	3462	924.0	4110

(1) Limited to 1.6 ksi (11.0 mPa)
(2) Limited to 30 ksi (207 mPa)
(3) Limited to 12.6 ksi (86.9 mPa)
(4) Limited to 40.89 ksi (282 mPa)

IBC 2016 and NYCBC 2014 allow a design steel stress of 38.8 ksi (268 mPa) for SAS and Stressbar Grade 97 steel bars, or other products that meet the criteria of AC 237. If the #28 bars were Grade 97 and met the requirements of AC 237, the allowable total load would be 895.8 kips 3985 kN). Note that in LRFD, nominal strength is computed as 0.85*(0.85*f'c*Ac+fy*As).

GROUT COVER AND BAR SPACING

Building Code Requirements for Structural Concrete - ACI 318 is an IBC code referenced document, which incorporates all provisions of ACI 318 into IBC. The commentary for ACI 318, 7.6 Spacing Limits for Reinforcement states "The minimum limits were originally established to permit concrete to flow readily into spaces between bars and between bars and forms without honeycomb, and to ensure against concentration of bars on a line that may cause shear or shrinkage cracking." ACI 318 sets the minimum clear spacing between parallel bars at the bar diameter, but not less than 1 inch (25.4 mm).

IBC Table 1808.8.2, Minimum Concrete Cover, sets the minimum cover at 1 inch (25.4 mm) for elements enclosed by a steel pipe, tube or permanent casing, 1.5 inches (38.1 mm) when enclosed by a stable rock socket and 2.5 inches (63.5 mm) when not enclosed by the above. The table makes no distinction between concrete and grout.

Eurocode 2 provides a method for computing minimum concrete cover. Factors include exposure class, design life, concrete strength, usage and bar size.

The Post-Tensioning Institute (PTI), in its Recommendations for Prestressed Rock and Soil Anchors, provides for a minimum 0.5 inch (13 mm) of grout cover. It is important to note that the steel within the tension elements covered by PTI is, typically, locked-off to a load of about 80% of the design load of the tension element. Hence, the steel is always under a high and constant tension load which is rarely the case for most micropile applications. Also, the utilization of high capacity tension elements as tiedown rock anchors in dams and structures subjected to high hydrostatic forces tend to be located within extremely "environmentally" challenging conditions which are rarely the case for micropiles.

STRAIN COMPATIBILITY AND ALLOWABLE STRESS IN STEEL

A fundamental of reinforced concrete design has been limiting the ultimate strain to 0.003. Many studies of reinforced concrete and steel-jacketed sections have shown that the strain at which concrete fails increases with confining pressure.

Grout Confinement Influence on Strain Compatibility in Micropiles, for the ADSC/DFI Micropile Committee focused on the use of Grade 150 (Fy=120 ksi, 827 mPa) bars in micropiles. The study considered confinement from soil, rock and casing. A water:cement ratio of 0.36, which resulted in grout strengths in excess of 9000 psi (62.1 mPa), was used to minimize shrinkage in test samples. Holman, et.al. recommends a design procedure using the results of the ADSC/DFI study.

Eurocode 2 provides a design procedure for increasing the usable yield stress on the basis of lateral confinement. The procedure allows the use of increased characteristic strength and strains based on the effective lateral compressive stress due to confinement. Confinement can be generated by cross-ties which reach the plastic condition due to lateral extension of the concrete. This is typically used for high capacity columns.

SAS Stressteel took a different approach by obtaining ICC approval for the use of Grade 97 reinforcing steel (Ghosh). A grout strength of 6000 psi (41.4 mPa) was used in their study. The ICC acceptance criteria are issued in AC237. A yield stress of up to 97 ksi (669 mPa)is permitted for threaded bars that meet the ICC conditions of acceptance that cover: bond, material properties, bar dimensions, bar bending, splices and anchorage. The ICC approval allows the use of Grade 97 reinforcing on projects governed by IBC codes. The New York City Building Department has issued directives that allow the use of 97 ksi (669 mPa) yield stress for threaded bars meeting AC 237. Both SAS Stressteel and Stressbar manufacture threaded bars meeting the AC 237 acceptance criteria. The authors are encouraging the other manufacturers to pursue this approach. We have been informed by both DSI and Skyline Steel that they have received ICC approval for selective bar sizes with Grade 100 steel.

PILE TESTING VS. VIDEO INSPECTION

Since 2008, the New York City Building Code has required that all small diameter caissons (Rock-socketed micropiles) be either inspected or load tested. Furthermore, the code allows rock sockets formed in competent bedrock to be designed for an allowable side friction of 200 psi. The Code defines competent bedrock as crystalline rocks, marble, serpentine, cemented shale and sandstone that may contain fracture and moderately weathered zones up to one inch (25.4 mm) wide spaced as close as 1 foot (305 mm) apart, and the RQD with a double tube, NX-size diamond core barrel is, generally, at least 35% for each 5-foot (1.5 m) run or a core recovery with a BX-size core of at least 35% for each 5-foot (1.5 m) run.

One advantage of video inspection of all rock sockets is assurance that rock sockets have been formed in stable bedrock. The video will show if the socket is in a boulder, any voids in the perimeter of the rock surface and any sediment that is settling to the bottom of the socket. Figures 1 and 2 show images of a small diameter rock socket in Manhattan obtained with a video camera.

LOAD SHEDDING

Load shedding is the transfer of load from the casing to the soil or bedrock. FHWA NHI-05-039 provides a design procedure for "plunging" in which the permanent casing is reinserted into a portion of the bond zone. The procedure results in a reduced load on the uncased portion of the pile by assuming that the pile load is transferred uniformly to the bond zone. Clearly, this requires a continuous layer of grout between the casing in the bond zone and the soil or rock in which the bond zone is formed.

The U.S. codes are silent on the issue of the direct transfer of compression load from the casing to the bedrock in which it is seated. In New York City, many foundation engineers have designed rock sockets on the assumption that some portion of the casing load is transferred to the bedrock. This has led to disputes on some projects where the contractor's bid was based on load shedding, but the owner's engineer has not allowed it.

Oweis and Hwang used PLAXIS to model the load transfer from the casing to bedrock based on the quality of the bedrock. Their analysis found that for good quality bedrock, the load transfer can be as high as 20% of the total load. Their method quantified bedrock strength using the geologic strength index (GSI). This may be very conservative for fractured rock if the grouting of the bond zone fills the fractures.

The authors recommend an instrumented load test program for projects where load shedding is used for design of rock sockets. The load test program would require the test pile to be run in compression, with the resistance provided by reaction piles drilled into the same bearing layer. The test pile and all reaction piles would be instrumented with a series of strain gages including one pair immediately above the bottom of casing, one pair immediately below the bottom of casing and another pair 3 feet (0.9 m) into the bond zone. The load shedding would be estimated by comparing the test pile and reaction piles on the basis of the load transfer between the gages immediately above and below the bottom of the casing.

CASE HISTORY- 33 CONGRESS SQUARE, BOSTON, MASSACHUSETTS

The interior of four structures were selectively demolished to allow for the internal addition of a 14 story structure. The foundations of the new office building will be supported on high capacity drilled micropiles, including 51 micropiles to support the new super columns, 67 micropiles to support the core of the new structure and 19 micropiles to support the tower crane foundation. This project was presented at the 2017 ISM in Vancouver, Canada, with emphasis on the core micropiles. Photos 7 thru 10 show some challenging conditions that had to be overcome to ensure the proper installation of these micropiles.

Two pile load tests were performed, one in compression to a maximum test load of 1010 tons (8.9 MN) and one in tension to a maximum test load of 458 tons (4.1 MN). The test results were excellent. Based on these results, the geotechnical engineers agreed to reduce the rock socket length by 50% from the original design. Photos 11 and 12 show the load test setup.

Two pile load tests were performed from March 28 to April 6, 2016 prior to the completion of the overall structural design. The tests were performed in a very tight open area adjacent to the project structures. The core piles were installed from January 6 to February 11, 2017. These piles were installed from a level about 25 ft. (7.62 m) below street level.

The original design loads for the micropiles were 325 tons (2.9 MN) in compression, 150 tons (1.3 MN) in tension and 11 tons (97.9 KN) lateral. The original micropile design consisted of the following: a 10 ¾ in. (273 mm) OD; 0.545 in. (13.8 mm) wall casing drilled down into stable rock; a core pipe [8.625 in. (219 mm) OD; 0.719 in.(19.8 mm) wall] to reinforce the rock socket plus 15 ft. (4.6 m) above the casing tip; a core pipe [7.0 in. (179 mm) OD; 0.50 in. (12.7 mm) wall in the upper 25 ft. (7.6 m) of the micropile to sustain the bending moment due to the lateral load at the top of the pile; a 2.5 in. (63.5 mm) Grade 150 bar to support the tension load; and 5000 psi (34.4 MPa) grout. Refer to Figure 1 for a detailed design sketch.

The length of the rock socket was specified by the Owner's Engineers to be 34 ft. (10.2 m) long. Bedrock consisted of hard, extremely fractured, slightly to moderately weathered diabase. The contractor opted to install the test piles with 25 foot long bond zones.

Two pile load tests were performed - one in compression to 1010 tons (8.9 MN) and one in tension to 458 tons (4.1 MN). The pile load tests were performed about three months before a wind tunnel study was performed which reduced all the design load components.

COMPRESSION TEST

The test pile arrangement consisted of four (4) reaction piles and the test pile in the middle. The test pile was drilled with a low headroom drill rig (DK-525) to provide drill rates for the casing to simulate the low headroom conditions anticipated for the production piles inside the buildings. The reaction piles were drilled with a Casagrande C-8 drill rig.

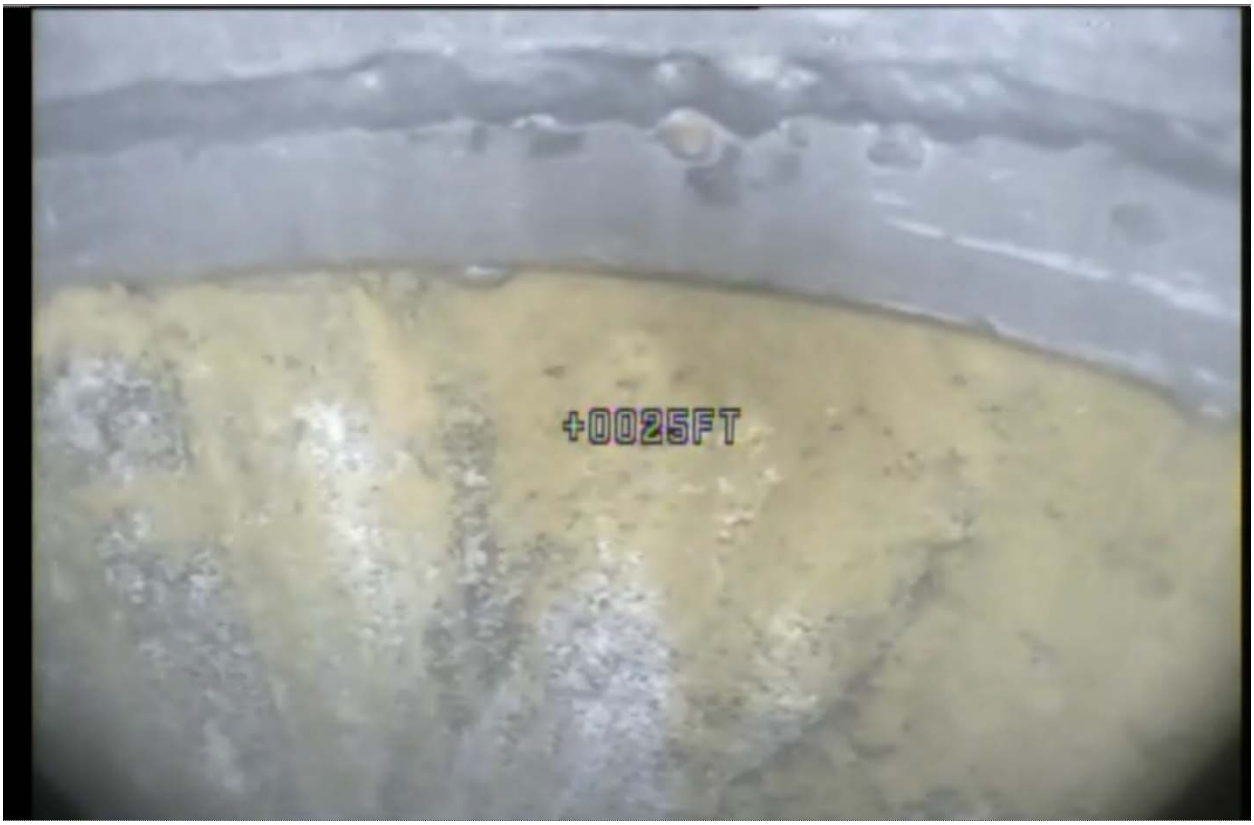


Figure 1: Casing Seated into Bedrock



Figure 2: Bottom of Rock Socket

Figure 3 shows the plot of pile settlement versus load for the test pile. The “curve” is essentially linear for the entire loading schedule. The total settlement of the pile was 1.471 in. (34.36 mm) at 650 tons (5.8 MN) and 2.656 in.(67.46 mm) at 1010 tons (8.9 MN). The net settlement after unloading from 1010 tons (8.9 MN) was only 0.372” (9.5 mm). The total creep movement at 1010 tons (8.9 MN) from 1 minute to 90 minutes was only 0.032 in. (0.813 mm).

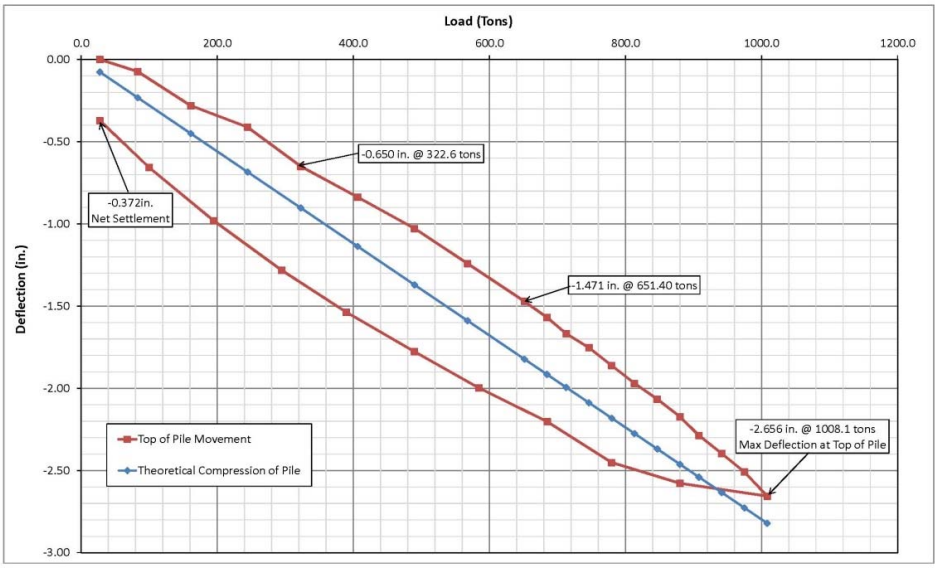


Figure 3: Compression test settlement versus load graph

Figure 4 shows the distribution of the test load throughout the full depth of the test pile. A total of 13 strain gauges were attached to the 2.5 in. (63.50 mm) Grade 150 bar. Geokon 4911 “sister bars” were utilized. Nine of the strain gauges were placed within the 25 ft. (7.6 m) rock socket.

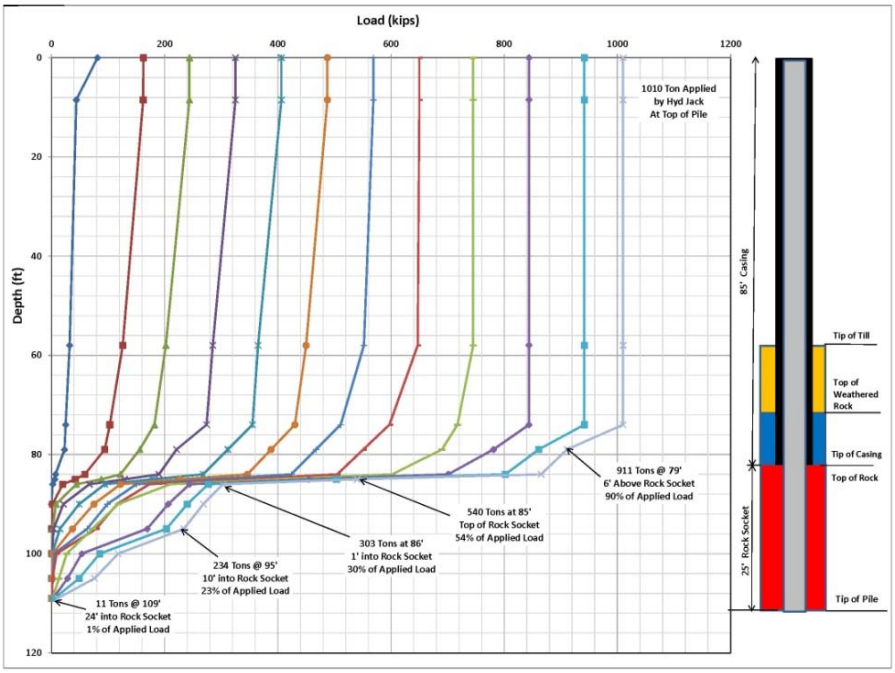


Figure 4: Compression test load distribution graph

The large number of strain gauges within the socket were utilized to confirm that a significant amount of the test load would be “shed” at or just below the casing tip. Note that 145 tons (1.29 MN) of the maximum test load was transferred above the casing tip within the weathered rock. There was 540 tons (4.8 MN) at the casing tip (54% of the test load) and only 303 tons (2.7 MN) at a depth of 1.0 ft. (0.3 m) below the casing. This is only 30% of the applied test load. Hence, 263 tons (2.3 MN) was “shed” in one foot below the casing tip and 562 ton from one foot above the casing to one foot below the casing. At 10 ft. (3.04 m) below the casing tip, 234 tons (2.1 MN) remained, or 23% of the max. test load.

TENSION TEST

One of the four reaction piles for the compression test was utilized to perform a pile load test in tension. The test (reaction) pile included a full length 3 in. (76.2 mm) Grade 150 bar; a 25 ft. (7.6 m) long rock socket; and three strain gauges and two tell-tales within the rock socket. Note that the bar was debonded with a PVC pipe close to the top of the rock socket. The depth to stable rock was 79 ft. (24 m).

Figure 5 presents the plot of test load vs elongation. The “curve” is essentially linear up to about 400 tons (3.6 MN) which is close to the minimum yield strength of the bar [~ 420 tons (3.7 MN)]. The bar begins to show plastic deformation beyond this point which accelerates between 450 tons (4.01 MN) and 458 tons (4.08 MN). The net “settlement” after unloading is 1.006 in. (25.55 mm) which is very close to the actual total movement at 458 tons (4.07 MN) less the theoretical elongation of the bar, if it were fully elastic at that load. The recorded elongation during the test was strictly due to the elongation of the bar, as evidenced by the recorded small movement [only 0.026 in. (0.661 mm)] at the tip of the pile.

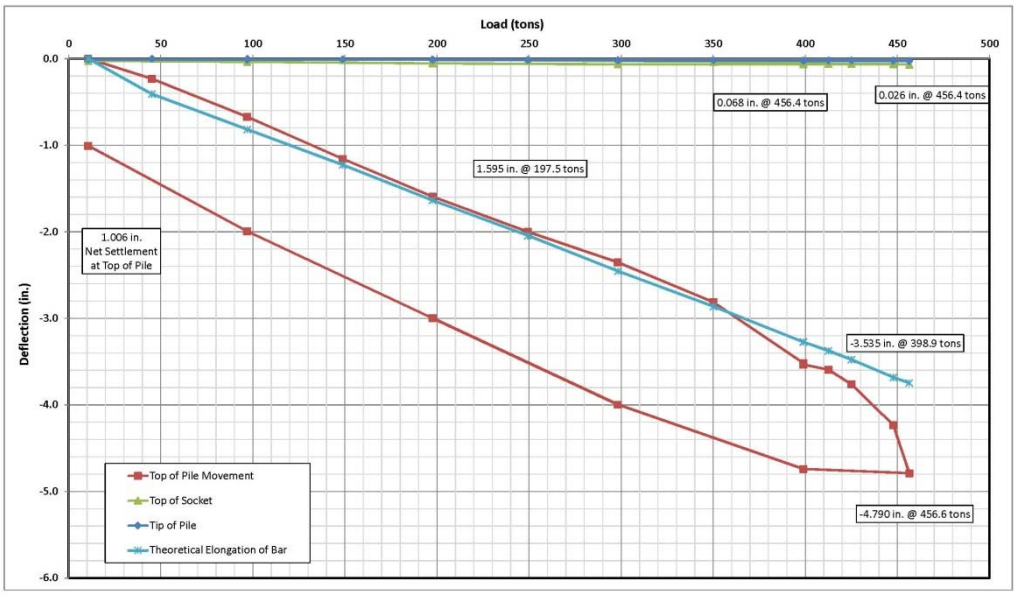


Figure 5: Tension test elongation versus load graph

Figure 6 presents the test load distribution thru the test pile. Note that all the drill casing had been extracted after the bar was installed and grouted. Also, the PVC sheathing that was utilized to debond the bar was installed to a depth of about 5 ft. (1.5 m) above the top of rock (we wanted to be 100% certain that the sheathing did not extend into the rock socket). The combination of both items explains why some of the test load was transferred above the top of rock. This resulted in 344 tons (3.1 MN) or 75% of the max. test load being transferred to the top of rock which is still significant. Approximately 115 tons (1 MN) were transferred one foot into the rock socket. Only 10 tons (89 KN) was recorded at a depth of 1.5 M (5 ft.) into the rock socket. Hence, a total of 334 tons (3.1 MN) was transferred in the upper 5 ft. (1.5 m) of the rock socket. This is 73% of the maximum test load. Note that the creep at the maximum test load was only 0.022 in. (0.558 mm) from 1 to 10 minutes.

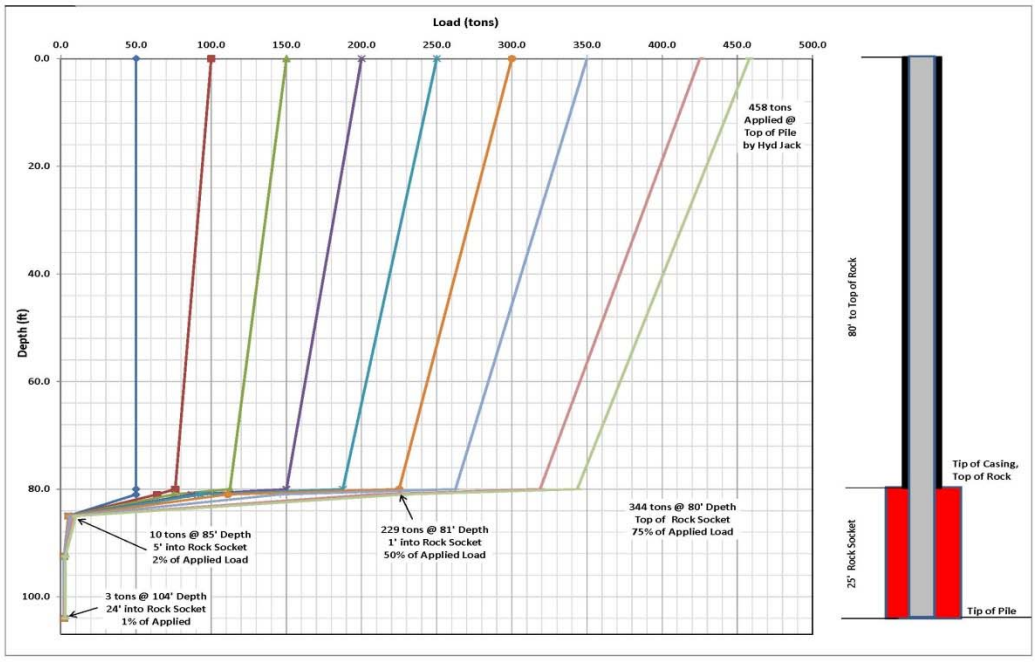


Figure 6: Tension Load test Distribution Graph

The strain gages located one foot below the bottom of the casing show that 50% of the total load was shed in the tension pile and 70% of the load was shed in the compression pile. Since the primary difference in load shedding is the bearing of the compression pile on bedrock, it is assumed that 20% of the total pile load was shed directly from the casing to bedrock. This is consistent with the Oweis study.



Figure 7



Figure 8



Figure 9



Figure 10



Figure 11



Figure 12

CONCLUSIONS

1. The Codes provide an unnecessarily wide range of structural capacities.
2. The maximum usable allowable stress of 1600 psi (11.0 mPa) in AREMA and the Massachusetts State Building Code should be dropped. None of the other codes limit the allowable stress on grout.
3. The silence of the codes on load shedding has led to contract disputes. The case history and the Oweis study both show about 20% of the total load being shed when the casing bears on competent rock. The authors recommend that load shedding from the casing to bedrock be allowed under the following conditions: (1) the casing is seated a minimum of 6 inches into competent bedrock, and (2) an instrumented load test is run that confirms the load shedding value. Load shedding should be used to both reduce the design load in the rock socket and reduce the length of the rock socket.
4. The codes do not account for the significant differences in material properties between fluid neat cement grout and concrete. The absence of aggregate gives the grout a much lower modulus, allows it to penetrate narrow spaces, and makes the grout a homogeneous material without the sharp edges of aggregate and with a uniform stiffness. The ACI commentary on bar spacing states "The minimum limits were originally established to permit concrete to flow readily into spaces between bars and between bars and forms without honeycomb, and to ensure against concentration of bars on a line that may cause shear or shrinkage cracking." The spacing requirement of 1 inch (25.4 mm) should be reduced for fluid neat cement grouts to account for the lack of aggregate and the much lower slump. The PTI recommendation of 0.5 inch (13mm) should become the minimum grout cover of core steel within rock sockets for micropiles.
5. The Codes allow the design of rebar with yield strengths greater than 80 ksi (552 mPa) for concrete that is confined in high capacity columns. Codes should allow this to be expanded to micropiles with engineering analysis. The article by Holman, Wolosich and Richards make a compelling case to increase the allowable stress in steel for micropiles that are confirmed within a permanent casing and in rock sockets. Note that the design for tension loads in m icropiles and for tension elements covered by PTI is based on 0.6 fy. We strongly recommend that this be the case for compression also and without any maximum allowable value.
6. Video inspection of rock sockets should be offered as an alternative to load testing where nearby test results are available.

REFERENCES

ADSC/DFI Micropile Committee, (2006) "Grout Confinement Influence on Strain Compatibility in Micropiles", ADSC.

Alperstein, R. and Zaad, M., (2005), "Down-Hole Caisson Inspection Using Remote Borehole TV", ADSC.

Frank, R., (2006) "Design of Pile Foundations Following Eurocode 7", Proceedings XIII Danube-European Conference on Geotechnical Engineering, Slovenian Geotechnical Society.

Holman, T. P., Wolosick, J. R. and Richards, T.D. (2016)"Design with High-Strength Steel Reinforcement in Micropiles – Clearing up the Misconceptions in Strain Compatibility Theory", Foundation Drilling.

ICC Evaluation Service, Inc., (2007) “AC 237 Acceptance Criteria for Threaded High-Strength Steel Bars for Concrete Reinforcement”.

FHWA NHI-05-039, (2005) “Micropile Design and Construction”, National Highway Institute.

Oweis, I., and Hwang, J., “Load Transfer to Micro Pile Rock Socket”, GeoFlorida 2010, ASCE.

Turner, M., (2010) “A Review of Current Micropile Design in the U.K. in Relation to Eurocode 7, ISM 2010, International Society for Micropiles.

AN APPROACH FOR OPTIMIZATION OF DRILLED SHAFT DESIGN IN DUBAI

Emad Y Sharif, B. Sc - M. Sc, GTC Lab Director, Dubai, UAE, +971504566264, emad.sharif@gtc-lab.com
Hardev Sidhu, Geotechnical Testing Expert, GTC Lab Manager, Dubai, UAE, +971544105943, hardev.sidhu@gtc-lab.com

ABSTRACT
Drilled shafts are widely used in Dubai as the main foundation option for high towers and bridges. Hundreds of meters of drilled shafts are installed in Dubai every day. Piling industry has grown widely in Dubai over the past 2 decades. Piles of large diameters as 2.5m and lengths up to 100m are common. It is evident that the current practice of geotechnical axial load capacity estimates in general is conservative, and actual pile axial load capacities as demonstrated by static and dynamic loading tests is much higher than the theoretical design capacities in almost the majority of cases.
The main purposes of this study is to review the shortcomings of the commonly used theoretical axial load estimate procedures, and examine the factors and parameters controlling the estimated axial capacity (input parameters). Optimization of the conservative design procedure is suggested by careful selection of main input parameters, and calibration to static loading tests.
Keywords: Drilled Shaft, Rock Mass Factor, Rock Compressive Strength, Load Transfer.

VERY BREIF BACKGROUND ON THE GEOLOGY OF DUBAI
The rock formations noticed in Dubai area are mostly the mid to upper Tertiary sediments of Berzman Formation, consisting of an interbedded sequence of carbonate rich arenaceous, argillaceous and rudite/ conglomeratic rocks. The weathered calcareous sandstones/ Calcarenites with thin interbeds of siltstone are noticed to a depth of 18 – 25 m, underlain by the dominantly argillaceous/ calci silttites with interbeds of polymictic conglomerates- with pebble to gravel size clasts of gabbros, chert, sandstones and carbonate rocks, Some deep-seated thick evaporate- gypsum beds associated with clays and mudstones are noticed beyond a depth of 80 – 100 m. These are continental shelf deposits with a depositional environment similar to the present day environment with frequent eustatic changes-fluctuations in the sea levels. The frequent sea level changes with harsh climatic conditions have given rise to the surfacial sabkah deposits during the quaternary times on wards along the coast lines.

ADVANTAGES OF DRILLED SHAFTS
The local geology in Dubai is characterized by extremely weak to weak (as per rock strength classification given in BS 5930 (1)) sedimentary rock of sandstone / siltstone / conglomerates / mudstone of compressive strength of 0.5-5.0 Mpa in general that is classified as an intermediate geo-materials (IGM) (2), or “Soft Rocks”.

The use of drilled shafts in Dubai is attractive due to relative ease of drilling and advancing stable boreholes through the “soft” sedimentary rocks (IGMs) with time and cost effective drilling methods using augers / buckets. Bentonite muds and chemical polymers are typically used to support the drilled holes for piles of different diameters (as large as >2m) and as deep as 100m. Temporary steel casing is advanced through the upper un-consolidated sandy soil. In many projects, were drilled hole through IGM is stable, water only is used as drilling fluid, as adopted in many projects. Drilled shafts in IGM resist the applied loads by skin friction as opposed to end bearing. Design maximum side friction resistance ranging between 200 to 600 kpa are typical, depending on the local rock strength, mass parameters, and pile installation details.

OVERVIEW OF THE BEHAVIOUR OF TYPICAL DRILLED SHAFTS UNDER COMPRESSIVE LOADING:
A description of axial load resistance behavior of drilled shafts in IGMs is given in FHWA-RD-95-172 - Load Transfer for Drilled Shafts in Intermediate Geomaterials (3), which presents a parametric finite element study to assess and evaluate the different factors affecting the performance of drilled shafts and load transfer mechanisms. This study was calibrated by the results of actual in-situ loading tests on instrumented piles. Some of important findings highlighted in this study are the determination of the

© 2018 Deep Foundations Institute

many factors that control the magnitude and development / mobilization of the side friction and understanding load transfer mechanism. The IGM-Shaft interface conditions and the compressive strength of the IGM were found to be of primary significance. A rough interface would mobilize as large as 4 times the max side friction as a smooth interface, as shown on the graph (Fig. 1) extracted from this important study. The side friction was found to be highly affected by the existing initial horizontal effective pressure at the shaft – IGM interface, and hence the pile concrete fluidity (Slump). Therefore, the determination of compressive strength as uni-axial strength will under estimate the strength of IGM materials, and compressive strength is better to be estimated with tri-axial tests (CIU) at confining/ consolidation pressure representing the in-situ conditions.

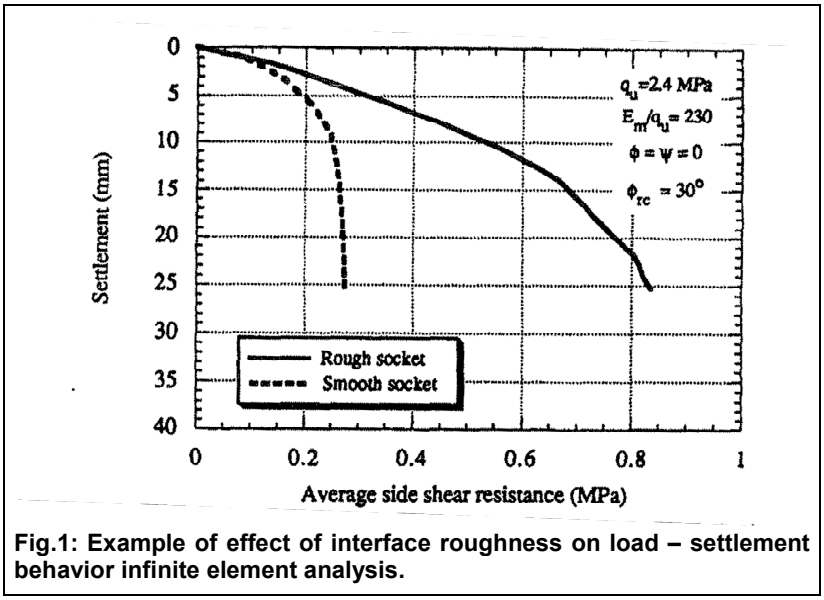


Fig.1: Example of effect of interface roughness on load – settlement behavior infinite element analysis.

FHWA-NHI-10-016 - Drilled Shafts Construction Procedures and LRFD Design Methods (4) also presents typical design procedure and performance prediction of drilled shafts based on actual behavior in static loading tests. The graph in Figure 2 illustrates the load transfer behavior of a drilled shaft of length L and diameter B subjected to an axial compression load Q_T applied to the butt (top) of the shaft (Figure a). Figure b shows the general relationship between axial resistance and downward displacement, and figure c shows the load transfer along the shaft of the pile and end resistance mobilization. Several important behavioral aspects of drilled shafts are illustrated in Figure 2. The first is that side and base resistances develop as a function of shaft displacement, and the peak values of each occur at different displacements. Maximum side resistance occurs at relatively small displacement and is independent of shaft diameter. Maximum base resistance occurs at relatively large displacement and is a function of shaft diameter and geomaterial type.

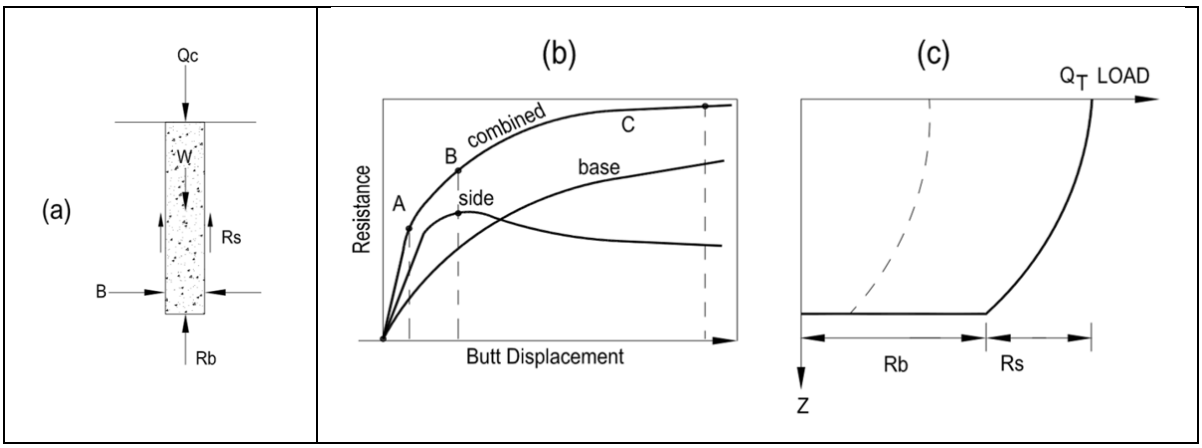


Fig. 2: Generalized Load Transfer Behavior of Drilled Shaft in Compression (FHWA-NHI-10-016).

ADDITIONAL DESIGN CONSIDERATIONS FOR ROCK SOCKETS:

A design decision to be addressed when using rock sockets is whether to neglect one or the other component of resistance (side or base) for the purpose of evaluating strength limit states. With regard to base resistance, AASHTO (5) Article C.10.8.3.5.4a states "Design based on side-wall shear alone should be considered for cases in which the base of the drilled hole cannot be cleaned and inspected or where it is determined that large movements of the shaft would be required to mobilize resistance in end bearing" (AASHTO, 2007). The philosophy embraced in the above comment gives a designer the option of neglecting base resistance. Under most conditions, the cost of quality control and assurance is offset by the economies achieved in socket design by including base resistance. Reasons cited for neglecting side resistance of rock sockets include (1) the possibility of strain-softening behavior of the sidewall interface, (2) the possibility of degradation of material at the borehole wall in argillaceous rocks, and (3) uncertainty regarding the roughness of the sidewall. Design for service limit states must, therefore, account for differences in side and base resistance mobilization as a function of axial displacement. Therefore, for drilled piles in Dubai, the side friction component provides the major contribution of axial load resistance and base resistance contribution is so limited and is ignored by many consultants. To enhance end bearing mobilization, methods as “base grouting” can be used (6), however, such techniques were not yet implemented in actual projects. Therefore, the following discussion is focused on optimization of side friction resistance only.

SETTLEMENT BEHAVIOUR AND LOAD TRANSFER PREDICTION:

Simple empirical correlations for drilled piles exist that provide a simple, yet accurate estimates of load – settlement behavior.

L1 - L2 Rule: Drilled Shaft Load - Settlement Behavior (Chen and Kulhawy, 2002).

Data base of high quality static loading tests has been used to establish the commonly known L1 - L2 rule (4); which describes the typical load – settlement and load transfer behavior of drilled shafts, as shown in the following schematic graph.

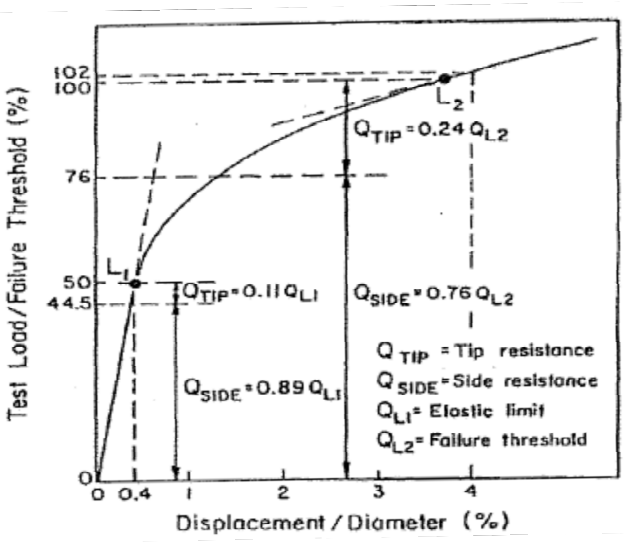


Fig. 3: Average Normalized Load-Displacement Curve that Forms the Basis of Load test Interpretation for Compression (Chen and Kulhawy, 2002).

The L1-L2 normalized curve presents typical behavior of drilled shaft under axial load, and showing the transition from linear to non-linear and includes a definition of failure load (at 3-5%D settlement for pile socketed in IGM). The L1-L2 criteria was found to be applicable to results of static loading tests in Dubai and can be used to evaluate results of static loading tests, and as a simple design tool.

LOCAL DRILLED PILE DESIGN PRACTICE:

The performance of drilled shafts in Dubai has been validated by many static loading tests on instrumented piles. In most cases, the results of static loading tests showed the actual capacity is much larger than the theoretical "nominal" design axial pile capacity. A study "Identification of soil and rock parameters by scientific interpretation of field measurements", 16th May, 2017 by Prof. Rolf Katzenbach was presented recently in Dubai showed a back calculation of results of static pile loading test showing that almost 50% of the pile length was only effective and necessary to resist the design load. The following graph shows results of many static pile loading tests conducted for piles within one major site in Dubai, plotted on the normalized L1-L2 graph, which indicates the actual capacity is much higher than the nominal design theoretical capcity.

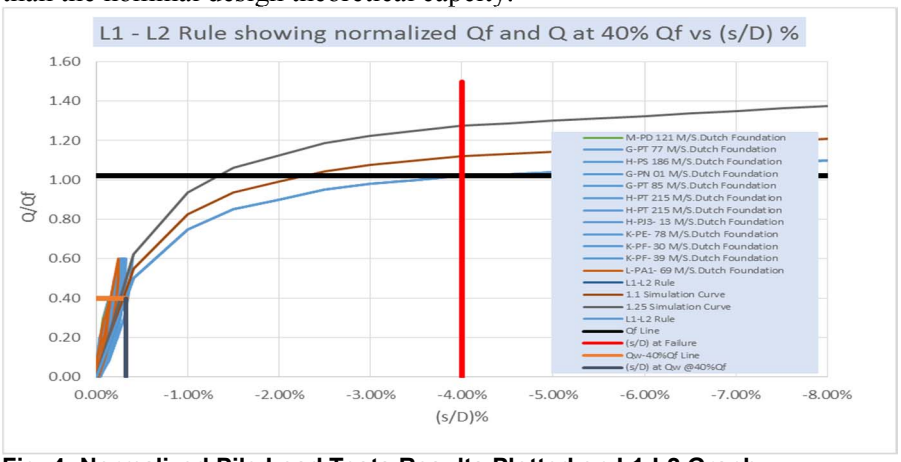


Fig. 4: Normalized Pile Load Tests Results Plotted on L1-L2 Graph.

The loading tests were conducted on working piles up to 150% of the nominal working load Qw. The nominal design is based on a global safety factor of 2.5, therefore, Qw = 0.4 Qf. By magnifying the L1-L2 simulation curve, it is found that the data fits with the 1.25 times magnified curve. Therefore, the actual pile design working load is >1.25 the adopted Qw, which leaves an important area for refinement of the theoretical design and make important savings. However, static loading tests conducted during construction stage on working piles are difficult to be used for design improvement. In few number of projects, tests are conducted on preliminary test piles during the design and pre-construction stage and has been effectively used to improve the theoretical design. Improvements of side friction resistance by >50% was achieved in several projects based on results of O-Cell pile loading tests during design stage. A typical example of 5 O-Cell tests conducted in one major project site showing maximum unit skin friction (fmax) versus theoretical estimated fmax from the site investigation results is shown in fig. 5.

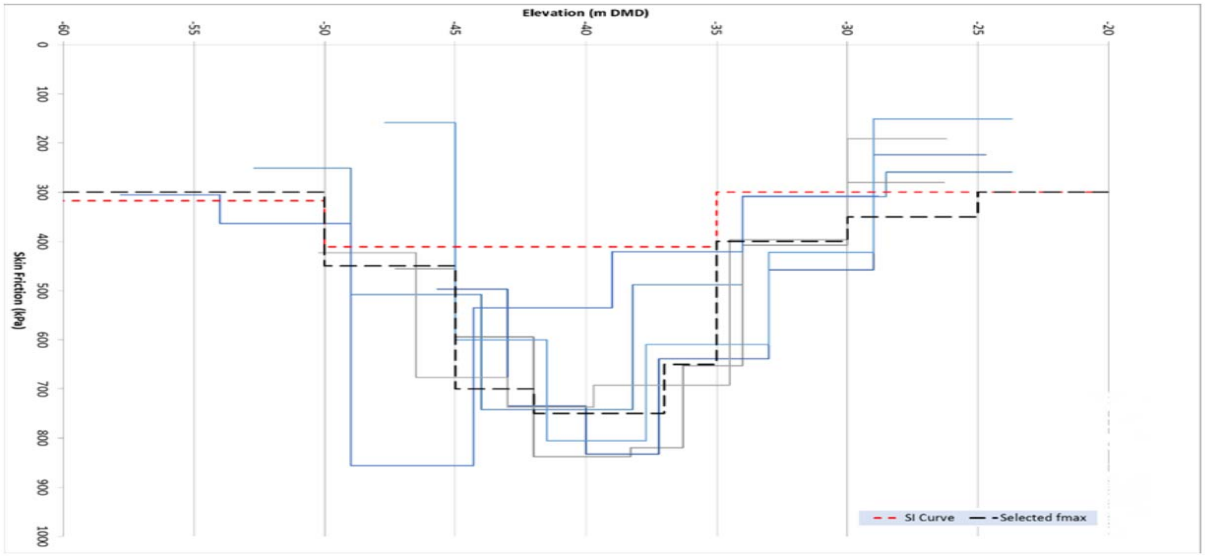


Fig. 5: O-Cell Tests on PTP piles showing Theoretical line (Red) and actual measured average unit friction.

The results of O-cell test for intervals far from the O-cell zone are under estimated because of limited development of friction resistance. Description of O-Cell tests & utilization of t-z curves for load test simulation and pile performance analysis are given in Fellenius (2014) :"Basic of Foundation Design (7) & Unipile software (8). The following set of unit friction mobilization versus displacement (t-z curves) from one of the above O-cell test results is presented below, that shows limited unit friction is mobilized away from the cell zone.

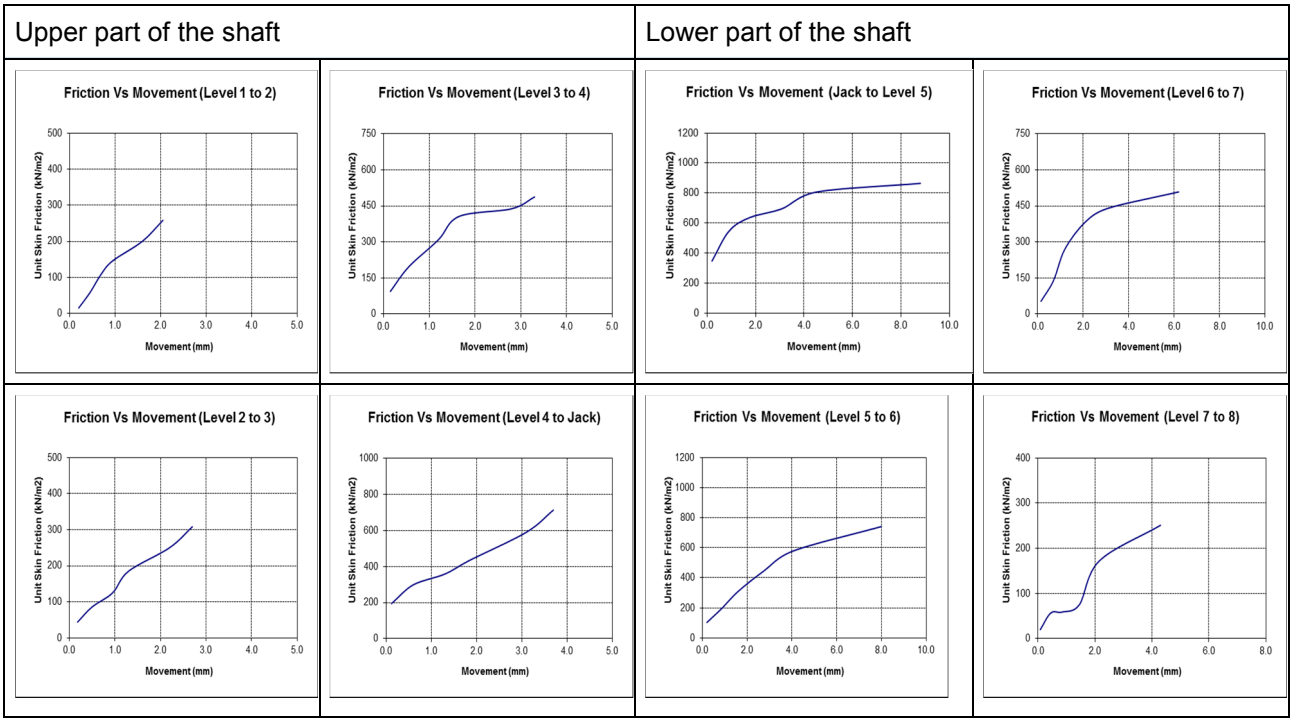
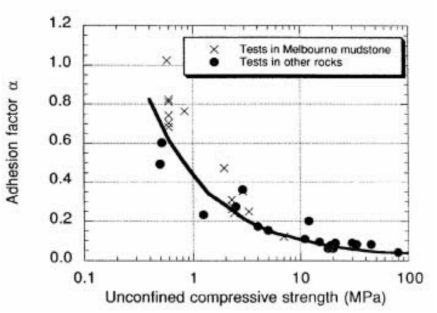


Fig. 6: Typical t-z curves for typical test pile (TP 8A – 1200m diameter).

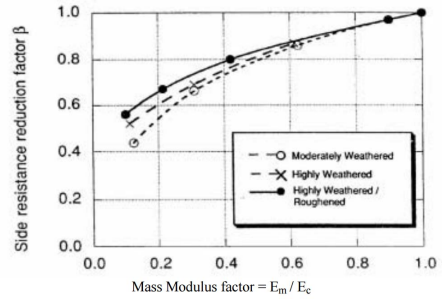
Therefore, optimization of the theoretical procedure for axial load estimate is of prime importance to bridge the gap between the conservative theoretical pile capacity estimates and actual pile behavior and achieve important savings. The use of preliminary tests piles is also encouraged as much as possible which provides reliable calibration of the theoretical assessed side friction and pile behavior.

THEORETICAL ASSESSMENT OF MAXIMUM SIDE FRICTION IN LOCAL PRACTICE:

In local practice, the max. side friction (fmax) is typically estimated with some empirical equation as Horvath and Kenney (9), however, the procedure of Williams and Pells (10) is more common. Williams and Pells proposed method for skin friction evaluation is described in (10 & 11). The relationship between compressive strength of rock in socket and side-wall shear resistance, or adhesion factor is presented below:

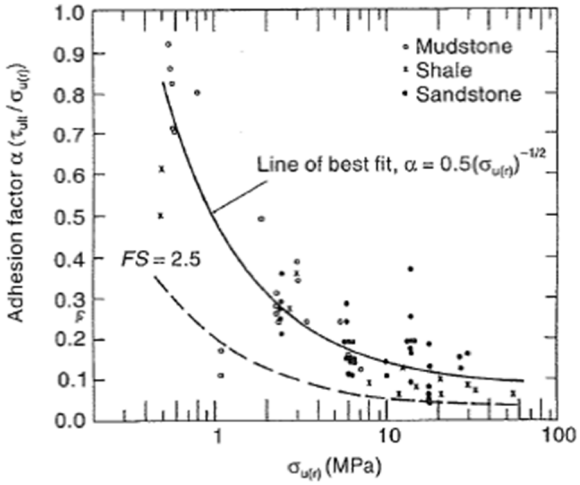


Adhesion factor α versus unconfined compressive strength (from Williams et al. 1980).



Side resistance reduction factor β versus mass modulus factor (from Williams et al. 1980).

A fitting curve is established as shown resulting in a simple equation as presented below:



Accordingly, *fmax = α.β UCS, where α = 0.5 (UCS)$^{-0.5}$, therefore,*
fmax = 0.5 β *(UCS)$^{0.5}$ Mpa, in which UCS is the unconfined compression strength in MPa.*

The reduction factor β represents rock mass discontinuities and Shaft – IGM interface roughness effects (e.g. use of bentonite vs chemical polymers, ..and other effects).

Fig. 7: Summary of Williams & Pells Method for Side Friction of Drilled Shaft (10 &11).

Bentonite Effect: The use of Bentonite slurry in advancing the pile shaft would cause the formation of bentonite cake causing smooth interface conditions. The use of other drilling fluids as chemical polymers would cause some improvement to skin friction. No data is available from local practice to provide an estimate of friction degradation due to method of pile installation. FHWA - NHI -10-016 (4), presents results of study (Brown 2002), in which side friction of piles advanced with different methods including dry polymer, liquid polymer, CAD (cased ahead), CFA (continuous Flight auger) and Bentonite, are compared.

In local practice, fmax is typically estimated assuming clean socket (where water or fluid polymer are used), however, where bentonite slurry is used, reductions of 20-30% are applied. The above Williams and Pells procedure provides a non-linear relationship (exponential) between the side friction adhesion factor and the rock strength. Non-linear relationships are more reliable than linear relationships as recommended by professional literature. According to Wiliams & Pells, procedure, the following main parameters determine the range of fmax:

a. Selection of representative Compressive Strength for each depth interval, and
b. Selection of reduction factor β,

For clean socket, the reduction factor β depends on (J) rock mass factor or modular ratio, as shown J-β relation (Williams & Pells) presented above.
In local practice, J is estimated from RQD (Rock quality designation) using the relationship (Bieniawski, 1984).
For most of the sites, RQD is <70% and hence a value of J <0.2 is selected. Accordingly, the value of β < 0.65 is also selected.

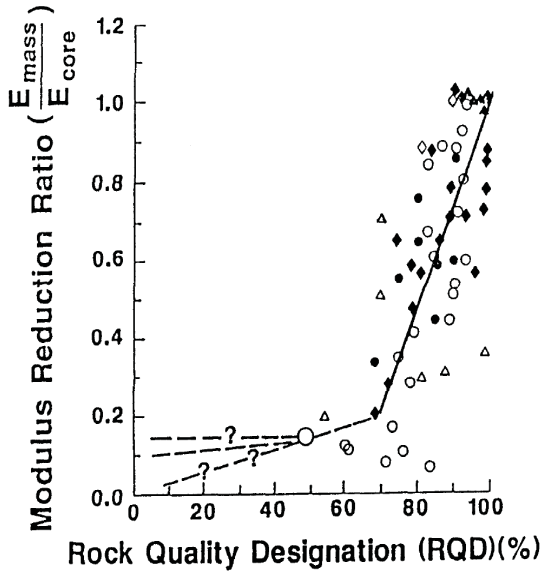


Fig. 8: Modulus Reduction Ratio as a Function of RQD (From Bieniawski, 1984).

Selection of design Compressive strength: The selection of compressive strength on the other hand is based on UCS (Uni-axial strength), which in the case of IGM provides a lower estimate of the rock strength. Further, large variations are typically obtained and therefore, the selection of design value for any depth interval becomes a difficult task!. The graph presents typical UCS profile and selected design curve for a major project in Dubai.

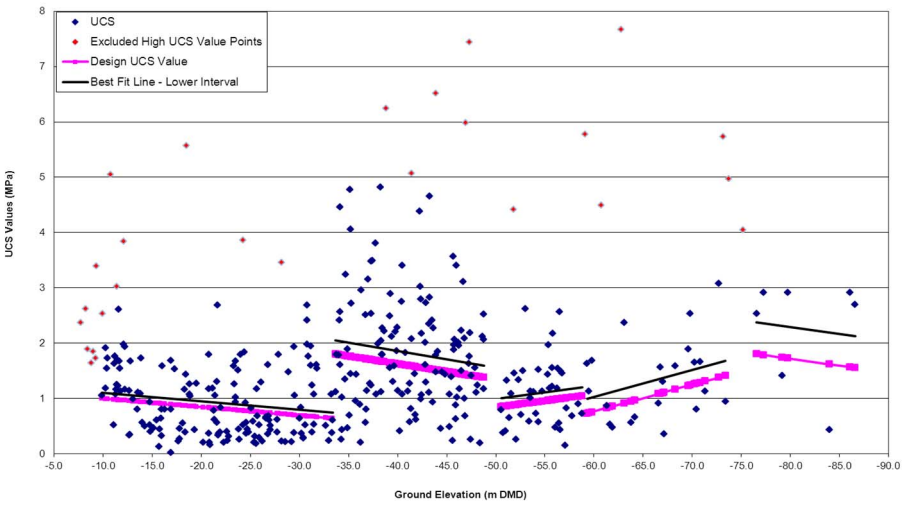


Fig. 9: Typical results of UCS tests profile showing large scatter of data, and showing selection of design UCS curve.

The graph shows that the profile is divided into "homogeneous" intervals, the extremely high UCS results are excluded, and design value which is less than the mean or best fit line depending on data variation and number of test data ("BS EN 1997-2004, Geotechnical Design, Part 1 – General Rules" and "A procedure for determining the characteristic value of a geotechnical parameter by A. J. Bond, Geocentrix Ltd., Banstead Surrey, United Kingdom".

The procedures for selecting both β and design UCS look satisfactory, however, the obtained fmax estimates are much less than actual resistance illustrated by actual loading tests.
Where preliminary pile loading tests (PTP) are conducted, a load test correction factor can be introduced as follows: fmax – corrected = $C_{correction}$ x fmax (from theoretical estimate).
However, for the general case, where PTP tests are not planned or considered, then the following optimization design steps are suggested.

OPTIMIZATION OF DESIGN PROCEDURE:
Selection of reduction factor β: The mass factor J is related to drilling parameters as fracture index or Fracture Frequency per meter in addition to RQD as shown on the following table (Tomlinson: Pile Design & Construction Practice (12)).

Table 1: Mass Factor J as Function of RQD and Fracture Frequency /m.

RQD (%)	*Fracture frequency per metre*	*Mass factor* j
0–25	15	0.2
25–50	15–8	0.2
50–75	8–5	0.2–0.5
75–90	5–1	0.5–0.8
90–100	1	0.8–1

It is noticed that the above J – RQD relation is less conservative than the above Bieniawski, 1984 relationship. The following typical example shows results of high quality drilling results in a tower site in Dubai showing the different drilling parameters, and indicating RQD is <50-60%

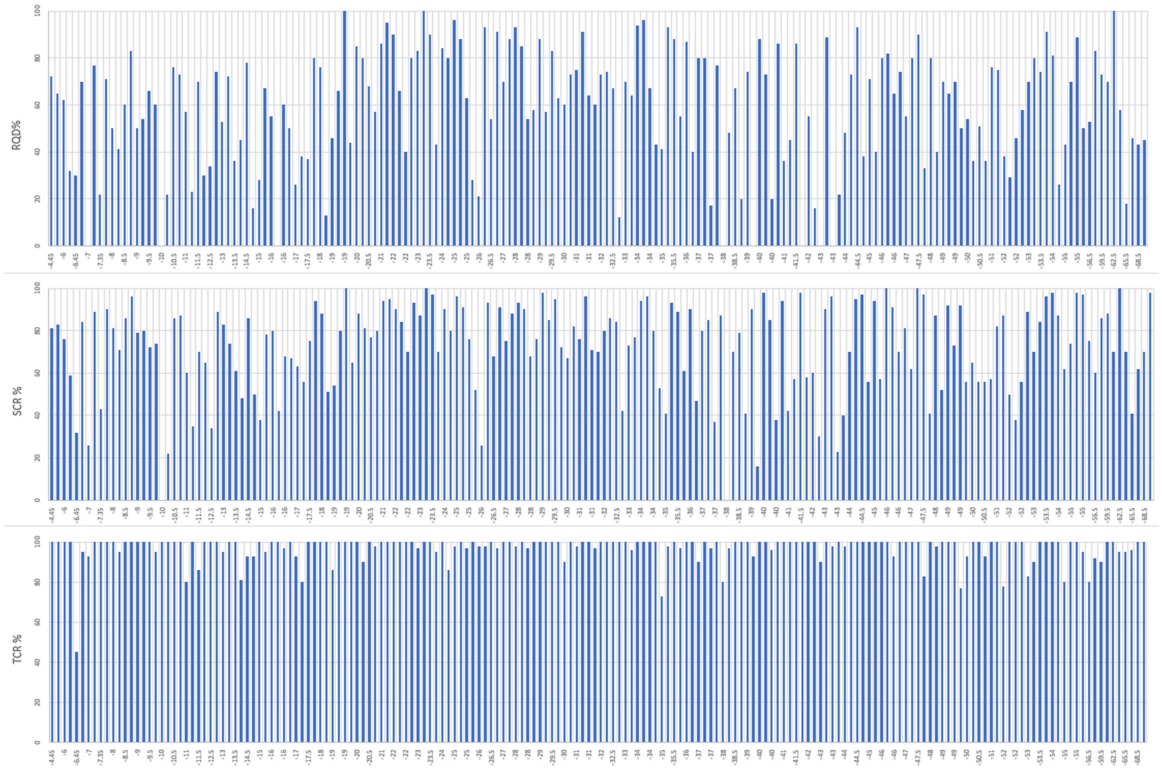


Fig. 10: Rock Core parameters – all BHs.

Fracture Index vs Fracture Frequency: Fracture Index for all the cores (number of natural fractures / core run) – as measured for all BHs is shown in the following figure.

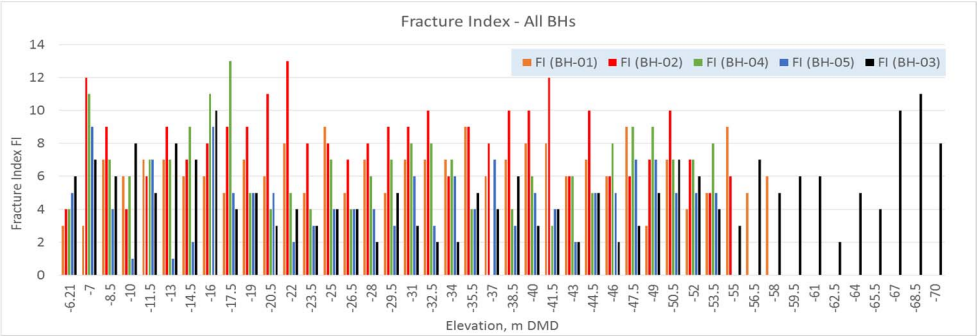
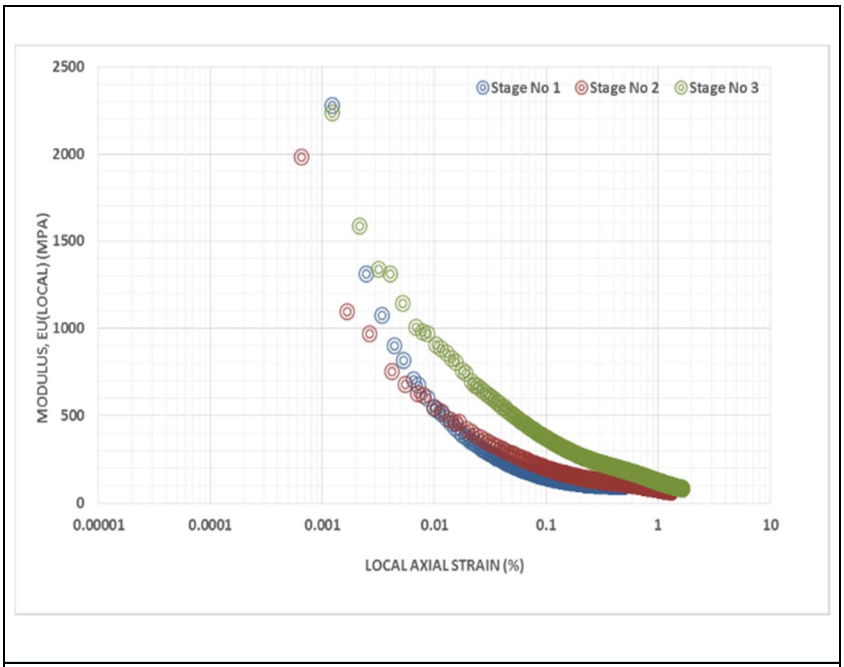


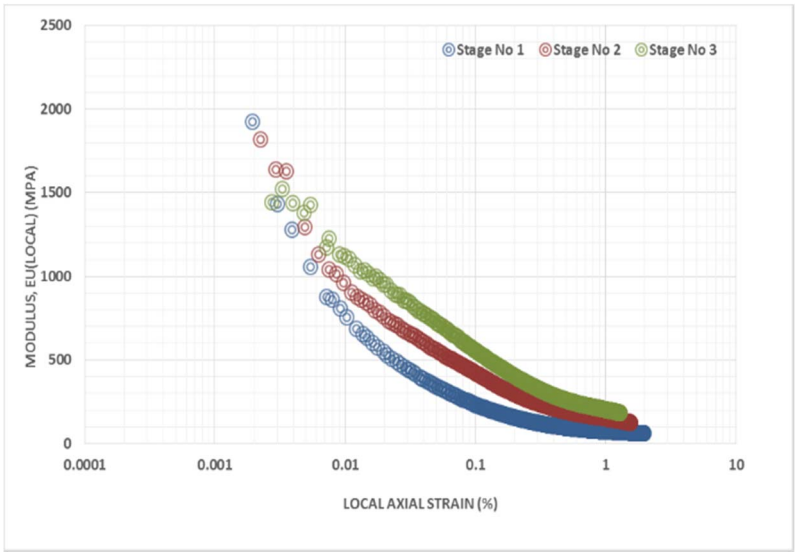
Fig. 11: Fracture Index (Fracture Frequency) vs Elevation – All Bhs.

Figure 11 indicates a representative Fracture Index of <8, noting the core run is 1.5m so the indicated results should be divided by 1.5 to five fracture frequency /m.
On the other hand J is defined as: E rock mass / E intact rock, and therefore it can be expressed as J= {(Vs-site)/(Vs-Lab)}^2, as Vs-lab represents shear wave velocity of intact core, and Vs-site represents rock mass quality. The ratio of Emass / Ecore may also represented by Er (re-loading modulus) measured with in-situ pressure-meter tests (PMT) to CIU laboratory tests (E at 0.1% axial strain). PMTs and in-situ shear wave velocity measurements are routinely conducted in Dubai but are not explicitly used for pile capcity design. For these tests results to be used to estimate the mass factor (J), CIU laboratory tests (consolidated undrained) tri-axial tests on intact core specimens of IGM with local strain and bender element tests shall be conducted. A typical result of multi-stage TX (CIU) test on IGM material is shown below presenting the local strain modulus vs axial strain. The results are very useful to estimate the representative modulus of IGM at given strain level, as 0.1% typically used for geotechnical analysis at service load level.



Extremely Weak Sandstone (Consolidation pressure: 150, 300, 600 kpa)

Fig. 12.1: Modulus degradation obtained from instrumented CIU Tri-Axial Test (Local Strain)



Very Weak Calciciltite (Consolidation pressure: 400, 600, 800 kpa)

Fig. 12.2 : Modulus degradation obtained from instrumented ClU Tri-Axial Test (Local Strain)

The following figure shows typical relationship obtained for the IGM modulus at 0.1 and 0.01% axial strain which represents small strain level.

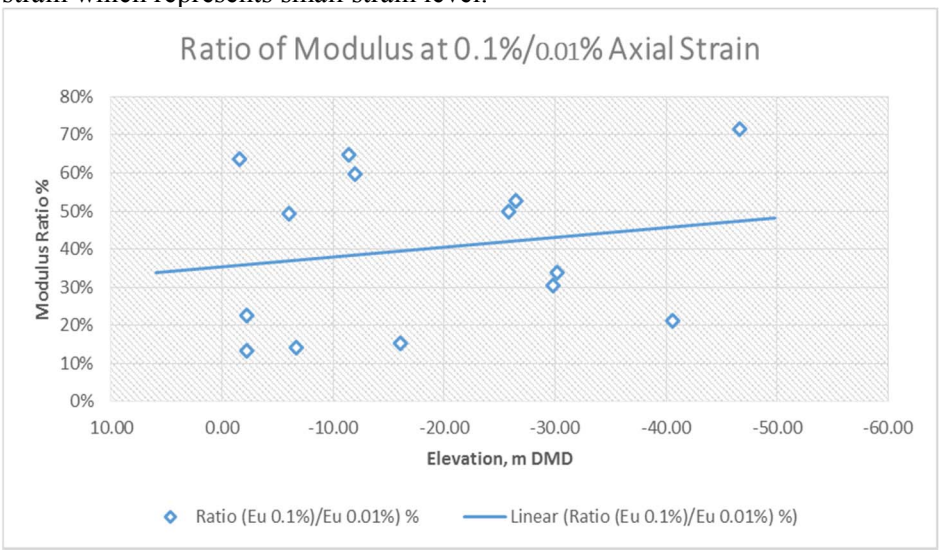


Fig. 13: Typical ratio of IGM modulus at 0.1to 0.01% Axial Strain obtained from Instrumented CIU Tri-axial tests.

Typical results from recently conducted investigation shows the correlation between PMT – Er and laboratory CIU modulus at 0.1% axial strain (local strain), which shows high ratio of about 1 between PMT – Er / Eu (local strain 0.1%), and indicating high mass factor J.

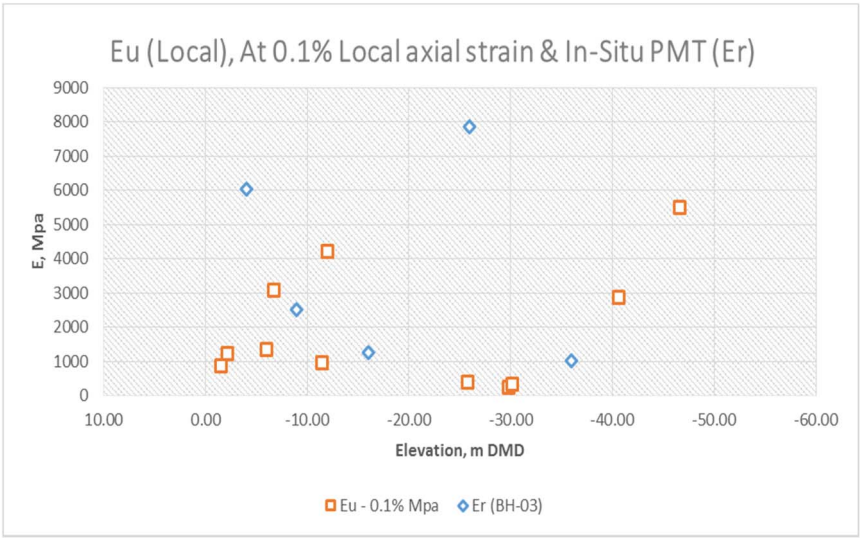


Fig. 14.1: Laboratory Modulus at 0.1% Axial Strain versus In-Situ Pressure meter Reloading Modulus – site 1.

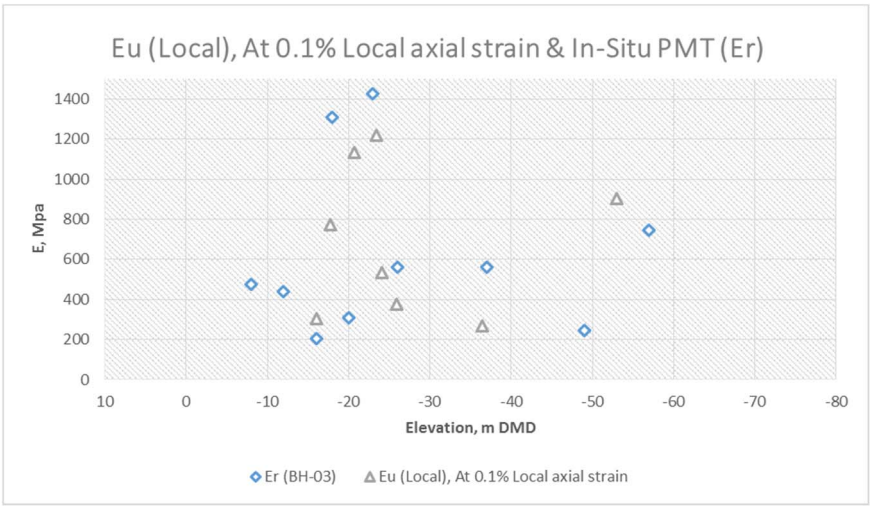


Fig. 14.2: Laboratory Modulus at 0.1% Axial Strain versus In-Situ Pressure meter Reloading Modulus – site 2.

The in-situ measured shear wave velocity is presented in the following typical profile recently measured in a prime site in Dubai.

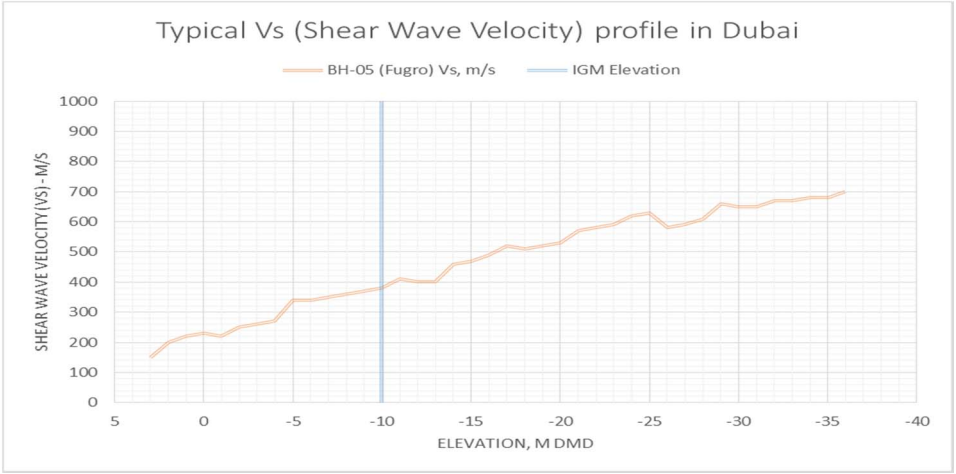


Fig. 15: Typical Down Hole Seismic Log of Shear Wave Velocity Profile in Dubai.

The laboratory measured Vs using bender element tests in CIU tests (after consolidation) ranged between 600 to 1000 m/s, giving J (Mass factor) = (Vs-site/Vs-lab)^2 of >0.4 in general for the sites included in this study.
Note: it is obvious that the global or total modulus typically measured and reported in standard site investigations from UCS tests is misleading and represents a fraction of the actual IGM stiffness. Measurements of global or total strain are affected by local stress concentration conditions near the ends of the test sample, and therefore, local strain is generally advised to be measured.

COMPRESSIVE STRENGTH OF IGM:
The uni-axial compressive strength is typically used to represent the strength of rocks. The compressive strength of Intermediate Geomaterials (IGMs), however, is highly affected by consolidation or confining pressure. High quality tests at GTC Lab in Dubai where recently conducted on many samples representing five main sites in Dubai showed a remarkable increase in compressive strength measured in CIU tests as consolidation pressure equal to in-situ overburden pressure (taking Ko = 1). The tests were conducted using computer controlled tri-axial testing equipment, on high quality samples with local strain and bender element tests. Photos of UCS and TX test machines are shown in Figure 16. All the tests were directly conducted by senior laboratory testing specialist (Hardev Sidhu).



Fig. 16: Photos of UCS and CIU tri-axial computer controlled testing machines (GTC-LAB, 2017)

Typical results are shown as follows: the CIU compressive strength is the deviatoric stress at failure. Linear trend line is added for each set of data for illustration only.

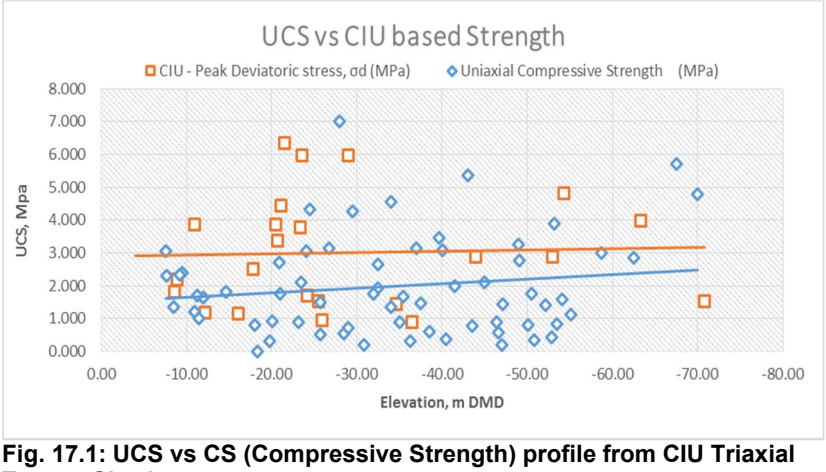


Fig. 17.1: UCS vs CS (Compressive Strength) profile from CIU Triaxial Tests – Site 1.

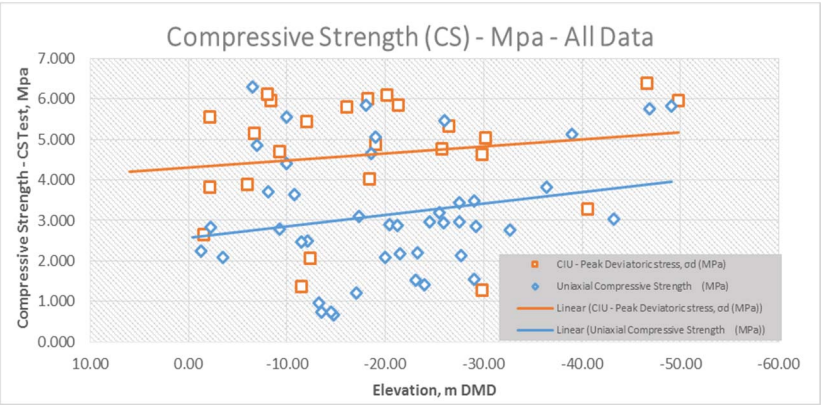


Fig. 17.2: UCS vs CS (Compressive Strength) profile from CIU Triaxial Tests – Site 2.

The compressive strength (CS) obtained from CIU tests is at least 50% greater than UCS tests for different rock types (Calcarenite, Sandstone, Conglomerates, Siltstone and Calcisitite).

The above strength profile represents the following typical site lithology.

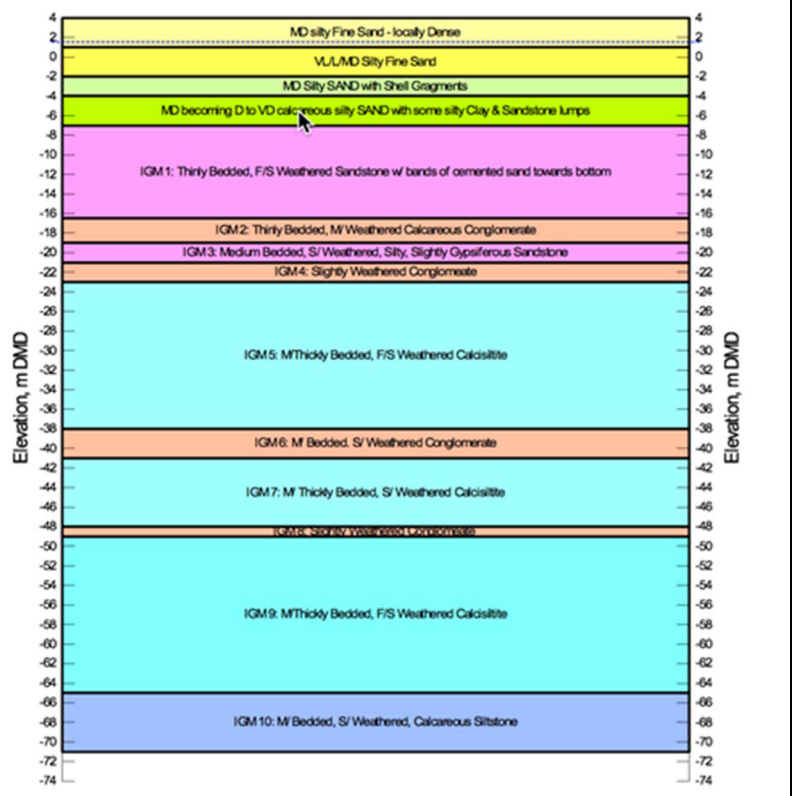


Fig. 18: Lithology of typical site in Dubai.

CONCLUSION:

Williams & Pells equation provides non-linear relationship with fmax, and includes parameters related to IGM (Intermediate Geo-Materials) -Shaft Interface (β), and rock strength. By combining the effects of proper selection of the mass factor J, and the use of Tri Axial based compressive strength, the following improvement is obtained:

Nominal maximum unit friction (fmax) = 0.5 β √UCS

For typical β = 0.65 normally selected, then fmax = 0.5x0.65 √UCS = 0.325 √UCS

By proper selection of mass factor J, then β would range between 0.7 to 0.75, and by using triaxial compressive strength (CIU) test values rather than uniaxial/unconfined compressive strength (UCS) test values, with CIU shown to be 1.5 UCS in Dubai, then
$f_{max} = 0.5x(0.7\text{-}0.75)x\sqrt{(1.5xUCS)}$, or $f_{max} = (0.42\text{-}0.46)x\sqrt{UCS}$
An improvement factor of 1.3 to 1.4 over nominal estimates of fmax. This level of improvement is substantial and is generally matching with results of static loading tests.

It must be however, pointed out that the use of this range of parameters requires that:
High quality drilling to be conducted such that realistic rock mass parameters are obtained.
In-situ PMTs and down-hole seismic tests to establish shear wave velocity and stiffness profiles representing the rock (IGM) mass.
Laboratory tri-axial (CIU) tests with consolidation pressure representing the overburden pressure, with local strain and few bender element tests.

Most of the above tests are typically conducted in site investigations for main projects in Dubai, however, the use of TX – CIU testing was used only in few projects.

The number of tests and locations, and estimate of representative strength and stiffness parameters for each homogeneous depth interval shall follow standard geotechnical evaluation methods and must be conducted by experienced geotechnical engineer, to be able to establish appropriate estimate of mass factor J and hence friction reduction factor β, in addition to selecting representative design compressive strength (CS) values for different layers.

The above procedure makes the application of Williams & Pells formula much more reliable and less conservative and approach results of actual static loading tests.

REFERENCES:

1. BS 5930:2015 – Code of Practice for Ground Investigations.
2. M.W O'neill, F.C Townsend, K.M Hassan, A. Buller, P.S Chan: "Load Transfer for Drilled Shafts in Intermediate Geomaterials. FHWA-RD-95-172.
3. Michael W. O'Neil and Lymon C. Reese (1999); "FHWA-IF-99-025. "Drilled Shafts: Construction Procedures and Design Methods"
4. Dan A. Brown, John P. Turner and Raymond J. Castelli; dated May (2010). "Drilled Shafts: Construction Procedures and LRFD Design Methods, FHWA - NHI -10-016 – Geotechnical Engineering Circular No. 10"
5. AASHTO LRFD Bridge Design Specifications, 4th Ed. 2007
6. Steven D. Dapp, Ph.D., P.E., Dan A. Brown & Associates Sequatchie, Tennessee, U.S.A Mike Muchard, P.E. :, "Experiences with Base Grouted Drilled Shafts in the Southern United Applied Foundation Testing, Tampaa, Florida, U.S.A."
7. Bengt Dr, H.. Fellenius (2014) :"Basic of Foundation Design" Bengt Dr, H.. Fellenius (2014) :"Basic of Foundation Design"
8. Unisoft Geotechnical Solutions Ltd : Unipile 5.0 (Pile Design Software)
9. Horvath, R.G. and T.C. Kenney. (1979). Shaft resistance of rock-socketed drilled piers. In Symposium on Deep Foundations, Atlanta, Oct. 1979, ed
10. A.F. Williams and P. J. N. Pells, (1981).Side Resistance rock sockets in Sandstone, mudstone and shale
11. Foundations on rock, 2nd ed., By Duncan C. Wyllie, 1999, Publisher: E & FN Spon)
12. Pile Foundation – Design and Construction Practice, By M.J Tomlinson, 4th Ed. 2004

BEHAVIOR OF LARGE DIAMETER BORED PILES IN CALCAREOUS CEMENTED SAND IN KUWAIT

Mohamed M. Al-Deab, Arup, Nottingham, UK, 004407444698544, Mohamed.Al-Deab@arup.com
Nabil F. Ismael, Kuwait University, Kuwait, nabil.ismael@ku.edu.kw

ABSTRACT

This paper outlines the behavior of large diameter bored piles in calcareous cemented sand in the state of Kuwait. This objective was achieved by investigating the characteristics of calcareous cemented sand in Kuwait, the reported capacities of large diameter bored piles (Diameter 0.6m to1.5m), estimation of pile capacity from pile load tests up to and/or near failure. Calibration of numerical models, constitutive laws and the corresponding soil parameters is an essential design stage to transfer the gained data from single pile load test to the design of the pile foundation. The ability of a Hardening Soil (H-S) model to represent the stress-strain behavior of calcareous cemented sand was checked and implemented to back-calculate the measured load-settlement performance of large diameter bored piles in calcareous cemented sand. The results show that the H-S model can reasonably represent the behavior of large diameter bored piles in calcareous cemented sand.

Keywords: calcareous cemented sand, H-S model, numerical analysis, bored piles, Load tests.

INTRODUCTION

Calcareous sands exist in many parts of the world where arid or semiarid conditions prevail. Competent deposits of cemented sands cover Kuwait city and parts of Saudi Arabia (Ismael et al. 1986; 1996, 1999). With major construction in Kuwait over the past 20 years, many multistory buildings, parking garages, housing projects, power stations and other structures were founded on this deposit and interest in the properties and behavior of calcareous cemented sands and behavior of large diameter bored piles in calcareous cemented sand have grown.

The properties of the calcareous cemented sand in Kuwait has been investigated by several researchers (Ismael et al. 1986; 1996, 1999). These investigations reveal that quartz is the major mineral phase and remaining mineral component is calcite. Stiffness increases with depth, and the reloading stiffness is greater than the virgin stiffness. Long term monitoring of Kuwait telecommunication tower, shows that the contact pressure and the pore water pressure beneath the ring foundation is almost constant. Regarding the behavior of bored piles in calcareous cemented sand in Kuwait, Ismael (1986, 1989, and 2001) reported values of the ultimate skin friction based of field test to the failure. Also, El-Mossallamy et al. (2006) estimated the ultimate base resistance of large diameter bored pile in calcareous cemented sand based on pile load test.

However, in the absence of an adequate information and field test results of the behavior of large diameter bored piles in calcareous cemented sand, local foundation is currently based on penetration tests and empirical correlations developed for other types of sand. This leads to uncertainty and conservative design. Therefore, a reliable approach of calculating the behavior of large diameter bored piles in calcareous cemented sand is required for rational design.

This paper outlines the implementation of Mohr-Columb (M-C) (Brinkgreve and P.A.Vermeer 1997) model and the Hardening Soil (H-S) (Brinkgreve and P.A.Vermeer 1997; Schanz et al. 1999) model in calculating the behavior of large diameter bored piles in calcareous cemented sand and validate the accuracy of these models against laboratory and field tests. The results shows limited capability of (M-C) model to calculate the behavior of calcareous cemented sand before failure, where the behavior is assumed linear. However, the calculated response by (H-S) model indicates very good agreement with the measured response at early loading stages and as well as the loading stages at yield. Also, the behavior of large diameter bored piles was analysed and discussed with emphasis on the calibration of numerical models and corresponding soil parameters. This is an essential design stage to transfer the gained data from single pile load tests to the design of the pile foundations.

© 2018 Deep Foundations Institute

CHARACTERISTICS OF CALCAREOUS CEMENTED SAND IN KUWAIT

Calcareous cemented sand is a complex material, which shows a highly non-linear behavior when subjected to stresses and stress changes. In order to model the behavior of the calcareous cemented sand, it is important to highlight the controlling factors of the behavior and then select appropriate model to represent this behavior. This section presents the main aspects, which control the behavior of calcareous cemented sand.

Stiffness

The stiffness of calcareous cemented sand is affected by three factor, the first factor is the stress level, where deeper samples show a higher stiffness than shallow samples Ismael (1999) and Al-Sanad and Ismael (1993). The second factor is the stress path, where the stiffness during the unloading is stiffer than primary loading Al-Sanad and Ismael (1993). The third factor is the density, where the denser the soil is, the higher the (peak) shear strength, but dense soils may show softening behavior after the peak, i.e. strength reduction towards a residual strength(Ismael 1999).

Drained Behavior and Time Dependency of Soil Behavior

Ismael and Al Sanad (1993) reported some typical values of permeability of calcareous cemented sand in Kuwait. They derived the obtained coefficient of permeability from the open hole tests, which were conducted in eight boreholes at different depth ranging from 12.0m to 40.0m. According to Ismael and Al Sanad (1993), the lowest value (~ 5 x 10-6 cm/sec) of the coefficient of the permeability measured by the falling head test was determined for silty fine sand layers between 35.0 and 40.0 m depth.

Also, Ismael and Al-Sanad (2001) presented the behavior of a ring raft antenna tower on calcareous cemented sand in Kuwait. The contact pressure under the raft was measured using pressure cells during the construction in 1988 and after construction in 1995. The reported performance included measurement of contact pressure and ground displacement below the tower foundation. The contact pressure was more or less stationary. The reported excess pore water pressures induced by loading of the ground by tower construction, were insignificant and the pressure cells responded mainly to the ground water table variation. Therefore, it is concluded that the behavior of the calcareous cemented sand is more or less a drained behavior.

NUMERICAL ANALYSIS

The numerical analysis scheme of the large diameter bored piles in calcareous cemented sand included five stages as follows. This section shows details of each stage

Stage 1: Selecting (M-C) and (H-S) Models to Represent the Response of the Calcareous Cemented Sand.

To calculate the stress strain response of the calcareous cemented sand in Kuwait, elasto- plastic models were considered to represent the irreversibility of a portion of the strains, stress-path dependency, and volume changes due to shear stresses (shear-dilatancy). Among elasto-plastic models, (M-C) and (H-S) models were selected. (M-C) model was selected because of its simplicity as a first order model, where it captures the failure behavior, while (H-S) model was selected because it can calculate both elastic and near failure behavior using plasticity framework and non-associated flow rule. In addition, (H-S) can simulate shear hardening and volumetric hardening. It provides stress dependency stiffness, and it represents the hyperbolic stress-strain response.

- ***Stage 2: Estimate and Derive Preliminary Model Parameters for (M-C) and (H-S) Models from the Published Soil Properties.***

Model parameters of both (M-C) and (H-S) model can be divided in two categories namely, basic model parameter and advanced model parameter. The Basic model parameters include the friction angle (ϕ), the cohesion intercept (c), and stiffness (E). the advanced soil parameters are unloading stiffness (E_u), reference stress level (P_{ref}), Poisson's ratio (u), Poisson's ratio for unloading and reloading (υ_{ur}), dilatancy angle (ψ), value of at rest earth pressure coefficient (K_0)in primary

one-dimensional compression (k^{nc}_0), the power of the stress-dependent stiffness formulation (m), and failure ratio that determines the strain level at failure (R_f). Table 1 shows (M-C) and (H-S) proposed preliminary model parameters as reported and concluded from the literature such as friction angle, loading and unloading stiffness, and cohesion.

For Poisson's ratio (υ), it is assumed that Poisson's ratio for drained condition varies in narrow range of 0.25 to 0.30 (Ismael, 1990). For unloading condition, Poisson's ratio assumed as 0.20. Coefficient K_0 in the primary consolidation calculated from k^{nc}_0=1-sin ϕ (Jaky, 1948), while for unloading path $K_0 = (1-\sin\phi)\ OCR^{\sin\phi}$ (Kulhawy, 1982). The dilatancy angle (ψ) assumed to be 0 - 2 degrees and it was estimated from $\phi_{max}=\phi_{cv}+0.8\ \psi$ (Bolton, 1986), where ϕ_{cv} estimated from (Kulhawy and Mayne, 1990) by assuming that calcareous cemented sand is angular medium dense poorly graded sand, and the quartz is the major mineral. In addition, Ismael (1993) reported that the residual friction angle is greater than peak angle by one to two degrees, which can substantiate the proposed range of the dilatancy angle. The value of the power of the stress-dependent stiffness (m) assumed as 0.5. (Ismael, 1990).The failure ratio (R_f) assumed as 0.9 and P_{ref} assumed as 100 kPa. (Kondner, 1963)

On the other hand, from practical design point of view, it is important to start the geotechnical design with preliminary soil parameter and then develop the design further according to the site specific soil parameters. Therefore, the parameters listed in Table 1 used to derive preliminary upper bound and lower bound parameters of the calcareous cemented sand. Table 2 shows the suggested preliminary upper and lower bound.

Stage 3: Verify the Back Calculated Response by (M-C) and (H-S) Models against Reported (CD) Triaxial Shear Test Results.

Ismael (1990) performed an isotropicaily Consolidated Drained (CD) triaxial tests with volume change measurements on calcareous sand samples under confining pressure of 140 and 630 kPa. The (CD) test results indicated no cohesion intercept and an angle of shearing resistance of 34 degree.

These strength parameters and the derived stiffness (E_{50}) from the (CD) test were used to back calculate the soil response by both (M-C) and (H-S) model. Table3 presents the parameters of M-C and H-S model. In Mohr -Coulomb model, two values of stiffness were estimated owing to the stress dependency stiffness limitation of (M-C) , therefore stiffness value of 15 MPa was estimated to simulate the behavior under confining pressure of 140 kPa. While, stiffness value of 33.25 MPa was estimated to simulate the behavior under confining pressure of 630 kPa. Figs 1 and 2 show the calculated stress-strain curve of the calcareous sand versus the measured stress-strain curve at confining pressure of 140 kPa and 630 kPa respectively.

- ***Stage 4: Estimate Preliminary Skin Friction and Base Bearing Values of Large Diameter Bored Piles.***

Ismael et. al (1986) reported that bored piles could develop a substantial skin friction in dense weakly cemented calcareous sand soil. They recommended value of 100 kPa based on results of five piles that have been tested to the failure. On the other hand, Ismael (1989) reported that bored piles in calcareous dense sand could develop low values of the skin friction.in order of 45-50 kPa. Also, Ismael (2001) reported that bored piles in weakly cemented calcareous sand could develop a significant skin friction of 94 kPa according to results of single pile load. These results were based on field tests on bored pile subjected to axial uplift. From these results, it could be concluded that cementation of the calcareous sand affect the magnitude of the developed skin fiction of the bored piles in the calcareous cemented sand. The skin friction ranges between 45 kPa to 100 kPa.

El-Mossallamy et al. (2006) reported Salmiya complex case study. This case study was about the behavior of large diameter bored piles in calcareous cemented in Kuwait. In Salmiya Complex, three pile load tests were conducted. These tests are two compression pile load test and one tension pile load

test. The results were analyzed (El-Mossallamy et al. 2006) and the ultimate average skin friction of 80 kPa and ultimate base resistance of 3.5MPa were estimated. The skin friction values by El-Mossallamy et. al. (2006) agrees with the results reported by Ismael et. al (1986), Ismael (1989), and Ismael (2001).

Table 1. Summary of derived preliminary parameters for (M-C) and (H-S) model.Parameter	**Value**	**Test Method**	**Sample Type**	**Depth, m**	**Reference**
Dry unit weight	17.47 to 18.6 kN/m3		Undisturbed	0.30 to 3.50 m	Ismael (1990,1993, 1996,1999)
Saturated Unit Weight	19.60-20.21 kN/m3		Undisturbed	0.30 to 3.50 m	Ismael (1990,1993, 1996,1999)
Young Modulus (E)	E 50= 14.8 MPa at confining pressure of 100 kPa	CD triaxial test	Undisturbed from large bulk sample	1m	Calculated from Ismael (1990)
	E50 = 17.47 MPa at confining pressure of 100 kPa	CU triaxial tests	Undisturbed from large bulk sample	0.3-1.0 m	Calculated from Ismael (1999)
Unloading-Reloading Young Modulus (E_{ur})	Reloading modulus can be assumed as 2 to 2.5 times that the virgin modulus according to plate load test results conducted by Al Sanad and Ismael (1993).				
Friction angle (ϕ)	34	CD triaxial tests	Undisturbed from large bulk sample	1m	Ismael (1990)
	35 degree	Direct shear	Undisturbed from large bulk sample	0.5	Ismael (1993)
	31 degree	CU triaxial tests	Undisturbed from large bulk sample	0.6	Ismael (1996)
	34.2 to 38.5 degree (range for four samples from different depths)	CU triaxial tests	Undisturbed (triple tube core barrel)	0.30 to 3.50 m	Ismael (1999)
Cohesion intercept (c)	0 kPa	CD triaxial tests	Undisturbed from large bulk sample		Ismael (1990)
	30 kPa	CU triaxial tests	Undisturbed from large bulk sample	0.6	Ismael (1996)
	90 kPa	CU triaxial tests	Undisturbed (triple tube core barrel)	3.5	Ismael (1999)

Table 2. Upper and lower bound of calcareous cemented sand

Parameter	Lower Value	Upper value	Unit
Material Type	Drained	Drained	--
γ_{dry}	17.47	18.60	kN/m^3
γ_{sat}	20.42	19.60	kN/m^3
E_{50}^{ref} (drained)	14.8	17.47	MPa
E_{oed}^{ref} (drained)	14.8	17.47	MPa
E_{ur}^{ref} (drained)	40	40	MPa
(m)	0.5	0.5	--
C^{ref}	1	80	kPa
ϕ (drained)	34	39	Degree
ψ	0	2	Degree
υ_{ur}	0.2	0.2	--
P_{ref}	100	100	kPa
$K_0^{nc} = (1-\sin\phi)$	0.441	0.3707	--

Table 3. (M-C) and (H-S) model parameters for back calculating the calcareous sand soil response

Parameter	(H-S) Model	(M-C) Model	Unit
Material Type	Drained	Drained	--
γ_{dry}	17.47	17.47	kN/m^3
γ_{sat}	20.42	20.42	kN/m^3
E_{50}^{ref} (drained)	14.8	--	MPa
E_{oed}^{ref} (drained)	14.8	--	MPa
E_{ur}^{ref} (drained)	40	--	MPa
(m)	0.5	--	--
E'	--	15/33.25	MPa
C^{ref}	1	1	kPa
ϕ (drained)	34	34	Degree
ψ	0	0	Degree
υ_{ur}	0.2	--	--
υ	--	0.3	
P^{ref}	100	--	kPa
K_0^{nc}	0.441	--	--

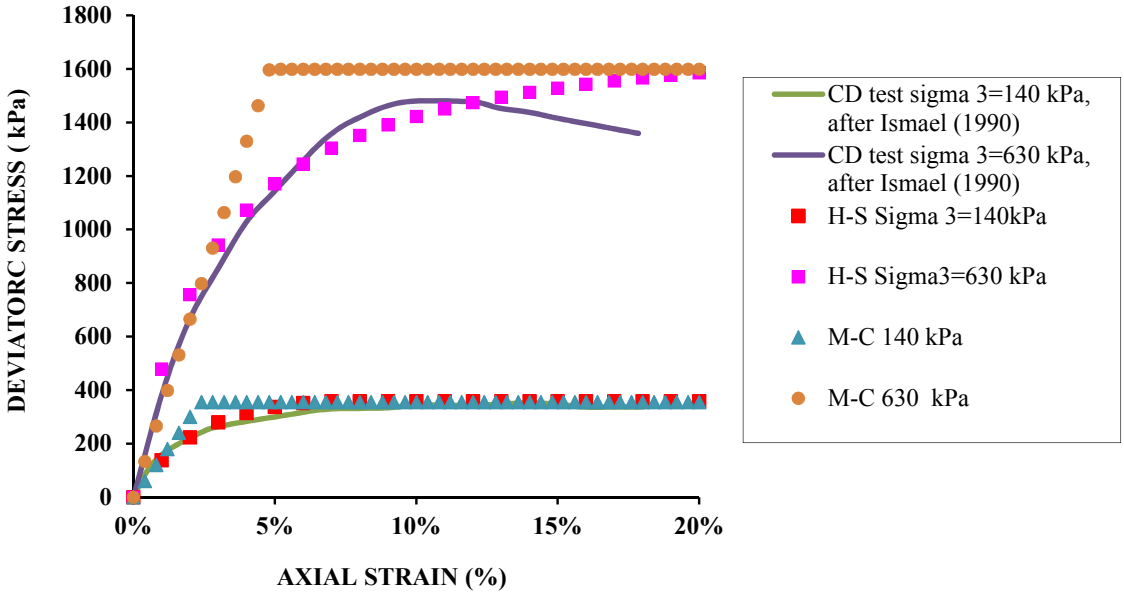


Fig.1: Verification of the back calculated stress strain (M-C) and (H-S) models

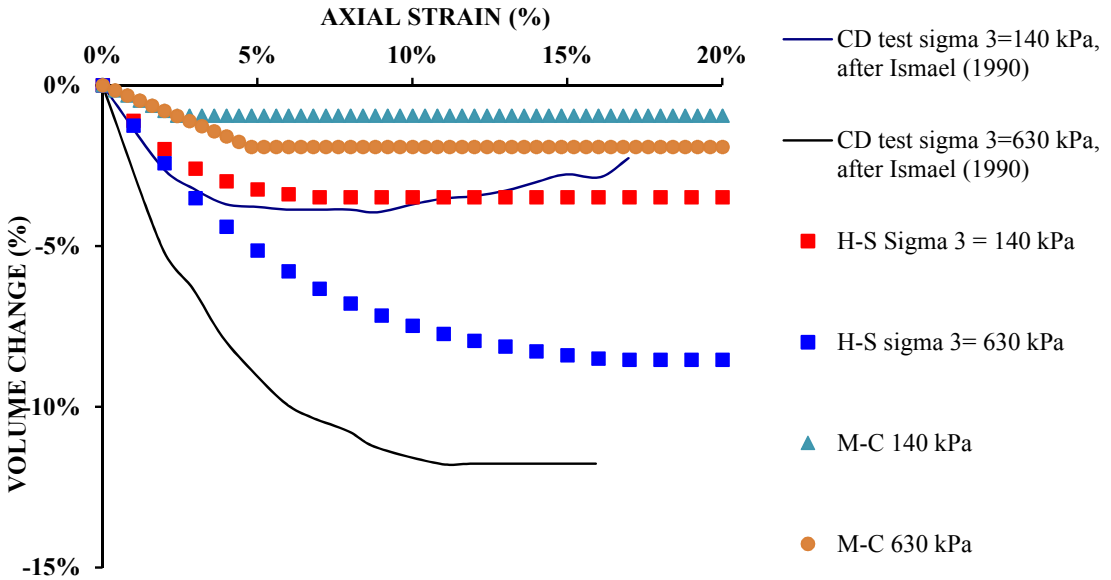


Fig. 1. Verification of the back calculated volume change by (M-C) and (H-S) models

- **Stage 4: Verification of estimated preliminary skin friction and base bearing values of large diameter bored piles**.

In 2005, Kuwait Bruckner Company Ltd. performed a near failure pile load test in calcareous cemented sand (H. Jarada and R. Bissinger, personal communication, July 2006). This pile load test was part of a testing program at Fintas area, Al Ahmadi province, Kuwait .The geotechnical information at the testing site indicated calcareous cemented sand up to 30 deep, with different degrees of cementation. The test pile was a bored pile with a diameter was 800mm, and a length of 22m. The maximum recorded

settlement during the pile load test was 73 mm, which is almost 10% of the pile diameter, which suggests near failure behavior and a significant base bearing had been mobilized. Figure 3 shows the load settlement curve for the test pile. This data was used to verify the preliminary design values presented in stage 4, where the verification included comparing the recorded ultimate load at approximately 10% of the pile diameter against two calculated ultimate loads .The first calculated ultimate load was the extrapolated ultimate load according to (Chin, 1970). The second calculated ultimate load was calculated in accordance with the ultimate skin friction and end bearing presented in stage 4.Table 4 shows a comparison between the measured and the calculated ultimate load.

Table 4. Summary of estimated pile capacity

Measured Ultimate Load [kN]*	Ultimate Load [kN] Extrapolated from (Chin 1970)	Ultimate Load [kN] Estimated from preliminary design values presented in stage 4
10000	12870	7279**

*Recorded at approximately 10% of pile diameter during the pile load test.

** (average skin friction= 100 kPa and bas bearing = 3.5 MPa)

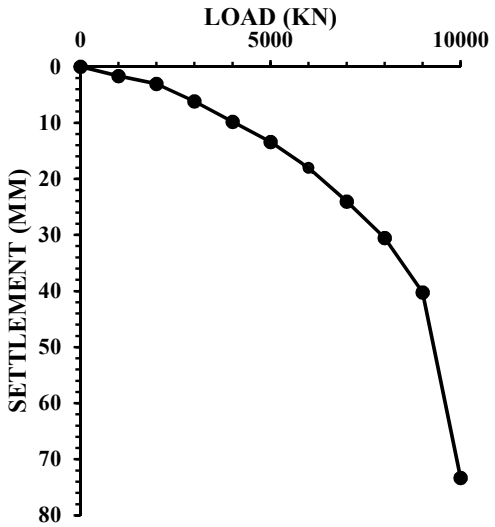


Fig. 2. Pile Load Settlement Results (800mm Diameter, Pile Length =22m), after (KBC, 2006)

- **Stage 5: Verifying and calibrating the back calculated pile response against reported pile load test results.**

In this stage, the preliminary parameters of (H-S) was calibrated against pile load test results conducted by Kuwait Bruckner Company (July 2005).This calibration aimed to overcome the lack of detailed site specific information of Fintas testing site and to verify the derived preliminary parameters for H-S models.

To model the large diameter bored piles, volume pile element were considered.to model the linear elastic behavior of the concrete material of the bored pile and the interface between the bored pile and surrounding soil considered as rough interface

The verification and calibration of this stage included finite element analysis by Plaxis 3D, where a working area of 20 m x 20 m x 40 m has been used. The pile was modeled as a volume element in the center of the mesh. The concrete material was modeled as linear elastic material with Young's modulus (E) of 30000 MPa. The loading of the volume piles was modeled as prescribed settlement at the pile top.

The Plaxis 3D results show that the calculated pile performance by the upper bound preliminary values is slightly different from the field response. This slight different indicates that the preliminary values can provide a preliminary pile response and this difference can be attributed to a slight difference in soil proprieties at the test site. Therefore, in order to calibrate the model parameters and to obtain better matching with the field result of the pile load test, the upper bound preliminary soil parameters were refined. The refined parameters as well as the upper values are presented in Table 5.

Table 5. Refined and Upper Values of the Calcareous Cemented Sand

Parameter	Refined Value	Upper value	Unit
Material Type	Drained	Drained	--
γ dry	18.64	18.60	kN/m3
γ sat	19.60	19.60	kN/m3
E50 ref (drained)	25	17.47	MPa
E_{ur} ref (drained)	65	40	MPa
(m)	0.5	0.5	--
C ref	30	80	kPa
ϕ (drained)	35	39	Degree
ψ	0	2	Degree
υ_{ur}	0.2	0.2	--
P_{ref}	100	100	kPa
K_0^{nc}	0.4264	0.3707	--

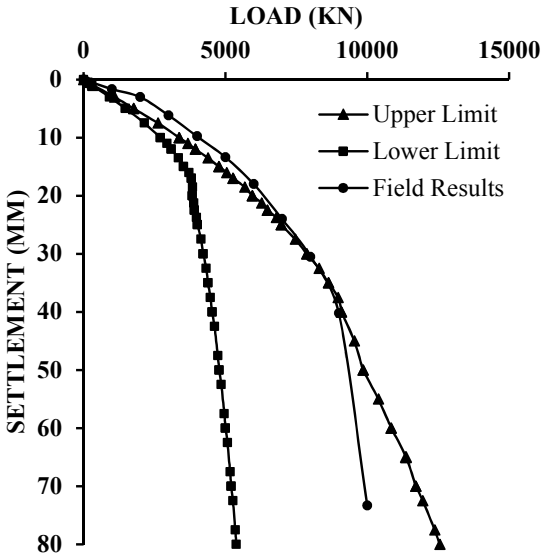


Fig. 3. Pile Load tests versus Upper bound and lower bound soil response.

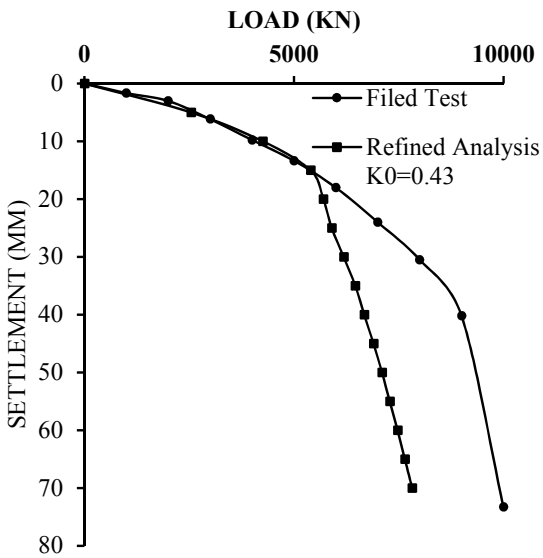


Fig. 4. Pile load response versus the refined analysis

DISCUSSION OF THE RESULTS

For the calculated behavior of the calcareous cemented sand, Figs. 1 and 2 show that the (H-S) model represent the response of the calcareous sand. At confining pressure of 140 kPa, the calculated response has a very good agreement with the measured response at early loading stages and as well as the loading stages at yield. However, at confining pressure of 630 kPa, the calculated response shows a slightly lower yield stress than the measured yield stress. In addition, Figs. 1 and 2 show the limited capability of (M-C) model to calculate the behavior before failure, where the behavior is assumed linear. For the volume change during shearing, both models overestimate the response.

For the calculated response of the large diameter bored piles, the results in Figs. 4 and 5 show stability of the analysis according to the input parameters. This stability can be seen as the upper parameters of the calcareous cemented sand result in higher pile capacity than the lower parameters. Also, the results of the upper soil parameters of the calcareous cemented sand agrees to some extend with the field results specially at the early stages of loading, which can be considered as working loads from practical point of view. However, the calculated pile response at late stages of loading of the volume pile was higher than the field results.

The calculated pile performance by the upper bound preliminary values is slightly different from the field response. This slight different indicates that the preliminary values can provide a preliminary pile response and this difference can be attributed to a slight difference in soil proprieties at the test site. The results of the volume piles after the refinement of the upper soil parameters show good agreement between calculated and measured values up to loads of 6000 kN. This refinement was achieved by refining the Young's modulus to match the slope of the first portion of the load settlement curve of the field load test, then refining the shear strength parameters (c, ϕ) to match the transition behavior of the pile from friction behavior to mobilize the end bearing.

Nevertheless, the volume pile element shows lower pile capacity than the field results. This difference between capacities may be attributed to the difference between the calculated initial stresses and the actual initial stresses. The results show that increasing the initial stresses when using (K_0) of 0.43 leads to a significant increase of the pile capacity.

CONCLUSIONS AND RECOMMENDATIONS

This research utilized the available information about the calcareous cemented sand to derive the required parameters of Mohr-Colum and Hardening Soil models. Hardening Soil model is a true second order model, where it can calculate both elastic and near failure behavior by using plasticity framework and non-associated flow rule. The following conclusions were reached:

1. Hardening Soil can simulate shear hardening and volumetric hardening; it provides stress dependency of the stiffness in addition to hyperbolic stress strain response as in triaxial test.
2. The Hardening Soil model shows its ability to simulate the load settlement of large diameter bored piles in calcareous cemented sand.
3. The analysis shows that the calibration of numerical models and corresponding soil parameters is an essential design stage to transfer the gained data from single pile load test to the design of the pile foundation. However, the presented numerical modeling has some assumptions and limitations. Additional laboratory testing, field testing, and pile instrumentation need to be done to overcome these assumptions and limitations.

ACKNOWLEDGEMENT

The study reported herein was performed during PhD program of the first author. Thanks to Prof. Dr. Fathalla El Nahhas, Professor of Soil Mechanics and Foundation and Prof. Dr. Yasser El Mossallamy, Professor of Soil Mechanics and Foundation, Soil Mechanics and Foundation Department for their kind supervision, sincere assistance and valuable guidance during the preparation of the PhD thesis and the abstract of this paper.

REFERENCES

1. Al-Sanad, H. A., and Ismael, N. F. (1993). "Settlement of Circular and Ring Plates in very dense calcareous Sand."Journal of Geotechnical Engineering, ASCE, 119(4), 622-638.
2. Brinkgreve, R. B. J., E.Engin, and W.M.Swolfs. (2012). Plaxis 3D, Plaxis bv, Delft, Netherlands.
3. Brinkgreve, R. B. J., and P.A.Vermeer. (1997)."Plaxis Finite Element Code for Soil and Rock." A.A. Balkema, Rotterdam.
4. Chin, F.K. (1970)."Estimation of the Ultimate Load of Piles from Tests not carried to Failure." Proceedings of the Second Southeast Asian Conference on Soil Engineering, 83-91.

5. El-Mossallamy, Y.M., El-Nahhs, F.M., Essawy, A.S. (2006)."Innovative Use of Piled Raft Foundation to Optimize the Design of High Rise Buildings." 10th Arab Structural Engineering Conference, Kuwait. 2006.
6. Ismael, N. F., Mollah, M. A., and Al-Khalidi, O. (1986)."Geotechnical Properties of Cemented Soils in Kuwait "Australian Road Research Journal, June.
7. Ismael, N. F. (1990). "Bearing Capacity of Footing on Calcareous Cemented Sand." Japanese Society of Soil Mechanics and Foundation Engineering, 30(3), 81-90.
8. Ismael, N. F., and Al-Sanad, H. (1993). "Plate Loading Tests on Weakly Cemented Surface Sand." Geotechnical Engineering, 124(133-150).
9. Ismael, N. F. (1996). "Loading Tests on Circular and Ring Plates in Very Dense Sand." Journal of Geotechnical and Geoenvironmental Engineering, ASCE, 122(4), 261-287.
10. Ismael, N. F. (1999). "Properties and Behavior of Cemented Sand Deposits in Kuwait." Japanese Society of Soil Mechanics and Foundation Engineering, 39(4), 47-57.
11. Ismael, N. F., and Al-Sanad, H. (2001). "Performance of Ring Raft for Antenna Tower on Cemented Sand in Kuwait." Kuwait Journal of Science and Engineering, 28(1), 94-113.
12. Kondner, R. L. (1963). "Hyperbolic Stress Strain Response: Cohesive Soil " Journal of Geotechnical and Geoenvironmental Engineering, ASCE, 89(115-143).
13. H. Jarada and R. Bissinger, personal communication, July 2006
14. Schanz, T., P.A.Vermeer, and Bonnier, P. G. (1999). "The hardening Soil Model: Formulation and Verification, " Beyond 2000 in Computational geomechanics-10 years of Plaxis, Balkema, Rotterdam.

COST-BENEFIT ANALYSIS OF FOUNDATIONS WITH REVIT-ASSISTED: CASE STUDY

Mateus N. Farina, Student, UniversityofPernambuco, Recife, Brazil, mateusfarina@gmail.com

Alexandre D. Gusmão, Professor, University de Pernambuco, Recife, Brazil, gusmao.alex@ig.com.br

ABSTRACT

This paper has the objective of demonstrating and analyzing the best alternative in relation to the cost-benefit of foundation in a residential building containing 11 stories. Some types of foundations were analyzed in order to obtain the best of the options previously chosen. Based on the construction in question and some factors (cost and productivity), an analysis was made to choose the most indicated types of foundation, and later the cost-benefit comparison was made. The chosen options were superficial foundation with footings (solution adopted in the work), and deep foundation through continuous flight auger piles or steel piles. The Revit program was used in the BIM platform to model all the alternatives, in order to assist in the visualization of the project, as well as in the respective quantitative ones. With study of the types of foundations, it was possible to verify which one would be the most suitable for the construction.

Keywords: foundations, footings, continuous flight auger pile, steel pile, Revit, BIM.

 © 2018 Deep Foundations Institute

INTRODUCTION

Importance of the project

The foundations area is of great importance in civil engineering, as any well-executed construction must begin with a suitable choice of foundation type. In order to choose the best option, a preliminary study of several factors, such as the analysis of the subsoil and the structure to be constructed, must be carried out. One of the major problems in today's construction is the choice of foundation type, where cost is taken into account without analyzing factors such as productivity and interference with neighbors.

This paper seeks the best foundation solution for the construction, where some factors are considered that bring impact, economically, and also to the neighborhood. Cost is one of the most important factors in choosing the type of foundation. It should always be analyzed among the options, which will have the lowest cost, taking into consideration the cost of execution of piles caps and piles, including the mobilization of equipment. But it should not be the primary factor of this choice, it should also be aligned with the deadlines, productivity, safety and technique used in each option. Each method of foundation has its particularity, both of equipment that will be used, as well as the form that will be done, causing it to demand more labor, or not. And lastly, consideration must be given to interference with neighbors, which can cause noise, vibration and particulate emissions. Therefore, each technique has its advantage and disadvantage, which will be addressed at this article.

The research aimed to choose the best type of foundation for the construction in question, with an analysis of cost, time / productivity and interference with neighbors. In addition, all this was done with the help of the Revit program on BIM platform, where all types of foundations were inserted and shaped for the construction in question. So, in the end, the exact quantity of materials was extracted from the program, taking into account the blocks and piles.

Evolution of the system CAD/BIM

In order to execute a construction, it is necessary to carry out several projects, from the most varied areas of engineering, ranging from architecture, installations to structural design.

A long time ago, these projects were executed manually, hand-drawn, with all the necessary details to be carried out correctly in the construction, without further questioning. With the passage of time and the advancement of technology, computer programs were created that aimed to streamline this process of making projects. What was once hand-drawn, was then drawn into computer programs, such as CAD (Computer Aided Design) tools, which are still widely used by architects and engineers, according to Crespo et al. (2007).

This tool is nothing more than the automation of drawings that were previously done manually. The designs in these types of programs are done on a 2D platform, and as before, all the necessary sections must be drawn one by one in order to obtain all the indispensable details.

This program on the CAD platform has brought many advantages to designers. It left the execution of projects much less laborious and more practical.

Approximately 15 years ago a concept of project design called BIM (Building Information Modeling) was created. It consists of 3D modeling, making it easier to analyze the projects, which are more faithful to the final result of the work. This concept involves the management of information within the construction, from its initial design phase, creating 3D models that covers all stages of construction, reported by Santos et al.(2009).

Engineers and architects think that this new concept of construction has come to stay. Because it brings many facilities to the users, and the program makes the execution of the project much more intuitive. In addition, another great advantage is the compatibility of all the projects of a construction.

The future of construction moves toward projects created on the BIM platform, making execution much more automatic and reducing errors.

Objective of the project

Analyze which type of foundation is most suitable for the construction studied. This paperwas carried out based on previous studies on the types of foundations and their characteristics.The BIM tool was used to assist in the creation of cost tables.

Thus, all selected alternatives of foundations for this projectwill be demonstrated in the Revit program, through created tables, with the cost of each option. In addition, at the end will be carried out a comparative study among all selections.

DEFINITIONS
Foundation engineering

Foundations engineering is an area of geotechnics that is based on studying the elements composed by the buried structure and the soil. The foundations are elements that have the function of transmitting the loads coming from the structure to the layers of the ground, within safety criteria involving the ultimate limit state (ELU), associated to foundation rupture, and service limit state (ELS) associated with the movements of the foundation.

According to Velloso and Lopes (2010), the design and execution of foundations - the Engineering of Foundations - requires knowledge of geotechnical and structural calculation (structural analysis and dimensioning of structures in reinforced and prestressed concrete, steel and wood) ; geotechnical engineering, on the other hand, covers engineering geology, soil mechanics and rock mechanics.

In order to carry out an adequate foundation engineering project it is necessary to have a general analysis of several factors. According to Velloso and Lopes (2010), the necessary elements for the development of a foundation project are:

a. Topography of the area

• Topographic survey (planialtimetric);
• Data on slopes and slopes in the site (or that can reach the site).

b. Geological-geotechnical data

• Underground research (sometimes in two stages: preliminary and complementary);
• Other geological and geotechnical data (maps, aerial and satellite photos, ae-rofotogrammetric surveys, articles on previous experiences in the area).

c. Data on neighboring constructions

• Number of floors, average load per floor;
• Type of structure and foundations;
• Foundation performance;
• Existence of subsoil;
• Possible consequences of excavations and vibrations caused by the new work.

d. Structure data to be built

• Type and use of the new work;
• Structural system (hyperstatic, flexibility, etc.);

• Construction system (conventional, pre-molded etc.);
• Charges (actions on foundations).

TYPES OF FOUNDATIONS

Superficial foundations

The superficial foundations, according to NBR 6122/2010 (2010), are elements in which the load is transmitted to the ground predominantly by the pressures distributed under the foundation.

These foundations are executed with a small excavation in the surface of the ground, and that does not require great equipment to execute it.The structure of superficial foundations can be realized in different ways, by blocks, footings and rafts.

Footings

According to NBR 6122/2010 (2010), it is superficial foundation elements that work in flexion, and because of this they require steel reinforcement, they present small height, and variable dimensions, depending on the requested load. It has on average an armor consumption of 40 to 60 kg of steel per m^3 of concrete. It is one of the most used surface foundation structures in constructions.

Deep foundations

According to NBR 6122/2010 (2010), deep foundations are elements that transmit the load to the ground by the tip surface (Rp) and also by the lateral surface of the pile (Rl). Because these elements usually have large depth and small tip area, the tip resistance is greater than the lateral resistance.

These foundation elements are most used in large constructions, as they can transmit larger loads to the ground.

There are some types of deep foundation elements and the most used type is pile. The choice of the type depends on the type of construction and the study of the soil, carried out by the geotechnical study.

Steel piles

According to NBR 6122/2010 (2010), they are elements composed of rolled or welded sections, folded sheet tubes (circular, square or rectangular section), seamless tube and rails. They have a maximum length of 12 m, but may receive splices. It is used in any type of soil, and can cross resistant layers of N_{SPT} between 50 and 60 blows. As they are covered by metallic material, they may be damaged by corrosion in the unearthed area, in which case, according to NBR 6122/2010 (2010), a protective coating or a covering must be made. In the case of the buried area of the pile, no type of anticorrosive treatment is necessary, but a sacrifice thickness must be obtained, which varies according to the type of soil that is inserted.

Like precast concrete piles, steel piles have shaft integrity, high load resistivity, can be unlimited in length, depending on driving equipment. However, for small buildings they are expensive.

Continuous flight auger piles

According to NBR 6122/2010 (2010), the continuous flight auger piles is a cast concrete in loco, executed by introducing a continuous helical thrust into the ground by rotation. Concrete injection is made by the central stem of the gate simultaneously with its withdrawal. The reinforced is always placed after the concreting.

CHARACTERISTICS OF THE BIM TOOL

The BIM tool consists of 3D modeling, making it easier to see the projects, which remain faithful to the final result of the work. This concept involves the management of information within the building, from its initial design phase, creating 3D models that cover all stages of construction.

The differential of this tool is that with it, it is possible to create exactly what will be executed on site. With modeling, 2D, 3D views, sections, facade view and all kinds of views are automatically created. (Santos et al. 2009).

BIM tool aggregates all of these modeling facilities, with information entered by the designers, such as the type of material to be used on a particular wall, its thickness, height, material manufacturers, and the cost of the components present. With the insertion of this information it is possible to obtain the exact quantitative of each material. However, it is possible that tables are created to obtain the budget precisely, thus minimizing the overhead for other sectors of project design.

With BIM it is possible to make changes to the projects without any major complications, since by making a change, it will be done automatically in every project, thus reducing possible incompatibilities between components.

Another interesting characteristic is the integration between the different types of project of a work, allowing the union in a single project, from the architectural, structural, facilities, etc. This causes the probability of errors to be decreased. The designer can make changes to the design, and automatically all drawings and documents will be updated, as well as the recalculated quantitative ones.

This automation of the processes allows greater productivity in the elaboration of the projects, bringing a significant decrease of errors, and consequently, saving of time and reduction of costs.

However, this tool has some disadvantages. The first is that an investment must be made to acquire the new software. And also the difficulty of learning the software, because it has many tools, so it requires more personal investment. Finally, because this tool is relatively new in the country, the number of companies that use it is small, so one of the advantages of integrating projects is not possible if all companies are not using the same tool.

However, analyzing the factors mentioned, the BIM tool has more advantages, making execution of projects much faster and simpler.

METHODOLOGY

In order to carry out the comparative study among the foundation options for the construction, a residential building, located in Recife/PE, Brazil,was used as a case study.

Initially information was collected from the construction in question, identifying the type of construction, the loads carried, the survey of the site, and the environment. From these data, it was then possible to analyze which types of foundations would be most suitable.

This study led to the conclusion that a more depth analysis should be done with the selected options, which were: superficial foundation (already existing in the construction), steel piles, and continuous flight auger piles(400 and 500mm diameter).

Already with the options defined, the load capacity of the pileswas calculatedby the method of Décourt (1996). From the SPT survey data, soil coefficients and parameters relating the foundation type to the soil type, the method calculates meter by meter, lateral, tip and total load capacity of the

foundation element. From the calculated ultimate load (Vrup), the allowable load (Vadm) is then determined, by the ratio of the ultimate load by the global safety factor two, determined by NBR 6122/2010 (2010).

From the allowable values of each piles option, it was possible to determine the number of piles in the caps of each column.

After studying the types of foundations and determining the required depth, the three foundation types were then inserted and modeled in the Revit program. Everything was inserted in the platform BIM, where they were modeled and taken into account the location of the columns, the piles caps or footings, and finally the piles.

Modeling of the solutions

The first foundation solution was the one used in site: superficial foundationwith footings and soil improvementwith compaction piles (sand and gravel piles).

The second solution was in continuous flight auger piles, presenting two options, one with 400 mm in diameter and one with 500 mm in diameter. The two options were modeled in Revit, separately.

Finally, the option was chosen in steel piles with laminated profile with section HP250x62.

To perform the modeling in Revit, another necessary data were the dimensions of the crowning blocks. A spacing between the piles equal to three times the diameter was set, and spacing between the edge of the pile to the edge of the blocks was set at 15cm.

In the case of deep foundations, it was determined in the project and according to the surveys that the piles would reach a depth of 16 meters, for both continuous flight auger piles and steel piles.

With the data of the depth of the piles and with the dimensions of the blocks it was possible to model the three types of foundations in Revit.

Budget

The BIM platform integrates several stages and processes of a construction (Santos et al. 2009). For civil engineers, one of the most important steps is the budget.

In the Revit modeling process, you can insert together with other data the cost of each material. After the complete modeling of the options, cost tables were generated, calculated automatically by the program, from the parameters reported.

The cost tables of the foundations options were created with data related to the size of the blocks and depth of the piles. In the table, the concrete volume data of each pile and volume of each block were requested. And finally, the total cost, taking into account the blocks, piles and balance beams.

Comparative study

The comparative study was based on the tables created by Revit, taking into account the cost of foundation blocks, piles and equilibrium beams, in the case of deep foundations. In the case of the superficial foundation, the cost of soil improvement, the footings and the balance beams were taken into account.

Next, the tables created by Revit were transferred to Excel, where it was possible to add the cost of mobilizing equipment.

To improve the study, other factors were taken into account in addition to cost. Deadline/productivity and interference with neighbors. Each of the foundation options was studied and analyzed in relation to these parameters. For that, notes were created from 1 to 5, with 5 being the best option and 1 being the worst. With these two factors added, an Excel table was created comparing cost-benefit among the three foundation options.

DESCRIPTION OF THE CONSTRUCTION

Characteristics

The buildingis located in Recife, Brazil. It is a residential building composed of 9 floors type (2 apartments per floor), and also has 2 floors cast for parking vehicles. The land area has 971.97 m² and a covered area of 494.55 m². It has 18 apartments, each with a private area of 96.33 m².

The structure is made of reinforced concrete and has 15 columns on the tower and 11 on its periphery.

Geotechnical investigation

The surveys were performed using the SPT method. Five drill holes were drilled, totaling 81.22m depth. With the survey it was possible to carry out a geotechnical profile of the subsoil, where the layers of soil were determined. The geotechnical profile can be seen in Fig. 1.

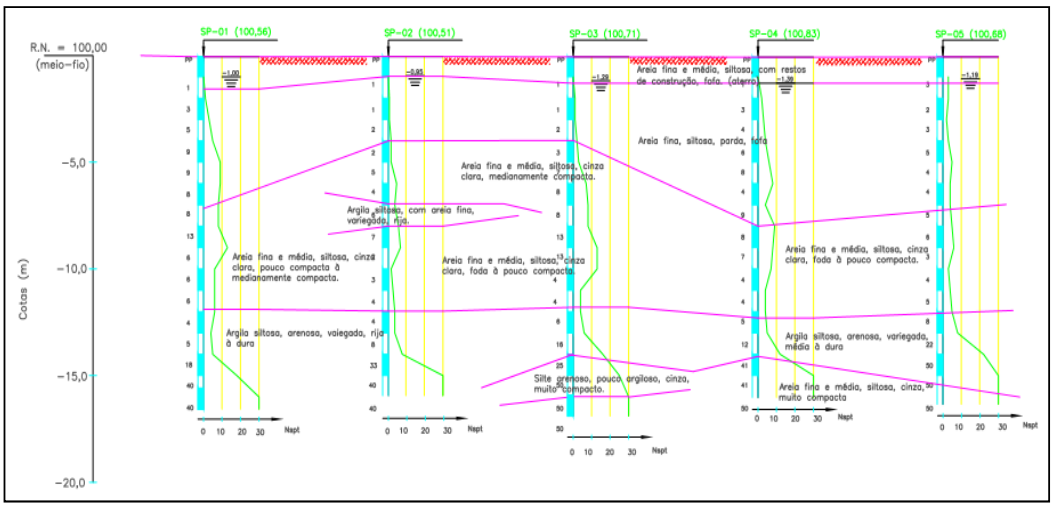


Fig 1. Geotechnical profile of the terrain.

The water level is approximately 1.16m depth. The first layer is fine, medium sand and silt, with demolition wastes (old embankment), with an average thickness of 1.29m, and average N_{SPT} equal to 1blow/30cm.

The second layer is composed of siltyfine sand, loose, with an average thickness of 5m, and an average N_{SPT} equal to 4blows/30cm.

The third layer consists of a fine and medium sand, with silt, loose to dense, with a thickness of approximately 6m, and an average N_{SPT} equal to 6blows/30cm. In the SP-02 boring, a layer of silty clay was found, hard, with thickness of approximately 1m, at a depth of 7m.

The fourth layer is formed by a silty clay, with fine sand, hard, presenting an average N_{SPT} equal to 22blows/30cm. In SP-03 boring a layer of sandy silt was found, very dense, with thickness of 1m.

Last layer is formed by a finesand, very dense, which is present only in SP-03, SP-04 and SP-05 borings with N_{SPT} equal to 47blows/30cm.

FOUNDATION DESIGNS

The following designs were executed in the Revit program, where the pile caps and the piles were modeled in the case of deep foundation. In the case of a superficial foundation, the footings and the soil improvement pileswere modeled as well.

For the concrete costs, the execution of each type of foundation and the mobilization of the equipment, the construction market of the city of Recife was taken as a basis, considering the cost of the reinforced concrete for the solutions of R$ 1,500.00 per cubic meter.

Superficial foundation

The superficial foundation was chosen in the initial project for the construction in question. The building's blade features 15 columns, and each column has a footing of different size. The superficial foundation design had a soil improvement with compaction piles (sand and gravel piles) with depths of approximately 6m each.

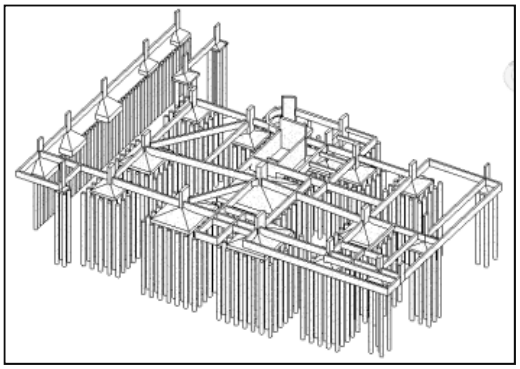


Fig. 2.3D representation of surface foundation modeled in Revit.

To carry out the cost quantification, it was considered that the improvement of soil with compaction piles would have an execution price of R$ 50.00/m, and a mobilization cost of R$ 10,000.00. The values of each service performed are shown below.

With the quantities extracted, the total cost of this type of foundation was reached, according to Table 2.

Table 1.Cost of soil improvement.

Improvement of soil with compaction piles				
	Volume (m³)	Area (m²)	Quantity (m)	Execution cost(R$)
Compaction piles	180.29	2,637.75	2,997.44	149,872.19

Table 2.Cost of balance beams and footings

Balance beam sand footings		
	Volume (m³)	Total cost (R$)
Balance beams	23.25	34,869.12
Blade footings	59.2	88,794.04
Periphery footings	9.21	13,822.30
Total	91.66	137,485.46

Table 3. Service costs

Service	Cost
Soil improvement	R$ 149,872.19
Mobilization	R$ 10,000.00
Balance beams	R$ 34,869.12
Footings	R$ 102,616.34
Total	R$ 297,357.65

Table 3 shows the total price of the services in the option of superficial foundation.

Continuous flight auger piles

For continuous flight auger piles were chosen, two options. One with 400mm in diameter and the other with 500mm.

Continuous flight auger piles (400mm diameter)

For this solution the mobilization cost of the equipment was R$ 15,000.00. And the cost of execution of the piles was R$ 130,00/m. Figure 3 is a graphical representation made by the Revit program.

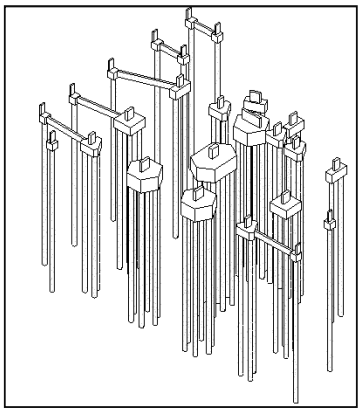


Fig. 3. 3D representation of continuous flight auger piles modeled in Revit.

With the modeling done, the program was then asked to create the cost tables of the foundation elements.

Table 4. Cost of the piles caps and balance beams

Material Blade Continuous flight auger piles 400mm - Piles caps + balance beams		
	Volume (m³)	Total cost(R$)
Balance beams	2.81	4,220.16
Blade pilescaps	62.04	93,003.15
Periphery piles caps	3.74	5,663.9
Total	68.59	102,887.21

Table 5. Pile costs

Material Blade Continuous flight auger piles 400mm - piles				
	Volume (m³)	Area (m²)	Quantity(m)	Execution cost (R$)
400mm blade pile	108.88	1,103.70	875.96	113,874.20
400mm Periphery pile	20.87	211.49	167.85	21,820.59
Total	129.76	1,315.20	1,043.81	135,694.79

Table 6. Service costs

Service		Cost
Mobilization	R$	15,000.00
400mm piles	R$	135,694.79
Balance beams	R$	4,220.16
Piles caps	R$	98,667.05
Total	R$	253,582.00

Table 6 shows the total cost that the continuous flight auger piles foundation will present, reaching R$ 253,582.00.

Continuous flight auger piles (500mm)

For this solution was used as equipment mobilization cost R$ 15,000.00. And for the cost of execution of the piles R$ 180.00/m.

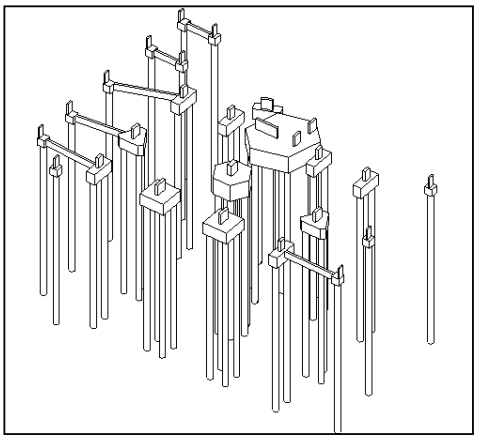


Fig. 4. 3D representation of continuous flight auger piles modeled in Revit.

Table 7. Cost of piles caps and balance beams

Material Blade Continuous flight auger piles 500mm - Piles caps + balance beams		
	Volume (m³)	Cost (R$)
Balance beams	2.89	4,341.55
Blade piles caps	80.62	120,930.00
Periphery piles caps	3.74	5,610.00
Total	87.25	130,792.13

Table 8. Piles cost

Material Blade Continuous flight auger piles 500mm- piles				
	Area (m²)	Volume (m³)	Quantity (m)	Execution cost (R$)
500mm blade piles	970.75	119.27	618.31	111,295.91
500mm Periphery piles	263.50	32.40	167.83	30,210.24
Total	1,234.25	151.67	786.15	141,506.16

Table 9. Service costs

Service	Cost
Mobilization	R$ 15,000.00
500mm piles	R$ 141,506.16
Balance beams	R$ 4,341.55
Piles caps	R$ 126,540.00
Total	R$ 287,388.39

With the cost table shown, separated by piles caps (table 7), piles (table 8) and beams of equilibrium (table 7). Finally, Table 9, being the total of services mentioned, with the increase of mobilization of the equipment.

Steel pile

The steel pile chosen was with laminated profile HP250x62. The cost of mobilizing equipment for the steelpile was R$ 15,000.00. For the execution cost was considered R$ 60.00/m, and the cost of the material was R$ 3.00/kg.

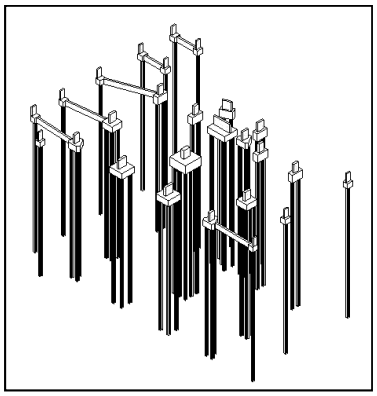


Fig. 5. 3D representation of steel pile foundation modeled in Revit.

Table 10. Cost of piles caps and balance beams

Material Blade Continuous flight auger piles 500mm - Piles caps + balance beams		
	Volume (m³)	Cost (R$)
Balance beams	2.98	4,479.20
Blade piles caps	20.74	30,672.00
Periphery piles caps	2.75	4,158.05
Total	26.47	39,309.25

Table 11. Piles cost

HP250x62 steel piles cost				
	Quantity (kg)	Piles cost (R$)	Driving cost (R$)	Total cost = Driving + piles
HP250x62 steel pile blade	48,973.80	146,921.40	47,394.00	194,315.40
HP250x62 steel pile periphery	10,298.20	30,894.60	9,966.00	40,860.60
Total	59,727.00	177,816.00	57,360.00	235,176.00

Table 12. Service costs

Service		Cost
Mobilization	R$	15,000.00
HP250x62steel piles	R$	235,176.00
Balance beams	R$	4,479.20
Piles caps	R$	34,830.05
Total	R$	289,485.25

COST-BENEFIT RATIO

Among the foundations options studied, the one that presented the best cost was the continuous flight auger piles with 400mm diameter, according to Table 13.

Table 13. Cost comparison

	Option	Cost
Surface foundation	Footings with soil improvement	R$ 297,357.65
Deep foundations	Continuous flight auger piles(400mm)	R$ 253,582.00
	Continuous flight auger piles(500mm)	R$ 287,388.39
	HP250x62 steel pile	R$ 289,485.25

In order to achieve a more in-depth study, not taking into account only the cost, other factors such as term/productivity and interference with neighbors were analyzed for each type of foundation. Which can be analyzed in Table 14.

For the superficial foundation solution, the execution of the footings is relatively time consuming and demands a large workforce involved in the service. In addition, a soil improvement was carried out, which brought a small increase to the service time, taking in average 2 minutes for each pile of improvement.

In relation to interferences with neighbors, the superficial foundation does not bring noises and vibrations, being a process without major problems. However, as there was soil improvement with sand and gravel piles, it may have caused noises to neighbors.

The solution in continuous flight auger piles has a fast execution. Depending on the equipment, an average of 250 meters of piles per day can be performed. This method almost does not affect the neighbors in the vibration issue, but it can bring some noise.

The method in steel piles has a good productivity, on average 100 meters of piles per day, but if splicing is necessary, the process takes longer. The process of driving the steel piles causes great vibrations and noises to the neighbors.

The following table shows all the factors analyzed for each type of foundation: 1 for the worst grade, and 5 for the best grade. The criterion adopted for choosing the banknotes was personal, analyzing the options and comparing them. The solution that had the highest score, is the one that presented the best cost-benefit.

Table 14. Cost-benefit of the options

	Option	Cost	Term / Productivity	Interferences with neighbours	Total
Superficial foundation	Footings with soil improvement	1	1	4	6
Deep foundation	Continuous flight auger piles (400mm)	4	4	3	11
	Continuous flight auger piles(500mm)	2	4	3	9
	HP250x62steel piles	3	2	2	7

Due to the study carried out based on the various parameters it is possible to conclude that the solution that presented the best result was the continuous flight auger pile with 400mm diameter.

CONCLUSIONS

This design step is usually executed on the CAD platform, but in the case of this project it was executed in Revit, and it was possible to notice a time gain compared to the other tool, since in the BIM platform, it is possible to perform modeling and obtain information automatically. Therefore the tool brought several benefits.

The present project had as objective to analyze the advantages of realizing the foundation project in the program Revit, in the platform BIM. With this first stage concluded it would be possible to later carry out the other projects related to the construction taking this as a basis

The BIM is much broader than actually executed in this project, in this case only a small step was made that if actually used later will bring benefits in the execution of the project.

This tool has great potential, but should be used more widely and by everyone involved in the construction.

This method of realization was determined by the engineers in order to obtain gains in project design and a cost estimate.

REFERENCES

Santos A. P.L., Witicovski L.C., Garcia L. E. M., Prof. Scheer S., 2009. A utilização do BIM em projetos de construção civil. Revista Iberoamericana de Engenharia Industria, vol.1, nº 2, p. 24-42.

Crespo C.C., Ruschel R.C., 2007. Ferramentas BIM: um desafio para a melhoria no ciclo de vida do projeto. Relatório Técnico, UNICAMP.

Décourt (1996). Análise e Projeto de FundaçõesProfundas. EmHachich, W., Falconi, F. F., Saes, J. L., Frota, R. G., Carvalho, C. S. e Niyama, S., Fundações: Teoria e Prática. EditoraPini. São Paulo. 1996b, 265-327p.
NBR 6122/2010 - Definições. Associação Brasileira de Normas Técnicas (ABNT) 2010.

NBR 6484/2001 - Procedimento. Associação Brasileira de Normas Técnicas (ABNT) 2001.

SCAC, 2013. Catálogo Técnico de Estacas Centrifugadas. São Paulo.

VELOSO, D. A; LOPES, F. R, 2010. Fundações: critérios de projeto, investigação do subsolo, fundações superficiais, fundações profundas. São Paulo: Oficina de textos.

DIAPHRAGM WALLS AND GROUND IMPROVEMENT ON THE OPEN-CUT EXCAVATION OF BOLOGNA HS RAILWAY STATION

Luca Utzeri, Italferr S.p.A., Rome, Italy, +39.0649752890, l.utzeri@italferr.it
Stefano Ciufegni, Francesco Sacchi, Italferr S.p.A. Rome, Italy, s.ciufegni@italferr.it, f.sacchi@italferr.it

ABSTRACT

Bologna new High Speed railway station extends underground along approximately 640m by a 56m width and a 25m depth.
The open-cut excavation to execute the underground station box was designed through an innovative structural system, which contemplates reinforced concrete diaphragm walls with unusual shape and static behaviour: the Vaults, diaphragm walls with an arched cross section absorbing thrust actions mainly by the compressive behaviour of the concrete, and the Buttresses, T-section diaphragm walls designed to react to actions transmitted by the Vaults by flexural behaviour. In order to ensure the stability of the excavation of such diaphragm elements, whose cross section area was about 10 square meters, a ground improvement around the perimeter of the excavation was provided through Cutter Soil Mixing technology.
An automatic geotechnical, structural and topographic monitoring system has allowed to detect the interaction between ground and structures during all construction phases and its impact on the adjacent urban context.

Keywords: Vault, Buttress, Cutter Soil Mixing

PREMISE

The construction of the High Speed/High Capacity (HS/HC) railway line crossing Bologna provided an opportunity to reorganise the entire configuration of the railway hub through a new subsurface station and major engineering works, such as the new bridges over the Reno and the tunnels crossing the city underground for over 10 km.

The new infrastructure will enhance the transport capacity of the entire railway hub, going from about 780 trains/day (approximately 80,000 passengers per day) to about 1,500 trains/day by completion of the HS/HC system and the regional transportation system (about 160,000 passengers expected, with 35,000 for HS).

The new HS train station is underground, but adjacent to the current station, so maintaining the advantage of being centrally located, close to the historic centre, and ensuring an easy interchange between HS and regional trains. Ordinary traffic runs along the current railhead, while the fast traffic runs almost entirely underground. The new structure will increase services, improving the mobility of citizens without taking additional space in the city area, and will limit the environmental impact of the passage of the new fast trains on the city.

THE STRUCTURAL SYSTEM OF THE UNDERGROUND STATION

The new Bologna HS railway station is placed underground below the last tracks of the existing Central Station; it extends along a stretch of approximately 640 m length and 56 m width (Fig. 1).

The HS rail level includes four tracks exclusively dedicated to HS trains and it is placed at a height of 19.10 m above sea level, 23.3 meters below the level of the surface rails.

© 2018 Deep Foundations Institute

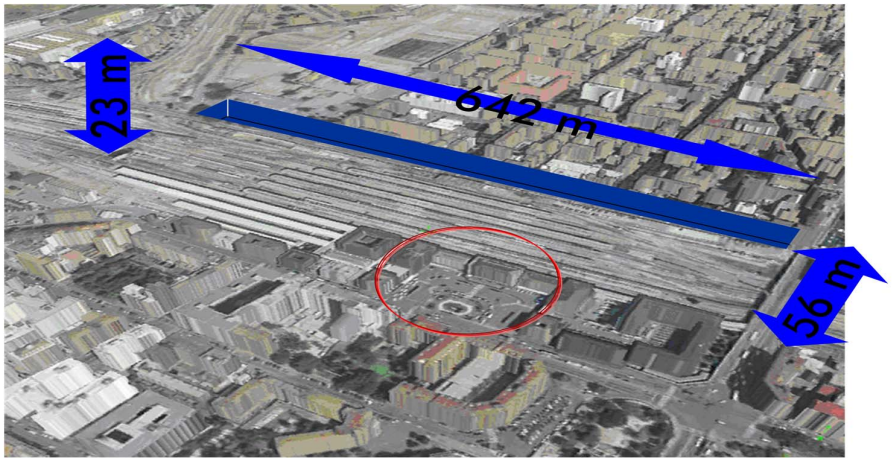


Fig. 1. Location and size of the new HS Station

The underground station is constructed through an open-cut excavation supported by perimeter diaphragm walls; the interfering surface tracks are temporarily removed.

The architectural and functional layout contemplates a succession of different floors placed at different levels and with specific functional purposes. The following can be identified, from top to bottom (Fig. 2):
- FS floor, at the level of the current station tracks, future site of the temporarily removed surface tracks;
- Kiss & Ride floor, about 7 m below the ground surface, which accommodates the passenger access road to the station;
- HS Hall floor, about 15 m below the ground surface, site of the HS hall, with ticketing and customer services;
- HS floor, about 23 m below the ground surface, site of the 4 HS tracks.

An additional underground floor is contemplated for passenger parking at the terminal sections of the station, approximately 11 m below the ground surface (Parking floor).

Stairway-and-lift groups descending from the FS floor to the HS platforms permit the access to the different levels.

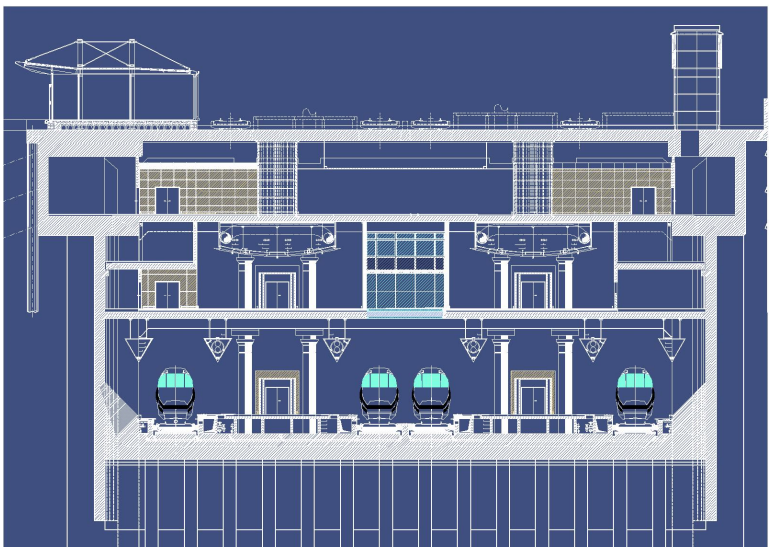


Fig. 2. Cross section and functional layout

The HS station structural system includes the retaining structures of the excavations (perimeter diaphragm walls and counteracting elements), foundations (slab base and anchoring elements) and elevation structures (frames, floor slabs, stairway-and-lift groups). Retaining walls, foundations and elevation structures are three distinct structural subsets that interact with each other in all phases of construction and operation, defining a single, complex geotechnical and structural system.

The perimeter diaphragm walls are the main innovative component of this work. They consist of structural elements with a particular shape and static behaviour, built using innovative methods and machining technologies: Vaults and Buttresses (Fig. 3).

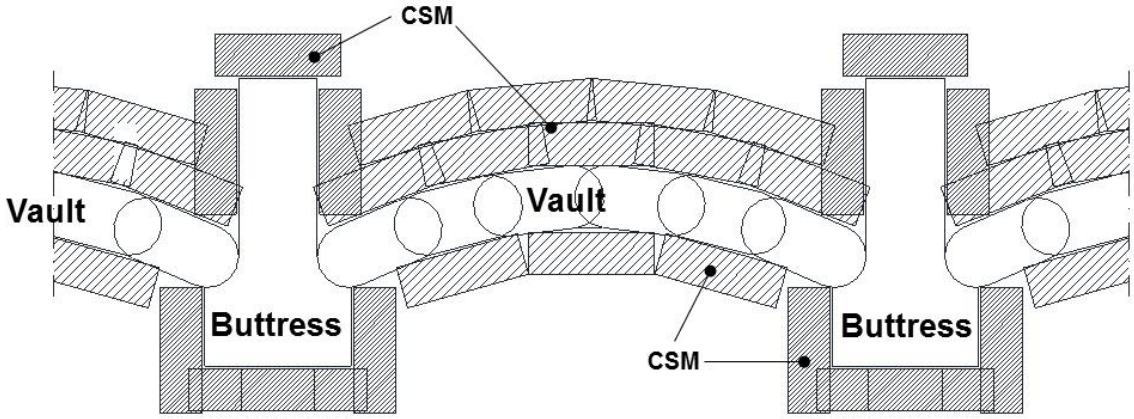


Fig. 3. Extract of Buttresses and Vaults plan

The Vaults are reinforced concrete diaphragm walls with an arched cross section, conceived to provide a "cave effect" to the interior walls, according to the criterion of the original architectural design; they are able to absorb the thrusts due to ground and water pressure by using mainly the compressive structural behaviour of the concrete. The Buttresses are reinforced concrete diaphragm walls with a "T"-shaped cross section; they are the main support elements absorbing the actions transmitted by the Vaults through a shear and bending structural behaviour.

Such peculiar structural configuration derives from the need of avoiding dam effects by providing diaphragm walls sufficiently short not to completely intercept the deep aquifer. Thus, the Vaults are only 23 m long, while the Buttresses, that require a deeper embedding, are 28 m long.

Buttresses and Vaults are placed in a regular sequence at a 12 m distance; the pairs of Buttresses opposing in the two longitudinal diaphragm walls at a 41 metre distance define the main cross alignments which subdivide the underground structural box into 53 fields.

Vaults and Buttresses are carried out from a working platform at 7m depth from the original ground surface; a temporary diaphragm wall, consisting of reinforced concrete piles of 800 mm diameter anchored by 3 or 4 orders of tie rods ("first stage" diaphragm wall) allows to reach the depth of the main working platform (Fig. 4).

The top beam of Vaults and Buttresses is a reinforced concrete element of large size, also working as a cable duct, characterized by a "C-shaped" cross-section, with top and bottom placed at the levels of the FS and K&R floors respectively (Fig. 5).

The structural elements that counteract the diaphragm walls are the steel struts, placed at the future underground floors and bound to the buttresses by steel plates, and the reinforced concrete base slab that forms the underlying support for the HS floor.

Before the completion of the base slab, the support for the Buttresses under the excavation temporary bottom is provided by the “cross walls”.

Cross walls are conceived as a continuous sequence of diaphragm panels of 25m depth from the working platform, that have to be demolished during the deepening of the excavation till the bottom is reached (Fig.4). Only the part of the cross walls below the base slab is a permanent work so it is made up of reinforced concrete.

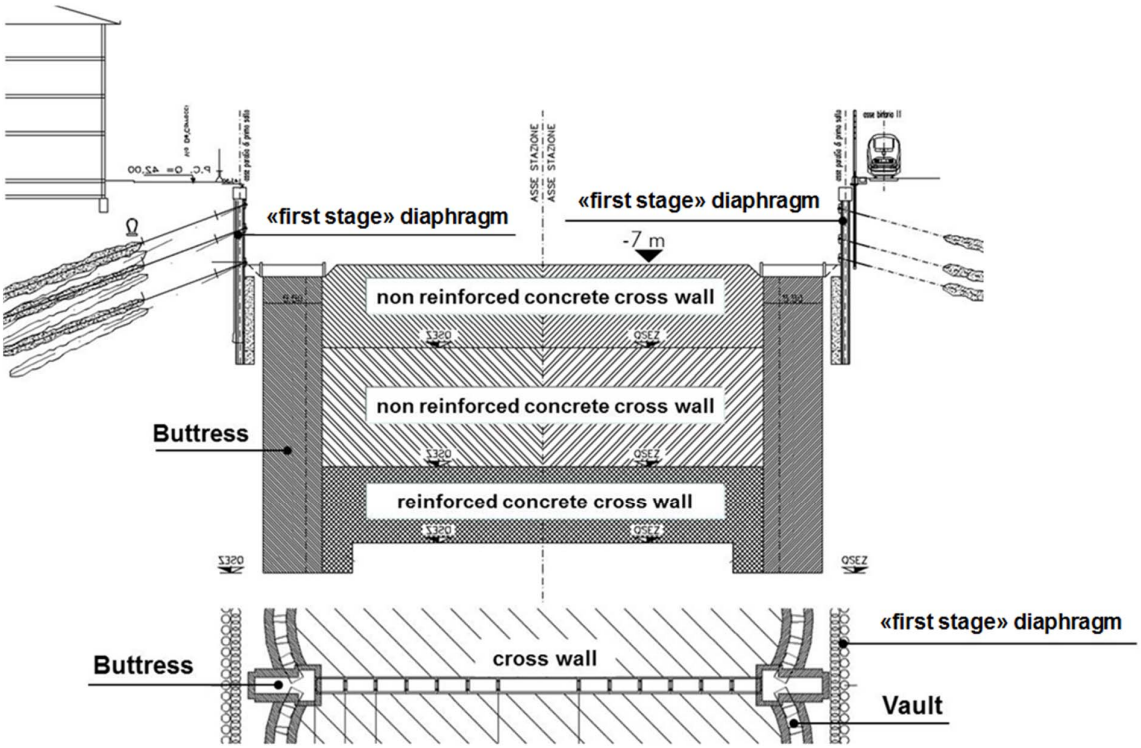


Fig. 4. Cross section and extract of plan of support works

In order to avoid the uplift of the slab due to the groundwater upward pressure, reinforced concrete piles and steel micro-piles are provided to anchor the slab itself.

The internal elevation structures consist of: vertical steel columns that rest on the reinforced concrete base slab and on inner elements of the cross walls; floor slabs supported by the steel beams that counteract the Buttresses starting from the excavation phase; reinforced concrete walls for stairway and lift groups.

The phases of excavation of the underground station, after the completion of the retaining structures, typically contemplates a “bottom up” sequence (Fig. 5); except for steel beams, all the internal elevation structures are executed from the bottom to the top after reaching the bottom of the excavation at a height of -23.5m from ground level.

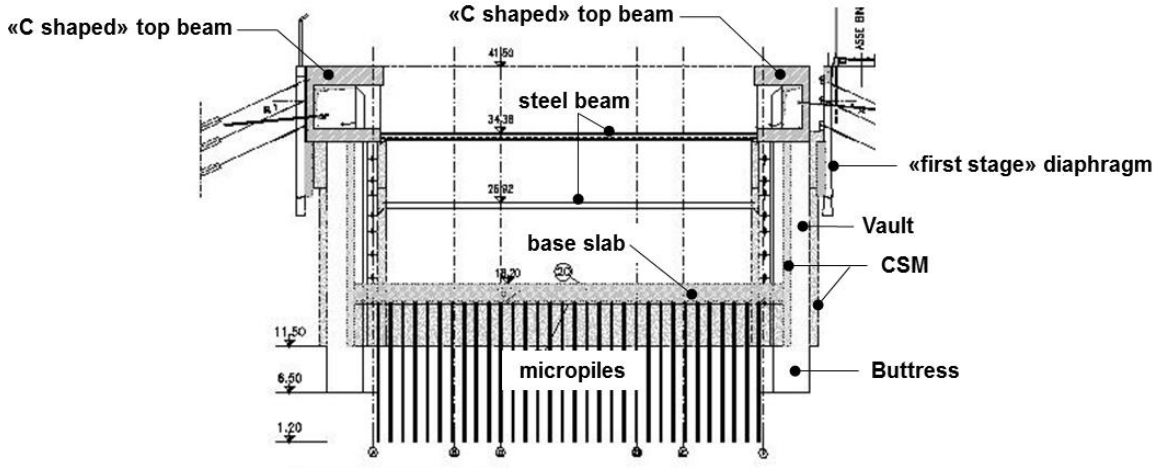


Fig. 5. Cross section "bottom up"

The transverse terminal walls of the underground structural box, through which the station connects to adjacent tunnels, consist in linear diaphragms that are supported by the floor slabs during all the excavation phases; at this scope, in these terminal sections all internal elevation structures are executed through a "top-down" sequence. Furthermore, linear diaphragms are provided instead of Vaults in the longitudinal terminal sections, in order to furtherly support transverse walls (Fig. 6).

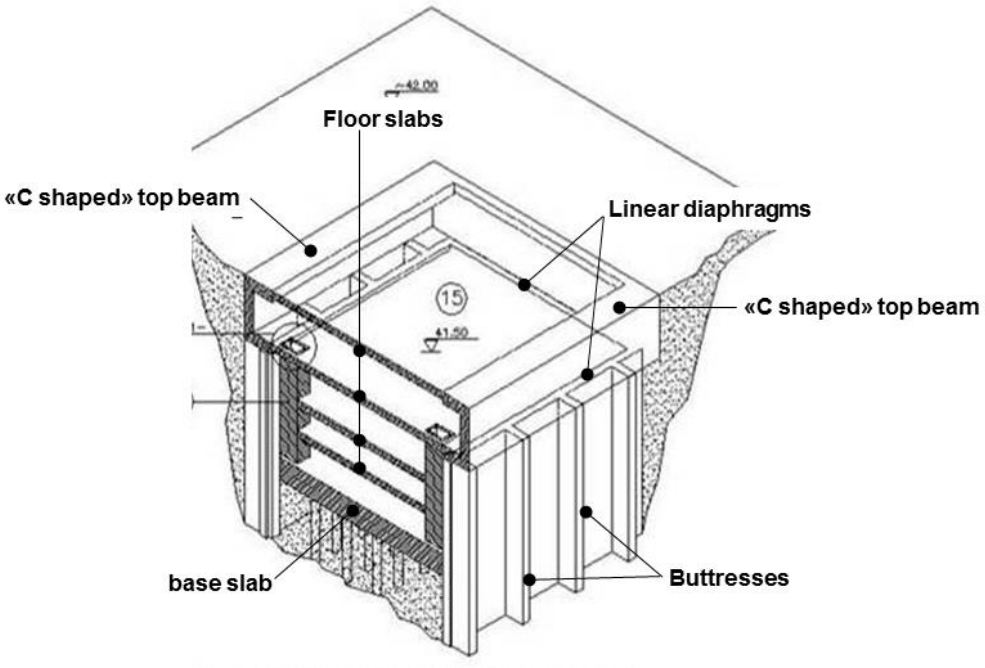


Fig. 6. Terminal section of the underground structural box

In order to improve the stability of the bottom of the excavation during the construction phases, a 5 m thick soil improvement is provided by jet-grouting technology, thus reducing the permeability and increasing the stiffness of the soil. At the terminal sections, the improved soil also performs as an additional strut at the base of the linear diaphragm walls. Dewatering wells are also provided along the inner perimeter of the excavation in order to reduce the water pressure under the layer of improved soil and prevent it to uplift.

THE HYDROGEOLOGICAL AND GEOTECHNICAL CONTEXT

Bologna subsoil is characterised by the presence of several layers with a grading composition that varies from high plasticity silty clay to silty sands and sandy gravel. The spatial distribution of the different layers, in particular of the sandy gravels, varies from one point to another, originating in the alluvial fan of the rivers and streams of the Apennines expanding towards the plain.

In the area of the HS railway station, clay and silty materials prevail; coarser-grained lenticular bodies are the final elements of the smaller streams alluvial fans and are composed primarily of sands, silty sands and sands with gravel.

Pore water pressure is determined by the specific influx and drainage conditions occurring case by case, depending on the infiltration in the layer that is in direct contact with the hilly relief, as well as on rainwater and leakages from networks; therefore, it varies almost randomly between minimum values close to zero and maximum values related to a hydrostatic groundwater table at a depth of 5m below the ground surface. The water flow occurs in a predominantly sub-horizontal direction.

Three mainly aquifers are detected, all confined by impermeable soil:

- the first at the surface, consisting of sands and silty sands, of a depth varying from 0m to 8m from surface level *(upper aquifer)*.
- the second, consisting of sands and gravels, between depths of 15m and 20m from ground level (*intermediate aquifer*).
- the third, consisting essentially of sands and silty sands, between depths of 25m and 38m from ground level (*deep aquifer*).

Due to the complexity of the stratigraphy detected from the initial investigation, a three-dimensional lithological model was developed using geophysical methods (electrical tomography and microtremors) and integrated with all geognostic boreholes performed at various stages of the design and execution. Fig. 7 shows the permeable layers.

The processing and the geo-referencing of existing information let construct a 3D grid representing the best fit of the entire set of data analysed: geological, lithological, hydrogeological, geognostic and geophysical. From the model obtained, three-dimensional images can be extracted (Fig. 7), or two-dimensional horizontal and vertical sections.

It was then possible to predict any potential critical situation during the excavation phases in such a variable environment and to define an intervention protocol.

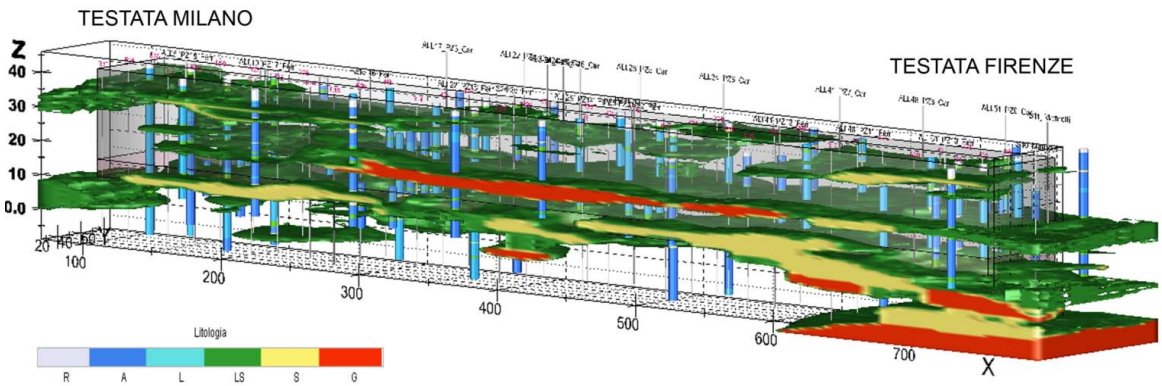


Fig. 7. 3D visualization of permeable bodies

THE DIAPHRAGM WALLS: VAULTS AND BUTTRESSES

The Vaults are diaphragm walls with a "arch shaped" cross section. Each Vault is made up of 6 diaphragm panels 1.20 m thick and 23 m deep, for an overall width of approximately 12 m between two successive buttresses (Fig. 8).

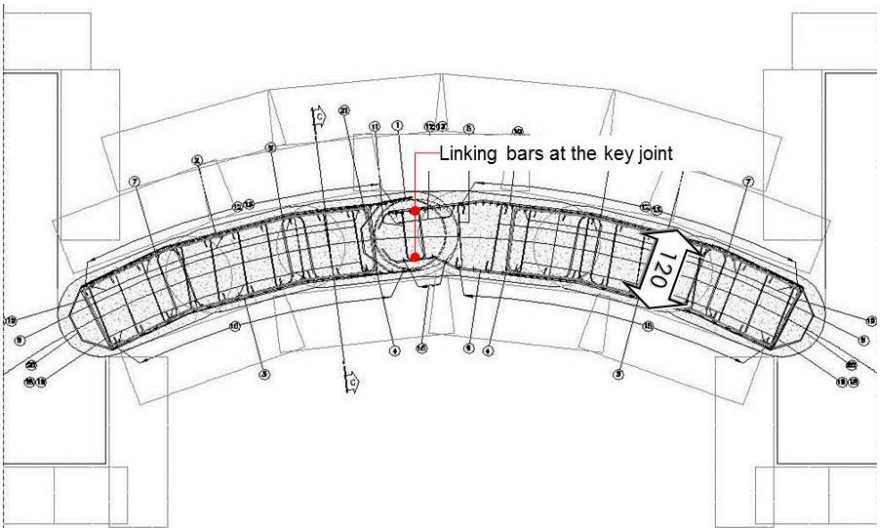


Fig. 8. The Vaults – Reinforced concrete cross section

Two half-vaults are completed in sequence, each consisting of 3 diaphragm panels, two primary side panels and one secondary central panel; the area of each half-vault cross section is close to 10 m^2. The reinforcement of each semi-vaults is pre-assembled in a single frame and inserted in the excavation before casting the concrete in a single phase.

A cylindrical PVC pipe of 1 metre diameter is prepared in the reinforcement frame of the first semi-vault at the key joint (Fig. 9); it is filled with dry material before the concrete is poured. The excavation of the second semi-vault causes the destruction of the PVC pipe, so the poured concrete replaces the volume of the dry material; the reinforcement frame of the second semi-vault has special linking bars at the key joint, in order to provide structural continuity to the whole vault.



Fig. 9. The reinforcement of the first half-Vaults

The Buttresses are diaphragm walls with a “T shaped” cross section (Fig. 10). Each Buttress is made up by excavating 3 diaphragm panels 1.5 m thick and 28 m deep, for an overall area of the cross section of over 10 m^2.

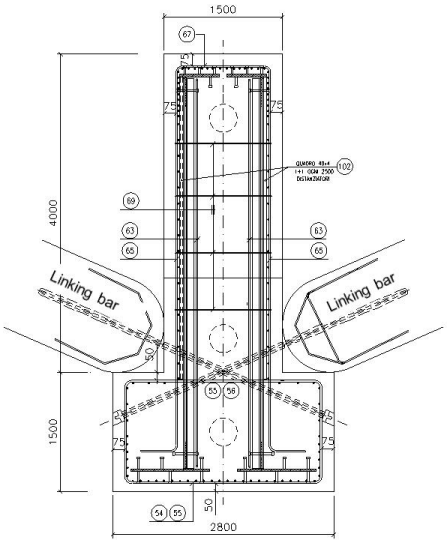


Fig. 10. The Buttresses - Reinforced concrete cross section

The main reinforcement of a single buttress consist of a reticular steel structure, weighing 70 tons, because of the high bending moment induced by the thrust applied by the adjacent vaults. The external reinforcement is designed to contain concrete cracking within the limits prescribed by the design.

Due to the limits of elevation of the overhead cranes serving the site, the buttresses reinforcement was divided into two portions, an upper one and a lower one, pre-assembled onsite and connected by bolted joints during the insertion in the excavation (Fig. 11).

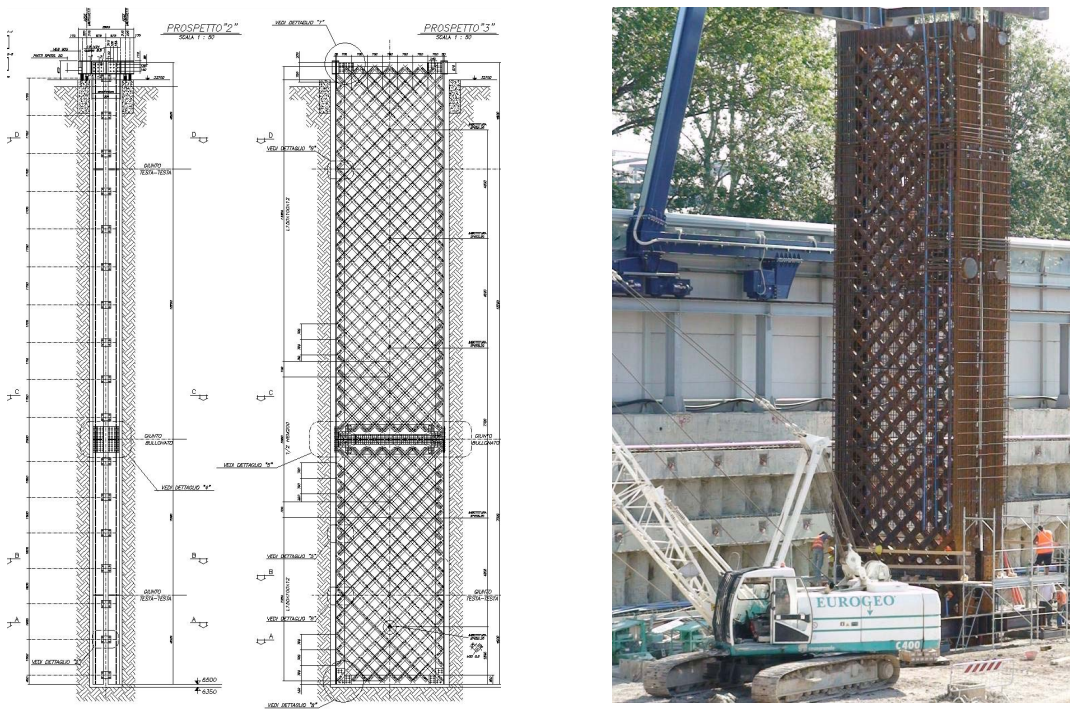


Fig. 11. Buttress reinforcement – Vertical sections and on-site moving

The excavation of the panels of Vaults and Buttresses is carried out by a clam shell bucket and contemplates the use of bentonite slurry. The large cross sections of the excavations, the urban location of the works and the heterogeneous composition of the subsoil require to consolidate the soil *a priori* along the perimeter of the panels, in order to ensure the stability of the excavation until the concrete casting (about 20 hours). In fact, a hypothetical partial collapse of the excavation during the insertion of the reinforcement would entail excessive time to re-establish the excavation safety (about 10-12 hours), while an instability phenomenon during the casting would irreparably compromise the integrity of the structures.

In order to ensure the contact between the structural elements along their whole depth, strict vertical tolerances (± 0.5%) are imposed and checked during execution. Before starting all operations, specific trial fields are carried out on full-scale sacrificial components, to analyse the execution methods for the Buttress-Vault joints and Vaults key joints.

THE GROUND IMPROVEMENT: CUTTER SOIL MIXING (CSM)

Ground improvement along the perimeter of the diaphragm panels is carried out using a technology set up a few years earlier (2003): Cutter Soil Mixing (CSM, Fig. 3, 5). CSM is able to provide a controlled geometry and to guarantee an absolute absence of discontinuities.

This technology started out as a combination of a technique of deep soil mixing and the hydromill for excavating diaphragms. It consists of milling batteries made up of toothed wheels, driven by a hydraulic motor, able to rotate independently both clockwise and anticlockwise, that excavate and mix soil with mortar.

During the insertion of the milling heads, the soil is broken up and a fluidifying agent is injected into the space between the heads themselves (Fig. 12a).

In the extraction phase (Fig. 12b) the milling heads rotate in such a way as to mix the grout with the soil to form a rectangular panel.

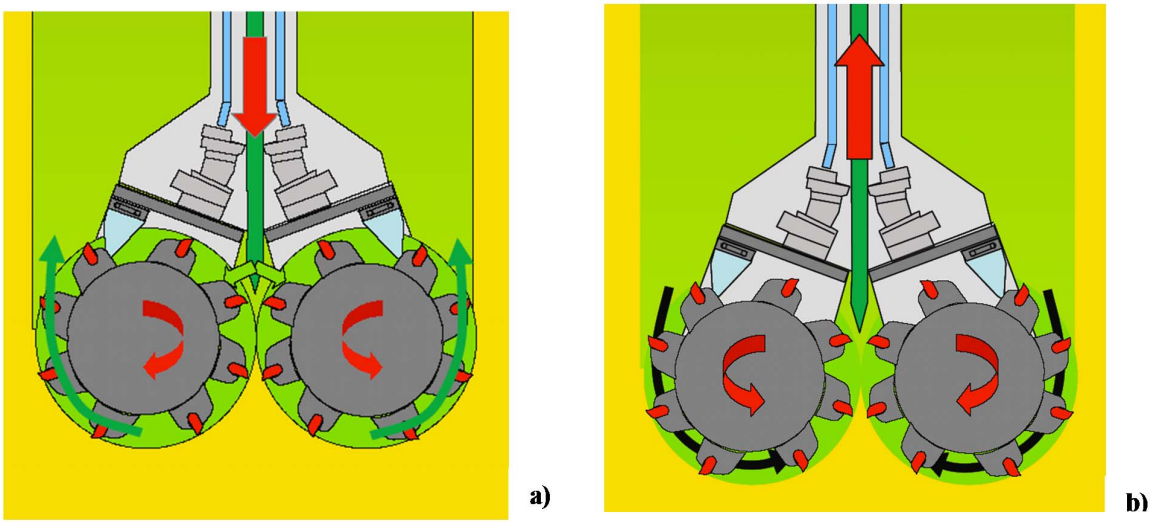


Fig. 12. CSM. Milling heads insertion (a) and extraction (b) phase

The mill is connected to a drill rod that allows to reach a 23m depth from ground level; the precision in positioning and verticality of the panels is ensured by monitoring instruments that allow the operator to correct the execution procedure in real time.

Due to the technological limitations at the time of the works, CSM is extended to the whole depth of the vaults (23m), but the final 5-metre stretch of the buttresses remains not protected; however, the soil

characteristics and the increased density of the sludge at that depth are such as to guarantee sufficient stability to the excavation walls.

All the working parameters (advancing and lifting speeds, volume and pressure of the drilling fluid and the injection mixture, verticality, etc.) are recorded and stored for each panel, after verifying the correct execution.

The grout injected is a cement/water mixture at a ratio of 400kg of cement per cubic metre of treated soil. The quantity of cement necessary to achieve the mechanical characteristics of the improved soil panels is determined carrying out an appropriate test field.

Since the intermediate aquifer level coincides in some points with the working platform level at -7m from surface, several test fields are performed in order to check that no well-bore caving is generated during advancing of CSM, which could cause subsidence outside the work area. At this scope, mature bentonite slurry is preferred to water as circulation fluid, because of the greater stability of the excavation and the higher speeding up of the advancement phase; no bad effect on the mechanical characteristics of the improved soil is detected due to bentonite.

The panels produced are 800mm thick by 2800mm long (Fig. 13).



Fig. 13. CSM panel from trial field

After execution of CSM, a series of boreholes are carried out on the improved soil panels to check the continuity of the panel and the required design strength by testing samples. The average compressive strength value, obtained by analysing approximately 260 samples, is 3.02 MPa.

THE AUTOMATIC MONITORING SYSTEM

The complexity of the works and their possible impact on adjacent urban structures required to provide an instrumentation set and a monitoring programme starting from the detailed design, in order to check the effects of the works and their compliance with the design provisions.

The monitoring system was designed in three basic components: a geotechnical one, concerning the excavation area, a structural one, involving the main structures, and a topographical one involving the buildings overlooking the perimeter of the station; it was aimed at checking possible deformations induced on the neighbouring structures and preserve them from damaging.

The configuration of the geotechnical and structural monitoring system provides n. 9 instrumented sections (Fig. 14), n. 6 “ordinary” (named “SO”) and n. 3 “special” (named “SS”) for the greater number of instruments.



Fig. 14. Monitoring Sections

Since the behaviour of complex structures interacting with soil is governed by many correlated parameters, monitoring system was designed for providing complementary measurements.

Also, the redundancy of the instruments and of the measures made possible to check the correct operation of each instrument and to have additional measures in the event of the failure of an instrument, as well as to better understand and interpret on-going phenomena.

These design criteria required a great automation of reading instruments and new technologies; a complex system of analysis and management was then developed and implemented such as to assure approval and validation of data in real time.

The possibility of increasing the instrumentation and having more sophisticated detection and transmission equipment allowed to reduce data collection time to a minimum.

A more effective management of data was achieved by working on the monitoring system through an interactive web platform, setting different hierarchical system access levels; it was then possible to remotely query the different in site instruments, obtain data in real time, early detect potentially critical situations, identify their causes and define proper interventions to be implemented.

The interactive setting was implemented on a remote server accessible via the Internet, with the following features:

- automatic collection and publication of the first data from the instruments (“raw” data) and/or from external databases (mainly manual instrumentation and robotic stations);
- publication of the final data in the form of graphs and tables after validation;
- full multi-user interactivity, based on site maps, to remotely query all the in site instrumentation in real time with options of setting system access by hierarchical levels;
- managing changes to the measurements plan and alarm thresholds approved by the Client;
- automatically managed alarms, sending out alerts (via e-mail, text messaging, etc.) to privileged users.

The recorded data were governed by a system management software dedicated for the purpose. Using signal stability control routines, acceptability ranges, etc., the data stored in the database were compared with pre-determined threshold values. In the event of exceeding these threshold values, the system would signal the anomaly.

A critical validation of all data allowed to separate the data set from any generated anomaly. This activity was carried out daily, while for anomalies or exceeding threshold values, it took place in real time. The special functions that the validation service performed were:

- coordinating monitoring activities for data validation;
- analysing and validating data before forwarding to the Client;
- interfacing with the Client for the analysis of both raw and validated data and of the exceeding of threshold values and for possible redefinition of the measuring frequencies based on the progress of the variables measured;
- managing alarms and any anomalous situations and informing the responsible;
- night and holiday-time availability for alarm management.

The software used can interface with commercially available software (Word, Excel, etc.) in such a way that information regarding both the "raw" and the processed the data can be viewed by all those involved in the monitoring process and in the construction of the station. The use of the web platform also allowed for immediate availability of all monitoring data without the need of paper format.

The database allowed to store data and display it graphically. At this scope, interactive maps were created with the location of each instrument, in order to display the data in real time, via Internet access, and prepare measurement reports.

Such monitoring system has made possible to manage approximately 3,200 instruments; about 2,500 instruments, most of which automatic, were used for geotechnical and structural monitoring, with frequencies of readings of even a few minutes, which generated a database of over 10 million data; about 700 instruments were used for topographic monitoring of the structures of the station and of the adjacent buildings and tracks in operation: topographical benchmarks (over 260), read with precision levelling, and optical targets (over 400), read via robotic stations, which generated over 1 million data.

On the basis of such monitoring organisation it was possible to interpret all phenomena occurred during each single phase of execution and complete the work in safety for both workers and for the outside environment.

Monitoring results

During the first excavation phase (December 2005 - December 2007), settlements of the ground were detected in the order of 4.5 cm upstream the edge of excavations (Fig. 15). This phenomenon was related to the perforation of the four orders of tie rods, as the "first stage" diaphragm wall did not undergo significant deformations.

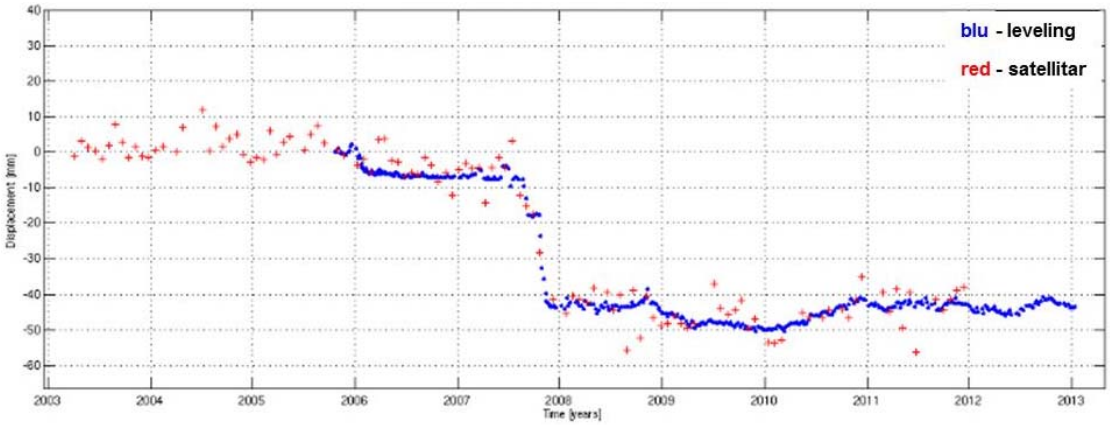


Fig. 15. Settlements of the ground upstream the first stage diaphragm wall. Leveling vs satellitar data

During the next excavation phases of the main underground box, a modest swelling of the ground upstream the diaphragm walls was detected, which showed its maximum value of about 1.5 cm in the central part of the box (Fig. 16) when the maximum depth of excavation was reached (November 2010). Such swelling attenuated near the terminals of the box and with the increasing of the distance from the excavation edge.

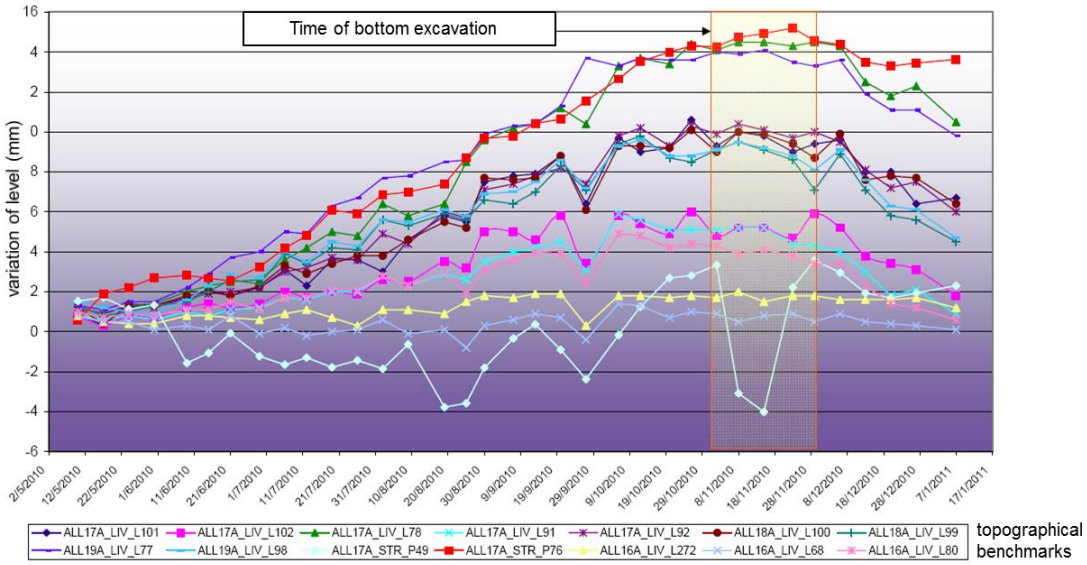


Fig. 16. Swelling of the ground upstream the edge of diaphragm walls during the final phase of excavation

The back analysis of the deformations developed by a Two-Dimensional Finite Elements Model matched the phenomenon in the central part of the box (Fig. 17), but overestimated it at the terminals, as the 2D FEM was unable to simulate the effects related to the actual three-dimensional configuration of the underground box.

The phenomenon was governed by two opposing contributions:

1) the elastic swelling of the soil around the excavation (with a maximum at the excavation bottom) that extended upstream the diaphragm walls due to the stiffness of the retaining structures;
2) the lowering of the water table due to the drainage effects induced by the excavation.

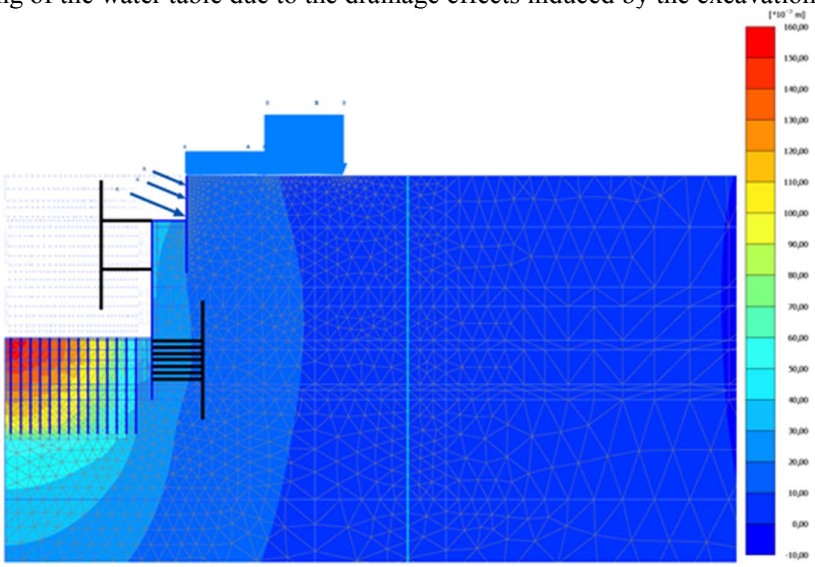


Fig. 17. Field of vertical displacements resulting from the 2D FEM of the excavation

SUMMARY AND CONCLUSIONS

The design and construction of Bologna new High Speed railway station represented a very hard challenge in the field of civil works in urban areas, which involved the largest urban open-cut excavation in Europe at the date of the works (2006-2010).

Limits to interference of the retaining structures with ground water lead to peculiar technical solutions characterized by innovation in conceptual design, in machining technologies and in automation of the monitoring system.

The diaphragm walls for the open-cut excavation were designed and executed through a regular sequence of special elements, Vaults and Buttresses, supported by steel struts and sacrificial diaphragms, that create a complex and very rigid structural system.

Due to the unfavorable geological and hydrogeological conditions, and to the irregular and very large cross sections of Vaults and Buttresses ("arch shaped" and "T shaped" respectively, about 10 m^2), a ground improvement was required around the perimeter of the diaphragm panels to ensure the stability of their excavation. The requirement to provide a controlled geometry without any discontinuity in soil improvement lead to choose the innovative technology of Cutter Soil Mixing, which combines a technique of deep soil mixing and the hydromill for excavating diaphragms.

No significant impact on the adjacent urban context was detected during the main excavation phases. The automatic geotechnical, structural and topographic monitoring system, set up for the purpose, confirmed the very rigid behaviour of the underground structural box, despite of the very large volume of total excavated soil, showing a modest swelling of the upstream ground of maximum 1.5 cm in the central part during the final phase of excavation. Such small effects were compatible with the serviceability of the neighbouring buildings and of the adjacent surface tracks on operation.

REFERENCES

M.D. Boscardin, E.G. Cording, 1989. Building response to excavation induced settlement. Journ. Geot. Eng. Div., Proc. ASCE, vol. 115, n. GT1, p. 1-21.

J.B. Burland, 1995. Assessment of risk of damage to buildings due to tunnelling and excavation. Invited Special Lecture, IS-Tokyo '95, 1st Int. Conf. On Earthquake Geot. Engineering.

R.B. Peck, 1969. Deep excavation and tunnelling in soft ground. State-of-the-Art Report, VII Int. Conf. SMFE, Mexico City.

M. Bringiotti, D. Nicastro, S. Ciufegni, F. Sacchi, 2012. Nuove Tecnologie per consolidamenti dei terreni nelle grandi infrastrutture Ferroviarie: il CSM e la stazione AV/AC di Bologna. Gallerie e Grandi Opere in sotterraneo n° 104

ESTIMATION OF THE LOAD BEARING CAPACITY OF ROOT PILES PARTIALLY EMBEDDED IN ROCK MASS RHYOLITE, USING EMPIRICAL AND SEMI-EMPIRICAL METHODS

Myckelle M. S. Ferreira, UFPE, Recife, Pernambuco, Brazil, +558121267526, myckellemichely@hotmail.com
Roberto Q. Coutinho, UFPE, Recife, Pernambuco, Brazil, +558121267526, robertoqcoutinho@gmail.com

ABSTRACT

Due to the different geotechnical conditions associated with the construction of PetroquímicaSuape, Pernambuco / Brazil, it was necessary to use root piles partially embedded in a rock mass. Through the research campaign, after the soil layer, a rock mass was found, consisting of stretches of rhyolite, basalt and intermediate material between rhyolite and trachyte. In general, the rock mass was occasionally extremely weathered with compressive strength ranging from 30 MPa $\leq q_u \leq$110 MPa. With the results of three static load tests, it was possible to compare the failure load obtained by interpreting the load-settlement curves, with the bearing capacity obtained by applying the methods of Horvath (1978), Poulos and Davis (1980), Rowe and Armitage (1984), Cabral and Antunes (2000) and España (2011), including the consideration of lateral strength of the soil section. The bearing capacity obtained by the soil contribution and application of the Horvath method (1978) to lateral rock bedding provided good estimates of the failure load, with a difference of -24% to +25%. By considering the lateral inlay and base of the pile in rock mass, using the method of España (2011), plus the contribution of the soil, this difference is between -30,5% and -8%.

Keywords: bearing capacity, root piles, rock mass

1. INTRODUCTION

Construction on rock substrates is a challenge for the professionals involved due to the level of loading imposed and the complex nature of the rock mass. In addition, in the case of deep foundations partially embedded in rock mass, how the load is transferred depends on several factors.

For some authors, the load applied to the top of the pile is absorbed only by the lateral socket in the rock mass and the strength of the pile base is mobilized only when a considerable slip occurs at the rock-pile interface. Also, the difficulty of ensuring an effective cleaning of the base of the hole eventually leads many designers to disregard the contribution of the base strength.

Likewise, the contribution of the soil section is usually overlooked by designers. However, by means of dynamic load test analyses, Juvêncio (2015) observed that in the piles where there was a profile with gradual weathering of the rock, the portion of resistance supported by the soil typically reached 40% of the applied ultimate load.

Considering the uncertainties inherent in the use of foundations embedded in rock mass, important studies have been made and enhanced in the attempt to evaluate the mechanism of load transfer and performance of the rock mass.

2. ESTIMATION METHODS OF LOAD BEARING CAPACITY OF PILES IN SOIL AND PARTIALLY EMBEDDED IN ROCK MASS

The axial load applied to the top of a pile partially embedded in a rock mass is transferred to the ground by means of the shear stress in the soil pile section, the side socket in rock mass and the compressive stress between the pile base and the rock. When a pile crosses heterogeneous layers, the deformations required to mobilize the strength in each section are different due to the rigid characteristics of the materials crossed.

© 2018 Deep Foundations Institute

In Brazil there are several semiempirical formulations used in the estimation of the bearing capacity of piles in soil. These methods look for correlations, mostly with dynamic penetration resistance values measured by standard penetration test (SPT). The portion of lateral strength in soil ($Q_{l,s}$) is given by the correlation shown in eq. 1.

$$Q_{l,s} = U \sum \tau_{l,s} \Delta L \qquad \text{(MN)} \qquad [1]$$

where U = perimeter of the cross section of the pile; $\tau_{l,s}$ = unit lateral strength of the soil section, and ΔL = thickness of the section considered.

The unit lateral strength of root piles, according to some methods is presented below:

Aoki-Velloso method (1975), eq. 2:

$$\tau_{l,s} = \frac{\alpha k N_L}{F_2} \qquad \text{(MPa)} \qquad [2]$$

Décourt-Quaresma method (1978;1996), eq. 3:

$$\tau_{l,s} = (3{,}33.\overline{N} + 10)\beta' \qquad \text{(MPa)} \qquad [3]$$

Cabral method (1986), eq. 4:

$$\tau_{l,s} = \beta_0 \beta_1 N_L \qquad \text{(MPa)} \qquad [4]$$

where: N_L = average penetration resistance index in ΔL; $\overline{N}$= mean value of N_{SPT} along the shaft; F_2, K and α = coefficients proposed by Aoki-Velloso (1975), β'= coefficient proposed by Décourt-Quaresma (1978, 1996), and β_0 and β_1 = coefficients proposed by Cabral (1986).

Concerning the estimated bearing capacity of piles embedded in rock mass, many authors concentrated their studies on finding correlations with parameters of the rock mass. The models that propose a correlation between the unit base strength ($q_{p,r}$) and or the lateral unit strength of the section in rock mass ($\tau_{l,r}$), with the simple compressive strength of the rock (q_u), can be expressed according to eq. 5 and eq. 6, respectively.

$$q_{p,r} = N\, {q_u}^{\rho} \qquad \text{(MPa)} \qquad [5]$$

$$\tau_{l,r} = \alpha {q_u}^{\beta} \qquad \text{(MPa)} \qquad [6]$$

where: α and N = factors related to the quality of the mass, and β and ρ = empirical parameters, as presented in Table 1.

Table 1. Coefficients of empirical methods to determine lateral and base strength.

Reference	α	β	N	ρ	q_u/P_{atm}
Rosenberg & Journeaux (1976)	0.37	0.51	-	-	5 - 400
Horvath (1978)	0.20	0.50	-	-	1 - 400
Meigh & Wolski (1979)	0.22	0.60	-	-	2 - 200
Poulos & Davis (1980)	0.05	1.00	0.20	0.5	-
Rowe & Armitage (1984)	0.45	0.50	1.00	1	4 - 400
Zhang & Einstein (1998)	0.40	0.50	3.00	1	5 - 550

The Cabral and Antunes (2000) and España (2011) methods propose further considerations to determine the bearing capacity of partially embedded piles in rock mass.

The Brazilian method proposed by Cabral and Antunes (2000) considers that the soil section can contribute to the bearing capacity of the pile partially embedded in rock mass. However, to do so it is necessary for the soil to have reasonable strength and an elastic deformation of more than δ_0, eq. 7.

$$\delta_0 = 2mm + 0{,}2\%\emptyset_s \quad \text{(mm)} \quad [7]$$

where: ϕs= diameter in soil of the pile in mm.

The unitary base strength of the pile, as well as the unit lateral strength of the section in rocky mass is presented by eq. 8 and eq. 9, respectively.

$$q_{pr} = n \cdot q_u \leq 0{,}4 f_{ck} \quad \text{(MPa)} \quad [8]$$

$$\tau_{l,r} = 2{,}5 \; a \; 3{,}5\% \; q_{p,r} < f_{ck}/15 \quad \text{(MPa)} \quad [9]$$

where: *n* = correction factor that takes into account the degree of change and small fractures, Table 2, and f_{ck} = the characteristic compressive strength of the concrete.

Table 2. Values of n second Cabral and Antunes (2000)

Rock type	Variation	Average
very weathered	0.07 - 0.13	0.10
weathered	0.24 - 0.36	0.30
slightly weathered - unaltered	0.48 - 0.60	0.54

The España (2011) method is found in the Guide to Foundations and Road Works prepared by the Spanish Planning and Infrastructure Department. This method does not apply to very fractured masses (q_u<1MPa), which present RQD <10%, or which have a considerable level of alteration.

According to the method, the pile bearing capacity is obtained based on admissible pressure, eq. 10.

$$P_{v,adm} = p_0 \alpha_1 \alpha_2 \alpha_3 \sqrt{\frac{q_u}{p_0}} \quad \text{(MPa)} \quad [10]$$

with: p_o as the reference pressure, adopted as 1MPa, α_1, α_2, α_3 are the dimensionless parameters that depend on the rock type, its degree of change and the spacing of the discontinuities, respectively.

These parameters must be representative to a depth of $1.5\phi_r$, measured from their support plane, where ϕ_r is the diameter of the pile embedded in rock mass.

The calculation of $q_{p,r}$ and $\tau_{1,r}$ from the admissible pressure $P_{v,\,adm}$, is given by eq. 11 and eq. 12.

$$q_{p,r} = 2P_{v,adm} \quad \text{(MPa)} \quad [11]$$

$$\tau_{l,r} = 0{,}1 q_{p,r} \quad \text{(MPa)} \quad [12]$$

In the cases where the length of the socket (L_r) is considerable, the method proposes the application of an embedding factor in the portion of strength at the pile base. This factor is found from Eq. 13:

$$d_f = 1 + 0{,}4 \frac{L_r}{\emptyset_r} \leq 2 \quad [13]$$

3. METHODS OF INTERPRETING STATIC LOAD TESTS

In view of the complexity involved in a design of piles partially embedded in rock mass, it is of the utmost importance to verify foundation performance by carrying out load tests. Several criteria have been proposed to define failure load, using the results of a static load test, among them the methods of Terzaghi (1943), Van der Veen (1953), Chin-Kondner (1970; 1971), Davisson (1972) and Décourt (1996).

The Terzaghi method (1943) determines the failure load from settlement corresponding to 10% of the pile diameter, while the Van der Veen method (1953) endeavors to find a vertical asymptote in the curve load-settlement, using exponential adjustment. The Chin-Kondner method (1970; 1971) considers that the load-settlement ratio is hyperbolic and the pile's failure load is obtained from the linear coefficient found by the graphic construction of the ratio between the settlement and the load versus the settlement. In the Davisson method (1972), the failure load is defined by the elastic shortening of the pile added to a base displacement, obtained through the pile diameter.

The Décourt method (1996) is based on the concept of rigidity. According to the author, a foundation's rigidity (R) is defined as the ratio between the applied load (Q) and the settlement (s) it undergoes.

Décourt (1996) states that the failure occurs when the spring constant or rigidity tends to zero. The physical failure load (Qu) is assumed to be the load that causes settlements that are close to the infinite and consequently produce rigidity values close to zero, as follows:

$$Q_u = \lim_{s \to \infty} \frac{Q}{s} \quad — \quad \frac{Q}{s} \to 0 \qquad [14]$$

In practice, the R values (Q/s) in ordinates, and the Q values, are plotted in abscissas. If the load test is conducted to very small R values, a linear or logarithmic extrapolation of the stretch where the curve becomes sub-horizontal would provide a good estimate of the physical failure load of the foundation. In most cases, simple linear extrapolation would be perfectly adequate. The failure can then be defined as the load corresponding to zero rigidity.

4. CASE STUDY

The entire geotechnical research campaign and consultancy and sizing of the foundations was guided and supervised by the second author of this work, based on an agreement between PetroquímicaSuape and the Federal University of Pernambuco (UFPE).

4.1 Study area

The area analyzed herein is located in the municipality of Ipojuca, Pernambuco State, Brazil, and corresponds to the site where PetroquímicaSuape, a large chemical plant, was built.

The PetroquímicaSuape plant is designed to produce purified terephthalic acid. This product is the raw material for producing polyester textile, PET resins, packaging, as well as industrial fibers used in the manufacture of tires, materials and equipment for the electric, automotive and oil industry sectors.

4.2 Site investigation

Since it is a large project and due to the complexity of the subsoil, the PetroquímicaSuape site was investigated using standard penetration tests (SPT) and mixed (SP and SM) drilling, CPTU, seismic CPTU, resistivity measurements, piezometer and undisturbed and disturbed soil and rock samples., The area was subdivided into nine sectors, as shown in Figure 1 in accordance with its geotechnical characteristics and the distribution of petrochemical structures.

The SPT tests were performed according to the ABNT standards (2001), using a manual system with a 65kg hammer and 72% driving power.

Laboratory tests were carried out on samples collected from the rock mass to determine the index properties of the rock (absorption, porosity, natural specific gravity and saturated specific gravity) and its mechanical properties (simple compressive strength of unaltered rock).

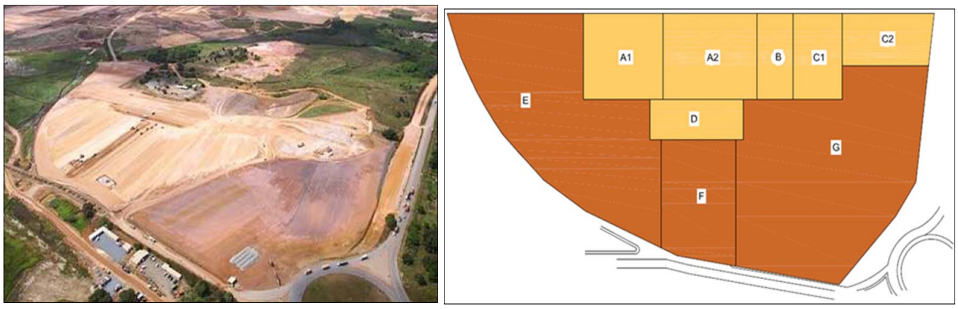


Figure 1. (a) View of the site after earthworks; (b) Subdivision of site in sectors.

Source: Coutinho (2008)

From the research carried out it was found that the area has quite a heterogeneous profile, generally consisting of layers of sandy silt, silty clay and silty fine sand. The rock mass is then found to consist of a matrix of rhyolite, basalt and intermediate material between the rhyolite and the trachyte. The natural ground surface terrain dimensions varied by about + 3 m to + 24 m above sea level, and after paving, the final average dimension is set to at + 7.8 m.

As demonstrated by Coutinho (2008), the rhyolite rock mass is slightly altered and occasionally fractured, while the average compressive strength found is 78 MPa. The rock mass sections of basalt have a rock matrix with a massive structure, ophitic texture and average compressive strength of 54 MPa. The intermediate section between the rhyolite and the trachyte has a massive structure and a texture classified as microporphyritic to porphyritic. The simple compressive strength values were 30 MPa $\leq q_u \leq$110 MPa.

In general, the rock mass in the PetroquímicaSuape site ranged from occasionally to extremely weathered and occasionally to moderately fractured, with a slope of discontinuities between 21º and 70º. In addition, by comparing the results of the laboratory tests and the values proposed in the literature, the strong influence of the state of alteration and fracture of the rock mass was verified in the values of porosity, specific gravity, degree of saturation, and simple compressive strength of the rock (Coutinho, 2008, Ferreira, 2017).

4.3 Construction characteristics of piles and load test results

In the PetroquímicaSuape foundation design, based on the subsoil characteristics and loading level imposed by the structure, two types of root piles partially embedded in rock mass, R1 and R2, were proposed, Figure 2.

The length embedded in the rock mass for the two pile types was defined as three to five meters, and in some situations, after a more accurate analysis of the site, or due to some executive difficulties, the embedded length was shortened.

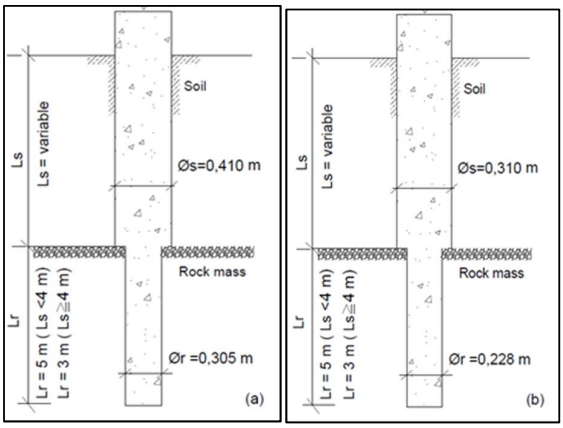


Figure 2. (a) General diagram of R1 root piles (b) General diagram of R2 root pile, both in PetroquímicaSuape. Source: Adapted from Coutinho (2008).

For this work, the analysis of the bearing capacity of root piles concentrated on data relating to three root piles implemented in the rock mass of PetroquímicaSuape. Table 3 shows the designations adopted for identifying the piles analyzed, their geometric characteristics and the work load for which they were designed.

Table 3. Design characteristics of the piles studied. Source: Adapted from Coutinho (2009).

Piles	ϕ_s (mm)	ϕ_r (mm)	L_s (m)	L_r (m)	Work load (kN)
E25	410	305	6.70	3.30	1000
E100	410	305	6.70	1.30*	1000
E110	310	228	6.70	3.30	750

Note: In this pile the stretch embedded in the rock mass had to be reduced due to executive problems.

The root piles studied were concreted with reinforcement in CA-50 steel with a diameter of 20-25 mm in the longitudinal rods, and CA-25 for the cross stirrups, with 8mm diameter. The strength of the concrete was specified with at least f_{ck} = 20 MPa.

Piles E25 and E100 were executed in sector A2, Figure 1 (b), and are sunk into a subsoil whose profile initially consists of a 2.65 m layer of sandy silt with a little medium compact clay, followed by very compact to compact silty fine sand with a thickness of 3.15 m, and a narrow 0.70 m layer of very compact fine silty sand. The rock mass described in Figure 3 (a) is found at 6.70 m deep.

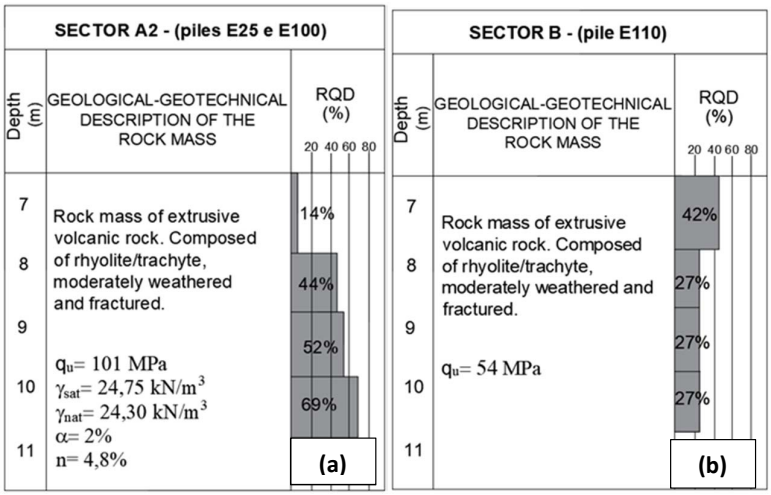


Figure 3. Description of rock mass into which the piles were socketed. Source: Adapted from Coutinho (2008).

With regard to the subsoil of sector B, into which pile E110 was inserted, a layer of clayey silt with fine sand is found, to give a medium to rigid condition. In the next 3 m, the layer has soft to medium consistency, followed by a 2 m layer of rigid to hard material. Then the rock mass of rhyolite/trachyte is found to have a greater degree of alteration compared to the mass of sector A2, Figure 3 (b).

The control of the root pile implementation in PetroquímicaSuape complied with Brazilian regulations. In relation to static load compression tests, these tests were carried out according to the specifications of the Brazilian standard ABNT (2006) for slow loading, with the test load achieving twice the work load of the piles.

During the static load test, pile E25 underwent a maximum load of 2000 kN, reaching a maximum settlement of 3.66 mm. After unloading, a residual settlement of 0.36 mm was observed, as shown in Figure 4. The static load test performed on pile E100 was applied to a 2000 kN test load with a total settlement of 3.85 mm and, after unloading, the residual setllement was 0.87 mm. For pile E110, the static load test reached a test load of 1500 kN, with a total settlement of 7.56 mm and a 2.27 mm residual settlement after unloading,.

The maximum settlements achieved in the tests for piles E25, E100 and E110 correspond to, 1.02%, 1.07% and 2.8%, respectively, of the average diameter of each pile.

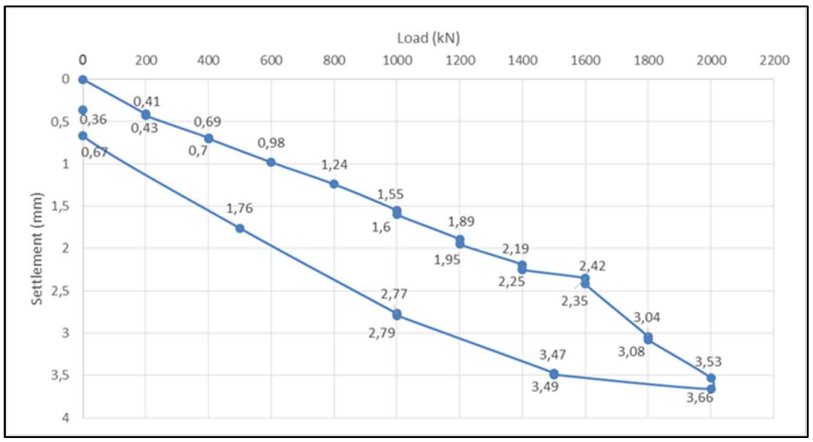


Figure 4. Load-settlement curve of pile E25. Source: Adapted from Coutinho (2009)

After analyzing the load tests, it was found that the piles in this study performed satisfactorily in relation to the design requirements, not reaching failure or significant settlement values for the established work load.

As demonstrated, the maximum settlements achieved ranged from 3.5 mm to 7.5 mm, while the permanent settlements were below 3 mm, that is, approximately 1% of the average shaft diameter of the piles. Thus, considering the evaluation by Reese and O'Neill (1988) and Osterberg (2000) that the mobilization of the strength of the pile base only runs for settlements of 10 mm, it is expected that in the piles studied, the pile toe strength has not been developed.

4.4 Estimation of the failure load from load tests

Even when the test load was twice the work load established in the design, no failure occrred in the piles. Extrapolation methods were applied in order to obtain the estimation of each pile's failure load.

These applied methods provide more accurate reuslts when the tests are taken to considerable settlement levels. However, in this study, the piles reached maximum settlements of relatively low 8 mm.

With this knowledge, the application of failure load estimation methods on piles E25, E100 and E110 enable an applicability analysis of the methods and results found, considering the circumstances.

By the fact that the Terzaghi (1943) and Davisson (1972) methods determined the failure load through a limit settlement, it was not possible to estimate the failure load from the load-settlement curves, since the displacements found in the tests were minimal and did not exceed the starting values of these methods. Therefore, only Van der Veen (1953), Chin-Kondner (1970, 1971) and Décourt (1996) methods were applied. The failure loads obtained for each pile analyzed by adopting the presented methods can be grouped in Table 4.

Table 4. Failure load obtained by load test interpretation methods.

Method	Failure load (kN)		
	Pile E25	**Pile E100**	**Pile E110**
Maximum load for load test (kN)	2000	2000	1500
Van der Veen (1943)	3750	2300	1600
Chin-Kondner (1970; 1971)	3846	3125	1820
Décourt (1996)	3880	2900	1830
Average failure load (kN)	3825	2775	1750

On analyzing the results, it was noted that, despite the low settlement level achieved in the tests, the failure load estimations of each pile are approximate.

In relation to the calculated average failure load, the Décourt method (1996) provided a percentage difference of +1.43% to +4.60%; the Chin-Kondner method (1970, 1971) differed between -0.55% and +12%, and estimations obtained from the Van der Veen method (1943) showed differences between -17% and -2%.

Considering the fact that the Décourt (1996) and Chin-Kondner (1970, 1971) methods give the most approximate results for every pile, it is more feasible to establish the failure load of each pile as given by the average of the estimations supplied only by these methods. Thus, the estimation of the failure load for piles E25, E100 and E110, is 3863 kN, 3012 kN and 1825 kN, respectively.

4.5 Estimation and analysis of bearing capacity of piles studied

In order to assess the pile bearing capacity, a comparison is made between the average failure load obtained from the load tests using the Décourt (1996) and Chin-Kondner (1970, 1971) methods, and the bearing capacity in four situations:

a) Consideration only of the lateral strength of the section embedded in rock mass, ($Q_{l,r}$), using the methods of Horvath (1978), Poulos and Davis (1980), Rowe and Armitage (1984), Cabral and Antunes (2000) and España (2011).

b) Consideration of the lateral strength of the stretch in soil, ($Q_{l,s}$), and lateral embedded in rock mass, ($Q_{l, r}$), using the methods of Cabral (1986), Horvath (1978), Poulos and Davis (1980), Rowe and Armitage (1984), Cabral and Antunes (2000) and España (2011).

c) Consideration of lateral strength of the soil section, ($Q_{l,s}$), lateral embedded in rock ($Q_{l,r}$) and the pile base, ($Q_{p,r}$), adopting the methods of Cabral (1986), Poulos and Davis (1980), Rowe and Armitage (1984), Cabral and Antunes (2000) and España (2011).

d) Consideration of the lateral strength embedded in rock ($Q_{l,r}$), and base of the pile ($Q_{p,r}$), from Poulos and Davis (1980), Rowe and Armitage (1984), Cabral and Antunes (2000) and España (2011).

According to the order of magnitude of the settlements reached in the load tests, as previosuly analyzed, for the piles in this study, it is probable that the tip resistance has not been mobilized when carrying out the load tests. However, since the methods of Poulos and Davis (1980), Rowe and Armitage (1984), Cabral and Antunes (2000) and España (2011) determine the bearing capacity by consideirng the lateral strength of the penetration and tip of the pile, the results were evaluated based on the situations presented in items c and d.

To adopt the aforementioned empirical methods, some considerations were made about the uniaxial compressive strength of the rock. The uniaxial compressive strength of the rock in sector A2 was obtained from a specific laboratory test, showing q_u=101 MPa. In relation to sector B, simple compression tests were not performed in this sector, so it was adopted that q_u=54 MPa, this value corresponds to the strength found in tests performed in other regions of the rock mass, for the same rock type in question and with the same degree of weathering.

When adopting the Horvath method (1978) the lateral strength is conditioned by the smaller value between q_u/P_{atm} and F_{ck}/ P_{atm}. The ratio proposed by Rowe and Armitage (1987) was established for soft rock with $q_u \leq 30$ MPa, so an analysis was made on the applicability of the method based on the characteristics found for the rock mass of PetroquímicaSuape. Accordingly, the value of the compressive strength of the rock matrix for E25, E100 and E110 piles was adopted as q_u=30 MPa.

For each of the four situations analyzed, the average failure load of the E25, E100 and E110 piles was compared to their bearing capacity obtained by applying the estimation methods. The results can be seen in Tables 5, 6 and 7.

Table 5. Percentage difference between the bearing capacity of pile E25, for the different methods, in relation to the average failure load of the pile.

Methods	Combinations for the bearing capacity of pile E25			
	$Q_{l,r}$	$Q_{l,r} + Q_{l,s}$	$Q_{l,s} + Q_{l,r} + Q_{p,r}$	$Q_{l,r} + Q_{p,r}$
Horvath (1978)	-27%	+3,5%	-	-
Paulos & Davis (1980)	+9%	+39%	+77%	+47%
Rowe & Armitage (1984)	+102%	+132%	+189%	+158%
Cabral & Antunes (2000)	-77%	-47%	-32%	-62%
España (2011)	-58%	-27%	-8%	-38%

Table 6. Percentage difference between the bearing capacity of pile E100, for the different methods, in relation to the average failure load of the pile.

Methods	Combinations for the bearing capacity of pile E100			
	$Q_{l,r}$	$Q_{l,r} + Q_{l,s}$	$Q_{l,s} + Q_{l,r} + Q_{p,r}$	$Q_{l,r} + Q_{p,r}$
Horvath (1978)	-63%	-24%	-	-
Paulos & Davis (1980)	-45%	-6%	+43%	+4.1%
Rowe & Armitage (1984)	+2%	+40%	+113.5%	+74.5%
Cabral & Antunes (2000)	-88%	-49%	-30%	-69%
España (2011)	-78.5%	-40%	-14%	-53.5%

Figure 7. Percentage difference between the bearing capacity of pile E110, for the different methods, in relation to the average failure load of the pile.

Methods	Combinations for the bearing capacity of pile E110			
	$Q_{l,r}$	$Q_{l,r} + Q_{l,s}$	$Q_{l,s} + Q_{l,r} + Q_{p,r}$	$Q_{l,r} + Q_{p,r}$
Horvath (1978)	+16%	+25%	-	-
Paulos & Davis (1980)	+72%	+81.5%	+100%	+91%
Rowe & Armitage (1984)	+219%	+228%	+295.5%	+286%
Cabral & Antunes (2000)	-75.5%	-66%	-54%	-63.5%
España (2011)	-55%	-46%	-30.5%	-40%

From the results, it is found that when the pile bearing capacity is determined only by considering the lateral stength of the section embedded in rock mass, the Horvath method (1978) provided the most coherent results with the failure load of piles E25 and E110.

When the pile bearing capacity is obtained by the contribution of the lateral strength of the soil section and the lateral embedded in rock mass, it is found that the Horvath method (1978), when associated to the estimation methods of lateral strength of the soil section, results in bearing capacity values of -24% to +25% of the failure load of E25, E100 and E110 piles.

In this same situation, the application of the Cabral and Antunes (2000) and España (2011) methods resulted in more conservative estimations, while, on the other hand, the methods of Poulos and Davis (1980) and Rowe and Armitage (1984) provided estimations far above the failure load obtained from the interpretation of the load tests.

With respect to the results for the bearing capacity comprising the lateral strength of the soil section, lateral socket in rock mass and base of the pile, the España method (2011) gave results reasonably close to the failure load of the piles and in favor of safety, with a different percentage in relation to the failure load, of -30.5% to -8% for the piles studied.

Complementing the analysis, of the methods used to determine the pile bearing capacity by considering the lateral strength of the section embedded in the rock mass and the pile base, the España (2011) and Cabral and Antunes (2000) methods provided the most conservative results.

5. CONCLUSIONS

The authors of this study understand that the analyses addressed in the article were based on a limited number of load tests, where neither failure or a considerable level of settlements was achieved .

Nevertheless, the aim was to address problems that many designers eventually encounter when designing piles partially embedded in rock mass. Moreover, the purpose was to analyze and compare the results by applying some calculation methods in the literature with real information gained from the project.

Thus, based on the results obtained from the load tests, it was found that the piles analyzed in this study showed a satisfactory performance in relation to the level of settlements found.

The methods to determine the failure load from the load-settlement curves provided fairly close results, and the estimated failure loads using the Chin-Kondner (1970; 1971) and Décourt (1996) methods were always higher than Van der Veen's estimations (1953).

Concerning the analysis for the best composition to estimate the pile bearing capacity studied, the best results were found to be obtained through the contribution of the soil section and application of the Horvath (1978) and España (2011) methods to the section embedded in rock mass.

The bearing capacity obtained by considering the lateral strength of the stretch in soil and by applying the Horvath method (1978) to the lateral embedded in rock mass, provided good estimations in relation to the failure load, with a difference of -24% to +25%. Where the bearing capacity is provided by the soil section's contribution of the section in mass, this difference is between -30.5% and -8%.

REFERENCES

ABNT 2006. Piles – Static Load – Test Performance Method - NBR 12131 - Brazilian Association of Technical Standards, Rio de Janeiro, 8 p (In Portuguese).

ABNT 2001. Soil – Simple test holes with SPT – Test Performance Method – NBR 6484 - Brazilian Association of Technical Standards, Rio de Janeiro, 17 p (In Portuguese).

Aoki, N. & Velloso, D.A., 1975. An approximate method to estimate the bearing capacity of piles. In: V Pan American Congress on Soil Mechanics and Foundations (Passmfe), Buenos Aires, Annals... Buenos Aires: Argentinean Society for Soil Mechanics and Foundation Engineering V5, p. 367-374.

Cabral, D.A., 1986. The use of root piles as foundation of normal works. In: Brazilian Congress of Soil Mechanics and Foundation Engineering. Porto Alegre/RS, v.6, p.71-82. (In Portuguese).

Chin, F.K., 1970. Discussion: Pile tests. Arkansas River Project, JSMFD, ASCE, v. 97, n. SM7, p. 930-932.

Chin, F.K., 1971. Discussion: of pile test. Arkansas River Project. Soil Mechanics and Foundation Engineering Journal, ASCE, vol. 97, SM 6, p.930-932.

Coutinho, R.Q., 2008. Technical Report III (Version 2) - Geotechnical interpretative report. Recife, Brazil.

Coutinho, R.Q., 2009. Technical Report II (Rev. 1) - Foundation Recommendations Report – General (ISBL+OSBL). Recife, Brazil.

Davisson, M.T., 1972. High capacity piles. Proceedings, Lecture Series. Innovations in Foundation Construction, ASCE, Illinois, Section, p. 52.

Décourt, L. 1996. Analysis of Deep Foundations: Piles. In: Foundations: Theory and practice, Hachich et al. (eds), Ed. Pini Ltda., São Paulo, Chap. 8.1, p.265-301. (In Portuguese).

Décourt, L. & Quaresma, A., 1978. Pile bearing capacity from SPT values. Proc. of VI Brazilian Congress on Soil Mechanics and Geotechnical Engineering (Cobramseg), Rio de Janeiro, Brazil, p. 45-53. (In Portuguese).

España 2011. *Guía de cimentaciones en obras de carretera. 3 ed. Madrid: Ministerio de Fomento. Centro de Publicaciones,* p.304.

Ferreira, M.M.S., 2017. Geomechanical classification and analysis of root piles partially embedded in rock mass – PetroquímicaSuape. Master of Science Dissertation. Federal University of Pernambuco, Recife, 242 p. (in Portuguese).

Hovarth, R., 1978. Field load test data on concrete-to-rock bond strength for drilled pier foundations. Publication 78-07. Toronto: University. of Toronto.

Juvêncio, E.L., 2015. Evaluation of the behavior of piles partly embedded in gneissic rock, Doctor of Science Thesis, UFRJ/COPPE, Rio de Janeiro, 225p. (In Portuguese).

O'Neill, M.W. & Reese, L.C., 1988. Drilled Shafts: Construction and Design, FHWA, Publication No. HI-88-042.

Osterberg, J., 2000. Side shear and end bearing in drilled shafts. In: Proceedings of GeoDenver Sessions - New technological and design developments in deep foundations, Denver, Colorado, Aug. pp. 72-79.

Poulos, H.G. & Davis, E.H., 1980. Pile Foundation Analysis and Design. New York: John Wiley and Sons. 397p. (Series in Geotechnical Engineering).

Rowe, R.K. & Armitage, H.H., 1984. The design of piles socketed into weak rock. In: Report GEOT-11-84, University of Western Ontario, London, Ontario, Canada.

Van der Veen, C., 1953. The bearing capacity of a pile. In: International conference of soil mechanics and foundation engineering, Zurich. Proceedings Zurich: Icosomef. v. 2. p. 84-90.

Innovative Design and Quality Control of Single Stage High Pressure Injection Micropiles, Waal-Compact-Piles

Floris Schokking, GeoConsult BV, Haarlem, The Netherlands,
Phone +31 23 526 9765, floris.schokking@geoconsult-haarlem.nl
Jan van der Wiel, Hektec B.V., Van 't Hek Group, Purmerend, The Netherlands
Phone +31 299 42 08 08, janvanderwiel@hektec.nl

ABSTRACT

The study of a series of load tests on single stage high pressure (80-100 bar) injection micropiles has led to an innovative design method for these piles with diameters up to 350 mm. An important issue in the new design approach is the development of a grout bulb in the soil under the high pressures, which could be observed after retrieval of the piles. During installation the formation of this bulb acts as a forced deformation on the surrounding soil and resulting from this are an increase in horizontal stress, strength and elasticity parameters. The bearing capacity of the piles in compression appears as a result in majority delivered by the developed skin friction and vertical displacements are observed to be low. Comparison of the static pile load test data with the results of finite element modelling (FEM) of the tests, incorporating the above described installation features, supported the load-deformation behaviour observed in the tests. The outcome of the modelling suggests that FEM could be used in future design for this type of micropiles, provided that a consistent dimension of the grout bulb in the soil can be secured.

To be able to guarantee the forming of an adequate grout bulb a quality control programme has been developed based on a set of parameters related to grout composition, grout velocity, grout pressures and the total volume of grout injected vs. the expected volume of the bulb. A first attempt is made to define guiding confidence boundaries for these parameters based on gained experience in recent installation projects.

Keywords: micropiles, grout injection, high pressure, FEM design, quality control, monitoring

INTRODUCTION

Micropiles were first introduced in the '50s of the previous century in Italy by Dr. Fernando Lizzi of Fondedile as "Pali radice" or root piles, for underpinning applications. Starting in 1957 'rectoli di pali radice", systems comprising multiple vertical and inclined micropiles, interlocked in three dimensional networks, were introduced and used for slope stabilization, reinforcement of
quay walls, protection of buried structures, and other soil and structure support and ground
reinforcement applications.

In The Netherlands the micropiles, under the product name Waalpaal or Waal-Compact-Pile, were first used for foundation improvement of old houses and buildings dating back to the 13th until the 19th century in Amsterdam. With small drilling rigs one could work inside the buildings in spaces with limited access and head room. Later the piles were used as well as tension elements in underground constructions, underpasses and tunnels in the construction phase. If required the piles could there serve as compression piles as well during the operational phase of the construction.

© 2018 Deep Foundations Institute

Single Stage High Pressure Injection Micropiles

The Waal-Compact-Pile system is typically used in granular materials, usually sands, which are overlain by soft cohesive layers, consisting of peat and clay. A steel tube (outside diameters 88,3 to 114,3 mm) fitted with a pointed head (Fig. 1), with diameters 150 to 250 mm, is drilled into the ground under low pressure injection of a low density cement grout (water/cement ratio of approx. 0,8)(Fig. 2a). The tubes consist of sections of 1,5 m to allow to work in spaces with limited height and which are coupled by a thread connection. These tubes stay in the ground after completion of the pile and form the structural support of the piles. After reaching the required end depth of the pile a dense cement grout with water/cement ratio of 0,4 is injected through the underside of the drill tube under continuous stationary turning of the screw point.



Fig. 1 Screw coupled tubes forming the drill stem with at the end the pointed drill head.

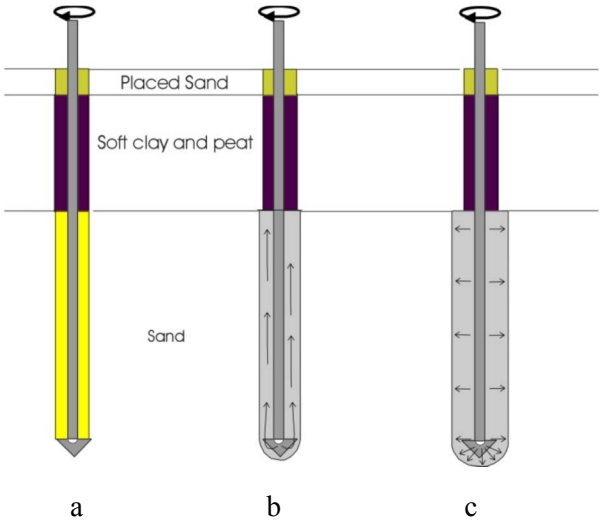


Fig. 2 a Drilling under low pressure injection of grout, b. Flow of grout at pressure up to 4 MPa to the soft clay and peat layers c. Forming of grout body under high grout pressures of 8,5 to 10 MPa with increasing diameter of grout body.

Before reaching the final pressure grout pressures range from 0,5 to 4 MPa with grout flow velocities from 15 to 20 liter/min. Under the high pressure of the grout it flows upward through and along the mixture of grout and sand until the cohesive overlying layers, acting as a hydrological barrier, where the grout flow is halted (Fig. 2 b). Resulting from the high pressure the grout/soil mixture deforms the surrounding soil horizontally and forms a grout body with a diameter which is a factor 1,4 to 1,5 larger than the point diameter of the drill (Fig. 2 c). Under an increasing densification of the grout it reaches final pressures of 8,5 to 10 MPa. The pile installation is completed with the placing of a head plate resting on a pre-welded ring on the last tube, which will support the concrete floors or foundation slabs to be applied later.

As far as the medium pressure grout application is concerned the piles may be compared with micropile systems described as Type B in the classification provided in FHWA, 1997. The final grout pressures are similar to the piles as applied in the Type D system from the same classification and referred to as IRS (Injection Répétitive et Sélective) introduced by the French Bustamante & Doix in 1985. The major difference of the Waal-Compact-Pile with that system being the direct application of the higher pressures at the end of the operation, where in the IRS system the second grouting stage is performed after hardening of the first stage grout application. What is similar in both systems is that from the high grout injection pressures a hardened grout "bulb" results in the soil. The Waal-Compact- Pile system is far more time efficient in forming this bulb as it is performed by a single stage injection operation. The forced deformation of the surrounding soil which accompanies the forming of the bulb is responsible for the high values of shaft resistance, which are characteristic for both the IRS system and the Waal-Compact-Pile.

FORMING OF GROUT BULB OR CYLINDER

The process of grout injection at the end of the drilling stage, the transport through the grout/sand mix along the drill pipe and the densification of the grout under increasing grout pressure induces a forced deformation of the grout-soil interface into the soil mass. After the grout is hardened a grout body like a bulb or cylinder has been formed. As far as the order of magnitude of the forced deformation is concerned a remarkable similarity appears to exist when comparing the IRS system and the Waal- Compact-Pile. Bustamente & Doix (1985) propose a parameter α = average grout injection bulb diameter/drill hole diameter. For various soil and rock conditions the authors give a range of α-values. For fine to course sand layers the α-values of 1,4 to 1,5 coincide with the measured diameters of grout bodies recovered after pile load tests at Wijdewormer and at Betuwelijn in The Netherlands and are related to the respective drill head diameters. Although the injection techniques are quite different for the two systems, the soil-pile interaction appears to be similar during installation and with respect to their load bearing behaviour.

Known theories of cavity expansion are applicable to the forming of the bulb or cylinder under the pressure of the grout. An increase in horizontal stress, angle of internal friction and stiffness of the soil results from the forming of a bulb. Zones with the decreasing of these effects away from the pile are developed. In Fig.8 the zones with increased horizontal stress around the pile are shown, as modelled with a finite element modelling (FEM) in PLAXIS. By derivation of the increase in strength parameters within these zones the distribution within the FEM grid could be established and a simulation of the static pile load tests at Wijdewormer (compression) and at Betuwelijn (compression) could be performed. The increase of the horizontal stress related to the in-situ vertical stress can be expressed in the realized K_h-values which are found to be ranging from 2 to 5. This is in accordance with various authors, such as Moller & Winding (1669, in Littlejohn, 1980), stating developed K_h-values ranging from 4 to 9 for soil anchors. The single stage micropile as described in this paper can be expected to behave under compressive loading similarly to the ISR type piles tested by Bustamente & Doix (1985), which is: at least 80 % of the load is carried by shaft friction and vertical displacements of the pile toes are low.

STATIC PILE LOAD TESTS AT WIJDEWORMER AND BETUWELIJN

A series of static pile load tests is performed on the single stage high pressure injection micropiles of which the main characteristics are presented in Table 1. At Wijdewormer the compression test was performed in a test area specifically designed for the installation and load tests. The piles were installed at a shallow depth of up to 10m - GL and in relatively low density Holocene sand layers with CPT cone resistance values ranging from Qc = 4 to 8 MPa (Fig. 3).

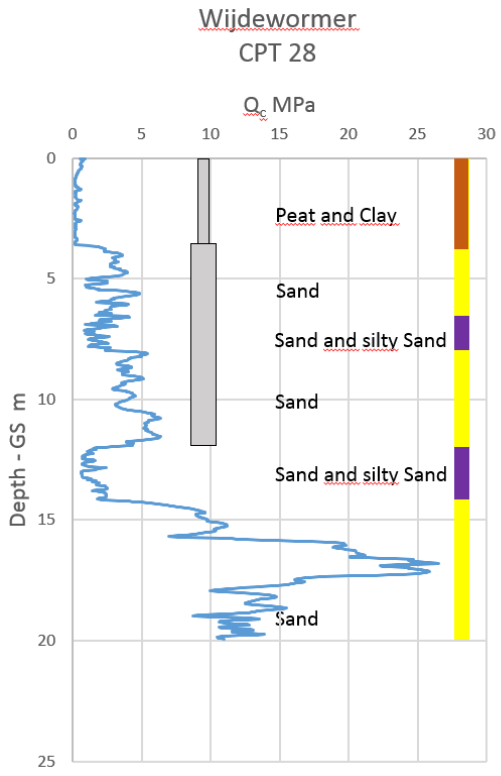


Fig. 3 CPT diagram at Wijdewormer

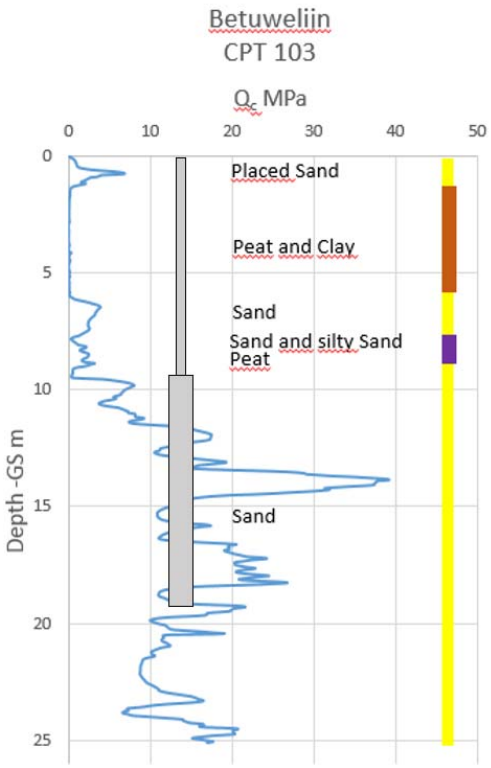


Fig. 4. CPT diagram at Betuwelijn

The tests at the Betuwelijn were performed to study the behaviour of the piles to be used under the approaches of a bored rail tunnel under the River Giessen. These piles reached a depth of 19 m -GL in Pleistocene medium dense to dense sand layers with CPT cone resistances of up to 38 MPa (Fig. 4).

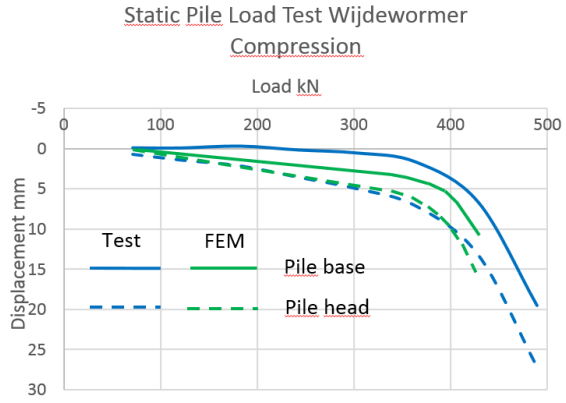
Table 1 Characteristics of static pile load tests at Wijdewormer and Betuwelijn

Location	Load	Max. load [kN]	Geotechnical * failure	CPT Cone Resistance [MPa]	Dimensions grout body		
					Length [m]	Diameter	
						Pile toe [mm]	Average [mm]
Tunnel Betuwelijn	Compression	2000	No	0 -38	7	261 – 325	263
	Tension	2000	No	0 -38	12	465 – 516	263
Test site Wijdewormer	Compression	480	Yes	4 – 8	4	282 - 347	220

*The piles show ongoing vertical displacements of the pile head of 10 to 20 mm at a static load during a time interval of 5 to 10 minutes.

Load-deformation behaviour

In Fig. 5 and 6 the load-deformation behaviour in the compression tests at Wijdewormer and Betuwelijn is presented.



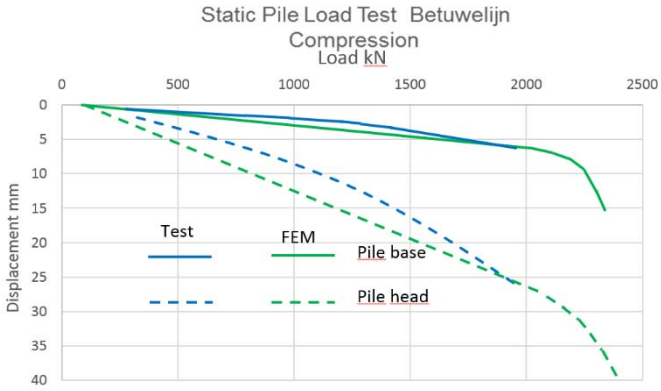


Fig. 5 and Fig. 6 Load-deformation behaviour of compression piles at Wijdewormer and Betuwelijn Field test data and Finite Element Model simulations

The pile at Wijdewormer began to fail at the applied load of 365 kN with a vertical deformation of the pile toe of 2 mm. Geotechnical failure occurred at 477 kN. From the final deformation at the pile toe of 2,9 mm a base resistance of 47 kN can be calculated. This means, that 420 kN of the pile bearing capacity is delivered by shaft resistance, which means 88 % of the pile bearing capacity. The shaft resistance is $\tau \approx$,085 MPa. Both the contribution to the shaft resistance and its value of $\tau \approx 0{,}085$ MPa with an average CPT value of 6 MPa correspond to the findings of Bustamente & Doix, 1985 (Fig. 8). The pile at Betuwelijn did not reach geotechnical failure. The maximum test load was kept at 2000 kN in order to prevent the steel yield limit to be reached and so to avoid structural failure of the pile. The vertical deformation of the pile toe at the maximum applied load was 7 mm. From the test at the Betuwelijn a minimum shear resistance $\tau \approx 0{,}35$ MPa can be derived. With a performed FEM modelling to be discussed later it is demonstrated that the maximum unit shaft resistance of $\tau \approx 0{,}4$ MPa lies well above the average values from the graph of Fig. 8.

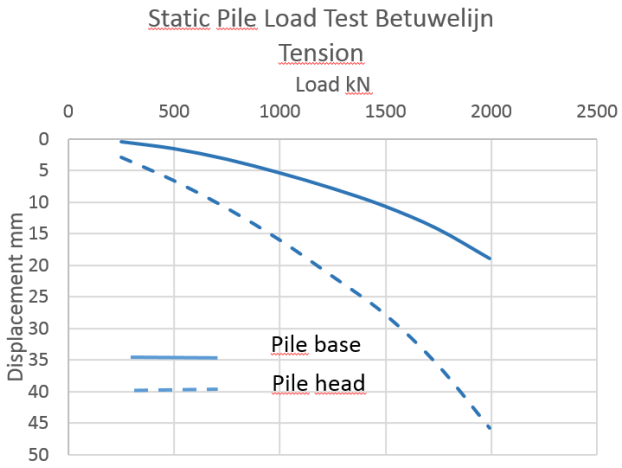


Fig. 7 Load-deformation behaviour of tension pile at Betuwelijn

In the tension test the geotechnical failure was not reached as well. The minimum unit shaft resistance of $\tau \approx 0{,}26$ MPa can be derived from this test.

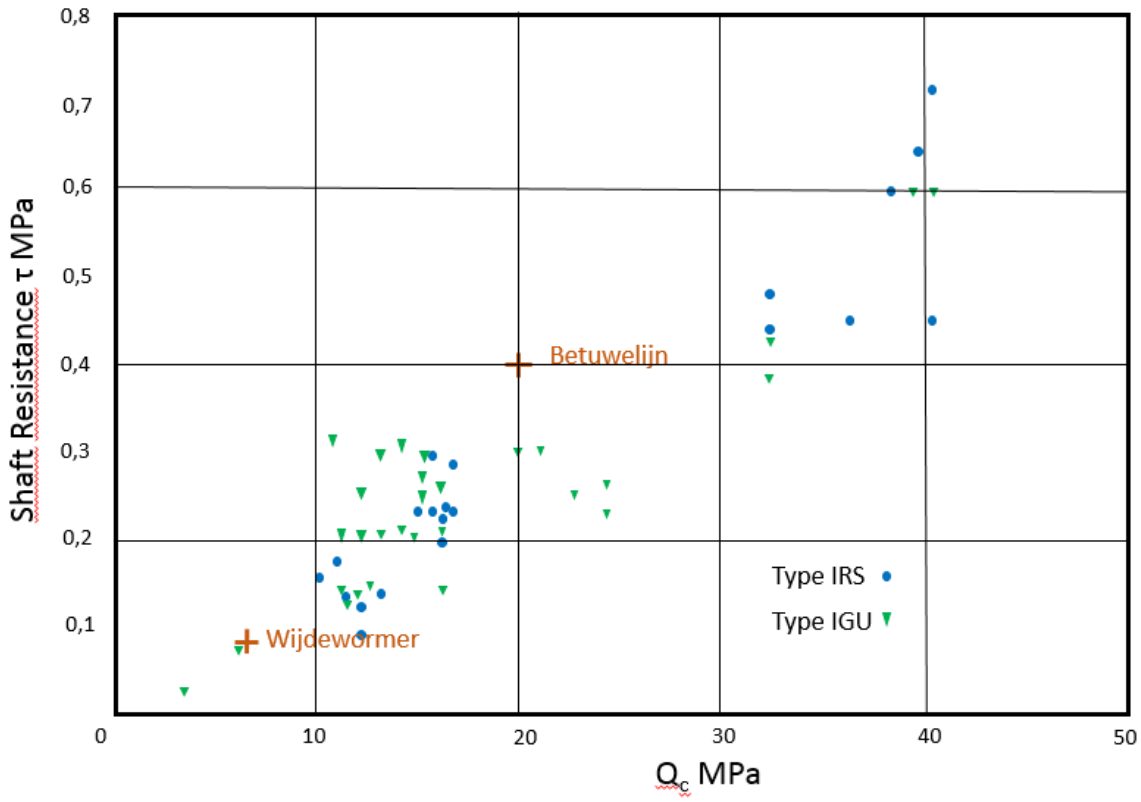


Fig. 8 Graph of Shaft Resistance vs Cone Resistance from load tests shear resistance developed of IRS and IGU (Injection Globale en presse Unifiée) type piles in sand and gravels with results of Wijdewormer and Betuwelijn (After Bustamente & Doix, 1985).

Performed laboratory test to compare the shear resistance of a grout to sand surface with that of the sand itself (Breure, & Evers, 2014) show that the shear resistance between the grout body and the soil is typically larger than the shear resistance of the soil. This phenomenon and the plotting of the unit shaft resistance values in the graph of Fig. 8 demonstrates that the single stage injection piles in this paper can be considered to be fully comparable with respect to their geotechnical behaviour with the IRS piles as described by Bustamente & Doix, 1985, although the multistage injection of the latter piles results in a differently shaped grout body within the soil. The forming of the grout bulb and the increase of strength properties of the soil around the pile resulting from the forced deformation of the soil is considered accountable for the major contribution of the shaft resistance to the bearing capacity of the pile in which respect both type of piles behave similarly.

INNOVATIVE DESIGN BY FINITE ELEMENT MODELLING

In most known design methods for micropiles the required dimensions of the piles are tailored to the estimation of the shear strength values as given in p.e. the diagram of Fig. 8 , or given in tables for specific soil or rock conditions.

By using as departing boundary condition the known diameter relationship with various sizes of the drill point diameter described in the foregoing, then the forced deformation of the soil which follows from it can form the outset for the calculation of developing horizontal stresses in the soil and the accompanying improvement of geotechnical parameters in the various soil layers surrounding the pile.

A finite element modelling approach to estimate the development of stress conditions and parameter distribution within the soil followed by a simulation of the loading of the pile appeared to be a suitable innovative method to determine the allowable loads on the pile and to obtain a feel for the corresponding vertical displacements.

Foundation design in The Netherlands is mainly based on the Cone Penetration Test (CPT). From this test the distribution of the soil can be derived digitally with the use of algorithms based on p.e. Robertson (2009) and Robertson & Cabal (2015) and applied to the FEM grid. After the new stress system related to the forced deformation is developed, the corresponding improved geotechnical parameters as angle of internal friction and Youngs modulus of elasticity can be estimated for the defined zones of soil improvement (Fig. 9). With known data on the pile stiffness, a combination of the stiffness of the steel drilling tube and the grout body, the load-deformation behaviour of the pile can be modelled with adequate accuracy.

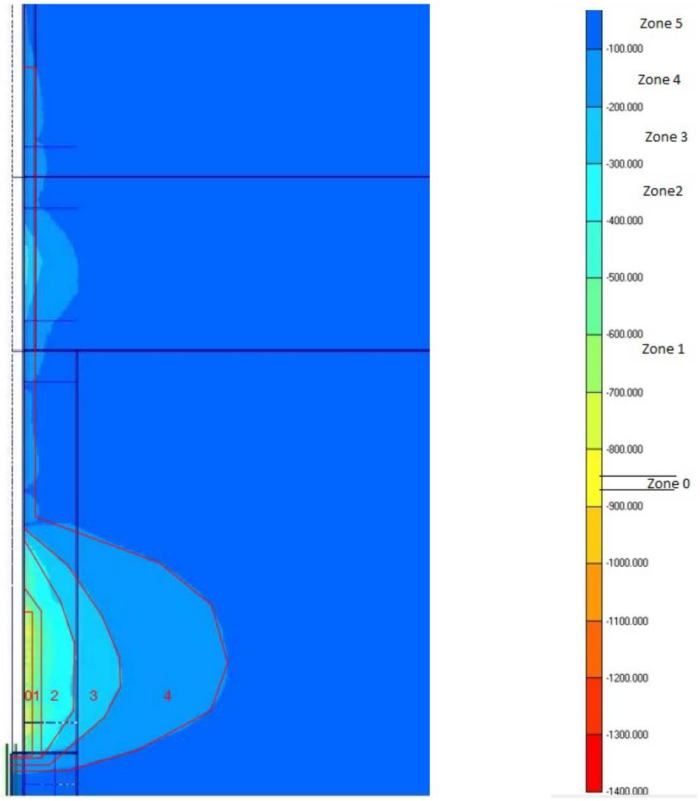


Fig. 9 Zones of increased horizontal stress and improved geotechnical parameters resulting from forced deformation by high pressure injection of the grout body.

In FEM modelling exercises with the PLAXIS programme the load-deformation behaviour of the load tested piles was simulated, with resulting curves as presented in Fig. 5 and 6. For the Wijdewormer test the observed geotechnical failure of the pile could accurately be modelled.

The modelling of the Betuwelijn load test resulted in a prediction of the load at which geotechnical failure occurred. The corresponding shear stress in the soil along the pile is approximately $\tau \approx 400$ kN/m^2 and lies well above the average line of the ISR tests in Fig. 8.

The use of this innovative more accurate design method will only lead to the use of reduced factors of safety provided that the assumed diameter and length of the grout body in the sand layer can be guaranteed to be formed consistently in the installation process. A study of the drilling and grout injection process allowed a first approach towards the development of an innovative quality monitoring procedure for the Waal-Compact-Pile.

DEVELOPMENT OF QUALITY MONITORING PROCEDURES

The consistent forming of a grout body with prescribed dimensions and depth in the sand layer must be guaranteed to meet the design requirements. Quality monitoring procedures are based on a series of parameters that can be measured during the drilling and grouting process. In Table 2 these process parameters are listed, with the measurements by which they are obtained.

Table 2 Measurements of process parameters for quality monitoring

	Process Parameters	Measurements
Drilling data	Depth in Bearing Sand Layer	a. Interpretation of drilling data b. Depth of pile toe c. Downward force and/or drilling moment
Grout data	Water/Cement Ratio	a. Weight of cement added to water volume in mixing vessel
	Grout Composition	b. Determination of volume weight of grout sample
	Grout Flow	c. Digital measurement on drilling machine
	Grout Pressure	d. Digital measurement on drilling machine
	Grout Volume	e. Digital measurement on drilling machine

Drilling data

a. If the depth of the layers as identified during the site investigation does not vary significantly over the site the CPT information will allow the determination of the required pile toe level and the length of the grout body.
b. If there exist significant variations in the thickness and depth of the bearing sand layer over the site the creation of a 3D-picture of the layers from the CPT information will be required to determine the intended pile toe level for all piles.
c. Changes in the downward force and the moment on the drilling tube may be used to check on the predicted levels of layers passed.

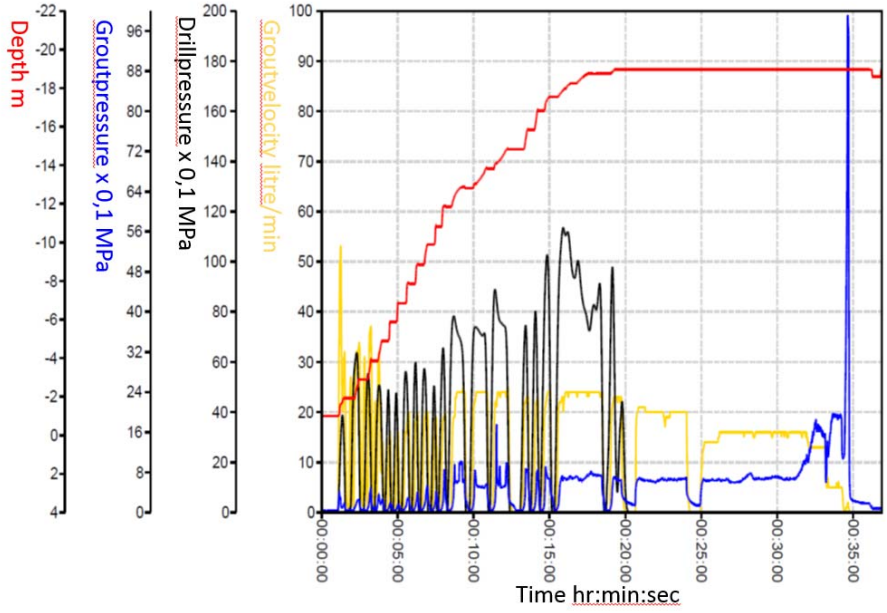


Fig. 10 Presentation of monitoring data during drilling and grout injection of Waal-Compact-Pile

Grout data

a. The water/cement ratio, in particular for the injection stage, is determined by measuring the increase of weight of the vessel resulting from adding the cement by means of a screw conveyor.
b. The required grout composition is checked by randomly sampling and determining the volume weight of the grout.
c. The grout flow during the final injection stage with a water/grout ratio of 0,4, should be continuous and at levels of approximately between 15 and 20 liter/min and should not show fluctuations or interruptions (Fig. 10).
d. Under continuous turning of the drill tube the injection pressure stays at levels of 0,5 to 4 MPa. When the required volume of grout is reached the injection pressure should steadily increase to its maximum between 8,5and 10 MPa and the drill will stall as a result of the increased density of the grout.
e. The total volume of grout applied during drilling and during injection appears the most important process parameter to judge the quality of the micropile. From compression tests on samples of the recovered Wijdewormer piles emerged concrete strength values of between 90 and 115 MPa . These strength values are corresponding to a water/cement ratio of approximately 0,2 as a result of water expelled from the grout at the higher grout pressures and so densifying the mix. The total volume of the grout mix with water/cement ratio of 0.4 can be calculated which is required to reach the volume of the grout body (consisting of a mix of pure grout and the drilled sand) that isrequired to a final water / cement ratio of 0.2. This Vgrout /Vgrout body value should ideally have a value of 1.

This has been tested on two sites in Amsterdam, of which the results are given in Fig. 11 and 12. For the smaller diameter (Dgrout body = 250 mm) piles at Gelderlandplein the Vgrout /Vgrout body values show slightly below 1, but with only a small variation. At the Brouwersgracht (Dgrout body = 350 mm) the values are well above 1 and with a larger variation. These are the first data sets that became available.

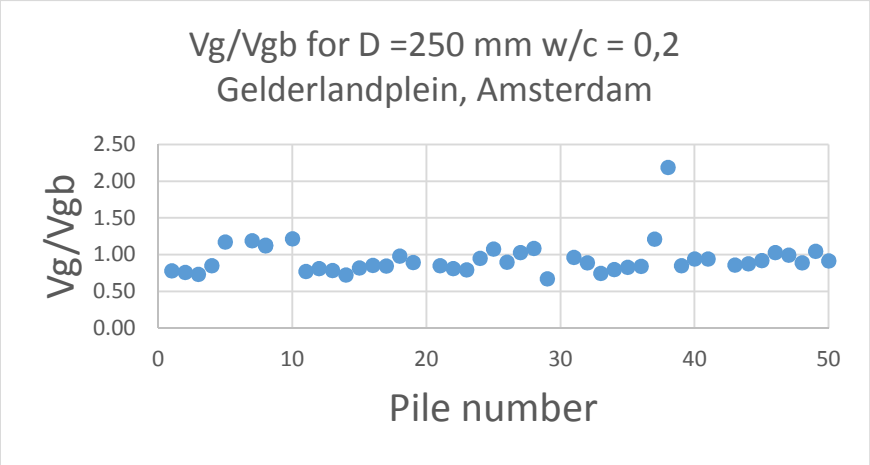


Fig. 11 Registred V_{grout} /$V_{grout\ body}$ values at Gelderlandplein, Amsterdam

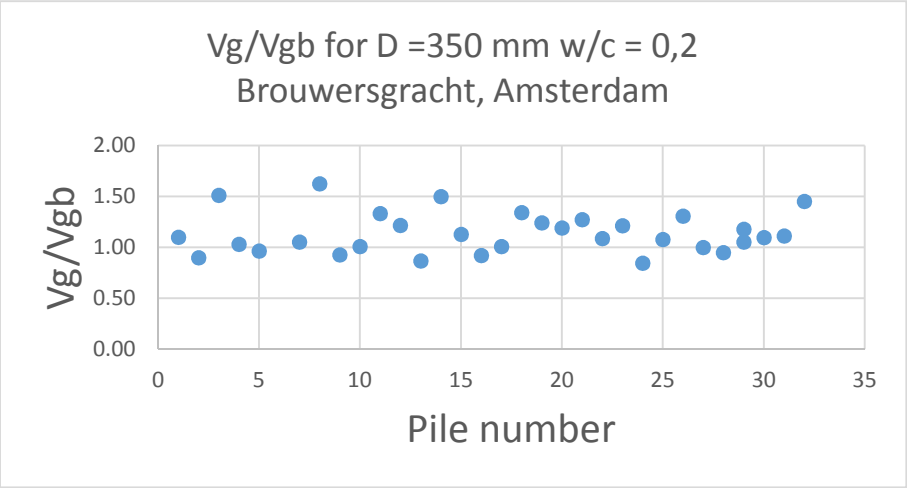


Fig. 12 Registered $V_{grout}/V_{grout\ body}$ values at Brouwersgracht, Amsterdam

Field tests, with recovering and measuring of the installed piles, are foreseen in the near future to establish $V_{grout}/V_{grout\ body}$ values for particular diameters and lengths of grout body developed. These will allow, with many more data sets to be analysed, to determine the boundaries between which the $V_{grout}/V_{grout\ body}$ values may vary to assure that the grout body meets the design specifications.

CONCLUSIONS EN DISCUSSION

The single stage high pressure micropiles discussed in this paper appear to be similar to the piles made with the Injection Répétitive et Sélective (IRS) method with respect to their geotechnical behaviour under loading conditions. The main difference between the two pile systems is the more simple and time effective installation of the Waal-Compact-Pile.

The series of investigation on the Waal-Compact –Piles and measurements of the grout body formed revealed a constant relationship between the diameter of the drill and the diameter of the grout body of $\alpha \approx 1{,}4$ to 1,5.

The graphs suggested by Bustamente & Doix, 1985, relating developed shaft resistance to soil density, show still a considerable scatter of results, where the Waal-Compact-Piles, installed in dense sand layers (Betuwelijn) give a higher value than the indicated average. This lead to try and find a more accurate design method for these piles.

The first exercises with FEM modelling of the installation and simulation of the loading of piles, which were statically load tested at two locations, were performed. The increase of horizontal stress and improvement of geotechnical properties could be modelled adequately, followed by the loading of the piles. It was demonstrated that with this innovative design approach allowable loads and accompanying settlements in the load tests could be estimated with acceptable accuracy.

The design approach with FEM modelling can only be used in a responsible way if the diameter and length of the expanded grout body in the soil can be guaranteed to be formed consistently during the installation process. From a series of process parameters to be monitored it appeared that the calculated volume of grout to be injected related to the expected volume of the grout body, is the most important parameter in the quality monitoring procedure. For this relationship, expressed in the formula Vgrout/Vgrout body, future research should be conducted to define confidence boundaries for its value for various expected diameters, length of grout body and soil conditions.

REFERENCES

Breure, W. & Evers, H.J., 2014, Schuifspannings verplaatsingsgedrag grout-zand *(Eng.: Shear stress deformation behaviour grout – sand)*, Geotechniek, Year 18, Vol. 3, July 2014, pp 68-71

Bustamante, M and Doix, B (1985), "Une Méthode pour le Calcul des Tirants et des Micropieux

Injectés". Bulletin de Liaison des Laboratoires de Ponts et Chaussées. LCPC, Paris, Nov-Dec, pp 75-92.

FHWA (1997), "Drilled and Grouted Micropiles, State-of-Practice Review", Bruce, D. A. and Juran, I., Reports No. FHWA-RD-96-016, 017, 018, and 019.

Moller, P. and Winding, S. (1969), "Anchoring in soil employing the Alvik, Lindo and JB drilling methods", 7th International Conference for Soil Mechanics and Foundation Engineering. Specialiy Session No. 15, pp 184 – 190, Mexico.

Littlejohn, G.S. (1970), "Soil Anchors", Institute of Civil Engineers, Ground Engineering Conference, London.

Robertson, P.K., 2009, Interpretation of Cone Pentration Tests – a unified approach, Can. Geotech. J., 46, pp 1337-1355.

Robertson, P.K. & Cabal, K.L., 2015, Guide to Cone Penetration Testing for Geotechnical Engineering, 6th edition, Gregg Drilling & Testing, Inc.

PERFORMANCE AND ANALYSIS OF A BRACED SECANT PILE WALL FOR A MULTI-STORY BUILDING IN MANHATTAN, NY

James D. Maniscalco, P.E.[1] & Evangelia S. Ieronymaki, Ph. D.[2]

ABSTRACT

This paper presents a case-study summarizing the construction and performance of a secant pile wall which served as the support of excavation during construction of two below grade basement levels for a multi-story building in Manhattan, NY. The secant pile wall was installed along the perimeter of the proposed building footprint (approximately125 ft by 123 ft) and was designed, along with multiple tiers of internal bracing, to support a 43 foot excavation below the existing ground surface. A 25-story residential building, directly adjacent to the west property line of the proposed building, provided a challenge during the installation of the west secant wall due to its close proximity to drilling equipment and was the main concern for settlement during the excavation. To monitor horizontal movement at the west secant wall during the excavation stages, two inclinometers (one at each corner of the adjacent building) were installed in the secant pile wall. A two dimensional finite element analysis of each stage of the excavation was retroactively performed, using the available soil information, and is compared to the measured inclinometer data obtained during construction.

INTRODUCTION

Due to the high density environment of Manhattan and limited space for new construction, it is common for owners and developers to look to below grade basement construction for additional space. The close proximity and sensitivity of adjacent structures as well as the relatively shallow ground water table encountered require the use of a support of excavation (SOE) system that will facilitate dewatering and essentially underpin adjacent structures by limiting ground movement and by preventing settlement of the surrounding area. For this reason, secant pile walls are an attractive option for earth retaining systems in Manhattan because they can provide both a rigid support of excavation system while also providing, if socketed into a relatively impermeable layer like clay or rock, water cutoff which allows for dewatering of the excavation.

The case study analyzed in this paper consists of a project in Manhattan where a secant pile wall, socketed into rock, was installed to serve as the support of excavation and water cutoff system for the construction of two below grade basement levels of an 11-story building. The secant pile wall and three levels of internal bracing, using corner struts, served as the temporary SOE system during the 43 foot excavation below surface grade. Upon completion of the excavation to its final depth, basement slabs were constructed which served as the permanent lateral support for the basement walls and the secant wall, in conjunction with an 8" concrete wall formed against it, served as the permanent basement walls. A concrete capping beam was formed on top of the secant wall which served to support the axial load of the perimeter columns of the building. Due to the presence of a 25-story residential building immediately adjacent to the west property line of the site, special measures had to be taken during construction of the west secant piles to avoid damaging the adjacent building and monitoring of wall deflections during subsequent excavation stages was performed. Continuous monitoring of lateral movement of the west wall was achieved by installing two inclinometers in secondary piles (one at each corner of the adjacent building) and measurements were taken as the excavation proceeded.

The scope of this paper is to discuss and analyze the construction and performance of the secant pile wall and bracing system for this project, specifically for the west wall adjacent to the 25-story

[1] Project Engineer, Underpinning & Foundation Skanska, Maspeth, NY
[2] Assistant Professor, Dept. Civil & Environmental Engineering, Manhattan College, Riverdale, NY
Research Affiliate, Dept. Civil & Environmental Engineering, Massachusetts Institute of Technology, MA

© 2018 Deep Foundations Institute

building. The overall construction process and challenge of installing piles so close to the adjacent building is discussed. A two-dimensional finite element analysis of the wall is also presented, using the commercial software PLAXIS, and the results are compared against the actual measured inclinometer data. The intent of this comparison is to determine if reasonable results can be obtained for wall performance using a simplified analysis and limited soil property information.

SITE CHARACTERISTICS

This paper focuses on the secant pile wall constructed for the New York University College of Nursing building at 433 First Avenue in Manhattan. As shown in Figure 1, the site is located just west of 1st Avenue with E. 26th Street to the north and E. 25th Street to the south. An existing 25-story reinforced concrete residential building supported on steel H-Piles is located directly adjacent to the western portion of the site while an existing 6-story brick building is located about 20 ft south of the site.

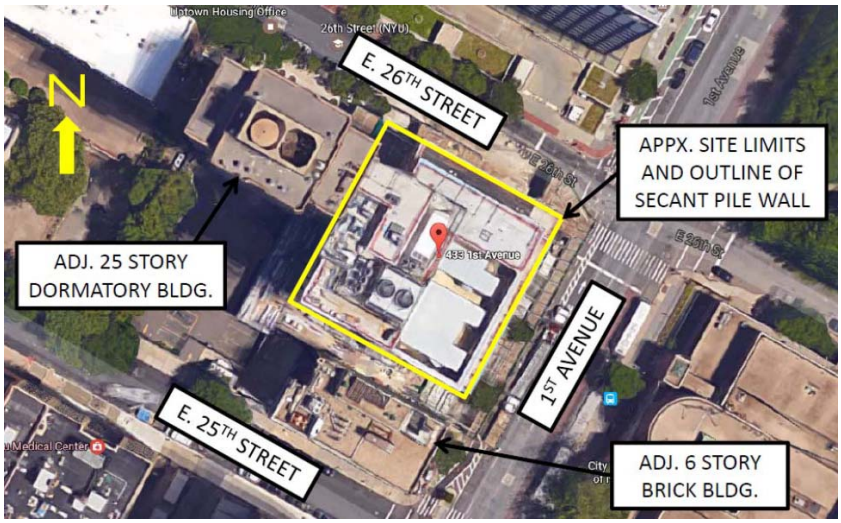


Figure 1: Site Location Plan (Image from Google Maps)

The building construction included two below grade basement levels which resulted in a required excavation depth of approximately 43 ft below existing grade while the depth to ground water was about 12 ft below grade. To provide excavation support and a relatively impermeable water cutoff system, both primary and secondary secant piles were socketed a minimum of 2 ft into competent rock or, if the bottom of excavation was deeper than the top of rock, extended 2 ft below the bottom of the excavation. Depth to rock varied across the site from 19 ft to 66 ft, while at the west wall specifically the depth to rock ranged from 40 ft to 66 ft, with an average depth of 53 ft below grade. Inclinometer 1 was installed in pile 164 and inclinometer 2 was installed in pile 184 with depths to rock of 54 ft and 45 ft, respectively (Figure 2).

The secant pile wall design consisted of using 39.4 in (1000 mm) diameter secant piles with 9 in (minimum) concrete overcut and 34 in (minimum) diameter rock sockets. Secondary piles were reinforced with W24x131 core beams spaced 5'-3/4" (maximum) on center. For the two secondary piles instrumented with inclinometers, 2.75 in (70 mm) diameter inclinometer casing was secured to the center of the core beam web and lowered into the pile prior to concreting. The design strength of the concrete mix used was 4,000 psi while the average 28-day compressive strength observed from actual field concrete break data was over 7,400 psi. Three levels of internal bracing, consisting of diagonal corner struts and continuous walers, were used to support the wall as the excavation proceeded.

The geotechnical site investigation consisted of twelve total borings and four test pits. The provided data consisted of SPT field N-values, visual classification of the soil by on site engineers and rock quality designation and recovery percentages, when rock was cored. The results and interpretations of the field data were presented in a Geotechnical Engineering Study [1].

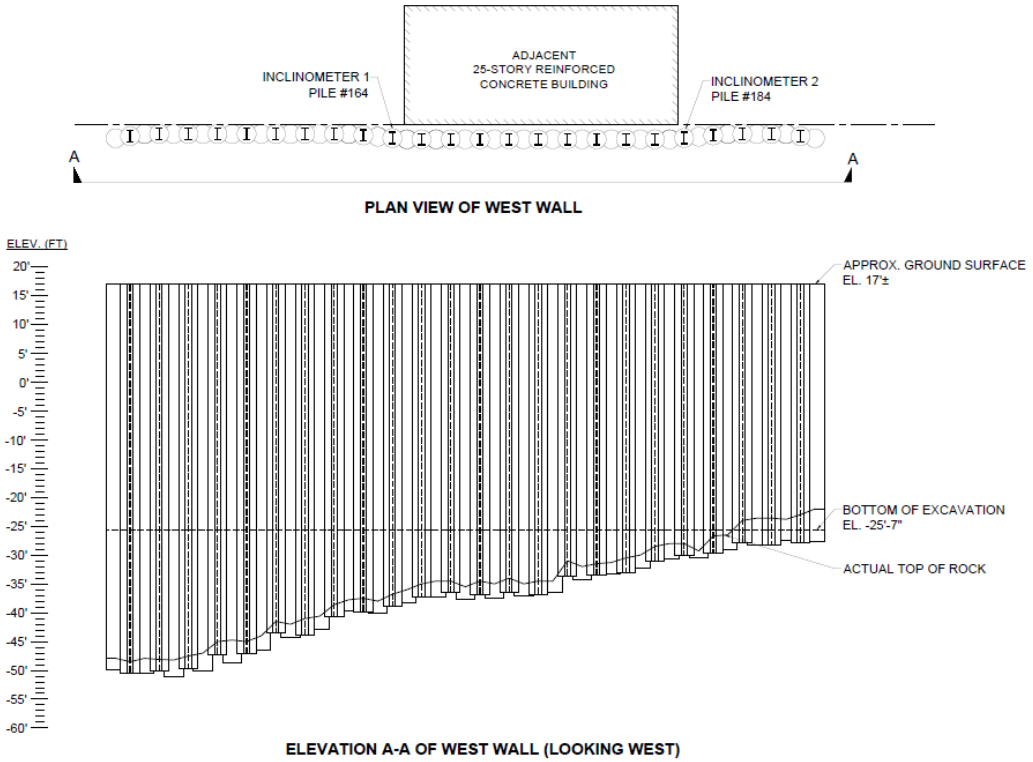


Figure 2: Elevation of West Wall and Inclinometer Locations

Based on the information obtained from the borings, the site stratigraphy comprises of manmade fill (typically encountered in Manhattan) consisting mostly of granular soil (gravel and sand) with varying amounts of construction debris, alternating layers of silty sand and sandy clay/clayey silt, highly decomposed mica schist rock (mostly blow count material) with varying amounts of clay and silt, and mica schist bedrock with an average recovery (REC) value of 83% and an average rock quality designation (RQD) value of 62% (Figure 5).

SECANT PILE WALL CONSTRUCTION

Construction Overview

Secant pile walls consist of drilled cast-in-place overlapping circular concrete shafts which form a continuous concrete wall along the excavation perimeter. Wall construction is sequenced by initially installing "primary" secant piles, allowing the concrete in these piles to harden and then subsequently drilling overlapping "secondary" piles in between the primary piles. Either a steel reinforcing cage or steel wide flange section is placed in the secondary piles to provide flexural rigidity to the wall and limit lateral deflections during the excavation stages. The continuous concrete overlap provides wall continuity which is crucial to the impermeability of the wall, acts as lagging between the steel reinforcing sections and adds to the overall rigidity of the wall system.

The 192 total secant piles were installed by twisting temporary 39.4 in (1000 mm) diameter Bauer sectional steel casing down through overburden material and to the top of rock. Soil was excavated inside the temporary casing as it was advanced into the ground using 35.4 in (900 mm) diameter tooling consisting of soil augers, drilling buckets and rock augers/core barrels (if drilling through

obstructions was required). An adequate soil plug was maintained at the casing bottom along with water head pressure inside the casing to prevent bottom heave of the soil into the casing during drilling. As the temporary casing provided lateral support of the soil during drilling, the drilling fluid consisted of water only and no polymer or bentonite slurry was required.

Once the casing was advanced to rock, it was seated approximately 6 inches into competent rock to ensure a good seal was achieved before rock socket drilling began. The rock sockets were drilled using both conventional 35.4 in (900 mm) tooling consisting of rock augers, core barrels and drilling/cleaning buckets and a 34 in diameter down-the-hole (DTH) hammer. At the completion of rock socket drilling, the sockets were cleaned of drill cuttings using a submerged mechanical clean out bucket and the core beams were placed into the pile (for secondary piles). A rigid tremie pipe system was then lowered through the water filled pile to the bottom of the socket (a "pig" or bottom plug is used to prevent water from entering the pipe prior to the start of concreting) and concrete was installed under gravity head while the temporary casing was simultaneously extracted. As the tremie pipe is lifted, the concrete under gravity head pressure pushes out the bottom plug and fills the shaft from the bottom which displaces the water and any suspended drill cuttings present and carries them up and out of the shaft as the tremie pour is completed.

Three drill rigs were used for secant pile installation consisting of a Liebherr LB-28, a Bauer BG-28 and a Bauer BG-24. The two more powerful rigs (the LB-28 and the BG-28) were used for temporary casing installation/extraction and overburden drilling while the BG-24 was dedicated to rock socket drilling. Higher torque capacity is required to twist and advance the temporary casing into the ground and overcut adjacent primary piles in the case of secondary pile drilling which is why the more powerful machines are used for this task. One rig was solely dedicated to rock socket drilling as this is the critical path of secant pile construction.

Construction Challenges at West Wall

The initial contract drawings showed the westernmost edge of the secant pile wall flush with the property line and the adjacent 25-story building. Installing secant piles immediately adjacent to an existing structure is not possible as parts of the drilling rig extend past the edge of the 39.4 in diameter secant pile. More specifically the casing drive adapter, shown in Figure 3, extends out 25.1 in from the center of the pile or 5.4 in past the edge of the pile. For this reason, the wall layout was revised to incorporate an 8 in clear distance from the edge of the secant pile to the adjacent building, which would result in 2.6 in clear from the outermost part of the drilling rig to the building. This was still not optimal clearance to the rig during construction, but the intent was to not lose valuable basement space.

Upon arrival at the site, it was observed that the adjacent building was actually leaning into the site and the 8 in clear distance would not be maintained above the ground level adjacent to the building. As the casing drive adapter is raised above the ground to facilitate casing installation, this would result in a conflict and potential damage to the adjacent wall. To mitigate this problem, a final revision to the west secant wall layout was used which involved the majority of the secant piles being flush with the west property line and locally tapering out the portion of the secant wall where the adjacent building encroached into the site in order to provide adequate clearance during drilling (Figure 4). For the tapered portion of the wall, the pile outer edge was moved an additional 2 in from the building (totaling 10 in clear from the edge of the piles) to account for the adjacent structures tilt.

This unusual and specific secant wall geometry was made possible by using a foam guide-wall template. This template, shown in Figure 4, provided the flexibility required to make adjustments in the field to the secant pile layout. The foam segments could be cut around the secant pile's circular outline and rotated to provide the wall taper where needed. This modified guide-wall layout allowed the piles to be installed with as much clearance as possible and, although the wall was still very close to the adjacent building, it allowed for successful installation of secant piles without damage to the adjacent structure.

FINITE ELEMENT MODELING

Soil Stratigraphy

Of the twelve borings at the site, the closest four to the west wall were used to determine the soil properties for the soil model analyzed in this paper. Figure 5 shows the interpolated soil stratification between the four boring locations. Due to the changing stratigraphy along the west wall, one generalized soil stratigraphy was considered in the analysis and was taken at the center of the adjacent building, between both inclinometer locations, to represent average soil conditions along the building.



Figure 3: Casing Drive Adapter

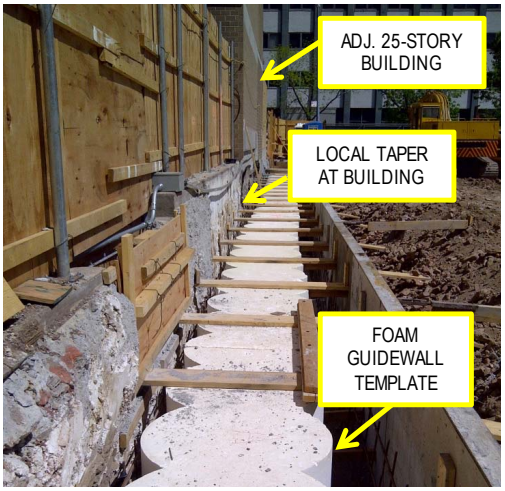


Figure 4: Guide-wall construction at West Wall

The manmade fill layer present in all four borings had N_{60} values ranging from 4 to 20 blows per foot (bpf) with an average of 10 bpf indicating a loose to medium dense condition as the higher N-values are most likely from construction debris encountered. A varved layer was present directly below the fill and consisted of alternating layers of silty/clayey sand and silty/sandy clay. The silty/clayey sand portion of the varved layer had N_{60} values ranging from 5 to 22 bpf with an average of 12 bpf; the silty/sandy clay portion of the varved layer had N_{60} values ranging from 4 to 23 bpf (generally increasing with depth) with an average of 13 bpf; a decomposed rock layer was present below the varved soils and had N_{60} values ranging from 9 to refusal (generally increasing with depth) with an average of 30 bpf. Competent mica schist bedrock was below the decomposed rock in three of the borings (boring B-1 was terminated before encountering rock), however the actual top of rock encountered in the field at each secant pile location is shown in Figure 5 and was used in the stratification considered in the analysis.

One of the issues with determining engineering properties for the cohesive portion of the varved soil layer was that two of the borings were inspected by one engineering consultant while the other two borings were inspected by a different consultant; the former classified the fine grained soil as clayey silt while the latter classified the fine grained soil as clay or silty/sandy clay. Due to the close proximity of the four borings to each other, it did not seem likely that the soil composition would vary that much between each boring so it was assumed that the cohesive soils were clay, as the cohesive soils in 8 of the 12 borings were classified as such. As the majority of the varved soil shown in the interpolated stratigraphy at the middle of the adjacent building is clay, the whole layer between fill and decomposed rock was considered to be clay in the analysis.

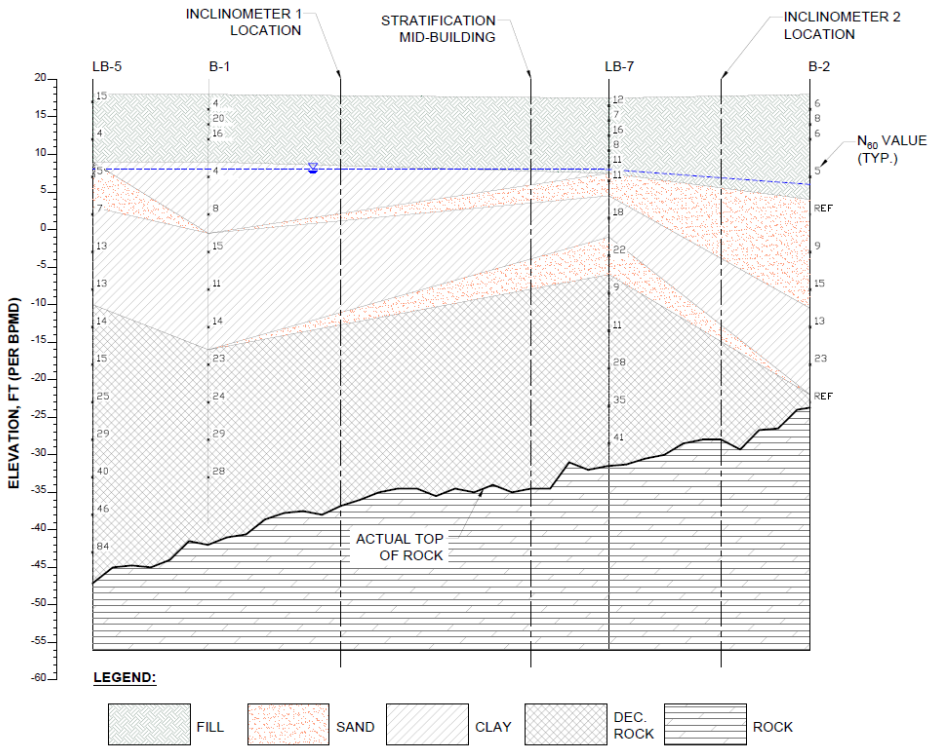


Figure 5: Soil Stratification Based on Boring Data at West Wall

Mohr-Coulomb Soil Model

The simple linear elasto-plastic Mohr-Coulomb (MC) soil model was used in the numerical analyses with five input parameters: Young's Modulus (E), Poisson's ratio (ν), Cohesion (c), Friction Angle () and Dilatancy Angle () (Table 1). The limitation of this soil model is that it cannot capture the small-strain stiffness that more advanced soil models can (hardening soil model, MIT-S1, etc.) but the latter require many more input parameters which are obtained from project specific lab testing. For this project, as is the case for many situations in practice, only SPT data and visual classification of the soil are available for use in determining the engineering properties of the soil. Due to the lack of data, the simplified MC model was selected and input parameters determined using empirical correlations and engineering judgement (Ameratunga et al., 2016; Kalhawy and Poulos, 1990). Details about estimating the soil properties from SPT data can be found in Maniscalco et al., (2018).

Since the soil property correlations used in this study depend solely on SPT N-values, it is important that the field N-values are corrected to 60% hammer efficiency as most of the correlations available in literature use this normalization standard to eliminate variation in data. The majority of correlations available for coarse grained soils using SPT data (to determine friction angle and modulus of elasticity) are for sands thus assumptions have to be made when using them to estimate the properties of the fill and decomposed rock layers. For clay, the correlations between SPT data and undrained shear strength are reasonable while correlations with modulus of elasticity are much more approximate and most references provide ranges of values based on qualitative consistency of clay. The soil properties input into PLAXIS are listed in Table 1.

Modelling of the Secant Wall and Internal Bracing

The secant pile wall was modeled by using a plate element with the equivalent elastic bending stiffness of the composite wall elements consisting of the steel core beam in secondary piles and concrete "lagging" in between. The overall moment of inertia was calculated for the wall per unit length based on the geometry of the secant wall while a composite modulus of elasticity accounted

for the presence of the steel beam by taking a weighted average of each materials contribution to the stiffness. Thus, the elastic modulus used was increased from that of concrete alone. The structural properties of the wall are shown in Table 2.

Table 1: Soil Property Input Parameters to PLAXIS

	Fill	Clay	Decomposed Rock	Rock
Soil Model	MC	MC	MC	Linear Elastic
Average N_{60}	10	13	30	-
Range of N_{60} Values	4 to 20	4 to 23	9 to REF	-
Drainage Type	Drained	Undr. B	Drained	Drained
Soil Unit Weight, γ *(kcf)*	0.120	0.115	0.140	0.176
Drained Elastic Modulus, E' *(ksf)*	400	158+9.2z	1555+132.5z	238,217
Poisson's Ratio, ν'	0.30	0.40	0.30	0.20
Cohesion, c' *(ksf)*	0.0	-	0.0	-
Friction Angle, ϕ'	32	-	38	-
Undrained Shear Strength, *Su (ksf)*	-	0.88+0.06z	-	-
Dilatancy Angle, ψ	0.0	-	0.0	-

Three levels of internal corner bracing were used to brace the secant wall as the excavation proceeded. As illustrated in Figure 6, the bracing system consisted of steel wide flange members diagonally bracing walers that spanned the full length of the wall. The member layout was the same for each bracing level but the member sizing varied per level. The bracing was modeled in PLAXIS using elastic anchor elements which capture the average bracing stiffness per level of bracing and per unit length of wall. The axial stiffness of the bracing per unit length of wall was calculating by determining the average equivalent perpendicular strut stiffness of each bracing level and then dividing that stiffness by the strut spacing. The structural properties of the bracing system are shown in Table 2.

Modelling of the Adjacent 25-Story Pile Supported Building

Limited information on the adjacent 25-story building and its foundations was available. From test pits excavated adjacent to the building during the geotechnical engineering study, it was clear that the building basement was founded on H-Piles (bottom of basement being 13 ft below existing grade). Based on the report description of the piles as 10.25 in deep with a flange width also of 10.25 in, the piles were assumed to be HP10x57 wide flange members. H-Piles are non-displacement piles typically used in New York City as end bearing piles, so they were assumed to be bearing on rock. The length of the building perpendicular to the secant wall was estimated based on Google maps images and the in plane spacing of the pile caps was assumed to be constant based on the limited portion of the adjacent foundations shown on the contract structural drawings.

To incorporate the effects of the adjacent buildings basement and its pile foundations on the west wall, 13 ft of soil behind the wall (for the length of the building perpendicular to the wall) was deactivated in PLAXIS and supported by a rigid box consisting of plate elements (representing the basement walls and bottom slab/pile caps). The rigid bottom plate was supported by representative pile groups (modeled as embedded beam rows in PLAXIS) which consisted of 8 piles in a square configuration. The properties of the embedded beam row were determined by considering the axial and flexural properties of the 8 HP10x57 piles in the layout shown the structural drawings. The building area load inputted to PLAXIS was calculated based on assuming a 200 psf area loading per floor for 25 floors plus the roof and basement and was applied at the bottom of the basement, 13' below grade, atop the rigid plate supported by the piles. The pile clusters (embedded beam rows) were connected to the rigid plate element by a hinged top connection and the bottom of piles extended to rock in the model. The properties of the embedded beam row are listed in Table 2.

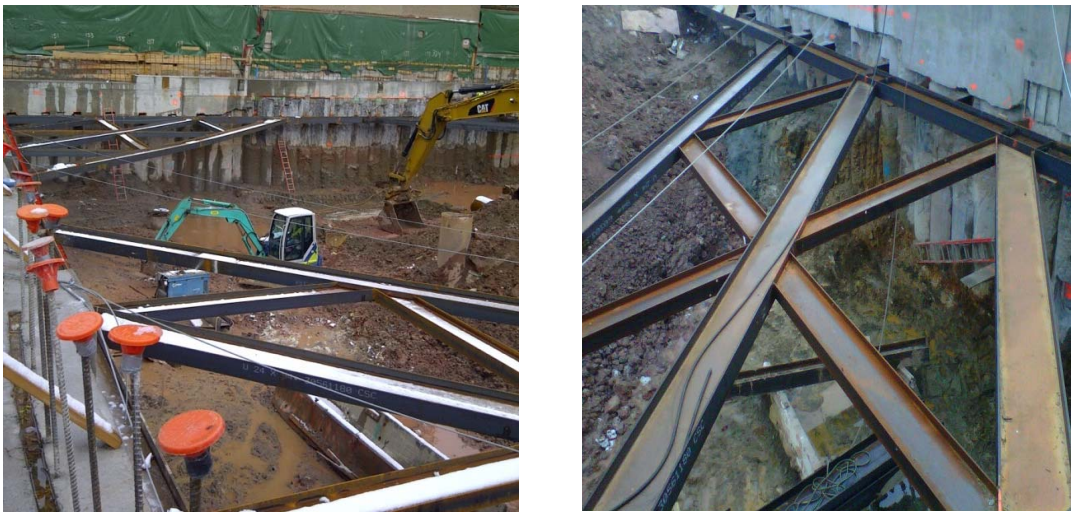


Figure 6: First Level of Internal Bracing.

Numerical Model Description

Figure 7 shows the full scale excavation at the final stage (43 ft cut with three bracing levels), illustrating the building adjacent to the west wall with its 13 ft basement and assumed pile foundation layout. The excavation stages were considered to be 2 ft below each bracing level as follows: 11 ft cantilever; 19 ft cut with brace at 9 ft depth; 32 ft cut with braces at 9 ft and 17 ft; 43 ft cut with braces at 9 ft, 17 ft and 30 ft. For excavation stages below the water level within the secant wall, water was assumed to be 2 ft below the excavation level to account for the sequential dewatering of the excavation as construction proceeded. Complete description of the numerical modeling can be found in Maniscalco et al., (2018).

Table 2: Structural Property Input Parameters to PLAXIS

	Secant Wall	Strut: Levels 1 & 2	Strut: Level 3	8 ea. Square Pile Group
Structure Type	Plate	F.E. Anchor	F.E. Anchor	Embedded Beam Row
Axial Stiffness, EA (kip/ft)	2,289,000	8,227	11,566	-
Bending Stiff., EI (kip-ft^2/ft)	1667000	-	-	-
Width, d (ft)	2.956	-	-	-
Poisson's Ratio, ν'	0.15	-	-	-
Modulus of Elasticity, E (ksf)	-	-	-	155,900
Unit Weight, γ (kcf)	-	-	-	0.136
Area, A (ft^2)	-	-	-	25
Moment of Inertia, I (in^4)	-	-	-	120.3
Spacing, $L_{SPACING}$ (ft)	-	15.92	15.92	14

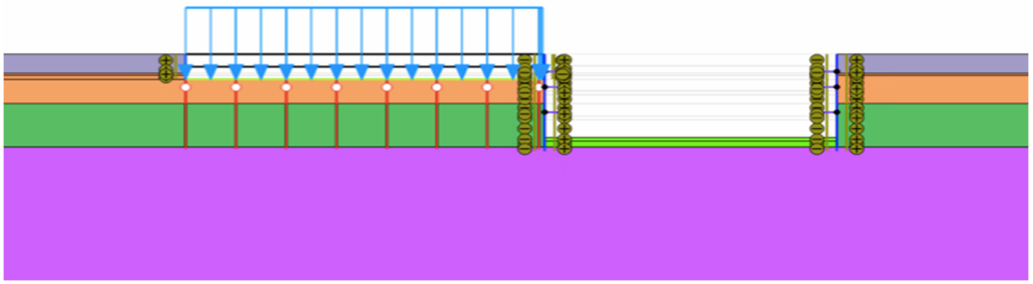


Figure 7: Two dimensional numerical representation of the excavation at 43 ft

DATA INTERPRETATION

The inclinometer data show horizontal displacements for the 19 ft excavation with one brace, the 32 ft excavation with two braces and the 43 ft excavation with three braces. The comparison between the measured data and the PLAXIS calculated deflections are shown in Figures 8 a) – c). It is observed that the calculated deflections match the inclinometer data well in terms of both shape and magnitude of deflections. The deflections calculated for the west wall, accounting for the presence of the adjacent 13 ft basement supported on piles, were significantly less than the deflections calculated for the opposite (east) wall of the model which had only soil adjacent to the wall (the deflection comparison is not shown in this paper). The fact that there was less wall deflections observed in the analysis when considering the 13 ft basement was expected as there is essentially no soil loading on the wall over that distance. The building vertical load is transferred down to rock by the pile foundations and horizontal loading on the building, due to relaxation of lateral soil support when excavating inside the secant wall is resolved by the buildings piles in lateral loading and also by passive resistance of the pile caps. Capturing this reduction in horizontal loading on the west wall was essential in generating realistic deflections as verified by the close match with inclinometer data.

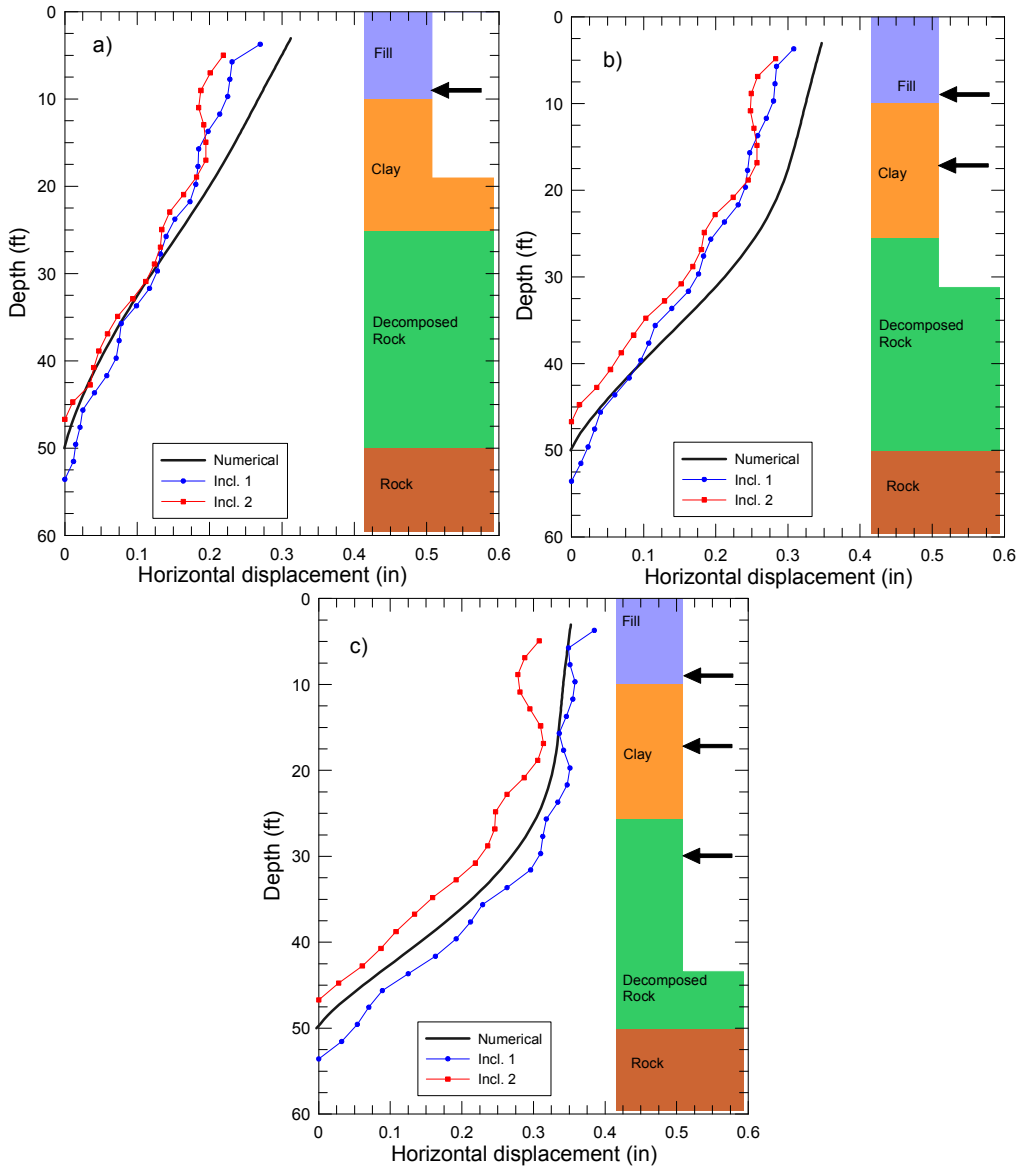


Figure 8: Comparison of measured and predicted horizontal wall movements for a) 19ft, b) 34ft and c) 43 ft excavation

CONCLUSIONS

As space is a limited and thus valuable commodity in populated urban areas like Manhattan, below grade construction is routinely used to maximize usable space for new buildings. With sensitive structures surrounding the deep excavations required for below grade construction, rigid support of excavation systems are needed to limit ground settlement while also helping control ground water during excavation stages. As exemplified in this project, the New York University College of Nursing building at 433 First Avenue in Manhattan, secant pile walls are often an attractive option for Support of Excavation as they can be installed very close to adjacent structures, provide water cutoff to facilitate dewatering of the excavation and provide a rigid wall to limit deflections during construction.

Based on the retroactive finite element analysis performed for this specific project, the complex and three dimensional real world problem of the west secant wall and the adjacent 25-story building was able to be modeled in a simplified two-dimensional model with reasonable accuracy. While there are many limitations to the Mohr-Coulomb model that limit its ability to capture the true nature of soil behavior, many times in practice there is limited geotechnical data available to justify using more complex soil models. However, as shown in this paper, engineers can still obtain reasonably accurate predictions for retaining wall analysis using SPT data, soil correlations and engineering judgement.

ACKNOLEDGEMENTS

The authors would like to thank Underpinning and Foundation Skanska (secant pile contractor) and Laquila Group, Inc. (foundation and excavation contractor) for providing construction challenges faced, secant pile as-built information and inclinometer data; Langan Engineering (geotechnical engineer) for soil investigation information. This work was accomplished during the graduate studies of the first author at Manhattan College.

RFERENCES

Ameratunga, J., Sivakugan, N. and Das, B. M., 2016. Correlations of soil and rock properties in geotechnical engineering (pp. 8-9). Springer.

Kulhawy, F.H. and Mayne, P.W., 1990. Manual on estimating soil properties for foundation design (No. EPRI-EL-6800). Electric Power Research Inst., Palo Alto, CA (USA); Cornell Univ., Ithaca, NY (USA). Geotechnical Engineering Group.

Langan Engineering, 2011. Geotechnical Engineering Report for NYU College of Nursing, College of Dentistry & Bioengineering Institute.

Maniscalco, J.D., Ieronymaki, E.S., Corral, G.J., 2018. Prediction of Secant Pile Wall Deflections for the Excavation of the NYU College of Nursing in Manhattan, New York, submitted to the ASCE Journal of Geotechnical and Geoenvironmental Engineering

PILE FOUNDATIONS OF TRIESTE'S NEW LOGISTIC PLATFORM

Alessandrini eng. Francesco, Alpe Progetti s.r.l. Società di Ingegneria – Udine – Italy
Fedrigo eng. Dario, Alpe Progetti s.r.l. Società di Ingegneria – Udine – Italy
Grillo eng. Luca, I.Co.P. S.p.A – Basiliano (UD) – Italy
Pedrini eng. Federica, Alpe Progetti s.r.l. Società di Ingegneria – Udine – Italy
Valusso eng. Diego, Alpe Progetti s.r.l. Società di Ingegneria – Udine – Italy

ABSTRACT

Design and construction of a seismically isolated very large slab on piles is shown.

As part of the implementation of the new logistic platform of Trieste Port, a piles supported dock is built. As an innovative feature, the dock is made by a wholly pre-compressed slab which shows a bidirectional continuity over an area of more than 70,000 m^2.

A group of over 800 in water-placed piles of large diameter will be realized for the support of the slab. The pile group has been studied together with the isolation system of the slab placed on the head of the piles themselves. During an earthquake, but also due to thermal deformations, the pile plus the seismic devices behaves as a single nonlinear element by exploiting partly the pile elasticity and partly the sliding friction of the isolator.

The study becomes more difficult due to the different lengths and consequent deformability of piles. In addition, the use of an increasing earth filling volume below the slab, changes the pile stiffness gradually over time as the filling grows, consolidating itself and the soil beneath.

keywords: pile foundation, seismic isolation, port dock

INTRODUCTION

Near the port area of Trieste, the construction of a new logistics platform, with a dock extension greater than 70000 m^2 has recently begun. The platform will be connected to the surrounding port areas and it will allow an increase in the sea traffic, opening to large commercial vessels. The construction of the platform is part of a wider planning activity which also involves the environmental decontamination of the area, new roads, railway and logistic activities, all linked together.

THE PLATFORM

The platform in construction consists of a monolithic post-tense reinforced concrete plate, with an almost trapezoidal plan shape: the sides (bigger / smaller) have a development of 460/160m, while the "height" is 280m.

The structure is continuous without joints, and is supported by a set of large diameter piles (Φ_{ext} = 1270mm), over double curved seismic isolators (friction pendulum system).

The plate structure is made up of 1.80m wide and 1.00m high main ribbings, perpendicular to the new coast line, spaced 10m to each other. The area in between is covered by a RC slab with a minimum thickness of 0.50 m. The single beam (rib) is cast into self-supporting formworks, and then post-tense by means of 32 super-0.6" polyethylene sheathed strands, with parabolic profile, which exert a total axial action of about 5000 kN.

Likewise, the slab is post-tense also in the perpendicular direction with strands spread on the area: on average there is 1 strand (equal to those used for the ribs) every 25cm, and all of them allow the exertion of an average compression action of 600 kN/m.

© 2018 Deep Foundations Institute

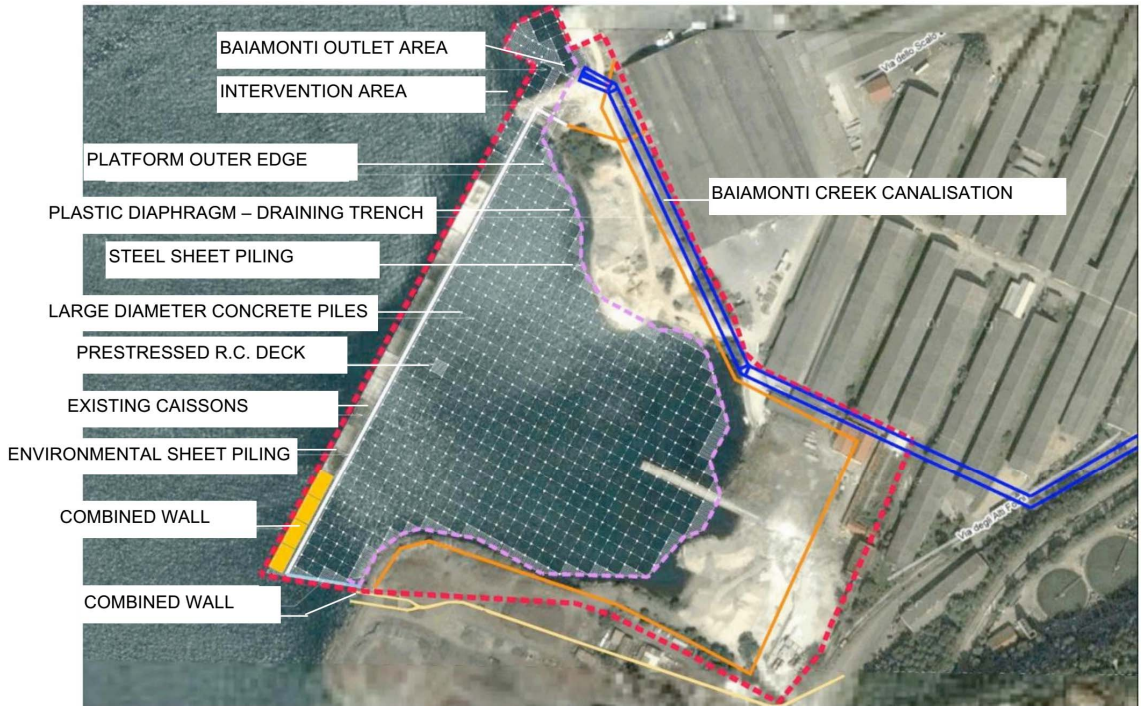


Fig. 1. Overall plan of the intervention area; the violet dashed line delimits the surface of the platform on piles

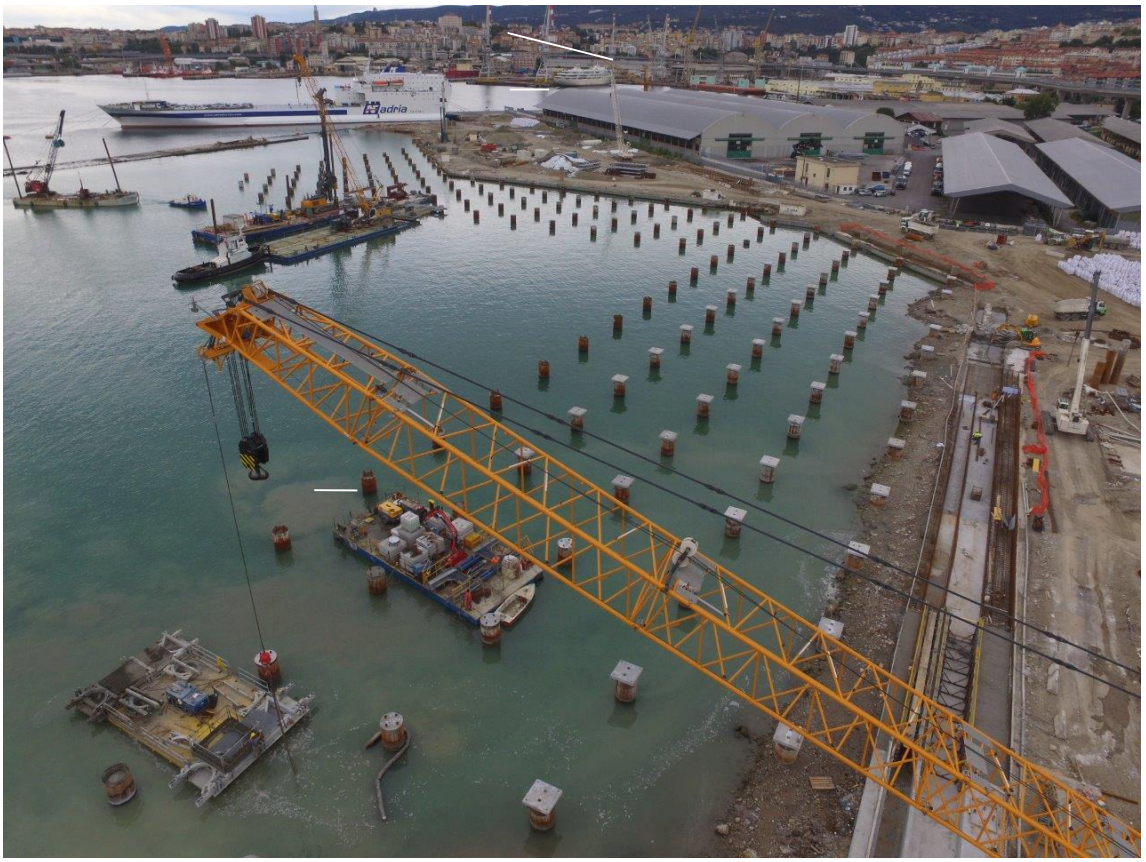


Fig. 2. Partial building phase of the piling that supports the platform; some pile heads have already been equipped with isolators

PREFABRICATION SYSTEM

The little time available for the construction has led, starting from the design stage, to the idea of using prefabricated elements settled on top of the foundation piles and then linked by a second stage concrete cast.

The main beams are obtained by using mixed steel-concrete beams (NPS® beams made by Tecnostrutture s.r.l.) as self-supporting formwork, which will be co-operating with the second phase casting. The base has a width of 1.80 m and a maximum thickness of 0.20 m. It incorporates the reinforcement (steel B450C) and the lower bars of the supporting trusses (S450 steel, 0.79m high, obtained with bars diameter ranging from 30mm to 42mm).

These "formworks" are mounted on an auxiliary prefabricated RC plate, 1.5x1.5x0.2m, which has the dual purpose of incorporating (in its lower face) the back plate of the isolators (otherwise difficult to position) and on the other, allow the inevitable adjustments required to compensate for the differences between the theoretical and real position of the elements (eg of the piles).



Fig. 3. Laying stage of the prefabricated main beams on the piles, waiting for the installation of prefabricated hollow core slabs, settled perpendicular in between the beams, realizing the formwork for the deck casting

On the edges of the main beams "formwork" are settled 30 cm thick prefabricated hollow core slabs, which have the task of supporting the second stage casting.

For the execution of the work plane on which to run the second phase casting (after the positioning of rebars and prestressing tendons), the following steps are carried out:

- phase 1 - execution of foundation piles with mesh 10x10m;
- phase 2 - positioning the isolator devices together with the prefabricated slab (Fig. 7);
- phase 3 - installation of NPS® beams;
- phase 4 – positioning of the prefabricated hollow core slabs.

FOUNDATION PILES

The foundational system adopted for the work consists of an almost regular piling, with sea piles of 1270mm outer diameter, realized according to a square mesh of 10m side.

The pile are of the drilled type, with a diameter of the drilling tool of 1180mm, and are equipped with a steel protection pipe, which acts as a formwork and support for the excavation.

The piles length is very variable, ranging from 22m to 45m, depending on the zone: this is due to the flysch bedrock depth on which they are founded, whose level degrades starting from the inner line of the coast to the outer sea, according to a North/East-South/West direction.

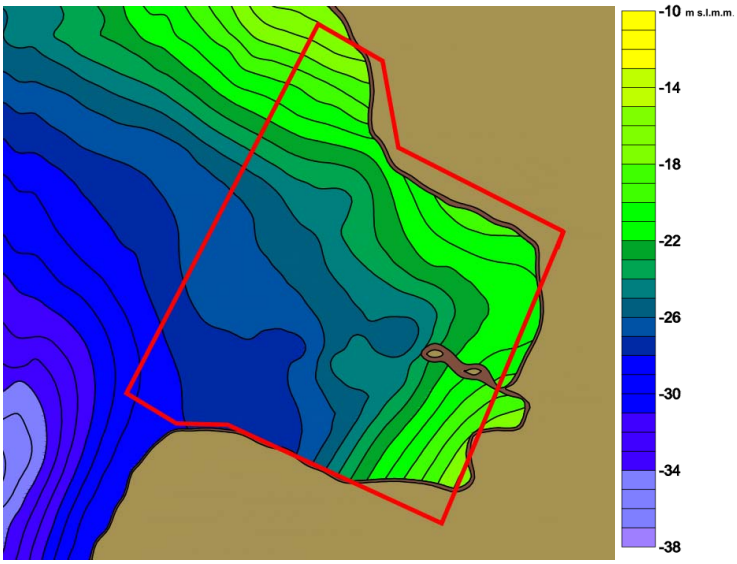


Fig. 4. Plan of the area with highlighted flysch top level contour lines

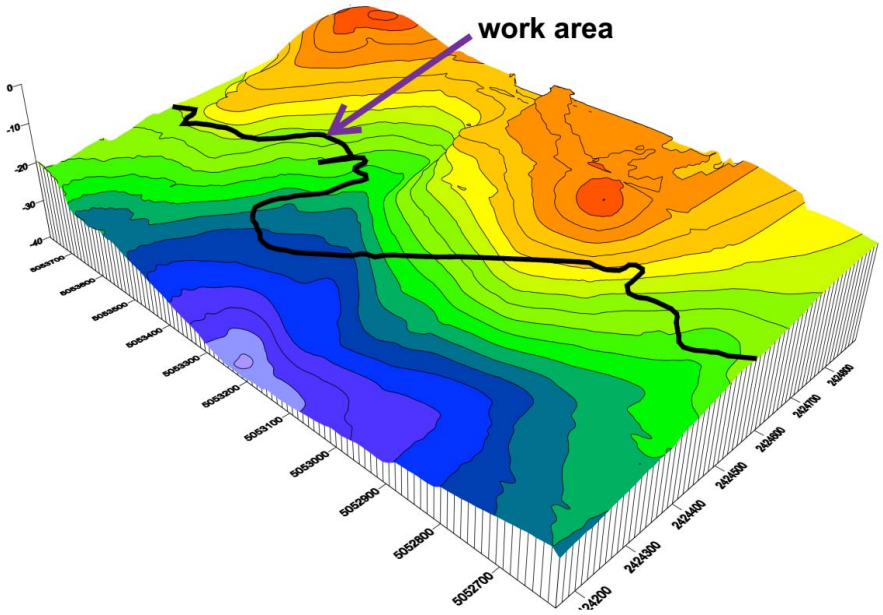


Fig. 5. Representation of flysch top level

From a constructive point of view, the realization takes place in the following phases:

• step 1 – positioning of a floating metallic template, with the aim of ensuring the accuracy of the relative distance between the piles (10m);

• step 2 - driving the protective steel pipe into the soil by vibroinfission; the length of the pipe is such as to exceed the level of the initial highly deformable and deformable soil layers (muds, low consistency silty clays) and reach the most consistent cohesive layer, approximately 5m over the bedrock;

• step 3 - execution of the excavation inside the pipe until reaching the design length of the pile; the deeper section of the excavation is supported by the use of polymers, without steel- pipe protection (suitable working method due to the better soil characteristics);

• step 4 - inserting the reinforcement cage and subsequent concrete casting.

The execution of these operations shows many different difficulties, such as ensuring the correct plan positioning of the pile, ensuring and maintaining an adequate verticality of the element, obtaining the right pile top level, always taking into account that the above described activities are made by pontoons carrying the heavy working equipment.

Figure 6 shows the main steps related to the pile's construction: the steel pipe insertion made through a vibrator (on the right), the drill runs inside of the pipe already in place (on the left), the insertion of the reinforcement steel cage in the drilled hole (in the center).

Production capacity was averaged at 2 piles per day.



Fig. 6. Overall view of the building steps of the piles

SEISMIC BEHAVIOUR

The platform is located in Trieste, commonly classified as zone 3 by the recent Italian regional

seismic classification, and therefore subject to a reduced seismic risk. However, considering the strategic function of the construction and the nominal life requirement of 100 years, the inertial accelerations become an important design parameter (a_g = 0.167g to LLS – Life Limit State).

The deck's behavior is in fact closely resembles a rigid diaphragm due to the large overall size, the absence of joints, the substantial compactness of the shape; with this hypothesis the inertial action associated with the design masses (dead weight of about 20 kN/m^2 and part of the live load of 42 kN/m^2) can be divided according to the stiffness of elevations only.

The stiffness of elevations was one of the problems encountered at the initial design stage, being very variable due to the different length of the elements.

A "traditional" link between the pile and the platform would have led to high load levels in the shortest piles (located predominantly in the north of the platform) and high horizontal displacements for long piles placed on the opposite side due to the twist coming out from the eccentricity between the center of mass gravity and the center of deck stiffness.

The alternative choice was then to introduce a device that would "rebalance" the system's behavior by reducing the stiffness of the shortest elements and thus also containing the torsional effects.

Therefore, double curvature seismic isolators (friction pendula) have been used, characterized by very low stiffness modulus (curvature radius of 8.7m), able to withstand high vertical design loads (8000 kN in service conditions), and simultaneously admit relative horizontal displacements of ± 240mm at the CLP - Collapse Limit State.



Fig. 7. Seismic isolator on the pile head with RC back slab, temporarily bound to the pile head

The choice of these elements and their characteristics was evaluated after a series of linear and non-linear, static and dynamic analyses that allowed to characterisation not only of the behavior of the single pile but also that of the piles' group.

These studies have highlighted how:

a. the system consisting of "*n*" piles of different length placed in series, with top isolator, behaves in a "selective" manner if we assume that the horizontal dock displacement, δ, is equal for all the elements. In the shorter piles, the reduced stiffness of the isolator device causes the pile to remain stationary and the displacement develops only in the isolator. In the longer piles, deformable in themselves, the isolator and the pile deforms depending on the relationship between the pile stiffness and the one of the isolator, up to the limit case where the pile is more deformable than the isolator (and in this case the isolator does not activate).

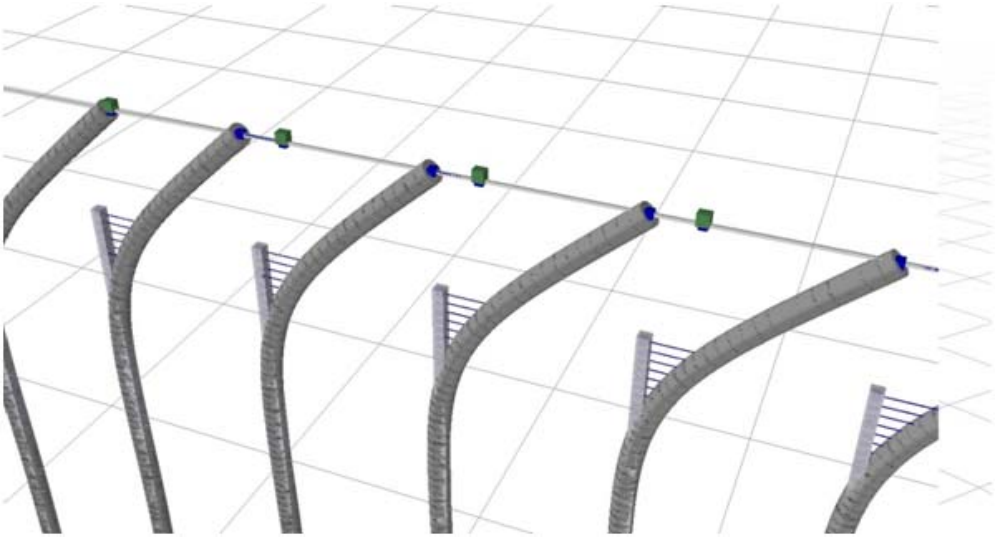


Fig. 8: results of non-linear static analysis of "n" piles (with different stiffness) coupled to the head: in the more stiff piles (on the right) the activation of the isolator is evident (green knot separated from the pile); in the longer pile (on the left) the isolator remains fixed on the pile head

b. the pile head isolator, thanks to its constructional features, acts almost as a "fuse" against the shear action transmitted to the pile: in fact, the force [1] is function of friction under dynamic conditions (mass by friction coefficient, assumed equal to 5%) and of a contribution inversely proportional to the curvature of the sliding surface (R = 8.7m in the present case, very high). With design data a maximum horizontal force of about 570 kN is reached.

$$F = Mg \bullet \mu + \left(\frac{Mg}{R} \right) \bullet d \qquad [1]$$

where Mg is the mass afferent to the device, μ is the friction coefficient, R is the curvature radius, d is the device displacement.

c. the overall behavioral evaluation was carried out through a series of 7 nonlinear dynamic analyses, each of which is associated with a natural accelerogram compatible with the seismogenic features of the area. Maximum average displacements of about 11 cm were found, with only few centimeters differences in the response between the various points of the perimeter.

d. it was also chosen to apply an alternative design approach based on displacement (Displacement Based Seismic Design) thanks to the stiffness uniformity of the elevations: in this case, starting from the elastic displacement response spectrum and taking into account the own period of the structure (appreciably assessed), two important results for design purposes come up. The first is that the expected displacement value has been found to be about 25cm; the second point is that this value represents an upper boundary, and thus constitutes a limit for perimeter joints and seismic isolators design.

e. an eventual greater stiffness of the geotechnical system (piles + soil) results in a greater number of isolators activated, thus a greater amount of dissipated energy and fewer overall displacements. Also in this case the action transmitted to the pile does not vary, as it is "guided" by the presence of the isolator.

The seismic calculations have been carried out through SEISMOSTRUCT (Seismosoft), a fiber non linear analysis software and the well known SAP2000 (Computer and Structures Inc) software, that allows non linear dynamic analysis using boundary links with hysteretic properties.

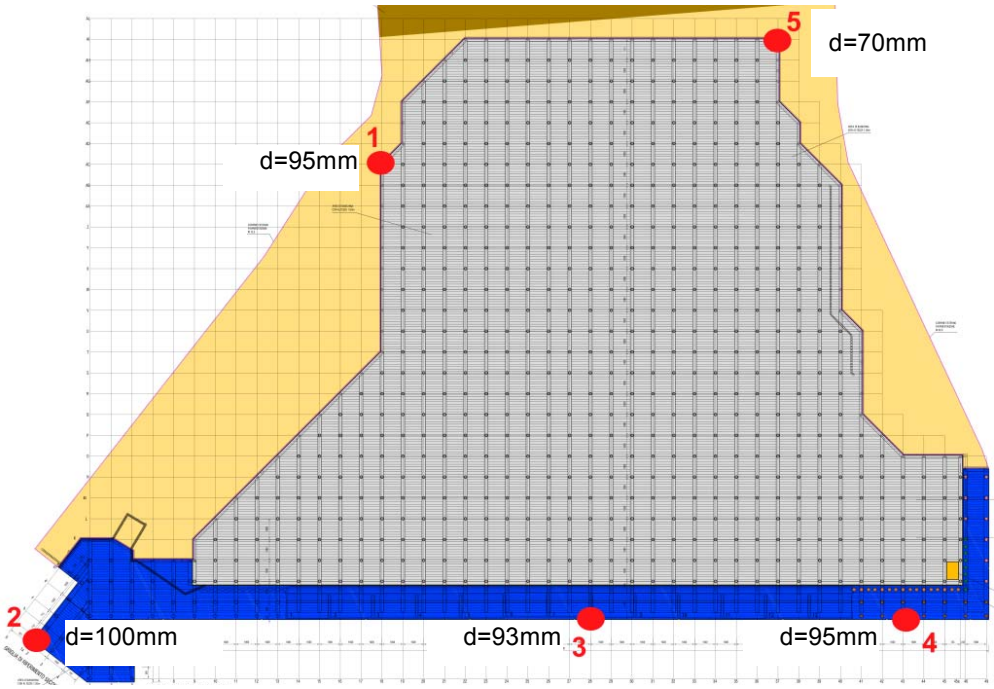


Fig. 9. General plan with highlighted checkpoints and the average displacements derived from the nonlinear dynamic analysis

PILE BEARING CAPACITY TESTS

The piles built in the area have been and will be subjected to different load tests, both in static and dynamic conditions, and a significant percentage (no less than 50%) of integrity tests (S.I.T. or P.I.T. test).

Specifically, before the start of the work, a design field test was carried out on a highly equipped pile with test strumentation. The pile, 34m long, was subjected to a maximum load of 2.5 times the service load (considering also a scale factor of 0.5, due to the smaller diameter of the test pile, 880mm, compared to the design piles, 1270mm). A static vertical load test, a horizontal static load test, and a heavy vertical dynamic load test (CASE) were performed.

During the building time more tests will be performed such as another coupled vertical static-dynamic load test and other 7 heavy dynamic load tests, all covering the minimum test number required by the Italian regulations for the total number of 856 piles.

CONCLUSIONS

The new logistic platform of Trieste Port includes a pile-supported dock with innovative features.

The main peculiarity is the construction of a wholly pre-compressed slab which shows a bidirectional continuity over an area of more than 70,000 m^2.

The slab, supported by a group of over 800 in water-placed piles of large diameter, is seismically isolated through friction pendula isolators placed on the top of the piles.

No common design calculations (displacement based method) have been carried out to evaluate the seismic behavior of the structure. The piles group has been studied together with the isolation system: during an earthquake, the pile plus the seismic devices behaves as a single nonlinear element by exploiting partly the pile elasticity and partly the sliding friction of the isolator.

The isolation system allowed an important reduction of the seismic horizontal loads on the pile tops and consequently a reduction of pile diameter from 1800mm initially expected to 1270mm of the final design.

REFERENCES

- AA.VV., 2016. Piattaforma Logistica di Trieste: Prove di carico su palo strumentato (The New Logistic Platform in Trieste:), 4Emme Service Spa.
- AA.VV., 2016. Piattaforma Logistica di Trieste: relazione di calcolo del sistema di isolamento sismico della Banchina (The New Logistic Platform in Trieste: platform seismic isolation system analysis report), Studio Calvi, Studio Altieri, Alpe Progetti Eng, 2016.
- Alessandrini F., Fedrigo D., Valusso D., 2016. Piattaforma Logistica di Trieste: relazione di preparazione e di calcolo delle prove di carico sul palo di prova Φ800 PP1 (The New Logistic Platform in Trieste: instrumented pile Φ800 PP1 load tests design report), Studio Altieri e Alpe Progetti Eng.
- Alessandrini F., Fedrigo D., Valusso D., 2016. Piattaforma Logistica di Trieste: Relazione sui risultati della prova di carico sul palo PP1 (The New Logistic Platform in Trieste: instrumented pile PP1 load tests results report), Studio Altieri e Alpe Progetti Eng.
- Brosolo M., 2016. Piattaforma Logistica di Trieste: relazione sulla prova non distruttiva ecometrica e vibrazionale eseguita su palo prova (PP1) (The New Logistic Platform in Trieste: test pile PP1 – ecometric and vibrational non destructive tests report).
- Priestley M.J.N., Calvi G.M., Kowalsky M.J., 2007. Displacement-Based Seismic Design of Structures, IUSS Press, EUCENTRE, Pavia.
- Solari N., 2016. Analisi ai carichi orizzontali di un palo trivellato in ambiente marino (Sea drilled horizontally loaded pile analysis), DPIA, Università degli Studi di Udine.
- Valusso D., Alessandrini F., Fedrigo D., 2017. Prove di carico su un palo-pilota di grande diametro ad elevata strumentazione nell'ambito del progetto della nuova banchina portuale a Trieste (PLT) (Load tests on a large diameter highly instrumented design pile for the New Logistic Platform in Trieste - PLT), Proceedings, 7th IAGIG, Catania, May 19-20, Vol. 1, pp. 114-119.

PILE LOAD TEST: ANALYTICAL METHODS FOR BEARING CAPACITY, INCLUDING BRAZILIAN METHODS

Denise I. S. Gomes Venturi, UFPE, Pernambuco, Brazil, +5511976994592, sasaki.denise@gmail.com
Roberto Quental Coutinho, UFPE, Pernambuco, Brazil, +558121268222, robertoqcoutinho@gmail.com

ABSTRACT

The prediction of the pile bearing capacity is an important item in deep foundation design. Based on this premise, the Brazilian standard for foundations determines the performance of static load–tests for pile assessment. However, as in the Brazilian standard, several other methods evaluate the pile bearing capacity from static load tests. This paper provides a comparison between some analytical methods for the pile bearing capacity from the load-settlement curves of static load tests. Some of the Brazilian methods will address the foundation standard (ABNT, 2010), rigidity by Décourt (1996) and comparable methods according to Massad (1992). Other comparable methods discussed are Davisson (1972), Chin-Kondner (1970) and Van der Veen (1953). Also, the method of the two straight lines (Massad & Lazo (1998) for short piles) will be addressed. The comparisons were made on nine static load tests on piles performed in Northeast Brazil (Pernambuco).

Keywords: pile, static load test, bearing capacity, deep foundations.

INTRODUCTION

Pile bearing capacity prediction is complex because several items influence the design of these foundations, ranging from soil conditions to the material and construction method of the piles in question. Therefore, it is essential to compare the pile's behavior after execution with the design requirements and it is especially necessary to check the ultimate load when the pile is put in place.

In order to do these checks, static load tests are normally performed on the piles. However, due to cost and time constraints, these load tests are not always carried out until the ultimate load (pile failure) and, in most cases, the tested piles are not instrumented in depth. So, the existing data are not enough to identify the failure load and without instrumentation it becomes harder to identify the performance of lateral friction and tip resistance.

There are several mathematical models in the literature that allow the analysis of the behavior of the load compensation curve obtained in the static load test. In this study, the analysis will be restricted to obtaining the failure load. Van der Veen (1953), Chin-Kondner (1970) and Davisson (1972) were approached because there was an interest in comparing the failure load obtained by these methods with those obtained from Brazilian methods, namely ABNT (2010), Décourt 1996) and Massad (1992). Moreover, the method of the two straight lines will be addressed (Massad & Lazo (1998) for short stacks), in addition to presenting the different characteristics of each method.

MATHEMATICAL MODELS

Van Der Veen (1953)

The Van der Veen (1953) method assumes the existence of an exponential relationship between the load applied to the top of the pile in a load test with the settlement obtained, according to Eq. [1].

$$Q = Q_u(1 - e^{-\alpha\delta}) \quad [1]$$

© 2018 Deep Foundations Institute

Where Q is the load applied to the top of the pile, Q_u is the failure load, δ is the settlement obtained in the load test, and α is the coefficient that defines the shape of the curve.

The α and Q_u values are constants obtained from an attempts process. For each value of Q_u adopted, a settlement is obtained and, then, a graph is plotted with the settlement δ in the ordinate axis against the $-\ln\left(1-\frac{Q}{Q_u}\right)$ in the abscissa axis. The graph closest to a line will indicate the desired value of the failure load (see **Figure 1**).

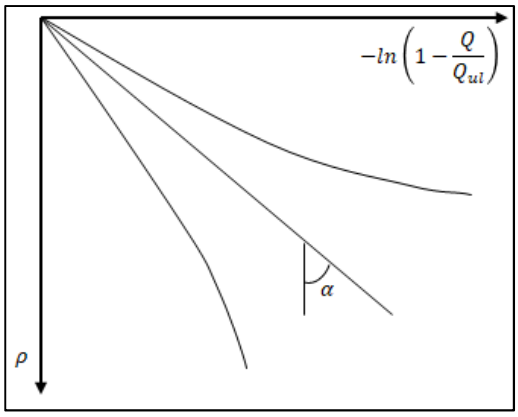


Figure 1 – Van der Veen (1953) graph: attempt process.
Source: Cintra et al (2013)

Chin-Kondner (1970)

The method proposed by Chin (1970) with the work by Kondner (1963, apud Fellenius, 2001) and considering the Chin-Kondner method (1970), begins from a graph in which the value results are plotted from the division of each displacement with its corresponding load in the abscissa axis against the settlement in the ordinates axis. Disregarding the initial points (small variations), it is found that the behavior of the graph resembles a straight line. The ultimate load is obtained from the inverse of the slope of this line.

$$Q_u = \frac{1}{C_1} \quad [2]$$

where Q_u is the failure load and C_1 is the slope of the straight line.

The Chin-Kondner method (1970) permits plotting of an ideal curve, given by the Eq.[3].

$$Q = \frac{\delta}{\delta C_1 + C_2} \quad [3]$$

where δ is the settlement, Q an applied load and C_2 the y-intercept of the straight line.

Figure 2 shows the straight line and ideal curve, using the Chin-Kondner method (1970).

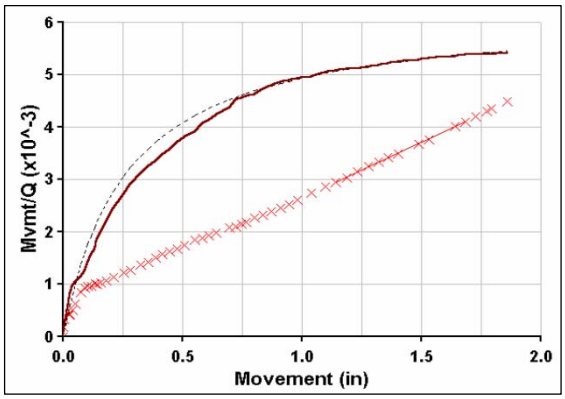


Figure 2 – Load test, ideal curve and straight line, the Chin-Kondner method (1970).
Source: Fellenius (2001a)

Davisson (1972)

Davisson's method (1972) consists of limiting a load corresponding to the settlement that exceeds the elastic deformation of the pile (taken as a free-standing column) by 4 mm (0.15 inch), plus a factor equal to the diameter of the pile divided by 120. This can be seen in Eq. [4] as follows

$$\delta = \frac{Q.L}{A.E} + \left(4 + \frac{\emptyset}{120}\right) \qquad [4]$$

where δ is the settlement, Q the applied load, L, A and $\emptyset$ the length, area and diameter of the pile, respectively, and E is the elastic modulus of the material of the pile.

According to Fellenius (2001a), the Davisson Offset Limit Method (1972) is probably the best-known and widely used method in North America.



Figure 3 – The Offset Limit Method (Davisson, 1972)
Source: Fellenius (2001a)

The Davisson offset limit load is, then, determined by crossing the line defined by Eq. [4] with the load-settlement curve obtained in the pile load test.

Massad (1992) and Massad & Lazo (1998)

Massad (1992) is a Brazilian author who developed a mathematical method for analyzing pile load tests, based on Cambefort ratios (1964).

Figure 4a shows the Cambefort ratios (1964) for excavated piles in the first load (P_h) as a confined load at the pile base, in case of a second loading or for root piles, and μ is equal to 1 for the first load on excavated piles. (See further information in Massad, 1992.)

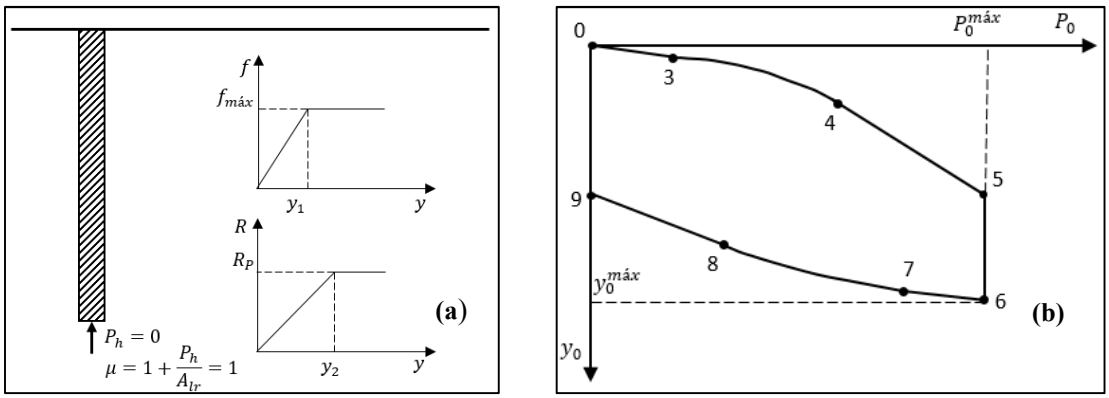


Figure 4. (a) Cambefort ratios (1964): Excavated piles, First Load; (b) Theoretical load-settlement curve. Source: Adapted from Massad (1992)

This author stated that the pile load test could be represented by a theoretical load-settlement curve, represented by three notable passages (**Figure 4**b), in the loading phase:

Section 0-3: Straight line. Corresponds to the pseudo-elastic phase of lateral friction mobilization. Point 3 indicates the moment when the lateral friction is saturated at the base of the pile.

Section 3-4: Curved excerpt (parabolic or exponential). It represents the advance of the saturation of lateral friction along the shaft, from the top downwards to the tip of the pile.

Excerpt 4-5: Straight line. Corresponds to the mobilization of the tip resistance.

Excerpt 5-6: Moment at which the failure occurs at the tip, with the tip reaction reaching its maximum value.

The sections formed by points 6 to 9 correspond to the unloading phase and will not be addressed in this study (further information to be found in Massad, 1992).

In this method, the author begins by classifying the pile as rigid, intermediate or long, from obtaining the parameter k (Eq. [5a].). In order to obtain parameter k, it is necessary to obtain the stiffness of the pile as a structural element (see Eq. [5b]).

$$\text{a)} \quad k = \frac{A_{lr}}{k_r . y_1} \qquad \text{b)} \quad k_r = \frac{E.S}{L} \qquad [5]$$

with A_{lr} = the lateral friction resistance at failure.

For short or rigid piles ($k \leq 2$) the two straight lines method can be used: a graphic method, easy to apply (see Massad & Lazo, 1998 and **Figure 5**). For long piles ($k \geq 10$), one should proceed with exponential adjustments of the section represented by points 3-4 to obtain lateral friction resistance (see Massad, 1992). Piles classified as intermediate should be analyzed with caution, according to the author.

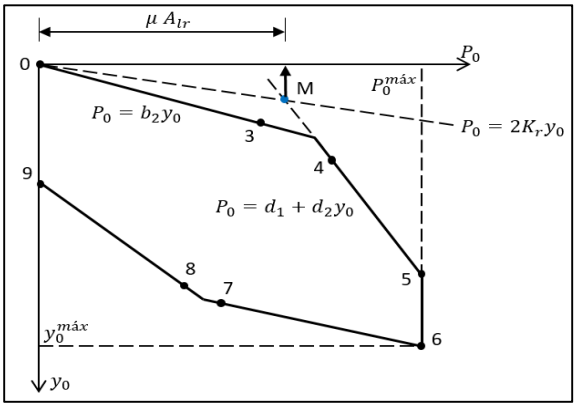


Figure 5 – Two straight lines (adapted from Massad & Lazo, 1998)

Décourt (1996)

The method of Décourt (1996), a Brazilian author, is based on the concept of stiffness. This stiffness is obtained from the division between each load Q applied to the top of the pile and the respective settlement δ obtained in the static load test Eq. [6].

$$RIG = \frac{Q_i}{\delta_i} \qquad [6]$$

where RIG is rigidity by a structural element, Q_i is a load applied to the top of the pile in a moment i and δ_i is the corresponding settlement obtained for the applied load Q_i.

Stiffness is plotted in the ordinates axis, against the applied force in the abscissa axis. It can be found that the stiffness of the structural element decreases with the evolution of the settlement, which represents a decreasing function.

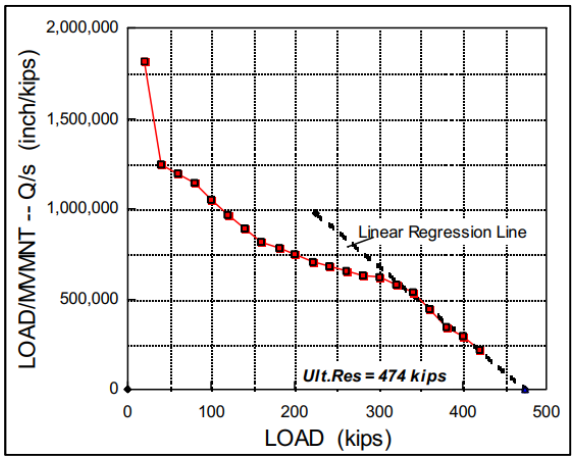


Figure 6 – RIG x Load: Décourt (1996)
Source: Fellenius (2001a)

In a physical failure model, the rigidity x load graph becomes linear and its extrapolation (of the linear section) determines the value of the ultimate load when intercepting the axis of the loads (see Figure 6).

The Décourt method (1996) also allows identification of the upper lateral friction range: the point where the graph becomes linear marks the saturation of the resistance of the top of the pile and the beginning of the straight development of lateral friction, from the shaft to the tip of the pile.

ABNT (2010)

ABNT is the abbreviation for Brazilian Association of Technical Standards. As with the method proposed by Davisson (1972), the extrapolation method provided in standard NBR 6122 (ABNT, 2010) determines the conventional breaking of the pile by the elastic shortening of the pile (as a structural element), plus a fixed settlement obtained as a function of its diameter, as can be seen from Eq. [7] and in Figure 7.
Similar to Davisson (1972), the limit load is to be mentioned rather than failure load.

$$\delta = \frac{QL}{AE} + \frac{\emptyset}{30} \qquad [7]$$

where δ is the settlement, Q the applied load, L, A and $\emptyset$ the length, area and diameter of the pile, respectively, and E is the elastic modulus of the pile material.

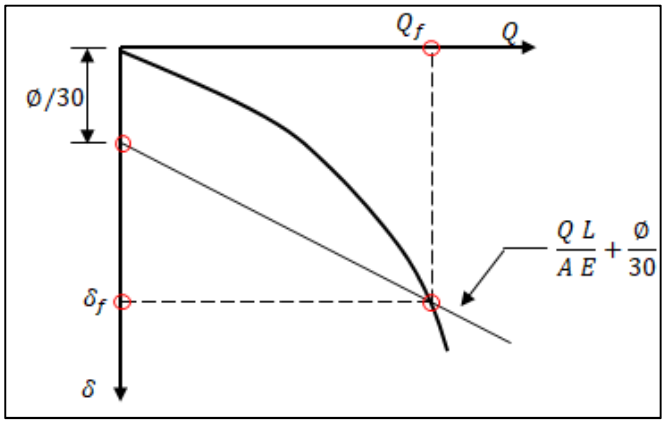


Figure 7: Limit load (adapted from ABNT, 2010)

STUDY AREA

The static load tests presented are part of a set of piles performed in Northeast Brazil (town of Ipojuca, in Pernambuco State). The load tests were carried out between 2009 and 2011, based on the ABNT standard (2006). The objective of the load tests was to validate the design load with safety coefficient 2 and so there is no in-depth instrumentation of these piles. All load tests performed were of the slow type, with 10 load increments in the loading phase and five load decreases in the unloading. They also had two or four reaction piles, depending on the range of the load tested. For root piles, they were socketed in a rock mass. In the analyses, the data used represented only the least resistant layer (soil). In relation to the material, all piles are in concrete with compressive strength of 20 MPa and elastic modulus estimated at 21 GPa.

STATIC LOAD TESTS

Figure 8 (a to i) presents the load-settlement curves of the static load tests in the study area. The tests were carried out on continuous flight auger piles and root piles (with final section embedded in more resistant material - rock mass). Both diameters and lengths ranged from x to y. Table xx summarizes these data as well as the test load.

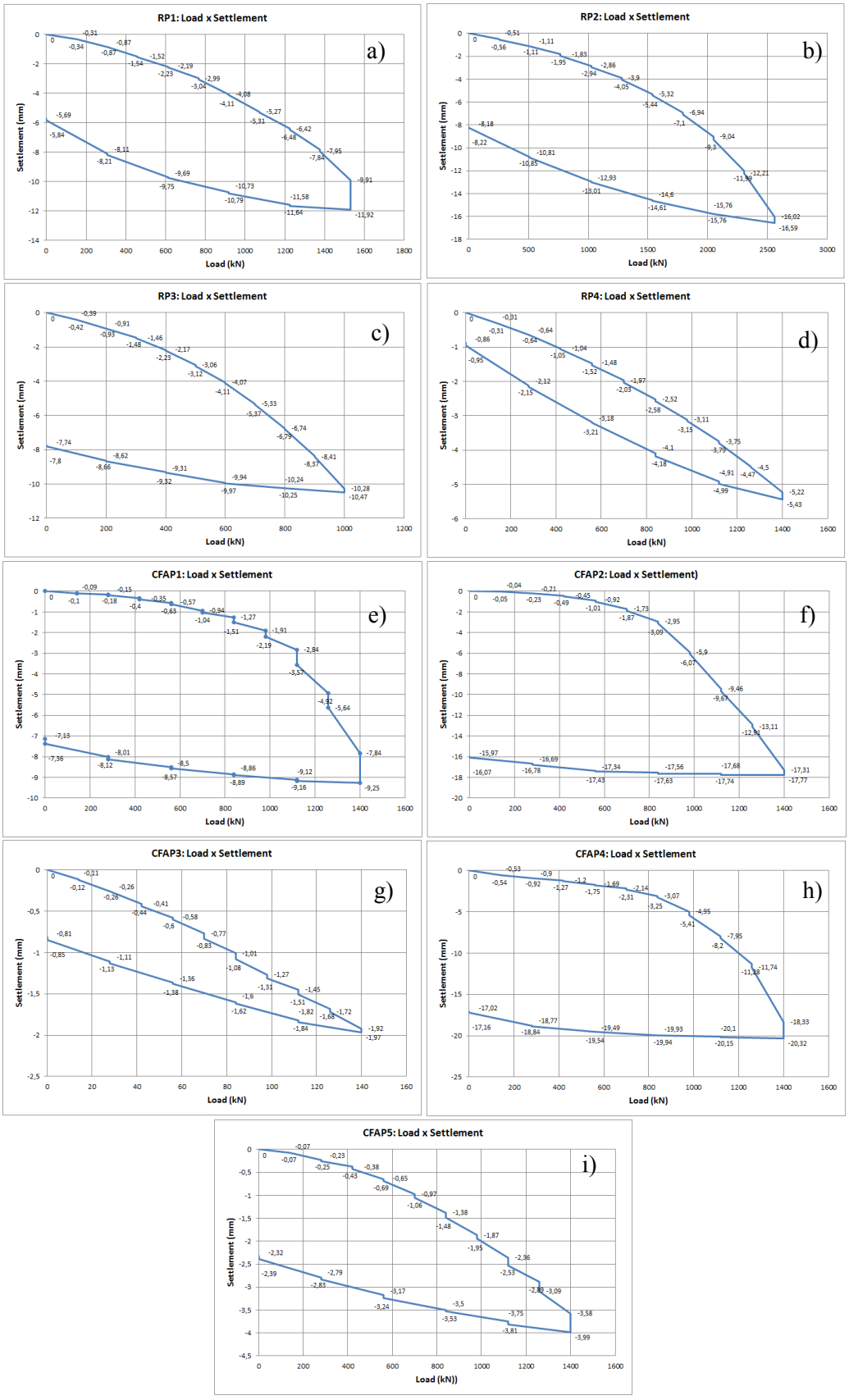


Figure 8: Load-settlement curves (a to d: root piles / e to i: continuous flight auger piles)

RESULTS AND DISCUSSIONS

Table 1 below presents a summary of the main characteristics of the piles tested, as well as the maximum load applied and its settlement.

Table 1. Piles – Summary Characteristics

Id	Pile	Φ (mm)	Design Load (kN)	Load Test (kN)	δ_{max} (mm)
A	Root	400	765	1530	11.92
B	Root	400	1280	2560	16.59
C	Root	310	500	1000	10.47
D	Root	400	700	1400	5.43
E	Continuous flight auger	600	700	1400	9.25
F	Continuous flight auger	500	700	1400	17.77
G	Continuous flight auger	600	700	1400	1.97
H	Continuous flight auger	600	700	1400	20.32
I	Continuous flight auger	600	700	1400	3.99

where δ is the maximum settlement in the load test.

As can be verified, the load tests were not carried out until the failure, since these tests were intended only to validate the safety coefficient 2 required by the Brazilian foundations standard (ABNT, 2010).

Table 2 below presents the results for analyzing the mathematical methods presented in this study.

Table 2. Summary of Results – Extrapolations in Load Testes

id	Type	FAILURE / ULTIMATE LOAD (kN)					LATERAL LOAD (kN)	
		Van der Veen	Chin-Kondner	Davisson	Décourt	ABNT	Décourt	Massad
a	Root	1680	2250	-	2420	-	1070	750
b	Root	2860	3700	-	3730	-	770	1700
c	Root	1240	1600	-	1660	-	400	580
d	Root	2200	3090	-	3280	-	420	980
e	Continuous flight auger	1430	1530	-	1490	-	420	240
f	Continuous flight auger	1500	1430	1170	1780	-	980	760
g	Continuous flight auger	3400	3360	-	8000	-	840	850
h	Continuous flight auger	1430	1650	1240	1630	-	420	820
i	Continuous flight auger	1700	1920	-	1800	-	280	540

Regarding the methods presented, the Brazilian methods of Décourt (1996) and Massad (1992) and Massad and Lazo (1998) are concerned with obtaining the lower and upper limits of lateral resistance, which is not possible to identify in the other methods addressed herein. Due to application restraints, this study only obtained the lateral strength using the method of Massad (1992) and Massad and Lazo (1998), not advancing the calculations until the ultimate load is obtained (to do so, it is also necessary to develop mathematical models for the unloading phase).

It is noticeable that the Davisson (1972) and ABNT (2010) methods are very similar, the Davisson method being more conservative than the ABNT method. It is worth noting that these methods are strongly influenced by the precision of the pile data (bearing in mind that the elastic modulus of the pile material is often estimated and not measured, for example). Of the nine load tests analyzed, with settlement varying between 2mm and 20mm, only two tests could be analyzed using the Davisson (1972) method (load tests

“f” and “h”) and none with the ABNT (2010) method. In addition, the values obtained by this method for the tested piles (1170 kN for "f" pole and 1240 kN for "h" pole) would not validate the safety coefficient 2 of the piles tested (which would lead to a stake of 1400 kN) as shown in Table 2.

In relation to the failure load, the results of the nine load tests presented in Table 2 were compared with the mathematical models of Van der Veen (1953), Chin-Kondner (1970) and Décourt (1996). It is found (see **Figure 9**) that the results showed very similar behavior, with the Van der Veen method (1953) providing values closer to the test load, whereas the values of the Décourt model (1996) were slightly higher than the other two methods.

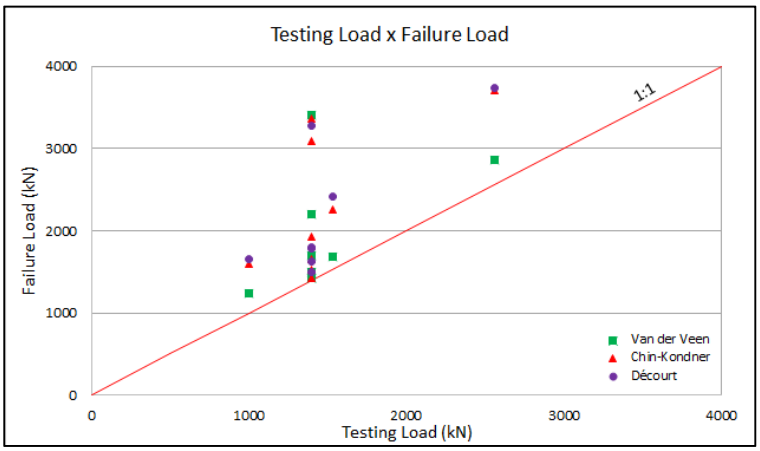


Figure 9: Testing Load x Ultimate Load Graph

Among the root type piles tested, the Van der Veen method (1953) presented more conservative values and closer to the values of the load test piles (values between 9.8% and 57% higher than the tested loads). The Chin-Kondner method (1970) and Décout method (1996) had values close to each other.

For the continuous flight auger, the Van der Veen (1953) and Chin-Kondner (1970) methods presented close values, while the Décourt method (1996) showed slightly higher values. Analyzing the values presented by the Chin-Kondner method, the range of values for the ratio between the load tested and the rupture load was between 2.1% and 37.1% (except for the "g" stake). It is worth noting that the "g" stake had similar behavior to that of the other stakes tested. This fact is perhaps due to some failure in the measurement of displacements or to some constructive failure, since this stake has the same characteristics as the other propeller-type pilots tested.

For the lateral loads (Table 2), the methods of Décourt (1996) and Massad (1992) presented different values among the piles in question, and it was not possible to reach a conclusion on the more conservative method.

Also, it is possible to find a similarity in the application of Chin-Kondner (1970) and Décourt (1996) models. While the former works with the inverse of the slope of the line from the points plotted in the graph settlement/load x settlement to obtain the ultimate load (after some initial variation), the Décourt method (1996) works with the projection of the line formed by the points of the graph load/settlement (rigidity) x load, at the moment when these points tend to present a linear trajectory.

The Décourt method (1996) also presents two other advantages: that of being able to predict the failure load even during the load test, from the projection of the line formed by the points of the above graph already at the beginning of the linear trajectory, and the other great advantage of this method is the identification of the part related to the lateral strength of the pile, at the moment of failure, represented by the point where the graph trajectory also becomes linear.

According to Fellenius (2017), the Chin-Kondner (1970) and Décourt (1996) extrapolation load is about 20% to 40% greater than the offset limit (Davisson, 1972). In this study the same occurred, with higher percentages of around 33% for the "h" load test and 22% and 52% for the "f " load test for the Chin-Kondner (1970) and Décourt (1996) methods respectively, for the only two load tests in which the Davisson (1972) limit load could be obtained.

CONCLUSIONS

Several mathematical models address the extrapolation of data obtained from the pile tests. Some methods are well known and easy to use (e.g. the Davisson method, 1972) and only a few are known, albeit disseminated in the literature and with more complex use (e.g. Massad, 1992).

Nevertheless, it should be analyzed that however refined the method is, any extrapolated value is a prediction. Thus, burst load values under pressure very far from the designed (and tested) values should be evaluated with caution.

In relation to the Brazilian methods, with the exception of the Brazilian standard, the authors seek to incorporate in their mathematical models the separation between lateral and tip resistance (values that can be obtained when the test uses in-depth instrumentation).

REFERENCES

ABNT 2006. Piles – Static Load – Test Performance Method - NBR 12131 - Brazilian Association of Technical Standards, Rio de Janeiro, 8 p. (In Portuguese).

ABNT 2010. Foundation Design and Performance - NBR 6122 - Brazilian Association of Technical Standards. Rio de Janeiro, 91 p. (In Portuguese).

Cambefort, M. 1964. *Essai sur le comportement en terrain homogène des pieux isoles et des groups de pieux*. Annales de I'Institut du Batiment et des Travaux Public, n.204, December 1964.

Chin, F.K., 1970. Discussion: Pile tests. Arkansas River Project, JSMFD, ASCE, v. 97, n. SM7, p. 930-932.

Davisson, M.T., 1972. High capacity piles. Proceedings, Lecture Series. Innovations in Foundation Construction, ASCE, Illinois, Section, p. 52.

Décourt, L. 1996. Analysis of Deep Foundations: Piles. In: Foundations: Theory and practice, Hachich et al (eds), Ed. Pini Ltda., São Paulo, Chap. 8.1, p.265-301. (In Portuguese).

Fellenius, B. H. 2001. What capacity value to choose from the results of a static loading test. Deep Foundation Institute. Fulcrum, p. 19-22.

Fellenius, B. H. 2017. Basics of foundation design. Electronic edition. www.Fellenius.net. 464p.

Massad, F. 1992. On the interpretation of pile load tests considering the residual point load and the reversion of the lateral friction. Part I: relatively homogeneous soils. Soils and Rocks Journal, Vol. 15 (2), São Paulo, pp. 103-115. (In Portuguese).

Massad, F. & Lazo, G. 1998. Graphical method for the interpretation of the load-settlement curve from vertical load tests on rigid and short piles. Proc. XI Brazilian Congress on Soil Mechanics and Geotechnical Engineering (Cobramseg), Brasilia, v. 3, p. 1407-1414. (In Portuguese).

Van der Veen, C. (1953). The bearing capacity of a pile. In: International Conference of Soil Mechanics and Foundation Engineering, Zurich. Proceedings Zurich: Icosomef. v. 2. p. 84-90.

A NEW METHOD OF QUALITY CONTROL FOR JET GROUTING

ONLINE VIBRATION MONITORING

Dipl.-Ing. Univ. Nikolaus Schneider, GuD Geotechnik und Dynamik Consult GmbH,

Darwinstraße 13, 10589 Berlin, Germany, +49 30 7890 89-0, schneider@gudconsult.de

Dr.-Ing. Silke Appel, GuD Geotechnik und Dynamik Consult GmbH,

Darwinstraße 13, 10589 Berlin, Germany,+49 30 789089 0, appel@gudconsult.de

SUMMARY

The innovative approach for this new method of quality control is based on vibration monitoring in hardened primary columns. The continuous rotation of the jet grouting rod produces a characteristic profile of vibration which can be measured in single columns and composed structures. Fast Fourier transformations (FFT) of recorded vibration signals allow to interpret the processed acceleration graphs to specify the degree and quality of overlap between primary and secondary columns as well as the diameter of single columns.

A BRIEF OVERVIEW OF JET GROUTING

Jet grouting is a geotechnical construction method in which the structure of soil is broken and eroded by a high pressure beam (figure 1).Cement slurry, which is jetted to the full reach of the beam, hardens and creates a column. Several columns may be composed to construction elements such as under-pinning bods or watertight slabs. The capability of the beam can be increased through an additional air nozzle. The high pressure beam may be either cement slurry or water. The jet grouting rod has several channels in which the inner one leads the high pressure fluid (figure 2).
Construction parameters such as pump pressure and volume, pull back time and revolution of the drilling rod are recorded during the process and compared with those of the test columns. The quality control of jet grouting is based on the premise that the geometry and compressive strength of columns in comparable soil layers can be achieved by repeating the construction parameters of the test column. If soil conditions change, however, the effect on the size of the column cannot be detected.



Figure 1: Jet grouting beam



Figure 2: Jet grouting rod

Jet grouting (figure 4) may be compared to a 3D printer as complex structures are comprised of repetitive, additive and identical construction elements (figure 5). The prerequisite is knowledge of location, geometry and properties of the material used.

3 D Printer:	Jet Grouting Process:
exact position of single elements	drilling deviation
exact measurement of single element	diameter of column
properties of material	compressive strength

© 2018 Deep Foundations Institute

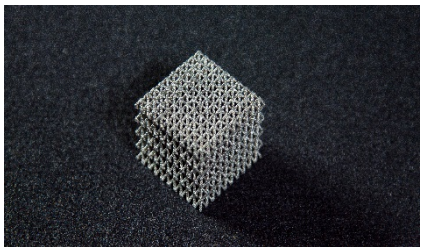


Figure 3: Additive constructed cube (source:www.siemens.com/presse)

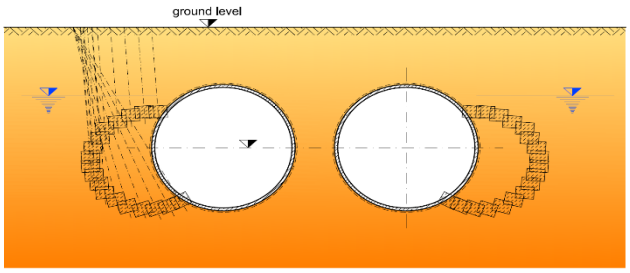


Figure 4: Metro station constructed with jet grouted columns

BERLIN IS A FOCUS LOCATION FOR JET GROUTING APPLICATION

The soil in Berlin is relatively consistent and primarily composed of fine sands which reach to a depth of approximately 60 meters. These sands were formed over three ice ages and deposited by glaciers which reached from Scandinavia to the region of Berlin.
Since the ground water level is generally at 3 meters below surface without a natural layer, the construction of a two level underground parking garage requires a special geotechnical approach.
Open draw down of ground water is generally not accepted by civic approval authorities to obtain a building permit as the ground water is protected and extraction volumes are limited.
Compliancy with the regulations for water management is achieved through excavation pits with a horizontal barrier. The lack of natural horizontal barriers in the soil necessitates construction of artificial barriers in the form of deep jet grouted (figure 5), injection or underwater concrete slabs.

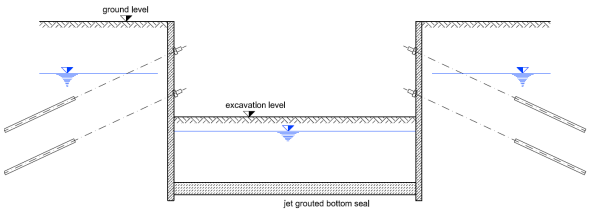


Figure 5: Deep jet grouted slab

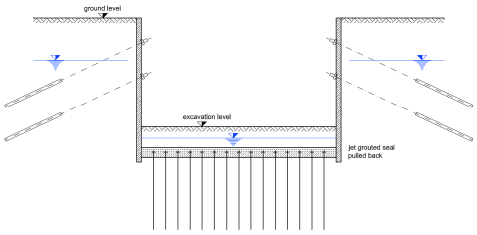


Figure 6: Jet grouted slab pulled back by micro piles

The sandy soil, high ground water level and building code regulations present a challenge which can only be technically managed through construction of horizontally sealed excavation pits. Jet grouted slabs, pulled back by micro piles (figure 6), have established themselves as the economically preferred method over injection slabs or underwater concrete slabs.

WHAT METHODS ARE CURRENTLY AVAILABLE TO VERIFY GEOMETRICAL CONFORMITY OF JET GROUTED COLUMNS?

The previous comparison of jet grouting with a 3D printer defined three quality criteria: exact position of each single element, the geometry of each element and the material properties.
Focus in this presentation is on the second of these three criteria, namely geometry of individual construction elements with special attention to the diameter.

An exact location of the jet grouted column may be verified with inclinometer sensors in the drilling equipment that transfer the exact location of each coupling onto the display of the operator. (figure 7)

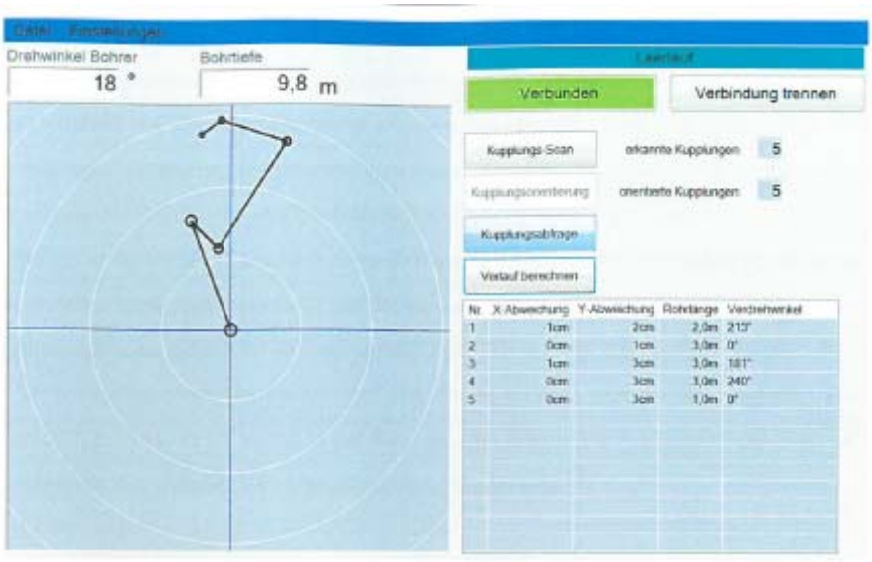


Figure 7: Plot of drilling rod alignment taken during drilling

The quality of material comprising the column may be established by taking samples in fluid state via pumps in the drilling rod.

What is the current approach used to verify the diameter of jet grouted columns?

- Test columns, which are dug free close to surface

But how are columns, which lie below the ground water level, verified?

- Test columns, whose diameter is recorded by distance sensors, lowered down into the soft column
- Test columns, whose diameter is measured with a Rover, operating out of the jet grouting rod
- Test columns, whose diameter is measured by contacts points in various distances
- Test columns, whose volume is measured by thermal calculations.

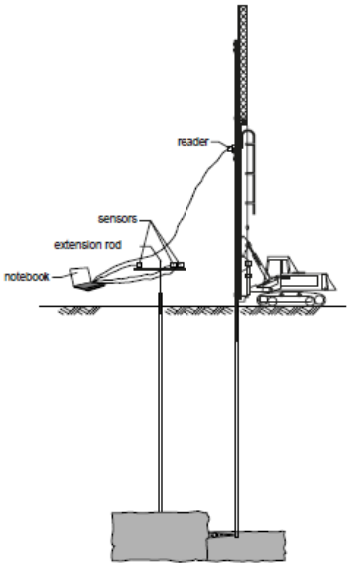
All of the above methods involve measurement of singular test columns which are executed in relevant and representative conditions. These methods assume that the achieved diameter can be repeated by maintaining the same construction parameters such as pressure, rotation, air pressure, etc. However, the soil conditions created by multiple glacial movements and melt are not homogenous. Therefore, the application of parameters from a given test column may not be transferrable, especially in the case of watertight construction.

THE NEW METHOD OF DIAMETER CONTROL BY VIBRATION MONITORING

The measurement is based on energy transfer from the jet grouting beam in the ground. Deformation is the main consequence of the high pressure beam moving through the soil as it is broken and mixed with suspension. A relatively small amount of energy is converted in the form of vibration, which is transmitted as space waves. The speed of the waves is dependent upon the mechanical properties of the soil. Once a column is hardened, it is able to transfer shear forces.

Hit by the powerful jet grouting beam, the column transfers energy along its axis to the top of the column where sensors can read the vibration (figure 8). Measurement of vibration transmitted into the primary column indicates whether the beam of a jet grouted column has encountered a hardened column or soft soil. The amplitude of speed or acceleration represents the key criteria as it differs

between a hardened column or soft soil. The acceleration in hardened material, i.e. jet grouted column results in a higher speed and lower reduction in amplitude. Knowing the time during which the grouting beam hits the column allows to calculate the missing link in a trigonometrical calculation (figure 9). Correlated to the rotation speed of the jetting rod provides the angle alpha and thus determines the diameter of the hardened column.



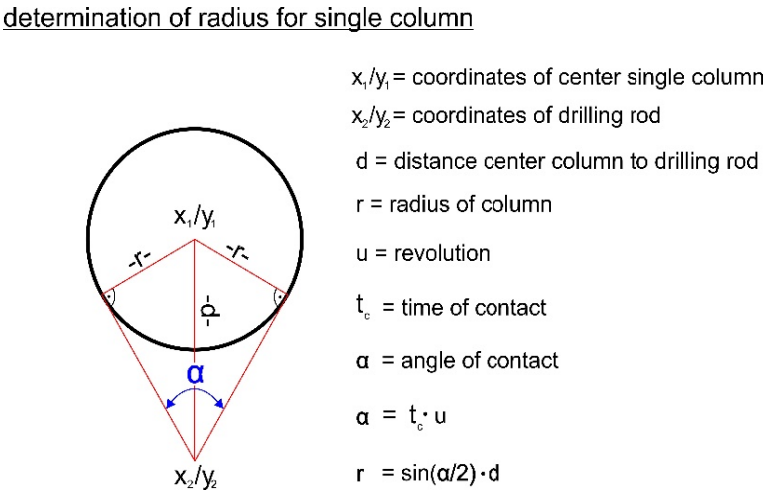


Figure 8: Set up for measurement **Figure 9: Trigonometrical relations**

FULL SCALE SITE TESTS IN BERLIN TO CONFIRM THE PRINCIPLES OF VIBRATION MONITORING

In August 2016 field test were carried out to compare calculated diameters with actual diameters of excavated columns (figure 10). A center column, already hardened, was hit by a jet grouted beam from the left and from the right inside an excavation pit. The distance of the columns to each other was known. A steel pipe with integrated vibration sensor was integrated into the center column. While jetting the adjacent columns against the center columns, the vibration induced in the center column was recorded.

Since the adjacent columns were constructed using a cement power beam, the middle column was covered on both sides with jet grouted bodies. The red spray paint makes it easier to see the difference between each column



Figure 10: excavated test columns



Figure 11: excavated primary column

After the adjacent columns were removed (figure 11), the geometry of the primary column was ready for onsite measurement. The comparison between the calculated radius using trigonometrical equations and the measured radius on site showed a very high degree of conformity

DATA COLLECTION OF VIBRATION

The acceleration sensor registered signals using the piezo electronic principle and was able to measure frequencies of at least 10 kHz. The recording was done at very high sampling frequency of over 20 kHz to capture information from the entire frequency range. Time signals were recorded. The high rate of data sampling produced a very large data size, which had been processed and reduced for further application.

Knowledge of the signal characteristics is extremely important to reduce the data volume without losing critical information. The following graphic (figure 12) shows the typical high frequency sampling of signals (left) as measured on the hardened primary column during jet grouting on a comparable project.

The spectrogram is shown on the right. Time intervals of T = 0.2 s are basis for a Fast Fourier Transformation (FFT) to show 256 spectra in relation to the time progress.

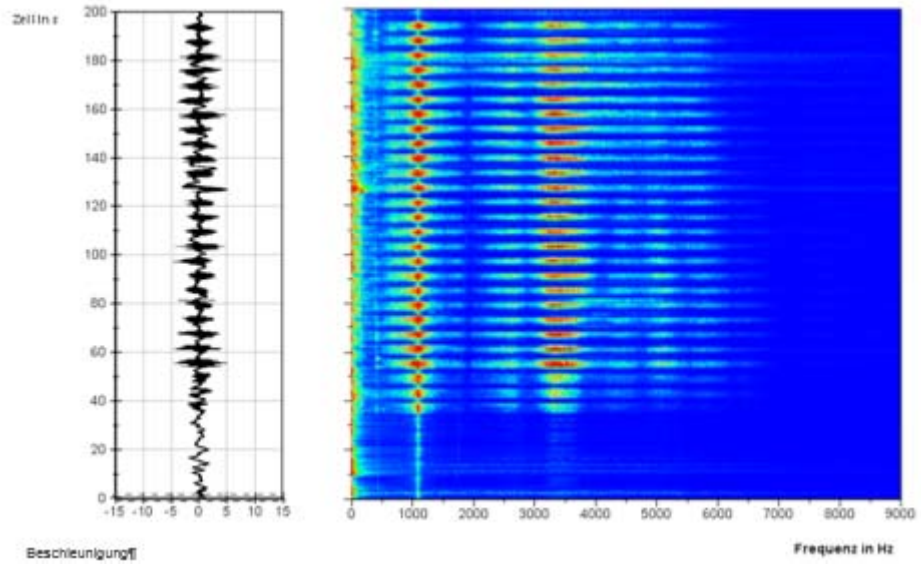


Figure 12 Time and spectrogram of acceleration during jet grouting against the primary column

The periodic repetitions (horizontal lines) in the spectrogram show a clear difference between the vibration into the primary column and the soil. It also shows frequency ranging at 1 kHz and between 2.3 kHz and 6 kHz while the beam had contact with the primary column. Signals up to approximately 1 kHz are also superimposed by other causal factors at the construction site such as the drilling equipment itself.

DATA PROCESSING

The example shown is based on frequency contents in the range of 2 kHz and 6 kHz. The whole signal is passed through a band pass filter (Butterworth 6. degree with Hanning-window).

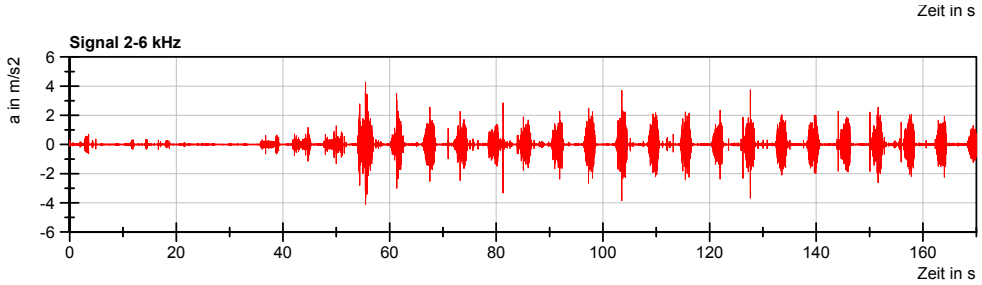


Figure 13: Filtered signals by Bandpass (2-6 kHz)

The advantage of using the addition of spectral elements (FFT of T = 0,2s) elements lies in a significant reduction of data volume, maintaining the key information in the graphs.

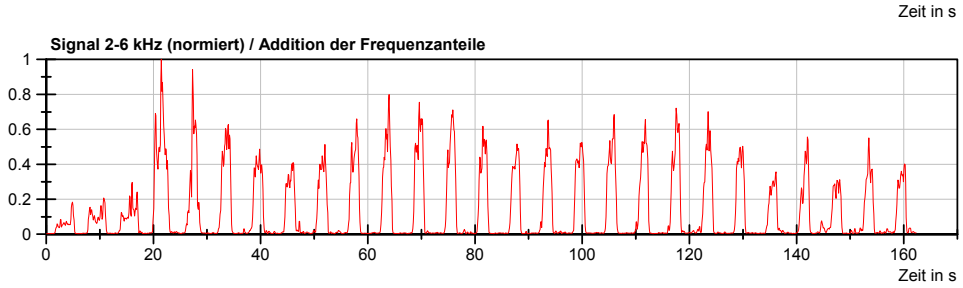


Figure 14: Retransformed data

INTERPRETATION OF RECORDED ACCELERATION ROUTINES

Based on the field tests to following conclusions can be drawn:

1) There is a significant difference between the jet grouting beam hitting a column or the soil
2) The vibrations induced by the high power beam are transferred along the axis of the hardened jet grouted columns and are recordable
3) The distance of the peaks confirm the rotation speed of the jet grouting rod
4) The contact time of the high power beam on the jet grouted column is readable under the acceleration peaks
5) The contact angle to calculate the radius of the jet grouted columns is very reliable
6) The value of the acceleration peaks varies according to the highly turbulent situation during jetting

VIBRATION MONITORING ON COMPOSED STRUCTURAL ELEMENTS

Watertight jet grouted construction slabs are usually constructed of primary columns “wet in wet” (figure 16). This means that the columns are constructed sequentially without waiting for the previous column to harden.
Secondary columns are jet grouted against the primary columns after they have hardened. Jetting energy is transferred in the drilling depth against a linear row of columns (figure 15).
This constructing sequence of primary and secondary rows of jet grouted columns allows to apply vibration monitoring to check on the overlap.
If a jet grouting beam penetrates soil alone, its vibrational energy dissipates over a relatively short distance as the individual sand grains absorb and dampen the affect.

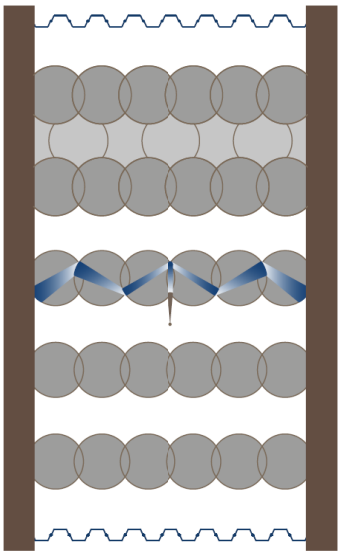


Figure 15: Vibration transfer

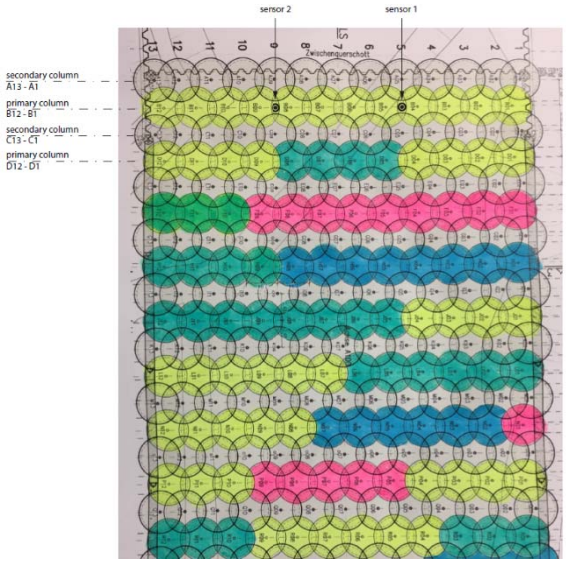


Figure 16: construction drawing

Alternatively, if the beam encounters an element of hardened primary columns, its high frequency vibration penetrates the element over a relatively longer distance. A jet grouting beam which encounters a hardened column will not result in deformation, rather a large portion of its energy will be transferred as a vibration impulse into the primary column (figure 15). The vibration will be transmitted within a row of column as structure borne noise.

Under this premise, a vibration monitor drilled into the hardened primary columns can deliver acceleration profiles which allow to determine if the high power beam reached to the hardened primary row. This “impact cone” (figure 19), designed with integrated energy source and data logger, can be set to record defined frequencies, in this case high frequency which is typical for transfer along a hardened primary row of columns.
These ideas carry the results gained on the vibration monitoring of single columns and were suitable to be tested on a construction site in the heart of Berlin.

SECTION 16. OF THE A 100 IN BERLIN, THE FUTURE CITY HIGHWAY BETWEEN NEU-KÖLLN AND TREPTOW

The traffic infrastructure in Berlin is designed with an inner city and outer highway ring. The inner city highway ring could not be completed during the division of Berlin between 1961 and 1989.
Construction of Section 16 finally commenced in May 2013 following long, political discussions. A piece of highway with 3 lanes in each direction over 3.2 km should join the Intersection Neu-Kölln with the exit at Treptower Park. Construction is planned from 2013 through 2022 with a budget of 473 million Euro. The project is divided into 7 lots. The investor is Bundesrepublik Deutschland. Contractor for lot 5 is company Porr with its partner for geotechnical works Stump.
The routing of the highway was planned into a 7 meter deep excavation pit, horizontally sealed, to comply with noise and air pollution standards. In addition, noise barriers with a height of up to 6 meters will be added.
All of the requirements together culminated in design of horizontal slab for lots 1 to 4 with underwater concrete and lots 5 and 6 with jet grouting method.
Jet grouting was applied to seal an area of approximately 12.000 m² in Lot 5 and approximately 2.500 m² in Lot 6, partially pulled back by micro piles.



Figure 17: Highway BAB 100 - 7 construction lots

Tests were made during the summer of 2017 in areas of Lot 5 to verify the integrity and overlap of jet grouted columns (figure 18)

SET UP OF TEST ARRANGMENTS ON THE CONSTRUCTION SITE

The overall concept for the test was set up to read the acceleration graphs in the row of primary columns using standpipes with integrated sensors. The row of primary columns was about 32 meters long with two monitoring locations. The recorders were installed approximately at the points of division into thirds in the row of primary columns axis. The diameter of the test column was 3,40 m. The secondary row A had 12 columns, the primary row B had 12 columns and the secondary row C had 13 columns.





Figure 18: Overall layout of the construction site

Figure 19: Data logger

The vibration sensors are constructed to fit into the standpipes. Once the monitoring stage is accomplished, these sensors are easy to retrieve and may be used again. They are not lost.

Figure 20 displays the processed acceleration graphs which were recorded while jetting column C 4. The time is recorded on the horizontal axis. The vertical axis shows the adjusted acceleration. The distance of the peaks reflects the rotation speed of the rod. The intensity of the signal distinguishes between the big and small nozzle.

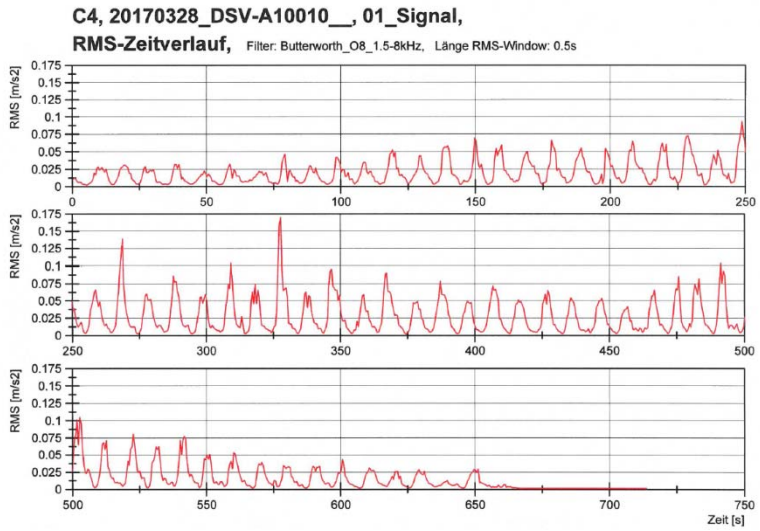


Figure 20: Vibration signals during the construction of secondary columns C 4

INTERPRETATION OF PROCESSED DATA

Hitting a single column shows a single peak in a symmetrical graph. However, hitting a sequence of columns, this geometry is reflected in a "double peak" as can be seen on the Figure 21 and 22. The double column shows the addition of two single column profiles which are essentially merged into one interlocking body

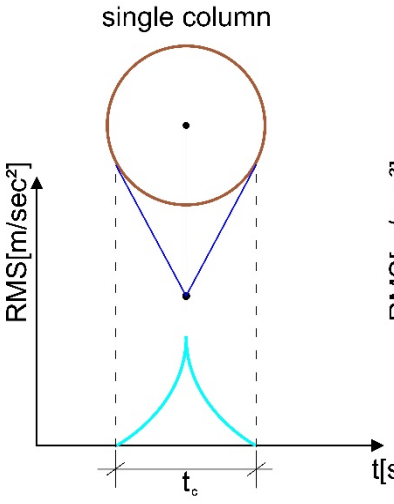


Figure 21: profile single column

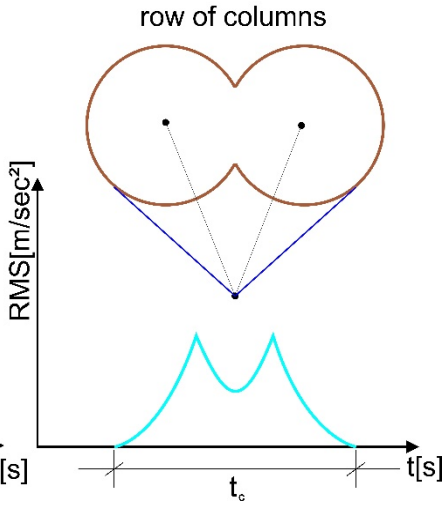


Figure 22: profile row of columns

Four basic profiles were extracted from the recorded acceleration values to determine the correlation criteria.

1. Column without contact

No significant vibration is measured if the jetting radius is not achieved to reach the primary column. The energy released does not reach to the column as it is absorbed in the soil.

2. Column without contact in the gap

If the jet grouting beam makes contact with a primary column, but the radius is not sufficient to erode soil in the gaps between the primary columns, then the soil remaining in those gaps will dampen the energy. In this case an energy drop is visible in the middle of the contact zone.

3. Regular column

The signal increases to a top value and decreases to the symmetric axis, confirming the basic profile of figure 22.

4. Oversized secondary column

If the secondary column has an unplanned wide diameter, then the beam has to cover a longer distance and exhibits longer contact time at unchanged rate of rotation.

.

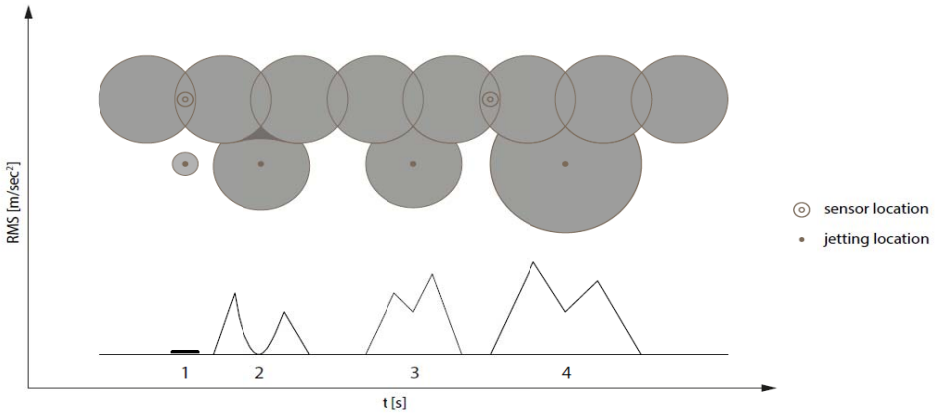


Figure 21: Graphs of possible signals

CONCLUSIONS DRAWN FROM THE TESTS ON SITE

Vibration monitoring on jet grouted columns opens a new type of quality supervision and supports the composition of new structural elements.

1) The actual diameter reached is focus of vibration monitoring for jet grouting rather than the compliance of execution parameters with test columns, as applied in the present state of the art. Thus the potential risk of unexpected ground condition is significantly reduced
2) Vibration monitoring on single columns allows diameter determination at any depth below ground level, without having to dig them free.
3) Vibration monitoring and sophisticated data processing provides an assessment of the interlock on composed jet grouted elements.
4) Vibration monitoring does not interfere with the production process on jet grouting.
5) Data loggers at every 5th column in the primary rows allows to cover the interlock of 100 % between primary and secondary columns.
6) Supporting structural elements for metro stations or emergency tunnels expands the future application range of jet grouting, if supervised by vibration monitoring.

.

REFERENCES

Studer J.A., Laue J. und Koller M.G. (2007) Bodendynamik, Springer Verlag Berlin Heidelberg

A NON LINEAR AND PLASTIC-HARDENING MODELLING OF VERTICALLY LOADED PILES

Maurizio Lenzi, ACMAR, Ravenna, Italy, maurizio.lenzi@acmar.it
Paola Campana, Studio Campana, Forlì, Italy, paola.geotech@libero.it

ABSTRACT

The non linear interaction between a vertically loaded single pile and the soil is deepened making use of the work-energy principle. It is shown that the pile behavior is governed at any elevation by the equality between the elastic strain energy stored by the axial load in the pile unit length and the sum of the strain energy stored by the tip reaction and the plastic-hardening work locally done by the friction reaction. This criterion provides an effective insight into the pile response through a nonlinear analytical model focused on the components of the pile settlements and on the load sharing among the pile bearing mechanisms. It allows one to evaluate the theoretical behavior of piles embedded in layered soils and the back analysis of the load tests results. It is also a control tool of complex models.

Keywords: non linear interaction, axial load, tip settlement, elastic shortening, work-energy principle, strain energy, plastic-hardening work.

INTRODUCTION

The development of a mathematical model of the pile-soil interaction includes two basic blocks such as general principles and constitutive relations. The general principles regard the equilibrium of the axial forces and the work-energy balance while the constitutive relations come from the experimental tests (Salsa, 2010). These lasts concern the linear elastic relations of the pile materials and the transfer curves of the axial load, here used to model the nonlinear behavior of the soil. Once selected these topics an analytical solution is searched as a function of the elastic shortening of the pile while varying the other one component of the pile settlement, namely the tip settlement. This last is in fact to be added at any elevation to the current elastic shortening of the underlying length of the shaft and, as a parameter, it plays the role of independent variable of the model. Following this approach the procedure leads to a solving work-energy equation in which the strain energy and the reciprocal work stored in a unit slice of the pile by the axial load component in equilibrium with shear stresses equals the plastic hardening work of the same shear stresses mobilized by the elastic shortening of the shaft.

In the paper firstly the case of a pile embedded in a homogeneous soil is analyzed then followed by the extension to the case of a pile interacting with a stratified soil in which the several segments of the pile, each embedded in a homogeneous soil layer, behave as a series of superimposed piles. The comparison with the results of case histories supports the validity of the analytical nonlinear model.

COMPONENTS OF THE PILE SETTLEMENT

The nonlinear behavior of the soil does not allow to obtain, for axially deformable piles, an explicit analytical correlation between the vertical loads and the pile settlements. To overcome this limitation a different paradigm is adopted making use as an independent variable not so much of the applied load (which is deduced as axial load at the head of the pile) but rather of the settlement of the pile tip. This choice allows to assign in a single section at the tip of the pile both the static and the displacement boundary conditions, removing in this way that limitation. Moreover the choice is appropriate taking into account that at any depth [z] the pile settlement [w] is the sum of the tip settlement [w_b], which acts as a free parameter impressing an uniform movement all along the pile, and of the settlement [w_e] due to the elastic shortening of the pile length $\boldsymbol{\zeta} = \mathbf{L-z}$, which extends from the pile tip up to the current section (Fig. 1). It follows that at any elevation the pile settlement is related to the two components of the vertical movements by the compatibility condition:

$$w(\zeta) = w_b + w_e(\zeta) \qquad [1]$$

© 2018 Deep Foundations Institute

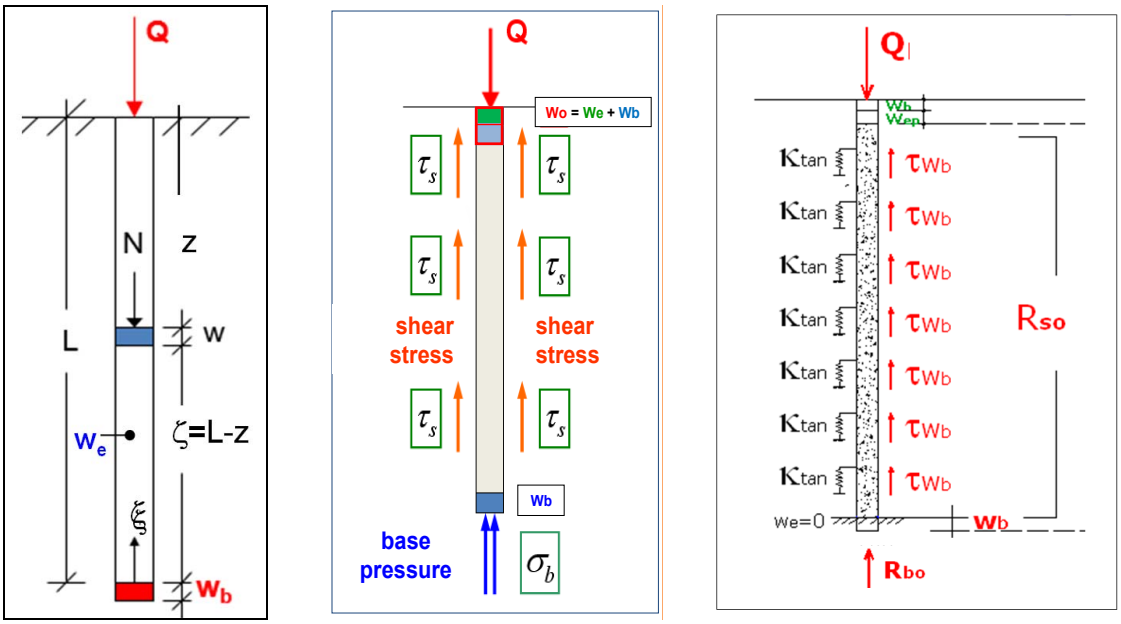


Fig.1. Nonlinear model of an axially loaded pile as a function of the elastic shortening [$w_e(\zeta)$]

CONSTITUTIVE RELATION OF THE PILE

The mechanical properties of the pile shaft are modeled in the linear elastic range because of the level reached by the compression stresses, usually limited even at the pile capacity. Therefore the constitutive relation that links the axial load [N] to the axial strain [$\varepsilon=dw_e/d\zeta$] takes the form:

$$N = EA \cdot \frac{dw_e}{d\zeta} \qquad [2]$$

In this equation [E] is the elastic modulus of the pile material while [A] is the area of the cross section of the pile. It follows that the density of the strain energy [U] stored in a unit slice of the pile during the loading process can be expressed by both the relations ($U = N \cdot \varepsilon/2$):

$$U = \frac{N^2}{2EA} = \frac{EA}{2} \cdot \left(\frac{dw_e}{d\zeta} \right)^2 \qquad [3]$$

CONSTITUTIVE RELATION OF THE SOIL

The nonlinear constitutive relations of the soil taken into account to link the shear stresses to the vertical displacements have all the typical property of a monotonic trend with a decreasing stiffness. This common feature of the constitutive relations implies that the two components [w_b , w_e] of the local vertical settlement find a counterpart in the two components [τ_{wb} , $\Delta\tau_{we}$] of the shear stress [τ_s]:

$$\tau_s(w) = \tau(w_b) + \Delta\tau(w_e) \qquad [4]$$

both activated by the friction mechanism (Fig. 2). When the pile is subjected to the rigid and uniform settlement [w_b] the local shear stress increases up to the value τ_{wb} making a work in the nonlinear field identified by the area OBAO shaded with a yellow color in the τ_s-w diagram. The sum of the tip reaction and of the shear stresses mobilized along the pile length ζ= L-z requires, for the vertical equilibrium to be satisfied, that the cross section of the pile provides the balancing axial force [N] which is enabled by the elastic strain [ε=N/EA] of the unit slice.

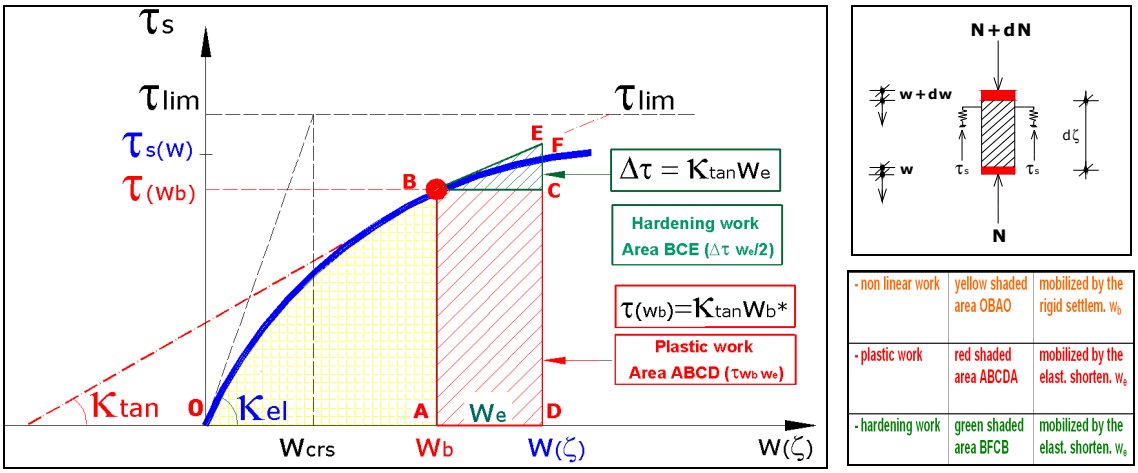


Fig. 2. Constitutive model of the shear stresses vs vertical settlements

The sum of all the elementary elastic shortenings [ε·dζ] of the underlying slices produces an additional settlement [w_e] at the elevation of the current section which in turn mobilizes a shear stress increase $\Delta\tau(w_e)$. The shear stresses components make thus an additional work that consists of a plastic work (area ABCDA shaded with a red color) performed by the shear stress component τ_{wb} and of a hardening work (area BFCB shaded with a green color) performed by the shear stress component $\Delta\tau_{we}$. Inside this frame the constitutive relation of the friction mechanism is expanded in the series:

$$\tau_s(w) \cong \tau(w_b) + \kappa_{\tan}(w_b) \cdot w_e \qquad [5]$$

in which the nonlinear component of the shear stress is confined directly in the term $\tau(w_b)$, that is an assigned function once selected the constitutive relation of the soil. The hardening path is in turn approximated by a linear stretch whose slope identifies the stiffness $\kappa_{tan}(w_b)$ of an equivalent elastic model performing the same elastic shortening. Il follows that the plastic-hardening work is the sum:

$$L_{p+h} = L_p + L_h \cong \tau(w_b) \cdot w_e + \kappa_{\tan}(w_b) \cdot w_e^2 / 2 \qquad [6]$$

of the plastic work (rectangular area ABCDA) which provides a lower limit and the hardening work of the linearized path (triangular area BECB), which provides an upper limit to the work of the shear stresses mobilized by the elastic shortening. Figure 3 shows as the hardening work is significant at the lower load levels while the plastic work becomes predominant when approaching to the pile capacity. As a consequence the theoretical response of the pile-soil system results to be bounded between two limit pushover curves, denoted *upper bound* and *lower bound* solutions, which usually delimit a narrow band of values which encloses the actual nonlinear solution (Fig. 4 – reference case study 1).

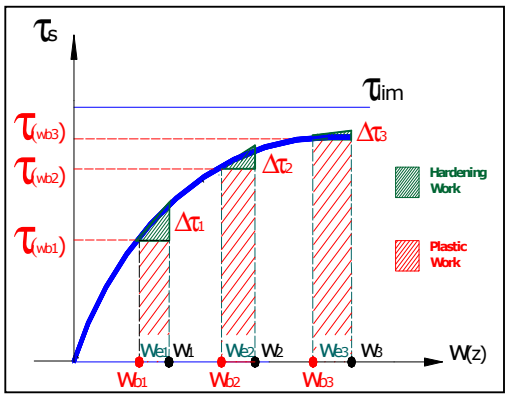


Fig. 3. Plastic and hardening shear work

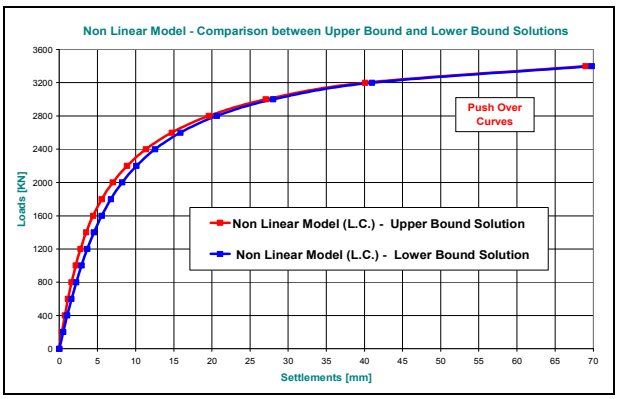


Fig.4. Upper Bound and Lower Bound Solutions

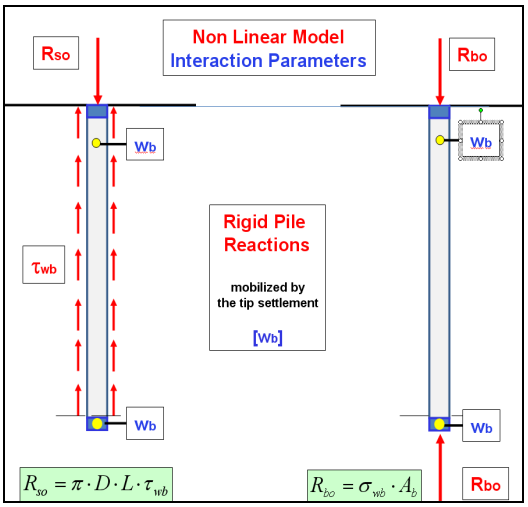


Fig. 5. Rigid pile reaction

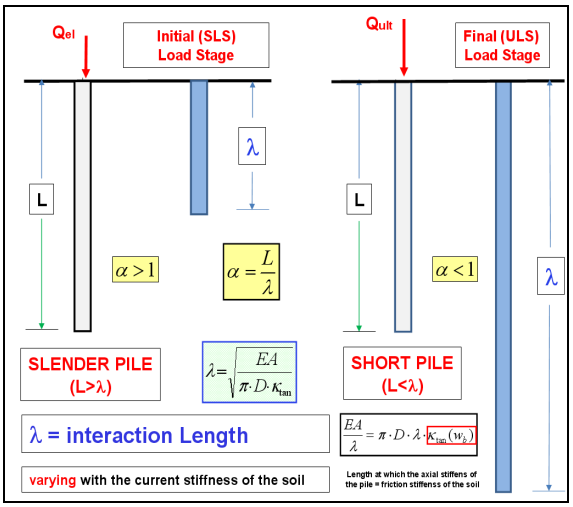


Fig. 6. Non linear interaction length

INTERACTION PARAMETERS

Once defined the main features of the constitutive relations of the soil in contact with the shaft, the representative parameters of the pile-soil behavior are then individuated. In this regard an appropriate choice when dealing with the coupling between geotechnical and structural systems is to select the dimensionless physical quantities that govern the interaction uniquely. It will be shown that these parameters are identified, for each load step, by the ratios:

$$\frac{R_{so}}{EA} = \frac{\pi \cdot D \cdot L \cdot \tau(w_b)}{EA} \qquad [7]$$

$$\frac{R_{bo}}{EA} = \frac{\sigma(w_b) \cdot A_b}{EA} \qquad [8]$$

between the rigid pile reactions [R_{so}] and [R_{bo}] mobilized by the tip settlement (Fig. 5) and the axial rigidity [EA], which takes into account of the elasticity of the pile material and the geometry of the pile cross section. Moreover the pile behavior depends on the characteristic length of interaction:

$$\lambda = \sqrt{\frac{EA}{\pi \cdot D \cdot \kappa_{\tan}(w_b)}} \qquad [9]$$

which is that particular length [λ] for which the axial elastic stiffness of the pile shaft [K_p=EA/λ] equals the current nonlinear stiffness of the friction mechanism [$K=\pi \cdot D \cdot \lambda \cdot \kappa_{tan}(w_b)$]. It is then possible to define, as related dimensionless quantity, the slenderness of the pile as the length ratio (Fig. 6):

$$\alpha = \frac{L}{\lambda} = \sqrt{\frac{\pi \cdot D \cdot L \cdot \kappa_{\tan}(w_b)}{EA/L}} \qquad [10]$$

between the geometric length [L] and the characteristic length [λ] of the pile. It also represents a stiffness ratio being the square root of the ratio between the actual stiffness of the friction mechanism and the elastic one of the shaft. This synthetic parameter well explains the current response of the pile distinguishing between *slender piles* (α>1) and *short piles* (α<1). That ratio in fact reduces as well as the current shear stiffness of the soil [$\kappa_{tan}(w_b)$] as the applied load increases. It follows that the behavior of a pile evolves during the loading process from that of a slender pile towards that of a short pile.

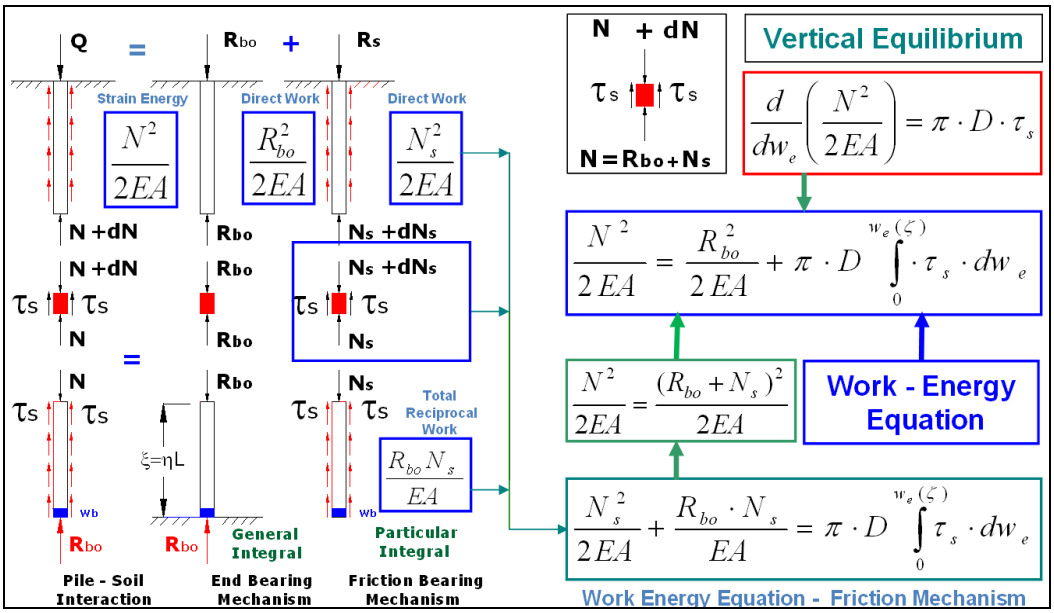


Fig. 7. Nonlinear analytical model of the pile soil interaction: work-energy criterion

WORK-ENERGY CRITERION AND NONLINEAR SOLUTION

To search for the nonlinear solution the principle that equals the strain energy to the work done by the external forces acting on a unit slice of the pile is applied. To this end firstly the vertical equilibrium of the slice is expressed as a function of the rate of change of the strain energy through the equation:

$$\frac{d}{dw_e}\left(\frac{N^2}{2EA}\right)=\pi\cdot D\cdot\tau_s \qquad [11]$$

It is coupled to the boundary conditions at the pile tip where the elastic shortening vanishes and the strain energy in the slice is that stored by the tip reaction, which gives a constant work contribution all along the pile. That relation provides the work-energy equation of the friction mechanism in the form:

$$\frac{N^2}{2EA}=\frac{R_{bo}^2}{2EA}+\pi\cdot D\int_0^{we(\zeta)}\tau_s dw_e \qquad [12]$$

It equals the strain energy stored by the axial load to the sum of the strain energy stored by the tip reaction and of the plastic hardening work of the friction shear stresses mobilized by the current elastic shortening of the shaft (Fig. 7). Making use of the constitutive relations it gives:

$$\frac{EA}{2}\left(\frac{dw_e}{d\zeta}\right)^2=\frac{R_{bo}^2}{2EA}+\pi\cdot D\cdot\left[\tau_{wb}w_e+\frac{1}{2}k_{\tan}w_e^2\right] \qquad [13]$$

This equation once solved provides the elastic shortening of the pile shaft [$w_e(\zeta)$]. It can be written in a more expressive dimensionless form as a function of the normalized elastic shortening [$w_e(\eta)/L$], which changes varying the normalized elevation $\eta=\zeta/L$ of the current section, and of the interaction parameters [R_{so}/EA, R_{bo}/EA, α], that are fixed values once assigned the tip settlement, finding:

$$\left[\frac{d}{d\eta}\left(\frac{w_e}{L}\right)\right]^2=\left(\frac{R_{bo}}{EA}\right)^2+2\cdot\left(\frac{R_{so}}{EA}\right)\cdot\left(\frac{w_e}{L}\right)+\alpha^2\cdot\left(\frac{w_e}{L}\right)^2 \qquad [14]$$

Taking into account of the boundary conditions at the pile tip, the nonlinear solution results to be:

$$w(\eta) = w_b + w_e(\eta) = w_b + \left\{ \frac{R_{so}\eta^2}{2} \cdot \left[\frac{2 \cdot (\cosh \alpha\eta - 1)}{(\alpha\eta)^2} \right] + R_{bo}\eta \cdot \left[\frac{\sinh \alpha\eta}{\alpha\eta} \right] \right\} \cdot \frac{L}{EA} \qquad [15]$$

$$N(\eta) = \frac{EA}{L} \cdot \frac{dw_e}{d\eta} = R_{so}\eta \cdot \left[\frac{\sinh \alpha\eta}{\alpha\eta} \right] + R_{bo} \cdot [\cosh \alpha\eta] \qquad [16]$$

It has a general validity, in the limits of the basic assumptions, not depending on a specific constitutive relation of the soil that may assume any plausible form included the elastic one. The main result achieved is that at any elevation the pile settlement and the axial load depend only on the interaction parameters [R_{bo}/EA, R_{so}/EA, α] and on the current deformable length normalized to the characteristic interaction length [$\alpha\eta=(L-z)/\lambda$]. All the terms are functions, through the selected tip settlement, of the rigid pile reactions R_{bo} and R_{so} which perform non linear and plastic work, amplified by factors (the terms inside the square brackets) which depend through the stiffness ratio [α] on the hardening work of the friction shear stresses that is mobilized by the pile elasticity. The *upper bound solution*, that collects the pile settlement [w_o] and the applied load [Q], results so to be (η=1):

$$\boxed{w_o = w_b + \left\{ \frac{R_{so}}{2} \cdot \left[\frac{2 \cdot (\cosh \alpha - 1)}{\alpha^2} \right] + R_{bo} \cdot \left[\frac{\sinh \alpha}{\alpha} \right] \right\} \cdot \frac{L}{EA}} \qquad \boxed{Q = R_{so} \cdot \left[\frac{\sinh \alpha}{\alpha} \right] + R_{bo} \cdot [\cosh \alpha]} \qquad [17]$$

The *lower bound solution* in turn, depending on the plastic work only, is found in the limit $\alpha \to 0$ in which all the hardening factors have unit value. It means uniform shear stresses and linear axial loads.

TRANSFER CURVES OF THE AXIAL LOAD

For the application of the model the soil constitutive relation has to be explicated. Specific relations apply to over-consolidated soils while a relation often valid in normally or light consolidated soils is the hyperbolic stress strain relation which shows an asymptotic behavior delimited by the soil capacity (Viggiani et al., 2012, Dalerci, Bovolenta, 2014). In the case of the hyperbolic relation the rigid pile reaction mobilized by the friction mechanism becomes (Lenzi, Campana, 2015):

$$R_{so} = Q_s \cdot \frac{w_b}{w_{crs} + w_b} \qquad w_{crs} = c_s \cdot D \qquad c_s = 2\tau_{lim} / G_s \qquad [18]$$

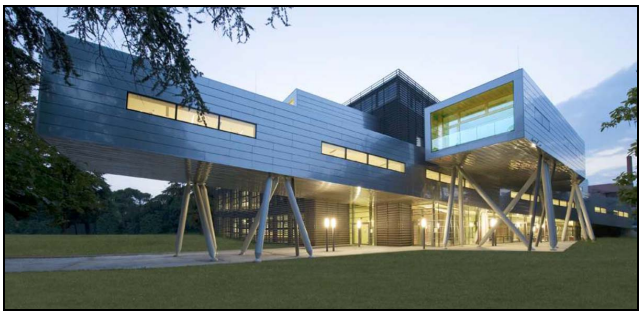
where $Q_s=\pi DL\tau_{lim}$ is the friction capacity while w_{crs} is the characteristic settlement which depends through the pile technology on the shear strength [τ_{lim}] and on the shear modulus [G_S] at low shear strain of the soil. Typical values of the ratio G_s/τ_{lim} varies in the range 400 (for clays) up to 1000 (for sandy soils). In a similar way the tip reaction is expressed by the relations:

$$R_{bo} = Q_b \cdot \frac{w_b}{w_{crb} + w_b} \qquad w_{crb} = c_b \cdot D \qquad c_b = 0.6 q_b / E_b \qquad [19]$$

where $Q_b=q_bA_b$ is the end bearing capacity while w_{crb} is the characteristic tip settlement which depends through the pile technology on the unit capacity [q_b] and on the elastic modulus [E_b] at low strain of the soil below the pile tip. Moreover the stiffness ratio [α] takes the form:

$$\alpha = \alpha_{el} \cdot \frac{w_{crs}}{w_{crs} + w_b} \qquad \alpha_{el} = \sqrt{\frac{K_s L}{EA}} \qquad K_s = \frac{Q_s}{w_{crs}} \qquad [20]$$

The procedure is so complete. For any increasing value of the tip settlement [w_b] the previous relations give the interaction parameters [R_{bo}, R_{bo}, α] and by means of the non linear model the elastic shortening [w_e], the pile settlement [w_o], the applied load [Q] and the load sharing [$R_s=Q-R_b$, $R_b=R_{bo}$].



w_b [mm]	R_{so} [KN]	R_{bo} [KN]	α [-]	w_e [mm]	w_o [mm]	Q [KN]	R_s [KN]	R_b [KN]
0.00	0	0	1.891	0.00	0.00	0	0	0
0.10	107	8	1.809	0.25	0.35	200	192	8
0.21	222	18	1.720	0.52	0.73	400	382	18
0.35	349	29	1.622	0.80	1.15	600	571	29
0.52	489	43	1.514	1.09	1.61	800	757	43
0.75	642	60	1.396	1.40	2.15	1000	940	60
1.03	808	82	1.267	1.74	2.77	1200	1118	82
1.42	988	110	1.128	2.10	3.52	1400	1290	110
1.95	1179	147	0.981	2.48	4.43	1600	1454	147
2.68	1373	193	0.832	2.89	5.56	1800	1607	193
3.69	1561	252	0.686	3.32	7.01	2000	1748	252
5.11	1736	324	0.551	3.77	8.88	2200	1876	324
7.12	1892	410	0.431	4.24	11.36	2400	1990	410
10.02	2025	511	0.328	4.73	14.75	2600	2090	511
14.37	2138	624	0.241	5.22	19.59	2800	2177	624
21.33	2230	749	0.169	5.73	27.06	3000	2252	749

Fig. 8. Case Study No.1: Nonlinear model of the piles

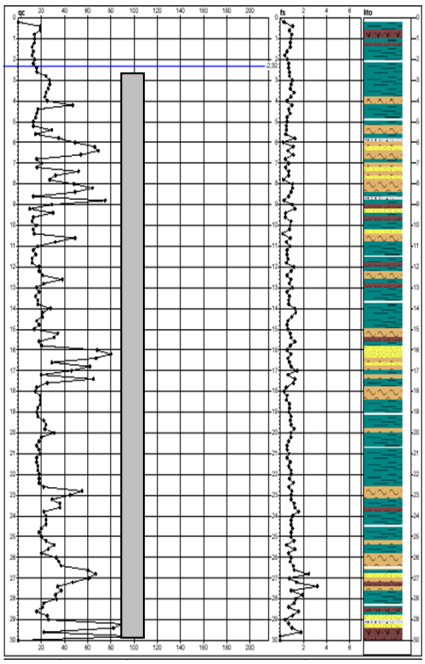


Fig. 9. CPT: tip resistance vs elevation

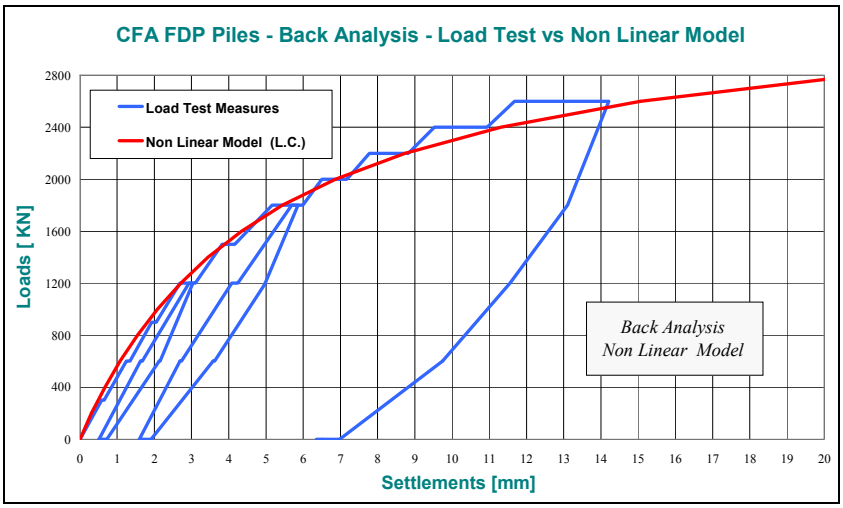
CASE STUDY No. 1 – PILE EMBEDDED IN A HOMOGENEOUS SOIL

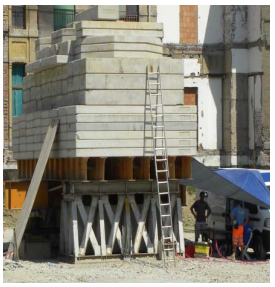
As an example the case study of the piles of the deep foundation of the Campus of the University of Forlì is illustrated (Fig. 8). The piles have a length of 26 m and a diameter of 0.60 m and they were drilled without extraction of the soil, that was pushed against the perimeter of the hole (CFA-FDP piles). The soil stratigraphy includes clayey silt and silty clay layers (Fig. 9) whose properties are assumed uniform all over the length of the pile. The average shear strength of the soil [τ_{LIM}] is set 50 KN/m^2 while the unit tip capacity [q_b] of the soil below the CFA pile is estimated to be 4.5 MPa. The pile design capacity thus amounts to 3725 KN. The elastic modulus [E] of the concrete is 30000 MPa. The geotechnical parameters used in the back analysis are summarized in Table 1.

Table 1. Case Study N$_o$.1 - Geotechnical parameters of the back analysis of the load test

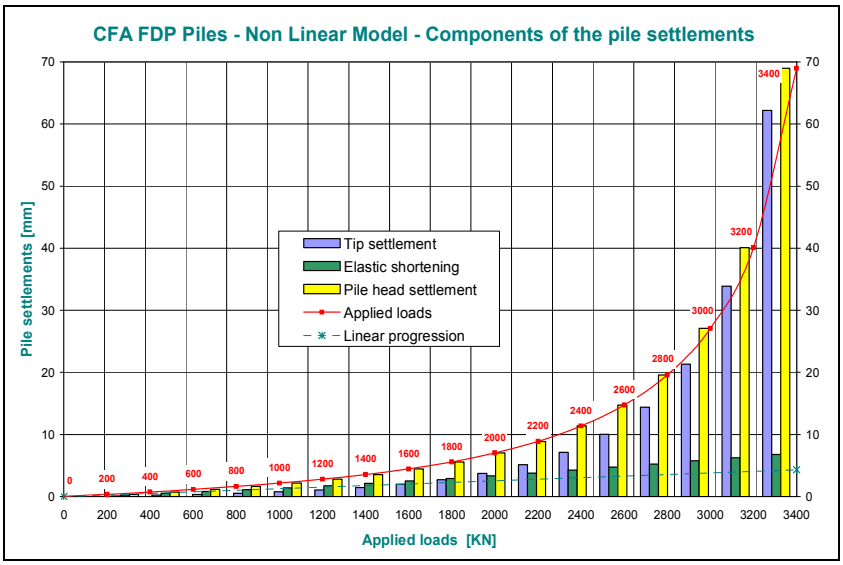
Friction Bearing Mechanism	*End Bearing Mechanism*
$Q_s = \pi D L \tau_{LIM} = 3.14 \cdot 0.60 \cdot 26 \cdot 50 = 2450$ KN	$Q_b = \pi D^2/4 \cdot q_b = 3.14 \cdot 0.60^2/4 \cdot 4500 = 1275$ KN
$c_s = 2\tau_{lim}/G_s = 0.0035$ (0.35%) ($G_s / \tau_{lim} \approx 600$)	$c_b = 0.6 q_b/E_b = 0.025$ (2.5 %) ($E_b / q_b \approx 25$)
$w_{crs} = c_s D = 0.0035 \cdot 600 = 2.1$ mm	$w_{crb} = c_b D = 0.025 \cdot 600 = 15$ mm
$K_s = Q_s / w_{crs} = 2450/2.1 = 1167$ KN/mm (elastic stiff.)	$K_b = Q_b / w_{crb} = 1275/15 = 85$ KN/mm (elastic stiff.)
$\alpha_{el} = [K_s L/EA]^{0.5} = 1.891$ (elastic interacion parameter)	$\beta_{el} = K_b L/EA = 0.260$ (elastic interacion parameter)

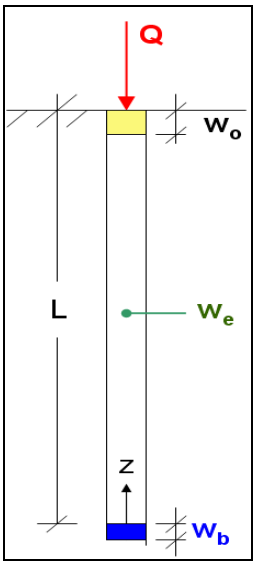
The results of the analysis are globally collected in Fig. 10, which makes evidence of a good agreement between the measures of the load test and the pushover curve provided by the nonlinear model. Moreover it shows as the elastic shortenings prevail at the first load levels and then they keep small values increasing the load, following a curve that does not deviate significantly from the straight one. Conversely the tip settlements dominate at values of the applied load next to the pile capacity. In turn the sharing of the test loads is initially governed by the friction mechanism that shows a high initial stiffness which mobilizes the friction capacity mainly by means of small elastic shortenings, then followed by a wide excursion in the plastic field increasing the applied loads. Instead the tip mechanism imparts an overall connotation of hardening type to the response as a whole of the pile, being that mechanism characterized by a low stiffness which involves large tip displacements to fully mobilize the end bearing capacity. The model also shows that the slenderness ratio reduces from the initial elastic value α_e=1.891 down to α=0.169 at 3000 KN. The actual behavior of the tested pile therefore progressively changed during the loading process from that of slender pile, which mainly mobilizes the friction mechanism, to that of a short end bearing pile.

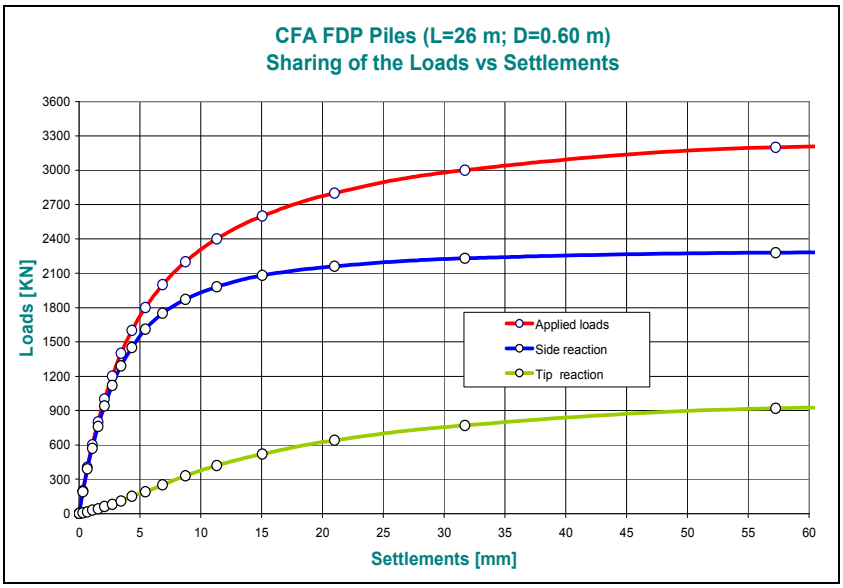












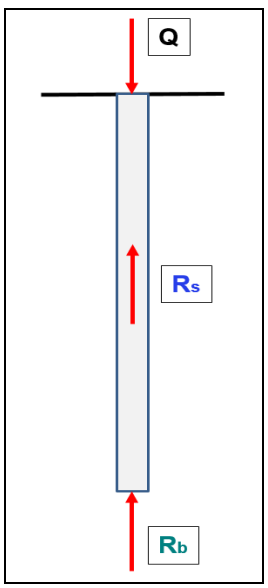


Fig. 10. Case study N$_o$. 1: a) load test; b) settlement compositions; c) load sharing

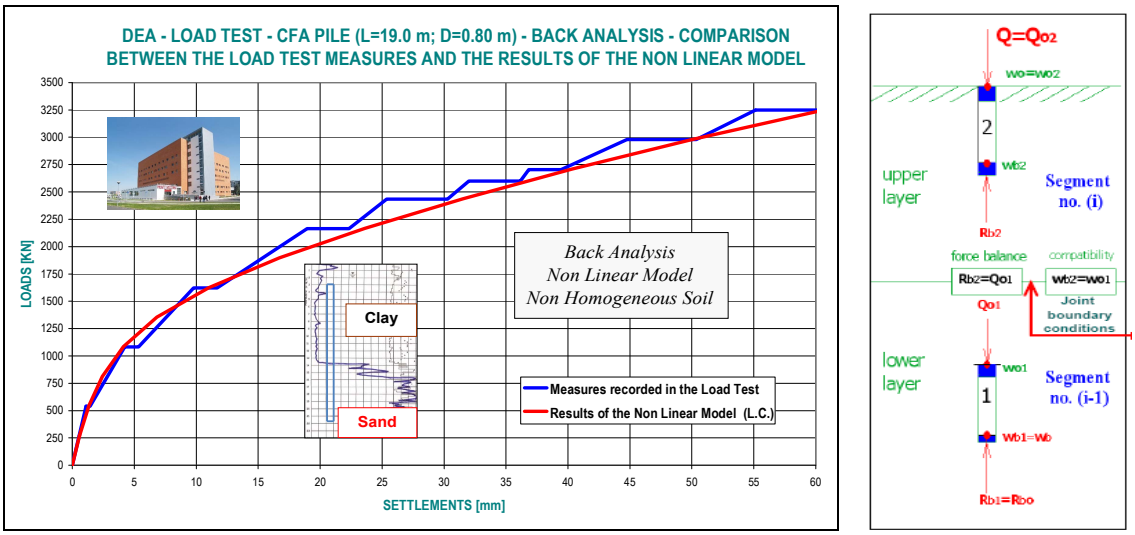


Fig. 11. Case study N$_o$. 2: Load test and nonlinear model of piles in non-homogenous soils

CASE STUDY No. 2 - PILE EMBEDDED IN A NON-HOMOGENEOUS SOIL

The nonlinear solution extends similarly to piles embedded in a non-homogeneous soil. Firstly the pile length is divided in number [n] of segments in each of which the nonlinear properties of the soil are on average homogeneous. The procedure starts from the tip segment (i=1) imposing the settlement [w_{b1}] and then it is replied up to the pile head (i=n) using for each element the recurrent relations:

$$w_{oi} = w_{bi} + \left[R_{so,i} \cdot \frac{\cosh \alpha_i - 1}{\alpha_i^2} + R_{bi} \cdot \frac{\sinh \alpha_i}{\alpha_i} \right] \cdot \frac{L_i}{EA} \qquad Q_{oi} = R_{so,i} \cdot \frac{\sinh \alpha_i}{\alpha_i} + R_{bi} \cdot \cosh \alpha_i \qquad \text{(i=1,n)} \qquad [21]$$

The quantities that appear in the previous formulas are evaluated, for each segment above the first one, by means of the relations:

$$w_{bi} = w_{o,i-1} \qquad R_{bi} = Q_{o,i-1} \qquad \text{(i=2,n)} \qquad [22]$$

The settlement and the axial force at the tip section of the upper segment marked by the index [i] are in fact equal in the common joint, due to compatibility and equilibrium conditions, to the settlement and to the axial force at the top section of the lower segment marked by the index [i-1]. It follows that a pile interacting with a non-homogeneous soil simply behaves as series of superimposed single piles.

As an example the case study of the piles of the deep foundation of the Department of Emergency and Acceptation (DEA) of the Ravenna City Hospital is shown in fig. 11. CFA-SCC piles D=0.80 m and 19 m long (from -3 m to -22 m) were drilled in a soil composed of two strata having a strong contrast of stiffness. It includes an upper layer of normally consolidated soft clay that reaches a depth of -13.5 m resting on a layer of very dense over-consolidated sand that extends down to -25 m and 3 m below the pile tips. The back analysis of the load test provides an effective insight on the load sharing (Fig. 12) and on the pile settlements (Fig. 13). The pile exploits at the service load (1300 KN) the 75% of the friction capacity that is mobilized mainly by the tip settlement inside the stiffer sand layer, which activates through the end bearing mechanism the further development of the pile capacity (3250 KN).

SUMMARY

The non linear behavior of axially loaded piles in a homogeneous soil was deepened through an analytical model based on the work-energy principle that equals the strain energy stored by the axial loads to the work of the tip reaction and the plastic-hardening work of the shear stresses. It applies also to non homogeneous soil in which case the pile segments behave as series of superimposed single piles each embedded in a homogenous soil layer. The case studies confirm the validity of the model.

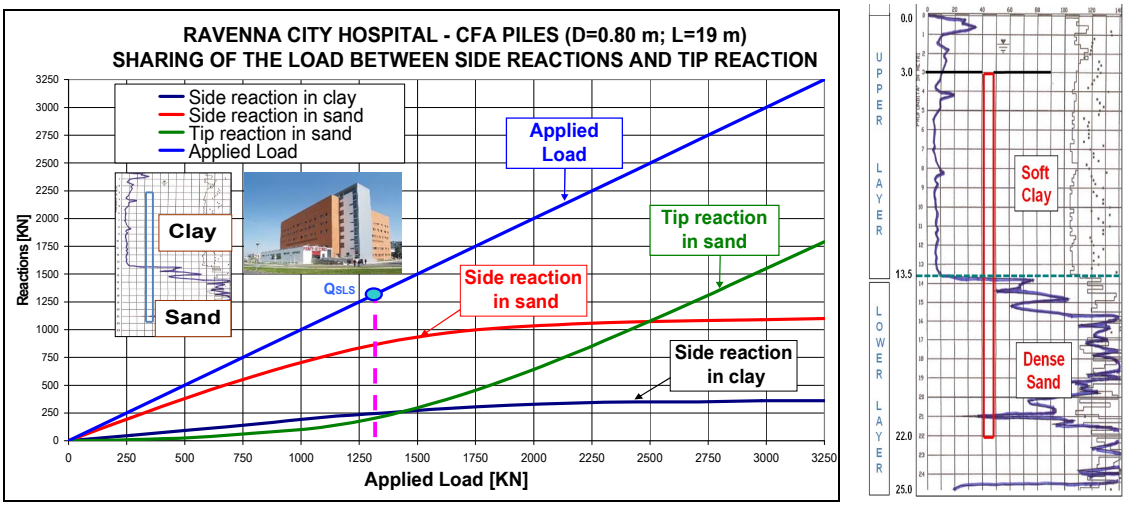


Fig. 12. Case study N_o. 2: sharing of the applied loads among side reactions and tip reaction

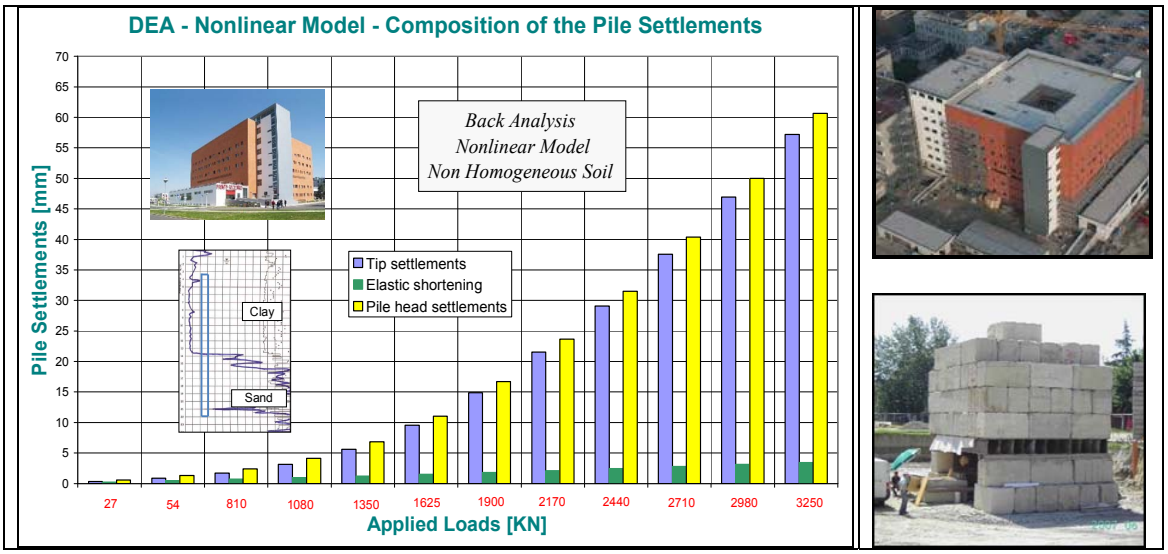


Fig. 132. Case study N_o. 2: components of the pile settlements vs applied loads

REFERENCES

Chou Y., Hsiung Y., 2009. Normalized equation of axially loaded piles in elastic-plastic soil. Journal of Geo-Engineering, Vol. 4, 1, 1-7.

Dalerci, G., Bovolenta, R., 2014. A new method for the evaluation of the ultimate load of piles by tests not carried to failure. International Journal of Geotechnical and Geological Engineering, Volume 22, Issue 6, 1415-1426.

Lenzi, M., Campana, P., 2012. Buckling analysis of partially embedded piles elastically restrained at their heads. DFI, Marine Foundation Committee, Seminar, Norfolk, Virginia, USA, December 5-7.

Lenzi, M., Campana, P., 2015. A nonlinear model for the analysis of pile foundations, 40th DFI Annual Conference on Deep Foundations, Oakland, California, USA, October 12-15, 299-308.

Salsa, S., 2010. Partial differential equations. Methods, models and applications, Verlag, Milan, 1-17.

Viggiani, C., Mandolini, A., Russo, G., 2012. Piles and pile foundations. Spon Press, London, 88-126.

ABOUT THE INFLUENCE OF TIME ON THE BEARING CHARACTERISTICS OF PRECAST DRIVEN PILES

Dr.-Ing. L. Vavrina, Aarsleff Grundbau, Hamburg
Dipl.-Ing. U. Plohmann, Aarsleff Grundbau, Eggenstein
Univ.-Prof. Dr.-Ing. habil. Chr. Moormann, Stuttgart University, Institute for Geotechnical Engineering
Dipl.-Ing. P. Wardinghus, Aarsleff Grundbau, Hamburg

ABSTRACT

The time-dependent increase of pile resistance is a known effect, which can be observed in cohesive and non-cohesive soils as well. In this contribution, approaches for the prediction of time-dependent increase of axial pile resistance are presented and compared with new field tests and project-related database results on precast piles in different soils. The aim of the evaluation is to develop a practical concept, for a reliable prediction of set up, which can be used as a tool for an a technically and economically optimized design of driven piles.

Keywords: driven piles, time-dependent increase, set-up, prediction

1. Motivation

Due to several recent investigations and publications, the increase of the axial pile resistance of precast driven piles after installation can be considered as well known. This time-dependent increase of resistance (known as 'set-up') can be significant and the magnitude greatly depends on soil type, but is influenced also by several further aspects like installation process and initial stress status in soil continuum. Reasons for this set-up are not yet fully understood especially in granular soils. In cohesive soils, set-up usually results from consolidation, i.e. degradation of installation-induced excess pore-water pressure, and creeping processes (e.g. Karlsrud et al. 2014). In non-cohesive soils set-up was initially considered to be caused by relaxation and changes to the inter-granular contact zone due to chemical processes. Recent research indicates that ageing effects of remolded soil might be the decisive process and that a complete understanding can only be achieved with appreciation of the micro-mechanical response of sand to the complex stress and strain paths induced during pile installation and subsequent equalization (Gavin et al. 2015). Bowman & Soga (2003) proposed a mechanism which allows the structure of a granular material to change over time as a result of creep strains and microstructural change. Due to Zhang & Wang (2014) the pile set-up in sand is mainly attributed to an increase in radial stress during pile loading as a result of soil ageing. Pile installation pushes the surrounding soil to the side, thereby imposing additional loading on the soil inside the influence zone. This loading action initiates an associated ageing (or creep) process during the set-up period; the ageing effects is considered to ultimately give rise to an increase in radial stress and pile shaft resistance. The measurements also reveal that the increase in ageing-induced soil stiffness is due to contact normal forces among soil particles gradually becoming more homogenized during the set-up period (Zhang & Wang 2014). Gavin et al. (2015) concluded that changes in stationary radial stress during set-up and enhanced dilation during loading appear to be the principal mechanisms controlling pile ageing in sand.

Apart from soil type, increase of axial pile resistance results only from increase of shaft friction. Pile toe resistance remains constant or decreases slightly.

Understanding and accurately predicting the time-depending increase of resistance is an important condition prior to an economic design of pile foundations. In order to predict the increase of resistance due to set-up, various approaches using empirical calculations are described in the literature. Most of them presuppose a direct relationship between time after end of driving and resulting increase of bearing resistance. The characteristics of soils are considered only indirectly, therefore, the aim is to derive an approach which allows to predict the time-dependent increase considering the soil type and soil properties. In this way an economic pile design could be realized.

© 2018 Deep Foundations Institute

2. Prediction of time-dependent increase of pile resistance

The set-up of driven piles in cohesive and granular soils has been decribed in several papers e.g. by Fellenius et al. (1989), York et al. (1994) Long et al. (1999) and Bullock et al. (2005). In recent years comprehensive studies and investigations on pile ageing effects mainly based on systematic field tests have been published, among others by Axelsson (2000a/b), Augustesen (2006), Gavin et al. (2013, 2015), Jardin et al. (2006) and Karlsrud (2012) resp. Karlsrud et al. (2014). These studies intend that the set-up factor $Q(t)/Q_0$ often lies in a range of 1.1 to 2.0 for a period of approx. 100 days after pile installation but might reach values of up to 3.0 within 1,000 days. Although there might be a distinct variability in the degree of set-up even within a construction site, long-term experience allows to derive empirical approaches for predicting the time-dependent increase of pile resistance.

Skov and Denver (1988) describe the relationship between time t after end of driving and increase of axial pile resistance $Q(t)/Q_0$ for sand, clay and chalk based on static and dynamic load tests on precast driven piles as a semi-logarithmic function [1].

$$Q(t)/Q_0 = 1 + \Delta_{10} \log_{10} (t/t_0) \qquad [1]$$

Q_0 is the axial pile resistance determined at reference time t_0 after end of driving and Δ_{10} is an empirical factor (set-up factor) which corresponds to the increase of axial pile resistance per logarithmic time step depending on the type of soil. The authors determine this factor for sand with $\Delta_{10} = 0.2$, for a clay with $\Delta_{10} = 0.6$ and for chalk with $\Delta_{10} = 5.0$. The corresponding reference time is $t_0 = 0.5$ days for sand, $t_0 = 1$ day for clay and $t_0 = 5.0$ days for chalk.

Karlsrud et al. (2014) found in large-scale studies a relatively good agreement with the approach of Skov and Denver (1988) for the determination of the increase of shaft resistance $Q_S(t) / Q_{S0}$ for cohesive soils, but therefore a reference time $t_0 = 100$ days shall be applied. In non-cohesive soils, Karlsrud et al. (2014) suggest - based on the results of large-scale static load tests on steel tube piles - that the time-dependent increase in shaft resistance could be described by a hyperbolic tangent function [2]:

$$Q_s(t) = Q_{s,ref} + a \tanh [b \cdot (t - t_{ref})] \qquad [2]$$

Based on empirical studies Karlsrud et al. (2014) found that the factor Δ_{10} increases with decreasing degree of overconsolidation ratio OCR and decreasing index of plasticity I_P as mentioned in [3]:

$$\Delta_{10} = 0{,}05 + 1{,}3 \, (1 - I_P/50) \, OCR^{-0{,}5} \qquad [3]$$

In other investigations Augustesen (2006) detected correlations between decrease of the factor Δ_{10} while undrained shear strength c_u decreases, so an application of undrained shear strengths of 10 kN/ m² $\leq c_u \leq$ 100 kN / m² results in values of $0.22 \leq \Delta_{10} \leq 0.29$.

$$\Delta_{10} = 1{,}24 - (c_u/60)^{0{,}03} \qquad [4]$$

3. Field tests

To quantify the time-dependent increase of axial pile resistance field tests were executed near the city Constance at Lake Constance and near Emden in Northern Germany.

In former investigations significant increases were observed, but the magnitude of these changes varied widely. In addition to natural scattering in soil characteristics, deviation between results of static and dynamic pile load tests, influences from repeated loading, variability caused by lack of limit resistance or the influence of different reference times could be adopted.

In order to limiting the mentioned variance, 6 piles with identical cross-sections, lengths and installation conditions were installed in a row with an internal distance of 2.0 m (e = 5.2 D_{eq}). The pile resistance of each pile was determined by dynamic load tests. The pile resistance was evaluated using the CAPWAP-Method.

All 6 test piles were installed at identical point of time t_0. Only pile no. 1 was subjected to a dynamic load test at time t_0. At the next time $t_1 > t_0$, pile 1 was repeated tested and pile 2 subjected to a first sample load. Next, piles 1, 2 and 3 were loaded; piles 1 +2 were repeatedly loaded and pile 3 was loaded the first time. This procedure was carried on in this way.

3.1 Field tests no. 1

Field test no. 1 was carried out at a location near the city of Constance at Lake Constance, where the following regional soil conditions were detected (Figure 1).

Under fillings and sandy deposits, the regional lacustrine clay called lake clay appears as a sandy clay in a predominantly very soft state with a natural water content close to the liquid limit of between 30 and 60%. The undrained shear strength of the clay was determined to be $c_u \leq 15$ kN/m². At a depth of 10 m below surface, a ground moraine of low plasticity follows, which shows in the upper 10 m a soft to stiff state (c_u = 20-50 kN/m²) and lower predominantly a semi-solid to solid state.

The cone resistance q_c, which was determined by two cone penetration tests (CPT), was almost zero at about 15 m under surface and then increased to $q_c \geq 10$ MN / m² in the semi-solid ground moraine. The shaft friction measured at the cone penetration test at depths between 15 m and 20 m was on average at f_s = 0.45 MN/m² and friction ratio was R_f = 4 to 6% (figure 1).

Figure 2 illustrates the results of the dynamic load tests on a semi-logarithmic scale, separated by shaft friction and toe resistance. At first, figure 2 shows that the measured initial shaft resistance with values of 150 kN to 200 kN is significantly lower than toe resistance with values of 600 to 700 kN. After 7 days shaft resistance increased to values between 540 and 620 kN.

The toe resistance remained constant for a period of 14 days. The increase in the shaft resistance 76 days after installation was on average more than 3 times with respect to t = 1d.

For the initial drive as well as restrikes a 70 kN hammer with drop heights between 30 and 40 cm were used. The pile toe was mobilized in all restrikes.

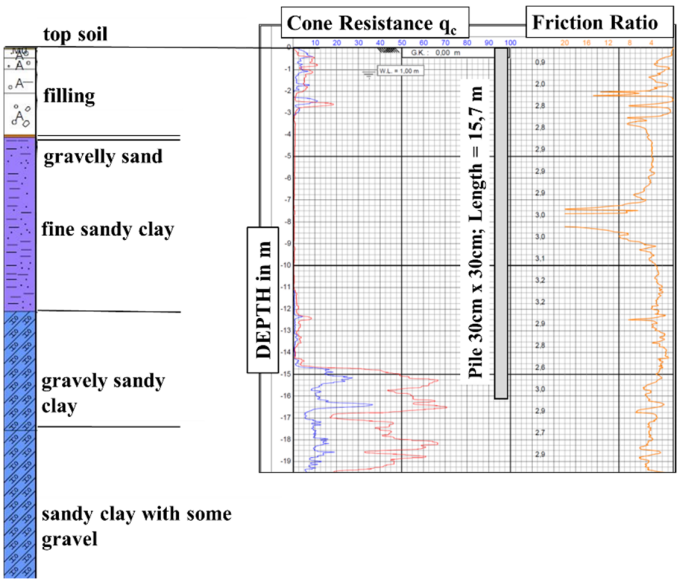


Figure 1: Soil profile at the investigation site no.1

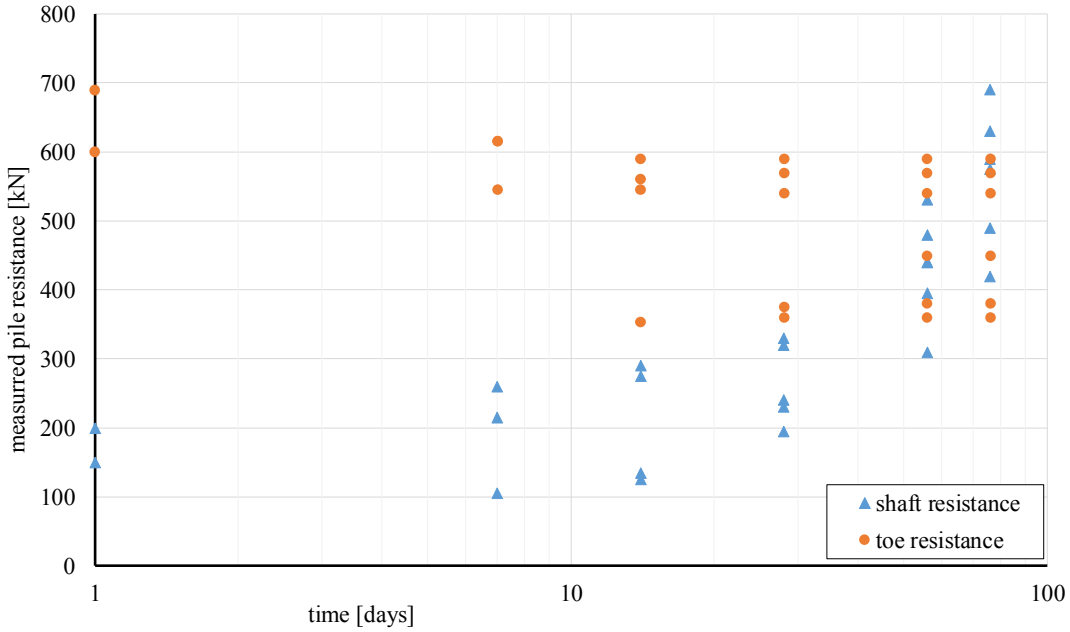


Figure 2: Results of dynamic load tests separated in shaft and toe resistance

3.2 Field test no. 2

At the site of the second field test near the city of Emden, organic soft layers (marine clay + peat) with thicknesses of up to 2.0 m are located fillings and sands underneath according to the ground investigation. Glacial loam and till are located with sand deposits of different thicknesses. The glacial till is a low plastic clay of a stiff consistency. The glacial till mixed with sandy deposits of different sizes were found (Figure 3). At depths from NN -20 m to NN -22 m embedded silt layers were found.

The results of dynamic load tests in Emden are shown in figure 4, separated in shaft resistance and toe resistance. In Constance, the proportion of shaft resistance with a value of 1.742 kN is higher than toe resistance with a value of 410 kN (t = 1d). After 7 days the measured pile shaft resistance was between the lowest value of 1.209 kN and the maximum value of 1.834 kN. The measured toe resistance was between 422 kN and 938 kN. In the further course of the testings, both shaft and toe resistance remained relatively constant, so that no relevant increase in the pile resistance could be detected.

In the investigations initial drive as well as restrikes were performed with a modern 70 kN hammer with drop heights between 50 and 60 cm. The sum of driving energy while initial drive was between 20.000 kNm/m and 30.000 kNm/m.

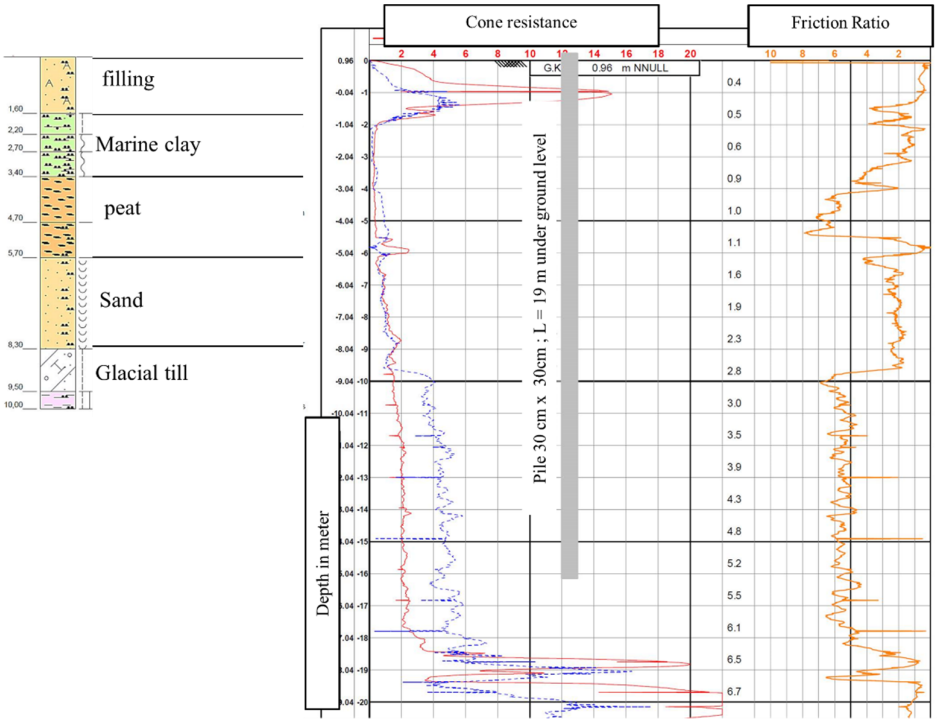


Figure 3: Soil profile at the investigation site no.2

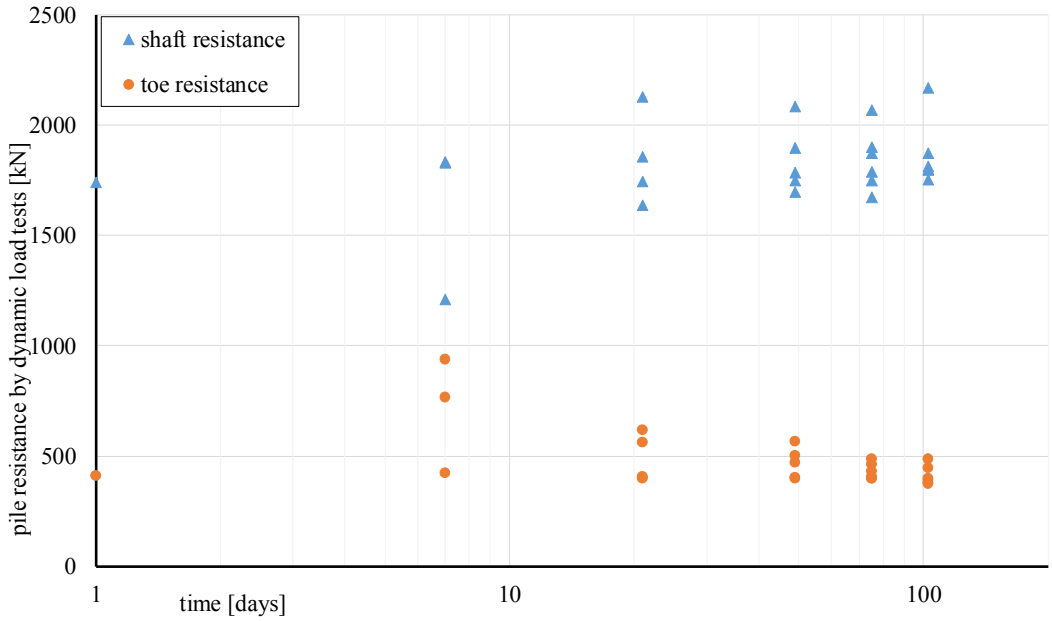


Figure 4: Results of dynamic load tests separated in shaft and toe resistance

4. Data based evaluation

In this chapter data of project based load tests on precast driven piles in cohesive and non-cohesive soils were compared with literature (Skov & Denver 1988, Jardine et al., 2006, Karlsrud et al., 2014 and Gavin et al. 2015).

Applied data of time-dependent increase in non-cohesive soils (Figure 5) were determined on precast driven piles, which were installed at various project sites in the area of the Elbe estuary between Hamburg and Cuxhaven. The detected subsoil was comparatively homogeneous with organic layers (peat and marine clay) and medium to dense sand underneath.

For the evaluation, values at reference time $t_0 = 0$ were determined by linear extrapolation. As a result of this calculation, some computational values are $Q / Q_0 < 1$.

Figure 5 shows data of time dependent pile resistance with the previously discussed large variance of measurement results. It has to be mentioned that test results are differentiated in single loaded and repeatedly loaded pile tests. However, results of dynamic load tests on single loaded piles show larger values of $Q / Q_0 \leq 1.84$ than test results, which were repeatedly loaded piles ($Q / Q_0 \leq 1.64$). The drawn minimum level indicates a moderate increase in the first 10 days that increases in half logarithmic scale exponentially (see Figure 5).

According to Skov & Denver (1988) the increase of axial pile resistance measured by static and dynamic load tests on single loaded piles with values of $2.0 \leq Q / Q_0 \leq 2.2$ forms the upper limit. The static tensile tests on steel tube piles in Dunkirk, France (Jardine & Standing, 2000) show an increase of $Q / Q_0 = 2.37$ while static tensile tests in Blessington (Garvin et al. 2015), within a period of 210 days show an increase of axial pile resistance about $Q / Q_0 = 2.1$.

For comparison,the results from the database with the prognosis according to equation eq. 1 are shown in figure 5 as well. It can be seen that up to approx. 80 days after installation the prediction is above the lower limit. From a time > 80 days, values of eq. 1 are below the lower limit of the measured values and thus eq. 2 leads to a prediction on the safe side in a sense of engineering.

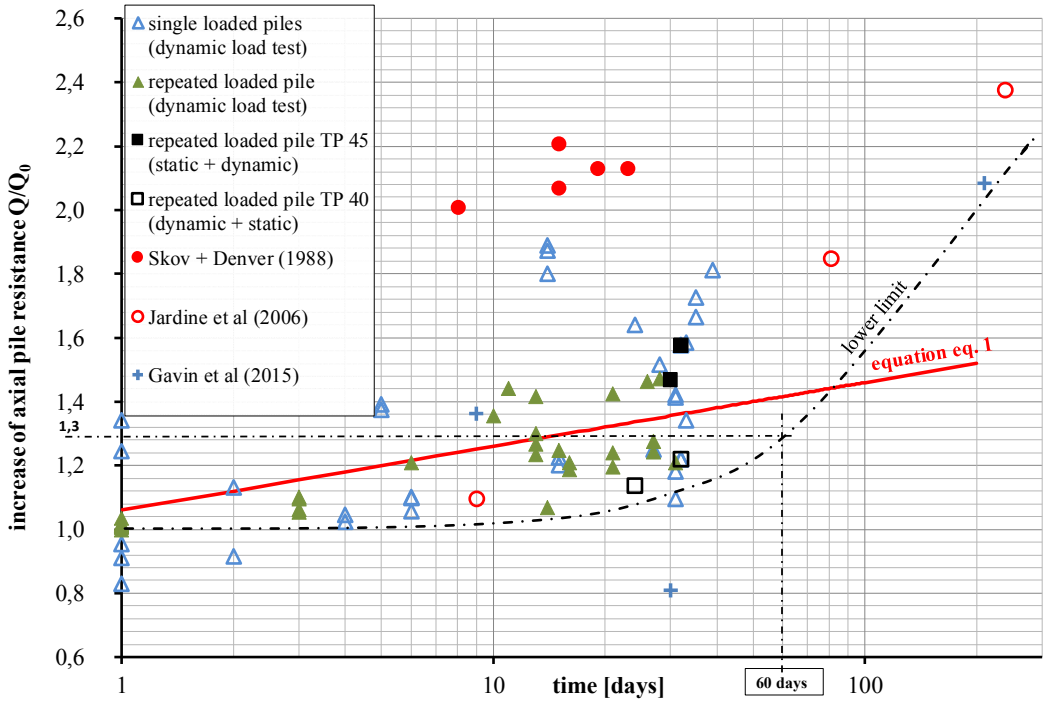


Figure 5: Data of project based load tests on precast driven piles in sands

Figure 6 shows the results of dynamic and static load tests in cohesive soils. One of these soils are over-consolidated tertiary clays with a rigid to semi-solid consistency and a classification of medium to high plasticity clay. The dynamic load tests, described in figure 7 as lake clay, were carried out on piles, which were driven into normally consolidated, very soft to soft clays. The increase of pile resistances is only moderate in that kind of soil, which is symbolized as lake clay + ground moraine.

Results of tertiary clay show within 50 days an increase of $Q / Q_0 = 1.08$ to 1.46. The results of dynamic load tests in clayey silt show significantly higher gains of up to $Q / Q_0 = 2.36$. An additional result of a static load test in clayey silt is also shown in figure 6. Prior to the static testing, a cyclic load was applied in 50 cycles. The increase in the load bearing capacity compared to the initial load capacity is smaller with $Q / Q_0 = 1.25$.

The observed increase in the pile resistance in lake clay after 8 days amounts to approximately $Q / Q_0 = 1.7$ and after 80 days to $Q / Q_0 = 2.2$.

The method described by Karlsrud et al. (2014) shows set-up factors depending on the ground conditions. The load tests carried out in low plastic, normally consolidated clays in Stöndal ($w_n = 0.3$; $I_P = 0.14$) show an increase of $Q / Q_0 = 1.9$ (after 65-175 days) to 2.7 (after 345-375 days). For the location Onsöy ($w_n = 0.6$, $I_P = 0.33$), values of $1.1 \leq Q / Q_0 \leq 1.3$ were determined in a normally consolidated, high plastic clay after up to 345 days. The results at the Cowden site ($w_n = 0.16$, $I_P = 0.18$), obtained in a low plastic over-consolidated ground moraine are of a similar order of magnitude as in Onsöy.

In Figure 6, the results of the data collection were compared with the prognosis showing a good conformity in normal consolidated soils. The measured values in over-consolidated soils are widely overestimated by the prognosis.

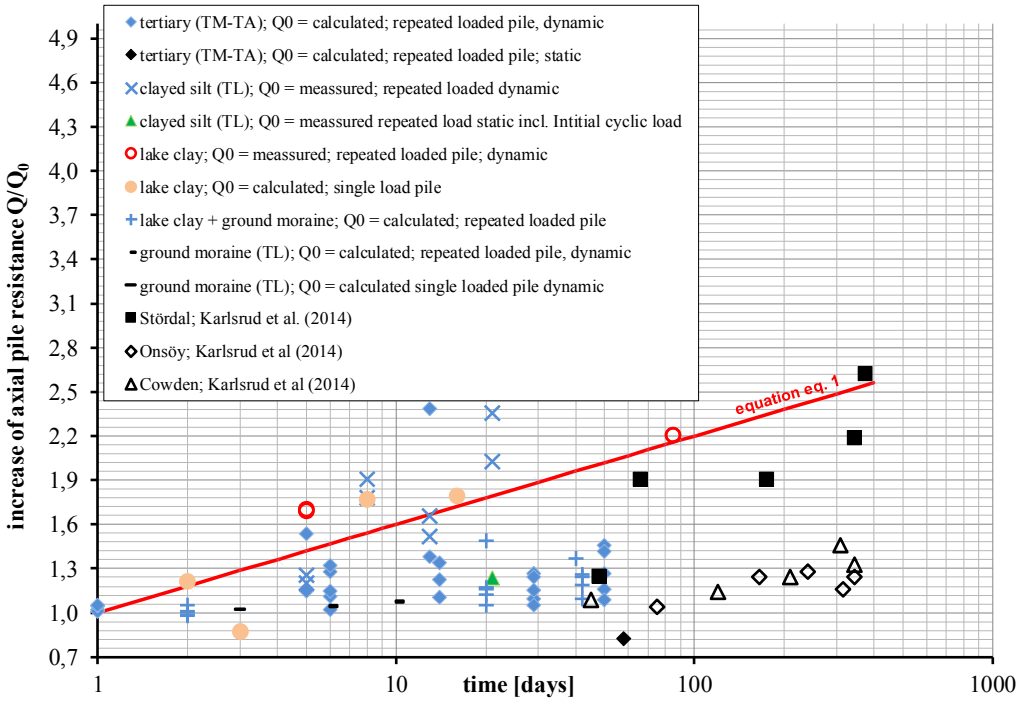


Figure 6: Data of project based load tests on precast driven piles in cohesive soil

5. Evaluation of prediction pattern

In the previous sections, results of increasing axial pile resistance Q / Q_0 on precast driven piles were presented. These results show that the increase in pile resistance can be attributed entirely to shaft friction. In cohesive soils in the first days after the pile installation, even a decrease of the toe resistance could be observed.

According to these evaluations, an increase of axial pile resistance $Q / Q_0 = 1.3$ can be assumed in sands, after ≥ 60 days. On average, growth was even at $Q / Q_0 = 1.5$ after 60 days. The application of equation eq. 2 yields an increase of axial pile resistance $Q / Q_0 = 1.4$ after 60 days with a gain factor of $\Delta_{10} = 0.2$

and a reference time of t_0 = 0.5 days. Thus the approach of an Q / Q_0 = 1.3 is confirmed after 60 days (see Figure 5).

The evaluation of the test results for cohesive soils confirms the approach according to Karlsrud et al. (2014) and shows that the set-up factor and the time increase with decreasing over-consolidation ratio OCR and decreasing plasticity I_P. The context according to Karlsrud et al. (2014) is shown in Figure 7, including set-up factors Δ_{10} for the field tests in Constance and Emden as well as clayey silt and ground moraine.

When evaluating set-up factors in Figure 8, however, it should be kept in mind that, according to eq. 4 the reference time is t_0 = 100 days. Since the duration of the project-related results was <100 days, the reference time t_0 = 1 day was calculated here based on Skov & Denver (1988).

The results of field test 1 (Constance) gave a set-up factor of Δ_{10} = 1.09 for the reference time of t_0 = 1 day and an initial shaft resistance of Q_{0s} = 141 kN. The set-up factor for the field results in Emden is also equal to t_0 = 1 day and an initial shaft resistance of Q_{0s} = 1.734 kN to Δ_{10} = 0.6. For clayey silt and ground moraine, set-up factor is Δ_{10} = 0.6 and Δ_{10} = 0.47 with initial shaft resistances of Q_{0s} = 1.597 kN and Q_{0s} = 244 kN respectively.

In total, the values for Δ_{10} calculated from the measurements are higher than determined by eq. 3.

There were no correlations found between the undrained shear strength and the increase Q / Q_0 (see Figure 8). Although the set-up factor decreases overproportionately with increasing shear strength, the overall growth factor here is in a different order of magnitude than by eq. 4.

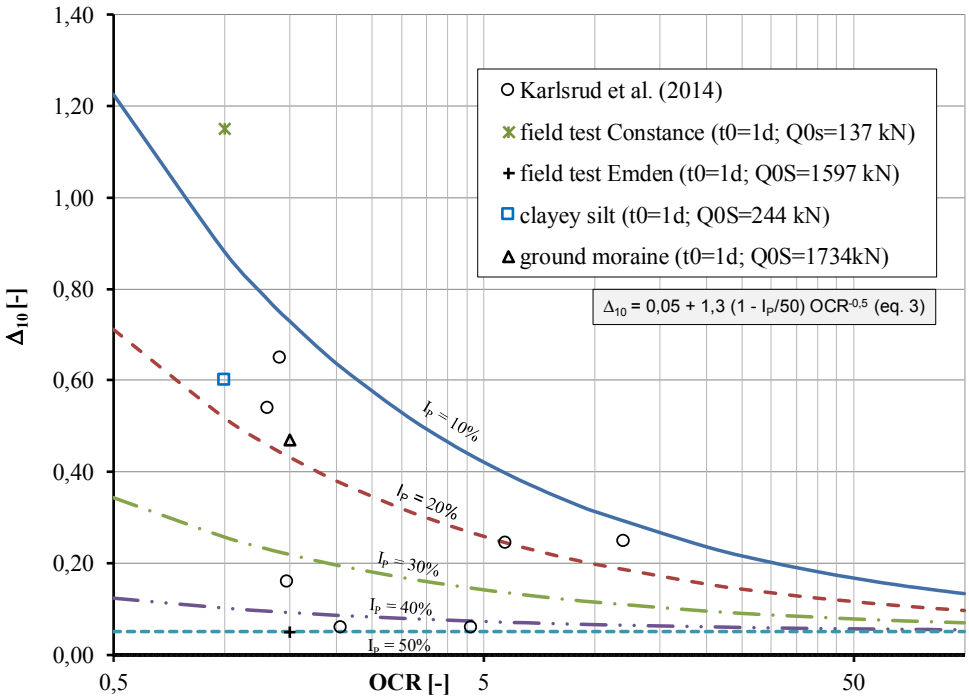


Figure 7: Connection of set-up, over consolidation ratio and plasticity index

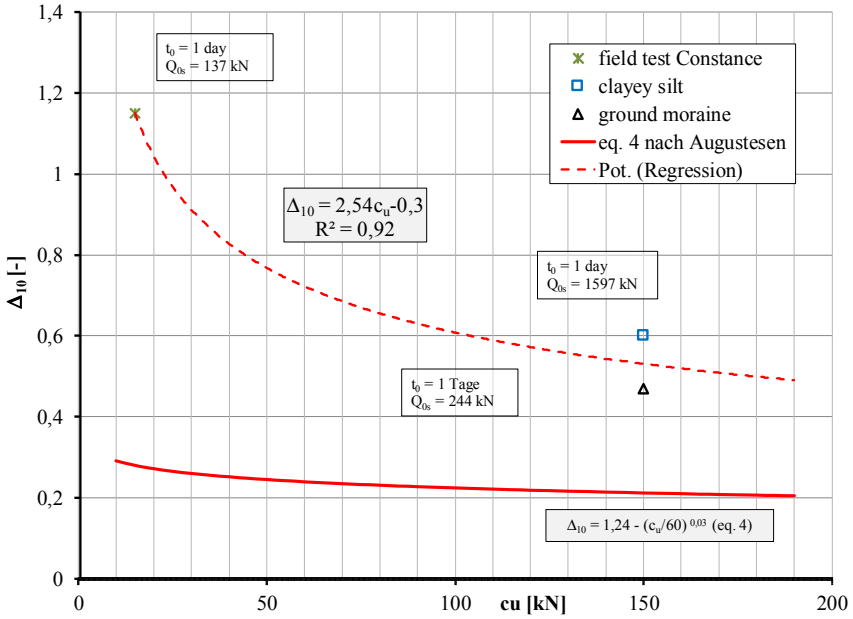


Figure 8: Connection of set-up and undrained shear strength

6. Conclusions

The presented pattern for prediction of time-dependent increase of pile resistance does not take the soil type or soil properties into account. Thus, equation eq. 1 differentiates between sand, clay and chalk and in comparison to the database equation eq. 1 shows a good conformity. However, for the prediction of time-dependent increase of pile resistance in cohesive soils, additional parameters should be noticed to consider the variability of cohesive soils.

If the consolidation ratio is taken into consideration , as predicted by Karlsrud et al. (2014) seems to be successful in comparison with results of the database whereas the approach based on undrained shear strength was not confirmed.

For a conceptual approach to the prediction of time-dependent axial pile resistance, the relevant period of observation must be defined first. In most construction projects, the full pile load usually occurs after the completion of the structural work, depending on the construction process, after at least 60 days. During this period, the short-term effects are usually completed depending on the type and characteristics of the soil, which is why a prediction for the period ≥ 60 days is important.

The following aspects can be considered a practical concept for pile design according to current knowledge:

• a prediction <60 days does not appear to be useful.

• in non-cohesive soils, an increase of 30% can be applied for time of ≥ 60 days or a prediction according to equation eq. 1.

• in cohesive soils, a distinction must be considered as follows:

- in case of normal consolidated soils, an increase of $Q / Q_0 = 2$ can be assumed after 60 days. equation eq. 1 has a good orientation for normal cohesive soils.

- In case of over-consolidated soils, an increase of $Q / Q_0 = 1.3$ can be expected after 60 days.

Generally, repeated load tests are recommended to prove a time-dependent increase in the resistance of precast driven piles or for further verification of prognosis, especially in cohesive soils.

References

Augustesen, A. (2006): The effects of time on soil behaviour and pile capacity: PhD Thesis, Department of Civil Engineering, Aalborg University, Denmark, (DCE Thesis; No. 4).

Axelsson, , G. (2000a): Long-term set-up of driven piles in sand, Ph.D. Thesis, Division of Soil and Rock Mechanics, Department of Civil and Environmental Engineering, Royal Institute of Technology, Stockholm, Sweden

Axelsson, G. (2000b): A conceptual model for pile set-up for driven piles in non-cohesive soil. Proc. Int. Deep Foundation Congress, Orlando, Florida, Vol. 1, Getotech. Special Publ., ASCE Vol. 116, 64-79

Bowman, E.T., Soga, K. (2003); Creep ageing and microstructural change in dense granular materials. Soils & Foundations, Vol. 43 (4), 107-117

Bullock, P.J., Schmertmann, J.H., McVay, M.C., Townsend, F.C. (2005): Side shear set-up. I: Test piles driven in Florida. J. of Geotech. and Geoenv. Eng., 131(3), 292-300

Fellenius, B.H., Riker, R.E., O´Brien, A.J., Tracy, G.R. (1989): Dynamic and static testing in soil exhibiting setup, J. of Geotechnical Engineering, ASCE, Vo. 115 (7), 984-1001

Gavin, K.G., Igoe, D.J.P., Kirwan, L. (2013): The effects of ageing on the axial capacity of piles in sand. Proc. of the ICE Geotech. Eng., Vol.166(2), 122-130

Gavin, K., Jardine, R. J., Karlsrud, K., Lehane, B.M. (2015): The effects of pile ageing on the shaft capacity of offshore piles in sand. Proc. Int. Symp. on Frontiers in Offshore Geotechnics III (ISFOG), Meyer (ed.), Taylor & Francis Group, Oslo, 129-151

Jardine, R.J., Standing, J.R., Chow, F.C. (2006): Some observations of the effects of time on the capacity of piles driven in sand. Géotechnique 56(4), 227-244

Karlsrud, K. (2012): Prediction of load-displacement behavior and capacity of axially loaded piles in clay based on analyses and interpretation of pile load test results. Thesis for the degree of Doctor Philosophiae. Norwegian University of Science and Technology

Karlsrud, K., Jensen, T.G, Lied, W.E.K, Nowacki, F.; Simonsen, A.S. (2014): Significant ageing effects for axially loaded piles in sand and clay verified by new field load tests. Proc. of Offshore Technology Conference, Houston, May 2014, Paper No. OTC-25197-MS

Long. J.H., Kerrgian, J.A., Wysockey, M.H. (1999): Measured time effects for axial testing of driven piling. Transport Research Board, 1663, No. 1, 8-15

Skov, R., Denver H. (1988): Time-dependence of bearing capacity of piles, 3rd Int. Conf. App. Stress-Wave Theory to Piles

York, D.L., Brusey, W.G., Clemente F., Law. S.K. (1994): Setup and relaxation in Glacial Sand. J. of Geotech. and Geoenvironmetal Eng., Vol. 120 (9), ASCE, 1498-1513

Zhang, Z., Wang, Y.H. (2015): Examing setup mechanisms of driven piles in sand using laboratory model pile tests. J. Geotech. and Geoenviron. Eng., 141(3), 04014114

DESIGN AND LOAD TESTING PROGRAM OF LARGE DIAMETER OPEN-ENDED PILES FOR A BRIDGE CONSTRUCTION PROJECT IN LOUISIANA

Murad Y. Abu-Farsakh, Ph.D., P.E.[1], Md. Nafiul Haque, Ph.D. [2], and Chris Nickel, P.E.[3]

[1]Research Professor, Louisiana Transportation Research Center, Louisiana State University, Baton Rouge, LA 70808. (Corresponding Author; Email: cefars@lsu.edu and Phone: 225-767-9147)

[2]Research Associate, Louisiana Transportation Research Center, Baton Rouge, LA 70808.

[3]Geotechnical Engineering Manager, Department of Transportation and Development, Baton Rouge, LA. 70804.

ABSTRACT

This paper presents the results from a pile load testing program for a bridge construction project at Chalmette, Louisiana. The load testing includes three 66-in. spun-cast post tensioned open-ended (O.E.) cylinder piles and one 30-in. square prestressed concrete (PSC) pile driven at four different locations along the bridge site. Both Cone Penetration Tests (CPT) and soil borings/laboratory testing were used to characterize the subsurface soil conditions. All test piles (TP) were instrumented with strain gauges to measure the load distribution along the length of the TPs and to measure the side and tip resistances, separately. Dynamic load tests (DLT) were performed on all TPs at different waiting periods after pile installations to quantify the amount of setup (i.e., increase in pile resistance with time). Case Pile Wave Analysis Program (CAPWAP®) analyses were performed on the DLT data to calculate the resistance distributions along the TPs. Static load test (SLT) was performed only on the PSC pile and statnamic load tests (SNLT) were conducted on both pile types. Design parameters such as the total stress adhesion factor, α, and the effective stress coefficient, β, were back-calculated. The α values ranged from 0.41 to 0.86, and the β values ranged from 0.13 to 0.29. The load test results showed that SNLT overestimated the tip resistance as compared to dynamic and static load tests. Moreover, the pile tip resistance was almost constant during the testing period, and setup was mainly attributed to increase in pile side resistance with time.

INTRODUCTION

Open-ended (O.E) cylinder piles are widely used for bridge foundations construction, as they provide superior moment resistance and high axial capacity (Szechy 1961, Paik and Salgado 2003). Small diameter (14" or less) O.E. piles are generally observed to plug early in the driving process and are thought to behave similar to closed-end piles. At larger diameters, however, O.E. piles usually "cut" through the soil instead of plugging, resulting in a column of soil within the pile whose height approaches the pile embedment depth. This transition to large diameter O.E. piles from PSC and small diameter closed–ended piles have brought to focus some of the gaps or inadequacies in current pile design procedures by American Association of State Highway and Transportation officials (AASHTO) and American Petroleum Institute (API). Available research works on large diameter O.E. cylinder piles mainly focuses on "plugging" and predicting pile capacity from CPT methods. However, very few full-scale field studies were conducted and reported on large diameter O.E. cylinder piles to examine their behavior during driving, load testing, soil setup process and predicting the axial capacity by total stress and effective stress methods.

© 2018 Deep Foundations Institute

TPs are usually instrumented with strain gauges to evaluate the load distribution along the pile length. Design parameters, such as the total stress adhesion factor, α, and the effective stress factor, β, that are typically used to estimate the side resistance of the pile can be back-calculated from the measured load distribution of the instrumented pile. Not enough studies were conducted to recommend the α and β values for large diameter O.E. piles as the instrumentation and performing load test on them are expensive.

The total stress adhesion factor, α, which is related to the undrained shear strengths (S_u) of clayey soils can be calculated from the method proposed by Tomlinson (1957) as follows:

$$\alpha = f_s / S_u. \quad \ldots(1)$$

where f_s = unit side resistance, and S_u = undrained shear strength. For cohesive soils, the value of α ranges from 0.4 to 1.0 (Tomlinson 1970). The β-method or effective stress method, which relates friction resistance to the effective overburden pressure was first proposed by Burland (1973) and is evaluated using the following relationship:

$$\beta = f_s / \sigma'_v \quad \ldots(2)$$

where, β is the effective stress coefficient and σ'_v is the effective overburden stress. Many researchers (e.g., Clausen 2005; Fellenius 2015) reported the back-calculated values of the β-coefficient, indicating that the value of β ranged from 0.15 to 0.35 for clays and ranged from 0.30 to 0.90 for sands (Fellenius 2015). The specific objectives of this study were: (a) instrument the TP with strain gauges to measure the side and tip resistances separately during load testing, (b) perform the laboratory and in-situ testing to characterize the subsurface soil condition, (c) conduct the load tests (i.e., DLT, SLT and SNLT) to measure the amount of setup with time, (d) calculate the rate of increase in pile resistance or setup, and (e) back-calculate the design parameters (α and β) for individual soil layers along the length of the piles.

PROJECT DESCRIPTION AND SOIL CONDITION

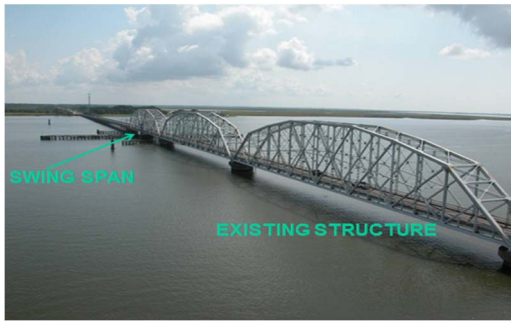
Test Site

This state project consisted of the construction of the new Rigolets Pass Bridge located in Orleans Parish along route US 90 in Chalmette, Louisiana, which is located northeast of New Orleans. The old bridge was damaged by Hurricane Katrina in August 2005, which required major repairs. In order to safely improve roadway and waterway traffic flow, a new two-lane high-rise structure was built west of the existing structure (Figure 1a). Four TPs were driven along the bridge in order to perform the load tests and verify the design methodology. Figure 1 shows the photos of the TPs, instrumentation and the hammer used for driving the piles. The width, length and hammer info of these four TPs are provided in Table 1.

Subsurface Geotechnical Conditions

Laboratory and in-situ testing programs were performed to characterize the subsurface soil conditions at the locations of the TPs. Boreholes were drilled at the four TP locations and high-quality 7.6-cm (3-in.) Shelby tube samples were extracted at different depths for comprehensive laboratory testing. The laboratory testing program included moisture content, Atterberg limits, and Unconsolidated Undrained (UU) triaxial tests. The in-situ testing program included performing both cone penetration tests (CPT) and standard penetration test (SPT) near the TP locations. The CPT provided measurements of cone tip resistance (q_c) and sleeve friction (f_s). The profile of CPT tests was used to classify the soil using the Zhang and Tumay (1999) probabilistic region estimation method. Figure 2 presents the soil boring log and CPT profile

for TP-2. The subsurface soil stratigraphy as revealed from boring and CPT profile showed that the soil at all the TP locations primarily consisted of clay with intermittent sand layers.



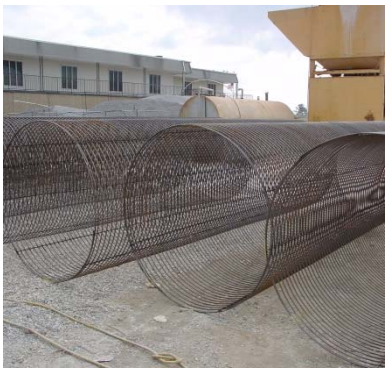
(a) Old bridge



(b) New bridge



(c) TP-1 (30 inch PSC test pile)



(d) Steel reinforcement

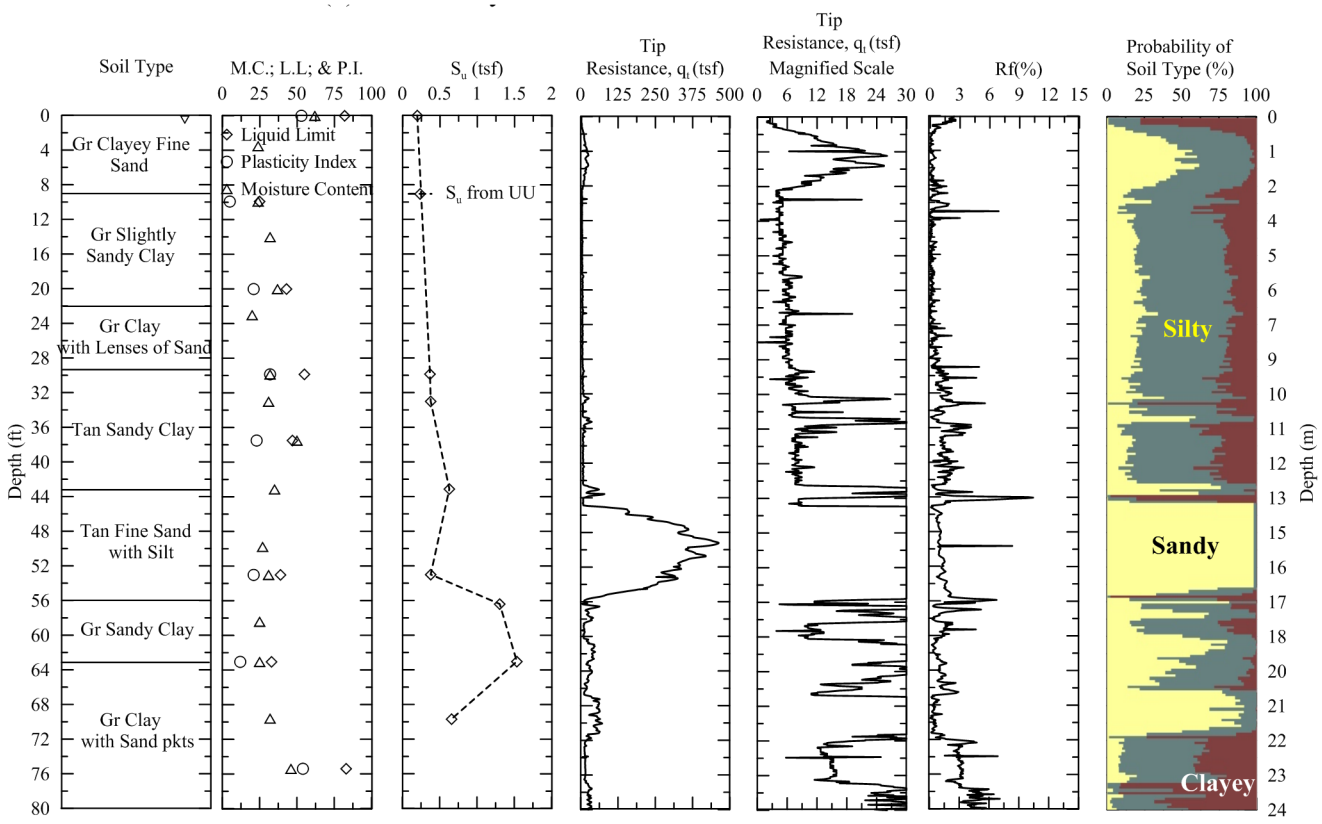


(e) 66 inch O.E. test pile

Figure 1: Project site, test piles, instrumentation and statnamic testing

Table 1: Test pile (TP) information

TP ID	Pile Type	Pile Width/ Diameter inch (mm)	Length ft. (m)		Hammer	Pair of Strain Gauges	Installation depth of Strain Gauges (Below GL) ft.
			Total	Penetration			
TP-1	PSC	30 (762)	57 (17.4)	41.5 (12.6)	Conmaco 300 E5	5	0, 13.5, 24, 34, 44.5
TP-2	Spun Cast Post Tensioned Cylinder	66 (1676)	153 (46.6)	119.8 (36.5)	Bruce SGH-3013 hydraulic	3	0, 56, 88.5
TP-3	Spun Cast Post Tensioned Cylinder	66 (1676)	183 (55.8)	174.9 (53.3)	Bruce SGH-3013 hydraulic	6	0, 51, 82.5, 114, 147, 173.5
TP-4	Spun Cast Post Tensioned Cylinder	66 (1676)	176 (53.6)	164.3 (50.1)	Bruce SGH-3013 hydraulic	5	0, 3, 51.5, 84, 116, 148



(b) Laboratory and CPT soil classification of TP-2

Figure 2: Soil profile, CPT profile and classification at test piles location

Pile Instrumentation and Installation

The TPs were instrumented with three to six strain gauge pairs to evaluate the load distribution along the length of the piles and to determine the side and tip resistances, separately. The locations of the strain gauges are presented in Table 1. TP-1 was driven with a Conmaco 300 E5 pile driving hammer. The O.E. cylinder piles (i.e., TP-2, TP-3 and TP-4) were driven using a Bruce SGH-3013 hydraulic hammer. The SGH-3013 has a rated hammer energy of 282.1 kip-ft. with a ram weight of 66-kips (294-kN) and a maximum stroke height of 4.3-ft. The pile driving resistances and the results of DLTs for all the TPs are presented in Figure 3. Plugging was not measured in this project due to the construction constraints.

LOAD TESTING PROGRAM

The load testing program was designed to confirm the pile resistance, study the pile setup behavior, and assess drivability. An extensive load testing program was carried out after pile installation using DLTs, SLT and SNLTs at this construction site. The SLT was performed only on the PSC TP (i.e., TP-1). It was decided that multiple restrikes and one SNLT would be used to study the setup behavior of O.E. piles (i.e., TP-2, TP-3 and TP-4). The test schedule for conducting DLTs, SLT and SNLTs are presented in Table 2. All the side (R_s), tip (R_{tip}) and total (R_t) resistances during each event is presented in Table 2.

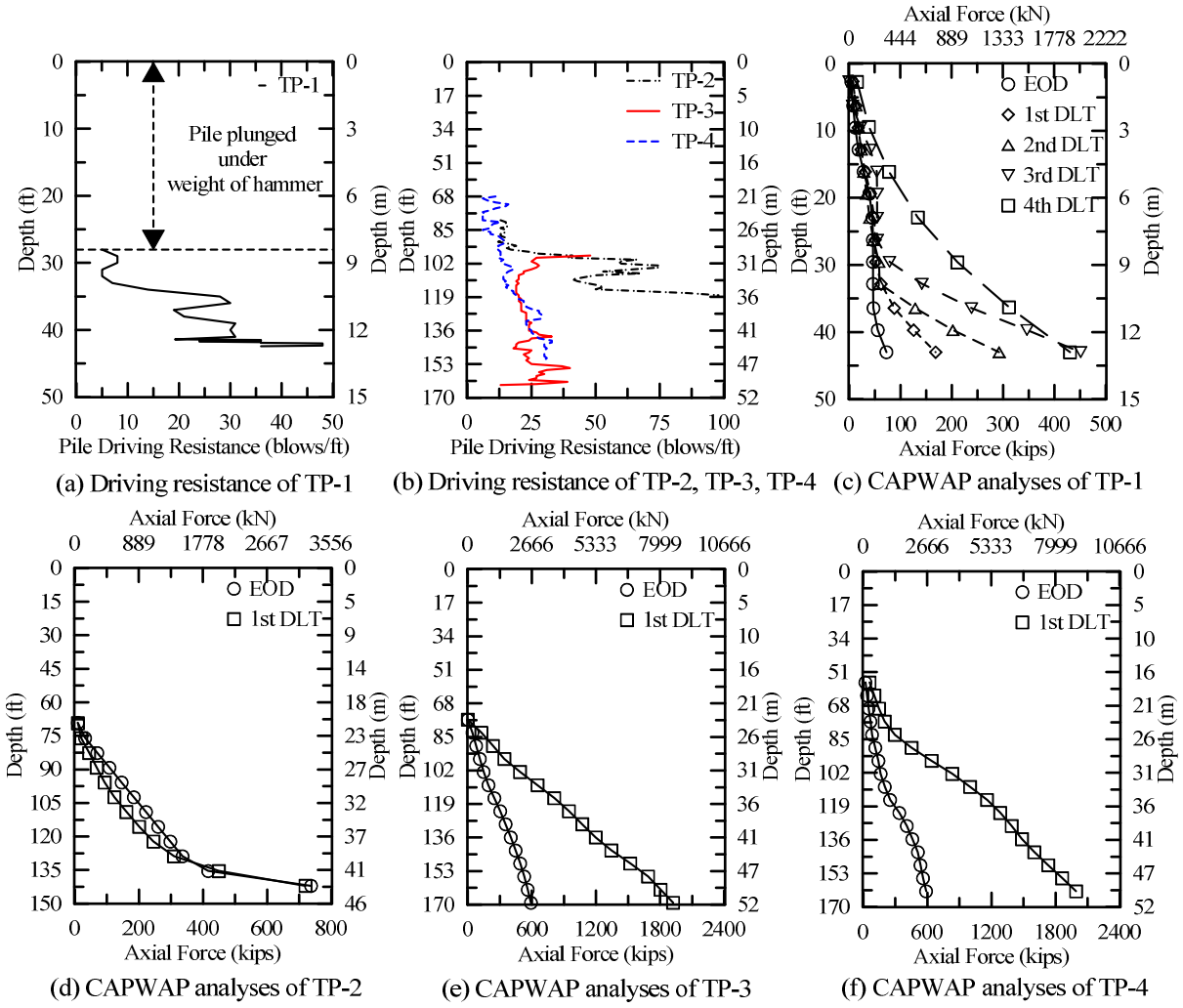


Figure 3: Driving resistance and CAPWAP® analyses of test piles

Table 2: Load test results for test piles

Pile ID	Events	Time	Side Resistance, R_s		Tip Resistance, R_{tip}		Total Resistance, R_t		Blow Count (blow/ft.)	Permanent Set (in.)
			kips (kN)	Ratio (R_s/R_{so})	kips (kN)	Ratio (R_{tip}/R_{tipo})	kips (kN)	Ratio (R_t/R_{to})		
TP-1	EOD	-	52 (231)	1.0	712 (3167)	1.0	764 (3398)	1.0	32	0.38
	1st DLT	23 min	220 (979)	4.2	714 (3176)	1.0	934 (4155)	1.2	27	0.44
	2nd DLT	60 min	274 (1219)	5.3	712 (3167)	1.0	986 (4386)	1.3	27	0.44
	3rd DLT	22 hr	438 (1948)	8.4	714 (3176)	1.0	1152 (5124)	1.5	36	0.33
	4th DLT	15 day	430 (1913)	8.3	630 (2802)	0.9	1060 (4715)	1.4	58	0.21
	SLT	14 day	694 (3087)	13.3	486 (2162)	0.7	1180 (5249)	1.5		
	SNLT	21 day	550 (2446)	10.6	884 (3932)	1.2	1434 (6378)	1.9		
TP-2	EOD	-	737 (3278)	1.0	975 (4337)	1.0	1712 (7615)	1.0	98	0.12
	1st DLT	36 hr	720 (3203)	1.0	525 (2335)	0.5	1245 (5538)	0.7	80	0.15
	SNLT	21 day	1655 (7361)	2.2	1311(5831)	1.3	2966 (13192)	1.7		
TP-3	EOD	-	591 (2629)	1.0	109 (485)	1.0	700 (3114)	1.0	19	0.63
	1st DLT	24 hr	1921 (8545)	3.3	109 (485)	1.0	2030 (9030)	2.9	69	0.17
	SNLT	22 day	2909 (12939)	4.9	168 (747)	1.5	3077 (13686)	4.4		
TP-4	EOD	-	588 (2615)	1.0	118 (525)	1.0	706 (3140)	1.0	31	0.39
	1st DLT	48 hr	1991 (8856)	3.4	125 (556)	1.1	2116 (9412)	3.0	125	0.10
	SNLT	30 day	2760 (12276)	4.7	555 (2469)	4.7	3315 (14745)	4.7		

Dynamic Load Tests (DLTs)

Restrike events were performed using Pile Driving Analyzer® (PDA®) including two accelerometers and two transducers for PSC piles attached to the pile top. Four accelerometers and four strain transducers were used for the O.E. piles. PDA® was employed to monitor the driving stresses. The DLTs were performed in accordance with the ASTM-D-4945-89. The Case Pile Wave Analysis Program (CAPWAP®) analyses of the measured stress and velocity data were performed on the selected EOD blow to determine the initial pile resistance, the side resistance distribution along the length of the pile and the tip resistance. The first high energy blow of each restrike event was also analyzed with CAPWAP® to determine the load distributions for restrike resistances. The CAPWAP® analyses of all the TPs along the length of the piles are presented in Figures 4c to 4f. Blow counts and permanent movement of each restrike events are also presented in Table 2. The CAPWAP® analyses showed that the tip resistance (R_{tip}) was almost constant during the restrikes except for TP-2. The side resistance (R_s) increased significantly for all the TPs except for TP-2, which contributed to the setup process that will be discussed later.

Statnamic Load Tests (SNLTs)

SNLTs were conducted on all the TPs. The statnamic device consists of a cylinder that supports reaction weights and was placed on top of the pile head. The device and reaction weights were initially supported by a reaction frame constructed around the TP. In this project, SNLT was accomplished with a 4,500 ton Statnamic device equipped with a gravel catching system. This device used a controlled burn of fuel to generate pressure which was transferred to the test shaft through a load cell. Load, acceleration and strain were monitored to obtain the foundation response during SNLTs. Figure 4 presents the load versus movement response for the TPs resulting from SLT and SNLTs.

The strain gauge readings obtained during the load tests were used to estimate the distribution of load transfer along the piles, as presented in Figure 5. To calculate the axial load distribution during load testing, the modulus of concrete was back-calculated for each load test using the strain data measured by the strain gauges that were installed at the ground level. A constant modulus of concrete was used for strain gauge data analysis in each load test. This constant modulus was determined using the strain data measured at the first load increment. The strains recorded at the gauge level near the pile tip comprise both the side and tip resistances of the bottom pile segments. In order to separate the side and tip resistances, the side resistance was extrapolated from the segment immediately above the bottom segment to the tip elevation of the pile, which is then deducted from the measured load to calculate the tip resistance.

RESULTS AND ANALYSES

Back-calculation of Total and Effective Stress Parameters

Table 3 presents the total stress adhesion factor, α and the effective stress coefficient, β calculated using the average peak unit side resistances obtained from the average strains at each gauge level (Eqs 1 and 2). The undrained shear strength (S_u) derived from UU was used to calculate the values of α. As observed from the table, the α values varied from 0.41 to 0.86 between the soil layers, which are within the range of published values (*e.g., 9*). The average value of α for all soil layers and all TPs range from 0.47 to 0.75, with an average of about 0.61.

Since the unit side resistances (f_s) were calculated from the load tests and the load tests were performed 14 to 30 days after EOD, the α values might be affected by setup process. Both the α and β value is lower for TP-2 compared to the other TPs. The damage at the bottom 33ft. (10-m) which was measured by PDA® may contribute to this lower value.

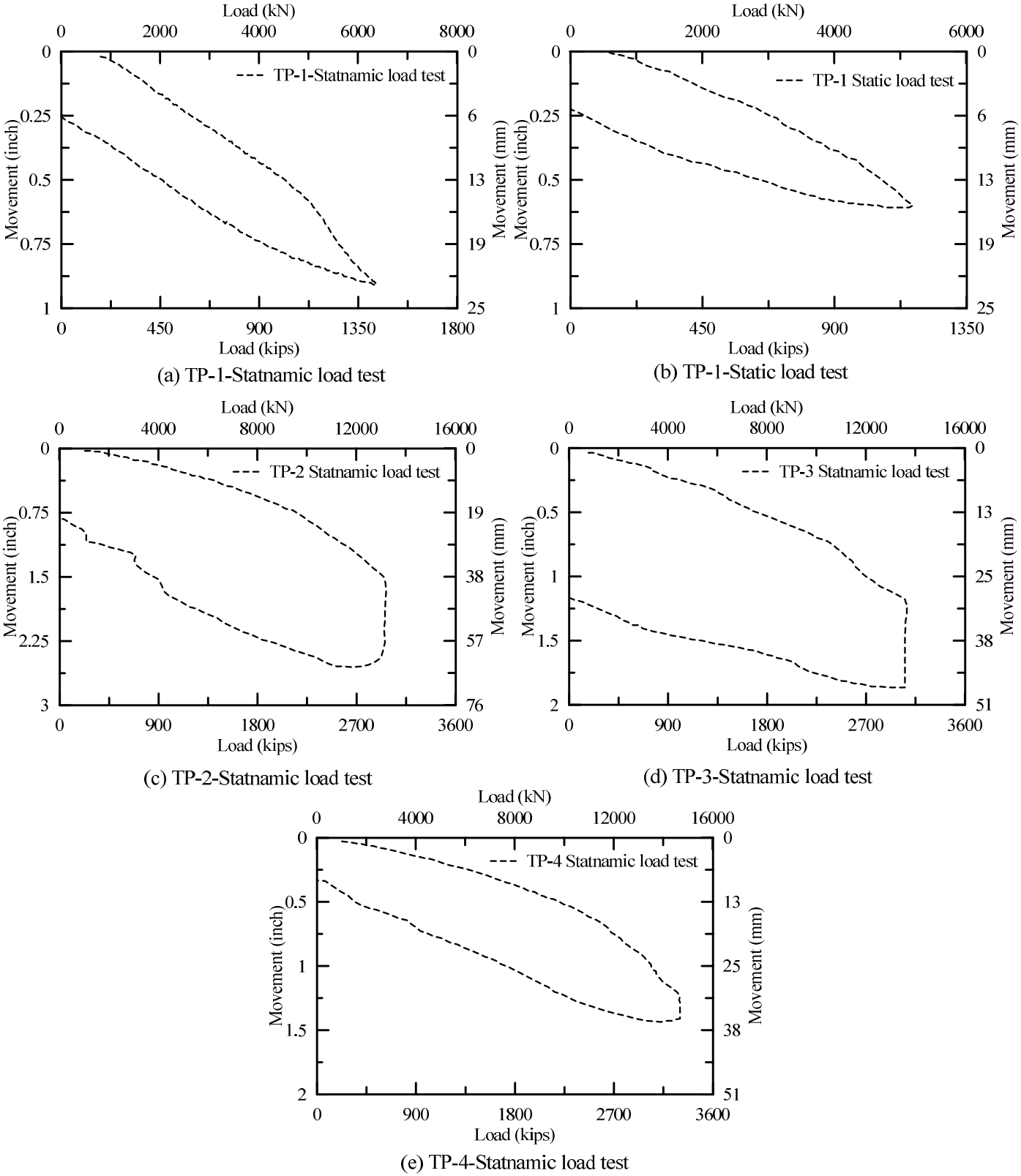
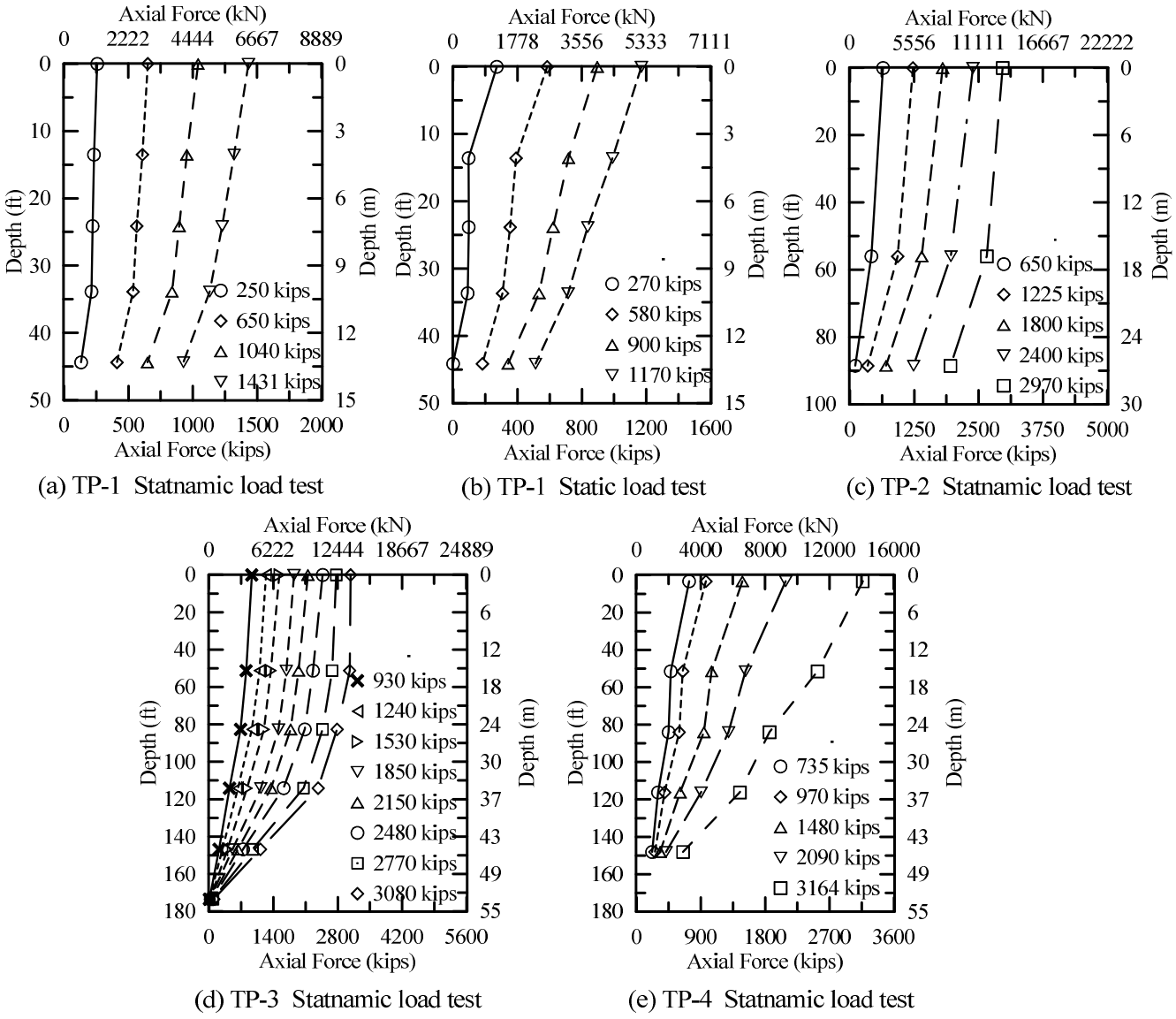


Figure 4: Load-movement plots from static and statnamic load tests



(a) TP-1 Statnamic load test (b) TP-1 Static load test (c) TP-2 Statnamic load test

(d) TP-3 Statnamic load test (e) TP-4 Statnamic load test

Figure 5: Load-distribution plots

Meanwhile, the calculated β-coefficients ranged from 0.13 to 0.29, which matches very well with reported values in the literature (e.g., Clausen 2005. Fellenius 2015). The average value of β-coefficients for all soil layers and all TPs is about 0.22. Figures 6a, 6b and 6c present the distribution of the unit side resistance, α factor, and the β coefficient along the length for all the TPs, respectively. Note that these values were plotted at the midpoint between the strain-gauge levels since the f_s, S_u and effective overburden stress (σ'_v) were also calculated in between the two gauge levels. Figure 6a indicates that the unit side resistance increased somehow linearly with depth.

Table 3: Back-calculated design (α and β) and setup parameters (A) for test piles

Pile ID	Segment length (ft.)	Design parameters, α and β		Setup Parameter "A' for Total Resistance, R_t	Setup Parameter "A' for Side Resistance, R_s
TP-1	0 – 13.5	0.62	0.14	0.10	0.28
	13.5 – 24.0	0.66	0.22		
	24.0 – 33.5	0.51	0.19		
	33.5 – 44.0	Sand	0.28		
TP-2	0 – 56.0	0.41	0.19	0.14	0.13
	56.0 – 88.5	0.54	0.23		
TP-3	0 – 51.0	Casing		0.23	0.24
	51.0 – 83.0	0.49	0.24		
	83.0 – 114.0	0.66	0.29		
	114.0 – 147.0	Sand	0.27		
	147.0 – 173.0	Sand	0.23		
TP-4	3.0 – 51.0	Sand	0.21	0.23	0.23
	51.0 – 84.0	0.86	0.13		
	84.0 – 116.0	0.56	0.18		
	116.0 – 148.0	0.83	0.26		
Average		**0.61**	**0.22**	**0.18**	**0.22**

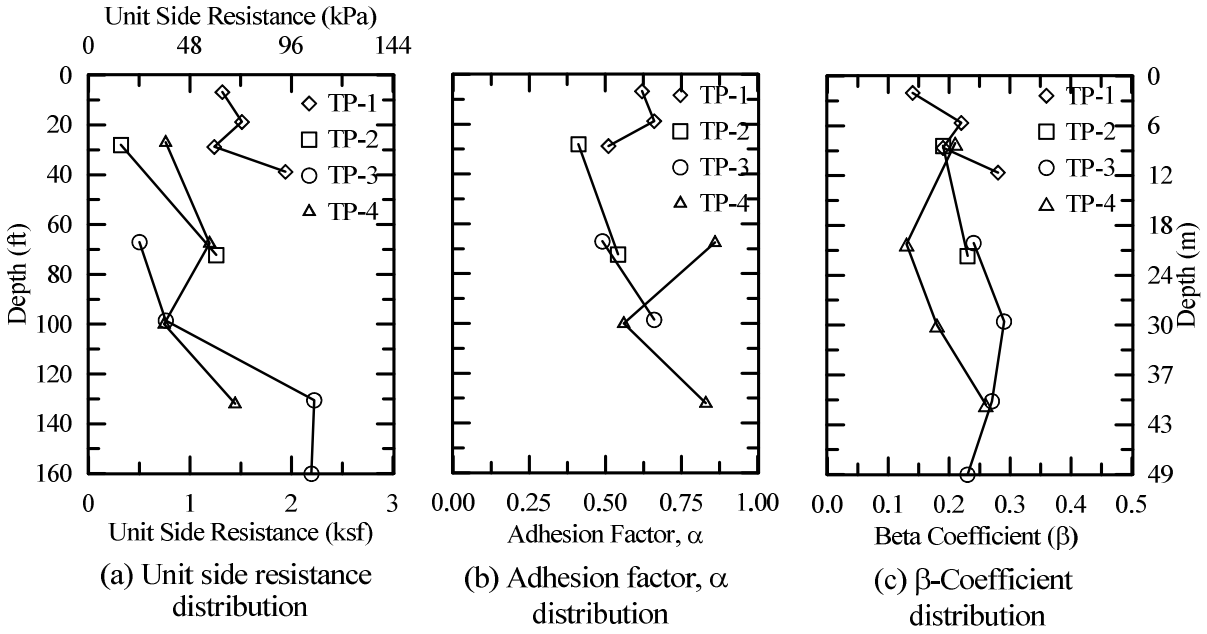
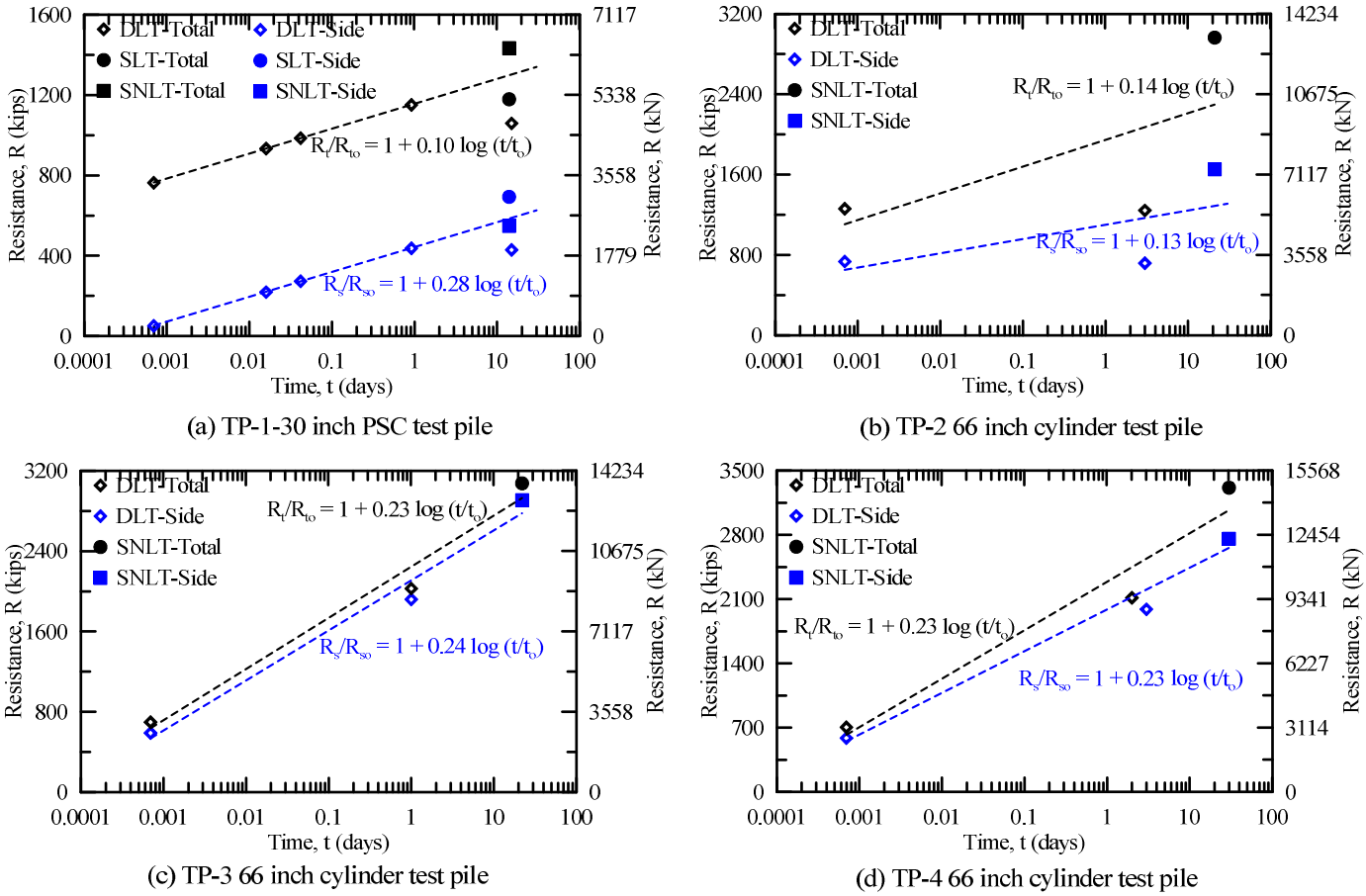


Figure 6: Distribution of (a) Unit side resistance (b) Adhesion factor, α (c) β-Coefficient

Increase in Pile Resistance or Setup

One of the main objectives of this study was to estimate the amount and rate of setup for O.E. piles, so that, it can be incorporated into the design of production piles. All the TPs were tested using DLTs at EOD and several restrikes after that and one SNLT or SLT at the end was performed to quantify the increase of resistance (or setup) with time. The total pile resistance (R_t) estimated using the PDA® and CAPWAP® from the DLTs as well as the resistances measured by the SLT and SNLT are summarized in Table 2. The setup ratio for side (R_s/ R_{so}), tip (R_{tip}/R_{tipo}) and total (R_t/R_{to}) resistances are also calculated for each TP and also presented in Table 2. The results of testing program showed that all the TPs exhibited significant amount

of setup. Figures 7a, 7b, 7c and 7d present the measured total (R_t) and side (R_s) resistances versus elapsed time for TP-1, TP-2, TP-3, and TP-4, respectively.



(a) TP-1-30 inch PSC test pile

(b) TP-2 66 inch cylinder test pile

(c) TP-3 66 inch cylinder test pile

(d) TP-4 66 inch cylinder test pile

Figure 7: Setup of side and total resistances of all test piles

Several methods (e.g., Skov and Denver 1988, Bullock et al. 2005, Ng et al. 2013) were developed to predict pile setup with time after EOD. Among the developed models, the relationship developed by Skov and Denver (1988) is considered to be the most popular method due to its simplicity and accuracy in estimating pile setup. They proposed the following equation:

$$\frac{R_t}{R_{to}} - 1 = A \log_{10} \frac{t}{t_o} \qquad \ldots(3)$$

where R_t = Pile resistance at time, t, R_{to} = Pile resistance at initial time, t_o, t = Time elapsed since end of initial pile driving, t_o = a reference initial time after which the resistance increases with the logarithmic increase of time, and "A" is the rate of pile resistance (R_t/R_o) increase per log cycle of time (t/t_o). In this study, t_o is selected as 1 day. As shown in Figure 7, both the total (R_t) and side (R_s) resistances were best fitted to a linear logarithmic time scale, which suggests a linear logarithmic time relationship similar to the models proposed by Skov and Denver (1988) and others (e.g., Bullock et al. 2005, Ng et al. 2013) do exist for this load testing program. The tip resistance (R_{tip}) did not change significantly during all the restrikes for all the TPs with the exception of TP-2. As mentioned earlier, damage was noticed at the bottom 33-ft. (10-m) of TP-2, which contributed to the lower tip resistance (R_{tip}) during the restrike for TP-2. However, for the other TPs, any change in the total resistance (R_t) was mainly due to

side resistance (R_s) setup, which is consistent with the findings in the literature (e.g., McVay et al. 1999, Ng et al. 2013) where the findings of load tests showed that the side resistance (R_s) mainly contributes to the setup process and the tip resistance (R_{tip}) stays constant over time during the load tests. The load test results also showed that for all the TPs (i.e., TP-1, TP-2, TP-3 and TP-4), the tip resistance (R_{tip}) was always over estimated during the SNLT compared to the tip resistance (R_{tip}) computed by the restrikes which lead us to conclude that the derived tip resistance (R_{tip}) from SNLTs are consistently greater those from DLT.

The calculated setup parameter "A" of total (R_t) and side (R_s) resistances for all TPs are tabulated in Table 3. It is interesting to observe that though both TP-3 and TP-4 were driven at two different locations; both TPs had similar setup ratios (R_t/R_{to} = 4.4 ~ 4.7) and rate of setup (A = 0.23 ~ 0.24). TP-2 had different amount and rate of setup compared to the other two O.E. piles (i.e., TP-3 and TP-4). We suspect the difference is due to the damage at bottom 33-ft. (10-m) of this pile. Since the setup of the PSC pile (TP-1) are mainly due to outside friction and the setup rate "A" for side resistance of the PSC piles and O.E. cylinder piles (TP-3 and TP-4) are close (i.e., A_{PSC} = 0.28 and $A_{OPEN\text{-}ENDED\ CYLINDER}$ = 0.23 ~ 0.24), one can postulate that no significant amount of setup was observed due to inside friction for the O.E. cylinder piles.

CONCLUSIONS

Based on this study, the following conclusions can be drawn:

1. The adhesion factor, α calculated from the statnamic load tests ranged from 0.47 to 0.75 with an average value of 0.61. The β-coefficient ranged from 0.20 to 0.26, and the average value of β for all soil layers in this study was 0.22. These values are comparable to results previous studies in literature.
2. The unit side resistances of most soil layers (determined using differentiation of loads between strain gauge levels) mostly exhibited strain softening behavior, which ensured that the side resistance was fully mobilized.
3. The distribution of unit side resistance and design parameters (α and β) with depth showed that the unit side resistance and design parameters (α and β) increased almost linearly with depth.
4. All the TPs (i.e., both open and close-ended pile) exhibited significant amount of setup which was mainly due to increase in side resistance. The tip resistance was almost constant for all TPs during the restrikes except for TP-2. The lower tip resistance for TP-2 can be attributed to the damage caused during driving at the lower 33-ft (10.0-m) of this pile.
5. The load test results showed that for all the TPs, the inferred tip resistances (R_{tip}) from SNLT were consistently greater than those determined from DLT in this particular site.
6. The logarithmic setup parameter "A" for all TPs were back-calculated for both total and side resistances, The results revealed that for the large diameter O.E. cylinder piles, the "A' parameter for side resistance was about 0.23 and that for PSC pile "A" was about 0.28 in this study. The difference was mainly due to size and shape of the piles.

ACKNOWLEDGEMENT

This research project is funded by the Louisiana Department of Transportation and Development (State SIO No. 30000134) and Louisiana Transportation and Research Center (LTRC Project No. 11-2GT). The authors want to appreciate the GRL engineers for their support and assistance to perform the analyses for the CAPWAP® data.

REFERENCES

1. Bullock, P, J., Schemertmann, J. H., McVay, M. C., and Townsend, F. C. Side shear setup I: Test piles driven in Florida. J. Geotech. Geoenviron. Eng., Vol. 131(3), 2005, pp. 292-300.
2. Burland, J. B. Shaft friction of piles in clay. Ground Engineering, Vol. 6(3), pp 30-42, 1973.
3. Clausen, C. J. F., Aas, P. M., and Karlsrud, K. Bearing capacity of driven piles in sand, the NGI approach. *Proc. of Int. Symp. on Frontiers in Offshore Geotechnics*, Perth, September, 2005, pp. 677-681.
4. Fellenius, B. H. Basics of foundation design. Electronic edition. Available at www. Fellenius. Net, 2015.
5. McVay, M. C., Schmertmann, J., Townsend, F., and Bullock, P. Pile friction freeze: A field investigation study. *Research Report No. WPI 0510632,* Vol. 1*,* Report submitted to Florida Department of Transportation, 1999.
6. Ng, K. W., Roling, M., AbdelSalam, S. S., Suleiman, M. T., and Sritharan, S. Pile setup in cohesive soil. I: Experimental investigation. *J. Geotech. Geoenviron. Eng.,* Vol. 139(2), 2013, pp. 199-209.
7. Paik, K. H. and Salgado, R. Determination of the bearing capacity of open-ended piles in sand. J. Geotech. Geoenviron. Eng., Vol. 129(1), 2003, pp. 46-57.
8. Skov, R. and Denver, H. Time dependence of bearing capacity of piles. Proc. of the 3rd Int. Conf. on the Application of Stress-Wave Theory to Piles, Canada, 1988, pp. 879-888.
9. Szechy, C. H. The effect of vibration and driving upon the voids in granular soil surrounding a pile. Proceedings to 5th International Conference on Soil Mechanics and Foundation Engineering, Paris, 1961, pp. 161-164.
10. Tomlinson, M. The adhesion of piles driven in clay. *Proceedings 4th Int. Conf. Soil Mech.,* London, Vol. 2, 1957, pp. 66-71.
11. Tomlinson, M. Some effects of pile driving on skin friction. *Proceedings of Conf. on behavior of Piles,* ICE, London, 1970, pp. 107-114.
12. Zhang, Z., and Tumay, M. T. Statistical to Fuzzy approach toward CPT soil classification. *Journal of Geo and Geoenv Engineering,* Vol. 125(3), 1999, pp. 179-186.

EVALUATION OF EFFECTIVENESS OF SLOPE STABILIZATION USING MONITORING TECHNIQUES: AN APPLICATION IN NORTHERN ITALY

Alessandro Micheli, Anas SpA, Rome, Italy, +39 06 44461, a.micheli@stradeanas.it
Maurizio Martino, Anas SpA, Rome, Italy, +39 06 44461, m.martino@stradeanas.it
Enrico Mittiga, Anas SpA, Rome, Italy, +39 06 44461, e.mittiga@stradeanas.it
Giorgio Ricci, Anas SpA, Rome, Italy, +39 06 44461, g.ricci@stradeanas.it

ABSTRACT

Evaluate the effectiveness of a massive slope stabilization work step-by-step through monitoring, both traditional (inclinometers) and innovative (terrestrial interferometry) for a huge embankment founded on a partially unstable rock slope.

Keywords: Interferometry, Monitoring, Observational Method, Slope Stability

INTRODUCTION

A huge embankment (up to 30 m from toe to top) was built between two tunnels along the alignment of a main road in Northern Italy in the valley of river Impero, in order to make possible road connections for some small communities around. Calculations made during this first design phase indicated that the slope upon which the embankment should have been built up would have been unstable under new massive earthwork loads. Therefore, it was decided to put the entire embankment on a massive reinforced-concrete (r.c.) slab, founded on micropiles and secured with prestressed-cable anchors. At the toe of the slope, along the bank of the river, no provisions against scouring were built up, as rock blocks are present. No monitoring was provided but works having finished in stages between 2008 and 2009, the embankment was in clearly stable conditions up to 2011, when small cracks were recorded at the top. In late 2012, however, after intense rainfall, severe displacements occurred and wide cracks appeared on the pavement of the roads at the top of the embankment, even if no collapse was reached. The shape of the entire crack was largely consistent with a failure mechanism involving the whole slope from toe to top. The presence of micropiles and anchors at the toe was not effective with respect of slope stability on the long run and, moreover, it added a brittle character to the whole stability (breaking of anchors). Roads and junction were forcedly closed to traffic and countermeasures had to be put in place.

GEOLOGICAL OUTLINES AND SOIL PROPERTIES

The site is situated in the southernmost part of Alps (Ligurian Alps), characterized by thick layers of sedimentary rocks (Flysch) that underwent to weak metamorphic processes and massive tectonic displacements. As a result, rock joints are close-spaced and, moving toward surface, materials become highly weathered and fractured. They present a relatively high permeability and are prone to seepage in respond to rainfall. At the top of these rock layers, there are colluvial and eluvial soils in highly variable thickness and heterogeneous range of sediments from rock blocks to silt and silty clays. Eluvio-colluvial soils, being mainly granular materials, are highly sensitive to water pore pressure, a topic not completely highlighted in the first design phase. The following table shows the geotechnical parameters of the mentioned soils.

© 2018 Deep Foundations Institute

Tab. 1. Soil mechanical parameters

	γ_k [kN/m^3]	φ'_k [°]	c'_k [kPa]	$(c_u)_k$ [kPa]	E [MPa]
Eluvial and colluvial soils	19.0	29	5	-	60
Altered Flysch soils	20.0	38	100	-	100
Bedrock Flysch soils	20.0	38	150	250	500

SITUATION

Several stabilizing structures were therefore planned (see Fig. 1), as described in the following, ranging from anchored piled-founded slabs to reinforced earth (RE) retaining walls at bottom, passing through drainage systems both on surface and in depth. As roads had to be at least partially reopen to traffic as soon as possible, in order to collect data both for safety warning during works and feedbacks about slope behaviour, a complex monitoring system was put in place. Both traditional survey techniques (inclinometers) and Terrestrial Synthetic Aperture Radar Interferometry (TinSAR) techniques were used. Interferometry made possible to achieve, continuously and from a remote point of view, the displacements of selected points on the slope along the instrument line of sight (LOS).

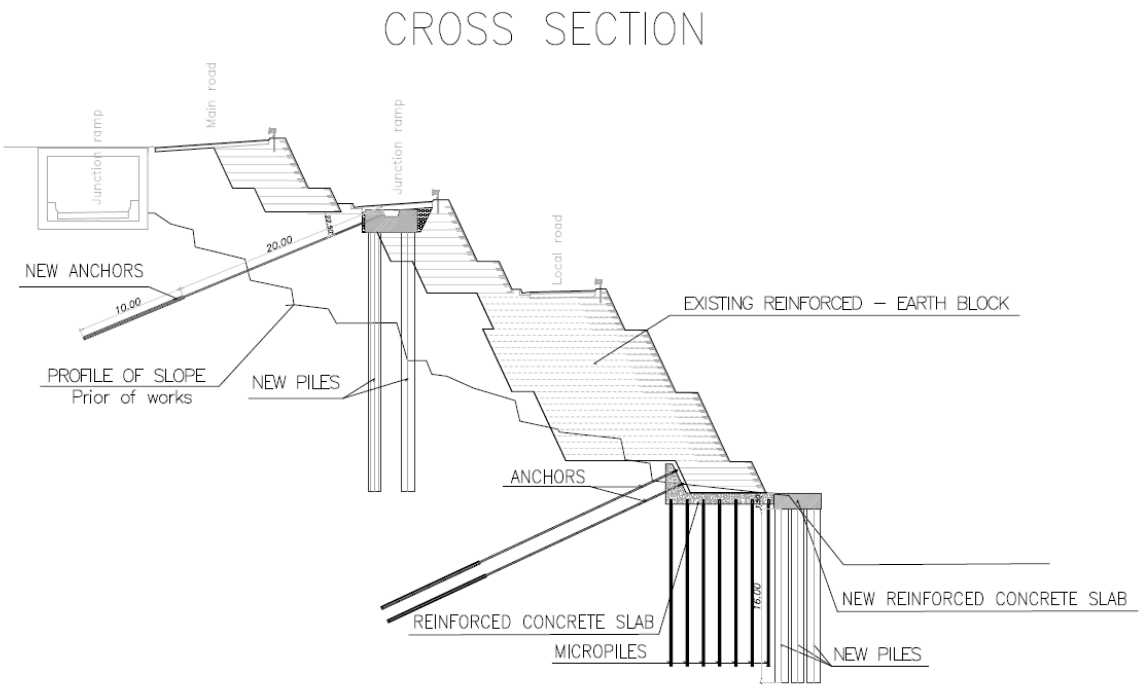


Fig. 1. Cross section of the slope including existing and new stabilizing structures

MONITORING

As said, the system for achieve measures of displacements of key-points on surface and in-depth was the centrepiece of the continuous monitoring of stability of the slope, within the limits of the area contoured by cracks on surface. Other goals of monitoring system were to measure piezometric levels in the slope and the values of load in particularly sensitive structures such as anchors.
A total of 17 inclinometer grooved pipes, 10 open-pipe and Casagrande piezometers and 4 magnet extensometers was installed, as well as load cells at the head of new anchors (see Fig. 2). The whole slope was monitored by TinSAR equipment, as well. As TinSAR monitoring was continuously carried out, it was quite easy to relate displacements of selected key points on the slope with implementation stages and pluviometry.

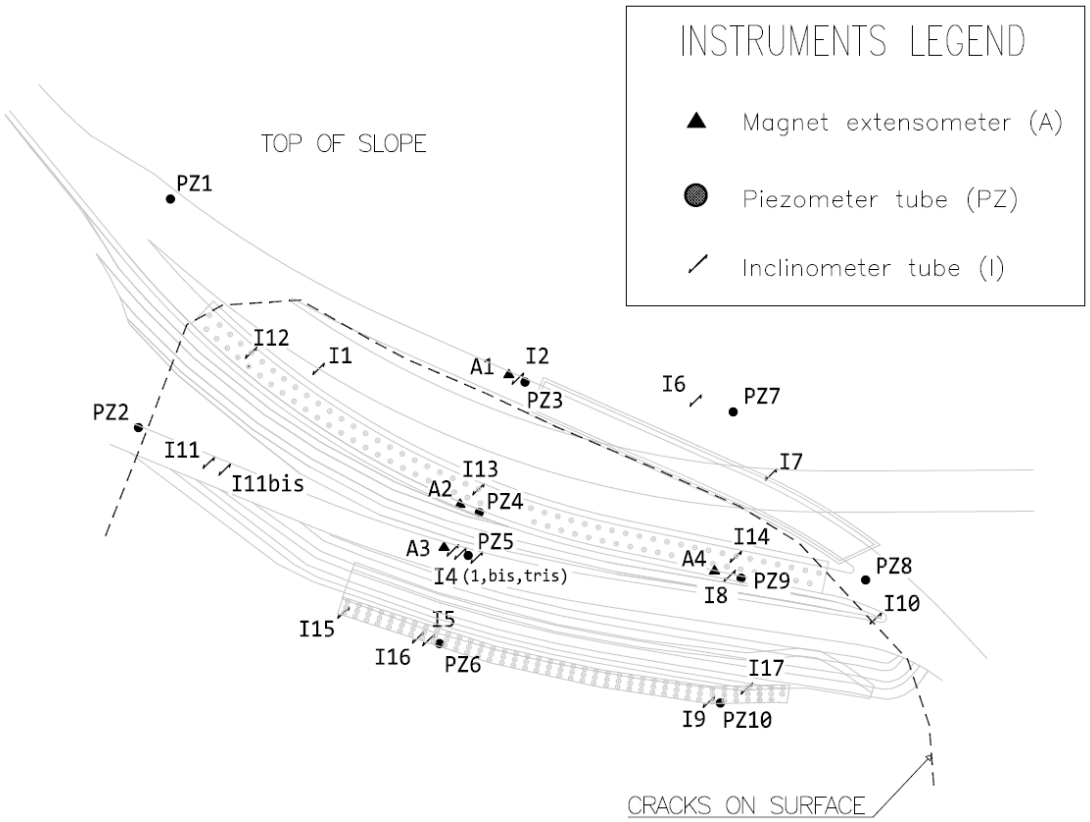


Fig. 2. Cracks on surface evidences and monitoring equipment

SAR (Synthetic Aperture Radar) terrestrial interferometry is a monitoring technique consisting in comparing two microwave signals emitted and received by two twined radar antennas, moving horizontally along a common rail over a length of few metres. Signals are compared referring to their phase. An appropriate location had to be chosen for TInSAR equipment, as interferometer needs to be in direct optical connection with its target (Mazzanti, 2011).
Data collected for many months from both inclinometers and interferometry were continuously compared each other, in order to better appreciate critical conditions. This technique was initially mainly oriented toward an "early warning" approach during work period, but it became a powerful tool to evaluate the steady growth of safety of the slope during stabilization structures construction and the actual effectiveness of each element (piles, anchors) just put in place and become

operational. In this way, it was possible to adjust the geometry of new elements (piles length, anchors pre-stress) while works were ongoing.
It is noteworthy that both monitoring techniques led to the same values for key-points displacements: data sets collected, after almost two years of monitoring period, continued to show a very strong correlation.

DESIGN BEFORE MONITORING

As shown in Fig. 3, stability of the slope was to be achieved by two groups of independent retaining structures. Namely, it was designed a concrete slab on bored piles, anchored to the depth of the slope through pre-stressed anchors and put almost in the middle of the slope and a line-up of bored piles at the toe of the slope, close to the existing anchored slab on piles. To be added at the end of the construction phase, a block of RE at the toe of the slope, juxtaposed to the existing RE retaining wall. The actual implementation of the latter element should have been subject to a critical design revision after first monitoring evidences.
The new RE retaining wall, in fact, should have become the most evident feature of the whole design, in terms of environmental impact, in a geographic area where these themes are strongly felt by population. The possibility to completely or even partially avoid the implementation of the retaining structure was therefore warmly welcomed, both on an environmental basis and, moreover, for saving money. Moreover, any work economies was immediately to be translated in money and time savings, with great advantages for the population.

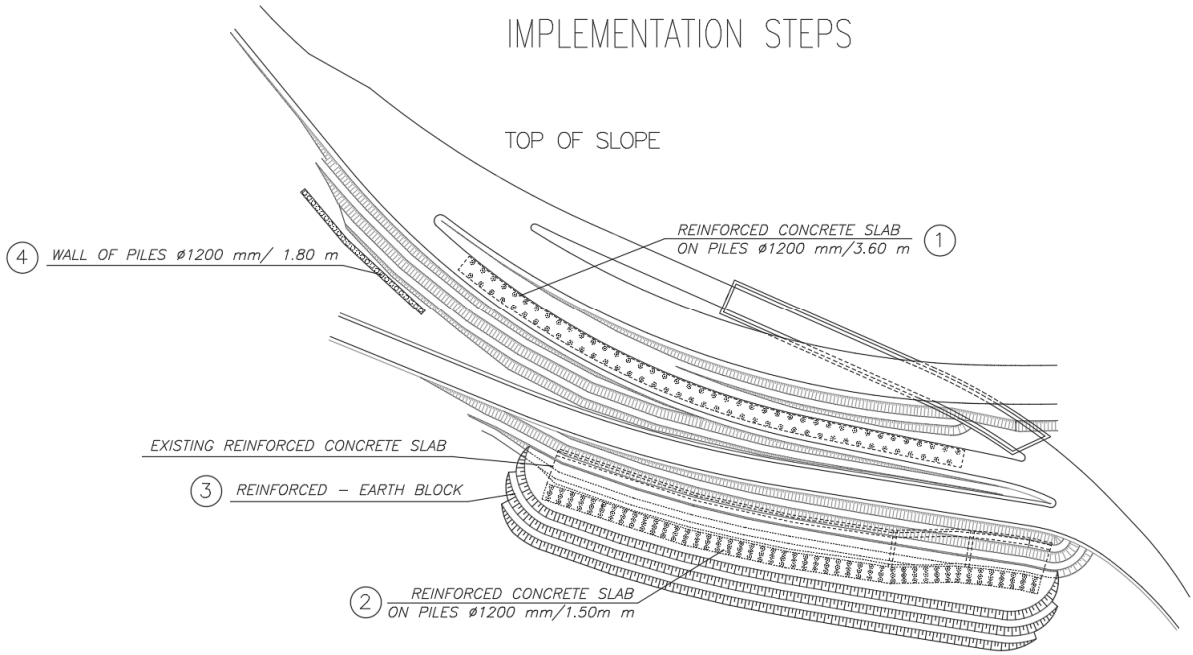


Fig. 3. Implementation stages

MEASUREMENTS

Measurements started in March 2013, just before the implementation phase. Key points, as targets of interferometry, are shown in Fig. 4.
The first step of implementation phase was the construction of the piled anchored slab at the middle of the slope (element 1 in Fig. 3). In this step, the targets showed a steady tendency to instability, with displacements growing with a slowdown ratio, due to the ever less important contribution of

pluviometry, going into spring and summer (see Fig. 5). One for all, the target P5, just in the middle of the slope on the left side, shows this typical tendency.

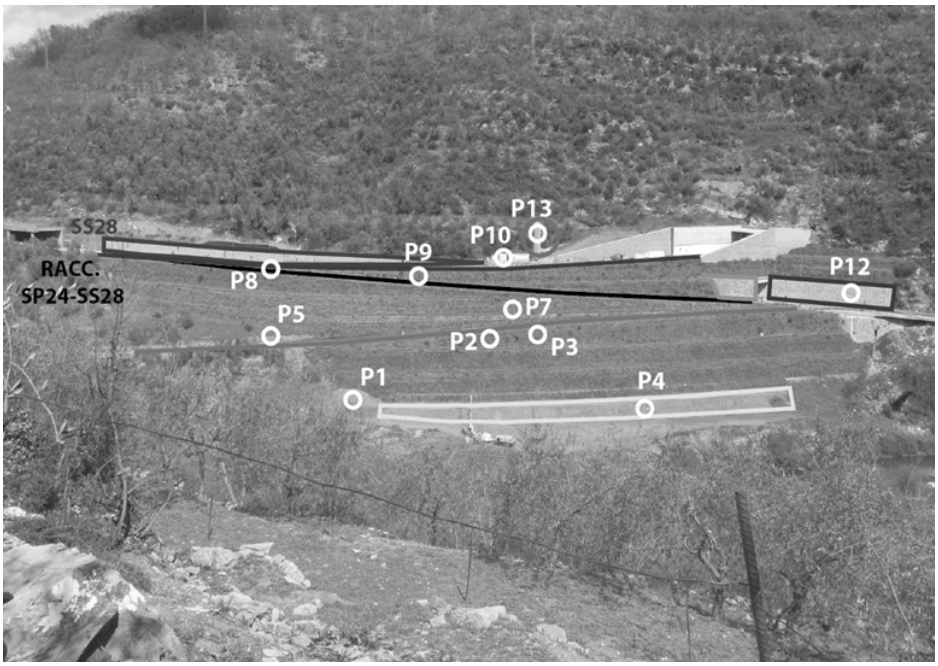


Fig. 4. Key points on surface as targets of interferometry

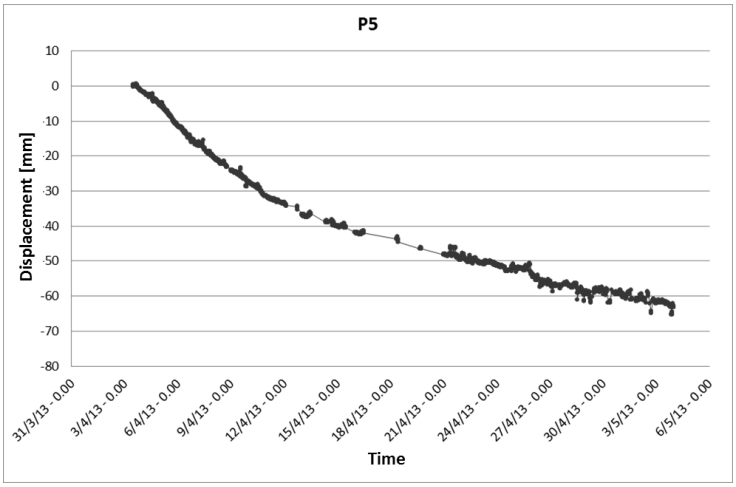


Fig. 5. Displacements measured for target P5 on slope – Before implementation phase

The effect of the implementation of the first stabilization structures, i.e. piles and anchors, is clearly visible, even if intense rainfall was recorded during autumn of 2013 (see Fig. 6). Other targets show similar tendencies.

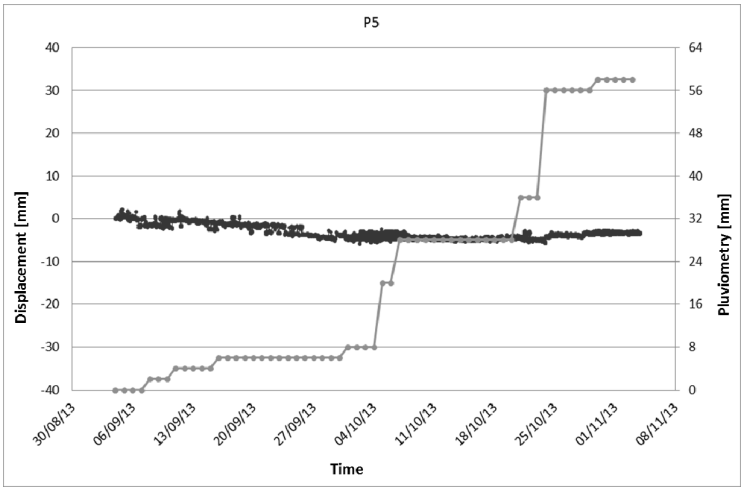


Fig. 6. Displacements measured for target P5 on slope – During implementation phase

As a whole, interferometry gave the same tendency for the slope, step by step. A typical weekly report is shown in Fig. 7, where comparison made between data freshly collected and the data already collected before implementation phase made possible to immediately appreciate every gain in stability.

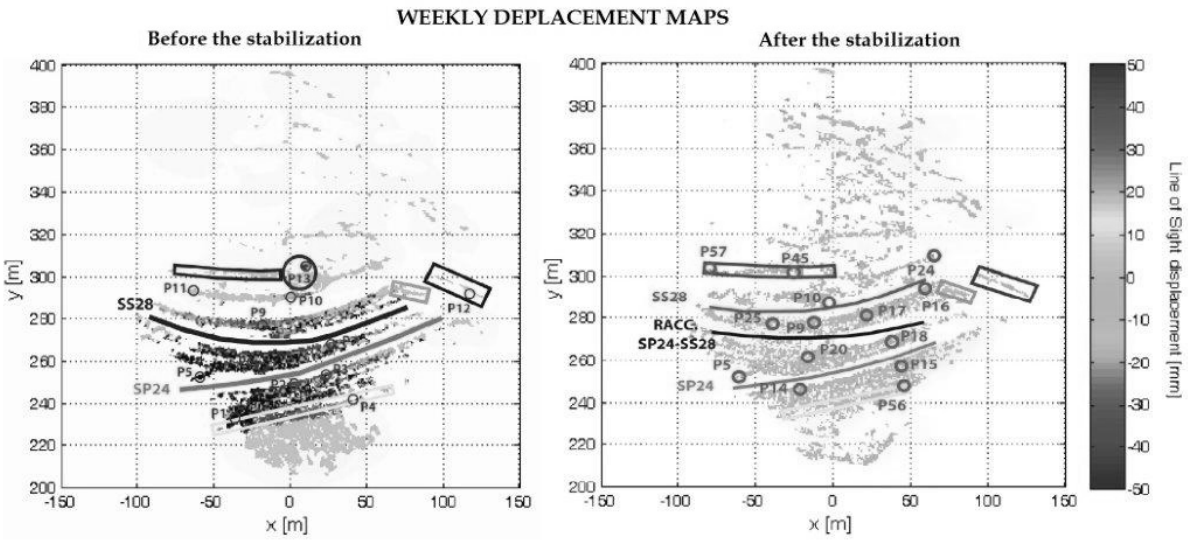


Fig. 7. An example of a weekly report of interferometry data and comparison with initial data

The consistency of interferometry data with direct measurement from inclinometer monitoring was checked step by step. In Fig. 8 is presented an example of this comparison, where displacement at the head of inclinometer I5 (at the bottom of slope) is compared with interferometry data on the same head as target for the same time frame, in conjunction with intense rainfall.

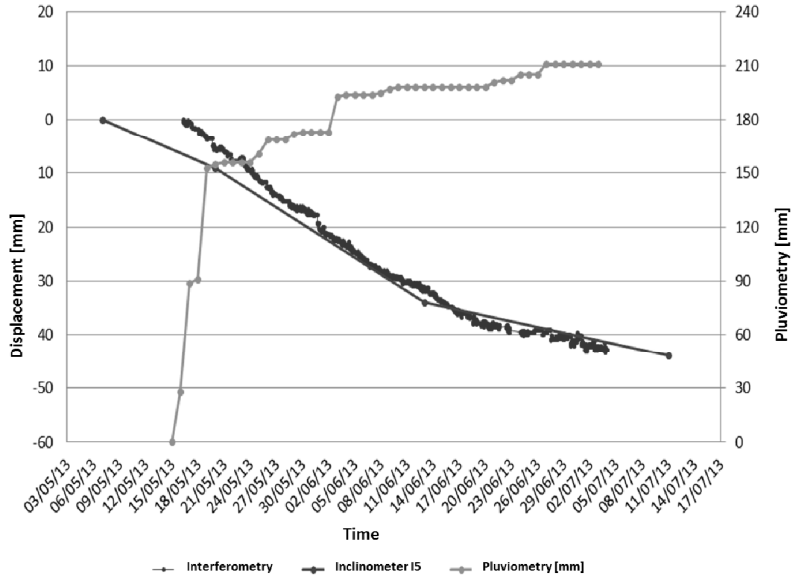


Fig. 8. A comparison between inclinometer (head of instrument) displacement and interferometry

DESIGN AFTER MONITORING

As shown, the steady growth of stability of the slope was clearly stated by monitoring. Even in presence of rainfall comparable to that of the previous years, in 2014 when implementation was almost completed, no displacements were recorded on the slope and cracks, meanwhile restored, never reappeared.
Therefore, it was decided to lighten the whole stabilization work, in order to achieve money savings and accelerate the complete restoration of the main road and the junction. The reinforced earth structure at the toe was almost completely built up, but a long extension of the piled anchored slab at the middle of the slope (element 4 in Fig. 3) was shelved.
Monitoring in 2014 displayed no displacements in any point of the slope, nor anomalous behavior of structures, such as increase or loss of loads in anchors.

CONCLUSIONS

As shown, the steady growth of stability of the slope was clearly stated by monitoring. Even in presence of rainfall comparable to that of the previous years, in 2014 when implementation was almost completed, no displacements were recorded on the slope and cracks, meanwhile restored, never reappeared.
Money and time savings were meanwhile achieved and this made the whole process a great success and an outstanding case history. Moreover, this application backed in a very favourable way applications of interferometry monitoring techniques in civil engineering works in Italy.
It has to be highlighted that, where traditional inclinometers are very likely to be put soon out of service (weathering of metallic pipe, damages by thirds, etc.), interferometric equipment will continue to be operational indefinitely. Data collected during lifetime of the structures and their real-time processing will guarantee the safe operational life of the main road.

REFERENCES

Mazzanti, P. 2011. Displacement Monitoring by Terrestrial SAR Interferometry for Geotechnical Purposes. Geotechnical Instrumentation News, June, pp. 25-28.

LATERALLY LOADED PILES IN AN EMBANKMENT OF DRY SAND

J.W.R. Brouwer, Geobest BV, Vianen, The Netherlands, +31650740785, roel.brouwer@geobest.nl

ABSTRACT

This article deals with the foundation design and construction of a sound barrier system for the Noord-Zuid subway line in Amsterdam. A foundation on open ended steel tubular piles had to be applied, resulting from high lateral loads due to the possible impact of crashing vehicles. An extensive soil investigation program was executed which consisted (a.o.) of Cone Pressure Meter tests. CPM tests were used to improve the lateral pile capacity calculations which resulted in a more economic design. Plaxis calculations were performed to analyze the lateral pile behavior close to slopes.
Steel tubular piles were installed by means of vibro driving to minimize construction noise. Installation proved to be difficult, as the piles had to be driven through very dense sand layers of an existing road embankment. On certain locations, full soil plugging during driving within the piles was observed, which is quite unusual for large tubular piles.

Keywords: sound barrier, piles, lateral, pressiometer, Plaxis, drivability

INTRODUCTION

In crowded urban areas in the Netherlands, the extended use of roads and railroads increases the noise level for the environment. The installation of sound barrier systems plays a vital role in (new) infrastructure projects and causes significant and necessary noise reduction for residents.

One of the finishing phases of the Noord-Zuid subway line in Amsterdam is the construction of a sound barrier system. This article describes the design and the construction of the foundation of a sound barrier system in the Northern part of Amsterdam, with a total length of approx. 2.6 km along the Nieuwe Leeuwarderweg (NLW) between highway A10 North and the Buiksloterdijk. The project location is presented in Fig 1. Sound barrier height varies from 1.0 m to 8.3 m. The red line in the figure shows the location with the highest barriers.



Fig. 1: location of proposed sound barrier system along the Nieuwe Leeuwarderweg. In red the location with the highest barrier (source: Google Earth)

The NLW was constructed in the year 1968 and consists over a substantial distance of a 10 m high embankment of sand. Several additions to the embankment have been constructed in the year 2005. The sound barriers are placed on top of this embankment. Further to the south of the project, the NLW has a deeper level and is constructed between sheet piles. The sound barrier will be placed directly on the sheet piles on these locations. This article focusses on the 8.3 m high barriers on the high embankments.

© 2018 Deep Foundations Institute

FOUNDATION SYSTEM

The sound barrier has a double function in this project: apart from the proposed noise reduction for the surrounding residential buildings and schools, the structure also functions as a traffic barrier. One of the client demands was that the complete system was able to resist lateral loads due to vehicles crashing into the barrier. As a result of this, high lateral loads and bending moments are acting on the foundation. The lateral loads combined with considerable axial loads and possible negative skin friction (drag down forces) caused by residual settlements of the NLW embankment requires a special foundation solution. The most economical solution was found in open ended steel tubular piles. Big advantage of this system is the application of a concrete plug in the top of the pile, where a structural connection between superstructure and pile is made. Due to the stringent client demands with respect to construction noise, it was decided to install the piles by means of vibro driving with an High Frequency, Variable Moment (HF-VM), vibro hammer. The foundation system is schematically shown in Fig. 2. Pile diameter varied due to the height and location of the sound barrier. Minimum pile diameter was 508 mm with a wall thickness of 7 mm. Maximum pile diameter was 914 mm with a wall thickness of 9 mm (slenderness D/t approx. 100). This article focusses on the large pile diameters.

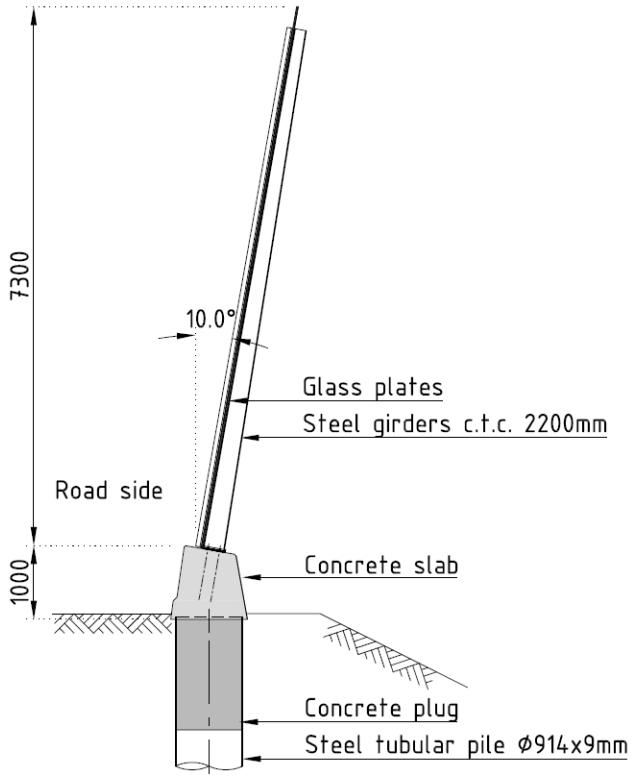


Fig. 2: Foundation system with open ended steel tubular piles

SOIL INVESTIGATION

Soil investigation programmes were carried out in different stages of the project and consisted in total of approx. 80 Cone Penetration Tests (CPT), 2 Cone Pressio Meter (CPM) tests with 4 tests per location, 4 soil borings and several laboratory tests. The laboratory program consisted of determination of unit

weight and water content, Consolidated Undrained Triaxial testing and oedometer testing on selected cohesive samples.
Typical spacing between test locations varied from 25 to 50 m, depending on observed variability of soil conditions.

The soil conditions are dominated by the existing NLW embankment which totally consists of sand material. Underneath, the typical Amsterdam soil conditions can be found, consisting of soft holocene layers (marine clay and the so called 'wadzand' formation), underlain by the 1st and 2nd sand layer. A thin layer of clayey sand (Alleröd) divides these sand layers. A typical profile is given in table 1.

Table 1. Typical Soil Profile

Layer no.	Depth [m below GL] From	to	Material
1	0.0	11.0	Sand, dense to very dense (old embankment)
2	11.0	12.0	Marine clay, firm
3	12.0	16.0	Sand and Silt (wadzand formation)
4	16.0	18.0	Sand, medium dense, silty
5	18.0	20.5	Sand, dense
6	20.5	21.0	Sand, clayey (Alleröd)
7	21.0	--	Sand, very dense

Ground water level is at approx. 10.0 m below ground level. Pile tip levels were chosen in the 1st sand layer with pile lengths up to 20 m. Interaction calculations were performed to determine the deepest level where negative skin friction would occur.

Lateral pile behavior was analyzed in an elasto-plastic model based on the theory of a beam supported by springs. The elastic behavior of the soil is usually described by means of the subgrade modulus K_h according to the theory of Ménard (1963). For piles with a radius larger than 300 mm, this equation is given by:

$$\frac{1}{K_h} = \frac{1}{E_m} \cdot \left[1.3 \cdot R_0 \cdot \left(\frac{2.65 \cdot R}{R_0}\right)^{\alpha} + \alpha \cdot R\right] \quad [1]$$

Where E_m = Ménard modulus, R_0 = reference pile radius (300 mm), R = pile radius and α = rheological coefficient.

The Ménard modulus is usually derived from the CPT cone resistance q_c. For sand, typical E_m values are 0.7 q_c to 1.0 q_c. In clays, this conversion factor varies between 2.0 to 3.0. This approach leads to safe but sometimes unrealistic low values. For this project it was decided to perform Cone Pressure Meter tests (CPM) to derive more realistic Ménard moduli enabling the project team to optimize the foundation design.

Pressuremeters are devices for carrying out in situ testing of soils and rocks for strength and stiffness parameters. They are generally cylindrical, long with respect to their diameter, part of this length being covered by a flexible membrane. The CPM is a combination of a normal CPT and a 'standard' pressuremeter and is entered into the ground by pushing.
Once in the ground, increments of pressure are applied to the inside of the membrane forcing it to press against the material and so loading a cylindrical cavity. A test consists of a series of readings of pressure and the consequent displacement of the cavity wall and the loading curve so obtained may be analyzed using standard solutions for cylindrical cavity expansion and contraction. Typical CPM results for this project are presented in Fig. 3.

From the CPM tests, the parameters G_{ini} (initial shear modulus), G_{ur} (unloading / reloading shear modulus) and c_u (undrained shear strength, cohesive soils only) can be derived. The Ménard modulus E_m can be derived from the shear moduli using the common relationship based on the Poisson's ratio ν. For this project, it was decided to use the initial shear modulus, derived from the initial loading curve, as input for the lateral pile calculations. For short term loading of crashing vehicles a 'dynamic' factor of 3.0 was applied to the static moduli, representing the stiffer soil behavior under very short loading conditions.

The sand material in the embankment has the largest contribution to the lateral stiffness of the foundation system, but also the marine clays at a lower level were tested. Elaboration of test results was performed according to the theory of Bolton (1999). The results are summarized in Table 2. Applied correlation factors are 1.0 for sands and 3.0 for clays, being the highest recommended factors.

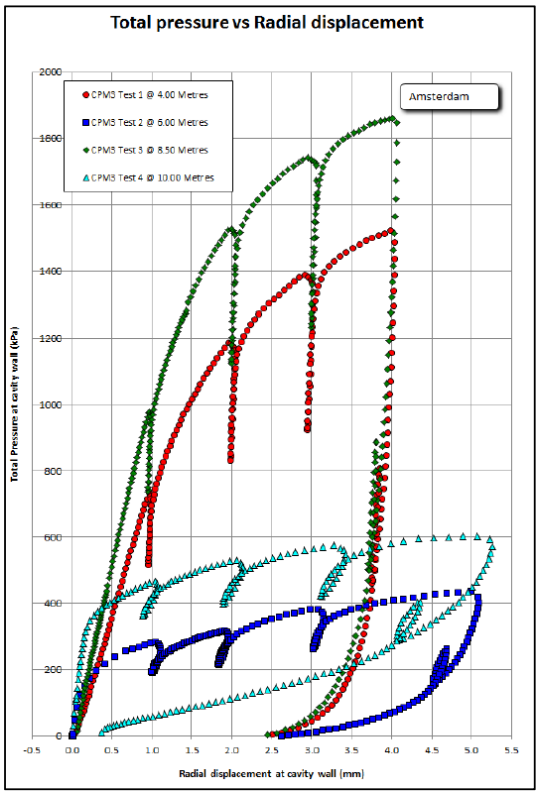


Fig. 3: CPM test results

Table 2. Ménard Moduli from CPM tests and correlation with cone resistance

Test no.	Depth [m]	Material	Cone resistance [MPa]	$E_{m,ini}$ (CPM) [MPa]	E_{ur} (CPM) [MPa]	E_m (correlation) [MPa]
CPM95-102	2.0	Sand	7.5	26.0	167.1	7.5
	3.5	Sand	20.0	24.4	144.7	20.0
	5.5	Clay	0.5	13.8	13.7	2.0
	7.5	Clay	0.5	12.0	38.8	2.0
CPM84-103	4.0	Sand	15.0	27.0	168.4	15.0
	6.0	Clay	0.5	3.4	19.9	2.0
	8.0	Sand	13.0	34.1	193.6	13.0
	9.5	Clay	1.0	12.0	13.3	2.0

The results show that large differences occur between the moduli based on correlation with cone resistance and moduli from CPM tests, even when the highest correlation factors are used. For the soils considered here, it is very conservative to use the 'standard' textbook correlation factors, especially lower or mean factors. Equation [1] shows that the relation between Ménard modulus and subgrade modulus is linear. A conservative estimate of the Ménard modulus will therefore lead to a very low value of the subgrade modulus and subsequent an unnecessarily large pile diameter and/or wall thickness. The investment of additional soil investigation by means of CPM testing pays off in a later phase of the project by means of a significant reduction on steel mass.

FINITE ELEMENT METHODS

The NLW embankment slope has an angle of approx. 27 degrees with the horizontal plane (2H/1V). This slope has to produce the passive resistance for piles subject to lateral wind forces and/or lateral forces from the impact of vehicles. A typical cross section with the NLW slope and the sound barrier system is given in Fig. 4. Piles are situated just near the slope. A water pond is present near the toe of this slope, which further reduces the soil resistance.

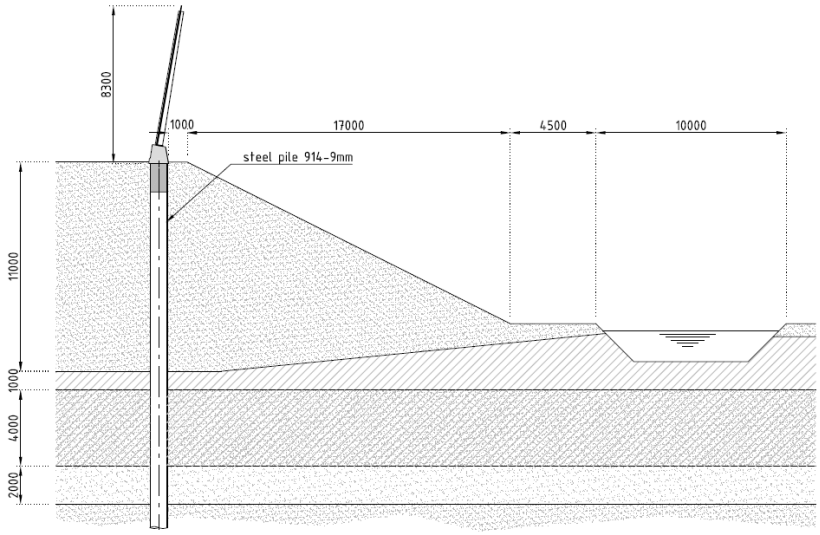


Fig. 4: sound barrier near slope of NLW embankment

Most computer programs based on spring supported beams have a tendency to overpredict the passive soil resistance of soil with steep slopes. Manual adjustments to this resistance are therefore often required, ranging from a reduction factor based on engineering judgement to totally neglecting the lateral resistance over the slope.

To get a closer insight in the influence of the slope on the passive resistance for this specific load case, Finite Element Method calculations were carried out with program Plaxis 2D. For comparison, calculations were carried out with a horizontal ground level and with a slope as given in Fig. 4. The differences in pile deflections and bending moments between the two sets of calculations were substantially high. Piles were first modelled as so called 'embedded piles', which simulates discrete elements at a certain centre to centre distance in a 2D plane. For comparison, the piles were also modelled as continous plates, where pile stiffness is corrected for the real centre to centre distance.

The results of the two sets of calculations are shown in table 3. An example of the Plaxis output for a pile near a slope is shown in figure 5.

Table 3. Results Plaxis calculations

Run no.	Situation	Pile condition	Maximum bending moment [kNm]	Deflection top of pile [mm]
1	Horizontal ground level	Embedded pile	149	15.5
2	Slope with water pond	Embedded pile	134	48.0
3	Horizontal ground level	Plate	112	3.5
4	Slope with water pond	Plate	115	14.7

The differences between the pile head deflection for a horizontal ground level and the 'slope with water pond' condition is remarkable high. Both approaches show that a reduction of approx. 70% of soil resistance applies to the 'slope with water pond' condition.

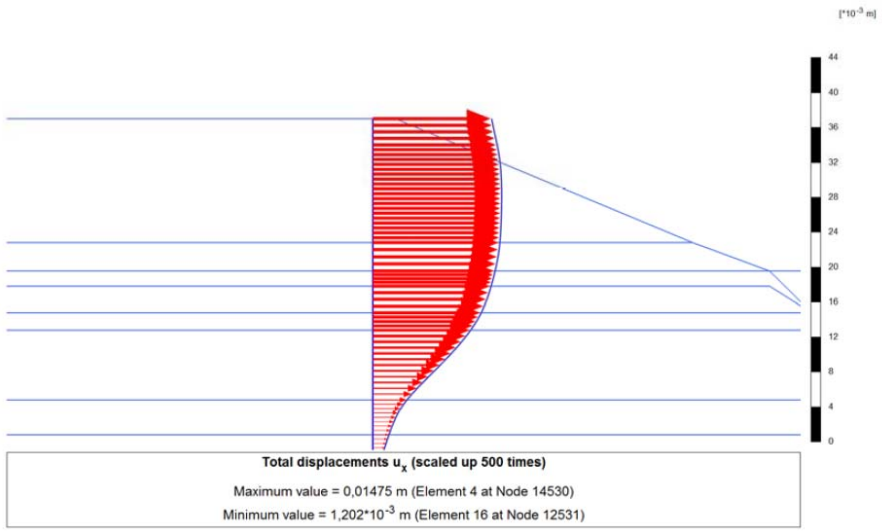


Fig. 5: Plaxis output for pile near slope

It was finally decided to perform all other calculations for large slopes with a spring based model and a horizontal ground level and an efficiency factor of 0.3 on the soil parameters. This means a reduction of 70% of the passive soil resistance over the height of the slope.

PILE DRIVING

As stated before, steel piles had to be installed by means of high frequency vibro driving. Piles were maximum 20 m long with a slenderness D/t of about 100. Drivability assessments had shown that soil resistance was relative high, due to the presence of thick layers of well compacted dry sand in the NLW embankment, but piles could be installed with a vibro hammer with an centrifugal force of approx. 1600 kN. In all assessments, coring behavior was assumed, where Soil Resistance during Driving (SRD) consists of inner and outer wall friction and tip resistance at the pile rim. This is common practice when driving open ended tubular piles with diameters larger than 600 mm. (Full) plugging during pile driving is hardly observed with piles of this diameter and was therefore not modelled.

The process of vibro pile driving on top of the embankment is shown in Fig. 6. During execution of the works, the SRD was rapidly increasing with increasing height of the embankment.

The sudden increase in SRD can be explained by Fig. 6., which shows the calculated SRD as a function of depth below Ground Level. The difference between coring SRD (inner and outer wall friction, dotted line) and plugging SRD (outer friction and full end bearing, striped line) is clearly visible. Plugging will lead to a drastic increase in SRD and therefore reduced pile advancement.



Fig. 6: Vibro driving of steel piles on top of the embankment

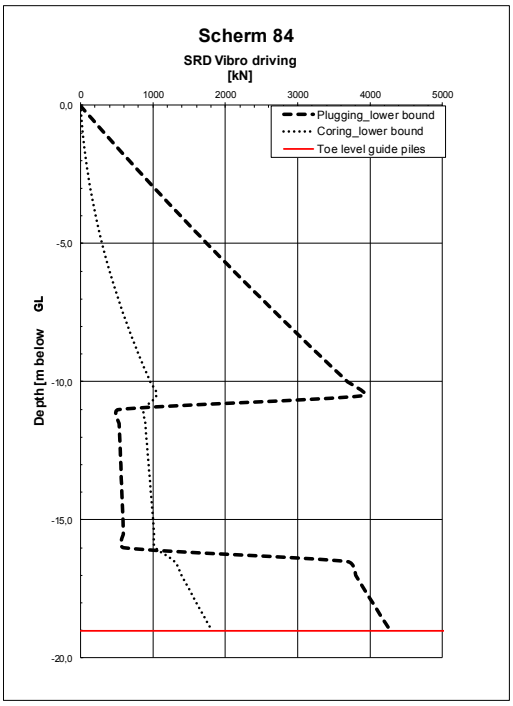


Fig. 7: difference between coring SRD and plugging SRD

At certain locations, obstacles (concrete lumps, stones, etc.) were found at a deep level, causing early refusal. At these locations it was required to move the position of the pile. At some other locations, it was observed that the soil level inside the pile after driving was up to 9 m lower. Naturally, this was observed relatively late in the pile driving process. Obviously, soil plugging had occurred within the pile, causing a severe increase in SRD which resulted in damage to the pile head due to the massive

energy transfer to the pile without sufficient pile penetration. The observed soil level reduction and damage to the pile head are shown in figure 8.



Fig. 8: soil plugging within a pile and pile top damage due to extensive vibro driving

Several mitigation measures were tried, such as the use of additional counter weights, the use of a larger vibro hammer, lubrication by means of adding small amounts of water inside and outside of the pile wall. Due to the strict client demands with respect to noise and vibration, pile installation by means of impact driving was not allowed.
Final solution was found in relief drilling by means of augering. The pile plug was removed to a level of approx. 6 m above pile toe level. The inner skin friction was decreased to acceptable values and piles could be driven to the design level.

CONCLUSIONS

- The use of tubular piles have proven to be a reliable and economic foundation type, especially when dealing with large lateral forces.
- The presence of slopes close to the pile location influences the lateral behavior of piles in a serious way, especially with high and steep slopes. To avoid uneconomic designs, it is highly recommended to perform Finite Element Analyses to get a better insight in the exact lateral pile behavior rather than use standard solutions.
- CPM testing can be beneficial in obtaining more reliable values of Ménard moduli and subsequent horizontal subgrade moduli, rather than using a standard correlation with cone resistance; the investment of this detailed soil investigation pays of further in the project because of the savings in pile diameter and/or wall thickness of the steel piles.
- (vibro) pile driving in dry sands may lead to early plugging behavior during driving, even with large pile diameters. This effect can lead to a sudden and dramatic increase in soil resistance during driving resulting in refusal and/or pile damage. Detailed drivability analyses with plugging behavior are recommended in these cases.

ACKNOWLEDGEMENT

The Author would like to thank Holland Scherm BV and the City of Amsterdam for the cooperation in the design and construction phase of this project and for permission to publish this article.

REFERENCES

Bolton M.D. , Whittle, R.W., 1999, A non-linear elastic/perfectly plastic analysis for plane strain undrained expansion tests, Géotechnique 49, No. 1, pp 133-141.

Ménard, L., 1963, Calcul de la force portante des fondations sur la base des résultats des essais Pressiométriques, Sols-Soils, 5, 9-28.

NNI, 2016, NEN9997-1, Eurocode 7, including Dutch National Annex.

MODELING THE EFFECT OF EXCESS PORE-WATER PRESSURE ON THE BEARING CAPACITY OF FULL DISPLACEMENT PILES IN GROUP: A CASE-STUDY IN PARMA (ITALY)

Simone F. Author, Freelance Engineer, Italy, francesco.simone.civileng@gmail.com
Guadagnini G. and Marchi G. and Cremonini C., Authors, ENSER S.r.l., Viale Baccarini 29, Faenza 48018 (RA), Italy, +39 0546 663423, ingegneria@enser.it
Marchi M. Contributors, DICAM, University of Bologna, Viale del Risorgimento 2, Bologna 40136, Italy, michela.marchi@unibo.it

ABSTRACT

Excess pore-water pressure development during installation of piles into saturated clays is of primary importance and strongly affects pile bearing capacity and settlements. Such a problem is well known in literature, but excess pore-water pressure magnitude prediction, and then that of the bearing capacity, is an open research topic. In addition, excess pore-water pressure may increase greatly when numerous piles are installed in a relatively small area - as in the case of a pile group foundation - thus leading to a non-negligible modification of stress conditions at the soil-pile interface and, as a consequence, to a temporary reduction of ultimate load-bearing capacity. The paper focuses on the interpretation of load-test data performed on several auger-screw piles (full displacement), part of an important soil improvement intervention in Parma (Italy). The analysis of load test showed low values of ultimate load bearing capacity of the tested piles. Hence, the need to investigate the evolution of excess pore-water pressure with time and its relationship with the ultimate pile bearing capacity.
In addition, special attention is dedicated to the study of possible mechanisms standing beneath the superposition of excess pore-water pressure effects among adjacent piles. Eventually, in order to give a consistent theoretical explanation of the recorded data, a simplified model is introduced. Such a model could be applied to similar case studies.

Keywords: soft soils, piles as settlement reducers, consolidation

1. INTRODUCTION TO THE CASE-STUDY

The case-study herein presented is an extensive soil improvement project performed by means of two identical adjacent raft foundations, standing over a total of 756 cylindrical full displacement piles made of non-reinforced concrete (L=32m, D=0.6m). The intervention aims at a reduction of the total and differential settlements, which would occur in saturated clayey subsoil. Each of the concrete slab (90 x 46 x 1.5m) stands over 378 piles and supports the load of 8 metallic silos used for wheat storage (Fig. 1). Piles were installed at different dates, and disposed according to a rectangular mesh (3.4 x 3.3m).
The pile installation technology- patented by *Trevi Group*- is *Discrepile* (auger-screw pile). Such a technology allows a huge lateral soil displacement, with consequent increase in lateral skin friction (Fig. 2). The pile installation is carried out in two different phases: 1) driving of the tool connected to the rotary head via a drill string by a combination of rotary and crowd forces, that are provided by a hydraulic rig; 2) tool withdrawal and simultaneous concreting up to the ground level, seamlessly, through the hollow center of the drilling string.

© 2018 Deep Foundations Institute

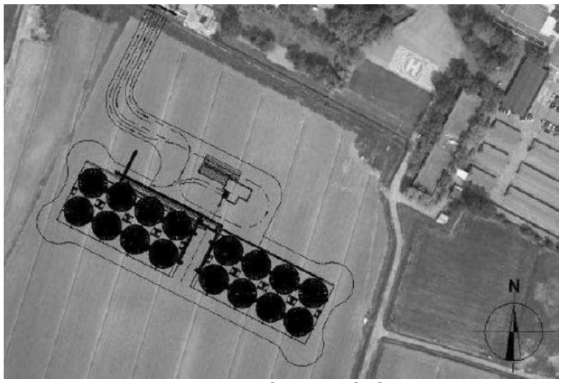


Fig. 1. Plan view of the raft foundations

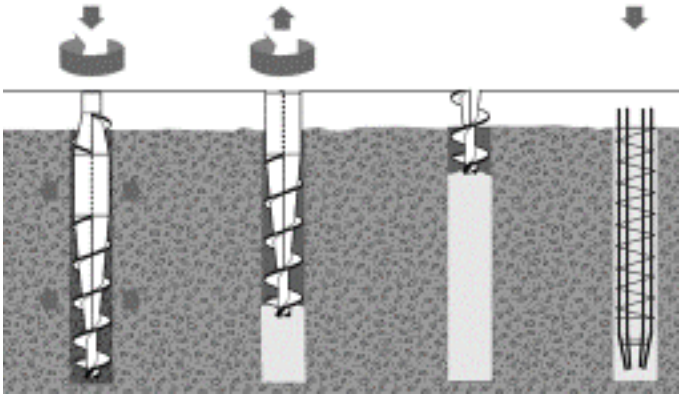


Fig. 2. Discrepile installation phases (TreviGroup online source, 2014)

The whole area was investigated between June and July, 2013 with 3 geognostic continuous boreholes and 6 cone penetration tests, 2 of which with seismic cone.
The soil is made of inorganic clays from medium to high plasticity; the units of interest are:

- Unit 1 (from 0 down to -10m) is basically made of clayey silt, with discontinuous intrusions of silty sands/sandy silts, OC;
- Unit 2 (-10m to -21m) presents silty clays and clayey silts with medium consistency, OC in the higher part;;
- Unit 3 (-21m to -34m) presents silty clays and clayey silts with low consistency, almost NC.

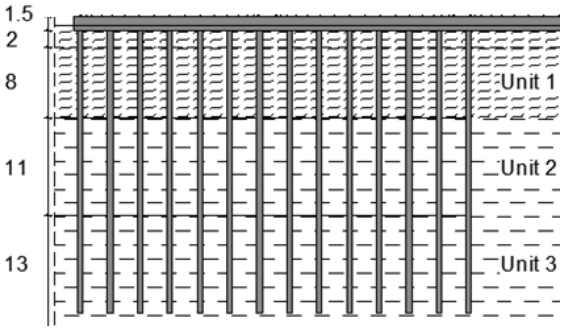


Fig. 3. Typical stratigraphic section

A typical stratigraphic section, geotechnical and consolidation parameters are shown in Fig.3, Tab.1 and 2. The subsoil is characterized by two different aquifers:

- An unconfined aquifer located between 1 and 2 m below the ground level, with a maximum seasonal variation of 1m;
- A confined aquifer inside the main gravel strata, with pressure head between +1 and +2m above ground level.

Table 1. Geotechnical design parameters, as deduced from in situ inspections

Geotechnical design parameter	**Unit 1** Silt OC	**Unit 2** Silty Clay lightly OC	**Unit 3** Silty clay NC
γ[kN/m^3]	19	19	19
φ'[deg]	25÷27	23÷25	22÷24
c'[kPa]	5÷10	4÷8	0÷5
s_u[kPa]	40÷50	1.36z+37	55÷60
E'[Mpa]	3.5÷4.5	0.13z+3.23	4÷4.5
M[MPa]	5÷6	0.18z+4.36	5.5÷6

Table 2. Consolidation parameters as deduced from oedometer tests

Depth [m]	**k[m/s]**	**c_v[m^2/s]**	**c_α**
20	1.34E-10	2.84E-08	6.03E-03
30.5	1.4E-09	8.17E-07	3.73E-03

2. LOAD TESTS PERFORMED ON SITE

Several static load tests were carried out on some of the piles at different timing, up to a value of 2.500 kN (reached with 10 constant load increments, each lasting one hour). In some cases, due to the unexpected high values of the settlements, this load value was not fully reached.
The first load test was done on a single test pile on September 2013, 48 days after pile installation, when the loss of undrained shear strength due to its execution was already partially regained. It showed a ultimate load bearing capacity value - interpreted with Chin's (1970) method - equal to Q_{exp}=3.440 kN and this value was used as the expected one for all the foundation piles that were going to be executed later on. Among them, in fact, seven piles were tested on May-June, 2014, after 30-45 days from the installation. They showed very high settlements for relatively small applied loads (Fig. 5*)*, and much lower values of ultimate load bearing capacity with respect to Q_{exp} (Tab. 3). In particular, a non-uniform behavior of the piles throughout the foundation was noticed. In order to investigate these general results, pile G7 was then tested two more times, 6 and 10 months after the execution, i.e. on Oct., 2014 and Feb., 2015. At that time, the raft had already been built (July-Sept., 2014); so, special attention was paid during its concreting to avoid linking the concrete slab to the pile G7 (a cylindrical void above the pile for the load to be applied independently from the raft).

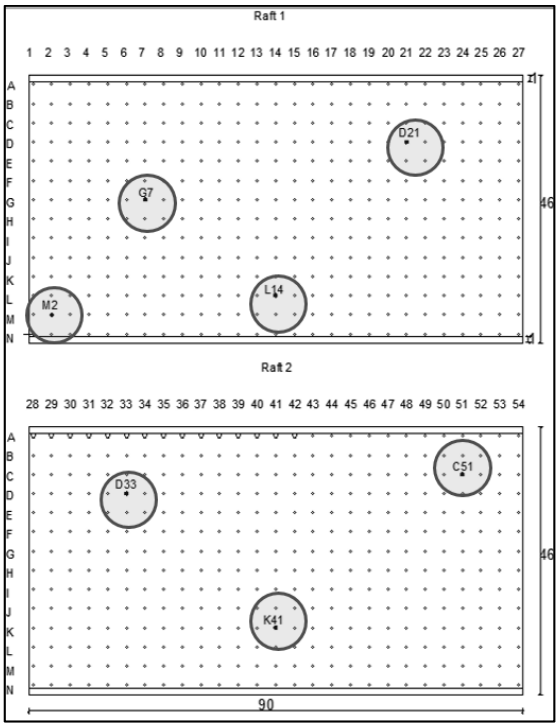


Fig. 4. Tested piles on each raft (plan view)

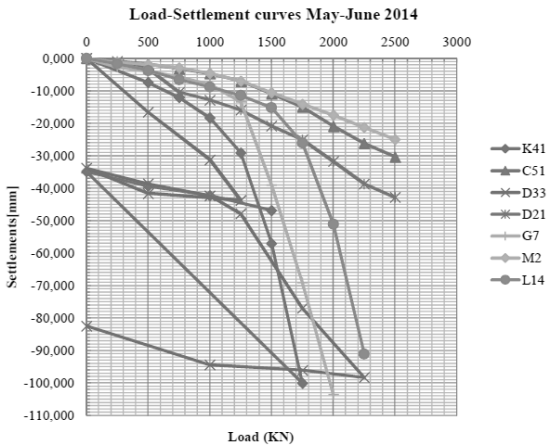


Fig. 5. Load-settlements curve from tests on May-June, 2014

Table 3. Load bearing capacity of piles and comparison with the expected value

Pile	Chin Q_{lim} [kN]	Q_{lim}/Q_{exp}
C51	2856	0.89
K41	1896	0.65
D33	2480	0.71
D21	3247	0.98
L14	2335	0.80
G7	1962	0.67
M2	3216	0.84

Those additional tests resulted in a substantial correspondence of the load-settlement curves between Oct., 2014 and Feb., 2015, and a much better behavior in terms of settlements and bearing capacity with respect to the first test on May, 2014 (Fig. 6). This may be due to two factors:

- The consolidation process and dissipation of excess pore-water pressure happened during a period of 5 months after the first test (from May to October, 2014);
- The full mobilisation of Q_p during the first test, due to the very high settlements reached on May, 2014 (104mm, which means 18% of the pile diameter).

Excess pore-water pressure was further analysed since it was believed to have a fundamental role in the test results (Denver 1988, Fleming et al. 2008, Karlsrud, 2012). Hence, the need for modeling the mechanisms of its dissipation.

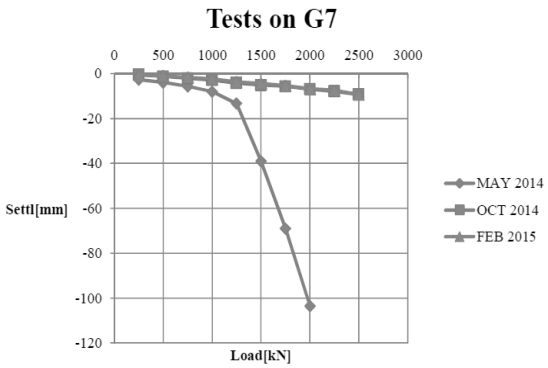


Fig. 6. Load tests on pile G7 on different dates

3. MODELING AND CALIBRATION

The proposed modeling approach accounts for the effect of the installation of single surrounding piles to the total pore-water pressure build-up around the tested ones. These single contributions - of non-negligible magnitude if summed all together, as described later on - are supposed to be a function of the time passed after the single pile installations and their distance from the tested pile (Randolph, 1979). In particular, even though the piles are part of a group foundation, they are treated as single piles, since most of the load tests were performed before the construction of the raft.

Once the total value of water pressure at the tested pile shaft is known, it is then related to the expected ultimate load bearing capacity by means of a unique constant coefficient calibrated according to the test results performed on site.

In order to handle the model with more ease, average values of undrained shear strength $c_u(0)$ and permeability k (as deduced from in situ and laboratory tests) were adopted:

$$k = 2.76 \text{ x } 10^{-6} [\text{m/day}] \quad [1]$$

$$c_u(0) = 48.5 \ [\text{kN/m}^2] \quad [2]$$

Moreover, the strain pattern of the soil was assumed to be similar to that generated by a driven pile.

Numerical analysis has been made, separately, for each of the tested piles, because they had different number of contributing piles (i.e. surrounding piles involved) and different execution and test dates. The whole procedure herein proposed can be roughly summarized as the application to some involved piles of the three inter-connected formulas [3], [4] and [5] described below. Each of them is a function of the previous one:

$$du(0) = 2c_u \ln\left(\frac{R}{r}\right) \quad [3]$$

$$du(t) = du(0) - 1.0362t + 0.0042t^2 - 8 * 10^{-6}t^3 + 5 * 10^{-9}t^4 \quad [4]$$

$$Q(t) = Q_{exp}\left(1 - K_i du(t)\right) = 3.400\ \text{kN}\left(1 - K_i du(t)\right) \quad [5]$$

The first of these three formulas (Randolph, 1979) describes the amount of excess pore-water pressure du(0) that is generated around a pile due to its execution, at time t=0 and at a distance r from the pile shaft (space variable); in particular, this initial value is maximum at the pile shaft and decreases until it becomes null at a distance equal to R, which is a function of the shear modulus of the soil, of undrained shear strength, and of the radius of the pile ro. A numerical value of R was found out according to (Karlsrud 2012) plots, that relate R/ro to pore water pressure for similar soils. Assuming almost null values of pore water pressure, the corresponding ratio R/ro in the graphs mentioned above equals 40; hence, R is found out to be 12m, being ro=0.3m. Substituting the assumed R=12m and $c_u(0)$, [3] becomes a function of r:

$$du(0) = 241 - 97\ln(r) \quad [6]$$

[6] is the decreasing law of pore pressure with increasing radial distance r from the pile, as shown in Fig. 7.
So, for each of the tested piles, only the piles around included within a circular area with radius R=12m were considered as contributing to the pore water pressure build-up of the tested piles and included in analytical computations (Fig. 8).
For instance, if a pile A is included in a circle centered in the tested pile B, with radius R, and the center to center distance between A and B is 3m, when A is executed, it will generate a contribution to pore pressure around B equal to:

$$du(0) = 2c_u \ln\left(\frac{12}{3}\right) \quad [7]$$

The second formula [4], which is specific for this case-study, describes the decreasing function of pore pressure du with days t (time variable). This curve is obtained entering the graph describing variation of pore pressure for different OCR (Randolph, 1979) with average values of permeability and initial undrained shear strength of the soil strata hosting the piles. For each of the tested pile (Fig.8), all contributions du(t) of surrounding ones were summed at some specific days after the execution of the tested pile (t=14, t=60, t=90, t=120, t=180, t=365 and t=730 days) and the total value finally related to Q(t) by means of the third equation [5], in the hypothesis of linear relationship between Q and du. In this latter formula, K_i is a constant parameter different for each of the tested piles *i* and it is determined by fitting, so that the bearing capacity expressed by [5] agrees with the value determined by Chin (1970)'s method on the pile load tests on May, 2014 (t is known). The calibration gave back 7 different values of K_i and their average value K_{av} was finally determined and adopted for plotting the Q(t) graph for each pile (Fig.9).

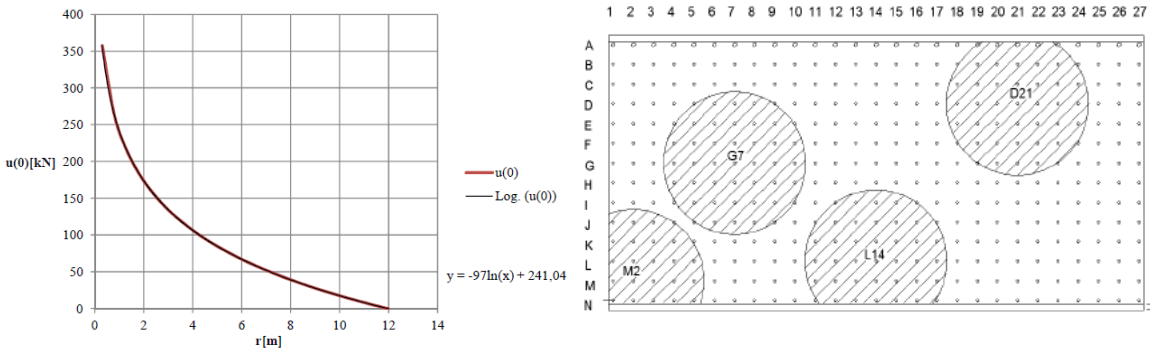


Fig. 7 and 8. Decrease of installation pore-pressure with increasing distance from the pile and piles contributing to the pore water pressure of the tested ones for raft 1

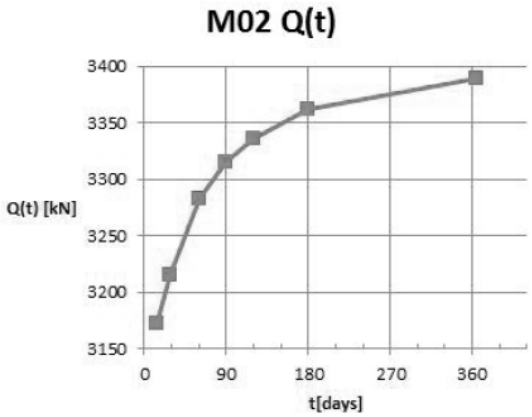


Fig. 9. Example of Q(t) graph for one of the tested piles (pile M2)

4. ANALYSIS OF THE RESULTS

Final du(t) and Q(t) plot for each pile showed two different possible shapes of the curves, as represented in Figures 10 and 11 for piles D33 and L14. Their symmetric shape is due to hypothesis of a linear correlation between the increasing values of excess pore-water pressure and the decreasing ones of the ultimate load-bearing capacity.

Piles C51, D33, M2 present values of du(t) always decreasing, with a corresponding always increasing Q(t). The curves increase and decrease, respectively, with a much higher rate within the first 90 days from the pile execution, and still with a considerable rate up to 5-6 months. After 180 days, in fact, the curve starts to tend to an asymptotic value, which means that, as excess pore-water pressure gets smaller and smaller, the corresponding load bearing capacity gets closer and closer to its final expected value Q_{exp}.

Differently, for piles K41, L14, G7, du(t) starts with a much lower value with respect to piles C51, D33 and M2, and, instead of decreasing due to the dissipation process, it increases very quickly up to a peak value around 30-45 days after the pile execution, more or less corresponding to the dates of the tests. After the peak value, that is of the same order of magnitude of the initial value of the aforementioned first group of piles, du(t) starts decreasing with the same rate of the first group of piles. The lowest value of load-bearing capacity is obviously attained where du(t) is at its peak value. These different behaviors can be due to:

- Different execution dates of the piles within a radial distance of R=12m from the tested ones (i.e. du from other piles started to contribute to the tested pile shaft in different moments; some of them hadn't even been executed yet at the date of the test, so their contribution was null);
- Different test dates (the piles were tested from 28 up to 34 days after their execution);
- Different number of piles contributing (i.e. internal piles have more contributing piles with respect to piles next to the border/corner of the raft).

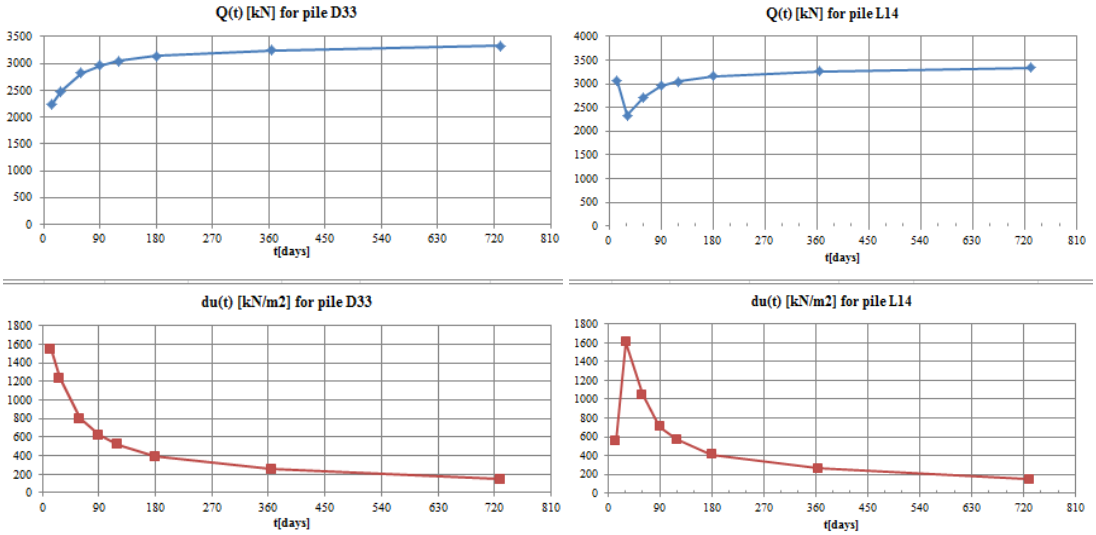


Fig. 10 and 11. Different behaviors of Q(t) for the tested piles (case of D33 and L14)

Table 4 summarizes the results of the computations and shows single values of K_i calibrated for each pile. Differently, the scatter in the results - that is the error of the model - is highlighted in the right-hand side of the table; in fact, when assuming a unique K_{av} as the average of the K_i obtained from data fitting, the difference in the prediction varies from -14% to 28%, with average error of the model in the order of +5.49%. The following plots relate the values of Q_u and du for each tested pile assuming the aforementioned coefficients K_i, thus creating a range of possible values of ultimate load-bearing capacity (Fig.12), given an initial value of du at the pile shaft.

Table 4. Results from fitting and errors for each pile

PILE	Ki	Q with Ki[kN]	Q_Chin	diff. perc.	Kav	Q with Kav[kN]	diff. perc.
C51	0,0001309	2885,24	2885,00	0,01%		2683,32	-6,99%
K41	0,0002762	1895,09	1895,00	0,00%		2441,33	28,83%
D21	0,000108	3245,70	3246,00	-0,01%		3118,78	-3,92%
D33	0,0002259	2479,51	2479,00	0,02%	0,000178543	2680,86	8,14%
L14	0,0002001	2335,21	2334,00	0,05%		2454,23	5,15%
G7	0,0002509	1963,24	1962,00	0,06%		2389,13	21,77%
M2	0,0000578	3215,52	3215,00	0,02%		2746,58	14,57%

The final formula representing the average linear correlation between Q_u and du for this case-study is expressed in [8]. As dissipation takes place, du tends to be null and, consequently, Q_u gets closer and closer to the expected final value of ultimate load bearing capacity Q_{exp} for the pile. The latter may be computed according to several theoretical formulations already available in literature and calibrated with eventual data from load tests.

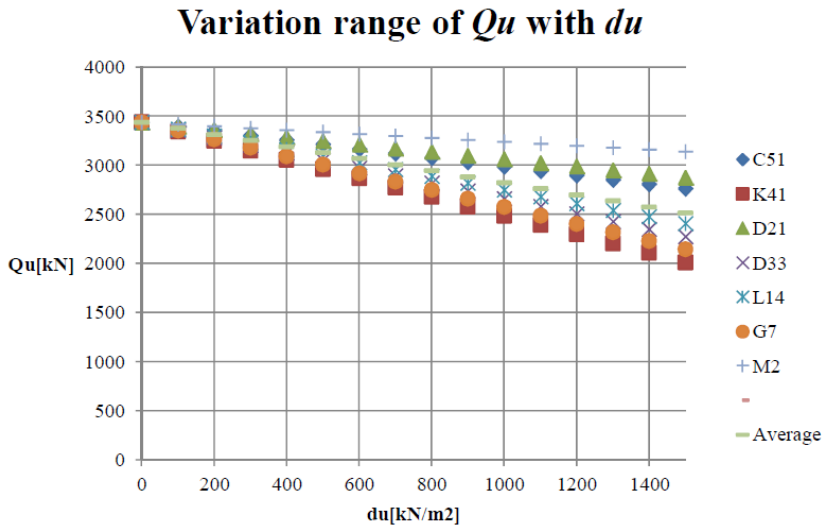


Fig. 12. Final variation range of Qu with du

$$Q_u = Q_{exp} - 0.6142\ du \qquad [8]$$

5. LIMITS OF THE MODEL

In order to handle the numerous parameters involved in consolidation issues easily, the model assumes the simplified hypothesis of constant permeability of the soil and constant undrained shear strength during consolidation and it is based on the theory of radial consolidation on single piles.
The first limit of the model is certainly represented by the relatively small number of load tests performed on the site, and by the possible errors in these data, that may arise from problems during testing procedure, unexpected soil characteristics, wrongly executed piles and interpretation method used to find Q_{lim}. The second main simplification is the hypothesis of assuming the superposition of pore-water pressure contributions as the algebraic sum of several contributions from other single piles, according only to their radial distance from them. This assumption may not consider the real dissipation paths/gradients of pore-water pressure in the soil.

6. CONCLUSIONS

The study presents a simple procedure in order to find a linear relationship describing the influence of excess pore-water pressure in time on the bearing capacity of full displacement piles in saturated clay, accounting for the contributions generated by the several piles of a group-pile foundation. The need for investigating the problem arises from a real foundation project, where load tests on piles enlightened a temporary loss of the load-bearing capacity, then re-gained in time, as pore-water pressure dissipation and consolidation took place.
The model assumes several simplified hypothesis and it ends up proposing a numerical procedure in order to find the average relationship between Q and du acting on a pile of a group foundation given the time passed after its execution, its position in the plan (i.e. number of surrounding piles), its geometry and soil properties.
The final formula is the result of a fitting operation with a limited number of test data. Therefore, the proposed modeling procedure - that seems to present an average error less than 6% - may need to be implemented with a higher number of data from pile tests performed in similar case-studies and verified by means of appropriate instrumentation.
The analysis of the pore pressure evolution during the installation process and the corresponding values of bearing capacity, anyway, needs further monitoring and numerical analysis, to take into account the complex stress-strain history induced in the soil by the pile installation.

REFERENCES

Chin, F. (1970). Estimation of the ultimate load of piles not carried to failure. *S.E. Proc. 2nd Asia Conf. on Soil Eng.*, (pp. 81-90).

Denver, S. A. (1988). Time Dependence of Bearing Capacity of Piles. *3rd International Conference on Application of Stress-wave Theory to Piles*, (pp. 879-889). Ottawa, Canada.

Karlsrud, K. (2012). *Prediction of load-displacement behaviour and capacity of axially loaded piles in clay based on analysis and interpretation of pile load test results.* Trondheim: PhD dissertation, NTNU.

Randolph, M. (1979). *driven piles in clay- the effects of installation and subsequent consolidation.* Géotechnique 29, No.4, 361-393.

Fleming, K., Weltman, A., Randolph, M., Elson, K. and Randolph, M. (2008). *Piling Engineering, Third edition.* Taylor & Francis. ISBN 9780203937648.

TreviGroup online source. (2014). Retrieved October 16, 2014, from http://www.trevispa.eu/viewdoc.asp?co_id=969.

THE IMPORTANCE OF ENERGY EVALUATION ON AN INDIVIDUAL PILE BASIS.

Julian P. Seidel. Foundation Specialists Group, Melbourne, Victoria, Australia, +61 417 501 275 jseidel@foundationspecialists.com.au

ABSTRACT

The relationship between hammer energy, pile capacity and pile movement (ECM relationship) is the common basis of all pile termination/acceptance criteria.

The energy delivered to a pile has historically either been assumed to be equal to the hammer potential energy, or has been assumed to be some fraction of the potential energy to account for various and wide-ranging losses in hammer drop and transfer through the helmet/cushioning system. With the advent of Pile Driving Analyzer (PDA) testing which became common in the early 1980s, true energy delivery to the tested pile could be measured.

However, regardless of whether energy losses were ignored, estimated or measured, it was and remains today effectively universal practice to assume that hammer efficiency and delivered energy does not vary. This is an assumption which is significantly incorrect and has significant consequences on achieved pile capacity.

This paper shows by way of a number of longitudinal studies of PDA energy measurement through projects that delivered energy routinely and randomly varies by 35% or more. The consequence of this degree of energy variability on pile capacity is established by reference to the normalized bearing graph approach.

The study concludes that effective pile driving control and pile acceptance criteria should account for energy variability on an individual pile basis.

Keywords: pile driving, dynamic formulas, pile acceptance, pile capacity

INTRODUCTION

On driven pile contracts prior to the advent of PDA testing, static load tests could not be relied on to provide reliable reference pile acceptance criteria, because these tests are necessarily conducted many days or even weeks after pile installation, when the capacity may be more or less than at the time of installation due to the effects of setup or relaxation respectively. There is therefore no direct relationship between installation characteristics and the capacity determined at a later time.

At that time, a small percentage of piles (which may or may not have been representative of the whole of a variable site) were tested statically. The vast majority of remaining piles were installed according to dynamic formulas which were known to be very unreliable and consequently were applied with high factors of safety.

Dynamic pile testing (Pile Driving Analyzer or PDA testing) has been in increasing usage in the United States since the 1980s, and has been progressively adopted as a primary quality assurance technique for driven pile projects internationally since then (Rausche et. al. 2008). The primary role for PDA testing, together with the associated analysis techniques, is estimation of pile capacity. However, PDA testing has other important construction control functions including measurement of delivered hammer energy.

Because PDA testing is relatively extensive (typically 3 to 15% of piles); can be undertaken at the time of installation; and allows delivered hammer energy to be measured, it fulfils a unique role as a reference for pile acceptance criteria for untested piles. Depending on local practice, the capacity of

© 2018 Deep Foundations Institute

these 85 to 97% of untested piles can be assessed by a variety of necessarily quick and simple methods – such as bearing graphs and dynamic formulas. These methods require basic site measurements of blow count, pile set or in some instances pile temporary compression (otherwise known as rebound), and observation of hammer stroke. Although the practice is far from universal, it is important that the bearing graphs or dynamic formulas which use these measurements and observations be correlated against the PDA testing results. Too often dynamic formulas continue to be specified in their original formulation, with no consideration of reference to the more reliable PDA tests.

The particular role, importance, limitation and reliability of dynamic pile testing in driven piling projects is described in principle in (Seidel, 2015). In the significant majority of projects, the predominant use of dynamic pile testing is to infer the axial compression capacity of piles, and this paper will focus on this use. These capacity estimates are most reliably determined for dynamic testing using one of a number of proprietary wave-matching algorithms in which the static and dynamic pile-soil interaction to a hammer impact are modelled. Progressive adjustment of the models to achieve the best correlation between measured and predicted responses to the impact are assumed to define the most appropriate static and dynamic soil models and hence the most likely static capacity mobilized during the dynamic event.

INFERENCE OF CAPACITY FROM INPUT AND RESPONSE

Pile capacity is inferred from all test methods by the interplay between input energy and pile response.

For a static load test, the input energy is derived from the applied pile head force, and the response is the measured deflection of the pile-soil system. The capacity is determined from analysis of the load-movement response which is open to various interpretations (Fellenius, 1980).

For dynamic tests, the input energy is the downward travelling wave from the hammer, and the pile response is the reflected upward travelling wave, which is the recommended reference for the analytical wave matching process.

For those piles not specifically tested, the assumed energy delivered to the pile is most reliably based on site-specific PDA testing relevant to the specific hammer-pile-ground combination. This energy can be adopted in Wave Equation Bearing Graphs for the site, or entered in various dynamic formulas in lieu of standard assumptions. Otherwise, different formulas may be based on the manufacturer's rating (potential energy), assumed drop efficiencies (kinetic energy) or calculated using various assumed and measured parameters to infer energy delivered to the pile (transferred energy) e.g. the Hiley Formula (Hiley, 1925).

THE NEXUS BETWEEN ENERGY, CAPACITY AND PILE MOVEMENT

In order that piles can be installed and accepted without testing, there is always an implied Energy-Capacity-Movement relationship that underlies the acceptance process. Without such a relationship, it would not be possible to install driven pile foundations without testing each and every pile. This Energy-Capacity-Movement relationship is expressed in dynamic formulas, bearing graphs or target sets.

Bearing Graphs

Figure 1 shows Bearing Graphs for a hypothetical case in which 5 different hammer strokes (from 0.4m to 0.8m) are analyzed. The hammer weight and the drop efficiency are important inputs to the analysis, but are not critical to this discussion.

Each Bearing Graph expresses the relationship between capacity and blow count for the specific hammer stroke, and the corresponding energy delivered to the pile. In other words the Bearing Graph

is an Energy-Capacity-Movement relationship, and there is a spectrum of energy-dependent bearing graphs.

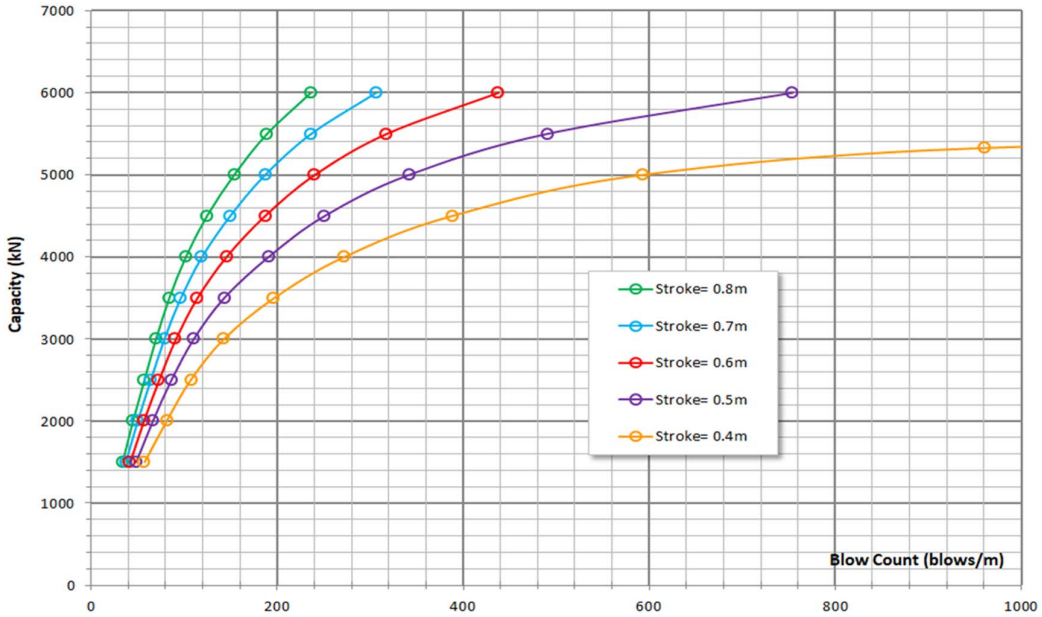


Fig. 1. Five Bearing Graphs for different hammer strokes and delivered energies

For any given (measured or assumed) energy, there is a relationship between capacity and pile movement. Any change in energy transferred to the pile correspondingly affects the capacity-movement relationship.

From Fig. 1, it can be seen that for a blow count of 200 blows/metre (equivalent to a set of 5mm/blow), then capacity may be as low as 3500 kN for a 0.4m stroke, but as high as 5650kN for a 0.8m stroke. These values are specific to the particular analysis assumptions. The range would be larger for a wider range of hammer strokes.

Measurement of pile movement, such as set or blow count is therefore an incomplete acceptance criterion unless energy is also measured or assumed. Refusal, which is a term often used to describe effective termination of driving, is therefore a relative term and does not provide an absolute value of pile capacity.

Dynamic Formula : Engineering News Record

The Engineering News Record formula from 1888 is given in Lawton et al. (1986) in the following form.

$$R_u = \frac{e_h E_h}{s + z}$$

The Capacity term is R_u. The energy term is $e_h E_h$, and the Movement term is $s + z$. The ENR formula is therefore an ECM relationship.

Dynamic Formula : Gates Formula

The original Gates Formula of 1957 is given in Lawton et al. (1986) in the following form

$$R_u = 27\sqrt{e_h E_H}\,(1 - \log s)$$

The Capacity term is R_u. The energy term is $\sqrt{e_h E_h}$, and the Movement term is $(1 - \log s)$. The Gates Formula is therefore an ECM relationship.

Dynamic Formula : Hiley Formula

The Hiley Formula from 1925 is given in Lawton et al. (1986) in the following form.

$$R_u = \frac{e_h E_h}{s + 1/2\,(c_1 + c_2 + c_3)} \frac{W + n^2 w}{W + w}$$

The Capacity term is R_u. The energy term is $e_h E_h \frac{W+n^2 w}{W+w}$,
and the Movement term is $s + 1/2\,(c_1 + c_2 + c_3)$. The Hiley Formula is therefore an ECM relationship.

Dynamic Formula : Modified Hiley Formula

In Australia and elsewhere it has been common practice for PDA testers to adopt a modified version of the Hiley Formula for correlation purposes. In this modification, the PDA measured energy EMX is used, and the set and temporary compression measured on the pile are adopted, hence

$$R_u = \frac{EMX}{s + c/2}$$

The Capacity term is R_u. The energy term is EMX ,and the Movement term is $s + c/2$. The Modified Hiley Formula is therefore an ECM relationship.

The context of ECM Relationships

Just as static load testing is the golden reference for the evaluation of a single pile capacity, the Energy-Capacity-Movement relationship which is intrinsic to the particular combination of piling hammer, driving system, pile and stratigraphy should be considered the golden reference for the determination of the capacity of the hammer-pile-foundation system. Naturally, if the stratigraphy changes and piles are significantly longer or shorter, or founded in different strata, the reference relationship will change accordingly.

Just as dynamic testing is subservient to properly performed static load testing for correlation purposes, so dynamic testing is also subservient to the Energy-Capacity-Movement relationship for evaluatio of the capacity of the foundation system as a whole. Each dynamic test and analysis provides an estimate of this underlying relationship, and the relationship is discovered by undertaking a holistic assessment of the set of dynamic test results. The individual dynamic test results must form a credible suite of results from which the relationship can be established to inform further piling.

A SYSTEM APPROACH USING A UNIFYING ENERGY-CAPACITY-MOVEMENT RELATIONSHIP

A properly implemented ECM relationship is necessary for a system approach to the piling process. Normally the ECM relationship would be developed over the first 5 or 6 piles tested, or over a smaller number of piles, but tested at different stages of driving which encompass a range of hammer energies and pile capacities.

Having established this unifying ECM relationship, thereafter, all piles – both tested and untested should be installed and accepted according to this standard. This is no different to normal practice for untested piles, except that the ECM relationship to which they are installed is rather constant, and is only modified on an 'as needs' basis as determined by subsequent testing.

The significant difference is that the tested piles are also accepted using the same ECM relationship determined in advance of the test, not based on the specific wave matching results for that pile. The underlying philosophy is that piles are not tested to provide contractual verification of isolated piles, but rather to provide an opportunity to review and if necessary amend the predetermined ECM relationship which underlies the whole foundation system.

It is important to understand this philosophy in the context of the following principles:

1. From a foundation system perspective, there is no particular significance of tested piles, as all piles should be installed with the same level of quality and risk to support the designated loads
2. The approval of piles should be on the basis of an integrated assessment in which the installation of untested piles is informed by the suite of test results, not segregated into piles which are approved according to different, unrelated and uncorrelated groups of piles separately verified by static testing, dynamic testing and dynamic formula approaches. Such an uncoordinated approach would result in piles being installed to different standards.
3. The vast majority of piles will be untested (typically 90 to 95%), and hence tested piles represent a relatively minor portion of the foundation system.
4. The highest priority should be given to establishing the unifying ECM relationship, and then ensuring that untested piles can be effectively monitored to ensure compliance of the whole foundation system.

Wave matching is still performed on the tested pile, but the analysis is undertaken in a timely manner, conducive to proper assessment of the data and with proper engineering judgement. As noted, the expectation is that the analysis will support the continuation of the ECM relationship being used to install piles generally, however, if the data indicates a distinct change in pile-soil interaction because of stratigraphic changes, the ECM relationship is revised accordingly. This approach results in a measured and holistic approach to the foundation system verification, and provides more consistent, stable and reliable pile acceptance criteria.

THE VARIABILITY OF DELIEVERED ENERGY

Having established the unifying Energy-Capacity-Movement relationship, it is necessary to implement this rigorously to determine capacity. That requires accurate assessment of pile movements (set and rebound as necessary depending on the relationship being used), and accurate measurement of energies being transferred to the pile.

As noted previously, various assumptions are made in relation to the energy delivered to untested piles. At best, these assumptions are based on actual measurements; at worst they are based on simplistic models of the pile driving event with poorly justified input parameters.

However what is common to all techniques in current practice is that the hammer efficiency is effectively assumed to be constant. As long as a hammer stroke is specified, the energy delivered is assumed to be constant to all piles. This assumption applies both to dynamic formulas and bearing graph approaches.

However, longitudinal studies of piling projects with dynamic testing measurements show that energy delivery varies considerably and unsystematically. In all cases presented, the nominated hammer stroke was constant for all pile tests. There was no intervention by the PDA operator to adjust the hammer energy, as may often happen when a tester encounters a lower than expected value based on

previous experience at the site. Therefore these cases represent unbiased samples of hammer performance, representative of the variability of hammer performance when untested piles are being installed.

Figures 2 to 4 show measurements of transferred energy from well-controlled projects with hydraulic hammers, and uniform hammer stroke requirements.

Case 1 in Fig. 2 is for a hydraulic hammer on a steel tube pile in near-shore conditions. Energy transfers varied by -16% / +20% about the average (36% range), with the minimum, average and maximum values being 265kJ, 316kJ and 380kJ respectively. The coefficient of variation (standard deviation/average) is 10.1%.

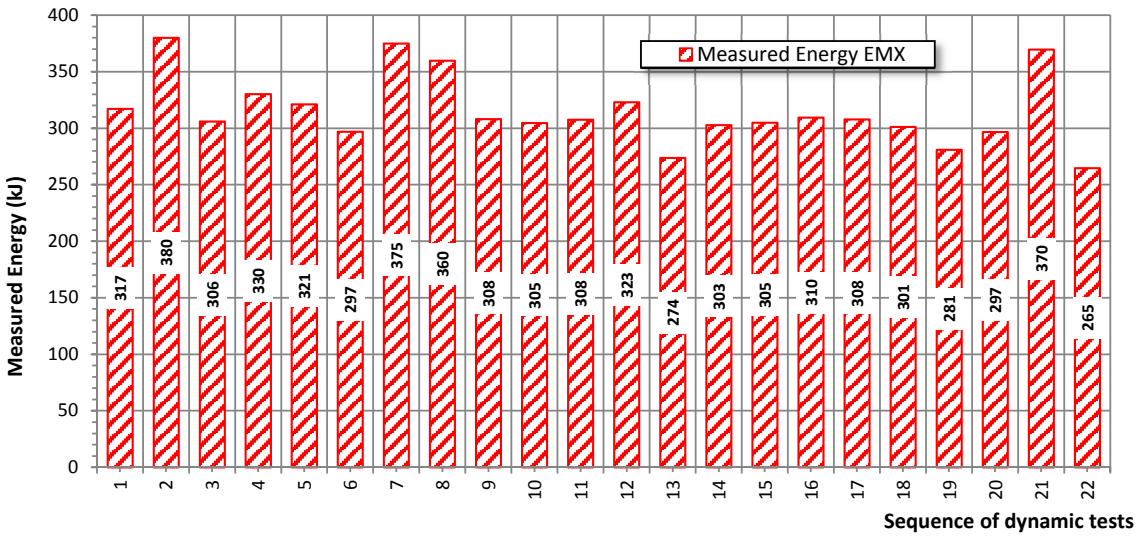


Fig. 2. Case 1 - Measured Energy transfers for hydraulic hammer on steel tube piles

Case 2 in Fig. 3 is for a hydraulic hammer on a steel tube pile, again in near-shore conditions. 43 piles were tested over the course of this project. Energy transfers varied by -20% / +20% about the average (40% range), with the minimum, average and maximum efficiencies being 69%, 86% and 103% respectively. The coefficient of variation (standard deviation/average) is 8.4%. The transferred energy efficiency of 103% implies that the actual stroke must have exceeded the nominated stroke. The histogram in Fig. 3 has a superimposed trendline which indicates that there was a progressive decline in the hammer performance over the course of the contract, on top of which there is random energy variability.

Case 3 in Fig 4. is for a hydraulic hammer on a prestressed concrete pile, for land-based piling. 155 piles were tested over the course of this project, and the results are shown in three separate histograms for clarity. Energy transfers varied by -46% / +31% about the average (77% range), with the minimum, average and maximum energy transfers being 37.5kJ, 69.2kJ and 91.0kJ respectively. The coefficient of variation (standard deviation/average) is 15.5%. The significantly higher range of energy transfer is likely primarily due to variable pile cushion thickness and condition.

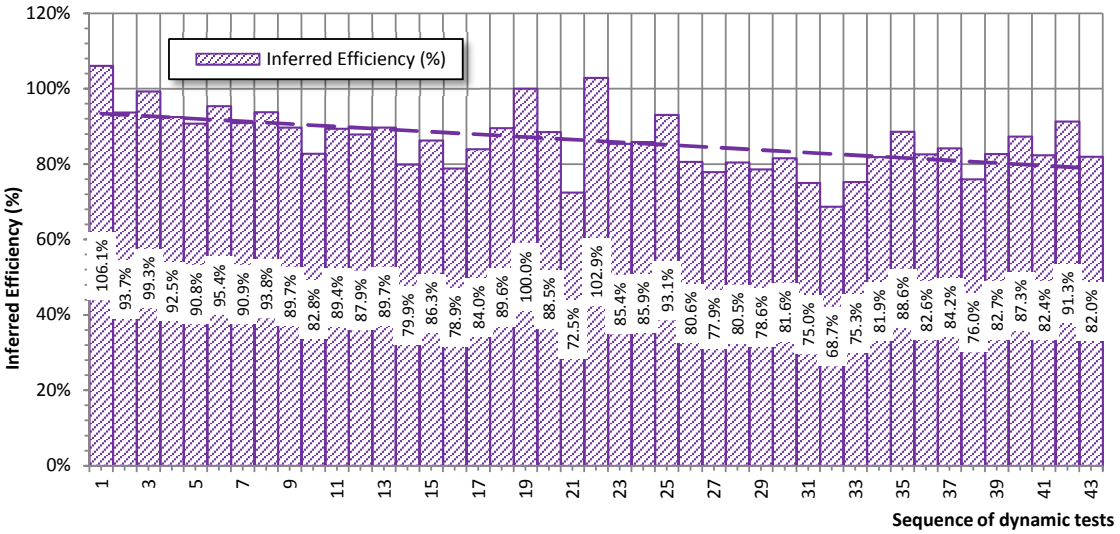


Fig. 3. Case 2. Measured Energy efficiencies for hydraulic hammer and steel piles

Causes of Hammer Variability

The potential causes of variability of hammer performance are likely to be extensive, but most importantly not recognized or detected by either the supervisory staff or the pile driving operators themselves. Reasons include

1. Inability to precisely control hammer stroke
2. Ambient temperatures
3. Length of continuous operation
4. Difficulty of driving
5. Temperature of the hydraulic circuits
6. Timing of the hydraulic controls
7. Hammer cushion condition
8. Pile cushion condition (concrete piles)
9. Wear / maintenance

CONCLUSIONS

Proper control of driven piling projects depends on development and implementation of an energy-capacity-movement relationship. Bearing graphs and dynamic formulas are all examples of energy-capacity-movement relationships used to accept untested piles. It is critically important that these methods are correlated to end of drive PDA testing.

In order to establish pile capacity, it is not sufficient to measure pile movements (e.g. blow counts, sets or temporary compression) – it is also necessary to know the delivered energy. Current practice is to assume hammer efficiency does not vary, only because there has been no practical way of estimating delivered energy for piles not specifically PDA tested.

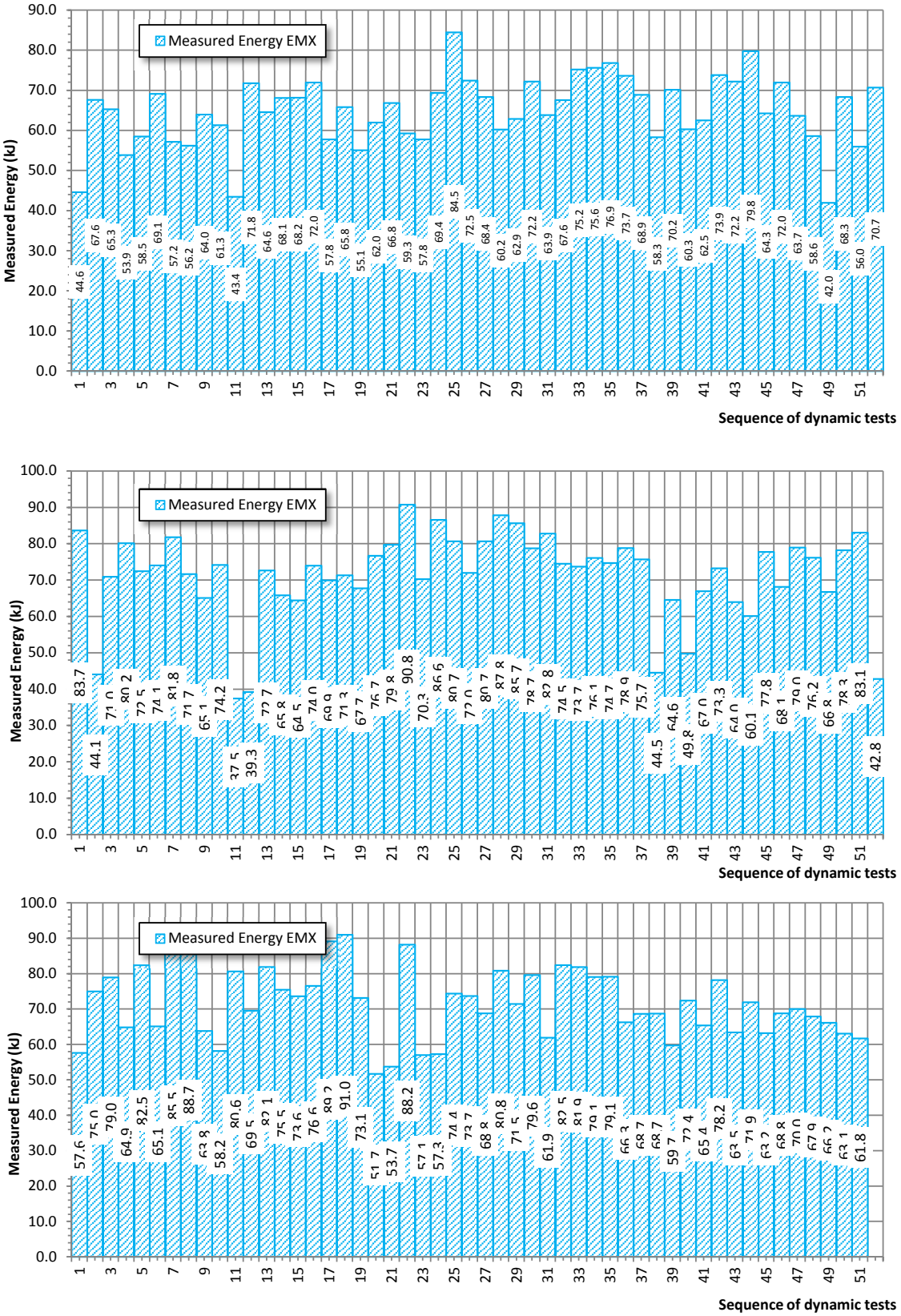


Fig. 4. Measured Energy transfers for hydraulic hammer and concrete piles

Longitudinal studies of energy transfers measured by PDA testing for 3 projects presented here show that transferred energies are not constant, but vary significantly and generally unpredictably over the course of a project. The two cases shown for steel piles show a 36% and 40% range. The case shown for concrete piles shows a 77% range.

The importance of verifying the energy delivered to each individual pile is demonstrated to be a necessary part of an effective QA system for driven pile foundations. Non-contact monitoring of piles using the Pile Driving Monitor (Seidel 2015) allows the movement-time response of piles to be measured with only the attachment of a reflective sticker on the pile. The velocity-time response of the pile can be derived from the movement, and the transferred energy can be correlated to the velocity response. This provides a practical way to monitor hammer performance and pile movements for every pile for implementation into the Energy-Capacity-Movement relationship.

REFERENCES

Fellenius, B.H. (1980). The analysis of results from routine pile loading tests. Ground Engineering, London, Vol. 13, No. 6, 19-31.

Hiley, A. (1925). A rational pile-driving formula and its application in piling practice explained. Engineering, 119 (3100) : 657-658.

Lawton, E. C., Fragaszy, R. J., Higgins, J. D., Kilian, A. P., & Peters, A. J. (1986). Review of Methods for Estimating Pile Capacity. In Transportation Research Record.

Rausche, F., Nagy,M. and Likins, G. (2008). Mastering the Art of Pile Testing. Proc. of the 8th Int'l Conf. on the Application of Stresswave Theory to Piles. Lisbon. J.A.Santos (ed) : 19-32

Seidel, J.P. (2015) Overview of The Role of Testing and Monitoring in the Verification of Driven Pile Foundations. 12th Australia New Zealand Conference on Geomechanics, Wellington, New Zealand.

THE MECHANISM OF GROUTING ACTION UNDER THE BASE OF BORED PILE

Adam Krasiński, Gdansk University of Technology, Faculty of Civil and Environmental Engineering, Poland, +48 58 347 10 44, akra@pg.edu.pl

Mateusz Wiszniewski, Gdansk University of Technology, Faculty of Civil and Environmental Engineering, Poland, mateusz.wiszniewski@pg.edu.pl

ABSTRACT

The grouting under the base of bored pile is carried out in order to reduce pile settlement and improve its bearing capacity. The principal aim of pressure grouting is to introduce an initial force between the soil and the pile base. In non-cohesive soil, the grouting can also enlarge the pile base area and therefore improve the base resistance. The example of static load tests on instrumented bored piles installed with and without grouting is presented. The interpretation and comparative analysis of both piles tests is carried out and gives interesting results. The conclusion of analysis is, that the grouting under the base primarily activates and increases the pile shaft resistance and thanks to it improves the characteristics of bored pile interaction with soil.

Keywords: pile foundation, bored pile, grouting under pile base, bearing capacity of pile

INTRODUCTION

Techniques for increasing the load-bearing capacity and stiffness of bored piles using cement injection under their bases have been practiced in Poland for about 20 years. Mostly used and well known are four technological solutions, that were described for instant by Gwizdała and Pinkowski (2007), Pinkowski and Gwizdała (2006), Gwizdała and Krasiński (2015). During the grouting injection, the following parameters are recorded: pressure and volume of the pressed grout or cement mortar, injection time, including the time of maintaining the maximum pressure and the value of the pile displacement in the upward direction. Values of these parameters in combination with static load test are essential for piles bearing capacity assessment. In order to evaluate the effectiveness of grouting, it would be more reliable to carry out comparative load tests on piles with and without grouting. Even greater reliability will be obtained when the load test is performed with detailed measurement of pile shaft and base participation in the external load transfer.

In this work, the essence of the grouting injection under the pile base was analyzed and an example of instrumented pile load test according to the above-proposed procedure was presented. The example concerns testing of large diameter piles, used for the foundation of the main bridge support over the Odra River in Wrocław (Poland). Two cases of piles were studied – one without and the other with the grouting under the base. Measurements of the axial force distribution in the pile core, carried out with the use of vibrating wire extensometers, provided valuable information on the pile-soil interaction and the grouting impact on that interaction.

THE WORK PRINCIPLE OF GROUTING UNDER THE BASE OF A BORED PILE

The purpose of the pressure grouting is an induction of some initial compressive force between the base of the pile and the subsoil. On the pile side, this force is absorbed by pile weight and by the soil friction along the pile shaft, which acts downwards (f_{s1} in Fig. 1). With respect to the soil underneath the pile base, strength of the injection causes its pre-stressing and consolidation. At the same time, relaxation and disturbance of the soil structure created during the drilling are also reduced. In non-cohesive soils, a certain volume of soil is additionally cemented and the effective area of the pile base increases. The injection pressure p_{in} should be adjusted, so that it causes the pile to be moved up (s_{p1}), however, but not more than 5 mm. In addition, the maximum pressure should be sustained for a specified period of time and held until the cement grout has hardened.

© 2018 Deep Foundations Institute

The value of a pre-generated force in the pile base cannot be calculated directly from the injection pressure. As a result of various pressure losses and as a result of soil consolidation under the pile base, the permanent force value in the base (Q_{b1}) is 30% to 50% lower than the initial value (calculated on the basis of the injection pressure p_{in}). In Fig. 1, values of resistance and displacement corresponding to the moment of injection activation are marked on the graphs by points A, and stabilized values (permanent) - by points B. The points A' and B' indicate the displacement (settlement) of the soil under the pile base, caused by the injection pressure, which are in fact not measurable.

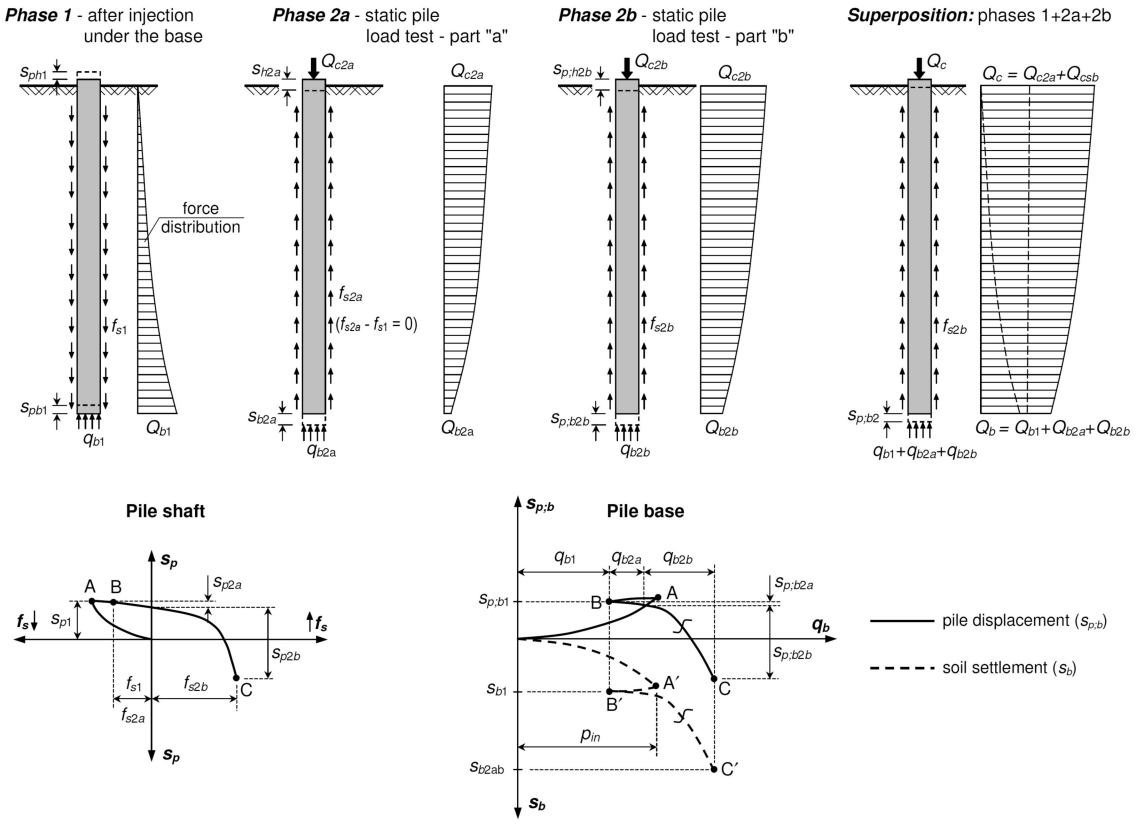


Fig. 1. Schematic work idea of the pressure grouting under the pile base

During the transfer of external loads (eg. during a load test), a significantly smaller settlement of the pile with injection than the pile without injection is observed. From the schematic diagram in Fig.1, it follows that the decrease in pile settlement value is primarily the result of the specific work of the pile shaft. When loading a pile, firstly shaft friction f_{s1} induced by the injection (directed downwards) is reduced to zero by friction f_{s2a}, and then the friction direction is reversed upwards and continuously mobilized to the value f_{s2b}. As a result, the resistance of the pile shaft, reaching in the final phase to point C, can even be doubled ($f_{s1} + f_{s2b}$). Additionally, when taking into account that soil during reloading behaves much stiffer then during primary loading, it results in greater stiffness of the pile in the initial load stages. Pile base resistance, during a static load test achieves a relatively small value ($Q_{b2a} + Q_{b2b}$) and also shows reduced stiffness, but it must be noted that this resistance is added to the already existing force generated by the injection (Q_{b1}).

It is believed, that the grouting injection increases the initial pile stiffness, but does not increase the load-bearing capacity of the pile R_{ult}. However, determining the design pile load capacity R_d, according to the criterion of allowable settlements, it can be concluded that the injection certainly increases the pile bearing capacity. On the other hand, the pile bearing capacity increases when as the injection result soil is cemented and the effective area of the pile base is increased.

A PRACTICAL EXAMPLE OF TESTING INSTRUMENTED BORED PILES WITH BASE GROUTING

The example refers to large diameter bored piles used for the foundation of suspended bridge over the Odra River in Wrocław. A detailed description of foundation, ground conditions, calculation analysis and the basic results of pile load tests are presented by Cudny et al. (2010), Dembicki et. al. (2013) or Krasiński and Sieńko (2010ab). 160 piles of diameter D = 1500 mm and effective length L = 18.0 m were used for the bridge slab foundation (Fig. 2). Piles were drilled in casing and with grouting base injection according to the Polish Road and Bridge Research Institute solution (see Fig. 3 and Gwizdała and Krasiński, 2015). The bottom of the foundation slab was placed at a depth of approximately 4.0 m below the ground level. Piles were installed in the ground, where the upper part consists of 5-7 m river sediments in the form of medium dense and dense sand and gravel. Below is a significant layer of hard pleistocene clays. The Fig. 2 presents charts of two cone penetration tests CPTU1 and CPTU2, which location in relation to the foundation plan is also shown. Clays showed no swelling properties.
Based on Polish Code PN-83/B-02482, design bearing capacity of pile was determined as $R_{c;d} \approx 7500$ kN. The influence of pile base injection was neglected in calculations. It was treated as an additional safety reserve and pile settlement reduction.

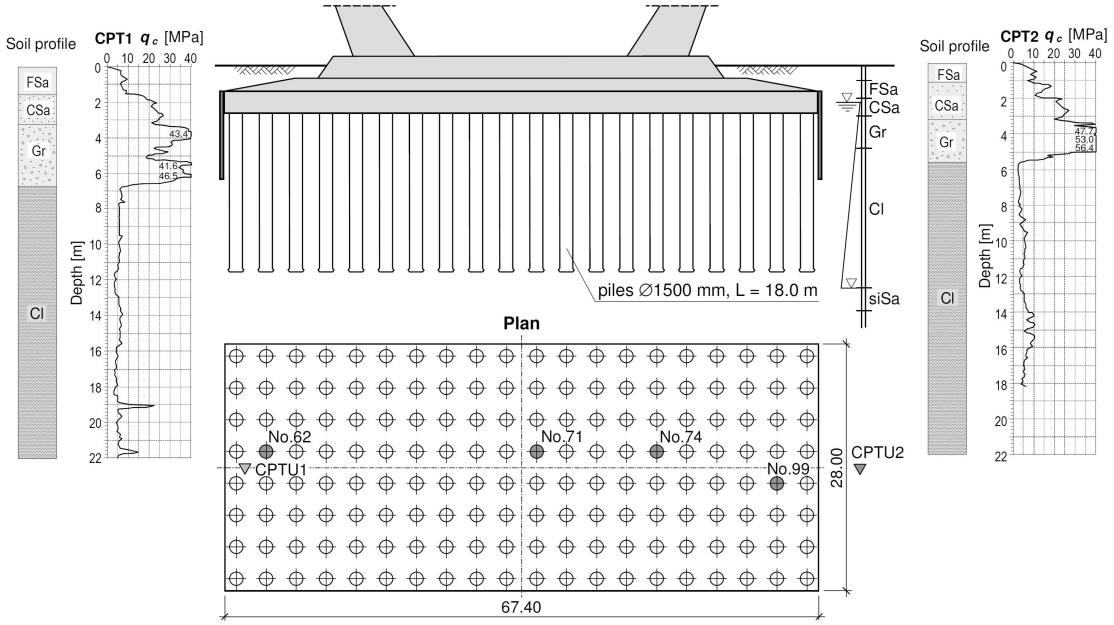


Fig. 2. Plan of the pile foundation of the main bridge support over the Odra River in Wrocław

As part of the research, static loads of four piles were carried out: No. 62, 71, 74 and 99. The basic settlements graphs are shown in Fig. 4. This article focuses on the results of two pile tests, No. 62 and 99. In general, both piles were installed in the same technology - by boring in casing. After steel casing tube installation, drilling in dry condition was carried out, so as not to cause excessive saturation of clayey soil and deterioration of their mechanical properties. For pile No. 62 base grouting was injected, while pile No. 99 was executed without injection. Grouting was carried out through injection tubes fitted in the lower part with rubber valves (manchetties) (Fig. 3). An injection instrumentation, fixed to the pile reinforcement and equipped with a separation membrane, was inserted into the pile hole just before concreting. During that process, injection tubes were filled with a bentonite suspension. About three weeks after, the injection process was carried out. Cement grout was pumped at a pressure of 1.5 MPa. During injection, which lasted 40 minutes, 420 liters of grouting mix were pumped in. Pile head lift 1.2 mm up. In the final phase, valves were closed at the upper tube ends and the pile was left for cement grout to harden.

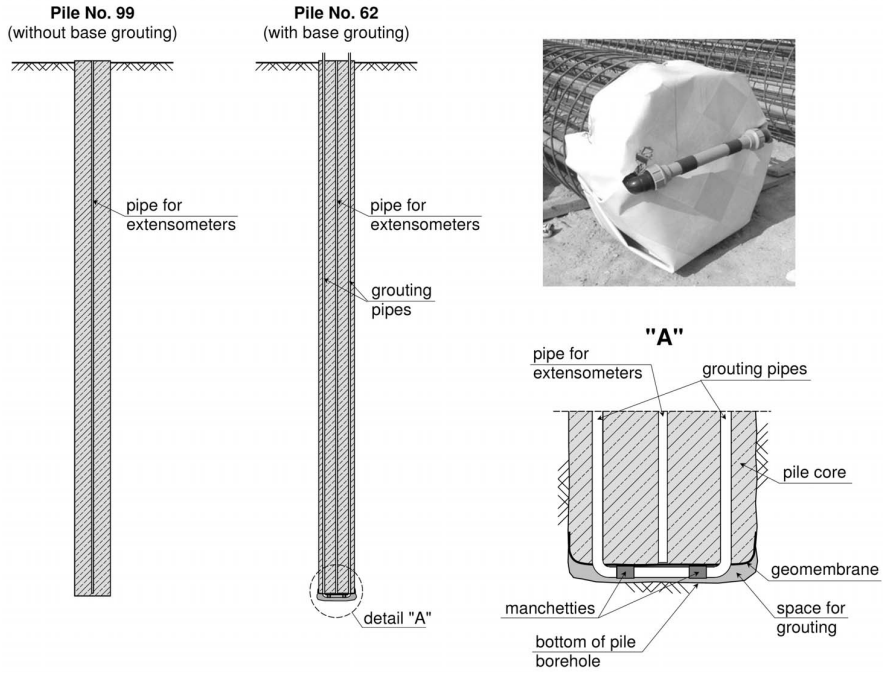


Fig. 3. Constructions of tested piles No. 62 and 99

Both piles were tested with the axial force distribution measurement. A vibrating wire extensometers were applied. It should be noted that these were the first static tests of this kind in Poland (in 2008). The operating principle of the measurement system is widely known. It has been described in detail in several publications (e.g. Bustamante and Doix, 1991; Fellenius, 2001, 2002; Krasiński and Sieńko, 2010), and also used several times in the author's subsequent research (Krasiński, 2011ab, 2012, 2013, 2014; Krasiński and Kusio, 2015b; Krasiński and Wiszniewski, 2017).

Fig. 4 shows a very clear and positive effect of the grouting. After exceeding the force value $Q \approx 4000$ kN, a larger settlement growth in the pale without injection is observed. For the force $Q_{max} \approx 11000$ kN, pile without injection showed about three times greater settlements ($s \approx 31{,}5$ mm) than piles with injection ($s = 10 \div 12$ mm). It should also be noted that settlement stabilization periods in individual load stages were shorter in case of piles with the injection under the bases.

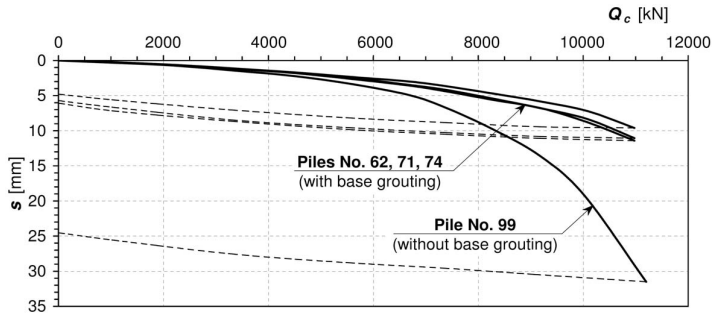


Fig. 4. Plots of foundation piles settlement from static load tests

MEASUREMENT RESULTS AND ANALYSIS

The applied measurement technique with the use of vibrating wire extensometers, made it possible to measure the strain in individual pile sections, during subsequent load stages. There were seven such sections in the tested piles (Figs. 5 and 6). Based on deformations, the values of axial forces Q_i, which were located in the middle of each section, were calculated. These forces were average values on the

length of individual sections. To calculate the forces, it was necessary to adopt the appropriate longitudinal pile core stiffness *EA*. The value of this stiffness, however, may change with strain and depth (eg. due to even small changes in the pile diameter). The adoption of a constant concrete stiffness modulus value *E* and its determination on the basis of general recommendations, e.g. from tables based on concrete class, is not very precise and leads to erroneous results interpretation (Fellenius et al., 2000; Fellenius, 2001; Kai et al., 2006; Lam and Jefferis, 2011; Sinnreich, 2011). In the analysis, the *EA* value was determined as strain and depth dependent, by using author's original iterative method, which is directly based on extensometer measurements. The method details will be published soon.

Another significant problem related to the interpretation of extensometer measurements concerns the occurrence of an initial axial force in the pile shaft. Determining the value of this force is difficult and complicated. The sensors are installed in the pile just before the load test and allow to register only the deformations, and consequently the forces in the pile shaft, occurring during the load test. Some propositions concerning the initial force value determination in the pile were presented by the author in publication (Krasiński, 2012). The problem of initial force is particularly important in the study of driven piles and piles with pressure grouting under the base. As mentioned earlier, the main task of the injection is to introduce such force into the pile shaft. The problems described above, as well as others, have been known since the beginning of the instrumented pile testing study and have been characterized in many papers (e.g. Chong, 2009; Fellenius et al., 2000; Fellenius, 2001, 2002; Kim et al., 2011; Sahajda, 2015; Siegel, 2005). The distributions of axial forces Q_i in piles No. 99 and 62 obtained from measurements and interpretation are shown in Figures 5 and 6.

It should be noted, that the axial force distributions shown in Figs. 5 and 6 differ slightly from the distributions from the same tests presented in previous publications (Cudny et al., 2010, Dembicki et. al., 2013 or Krasiński and Sieńko, 2010ab). The differences result from the concrete stiffness modulus taken to interpret the measurement results. Graphs presented in above mentioned papers were obtained assuming a constant value of the concrete modulus *E*, determined on the basis of concrete class.
In addition, during testing of both piles, measurement problems occurred, which were discovered during the interpretation. They consisted of too weak anchoring of some extensometer gauges and the phenomenon of anchors "slipping" inside the tubes. For this reason, when interpreting the measurements from the pile No. 99, the measured values from gauges G1 and G2 and also G4 and G5 were summarized (see Figs. 5 and 7). Whereas, when interpreting the measurements from the pile No. 62, the measured values from the G2 and G3 gauges were summarized (see Figs. 6 and 8).

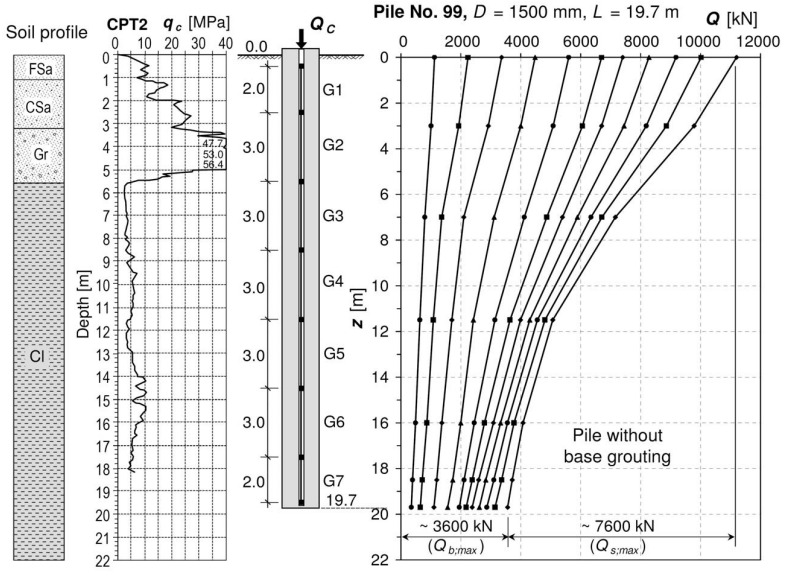


Fig. 5. The axial force distribution in pile No. 99

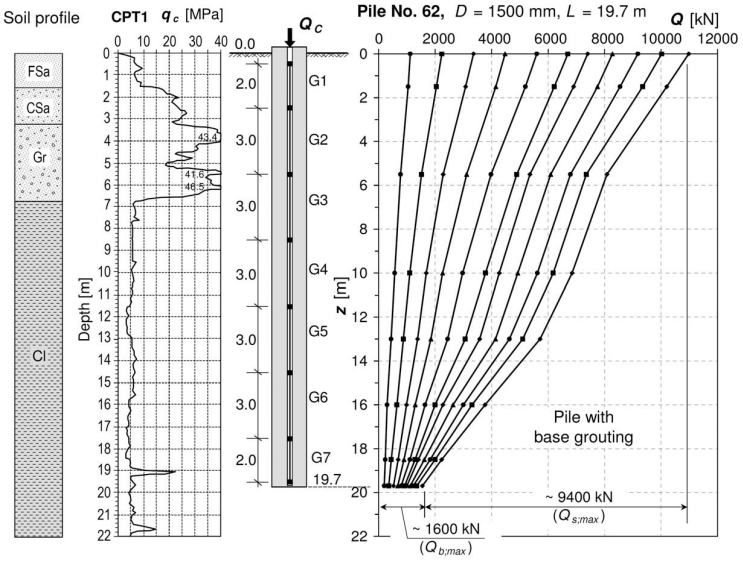


Fig. 6. The axial force distribution in pile No. 62

Even a cursory analysis of the graphs presented in Figs. 5 and 6 allows to notice a significant difference in their shapes, which results from a different distribution of external load carried by pile shaft (Q_s) and pile base (Q_b) in both studied piles. In the pile No. 99 (without base grouting), the load part carried by the base in the final testing phase reached the value $Q_{b;max} \approx 3600$ kN, and in the pile No. 62 (with the base grouting) less than a half of that value, reaching $Q_{b;max} \approx 1600$ kN. The reverse relation is of course in the loads transferred by the pile shaft resistance Q_s.

Therefore, it can be concluded that the grouting injection under the pile base, ideologically illustrated in Fig. 1, has been confirmed. Figures 7 and 8 present the results of further test interpretations in the form of soil unit resistance mobilization diagrams in relation to pile displacement, resistance along the pile shaft f_s and resistance under the pile base q_b. The f_{si} values should be understood as an averaged from the length of individual measurement sections, which, however, do not always coincide with the soil layers in the substrate.

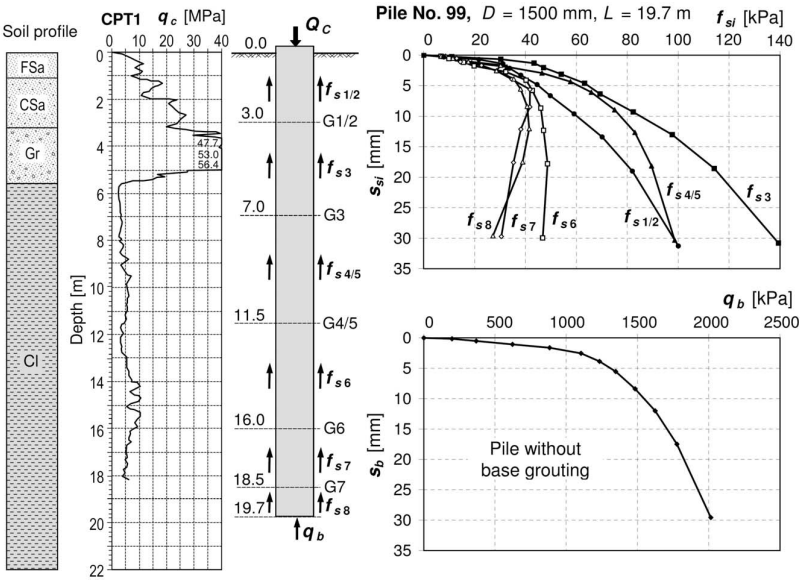


Fig. 7. Plots of soil resistance along the shaft and under the base of pile No. 99

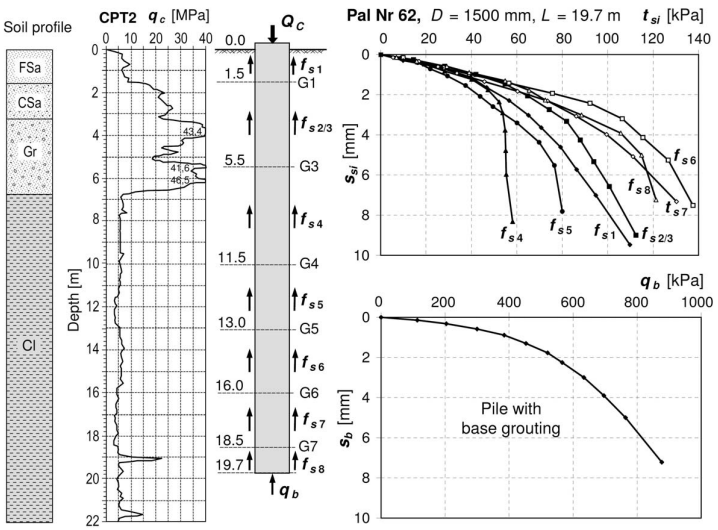


Fig. 8. Plots of soil resistance along the shaft and under the base of pile No. 62

From the results presented above, the values of unit resistance f_{s6}, f_{s7} and f_{s8}, registered in the lower sections of piles in the clay layer, are of particular interest. In the pile No. 99 (Fig. 7), these resistances reach maximum values of 40 kPa, with displacements of 5-10 mm and are subjected to reduction with further displacements, which is typical for this type of soil. However, in the pile No. 62 (Fig. 8), the same clay resistances f_{s6}, f_{s7} and f_{s8} were recorded at values about three times higher, about 120-140 kPa and which, with displacements of around 8 mm, have not yet achieved full mobilization.

It can therefore be concluded, that as a result of pile base grouting injection, the frictional resistance f_s of clay in the lower pile sections has more than doubled. This increase may additionally result from differences in mechanical parameters of soils around both piles, as well as from the effect of soil strengthening in the lower zone of pile, caused by the grouting pre-stressing.

In Fig. 9, resistance curves q_b of both piles are presented in the same stress and displacement scale. Results were plotted in such a way that the graph from pile No. 62 was relatively smoothly transformed into the graph of the pile No. 99. Therefore, with a large approximation, the value of permanent stress $q_{b1} \approx 700$ kPa was estimated in the ground under the pile base. According to the machine data, the pressure of cement grout during the injection was equal to 1500 kPa. It can consequently be concluded that the lasting effect of this pressure, in the studied case, more or less decreased by half.

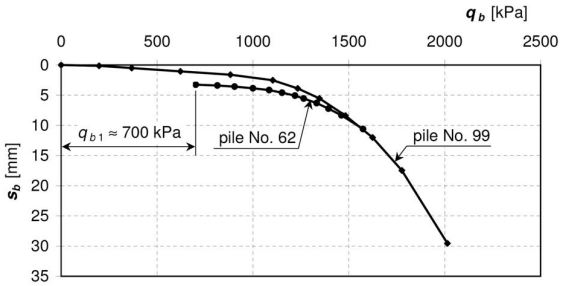


Fig. 9. Estimation of the initial stress q_{b1} under the pile base, generated by grouting injection

CONCLUSIONS

The tests described in the article showed that the grouting injection under the base of a bored pile is reasonable and significantly increases stiffness and design bearing capacity of piles. A reliable statement of this fact requires a construction of comparative pile load tests with the base injection and without.

The practical example presented in the article also indicates that it is very expedient to perform pile testing with the measurement of axial force distribution along pile shaft. Such a measurement not only allows to more accurately verify the effectiveness of grouting injection, but also to get to know the essence of its operation and the characteristics of soil structure interaction.

Although the primary purpose of base injection is to pre-stress its substrate, it has been found that this treatment also activates increased soil resistance along the pile shaft. According to theoretical analysis, the resistance along can increase twice and according to the research - even three times, especially in the lower pile sections.

The example described in the article concerns a single case of testing an instrumented bored pile with grouting injection and it was one of the first such a research in Poland. The obtained results do not allow yet to formulate main conclusions and to propose generalizations. The author, however, is convinced that this type of research will gain more popularity and after collecting a sufficient database, more generalization will be possible. After that, a long-awaited, reliable method for design of piles with base grouting and prediction of their behavior in the soil will be developed.

REFERENCES

Bica A.V.D., Prezzi, M., Seo, H., Salgado R. and Kim D., 2013. Instrumentation and Axial Load Testing of Displacement Piles, Lyles School of Civil Engineering Faculty Publications, Paper 6.

Bustamante M. and Doix B., 1991. A new model of LPC removable extensometers. Proceedings of 4th Int. Conf. on Pilling and Deep Foundations, STRESA, Italy, April 7-12.

Chong Y.W., 2009. Use of Instrumented Static Pile Load Test Results as a "Crystal Ball", Proceedings of the 17th International Conference on Soil Mechanics and Geotechnical Engineering, 5-9.10.2009, Alexandria, Egypt.

Cudny M., Krasiński A., Załęski K. and Dembicki E., 2010. Fundament pylonu mostu podwieszonego w ciągu autostradowej obwodnicy Wrocławia (A8). [Pylon foundation of a cable stayed bridge at the motorway rig road of Wrocław (A8)]. Mosty, nr 2, pp. 36-41 (In Polish).

Dembicki E., Cudny M., Krasiński A. and Załęski K., 2013. Pylon foundation of a cable stayed bridge at the motorway rig road of Wrocław. Proceedings of the 18th International Conrefence on Soil Mechanics and Geotechnical Engineering, Paris, pp. 2715-2718.

Fellenius, B.H., Brusey, W.G. and Pepe, F., 2000. Soil setup, variable concrete modulus, and residual load for tapered instrumented piles in sand. ASCE Specialty Conf. on Performance Confirmation of Constructed Geotech. Facilities, University of Massachusetts, Amherst, USA, April 9-12, 2000.

Fellenius B.H., 2001. From strain measurements to load in an instrumented pile. Geotechnical News Magazine, Vol. 19, No. 1, 2001, pp. 35-38.

Fellenius B.H., 2002. Determining the resistance distribution in piles, Part 1: Notes on of no-load reading and residual load. Part 2: Method for determining the residual load. Geotechnical News Magazine. 20(2): pp. 35-38 and 20(3): pp. 25-29.

Gwizdała K. and Pinkowski A., 2007. Wpływ iniekcji pod podstawą na osiadanie pali wierconych w piaskach. [The influence of grouting under the base on bored piles settlement in sands]. Inżynieria i Budownictwo, r. 63, nr 7-8 (In Polish).

Gwizdała K. and Krasiński A., 2015. Zastosowanie pali wierconych wielkośrednicowych w fundamentowaniu obiektów mostowych. [The application of large diameter bored piles in bridge foundation]. Mosty, nr 4, pp. 24-29 (In Polish).

Kai S. L., Kian T. L. and Huat T. A., 2006. Analysis of strain-dependent concrete modulus from mass instrumented test pile samples, 10th Int. Conf. on Piling and Deep Foundations, June 2006, Amsterdam.

Kim, S.R., Chung, S.G., and Fellenius, B.H., 2011. Distribution of residual load and true shaft resistance for a driven instrumented test pile. Canadian Geotechnical Journal, (48)4, pp.583-598.

Krasiński A. and Sieńko R., 2010. Pomiar pionowego rozkładu siły w palu podczas testów statycznych. [The measurement of vertical force distribution in the pile during a static load tests]. 56 Konferencja Naukowa Kielce – Krynica 19-24.09.2010. (In Polish).

Krasiński A. and Sieńko R., 2010. Wykorzystanie pomiaru pionowego rozkładu siły w palu do interpretacji testów statycznych [Use of vertical force distribution measurement in pile to static load tests interpretation]. Magazyn Autostrady, nr 11, pp. 24-28. (In Polish).

Krasiński A., 2011. Advanced field investigations of screw piles and columns. Archives of Civil Engineering, LVII, 1, pp. 45-57;

Krasiński A., 2011. Wyniki badań terenowych pali i kolumn wkręcanych [The results of field tests on screw piles and columns]. Inżynieria Morska i Geotechnika nr 6, pp. 516-530 (In Polish).

Krasiński A., 2012. Problematyka interpretacji pomiarów rozkładu siły osiowej w trzonie pala podczas próbnych obciążeń statycznych. [Problems with the interpretation of axial force distribution measurements during static pile load tests]. Inżynieria Morska i Geotechnika, nr 2, pp. 118-124 (In Polish).

Krasiński A., 2013. Pale przemieszczeniowe wkręcane. Współpraca z niespoistym podłożem gruntowym. [Screw displacement piles. Interaction with non-cohesive soil]. Monografie, Nr 134, Wydawnictwo Politechniki Gdańskiej, Gdańsk, p. 250 (In Polish).

Krasiński A., 2014. Numerical simulation of screw displacement pile interaction with non-cohesive soil. Archives of Civil and Mechanical Engineering. Vol. 14, No 1. pp. 122-133.

Krasiński A. and Kusio T., 2015. Pile model tests using strain gauge technology. Studia Geotechnica et Mechanica, 37 (3) pp. 49–52.

Krasiński A. and Wiszniewski M., 2017. Static load test on instrumented pile - field data and numerical simulation. Studia Geotechnica et Mechanica, Vol. 39, No. 3, pp. 17–25.

Lam C., Jefferis S. A., 2011. Critical assessment of pile modulus determination methods, Canadian Geotechnical Journal, Vol. 48, No. 10: pp. 1433-1448.

Omer J.R., Delpak R. and Robinson R.B., 2002, Instrumented load tests in mudstone: pile capacity and settlement prediction, Can. Geotech. J., 39, pp: 1254–1272.

Pinkowski A. and Gwizdała K., 2006. Analiza wpływu iniekcji pod podstawami pali wierconych. [The

analysis of grouting under the bases of bored piles]. Zeszyty Naukowe Politechniki Białostockiej. Budownictwo, 2006, nr 28. XIV Krajowa Konf. Mech. Gruntów i Fundamentowania, Augustów-Białystok, t. 2 (In Polish).

Sahajda, K., 2015. Siły rezydualne w ocenie nośności i osiadań żelbetowych pali wbijanych [Residual forces in the assessment of bearing capacity and settlement of reinforced concrete driven piles]. PhD Thesis. Warsaw University of Technology. (In Polish).

Siegel, T.C. and McGillivray, A., 2009. Interpreted residual load in an augered cast-in-place pile. 34th Annual Conference on Deep Foundations, Deep Foundations Institute, 173-182.

Sinnreich J., 2011. Strain Gage Analysis for Nonlinear Pile Stiffness, Can. Geotech. J., 35, No. 2

THE NORMALIZED BEARING GRAPH AND DYNAMIC REDUCTION FUNCTION CONCEPTS IN PILE ACCEPTANCE

Julian P. Seidel. Foundation Specialists Group, Melbourne, Victoria, Australia, +61 417 501 275 jseidel@foundationspecialists.com.au

ABSTRACT

As discussed in a companion paper to this conference, Wave Equation bearing graphs, and pile driving formulas are all forms of an Energy-Capacity-Movement (ECM) relationship which are used to accept driven piles which are not specifically tested. As it is generally impractical to test every pile, all these approaches have in common that they can be applied on site in real time using very basic measurements of pile movement and observations of hammer stroke.

The Wave Equation concept provides a more realistic model of the dynamic interaction of the hammer, pile and soil. From this analysis, the relationship between Capacity and Blow Count is shown graphically as a so-called Bearing Graph. There is actually a suite of Bearing Graphs for different hammer efficiency assumptions. Bearing Graphs can be considered to provide a reference ECM relationship against which the reliability of dynamic formulas can be evaluated.

This paper is based on a parametric study using the Wave Equation program, GRLWEAP (2003). The study shows that the modified Hiley Formula, duly corrected by a Dynamic Reduction Factor (DRF) reproduces the Wave Equation-predicted capacity-blow count relationships.

This paper also demonstrates how a suite of Wave Equation bearing graphs can be reduced to a single normalized graph.

Keywords: pile acceptance, pile driving formula, GRLWEAP, PDA, DRF

INTRODUCTION

Prior to the development of the Wave Equation concept by Smith (1960) and instrumentation that allowed stresswaves to be measured during installation, pile driving formulas were used in conjunction with static load testing for pile driving control. Dynamic (PDA) pile testing (Rausche et al., 2008) has been in common use since 1980s. Because the tests can be concurrent with the driving process, they provide the opportunity for establishing a direct relationship between hammer energy, pile capacity and pile movement (ECM relationship). The ECM relationship is the fundamental basis of pile termination/acceptance as discussed in a companion paper to this conference by Seidel (2018).

Pile driving formulas are used internationally as a form of construction control and pile acceptance, because there is a need for simple methods of pile acceptance for the majority of piles which are untested. However, these formulas are generally based on simplistic models of pile driving. The reliability of the better known pile driving formulas has been compared with static load tests by many researchers, typically with confusing and disappointing results. Some of the reasons for the poor reliability of dynamic formulas are discussed in the following.

HISTORICAL EVALUATION OF DYNAMIC PILE DRIVING FORMULAS

Much of the literature on the reliability of pile driving formulas predates the common use of PDA testing, which began to be used on driven piling projects in the 1980s. The studies were necessarily limited to the technologies available at that time.

Fundamentally, pile driving formulas seek to equate the energy applied by the hammer to the pile with the work done overcoming the resistance of the soil, which is taken to be the capacity of the pile. The

© 2018 Deep Foundations Institute

pile movement is the pile response to the applied hammer energy, which all pile driving formulas seek to interpret in terms of pile capacity.

Hammer Energy

In considering the interpretation of a pile driving event, what is important is the actual energy transferred from the hammer to the pile through the capblock, hammer and pile cushions. Since the advent of dynamic pile testing, it has been possible to measure actual energy transfer to the pile, but prior to that the energy delivered to the pile was unknowable. Different formulas therefore use manufacturer's rated energy (potential energy), or assumed drop efficiencies (giving the impact kinetic energy) or attempt to simplistically calculate the transferred energy by considering relative hammer and pile weights and the energy loss in the transfer.

It is now known that different hammer types have different but broad normal efficiency ranges and that the transferred energy not only depends on many variables of hammer operation, but also on the pile and soil characteristics, none of which can be captured in a formula approach.

Therefore, in historical studies of pile driving formulas, the adopted energy assumptions were inevitably unreliable.

Reference Static Capacity

The reference capacity used in evaluations of pile driving formula are typically static load tests. Fellenius (1980) has discussed both the potential errors in loads inferred from the pressure of hydraulic jacks and that the many methods of interpretation of static load testing cited in the literature can result in a wide range of inferred static capacities. These significant issues with the reference capacity value will not be considered further here.

What is not generally considered, however, is that the static load testing is conducted many days or even weeks after the pile installation. Static load testing therefore provides a reference capacity specifically relevant to the time of the test, which will normally be different to the capacity of the pile at the time of installation due to the phenomena of pile set-up or relaxation which is well documented (e.g. Samson and Authier (1986) amongst many others).

On the other hand, any pile capacity assessments at end of drive, whether by PDA test or by pile driving formula will be particular to the soil resistance only at the time of installation. It is valid to compare pile driving formulas with PDA tests (which estimate capacity at the same time). However, directly comparing pile driving formulas with static load tests is not valid unless there is no setup or relaxation.

Driving Resistance

The form of the pile driving formulas implies that the capacity which is predicted is the static capacity of the pile (at the time of installation). However, as is well understood from the work of Smith (1960) the resistance to driving is not only static, but also includes a dynamic component which is not present during subsequent static loading from the supported structure.

The primary challenge of dynamic pile testing methods and associated Wave Matching analysis techniques is to isolate the dynamic component of the driving resistance so that a reliable static capacity can be inferred from the pile driving event.

Pile driving formulas therefore do not predict static capacity, but predict driving resistance, and therefore should be corrected so that the effect of the dynamic resistance is removed.

Poor Correlations

The physical models which underlie dynamic formulas are simplistic representations of a complex dynamic hammer-pile-soil event, much more appropriately modelled using a one-dimensional wave theory analogy. It would be unreasonable to assume that these simple models can reliably predict pile capacity.

However, the problems with historical comparisons of pile driving formulas with static load testing are in large part a result of the assumptions inherent in those comparison studies, as noted above.

The use of pile driving formulas should always be correlated or referenced to Wave Theory-based approaches.

AN ALTERNATIVE APPROACH TO EVALUATING PILE DRIVING FORMULAS

Given the fundamental difficulties with historical studies of pile driving formulas discussed above, it is clear that two of the primary difficulties can be overcome by undertaking a comparison of the pile driving formulas with dynamic pile testing and associated Wave Matching analysis of pile capacity (Rausche et al., 1985).

Comparison of Pile Driving Formula with PDA Testing

For comparisons with PDA testing, both the actual transmitted energy is known (the PDA EMX parameter) and the pile driving formula and Wave Equation estimate of capacity both reference the same capacity which exists at the time of the test. What remains to be assessed is the reliability of the pile driving formula, and the overestimation due to the formula's computation of driving resistance rather than static capacity.

In fact, when as is common in PDA practice in Australia, a correlation factor is applied to the modified Hiley Formula, subsequently described as the Energy Formula (Paikowsky and Chernauskas, 1992), this comparison is being undertaken, and the derived correlation constant encapsulates errors in both the model and the dynamic resistance embedded in the pile driving formula.

The modified Hiley Formula or Energy Formula is as follows. EMX is the transferred energy to the pile from PDA measurements, and the set, s and temporary compression, c are measured on the pile. As noted previously, R_u is generally assumed to be the estimate of static capacity, whereas it is in fact the driving resistance.

$$R_u = \frac{EMX}{s + c/2}$$

Figure 1 compares the ratio of Modified Hiley Formula to wave-matched dynamic pile testing capacity estimates for a long floodplain bridge project. Each data point represents an individual comparison, and the trendline, and ±10% trend-lines are superimposed. By conventional practice, an average correction constant of between 0.71 (or 1/1.4) and 0.77 (or 1/1.3) might be applied to the Modified Hiley capacity estimates.

However, it can be observed that the ratio is not constant, but tends to increase with increasing pile set, which suggests an increasing contribution of dynamic resistance as a component of overall driving resistance, requiring a larger correction.

Secondly, it is well known that wave matching does not result in a single unique capacity estimate. In the author's experience, for normal data, valid matching solutions will have total capacities within a ±10% range. The ±10% bands on the trend-line demonstrate that with few exceptions the ratios fall within these bounds.

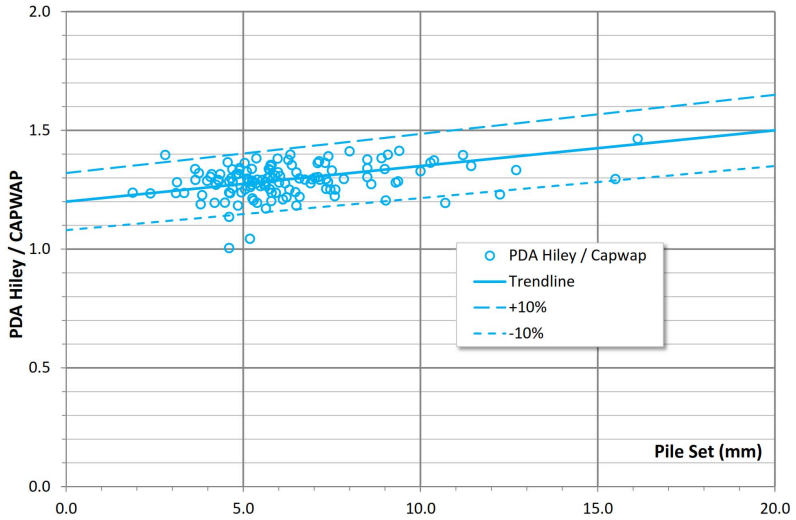


Fig. 1. Typical relationship between Modified Hiley Formula and Capwap

In fact, as shown in Fig. 2, it is quite reasonable that at higher pile sets, the overall driving resistance has a more significant dynamic resistance component, and that the pile driving formula estimate must be discounted by an increasing amount with higher set.

In hard driving, when pile sets are low, pile motion is limited, and dynamic resistance is low – the classic example would be a pile driven to strong rock, where high end bearing can be mobilized at low deflections, and with minimal toe velocity. On the other hand, during easy driving, the static capacity of the pile is relatively low, but dynamic resistances will be high because of the significant pile motion.

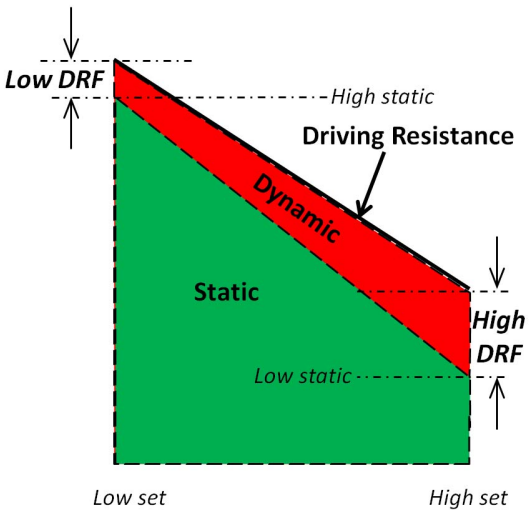


Fig. 2. Schematic representation of the variation of static and dynamic resistance components of overall driving resistance as a function of pile set

The Dynamic Reduction Factor (DRF) is defined as the ratio of Driving Resistance to Static Resistance. Personal experience suggests that the DRF can be assumed to be a linear function up to a set of approximately 12mm per blow, and has the form

$$DRF = DRF_0 + DRF_s * s$$

DRF_0 is the reference value at a theoretical set value of 0. Typical values are between 1.25 and 1.50, but can range from 1.0 to 2.5 or more depending on the hammer, pile and soil conditions.

DRF_s is the set-multiplier, and typically varies between 0.03 and 0.06 for sets measured in millimeters, but can be less than 0.03 in some circumstances.

The author has used the DRF approach in his standard practice of driven piling construction control for more than 5 years. For reasons which will become evident, the resulting Pile Driving Formula shown hereafter is called the Bearing Formula.

$$R_u = \frac{EMX}{DRF\ (s + c/2)}$$

COMPARSION OF PILE DRIVING FORMULAS WITH BEARING GRAPH

For the purpose of comparing the ECM relationships implied by Pile Driving Formulas and Wave Equation Analysis without the potentially confusing influence of variable ground conditions, it is convenient to extract the relevant parameters for the Pile Driving Formulas from the Wave Equation Analysis (WEA) results. WEA provides estimates of transferred energy, pile set and maximum pile-top displacement, from which temporary compression is simply calculated. The pile driving formula driving resistance estimates can therefore be computed for each defined static pile capacity in the WEA. Although the particular program used for this study was GRLWEAP (2003), alternative programs would presumably yield similar outcomes.

A series of parametric studies were undertaken simulating hydraulic hammers on steel pipe piles and prestressed concrete piles. Hammer drop efficiencies were assumed constant and according to GRLWEAP default values. A range of hammer strokes from 0.4 to 0.8m were adopted in the study, and bearing graphs (capacity vs blow count) compared between WEA and various pile driving formulas.

Case 1 : Prestressed Concrete Pile example

Case 1 is the analysis of a 14 tonne hydraulic hammer driving a 20m long 550mm octagonal prestressed concrete pile. The hammer and pile cushions were a nylon compound and plywood respectively. Fig. 3 shows the standard WEA bearing graphs for each stroke/energy for 10 capacities between 1500kN and 6000kN.

In Fig. 4, in addition to the WEA bearing graphs, 5 additional bearing graphs are shown based on application of the uncorrected Energy Formula to the energy, set and temporary compression values predicted by the WEA. It is clear that the Energy Formula significantly overestimates the capacities across all strokes/energies.

In Fig. 5, in addition to the WEA bearing graphs, 5 additional bearing graphs are shown based on application of the corrected Energy Formula to the energy, set and temporary compression values predicted by the WEA, using a single correction factor of 0.625 (or 1/1.60) which is the average for all computed ratios. Although the corrected Energy Formula is in reasonable agreement with the WEA at blows counts of between 100 and 150 blows/m, it overpredicts capacity at lower blow counts and underestimates capacity at higher blow counts, neither of which is desirable.

The WEA can also be used to determine the DRF equation parameters. Figure 6 shows the ratio of the Energy Formula and WEA capacities for all hammer strokes. The derived linear trend-line is the DRF equation used for correction of the Energy Formula.

$$DRF = 1.30 + 0.032 * set$$

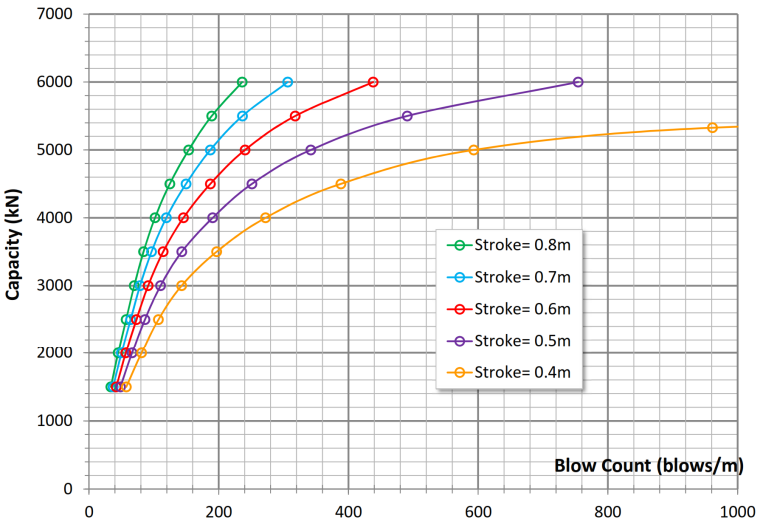


Fig. 3. Case 1 : Bearing Graphs for 5 hammer strokes from 0.4 to 0.8m

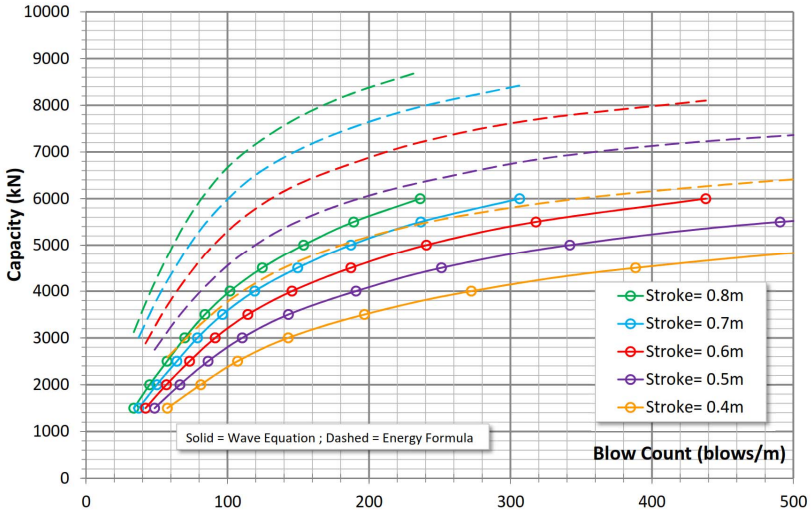


Fig. 4. Case 1 : Comparison of WEA and uncorrected Energy Formula

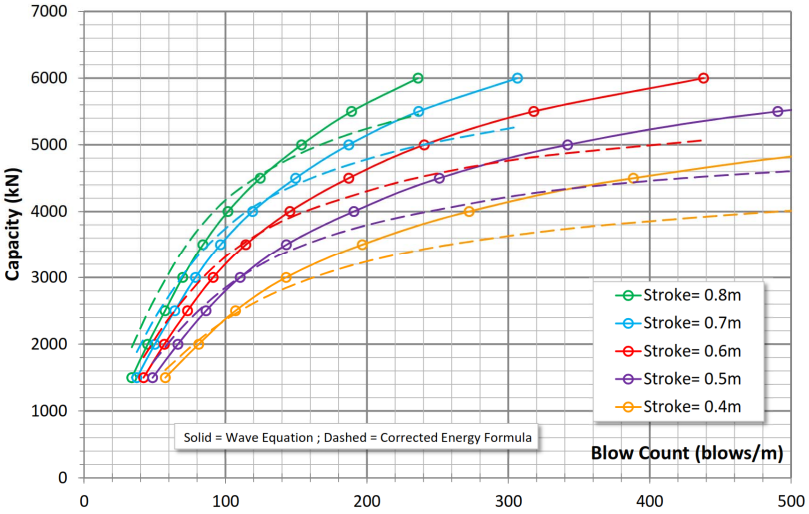


Fig. 5. Case 1 : Comparison of WEA and corrected Energy Formula

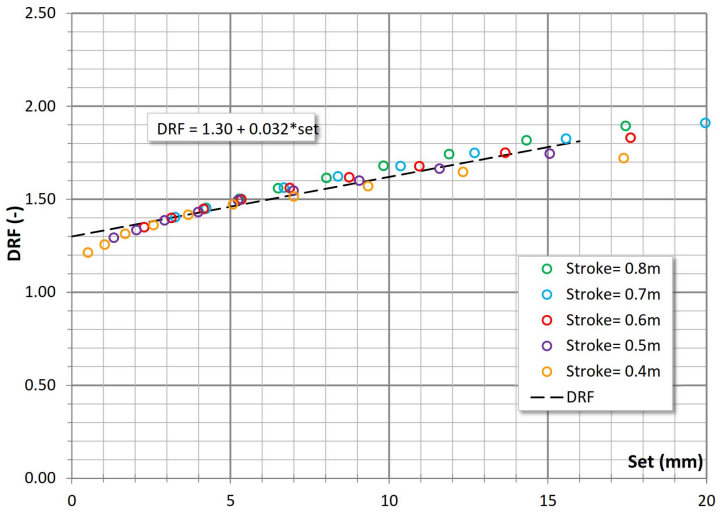


Fig. 6. Case 1 : Ratio of Energy Formula and WEA capacities for all capacities and strokes

This DRF equation is used to develop the Bearing Formula for this data set, i.e.

$$R_u = \frac{EMX}{(1.30 + 0.032s)\,(s + c/2)}$$

Figure 7 compares the WEA Bearing Graph with the Bearing Formula. It can be seen that there is excellent correlation between the two approaches, validating the concept of increasing dynamic resistance with increasing pile set, and the need for a set-dependent correlation factor.

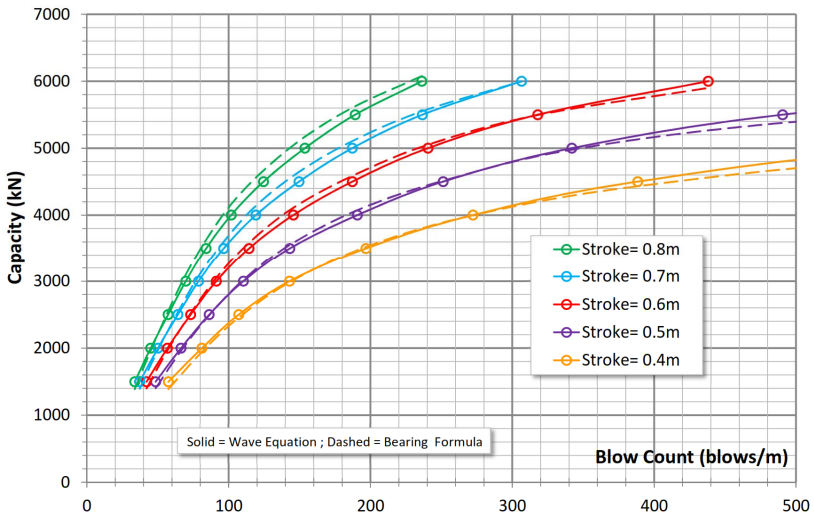


Fig. 7. Case 1 : Comparison of WEA Bearing Graph and Bearing Formula

Case 2 : Steel Pipe pile example

Case 2 is the analysis of a 16 tonne hydraulic hammer driving a 1050mm diameter x 24mm wall thickness steel pile. As for Case 1, the hammer cushion was a nylon compound. The data was analyzed for capacities between 3000kN and 12000kN, and hammer strokes were varied between 1.0m

and 1.4m. Figure 8 shows the ratio of the Energy Formula and WEA capacities for all hammer strokes. The derived linear trend-line is the DRF equation used for correction of the Energy Formula.

$$DRF = 1.17 + 0.045 * set$$

Figure 9 compares the WEA Bearing Graph with the Bearing Formula. It can be seen that there is again excellent correlation between the two approaches.

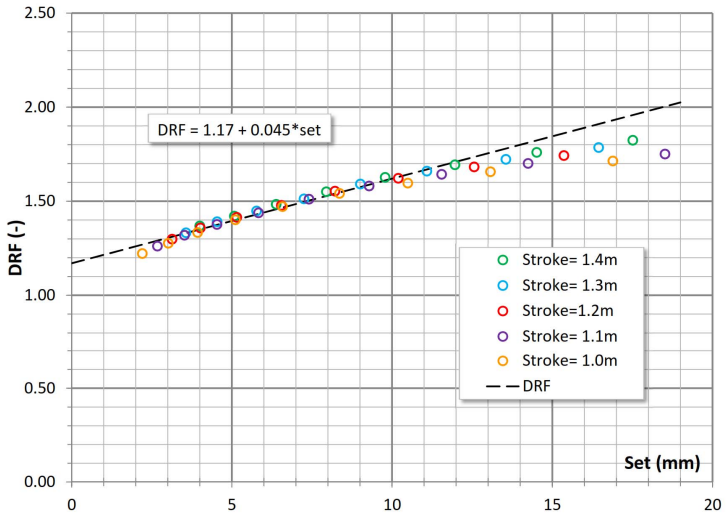


Fig. 8. Case 2 : Ratio of Energy Formula and WEA capacities for all capacities and strokes

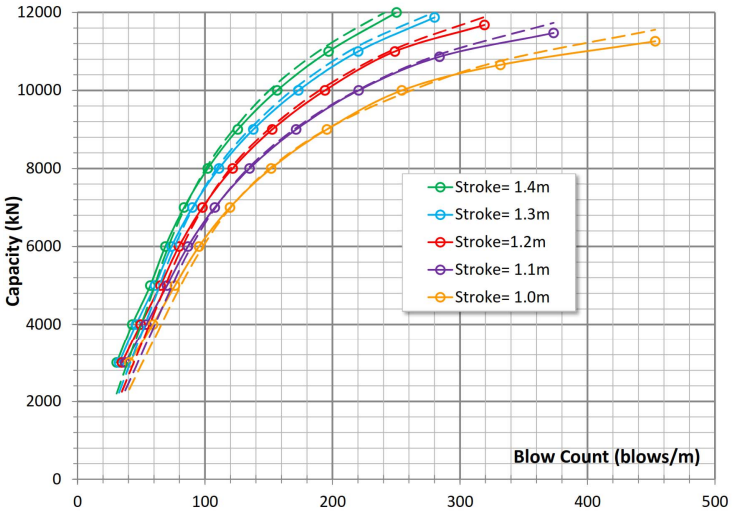


Fig. 9. Case 2 : Comparison of WEA Bearing Graph and Bearing Formula

NORMALIZED BEARING GRAPHS

As shown in Fig.1 and elsewhere, the WEA Bearing Graphs form a suite of energy-dependent capacity-blow count curves. These curves can be condensed to a single curve by normalizing each curve by the corresponding capacity at any given common blow count. For instance Fig. 10 shows the normalization capacities to be applied to each curve based on a blow count of 200 blows/m.

After normalization, the curves are all replotted, resulting in a unique curve of normalized capacity (at the reference blow count) against blow count as shown in Fig. 11.

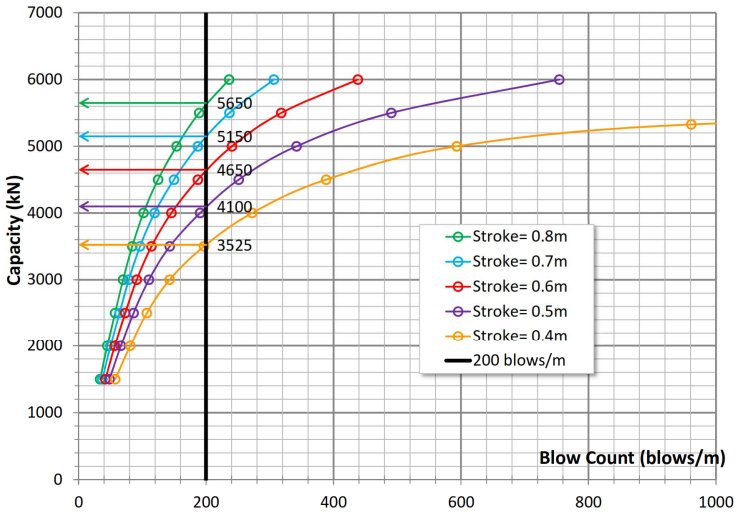


Fig. 10. Case 1 : Normalization values using reference blow count of 200 blows/m

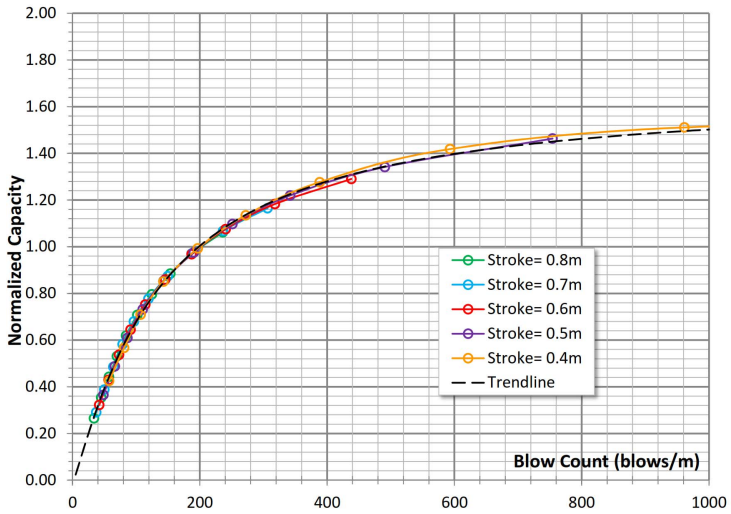


Fig. 11. Case 1 : Normalized capacities using reference blow count of 200 blows/m

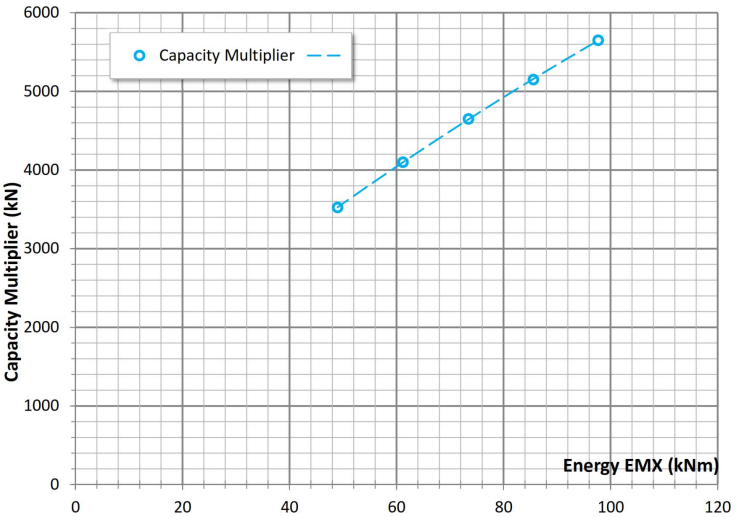


Fig. 12. Case 1 : Capacity Multiplier Equation

The normalized Bearing Graph of Fig. 11 is designated the Relative Capacity Curve for the particular combination of pile and hammer at that site, and shows the variation of relative or non-dimensional capacity with blow count, independent of hammer energy. The capacity of any pile is the product of the relative capacity at any given blow count and the Capacity Multiplier shown in Fig. 12 for the relevant energy. Current practice is to adopt an energy based on assumed efficiency or energy measured during PDA testing. The companion paper discusses the significant variability of piling hammer efficiency, and the importance of evaluating energy transfer on an individual pile basis.

The equations for the normalized bearing graph and the capacity multiplier equation can be used to implement improved construction control with a device such as the Pile Driving Monitor (PDM) which can extend the benefits of PDA testing to every pile on a project.

CONCLUSIONS

A new pile driving formula, called the Bearing Formula is introduced. The Bearing Formula can be developed by correlation with Wave Equation Analysis or PDA testing. The Bearing Formula is a modification of the Energy Formula, with correction for dynamic resistance implemented by a variable correction factor which is a function of pile set. The method is general and applies equally to end-bearing and friction piles. The correspondence between Wave Equation Analysis Bearing Graph and the Bearing Formula demonstrates that the Formula effectively accounts for dynamic resistance, and produces near identical capacity-blow count relationships. Although Wave Equation Analysis also has limitations, it represents the current best practice approach for simulating pile driving.

In addition, it was demonstrated that a Wave Equation Bearing Graph can be reduced to a single normalized relationship that is common across all hammer strokes and energies. These approaches can be implemented into improved construction control for driven piling. PDA testing combined with PDM monitoring can significantly improve overall pile foundation system reliability.

This approach can be applied equally to driving and restrike testing – different relationships may apply as a result of generally higher damping on restrike. However although test piles may be subjected to restrike testing, it is not normal practice to restrike untested piles because of the associated delays. Therefore, in general pile setup or relaxation effects after driving should be accounted for separately.

REFERENCES

Fellenius, B.H. (1980). The analysis of results from routine pile loading tests. Ground Engineering, London, Vol. 13, No. 6, 19-31.

Goble, G., Rausche, F., & Likins, G. (2003). GRLWEAP Manual, GRL Engineers. Inc., Cleveland, OH, USA

Lawton, E. C., Fragaszy, R. J., Higgins, J. D., Kilian, A. P., & Peters, A. J. (1986). Review of Methods for Estimating Pile Capacity. In Transportation Research Record.

Paikowsky, S. G., and Chernauskas, L. R. (1992). Energy approach for capacity evaluation of driven piles. In Fourth International Conference on the Application of Stress-Wave Theory to Piles (pp. 21-24). September.

Rausche, F., Goble, G. G., & Likins Jr, G. E. (1985). Dynamic determination of pile capacity. Journal of Geotechnical Engineering, 111(3), 367-383.

Rausche, F., Nagy,M. and Likins, G. (2008). Mastering the Art of Pile Testing. Proc. of the 8th Int'l Conf. on the Application of Stresswave Theory to Piles. Lisbon. J.A.Santos (ed) : 19-32

Samson, L., & Authier, J. (1986). Change in pile capacity with time: case histories. Canadian Geotechnical Journal, 23(2), 174-180.

Seidel, J.P. (2018). The Importance of Energy Evaulation on an Individual Pile Basis. Accepted for DFI-EFFC Intl Conference on Deep Foundations and Ground Improvement, Rome, June 2018.

Smith, E.A.L. (1960) Pile Driving Analysis by the Wave Equation. Journal of the Soil Mechanics and Foundations Division, ASCE, 86, 35-64.

ANCHOR HEAD MODELS : CLASSIFICATION, ADAPTABILITY & DESIGN

M. Ansriou, Franki Foundations Belgium, Engineering Department, Saintes, Belgium, mohamed.ansriou@ffgb.be
T. Wulleman, Franki Foundations Belgium, Engineering Department, Saintes, Belgium, thomas.wulleman@ffgb.be
C. Rabeux, Ecole Centrale des Arts et Métiers (ECAM), Brussels Engineering School, Brussels, Belgium, a.ouaar@ecam.be
A. Ouaar, Ecole Centrale des Arts et Métiers (ECAM), Brussels Engineering School, Brussels, Belgium, clement-rabeux@hotmail.com

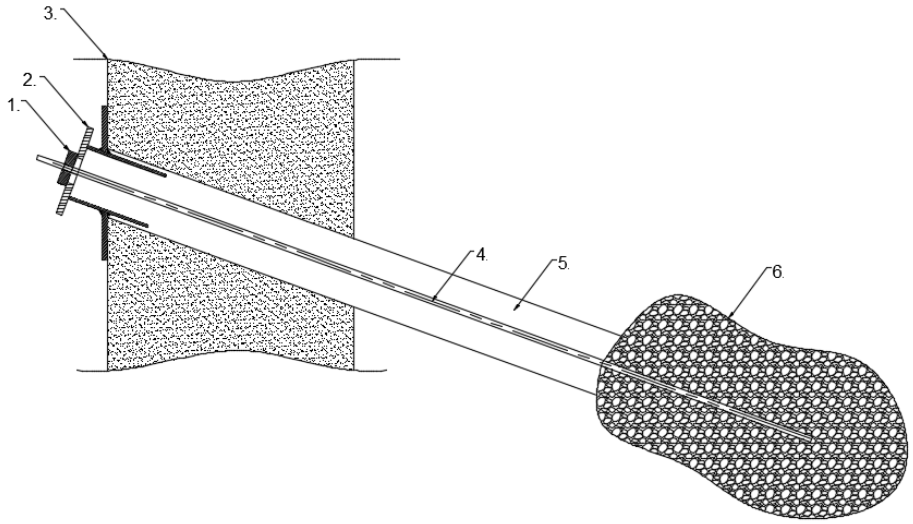
ABSTRACT

Tieback anchors are elements made of reinforcement, composed by bars or tendons, introduced in a small diameter borehole and sealed into the ground by grout or mortar injections. Those systems are generally used to limit the top displacement of retaining structures. The geotechnical design of those elements is today well controlled but few publications showing the different models and their characteristics exist. The goal of this publication is, at first, to make a synthesis of the mostly used head anchors. Secondly, to show their adaptability as a function of the nature of the retaining structure. Finally to propose, by using an example, a methodology to design them. A parametric study is also performed by evaluating the required thickness of the different steel plates by varying the ULS (Ultimate Limit State) load and the tieback anchor inclination.

Keywords: geotechnics, anchors, anchor heads, retaining structures, FEM (Finite Element Modelling).

1. INTRODUCTION

Anchor heads are all intermediate elements that safely aid the transfer of loads from the wall or retaining structure to the reinforcement (**Fig 1**). There are different types of anchor heads, which type is adopted will depend on the prevailing technical challenge to be addressed.



1. Locking tool
2. Anchor head
3. Wall
4. Bar
5. Drill hole
6. Sealing grout

Fig 1. Tie rod general diagram

© 2018 Deep Foundations Institute

2. BAR OR STRANDS REINFORCED ANCHORS ?

Reinforcement for tieback anchors are usually of two types : bars or strand tendons. The use of hollow bar reinforcement anchors makes it possible to execute the drilling and insertion of reinforcement in that order. For strand tendons, a substitution step is needed to replace the drill rod with strand tendons what always affects the execution procedure.

The unit cost for bar tendons is cheaper. However, in terms of strength mobilized per sectional area, strand tendons offer better performance attributable to their much higher elastic strength property.

Table 1. Elastic limit state for bars and strand tendons

	Bars tendons	**Strand tendons**
Elastic limit stress	Up to 600 MPa	Up to 1700 MPa

Taking into account the execution and material cost in Belgium, when the SLS (Service Limit State) service load is higher than 400 kN, strand tendons are cheaper than hollow bars. In this paper, low loaded anchors refer to anchors whose SLS load is up to 400 kN while high loaded anchors overburden service load higher than 400 kN.

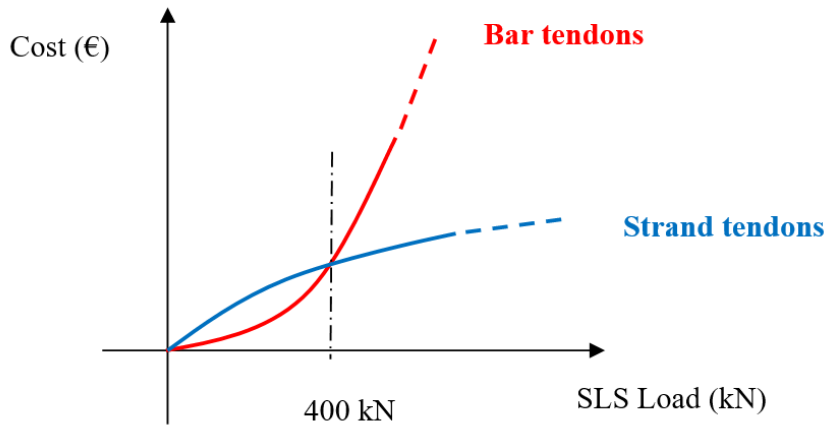
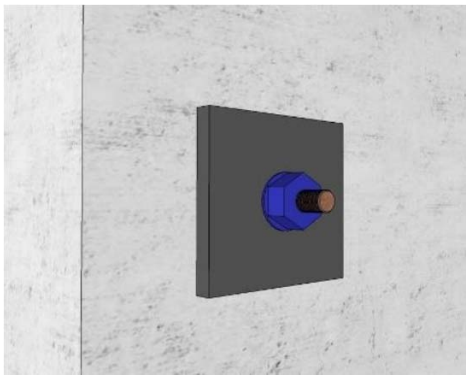


Fig. 2. Cost vs. Service Load in Belgium

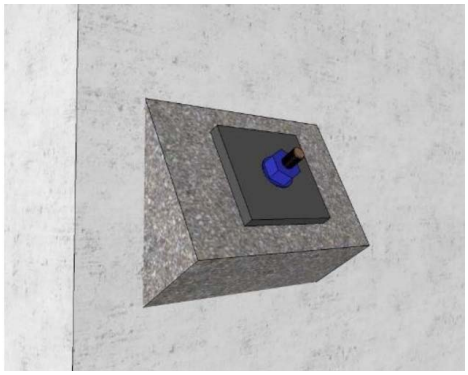
The selected reinforcement type will affect the design of the anchor head. When tendon strands are used, the anchor is generally considered as high loaded (> 400 kN) and the anchor head must be robust to ensure correct load transfer to the reinforcement (Models 3 & 4). In contrast, when a rebar is used as reinforcement, the anchor is considered as low loaded (< 400 kN) and the anchor head model can be lighter (Models 1, 2,5 and 6).

3. HEAD ANCHOR MODEL TYPES

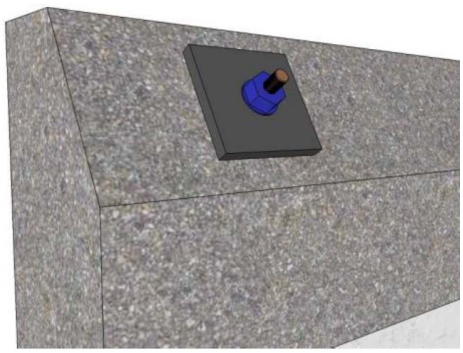
This section presents the results obtained from various project sites in Belgium, with a view to discussing the different anchor head models. The anchor head models can be either *punctual models*, which are models not linked to each other, with a localised application on the wall or *distributions models* which are systems linked to each other (usually by a profile) and for which the effect is more distributed along the wall. This article focuses only on *punctual models*. Distribution models will not be discussed.



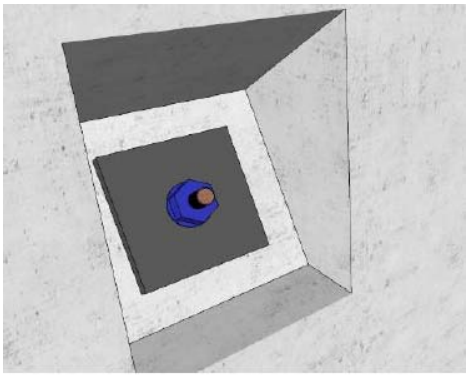
Model 1a : This is the simplest model. It is composed of a blocking piece and a distribution plate. This model doesn't allow for an angular deviation and is well adapted when the mobilised soil matches the horizontal axis of the anchor.



Model 1b : This model is similar to model 1a but a concrete base is added to the existing wall. This can be adopted when it is not possible to install anchor heads within the wall (because of an important punching in the wall) or when the contact surface between the distribution plate and the wall has to be improved. This configuration allows for installation of anchors with angular deviation.

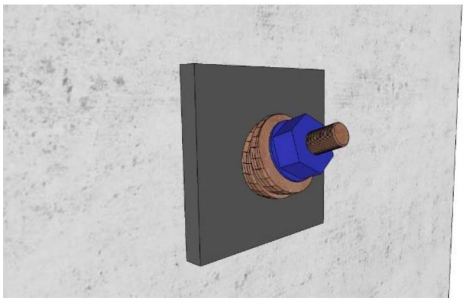


Model 1c : When the anchor has to be installed on top of the wall, it may be better to use a distribution beam. This is also interesting when the wall to be anchored is not to be damaged.



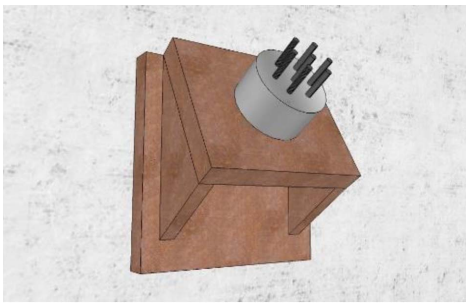
Model 1d : A opening can be made during the design of the wall or by coring within an existing one. The mechanical working of this model is the same as the models 1a to 1c but with the advantage that it allows for a better anchor head protection against corrosion and suitable for permanent anchor system.

3.1 Model 1 : Square or circular distribution plate



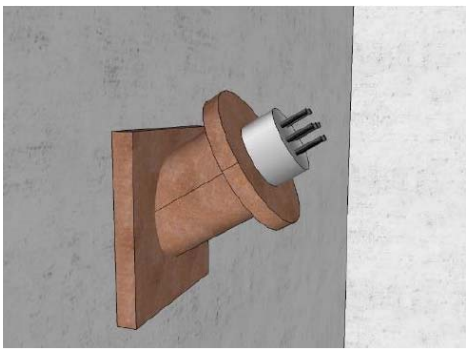
Model 2 : The use of biased wedge has two main advantages ; it allows for the installation of an inclined anchor system that exerts reduced stress on the reparation plate arising from the stress distribution effect of the biased wedge.

3.2 Model 2 : Biased wedge



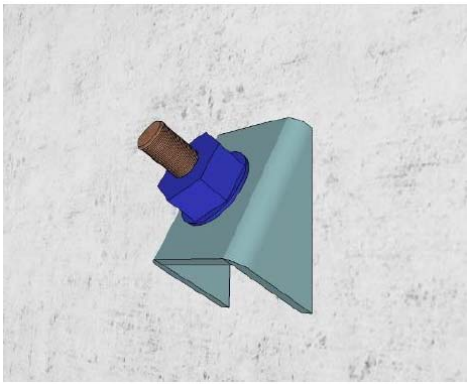
Model 3 : This model assembles two triangular and one square steel plates. It is quite robust but also heavy and allows for anchor heads with an angular deviation. The advantage of this model resides in the fact that the plate that is in contact with the wall is not subject to bending stresses.

3.3 Model 3 : Steel bracket



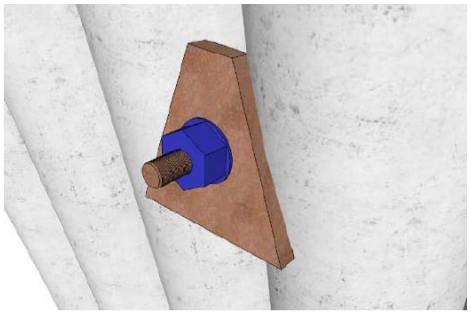
Model 4 : This model is similar to model 3 but the deviation angle results from the scabbard inclination. The scabbard is attached to the distribution plate and to a circular plate supporting the anchor block.

3.4 Model 4 : Scabbard



Model 5 : The steel clamp model is well adapted for low loaded anchors. It is composed of a blocking piece mounted on a folded steel plate. The steel plate gives the deviation angle. The absence of distribution plate allows for a higher punching stress on the wall.

3.5 Model 5 : Steel clamp



Model 6 : Designed for secant piles, the angular deviation is determined by the plate and the wall itself. This model is appropriate for light load anchors.

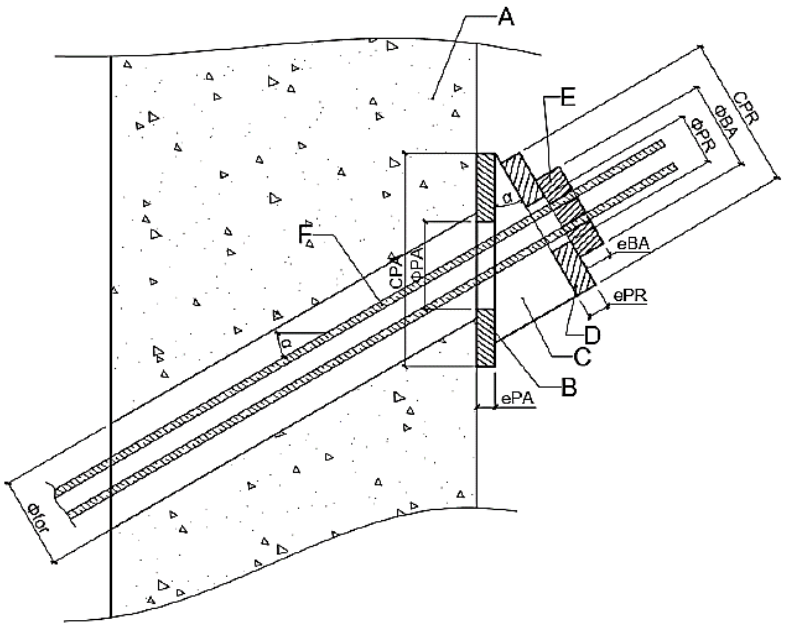
3.6 Model 6 : Trapezoidal steel plate

Table 2. Adaptability of the anchor head model in function of the retaining wall type.

Wall type	Adaptability							
	Model 1a	Model 1b	Model 1c	Model 1d	Model 2	Model 3	Models 4 &5	Model 6
Sheet walls	V	X	V	X	V	V	V	X
Diaphragm walls	V	V	V	V	V	V	V	X
Strutted trenchs	V	V	X	V	V	V	V	V
Secant & tangent pile walls	X	V	V	V	X	X	X	X
Soil mix walls	V	V	V	V	V	X	X	X
Berliner walls	X	X	X	X	X	X	X	X
Nailed walls	V	V	X	X	V	X	X	X
Existing walls	V	V	V	V	V	V	V	X

V **Adaptable**
X **Not Adaptable**

4. ANCHOR HEAD DESIGN EXAMPLE



A. Retaining structure
B. Distribution steel plate
C. Triangular steel plate
D. Rectangular repartition plate
E. Locking tool
F. Reinforcement

Φ_{for} : 150 mm
C_{PA} : 350 mm
Φ_{PA} : 100 mm
Φ_{PR} : 85 mm
C_{PR} : 250 mm

Fig. 3. Sectional representation of Model 3

To ensure the stability of the system, the following verifications have to be checked :

A. Design of the area of the plates to avoid punching of the retaining structure according to 6.4.3 of Eurocode 2 [5].
B. Design of the support steel plate thickness according to Von Mises criteria
C. Design of the triangular steel plate thickness according to Von Mises criteria
D. Design of the rectangular steel plate thickness according to Von Mises criteria

When the stresses on one point of the material are multidirectional, it is necessary to define the ultimate limit state parameters taking into account the directions of all stresses. This is made, for ductile materials, by comparing a fictitious stress, called stress of Von Mises, to the limit elastic stress of the steel quality.

Verification A. will be considered as fulfilled and will not be detailed in this article. Verifications B to D will be checked for an elastic limit stress of 235 MPa.

$$\sigma_{VM} = \sqrt{\sigma^2 + 3 \times \tau^2} < f_y = 235\ MPa$$

The design can also be performed following an analytical way by calculating a bending moment and the required thickness but the results lead to significant amount of steel which, besides being expensive, is not suitable for practical applications.

To take into account the plastic behaviour of the material, it is admitted that failure is reached when the limit elastic stress is obtained on the average stress at a distance equal to the thickness of the steel element in the most solicited area (**Fig. 4**).

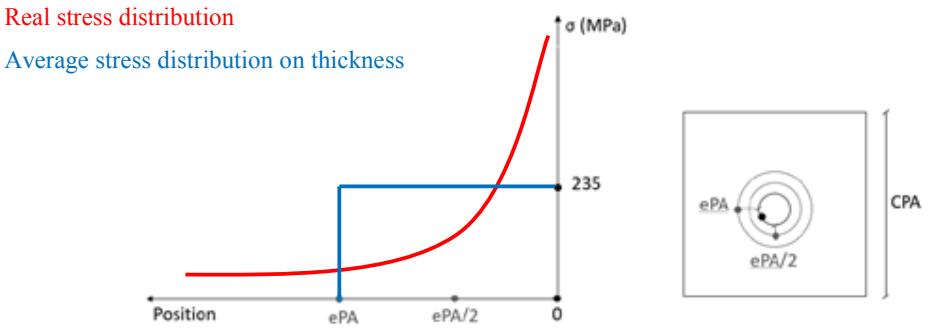


Fig. 4. Real vs average stress distribution.

Hypothesis of the finite element modelling :

1. All materials are considered as infinitely elastic.

Table 3. Material properties

	Concrete elements	Steel elements
Young Modulus	30 000 N/mm²	210 000 N/mm²
Poisson coefficient	0.2	0.3

2. Two types of contact law are used. Tie contact, which is a perfect contact with total strain transmission, is used between the steel pieces. Tangential and normal contact laws, which are used between the support steel plate and the concrete wall, allow displacement between two surfaces. The friction coefficient adopted is 0.8. The separation between the wall and the anchor head surface is also authorized.

3. Hexahedron elements are used for the mesh. The mesh is refined on the anchor head elements but less refined on the wall to optimize the time calculation. The number of elements varies from 22 000 to 25 000 elements with a time calculation varying from 1,3 to 20 seconds.

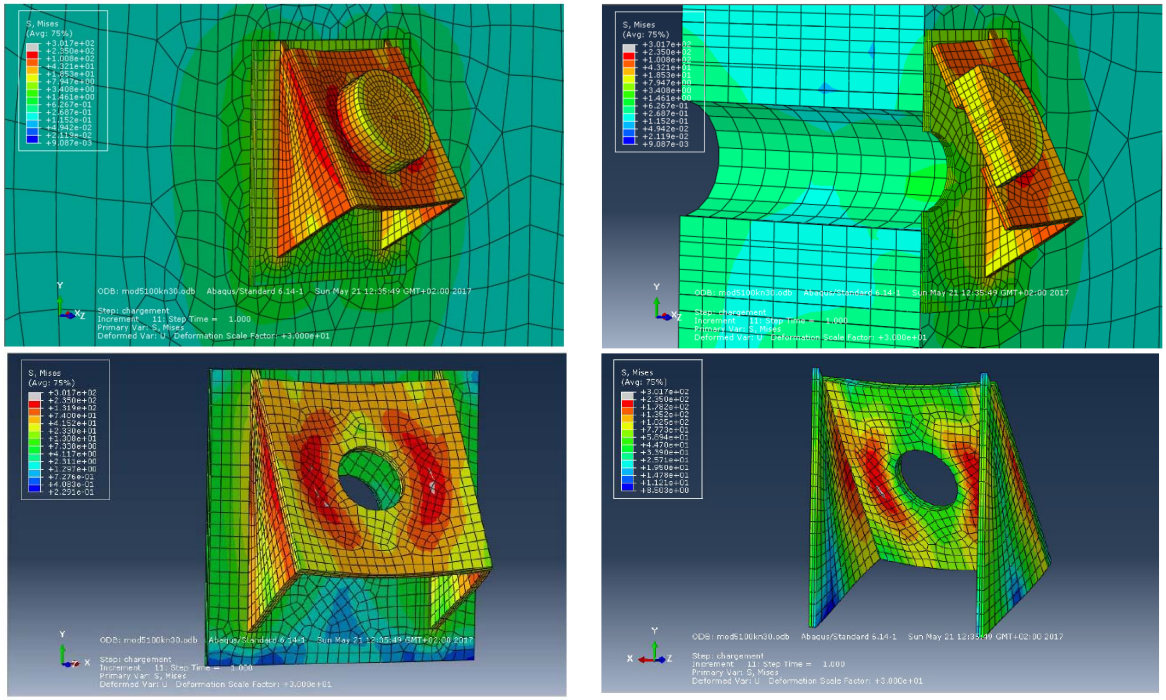


Fig. 5. Results of FEM for a load of 1000 kN and an angle of 30°.

Qualitatively, the maximum bending moment appears in the rectangular repartition plate (D). The important stress (235 MPa) obtained in the two triangular steel plates (C) partially originates from the bending of the rectangular repartition plate (D) due to the welding that links those parts. The repartition role of the distribution steel plate (B) on the concrete wall leads to low solicitations. The results of a parametric study evaluating the required thickness of the different parts by varying the ULS load and the tieback anchor inclination are shown on the diagrams in the **Fig. 6**, **Fig. 7** and **Fig. 8**. The goal is to optimize the use of steel for each part of the anchor block model.

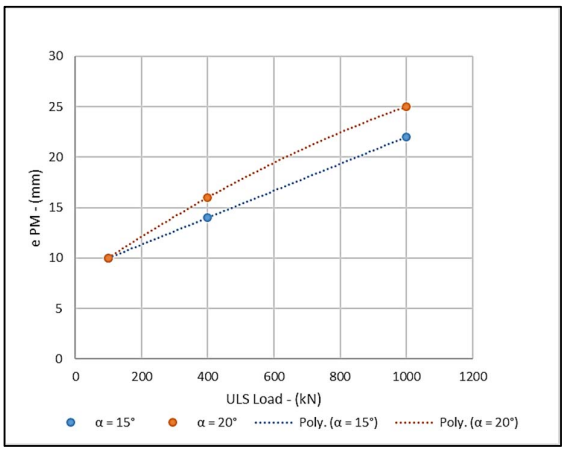


Fig. 6. Triangular steel plate thickness vs ULS Load

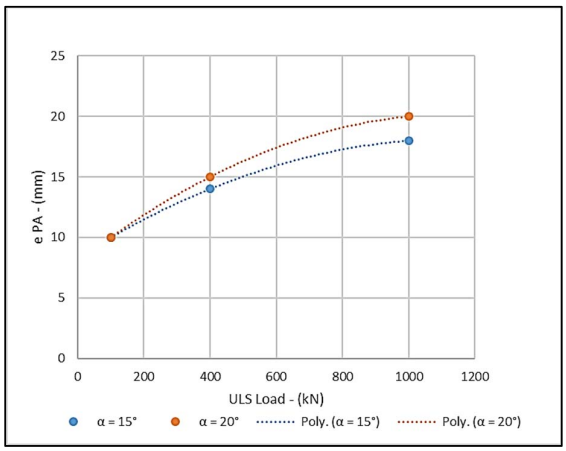


Fig. 7. Distribution steel plate thickness vs ULS Load

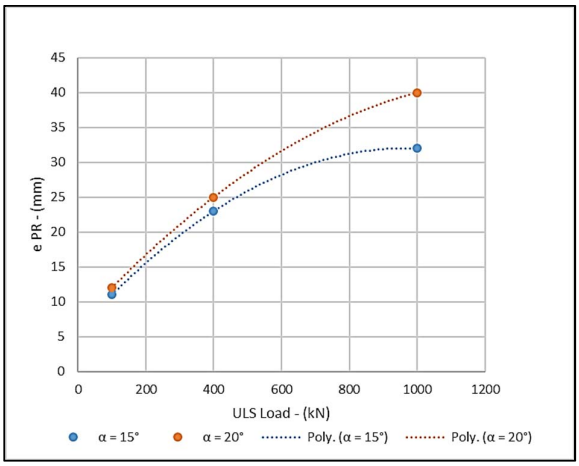


Fig. 8. Repartition steel plate thickness vs ULS Load

The parametric study shows that the anchor inclination has no significant influence on the thickness calculation of the different parts for ULS loads below 400 kN. The required thickness of the repartition steel plate (D) is always higher than that of the other plates because of significant bending combined with stress concentration due to the opening in this plate (**Fig. 8**). The triangular steel plates (C) are mainly subject to compression loads which explain the proportionality between the load and the thickness on **Fig. 6**. Punching stresses, coming from the triangular steel plate, are particularly critical for the thickness design of the distribution steel plate (**Fig. 7**). Optimisation of the distribution plate (B) thickness can be done by increasing the thickness of the triangular steel plate which will decrease the punching stress and reduce the thickness of the support steel plate.

5. CONCLUSION

The paucity of data on anchor head systems made this research very challenging. Exploratory visits to some construction sites and interviewing persons with prior knowledge of these systems provided the information used in preparing this anchor head classification. This paper is a preliminary *state of the art* giving the designer a first tool to make a wise choice on the most appropriate anchor head model to adopt according to the design context. The influence of the type of anchor reinforcement on the robustness of the model was discussed. A parametric study was also performed by calculating the thickness of the several parts of model 3 by varying both the ULS load and the tieback anchor inclination. This study shows that the inclination has no significant influence on the thickness design of model 3 when the ULS load is below 400 kN. Bending moments and opening in the distribution plate produce significant stresses that increase the required thickness. Similar parametric studies can be done on various models allowing the creation of diagrams that may help designers to quickly find the required thickness of the different parts of the chosen anchor head model. Specially for high loaded anchors, the finite element analysis is useful to optimize the overall steel weight which besides economic factors, facilitates handling on site.

ACKNOWLEDGMENTS

The authors thank Jean-Louis Vieslet, Dimitri Timbremont and Xavier Raucroix for their advices on this study.

REFERENCES

[1] RABEUX, C. (2016), Etude comparative des têtes d'ancrage, ECAM, Brussels Engineering School, 1-100

[2] Departement of Transportation Federal Highway Administration (2016), Geotechnical Engineering Circular n°4 Ground Anchors And Anchored Systems.

[3] Comité Français de la Mécanique des Sols et des Travaux de Fondations (1995), Tirants d'ancrage – Recommandations concernant la conception, le calcul, l'exécution et le contrôle, Eyolles.

[4] European norm, (2005) Eurocode 3: Design of steel structures - Part 1-1: General rules and rules for buildings, European committee for standardization.

[5] European norm, (2005) Eurocode 2: Design of concrete structures - Part 1-1: General rules and rules for buildings, European committee for standardization.

DAMAGING OF THE ST. BENEDETTO TUNNEL AFTER THE QUAKE OF OCTOBER 30, 2017: STUDY AND REPAIR

Alessandro Micheli, Anas S.p.A., Rome, Italy, +390644466229, a.micheli@stradeanas.it
Luca Cedrone, Anas S.p.A., Rome, Italy, +390644466405, l.cedrone@stradeanas.it
Maurizio Martino, Anas S.p.A., Rome, Italy, +390644466748, m.martino@stradeanas.it

ABSTRACT

The earthquake occurred on 30 October 2016 in Central Italy (magnitude M_w 6.5 with epicenter between Norcia and Preci), damaged road platform and main engineering structures on different sections of the State Road S.S. 685 "delle Tre Valli Umbre".

Damages have led to the closure of the whole S.S. for practicability and safety problems. Particularly, for the St. Benedetto Pass Tunnel, the main damages have occurred at the concrete lining and at the road platform, at about 920 m from Norcia side entrance.

Technical inspections of damage have been made and all the activities necessary to obtain information regarding the characteristics of the tunnel, the state after the earthquake and the characteristics of the materials, have been promptly started.

The seismic swarm that struck the Central Apennine in the period August to October 2016, has led to a decimetric breakthrough of a huge crustal volume in the area. Breakthrough has involved the mobilization of preexisting faults and new breaks (cosismic). Maybe one of these faults, on the morning of October 30, intercepted, dislodging it, the St. Benedetto tunnel.

With the information acquired, the final designs for the repair of the tunnel have been drawn up and work is still ongoing.

Keywords: earthquake, Norcia, fault, tunnel, damage, repair.

DESCRIPTION OF THE SITE

The State Road S.S. 685 "delle Tre Valli Umbre" (Spoleto-Norcia-Arquata del Tronto) suffered damages and deformations at the road platform and at main engineering structures on different sections, due to the magnitude M_w 6.5 seismic event, occurred on 30 October 2016, at 7:40 am, within the sequence started in Central Italy with the earthquake of 24 August 2016.

Damages have led to the closure to the traffic for practicability and safety problems. Particularly, the St. Benedetto Pass Tunnel, located between Norcia and Arquata del Tronto, has been affected by significant damages to the concrete lining and to the road platform, principally in one section.



Fig. 1 Geographic location of the area

© 2018 Deep Foundations Institute

The inspection by Anas engineers, just after the quake, highlighted significant damages located approximately 920 m from Norcia side entrance (at about K.P. 10+970), with the breakage of the final lining in multiple points, and the lifting of the road platform of about 0.24 m. A provisional intervention, which would allow for the extraordinary practicability of the tunnel, for all the activities required for the design of the restoration intervention (reliefs, surveys, etc.), has been detected.

At the time of writing this text, all the investigations needed to define the actual state, the quality and the condition of the materials in place and the process for designing the restoration of the tunnel, have been completed; the work for its implementation is now in progress.

DESCRIPTION OF THE SEISMIC EVENT

The seismic swarm that struck the Central Apennine in the period August to October 2016, besides the lifting of the Vettore Mt. area, has led to a decimetric breakthrough of a huge crustal volume in the Norcia-Castelluccio area, and so in the St. Benedetto tunnel area. Breakthrough has involved the mobilization of pre-existing faults and new breaks (cosismic). There is therefore the possibility that one of these faults, on the morning of October 30, intercepted, dislodging it, the St. Benedetto tunnel (Galli et al 2017).

While it is certain that the phenomenon has been cosismic, less clear is the nature of the shear plan, which is the subject of further studies that Anas is carrying out with the Department of Civil Protection and with the University of Rome "Sapienza".

The event that caused the damage of the St. Benedetto tunnel is part of a seismic sequence triggered by the earthquake of August 24, with its epicenter between Amatrice and Accumuli, illustrated in the following figure, from the website of the National Institute of Geophysics and Vulcanology (INGV).

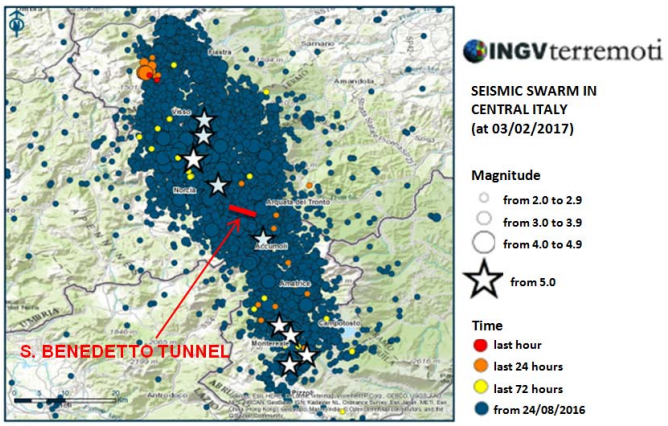


Fig. 2 Seismic swarm of central Italy updated at 03.02.2017 (from INGV)

A series of differential interferograms, obtained from European satellite Sentinel-1 radar data, cover the period of earthquakes recorded between October 26 and 30.

The interferogram of Fig. 3a) shows the soil deformation caused by the series of recorded events: the stars indicate the epicenter of the strongest shocks, the yellow symbols show the direction of the displacement of the ground (+ for uplift, - for settlement), the ellipse locates the lowering area.

In the area near the epicenters there is a very complex stretch of deformation, about 30 km long and about 10 km wide, with negative displacement values and very high deformation gradients up to 0.3 m/km. In this area, near the plain of Castelluccio, the maximum reduction of about 0.8 m is observed. The long green eastern line follows the location of Vettore Mt. – Bove Mt. fault.

Fig. 3b) shows the map of the active faults known in the area (in red). The stars indicate the location of the three main events. The colored bands indicate the areas of the fault system along which cosismic cracks have been produced at the event marked with the same color.

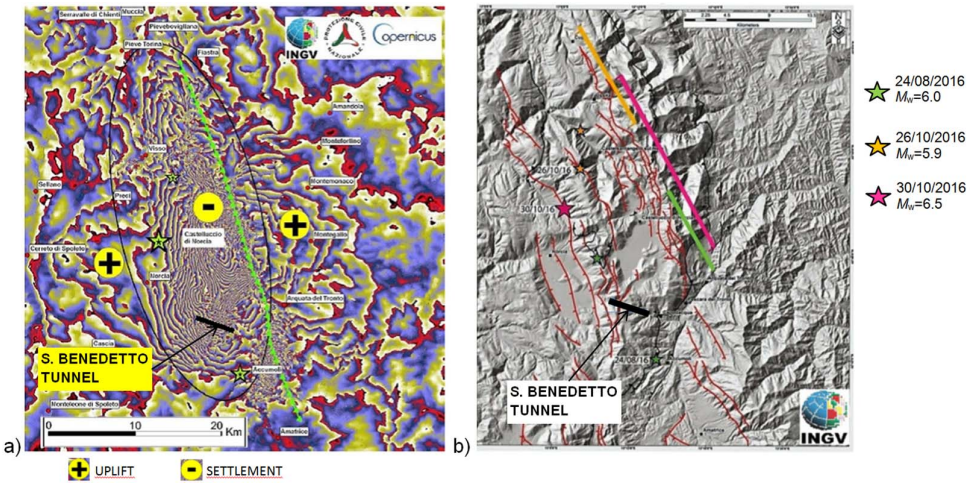


Fig. 3 a) Interferogram from satellite Sentinel-1, b) map of the active faults

Difficulties related to the presence of a very hard vegetation have not allowed to recognize clearly fractures at surface above the crack inside the tunnel. On the other hand, both on the northern and southern continuation of the supposed deep fault, numerous clues and evidence associated with the break-up, although discontinuous, were recognized. Among the most significant, a set of fairy fractures with a rejection of 0.10-0.20 m to the east, was followed continuously for about 600 m on Serra Mt. This set is compatible with the rupture observed in the tunnel (Galli et al 2017).

CASE HISTORIES

What happened to the tunnel in question is an uncommon occurrence, for which there is a limited case histories and few experience of repair intervention. As is known, in Italy and in most of the countries with high seismic activity, surface faulting is a very rare phenomenon, because it is associated, with certain exceptions, with surface earthquakes of high magnitude (M_w> 6). The prospect that faulting may interest an anthropic artifact is even smaller (Galli et al. 2017).

A previous Anas experience dates back to earthquake that occurred in L'Aquila area, culminating in the event of April 6, 2009 (M_w 5.9), which damaged the Monteluco tunnel on S.S. 17 (Valente 2010).

In that case, a detailed study of the cracking framework induced on the lining of the tunnel was made, finding that the energy due to the intense seismic event had been absorbed mainly through the dislocation of the segments at the casting. The tunnel had contained the effects through a widespread cracking, with benefit for structural strength and functionality, which had not been compromised.

Coriglioni (2017) shows that in literature there is a database of similar events (Powell et al. 1998), where data are reported in terms of the M_w of the earthquake and the location of the tunnel, for a total of 204 cases involving 10 seismic events. This collection, updated over time, points out that only quakes of M_w>6, depending on the distance from the epicentre, have damaged underground constructions.

The causes of damage, according to Dowding and Rozen (1978), can be divided into three categories:

- damage due to shaking;
- damage due to failure shift (tectonic displacement);
- damage resulting from instability that occurs in the soil (liquefaction, landslides, etc.).

Starting from November 1, 2016, Anas has been involved in technical inspections and research with the aim of acquiring all the information necessary for the design of an intervention to restore safety conditions of the infrastructure. Besides, Anas has started investigations and studies aimed at the recognition and reconstruction of the dynamics that caused the state of the damage found and, eventually, to verify whether the cause is attributable to one of the cases suggested in the literature.
Unfortunately there are not instrumental data available of the state of the tunnel before the earthquake.

ORIGINAL DESIGN OF TUNNEL

An investigation activity has been launched aimed at the recovery of data relating to the original design and construction of the structure, focused on the design solutions used according to the geological model adopted and on the issues encountered during the construction work.

From the documentation provided by the construction company "Società Italiana per Condotte d'Acqua", it was learned that the construction of the tunnel was preceded by the execution of a pilot pipe (Φ3.6 m TBM, centrally located in the crown area, along the entire length of the tunnel), with the aim of identifying preventively the problems that would have been encountered during excavation. Subsequently, the excavation of widening was made with explosive, using the presence of the central perforation, created by the pilot tunnel, as a venting area for the explosion.



Fig. 4 Detail of TBM Wirth tb1l 360h with full cross section cutterhead used for the "pilot" tunnel (extract from Ricci 1986)

The first stage lining consists of radial bolts, electrowelded mesh and spritz-beton, while the final lining was made with non-reinforced concrete; between the two coatings was put in place a PVC waterproofing mantle. In the crown, there is also a suspended ceiling slab for the ventilation system.

The St. Benedetto tunnel is a two-way gallery, with Capodacqua side entrance at 1014 m s.l.m. and Norcia side entrance at 1001 m s.l.m., with a constant level of 0.29 % and a max coverage of 600 m.

From the geological point of view, soils belong to the stratigraphic succession of the Umbro-Marchigian series. From the geotechnical report, attached to the final design, were extracted the main aspects that characterize the area concerned by the work.

The tunnel excavation involves rock formations consisting of a calcareous stratigraphic succession: starting from the Norcia side entrance there is a section crossing the massive limestone, followed by Corniola with Megabrecce and finally Corniola.
The transition between the various lithologies were found during the excavation at the following distances from the Norcia side entrance:

- at 720 m, from massive limestone to Corniola with Megabrecce;
- at 1460 m, from Corniola with Megabrecce to Corniola.

In the section between 550 m and 720 m from the Norcia side entrance, frequent faults and cutting areas have been detected, close to contact with Corniola with Megabrecce, with an immersion that forms an angle of about 320° with the axis of the tunnel. Starting from the distance of 1440 m from Norcia side entrance, towards Capodacqua, excavation takes place completely in Corniola.
The characteristics of the crossed formations have been investigated during the design phase.

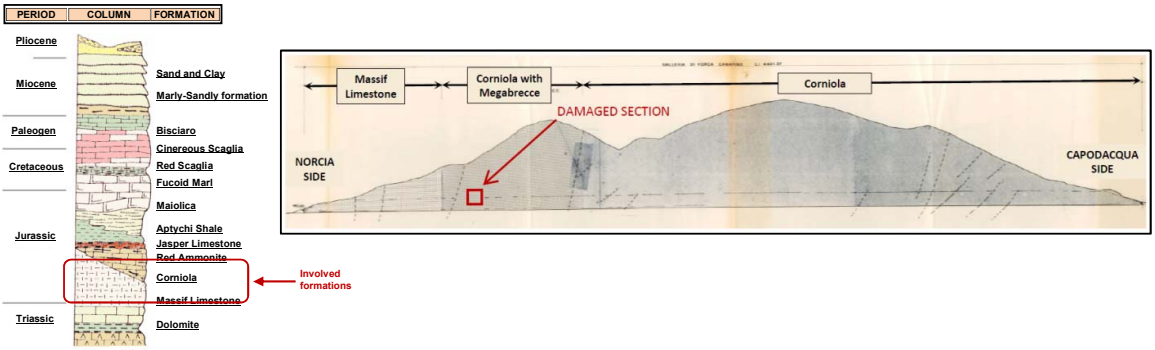


Fig. 5 Stratigraphic succession of the Umbro-Marchigian series (on the left) and extract of the geological section from the final design (on the right).

Under the hydraulic aspect the horizontal survey confirmed that the water table is below the tunnel, but water presence was observed during the excavation, and between the prog. 3690 m and 3750 m it required the introduction of a modification of the hydraulic arrangement of the road construction superstructure, in order to channel and drain the intercepted water flow, part along the Marche side and part along the Umbrian side.

After the seismic event, a reduction of this water flow has been observed, until the disappearance, as a sign of a probable change in the hydraulic regime of the area. By contrast, local authorities have faced a sudden increase in water in the San Pellegrino stream, much more downstream and west of the tunnel.

To put the area of the St. Benedetto tunnel in a more general context, since the area is not covered by the geological map of Italy at 50000, reference was made to the thematic mapping of literature: in particular the geological map of the Sibillins Mountains in scale 1:40000 (Pierantoni et al. 2002), of which the Fig. 6 is an extract. It also reports the axis of the tunnel and the area of the damage.

It is noted that the tunnel is located in the formation of massive limestone, in the western part, and Corniola, elsewhere. However, from the reliefs made, a much more complex situation has emerged, then the one of the tunnel's design and in the official bibliography, even in relation to the different scales of representation.

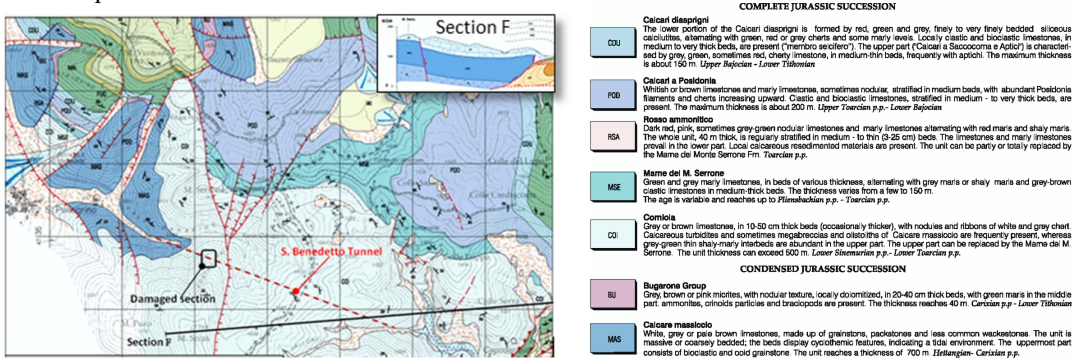


Fig. 6 Extract from "Geological map of the Sibillini Mountains"

STATE OF THE TUNNEL AFTER THE MAINSHOCK

Important damages are located at approximately 920 m from Norcia side entrance (about 25 m from K.P. 10+981 to K.P. 10+956), with the breakage of the final lining, in multiple sections, and with the lifting of the road platform of about 0.24 m. The following figures illustrate what happened:

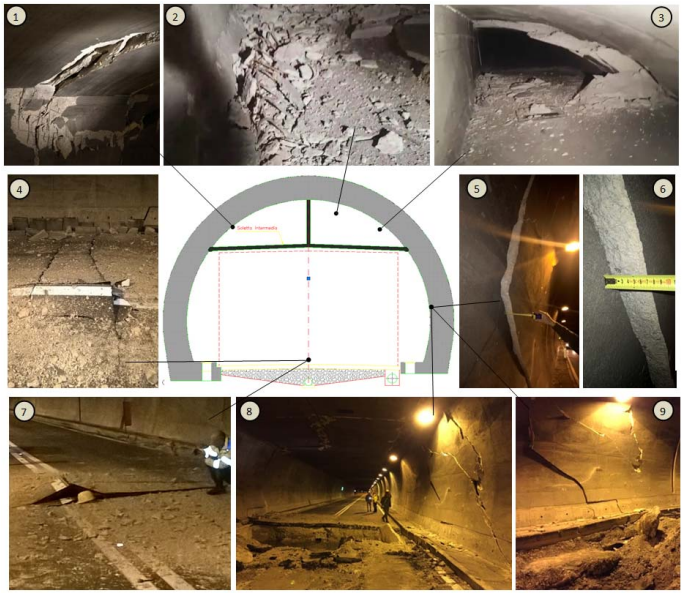


Fig. 7 Cracks detected in tunnel: photos 1, 2, 3 e 8 were taken with the back to Norcia, photos 5, 6, 7 e 9 with the back to Capodacqua, photo 4 is transversal to the road with Norcia to the left

An investigation of the cracking of the final lining has been carried out during the investigation; in Fig. 8 you will find the relief of the lesions found on the valley (top) and mount (below) side. In Fig. 9, the integer shape (black full line) and the deformed one caused by the earthquake (red dotted line) are compared. The relief has also highlighted, as shown in Fig. 10, a lift in the middle of the road surface of about 0.24 m of the Norcia side compared to the Capodacqua side.

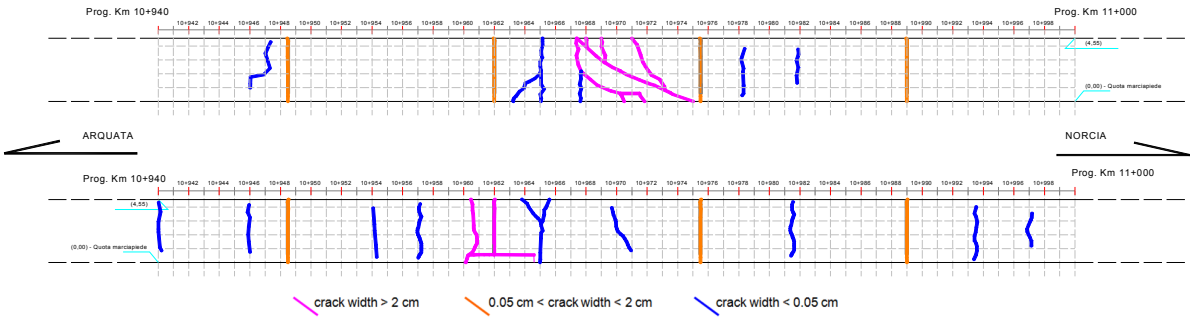


Fig. 8 Tunnel relief in the area of interest

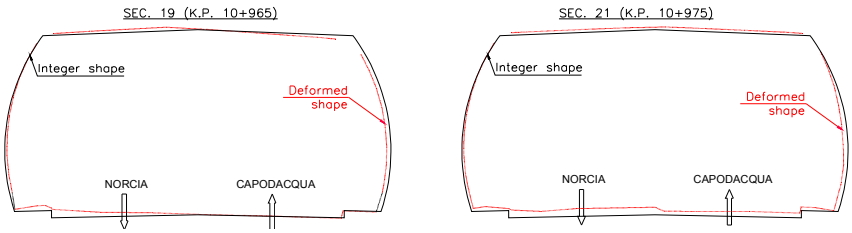


Fig. 9 Comparison between integer and deformed cross section

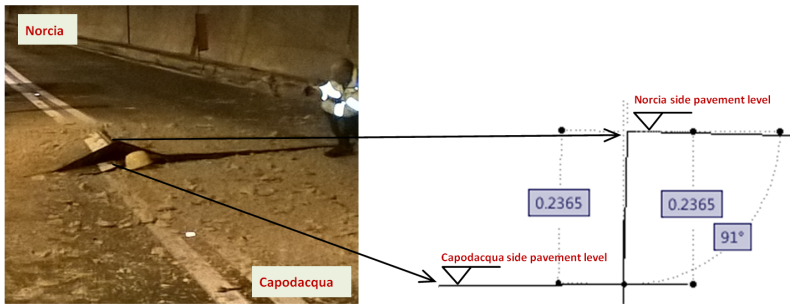


Fig. 10 Detail of the lift of the road surface and detail of topographic survey

After the survey phase, temporarily safety procedures were initiated by shoring the most damaged tunnel section, with the aim of making the area convenient for the workers involved in investigations and for the exceptional transit of Colfiorito plain farmers. The figure below shows the action taken.



Fig. 11 Intervention to ensure the safety temporarily

INVESTIGATIONS FOR THE RESTORATION INTERVENTION DESIGN

A survey plan has been elaborated with particular attention to the study of the connection between the geological characteristics of the area and the type of damage found, which is mainly concentrated in a very narrow range of the tunnel and has suggested the possible action of a fault or a system of faults. The survey plan has been drawn up after the acquisition of available project data and many site visits. The surveys carried out are listed below and are shown in the following figures:

- logging drillings with *in-situ* testing and sampling for laboratory tests for a total of 75 ml;
- geophysical surveys, articulated in georadar and electrical tomography, for two different heights heights along mountain and valley side for a development of 100 m each (for a total of 400 m), and refractive seismic surveys along mountain and valley side for a development of 100 m each (for a total of 200 m).
- *In-situ* tests consisted of flat jacks on the final lining, lugeon tests, dilatometric tests.
- Laboratory tests aimed at the definition of the geotechnical-geomechanical reference model.

Some tests have been studied and localized also through the first findings of geophysical surveys carried out simultaneously with the elaboration of the survey plan.

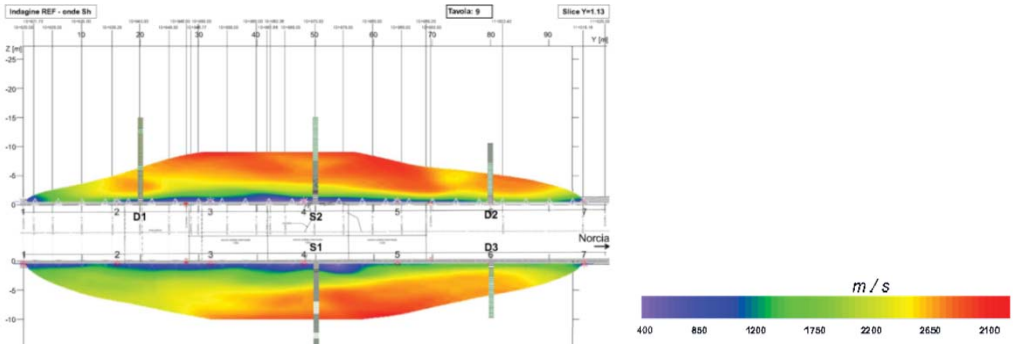


Fig. 12 Graphic return of refractive seismic survey – Shear waves

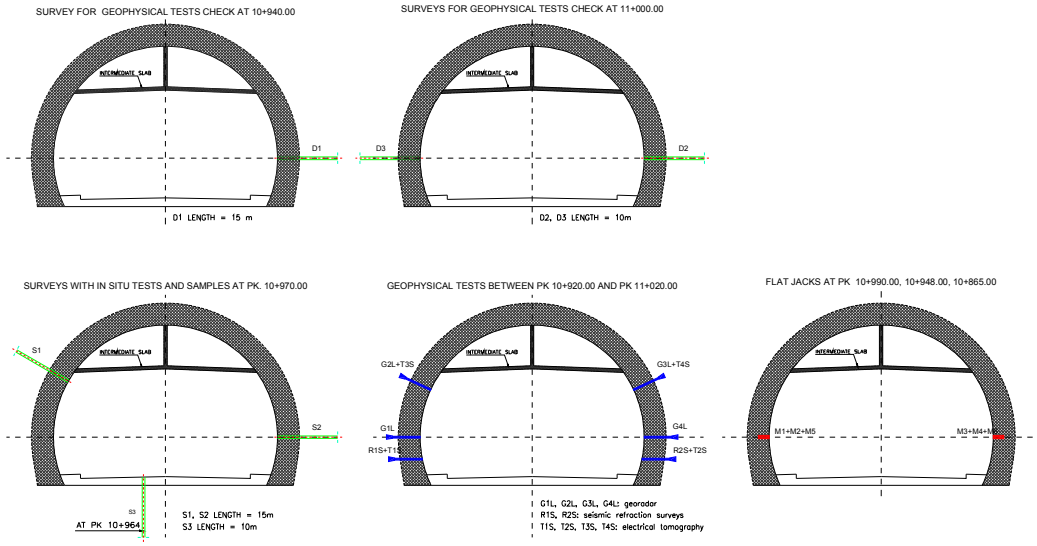


Fig. 13 Location of surveys in section (view towards Capodacqua)

The georadar surveys have allowed to detect the thickness of the final lining in 1.0 m for the first 10 m from Norcia side and in 1.3 m elsewhere. Metal structures, such as sheet metal, have not been found.

A detailed geological-structural relief has been also carried out, aimed at the identification and characterization of surface cosismic evidence, possibly related to the effects found in the tunnel.

The stratigraphies obtained from geognostic surveys have highlighted a band around the excavation section defined as "destructured rock" characterized by near-zero RQD values. This band extends for 5.0 m in S2 and S3 surveys, while appearing to be smaller (2.0 m) in S1 survey (section A-A, on the left of Fig. 14). In section B-B (on the right of Fig. 14), the data, though less complete, appears more homogeneous with the band extending around the tunnel in both D2 and D3 surveys equal to 3.0 m. Elsewhere, beyond the destructured band, the "intact rock" was identified with appreciable RQD values, only locally elevated. Probably, such a unit corresponds to the rock that didn't suffer clearly from detachment produced by the explosive wreck excavation.

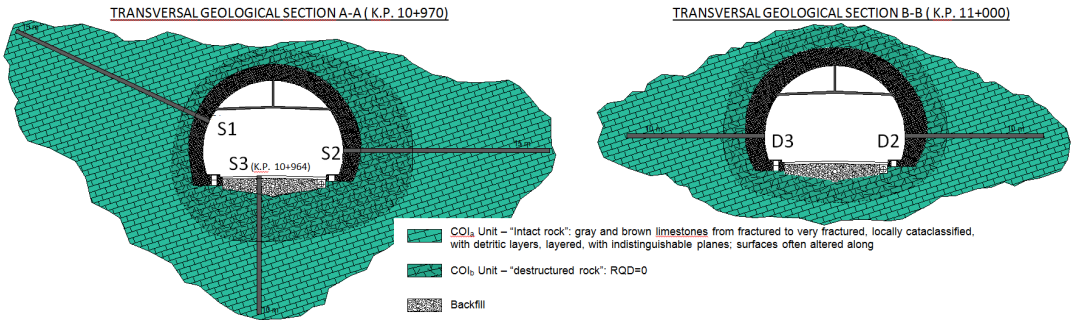


Fig. 14 Geological sections reproduced through surveys

During the drilling of the S2 survey, 4 specimens were subjected to uniaxial compression tests in the laboratory and along the S1, S2 and S3 surveys, dilatometric tests were performed at different depths; the obtained data allowed to derive the mechanical properties of the interested rock, which do not deviate from what was hypothesized in the original design project for the construction of the tunnel.

DESCRIPTION OF INTERVENTIONS

The interventions for the repair of the tunnel consist on the demolition of the existing final lining and related works (slab for the ventilation system, sidewalk, pavement) and their following reconstruction. These operations are carried out in the section most affected by the disadvantages (about 25 m from K.P. 10+981 to K.P. 10+956), where important cracks were detected, resulting in the disjunction of existing lining portions. In this area, the lesions affected the entire thickness of the lining with relative displacements on the transverse plane to the axis of the tunnel also greater than 0.10 m.

The intervention is performed by range and is described in the following operating steps:

- demolition:
  - demolition of the intermediate slab, sidewalk and pavement for range of 2.0 m as maximum;
  - in this 2 m, setting up of a provisional support system of the existing final lining consisting of steel ribs (2 IPE180/1 m) and fiber-reinforced spritz-beton (thickness 0.10 m);
  - completion of the two previously phases, in the 25 m of interest;
  - cavity consolidation by fiberglass bolt (Φ60/40, 1 valve/m) with improved adherence of variable length from 3 to 9 m, arranged at a radius of 2 m and a longitudinal distance of 1 m with a staggered arrangement (quincunx);
  - removal of provisional support (ribs and spritz-beton) previously in operation, for advancing range of a maximum length of 2.0 m;
  - in this 2 m, demolition of the final existing lining;
  - in the same 2 m, fast execution of a layer of fiber-reinforced spritz-beton 0.1 m thick;
  - installation of the first stage lining (2 IPE180/1 m + fiber reinforced spritz beton up to the inner thread of the ribs), in the same range of 2 m in length;
  - completion of the demolition of the existing final lining, execution of the fiber-reinforced spritz-beton layer and installation of the first stage lining for the entire 25 m of interest.
- Building of the invert:
  - excavation of 2.5 m respect to project level, for range of 7.0 m as maximum;
  - positioning the necessary reinforcements and casting of the tunnel invert and of the side walls for segments of 3.0 m length. It is foreseen a thickness of the tunnel invert of 0.70 m with reinforcement incidence of 140 kg/m^3. Between a segment and the other one, it is necessary to lay out tiles in neoprene of thickness of 10 mm.
- Building of the final lining:
  - setting up a waterproofing system with a layer of non-woven fabric and a 2 mm thick PVC waterproofing fabric. At the extrados of the side walls is planned to position a micro-wetted PVC pipe for the collection of percolation waters;
  - installing the necessary reinforcements, casting of the piers and of the crown according to the same sequence and the same size of the segments prescribed for the realization of the tunnel

invert. It is foreseen a thickness of 0.90 m with reinforcement incidence of 130 kg/m^3. Between a segment and the other, it is necessary to install neoprene sheets of thickness of 10 mm in continuity with the casting of the tunnel invert and the side walls.

- Finishes and completions works:
  - renovation of the intermediate floor and the ventilation system;
  - repairs of sidewalk and road pavement, with its hydraulic system;
  - refurbishment of the lighting system.

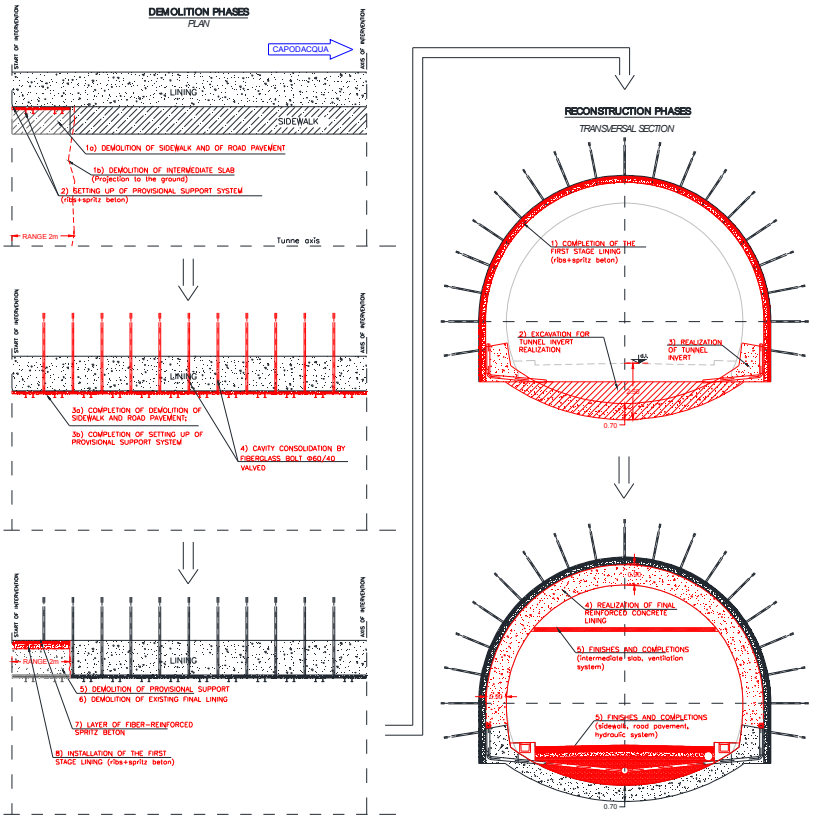


Fig. 15 Constructing phases

The demolition phases have been planned in such a way that the maneuvering and machines used always operate under safety conditions. For this reason, demolition operations will always be carried out for very small feed fields and under systems support and/or shoring.
The demolition operations of the existing lining have also made it possible to discover the conditions of the rock and in particular to detect the presence of gaps between the final lining and the profile of the excavated rock, as seen in the following images:



Fig. 16 Gap between the final lining and the profile of the excavated rock

At the time of writing this text works are being completed; below are some photographs of the workings performed.



Fig. 17 Completion of the demolition of the intermediate slab and setting up of the provisional support system



Fig. 18 Completion of the setting up of the provisional support system and cavity consolidation



Fig. 19 Demolition of the final existing lining (in progress at the date of this text)



Fig. 20 Detail of th demolition of the final existing lining



Fig. 21 Final completion operations

CONCLUSIONS

Geological studies, ongoing with the Department of National Civil Protection of Rome and the Department of Earth Sciences, University of Rome " Sapienza", show different characteristics of the rock around the existing concrete lining damaged by the earthquake, with consequent different mechanical behavior.

From an engineering point of view, the information obtained leads to the conclusion that the damage to the tunnel is due to the presence of specific concomitant factors linked to the particular seismic event and to the characteristics of the tunnel and the area where it is located; in the state of the current knowledge, they can be synthesized through the following four points:

- the high intensity of the seismic event, $M_w > 6$;
- the proximity of the tunnel to the epicenter of the earthquake;
- the non-homogeneous mechanical characteristics of the area concerned;
- the geometric characteristics of the structure.

The study of the cracking surface showed the presence of longitudinal lesions inclined by about 45°, due to the effects of shear action, typically induced by the earthquake. It has also been argued that the cracking surface has been significantly influenced by the particular geometry of the section of the tunnel, in particular by the presence of the suspended ceiling slab for the ventilation system.

ACKNOWLEDGMENTS

The activity of finding the data on the construction of the gallery was possible thanks to the availability and collaboration of “Società Italiana per Condotte d’Acqua S.p.A.”, through Eng. S. Oliva and Mr. Eng. Santarelli.

We also thank Eng. Annalisa Andreacchio of Anas S.p.A. for the valuable contribution given to the writing of the article.

REFERENCES

Corigliano, M., 2017. Progettazione di gallerie profonde in zone sismiche. MIR, Torino.

Dowing, and Rozen, 1978. Damage to rock tunnels from earthquake shaking. American Society of Civil Engineers, Journal of Geotechnical Engineering Division, 104 (2 Feb.), 175-191.

Galli, P., Galderisi, A., Martino, M., and Scarascia Mugnozza, G., 2017. GNGTS, 36° Convegno Nazionale Trieste 14-16 novembre 2017, L'eccezionale caso della fagliazione della galleria San Benedetto (in print).

Pierantoni, P.P., and Cicora, S., 2014. Caratteri geologico-strutturali dell'Appennino umbro-marchigiano e implicazioni sulla circolazione idrica profonda: l'area idrotermale di Acquasanta. Convegno Nazionale Acquasanta Terme (AP), Università di Camerino.

Pierantoni, P.P., et Al., 2002. Geological map of Sibillini Mountains.

Power, M.S., Rosidi, D., and Kaneshiro, J.Y., 1998. Seismic vulnerability of tunnels and underground structures revisited. Proceedings of North American Tunneling '98, Newport Beach, CA, Balkema, Rotterdam, 243-250.

Ricci, P., 1986. Galleria "San Benedetto", S. Pellegrino di Norcia (PG), Rassegna dei Lavori Pubblici del Maggio 1986.

Società Italiana per Condotte d'Acqua S.p.A., 1986. Progetto Esecutivo Galleria S. Benedetto.

Valente, A., Micheli, A., Cedrone, L., and Bardani, C., 2010. La galleria Monteluco (L'Aquila): un caso di galleria soggetta a sisma, Gallerie, 93.

http://www.ingv.it/it/

FINITE ELEMENT NUMERICAL ANALYSIS TO EVALUATE THE LATERAL BEHAVIOR OF THREE PILE GROUP CONFIGURATIONS

Murad Abu Farsakh, Research Professor, Louisiana State University, Baton Rouge, LA, cefars@lsu.edu.

Ahmad Souri, Ph.D. Research Associate, Louisiana State University, Baton Rouge, LA, asouri2@lsu.edu

George Voyiadjis, Boyd Professor, Louisiana State University, Baton Rouge, LA, cegzv1@lsu.edu

This paper compares the static lateral behavior of three pile group configurations: vertical piles, battered piles, and a mix of vertical and battered piles. The study is based on a previous investigation for the lateral behavior of M19 battered pile group at the I-10 Twin Span Bridge, in which a static lateral load test and 3-D finite element (FE) simulation was conducted. The battered pile group FE model was used as a basis for developing the FE models of vertical and mixed pile groups in the current study. The nonlinear material behavior was accounted for using elastoplastic constitutive models such as the Concrete Damaged Plasticity model and the Anisotropic Modified Camclay model. The pile groups behavior was investigated in terms of load-displacement, axial reaction, and *p-y* curves and *p*-multipliers. The results showed that the battered and mixed pile group stiffness was 120% and 50% higher than the vertical pile group, respectively. The largest lateral load share was unevenly distributed among the rows and different in each pile group configuration. For the axial reaction, the significant percentage was mainly in two rows in the vertical and the battered pile groups, while it was in four rows in the mixed pile group. The back-calculated *p*-multipliers was found different in each pile group with the highest values in the battered pile group.

INTRODUCTION

Bridge piers and offshore structures are usually supported by pile foundations that are designed to resist vertical and lateral loads. The lateral behavior of pile-soil system depends on both the pile stiffness and the soil reaction. The soil reaction is a nonlinear function of deflection, depth, pile stiffness, and soil stiffness and strength. The established methods for predicting the lateral capacity of single pile are: the *p-y* curve method (e.g., Matlock 1970; Reese et al. 1974), elastic solution (Poulos and Davis 1980), the strain wedge model (Ashour et al. 2004), and the finite element (FE) method (Brown and Shie 1990; Trochanis et al. 1991; Comodromos and Pitilakis 2005). Pile foundations are usually used in groups, in which the lateral capacity of a pile in the group is less than the case of isolated single pile. The soil in front of the pile in interest is weakened by the overlap of stress zones from surrounding piles, which is referred to as the group effect. Pile group solutions based on the *p-y* curve method accounts for the group effect using empirical factors called "*p*-multipliers" (Brown et al. 1988). Site specific *p*-multipliers are estimated thru iterative procedure to match the experimental load-displacement curve of the pile group with the curve from the prediction. Several studies suggested values for *p*-multipliers for vertical pile groups based on soil type and pile-pile spacing (McVay et al. 1995; Ruesta and Townsend 1997; Rollins et al. 2005). Additionally, the lateral capacity of vertical pile groups is also influenced by vertical load, piles arrangement, and slenderness ratio (e.g., Rao et al. 1998; Ilyas et al. 2004; Hussien et al. 2012).

In contrast to vertical pile groups, there are limited number of experimental studies available for battered pile groups (Ranjan et al. 1980; McVay et al. 1996; Zhang et al. 2002; Abu-Farsakh et al. 2011). Numerical studies for battered piles and battered pile groups are found in literature, but with no direct comparison to evaluate the differences between the vertical and battered configurations. In the present study, the lateral

© 2018 Deep Foundations Institute

behavior of three pile group configurations (vertical, battered, and mixed) is investigated using 3-D FE modeling. The study is an extension to the previous field and numerical investigations for the lateral behavior of the M19 pier battered pile group foundation of the I-10 Twin Span Bridge (Souri et al. 2015). The vertical and mixed pile groups FE models are based on the battered pile group FE model, in which the same pile cap size, pile size and spacing, material models, concrete and soil parameters were used. The FE results for the three pile groups were compared in terms of load-displacement curves, axial reaction, back-calculated *p*-*y* curves and *p*-multipliers.

The Static Lateral Load Test of Pier M19

The field test was conducted on the M19 pier foundation in 2007 and is briefly described here (Abu-Farsakh et al. 2011). The pier foundation was built of 24-battered piles inclined at 1H:6V slope. The square prestressed concrete piles had 0.9 m width and 34 m length, and were arranged in a 6x4 configuration at uneven pile spacing (Figure 1d). The eastbound and westbound piers were pulled toward each other using two high capacity strand jacks and steel tendons. The lateral load was applied in 0.9 MN increments and reached a maximum value of 8.3 MN. Two types of instrumentation were installed in selected piles: a series of six inclinometers for piles' slope and deflection measurements, and two pairs of strain gages for bending moment calculations. The in-situ soil conditions were obtained from the CPT sounding, which revealed a clay-dominated soil profile with a medium sand layer at 11.6-14.9 m and dense sand layer at depths greater than 30 m from the mudline (Figure 2). A layout map for piles numbering shown in Figure 1d is used throughout the study. Each pile was labeled according to its row (L, ML, MT, T) and column number (1, 2, … 6). A row refers to the piles arranged transversely to the load direction, whereas a column refers to the piles arranged parallel to the load direction.

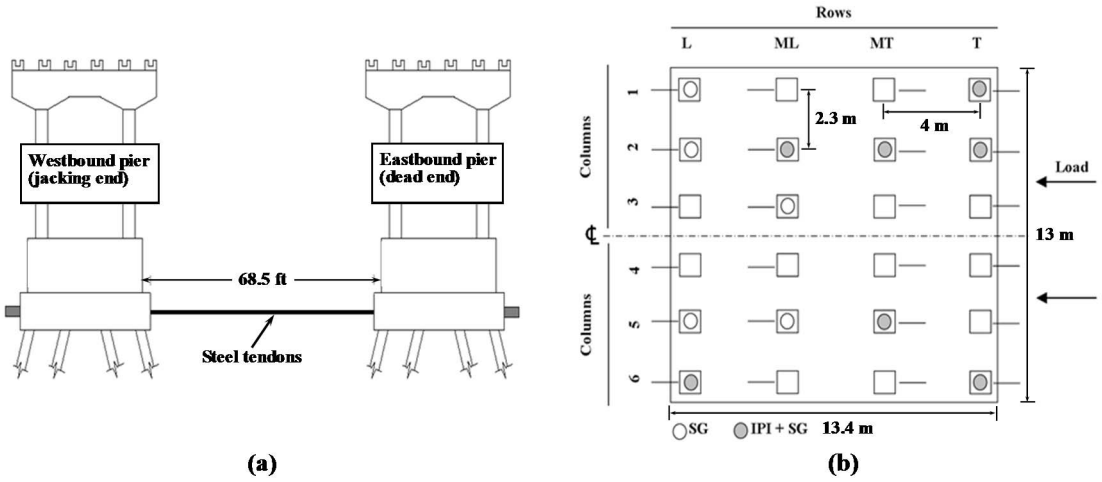


Figure 1. (a) Sketch of lateral load test, (b) plan view for piles' arrangement and labeling

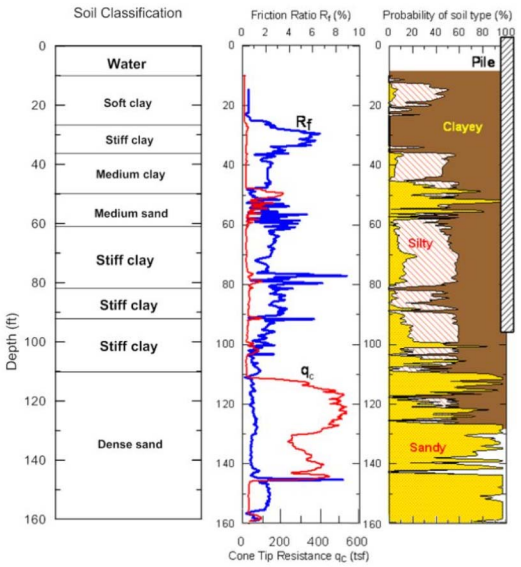


Figure 2. CPT sounding and soil profile for the M19 pier

DESCRIPTION OF THE FINITE ELEMENT MODELS

Geometry and FE mesh

Three FE models were developed in Abaqus v6.12 for three pile group configurations: Vertical, Battered, and Mixed. Following the FE study by Souri et al. (2015), the vertical pile group and mixed pile group models were developed based on the verified battered pile group FE model of the M19 pier foundation. The FE models resembled half of the foundation geometry to take advantage of the symmetry and reduce the solution cost. The pile group and soil body were created from two separate meshes using the linear solid continuum element (C3D8R). The number of elements for the pile group mesh was ~10500, and ~72000 for the soil mesh. The geometry, mesh, and dimensions of the three FE models are shown in Figure 3. The soil domain boundaries were located far away (30D from the group edge) from the pile group to eliminate their influence. The piles were placed in pre-bored holes in the soil mesh (i.e. wish-in-place) and the pile-soil interaction was facilitated using the interface model. The connection between the piles and the cap was assumed as fixed-head connection.

The main steel reinforcement in the piles was included in the FE models to introduce the prestress force. This was achieved using the embedded shell elements technique (Abaqus 2011). Each row of steel tendons in the pile section was compensated by one shell so that a total of four shells is used per pile in box shape (Figure 4). The interaction between the pile's solid elements and the shell elements was governed by the strain compatibility condition between the elements' nodes.

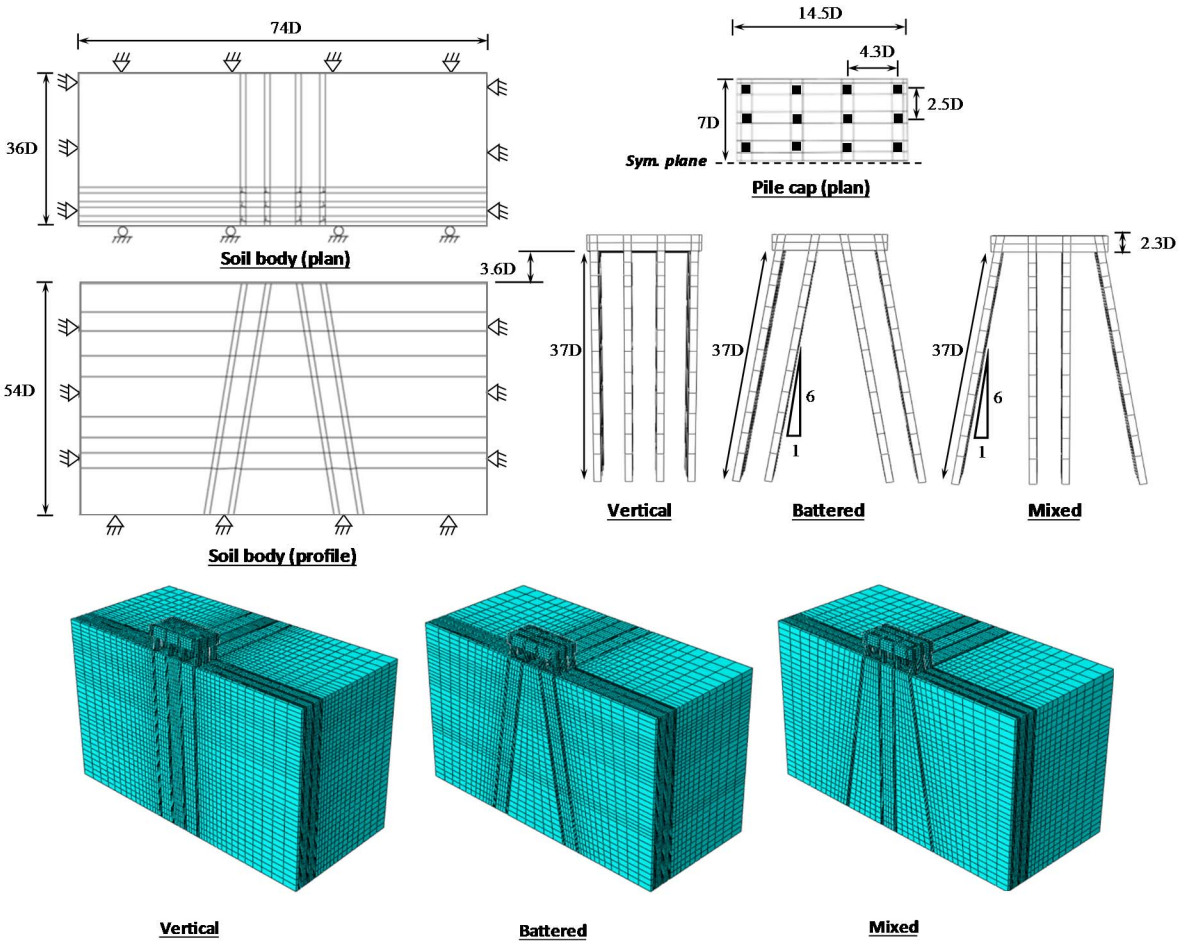


Figure 3. Geometry and mesh of the pile groups' FE models (D is pile width = 0.9 m)

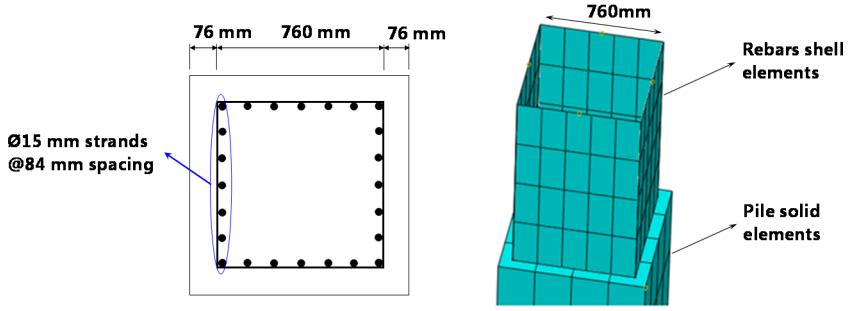


Figure 4. Arrangement of main steel in the pile's section and the FE reinforcement model

Material constitutive models

The nonlinear material behavior of the pile and soil materials was accounted for using elastoplastic constitutive models. For piles' concrete material, the concrete damaged plasticity (CDP) was used (Abaqus 2011). The CDP model incorporates the distinct stress-strain behavior in tension and compression regions, and the material stiffness reduction as a way to compensate for cracks formation. The material stiffness reduction is introduced by the scalar damage parameter *d* as

$$D^{el} = (1 - d)D_0^{el}$$

where D^{el}, D_0^{el} are the damaged and undamaged elasticity matrices, respectively.

The scalar damage parameter d is estimated by an averaging function for the distinct damage parameters (d_t, d_c) for the tensile and compression regions. The two parameters (d_t , d_c) are a function of strain, and were estimated using analytical concrete models from literature (Mander et al. 1988; Gupta and Maestrini 1990; Cicekli et al. 2007). The parameters use for CDP were $E_c = 35$ MPa for compressive strength $f_c' = 55$ MPa (ACI 318), and Poisson's ratio $\nu = 0.2$. The yield stresses in tension and compression regions were determined after Mander et al. (1988) and Gupta and Maestrini (1990), respectively.

For clay soils, the Anisotropic Modified Camclay (AMCC) model was used (Dafalias et al. 2006). It is based on the original Modified Camclay model, and incorporates the anisotropic soil behavior thru the rotational hardening rule for the yield surface (e.g., Voyiadjis and Song 2000; Abu-Farsakh et al. 2015). The elastic stiffness of soil in AMCC model is dependent on the mean stress, and therefore it increases linearly with depth. The plastic behavior is triggered by the yield surface, and an associative flow rule was adopted for the evolution of plastic strains. The AMCC model parameters used in the study are summarized in Table 1.

The Drucker Prager (DP) model was used for sand layers, which is well known for modeling the behavior of pressure dependent materials (Chen and Han 2007). The elastic stiffness is dependent on the mean stress, similar to AMCC model, and the plastic behavior is triggered by the DP yield surface with non-associative flow rule to control the dilation. The DP model parameters used in the study are shown in Table 1.

Table 1. Parameters for AMCC and DP models

Soil Type	Depth from Mudline (m)	Unit Weight (γ) (kN/m^3)	Undrained shear str. (S_u) (kPa)	AMCC						DP		
				κ	λ	M	α_{ini}	x	C	κ	β	d' (kPa)
Soft Clay	0-4.5	19.3	12	0.03	0.14	0.9	0.034	1.33	4	-	-	-
Stiff Clay	4.5-7.6	18.7	75	0.01	0.12	1.1	0.111	1.33	4	-	-	-
Medium Stiff Clay	7.6-11.6	17.0	53	0.02	0.13	1.0	0.219	1.33	4	-	-	-
Medium Sand	11.6-14.9	18.8	-	-	-	-	-	-	-	0.003	53	0.5
Stiff Clay	14.9-21.3	17.7	74	0.01	0.12	1.2	0.271	1.33	4	-	-	-
Stiff Clay	21.3-24.5	19.1	151	0.01	0.12	1.2	0.271	1.33	4	-	-	-
Stiff Clay	24.5-30.1	20.1	86	0.01	0.12	1.2	0.363	1.33	4	-	-	-
Dense Sand	> 30.1	19.4	-	-	-	-	-	-	-	0.003	58	0.5

* κ is slope of reload line in e-log p' plot; λ is slope of virgin consolidation line in e-log p' plot; M is slope of critical state line; α_{ini} is initial anisotropy; x and C are model constants; β is the friction angle in DP model; d' is soil cohesion in DP model

Pile-soil interface model

The interface model allowed the simulation of gap formation at the pile-soil interface and the transfer of normal and shear stresses. In the normal direction, the pile-soil interpenetration was prevented when the pile moves into the soil with the transfer of interface normal stress. When the pile moved away from the soil, the normal stress vanished and the gap formed behind the pile. In the tangential direction, pile-soil sticking or slipping was allowed with the transfer of interface shear stress. The slipping at the interface was triggered when the interface shear stress (τ_i) reached the stress limit (τ_{lim}), which was governed by the Coulomb friction criteria (τ_c) and the ultimate friction stress (τ_{max}), as shown in Figure 5.

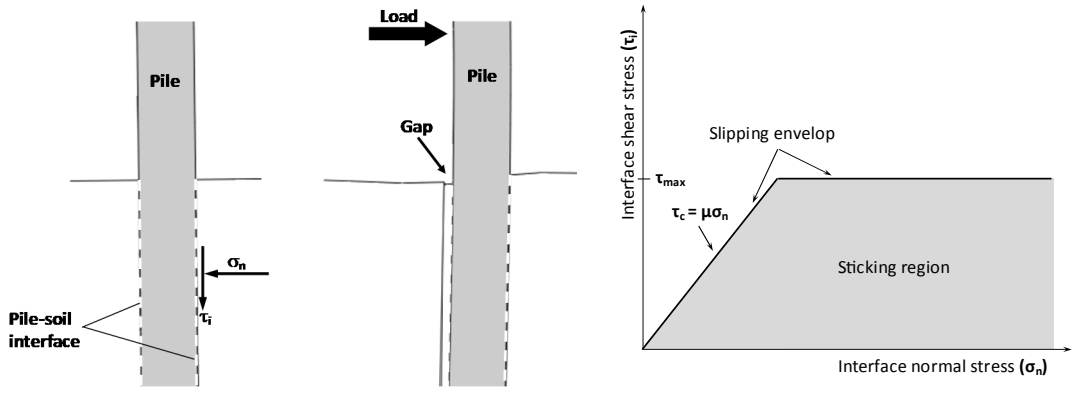


Figure 5. Pile-soil interface model characteristics

where σ_n is the normal stress at the interface, μ is the friction coefficient with assumed value of 0.5, and τ_{max} was assumed as the undrained shear strength for each layer.

It should be noted that the sensitivity of the FE model to the interface model parameters was found negligible for the lateral behavior of piles as similarly reported in the study by Mroueh and Shahrour (2009).

Loads and boundary conditions

The loads applied in the FE models were: gravity, weight of superstructure, and lateral load. The gravity load established the geostatic stress equilibrium in the soil body, and was applied by defining the gravitational acceleration g = 9.81 m/s^2. The dead load due to superstructure weight was applied as uniform distributed load on top of the cap in the global vertical direction. The lateral load was applied as uniform distributed load on the side of the cap in the global horizontal direction, and reached a maximum value of H_{max}= 25 MN. For boundary conditions, the soil body boundaries were constrained using pin-type displacement constraint on the far sides and bottom boundaries of the soil mesh and using roller-type constraint on the symmetry plane. The FE solution proceeded in the following steps; in the first step, the gravity load was activated to establish the geostatic stress in the soil and initial equilibrium. Then, the dead load of the superstructure was activated in the second step. Finally, the lateral load was applied in a stepwise scheme as follows: 2.5, 3.4, 4.3, 5.2, 7.0, 7.7, 8.3, 11.1, 15.5, 20.0, 25 MN.

RESULTS

Load-displacement response and lateral stiffness

Comparison of the load-displacement curves for the three pile groups is shown in Figure 6. Under the same lateral load, the vertical pile group (PG) exhibited the lowest lateral resistance compared to the battered and mixed PGs. For instance, at the maximum load, the displacement in the vertical PG was 280 mm compared to 76 mm for the battered PG and 165 mm for the mixed PG, which is due to the greater resistance from battered piles. The figure also depicts the average lateral load carried by each row in the PGs. It is noticeable that the load distribution is affected by the presence of battered piles. In the vertical PG, the largest load share was carried by the leading row L (31% at max load) followed by rows ML (24%), MT (23%), and T (22%). For the battered PG, middle rows carried larger share with 31% and 28% for rows ML and MT, and 22% and 19% for rows L and T, respectively. For the mixed PG, the load share distribution was 36%, 17%, 18%, and 29% for rows L, ML, MT, T, respectively. The load share percentages indicate that the lateral load is closely to be uniformly distributed in vertical PGs, and nonuniform distribution for the cases of battered and mixed PGs.

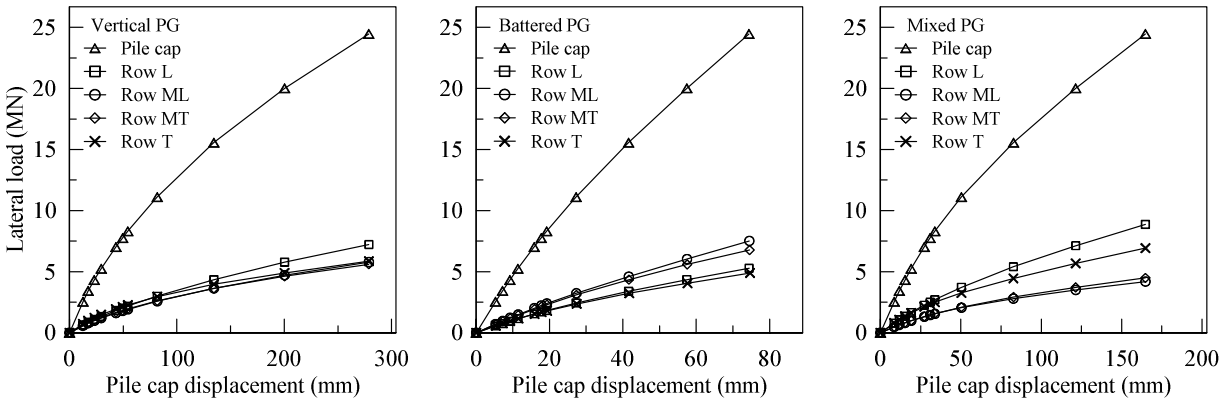


Figure 6. Load-displacement response and average load per row

The lateral stiffness and relative stiffness with respect to the vertical PG are presented in Figure 7. It is noticeable that the lateral stiffness decreased nonlinearly with lateral displacement at a similar rate in the PGs. This decrease can be possibly attributed to the progressive damage in the piles and soil yielding at the front of the PGs. The relative stiffness was estimated in respect to the vertical PG, and the results shows a significant increase in the lateral stiffness in the battered (+120%) and mixed (+50%) PG configurations.

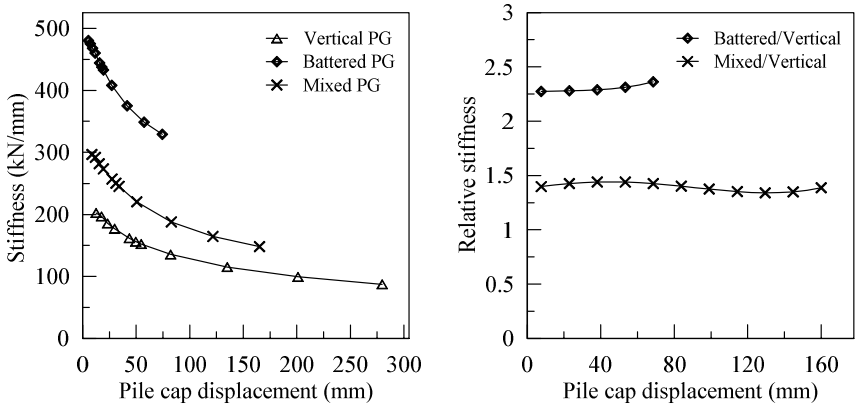


Figure 7. Comparison of PGs lateral stiffness

Axial reaction in piles

The lateral load applied on the PG generated axial reaction in the piles, and the results are shown in Figure 8. The results were normalized using the group lateral load (H) for better understanding. In the figure, a positive value for the axial reaction means it has compressive action (i.e. push in), while for a negative value the action is tension (i.e. pull out). First, it is noticed that the axial reaction in a pile and its mirror pile was similar in magnitude, assuming that the mirror axis passes between the middle rows and perpendicular to the load direction. For example, the axial reaction carried by pile L1 and its mirror pile T1 was similar in magnitude but different in the sign. Second, in any row for all PGs, the axial reaction was largest in the edge column (i.e. column 1), which was due to the lesser influence from the group effect. Third, the axial reaction per pile row differs between the PGs. In the vertical PG, the axial reaction was largest in the leading and trailing rows (L and T) with an average percentage of 8% per pile, and it stabilized with increased lateral load. In the battered PG, the axial reaction was largest in the middle rows (ML, MT) with an average of 11% per pile, and increased linearly with lateral load. For the mixed PG, the largest axial

reaction was observed in rows L and T with an average of 8.5% per pile. One interesting observation is that the axial reaction was compressive in row MT and tensile in row ML in the mixed PG, which is the opposite in load sign for the same rows in the vertical and battered PGs.

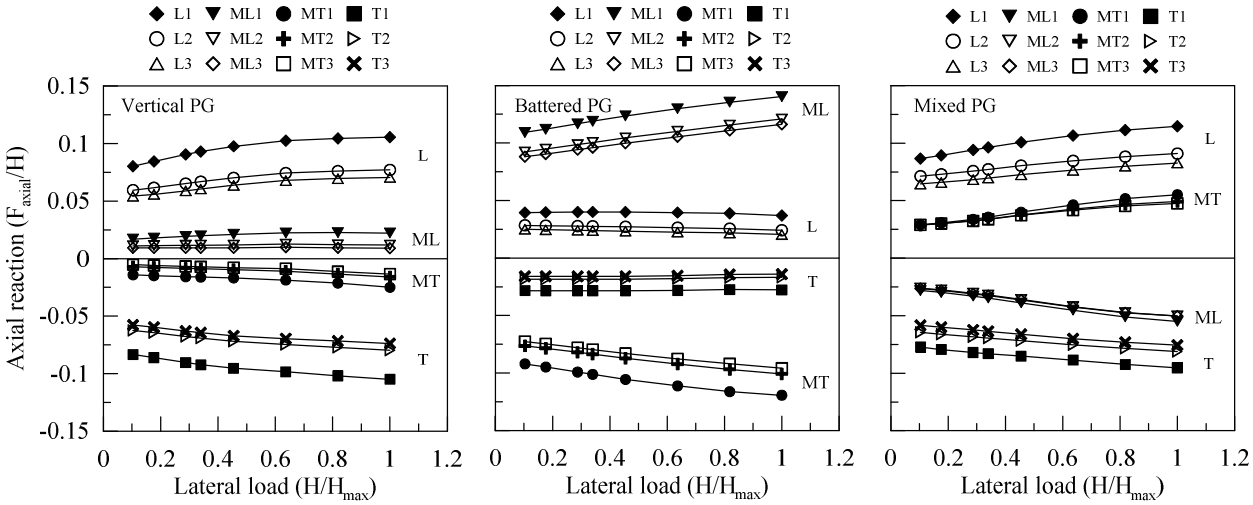


Figure 8. Axial reaction results

P-y curves

The variation of soil resistance (*p*) with lateral pile displacement (*y*) at certain depth is called the "*p-y* curve". In the current study, the *p-y* curves are back-calculated using the soil resistance and the lateral pile displacement at several depths. Figure 9 shows the *p-y* curves for columns 1 and 2 (column 3 was similar to 2, not shown) at selected depth z/D = 4.5 from the mudline. The *p-y* curves for isolated single pile cases (vertical, positive battered, and negative battered) are also presented in each sub-figure. Note that the *p-y* curves for the single pile cases in all sub-figures are the same, and may look different due to the difference in the horizontal scale. The influence of the group effect is clearly noticeable in all PGs; the *p-y* curves in the PGs are softer compared to the single pile case at the same displacement level. Also, columns 2 and 3 piles had a noticeable softer *p-y* curves than column 1 piles, which was due to the higher influence of the group effect on the interior piles.

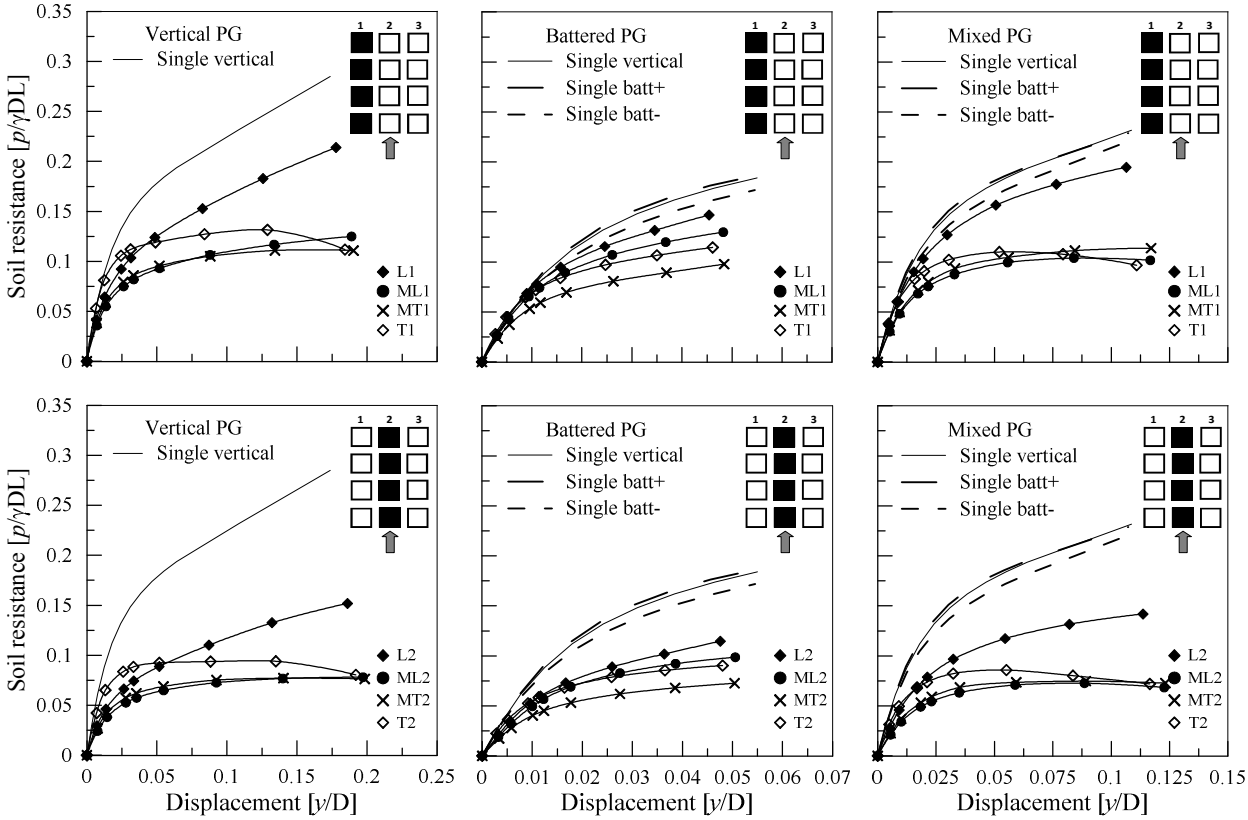


Figure 9. Back-calculated *p-y* curves for depth z/D = 4.5 from mudline

The *p-y* curves from the FE results allow back-calculating the *p*-multipliers, which provide quantitative measure for the group effect. The *p*-multiplier is defined as the ratio of soil resistance for a pile-in-group (p_g) to the soil resistance for the isolated single pile (p_{single}) at the same displacement level (y), and typically assume a value less than unity. Figure 10 shows *p*-multipliers variation with displacement for columns 1 and 2 in all PGs. Overall, the *p*-multipliers were highest in the battered PG, which was mainly due to the increased pile-pile spacing with depth.

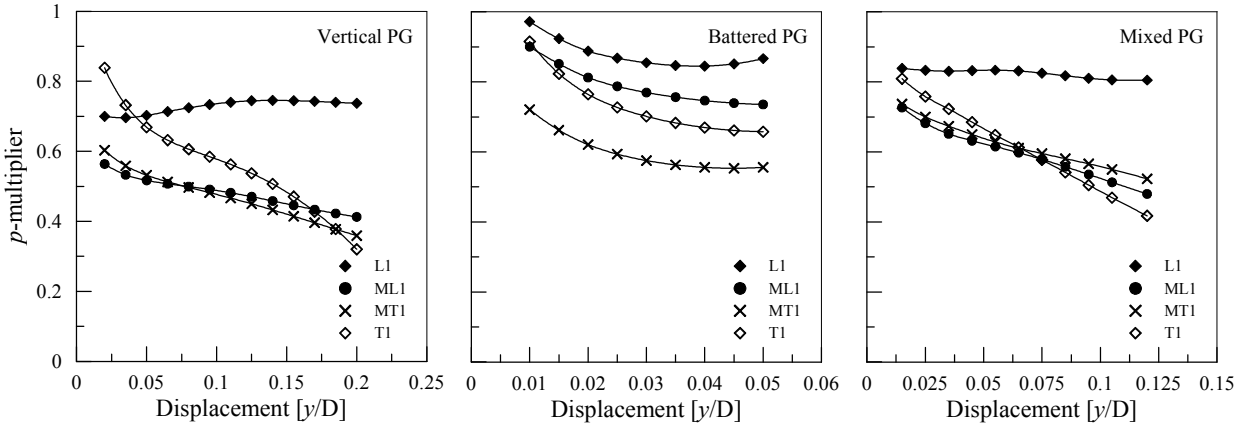


Figure 10. Back-calculated *p*-multipliers for depth z/D= [4 – 5] from mudline

The *p*-multipliers were averaged over the displacement range of 25-50 mm and summarized in Table 2. The *p*-multipliers for column 1 (edge column) are notably higher than columns 2 and 3 in all PGs with a

difference of 0.15-0.2. This observation leads to the conclusion that the average *p*-multiplier for a row would decrease with increasing number of pile group columns. This is following the fact that there are only two exterior columns in any PG, and their influence on the average *p*-multiplier would diminish with increasing the number of interior columns. The majority of past pile group experiments estimated the *p*-multipliers from pile groups having three or less columns in total (e.g., Ilyas et al. 2004; Chandrasekaran et al. 2010).

Table 2. Average *p*-multipliers for depth z/D= 4.5

		Row			
	Column	L	ML	MT	T
Vertical PG	1	0.73	0.49	0.48	0.59
	2	0.51	0.32	0.34	0.44
	3	0.49	0.30	0.32	0.42
	Row average	0.58	0.37	0.38	0.48
Battered PG	1	0.89	0.81	0.62	0.77
	2	0.67	0.60	0.46	0.61
	3	0.64	0.55	0.43	0.58
	Row average	0.73	0.65	0.51	0.65
Mixed PG	1	0.87	0.54	0.57	0.61
	2	0.63	0.37	0.39	0.47
	3	0.61	0.35	0.37	0.44
	Row average	0.70	0.42	0.44	0.51

The *p*-multipliers for the leading and trailing rows are compared to the recommended values from literature in Figure 11. The recommended values of *p*-multipliers from literature are given as function of pile spacing in the loading direction (S_L) only, and assumes similar pile spacing in the transverse direction ($S_T = S_L$). In the current study, the *p*-multipliers for all PGs are below the recommended values except for the trailing rows. This is possibly because the pile spacing was non-symmetric at the cap level in all PGs (S_L = 4.3D, S_T = 2.5D). The smaller spacing in the transverse direction resulted in greater influence from the group effect. Finally, the large number of columns was another factor that lowered the average row *p*-multiplier, as discussed previously.

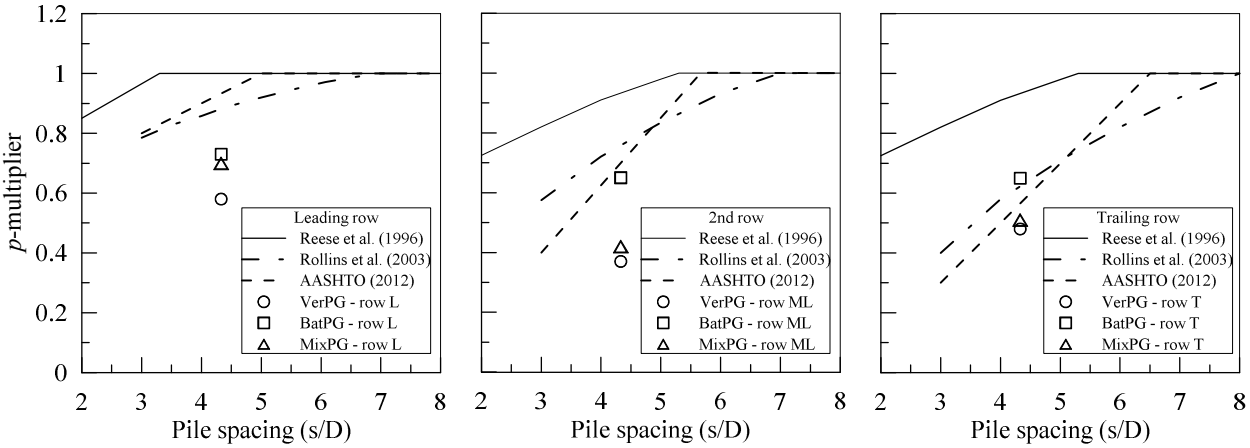


Figure 11. Comparison of *p*-multipliers with the recommended values in literature.

SUMMARY AND CONCLUSIONS

The static lateral behavior of three pile group configurations (vertical, battered, mixed) was studied using 3-D FE simulations. The FE models resembled prestressed concrete pile groups in 4x6 arrangement. The vertical and mixed pile groups were based on the FE model for the battered pile model, which was verified in previous case study. The FE models accounted for the nonlinear material behavior using nonlinear constitutive models, and for the pile-soil gapping using the interface model. The lateral behavior of the pile groups was compared in terms of load displacement curves, axial reaction, *p-y* curves, and *p*-multipliers. The results showed that:

- In reference to the vertical pile group, the battered and mixed pile groups had significantly higher lateral stiffness; +120% and +50% respectively.
- The lateral load share per row was different in the pile groups. In the vertical pile group, the lateral load share was closely distributed in all pile rows except in the first row which was higher by 7%. In the battered pile group, the middle rows (second and third) had the highest load share with 7-9% higher share than the first and last rows. For the mixed pile group, the largest load share was highest in the first and last rows with 11-18% higher share than the middle rows.
- Piles' axial reaction results indicated that only two rows carried significant load percentage in the vertical and battered pile groups cases, while it was the four rows in the mixed pile group. An interesting observation was that the leading rows (first and second) in the vertical and battered pile groups were subjected to compressive axial reaction, whereas for the mixed pile group it was in the first and third rows.
- The back-calculated *p*-multipliers were notably higher in the battered pile group, and fairly similar for the vertical and mixed pile groups except in the leading row of the mixed pile group. The exterior columns in all pile groups had higher *p*-multiplier compared to the interior columns with 0.15 to 0.2 difference. This lead to the conclusion that the *p*-multipliers would decrease when the total number of pile group columns increased.

REFERENCES

Abaqus. (2011). *Abaqus Documentation*. Dassault Systèmes, Providence, RI.

Abu-Farsakh, M., Rosti, F., and Souri, A. (2015). "Evaluating pile installation and subsequent thixotropic and consolidation effects on setup by numerical simulation for full-scale pile load tests." *Canadian Geotechnical Journal*, 52(11), 1734–1746.

Abu-Farsakh, M., Yu, X., Pathak, B., Alshibli, K., and Zhang, Z. (2011). "Field testing and analyses of a batter pile group foundation under lateral loading." *Transportation Research Record: Journal of the Transportation Research Board*, 2212, 42–55.

Ashour, M., Pilling, P., and Norris, G. (2004). "Lateral behavior of pile groups in layered soils." *Journal of Geotechnical and Geoenvironmental Engineering*, 130(6), 580–592.

Brown, D., Reese, L., and O'Neill, M. (1988). "Lateral load behavior of pile group in sand." *Journal of Geotechnical Engineering*, 114(11), 1261–1276.

Brown, D., and Shie, C. (1990). "Three dimensional finite element model of laterally loaded piles." *Computers and Geotechnics*, 10(1), 59–79.

Chandrasekaran, S. S., Boominathan, A., and Dodagoudar, G. R. (2010). "Group Interaction Effects on Laterally Loaded Piles in Clay." *Journal of Geotechnical and Geoenvironmental Engineering*, 136(4), 573–582.

Chen, W., and Han, D. (2007). *Plasticity for Structural Engineers*. J. Ross Publishing.

Cicekli, U., Voyiadjis, G., and Abu Al-Rub, R. (2007). "A plasticity and anisotropic damage model for plain concrete." *International Journal of Plasticity*, In honor of Professor Dusan Krajcinovic, 23(10–11), 1874–1900.
Comodromos, E. M., and Pitilakis, K. D. (2005). "Response evaluation for horizontally loaded fixed-head pile groups using 3-D non-linear analysis." *International Journal for Numerical and Analytical Methods in Geomechanics*, 29(6), 597–625.
Dafalias, Y., Manzari, M., and Papadimitriou, A. (2006). "SANICLAY: simple anisotropic clay plasticity model." *International Journal for Numerical and Analytical Methods in Geomechanics*, 30(12), 1231–1257.
Gupta, A., and Maestrini, S. (1990). "Tension-stiffness model for reinforced concrete bars." *Journal of Structural Engineering*, 116(3), 769–790.
Hussien, M. N., Tobita, T., Iai, S., and Rollins, K. M. (2012). "Vertical loads effect on the lateral pile group resistance in sand." *Geomechanics and Geoengineering*, 7(4), 263–282.
Ilyas, T., Leung, C., Chow, Y., and Budi, S. (2004). "Centrifuge model study of laterally loaded pile groups in clay." *Journal of Geotechnical and Geoenvironmental Engineering*, 130(3), 274–283.
Mander, J., Priestley, M., and Park, R. (1988). "Theoretical stress-strain model for confined concrete." *Journal of Structural Engineering*, 114(8), 1804–1826.
Matlock, H. (1970). "Correlation for design of laterally loaded piles in soft clay." Offshore Technology Conference, Houston, TX.
McVay, M., Casper, R., and Shang, T. (1995). "Lateral response of three-row groups in loose to dense sands at 3D and 5D pile spacing." *Journal of Geotechnical Engineering*, 121(5), 436–441.
McVay, M., Shang, T., and Casper, R. (1996). "Centrifuge testing of fixed-head laterally loaded battered and plumb pile groups in sand." *Geotechnical Testing Journal*, 19(1), 41–50.
Mroueh, H., and Shahrour, I. (2009). "Numerical analysis of the response of battered piles to inclined pullout loads." *International Journal for Numerical and Analytical Methods in Geomechanics*, 33(10), 1277–1288.
Poulos, H., and Davis, E. (1980). *Pile foundation analysis and design*. Series in geotechnical engineering, Wiley, New York.
Ranjan, G., Ramasamy, G., and Tyagi, R. (1980). "Lateral response of batter piles and pile bents in clay." *Indian Geotechnical Journal*, 10(2), 135–142.
Rao, S. N., Ramakrishna, V. G. S. T., and Rao, M. B. (1998). "Influence of Rigidity on Laterally Loaded Pile Groups in Marine Clay." *Journal of Geotechnical and Geoenvironmental Engineering*, 124(6), 542–549.
Reese, L., Cox, W., and Koop, F. (1974). "Analysis of laterally loaded piles in sand." *Offshore Technology Conference*, Houston, TX.
Rollins, K., Lane, J., and Gerber, T. (2005). "Measured and computed lateral response of a pile group in sand." *Journal of Geotechnical and Geoenvironmental Engineering*, 131(1), 103–114.
Ruesta, P., and Townsend, F. (1997). "Evaluation of laterally loaded pile group at roosevelt bridge." *Journal of Geotechnical and Geoenvironmental Engineering*, 123(12), 1153–1161.
Souri, A., Abu-Farsakh, M., and Voyiadjis, G. (2015). "Study of static lateral behavior of battered pile group foundation at I-10 Twin Span Bridge using three-dimensional finite element modeling." *Canadian Geotechnical Journal*, 53(6), 962–973.
Trochanis, A., Bielak, J., and Christiano, P. (1991). "Three-dimensional nonlinear study of piles." *Journal of Geotechnical Engineering*, 117(3), 429–447.
Voyiadjis, G., and Song, C. (2000). "Finite strain, anisotropic modified cam clay model with plastic spin. I: theory." *Journal of Engineering Mechanics*, 126(10), 1012–1019.
Zhang, L., McVay, M., Han, S., Lai, P., and Gardner, R. (2002). "Effects of dead loads on the lateral response of battered pile groups." *Canadian Geotechnical Journal*, 39(3), 561–575.

INFLUENCE OF THE LOADING DURATION ON UNDRAINED SHEAR RESISTANCE OF SOFT CLAYS OBSERVED DURING THE CONSTRUCTION OF A ROADWAY

Giana Laport Alves de Souza, PhD student, UERJ, giana.laport@gmail.com
Marcus Peigas Pacheco, PhD, Professor, UERJ, marcus_pacheco@terra.com.br
Rubenei Novais Souza, PhD, PETROBRAS, rubenei@petrobras.com.br

ABSTRACT

This paper presents a brief research on the influence of loading duration or strain rate on the undrained shear resistance of soft clays and reports the case observed during the construction of the Via UHOS, a roadway built in Rio de Janeiro metropolitan area for traffic of special vehicles transporting ultra heavy over size equipment. Based on the Via UHOS experience and the conducted research it was proposed a new procedure for designing of embankments on soft soils taking into account the influence of loading duration on undrained shear resistance. The new procedure makes possible more cost-effective solutions for projects of road embankments subject to exceptionally high loads traffic than those resulting from the use of the current methodology that considers such charges permanent.

Keywords: embankments on soft soils, loading duration, strain rate.

INTRODUCTION

The technological and economic development of a country usually imposes the need of constructions of ports, roads and industrial and energy plants. This kind of construction may demand transport of ultra-heavy equipment. In order to make possible the traffic of special vehicles for transport of these equipment, mostly in coastal lowlands, in many cases it is necessary to build stretches of roads designed exclusively for this purpose. When these roads cross areas with soft soils, the application of conventional embankment design methodology usually results in the need of soft soil treatment or inclusion of reinforcements in embankments, which may be very expensive.

Because of the traffic of these special vehicles implies relatively high loads of very short duration and considering that some academic papers have shown that the larger the strain rate the higher the undrained shear resistance of soft clays, it is conjectured that the use of an undrained shear resistance determined specifically for this condition, loading duration of only few seconds, may result in more economic projects than those designed according the conventional methodology, which considers the loading due to special vehicles as permanent load.

In this context, this papers presents a brief literature review on the influence of loading duration or strain rate on the undrained shear resistance of soft clays and reports a practical case of the observation of this phenomenon during the construction of the Via UHOS, a road built in Rio de Janeiro metropolitan area for traffic of special ultra-heavy vehicles.

INFLUENCE OF STRAIN RATE ON UNDRAINED SHEAR RESISTANCE

The influence of strain rate on undrained shear resistance of soft clays has been discussed since the beginning of the soil mechanics as a science. Terzaghi (1941) and Taylor (1942 and 1948) presented the first considerations about this topic and it is from Taylor (1948) the first expression of the undrained shear resistance considering two parts, one due to friction and other due to viscosity, which was considered as a function of shear strain rate. Bishop and Henkel (1962) analyzed the influence of strain rate of the soil on the representativeness of the results of triaxial tests concluding that in undrained tests there is a reduction of the shear resistance with the increasing of the duration of the test, which is negligible for sands but tends to be meaningful to some clays, reaching about 5% decrease in the tangent of the effective friction angle for each increase of 10 times in the duration of the test. Lerouil et al. (1985) presented a study showing that the strain rate of a clay in oedometer tests with controlled strain affects the effective vertical stress x vertical strain curve and, consequently, the preconsolidation stress. As the undrained shear resistance of soft clays is proportional to the

© 2018 Deep Foundations Institute

preconsolidation stress (Mesri, 1975 and 1989), it is concluded that the studies of Lerouil et al (1985) also show the influence of strain rate of clayey soils in their undrained shear resistance. Pinto (2000) presented results of undrained triaxial compression tests on samples of a clay with different loading times up to rupture, that implies different strain rate of the soil. It was demonstrated that the slower the loading the lower the undrained shear resistance. The results presented by Pinto (2000) also show that the strain rate affects the rigidity of the soil as well. Is was observed that the slower the loading the lower the rigidity of the soil.

Martins (1992) and Martins et al. (2001) presented the most complete known studies on the influence of strain rate on undrained shear resistance of clayey soils. These authors not only established a constitutive model of the behaviour of clayey soils considering the undrained shear resistance composed by one part due to friction and other due to viscosity, which is proportional to strain rate, but described the physical phenomenon associated with this behavior. Based on the studies of Terzaghi (1941) and Taylor (1942 and 1948), Martins (1992) considers that all the solid particles of the saturated clayey soils are wrapped by a layer of adsorbed water. The part of this adsorbed water close to the surface of the grain is solid and strongly adhered to it. As it moves away from the surface of the grains, the viscosity of adsorbed water decreases gradually until to reach the properties of the common water. Thus, the soil structure contemplate two types of contact between the grains: the contact type "solid bond" between the grains that only adsorbed water in solid form occurs and the contact type "bond film" between the grains that besides the adsorbed water in solid form there is a film or layer of adsorbed water in the liquid form. Considering such soil structure, it can be concluded that a potential shear surface will include both types of contact and the quantity of each type will depend on the soil structure and physical and chemical characteristics of the soil particles and water. Figure 1 presents the model of an element of soil considered by Martins (1992).

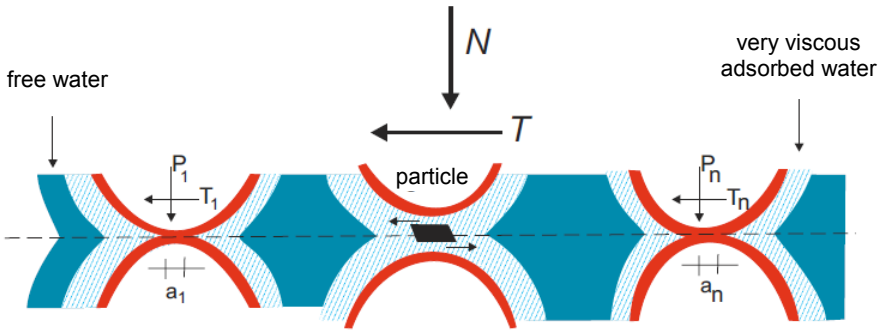


Figure 1: Element of soil (Martins, 1992)

Considering the soil element model shown in Figure 1 and assuming the balance of forces in the shear plane, Martins (1992) established the expression [1].

$$\tau = \underbrace{\sigma' \tan \phi'_{mobized}}_{\tau_f\,(friction)} + \underbrace{\eta(e)\frac{d\gamma}{dt}}_{\tau_v\,(vis\cos ity)} \qquad [1]$$

where:

τ = undrained shear resistance

σ' = effective normal stress on rupture plan

$\phi'_{mobilized}$ = mobilized effective friction angle of the soil

$\eta(e)$ = coefficient of viscosity of the soil

$\frac{d\gamma}{dt}$ = shear strain rate

Expression (1) shows that the shear stress τ is resisted internally by a part due to friction τ_f and other part due viscosity τ_v. The coefficient of viscosity of the soil $\eta(e)$ represents the overall effect of the viscosity of the adsorbed water and the soil structure, in particular the void index, which sets the proportion of solid and viscous contacts in the shear plane. As can be seen, the determination of the viscous resistance directly from the parameters of expression (1) is not practical. However, it can be achieved in conventional triaxial compression test. As shown by Martins (1992), Alexandre (2006) and Aguiar (2014), in triaxial compression tests of type consolidated undrained (CU), during the beginning of the application of the deviator stress, when there is no displacement for mobilizing frictional resistance nor excess of pore pressure, all resistance mobilized is viscous. Thus, in principle, it is possible to identify the part of viscous resistance of the soil in a conventional CU test, as shown schematically in Figure 2 from Aguiar (2014), which presents the typical total and effective stress paths for a conventional CU test. However, despite of the solidity conceptual, because of the interference of adjustment strain of the system and inaccuracy of measurement of pore pressure, in many tests is not possible to catch the amount of deviator stress applied before the beginning of the excess of pore pressure, corresponding to the segment AB in Figure 2.

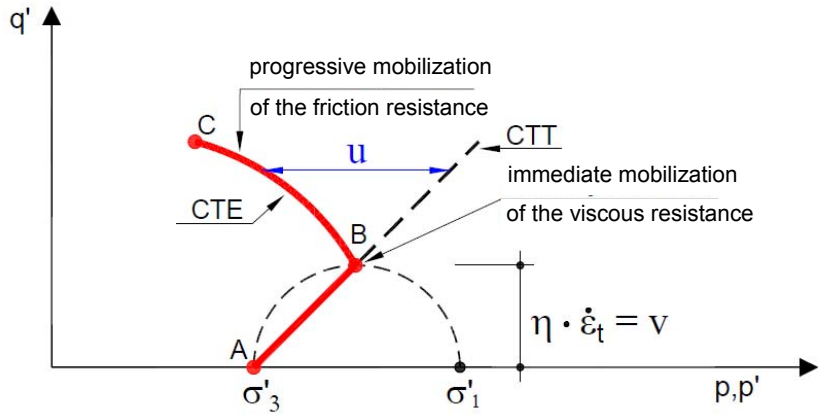


Figure 2: Immediate activation of viscosity resistance (Aguiar, 2014)

Based on the exposed above it can be concluded that, in fact, saturated clayey soils present a part of the undrained shear resistance that is due to viscous contacts between layers of water adsorbed to soil particles and that this part of resistance is proportional to the strain rate of the soil during the shearing. These conclusions imply that, in cases of short-term loading, where the rupture would occur necessarily at high strain rate, otherwise the loading is removed before it is reached a level of deformation characteristic of rupture, it is possible to take in count the viscous resistance corresponding to a high strain rate compatible with the short duration of loading.

SHORT DESCRIPTION OF THE DESIGN AND CONSTRUCTION OF VIA UHOS

Via UHOS (Ultra Heavy Over Size) is a road of about 18 km long built for the transportation of large equipment needed to assemble a new refinery in Rio de Janeiro metropolitan area. The road connected Guanabara Bay to the a existent road which is the main access to the area of the mentioned industrial plant. Figure 3 presents the location of the work.



Figure 3: Location of Via UHOS

Via UHOS crosses some small rivers where was found compressible layer of soft clay. The occurrence of this material was also been found in other stretches of the road, where probably existed watercourses in past geological periods. Where the route of Via UHOS coincided with existent roads, urban areas or the old Ferrovia Centro-Atlântica (FCA), the soft clay layer underlying the existing embankment about 2 m thick. In other stretchs, where Via UHOS was the first element of the infrastructure of transportation, the soft clay was outcropping. The thickness of the soft clay layer was variable, in some cases exceeding 10 m.

The transport of the ultra heavy and/or large dimensions equipment was performed using special multi-hubs vehicles, which applied on the ground loads corresponding to equivalent distributed vertical stress ranging from 30 kPa to 70 kPa. Figure 4 shows pictures of one of these vehicles carrying the two heaviest equipment of the plant.

The stabilisation solutions of the soft clay layer adopted at Via UHOS included removing and replacing the soft soil, acceleration of the consolidation with wickdrains, reinforcement of the embankment with geogrids and reinforcement of soft clay layer with gravel columns depending on the undrained shear resistance and thickness of the soft clay layer as well as the admissible ground displacement in each stretch of the road.



Figure 4: Special multi-hubs vehicle carrying ultra heavy equipment at Via UHOS

As is typical in road design, the 18260 m of extension of Via UHOS were divided into 913 segments of 20 m (stakes E-000 to E-913). In the segments between E-692 and E-696, which are part of the stretch of the old Centro-Atlântica railway, based on standard penetration tests (SPT) carried out

nearby, the original geotechnical design admitted the occurrence of a soft clay layer of 4 m thickness and undrained shear resistance constant with depth equal to 12 kPa and a embankment of 1.5 m thick in part of the section of the road. Considering this geotechnical profile it was designed and executed a new embankment reinforced with geogrids, whose thickness was 2 m at the part above the existing embankment and 3.5 m on the outcropping soft clay, fashioning a 16 m wide platform on which would be executed a 40 cm thick gravel layer of 10 m wide.

After the execution of the new embankment, in order to meet the refinery installation schedule, it was started traffic of the special vehicles with distributed load equivalent to 30 kPa before the execution of 40 cm thick gravel layer.

Two of these vehicles crossed the mentioned stretch and the entire route without any problem. After that the 40 cm thick gravel layer was executed corresponding to a distributed load of about 8 kPa. In the day after the execution of this layer was observed cracks and lateral displacement on the embankment and elevation of the top of the downstream land compatible with the beginning of a process of rupture of the soil foundation. Figure 5 shows pictures of mentioned stretch taken on the morning of the day after the execution of the 40 cm thick gravel layer.



Figure 5: Imminence of rupture of the soil foundation at the stretch between E-692 and E-696

The finding of the imminence of soil foundation rupture in the stretch between E-692 and E-696 showed a behavior incompatible with the subsoil profile adopted in the design. In addition, the signs of exhaustion of the soil foundation resistance for a permanent surcharge of about only 8 kPa after good performance under a short-duration loading of about 30 kPa, corresponding to the distributed load equivalent of the first two special vehicles that crossed Via UHOS, indicated a likely influence of the loading duration on the undrained shear resistance of the soft clay layer.

Immediately after the imminence of rupture shown above it was removed part of the new embankment and provided a complementary geotechnical investigation, which contemplated standard penetration tests (SPT), cone penetration test with measurement of pore pressure (CPTU), vane tests (VT) and extraction of undisturbed samples type shelby for laboratory tests. The results of the 'in situ' tests were used for reviewing of the design as soon as possible and the laboratory tests were included in a more extensive work, intended to study in more detail the influence of loading duration on undrained soil resistance, what exactly is the object of this paper.

COMPLEMENTARY GEOTECHNICAL INVESTIGATION

The complementary geotechnical investigation in the stretch between E-692 and E-696 was concentrated close to E-694 section, which was located at the center of the unstable stretch. Initially it was carried out two standard penetration tests approximately at the road axis, whose results showed that the thickness of the soft clay layer was greater than 12 m and the its consistency was very soft. It was also carried out two vane tests, VT-28 at the road axis where there was the embankment and VT-29 located about 6 m away from the edge of the embankment where the soft clay layer was outcropping. The results of this tests in terms of undrained shear resistance S_u are shown in Table 1. In VT-28 it was not possible to determinate the undrained shear resistance S_u in the first meter of the soft clay layer. The values in red underscores shown in Table 1 have been extrapolated based on the

evaluation of all the measurements available. Table 1 also shows the values of the undrained shear resistance S_u corrected by vane test correction factor μ of Bjerrum (1973) equal to 0.7 according to results obtained in retroanalysis held by Souza et al (2014) in rupture occurred in the section E-357 of Via UHOS.

Next to the location of VT-29 it was also carried out a CPTU, whose full results can be analyzed in Souza (2017). In order to obtain a very representative subsoil model, the results of the vane tests and CPTU were analyzed conjunctly. As shown by Souza (2017), the combination of the results of these two types of tests to obtain the profile of the undrained shear resistance of soft soils constitutes a good practice because they have complementary characteristics in terms of representativeness of the soil behavior on this parameter. While through vane test it is possible to obtain directly the undrained shear resistance, without correlations, but it does in certain depths, the CPTU test demand the use of empirical correlations from the cone tip resistance (q_t) to obtain this parameter, but such achievement is obtained continuously throughout the entire depth tested.

Table 1: Undrained shear resistance S_u profile obtained from the results of the vane test carried out in the E-694 section

Depth	*VT-28*	*VT-29*	*VT-29 (corrected)*	*VT-28 (corrected)*
[m]	[kPa]	[kPa]	[kPa]	[kPa]
1	13	9	6,3	9,1
2	13	9	6,3	9,1
3	13	9	6,3	9,1
4	13,5	9,5	6,65	9,45
5	15	11	7,7	10,5
6	16,5	12,5	8,75	11,55
7	19	14	9,8	13,3
8	19	15	10,5	13,3
9	16,5	16	11,2	11,55
10	21,5	17,5	12,25	15,05
11	23	19	13,3	16,1

Figure 6 presents undrained shear resistance profiles obtained from the results of the mentioned vane tests and CPTU. VT-29 and CPTU, which were carried out on outcropping soft clay, represent the part of the subsoil without the action of the existing embankment, where the soft clay layer was called Soft Soil 1. The VT-28 test, performed on the road, where there is a embankment of the old railway, represents the part of the subsoil that suffered the action of the existing embankment, where the soft clay layer was called Soft Soil 2. As can be seen, there is a good approximation between the profile of S_u obtained from CPTU test considering the N_{kt} coefficient equal to 12 with that corresponding to the result of VT-29 corrected.

Based on the limits of the unstable surface observed in the field and results of the complementary geotechnical investigation, specifically the thickness of the soft clay layer and the pattern of the undrained shear resistance profile, which is constant up to about 4 m deep and linearly growing from that depth, it was done the retroanalysis of the rupture presented on the Figure 7. The mentioned retroanalysis and all other stability analyses presented in this paper were performed using the GeoStudio software 2007-SLOPE/W®, taking the results corresponding to the method of Morgenstern-Price. The result of the retroanalysis indicated undrained shear resistance profiles of Soft Soil 1 and Soft Soil 2 lightly higher than that obtained from the vane tests and CPTU.

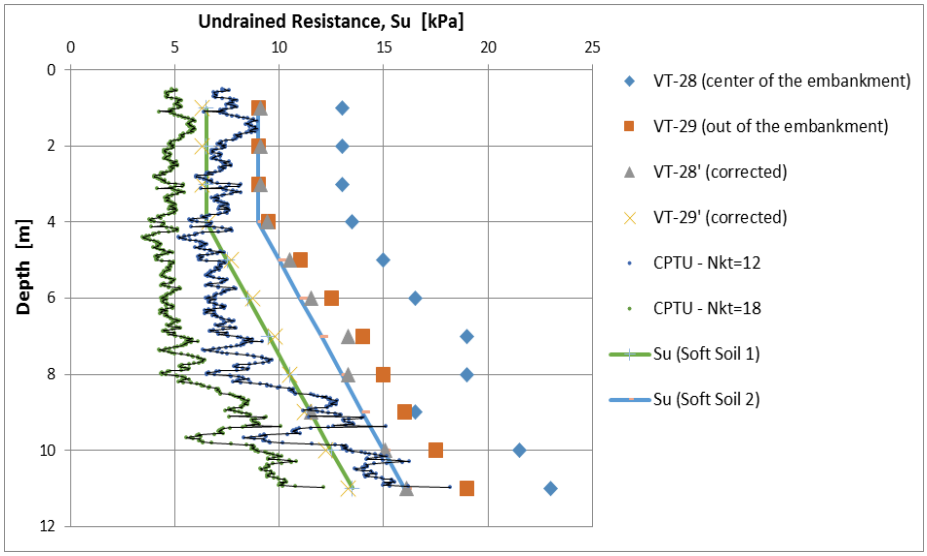


Figure 6: Undrained shear resistance profiles S_u obtained from the results of the vane tests and CPTU

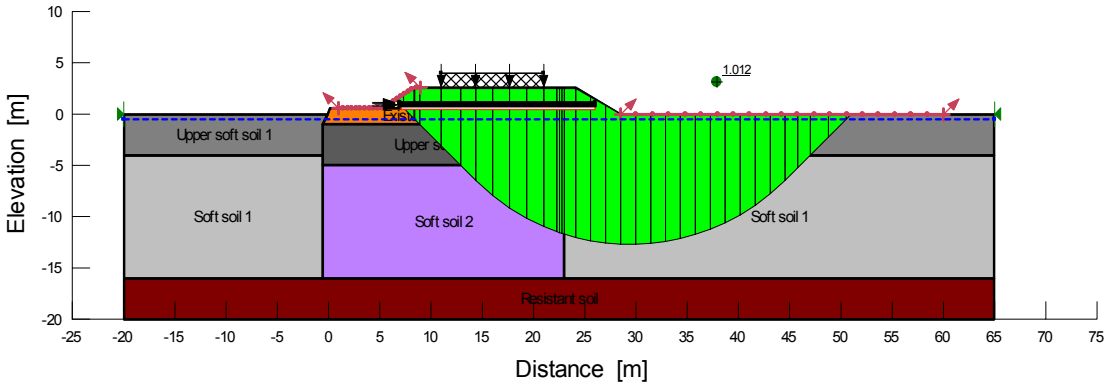


Figure 7: Retroanalysis of the original E-694 section considering surcharge of 8 kPa corresponding to gravel layer 40 cm thick

Next to the location where were performed the test vane test VT-29 and CPTU it was collected undisturbed samples of the soft clay for laboratory tests, whose main purpose was to reproduce in more well controlled boundary conditions the verification of the influence of the loading duration on the undrained shear resistance of the studied soft clay. As shown by Souza (2017), the influence of loading duration on the undrained shear resistance of the clayey soils can be examined through the study of the influence of the strain rate. As of the soils present increasing of the strain during the loading until the rupture, if the short-term loading is large enough to cause rupture, it necessarily occurs with high strain rate, otherwise the loading is removed before the rupture strain is reached. Thus, in the present case, in addition to the characterization tests, it was done two isotropically consolidated undrained triaxial compression tests (CIU) with different strain rate. In the first one, the strain rate was 0.026 mm/min, considered conventional for the soft clay studied. In the second test, the adopted strain rate was ten times higher, 0.260 mm/min. Both tests were performed with confining stress of 50 kPa 25 kPa and 100 kPa. Other details of the execution of such tests can be found in Souza (2017). The results obtained confirmed the increase of the undrained shear resistance in the accelerated test and, taking in count relationship between confining effective stress and the undrained shear resistance, it was possible to establish the undrained shear resistance profiles for Soft Soil 1 and Soft Soil 2 presented in Figure 8. It should be noted that the undrained shear resistance profile for the case of the short-term duration loading obtained from the triaxial test represent only a minimum value to be considered in the analysis since in the actual problem, because of the passage of the vehicles in

each section takes only about 30 seconds, that would imply in a strain rate of the soil during the shearing much bigger than 0.26 mm/min, the viscous resistance would be greater than the measured on accelerated CIU test.

Considering the results of the complementary geotechnical investigation, including laboratory tests, it can be adopt as representative of the subsoil the undrained shear resistance profiles presented in Figure 8, keeping in mind that in case of short-term duration loading the resistance profiles represent only minimum values confirmed, being the actual values probably much bigger.

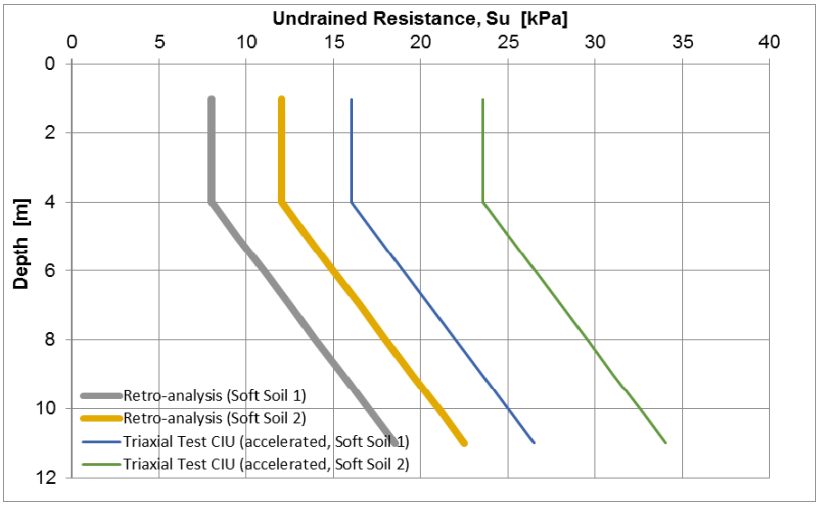


Figure 8: Undrained shear resistance profiles representative for permanent and short duration loading conditions

EVIDENCE OF THE OCCURRENCE OF THE PHENOMENON IN VIA UHOS

The evidence of the influence of the loading duration on undrained shear resistance of the soft clay layer at E-694 section of Via UHOS can be demonstrated through the of stability analyze of the embankment considering the representative undrained shear resistance profiles indicated in Figure 8. Initially it is shown that, for the existing permanent loading before applying the gravel layer 40 cm tick the system was stable, as can be observed in Figure 9. When it was added the permanent load corresponding to the mentioned gravel layer the system became unstable, as shown in Figure 7.

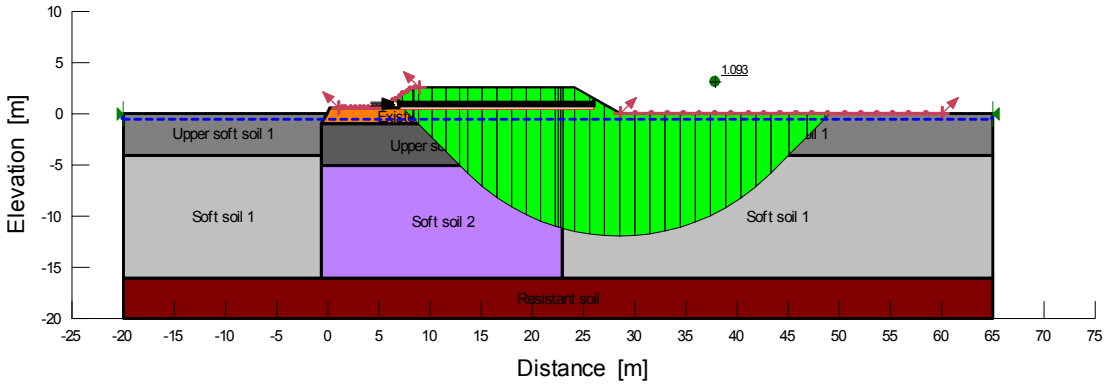


Figure 9: Stability analysis of the original E-694 section without surcharge considering the retroanalyzed undrained shear resistance profiles

Figure 10 and Figure 11 present the stability analyses of the original E-694 section considering surcharge of 30 kPa, corresponding to the passage of the first two special vehicles multi-hubs, and the undrained shear resistance profiles for permanent and short-term duration loading respectively. As can be observed, adopting the resistance profiles for permanent loading the safety factor is only 0.82, indicating rupture. When it is adopted the resistance profiles for short-term duration loading the

safety factor is higher than 1.03, indicating stability. Thus, it can be concluded that the stability analyses presented in Figure 10 e Figure 11 demonstrate unequivocally the influence of the loading duration undrained shear resistance of the soft clay at the E-694 section of Via UHOS. These stability analyses also demonstrate that the passage of the first special vehicles with distributed load equivalent to 30 kPa without problem was thanks to viscous resistance portion, due to the high strain rate of the soil or to the short duration of loading, since according to the conventional analysis it would occur rupture.

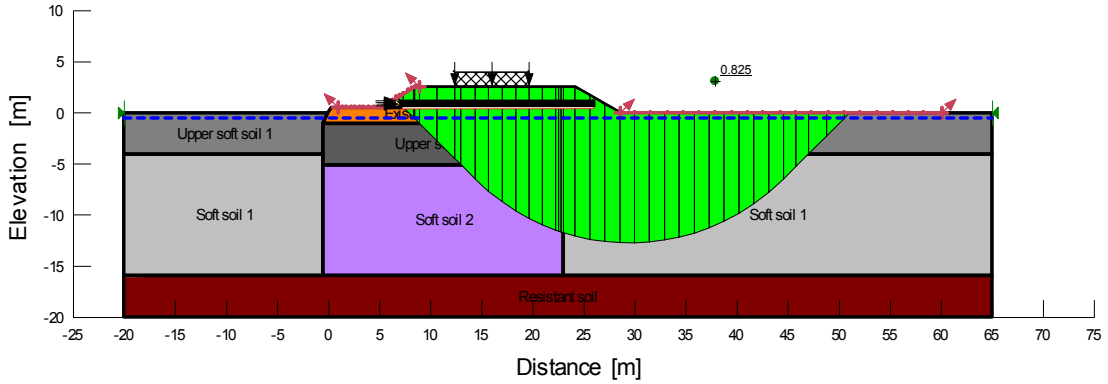


Figure 10: Stability analysis of E-694 section considering surcharge of 30 kPa and undrained shear resistance profiles for permanent loading

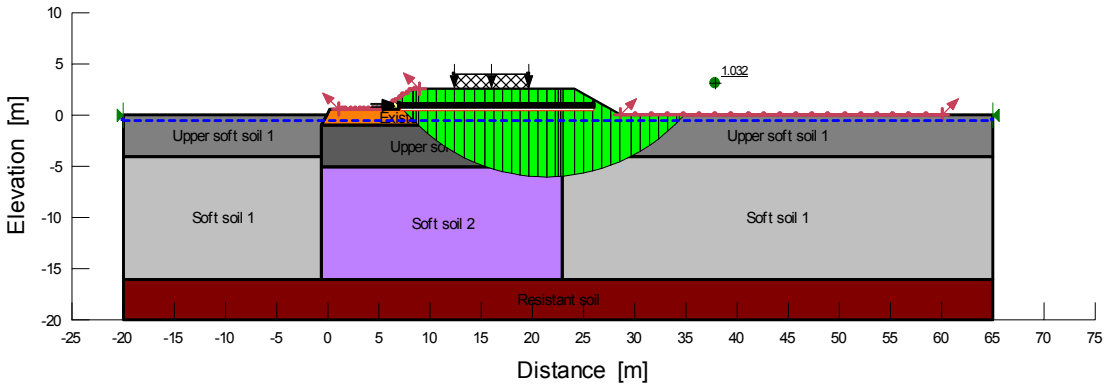


Figure 11: Stability analysis of E-694 section considering surcharge of 30 kPa and undrained shear resistance profiles for short-term duration loading

ADJUSTMENT OF THE EMBANKMENT DESIGN IN THE E-694 SECTION OF VIA UHOS

Based on the results of the complementary geotechnical investigation and on the empirical observation of the significant influence of the loading duration on the undrained shear resistance of local soft clay layer, it was done an adjustment of the embankment design in the E-694 section, basically reducing the height and increasing the width of the embankment. Figure 12 and Figure 13 present the stability analyses of this new section considering the maximum load of the special vehicles, 70 kPa, and the undrained shear resistance profiles for permanent and short-term duration loading respectively. As can be observed, adopting the resistance profiles for permanent loading the safety factor is only 1.06. When it is adopted the resistance profiles for short-term duration loading the safety factor is higher than 1.41. Considering that the solution of adjustment of the embankment design implied that the loading on soft clay layer was predominantly of short duration, it was considered sufficiently safe. Thus, the construction was concluded and the traffic of the special vehicles was restarted and completed without problems. Figure 14 shows two of the authors of this paper following the passage of the last and heaviest special vehicle by the E-694 section.

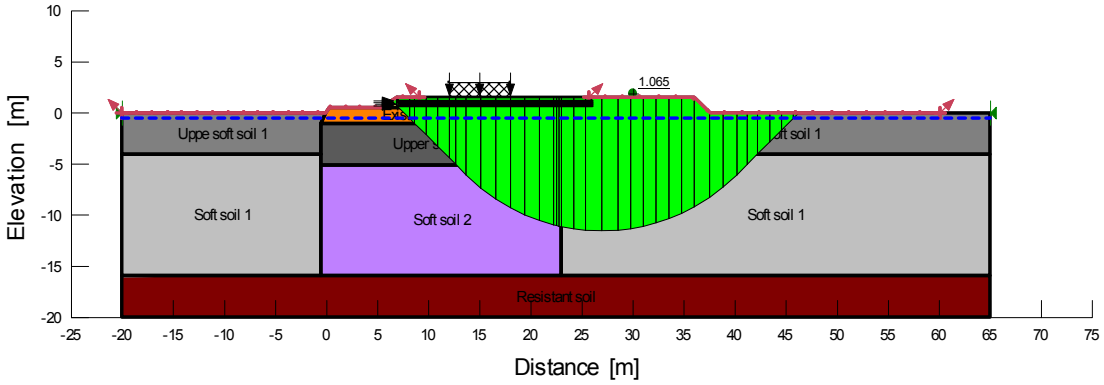


Figure 12: Stability analysis of the E-694 section after the adjustment of the design, considering undrained shear resistance profiles for permanent loading

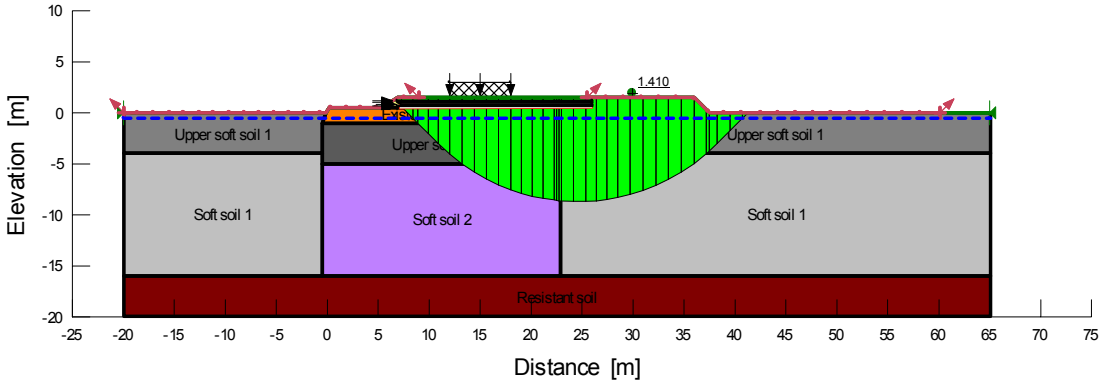


Figure 13: Stability analysis of the E-694 section after the adjustment of the design, considering undrained shear resistance profiles for short-term duration loading



Figure 14: Passage of the last and heaviest special vehicle by the E-694 section of Via UHOS

PRELIMINARY PROPOSAL FOR A NEW DESIGN METHODOLOGY

The experience on Via UHOS and the research realized confirms the importance and feasibility of establishing a new design methodology for special road embankment on soft soil, which makes possible to take into account the influence of loading duration on undrained shear resistance of the soft soil. Presently it is being conducted at UERJ – University of State of Rio de Janeiro a doctorate research for achieving this objective. Preliminarily it is considered that the new methodology should incorporate a geotechnical data acquisition plan that includes the collection of undisturbed samples of good quality, representative of the studied layer, for performing four triaxial tests CIU. Each test should be done with a different strain rate. The first test should be carried out with the conventional

strain rate, representative for permanent loading, about 0.026 mm/min in the case of the soft clay of Via UHOS. The other 3 CIU tests should be conducted at strain rates of 10, 50 and 100 times the conventional. Each test should contemplate the rupture of 3 specimens, each one with a different confining stress, to cover the range of effective stresses of the design. In all 4 tests should be adopted the same 3 confining stresses.

The procedure described briefly above will give 4 envelopes of resistance in terms of effective stresses, each one corresponding to a different soil strain rate, 3 curves undrained shear resistance x strain rate for the same confining effective stress, plus curves $(\sigma_1 - \sigma_3)$ x ε for each specimens tested. From these results and also in situ tests such as CPTU and vane test, whose main purpose is validate the results of the laboratory tests and extrapolate these results along the depth, the designer will can set the undrained shear resistance profiles representative of the permanent loading condition (conventional) and short-term loading duration condition (accelerated) applicable to the project.

On the basis of the two undrained shear resistance profiles defined above, the geotechnical design should contemplate two stability analyses. In the first one it should be considered the conventional undrained shear resistance profile and all permanent loading. In the second stability analysis it should be considered the total loading, including the short-term loading duration, and the undrained shear resistance profile representative of the short-term loading duration. The safety factor to be considered for possible adjustment of the studied section will be the smaller one.

CONCLUSIONS

Based on what was exposed in this paper it can be concluded that the influence of the strain rate or loading duration on the undrained shear resistance of soft clayey soils is already a established conceptual and experimental knowledge. It is known that saturated soft clay soils present a significant portion of viscous resistance, which grows with the increasing of strain rate or the reduction of the loading duration. This paper also showed the case studied of the influence of loading duration on undrained shear resistance of the soft clay of the E-694 section of Via UHOS. In that case, the consideration of the influence of loading duration on undrained shear resistance of the soft clay in the adjustment of the embankment design made possible the adoption of a more economical solution than that would result from a conventional design, where loading of short duration are also considered as permanent loading in stability analyses.

Based on the experience in Via UHOS and the research carried out was possible to present the preliminary proposal of a new design methodology for special road embankment on soft soil, which makes possible to take into account the influence of loading duration on undrained shear resistance of the soft soil embankment. This new design methodology allows design solutions of road embankments subject to exceptionally high loads traffic that are cheaper than those obtained using the current methodology, in which such charges are also considered permanent.

REFERENCIAS BIBIOGRAFICAS

Aguiar, V.N. (2014) – “Contribuição ao estudo das relações tensão-deformação-resistência-tempo das argilas moles”, Tese de Doutorado, COPPE/UFRJ, Rio de Janeiro-RJ, Brasil.

Alexandre, G.F. (2006) – “Contribuição ao entendimento da fluência não drenada”, Tese de Doutorado, COPPE/UFRJ, Rio de Janeiro- RJ, Brasil.

Bishop, A. W. e Henkel, D.J. (1962) – “The measured of soil properties in the triaxial test”, Edward Arnold, 2° Edição.

Leroueil, S; Kabbaj, M; Tavenas, F. e Bouchard, R. (1985) – “Stress-strain-strain rate relation for the of sensitive natural clays compressibility”, Géotechnique , 35, N°. 2, 159-180.

Martins, I.S.M. (1992) – “Fundamentos de um modelo de comportamento de solos argilosos saturados”, Tese de Doutorado, COPPE/UFRJ, Rio de Janeiro-RJ, Brasil.

Mesri, G. (1989) – “A reevaluation of $S_{u\,(mob)}$=0,22 σ'_p using lapboratory shear tests, Department of Civil Engineering University of Illinois at Urbana-Champaign, Urbana, IL, U.S.A.

Pinto, C.S. (2002) – "Curso Básico de Mecânica dos Solos em 16 aulas" Oficina de Textos, São Paulo-SP, Brasil.

Souza, G.L.A. (2017) – "Estudo da influência da duração do carregamento em projetos de aterros sobre solos moles destinados à construção de vias sujeitas ao tráfego de veículos especiais ultra-pesados", Dissertação de Mestrado, UERJ – Universidade do Estado do Rio de Janeiro, Rio de Janeiro-RJ, Brasil.

Souza, R.N.; Pinto, T.C.; Souza, G.L.A.; Soares, A.S. e Viana, E.A. (2014) – "Propriedades geotécnicas das argilas moles da estrada de transporte de equipamentos pesados do COMPERJ", XVII Congresso Brasileiro de Mecânica dos Solos e Engenharia Geotécnica, Goiania-GO.

Terzaghi, K. (1941) – Undisturbed clay samples – Contributions to the Soil Mechanics.

Taylor, D.W. (1942) – Research on consolidation of clays. Department of Civil and Sanitary Engineering, Massachussets Institute of Technology, Serial 82, August.

Taylor, D.W. (1948) – Fundamentals of Soil Mechanics, New York, John Wiley & Sons.

METHOD FOR ASSESSING DAMAGE INDUCED IN UTILITIES DUE TO GROUND MOVEMENTS FROM MAJOR INFRASTRUCTURE PROJECTS

Francesc Mirada, Arup, London, United Kingdom, +44 20 7755 5529, francesc.mirada@arup.com
Riccardo Impiumi, Arup, London, United Kingdom, +44 20 7755 5604, riccardo.impiumi@arup.com
Zeena Farook, Arup, London, United Kingdom, +44 20 7755 5789, zeena.farook@arup.com

ABSTRACT

Geotechnical Engineers are faced with huge challenges in predicting the movements caused by tunnelling and excavations and their impacts on utilities. Furthermore the number of parties involved in infrastructure projects often requires multiple iterations to come to a common solution, making the analyses very labour intensive, locking resources and budget from other parts the project. The ground movement induced in utilities due to major infrastructure projects is to be assessed by means of the Oasys software Xdisp. The stakeholders comprise various utilities providers, each with unique criteria and a variety of asset dimensions to be assessed. Ground movements generated by three phases of works (demolition of buildings, installation of temporary and permanent retaining walls, excavation behind the walls and tunnelling) are calculated using a combination of Oasys Pdisp and Xdisp. Displacements are calculated for each phase and imported in the subsequent phase, for the utility assessment to be undertaken. Asset information provided in GIS format, which included the geo-referenced position of the asset, function, dimensions and material in order to identify the limiting criteria to be applied. Due to the number of assets and expected iteration typical of this kind of analysis a fluid solution consisting of tailoring the software XDisp to adapt it to the requirements of the different asset holders is adopted. The output can then be manipulated with a relatively sophisticated geospatial process for direct input in GIS for improved settlement visualisation based on strain and displacement set criteria. It is estimated the process can save up to 60% of the computing time, based on size of the project, compared to standard methods of calculation using the same software.

Keywords:

INTRODUCTION

Background

For large infrastructure projects, it is common to use a phased methodology to for assessing the utilities affected by ground movement from works. A three-phased process is proposed. Phase 1 considers the magnitude of likely ground movements only. Phase 2 determines the potential utility strain, pull-out and joint rotation assuming the utilities follow the ground movement (i.e. the utilities have negligible structural stiffness). Reduction factors can be used to consider axial slip between the grounds and pipe as appropriate. Phase 3 consists of a more detailed analysis in which the assumption made in Phases 1 & 2 are re-assessed and more complex methods like Finite Elements that consider soil-structure interaction are used.

Recent developments

This paper describes the proposed methodology used and implemented in Xdisp for assessing damage induced in utilities due to ground movements arising from major infrastructure projects. Given the number of utilities required to be assessed this paper presents further developments that have been achieved using database and GIS based system to semi-automate the process (Devriendt, et al. 2012).

GROUND MOVEMENTS

Loading and unloading

Oasys Pdisp, in combination with Oasys Xdisp, was used to predict settlements due to loading and unloading near buildings and utilities. Within the program, the Boussinesq method was utilised.

© 2018 Deep Foundations Institute

The method has the advantage that it gives a report of stresses in the ground in addition to displacement. The software uses integrated forms of the well-known equations derived by Boussinesq (1885). Strains are calculated within the strata. Displacements are then defined by integrating vertical strains. However, the method is not able to calculate horizontal displacements.

The program was also enhanced to consider polygonal loads, where previously only rectangular and circular loads could be inputted. The Polygon Wizard within the program is used to fit rectangles to the load's polygon

In order to generate rectangles from a polygon the polygon is first expanded into trapezoids. Each trapezoid is then expanded into one or more rectangles. The rectangle Tolerance is defined as the total "overlap" and "underlap" of rectangles within each trapezoid, as a proportion of the total area of that trapezoid. Due to the methodology used, trapezoids with greater differences in length of their parallel edges will generate more rectangles than those of lesser difference - even though those with lesser difference may have larger areas.

Retaining wall installation and box excavation

Retaining wall installation and excavation are calculated in accordance with Ciria Guide C580, now updated to C760. Movements at corners are calculated using the methodology outlined in Fuentes R. and Devriendt M. (2010).

Tunnels

Greenfield ground movements due to the excavation of a tunnel can be predicted assuming the transverse settlement trough approximated by a normal Gaussian curve and the longitudinal trough corresponding to a cumulative probability curve as described by Atterwell & Woodman (1982) and O'Reilly & New (1982).

The geometry of the settlement trough is defined by the volume loss due to tunnel excavation, which is the order of 2% of tunnel diameter for tunnels in London Clay, and the depth of the tunnel relative to the level at which displacements are to be measured.

Pipe Strains

The initial assumptions made in Oasys Xdisp were the same as the ones described by Bracegirdle et al. (1996). Bending strains along the pipe are calculated assuming the pipe follows the ground movements; the horizontal strain consider the soil-pipe interaction by decreasing the strain on the pipe by a reduction factor. This methodology does not allow for slip at soil-pipe interface and can be quite conservative.

Welded pipes can be treated as a continuum therefore not allowing for stress concentration at joints. Consequently, the strain calculations for welded pipes remained the same. For jointed pipes, the analysis assumed all rotation to happen at the joint between adjacent pipe segments. The envelope of flexural strains deriving from the worst combination of joints location relative to the tunnel axis should therefore be considered. Axial strains should be considered in terms of pullout at axis level between two consecutive segments. This is done by considering the resultant of strains along the pipe segment as in Figure 1. Different pullout combinations should be considered as in Figure 2.

$PO = P_{length} \times \Sigma_{\epsilon axial}$

Where:

PO = pullout

P_{length} = length of pipe segment

$\Sigma\varepsilon_{axial}$ = sum of axial strain along pipe segment

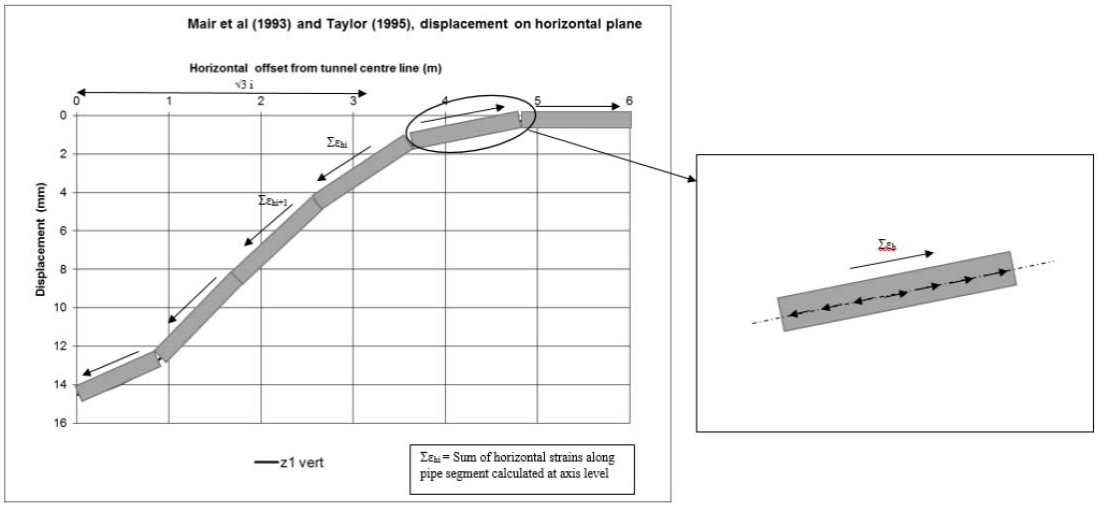


Fig. 1 - Example of strain distribution along pipe segment

The pullout for a segment is then be added to the pullout from adjacent segment to a joint to obtain the total pullout for that joint (Figure 2). No friction between pipes or interlocking due to flexion at joint are considered.

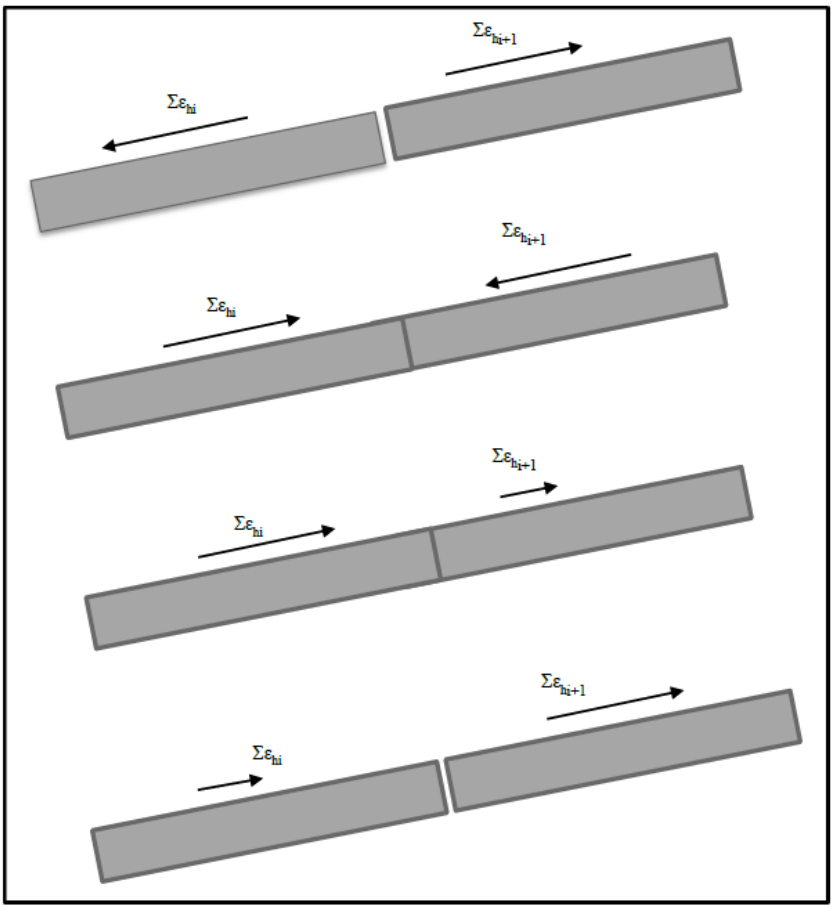


Fig. 2 – Pullout at joints

The maximum strain at the joint is the combined action of axial and flexural strain. These are added together according to the sign convention stated above.

THREE PHASE ASSESSMENT

Phase 1: Asset screening assessment

Phase 1 determines the magnitude of settlement and maximum ground slopes only based on the greenfield surface settlement contours. This phase identifies the zone of influence (i.e. 1mm settlement contour). This is used to identify the utilities that are at negligible risk of damage and therefore screened out of from further assessment. Those utilities considered to be flexible are also screened out at this phase of the assessment.

Phase 2: Assessment of buried assets

Oasys Xdisp software automates the calculation of the ground movements and carries out utilities damage impact assessments according to the methodology proposed by Bracegirdle et al. (1996). Figure 3 shows a snapshot of the Xdisp model used for the utilities assessment.

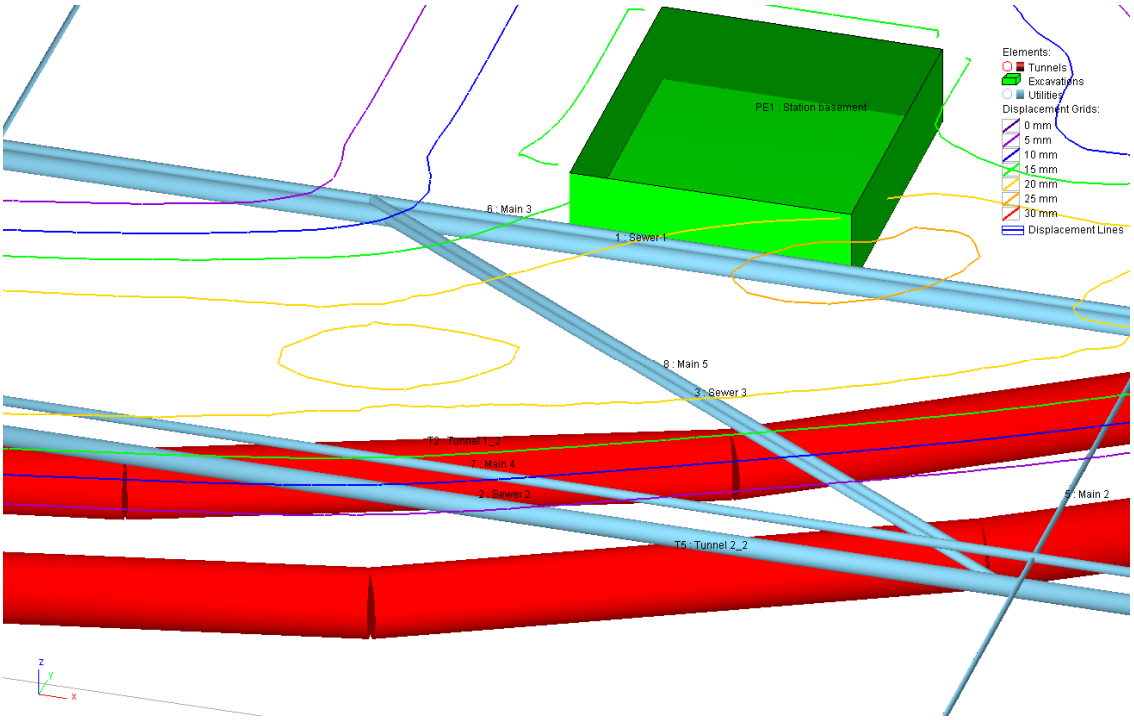


Fig 3. Snapshot of Xdisp model with ground movement contours

Phase 3: Re-assessment of Phase 2 hypothesis or more complex analysis and mitigation measures

Conservative parameters like the volume loss or ground settlement calculation method can be adjusted in order to adopt a more realistic approach. Other methods like Finite Element analysis that account for soil-structure interaction could be used to refine the results if needed.

If the potential for damage induced to the utility is considered to be unacceptably high, engineering judgement must be made to understand whether mitigation is possible and appropriate. When considering the mitigation, account must also be taken for the potential negative impact it may have. (i.e. ground movements arising from the installation of Tubes-a-Manchette (TAMs) could influence ground movements) and result in greater damage to the utility.

USE OF DATABASE AND GIS BASED SYSTEMS FOR AUTOMATION

Given the number of utilities required to be assessed on large infrastructure projects, the use of database and GIS based systems for automating the process linked with specifically designed ground movement impact assessment software such as Oasys Xdisp and Pdisp, enables time and cost savings to be made.

FME (Feature Manipulation Engine) can transform or translate sets of data from one format to another. The results of the assessment are incorporated into the GIS database, reports and graphs along the asset chainage to show axial and flexural strains, combined tensile and compressive strains, and the displacements along and perpendicular to the utility can be automatically generated. In Figure 5 there is a snapshot of the FME workflow used for the generation of output results.

Moreover, utilities companies are now using contents of the GIS database, producing utilities drawings with associated information such as material, diameter, age, etc. Designers can therefore take advantage of the pool of information provided to automate the calculation process by pre-setting different software to exchange information directly, without the need to enter items manually. The same process can then be utilised once the calculations are complete to update drawings providing the client with an even greater pool of information, it being the output of the analyses. The typical output consists of drawings including settlement contours, showing the utilities labelled with “exceeding” or “not exceeding” the agreed criteria.

Figure 4 summarises the process of GIS database automation linked with Oasys geotechnical software. A semi-automatic process was achieved to generate the visual assessment output as shown in Figure 5 using combination of Pdisp for demolition heave and Xdisp for excavations and tunnels together with digital tools like GIS and FME.

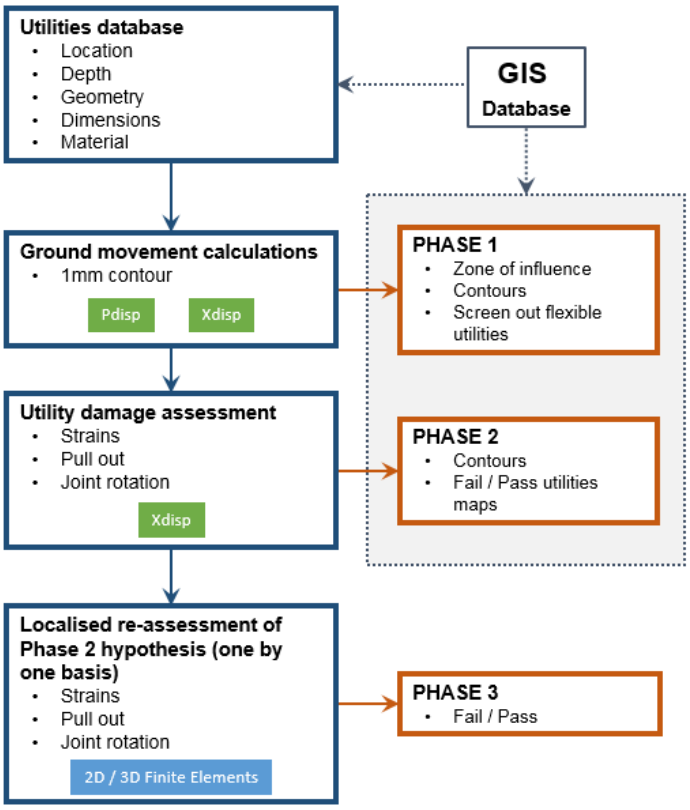


Fig. 4. Diagrammatic process of database and GIS automation linked with Oasys Pdisp and Xdisp

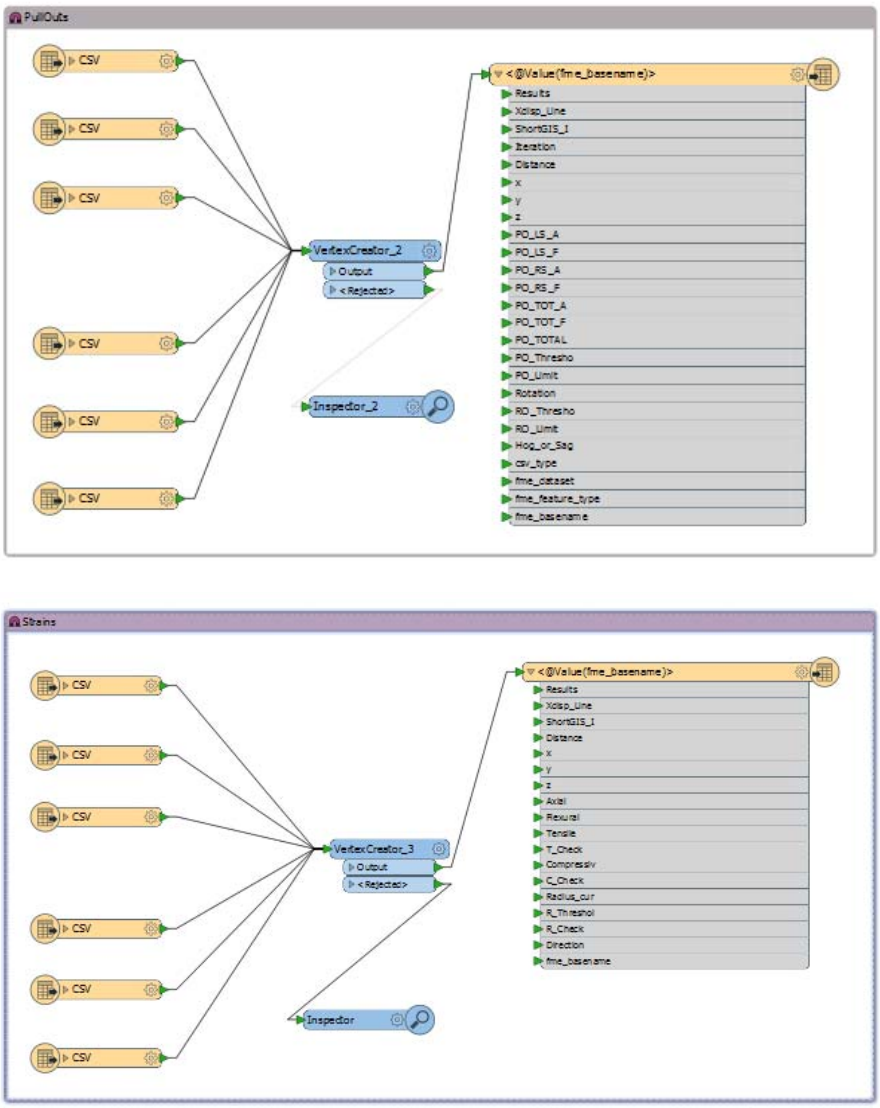


Fig. 5. Automation of the output generation using FME.

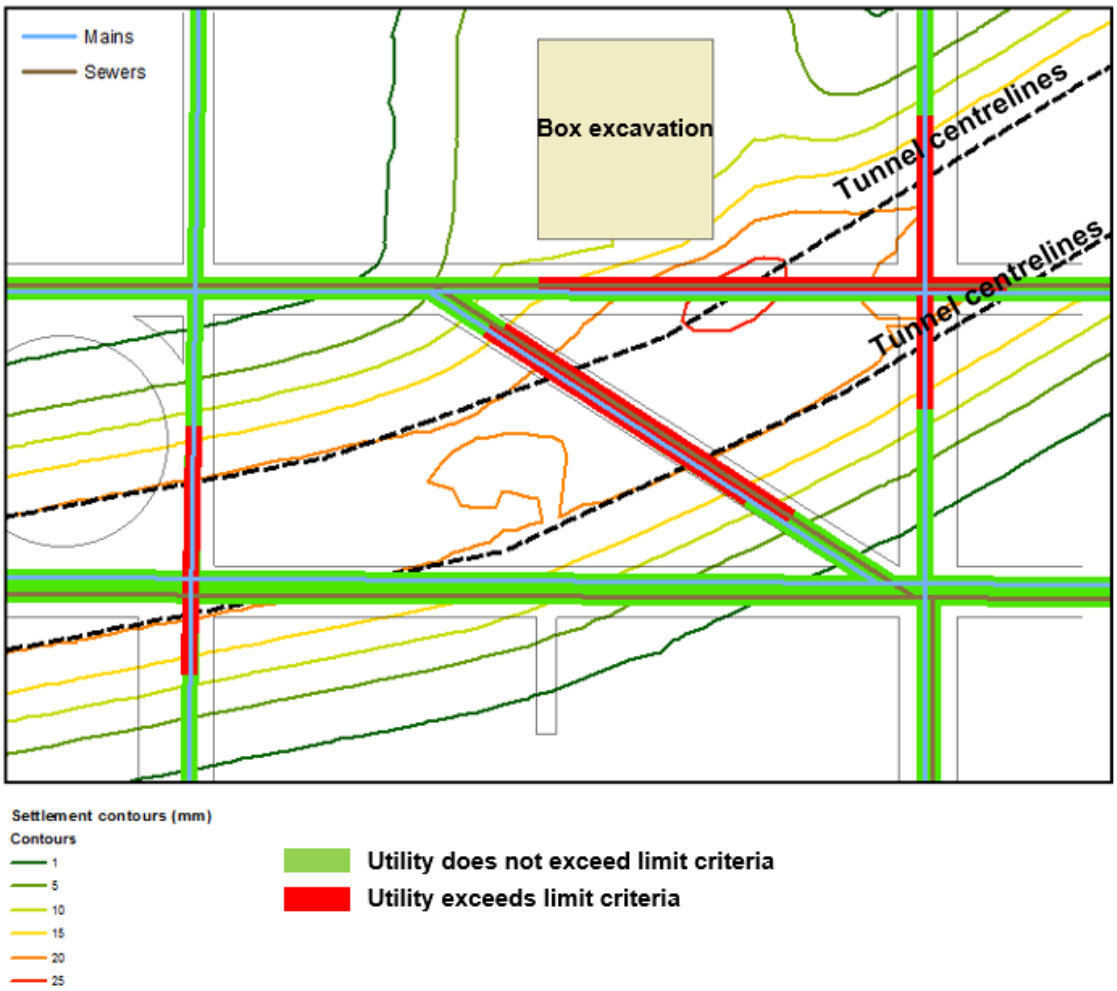


Fig. 5. ArcMap assessment output example with settlement contours and pass/fail criteria

CONCLUSIONS

Time and cost savings

The automation of processes described in this paper not only allows evident time savings connected with direct input of data from one software to another, but reduces the risk of committing mistakes and omitting information which are typical of jobs involving manipulation of big amount of data.

Time savings has been estimated to the number of iterations needed to complete the project. It is typical in project with many stakeholders to reach upwards of ten iterations by Phase 2. The time saved, also allows the Engineer to add value by providing the Client with alternative scenarios, for example dealing with different Volume losses hypothesis, different retaining wall movements, etc.

REFERENCES

Attewell P B and Woodman J P. 1982. Predicting the dynamics of ground settlement and its derivatives caused by tunnelling in soil. Ground Engineering, November 1982, 13 - 36.

Bracegirdle A and Mair R J, Nyren R J, Taylor R N. 1996. A methodology for evaluating potential damage to cast iron pipes induced by tunneling – Geotechnical Aspects of Underground Construction in Soft Ground, Mair & Taylor (eds), 1996 Balkema, Rotterdam, pp 659-664.

Boussinesq, J. 1885. Applications des potentials a l'etude de l'equilibre et de movement des solides elastiques. (Gouthier-Villars, Paris)

CIRIA Report C580. 2003. Embedded retaining walls - guidance for economic design.

Devriendt, M., Waterson, E., and Gates, J. 2012. Automatic cost saving. Ground Engineering, June 2012, p. 18.

Fuentes R. and Devriendt M. 2010. Ground movements around corners of excavations - An empirical calculation method. Journal of Geotechnical and Geoenvironmental Engineering. Volume 136, Issue 10, pp. 1414-1424.

O'Reilly M P and New B M. 1982. Settlements above tunnels in the United Kingdom - Their magnitude and prediction. Proc. Tunnelling '82, ed Jones M P. IMM, London, pp 137-181.

PILE GROUPS WITH NEGATIVE SKIN FRICTION

Francesco Basile, Geomarc Ltd, Messina, Italy, tel +39 338 7038381, francesco.basile@geomarc.it

ABSTRACT

An efficient analysis method is presented for assessing the response of single piles and pile groups subjected to negative skin friction (NSF). The method involves two separate steps: (1) estimate of the free-field ground movements in the consolidating soil, and (2) analysis of the piles subjected to the computed free-field ground movements by means of PGROUPN, a computer program based on a 3D non-linear boundary element solution. The impact of various factors which affect the response of piles to NSF is examined, including the number of piles, the pile spacing, the additional presence of pile-head loading, and the influence of soil nonlinearity and pile-soil slip. Results provide insights into the correct understanding of NSF effects on pile behaviour and show the importance of considering such aspects as pile-soil slip and group interaction effects. In particular, it is demonstrated that the usual detrimental effect of group interaction among piles is diminished by the beneficial group effect for piles under NSF, thereby resulting in a lower values of drag force and drag settlement as compared to a single isolated pile.

Keywords: piles, pile groups, BEM, negative skin friction

INTRODUCTION

Pile foundations embedded within a consolidating soil layer are subjected to negative skin friction (NSF), i.e. negative shear stresses caused by the downward movement of the soil relative to the pile. Misconception remains among some pile designers that NSF will reduce the geotechnical axial capacity of a pile. However, it should be recognized that NSF pile design is mainly a settlement rather than a geotechnical capacity issue, and therefore it should be approached from a serviceability viewpoint by means of a pile-soil interaction analysis. Indeed, as pointed out by many researchers (e.g. Poulos, 2008; Fellenius, 2017), geotechnical failure implies that the entire pile moves past the soil and therefore NSF cannot be present at this point (given that NSF requires the soil to move past the pile). In such a case, NSF actually turns into positive shaft resistance and thus should generally not be considered in assessing the pile geotechnical capacity (unless there is significant strain softening of the interface friction, which is unlikely in the common situation of NSF in soft clay).

The main concerns for pile design in the presence of NSF are therefore two-fold:

1) ULS — the additional force ('*drag force*') induced in the pile by NSF at the neutral plane location (i.e. the depth at which the friction changes from negative to positive), and its effect on the pile structural strength;

2) SLS — the additional pile settlement ('*drag settlement*') caused by NSF, and its effect on the serviceability limit state design, i.e. settlements and differential settlement must remain within acceptable limits.

In addition, the pile geotechnical capacity must clearly be adequate for the head load (i.e. dead load and live load), while ignoring the NSF effect. In practice, the NSF effect on pile structural capacity only becomes significant for end-bearing piles (i.e. those which terminate in relatively impenetrable material such as rock or very dense sand or gravel), whereas, in the case of floating piles, the serviceability problem is usually prevailing and governs the design.

© 2018 Deep Foundations Institute

Current design practice for piles subjected to NSF is often unduly conservative because of the following reasons:

1) The drag force induced by NSF is incorrectly treated as an *external* unfavourable action (usually at the pile-head level) that reduces the pile geotechnical capacity; however, as discussed above, this is a faulty concept and can lead to an overconservative or even erroneous (Fellenius, 2017) design. The drag force should instead be regarded as an *internal* force associated with the development of static equilibrium of the pile-soil system. The use of "force" instead of "load" is intentional to make a distinction that the drag force should not be considered as an applied load on the pile head in design.

2) The drag force caused by NSF is usually evaluated on the assumption of full pile-soil slip, i.e. it is assumed that NSF is fully mobilized above the neutral plane regardless of the magnitude of ground movement. This can be an overconservative assumption when the ground movements are expected to be small, such as in a matured or treated (e.g. with vertical drains) reclaimed land. Similarly, the depth to the neutral plane (which actually is the result of a complex pile-soil interaction problem) is often determined in an empirical manner (e.g. at the base of the settling soil) and disregarding the magnitude of ground movements. As a result, the depth may be overestimated and thus the drag force would be further exaggerated.

3) Beneficial group effects are ignored — in contrast to conventional axial loading at pile-head level, pile-to-pile interaction effects have a favourable effect in the case of NSF, i.e., as compared with a single isolated pile, there is a tendency for reduced drag forces and drag settlements in the group, especially for the inner piles.

The above shortcomings may be overcome by adopting a more fundamental approach in which the NSF-induced ground settlement is actually treated as a 'geotechnical' action on the pile group and a pile-soil interaction analysis is carried out (clearly the presence of any direct loading at the pile head should also be included). This would allow a more realistic (and often more economic) assessment of the key features of pile response to be used in design, i.e. the pile-group settlement, the drag force, and the depth to neutral plane. It is encouraging to observe that such an approach is starting to become recognized (at least partially) by some modern codes, e.g. in Eurocode 7 the designer is given the option to allow for NSF by using pile-soil interaction analysis when the ground settlements are expected to be relatively small (and thus the "traditional" design for NSF would be too conservative).

A rigorous pile-soil interaction analysis including the NSF problem can be based on continuum approaches, such as the finite element (FEM) and the finite difference (FDM) methods. Such "complete" solutions allow for the proper modelling of the consolidation process, and hence the development of NSF-induced ground settlements is computed within the analysis by the application of surcharge loading (e.g. Comodromos and Bareka, 2005; Lee et al, 2009; Tan and Fellenius, 2016). However, even though FEM and FDM analyses are most powerful numerical tools, their use would be unpractical in the routine design of piles (and pile groups) under NSF due to the excessive complexity and high computational costs involved, particularly considering that accounting for pile-soil slippage and non-linear soil behaviour is essential. In the NSF problem, such limitations are further exacerbated by the increased computing time required by a consolidation analysis and also by the consideration that this level of complexity may not always be warranted because of the often limited available information related to ground movements and how they are developed (Poulos, 2017).

A more practical solution to deal with the analysis of piles under NSF is provided by simplified approaches involving initial separation of the soil and the pile domains so that the soil movements are first computed and then imposed on the piles. The approach is based on two separate steps:

(1) evaluation of the free-field downward ground movements in consolidating soil;

(2) analysis of the pile group subjected to the computed free-field ground movements (and to any direct load at the pile cap level).

(1) Estimation of ground movements

The magnitude of consolidation settlements, such as those induced by surcharge loading or dewatering, can be estimated using conventional settlement analysis, for example Terzaghi's one-dimensional consolidation theory. Although the time-rate of consolidation settlements may also be considered, end-of-consolidation settlements is often assumed in practice. Consolidation settlements are generally evaluated in free-field conditions, i.e. in the absence of the piles. This generally is a conservative assumption as the presence of the piles increases the soil stiffness, thereby reducing the induced ground movements (e.g. Mroueh and Shahrour, 2002).

(2) Analysis of pile response

The second step of the procedure can be carried out by a boundary element (BEM) analysis of the single pile or the pile group subjected to the NSF-induced ground movements evaluated above. BEM solutions are quite fitting for the NSF problem as they provide an effective means of retaining the essential aspects of pile interaction through the soil continuum, without incurring the high costs and complexity of FEM and FDM solutions. Examples include the simplified BEM approach for single piles and symmetrical pile groups proposed by Kuwabara and Poulos (1989) and a similar solution by Teh and Wong (1995). In this paper, a more general BEM approach is proposed which provides a complete 3D non-linear solution of the soil continuum, while retaining a computationally efficient code.

PGROUPN ANALYSIS

The proposed method is based on the two-step approach described above (as depicted in Figure 1) and is carried out within PGROUPN (Basile 2003), a numerical code for pile-group analysis which is commonly used in design through the software Repute (Bond and Basile, 2017). The analysis takes into account the simultaneous influence among all elements of all piles in the group, i.e. a "complete" solution of the soil continuum is provided. Pile-group effects are therefore evaluated as a matter of course, thereby overcoming the approximations of traditional interaction factor approaches and the fundamental limitations of Winkler models (based on empirical multipliers to account for group action). In addition, by retaining soil continuity, the input soil parameters have a clear physical meaning (e.g. the soil Young's modulus and strength properties) and can be measured directly in soils investigation. The basic influence of pile-soil slip and soil nonlinearity is modelled using a hyperbolic continuum-based interface model, while completely general direct loading conditions (axial, lateral, and moments) on the pile group can be examined, in addition to the profile of external ground movements which is computed separately as at Step (1) above.

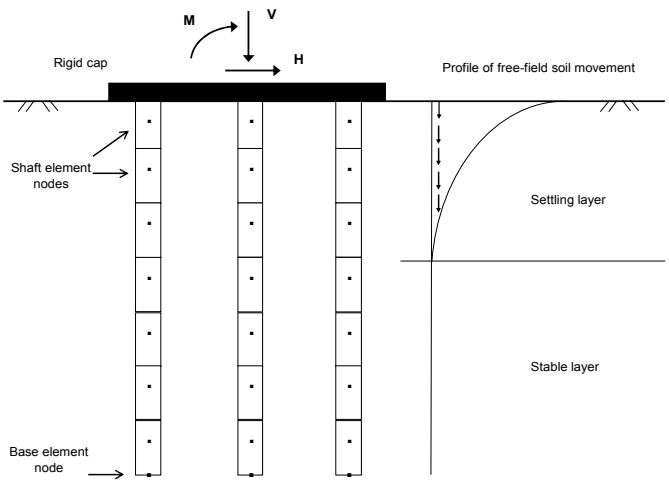


Fig. 1. BEM schematisation of the problem

It is noted that the PGROUPN analysis may be employed not only in the consolidation case described herein but in many circumstances in which pile foundations are subjected to "passive" loadings arising from vertical and/or horizontal movements of the surrounding ground. Examples include tunnelling (Basile 2014), kinematic effects induced by earthquakes (Basile 2012), slope movement, excavation, swelling of an expansive clay, and construction of adjacent piles or buildings.

The general capabilities of the PGROUPN code are summarized below:

- based on 3D complete BEM solution of the soil continuum;
- models all relevant interactions (i.e. pile-soil, pile-pile, raft-soil and pile-raft);
- piles in any configuration and having different characteristics within the same group (e.g. stiffness, length, rake, shaft and base diameter);
- piles connected by rigid and, if appropriate, ground-contacting cap;
- multi-layered soil profiles;
- linear elastic, elastic-plastic or non-linear continuum-based soil model;
- general 3D loading conditions, including any combination of vertical, horizontal, moment, and torsional loading acting on the pile cap;
- externally imposed vertical and/or horizontal ground movements;
- output includes the distribution of displacements, stresses, forces and moments along the piles, plus the normal stresses, displacements and rotations of the pile cap.

A detailed description of the theoretical formulation of PGROUPN has been presented elsewhere (Basile 2003, 2014) and hence only a brief outline is given below. The analysis involves discretization of only the pile-soil interface into a number of cylindrical boundary elements, while the base is represented by a circular (disc) element, as illustrated in Figure 1. The behaviour of each element is considered at a node (located at the mid-height of the element on the centre line of the pile), with the distributions of the stress components at the pile-soil interface which are assumed to be uniform over each element. The method employs a sub-structuring technique in which the piles and the surrounding soil are initially considered separately and then coupled by imposing the displacement compatibility ($u_s = u_p$) and stress equilibrium ($t_s = -t_p$) conditions at the pile-soil interface.

Soil domain

Assuming purely linear elastic soil behaviour, the soil displacements, arising both from the stresses caused by pile-soil interaction and the external source of ground movement, may be expressed as:

$$\{u_s\} = [G_s]\{t_s\} + \{u_e\} \qquad \text{(Equ. 1)}$$

where u_s are the soil displacements, t_s are the soil stresses, G_s is the soil flexibility matrix obtained from Mindlin's (1936) solution, and u_e are the external soil movements. It is noted that Mindlin's solution is rigorously applicable to homogeneous soil conditions. In practice, however, this limitation is not strictly adhered to, and the influence of soil non-homogeneity can be approximated using a weighted average value of soil modulus at the influencing and influenced pile nodes (e.g. Yamashita et al., 1987; Poulos, 2009).

Pile domain

If the piles are assumed to act as simple (elastic) beam-columns which are fixed at their heads to the pile cap, the pile displacements may be written as:

$$\{u_p\} = [G_P]\{t_p\} \qquad \text{(Equ. 2)}$$

where u_p are the pile displacements, t_p are the pile stresses, and G_p is a matrix of coefficients obtained from the elementary (Bernoulli-Euler) beam theory.

Limiting stress and non-linear soil behaviour

The foregoing procedure is based on the assumption that the soil behaviour is linear elastic. However, it is essential to ensure that the stress state at the pile-soil interface does not violate the yield criteria. This can be achieved by specifying the limiting stresses at the pile-soil interface, for example using the classical equations for the ultimate shaft and base resistance (e.g. Basile 2003). Non-linear soil behaviour is modelled by assuming that the tangent soil Young's modulus (E_{tan}) varies with the pile-soil interface stress (t) according to the common hyperbolic stress-strain law:

$$E_{tan} = E_i(1 - R_f t/t_{lim})^2 \qquad \text{(Equ. 3)}$$

where E_i is the initial soil modulus, R_f is the hyperbolic curve-fitting constant and t_{lim} is the limiting value of pile-soil stress. Thus, the soil and pile equations described above for the linear response are solved incrementally using the modified values of soil Young's modulus of Equ. 3 within the soil matrix [G_s], while enforcing the conditions of yield, equilibrium and compatibility at the pile-soil interface. For the pile-soil interface elements which have yielded, no more increment in stress is permitted and any increase in load is therefore redistributed between the remaining elastic elements until all elements have failed.

NUMERICAL RESULTS

Validity of the proposed analysis is confirmed through a comparison with published results from well-established numerical solutions.

Comparison with Poulos (2006)

In order to illustrate the crucial difference between the effects of loading induced by external ground movements and direct applied load at the pile-head, a single pile in a two-layer soil profile is analysed under the following types of loading (Fig. 2):

(a) An axial load of 1 MN applied at the pile head;
(b) A downward ground movement profile linearly decreasing from 100mm at the ground surface to zero at a depth of 12m.

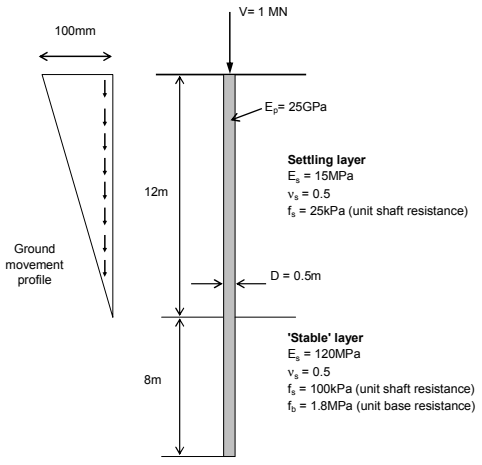


Fig. 2. Pile in two-layer soil system

The resulting axial force distribution computed by PGROUPN for loading types (a) and (b) is reported in Fig. 3, showing a favourable agreement with the results obtained by Poulos (2006) using a similar BEM approach with an elastic-perfectly plastic interface model (in practice corresponding to the use of R_f =0 in Equ. 3). Figure 3 also reports the distribution generated by the two type of loadings (a) and (b) acting together, and the distribution resulting from the addition of the two profiles of axial force obtained for loadings (a) and (b). The following features of behaviour are shown:

(a) The distribution of axial force in the pile due to direct loading is very different from that induced by ground movements. In the former case, the maximum axial force occurs at the pile head, whereas in the latter case, the maximum axial force (i.e. the drag force) occurs near the bottom of the layer subjected to ground movement. This consideration further shows the fallacy of treating the NSF as a force applied at the pile head, as still adopted by some pile designers.

(b) The simple addition of the two profiles of axial force obtained for loadings (a) and (b) would be unconservative, i.e. it yields axial forces which are less than those arising from the simultaneous application of loadings (a) and (b). This is because the downward ground movement has caused full slip at the pile-soil interface of the upper settling layer (i.e. the limiting unit shaft resistance is reached) and hence the superposition principle does not apply.

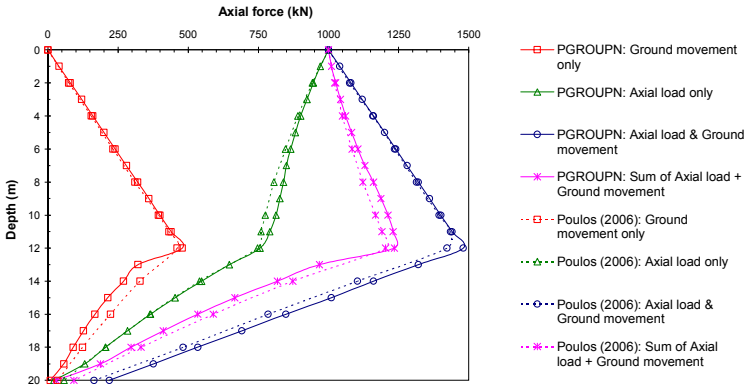


Fig. 3. Comparison of axial force distribution with Poulos (2006)

Effect of soil slip

Consideration of soil nonlinearity (including soil slip at the pile-soil interface) is essential in NSF pile design since soil slip can develop under relatively small ground movements. This results in a smaller drag force (and drag settlement) than that computed using a linear elastic (LE) model because only limited shear stress is permitted to transfer from the consolidating soil to the pile. Indeed, the LE model does not allow slip to take place at the pile-soil interface (i.e. it does not impose any limiting

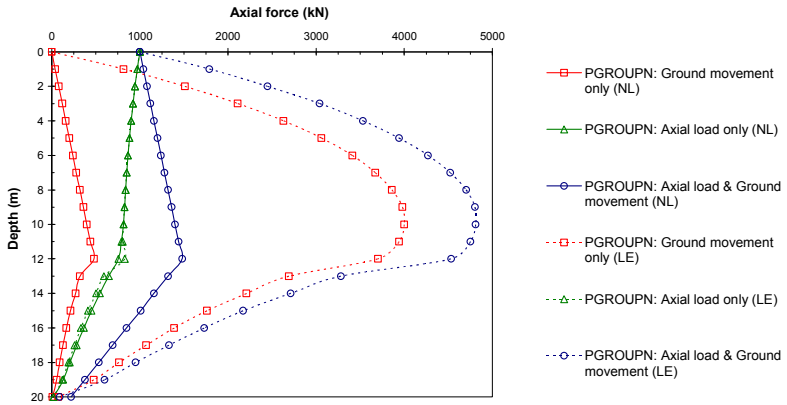


Fig. 4. Comparison of LE vs. NL analysis

values for the shear stress), thereby resulting in unrealistically large values of shear stress and thus drag force (and drag settlement). For the test case reported in Fig. 2 under loading (b) from ground movements only, the NL analysis computes that the unit shaft resistance is fully mobilized along the portion of the pile in the settling zone, thereby causing slippage at the pile-soil interface. Figure 4 shows that use of the NL analysis leads to a 88% reduction of the maximum drag force (i.e. from 3940 kN to 490 kN), as compared to the LE analysis.

Comparison with Poulos (2008)

Two hypothetical but typical problems reported by Poulos (2008) are analysed, as shown in Fig. 5. The first case involves an *end-bearing* pile embedded into a 20m thick settling soft clay layer, underlain by a "stable" stiff clay layer with a length of pile in the stable zone equal to L_c = 6m (giving a total pile length of 26m). The second case relates to a *floating* pile embedded into an identical settling layer as for the end-bearing pile, while the underlying stable layer is a medium clay layer (with significantly smaller strength and stiffness than in the first case) and the pile length in the stable zone is L_c = 18m (i.e. a total pile length of 38m). Both piles are subjected to an identical ground settlement profile linearly decreasing from a maximum value (S_o) at the ground surface to zero at a depth of 20m, whereas the applied loads (e.g. dead load) at the pile head are 1.5MN and 0.8MN for the end-bearing and floating pile, respectively.

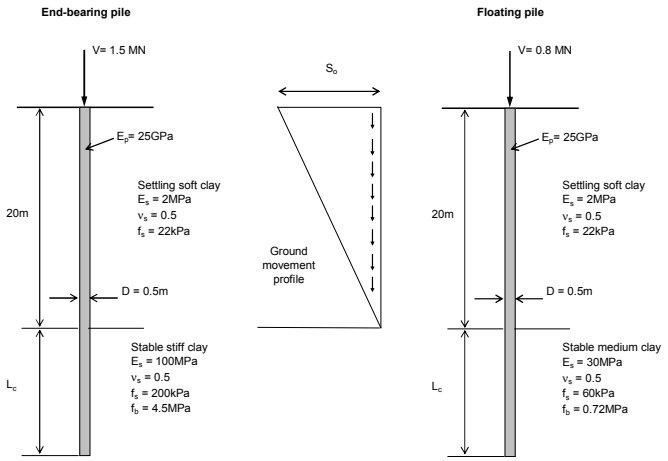


Fig. 5. End-bearing and floating pile in two-layer soil system

In order to emphasize the importance of accounting for the actual magnitude of the ground movements in the design of piles under NSF, attention is initially concentrated to the case in which the piles are only subjected to the ground settlement profile. Figure 6 shows the development of the maximum drag force and pile settlement (i.e. drag settlement) with increasing soil surface settlement (S_o). It is noted that, not only the maximum drag force, but also the pile drag settlement reaches a limiting value, regardless of the soil surface settlement — this is a most critical feature of behaviour which has to be recognized during the SLS check. Figure 6a also reports the limiting value f_sA_s = 691 kN (where A_s is the shaft area of the pile upper portion) which would generally be considered in a traditional NSF design under the assumption of full mobilization of the shear stress above the neutral plane (which is considered to be located at the base of the settling layer). It is observed that, only for soil surface settlements greater than about 200mm, the above assumption would be realistic. However, for smaller ground movements (e.g. S_o = 50mm), the maximum drag force is much less than that based on the simplistic full skin friction assumption. Figure 6 further proves that, in contrast to the case of conventional axial loading at the pile-head, the development of pile-soil slip is beneficial as it results in reduced drag forces and drag settlements as compared with a purely linear elastic interface condition. Indeed, pile-soil slip start to develop when the soil surface settlement is about 50mm and is almost complete at about 200mm. Thus, linear elastic theory would seriously overestimate the pile drag force and drag settlement for soil surface settlements in excess of about 50mm.

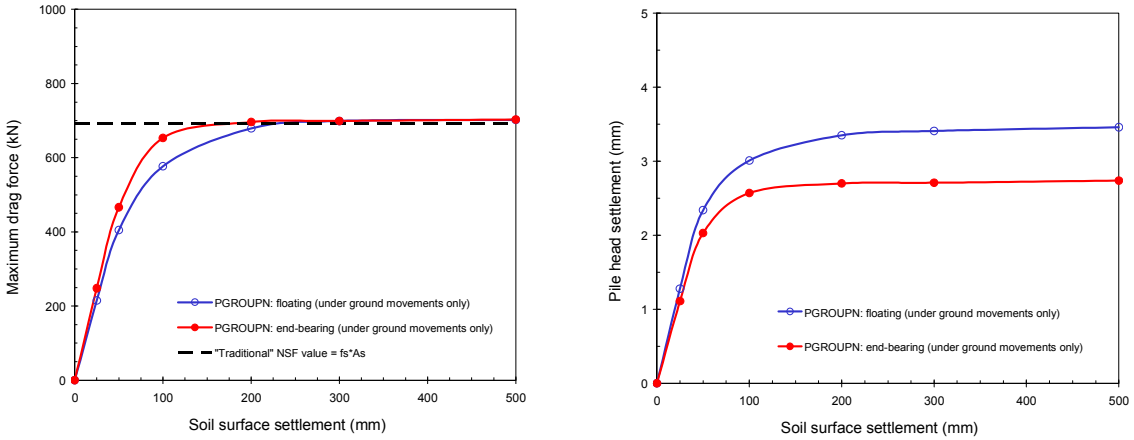


Fig. 6. Piles subjected to ground movement only: (a) Max. drag force; (b) Pile settlement

In Fig. 7, attention is turned to the more practical case in which the piles are subjected to both the ground settlement profile and the pile-head loads reported in Fig. 5. The non-linear correlation between pile drag force/settlement and ground settlement is similar to that discussed above, thereby confirming the value of accounting for soil slip via a pile-soil interaction analysis in order to achieve a more realistic assessment of pile response. For a soil surface settlement S_o = 100mm, Fig. 7b shows a good agreement of the pile head settlement values computed by PGROUPN with those reported by Poulos (2008) using the BEM approach described earlier.

Figures 8a-8c show the profiles of pile axial force, settlement, and interface shear stress, respectively, as obtained by PGROUPN for the floating pile subjected to the head load of 0.8MN and to two different ground settlement profiles (as reported in Fig. 8b). It is noted that the analysis is capable of consistently identifying the location of the neutral plane (NP), which can be defined as the plane where there is no relative movement between the pile and surrounding soil (i.e. where pile and soil settlement become equal). Indeed, the NP is also the location of the maximum force in the pile and where the direction of the pile shear stress reverses from negative to positive. Figures 8a-8c demonstrate that, for the same axial load, the larger ground settlements lead to an increased extent of soil slip along the pile, thereby resulting in a deeper NP location (i.e. from 17.5m to 19.5m depth), while the pile axial force and settlement are increased, as expected. It is noted that, due to the full mobilization of shear stress above the NP location, the transition zone from full NSF to positive shaft resistance becomes sharper and smaller for increasing ground settlement, as also obtained by Tan and Fellenius (2016) using a rigorous FEM analysis.

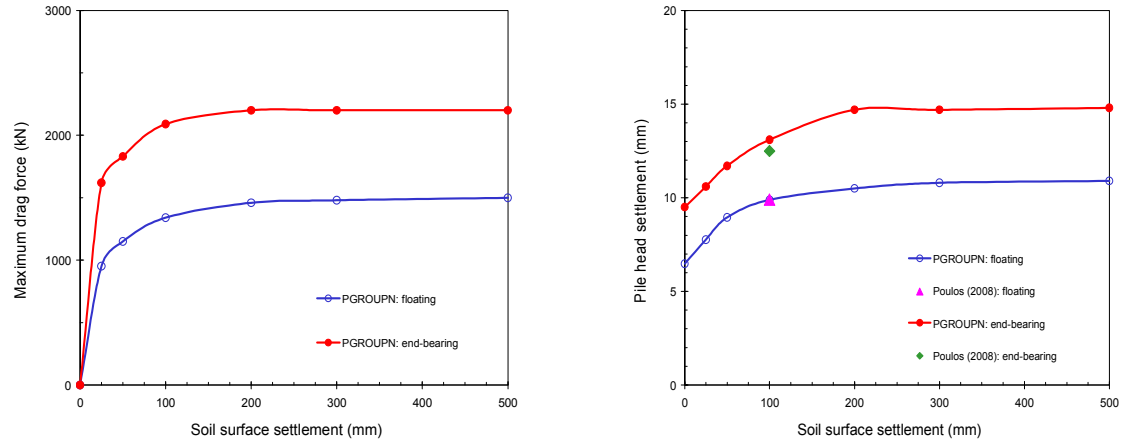


Fig. 7. Piles with head load & ground movement: (a) Max. drag force; (b) Pile settlement

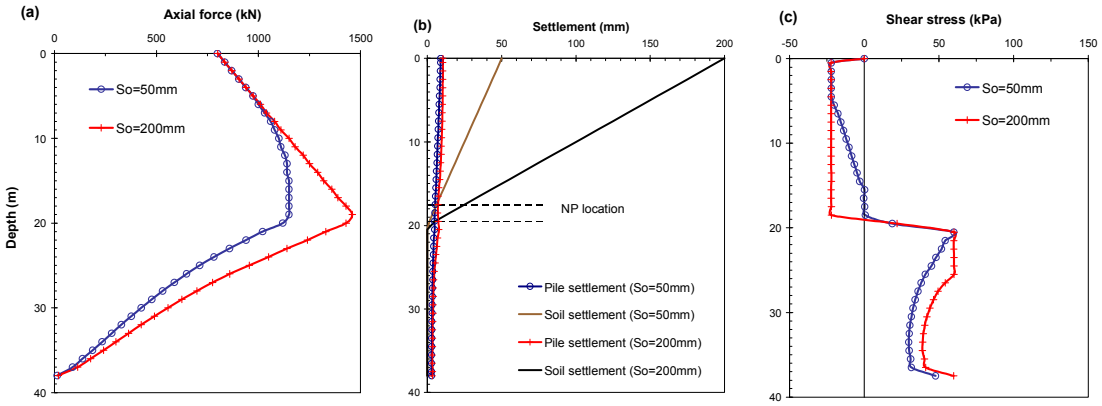


Fig. 8. Floating pile with head load & increasing ground movement

Comparison with Comodromos and Bareka (2005)

The behaviour of single pile and pile groups embedded in a multi-layered soil profile and subjected to direct head load and/or NSF-induced ground movements is investigated through a comparison of PGROUPN with the results obtained by Comodromos and Bareka (2005) using the more rigorous finite difference software FLAC-3D. The soil profile consists of a soft clayey silt 6m thick, underlain by highly plastic soft clay extending to a depth of 18.0m. Under this, a layer of medium stiff clay with a thickness of 24m, underlain by very dense sandy gravel extending to the end of the borehole at a depth of 80.0m. The soil profile and parameters used in the PGROUPN analysis are those reported by Comodromos and Bareka and are summarized in Fig. 9. The FLAC-3D non-linear analysis was based on secant values of soil modulus (E_{sec}), whereas the PGROUPN non-linear model adopts a soil modulus approaching the initial tangent value (E_i). Thus, in order to ensure consistency between analyses, a back-analysis of the single pile results has been carried out and a correlation equal to $E_i = 5E_{sec}$ is adopted (with hyperbolic factors of $R_f = 0.6$ for the shaft and $R_f = 0.99$ for the base, as per Equ. 3). In FLAC-3D, the consolidation settlement of the ground is computed within the analysis by means of the application of surface loading (corresponding to different heights of embankment), as reported in Fig. 12. The PGROUPN analyses have therefore been carried out using the ground movement profiles computed by FLAC-3D as an input.

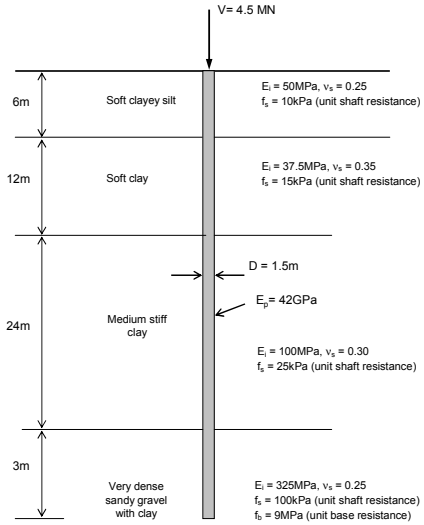


Fig. 9. Soil profile and design parameters used in PGROUPN analysis

Figures 10, 11, and 12 report the profiles of pile shear stress, drag force, and drag settlement, respectively, predicted by PGROUPN and FLAC-3D. A substantial agreement between results is found for all three types of loading conditions, i.e. direct head load (V = 4.5 MN), surface loading (S.L. = 5, 100 kPa), and a combination of V and S.L. Results show that larger surface loads (and thus larger ground settlements) result in a deeper NP location, while the pile drag force and drag settlement are increased, as expected. It is important to note that, even for the relatively small surcharge load S.L. = 5kPa (corresponding to a ground surface settlement of only about 8mm), negative shear stress are developed along a considerable portion of the pile length (the NP is over 30m deep), while the drag force attains a value of nearly 1MN. With increasing surcharge load to S.L. = 100kPa, NSF is fully mobilized for almost the entire pile length and the drag force reaches a value of about 3.5MN, while the pile approaches the end-bearing configuration (i.e. NP location at about 40m depth). In addition, Fig. 13 shows the combined effect of head load (V = 4.5 MN) and surcharge load S.L. = 50kPa (corresponding to the surcharge load of the bridge approach embankment), resulting in a maximum axial force from PGROUPN of 7.4MN with a NP location at 33m depth. Thus, the additional effect of head load is an increased value of the maximum axial force and a reduced depth to NP location, as compared to the case in which only the surcharge load S.L. = 50kPa is acting (refer to Fig. 11).

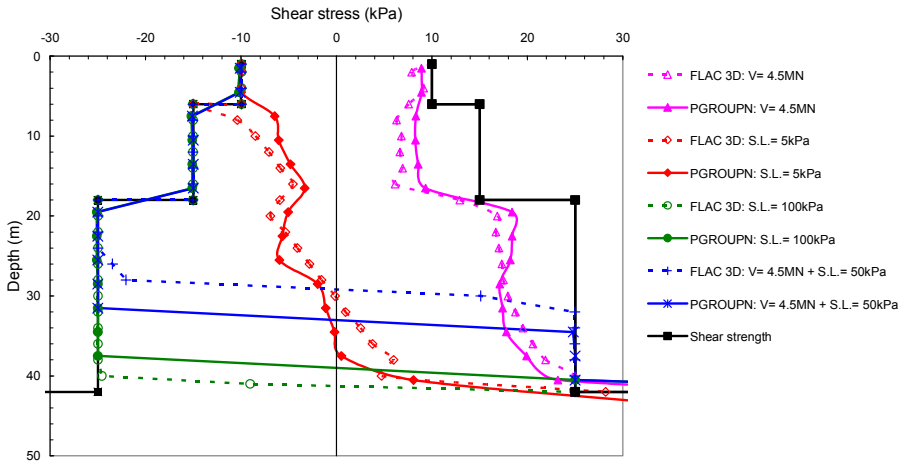


Fig. 10. Shear stress along single pile for various surface loads (S.L.) and/or head load (V)

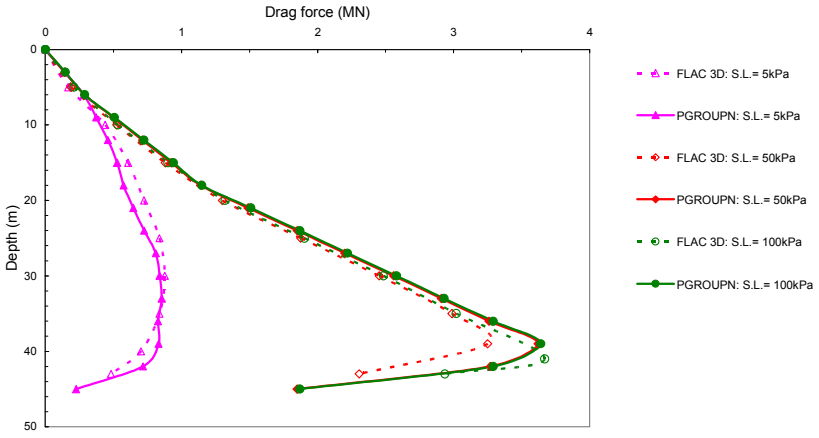


Fig. 11. Drag force along single pile for various surface loads (S.L.)

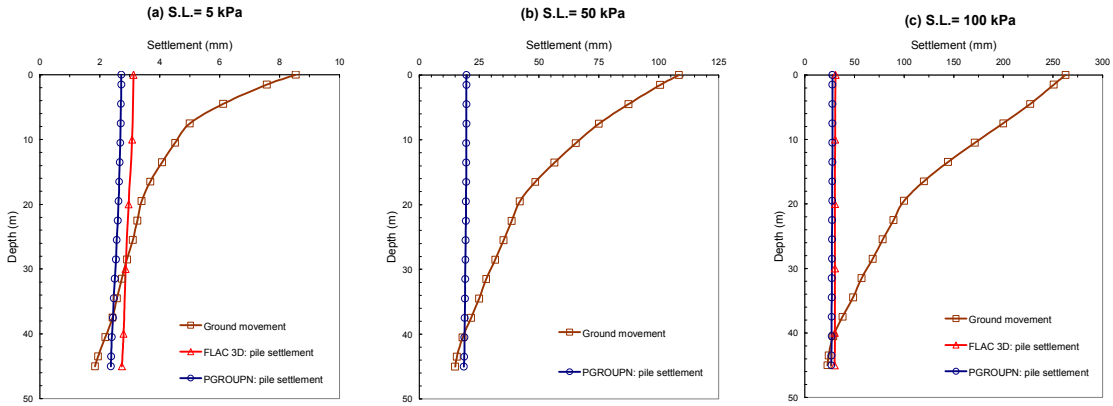


Fig. 12. Pile and ground settlement for various surface loads: (a) 5kPa, (b) 50kPa, (c) 100kPa

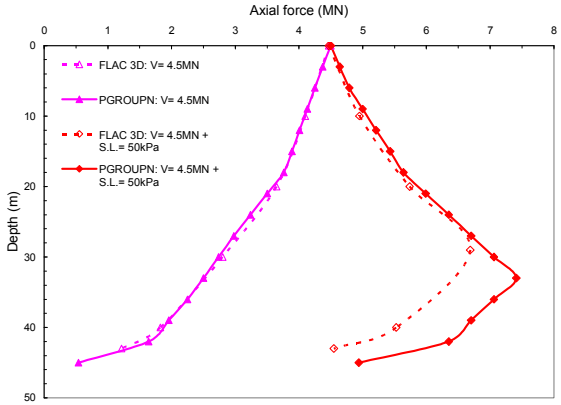


Fig. 13. Axial force along single pile for head load (V) and/or surface load (S.L.)

In order to investigate the effects of group interaction, the single-pile analysis is extended to a fixed-head group of piles in a 3x3 configuration at a pile spacing of 3D (see inset to Fig. 14). The pile cap is assumed to be fully rigid and, owing to the ground settlement, not interacting with the ground. In order to concentrate our attention to the NSF problem only, it is initially assumed that no external load is acting on the pile cap, while the NSF-induced ground movements are those corresponding to a surface load of 50kPa (refer to Fig. 12b).

Figure 14 shows that, in contrast to conventional axial loading at pile-cap level, group effects stemming from pile-to-pile interaction have a beneficial effect in the case of NSF problems, resulting in a reduction of the maximum drag force by 14% in the corner pile and by 31% in the centre pile, as compared to the corresponding single pile. The above results and trend of behaviour from PGROUPN are in good agreement with those predicted by the FLAC-3D analysis. The reduction of the maximum drag force becomes more marked with increasing the number of piles in the group, leading to a 25% reduction on the corner pile, as compared to the single pile, in the case of a 4x4 pile group. It is also noted that, due to the assumption of fully rigid cap, all piles in the group have developed a NP at the same depth (as correctly modelled by PGROUPN), with the NP location moving upward from 39m for the single pile to 36m for the 3x3 pile group. The above features of behaviour therefore offer the prospect of a more economical design for piles in a group given that the reduced maximum drag force (for example that on the corner pile) and the reduced depth of NP location, as compared to a single isolated pile, may be used for the ULS check of pile structural strength. It is also noted that some tensile force is developed at the corner pile near the pile-head, a behavioural feature which has also been reported by several researchers (e.g. Kuwabara and Poulos, 1989, Teh and Wong, 1995; Lee et al, 2009). In practical cases, however, the tensile force will be eliminated by the usually greater effect of the dead load, as numerically illustrated in Fig. 16.

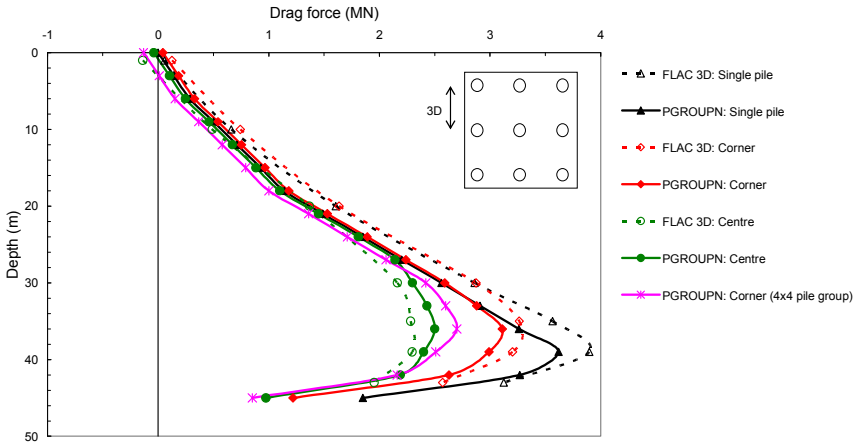


Fig. 14. Drag force distribution for 3x3 pile group with 3D spacing and surface load of 50kPa

Figure 15 shows that the beneficial group effects for piles under NSF decrease with increasing pile spacing (due to the reduced pile-to-pile interaction) and become almost negligible for the group at wider pile spacing (6D), where the reduction in maximum drag force on the corner pile is only 11%, as compared to the single pile.

In order to investigate the more practical case in which both the head load and the NSF are acting, the 3x3 group at 3D spacing is subjected to a total load at pile-cap level of 40.5MN (i.e. an average load of 4.5MN per pile) in addition to the surcharge load S.L. = 50kPa. Figure 16 confirms (even though reduced) the beneficial NSF group effects observed in Fig. 14 in the absence of external cap load, leading to a reduction of the maximum axial force by 4% in the corner pile and by 22% in the centre pile, as compared to the corresponding single pile. Similarly to the single-pile results, the additional effect of external cap load is an increased value of the maximum axial force and a reduced depth to NP location, as compared to the case in which only the surcharge load is acting.

Finally, it should be observed that, even for the larger 4x4 pile group, the computational time required by the PGROUPN analysis is a matter of only a few seconds on an ordinary computer, thereby confirming the value of PGROUPN as a practical numerical tool for the design of pile groups subjected to NSF conditions.

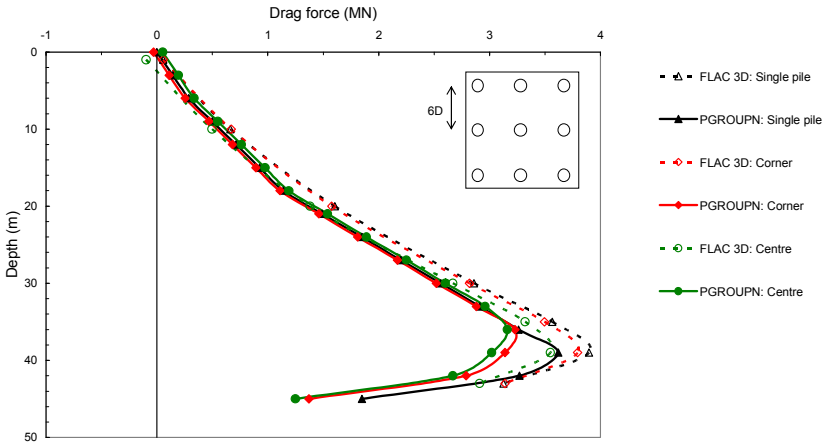


Fig. 15. Drag force distribution for 3x3 pile group with 6D spacing and surface load of 50kPa

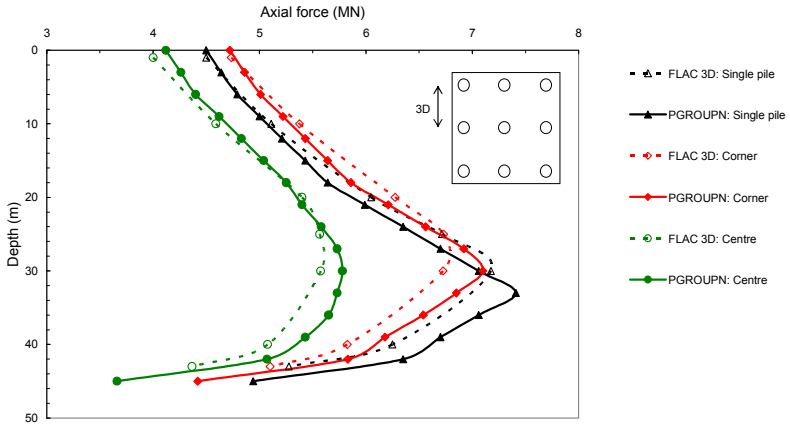


Fig. 16. Axial force in 3x3 pile group under total cap load of 40.5MN and surface load of 50kPa

CONCLUSIONS

Pile design in NSF conditions is mainly a settlement rather than a geotechnical capacity issue, and therefore it is best approached from an SLS viewpoint by means of a pile-soil interaction analysis. For this purpose, this paper has introduced a practical two-stage procedure, based on the 3D non-linear BEM solution implemented within the PGROUPN code, for estimating the response of piles and pile groups subjected to NSF-induced ground movements and to any direct load at pile-head level. Based on the results presented in the paper, a number of considerations may be made:

● The proposed numerical approach is capable of generating reasonable predictions of pile-group response under NSF with negligible computational costs, thus offering a practical compromise between the simplistic full skin friction assumption generally invoked in routine practice and the complexity and time-consuming nature of 3D FEM and FDM solutions.

● PGROUPN is able to model with sufficient accuracy the partial shear stress mobilization corresponding to the actual NSF-induced ground movements, thereby resulting in a reduced pile drag force and drag settlement as compared to the traditional full mobilization assumption. It should again be emphasized that drag force is an *internal* force associated with the development of static equilibrium of the pile-soil system, and therefore it is only a matter for the pile structural strength, i.e. it should not be lumped in with the load from the structure for the assessment of pile geotechnical capacity.

● Consideration of soil nonlinearity (including soil slip at the pile-soil interface) is advantageous in NSF pile design since soil slip can develop under relatively small ground movements, thereby resulting in reduced pile drag forces and drag settlements as compared with a purely linear elastic interface condition.

● In contrast to conventional axial loading at pile-cap level, group effects stemming from interaction among piles have a beneficial effect in the case of NSF problems. As compared with a single pile, there is a tendency for reduced drag forces and a reduced depth of NP location in the group piles, thereby offering the prospect of a more economic and theoretically sound design for piles in NSF conditions.

REFERENCES

Basile, F., 2003. Analysis and design of pile groups. In Numerical Analysis and Modelling in Geomechanics (ed. J.W. Bull), Spon Press, pp. 278-315.

Basile, F., 2012. Pile-group response under seismic loading. Proc. 2nd Int. Conf. on Performance-Based Design in Earthquake Geot. Eng., Paper No. 11.01, Taormina, Italy, pp 1185-1200.

Basile, F., 2014. Effects of tunnelling on pile foundations. Soils and Foundations, Vol. 54, No. 3, pp. 280-295.

Bond, A.J. and Basile, F., 2017. Repute 2.5, Software for pile design and analysis. Reference Manual, Geocentrix Ltd, Surrey, UK, 52 p.

Comodromos, E.M. and Bareka, S.V., 2005. Evaluation of negative skin friction effects in pile foundations using 3D nonlinear analysis. Computers and Geotechnics, Vol. 32, pp. 210-221.

Fellenius, B.H., 2017. Basics of foundation design – a textbook. Pile Buck International, Inc., Vero Beach, FL, Electronic Edition, www.fellenius.net, 464 p.

Kuwabara, F. and Poulos, H.G., 1989. Downdrag forces in groups of piles, ASCE J. Geot. Eng. Div., Vol. 115, No. GT6, pp. 806-818.

Lee, C.J., Ng, C.W.W., and Jeong, S.S., 2009. The effect of negative skin friction on piles and pile groups. In Linear and Non-linear Numerical Analysis of Foundations (ed. J.W. Bull), Spon Press, pp. 181-230.

Mindlin, R.D., 1936. Force at a point in the interior of a semi-infinite solid. Physics, Vol. 7, pp. 195-202.

Mroueh, H. and Shahrour, I., 2002. Three–dimensional finite element analysis of the interaction between tunnelling and pile foundations. Int. J. Numer. Anal. Meth. Geomech., Vol. 26, pp. 217-230.

Poulos, H.G., 2006. Ground movements – A hidden source of loading on deep foundations. John Mitchell Lecture, Proc.10th DFI Int. Conf. on Piling and Deep Foundations, Amsterdam, pp. 2-19.

Poulos, H.G., 2008. A practical design approach for piles with negative friction. Proceedings of the Institution of Civil Engineers, UK, Vol. 161, No. 1, pp. 19-27.

Poulos, H.G., 2009. Program CLAP (Combined Load Analysis of Piles). Users Manual, v. 6.2, Coffey Geotechnics Pty. Ltd, 45 p.

Poulos, H.G., 2017. Tall Building Foundation Design. CRC Press, 532p.

Tan, S.A. and Fellenius, B.H., 2016. Negative skin friction pile concepts with soil-structure interaction. ICE Geotechnical Research Journal, UK. Paper 16.00006. pp. 1-11.

Teh, C.I. and Wong, K.S., 1995. Analysis of downdrag on pile groups, Géotechnique, Vol. 45, No. 2, pp. 191-207.

Yamashita, K., Tomono, M. and Kakurai, M., 1987. A method for estimating immediate settlement of piles and pile groups. Soils and Foundations, Vol. 27, No. 1, pp. 61-76.

SEISMIC PERFORMANCE OF A PILED RAFT FOUNDATION WITH GRID-FORM DMWS CONSIDERING SOFTENING OF STABILIZED SOIL

Yoshimasa Shigeno, Takenaka Corporation, Tokyo, Japan, +81-80-6720-6263, shigeno.yoshimasa@takenaka.co.jp
Kiyoshi Yamashita, Takenaka Corporation, Tokyo, Japan, yamashita.kiyoshi@takenaka.co.jp
Junji Hamada, Takenaka Corporation, Tokyo, Japan, Hamada.junji@takenaka.co.jp

ABSTRACT

The seismic performance of a piled raft foundation with grid-form deep mixing walls (DMWs) in soft ground under strong earthquake loads is numerically evaluated in this study. A base-isolated 12-story building located in Tokyo is modeled as a detailed three-dimensional finite element soil structure interaction model. In the previous study, the model was calibrated using the records of the 2011 off the Pacific coast of Tohoku Earthquake. Based on this result, seismic response analyses under strong earthquake loads are conducted in this study. Artificial earthquakes that are officially notified for performance design in Japanese building design codes are used as strong earthquakes. For the constitutive model of stabilized soil, the elasto-plastic model that is able to evaluate shear and tension failure is used, and it is also able to evaluate the post-peak tension-softening assuming the energy release during the formation and opening of cracks in the DMWs. Based on the analysis results, it is found that even though the induced stress in the DMWs reaches the tensile strength and softens, the grid-form DMWs are quite effective at reducing the bending moment of the piles to an acceptable level under the strong earthquake load.

Keywords: piled raft foundation, deep mixing walls, soil and structure interaction analysis

INTRODUCTION

In recent years, piled raft foundations have been used in many countries as building foundations. The effectiveness of piled rafts at reducing average and differential settlements has been confirmed on soft clay and even on liquefiable sand with grid-form cement deep mixing walls (DMWs) (Yamashita et al. 2011, 2013, 2016). The grid-form DMWs work as a countermeasure for liquefaction by increasing the resistance of unstabilized soil. However, adding the grid-form DMWs as a new component of the foundation, the seismic behavior becomes more complicated and the necessity for detailed evaluation increases.

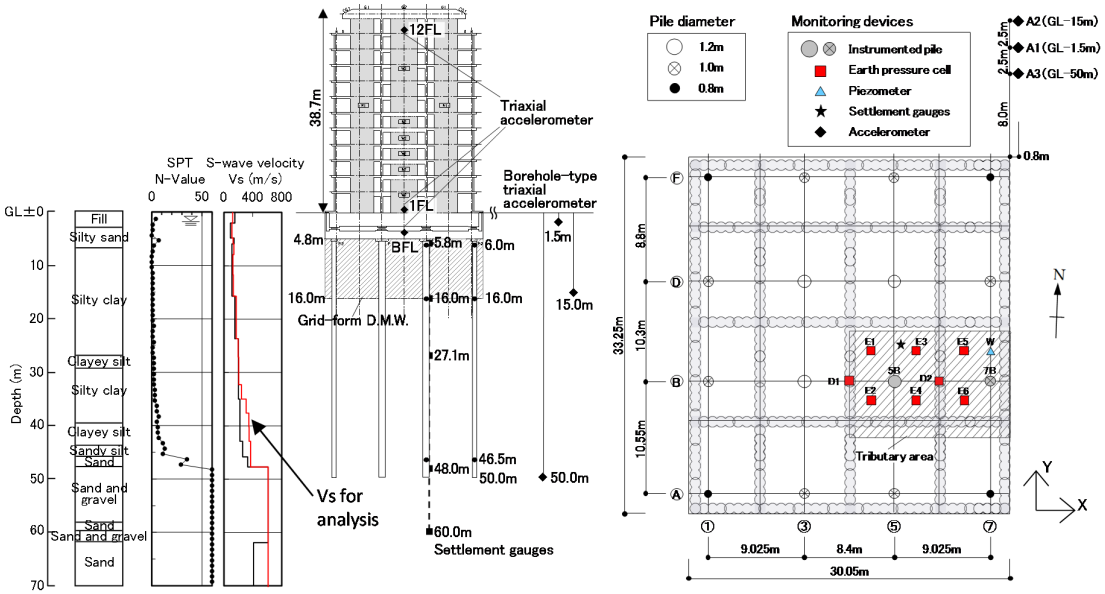
Field monitoring has been performed on a piled raft foundation with grid-form DMWs in soft ground supporting a 12-story building. The seismic response of the soil-foundation system was successfully recorded at the time of the 2011 off the Pacific Coast of Tohoku Earthquake (Yamashita et al. 2012). In the previous studies, seismic response analysis using a detailed three-dimensional (3D) finite element (FE) model was conducted for observation records (Hamada et al. 2014, Shigeno et al. 2017). In the analyses, the numerical model was well calibrated, and the model was able to reproduce the observation records in adequate accuracy. Furthermore, the seismic performance of the foundation under strong earthquakes was evaluated considering the tensile strength of the DMWs (Shigeno et al. 2017). In the study, the soundness of the piles was confirmed even though the grid-form DMWs were partially failed by tension. However, softening of the stabilized soil was not considered in the analysis and the results might be a little optimistic. Then in this study, the softening after the peak strength of the stabilized soil is considered in the evaluation of the seismic performance of a piled raft foundation with grid-form DMWs under a strong earthquake. For the constitutive model, the elasto-plastic model

© 2018 Deep Foundations Institute

that has the both tensile and shear criteria, and also is able to consider the softening is applied. The effect of the softening of the DMWs caused by the strong motion on the sectional force of the piles is mainly discussed.

BUILDING AND GROUND CONDITIONS

Figure 1 shows a schematic view of the building and its foundation with the soil profile (Yamashita et al. 2012). The building analyzed is a 12-story residential building located in Tokyo. The height is 38.7m above the ground, and the cross section of the first floor is 33.25 m by 30.05 m. The building is a reinforced-concrete structure with a seismic base-isolation system; it was completed in 2008.
The soil down to a depth of 44m is alluvial stratum. The upper 7m is fill, soft silt and loose silty sand. The rest is very soft to medium silty clay. The stratum deeper than 44 m is diluvial sand and a gravel layer with SPT N-value of 60 or higher. The ground water table appears approximately 1.8 m below the ground surface. The building is supported by a piled raft with grid-form DMWs which were employed to prevent liquefaction of the silty sand from GL -3 m to -7 m as well as to improve the bearing capacity of the raft foundation. The spacing between the DMWs is about 6 to 9 m, and the area replacement ratio is 25%. The locations of the seismic monitoring devices are also shown in Fig. 1. At the time of the 2011 off the Pacific Coast of Tohoku Earthquake, the seismic response of the soil-foundation system, i.e., axial force and bending moment of two piles, contact pressure and pore water pressure beneath the raft, and accelerations of the ground and structure, was successfully recorded.



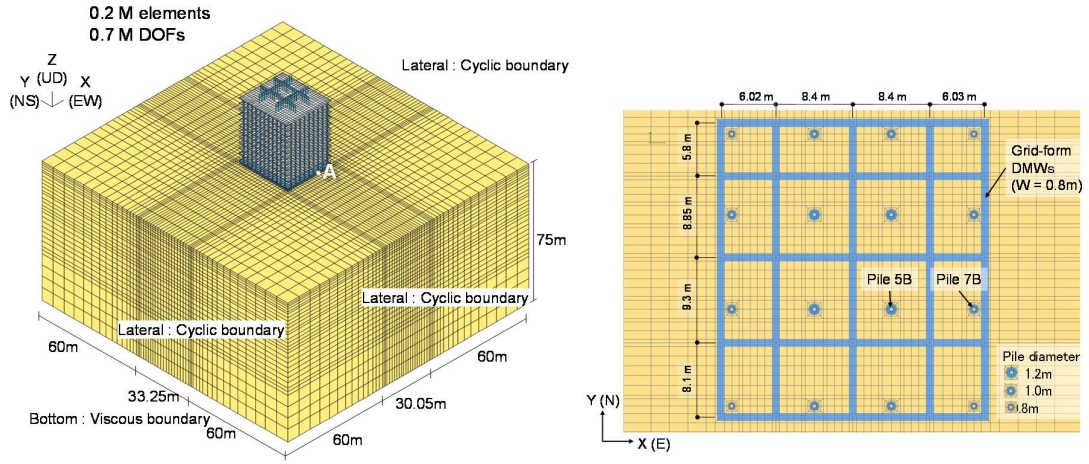
(a) Ground profile and cross section of building (b) Foundation plan with location of devices

Fig. 1. Schematic view of building and monitoring devices

FINITE ELEMENT MESH

Figure 2(a) shows the finite element (FE) mesh, which has 213,622 elements and 656,543 degrees of freedom. The superstructure is modeled using elastic bars and shells, and the piles are modeled using

elastic bars. Table 1 shows the material properties of the piles. The raft is modeled using elastic solid elements with the modulus of concrete. Rayleigh damping is applied to these components at a damping ratio of 2%. Figure 2(b) shows a top view of the FE mesh beneath the raft. To consider the shape and volume of the piles, cavities in the shape of the piles are made in the model. The nodes of the piles and the adjacent ground nodes at the same depth are bound by rigid bar elements. The base isolation system is modeled using a tri-linear spring. The lateral boundaries are periodic boundaries, and are positioned 60 m outside of the building to reduce the boundary effect. The bottom is a viscous boundary at a depth of 75 m from the ground surface. The software is an in-house program called MuDIAN (Shiomi et al. 1998). It is parallelized using the hybrid parallel method and is able to analyze a large-DOF model at high speed (Shigeno 2014).



(a) General view **(b) Magnified top-down view under the raft**

Fig. 2. Finite element model

Table 1 Pile properties

Pile diameter	(mm)	800	1000	1200
Young's modulus	(MN/m^2)	40000	40000	40000
Damping	(%)	2.0	2.0	2.0
A_e*1 of SC pile*3	(m^2)	0.3268	0.4649	0.6714
I_e*2 of SC pile	(m^4)	0.02199	0.04899	0.10316
A_e of PHC pile*4	(m^2)	0.2441	0.3633	0.5054
I_e of PHC pile	(m^4)	0.01455	0.03437	0.06958

*1 A_e : Equivalent cross-sectional area
*2 I_e : Equivalent moment of inertia of area
*3 SC pile : steel pipe–concrete composite pile
*4 PHC pile : prestressed high-strength concrete pile

INPUT MOTION

An artificial wave is used for a strong earthquake called 'Level 2 earthquake' that is officially notified in Japanese building design code for performance design. The recurrence interval is considered to be about 500 years. The wave is defined by the acceleration response spectrum as shown in Fig. 3. The input wave is generated using phase data. In this paper, the wave is generated using the Hachinohe phase data at the Tokachi Oki Earthquake in 1968 recorded at Hachinohe bay. Hachinohe wave is the typical subduction zone earthquake, and strong motion continues during long period. And also the total input energy is large among Level 2 earthquakes. The NS direction wave is used, and one directional

input motion (NS direction) is applied in this study. Figure 4 shows the input motion, and the maximum acceleration is 337 gal.

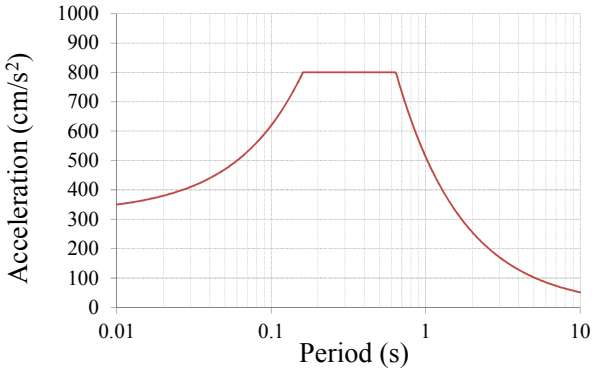


Fig. 3. **Acceleration response spectrum of Level 2 earthquake**

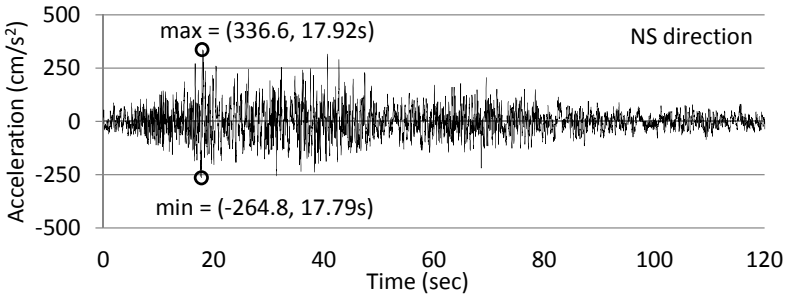


Fig. 4. **Input acceleration wave (Hachinohe wave) at a depth of 75 m (2E) in the NS direction**

MODEL FOR SOIL AND STABILIZED SOIL

The Yoshida model for multi-dimension (Tsujino et. al., 1994) is used as the constitutive model for the soil. The Yoshida model is a two-surface nonlinear elastic model and is characterized using G-γ and h-γ characteristics directly as input data.

The profile of shear wave velocity (V_s) of the ground for the analysis is shown in Fig. 1 by the red line together with data derived from P-S logging. The V_s profile for analysis was obtained by calibration analysis using the observed records at this site (Shigeno et. al. 2017). The other soil properties are reported in Shigeno et al. (2017). Initial damping other than the hysteresis is assumed to be 1% Rayleigh damping.

In the previous study, the importance of considering the tensile criterion for stabilized soil was shown (Shigeno et. al., 2017). However, softening after failure was not considered although stabilized soil exhibits strain localization after the peak tensile strength. In this study, the elasto-plastic model proposed by Namikawa et al. (2006a) that has tensile and shear criteria and also be able to evaluate softening after failure is applied.

The tensile failure of stabilized soil exhibits strain localization after the peak strength, and the deformation concentrates inside a strain localization zone. For concrete, the methods assuming the energy release during the formation and opening of cracks are proposed to determine the post-peak tension-softening (Niwa et al. 1998). This assumption implies that the amount of energy released per unit area for widening the cracks corresponds to the area formed by the tension-softening curve. The

energy consumed per unit crack area is defined as the fracture energy G_f. Namikawa evaluated the fracture energy G_f of the stabilized soil using three-point bending tests, and estimated the relationship of the stress and opening crack displacement using 1/4 bilinear model proposed by Rokugo et al. (1989) for concrete.

The tensile strength T_f considering softening using a damage parameter ω is expressed by the second invariant of deviatoric stress J'_2, the mean stress σ_m and Lode angle θ (note that tension is positive).

$$\frac{2(J'_2)^{\frac{1}{2}}}{\sqrt{3}}\sin\left(\theta+\frac{2\pi}{3}\right)+\sigma_m = T_f(1-\omega) \qquad [1]$$

The damage parameter ω for tensile failure is expressed as the function of the maximum plastic principal strain ε_1^p using 1/4 bilinear model. The stress and plastic strain relation for tension is defined by the ratio of the crack opening displacement and the width of failing region assuming the distributed cracks model.

$$\begin{aligned} &\omega = l_m \frac{T_f}{G_f}\left(\varepsilon_1^p - \varepsilon_{1peak}^p\right) \quad \omega \le 0.75 \\ &\omega = \frac{12}{17} - \frac{1}{17} l_m \frac{T_f}{G_f}\left(\varepsilon_1^p - \varepsilon_{1peak}^p\right) \quad 0.75 < \omega \le 1.0 \end{aligned} \qquad [2]$$

Where, G_f is fracture energy, $\varepsilon_1{}^p{}_{peak}$ is the peak plastic principal strain and l_m is the parameter that depends on the mesh size of the finite element model. The parameter l_m is introduced to remove the mesh size dependency by the strain localization.

The Mohr–Coulomb criterion is used for shear strength, and the criterion is also expressed using the stress invariants, friction angle ϕ and cohesion c.

$$\begin{aligned} &(J'_2)^{\frac{1}{2}} + \Gamma(\theta)\left\{\sigma_m - \frac{c(1-\omega)}{\tan\phi}\right\}k_y = 0 \\ &\Gamma(\theta) = \frac{\cos\theta}{\sin\phi} - \frac{1}{\sqrt{3}}\sin\theta \end{aligned} \qquad [3]$$

Where k_y is the internal state variable that determines the size of the loading surface, and it is assumed to be the hyperbolic function of the second invariant of the deviatoric plastic strain $\bar{\varepsilon}^p$ as follows.

$$\frac{k_y - k_0}{k_f - k_0} = \frac{\dfrac{\bar{\varepsilon}^p}{e_y}}{1+\dfrac{\bar{\varepsilon}^p}{e_y}} \qquad k_0 = \frac{T_f}{\sigma_m - \dfrac{\alpha c}{\tan\phi}} \qquad [4]$$

Where k_f is the coefficient of the normal-yield surface, e_y and α are the hardening parameter.

The damage parameter for shear failure of the stabilized soil was obtained from the plane strain compression test as follows (Namikawa et al. 2006b).

$$\omega = 1 - \exp\left\{-\frac{R_l\left(\bar{\varepsilon}^p - \bar{\varepsilon}^p_{peak}\right)}{e_r}\right\} \qquad R_l = \frac{l_m}{l_c} \qquad [5]$$

Where, l_c is the characteristic length that specifies the size of the failure region, and e_r is the parameter. The damage parameter ω is the common for both tensile and shear criterion, and the loading surface reduces in the both criterion after stress reaches the strength.

The design standard compressive strength F_c is used as the compressive strength of the stabilized soil. The value of F_c is calculated using the average compressive strength of in-situ core samples q_{uf} and its variation V_{quf} referred to BCJ (2002) as follows.

$$F_c = (1 - 1.3V_{q_{uf}})q_{uf} \qquad [6]$$

The value of q_{uf} and V_{quf} are 3.8 MPa and 0.25 that are the average and variance of 36 core samples

aged 28 days (Yamashita et al., 2015), and the value of F_c becomes 2.6 MPa. The tensile strength is $0.2F_c$, the cohesion is $0.3F_c$., the friction angle is 30 degrees and the Poisson's ratio is 0.26 referred to the proposal by BCJ (2002). As for the initial stress in the DMWs, isotropic stress of 170 kPa is given by considering the measured vertical pressure between the raft and the DMWs of 300 kPa (Yamashita et al, 2015) and the horizontal stress calculated using the coefficient of earth pressure at rest. The initial shear modulus (G_0 = 500 MPa) was determined by the calibration analysis targeting the observation records of the 2011 off Pacific Coast Tohoku Earthquake (Shigeno et al., 2017). The strength parameters of the stabilized soils are listed in Table 2.

The properties and parameters of the Namikawa model was determined by the three-point bending test and the plane strain compression test of the stabilized soil (Namikawa et al. 2006b), and they are listed in Table 3. Figure 5 shows the simulation result of the uniaxial extension test. The lateral axis is the maximum principal stress, and the horizontal axis is the maximum principal strain. Properties of Table 2 and 3 are used. The initial stress is zero, and the extension is given under strain constrained condition. The stress degrades after it reaches the initial tensile strength σ_{t0} = 520 kPa.

Table 2. Parameters of stabilized soil related to strength

Compressive strength	F_c	MPa	2.6
Tensile strength	$0.2F_c$	kPa	520
Cohesion	$0.3F_c$	kPa	780
Friction angle	ϕ	degree	30
Poisson's ration	v		0.26
Density	ρ	t/m^3	2.0
Initial shear modulus	G_0	MPa	500

Table 3. Parameters for Namikawa model

Hardening parameter	α		0.9
Hardening parameter	e_y		0.0001
Fracture energy	G_f	N/m	96.0
Softening parameter for shear	e_r		0.4
Dilatancy coefficient	D_c		0.0
Localization size	l_m	mm	1000
Characteristics length	l_c	mm	0.6

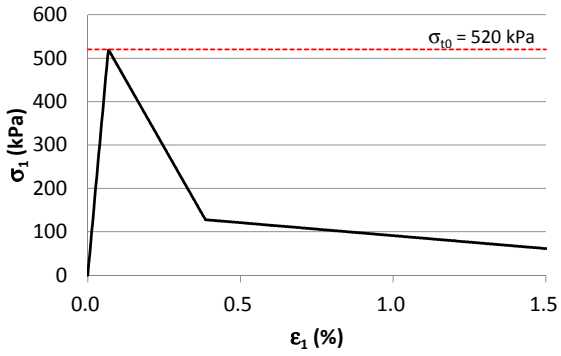
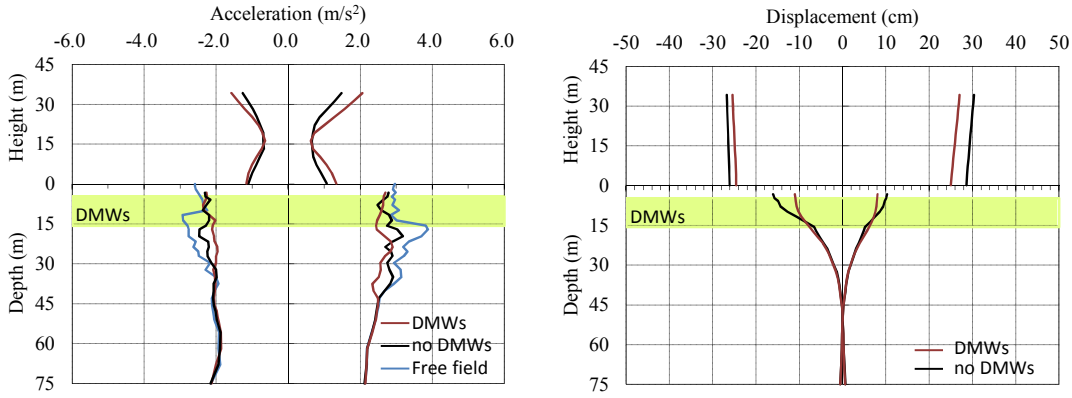


Fig. 5. Numerical uniaxial extension test of stabilized soil

RESULTS OF SEISMIC RESPONSE ANALYSIS

The case without DMWs is also analysed to clarify the effect of them. Figure 6(a) shows the profiles of the peak acceleration at the center of the superstructure and the raft in the NS direction together with those of the ground at point A (Fig. 2(a)). The peak acceleration profile of the soil column model is also shown as 'Free field' by the blue line. The PGA at the surface of the far field is 296 gal. In the case with DMWs, the peaks are 325 gal at the raft and 131 gal on the first floor. The reduction rate by the base isolation system is 40%. In the case without DMWs, the peaks are 275 gal and 111 gal. The peak of the raft is slightly larger in the case with DMWs in this case. Figure 6(b) shows the profiles of the peak displacement. The displacement is relative to GL -49.9 m and in the NS direction. The peaks at the bottom of the raft are -10.9 cm and 8.0 cm in the case with DMWs, which are smaller than -15.7 cm and 10.1 cm in the case without DMWs. The ground deformation beneath the raft is reduced by the grid-form DMWs, and this affects the sectional force of the piles.



(a) Acceleration **(b) Relative displacement (to GL-49.9 m)**

Fig. 6. Peak response profiles of superstructure at center and ground at point A (NS-direction)

Figure 7 illustrates the extent of tensile failure in the grid-form DMWs during the earthquake in two points of view. Elements are colored according to the number of Gauss points where the induced stress reaches the tensile strength. Number of Gauss points is eight in each element, and then the maximum value is 8. The tensile failure is seen mostly in the lower part of the longitudinal walls to the shaking direction, and this is due to shear deformation. In the most of the upper part of the longitudinal walls, tensile failure elements are not seen because the deformation is restricted by the raft. In the transverse walls, some elements at the bottom of grid crossing corners fail clearly due to bending. Compared to the results of no softening case in the previous study (Shigeno et al. 2017), the extent of tensile failure shown is larger. This result is reasonable because the unbroken elements have to share the released stress of the broken element and results in the extension of failure zone in the softening considering case.

Figure 8 shows the time histories of the maximum principal stress σ_1, strain ε_1 and the tensile strength of the elements shown in Fig. 7. The values at Gauss point No.1 are specified. The red dot line is the initial tensile strength σ_{t0} = 520 kPa. In element 1, which is near the head of the DMWs, the peak maximum principal stress reaches σ_{t0}. And the induced maximum tensile strain is 0.06%. The tensile strength degrades after the stress reaches σ_{t0}. However, the degradation ratio is as small as 3%. In element 2, the stress does not reach the tensile strength, and then the softening can't be seen at this point. In element 3, the stress also reaches the tensile strength and softening occurs. The maximum tensile strain is 0.11%, and the tensile strength degrades to one hundredth of the initial strength that is the limitation value given as a parameter. These results show the colored regions in Fig. 7 are not the

parts where the strength is totally degraded. It is important to note that the elements have different residual strength, even though they specify the same color in the contour map.

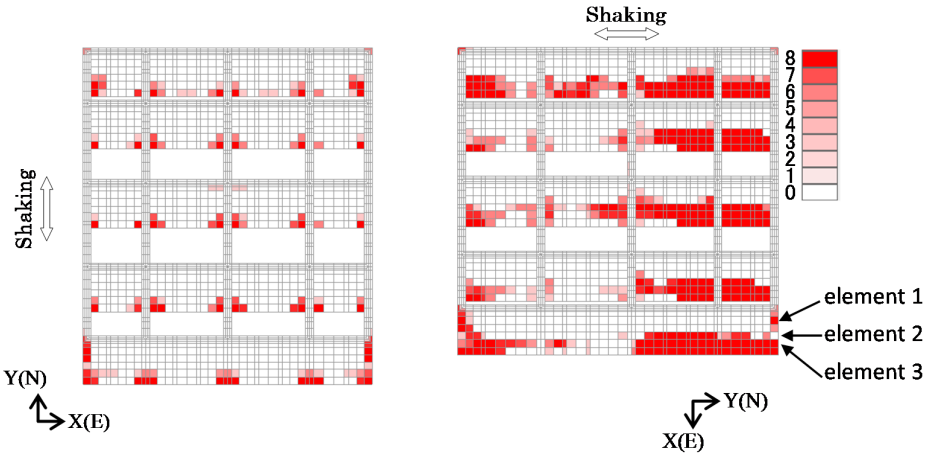
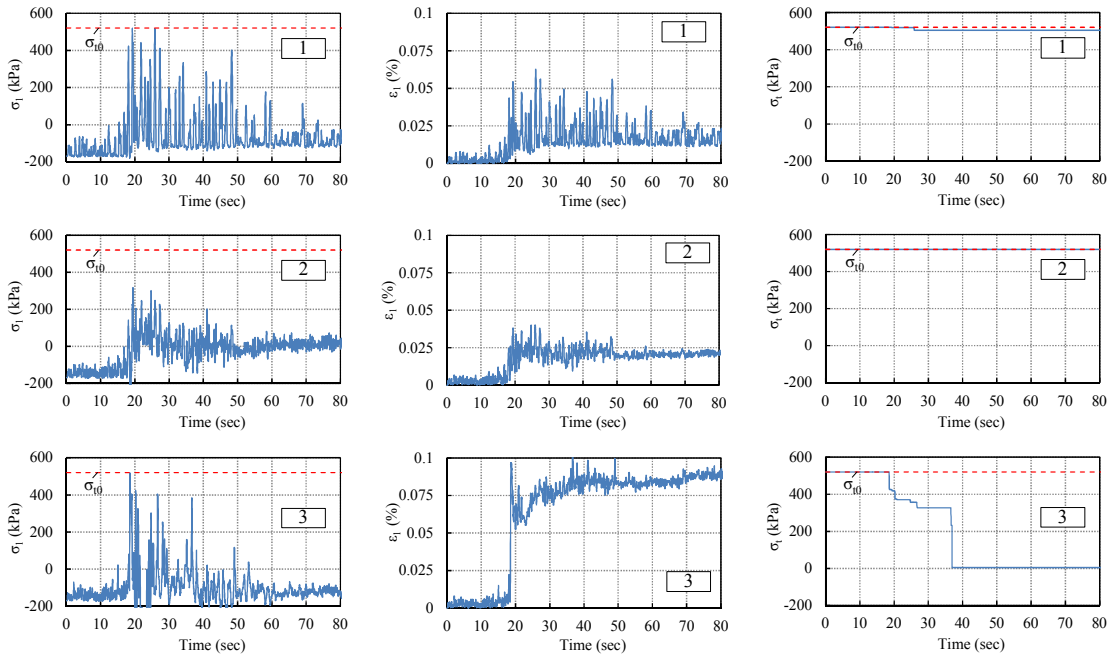


Fig. 7. Contour map of tensile failure Gauss points in grid-form DMWs



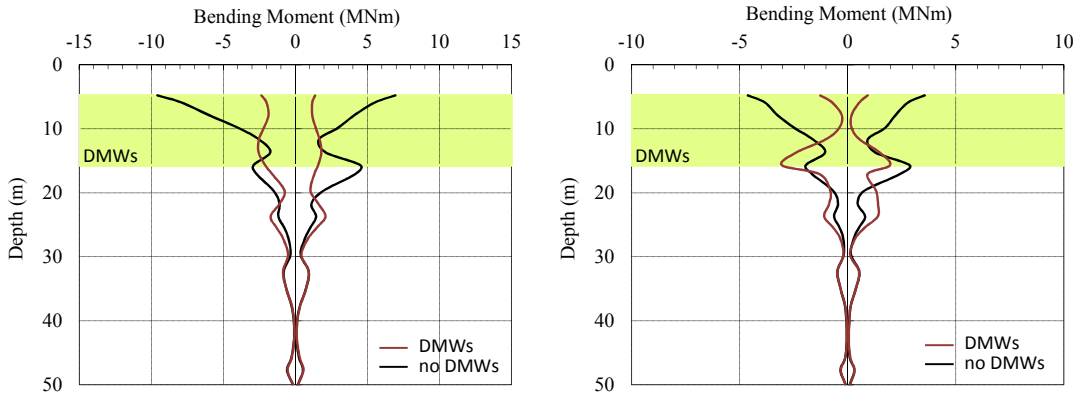
(a) Maximum principal stress (b) Maximum principal strain (c) Tensile strength

Fig. 8. Time histories of tensile stress, strain and tensile strength

Figure 9 shows the profiles of the peak bending moment in piles 5B and 7B showed in Fig. 2(b) in the NS direction. The peak value near the pile head in the case with DMWs is remarkably smaller than those in the case without DMWs. In the case with DMWs, the deformation of the soil enclosed by the DMWs is small and results in a small bending moment near the pile head. However, the moment at the bottom of the DMWs is large, because the curvature of displacement becomes large due to the high rigidity of the DMWs at this point. On the other hand, in the case without DMWs, the deformation of the soil near the pile head is large and asymmetric in the peak profile. This results in the large and asymmetric bending moment at the pile head. These results show the same tendency as the case

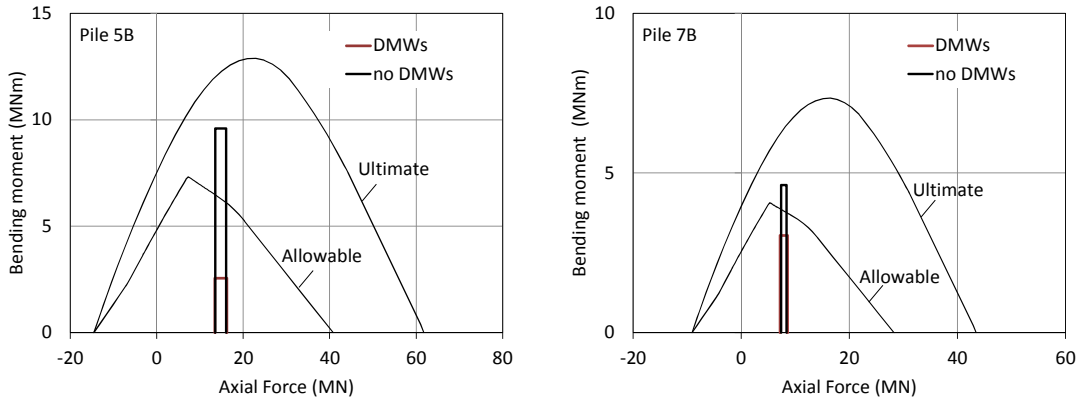
without softening of the DMWs (Shigeno et al. 2017).

Figure 10 shows the relationship between the axial force and the bending moment of Piles 5B and 7B, together with the design interaction curves of the steel pipe–concrete composite (SC) pile (Japan pile 2011) which is used in the top portion at 12 m. Here, the axial force means the sum of the statically measured pile head load and the maximum and minimum dynamic incremental force in the analysis, and the bending moment means the maximum value along the SC pile. The analytical results show that the maximum bending moment in the case with DMWs is below the allowable criterion (the unit stress at the edge of the concrete is in the elastic condition). In contrast, the maximum bending moments in the case without DMWs are close to the ultimate criterion (the unit stress at the edge of the concrete reaches the compressive strength). Hence, the grid-form DMWs are quite effective at reducing pile bending moment to an acceptable level, although the induced stress in the stabilized soil partially reaches the tensile strength and softens under the strong earthquake load. This indicates that the grid-form DMWs can be designed more rationally by the performance-based design method in which a partial failure of the DMWs is accepted.



(a) Pile 5B **(b) Pile7B**

Fig. 9. Profiles of peak bending moment of piles



(a) Pile 5B **(b) Pile7B**

Fig. 10. Calculated maximum moment along pile and design N–M interaction curves of SC piles

CONCLUSION

Seismic response analysis of a piled raft foundation with grid-form DMWs using the three dimensional nonlinear finite element model under a strong earthquake load is carried out considering

after peak softening of the DMWs. As a result, the induced stress reaches the tensile strength in some lower parts of the DMWs, and the extent of failure zone is larger compared to the no-softening case. However it is found that the DMWs are quite effective in reducing sectional force of the piles to an acceptable level. And the results also suggest that the possibility the performance-based seismic design of piled rafts with grid-form DMWs can be specified by the presented nonlinear 3D FE model.

References

Building Center of Japan, 2002. *Specification for design and quality control of cement treated soil* (in Japanese).

Hamada, J., Shigeno, Y., Onimaru, S., Tanikawa, T., Nakamura, N. and Yamashita, K. 2014. Numerical analysis on seismic response of piled raft foundation with ground improvement based on seismic observation records, *Proc. of the 14th IACMAG*, Kyoto, Japan.

Japan pile corporation, 2011. *Pile foundation design materials* (in Japanese)

Namikawa, T. 2006a. Study on tensile and shear failure characteristics of cement-treated sand, *Doctor Thesis, Univ. of Tokyo* (in Japanese)

Namikawa, T. and Koseki, J. 2006b. Experimental determination of softening relations for cement-treated sand, *soils & foundations*, Vol.46, No.4, 491-504.

Namikawa, T., Koseki, J. and Suzuki, Y. 2007. Finite element analysis of lattice-shaped ground improvement by cement-mixing for liquefaction mitigation, *Soils & Foundations*, Vol.47, 559-576.

Niwa, J., Sumranwanich, T. and Tangtermsirikul, S. 1998. New method to determine tension softening curve of concrete, *Proc. FRAMCOS-3*, 347-356.

Rokugo, K., Iwasa, M., Suzuki, T. and Koyanagi, W. 1989. Testing methods to determine tensile strain softening curve and fracture energy of concrete, *Fracture Toughness and Fracture Energy*, Balkema, 153-163.

Shigeno, Y., Hamada, J. and Nakamura, N. 2014. Hybrid parallelization of earthquake response analysis using K computer, *Proc. of the 14th IACMAG*. Kyoto, Japan

Shigeno, Y., Yamashita, K., Hamada, J. and Nakamura, N. 2017. Numerical evaluation of seismic performance of piled raft with grid-form DMWs under large earthquake loads, *Design and analysis of pile raft foundations -2017*, Tamkang University Press, 109-127.

Shiomi, T., Shigeno, Y. and Zienkiewicz, O. C., 1993. Numerical prediction for model No. 1., *Verification of Numerical Procedures for the Analysis of Soil Liquefaction Problems*, Balkema, 213-219.

Tsujino, S., Yoshida, N. and Yasuda, S. 1994. A simplified practical stress-strain model in multi-dimensional analysis, *Proc. of International Symposium on Pre-failure Deformation Characteristics of Geomaterials*, Sapporo, Japan, 463-468.

Yamashita, K., Yamada, T., and Hamada, J. 2011. Investigation of settlement and load sharing on piled rafts by monitoring full-scale structures, *Soils & Foundations*, Vol. 51 (3), 513–532.

Yamashita, K., Hamada, J., Onimaru, S. and Higashino, M. 2012. Seismic behavior of piled raft with ground improvement supporting a base-isolated building on soft ground in Tokyo, *Soils & Foundations*, Vol. 52, 1000–1015.

Yamashita, K., Wakai, S. and Hamada, J. 2013, Large-scale piled raft with grid-form deep mixing walls on soft ground, *Proc. of the 18th Int. Conference on SMGE*, Paris, France, 2637-2640.

Yamashita, K., Tanikawa, T., Shigeno, Y. and Hamada, J. 2015. Vertical load sharing of piled raft with grid-form deep mixing walls, *Conference on Deep Mixing 2015*, San Francisco, USA, 437-446.

Yamashita, K., Hamada, J. and Tanikawa, T. 2016. Static and seismic performance of a friction piled combined with grid-form deep mixing walls in soft ground, *Soils & Foundations*, Vol. 56, 559-573.

SOIL IMPROVEMENT BY EXPANDING POLYURETHANE RESINS

Andrea Dominijanni, Assistant Professor, Politecnico di Torino, Torino (Italy), Ph: +39 011 090 4820, E-mail: andrea.dominijanni@polito.it
Nicolò Guarena, PhD Candidate, Politecnico di Torino, Torino (Italy), Ph: +39 011 090 7705, E-mail: nicolo.guarena@polito.it
Mario Manassero, Full Professor, Politecnico di Torino, Torino (Italy), Ph: +39 011 090 4820, E-mail: mario.manassero@polito.it

ABSTRACT

In recent years, polyurethane resins have frequently been used to improve the mechanical behaviour of soils and to recover foundation settlements after subsidence. Such resins are characterized by the ability to swell when they are exposed to water. As a consequence, in the presence of a confinement, such as that which occurs after injection in the subsoil, the expansive capacity of the resin produces the compaction of the surrounding soil or the propagation of a fracture. In order to supply design tools for this type of intervention, the physico-chemical properties of polyurethane resins are described and the injection modalities, for different types of soil, are illustrated, through basic experimental tests. A simple theoretical approach, which is based on the cavity expansion model in an elastic-plastic medium, is presented in the case of a coarse-grained soil, in order to predict the volume increase of the treated bulb after the injection of the polyurethane resin, when equilibrium is reached with the surrounding soil. Finally, a calculation example is provided, aiming at illustrating the results that can be obtained from the application of this theoretical approach.

Keywords: soil consolidation, settlement remediation, cavity expansion theory, analytical solution

INTRODUCTION

Until the end of the eighties, soil consolidation and reinforcement systems were conceived and developed on the basis of the advancements that had been made to the stream of knowledge pertaining to the mechanical, hydraulic and physical/chemical behaviour of soils. After this period, a basically technological development prevailed, in which the most important progresses emerged in terms of the depth and distance that could be reached by probes, of productivity and of the control of the equipment. In recent years, studies and in-depth investigations have again become fashionable due to the changed economic context, as well as to the necessity of reducing the environmental impact and of conserving the original stability and functionality of the structures which interact with the soil.

According to various authors, soil consolidation treatments with expansive resins seem to fit well into this new tendency, as they are not very invasive and have shown great flexibility, low energy consumption and extremely reduced environmental impacts, in particular as far as the executive phase is concerned. On the other hand, the design of this type of intervention, but also of almost all the other soil consolidation and reinforcement typologies based on the injection of fluids into the subsoil, has till now always simply referred to purely empirical approaches that are able to offer rough estimates, at a basically qualitative level, and which need to be further validated through test campaigns prior the realization and continuous monitoring during all the executive phases. In light of all the aforementioned considerations, the present paper has the aim of simply attempting to draw up an overview of a suitable theoretical approach, able to model the interaction between the injected bulb and the surrounding soil in light of the basic principles of the mechanics of porous media.

PHYSICAL AND CHEMICAL PROPERTIES OF POLYURETHANE RESINS

Urethane and polyurethane polymers are part of a vast family of polymers that can be characterized by various physical properties, including the capacity to expand (i.e. to swell). Expanding polyurethane resins are produced from the exothermic reaction that occurs between a polyol and an isocyanate, which are mixed in volumetric proportions that are established according to the particular production

© 2018 Deep Foundations Institute

needs. During the reaction, a great quantity of carbon dioxide is generated, and this determines the volumetric expansion of the mixture and the formation of a spongy structure within which gas bubbles are trapped. In a very short period of time (from some seconds to some minutes), the mixture hardens, passing from a liquid state to a solid one. The confining pressure, exerted by the surrounding soil on the resin during swelling, as well as the final density of the resin depend on the gas production rate before hardening.

Numerous laboratory tests have been conducted on the GeoPlus® resin utilized by Uretek, in order to determine its main physical and mechanical properties (Favaretti et al. 2004). The relationship between the swelling pressure and the density of the resin (or specific weight) has in particular been studied under oedometric conditions, by use of a specific apparatus that allows the resin to be inserted into a rigid cylindrical mould, equipped with a piston. Immediately after being injected, the resin starts to expand, and, because of the elevated stiffness of the testing apparatus, the swelling phenomenon can only take place in the vertical direction. The mixture is allowed to swell freely over a few centimetres, and the piston is then blocked by a transversal contrast equipped with a manometer.

The swelling pressure has been determined as the pressure the transversal contrast has to apply in order to prevent the piston from moving upward. The following empirical relationship between the swelling pressure and the density of the resin has been obtained by fitting the experimental results:

$$P = \exp\left[0.23 \cdot \left(\gamma_{rf} - 0.36\right)\right] - 1 \qquad [1]$$

where:

P = the swelling pressure, determined under oedometric conditions (expressed in MPa);
γ_{rf} = the weight per unit volume (or specific weight) of the expanded resin (expressed in kN/m^3).

During the conducted tests, swelling pressure values between 0.40 and 10.00 MPa were measured in the investigated density range (γ_{rf} = 2.00÷10.00 kN/m^3). Moreover, Buzzi et al. (2008) have found a specific weight γ_{rf} = 0.36 kN/m^3 under free swelling conditions of the resin, that is, without applying any confining pressure. The empirical relationship, Eq. 1, was obtained by minimizing the approximation error of the data provided by Favaretti et al. (2004) and by imposing γ_{rf} = 0.36 kN/m^3 for P = 0 MPa.

Starting from Eq. 1, it is possible to determine the relationship between the expanded volume of the resin (final volume of the resin, V_{rf}) and the initial volume of the mixture injected into the soil in a liquid state (initial volume of the resin, V_{ri}). In fact, since the resin mass basically remains unchanged when it passes from the liquid state to the final expanded solid state, the swelling ratio, defined as V_{rf} / V_{ri}, can be expressed in the following way:

$$\frac{V_{rf}}{V_{ri}} = \frac{\gamma_{ri}}{\gamma_{rf}} = \frac{10.5}{0.36 + \frac{1}{0.23} \cdot \ln\left[1+P(MPa)\right]} \qquad [2]$$

where:

γ_{ri} = 10.5 kN/m^3 = the specific weight of the resin at a liquid state.

The ratio between V_{rf} and V_{ri}, obtained through this procedure, is shown in Fig. 1. Whenever the polymerization reaction takes place in an unconfined environment (i.e. in the open air), the resin solidifies with a specific weight equal to 0.36 kN/m^3 and with a volumetric expansion degree equal to about 30 (Dei Svaldi et al. 2005). The relationship reported in Fig. 1 takes on a particularly important role in the evaluation of the injection of resins into the soil (Foti and Manassero 2009).

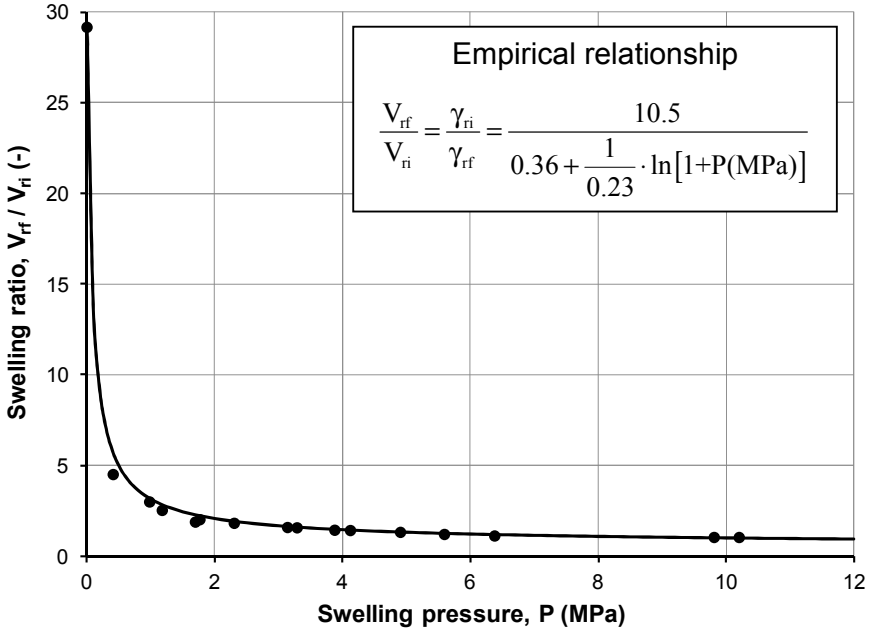


Fig. 1. Experimental relationship between the swelling ratio and the swelling pressure for the GeoPlus® resin.

INJECTION OF POLYURETHANE RESISNS IN SOILS

Injections of expanding polyurethane resins are used above all for improving the mechanical properties of soils and for recovering the absolute and/or differential settlements of surface foundations. The theoretical approach adopted in the design of such interventions depends on the grain size distribution of the soils wherein the consolidation treatment has to be carried out.

In the case of coarse-grained soils (medium/large size grained sands and gravels), the hydraulic conductivity is sufficiently high to allow the resin to penetrate the pores, with the consequent formation of a bulb of grouted soil, which expands until it reaches a state of equilibrium with the confining stress generated by the surrounding soil. In the case of fine-grained soils (fine sands, silts and clays), the resin is not able to penetrate the pores, and its expansion determines the formation of fractures, whose direction depends above all on the homogeneity and isotropy of the soil and on the initial stress state. The resin propagates into the fractures, thus determining variations in the soil density state and significant displacements of the surrounding soil.

The drainage conditions, which also depend on the grain size of the treated soil, are very important for the analysis of the effects produced by the injection of polyurethane resins. Drained conditions are assumed in coarse-grained soils, since the dissipation of the interstitial overpressures generated by the expansion of the injected bulb is very quick. Instead, in fine-grained soils, the expansion of the resin takes place in undrained conditions, with the development of interstitial overpressures, which dissipate over an appreciable period of time. In this case, it results that variations in the effective stress state occur over time, and this can lead to the necessity of further injections later on to obtain the pre-established consolidation objectives. As it is very difficult to evaluate the interstitial overpressures caused by the expansion of the resin, resort is usually made to a total stress analysis, in which the soil is assimilated to a mono-phase medium characterized by a Tresca strength criterion (purely cohesive material). In this way, it is possible to estimate the effects of the injection in the short term, in terms of variations in the total stress state and in terms of displacements induced within the soil.

Influence of soil grain size

Expanding polyurethane resins show different behaviours depending on the grain size distribution of the soil into which they are injected. In order to evaluate the different behaviours, even from just a visual point of view, a series of point injection tests has been conducted on a fine-grained soil (a compacted clay) sample and on a coarse-grained soil (a dry, gravity deposited sand) sample, utilizing cylindrical steel moulds characterised by a diameter of 27.5 cm and a height of 50 cm. During the preparation of the samples inside the moulds, the upper surface of the soil was levelled to a height just below the top of the mould, leaving a free volume at the top corresponding to a gap in height of about 3 cm. This procedure was adopted in order to avoid excessively high pressures being reached inside the mould, once the top had been closed, taking into account the swelling ability of the resin. A quantity of 4 kg of GeoPlus® resin was injected into each mould to a depth of about 15 cm from the upper cover of the mould. The injection was performed in different stages, each of which lasted between 2 and 4 seconds, with a pause in between of 2 seconds.

During the resin injection inside the compacted clay, the expulsion of water was observed from the bottom of the mould, thus demonstrating that the expansion of the resin determines the development of interstitial overpressures in the compacted soil. Once the injection phase had been completed, the upper cover of the mould was removed and a cap of resin was observed in the gap left free during the preparation phase of the sample. Instead, when the lower cover was removed, a fracture in the soil was observed, inside which the resin had propagated, as can be seen in Fig. 2a. Subsequently, on removal of the soil from the mould, two main fractures were observed (Fig. 2b), starting from the point of injection, inside which the resin had propagated along the entire available height, and had in part reached the lateral walls, until it partially took on the form of the mould, as can be seen in Fig. 2c.

A very different result was obtained from the test on the injection of the sand sample. Neither fractures nor the presence of resin at the bottom were observed on removal of the lower cover. After proceeding once again with the removal of the soil, a bulb shaped mass of resin was found, starting from a certain depth (Fig. 3a). The subsequent removal of the sand made it possible to remove the bulb shaped mass (Fig. 3b), which terminated in a plug made up solely of resin. The bulb was about 30 cm long (while the length of the mould was 50 cm). The bulb shaped mass was then sectioned using a circular saw, in order to enable the observation of the internal composition. A photograph of the bulb that had been cut along a transversal section close to the injection point is shown in Fig. 3c, from which it can clearly be seen that the resin has penetrated between the sand grains and has formed a mass. Therefore, on the basis of this evidence, it is possible to deduce that a very rapid penetration process of the resin occurs among the grains of coarse-grained soils, and this determines the formation of a bulb, which, during solidification, increases its volume and compacts the surrounding soil.



Fig. 2. Injection of the polyurethane resin into the compacted clay sample: (a) traces of two main fractures propagating to the very edge of the mould; (b) solidified resin inside the fractures propagating in the clayey soil; (c) removal of the resin from the mould.

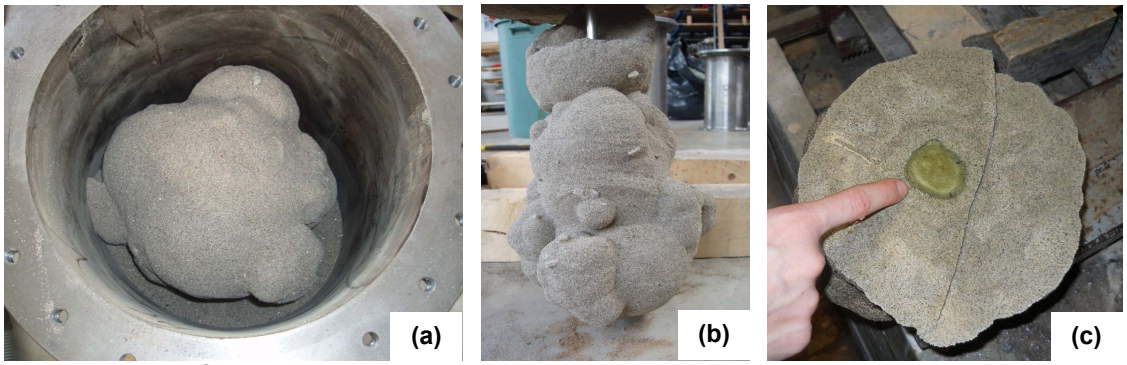


Fig. 3. Injection of the polyurethane resin into the sand sample: (a) bulb shaped resin mass; (b) treated soil after removal from the mould; (c) transversal section of the bulb shaped mass, cut close to the injection point.

The different behaviour of the resin versus the different grain size distribution of the two soil samples would seem to suggest that the development of a theoretical approach, suitable for modelling the compaction obtained after expansion of the resin, should consider the properties of the soil wherein the injection takes place. Specifically, in the case of sands and gravels, the formation of the bulb seems to result from the penetration of the resin in liquid state into the soil pores, which is followed by an expansion phase as the resin solidifies. Therefore, the modelling of the volume increase of the bulb can be carried out referring to the study of the expansion of a cavity (spherical or cylindrical) inside an elastic-plastic medium.

THEORETICAL MODELS FOR COARSE-GRAINED SOILS

The behaviour and propagation of expanding polyurethane resins in coarse-grained soils (medium/coarse sands and gravels) can be based on the theory of the expanding cavity in elastic-plastic media. It should be pointed out that all the reported correlations have been obtained with reference to analyses performed in drained conditions. Accordingly, the related stress components defined in the following paragraphs should be regarded as effective stresses.

Initial permeation

Owing to the elevated permeability of these soils, an initial significant effect of permeation is encountered during the injection phase, which depends on the viscosity of the resin and on the number and dimensions of the pores in the soil. In particular, on the basis of Darcy's law and of the mass balance of the fluid phase, the following equations can be obtained for the initial radius of the bulb, a_0 [m], which can be used for the case of injection from a spherical source (Eq. 3) and from a cylindrical source (Eq. 4), respectively:

$$a_0 = \sqrt[3]{\frac{3 \cdot a_f \cdot k_r \cdot \Delta H \cdot t}{n} + a_f^3} = \sqrt[3]{\frac{3 \cdot a_f \cdot K \cdot p_i \cdot t}{n \cdot m_r} + a_f^3} \quad [3]$$

$$a_0 = \sqrt{\frac{2 \cdot k_r \cdot \Delta H \cdot t}{n \cdot \ln\left(\frac{a_0}{a_f}\right)} + a_f^2} = \sqrt{\frac{2 \cdot K \cdot p_i \cdot t}{n \cdot \mu_r \cdot \ln\left(\frac{a_0}{a_f}\right)} + a_f^2} \quad [4]$$

where:

k_r = the hydraulic conductivity coefficient of the soil to the resin [m/s];
ΔH = the differential hydraulic head generated by the injection pressure, p_i [m];
n = the soil porosity [-];
$p_i = \gamma_{ri} \Delta H$ = the injection pressure of the resin [Pa];

K = the intrinsic permeability of the soil [m^2];
μ_r = the dynamic viscosity of the resin [Pa·s] (Vinson and Mitchell 1972);
a_f = the radius of the injection hole [m];
t = the reaction time of the resin [s].

Equilibrium pressure

During the injection phase of coarse-grained soils, the polyurethane resin is able to penetrate the soil pores in a liquid state, forming a bulb of treated soil, whose shape depends on the injection modality. In the case of point injection, the bulb takes on a spherical shape, while the bulb takes on a cylindrical shape for a columnar treatment. In the subsequent solidification phase, the resin, and consequently the bulb of treated soil, expands until it reaches a state of equilibrium with the surrounding soil. The swelling pressure of the resin decreases as the radial deformation of the bulb increases, while the radial confining stress of the surrounding soil increases. The expansion process stops when an equilibrium state, in which the swelling pressure of the resin is equal to the confining radial stress of the soil, is reached. In order to determine the confining stress generated in the soil at equilibrium, it is possible to refer to the theory of the expanding cavity in an elastic-plastic medium, which Yu and Houlsby (1991) have dealt with. In their study the theoretical developments, set up to take into consideration the large deformations determined in the plasticized soil area, are reported.

The behaviour of a coarse-grained soil, close to the peak strength conditions, can be simulated referring to a frictional and cohesive material showing a Mohr-Coulomb yield criterion. By indicating the yield function with f, the radial stress with σ_r, the tangential stress with σ_θ, the soil friction angle with φ and the soil cohesion with c', the strength criterion can be expressed in the following way:

$$f = \sigma_r - N \cdot \sigma_\theta - Y = 0 \qquad [5]$$

where:

$$N = \frac{1 + \operatorname{sen}\varphi}{1 - \operatorname{sen}\varphi} \qquad [6]$$

$$Y = \frac{2 \cdot c' \cdot \cos\varphi}{1 - \operatorname{sen}\varphi} . \qquad [7]$$

The behaviour of a coarse-grained soil, at the critical state, can be simply simulated by assuming a Mohr-Coulomb strength criterion for a purely friction-type material, that is, by setting Y=0 in Eq. 5. Moreover, the following geotechnical parameters were adopted:

- Young's modulus, E', and the Poisson coefficient, ν, for the characterization of the elastic behaviour of the soil;
- dilatancy angle, ψ, for relating peak and critical state strength.

In order to obtain the relationship between the dimensionless swelling ratio, V_{rf} / V_{ri}, as defined in Eq. 2, and the confining stress generated in the soil, it is first necessary to determine the radius of the cavity, a, under the action of the generic internal pressure, P. The confining pressure on the cavity wall is made equal to P, in order to guarantee equilibrium. The radius of the cavity can be determined through the following equation:

$$a = \begin{cases} a_0 & P \le P_0 \\ a_0 + \dfrac{(P - P_0) \cdot a_0}{2 \cdot m \cdot G} & P_0 < P \le P_1 \\ a_0 \cdot R_a & P > P_1 \end{cases} \qquad [8]$$

where:

a_0 = the initial radius of the cavity, that is, the bulb of treated soil;
P_0 = the initial pressure at the cavity wall, assumed equal to the horizontal geostatic stress in the case of a cylindrical cavity and equal to the mean geostatic stress in the case of a spherical cavity;
P_1 = the first plasticization pressure at the cavity wall, which can be evaluated through the following expression:

$$P_1 = \frac{m \cdot \left[Y + (N-1) \cdot P_0 \right]}{m+N} + P_0 ; \qquad [9]$$

m = the geometrical coefficient, which should be assumed equal to 1 in the case of a cylindrical cavity and equal to 2 in the case of a spherical cavity;
G = the shear modulus, which can be evaluated as $G = \frac{E'}{2 \cdot (1+\nu)}$;
R_a = the ratio of the radius of the cavity, a, at a generic pressure $P > P_1$ to the initial radius of the cavity, a_0.

The R_a parameter can be determined by referring to either the solution by Carter et al. (1986), which is based on the hypothesis of small deformations, or the Yu and Houlsby (1991) solution, which is based on the hypothesis of large deformations in the plastic zone (whose extent is given by the plastic radius, b) and small deformations in the more external elastic zone. When the hypothesis of small deformations is adopted, R_a can be determined in the following way:

$$R_a = 1 + \left[\delta + \frac{N \cdot M \cdot \xi}{m \cdot (N+M) + N \cdot M \cdot (1-m)} - \frac{M \cdot \ln(\eta)}{M+m} \right] \cdot \left(\frac{b}{a_0} \right)^{1+\frac{m}{M}} + \frac{M \cdot \ln(\eta)}{M+m} - \frac{N \cdot M \cdot \xi}{m \cdot (N+M) + N \cdot M \cdot (1-m)} \cdot \left(\frac{b}{a_0} \right)^{\frac{m \cdot (N-1)}{N}} \qquad [10]$$

where:

$$\frac{b}{a_0} = R^{\frac{N}{(N-1)m}} \qquad [11]$$

$$R = \frac{(m+N) \cdot \left[Y + (N-1) \cdot P \right]}{N \cdot (1+m) \cdot \left[Y + (N-1) \cdot P_0 \right]} \qquad [12]$$

$$\delta = \frac{Y + (N-1) \cdot P_0}{2 \cdot (m+N) \cdot G} \qquad [13]$$

$$\xi = \frac{\left[1 - \nu^2 \cdot (2-m) \right] \cdot (1+m) \cdot \delta}{(1+\nu) \cdot (N-1) \cdot M} \times \left[N \cdot M + m \cdot (1-2 \cdot \nu) + 2 \cdot \nu - \frac{m \cdot \nu \cdot (N+M)}{1 - \nu \cdot (2-m)} \right] \qquad [14]$$

$$\eta = \exp\left\{ \frac{(M+m) \cdot (1-2 \cdot \nu) \cdot \left[Y + (N-1) \cdot P_0 \right] \cdot \left[1 + (2-m) \cdot \nu \right]}{E' \cdot (N-1) \cdot M} \right\} \qquad [15]$$

$$M = \frac{1+\operatorname{sen}\psi}{1-\operatorname{sen}\psi} . \qquad [16]$$

Under the hypothesis of large deformations in the plastic zone, the evaluation of R_a is more complex and requires the evaluation of an integral that cannot be solved in closed form. Yu and Houlsby (1991) supplied an approximate solution in the following form:

$$R_a = \left\{ \frac{R^{-\frac{N\cdot(M+m)}{m\cdot(N-1)\cdot M}}}{(1-\delta)^{\frac{(M+m)}{M}} - \frac{N\cdot(M+m)}{\left[m\cdot(N-1)\cdot M\right]\cdot\eta}\cdot\Lambda_1(R,\xi)} \right\}^{\frac{M}{(M+m)}} \qquad [17]$$

in which:

$$\Lambda_1(R,\xi) = \sum_{n=0}^{\infty} A_n^1 \qquad [18]$$

$$A_n^1 = \begin{cases} \dfrac{\xi^n}{n!}\cdot\ln R & \text{if } n = \dfrac{N\cdot(M+m)}{m\cdot(N-1)\cdot M} \\ \dfrac{\xi^n}{n!\cdot\left(n - \dfrac{N\cdot(M+m)}{m\cdot(N-1)\cdot M}\right)}\cdot\left[R^{n-\frac{N\cdot(M+m)}{m\cdot(N-1)\cdot M}} - 1\right] & \text{if } n \neq \dfrac{N\cdot(M+m)}{m\cdot(N-1)\cdot M} \end{cases} . \qquad [19]$$

Starting from the radius of the cavity, a, it is possible to determine the final volume of the bulb, V_{bf}:

$$V_{bf} = \begin{cases} \pi\cdot a^2\cdot H & \text{cylindrical cavity} \\ \dfrac{4}{3}\cdot\pi\cdot a^3 & \text{spherical cavity} \end{cases} \qquad [20]$$

where H represents the height of the cylindrical cavity, which is equal to the height of the section of column into which the resin is injected.

Once the initial volume of the bulb is known, which is given by

$$V_{bi} = \begin{cases} \pi\cdot a_0^2\cdot H & \text{cylindrical cavity} \\ \dfrac{4}{3}\cdot\pi\cdot a_0^3 & \text{spherical cavity} \end{cases} , \qquad [21]$$

it is possible to determine the variation in volume that the bulb undergoes, in function of pressure, P:

$$\Delta V_b = V_{bf} - V_{bi} . \qquad [22]$$

Assuming that the variation in volume of the bulb is only due to the expansion in volume of the resin, it is possible to obtain the final volume of the resin, V_{rf}, through the following relationship:

$$V_{rf} = V_{ri} + \Delta V_b . \qquad [23]$$

Once the volume of the injected resin is known, it is possible to determine the relationship between the V_{rf} / V_{ri} ratio and the confining stress that is generated at the cavity wall, which has to be balanced by the swelling pressure of the resin bulb in order to satisfy the equilibrium condition.

As a calculation example, the case of a dry sand, to which the following geotechnical parameters are assigned, is reported:

- specific weight of the soil, $\gamma_t = 19$ kN/m^3;
- Young's elastic modulus, E' = 30 MPa;
- Poisson coefficient, $\nu = 0.25$;
- intercepted cohesion, c' = 0 kPa;
- peak friction angle, $\varphi_P = 32°$;
- friction angle at the critical state, $\varphi_{CV} = 32°$;
- dilatancy angle, $\psi = 0°$;
- over-consolidation ratio, OCR = 1.

Let us design an injection of expanding polyurethane resin, at a depth of 3.5 m; it is assumed that an overload q = 10 kPa is present at the ground level. Moreover, it is hypothesized that the resin expands as a cylindrical cavity (therefore m = 1), with a height H = 3 m; an initial radius of the bulb, $a_0 = 0.1$ m, is assumed. The initial volume of resin, V_{ri}, is equal to 0.019 m^3 (which corresponds to an injected mass of about 20 kg, for a soil porosity n = 0.3). The rheological law of the resin and the relationship between the V_{rf} / V_{ri} ratio and the confining stress that is generated in the soil, calculated on the basis of the cavity expansion theory, under the hypothesis of both small and large deformations in the plastic zone, are reported in Fig. 4.

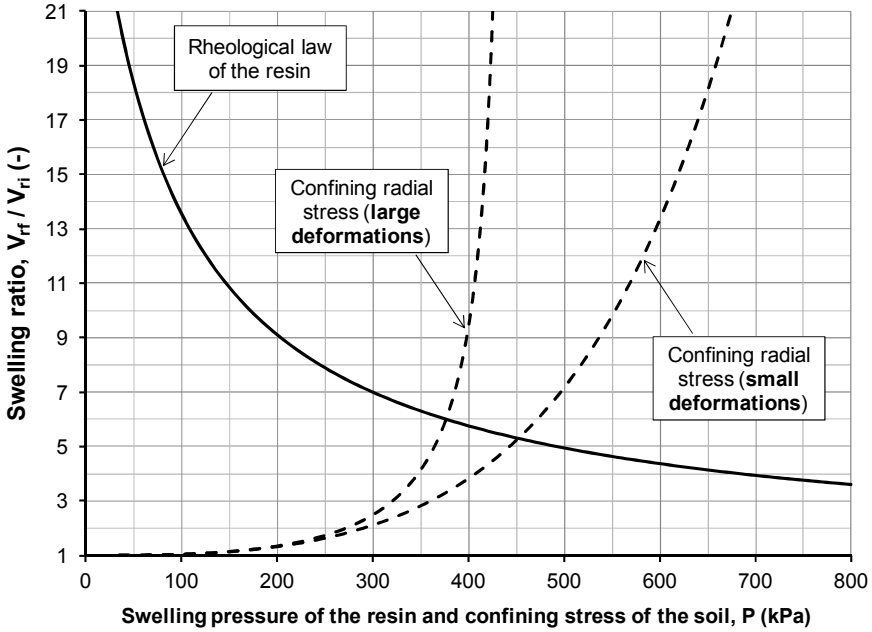


Fig. 4. Swelling ratio versus the swelling pressure of the resin and the soil confining stress, under the hypothesis of both small and large deformations.

As can be observed in Fig. 4, the swelling pressure appears very high in correspondence to values of the V_{rf} / V_{ri} ratio just above 1, while the confining stress is close to the horizontal geostatic stress, thus determining a non-equilibrated condition that induces a further deformation of the bulb, with a consequent increase in the V_{rf} / V_{ri} ratio. The equilibrium is reached when the swelling pressure of the resin equals the confining stress exerted by the soil surrounding the bulb: the latter condition can be graphically identified with the intersection point between the two curves and, therefore, the corresponding pressure value represents the final equilibrium value. The intersection point of the two curves is obtained in correspondence to an equilibrium pressure, $P \cong 450$ kPa, to which, in the case of small deformations, a V_{rf} / V_{ri} ratio $\cong 5.3$ is related. In the case of large deformations, $P \cong 375$ kPa is obtained in the plastic zone, to which a V_{rf} / V_{ri} ratio $\cong 6$ corresponds. It can be observed that when the hypothesis of small deformations in the plastic zone is introduced into the analysis, basically the equilibrium pressure is over-estimated and the swelling ratio is under-estimated.

CONCLUSIONS

Interventions with expansive polyurethane resins are increasingly used in the engineering practice to recover the settlements of surface foundations, as well as to improve the mechanical properties of soils. Since the design of such soil treatments is mainly based on purely empirical approaches, an attempt has been made in order to develop a theoretical model, suitable for analysing the interaction of the injected resin with the surrounding soil. After a brief overview of the different behaviours that polyurethane resins may show, depending on the grain size distribution of the soil into which they are injected, analytical solutions have been presented in the case of coarse-grained soils, by applying the cavity expansion theory for an elastic-plastic medium. The equilibrium pressure is obtained from the intersection of the cavity expansion curve and the rheological law of the expanding resin. Through a calculation example, the error associated with the hypothesis of small deformations has been highlighted, with respect to the formulation that accommodates large deformations in the plasticized soil area. In particular, the equilibrium pressure at the cavity wall results to be over-estimated by about 20%, whereas the swelling ratio is under-estimated by about 12%. Finally, it is worth noting that the proposed theoretical model can be further developed in order to evaluate the variations in the stress state, which are induced in the soil surrounding the injected bulb, and the volumetric strain within the plastic zone.

ACKNOWLEDGMENTS

The authors would like to express their gratitude to Uretek Italia S.p.A. for providing financial support in this study.

REFERENCES

Buzzi, O., Fityus, S., Sasaki, Y., and Sloan, S.W., 2008. Structures and properties of expanding polyurethane foam in the context of foundation remediation in expansive soil. Mechanics of Materials, 40(12) 1012-1021.

Carter, J.P., Booker, J.R., and Yeung, S.K., 1986. Cavity expansion in cohesive frictional soils. Géotechnique, 36(3) 349-358.

Dei Svaldi, A., Favaretti, M., Pasquetto, A., and Vinco, G., 2005. Analytical modelling of the soil improvement by injections of high expansion pressure resin. Proceedings of the 6th International Conference on Ground Improvement Techniques, Coimbra, July 18-19, pp. 577-584.

Favaretti, M., Germanino, G., Pasquetto, A., and Vinco, G., 2004. Interventi di consolidamento dei terreni di fondazione di una torre campanaria con iniezioni di resina ad alta pressione d'espansione. Atti del XXII Convegno Nazionale di Geotecnica, Palermo, September 22-24, pp. 357-364.

Foti, S., and Manassero, M., 2009. Rinforzo e adeguamento delle fondazioni per sollecitazioni statiche e dinamiche. Atti della XXII Edizione delle Conferenze di Geotecnica di Torino, Torino, November 18-19, 52 p.

Vinson, T.S., and Mitchell, J.K., 1972. Polyurethane foamed plastics in soil grouting. Journal of the Soil Mechanics and Foundations Division, 98(SM6) 579-602.

Yu, H.S., and Houlsby, G.T., 1991. Finite cavity expansion in dilatant soils: loading analysis. Géotechnique, 41(2) 173-183.

Challenges in the design of jet grouted structures

Alessandro Flora, Giuseppe Modoni**, Stefania Lirer***, Valeria Nappa**

* University of Napoli Federico II, Italy
** University of Cassino and of Southern Lazio, Italy
*** University Guglielmo Marconi, Rome, Italy

Abstract

The authors have worked on the design and control of jet grouted structures for years, collecting a relevant amount of experimental data and characterizing the variability of the properties of the single columns with probabilistic models. In time, they have proposed deterministic, semi-probabilistic or probabilistic methods to include the observed and unavoidable randomness of columns properties in the design of jet grouted structures. Starting from the gained mass of information and experience, this paper sorts out the main issues for the design of two of the most relevant examples of jet grouted structures: massive jet grouted bottom plugs and foundation reinforcement with isolated columns. Design considerations will be drawn considering the characteristics of jet grouting within the framework of EC7, discussing pros and cons of the use probabilistic and determinist approaches.

1 Introduction

Jet grouting is a powerful ground improvement technology, that provides solution to a wide variety of geotechnical problems. Direct observations (e.g. Croce and Flora, 2000, Croce and Modoni, 2007; Modoni and Bzowka, 2013) have proven that the geometrical and mechanical properties of columns are variable, usually much more than for other traditional reinforcement technologies, being ruled by the interaction during execution of the jet with the natural soil. The jet grouting columns are far from being perfectly cylindrical and homogeneous treated bodies, and their axes may randomly deviate from the assigned position. Therefore, whatever the considered technology (single, double or triple fluid jet grouting), the most relevant issues are by far the ability to predict and control the properties of the single column and their scatter, as well as the need to take such a scatter into account at the design stage. The design procedure used to this aim differs from country to country. Eurocodes have introduced in Europe the *partial factors design* approach, which is essentially a deterministic (of semi-probabilistic origins) approach, that for *Ultimate Limit States* failure checks imposes:

$$\gamma_R \cdot R_d\left(\frac{M_{i_k}}{\gamma_{Mi}}\right) \geq \sum_i \gamma_{ai} \cdot E_i \qquad (1)$$

where $\gamma_R \leq 1$ is the global reducing factor to be applied to the design resistance R_d, computed as a function of the *characteristic* parameters (e.g. the material strength parameters M_{i_k}), each factored with reducing partial coefficients ($\gamma_{Mi} \leq 1$). The factored material strength parameters are called the design parameters ($M_{i_d}=M_{i_k}/\gamma_{Mi}$).The effects of nominal loads E_i (dead, live etc.) are also multiplied by partial factors γ_{ai} ($\gamma_{ai} \leq 1$ for favourable loads and $\gamma_{ai} \geq 1$ for unfavourable loads). The overall combination of parameters depends on the specific mechanism under consideration, and on the kind of approach adopted (generally named "geotechnical" when scaling down the material strength parameters without modifying the effects of nominal loads, and "structural" when

© 2018 Deep Foundations Institute

introducing partial factors on the latter without modifying M_{i_k}). With this approach, Mi_k can be associated with an acceptable probability of failure computed with probabilistic models as follows:

$$M_k = M_{pf} = M_m \cdot \left(1 - \omega \cdot CV(M)\right) \quad (2)$$

where Mm and CV(M) are respectively the mean value and the coefficient of variation of the considered strength variable, and ω is a parameter whose value depends on the tolerated probability for the property to have a lower value (for a risk level of 5% and a sufficiently large number of data, ω=1.645). Alternatively, Mk can be derived from previous experiences or from literature. The values of the partial factors γM should take into account the reliability of the estimate of Mk (being higher for characteristic values assumed from experience or literature, and lower for values calculated on the basis of experimentation and probabilistic distributions).
With this semiprobabilistic approach, if a geometrical variability is expected (and this is certainly the case for both the diameter D and the deviation from the ideal position of a jet grouted column), EC7 allows to design modifying the characteristic value of the generic geometric variable "a" in a conservative way as follows:

$$a_d = a_k \pm \Delta a \quad (3)$$

With reference to jet grouted columns, considering that probabilistic distributions are known for both the diameter and the inclination parameters, consistently with the formal disequation (1) in the following eq. (3) will be expressed as:

$$a_d = \frac{a_k}{\gamma_a} \quad (4)$$

where γ_a (≥1) is a factor accounting for the uncertainty in the calculation of a_k (that can be calculated from a probabilistic distribution or just assigned on the basis of previous knowledge or personal experience). In spite of its relative simplicity, this approach has the main drawback of not allowing a correct perception of the real safety margins, being not always easy to foresee the combined effects of the different variables on the overall risk.
If sufficient information on all the involved random variables and on their probabilistic distributions are known, a fully probabilistic approach may be better suited to design jet grouted structures. With a fully probabilistic approach, in fact, an overall risk is assumed based on the performance of the structure, thus with a much more sound consideration of the real risk. In such a way, eq. (1) does not hold anymore, being not possible to define a characteristic value of the involved random variables. The equilibrium is then granted by using the same disequation, with random values of the variables and without partial factors.
In this paper, the two alternative approaches will be presented and discussed with reference to two completely different applications of jet grouting: jet grouted bottom plugs and vertically loaded single columns.

2 Characteristic properties of jet grouted columns

2.1 Diameter of columns

The first step for the design of any jet grouted structure is the prediction of the diameter of the columns, which depends on jet hydrodynamic properties as well as on the soil resistance to erosion. At the design stage, it is very important to take into account the variation of the diameter of the jet grouted columns with depth, connected to both the increase in soil shear strength and local

variability. It is thus suggested to consider the diameter as a stochastic variable having a probability distribution. An effective design procedure should quantify in the most comprehensive form the size of columns based on accurate predictions of the mean diameter (D_m) and of the scattering around this value. D_m can be either verified through field trials or predicted, for instance with the analytical expression suggested by Flora et al. (2013).
The random variability of diameter can be inferred from the statistical analysis of experimental data obtained from field trials. A Gaussian probability function can be conveniently assumed to simulate this variability and provide typical values of the coefficients of variation CV(D) (Tab. 1) as a function of a qualitative indication of soil heterogeneity.
Once the statistical parameters of the distribution are known, in the semiprobabilistic approach the characteristic value D_k can be calculated assigning a 5% percentile of the normal distribution as follows:

$$D_k = D(5\%) = D_m(1 - 1.645 \cdot CV(D)) \quad (5)$$

Table 1. Typical values of the coefficients of variation CV(D) of the diameter of jet grouted columns, as a function of soil heterogeneity (after Croce et al., 2014)

	Soil Heterogeneity		
	Low	Medium	High
CV(D)	0.02-0.05	0.05-0.10	0.05-0.20

2.2 Deviation of the columns axis

A relevant problem of jet grouted columns is the possible deviation of the axis from its design position, with obvious effects on the performance of those jet grouted structure for which continuity is a fundamental requirement (e.g. bottom plugs, cutoff barriers, provisional lining of tunnels). The magnitude of such a deviation depends on the quality of equipment, on subsoil characteristics and on perforation direction and length. The misalignment of columns can be quantified by an azimuth α anda deviation β angle (Figure 1). In the case of no systematic errors, the angle α is equally probable and characterized by a uniform probabilistic function (i.e. there is no statistical parameter to assign to figure the distribution out), while the deviation β follows a gauss type distribution around the nil value (β= 0) (Croce et al., 2014). According to previous experience (Croce et al., 2014), the standard deviation SD (β) of the inclination may be assumed to range between 0.1° and 0.6°, with the largest values occurring in particularly unfavorable conditions (low-quality equipment, no measurement of drilling inclination and very heterogeneous and/or coarse-grained soils). If a sufficiently large set of measured data is available, in the semiprobabilistic approach the characteristic value of the deviation angle β_k can be computed by fitting the experimental data with a normal probabilistic distribution and by computing the value correspondent to a 5%risk level as:

$$\beta_k = 1.645 \cdot SD(\beta) \quad (6)$$

2.3 Mechanical properties of the jet grouted material

The mechanical properties of jet-grouted material depend on characteristic of the grout, original soil composition, environmental factors and treatment system (Terashi et al. 1997). In addition, it must

be expected that these properties vary from point to point. Therefore, experimental results obtained from small cored samples cannot be considered representative of larger jet grouted elements.

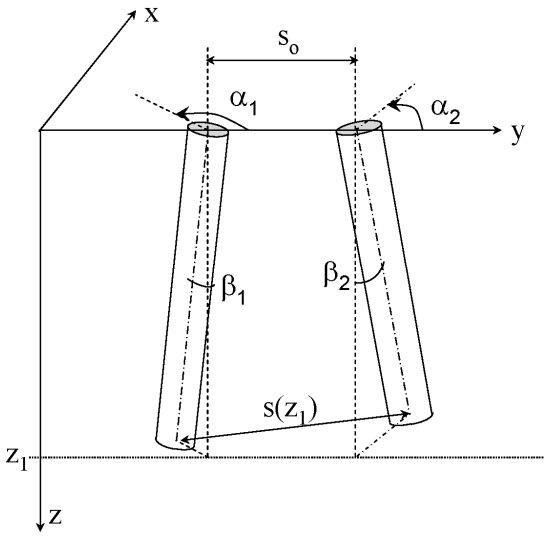


Figure 1. Deviation of the column axis from verticality: inclination β and azimuth α angles.

In most of the usual jet grouting applications, a linear elastic-perfectly plastic model is sufficient to represent its mechanical behaviour. Since the shear strength of jet grouted material is usually analysed via its unconfined compressive strength $q_{u,jg}$, for the sake of simplicity Modoni et al. (2016) suggest to assume that τ is a constant not depending on the confining stress, thus considering an equivalent Tresca failure model. With reference to a linear Mohr-Coulomb failure criterion, this means that:

$$\tau_{max} = c'_{jg} = \frac{q_{u,jg}}{2 \cdot \tan\left(\frac{\pi}{4} + \frac{\varphi' jg}{2}\right)} = \delta \cdot q_{u,jg} \tag{7}$$

In which c'_{jg} and φ'_{jg} are respectively the cohesion and shear strength angle of the jet grouted material, and δ the parameter summarizing the effect of φ'_{jg} on the proportionality between the assumed shear strength and the unconfined compressive strength. Toraldo et al. (2017) report experimental values of φ'_{jg} included in a wide range ($25° \leq \varphi'_{jg} \leq 58°$), with most of them in the range $25° \leq \varphi'_{jg} \leq 45°$ (which implies that $0{,}32 \geq \delta \geq 0{,}21$). Even though the lower values are usually related to fine grained soils and the higher ones to coarse soils, this is not a general rule, being the value of φ'_{jg} not necessarily related to that of the untreated soil. The variability of δ introduces an additional uncertainty in the calculation of shear strength, which is however related to a lack of knowledge and not to the possible randomness of the shear strength angle, which is taken into account in the quantification of $q_{u,jg}$. As well known (Croce et al., 2014), $q_{u,jg}$ has a lognormal distribution. Assuming that the characteristic value $q_{u,jg,,k}$ is the value corresponding to a 5% risk of being higher than the experimental value, with the semiprobabilistic approach it can be expressed as:

$$q_{u,jg,k} = q_{u,jg}(5\%) = exp\left\{\ln\left(q_{u,jg,m}\right) - 0{,}5 \cdot ln\left[1 + \left(CV(q_{u,jg})^2\right] - 1.645 \cdot \sqrt{ln\left[1 + \left(CV(q_{u,jg})\right)^2\right]}\right\} \tag{8}$$

The mean value $q_{u,jg,m}$ does not depend on the area to which it refers (i.e. the value $q_{u,jg,m}$ calculated using the experimental data obtained on small specimens reliably represents that related to larger jet grouted elements, like columns or even plugs for instance). This is not the case for $CV(q_{u,jg})$, which is size dependent. The large variability observed in laboratory (Tab. 2) cannot be used to determine the mechanical properties of larger element, in which interaction between weaker and stronger portions might play some role and reduce variability. For instance, increasing the size of the sample there is a progressive tendency to reduce skewness, as the strength of the smallest samples is scattered with an asymmetric statistical distribution, while the distributions for the larger samples become progressively more symmetrical, asymptotically tending to the normal distribution.

Table 2.Experimental variability of the compressive strength qu of the jet grouted material at the lab scale (after Toraldo et al., 2017).

No.	Soil type	Number of data	Mean: MPa	Standard deviation: MPa	Variation coefficient	Skewness	Kolmogorov–Smirnov goodness-of-fit tests*	Reference
a	Cohesive soil	342	2·8	1·35	0·48	0·55	0077 (0·074)	Shibazaki *et al.* (1996)
b	Clay soil	55	2·14	1·33	0·75	0·49	0·090 (0·183)	Nikbakhtan & Osanloo (2009)
c	Sandy soil	298	12·75	5·55	0·44	0·84	0·084 (0·082)	Shibazaki *et al.* (1996)
d	Silty sand	26	8·14	3·26	0·40	0·23	0·106 (0·267)	Croce & Flora (1998)
e	Gravel	26	10·49	3·77	0·36	0·90	0·051 (0·267)	Croce *et al.* (1994)
f	Gravel	71	13·06	6·14	0·47	0·58	0·110 (0·161)	Mongiovì *et al.* (1991)

*The values within brackets represent acceptance values with 0·05 significance level.

Considering the very large coefficients of variation $CV(q_{u,jg})$ shown by laboratory tests (see for instance Croce et al., 2014) and neglecting this size dependence of the coefficient of variation would be too conservative in design. In particular, $CV(q_{u,jg})$ reduces as the area increases (i.e. for the entire column it is lower than the one calculated from laboratory tests on small specimens). Toraldo et al. (2017) propose to calculate $CV(q_{u,jg})$ of the structure as:

$$CV(q_{u,jg})_{structure} = \lambda \cdot CV(q_{u,jg})_{specimen} \quad (9)$$

whre λ is a reduction factor depending on the geometrical properties of the element to which it refers (see Toraldo et al., 2017 for the details). For typical geometrical characteristics of jet grouted plugs, $0{,}4 \leq \lambda \leq 0{,}55$, with the lower values pertaining to thicker plugs. For jet grouted isolated columns having diameters not higher than 1.5 m, $\lambda \approx 0{,}7$.

3. Design approaches

3.1 Deterministic approach

With this approach, partial factors have to be introduced to pass from the characteristic to the design values of all the random variables. As discussed in §2, therefore, values of the coefficients γ_D, γ_β, $\gamma_{qu,jg}$ differing from one may have to be assigned, depending on the considered kind of check ("geotechnical" or "structural"). Tables 3, 4 and 5 suggests values of these factors coming from the authors' personal experience and previous theoretical works (e.g. Croce et al., 2014).

Table 3- Suggested values of the partial factor γ_D.

Application	Derivation of characteristic value D_k	γ_D		
		Low soil heterogeneity	Medium soil heterogeneity	High soil heterogeneity
Isolated columns or thin structures	Literature	1.10	1.15	1.20
	By field trials	1.00	1.00	1.05
Massive treatments	Literature	1.05	1.10	1.20
	By field trials	1.00	1.00	1.05

Table 4.- Suggested values of the partial factor γ_β.

Application	Derivation of characteristic value β_k	γ_β
Isolated columns	Literature	1.05
	Field trials	1.00
Massive treatments or thin structures	Literature	1.10
	Field trials	1.05

Table 5.- Suggested values of the partial factor $\gamma_{qu,jg}$.

Application	Derivation of characteristic value $q_{u,jg,k}$	$\gamma_{qu,jg}$	
		Low soil heterogeneity	Medium/High soil heterogeneity
Isolated columns or thin structures	Literature	2	3
	Field trials	1.5	2
Massive treatments	Literature	2	2.5
	Field trials	1.5	2

3.2 Probabilistic approach

If a statistically meaningful sample of the relevant geometrical and mechanical properties of jet-grouted columns is available, a possible alternative is to model the observed distributions with probabilistic functions and to introduce them in a fully probabilistic analysis of the response of the jet-grouted structure. The Monte Carlo method (Haldar and Mahadevan, 2000, Fenton and Griffiths, 2008) can be used to this aim. With this procedure, a large number of structures is numerically generated, their mechanical or hydraulic performance are quantified with predictive tools and the probability of failure is quantified as the fraction of unsuccessful cases. This approach is only apparently more cumbersome, being nowadays easy to implement it. Since it can be carried out with an explicit reference to a risk level, it does not need the introduction of partial factors.

4. Design of a bottom plug

4.1 General issues

In the case of permeable soils, underwater excavations can be conveniently performed by sealing their bottom with massive horizontal barriers (bottom plugs) made of partially overlapped jet grouted columns (e.g. Flora et al. 2012, Modoni et al., 2016). With regard to the static performance, the design of such structures must be carried out considering the following failure mechanisms (Figure2):

- overall uplift failure (Fig. 2.b.1): the uplift action of the water is not adequately counterbalanced by the sum of the self-weight of the whole structure (plug and retaining structure) and of the shear strength at the interface between the retaining structure and the soil;
- plug uplift failure (Fig. 2.b.2): the failure consists in the vertical translation of the plug because of insufficient self-weight and shear strength at the interface with the retaining structure;
- plug's structural failure (Fig. 2.b.3): the plug is too slender and the failure is due to a bending mechanism, unsuited to the jet grouted material,with zero tensile strength (cracking failure).

In Figure 2.a, $h_p=h_s+h_{jg}$indicates the thickness of the plug, with $h_s$and h_{jg}respectively representing the untreated and jet grouted portions of the plug.

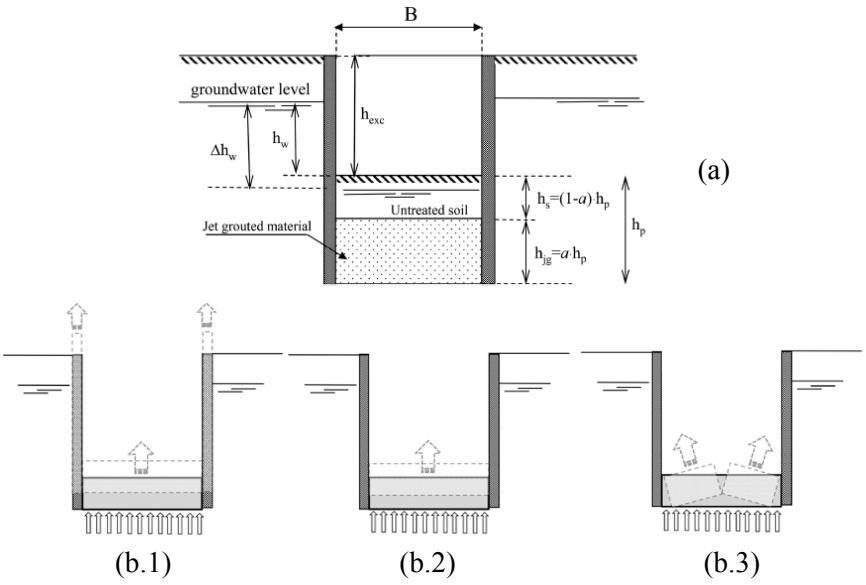


Figure 2. Scheme of the jet grouted bottom plug (a) and possible failure mechanisms of a bottom plug (b.1. uplift of the earth retaining structure and the plug; b.2 uplift of the plug only; b.3 structural collapse of the plug).

Once the thickness of the plug has been assigned on the bases of equilibrium conditions, the design of the plug has to be carried out assigning a value to Dm and then to the spacing s, in such a way that the water inflow is nihil or tolerable. To this aim, the value of hjg has to be verified and eventually increased, if needed for hydraulic reasons. In the following, these design steps are shown and discussed in some detail.

4.2 Height of the plug – deterministic calculation

With reference to typical excavations for which jet grouted plugs are adopted, the overall uplift equilibrium (Fig. 2.b.1) is usually satisfied with large safety margins, and does not need a deeper insight. In this work, some considerations will be done on the uplift of the plug (Fig. 2.b.2) and on the structural failure by cracking propagation (Fig. 2.b.3).
With reference to EC7 indications (eq. 1), whatever the mechanism,the assessment of equilibrium of the plug can be written as:

$$\gamma_R \cdot R_d\left(\frac{M_{i_k}}{\gamma_{Mi}}\right) \geq \gamma_v \cdot V_k - \gamma_G \cdot G_k \qquad (10)$$

V_k being the characteristic value of the destabilising action of the water pressure (pushing the plug upwards), G_k the characteristic value of the stabilising action provided by the structure's self-weight and R_d the design value of the stabilising action (lateral shear resistance of the jet grouted materialat the interface with the retaining structure in the uplift mechanism, or the stabilising moment caused by the uniaxial compressive strength in the structural failure mechanism).
The partial factors γ_R, γ_V and γ_G should stem from considerations on the reliability of the quantification of V_k, G_k and R_d, and on the criticality of the investigated mechanism.
For uplift limit states (UPL), considering V_k and G_k respectively as permanent unfavourable and favourable actions, EC7 imposes γ_V=1 and γ_G=γ_R =0.9. Such values of γ_V and γ_G can be considered well suited for the case of bottom plugs, because water pressure can be known reliably (and considered as a permanent action), and the defects of columns dimensions and position have basically no effect on the weight of the plug, being usually the unit weight of the jet grouted soil very close to that of the untreated soil (with the exception of double fluid system, for which some decrease of the unit weight is observed), and being the overall untreated volume an extremely small portion of the plug.
On the contrary, γ_R should be lower than the suggested value (γ_R=0.9) to take into account that the jet grouted plug has not the same precise lateral dimensions that an equivalent cast concrete structure would have, and thus the calculation of R_d is somehow more uncertain than for traditional concrete structures. The value γ_R=0.8 would be probably better suited. As usual in geotechnical checks, EC7 also imposes partial coefficients γ_{Mi} to the strength parameters for geotechnical checks. In this case, reference will be done to the uniaxial compressive strength of the jet grouted material q_u; values of γ_{qu} suggested by the Authors are reported in Table 5. Such values are higher than the ones indicated by EC7 for the geotechnical shear strength parameters, to take into account the uncertainty in the quantification of δ (eq. 7) and λ (eq. 9).
For structural bending check, which is usually overlooked by practitioners, a structural approach seems better suited. Then, EC7 indicates γ_V=1.35, γ_G=γ_R=γ_{qu}=1.

Uplift check (Fig. 2.b.2)

In this case, the design resistance can be expressed as:

$$R_d = p\int\tau_{max,d}\cdot dz \tag{11}$$

where p is the perimeter of the plug and $\tau_{max,d}$ the characteristic shear strength at the plug-retaining wall interface (whose area is $2\cdot h_{jg}\cdot(B+L)$, being B and L the width and length of the plug). The integral is extended to the thickness of the jet grouted part of the bottom plug ($h_{jg}=\alpha\cdot h_p$, Fig. 9.a), conservatively neglecting the shear contribution of the untreated part. Considering eq. (7), eq. (11) than becomes:

$$R_d = p\cdot\int\frac{\delta\cdot q_{u,jg,k}}{\gamma_{qu,jg}}\cdot dz \tag{12}$$

If $q_{u,jg,k}$ is constant along the height of the plug (reasonable in the case of an homogeneous soil), R_d can be finally written as:

$$R_d = 2\cdot(B+L)\cdot h_{jg}\cdot\delta\cdot\frac{q_{u,jg,k}}{\gamma_{qu,jg}} \tag{13}$$

Which means that R_d depends on a number of geometrical and mechanical parameters as follows:

$$R_d = R_d\left(L, B, h_{jg}, \delta(\varphi), \lambda(h_{jg}), q_{u,jg,m}, CV(q_{u,jg})_{specimen}, \gamma_{qu,jg}\right) \quad (14)$$

In eq. (14) the lack of knowledge may reflect into the uncertainty on the values of h_{jg}, $\delta(\varphi)$, $\lambda(h_{jg})$, and $q_{u,jg,m}$, and the statistical randomness in the values of $CV(q_{u,jg})_{specimen}$.
Considering the symbols adopted in Fig. 2.a, inequality 10 can be considered as an equality and rearranged to calculate the height of the jet grouted part of the plug h_{jg} as follows:

$$h_{jg} = \frac{\gamma_V \cdot (h_w \cdot \gamma_w) + (\gamma_V \cdot \gamma_w - \gamma_G \cdot \gamma_s) \cdot h_s}{\gamma_R \cdot \left(2 \cdot \frac{B+L}{B \cdot L} \cdot \delta \cdot \frac{q_{u,jg,k}}{\gamma_{qu,jg}}\right) + \gamma_G \cdot (\gamma_{jg}) - \gamma_V \cdot (\gamma_w)} \quad (15)$$

For a fully treated plug, h_s=0.

Structural cracking check (Fig. 2.b.2)

In this case, equilibrium is imposed considering the simple 2D scheme reported in Fig. 3. The value of h_{jg} is then:

$$h_{jg} = \frac{-b + \sqrt{b^2 - 4 \cdot a \cdot c}}{2 \cdot a} \quad (16)$$

where:

$$a = \gamma_R \frac{3}{16} \frac{q_{u,jg,k}}{\gamma_{qu}} \quad (17.a)$$

$$b = \left(\gamma_G \cdot \gamma_{jg} - \gamma_V \cdot \gamma_w\right) \frac{B^2}{8} \quad (17.b)$$

$$c = -\frac{B^2}{8}\left[\gamma_V \cdot \gamma_w \cdot h_w + (\gamma_V \cdot \gamma_w - \gamma_G \cdot \gamma_s) \cdot h_s\right] \quad (17.c)$$

Again, for a fully treated plug, h_s=0.

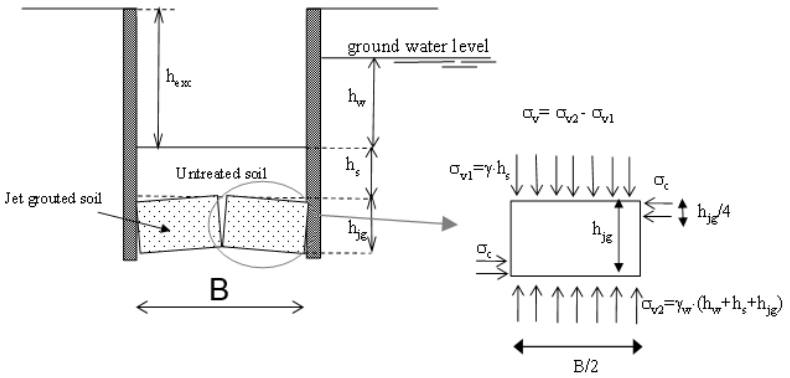


Figure 3. Mechanical scheme considered to calculate the minimum value of h_{jg} needed to avoid bending failure because of cracking propagation (structural check of the plug).

Height of the bottom plug for equilibrium

The minimum value of h_{jg} to use in design must be the highest given by eqs. (15) an (16). In order to draw some considerations on which of the two mechanism is the most critical in real cases, some calculations have been carried out with eqs. (15) and (16) and also, for comparison, with the FEM code Plaxis2D (Brinkgreve et al., 2018). With this latter, the jet grouted part of the plug has been modelled in two different ways: considering the Tresca criterion represented by eq. (7) (i.e. a purely cohesive material), or a material having a Mohr-Coulomb failure locus defined by the values of c' and φ' used in eq. (7). This latter approach is obviously more realistic and less conservative. The first calculation refers to the following set of geometrical conditions and mechanical parameters: $L=\infty$ (2D calculation), B=30 m, h_w=15 m,h_s=0 m, γ_{jg}=18 kN/m^3, $q_{u,jg,m}$=8 MPa, $CV(q_{u,jg})$=0.45 (sandy soil), λ=0.55. The analysis has been carried out considering $0\leq\delta\leq0.4$ to check the influence on the overall result of this mechanical parameter, difficult to quantify.All the partial coefficients have been posed equal to 1.Fig. 4.a shows the analytical and numerical results in a δ vs h_{jg} plane.

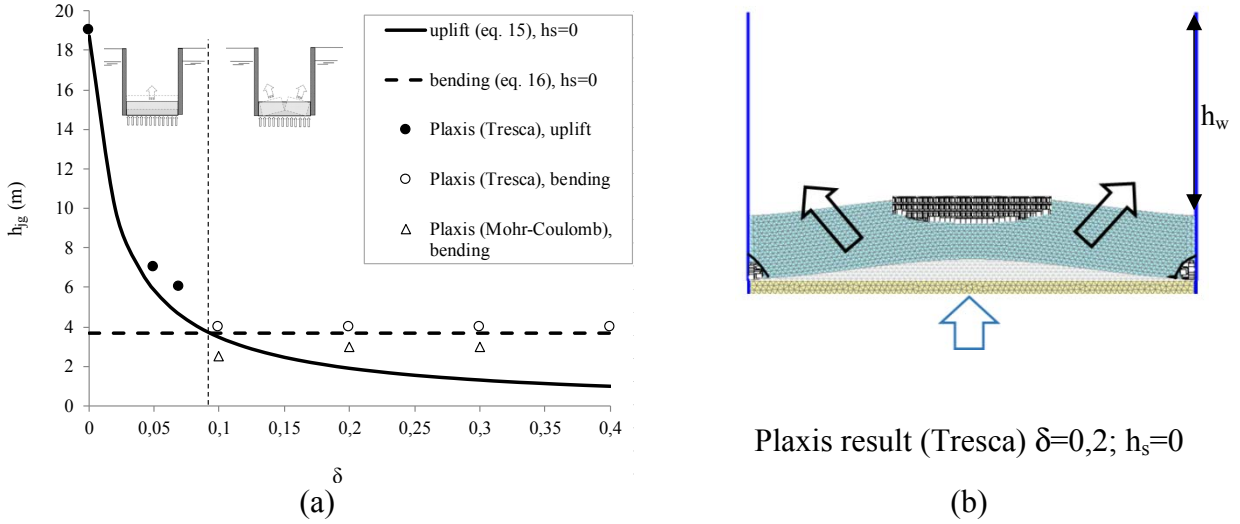


Figure4. Height h_{jg} of the jet grouted part of the bottom plug for equilibrium: a) comparison among analytical solutions (eq. 15 and 16) and numerical results, with the indications of the range of values of δ for which each mechanism is governing; b) plastic points (white) in the Plaxis simulation of one of the cases with bending structural failure.

The points corresponding to the numerical analyses are close to the analytical solutions, thus confirming the reliability of eqs. (15) and (16). As expected, the analyses carried out with the Mohr-Coulomb model are less conservative than the ones with the Tresca model, plotting a little below the analytical solutions. Fig. 4.b shows the plastic points in the numerical analyses, at a stage close to the final one, for one of the cases of bending failure. The figure demonstrates that the failure mechanisms triggered by the water pressure are exactly those assumed in eqs. (15) and (16). The comparison between numerical and analytical results also shows that, for the analysed case, the bending mechanism is the most critical one for any value of δ higher than 0.1. Fig. 5.a reports the analytical solutions for different values of B (=15, 30, 45 m) keeping h_s=0, and Fig. 5.b reports the same solutions for h_s=4m. Interestingly, the effect of B is to increase the demand for a higher value of h_{jg}, without changing the value of δ for which there is a switch between the uplift mechanism (in this case for $\delta<0.1$) and the bending structural failure (in this case for $\delta>0.1$). Figs. 5.b and 5.d show that having an untreated part of plug on top of the jet grouted part is effective only for low values of h_w, while it has little or no effect for higher values of the water pressure. By changing the values of B and h_w in a large range ($5\text{ m}\leq(B, h_w)\leq40$ m) with all possible combinations, it is found that in all

cases the structural bending failure is the most critical one for the range of more realistic values of δ (0.2≤δ≤0.3). In other words, the cohesive resistance along the perimeter of the plug soon starts to be so relevant to equilibrium that the uplift check (eq. 15) is easily satisfied with extremely low values of h_{jg}. This is interesting, as most times practitioners design plugs accounting only for the uplift mechanism, which as shown is not a realistic one, considering that for water tightening reasons there is usually an overtreatment along the perimeter, and thus a relevant cohesive interaction with the surrounding retaining structure has to be expected.

All these considerations have been done with reference to the plots reported in Fig. 5, obtained assuming λ=0.55. Fig. 6 shows the effect of different values of λ (=0.4, 0.55, 1) for B=30 m. The lower values of λ lead to very similar results, indicating that the exact quantification of this parameter (which is not an easy task) is not necessary. The value λ=1 (i.e. considering for the plug the same variability of $q_{u,jg}$ observed on small specimens) results in higher, overconservative values of h_{jg}. It can be concluded that the conservative but reasonable value λ=0.55 should be considered.

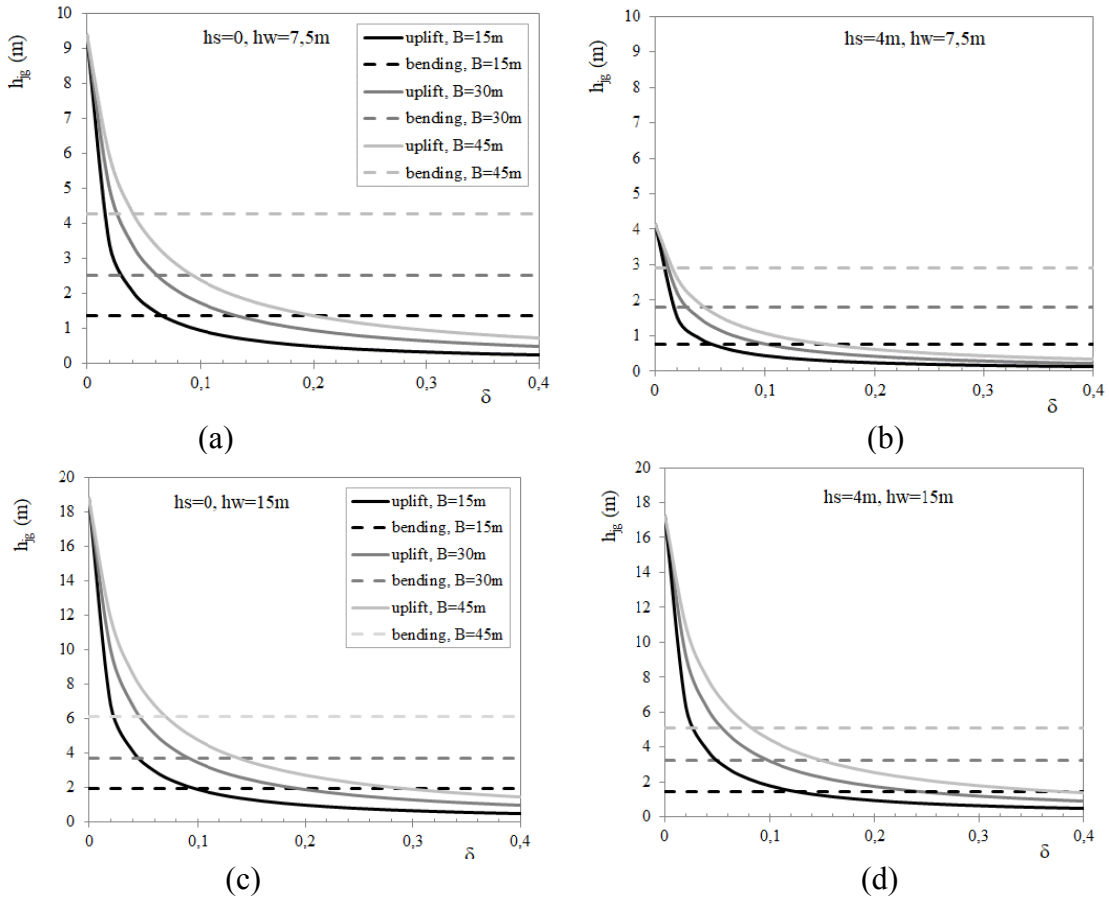


Figure 5. Height of the bottom plug h_{jg} for equilibrium, for different values of B(15, 30 and 45 m), h_w (7.5 and 15 m)and h_s (0, 4m).

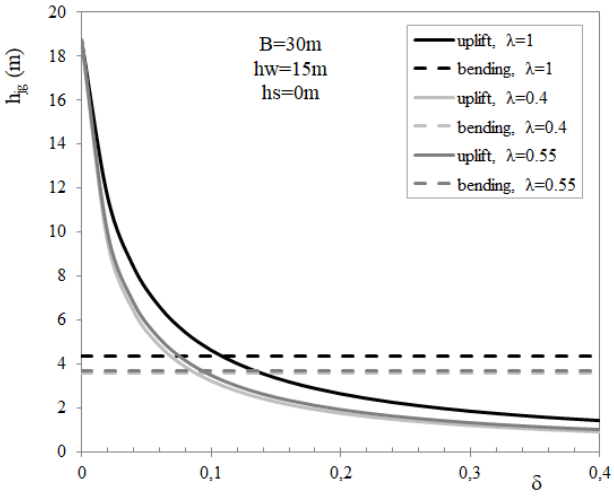


Figure 6. Effect of different values of λ on the calculated value of hjg. In the range of more realistic values (0.4≤λ≤0.55), the exact value of this parameter has little or no effect.

A final comment on the partial factors to be adopted: in all cases, the most critical combination is the "geotechnical one". As a consequence, the geotechnical combination of partial factors should be adopted even in the bending check, that may seem more of a structural one.

4.3 water inflow –probabilistic calculation

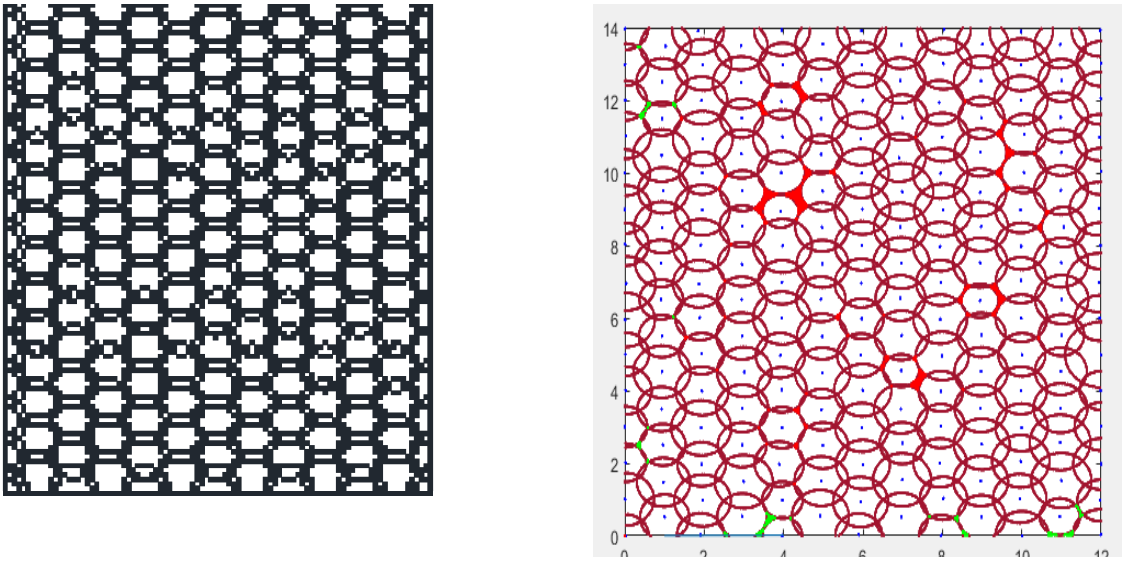
Once equilibrium is granted, the design of a bottom plug has to be completed by assigning a diameter D and a spacing s to the jet grouted columns. In this step, the design goal is to have a tolerable seepage through the plug, manageable with current drainage and pumping systems, more than having a completely impermeable structure. In fact, impermeability may lead to overconservative design. Water seepage does not necessarily entail dramatic consequences, depending essentially on the volume and velocity of the water flowing into the excavation area. Therefore, specific calculations should quantify the water flow rate Q passing through the possibly defective plug.Defining a unique value for the tolerable flow rate is not easy, as it should depend on the systems available for drainage, but a limit value of 2÷3 l/s over 1000 m^2 is suggested in different codes of practice. In the short term (i.e. during excavation), seepage occurs only through the untreated portions of the plug (if any), characterised by the typical high permeability coefficients of cohesionless soils, and not in the jet grouted material (which has a coefficient of permeability at least two or three orders of magnitude lower than that of the untreated soil). The flow rate Q can be computed as:

$$Q = k_s \cdot \frac{h_w}{h_{jg}} \cdot A_{un} \tag{18}$$

where k_s is the Darcy coefficient of permeability of the untreated soil and A_{un} is the untreated area at the top of the jet grouted part of the plug. In the long term, water will also flow through the jet grouted part, and waterproofing has to be granted with other devices (like impermeable linings).
Then, the design problem is to calculate A_{un} as a function of the diameter and spacing of the columns, as well as of the depth of the plug. Because of the random variabilities of diameter and inclination of the columns, the only way to deal with this problem quantifying the risk is by a fully probabilistic approach. The authors have developed a numerical code (named *Jetplug*) able to deal with this problem for any number of columns. The code calculates probabilistically the total

untreated area at any depth for an assigned given risk level, giving for each iteration, at any depth, an output similar to that reported in Fig. 7.b. Therefore, *Jetplug* allows to know both the total value of A_{un} and also the single areas of the different untreated parts. Since the calculation may be time consuming, the problem arises of the minimum number of columns needed to represent reliably the overall problem. Considering the simple case of a square plug (B=L), Fig. 8 shows the ratio A_{un}/BL at the top of the plug for a given set of statistical, mechanical and geometrical parameters. Interestingly, it is noted that the value of A_{un}/BL is overestimated if a reduced number of columns is considered. For more than 40 columns,the value of A_{un}/BL seems independent of the number of columns. Even though this may not be considered as a general rule, it seems a reasonable indication to compute A_{un} by using not more than 40-50 columns.

In this work, the statistical distribution of $A_{un}(z)/BL$ and its dependence on the diameter and inclination of columns was computed with the Monte Carlo method, adopting the procedure described by Modoni et al. (2016). The calculation was performed for s/D_m=0.75 and 0.80, assuming CV(D)=0.1, 0.2 and DS(β)=0.1°, 0.2° and 0.3°.



(a) (b)

Figure 7. Example of *Jetplug* calculation output: ideal (a) and probabilistic (b) disposition of the columns at the top of a jet grouted plug, for a given set of statistical parameters. The shaded areas in Fig. 6.b indicate the untreated parts.

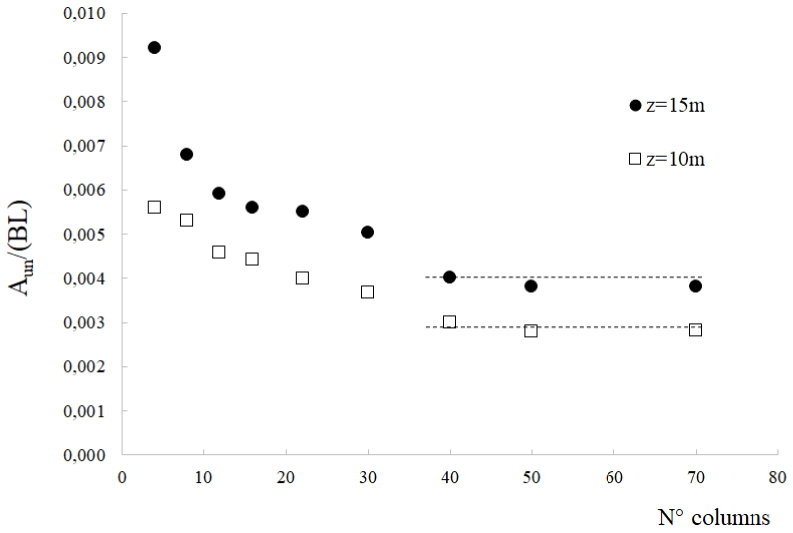


Figure 8. Effect of the number of columns considered in the probabilistic calculation of the ratio A_{un}/(B·L) at the depth of excavation (z=10, 15 m).

For each combination of parameters, 1000 iterations were performed to obtain a meaningful statistical sample, and for each iteration the variation with depth of the untreated area ratio was computed. Only the portions of untreated material connected with the surrounding water-bearing soil were considered in the computation of A_{un}/BL. The value of $A_{un}(z)/(B\cdot L)$ for a risk level of 5% at each depth was computed and plotted versus the dimensionless depth z/D. Fig. 9 shows larger imperfections of the plug for increasing depth, spacing and defects of columns (i.e. variability of diameter and inclination), and clearly demonstrates the beneficial effect of using larger values of D. The plots of Fig. 9, drawn for quite usual values of s/D, can be used as a simple immediate design tools: once the depth of excavation is known, and the statistical variabilities have been estimated, the best choice of D and s can be done to reduce the water flow Q to tolerable values.The plots in 8 show that, for the typical depths of excavation and diameters of the columns, the values of $A_{un}/(B\cdot L)=Q/(k\cdot B\cdot L\cdot h_w/h_{jg})$ (i.e. the dimensionless values of the water flow) are generally small (mostly in the range of 0.1-1%), and is therefore easy to comply with the limit water flows previously indicated (2÷3 l/s over 1000 m^2) without needing to have a totally impermeable plug. In case the height of the treated part hjg assigned for equilibrium is too small (thus leading to extremely high hydraulic gradients h_w/h_{jg}), the water flow can be reduced also by increasing h_{jg}.

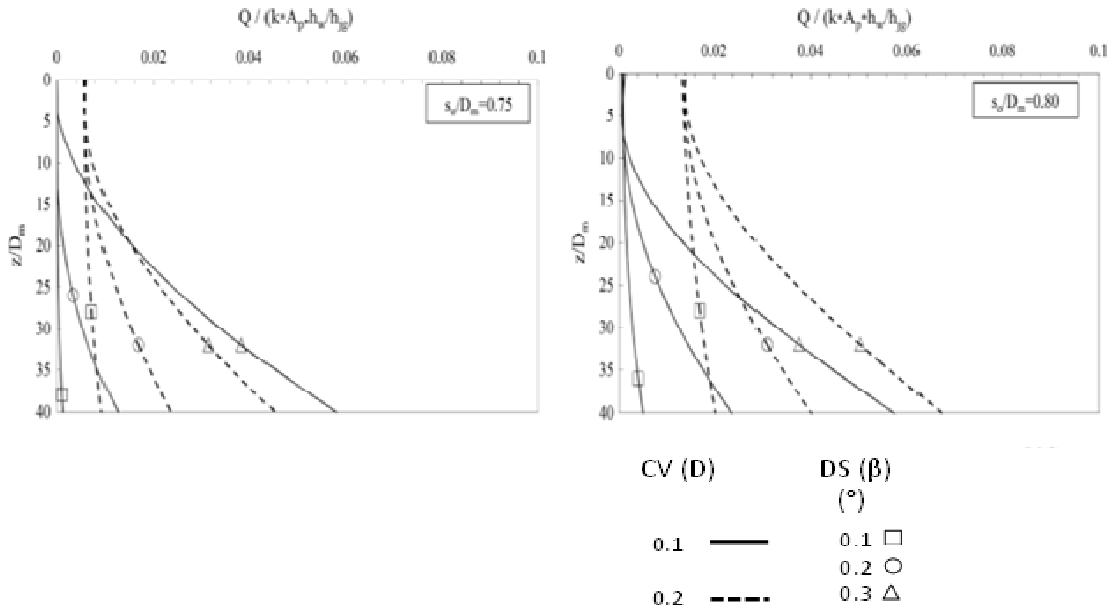


Figure 9. Design charts to assign the best value of D_m and to check that h_{jg} found for equilibrium (eqs. 15 and 16) is large enough to reduce Q to tolerable values. Charts for s_0/D_m=0.75, 0.80. In the x axis title, A_p is the area of the plug (A_p=BL).

5. Design of a vertically loaded isolated column

Jet grouting isolated columns have been successfully adopted in various cases both as foundations of new buildings (e.g. De Paoli et al., 1989) or for underpinning of pre-existing structures (e.g. Shibazaki and Ohta, 1982; Wanik, 2013). Even though it has previously been shown that the jet grouting columns are affected by unavoidable geometrical and mechanical defects, their performance can be satisfactory as vertical load bearing reinforcements, provided that such defects are conveniently taken into account. Starting from a well documented field trial on axially loaded single columns, a procedure is proposed herein to calculate the bearing capacity of jet grouting columns, and a comparison is carried between the results obtained via a deterministic and a probabilistic approach.

Back analysis of axial load tests on jet grouting columns

Modoni and Bzòwka (2012) back analyzed with a FEM code a full scale loading tests (D=1.8 m, L=7.0 m, double fluid jet grouting in a homogenous sandy soil deposit) carried out in Poland (Fig. 10). They found that the tip resistance p_L could be well interpreted with the approach suggested by Wright and Reese (1977) for large diameter bored piles (Fig. 11.a). On the contrary, the lateral resistance s_L is higher than that predicted with the method proposed by the same authors, and nicely fitted by the relation proposed for jet grouting columns by Bustamante, 2002 (Fig. 11.b). The difference in lateral resistance between jet grouting columns and bored piles can be explained as a positive effect of the non-cylindrical shape of the columns (Modoni and Bzówka, 2012). Following the approach proposed by Modoni and Bzòwka (2012), the lateral and tip unit shares p and s of the load can be expressed as functions of p_L and s_L, as well as of the settlement w and of the diameter of the column, in a way in all similar to that used for piles as:

$$\frac{p}{p_L} = \frac{w}{D_t} \cdot \frac{1}{0.029+0.428 \cdot \frac{w}{D_t}} \tag{19}$$

$$\frac{s}{s_L} = \frac{w}{D_i} \cdot \frac{1}{0.0063+\frac{w}{D_i}} \tag{20}$$

where p_L and s_L are taken from Figs. 11.a and 11.b as a function of soil strength (expressed in terms of q_c or N_{SPT}), D_t is the diameter of the column's tip, D_i is the diameter at the generic depth. Eqs. (19) and (20) can be combined to estimate the Q-w curve, with the so called load transfer curve method, as:

$$Q(w) = p(w) \cdot \frac{\pi \cdot D_t^2}{4} + \pi \cdot \int D_i \cdot s(z,w) \cdot dz \tag{21}$$

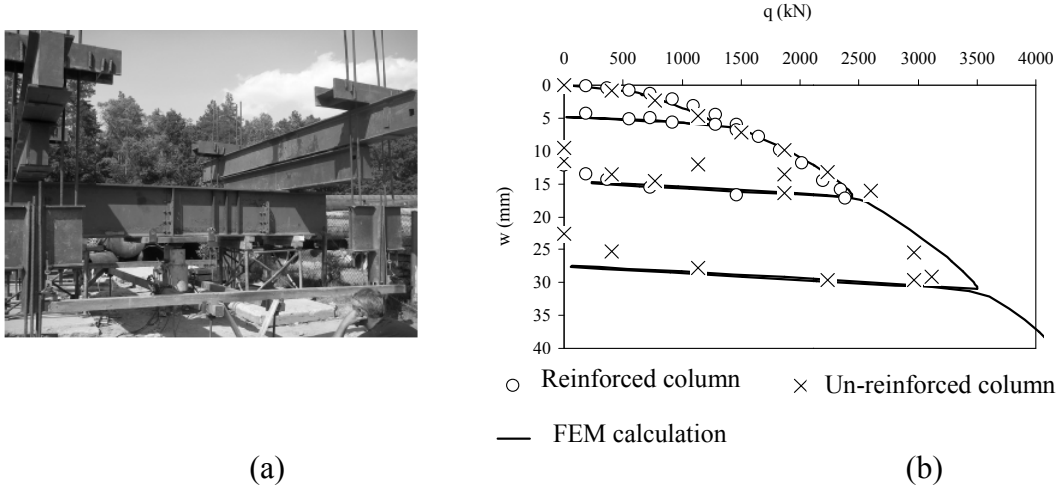


Figure 10. Results and simulations of the axial loading tests from Bzówka 2009; (a) experimental set-up; (b) load settlement curves and FEM back-analysis.

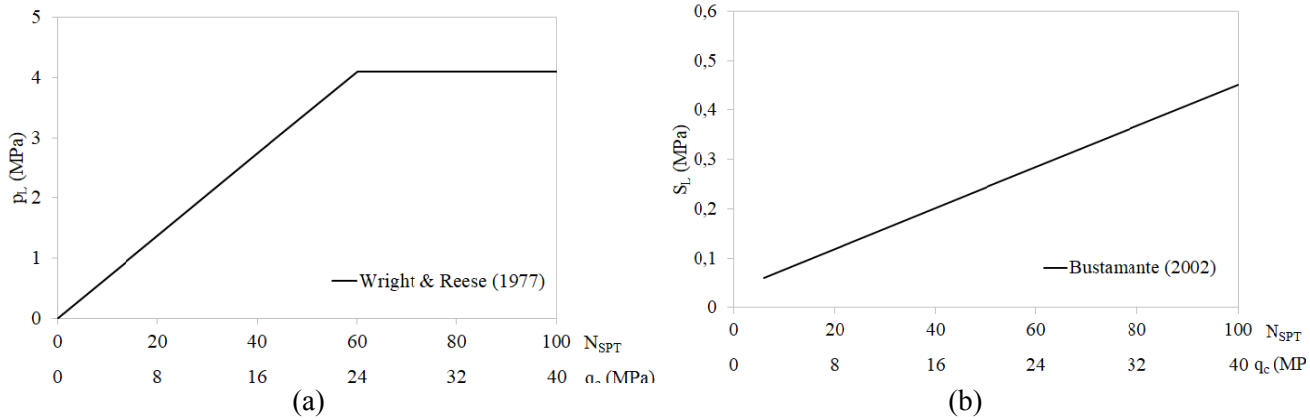


Figure 11. Charts for the calculation of p_L and s_L (eqs. 19 and 20).

In the following, using this formulation a parametric study is presented to evaluate the effects of different possible design approaches (deterministic or probabilistic) on the prediction of the response of an axially loaded single column. The analyses have been carried out with the load transfer curve method and parameters defined above, identifying as limit condition the one giving a

settlement of 5 cm (5% of the mean diameter), similarly to what is typically assumed for large diameter piles. An interesting issue related with this application for jet grouting columns is that failure can be ruled either by the attainment of the limit settlement or by the structural failure of the column occurring where the normal force equals in a cross section the limit strength. This will not necessarily happen in the upper part of the column, as there may be deep sections having locally lower values of $q_{u,jg}$.

Bearing capacity – deterministic approach

The load-settlement curves for columns having constant diameter and uniaxial strength (the mean values D_m=1 m, $q_{u,jg}$=8 MPa are here taken as reference) and different lengths are reported in Fig.12. They show that the limit load increases with column length up to some level (in this case, with all partial factors equal to 1, about 6.3 MN). Afterwards, the structural collapse of the column becomes predominant and any further increase of the length is ineffective. The length corresponding to the plateau of the load settlement curve (named L_{opt} in the following) at a w/D=5% can be thus identified as the maximum achievable reinforcement for the foundation. In the case of Fig. 12, L_{opt} is much higher than the usual values adopted in practice for jet grouted columns. Thus, in this case structural failure seems not to be a real issue. However, this calculation has been carried out without introducing any partial factor, thus looking only to mechanisms. The calculation has then be repeated using some of the values of the partial factors γ_D and γ_{qu} given in Tables 4 and 5. Depending on soil heterogeneity and on the derivation of the mean values, whether from literature of from a field trial, γ_D ranges from 1 to 1.2, and γ_{qu} from 1.5 to 3.

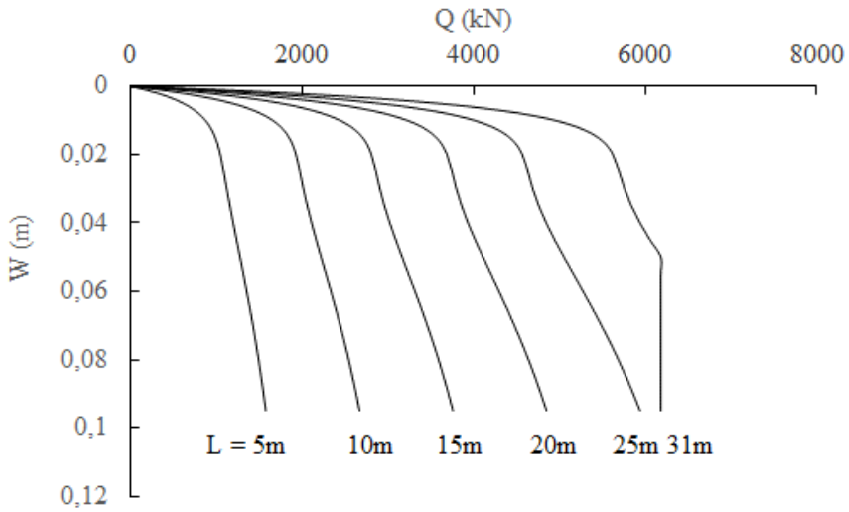


Figure 12. Load settlement curves for jet grouting columns of different length.

The influence of this choice on the limit load and on the optimal length of the column can be immediately seen in Fig. 13, in which the limit load is expressed as a function of the column length for some typical combinations of partial factors and for the reference condition with unit partial factors (γ_D=1 and γ_{qujg}=1) reported in Fig. 12. Fig. 13 clearly shows that partial factors may cut L_{opt} to values much lower than 31 m. This means that for vertical load bearing columns, a detailed knowledge of the jet grouting properties from field trials is necessary to choose the consistent values of the partial factors and to reduce the over conservativeness of design.

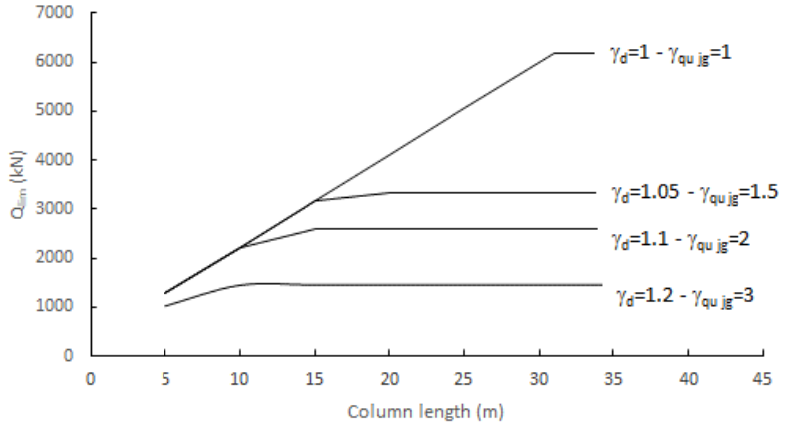


Figure 13. Dependency of the limit load on the column length for different partial factors.

In order to have an optimum design (i.e. using the column to its maximum contribution prior to reach structural failure), the conclusions observed in Figs. 12 and 13 for a specific case (D_m=1 m, $q_{u,jg}$=8 MPa) can be generalized, to find for different ground conditions which is the maximum length L_{opt} a jet grouted column can have to fully mobilize its bearing capacity Q_{lim} (obtained using eq. (21) for $p=p_L$ and $s=s_L$) without reaching structural failure. Fig. 14 shows design charts which give such a maximum value L_{opt}/D as a function of soil properties, jet grouted material uniaxial strength and possible values of the relevant partial factors (γ_d, $\gamma_{qu,jg}$). It is shown that as soil shear strength increases, L_{opt} decreases. Whatever the soil, for $L>L_{opt}$ the bearing capacity of the column is $q_{lim}=0.25\cdot\pi\cdot D^2\cdot q_{u,jg}$, i.e. the critical mechanism is structural failure. If for design needs higher values are desired, a higher jet grouted material strength has to be reached within the column.

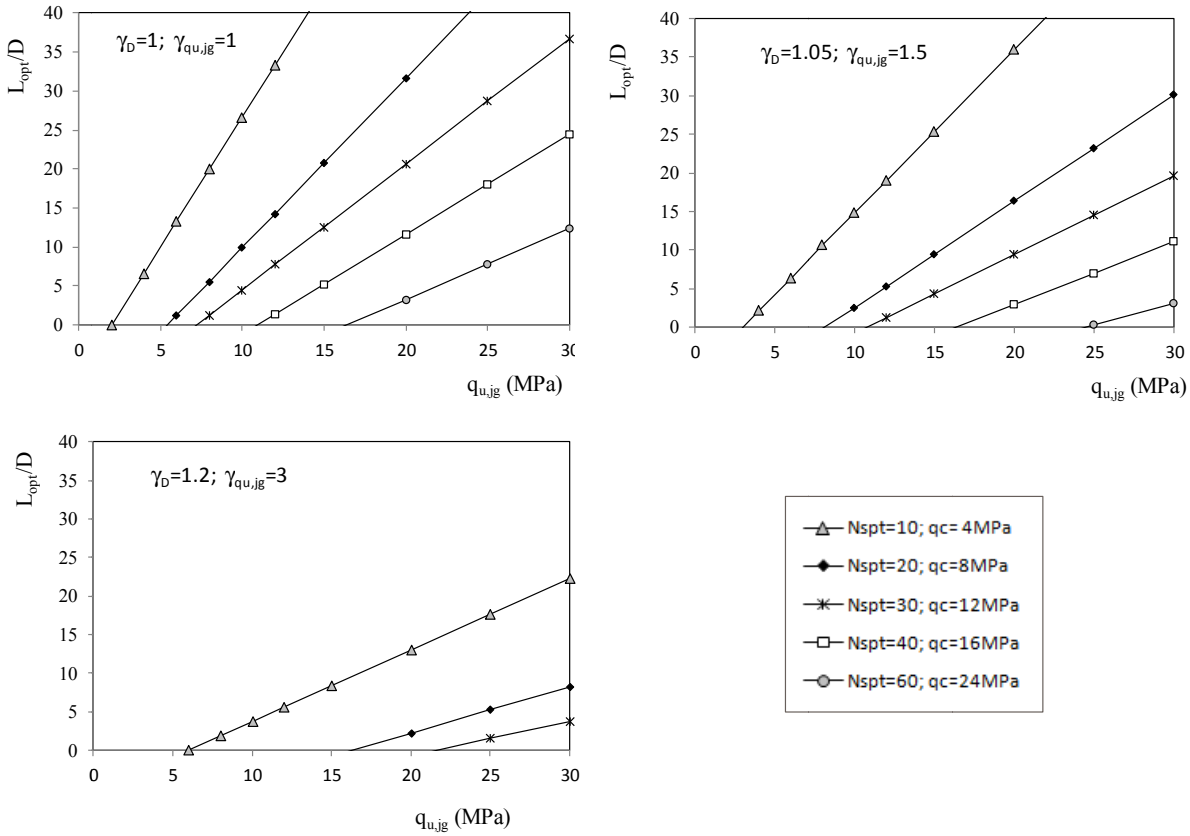


Figure 14. Charts to calculate L_{opt} as a function of partial factors, q_{ujg} and soil properties.

Bearing capacity - probabilistic calculation

The probabilistic calculation has been performed varying randomly the diameter and resistance of the columns and computing the limit load of the columns. As in the previous example of the bottom plug, the calculation has been performed with the Monte Carlo method, assuming CV(D)=0.05÷0.2 and CV(q_{u_jg})=0.15÷0.45. For each combination of parameters, one thousand columns are generated, computing the limit load for each of them and taking the values correspondent to a 5% fractile of the distribution (i.e. to a 95% level of confidence) as the result of the probabilistic calculation. The coefficient of variation CV(q_{u_jg}) has been scaled assuming in this case λ=0.7 (eq. 9). This value is

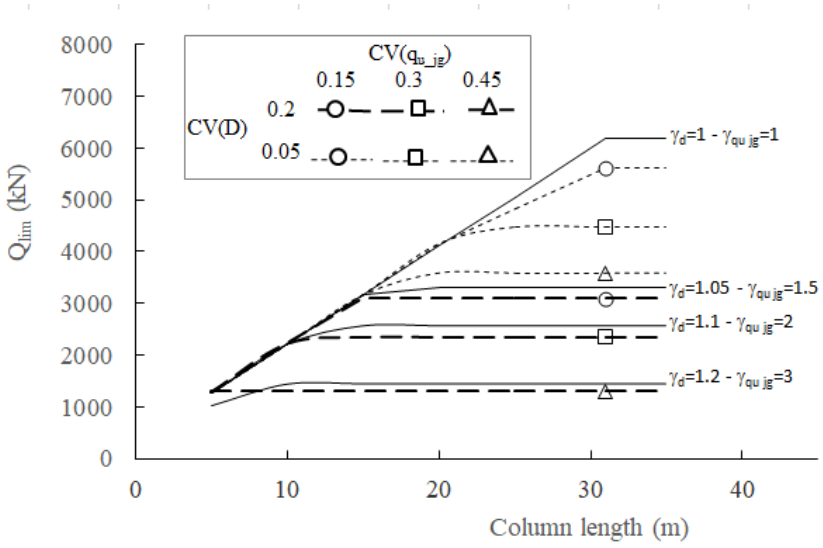


Figure 15. Effect of column length on bearing capacity. Comparison between deterministic and probabilistic (5% risk level) results.

higher than the one pertaining to bottom plugs because the involved dimensions (diameter of the column vs lateral surface of the plug) are smaller. The results, plotted as functions of column length, are compared in Fig. 15 with those previously obtained with the deterministic approach and the use of partial factors (see Fig.13).

The plot shows that the main effect of the scatter of the random variables is a reduction of L_{opt}. It also indicates that for the case of higher variability of parameters (soil with high heterogeneity, CV(D)=0.2, CV($q_{u,jg}$) = 0.45), the results plot very close to the deterministic curve with the highest considered values of the partial factors (γ_d=1.2 and $\gamma_{qu,jg}$=3). This means that the range of behaviors depicted in Fig. 14 by the deterministic curves covers all the range of possible probabilistic results at 5% risk. In order to use the deterministic approach, then, the partial coefficients have to be assigned taking into account the heterogeneity of the soil.

6. Conclusions

The paper has presented two typical applications of jet grouting, bottom plugs and axially loaded isolated columns, discussing the design challenges for both of them. It is recognized that the

random variability of the diameter and position of the columns, as well as that of the uniaxial strength of the treated material, cannot be overlooked. However, not all the calculations have to be carried out with a probabilistic approach, and a simpler deterministic (or semiprobabilistic) approach may be adopted, provided the partial factors are carefully assigned.

For the case of a well designed bottom plug (i.e. with a tolerable water inflow), for instance, being it a massive structure with a very low percentage of untreated material, the random defects do not affect the overall static behavior. Then, the deterministic approach can be conveniently adopted, provided some care is introduced in the choice of the mechanical properties of the jet grouted materials and of the partial factors. A relevant role is played by the parameter δ, ruling the shear interaction between the plug and the surrounding retaining structure: neglecting this shear interaction (i.e putting $\delta=0$) would result into an extremely overconservative design. For the most realistic values of this parameter ($0.2\leq\delta\leq0.3$), the ruling mechanism is not uplift but bending structural cracking, which must be therefore considered as the design check to be carried out. Even though this may seem as a structural rather than a geotechnical mechanism, the geotechnical combination of partial factors is always the most critical one. Therefore, the strength parameters have to be scaled without amplifying the unfavourable actions. On the contrary, the evaluation of water inflow cannot be but probabilistic. Simple charts are reported to this aim, for some typical values of s_0/D_m.

For the case of vertically loaded isolated columns, it has been shown that their performance can be satisfactory as reinforcements, provided the column structuralstrength is not attained. Since this may be the case because the jet grouted material is a poor concrete, there is an upper bound of the bearing capacity Q_{lim} which corresponds to structural failure, and to an optimum design column length L_{opt}. Having longer columns would be useless. This limit length may sharply reduce if high variabilities are expected for the mechanical and geometrical parameters of the column, which in turn are strictly related to soil heterogeneity and characteristics. The deterministic approach with partial factors is able to reproduce similar results, but the choice of the partial factors is extremely critical. For heterogeneous soils, high values have to be selected.

References

Bustamante, M. (2002). Les colonnes de jet grouting. Report of the Seminar: Pathologies des Sols et des Foundations, http://www.keller-france.com/rechercheet- developpement/theses-et-publications: 6 p [in French].

Brinkgreve, R.B.J., Kumarwamy, S., Swolfs, W.M., Foria F. 2018. Plaxis, Reference Manual, The Netherlands.

Croce, P. and Flora, A. (2000) Analysis of single fluid jet-grouting. Geotechnique, 50, No.6: 739-748.

Croce P., G. Modoni (2007). Design of Jet Grouting Cut-offs. Ground Improvement – Thomas Telford, vol. 11-1, pp. 11-19.

Croce P., Flora A. and Modoni G. (2014). Jet Grouting. CRC Press, Taylor & Francis Group, 284 pp.

de Paoli, B., R. Tornaghi, and D. A. Bruce. (1989). Jet grout stabilization of peaty soils under a railway embankment in Italy. Foundation Engineering: Current Principles and Practice, New York: ASCE: pp. 272‑290.

ENV 1997-1 Eurocode 7: Geotechnical design — part 1: general rules. European Committee for Standardisation (CEN), Brussels (1997)

Fenton, G.A. and Griffiths, D.V. (2008). Risk Assessment in Geotechnical Engineering, John Wiley & Sons inc., New York, 461 pages.

Flora, A., Lirer, S. and Monda, M. (2012). Probabilistic design of massive jet grouted water sealing barriers. Proceedings of the IV International Conference on Grouting and Deep Mixing, New Orleans (USA), Vol. 2, Johnsen L.F., Bruce D.A., Byle M.J. Ed, ASCE: pp. 2034-2043.

Flora A., G. Modoni, S. Lirer, P. Croce (2013). The diameter of single, double and triple fluid jet grouting columns: prediction method and field trial results. Géotechnique, pp. 934-945.

Haldar, A. & S. Mahadevan, (2000). Reliability Assessment Using Stochastic Finite Element Analysis, John Wiley & Sons, Inc., New York.

Modoni, G. and J. Bzowka. (2012). Design of jet grouting for foundation. ASCE Journal of Geotechnical and Geoenvironmental Engineering 138(12), pp. 1442‑1454.

Modoni G. and Bzówka J. 2013. "Analysis of Foundations Reinforced with Jet Grouting". Journal of Geotechnical and Geoenvironmental Engineering , ASCE, 1442-1454.

Modoni, G., Flora, A., Lirer, S., Ochmański, M., Croce, P. (2016). Design of Jet Grouted Excavation Bottom Plugs. Journal of Geotechnical and Geoenvironmental Engineering, ASCE, 142(7).

Shibazaki M., Ohta S. (1982). A unique underpinning of soil solidification utilizing super-high pressure liquid jet. Proc. of the Conference of Grouting in Geotechnical Engineering, New Orleans, pp. 680-693.

Terashi, M. (1997). Theme lecture: deep mixing method – brief state of the art. In Proceedings of the 14th international conference on soil mechanics and foundation engineering, Hamburg, Germany, vol. 4, pp. 2475–2478. Rotterdam, the Netherlands: Balkema

Toraldo C, Modoni G., Ochmansky M and Croce P. (2017). The characteristic strength of jet-grouted material. Geotechnique.

Wanik K. (2013). Use of jet grouting technique to realize substructures of hystoric buildings: the example of an apartment building in Warsaw. Proc. of the second international symposium on Geotechnical Engineering for the Preservation of Monuments and Historic Sites. Bilotta, Flora, Lirer & Viggiani editors. Taylor and Francis Group.

Wright, S. J. and L. C. Reese. (1977). Construction of Drilled Shaft and Design for Axial Loading; Manual on Drilled Shaft 1: Washington, DC: U.S. Department of Transportation: 140 pages.

A GROUND IMPROVEMENT TREATMENT FOR TWO RAISE BORED ELEVATOR SHAFTS IN A HISTORICAL SITE OF CENTRAL ITALY

Massimo Grisolia, Sapienza Università di Roma, Rome, Italy, +39 06 44585022, massimo.grisolia@uniroma1.it
Ignazio P. Marzano, Sapienza Università di Roma, Rome, Italy, +39 06 44585827, paolo.marzano@uniroma1.it
Giuseppe Iorio, AGiS Ingegneria S.r.l., Rome, Italy, +39 06 92597141, iorio@agisingegneria.it
Giuseppe Panetta, AGiS Ingegneria S.r.l., Rome, Italy, +39 06 92597141, panetta@agisingegneria.it
Ferruccio Cribari, TREVI S.p.A., Cesena, Italy, +39 0547 319311, fcribari@trevispa.com
Giuseppe Trovato, TREVI SpA, Cesena, Italy, +39 0547 319311, gtrovato@trevispa.com

ABSTRACT
The paper concerns special ground improvement works to allow the execution of two vertical elevators inside a cliff on which rest a city of high historical and architectural value. The soils to be excavated and subjected to ground improvement are constituted by an alternation of pyroclastic soils and tuffs of different consistency and cementation degrees. The ground improvement has been carried out by some series of guided jet-grouted columns performed in order to preconfigure a connection room with an access tunnel. The effectiveness and continuity of the treatment was verified by direct control tests and geophysical surveys. In order to limit the environmental and work impacts on the historical city center, the excavation of the vertical shafts have been performed by a special raise boring machine. A sophisticated monitoring system allowed to verify the effects of vibrations on the historical and artistic buildings during both the ground improvement and the shaft excavation phases.

Keywords: Ground improvement, jet-grouting, historical center, raise boring machine.

INTRODUCTION
Located between the southern borders of the Tuscan Maremma and Rome, Viterbo is a site of high historical and architectural value in Central Italy characterized by one of the richest and best preserved heritage of medieval constructions. Churches and palaces, buildings dating back to the 11th, 12th and 13th centuries and the impressive city walls which still fully encircle the historical center.



Fig. 1. San Lorenzo square: Duomo of San Lorenzo and Palazzo dei Papi over San Lorenzo hill

In this landscape of volcanic origins, a special area in the city is placed over the San Lorenzo hill, in the namesake square where the famous Palazzo dei Papi (Papal Palace, set around the square below with its elegant arches) and the Romanesque Duomo of San Lorenzo are (Fig. 1).
To connect by a pedestrian touristic crossing the lower area of the city (Faul valley) to the San Lorenzo square (Fig. 2a), a base tunnel and two vertical elevator shafts were to realize. As illustrated in the section reproduced in Fig.2b, other two minor intermediate entries were also to be constructed.

© 2018 Deep Foundations Institute

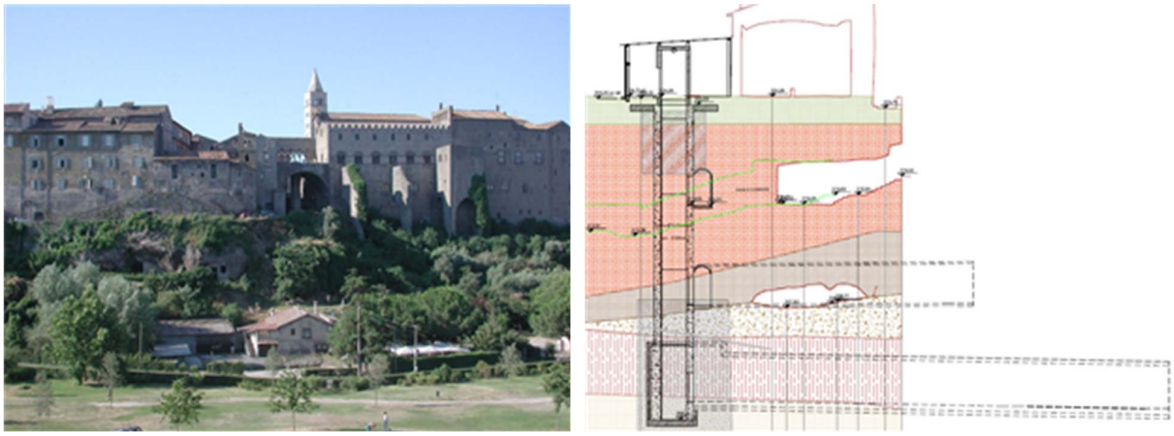


Fig. 2. a) View of the cliff; b) Section of the connections.

MAIN FEATURES OF THE WORK

GEOTECHNICAL FRAME

According to the geological genesis and development of the site, the terrains are of volcanic nature and characterized by an alternation of pyroclastic soils and tuffs of different consistency and cementation degree (Fig. 3).

Under a first shallow layer of manmade soils, the upper tuff stratum ("TRS") has an important thickness and it is constituted by red tuffs with black slags. It shows a medium-high level of cementation, which is reflected in overall good properties in terms of strength and stiffness.

Beneath it, two layers of black pozzolanic soils have been found, distinguished between an averagely cemented level ("PNL") and a looser one ("PNA"). These constitute a second facies of the same upper formations, and can be seen as a transition zone.

The bottom formation ("TC" - "TSC"), ascribable to an elder effusive period, is mainly made of tuffs with ashes, also including different intercalations of sandy tuffs. The cementation degree can strongly and irregularly differ in a few meters, and variable inclusions are often present.

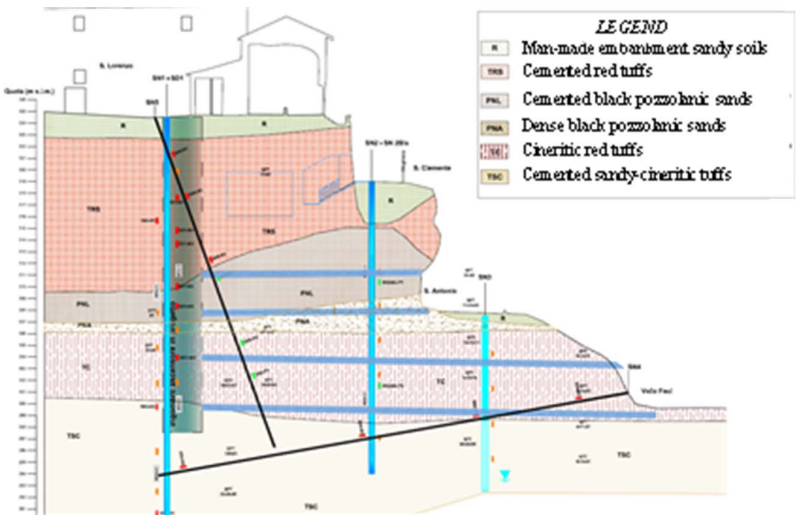


Fig. 3. Geotechnical section of the soils encountered by the works

THE FAUL BASE TUNNEL

The base connection to reach the lifts to the upper square, is a traditional blind hole tunnel of about 36 meters in length, dug in lower "TC" soils (Faul tunnel). The excavation phases provided, after a typical excavation step of about 1.0 m of length, a preliminary lining in shotcrete reinforced with IPE 140 steel ribs placed at 1.0 m interaxis (Fig. 4a) and a final 30 cm thick reinforced shotcrete lining (Fig.4b).



Fig. 4. a) Preliminary lining; b) Final lining.

The different geometries needed at the end of the tunnel to allow the execution of the enlargement of the waiting area in front of the lifts shafts, led to a different lining layout. In this area the preliminary lining was made by double IPE 140 steel ribs and shotcrete (Fig. 5a). The final lining of the waiting area presents two circular areas lightly reinforced in correspondence of the shafts to be realized, in order to speed up further drilling operations.



Fig. 5. Enlarged waiting area at the end of Faul tunnel - a) preliminary lining; b) reinforcement bars of final lining above sprayed waterproofing

VERTICAL SHAFTS

The lifts provided for the vertical connection are placed inside two 3.13 m diameter circular vertical shafts, with 4.13 m interaxis, and 25 m total height.

The drilling technique employed for the shafts was the so called “raise boring”. The raise boring method is a process used in underground mining to create a circular hole between two levels with no need for explosives, suitable for production of vertical or inclined shafts from bottom to top. The raise boring machine was set up on the upper level of the two areas to be connected, on a concrete pad (Fig. 6a). A 300 mm diameter hole (pilot hole) was drilled to the Faul tunnel. Once the drill broke into the shell of the tunnel, the bit was removed and a 3130 mm diameter reamer head was attached to the drill string and raised back towards the machine (Figs. 6b - 6c). The drill cuttings from the reamer head fall to the floor of tunnel, so reducing the traffic of heavy trucks related to disposal of mucking materials into the upper historical square.



Fig. 6. Raise boring method - a) raise boring machine on the upper level - b) connection of the reamer head to the drill string on the Faul tunnel shell - c) end of excavation of a shaft seen from above

According to the working phases, after the execution of the first shaft a square box-shaped steel modular structure (Fig. 7a), in which lift would be placed, was lowered down and finally fixed by concrete casting in the annular space around it (Fig. 7b-7c).



Fig. 7. a) Square box-shaped steel modular structure inside the shafts - b) lifting - c) placing inside the first shaft

GROUND IMPROVEMENT WORKS

THE FAUL TUNNEL

In order to prevent any kind of effects induced on surface by excavation works of the Faul tunnel, due to the heterogeneity of the pyroclastic soils at the lower level and considering the presence of cavities above it, design provided a number of soil improvement works around and on the face of the tunnel.

Around the tunnel, a shield made of 600 mm diameter interpenetrated columns was realized by guided sub-horizontal jet-grouting technique (Figs. 8a,8c). This layout was further stiffened in the first 8 meters by a second external row of columns, as illustrated in Figure 8b. At the base, elliptical jet grouting treatments were provided in order to create a reliable foundation support for the shield and preliminary lining ribs.

To consolidate the advance core, a number of seven 34 m long, cemented microcolumns reinforced with glass-fiber structural elements was adopted.

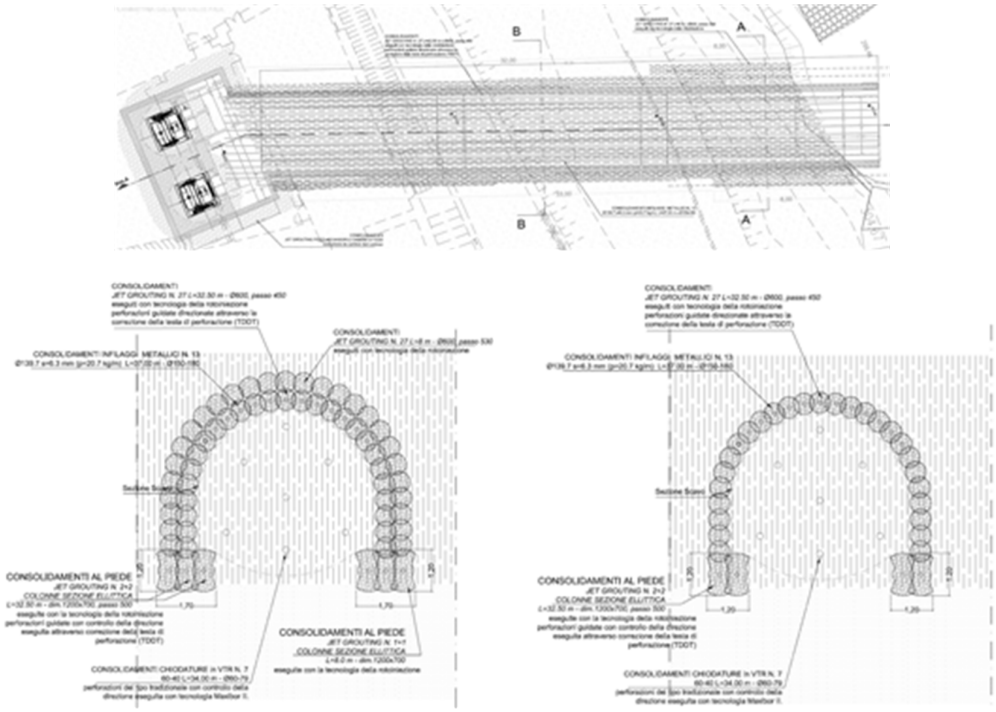


Fig. 8. Ground improvement preliminary works on the Faul tunnel - a) Plan - b) Typical section of stiffened layout - c) Typical section of ordinary layout

To speed up the excavation works, columnar treatments have been realized from outside, before starting to dig. To make it possible ensuring at the same time the right provided geometries, a special technology named "TDDT - Trevi Directional Drilling Technology" based on the HDD (Horizontal Directional Drilling) technologies used to lay utilities (usually cables and pipes) underneath surface obstacles (watercourses, roads, railways, structures, buildings, etc.) was used. This application enabled to drill small-diameter boreholes (50-200 mm) of considerable length (about 30 m) thanks to the preliminary generation of a magnetic field, which acted as a geometric guidance for the drilling machinery. In this way, during drilling operations in progress, a continuous check of the drill string 3D coordinates was available, so that the final geometric layout of the ground improvement columns could utmost fit the design schemes.
Figure 9 shows a graphic representation of the final spatial layout of jet grouting columns, widely within the limitations fixed by preliminary defined geometric tolerances.

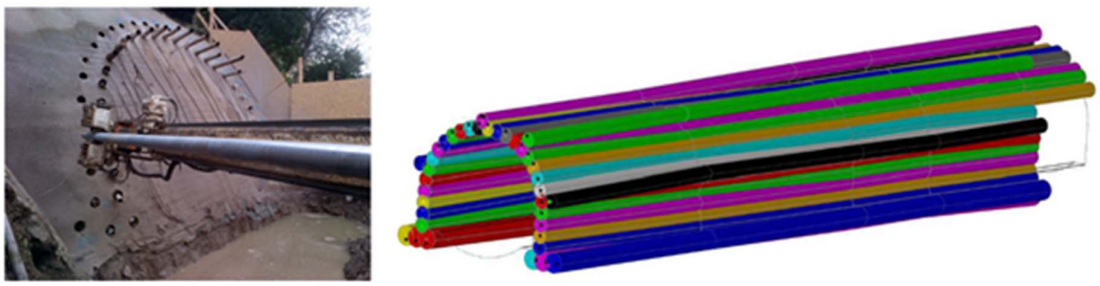


Fig. 9. Preliminary jet grouting columns - a) Outside view - b) 3D layout of executed treatments

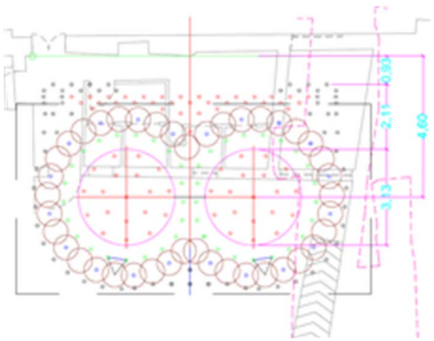
VERTICAL SHAFTS

The application of "raise boring" technique for the two shafts excavation required the preparatory execution of a number of ground improvement works on the volcanic soils involved in the digging operations, aimed to confer them adequate properties in terms of homogeneous cementation and strengths, along with potential cavities clogging.

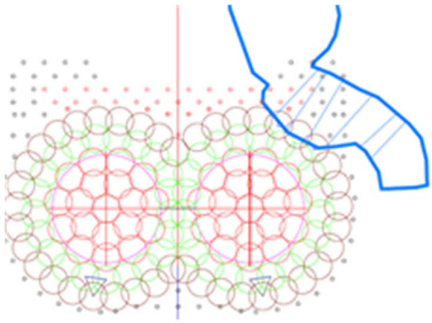
Soil treatments were executed both in soil volumes around the waiting room of the lifts, and on top of the shell of the final enlargement of the tunnel. Partially interpenetrated 800 mm diameter jet grouting columns have been created in a geometric pattern specifically studied to reach the different areas.
In Figure 10, the whole ground improvement works are represented for horizontal sections at different depths, as explained in table 1.

Table 1. Vertical shafts jet grouting improvement layout

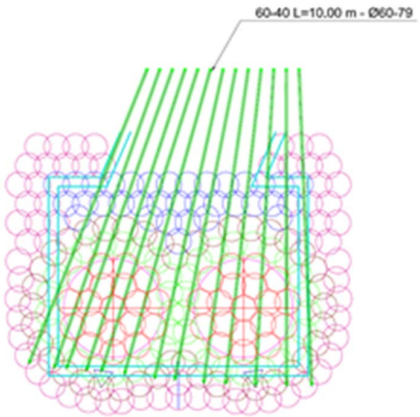
Aim of the treatment	*Number of columns (colour)*	*Columns length*	*Blank drilling length*	*Figure*
Shallow protection of buildings foundation	41 (brown)	4 m	1 m	10a
Protection around enlargement area excavation	65 (purple)	14 m	16 m	10c- 10d
Enlargement area shell	34 (blue)	6 m	14 m	10c
Improvement of soils to excavate - outline shafts area	41 (brown)	14 m	8 m	10b -10c- 10d
	42 (green)	7 m	13 m	10b-10c
Improvement of soils to excavate - inner shafts area	38 (red)	6 m	14 m	10b-10c



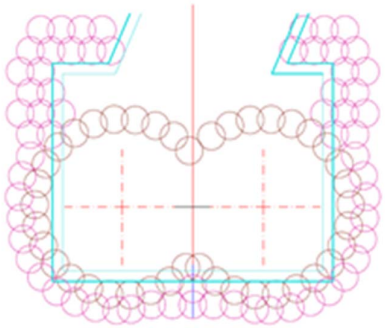
10a - Section at level -1 m b.g.l.



10b - Section at level -14 m b.g.l.



10 c - Section at level -18 m b.g.l.



10b - Section at level -24 m b.g.l.

Fig. 10. Horizontal sections of jet grouting columns in shafts area

MONITORING PROGRAM

To check the quality and the effects induced by ongoing activities, a considerable monitoring program has been implemented.

In order to obtain direct information about global response of the cavity and tunnel structures, and potential settlements induced by excavation, four sections (S1-S2-S3-S4) properly arranged along the Faul tunnel at interaxis ranging between 5 and 7 m according to morphological and geotechnical boundary conditions. Each section was instrumented with a simple topographical monitoring system of fixed points on the preliminary lining ribs to highlight possible strains of the excavated core, calculated by mutual distances variation (Fig. 11a). Measures of chords variations and shell settlements were considered and checked to ensure compatibility of performances with regard to design assumptions. At the same time, 3D displacements of external benchmarks placed on the hill above the tunnel were noted through classical topographic monitoring (Fig. 11b).

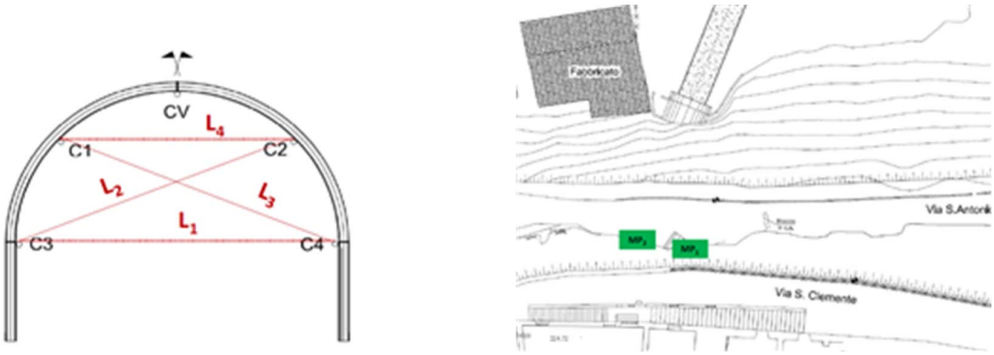


Fig. 11. Faul tunnel monitoring system - a) Typical layout of benchmarks on preliminary lining ribs - b) External observation instruments for topographical survey

A second monitoring system was installed on the existing buildings in the square at the top of the shafts, in the area adjacent to the San Lorenzo square, including both a dynamical control of induced vibrations, and a static monitoring of displacements and tilting on facades.
Vibrations levels related to shafts drilling operations were recorded by means of three triaxial accelerometers fixed on buildings closest to the shafts and connected to a continuous data acquisition system, as illustrated in Figure 12.

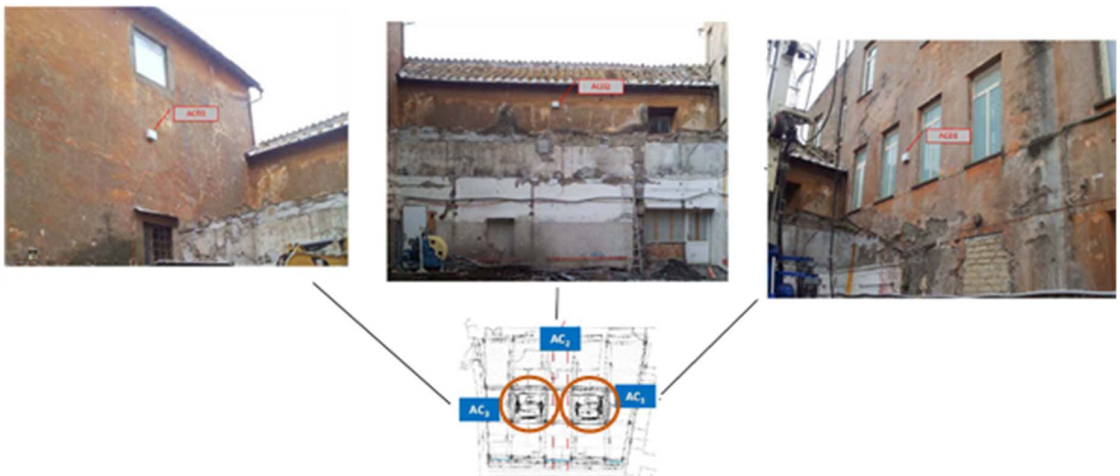


Fig. 12. Accelerometric monitoring system on buildings around shafts

Static monitoring was aimed to have information about potential settlements and rotations that could affect the buildings. Movements across surface of existing cracks on two facades were monitored, too.
The vertical displacements control of the buildings was entrusted to a special hydraulic settlement system (Fig. 13a), composed by a number of seven gauges hydraulically connected (T1-T7). All gauges were linked to the reference tank (T1), so any vertical displacement of gauges was measured as a change of pressure generated from the variation of liquid column. The system allowed to monitor absolute and relative vertical displacements, and was connected to a data acquisition system where both pressure (level) and temperature were stored for temperature compensation.
The measurement of inclination was carried out by means of one biaxial self-compensated tilt meter (CE1) based on MEMS technology, applied on front building façade as depicted in Figure 13b.

Taking advantage of the presence of cracks on buildings facades, also two electrical crackmeters (MG1 - MG2) were installed, anchored on the opposite sides of the joint, to measure the changes in the distance between the anchors (Fig. 13c).



Fig. 13. San Lorenzo square monitoring system - a) settlement measure hydraulic system - b) Tiltmeter - c) Crackmeters

MONITORING OF FAUL TUNNEL

The measures from topographical monitoring on ground level above Faul tunnel showed very slight displacements, with maximum settlements and horizontal displacements around 2-3 mm (Fig. 14).

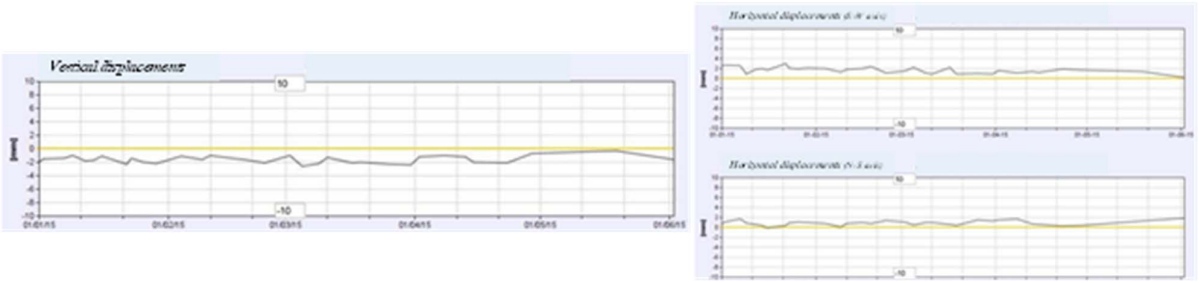


Fig. 14. Topographical monitoring (MP2) on ground level above Faul tunnel

Monitoring measures relative to benchmarks inside the tunnel likewise confirmed same results: in all the sections, absolute and relative displacements of monitored points showed small values. Maximum displacements were obtained in section S1, represented in graphs of Figure 15, with inner convergences limited to maximum values of 2 mm and shell settlements at most of 3 mm.

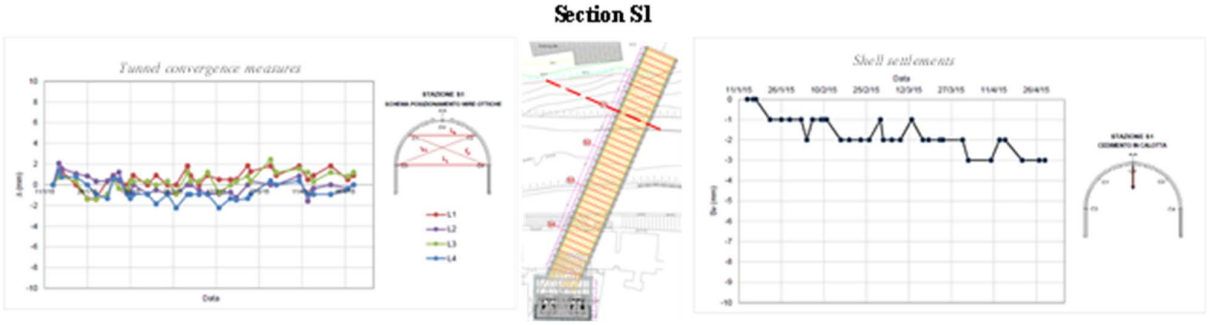


Fig. 15. Faul tunnel convergences and shell settlements for section S1

VERTICAL SHAFTS INDUCED EFFECTS

From the perspective of dynamical effects induced by shafts excavation with raise boring machine, vibrations recorded by accelerometers resulted extremely low and widely under preliminary fixed limit values. Maximum velocity of vibrations averagely reached 0.5 - 1.0 mm/s, in the face of tolerable entities of 5.0 mm/s, also according to international standards indications. Higher values were recorded for short-term occurrence, related to impulsive action for machine movement and adjustment. Anyway, also in this case limits were broadly respected. Some interesting aspects noticed regarded the increase of vibrations for the second shaft drilling, and the isotropic diffusion of waves, which led to same velocities of vibration in every direction. Next graphs (Fig. 16) show the trend of velocity of vibration in the 3 axis recorded by the same accelerometer (AC2) for both shafts drilling operations. Red dashed lines indicate fixed threshold values.

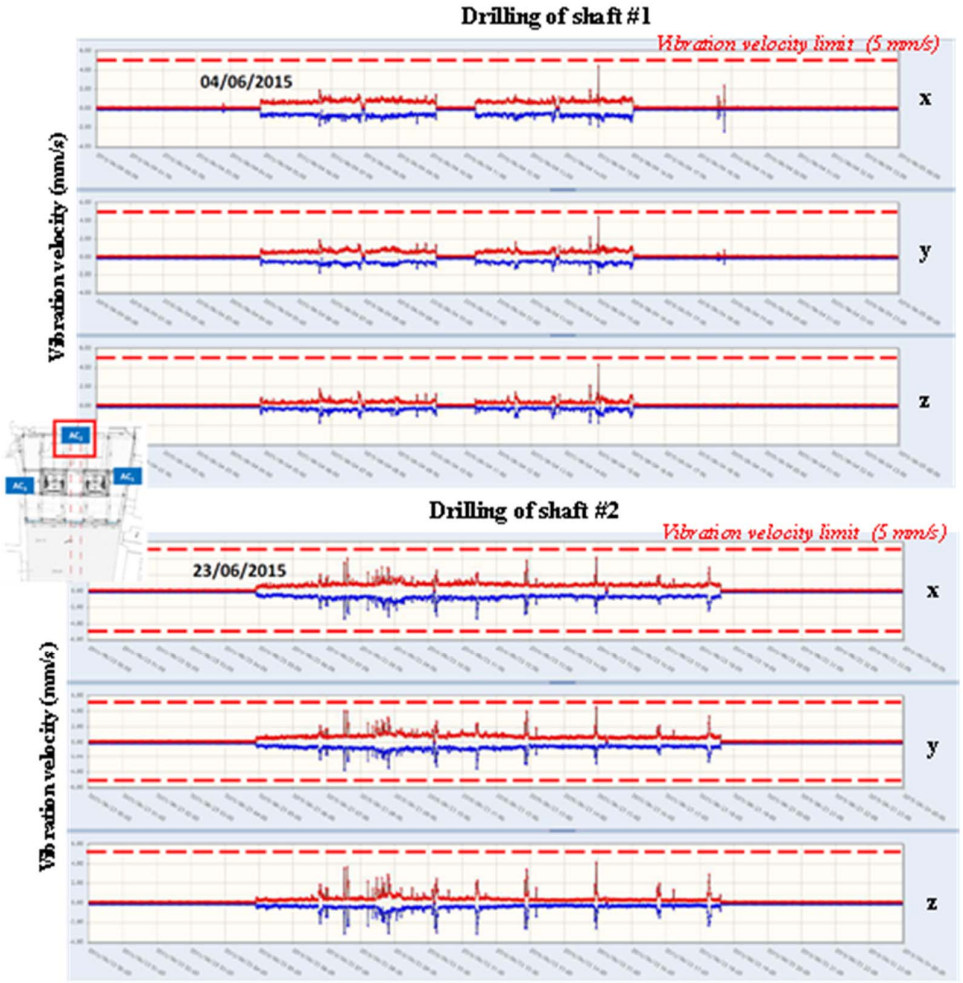


Fig. 16. Accelerometric measures in terms of velocities of vibration

Data obtained from monitoring system installed on existing buildings on top of the hill indicated coherently no practical effect induced by shafts drilling. Higher settlements recorded by hydraulic instruments resulted substantially negligible, under 1 mm, with no kind of trend or evolution during the whole working period. Measures recorded by instrument T3, by way of example, are reported in the following Figure 17. In the same way, tilmeters provided constantly null rotations during shafts drilling (Fig. 18). Crackmeters could not point out any meaningful variation of cracks width, neither (Fig. 19).



Fig. 17. Building settlement recorded by instrument T3



Fig. 18. Building tilts recorded by instrument CE1

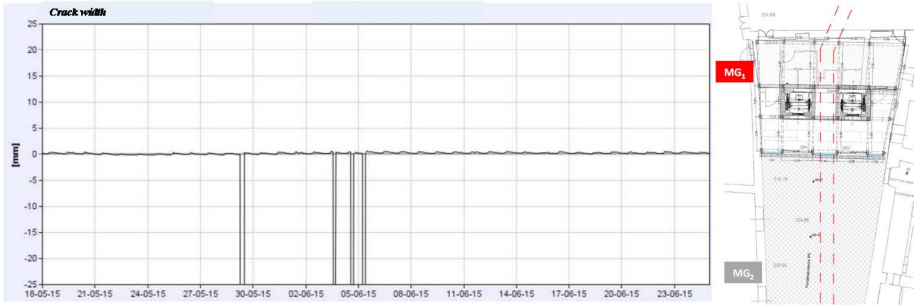


Fig. 19. Building crack width recorded by instrument MG1

CONCLUDING REMARKS

The construction of two new elevators to the hilltop city of Viterbo posed very interesting and sensitive issues mainly related to the high sensible historical and artistic value of the local urban context.
Innovative ground improvement based on the use of directional drillings carried out around the horizontal Faul tunnel, successfully restricted potentially dangerous displacements related to the excavation phases.
For the two lift shafts, the properly adopted raise boring drilling technique, together with a very extensive and focused soil improvement, allowed the excavation of two parallel circular big diameter shafts under absolute secure conditions, without any practical effects induced on the surrounding old historical buildings.
A particularly extensive monitoring system allowed an effective continuous control of interaction with the buildings heritage during the whole construction stages and the excellent soils response once improved.
The experience may constitute a meaningful reference for other similar requalification works of esteemed sites, which characterize Italian framework.

REFERENCES

Burke G.K. (2012). "The State of Practice of Jet Grouting". Proc. of the 4th International Conference on Grouting and Deep Mixing. Geotechnical Special Publication No. 228.

Croce P., Flora A., Modoni G. (2014). "Jet-Grouting – Technology, Design and Control". CRC Press ISBN: 9780415526401

DIN 4150-3:1999 : "Structural Vibration. Part 3: Effects of vibration on structures"

CEMENT AND SUPERABSORBENT POLYMER TO SOLIDIFY SLURRY

Jinyuan Liu and Ali Ahmad
Department of Civil Engineering, Ryerson University, Toronto, Ontario, Canada

ABSTRACT

This paper presents an experimental investigation of the geotechnical properties of cement and superabsorbent polymer (SAP) solidified slurry, particularly the unconfined compressive strength (UCS) and consolidation properties. The ultimate goal of this research is to apply SAP in treating soils with high water contents, like hydro-excavation slurry or mine tailing. Different dosages of cement and SAP are used in this study to solidify and strengthen the treated samples. The samples are cured before the tests for different curing times. For this study, the constant rate of strain (CRS) consolidation tests is used to evaluate the compressibility of solidified slurry. Based on the results, it is found that SAP can solidify slurry quickly and cement increases the strength of treated samples over time. There is an optimum SAP dosage issue. SAP inside the mixture behaves as a water resource to facilitate the hydration process of cement, while overdosage of SAP will weaken the bonding between particles inside the samples. The test results confirm that SAP is a promising material for the ground improvement of problematic soils with a high-water content.

Keywords: Superabsorbent Polymer, Slurry, Solidification, Soil Mixing

INTRODUCTIONS

Slurries are normally generated by processing and extracting a mineral from its elements of interest and construction operations, like hydro excavation (HydroVac). A conservative estimate of the annual total worldwide production of soil slurries is about 1-billion cubic meters (Edil & Fox, 2000). With this massive amount of slurries, researchers have been looking for ways to recycle the slurries rather than disposing them. For example, cement has been used to improve the strength of various types of slurries, such as dredged clay, to allow them to be used for earthwork and embankment (Wang et al. 2014).

Many studies have been conducted to investigate improvements in strength and compressibility of cemented clay (Bennert et al., 2000; Edil & Fox, 2000; Horpibulsuk et al., 2004). However, it is well recorded in these previous studies that strength decreases significantly when the slurries have a high-water content (Horpibulsuk et al., 2004; Miura et al. 2002). To address this challenge, a new material called superabsorbent polymers (SAPs) was recently introduced to take care of excess water in the slurry to facilitate strength improvement. SAPs are functional macromolecules with the ability to absorb water (Buchholz & Fredric, 1996). When the SAP particles are mixed with the slurry, they absorb water and transform themselves into hydrogels. These SAP hydrogels act as water reservoirs and they are also capable of going through hydration/dehydration cycles.

This research investigates SAP and cement to solidify slurries from HydroVac operations. The conventional method is to transport the slurries with HydroVac tankers to a liquid receiving site. Currently, SAPs are being used to turn slurries into solid or semisolid, which allows spoil transportation by using dump trucks rather than vacuum trucks. This solidification process has generated a considerable amount of savings in transportation and disposal costs. However, the SAP solidified spoil still needs to be transported to dump sites due to the lack of test data to support its use as a backfill material. New backfill materials are brought to the job site from elsewhere, which is both a time-consuming and an uneconomical process. Thus, this research evaluates the feasibility of recycling SAP solidified slurry into a backfill material through a series of geotechnical laboratory tests.

© 2018 Deep Foundations Institute

MATERIALS USED IN THIS STUDY

Slurry from a HydroVac job site in Ontario

The slurry used in this study was obtained from a HydroVac job site near Niagara-on-the-Lake, Ontario, as shown in the right-hand side of Fig. 1. The specific gravity was 2.6 per ASTM D854 (ASTM, 2014). The Atterberg limits were measured at 30.9% for the liquid limit and 19.9% for the plastic limit as per ASTM D4318 procedures (ASTM, 2017b). The slurry had a water content of about 95% and a wet unit weight of about 14.4 kN/m^3.

Cement and SAP used in this study

The sodium polyacrylate type SAP with a dry bulk density of 360 – 470 (kg/m^3) and pH of 5.5-6.5 was used as the binder to solidify the slurry. The SAP material was donated by MetaFLO Technologies Inc. The semi-plastic slurry treated by SAP is shown in the left-hand side of Fig. 1. In this experiment, ordinary Portland cement (Type I) was used in all the mixings.

SAMPLE MIXING AND PREPARATION

Test specimens were prepared with the designed additive according to Table 1. First, the dry form of SAP and cement were mixed. Then, the mix of SAP and cement was added to the slurry for 5 minutes of mixing using a high-speed paint mixer connected to an electric hand drill. For the samples used for unconfined compression tests, mixed slurry was poured without compaction into 3-inch diameter and 6-inch height plastic molds. Each mold was filled in three portions with a certain amount of vibration applied at each portion filling. Afterwards, the filled mold was capped with a lid and put in a humid container for curing.

For consolidation test samples, manual mixing was used due to the fact that a small quantity of mixture was needed for each sample. First, the pre-calculated portion of cement and polymer were added to the slurry and the specimen was then manually mixed thoroughly for 5 minutes using a spatula. Then, the mixture was poured directly into a consolidation ring and trimmed with a wire saw for a flat surface. At the final stage, each sample was wrapped in soft nylons and kept sealed in the lab environment for curing before testing.



Fig. 1 Slurry before (RHS) and after (LHS) mixing with SAP

UNCONFINED COMPRESSIVE STRENGTH (UCS) TESTS

A total of 36 samples were prepared according to Table 1 with different cement and SAP dosages: Three cement dosages (12%, 10%, 8%) and six SAP dosages (0, 0.4%, 0.6%, 0.8%, 1.0%, 1.6%). The dosages are calculated by the wet weight of the sample. The unconfined compressive strength (UCS) value of each test is also included in the table.

Table 1. Summary of samples for UCS tests

Specimen #	Cement content (%)	SAP content (%)	Curing time (day)	Peak UCS (kPa)	Specimen #	Cement content (%)	SAP content (%)	Curing time (day)	Peak UCS (kPa)
1	12	0	7	371	19	10	0.8	7	325
2	12	0	28	681	20	10	0.8	28	509
3	12	0.4	7	381	21	10	1	7	311
4	12	0.4	28	631	22	10	1	28	509
5	12	0.6	7	389	23	10	1.6	7	97
6	12	0.6	28	685	24	10	1.6	28	155
7	12	0.8	7	435	25	8	0	7	168
8	12	0.8	28	758	26	8	0	28	334
9	12	1	7	404	27	8	0.4	7	221
10	12	1	28	664	28	8	0.4	28	374
11	12	1.6	7	363	29	8	0.6	7	220
12	12	1.6	28	702	30	8	0.6	28	359
13	10	0	7	289	31	8	0.8	7	212
14	10	0	28	489	32	8	0.8	28	338
15	10	0.4	7	286	33	8	1	7	207
16	10	0.4	28	511	34	8	1	28	330
17	10	0.6	7	275	35	8	1.6	7	119
18	10	0.6	28	509	36	8	1.6	28	325

In most cases, a shear plane was found to be formed at an angle to the horizontal, while a conical failure mode was also observed in some samples. Typical stress-strain curves of the UCS tests are shown in Fig. 2. Each sample is noted first by cement dosage, followed by SAP dosage in percentage and then curing time. For example, the 12C+0.8P_7D sample means that the sample was mixed with 12% cement, 0.8% SAP, and cured for 7 days. Most samples reach their peak strengths at a failure strain value of about 2%. After that, the strengths drop significantly with increasing shear strain. The non-lateral confinement in the UCS test may contribute partially to this strain softening behavior. A more thorough study is needed to study its stress-strain behavior under lateral confinement condition.

The influences from cement, SAP, and curing time on the UCS are shown in Fig. 2. It is as expected that the strength of a cement and SAP-treated sample increases with increasing curing duration. For example, under the same dosage condition, the UCS results from the 28 day curing samples were higher than the corresponding 7 day curing samples. UCS is also increased with an increasing cement dosage. For example, a significant increase in UCS values is observed when the cement dosage is increased from 8% to 10 %.

However, the UCS does not increase with increasing SAP dosage. The maximum UCS values were obtained in the samples with a SAP dosage of either 0.6 % or 0.8%. Comparing the samples with and without SAP content, it can be found that SAP can facilitate strength increase by acting as a resource of water for facilitating cement hydration. However, there is an optimum SAP dosage issue. Over-

dosage SAP likely occupies more spaces inside the soil sample and weakens the cement bonding between particles.

Based on the test results, it can be concluded that the optimum dosages for the studied slurry is about 10% cement along with a range of 0.6-0.8 % SAP content.

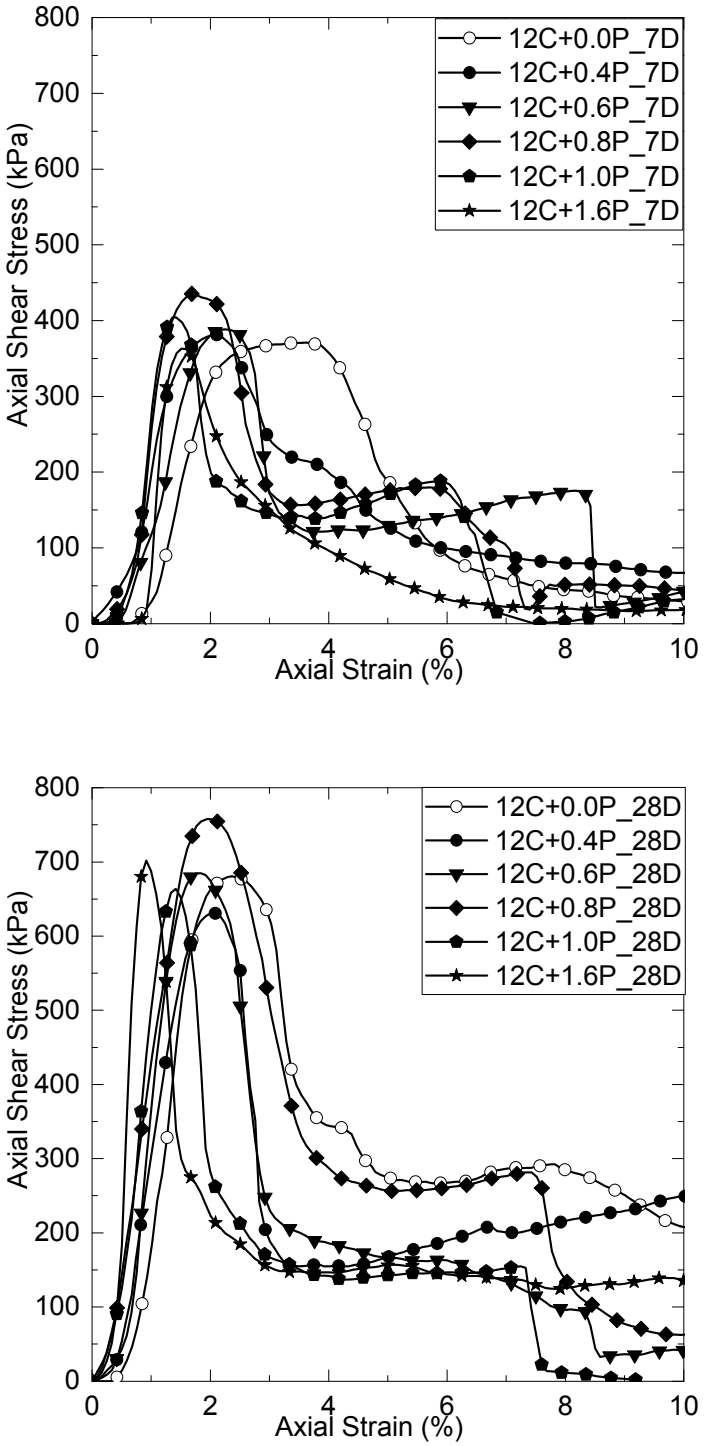


Fig. 2 Typical stress-strain curves of UCS tests on cement and SAP treated samples

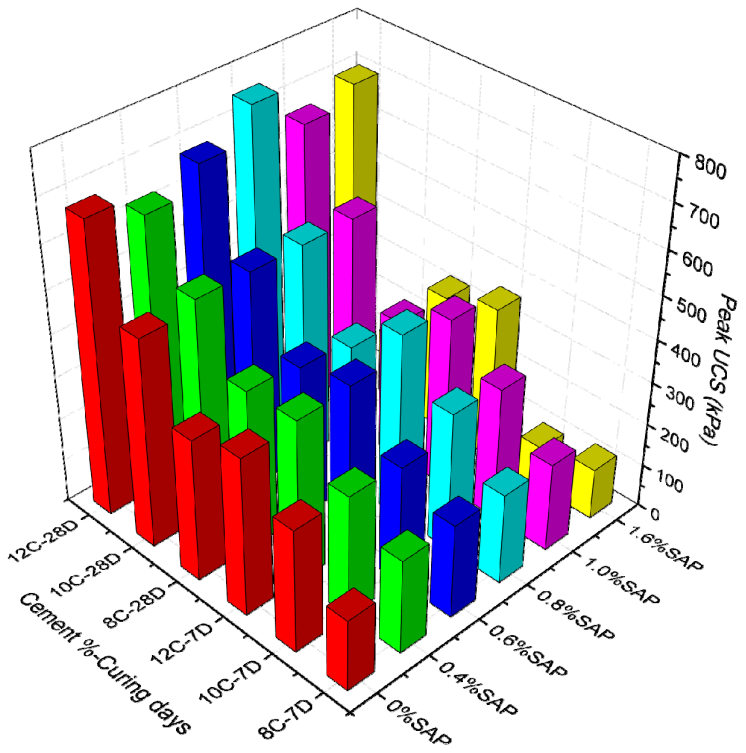


Fig. 3 Influences on UCS values from dosage and curing

CONSTANT RATE OF STRAIN CONSOLIDATION TESTS

A total of eight different specimens were tested by the constant rate of strain (CRS) consolidation tests to study the compressibility of treated samples under different cement and SAP dosages. Compared to the conventional incremental loading (IL) consolidation (oedometer) tests, the CRS test method has several advantages, including more accurate test curves and less secondary consolidation influence on the results. The CRS testing machine used for this study was manufactured by GEOTAC (Trautwein, 2001). A loading rate of 1% per hour was applied in all the tests along with a lower unloading rate for obtaining more test points during unloading stages.

Through oven drying, each component of samples can be obtained given the known cement and SAP dosage of the sample. The void ratio of the treated samples was calculated based on the quantity of each component (SAP, cement, soil, and water). This method is confirmed by a consistent degree of full saturation for each sample.

Typical *e-log p* curves of all specimens with 12% cement dosage are shown in Fig. 4. Comparing the initial void ratio of the samples, the higher dosage of SAP, the lower the initial void ratio due to the low specific gravity of SAP. Due to the same dosage of cement, the slope of compression curve, Cc, is similar for all the tests. The curing time did not show a significant effect on compression indices and rebound indices of the samples. That means the cement and SAP can strength the solidified slurry within a very short time. The consolidation indices of solidified samples are shown in Table 2. The low rebound indices show the feasibility of compaction of cement and SAP solidified samples for backfill applications.
However, the influence of curing time can be seen in the yield strength of the sample, *Pc*. The yield strength is determined by the Pacheco Silva's (1970) method due to its simplicity and scale

independence (Clementino, 2005). The yield strength of over 700 kPa from 7-day cured samples shows the feasibility of using cement and SAP solidified samples for most backfill cases. The yield strength is increased with an increasing curing time. For example, the yield strength of a 14-day cured sample is higher than the corresponding 7-day cured sample under the same cement and SAP dosages condition, as shown in Fig. 5. Generally speaking, the addition of SAP increases the yield strength of a sample compared to a sample without SAP. However, there seems to be no linear relationship between yield strength increase and dosage of SAP.

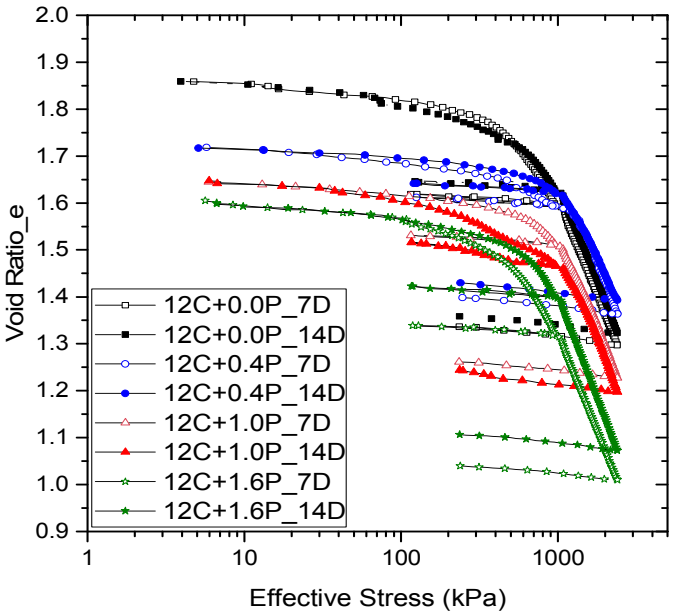


Fig. 4 Typical e-log p curves for cement and SAP treated slurry samples

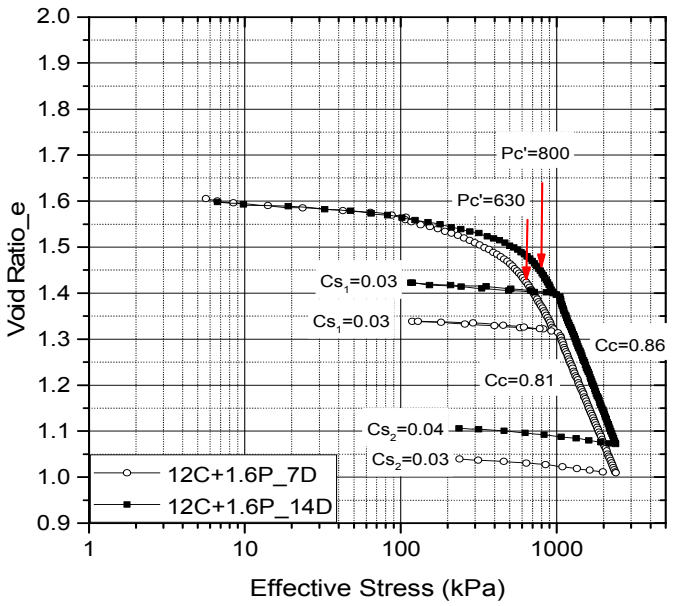


Fig. 5 Comparison of samples with different curing time

Table 2: Samples tested under CRS

Specimen #	Cement Dosage (%)	SAP Dosage (%)	Curing (Days)	Yield Strength (kPa)	Compression Index (Cs)	Rebound Index (CS_1)	Rebound Index (CS_2)
1	12	0	7	560	0.86	0.02	0.04
2	12	0	14	650	0.86	0.03	0.04
3	12	0.4	7	1020	0.96	0.02	0.03
4	12	0.4	14	1000	0.69	0.02	0.04
5	12	1	7	1000	0.99	0.02	0.03
6	12	1	14	1020	0.68	0.03	0.03
7	12	1.6	7	630	0.81	0.03	0.03
8	12	1.6	14	800	0.86	0.03	0.04

MAIN CONCLUSIONS AND DISCUSSIONS

This paper presents a series of geotechnical laboratory tests on the properties of superabsorbent polymer (SAP) and cement solidified slurry, including unconfined compressive strength (UCS) tests and consolidation tests. Based on the test results, the following conclusion can be drawn.

1. SAP is a promising material to solidify soil with a high water content. SAP and cement can significantly improve the compressive strength of solidified slurry. The results of the UCS tests confirm an improvement in the shearing strength of specimens. The strength increase is dependent on many factors, including SAP and cement dosage, and curing time. There is an optimum dosage issue. Based on this study, the optimum dosages of cement and SAP are concluded to be 10% cement along with a 0.6-0.8 % SAP calculated by wet weight of slurry.

2. Water trapped in SAP would be a good source of water for cement hydration. This may explain a higher compressive strength recorded from samples containing SAP compared to corresponding samples without SAP. However, the optimum dosage is crucial since extra water inside the samples will weaken the structure of soil and result in a lower strength. Soil containing SAP is compressible with only limited rebound after stress relief.

3. The cement and SAP solidified slurry exhibits a similar compressibility of natural soils. The low rebound index and high yield strength of treated samples prove its feasibility for compaction as a backfill material in the field. It is apparent that more research is needed to compare the properties of SAP solidified slurry and regular backfill materials.

In summary, this paper presents an innovative SAP in treating soil with a high water content. The results confirm the promising applications of SAP in the geotechnical engineering field.

ACKNOWLEDGEMENTS

The authors acknowledge the financial support of the Engage program of the Natural Sciences and Engineering Research Council of Canada and the support of MetaFLO Technologies Inc. Mr. Filipe Batista of Ryerson University supported the experimental work. Filipe was funded through 2016-2017 Fall/Winter Work Study Research Assistant Program at Ryerson University.

REFERENCES

ACI, 2005. ACI 229R-99 Controlled Low-Strength Materials, 99(Reapproved), 1–15.

ASTM, 2012. D4186/D4186M-12. Standard test method for one-dimensional consolidation properties of saturated cohesive soils using controlled-strain loading. American Journal of Engineering and Applied Sciences., 2458000, 1–18. http://doi.org/10.1520/D4186

ASTM, 2014. Standard Test Methods for Specific Gravity of Soil Solids by Water Pycnometer. American Society for Testing and Materials. http://doi.org/10.1520/D0854-14

ASTM, 2017a. Standard Test Method for Preparation and Testing of Controlled Low Strength Material (CLSM) Test Cylinders 1. American Society for Testing and Materials. http://doi.org/10.1520/D4832-16

ASTM, 2017b. Standard Test Methods for Liquid Limit, Plastic Limit, and Plasticity Index of Soils. American Society for Testing and Materials. http://doi.org/DOI: 10.1520/ D4318-17

Bennert, A., Maher, M., Jafari, F., & Gucunski, N., 2000. Use of Dredged Sediments from Newark Harbor for Geotechnical Applications. American Society for Testing and Materials, 18(10), 14.

Buchholz, & Fredric L., 1996. Superabsorbent Polymers: An Idea Whose Time Has Come. Retrieved from http://pubs.acs.org/doi/pdf/10.1021/ed073p512

Clementino, R. V., 2005. Discussion of " An oedometer test study on the preconsolidation stress of glaciomarine clays " 1. Canadian Geotechnical Journal. http://doi.org/10.1139/T05-010

Edil, T. B., & Fox, P. J., 2000. Geotechnics of High Water Content Materials. American Society for Testing and Materials. West Conshohocken. http://doi.org/10.1520/STP1374-EB

Horpibulsuk, S., Miura, N., & Bergado, D. T., 2004. Undrained Shear Behavior of Cement Admixed Clay at High Water Content. Journal of Geotechnical and Geoenvironmental Engineering, 1096. http://doi.org/10.1061/(ASCE)1090-0241(2004)130:10(1096)

Jia, R., 2010. Consolidation behavior of Ariake clay under constant rate of strain. Retrieved from http://portal.dl.saga-u.ac.jp/bitstream/123456789/117863/5/jia_201009.pdf

Miura, N., Horpibulsuk, S., & Nagaraj, T. S., 2002. Engineering behavior of cement stabilized clay at high water content. Soils and Foundations, 41(5), 33–45. http://doi.org/10.1248/cpb.37.3229

Trautwein., 2001. Sigma-1 CRS- Instruction Manual (ver 1.01.0). Houston, TX: Trautwein Soil Testing Equipment Company.

Wang, Z.-F., Shen, S.-L., Yin, Z.-Y., & Xu, Y.-S., 2014. Rapid field evaluation of the strength of cement-stabilized clayey soil. Bulletin of Engineering Geology and the Environment, 74(3), 991–999. http://doi.org/10.1007/s10064-014-0643-3

FOUNDATION SHAFT EXECUTED WITH JET GROUTING

G. Modoni, Università di Cassino and Southern Lazio
M. Ochmański, Università di Cassino and Southern Lazio and Silesian University of Technology
E. Salvatore, Università di Cassino and Southern Lazio
Ahn Dan L. Q. A. D. California Department of Transportation
P. Croce, Università di Cassino and Southern Lazio

ABSTRACTS

The paper analyses the use of jet-grouting for the execution of shaft foundations. Such a solution is sometimes used to transfer the loads from high bridges and viaducts to deeper competent subsoil strata. In this application jet grouting is used with the dual function of supporting the surrounding soil and sealing the excavation where the foundation is housed. The structure is then formed by a continuous two-dimensional wall having a circular planimetric layout and a massive bottom plug made of overlapped jet grouted columns. In the first part of the manuscript, a real case study is presented where a shaft is built for the foundation of the pier of a highway viaduct. The surveys and tests carried out both in the design phase and during construction are also reported. Starting from this case, the second part of the paper is dedicated to some possible methods for the analysis of the jet grouting wall considering the characteristics of the jet grouting columns. The presented method aims to simulate in the most realistic and rational way the variability of the geometric and mechanical properties of the jet grouting columns.

INTRODUCTION

In recent years, the development of transportation infrastructures in Italy passing predominantly through mountainous morphologies has led to the construction of numerous roadway and railway viaducts of considerable size. From the structural viewpoint there is a tendency to create continuous beams, with pillars spanned at remarkable distances for which it is essential to ensure very small settlement. Consequently, deep foundations made with piles or larger concrete shafts are frequently applied. The latter solution is predominantly adopted when the subsoil stratigraphic is characterized by a sequence of layers made of soft soils underlain by bedrock with the roof located at the depth of several dozen meters.

For such shaft foundations, the jet grouting technique is frequently used with the main purpose to ensure stability of the walls and prevent water inflow into the excavation (Balossi Restelli and Profeta, 1985; Balossi Restelli et al., 1986). For this purpose, the jet grouted columns are arranged in single or double rows to form a cylindrical wall with columns of approximately cylindrical shape. In this application, the jet grouting columns are often reinforced by the insertion of the hot-rolled steel profiles. Moreover, additional jet grouted columns can be created at the bottom of the shaft with the purpose of reducing the excavation depth, reducing the volume of concrete required to fill the shaft and, at the same time, ensure the watertightness of the structure. This second type of element is commonly referred as “bottom plug”.

The paper presents the case study of a shaft foundation created across the Bormida river for the construction of a highway viaduct. From this example, a guideline has been derived for the analysis of the mechanical behaviour of the jet grouting wall during the different construction phases. Additionally, some remarks for designing are given taking into account the variable characteristics of the jet grouted columns.

© 2018 Deep Foundations Institute

SHAFT FOUNDATION OF THE BORMIDA HIGHWAY VIADUCT

The viaduct over the Bormida River was built several years ago to create an alternative to the existing Torino-Savona highway. The viaduct has five spans with variable length up to 115 m and reaches a total length of 410 m (see Fig. 1.a). The structure of the viaduct is very peculiar, being the beams created with the DYWIDAG technology, and therefore it was necessary to guarantee very little settlements to the foundation.

To achieve this goal the two highest pillars (no 1 and 2) were placed on shaft foundations built with the jet grouting technique. In particular, the pillar # 1 is 65 m high and its foundation is located in the Bormida riverbed, and thus requires special attention during both design and construction (Fig. 1.a).

The subsoil stratigraphy (Fig. 1.b) at the location of pillar # 1 is characterized by alluvial deposits having an average thickness of about 15 m. Specifically, the subsoil in this position is made from the top to the bottom of an about 3 meters thick layer of sandy limestone, underlaid by mostly gravely material interbedded with limestone and randomly distributed cobbles and boulders. Below the alluvial deposits there is a formation of intensely fractured carbonate rock whose roof is very irregular and strongly inclined.

From the structural analysis the pillar no 1 transfers to its foundation a vertical load of about 78000 kN, a horizontal load equal to 17000 kN and a bending moment of 2300 kN*m. As a normal practice, the design solution has been conceived taking into account both the structural requirements of the works and the construction problems, with careful consideration for the different construction phases.

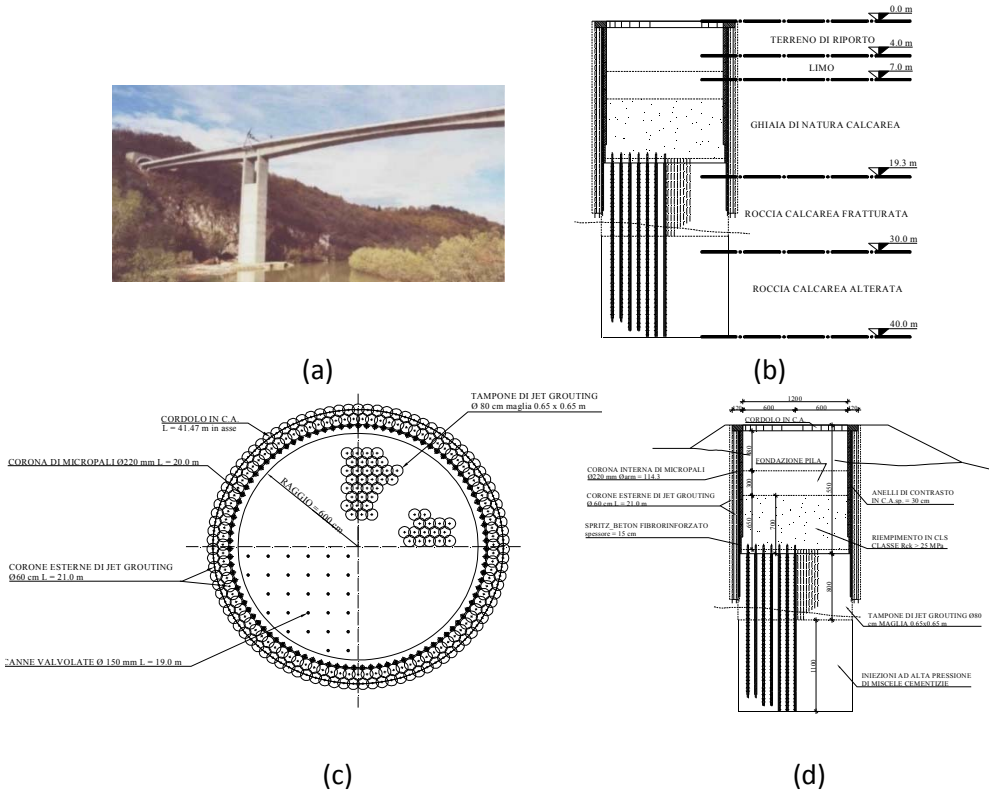


Fig. 1. Pillar #1 of the viaduct over the Bormida River (a. view of the viaduct; b. subsoil stratigraphy; c. horizontal cross-section; d. vertical cross-section)

The foundation shaft has a diameter of 12 m and is enclosed by a jet grouting wall, consisting of two concentric rows of 85 jet grouting columns each (double wall). The columns have a nominal diameter of 0.6 m (Fig. 1.c and d). In order to ensure continuity of the structure, the injection holes were located at a mutual distance of 0.44 m. The columns have a length of 21 m which allowed to reach the lower bedrock. In order to give the walls an ability to absorb bending moments in the vertical direction, some steel tubular elements were inserted during columns execution at the inner row of the shaft wall. At the bottom of the excavation, a bottom plug of 8.5 m height were constructed with partly overlapped jet grouting columns having a diameter of 0.80 m and drilled at a mutual distance of 0.65 m. The button plug has the dual purpose of ensuring the bottom water-tightness and consolidating the ground of variable thickness overlaid to the rock formation. The reinforcement of the button plug was completed by inserting numerous hot-rolled tubular elements of 19 m length. Through these tubes, high pressure cement injection were carried out with the aim of filling possible fractures and/or cavities in both pre-consolidated jet grouting material and fractured rock stratum.

The construction of the foundation was planned for the later stage. Specifically, at a preliminary stage of the works, a small circular isle with a height of 4.00 m was built within the riverbed. Subsequently, the jet grouting wall and bottom plug were executed and steel tubes inserted into the wall. The treatment of the bottom plug was performed just drilling the hole in the upper section, i.e. for the first 15 m, and further injection up to a depth of 23.5 m (considering both these depths from the top of the new ground surface).

The shaft was excavated with the technique of "underexcavation" which consists in construction parallel reinforced concrete rings 1.50 m high and 0.30 m thick one below the other. The steel tubes for the injection of the bottom were placed later working directly from the floor of excavation. Finally, the foundation works were completed with a concrete casting inside the shaft.

The execution of the foundation was anticipated by an intense experimental activity. With regard to the jet grouting, the choice of the most appropriate values of the treatment parameters and the overlapping distance between the adjacent columns was accomplished, as usual in this case, by carrying out a field trial. In particular, various treatment parameters were applied for different groups of columns, each consisting of three columns in staggered configuration, to form a wall unit module. The penetration of the columns was assessed by core sampling at the centre of each group together with the verification of the treatment continuity. Finally, a single-fluid system was adopted for the wall, injecting a mixture of water/cement with a ratio of equal approximately to 1.0, three nozzles of 1.8 mm diameter each and injection pressure of 450 bar in order to give a flow rate of about 150 l/min. The withdrawal of the JG monitor took place with an average speed of about 50 cm/min and a rotation speed of 20 rpm.

Always as a part of the field test, the mechanical strength of the improved soil was determined by performing uniaxial compression tests on samples taken from different depths. The measured values of uniaxial compressive strength were between a minimum of 8.5 and a maximum of 19.6 MPa with a significant variability.

Subsequently, after the execution of the jet grouting treatment, specific control tests were carried out before excavation. These tests mainly aimed at verifying the continuity of the wall and the bottom plug. With this aim a series of a sonic tomography tests were performed providing satisfactory results, even considering the natural variability of the jet grouting material.

The positive outcome of the treatment was finally confirmed during the execution phase, especially considering that the natural soil was very permeable and groundwater was fed directly from the overflowing river.

STRESS AND DEFORMATION ANALYSIS OF THE WALL

The previously described case study is the inspiration for a analysing the structural behaviour of the jet grouting wall during the different excavation phases. In the preliminary analysis, the shaft can be conceptualized as formed of identical, perfectly cylindrical and overlapped columns, and thus the wall can be schematized as a cylindrically shaped body made up of a series of longitudinal elements (columns) and a series of transverse elements formed by the circularly interconnected rings (Fig. 2). In this scheme, the soil pressure surrounding the shaft is partly absorbed by the longitudinal elements due to its own flexural rigidity and partly by the transversal elements able to turn soil pressure into compression thanks to the arch effect. For simplicity, it has been stated that the pressure acting on the shaft is produced by the subsoil at rest (K_o) conditions, i.e. in absence of any transversal dilatation or contraction. In particular, the pressure from the surrounding soil is transferred from the outside into inside of the shaft and is proportional at all points to the depth from the ground surface. Whereas, the pressure of the soil located inside the shaft is transferred in opposite direction, from the inside to the outside and is function of a depth from the bottom of the excavation.

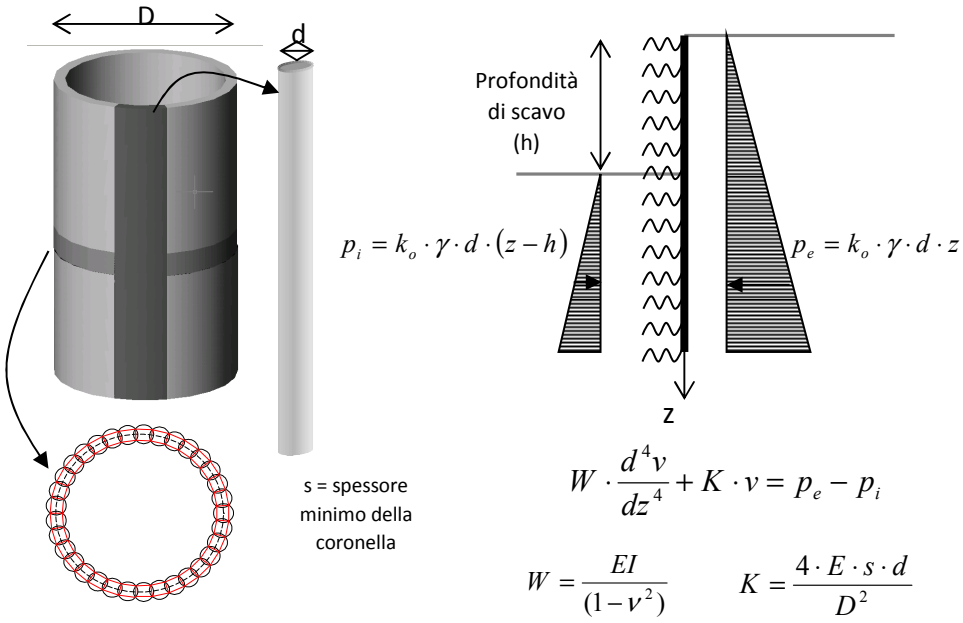


Fig. 2. Simplified structural scheme of the JG shaft wall.

Considering equilibrium and consistency between these elements, it is possible to derive for each longitudinal element the relation given in Fig. 2, in which v is the horizontal displacement of the generic point, W is the flexural rigidity of the longitudinal elements and K is the compressional stiffness of the transverse rings.

The solution for the given equation was obtained using the algorithm of the finite difference method for the case of a single wall of the same size as the shaft on the Bormida river, i.e. a diameter of 12.0 m and a length

of 21.0 m. In particular, a typical value of the stiffness modulus of 2500 MPa and a Poisson ratio of 0.2 was applied for the JG material. Similarly to the previously examined case, the column diameter was equal to 0.6 m and the overlapping distance to 0.44 m necessary to ensure the minimum wall thickness of 0.51 m. For the calculation of soil pressure, it was assumed for simplicity that the surrounding soil is dry and has a unit weight of 20 kN/m^3 and the at-rest earth pressure coefficient K_0 is equal to 0.5.

The diagram of the bending moments calculated at different depths of excavation is shown in the Figure 3. In general, it can be observed that the maximum value is reached, from time to time, at the bottom of current excavation and the overall values of bending moments are relatively low.

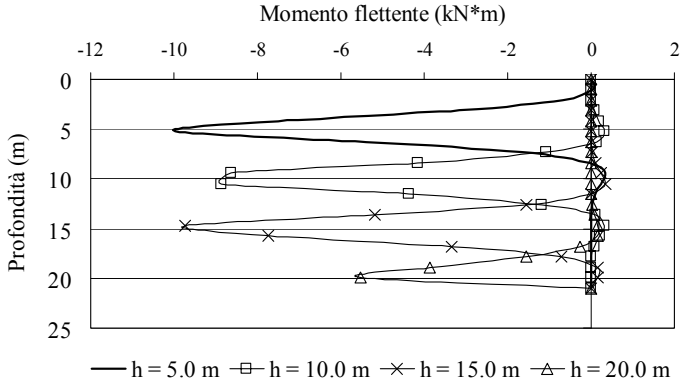


Fig. 3. Bending moments acting on the longitudinal elements of a cylindrical wall for the different excavation depths (h = depth of excavation).

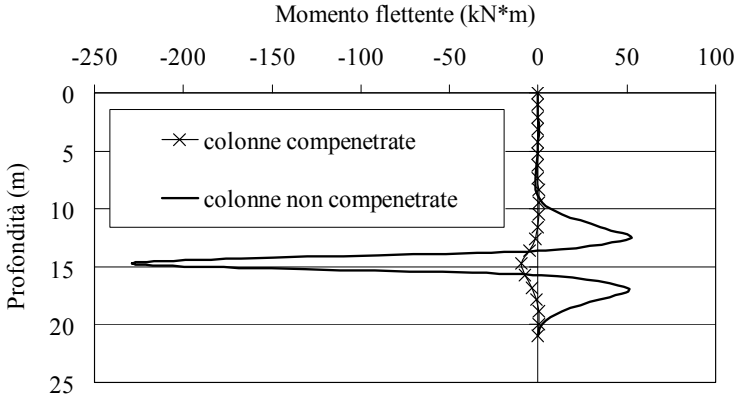


Fig. 4. Bending moments obtained for the case with perfectly overlapped columns and for the case with a lack of the structural continuity at a depth of 15.0 m (excavation depth = 15.0 m).

However, it must be noted that steel reinforcement is needed to absorb the bending moments, especially in the upper part where the normal stress in the columns produced by the weight of the structure is relatively small.

The previously carried out analysis omits the occurrence of the structure defects. It is therefore interesting to observe what happens if a transversal section of the shaft losses the structural continuity. From the numerical point of view, this situation can be simulated by eliminating a transversal element rigidity at a generic depth. Figure 4 shows the diagram of the bending moments obtained under the previously analysed

conditions, assuming the excavation depth of 15.0 m and an interruption at the same depth of the horizontal continuity of the wall. Comparing the two diagrams of bending moments it is immediately seen that this interruption produces a remarkable increase of the bending moment, which becomes about 23 times higher than those computed with no structural defects.

CALCULATION PROCEDURE

The previous analysis highlights the importance of assessing the stress state produced in the jet grouted material in the transverse sections (arching effect), as it rules the entire function of the entire support work. This verification can be performed with the different computational approaches. In accordance with the most classical, deterministic approach, a structural calculation is carried out assuming that geometrical and mechanical characteristics are constant. For example, using the Mariotte formula commonly used for the calculation of pipes, it is possible to calculate the depth of the shaft (Z_{lim}) at which the jet grouted material reaches the limit value of the uniaxial compressive strength σ_c:

$$Z_{\lim} = \frac{2 \cdot \sigma_c \cdot \sqrt{d^2 - i^2}}{k_o \cdot \gamma \cdot D} \qquad (1)$$

where D is the outer diameter of the wall, d and I are the diameter and the distance between adjacent columns, K_0 and γ are respectively the at-rest earth pressure coefficient and the unit weight of the subsoil considering that the shaft is entirely above the groundwater table. If these values are assumed to be the same as adopted in the previous paragraph and the compressive strength of jet grouted material is set to σ_c = 13.38 MPa, equal to the experimentally measured average value in the case of the shaft on the Bormida River, it is possible to create a single wall structure up to the depth of about 90 m. Obviously, it is necessary to introduce some reduction coefficient to ensure the structural safety. However, it is easy to understand how arbitrary and uncertain is this choice since there is no sufficient practice for the jet grouting applications.

One of the possible alternative solutions is to model the variability of the geometrical and mechanical characteristics of the jet grouting columns (Croce and Modoni, 2002) starting from a statistical analysis of the relevant quantities and introducing them in the calculation. With this purpose, the statistical analyses of numerous experimental data collected by the authors concerning the geometrical and mechanical characteristics of the jet grouting columns are summarized in Figure 5. For the details of these analyses the reader is referred to Croce et al. (2004). In particular, Fig. 5a depicts the frequency distributions of the jet grouting columns diameters measured in a test field (Croce & Flora, 1998). The values of the diameters measured on each column at different depths, are related to the mean value of the same column to highlight the variability of the diameters within columns with use of the variation coefficient. From this figure it is possible to see that the diameter of the columns is not constant but randomly and symmetrically varies around its mean value. It can be also seen that the variation coefficient strongly depends on the heterogeneity of the treated soils (Croce et al., 2004). Based on the results from the statistical analysis it is proposed to model the variability of the diameter with a function of normal distribution:

$$f(x) = \frac{1}{\sqrt{2\pi\sigma_x}} \exp\left[-\frac{1}{2}\left(\frac{x - \mu_x}{\sigma_x} \right)^2 \right] \qquad (2)$$

This model allows to calculate the probability associated with a given variable x by defining two parameters (e.g. mean μ_x and the variation coefficient $CV(x)=\sigma_x/\mu_x$).

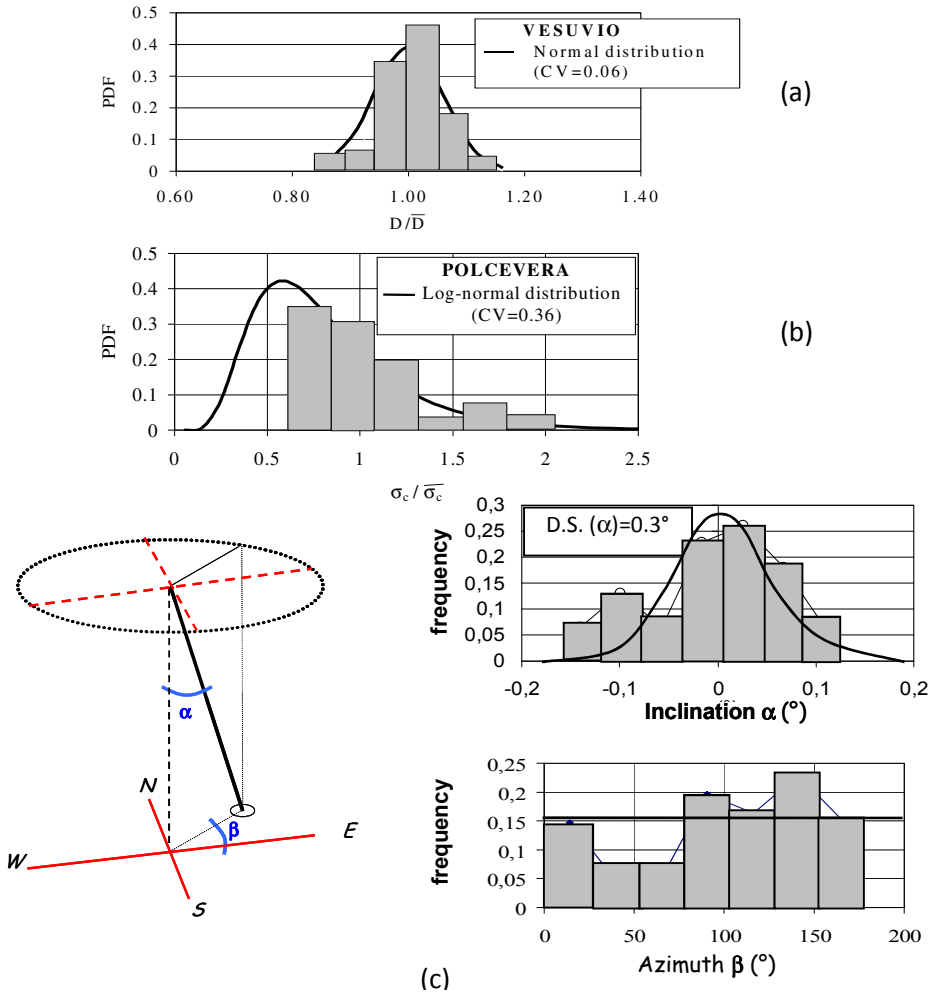


Fig. 5. Statistical analysis of the geometrical and mechanical characteristics of jet grouting columns (a. column diameter; b. uniaxial compressive strength of the JG material; c. columns inclination).

The statistical analysis of the data on the uniaxial compressive strength of the jet grouted material is shown in Fig. 5b where reported the results of a field tests (Polcevera, Croce et al., 1994). From this Figure it can be noticed that the variability of the values of the compressive strength is much higher than that for the diameters. These circumstances, together with the observation that the most probable values of the compressive resistance are the lowest ones and considering that compressive strength can only have the positive value, initiated the idea of simulating that variability with a log-normal function expressed as follows:

$$f(x)=\frac{1}{\sqrt{2\pi}\varsigma_x}\exp\left[-\frac{1}{2}\left(\frac{\ln(x)-\lambda_x}{\varsigma_x}\right)^2\right] \qquad (3)$$

This model postulates a normal variation of the generic x and introduces the parameters (λ_x and ζ_x) correlated to the mean μ_x and to the CV (x) variability coefficient of x.

The last characteristic feature, particularly important for the continuity of the wall is the column inclination from the vertical axis. This aspect was analysed in the Figure 5c presenting the data from the Serafini Island test fields (Croce and Modoni, 2005) for which the drilling inclination of was evaluated on the large number of columns.

To take into account this aspect two geometric variables are considered, the angle of column inclination α with respect to the vertical column axis and the azimuth β which orientates the column to the orthogonal plane (NS-EW). Therefore, it has been observed that while for the α angle there is a symmetrical statistical distribution on both sides of the nil value, for the β angle there is no preferable value since all the directions are equally probable.

Once the parameters and appropriate risk factors (FR) are chosen these probabilistic models allow to assign for each parameter the design value unique for all columns and to perform calculation in the same way as for the deterministic method (semi-probabilistic method). For example, with reference to the geometry of the previously studied case, calculation of the wall was performed assigning to each parameter a design value calculated using the above introduced probabilistic model. In particular, average values were assigned to the variables previously assigned in the deterministic method ($D_{_medio}$=0.60 m, σ_{c_medio}=13.38 MPa, α_{medio}=0), a risk factor for all variables equal to 0.05 together with different values of the variability coefficients CV (d), CV (σ_c) and D.S.(α).

For the β azimuth, it was assumed that the axis of each column diverged from the axis of the wall in the plane containing both axes. According to the previous hypothesis, the wall sections are still circular and thus it is possible to calculate the limit value of the excavation depth Z_{lim} using the eq. 1 at which collapse of the jet grouted material occurs. The values of Z_{lim} are presented in the diagram given in Fig. 6 by varying values of the CV (d), CV (σ_c) and D.S.(α). It is immediate to note that with greater variability of geometrical and mechanical characteristics of the columns the smaller the depth that determines the shaft collapse. In particular, depth at collapse occur is significantly reduced that when comparing with the previously evaluated value from the deterministic method.

Another possible approach is to consider the geometrical and mechanical characteristics of the columns that form wall no longer constant but variable according to previously introduced probabilistic models.

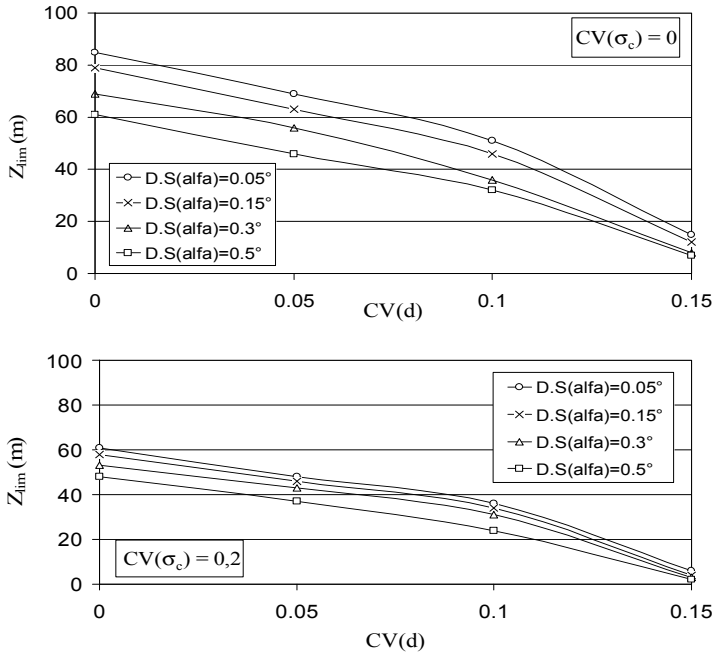


Fig. 6. Semi-probabilistic calculation of the jet grouting wall.

This last procedure, carried out with a probabilistic method, consists in the random generation of columns with the Monte Carlo technique. In particular, blocks with the length equal to the column mean diameter are randomly generated for each column with a value of azimuth β and angle of inclination α. For each block within the single column a value of diameter d and uniaxial compressive strength σ_c are assigned according to the selected model. With this method it is possible to generate any number of shafts and for each of them the transversal sections at different depths are studied (Fig. 7a). Since the deepest section generally has no more a circular shape it is not possible to evaluate stress state in the subsoil with the previously used formula (eq. 1), thus more sophisticated calculation methods are needed. For the analysed case, a finite element code (SAP 2000, ver. 6.11) was used schematizing each transversal section with a set of blocks as shown in Fig.7c. For each generated wall it is possible to evaluate the value of Z_{lim} defined as the depth at which the overlapping between the adjacent columns does not occur or where the limit strength of the jet grouted material is reached at least in one point. By analysing a sufficiently large number of cases (N) and assuming a specific risk factor (FR) it is possible to calculate the correspondent Z_{lim} depth of the wall (Fig. 8).

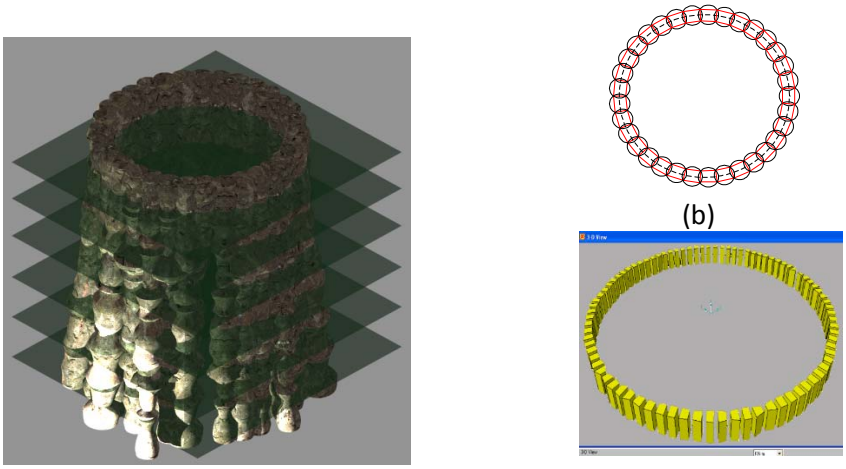


Fig. 7. Schematization of the jet grouted shaft for the calculation of transverse sections (a) Three-dimensional visualization of a randomly generated shaft; b) Example of transversal section; c) Schematization of the section for the numerical calculation).

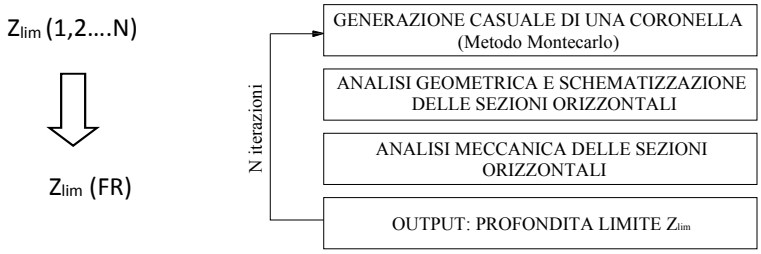


Fig. 8. Flowchart of the probabilistic approach.

The Figure 9 shows the results obtained with this method adopting the same values as in the previously performed semi-probabilistic calculation. Again the significant reduction of limit excavation depth caused by the random variability of column characteristics can be seen. Certainly, by comparison of the results from the probabilistic method with those from the previous semi-probabilistic calculation (Fig. 6) it is noted that the first leads to the significantly smaller limit depth. This result comes from the fact that the shape of the wall transversal sections studied with the probabilistic approach is not circular and for this reason the stresses in the subsoil are significantly higher.

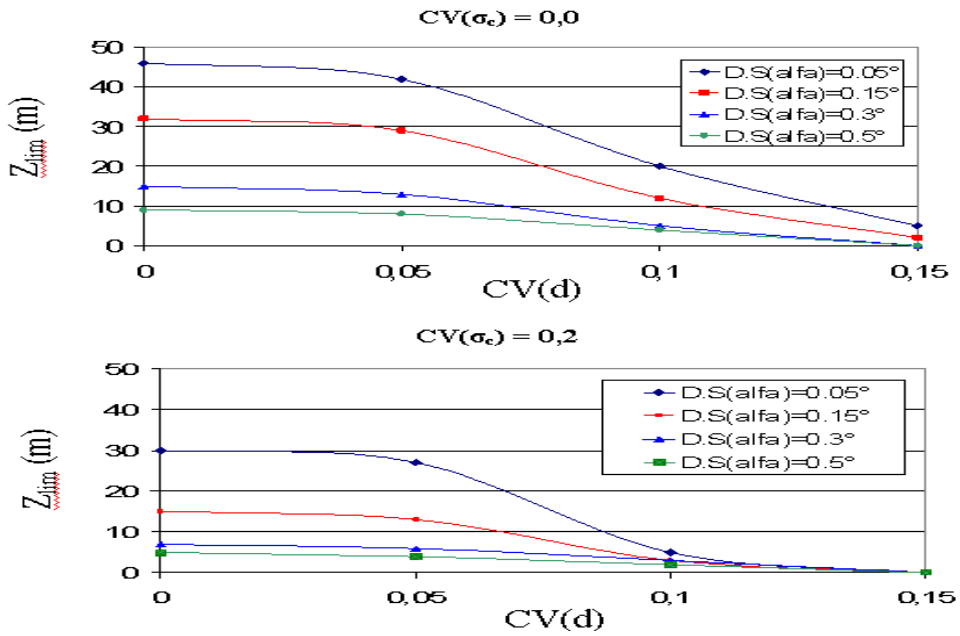


Fig. 9. Probabilistic calculations of the jet grouted shaft.

CONCLUSIONS

Starting from the case study of a shaft foundation created with the jet grouting technique, the supporting function of jet grouted shafts has been analysed. The study of the stress state produced in the shaft walls during the excavation phase clearly highlights the importance of the arch effect generated by the overlapped columns. Furthermore, the stress state analysis in the transversal section of the wall has been performed using the deterministic, semi-probabilistic and probabilistic methods. The comparison of the results obtained from the application of these methods reveal that the probabilistic approach has the highest level of rationality which allows to take into account all the geometrical and mechanical aspects with the remarkable variability of the column properties.

BIBLIOGRAPHY

Balossi Restelli A., Profeta M. (1985) "Autostrada Udine-Tarvisio. Trattamenti speciali per fondazioni e difese fluviali" Industria delle Costruzioni.

Balossi Restelli A., Colombo A., Gervaso F., Lunardi P. (1986) "Tecnologie speciali per il preconsolidamento di scavi nelle alluvioni di Milano in occasione della costruzione della linea 3 della Metropolitana", Congresso Int. "Grandi Opere Sotterranee", Firenze, 8-11 giugno.

Croce P., Gaio A., Mongiovi' L., Zaninetti A., (1994) "Una verifica sperimentale degli effetti della gettiniezione" Rivista Italiana di Geotecnica.

Croce P., Flora A., (1998) "Effetti della gettiniezione in terreni piroclastici" Rivista Italiana di Geotecnica, N.2, pp.5-14.

Croce P., Modoni G., (2002) “Numerical modelling of jet-grouting foundations”, Proc. of the V European Conference on Numerical Methods in Geotechnical Engineering, Paris.
Croce P., Flora A., Modoni G. (2004) Jet grouting, Hevelius editore, Benevento.

Croce P., Modoni G. (2005). Design of Jet Grouting Cut-offs. 6th Int. Conf. on Ground improvement Technique, July, Coimbra (Portugal).

COMPACTION GROUTING INTERVENTION FOR THE MITIGATION OF SOIL LIQUEFACTION RISK WITHIN THE EARTHQUAKE-STRICKEN AREA OF EMILIA IN 2012

Claudio Asioli, Trevi S.p.A.-Design, Research & Development Dept., Cesena (FC), Italy, casioli@trevispa.com
Federico Fanti, Trevi S.p.A.-Design, Research & Development Dept., Cesena (FC), Italy, ffanti@trevispa.com
Paolo Zuffi, Trevi S.p.A.-Design, Research & Development Dept., Cesena (FC), Italy, pzuffi@trevispa.com

ABSTRACT

In order to reduce the liquefaction risk, it is common practice to modify the mechanical features of natural soils by means of active interventions.

Compaction Grouting is one of the most widely used technologies, since it generally achieves very good results in terms of costs/advantages.

The paper describes the design criteria employed and the achieved results for the soil consolidation intervention carried out within the earthquake-stricken area of Emilia (May 2012); upon said area a new primary school and kindergarten were built.

In addition to the liquefaction analyses – which were carried out according to the simplified method proposed by NCEER and which show the presence of a potentially-liquefiable layer of saturated silty sand between 1.8 m and 7.0 m from ground level – the paper also illustrates the calculation procedure developed for the compaction grouting columns' design.

In particular, the text focuses on the two phases into which the design can be divided: assessment of the minimum soil strength to be obtained in the liquefiable layer in order to guarantee the safety factor required; setting out of columns' geometry (pattern, diameter and spacing) to be adopted in order to reach the requested density degree.

Similarly to the liquefaction potential index (LPI) defining the degree of risk, a new index soil improvement index (SII) is proposed to provide directions on the soil improvement that needs to be obtained.

Moreover, said index can be employed also to assess the effectiveness of the accomplished intervention.
Finally, the paper describes monitoring and additional soil investigations results, both for the assessment of the preliminary test field – which is necessary to validate the design theoretical analyses – and for the final control tests.

Keywords: liquefaction, compaction grouting, soil consolidation, soil improvement index, test field.

THE COMPACTION GROUTING TECHNOLOGY

Compaction grouting, also known as low mobility grouting, consists in inserting into the soil, by rotary drilling or driving, a steel casing through which, once the design depth is reached, mortar or concrete is injected. Simultaneously with the casing's extraction, the injection takes place in a slow and controlled way usually by stages.

The ideal grouting process should involve in-situ soil horizontal displacement without permeation or fractures, in order to obtain a densification of the natural soil surrounding the injection point, with consequent increase in its shear strength.
Such a result is achieved by using a highly consistent mortar or concrete (Class S1 with a 4÷5 cm slump) with an unconfined compressive strength equal to 4÷10 MPa.

© 2018 Deep Foundations Institute

GEOTECHNICAL SITE CONDITIONS

The geotechnical site conditions were defined according to the soil investigations provided by the tender documents together with an additional soil investigations performed before the beginning of works. The soil stratigraphy, as indicated in Figure 1, consists of an alternation of fine-grained and coarse-grained materials typical of Pianura Padana's alluvial deposits. In particular, a clayey silt lens was encountered in a small area of the site.

The ground water table was encountered at a depth ranging from 1.5 to 2.3 m from natural ground level according to the seasonal variations.

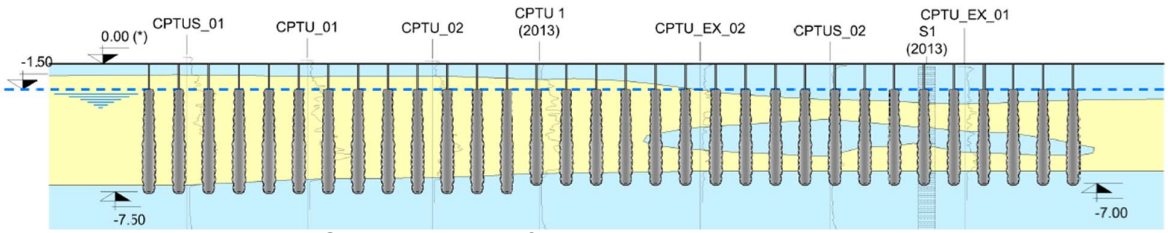


Fig. 1. Stratigraphic Profile with the executed intervention

LIQUEFACTION ANALYSIS AND COMPACTION GROUTING DESIGN

The safety factor relevant to liquefaction phenomena was assessed according to the simplified method suggested by Youd T.L. and Idriss I.M. (2001), which allows to estimate the soil's cyclic shear resistance starting from the results of the piezocone CPTU tests.
The safety factor employed for the calculations was 1.25, pursuant to the requirements of Eurocode 8.

According to the performed analyses, an average safety factor equal to 0.75 was found in the layer of saturated silty sand at a depth between 1.5 m (maximum water table level) and 7.0 m from ground level, hence it turns out to be potentially liquefiable.

The liquefaction potential index (LPI) evaluated according to the method of Iwasaki et al. (1982), for the 10 CPTU tests available, ranges from 3.7 (silty clay lens area) to 12.3, corresponding to a moderate/high liquefaction risk.

As far as compaction grouting columns' design is concerned, a calculation procedure starting from the design cyclic stress ratio (CSR) and reversing the formulas employed for liquefaction analysis was developed. Said procedure allows to define the "minimum CPTU cone resistance profile" ($qc_{,MIN}$) that has to be obtained to achieve the required safety factor. The adopted procedure implies that the soil behaviour index (IC) is kept fixed.

Once the minimum cone resistance has been determined, the minimum relative density to be obtained in-situ was assessed. That allowed to define the consolidation's geometry by means of the relation proposed by Mitchell J.K. (1981), which is based on the following hypotheses:

- The volume of the injected material displaces the soil, thus inducing a decrease in the void volume equal to the injected volume;
- Soil displacement occurs only in the radial direction, hence no upheaval of the ground level has to take place.

According to the aforementioned hypotheses, the initial design geometry of compaction grouting columns consisted of a square pattern with 1.75 m spacing and with an average equivalent diameter ranging from 500 mm (upper 1.5 m section), to 600 mm (remaining 3.5÷4.0 m of columns).
A total of 888 columns was expected to be constructed on a 2700 m2 area, so that the corresponding replacement ratio was equal to about 9%.
The presence of the columns in the soil has two additional beneficial effects:

- Since the columns are composed of a cement mortar, their shear resistance could be taken into account.
- The columns' higher shear stiffness should attract a higher seismic shear stress lowering the seismic stress (CSR) acting on the surrounding soil (Baez 1995).

"On the safe side", these two effects have been completely disregarded in the design where only the densification treatment effect was considered.

TRIAL TEST FIELD

The validity of design assumptions and the suitability both of the equipment and of the technological and construction parameters were assessed by means of an in-situ preliminary trial test field, which allowed to check the soil consolidation degree obtained with three different column spacing: 1.75 m (envisaged design spacing), 1.50 m e 2.00 m. A large trial test field, with 16 columns performed for each spacing, was carried out in order to involve an adequate soil volume also during the test stage.

During columns' execution, a topographic monitoring of the ground level was executed revealing an average upheaval equal to 10 cm for the 1.75 m spacing, 15 cm for the 1.50 m spacing and 6 cm for the 2.00 m spacing. For all three tested patterns, up to a depth of approximately 4.5 m from ground level, post-consolidation CPTU tests showed that cone resistances were higher than the minimum value required.

The only pattern always showing resistance values equal or higher than the minimum ones, was that with the 1.50 m spacing. In the treatment's deepest portion, for about 0.5÷1.0 m from the lower clay level, no test has ever reached the minimum required resistance level.
However, the design pattern, with a 1.75 m spacing, obtained a remarkable improvement as far as resistance was concerned, even though it didn't reach in all parts the minimum value required.

The above mentioned effects highlighted the following aspects:
- Upheaval of the ground level implies a volume loss of injected material, thus disputing Mitchel's first hypothesis, which consequently determines a lower densification of the soil situated between the columns;
- The soil's upward displacement induces overpressures that, in any case, produce soil consolidation next to the upper part of the treatment;
- With the first injection step, in the deepest part of the column, soil displacement occurs not only in the radial direction (Mitchell's 2nd hypothesis) but also downward; that's why, even in this area, a lower soil consolidation is obtained.

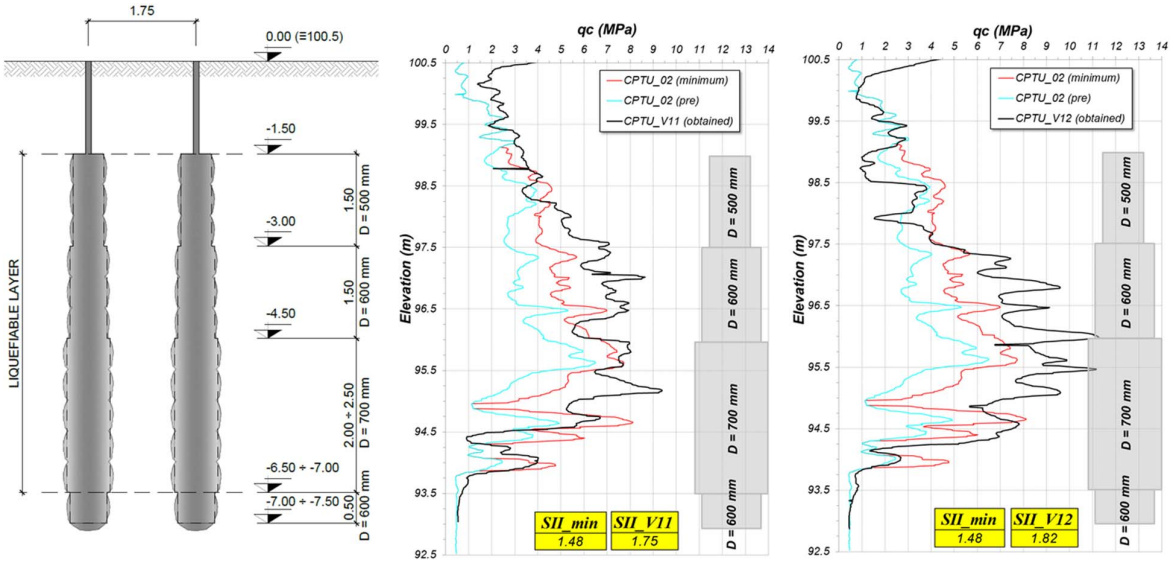


Fig. 2. Typical section of the columns and cone resistances obtained in the additional test field

According to said considerations, the column's geometry was modified by keeping a 1.75 m spacing and by increasing the columns' diameter to 700 mm for the lowest 4.5 m of the columns. Moreover, a further injection step was added below the liquefiable layer, extending columns for 50 cm into the lower clay layer.

Figure 2 shows the final geometry adopted, together with the results of two additional penetrometer test obtained in the additional test field performed to validate the new design hypotheses.

CONSIDERATIONS ON THE SOIL BEHAVIOR INDEX OF THE POST-TREATMENT TESTS AND CONTROL CRITERIA OF THE OBTAINED RESULTS

The analysis of post-treatment penetrometer tests carried out in the trial test field's area (and, eventually, also for the final tests) highlighted a systematic decrease in the Ic soil behavior index which was evaluated according to the 1990 Robertson's classification.

The treatment produces both an increase in the qc cone resistance and in the fs sleeve friction. Due to such effect, the normalized friction ratio FR(%) is kept unchanged during pre and post treatment as shown in Figure 3.

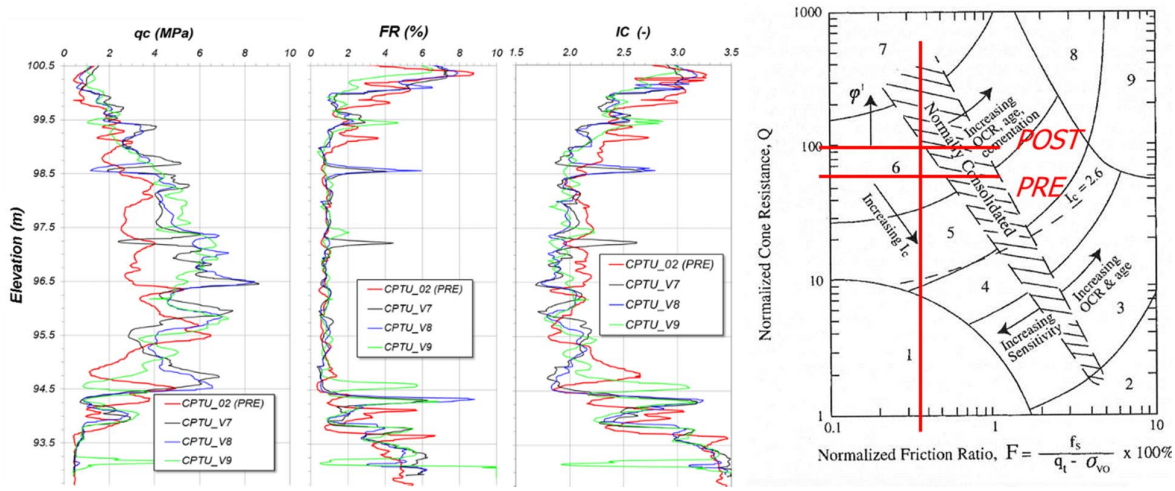


Fig. 3. Qc, FR and Ic comparison calculated for three control tests of the field and Robertson Graph 1990.

According to the 1990 Robertson's graph, with a doubled normalized cone resistance and an unchanged friction ratio, a lower Ic value is obtained.

Consequently, the soil's fine content turns out to be "coarser" compared to its initial condition.
From a physical perspective, that would lead to an absurd result, since, by inserting a stiff element into the soil, the soil's granulometric structure should not change.

The decrease in the Ic value clashes with one of the adopted basic design hypotheses, according to which the Ic value is kept unchanged, since it is strictly bound to the soil's granulometric nature.

Said interpretation would lead to a soil more susceptible to liquefaction than it was initially; that explains the choice of using the post/pre cone resistance ratio, defined as Soil Improvement Index (SII), as a control criterion of the result obtained, rather than repeating the liquefaction analysis using the CPTU tests.

RESULTS OBTAINED WITH THE TREATMENT

Two different working phases were carried out; during the 1st one, from the end of May until mid July 2014, 591 compaction grouting columns were executed, while in the second phase, from mid May to mid-June 2015, after the construction of the school's first lot, the remaining 297 columns were executed, for a total of 888 elements.

Results in terms of mechanical resistance

16 CPTU tests and 1 seismic tomography were carried out in order to assess the achieved compaction degree. Control tests were performed next to the ones carried out before consolidation, using the same testing probe.
Very positive results were obtained as far as cone resistances were concerned (see Figure 4 quoting the results of 3 CPTU tests).

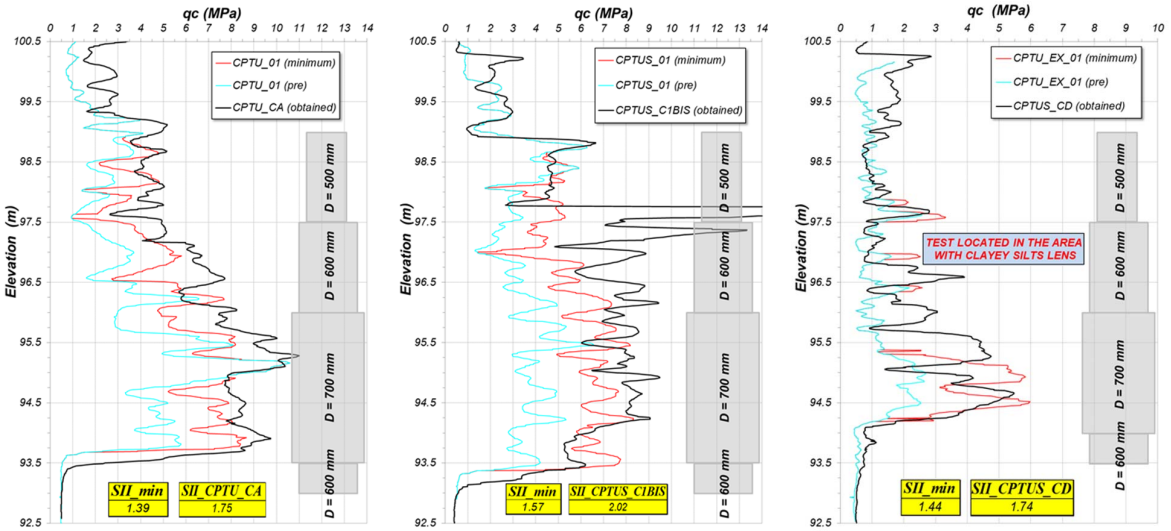


Fig. 4. Cone resistance of three control tests.

The less satisfactory results in terms of resistance were obtained close to the area where a lens of clayey silts was detected within the liquefiable layer; in such areas the LPI pre-treatment index turned out to be lower than 5 (moderate risk). This phenomenon probably depends on a thinner sandy layer which was also confined between two more compressible clayey layers.

Results in terms of shear waves' velocity

Very interesting results were obtained from the seismic tomography. Figure 5 shows the comparison between pre and post treatment shear waves velocity (Vs). The measured Vs increment in the consolidated area ranges from about 100 m/s and 200 m/s, with post treatment values that generally range from 200 to 350 m/s.

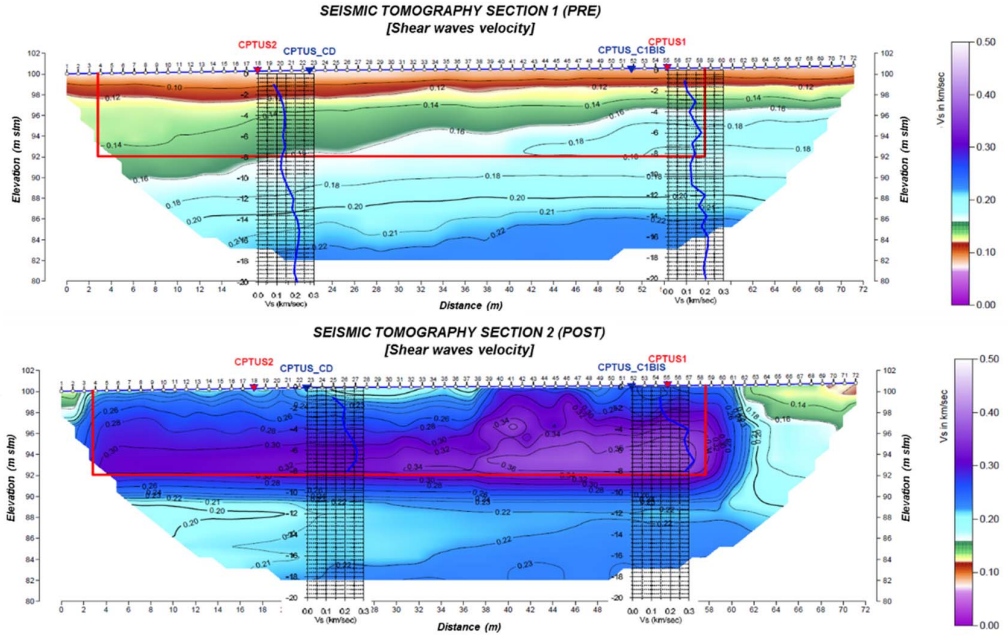


Fig. 5. Pre and post treatment shear waves velocity obtained from Seismic Tomography

Seismic CPTUS tests allowed to confirm the Vs increase obtained through the tomography. In particular, by carrying out a tomography's section next to the CPTUS tests position, the values obtained are generally higher than those directly measured by the seismic cone tests (Figure 6a).

Such result may probably be attributed to the fact that, with tomography, the shear waves are much more affected by the presence of stiffer columns, hence the Vs value obtained turns out to be higher.

Figure 6b shows the comparison of pre and post-intervention Vs values with the average Vs values obtained by a correlation with the qc cone resistance (Jamiolkowsky et al.1989). It is worth observing that the red curve relevant to the initial natural soil condition perfectly matches the CPTUS values, especially for the cohesionless layers, whereas the blue curve concerning correlations drawn from post-treatment tests significantly deviates from CPTUS's measurements and does not allow to highlight the obtained soil improvement.

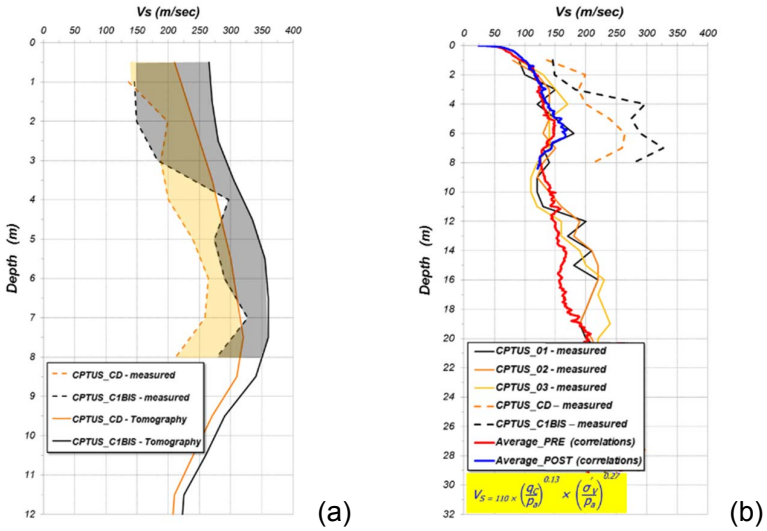


Fig. 6. Comparison of the Vs obtained from CPTUS and Seismic Tomography (6a) and Vs comparison obtained from qc resistance-based correlation (6b) for pre and post CPTUS.

A liquefaction Analysis on post treatment conditions, based on the Vs values drawn from CPTUS tests and from the tomography, was finally carried out pursuant to the procedure suggested by Andrus and Stokoe 2000 and 2003. Such analysis confirmed the effectiveness of the performed treatment (Figure 7).

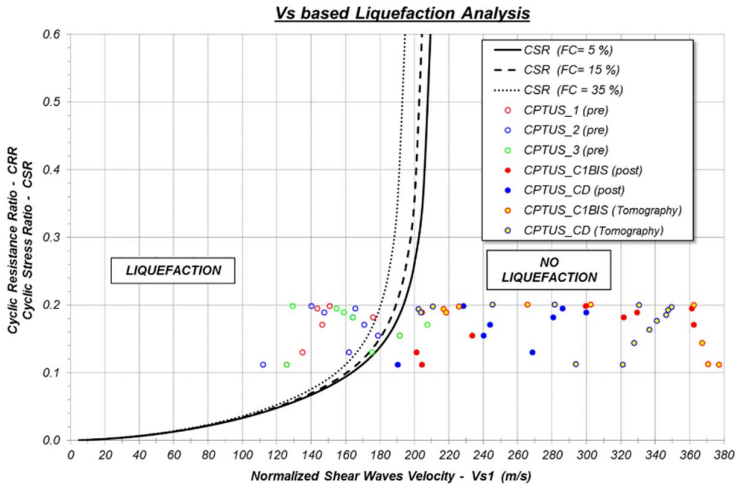


Fig. 7. Post-treatment liquefaction analysis based on shear waves velocity.

MONITORING

During the working phases, the following topographic monitoring was carried out:
- Records of ground level upheavals next to each column;
- Topographic precision survey next to 5 columns;
- Pre and post intervention topographic survey for the assessment of the total induced upheavals.

The assessment of upheavals during the single columns' injection phases was carried out by employing a laser level. The laser level was placed at a proper distance from the injection point, while the receiver stood as close as possible to the drilling point, compatibly with the space occupied by the equipment. During the injection steps, the upheaval values measured with the laser level at the various depths were recorded. In this way, it was possible to make sure no anomalous upheavals - higher than those recorded during the test field - took place, in order to avoid mortar's volume losses, which would determine lower densifications than the design ones.

In addition, a topographic precision control for 5 vertical points was carried out. The topographic survey device was made up of 2 robotized stations for data measurement and of 19 topographic targets installed along two orthogonal directions on concrete cubes directly resting on the soil as shown in Figure 8.

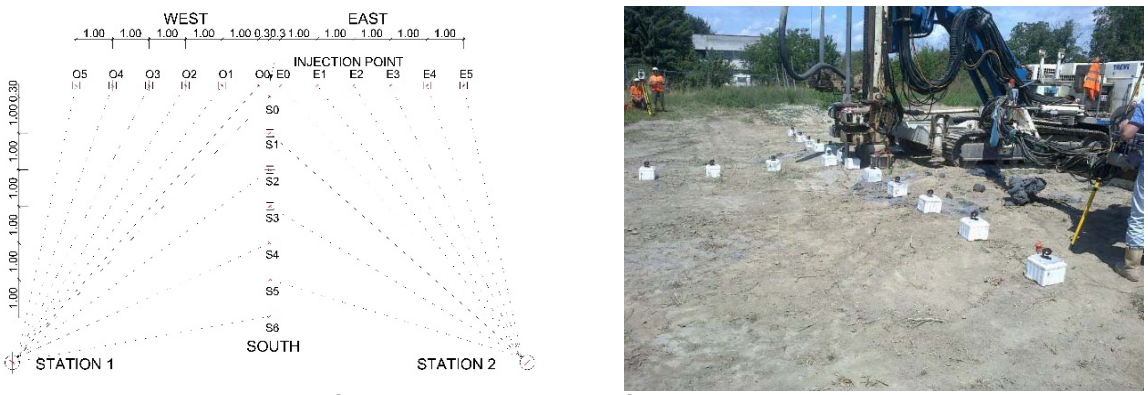


Fig. 8. Arrangement of the monitoring system for the precision topographic survey

Figure 9 shows the upheavals measured for 2 out of 5 measured points. Comparison between the precision survey and the upheaval measured by the laser level allows to confirm that even this monitoring system, despite being less accurate, succeeded in providing reliable data on the upheaval degree.

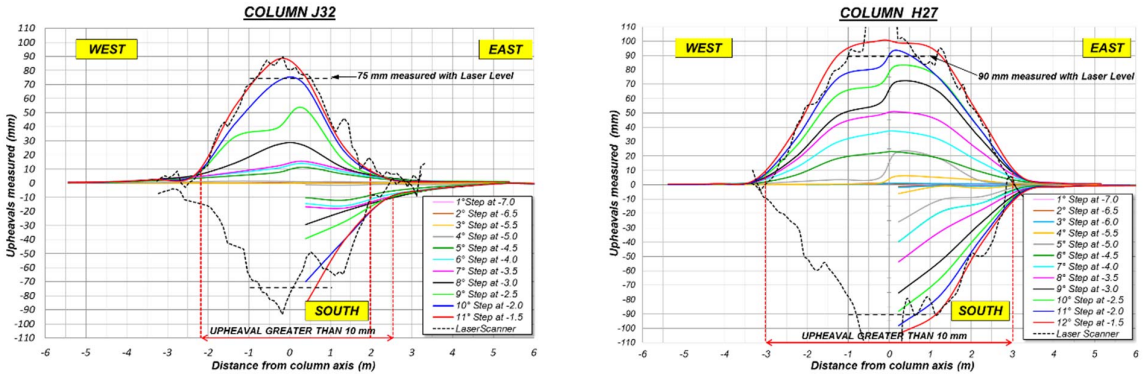


Fig. 9. Upheavals measured with the precision topographic survey concerning two different points

The analysis of graphs shown in Figure 9 allows to state that, at a depth greater than 3.5÷5.0 m in free field condition, upheavals are lower than 20 mm.

Moreover, it is worth observing that the upheaval's cone of influence is kept nearby the compaction grouting column with a maximum radius equal to approximately 2.5 ÷ 3 m.
Upon finalization of works, a topographic survey of the treated area's surface was carried out and compared with the pre-treatment survey, thus allowing to draw up a contour curves upheavals' map, (Figure 10).

Apart from a few points where a localized peak with a maximum value of 29 cm was detected, all measured upheavals generally ranged between 10 and 20 cm.

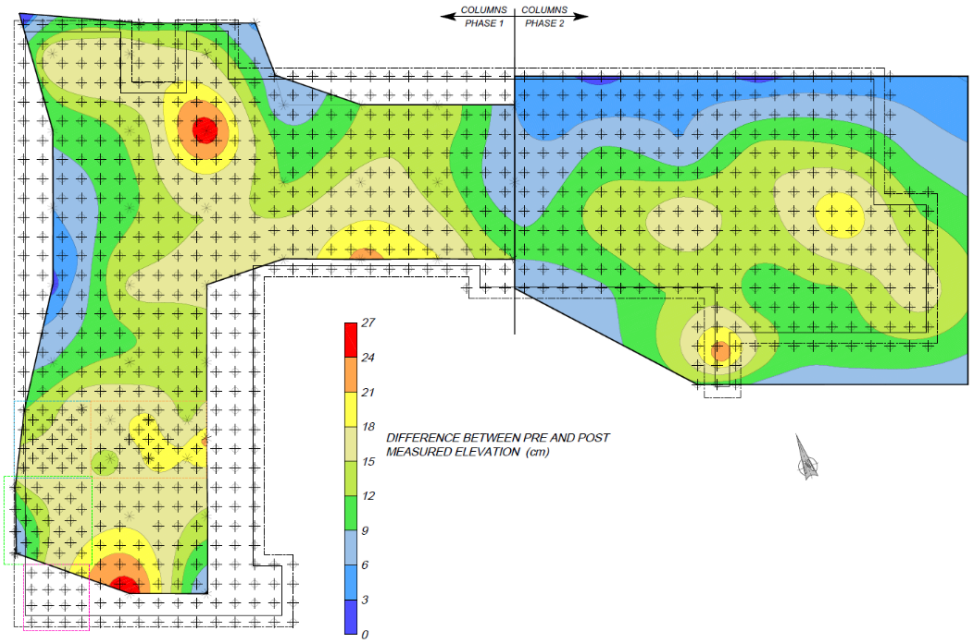


Fig. 10. Upheavals measured with the pre and post treatment topographic survey

KNOWLEDGE ACQUIRED FROM SITE EXPERIENCES

The analysis of available data and site experience leads to the following conclusions:

- The soil densification obtained through the compaction grouting treatment must be checked by comparing the pre and post-treatment cone resistance by means of the Soil Improvement Index (SII) and without repeating the CPTU-based liquefaction analyses which, in our opinion, due to the different soil behavior index obtained from the post-treatment penetrometer tests, are not correct.

- The post-treatment liquefaction analyses can be carried out by employing the shear wave velocity values measured by means of penetrometer tests with seismic cone (CPTUS) or, better, through Seismic Tomography, but not through Vs correlations.

- The Compaction Grouting technology can be used next to (or within) buildings or structures only if the treatment depths are located 4÷5 below the ground level.

- For less deep treatments (up to 1.5 m from ground level) it is better to remain at a distance of 3÷4 m from nearby structures.

REFERENCES

Asioli C., Fanti F., Del Monte D., Zuffi P., (2014). Progetto di un intervento di compaction grouting per la mitigazione del rischio di liquefazione dei terreni in un'area dell'Emilia investita dal sisma del 2012. XXV Convegno Nazionale di Geotecnica, Baveno 4-6 Giugno 2014.

Andrus, R.D., Stokoe, K.H., II, (2000). Liquefaction resistance of soils from shear-wave velocity. Journal of Geotechnical and Geoenvironmental Engrg., ASCE, 126(11), 1015-1025.

Andrus, R.D., Stokoe, K.H., II, Chung, R.M., Juang, C.H, (2003). Guidelines for evaluating liquefaction resistance using shear wave velocity measurements and simplified procedures. NIST GCR 03-854, National Institute of Standards and Technology, Gaithersburg, MD.

Baez J.I.,1995. "A design model for the reduction of soil liquefaction by vibro-stone columns". Ph.D. dissertation, University of Southern California

Iwasaki T., Tokida K., Tatsuoka F., Yasuda S., Sato H., (1982). Microzonation for soil liquefaction potential using simplified methods. Proc. 3rd International Conference on Microzonation, Seattle 1982, (3), 1319-1330.

Jamiolkowski M. et al. (1989), "Italian experience in assessing shear wave velocity from CPT and SPT", XII° ICSMFE, Rio de Janeiro.

Mitchell, J.K., (1981). Soil Improvement – State-of-the-Art Report. Proc. X° ICSMFE, Stockholm (1981), (4) pp. 509 - 565.

Robertson P.K., (1990). Soil classification using the cone penetration test. Canadian Geotechnical Journal, Vol. 27 pp.151 – 158.

UNI EN 1998-5, (2005). Eurocodice 8: Progettazione delle strutture per la resistenza sismica – Parte 5: fondazioni, strutture di contenimento ed aspetti geotecnici. UNI Ente Nazionale Italiano di Unificazione, Milano.

Youd T.L., Idriss I.M., (2001). Liquefaction resistance of soils: summary report from the 1996 NCEER and 1998 NCEER/NSF workshop on evaluation of liquefaction resistance of soils. ASCE Journal of Geotechnical and Geoenvironmental Engineering, 127 (4), 297-311

DEEP JET GROUTING FOR THE CONSTRUCTION OF MRT BLUE LINE EXTENSION IN BANGKOK

Bruno Vingiani, Trevi S.p.A., Cesena, Italy, +39 0547 319147, bvingiani@trevispa.com
Maurizio Siepi, Trevi S.p.A., Cesena, Italy, +39 0547 319318, msiepi@trevispa.com

ABSTRACT

A 37 m deep ground treatment by jet grouting has been recently completed in relation to MRT Blue Line Extension Project in Bangkok. Scope of the work was the improvement of the mechanical and hydraulic characteristics of different soil strata to allow the safe (mined) excavation of two short tunnels connecting Intervention Shaft No. 2 (IVS.2) with the adjacent twin bored tunnels. After a brief description of the nature and characteristics of the different formations to be treated, the paper deals with the results of a preliminary 43.5 m deep trial field performed in the area aimed to define and optimize jet grouting procedures and parameters. The main equipment utilized and the specific logistic constraints characterizing the intervention are also described here with.

Keywords: underground, metro, jet grouting, soft clay, Bangkok

INTRODUCTION

The MRT Initial System Project (Chaloem Ratchamongkhon Line, also known as Blue Line) was the first underground metro line in Bangkok (completed and opened in July 2004). Consisting of 18 underground stations, it runs for 27 km from Hua Lamphong Station to Bang Sue Station, crossing the main business district of the metropolis. In 2010, the Mass Rapid Transit Authority (MRTA) of Thailand awarded the construction of 27 km of new line, as part of the MRT Blue Line Extension Project, towards south, from Hua Lamphong to Bank Khae. The extension includes a 5.5 km underground section with four stations and three intervention shafts (Figure 1), while the remaining 21.5 km are elevated with fifteen stations.

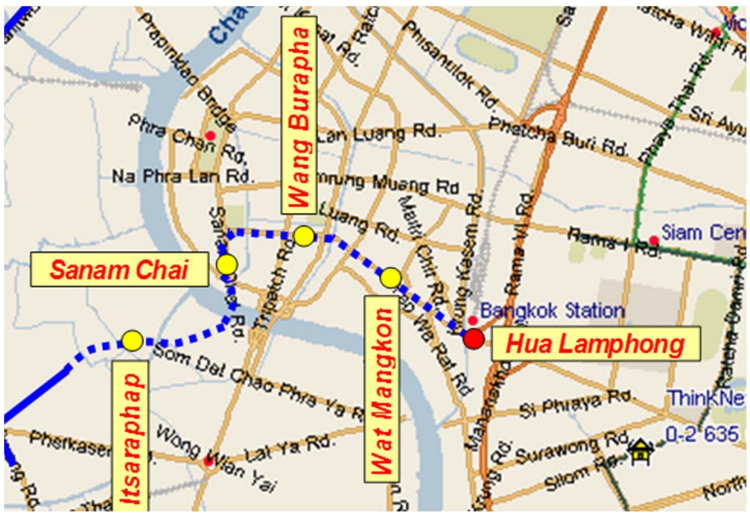


Fig. 1. Scheme of the underground section of MRT Blue Line Extension Project

Passing underneath the Chao Phraya, the main river crossing the city, this underground section will serve one of the most populated and traffic congested area of Bangkok, the Old China Town District (Yao Warat). Considering the particular nature of Bangkok subsoil and the presence of sensitive buildings at the surface, the construction of single-track twin bored tunnels performed by EPB shield has been the tunneling solution adopted for this underground section. The works are currently in a very advanced stage and the whole extension is planned to be opened within 2020. The contract for

© 2018 Deep Foundations Institute

the execution of the underground civil works relevant to the section Hua Lamphong-Sanam Chai has been awarded by MRTA to Italian-Thai Development PCL of Thailand. Within this section, a deep ground treatment by jet grouting has been recently performed by a Joint Venture between Trevi Construction Co. Ltd. of Hong Kong and Italthai Trevi Co. Ltd. of Thailand.

HYDRO-GEOLOGICAL CONTEXT

The city of Bangkok lies in the delta basin of the Chao Phraya River. The area presents a generally plane topography with a ground level resting 0.5 to 1.5 m above the sea level. The subsoil is characterized by a sequence of clayey and sandy deposits down to 400 m and more. Subsoil conditions along the underground section of the MRT Blue Line Extension Project have been extensively explored at the design stage of the project by field investigations and laboratory tests (Figure 2).

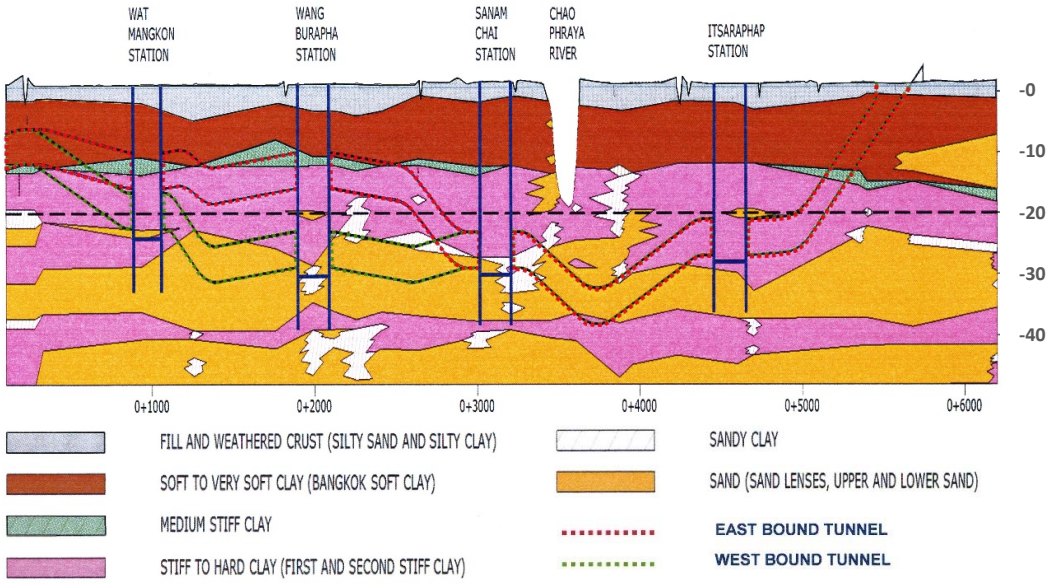


Fig. 2. Soil profile along the underground section of MRT Blue Line South Extension

The soil profile can be schematically summarized as follows (after *S. Tian Ho et al.*, 2006):

Weathered Crust and Backfill Material (1st layer): This uppermost layer has a variable thickness of 1 to 2 m. The fill material is mainly constituted by very loose to medium dense silty sand, while the weathered crust is a medium to stiff silty clay of yellowish color. The groundwater table was resting within this stratum until the Eighties.

Very Soft to Soft CLAY (2nd layer): This formation, so-called "Bangkok Soft Clay", is the first undisturbed layer and is present at depths between 2 and 12 m. It is a cohesive formation characterized by high plasticity, high compressibility and low strength. The undrained shear strength varies from 10 to 25 kPa, while the natural water content (60 to 150%) is close to the liquid limit. The groundwater table currently rests at the bottom of this layer.

Medium Stiff CLAY (3rd layer): A thin seam of dark grey to brownish grey medium stiff clay is occasionally found as third layer underneath the Bangkok Soft Clay.

Stiff to Hard CLAY (4th layer): This formation, present at depths between 14 and 25 m, consists of a yellowish to light greyish brown stiff to very stiff clay.

Medium to Very Dense SAND (5th layer): This formation, so-called "Upper Sand", consists of a medium dense to very dense clayey and silty sand of yellowish to greyish color. It is present at depths between 35 and 40 m.

Very Stiff to Hard CLAY (6th layer): This layer is found underneath the Upper Sand and has a thickness of 10 to 12 m.

Very Dense SAND (7th layer): This formation, so-called "Lower Sand", consists of very silty sand of yellowish brown to brownish grey color. It has been detected down to 65 m depth (bottom of the deepest investigation boreholes). The water table is generally close to the ground level and water pore pressure is hydrostatic only up to a depth of around 10 m. In fact, the intensive well pumping from the deeper sandy strata has progressively led to an under drainage of the deeper soil strata, as shown in Figure 3.

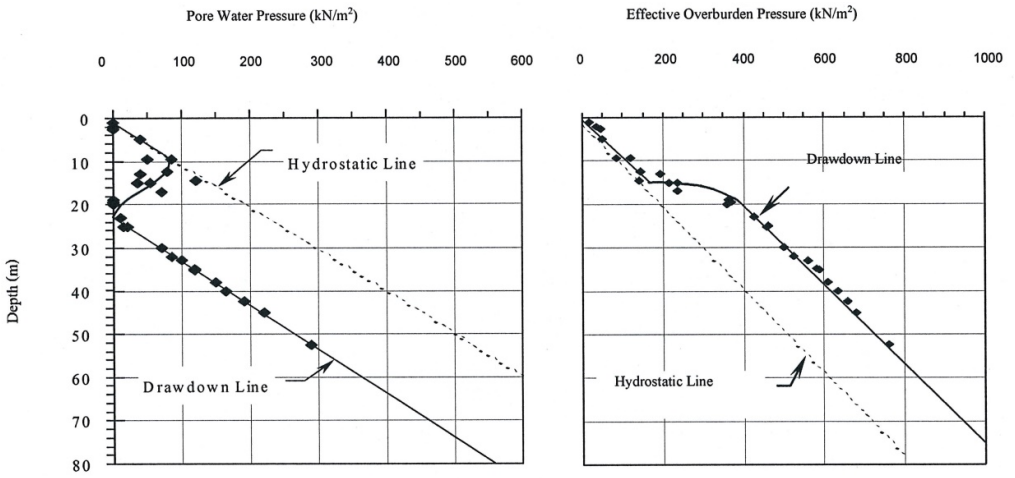


Fig. 3. Water pore pressure and effective overburden pressure in Bangkok (after Teparaksa, 1999)

SCOPE AND SPECIFIC REQUIREMENTS OF THE GROUND TREATMENT

From Wang Burapha station to Sanam Chai station, the MRT Blue Line Extension Project runs underneath Charoenkrung Road, a five lanes artery deemed to be one of the most traffic congested of Bangkok. In this section of the track, the twin bored tunnels run in parallel one above the other, being the lower tunnel at an approx. maximum depth of 35 m. The Intervention Shaft 2 (IVS.2) has been located in a small courtyard surrounded by buildings resting on the northern side of Charoenkrung Road. In correspondence of the shaft, the twin bored tunnels are to be connected to the shaft by two short mined tunnels.

Taking into account the nature of soil formations to be excavated and the requirement of limiting the settlements at the surface at the minimum, the design foresees the execution of a ground treatment (by jet grouting) to improve mechanical and hydraulic features of the involved soil volume (Figure 4).

The following characteristics, at 28 days of curing, were prescribed for the treated soil by project specifications:

- unconfined compressive strength (UCS) in the range 500-2,500 kPa
- hydraulic conductivity (k) lower than 10^{-6} m/s.

The achievement of a high homogeneity of treatment, to be confirmed by fully cored boreholes inside the consolidated soil mass, was also specified as an essential requirement.

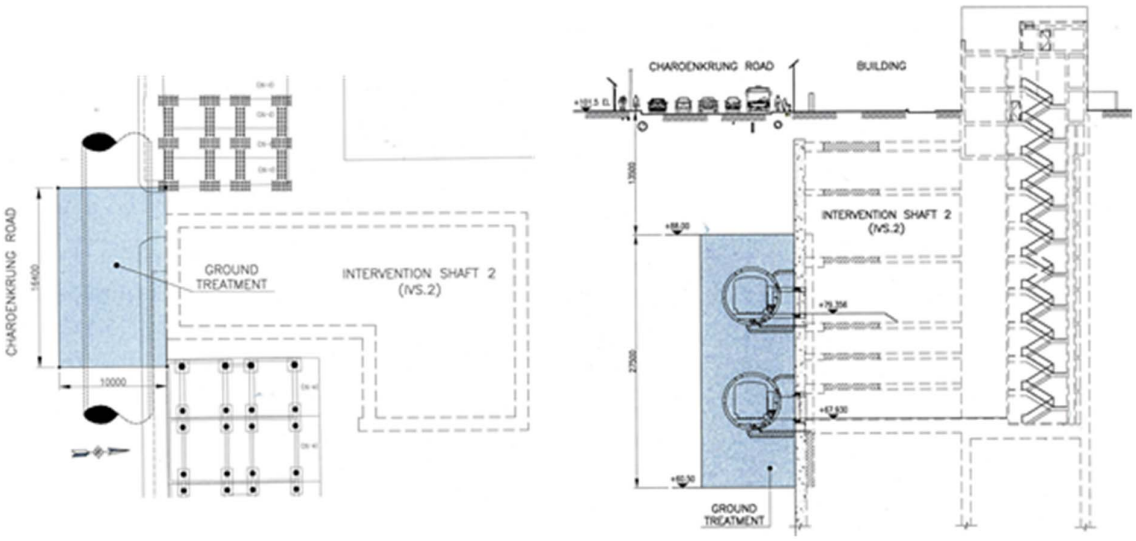


Fig. 4. Plan view and section of the ground treatment foreseen at IVS.2

JET GROUTING TRIAL FIELD

The actual soil profile and in-situ characteristics in the area of IVS.2 have been investigated by three boreholes. Location and resulting soil profiles are shown in Figure 5.

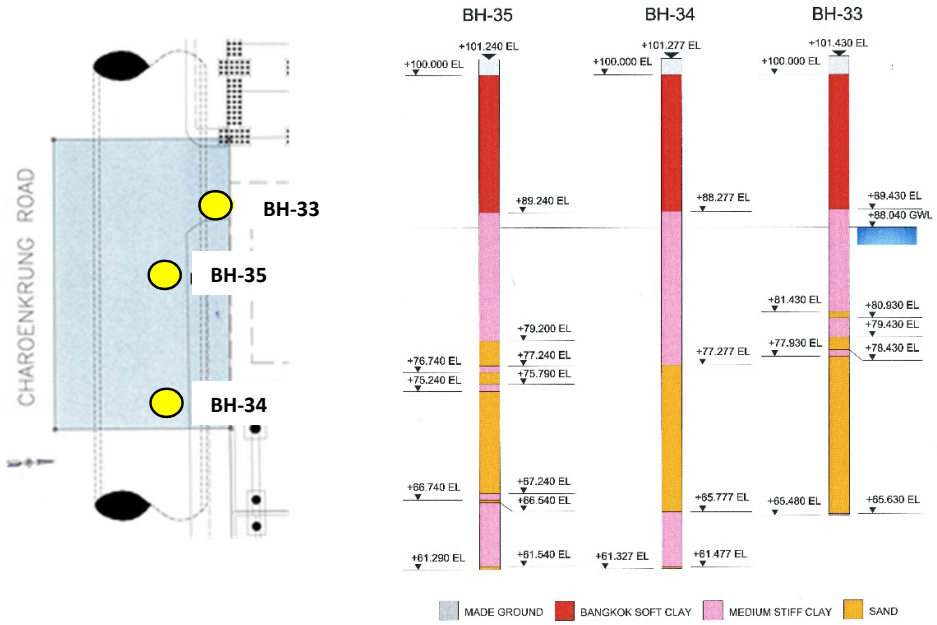


Fig. 5. Location and schematic logs of the specific soil investigation carried out at IVS.2

As can be noted, although the short distance, the identified soil profiles are not completely in accordance. This localized variability is typical of Bangkok geological context. Taking into account the outcome of the soil investigation and the remarkable depth of the treatment, the Foundation Subcontractor has envisaged the application of the "double-fluid" jet grouting method (Figure 6) to achieve the minimum target diameter of 1.6 m of the treated soil columns.



Fig. 6. Scheme and principle of jet grouting "double-fluid" method

Jet grouting trial field has been located inside the courtyard where the IVS.2 had to be successively constructed. To determine the collateral effects caused by jet grouting on the buildings at the surface and the underground utilities also present in the area, a monitoring network has been implemented prior to starting any drilling activity in the area. The monitoring system included the following instrumentation (Figure 7):

- a network of settlement/heave markers (topographically surveyed) placed at the ground surface and on the surrounding buildings;
- one vibrating wire piezometer (42.5 m deep), placed at about 1 m from one of the jet grouting trial columns;
- one inclinometer (42.5 m deep), placed at about 1.5 m from another of the jet grouting trial columns.

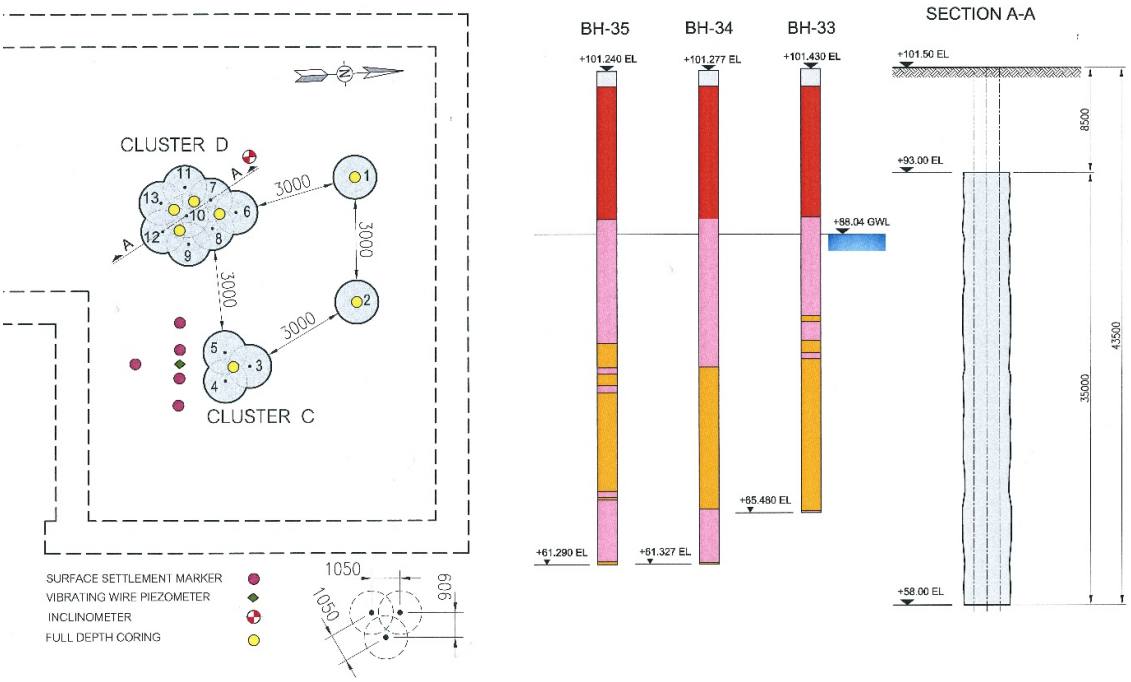


Fig. 7. Plan view and typical section of the trial field at IVS.2

Monitoring data have been systematically collected at fixed intervals during drilling and jet grouting operations.

The trial field consisted in the execution of thirteen jet grouting columns, distributed as follows (Figure 7):

- two single columns;
- one cluster of three overlapping columns disposed according to a triangular equilateral grid with a center to center spacing of 1.05 m;
- one cluster of eight overlapping columns disposed according to the same grid of the cluster of three columns.

All jet grouting trial columns have attained the maximum depth of 43.5 m, in order to assess the achievement of the target minimum diameter of 1.60 m also in the lower stiff clay formation which upper limit was detected at El. +65.50 approx. As part of the experimental program, the following procedures and parameters have been "varied" during the execution of the trials:

- preliminary "pre-cutting by water" procedure (i.e. "while drilling", in "up-stage" and in "down-stage");
- "pre-cutting by water" pressure (in the range 20-30 MPa);
- quantity of grout per linear meter of column (in the range 1,050-1,200 l/m);
- specific energy per linear meter of column (in the range 48-60 MJ/m);
- water/cement ratio of the grout (in the range 1.0-1.1 by weight).

During the execution of the jet grouting columns, in view of the presence of buildings and underground utilities close to the trial area, particular attention has been devoted and special precautions have been taken to ensure a constant free flow at the surface of the surplus mixture of grout and soil particles (so-called "spoil"), which is a peculiarity of jet grouting technique. Drilling and jetting parameters have been recorded by a last generation monitoring and recording system (SOILMEC DMS-JG) mounted on the rig.

Furthermore, the deviation of each jet grouting column has been measured and recorded during the drilling phase by a SOILMEC DPS down-the-hole inclinometer. Assembled inside a diamagnetic rod segment that can be fitted just above the jetting monitor, this device contains a compass and two accelerometers, which allow measuring the inclination on two orthogonal planes and the azimuth in the direction of the magnetic north.

In compliance with the project specifications, a comprehensive in-situ and laboratory tests program has been carried out to appraise the effectiveness of the applied method. In addition to the routinely quality controls (on materials and execution processes) carried out during drilling, pre-cutting and jetting, the following in-situ and laboratory control tests were executed after the completion of the trials:

- core holes (with TCR measurement), at the center of the single jet grouting columns and in correspondence of the overlapping area between two or three columns, to assess the homogeneity of the treatment;
- Standard Penetration Tests (SPT) at pre-determined depths inside the holes, to qualitatively evaluate the stiffness of the treated soil;
- in-situ permeability tests ("constant head" type) at predetermined depths inside the holes, to estimate the hydraulic conductivity of the treated soil mass;
- laboratory tests, at minimum 28 days of curing, on treated soil samples selected from the core boxes, to determine treated soil density, water content and UCS (as per ASTM D 2166:00);

– laboratory tests (as per ASTM D 5084:00), at minimum 28 days of curing, on treated soil samples selected from the core boxes, to determine the hydraulic conductivity of the treated soil.

In Figure 8, a summary of the laboratory test results vs. depth is shown.

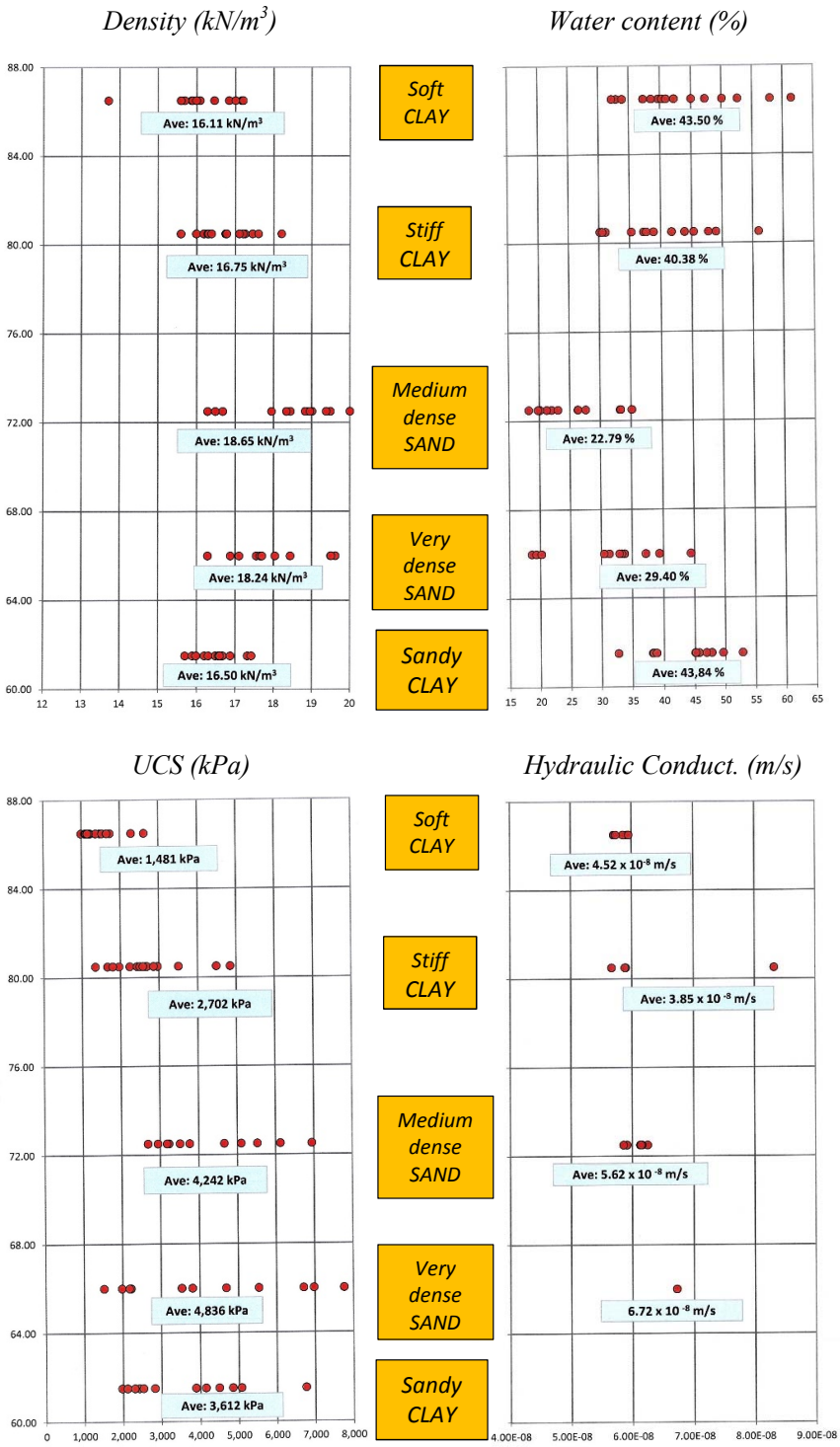


Fig. 8. Laboratory test results: Density, Water Content, UCS and Hydraulic Conductivity vs. depth

The analysis of the laboratory test results has led to the following conclusions:

- in any soil formation, the hydraulic conductivity is much lower than the required maximum value of 10^{-6} m/s;
- in correspondence of the upper clay formation, the UCS average value is virtually within the specified range (500 to 2,500 kPa);
- in correspondence of all other formations, the UCS average value is exceeding the upper limit of 2,500 kPa.

Nevertheless, jet grouting method, procedure and pre-cutting/jetting parameters proposed by the Foundation Subcontractor as result of the trial field (Table 1) have been approved by the Designer and the Construction Supervision Consultant and adopted for the execution of the ground treatment at IVS.2.

Table 1. Approved pre-cutting/jetting parameters.

J.G. Method	Pre-cutting(*) pressure (MPa)	w/c ratio (-)	Grout pressure (MPa)	Grout flow rate (l/min.)	Grout volume (l/m)	Air pressure (MPa)	Air flow rate (l/min.)	Specific Energy(+) (MJ/m)
double fluid	30	1,11	40	350	1,050	~ 1.3	~ 14,000	~ 60

(*) performed in "*down-stage*" after drilling

(+) excluding pre-cutting energy

The layout adopted for the execution of trial clusters (triangular equilateral grid with a center to center spacing of 1.05 m) was also approved. It is finally worth mentioning that the settlement/heaves recorded on the buildings surrounding the area during the execution of the trial columns, were always within the specified trigger limits.

MAIN EQUIPMENT

For performing the work, a newly conceived drilling/jetting rig type SOILMEC SM-28 (Figure 9) was mobilized at site. Equipped with an alloy telescopic boom and a twisting carousel containing up to 27 m of additional rods, this 35-ton drilling rig can perform uninterrupted jet grouting columns up to 34 m.



Fig. 9. Drilling/Jetting rig SOILMEC SM-28 in action at IVS.2

Other key components of the jet grouting plant used at site were:

- one 25 m^3/h capacity automatic grout batching plant type SOILMEC GM-25;
- one 10 m^3 capacity grout stirrer type SOILMEC SGA-100;
- one high pressure grout pump type SOILMEC 7T-600J;
- one 25.5 m^3/min. at 2.5 MPa capacity air compressor type AIRMAN PDSK 900S.

A skid mounted rotary rig type LONGYEAR 38 was also utilized at site for performing the core holes and the SPT inside the trial columns.

GROUND TREATMENT FINAL DESIGN AND EXECUTION

The initial design of the ground treatment by jet grouting at IVS.2 (Figures 4) was finally revised according to the outcomes of the additional soil investigation carried out in the area. In fact, the Designer determined as not necessary the treatment of the upper and lower stiff clay formations.

Consequently, the maximum drilling depth was reduced to 37 m and the jet grouting column's length to 16 m (Figure 10), thus limiting the soil treatment to the sandy formation only.

Furthermore, as additional precautionary measure to avoid the development of excessive stresses on the foundations of the two closest buildings due to the use of compressed air, two lines of 0.8 m "single-fluid" jet grouting columns were performed in correspondence of both northern corners of the soil volume to be treated.

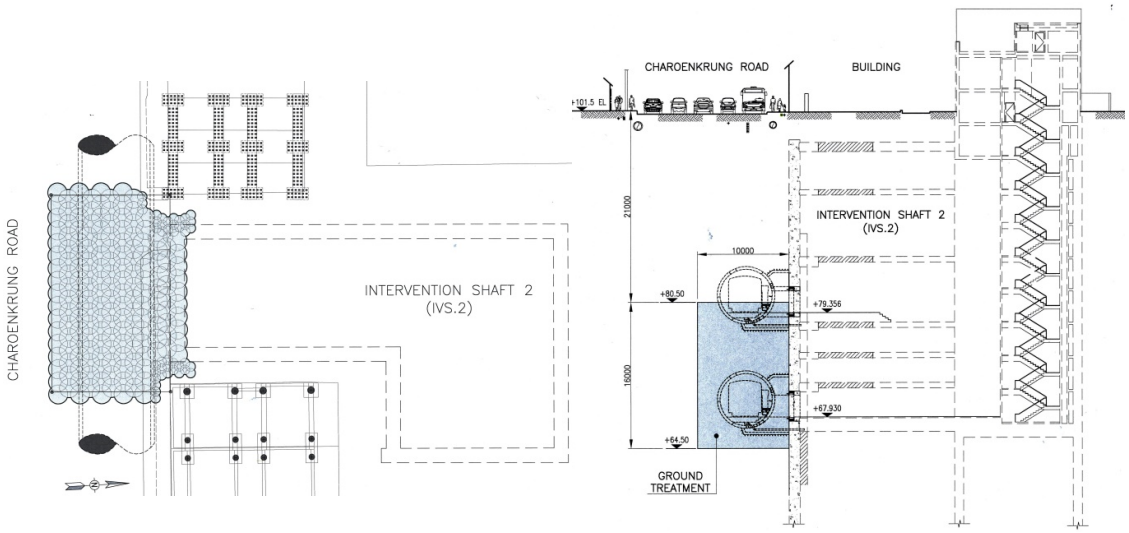


Fig. 10. Plan view and section of ground treatment at IVS.2 (final design)

As per final design, a total of 176 "double-fluid" and 43 "single-fluid" jet grouting columns were performed at IVS.2, achieving a total treated soil volume of 3,135 m^3. In order to minimize the traffic disruptions along Charoenkrung Road, the intervention was divided in two phases. For the same purpose, working activities were performed in extended 12-hour shifts for six days a week.

Besides the above, the major logistic constrain faced during the execution of the ground treatment was due to the large quantity of spoil produced by the jet grouting process during the jetting phase (Figure 11).



Fig. 11. Surplus quantity of soil and cement arising at the surface as result of the jet grouting process

The management of this spoil at site included its timely removal from the working platform, its temporary stock in dedicated ponds and steel tanks and its final disposal off site. All these operations required the use of considerable resources.
Notwithstanding the logistic constraints imposed by the limited working area and the striving associated to the spoil management, the excellent cooperation between the Main Contractor and the Foundation Subcontractor allowed the achievement of an average production rate of 2.5 columns per day and the completion of the works on schedule.

CONCLUSIONS

The deep ground treatment carried out at IVS.2 in Bangkok has confirmed once again the effectiveness and reliability of jet grouting method and technology for the improvement of the mechanical and hydraulic characteristics of soils of different nature. In fact, the implementation of state-of-the-art equipment, last generation recording devices and the adoption of stringent quality control procedures have steered the positive accomplishment of the treatment, in spite of several logistic constraints. Jet grouting technique, 30 years after its conception and application in geotechnical engineering, still remains the preferred method for treating fine grained soils where the presence of silt and clay particles make technically uncertain and economically inconvenient the use of permeation grouting.

In this connection, it is worth mentioning that execution of a sufficiently wide-ranging and comprehensive preliminary test field is of utmost importance for the definition of the optimal executive parameters from both technical and economic (i.e. execution times and cement consumption) aspects.

ACNOWLEDGEMENTS

The Authors wish to express their gratitude to MRTA of Thailand, CSCBL Consortium and Italian-Thai Development PCL for their contribution to the successful completion of the works described in this paper. Special thanks are presented to Mr. Pairach S. and Mr. Prakin A. of Italian-Thai Development PCL for the time dedicated to the revision of this paper.

REFERENCES

N. Thasnanipan et al., 2009. Diaphragm wall support deep-excavations in Bangkok. Proceedings of the ITA-AITES World Tunnel Congress, 23-28 May 2009, Budapest, Hungary.

C. Photayanuvat et al. 2006. Outline design of the Blue Line South underground section – Extension of the existing Bangkok MRT subway Line. Proceedings of the International Symposium on Underground Excavation and Tunneling, 2-4 February 2006, Bangkok, Thailand.

S. Tian Ho et al., 2006. Geotechnical investigation of 3 MRT lines in Bangkok. Proceedings of the International Symposium on Underground Excavation and Tunneling, 2-4 February 2006, Bangkok, Thailand.

W. Teparaksa et al., 2006. Design of subway tunnel under the Chao Phraya river for Bangkok South Blue Line Extension. Proceedings of the International Symposium on Underground Excavation and Tunneling, 2-4 February 2006, Bangkok, Thailand.

P. Chotidilok, S. Suwansawat, 2009. Ground improvement design and technique for supporting the construction of Bangkok Blue Line South Extension subway. Proceedings of the ITA-AITES World Tunnel Congress, 23-28 May 2009, Budapest, Hungary.

INTERVENTION FOR IMPROVING CHARACTERISTICS IN FAULT ZONE IN TUNNEL ALIGNMENT - CONSOLIDATION USING CHEMICAL GROUTING WITH MONO AND BI-COMPONENT RESINS

Pasquale Petrocelli, CIPA S.P.A., Rome, Italy
Aldo Bellone, CIPA S.p.A., Rome, Italy
Francesca Rossano, CIPA S.p.A., Rome, Italy
Marco Aurelio Piangatelli, CIPA S.P.A., Rome, Italy

ABSTRACT

During the excavation of the underground works for the execution of the new TERNA S.p.A. 380kv power line, that connects Sicily and Calabria, a 12% inclined and 2.8 km long tunnel was made. It finished in a vertical shaft that was 300 m deep and 7 m diameter.

This tunnel excavation, which was executed by means of a double-shield TBM (Tunnel Boring Machine) with 4.1 m diameter, passed through a large part of the Calabro Arch's crystalline-metamorphic base. The scientific literature used to draft the preliminary project and the geological surveys done during the project phase confirmed that the geological properties led to Calabro Arch's crystalline-metamorphic base.

However, the nature of some parts of the terrain in some excavation areas, showed how this type of rock mass can present extreme variations. It showed fault areas with extremely high grades of broken rock, with very low GSI (Geological Strength Index) values. It also showed a granulometry similar to a sand-consistency, sometimes similar to a clay-consistency, with a significant quantity of water.

These fault areas, with a massive quantity of water moving inside them, gave huge problems during the tunnel excavation. They created very low progress areas and three "geological events" which caused TBM interruption in the tunnel.

As shown in this paper, the three TBM interruptions required particular and delicate work, which could only be carried out after some interventions to condition the rock mass property by the use of mono and bi-component chemical grouting using resins. These interventions aimed to improve geo-mechanical properties and allow excavating small tunnels to "unlock" the TBM and then the crossing of fault areas.

INTRODUCTION

The work is constituted of a tunnel that is 2850 meters long with a 12% slope and by a 300 meter deep shaft (Fig. 1) . The TBM passed through heterogeneous areas with strong water presence and faults.

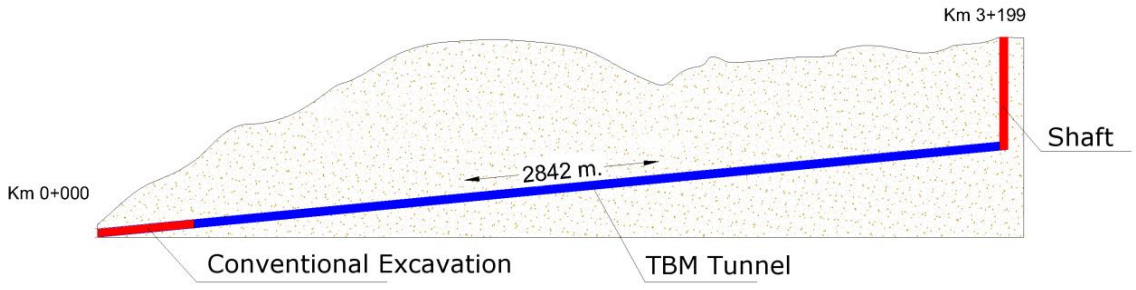


Fig. 1. The tunnel and the shaft.

© 2018 Deep Foundations Institute

These "fault" zones blocked the TBM and required unlocking interventions. Four major geological events required heavy soil treatments (Fig. 2).

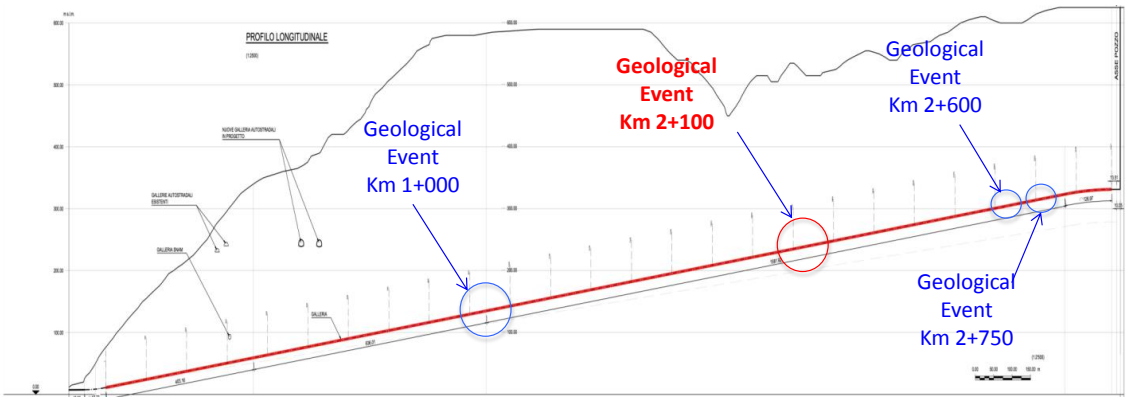


Fig. 2 Geological event occurrences.

THE GEOLOGICAL EVENT AT THE Km 2+100 ON 12th DECEMBER 2014

The geological event at Km 2+100 presented complex geological situations. All other cases are attributable to this, but have shown operational difficulties and conditions that were less prominent.

Block mechanisms

Three kind of block mechanisms occurred during the geological events:

- Rotating head block
- Excavation chamber filling
- Front shield filling

The TBM went through zones of highly altered rocks and with a lot of water where the three mechanisms occurred in rapid succession, triggering a loop process that required additional interventions to restart the TBM.

The TBM crossed a clay diaphragm a few meters thick, entering in a zone that in the geomechanical profile was referred to as the main fault.

After the TBM head of passed this diaphragm, the considerable presence of pressurized water caused a siphoning phenomenon.

A significant amount of material was carried into the excavation chamber, the front shield and the rear shield of the TBM.

In the end the material completely filled the machine, causing an instant block.

The situation differed from the first event at km 1+000:

- The material that flowed into the TBM was predominantly a clay matrix
- The presence of water was considerably higher than the first case
- Contrary to the first case, the phenomenon of the material inflow continued spontaneously and cyclically, without interruptions.

The phenomenon triggered by the diaphragm breakage was of considerable size.
After several days, the phenomenon did not seem to finish and after the attempts at TBM cleaning, it resumed vigorously, causing serious worries to the technicians. The zone of altered rocks was more than 20m thick.

The water flow changed cyclically, from 50 l/s to 80 l/s and water pressure at the TBM head was about 13 bar.

Immediately after the event, the material entering into the TBM had temporarily blocked the phenomenon (Fig. 1), so that it seemed to have stopped, but the water flowing into the TBM was always cloudy, indicating a transport of material, so it was assumed that the phenomenon could not be considered exhausted.



Fig. 3. The material flowed into the TBM.

The attempts to clean the shields and the excavation chamber caused the spontaneous return of material into the TBM, with force and intensity.

The TBM, before encountering the fault, had met a clay diaphragm that had created a waterproof barrier that allowed the water to reach high pressure.

Prior to starting with the consolidation actions, an attempt was made to find out the fault thickness and to reduce the hydraulic pressures by draining the area to be treated.

The TBM shield is provided with n.8 holes Ø89mm to make destructive drillings. A "Beretta T43" drill rig was mounted on the erector slide. The drill rig had been modified and adapted to work in narrow spaces and it could do every kind of intervention (destructive drillings, drainages with steel casings, bolts and injections, etc.). This machine proved very effective.



Fig. 4. The "Beretta T43"drill rig

Some destructive perforations were made, recording the push pressure, the rotations and the time needed for the penetration, in order to determine the thickness of the fault. All these values have been recorded and interpreted by engineers and geologists to rebuild the most plausible scenario (Fig. 5. and Fig. 6).

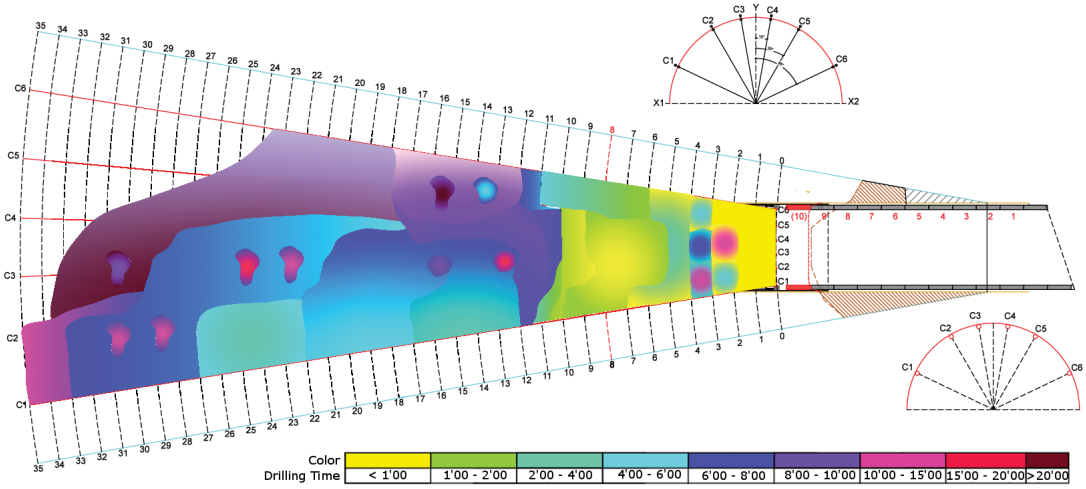


Fig. 5. Chromatic representation of the time needed to the drillings to go through the soil.

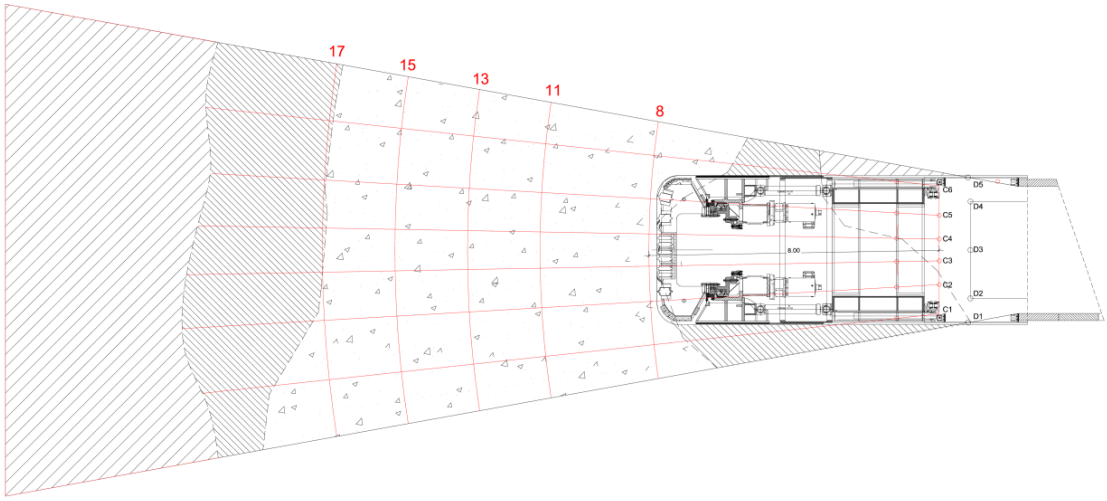


Fig. 6. Reconstruction of the fault geometry

With constant drainage it was possible to reduce the pressure of the water, but performing continuous and constant drainage was not a simple task, because the clay layer often behaved as a plug and therefore the drained water decreased over time and pressure increased again.

This issue was resolved adopting self-drilling drainage pipes, with big water-soluble valves (more than a centimetre in diameter) and therefore hard to be obstructed by fine materials (Sidra Drain, Fig. 7).



Fig. 7. Continuous drainage with self-drilling drainage pipes, with water-soluble valves.

With this method, the area to be treated with resins was well drained of the water that would have reduced the effectiveness of the resin injection. Also, the pressure decreased and the phenomenon of the cycling water flush and material inflow ended.

INJECTIONS WITH MONO-COMPONENT AND BI-COMPONENT RESINS

Resin injections had been hypothesized by using PVC pipes with "manchettes" valves. This would have allowed injections of each type of resin to the various set distances, by the use of packers to isolate the different injection portions.

Unfortunately, all attempts to install these pipes failed because the presence of water allowed the material to flow into the casing. This material prevented the pipe from being installed, or dragged it out during the casing extraction to expose the valves.

After several attempts, the adopted solution was the direct injection into self-drilling bolts. After the injections, the bolts were extracted for a subsequent re-drilling that allowed a new injection to a new distance.

The general criterion followed was:

- Try to consolidate areas whose time for drilling had been less than 10 minutes;
- Try to differentiate the injections according to the following guide lines:
    - Filling injections to protect TBM shield with the mono component resin “Basf MRoc MP 355 (MS) 1K DW”;
    - Consolidation injections with the bi-component resin “Basf MRoc MP 355 (MS) PTA + PTB”.

The conditions round the TBM were unknown and the behaviour of the resin in those particular conditions was not foreseeable, so the technicians implemented a scale model of the area to be treated to simulate the behaviour of the resin in the presence of large amounts of water (moreover in drainage condition, Fig. 8).

In the box where the tunnel excavation material was accumulated, an experimental study was conducted by simulating multiple bi-component resin simulations combining two different factors:

- Amount of water;
- Different mix-designs involving resin, accelerator and water quantities.

The various mix-designs were injected into the soil with the same technique and the same lengths as for the real case, and then results were analysed after dissecting the treated areas (Fig. 9). It was possible to determine the right mix-design to achieve two results:

- Good mechanical strength of the combination rock + resin in order to create an arc effect at the passage of the TBM;
- Good set speed to allow the resin to travel in the tube and expand around a significant injection area without getting dragged by flowing water.



Fig. 8. Test field for mix-designs.



Fig. 9. Some tests for mix design.

Once the mix design, modes and timing had been defined, the real intervention started. In order to perform an effective intervention, the volume to be injected was shared into a two-dimensional grid (Fig. 10 and Fig. 11), also taking into account the forced inclination of the holes in the gripper shield.

The two-dimensional grid was designed with a 1m x 1m mesh according to the following items:

- The injections should be carried out by the injection of self-drilling bars R32 with three-hole drilling head.
- Each bar could be injected only from the bottom and only one injection could be carried out per each bar.
- Range of action. The test field showed that the resin solidified in a diameter of about 1-1.5 m.

Intervention sequence:

1. Insertion of the bar at the set depth;
2. Injection of the resin up to saturation or up to a predetermined volume;
3. Pull back of the bar used for the injection;
4. New drilling at a lower depth

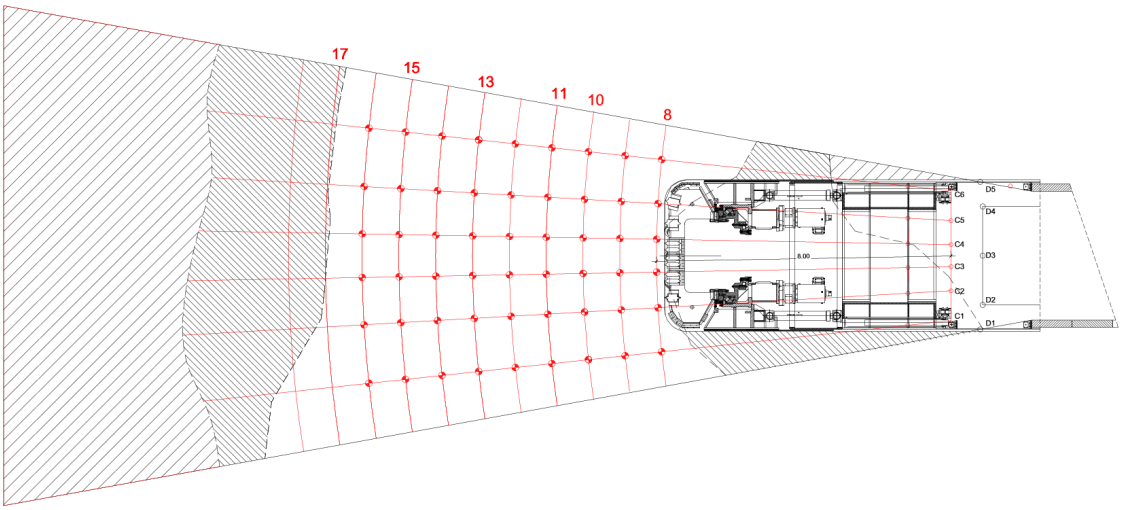


Fig. 10. The injection grid – Plan view.

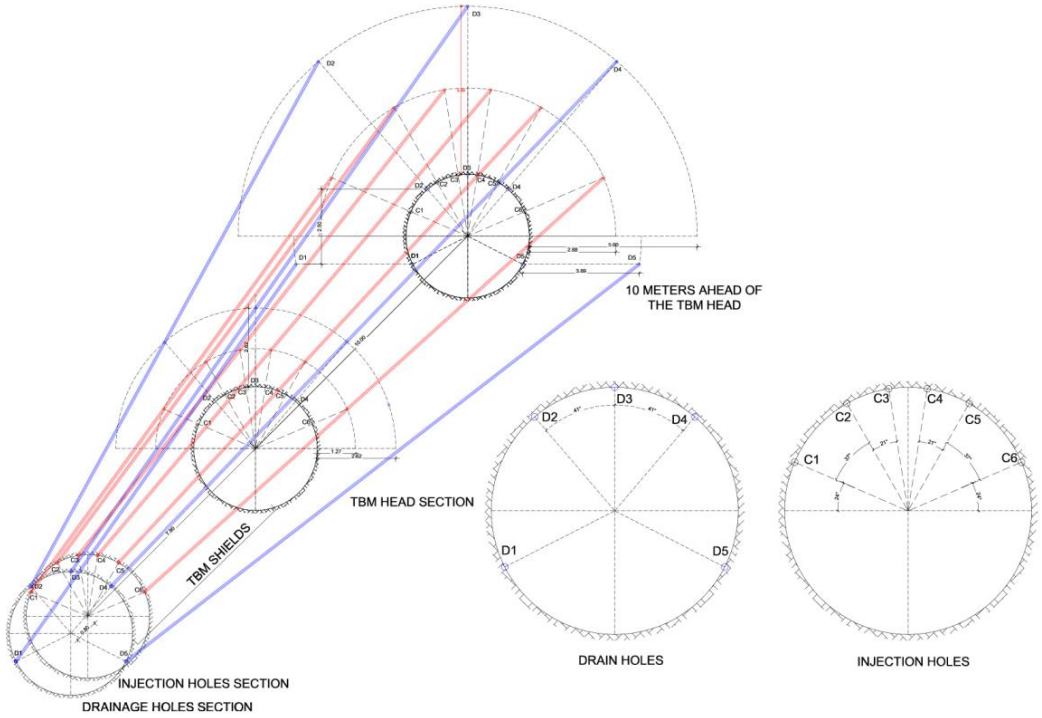
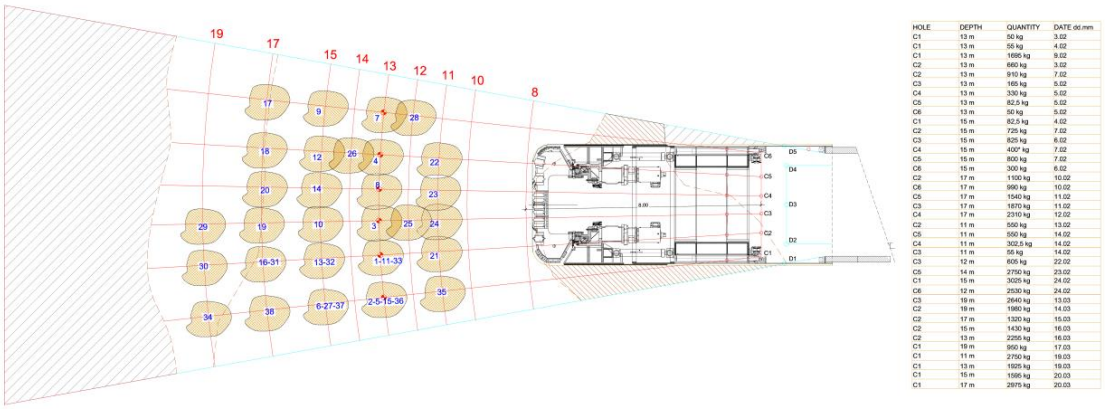


Fig. 11. 3D projection of drains and injections.

For each injection hole, identified with C1÷C6, at least 8-9 perforations had to be made. Due to the injection time, it was decided to make the first consolidations up to 19 m, then to evaluate the result by using a local tomography that returned the physical characteristics of the combination soil + resin.

At the end of this step, the scheme of the injections is shown in Fig. 12.



HOLE	DEPTH	QUANTITY	DATE dd.mm
C1	13 m	50 kg	3.02
C1	13 m	55 kg	4.02
C1	13 m	1685 kg	9.02
C2	13 m	660 kg	3.02
C2	13 m	910 kg	7.02
C3	13 m	165 kg	5.02
C4	13 m	330 kg	5.02
C5	13 m	82,5 kg	5.02
C6	13 m	50 kg	5.02
C1	15 m	82,5 kg	4.02
C2	15 m	725 kg	7.02
C3	15 m	825 kg	6.02
C4	15 m	400* kg	7.02
C5	15 m	800 kg	7.02
C6	15 m	300 kg	6.02
C2	17 m	1100 kg	10.02
C6	17 m	990 kg	10.02
C5	17 m	1540 kg	11.02
C3	17 m	1870 kg	11.02
C4	17 m	2310 kg	12.02
C2	11 m	550 kg	13.02
C5	11 m	550 kg	14.02
C4	11 m	302,5 kg	14.02
C3	11 m	55 kg	14.02
C3	12 m	605 kg	22.02
C5	14 m	2750 kg	23.02
C1	15 m	3025 kg	24.02
C6	12 m	2530 kg	24.02
C3	19 m	2640 kg	13.03
C2	19 m	1980 kg	14.03
C2	17 m	1320 kg	15.03
C2	15 m	1430 kg	16.03
C2	13 m	2255 kg	16.03
C1	19 m	950 kg	17.03
C1	11 m	2750 kg	18.03
C1	13 m	1925 kg	19.03
C1	15 m	1595 kg	20.03
C1	17 m	2975 kg	20.03

Fig. 12. The injection grid – The injection distribution at the end of the first step.

Before the TBM restarting, a series of tomography and seismic tests were carried out within the drainage pipes to determine the resulting physical characteristics (Fig. 13 and Fig. 14).

The results obtained were encouraging, so another series of injections were made on the left side, that resulted less consolidated. After this second step, new tests were carried out (Fig. 15).

CONCLUSION

A new power-line tunnel in Italy was drilled by a Tunnel Boring Machine (TBM). During the TBM drilling, four fault zones were encountered, each causing TBM stoppages. This paper describes the worst stoppage.

The method for repairing the fault zone was chemical grouting using resins. Prior to the injections, the hydraulic pressure on the TBM head was lowered by a drainage system, increasing the efficiency of the resins. The injection of the mono-component resins filled the cavities and protected the TBM from the subsequent injections of structural resins. The bi-component resins for structural purposes were used to consolidate the altered and collapsed soil that in the presence of water would have prevented the TBM passage. All the combined techniques allowed the TBM to overcome the fault.

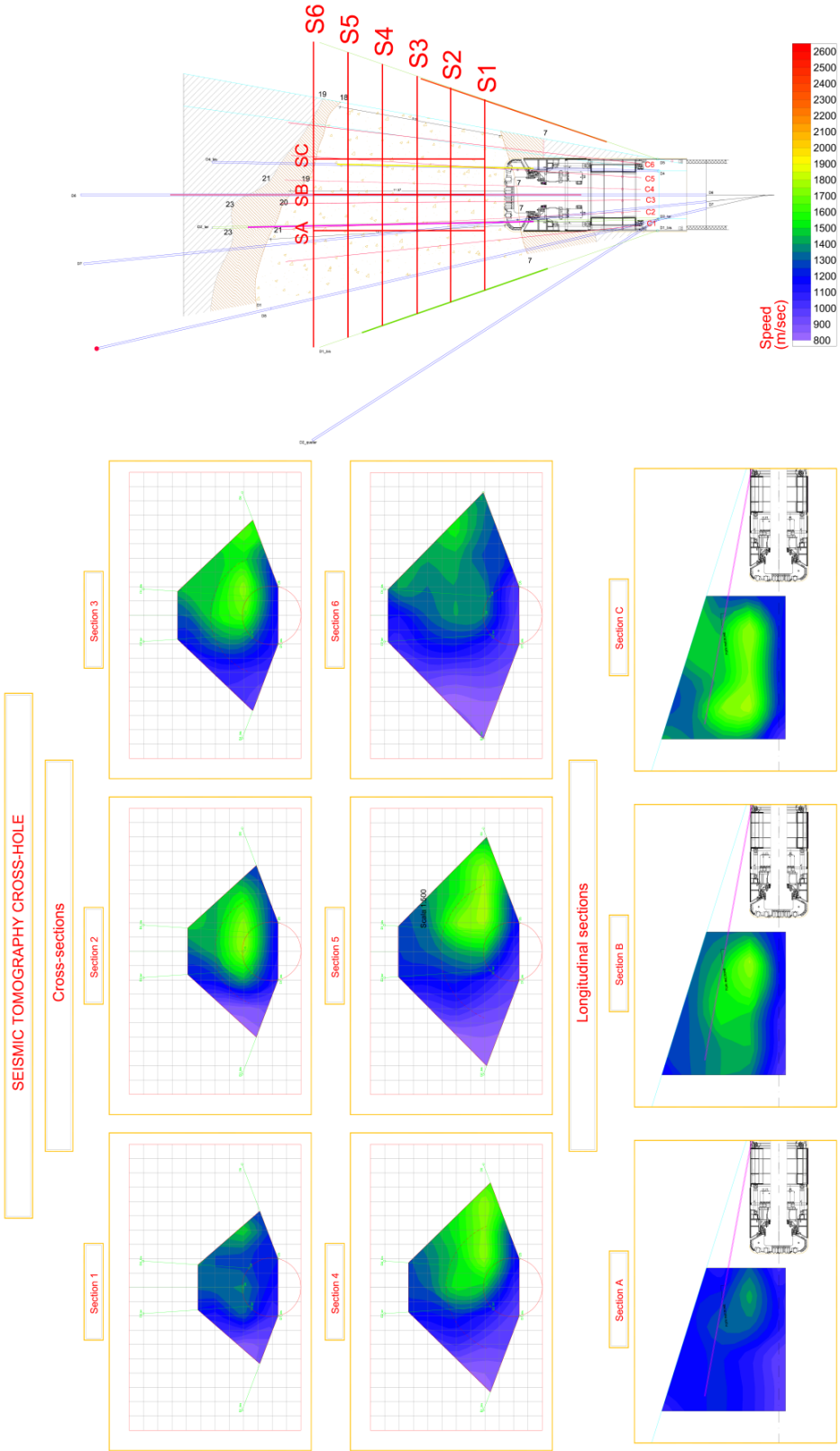


Fig. 13. Schematic results of the seismic tomography tests of the first step.

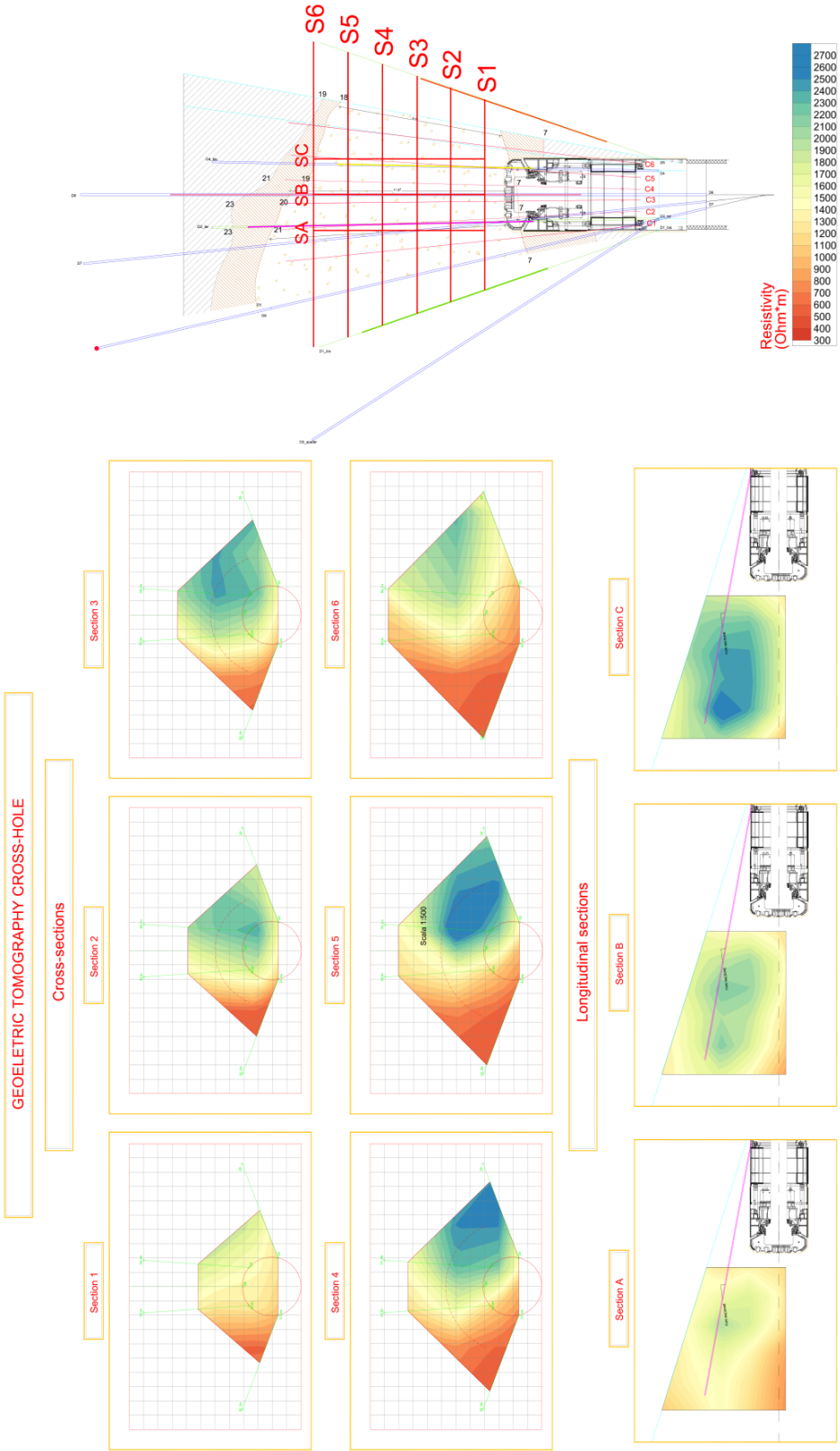


Fig. 14. Schematic results of the geoelectric tomography tests of the first step.

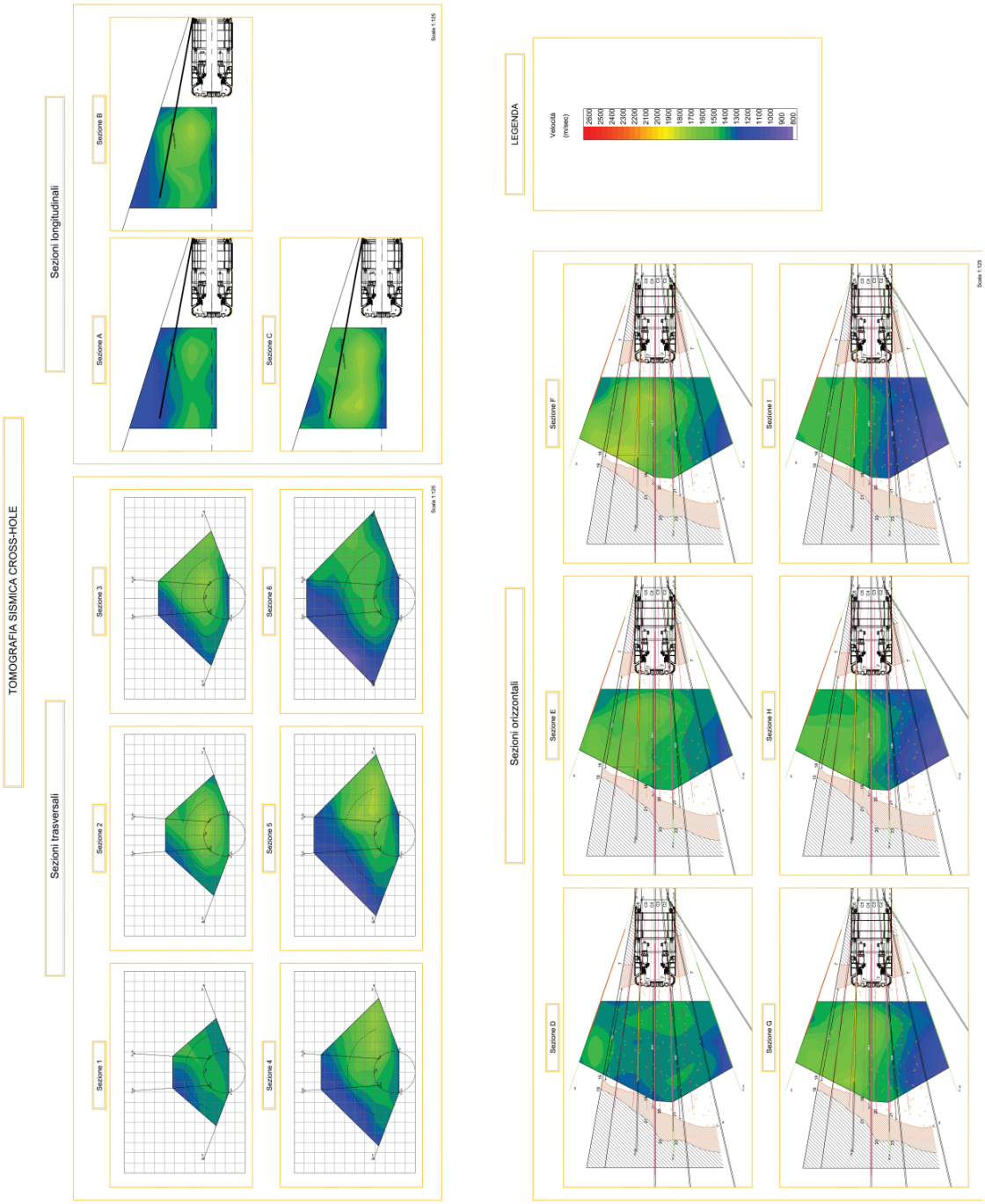


Fig. 15. Schematic results of the seismic tomography after the second step.

LATTICE-SHAPED JET GROUTING CONFIGURATION TO PREVENT SOIL INDUCED LIQUEFACTION AT CHRISTCHURCH TOWN HALL – NEW ZEALAND

Cristóvão, António; *JETsj Geotecnia Lda, Lisboa, Portugal, acristovao@jetsj.com*
Brito, David; *JETsj Geotecnia Lda, Lisboa, Portugal, dbrito@jetsj.com*
Nogueira, Abílio; *KGA- Geotechnical Group Ltd, Christchurch, New Zealand, abilio@kga.co.nz*

ABSTRACT

Soil improvement techniques are commonly used to mitigate one of the major and most complex problems that can occur during and after a seismic event – liquefaction triggering of soil deposits. Following several research programs and efforts of the scientific community to find methods to mitigate the liquefaction hazard, stone columns and jet grout columns were found to be the most common solutions used to decrease the likelihood and severity of foundation movements caused by earthquake-induced soil liquefaction and lateral spreading. The stone column method relies on additional drainage and the densification of the soil around the column, resulting in the reduction of pore water pressures and shear stress levels during seismic excitation. The jet grout columns, when forming cells (lattice structure), contain the soil during the seismic demand; this greatly reduces the shear stresses in the soil, with the consequent reduction on the liquefaction potential of the treated soil block.

Several authors have published technical papers offering guidance and field data related to seismic improvement techniques, including:

- "Seismic response evaluation of sites improved by deep mixing": Results from centrifuge tests that measured pore water pressure responses of many deep mixing treatment configurations and a field case have been used to verify the applicability of the proposed simplified approach using deep-mixing technique [1];
- "Design and Installation of Soil Improvement against Liquefaction in Reclaimed Ground with Coal Ash": the reduced displacement type of the cement deep mixing (CDM) method was selected, to avoid the lateral deformation of surrounding structures. The validity of the numerical analysis was firstly checked based on previous conducted laboratory tests results, followed by a proper calibration of the analytical model with parameters [2].

Liquefaction susceptibility can be evaluated based on semi-empirical methods using both SPT and CPT data (alongside geophysical data, DMT, etc). However, numerical analysis of ground response of the soil deposit is also a very powerful tool, especially when calibrated with data of a recent earthquake sequence as observed in the Canterbury region.

This paper outlines the philosophy adopted for the ground stabilization study preliminary design as part of the Christchurch Town Hall Conservation Project. The proposed ground improvement method comprises the formation of lattice-shaped jet grout columns to mitigate the soil liquefaction, lateral spreading and associated surface subsidence on existing buildings and infrastructures.

 © 2018 Deep Foundations Institute

1 - INTRODUCTION

The Christchurch Town Hall has been significantly damaged by the earthquake sequence that occurred between 2010 and 2011, particularly liquefaction related damage and lateral spreading. As part of the building remediation works, it is intended to create a stabilized soil block to decrease the likelihood and severity of foundation movements caused by future earthquake-induced soil liquefaction and lateral spreading.

The design concept is based on the construction of overlapping jet grout columns to form a cellular structure, reducing the overall deformability of the ground and limiting the development of major shear strains.

Liquefaction behaviour of the ground beneath the Town Hall building was simulated using a combination of soil parameters and jet-grouting columns subjected to the seismic motion registered during the 4th of September 2010 at Christchurch Resthaven Station (REHS). For this purpose, the soil response was investigated through a parametric analysis using an effective stress based model UBC-SAND (PLAXIS2D). To assess the effectiveness of jet-grout columns as a soil stabilization technique to increase liquefaction resistance, several cellular arrangements of jet grouting columns were modelled and pore water pressures were measured in the model.

2 - SITE LOCATION

The Christchurch Town Hall for Performing Arts complex is located at 86-95 Kilmore Street, Christchurch – New Zealand (Figure 1). It is located in central Christchurch, enclosed by Colombo Street to the east, Kilmore Street to the north, the Avon River and Victoria Square to the south and the Crowne Plaza Hotel to the west.

The complex consists of a 2500 seat Auditorium, 1000 seats in James Hay Theatre, a lobby area, a restaurant and function rooms.

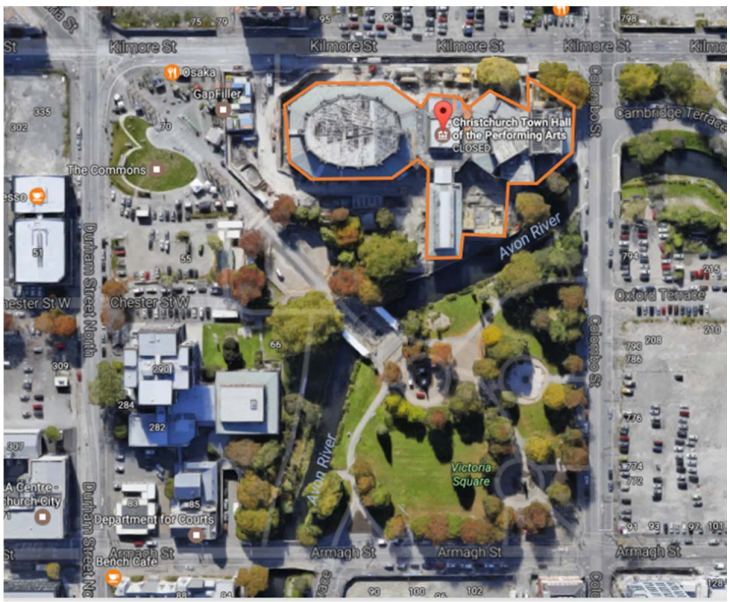


Figure 1 – Town Hall Location Plan

After the 22th February Canterbury Earthquake, the building and surrounding area showed evidence of widespread liquefaction, and lateral spreading cracks were noted on the north bank of the Avon River.

Liquefaction and lateral spreading of the underlying soils have caused differential settlements and distortion of the building and foundation elements, compromising the serviceability of the structure. Post-earthquake survey data indicated building foundation settlements of 240mm to 630mm, and typically between 300mm to 500mm [3].

According to the published geological map ("Geology of the Christchurch Urban Area"), the Town Hall site is underlain by alluvial sand and silt overbank deposits of the Springston Formation. This formation is characterized by post-glacial fluvial channel and overbank sediments containing gravel, sand and silt.

3 - MODELLING PROCEDURES

3.1 - In situ data

The ground investigation available for this site was part of an extensive research project with a broader scope for the affect seismic areas in Christchurch. Geotechnical field investigations included standard penetration test (SPT) and cone penetration test (CPT) data around the perimeter of the building, complemented by the installation of several piezometers, providing enough data for a better understanding of the site geology and lithology. For one of the several campaigns, the CPTs reached depths ranging from approximately 5.2m to 8.0m below the existing ground surface. At these depths, a dense gravelly sandy layer was encountered causing probe refusal. The results from CPTs indicated that the subsoil conditions comprised mainly silty sand and sandy silt layers overlying loose to dense sand and gravel materials. Groundwater was recorded between 1.5m and 2.5m below ground level. [3]. The ground investigation campaign occurred after the seismic events of 2010 and 2011 Canterbury earthquakes.

The following generalized geotechnical model was proposed for the site based on the interpretation of the collected in situ data obtained during the field investigations:

Table 1 – Generalised subsurface profile [4]

ID	Level of top of layer (m, CDD)	Depth below Kilmore St level (m)	Layer thickness (m)	Material Description	Typical SPT N	Typical CPT q_c (MPa)
1	14.7 to 13.4	0.0 to 1.1	0.4 – 1.9	Fill	N/A	N/A
2	13.0 to 12.8	1.5 to 1.7	2.8 – 5.5	Silt with minor sand and sandy silt	4 - 7	1 - 7
3	10.3 to 7.3	4.2 to 7.2	2.0 – 10.0	Interbedded gravel, sandy gravel and sand	15 - 50	5 - 30
4	5.5 to -0.5	9.0 to 15.0	0.5 – 2.0	Interbedded organic silt and peat	1 – 5	1 - 5
5	4.5 to -1.1	10.0 to 15.6	3.8 – 11.1	Silty sand and sand	20 - 40	5 - 30
6	-4.8 to -1.1	19.3 to 21.5	0.5 – 1.5	Silt (aquaclude)	1 – 5	1 - 5
7	-5.7 to -8.1	20.2 to 22.6	7.0 – 9.0	Interbedded gravel, sandy gravel and sand	30 - 50	N/A
8	-13.9 to -15.9	28.4 to 30.4	Unproven	Interbedded silt and peat	10 - 30	N/A

Following the February 22nd Christchurch earthquake (2011), evidence of liquefaction in the form of sand boils was observed on the ground surface around the Town Hall complex as well as on the roads and properties in the immediate surroundings. The same hazards were reported after the 13th June 2011 earthquake [5].

In order to model the effects of earthquake propagation waves on soils, a real accelerogram was used for the numerical analysis. The seismic motion registered during the 4th September 2010 earthquake at the REHS Station was obtained from "GeoNet" database. Ground motions recorded show that soil type and stratigraphic characteristics modify appreciably the rock motion characteristics. Soil thickness variations, for similar geotechnical conditions can lead to different outcomes. The recorded station was close enough to the Town Hall and the ground conditions were very similar between the station and the site; however the study of soil behaviour for three or four additional signals would have been beneficial to provide robustness to the model. This would have been done if we were given the opportunity to proceed for the detailed design.

A magnitude (M_W) of 7.1 and peak ground acceleration (PGA) of 0.25g were recorded during the 2010 earthquake. The performance of the soil stabilisation modelling was analysed for a scaled design earthquake event with a PGA of 0.44g and a magnitude of 7.5, using the methods outlined by Idriss and Boulanger [6]. The signal was scaled only to PGA values. This is shown in Figure 2.

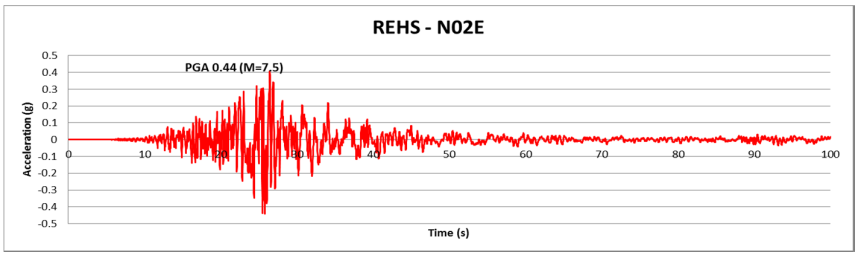


Figure 2 – Scaled seismic input signal: Acceleration time history

3.2 - 2D finite element modelling

The seismic response of the jet-grout columns cellular arrangement was investigated by means of an undrained and drained effective stress analysis and considering that pore water pressures build-up due to cyclic loading. The pore water pressure response (for liquefaction) is a widely used engineering response indicator [1].

The analysis was undertaken using finite element software PLAXIS2D. Soil behaviour was modelled according to the *Hardening Soil* constitutive model and the *UBC3D-PLM* constitutive soil model [7], which is a 3D reformulation of that originally proposed by Puebla *et al.* [8] designated as UBCSAND [9].

All the non-liquefiable layers were defined as per the *Hardening Soil (HS)* model. The *HS* is an advanced model allowing the simulation of different soil types behaviour for both soft and stiff soils (Shanz, 1999). In contrast to an elastic perfectly-plastic model, the yield surface of a hardening plasticity model is not fixed in a principal stress space, but can expand due to plastic straining. Within this model, damping can be modelled by means of Rayleigh damping. Rayliegh damping intends to model viscous damping, since it contributes to the velocity term in the dynamic equation by considering a percentage of the mass (α[M]) and a percentage of the stiffness (β[K]), where [M] is the mass matrix, [K] the stiffness matrix and α/ β the Rayleigh coefficients. To calibrate these coefficients, it is necessary to define the target damping ratios and the related frequencies.

Hardening Soil small Strain (HSsmallStrain) should also be suitable to model the non-liqueafiable layers. It handles with strong stiffness variation (increasing shear strain amplitudes in the domain of small strains) and hysteric behaviour, through a non linear elastic stress-strain relationship. These features allow the HSsmallStrain to produce accurate and reliable approximation of displacements for dynamic applications. Nevertheless, the additional parameters associated with this model couldn't be calibrated with the available ground investigation data.

Soil parameters were based on the results obtained from CPTs performed at the site. The confining stress dependent stifness modulus for primary loading (E_{50}) was assessed by correlation with the CPT data using the proposal after Robertson and Campanela (1983). It was later correlated to the secant stiffness modulus (E_{50ref}), corresponding to the reference confining pressure (pref=100 kPa), using the expression established by Brinkgreve (2014):

$$E_{50} = E_{50}^{ref}\left(\frac{c'\cdot cot\, g\varphi' - \sigma_3'}{c'\cdot cot\, g\varphi' + p^{ref}}\right)^m \quad [1]$$

where (c') is the efective cohesion; (φ') is the soil internal friction angle; (σ_3') is the minor principal stress (confining stress in a triaxial test); (m) is the stress dependent stiffness parameter; and (p^{ref}) is the reference confining pressure correspondent to 100 kPa.

The amount of stress dependency corresponding to the power (m) was considered to be 0.7 for the silts and 0.6 for the silty sand layer. In the absence of oedometer test results and considering the frictional nature of the materials, the oedometer modulus (E_{oed}^{ref}) was assumed to be equal to E_{50}^{ref}. To allow for the loading and unloading stress paths, the unload-reload modulus was set to 1.

The liquefiable layers were modelled using the cyclic soil behavior of the constitutive model UBC3D-PLM. This involves two yield surfaces of the Mohr-Coulomb type. The primary surface evolves according to an isotropic hardening law, while a simplified kinematic hardening rule is used for the second yield surface. The plastic flow rule is non-associated and is based on the Drucker-Prager´s law and Rowe´s stress dilatancy hypothesis. Two of the model parameters are of special interest for this study: fac_{hard} - that controls the evolution (hardening) law of the secondary yield surface to cyclic loading (K_0 effect); and fac_{post} - that governs the soil stiffness after onset of cyclic mobility when the mobilized friction angle reaches the peak friction angle. In other words, fac_{post} counterbalances the underestimation of resistance for "very dense" sands by increasing the stiffness of soil after cyclic loading and fac_{hard} is affected by levels of initial

vertical stress as function of $N_{1,60}$ as well as the predicted / empirically proposed $K\sigma$. The smaller the value of fac_{hard}, the greater the excess of pore water pressure and the lesser the liquefaction resistance. The smaller the fac_{post}, the less stiff the post-failure response will be [9].

3.3 - Calibration

Beaty and Byrne [10] proposed a set of equations to calibrate the UBCSand model parameters, based on only the corrected SPT value $(N_1)_{60}$.

The aforementioned calibrations suggested default values of 1.0 for both the hardening and post-liquefaction factors (fac_{hard} and fac_{post}, respectively). However, different investigators such as Makra [11], after calibrations with laboratory tests and field observations of the performance of the San Fernando Dam after 1971 San Fernando earthquake, have suggested that those factors are 0.45 and 0.02 respectively. Without additional seismic results from in situ tests, those values were considered appropriate for the project. Due to dependency of the models to different stress paths, it is recommended that the calibration of elasto-plastic models used for dynamic analysis should be done using cyclic loading tests such as triaxial torsional shear or simple shear tests (unavailable for the time being). The laboratory tests can properly simulate the loading conditions present in the field. The calibration can be obtained when then the cyclic stress ratio is compared with the number of loading cycles required to cause liquefaction.

The values for the Hardening Soil and UBCS and materials are listed below in Table 2.

Table 2 – Relevant geotechnical soil parameters

	Layer	1	2	3A	4	5A	5B	6	7
Plaxis model		HS	UBC_{SM}	UBC_{SM}	HS	UBC_{SM}	UBC_{SM}	HS	HS
Drainage type		U	U	U	U	U	U	U	D
Unsaturated unit weight (kN/m^3)	γ_{unsat}	18.00	17.00	18.00	14.00	17.00	17.00	14.00	18.00
Saturated unit weight (kN/m^3)	γ_{sat}	20.00	18.00	19.00	18.00	18.00	18.00	18.00	21.00
Constant volume friction angle (degrees)	$Ø'_{cv}$	30	27	40	26	30	40	26	38
Peak friction angle (degrees)	$Ø_p$	-	28	48	-	31	48	-	-
Cohesion (kN/m^2)	c'	-	0.01	0.01	-	0.01	0.01	-	-
Triaxial stiffness (kN/m^2)	E_{50}	12000	-	-	2000	-	-	12000	40000
Oedometer loading stiffness (kN/m^2)	E_{oed}	12000	-	-	2000	-	-	12000	40000
Triaxial unloading stiffness (kN/m^2)	E_{ur}	36000	-	-	6000	-	-	36000	120000
Elastic shear modulus number	K_G^e	-	867	1,431	-	993	1,418	-	-
Plastic shear modulus number	K_G^p	-	267	5,665	-	529	5,311	-	-
Elastic bulk modulus number	K_B^e	-	607	1,002	-	695	993	-	-
Power for stress dependent	me	0.50	0.50	0.50	1.00	0.50	0.50	0.70	0.50
Power for stress dependent	ne	-	0.50	0.50	-	0.50	0.50	-	-
Power for stress dependent	np	-	0.40	0.40	-	0.40	0.40	-	-
Failure ratio	Rf	0.90	0.81	0.64	0.90	0.62	0.62	0.90	0.90
Reference stress	Pa	100	100	100	100	100	100	100	100
Densification factor	fac_{hard}	-	1.00	1.00	-	0.45	0.45	-	-
Corrected SPT blowcount	$(N_1)_{60}$	-	8	36	-	35	35	-	-
Post liquefaction factor	fac_{post}	-	1.00	1.00	-	0.02	0.02	-	-
Lateral earth pressure coefficient	Ko	0.5	0.5	1	0.56	1	1	0.56	0.38
Permeability (m/s)	Kx, Ky	10	10^{-4}	10^{-3}	10^{-3}	10^{-4}	10^{-4}	10^{-4}	100

To perform a dynamic analysis in PLAXIS 2D, special boundary conditions were applied to simulate a semi-infinite medium. The purpose of these boundaries is to impede wave reflection at the model boundaries, avoiding model perturbations. For that purpose, lateral boundaries were placed at a considerable distance from the building area in order to minimize possible interferences. These were also defined as "free-field" boundaries and a compliant base was used for the input of the earthquake motion.

The selected time history was applied at the elevation of the assumed firm strata, coincident with the top of the very dense gravelly soils. It is the same location where the seismic motion of the outcropping rock was recorded, scaled to achieve the required seismic design accelerogram. For the Hardening Soil layers, the Rayleigh damping coefficients associated with small damping ratios were selected. In this formulation, the damping matrix is a function of the mass and the stiffness matrices which are modified by the Rayleigh coefficients α and β. The two coefficients are calibrated based on damping ratios and two sets of natural frequencies of the free field soil.

Calibration of numerical models is essential to check the reliability of the adopted analysis approach. In order to achieve this, a comparison between the numerical model, without ground improvement, and CPT based simplified methods, enabled the identification of the presence of liquefiable layers. This procedure has demonstrated an agreeable matching for both methodologies used. In this case, the FEM analysis produced pore water pressures ratios near one (r_u=1) for the same liquefiable layers as with the CPT data when analysed with the CLiq program using the Boulanger and Idriss (2014) method. This method is well calibrated with abundant data collected after the recent Canterbury Earthquake Sequence in 2011. However, it is not necessary to reach pore pressure ratios of 1.0 to demonstrate that liquefaction occurs. Beaty and Perlea [12] suggested that liquefaction is triggered for pore pressure ratios above 0.85. The technical specification for this project required an excess of pore water pressure ratio on the improved soil block up to 0.5.

4 - RESULTS

4.1 - Design Rationale for Ground Improvement Intervention

The ground improvement created by the lattice shaped jet grout columns will form a stiff block that will reduce the overall deformability and potential liquefaction susceptibility of the soil. This was proposed by the Council Geotechnical Consultant based on research and evidence from the Christchurch earthquakes showing that when a thick non liquefiable crust is present below the building foundations the observed damage after a major seismic event is limited. While global settlements are still expected to occur under such destructive circumstances, the effects on surface structures should be relatively non-damaging.

Professor Ishihara [13] has collected data from numerous case studies and has proved that there is an inverse relation between the thickness of a mantle of non-liquefiable soils and the liquefaction damage observed at the surface. If the non-liquefiable crust is sufficiently thick, the uplift force due to the excess water pressure will not be strong enough to cause a breach in this layer. Hence there will be no surface manifestation of liquefaction even it occurs deep in the sub-soil.

4.2 - Liquefaction Mitigation

To demonstrate the effectiveness of the lattice structured jet grout columns in the reduction of liquefaction potential, the FEM numerical analysis was carried out for different cellular arrangements. The modelled configurations were:

i. Wall clear spacing: A=8.0m; B=8.0m (Figure 3);
ii. Wall clear spacing: A=6.0m; B=6.0m (Figure 3);
iii. Wall clear spacing: A=4.0m; B=4.0m (Figure 3);
iv. Wall clear spacing: A=7.0m; B=7.0m with a 2.5m diameter central column (Figure 4).

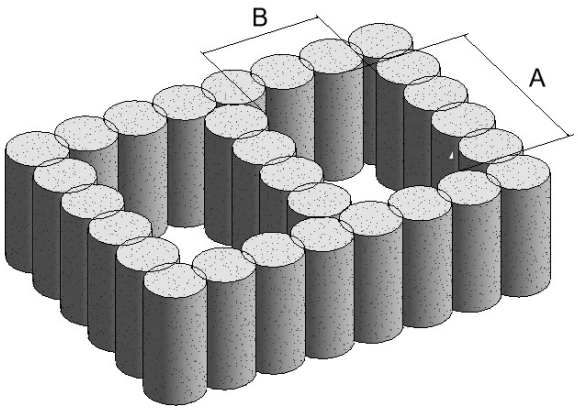


Figure 3 – 3D perspective of lattice cellular structure with spacing A x B

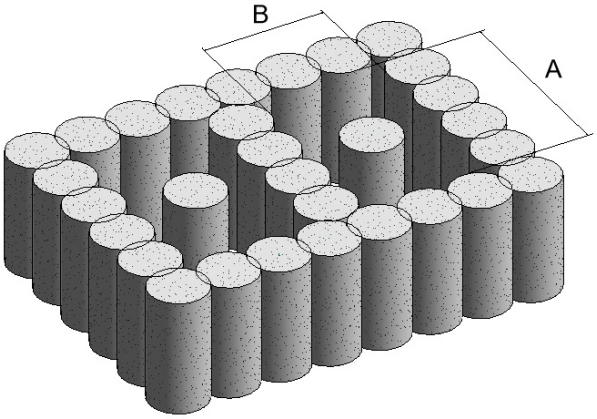


Figure 4 – 3D perspective lattice cellular structure with spacing A x B and additional central column

The UBCSAND model allows the software to compute the generation of excess pore water pressures throughout the soil deposit, including the treated soil block, taking into account the different effective stress levels experienced by the soil during a seismic event. The development of excess pore water pressure is expressed in terms of the excess pore water pressure ratio (r_u). The jet grout columns reduce the ratio r_u, by reducing the shear strains in the soil, inside the treated block. This ratio at a given depth in the soil profile typically represents the development of excess pore water pressure in relation to the initial vertical effective stress. The ratio r_u is given as follows:

$$r_u = 1 - \sigma'_v/\sigma'_{v0} \quad [2]$$

The undertaken analysis has demonstrated that the lattice cellular structure with 8m x 8m and 6m x 6m configurations (clear space between jet grout walls) is not effective at mitigating liquefaction in Layer 2, as pore pressure ratios between 0.85 and 1 were obtained. This means that full liquefaction triggering can be expected.

However, the remaining two arrangements, characterized by a lattice cellular structure with 4m x 4m and 7m x 7m configurations plus a 2.5m diameter central column, demonstrated that these solutions could be effective in terms of liquefaction mitigation. The results show that most of Layer 2 will experience pore pressures ratios ranging between 0.5 and 0.7. This means that, whilst liquefaction is unlikely to occur, some settlement is expected during and after the seismic excitation based on the development of the pore water pressure profiles. The next two figures show the pore pressure ratio results obtained for both efficient solutions.

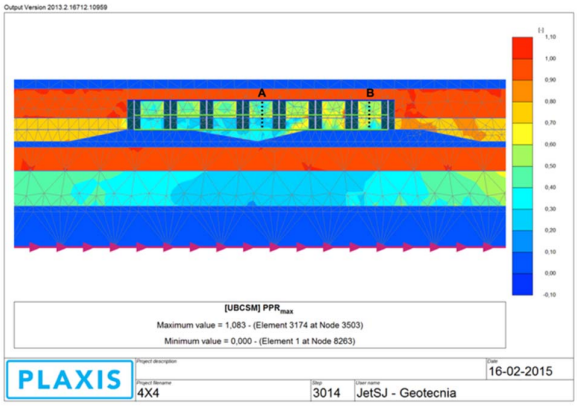


Figure 5 – Maximum Pore Pressure Ratio (4m x 4m configuration)

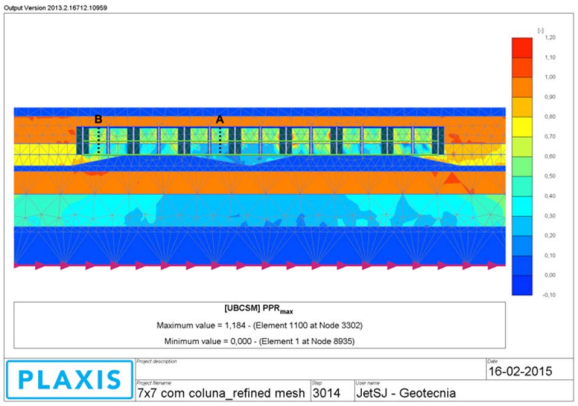
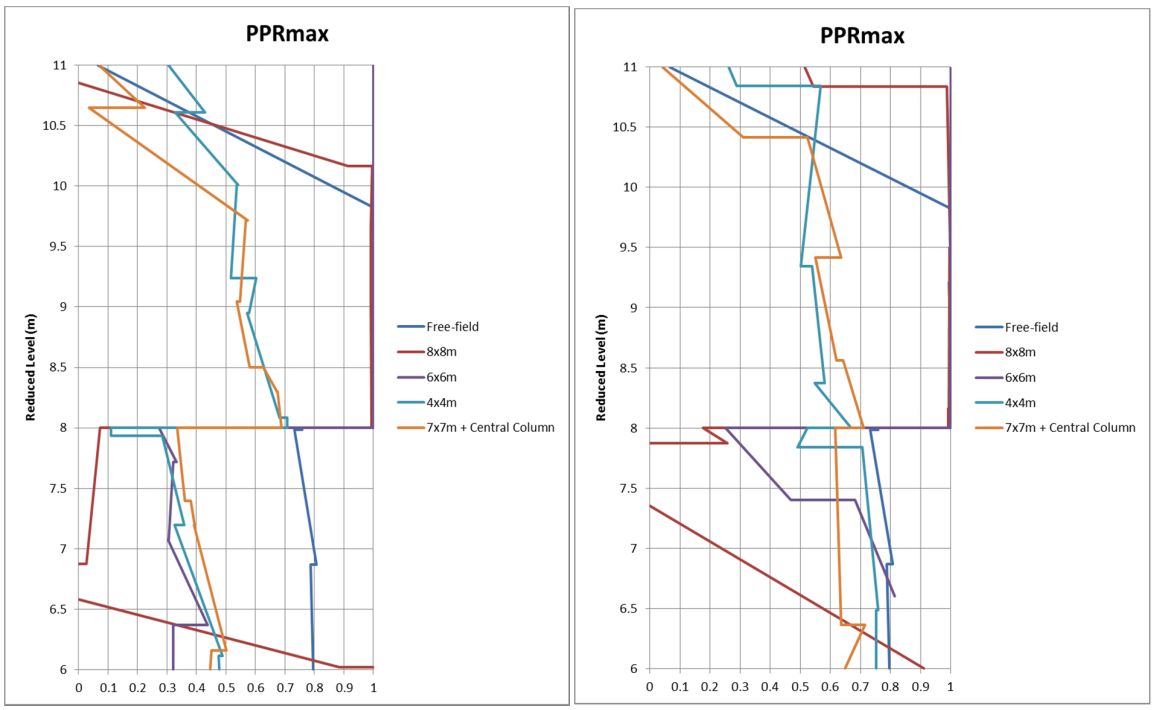


Figure 6 – Maximum Pore Pressure Ratio (7m x 7m configuration + Central Column)

Detailed pore water pressure ratio results for all the analysed jet grout columns cellular configurations (including free field, 8m x 8m and 6m x 6m arrangements) are summarized in Figure 7. Pore water pressure results (PWPR) are given for the following sections within the treated soil block:

I. Centre of the treated soil block (section A in Figure 5 and Figure 6).
II. Edge of the treated soil block (section B in Figure 5 and Figure 6).



I. Centre of the treated soil block

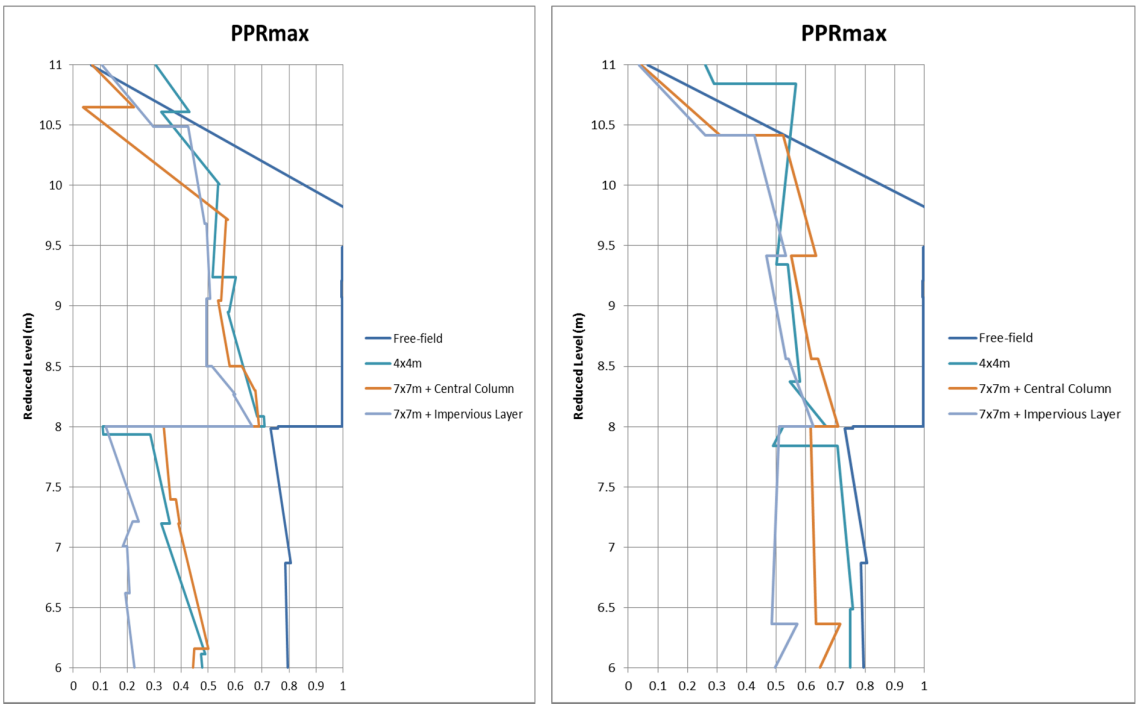
II. Edge of the treated soil block

Figure 7 – Pore Pressure Ratios Results for Section A and B

A complementary analysis was conducted in order to check if the efficiency of the solution improves if the jet grout walls are supported by a non-liquefiable layer and especially if this layer is of low permeability. In such scenario, it was found that the lattice shaped jet grouting walls will not only reduce the overall ground deformations, they will also contribute to control the potential for the excess pore pressure to migrate upwards into the treated block area. In order to simulate this effect, an additional model was developed to include a low permeability soil layer (Layer 4), with a permeability of $k=10^{-7}$ m/s, extending up to the base of the treated soil block. In this case, the results showed that the effects inside the treated soil block are more homogeneous and that the obtained pore pressure ratio is consistently around 0.5 or less, meaning that no liquefaction is expected to occur.

Figure 8 compares the maximum pore pressure ratio results for the most effective solutions with this last additional scenario. The results show the effectiveness of the ground improvement solutions, highlighting the importance of the soil permeability in the global soil behaviour.

I. Centre of the treated soil block (section A in Figure 5 and Figure 6).
II. Edge of the treated soil block (section B in Figure 5 and Figure 6).



I. At centre of the treated soil block II. At the edge of the treated soil block

Figure 8 – Pore Pressure Ration Results for jet grout walls founded on a low permeability layer - sections A and B

4.3 - Lateral Spreading Resistance

The soil stabilization works were restricted to the Town Hall building footprint and would not restrain the riverbank between the foundations and the river, thereby allowing for lateral spreading. The lateral spreading mechanism will develop within and above Layer 2 due to the high susceptibility of this layer to liquefaction and loss of lateral confinement. Despite that, no damage is expected to occur to the stabilized block as a result of the horizontal soil movement. The stabilized block was considered to be "anchored" in Layer 3, once a few discrete lenses of soil were expected to liquefy.

The jet grout columns allow for the vertical load imposed by the building as well as for the lateral shear stress imposed by the seismic motion. The external jet grout columns wall, adjacent to the river, is expected to suffer higher demand of shear forces in case the river bank moves away from the building, as the lateral soil support becomes ineffective.

In the Design Features Report [4], the shear stress on the jet grout wall resulting from the load imposed to the building is 123kPa for a 1m diameter column, considering a maximum vertical line load of 244 kN/m. With the proposed configuration, with columns of 2.5m diameter, the shear stress on the jet grout wall due to the vertical structural load shall reduce to 49 kPa.

The maximum shear stress in the peripheral wall, consequence of the seismic motion, was found to be 435kPa (Figure 9).

Turan [13] proposes the following equation to assess the shear strength of a composite soil-cement column:

$$\tau_{rd} = 0.3\sqrt{UCS} \quad [3]$$

where τ_{rd} is the compressive strength of the soilcrete material, determined by laboratory tests; and UCS is the unconfined compression stress of the composite soil cement material.

According to unconfined compressive tests results, relying on several cylindrical core samples retrieved from "in situ" jet grout columns, an average value of UCS_{AVE}=9.5MPa has been set. As $UCS_{design}=UCS_{AVE}/SF$, the ultimate limit state of the jet grout material against shear was verified, assuming a SF=2.0.

$$UCS_{design} = 4.75MPa$$

$$\tau_{rd} = 0.63\ MPa = 630kPa$$

$$\tau_{rd} = 630\ kPa > \tau_{sd} = 435 + 43 = 484kPa$$

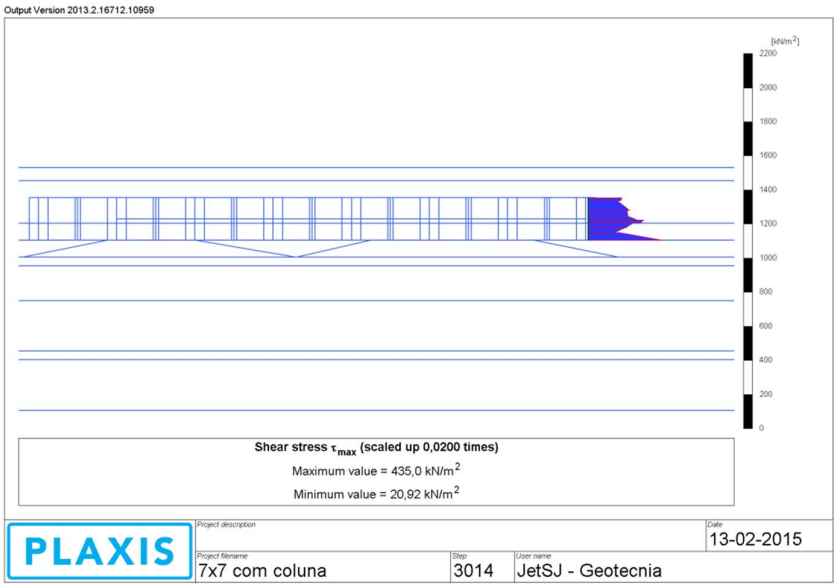


Figure 9 – Shear stress on the perimeter wall due to the design seismic motion

5 - CONCLUSIONS

The determination of the liquefaction potential of soils is still a major technical challenge. Ground failures associated with soil liquefaction often cause damages that can severely affect citizens and infrastructures. It is important to understand the soil behaviour under extreme seismic demand in order to allow for foundation and structural design to prevent the loss of building support and integrity.

The inherent complexity of a constitutive soil model, capable of accurately simulating the stress-strain behaviour experienced during a seismic event, relies on the identification of several elements, such as: the soil conditions; stress-strain history; anisotropy; stress level dependency of stiffness, amongst others. The UBCSAND (PLAXIS) model provides satisfactory interpretation of soil behaviour when submitted to severe seismic actions by analysing shear stresses, shear strains and excess pore water ratios.

In the present study, a series of numerical analysis were performed to investigate the effectiveness of different jet grout columns lattice configurations and prevent liquefaction triggering.

The results of the numerical analysis were evaluated in terms of pore water pressure ratios depending on the different cell configurations. It was demonstrated that, for the present case study, 8m x 8m and 6m x 6m spacing configurations are ineffective in terms of liquefaction mitigation. However, the cellular jet grout arrangements with configurations of 4m x 4m and 7m x 7m with an interior isolated jet grout column showed visible improvement in the soil response to seismic action and subsequent reduction of pore water pressures values.

In addition to numerical analysis, it is important to monitor and observe the behaviour of constructions when submitted to real seismic events. This will allow for a better understanding of such a complex phenomenon and consequently improve the geotechnical designs and solutions to be implemented according to different geological and seismic scenarios.

ACKNOWLEDGEMENTS

The authors acknowledge Mainmark for the collaboration and data made available for the present study and Mr Nick Traylen of Geotechnical Consulting Ltd, as the design peer reviewer, for his input and assistance during design process.

REFERENCES

[1] R. V. Siddhartan and A. Porbaha, "Seismic response evaluation of sites improved by deep mixing," ICE: Institution of Civil Engineers, 2008.

[2] K. Ogura, H. Kawamura, M. Y. Yoshida and T. Harada, "Design and Installation of Soil Improvement against Liquefaction in Reclaimed Ground with Coal Ash," Proccedings of the 22th (2012) International Offshore and Polar Enginneering Conference, 2012.

[3] Tonkin and Taylor Ltd, "Post earthquake assessment and conceptual geotechnical design report," February 2012.

[4] Tonkin and Taylor, "Design Features Report for Overall Geotechnical Design," 2014.

[5] Tonkin and Taylor, "Geotechnical Factual Report," 2014.

[6] R. Boulanger and I. Idriss, "CPT and SPT based liquefaction triggering procedures," 2014.

[7] V. Galavi, A. Petalas and R. Brinkgreve, "Finite element modeling of seismic liquefaction in soils," *Geotechnical Engineering Journal of the SEAGS & AGSSEA,* vol. 44, no. 3, pp. 55-64, 2013.

[8] H. Puebla, P. Byrne and R. Philips, "Analysis of CANLEX Liquefaction Embankments: Prototype and Centrifuge Models," *Canadian Geotechnical Journal ,* pp. 641-657, 1997.

[9] N. GEROLYMOS, P. TASIOPOULOU and G. GAZETAS, "Seismic performance of block-type gravity quay-wall: numerical modeling versus centrifuge experiment," *SECED 2015 Conference: Earthquake Risk and ENgineering towards a Resilient World,* 9-10 July 2015.

[10] M. Beaty and P. Byrne, "UBCSAND constitutive model, Version 904aR," *Documentation Report: UBCSAND constitutive model on Itasca UDM Web Site,* p. 69, 2011.

[11] A. Makra, "Evaluation of the UBC3D-PLM Constitutive Model for prediction of Earthquake Induced Liquefaction on Embankment Dams," *Delft Univertisy of Technology,* 2013.

[12] M. Beaty and V. Perlea, *Effect on ground motion characteristics on liquefying sand dams,* 2012, pp. 2108-2117.

[13] K. Ishihara, "Stability of natural deposits during earthquakes," *11th ICSMFE,* vol. Vol. 1, pp. 321-376, 1985.

[14] D. H. Turan, *Utilization of High Modulus Columns in Foundation Enginnering Under Seismic Loadings,* 2004.

STUDY ON THE QUALITY OF MULTIFAN SHAPED JET GROUTING

Takashi Shinsaka, Sanshin Corporation, Tokyo, Japan, t-shinsaka@sanshin-corp.co.jp.
Junichi Yamazaki, Sanshin Corporation, Tokyo, Japan, j-yamazaki @sanshin-corp.co.jp.
Yasuharu Nakanishi, N.I.T. Inc., Tokyo, Japan, nakanishi@nitjet.com.
Kazuhito Komiya, Chiba Institute of Technology, Chiba, Japan, hisho-stf@it-chiba.ac.jp.

ABSTRACT

Jet grouting is a technique for ground improvement which employs high pressure cement slurry and high pressure air. Because of the high energy with which the cement slurry is injected into the ground, the soil structure breaks up and mixes with the soil particles in situ, creating a high-strength soil-cement material. However, this creates a large amount of industrial waste during construction, which is a problem because of the effect on construction costs and environmental factors. Based on this background, a new jet grouting method (the MultiFan method) for wall-form ground improvements was developed in order to reduce the amount of redundantly improved soil. This method is comprised of partially formed, fan-shaped columns. In this paper, we geometrically examined the effectiveness of the MultiFan shape column for wall-form ground improvement. The effectiveness of the MultiFan column was verified by comparing it with round and oval columns created by conventional jet grouting methods. Consequently, the ground improvement work utilizing the MultiFan columns could be carried out more effectively than round or oval shapes. In addition, we developed a new control device for this method of ground improvement and conducted field tests to confirm its workability and quality. Consequently, we were able to confirm our assumption that it is possible to construct MultiFan shape columns for ground improvement work. Furthermore, core borings were carried out and column strength and variation were confirmed by uniaxial compression tests. The results showed that there was almost no difference in strength between the large diameter part and the small diameter part of the fans, and the variation was small. Therefore, it was confirmed that a homogeneously improved soil body could be produced by the MultiFan shape jet grouting method.

INTRODUCTION

Double fluid jet grouting is a technique for ground improvement which employs high pressure cement slurry and high pressure air (e.g. Shinsaka & Yamazaki, 2013). Because of the high energy with which the cement slurry is injected into the ground, the soil structure breaks up and mixes with the cement slurry in situ, creating a high-strength soil-cement material. This technique has been applied in various types of work, such as excavation support and the protection of departure and arrival shafts in tunnels. However, after the 2011 Great East Japan Earthquake, applications for liquefaction mitigation through a lattice and wall-form arrangements of columns have increased (Yamauchi et al., 2014; Uchida et al., 2014). Until now, lattice and wall-form improvements were constructed with round columns generated by jet grouting. Because the columns were round, more soil was improved than what was actually required, and more cement slurry was used than what was required. Furthermore, the cost of industrial waste disposal was high. Therefore, round columns are not economically viable with respect to cost and environmental factors. Consequently, the MultiFan jet grouting method of ground improvement was developed in order to reduce the amount of redundantly improved soil (Shinsaka et al., 2017). This method is comprised of fan-shaped columns that consist of different diameters. There are other various types of jet grouting methods, such as “Caramella”, “Candy Jet”, “Bow Tie Jet” or “Elliptic Jet”, which are columns with a similar fan shape. These have also been constructed in Europe and the USA in actual constructions for bottom plugs and cutoff walls (e.g. Leoni and Pianezze, 2017, Leoni et al., 2016).

In this study, we geometrically examined the effectiveness of the MultiFan-shaped column created from two different diameters. This is the simplest shape for lattice and wall-form ground improvements. In addition, we developed new equipment for this ground improvement method, and conducted field tests to confirm its workability.

© 2018 Deep Foundations Institute

VERIFICATION OF THE EFFICIENCY OF DIFFERENT CROSS SECTIONS

Cross Sectional Shapes of Existing Jet Grouting Techniques

When the jet grouting monitor is continuously rotated while being lifted up, round columns are formed. Therefore, round soil-cement columns are typically formed. Because the jet grouting method uses fluid and not mixing blades, as in the mechanical mixing method, the slurry is mixed in situ and the adjacent improved soil bodies can overlap and adhere to each other. Because of such advantages, jet grouting offers a very wide range of applications.

Fig. 1 shows the representative arrangements of jet grouting columns. Sealing slabs are constructed by overlapping the columns (Fig. 1(a)). In this arrangement round columns are effective. On the other hand, when wall- (Fig. 1(b)) or lattice-form (Fig. 1(c)) structures are constructed with round columns, a considerable amount of redundantly improved soil body exists as part of the structure. When there is an increase in the redundantly improved soil body, there is a high cost associated with materials and industrial waste disposal. Additionally, construction time is longer, which, together with unnecessary materials being produced and disposed of, can have a negative impact on the environment. Therefore, there are various problems associated with round columns.

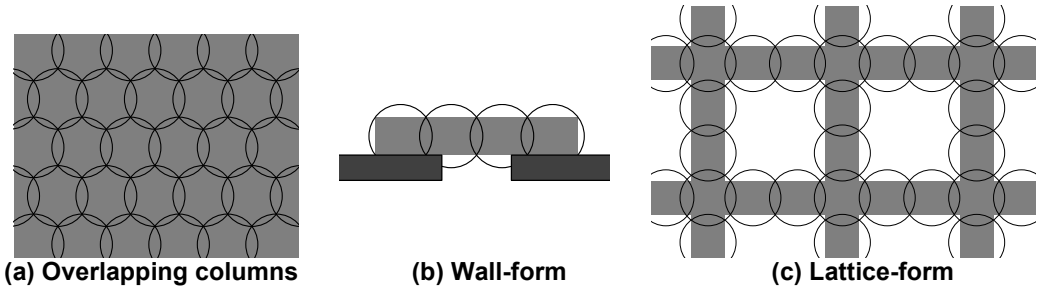


Fig. 1. Representative arrangements of jet grouting

In response to these problems, wall form ground improvements with oval columns have recently been constructed (Ota et al., 2015). When oval columns are used, the amount of redundantly improved soil body is smaller than with round columns, but the effective thickness of the overlapping sections becomes thinner. In other words, when the same thickness of wall form ground improvement is constructed, the spacing between oval columns is less than that of round columns (Shinsaka et al., 2017).

In this study, we geometrically examined the effectiveness of the MultiFan-shaped column—a partially formed, fan-shaped column (Fig. 2)—and verified its effectiveness by comparing it with round and oval columns.

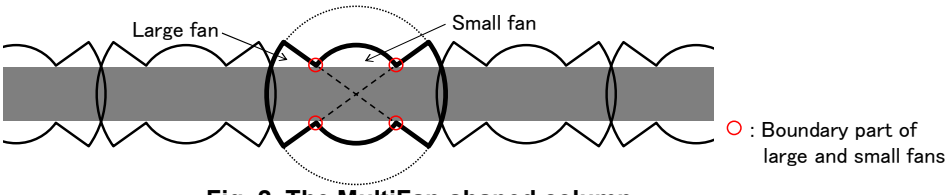


Fig. 2. The MultiFan-shaped column

Method of controlling the column shape

The jet grouting method has different parameters, such as grout pressure, grout flow rate and withdrawal rate, and there are various specifications depending on the method used. However, within the same method of jet grouting, these specifications have many fixed values depending on the soil

condition of the target ground. Given that grout pressure, grout flow rate and withdrawal rate are fixed, column diameter can be controlled by the rotation cycle of the monitor.

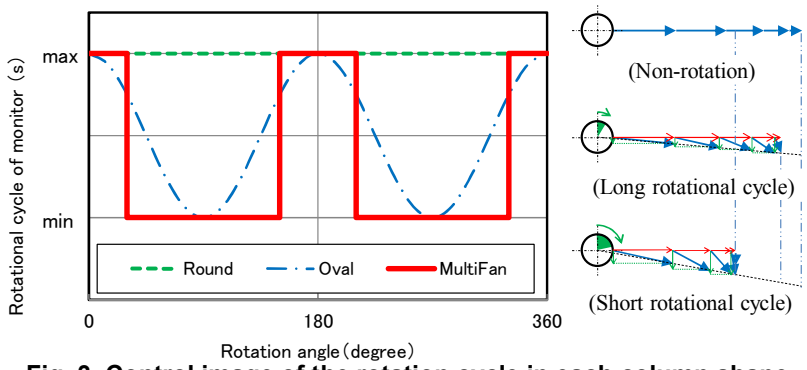


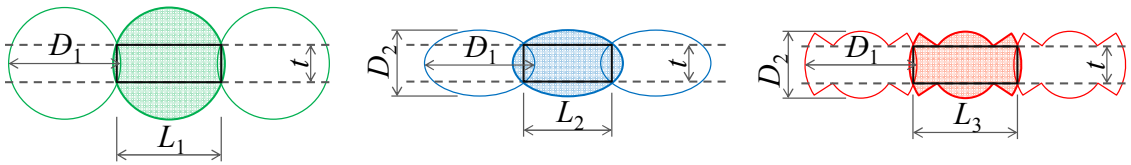
Fig. 3. Control image of the rotation cycle in each column shape

Fig. 3 shows the control image of the rotation cycle for each of the column shapes. The diameter of the round column is determined by the maximum capability of the jet grouting method. At this time, the rotation cycle is set at the maximum value. The maximum diameter part of the oval and MultiFan columns is set at the same value as that of the round columns. However, the diameter of each of these shapes can be reduced by shortening the rotation cycle. When the rotation cycle is set at the minimum value, the diameter of these shapes is the minimum. When the rotation cycle is continually changed to trace a sine curve between the maximum and minimum values, an oval column is produced. On the other hand, when the rotation cycle is changed intermittently between the maximum and minimum values, a MultiFan column is created. Accordingly, a complex control device is necessary to construct an oval column, but a MultiFan column can be constructed using a simple control device.

Column arrangement for a wall-form

Fig. 4 shows the relation between the "large diameter" (D_1), "small diameter" (D_2), "thickness of wall form" (t), and "spacing of columns" (L), in the cross sections of the three different column shapes. Hereafter, the small diameter is normalised by the large diameter (D_1) and is referred to as the "coefficient of small diameter" (C_{sd}), which is $C_{sd}= D_2/D_1$. The thickness of the wall form (t) is normalised by the large diameter (D_1) and is referred to as the "coefficient of wall thickness" (C_{wt}), which is $C_{wt}=t/D_1$. The values of C_{wt} and C_{sd} are changed and each cross section is compared. Because the shape of the improved soil body in jet grouting is columnar, examination of the improved body in this paper will be based on its cross section rather than its volume.

For a round column, which is the basic shape created by jet grouting, the necessary thickness of the wall form (t) determines the column spacing (L). Similarly, for oval columns the thickness of the wall form (t) also determines the column spacing (L). However, the spacing of oval columns (L_2) is smaller than that of round columns (L_1). On the other hand, when MultiFan columns are constructed, the thickness of the wall form (t) is determined by the thickness of the boundary part of the small and large fans (Fig. 2). That is, the central angles of the large and small fans are decided by setting a small diameter (D_2) for the thickness of the wall (t). At this time, the spacing of the MultiFan-shaped columns (L_3) can have the same value as that of the round columns (L_1).



(a) Round shape **(b) Oval shape** **(c) The MultiFan shape**

Fig. 4. Relation between different column cross sections

Fig. 5 shows the relation between the coefficient of wall thickness (C_{wt}) and the cross sectional "area of improved body by jet grouting" (A_{jg}). For ease of comparison, the cross sections of the improved soil bodies in the graph are calculated with the large diameter (D_1), set at a value of 1. In a round shape, as noted above, the thickness of the wall changes in relation to the spacing of the columns, but the cross section of each column is the same. On the other hand, the cross sections of both the oval and MultiFan shapes are smaller than that of the round shape. Moreover, as the coefficient of small diameter (C_{sd}) decreases, the cross section of the improved soil body (A_{jg}) also decreases. When comparing the results that used the same coefficient of small diameter (C_{sd}) with the cross section of the MultiFan shape, as the coefficient of wall thickness (C_{wt}) decreases, the cross section of improved soil body (A_{jg}) also decreases. For the oval shape, however, even though the coefficient of wall thickness (C_{wt}) changes, the cross section of the improved soil body (A_{jg}) remains the same.

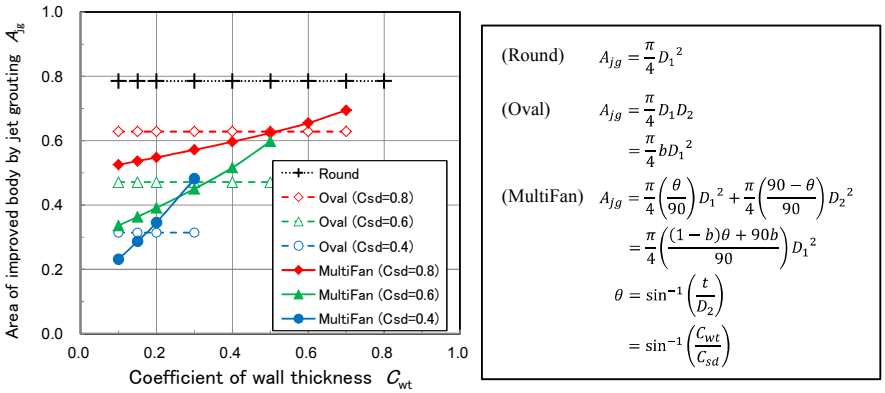


Fig. 5. Relation between the coefficient of wall thickness and cross section of improved soil body

Next, we examined the influence on the spacing of columns of the three different column shapes. Fig. 6 shows the relation between the coefficient of wall thickness (C_{wt}) and the "column spacing ratio", which is the value normalised by the large diameter D_1 (L/D_1). In round and MultiFan shape columns, the column spacing ratio decreases as the coefficient of wall thickness increases. The values of the round and MultiFan shapes are the same. By contrast, this tendency is the same for oval columns, but the value is smaller than it is for the round and MultiFan shapes.

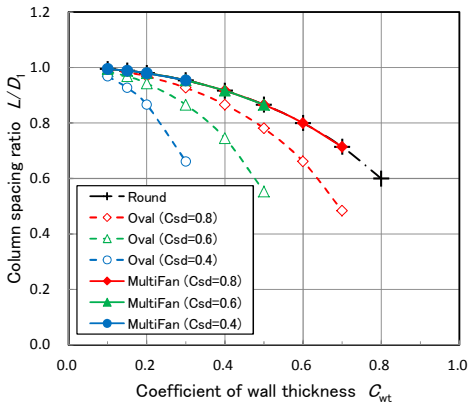


Fig. 6. Relation between the coefficient of wall thickness and column spacing ratio

Fig. 7 shows the relation between the coefficient of wall thickness (C_{wt}) and the "column number ratio" (n). Here, the number ratio refers to the number of columns in one line, and when the thickness of the wall is the same for the different column shapes, the number of the round columns was set to 1. From this graph, it is clear that the value of the MultiFan shape is the same as that of the round shape. However, the value of the oval shape tends to be greater than those of the round and MultiFan shapes.

In particular, the number ratio of the oval shape increases greatly as the coefficient of wall thickness (C_{wt}) increases.

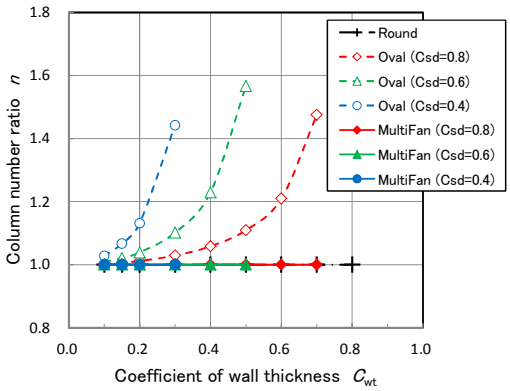


Fig. 7. Relation between the coefficient of wall thickness and column number ratio

Therefore, the spacing of oval columns is smaller than it is for round columns, although the area of an oval column is smaller than that of a round one. Consequently, the effective area of a wall constructed with oval columns decreases when compared with one made with round columns, while the number of necessary columns increases. Because the number of columns increases, the cost of materials and industrial waste disposal may rise. By contrast, because the number of MultiFan and round columns is the same, the cost of materials and industrial waste disposal decreases with MultiFan columns.

Next, we compared the quantity of grout materials needed to construct a wall of the same volume using round, oval and MultiFan-shaped columns. Fig. 8 shows the relation between the coefficient of wall thickness (C_{wt}) and "the redundant ratio" (β). The redundant ratio (β) is calculated using Eq. [1]:

$$\beta = \frac{(A_{jg} - A_w)}{A_w} \qquad [1]$$

where, A_{jg} is the cross sectional area of the improved soil body; A_w is the effective cross sectional area of the wall. From Fig. 8, it is clear that the MultiFan and oval columns demonstrated smaller values of redundantly improved soil body than that of round columns. Furthermore, the MultiFan columns had a smaller value of redundantly improved soil body than that of oval columns. In other words, we identified the point at which unnecessary construction for the wall body becomes small.

This revealed that ground improvement work could be carried out more effectively with MultiFan columns than with oval or round columns.

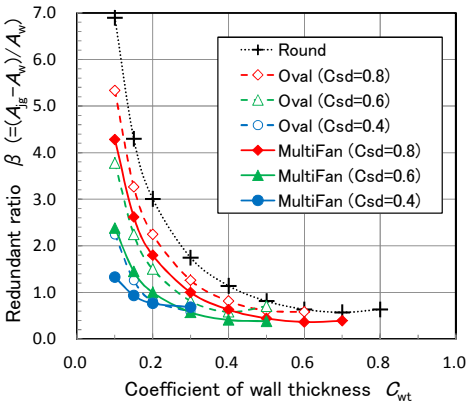


Fig. 8. Relation between the coefficient of wall thickness and redundant ratio

FIELD TEST OF MULTIFAN-SHAPED COLUMNS

Purpose of field test

We developed new equipment to construct MultiFan columns for ground improvement work (Fig. 9). This equipment could intermittently change the rotational speed of the monitor depending on the nozzle angle (Fig. 10). It could also control the radius and central angle of the fan. Field tests with this equipment were carried out to confirm its workability (Hontani et al., 2017).



Fig. 9. New equipment to construct MultiFan columns

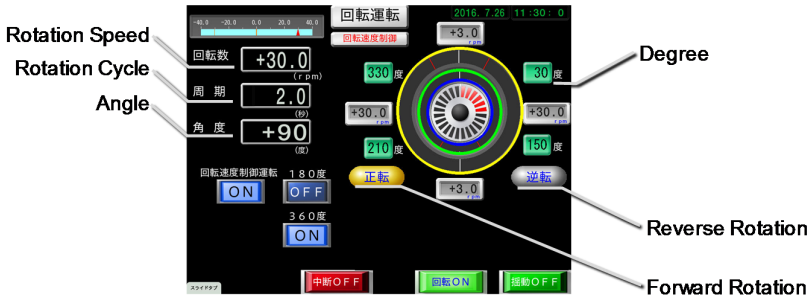


Fig. 10. Control monitor of new equipment

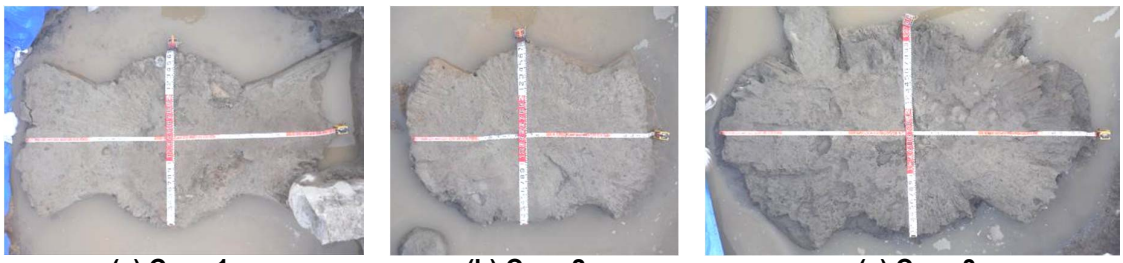
Overview of field test and results

In the target ground for the field test, the SPT-*N* values were 3 or less, and the target ground was classified as cohesive silt with sand. Table 1 summarizes the construction parameters adopted in this test. Cases 1 to 3 are those in which the effective wall thickness is set to 1.0m (3.3ft), 1.5m (4.9ft), and 2.0m (6.6ft). The diameter and central angle of the small fans are changed, but the diameter of the large fans in all cases are set to 4.0m. Preliminary experiments for determining the construction specifications were carried out before the test. The rotational cycle of the small diameter part was changed in stages, and the diameter of the fans were confirmed by using the JWM system (Shinsaka & Yamazaki, 2013). The JWM (Jet Wave Monitoring) system was developed to enable the confirmation of jet grouting ground erosion conditions.

Table 1. Construction parameters in field test

Construction parameters		1	2	3
Water-cement ratio (W/C)	[%]	106	106	106
Grouting pressure	[MPa]	35	35	35
	([psi])	(5076)	(5076)	(5076)
Flow rate	[L/min]	360	360	360
	([ft^3/min])	(12.7)	(12.7)	(12.7)
Air flow rate	[Nm^3/min]	10.0~12.0	10.0~12.0	10.0~12.0
	([Nft^3/min])	(353~424)	(353~424)	(353~424)
Withdrawal rate	[min/m]	6.67	8.00	9.33
	([min/ft])	(2.0)	(2.4)	(2.8)
Central angle (Large D./Small D.)	[Deg.]	(60/120)*2	(80/100)*2	(90/90)*2
Monitor rotation (Large D./Small D.)	[rpm]	3.4/30.0	3.4/24.0	3.4/15.0
Rotational cycles of monitor (Large D./Small D.)	[s]	17.5/2.0	17.5/2.5	17.5/4.0

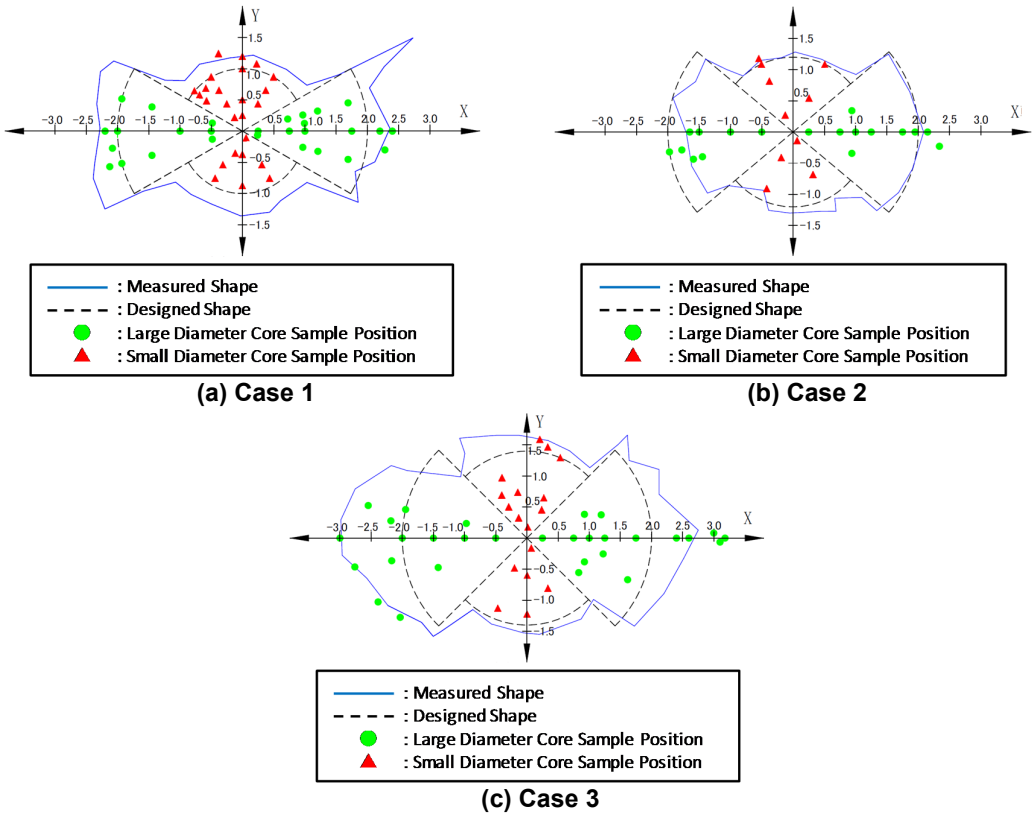
After jet grouting, we excavated the ground to reveal the top of the columns and inspected their shape. Consequently, we were able to confirm our assumption that it is possible to construct MultiFan-shaped columns for ground improvement work, as shown in Fig.11.



(a) Case 1 (b) Case 2 (c) Case 3

Fig. 11. The MultiFan-shaped column from the field test

In addition, core samples were gathered by core boring at the positions shown in Fig. 12. Then, the condition of the core was observed and the strength was confirmed by unconfined compression tests. Fig. 13 shows the histograms of the large and small diameter parts of the fan, and the whole of the MultiFan column. From this graph, there is no significant difference in the average strength between the large and small diameter parts of the fans. According to the coefficient of variation, which is an indicator of the quality of the improved soil body, the large fan was 37.5%, the small fan was 36.8%, the whole of the MultiFan column was 37.9%. From this result, a difference between the large and small diameter part of the fans could not be recognized. Moreover, these values are almost the same as the coefficient of variation of strength in the in-situ treated soil created by the slurry-based deep mixing method. It was also confirmed that the quality is comparable to that of the conventional jet grouting method.



(a) Case 1 (b) Case 2

(c) Case 3

Fig. 12. Core boring at different positions

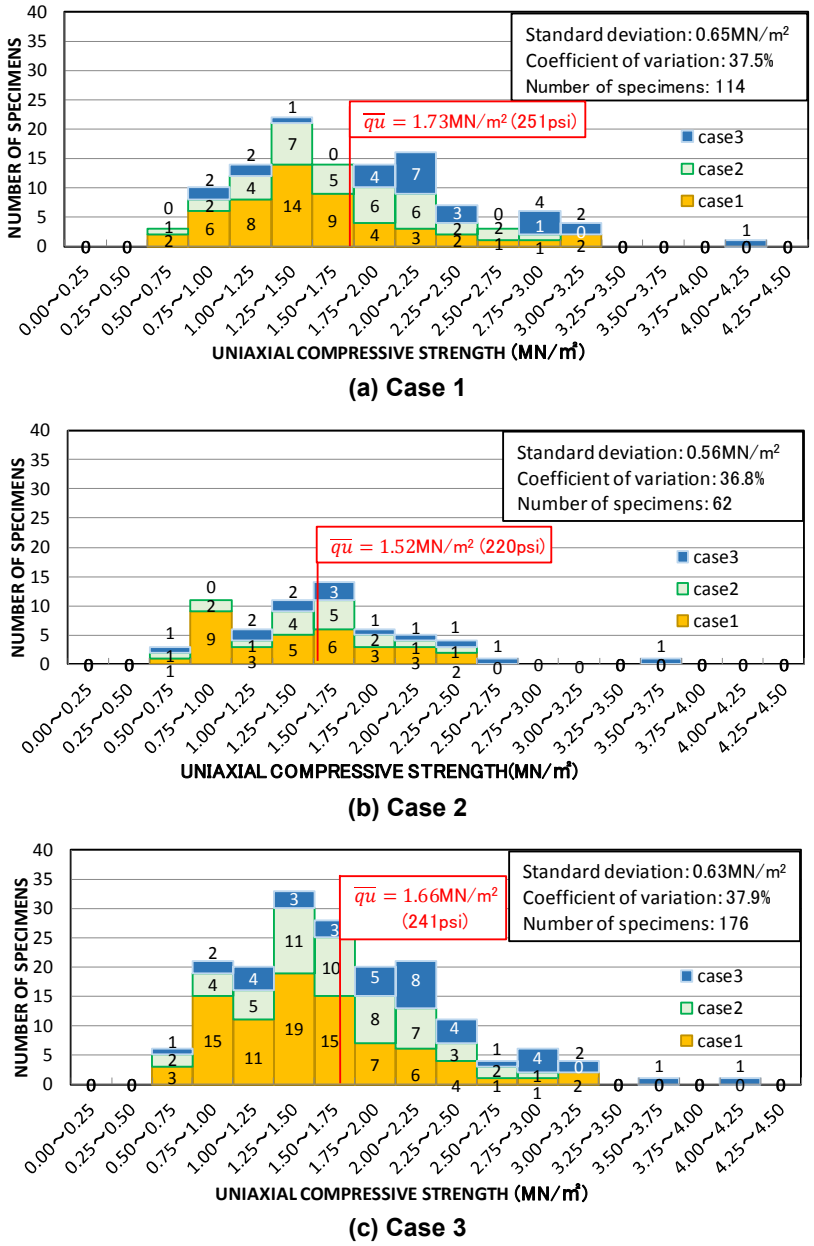
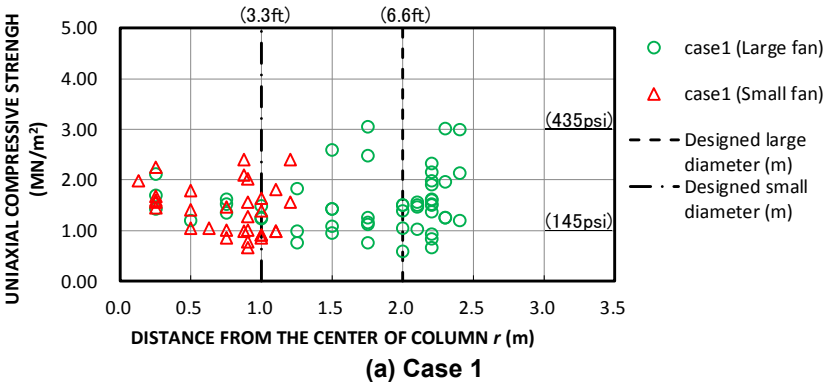
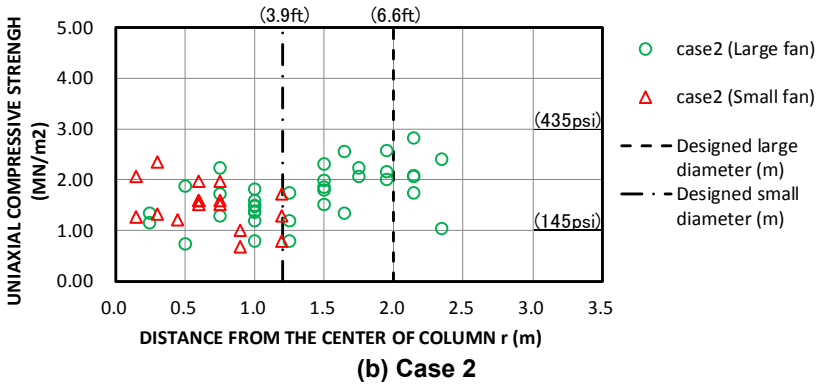


Fig. 13. Histograms of the large and small diameter parts of the fan, and the whole of the MultiFan column

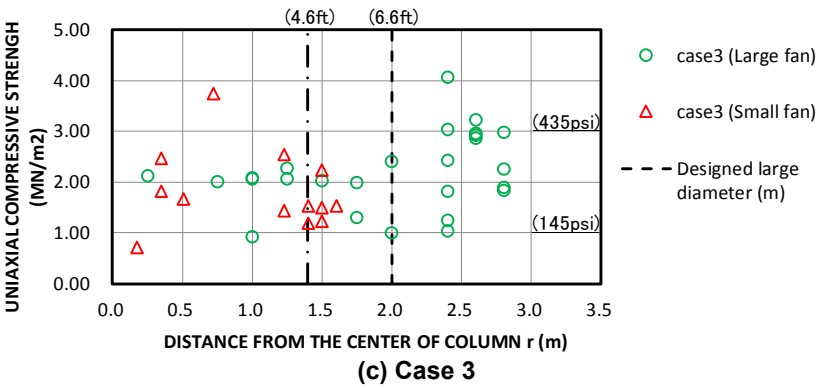
Fig. 14 shows the relation between the distance from the center of the column and compressive strength. From this graph, the uniaxial compressive strength is distributed in the range of 1.0 to 3.0 MN/m^2 (145 to 435 psi). Regardless of the size of the effective diameter in each case, there was almost no difference between the distance from the center and the strength.



(a) Case 1



(b) Case 2



(c) Case 3

Fig. 14. relation between the distance from the center of the column and compressive strength

The results showed that there was almost no difference in strength between the large diameter part and the small diameter part of the fans, and that the variation was small. Therefore, it was confirmed that a homogeneously improved soil body could be produced by the MultiFan shape jet grouting method.

CONCLUSION

When the wall form improvements were constructed, the MultiFan and oval columns demonstrated smaller values of redundantly improved soil body than the round columns. On the other hand, when the same thickness of wall form ground improvement was constructed, the spacing of the oval columns was smaller than those of the MultiFan and round columns. In other words, more oval columns were required than MultiFan or round columns. This revealed that improvement work could be carried out more effectively with MultiFan columns than with oval or round columns. Furthermore,

we developed new equipment for this work, and carried out field tests to confirm its workability. The fan radius and central angle were controlled by changing the rotational speed and angle at which the equipment was used. Consequently, we were able to confirm our assumption that it is possible to construct MultiFan columns for ground improvement work. Recently in Japan, MultiFan shaped jet grouting has been utilized to construct wall-form improvements and as a guide wall of a diaphragm wall (Shinsaka et al. 2018). Moreover, MultiFan columns have been successfully constructed in Europe and the USA in constructions for bottom plugs and cutoff walls (Leoni and Pianezze, 2017).

REFERENCES

Hontani, Y., Shinsaka, T. & Yamaguchi, H. (2017). Development of Jet Grouting Method for Existing House Estates - Performance Confirmation Tests -, 52th Japan National Conference on Geotechnical Engineering, Nagoya, Japan, 703-704.

Leoni, F.M., Pianezze G. & Bertero A. (2016). Comparison of the Pre-Construction and Production Qc Test Results for the Sela-22 Elliptical Jet Grouting Project (New Orleans, La), Proceedings of the International Conference on Deep Foundations, Seepage Control and Remediation (41st Annual), 2016, New York, NY, (DFI).

Leoni, F.M. & Pianezze G. (2017). Elliptical Jet Grouting: An innovative, Viable and Effective Solution: The Example of the Bottom Plugs for the SELA Projects in New Orleans, LA, Proceedings of the International Grouting Conference GROUTING 2017, ASCE, Hawaii, USA, 11-20.

Ota, K., Yamauchi, T., Kawanishi, A., Tezuka, H. & Miya, A. (2015). Development of Jet Grouting Method for Existing House Estates - Performance Confirmation Tests -, 50th Japan National Conference on Geotechnical Engineering, Hokkaido, Japan, 1789-1790.

Shinsaka, T., Shimano, A., Mansho, T. & Umezu, D. (2018). MultiFan Shaped Column of Jet Grouting Method Utilizing of Swing Type Rotation Control Device, 53th Japan National Conference on Geotechnical Engineering, Kagawa, Japan.

Shinsaka, T. & Yamazaki, J. (2013). Development of high-speed type jet grouting. Proceedings of the 2nd International Conference GEOTEC HANOI 2013, Ed. by Phung Duc long, Hanoi, Vietnam, 425-232.

Shinsaka, T., Yamazaki, J., Nakanishi, Y. & Komiya, K. (2017). Development of the MultiFan-shaped jet grouting method of ground improvement. Proceedings of the International Grouting Conference GROUTING 2017, ASCE, Hawaii, USA, 1-10.

Uchida, A., Taya, Y., Konishi, K., Noguchi, T., Abe, H., Yamanaka, R. & Tokimatsu, K. (2014). Field test about grid-form ground improvement for roads and houses of residential area (Part 2). Proceedings of the 11th National Symposium on Ground Improvement, Sendai, Japan, 323-326.

Yamauchi, T., Tezuka, H. & Tsukamoto, Y. (2014). Development of rational soil liquefaction countermeasure consisting of lattice-shape soil improvement by jet grouting for existing housing estates. Proceedings of the 11th National Symposium on Ground Improvement, Sendai, Japan, 221-228.

THE MULTI-PURPOSE BOTTOM PLUG: AN INNOVATIVE SOLUTION FOR THE GALATAPORT PROJECT IN ISTANBUL, TURKEY.

Salvatore Miranda, Trevi SpA, Istanbul, Turkey, +39 3478702222, smiranda@trevispa.com
Claudio Asioli, Trevi SpA, Cesena, Italy, +39 3460954407, casioli@trevispa.com
Claudio Nastasi, Trevi SpA, Istanbul, Turkey, +90 5536767645, cnastasi@trevispa.com

ABSTRACT

The paper describes an innovative geotechnical engineering solution that has been provided within the scope of the Galataport Project, in Istanbul, Turkey. Among all interesting geotechnical works included in the Project, this paper presents the design principle, adopted technologies and performance controls related to the Multi-Purpose Bottom Plug (MPBP). This original geotechnical engineering solution has been employed for the deep basement excavation in Karaköy and consists of a combination of seepage control, ground improvement, and load bearing elements, which have been executed with double-fluid jet grouting, pseudo-elliptical jet grouting and permanent micropiles, respectively. The paper highlights the importance of employing cutting-edge technologies within the foundation engineering field and state-of-the-art electronic control devices, in parallel with the essential human expertise, in order to obtain the desired results in this high profile Project. The results of an in-situ test carried out on the single element of the foundation system are also presented.

Keywords: Ground improvement, Elliptical Jet grouting, Bottom Plug, Liquefaction, Seepage control, Micropiles

INTRODUCTION

The Port of Istanbul is a passenger terminal for cruise liners, which is situated at Karaköy neighbourhood of Beyoğlu district in Istanbul, Turkey. The Port has up to 1,200 m of coastline and covers an area of approximately 100,000 m^2. It consists of two adjoining quays, the Karaköy (or Galata) quay and the Salıpazarı quay, extending from the Galata Bridge on the Golden Horn to Salıpazarı on the west coast of the Bosphorus. The construction of Karaköy quay began in 1892, and was completed in 1900. Two warehouses were built in 1910, and three more were added in 1928. The Salıpazarı quay was built in 1957 by the Ministry of Public Works. The Port of Istanbul served as the country's biggest seaport for import cargo until 1986 when it became obsolete due to the increase of container shipping. In 1988 the Port was converted into a passenger terminal for cruise liners and in 2007 it was extended in order to meet the growing demand for cruise tourism.





Quay	Length	Depth	Height [msl]
Karaköy	523 m	7 ÷ 9 m	0.5 ÷ 1.5 m
Salıpazarı	627 m	10	2.0 ÷ 2.5 m

Figure 1. Area of Project

Doğuş Group was awarded the Salipazarı Cruise Port tender on May 16, 2013 and in February 2014 entered into a partnership with BLG Capital, affiliate/group company of Bilgili Holding. Through this partnership, Salıpazarı Liman İşletmeciliği ve Yatırımları A.Ş. (SLI - Salıpazarı Port Management Inc.) was founded for the development and operation of the area. In February 2014 the port area was taken over and the operations began. The project involves the construction of a modern terminal for cruise ships, the construction of promenade by the coastline that has been closed to public for nearly 200 years, the reconfiguration of Tophane square, the restoration of historical buildings and redevelopment of the Salıpazarı section of the port area. The

© 2018 Deep Foundations Institute

new terminal will play a pivotal role in the project, since it is designed to be a world-first in underground boarding bridge systems for ships. Passengers will exit at boarding bridges, arriving at the terminal area through the tunnel which will be built along the pier. By moving all terminal operations and the customs areas underground, the coastline will be given back to the city.

The Geotechnical Works Contract is divided into two packages: Salıpazarı and Karaköy, which were firstly issued as two different tenders and were both eventually awarded to Trevi. The concept tender design was deeply studied by the engineers of Trevi Design, Research & Development office, who proposed several technical improvements and alternative solutions, which resulted in a significant value engineering. Therefore, Trevi acts as both main contractor and proposal designer.

The difficult hydraulic and geotechnical condition, the high seismic hazard of the site, the presence of historical buildings that need to be restored and strengthened, the simultaneous execution of the new quay by other Contractors and the continuative operation of the port while construction activities are ongoing, require the employment of cutting-edge technologies within the foundation engineering field and cause additional difficulties to this high profile Project. Construction activities started in July 2016 and are still going on while this paper is being written.

THE SALIPAZARI SITE

The Salıpazarı package includes the construction of an underground cruise port terminal, for which the whole 65,000 m^2 large site needs to be excavated down to approximately 15 m below ground level (13 m below sea level). The ground surface on top of terminal will be designated for a seaside promenade, walking paths and public squares.

The related foundation works envisage the execution of a 1,200 mm thick diaphragm wall, to be obtained by both mechanical grab and hydromill, (50,000 m^2 of D-Wall), a massive soil improvement against liquefaction by vibro-replacement (100,000 m of columns) and soil mixing with TurboJet (250,000 m^3 of treated soil), a pile foundation composed of 1,000 mm diameter bored piles (35,000 m) and the implementation of a dewatering system for the whole site (Fig. 2). The diaphragm wall at land-side is executed in natural soil/rock conditions and is supported by ground anchors (total 30,000 m). At sea-side, instead, the diaphragm wall is constructed in a filled area and is connected to the new quay wall through a special design scheme, which envisages a preliminary improvement of the soil by Turbojet (deep soil mixing).

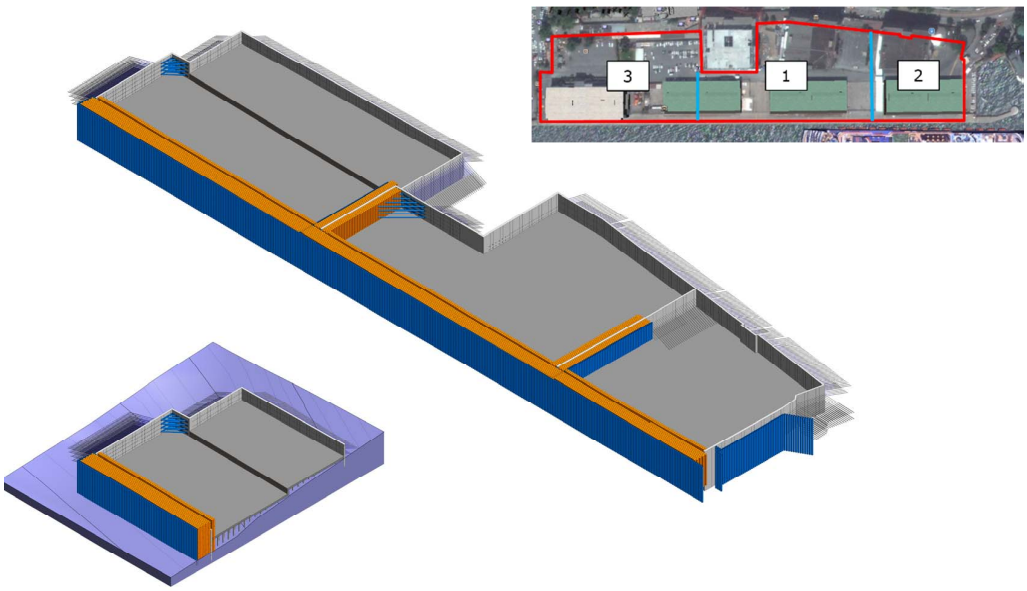


Figure 2. Schematic view of Salıpazarı site

THE KARAKOY SITE

The Karaköy package, in addition to the re-construction of its portion of quay, consists in the refurbishment of an area that was fully occupied by five buildings. Two historic buildings have been completely preserved, other two buildings have been partially demolished, while one non-historic building has been completely demolished.

The foundation works within the footprint of demolished buildings consist of a 1,000 mm thick propped diaphragm wall/secant pile wall, to be executed by mechanical grab and rotary piling rig (18,000 m^2 of D-Wall and 7,000 m of secant piles, with 200 steel props), a hydraulic bottom plug in order to reduce groundwater flow during excavation and related settlements of adjacent buildings, to be executed by 2,000 mm diameter double-fluid jet grouting overlapping columns (45,000 m^3 of treated soil), a lattice-type soil improvement against liquefaction composed of elliptical jet grouting columns (50,000 m^3 of treated soil) and a mesh of permanent tension micropiles against uplift, consisting of Double Corrosion Protected (DCP) steel bars (10,000 m).

As far as the preserved historical buildings are concerned, the related foundation works had to be conducted from inside the buildings, with reduced headroom, and consisted of a massive soil improvement against liquefaction by means of 1,500 mm single-fluid jet grouting (40,000 m^3 of treated soil) and structural underpinning by means of micropiles, in order to allow the excavation of a partial basement underneath.

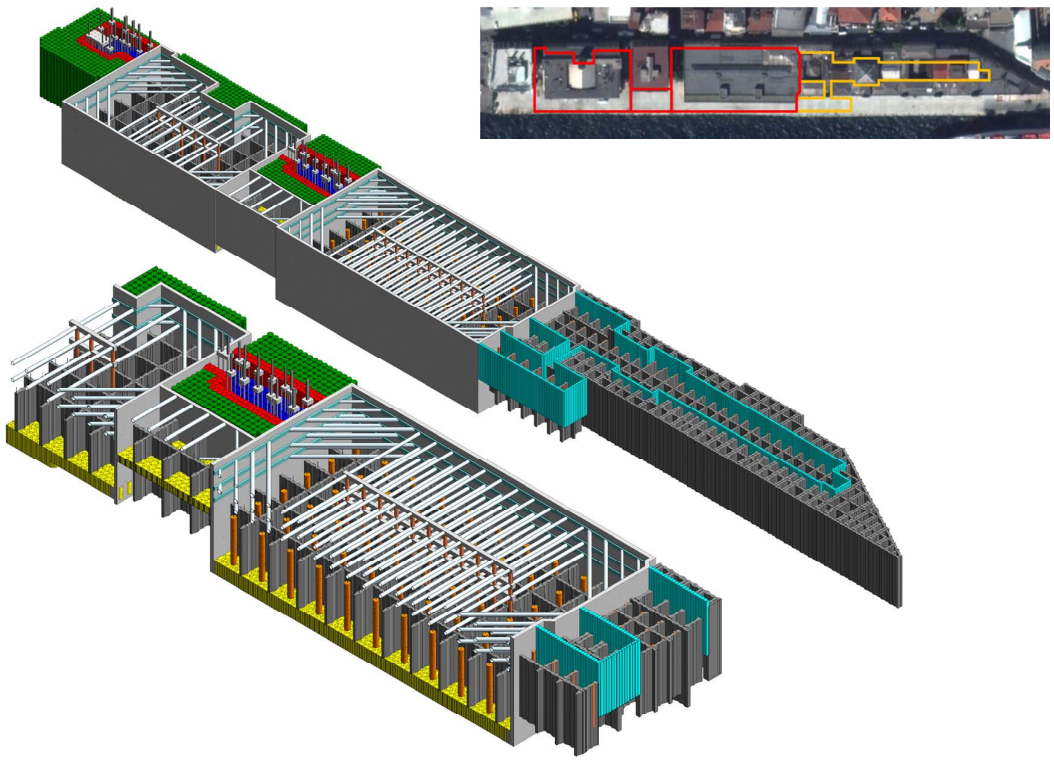


Figure 3. Schematic view of Karaköy site

An extensive monitoring system was installed in order to control the movement and forces acting on the different components of the foundation system, the surrounding soil and existing buildings. All the aforementioned activities were executed almost simultaneously, which caused additional difficulties with the project.

As far as the soil conditions are concerned, in Karaköy site a 25 m thick layer of man-made fill (uncontrolled mixture of materials from clay to cobbles size) is present in the whole area, followed by an approximately 5 m to 10 m thick layer of very loose liquefiable silty sand. The bedrock is very strong, very fractured greywacke

(UCS = 100 ÷150 MPa) and it is located between 35 m to 45 m below ground level, which is always deeper than the geotechnical activities involved in this area. Therefore, all structures were executed within the man-made fill and the underlying marine sand layer. The thick fill/sand layer contains a low amount of fine material and is classified as loose to very loose (NSPT = 0 ÷ 15, qc = 0.5 ÷ 3.0 MPa), with a high liquefaction risk.

THE MULTI-PURPOSE BOTTOM PLUG

Among all interesting geotechnical works included in Karaköy site, this paper focuses on the design principle, adopted technologies and performance controls executed on the Multi-Purpose Bottom Plug (MPBP). This innovative geotechnical solution is a combination of seepage control, ground improvement, and load bearing elements (Fig. 4), which was adopted to allow the deep excavation within the footprint of demolished buildings. Excavation depth was approximately 12.5 m below the working platform (11.0 m below sea level).

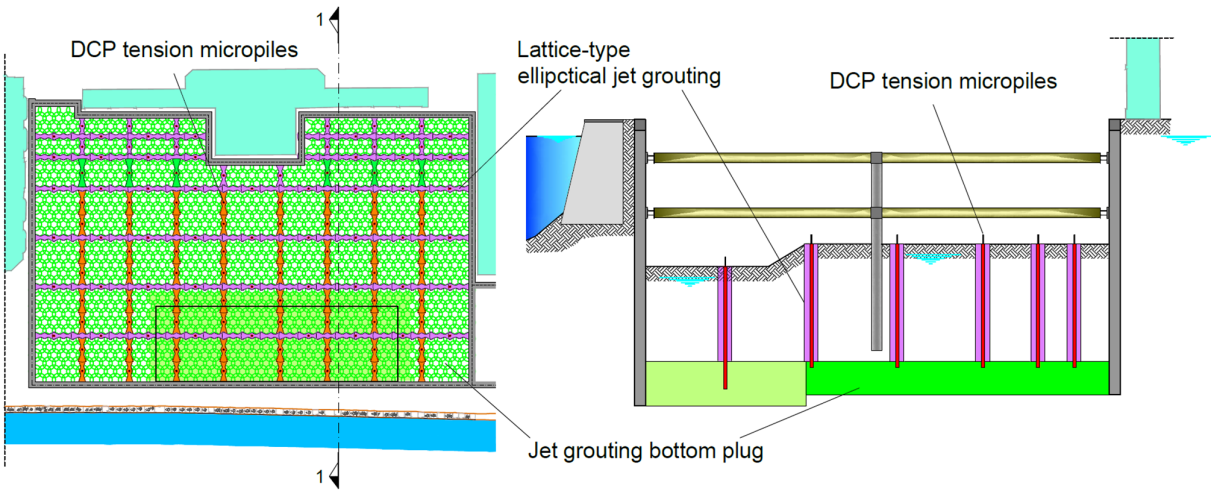


Figure 4. Plan and section view of MPBP

The main body of the bottom plug is composed of overlapping jet grouting circular columns, executed with the double-fluid method and designed to have a 2,000 mm diameter. Columns are executed on a triangular pattern with an average centre to centre spacing of 1,500 mm. The bottom plug's thickness is the one strictly necessary to ensure the hydraulic stability of the excavation.

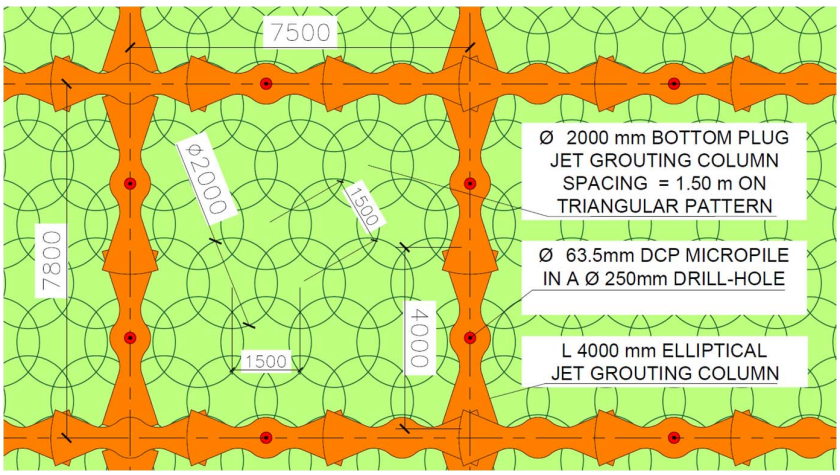


Figure 5. Detail of single MPBP element – Plan view

Subsequently, pseudo-elliptical jet grouting columns are executed from the top level of the bottom plug up to the excavation level on a lattice-type pattern, in order to act as a mitigation element to liquefaction. In particular, the pseudo-elliptical shape of jet grouting columns was chosen instead of the circular one in order

to optimize the lattice geometry, by minimizing the amount of jetting and related time of execution. The lattice-type jet grouting treatment also acts as a foundation for the future building and will carry the vertical structural loads in permanent conditions. Average width in plan of elliptical jet grouting column is 4.0 m.

Finally, the stability against uplift in temporary conditions (prior to building construction) is ensured by permanent Double Corrosion Protected (DCP) steel bars, which are installed as drilled and grouted micropiles through the previously-executed elliptical jet grouting columns. DCP steel bars have a diameter of 63.5 mm and are installed within a 250 mm diameter drill-hole.

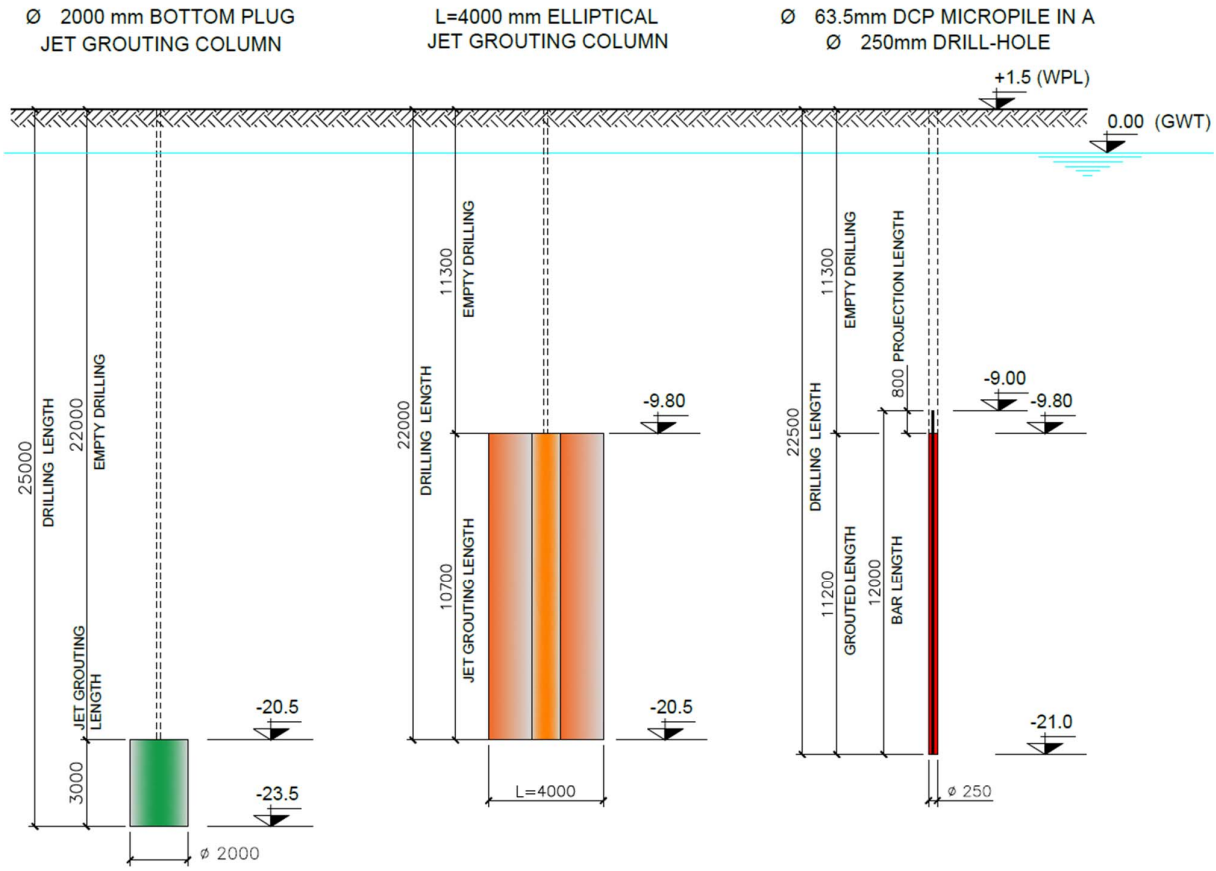


Figure 6. Detail of single MPBP element – Vertical section

Lattice-shaped ground improvements using soil-cement mixtures have been often developed as solution against soil liquefaction. The idea is to create a grid of treated soil in order to retain the untreated soil in between and to control its shear deformation during an earthquake, preventing the rising of excess pore water pressure and a possible liquefaction phenomena.

The good performance of this method was confirmed at the time of the 1995 Hyogo-ken Nanbu (Kobe) earthquake and applications of such design concept have increased since then. There are several studies on efficacy of lattice-type soil improvement as mitigation to liquefaction. These include both laboratory tests (such as shaking table tests and centrifuge experiments) and numerical analyses (such as dynamic 3D FEM/FDM analyses).

In order to design the unit cell of MPBP, a non-linear time history 3D FDM analysis was carried out by means of the FLAC3D software. The liquefaction potential of the natural soil was analysed on a 35 m deep, 2m x 2m sand column bordered by periodic boundaries (Fig. 7). The seismic input was applied at a bedrock elevation of -35.0 m msl (quite boundary). With regard to the assessment of the mitigation effect of the treated soil, three different cell net sizes were considered, namely: 5m x 5m; 7m x 7m and 10m x 10m. Main details of the models are shown in Fig. 8.

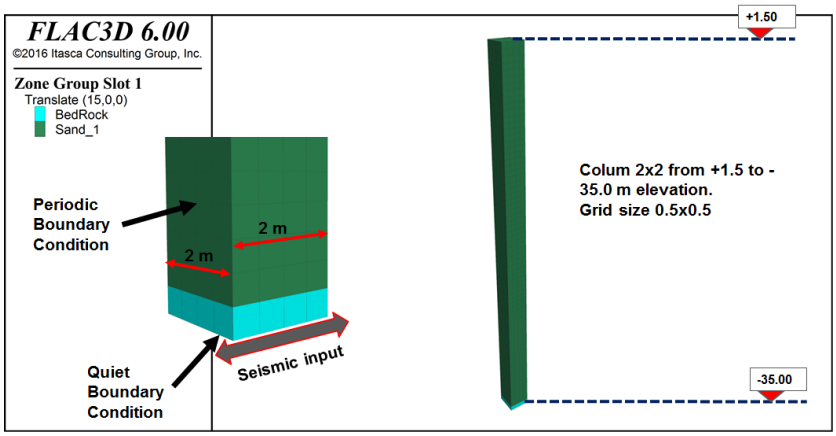


Figure 7. FDM model of natural soil for non-linear time history analysis

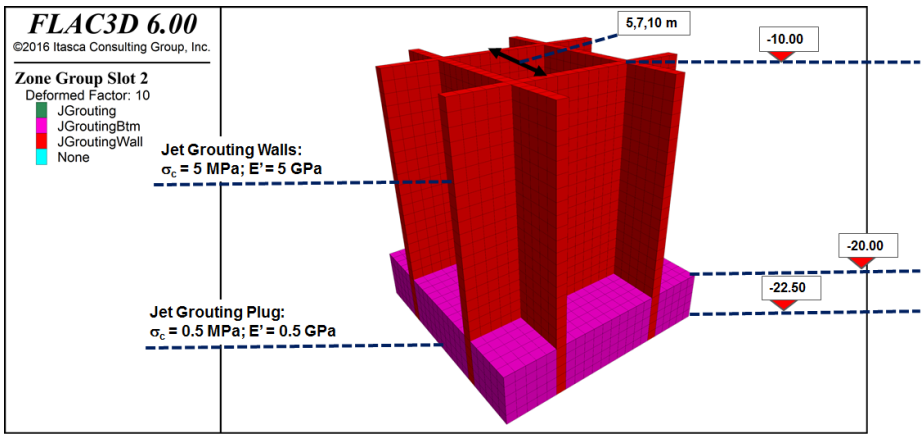


Figure 8. FDM model of lattice type jet grouting cell for non-linear time history analysis

The seismic input considered for the analysis was the Izmit-Kocaeli event of 17 August 1999 (Source: PEER NGA strong motion database record). Main analysis results are shown in Fig. 9 and Fig. 10: the red points are those where the ratio R_u, between the excess pore pressure and the effective vertical stress reaches the value of 1. It is possible to notice that, in natural soil, the liquefaction occurs down to 24 m below water table. Instead, in presence of soil improvement, R_u approaches 1 just in a thin band underneath the soil treatment. The 7m x 7m grid was selected, even though the 10m x 10m option provided satisfactory results too.

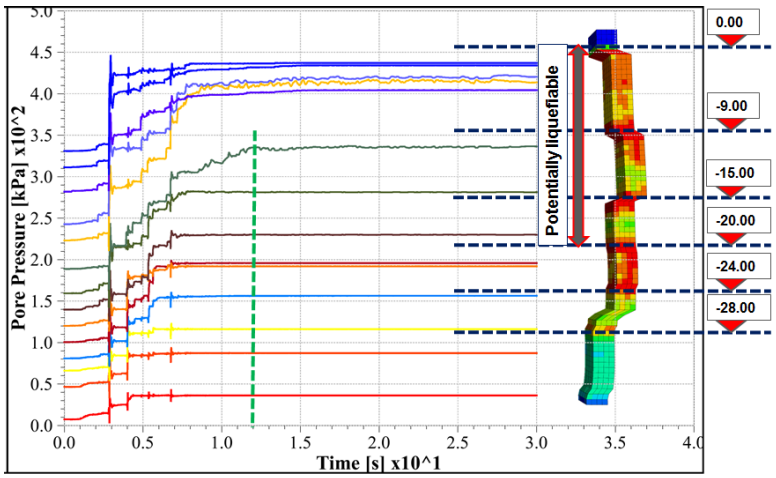


Figure 9. Pore pressure history and Max Ru in natural soil

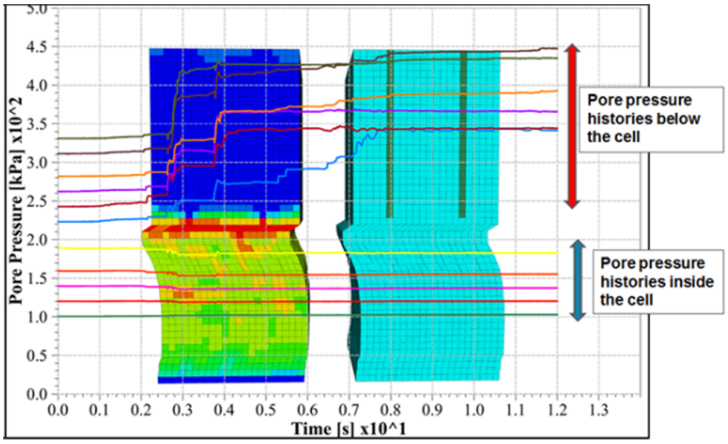


Figure 10. Pore pressure history and Max Ru in improved soil

The technologies involved and the electronic control devices employed for the execution of MPBP are of latest-generation. In particular, for the execution of the double fluid jet grouting bottom plug, the drilling rigs were equipped with the "Jet-Vision System" and with the "Drilling Position System" (DPS) electronic devices. The former controls and monitors the automatic rising of the drilling tool/rods during the jetting phase; the latter controls the 3D position of the drilling tool during the drilling phase, which is of basic importance to ensure the overlapping between the jet grouting columns and the consequent successful execution of the bottom plug. For the execution of pseudo-elliptical jet grouting columns, the Jet-Vision system was provided with the "orbital jet" option, which allows to modify the rotation speed during the jetting phase in a planned way. The rotation speed varies from V_{r1} to V_{r2} to create variable radius sectors (Fig. 11).

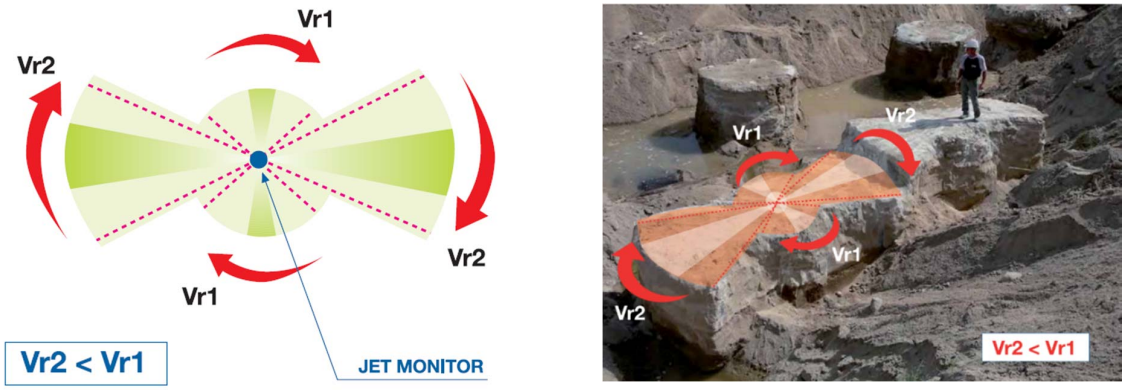


Figure 11. Pseudo-elliptical jet grouting (Photo from Gioia Tauro Port Project - Trevi)

The DPS was also used during the execution of both elliptical jet grouting columns and DCP micropiles. This allowed to locate jet grouting columns at the bottom of excavation (blue in Figure 12) and at the bottom end of columns (magenta in Figure 12) and to make sure that DCP micropiles (red in Figure 12) were always installed within the jet grouting columns.

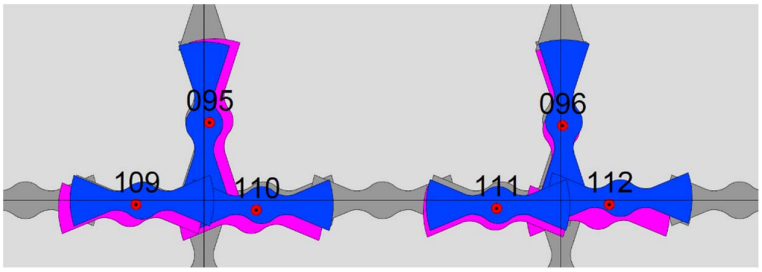


Figure 12. As-built elliptical jet grouting and DCP micropiles by using DPS

This was important since micropiles had been designed as “fully embedded in elliptical jet grouting”, considering an ultimate micropile-to-jet grouting skin friction of 400 kPa. Taking into account that all activities were executed from the original working platform, prior to the start of excavation, the correct position of micropiles could not be ensured by visual inspection, but had to rely only on the executed DPS measurements.

The elliptical jet grouting forming the MPBP has been designed in order to create a stiff grid that will prevent the loose sand from liquefying in case of earthquakes. For this reason, it was specified that soil improved by jet grouting should have an average unconfined compressive strength higher than 5 MPa and an average elastic modulus higher than 5 GPa. This was verified by laboratory tests on cored samples taken from both preliminary field trial tests and final QA/QC checks, which provided satisfactory results (Figure 13).

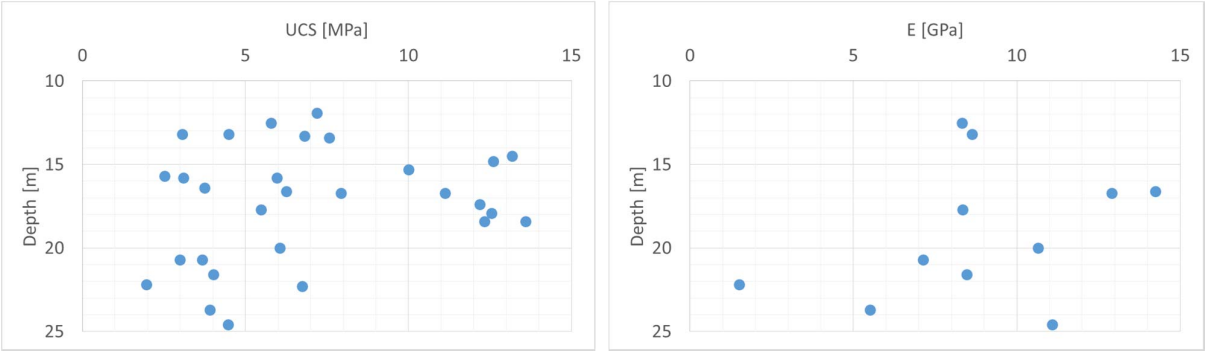
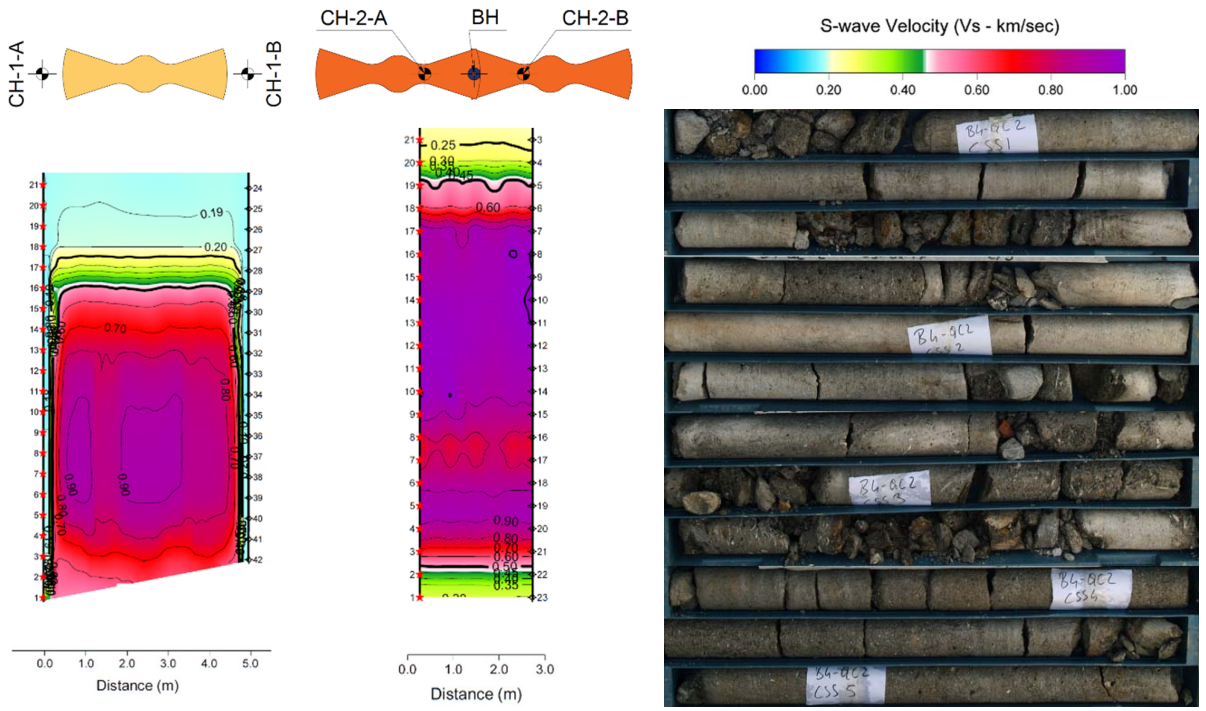


Figure 13. UCS and elastic modulus of laboratory tested elliptical jet grouting samples

During the preliminary field trial tests, it was also verified that the design column width in plan of 4 m could be obtained. This was an ambitious goal, since it was rarely achieved in previous experiences. The length in plan of elliptical jet grouting column was assessed by means of seismic cross-hole tomography on both single column (Fig. 14.a) and overlapping columns (Fig. 14.b). Results show an estimated column’s width in plan greater than 4 m. Moreover, a continuous coring was executed on the joint between two columns, which shows a continuous overlapping and a good quality of samples (Fig. 14.c).



(a) **(b)** **(c)**

Figure 14. Seismic cross-hole tomography and cored samples on elliptical jet grouting columns

Finally, also the tension capacity of DCP micropile was assessed through the on-site preliminary static load test. A 7 m deep, 4 m wide, jet grouting column was executed up to near ground surface and was equipped with steel rebars in order to record its uplift during testing (Figure 15.a). An instrumented DCP micropile was installed at its centre (Figure 15.b) and a static tension load test was carried out after 20 days from micropile execution (Figure 15.c). Maximum test load was 2,000 kN. Which corresponds to an applied micropile-to-jet grouting skin friction of about 400 kPa (on the ϕ 250 mm diameter micropile shaft).



(a) (b) (c)

Figure 15. Arrangement of tension load test on DCP micropile

General instrumentation layout is shown in Figure 16.a. In order to monitor the strain development along the micropile shaft, two sets of Vibrating Wire Miniature Embedment Strain Gauges (Fig. 16.b) were installed at 4 levels along the DCP bar, namely: -6.00, -4.25, -2.50 and -0.75 msl. Instead, for measuring the strain development inside the jet grouting column, two sets of 4 nos. EXT2strain retrievable extensometers (Fig. 16.c) were installed at the distance of 0.5 m (EXT-B) and 1.5 m (EXT-A) from micropile axis. Extensometers were inserted inside 2" steel pipes, previously drilled and grouted. Two tell tale rods were used to measure the tip movements and 14 nos. displacement transducers to monitor the uplift at surface. An automated digital survey level was used for monitoring the movement of reference beam during test to a precision of +/-0.01mm. Displacement, load and strain data were automatically recorded at 30 seconds intervals.

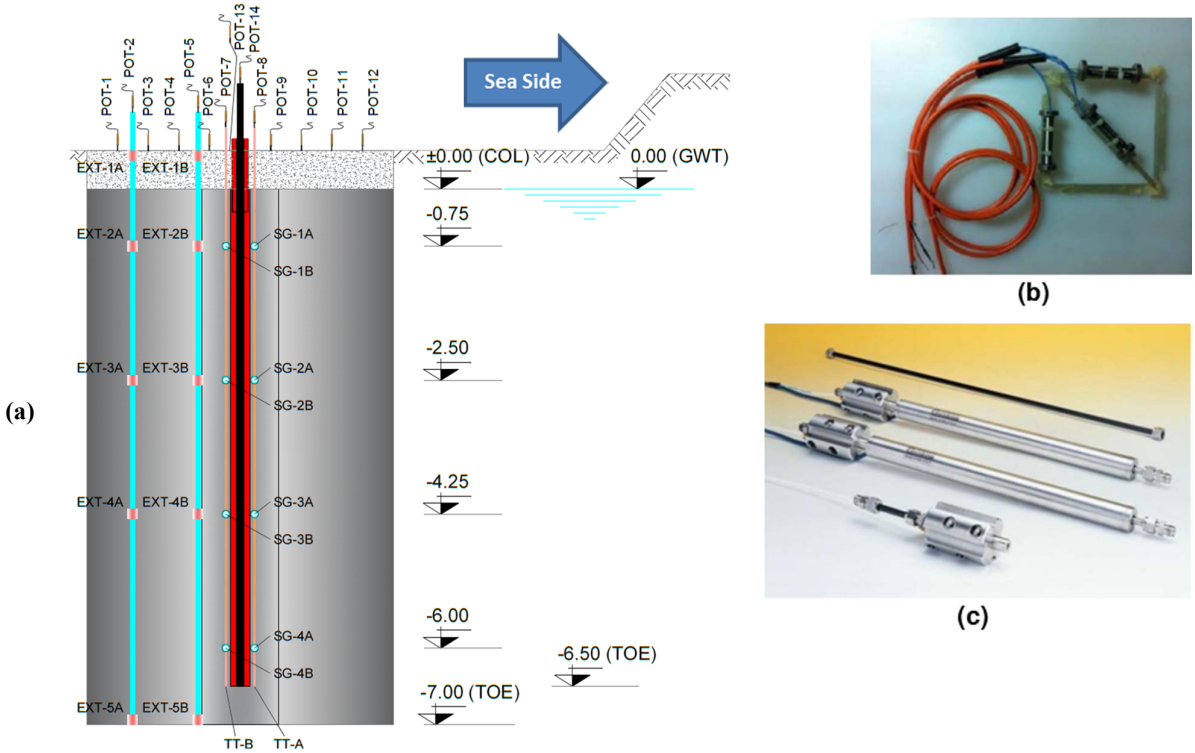


Figure 16. Instrumentation used for tension load test on DCP micropile

Test was successfully conducted to the specified test load and showed a non-uniform uplift of the jet grouting column, which varied between 3 and 6 mm, as represented in Fig. 17.a. This is possibly due to the irregular shape and mechanical properties of the jet grouting column.

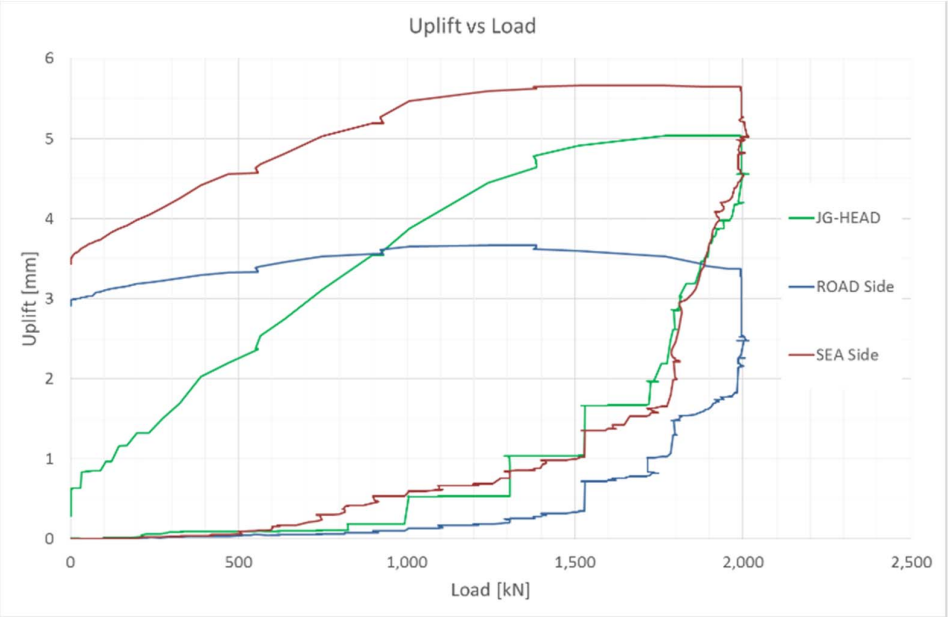


Figure 17. Tension load test results- Measure uplift

For what concerns the strain measurement, due to the mobilized high tension strain concentrations, the miniature embedment type strain gauges didn't perform satisfactory starting from low levels of load. The average total strain calculated from tell tales along the micropile was quite in line with the total strain values measured by extensometer EXT-B. That's why EXT-B strain values taken into account for shaft friction and load distribution calculations along micropile shaft. Measured Δmicrostrains are shown in Fig. 18, from which it is possible to notice that the micropile tip was just slightly mobilize, while concentrated cracks occurred at the top of micropile. Also, strain concentration decreases moving from micropile to jet grouting column edge.

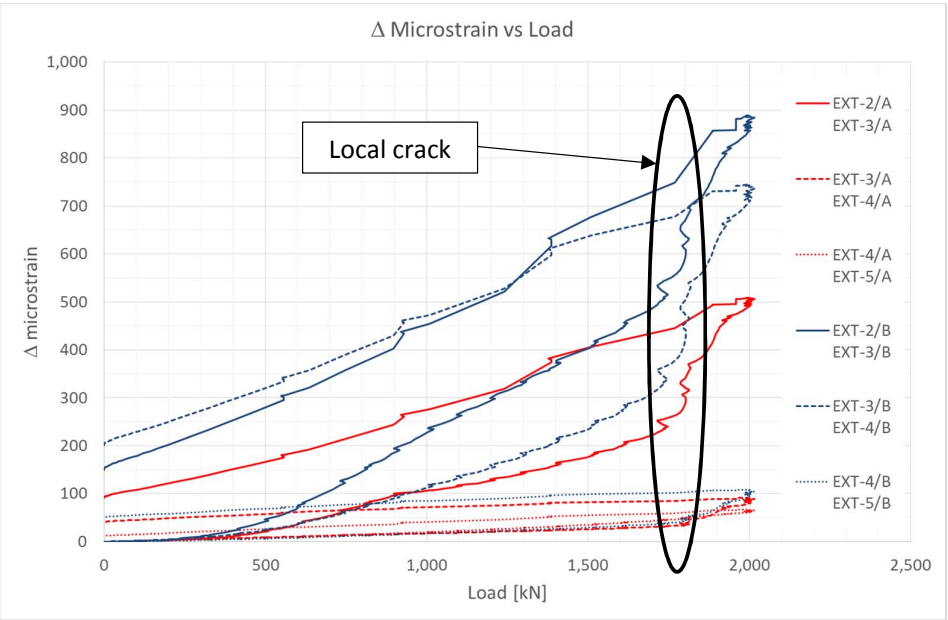


Figure 18. Tension load test results- Measure strain along jet grouting column

CONCLUSIONS

The design principle, chosen technologies and performance controls related to the Multi-Purpose Bottom Plug (MPBP) of Karaköy have been described. In order to obtain the desired results in this high profile Project, it was necessary to rely on the best combination of:

- Most advanced geotechnical analysis and design software: the design of MPBP was carried out through a non-linear time history 3D FDM analysis by means of the FLAC3D software;
- Cutting-edge technologies within the foundation engineering field: technologies like pseudo-elliptical jet grouting requested the use of the latest drilling rigs, specifically designed by Soilmec for these activities;
- State-of-the-art electronic control devices: the "Jet-Vision System" system allowed to control and monitor the automatic rising of the drilling tool/rods during the jetting phase and, thanks to the "orbital jet" option, it was possible to automatically modify the rotation speed during the jetting phase in a planned way for the pseudo-elliptical jet grouting. Moreover, the "Drilling Position System" (DPS) allowed to monitor the 3D position of both jet grouting columns and micropiles, which was of basic importance for the successful execution of the bottom plug and to make sure that micropiles were installed within the previously-executed jet grouting columns. Finally, the complex monitoring system used during the preliminary static load test on DCP micropile installed within an elliptical jet grouting column, allowed to assess the general behaviour of micropile under tensile load and to estimate the load transfer curve along micropile shaft and to measure the strain concentration along jet grouting column.
- Last but not least, the human expertise played a pivotal role for the correct execution of the MPBP and, more in general, for the successful completion of this high profile Project.

This paper also confirms that it is possible to obtain elliptical jet grouting columns up to 4.0 – 4.5 m wide in plan, if the soil condition is favourable (i.e. very loose sand). It is also possible to design the jet grouting columns as structural elements; however, a greater safety factor should be considered in order to take into account intrinsic heterogeneity of improved soil. In the present case, the grouting columns were used as bearing element for tension micropiles and an ultimate micropile-to-jet grouting skin friction greater than 400 kPa was obtained.

Excavation is ongoing while this paper is being written. Updates to follow.

ACKNOWLEDGMENTS

The authors appreciated the continuos assistance provided by the Client (SLI) and their Geotechnical Consultant ENAR. At design stage, the collaboration between TREVI R&D Office and ITASCA has been also important for the detialed analysis and design of MPBP, while the support of GEOGRUP has been fundamental for the correct execution of the on-site micropile load test.

ASSESSING THE EFFECTIVENESS OF RIC/RDC TECHNIQUE FOR DEEP FILL COMPACTION APPLICATION

Aymen Brik, Trevi G.E, Technical Manager, United Arab Emirates, aymbb@hotmail.com
Emmanouil Spyropoulos, Saudi Aramco, Geotechnical Engineer, Kingdom of Saudi Arabia, Emmanouil.spyropoulos@aramco.com

ABSTRACT

Rapid Impact/Dynamic Compaction (RIC/RDC) is a recently developed ground densification technique that offers cost-effective alternatives among other conventional compaction methods (i.e roller compaction) and deep densification techniques (i.e Dynamic Compaction, Vibro Compaction).
The use of Rapid Impact/Dynamic Compaction (RIC/RDC) technique is fast-growing in the Middle East due to substantial time and cost saving benefits especially in large scale projects.
A special trial program has been developed in the kingdom of Saudi Arabia as to identify the potential of RIC/RDC in compacting fill material of considerable thickness in a single run, based on different options of locally available material.
The present paper discusses results and recommendations obtained from the trial.

Keywords: Rapid Dynamic Compaction, Rapid Impact Compaction, Fill Compaction, CPT

INTRODUCTION

Dynamic compaction (DC) is a ground improvement technique that has been used on thousand projects in the Middle East and worldwide and for over 50 years.

Dynamic Compaction (DC) method is applicable for a wide variety of soil conditions, particularly saturated/unsaturated loose sands, dune sands, non-organic fill, reclaimed soils with variable characteristics and sizes even with the presence of large sized boulders, landfills deposits and collapsible soils. This method has been frequently used to densify loose soils to significant depths in order to increase its bearing capacity, decrease post construction settlements and mitigate liquefaction risks in case of seismic events.

Rapid Impact/Dynamic compaction (RIC/RDC) technique has been recently developed to offer viable and cost effective alternatives for fill compaction applications. Many meters of fill can be compacted in one lift/stage using this method, instead of compaction by several lifts of thin layers, as per conventional method. The capacity of RIC/RDC equipment has been recently enhanced to allow using higher hammer weights and larger compaction foots (i.e. compaction energy of 16 tons.m as against 9 tons.m for standard RDC/RIC equipment), which resulted in deeper treatment depths and larger domain of applicability.

The main difference between DC and RIC/RDC results in the rate of application of energy and way of propagation into the ground. With dynamic compaction, the compaction energy (1 to 2 drops per minute) is propagated from the surface to the underlying soil by means of Rayleigh (surface) waves and transverse (shear) waves, whereas with RIC/RDC, the rate can be as high as 40 to 80 drops per minute and Rayleigh waves have the largest energy content (at surface).

The Rapid Impact/Dynamic Compaction (RIC/RDC) technique is very efficient and economical when used as a “fill” compaction technique, in order to compact many meters of fill “on a single run” instead of compacting it by thin layers, as per conventional method.

© 2018 Deep Foundations Institute

ADVANTAGES/BENEFITS OF RIC/RDC METHOD

There has been a growing trend in the world (mainly in the Middle East Area) to backfill undulating sites using engineering fill and bring them to a more or less uniform level before general construction works. These activities are in general included within early site preparation contracts. Within such projects filling operations of variable thicknesses are taking place for attaining the project's final grade levels. These activities are either developed by backfilling in soil layers with subsequent compaction (on-shore areas) or by dredging and reclamation (off-shore areas).

For offshore applications, the conventional surface compaction techniques are not appropriate. Deep consolidation process shall take place after completion of filling operations in order to improve the recent fill deposits and to guarantee the stability of the structures to be built upon it. Dynamic Compaction (DC) and Rapid Impact/Dynamic compaction (RIC/RDC) techniques offers more flexibility for reclamation fill specifications mainly in terms of percentages of fines, which allow to reduce the control of fines generated during reclamation works.
In general, RDC/RIC technique can be used partially in combination with vibro compaction method or as standalone technique in case of shallow depths (less than 6m).

Within the on-shore areas, backfilling operations are following guidelines provided within various industry practices and standards which relates to the soil placement, compaction, and inspection. More specifically:

- Fill material shall be placed in uniform loose lifts not exceeding 200mm/300mm maximum in loose depth respectively, provided that the specified compaction is achieved for the full depth.
- Compaction of each lift shall be performed with equipment compatible with soil type. Fill material shall follow the Relative Density specifications stipulated within various international practices (as determined by ASTM D4253 and ASTM D4254 for cohesion less granular soils that do not exhibit well-defined moisture density relationship).
- Quality control of each lift shall be performed through field control tests where the in-place density and moisture content of soils are determined. Testing shall be performed at certain frequencies for each lift following industry practices.

The traditional backfilling operations impose various disadvantages in relation to:

- The time required for completion of the project especially at places where thick fills are essential. For example a fill of 5m thickness requires placement and compaction of 25 different layers of 200mm and associated in situ testing for each layer lift.
- The cost associated since it involves surface rolling activities which are normally charged on square meter rates. Therefore, area of all lifts shall be accumulated implying a compaction cost which exceeds the cost of a single compaction effort from the top surface by utilizing a different compaction approach.
- Handover issues between the site preparation Contractors and the subsequent construction Contractors which may lead to claim situations. Such matters have been observed within various projects where construction Contractors questioned the density degree of the soils which have been placed/compacted through the traditional procedures.

Rapid Impact/Dynamic Compaction (RIC/RDC) has proved to be a viable alternative to traditional roller compaction method. Considering the size of the infrastructure projects which has developed recently in the Middle East Area and for areas covering up to over few millions square meters, it would not be possible to meet the project schedule and cost requirements without the use of RIC/RDC for fill compaction.

The benefits acquired by employing the Rapid Impact/Dynamic Compaction (RIC/RDC) method comparing to the conventional procedure (mainly for areas requiring various backfilling operations) are below summarized:

- The cost of the project scheme is reduced by using the RIC/RDC method because a bulk placement of significant soil thickness is taking place followed by a compaction which is undertaken at the top formation instead of placement/compaction of thin lifts (200mm).
- Handover issues between the site preparation contractors and the subsequent contractors generated by the density degree of the soils can possibly be removed by including the site preparation works within the construction contractors scope due to the limited time required for RIC/RDC.
  Performance criteria, by means of bearing capacity and settlement for foundations, can be guaranteed as part of the fill compaction rather than density criteria.
- Very high productivity (70,000-100,000 sqm/month/rig, double shifts basis) as against 10,000 sqm for the traditional method.
- Treatment can be carried out in closer proximity to existing structures and services vulnerable to vibration damage.
- Flexibility in the backfilling material requirements (material gradation and plasticity requirements) : experience has proven that wide range of material can be compacted using RIC/RDC method, such as poorly graded sands, fine sands, dredged material and dune sands, subject to not exceed a maximum percentages of fines of about 15%. Whereas, material should be well graded in case of conventional method.
- Ensures proper compaction at the soil surface, since the energy is more efficiently transferred through the compaction foot which remains in contact with the ground.
- RDC technique can be used a standalone ground improvement or fill compaction technique, as applicable to granular soils down to 6 meters.
- Due to less amount of equipment involved this method requires less supervision and eliminates major safety concerns in traffic management during compaction, while also giving more flexibility to the Contractor.



Fig. 1. Rapid Impact/Dynamic Compaction (RIC/RDC) works

RIC/RDC EQUIPMENT

The RIC/RDC device consists of an excavator-mounted hydraulic hammer striking a circular compaction foot that rests on the ground. The tamper typically strikes the foot at the rate of 40 to 80 blows per minute.

The hammer (ranged from 7 tons to 16 tons weight) is hydraulically raised to a maximum height of 0.5-1.2m and then allowed to free-fall, resulting in a maximum energy of about of 20 tons.m per blow.

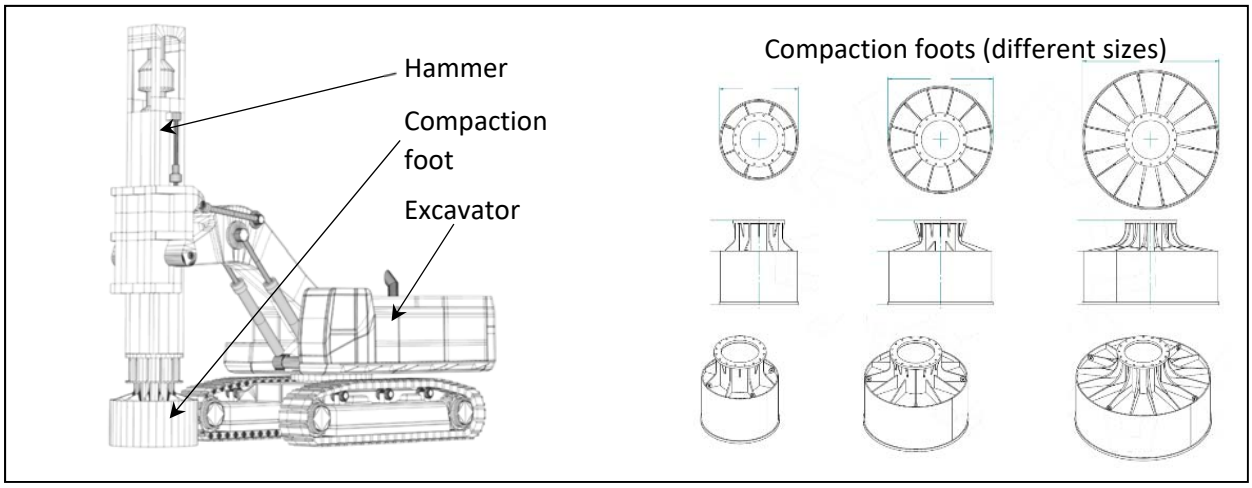


Fig. 2. Equipment Details

The maximum number of blows for each point is generally linked to the capacity of equipment used and site conditions. Stopping criteria is always defined as: maximum foot travel of 80-120cm and/or 50-60 blows per point per pass.

An automated record is essential for RIC/RDC procedure to allow proper monitoring and adjustment of all execution parameters (height, number of phases/blows, foot dimeter, final penetration, grid spacing) in accordance with the ground response during compaction and based on a defined stopping criteria. A systematic assessment of the achieved results using Cone Penetration testing (CPT) is also necessary to make sure that the appropriate amount of energy is transferred to the ground and project criteria area reached.

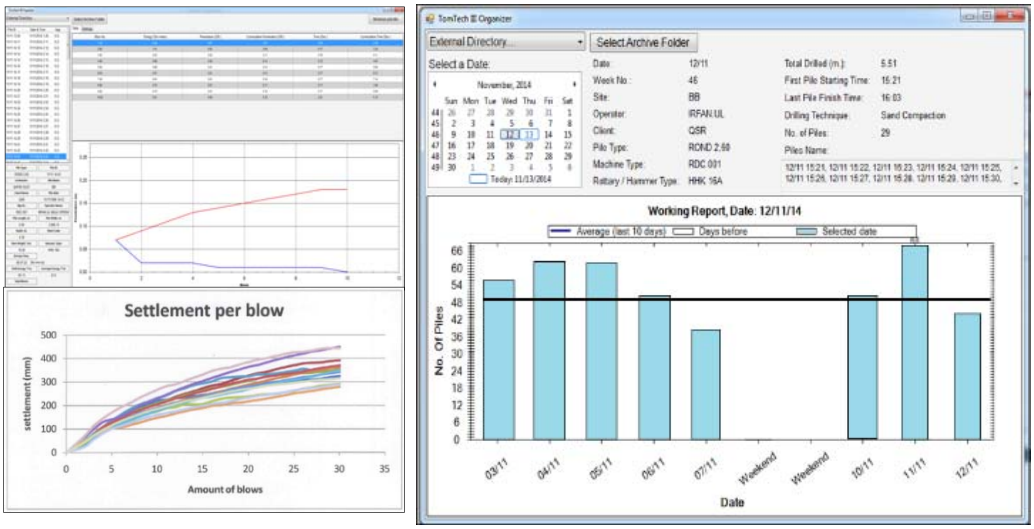


Fig. 3: RDC's Monitoring software

TRIAL AREAS

A large scale trial area has been developed within the framework of large scale infrastructure project in the Kingdom of Saudi Arabia, involving embankment works for several millions of cubic meters. The main purpose of this trial area is to identify the potential of Rapid Impact/Dynamic Compaction (RIC/RDC) technique in compacting fill material of considerable thickness in one go as a cost effective alternative to traditional method by Roller Compaction.

The intended objectives of the trial areas include also the confirmation of the effectiveness depth and maximum achievable criteria according to different types of filling material.
Trial areas have been divided into two (2) locations according to the type of material to be used:

1- Trial A : Dune Sands, with fines content as high as 8%,

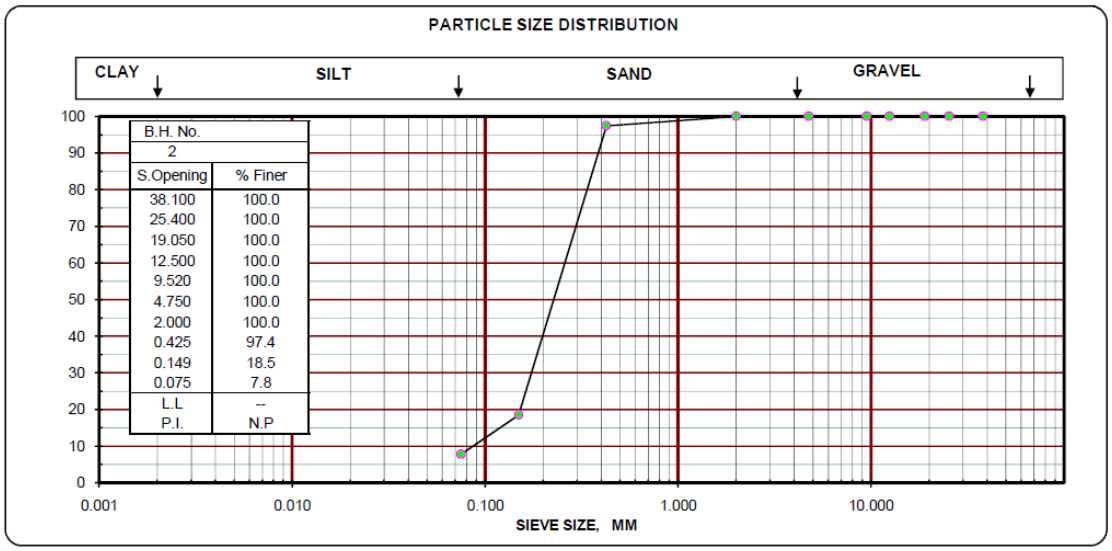


Fig. 4: Sieve Analysis for material in trial Area A

2- Trial B : Dune Sands, with fines content as high as 15%,

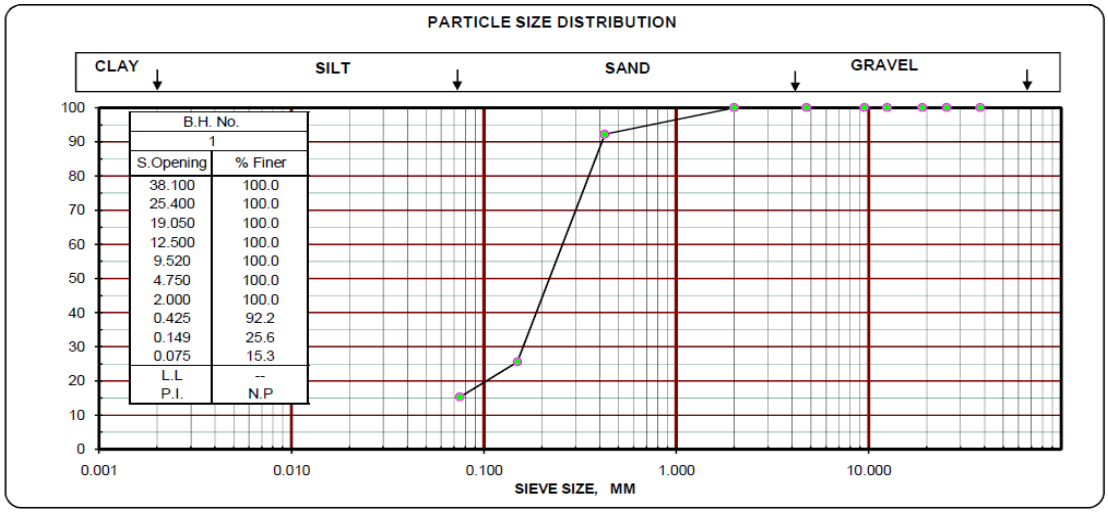


Fig. 5: Sieve Analysis for material in trial Area B

A pre-compaction testing campaign was carried out at site in order to check the quality of filling material, confirm the depth of improvement and define the initial compaction parameters, including cone penetration tests (CPT) and boreholes with soil sampling for sieve analysis tests.

COMPACTION PROCEDURE

Applying RIC/RDC shall include compaction at different phases (grids) and passes (number of compaction times on each impact point), with use of different compaction foot and different diameters, in order to effectively reach the deepest influence and maximum compaction degree.

The compaction was performed repetitively following three grids, starting from a large grid of 6x6 m spacing, by using small dimeter foot, then ending to a closer grid with 3x3m spacing, with larger foot, as shown in the following sketch:

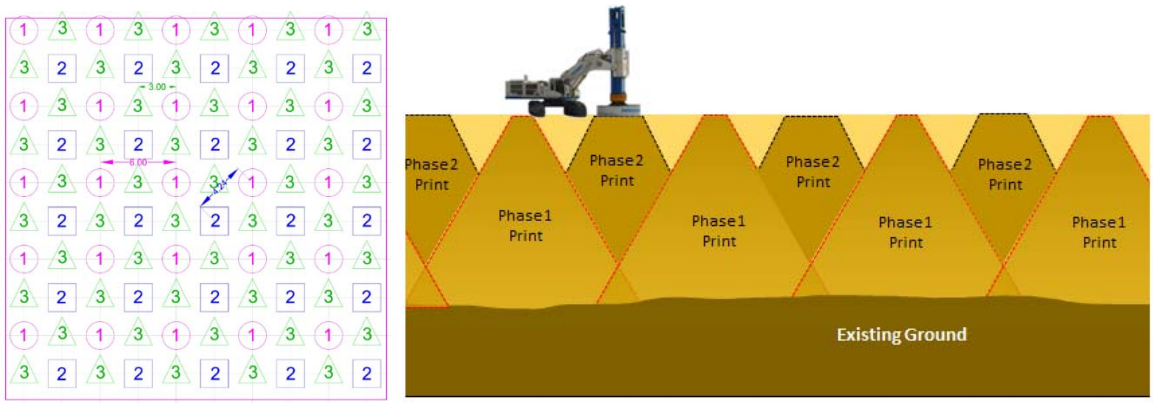


Fig. 6. RDC compaction Procedure

The main execution parameters used for the trial areas, can be summarized herein below:

- Phase 1 (primary grid): Total number of 40 to 60 blows (height ranging between 0.5 and 1m), using 1.5m dia foot and 16tons-Hammer.
- Phase 2 (secondary grid): Total number of 40 to 60 blows (height ranging between 0.5 and 1m), , using foots of 1.5-2m diameter and 16tons-Hammer.
- Phase 3 (tertiary grid): Total Number of 20 to 40 blows (height ranging between 0.5 and 0.7m), using foot of 2.5m diameter and 16tons-Hammer.

ASSESSMENT OF RDC EFFECTIVENESS BASED ON CPT RESULTS

Following RIC/RDC works, a set of three (3) CPT tests per trial was carried out in order to quantify the increase in cone tip resistance with depth and confirm the maximum achievable compaction degree. The comparison between pre and post compaction test results shows a massive improvement of the cone resistance and sleeve friction values varying between 100% to 500%, comparing to the pre-compaction results :

Trial A : fines content (passing sieve # 200) as high as 8%	Trial area B : fines content (passing sieve # 200) as high as 15%

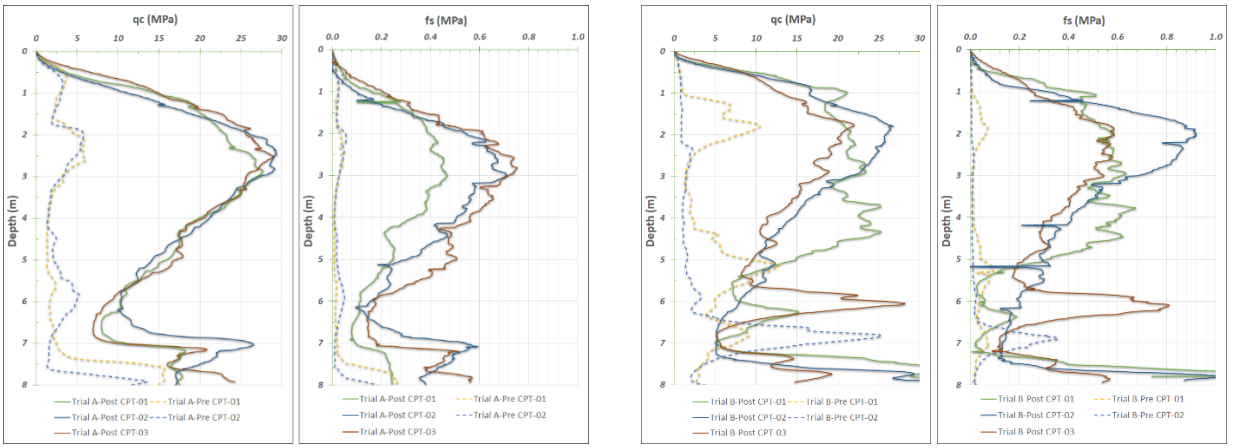


Fig. 7. Comparison between Pre and Post CPT results

The targeted acceptance criteria for the Rapid Impact/Dynamic Compaction (RIC/RDC) works are mainly based on the Relative Density (Dr) specifications as described within various industry practices. Performance Lines have been created by back calculating the required degree of Relative Density to cone tip resistance values of Cone Penetration Tests (CPT) by using different correlations. The average of the Performance Lines is compared to the post soil improvement Cone Penetration Tests (e.g. cone resistance values, qc) for identifying compliance to the acceptance criteria. Post Cone Penetration Tests (CPT) are undertaken between the compaction prints.

For this project in specific, averaged values from performance lines (corresponding to Dr = 70%) are created using the three methods mentioned below :

i. Baldi et al (1986)modified by Lune(2006) : $D_r = \frac{1}{C_2} \ln\left(\frac{q_c}{C_0(\sigma'_{v0})^{C_1}}\right)$ [1]

C_0=157, C_1=0.55, C_2=2.41

A correction factor for the relative density equal to 1.2, 1.4 and 1.5 should be used with estimated relative densities of smaller than 40%, 40 to 60%, and greater than 60%, respectively.

ii. Jamiolkowski et al.(1985) : $D_r = -98 + \left(66.\log_{10}\frac{q_c}{[\sigma'_{v0}]^{0.5}}\right)$ [2]

iii. Schmertmann et al. (1978) :

The relative density can be correlated based on the achieved cone resistance (qc) value and vertical effective stress (σ'_{v0}), using the following chart :

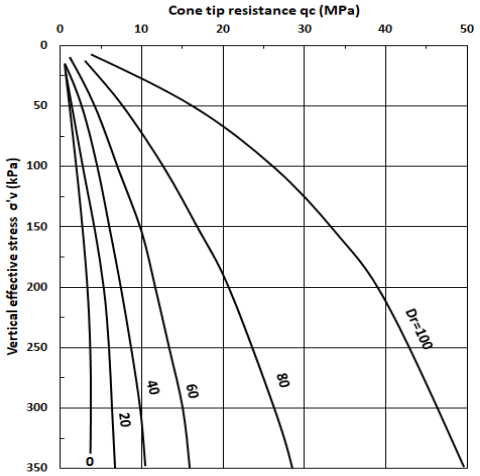


Fig. 8. Relative density curves by Schmertmann et al. (1978)

The average performance line has been considered the targeted criteria for fill compaction works.

Based on the obtained results, the followings conclusions are pointed-out :

- Trial Area A:
  - A minimum Relative Density of 70% has been attained down to the depth of 6m by Post CPT 1 (Print) and Post CPT 2 (Intermediate soil).
  - Minimum Relative Density of 70% till depth 5.75m was achieved by Post CPT 3 (Intermediate soil).
  - Although a substantial growth in stiffness was detected between 6m to 7m depth, the Relative Density criterion of 70% was not achieved.
  - An increase of the soil stiffness is also found at the bottom of the loose soil formations (from 7m to 8m depth).
  - The estimated elastic modulus and friction angle, from post-compaction CPTs, are as high as 100 MPa and 45 degrees (respectively).

- Trial Area B:
  - A minimum Relative Density of 70% has been attained down to the depth of almost 5.5m.
  - The consequence of compaction is also shown at depth 5.5 to 6m however, it is not adequate to achieve a degree of 70% Relative Density.
  - An increase of the soil stiffness is also found at the bottom of the loose soil formations (from 7m to 8m depth).
  - The estimated elastic modulus and friction angle, from post-compaction CPTs, are as high as 75 MPa and 45 degrees (respectively).

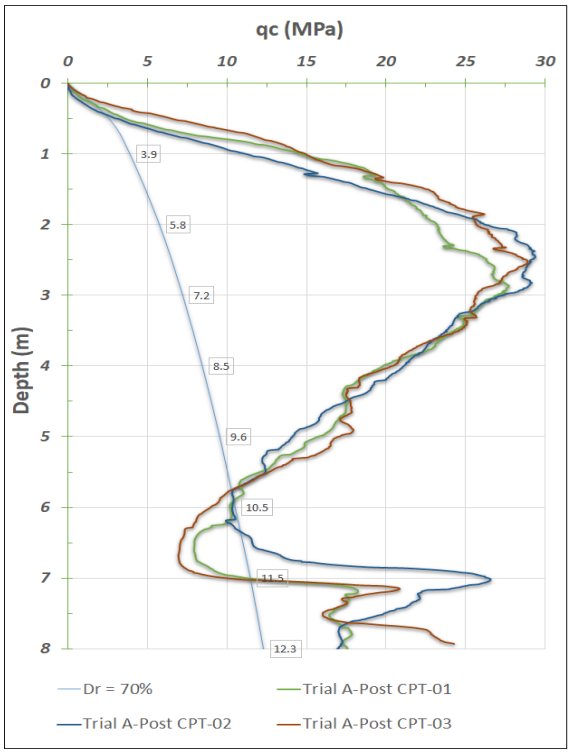


Fig. 9. Comparison between Post CPT results and Performance Lines for trial area A

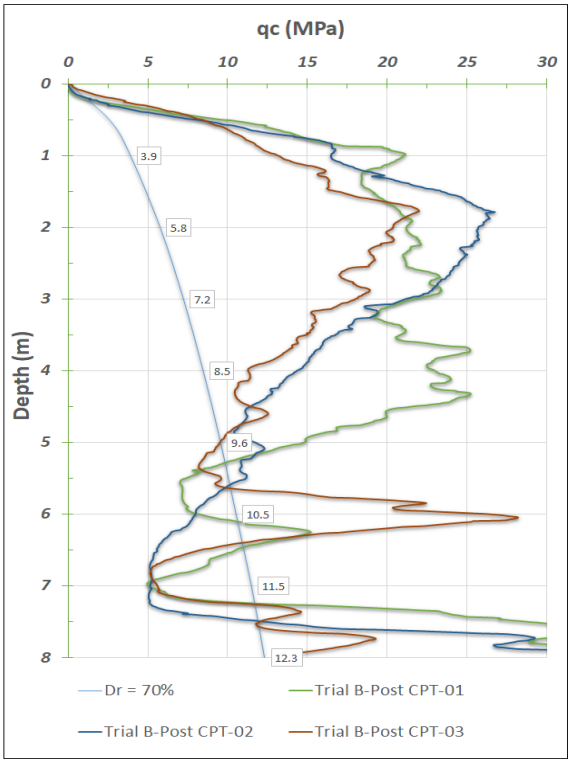


Fig. 10. Comparison between Post CPT results and Performance Lines for trial area B

CONCLUSION

Technical evaluation and benefits of the Rapid Impact/Dynamic Compaction (RIC/RDC) and its ability to compact subsurface soils to various depths based on respective soil compositions have been presented in this paper. This study concentrates to the adoption of the Rapid Impact/Dynamic Compaction (RIC/RDC) as alternate to the traditional backfilling operations within the on-shore areas. RIC/RDC provides compaction - from the top surface - of a single soil lift to the specified tolerances as provided within various industry practices.

The RIC/RDC method has successfully piloted at a special trial area in Saudi Arabia, for sandy granular materials, with fines content (passing sieve # 200) as high as 15%.

This method (RIC/RDC) considerably cuts down on time and schedule, by far more than 50%, allowing the early start of construction activities. Furthermore, the net cost per meter for this activity reduces dramatically when compared to the net cost per meter applicable to the traditional backfilling operations, a net reduction of around 50%, making this alternative not only practical, but effective.

In addition, due to less amount of equipment involved this method requires less supervision and eliminates major safety concerns in traffic management during compaction, while also giving more flexibility to the Contractor.

To conclude, Rapid Impact/Dynamic Compaction (RIC/RDC) technique can be safely and efficiently used for mitigating loose granular fill materials of considerable thickness in a single lift bulk placement as a cost and time effective alternative to the traditional method by Roller Compaction.

REFERENCES

B.T. SCOTT & M.B. JAKSA, *The University of Adelaide, Australia, 2014, Evaluating rolling dynamic compaction of fill using CPT*

K. Rainer Massarsch, *Geo Risk & Vibration AB, Bromma, Sweden, 2014, Use of CPT for design, monitoring, and performance verification of compaction projects.*

US DEPPARTEMENT OF TRANSPORTATION, FEDERAL HIGHWAY ADMINISTRATION. *1995, Geotechnical Engineering Circular No.1 Dynamic Compaction*

M. MOHAMMED MOHAMMED*, 2010, Effective improvement depth for ground treated with rapid impact compaction*

BASHAR TARAWNEH, *2014, Performance of Rapid Impact Compaction as a Middle-Deep Ground Improvement Technique*

TREVI GROUND ENGINEERING, *2017, Fill Compaction using DC/RDC technique Brochure*

G.L. SIVAKUMAR BABU *NPTLE Course Lecture 6: Ground Improvement*

TERRASYSTEMS INCORPORATED, TerraNotes: *Rapid Dynamic Compaction, Another form of dynamic Compaction?*

WORKSHOP ISSMGE TC 211 GROUND IMPROVEMENT, *2015, Quality Control of Ground Improvement Works by In Situ testing. Case Studies in Portugal, Togo, Poland, UAE and Qatar*

P. K. ROBERTSON AND K.L. CABAL (ROBERTSON), 2015, Guide to Cone Penetration Testing for GeoTechnical Engineering. Gregg Drilling & Testing, Inc

CASE STUDIES OF GROUND IMPROVEMENT USING RAMMED AGGREGATE PIERS IN PROBLEMATIC SOILS ALLOWING FOR CONVENTIONAL FOUNDATION

Roberto Avendano, B.Eng., P.Eng., GeoPacific Consultant Ltd., Vancouver, British Columbia, Canada, (604) 439-0922, avendno@geopacific.ca

Matt. J. Kokan, M.A.Sc., P.Eng., GeoPacific Consultant Ltd., Vancouver, British Columbia, Canada, (604) 439-0922, kokan@geopacific.ca

ABSTRACT

Rammed Aggregate Piers or Aggregate Piers (AP) elements have become an effective alternative to deep foundations or large contiguous raft foundations in soft soils. AP elements with a diameter of 600 mm are concentrated under rigid foundation elements extending through the soft or compressible soil layers. This paper will present two case histories where AP elements were utilized in soft and compressible soils to replace costly deep foundation options and permit the use of a conventional foundation systems at relatively high bearing pressures. The first case history presented in this paper details the use of AP elements at a new Fine Arts University building in Vancouver, British Columbia, where the subsurface soil conditions consisted of loose granular fills underlain by soft glaciomarine deposits. The second case history involves a new police services station in Kelowna, British Columbia, where the subsurface conditions generally consisted of several metres of fill over natural soils comprising of loose to compact sand to sandy silt over clayey silt with thin zones of sandy silt. In both of the case histories, the AP elements were load tested and results showed excellent performance, with deflection tolerance met during testing. The results confirm that AP elements are an effective alternative to deep and raft foundations.

Keywords: **rammed aggregate piers, RAP, densification, ground improvement, conventional foundations, case history**

INTRODUCTION

Granular stone columns, specifically Rammed Aggregate Piers or Aggregate Piers (APs), are being used in many sites in British Columbia, Canada as an effective alternative to deep foundations or large contiguous raft foundations in problematic soils. Hughes et al. (1975) states that the bearing capacity of granular columns is dependent upon the bulging of the column; the ultimate load is dependent on the friction angle of the gravel used to form the column and the lateral restraint of the soil around the gravel column. Unlike conventional stone columns constructed by the vibro-replacement method studied by Hughes and Withers (1974) and Hughes et al. (1975), APs are constructed by ramming aggregate into the ground with vertical compactive energy using a beveled tamper head. It has been shown that this method of construction results in friction angles of 45 to 52 degrees within the constructed gravel column or AP element, and an increase of the lateral stress in the soil surrounding the column (White et al. 2000; Handy 2001; Wissmann et al. 2001).

Many regions of British Columbia are underlain by loose, soft, compressible and sometimes liquefiable soils, requiring the use of an effective ground improvement technique. AP elements have been used to reinforce and improve the bearing capacity of problematic soils, replace costly deep foundation options and permit the use of a conventional foundation systems at relatively high bearing pressures. This paper will present a case history of two sites where AP elements were utilized to replace costly deep foundation options and permit the use of a conventional foundation systems. The first site is located near downtown Vancouver, British Columbia, in an area called the False Creek Flats where a proposed Fine Arts University building is to be situated. The second site is located in downtown Kelowna, British Columbia, where a new police services building was proposed.

© 2018 Deep Foundations Institute

SITE AND SOIL CONDITIONS

Site 1 - Fine Arts University Building in Vancouver

The new Fine Arts University building is located at a site that was previously an industrial area known as the False Creek Flats, just east of downtown Vancouver. The soil profile at the site was determined by completing an exploration program consisting of a total of 8 auger test holes and 11 electronic Cone Penetration Tests (CPTs). The auger test holes were drilled to depths of 6.m to 10.4 m below the current site grades and the CPTs were advanced to refusal at depths ranging between 4.4 m to 10.7 m below existing site grades. The soil profile at the site consists of 2 m to 6 m of fill. The fill generally consists of compact to dense sand and gravel to compact sand. The fills were underlain by glaciomarine deposits that extend to depths between 4 m to 10 m. The glaciomarine deposits consist of sandy silt to silt. The silt is inferred to be firm to stiff, with a moisture content of between 20 and 40 percent. The characteristic undrained shear strength of the silt is between 50 kPa and 100 kPa in the upper 2 m, decreasing to as low as 25 kPa between 7 m and 10 m depth. The silt is lightly over-consolidated relative to current in-situ stresses. The glaciomarine deposits are further underlain by very dense glacial till to sandstone deposits at depths ranging from 4 m to 11 m below the existing site grades. Figure 1 provides a CPT soundings plot of the subsurface soil conditions at the site.

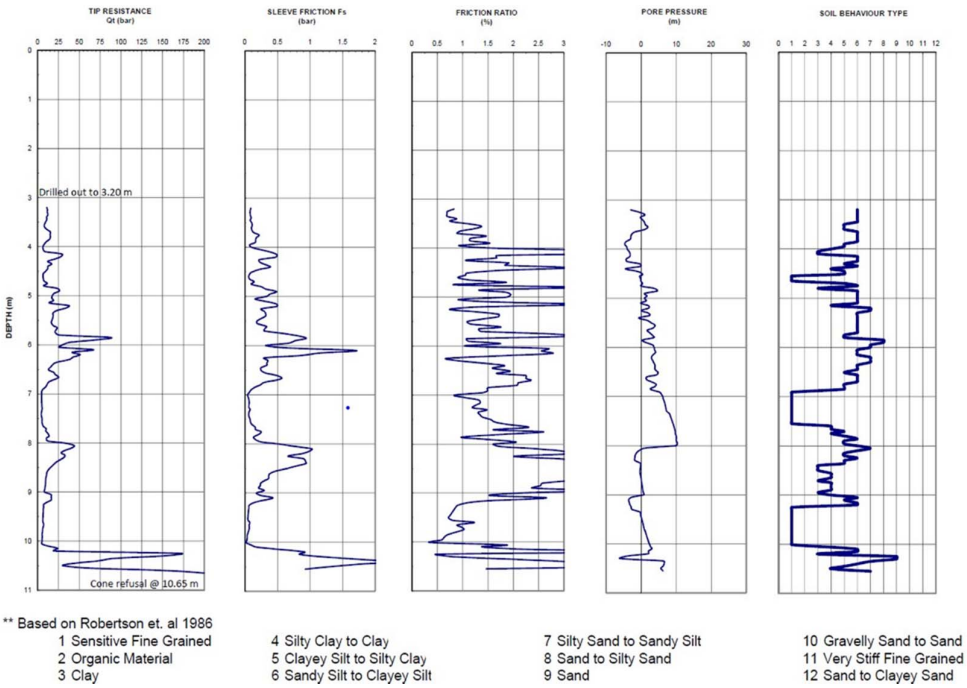


Fig. 1. Typical CPT sounding of the soil profile of the False Creek Flats

Site 2- Police Services Building in Kelowna

The new police services building was proposed in the downtown area of Kelowna, British Columbia. Kelowna is a city of 200,000 residents located about 450 km east of Vancouver, British Columbia. The downtown area of Kelowna fronts the Okanagan Lake and thus the soil conditions mainly consist of lake deposited silts and clays to sands. The soil profile at the site was determined by completing an exploration program consisting of a total of 7 auger test holes and 3 electronic CPTs. The auger test holes were drilled to depths of 6.1 m to 7.6 m below the current site grades and the CPTs were advanced to depths ranging between 28 m to 32 m below current site grades. The subsurface conditions at the site generally consist of 1 m to 3 m of variable medium dense granular fills. The fills are underlain by the native silty sand to sandy silt extending to a depth of about 6 m to 9 m below existing grade and is

generally compact to medium dense with interbedded layers of loose material. The silty sand to sandy silt is underlain by a slightly over-consolidated clayey silt layer to depths of about 14 m. The clayey silt layer is further underlain by sandy silt to silty sand to depths greater than 30 m. Groundwater levels were measured at a depth of about 2 m below the ground surface. Figure 2 provides a CPT sounding plot of the subsurface soil conditions at the Kelowna site.

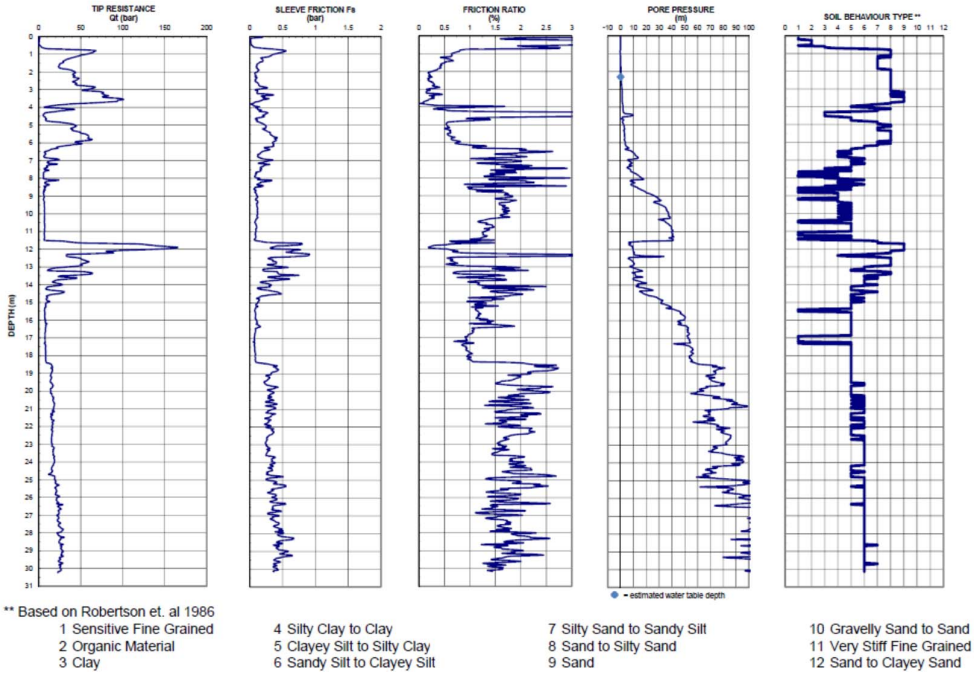


Fig. 2. CPT soundings plot of the Kelowna police services building soil profile

PROPOSED DEVELOPMENT AND RECOMMENDED ALTERNATIVE DESIGN

Site 1 - Fine Arts University Building in Vancouver

The proposed fine arts building consists of a four storey structure constructed at the existing site grades. Construction utilized a mixture of reinforced concrete and steel frame with heavy superstructure loading. Column loads were in the range of 5,000 kN to 8,000 kN and wall loading in the range of 600 kN/m or less. The original design of the building called for the superstructure loads to be supported on pile foundations, where the piles would be driven through the fills and native glaciomarine deposits into the underlying dense to glacial till or sandstone layers. However, due to schedule and cost constraints, the proposed deep foundation option was not feasible at the site. Thus, an alternative solution was required for the foundation system of the building.

The alternative design consisted of dynamically compacting the upper fills and installing a total of 2,158 stone columns consisting of 600 mm diameter APs concentrated under the foundation elements of the building. The AP elements extended through the fills and glaciomarine deposits down to the dense glacial tills or sandstone. The APs were designed to be concentrated around foundation elements allowing for an increase in the soil bearing capacity at the foundation locations. The foundation design now allowed the building to be supported with a conventional foundation system, consisting of pad and strip footings. Figure 3 shows the proposed AP design.

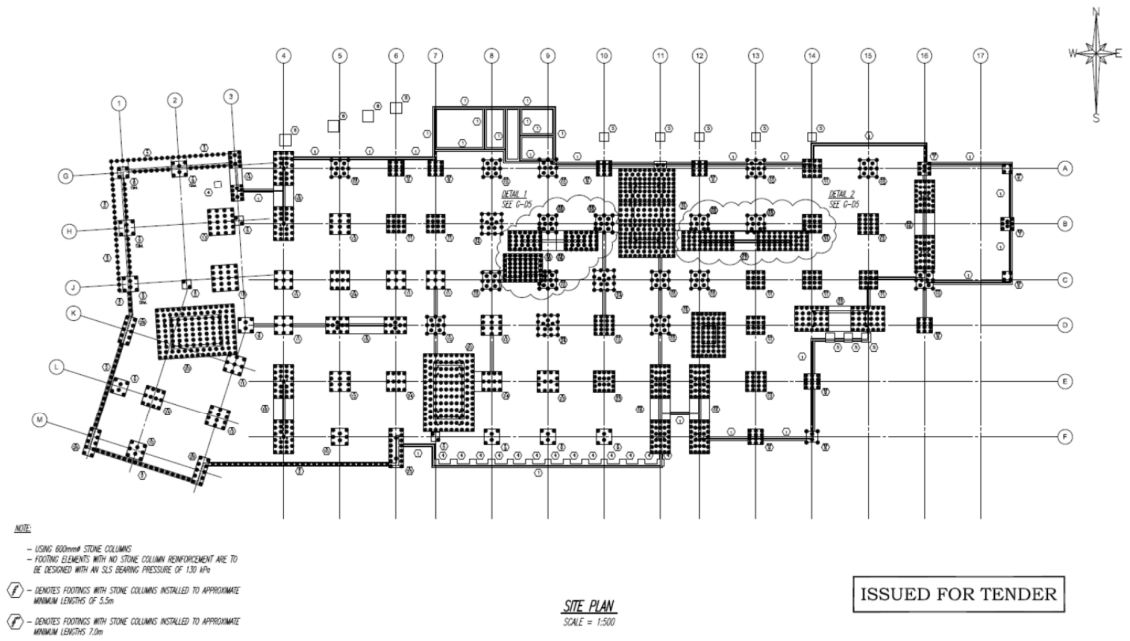


Fig. 3. Densification drawing showing the recommended 2,158 AP elements concentrated below the footings

The AP element depths ranged from 4 m to 14 m below the existing site grades. The APs were installed in 45 working days allowing for a reduction in schedule of about 2 months. Furthermore, the conventional foundation design also facilitated the ability to allow of overlapping activities during construction, thus accelerating the overall schedule of construction.

Site 2- Police Services Building in Kelowna

The proposed police services building consists of a four storey structure constructed at the existing site grades. Construction utilized a mixture of reinforced concrete and steel frame for the building. The superstructure loads were moderately heavy, with column loads in the range of 2,000 kN to 5,000 kN and wall loading in the range of 600 kN/m or less. The original design of the building called for preloading the building and then supporting the structure on a large contiguous raft foundation. However, due to schedule and cost constraints, the proposed preload and raft option were not feasible at the site. Therefore, an alternative solution was required for the foundation system of the building.

Once again, the alternative design consisted of dynamically compacting the upper fills and installing a total of 673 stone columns consisting of 600 mm diameter APs under the foundation elements of the building. A design depth of the APs of 8 m below the foundation elements was provided to improve the upper soil profile. The APs were designed to be concentrated around foundation elements allowing for an increase in the soil bearing capacity at AP locations. The foundation design now allowed the building to be designed with a conventional foundation system, consisting of pad and strip footings. Figure 4 shows the proposed AP design.

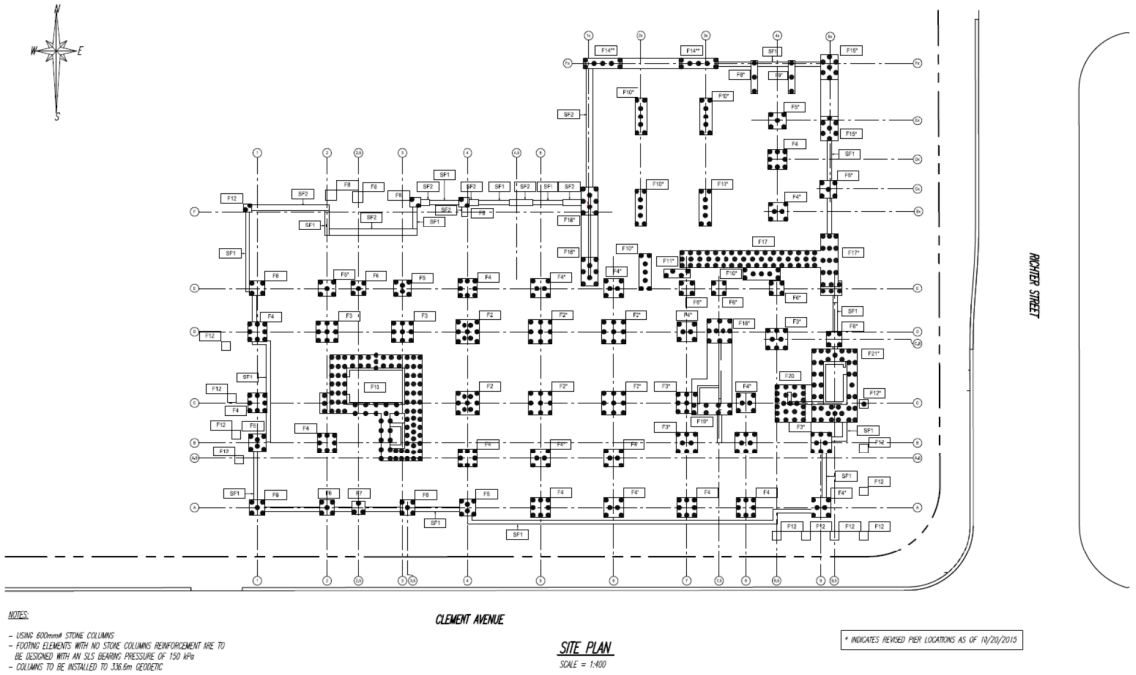


Fig. 4. Densification drawing showing the recommended 673 AP elements concentrated below the footings

TESTING AND RESULTS

At both sites load tests were performed in accordance with ASTM D1143/D1143M (Test Methods for Deep Foundations Under Static Axial Compressive Load). The full-scale load tests were performed using steel reaction beams secured with helical anchors. All tests were performed using a 200-ton hydraulic ram with a 15-cm stroke. The load tests were used to evaluate the stiffness and capacity of individual AP elements to confirm the initial design assumptions.

Test Results at Site 1 - Fine Arts University Building in Vancouver

A total of three load test were performed at the Fine Arts building. Creep load tests were performed at the service design load of the AP of 200 kN and the total creep displacement was approximately 0.76 mm. The creep displacements were less than the generally accepted value of 1 mm during 10 minutes of holding time.

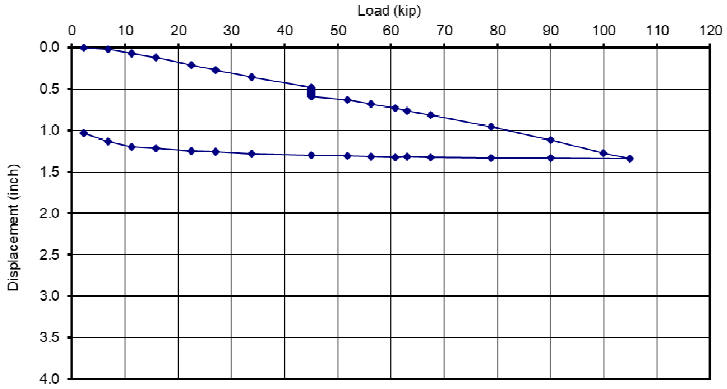


Fig. 5. Load test results at the Vancouver site

The test showed that at the design load of 200 kN with a top-of-pier stress of 700 kPa the total measured displacement was 15 mm. At the maximum load applied to the test pier of 466 kN corresponding to a top-of-pier stress of 1650 kPa the total displacement of 34 mm was measured.

Test Results at Site 2 – Police Services Building in Kelowna

Creep load tests were performed at the service design load of the AP of 200 kN and then taken to a maximum test load 490 kN. The total creep displacement at 200 kN was approximately 0.14 mm and the total creep displacement at 490 kN was 0.44 mm. The creep displacements at each load were less than the generally accepted value of 1 mm during 10 minutes of holding time.

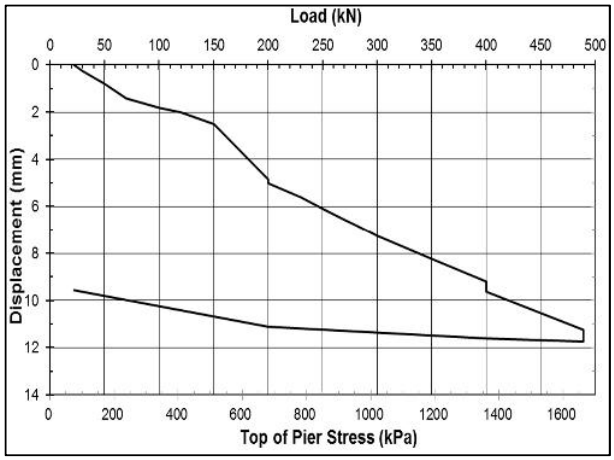


Fig. 6. Load test results at the Kelowna site

The test showed that at the design load of 200 kN with a top-of-pier stress of 700 kPa was achieved with a total measured displacement of 4.5 mm. At the maximum test load of 490 kN with a top-of-pier stress of 1,676 kPa the total measured displacement was 12 mm.

CONCLUSION

At both sites the alternative design consisting of AP elements concentrated under the buildings foundations was implemented. The alternative design improved the poor soils conditions at both sites allowing for a significant increase in the design soil bearing pressures. For both the Fine Arts University building in Vancouver and the police services building in Kelowna, the design limit equilibrium bearing capacity was able to be increased from 150 kPa to 300 kPa. The increase in bearing capacity allowed for the use of a conventional foundation system consisting of pad and strip footings, replacing the previously recommended pile and raft foundations. The field testing performed at both sites confirmed that the AP design effectively improved the soil bearing capacity while maintaining the required foundation settlement criteria of less than 25 mm. Figure 6 shows the nearly completed Fine Art University building which opened in August of 2017. Figure 7 shows the completed police services building which opened in June 2017.



Fig. 7. Fine Arts University building in Vancouver, British Columba



Fig. 8. Police services building in Kelowna, British Columba

Summary

The two noted case histories, the Fine Arts University building in Vancouver and the police services building in Kelowna, are excellent examples of how ground improvement techniques can be used as an effective alternative to deep and raft foundations. Both projects demonstrate that APs can be used under foundation elements in complex soil profiles to provide an increase in the soil bearing capacity allowing for an implementation of conventional foundation systems. The field test results confirmed that the AP design achieved the required service bearing capacities within the required settlement criteria. The two case histories demonstrate how soil improvement techniques can be used for ground improvement urbanized areas with difficult soil conditions.

ACKNOWLEDGMENTS

"TBA"

References:

Handy, R. L. 2001. Does Lateral Stress Really Influence Settlement?, Journal of Geotechnical Engineering, ASCE, 127(7): 623-626.

Hughes, J.M.O., Withers, N.J., and Greenwood, D.A. 1975. A field trial of the reinforcing effect of a stone column in soil, Geotechnique, 256(1): 31 - 44.

Hughes, J.M.O., and Withers, N.J. 1974. Reinforcing of soft cohesive soils with stone columns, Ground Engineering, May, 42-49.

White, D.J., Lawton, E.C., and J.M. Pitt, J.M. 2000.Lateral Earth Pressure Induced by Rammed Aggregate Piers, Proceedings, 53rd Annual Canadian Geotechnical Conference. Montreal, Canada.

Wissmann, K.J., Moser, K. and Pando, M.A. 2001. Reducing Settlement Risks in Residual Piedmont Soils using Rammed Aggregate Pier Elements, Proceedings, ASCE Specialty Conference. Blacksburg, VA. June 9- 13.

DYNAMIC COMPACTION OF ROCKFILL ON LAND AND UNDER WATER AT STOCKHOLM NORVIK PORT

Sölve Hov, GeoMind, Stockholm, Sweden, +46 70 240 29 05, solve.hov@geomind.se
Håkan Eriksson, GeoMind, Stockholm, Sweden, +46 70 556 04 11, hakan.eriksson@geomind.se
Carl Wersäll, KTH Royal Institute of Technology, Sweden, +46 8 790 80 24, carl.wersall@byv.kth.se

ABSTRACT

A case study is presented on dynamic compaction of rockfill during construction of the new Stockholm Norvik container and ro-ro port, due to open in 2020. The compaction on land was performed with a 20-tonne pounder using a drop height of 20 metres. Because of the soil type, soundings could not be used to evaluate the compaction effect. The maximum depth of influence was therefore measured using inclinometers and extensometers and was found to be around 10 m, in line with expected depths. The dynamic response of the rockfill was measured with an accelerometer mounted on the pounder. From the derived stress vs. displacement curves, a displacement modulus was evaluated and incorporated in the superstructure design. The dynamic compaction under water was performed using the same pattern, but due to limited water depths the drop height was 10 m. An attempt to estimate the maximum depth of influence was made by adjusting the well-known Menard empirical relationship between drop height, weight and compaction depth. This was done to take into account the buoyancy effect and water resistance resulting in a lower velocity at impact. Accelerometer measurements of the underwater compaction was also performed to evaluate the dynamic response. As on land, the measurements were used to derive a stress vs. displacement curve intended to predict the deformations of the compacted rockfill during construction of the ro-ro quay L-walls. The modulus of the rockfill after compaction was also evaluated by monitoring the craters created during compacting, followed by a back calculation of the change in density index. Based on the density index, the modulus could be assessed and compared to the same parameter from accelerometer measurements. Predicted and measured deformations will be compared during the construction of the L-walls as well as during placing of additional fill on the harbour area.

Keywords: dynamic compaction, accelerometer measurements, under water compaction

INTRODUCTION

This paper describes the dynamic compaction of an existing loose rockfill during the construction of the new Stockholm Norvik Port. Dynamic compaction was chosen as the preferred ground improvement method due to large depths to bedrock and large boulders in the rockfill, ruling out other methods for compacting coarse-grained soils, and because of small settlement tolerances within the container port. GeoMind, a Swedish specialist geotechnical consultancy firm, was engaged to design the geotechnical works, including follow up during construction.

Dynamic compaction has previously successfully been utilized on similar rockfill material in Scandinavia, e.g. Hansbo (1977, 1978), Bjølgerud & Haug (1983), Stordal & Simonsen (1993).

The maximum depth of influence, d_{max}, is normally estimated empirically by the relationship originally formulated by Ménard & Broise (1975) and later modified by Leonards et al. (1980), Mayne et al. (1984), Lukas (1995) and others:

$$d_{max} = k\sqrt{WH} \quad [1]$$

Where, k = empirical constant, W = weight of pounder in metric tonnes, and H = drop height in m. The constant k normally varies between 0.4 and 0.8 and depend mainly on the soil type, ground water level and dropping mechanism. Mayne et al. (1984) compiled results from a large number of projects and concluded that $k \approx 0.5 - 0.6$ is a good average. The degree of soil improvement varies from the

 © 2018 Deep Foundations Institute

surface down to d_{max} and is considered to give a maximum effect at critical depth, d_c. Normally, d_c can be assumed to be around one half of d_{max} (Mayne et al. 1984).

Typical control methods for dynamic compaction are different kinds of penetration tests. In this project however, it was impossible to perform these kinds of tests as the rockfill contained large boulders, see Fig 1. It was therefore in an early stage decided to use accelerometers mounted on the pounder as a control method, in addition to inclinometers, extensometers, and measuring of crater depths.

Several researchers have previously used accelerometers to measure the deceleration at impact to evaluate the soils dynamic response, e.g. Hansbo (1977; 1978), Chow et al. (1990), Bo et al. (2009), Lopez et al. (1998), Holeyman and Vannesta (1987). At Stockholm Norvik, deceleration measurements were also performed for the dynamic compaction under water.

STOCKHOLM NORVIK PORT

The municipal company Ports of Stockholm is building a harbour for rolling goods and containers. The port is designed to be the Baltic Sea freight port of the future and will ensure efficient supply of goods to the Stockholm region, one of Europe's fastest growing capital cities. With this type of growth, long-term investment in a well-functioning infrastructure is essential and the port is an important part of this development. The port is located 60 km south of Stockholm and will open in 2020. The total harbour area will be approximately 400,000 m^2.

The area initially comprised an island surrounded by water. During the construction of an oil refinery in the neighbouring area in the 1980s, the blasted rock was dumped in the sea close to Norvik. New land was reclaimed by allowing end-dumped rockfill to displace the very soft clay overlaying moraine and rock. During the reclamation of the new land, up to 300,000 m^3 of clay was contained, partly overlain by crushed rock. The clay was improved by dry deep mixing and jet grouting in a separate contract and is not dealt with in this paper.

The thickness of the rockfill varies from just a few metres to more than 20 metres, and includes large boulders, see Fig. 1.



Fig. 1: Variation of the rockfill used when reclaiming the new land.

DESIGN AND EXECUTION OF COMPACTION WORKS

Deep compaction was necessary for the majority of the harbour area with rockfill down to moraine or bedrock, both below and above water, in order to fulfil the contract requirements for containers stacks, water and sewer systems as well as the quay walls which partly were designed as retaining structures. The maximum allowable differential settlement on the harbour area was by the client set to ± 30 mm over a distance of 10 m, and/or a maximum allowable total settlement of 75 mm.

To evaluate the mechanical properties of the rockfill, especially the constrained modulus, two test embankments with rockfill were constructed in 2012. The geometry of the embankments was approximately 30 m x 30 m x 5 m. Settlement and ground water level were monitored versus depth and time, both before, during, and after the construction of the embankments. Due to the coarseness of the rockfill, the groundwater pressure under the embankment corresponded directly with the sea level. The majority of the initial settlement, around 150 mm, occurred after the first two weeks followed by creep that added another 100 mm of settlement after 4 years. Based on the monitoring, the constrained modulus was evaluated to follow a common square root increase versus depth reaching around 10 MPa at 10 m depth.

As a comparison, two additional test areas were compacted using dynamic compaction. The foot print was roughly the same size as for the fill test embankment. A rectangular 20,000 kg pounder was dropped from 20 m height repeatedly. A rectangular pattern with a final spacing of 2 m was used. The settlement was measured at the top of the pounder after each drop. Laser scanning was also performed for these test areas before starting the compaction and after the finalised compaction. A comparison of scanning before and after compaction gave an average settlement within the area of 1.2 m which roughly corresponds to 10 % compressive strain if the affected depth is 10 to 12 m. Up to ten drops per print was tested and the effect of each drop reduced after the 5th drop.

Design of the dynamic compaction was based on the trial compaction, but the spacing was increased to 2.5 m in a rectangular pattern, keeping the same weight and drop height. This is still perhaps a relatively close grid spacing, but was performed to obtain a high energy per area compaction. Other trial tests, specifically intended to evaluate d_{max} and the dynamic response of the rockfill, were performed at the start of the compaction works in 2017. Dynamic compaction was also performed under water for the foundation of the quay walls. An aerial photograph of the dynamic compaction on land is seen in Fig. 2.

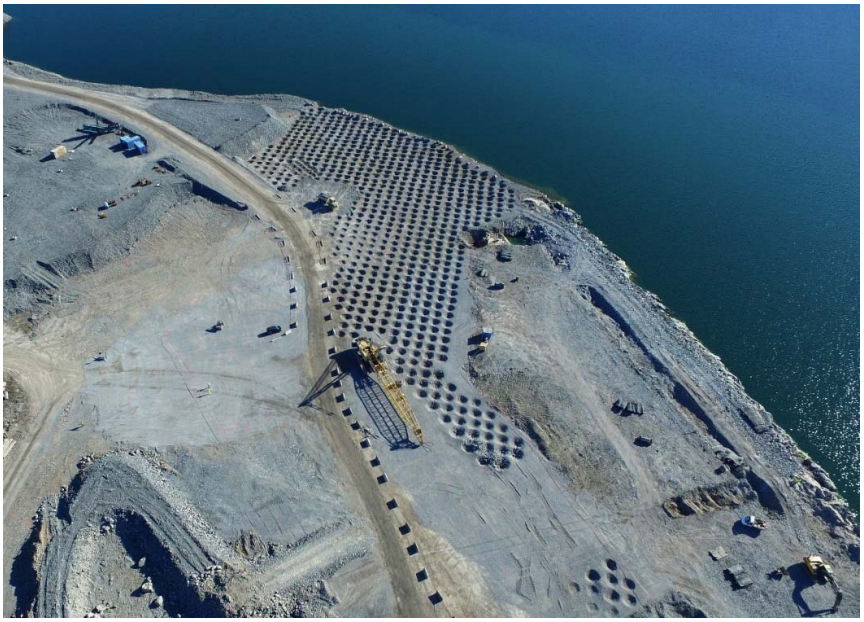


Fig. 2: Aerial photograph of the dynamic compaction on land (photo courtesy of NCC).

The rockfill material is governed by very large particle sizes and a significant angularity since it is a by-product of blasting underground excavations. These aspects lead to high requirements for the compaction method. The chosen dynamic compaction method utilized in this project was considered to produce sufficient compaction energy to overcome contact stresses and has been applied successfully in other similar compaction works reported in the literature, as discussed above.

TRIAL TESTS ON LAND

Depth of influence

To investigate d_{max}, inclinometers and extensometers were installed. The inclinometers were installed down to bedrock at around 20 m depth, and the extensometers at different depths protected by a casing. A trial test area was set up, see Fig. 3a, where dynamic compaction was performed in a specific order whilst alternatingly measuring the inclinometers and extensometers.

From the inclinometer measurements, Fig. 3b, it could be shown that the d_{max} was around 10 m, giving $k \approx 0.5$ according to Eq. 1. The extensometers gave similar results, and is in line with results published by other authors.

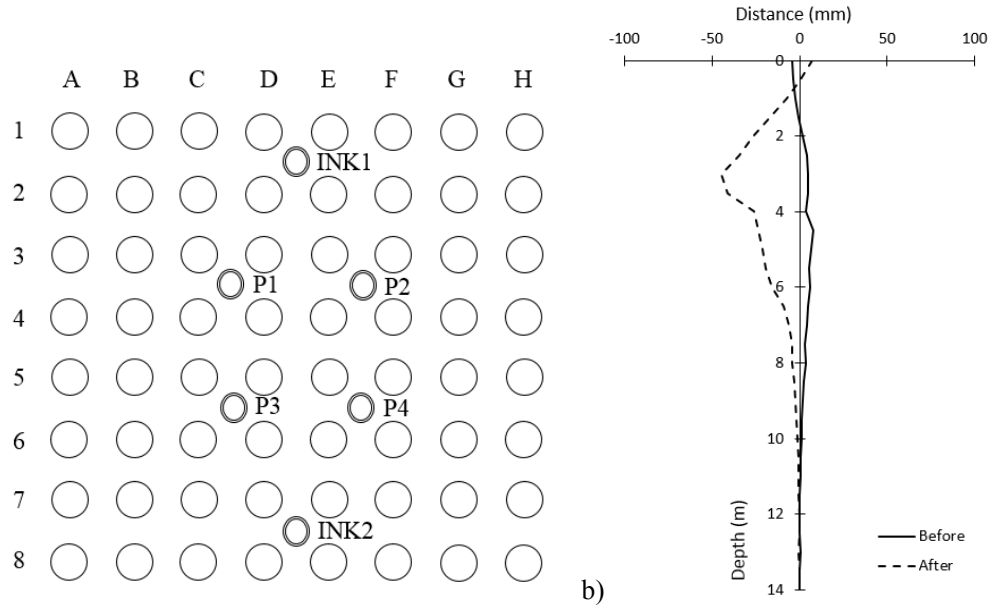


Fig. 3. a) Schematic plan of trial tests (P1-4 = extensometers, INK1-2 = inclinometers). b) Results from measurements of inclinometer INK2, before and after compaction of prints in rows 1 – 6, i.e. to a distance of 3.75 m from the inclinometer. When compacting in row 7, the inclinometer was destroyed and could not be measured.

Deceleration measurements

In an attempt to investigate the soil deformation properties, deceleration measurements were performed using an accelerometer mounted on the top of the pounder. During the trial tests, the acceleration during fall, and deceleration during impact, were measured during up to 8 drops in a number of prints.

The output from the measurements are given in time vs. deceleration. By integrating this curve, a velocity curve is obtained, and by double integration a displacement curve is obtained. This integration creates integration constants which can be solved by using the known velocity at impact and at rest, in addition to the total displacement for each drop, i.e. the crater depth. The results can be calculated to a

stress vs. displacement curve by Newton's second law, where the stress corresponds to the stress between the pounder and the soil, and the displacement corresponds to the soil displacement ending up at the crater depth.

Previous studies, e.g. Hansbo (1977; 1978), have shown that this stress vs. displacement curve obtained from deceleration measurements of dynamic compaction, after some initial adjustments with regards to dynamic effects, roughly can be assumed to be the same as for static load tests. This assumption is connected with several uncertainties, but nonetheless gives indications of the soil deformation properties.

Other researchers, e.g. Orrje (1996), have attempted to derive a modulus of shear and elasticity via impedance and elastic theory, but this approach has in this case given unrealistic results. Other methods include calculation of different dynamic soil moduli, described in for example Poran et al. (1991; 1992), and interpretation using numerical wave equation models as described in e.g. Chow et al. (1990).

A few results of the measured deceleration during impact are shown in Fig. 4. The maximum deceleration was measured to be around 100 – 120 g. The acceleration during the drop was around 0.5 g, which is relatively low compared to other published results (e.g. Holeyman and Vannesta, 1987).

The velocity at impact, calculated from the measured deceleration was compared to analyses of video photography and to theoretical calculations based on free falling objects. For the 20 m drop height, a falling time of 2.6 – 3.1 s and a velocity at impact of 13 – 14 m/s was calculated from the acceleration measurements, in agreement with analyses of video photography. This is to be compared to a theoretical falling time of appr. 2 s and a velocity at impact of appr. 19.8 m/s. This corresponds to around 70 % efficiency in velocity at impact, which is relatively low compared to other published results (Lukas, 1995).

The crater depths during the trial tests were measured using surveying equipment and were used to calibrate the evaluation of the deceleration measurements. The crater depths after 6 drops were around 0.6 – 0.7 m for the trial tests. During production, however, they were up to, and occasionally over, 1.5 m.

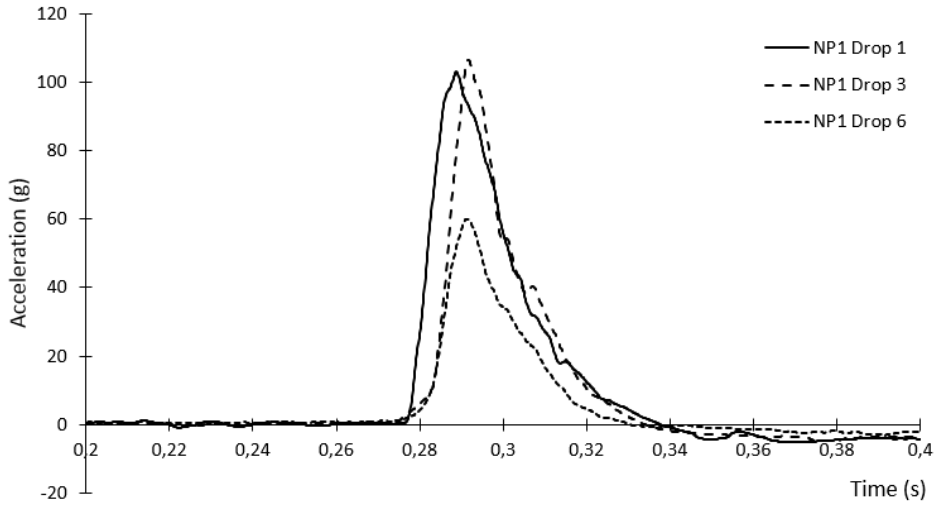


Fig. 4. Example of deceleration measurements of three drops, 1st, 3rd and 6th, in one trial test print (NP1). The reason for the lower deceleration for the 6th drop is probably because the pounder hit the crater wall.

TRIAL TESTS UNDER WATER

Estimation of depth of influence

No documented experience from estimating d_{max} during under-water dynamic compaction has been published in the literature, to the best of the authors' knowledge. The Menard empirical relationship for estimating d_{max}, Eq. 1, based on weight and drop height, could not be used since the pounder is affected by a buoyancy effect and a drag force lessening the velocity at impact. However, as the term WH is directly proportional to the kinetic energy at impact, KE, it can be assumed that a reduction in KE at impact can be taken into account by an equal reduction in WH in Eq. 1 to calculate d_{max} at under-water compaction. This approach is also based on the assumption that the empirical constant k is equal on land and under water. The compaction on land and under water was performed on the same type of rockfill material, using the same dropping mechanism and, in both cases, primarily involved compaction of soil under water as the ground water table on land was only at around 2 m depth.

The KE at impact can be calculated as:

$$KE = \frac{1}{2} m' v^2 \qquad [2]$$

Where m' = effective mass in kg, and v = velocity at impact in m/s.

Under water, the effective mass, i.e. the pounder weight corrected for buoyancy effect, was appr. 14,000 kg. The velocity under water is lessened by a drag force which is dependent on the cross-sectional area, the actual velocity, the density of water, and a drag coefficient. The drag coefficient is in turn dependent on the geometry of the pounder and type of flow of water around the pounder, e.g. turbulent flow. This drag force creates a terminal velocity as it increases with increasing velocity, and reaches equilibrium with the gravity force at the terminal velocity. This terminal velocity, reached at around 30 m fall in water, was theoretically calculated to be appr. 10.6 m/s. At 10 m drop height, the velocity was theoretically calculated to be appr. 9.6 m/s.

The measured acceleration, however, was slightly over 0.2 g during the falling time of appr. 2.7 s, giving an actual velocity at impact around 5.5 m/s. This equals appr. 60 % effectiveness of the theoretical velocity at impact for the under-water compaction, and gives a KE of around 220 kJ/blow at impact. On land, the velocity at impact was 13 – 14 m/s, giving a KE of around 1,800 kJ/blow at impact, which is within published values (Greenwood and Kirsch, 1983).

The KE at impact under water was thus calculated to be around 12 % of the kinetic energy of compaction on land where $d_{max} \approx 10\,m$ was measured. d_{max} under water will then be reduced by $\sqrt{0.12} \approx 0.35$ giving $d_{max} \approx 10 \times 0.35 \approx 3.5\,m$. This is to be compared with theoretical values of velocity at impact where the reduction in KE is approximately 17 %, giving $d_{max} \approx 4\,m$. This approach is of course associated with uncertainties and have not been verified by any measurements, but seems reasonable, if not a bit too low compared to crater depths which were measured to be mainly around 0.4 – 0.6 and occasionally over 0.8 m after 6 drops.

Deceleration measurements

The underwater pounder with the mounted accelerometer is shown in Fig. 5. The cylindrically shaped pounder consisted of a steel frame filled with concrete. In some internationally published case studies, under water compaction have been performed using square pounders with holes to reduce the underwater drag force, e.g. Yee and Varaksin (2012). How these compare to this solid cylindrical pounder is not known, but clearly the compaction effect is mainly dependent on the energy at impact, which again is a function of the effective weight, cross-sectional area and shape of the pounder. The pounder can thus be designed in different ways, as long as sufficiently high energy at impact is obtained.

As well as on land, the acceleration and deceleration were measured during drop and impact. An example of results for measurements during impact is shown in Fig. 6. The maximum acceleration was around 10 g, roughly one-tenth of that on land.

Evaluation of the results was performed the same way as with the results from measurements on land. However, the crater depth could not be measured with the same accuracy. Rough estimates of crater depths were obtained by a cable wire measuring system and from multi-beam echo sounding. The calculation methods for the deceleration at impact, however, were calibrated and adjusted when evaluating the on-land deceleration measurements, so the evaluated parameters is believed to be representative. The calculated and measured crater depths were within the same order of magnitude.



Fig. 5. Pounder used for under water dynamic compaction. The accelerometer is mounted on the side of the weight (left side in this picture) to avoid damage from chains.

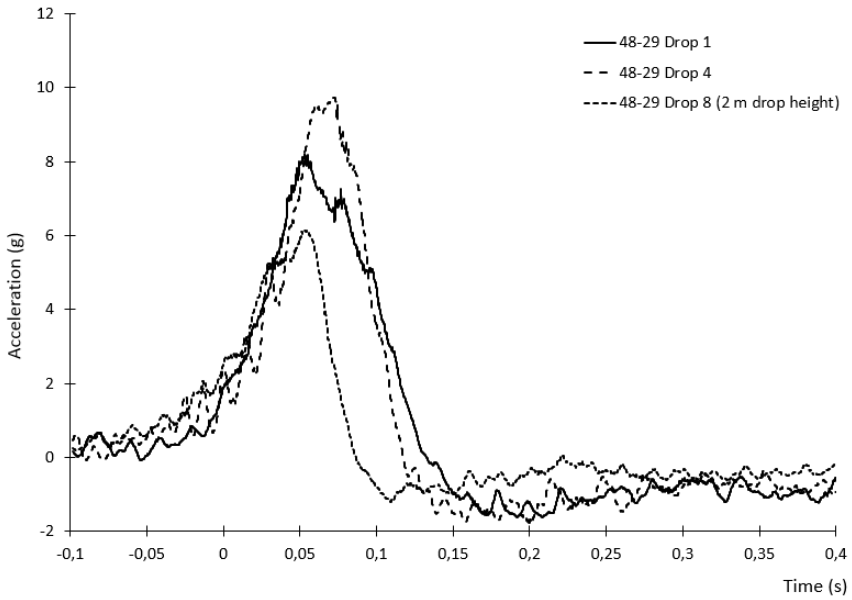


Fig 6. Example of deceleration measurements under water of three drops, 1st, 4th and 8th, in point 48-29. The drops were done with 10 m drop height, except the 8th drop which was done from 2 m.

Results from a number of stress vs. displacement curves are shown in Fig. 7. The initial steep inclines of the curves are seen as dynamic effects, and a settlement modulus was interpreted from the straight part down to the maximum contact stress. It can be seen that the inclines are similar for all drops, even for 2 m drop height. As described, this stress vs. displacement relationship has been shown to be roughly similar to that of a static load test. Holeyman and Vannesta (1987) suggested to use the slope of the unload/rebound curve, but this was seen as too unconservative for use in the design.

The displacement modulus, here denoted DM, is defined as:

$$DM = \frac{\Delta\sigma}{\Delta s} \quad [3]$$

Where $\Delta\sigma$ = change in contact stress between pounder and soil, Δs = displacement of pounder and soil.

The modulus was interpreted to be around 3,500 – 4,000 kPa/m for the under-water compaction. On land, the modulus was calculated to be around 50,000 – 80,000 kPa/m, which is in agreement with results obtained by Hansbo (1977; 1978).

The evaluated DM values were checked with a parametric study using the density index, D_r. Rough estimates using assumed values of $e_{max} = 0.45$, $e_{min} = 0.25$, initial $D_r = 15$ %, $d_{max} = 3.5\ m$, and an average settlement during compaction of 0.3 m, gives a final $D_r \approx 75$ %, corresponding to a modulus of elasticity around 30 – 50 MPa for this type of rockfill (Bergdahl et al. 1993).

Several methods have been suggested which aims to calculate the reduction in void ratio as a result of dynamic compaction (Poran et al. 1992; Oshima & Takada 1997). These are, however, theoretical in nature and have only been tested on homogeneous soil conditions, often in laboratory conditions. Hence, they have not been used in this study.

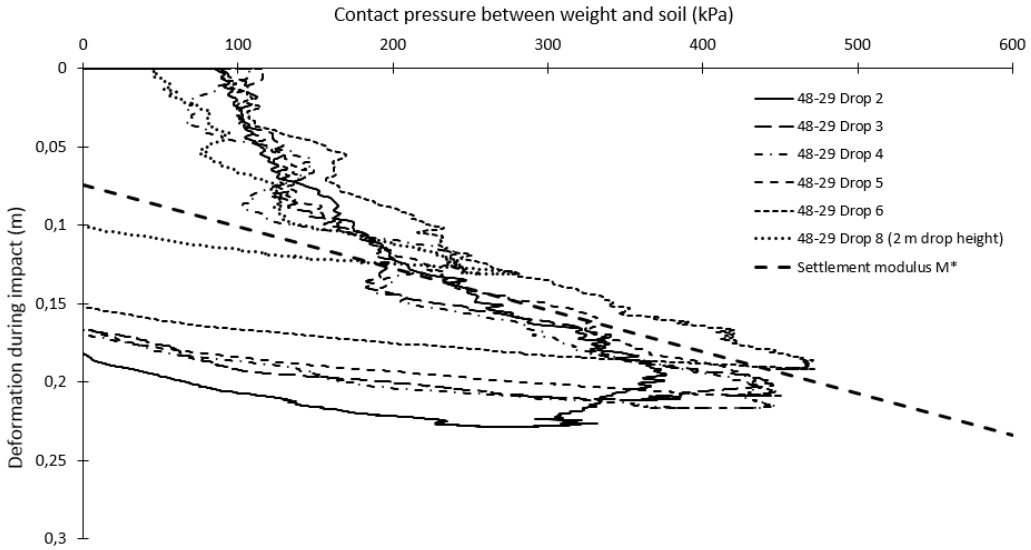


Fig. 7. Stress vs. displacement curves and evaluation of the settlement modulus M*

Evaluation of settlement at loading

The evaluated DM for the under-water compaction is assumed to be representative for additional static loads such as quay L-walls and back fill. The quay L-walls including the backfill will generate around 150 kPa load on the dynamic compacted rockfill under water. The estimated $DM \approx 4{,}000$ kPa/m will give a settlement of around 0.05 m during construction. This calculation does not however take into

account the looser compacted rockfill between the prints. Using the derived modulus of elasticity, the settlement will be around 0.05 – 0.1 m, and is in agreement with the calculations using DM.

Deformations in the back fill itself has not been calculated since long-term creep settlements will be minimised using temporary preloading. Creep settlements in the dynamic compacted rockfill is thought to be neglectable.

It should be noted that the evaluation of results and calculation of settlement is associated with large uncertainties, e.g. in calculation methods, inhomogeneity in rockfill after compaction, etc. They are however considered to be good enough for engineering purposes, and will be compared to measured settlement during construction of the quay walls.

CONCLUSIONS

Deep dynamic compaction of rockfill on land was performed over an area of approximately 85,000 m^2 and 14,000 prints. Under water, dynamic compaction was performed in three layers, in total around 30,000 m^2 and 5,000 prints. With a number of trial tests, including large scale trial compaction at an early design stage, the design and compaction works could be optimized to fulfil the design criteria. The compaction works are successfully being executed.

As a part of the trial tests, accelerometer measurements were performed to evaluate the dynamic response of the rockfill, both on land and under water. The novel underwater measurements gave insights to obtained impact stresses and compaction effect of underwater compaction. The maximum acceleration under water was around one tenth of that on land, approximately 10 and 100 – 120 g, respectively.

An attempt was also made to evaluate the maximum depth of influence for the underwater compaction by using a measured relative reduction in kinetic energy, subsequently applied in the Menard empirical relationship. The kinetic energy under water was calculated to be around 12 % of that on land, corresponding to around 35 % of the maximum depth of influence.

Stress vs. displacement curves were derived and used to predict settlements of around 0.05 – 0.1 m due to around 150 kPa of load from additional fill and quay L-walls.

The authors hope that the work presented herein will encourage more research on deceleration measurements and the evaluation of the depth of influence for under water compaction. Especially, it should be investigated how the Menard empirical relationship can be modified to take into account a change in the energy impact, perhaps reformulating the relationship to be based on a scientific parameter such as kinetic energy, making it also applicable for under water compaction.

ACKNOWLEDGEMENTS

The authors are grateful to the Port of Stockholm for the understanding of the importance of doing large scale trial tests and also advanced measurements during the compaction works. The authors also wish to thank the contractor Trevi, who has been very cooperative, and Kent Allard and Kent Lindgren for assisting with the accelerometer measurements.

REFERENCES

Bjølgerud, O. and Haug, A., 1983. Dynamic Compaction of Rockfill at an Oil Refinery. Proceedings of the 8th European Conference on Soil Mechanics and Foundation Engineering, Helsinki, Vol. 1, pp. 213-218.

Bo. M. W., Na, Y. M., Arulrajah, A. and Chang, M. F., 2009. Densification of granular soil by dynamic compaction. Proceedings of the Institution of Civil Engineers Ground Improvement, Vol. 162, pp. 121-132.

Chow, Y. K., Yang, D. M., Yang, K. Y. and Lee, S. L., 1990. Monitoring of dynamic compaction by deceleration measurements. Computers and Geotechnics, 10, No. 3, 189-209.

Greenwood, D. A. and Kirsch, K., 1983. State of the art: Specialist ground treatment by vibratory and dynamic methods. Piling and ground treatment for foundations, Thomas Telford, London, pp. 17-45.

Hansbo, S., 1977. Dynamic consolidation of rockfill. Proceedings of the 9th International Conference on Soil Mechanics and Foundation Engineering, Tokyo, Vol. 2, pp. 241-246.

Hansbo, S., 1978. Dynamic consolidation of soil by a falling weight. Ground Engineering, Vol. 11, No. 5, pp. 27-36.

Holeyman, A. and Vanneste, G., 1987. A new approach to the execution and control of dynamic compaction. Compaction Technology, Thomas Telford, London.

Leonards, G. A., Cutter, W. A. and Holtz, R. D., 1980. Dynamic compaction of granular soils. Journal of the Geotechnical Engineering Division, ASCE, 106, No. GT1, 35-44.

Lopez, R. A, Francis, M. J., Rollins, K. M., Davis, S. W. and Batchko, Z., 1998. Composite ground modification system: Vibroreplacement and dynamic compaction, Salt Lake County Detention Center, Utah. Proceedings of the 4th International Conference on Case Histories in Geotechnical Engineering, St Loius, pp. 895-900.

Lukas, R. G., 1995. Geotechnical Engineering Circular No. 1: Dynamic compaction. Federal Highway Administration, Washington, DC, FHWA-SA-95-037.

Mayne, P. W., Jones, J. S. And Dumas, J. C., 1984. Ground response to dynamic compaction. Journal of Geotechnical Engineering, ASCE, 110, No. GT6, 757-773.

Menard, L. and Broise, Y., 1975. Theoretical and practical aspecrs of dynamic consolidation. Géotechnique, 25, No. 1, 3-16.

Orrje, O., 1996. The Use of Dynamic Plate Load Tests to Determining Deformation Properties of Soil", Doctoral Thesis, KTH, 249 p.

Oshima, A. and Takada, N., 1997. Relation between compacted area and ram momentum by heavy tamping. Proceedings of the 14th International Conference on Soil Mechanics and Foundation Engineering, Hamburg, 3, 1641-1644.

Poran, C. J., Heh, K. S. and Rodriguez, J., 1991. Impact respons of granular soils. Proceedings of the 2nd International Conference on Recent Advances in Geotechnical Earthquake Engineering and Soil Dynamics, St Loius, 2, 1387-1398.

Poran, J. C., Heh, K.S. and Rodrigues, J. A., 1992. Impact behaviour of sand. Soils and Foundations, Japanese Society of Soil Mechanics and Foundation Engineering, Vol. 32, No. 4, 81-92.

Stordal, A. and Simonsen, A. S., 1993. Dypkomprimering av steinfylling i Njupsvikane på Kollsnes (In Norwegian). Geoteknikkdagen, Norges Geotekniske Forening, s. 21.1-21.14.

Yee, K. and Varaksin, S., 2012. Ground reinforcement in deep water. Proceedings of the International Conference on Ground Improvement and Ground Control, pp. 575-585.

EFFECT OF STEEL FIBRES ON THE BEHAVIOUR OF A CHEMICALLY STABILISED SOIL

Correia A.A.S., CIEPQPF, Dep. Civil Engineering, Univ. of Coimbra, Portugal, aalberto@dec.uc.pt
Venda Oliveira P.J., ISISE, Dep. Civil Engineering, Univ. of Coimbra, Portugal, pjvo@dec.uc.pt
Teles J.M.N.P.C., Dep. Civil Engineering, Univ. of Coimbra, Portugal, jmcidteles@hotmail.com

ABSTRACT

The paper describes the effect of fibre quantity on the mechanical behaviour of a soft soil stabilised with binders and reinforced with steel fibres. Two types of tests were carried out – unconfined compressive strength (UCS) and direct tensile strength (DTS) tests. The results obtained showed that the compressive strength, tensile strength and stiffness changed with the fibre quantity depending on the strain mechanism of each test. In general, the presence of a low quantity of steel fibres had a detrimental effect in terms of UCS while a beneficial effect was found for DTS tests. As the fibre quantity was increased, the UCS tests revealed a decrease in brittleness, while the DTS tests showed brittle behaviour with an abrupt and complete loss of tensile strength after failure. The relationships between compressive and tensile strengths are presented in the paper.

INTRODUCTION

The technique chemical stabilisation of soils has become widespread around the world since the 1960s, and it is applied to many fields such as: foundations of structures and embankments, stability of slopes, vibrations induced by high-speed trains or industrial equipment, liquefaction, soil mixing walls (Terashi, 2005; Holm, 2005; Terashi and Kitazume, 2009) and stabilisation/solidification of contaminated soils (Al-Tabbaa et al, 2009; Hernandez-Martinez et al., 2009).

In general, the mechanical behaviour of chemically stabilised soils is characterised by a good compressive strength but poor tensile strength (Sukontasukkul and Jamsawang, 2012) associated to a brittle behaviour (Consoli et al., 2009; Sukontasukkul and Jamsawang, 2012; Olgun, 2013). In some cases, tensile strength is required to prevent failure under tension, such as when deep mixing columns (DMCs) are subjected to horizontal displacements, seismic loads and/or lateral earth pressures (as for deep-mixed soil walls). The tensile strength can be increased by the inclusion of fibres in the soil-binder-water mixture, in a similar way as used in concrete.

Even know that the effect of steel fibres in concrete has been studied by many authors (Haktanir et al., 2007; Chalioris and Karayannis, 2009; Paultre et al., 2010; Caverzan et al., 2012; Madhkhan et al., 2012; Perrot et al. 2013; Carneiro et al., 2014; Kaïkea et al., 2014; Khaloo et al., 2014), the effect of this type of fibres on the behaviour of chemically stabilized soils has also been largely ignored by the scientific community provably due to corrosion problems. The study made by Sukontasukkul and Jamsawang (2012) has revealed that the inclusion of short steel fibres in a soft soil stabilized with high-binder contents (>10%), induces a reduction in the flexural strength, while Gülü and Khudir (2014) have shown that the use of short steel fibres in a low-plasticity silt stabilized with 4% of lime causes an increment in the compressive strength.

© 2018 Deep Foundations Institute

The aim of this work is to contribute to a better knowledge of the compressive and tensile behaviour of stabilised soft soils with a high-binder content and reinforced with steel fibres. The influence of the fibre quantity was evaluated through the performance of two different type of tests: unconfined compressive strength (UCS) and direct tensile strength (DTS) tests. Based on the results achieved possible relationships between the compressive strength and the tensile strength were evaluated, which may be helpful for design.

TESTING PROGRAMME

Materials

The soil selected for the laboratory work is a soft soil collected from the "Baixo Mondego" area (near the city of Coimbra, Portugal). The soil deposit was formed more than 20 000 years ago in a fluvio-marine depositional environment and presents a thickness of +/- 20 m. The grain size distribution of the natural soil is mostly composed of silt (61%) with a reasonable amount of clay (25%) and some sand (14%). It has a unit weight of only 14.6 kN/m^3, a void ratio higher than 2.0, a natural water content of 80.9%, and a high organic matter content, around 13.1%. These characteristics induces high compressibility and plasticity indexes (w_L= 68.0%; w_P = 41.9%) and a low undrained shear strength (< 25 kPa) (Coelho 2000; Venda Oliveira et al. 2010, 2012, 2013, 2014; Correia 2011; Custódio 2013; Teles 2013). According to the ASTM D 2487 (1998) standard this soil is classified as a clayey-silt organic with a high plasticity, OH.

The soft soil was stabilized with a composition of Portland cement Type I 42.5 R and blast furnace granulated slag, mixed in a dry weight proportion of 3/1 applied in a quantity (dry weight of binder per volume of untreated soil) of 375 kg/m^3. While the Portland cement reacts immediately with water producing a high quantity of reaction products in the short term, the slag promotes the development of pozzolanic reactions, which are responsible for the improvement of the mechanical properties in the long-term (Taylor 1997; Janz and Johansson 2002).

The stabilized soil was reinforced with commercial crimped steel fibres with a length of 30 mm, a width of 2.1 mm, a thickness of 0.4mm, a tensile strength higher than 700 MPa and an elasticity modulus of 200 GPa (in accordance with the data supplied by the manufacturer). The fibres are crimped in shape which maximizes the friction with the surrounding material but increases the deformability of the fibre when it is stretched. The steel fibres were applied in five different quantities (0; 25; 50; 100 and 150 kg/m^3).

Specimen Preparation and Testing

The reinforced and chemically stabilized soil samples were prepared according to the procedure presented in EuroSoilStab (2001) and the procedures established by Correia (2011) and Correia et al. (2015 and 2017). To assure constant soil properties (w_{nat} and organic matter content), the experimental work started with the homogenization of the soil. Then, the soil was mixed in a mechanical mixer at a speed of 142 rpm for 4 minutes with a slurry of the binders (the water content was increased from 80.9% to 113% in order to ensure the best compromise between strength and quality of the samples, Correia (2011)) and with the specified content of fibers. The resulting mixture was then placed into cylindrical PVC moulds (200mm height and 100mm diameter). In order to ensure uniformity throughout the samples the mixture was placed in 3 layers in the moulds. Each layer was compacted following a 3 step

procedure: first was lightly tapped by hand, after, a vibration was applied with a hand drill near the inner surface of the mould and, finally, the layer was compacted with a pressure of 100kPa for 10 seconds. Before placing another layer the surface of the paste was lightly scarified. The samples produced were immediately stored in a humidity room (temperature of 20±2 °C and relative moisture of 95±5%). All the samples were extracted from the moulds 7 days later and after 28 days of curing time they were tested in a universal testing machine. The UCS and DTS tests were performed by imposing a constant strain rate of 1%/min in accordance with BS 1377-7 (1990) and ASTM D 2166 (2000). Throughout the entire test the load cell and strain gauge readings were recorded by an automatic data acquisition system. Every test was repeated twice to verify the reliability of the procedure.

RESULTS

The effect of the fibre quantity (FQ) in terms of compressive (UCS tests) and tensile behaviour (DTS tests) is summarized in Table 1 and Figures 1 and 2. Figure 1 depicts the stress-strain behaviour evaluated from UCS and DTS tests, while Figure 2 summarizes the effect of FQ in terms of stiffness, compressive and tensile strength, obtained from the two types of tests.

Tabel 1. Summary of the results obtained from UCS and DTS tests.

Fibre Quantity (kg/m^3)	Test code	UCS				DTS			
		q_u (kPa)	$\mathbf{q_u^{av}}$ (kPa)	$\mathbf{E_{u\,50}}$ (MPa)	$\mathbf{E_{u\,50}^{av}}$ (MPa)	f_{ct} (kPa)	$\mathbf{f_{ct}^{av}}$ (kPa)	$\mathbf{E_{u\,50}}$ (MPa)	$\mathbf{E_{u\,50}^{av}}$ (MPa)
0	FQ = 0, T1	2760.9	2623.4	193.5	190.3	411.2	378.6	1316.7	1379.7
	FQ = 0, T2	2485.8		187.1		345.9		1442.7	
25	FQ = 25, T1	2133.6	1971.9	147.3	140.6	436.0	436.0	1352	1352
	FQ = 25, T2	1810.2		133.9		*		*	
50	FQ = 50, T1	1774.5	1851.1	192.1	201.1	454.1	482.7	1366.7	1391.9
	FQ = 50, T2	1927.7		193.7		511.2		1417.1	
100	FQ = 100, T1	2116.9	2209.9	172.8	169.6	448.5	478.0	1481.1	1449.0
	FQ = 100, T2	2302.7		166.4		507.4		1416.8	
150	FQ = 150, T1	1953.7	1994.9	124.2	142.0	396.1	365.1	1427.7	1408.0
	FQ = 150, T2	2036.2		159.7		334.1		1388.3	

* Problems during testing.

In general, the UCS (Figure 1a) tests reveal that the increase in the fibre quantity changes the behaviour of the soil-binder paste, inducing a decrease in the brittleness and an increase in the residual strength, due to the mobilization of the tensile strength of the steel fibres. This behaviour is not replicated by the DTS tests (Figure 1b), since all the results, independently of the fibre quantity, indicate a brittle behaviour with abrupt loss of strength after failure. In fact, due to the failure mechanism imposed by the DTS test, the stresses applied immediately after failure will be instantaneously transferred to the steel fibres, which are unable to support the external load, either because they break, or have insufficient anchorage length.

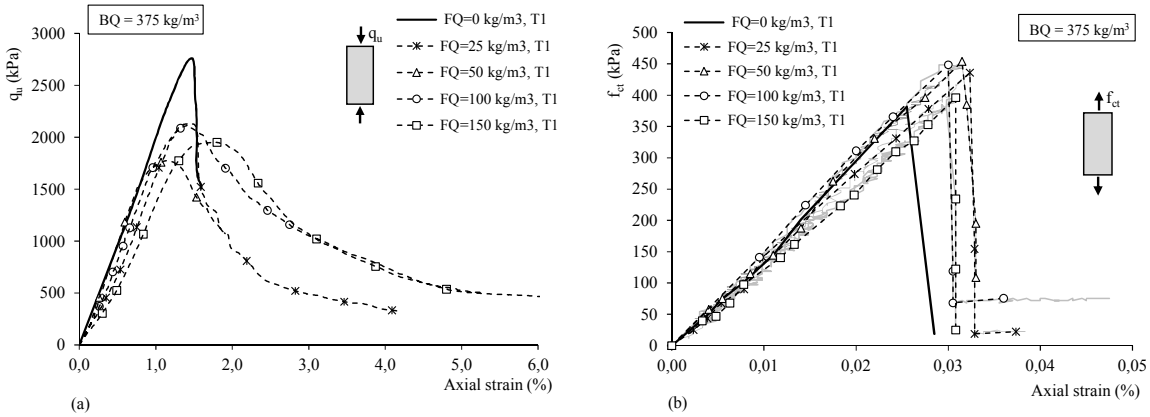


Fig. 1: Stress-strain plots – effect of fibre quantity: a) UCS test; b) DTS test.

Figure 2 summarizes the effect of FQ in terms of stiffness, compressive and tensile strength, obtained from the two types of tests. In general, all the tests do not show a linear trend, both in terms of strength or stiffness, indicating an optimum amount of fibres, which is different from one test to the other. The results of the UCS (Figure 2a) and DTS (Figure 2b) tests show an evolution in the opposite direction, since the addition of any FQ for the UCS tests always has a detrimental effect (with a minimum compressive strength for 25-50 kg/m^3 of FQ), while the DTS tests reveal a maximum tensile strength when 50-100 kg/m^3 of fibres are added to the mixture. These results indicate that the mobilization of the tensile strength of the fibres in the UCS tests does not compensate the reduction of the cement bonds due to the presence of the fibres while, in the DTS tests, there is a mobilization of a significant tensile strength, even for low strain levels ($\varepsilon_{ax} \cong 0{,}03\%$, Figure 1b). The evolution of the stiffness, expressed by the undrained secant Young's modulus for 50% of strength E_{u50}, from the UCS and DTS tests shows a similar behaviour, described by a decrease with the inclusion of 25 kg/m^3 of fibres, followed by a slight recovery of E_{u50} when 50 kg/m^3 of steel fibres are added (optimum value), after which it decreases continuously until the minimum for higher FQ.

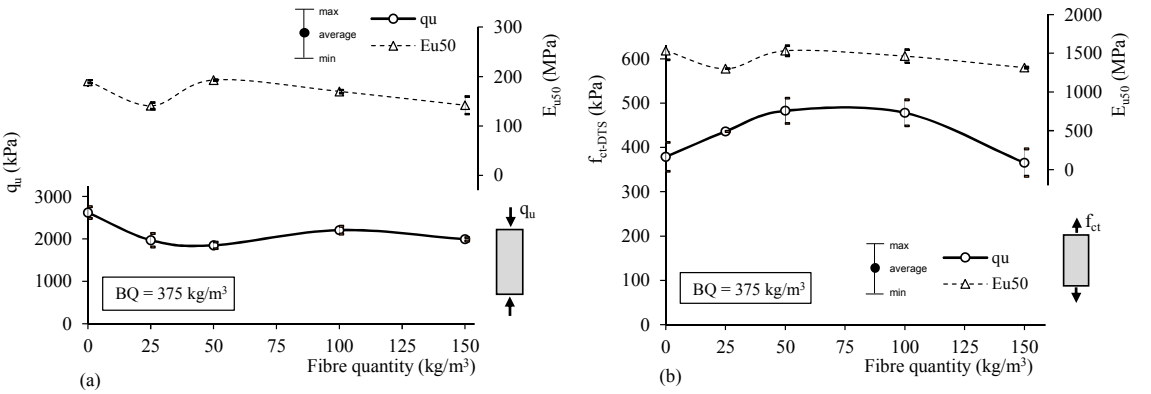


Fig. 2: Effect of the fibre quantity on stiffness, compressive and tensile strength: a) UCS test; b) DTS test.

The effect of the fibre quantity on the evolution of the relationship between the compressive and tensile strength ($f_{ct\text{-}DTS}/q_u$) is depicted in Figure 3. The ratio $f_{ct\text{-}DTS}/q_u$ increases with the fibre quantity reaching

a maximum (0.26) for the fibre quantity of 50 kg/m^3, followed by a continuous decreases until the minimum for higher FQ. For design purposes, a relationship $f_{ct\text{-}DTS}/q_u$ of 0.2 can be taken as a conservative value when steel fibres are added to the stabilized soil.

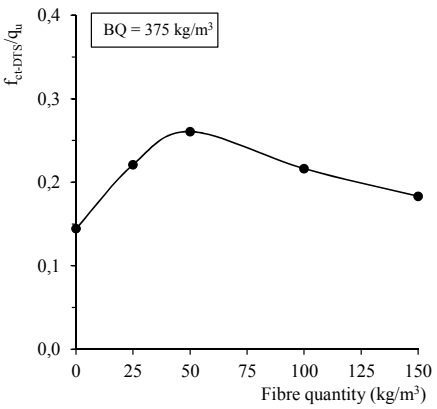


Fig. 3: Effect of fibre quantity on the ratio of peak strength: $f_{ct\text{-}DTS}/q_u$.

CONCLUSIONS

In this work it was studied the effect on the mechanical behaviour of adding steel fibres to a chemically stabilized soft soil. The UCS tests results have shown that the addition of steel fibres to the mixture tends to decrease its brittleness. However, the results of the DTS tests continue to show a brittle behaviour characterised by an abrupt loss of strength after failure, which is due to the failure mechanism that induces the instantaneous transfer of the external load applied on the stabilised soil matrix to the fibres, which are unable to support the external load, either because they break, or have insufficient anchorage length.

The effect of the increment of the steel fibre quantity also depends on of the type of tests. The results of the UCS tests show, for any amount of fibres, a reduction of the compressive strength for the inclusion of 25-50 kg/m^3 of fibres. The results of DTS tests show a beneficial impact of the fibres, leading to a maximum tensile strength for 50-100 kg/m^3 of fibres. These differences are due to the distinct failure mechanisms of each test and to the mobilization of the tensile strength of the steel fibres.

Based on all results, it is proposed a relationship $f_{ct\text{-}DTS}/q_u$ of 0.2 for design purposes.

Further studies should be done in order to corroborate the results here presented, and at the same time, to improve the characterization of the tensile behaviour of soils stabilized chemically and reinforced with steel fibres.

ACKNOWLEDGEMENTS

The authors would like to express their thanks to CIMPOR and to Biu International for supplying, respectively, the binders and the fibres used in the work and to the institutions that financially supported the research: POCI-01-0145-FEDER-007633 (ISISE) and UID/EQU/00102/2013 (CIEPQPF).

REFERENCES

Al-Tabbaa, A. Barker, P., Evans, C.W. (2009). "Keynote Lecture: Design of deep mixing in infrastructure applications". International Symposium of Deep Mixing &Admixture Stabilization. Okinawa, Japan.

ASTM D 2487 (1998). *Standard classification of soils for engineering purposes (UnifiedSoil Classification System).* American Society for Testing and Materials.

ASTM D 2166 (2000). *Standard test method for unconfined compressive strength of cohesive soil*. American Society for Testing and Materials.

BS 1377-7 (1990). *Methods of test for soils for civil engineering purposes – part 7: Shear strength tests (total stress)*. British Standards Institution, London.

Carneiro, J.A.; Lima, P.R.L.; Leite, M.B.; Filho, R.D.T. (2014). Compressive stress-strain behaviour of steel fiber reinforced-recycled aggregate concrete. *Cement & Concrete Composites,* 46: 65-72.

Caverzan, A.; Cadoni, E.; Prisco, M. (2012). Tensile behaviour of high performance fibre-reinforced cementitious composites at high strain rates. *International Journal of Impact Engineering*, 45: 28-38.

Chalioris, C.E.; Karayannis, C.G. (2009). Effectiveness of the use of steel fibres on the torsional behaviour of flanged concrete beams. *Cement & Concrete Composites*, 31: 331-341.

Coelho, P.A.L.F. (2000). Geotechnical characterization of soft soils. Study of the experimental site of Quinta do Foja. M.Sc. thesis, Department of Civil Engineering, University of Coimbra (in Portuguese).

Consoli, N.C.; Vendruscolo M.A.; Fonini, A.; Rosa, F. D. (2009). Fiber reinforcement effects on sand considering a wide cementation range. *Geotextiles and Geomembranes*, 27(3): 196-203.

Correia, A.A.S. (2011). "Applicability of deep mixing technique to the soft soil of Baixo Mondego". Ph.D. dissertation, University of Coimbra, Coimbra, Portugal (in Portuguese).

Correia, A.A.S.; Venda Oliveira, P.J.; Custódio, D.G. (2015). Effect of polypropylene fibres on the compressive and tensile strength of a soft soil, artificially stabilised with binders. *Geotextiles and Geomembranes*, 43(2): 97-106.

Correia, A.A.S.; Venda Oliveira, P.J.; Teles, J.M.N.P.C. and Pedro, A.M.G., 2017. "Strength of a stabilised soil reinforced with steel fibres". *Proceedings of ICE - Geotechnical Engineering* (doi: 10.1680/jgeen.16.00200)

Custódio D. G. (2013). Mechanical behaviour of a stabilized soft soil with polypropylene fibres. M.Sc. dissertation, University of Coimbra, Coimbra, Portugal (in Portuguese).

Eurosoilstab (2001). "Development of design and construction methods to stabilise soft organic soils. Design guide soft soil stabilization". CT97-0351, EC Project No. BE 96-3177, Industrial & Materials Technologies Programme (BriteEuRam III), European Commission, pp. 94.

Güllü, H.; Khudir A. (2014). Effect of freeze-thaw cycles on unconfined compressive strength of fine-grained soil treated with jute fiber, steel fiber and lime. *Cold Regions Science and Technology*, 106-107: 55-65.

Haktanir, T.; Ari, K.; Altun, F. Karahan, O. (2007). A comparative experimental investigation of concrete reinforced-concrete and steel-fibre concrete pipes under three-edge-bearing test. *Construction and Building Materials*, 21: 1702-1708.

Hernandez-Martinez, F.G., Sparrevik, M., Kvalvåg, □., Eggen, A., Kvennås, A., Grini, R.S. (2009). "Stabilization/solidification of two contaminate marine sediments". International Symposium of Deep Mixing &Admixture Stabilization. Okinawa, Japan.

Holm, G. (2005). "Keynote Lecture: Towards a sustainable society – recent advances in deep mixing". International Conference on Deep Mixing – Best Practice and Recent Advances: k13-k24. Swedish Deep Stabilization Centre. Stockholm, Sweden.

Janz, M., and Johansson, S.-E. (2002). "The function of different binding agents in deep stabilization". Swedish Deep Stabilization Research Centre, Report 9, Linköping, Sweden.

Kaïkea, A.; Achoura, D.; Duplan, F.; Rizzuti, L. (2014). Effect of mineral admixtures and steel fiber volume contents on the behaviour of high performance fiber reinforced concrete. *Materials and Design*, 63: 493-499.

Khaloo, A.; Raisi, E.M.; Hosseini, P.; Tahrisi, H. (2014). Mechanical performance of self-compacting concrete reinforced with steel fibers. *Construction and Building Materials*, 51: 179-186.

Madhakhan, M.; Azizkhani, R.; Harchegani, M.E.T. (2012). Effects of pozzolans together with steel and oplypropyline fibers on mechanical properties of RCC pavements. *Construction and Building Materials*, 26: 102-112.

Olgun, M (2013). Effects of polypropylene fiber inclusion on the strength and volume change characteristics of cement-fly ash stabilized clay soil. *Geosynthetics International*, 20(4): 263-275.

Paultre, P.; Eid, R.; Langlois, Y.; Lévesque, Y. (2010). Behavior of steel fiber-reinforced high-strength concrete columns under uniaxial compression. *Journal of structural Engineering*, 136(10): 1225-1235

Perrot, A., Lecompte, T., Estellé, P., & Amziane, S. (2013). Structural build-up of rigid fiber reinforced cement-based materials. *Materials and Structures*, 46(9), 1561–1568.

Sukontasukkul, P., Jamsawang, P. (2012). Use of steel and polyprolylene fibers to improve flexural performance of deep soil-cement column. *Construction and Building Materials*, 29(1): 201-205.

Taylor, H.F.W. (1997). Cement Chemistry. 2nd edition, Thomas Telford.

Teles, J.M.N.P.C. (2013). Mechanical behaviour of the soft soil of Baixo Mondego chemically stabilised with the addition of mettalic fibres. M.Sc. dissertation, University of Coimbra, Coimbra, Portugal (in Portuguese).

Terashi, M. (2005). Keynote Lecture: Design of deep mixing in infrastructure applications. International Conference on Deep Mixing – Best Practice and Recent Advances: k25-k45. Swedish Deep Stabilization Centre. Stockholm, Sweden.

Terashi, M., Kitazume, M. (2009). “Keynote Lecture: Current practice and future perspective of QA/QC for deep-mixed ground”. International Symposium of Deep Mixing &Admixture Stabilization. Okinawa, Japan.

Venda Oliveira, P.J., Lemos, L.J.L. Coelho, P.A.L.P. (2010). Behavior of an atypical embankment on soft soil: field observations and numerical simulation. *Journal of Geotechnical and Geoenvironmental Engineering*, 136(1): 35-47.

Venda Oliveira, P.J.; Correia, A.A.S.; Garcia, M.R. (2012). Effect of organic matter content and curing conditions on creep behaviour of an artificially stabilized soil. *Journal of Materials in Civil Engineering*, 24(7): 868-875.

Venda Oliveira, P.J.; Correia, A.A.S.; Garcia, M.R. (2013). Effect of stress level and binder composition on secondary compression of an artificially stabilized soil. *Journal of Geotechnical and Geoenvironmental Engineering*, 139(5): 810-820.

Venda Oliveira, P.J.; Correia, A.A.S.; Lopes T. J.S. (2014). Effect of organic matter content and binder quantity on the uniaxial creep behaviour of an artificially stabilized soil. *Journal of Geotechnical and Geoenvironmental Engineering*, 140(9): 04014053-1: 04014053-10.

GROUND IMPROVEMENT BY INCLUSIONS IN UNSTABLE SLOPES

Carlos S. Oteo, Prof. on Ground Eng. Retired (A.G.I., S. L., Spain)
Javier Oteo, (A.G.I., S. L., Spain) Ing. C. C. y P.
Pedro Sola, I.I.T., S.L.(Spain), Ing. C. C. y P.

ABSTRACT

In order to solve problems related to the instability of natural slopes or hillsides, diverse techniques in terrain treatment have been employed: jet-grouting, micropiles, wall or anchored piles, etc. Amongst these systems, the use of more or less rigid inclusions, with or without anchors and introduced on both sides of the fracture surface, can be distinguished. This paper describes the possibilities of the use of resistant, discontinuous "buttresses" to increase the stability of the embankments on the natural slopes analysed. These "buttresses" can be formed by close reinforced injections up to pile rectangular modules (5 × 1 m, plan view). Real examples of the application of these "buttresses" with differing rigidities are included.

Keywords: Slope instability, ground improvement by inclusions

INTRODUCTION

The use of micropiles to reinforce the stability of slopes is already a classic technique. But when there is more than one injection, reinforced features (inclusions) can be discussed in which, around the metal tube or the framework applied to the ground, both the injection and the framework count. The grouting must be made through valves or pipe sleeves ("Tubes-à-manchettes", T.A.M.) installed in the metal pipe. In these cases, the objective does not have to be to withstand vertical loads; these inclusions can work by bending and / or shear stress. Therefore, they incorporate the ground in which not only the resistance of their piping is included, but also that of the whole in which the injection penetrates and reinforces ("breaking" the ground, penetrating it and improving the earth mass).

A particular case would be that of "reinforced injections" executed with PVC piping with IR or IRS injection. In that case, the role of the reinforcement becomes relatively unimportant, due to its lower resistance to the cut with respect to that of the metal tubes. The improvement, therefore, corresponds only with the injection. With metal reinforcement, screen walls have been set up for small-depth excavations (such as case of an underground car park in Seville, designed by A. Santos). At first, injections with T.A.M. they try to treat the land and not get a foundation. When you want to get more advantages, you can continue to increase to micropiles with medium or minimum diameter. Another special case of "reinforced" inclusions could be jet-grouting columns, in which - just after completion - a metal framework, Ø32 mm type or an open metal pipe, of the order of Ø80-90 mm, is inserted, although this is not always easy to perform.

THE EFFECT OF GROUTING

The intake of grout depends on the pressures applied, the injection rate and the properties of the ground. Through a survey among specialised Spanish companies, the relationship between the intake of grout and the pressures applied has been estimated in terms of the deformability of the ground. According to this data, volumes of up to almost 400 l / m.l can be introduced for areas of low compactness, to 2-3 bars. (BOTELLO, 2015). In areas of medium deformability, volumes of less than 100 l / m.l may be introduced (in several accumulated phases), even if pressures of 5 to 10 bar are used. Larger compartments clearly need fracturing, with pressures of 10-20 bars and volumes of only 25-30 l / m.l.

A sort of crown (more or less continuous or with pseudopods, according to diagram Fig. 1) from ground improved by the injection can be created, both by the effect of the applied pressure and by the binding effect of the supplied grout. This effect was already studied by DE ASSIS (2005) and

© 2018 Deep Foundations Institute

evaluated by studies with the PLAXIS Code and adjusted with actual values of movements. From DE ASSIS´ concept of "equivalent column", concerning the inclusion and the results of the aforementioned survey, the effects of the injection around the inclusion or IR type and IRS micropile can be estimated. The result is shown in Fig. 2 (BOTELLO, 2015).

Experience shows that the effect of the injection surrounding such an inclusion is terminated at a distance of about 1.5-2.0 m from the drill shaft, the main improvement being in the first half of that area. This is what is indicated, in a somewhat hypothetical and somewhat real way, in Fig. 3, where we try to make a recommendation on the variation of cohesion, c, and friction, tg φ, of a soft terrain by the effect of injection, depending on the distance to the shaft of the injected bore. It has been considered that cohesion can be doubled and that tg φ can increase to 1.5 (which is equivalent to moving from one land with φ = 20° to another with φ = 25°, approximately). With this recommendation, the effect of inclusion in soft ground with a finite element code can be studied, replacing the terrain around the inclusion by a ground mass improved with those properties.

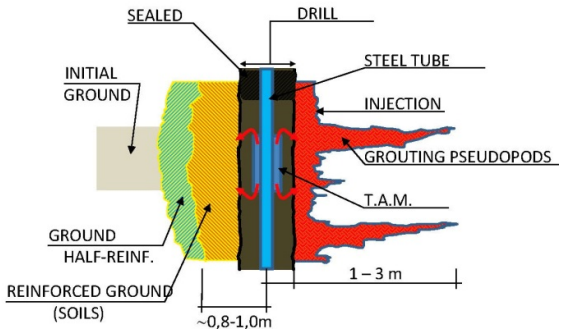


Fig. 1. Outline of ground improvement around a reinforced inclusion (OTEO, 2016)

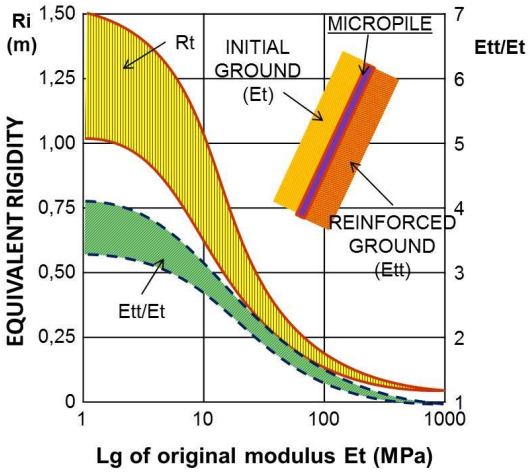


Fig. 2. Estimate of the effects of the injection around the micropile (IR or IRS) (BOTELLO, 2015)

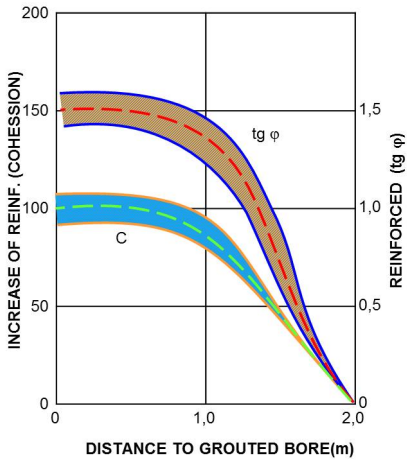


Fig. 3. Outline of land improvement around an injected micropile (BOTELLO, 2015) (Cohesion is pendent and that the friction angle in ratio)

AFTES (in its recommendations for the design and realization of soil and rock injection work, document GT8R1F1) indicates that the spacing between holes should be of the order of 3-7" in fissured rock; of 1.5-2.0 m in rocks with fine cracks; 1.0-1.2 m in sands and 0.8-1.0 m in silty sand. This can improve the distribution of injections.

These values correspond more to impregnation injections than to the IRS type of the reinforced inclusions, since in the latter there may be fracturing and, with the appropriate pressures, the holes can be separated somewhat more than AFTES indicates. However, if the conditions of resistance to the cut are weak, these conditions can be applied without affecting the parameters.

In many cases, protection quasi-continuous screens have been used between tunnels and buildings with reinforced injections or with inclusion of jet-grouting columns (OTEO, 2016). Sometimes, the screen has even been mixed: Micropiles on the side of the building and jet-grouting on the side of the tunnel, to reduce the impact of the injection on the building, in separate columns.

REINFORCED INCLUSIONS IN EMBANKMENTS AND HILLSIDE STRUCTURES

The technique of micropiles with single or repeated injection - or reinforced injected inclusions - has been widely used in Spain to solve problems related to the instability of hillsides. The most commonly adopted solution is that of a discontinuous display of reinforced inclusions or micropiles, inclined in two or three directions (towards the embankment, vertical and towards the levelled ground), with slopes 1 (H): 3 (V) to 1 (H): 4 (V), with separations of 0.40-0.80 m between each micropile. This gives a certain improvement of the terrain (if the IRS type is injected, with valves), plus a "reinforcement" in the area of the emerging fracture surface under the embankment. This solution, widely employed (HERNÁNDEZ DEL POZO and others, 2002; SANTOS, 2003), has limitations: The pile length above the surface of the embankment shall not be less than 6-9 m; the embedding below that surface must be of that order of magnitude; the section of the metal tube should be of the order of 10-20 cm^2, the area injected, at least 60% of the length of the inclusion, (area of the fracture surface); in the simplest cases, it can be an UI-type injection, etc. (Fig. 4).

BOTELLO (2015) has simulated numerically the reinforcement of an unstable embankment by means of a microscreen with two inclinations, comparing them successfully with various field measures.

If these conditions are not fulfilled - especially the first two - the flexibility of the inclusions may be excessive and, therefore, their influence is small. Indeed, the ground on which the inclusions are introduced tends to mobilise the maximum shear strength and becomes deformed, partly dragging the inclusions. In these cases, the diagram of Fig. 4 cannot be used, and a micropile grid must then be designed which transforms the reinforcement into a real mass of treated and "reinforced" soil or even more rigid inclusions employed. If they are injected at the top, the injection can come out at the end of the hole. In other situations, these examples should not be used for liquid injections, although you can use these injections as an improvement of their conditions.

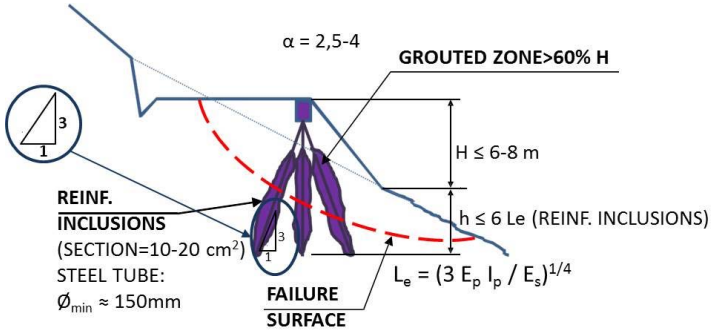


Fig. 4. Use conditions for micro barriers of micros or reinforced inclusions on the edge of the embankment

The other generic solution is to distribute the inclusions in "knives" or "buttresses" perpendicular to the axis of the embankment or to the wall whose backfill is to be treated. In the case shown in Fig. 5, the inclusions (in which the effect of ground improvement was especially sought) should be distributed in buttresses, distanced at 4-6 m. In case of major instabilities, a "buttress" device such as that in the Fig. 6, formed by two-three rows of inclusions with the staggered holes may be used, separated by 1.5 m in the same row. The metal tubes can be joined with a reinforced concrete slab in their upper part, as a "bridge" that happens to constitute the base (plus the tread layer).

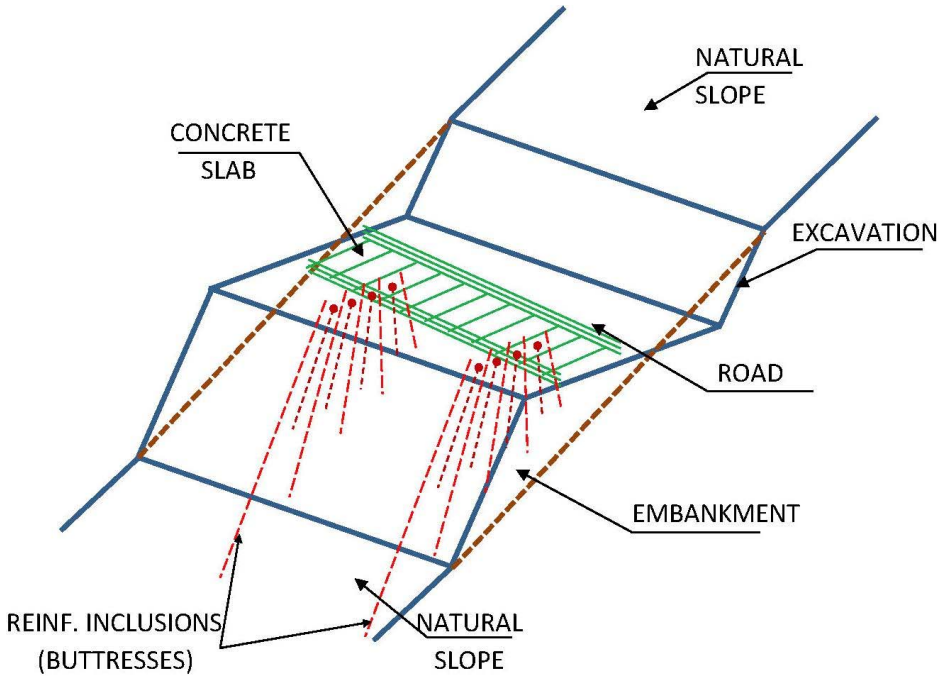


Fig. 5. Reinforcement of a embankment on slopes with "knives" of reinforced inclusions

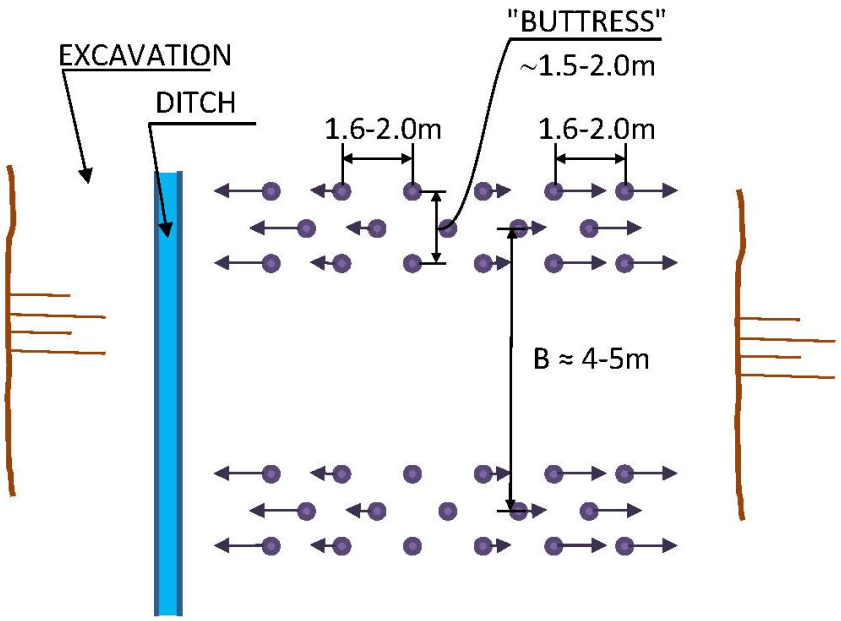


Fig. 6. Detail of a possible reinforcement with "knives" or buttresses of reinforced inclusions

This reinforcement role in which the injection predominates, increasing the cohesion and ground friction, is the basis of the treatment that we have undertaken in several cases: At the bottom of a piled wall, with four levels of anchors, where the ground at the base was not the intended rock, but a very altered material (CARRERAS et al., 2016), on unstable hillsides, etc.

In this case, as in others, the area of the buttress or knife can be represented as a new type of ground: The soil treated or improved, with an apparent density, γ^*_{ap}, an apparent cohesion, C^*, and an apparent friction, tg φ^*. If the separations between the ends of the holes are of the order of 3 m within the same row and 1.60 m between those of two different rows, it can be considered that γ^*_{ap} attains the same value as the apparent density of the terrain (or which increases by 10% overall). The cohesion, C *, can be taken equal to double-triple of that of the terrain and that tg φ * is in the order of 150% of the tangent of the angle of internal friction of the terrain, φ. This recommendation may be applicable to other similar cases.

The use of "buttresses" of reinforced inclusions has some advantages:

- By concentrating the reinforcement in areas, the water can pass through the intermediate terrain, so that the injection does not waterproof the whole.

- The drainage, if necessary (and it almost always is) must be done with drainage ditches and / or vertical wells (Ø 1.20-1.50 m, with radial drains).

- The reinforcement is achieved both by the injection and by the presence of the reinforcements that carry the inclusions.

- They can be used for H values (Fig. 7) clearly greater than 6-8 m. In that case the embedding becomes less important, since the effect of the injection may predominate.

If we employ "buttresses" and the inclusions are close enough, the injected-inclusions terrain body can be considered as sufficiently rigid to be moved as a single body. In this case, as indicated by Fig. 7, a simplified analysis can be made, considering that: a) The part of the treated area above the potential fracture surface behaves as a rigid solid. b) The total thrust of the ground on the buttress corresponds to a width equal to twice the width of the buttress, B. c) That rigid block rests on the inclusions continuing below, in the area of best and not unstable terrain.

Therefore, this rigid zone transmits compressions or tractions to the inclusions, which must have (below the well-injected area), a $L_{mín}$ length the value which will be at least 4.0 m, whereby with H_M=10 m, the compression and tensile load on the underside of the inclusions is of the order of 30 T (they would require a section on the order of 13-14 cm^2 of steel and a minimum length of 4.0 m).

However, if the embankment is large (height, width, etc.) or the slope of a clearing, these solutions of reinforced inclusions with injection must overcome even more rigid features, in which the resistant feature and not the injection predominates. Reinforced concrete elements, medium and large piles or slurry walls modulis (4 × 1 or 5 × 1 m) can be used, as in the case of the Diezma slope, (OTEO, 2016); there are often called "bolts", and are no more than rigid "reinforced inclusions".

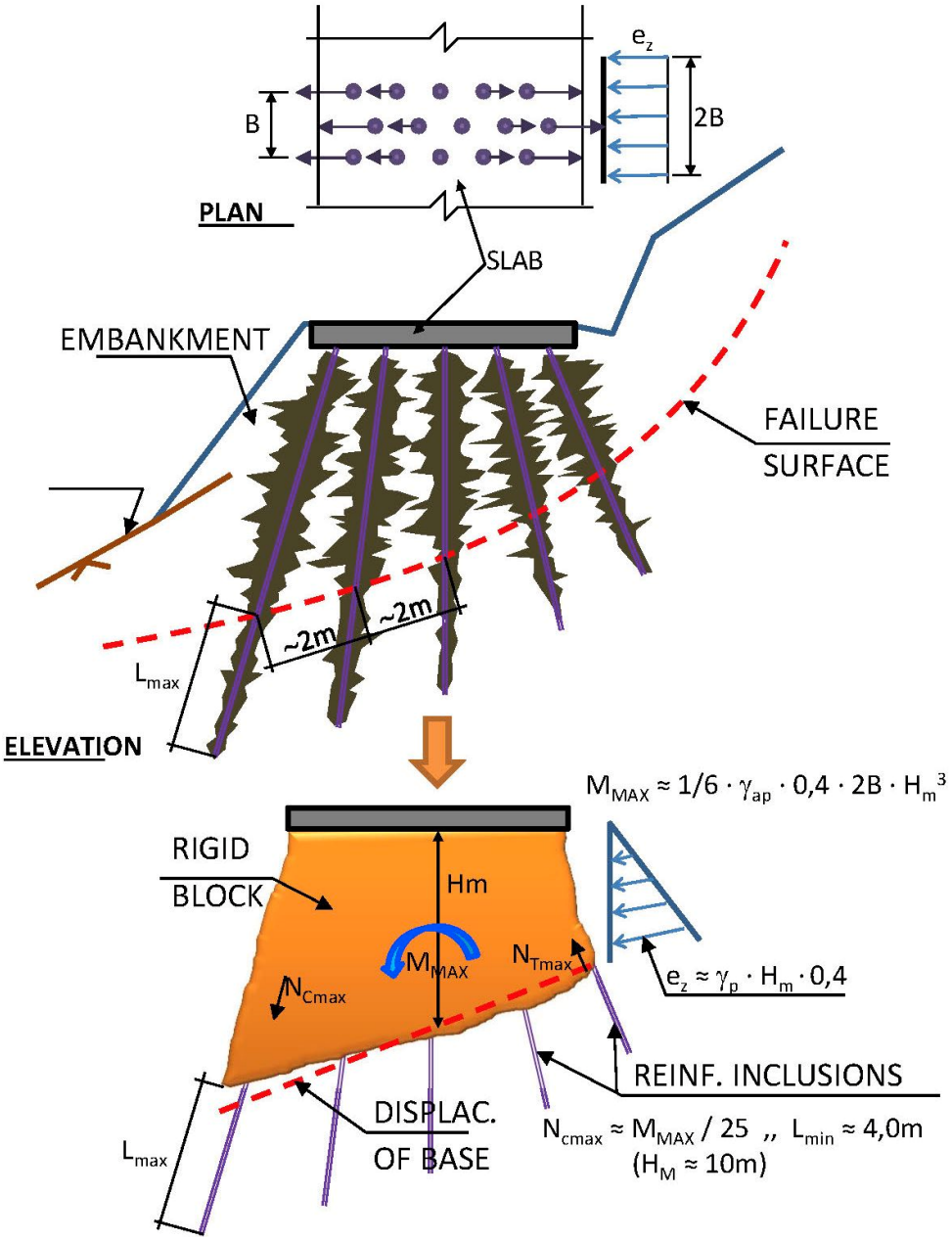


Fig. 7. Simplified analysis of a buttress

EVOLUTION OF REINFORCED INCLUSIONS

In Fig. 8, the evolution of the reinforced inclusions is shown: from the screen to the outer edge of the embankment (three inclinations), to the discontinuous screen module (the real "bolt"), with or without additional anchorage, passing through the "knife" of inclusions and the discontinuous screen of the nearby piles (with or without anchorage). That is, from lower to higher rigidity. The maximum bending moments will also be very different in each case. It is possible to indicate that H is the maximum ground thickness that moves (where the inclusions are located) and Le is the elastic length of the inclusion-terrain system defined in Fig. 4 (which may be 0.6-1.0 m in a micropile and 10-12 m in a slurry wall moduli, as determined by BOTELLO et al., 2007): For H / Le less than 5, inclusions must be display modulis. Between 5 and 10-11 m, large and medium diameter piles and for H / Le> 10-11 m are the micropiles.

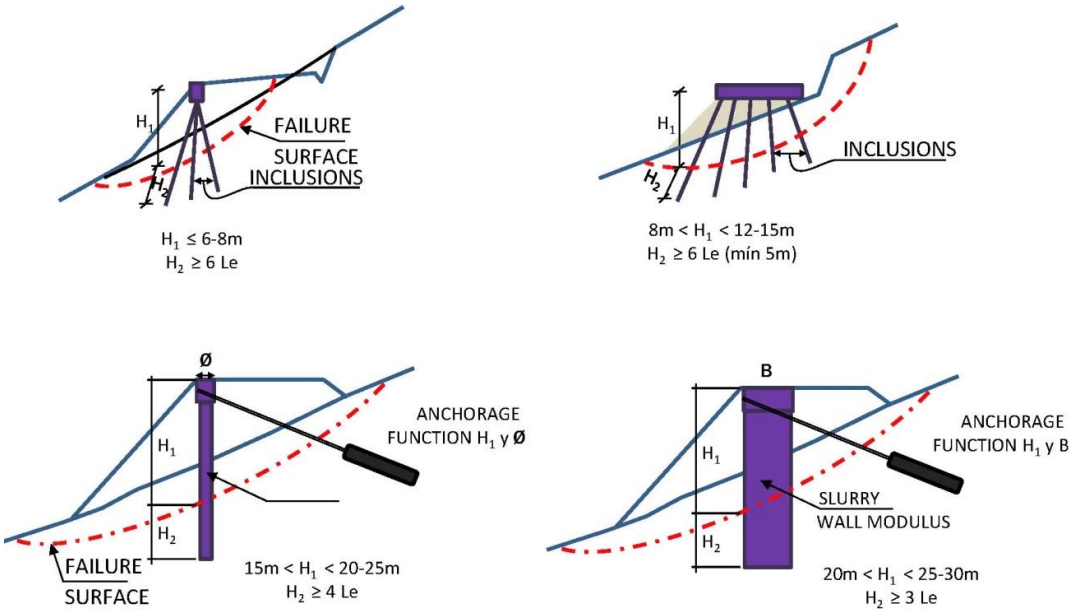


Fig. 8. Diverse solutions of "reinforced inclusions"

EXAMPLE OF TREATMENT WITH BUTTRESSES

Various examples of buttress treatments can be seen in OTEO (2016). This section includes another example of recent action (FERNÁNDEZ-NESPRAL and others, 2017).

The route of the CN-630, in its descent towards Oviedo (North of Spain) near the port of Pajares, runs on a hillside, with its platform in a clearing and on a medium to average height embankment. Towards its PK 85 + 250, a section of about 70 m in length had been suffering, for considerable time, continuous descents that were obliging frequent reinforcement in the road.

In the spring of 2015, by increasing the instability symptoms of that section, four continuous dynamic penetration DPSH tests were carried out, two mechanical borehole drillings, on both sides of the roadway, in order to recognise the terrain and install inclinometric casing to measure the horizontal displacements of the land. In addition, topographic references were placed on the screed. The results of these reconnaissance and auscultation revealed an emerging instability of slow downhill creep, affecting the hillside-road body, with its top in the clearing slope upstream, with thicknesses of 3 to 12 m under the road increasing downhill, and with its possible exit about 60 m further down the old landfill. In the summer of 2015, the speed of movements increased (4 mm / month).

The results of the geotechnical information obtained (augmented with geophysical profiles) have been collected in Fig. 9: a) Quaternary coating of anthropic fills and colluvial soils of silts, clays and gravel, all with thicknesses of 3 to 15 m; b) Carboniferous substrate of the Lena Group, consisting of slates, siltstones and sandstones with some karstified limestone banks, bounded to E-SE and its beginning highly altered, grade IV to VI.

Quaternary soils have been characterised by pressure wave velocities of less than 1200 m / s in seismic refraction and in electrical tomography, by resistivities less than 200 ohm·m for man-made fills and greater than that for colluvium; the SPT trials had very variable and dispersed values between 5 and 15. The contact with the underlying strata was established assigned to siltstones and shale altered speeds from 1200 to 1750 m / s, and altered limestones and sandstones from 1750 to 2000 m / s, and resistivities less than 100 omh·m, and greater than 100 ohm·m for those same properties; low velocity rock was assigned velocities of 2000 to 2300 m / s, and sound rock velocities above this last value, the ceiling of the latter appearing at depths between 13 and 16 m under the road; the SPT trials recorded

values of 30 to 50 at the altered onset of the rock and rejection at the sounder levels. The groundwater table is infrequent in summer.

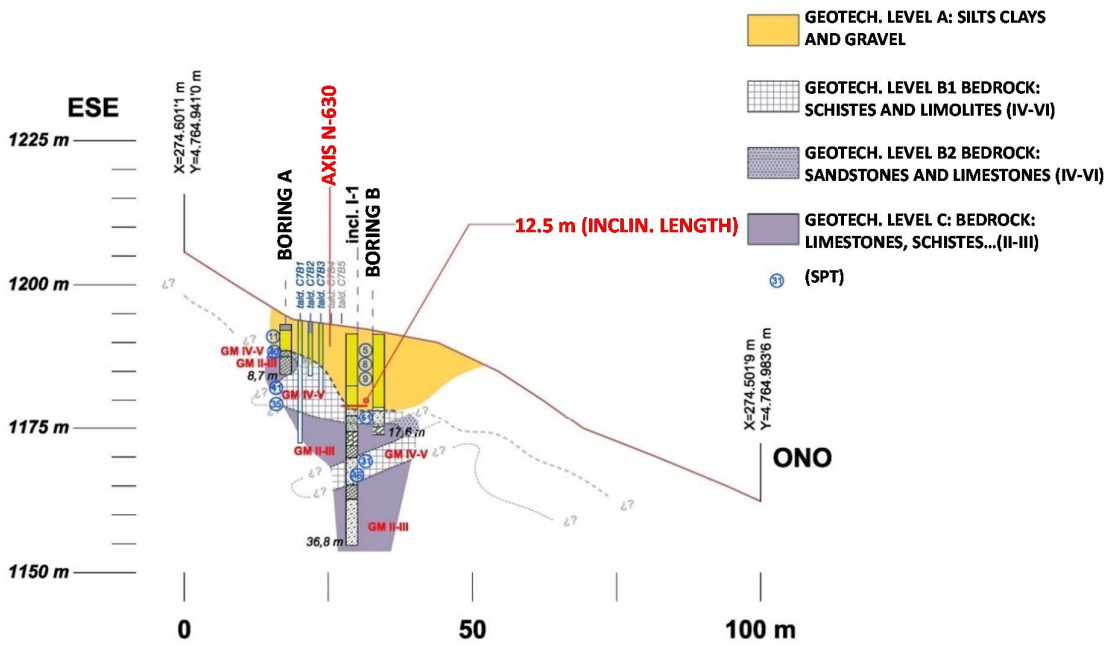


Fig. 9. Geological-geotechnical representative profile (Puerto de Pajares, F. NESPRAL et al, 2017)

Calculations were made using the SLIDE code of RocScience to adjust the initial "estimated" values of the shear strength parameters to a safety factor between 1 and 1.1.

The only way to occupy a road lane was to opt for the planned solution, which included: a) Reinforced injections on buttresses, with steel tube-pipe sleeve and concrete grout, to improve and reinforce the unstable ground under the roadway; (Fig. 10); b) Reinforced concrete slab; c) Vertical large diameter wells, connected to each other and with radial fans of sub-horizontal bores, to drain the ground above the stable rock, and gravity evacuation of the captured water.

Each buttress comprised 15 injection bores arranged in three separate parallel rows at 0.8 m, with 5 holes in each, and located staggered with intervals of 1,8 m inside each row (Fig. 11). The lengths for the holes resulted from the need to traverse the quaternary covering and the very altered beginning (grade IV to VI) of the rock substrate, until 1 m into the least disturbed rock (grade III to IV). The reinforced concrete slab that clamps the steel tubes of the injection drills had a 0.4 m edge. The injection pressures were 1.5-2.0 MPa in the altered substrate and 0.7-1.5 MPa in the quaternary coating.

The drainage wells should capture the groundwater that flows through the bottom of the quaternary coating and the beginning of the highly altered rocky substratum, and this should be prevented from penetrating under the road; therefore, the intended barrier was located near the ridge upstream of the slope (Fig. 10). The distance between buttresses was established at 4 m, approximately twice the width of the buttress itself.

The stability analysis, including the reinforcement gave minimum safety factor values of 1.49 to 1.39, depending on whether it assumed an interstitial pressure factor, r_u, of 0 or 0.1.

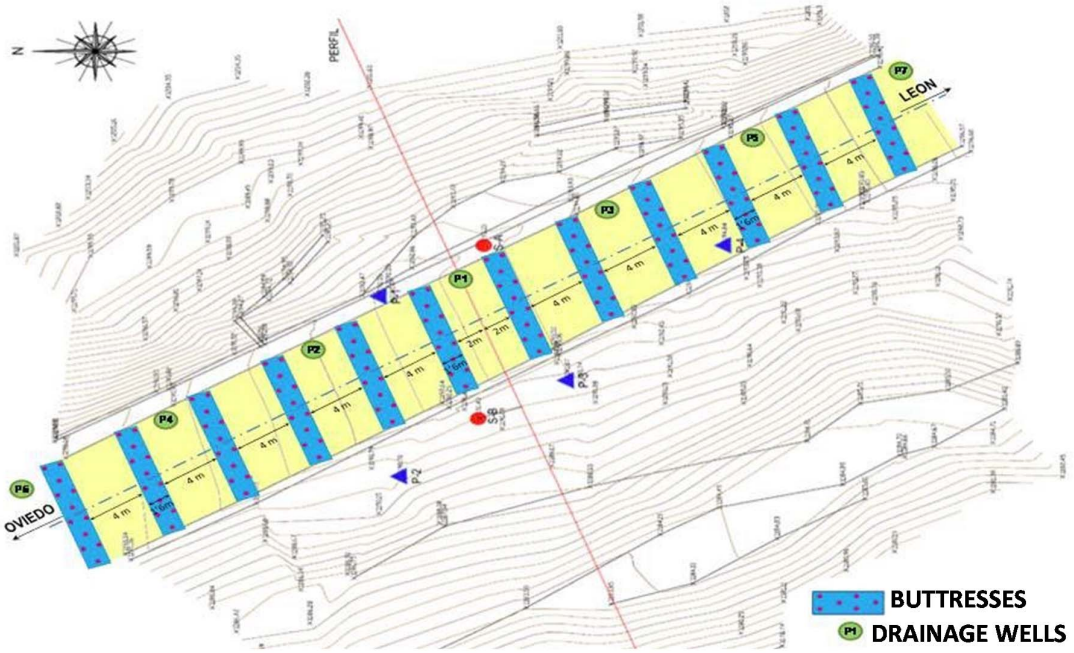


Fig. 10. General floor with buttresses of reinforced injections and drainage wells (F. NESPRAL et al, 2017)

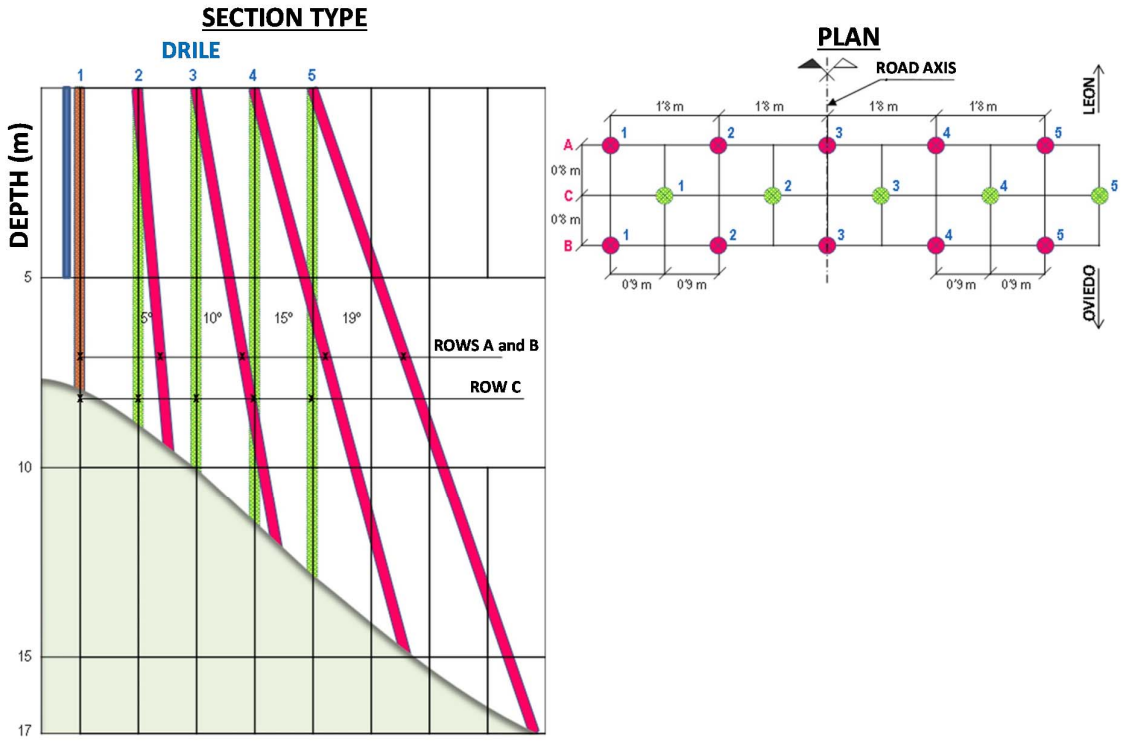


Fig. 11. Details of injection holes in a buttress (F. NESPRAL et al, 2017)

During the injection work, there were certain movements (4-10 mm), compatible with the solution used. Once the reinforcement work was completed, the movements stabilised (F. NESPRAL, et al, 2017).

CONCLUSIONS

By way of conclusions, it can be stated:

- The use of reinforced inclusions may be a suitable solution to solve problems of instability of slopes and embankments.

- Separating the buttresses enables the drainage of water that may come down the slope.

- Reinforced inclusions with low rigidity (metal tubing with pipe sleeve) can be used up to display modules (5 × 1 m), anchored.

- Replacing the treated area with equivalent terrain can simplify the theoretical analysis of instability.

ACKNOWLEDGEMENTS

The authors would like to thank the General Directorate of Highways of the Ministry of Public Works of Spain, the Andalusian Government, etc., for having permitted, at the time, the solution of reinforced inclusions to be employed.

REFERENCES

AFTES (2005) "Recommendations pour le design et realization of travaux d'injection dans sols and roches". Doc. GT8R1F1.

BOTELLO, A. (2015). "Sobre el comportamiento de micropilotes trabajando a flexión y/o cortante en estructuras de tierra". Doctoral Thesis. Polytechnical University of Madrid (UPM).

BOTELLO, A., DE LA FUENTE, P., & OTEO, C. (2007). "Los pilotes y micropilotes como solución para estabilizar taludes". V Congreso Andaluz de Carreteras. Jaén, Spain.

CARRERAS, J. L., SOLA, P., OTEO, C., & LEIRA, J. A. (2016). "The behavior of a pile wall for to contain a hill excavation in Asturias (Spain) ". 12th International Symposium on Landslides. Napoli.

DE ASSIS, S. (2005). "Optimización de los diferentes sistemas de protección de estructuras respecto de la excavación de túneles". Doctoral Thesis. Polytechnical University of Madrid (UPM).

FERNÁNDEZ-NESPRAL, C., OTEO, C., & SOLA, P. (2017). "Estabilización de un deslizamiento en el Puerto de Pajares". IX Simposio Nacional sobre Taludes y Laderas Inestables. Santander.

HERNÁNDEZ DEL POZO, J. C., OCETE, I., LAMAS, F., & HERNÁNDEZ, J. C. (2002). "Micropilotes inyectados: Técnica y Cálculo". Departamento de Ing. Civil. University of Granada, Spain.

OTEO, C. (2015) "Quince lecciones y un epílogo sobre Geotecnia de Obras Subterráneas" Asociación Técnica de Carreteras (AIPCR). Madrid.

OTEO, C. (2016). "La mejora del terreno: De las cimentaciones profundas a las inclusiones y pasadores". Monografía del CEDEX. Spanish Ministry of Public Works, Spain.

GROUND IMPROVEMENT INSTEAD OF PILING – EFFECTIVE DESIGN SOLUTIONS FOR HEAVILY LOADED STRUCTURES

Michał Topolnicki, Keller Polska, Gdynia, Poland, +48 58 7697540, mtopolnicki@keller.com.pl

ABSTRACT

It is shown that well designed ground improvement schemes may effectively replace conventional foundation solutions for a wide range of applications involving heavy loads and structures sensitive to settlement. This is achieved without compromising stringent design criteria. The presented case studies illustrate the use of four ground improvement methods: deep vibro-compaction, vibro-replacement (stone columns), wet deep soil mixing and jet grouting. These methods were used in different projects and soil conditions, alone or in combinations. Beneficial returns in terms of construction costs, shortening construction time and reducing CO_2 emission are discussed where applicable.

Keywords: ground improvement, vibro compaction, deep soil mixing, jet grouting, alternative design

INTRODUCTION

In standard design practice, a distinct gap exists between piling and ground improvement (GI) solutions used for foundation support. Piling is typically adopted for heavily loaded structures, such as high rise buildings, bridges, large commercial centres, silos and other industrial objects, for which stringent bearing capacity, stability and settlement criteria must be satisfied. Conversely, GI solutions are usually considered to be of no or limited use for heavily loaded structures, mainly due to the perceived inability to limit total and differential settlements to an acceptable level.

Undoubtedly, the predominant use of piling for foundation of heavily loaded structures is reasonable and has a long tradition. It should be noted, however, that there is also a range of applications where piling and GI solutions may actually overlap. This is illustrated in Fig. 1, which shows indicative ranges of GI and piling solutions in a schematic load vs. settlement graph. For an exemplary GI design, marked with point 1, the associated settlement corresponds to a relatively susceptible foundation support. For the same foundation and loading, a significantly stiffer GI design can be also applied, for example by increasing the area improvement ratio of the treatment. The resulting reduced settlement is represented by point 2. Between points 1 and 2, other GI solutions exist for the same loading. Taking into account different combinations of foundations, loads and GI methods a range of possible GI solutions can be encircled by connecting a family of corresponding points '1' and '2'. A complementary range of piling solutions can be drawn in a similar way. The combined figure obtained reveals an overlapping area where piling and GI solutions may both be applicable in the same range of loads without compromising functional design criteria. In this respect, it should be noted that GI solutions usually offer shorter execution times and lower construction costs, and therefore are attractive for clients and contractors. In many situations they also reduce a project's carbon footprint.

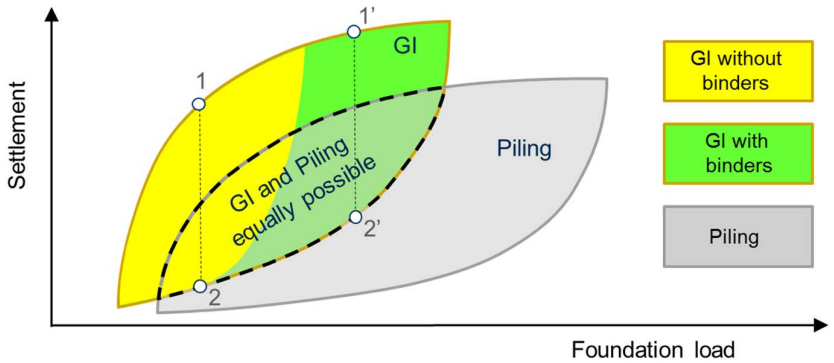


Fig. 1. Tentative ranges of piling and ground improvement solutions for foundation support

© 2018 Deep Foundations Institute

Subsequent parts present selected design-and-build project case studies to illustrate the efficiency of tailored GI solutions as compared to conventional piling designs. The ground treatment technologies considered were vibro compaction and vibro replacement (bottom feed) processes, and methods utilizing binders to stabilize soil, such as wet deep soil mixing and jet grouting (soilcrete). Detail descriptions of these technologies can be found in Kirsch and Bell, 2013. The underlying projects involve different ground conditions, structures sensitive to total and differential settlements, and heavily loaded foundations in the form of slabs and separated footings.

APPLICATION OF VIBRO COMPACTION (VC)

Densification of a loose cohesionless soil deposit by the VC process is one of the most effective GI methods. Figure 2 illustrates the use of VC to support a high rise building (Sea Towers) in Gdynia, constructed behind a gravity-type quay wall. The area was a dredged zone of backfilled marine sediments in a loose to medium dense state, composed of fine/medium/coarse sands with some silty inclusions in deepest parts of the dredged zone. While the concentrated loads from both towers were mainly taken by purposely located diaphragm walls, the design aimed to optimize the thickness of the foundation slab utilizing subgrade reaction. To increase ground stiffness below the slab, VC was applied to a depth of 5 to 8 m below the working level, and in two grids of 2 and 3m c/c spacing. A significant improvement was achieved, allowing use of an average constrained compression modulus E_s of 160 MPa in the design. The GI design was based on FEM 3D soil-structure interaction analyses. The observed settlements were in a good agreement with the prediction (Fig. 3). The VC solution was an alternative to the original design, which comprised 1,312 no. stabilized columns diameter 0.8 m, and 3.5 m long in average. The applied scheme was more than 3 times cheaper than the original solution, and also shortened the construction schedule.

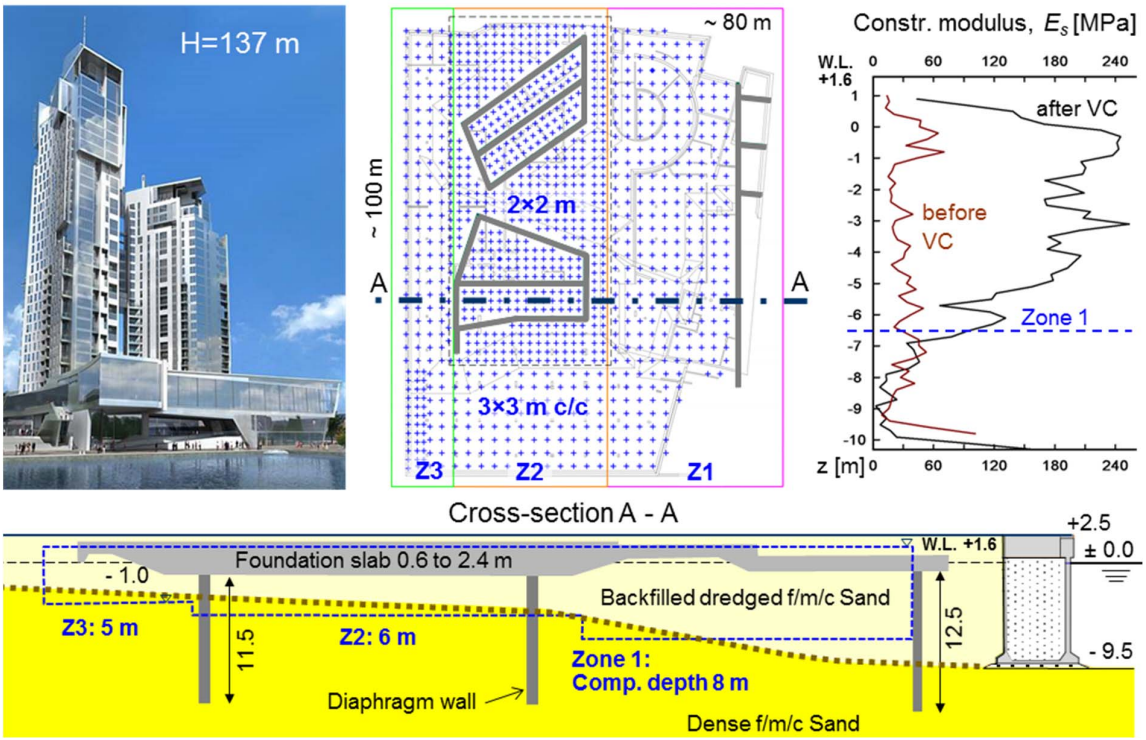


Fig. 2. Compaction of dredged soil with VC to enhance slab-subgrade interaction

In a similar project, VC was used to improve soil to exclusively support the foundation of a high rise building (Florido Tower) in Vienna, as presented in Fig. 4. Although below the planned foundation level there was a competent subsoil, composed of gravel and stiff tertiary clay and capable of accommodating a mean characteristic bearing pressure of 400 kPa, there was a risk of excessive foundation tilt because

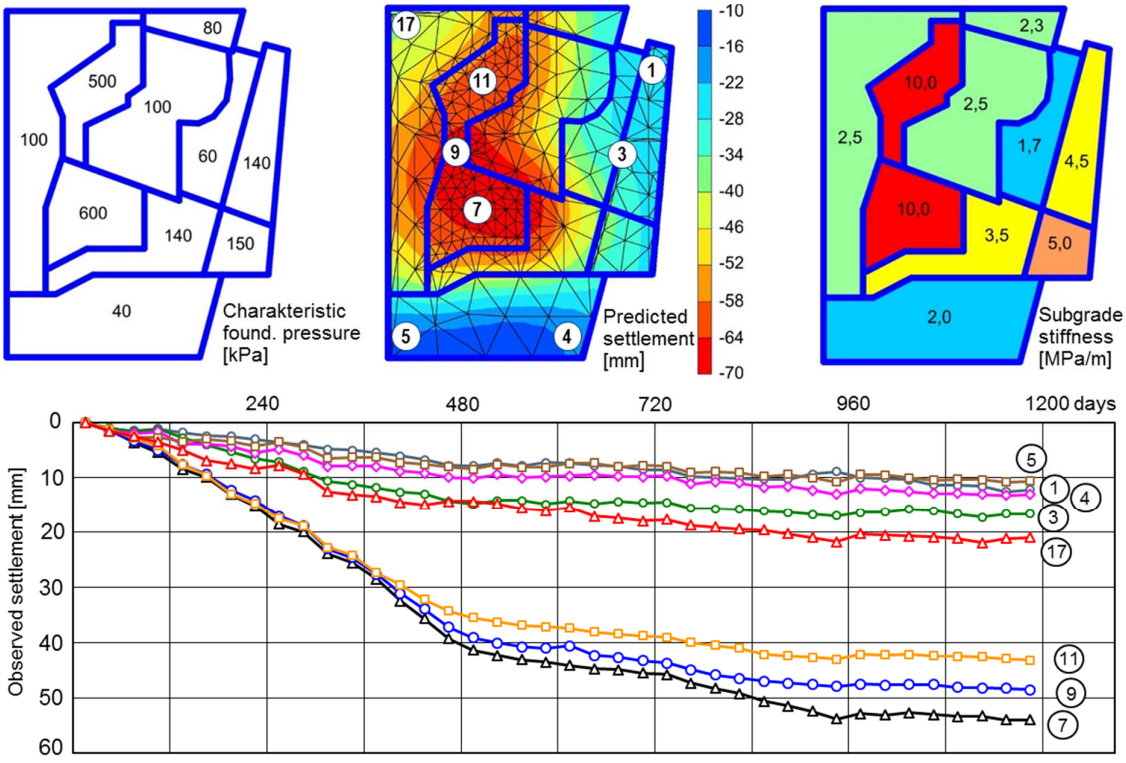


Fig. 3. Predicted and observed settlement of the foundation slab of Sea Towers building

of a strongly varying thickness of the underlying gravel layer. Instead of a typical piling solution to mitigate tilt, a GI scheme was implemented. The shallower parts of the tertiary clay were excavated and replaced with loosely placed gravel to construct a 'cushion' with a uniform thickness under the entire foundation slab. The gravel zone was subsequently intensively treated with VC to achieve a well compacted and relatively uniform subbase layer, while in each treatment location the poker vibrator was forced to penetrate as far as possible into the underlying clay layer to assure ground improvement also in the transition zone between gravel and stiff clay. Predicted maximum settlement was 60 mm, while the measurements indicated 55 mm in average.

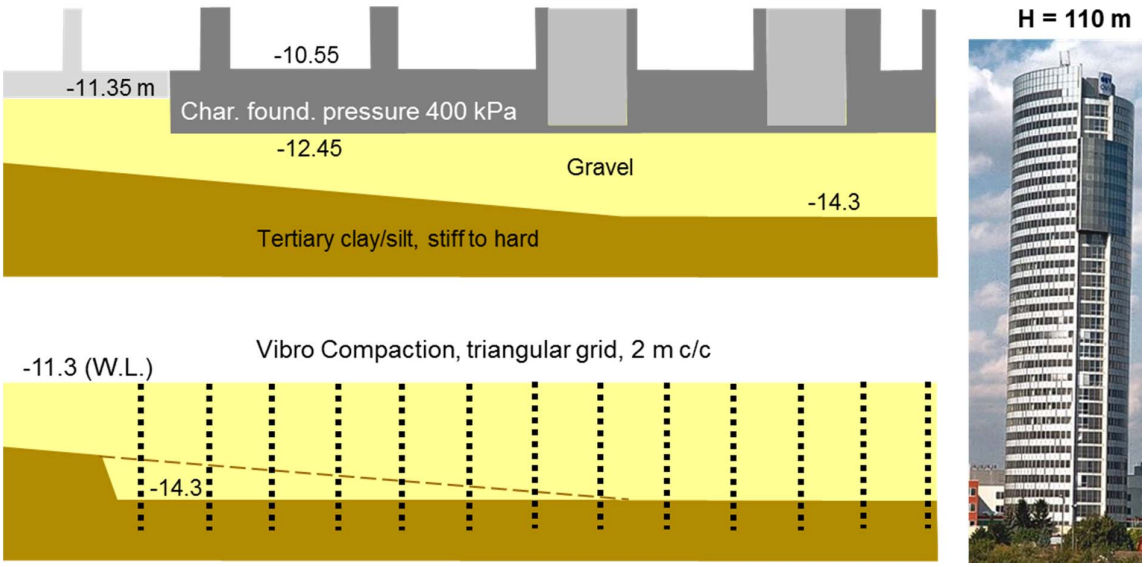


Fig. 4. Ground improvement solution adopted for the foundation of Florido Tower

APPLICATION OF VIBRO REPLACEMENT (VR)

A multistory building with a glass facade (LOT HQ in Warsaw) was built on a construction site with varying soil conditions below the foundation level. Almost half of the foundation slab was located in a soft clay area, whereas the remaining part was located in a stiff sandy clay or compacted sand zone (Fig. 5). Because of the sensitivity of the structure, there was a stringent design requirement to limit settlements to 25 mm. Initial analyses predicted 29 to 56 mm of settlement for a shallow foundation on the existing ground, indicating a tendency to tilt. Therefore a piling solution was initially considered by the client, comprising of 720 no. CFA piles diameter 0.5 m with a total length of 7,920 lm. Noting that part of the ground was competent for a shallow foundation, an alternative GI system was proposed. The design included gravel columns with a total length of 3,590 lm; 7 times cheaper and much faster than piling. Monitoring validated the GI solution, showing uniform settlements less than 20 mm (Fig. 6).

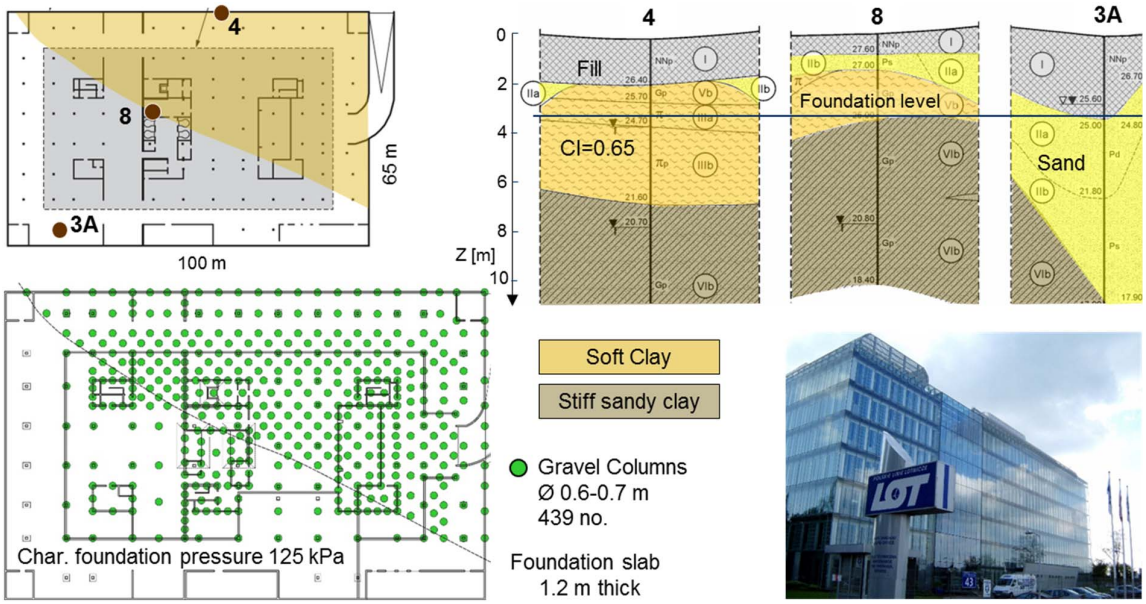


Fig. 5. Gravel columns applied to control differential and total settlement of a sensitive building

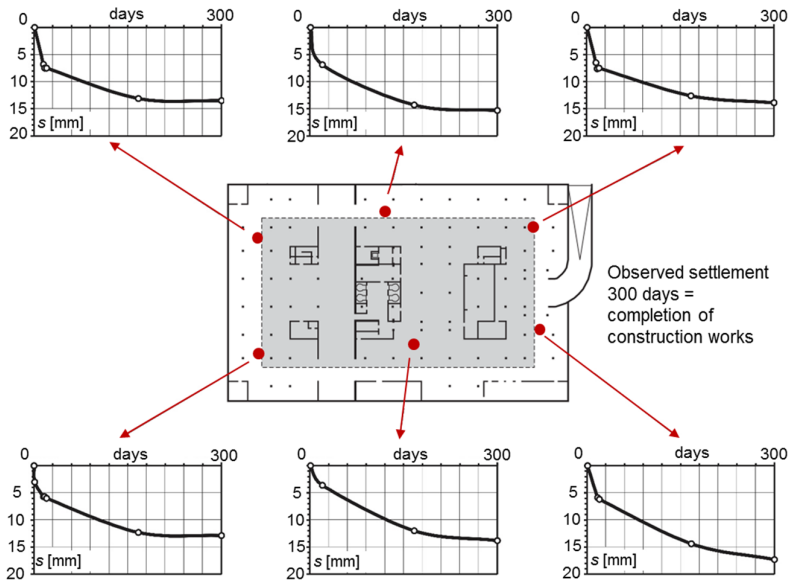


Fig. 6. Measured settlement of LOT building until completion of construction works

APPLICATION OF WET DEEP SOIL MIXING (DSM)

The GI methods of soil stabilization with cementitious binders offer competitive solutions for a variety of challenging applications. Figure 7 illustrates the use of DSM for the foundation of a large residential and commercial complex in Warsaw, comprising attached buildings with differing heights. The ground below the foundation level consisted of medium and coarse sands to a depth of about 20 m, underlain by a stiff clay. The initial design adopted a shallow foundation system, with a continuous slab of considerable thickness needed to accommodate high concentrated loads. The 20-story buildings required the slab to be 1.6 m thick. Aiming to reduce the volume of foundation concrete, an alternative GI system was proposed with 705 no. DSM columns diameter 1.2 m, strategically arranged in groups and rows to support heavily loaded pillars and structural walls. The columns were 5 to 7.5 m long, and the total column length was 4,350 lm, measured from the working platform level 0.6 m above the foundation level to allow for column trimming. The adopted characteristic compressive strength of the stabilized soil was 5.5 MPa, and partial safety factor for material strength was 2.5. The implemented GI solution resulted in a reduction of the slab volume of about 4,000 m^3 without compromising design requirements.

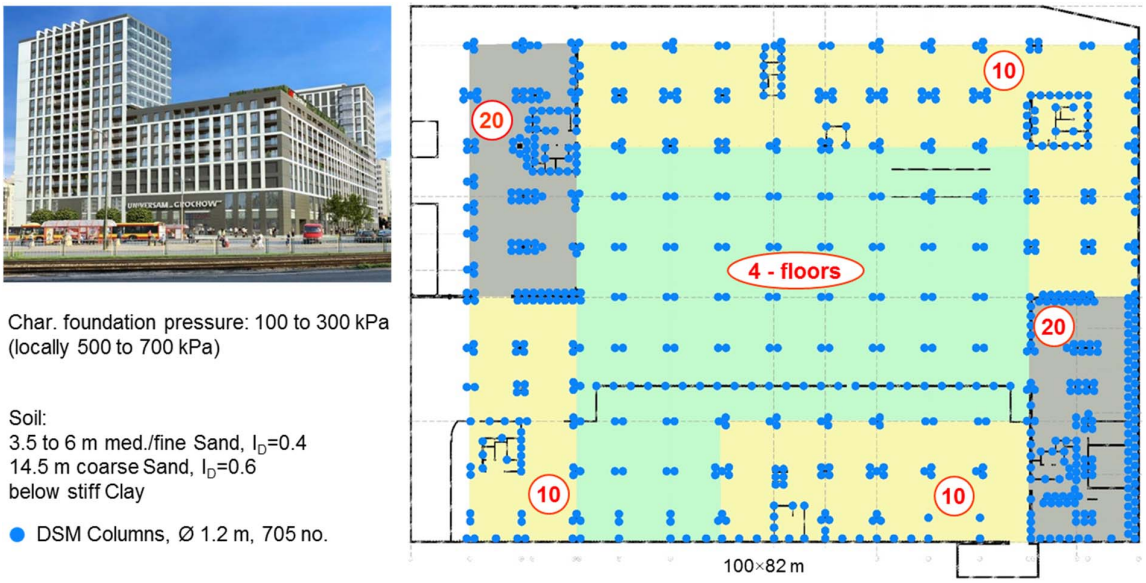


Fig. 7. Foundation solution with DSM columns for a large residential and commercial complex

The application of wet DSM for foundation of a large shopping center Rybnik PLAZA, supported on pad foundations, is presented in Fig. 8. The characteristic bearing pressures varied between 330 to 550 kPa, resulting in the maximum foundation load of 14,420 kN. The subsoil consisted of a loose fill to the depth of about 2 m, followed by a soft silty clay layer, about 4.5 m thick, underlain by bearing coarse sand and stiff clay deposits. The foundation level for the majority of the footings was at the depth of 2, 2.1 and 2.3 m. Because of the presence of a soft clay layer below the foundation level, a conventional piling solution was initially designed to control bearing capacity and differential settlements to less than 1:550, i.e. to a maximum difference of 15 mm between adjacent pad foundations arranged in a main grid of 8.6×8.6 m. The details of the original design with CFA piles diameter 0.8 m are presented in Tab. 1.

The alternative GI solution with DSM columns diameter 0.9 m, arranged tangentially in groups of 3 to 36 columns to support nine types of foundation pads, F1 to F9, is shown in Fig. 8. For the most unfavorable combination of characteristic loads, the calculated maximum compressive stress in DSM column was 764 kPa. In relation to the adopted characteristic strength of stabilized soil equal 2.2 MPa, the resulting partial safety factor for material strength was 2.88. Settlement calculations, comprising different combinations of adjacent foundation pads and soil conditions, determined based on the nearest soil investigation profile, revealed that total and differential settlements were within the prescribed limits. An example result is shown in Fig. 8 for three selected pads, type F7, F6 and F3, with significantly different geometries, loads and patterns of DSM columns.

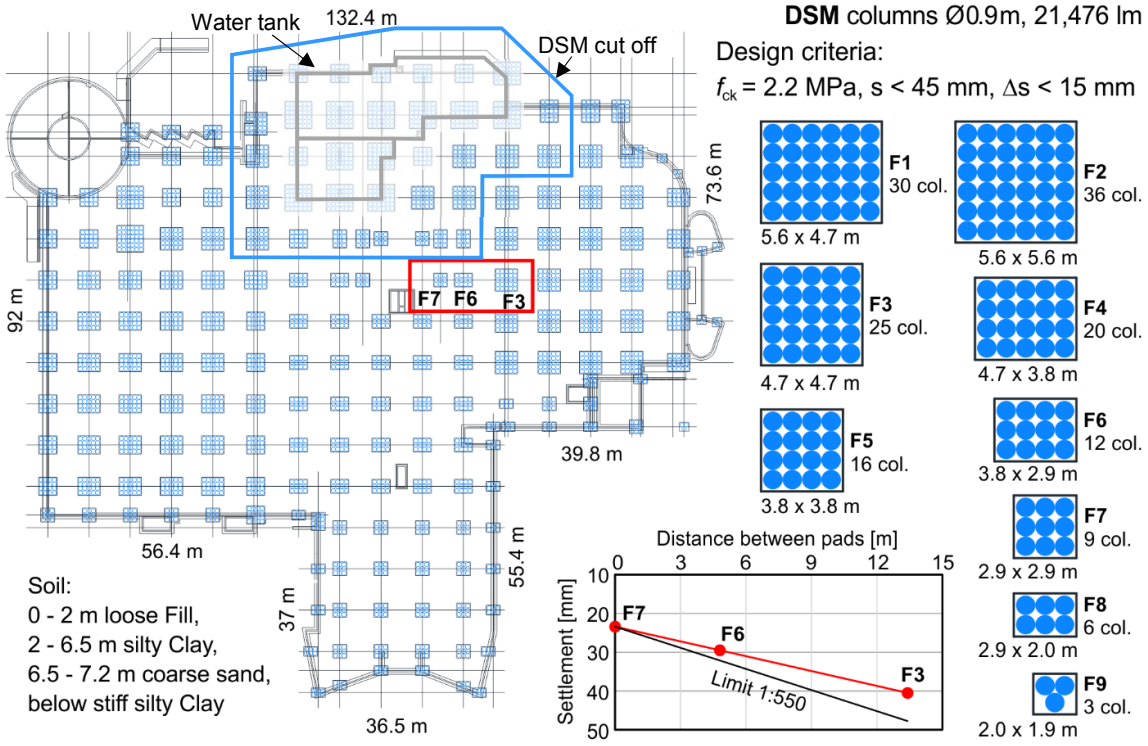


Fig. 8. Shopping center PLAZA founded on 205 pad foundations supported on DSM columns

Compared to original piling design, the alternative proposal offered a significant overall cost saving of about 45% (Tab. 1), arising from a lower unit rate of DSM columns (despite increased total length), reduction of the total volume of foundation pads, and the reduction of steel reinforcement due to a more uniform support of pad foundations. During construction works a further optimization of the foundation design took place. A cut off wall, composed of overlapping DSM columns diameter 0.8 m with an axial spacing of 0.6 m, was constructed around the firefighting water tank planned at the depth of 6 m (Fig. 8). The cut off wall made it possible to excavate the soil in a dry pit, exchange the remaining soft clay below the foundation level, and to construct the tank. The tank structure was subsequently used to underpin several pillars initially founded on DSM supported pad foundations. This illustrates the flexibility of DSM technology, which can be used for different purposes.

Table 1. Comparison of piling and DSM foundation solutions for the PLAZA center

Foundation solution	Number	Mean length	Total length of piles / columns	Foundation volume [m^3]	Reinforcement [kg]
CFA piles, Ø0.8 m	1,154	12.0[2] m	13,848 m	4,535	227,000
DSM col., Ø0.9 m **- 45%**	3,304[1]	5.5[2] m	18,172 m **+31%**	3,292 **-27%**	132,000 **- 42%**

[1] before optimization related to foundation of the water tank; [2] measured from working platform level

The next example demonstrates a combined use of VR and DSM to support a large silo in CHP Siekierki power plant in Warsaw, with a height of 70 m and a capacity of ash storage of 20,000 m^3 (Fig. 9). The silo was constructed on a ring foundation, with an axial diameter of 23.6 m and a width of 5 m, exerting a mean characteristic bearing pressure of 1,125 kPa (or 5,625 kN/m) when fully loaded, or 324 kPa (1,620 kN/m) when empty. To limit the settlements to 200 mm during operations, it was necessary to apply standard piles or to design and execute a tailored GI solution. The GI works were conducted in two stages (Fig. 10). In the first stage, 279 no. sand/gravel columns were installed in a circular pattern to the depth of about 12 m below the working level. The purpose of VR treatment was to increase the bearing capacity and to equalize the susceptibility of the sand layer under the silo to reach an equivalent minimum constrained compression modulus of E_s= 80 MPa (cf. Fig. 9).

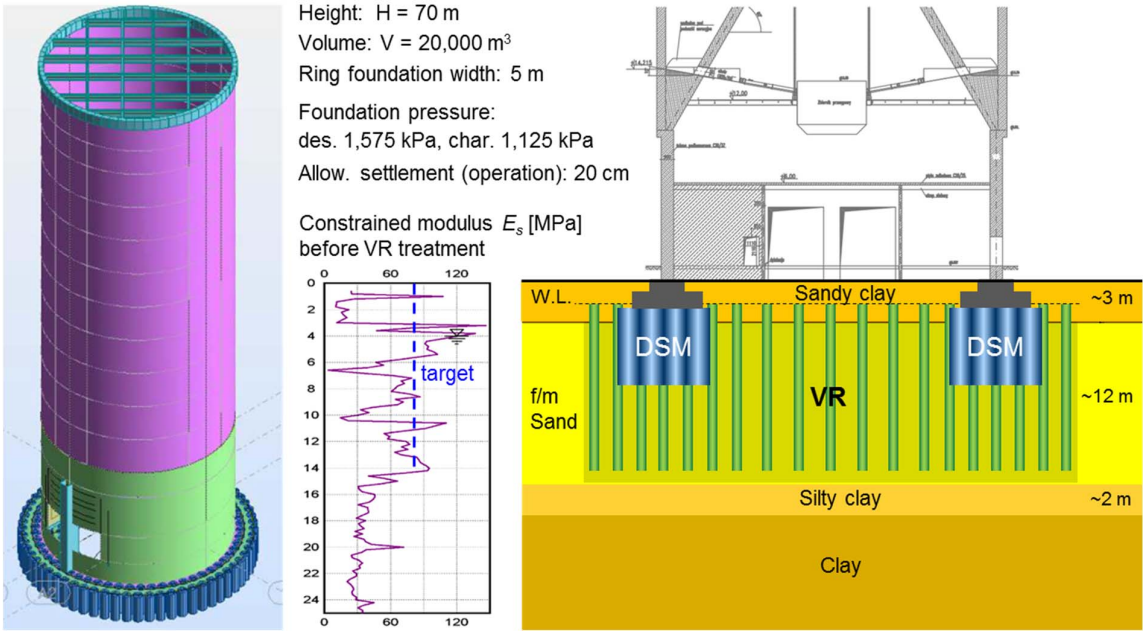


Fig. 9. Ash container in CHP Siekierki, and the adopted GI scheme with combined VR and DSM

In the second stage, 216 no. DSM columns diameter 1.2 m were installed to support the ring foundation. The maximum design column load was 2,774 kN, resulting in a design compressive stress of 2.45 MPa. The FEM analyses revealed ring settlement of 245 mm under the full load and 50 mm for the empty silo, indicating a settlement of 195 mm during operation, which was within the allowable design limit.

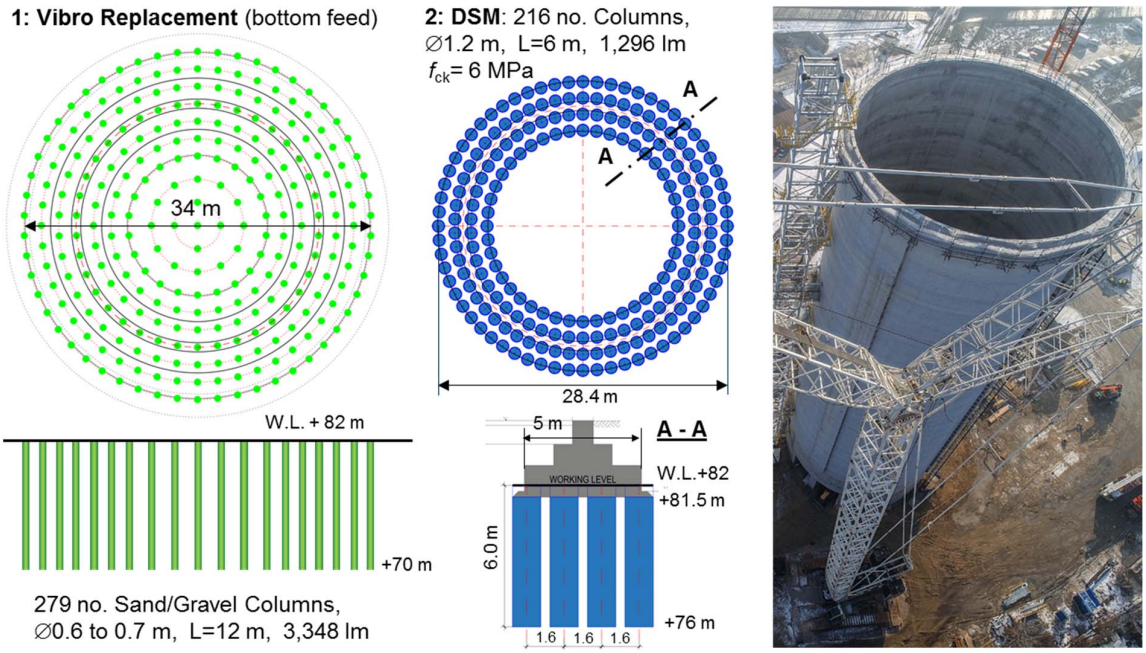


Fig. 10. The arrangement of VR and DSM columns, executed in two consecutive stages

APPLICATION OF JET GROUTING (JG or Soilcrete)

A high rise building Olivia Star in Gdańsk, 156 m high and almost rectangular in plan above the ground level, was constructed on a site constrained within the existing development (Fig. 11). Noting that the

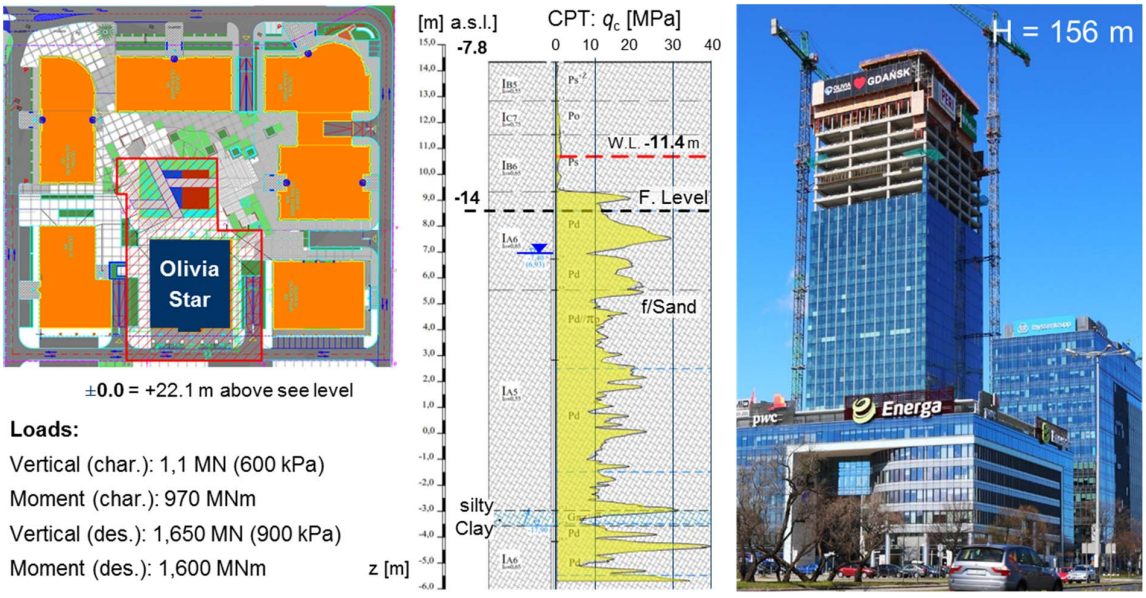


Fig. 11. Olivia Star in Gdańsk, founded on slab-soil interaction system with JG columns

ground consisted of a competent fine sand with a relative density of 0.5 to 0.7, an optimized GI foundation system was proposed instead of conventional piling. The design utilized 124 no. soilcrete columns diameter 1.8 m, purposely arranged below the foundation slab to effectively support heavily loaded pillars and structural walls, and the soil-slab interaction to transfer part of the load to the subsoil. The columns extended 5, 11 and 13 m below the foundation level at -14 m, and were executed from a working platform at -1.4 m inside the construction pit (Fig. 12). The JG technology was favorable because a smaller rig could be used in the excavation, which was also needed to construct underpinning soilcrete columns along a short sidewall of the adjacent building, supported on a strip foundation at the depth of -12.9 m. Furthermore, overlapping soilcrete columns diameter 1.8 and 2.5 m were also used to construct a deep shaft in the central part of the building, comprising a peripheral wall and a bottom plug to facilitate excavation in dry conditions. Ten columns along the shaft wall were reinforced with soldier profiles IPE500, installed in fresh elements to increase bending resistance.

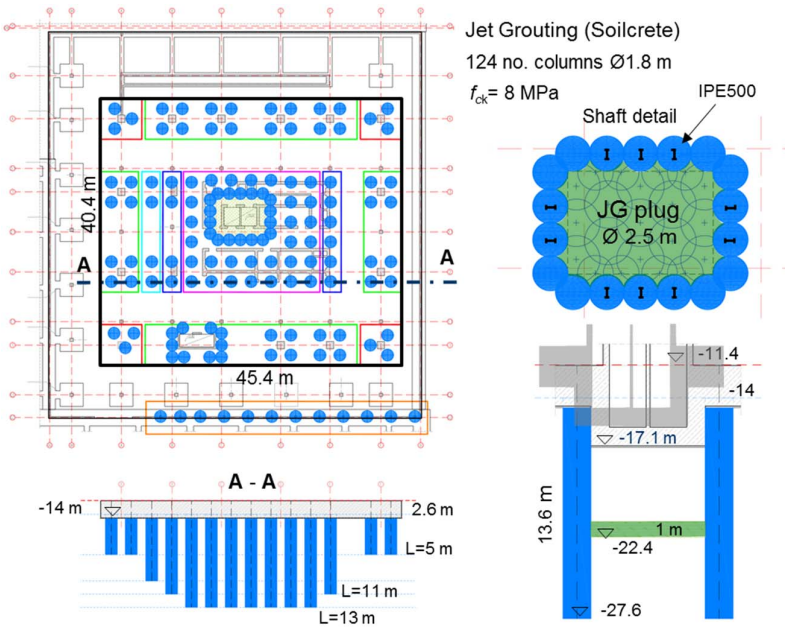


Fig. 12. Arrangement of JG columns below the foundation slab and around the central shaft

Advanced design analyses were conducted to predict foundation settlement which had to be limited to 50 mm. Example results are presented in Fig. 13. The foundation stiffness was derived from FEM calculations with PLAXIS, and was subsequently transformed to a simplified 'stiffness map' which was used in the structural design of the foundation slab. The calculations revealed that the overall load was distributed between the JG columns and the subsoil in a ratio of about 60 to 40% (the ground surface below the foundation slab was re-compacted before placing lean concrete). The maximum characteristic compressive force acting on a single soilcrete column was found to be 6,800 kN.

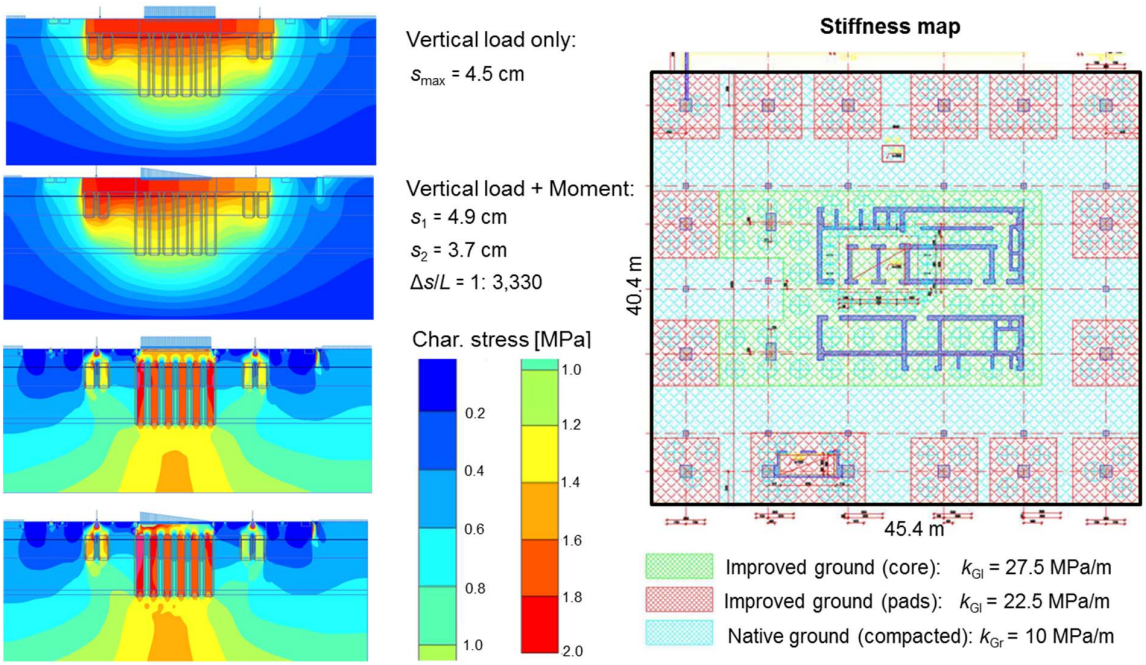


Fig. 13. Results of analyses carried out for the soil-structure interaction model with JG columns

To verify the stiffness of soilcrete columns adopted in the design, as well as to confirm the quality of the executed columns, a loading test was conducted on site to a high load reaching 150% of the maximum column load (Fig. 14). The observed settlement corresponding to the maximum load was only 5 mm, exceeding expectations. The soilcrete material was able to withstand a compressive stress of 3.9 MPa during the maximum loading stage without a noticeable creep deformation.

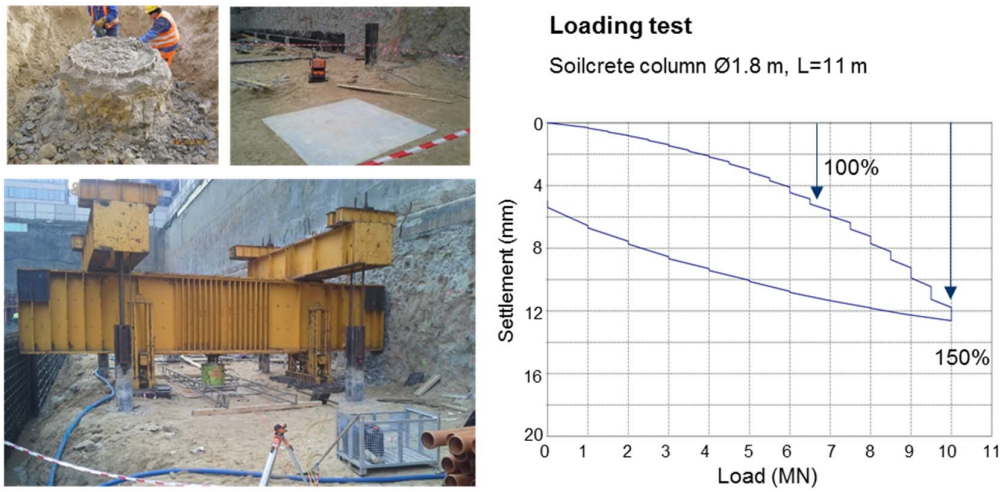


Fig. 14. Static loading test of JG column up to 10 MN

CARBON FOOTPRINT OF FOUNDATION SOLUTIONS

The examples of LOT building and PLAZA shopping center projects can be utilized for a comparison of carbon dioxide emissions associated with different geotechnical approaches within the same project. The calculations of CO_2 emissions were conducted using a standardized excel spreadsheet tool (Carbon Calculator v.3), jointly developed by EFFC and DFI. The emissions related to the materials and energy consumed, freight and personnel transportation were calculated based on project specific input data, whereas the emissions linked to mobilization/demobilization, assets and wastes produced were estimated using default settings. All calculations were based on the application of slag cement type CEM III/A for construction of piles, foundation caps and for soil mixing, with a default GGbs content of 51%, and a default factor of 41% was also used for recycled steel. The results are presented in Fig. 14.

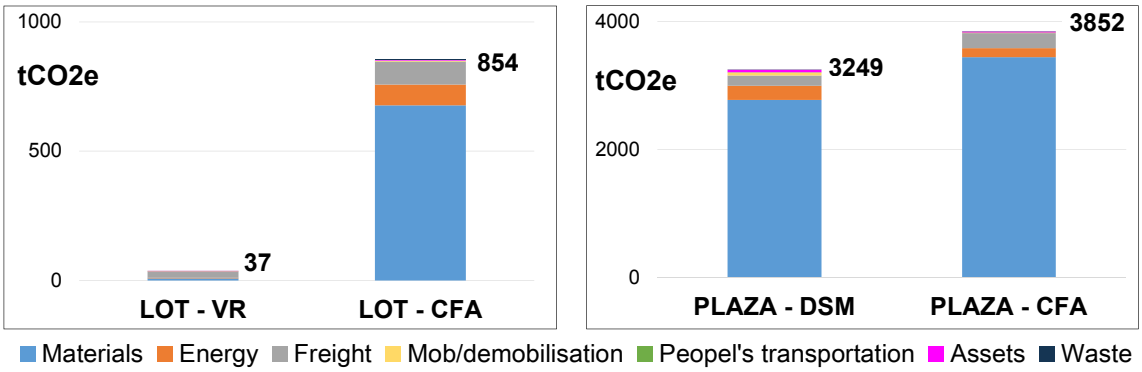


Fig. 14. Carbone dioxide emission associated with piling and GI designs for two selected projects, namely the LOT building and the PLAZA shopping center

In case of LOT building, there is a dramatic difference in CO_2 output in favor of the GI solution, arising from a combination of an environmentally-friendly technology (VR) with an optimized GI design, applied only under a portion of the same foundation slab. The PLAZA center project is more complex. In this case the comparison of CO_2 emission includes not only different designs with CFA piles and DSM columns, but also takes into account the associated changes in the overall volume of foundations and the amount of reinforcement, which have a significant impact on the combined emission output. Also in this case the GI solutions leads to a distinct reduction of carbon dioxide emission as compared to standard piling design (-16%).

CONCLUSIONS

It has been demonstrated based on practical design-and-build experience that creative geotechnical designs involving the use of contemporary technologies of ground improvement, applied alone or in combination, offer attractive alternative solutions to a wide range of foundation problems associated with heavily loaded and settlement sensitive structures, and are therefore appealing to clients and contractors. The benefits of GI solutions typically comprise shorter construction times and lower construction costs, but may often also include important reduction of project-related carbon dioxide emissions. It is therefore expected that the role of unconventional GI solutions in civil engineering practice will grow in the future, offering also new and interesting possibilities for researchers, geotechnical designers and specialized contractors.

REFERENCES

Carbon Calculator Tool v3.0, EFFC and DFI, http://www.geotechnicalcarboncalculator.com/de
Kirsch, K. and A. Bell (editors), 2013. Ground Improvement. CRC Press, London.

INNOVATIONS IN GROUND IMPROVEMENT: CREATING COMPOSITE GROUND WITH DRILL DISPLACEMENT COLUMN™ AND AUGER CAST COLUMN™

Tom Farrell, MS, GE, Farrell Design-Build, Placerville, California, USA
John Ho, PhD, GE, Farrell Design-Build, Irvine, California, USA
Neville Su, GE, AECOM, Los Angeles, California, USA
Sam Warren, PE, Farrell Design-Build, Irvine, California, USA

ABSTRACT

Within the geologically diverse and seismically active region of the western United States, innovations in ground improvement have developed to provide composite ground that support heavy structures, increase soil stiffness and bearing capacity, control settlement, and reduce the damaging effects of soil liquefaction. This paper provides a description of construction methods, design considerations, and case histories of successful applications of rigid inclusions (RI) used to create composite ground. Within California, Rigid inclusions are commercially known by the authors as Auger Cast Column™ (ACC) and Drill Displacement Column™ (DDC). This paper outlines geotechnical and structural design considerations associated with the ACC/DDC rigid inclusion system, and addresses the unique engineering, geologic, environmental, and regulatory challenges for projects in California.

Keywords: Rigid Inclusion, Settlement Control, Composite Ground, Ground Improvement, Drill Displacement Column, DDC, Auger Cast Column, ACC, Grout, Concrete

© 2018 Deep Foundations Institute

INTRODUCTION AND DESCRIPTION OF AUGER CAST COLUMN™ AND DRILL DISPLACEMENT COLUMN™ RIGID INCLUSIONS

Within the past 10 years in the western United States, rigid inclusion foundation support has become an acceptable and prevalent alternate to conventional deep, intermediate, and shallow foundations. Rigid inclusions have been used in Europe for decades (Simon, 2014; Rathmeyer, 1975; Combarieu, 1974, 1988) which included the first use of concrete pile supported bridge approach embankment (Reid and Buchanan, 1984). The first use of vibro concrete column in the United States was the Waterway Terminal in Philadelphia in 1994 (U.S. FHWA-NHI-16-028, 2017). In recent years, the adoption of rigid inclusions for use in foundation support has accelerated in California.

The authors uses the trade names Auger Cast Column™ (ACC) and Drill Displacement Column™ (DDC) to denote 2 different construction methods for installation of rigid inclusion ground improvement. Both methods are described further in the Construction Methods section. Advances of ground improvement support of heavy foundations in California, including the use of DDC, was previously presented by the authors (Farrell et al., 2016). The following paper outlines the ACC/DDC construction process and the current state of the design practice in California. Several brief case histories are used to illustrate successful uses of ACC/DDC as an alternate to driven piles, torque-down piles, auger cast piles, drill displacement piles, aggregate piers, stone columns, soil mixing, and engineered fill. Design and construction considerations are also included to provide the practicing engineer a description of ACC/DDC used to support heavy foundations on composite ground in California.

Prevalence of Deep Foundations and Ground Improvement in California

Recent California building code updates (2013 CBC and 2016 CBC) have increased the need for deep foundations or ground improvement support in seismically active regions where liquefaction settlement has become increasingly important due to higher Peak Ground Acceleration (PGA) adopted in the recent seismic code updates. Various levels of ground shaking in terms of PGA values have been used by engineers in soil liquefaction evaluations historically, ranging from 10% probability of exceedance in 50 years (corresponding to a return period of 475 years) in the Uniform Building Codes in the 1990s, to 2% in 50 years (2,475 years return period) in the recent California Building Codes. California Department of Transportation (Caltrans Geotechnical Manual, December 2014) uses 5% in 50 years (975 years return period). Seismic design provisions have been transformed and have become more stringent from the ASCE 7-02 and ASCE 7-05 to the current design standard, ASCE 7-10. Significant changes were made to the seismic ground motion maps in ASCE 7-10 in several ways that affect geotechnical evaluations and ground improvement designs in California (Farrell et al. 2016).

In addition to code-driven requirements, socioeconomic pressure continues to drive growth in urbanized environments. Owners are developing larger structures in constrained geography. Geotechnical and structural engineers are faced with challenging site conditions due to the diverse geology, environmentally impacted redevelopment, and the limits of readily developable land. Many sites in the greater San Francisco Bay area and greater Los Angeles area require the support of heavy loads on sites with soft or loose soils, contaminated soils, or undocumented fill that necessitate ground improvement to safely support the structure. Composite ground, created by ACC/DDC, is used more and more as a shallow or mat foundation support option to address the structure load and geologic hazard concerns.

Construction Method

ACC/DDC construction utilizes a partial or full displacement auger tool to produce and expand a cavity in the soil during drilling, followed by pressurized grouting of the cavity during withdraw, to form a well-defined, engineered grout, rigid inclusion within the ground (Figure 1). The combined mechanical displacement of soil and pressure grouting forms “composite ground,” a ground improvement effect that enhances the engineering behavior and properties of the improved soil or the composite ground cell. ACC/DDC diameter, length, and on-center spacing can be varied to satisfy project-specific design parameters, such as liquefaction mitigation, settlement control, and improved bearing capacity.

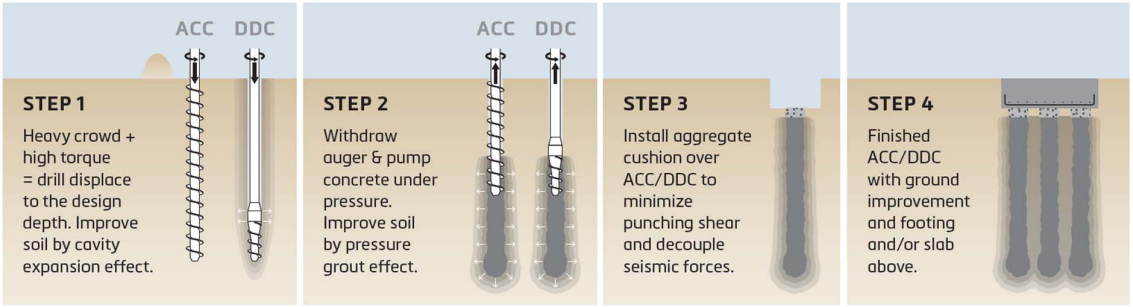


Figure 1. ACC/DDC Four-Step Construction Process

Composite ground, using Auger Cast Column™ (ACC) and Drill Displacement Column™ (DDC) ground improvement, bridges the gap between deep stiff piles, intermediate semi-stiff aggregate pier or stone column ground improvement, and shallow flexible engineered-fill. The gap is defined as "resisting heavy structure loads" over: 1) deep compressible soil, 2) mixed compressible, alluvial soil with layered liquefaction potential, 3) compressible soil with contamination concerns and/or liquefaction potential, and 4) all of the above in dense urban regions where noise and vibrations are undesirable. The well-defined engineered grout column of the ACC/DDC, used to create composite ground, provides the long-term confidence and reliability for foundation support if geotechnical and structural design considerations are adequately addressed by the design engineer.

Fixed-mast drill rigs weighing approximately 100 to 200 kips (445 to 890 kN) are generally used for installation of ACC/DDC rigid inclusions in California. The drill torque required to advance partial and full displacement tooling ranging from 12 to 24 inches (0.30 to 0.61 m) in diameter into the soil is generally between 75 to 220 kip-ft (100 to 300 kN-m). Soil properties, soil stratigraphy, and tool diameters have a profound effect on the required torque and vertical progression of ACC/DDC construction. Fixed-mast drill rigs, rather than crane-mounted augers on swinging leads, are used for the following reasons:

1) Fixed-mast drill rigs provide a fixed/rigid frame from which high-torque can be applied to a partial or full displacement drill tool.
2) Weight of the fixed-mast drill rig, in combination with mechanical crowd force from a winch operated drill carrier, imposes large downward force to the tool during the drilling operation.
3) The fixed-mast platform allows for accurate horizontal control of ACC/DDC locations.

Benefits of ACC/DDC include:

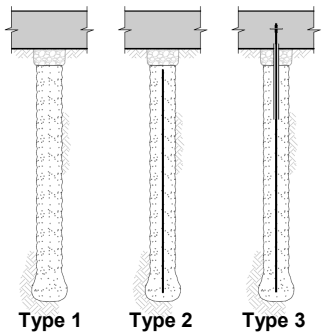
1) The ability to create an engineered reinforced soil mass beneath foundations, referred to by the authors as, “Composite Ground”.
2) Well-defined, high-quality, grout or concrete columnar inclusions within the soil.
3) Low noise and no vibrations produced with the hydraulically-powered drill installation.
4) Increased bearing capacity can result in reduced foundation sizes.
5) Very low soil cuttings are generated with the displacement auger for DDC, especially on sites with environmentally-impacted soil or undocumented fill materials.
6) Ground improvement effects during construction, by means of cavity expansion, can be developed using full-displacement auger tool for DDC.
7) Reduced soil displacement with ACC, using partial displacement augers, can be used adjacent to sensitive utilities and structures. ACC also provides a means to penetrate overlying competent soil to improve deeper compressible or liquefiable soil layers.
8) For project sites that are environmentally impacted, ACC/DDC provides a low permeability improved zone. This condition is desired by regulatory agencies in California to reduce the possibility of cross-contamination of water between aquifers in water bearing zones and the infiltration of surface water into clean groundwater at depth.

Challenges of ACC/DDC include:

1) Mobilization of large, heavy, fixed-mast drill rigs can be hard to maneuver for small sites, and can be cost prohibitive for small projects.

2) Ground heave caused by drill displacement and pressure grout effects need to be closely monitored. The ACC system can be employed to reduce heave when required.
3) Availability of ready-mix grout for smaller projects.
4) Laydown area required for on-site grout batch plant for larger projects.
5) Stability and resiliency of construction pad due to frequent movement of heavy equipment.

Construction of ACC/DDC may also incorporate reinforcement to accomplish additional design objectives. The purpose of the reinforcement is described in the following sections. The authors identify the configuration of reinforcement within ACC/DDC using the following terminology (Figure 2):



Type 1 ACC/DDC	Unreinforced rigid inclusions.
Type 2 ACC/DDC	Rigid inclusions with a center reinforcement bar.
Type 3 ACC/DDC	Rigid inclusions with a center reinforcement bar, anchored into the foundation to provide uplift resistance.

Fig. 2. ACC/DDC Reinforcement Configurations

STATE OF PRACTICE OF DESIGN IN CALIFORNIA

Serviceability (Settlement Evaluation)

Controlling settlement is the primary reason for the use of ground improvement and ACC/DDC rigid inclusions in California. The added benefits of higher bearing capacity and reduction in liquefaction potential are secondary to the overall benefit of settlement control of the structure being supported. The calculation of settlement of ACC/DDC composite ground uses the techniques similar to those for pile foundations. However, instead of transferring the majority of structural loads to deeper soil strata as accomplished with deep foundations, ACC/DDC derives support from soils within the treatment zone (composite ground zone), as well as transferring a portion of the structural loads to deeper soils below the treatment zone (lower zone). A complex soil-structure interaction within the composite ground zone involves many variables that may be challenging for design engineers to adequately address within the typical project time and budget constraints. The authors have found success in utilizing Finite Element Analysis (FEA) software to model the soil-structure interaction of foundations supported by composite ground for relatively large projects. However, for practical deliveries of most projects, a two-zone (an upper/improved zone and a lower/unimproved zone) approach is generally used without performing FEA analysis. The upper zone consists of the rigid inclusion/soil composite; and the lower zone consists of unimproved soils. Total settlement is the sum of the upper and the lower zone settlements. Several methods to estimate settlement of the upper zone have been described in literature (Combarieu, 1988; Siegel, 2011; Varaksin et al., 2016; Majchrzak et al, 2004). Neutral plane concepts related to piled foundations, while not fully appropriate for rigid inclusions without modification, can be used estimate lower zone settlement (Hannigan, 2016; Brown, 2006; Fellenius, 2004; Siegel, et al., 2014).

The key concept for all settlement estimates pertaining to piles and rigid inclusions is that of the neutral plane. The neutral plane is the location of force and displacement equilibrium along the rigid inclusion within the soil. Positive and negative resistances along the shaft are balanced at the neutral plane, resulting in zero relative movement between the rigid inclusion and soil. Above the neutral plane; soil moves downward relative to the rigid inclusion. Below the neutral plane the rigid inclusion moves downward relative to the soil. Settlement analysis of ACC/DDC following this concept includes estimating the neutral plane location, calculating the settlement in the composite zone above the neutral plane, calculating the compression (seating) of the load transfer platform, and calculating settlement below the neutral plane in the lower zone. The authors recommend several methods be used to envelope settlement.

Strength (Capacity)

An area load test is used to confirm the ultimate geotechnical resistance of a unit cell of composite ground. The authors accomplish this by using an equivalent cell area over the ACC/DDC composite ground consisting of a 4 feet by 4 feet (1.2 m by 1.2 m) equivalent footing. The concept is similar to a pile load test conducted in general conformance with ASTM D1143 Procedure A with minor modifications. The load test is run to 100% of the design load and then held for up to 60 minutes at 100%, then is loaded to 200% of the design load, and then slowly rebounded back to zero load. Several load-unload-reload cycles can be used during the load test, depending on the project objectives, to understand the components of elastic and plastic deformation. Composite modulus of the composite ground can be estimated from the load deflection curve at 100% design test load in sandy and silty soil profiles where porewater pressure can stabilize within the duration of the test. In predominantly clay profiles, longer test durations are needed to estimate the composite modulus. Maintained tests are often cost prohibitive for projects. Therefore, the authors use full-scale load testing to verify ultimate geotechnical resistance (ultimate bearing capacity) and rely on conventional geotechnical calculations to estimate long-term settlement of the composite ground.

The structural capacity of the rigid inclusion, a structural limit state, needs to be checked for compression, shear, and moment. Large embankments, new structures adjacent to rigid inclusions, and kinematic bending effects from seismically induced shear waves can impose lateral displacements and curvature that must be considered in rigid inclusion design (Briet and Morel, 2015; Gingery, et al., 2009). Based on the author's experience, more research is needed to establish minimum code requirements for structural calculations of semi-rigid and rigid ground improvement.

Foundation Interface with ACC/DDC rigid inclusions

To provide stiffness compatibility of ACC/DDC rigid inclusions and a true composite ground effect, a cushion or load transfer platform (LTP) must be placed between the foundation and the ACC/DDC composite ground. The integration of a compressible cushion between the ACC/DDC and foundation helps to engage the soil before the resistance capacity of the rigid inclusion is fully developed (Siegel, 2011). The cushion or LTP has been referred to as "aggregate cushion" or just "cushion" in California and serves the following performance and compatibility purposes:

1) Disconnect the ACC/DDC from the foundation to provide a seismic break.
2) Normalize the stiffness ratio between the ACC/DDC and soil.
3) Provide protection of completed ACC/DDC work.

Cushion thickness generally ranges from 6 to 24 inches (0.15 to 0.61 m) with a diameter ranging from 16 to 36 inches (0.41 to 0.91 m). The cushion is generally comprised of select frictional material like sand, 3/8-inch (10 mm) crushed rock, 3/4-inch (19 mm) crushed rock, and 3/4-inch (19 mm) Class 2 aggregate baserock.

The primary cushion performance and compatibility requirement in California is a seismic break. The cushion provides a preferential shearing plane at the foundation concrete interface with the ACC/DDC composite ground during seismic shaking. Without a cushion and seismic break, the rigid inclusion will be cast and be bonded to the foundation concrete and will behave more like an unreinforced pile during seismic shaking. In such a condition, an unpredictable shear mechanism can develop in the grout that can result in brittle cracking of the rigid inclusion system. In order to provide a ductile response and protect against excessive cracking, a seismic break must be utilized. In high vertical stress applications and low lateral confinement conditions such as liquefiable soil layers, type 2 ACC/DDC have been used to provide higher strength and ductility within the rigid inclusion. Type 2 ACC/DDC rebar reinforcement increases the shear and moment capacity by 5 to 10 times the unreinforced case. However, the use of type 2 ACC/DDC does not negate the requirement of cushion.

The secondary cushion performance and compatibility requirement is stiffness compatibility with the compressible soil. The use of cushion allows for the normalization of the subgrade stiffness under the foundation. Rigid inclusions are stiff relative to the soil matrix (Varaksin 2014), and thereby resist most of the load at the foundation interface. A well-constructed cushion will allow seating (deflection) at the foundation interface that serves to reduce hard points and to facilitate strain compatibility between the

composite grout materials with dissimilar stiffness. Analogous to a mattress over coil springs, the aggregate cushion softens the reaction of very stiff ACC/DDC springs to allow for a normalized composite behavior. A small settlement enables the foundation to fully engage the improved composite ground before engaging the ultimate capacity of the ACC/DDC.

The third performance and compatibility requirement is the protection of ACC/DDC to ensure the reliability of the composite ground. Excavation of foundations and excessive rutting from equipment can impose lateral displacements on the ACC/DDC which may develop excessive cracks and compromise the integrity of the grout. A cushion or LTP facilitates protection of completed work by constructing the grout elevation lower than the maximum excavation depth.

Uplift Resistance

A benefit available to the ACC/DDC system is the use of high strength rebar to resist uplift forces. Structural engineers in California have utilized the rigid inclusion as a ground anchor to resist net uplift at foundations. Martin Luther King Hospital Parking Structure in Los Angeles County, discussed in the following case histories, utilized type 3 DDC for uplift resistance. Foundation concrete was reduced by using type 3 DDC by reducing massive concrete gravity load to resist the uplift forces. Type 3 ACC/DDC anchor reinforcement is wet-stabbed into the fresh grout. A bond-break along the anchor, also referred to as the unbonded zone, is provided at the foundation interface by means of an oversized PVC pipe through the cushion. The unbonded length must be sufficiently long to ensure seating of the cushion does not damage or cause the anchor to yield in compression. The unbonded zone can be adjusted to provide project-specific ductility requirements for foundations subject to overturning. To ensure the anchor does not participate in resisting lateral loads, the unbonded zones annulus must be oversized allow lateral translation of the foundation and anchor during seismic shaking. Type 3 ACC/DDC is designed such that the geotechnical limit state in uplift is greater than the strength limit state of the bar. Multiple type 3 ACC/DDC can be used for uplift resistance at foundations supporting shear walls, braced frames, and moment frames.

Footing and Slab Design

The use of aggregate cushion as presented above prevents hard points at the foundation interface and closely simulates an inverted bearing capacity effect where the ACC/DDC moves into the load transfer platform below the foundation base. The concentrated load is spread out at the foundation, reducing the need to design the foundation like a pile cap. Without the aggregate cushion, hard points may cause overstress in the foundation concrete and possibly excessive cracking in ACC/DDC under design loads. Other design considerations for foundation and slab support include the ground improvement area replacement ratio, ACC/DDC to soil stiffness ratio, ACC/DDC to foundation stiffness ratio, allowable total and differential settlements, and static versus seismic bearing capacities.

In California, footings are typically supported by 16 to 24 inches (0.41 to 0.61 m) diameter ACC/DDC at a spacing ranging from approximately 4 to 6 feet (1.2 to 1.8 m) on center, with allowable bearing capacities ranging from 5,000 to 10,000 pounds per square foot (240 to 479 kPa). Typical area replacement varies from 8% to 15% for foundation support. Slab and mat foundations are typically supported by ACC/DDC ranging from 6 to 12 feet (1.8 to 3.7 m) on center. ACC/DDC load-deflection behavior is predicted during design and verified with full-scale load tests.

In addition to full-scale load testing, pre- and post-ground-improvement verifications, using Cone Penetration Testing (CPT) in sandy soils and dilatometer testing (DMT) in clays and silts, are sometimes conducted to verify ground improvement effects that have been used in the design. Depending on the rate pore pressure dissipation, CPT testing in silts and clays may not result in apparent "improvement" in terms of an increase in the post-mitigation resistances. In some cases, excess pore pressures generated during installation may cause a temporary decrease of cone resistance. A long-term monitoring program may be required to demonstrate improvement at these sites. Alternatively, post-ground-improvement CPT and DMT are not required if the ground improvement design analyzes the ACC/DDC composite ground with pre-ground-improvement soil parameters.

Rigid Inclusion Design in California

ACC/DDC performance-based design is typically executed by a specialty design-build geotechnical contractors (geocontractor) and requires participation among the project geotechnical engineer, structural engineer, and the general contractor. The geocontractor joins the design team as the Engineer of Record for the ground improvements in addition to joining the contracting team as a subcontractor to construct the work. Based on the author's experience, the design-build workflow is widely accepted for private commercial, industrial, and residential projects and is gaining acceptance in public contracts.

In California, ACC/DDC techniques are currently used and approved by Federal Transportation Board (FTB), Bay Area Rapid Transit / Valley Transit Authority (BART/VTA), Los Angeles County, University of California (UC), California State University (CSU), and several city and county jurisdictions. ACC/DDC have not been approved for hospitals, schools, and bridges regulated by Office of Statewide Health Planning and Development (OSHPD), Division of the State Architect (DSA), and California Department of Transportation (Caltrans), correspondingly.

CASE HISTORIES

Stanford Campus at Redwood City, Redwood City, CA

The Stanford Redwood City campus is located across from the Stanford Medicine Outpatient Center off Highway 101 (Figure 4). The 35 acre (14 hectare) site is 5 miles (8 km) from the main Stanford campus. Phase one of the new campus is composed of 9 new structures that include 4 to 6 story high tech offices, a parking structure, and central utility plant. Geotechnical conditions range from soft compressible clay with ancient dissected sloughs that were naturally filled with loose sand deposits. The San Andreas fault is 5 miles (8 km) to the west of the site and the Hayward fault is 13 miles (21 km) to the east, resulting in active faults generating an estimated earthquake of M=6.7 and PGA=0.623g. The geotechnical and geologic hazards range from excessive site settlement from new structural loads, liquefaction settlement of 2-3 inches (51 to 76 mm), and liquefaction related ground rupture. Typically, vibro stone columns (VSC) would be used to manage the liquefaction related geologic hazards. However, VSC were excluded because of vibration concerns for the active medical facility across the street and the presence of environmentally impacted areas on the site. Drill Displacement Column (DDC) was proposed by the geotechnical engineer to control settlement, increase bearing capacity, reduce liquefaction settlement, eliminate ground rupture, and to plug any concerns of cross water contamination by virtue of the displaced ground and grouted columns.



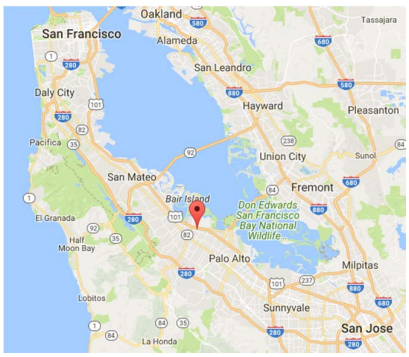


Fig. 3. Stanford Campus at Redwood City

Full-scale test sections (Figure 5) were performed to determine the optimum DDC spacing for ground rupture control. DDC spacing of 5 feet (1.5 m), 6 feet (1.8 m), and 7 feet (2.1 m) on center in equilateral triangle layouts were tested to depths of 35 feet (10.7 m) below grade. The DDCs have a neat diameter of 18 inches (0.46 m) with finished diameters approaching 20 inches (0.51 m) with pressure grout effects. Quality control and quality assurance of DDC construction utilizes Automated Monitoring Equipment (AME) installed on the drill rigs, in addition to analog hand records kept by a full-time quality control representative. Post-treatment cone penetration test results showed that 6 feet (1.8 m) on center increased the density of loose sand enough to control ground rupture and to reduce liquefaction related settlement to less than ¾ inches (19 mm). Full-scale load tests (Figures 5a, 5b, and 6)

demonstrated that the original designed allowable bearing capacity of 5,000 psf (240 kPa) could be increased to 6,000 psf (287 kPa) for static loads. Total settlements for the multi-story structures are estimated to be less than 1 inch (25 mm) for static and seismic settlements combined. Over 7,000 DDC were installed to depths ranging from 30 to 35 feet (9.1 to 10.7m).

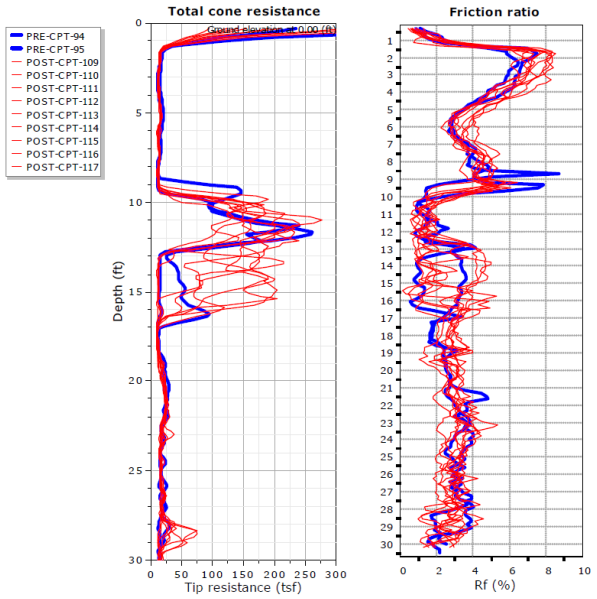


Fig. 4a. Pre- and Post-Ground-Improvement CPTs

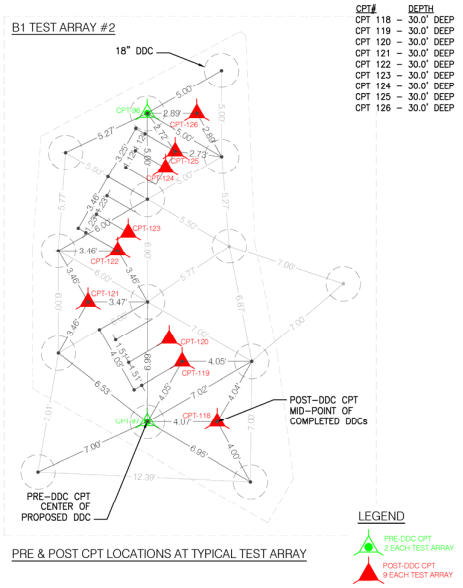


Fig. 4b. Test Array



Fig. 5a. Full-Scale Load Test of Composite Ground

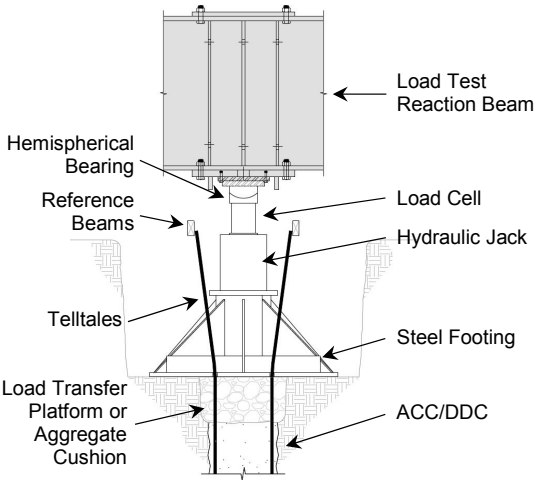


Fig. 5b. Load Test Schematic

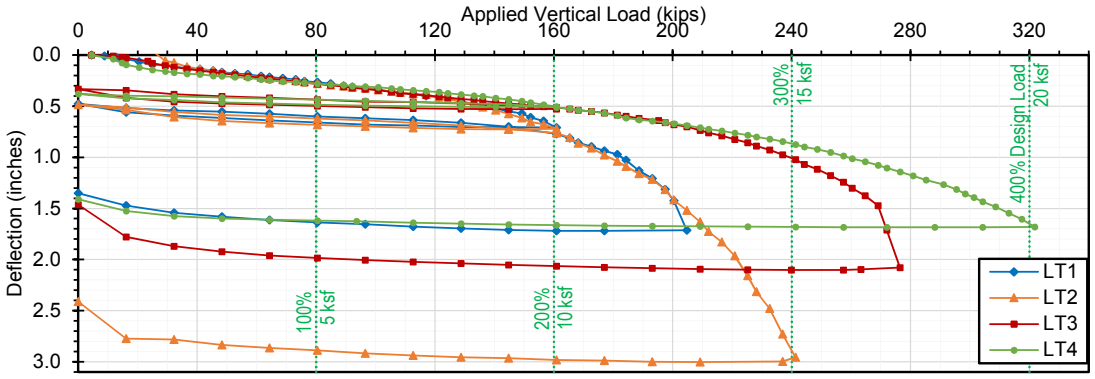


Fig. 6. Bearing Load Test Results: Applied Vertical Load vs. Deflection

Martin Luther King Hospital East Parking Structure, Los Angeles, CA

The Martin Luther King Hospital East Parking Structure is located off South Wilmington Avenue in Los Angeles County just north of Compton on the east side of the hospital campus (Figure 8). The new 6-story parking structure has over ten active faults within 15 miles (24 km) of the site with the Newport-Inglewood (Los Angeles Basin) at less than 3 miles (4.8 km) from the site with a maximum estimated Mw=7.1. The design earthquake was considered with Mw=6.61 and a corresponding PGA_M=0.636g. The geotechnical and geologic hazards range from 15 feet (4.6 m) of undocumented fill, excessive site settlement from new structural loads, seismic/liquefaction settlement up to 2.6 inches (66 mm), and small contaminated soil areas at the site. Aggregate piers and drilled piers were recommended for improving the site or extending to depths below the fill for foundation support. Drill Displacement Column™ (DDC) were proposed by the design-build contractor to improve the site soil and reduce static and seismic settlement to less than 1 inch total (25 mm). The DDC system also provided the benefits of no-vibration at the hospital campus, high bearing capacity, uplift resistance at moment frames, and to plug any concerns of cross water contamination by virtue of the displaced ground and grouted columns. Type 2 DDC were used to increase the bearing capacity to 8,000 psf (383 kPa) at all footings. Type 2 DDC was selected for the project to provide increased ductility of the rigid inclusion in potentially liquefiable soil layers and to provide the confidence that DDC would retain its reliability through multiple strong seismic shaking events without sacrificial confinement rows (confinement rows at footing edges as required for aggregate pier systems). Type 3 DDC with high-strength rebar were also used to resist tension forces at the ends of seismic resisting moment frames.

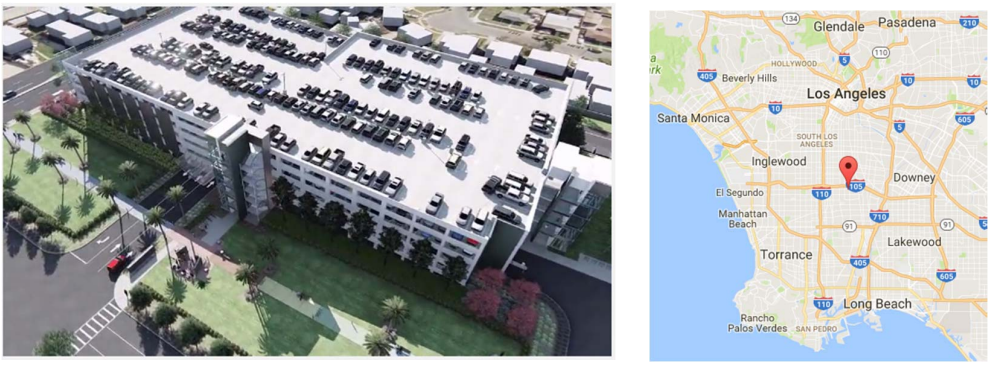


Fig. 7. Martin Luther King Hospital East Parking Structure

Two full-scale load tests (Figure 9) were performed to prove the increased bearing capacity over a 4 feet by 4 feet (1.2 m by 1.2 m) area of composite ground with one 16-inch (0.41 m) by 27-foot (8.2 m) long DDC in the center of the composite ground. The composite ground load tests showed less than ½ inch (13 mm) deflection at the 128 kips (569 kN) design load. The tension load test showed less than ½ inches (13 mm) deflection at 172 kips (765 kN) tension load. Total settlements for the multi-story parking structure are estimated to be less than 1 inches (25 mm) for static and seismic settlements combined. Over 500 DDC were installed to depths ranging from 30 to 35 feet (9.1 to 10.7 m). Pre- and post-ground improvement Cone Penetration Test results are shown in Figure 9.

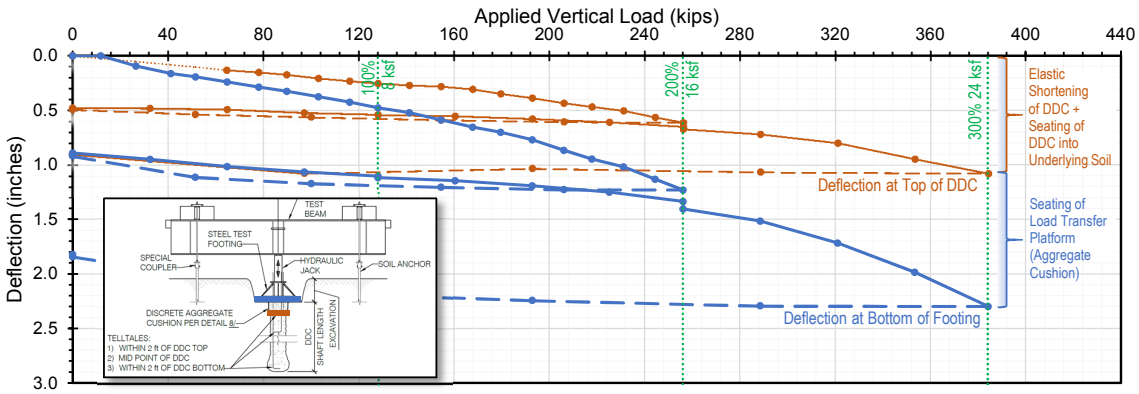


Fig. 8. Bearing Load Test Results: Applied Vertical Load vs. Deflection

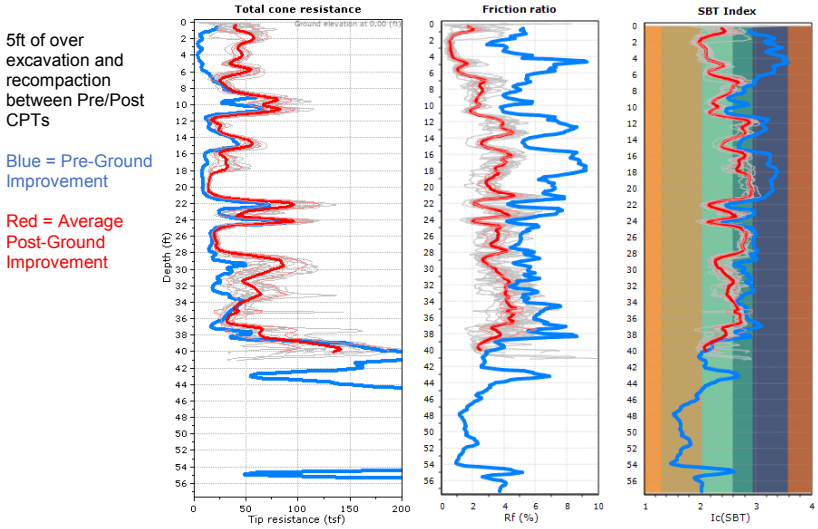


Fig. 9. Pre- and Post-Ground-Improvement Cone Penetration Tests

Maxwell Field Parking Structure, Berkeley, CA

Maxwell Field Parking Structure is located within the University of California, Berkeley campus (Figure 11). The University of California at Berkeley planned to replace the old practice field just north of Memorial Stadium with a new two-story parking structure and a new practice field on the roof. The site is situated just 75 feet (23 m) south and west of the Hayward fault. In addition, the site rests over a canyon fill on the historic Strawberry Creek. Since the 1930s, the "Little Inch" box culvert has been the main drainage channel for Strawberry Creek and it rests between 20 to 34 feet (6 to 10 m) below the ground surface directly under this site. The main project geologic hazards were seismic settlement, static settlement, and foundation support, and to protect the still active Little Inch box culvert.

The ACC and DDC solution was selected for foundation support for the following reasons: 1) the DDC system is a displacement method that will compact soil laterally thus reducing seismic settlement between and around each DDC, 2) the ACC installation is drilled with no vibrations and partial displacement, thus protecting Little Inch during the construction, and 3) the engineered grout mix acts as a plug to prevent cross-water contamination at the site.

The challenge for the structural engineer and the design team was to creatively position structural columns and foundations to straddle the Little Inch and Big Inch culverts. The sloping bedrock profile with a survey of Little Inch was modeled by Farrell and presented to the structural engineer and design team with proposed ACC/DDC locations around Little Inch, see Figure 11. Over 480, 18-inch (0.46 m) diameter ACC/DDCs were installed to depths of 8 to 40 feet (2.4 to 12.2 m). Load test results and post-installation CPT and DMT tests (Figures 12 and 13) showed acceptable performance of the ACC/DDC system and the soil that was improved within two diameters around the DDCs.

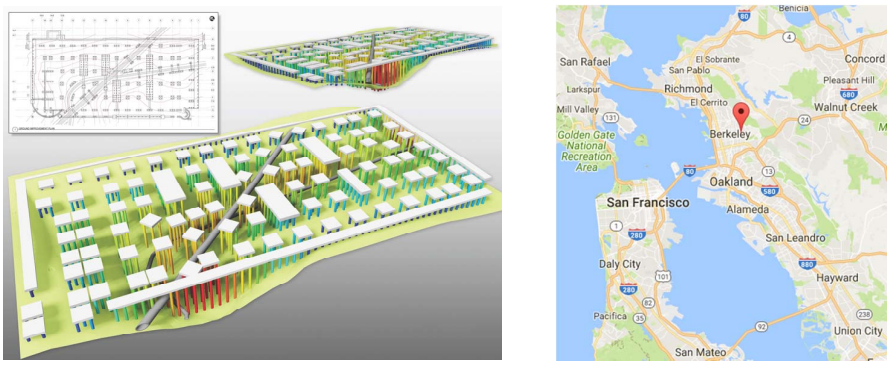


Fig. 10. Maxwell Field Parking Structure 3D Map for Foundation Coordination

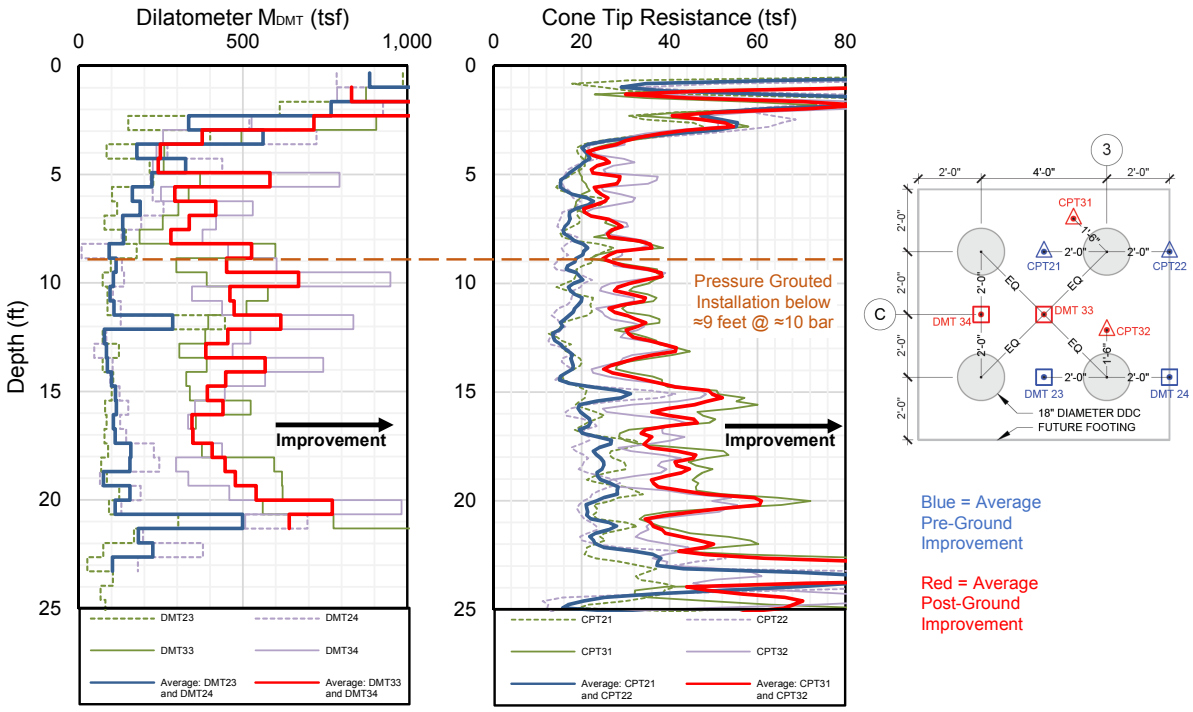


Fig. 11. Pre- and Post-Ground-Improvement Dilatometer and Cone Penetration Testing

DESIGN AND CONSTRUCTION CONSIDERATIONS

Geotechnical and Structural Engineering Questions in Seismic Regions

Key questions and considerations that the geotechnical and structural engineer need to know about ACC/DDC rigid inclusions in seismic regions include:

1) What is the stiffness of the composite ground?
2) Is the composite stiffness compatible with the intended settlement control?
3) Will the composite ground shear or bulge under static and seismic loads?
4) Does the composite ground need to be confined within liquefiable soil zones to provide reliable support? Confinement is sometimes overlooked by geotechnical engineers with aggregate pier and stone column systems.
5) Will composite ground behave uniformly or vary across the project site?
6) Is the increased bearing capacity uniform under a conventional spread footing?
7) How does the subgrade modulus (stress and settlement) vary across a large mat foundation?
8) Does the composite ground reduce total and differential settlement to tolerable limits?
9) Is a structural slab required or can composite ground support a slab-on-grade?
10) Does composite ground improve sliding friction and passive lateral resistance of the foundation?
11) Can the composite ground provide ground anchorage to resist overturning forces?

These questions are often answered by geotechnical engineers and specialty geocontractor engineers in today's building industry in California. (Farrell et. al. 2016).

SUMMARY AND CONCLUSIONS

This paper illustrated the use of ACC/DDC, their construction process, and the current state of the design practice in California. Several case histories are used to illustrate the prevalence of ACC/DDC as an alternate to driven piles, torque-down piles, auger cast piles, drill displacement piles, aggregate piers, stone columns, soil mixing, and engineered fill. The design methods of ACC/DDC are different from those of piles due to the aggregate cushion that separates the foundation from the rigid inclusion

and the resulting composite ground effect of the rigid inclusion and soil mass. Design and construction considerations, in addition to industry-specific issues, are included to provide an overall picture of ACC/DDC used to support heavy foundations on composite ground in California.

ACC/DDC have been used to control static settlements for buildings ranging from several stories to 20 to 30 stories with success, and have been used for other purposes including soil liquefaction mitigation, lateral spread mitigation, and slope stabilization. Multiple rows of alternating type 2 ACC/DDCs have been used as stabilizing buttresses for slope stabilization and for lateral spread mitigation. Design and construction can be improved upon further research and discussions among academic researchers, design engineers, constructors, regulators, code writers, and insurance industries to implement site mitigation criteria and standards.

REFERENCES

Briet, Samuel and Jean Francois Morel, 2015. Construction of Highway Embankment Using Controlled Modulus Columns. Conference of the Transpiration Association of Canada, Charlottetown, PEI.

Brown, D.A., et al., 2007. Geotechnical Engineering Circular No. 8 Design and Construction of Continuous Flight Auger Piles, Office of Technology Application, Office of Engineering/Bridge Division, Federal Highway Administration, U.S. Department of Transportation, Washington, D.C.

Combarieu, O. 1988. Amélioration des sols par inclusions rigides verticales. Application à l'édification de remblais sur sols médiocres. Revue Française de Géotechnique, 44, 57-79.

Farrell, et al., 2016. Advances in California - Ground Improvement Support of Heavy Foundations. Convention Proceedings Structural Engineers Association of California, Maui, Hawaii, p.20.

Fellenius, B.H., 2004. Unified design of piled foundations with emphasis on settlement analysis. Honoring George G. Goble — "Current Practice and Future Trends in Deep Foundations" Geo-Institute Geo-TRANS Conference, Los Angeles, July 27-30, 2004, Edited by J.A. DiMaggio and M.H. Hussein. ASCE Geotechnical Special Publication, GSP 125, pp. 253 - 275.

Gingery, J.R. et al., 2009. Addressing Kinematic Pile Bending Design Requirements in the International Building Code. Contemporary Topics in In Situ Testing, Analysis, and Reliability of Foundations. GSP 186. 2009

Hannigan, P.J., et al., 2016. Design and construction of driven pile foundations. FHWA-NHI-16-009, National Highway Institute, Federal Highway Administration, U.S. Department of Transportation, Washington, D.C.

Majchrzak et al, 2004. Settlement of Shallow Foundations Constructed over Reinforced Soil: Design Estimates vs. Measurements. Proceedings: Fifth International Conference on Case Histories in Geotechnical Engineering, New York 2004.

Reid, W.M. and Buchanan, N.W., 1984. Bridge Approach Support Piling. Piling and Ground Treatment, Thomas Telford Ltd, London, UK.

Siegel, T., Technical Note: Simplified Settlement Model for Shallow Foundation on Composite Ground with Rigid Piles, DFI Journal, Volume 5, No. 1 June 2011.

Siegel, Timothy and Willie NeSmith, 2010. Large-scale Plate Load Testing of Ground Improved Using Displacement Grout Columns. GeoFlorida 2010: Advances in Analysis, Modeling & Design, GSP 199, pp. 2398 – 2405.

Siegel, T. C., et al., 2014. Neutral Plane Method for Drag Force of Deep Foundations and the AASHTO LRFD Bridge Design Specifications.

Simon, Bruno, 2014. General report S5 Rigid Inclusions and Stone Columns. ISSMGE – TC 211 International Symposium on Ground Improvement IS-GI Brussels, May 31 – June 1, 2012.

U.S. Department of Transportation Federal Highway Administration, FHWA-NHI-16-028, 2017. Ground Modification Methods Reference Manual – Volumes I and II, April 2017.

Varaksin, et al., 2014. The thin line between deep foundations and soil improvement abstract. PNRPU Construction and Architecture Bulletin. 9-32. 10.15593/2224-9826/2014.3.01.

Varaksin, et al., 2016. Ground Improvement vs. Pile Foundations? ISSMGE – ETC 3 International Symposium on Design of Piles in Europe. Leuven, Belgium, April 28 & 29, 2016.

LONG TERM MECHANICAL PROPERTY OF CEMENT TREATED LOAM USED IN ROAD EMBANKMENT

Yukika Miyashita, Public Works Research Institute, Tsukuba, Ibaraki, Japan, +81-29-879-6759, y-miyashita@pwri.go.jp
Genki Inoue, Kiso-Jiban Consultants Co. LTD. (formerly Public Works Research Institute), Koto-ku, Tokyo, Japan, +81-3-5632-6823, inoue.genki@kiso.co.jp

ABSTRACT

To investigate long term mechanical property of cement treated loam, a boring survey was conducted on a large embankment with its volume of about 0.4 million cubic meters and maximum height of about 40 meters, after 9 years from its construction. Strength distribution of the undisturbed core sample with the length of 18 meters was obtained by unconfined compression and penetration tests. It was found that the unconfined compressive strengths in the whole length of the sample were larger than the designed values. According to the comparison of unconfined compressive strength at a certain depth, strength obtained in this study was hardly increased from the strength nine years ago.

Keywords: long term mechanical property, cement treated loam, road embankment, unconfined compressive strength

INTRODUCTION

To promote re-utilization of construction generated soils which are generated by cutting and excavations, it has been required them to be reused more efficiently. As one of the efforts, the construction generated soils with less strength or trafficability have been adopted to use widely by applying chemical stabilization using cement or lime. Currently in Japan, construction generated soils have been occupied about 90 % of the whole soils employed in earthworks, according to the survey of construction by-product which was conducted by the Ministry of Land, Infrastructure, Transport and Tourism, Japan (hereafter denoted as MLIT) in 2012.

These treated soils have been used frequently as fill materials of road embankment. Types or the amounts of the binders are determined by proportioning laboratory tests to achieve a design strength after a short period of time. In general, it is well known that the strength of the treated soils increase with curing time under controlled laboratory conditions, due to the chemical reactions between soil and binders. On the other hand, it was also recognized that the in-situ strength can be affected by several conditions, including variation of soils, the degree of mixing, curing temperature and exposure conditions. There are many studies based on the site investigations of the treated soils having large design strength or amount of cement, such as cement columns made by deep mixing method (e.g., Hayashi et al., 2003; Ikegami et al., 2010). However, fewer studies were conducted on the treated soils whose design strengths were several hundred (kN/m^2) levels, that is, the treated soils which were utilized as a fill material of high embankment or in the shallow ground improvement.

In this study, therefore, site investigation of a large embankment made of cement treated loam was conducted after 9 years from its construction. A boring survey was conducted to obtain an undisturbed core sample of the treated loam with a length of about 18 m, from the middle height of the embankment where the maximum height of about 40 meters. Visual observation combined with the application of phenolphthalein solution was conducted to check the uniformity and the mixing condition of cement in the treated loam. To obtain the strength distribution of the whole height of the sample, unconfined compressive strengths were measured in every 2 meters, while penetration resistances were measured in every 10 centimeters. Long term mechanical property of the treated loam was discussed based on the strength distribution obtained from this survey, design strength after 28 days, and the set of unconfined compressive strengths at a certain depth after 56 days.

SITE INVESTIGATION AND LABORATORY TEST

Overview of road embankment investigated

The boring survey was conducted at a large embankment made of cement treated soil, after 9 years from its construction. This embankment whose volume of 414340 m^3 and the maximum height of about 40 m was made to fill a valley to construct a highway in Shizuoka prefecture, Japan (Nishimi, 2009). 29 types of soils which were generated in neighboring

© 2018 Deep Foundations Institute

construction sites were used as the fill materials of the embankment. One of the major soils was a loam having high water content and small cone penetration resistance. Cement treatment was applied to improve the quality and the strength of the soil. Unconfined compressive strengths after 28 days curing, q_{u28_design}, were determined as shown in Table 1 by considering the result of slope stability analysis of the embankment. Stationary plant at the construction site was selected to mix cement with the soils as uniform as possible. Amount of the cement was in the range of 32 to 225 kg/m^3. It was decided by the proportioning laboratory test on the soil whose quality was the worst in each day, while several types of soils were irregularly provided to the plant every day. Ranges and average values of the unconfined compressive strengths obtained at the plant after 28 days are indicated in Table 1 as q_{u28_plant}.

Table 1. Unconfined compressive strength in designing and proportioning (modified after Nishimi, 2009)

Parts of embankment	Upper part	Lower part
Design strength after 28 days, q_{u28_design} (kN/m^2)	190	500
Strength obtained at plant, q_{u28_plant} (kN/m^2)	239 - 1654 (914 on average)	562 - 1584 (1022 on average)

Procedure of boring survey and laboratory tests

Cross section of the embankment and the position of the bore hole are presented in Fig. 1. The blue node indicates the place where the unconfined compressive strength at the time of the construction could be identified. Those strength were obtained as one of the data for quality control of the embankment. The positon of the bore hole was selected to be adjacent to this place at the depth of about 18 m. The boring was started from the middle height of the embankment to a depth of the original ground. The undisturbed core sample was taken with a diameter of 70 mm and a length of 21 m.

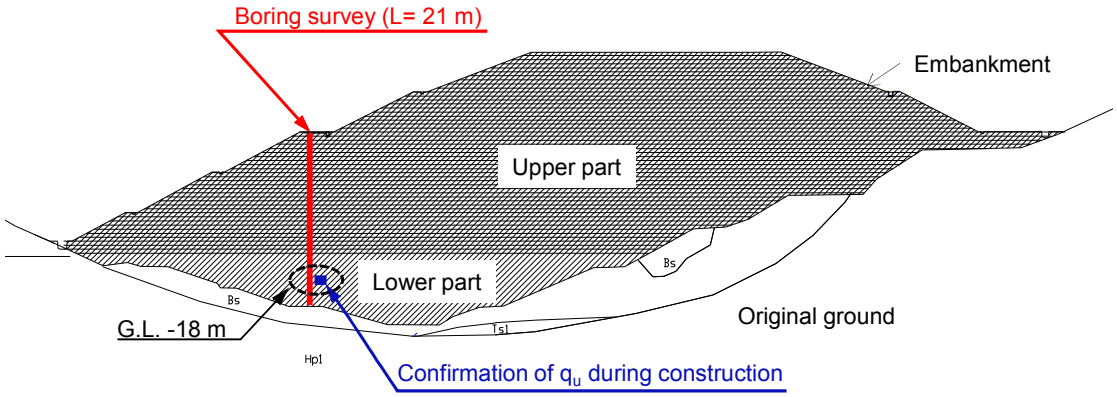


Fig. 1. Cross section of road embankment investigated in this study

Visual observation combined with the application of phenolphthalein solution was conducted to check uniformity and alkalinity of the fill material. To obtain strength distribution of the whole length of the sample, three types of mechanical tests were conducted; unconfined compression test (JIS A1216), soil hardness test (JGS 1441) and needle penetration test (JGS 3431) based on Japanese Geotechnical Society (2013). Unconfined compressive strengths were measured around 2 m intervals, while soil hardness and needle penetration tests were applied around 100 mm intervals.

A portable (Yamanaka-type) soil hardness tester having a cone with its diameter of 18 mm and length of 40 mm was used to obtain the length of the cone penetrated in the soil sample which was called hereafter as hardness index. The hardness index was converted to unconfined compressive strength using the equation [1]. It was defined by the test results of cement treated soils whose maximum strength level is about 500 kN/m^2 (Japanese Geotechnical Society, 2013).

$$D = 6.10 \ln(q_{u_D}) - 8.50 \quad [1]$$

Where D= hardness index (mm) and q_{u_D}= unconfined compressive strength converted from D (kN/m^2).

A portable needle penetration tester (Maruto Testing Machine Company, SH-70) having a needle with its diameter of 0.84 mm and length of 10 mm was used to obtain the gradient of needle penetration as shown in the equation [2].

$$N_P = P/L \quad [2]$$

Where N_P= gradient of needle penetration (N/mm), P= penetration resistance (N) and L= length of needle penetrated in the sample (mm).

N_P was then converted to unconfined compressive strength q_{u_NP} using the equation [3]. It was proposed by the manufacturer considering the test results on natural rocks and cement treated soils whose range in strength was about from 300 to 4000 kN/m^2.

$$\log(q_{u_NP}) = 0.978 \log(N_P) + 2.621 \quad [3]$$

Result of visual observation in laboratory

Figure 2 shows a photograph of the whole core sample at the depth from 3 to 21 m. Ground water level was confirmed at the depth of 15.2 m. It was estimated that the horizontal cracks in the sample were made due to the boring survey. In general, the sample was well cemented except for the cracks and the part shallower than 3.4 m which was coincided with surface soil. Varieties of colors, types and diameters of gravels, and structures of soil particles were observed throughout the height of the sample, as it was explained before that the type of soils used in the embankment was not unique.

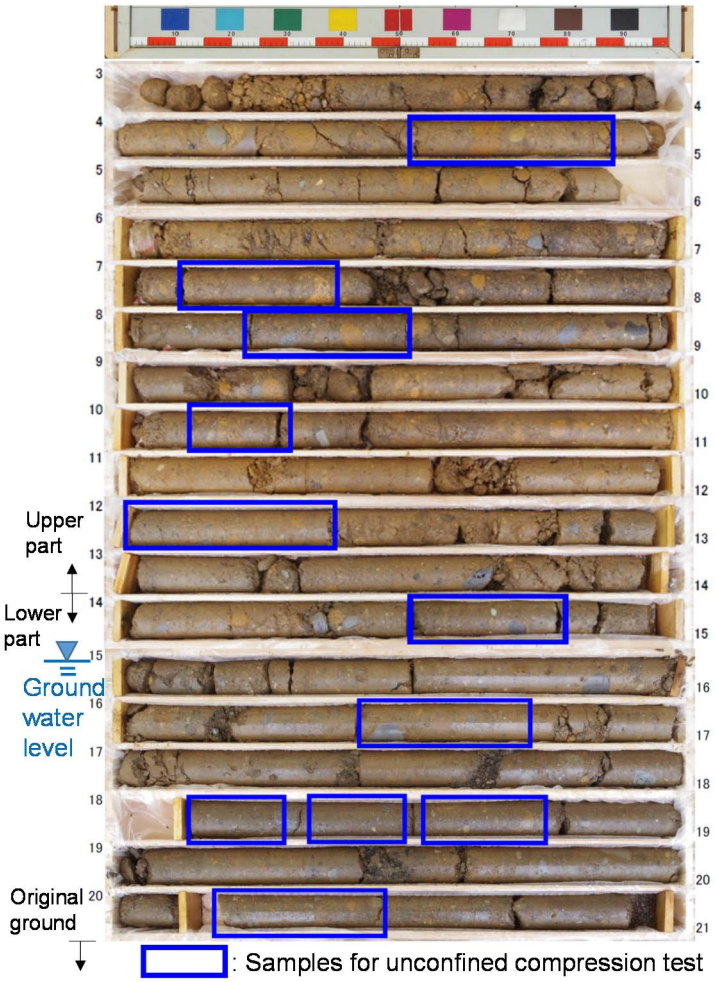


Fig. 2. Photograph of whole core sample

A typical example for the comparison between before and after applying phenolphthalein solution to the sample is presented in Fig. 3. It was observed that the color of the surface and the cross sections of the whole sample which was deeper than 3.4 m changed to red-purple as shown in Fig. 3. Such change in color suggested the alkalinity of the sample by the reaction of phenolphthalein, even after 9 years from the construction of the embankment. It was inferred from the result that the cement and soils had been mixed very well throughout the entire period of construction.

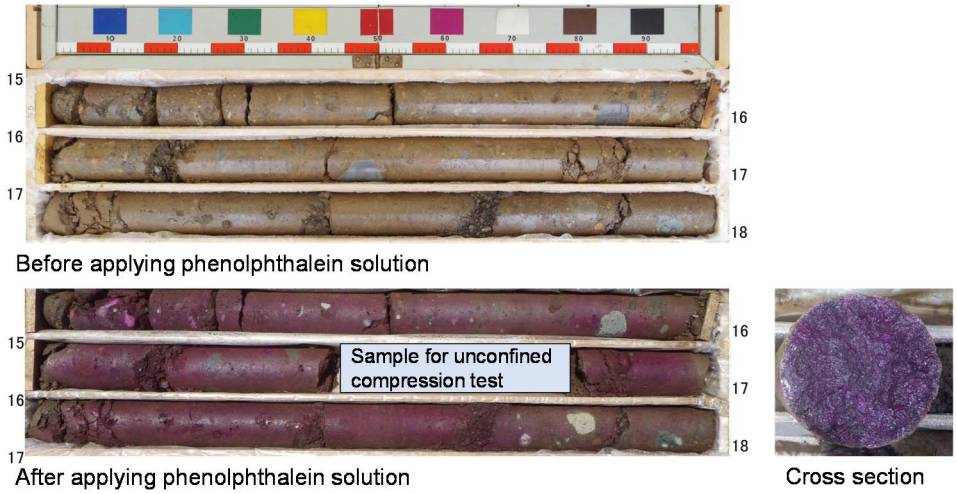


Fig. 3. Typical observation result concerning alkalinity of the sample using phenolphthalein solution

Result of mechanical tests in laboratory

Results of unconfined compression tests are summarized, with the distribution of unconfined compressive strength, q_{u_UC} and the relationships between q_{u_UC}, water content and dry density, as shown in Fig. 4a, b and c respectively. All the q_{u_UC} values exceeded design strengths for upper and lower part of the embankment which were indicated with a red broken line in Fig. 4a. It should be mentioned that several large particles were contained in most of the specimens, although the effect of those particles on the strength could not be identified. Despite the differences in the types of soils, macro structures of soil particles and amount of cement, q_{u_UC} values correlated with water contents and dry densities as shown in Fig. 4b and c. That is, q_{u_UC} increased with the decrease in water content and increase in dry density.

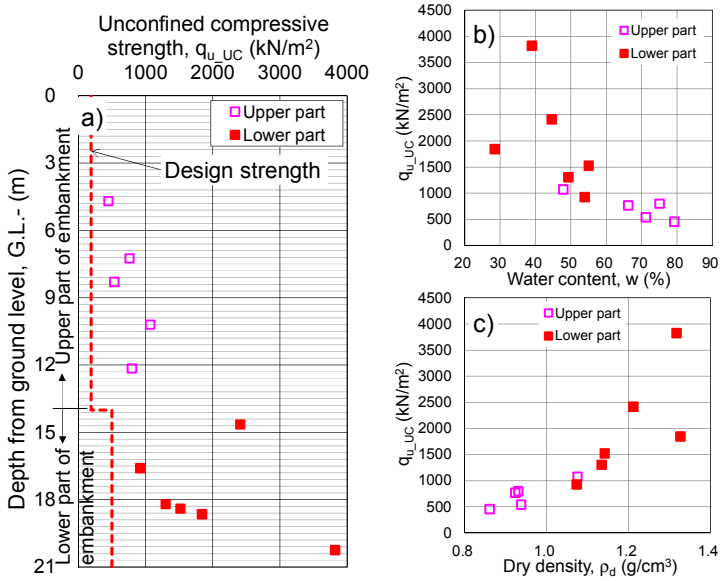


Fig. 4. Distributions of unconfined compressive strength (a), relationships between unconfined compressive strength and water content (b) and dry density (c)

Distribution of hardness index, D and unconfined compressive strength converted from D, q_{u_D} in the direction of depth of the sample are shown in Fig. 5a and b, respectively. Design strength and the results of unconfined compression test, q_{u_UC} are also indicated in Fig. 5b. D values were larger than approximately 30 mm in most of the cases, while the converted q_{u_D} values were not larger than 2000 kN/m^2. The portable soil hardness tester had been developed originally for the field survey in agricultural engineering. Considering the D values measured on the sample, the maximum strength level of the cement treated soils to define the equation [1], and the capacity of the tester, it was difficult for this test method to estimate the strength of 1000 kN/m^2 level accurately.

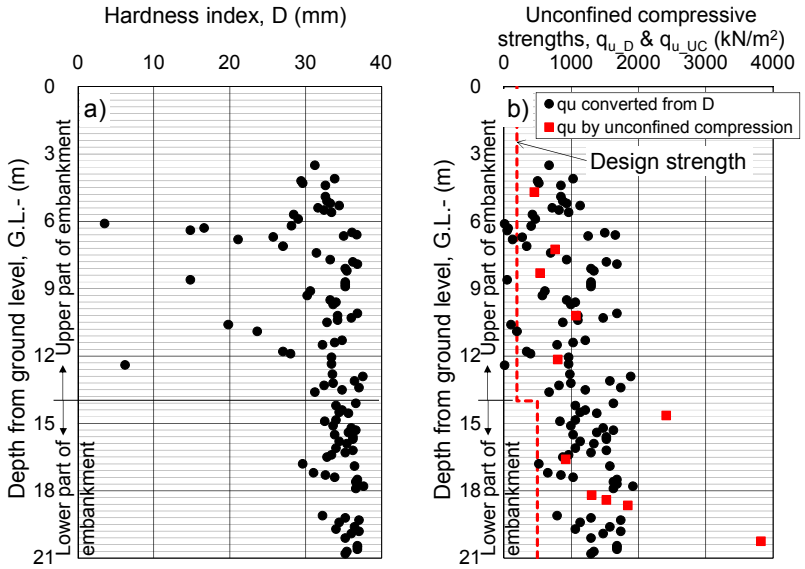


Fig. 5. Distributions of hardness index (a) and unconfined compressive strengths (b)

Fig. 6a shows the distribution of needle penetration gradient, N_P. Fig. 6b shows the unconfined compressive strength converted from N_P, q_{u_NP} in the depth direction of the sample with exhibiting the design strength and q_{u_UC}. N_P values obtained shallower than 14 m were in the range of 1 to 10 N/mm, while the range of N_P values obtained deeper than 14 m shifted to slightly higher level and varied in wider range. q_{u_NP} values greater than 4000 kN/m^2, i.e., N_P values bigger than 10 N/mm were finally eliminated in Fig. 6b, by referring the maximum strength level of the geomaterials to define the equation [3] and the range of q_{u_UC} values.

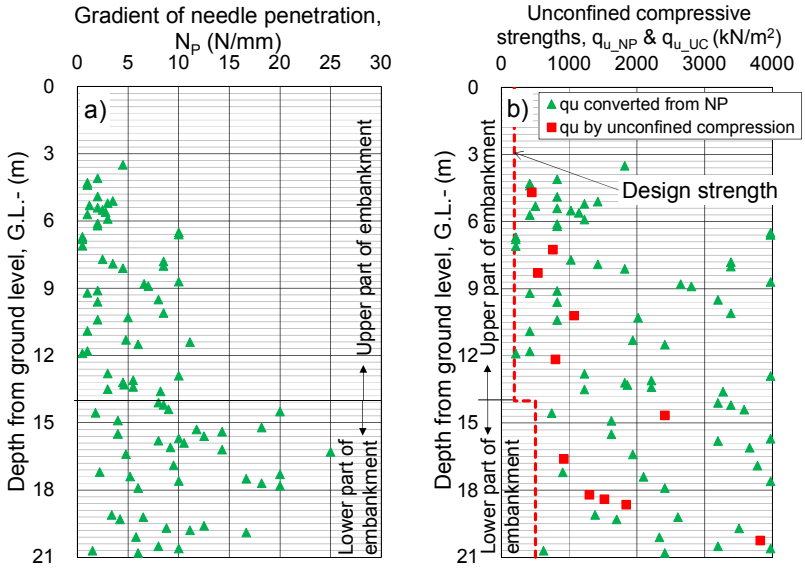


Fig. 6. Distributions of needle penetration gradient (a) and unconfined compressive strengths (b)

Relationships between q_{u_D}, q_{u_NP} and q_{u_UC} are presented in Fig. 7. Values of q_{u_D} and q_{u_NP} corresponding to a q_{u_UC} value at a certain depth were picked up from the nearest depth with each other. It could be seen that q_{u_D} and q_{u_UC} exhibited tolerable agreement when the value of q_{u_UC} less than 2000 kN/m^2. On the other hand, the relationship between q_{u_NP} and q_{u_UC} had large dispersion. One of the possible reasons might be the variation of the needle penetration test result. The existence of gravels close to the surface of the sample would be affected to N_P values. To improve the above relationships, it is required to evaluate the applicability of equations [1] and [3] in detail based on several types of treated soils including the sample in this study.

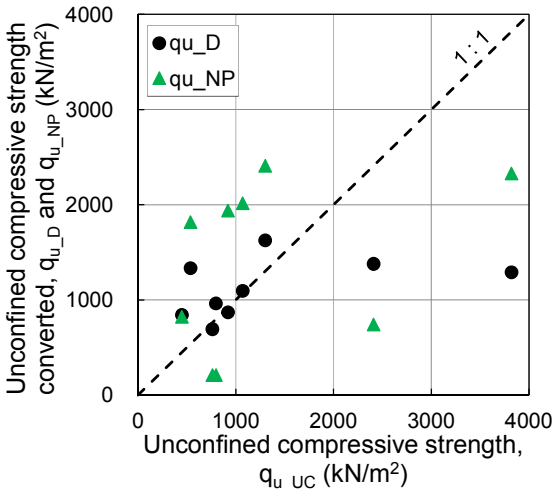


Fig. 7. Relationships between unconfined compressive strengths obtained by soil hardness, needle penetration and unconfined compression tests

DISCUSSION

Distributions of unconfined compressive strengths obtained in this study are summarized in Fig. 8. It could be judged in general that the unconfined compressive strength after 9 years was larger than the design strengths, throughout the whole length of the sample. It was found that some of the q_u values were much larger than the design strength. It might be mainly due to the variation of soils and the way of assessing the amount of cement at the time of construction, rather than the increase in strength during 9 years as explained below.

q_{u_UC} values obtained at the depth of 18 m after 56 days and 9 years from construction are compared in Fig. 9. Average value of q_{u_UC} after 56 days was 1319 kN/m^2. After 9 years, it had been increased by 1.2 times with a strength value of 1553 kN/m^2. The strength increment exhibited under this study was smaller as compared to that of cement columns (Committee of Geocement, 2014) as shown in Fig. 9. These cement columns with a diameter of 450 mm and a height of 2 m were made by filling a mixture of volcanic clay and cement slurry to a site above the ground water level. Characteristics of material, construction technique, amount and type of cement, and curing condition were different from the situations of this study. These factors would be affected to their long term mechanical properties. Especially on the properties obtained deeper than ground water level in this study, the effect of water and its quality might not be negligible as pointed out in the several previous studies on deterioration of treated soils caused by leaching of calcium ion (Catinaud et al., 2000; Kitazume et al., 2003; Ghobadi et al., 2014). It was not possible to investigate the long term mechanical property more in detail, as the other mechanical properties such as stress-strain relationships to obtain stiffness, physical and chemical properties at the time of construction could not be found in this study.

13 case histories in 12 previous studies on long term mechanical property of chemically treated soils are summarized by the relationships between the ratio of q_u*/ q_{u28}, and q_{u_UC} after 28 days, q_{u28}, as shown in Fig. 10 (Committee on properties and testing methods of cement treated soils, 2005). q_u* was defined as the q_{u_UC} value obtained after more than 10 to 20 years. The data of the previous studies were classified by the types of investigation (laboratory testing or site investigation) and in-situ construction methods, while the types of soils, type and amount of cement were not considered in the classification. According to the report, they had been obtained without or with less effect of deterioration due to exposure

conditions. The q_u*/q_{u28} value in this study was defined by the average of q_{u_UC} values at the depth of 18 m after 9 years (1553 kN/m^2) and the range of q_{u28} values of lower part of the embankment obtained at the stationary plant (562 - 1584 kN/m^2). It was calculated as the range of 1.0 to 2.8 and then plotted in Fig. 10 with the red rectangle. q_u*/q_{u28} values in the previous studies based on the site investigation were in the range of 1.8 to 4.6 when the q_{u28} values were larger than 1000 kN/m^2. The range of q_u*/q_{u28} value of this study was not high as shown in Fig. 10. Exposure condition at the depth of 18 m in this study, that is, the effect of ground water might be influenced the strength after 9 years as already pointed out in Fig. 9, while several other factors might be affected too. Further investigation including laboratory tests are required to clarify the major factors on the long term strength increment.

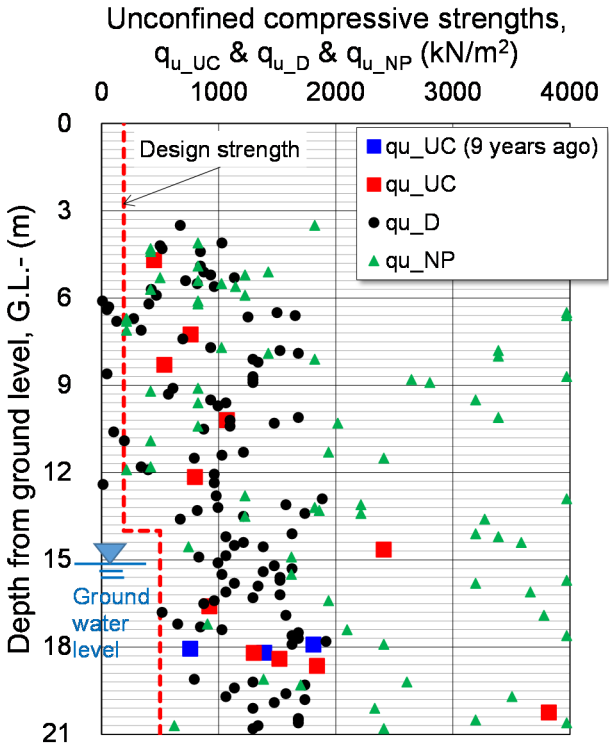


Fig. 8. Distribution of unconfined compressive strengths of whole sample

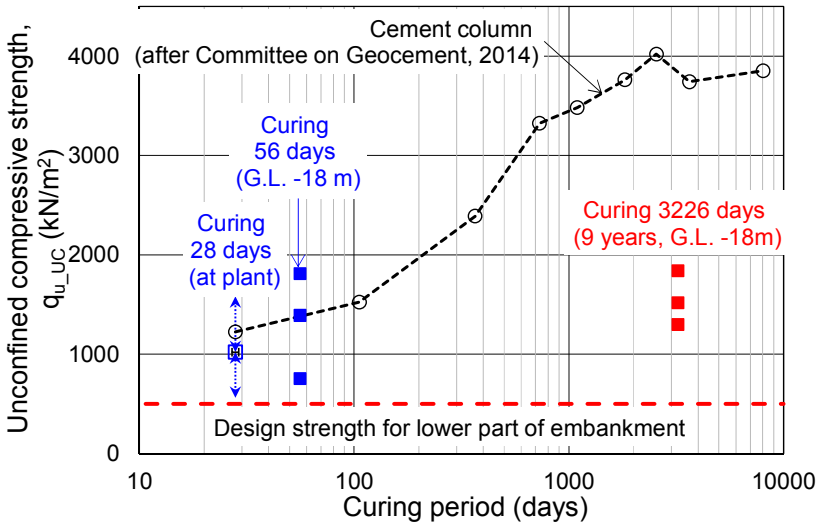


Fig. 9. Relationships between unconfined compressive strength and curing period of the sample at depth of about 18 m

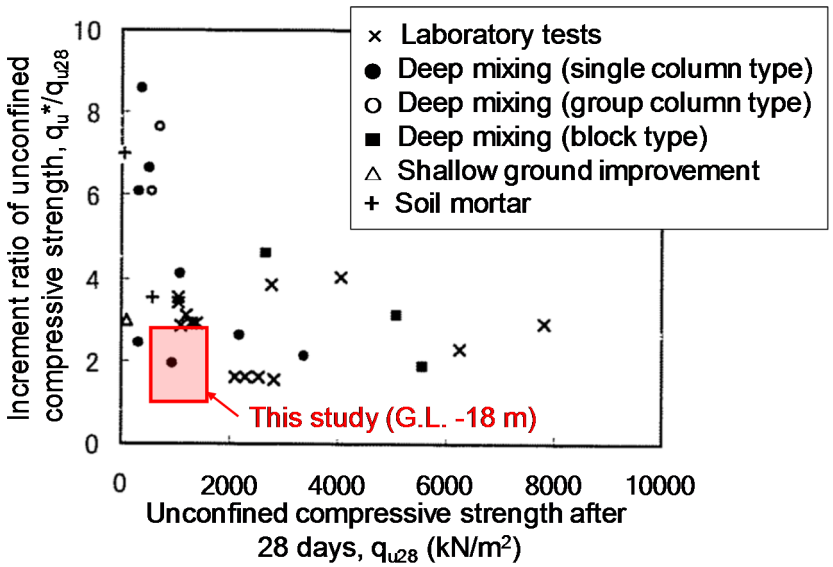


Fig. 10. Increment ratio of unconfined compressive strength after more than 10 years in previous study and that after 9 years in this study (modified after Committee on properties and testing methods of cement treated soils, 2005)

SUMMARY

A site investigation on a road embankment which had been made of cement treated loam was conducted after 9 years from its construction. It was found that the unconfined compressive strengths in the whole length of the undisturbed core sample were larger than the design strengths.

According to the comparison of strength at a certain depth below the ground water level, unconfined compressive strength after 9 years was 1.2 times larger than that of 56 days. The strength increment which was exhibited under this study was not high, when comparing the results of the previous studies on the long term mechanical property of the cement treated soils without or with less effect of deterioration due to exposure conditions.

ACKNOWLEDGEMENTS

The authors would like to thank Numazu office of river and national highway, Chubu Regional Development Bureau, MLIT, Japan and Nishimatsu Construction Co., LTD., for the assistance of site investigation and providing all the related information.

REFERENCES

Catinaud, S., Beaudoin, J.J. and Marchand, J., 2000. Influence of limestone addition on calcium leaching mechanisms in cement-based materials. Cement and Concrete Research, Vol. 30, pp. 1961 - 1968.

Committee on Geocement, 2014. A study on long term stability of soil-cement columns treated by geocement. Cement and Concrete, Monthly Journal of Japan Cement Association, No.804, pp. 9 - 14 (in Japanese).

Committee on properties and testing methods of cement treated soils, 2005. Report of committee on properties and testing methods of cement treated soils. Proceedings of the symposium on the investigation, design and construction methods of cement treated soils and evaluation of their properties, pp. 163 - 166 (in Japanese).

Ghobadi, M. H., Abdilor, Y., and Babazadeh, R., 2014. Stabilization of clay soils using lime and effect of pH variations on shear strength parameters. Bulletin of Engineering Geology and the Environment, Vol. 73, No. 2, pp. 611 - 619.

Hayashi, H., Nishikawa, J., Ohishi, K. and Terashi, M., 2003. Field Observation of Long-term strength of cement treated soil. Proceedings of the Third International Conference on Grouting and Ground Treatment, New Orleans, February 10 - 12, ASCE, pp. 598 - 609.

Ikegami, M., Ichiba, T., Ohishi, K. and Terashi, M., 2010. Lon-term properties of cement treated soil 20 years after construction. Proceedings of the sixteenth International Conference on Soil Mechanics and Geotechnical Engineering, Japanese Geotechnical Society, 2013. Geotechnical and Geoenvironmental Investigation Methods, pp. 1199 - 1202.

Kitazume, M., Nakamura, T., Terashi, M. and Ohishi, K., 2003. Laboratory Tests on Long-Term Strength of Cement Treated Soil. Proceedings of the Third International Conference on Grouting and Ground Treatment, New Orleans, February 10-12, ASCE, pp. 586 - 597.

Nishimi, N., 2009. Quality control of fill using cement mixed soil. Annual technical report of Nishimatsu Construction Co., LTD., Vol. 32, pp. 67 - 72 (in Japanese).

MEGA SOIL IMPROVEMENT CASE STUDY:
IMPROVEMENT OF SOFT SOIL USING PREFABRICATED VERTICAL DRAINS

Robert Thurner, Keller Grundbau GmbH, Austria – Dubai email: r.thurner@kellerme.com
Mohamed Ayeldeen, Keller Grundbau GmbH, Dubai email: m.ayeldeen@kellerme.com

ABSTRACT

A huge industrial area in Egypt of more than 60 km^2 was found to contain very soft clays up to 50 m depth. The ideal solution to achieve the required goals for the soil improvement is to install some hundred million meters of prefabricated vertical drains (PVD) in combination with a surcharge of a height of 6.5 m. One of the biggest challenge was to build up a simple design model throughout this huge area with wide variation in the soil properties/conditions. Next to the locally available experience regarding the soil conditions and the primary soil investigation, a quite intensive soil investigation campaign with more than 150 CPTUs and 600 dissipation tests was going on parallel to the installation to adapt the preliminary design. It was essential to build a trial field including several types of instrumentations for intensive monitoring of the occurred deformation. The collected data was used to predict the soil behavior and the development of the settlement. Simple to sophisticated calculation models have been used to evaluate the effectiveness of the works that were executed. Some standard methods such as Sherif and Asaoka were applied using the settlement measurements, while for the trial field, a combined evaluation and check of the concepts applied has been done using multiple-level piezometers, inclinometers, extensometers and other instrumentation. This has been combined with 3D-FEM analyses to understand the behavior of the entire system and to optimize the soil improvement scheme. In the proposed paper an overview and some interesting details will be given about the multiple tasks during the design, evaluation of the trial field and execution of the geotechnical works. Some equations and models have been developed and verified with the measured parameters.

Keywords: prefabricated vertical drains, soft clay, soil improvement, consolidation, preloading

INTRODUCTION

Soft soil deposits can be found in many places all over the world, especially coastal areas, which are recognized by a high compressibility and a low shear strength [1], [2]. It became essential to find the appropriate method to improve the softly soil characterizations in order to meet the needed engineering requirements for construction. One of the most well-known method used to improve the soft soils is preloading over vertical drains. This approach can be used effectively to reduce the post-construction settlement and improve the soil shear strength as well. By considering the very low vertical permeability of the soft soils, the time required to achieve the required settlement will be too long compared to the available time for the construction. Moreover, the horizontal permeability of soft clay is much higher than the vertical permeability. Therefore, using vertical drains in soft soils will reduce the drainage path from the thickness of the soil layer (in case of vertical consolidation) to half of the drain spacing (in case of horizontal consolidation) [3], [4].

SOIL PARAMETERS AND DESIGN REQUIREMENTS

The preliminary soil investigation was based on 8 CPTus performed in the upper zone including 4 dissipation tests for each CPTu. The preliminary soil profile can be seen in Figure 1. The first 15 meters can be defined as silty clays to sandy silts, where the over consolidated ratio, *OCR* is varying from 1.1 to 2.25 and the coefficient of horizontal consolidation, C_h was estimated to be over 10 m^2/year. However, the lower layer – from 15 m to about 50 m - can be considered as silty clays to clays, with *OCR* value of 1.1 – 1.2 and C_h of 3.0 m^2/year. Based on these soil parameters a calculation model taking into account the stepwise settlement calculation over the depth and the decisive parameters are given as in table 1.

© 2018 Deep Foundations Institute

Table 1. Calculation model for preliminary design

Depth [m]	Preliminary Lead Design Zone B – Stage 1		
	E_s [kN/m²]	C_v [m²/year]	C_h [m²/year]
0 – 10	5000	1.0	10.0
10 – 15	2750	1.0	10.0
15 – 25	3500	1.0	3.0
25 – 50	5250	1.0	3.0

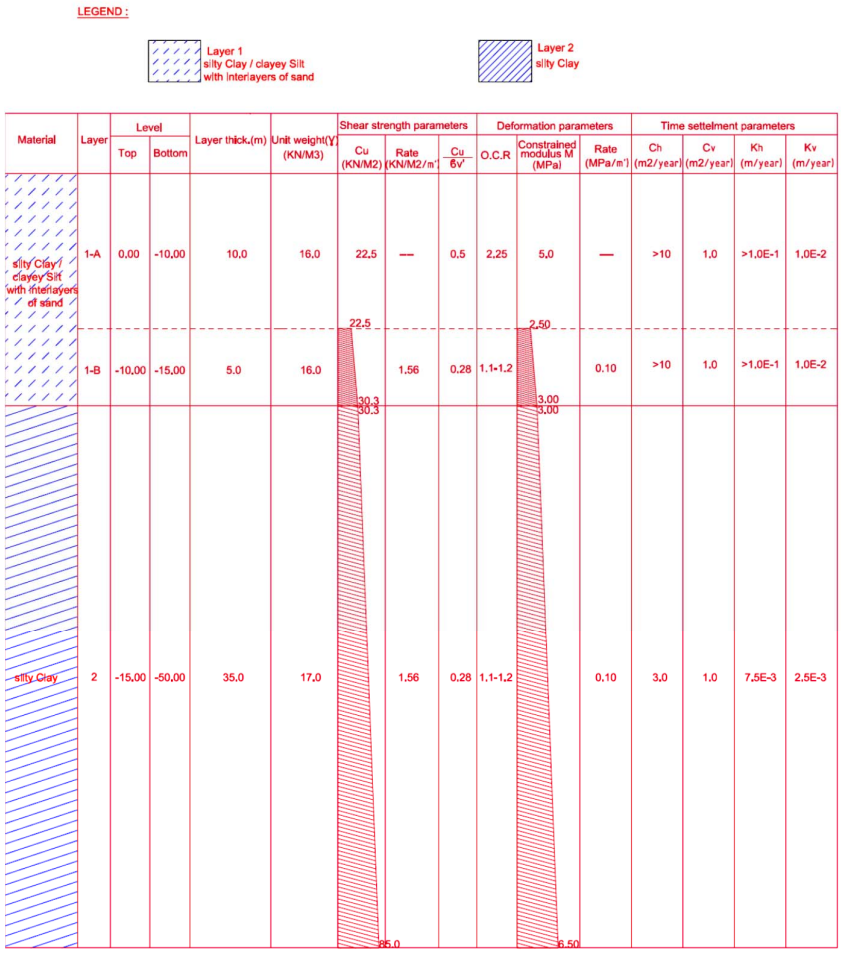


Figure 1. Preliminary geotechnical design parameters.

By considering the above soil profile, the agreed design was 25 m depth PVD installed from the one meter thick working platform. The vertical drain spacing is 1.5 m in triangular shaped grid. The mentioned design and assumptions will be confirmed by measurements from the field trial zone, to be installed on site with sophisticated monitoring system. Moreover, due to the huge area of the project, more than 150 CPTus with about 600 dissipation tests will be performed all over the site to confirm the homogeneity of the assumed soil profile. Another 100 post CPTus will be performed later on.

Several methods were used in the design including simplified Hansbo method [5], [6] and some other finite element software. The expected settlements for the different methods were compared in Table 2, where it can be seen that the expected settlements after six months preloading is up to more than 200 cm, and the remaining settlement after 20 years is about 13 cm.

Table 2. Comparison between different design methods

Value of settlements, cm	Method 1: conventional analysis	Method 2: Finite difference (Settl3-D)	Finite element	
			Equivalent vertical permeability approach	Equivalent horizontal permeability approach
1-Case of applying of stress 91 kN/m^2 for six months	210	220	210	216
2-Effective settlement for a period of 20 years after applying a stress of 70 kN/m^2	11	12	15	12

TRIAL ZONE

The general concept is to start the project with the approved preliminary lead design. Simultaneously, an extensively monitored trial zone will be executed and monitored according to the proposed schedule. Based on the received results, soil parameters shall be figured out, which will be used later on to verify and adopt the preliminary lead design. Moreover, this process shall lead to a better understanding of the Soil-PVD-Surcharge interaction and therefore allow to optimize the design. The designed area dimensions for the trial zone are 250 m x 250 m. Additional soil investigation was provided for this area including 3 CPTus with four dissipation tests for each CPTu and two boreholes up to 70 m depth. Directly after the installation of the PVDs, preloading fill (surcharge) sized 150 x 150 m was executed. The surcharge was applied in layers with total height of 6.5 m (from the virgin soil level), with an average unit weight of 1.64 t/m^3. Monitoring systems were installed including 21 pieces of Ground Measurement Points, *GMP*, 2 pieces of extensometers, *EXT*, 3 pieces of piezometers, *PWP* and 2 pieces of inclinometers, *INK* ,to fully monitor the trial zone behavior during consolidation stages, as shown in Figure 2. Beside the mentioned systems, one GMP was installed next to each instrument (EXT, PWP and INK) for measurement calibration purpose. Four open pits were installed to monitor the ground water table for the hydrostatic PWP calculations. Six deeply fixed points (up to 60 m depth) were distributed all over the site to be used as reference level for the surveying measurements.

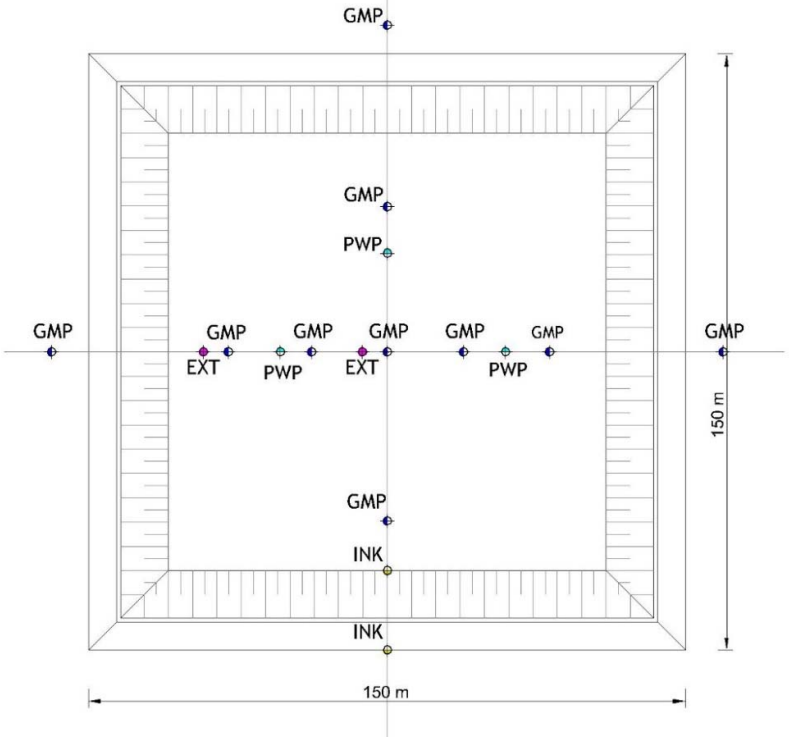


Figure 2. Layout for the trial zone

TRIAL ZONE SOIL PROFILE

In order to have a clear understanding of the soil profile in the trial zone before the improvement, the results for the performed 3 CPTus were compared with the previous 8 CPTus, while intensive laboratory tests were done on the obtained samples. The results for the first borehole were in a good agreement with the chosen design soil profile (Figure 1). This means that the current design is still valid at the moment, and the trial zone results after improvement will be sufficient enough to adjust the design if needed.

EMBANKMENT CONSTRUCTION AND STAGE OF LOADING

The platform in the trial zone was ready three months before the PVD installation with a thickness of 1 m, which can be considered as a first stage of preloading and will be taken in the account later on in the modeling. The duration of the PVD installation was about 1month to cover all the trial area of 250 x 250 m. The third stage was constructing the embankment to a height of 5.5 m above the platform. The embankment construction was done in layers with an average thickness of about 1.0 m, while the setup of the whole embankment took another month. All the embankment was built from medium sand with a fines content less than 5%. Roller compactors were used for each layer to ensure the homogeneity of the surcharge unit weight, with four sand cone tests for each layer. After completing the total height, a wide open pit was executed till the bottom of the embankment and the actual field unit weight was measured again and it was found to be in average of 16.4 kN/m^3.

TRIAL ZONE RESULTS

Intensive monitoring systems were adjusted to follow up to the behavior with high accuracy. All the instrumentations and the settlement points were measured on a daily basis during embankment construction and for two weeks after finishing the construction. Starting from the third week, the readings were taken three times per week, to be reduced after another two weeks to be twice a week for the next 5 months. Finally, after 6 months from the embankment construction, the readings will be measured weekly till the end of the first year.

Ground measurement point, GMP

One of the biggest challenges on a mega site (especially when settlements are expected to occur everywhere), was to define a trustable fixed point as a reference in the GMP readings. Installing 60 m deep micro piles with an optimized distribution to cover the entire site was the most accurate method for this. A typical settlement characteristic is shown in Figure 3. A logical matching between the surcharge construction and the early settlement was observed where high settlement of 83 cm occurred in the first month during the embankment installation. Reduction in the settlement slope can be observed with time, which reflects the fact of increasing the degree of consolidation and reducing the settlement rate.

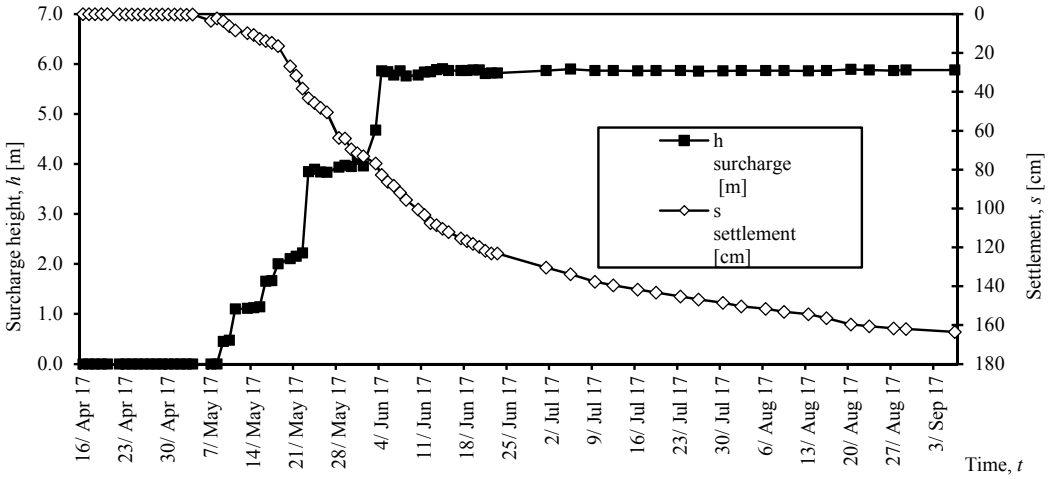


Figure 3. Settlement and surcharge height with time for GMP 6

Pore-water pressure, PWP

It was necessary to observe and analyse the total and excess pore pressure during the consolidation process, however excess water pressure readings can be misleading. The distance between the piezometer and the drains can severely affect the results [7]. In the current trial zone, three piezometers were installed, the results of only two are reliable and are therefore used in the analysis. In all the three piezometers, four levels were chosen for the study (10, 20, 35 and 50 m). One extensometer was set up at the same level to be used later in order to adjust the piezometers levels. The excess pore water pressure was calculated and compared twice; first by considering the initial piezometer readings before the surcharge and second by considering the hydrostatic pressure from the open pits. The values for both methods were a bit different. This could be the effect of several sources such as the piezometer calibration, the floating of the cell in a limited distance or the capillarity effect on the water table in the pit. However, the overall trend for both methods was the same and in compliance with the literature [7], [8]. Figure 4 presents the excess PWP for piezometer 2. The increase in the excess pressure with increasing surcharge differs with depth, however for the first two gauges it is almost equivalent. While the dissipation is obvious with time, the dissipation rate in the first gauge in higher than in the others, for which the first layer is close to the upper sand filter with shorter water pass. The dissipation rate in the second and third gauges are less in the same order with depth, and as what was expected for the fourth gauges (located in the sand layer) the excess pressure is almost zero.

Inclinometer, INK

Beside the piezometers, two inclinometers were installed as well to measure the lateral deformation close to the slope edge. It can be seen from Figure 5 the noticeable increasing in the lateral deformation with time in the two months (April to June), while the increasing in lateral deformation decline later on (June to August), and it was almost stopped in the last month in the presented chart (September).

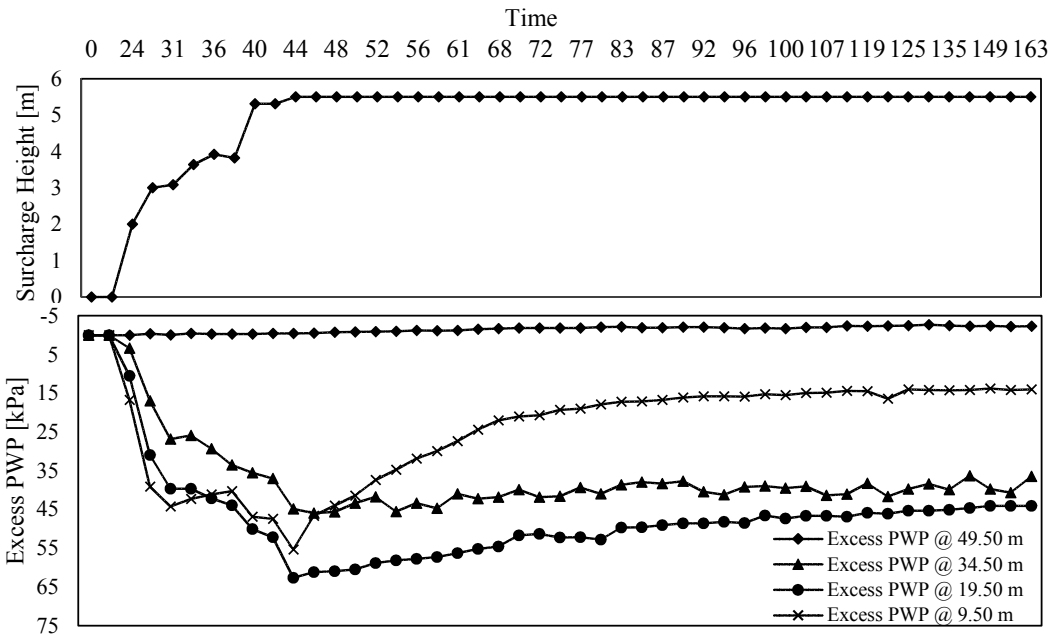


Figure 4. Pore-water pressure for piezometer 2

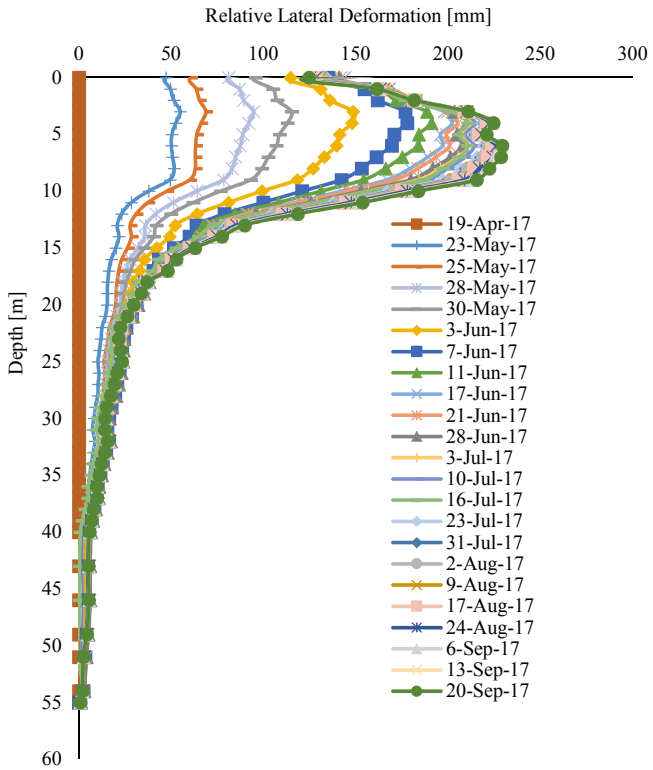


Figure 5. Lateral deformation with depth from INK 1

MEASUREMENT ANALYSIS

Settlement rate

The first step in the analysis is to estimate the settlement rate as it can be a clear acceptance criterion to judge the efficiency of the improvement. Figure 6 is showing the average settlement rate during and after the embankment construction. It is clear that there is a huge difference in the slope rate in both stages. While the rate reduced from 2 cm/day in the first week to about 1cm/day in the fourth week, the settlement rate after construction was almost about 0.4 cm/day from week number 10 until week number 18. Obviously, the settlement rate is reducing with time, however it cannot give a clear answer about when to expect the end of the primary consolidation.

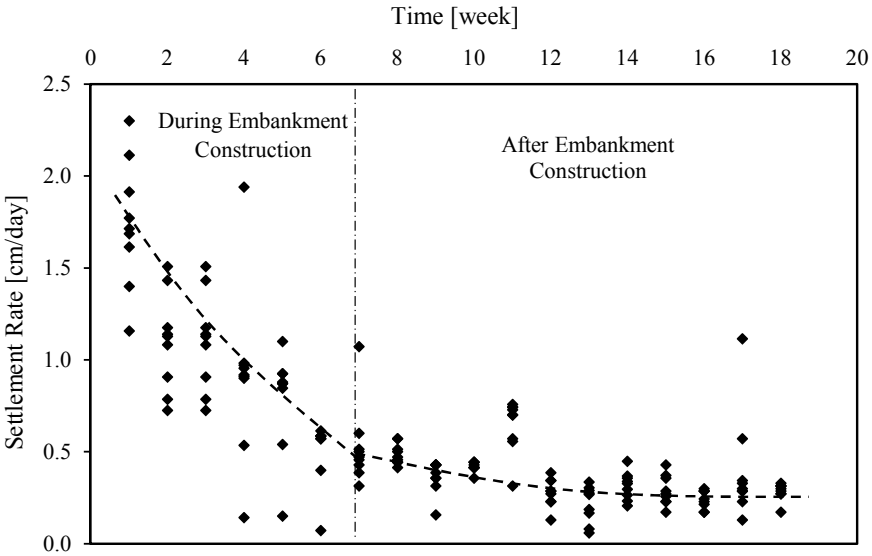


Figure 6. Average settlement rate per day during the preloading

Asaoka method

Although Asaoka method is considered to be one of the most common methods to estimate the total settlement during preloading, the application of Asaoka in the current case was not possible [9]. As Asaoka is an analytical method based on the relative deformation between two consecutive settlements (Sn and Sn+1) at the same time interval, the estimated settlement can easily vary up to the applied duration. It is worth to mention that it can be the case for the presented project. Due to the limited monitoring time until the present moment, the estimated settlements using Asaoka was on average 160 cm, as shown in Figure 7. This means that more than 98% consolidation degree is achieved. However, by considering the actual settlements and the calculated settlement rate this seems not realistic in a first evaluation.

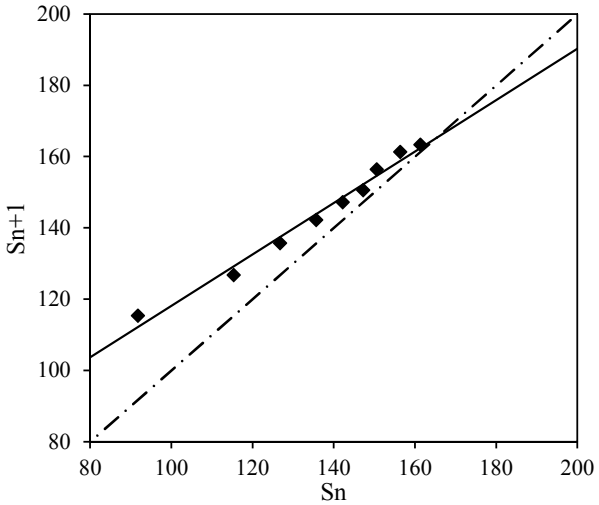


Figure 7. Asaoka method application for GMP 6

Sherif method

This method was adopted to estimate the total settlement during preloading, which is based on the ratio of the time and the value of t * h/s, where *s* is the settlement at time *t* and *h* is the surcharge height[10]. By applying the Sherif method as shown in Figure 8, the final settlement can be calculated as:

$$S_{final} = [\Delta t / \Delta(t * h/s)] \times h_{max}$$

where h_{max} is the maximum surcharge height.
From the application of the previous equation after Sherif, the expected settlement is about 220 cm, which means that the degree of consolidation using the data shown in Fig. 8 is about 70%.

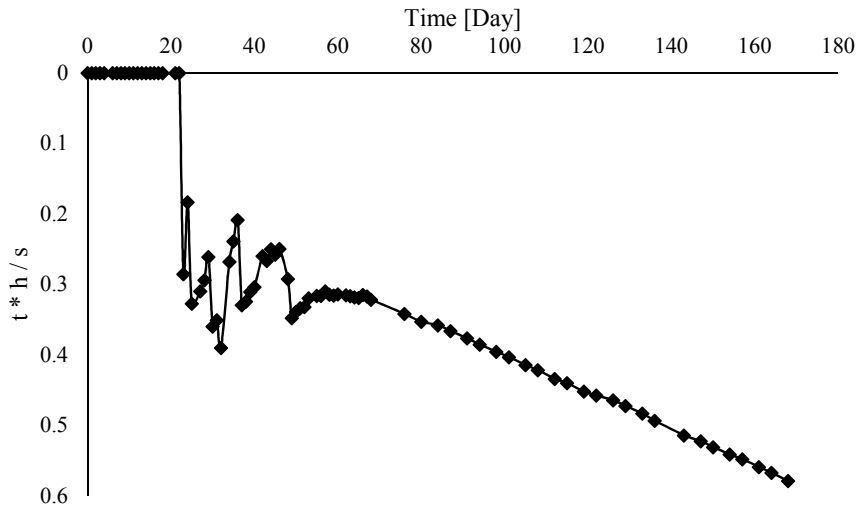


Figure 8. Sherif method application for GMP 6

DEGREE OF CONSOLIDATION COMPARISON

Besides the previously mentioned methods, a new method was used (Li method, based on Asaoka) by considering the early stage of the preloading [11]. Using the Li method did not affect the final expected settlement from Asaoka, but, as shown in Figure 9, the behavior in the first 40 days changed to a more reasonable one.

Excess pore pressure results were also used to calculate the current degree of consolidation from the remaining excess pressure before dissipation [3], [8]. The estimated degree of consolidation from excess pressure was about 65-80%, which is in a good agreement with Sherif method expectations. For more investigation, classical Terzaghi equations were applied considering the soil parameters from the soil investigation (CPTu and boreholes), where the calculated degree of consolidation is about 85%. A numerical model using Plaxis 2D was also adopted to simulate the case of using multiple stages of construction. The soil parameters used in the model were the same as the ones used in Terzaghi's classical equations, while a soft soil model was used to simulate the soft clay material. The achieved degree of consolidation is about 67%.

CONCLUSION

Several methods were used to estimate the final settlements and the current degree of consolidation, however it is essential to have a clear idea about the limitations for each method. From the measurements until the submission of this paper, it seems that the behavior of the system Soil-PVD-Surcharge is in line with the outcome of the preliminary lead design. Although some methods have obtained the same degree of consolidation, more measurements should be considered for longer period as 3 months of preloading is still not enough. The evaluation of the entire system including developing a site specific geotechnical model will be done based on this and future measurements.

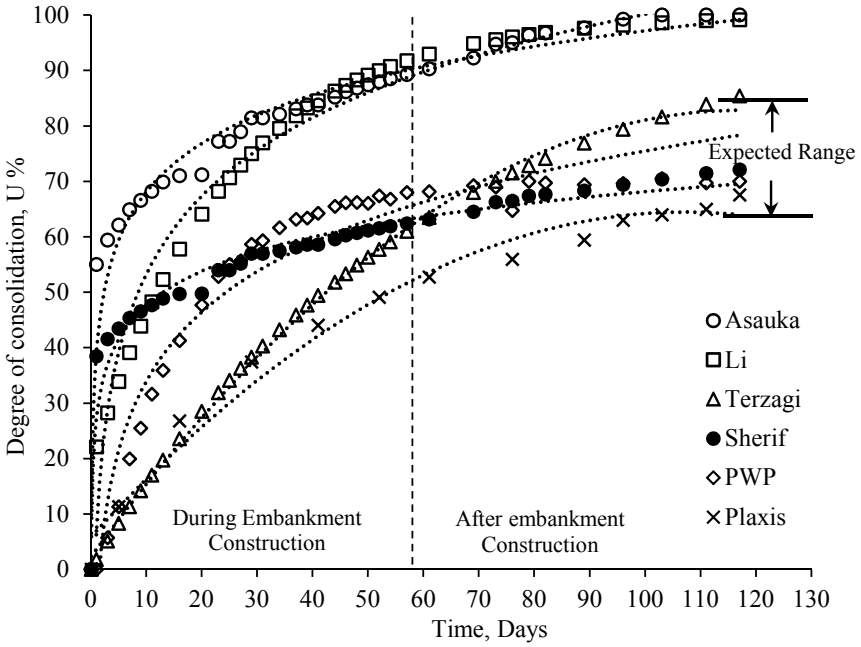


Figure 9. Degree of consolidation calculations

REFERENCES

[1] M. Salem and R. El-sherbiny, "Comparison of measured and calculated consolidation settlements of thick underconsolidated clay," *Alexandria Eng. J.*, vol. 53, no. 1, pp. 107–117, 2014.

[2] M. Ayeldeen and M. Kitazume, "Using fiber and liquid polymer to improve the behaviour of cement-stabilized soft clay," *Geotext. Geomembranes*, vol. 45, no. 6, pp. 592–602, Dec. 2017.

[3] B. Indraratna, C. Rujikiatkamjorn, A. S. Balasubramaniam, and G. McIntosh, "Soft ground improvement via vertical drains and vacuum assisted preloading," *Geotext. Geomembranes*, vol. 30, pp. 16–23, 2012.

[4] Buddhima Indraratna, C. Rujikiatkamjorn-, and Jian Chu, "Critical Review of Analyses in Soft Clay Stabilisation with Geosynthetic Vertical Drains beneath Road and Railway Embankments," *Adv. Meas. Model. Soil Behav.*, 2007.

[5] S. Hansbo, "Consolidation of clay by band-shaped prefabricated drains," *Gr. Eng.*, vol. 12, no. 5, pp. 16–25, 1979.

[6] H. M. Abuel-Naga, M. J. Pender, and D. T. Bergado, "Design curves of prefabricated vertical drains including smear and transition zones effects," *Geotext. Geomembranes*, vol. 32, pp. 1–9, 2012.

[7] B. Indraratna, Jian Chu, and C. Rujikiatkamjorn, *Ground Improvement Case Histories: Embankments With Special Reference To Consolidation And Other Physical*. Elsevier Ltd., 2015.

[8] D. T. Bergado, A. S. Balasubramaniam, R. J. Fannin, and R. D. Holtz, "Prefabricated vertical drains (PVDs) in soft Bangkok clay: a case study of the new Bangkok International Airport project," *Can. Geotech. J.*, vol. 39, no. 2, pp. 304–315, 2002.

[9] A. Asaoka, "Observational procedure for settlement prediction," *SOILS Found. Found.*, vol. 18, no. 4, pp. 87–101, 1978.

[10] G. Sherif, "Setzungsmessungen an Industrie- und Hochbauten und ihre Auswertung, Veroffentlichung des Institutes fur Grundbau und Bodenmechanik der TH Aachen," 1973.

[11] C. Li, "A simplified method for prediction of embankment settlement in clays," *J. Rock Mech. Geotech. Eng.*, vol. 6, no. 1, pp. 61–66, 2014.

PERFORMANCE OF A NEW DRIVEN BATTERED MICROPILES SYSTEM IN SAND

Amirhassan Mehdizadeh, The University of Melbourne, Melbourne, Australia, +61 424 923 392, amehdizadeh@unimelb.edu.au
Mahdi M. Disfani, The University of Melbourne, Melbourne, Australia, mmiri@unimelb.edu.au
Chin F. Tsang, The University of Melbourne, Melbourne, Australia, c.tsang@student.unimelb.edu.au
Guillermo A. Narsilio, The University of Melbourne, Melbourne, Australia, narsilio@unimelb.edu.au
Robert Evans, Swinburne University of Technology, Melbourne, Australia, robertevans@swin.edu.au
Emad Gad, Swinburne University of Technology, Melbourne, Australia, egad@swin.edu.au

ABSTRACT

A new concrete-free driven micropile footing system that consists of a steel pile cap and a number of inclined small diameter steel micropiles has been tested. This new footing system is light enough to be manually handled and can be installed in a short time-frame using small jackhammers. There is minimal soil disturbance and no need for any excavation making it a smart solution for supporting light structures. This paper presents the performance of this new footing system in a medium dense sand formation under vertical compressive and tensile pull-out forces. Two different combinations (with different embedment depths) were tested. Ultimate bearing and pullout capacities were determined using a range of methods. A plate load test was also performed as a benchmark for shallow foundation capacity. The recorded pullout capacity was approximately 27 per cent of the bearing capacity showing that there are other parameters such as the reinforcing effect of battered micropiles enclosing the soil in between that contribute to the improved bearing capacity. These influential parameters need to be applied in the current engineering approach as the ultimate bearing capacity is underestimated. A negative group effect was also found that needs to be considered in estimating both tensile and compressive loads.

Keywords: battered micropile, field static micropile test, pullout and bearing capacities

INTRODUCTION

Micropile technology is a low impact construction techniques commonly used for retrofitting of existing foundations or new construction where using heavy equipment such as piling rigs is impossible due to limited access or risk of soil instability. Micropiles are piles with small diameter of less than 300 mm which can be driven, drilled or casted in place depending on the micropile type, soil condition and construction requirement. In early 1950s, they were used first for underpinning damaged historical buildings after World War II (Mason and Bruce 2001). However, micropiles application was soon employed in other geotechnical applications such as retaining structures, shoring and ground improvement due to their flexibility in construction, dimension and layout (Bruce et al. 1997; Schlosser and Frank 2004). Among different types of micropiles, a new steel (concrete-free) driven battered micropiles system is gaining popularity due to its light weight, quick installation (normally less than 15 minutes) with minimal soil disturbance. This new micropiles system is known as Surefoot and comprised a galvanized steel top plate that sits on the ground surface and a number of galvanized steel hollow micropiles. The tubular micropiles with outside diameter of 40 mm are driven outward at 25° from vertical through guiding sleeves connected to the top plate using hand-held jackhammers (Fig. 1). Depending on required capacity, size of the top plate and number and length of micropiles can be changed. They can also be connected to each other through a capping system to make a composite system capable of carrying much higher loads.

© 2018 Deep Foundations Institute

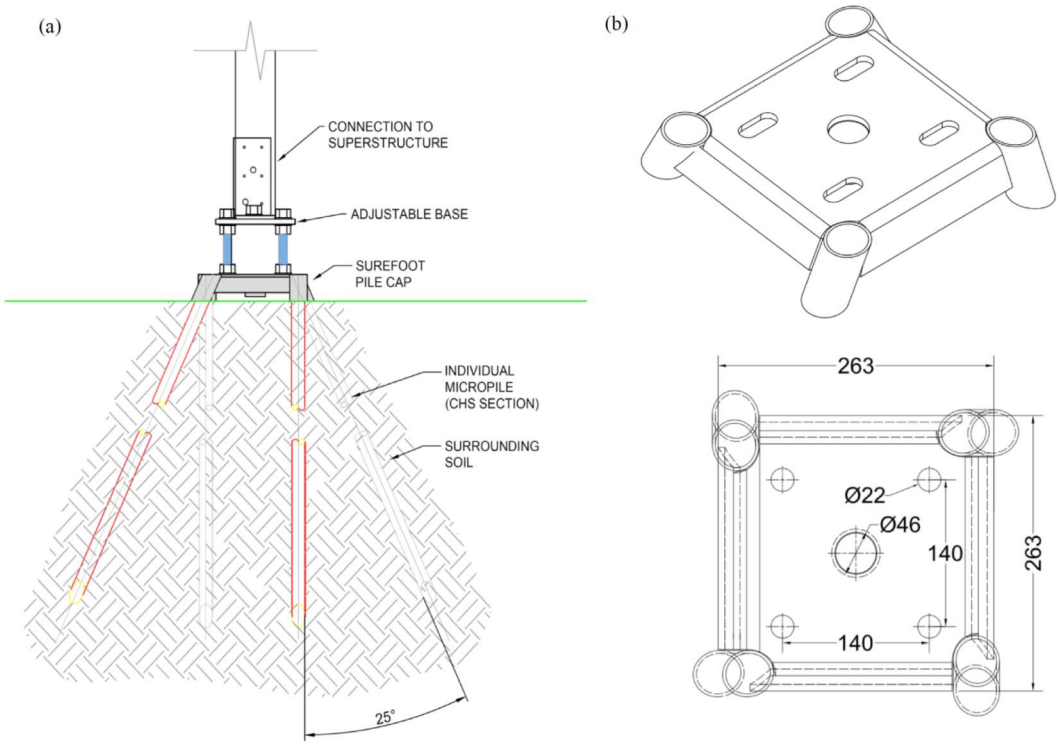


Fig 1. (a) New driven battered micropile system with surrounding soil and (b) S250 top Cap

Generally, the geotechnical capacity of micropiles are based on skin friction and toe bearing. However, end bearing is normally disregarded due to small toe area (e.g. Bruce and Yeung 1984; Juran et al. 1999; Cadden et al. 2004) except when micropiles sit on hard rock (Cadden et al. 2004 and FHWA 2005). In a battered micropile system, other mechanisms such as internal reinforcement and arching provided by the micropiles and surrounding soil need to be considered. Takahashi (1985) proposed an analytical method to examine the flexural behaviour of a battered pile. He found that the maximum bending moment was related to the settlement of the ground surface and the inclination of the pile. Behaviour of battered micropiles in very dense sand was investigated by Ishito et al. (2003). Laboratory test results indicated that a positive network effect was mobilized under inclined loads and increased gradually with settlement. Shaft resistance of vertical and battered piles in sand subjected to vertical loading was studied theoretically and experimentally by Hanna and Nguyen (2003). It was found that an increase in pile inclination up to 30° with respect to the vertical direction decreased the ultimate shaft resistance slightly. Tsukada et al. (2006) investigated mechanism of bearing capacity of spread footings reinforced with battered micropiles by conducting a series of model tests. An interaction between the footing and a group of micropiles was recognized. This interaction improved the bearing capacity of foundation more than twice the summation of the individual bearing capacity of the footing and the micropiles group. Vertical and uplift capacities of a single and a group of battered micropiles in sand were examined using physical modelling and field testing by Kyung et al. (2016) and Kyung and Lee (2017), respectively. Kyung et al. (2016) showed that vertical capacity increased initially by an increase in installation angle with maximum value at 15° and then decreased gradually. However, the vertical capacity of a micropiled raft was affected by both angle of installation and micropiles spacing. This finding was slightly different for the maximum uplift capacity. Although the same trend was followed but the maximum uplift capacity was observed for the installation angle of 30°.

The current engineering approach is simplistic and is based on a combination of shallow and deep foundation design principles (Mehdizadeh et al. 2016). However, literature shows that there are uncertainties in the behaviour of a battered micropile system that cannot be explained by conventional theories alone. To assess the engineering design principles and the ultimate capacity of this new battered micropile system in noncohesive soil, static field load tests were performed as being the most reliable

approach. It is worth mentioning that the performance of this new footing system in clay was previously studied and presented by Mehdizadeh et al. (2016).

A series of static load tests were performed on a range of Surefoot systems to evaluate both compression and pull-out capacities. These tests were all conducted in an area comprising quaternary Holocene to Pleistocene dune sand deposits, located in Fingal (a suburb south of Melbourne). This paper presents *in-situ* geotechnical test results along with the field static load tests. The field test results are back-analysed using a range of available methods (from current literature) to determine the failure load. Achieved ultimate capacities were then compared with the current design approach and discussed.

SITE DESCRIPTION AND TEST PROGRAM

The test site was located in Melbourne's southern suburb of Fingal in Victoria; Australia. A series of *in-situ* geotechnical tests were conducted near the testing area, which include Cone Penetration Test (CPT) at five locations and Standard Penetration Test (SPT) in three boreholes down to 10 m below ground surface.

It was revealed that the site consisted of silty sand with organic root matter present in the first 400 mm. Relative density of the silty sand was found to increase with depth and varied from loose to dense. No water table was observed down to the bottom of the boreholes. Multiple disturbed specimens were taken to a depth 6 m to measure moisture content. To compare the performance of this new battered micropile system against a standard shallow foundation, a Plate Load Test (PLT) 760 mm in diameter was performed. On the contrary to the CPT and SPT, the PLT was set up at the bottom of a trench 400 mm below ground surface to remove the possible influence of the organic matter and inconsistency of this top layer. Normalized CPT cone resistance and friction ratio and SPT corrected values (N'_{60}) are presented in Fig. 2. It is evident that down to the bottom of the micropiles (maximum embedment depth of 1.5 m plus trench depth of 0.4 m), all CPT and SPT results show uniformity in trend and magnitude. The average soil parameter values for the upper 2 m layer, which were correlated from CPTs and SPT results and laboratory tests are indicated in Table 1. It is worth mentioning that a ground surface survey was carried out to correlate the *in-situ* tests results.

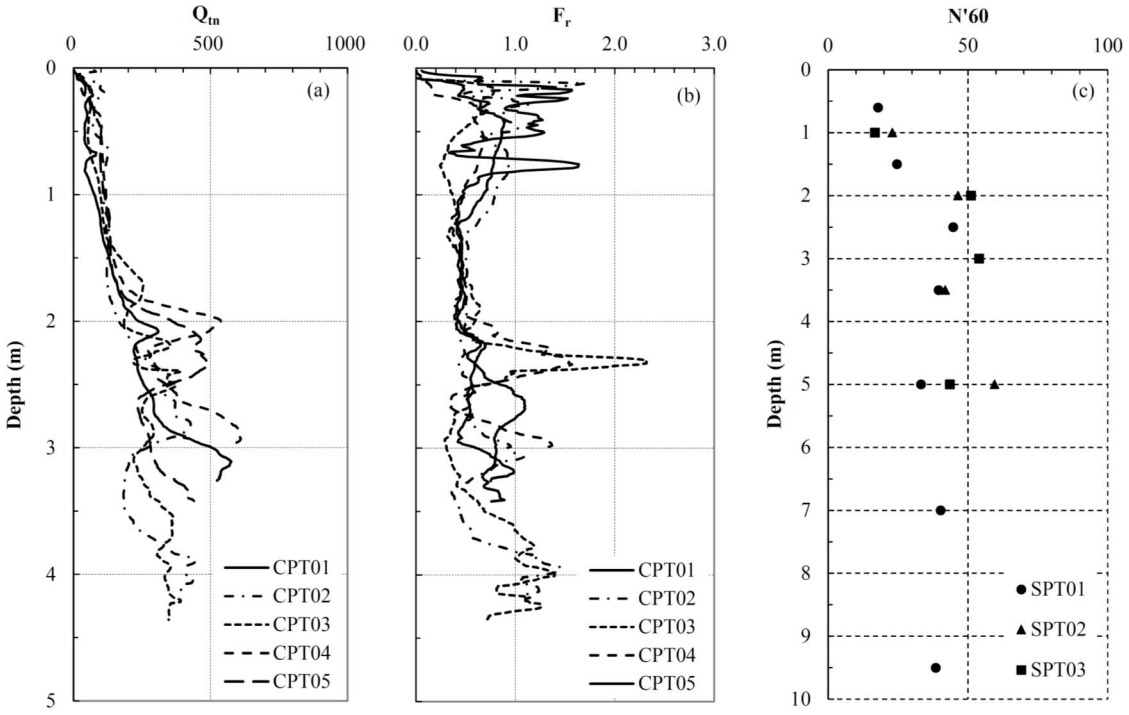


Fig. 2. (a) Normalized CPT cone resistance, (b) normalized CPT friction ratio and (c) corrected SPT values

Table 1. Average values of soil parameters based on CPT, SPT and laboratory measurement

Soil Parameter	Soil Depth (m)	CPT	SPT	Lab
Friction Angle (°)	0-1	36	-	-
Young's Modulus (MPa)		3.7	-	-
Moisture Content (%)		-	-	-
Soil Unit Weight (kN/m^3)		16.2	-	-
Friction Angle (°)	1-2	38	32	-
Young's Modulus (MPa)		17.7	9.5	-
Moisture Content (%)		-	-	2.4
Soil Unit Weight (kN/m^3)		17.2	-	-

The testing program included determination of bearing and pull-out capacities of two types of this new footing system (S250 and S400) (Table 2). For each type, two different embedment depths (1.2 and 1.5 m) typically used in practice were chosen. In total, eight static load tests were performed on four footings. Each footing was subjected to both compressive and tensile loads. A one day time interval was employed between two consecutive tests to allow the soil relax. To apply the compressive load to the micropile footings, a stronger Surefoot footing (S500) was used as a reaction support. Table 2 details the specification of installed footings. To eliminate the effect of the organic root matter, a 400 mm deep trench was excavated and the test footing systems were installed at the bottom of the trench. The test layout is shown in Fig. 3. Since no creep deformation or considerable consolidation settlement was expected for this site material, the Quick Maintained pile load test method (QM Test) according to FHWA (2005), ASTM-D1143 (1994) and D3689 (1990) with some modifications was used in this research. Eight percent of anticipated ultimate capacity was applied to the top plate and held for 15 minutes. Continuous jacking to maintain the applied load was considered as failure and termination criteria. Finally, the system was unloaded in three to four steps except for the S400-1500 due to malfunction of the jack. Fig 4 shows the compression test set-up for S400-1500.

Table 2. Specification and details of the installed reaction and test footings

Footing Type	Embedment Depth (m)	Type of Footing	Number of Micropiles	Total Embedment Length (m)	Top Plate Width (mm)
S500-2000	2	Reaction	9	18	480
S250-1200	1.2	Main	4	4.8	260
S250-1500	1.5	Main	6	6	260
S400-1200	1.2	Main	4	7.2	380
S400-1500	1.5	Main	6	9	380

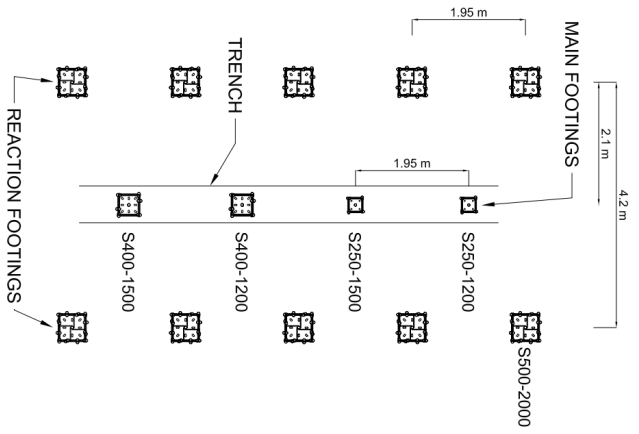


Fig. 3. Tests Layout



Fig. 4. Compressive Test Set-up on S400-1500

TESTS RESULT

The load-settlement diagram for each footing under compressive and tensile load is shown in Fig. 5. S250-1200 and S400-1200 footings were subjected to the tensile load first while S250-1500 and S400-1500 experienced compressive load first. As the main aim of this research was to investigate the ultimate capacity and not settlement measurement, each test was continued until failure. This was evident during the early stages of loading where residual settlements of the previous test needed to be compensated before soil resistance picked up again. This was more obvious for footings that were subjected to the tensile load first (Fig. 5). A considerable difference between bearing and pull-out capacities was noticed for this new battered micropiles system. This indicates that the skin friction and lateral pressure on the micropiles could not be the main resisting components of this new driven battered micropile footing. As the toe capacity of the micropiles is small, it seems that there are other parameters such as the reinforcing effect of battered micropiles enclosing the soil in between or soil arching which may contribute to the improved bearing capacity. Regardless of whether the pull-out test was performed first or not, no obvious difference in ultimate capacity and final settlement was observed in pull-out tests. This confirms that soil disturbance or the loose contact at soil-micropile shaft (which was developed during the first test) had no noticeable impact on the skin resistance in the second test.

There are different methods in the literature (e.g. Brinch and Hansen 1963; De Beer 1972; Fuller and Hoy 1970; Chin 1971; Mazurkiewics 1972; Butler and Hoy 1977; GCP-18 2015) that can be used to back-analyse the ultimate capacity from the field static test. However, depending on the type of pile or micropile, some of them may not be applicable or may overestimate the ultimate capacity. According to the authors' experience, De Beer (1972), Fuller and Hoy (1970) and GCP-18 (2015) determine the ultimate capacity of this new battered micropiles system better than other methods. Table 3 presents the ultimate bearing and pull-out capacities of each footing. As expected, by an increase in number and embedment depth of micropiles, ultimate capacity of footings increased except for S400-1200, which showed the same capacity as the S250-1500 and will be discussed in the next section. The ratio of bearing capacity to pull-out capacity was found to vary from 4.25 to 3.55 with a decreasing trend when the number and embedment depth of the micropiles increased.

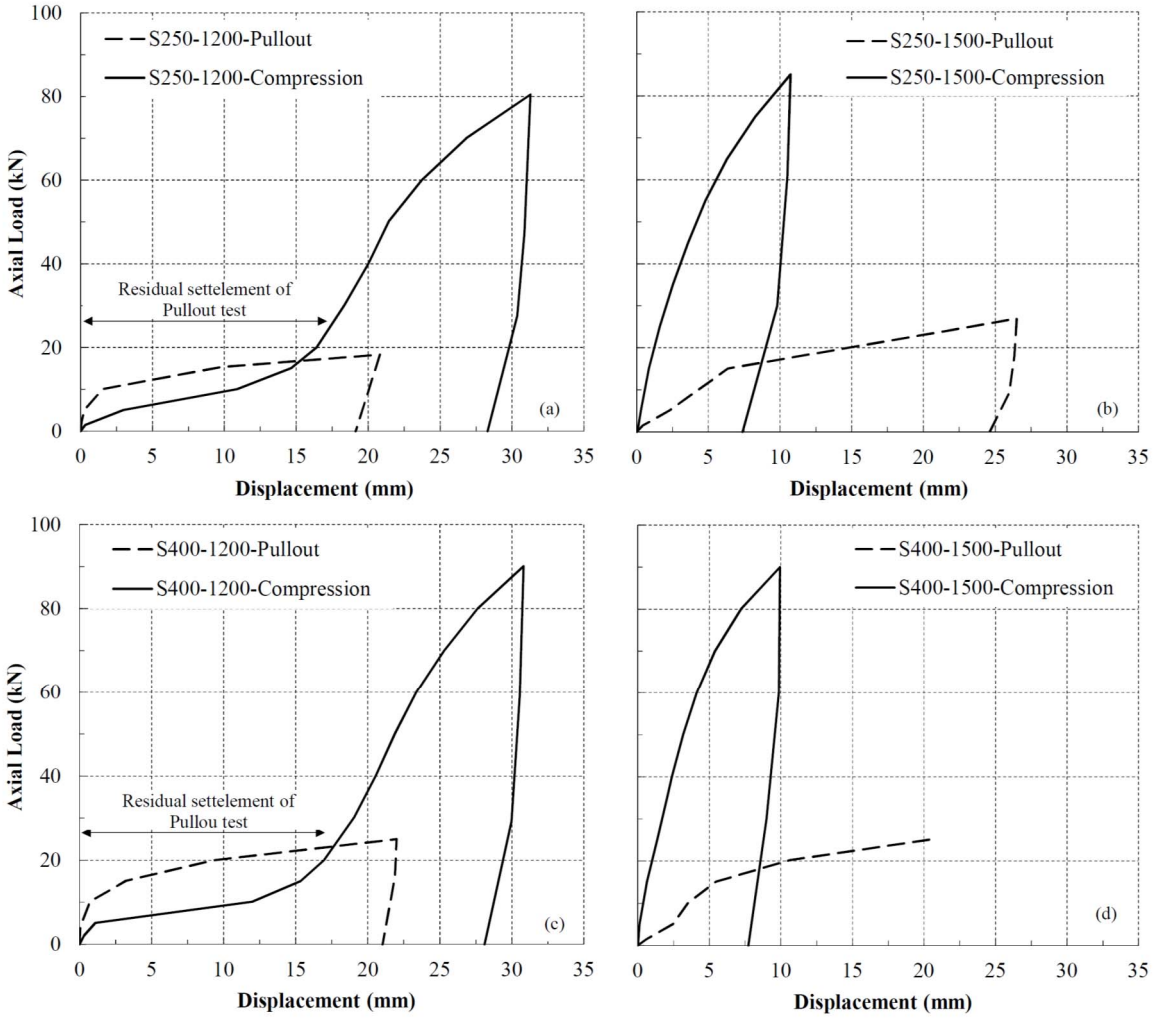


Fig. 5. Load-settlement diagram for compressive and tensile loads (a) S250-1200, (b) S250-1500, (c) S400-1200 and (d) S400-1500

Table 3. Analysis of ultimate capacity

No.	Footing	Ultimate		Q_{ub}/Q_{up}
		Bearing Capacity, Q_{ub} (kN)*	Pull-out Capacity, Q_{up} (kN)*	
1	S250-1200	51	12	4.25
2	S250-1500	60	16.6	3.61
3	S400-1200	60	16	3.75
4	S400-1500	71	20	3.55

*: Average value calculated from all appropriate methods

It was mentioned earlier that to compare the capacity of this new battered micropile system with a shallow foundation; a plate load test was performed. Fig. 6 illustrates the load-settlement graphs from the PLT for footings S250-1500 and S400-1500, which were subjected to compressive load first. The PLT and both footings were installed 400 mm below the ground surface. The diameter of the biggest plate for PLT was 760 mm which can simulate a square concrete footing with approximately 670 mm width. It is evident from Fig. 6 that the tested footing systems yielded a bearing capacity at least twice that of an equivalent square concrete footing in non-cohesive material. For instance, the bearing

capacities of 20, 40 and 44 kN were mobilized for the tested plate, S250-1500 and S400-1500, respectively, during the first 3 mm of settlement. Moreover, soil stiffness was also enhanced significantly due to the reinforcing effect of the micropiles, which can be seen from the slope of the loading curves. This shows that this new battered micropile system can be considered as an engineering alternative for shallow and semi-deep foundations, saving construction cost and time. The same improvement can also be expected under tensile loads when a 670 mm wide concrete block can only resist approximately 4 kN (regardless of friction over its sides) when the pull-out capacity of the smallest footing was measured fourfold higher.

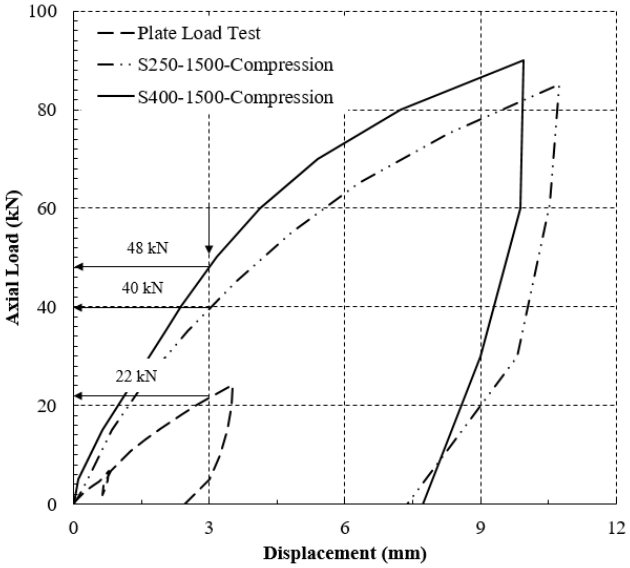


Fig. 6. Load-settlement diagram for plate load test, S250-1500 and S400-1500

DISCUSSION

It was mentioned that Surefoot's current engineering design principle is based on the conventional theories of skin friction and bearing capacity (Mehdizadeh et al. 2016). Kyung et al. (2016) and Kyung and Lee (2017) showed that for a battered micropile, ultimate bearing and pull-out capacities can be calculated from Eqs. 1 and 2, respectively.

$$P_{ub} = \left(P_{ti} + P_{fi}\right)\cos\theta + (P_{h1} - P_{h2})\sin\theta \quad [1]$$

$$P_{up} = \left(P_{fi} + W_f\cos\theta\right)\cos\theta + (P_{h1} - P_{h2} + W_f\sin\theta)\sin\theta \quad [2]$$

Where P_{ti} is toe resistance, P_{fi} is skin resistance, P_h is lateral pressure that can be calculated according to Broms (1964), Petrasovits and Award (1972), or Prasad and Chari (1999). W_f is the micropile weight and θ is the installation angle from vertical.

Kyung et al. (2016) and Kyung and Lee (2017) then suggested that the capacity of a group of micropiles is equal to the capacity of one micropile times number of micropiles in the group times an appropriate group effect factor. Fig. 7 presents the bearing and pull-out capacities of the tested footings based on this method without applying any group effect factor, if using the lateral pressure distribution suggested by Prasad and Chari (1999). It can be seen that this method underestimates the bearing capacity of this new footing system but provides a realistic prediction for pull-out capacity. Calculations confirm the suggested hypothesis that there are other contributing factors such as the reinforcing effect of battered micropiles; arching or block action which increase the bearing capacity of this system and not only skin resistance and toe bearing. The suggested method in this paper calculates the bearing capacity of a battered micropile system based on individual micropiles (toe resistance, skin friction and lateral pressure applying on inclined micropile) and does not take into account enclosing the soil between

micropiles that may act as a block. Moreover, the lateral pressure distribution on the battered micropiles is highly dependent on the stiffness of micropiles, soil type and fixity of the micropile toe. Therefore, without field instrumentation or a validated numerical model it is hard to find out micropile deformation patterns and inflection points.

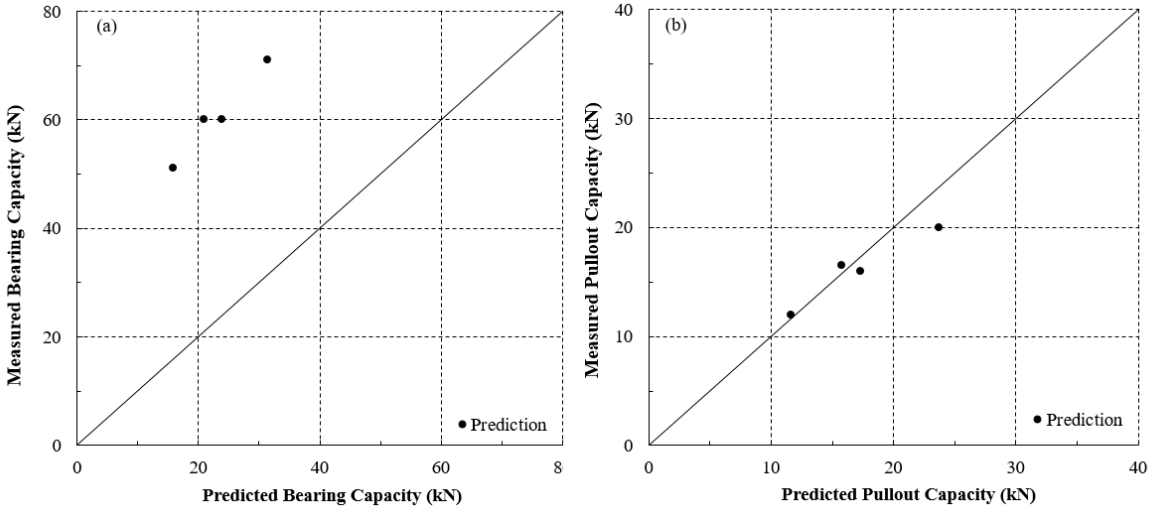


Fig. 7. Accuracy of current engineering approach in predicting (a) bearing and (b) pull-out capacities of this new battered micropile

The impact of micropiles on each other in the group and how they work together toward ultimate capacity also needs to be considered. Table 3 showed that the bearing and pull-out capacities did not change between S250-1500 and S400-1200 although the total embedment depth of S400-1200 was higher. Since the geotechnical investigation did not show any non-uniformity in soil layers and properties and footings were installed close to each other with two meters spacing, the reduction in capacity of S400-1200 could not be related to soil parameters. It implies that there exists a negative group effect with increasing number of micropiles. reducing capacity, while the number of micropiles increased to six for S400-1200 in comparison to four for S250-1500 (Fig. 8). Field tests on a single battered micropile will provide a better understanding on the group effect.

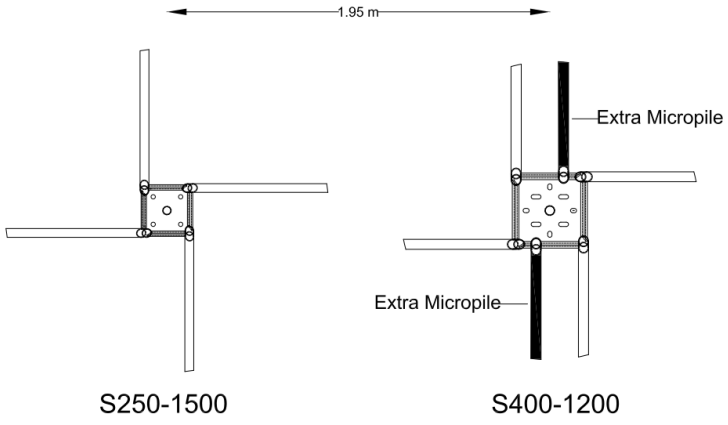


Fig. 8. Micropiles layout in the tested Surefoot systems

CONCLUSION

The ultimate bearing and pull-out capacities of a new driven battered micropiles system in a non-cohesive material was investigated through performing field static load tests. The current engineering approach then was examined based on the field data. The research achievements and recommendations are summarized below:

- This new battered micropile system can be considered as an engineering alternative for shallow footings as the ultimate bearing and pull-out capacities were found to be well above the traditional shallow foundations.

- It was found that conventional theories fall short in predicting the ultimate bearing capacity of this battered micropile system as the reinforcing effect of the micropiles is overlooked. This reinforcing effect can be investigated using a 3D numerical modelling verified by field test results.

- The pull-out capacity of this new driven battered micropile system can be calculated reasonably well in non-cohesive material according to Kyung and Lee (2017) if lateral pressure distribution is applied using the approach taken by Prasad and Chari (1999).

- Micropile instrumentation for future field testing will provide a valuable insight regarding micropile deformation pattern.

- A negative group effect needs to be considered further and more field tests need to be performed to validate and improve the current engineering principle.

ACKENOWLEDGEMENT

This research was funded by the Australian Research Council Linkage scheme (project ID LP160100828). In addition, the authors acknowledge the financial and in-kind support provided by Surefoot Pandoe Pty Ltd. Camilo Pineda, senior structural engineer at Surefoot is acknowledged for his contribution to this research.

REFERENCES

ASTM-D1143, 1994. Standard test method for piles under static axial compression load. ASTM International, DOI: 10.1520/D1143_D1143M

ASTM-D3689, 1990. Standard test method for individual piles under static axial tensile load. ASTM International, DOI: 10.1520/D3689_D3689M

Brinch, H. and Hansen, J., 1963. Discussion Hyperbolic Stress-Strain Response. Cohesive Soils. Journal of Soil Mechanic and Foundation, ASCE, 89(4) 241-242.

Broms, B.B., 1964. Lateral resistance of piles in cohesionless soils. Journal of Soil Mechanic and Foundation, Div., 90(3) 123-158.

Bruce, D.A., and Yeung, C.K., 1984. A review of minipiling with particular regard to Hong Kong applications. Hong Kong Engineer, 12(6) 31-54.

Bruce, D.A., Dimillio, A.F., and Juran, I., 1997. Micropiles: the state of practice. Ground Improvement, 1(1) 25-35.

Butler, H.D. and Hoy, H.E., 1977. Users Manual for the Texas Quick-Load Method for Foundation Load Testing. Federal Highway Administration, Office of Development, Washington, DC.

Cadden, A., Gomez, J., Bruce, D., and Armour, T., 2004. Micropiles: recent advances and future trends. In Current practices and future trends in deep foundations. ASCE, 140-165, DOI: 10.1061/40743(142)9.

Chin, F.K., 1970. Estimation of the Ultimate Load of Piles not Carried to Failure. Proceedings 2th Southeast Asian Conference on Soil Engineering, Singapore, 81-90.

De Beer, E.E. and Wallays, M., 1972. Franki Piles with Overexpanded Bases. La Technique des Travaux, 333, 48.

Federal Highway Administration (FHWA), 2005. Micropiles design and construction. Report No. FHWA NHI-05, 39.

Fuller, F.M. and Hoy, H.E., 1970. Pile Load Tests Including Quick-load Test Method Conventional Methods and Interpretations. 333, 78-86.

Geotechnical Control Procedure (GCP-18), 2015. Static pile load test manual. Department of transportation, Geotechnical Engineering Bureau, Report 18, New York.

Hanna, A., and Nguyen, T.Q., 2003. Shaft resistance of single vertical and batter piles driven in sand. Journal of Geotechnical and Geoenvironmental Engineering, 129(7) 601-607.

Juran, I., Bruce, D.A., Dimillio, A. and Benslimane, A., 1999. Micropiles: the state of practice. Part II: design of single micropiles and groups and networks of micropiles. Ground Improvement, 3(3) 89-110.

Kyung, D., Kim, D., Kim, G., and Lee, J., 2016. Vertical load-carrying behavior and design models for micropiles considering foundation configuration conditions. Canadian Geotechnical Journal, 54(2) 234-247.

Kyung, D., and Lee, J., 2017. Uplift Load-Carrying Capacity of Single and Group Micropiles Installed with Inclined Conditions. Journal of Geotechnical and Geoenvironmental Engineering, 143(8) 04017031.

Mason, J., and Bruce, D., 2001. Lizzi's structural system retrofit with reticulated internal reinforcement method. Transportation Research Record: Journal of the Transportation Research Board, (1772) 107-114.

Mazurkiewicz, B.K., 1972. Test Loading of Piles According to Polish Regulations. Royal Swedish Academy of Engineering Sciences Commission on Pile Research, Report No. 35, Stockholm, 20

Mehdizadeh, A., Disfani, M.M., Evans, R., Gad, E., Escobar, A., and Jennings, W., 2016. Static load testing of concrete free reticulated micropiles system. Proceedings of the 5th International Conference on Geotechnical and Geophysical Site Characterisation, ISC 2016, 2 1353-1358

Petrasovits, G., and Award, A., 1972. Ultimate lateral resistance of a rigid pile in cohesionless soil. Proc., 5th European Conf. on SMFE 3, The Spanish Society for Soil Mechanics and Foundation, 407-412.

Prasad, Y.V.S.N., and Chari, T.R., 1999. Lateral capacity of model rigid piles in cohesionless soils. Soils and foundations, 39(2) 21-29.

Schlosser, F. and Frank, R., 2004. FOREVER (FOndations REnforce´es VERticalement): Synthe`se des re´sultats et recommandations du Projet national sur les Micropieux. Presse de l'ENPC, Paris.

Takahashi, K. 1985. Bending of a batter pile due to ground settlement. Soils and foundations, 25(4) 75-91.

Tsukada, Y., Miura, K., Tsubokawa, Y., Otani, Y., and You, G.L., 2006. Mechanism of bearing capacity of spread footings reinforced with micropiles. Soils and foundations, 46(3) 367-376.

You, G.L., Miura, K., and Ishito, M., 2003. Behavior of micropile foundations under inclined loads in laboratory tests. Lowland Technology International, 5(2) 16-26.

PROPERTIES OF GROUND IMPROVEMENT USING LOW CO_2 EMISSION CEMENT

Takao Kono, Takenaka Research and Development Institute, Takenaka Corporation, 5-1-1, Otsuka, Inzai, Chiba, 270-1395, JAPAN, +81-80-2454-9088, koono.takao@takenaka.co.jp
Masamichi Aoki, Takenaka Research and Development Institute, Takenaka Corporation, 5-1-1, Otsuka, Inzai, Chiba, 270-1395, JAPAN, +81-80-1181-7014, aoki.masamichi@takenaka.co.jp

ABSTRACT

The reduction of CO_2 emissions is an important issue concerning global climate change. In Japan, CO_2 emission owing to cement production comprises approximately 3% of the total CO_2 emissions. This study reports a technology system that can substantially reduce the emitted energy and CO_2 from cement production using energy CO_2 minimum (ECM) cement. Herein, ECM cement with a slag content of over 60% was developed and its applications for concrete structures and ground improvement were studied. The CO_2 produced when producing the newly developed cement was 70% and 40% less than the CO_2 produced when producing ordinary Portland cement and conventional blast-furnace cement type B, respectively. This study also presents laboratory test results of ground improvement using ECM cement. In the laboratory test, the hydration heat characteristics, compressive strength, and dissolution of hexavalent chromium Cr(VI) of improved soils were investigated. Thereafter, the ECM cement was applied for the ground improvement of a construction project in the Osaka Bay area, Japan. The strength and deviation of strength of the improved soil on site were also studied, and based on the laboratory and in situ results, the ECM cement was considered to be suitable for ground improvement.

Keywords: ground improvement, CO_2 emission, blast furnace slag

INTRODUCTION

The total emissions of CO_2 in Japan were 1.3 billion tons in 2015 (JCCCA, 2017). Because of these high emissions, it has become paramount to reduce the CO_2 output by improving the climate change policies. The production of cement in Japan was a maximum of 99.6 million tons in 1996, but recently, the production declined and in 2015 it was 59.3 million tons (Japan Cement Association, 2017a). And in 2015, 29.2 million tons was used for concrete (Japan Cement Association, 2017b) and 7.8 million tons was used for ground improvement (Japan Cement Association, 2017c). In addition, CO_2 emissions from cement production in Japan currently comprise approximately 3% of the total CO_2 emissions of Japan. Theoretically, if CO_2 emissions from the production of cement for concrete manufacture and ground improvement are reduced, the CO_2 emissions in Japan can also be reduced.

Current research suggests that blast-furnace cement may be effective in reducing CO_2 emissions. Blast-furnace slag cement types A, B, and C used in Japan are defined in JIS5211 depend on the chemical compositions of blast-furnace slags. Blast-furnace slag cement that are produced by incorporating blast-furnace slags tend to exhibit low early-age strengths, high drying shrinkage, and high carbonation rate. Therefore, slag cement has not been so utilized in concrete structures. In the case of ground improvement, cement– based solidifying material are often utilized to prevent the elution of Cr(VI).

To reduce CO_2 emissions during cement production, new slag cement (ECM cement) containing >60% blast-furnace slag have been developed (Yonezawa et al., 2013). In this development, the reduction of CO_2 emissions are trying to achieve in cement production by replacing the OPC in concrete with ECM cement and replacing cement-based solidifying material with ECM cement in ground improvement.

© 2018 Deep Foundations Institute

In order to apply ECM cement for concrete, they considered application to high-strength reinforced concrete (Tuji et al., 2014), civil-engineered concrete (Hashimoto et al., 2014), cast in place piles concrete (Ogawa et al., 2014) have been examined (Fig. 1). High-strength concrete can significantly reduce carbonation, and civil-engineered concrete have thick covers, cast in place piles concrete are unlikely to have carbonation and drying shrinkage occurrence because it is placed into the ground. And in order to apply ECM cement for ground improvement, it is necessary to investigate the strength characteristics and elution characteristics of Cr(VI).

This study describes the profile of ECM cement and evaluates the properties of ground improvement using laboratory tests. Furthermore, an application focused on preventing liquefaction of the ground improvement for building foundations has been described.

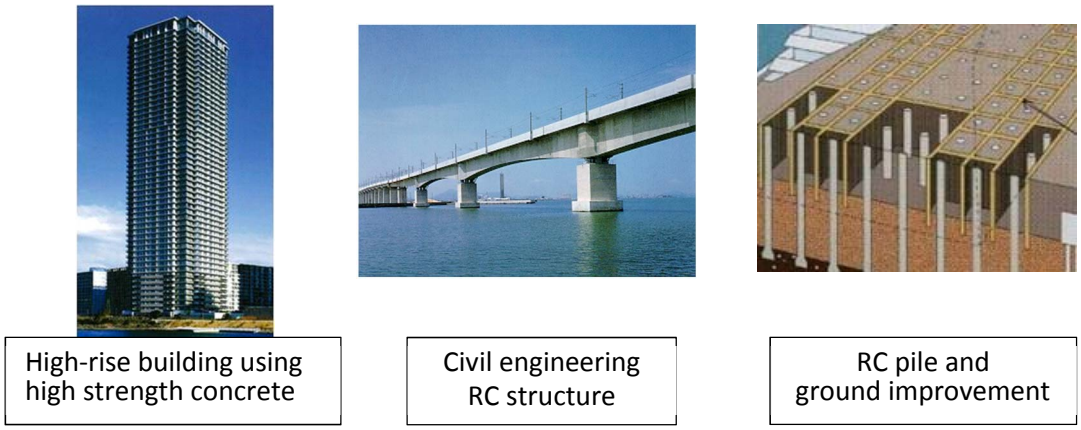


Fig. 1. Target structures using ECM cement

PROFILE OF THE ECM CEMENT

Yonezawa et al. (2013) showed the relation between slag hydration and content ratio of the ordinary Portland cement (OPC). Based on their experimental results, they suggested that slag cement may possess stable hydration only when the OPC content is greater than 15%. Kono et al. (2016) also showed the relation between the compressive strength of ground improvement and the amount of anhydrite gypsum (CS). CS content of 3%–10% was effective at increasing the initial compressive strength. CS content of 6%–10 % was effective at increasing the long-term (>28 days) strength. To harness the ECM cement, it is paramount that the cement contains a gypsum content of 3%–10%.

The OPC had low concentrations of Cr(VI), but Cr(VI) was not eluted from the concrete structure. A cause may be that Cr(VI) was eluted into the ground because the ground improvement was highly porous and had low compressive strength. Considering this effect, the amount of elution of Cr(VI) from the ground improvement is regulated in Japan (Environment Agency of Japan, 1991) because of the toxicological effects of the heavy metal. Ida et al. (2010) showed that Cr(VI) was immobilized when the BFS content was >60% and the OPC content was >30%.

These experimental results determined the composition of the ECM cement that is suitable for ground improvement. Moreover, Fig.2 shows the CO_2 emissions of the specific type of cement. In this CO_2 emissions, material and production of OPC, BFS and CS are taken into account, but transport is not. Using ECM cement may reduce the CO_2 emissions by 45% and up to 65% as compared with BB cement and OPC, respectively.

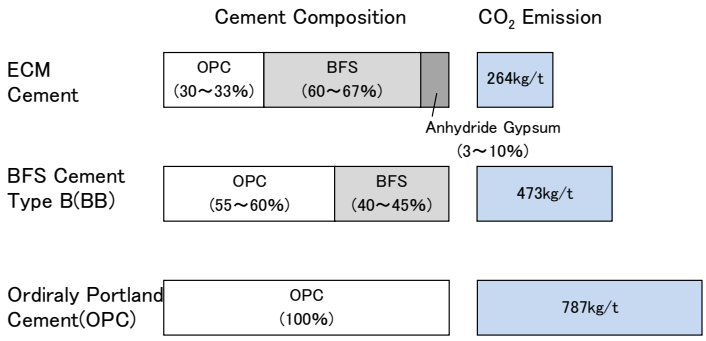


Fig. 2. Composition of ECM, BB and OPC cement and CO_2 emission

PROPERTIES OF GROUND IMPROVEMENT USING ECM CEMANT IN LABORATORY

To investigate the influence of the hydration reaction on the strength of ground improvement, a simplified adiabatic test was performed. In addition, laboratory strength and elution characteristics of hexavalent Cr(VI) experiments were conducted to investigate the characteristics of ground improvement using ECM cement.

Materials

The compositions of various types of cement and soil used for the test are shown in Table 1 and Table 2, respectively. ECM cement and blast-furnace cement type B (BB cement) were used for the laboratory test. In addition, artificial sand ground was adopted for the simplified adiabatic test to investigate the temperature increase of ground improvement. The strength and elution characteristics of the hexavalent Cr(VI) experiment focused on soil samples that were obtained from two major cities, Tokyo and Osaka.

Table 1. Chemical composition of the cement

	SiO_3	Al_2O_3	Fe_2O_3	CaO	MgO	SO_3
ECM	28.60	11.09	1.13	48.59	4.72	3.55
BB	26.21	9.32	1.79	53.25	4.07	2.42

Unit; %

Table 2. Soil properties

Type of soil	Test type	Wet density (g/cm^3)	Water content (%)	Grain size (%)			
				Clay	Silt	Sand	Gravel
Artificial Sand	simplified adiabatic test	1.80	25.0	8.3	1.7	90.0	0.0
Tokyo Clay	compressive strength test	1.65	58.6	39.5	53.0	7.6	0.0
Osaka Clay		1.70	50.1	37.1	57.1	5.8	0.0
Osaka Sand		1.82	32.8	11.0	6.0	83.0	0.0

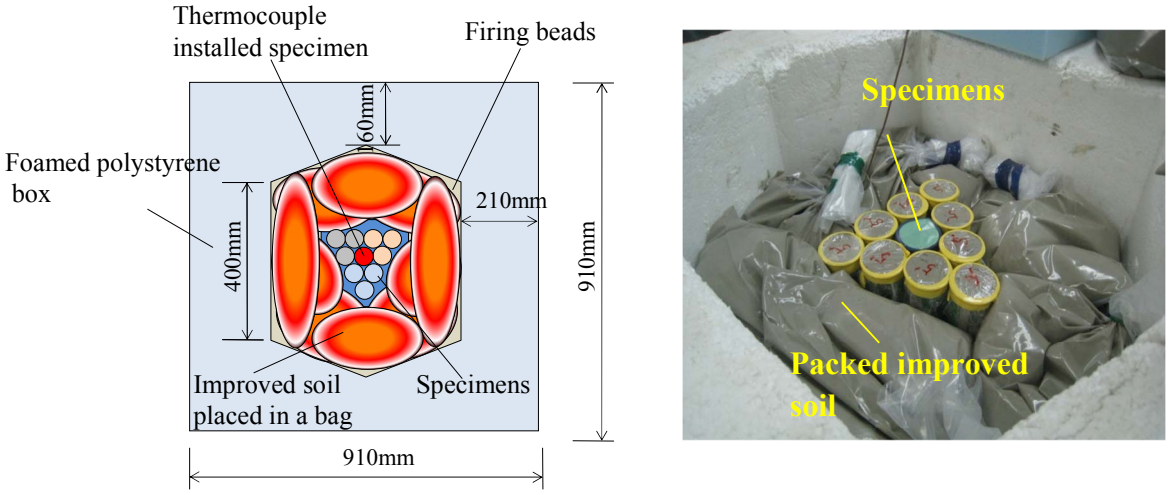
Simplified Adiabatic Test

The outline of the specimen in the simplified adiabatic test is shown in Fig. 3. Considering a practical ground improvement diameter of 1.0 m, the size of the foamed polystyrene box for the test was selected as 910 mm × 910 mm × 800 mm. Ten specimens of Φ 50 mm × h 100 mm were then placed in the center of the polystyrene box, in which the specimens were prepared according to JIS R 5201.

Muronoi et al. (2010) pointed out that the volume ratio of the improved soil and foamed polystyrene box

needed more than 5% for the simplified adiabatic test. Therefore, in this test, the improved soil made under the same condition as the test specimen was placed in a polyethylene bag and around the specimen, and the volume ratio was set to more than 5%. In addition, firing beads were filled in the space between the specimen and the polyethylene bag.

The temperature increase in the simple thermal insulation test was measured up to 11 days by installing a thermocouple at the specimen that was at the center of the 10 specimens. The specimens were then taken out of the polystyrene box after the 12th day and cured under at a temperature of 20 ± 3°C and a humidity of around 95%. To ascertain the relation between the temperature increase due to the hydration reaction and the strength, the uniaxial compressive strength at the age of 28 days was investigated.



(a)Plan view **(b) Installation status of specimens**

Fig. 3. Test apparatus for the simplified adiabatic test

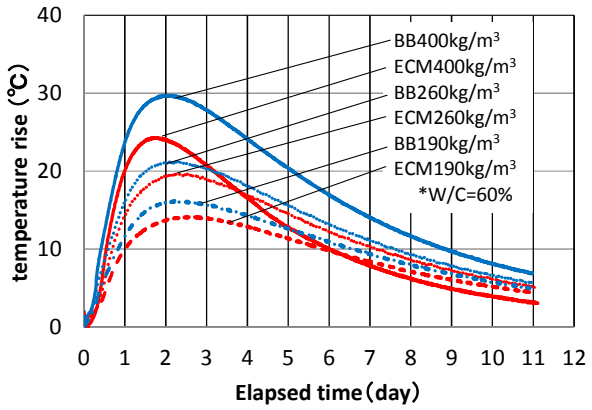


Fig.4 The relation between time and temperature increase

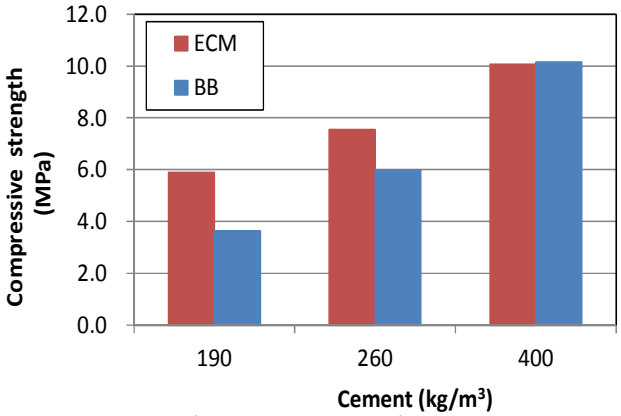


Fig.5 The compressive strength

Fig. 4 shows the relation between the time and temperature increase of the ground improvement in the simplified adiabatic test. The degree of temperature increase of the ground improvement shows the temperature was maximum after approximately 2 days and then gradually decreased. The maximum temperature increase ranged from 13.7°C to 29.7°C, and it increased with increasing cement content. In addition, comparing ECM and BB, the maximum temperature increase of the ground improvement using ECM was lower by 1.5° C–5.4°C than the maximum temperature increase of the ground improvement of BB.

Fig. 5 shows the compressive strength after curing for 28 days. The figure shows that the compressive strength using ECM was higher than the compressive strength using BB even if the degree of temperature increase was smaller.

Compressive Strength and Dissolution Experiment of Cr(VI)

Fig. 6 shows the compressive strength of the improved soil. The strength was strongly influenced by the type of soil and the type of cement. In addition, the strength of the ECM cement was higher than that of the BB cement. Fig. 7 shows the results of the dissolution experiment of Cr(VI) from the improved soil. In the Osaka clay sample, Cr(VI) was not eluted from the ECM cement even when it was eluted from the using the BB cement. In conclusion, the use of ECM cement as a ground improvement was confirmed to be effective in immobilizing Cr(VI).

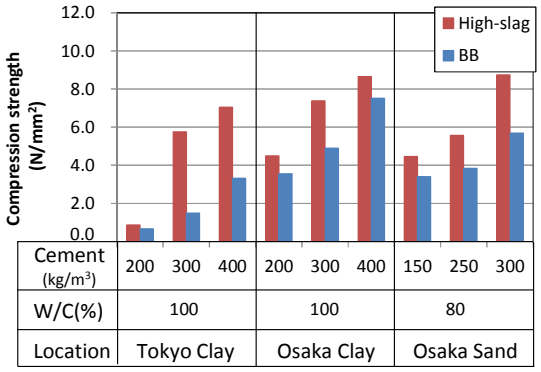


Fig. 6. Compressive strength of improved soil

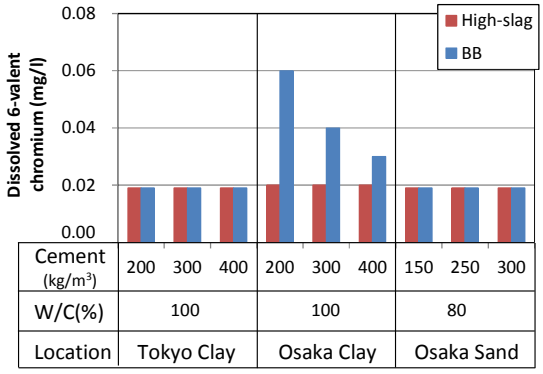


Fig. 7. Cr(VI) dissolution of improved soil

APPLICATION TO THE CONSTRUCTION PROJECT

Building Outline

This building is the factory manufacturing a precision electronics instrument. Fig. 8 shows the plan view of the building (Kono et. al, 2017). This building is located in the bay area of Osaka, and this area has a possibility of liquefaction during an earthquake. To prevent liquefaction, it is necessary to construct ground improvement under this building. This is the first demonstration of the application of ECM cement to practical ground improvement; consequently, ECM cement is applied to a 1/6 range (see Fig. 9) and BB cement is applied to a 5/6 range.

Soil Profile and Ground Improvement Specifications

Fig. 9 (Kono et. al, 2017)displays the soil profile of the construction site. It comprises a composite material containing size fractions ranging from gravel to silt. A 14-m thick ground improvement ranging between a depth of 3 and 17 m was constructed. The planned shape of the ground improvement was a 9 m × 9 m grid (see Fig. 9). The design compressive strength of the ground improvement varied with depth. Between the depth of 3 and 10 m, the design compressive strength was F_c = 1.5 MPa, and between the depth of 10 and 17 m, it was F_c = 2.1 MPa.

Laboratory Experiments

Laboratory experiments were conducted on the soil samples obtained from the construction site to evaluate the compressive strength of the ground improvement and analyze the amount of Cr(VI) dissolution from the improvement. The target compressive strength in the laboratory (The Building Center of Japan, 2002) was X_L = 2.2 MPa for F_c = 1.5 MPa and X_L = 3.1 MPa for F_c = 2.1 MPa. Soil samples were collected from depths of 4–16 m, and the composites of these depths were used for the laboratory experiment. Table 3 shows the characteristics of the soil sample. Fig. 10 shows the results of the compressive strength of the improved soil. The compressive strength using the ECM cement was

higher than that of the BB cement. In addition, the amount of Cr(VI) elution from the improved soil was less than the value of regulation (0.05 ppm) (Kono et al., 2017).

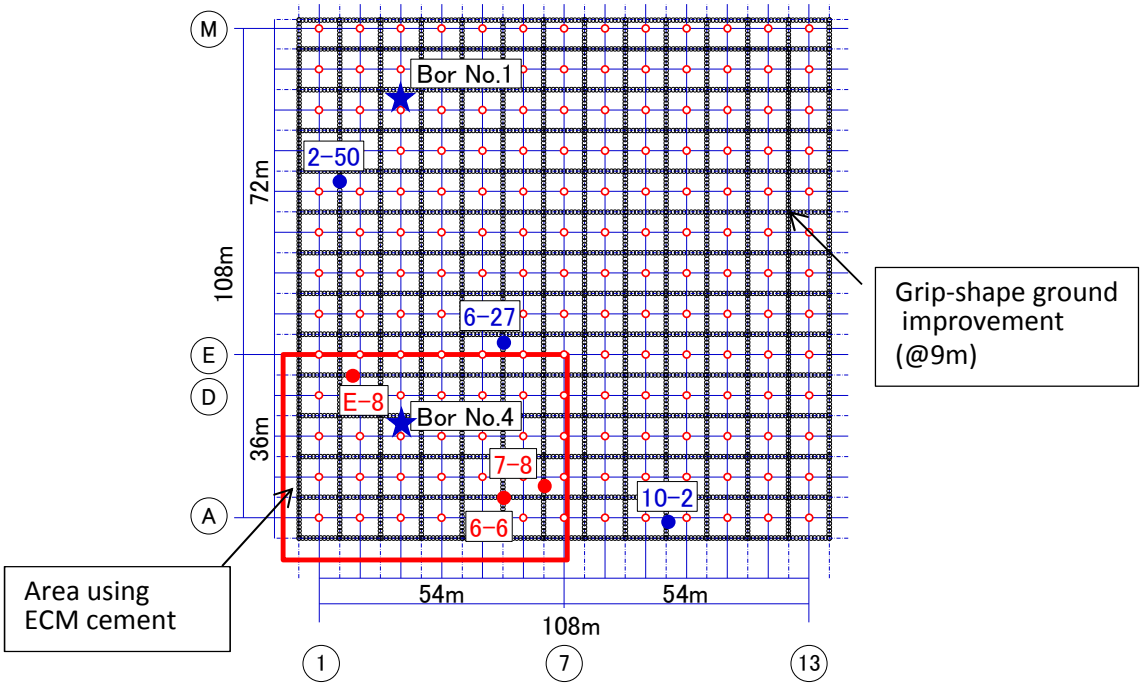


Fig. 8. Plan view of the building (Kono et al., 2017)

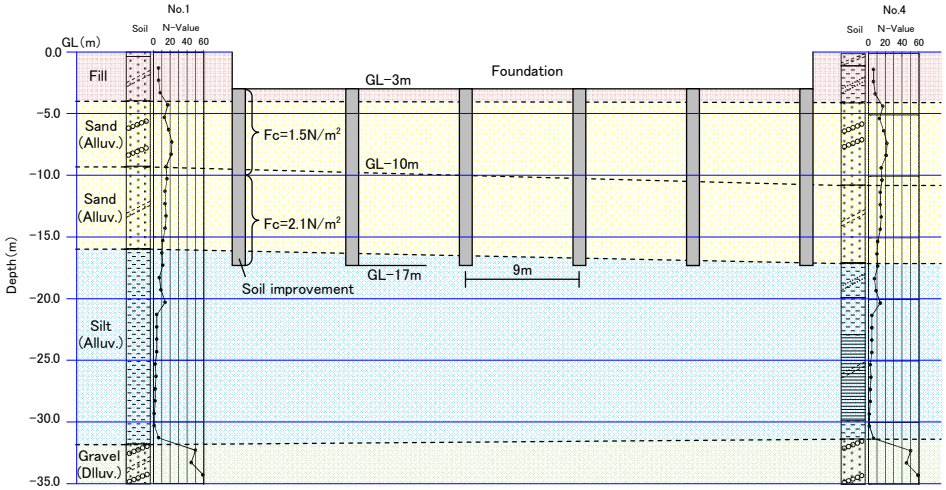


Fig. 9. Soil profile and specification of ground improvement (Kono et al., 2017)

Table 3. Soil sample characteristics

Soil type	Wet density (g/cm^3)	Water content (%)
Sand (4-16 m)	2.04	21.3

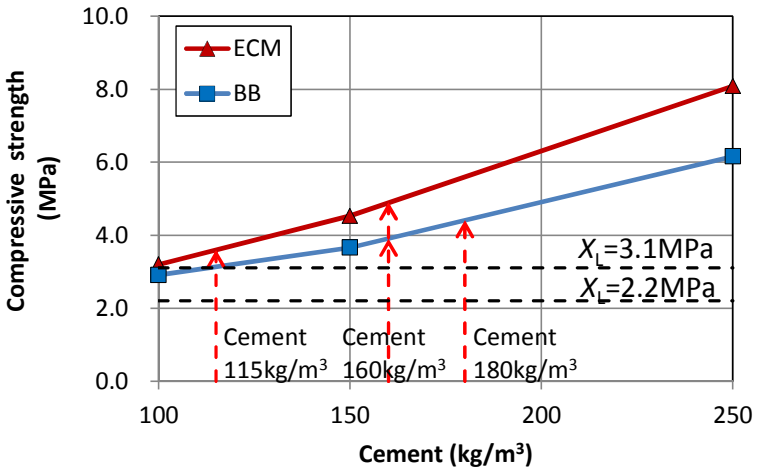


Fig. 10. Compressive strength of improved soil

Construction Method

The ground improvement was constructed using the cement deep-mixing machine (CDM machine). The CDM machine comprises two mixing shafts with 1-m diameter blades. Photo 1 shows an overview of the CDM machine, and Photo 2 shows the details of the blades.



Photo 1. Overview of the CDM machine



Photo 2. Details of the blades

Results of In Situ Experiment

Table 4 shows the in situ construction conditions, which were determined via the strength test results in the laboratory. As the N value of the sand layer from the depth between 6 and 10 m was relatively high, the resistance to the rotation of the shaft increased; thus, it is difficult to ascertain proper mixing. The quantity of cement was increased to facilitate proper fluidity.

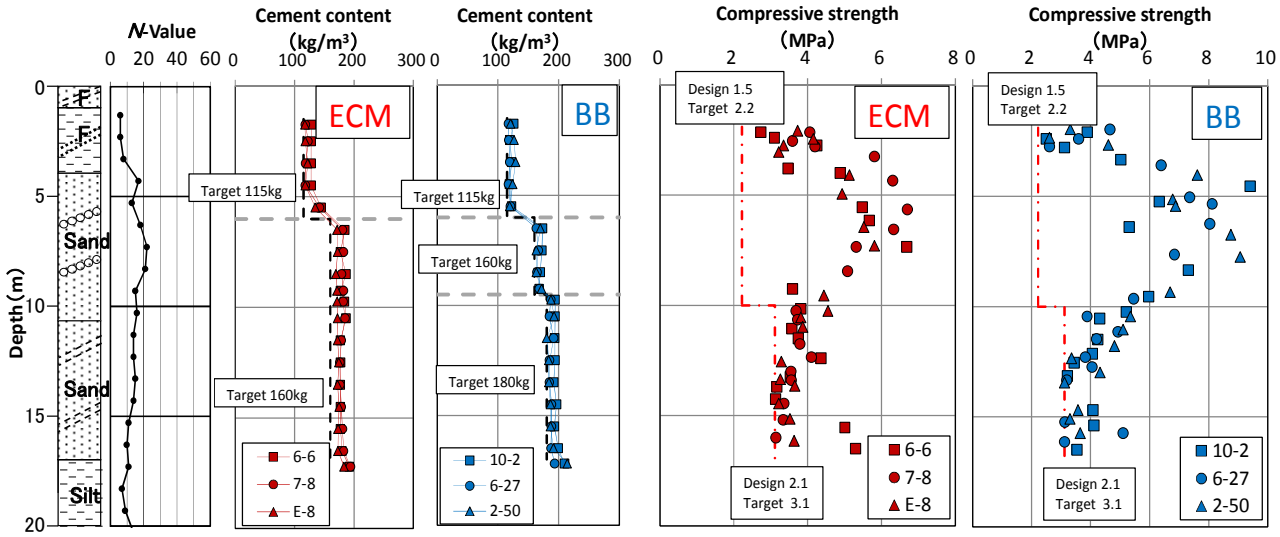
The core samples between the depth of 3 and 17 m were collected to investigate the quality of the ground improvement in the field. Core samples were collected 10 to 12 days after construction. Fig. 8 shows the location of the core sample extraction point. Fig. 11 shows the depth distribution of cement amount in the injected cement milk and compressive strength of ground improvement. It shows that the amount of cement was well controlled at the construction.

Table 5 summarizes the investigation results. In both the ECM and BB cements, the compressive strengths of the ground improvements were greater than the target compressive strength. The table also shows that for both ECM and BB cements, the coefficient of the strength variation was less than the target value of 25% (The building center of Japan, 2002b) except between the depth of 3 and 10 m. In the layer of 3-6 m, it is considered that the variation of the ground condition was relatively high, so the variation of the strength of the ground improvement was also increased. The strength of ECM was lower than BB, although the strength of ECM was higher than the BB in the laboratory tests.

Table 6 shows the relation of the compressive strength of the core sample and laboratory test results. The laboratory compressive strength of same amount of cement as practical construction was estimated from the relation of cement content and compressive strength at the laboratory test result (see the red dotted line in Fig. 4). The ratios of the strength of core sample and the strength of the laboratory test were about 0.7 to 1.2 in the case of the ECM cement and about 0.9 to 1.8 in the case of the BB, the strength ratio of the core sample and laboratory was bigger than the target value of 0.6 to 1.0 (The building center of Japan, 2002c).

Table 4. Construction condition

Depth (m)	Design strength (MPa)	Soil condition	N-value	Water cement ratio (%)	Cement(kg/m^3)	
					ECM cement	BB cement
3-6	1.5	Gravel	<10	80	115	115
6-10	1.5	Sand	20	80	160	160
10-17	2.1	Sand	10	80	160	180



(a)Cement content **(b) Compressive strength**

Fig. 11. Distribution of cement content and compressive strength in the field

Table 5. Summary of strength in the field

Depth (m)	Design strength (MPa)	Target strength (MPa)	Compressive strength (MPa)		Coefficient of variation (%)	
			ECM cement	BB cement	ECM cement	BB cement
3-6	1.5	2.2	4.4	5.3	25.3	39.6
6-10	1.5	2.2	5.4	7.1	16.5	18.3
10-17	2.1	3.1	3.7	4.0	14.1	17.2

Table 6. Ratio of the core sample strength and the laboratory test strength

Depth (m)	Estimated Compressive strength based on laboratory test results for target cement content (MPa) (Fig. 10)		Ratio of the core sample strength and the laboratory test strength	
	ECM cement	BB cement	ECM cement	BB cement
3-6	3.6	3.1	1.2	1.7
6-10	4.9	3.9	1.0	1.8
10-17	4.9	4.4	0.8	0.9

Effect of CO_2 Emission Reduction

Table 7 shows the amount of reductions in CO_2 emissions in this project. In this project, CO_2 emission from the construction of the ground improvement using ECM cement is 40 kg/m^3. Using ECM cement in place of BB cement, CO_2 emissions can be reduced by 45%.

Table 7. CO_2 emission reduction

Cement type	Average cement (kg/m^3) (Table 4)	CO_2 emission of cement (kg/t) (Fig.2)	CO_2 emission of ground improvement (kg/ m^3)
ECM cement	150	264	40
BB cement	160	473	76

SUMMARY AND CONCLUSIONS

This study describes the development of the ECM cement containing >60% blast-furnace slag appropriate for ground improvement to reduce CO_2 emissions. The compressive strength of the ECM cement was higher than that of the BB cement, and the use of ECM cement as a ground improvement was confirmed to be effective in immobilizing Cr(VI). Using ECM cement in place of BB cement, CO_2 emissions can be reduced by 45%.

ACKNOWLEDGMENTS

This development is part of the "Research and Development of Energy CO2 Minimum (ECM) Cement Concrete System" from the New Energy and Industrial Technology Development Organization (NEDO). We would like to show our appreciation for NEDO.

REFERENCES

Environment Agency of Japan, 1991. Environment Agency Notification, No.46. (in Japanese)

Hashimoto Manabu, Sakata Noboru, Etsuo Sakai and Toshio Yonezawa, 2014. Study on Concrete For Civil Engineering Using Blast Furnace Slag High Containing Cement, Proceedings of The 69th Japan National Conference of Soil Mechanics and Foundation Engineering, pp.601-602. (in Japanese)

Japan Cement Association, 2017a. http://www.jcassoc.or.jp/cement/3pdf/jh2_0900.pdf (in Japanese)

Japan Cement Association, 2017b. http://www.jcassoc.or.jp/cement/3pdf/jh3_1600_b.pdf (in Japanese)

Japan Cement Association, 2017c. http://www.jcassoc.or.jp/cement/3pdf/jh6_0800.pdf (in Japanese)

Japan Cement Association, 2015. Role of the Soil Improvement by Cement for Large-Scale Disasters, pp. 94-98. (in Japanese)

Japan Center for Climate Change Actions, 2017. http://www.jccca.org/chart/chart04_01.html (in Japanese)

Kono Takao, Aoki Masamichi and Yonezawa Toshio, 2016. Development of Low CO2 Emission Soil Improvement Using High-Slag Cement, Civil Engineering Conference in the Asia Region CECAR7 (CD-ROM).

Kono Takao, Aoki Masamichi, Miyamoto Yuki and Ueda Masahiro, 2017. Grid-Formed Ground Improvement Using Low CO_2 Emission Cement, Kiso-ko, Vol.45, No.6, pp. 37-40. (in Japanese)

Ogawa Akiko, Inoue Kazumasa, Tsuji Daijiro, Murakami Hiroki, Aoki Masamichi, Hirai Yoshio, Onishi Naohiro and Sato Kazuhide, 2014. Field Construction Tests of Cast-in-place Concrete Piles using High Slag Cement, Summaries of Technical Papers of Annual Meeting, AIJ, pp.333-334. (in Japanese)

The building center of Japan, 2002a. Design and Quality Control Guidelines of the Soil Improvement for Building, pp. 218-226. (in Japanese)

The building center of Japan, 2002b. Design and Quality Control Guidelines of the Soil Improvement for Building, p 38. (in Japanese)

Tsuji Daijiro, Murakami Hiroki, Sato Kazuhide and Sakata Noboru, 2014. Experiment of Actual Column Construction of 100 N/mm^2 Class High Strength Concrete Using Blast Furnace Slag High Cement, Cement Science and Concrete Technology, Proceedings of the Japan Concrete Institute, Vol. 36, No.1, pp.1702-1707. (in Japanese)

Yonezawa Toshio, Sakai Etsuo, Koibuchi Kiyoshi, Kanda Tetsushi, Dan Yasuhiro and Sagawa Takahiro, 2013. High-slag Cement and Structures for Substantial Reduction of Energy and CO2, Proceedings of the Third International Conference on Sustainable Construction Materials and Technologies-SCMT3, pp. 1-10.

Youya Ida, Etsuo Sakai and Yoko Ooba, 2010. 6-Valent Chromium Immobility using Slag High Content Cement, Cement Science and Concrete Technology, JCA, No.64, pp. 180-181. (in Japanese)

SECANT PILES SHAFTS AND DIRECTIONAL DRILLING (SPDD) FOR A MODULAR DRAINAGE SYSTEM

Marco Angelici, TREVI SpA, Cesena, FC, Italy, +39 348 1450274, mangelici@trevispa.com

ABSTRACT

In order to control the landslide movements in the vicinity of the small centre of Santa Maria Maddalena in centre-north Italy, SPEA Engineering S.p.A designed a large drainage system for "Autostrade per l'Italia" S.p.A.. The stability problems afflicted also the piles foundations of a viaduct of A1 motorway, where movements are directly linked to the amount of precipitations were discovered.
The studies discovered that the area was affected by the reactivation of a massive "paleofrana" (ancient landslide) deposit area, for which a shear surface was detected at a depth varying from 15 to 40 m.
In order to solve the problem, a complex and modular system of 5.6 m diameter collecting circular shafts. A complex scheme of 50m long radial drains has been foreseen to control the ground water level.
The collecting shafts are then connected each other by 2 or more conduits at the bottom, while the lowest shafts are connected to the nearest watercourse for final discharge of the drained water.
The use of directional drilling was imperative because of the high accuracy required, and the length of the boreholes between the shafts or the discharge leg (up to 213 m).

Keywords: Directional Drilling, landslide, shaft, secant piles, drainage, drain, well, large diameter well, main well, discharge point.

DEEP DRAINAGE SYSTEM, STATE OF ART

The principle of enhancing slope stability by draining the ground-water has been applied for decades. However traditional solutions, such as small diameter drains and dewatering wells, are not generally practical or economic where unstable masses are deep and cover large areas, or where sensitive urban developments and underground services preclude their use. In the past, to overcome such a problem, a technique was applied with success to stabilize urban areas threatened by deep active slide zones in Italy. Large diameter (up to 2 m) shafts were drilled vertically, at centres of 5 to 9 m. Each shaft is connected to its neighbour by a horizontal, small diameter, drill hole, drilled just above the shaft base. Thus, all water attracted and intercepted by these large drainage columns is transmitted by gravity to a convenient draw off point.
This system had major operational, environmental, technical and cost advantages, and it was used to depths of over 50 m. A key feature was that the array geometry can be readily modified and adapted to the geology, structure and permeability of the unstable mass revealed during construction. As the system is not continuous, say like a drainage trench, It is particularly convenient when shallow obstructions are present, typically in urban areas. Other advantages of the system were that it was: efficient in restricted areas environmentally, compatible and safe cost effective, in comparison with equivalent drainage systems, such as continuous drainage trenches (for depth higher than…) possible to adapt the layout to the actual geometry and geology of the unstable slope, as revealed during construction.
In the figure (Fig. *1*), were Rodio applied the Rodren wells, the scheme of such "modular solution" is resumed.

© 2018 Deep Foundations Institute

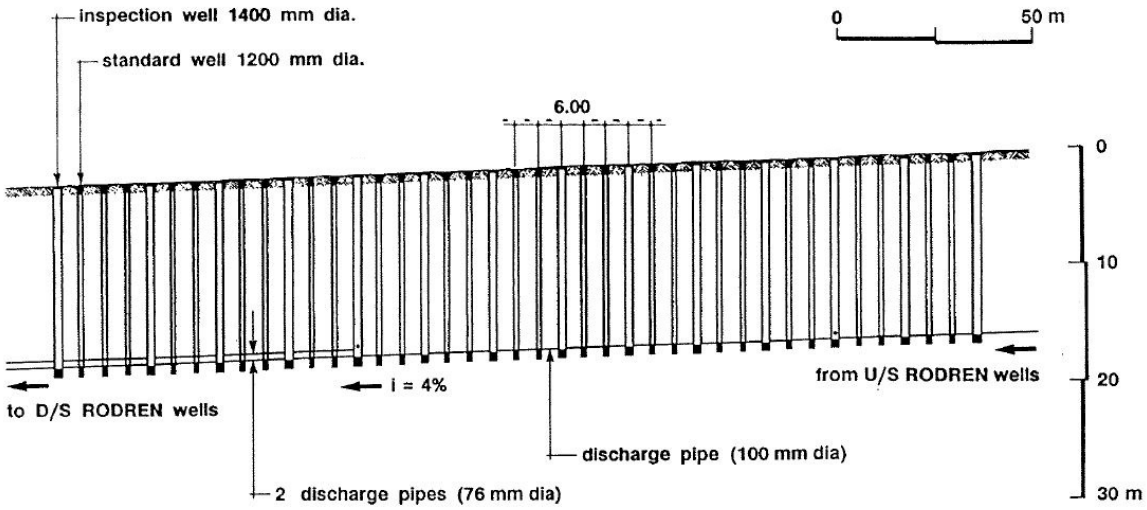


Fig. 1: Rodren's wells disposition.

Once wells were ultimate, a special rig having a circular frame sized, to operate inside the vertical steel liner and to safeguard the operator (Fig. *2*) were lowered into each well, to drill horizontal connections. All engines and power packs were placed outside the shaft (fig. 1)

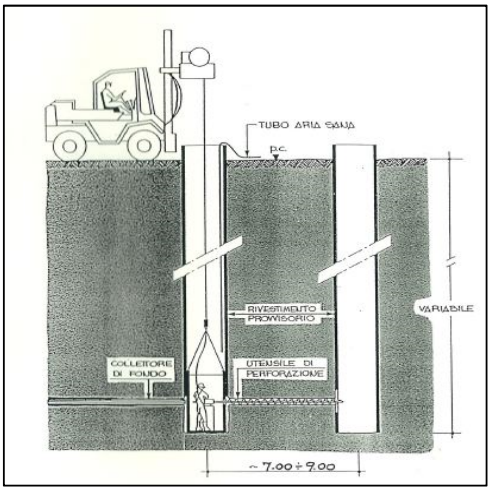


Fig. 2: special rig operating to connect wells.

Limitations

The main limitation of the system above depicted, is the safety conditions work, that are not in line with the actual regulation. The rig operator must handle drilling staff at a great depth from the surface in a very restricted environment. In case of emergency there are no possibility of help from another worker and the rescue from the shaft, if the alarm is not activated, can be decided only if the surface crew detects an anomalous situation.
In such a limited space, preventer use is not allowed, so a propaedeutic dewatering, in case of significant water pressure condition, is always necessary.
The continuity of the whole system is guaranteed by mean the possibility of connect wells each other, this means that distances higher than those allowed by the small special rig, do not allowed the natural

water discharge, and requires a pump out system. This situation may occur in case of surface obstacles as well as a building, as shown in (Fig. 3).

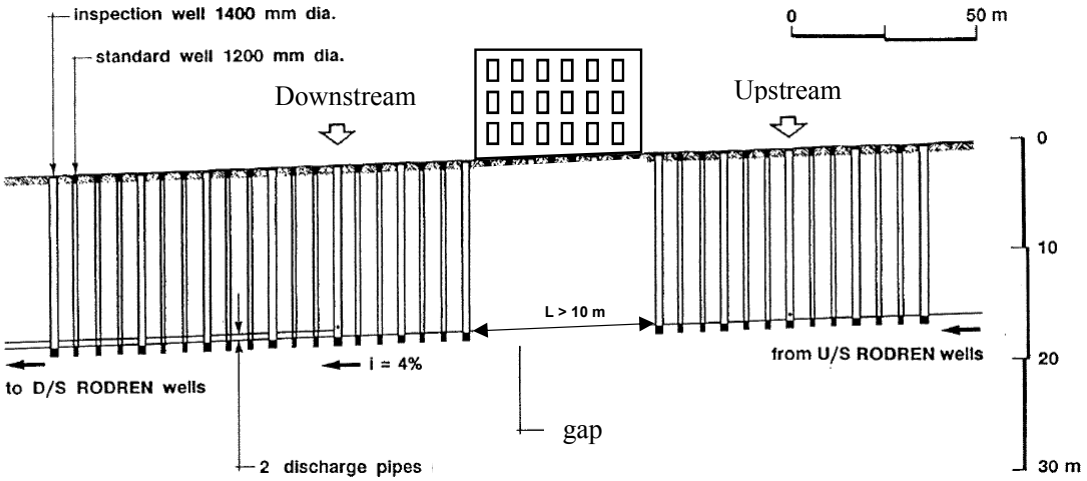


Fig. 3: surface obstacle may create an interruption of the discharge line.

Any precision drilling (+/- 30 cm) of a length higher than 10 m, should be performed by using a directional method, taking in account two relevant aspects: the alignment rig error at such a depth and small working area, the eventual presence of chaotic formations, as well as boulders in soft matrix. Anyway, a steerable down the hole assembly and/or a directional rig, couldn't be handled inside a so reduced working area, constituted by a 1.2 – 2.0 m diameter steel casing.
Another point of weakness of the system is represented by the formations that can be drilled with the "shaft rig". Rocky formation, that requires high "weight on bit", may be drilled very slowly, considering that a down the hole hammer cannot be used, because of the large amount of spoil powder released inside the small well.
The last relevant problem concerns the maintenance operations. In fact, because of the high depth and the confined space available, actions, as substitution of occluded drains or insufflation of water or air to clean drain slot, requires special and dedicated equipment, besides a specialized team.

INTRODUCING THE CSP + TDDT MODULAR SYSTEM

The Modular Elements

Each element is constituted by a CSP main shaft (structural or not), a number of interconnected draining elements (such as gravel piles), a number of draining conduits (provisional or not).
The basic concept is that from each main shaft, a number of drilling may be launched for different purposes. Such a drilling can be traditionally executed or directionally controlled in order to reach long distances and a high precision positioning. The directional option is required whenever draining isolated elements (gravel piles or draining wells) have to be interconnected, long drainage pipes have to be installed, main shaft have to be connected each other or to a discharge point. Fig. 4 depicts the basic module projected for the case history of the present paper. In the same is present a plan view in which a two lateral lines of gravel piles depart from the main shaft (MS) intercepting several gravel piles. Those "lateral wings" of drainage, depart from the opposite side of the MS in order to constitute a permeable barrier generally oriented perpendicularly in respect to the slope and the groundwater flow. It is also possible to note four schematized radial drainage conduits, that can be used for provisional (lowering the ground water level during the shaft excavation) or definitive purposes.

Gravel piles are generally realized by means of bored piles technique, and filled up with granular material (Fig. 5). The same are plugged, on the top, by means of a concrete plate (top plug, TP), while the bottom is isolated, by means a concrete bottom plug (BP).

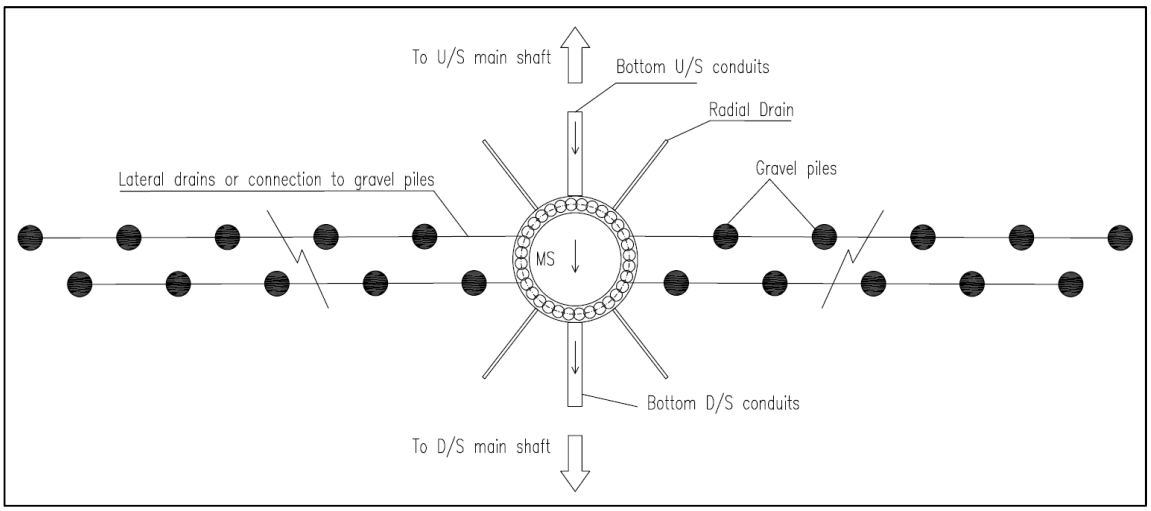


Fig. 4: plan view of a modular element

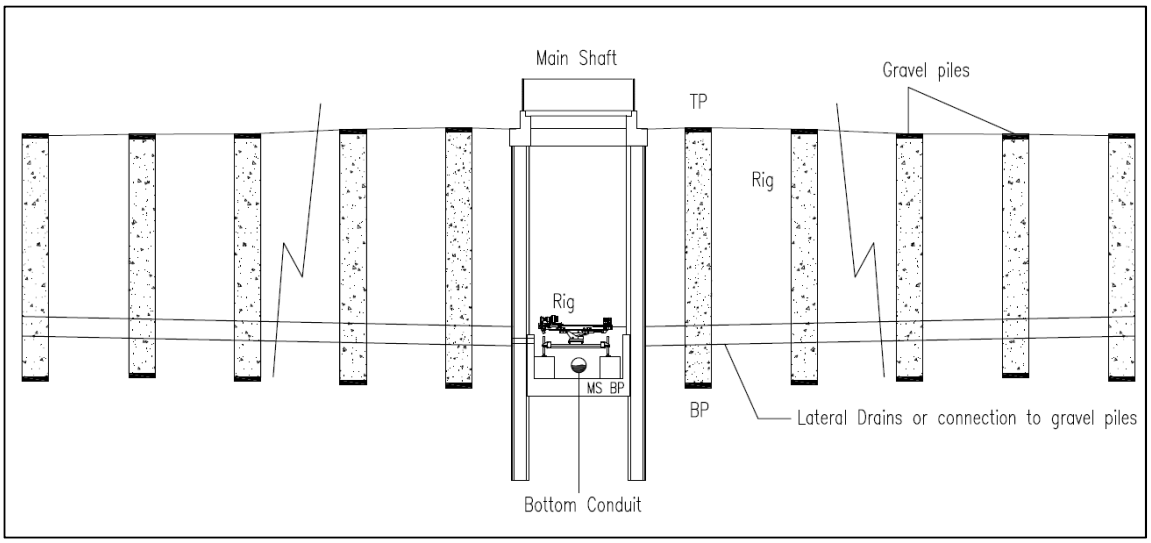


Fig. 5: section view of a modular element

Main Shafts

Main shaft, as above explained, is constructed by means the Cased Secant Piles technique Fig. 6, through which is possible to reach a maximum depth of around 26 m. The action of two counter rotating rotaries, allows the simultaneous advancing of both auger and casing. This permits a quick rate of penetration avoiding the use of drilling fluid. Such a "dry way" of excavation is particularly safe in landslide zone, where fluid addiction can worsen stability conditions. Anyway, in case of higher depth of excavation was required, the main shaft can be realized by mean of other techniques, as well as bored piles or diaphragm walls. The internal diameter of the main shaft may vary from 3,5 to 6 m, depending on both the length and the diameter of the boreholes to execute. Those two parameters, and the type of soil to be drilled, influence the rig specifications and dimensions. In case of the water pressure requires the use of a preventer, an extra length of around 1 m has to be considered. In general, the shaft

dimensions allow a crew of more than 2 people operating in the working area, respecting all the safety rules. Distance between shafts can exceed 300 m, and the bottom connection conduits may have large diameter (up to 500 mm) in order to guarantee a high volume of water discharge and a low risk of obstruction. As depicted in Fig. 7Fig. 7:, from a main shaft, different type of conduits may be installed.



Fig. 6: preparatory phases of the CSP: the "concrete guide beam"

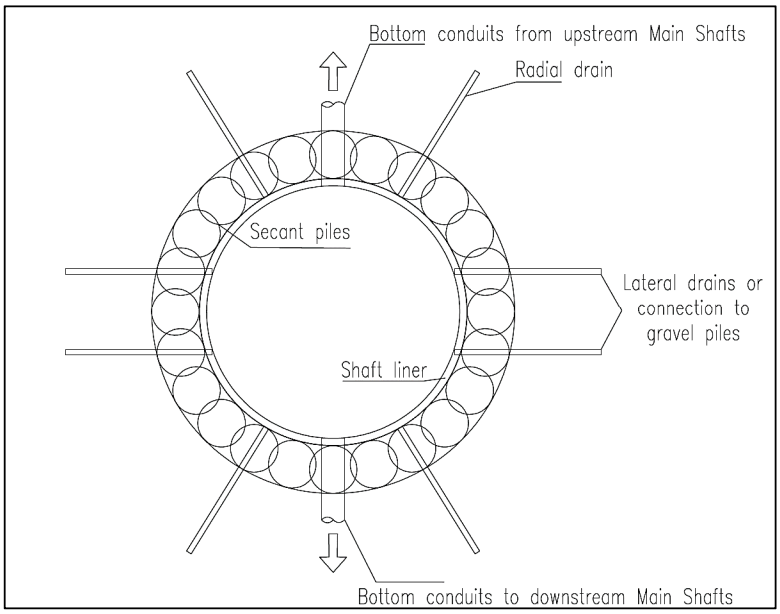


Fig. 7: plan view of a typical main shaft built for Lagaro's project.

To guarantee access operations and safety manoeuvres, the MS is equipped with a fixed ladder with safety cage, and an axial flow fan to circulate clean air. A permanent suspended winch, at the top of the shaft, is required in case of emergency, to quickly lift up injured people.



Fig. 8: birds eye view of the shaft. In the left, high corner, the fixed ladder and the big bottom end of the fan. The special drilling rig, PSPR 20, and the crew are also visible.

Gravel piles

To increase the volume of the intercepted water at a different elevation a number of gravel piles may be executed. The scheme of Fig. 4, depicts a lateral disposition of two parallel lines of piles. Different configuration may be foreseen as well as "divergent lines" shown in Fig. 9

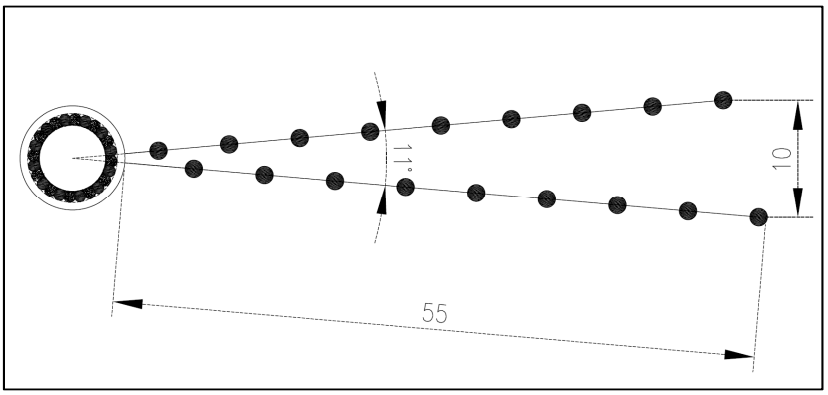


Fig. 9: radial disposition

Piles are normally excavated by using the "bored pile" technique. In order to avoid that water intercepted may filtrate in deeper soil zones, the base of each pile needs to be isolated by a bottom plug, casted before gravel is lowered by mean a tremie pipe. In the same manner, once the pile has been filled up, a top plug will be created at the ground level to avoid ingress of surface water in to the soil. The thickness of the gravel backfill can be variable, and different design solutions can be assumed to insulate different elevation aquifers from each other. In other ends, the pile filling can be zonate, and made of an alternation of permeable and not permeable levels.

Lagaro Case History

The small centre of Lagaro, central Italy (Bologna), was affected by surface movement that have increased in the past 3 years. In the occasion of a highway tunnel construction for the "A1 variante", the centre has been monitored by mean the installation of different topographic survey systems. In the same occasion, the monitoring has been extended also to the viaduct pile of the existing A1 highway. Thanks to these measures, a correlation between ground water level oscillation and movements has been deduced and a system to drain large amount of water till a depth of 20 m was projected. Thanks to a previous successfully intervention in Rome (Third Lane construction of the Raccordo Anulare)[1], where three drainage shafts were connected each other and to a discharge point, the solution in object was evaluated to be effective. In this case, to extend the draining surface, a number of gravel piles arranged in a double line was foreseen, so to create something very similar to a continuous barrier without the negative effect of it in terms of stability. In many circumstances, in fact, a deep drainage trench, oriented perpendicularly to the slope, may induce a preferential way for "tension crack" enucleation. A number of aligned circular bodies, offers a large drainage surface, but the discontinuity of the cut surface together with a slight angle between the piles raw axis and the slope contour lines, doesn't afflict the slope stability.
The complex geology of the zone, characterized by a strong heterogeneity has been the main issue from a productivity point of view. The heart volume representing the landslide body, is constituted by calcareous marlstone interbedded with sandstone and together are part of the Monghidoro and Montevenere formations (late Cretaceous – Paleocene). In this area, such a formation, are strongly weathered and mixed up by ancient landslide phenomenon, that transformed the sequence in a chaotic mass, constituted by hard boulders immerged in a soft silty-clay matrix.

The project layout

After a deep shear surface has been detected (Fig. 10), a number of modular unities was designed in order to influence three different zones of the hill slope (Fig. 11).

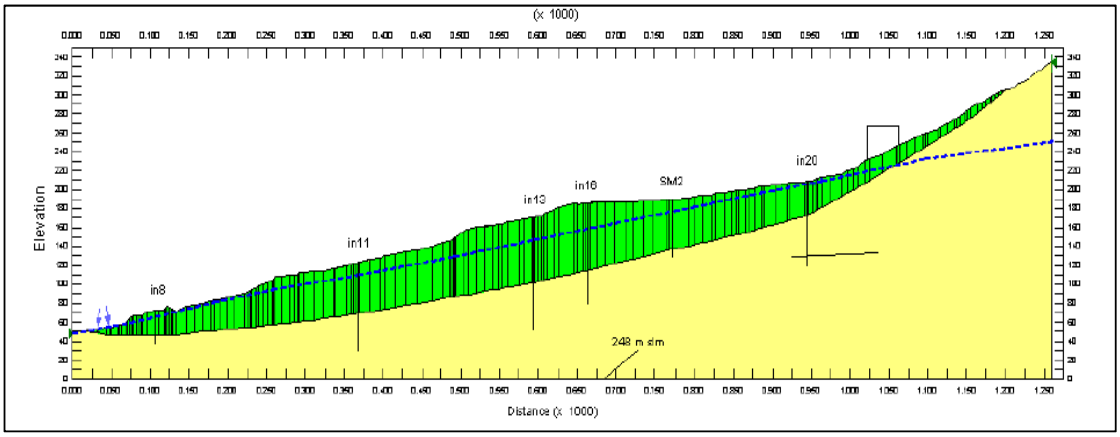


Fig. 10: The proposed model for the shear zone. A section through 1.2 Km of the interested area. The body involved in the landslide is represented in green. The dot blue line is the water level table.

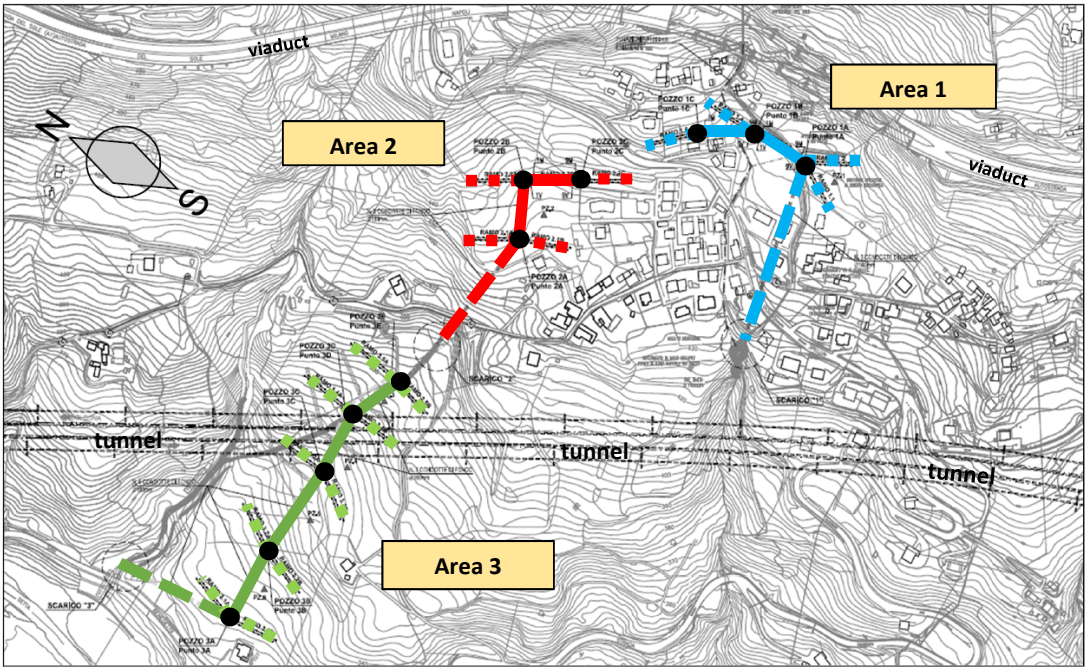


Fig. 11: the three areas represented in the topographic map. Black dots are the main shafts, continuous lines are the bottom conduits, small dot lines are lateral connections to gravel piles (not represented), long dot lines are the discharge conduits to a stream.

Fig. 11 depicts the general layout of the intervention and the three areas in which the modulus was built with 5 and 3 main shafts for Area 1 and Area 2 and 3 respectively. In total 11 main shafts, were located in the critical zones of the slope.

	N.	Total Length (m)	Diameter (mm)
Drilling for lateral drains	88	4399	131
Drilling for bottom conduits (m)	29	2884	320
Main Shafts (n.)	11	264	7600 (external)
Gravel Piles (m)	792	19000	1500
Secant Piles for Main Shaft	264	6336	1000

Fig. 12: the table resumes the quantities of each modular component for the three areas

Construction Details

Main Shaft

The main shaft was projected in order to host a drilling rig able to launch boreholes up to 70 m, with a diameter up to 160 mm, in difficult terrains. The internal diameter of 5.6 m, was reached by means of 24 secant piles, of 1 m diameter. The rig was conceived inner the company and the features enable to orient the mast by both shifting and rotational movements of the base.

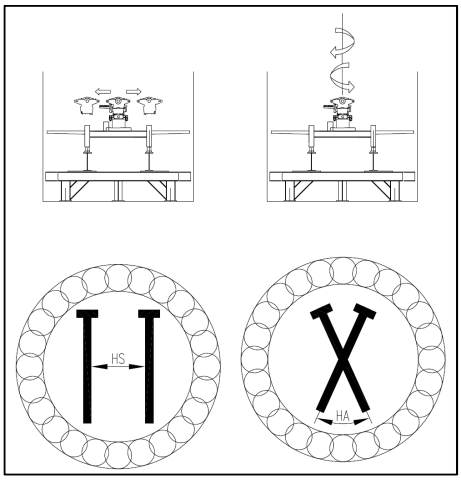


Fig. 13: special rig hosting; main shaft vertical section and plan view

The interception of the gravel piles, was considered to be done by mean of two conduits per line of pile. This was conceived in order to have always at least one pipe working, in case the other got plugged by sedimentation material, or particles passed through the filter.

Gravel piles and drain conduits

The geometry of the complex "drain pipes + gravel piles" determines the capability of catch water from the ground. In this project, the drain pipes were constituted by a slotted part (through the gravel piles) and a blind part, in the between (Fig. 14).

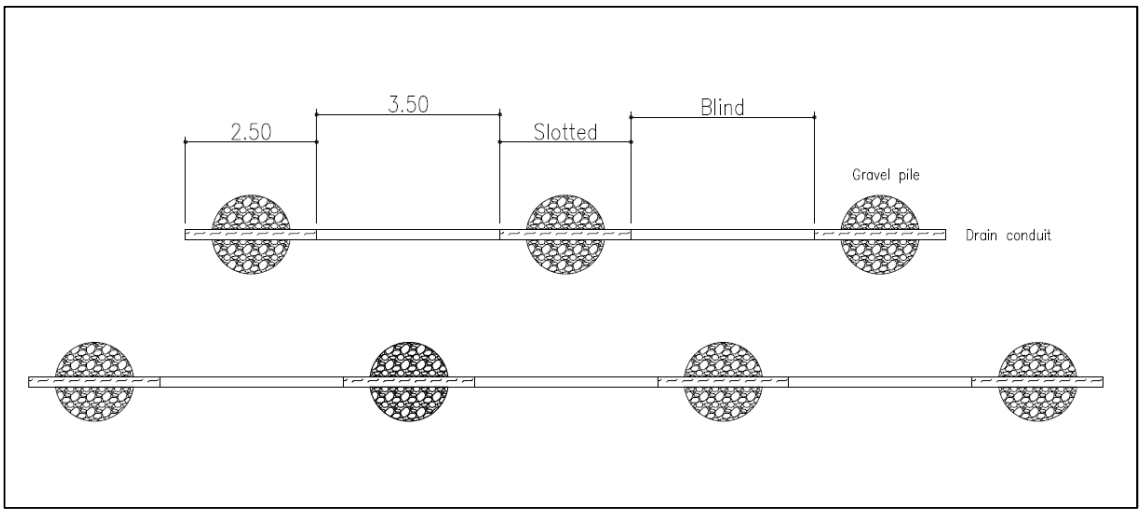


Fig. 14: typical arrangement for the lateral wings of each main shaft. 1.5 m diameter gravel piles are spaced 6 m centre to centre.

The pipes were HDPE made, wrapped on geotextile tissue, and contained in a larger steel pipe, in order to be retrieved and substituted if problem due to occlusion occurred. Diameters of the pipes above mentioned, were 88.9 and 131 mm respectively. Installation was done by casing the directional pilot hole with the final product itself (131 mm steel pipe).

Bottom conduits

The longest drillings were made in order to place the bottom conduits. Diameters also were larger than that of the lateral drainage pipes, considering that the pipes to install were 160 and 225 mm respectively. For the downstream main shafts, where the amount of water to discharge was higher, 3 pipes were foreseen (two 160 mm and one 225 mm diameter). For the upstream main shafts, one 225 mm and one 160 mm were foreseen. Installation was done by using the back-reaming technique as well as in the horizontal directional drilling (HDD) applied to river crossing, or other traditional HDD application. The difference in respect to those applications, were in the reduced space to assemble the conduit. In fact, while in a open space the whole length of pipe can be assembled on the surface by mean of a head to head welding procedure, the only possibility, having to pull back the pipe from a shaft, was to using special fast connections, in order to add 3 m long piece at once.

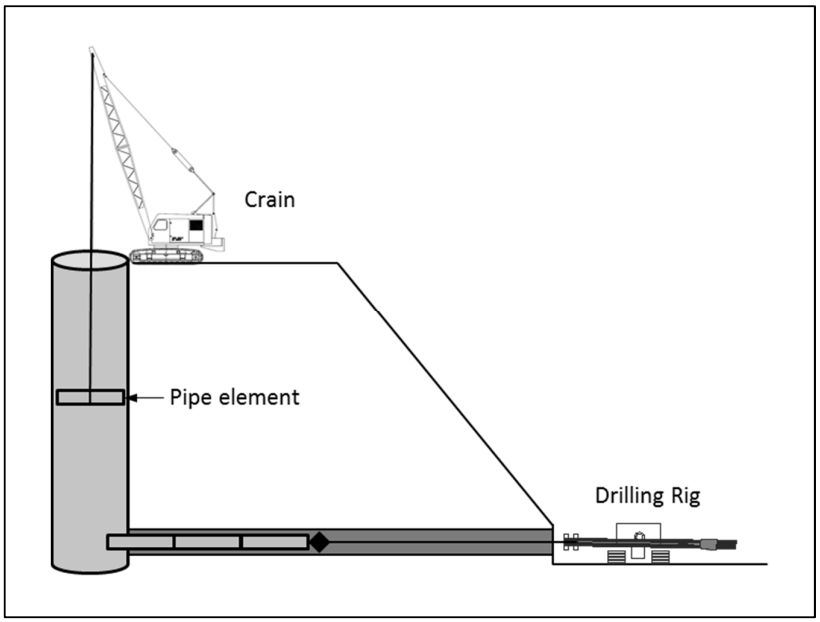


Fig. 15: procedure to assemble the product pipe from inside the shaft while pulling back operation

Summary and conclusions

Comparisons with traditional methods, where possible, shows that the SPDD is particularly convenient with the increasing of the length to treat and volumes of water to discharge. In case of medium to long distance (60 – 200 m) from the last collecting shaft to a discharge point, the SPDD technology to install a bottom conduit (at 20 m average depth) results cheaper in respect to traditional technology. In fact, with SPDD no intermediate shafts are required to connect two generic points.

For all the work duration no effects on surface have been noted, as well as no increments in landslide movements. After completion of the area n.3 (the earlier completed) measurement on volume collected at the discharge point was positively correlated to amount of precipitation.
The groundwater level has been also monitored with a consistence reduction of the seasonal oscillations.

From a technology development point of view, great improvements have been done in the way of drilling in presence of problematic soils. The nature of the “in situ” formation has been already discussed; to steer boreholes in this condition different tool have been used. Traditional tools as well as slant face bit or fixed bent sub could be used only in the lower part of the area where rock boulders

were rare, and marl-claystone represented the most of the formation. As the weathered rocks become predominant, other tools were required as well as Wassara hammer specially to pass throughout the gravel piles, and mud motor, where the boreholes presented a length higher than 100 m. In presence of rock and no possibility to recycle water (during the summer season) also an air hammer has been used. Consequent problems were connected to the ability of change quickly the bottom hole assembly and the subsidiaries plant: high pressure – high volume pumps, air compressors, desander groups.

UNDERGROUND CAR PARK IN THE ANCIENT "MORELLI" CAVERN IN NAPLES

Massimiliano Bringiotti, CIPA S.P.A., Rome, Italy
Aldo Bellone, CIPA S.p.A., Rome, Italy
Francesca Rossano, CIPA S.P.A., Rome, Italy

ABSTRACT

In 2004 works started for the now completed seven-level automated car park accommodating 480 parking spaces inside the pre-existent "Morelli cave", located in a strategic area in Naples. Since 470 BC Greeks initiated the growth of the fascinating world of the underground Naples, of which this cave belongs.

It seems that once here the god Mithras was worshiped. it's also became a quarry for tuff extraction and in 1600s it became an aqueduct serving the area. In 1853 the Bourbon Tunnel, a project commissioned by King Ferdinand II of Bourbon to allow easy escape from the Royal Palace in case of riots, was connected to this network of tunnels.

The cavern became an air raid shelter during the Second World War, then a deposit of cars and motorcycles in the '50s and' 60s, a disposal area and it has been abandoned in the last 40 years before it's new utilization..

INTRODUTCION

Over time, the overcrowding and congestion of major cities' historic centres has led to seeking spaces underground that can accommodate activities and car parks, as in the case of the Morelli cavity, site of the future car park by that name.

Before describing its characteristics, design solutions, and executive problems, it is necessary to introduce the site historically into the broader landscape of the cavities present below ground in the municipality of Naples.

The province of Naples, which includes the area of the Municipality of Naples, has a large number of cavities.

The existence of "Naples underground" is connected with the morphological and geological conformation of its territory, consisting of tuff stone which has entirely special features of lightness, brittleness, and stability.

The first transformations in the territory's morphology, taking place thanks to the Greeks starting from 470 BC, initiated the growth of the fascinating world of Naples underground. These transformations were dictated by water provision requirements, which led to the creation of underground cisterns to collect rainwater, and by the need to recover construction material to erect the buildings of Neapolis. In subsequent centuries, the city's expansion led to the construction of a proper aqueduct, which allowed drinking water to be collected and distributed thanks to a series of cisterns linked to a dense network of tunnels. During Roman rule, the existing aqueduct was expanded and perfected, but with the rise of the Angevins in 1266, the city saw great urban expansion, which obviously corresponded with increased extraction of tuff from the subsoil to construct new buildings. This confirmed a particular feature of Naples: that of having been generated from its own innards, with buildings rising directly above the quarry that provided their building material.

Decisively impacting the destiny of Naples underground were some edicts between 1588 and 1615, which prohibited introducing building materials into the city in order to stem Naples's uncontrolled expansion. To avoid punishment while still meeting the need for urban expansion, the citizens had the

© 2018 Deep Foundations Institute

idea of extracting the tuff beneath the city, by using pre-existing shafts, enlarging the cisterns designed to contain drinking water, and digging out more. Extraction of this kind, which took place from top to bottom, required special techniques in order to guarantee the stability of the subsoil and prevent undesired collapses.

Only in 1885, after a terrible cholera epidemic, was the use of the old water distribution system abandoned in favour of adopting the new aqueduct, which is still in operation.

The most recent underground project dates back to the Second World War, when to offer safe refuge to the population, the decision was made to adapt the ancient aqueduct's structures to the citizens' needs. Throughout Naples, 369 shelters in the caves and 247 collapse-proof shelters were set up. An official list from the Ministry of the Interior from 1939 lists 616 addresses that led to these 436 shelters, some of which with more than one access. The arrangement of the shelters led to an additional splitting-up of the ancient aqueduct.

At War's end, given the dearth of means of transport, almost all the rubble was unloaded into the subsoil, almost as if wishing to bury with it all the memories of that sad period. Until the late 1960s, there was no more talk of Naples underground, even though many went on using the shafts as dumps.

However, starting in 1968, some instabilities began to occur, due essentially to ruptured sewers, or leaks in the new aqueduct. In all the world's cities, these problems are seen when sewage gurgles to the surface, or with flooding; but in Naples, precisely because of the vast, hollow subsoil, the same problems become evident with large sink holes. This is due to the fact that aqueduct water or sewage almost always finds a preferential path towards the old shafts, where all those incoherent materials at the roof of the tuff and surrounding the leaks liquefy. This causes a void, which proceeds upwards and becomes evident only when the final layer – consisting of slabs of terrain or of roadbeds– collapses into it.

Coming to the subject hereof, the "Morelli cave" (see Figure 1.) is located in one of the most strategic areas of the city of Naples (see Figure 2.), just a few hundred metres from the downtown Piazza Dei Martiri, Villa Comunale, and Via Caracciolo; a "Bourbon-era" tunnel, which in the Neapolitan circulation plans will connect with Piazza del Plebiscito and the Via Toledo area, departs from it.

For years the car park was used on "on grade level" at about 9.00 m above sea level, with extremely limited capacity.

However, the project developed a total of 435 spaces, 225 of which for rotation parking and 210 for private garaging. It bears mentioning in any event that the original plan called for 673 car spaces, and many of them (no fewer than 238) were sacrificed in drawing up a design that respected the safety and stability needs, as well as the state of the locations, to the maximum extent possible.

The general layout of the car park located within the Morelli cavity (see Figure 3.) consists of a structure in reinforced concrete cast onsite, and is organized in 14 modules, seismically jointed together.

Each module has a total of 6 decks in elevation and a foundation with plinths and a connection slab – except for the smaller ones to be done in rather special points in the cavity, such as niches and enclosed spaces between the existing masonry works. A newly-built tunnel serves the car park, with an entrance from the arcades of the building at Via Morelli. This tunnel, which entailed considerable difficulties connected essentially with having encountered additional cavities – often full of detritus – along the route, has a mezzanine that allows pedestrians to access the structure.



Figure 1. Pictures of the "Morelli" cavern.



Figure 2. "Morelli" cavern location into the urban context of Naples.

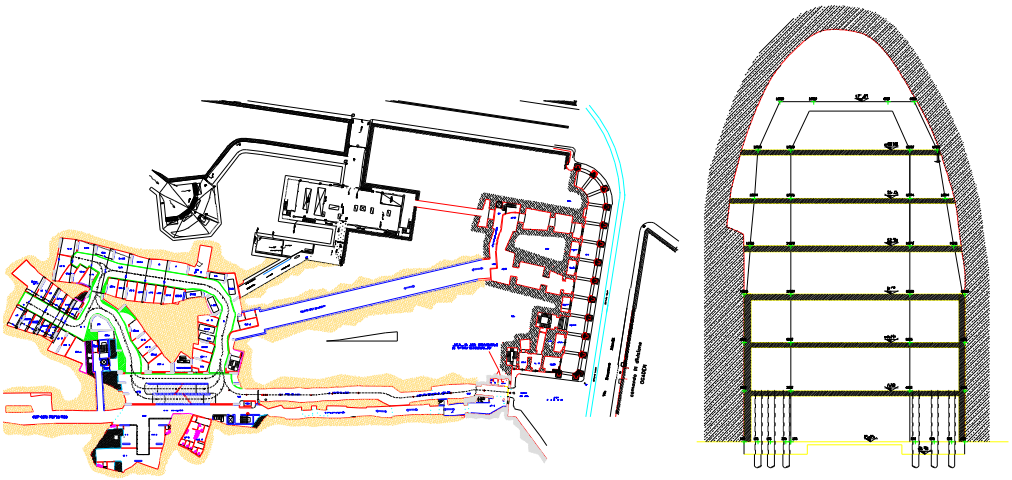


Figure 3. General layout of the parking and a typical section.

STRATIGRAPHY OF THE SUBSOIL

The Morelli cavity develops entirely in the setting of the tuff mass of the Monte Echia promontory, where the presence of a series of buildings over it in fact hampered the execution of systematic probes from above to define the tuff roof's development in detail.

The stratigraphy of the subsoil was thus gleaned both from direct observations conducted on the walls of the Morelli cavity, and from the results of the ongoing core sampling, which was possible to perform both in the same cavity and in some yards above it. Based on these observations, it may be said, with a sufficient degree of approximation, that the tuff coverage is no less than about 4.0 m with respect to the highest part of the cavity.

Above the tuff mass, practically to ground level, are loose pyroclastic soils and, to a lesser extent, landfill.

The free surface of the groundwater, based on some observations made in the car park area, is at about +1.5 m above sea level.

GEOTECHNICAL CHARACTERIZATION OF THE SUBSOIL

Degree of fracturing of the mass

The degree of fracturing of the rock, as obtained from the examination of the various probes performed in the Morelli cavity's tuff walls, is generally rather contained. Rather high RQD (Rock Quality Designation) levels were in fact obtained, mostly between 90 and 100%; only in a few cases, near individual discontinuities, was an RQD value of less than 50÷60% found.

Moreover, as far as is visible to the naked eye inside the Morelli cavity, there are no real families of discontinuity, but only localized cracks. However, it cannot be ruled out that in some areas, the mass, on the inside, may in fact be characterized by a higher level of fracturing than appears from an examination of the exposed surfaces, or that there might not be discontinuities parallel or sub-parallel to the cavity walls, produced by the release of tension due to the making of the cavity itself.

Physical-mechanical properties of the soils and rocks

For the purposes of the performance and the stability of the works in question, the loose pyroclastic soils present above the roof of the tuff formation are doubtlessly of little importance, in both geotechnical and applicative terms. As for the tuff, on the other hand, it bears mentioning that in the case in point, it is of the utmost importance to define its resistance characteristics not only at the level of the individual samples, but also and above all on the scale of the mass.

Starting from the results of the laboratory tests as reported in the 2001 document drawn up by the Department of Geotechnical Engineering (Dipartimento di Ingegneria Geotecnica – DIG) of Università di Napoli Federico II, it is found that the weight of the unit of dry volume equals on average 10.8 kN/m^3. Depending on the natural water content, equalling 0.20, a weight of the unit of volume of the tuff equal to about 13.0 kN/m^3 is obtained.

The average value of the breaking strength is approximately 3.5 MPa for samples subjected to testing after having been air-dried, and 2.6 MPa for samples subjected to testing in saturation conditions. It is then observed that the saturation leads to a reduction in resistance equal to about 25%, while in both cases the standard deviation is about 0.7 MPa. Based on statistical considerations, one may then take into account a characteristic value (obtained by subtracting twice the standard deviation from the average value) of the uniaxial compressive strength equal to about 2.1 MPa for the dried samples, and 1.2 MPa for the saturated samples.

As for the breakage envelope and the relative parameters c' and ϕ', the results of the triaxial CID compression tests performed at DIG, Università di Napoli Federico II, were taken into consideration. In the σ'_1-σ'_3 plane, the values of the breaking strains obtained by the tests performed on saturated samples, with the exclusion of some clearly anomalous results, yielded an effective cohesion value of 0.74 MPa and a 17° angle of friction.

However, it is stressed that this angle of friction value is far below the typical range of values obtained for yellow Neapolitan tuff in the abundant experimentation performed at DIG, Naples. Based on these tests, in fact, in may be said that the angle of friction always exceeds 20°, with typical values between 24° and 30°.

The first one obtained is thus to be considered an anomalous value which is probably influenced by the limited number of tests performed and the strong heterogeneity of samples tested, as proved by the marked variability of the uniaxial compressive strength found among the tested samples.

The tuff's resistance parameters are cross-correlated with the negative degree of correlation (Aversa 1989); that is, increased cohesion often corresponds with a diminished term of friction. Since the stability of the excavations depends highly on the cohesion value, the preference was to assume a higher value (25°) for the angle of friction and to obtain the cohesion with the compressive strength characteristic of the dried material, thus obtaining $c'_k = 0.66$ MPa. On the other hand, the analogous value for saturated tuff equals about 0.40 MPa.

As concerns deformability, the uniaxial tests also yielded a Young's modulus between 1500 and 3500 MPa.

As rock mechanics tells us, to carry out the mechanical characterization of a mass, once the properties of the material of which it is made are known at the scale of the samples used in the lab, it is necessary to assess certain factors that influence and determine their behaviour on a larger scale. Of these, the most important ones are the so-called "size effect" and the degree of fracturing of the mass.

In particular, *"size effect"* is essentially linked to the material's inhomogeneity and to the possible presence of micro-cracks. In this regard, special laboratory tests have clearly shown that with increased sizes of the sample subject to rupture testing, the cohesion and the elastic modulus tend to diminish to an asymptotic value. To take this diminution into account, in the case of yellow tuff a reductive coefficient equalling about 0.7 ought to be considered.

The *degree of fracturing*, however, is linked mainly to the development of the cooling and cementation processes of the loose pyroclastic material from which the tuff originated, as well as to later seismic and/or tectonic phenomena and, in the final analysis, to states of overstressing caused by humans, which may have caused the rock to break locally. The influence of the degree of fracturing on the overall behaviour of a rock mass is extremely important: one need only consider that in the presence of two or more families of discontinuity, each with an interaxis between cracks on the order of one decimetre (a rather frequent case, for example, in highly tectonized rock), the behaviour at excavation is no longer that of a rock, rather than that of a gravel, or at any rate of a fundamentally noncohesive soil.

Aside from this extreme case, rock fracturing results in a reduction both of cohesion and of the elastic modulus, which of course grows more accentuated as the rock's integrity lessens. In the specific case, the high RQD values found with the investigations performed result in reductive factors that may be estimated at about 0.85÷0.90.

Therefore, in conclusion, the tuff mass in question may be characterized with a constitutive elastic/perfectly elastic rule, with the criterion of Mohr-Coulomb yield point and non-associated flow rule, or an elastic-plastic model with hyperbolic type tension/deformations bond, using the average values of the parameters in Table 1.

Table 1. Average values of the tuff parameters.

Parameters	tuff above the water table	tuff below the water table
weight of unit of volume:	14 kN/ m^3	14 kN/ m^3
angle of friction:	25°	25°
effective cohesion:	350÷400 kPa	250÷300 kPa
tensile strength:	70÷100 kPa	40÷60 kPa
elastic modulus:	1000 MPa	800÷1000 MPa
Poisson's ratio:	0.25	0.25
dilatancy angle:	0	0

DESCRIPTION OF BEARING STRUCTURES

The vertical structures consist of septa 40 cm thick and variable in length, placed, for the first useful elevations, crosswise against and longitudinally with the cavity's axis of development. They are conceived as collaborating with the tuff walls up to an elevation of +9.65 m; for the remaining parts as well, the septa are connected to the very walls of the cavity.

Deck slabs

The slabs are to be understood as cast full slab on site, with two-way reinforcement, for a total thickness of 35 cm.

Foundations

The foundations consist of plinths 80 cm thick, in some cases on piles 400 mm in diameter and 6.00 m in length above the plinths' level of installation. The plinths are joined to a connection slab about 40 cm thick, and upper surface coinciding with the upper surface of the plinths. The indicated upper surface elevation is set at +0.50 m.

As regards only the boreholes, the piles were made from the work site elevation, appropriately levelled to +3.20 m, except for the already-indicated piles/piers, which instead shall be complete with reinforcement and casting up to the borehole mouth level, as they had have to function as provisional support for the first three slabs.

CONSTRUCTION PHASES

The works to build the Morelli car park began in June 2004. Hereunder, the modes of operation and design for each working process shall be described, highlighting the problems faced in so particular a site, which have prolonged the working operations.

Working operations began with the bench and stabilization of the walls and of the cavity crown.
This stabilization was done through the insertion of structural elements, threaded bars and Ct-Bolts, suitable for improving the geomechanical characteristics of the mass, and whose characteristics are to be analysed in greater depth below.

An additional intervention was carried out in correspondence with the cavities' crowns. In some sections, these were reinforced with lattice ribs (see Figure 4.), constituting a kind of lining; of course, since the cavities, once the excavation is done, reach heights up to a maximum of 30 metres, for the installation of these ribs, as well as for the stabilization on its own, scaffolding was erected ad hoc, with irregular geometries adapted to the cavity's morphology, making it possible to reach these heights (see Figure 5.).

The operations were completed with the installation of wire mesh and shotcrete.



Figure 4. Lattice grids that fit the crown.



Figure 5. A view of part of the scaffolding.

CAVITY STABILIZATION: CT-BOLT

The cavity was consolidated, in accordance with precise needs, using various techniques, such as appropriately grouted Dywidag anchor bars, but particularly worthy of mention is the additional system known as CT-Bolt, one of the systems most widely used to support and consolidate rocky walls (see Figure 6.).

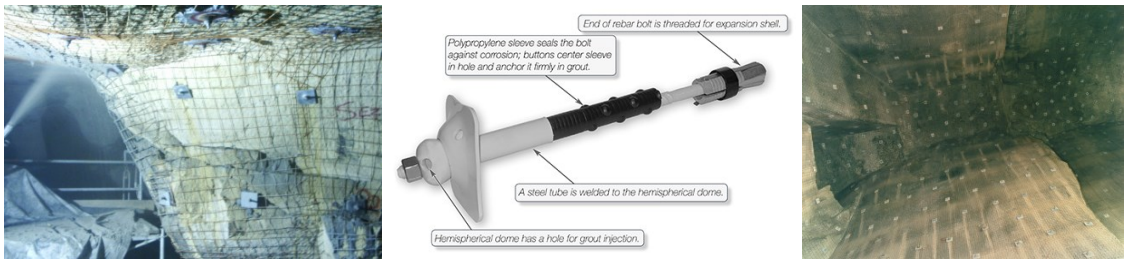


Figure 6. CT-Bolt on the crown before they are covered by a shotcrete layer.

The purpose of a system conceived in this way is to contain the deformation phenomena and, in the event there are disarticulated prisms of rock, to support them.

Of course, the choice of anchoring type is closely linked to the type of rocky mass and, in addition to the specific work site conditions, to technical and economic considerations. CT-Bolt is a corrosion-resistant anchoring that is installed following the geomechanical principle of temporary and immediate rock support using an expansion shell and then grouted to give it permanent anchoring characteristics. This system presents considerable differences in technique, performance, and cost (of the element and of its installation) from other types of anchoring. A rigid sleeve in polyethylene placed between the steel bar and the rock guarantees the seal, eliminating the corrosive action of water, and is at the same time used as grouting conduit.

The sleeve's particular shape also acts as a continuous centring device for the bolt in the borehole, keeping water from coming into contact with the steel and guaranteeing an anti-friction effect against slippage. The CT-Bolt comes with a dome-shaped body that has two functions: it supports and distributes the load on the bolt plate and serves as a grouting chamber.

The grout is pumped into the mixing dome and through the polyethylene sleeve; at the upper end it flows between the sleeve and the rock until escaping from the bolt plate. The characteristics are shown in Table 2.

Table 2. CT-Bolt characteristics.

Model	Bar diameter	Ultimate tensile strength, point anchored	Ultimate tensile strength, fully grouted
C-TUBE M20	18.6 mm	150 kN	180 kN
C-TUBE M22	21.6 mm	250 kN	318 kN
Standard length	From 1.5 m to 8.0 m (others upon request)		
Boring diameter	From 45 to 51 mm		

BUILDING OF THE MORELLI TUNNEL

The excavation of the entrance tunnel to the Via Domenico Morelli car park was done first in full face, supporting the excavation cross section with bolts and the installation of electrowelded mesh (see Figure 7.).

Then, in September 2005, intercepting a cavity filled with loose debris required changing the mode of excavation; in fact, after having grouted with lean concrete to allow the cavity to be filled after stabilizing the excavation face with shotcrete, the decision was made to excavate a truncated conical cross section with double forepoling on the crown, reinforcement pipes diam. 139.7, 8 mm thick, with an interaxis of approximately 25 cm, to allow this problem to be overcome.

Subsequently, the first-phase lining was made (ribs and shotcrete), as well as sealing, formwork reinforcement and the casting of the final lining, later completed in June 2006 with the grouting of an intermediate slab allowing the upper portion of this tunnel to be used by pedestrians.



Figure 7. Excavation done by roadheader and supported by electrowelded mesh and CT-Bolts.

BUILDING OF THE STRUCTURE IN ELEVATION

The building of the structures constituting the car park began in July 2006 from module A, continuing with the construction of modules I and H, B and G; for the other modules, the plan was to proceed alternately to the current cavity entrance from Largo Morelli.

This is all to build a encirclement of the central pier in natural tuff which characterizes the cavity itself.

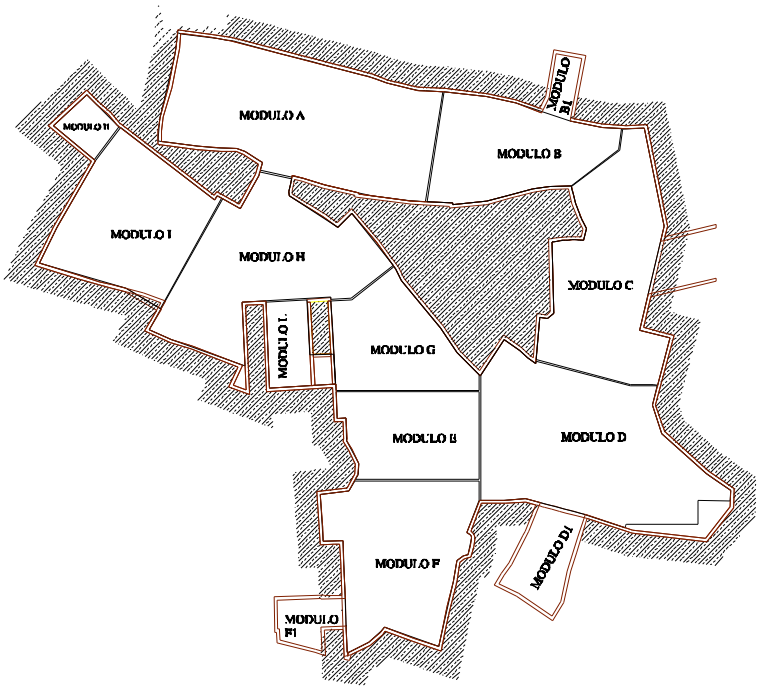
To pursue this purpose, for modules A, B, B1, I, H, G, and F, the floors at elevations +6.60 m, +9.65 m, and +3.55 m were made before excavating to the foundation level in such a way as they may function as struts against the tuff walls, particularly for module F, at an elevation of approximately +7.50 m (see Figure 8). This was dictated by the need to counter a barbican whose foundation is

presumed at an elevation of +3.00 – an elevation where the tuffs settle, as confirmed by the latest probes on November 28, 2006.

As regards the procedures for building these floors, as already discussed, by exploiting the deep foundation type, already at an elevation of +3.20 m pile-piers were built, constituting the vertical support of the deck at that elevation.

This is followed by the reinforcement and the casting of the setpa which support the floors at an elevation of +6.60 m and +9.65 m. Having completed these two phases, after appropriate curing of the castings, the excavation took place by indenting the existing tuff bank, which was further lowered to the installation elevation of the connection slab in the foundation, to be followed by the set section excavation to build the plinths.

As may be easily intuited, these cases considerably slowed the working operations; it must not in fact be forgotten that the need to make the decks to an elevation of 9.65 before reaching foundation level led to excavations under cover, with the use of appropriate equipment. Additional provisional works (plating and mini-piles) were needed to stabilize the masonry septa nearest to module I, even if not provided for in the design phase.



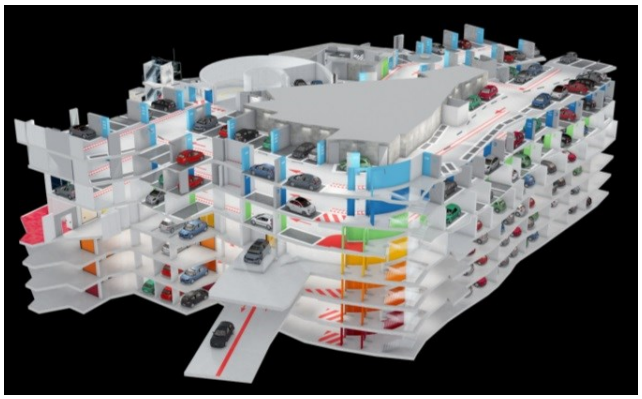


Figure 8. Layout of the modules of the parking and a 3D rendering.

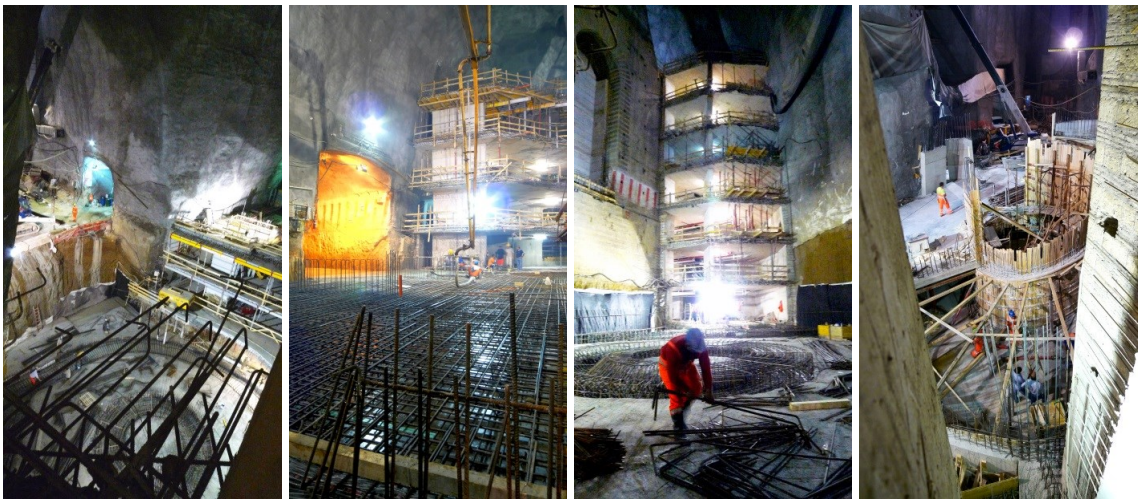


Figure 9. Pictures of the construction of structures.



Figure 10. Old vehicles found during the works.

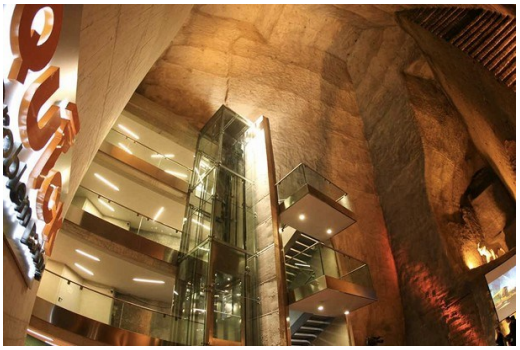


Figure 11. The parking today.

REFERENCES

Evangelista, A., Aversa, S. 1994. *Experimental evidence af non-linear and creep behavior of pyroclastic rocks*. Proc. Course on Visco-plastic behaviour of geomaterials.

Aversa, S. 1989. *Comportamento del Tufo Giallo Napoletano ad elevate temperature*. Tesi di dottorato di Ricerca in Ingegneria Geotecnica, Università di Napoli.

Evangelista, A. 1980. *Influenza del contenuto d'acqua sul comportamento del tufo giallo napoletano*. Atti del XIV Convegno Nazionale di Geotecnica, Firenze.

BIBLIOGRAPHY

Bringiotti, M. 2003. *Guida al Tunneling 2nd ed.* PEI.

Bringiotti, M., and Bottero, D. 1999. *Consolidamenti e fondazioni 2nd ed*. PEI.

VACUUM PRELOADING WITH DRAIN TO DRAIN METHOD FOR THE NEW INTERNATIONAL AIRPORT OF MEXICO CITY

Vito Nicola Ghionna, Former Professor at Technical University of Turin, now at Studio Geotecnico Italiano, Milan, Italy, phone: +39-02-5220141, email: v.ghionna@studiogeotecnico.it

Luiz Guilherme de Mello, POLI Universidade de São Paulo and Vecttor Projetos, São Paulo, Brazil, phone: +55-11-30342333, email: lgmello@vecttor.com.br

Valeriano Pastore, Studio Geotecnico Italiano, Milan, Italy, phone: +39-02-5220141, email: v.pastore@studiogeotecnico.it

Roberto Andrighetto, Studio Geotecnico Italiano - Milan, Italy, phone: +39-02-5220141, email: r.andrighetto@studiogeotecnico.it

Lucas Pereira Cammarota, Escritorio Geotecnico Brasileiro, São Paulo, Brazil, phone: +55-11-30342333, email: lucas@escritoriogeotecnico.com.br

ABSTRACT

The paper describes the performance of an extensively instrumented trial field of vacuum assisted fill loading with prefabricated vertical drains in the area of Texcoco Lake (2228 m a.s.l.) for the construction of the new International Airport of Mexico City. A vacuum preloading of approximately 60 kPa was applied on top of drains over a period of 180 days using the drain to drain technique combined with cylindrical capped drains (Star Drains) installed at 1.2 m interval on a triangular grid. The loading fill consisted of 2 m thick locally available low density volcanic material ("Tezontle"). Soil profile in the area is characterized by very soft Mexico City clay having notoriously very poor geotechnical properties. A final settlement close to 2 m was recorded at the central point of the fill corresponding to a consolidation degree of approximately 70%. Settlements measured both on the ground surface and at depth were in good agreement with predictions by numerical analyses.

Keywords: trial field embankment, vacuum preloading, drain, Mexico Clay, consolidation settlement

INTRODUCTION

The new International Airport of Mexico City is located in the area of the Texcoco Lake; this area is subjected to land subsidence due to a huge deep pumping program in the lower aquifers located below 60 m depth started at industrial scale in 1930. The site rests over a deep formation of Mexico City clays, which are extremely plastic materials exhibiting notoriously large natural void ratios and water contents, with very poor geotechnical properties. The ground water level is rather shallow. Without a suitable soil improvement, excessive differential settlements and stability problems of runways and taxiways would be expected along with detrimental effects on airport buildings. To this purpose, a system of prefabricated vertical drains (PVD) with combined vacuum and surcharge preloading was considered: a trial field was then planned using the technique of vacuum preloading with the "drain to drain" (membraneless) method, where the vacuum is individually applied to each drain through specifically designed connection caps. This system has been extensively applied throughout the world in many infrastructural works. In Mexico Star Drains have been recently successfully adopted by Odebrecht Co. for the Etileno XXI project in Coatzacoalcos, State of Veracruz, in similar subsoil conditions.

TRIAL FIELD AND PVD DRAINS DESCRIPTION

The test embankment had a footprint of 76 m in length and 56 m in width and a final height of 2 m (Figs.1÷2). It was composed of two layers of a lightweight gravelly-sized material of volcanic origin ("Tezontle"), compacted to a dry unit weight (γ_t) of approximately 12.2 kN/m^3, separated by a thin layer

© 2018 Deep Foundations Institute

of the same material with finer (sandy) grain size ("Tezontle fino"), having the function of protecting the vacuum lines. In overall a vertical pressure of about 24.4 kPa was imposed on the ground surface by the surcharge fill. A reinforcing geogrid was laid at the base of the embankment to prevent failures and ensure more uniform settlements, while an underlying geotextile fabric was adopted to prevent intrusion of clayey particles into the first Tezontle layer.

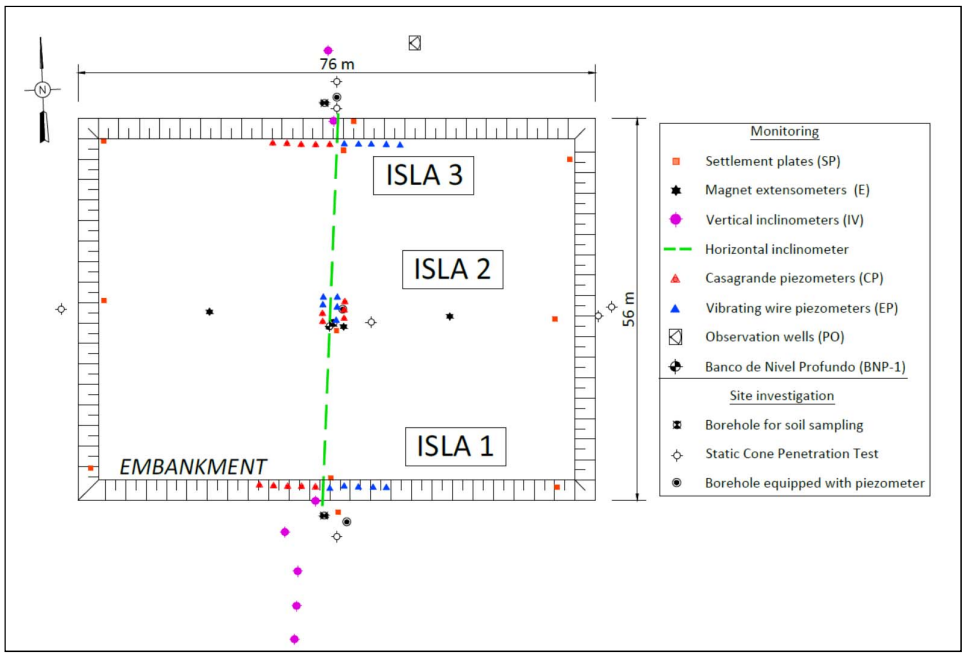


Fig. 1 – Plan of test embankment with location of monitoring instrumentation and of site investigations

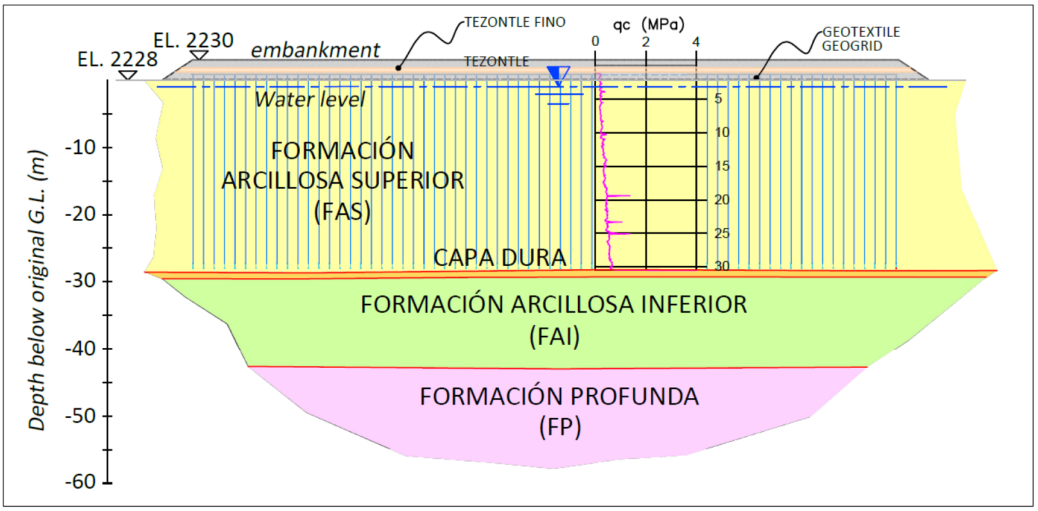


Fig. 2. Schematic cross section of test embankment and stratigraphy

The drains system consisted of partially penetrating vertical pipes of plastic material having a star shaped internal core wrapped by a protective geotextile filter ("Star Drains") (Fig.3); the drains have an outer diameter of 30 mm and are installed by a steel mandrel having an outer diameter of 60 mm. The first 3 m of the pipes from the top cap were sealed by an impermeable plastic tape to reduce the risk of air inflow from ground surface. PVD drains were installed at a depth of 28 m from ground level (GL) that, in the test fill area, is located at 2228 m a.m.s.l. The bottom of drains was 2 m above the deep formation named Capa Dura (Fig.2). Drains were arranged according to a triangular pattern with a spacing of 1.2

m. The installation was carried out from the top of the first layer of Tezontle. Special laboratory tests were carried out to measure the well resistance of the drains under different confinement pressures. Such tests gave very high values of discharge capacity: $q_w = 60 \bullet 10^{-4}$ m^3/sec at a confinement pressure of 300 kPa. However, in the numerical analyses carried out to model test fill behavior such value was reduced to take into account possible effects caused by negative long term phenomena such as buckling, kinking, and clogging phenomena (Miura et al., 1998; Aboshi et al., 2001; Lee and Karunaratne, 2007).

VACUUM SYSTEM

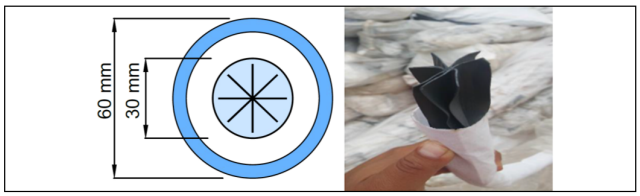


Fig. 3 – StarDrains



Fig. 4 – Drain layout

The vacuum system consisted of 6 vacuum pumps aligned along the southern side of the embankment, each one feeding 10 lines of solid, air and water tight, plastic pipes laid horizontally on the surface of the first Tezontle layer (Fig.4). Once all drains were installed, each drain cap was individually connected to the relevant vacuum line. An air-water separator tank was used at each pump location in order to draw apart the water contained in the air-water mixture abstracted from the drains and detect its amount. The vacuum pressure recorded at pump manifolds was on average 70 kPa. Taking into account that the atmospheric pressure at the trial fill site is about 78 kPa, the efficiency of the pumps was about 87%, with no single pump working below 80%. An average head loss of approximately 30% was detected between the pumps and the terminals of the vacuum lines on top of their farthermost drains and approximately 15% on top of drains located at mid points of the vacuum lines. The average delivered vacuum pressure at the drains top connection is therefore taken as 60 kPa (intermediate between pump manifold and vacuum line end).

GEOTECHNICAL INVESTIGATION AND SOIL PROPERTIES

Field investigation

An intensive site investigation was conducted in the area of test fill before its construction in order to determine soil stratigraphy and geotechnical properties of soil layers. Site investigations included (Fig. 1): 3 drilling boreholes with continuous coring (BH) for high quality soil sampling; 3 boreholes with SPT tests in sandy layers; 7 CPTU with dissipation tests; 22 Field Vane tests carried out in 4 boreholes.

Soil profile and groundwater level

Field investigation evidenced a relatively uniform soil profile consisting of the following units (Fig.2):

- Formacion Argilosa Superior (FAS): highly plastic and extremely compressive soft clay of lacustrine origin with water content ranging from 150% to 300% and void ratios ranging from 4 to 8; the unit extends approximately from 0 to 30 m from ground level (GL);
- Capa Dura (CD): very dense to hard slightly cemented sandy silt layer from 30 to 31.5 m from GL; the number of SPT blows is usually very high;
- Formacion Argilosa Inferior (FAI): soft clay of lacustrine origin with occasionally interbedded lenses of fine sands and volcanic ashes of centimetric thickness, extending from 31.5 m to 45

m below GL; as this unit is deeper than FAS, it exhibits higher strength and lower compressibility due to the increase in overburden;

- Formacion Argilosa Profunda (FAP): soft clay with characteristics similar to FAI extending at depths below 45 m from GL; this unit is similar to FAI and FAS but it exhibits lower void ratios and natural water contents due to water pumping in the deeper acquifers.

The ground water table (GWT) was found at very shallow depths, approximately 1 m from GL.

Laboratory tests

Particular attention was devoted to the one dimensional compressibility properties of cohesive layers at short and long term: the test program included 21 stress controlled oedometer tests and 11 long duration "creep" tests. Unconsolidated undrained triaxial tests (TX-UU) were also conducted to have supplementary data on the undrained shear strength (c_u) of fine grained materials.

Soil properties

The most relevant soil properties obtained are summarized in Figs. 5 to 8.
The pore water pressure (u) profile measured by piezometers is shown in Fig.6. The deviation from the hydrostatic trend observed in the lower portion of the curve is an effect of the deep pumping.

The high variability of e-logσ'_v compression curves in Fig. 8 is in relation with the pronounced variability of initial void ratios and natural water contents, as evidenced in Fig.5. Using data of virgin compression lines, a relationship was found between the permeability coefficients in vertical direction (k_v) and the void ratio (e), that was in agreement with Taylor (1948) law written in semi-logarithmic version: $\log k_v = \log k_{v,0} - (e_o - e) / C_k$. In such expression $k_{v,0}$ is the permeability coefficient at the in situ void ratio (e_0) whereas C_k is a permeability change index. Tavenas (1983) proposed to link C_k to the in situ void ratio through the following equation: $C_k = 0.5 \bullet e_0$. However, for the investigated samples more appropriate values of C_k/e_0 were the following: $C_k/e_0 = 0.35$ for FAS formation and $C_k/e_0 = 0.45$ for FAI formation. These values were used in the numerical analyses.

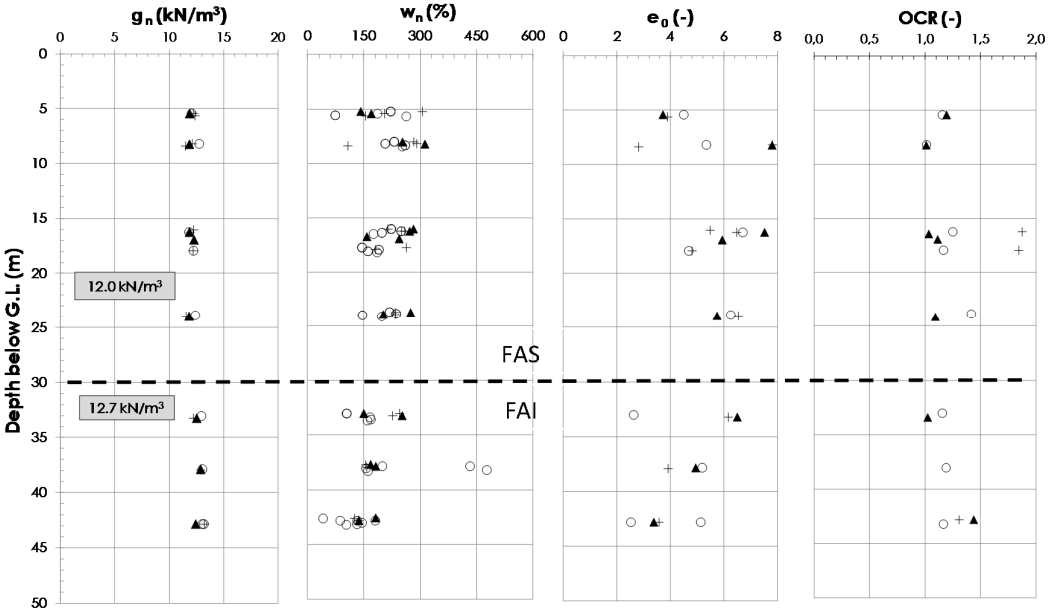


Fig. 5. Index properties for FAS and FAI layers: unit weight, water content, void ratio, overconsolidation ratio (Legend ○=BH1, ▲= BH2, +=BH3)

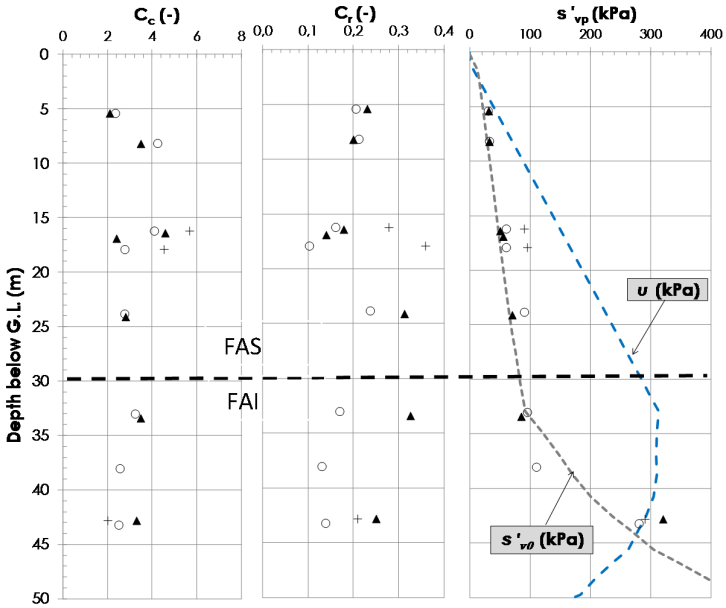


Fig. 6 - Cc and Cr from oedometer tests; groundwater pressures from piezometers and evaluated vertical obverburden stresses (Legend ○=BH1, ▲= BH2, +=BH3)

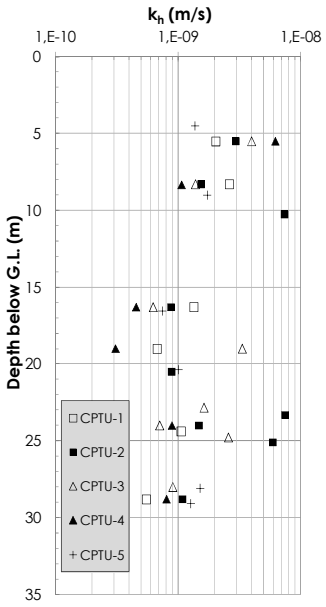


Fig. 7 – Horizontal permeability coefficients from CPTUs

MONITORING SYSTEM AND INSTRUMENTATION

An intensive monitoring program was conducted in the test area in order to follow the consolidation process during the whole test period. The following instrumentation was installed (Fig.1):

a) 246 superficial benchmarks installed on top of the test fill and all around the boundaries of the embankment;

b) 9 settlement plates placed at the base of the first Tezontle layer with the aim to monitor settlements of the original ground surface from the beginning of the construction works;

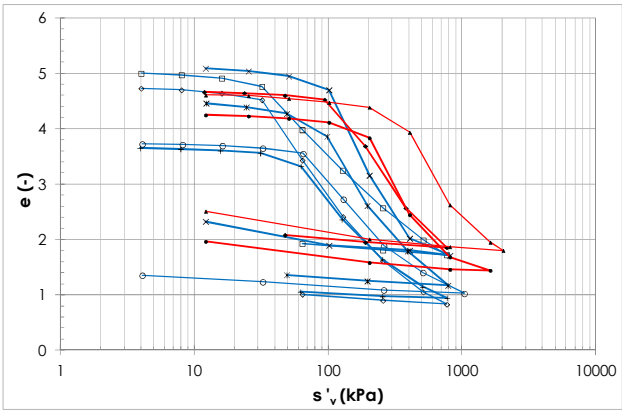


Fig. 8 – Results from oedometric tests: blue lines refer to FAS samples, red lines to FAI samples

c) a horizontal inclinometer laid below the embankment along the transverse centerline of the improved area, to detect the deformed shape of the ground close to base of the fill during the test;

d) a steel pipe inserted in a 47 m deep borehole to measure (by precision leveling on the top) the settlements in the deep sediments, i.e. the area subsidence;

e) 18 magnetic extensometers installed in 3 boreholes aligned along the longitudinal centerline of the test fill in the E-W direction. Each boring contained a multipoint extensometer with 6 measuring magnets positioned at depths ranging approximately from 2 m to 47 m from GL;

f) 7 vertical inclinometers installed close to the external boundaries of the test embankment;

g) 15 piezometers installed in 3 different clusters ("islas") located along the transverse centerline of the test fill; each cluster included 5 couples of piezometers each formed by a Casagrande piezometer and an electric vibrating wire piezometer;

h) 2 deep observation wells (PO), to detect possible variations of ground water level (GWL). No significant variations were observed in the whole test period;
i) manometers installed at pump manifolds and at selected terminals of vacuum lines on top of drains to check vacuum pressures supplied by each pump and head loss along the vacuum lines;
j) mechanical calipers installed over the tension cracks opened on ground surface close to the fill edge to monitor their evolution with time.

Precision leveling of benchmarks and measurements of the other instruments were carried out daily.

CONSTRUCTION PHASES AND LOADING HISTORY

The construction sequence involved the following phases:

i. placing the first layer of Tezontle (height= 0.6 m);
ii. installing Star-drains from top of Tezontle layer;
iii. positioning vacuum lines and connecting drain caps to them;
iv. placing the protective layer of fine Tezontle on the vacuum lines (height=0.3 m);
v. activation of vacuum pumps and checks of vacuum system performance;
vi. placing the final layer of Tezontle (height = 1.1m).

The overall duration of vacuum application was 180 days. Monitoring data continued to be collected for a period of 60 days after vacuum switch-off.

ANALYSIS OF MONITORING DATA

Settlements at the centre of the embankment

Fig.9 illustrates the time history of settlements measured in the centre of test fill. A final settlement of 1.97 m was obtained in six months. Settlements stopped very quickly after the vacuum pumps were switched off. Based on results of a previous field test conducted in an adjacent area with a traditional surcharge fill without vacuum, the performance of the new test fill with vacuum can be considered very satisfactory and even better in terms of time to reach the same settlement.

Differential settlements along the transverse centerline

Fig.10 summarizes data obtained from the horizontal inclinometer. Curves evidence isochronic settlement profiles that have almost symmetrical shapes and trends similar to that exhibited by traditional embankments. The differential settlements between the center and the boundaries of the embankment are influenced by the inward movements of the lateral boundaries caused by vacuum. Boundary settlements vary linearly with the corresponding ones detected at the centre. It must be clarified that the endpoints of the horizontal inclinometer are located each one about 5 m apart from the top edge on the preload embankment. Along the transverse centerline a ratio equal to about 0.55 between lateral and central settlements was observed, whereas a ratio of 0.6 was observed from settlement plates measurements: the latter value is practically coincident with that predicted by the elastic theory for traditional embankments.

Deep settlements at centre of fill

Fig.11 shows the trend with depth and time of the vertical settlements measured through the magnet extensometers at the center of the trial embankment.

Negligible settlements were measured in the 60 days after vacuum switch-off: the last two lines in the figure are practically coincident.

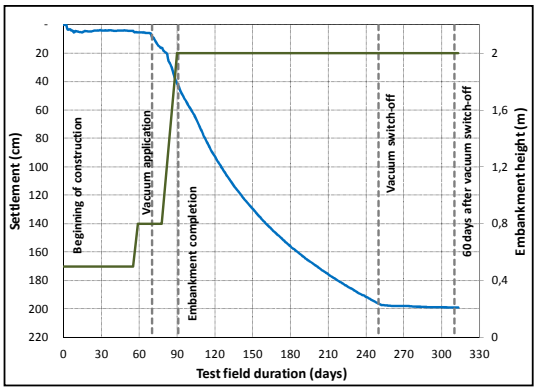


Fig. 9 – Settlement at center of test field. The green line shows embankment construction sequence.

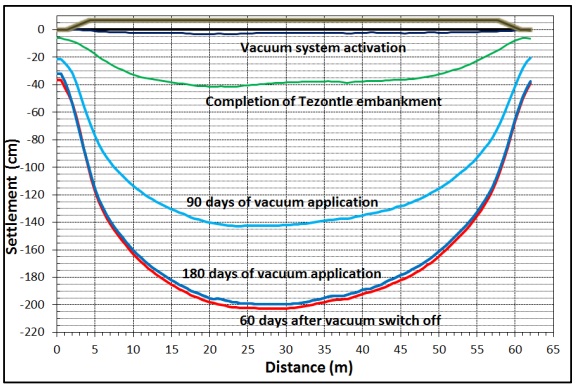


Fig 10 – Time history of settlements measured by horizontal inclinometer

Horizontal displacements outside the vacuum treated area

Fig.12 summarizes the time trend of the lateral displacements measured by vertical inclinometers. The following comments can be made:

a) vacuum application induced significant horizontal displacements directed towards the embankment body; the displacements extended to significant depths reaching, in some cases, points near the bottom of the casings;

b) the placement of the final layer of Tezontle caused lateral displacements in the outward direction with strong deformations on top of casing;

c) after vacuum switch off, the inward lateral movements manifested a slight tendency to reduce or even revert;

d) the maximum values measured at ground surface at the end of the test in the inclinometers installed nearest to the fill ranged between 170 and 270 mm, gradually reducing in magnitude moving away from the improved area; appreciable values (of the order of 50 mm) were still detected at a distance of 20 m from the border of the embankment.

According to Mesri and Khan (2012) the ground surface horizontal displacements at the boundary of the vacuum treated area are in some relationship with the settlements at the

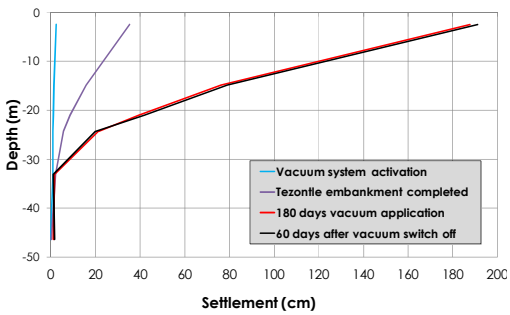


Fig. 11 – Settlement at center of test field measured by magnet extensometers

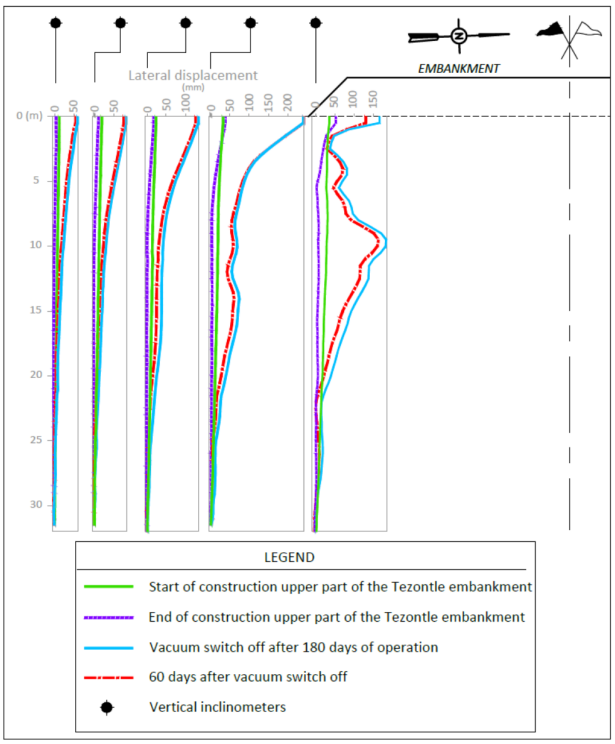


Fig. 12 – Cumulative displacements measured by a series of vertical inclinometers located at 5 m spacing

centre of fill. This has been confirmed by data gathered in the present trial field; nevertheless, the observed trend remained below those inferred by the aforementioned authors from the analyzed case histories.

Tension cracks close to the outer boundaries of the fill.
Negative pressures applied by vacuum in soil below the test fill tend to develop tension cracks on ground surface close to the improved area (Seah,2006). Theoretical reasons explaining the formation of such cracks have been presented by Chai et al. (2005). Local cracks developed along the two minor sides of the embankment. Five cracks were observed that were oriented approximately parallel to the sides of the embankment, reaching, at the final stage, lengths up to 420 mm and opening sizes up to 35 mm.

Pore water pressures variations
Pore pressures variations measured by piezometers under vacuum application are influenced, among other parameters, by the distance of the piezometer tips from the drain pipes. The real position of the piezometers with respect to the drain pipes can be affected by possible deviations from the vertical of both instruments and drains. This can give rise to unpredictable discrepancies between piezometers readings and theoretical predictions.
The variations of pore pressures measured by piezometers at the center of the fill can be observed in Fig. 13. Pressure variations in this figure are corrected for the settlements of the piezometers tips. It is worthwhile to point out that both the values and the shapes of the curves in the figure depict pore pressures in soil surrounding the drains that are affected by all the uncertainties described above. In particular they are not indicative of the vacuum distribution inside the drains.

Water discharge from the vacuum system
In a one dimensional consolidation process a direct relationship exists between the settlement rate (ds/dt) of the ground surface and the flow rate (q_w) of water flushed out from the soil. Basing on such premise, the daily flow rates $q_w(t)$ of water extracted by the vacuum pump feeding the central portion of the embankment have been plotted in Fig.14 versus the settlements of the centre of the embankment. As can be seen the two curves show a similar trend that can be satisfactorily described by an exponential law.

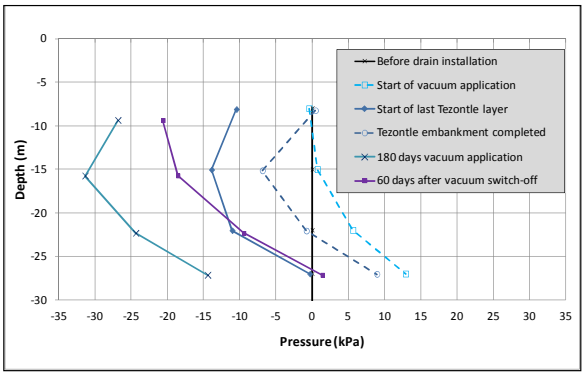


Fig. 13 – Variation of water pressure (average from Vibrating-Wire and Casagrande piezometers at the center of the embankment) during works. Settlements of piezometers are taken into account

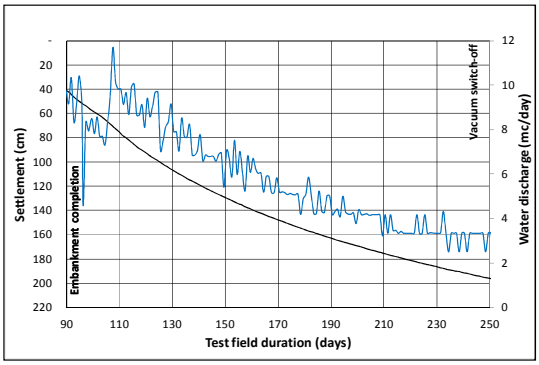


Fig 14 – Embankment settlement at the centre of the fill (black line) vs water discharge from pumping system (blue line)

NUMERICAL MODELING

Theoretical analyses of soil improvement using vacuum assisted surcharge fills with drains has formed the object of numerous investigations. According to the nature and properties of the treated soils along with the design requirements of the structures/building to be built on them, several methods have been proposed to model fill behavior, such as: analytical solutions based on radial consolidation theory

applied to single drain axisymmetrical unit cell approach (Chai et al, 2010; Chai and Carter, 2011; Perera et al., 2016; Geng et al. 2012); unit cell approach implemented in numerical codes using the finite difference method (FDM) (Khan, 2010; Mesri and Khan, 2010) or the finite element method (FEM) (Indraratna et al, 2005); simplified 2-D and 3-D FEM analyses of multi drain nets (Rujikiatkamjorn et al., 2008). In the following only a general information on the adopted code and the results obtained is given.

Numerical code adopted

Numerical analyses were carried out by ILLICON code developed at Department of Civil and Environmental Engineering of Illinois University, Urbana-Champaign (USA) (Funk and Mesri, 2014). The code is a finite differences software based on the one-dimensional consolidation theory for clay proposed by Mesri and Rokhsar (1974) and further enlarged by Choi (1982). Among the key features of the code we mention (Khan, 2010; Mesri and Khan, 2010, 2012): multi layer soil profile, totally and partially penetrating drains, presence of horizontally draining layers, anisotropy of the hydraulic conductivity of soil layers, changes in compressibility and permeability during primary consolidation, variations of permeability and compressibility inside the smear zone, submergence of ground surface during consolidation, well resistance of drains, vacuum pressure distribution inside the drains, any loading history including combinations of fill surcharge and vacuum.

Model assumptions

Pore water pressure profile and initial overburden stress profile were assumed in accordance with Fig. 6. Soil parameters of sub-layers were inferred from data reported in Figs. 5 and 6. The complete compression curves shown in Fig. 8 were directly input in the calculations, thus allowing to avoid any external interpretation of the deformability parameters of the soil and any discrepancy with the selected laboratory data. The in situ initial horizontal permeability coefficients $K_{h,o}$ were assumed to coincide with those gathered from CPTU dissipation tests (Fig. 7). Taylor (1948) equation with c_k values previously reported was adopted to describe the variation of k_h with void ratio.
Drains system was characterized by the following parameters: length of drain: L =28 m from GL ; drain diameter: D_w= 30 mm; mandrel diameter: D_m= 60 mm; equivalent diameter of the unit cell : D_e=1.26 m; diameter of the smear zone: D_{smear}= 2• D_m ; operational in situ drain discharge capacity: q_w=75 m^3 per year ; sealed length on the upper portion of drains: 2 m below GL. Horizontal conductivity in the smear zone ($k_{h,sm}$) was assumed to vary linearly with radius and the ratio $k_{h,sm}$ / k_h was taken, on average, equal to 0.6. Compressibility properties in the smear zone was considered to correspond to those of fully remolded samples defined by the intrinsic compression line proposed by Burland (1990).
According to Chai et al. (2010) for one way drainage case, a trapezoidal vacuum pressure distribution inside the drains was assumed to account for the presence of the upper sealed portion; after a linear trend near the top, a constant vacuum pressure distribution was considered in the remaining part with a value corresponding to the vacuum pressure measured on top of drains at connections with the vacuum lines: 60 kPa in stabilized conditions.

Results of numerical analyses

Fig. 9 shows the trend with time of surface settlements in the centre of fill predicted by numerical analyses along with those evaluated at the elevations at which magnet extensometers were installed. In fig 15 the same data are plotted against the depth for different construction steps. In both cases the agreement is very satisfactory. The average consolidation degree predicted by ILLICON code was approximately 70%. It is noted that this value is consistent with the average value of variation of pore water pressure at the time of vacuum shutdown. In fact, taking as 60 kPa the delivered value of vacuum pressure (negative) and 24.4 kPa the maximum excess pore pressure (positive) induced by the Tezontle embankment, 70% of consolidation degree corresponds to approximately 35 kPa of average negative pore pressure variation. This figure is not so different from the recorded values at the piezometers

(around 30 kPa), considering also the uncertainty of the position of piezometric cell compared to the position of the drains.

CONCLUSIONS

The main purpose of the trial test was to verify the capability of a drain to drain vacuum application method combined with a preloading fill to be successfully applied under extremely difficult soil conditions such as those existing in the construction area of the new International Airport of Mexico City. StarDrains were adopted to accelerate soft soil consolidation. To this aim an intensive monitoring program was carried out to control the effects induced in the subsoil by the consolidation process. Monitoring comprised all the period of construction and also a period of 60 days after vacuum switch off. During this period the instrumentation installed provided a conspicuous amount of data allowing to draw the following conclusions:

a) The drain to drain vacuum system adopted proved able to maintain the vacuum pressure almost constant, on average 70 kPa at the pump manifolds, for the whole duration of the trial field.

b) The vacuum assisted preloading fill with drains was very effective inducing settlements that, at the centre of fill, reached a value close to 2 m and an average consolidation degree approximately equal to 70%. This result was obtained with limited embankment preload (2.0 m of light material – Tezontle – with total load of 24.4. kPa).

c) A much longer time would have been necessary for a traditional preloading system without vacuum to cause the same settlements as demonstrated by results gathered by a traditional surcharge embankment tested before in the same area. The trial field with drains and conventional surcharge was carried out by GACM (Grupo Aeroportuario de la Ciudad de México) under the technical and scientific supervision of II-UNAM (Instituto de Ingenieria – Universidad Nacional Autonoma de Mexico). The conventional preloading was about 45 kPa (1 m of Tezontle + 1.8 m of heavier material – Tepetate) with 2.0 m wick drain spacing. More than one years was needed to reach a settlement in the center of the trial field equal to 200 cm.

d) Settlements at the internal boundaries of the fill varied linearly with the settlements at the fill centre remaining confined in a ratio of approximately 0.4 to 0.6 with respect to the latter one. Significant settlements (of the order of various centimeters) were still detected at a distance of 20 m from the border of the embankment.

e) Lateral displacements outside the fill were influenced by construction history and vacuum application, relatively small and directed towards the fill. The maximum values observed at ground surface on the inclinometers located nearest to the embankment ranged between 170 and 270 mm. Significant values were still observed at a distance of approximately 20 m from the embankment.

f) Pore pressures variations measured by Casagrande and vibrating wires piezometers were in acceptable agreement, the latter showing a prompter response to loading and vacuum application.

g) Ground surface settlements and deep settlements predicted by numerical analyses were in good agreement with the corresponding ones measured at the center of fill. This shows the possibility to extend trial field results to the design of larger embankments.

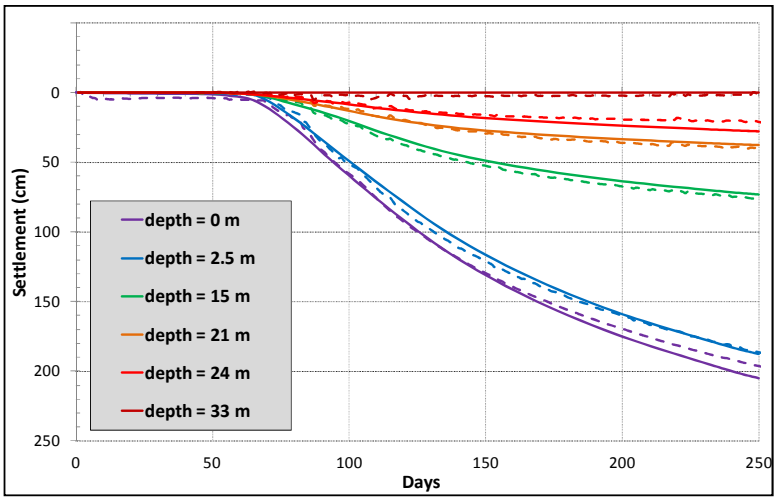


Fig. 15 – Evolution of settlement with time: comparison between numerical predictions (continuous lines) and field measurements (dotted lines) from extensometers at different depths.

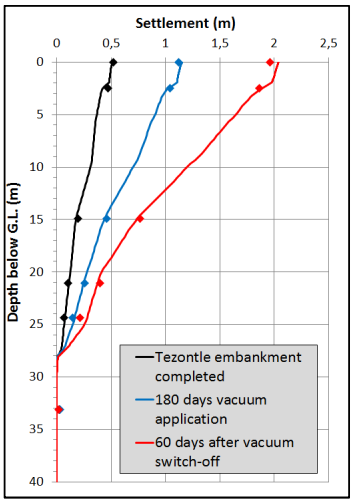


Fig. 16 - Comparison of measured (diamonds) and predicted (continuous lines) settlements at field centre.

REFERENCES

Aboshi, H., Sutoh, Y., Inque, T. and Shimizu, X. 2001. Kinging deformation of PVD under consolidation settlement of surrounding clay. Soils and Foundations, 40 (5): 25-32

Burland, J.B. 1990. On the compressibility and shear strength of natural clays. Geotechnique, 40 (3)

Chai, J. and Carter, J.P. 2011. Deformation analysis in soft ground improvement. Geotechnical, Geological and Earthquake Engineering, 18: 109-171

Chai, J., Carter, J. P. and Hayashi, S. 2005. Ground deformation induced by vacuum consolidation. Geotechnical and Geoenvironmental Engineering, ASCE 131 (12): 1552-1561

Chai, J., Hong, Z. and Shen, S. 2010. Vacuum-drain consolidation induced pressure distribution and ground deformation. Geotextiles and Geomembranes, 28: 525-535

Chai,J., Miura, N. and Bergado, D.T. 2008. Preloading clayey deposit by vacuum pressure by cap- drain: analyses versus performance. Geotextiles and Geomembranes, 26 (3): 220-230

Choi, Y.K. 1982. Consolidation behavior of natural clays. Ph.D. thesis, Univ. of Illinois at Urbana Champaign, Illinois

Dykstra, C. 2015. Design, construction and monitoring of 18 m thick embankment on top of very soft peat using BeauDrain vacuum consolidation. Proc. XVI European Conference on Soil Mechanics and Geotechnical Engineering, ICE publishing: 247-252

Funk, J.R. and Mesri, G. 2014. ILLICON User Guide, Dept. of Civil and Environmental Engineering, Univ.of Illinois at Urbana Champaign, Illinois

Geng, X., Indraratna, B. and Rujikiatkamjorn, C. 2012. Analytical solutions for a single vertical drain with vacuum and time-dependent surcharge preloading in membrane and membraneless systems. International Journal of Geomechanics, 12 (1): 27-42

Indraratna, B., Rujikiatkamjorn, C. and Sathananthan I. 2005. Analytical and numerical solutions for a single vertical drain including the effects of vacuum preloading. Canadian Geotechnical Journal, 42(4): 994-1014

Khan, A.Q. 2010. Ground improvement using vacuum preloading together with prefabricated vertical drains. Ph.D. thesis, Univ. of Illinois at Urbana Champaign, Illinois

Lee, S.L. and Karunaratne, G.P. 2007. Treatment of soft ground by Fibredrain and high-energy impact in highway embankment construction. Ground Improvement, 11 (4): 181-193

Mesri, G. and Khan, A.Q. 2010. Interpretation of vacuum preloading with ILLICON methodology. Proc. Int. Conf.on Geotechnical Engineering. Pakistan, Geotechnical Engineering Society, Lahore

Mesri, G. and Khan, A.Q. 2012. Ground improvement using vacuum preloading together with prefabricated vertical drains. Journal of Geotechnical and Geo-environmental Engineering, 138 (6): 680 – 689

Mesri, G. and Rokhsar, A. 1974. Theory of consolidation of clay. Journal of Geotechnical Engineering, ASCE, 100 (8): 889-904

Miura, N. and Chai, J. 2000. Discharge capacity of prefabricated vertical drains confined in clay. Geosynthetic International. 7(2): 119-135

Perera, D., Indraratna, B, Leroeil, S., Rujikiatkamjorn, C. and Kelly, R. 2015. Analytical model for vacuum consolidation incorporating soil disturbance caused by mandrel-driven drains. Canadian Geotechnical Journal, 54: 547-560

Rujikiatkamjorn, C., Indraratna, B. and Chu, J. 2008. 2D and 3D numerical modeling of combined surcharge and vacuum preloading with vertical drains. International Journal of Geomechanics, 8 (2): 144-156

Seah, T.H. 2006. Design and construction of ground improvement works at Suvarnabhumi Airport. Geot. Eng. Journal of Southeast Asian Geotechnical Society, vol. 37: 171-188

Tavenas F., Jean, P., Leblond, P. and Leroueil, S. 1983. The permeability of natural soft clays.Part II: Permeability characteristics. Canadian Geotechnical Journal, 20 (4): 645-660

Taylor D.W., 1948, “Foundamental of soil mechanics” John Wiley & Sons Inc., New York

A DEEP SOIL MIXING APPLICATION FOR A ROAD SLIP FAST REPAIR

Massimo Grisolia, Sapienza Università di Roma, Rome, Italy, +39 06 44585022, massimo.grisolia@uniroma1.it
Ignazio P. Marzano, Sapienza Università di Roma, Rome, Italy, +39 06 44585827, paolo.marzano@uniroma1.it
Giuseppe Iorio, Soilmixing S.r.l., Rome, Italy, +390692597141, iorio@soilmix-ing.it
Raffaele Papa, Soilmixing S.r.l., Rome, Italy, +390692597141, papa@soilmix-ing.it
Giuseppe Panetta, AGiS Ingegneria S.r.l., Rome, Italy, +390692597141, panetta@agisingegneria.it

ABSTRACT
Due to main geomorphological characters, in many Italian Regions hillside roads often suffer of slips settlements due to weak soil properties of superficial altered soils and unfavorable local pore water pressure conditions. Traditional stabilization works, such as retaining walls or piles associated with drains are difficult to make, too expensive related to the actual stability problem and implicate car traffic limitations for a long period. The paper presents a case study regarding the stabilization works of a hillside road slip on National Italian Road in central Italy based on the application of the soil mixing method to improve the road stability. The solution was relatively simple and fast with a short and only partial traffic interruption. Slope stability analyses and an original and specifically made quality control procedure are presented too.

Keywords: Ground improvement, soil mixing, road slip repair.

INTRODUCTION

A section of about 80 m of National SR2 Cassia Road near Siena-Central Italy interferes with an important and widespread slide movement affecting the slope below. Such situation led to progressive deformations on the road embankment with the appearance of depressions on the pavement of the valley lane. This condition forced the Road Manager to perform periodically road surface compensation by laying new hot-rolled asphalt layers.
At the beginning of the 2017, the problem appeared to be greatly accentuated showing precarious conditions of stability with a well formed system of cracks extending for about 60 m along the road valley lane (Fig. 1). The horizontal displacement of the lane, highlighted by the manifest curvature of the road safety guardrails, reached about 50-80 cm in correspondence of the maximum sliding zone. The valley lane was then closed for safety reasons and the traffic temporarily diverted on the upstream lane (Fig. 2) that appears also to be affected by the formation of a wider crown of circular cracks (Fig. 3a). No signs of movement or instability were noted on the outer edge of the road and especially in the roadside ditch lined with concrete blocks (Fig. 3b).



Fig. 1. Detachment area on the downstream lane

© 2018 Deep Foundations Institute



Fig. 2. Diversion on the upstream lane



Fig. 3. a) Cracks on the upstream lane; b) upstream roadside ditch lined with concrete blocks

STRATIGRAPHIC SEQUENCE AND GEOTECHNICAL MODEL

The stratigraphic sequence and the associated geotechnical model were evaluated from a specifically made geotechnical survey. The stratigraphic sequence consists of four main layers (Fig. 4): a) road pavement system; b) road embankment; c) landslide deposits; d) basal Early – Middle Pliocene grey pelitic deposits.

The pavement structure is a combination of sub-base, base, binder and surface course placed on the embankment to support the traffic load. The upper layer of the flexible pavements is constituted by bituminous layers of about 0.5 m to 1.1 m of thickness as a consequence of the periodical compensation works of the road surface. The underlying sub-grade layer, about 1.0 m thick, consists of a combination of high quality aggregates, such as crushed stones, gravel and sand.

The road embankment material is classified as silty sand with gravel.

The basal complex constituted by Early-Middle Pliocene grey pelitic deposits may include in the upper zone some calcareous cemented layers of few centimeters of thickness. It is very stiff and characterized by high strength values (generally Nspt>100).

In this area the morphodinamic processes are characterized by superficial soil slips caused by the erosion of the slope toe by the Formoncino creek. The unstable deposits consist of weathered and rearranged clay levels.

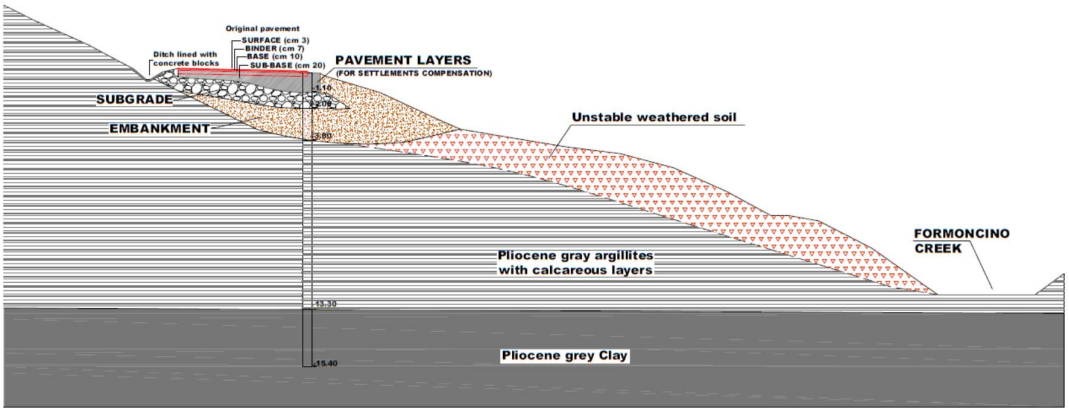


Fig. 4. - Geotechnical model

SOIL MIXING DESIGN

In this context, to achieve acceptable stability conditions of the road embankment in the quickest way maintaining compatibility with traffic requirements, a flexible, economic and fast ground improvement technique was proposed.
The solution is based on a soil mixing procedure executed directly from the road surface and constituted of columnar elements, isolated or secant, of 600 mm diameter and variable depth ranging between 3.5 m and 6.2 m from the ground level.
The technical solution was selected with the double aim of supporting the road embankment and enhancing the shear resistance of the foundation soils. To achieve that, three kind of column pattern were installed. On the upstream lane, a light ground improvement intervention constituted of a 25 isolated columns, 3.5 m long, aligned and spaced 3.2 m positioned on the lane axes was adopted (Fig. 5 and 6). For the downstream lane, two different installation pattern were implemented. Near the upstream lane, a triangular shape pattern composed by 49 columns, 4.6 m long with minor and major spacing of 1.2 m and 3.2 m respectively was adopted (Fig. 5 and 6). For the more external part of the downstream lane, shear walls made of two or three secant columns, 6.2 m long were installed at 1.6 m spacing (Fig. 5 and 6).

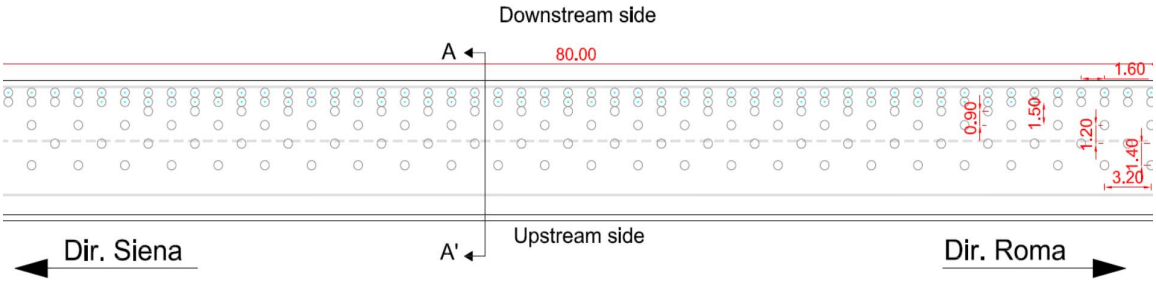


Fig. 5. Ground improvement geometry and column patterns

Portland cement 42.5 was selected as stabilizing agent and to increase the shear resistance of the shear walls, one or two columns (for shear walls made of two or three columns respectively) were reinforced with tubular armor of diameter Φ = 88,9 mm and thickness 9,5 mm placed just after the treatment execution when the soil mixed material was still fresh and relatively fluid.
Based on the expected work rates and the physical characteristics of the soils to be treated, an average design compression strength of 2.0 MPa after 28 curing days was assumed in the design for the soil mixed material.

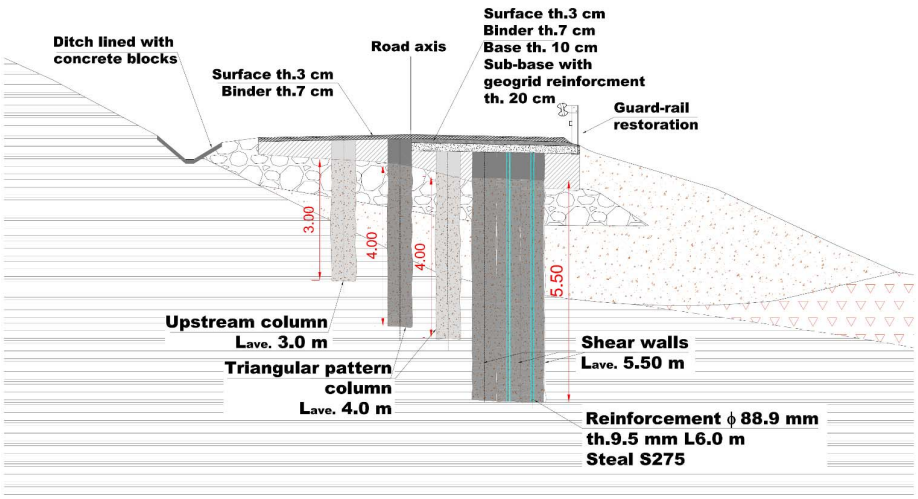


Fig. 6. Cross section of the designed ground improvement works

STABILITY ANALYSIS

Specifics finite element analysis were carried out with Plaxis 2D to evaluate the beneficial effects of the designed ground improvement works on the overall stability of the road body.
The model simulates the average cross-section of the hillside, extrapolating the set of available stratigraphic and geotechnical data with the result of a topographical survey, considering the effects of the occurred settlements of the road embankment over time.
The ground was assimilated to an elasto-plastic material with isotropic hardening regulated by volumetric ε_{pv} and plastic shear strain γ_p (Hardening Soil model).
The behavior in the elastic field was defined by a Young modulus E', function of the actual effective stress state, as follow:

$$E' = E'_{ref} \cdot \left(\frac{c' \cot \varphi' + \sigma'_3}{c' \cot \varphi' + p_{ref}} \right)^m$$

where p_{ref} = 100kPa is the reference pressure, E_{ref} is the Young modulus for a value of the minor principal effective stress σ'_3=100kPa, and the power *m,* which regulate the amount of stress dependency, is a soil dependent factor.
For a stress path starting from isotropic and normal consolidated conditions, the E_{50}, defined by the following relation, correspond to the secant Young modulus at 50% of the ultimate deviatoric stress q_f.

$$E'_{50} = E'_{50ref} \cdot \left(\frac{c' \cot \varphi' + \sigma'_3}{c' \cot \varphi' + p_{ref}} \right)^m$$

where E'_{50ref} is a reference secant stiffness modulus corresponding to the reference confining pressure p_{ref}.
The oedometer modulus E'_{0ed}, is a tangent stiffness modulus obtained from an oedometer test and regulate the volumetric strain due to compression loads. It is function of the actual stress state and could be expressed as follow:

$$E'_{0ed} = E'_{0edref} \cdot \left(\frac{c' \cot \varphi' + \sigma'_1}{c' \cot \varphi' + p_{ref}} \right)^m$$

where E'_{0edref} is the tangent stiffness modulus obtained from an oedometer for a value of the major principal effective stress σ'_1=100kPa

The numerical model was first aimed to simulate the progressive softening of the upper layers of soil that led to the road section instability. This operation was specifically useful to back analyze the geotechnical parameters of the unstable weathered soils. Afterwards the effects of the ground improvement works were simulated giving to the treated area, equivalent stiffness parameters obtained in function of the area improvement ratio (a_s) and treatment geometry.

Assuming the design unconfined compression strength of the improved ground equal to f_{cd} = 2.0 MPa, the average shear strength in the numerical analysis ranged between 106 and 212 kPa in function of the different a_s proposed.

The analysis allowed to simulate the phenomenon of instability affecting the slope and the consequent slip of a roadway section (Fig.7 and 8). Moreover, the model was able to well simulate the current configuration of the deformed road body thus providing an accurate estimation of the displacements along the slope (Fig.7 and 8).

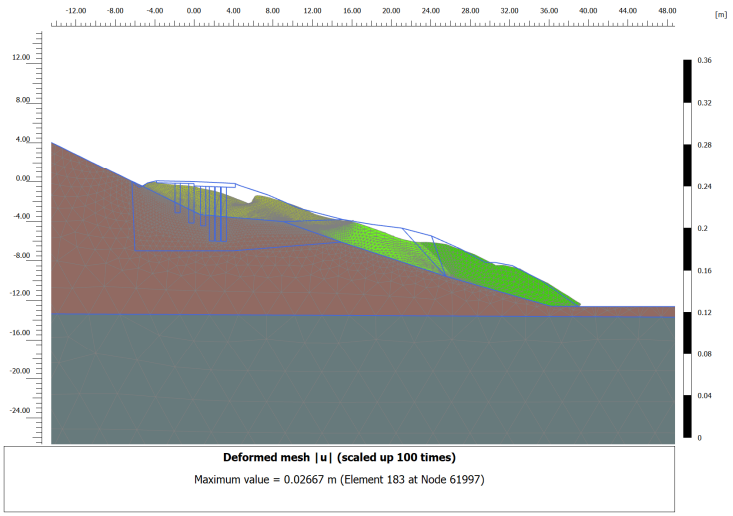


Fig. 7. FEM results - Slope strains without improvement

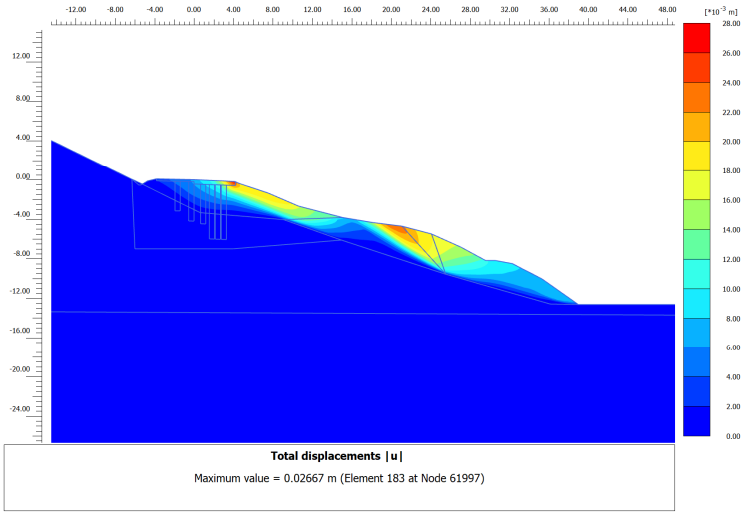


Fig. 8. FEM results – Slope displacements without improvement

Once recreated the initial conditions, the model was used to simulate the beneficial effect of the ground improvement works on the roadway stability.

The carried-out analyses show that a clear overall improvement of the road stability conditions should be expected after the designed intervention (Fig. 9). In particular, the soil mixed columns will help to transfer the load of the new road pavement to the deeper ground characterized by better mechanical properties and presumably not affected by past deformation phenomena.

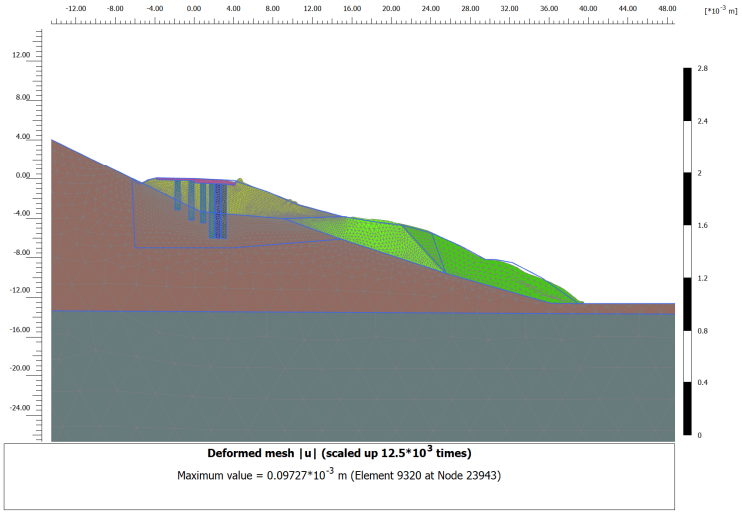


Fig. 9. FEM results - Slope strains with beneficial effect of ground improvement works

As can be clearly seen from the figure below (Fig. 10), after the treatment there are practically any expected displacement on the roadway, indicating a substantive achievement of suitable stability conditions. From the other hand, as expected, the movement of the weathered soil layer outside the consolidated area, will not experience any practical attenuation. This evidently confirms, as mentioned above, that the proposed interventions do not constitute a definitive solution to the bigger problem of the safety of the slope on which the road is set. This last issue could only be achieved by targeted and broad interventions that require a much higher economical commitment.

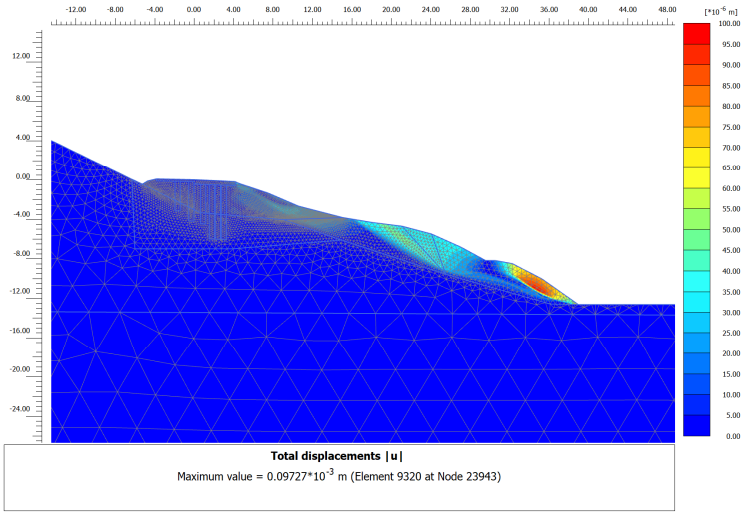


Fig. 10. FEM results - Slope displacements with beneficial effect of ground improvement works

EXECUTION AND QUALITY CONTROL

The soil mixed columns were installed by a Soilmec PSM 1360 with a mixing tool specifically designed to well perform in the presence of different kind of artificial and natural soils along the depth. The tool was equipped with two additional shear blades, featured with a rapid attachment system, for the additional support necessary to treat the encountered harder and stiffer soil layers.
Prior to the soil mixing works, the road surface was accurately prepared and leveled allowing the position of the shear walls and improved columns to be visibly marked (Fig. 11).



Fig. 11. Prepared road surface

The following pictures show the phases of installation of shear walls and isolated columns together with a clean head of a single column to appreciate the quality of the mixing at surface.



Fig. 12. Phases of column installation: a) shear walls, b) single columns, c) clean single column head

During the execution, the operational parameters of the treatment were real time monitored and adjusted to the encountered ground conditions.
To assess the mechanical characteristics of the installed columns, specifically developed undisturbed wet grab samplers were employed to avoid possible uncertainties related to the molding phases. These samplers are made by a pvc pipe with inner diameter equal to the specimens to be tested in laboratory. The choice of the inner diameter strictly depends on the workability of the soil cement mixture. In this case the diameter of Φ= 46 mm was proven effective by a core recovery greater than 95% and a neglectable variability of the recovery percentage between different samples. The sampler was hand

pushed in the fresh soil cement column and then retrieved with the help of steel cables. The sampler is equipped with a non-return valve to prevent air to enter and thus allowing the undisturbed fresh soil cement sample to be successfully retrieved. After the retrieval, the sampler was then sealed and left to cure in controlled laboratory conditions. After 28 curing days, the sample was cut into sections respecting the H/D ratio of 2/1 and the obtained specimens freed from the plastic casing before being subjected to unconfined compression tests.
This newly sampling method, makes easier and more efficient the onsite operations of quality control and assurance, giving at the same time more representative and reliable specimens than that obtained by "classic" wet grab procedures.
The so prepared specimens were then subjected to unconfined compression (UC) tests at a rate of 1.0 mm/min. Fig. 13 show an example of stress-strain curve acquired and the relative broken specimen.

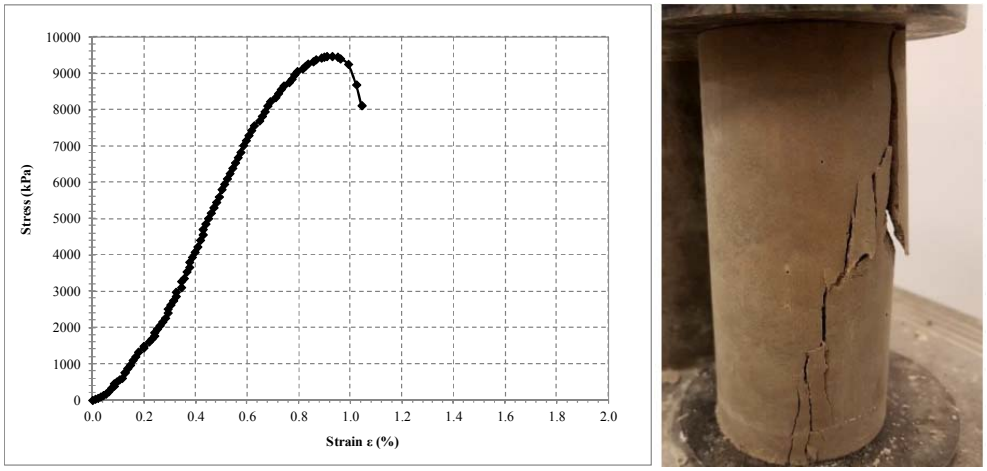


Fig. 13. Stress strain curve and broken specimen

The results obtained on the specimens so far tested are reported together with the relative physical properties in following table.

Table 1. Physical properties and UCS of the tested specimens

Sample	Spec. N°	Diameter (mm)	Height (mm)	γ (KN/m^3)	q_u (kPa)
US1	1	46	102.0	17.91	8,406
	2	46	99.5	17.68	8,183
	3	46	95.8	17.47	9,471
	4	46	99.5	16.82	7,937
	5	46	99.6	18.10	5,879
	6	46	99.4	18.26	7,148
	7	46	102.0	17.80	7,425
	8	46	99.4	18.33	6,642
US2	1	46	96.0	18.13	7,588
	2	46	97.9	17.89	8,460
	3	46	98.1	17.74	8,785
	4	46	98.3	18.33	5,271
	5	46	98.1	17.79	7,594
	6	46	99.4	18.02	7,822

The assessment of the characteristic compressive strength of the stabilized soil, f_{ck}, was based on a statistical evaluation. Particularly, by assuming a lognormal distribution of the data the characteristic compressive strength, f_{ck}, may be related to the mean, f_{cm} $(ln\, f_c)$, and the standard deviation, s_d $(ln\, f_c)$, of the natural logarithm of the strength of field samples using the following equation:

$$f_{ck} = \min \begin{bmatrix} \exp\left[f_{cm}(\ln f_c) - m\, s_d(\ln f_c) \right] \\ \leq 12 \text{ MPa} \end{bmatrix}$$

where:

$$f_{cm}(\ln f_c) = \frac{1}{n}\sum_{i=1}^{n} \ln(f_{ci})$$

represents the mean value of $ln\ (f_{ci})$, and

$$s_d(\ln f_c) = \sqrt{\frac{1}{n-1}\sum_{i=1}^{n} \left(\ln(f_{ci}) - f_{cm}(\ln f_c)\right)^2}$$

is the standard deviation of $ln(f_{ci})$, and
n - represents the number of samples in a population; statistical evaluation is used if n≥8.
The m-value determines the confidence (probability) that any measured compressive strength of the stabilized soil f_{ci} is equal or greater than f_{ck}. For wet deep mixing using cement as binder, m = 1.28 (corresponding to 90% of confidence) has been initially introduced in Japan before gaining wider international acceptance and being adopted by the recent DIN 4093 (2015).
From the statistical analysis of the obtained results, shown in Fig. 14, an average compressive strength f_{cm} = 7.6 MPa and a characteristic compressive strength f_{ck} of about 6.16 MPa have been evaluated.

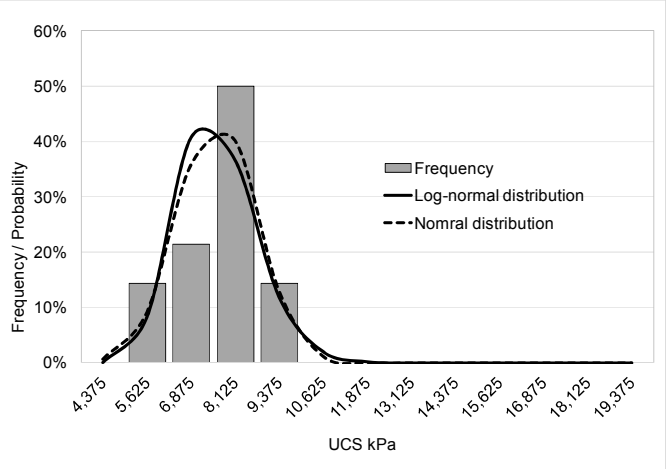


Fig. 14. Statistical analysis of the results.

The design compressive strength of stabilized soil, f_{cd}, which was used in ultimate limit state (ULS) analysis, was calculated as follows (cf. DIN 4093):

$$f_{cd} = \alpha_{cc} \frac{f_{ck}}{\gamma_m}$$

where:
α_{cc} = reduction factor for potential long-term effects affecting strength of the deep mixed soil, in Italy (cf. NTC08) equal to 0.85,
γ_m = partial safety factor for the deep mixed soil, in Italy (cf. NTC08) equal to1.5.
According to the previous equations, the design compressive strength resulted to be equal to f_{cd} = 3.49 MPa which is an acceptable and very good results if compared to the minimum expected by the design calculations.

CONCLUDING REMARKS

The stabilization works of the hillside road slip on Regional Road n° 2 "Via Cassia" near Siena based on soil mixing method showed advantages in terms of rapidity of execution, impact on the road usability and costs. The use of various columns patterns was able to fix multiple mechanisms of instability. In any cases, the consolidation works must be intended as preliminary intervention to solve the urgent road stability problem. A definitive slope stabilization solution, extended from the downstream torrent to the entire sliding area, must be based on more comprehensive geotechnical investigation and on much higher economical commitment.

ACKNOWLEDGEMENT

The authors would like to thank the client, Calzoni S.p.A., for allowing the publication of the results and for providing financial support to the scientific activities carried out during the project.

REFERENCES

DIN 4093/2015. Bemessung von verfestigten Bodenkörpern - Hergestellt mit Düsenstrahl, Deep-Mixing- oder Injektions-Verfahren, Beuth Verlag GmbH, Berlin.

Denies, N., Van Lysebetten G., Huybrechts, N., De Cock, F., Lameire, B., Maertens, J., Vervoort, A. (2013). "Design of Deep Soil Mix Structures: considerations on the UCS characteristic value". Proceedings of the 18th International Conference on Soil Mechanics and Geotechnical Engineering, Paris 2013.

FHWA, 2013-11. Federal Highway Administration Design Manual: Deep Mixing for Embankment and Foundation, Support Publication No. FHWA-HRT-13-046.

Filz, G. (2012). "Guidance for specifying the strength of deep-mixed ground". Deep soil mixing specialty short course, forth International conference on Grouting and Deep Mixing, Marriott New Orleans, LA February 16-18, 2012.

Grisolia M., Kitazume M., Leder E., Marzano I.P., Morikawa Y. (2012) "Laboratory study on the applicability of molding procedures for the preparation of cement stabilised specimens". International Symposium & short courses on Recent Research, Advances & Execution Aspects of ground improvement works. May – 2 June 2012 Brussels.

Grisolia M., Leder E., Marzano I.P., (2013). "Standardization of the molding procedures for stabilized soil specimens as used for QC/QA in Deep Mixing application". Proceedings of the 18th International Conference on Soil Mechanics and Geotechnical Engineering, Paris 2013.

Kitazume M., Grisolia M, Leder E., Marzano I.P., Alberto A.S. Venda Oliveira P.J., Åhnberg H., Andersson M. (2015). "Applicability of molding procedures in laboratory mix tests for quality control and assurance of the deep mixing method". Soils and Foundations. Vol. 55, No. 4. pp. 761-777.

Marzano I.P., Osman A.A-M., Grisolia M., Al-Tabbaa A. (2009). "Mechanical performance of different stabilised soils for application in stratified ground". Proceedings of the 17th International Conference on Soil Mechanics and Geotechnical Engineering: The Academia and Practice of Geotechnical Engineering.

Marzano, I.P., Al-Tabbaa, A., Grisolia, M. (2009). "Influence of curing temperature on the strength of cement-stabilised artificial clays". Geotechnics of Soft Soils - Focus on Ground Improvement - Proceedings of the 2nd International Workshop on Geotechnics of Soft Soils.

Marzano I.P., (2017). "Soil Mixing – Tecnologie esecutive, progetto e controlli". Ed. Hevelius 112p. (in Italian).

Terashi, M., 2002. Long-term strength gain vs. deterioration of soils treated by lime and cement, Proc. Deep Mixing Workshop 2002, Tokyo, Port and Airport Research Institute & CDIT.

Terzaghi, S., Okada, W., Houghton, L.D., Quickfall, G. (2006). COLMIX - Deep Soil Mixing in New Zealand – An update. Hiway Geotechnical New Zealand.

Topolnicki, M. (2016). "General overview and advances in Deep Soil Mixing". Proc. Conferenze di Geotecnica di Torino XXIV Ciclo, 25, 26 February.

A NEW QUANTITATIVE APPROACH IN THE EVALUATION OF HOMOGENEITY IN DEEP MIXING

Diego Bellato[1], Paolo Fania[2] and Ulli Wiedenmann[3]

[1] Project manager, International Projects and Services Department, BAUER Spezialtiefbau GmbH; Bauer Straße 1, Schrobenhausen, Germany; e-mail: diego.bellato@bauer.de
[2] Project engineer, International Projects and Services Department, BAUER Spezialtiefbau GmbH; Bauer Straße 1, Schrobenhausen, Germany; e-mail: paolo.fania@bauer.de
[3] Senior project manager, International Projects and Services Department, BAUER Spezialtiefbau GmbH; Bauer Straße 1, Schrobenhausen, Germany; e-mail: ulli.wiedenmann@bauer.de

ABSTRACT

Deep mixing methods have been becoming in the last decades more and more common techniques in the field of geotechnical engineering and have been applied to many different contexts for a wide range of applications like ground improvement, foundation elements, slope stability, soil liquefaction mitigation, cut-off and/or retaining structures etc. Despite the extensive use of such methods and the general definition of homogenization provided to describe this ground improvement procedure, the concept of homogeneity in deep soil mixing is still not well investigated and, in most of the cases, the achievement of a predefined target value of jobsite-specific quality indexes, e.g. the blade rotation number, is assumed as indication that an homogeneous mass of treated soil has been produced in-situ. In other cases, the required homogenization is confirmed only indirectly by means of strength laboratory tests on wet-grab samples and/or cores. This paper summarizes and discusses the concept of homogenization in deep soil mixing and the findings of previous research studies on this topic. In addition, it provides a new quantitative approach for a direct estimation of the degree of homogeneity achieved within the soil mixed elements allowing for further statistical analyses and an overall better understanding of the amount and type of untreated soil particles within the improved soil matrix.

KEYWORDS: deep mixing, QA/QC, homogenization

INTRODUCTION

Deep mixed ground is a composite system consisting mainly of original soil, binder (usually cement) and, possibly, admixtures. Therefore, its behavior is not easily predictable and it is influenced by many factors, such as type of natural soil and its rheology, chemical characteristics of the binder, curing conditions and so on.
To assess the quality of improved areas, QA/QC procedures are often used on site as required by design specifications. QA/QC programs can vary greatly from country to country due to the

© 2018 Deep Foundations Institute

complexity of the mixed material and the great variety of existing investigation techniques, like penetration methods, field load and hydraulic conductivity tests, geophysical methods, and visual examinations. Laboratory trials are also frequently adopted due to their cost effectiveness, although they may not be representative of the real treated ground. However, none of the existing QA/QC methods allow for a quality monitoring during production, except for the process parameter called blade rotation number, which is part of the European standards since 2005 (EN 14679:2005).

It is worth noticing that, despite the intrinsic mixing nature of the construction method, design specifications rarely include a control on the homogeneity of the final product, which is usually confirmed only indirectly through mechanical/hydraulic tests performed in-situ or on laboratory samples. By studying the mixing mechanism in details, other parameters seem to be more suitable to describe the correlation with the mixing efficiency, but only limited research on this subject is currently available in the international literature.

One of the most important aspects in the context of deep mixing applications is related to a proper understanding of the concept of "homogeneity". According to Larsson (2001), a mixture can be regarded as "homogenized" when the composition of all its ingredients is uniform throughout its volume. From a practical perspective, this definition shall be applied to a suitable "scale" in order to have a physical sense. In this respect, a "scale of scrutiny" may be introduced and it represents the minimum size of the regions of segregation in the mixture that would cause it to be regarded as imperfectly mixed. The scale of scrutiny is logically linked to other two concepts schematically sketched in Figure 1 and illustrated as follows:

- scale of segregation: it is a measure of the average size of the unmixed regions;
- intensity of segregation: it depicts the difference in concentration between adjacent regions and can also be interpreted, in this specific case, as the effect of the molecular diffusion of a binder in a mixture.

The scale of scrutiny shall normally be larger than the scale of segregation to account for the real variation of concentration in the investigated material.

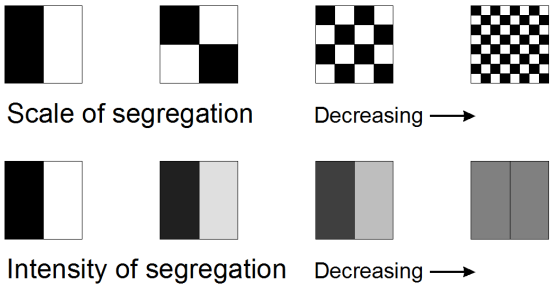


Figure 1: Conceptual representation of the scale and intensity of segregation

By using the dispersion of binder as main parameter representative of the homogenization effect attained at the end of the treatment, the mixing quality can be expressed through statistical coefficients, given a series of n observations of the binder concentration X, the sample mean, $\bar{x}$, and the sample variance, s^2.

Statistical analyses have shown that the sample variance of a completely segregated mixture, s_0^2, can be defined as

$$s_0^2 = \bar{x}(1-\bar{x}) \quad (1)$$

and the intensity of segregation, Υ, by

$$\Upsilon = \frac{s^2}{s_0^2} = \frac{s^2}{\bar{x}(1-\bar{x})} \quad (2)$$

where Υ is equal to 1 for a completely segregated mixture and 0 for a uniform mixture.
Another theoretical indicator that can be used to investigate the degree of homogenization is the sample concentration variance of a completely random mixture with particles of equal size, i.e. of a mixture in which particles (here assumed binder) can be found in any random position within the sample:

$$s_R^2 = \frac{\bar{x}(1-\bar{x})}{n_p} \quad (3)$$

with n_p representing the number of binder particles in the sample. It is clear from Equation (3) that a higher number of binder particles (i.e., higher binder content) leads to a more even distribution of the agent and to an overall better mixing quality.
This previous statistical approach contributes to the definition of a new mixing index:

$$\mathrm{I_{mix}} = \frac{\text{amount of mixing that has occurred}}{\text{amount of mixing that could occur}} = \frac{\mathrm{s_0^2 - s^2}}{\mathrm{s_0^2 - s_R^2}} = 1 - \frac{\mathrm{s^2}}{\mathrm{s_0^2}} \quad (4)$$

where $s_0^2 = \bar{x}(1-\bar{x})$ is the initial sample variance of a completely segregated mixture. The mixing index indicates how far the mixture is from the initial state. For a completely segregated mixture, it is equal to 0, while for a completely random mixture it is 1.
This approach, while very simple and intuitive, can present some downsides. The first is related to the fact that the total variance is biased by the variances due to analytical and sampling errors, which can be significant and, unfortunately, difficult to be estimated. A better determination of the sample variance due to imperfect mixing is only possible when a proper sampling procedure is established. In addition, the mixing index of Equation (4) is relatively insensitive to the mixture quality, but this issue can be solved by using a more sensitive parameter such as the standard deviation, instead of the variance. By assuming the variance for a completely random fluid mixture, $\mathrm{s_R^2}$,equal to 0 (Miles, 1962), Equation (4) can be modified to provide a simple statistical tool for the determination of the degree of mixing, based on the amount of binder in the mixed material:

$$\mathrm{I_{mix}} = 1 - \frac{\mathrm{s}}{\mathrm{s_0}} \quad (5)$$

Notwithstanding its theoretical background, the mixing index of Equation (5) cannot be used in practical deep mixing applications because of the very expensive and time-consuming laboratory analyses to be performed in order to obtain the binder concentration from samples (more than 30 for statistical representativeness) of each constructed element to be investigated.
A number of alternative mixing indexes and methods were developed in the past for a simple quality control of the mixing process at jobsites. Three main approaches can be individuated, namely related to QA/QC procedures to be applied in advance of, during, and after production.

QA/QC IN PRE-PRODUCTION PHASE

The only possible investigation in this phase consists of laboratory tests and, usually, its purpose is to assess if the mix design initially conceived is leading to the targets set by the client. One of the most important parameter controlling the efficacy of the treatment is the water content of the soil-binder mixture.
According to some studies (Bell, 1988; Rathmayer, 1996), a limited increase (up to a specific value) in the degree of liquidity of the soil being mixed causes a gain in both strength and uniformity of the blended material. For this reason, many new mixing technologies rely upon wetting up and fluidizing the soil formations. Some researches were carried out in the past in an effort to determine the optimum water content in the target soil.
Kitazume (2005) stated that the ideal consistency for optimum mixing lies slightly beyond the liquid limit content of the original soil. Kitazume and Terashi (2013) reported about a study conducted by Terashi et al. (1977) in which the maximum strength of the investigated stabilized materials was shown to be achieved at around the liquid limit of the original soil, but only for short term samples at 3 days curing. With longer curing periods, an indirect relationship between unconfined compressive strength and initial water content appears clearly, with the optimum water content shifting towards the dry side.
Szymkiewicz et al. (2013) observed that the workability limit in clayey soils can be assumed equal to the liquid limit because, in this form, the material is still viscous and dense and allows the paddles to easily disperse the binder through their shearing action. According to the results obtained by the authors, working above this limit would ensure a good degree of homogeneity as well as good strength values, which can be expected higher than the ones achieved when working below it.
Discrepancies on the optimum water content associated with the maximum strength in treated soils can be explained by the different nature of the materials (soil and binder) investigated by several researchers and, more likely, by the particular chemical reactions between binder and clay. Higher water contents promote a better homogeneity of the mixture, hence allowing a smooth ion exchange between cement and clay, but increase concurrently the proportion of free water leading to a higher porosity in the final product. Reduced water content slows down the cation exchange phenomenon, but, at the same time, lowers the porosity of the mixed element, leading to higher strength values. For this reason, the optimum water content can be interpreted as a compromise between workability and target values in terms of strength and permeability to

be achieved. Despite these studies, many difficulties still exist in directly correlating the results obtained from specimens prepared in the laboratory with samples obtained from the site.

QA/QC DURING PRODUCTION PHASE

The most popular standardized on-site quality index that can be correlated to the degree of mixing is the blade rotation number (BRN), introduced by Yoshizawa et al. (1996) and subsequently defined in the EN 14679:2005 as the total number of mixing blades passing during 1 m of shaft/tool movement:

$$BRN = \sum n_B \left(\frac{N_d}{V_d} + \frac{N_u}{V_u}\right) \tag{6}$$

where $\sum n_B$ is the total number of mixing blades, N_d and N_u are the rotational speeds (rpm) of the blades during penetration and withdrawal, and V_d and V_u are the mixing blade velocities (m/min) during penetration and withdrawal phases, respectively.

Good logarithmic correlation between the BRN and the mixing quality have been proven by many researchers in the past (Larson, 2005, Topolincki, 2009, Bohem, 2012, etc.), although several limitations occur. In particular, at the base of the mixed columns, the blade rotation number is not automatically guaranteed (Kitazume and Terashi, 2013), since only some of the blades are involved in the mixing process of the bottom layers. The main downside though lies in the fact that this factor is closely related to the specific geometry of the selected mixing tool and does not apply to new techniques such as the Cutter Soil Mixing. A formula for the calculation of the specific mixing energy (expressed in kNm/m³) was defined (Bellato et al., 2017) as follows:

$$E_i = \frac{\left|\left(T_{d,i} \cdot R_{d,i} \cdot t_{d,i} \cdot \varphi_d\right) + \left(T_{u,i} \cdot R_{u,i} \cdot t_{u,i}\right)\right| \cdot 2\pi}{V_c} \tag{7}$$

where $T_{d,i}$ and $T_{u,i}$ represent the average torque applied to the two wheels during penetration and withdrawal, respectively (in kN·m), $R_{d,i}$ and $R_{u,i}$ are the average rotational speed of the two mixing wheels during penetration and withdrawal, respectively (in rpm), $t_{d,i}$ and $t_{u,i}$ are the overall time durations taken by the mixing wheels to blend the soil with the binder suspension during penetration and withdrawal, respectively (in min), and V_c is the reference volume occupied by the mixing tool. The subscript *"i"* indicates that all quantities are referred to a specific depth interval *i* in the element (assumed equal to 1 m). The parameter φ_d is called *phase factor* and allows to take into account the particular construction method used on site for the installation of the panels (Bellato et al., 2012). Its value is 1 for a single-phase construction sequence or 0.5 for a two-phase construction sequence.

The specific mixing energy is probably a key parameter by which different techniques equipped with different mechanical mixing tools could be theoretically directly compared. However, further researches in this direction is required.

QA/QC IN POST-PRODUCTION PHASE

The most reliable and common QA/QC procedures consist in post-production investigations, i.e. tests carried out on the stabilized soil (cores or wet grab samples) after a certain curing of the material has occurred. The selection of the unconfined compressive strength, *UCS*, and its coefficient of variation as reference parameters is a routine choice (Kawasaki et al., 1981; Burke and Sehn, 2005; Larsson, 2005). In accordance with EuroSoilStab (2002), a specific mixing index called stabilization effect is proposed for cohesive soils. This index is based on the undrained shear strength of the treated and untreated cohesive soil and its formula is given as:

$$S_{eff} = \frac{s_{u,untr}}{s_{u,treated}} \quad (8)$$

where $s_{u,untr}$ and $s_{u,treated}$ are the undrained shear strengths of the untreated and treated material, respectively. This definition assumes implicitly that there is a relationship between binder content and strength.

In order to evaluate the mixing efficiency of different deep mixing methods, Baghdadi and Shihata (1999) suggested the use of the efficiency of mixing, η_{mix}, given by

$$\eta_h = \frac{UCS_{field}}{UCS_{lab}} \times 100\% \quad (9)$$

where UCS_{field} and UCS_{lab} are, respectively, the unconfined compressive strength of samples collected directly at the field (jobsite) and expressly prepared at the laboratory.

Another type of mixing index was developed to determine the efficiency of mixing by comparing the strength of samples prepared in the laboratory with that obtained from samples collected at the site. The resistance ratio, R_r, interpreted as the dimensionless ratio of the measured to design strength, is based on the hypothesis that the strength and deformation properties derived from tests on laboratory prepared specimens are the best attainable. This hypothesis, validated by many experimental studies, leads to the quality index:

$$I_{mix} = \frac{\bar{R}_r - 1}{s_R} \quad (10)$$

where $\overline{R_r}$ is the expected value of R_r and s_R is the corresponding expected standard deviation. This index describes the number of standard deviations separating the best estimate of R_r from its limiting value of 1. It is worth mentioning that Bellato et al. (2017) have dealt with cases where the in-situ strength results were higher than those attained in the laboratory by using the same materials and mix design applied at the site.

NEW QUANTITIVE APPROACH FOR THE ESTIMATION OF HOMOGENEITY

The QA/QC methods described above were all, to a certain extent, relating the quality of deep mixing to the strength achieved rather than to the actual homogeneity. For this reason, a new

approach has been developed to give site engineers the possibility to quantify directly the degree of mixing within the constructed elements in terms of statistical distribution of untreated soil inclusions, especially in difficult ground condition like clayey soils.
The main assumption is that soil-mixed elements can be regarded as composed of two main phases, i.e. a homogeneous mixture between soil and binder slurry without any clump and, in minor part, untreated soil inclusions. To estimate the spatial distribution (in planar direction and over depth) of the latter, a series of cores shall be drilled throughout the predefined investigation depth and at different locations in order to comply with the requirements of statistical significance. Moreover, randomness in the position of the clumps within the cores is assumed, which means that the maximum size of the intercepted inclusion is supposed to be representative of its actual size.
The cores are then cut diametrically and processed by means of accurate image-processing tools, capable of filtrating particles or clumps smaller than a certain fixed value (background noise). This analysis shall be performed only after the surface of one of the two available halves has been properly cleaned and dried up with the purpose of observing more clearly the difference in colour between the homogeneous mixture and the inclusions. To avoid undesired disturbance and to obtain the best quality in the images, the cores shall be characterized by a sufficient strength able to sustain cutting without falling apart.
Due to possible different lengths of the core runs obtained from a single column, a length-weighted average of the percentage of soil lumps with respect to the complete treated area, P_{av}, may be computed according to the following relationship:

$$P_{av} = \frac{\sum_i^n l_i \cdot P_i}{\sum_i^n l_i} \tag{11}$$

where P_i represents the percentage of inclusion with respect to the area of the i^{th} core and n is the number of cores obtained from a single vertical of investigation. This formula has been used for a test trial on clayey soils in a research study, giving the results showed in Figures 2, 3 and 4 and Table 1.

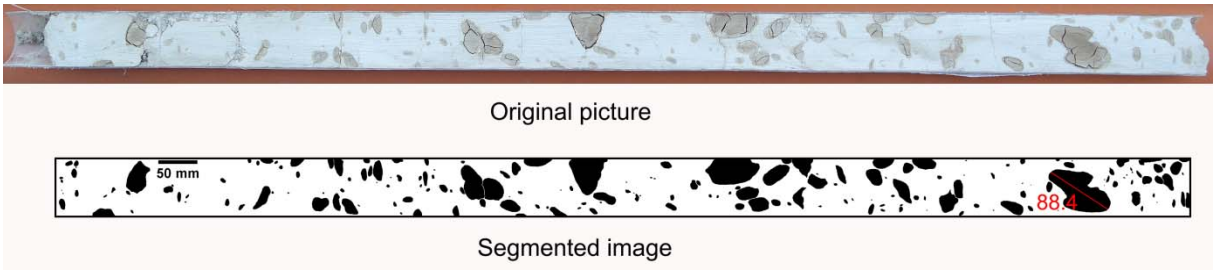


Figure 2: core – original picture and segmented image obtained by means of image processing

Beside locating and measuring the largest imperfection within the cores, this method provides the possibility to determine the percentage of inclusions with respect to the core area, any

correlation between amount of inclusions and depth and to calculate the average percentage of clumps with respect to the total cored area, as shown in Figure 3.

Table 1: results of the image processing on the core of Figure 2

Parameter	Value
Depth interval from drilling level (m)	0.00-1.50
Percentage of clay inclusions (%)	20.3
Max size of the clay clumps (mm)	88.4
Length of the core (mm)	1442.9

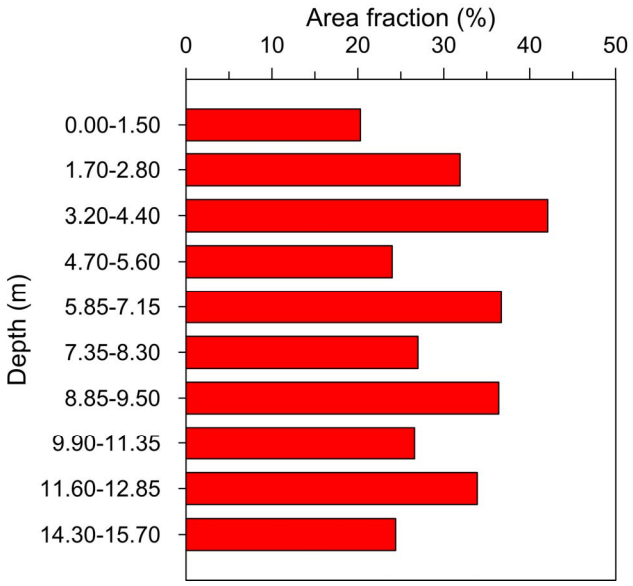


Figure 3: example of the area fraction of untreated inclusions over depth

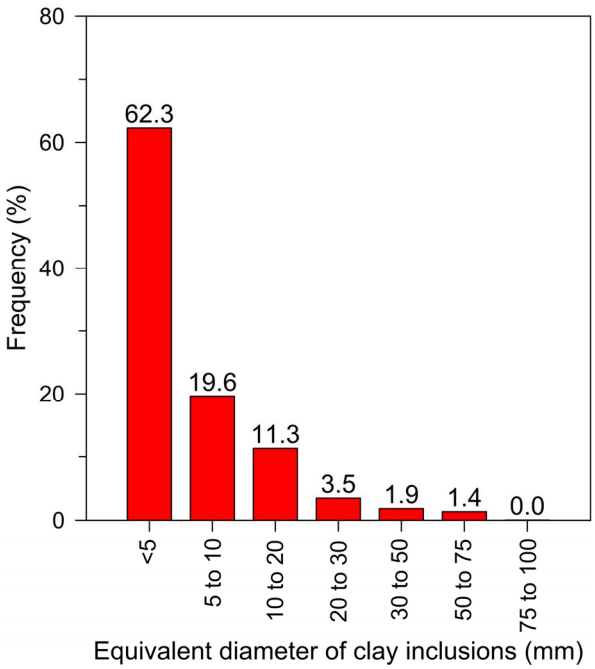


Figure 4: particle size distribution of the inclusions

In addition, individual particle analyses can be carried out to evaluate the most relevant characteristics of the 2D clay inclusions recognized from the segmented diametrical section of each core. Their equivalent diameter, D_{eq}, is computed according to the following formula:

$$D_{eq} = \sqrt{\frac{4A}{\pi}} \tag{12}$$

where A represents the area of the i^{th} inclusion. This parameter represents the diameter of an equivalent circle having the same area of a specific inclusion and is, in general, different from its maximum size measurable on the sample. The individual particle analysis is, in many cases, a very useful tool that helps to assess the proportion of inclusions above or below a certain threshold size. For example, in Figure 4, the results of the analysis show that more than 80% of

the clay inclusions had an equivalent diameter lower than 10 mm, indicating the good quality of the mixing operations, especially compared with the scale of the element (2.4 m in diameter) and the scale of scrutiny assumed for this study, i.e. 1/10 of the column diameter.

CONCLUSION

The European standards, as well as the international codes, do not usually consider the homogeneity of the deep mixing process as a typical design requirement. QA/QC procedures are generally focused on pre- and post-production tests, and the usual purpose is to determine the strength value, assuming that, if the target resistance is achieved, then also the element was correctly executed. The only parameter that can help during production is the BRN, but even that has shown some limitations when addressing mixing tools characterized by a geometry different from ordinary vertical shaft equipped with blades. The energy approach could be a better solution for the future, but in lack of additional studies, the investigation method here presented can represent a good alternative, providing useful post-production analyses that can really allow an overall control of the mixing quality from a homogeneity point of view.
Assuming that a statistically significant number of cores are carried out at a predefined spacing, it is possible to obtain a good perception of the performance of the technique used at the site. At the same time, statistical quantities can be derived to prove the quality of the works or to identify critical areas with high number of inclusions, which could lead to permeability issues or even possible failures. A further advantage of this approach is the capability to produce a clearer picture of the mixing process executed on site to be utilized as a basis for optimization of the mixing tools/procedures. Finally, the analysis of the cores can provide useful information to calibrate and understand in a more representational way the relationship between mixing quality indicators like the BRN or the specific mixing energy and the homogeneity of the mixed product.
In order to deepen the knowledge on homogeneity of deep mixed elements and to validate this experimental methodology, further studies are required in different ground and binder conditions.

REFERENCES

Baghdadi Z and Shihata S (1999). On the durability and strength of soil-cement. *Proceedings of the ICE – Ground Improvement*, 3(1), pp. 1–6.

Bell F (1988). Stabilization and treatment of clay soils with lime – Part 1 – Basic principles. *Ground Engineering*, 21(1), pp. 10–15.

Bellato D, Dalle Coste A, Gerressen F-W, and Simonini P (2012). Long-term performance of CSM walls in slightly overconsolidated clays. *Proc. of the International Symposium on Ground Improvement – Recent Research*, Advances and Execution Aspects of Ground Improvement Works, ISSMGE Technical Committee TC 211 Ground Improvement, Bruxelles, Belgium.

Bellato D, Marzano IP and Simonini P (2017). A new parameter for the evaluation of mixing quality in deep soil mixing. *5th International Grouting Conference* - Honolulu, Hawaii

Boehm DW (2012). Dry Deep and Mass Mixing – current Methods and Applications. *Proc. Deep soil mixing specialty short course, 4th International conference on Grouting and Deep Mixing*, Marriott New Orleans, LA (USA).

Burke GK and Sehn AL (2005). An analysis of single axis wet mix performance. *Proc. Int. Conf. On Deep Mixing - Best Practice and Recent Advances*. Swedish Deep Stabilization Research Centre, Stockholm, 41-46.

EN 14679:2005 (2005) Execution of special geotechnical works – Deep mixing. Technical Committee CEN/TC 288

EuroSoilStab (2002). Design guide: soft soil stabilisation – Development of design and construction methods to stabilise soft organic soils. *Tech. rep.*, IHS BRE Press.

Kawasaki T, Niina A, Saitoh S, Suzuki Y, and Honjyo Y (1981). Deep mixing method using cement hardening agent. *Proceedings of the 10th International Conference on Soil Mechanics and Geotechnical Engineering*. Stockholm (Sweden), pp. 721–724.

Kitazume M (2005). State of practice report – Field and laboratory investigations, properties of binder and stabilized soil. *Proceedings of the International Conference On Deep Mixing – Best Practice and Recent Advances*, vol. 2. Swedish Deep Stabilization Research Centre, Stockholm (Sweden), pp. 660–684.

Kitazume M and Terashi M (2013). The deep mixing method. CRC Press

Larsson S (2001). Binder distribution in lime-cement columns. *Proceedings of the ICE – Ground Improvement*, 5(3), pp. 111–122.

Larsson S (2005). State of Practice Report – Execution, monitoring and quality control. *Proc. International Conference on Deep Mixing - Recent Advances and Best practice*, Stockholm, Sweden.

Miles SR (1962). Heterogeneity of seed lots. *Proc. of the International Seed Testing Association*, 27(2), pp. 407-413.

Rathmayer H (1996). Deep mixing methods for soft subsoil improvement in the Nordic countries. *Proceedings of the 2nd International Conference On Ground Improvement Geosystems*, vol. 2. Tokio (Japan), pp. 869–877.

Szymkiewicz F, Tamga F, Le Kouby A. and Reiffsteck P (2013). Optimization of strength and homogeneity of deep mixing material by the determination of workability limit and optimum water content. *Can. Geotech. J. 50*: 1034–1043.

Terashi M, Okumura T and Mitsumoto T (1977). Fundamental properties of lime-treated soils. Report of the Port and Harbour Research Institute. 16(1), pp. 3-28 (in Japanese).

Topolnicki, M. (2009). "Design and execution practice of wet Soil Mixing in Poland". *Proc. International Symposium on Deep Mixing & Admixture Stabilization*, Okinawa, Japan.

Yoshizawa, H., Okumura, R., Hosya, Y., Sumi, M. and Yamada, T. (1996). "JGS TC Report: Factors affecting the quality of treated soil during execution of DMM". *Proc. Of the IS-Tokyo´96, 2nd Int. Conf. on Ground Improvement Geosystems*, Tokyo, Japan.

AN INNOVATIVE SOIL MIXING TREATMENT TO UNDERPIN EXISTING BUILDINGS

Massimo Grisolia, Sapienza Università di Roma, Rome, Italy, +39 06 44585022, massimo.grisolia@uniroma1.it
Ignazio P. Marzano, Sapienza Università di Roma, Rome, Italy, +39 06 44585827, paolo.marzano@uniroma1.it
Giuseppe Iorio, Soilmixing S.r.l., Rome, Italy, +390692597141, iorio@soilmix-ing.it
Raffaele Papa, Soilmixing S.r.l., Rome, Italy, +390692597141, papa@soilmix-ing.it
Giuseppe Panetta, AGiS Ingegneria S.r.l., Rome, Italy, +390692597141, panetta@agisingegneria.it

ABSTRACT

An original soil mixing treatment was chosen to improve the foundation performance of three existing buildings founded on isolated shallow footings and affected by severe damages caused by differential settlements. The settlements were due to the variable presence of a thick manmade ground layer overlaying a layer of alteration of the basal marly-arenaceous Flysch. Thanks to a specifically developed mixing tool with controlled variable diameter, it was possible to drill small holes in the plinths of the existing shallow foundations and to realize beneath them, larger diameter soil mixed bearing columns in direct contact with the existing structures. The tool final shape, the feasibility and the working parameter of the treatment were selected according to the results obtained in specific field trials. The results of the field trials and the outcomes of specific QC/QA procedures employed during the works are also presented.

Keywords: Ground improvement, soil mixing, differential settlements, existing buildings.

INTRODUCTION

The treatment regards three buildings respectively named B/C, D and F, belonging to a residential complex built at the end of the 1960s in Civitavecchia, a little town near Rome in Central Italy. The buildings plans are "L" or "C" shaped with major dimensions ranging between 75 m (D, F) and 95 m (B/C), and 15-25 m in transverse direction, with three-story elevation and a basement level used as car garage (Fig 1)

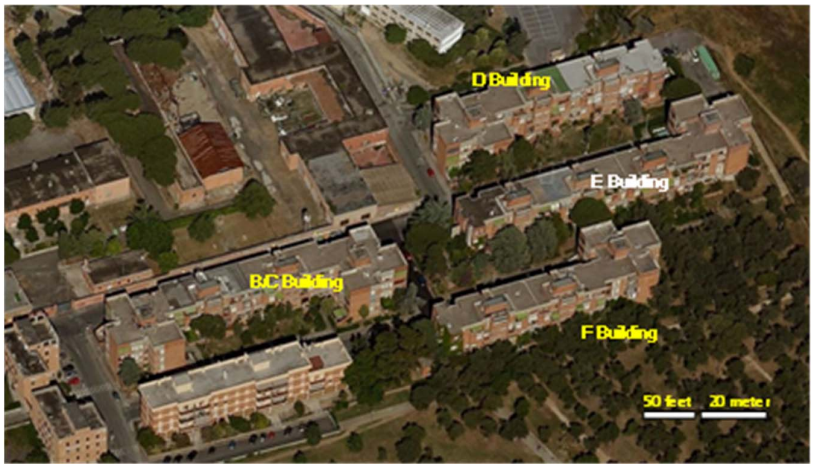


Fig. 1. Residential complex "Civitavecchia 70"- General plan

From a structural point of view, the buildings are reinforced concrete framed structures with typical span of about 4 and 5.5 meters between columns. Reinforced concrete and hollow tiles mixed floor have a global thickness of 20 cm. The global geometry of a building (F named) is shown in next figure, extracted from a structural model built to assess the average local load on footings.

© 2018 Deep Foundations Institute

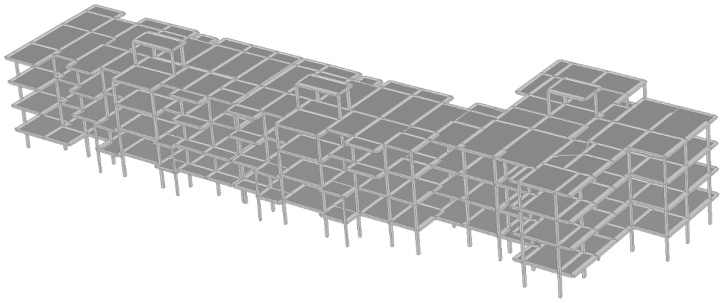


Fig. 2. Building F – Structural model

A plan of footings is presented in Fig. 3: footings are made by square shallow foundation plinth located at about 0.6-1.0 meters below the garage level. Five types of footing can be distinguished, with side B variable between 0.95 and 1.45 m (Fig.3). According to the detailed assessment carried out, medium characteristic soil pressure resulted variable between 275 kPa (Type 1: B=1.45 m) and 415 kPa (Type 4-5: B=0.95-0.90 m) while is approximately equal to 350 kPa for footings with dimension B=1.15 m and 1.30 m (type 2 and 3).

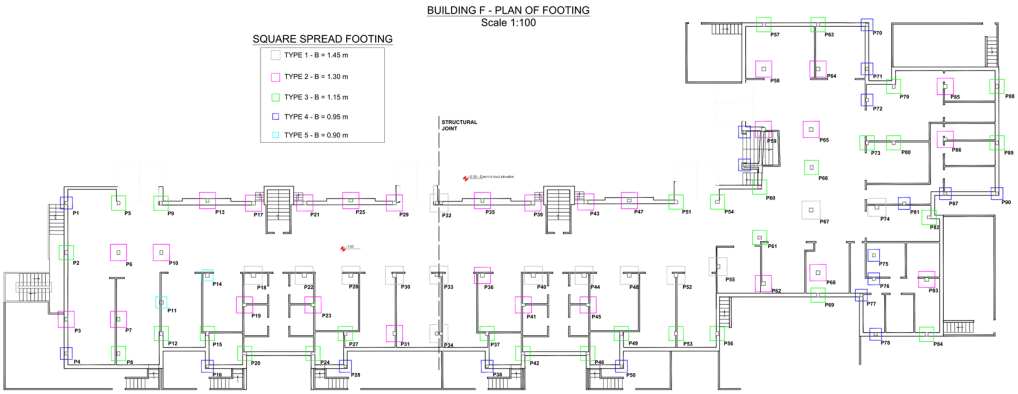


Fig. 3. Building F – Plan of footings

Soils stratigraphic sequence in the area generally consists of three layers, as shown in figure 4. An upper layer, with a thickness varying between 1.0 m and 4.0 m constituted by manmade soils classified as sandy gravel ("R1"), gravelly silt and clay ("R2") and clayey silt ("R3"). In the silty-clayey layers, widespread carbonate patinas, due to water infiltration (R2*/R3*) are present. The second underlying layer consists of an alteration of the basal marly-calcareous-arenaceous "Tolfa Mountain Flysch", constituted by silty clay and clayey silt with sand ("DA") and calcareous marl cobbles (DA2). This stratum may include some weathered and oxidated clay levels (DA*) and cemented layers of few centimeters of thickness (TSF) at the roof. It generally possesses very high consistency (Ic=1.4-1.8) and apparent low compressibility. The underlying basal Flysch is very competent and characterized by high strength (generally N_{SPT}>50).

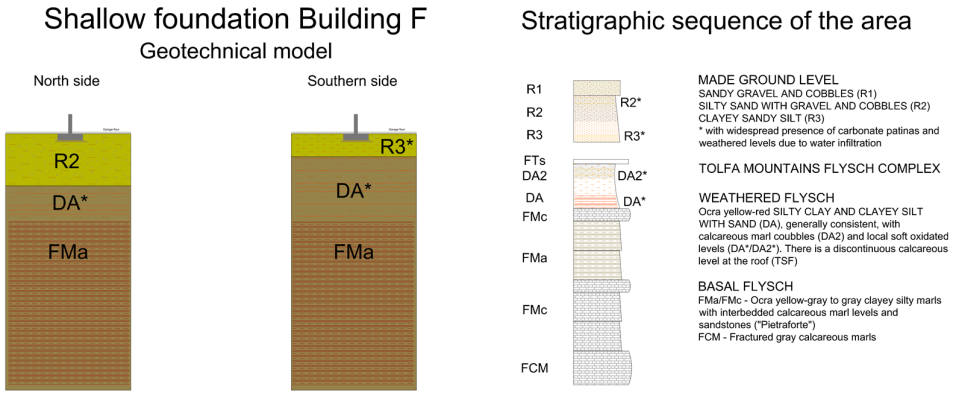


Fig. 4. Building F - Stratigraphic sequence and geotechnical model of footings

The thickness and the geotechnical properties of the upper manmade layer may significantly vary, even within a small area. According to the moderate-high strength of the silty clay and clayey silt when dry, all the low-rise buildings in the district were constructed on shallow foundation, founded on the fills (R2 and R3).
However, since the first years after construction, the behavior of these foundation layers was very sensitive to change of water content. Some laboratory and field investigations confirmed this behavior. When the soil moisture changed due to rain and wastewater loss from the buildings, the footings encountered slow settlements. Besides, considering the variations in the thickness of the fills, differentiated distribution of loads and the lack of connections between single footings, differential settlements between parts of the buildings occurred. Cracks on nonstructural elements were clearly seen and progressively propagated in the majority of the flats. The average crack width was in the order than 0.2-0.4 mm (Figure 5).

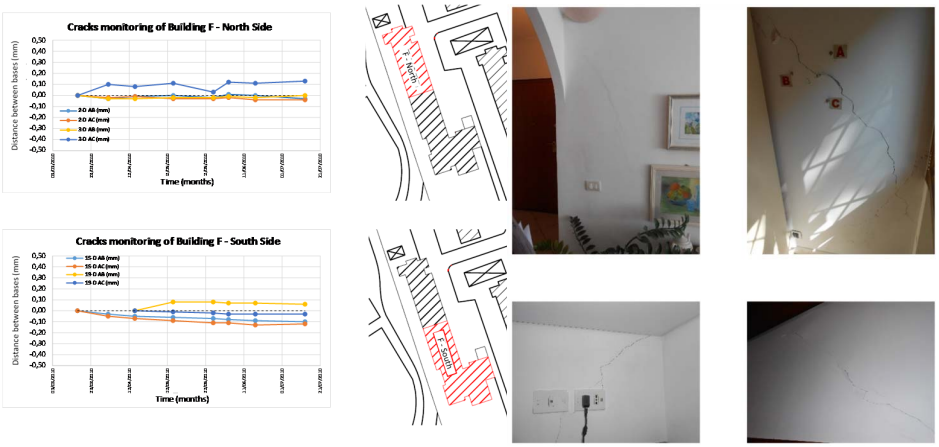


Fig. 5. Building F - Temporal trends of cracks in nonstructural elements

In this case, to strengthen the bearing capacity and minimize the settlements, a very expensive and complex to do reinforced concrete raft has been realized.
In order to evaluate alternative solutions, the Client, with the aim of assessing the effectiveness of deep mixing method to limit the settlements, entrusted a preliminary study for the buildings B/C, D and F.
A preliminary field trial was carried out between March and April 2016 to evaluate the efficacy of an innovative soil mixing procedure, based on the development of specifically designed spreadable tools, to improve the foundation soils of the three buildings. To confirm the achievable field strength and to select the more efficient and performing mixing tool in such complex ground conditions, three different types of trial columns were installed (Figure 6 and 7), namely DM1 (standard single vertical axis mixing tool, 200 mm in diameter and three pairs of mixing blades), DM2 (spreadable single vertical axis mixing tool, 330 mm in diameter fully opened from the surface to the bottom, with three mixing blades) and DM3 (same tool as DM2 but closed at the surface, 170 mm in diameter, and fully opened at the depth of 0.80 m from the ground surface corresponding to the footing level of the buildings). For each case, the soil was mixed with a Portland Cement slurry with W/C ratio of 0.6 and the operational parameters (penetration and withdrawal speed, injection pressure and flux etc.) set to achieve a final binder content of about 500 kg/m^3.



Fig. 6. Spreadable tool used in the field trial

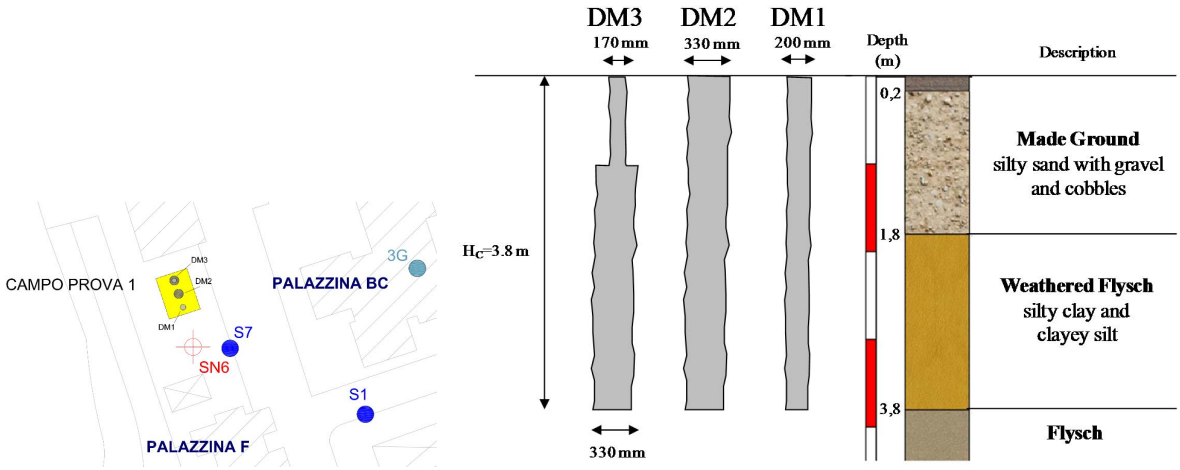


Fig. 7. Field trials plan, stratigraphy and layout.

A series of tests were carried out on three kinds of samples obtained from laboratory mixing, cored columns and in situ cured 4 m long cased pipe samples with inner diameter of 95 mm. The cased pipe sampler was pushed into the selected DM2 type column when the stabilized soil mixture was still fresh and relatively fluid. The analysis of the results reported in Marzano et al. 2017, (Figure 8) clearly show that the cased-pipe samples better represent the actual mechanical characteristic of the soil mixed material as compared to the cored ones. The characteristic UCS strength values of stabilized soil based on a statistical elaboration (Topolnicki, 2016) was f_{ck} = 3.65 MPa.

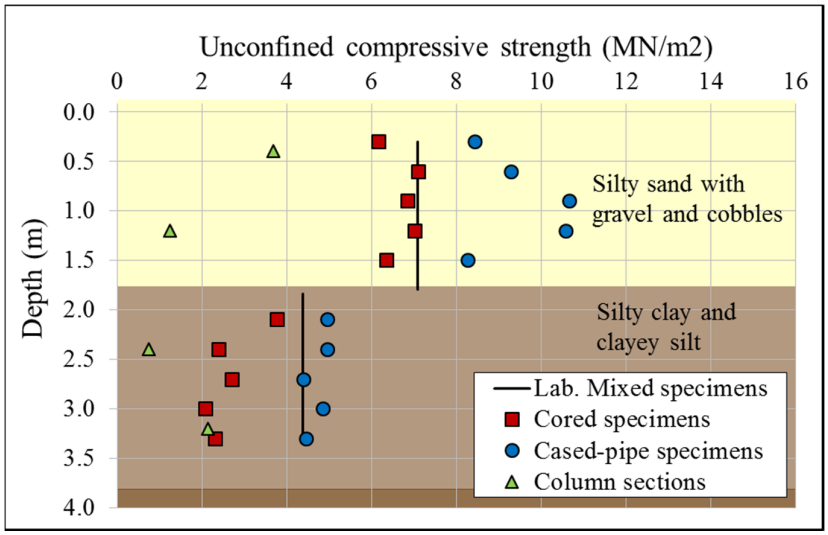


Fig. 8. Strength distribution of treated soils with depth at 28 curing days (Marzano et al. 2017).

FOUNDATION GROUND IMPROVEMENT DESIGN

The foundation reinforcement required the connection of the soil-mixed columns to the existing plinths to transfer vertical loads to the bedrock. The reinforcing columns were obtained by a spreadable tool that includes an automatic system for opening and closing blades, just to vary the diameter along the column depth. To connect the bearing soil mixing columns it was sufficient to make some little holes into the existing shallow foundations and realize columns with larger diameter in direct contact with the existing structures. Two types of treatment were generally adopted with two or four columns for each plinth. The corresponding improvement area ratio a_s ranged from approximately 8 to 13% for larger spread foundations (B=1.15÷1.45 m) and in the order of 35-40% for the other ones (Fig. 9).

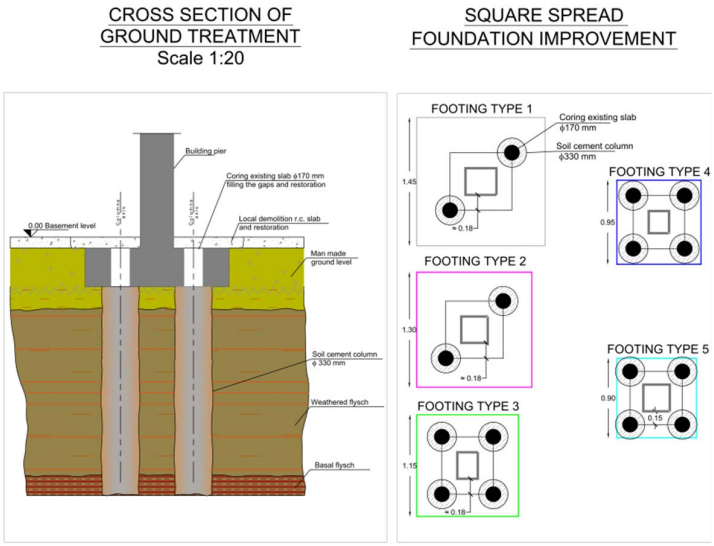


Fig. 9. Building F – Soil mixing foundation ground improvement: section and typical plans

The design characteristic UCS strength for the stabilizing column, f_{ck} , was 2 MPa for the silty clay layers. In the case of Building "F" ground improvement treatment involved about 90 footing, and more than 270 soil cement columns to be realized (Figure 10).

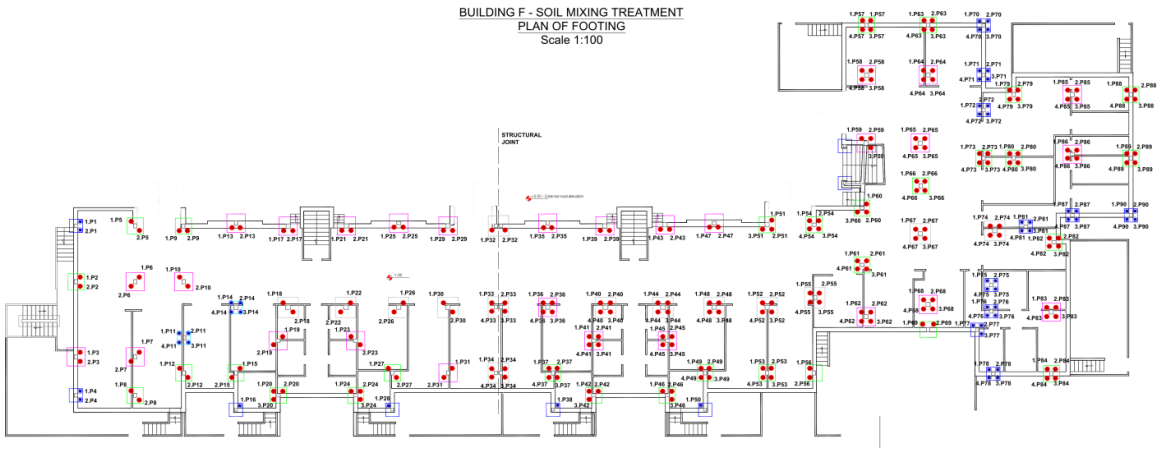


Fig. 10. Building F – Soil mixing foundation ground improvement sketch

CONSTRUCTION AND QUALITY CONTROL PROCEDURES

The soil treatment includes the following steps:

- demolition of a portion of the existing pavement placed directly above the spread foundation slab;
- coring of the existing spread foundation (diameter 170 mm) to allow the passage of the mixing tool;
- execution of larger soil cement columns of minimum diameter 330 mm by the specifically designed spreadable tool;
- filling the gaps of coring and final restoration of the existing slab.

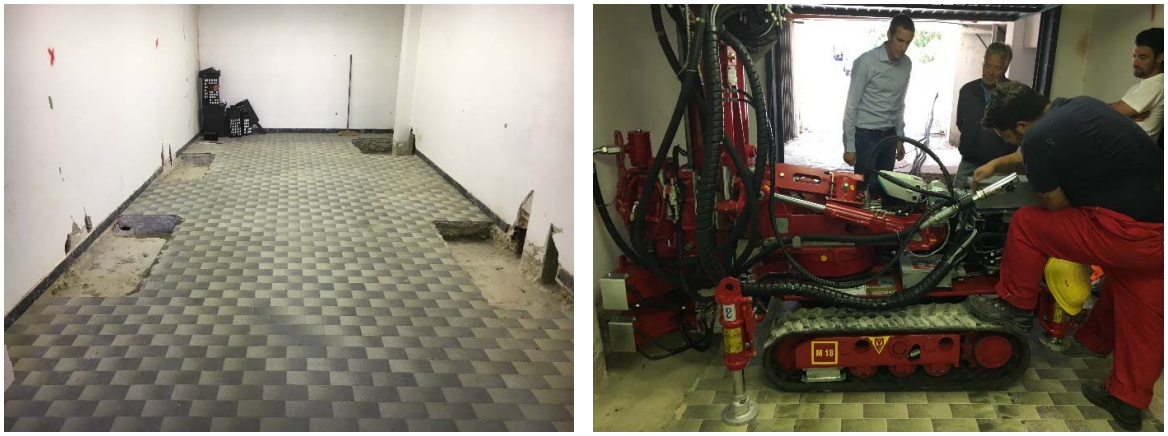


Fig. 11. Building F – Soil mixing foundation ground improvement steps: a) ultimate demolition of existing slab b) coring of the footing (diameter 170 mm) for the passage of the spreadable tool

Thanks to the use of a compact machinery, it was possible to work in limited spaces, under low headroom conditions and to make the treatments in adherence to the existing foundation piers.
During the treatment, the SM Machine was also equipped with a construction quality control system, which enables the real-time monitoring and control of execution parameters (such as penetration/retrieval speed, inclination, torque, RPM, tool geometry, pressure and flux of binder) to ensure reliable stabilized soil columns. The spoil return from the treatment was limited and easily handled.



Fig. 12. Building F – Soil mixing foundation ground improvement steps: c) execution of soil cement columns d) "light" soil mixing treatment completed



Fig. 13. Building F – Soil mixing foundation ground improvement steps: e) fill holes gaps and f) final works and restoration of the existing slab

QUALITY ASSURANCE

The quality assurance (QA) of soil mixing treatment involved the installation of trial columns and the execution of unconfined compression tests on samples retrieved by the cased-pipe sampler as successfully employed in the preliminary field trials.
For these purposes very significant results were obtained by two adjacent realized columns, namely SMC1 (spreadable single vertical axis mixing tool, 330 mm in diameter opened from the surface, before the column installation the concrete slab was removed) and SMC2 (same mixing tool fully opened from the concrete slab to the bottom, with three mixing blades) shown in Fig.14.

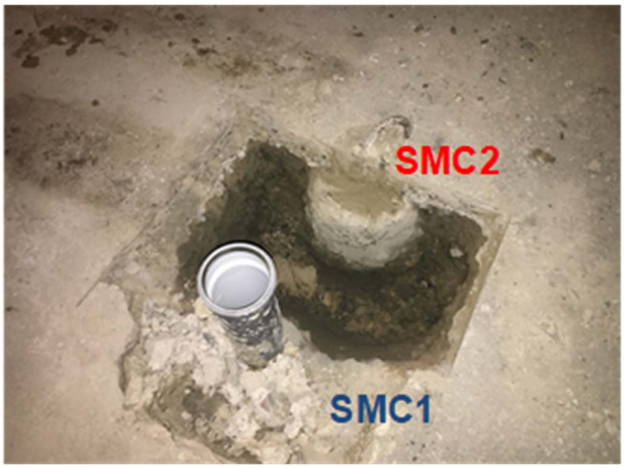


Fig. 14. Building F – Soil mixing trial columns

The soil was mixed with a Portland Cement slurry with W/C ratio of 0.6 and the operational parameters (penetration and withdrawal speed, injection pressure and flux etc.) set to achieve a final binder content (defined as ratio of weight of dry binder to the volume of soil to be treated, kg/m^3) of about 500 kg/m^3.
Shortly after column installation, a cased pipe sampler (2,70 m long cased pipe with inner diameter of 95 mm) (Marzano et al. 2017) was pushed into the SMC1 column when the stabilized soil mixture was still fresh and relatively fluid. The position of the sampler was carefully chosen to avoid the center of the column notoriously containing highest amount of binder material. Some hours after the installation, a shear surface at the base of the sampler was created by twisting the inner pipe of 180° in order to facilitate the sample retrieval at the desired curing time.
After about 25 days of curing, the installed columns were fully exposed (Figure 15) to have a visual inspection of them. The visual control confirmed that the column with larger diameter is in perfect direct contact with the existing continuous slab at the basement level



Fig. 14. Building F – Preliminary field trial: enlarged soil mixing columns

At the same curing time, the internal pipe, containing the undisturbed core, was pulled out by means of steel cables and brought to the laboratory. Here, to obtain representative specimens for the UC tests, it was divided into sections (respecting the aspect ratio, height to diameter H/D, of 2), trimmed and then freed from its plastic skin. After a curing time of 28 days, the specimens were subjected to unconfined compression (UC) tests at a rate of 1.0 mm/min.
The results obtained show relatively small scatter with the depth (as shown in Fig. 15), perfectly in agreement to the ones obtained from the preliminary field trial samples (see Fig. 8) demonstrating once again the good quality and homogeneity of the treated soil.

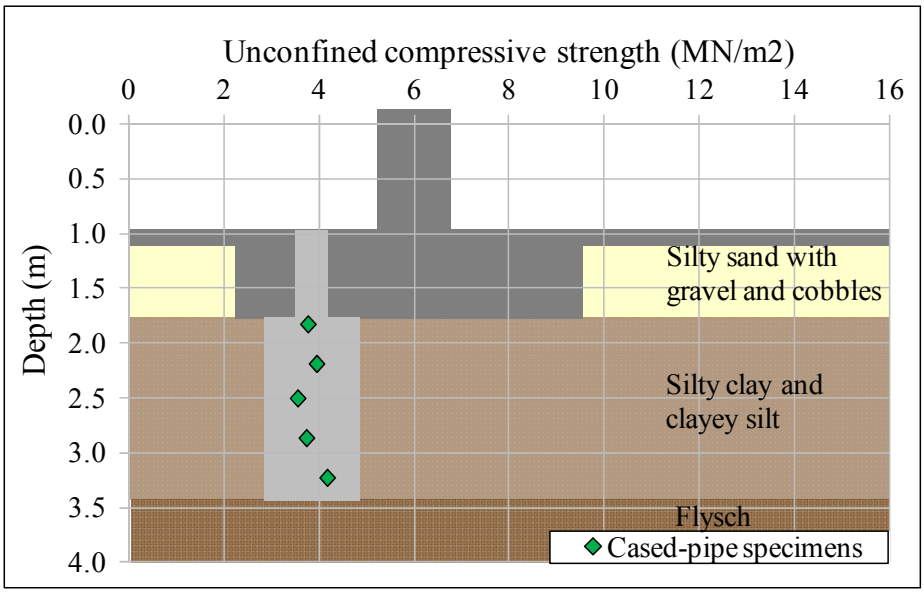


Fig. 15. Building F – Tested column - Strength distribution of treated soils with depth.

Moreover, the overall quality of the retrieved specimens, shown in Fig. 16, and the relative homogeneity of the results clearly confirm the ability of the cased-pipe sampler to retrieve high quality "undisturbed" in situ cured samples.

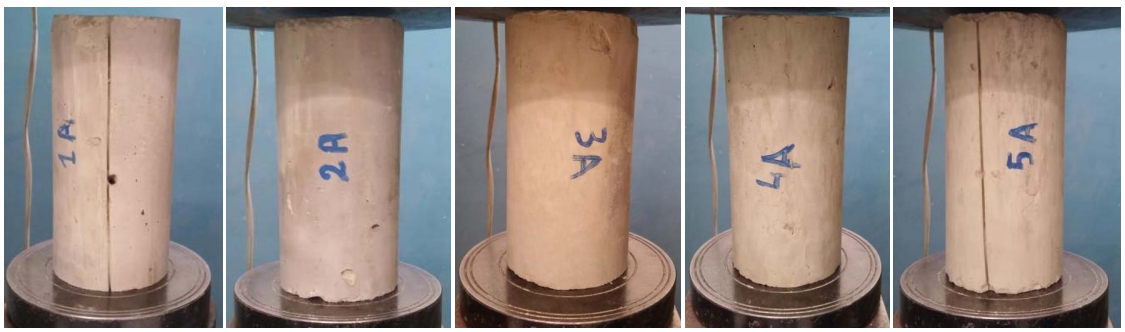


Fig. 16. Building F – Tested column – Cased-pipe retrieved specimens.

CONCLUSION AND PERSPECTIVES

The underpinning of buildings shallow footings by a soil mixing treatment using a tool with controlled variable diameter may be considered a good, economic, simple and fast solution to improve and uniform foundation performances.
The contact with the existing slab and the enlarged column was proved effective and very well executed with minor disturbance caused to the existing structure.
The results of specifically executed field trials and a preliminary structural analysis of each building allowed a detailed design.

The innovative QA procedures based on the use of cased-pipe sampler, allowed retrieving high representative undisturbed and in situ cured soil cement specimens.
The QC procedures implemented during the execution phases allowed adjusting real time the working parameters to the encountered sub-soil conditions for the installation of high quality mixed columns.
The results of an ongoing monitoring program will be useful to control the immediate and long-term effects.

ACKNOWLEDGEMENT

The authors would like to thanks the client, Condominio CV70, for allowing the publication of the results and for providing financial support to the scientific activities carried out during the project.

REFERENCES

Bruce, D.A., Bruce, M.E.C., Di Millio, A.F. (2000). "Deep Mixing: QA/QC and Verification Methods." Proc. of the 4th International Conference on Ground Improvement Geosystems. Finnish Geotechnical Society, Helsinki, Finland, pp. 11-22.

CDIT (Coastal Development Institute of Technology). (2002). The Deep Mixing Method - principle, design and construction. A.A. Balkema Publishers, Lisse, Abingdon, Exton (PA), Tokyo.

Denies, N., Van Lysebetten G., Huybrechts, N., De Cock, F., Lameire, B., Maertens, J., Vervoort, A. (2013). "Design of Deep Soil Mix Structures: considerations on the UCS characteristic value". Proceedings of the 18th International Conference on Soil Mechanics and Geotechnical Engineering, Paris 2013.

DIN 4093 (2015). Bemessung von verfestigten Bodenkörpern - Hergestellt mit Düsenstrahl, Deep-Mixing- oder Injektions-Verfahren, Beuth Verlag GmbH, Berlin (In Tedesco).

Grisolia, M. , Leder, E. and Marzano, I.P. (2013). "Standardization of the molding procedures for stabilized soil specimens as used for QC/QA in Deep Mixing application." Proc. of the 18th International Conference on Soil Mechanics and Geotechnical Engineering.

Grisolia, M., MarzanoI.P., De Lentinis D., Leder E. (2010). "Performance of CSM stabilised soils in geotechnically complex formations". Proc. Geotechnical Challenges in Megacities, Moscow (Russia)

Han, J., Yang, X.M., Chen, J.F., and Porbaha, A. (2009). "Settlement calculation of deep mixed foundations". Proceedings of International Symposium on Deep Mixing and Admixture Stabilization, Okinawa, Japan, May 19–21.

Kitazume, M., & Terashi, M. (2013). The deep mixing method. Boca Raton: CRC Press.

Marzano I.P., (2017). "Cased-Pipe Sampling for Quality Assurance of Deep Mixing Method: A Case Study". Proc. International Conference Grouting 2017 – Jet grouting, Diaphragm Walls, and Deep Mixing. Honolulu

Marzano I.P., (2017). "Soil Mixing – Tecnologie esecutive, progetto e controlli". Ed. Hevelius 112p. (in Italian).

Marzano, I.P., Osman, A.A-M., Grisolia, M., Al-Tabbaa, A. (2009). "Mechanical performance of different stabilised soils for application in stratified ground". Proc. of the 17th International Conference on Soil Mechanics and Geotechnical Engineering: The Academia and Practice of Geotechnical Engineering. Alexandria (Egypt).

Mosser, J., Arcos, J. (2012). "Deep mixing columns with a spreadable tool". Proc. of the forth International conference on Grouting and Deep Mixing, Marriott New Orleans, LA February 16-18, 2012.

Pooranampillai, S., Parmantier, D., Dawson, K., and Shin, S. (2012). "A Case History on the Design, Construction, and Field Quality Control of Cement Deep Soil Mixing."Proc.of the 37th Annual Conference on Deep Foundations, Houston, TX.

PWRC (Public Work Research Center). (2004). Design and construction manual on deep mixing method for inland construction, 326p. (in Japanese).

Topolnicki, M. and Pandera, P. (2012). "Design of in-situ soil mixing". International Symposium on Recent Research, Advances & Execution Aspects of Ground Improvement Works, Brussels, Belgium 30 May - 1 June, 2012.

Topolnicki, M. (2016). "General overview and advances in Deep Soil Mixing". Proc. Conferenze di Geotecnica di Torino XXIV Ciclo, 25, 26 February.

Applications of Cement Stabilization for Mitigating Earthquake Disaster

Masaki KITAZUME, Tokyo Institute of Technology, 2-12-1 Ookayama, Meguro, Tokyo, +81 3 5734 2798, kitazume@cv.titech.ac.jp

ABSTRACT

In Japan, soft alluvial clay ground has frequently been encountered in on land and marine constructions, which is so soft and compressible that large ground settlement and failure are concerned. Sandy soil has relatively desirable properties for compressibility and stability, but liquefaction may happen during earthquake in a case of loose and saturated condition. In fact, port and harbor facilities at Kobe Port were heavily damaged in the 1995 Hyogoken-Nambu earthquake. In the earthquake, gravity type of sea revetments displaced a couple of meters toward sea together with large ground settlement at backfill yard. There are many kinds of soil stabilization techniques that were developed and available in Japan for countermeasure of stability, ground deformation and liquefaction. Among them, cement admixture stabilization techniques have frequently been applied to improvement of clayey and sandy soils. In this paper, some applications of three cement stabilization techniques to earthquake disaster mitigation are briefly introduced.

Keywords: cement stabilization technique, earthquake, disaster mitigation

INTRODUCTION

In Japan, soft alluvial clay ground has frequently been encountered in on land and marine constructions. The ground is so soft and compressible that large ground settlement and failure can take place. Sandy soil has relatively desirable properties for compressibility and stability, but liquefaction may happen during earthquake in a case of loose and saturated condition. In fact, port and harbor facilities at Kobe Port were heavily damaged in the Hyogoken-Nambu earthquake in 1995. In the earthquake, gravity type of sea revetments displaced a couple of meters toward sea together with large ground settlement at backfill yard. In the Tohoku earthquake in 2011, liquefaction took place at large area in Chiba Prefecture which caused serious damages on the urban infrastructures. Table 1 shows the amount of damage to port facilities caused by strong earthquake (Noda, 1991), and demonstrates quite large difference in the damage between with and without liquefaction. According to the table, the amount of damage when liquefaction took place is about 20 to 50 times larger than that without liquefaction. This highlights the importance of liquefaction mitigation to minimize earthquake disaster.

There are many kinds of soil stabilization techniques that were developed and available in Japan for countermeasure of ground stability, ground deformation and liquefaction. Among these techniques, cement stabilization techniques have frequently been applied to improve clayey and sandy soils for reinforcement of foundation and liquefaction prevention, *etc*. In this paper, some applications of stabilization techniques, Deep Mixing Method, Premixing Method and Lightweight Treated Soil Method, to earthquake disaster mitigation are briefly introduced.

Table 1. Comparison of amount of damage (Noda, 1991)

Earthquake	Magnitude	Port	Soil type	Max. accel. (gal)	Liquefaction	Damage (million yen)
Niigata, 1964	7.5	Niigata	Sand	159	Yes	49,980*
Tokachi Oki, 1968	7.9	Hachiohe	Sand	233	No	1,980*
Miyagiken Oki, 1978	7.4	Shiogama	Clay	273	No	160*
Miyagiken Oki, 1978	7.4	Ishinomaki	Sand	195-210	Yes	3,008*
Urakawa Oki, 1982	7.3	Muroran	Sand	164	No	120
Nihonkai Chubu, 1983	7.7	Akita	Sand	205	Yes	6,400

* converted into 1978 prices.

© 2018 Deep Foundations Institute

DEEP MIXING METHOD

Outline of the method

In the deep mixing method, soft soil is stabilized in situ with binder without compaction. The deep mixing method (DMM) has usually been applied to improvement of soft clays and organic soils for various purposes such as stability increase, settlement reduction, excavation support and seepage control (CDIT, 2002; Kitazume and Terashi, 2013). The deep mixing method originally developed in Japan and Nordic countries has now gained wide popularity in the worldwide market. During the past four decades, a variety of deep mixing processes has been developed by contractors as their proprietary techniques. The mixing processes are classified by the introduction of binder, wet or dry method, and type of mixing tool, mechanical mixing and high pressure injection method, *etc*.

The mechanical deep mixing method was put into practice in Japan in the middle of 1970s to improve soft marine deposits, then was spread into China, South East Asia, and recently to the other part of the world. Four decades of practice have made equipment improved, binders changed, and applications diversified. Figures 1(a) and 1(b) show the deep mixing machines of the mechanical and high pressure injection methods, respectively. In the mechanical mixing method, the special machines used to stabilize soft soil are basically composed of several mixing shafts and blades, and a binder supplying system. In one operation, a column of stabilized soil is constructed in a ground. Through a series of construction procedures, any arbitrary shape of improved soil mass (such as block, wall and grid types) can be formed in the ground. In the high pressure injection method, the binder slurry is injected at a high pressure of 10 to 60 MN/m^2 through the nozzle into a ground. The binder slurry is mixed with the soil while the injection pipe is slowly rotated and withdrawn to the ground surface. The injection tool is designed to withstand high injection pressures using proper materials as well as the specialized seals between the rod joints. Basically, there are three types of the techniques: single fluid technique, double fluid technique and triple fluid technique. For liquefaction mitigation, the block and grid types of DMM have been applied irrespective of the type of mixing tool.





(a) Mechanical mixing method **(b) High pressure injection mixing method**

Fig. 1. Deep mixing machine

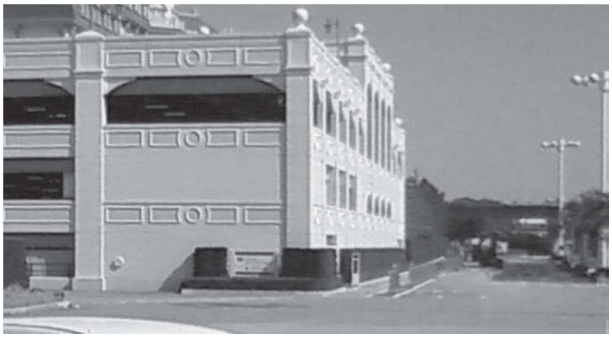
Application of mechanical DM method to building foundation

Figure 2(a) shows an example of the mechanical deep mixing applications to a building foundation, which is a four-story parking facility (Uchida *et al*., 2012; 2013; 2014). Figure 2(b) shows the ground condition and the SPT *N*-value distribution along the depth, where a fill layer and an Alluvial sand layer are deposited over the Alluvial layers from the surface to a depth of GL -14 ~ 16 m. The bearing stratum with the SPT-*N* value larger than 50 is found at GL -39 m to GL -72 m. The fill layer and the Alluvial sand layer are in the loose and saturated condition with the SPT *N*-value of around 10. Figure 2(c) shows the safety factor of liquefaction, F_L, along the depth, which is calculated according to the recommendations by the Architectural Institute of Japan (AIJ, 2006) for the case of the surface

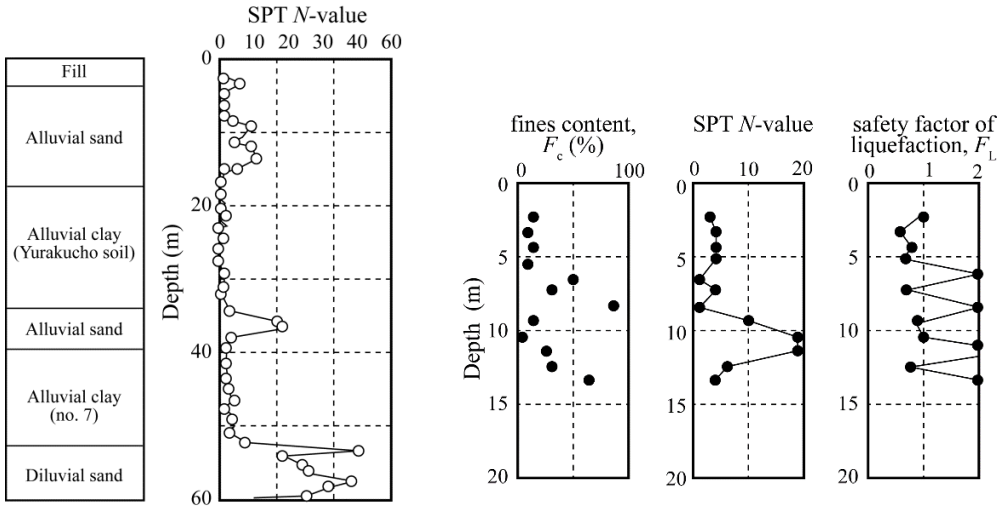
acceleration of 200 cm/s^2. The figure shows that the F_L value is lower than 1.0 at the depth of GL -1.8 m to GL -12 m, which indicates that liquefaction is likely to occur during large earthquake.

Based on the ground survey, two countermeasures were applied to the building and ground: the pre-stressed high-strength concrete piles with the diameter from 500 mm to 1000 mm and the length from 33 m to 60 m were driven to minimize the settlement of building, and the grid type deep mixing method was applied in order to prevent liquefaction. The grid type deep mixing method was successfully applied to the 14-story building in Kobe for liquefaction prevention (Tokimatsu *et al*., 1996; Suzuki *et al*., 1996). The grid spacing and the unconfined compressive strength of the stabilized soil were designed as 15.6 m by 16.5 m and 1.8 MN/m^2 respectively, based on the AIJ recommendations for ground improvement (Architectural Institute of Japan, 2006) and the simplified method proposed by Taya *et al*. (2008). The ground improvement was performed by the mechanical mixing deep mixing machine with two mixing shafts. After completion of the ground improvement, the unconfined compressive strength of the field stabilized soil was measured at four weeks curing and was 3.3 - 9.8 MN/m^2 with an average of 5.8 MN/m^2.

The building and the improved ground were subjected to the large seismic force in the 2011 Tohoku earthquake. Though extensive soil liquefaction took place at the surrounding land reclamation area without ground improvement in Urayasu city, the building and the improved ground were not damaged by the earthquake, as shown in Fig. 2(a), which was taken at two days after the earthquake. This reveals the successful application of the grid type deep mixing to liquefaction mitigation.



(a) Building on grid type deep mixing improved ground.



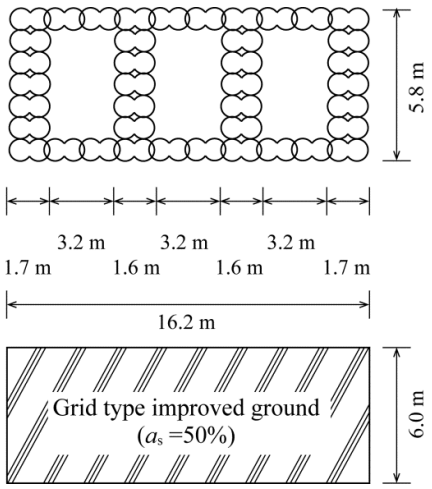
(b) Ground condition (Boring No. 2). (c) Safety factor for liquefaction, F_L (Boring No. 6).

Fig. 2. Application of grid type deep mixing improved ground (Uchida *et al*., 2012).

Applications of mechanical DM method to road foundation

Soon after the aftermath of the 2011 Tohoku earthquake and tsunami, the Cement Deep Mixing Association, the Dry Jet Mixing Association and Chemical Grouting Co. Ltd. conducted field surveys in the Tohoku and Kanto areas together to investigate any deformation and damage in the deep mixing improved ground and the performance of the improved grounds. Though few slight deformations were found in some grounds, as a whole neither serious deformation nor damage was found in the improved grounds and superstructures even they were subjected to the quite large seismic force (Kitazume, 2012; Tokunaga *et al*., 2015.). Here, one of the applications in the field survey is briefly introduced.

The road embankment at Soga, Chiba Prefecture, was improved by the grid type deep mixing method for liquefaction prevention. The original ground beneath the embankment contained large amount of fine sand to the depth of -7 m, which was anticipated to be liquefied due to earthquake motion. The improved ground had about 5.6 m in width, 6.0 m in height, and the improvement area ratio of 50%, and whose unconfined compressive strength, q_u was 200 kN/m^2 (Fig. 3(a)). The site was subjected to the large seismic force in the 2011 Tohoku earthquake. No damage was found in the embankment and the improved ground as shown in Fig. 3(b), even it was subjected to the seismic force of 5.0 upper in Japanese Magnitude-Shindo (seismic intensity scale). As contrast, Figure 3(c) shows heavy damage of road without ground improvement due to liquefaction located in the neighborhood (Kitazume, 2012).



(a) Layout of ground improvement, plane and sectional views.





(b) Road at improved are after earthquake. **(c) Road at unimproved area after earthquake.**

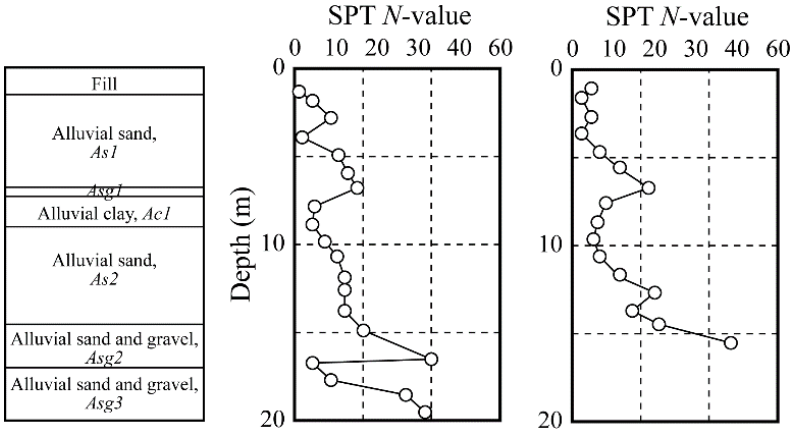
Fig. 3. Ground improvement at Soga, Chiba Prefecture,.

Application of high pressure injection DM method to building foundation

The Osaka Prefectural Nakanoshima Library is designated as National Important Cultural Property, where the Neo-baroque style is enhanced with four massive columns standing at the building's front entrance and the copper roof dome (Fig. 4(a)). The building was build in 1904 as a donation by Kichiuemon Sumitomo and was followed by the construction of exterior appearance in 1922. The ground condition is shown in Fig. 4(b), where several soil layers are deposited at the site: the fill layer at the top, underlain by the Alluvial sand layer, *As1*, and the Alluvial sand and gravel layer, *Asg1*, the Alluvial clay layer, *Ac1*, the Alluvial sand layer, *As2*, and the Alluvial sand and gravel layers, *Asg2* and *ASsg3*. Figure 4(b) also shows the SPT *N*-value distributions along the depth (Japan Cement Association, 2015). As the SPT *N*-values of the *As1* and *Ac1* layers are relatively small, liquefaction is likely to take place in the layers which may cause serious damage to the building.



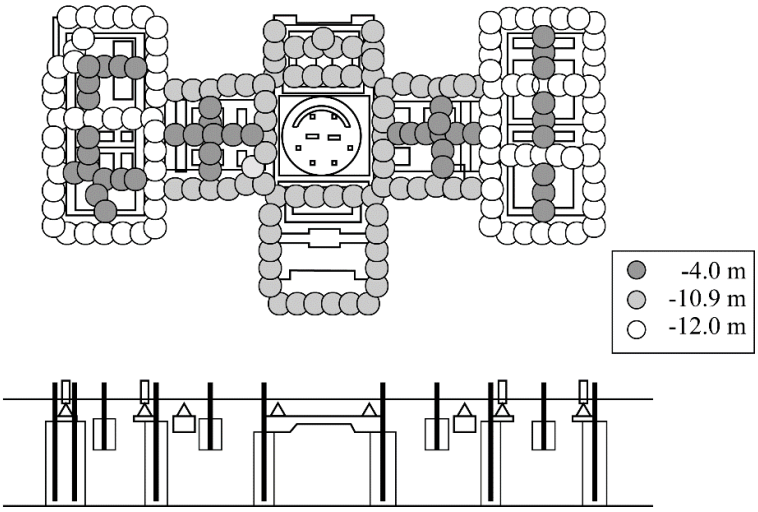
(a) Library building.



(b) Ground condition, ground stratum and SPT *N*- values.

Fig. 4. Osaka Prefectural Nakanoshima Library (Japan Cement Association, 2015).

The stabilized soil columns were constructed beneath the building piles and slabs to increase the bearing capacity of the building piles, as shown in Fig. 5. Additional stabilized soil columns were constructed between the building piles to form the grid type improved ground to prevent the liquefaction. In the figure, the length of columns are distinguished by different colors. The grid spacing was designed as L/d = 1.4, where L and d are the grid spacing and the thickness of liquefiable layer, respectively. As the ground improvement should be carried out beneath the existing building, the jet grouting method was applied instead of the mechanical deep mixing techniques. One of the double fluid techniques was applied, where the diameter and design strength of the jet grouting column were 3 m and 1,600 kN/m^2 ,respectively



(a) Layout of ground improvement.



(b) Double fluid type high pressure injection method.
Fig. 5. Ground improvement by high pressure injection deep mixing method.

PREMIXING METHOD

Outline of the method

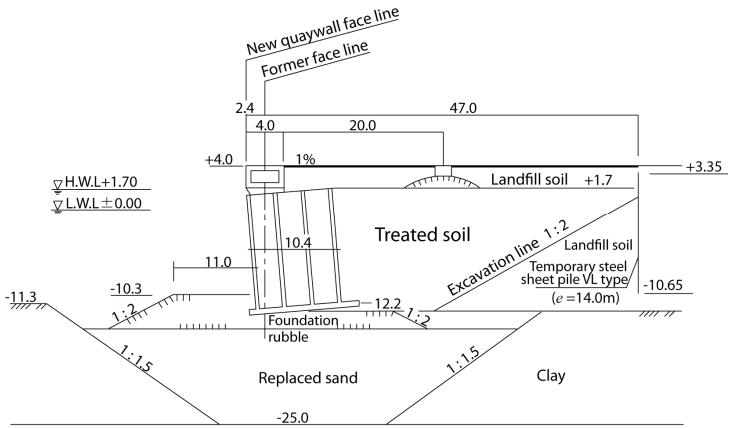
Sandy soil has often been used as a land reclamation material. However, sandy soil is usually stratified in the loose condition, especially in reclamation at coastal area. Any ground improvement is usually required for the loose stratified reclaimed land after reclamation in order to prevent liquefaction. Premixing Method has been developed for liquefaction mitigation, where a small amount of binder and chemical additive are mixed with sandy material (CDIT, 2003). Recently, it has been also frequently applied for reducing the earth pressure acting on the revetment, backfilling behind sheet walls and concrete caisson. After mixing these materials in a mixing plant at field, the stabilized soil is transported to and placed at a designated area to construct a stabilized reclaimed ground (Zen *et al*., 1990). The basic principle of the method is that the shear strength of stabilized soil is not decreased to zero and liquefaction does not take place even if the pore water pressure is generated up to the overburden pressure.

In the execution, sandy soil is mixed with binder and separation inhibitor and then is placed at site, where belt conveyor mixing with dumper chutes and mechanical mixing by screw type mixer are

available. In the placement of stabilized soil, spreading, chute and direct placement methods are available.

Application to sea revetment earthquake for disaster restoration

Figures 6(a) and 6(b) show an application at Kobe port where the concrete type quay wall was damaged in the Hyogoken-Nambu earthquake. The concrete caisson displaced horizontally and titled toward the sea. As the amount of displacement were within the allowable level to function as a quay, the caisson was used without re-positioning but the backfill was excavated and replaced by the stabilized soil in order to prevent liquefaction and reduce the static and dynamic earth pressures acting on the caisson. The design strength of the stabilized soil was 100 kN/m^2 and blast furnace cement type B of 7.5 % in binder content was mixed with the soil as well as separation inhibitor agent of 75 mg per unit dry weight of sand (kg) to achieve the design strength.



(a) Section view



(b) Execution of improvement at site

Fig. 6. Application of Premixing Method at Kobe port

LIGHTWEIGHT TREATED SOIL METHOD

Outline of the method

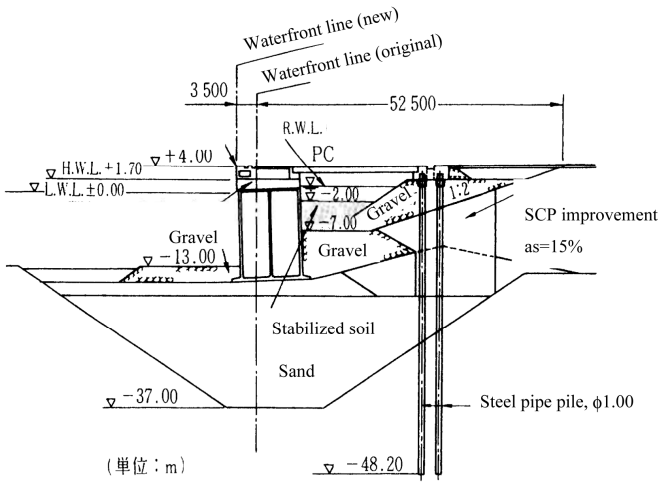
Lightweight Treated Soil Method was developed to reduce residual and uneven settlement, decrease earth pressure, prevent lateral displacement and improve earthquake resistance of port and airport facilities, in which dredged soil is mixed with binder and either air foam or expanded polystyrene (EPS) beads of 1 to 3 mm in diameter (CDIT, 2004). The density of stabilized soil can be obtained

from 6 and 15 kN/m^3 by controlling the amount of air foam or polystyrene beads, and the water content of soil. As dredged soil to be stabilized has a relatively high water content in many cases, the stabilized soil has high liquidity at mixing stage and then looses liquidity quickly. The execution procedure of the method is very similar to Premixing Method, which includes dredging, transporting, mixing, placing and curing steps.

The earth pressure of the stabilized soil can be very small by the effect of its relatively large strength as well as the light-weight property, which can downsize superstructure such as caisson and sheet wall. The method has been applied to landfill or backfill behind a newly constructed quay wall, reinforcement of existing structure, embanking of adjacent work, and submerged backfill and embanking on soft ground.

Application to sea revetment earthquake for disaster restoration

Figure 7 shows an application of the method at Kobe port where the concrete type quay wall was damaged by the Hyogoken-Nambu earthquake (Wako *et al*., 1998). The concrete caisson displaced horizontally and titled in the earthquake. As the amount of displacement was within the allowable level, the caisson was used without re-positioning but the backfill was partially excavated and replaced by the stabilized soil in order to reduce the static and dynamic earth pressures acting on the caisson. The design unit weight and strength of the stabilized soil were 14 kN/m^3 and 100 kN/m^2 respectively.



(a) Section view



(b) Execution of improvement at site

Fig. 7. Application of Lightweight Treated Soil Method at Kobe port

CONCLUDING REMARKS

In this manuscript, several applications of three soil admixture stabilization techniques, Deep Mixing Method, Premixing Method and Lightweight Treated Soil Method, to earthquake disaster mitigation are briefly introduced. The improvement type and mechanism of the technique are different each other. However, the applications introduced in the manuscript clearly reveal that all the methods have the high applicability to earthquake disaster mitigation. These stabilization techniques have been applied successfully to various site and improvement purposes in the past and are expected to develop further for more various sites and improvement purposes in the future.

REFERENCES

Architectural Institute of Japan. 2006. Seismic response analysis and design of buildings considering dynamic soil structure interaction (in Japanese).

Coastal Development Institute of Technology. 2002. The Deep Mixing Method - principle, design and construction -, Balkema publishers, 123 p.

Coastal Development Institute of Technology. 2003. The Premixing Method - principle, design and construction -, Balkema publishers, 140 p.

Coastal Development Institute of Technology. 2004. The Lightweight Treated Soil Method - new geomaterials for soft ground engineering in coastal areas -, Balkema publishers, 120 p.

Japan Cement Association. 2015. Role of cement type of soil stabilization binder for preventing large scale disasters. 113 p. (in Japanese).

Kitazume, M. 2012. Soil mixing performance in the 2011 Tohoku earthquake, The Magazine of the Deep Foundations Institute, pp. 77-78.

Kitazume, M. and Terashi, M. 2013. The Deep Mixing Method. CRC Press, Taylor and Francis Group, 410 p.

Noda, S. 1991. Waterfront development and liquefaction, Journal of the Japanese Society of Soil Mechanics and Foundation Engineering, 'Tsuchi-to-Kiso', Japanese Geotechnical Society, Vol. 39, No. 2, pp. 1-4 (in Japanese).

Suzuki, Y., Saitoh, S., Onimaru, S., Kimura, G., Uchida, A. and Okumura, R. 1996. Grid-shaped stabilized ground improved by deep cement mixing method against liquefaction for a building foundation, Journal of the Japanese Society of Soil Mechanics and Foundation Engineering, 'Tsuchi-to-Kiso', Japanese Geotechnical Society, Vol. 44, No. 3, pp. 46-48 (in Japanese).

Taya, Y., Uchida, A., Yoshizawa, M., Onimaru, S., Yamashita, K. and Tsukuni, S. 2008. Simple method for determining lattice intervals in grid-form ground improvement, Electrical Journal of Geotechnical Engineering, 3(3), pp. 203-212 (in Japanese).

Tokimatsu, K., Mizuno, H. and Kakurai, M. 1996. Building damage associated with geotechnical problems, Soils and Foundations, Special Issue 1. pp. 219-234.

Tokunaga, S., Kitazume, M., Morikawa, Y., Takahashi, H., Nagatsu, T., Honda, N., Onishi, T., Asanuma, T., Kubo, S. and Higashi, S. 2015. Performance of cement deep mixing method in 2011 Tohoku earthquake, Proc. of the Deep Mixing 2015. pp. 1071-1080.

Uchida, A., Odajima, N. and Yamashita, K. 2013. Performance of building foundation with grid-form ground improvement during the 2011 Tohoku pacific earthquake, Architectural Institute of Japan Journal of Technology, 19(42), pp. 481-484 (in Japanese).

Uchida, A., Tsukuni, S., Akashi, T., Ohashi, M. and Arai, H. 2014. Simplified evaluation method about effect of liquefaction countermeasure for the grid-form deep mixing walls, Architectural Institute of Japan Journal of Technology, 20(46), pp. 921-924 (in Japanese).

Uchida, A., Yamada, T. Odajima, N. and Yamashita, K. 2012. Piled raft foundation with grid-form ground improvement subjected to the 2011 earthquake, Proc. of the 9th International Conference on Urban Earthquake Engineering/4th Asian Conference on Earthquake Engineering, pp. 151-156.

Wako, T., Tsuchida, T., Matsunaga, Y., Hamamoto, K., Kishida, T. and Fukasawa, T. Use of artificial light weight materials (Treated soil with air form) for port facilities, Journal of the Japan Society of Civil Engineers, No.602/6-40, pp. 35-52 (in Japanese).

Zen, K., Yamazaki, H., and Sato, Y. 1990. Strength and deformation characteristics of cement treated sands used for premixing method, Report of the Port and Harbour Research Institute, Vol. 29, No. 2, pp. 85-118 (in Japanese).

CUTTER SOIL MIXING AS GROUND IMPROVEMENT TECHNOLOGY IN UNDER-CONSOLIDATED CLAYS

Sandro Gomes, Intrafor Hong Kong, Hong Kong, sandro.gomes@vsl-intrafor.com
Joao Nunes, Intrafor Hong Kong, Hong Kong, joao.nunes@vsl-intrafor.com
Franz-Werner Gerressen, Bauer Maschinen GmbH, Germany, franz-werner.gerressen@bauer.de
Thomas Vohs, Bauer Maschinen GmbH, Germany, thomas.vohs@bauer.de

ABSTRACT

Cutter Soil Mixing (CSM), a deep soil mixing method, was used to improve the soil conditions at a jobsite in Lantau Island (Hong Kong), acting as deep guide wall and trench support for the further diaphragm wall works, on a project that required the construction of two ventilation shafts for tunnels built by Tunnel Boring Machine technology. The geological profile of the reclamation area where the works were carried was composed by a layer of fill (sand) and 15 to 20 meters thick layer of very low cohesion, under-consolidated, marine deposits (soft clay), varying from virtually 0 kPa at the top to 30 kPa at the bottom, at the top of an alluvium deposits layer.It was the marine deposits layer that required to be treated otherwise there was the risk of its intrusion into the excavated diaphragm wall panels and trench collapse.

The paper describes the necessary approach to apply Cutter Soil Mixing under the specific site conditions and discusses also the results obtained from tests carried on site.

Keywords: Cutter Soil Mixing, Marine Deposits, Under-consolidated Clays; Ground Improvement

INTRODUCTION

Cutter Soil Mixing (CSM) is an advanced deep soil mixing method and, with hundreds of completed projects worldwide. It has become very popular methodology, especially for ground improvement, cut-off walls and rehabilitation and upgrading of dams and dikes. The state-of-the-art CSM equipment allows the mixing of natural ground with a cementitious binder in order to economically install high quality vertical structures.

In order to avoid the dispersion of marine deposits and limit the pollution from its dispersion, it was prohibited to dredge the soft clays for the reclamation works. Due to the need of working in a newly reclaimed area, created by backfilling directly on top of non-dredged marine deposits (soft clays), in combination with time constraints which did not allow waiting for consolidation of the soft clay under the load induced by the newly placed Fill, all diaphragm wall works needed to be excavated through under-consolidated clays. The ground improvement was then a need to carry out in order to ensure all following works can be carried out safely.

Intrafor Hong Kong Ltd., Hong Kong based subsidiary of VSL International and part of the Bouygues Construction Group, specialized in Ground Engineering works, proposed to use the CSM method for ground improvement and was awarded with a first contract in 2016, which is in the base of this paper's subject.

The CSM method was chosen rather than other ground improvement methods, including Triple-Shaft Deep Soil Mixing and Jet-Grouting, due to its ground improvement capabilities at very economically conditions having in mind the *in situ* soil characteristics, as well its versatility to be used in a wide range of soils, allowing Intrafor to expand its range of ground improvement solutions.

© 2018 Deep Foundations Institute

CUTTER SOIL MIXING

Deep soil mixing

Cutter Soil Mixing is an alternative method of deep soil mixing where the soil is mixed in situ with cementitious binder slurry by mixing tools. This creates a mortar-like material with the soil particles becoming the aggregates. Thus one of the major advantages of CSM method is to save the transport and purchasing of aggregates. The mass of excavated material and spoil that needs to be treated, transported and hauled and dumped off site is – depending on the ground conditions – also significantly reduced. That makes the method not only environmentally friendly but also economic, as it shows a much higher performance than a two phase cut-off wall or even a secant pile wall, where the soil has to be excavated in a first step and the excavation has to be filled in a second step, often under water or a supporting fluid.

Clays of high plasticity and very hard rock formations are unfavorable soil conditions. Organic soils are limited in their suitability as well due to their negative effects on hydration when dispersed in the soil-cement mortar, leading to reduced strength, especially at an early age.

Construction method

Based on the experience gained with the in-house developments of trench cutters and deep soil mixing with continuous flight augers (Mixed-In-Place, MIP), the development started back in 2003 to combine both methods, called “Cutter Soil Mixing”. While in trench cutting, the bentonite slurry is used to transport the excavated material out of the trench in addition to its function in supporting the trench, with Cutter Soil Mixing (CSM), cementitious slurry is pumped to the actual location of the CSM tool. The CSM tool essentially consists of four wheels, the gearboxes driving the wheels, shear plates and a slurry nozzle (Figure 1).

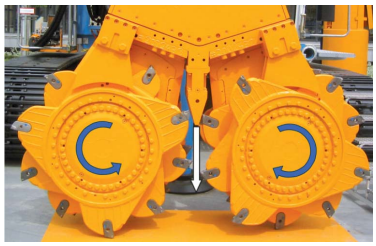


Fig. 1. - CSM tool showing slurry flow (white arrow) and direction of rotation of the cutter wheels (blue arrows) [1]

The in situ soil or rock is cut by the CSM wheels. The slurry is discharged from the nozzle between the wheels and is mixed with the soil by the CSM wheels turning against the slurry flow. The cutting or mixing teeth push the soil particles through the shear plates creating a kind of compulsory mixer.

A panel is installed in the following main steps:

After positioning of the CSM tool at the specified panel location, penetration takes place to the final depth. For slow penetration speeds or large depths, bentonite slurry or water (in clayey soils) is used (so called two-phase system). In case of higher penetration speeds and/or small depths, cementitious slurry can be used from the beginning (so called one-phase system). After reaching final depth, withdrawal process starts. Cementitious slurry is added and mixed with the soil. For the two-phase system, the total amount of cement is mixed into the soil in this step. For the one-phase system, only the difference between the calculated

cement mass and the mass already introduced during penetration is added. In either case, the mix is further homogenized.

The panels can be installed either in a fresh-in-fresh or in a hard-in-hard sequence (Figure 2). Fresh-in-fresh means that each secondary panel (S) is cut in the gap between the most recently produced and still wet primary panels (P). Subsequently, the next primary panel is installed (sequence P – P – S – P – S – ...). When the hard-in-hard sequence is used, first a number of primary panels are produced and subsequently the gaps are filled, over-cutting the already set primary panels (sequence P – P – P – ..., S – S – S – ...).

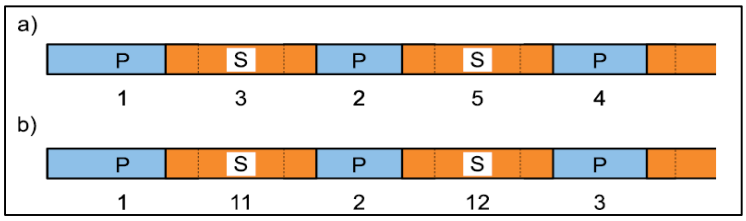


Fig. 2. - Construction sequences of continuous walls with primary (P) and secondary (S) panels: a) "fresh in fresh", b) "hard in hard"

Construction materials

The materials used in Cutter Soil Mixing are cementitious binder, which is typically a mixture of ordinary Portland cement (OPC), ground granulated blast-furnace slag (GGBFS), bentonite for stabilization and water, and possibly also chemical admixtures like plasticizers and retarders. Polymer additives can also be used, both to increase viscosity and decrease fluid loss.

The composition of the cement (bentonite) slurry used and its dosage strongly depend on the in-situ ground conditions and the purpose of the designed geotechnical structure. Additionally, a key factor is the quantity of water needed to lubricate the soil to achieve sufficient workability (consistency). Workability in the fresh stage has a strong impact on the quality of the hardened soil mortar.

Application, advantages and limitations

Cutter Soil Mixing – like other methods of deep soil mixing – can be used for soil improvement, installation of cut-off walls and also for retaining walls if subsequently reinforced. A compressive strength up to 15 MPa for retaining walls and permeability in the magnitude of $1 \cdot 10$–8 m/s for cut-off walls can be achieved within an economic product range. In additional to the advantages shared with other deep soil mixing methods, the CSM method provides further advantages:

– The method can cope with many soil types including rocks since harder soil formations can be penetrated, broken down and mixed. Even fine-grained soil can be homogenized as the cutter wheels together with shear plates act as a kind of compulsory mixer.
– A high degree of verticality of wall panels is achieved by counter-rotating mixing wheels.
– The cutter principle ensures construction of clean and trouble-free panels and joints, even between wall panels of different construction age.
– Small base units can generate a high daily output and very deep panels.
– By producing rectangular panels, the entire wall section can be considered for structural design and permeability.

PROJECT BACKGROUND

The ground improvement works which constitutes the subject of this paper took place in Hong Kong, China, integrated in the biggest project ever awarded in this city, and still ongoing. Following, brief description of main project and INTRAFOR scope of works.

Main project overview

The main project will provide a strategic link connecting the Northwest New Territories (NWNT) with an interface hub in Lantau Island and the Hong Kong International Airport (HKIA) (Figure 3).



Fig. 3. - Hong Kong map with jobsite identification

The total length of this new route is about 9 km, consisting of two sections. The first one will connect North Lantau Highway (NLH) at Tai Ho and the new reclamation area in Lantau Island, situated at the northeast waters off the HKIA. The second one will connect Lantau and Tuen Mun.

This link will reduce the journey time between NWNT and Lantau. As compared to the current route, the traveling distance between Tuen Mun South and HKIA will be reduced by about 22 km. The traveling time will also be shortened from 30 minutes to 10 minutes. This new road link not only helps divert traffic flows to relieve the existing traffic conditions of NLH, Lantau Link and Tuen Mun Road, but also provides as an alternative route to the HKIA, thus reinforcing the HKIA as a regional aviation hub.

Scope of works – Diaphragm Walls and Cutter Soil Mixing

As part of the main project, the main contractor was awarded with the construction of two 5 km long sub-sea tunnels. INTRAFOR was chosen by the main contractor in order to carry all the foundation and ground improvement works associated to the tunnel works (ventilation shafts and temporary parking plug for TBM) in the new reclamation area at Lantau Island.

The foundation works consisted in around 32,500 m^2 of diaphragm walls, to make two ventilation shafts and a parking plug where the TBM will stop waiting the completion of other civil works prior completion of the tunnels. However, due the geological conditions, it was required to execute some ground improvement works consisting in around 49,500 m^2 of CSM.

Ground conditions

Following, brief description of ground conditions. Figure 4 shows a typical cross section of the treatment area as well as a shear strength profile.

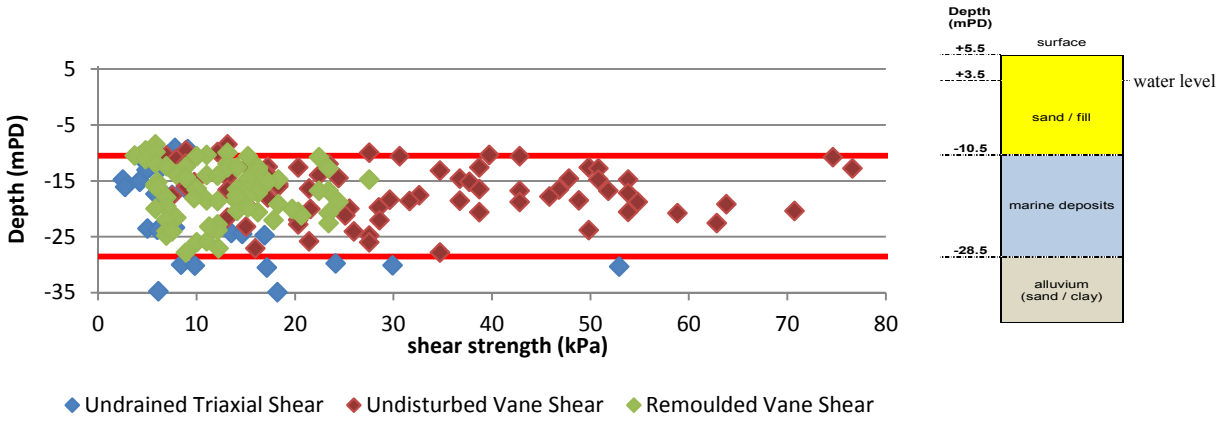


Fig. 4. - Typical soil profile and shear strength values

The jobsite consists in an artificial island created by backfilling straight on top of marine deposits that were not allowed to be previously dredged due environmental restrictions, as well due the lack of available sites for depositing it.

The top layer consists in public fill (sand) with around 16 meter thickness, followed by a thick layer of marine deposits (under-consolidated soft clays), with an average 18 meter thickness, of very low cohesion, varying from virtually 0 kPa at the top and 30 kPa at its bottom. Below the marine deposits is a layer of alluvium deposits (sand and clay) with an average SPT N=50 and a maximum SPT N=163. The average thickness is 25 meter. At the bottom there was a very stiff layer of decomposed siltstone of more than 50 meter thickness, where the diaphragm wall panels were founded.

Geotechnical problem and solution

The marine deposits layer, due its nature of under-consolidated soft clays, presented a hazard for the execution of the required diaphragm wall works, with high risk of intrusion of marine deposits into the excavated panels, as well the collapse of the trench during the excavation process. Vertical drains had been installed to accelerate the consolidation of the newly installed landfill, however due the work scheduling constraints the diaphragm wall works needed to start almost immediately after the backfilling, not allowing the drains to produce their effect of excess pore pressure dissipation.

In order to overcome the issue above mentioned and allowing the start of the diaphragm wall works as per schedule it was decided to carry out ground improvement using CSM, in order to provide enough stability and security for the further diaphragm wall works.

GROUND IMPROVEMENT WORKS

The CSM works consisted in building two rows on each side of and along the alignment of the diaphragm wall and inside the diaphragm wall closing panels, in a total of 540 panels. The CSM panels, reaching depths between 32 and 36 meter, would act as deep guide wall for the diaphragm wall panels, providing the required trench stability for safe execution of diaphragm wall works. A detail of the layout is shown in figure 5.

The acceptance criteria for CSM ground improvement were then defined as:

– Continuity and homogeneity of the wall;

– Minimum wall thickness of 230 cm;
– 28-day unconfined compressive strength (UCS) of 1.0 MPa in the marine deposits.

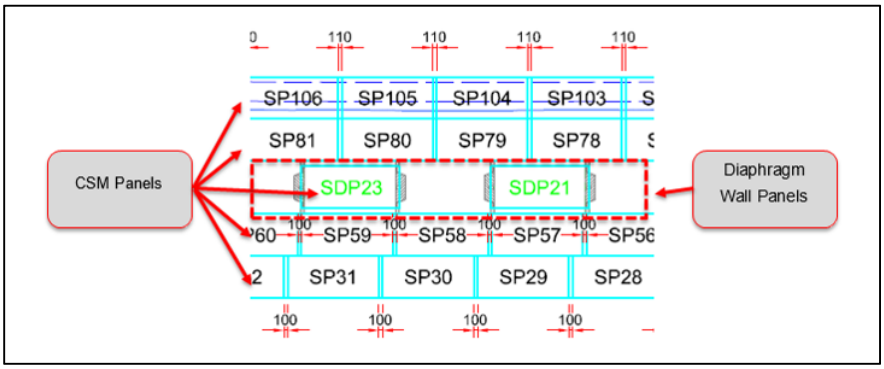


Fig. 5. - Simplified schematics of CSM / Diaphragm Wall Panels pattern

The CSM panels were installed using two BCM 10 mixing units and rectangular Kelly bar. The rigs were equipped with on-board monitoring and controlling system B-Tronic, which enables the operator to control the verticality and pumped slurries volume during production, amongst other parameters requires for the normal and proper operation of the rig, and record data allowing the respective quality control.

The panels were installed using the two-phase system, using bentonite and water for the penetration, respectively on the sand and marine deposits layers, and cement grout for the withdrawal. The volume pumped during the penetration phase was variable, depending on the ground conditions, being the main concern of the operator during this phase the control of verticality of the panel. During the withdrawal phase, the retrieval speed was adjusted by the operator using the B-Tronic system in order to ensure that a uniform cement grout distribution is achieved along all extension of the panel.

The wall was constructed hard-in-hard with the secondary panels installed at a minimum of 12 hours gap after the adjacent primary panels' installation. This process was chosen in order to avoid the contamination of the already installed panels by the water or bentonite slurry using during the penetration phase. The continuity of the wall was achieved by overlapping primary and secondary panels by a minimum of 100 mm.

In order to contain the excess slurry and spoil from penetration phase, it was excavated a small trench, being the spoil disposed from this trench to a spoil truck, using an excavator.

Due to its high resistance to chloride the cement grout used consisted of slag cement (CEM III/A 42.5N). Also, the slag would lead the mix to harden slowly in the first days, allowing a better junction between primary and secondary panels. The bentonite slurry was used to provide stability for the sand layer during the penetration phase.

All grout and bentonite slurry fabrication equipment were installed on barge, due local environmental restrictions, imposing additional challenges to overcome. Two batching plants with grout production capacity of 30 m^3/hour were used to mix the cement grout and bentonite slurry. Each batching plant was fed by two horizontal silos for cement and one horizontal silo for bentonite. After fabrication both bentonite slurry and cement grout were pumped to land, where agitators, tanks and pumps were installed in order to supply slurry for both rigs. The pumps feeding the rigs had the possibility of being remotely controlled by the operator, allowing him to ensure the proper flows, according to the needs, on both phases.

TESTING

In order to ensure the quality of works according to requirements, a testing program was implemented, for cement grout, bentonite slurry and for the installed panels.

Cement Grout and Bentonite Slurry testing

The cement grout density was tested both in the batching plant every 5 batches as well as 3 times per panel at the pump output to the rig, in order to ensure the quality of every single panel.

The bentonite slurry was tested for density, viscosity and pH daily at the main storage tank, and also during the excavation of each panel at the pump output to the rig. The control of the bentonite slurry was essential to avoid excavation related problems, such as getting the tool stuck or having trench collapse.

The volumes injected either water or bentonite during the penetration or cement grout during withdrawal were measured with a flow meter installed on the base machine, monitored and recorded by the B-Tronic.

Pre-production testing

In order to assess the cement type and grout mixture design to be used during the CSM production phase, laboratory tests had been carried with the goal of performing Unconfined Compressive Strength (UCS) tests at 7, 28 and 56 days. The targeted UCS at 28 days for the marine deposits was 1 MPa.

Nine different mixtures were tested using various types of cements as well as various dosages. A total of 52 cubes were casted, with marine deposits collected from the area targeted to be treated, using piston sampling method. Table 1 shows the characteristics of the marine deposits samples used. The characteristics are the same as encountered on the targeted treatment area.

Table 1 - Marine deposit samples characteristics

sample	depth (mPD)	moisture content	WL (%)	WP (%)	PI (%)	particle density (mg/m^3)
A	-13.5	72%	76%	32%	44%	2.67
B	-11.5	66%	76%	34%	42%	2.63
C	-12.5	78%	76%	62%	14%	2.65
D	-24.5	56%	57%	24%	33%	2.64
E	-19.5	31%	non plastic			2.66
F	-8.5	44%	32%	19%	13%	2.67
G	-11.5	61%	54%	25%	29%	2.68
H	NA	83%	61%	24%	37%	2.69
I	NA	63%	61%	24%	37%	2.68
J	-14.5	72%	74%	29%	45%	2.65
K	NA	62%	62%	24%	38%	2.68

Based on the trials done and the results obtained and the cement characteristics, that are more suitable for the type of ground to be treated, it was chosen to use CEM III/A, which at 28 days presents an estimated UCS value about 41% higher than using OPC (Figure 6), allowing using less cement for the same strength.

As per estimation presented on the previous graphic (Figure 6), the average strength for CEM III/A at 28 days is 2.58 (±1.07) MPa, while for OPC the average strength at 28 days is 1.71 (±1.03) MPa.

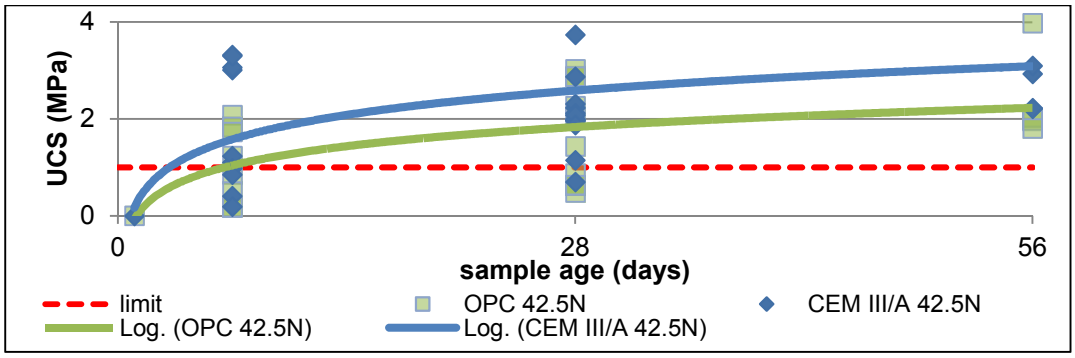


Fig. 6. - Comparison of UCS results between CEM III/A and OPC

Quality control testing

In order to assess the performance of works, it was initially decided to take wet samples in all panels, however, this method was unsuitable, due the cohesive characteristics of the soil, not providing representative or consistent data for quality control and acceptance purposes [2].

The adopted solution to overcome this issue and demonstrate undoubtedly the quality of treatment and achievement of requirements was the adoption of 4C-MLC triple tube barrel coring. Core samples were retrieved either from the center of the panels and from the overlapping area between primary and secondary panels, in order to demonstrate also the continuity of the treatment. In total 16 cores were taken, spread across the different treatment areas. In addition, two permeability tests were carried out *in situ*, for internal purposes only, with results on the magnitude of 10^{-9} m/s. This test is a good indication for the integrity of the ground treatment.

The final acceptance of the ground improvement works was based on the results obtained by coring.

Testing results

To assess the quality of the ground improvement works 16 panels were cored, representing 3% of the installed panels [2]. These were spread across the treatment area, resulting in 55 samples. The sample age varies from 29 days to 229 days. Due to constraints on site it was not possible to have all cores done on time and the samples tested at 28 days.

As seen on the figure 7, two individual samples failed to achieve 1.0 MPa, with failure due to cracks but not due material failure, as per laboratory reports, with the average for each panel being always superior to the minimum required of 1.0 MPa. Although the results obtained by coring are higher than contractual requirements, it is expected that the actual strength in situ to be even higher, as the results obtained by coring can be influenced by micro fissures caused by the drilling and extraction process, by different curing conditions for samples and for *in situ* ground treated, as well by the samples handling on site and between site and laboratory [3].

At 7 days the estimated strength of the treated ground is already 52% of the 28 days strength (0.69 MPa / 1.33 MPa), increasing this value to 76% at 14 days (1.01 MPa / 1.33 MPa). It was also noticed that the strength keeps increasing considerably until almost 10 months after the panels' installation. This strength increase was still notable at slower rate up to 25 months.

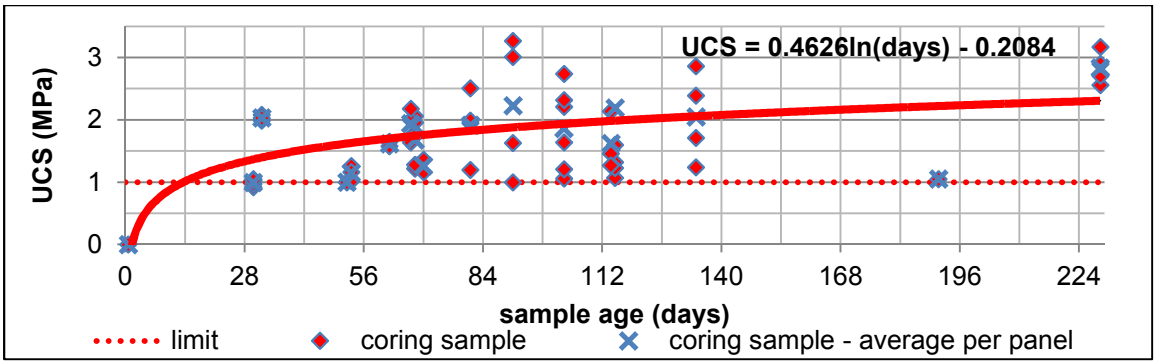


Fig. 7. - UCS for coring samples

The treated ground presents a good homogeneity, possible to see in the cores recovered (Figure 8), with an average core recovery rate of 97.7%, which represents an exceptional recovery rate for the type of soil in question, being an acceptable limit defined at 90% [3].



Fig. 8. - Section of core

Correlation between wet grab samples and coring samples UCS

Even though the wet grab samples were not taken into account for quality control, it was taken the chance to study the UCS correlation between wet grab samples and cored samples (Figure 9).

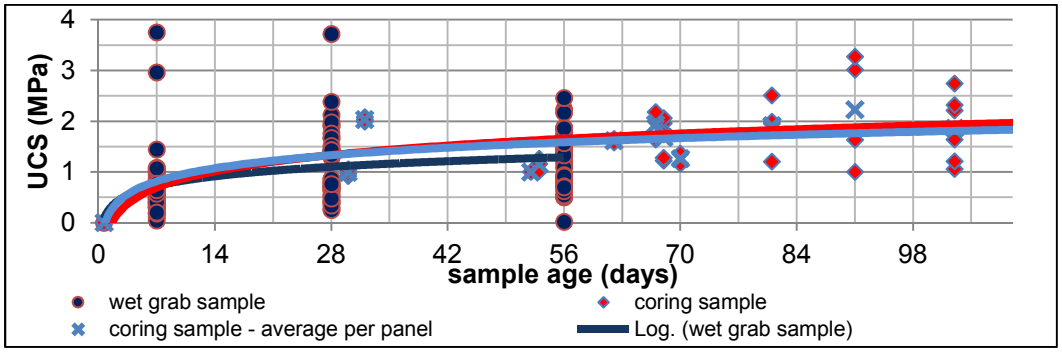


Fig. 9. - UCS for wet grab and coring samples

The wet grab samples were collected at a depth of -24.5 mPD, i.e. 30 meters from ground level, right after the panel completion. Samples were casted in cubes (100mm x 100mm x 100mm) which were cured on site prior transportation and demolded in laboratory for testing.

However, due the characteristics of the sampler device, not allowing defining or controlling the depth where the sample was collected, and as well the cohesive nature of the soil, it was very difficult to obtain proper samples to be casted. Moreover, most of the samples were being contaminated by material prevenient from

the first meters of the panel, which was being trapped inside the sampler on its way down. In addition, the targeted depth for sample collection was also a challenge itself, once it was the double of the depth for which the type of sampler collector used had been previously applied in other projects. To overcome the above-mentioned issue it was studied an alternative solution for the samples collection by modifying the sample collection device. However, the cost required, as well the lack of certainty in solving the problem, linked with the cohesive nature of the soil, lead to the abandon of this solution and the implementation a coring campaign, to provide the required quality control results.

At 28 days, the average estimated UCS for coring samples is 20.6% higher than the average UCS for wet grab samples, increasing this value to 22.9% at 56 days. Taking into account only the results for the panels with both results from wet grab and cored samples (Figure 10), the difference will increase to 115.3%, favorable to the results obtained by cored samples.

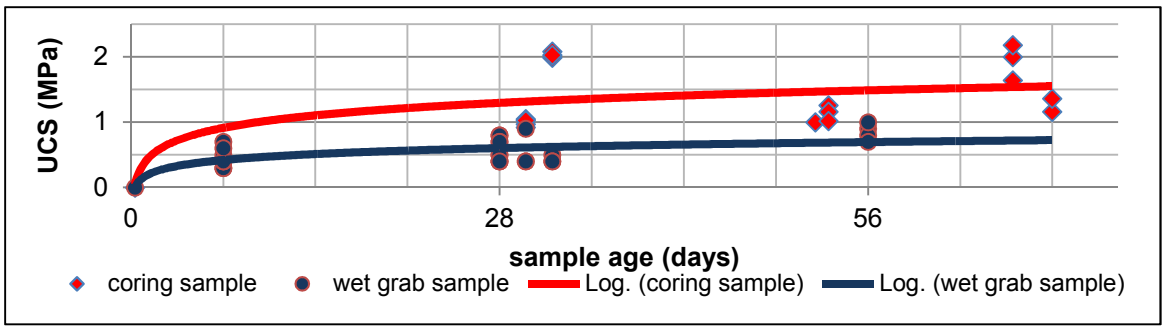


Fig.10. - UCS for panels with both wet grab samples and coring samples

The difference observed is consistent with observations previously done on this subject [3] and in this case can be justified by the extremely high cohesive nature of the ground, making the wet grab sample collection difficult, limiting the quality of the collected material to make proper samples for testing.

SUMMARY

The paper demonstrates that Cutter Soil Mixing was a very suitable method to provide the required ground improvement in order to proceed with further diaphragm wall works in safe condition.This deep mixing method had succeeded to overcome the challenging conditions encountered on site, namely due the geological conditions on the area to be treated, being all the diaphragm wall works already completed without any trench stability issues noticed. Intrafor Hong Kong was awarded a new works order, under the same contract, in order to carry the ground improvement works for the foundation slab of the future tunnel ventilation building. This demonstrates the reliability of this method and satisfaction of the client with the product and the method as well.

REFERENCES

[1] Bauer Maschinen GmbH: CSM Cutter Soil Mixing, Process and Equipment, 2009.

[2] Mary Ellen C. Bruce, Ryan R. Berg, James G. Collin, George M. Filz, Masaaki Terashi, David S. Yang, "Federal Highway Administration Design Manual: Deep Mixing for Embankment and Foundation Support – FHWA-HRT-13-046", 2013

[3] D.A. Bruce, M.E. Bruce, A.F. DiMillio, "Deep Mixing: QA/QC and Verification Methods", 2000, Grouting Sol Improvement, Geosystems Including Reinforcement. Proceedings of the 4th International Conference on Ground Improvement Geosystems. Finnish Geotechnical Society, Helsinki, Finland.

LIQUEFACTION COUNTERMEASURES USING FLOATING GRID-FORM SOIL IMPROVEMENT FOR THE CONTAINER YARD LOCATED IN HARBOR AREA

Shoichi Tsukuni, Takenaka Civil Engineering & Construction Co., Ltd., Tokyo, Japan, +81-3-6810-6215, tsukuni-s@takenaka-doboku.co.jp
Takahiro Sugano, Nagoya Institute of Technology, Nagoya, Japan.
Takahiko Masumoto, Takenaka Civil Engineering & Construction Co., Ltd., Tokyo, Japan, +81-3-6810-6215, masumoto-t@takenaka-doboku.co.jp
Kazuhiro Kaneda, Takenaka Corporation, Tokyo, Japan, kaneda.kazuhiro@takenaka.co.jp
Yoshio Hirai, Takenaka Corporation, Tokyo, Japan, hirai.yoshio@takenaka.co.jp

ABSTRACT

This study investigates the effect of using floating grid-form soil improvement (FGFSI) technique which is constructed in the shallow region of a liquefied layer. Using FGFSI to mitigate liquefaction below a container yard, two dynamic centrifuge model tests were conducted using the Nankai Trough earthquake as the input motion, with the aim of assessing the countermeasure effects. One test involved no countermeasure, whereas the other used FGFSI with 5 m high grid walls and a grid spacing of 6 m or 12 m. The average container settlement without countermeasures was 0.571 m, whereas that with the 6 m grid FGFSI was 0.280 m; the settlement with countermeasures was reduced to 49% that without countermeasures. A relatively large free-field settlement of 0.308 m occurred without countermeasures. However, no liquefaction was recorded within FGFSI region because it was suppressed by the contact pressure of the container. With less space between the grid walls, there was less difference between the container and ground surface settlements.

Keywords: liquefaction, floating grid-form soil improvement, dynamic centrifuge model test, settlement

INTRODUCTION

The grid-form soil improvement technique (Fig.1) is used in Japan to prevent liquefaction near levees and buildings foundations (Cooperative Research Reports of PWRI 1999). The effectiveness of this technique was demonstrated during the 1995 Kobe earthquake (Suzuki et al 1996) and the 2011 Tohoku earthquake (Uchida et al., 2012). Conventional grid-form soil improvement involves constructing a grid of walls throughout the entire liquefied layer; this is turn involves a high volume of improved soil and consequently high construction cost. By contrast, floating grid-form soil improvement (FGFSI) involves a lower volume of improved soil because the grid walls are constructed only in the shallow region. However, FGFSI cannot mitigate liquefaction below the floating grid-walls. Therefore, FGFSI affords less liquefaction mitigation compared to conventional grid-form soil improvement.
Previous research into FGFSI includes the following. Dynamic centrifuge tests in which the height and spacing of the grid walls were varied have been conducted to investigate the mitigation of liquefaction within and below the grid walls (Takahashi et al., 2012). Separately, dynamic centrifuge tests have been conducted in which grid-form soil improvement and FGFSI were combined to enhance the liquefaction; a relationship was established between the height of the floating grid walls and the settlement of the ground surface (Takahashi et al., 2012). Those studies focused only on accumulation of excess pore pressure (EPP) within the floating grid walls and on ground surface settlements. Structures constructed above the FGFSI were not modeled in the experiments.

© 2018 Deep Foundations Institute

The purpose of the present research was to investigate liquefaction mitigation when FGFSI is applied to a container yard in a harbor area. This was done with dynamic centrifuge tests using the Nankai Trough earthquake as the input motion. In experiments, aboveground containers were modeled, and their settlement was measured. Two dynamic centrifuge tests were conducted. One used no countermeasures, whereas the other used FGFSI in which the height of the grid walls was 5 m and the spacing was 6 and 12 m.

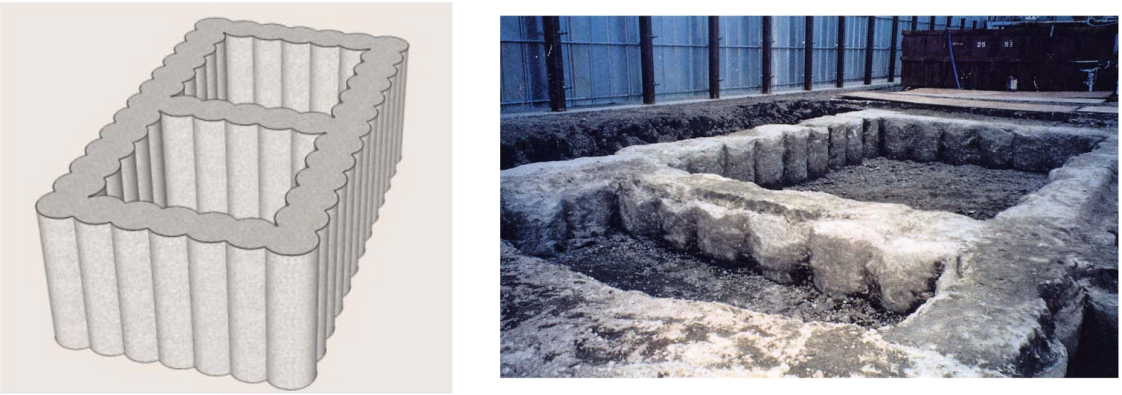


Fig. 1. Grid-form soil improvement.

EXPERIMENTAL CONDITIONS

The dynamic centrifuge tests were conducted under an 80 g field using a rigid box that was 1,100 mm long in the earthquake direction, 400 mm wide, and 290 mm tall; this corresponds to a span of 88 m, a width of 32 m, and a height of 23.28 m. The model was scaled subsequently to reflect estimates of the true scale. An actual container spans 2.4 m is 12.2 m wide in the orthogonal direction, and is 2.6 m tall. In the experiments, we modeled six actual containers in the earthquake direction and four vertically. The container model was divided into three model containers, each of which modeled two actual containers in the earthquake direction and four vertically. The spacing between any two adjacent model containers was 0.3 m. Consequently, the container part spanned 15 m, was 12.2 m in the orthogonal direction, and was 10.4 m tall. The container contact pressure was 42.89 kPa.

Table 1 lists the experimental cases. Case-1 involved no countermeasures. Case-2 modeled FGFSI at 1.5-6.5 m below ground level (i.e., 5 m tall grid walls) and with grid-wall spacing of 6 and 12 m. The grid-wall spacing is defined as the horizontal distance between the center of facing grid walls. The groundwater level was 2.8 m below ground level (GL). Figure 2 shows plan and cross sectional views of the ground model. The ground model between GL and GL -20 m comprised Iide silica sand No.6 (Dr = 72%) which has maximum and minimum void ratios of emax = 0.872 and emin = 0.514, respectively. The liquefaction strength of this sand is 0.227, which corresponds to a 2.5% axial strain with a simple amplitude with 20 cycles. The liquefied layer was 17.2 m thick because the groundwater level was GL- 2.8 m. The ground model between GL- 20 m and GL- 22 m comprised Iide silica sand No.6 (Dr = 90%). This dense non-liquefied layer was formed using the aerial drop method, and silicone oil was used as the pore fluid to satisfy the similarity rule. In the experiments, we measured the settlement of the containers and ground surface (GL0 m), the horizontal acceleration, and the EPPs at GL- 5 m, GL- 10 m, GL- 15 m, and GL- 20 m. The measurement of horizontal acceleration included that at the ground surface and the top of the container.

Table 1. Experimental cases.

Case	Spacing of grid wall	Container settlement (m)			
		Left	Center	Right	Average
Case-1	Without countermeasures	0.513	0.619	0.582	0.571
Case-2	6 m	0.265	0.276	0.299	0.280
	12 m	0.344	0.359	0.370	0.358

Figure 3 shows the ground model for Case-1 and the process used to produce the ground model for Case-2; in the latter case, the FGFSI grid was made of glass epoxy.

An earthquake wave derived from the Nankai Trough earthquake was used in the experiments. Figure 4 shows the time history of horizontal acceleration measured from the in Case-1. The maximum measured horizontal accelerations were 0.253 g for Case-1 and 0.248 g for Case-2.

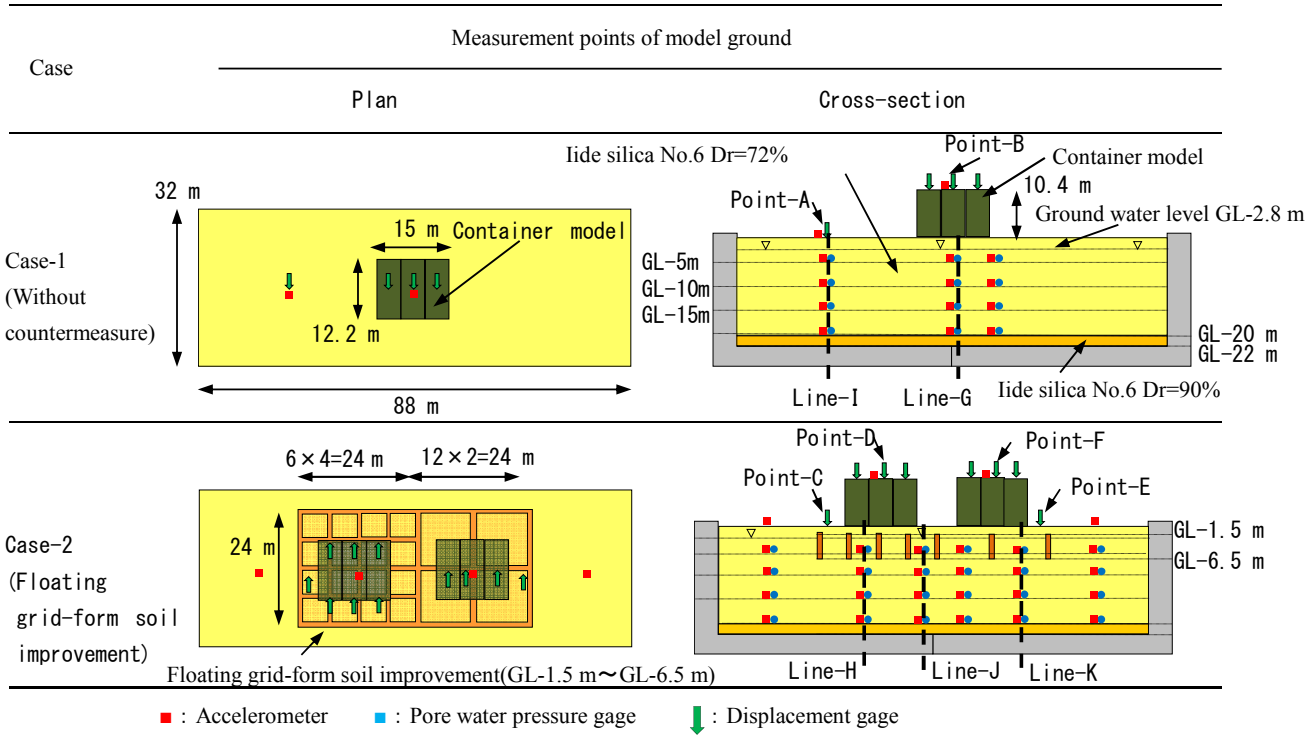
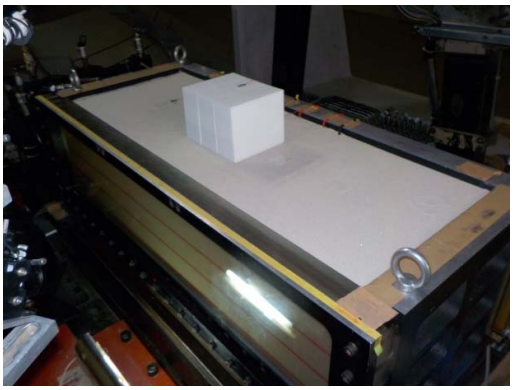
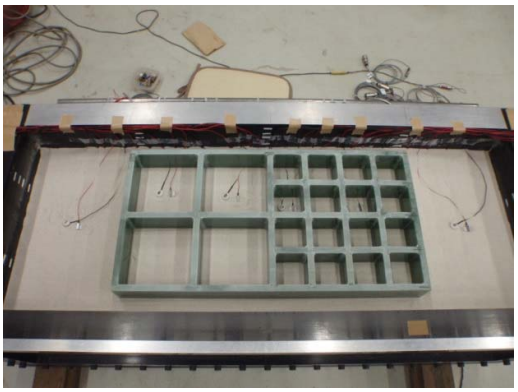


Fig. 2. Illustration of experimental cases.



Ground model of Case-1



Production process of Case-2

Fig. 3. Process of producing the ground models.

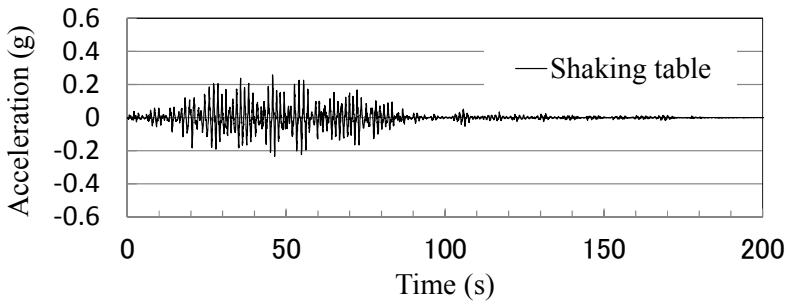


Fig. 4. Time history of horizontal response acceleration; shaking table.

EXPERIMENTAL RESULTS

The experimental results reflect the true scale.

(1) CONTAINER SETTLEMENT

Table 2 lists the settlement of the container models as measured after dissipation of EPP in the liquefied layer. The settlement obtained without countermeasures (Case-1) was 0.571 m, whereas those obtained with FGFSI (Case-2) were 0.280 m for the 6 m grid and 0.358 m for the 12 m grid. The settlements with the 6 and 12 m grids were 49% and 63%, respectively, of that without countermeasures. The maximum difference in settlement among three container models was 0.106 m in the case without countermeasures; the FGFSI differences were 0.034 m and 0.026 m for the 6 and 12 m grids, respectively. Clearly, smaller settlement differences were obtained with FGFSI than without.

Figure 5 allows comparison between the settlement time history measured at the free-field ground surface (Point-A in Fig. 2) and that at the top center of the container (Point-B in Fig. 2). The free-field ground settlement (0.308 m) was larger than the container settlement (0.619 m). The settlement of the container relative to the free-field ground surface was 0.311 m.

Table 2. Container settlement.

Case	Spacing of grid wall	Container settlement (m)			
		Left	Center	Right	Average
Case-1	Without countermeasure	0.513	0.619	0.582	0.571
Case-2	6 m	0.265	0.276	0.299	0.280
	12 m	0.344	0.359	0.370	0.358

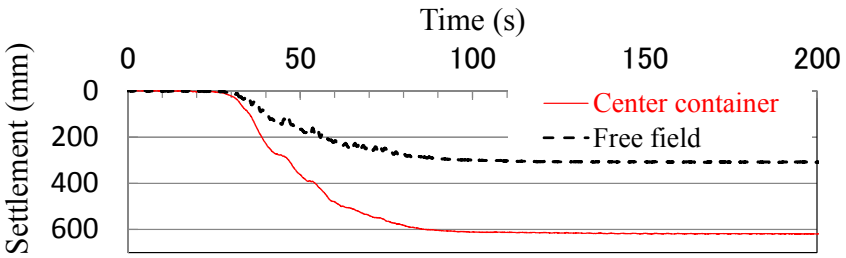


Fig. 5. Settlement time histories of container and free field ground surface; without countermeasures (Case-1).

Figure 6 allows comparison between the time histories of ground surface and container settlement measured in Case-2 (i.e., with FGFSI). The container settlement time histories were measured at Point-D for the 6 m grid and Point-F for the 12 m grid; the ground surface settlement time histories were measured at Point-C for the 6 m grid and Point-E for the 12 m grid (see Fig. 2). The ground surface and container settlements with the 6 m grid were 0.272 m and 0.276 m, respectively, which means that the subsidence (the difference between the ground surface and container settlement) was very small (0.004 m). By contrast, with the 12 m grid, ground surface and container settlements were 0.223 m and 0.359 m, giving a much larger subsidence (0.136 m) than that for the 6 m grid.

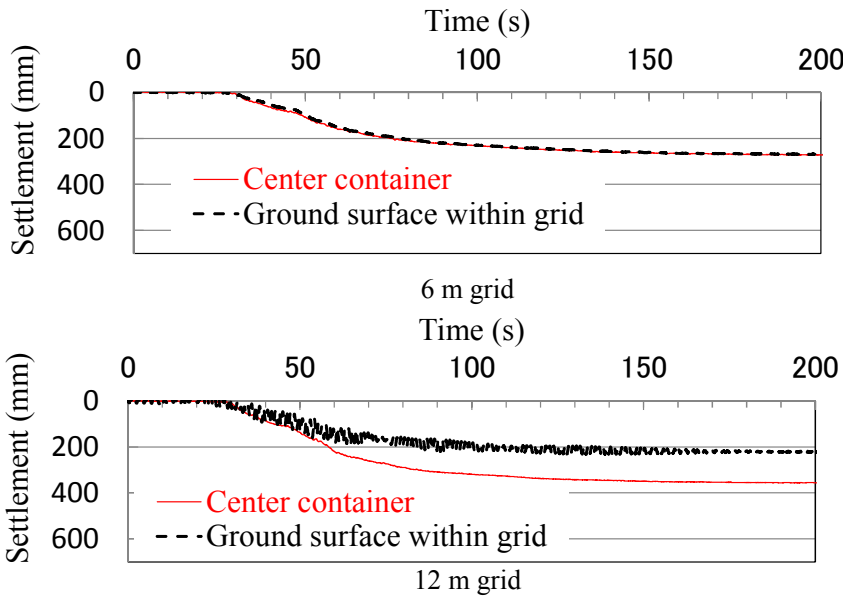


Fig. 6. Settlement time histories of container and free field ground surface; with floating grid-form soil improvement (Case-2)

(2) HORIZONTAL ACCELERATION

Figure 7 shows time histories of horizontal acceleration measured below container center (Line-G in Fig. 2) without countermeasures. For GL- 15 m, the horizontal response acceleration was almost the same as that of the shaking (see Fig. 4), so we reason that no liquefaction occurred below GL- 15 m. At GL- 5 m, the horizontal response acceleration decreased after 60s, so we reason that liquefaction occurred between GL- 5 m and GL- 15 m.

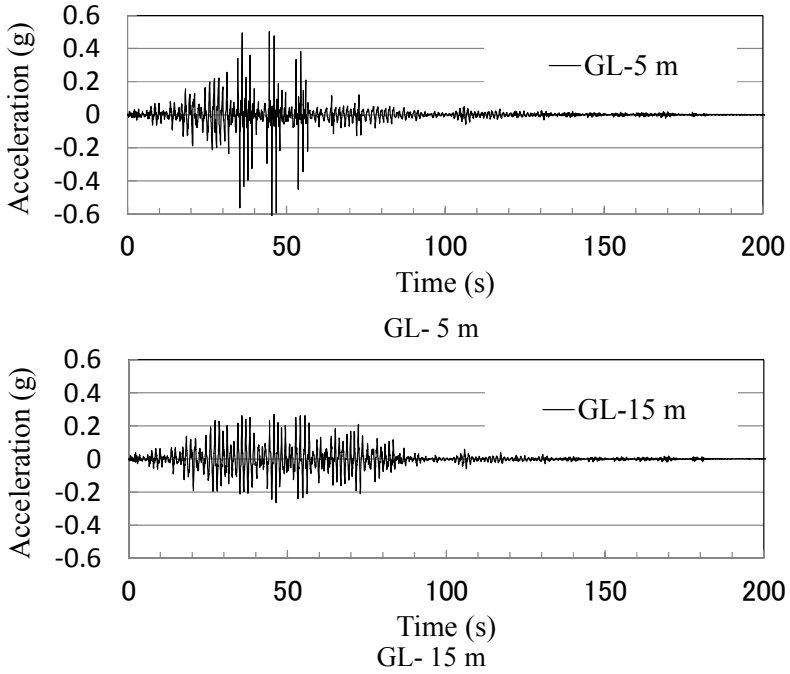


Fig. 7. Time histories of horizontal response acceleration; Line-G (see Fig. 2) without countermeasures (Case-1).

Figure 8 shows time histories of horizontal response acceleration measured below container center (Line-H in Fig. 2) with FGFSI with the 6 m grid. At GL- 15 m, the horizontal response acceleration was almost the same as that without countermeasures, so we reason that no liquefaction occurred below GL- 15 m. However, at GL- 5 m, the horizontal response acceleration was lower than the input motion. Hence, the FGFSI could not stop liquefaction occurring between GL- 5m and GL- 15 m.

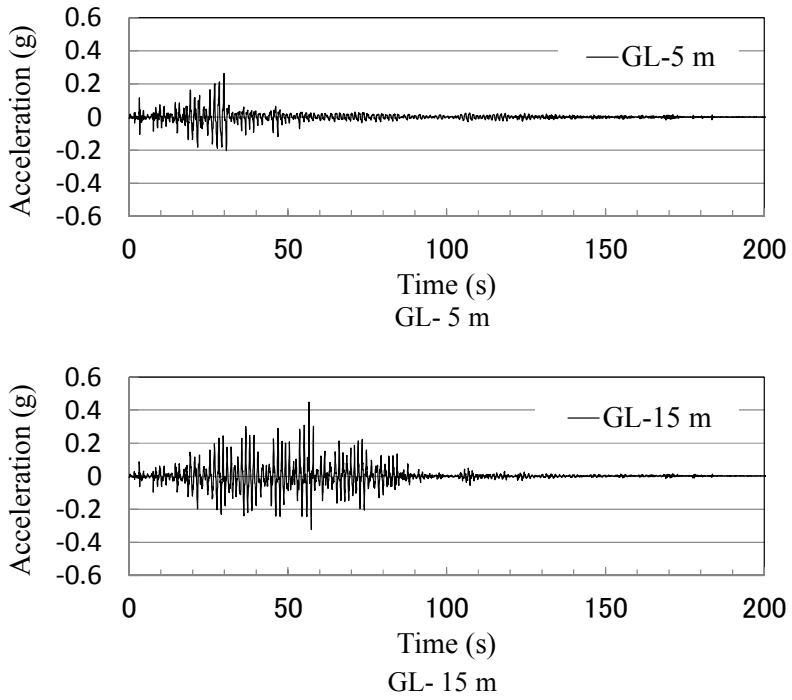
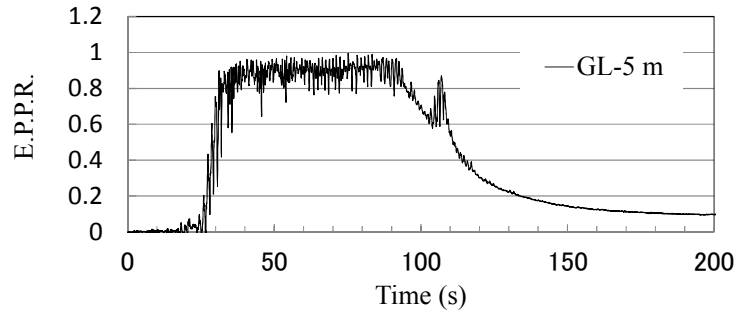


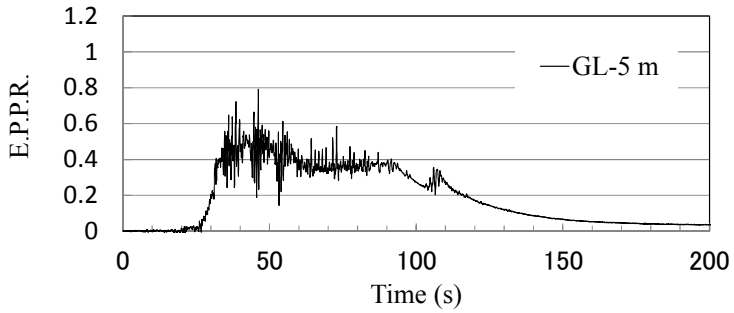
Fig. 8. Time histories of horizontal response acceleration; Line-H (see Fig. 2) with FGFSI (Case-2) with 6 m grid.

(3) EXAMINATION OF EXCESS PORE PRESSURE

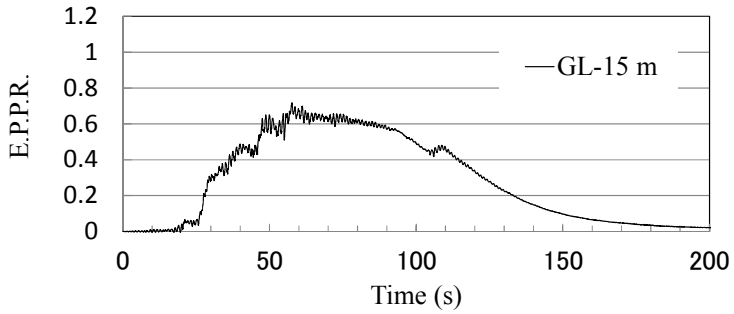
Figure 9 shows time histories of EPP ratio obtained without countermeasures at measurement points in the free-field (Line-I in Fig. 2) and below container center (Line-G in Fig. 2). The vertical effective stress, which is used to calculate EPP ratio below container center, includes the contact pressure of the container. At GL- 5 m in the free field, EPP started to accumulate after roughly 25 s, and liquefaction occurred after 30 s because the EPP reached 1.0. By contrast, at GL- 5 m and GL- 15 m below container center, the maximum EPP ratios were 0.79 and 0.72, respectively. Figure 10 shows distributions of maximum EPP ratio with depth measured in the free field and below container center. The horizontal response acceleration at GL- 5 m below container center was small because the liquefaction that occurred around the container attenuated the input motion.



Free field GL- 5 m (Line-I)



GL- 5 m (below center container, Line-G)



GL- 15 m (below center container, Line-G)

Fig. 9. Time histories of excess pore pressure ratio; without countermeasures (Case-1).

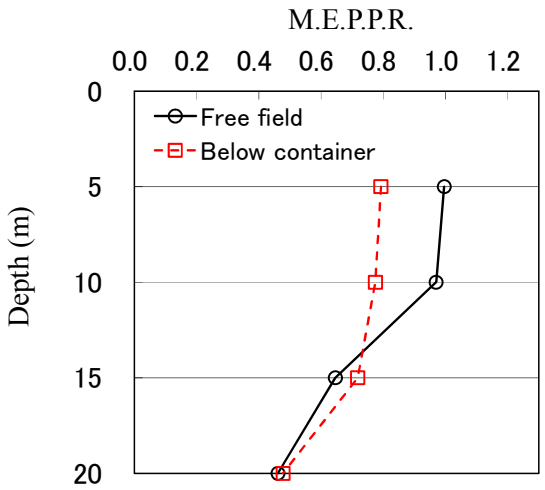
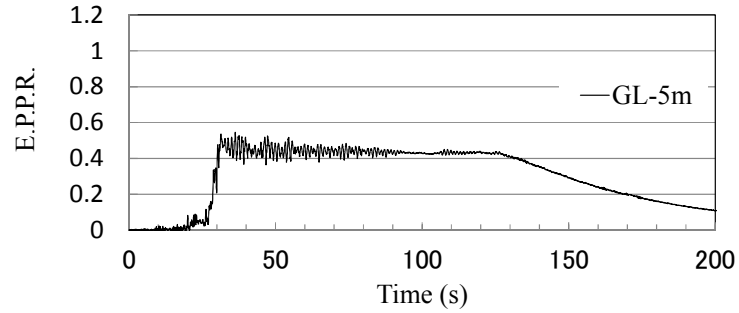
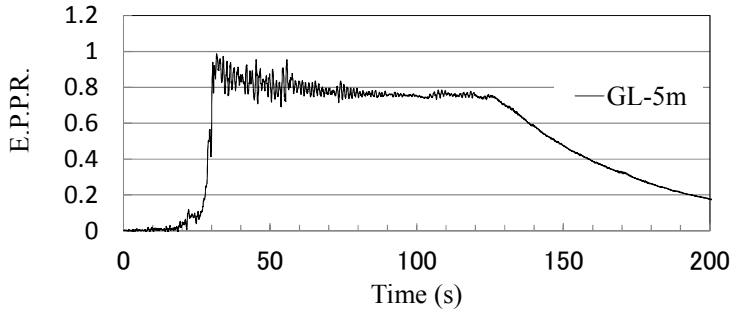


Fig. 10. Distributions of maximum of excess pore pressure ratio with depth; without countermeasures (Case-1).

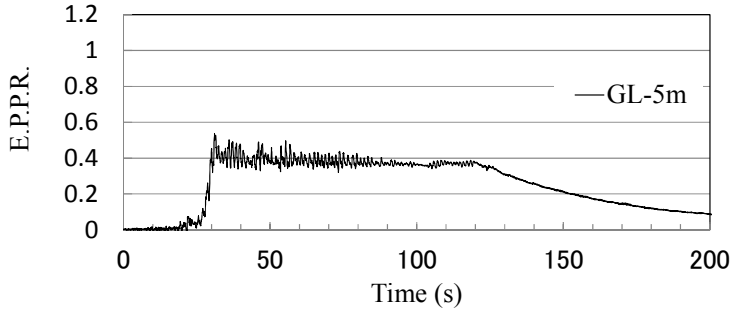
Figure 11 shows time histories of EPP ratio obtained the FGFSI. In the case of the 6 m grid, we compared between Line-H (vertical effective stress with container contact pressure) and Line-J (vertical effective stress with container contact pressure) and Line-J (vertical effective stress without container contact pressure). The maximum EPP ratio on Line-H was 0.55; we reason that the container center contact pressure prevented liquefaction. In contrast, the maximum EPP ratio obtained on Line-J was 0.99; we reason that liquefaction occurred despite the narrow 6 m grid-wall spacing. In the case of the 12 m grid, the maximum EPP ratio obtained on Line-K below the container was 0.54; we reason that no liquefaction occurred FGFSI because it was mitigated by the vertical effective stress augmented by container contact pressure.



Below container with 6 m grid GL- 5 m (Line-H)



Side of container with 6 m grid GL- 5 m (Line-J)



Below container with 12 m grid GL- 5 m (Line-K)

Fig. 11. Time histories of EPPR; with FGFSI (Case-2).

Figure 12 shows the distributions of maximum EPP ratio with depth below container center along Line-H (6 m grid) and Line-K (12 m grid). For both the 6 and 12 m grids, the maximum EPP ratio was small at GL- 5 m and did not 1.0 below GL- 10 m. Although there was little difference between the distributions for the 6 and 12 m grid, the container settlement with the 12 m grid was larger than that with the 6 m grid. This difference in container settlement can be explained as follows. As shown in Fig. 2, container was supported more by the 6 m grid than by the 12 m grid. Within the 12 m grid, liquefaction occurred where the container was unsupported not where it was supported. Consequently, there was a difference in subsidence between the 6 and 12 m grids; the larger subsidence with the 12 m grid caused larger settlement of container.

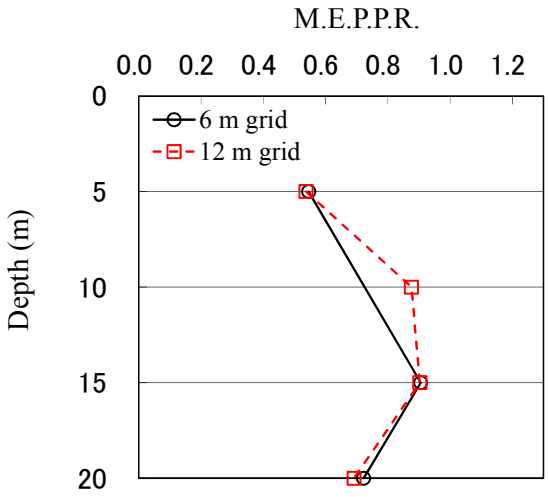


Fig. 12. Distributions of MEPPR with depth; with FGFSI (Case-2).

CONCLUSIONS

1. Without countermeasures, the container settlement was larger than that of the free field.
2. For FGFSI with 5 m high grid walls, the difference in settlement between the container and the free field was smaller than that without countermeasures. The FGFSI was able to mitigate the subsidence of the container.
3. In the FGFSI, having less space between the grid walls resulted in less container settlement.

References

Cooperative Research Reports of PWRI, 1999. Design and Construction Manual of Countermeasures Against Liquefaction, Vol. 186 (in Japanese).

Suzuki, Y., Saito, S., Onimaru, S., Kimura, T., Uchida, A. and Okumura, R., 1996. Grid-shaped stabilized ground improved by deep cement mixing method against liquefaction for a building foundation, Tsuchi-to-Kiso, JGS, Vol. 43, No. 3, pp. 46-49 (in Japanese).

Uchida, A., Yamashita, K., Odajima, N., 2012. Performance of Piled Raft Foundation with Grid-Form Ground Improvement During the 2011 off the Pacific Coast of Tohoku Earthquake, Journal of Disaster Research Vol.7 No.6, pp.726-732.

STRENGTH DESIGN OF CEMENT-TREATED PILES SUBJECTED TO LATERAL FLOW OF LIQUEFIED GROUND

H. Takahashi, Port and Airport Research Institute, Yokosuka, Japan, takahashi-h@pari.go.jp
W. Tsuda, Sumitomo Mitsui Construction Co., Tokyo, Japan, wakakitsuda@smcon.co.jp
N. Takahashi, Sumitomo Mitsui Construction Co., Nagareyama, Japan, tnaoki@smcon.co.jp
M. Fuchiyama, Sumitomo Mitsui Construction Co., Nagareyama, Japan, m-fuchiyama@smcon.co.jp
Y. Morikawa, Port and Airport Research Institute, Yokosuka, Japan, morikawa@pari.go.jp
I. Towhata, Kanto Gakuin University, Yokohama, Japan, towhata.ikuo.ikuo@gmail.com

ABSTRACT

The lateral flow of the ground due to liquefaction has caused severe damage to many varieties of facility. In past papers, the authors proposed a pile-type improvement method applying a new pile arrangement, wherein deep mixing piles were arranged with being shifted to prevent the lateral flow of liquefied ground in all directions. Additionally, the tops of the piles were connected by stabilised shallow ground. This method allows liquefaction, but the piles decrease the amount of lateral flow, and the stabilised shallow ground can be used immediately after the earthquake. However, the efficacy for ground behind quay walls has not been examined. In this study, the method's efficacy behind quay walls was examined and the design method of the cement-treated piles was discussed. Centrifuge model tests showed that the lateral flow was dramatically restricted in the improved area, and the settlement of the ground surface could be reduced. The moments in the tests were significantly smaller than those of the proposed method for all piles and periods. It could be said that the proposed method calculates a safety-side moment. Although the strengths in the model were rather smaller than those of the proposed design, the cement-treated soil had no failures.

Keywords: lateral flow, liquefaction, pile improvement, quay wall, strength design

INTRODUCTION

In past huge earthquakes, the lateral flow of the ground due to liquefaction has caused severe damage to many varieties of facility. The most effective countermeasure is to completely prevent the liquefaction itself; however, this requires an extensive budget, especially to improve a large area. The concepts of liquefaction allowance and damage reduction might be suitable for a liquefaction countermeasure. The authors (Takahashi et al., 2013) proposed a pile-type improvement method applying a new pile arrangement, wherein deep mixing piles were arranged with being shifted to prevent the lateral flow of liquefied ground in all directions (Fig. 1). Additionally, the tops of the piles were connected by stabilised shallow ground. The piles can resist the horizontal force of the lateral flow because their bottoms and tops are sustained by the bottom layer and the stabilised ground, respectively. This method allows liquefaction, but the piles can decrease the amount of lateral flow,

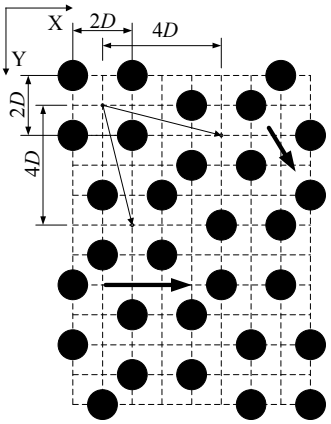


Fig. 1. Proposed pile arrangement to prevent lateral flow in all directions

© 2018 Deep Foundations Institute

and the stabilised shallow ground can be used immediately after the earthquake. The efficacy of this method was demonstrated by the authors, based on numerical analyses and model tests in gravitational and centrifugal fields (Morikawa et al., 2014; Takahashi et al., 2016). However, these studies focused only on improvements for sloped ground; their efficacy for ground behind quay walls has not yet been examined.

In this study, the efficacy of the pile-type improvement is examined for ground behind quay walls with the help of centrifuge model tests. Additionally, a design method for cement-treated piles is discussed, based on measured bending moments using acrylic pipes. A model test using cement-treated soil for piles and shallow ground was also conducted to verify the strength design. In centrifuge model tests, the lateral flow of the ground was generated by shaking and liquefying the model ground, and inclining the sheet-pile quay walls. It should be noted here that this improvement is not intended to enhance the stability of the quay walls. The objectives of the improvement are to reduce the amount of lateral flow and secure the ground surface, even if the ground is liquefied.

CENTRIFUGE MODEL TEST PREPARATION

Model ground

The machine used in the study was a PARI Mark II centrifuge, developed by the Port and Airport Research Institute (Kitazume & Miyajima, 1995). The size reduction ratio was 1/50, so that the centrifugal acceleration was 50 *g*. Table 1 lists the test cases in a prototype scale: unimproved without piles (Case UN), improved with acrylic piles and board (Case I2d-a), and improved with cement-treated soil (Case I2d-c). Figure 2 shows the cross-sectional schematic views of Cases I2d-a and I2d-c, including the sensor arrangement. First, a stainless-steel board simulating the sheet piles was placed on the bottom of a container, but not fixed there. Then, sandy ground was manufactured using a sand-raining technique in the air (e.g., Takahashi et al., 2006). The bottom layer of the model ground was 85-mm thick, and its material and relative density were Iide sand No. 7 (D_{50} = 0.17 mm and Uc = 1.5) and approximately 90%, respectively. After embedding piles into the bottom layer, the backfill ground was manufactured. The piles were placed apart from the board not to affect the displacement of the quay walls. The backfill ground was a liquefiable layer 195 mm thick. The sand material was Soma sand No. 5 (D_{50} = 0.35 mm and Uc = 1.6), and the relative density was approximately 50%. The stainless-steel board was attached to the container support during the backfill-ground preparation in order not to disturb the ground.

Table 1. Test cases

Case	Pile	Distance of piles	Measured acceleration of main shaking	Period of main shaking
UN	Nil	–	1.86 m/s^2	25 s
I2d-a	Acrylic pipe	4 m (2D) *	1.60 m/s^2	25 s
I2d-c	Cement-treated soil	4 m (2D) *	1.71 m/s^2	25 s

* D is diameter of a pile

Model piles

In Case I2d-a, acrylic pipes were used to improve the ground instead of cement-treated piles. This enabled the measurement of the bending moments of the pipes subjected to a horizontal force induced by the lateral flow. The outer and inner diameters were 40 mm and 28 mm, respectively. The outer diameter corresponded to 2 m in a prototype scale. The mean density of the pipe was adjusted to become the same as cement-treated soil by filling it with silicon and steel bars. Strain gauges for measuring the strains were affixed to the pipe surfaces at positions P1, P2, and P3 (Fig. 2). The bottom of a pipe was embedded into the bottom layer to the depth of a diameter; the top of the pipe was fixed

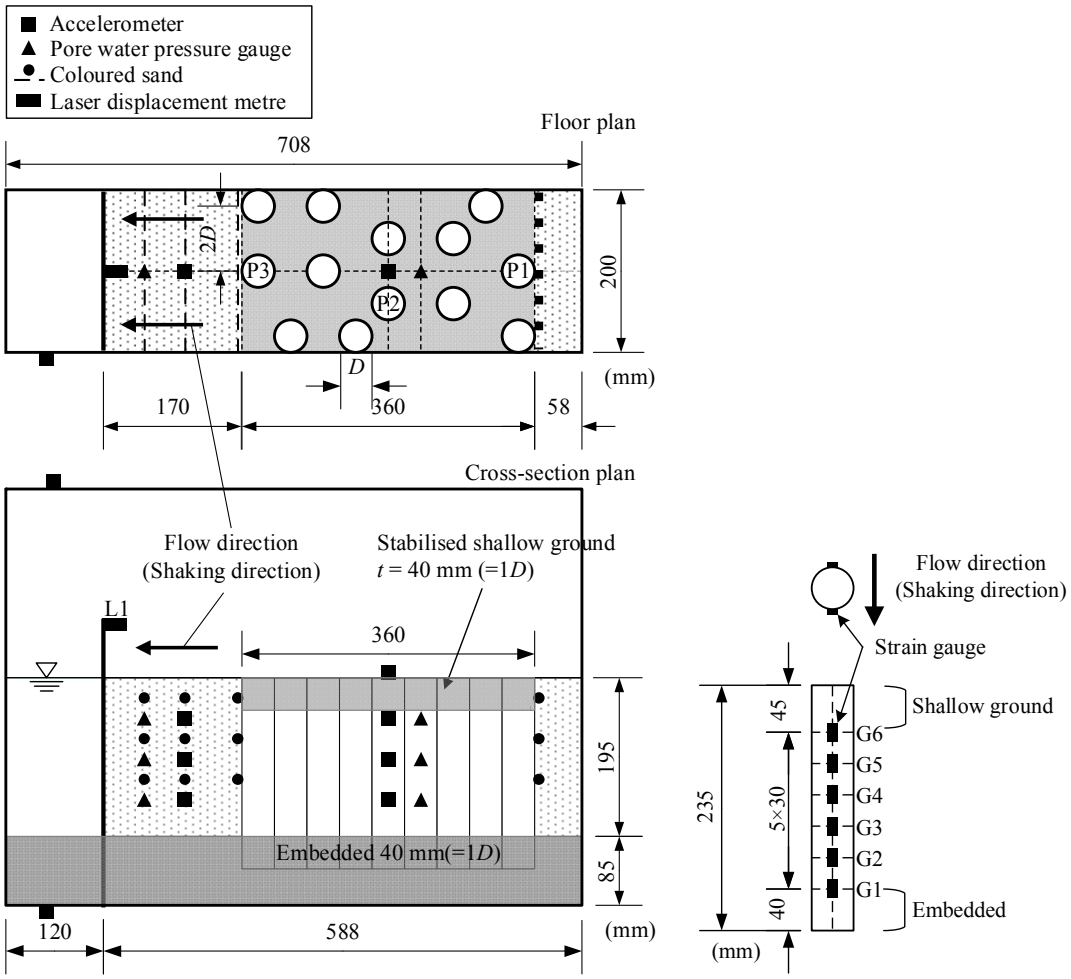


Fig. 2. Cross-sectional schematic view of models

to the shallow ground with an adhesion bond. The stabilised shallow ground was modelled by piling stainless-steel and acrylic boards, which were bundled with the help of epoxy resin. The density was almost the same as cement-treated soil, and the thickness was set to 40 mm, in accordance with the diameter of a pipe, corresponding to 2 m in a prototype scale.

In Case I2d-c, cement-treated soil was used to model the piles. The diameter was also 40 mm. Each pile contained a carbon rod with a 3-mm diameter, referring to Kitazume & Maruyama (2007). An electric current flows through the rod during the test, and is interrupted if the treated pile breaks. This helps detect pile breakage. Piles were embedded into the bottom layer, and their tops were fixed to the shallow ground. The shallow ground was also stabilised by cement. Figure 3 shows a model of the piles and stabilised shallow ground. Forty-mm-diameter piles were inserted into 50-mm-diameter holes in the stabilised shallow ground. The gap between the pile and the hole was filled with epoxy resin. The unconfined compressive strength of the treated cement was determined by the measured data and the design method proposed by Morikawa et al. (2014). In this method, a horizontal force induced by the lateral flow was first assumed to be 30% of the total overburden pressure. Next, the external and internal stabilities of the cement-treated soil were examined using the assumed horizontal force. The external stability assessment consists of sliding and overturning the treated soils, and bearing capacity failure of the bottom layer; the internal stability assessment consists of bending, shear, and compression failures of the piles, and bending and shear failures of the stabilised shallow ground. The top and bottom of a pile were movable and hinged supports, respectively.

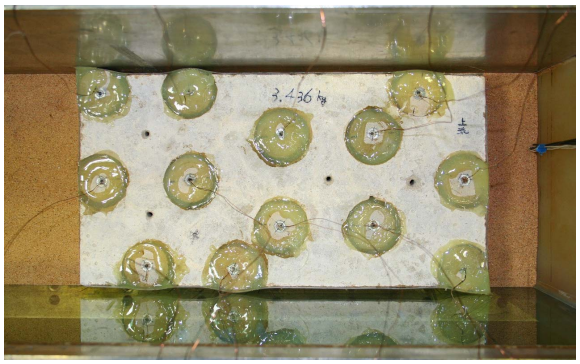


Fig. 3. Model piles and stabilised shallow ground

Pore fluid and test method

To equalise the similitude time ratios regarding the dynamic behaviours and the percolation of the pore fluid, a viscous fluid is often used in a centrifuge model test. The viscosity slows the fluid current and liquefies loose sandy ground. Viscous fluid was also used in the present tests, and 50-times viscosity was made by adding water-soluble cellulose ether into de-aired water. Viscous fluid was percolated from the bottom of the ground under a centrifugal acceleration of 30 *g*. The percolation under centrifugal acceleration can produce highly saturated ground (Okamura & Inoue, 2012). The model ground was fully submerged.

After the percolating fluid, the centrifugal acceleration was increased to 50 *g*, and the model ground was shaken by a shaking table. The target frequency and acceleration of the input wave were 2 Hz and 2.0 m/s^2 in a prototype scale. The shaking consisted of two periods: main and subsequent. The period of each shaking was 25 s, and the magnitude of the subsequent shaking was one-third of the main shaking. Table 1 includes the acceleration measured at the shaking table. The response acceleration and pore-water pressure were measured by sensors embedded in the ground, and the ground displacement was examined after the shaking test by observing coloured sand embedded in the ground.

EFFECT OF IMPROVEMENT ON THE DISPLACEMENT

Before examining the effect of the improvement on the displacement, the full liquefaction of the ground was first confirmed. Figure 4 shows the time histories of the excess pore-water pressure ratio in a prototype scale. The ratio reached 1.0 in all test cases; thus, it could be confirmed that the ground was fully liquefied. Figure 5 shows the displacement time histories at the top of the steel board in a prototype scale. As shown in the figure, the magnitudes of the maximum displacement of all test cases were almost similar. This was because the board was sufficiently separated from the improvement area. The fluctuation after shaking would be caused by a swing of the liquefied ground.

Figures 6 and 7 show the horizontal displacement at a depth of 1.25 m and the settlement of the ground surface, respectively. The distribution of the horizontal displacement was measured by coloured sand bars embedded in the ground. The displacement of Case I2d-a was not measured because it would be almost the same as that of Case I2d-c. As shown in Fig. 6, the horizontal displacement of Case I2d-c was significantly smaller than that of Case UN. Even at the downstream end, the displacement of Case I2d-c was 23% of that of Case UN. The lateral flow was dramatically reduced by enhancing the ground. Figure 7 indicates that the settlements of Cases UN and I2d-c in the improvement area were 0.4 and 0.0 m, respectively. The settlement could also be reduced. Thus, the efficacy of the improvement was verified. The point is that the stabilised shallow ground will not be displaced vertically, owing to the piles sustaining it, if a gap occurs between the shallow and sandy ground. The ground surface can be used immediately after the earthquake. This gap, however, was not observed in the present model tests. Moreover, the settlement of Case I2d-c was larger than that of

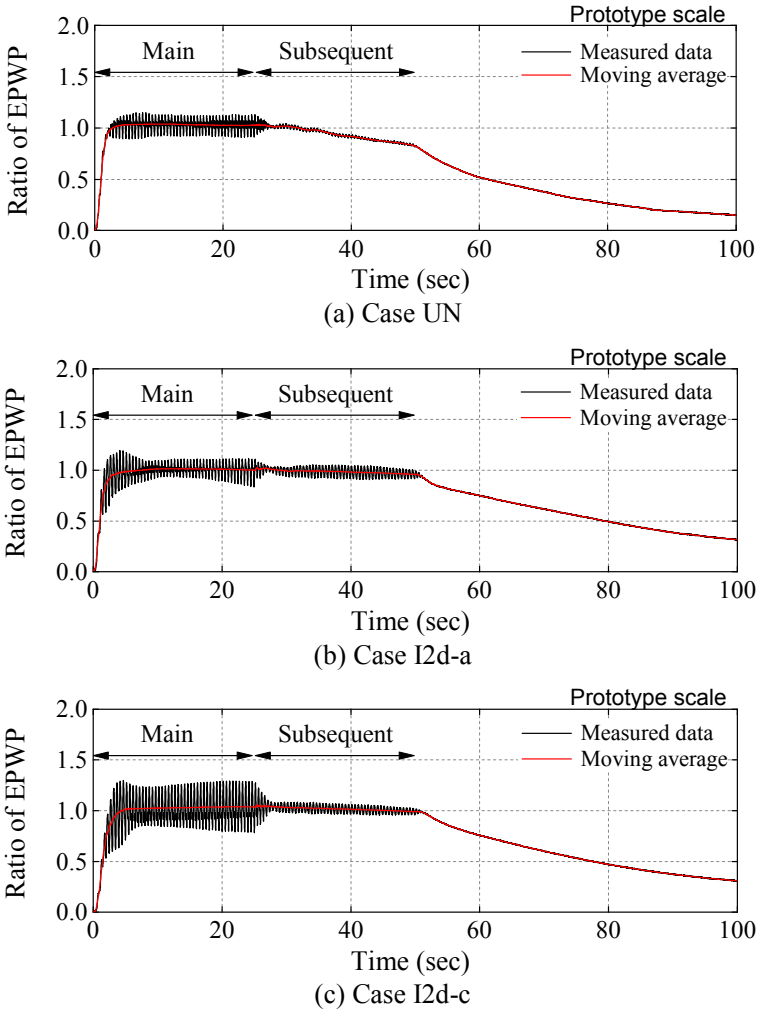


Fig. 4. Time histories of excess pore water pressure ratio (EPWP)

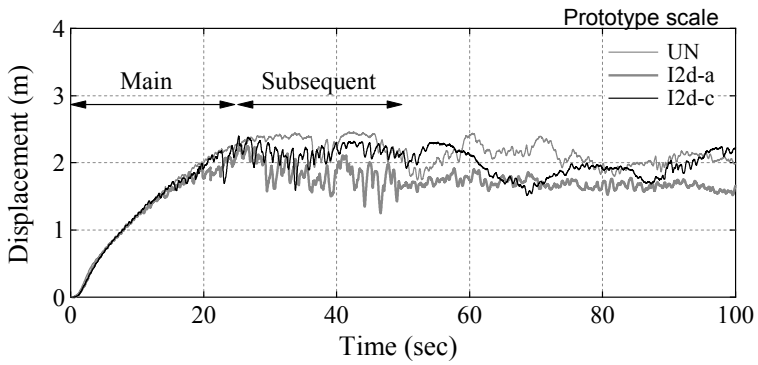


Fig. 5. Time histories of displacement at the top of sheet pile

Case UN in the downstream area outside the improvement area. This is because no lateral flow occurred from the improvement area to the downstream area.

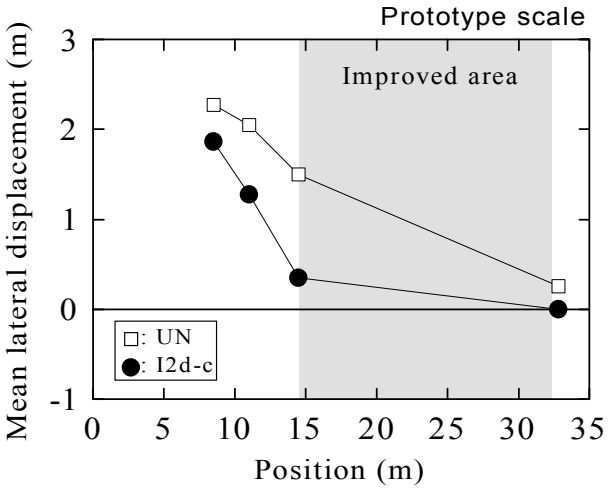


Fig. 6. Horizontal displacement at depth of 1.25m

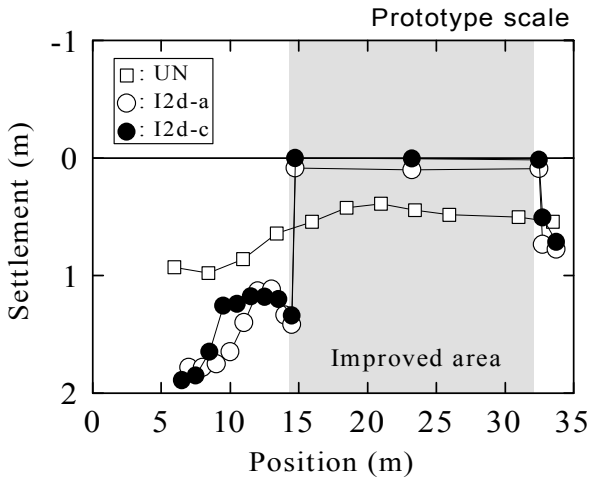


Fig. 7. Settlements of ground surface

DISCUSSION OF PILE STRENGTH DESIGN

Figure 8 shows the time histories of the bending moments obtained at the positions showing the maximum values. The pile strains were measured in Case I2d-a by using acrylic pipes P1–P3. The bending moments were calculated by multiplying the measured strains, section modulus, and elastic modulus. The positive moment represents the bending of a pile wherein the upstream side of the pile extends. During the main shaking, the moment fluctuated between the positive and negative sides. The absolute value of the peak moment of the negative side was larger than that of the positive side; the bending appeared to extend the downstream side of the pile. This would be due to a downstream horizontal force induced by the lateral flow. The negative moment remained even after subsequent shaking in piles P1 and P3, which were located on the upstream and downstream edges, respectively. In contrast, the moment did not remain in pile P2, which was located in the centre of the improvement area. This indicated that the bottom of P2 moved or the stabilised shallow ground was deformed. The reason is unclear at the present stage, but pile crowding around P2 might affect the result.

Figure 9 shows the depth distributions of the bending moment in a cycle around the time when the absolute value of the bending moment became a maximum. The discrete moments were interpolated using the cubic smoothing spline method. The figure includes the bending moment that was calculated by the proposed method (Morikawa et al., 2014). As mentioned previously, the horizontal force induced by the lateral flow was assumed to be 30% of the total overburden pressure, and the top and

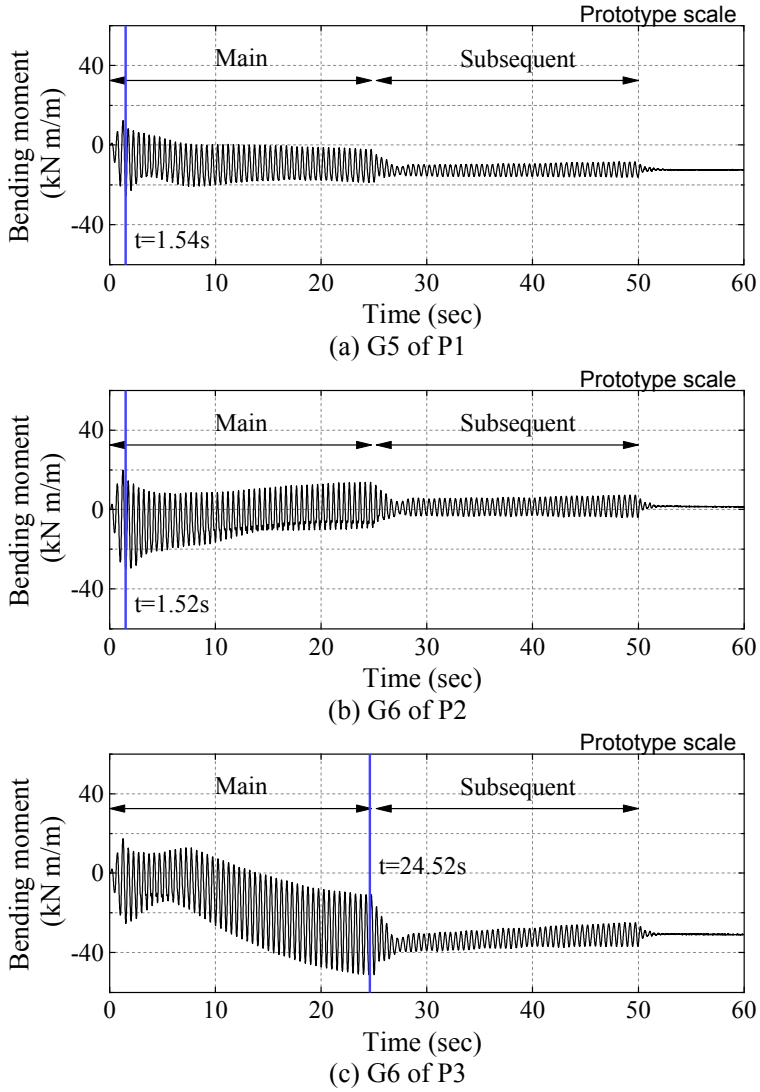
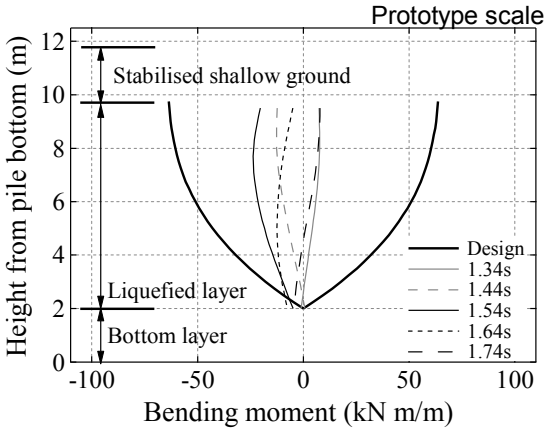


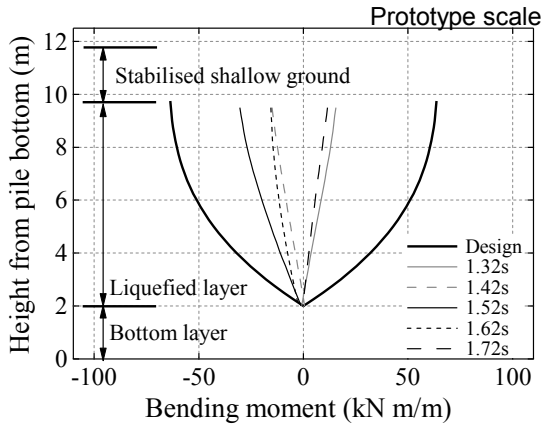
Fig. 8. Time histories of bending moment of piles

bottom of the pile were movable and hinged supports, respectively. The figure demonstrates that the moments in the tests were significantly smaller than those of the proposed method for all piles and periods. It could be said that the proposed method calculates a safety-side moment. However, the proposed method does not consider the inertial force of the pile itself. It should be noted that the moment might exceed the value calculated by the proposed method, if the weights of the piles and the stabilised shallow ground are sufficiently large.

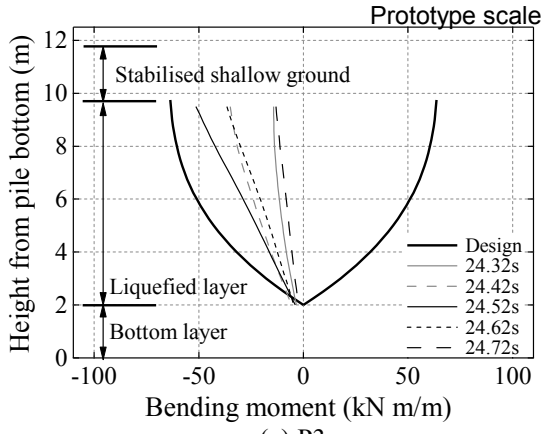
In Case I2d-c, cement-treated soil was used to model the piles and shallow ground. The unconfined compressive strengths required for the pile and shallow ground were 7.4 MPa and 2.2 MPa in the proposed design, respectively; the strengths of the pile and shallow ground used in the model were 6.1 MPa and 2.0 MPa, respectively. The reason why they were set to be small was that the strengths estimated by the moments in Case I2d-a were smaller than those in the proposed design. The estimated strengths were 6.7 MPa and 2.0 MPa. In the present study, the soundness of piles was evaluated in a severe condition. Although the strengths in the model were rather small, the cement-treated soil had no failures, according to visual observations and the electric conduction in the carbon rods embedded in the piles. Thus, the efficacy of the strength design could be verified. However, the strength obtained by the proposed design will have a margin for failure, and the required strength is considerably high, considering the general strength in a real execution. A more reasonable design is needed in the future.



(a) P1



(b) P2



(c) P3

Fig. 9. Depth distribution of bending moment

CONCLUSIONS

In this study, the efficacy of a pile-type improvement was examined for the ground behind quay walls. Additionally, a design method for cement-treated piles was discussed, based on the measured bending moments using acrylic pipes. A model test using cement-treated soil for piles and shallow ground was also conducted to verify the strength design. The results can be summarised as follows:

1) In centrifuge model tests, the lateral flow of the ground was generated by shaking and liquefying the model ground, and inclining the sheet-pile quay walls. The test results showed that the lateral flow was dramatically restricted in the improvement area, and the settlement of the ground surface could be reduced.

2) In the proposed design, the horizontal force induced by the lateral flow was assumed to be 30% of the total overburden pressure, and the top and bottom of a pile were movable and hinged supports, respectively. The moments in the tests were significantly smaller than those of the proposed method for all piles and periods. It could be said that the proposed method calculates a safety-side moment.

3) Although the strengths in the model were rather smaller than those of the proposed design, the cement-treated soil had no failures. Thus, the efficacy of the strength design could be verified. However, a more reasonable design is needed in the future.

REFERENCES

Kitazume, M. and Maruyama, K. 2007. Internal stability of group column type deep mixing improved ground under embankment loading. Soils and Foundations, 47(3) 437-455.

Morikawa, Y., Takahashi, H., Tsuda, W., Takahashi, N., Tomura, G., and Towhata, I. 2016. Development of countermeasure method using pile-type stabilization against lateral flow due to liquefaction. Technical Note of the Port and Airport Research Institute, No. 1326, 54 p. (in Japanese)

Morikawa, Y., Takahashi, N., Tsuda, W., Towhata, I., Takahashi, H., Sassa, S., and Kohama, E. 2014. Dynamic centrifuge test on the reduction of lateral flow of liquefied ground by column type stabilization. Proceedings of International Conference on Piling and Deep Foundations, Stockholm, May 21-23, pp. 203-712.

Okamura, M. and Inoue, T. 2012. Preparation of fully saturated models for liquefaction study. International Journal of Physical Modelling in Geotechnics, 12(Issue 1) 39-46.

Takahashi, H., Kitazume, M., Ishibashi, S., and Yamawaki, S. 2006. Evaluating the saturation of model ground by P-wave velocity and modelling of models for a liquefaction study. International Journal of Physical Modelling in Geotechnics, 6(Issue 1) 13-25.

Takahashi, H., Takahashi, N., Morikawa,Y., Towhata, I. and Takano, D. 2016. Efficacy of pile-type improvement against lateral flow of liquefied ground. Geotechnique, 66(Issue 8) 617-626.

Takahashi, N., Derakhshani, A., Rasouli, R., Towhata, I., and Yamada, S. 2013. Shaking model tests on mitigation of liquefaction-induced ground flow by new configuration of embedded columns. Proceedings of the 18th International Conference on Soil Mechanics and Geotechnical Engineering, Paris, September 2-6, pp. 1623-1626.

TESTING AND EVALUATION OF RESIDUES AS A BINDER COMPOENT FOR DEEP MIXING AND JET GROUTING

Per Lindh, Swedish Geotechnical Institute, SGI, per.lindh@swedgeo.se

Håkan Eriksson, Geomind, hakan.eriksson@geomind.se

ABSTRACT

ABSTRACT

The Ports of Stockholm is building a new port for rolling goods and container traffic. The Stockholm Norvik Port will open in 2020 and is will be the Baltic Sea freight of the future. The new area was a bay that was filled with crushed bedrock in the 1980s. During the construction two large volumes of approximately 300 000 m^3 of very soft clay was trapped inside the fill. Due to the procedure for placing the fill, two thirds of the clay were covered with crushed rock whereas for the remaining part the clay reached the surface. To improve the shear strength of the clay two different improvement techniques were employed. In the case with very soft clay all the way up to the surface, deep mixing was applied and in areas were the clay was superimposed with crushed rock, jet grouting was used. In the deep mixing area, the columns were 800 mm in diameter and the total area ratio was 70 %. The total length of the columns were approximately 200 000 meters. The jet grouting was designed with a diameter of 1.5 meter and a spacing of 2.5 meters and a total length of 40 000 meters. The main goal was to find a cost efficient and environmental friendly binder combination for deep mixing as well as for the jet grouting at The Stockholm Norvik Port.

Keywords: Deep mixing, jet grouting, residues binder

Deep Mixing and Jet grouting

This study consists of two parts with laboratory results from respective improvement method. The first part deals with deep mixing with the dry mixing technique and the second part deals with jet grouting. The two different improvement methods use dry respective wet methods and thereby differ in binder components and strength requirements.

Deep mixing

To evaluate the optimum binder combinations for the deep mixing a simplex lattice design for three binders was applied (Montgomery, 1996; Myers and Montgomery, 1995). For the deep mixing three different binder components were tested. These were cement, quick lime (Ql) and lime kiln dust (LKD). Three different binder amounts were tested, 80, 100 and 120 kg binder per cubic meter of clay. Since the reactivity of the three different binder components varied, the experiments were designed with a constrained boundary to maximize the LKD proportion to 50% of the total binder content, see Figure 1.

© 2018 Deep Foundations Institute

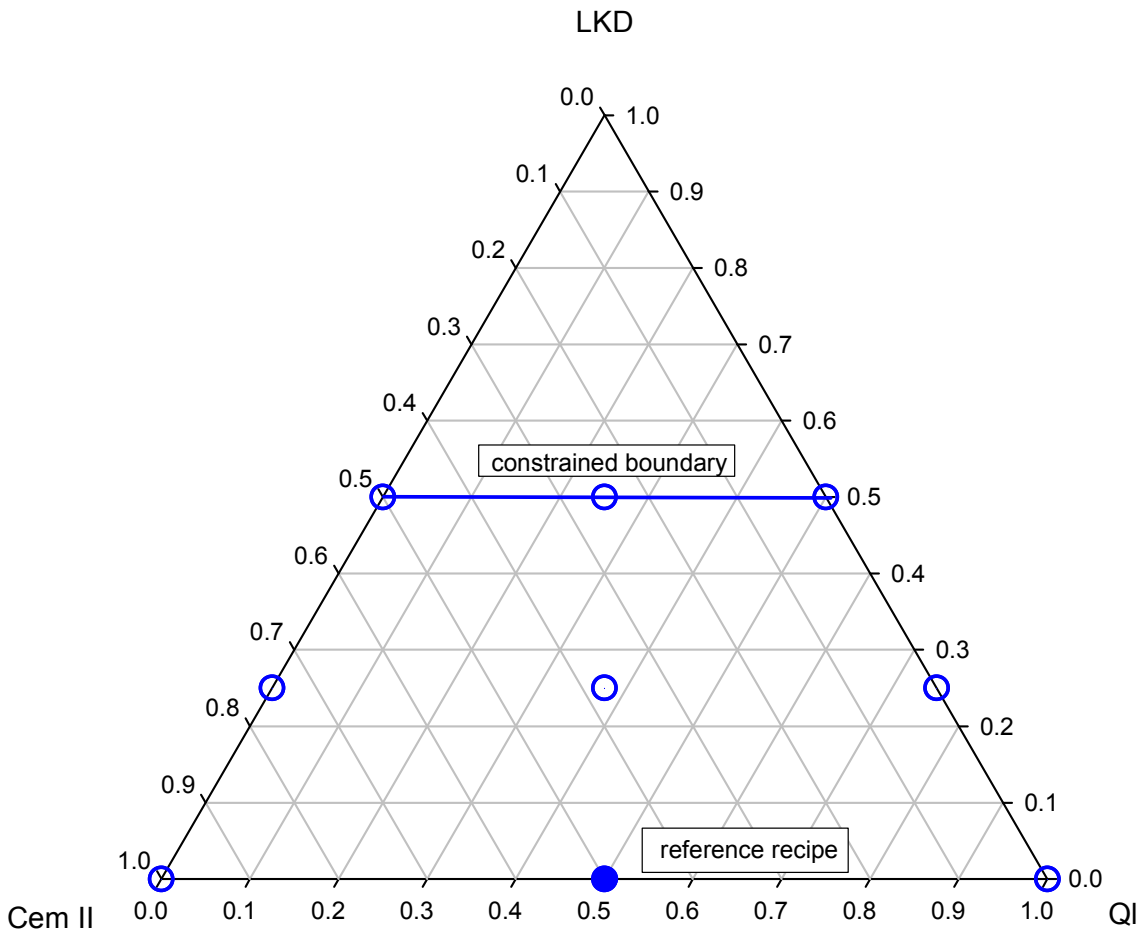


Figure 1. A constrained simplex design with a boundary that maximizes the LKD content to 50% of the mix. The filled blue circle represents a reference recipe consisting of 50% cement and 50% quick lime. This is a commonly used recipe for deep mixing in Sweden.

The ternary plot should be interpreted as an experimental surface where each point represents 100% of binder but the distribution of the binder components varies, e.g. in the left corner the binder consists of 100% cement and in the middle of the lower boundary, at the reference recipe, the blend consists of 50% cement and 50% quick lime.

Since there were three different binder amounts, three different simplex designs were performed. Each design consisted of nine different recipes with replicate sample which gives eighteen specimens plus two extra in the middle of the design. For each binder amount 18 samples were prepared except for the binder content of 100 kg where 32 samples were prepared.

After 28 days of curing in 7 ºC the samples were tested with free-free resonant column and then the shear strength was evaluated (Rydén *et al*; 2006). The free-free resonant column tests were performed to compare laboratory prepared specimens with in situ conditions. The shear strength from the UCS testing is presented in Figure 2, Figure 3 and Figure 4. In the header of the following figures the model and R-squared values is shown. Figure 3 is an augmented design and the response surface model is evaluated as a special cubic model. In the augmented design the nonlinear effects is more pronounced probably due to higher resolution in the design.

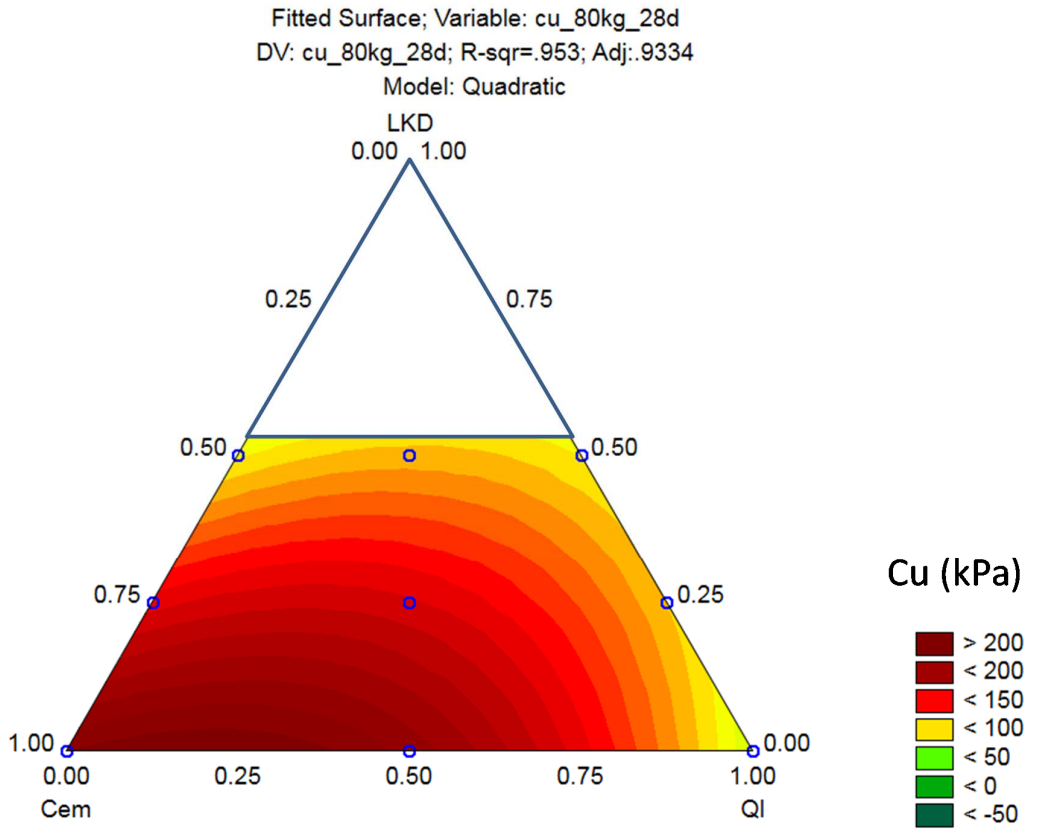


Figure 2. Graph showing the shear strength for different binder blends with a total of 80 kg of binder per cubic meter of clay. The samples were cured for 28 days at 7 °C. The results show that a combination of 80% cement and 20% lime gives the highest shear strength.

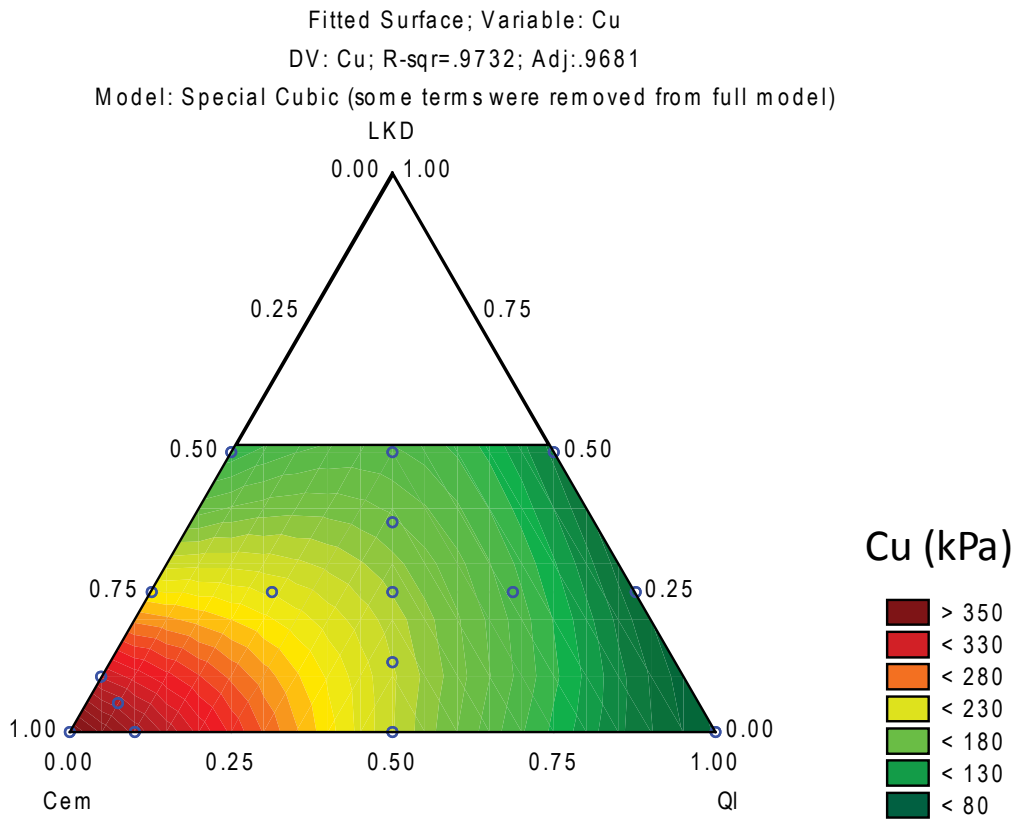


Figure 3. Graph showing the shear strength for different binder blends with a total of 100 kg of binder per cubic meter of clay. The samples were cured for 28 days at 7 °C. The results show that 100% cement gives the highest shear strength after 28 days. The design consists of some extra interior test points.

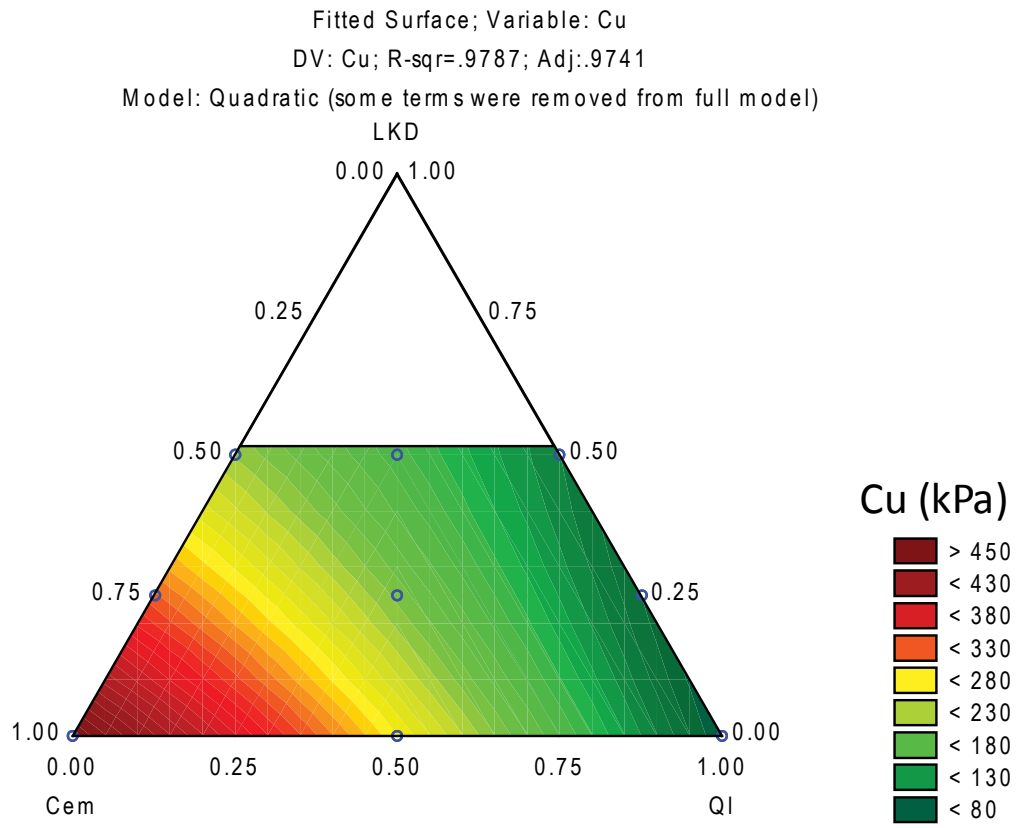


Figure 4. Graph showing the shear strength for different binder blends with a total of 120 kg of binder per cubic meter of clay. The samples were cured for 28 days at 7 °C. The results show that 100% cement gives the highest shear strength.

From Figure 2, 3 and 4 cement gives the highest shear strength. The limit value for the samples was a shear strength of minimum 200 kPa after 28 days of curing at 7 degrees Celsius. It is clear from the figures that the limit value is fulfilled for all samples stabilised with cement with 80, 100 and 120 kg of binder per cubic meter of clay. However, for higher binder content than 80 kg/m^3 of clay it could be seen that a large variety of binder combinations with cement, lime and LKD full fill the strength requirements and this gives the designer more freedom to choose a more environmental friendly alternative.

In this study, free- free resonant column technique was employed. The test method means that the specimen is placed on a soft foam and an accelerometer is attached to the specimen. Then the specimens eigenfrequency is measured and the P-wave velocity is calculated. The results from the free-free resonant column correlated to the shear strength test evaluated from UCS tests is shown in Figure 5. The figure shows a good correlation between P-wave and shear strength.

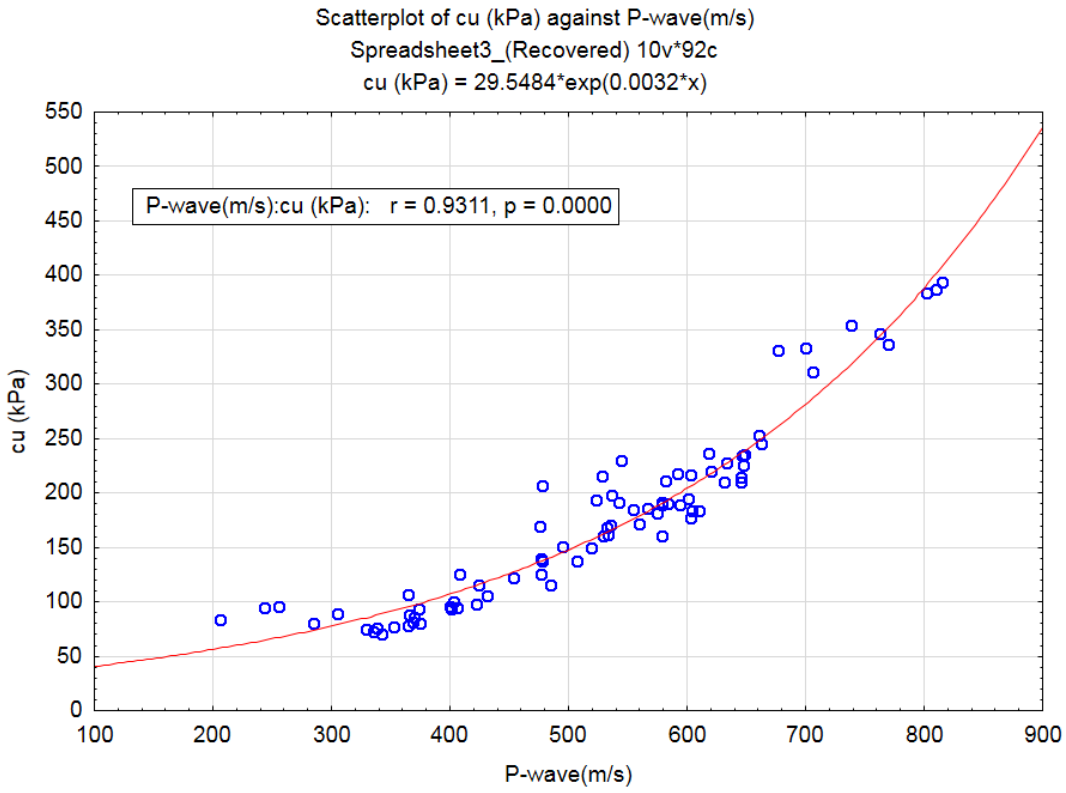


Figure 5. Graph showing the shear strength as a function of P-wave velocity for the deep mixing samples.

Jet grouting

The different binder components for the jet grout were, cement, cement kiln dust (CKD), LKD and lime stone filler. The jet grout recipes were tested with different clay contents. The clay contents were 0, 17, 37.5 and 58 % of clay in the mix, see Table 1.

Table 1. Tested binder combinations for jet grouting. Y= test performed

Recipe	Cement (%)	LKD (%)	CKD (%)	Water binder ratio	Clay content 0%	Clay content 17%	Clay content 37.5%	Clay content 58%
A	100			1.0	y	y	y	y
B	70	30		1.0	y	y	y	y
C	80		20	1.2	y	y	y	y

The limit value for the jet grouting recipe was an unconfined compression strength (UCS) of 3 MPa after 28 days of curing with a clay content of 58%. Due to higher binder content the exotherm reaction is higher and thereby the curing temperature was chosen to 20 °C The results from the strength testing is shown in Figure 6, Figure 7 and Figure 8.

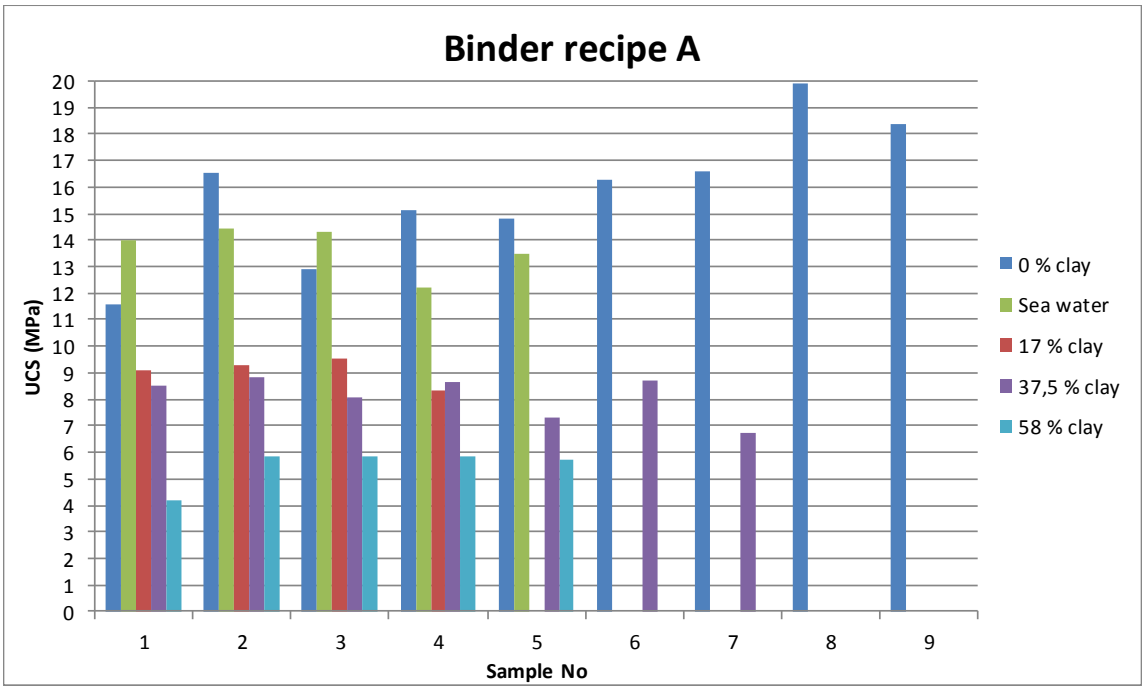


Figure 6. Graph showing the UCS strength for recipe A after 28 days of curing at 20 °C. In this combination, the recipe was also tested with sea water to ensure that there were no harmful components in the sea water.

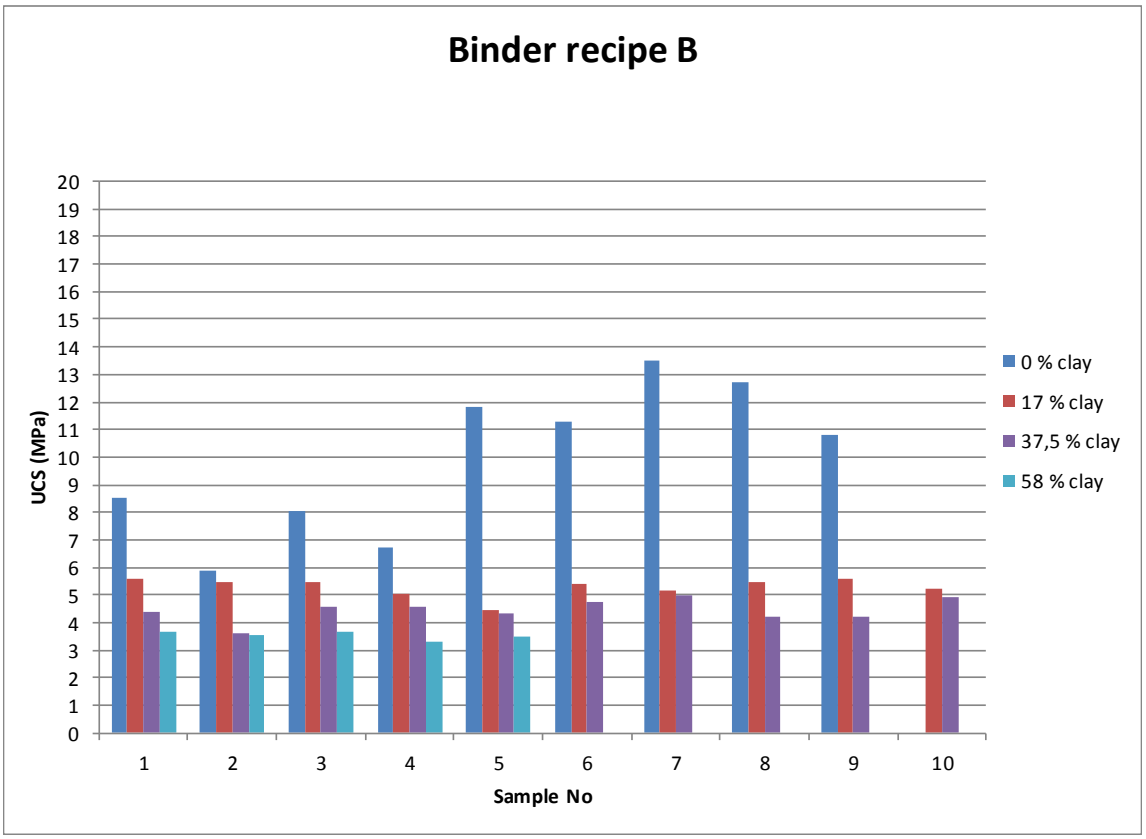


Figure 7. Graph showing the UCS strength for recipe B with 70% cement and 30% slag after 28 days of curing at 20 °C.

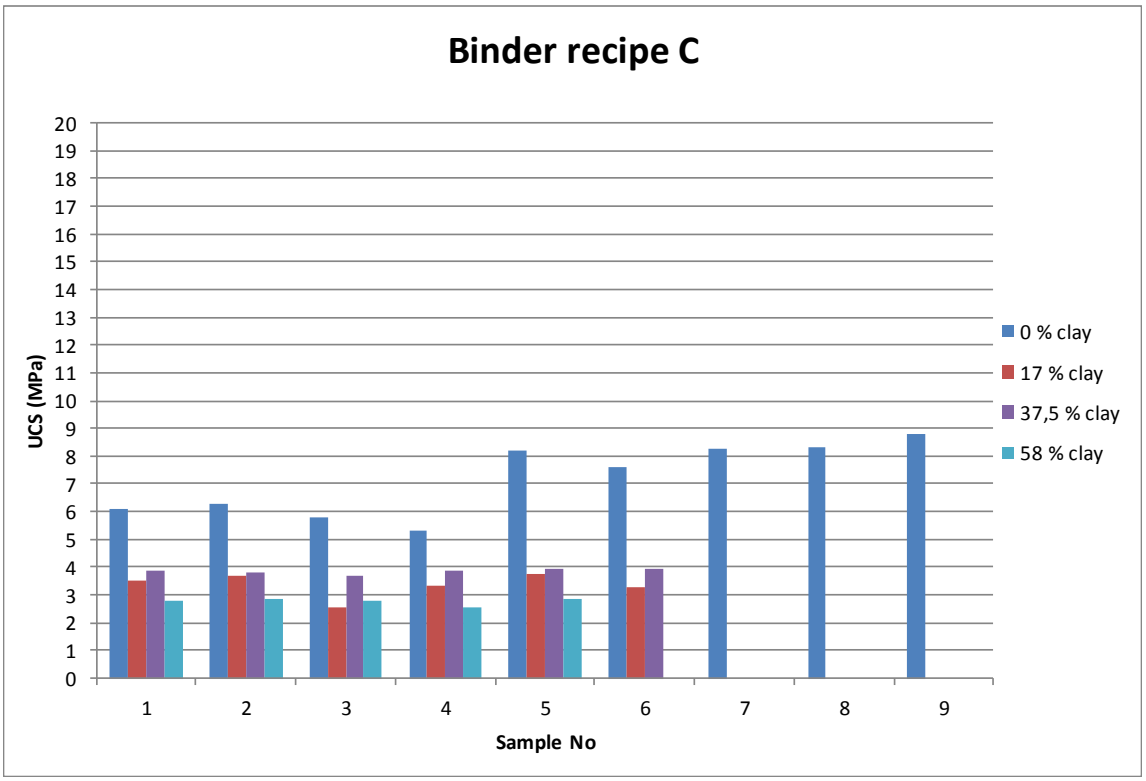


Figure 8. Graph showing the UCS strength for recipe C with 80% cement and 20% LKD after 28 days of curing at 20 °C.

The results show that the binder recipe A and B fulfill the limit value of 3 MPa with a clay content of 58%. The results for recipe C falls just below the limit value.

To validate the laboratory results, the samples with 58% clay content were measured with free-free resonant column test to follow the strength development during the curing period, see Figure 9. The results from the seismic testing could then be compared with results measured in situ. The results validate the shear strength results with the highest strength for recipe A followed by recipe B and C.

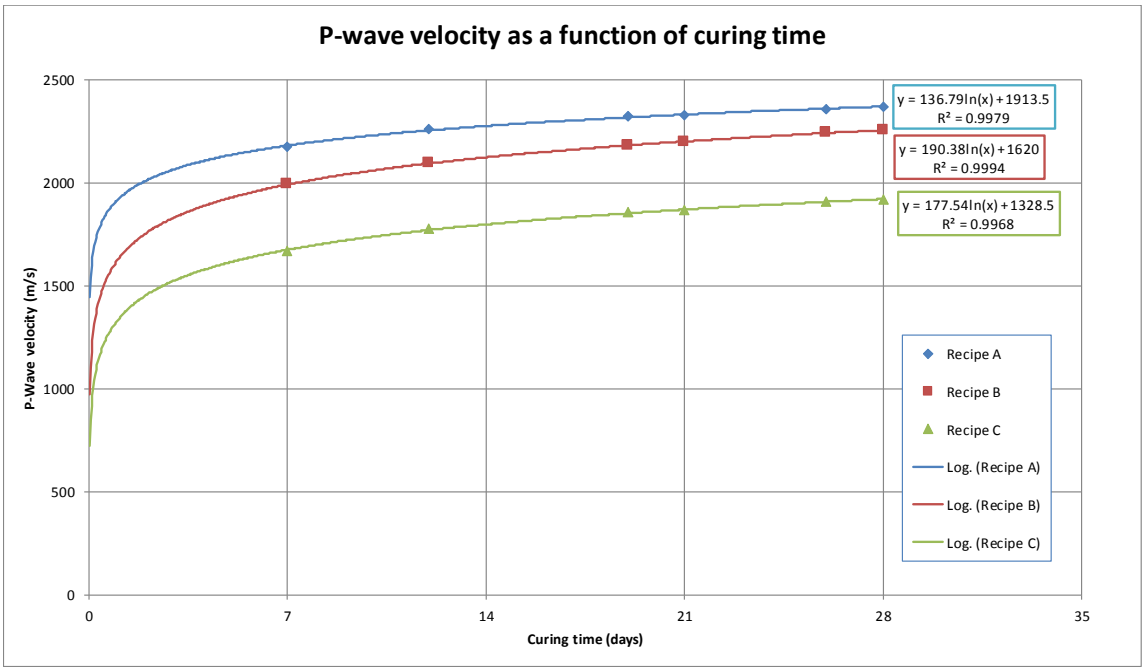


Figure 9. P-wave velocity as a function of curing time for recipe A to C with a clay content of 58%.

Conclusion

From the results above residues as LKD and CKD could be an alternative to the traditional binders in both the dry mix method and in jet grouting. There are many advantages to use more residues in combination with traditional binders. The two main factors are economy and environmental considerations since both the cost and the carbon footprint from the residues is much lower compared to the traditional binders. However, the limiting factors are availability, how much will be in stock and where is it located and how far it could be transported without losing the environmental advantage compared to the traditional binders.

Acknowledgement

The authors will hereby thank the Ports of Stockholm, CEMEX and SMA for their contribution to this study.

References

Montgomery, D. C. (1996) Design and Analysis of Experiment. Wiley.

Myers, R. H. and Montgomery, D. C. (1995) Response Surface Methodology. Wiley.

Ryden, N., Ekdahl, U., Lindh, P. (2006) Quality control of cement stabilised soil using non-destructive seismic tests. *DGZfp – Proceedings BB102-CD, Lecture 34, Advanced Testing of Fresh Cementitious Materials, Stuttgart*. The German Society for Non-Destructive Testing, Berlin, Germany

UNCONFINED COMPRESSION TESTS OF CEMENT-TREATED SOIL CONTAINING UNMIXED SOIL

Tsutomu Namikawa, Shibaura Institute of Technology, Tokyo, Japan, 81-3-5859-8358, namikawa@shibaura-it.ac.jp
Sae Suzuki, Shibaura Institute of Technology, Tokyo, Japan, 81-3-5859-8358, ah13041@shibaura-it.ac.jp

ABSTRACT

Cement-treated columns constructed by deep mixing method are likely to contain incompletely mixed material, that is, in-situ soils unmixed with cement. Such unmixed soil should affect the mechanical performance of the cement-treated column. This paper presents unconfined compression tests of cement-treated clay specimens containing unmixed clay. The specimens used in this study were prepared by mixing cement, water and Fujinomori clay in the laboratory. On the procedure of preparing the specimens, untreated clay pieces representing unmixed soils were intentionally inserted into the cement-treated clay slurry in the mold. The volumetric proportions of untreated clays are 1% and 2%, and the locations of those are determined randomly. The test results indicated that the untreated clay considerably affects unconfined compressive strength (UCS) of the cement-treated clay. UCS of the specimen for the untreated clay content of 1% is reduced by about 9% as compared to that of the specimen without untreated clay. UCS of the specimen for that of 2% is reduced by about 13%. This experimental result indicates that the influence of unmixed soil cannot be neglected when determining the design strength of the ground improved by cement mixing method.

Keywords: Cement-treated soil, Unmixed soil, Unconfined compressive strength

INTRODUCTION

The ground improvement by deep mixing has been widely used for structure foundations, retaining walls and liquefaction mitigations. The strength of the cement-treated soil constructed by deep mixing method varies greatly, even at a single column, owing to the variability of in situ soil properties, the variability of mixing effectiveness, and other factors. Namikawa and Koseki (2013) conducted finite element analyses incorporating random-field theory to simulate the unconfined compression behavior of full-scale column samples in which the material properties vary. The simulation results provided a rational explanation for the difference between the mean strength of cored samples and the overall strength of a full-scale column. Moreover, cement-treated columns constructed by deep mixing method are likely to contain incompletely mixed material, that is, in-situ soils unmixed with cement. Such unmixed soil should affect the mechanical performance of the cement-treated column. Current quality assurance procedures allow a small percentage of incompletely mixed material represented by core recovery ratio. The core recovery ratio of 90 - 95% is allowable in the Japanese quality assurance (BCJ 1997). This criterion allows implicitly some amount of unmixed soil remaining in the cement-treated column. However, there is little study on the influence of the unmixed soil on the mechanical behavior of the cement-treated soil.

This paper presents unconfined compression tests of cement-treated clay specimens containing unmixed soils. The cement-treated clay was examined in this study because clay layers cannot be effectively mixed with cement slurry and incompletely mixed clay lumps often remain in cement-treated columns. The specimens used in this study were prepared by mixing cement, water and Fujinomori clay in the laboratory. On the preparation procedure of the specimens, small untreated clay pieces representing unmixed soils were intentionally inserted into the cement-treated clay slurry in the mold. The volumetric proportions of unmixed parts are 1% and 2%, and the locations of untreated clays are determined randomly. The test results indicated that the untreated clay considerably affects unconfined compressive strength (UCS) of the cement-treated clay. The experimental result indicates that the influence of unmixed soils cannot be neglected when determining the design strength of the

© 2018 Deep Foundations Institute

ground improved by cement mixing.

EXPERIMENTAL PROGRAM

Unconfined compression tests were conducted on the cement-treated clay specimens prepared in a laboratory. The composition of the cement-treated clay used in the test is shown in Table 1. This table shows the weight ratio of the materials composing the specimen. Portland cement and Fujinomori clay were used in this study. The consistency of Fujinomori clay is shown in Table 2. The clay used as the unmixed parts was prepared by consolidating the slurry of Fujinomori clay. The clay slurry was made by mixing the Fujinomori clay powder and water. Thereafter, the clay slurry was poured into a cylindrical mold of 100 mm in diameter and 120 mm in height, and consolidated under the loading pressure increased step by step. The final consolidation pressure is 38 kPa. UCS of the consolidated clay is about 40 kPa. The consolidated clay was cut into small pieces used as the unmixed parts. The small pieces are cubes having about 5 mm sides. A clay piece used as the unmixed parts is shown in Fig. 1(a). It should be noted that the size of the unmixed parts is not changed in this study. The size of unmixed parts is likely to affect the overall strength of the cement-treated soil. Further study is required to investigate the effect of the size of unmixed parts on the overall strength.

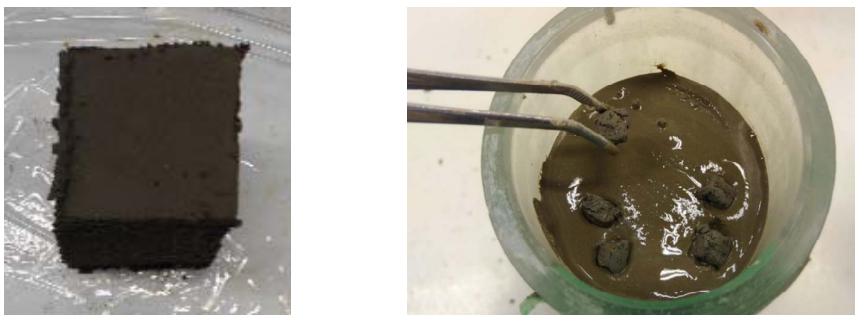
Table 1 Mixing properties of cement-treated soil (weight (%))

Water	Portland Cement	Fujinomori Clay
35.5	7.8	56.7

Table 2 Consistency of Fujinomori clay

Plastic limit	Liquid limit	Plasticity index
23%	49%	26

Based on the Japanese Geotechnical Society standard JGS0821-2009 (JGS 2017), the specimen was prepared by the following procedure. All the materials shown in Table 1 were mixed thoroughly. The mixed material was put into a cylindrical mold in 5 separate stages. The mixed material was compacted by vibration at each time to reduce air bubbles in the slurry. In the preparation of the specimens containing the unmixed parts, the untreated clay pieces were put in the mixed soil cement slurry before compacting at each time (see Fig. 1(b)). Thereafter, the specimens were cured under wet condition. The curing times are 7 days. A cylindrical specimen of 50 mm in diameter and 100 mm in height was used in the tests.



(a) A clay piece (b) Putting clay pieces in cement-treated clay slurry

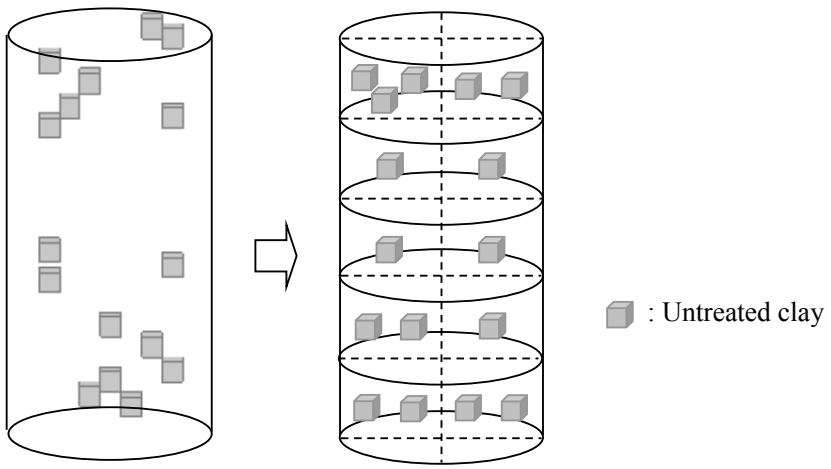
Fig. 1 Clay piece used as unmixed part

In the unconfined compression tests, both the top and bottom ends of the specimen are capped with gypsum. The loading rate is 1 mm/min. The load in the vertical direction is measured by an inner load cell that is free from the effects of friction at the bearing. The displacement of the loading shaft is measured by a displacement transducer. The axial strain is evaluated from the displacement measured by this transducer.

The specimen conditions for the unconfined compression tests are summarized in Table 3. The specimens of which the volumetric proportions of untreated clay are 0%, 1% and 2% were examined in this study. The specimens contain 16 untreated clay pieces in Case 1% and 32 pieces in Case 2%. The locations of untreated clay pieces are randomly determined by the Monte Carlo simulation. An example for the locations of untreated clay pieces in Case 1% is shown in Fig. 2. Fig. 2 (a) shows the locations determined by the Monte Carlo simulation. In practice, the cylinder is divided into 20 parts as shown in Fig. 2 (b) and the clay pieces were put in the parts corresponding to the locations calculated by the Monte Carlo simulation in the compaction process. The locations of untreated clay pieces were calculated for each specimen; those locations differ between the specimens. Six specimens were tested in all the cases. Although the number of specimens is not enough for the statistical sample size, the characteristic of the compression behavior of the cement-treated soil including the untreated parts could be clarified from the results with the six specimens.

Table 3 Specimen conditions

Case	Volumetric proportions of untreated clay	Size of untreated clay	Number of untreated clays	Number of specimens
0%	0%	-	-	6
1%	1%	5 × 5 × 5 mm	16	6
2%	2%	5 × 5 ×5 mm	32	6



(a) Simulated location (b) Practical location in the test

Fig. 2 An example of untreated clay locations

EXPERIMENTAL RESULTS

The stress-strain relationships for Case 0% are shown in Fig. 3(a). The stress-strain relationship is almost linear during the initial loading process and the strain-hardening behavior is observed before the peak stress state. There is a little variability in the stress-strain curves of 6 specimens.

UCS defined as the peak stress is in the range of 1.69 MPa to 1.79 MPa. The axial strain at the peak stress is around 0.6 %.

The stress-strain relationships for Case 1% are shown in Fig. 3(b). These stress-strain relationships are similar to those for Case 0% shown in Fig. 3(a). However, the peak stresses in Case 1% are smaller than those in Case 0%. UCS for Case 1% is in the range of 1.46 MPa to 1.71 MPa. This reduction of strength is attributed to the inclusion of the untreated clay. Moreover, the axial strains at the peak stress in Case 1% are smaller than those in Case 0%.

The stress-strain relationships for Case 2% are shown in Fig. 3(c). These stress-strain relationships are similar to those obtained in Case 0% and Case 1%. The peak stresses in Case 2% are smaller than those in Case 1%. UCS for Case 2% is in the range of 1.45 MPa to 1.57 MPa. The axial strains at the peak stress in Case 2% are almost same as those in Case 1%.

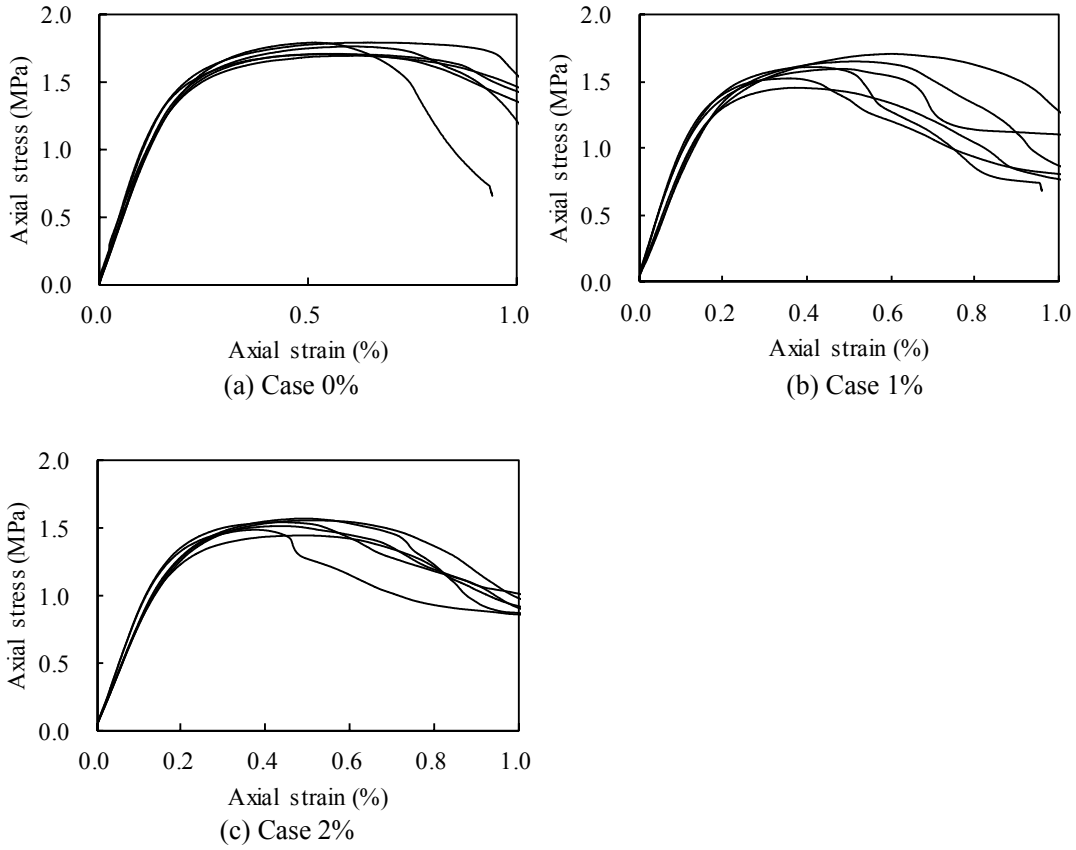


Fig. 3 Stress-strain relationships

The comparison of the typical stress-strain relationships for the three cases is shown in Fig. 4. It can be seen that there is some difference between the three stress-strain relationships. The initial inclination and the peak stress decrease as the untreated clay content increases. The typical specimens after the tests are shown in Fig. 5. Vertical cracks are observed on the specimen surfaces in the three cases. There is no significant difference between the fracture patterns of the three specimens.

UCS is summarized in Fig. 6. The strength clearly decreases with the untreated clay content. The mean values of UCS are 1.74 MPa, 1.59 MPa and 1.52 MPa for Case 0%, Case 1% and Case 2%, respectively. On the basis of these mean strengths, 1% content of the untreated clay causes about 9% reduction in strength and 2% content of that causes about 13% reduction in strength. This result indicates that a few per cent content of the unmixed soil is likely to cause a meaningful reduction in

strength of cement-treated soil.

While the variance of UCS in Case 1% is larger than that in Case 0%, that in Case 2% is not clearly larger than that in Case 0%. The locations of the untreated clays differ between the specimens in Case 1% and Case 2%. Therefore, the variance of UCS in Case 1% and Case 2% was expected to become larger than that of the specimens without the untreated clay in Case 0%. However, there is no significant difference between the variance of UCS in Case 0% and Case 2%. This result implies that the locations of the untreated soils do not considerably affect the strength when the untreated soils distribute randomly.

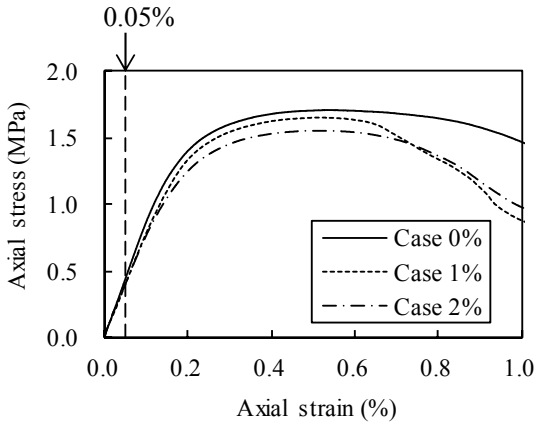


Fig. 4 Comparison of stress-strain relationships



(a) Case 0% (b) Case 1% (c) Case 2%

Fig. 5 Example of specimens after failure

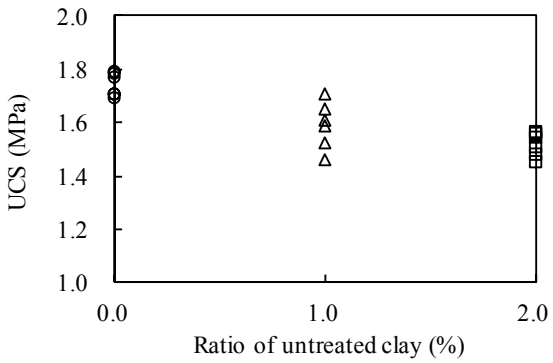


Fig. 6 Influence of untreated clay on UCS

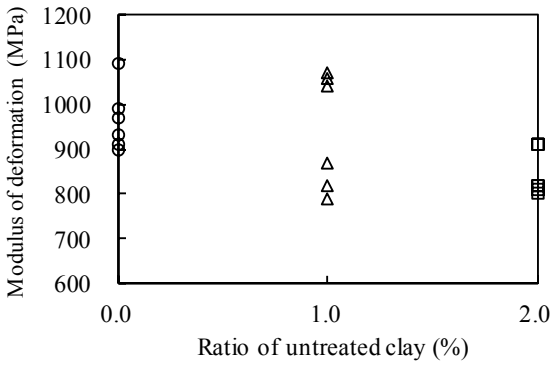


Fig. 7 Influence of untreated clay on modulus of deformation at axial strain of 0.05%

Modulus of deformation is summarized in Fig. 7. The modulus of deformation is evaluated at the axial strain of 0.05% shown in Fig. 4. The modulus of deformation decreases with the untreated clay content. The mean values of the modulus of deformation are 970 MPa, 940 MPa and 850 MPa for Case 0%, Case 1% and Case 2%, respectively. On the basis of these mean values, 1% content of the untreated clay causes about 3% reduction in modulus of deformation and 2% content of that causes about 12% reduction.

The experimental results show that a few per cent content of untreated soil affects considerably the strength and the modulus of deformation of the cement-treated soil. This implies that the content of the unmixed soil should be considered when determining the strength and the modulus of deformation in the design and quality assurance procedures of the deep mixing method.

CONCLUSIONS

The unconfined compression tests were conducted on the cement-treated clay specimens containing the untreated clay to investigate the influence of the unmixed soil on the strength of the cement-treated soil column. The test results indicated that the untreated clay considerably affects unconfined compressive strength (UCS) of the cement-treated clay. UCS of the specimen for the untreated soil content of 1% is reduced by about 9% as compared to that of the specimen without untreated soil. UCS of the specimen for the untreated soil content of 2% is reduced by about 13%. This experimental result indicates that the influence of unmixed soil cannot be neglected for determining the design strength of the ground improvement by cement mixing.

REFERENCES

Building Center of Japan (BCJ), 1997. Design and quality control guideline for building foundation treatment: Deep/shallow soil mixing methods with cement admixtures. (in Japanese).

Japanese Geotechnical Society (JGS) (2017): Japanese Geotechnical Society Standards Laboratory Testing Standards of Geomaterials. Practice for making and curing statically compacted stabilized soil specimens.

Namikawa, T. and Koseki, J., 2013. Effects of spatial correlation on the compression behavior of a cement-treated column. Journal of Geomechanics and Geoenvironmental engineering, **139**(8), pp. 1346-1359.

BIM – A UK FOUNDATION SUB-CONTRACTORS PERSPECTIVE

Mark Pennington – Technical Director, Balfour Beatty Ground Engineering and Chairman FPS Technical Committee, Basingstoke, UK, mark.pennington@balfourbeatty.com.
Tracey Fitch – Principal Technician, Balfour Beatty Ground Engineering, Basingstoke, UK, tracey.fitch@balfourbeatty.com.

ABSTRACT

Over the past five years there has been a big shift in the construction and engineering worlds as digital technologies and processes have bought time, cost and safety benefits to many. It has been widely stated that digital development will change the way the construction industry works over the next five years more than it has changed over the last twenty five years. The implementation of Building Information Modelling (BIM) has developed at different rates in different parts of the industry. There is a perception in the UK that the foundation industry is lagging behind others in BIM development. It is important to understand the definition of BIM to assess progress. This paper presents the outlook from the perspective of a UK foundation contractor on BIM development and achievement. This includes the definition and explanation of BIM, the current codes available, current and future progress and opportunities. It also provides some recommendations on how the rate of development can be improved.

1.0 INTRODUCTION

Many people have heard the buzz over BIM during the last few years; Building Information Modelling led many to believe this was based around a model. Initially many thought a 3D model was necessary for this to work but further understanding shows that a model is simply an output of the data available. This acronym is misleading, BIM is about data and how we create, share and manage it in a way that benefits projects at all stages in the project life cycle. Replacing Building with Better and Modelling with Management is a different way of explaining what BIM is aiming to achieve. Many have stopped using the term and replaced it with digital terms more aligned with what is being used. Within this paper BIM and digital data transfer or management should be read as one and the same. General statement within this paper are based on the authors experience and interface with other foundation sub-contractors within the FPS.

A significant part of BIM development over the past few years is to enable whole life costing for structures. Many foundation solutions are not maintainable assets; they are hidden structures with a defined design life. From a foundation perspective whole life costing can be thought about in terms of providing good records for possible re-use or future development of the site. Understanding existing conditions and site constraints is critical for designing and constructing foundation works.

Any digital technology developed and utilised to aid in the design, planning, construction and recording of data related to foundation engineering is considered as BIM or digital data management development.

Within the foundation contracting industry in the UK progress in digital data management has been made in many areas. This has been by individual foundation contractors and also as an industry and this progress is yielding benefits. However, progress is too slow and the foundation industry is falling behind others in this development. Understanding the current state of development, the key blockers to development and future opportunities is needed to accelerate progress.

2.0 WHAT IS CURRENTLY IN PLACE TO ALLOW BIM COMPLIANCE

2.1 Introduction

In order to understand BIM compliance it is necessary to appreciate the key codes of practice and documents that are available to help define digital data management.

© 2018 Deep Foundations Institute

2.2 Codes of Practice

The following standards define BIM protocols in the UK:

- BS 1192:2007 - Collaborative production of architectural, engineering and construction information. Code of practice
- PAS 1192-2:2013 - Specification for information management for the capital/delivery phase of construction projects using building information modelling
- PAS 1192-3:2014 - Specification for information management for the operational phase of assets using building information modelling
- BS 1192-4:2014 - Collaborative production of information. Fulfilling employer's information exchange requirements using COBie.
- PAS 1192-5:2015 - Specification for security-minded building information modelling, digital built environments and smart asset management
- CIC BIM Protocol - The BIM Protocol is a supplementary legal agreement that is incorporated into professional services appointments and construction contracts by means of a simple amendment

Within the foundation industry in the UK the key codes are BS 1192:2007 and PAS 1192-2:2013. In the author's opinion the industry can independently comply and in most cases does comply with BS1192:2007. Compliance with PAS documents has more reliance on the overall project workflows and protocols. These are defined within individual project execution plans. These are now regularly produced on a number of projects, however, experience from FPS members indicates there is rarely a contractual requirement for the foundation contractor to comply with the standard. This potentially gives an explanation to slow development of digital data management processes within the UK foundation market.

The ICE Specification for Piling and Embedded Retaining Wall 2017 (SPERW) sets out the data that is required to be captured for each of the different piling techniques used in the UK; this is a very good starting point for foundation related digital data capture. Individuals responsible for drafting project execution plans which include foundation solutions should refer to Table B1.1 within SPERW 2017.

2.3 Technology

In order to enable successful digital data transfer the correct technology needs to be in place. This can come in the form of correct hardware and software together with specific applications and data storage. There are a number of software packages in place.

The best example of this is AGS data which currently captures and presents all site investigation information in a digital format. This has been around for many years and is used extensively through site investigation communities and consulting engineers within the UK. Experience within the FPS shows that AGS format is not used typically on the vast majority of foundation schemes by the foundation contractor. This shows that even when the technology is in place the workflows and transmission of this information needs to be improved for this to work at all levels.

Technology also has to develop to allow the storage and easy identification and location of all digitally captured data. Common data environments exist in many forms. These are typically established on a project by project basis (Projectwise, Business Collaborator, Aconex). The criteria for a common data environment is to provide a single-source of information for any given project, used to collect, manage and disseminate all relevant approved project documents and data for multidisciplinary teams in a managed process.

2.4 Tier 1 Contractor Compliance

Tier 1 contractors within the UK are now generally BIM compliant. Workflows adopted and digital information stored is compliant with BS 1192:2007 and PAS 1192-2:2013. This is a significant step forward within the construction industry and shows how digital data is progressing.

Project BIM execution plans are also common place. These define how digital information should be captured and transferred on each project. These define how PAS 1192:2 should be adopted on that particular project.

3.0 PROGRESS TO DATE

3.1 Introduction

There is much in place to enable digital data transfer on construction projects within the UK. The foundation industry recognises the clear benefits of adopting digital techniques. These are developing at different rates within different companies and different sectors within the industry. There is no standard approach to digital data capture and currently it is not adopted as widely as it could be. In this section of the paper we will elaborate on three areas where digital development has significantly enhanced the foundation industry: Specific Industry guidance, modelling and capturing field data digitally.

3.2 Federation of Piling Specialists Guidance

In February 2013 the FPS recognised the benefit of developing some industry guidance into the capture and management of digital data within the foundation industry. Following consultation with key stakeholders including consulting engineers, tier 1 contractors and other professional industry body's five guidance notes were produced:

- Guidance Note 1 – How can BIM help industry problems?
- Guidance Note 2 – BIM Introduction and Workflow
- Guidance Note 3 – Definition of BIM Compliance
- Guidance Note 4 – Information, Classification and Exchange of Piling Data
- Guidance Note 5 – Software Guidance for BIM

The target audience for the guidance notes is both FPS members and any stakeholders involved in construction projects where foundations are an element. The aim of the guidance is to inform, provide a baseline and give some guidance on the development of workflows. This inevitably will involve changes to existing working procedures.

Guidance note 1 identifies the clear benefits that can be gained on a foundation element of a project at pre-award, pre-construction, construction and handover phases. It was easy to define and explain benefits, it was difficult quantify these in terms of commercial gain without running projects using digital workflows vs conventional workflows concurrently.

Managing data correctly is the key behind successful implementation. Guidance note 2 gives an example of digital data transfer could look like on a project. This is provided in Figure 3.1 below. A key element in this is a standardised method for the input data to start the workflow. The FPS have developed a standard electronic spreadsheet that is used by the project Engineers. This ensures that information passed to the foundation contractor is in a standard format to feed into the foundation digital workflow. From a foundation contractor's perspective, this standard way of specifying piling information is not used as widely as it should be. If this requirement is embedded into a fixed workflow, ie. it has to be in this format for the digital workflow to work, the importance of the spreadsheet will increase as would the usage.

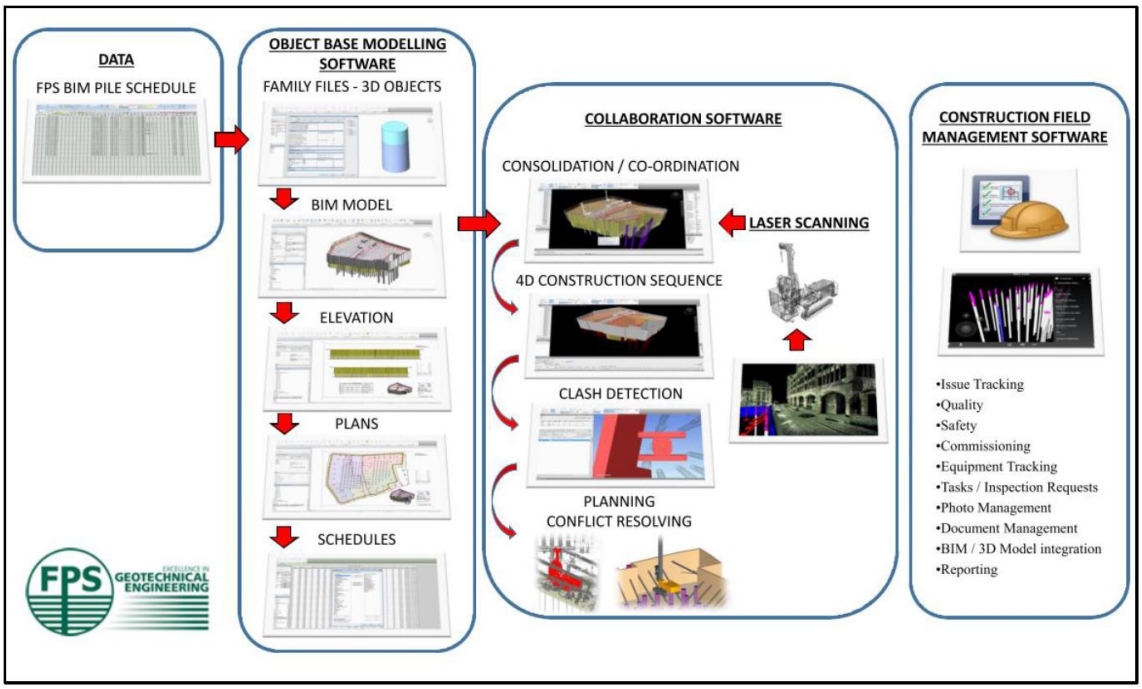


Figure 3.1 – BIM Data Workflow, FPS Guidance Note 2

It is important to have standards and benchmarks to understand the level of BIM compliance. This is set out in guidance note 3, from basic existing production and transfer of information to intelligent, interactive data sharing.

To use digital data transfer effectively pieces of data need to be coded so that they can be linked together and searched for in a consistent way. Uniclass coding is recognised within the UK as the standard method to classify construction works and elements. UNICLASS 2015 is a development of CPIc's UNICLASS 2 and is now cited in the UK National foreword to ISO 12006-2 Building construction – Organisation of information about construction works as the UK response to that International Standard. Guidance note 4 summarises the classification for foundation elements. In addition this guidance note sets out the key digital data requirements at various stages throughout the foundation construction process. This links with the requirements set out in SPERW.

Computer software (in particular a 3D model) is often seen as the key component around BIM. Software is important but the common data environment and the workflows around the transfer and management of the data is more critical. There are many different software packages available to enable the production, manipulation and transfer of data, the key is to understand how these all link together. The use of Industry Foundation Classes (IFC) as a transfer format is a means of achieving this. IFC is a platform neutral, open file format specification that is not controlled by a single vendor or group of vendors. It is an object-based file format with a data model developed by buildingSMART to facilitate interoperability in the architecture, engineering and construction industry, and is a commonly used collaboration format in Building information modelling based projects.

3.3 Modelling

The use of 3D and 4D modelling is wide spread within the foundation industry. This is the most visual and easily presentable element of the digital data transfer process. Its uses and benefits are vast at the design, planning and construction phases of the works. In foundation engineering there are three key areas where modelling yields significant advantages: ground modelling, designing and construction / logistics planning.

In most construction and also mechanical engineering solutions it is possible to model just what is going to be built and/or manufactured. In foundation engineering there is a necessity to model the existing ground, this adds a significant complication. The ground profile is modelled by interpolation between the site investigation locations. This interpolation can lead to errors; by continually improving the 3D modelling of the sub-surface conditions it is possible to reduce these errors. Certain parts of the UK have had substantial site investigations carried out. Applications are now available to combine all of this information together and plot a 3D ground profile accurately.

Designing foundation elements in 3D has been around for some time. These are typically used in isolation to develop an efficient design solution. The use of finite element 3D software (eg PLAXIS) to model soil structure interaction allows good visualisation of the solution. Currently this level of design is used within foundations but the data output is not captured digitally into the project data set. Section 4.0 of this paper goes further into benefits possible from developing this further.

Perhaps the biggest benefit of progressing modelling for the foundation industry is in the logistical planning of the works. This has seen the development of intelligent 3D, 4D and 5D models which enable virtual construction of the work. The benefit of intelligent models is that material and plant costs are included allowing accurate cost plans to be produced. Many sites within the UK are constructed with large plant in a small area. Accurate planning of the work can yield significant savings.

Figure 3.2 provides an example of using designed foundation elements (both temporary and permanent works) to plan a diaphragm wall construction in a constrained site in London. The detail is critical when planning cage installation and concreting arrangements in diaphragm walls. It is important that the actual designed permanent works elements are used when planning any temporary works.

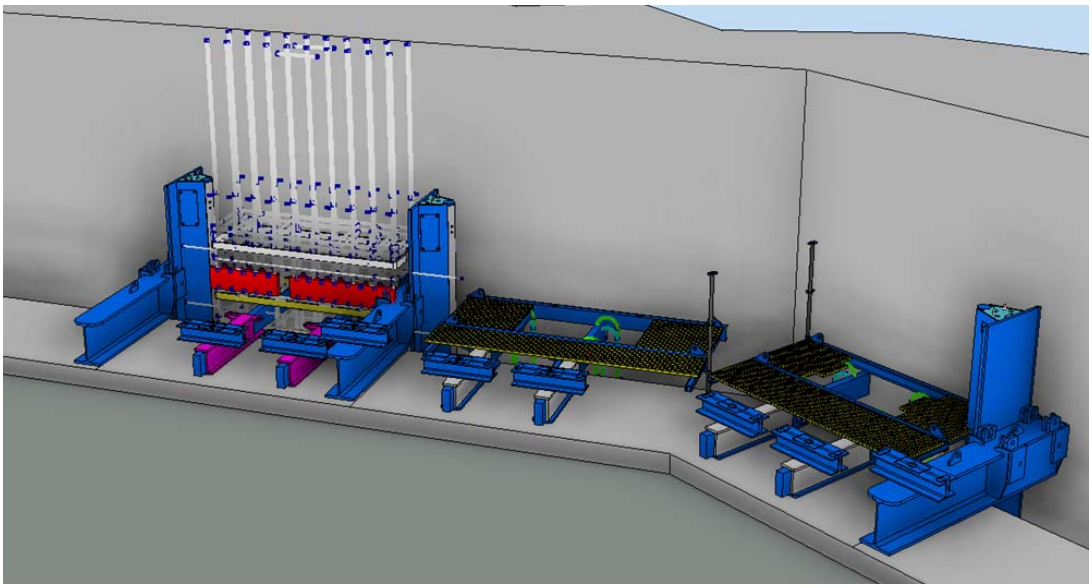


Figure 3.2 – Example of modelling permanent and temporary works to achieve a solution

3.4 Capturing Data Digitally

A significant advantage of digital data management is the ability to transfer information into the field electronically, record construction records digitally and have instantaneous visibility of site progress from anywhere in the World. With the development of tablet technology and cloud storage this has now become easily achievable. The advantages in the reduction of paper records, standardisation of records, improved quality of records and improved speed of monitoring site progress means that implementation of this technology will quickly grow and become standard.

Within the UK there is not one system that is universally adopted. Like any software available there are many different applications that can do the same thing. The key is to get the workflow properly planned to ensure the correct information is passed to the field and then the correct information captured.

In the most simplistic form data capture is possible with standard spreadsheets and writable forms stored in suitable cloud storage. This allows access and updates from any location. Care needs to be exercised using this approach as data can be over written and lost. Contractors within the UK have developed their own applications that suit their individual construction processes. This allows version control and critical hold points to be built into the process. This may involve taking a record photograph of a certain time in the process before progressing.

The format of the data capture and how this is translated and then stored to be transmitted later is important. AGS data is the standard accepted format for site investigation data, as discussed in Section 2.3. The FPS and the AGS are currently looking at developing the AGS format further to include foundation construction information. This would have the benefit of providing us with as built data format for all site investigation and foundation information. This would provide useful information for any re-use of the site.

It is not only the development of hand held tablets to capture data on sites that has progressed. Other developments such as drones and laser scanning have also improved digital data capture, reduced construction risk, improved productivity and improved safety on site. Information from laser scanning and drone images can be linked with other project data if captured in a standard format.

Laser scanning has been used to confirm as built profiles of retaining walls and excavations to quickly allow construction tolerances to be accurately measured and compared in 3D with the design. Laser scanning has also been used to accurately measure existing facades in city centre sites. This not only allows for clash detection to be checked and connection details developed for the permanent and temporary works but also enables construction plant to be correctly planned and positioned for construction. Figure 3.3 below is an example of a laser scan point cloud data for the Olympic Stadium in London. It is clear that accurate information can be obtained quickly for existing structures.

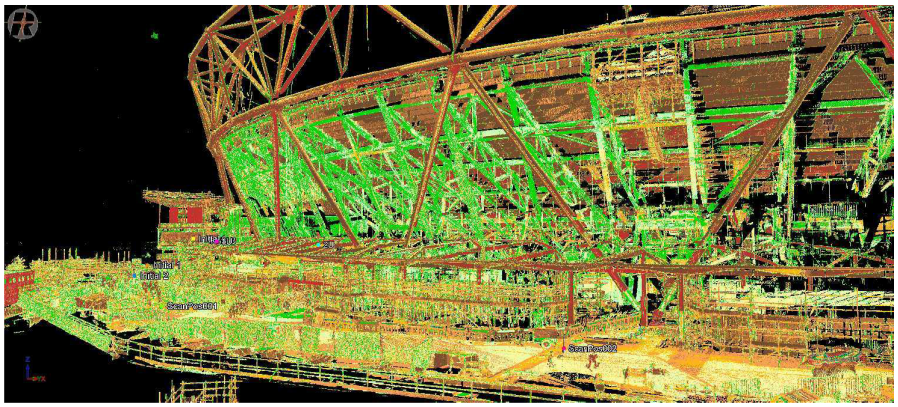


Figure 3.3 – Laser scanning image for the Olympic Stadium, London

Drones have been used to inspect tall plant as part of the preventative maintenance programme. This reduces the amount of time piling rigs / cranes need to be stopped, reduces working at height and provides an accurate record of the inspection. The development of easily usable drones and high quality imagery means that good piling rig / crane inspection records can be captured. Figure 3.4 below is an example of a drone image of the top of a piling rig.

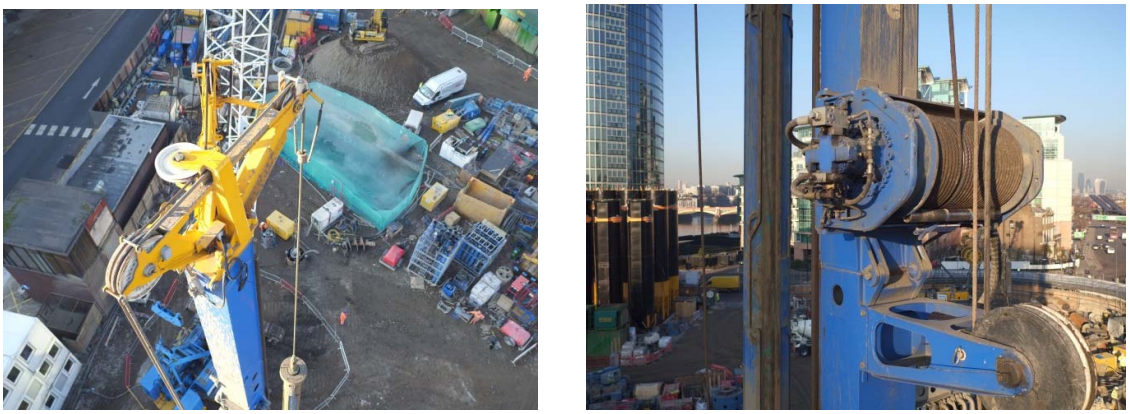


Figure 3.4 – Drone images for preventative maintenance inspections of piling rigs

4.0 OPPORTUNITIES

4.1 Introduction

The opportunities within digital data management are significant. Within this section the author will cover some of the technologies that are currently being developed but not used commercially within foundation engineering in the UK at the moment. The Author will also cover areas where improved collaboration would, in the opinion of the author, yield significant benefits.

4.2 Technologies

Technology will continue to develop and this will lead to improved ways of planning and executing foundation work. Virtual Reality is one area of development. Virtual Reality headsets are now common place in the gaming and personal market. This will develop uses into construction and foundation engineering in a number of ways.

It is already possible to train plant operators to use certain items of plant in a virtual world. This will be invaluable within the foundation industry where large items of plant are regularly used. This will provide the ability to train drivers virtually at site level to understand the controls and limitations of specific pieces of plant and identify site specific blind spots. People plant interface is a leading safety consideration within the industry. The ability to work virtually within a piece of plant and work out safe areas for people to move and work around it will be a big step in reducing people plant interface accidents. Figure 4.1 presents training in progress where views can be switched from inside to outside the cab.



Figure 4.1 – Example of virtual control of an excavator

It is also possible to construct sites in a 3-D model and then virtually move around in the model to get spatial appreciation and highlight unsafe areas. As this develops further it could be used to plan the works in detail to improve production in a safe and controlled environment. Figure 4.2 provides an example of a virtual site where it is possible to move around to get a realistic view.

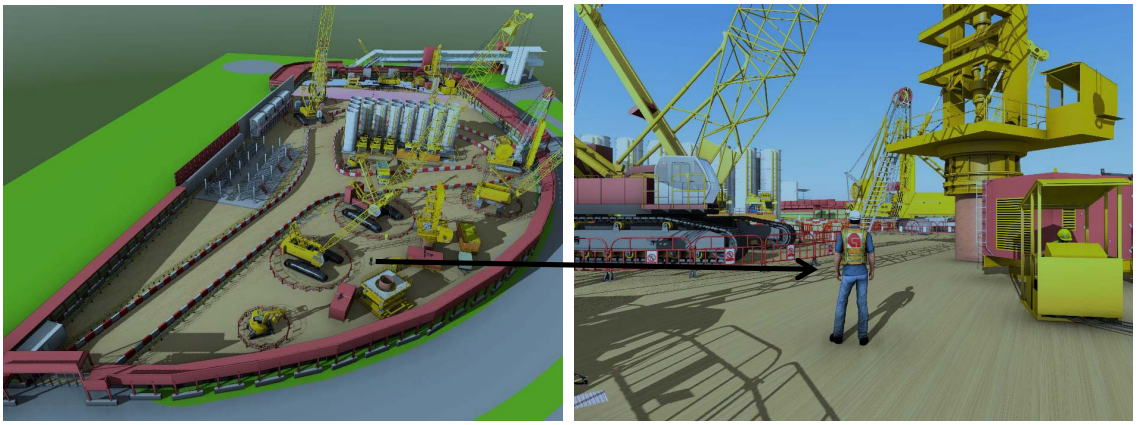


Figure 4.2 – Example of moving around a site in virtual reality

Not only is Virtual Reality possible but mixed reality can also be used to plan and manage work. There are many benefits of being able to see the site develop in a virtual world; planning, clash detection, impact on what is on the site, safety planning, site staff briefings, client briefings, collaboration with other parties on the site and many more. Figure 4.3 below shows a crane virtually superimposed on a site viewed through a virtual headset.



Figure 4.3 – Example of mixed reality

3D design software is currently used extensively within the UK. If the output from the design software could be linked to the project data set and ultimately 4D or 5D model then this would allow immediate assessment of design variations. All too often a late change in foundation design is implemented without a full understanding on the impact on the rest of the structure. Foundation design is about managing the ground risk. In many cases many iterations of the design are required to find the correct solution which brings value but also minimises risk. It will be a significant improvement to see the time and cost impact of a change linked directly to the design.

Many foundation rigs have a significant amount of digital instrumentation. Within the UK foundation industry this is used to varying degrees. However, this information is not being used as a direct digital link between the rig and the as-built records. Clearly as the digital recording of foundation construction information improves then the next step is to link the rig information directly to the construction records. This will provide factual, clear results that do not have the risk of errors in human interpretation.

4.3 Collaboration

Collaboration is a key element of any original BIM development. Level 3 BIM is defined as full collaboration between all disciplines by means of using a single, shared project model which is held in a centralized repository. All parties can access and modify that same model and data, and the benefit is that it removes the final layer of risk for conflicting information. This is known as 'Open BIM'. Current nervousness in the industry around issues such as copyright and liability are intended to be resolved – the former by means of robust appointment documents and software originator/read/write permissions, and the latter by shared-risk procurement routes such as partnering.

Within the foundation industry in the UK there is a long way to go to reach this level. The first step is to ensure that foundation contractors have a contractual obligation to comply with project specific digital data management plans (or BIM execution plans). Without this implemented widely across the UK then digital development in foundations will continue slowly.

5.0 RECOMMENDATIONS

Digital technology will continue to develop both inside and outside the construction industry. Digital developments within foundation engineering need to continue to match or exceed this. The acronym BIM is not clearly enough defined to facilitate this development. Any digital development should be viewed as a development of BIM. As more and more data is captured digitally it will be possible to combine this data for greater benefit.

It is important within the UK that all documentation is compliant with the requirements of BS 1192:2007. This is fundamental to ensure document consistency enabling digital searching of documents.

In defining the benefits of changing to a digital workflow it is difficult to quantify the commercial gain. It is important to clearly document actual benefits gained in order to ensure digital improvements across all levels of foundation engineering is adequately supported to develop at the required rate. Full implementation and development will not happen until compliance of digital data transfer is a contractual requirement at project level.

6.0 REFERENCES

British Standard Institution (2007). Code of Practice. Collaborative production of architectural, engineering and construction information: BSI, BS 1192 + A1 (2015) + A2 (2016).

British Standard Institution (2013). Publically Available Specification. Specification for information management for the capital/delivery phase of construction projects using building information modelling: BSI, PAS 1192-2.

British Standard Institution (2014). Publically Available Specification. Specification for information management for the operational phase of assets using building information modelling: BSI, PAS 1192-3.

British Standard Institution (2014). Code of Practice. Collaborative production of information. Part 4 Fulfilling employer's information exchange requirements using COBie: BSI, BS1192-4.

British Standard Institution (2015). Publically Available Specification. Specification for security-minded building information modelling, digital built environments and smart asset management: BSI, PAS 1192-5.

British Standard Institution (2015). International Standard. Building construction – Organization of information about construction works. Part 2: Framework for classification. BSI, BS ISO 12006-2:2015.

Construction Project Information Committee (2015). Uniclass 2 Toolkit. Available at http:/www.cpic.org.uk/uniclass2.

FPS (various). Building Information Modelling guidance notes (Number 1 to 5). Available at http://www.fps.org.uk.

Institution of Civil Engineers (2017). ICE Specification for piling and embedded retaining walls. Third Edition: Thomas Telford.

DATA MANAGEMENT, ANALYSIS, AND REPORTING FOR SMALL FOUNDATIONS

Jamey Rosen, Geosyntec Consultants. jrosen@geosyntec.com
Andrew Higgins, Geosyntec Consultants. ahiggins@geosyntec.com

Keywords: excavation, trench, verticality, tolerance, database, GIS, visualization

Data management technologies and applications in the Deep Foundations industry are no longer limited to large projects with detailed specifications. This paper will demonstrate how some of the same technologies developed for larger projects are being scaled down to apply to small-scale grout curtains, slurry and diaphragm walls, and other subsurface applications. "Small", in this case, can refer to either the size of the construction, or the level of detail and requirements in the specifications. Examples will include use of mobile field data collection and web based tools that can quickly collect basic field observations and automatically generate statistics, daily reports, and as-built drawings; allowing high quality control on both data collection and interpretation.

INTRODUCTION

This paper discusses the application of modern data management and visualization tools to small-scale deep foundation construction projects. Careful collection and organization of data is essential to ensuring that foundations are constructed with acceptable quality. In the past 5 years, project specifications in the United States for federal deep foundation projects, including barrier walls and grout curtains, have increasingly included requirements for data management. These specifications detail how contractors need to collect, organize, visualize and transfer data to the owner. The intent of the specifications is generally such that the owner can view the data in a quick and high-quality manner, based on simple principles of good data management. The propensity of these specifications in large government projects might suggest that these principles and techniques are only applicable to large projects. However the same principles and techniques can be applied to projects at any scale, allowing contractors to perform efficient quality control on their data, generate quick or automatic reports and as-built drawings, and ultimately use their data to increase the quality of their construction.

The remainder of this paper describes some scalable data management concepts and workflows and then provides some examples of how these can be applied to "small" foundation projects.

THE NEED FOR DATA MANAGEMENT

Data management includes the use of databases to store, validate, and organize data; tools to populate the database (e.g., forms and instrument file transfer tools); tools to analyze the data (e.g., statistical and spatial analysis); tools to visualize data (e.g., maps and graphics); and tools to access the data (e.g., interactive websites). Foundation projects require some or all of these tools, and they are frequently applied when there is a specific need driven by one or more factors:

- Field decision making, including the need for a specific analysis of existing data to determine how to proceed with the next phase of work. For example, analysis of grout take trends across a grout curtain determine where to drill additional grout holes;
- Specification compliance, including the need to quickly to and transparently generate reports and as-built drawings for submission to the owner; and
- Contractual obligation, including the requirement for a contractor to submit organized data in a specific format to the owner.

© 2018 Deep Foundations Institute

PRINCIPLES OF DATA MANAGEMENT

Good data management on geo-foundations projects simply refers to having a process for collecting data into a single system (generally a database), reviewing those data for errors or omissions, and visualizing the data in a common context (generally graphs and maps). The data quality can be maximized by following principles including the following:

- Single Source Data – All information officially "lives" in a single place. This means that the database represents the single authoritative repository of project information, and any other documents that contain data (spreadsheets, for example) are understood to be exports or copies of the master database.

- Untouched Data – Once data exist in a digital format, some manual or automated system (generally referred to as the database management system, DBMS) facilitates any transfer of those data into and out of the database, minimizing or eliminating any manual transcription or other operations on those data.

- Data Storage Rules – Data are limited to specific data types (date, text, numeric, etc.) and specific rules or ranges (e.g., grout take volumes can not be negative) to maintain quality and usability of data in the database.

- Non-Proprietary Data Formats – Whenever and wherever possible, file types should be in industry-standard (e.g., Microsoft Excel, gINT) or otherwise universally accessible formats (e.g., ASCII text). Data should thus not be kept in a binary file format, or a file format that requires some specific modeling or other software to view. Instead, data should be kept in standard database or text (ASCII) format.

- Spatial Consistency – To the extent necessary and depending on the source of the data, all spatially-enabled data should be in a consistent coordinate system or have metadata that allows conversions to a standard system.

- Transferability – The master database should be designed to ultimately serve as a complete project archive and should be easily "packaged" and documented in expectation of long-term use.

- Documentation – Every file, table, field, and relationship should have embedded documentation that ensures correct schema usage. Every record should be "stamped" with its source, date of creation, author, usage limitations, etc.

The above principles can be applied to projects at any scale. For example, the act of making a field measurement of the temperature of concrete prior to placement results in a series of entries (contractor name, date/time, temperature) into a log book. These values are then typed into a simple industry-standard format spreadsheet [*Non-proprietary Data Formats*] that is maintained through the project as the official record of concrete data [*Single Source Data*], and that spreadsheet row is annotated with the date and time of data entry [*Documentation*]. A few simple formulas and column criteria rules in the spreadsheet automatically provide errors to the user if the temperature measurement date is not a recognized date or occurs before the start of the project (suggesting a data entry or logbook error) [*Data Storage Rules*]. The spreadsheet is also used as a "live" data source for a graph of concrete control chart (graph of temperature vs. time) [*Untouched Data*], and at the end of the construction the spreadsheet and linked chart are provided to the owner [*Transferability*].

DATA MANAGEMENT WORKFLOWS

The above principles are generally applied through the design and development of basic workflows that allow data to be collected into a database and then served from the database to models, analyses, visualizations, CAD, and mapping systems. A generic workflow, illustrated below, contains three basic categories of activities or objects:

Inputs – data sources either typed into a spreadsheet or form (hand entry); generated from an instrument; or produced from some existing process.

Storage – the database and its components. This consists of a database ("enterprise" if the database is accessible over an intranet or the internet), the Database Management System (DBMS) (which contains the "tools and rules" and automation to facilitate populating the database and serving the data to the outputs), and potentially a document library, which can be a separate database optimized for handling documents.

Access and Outputs – tools to analyze, visualize, and interact with the data in the database.

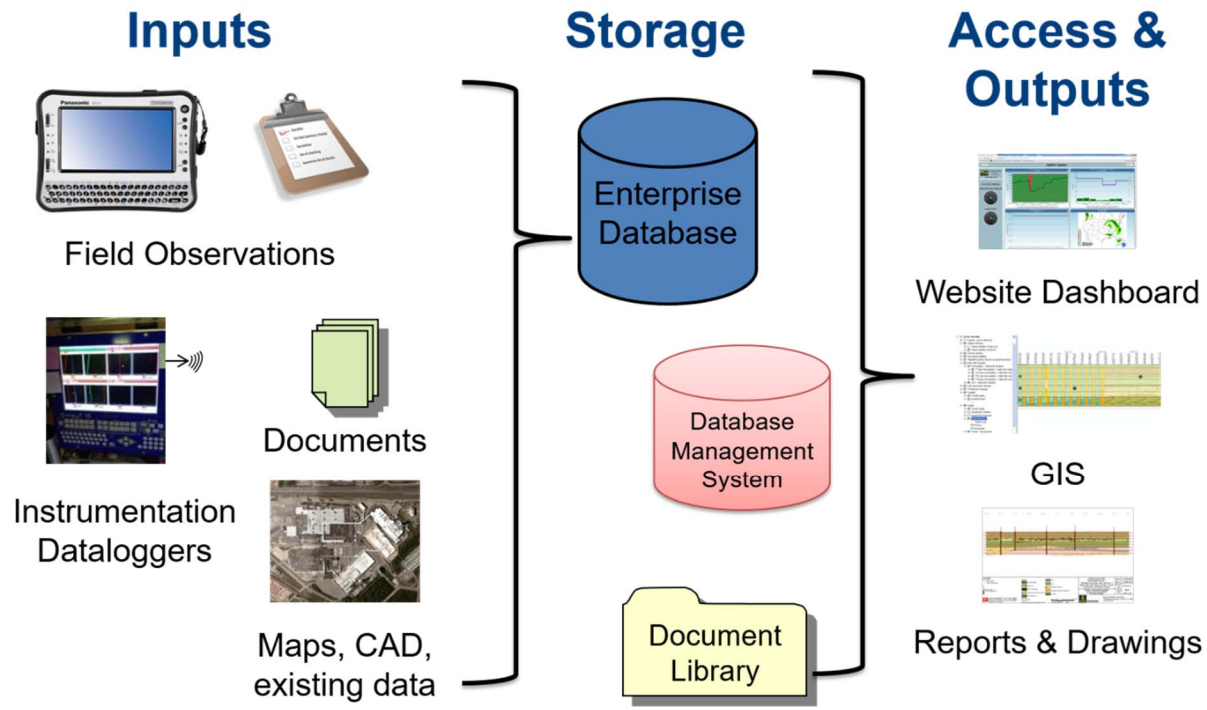


Fig. 1. Generic Data Management Workflow

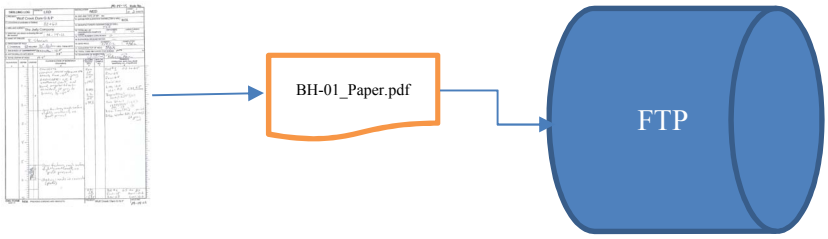
EXAMPLES AND CASE STUDIES

The examples below contain "step by step" instructions showing the principal components of data management applied to the scenario. Elements of the workflow are provided as embedded flow charts.

Exploratory Borehole Array

In this example (based on several recent exploratory borehole investigations), data management principles are applied to compilation and visualization of data in geological borehole logs.

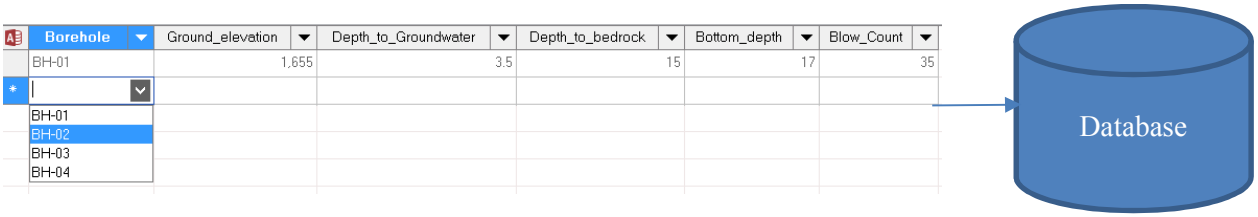
1. Paper Borehole Log



While electronic entry of borehole data during logging is possible, most geologists in the foundations industry prefer to document their core logging by hand for ergonomic and other preferential reasons. In this scenario, the geologist creates a paper log which is later scanned (or photographed). The scanned log is given a filename that references the hole (e.g. BH-01_Paper.pdf) and uploaded to a file transfer protocol (FTP) site or other web-accessible document library.

2. Electronic Logging of Major Details

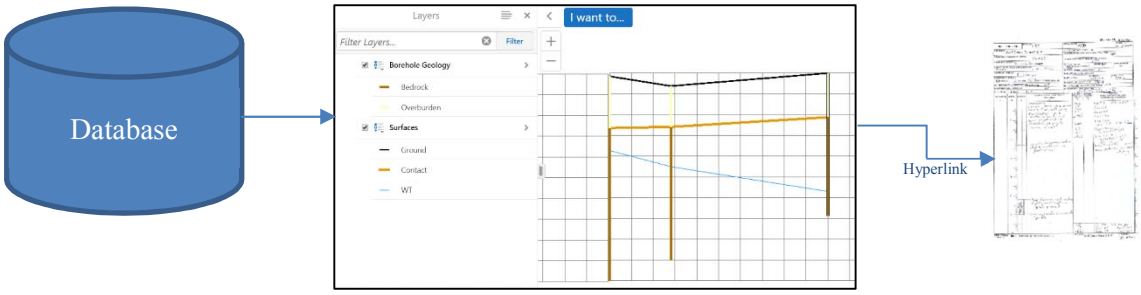
In the interest of time and efficiency for this small project, the only details from the borehole logging that are selected for digital entry are the top elevation of the hole, the depth to groundwater, the depth to the top of bedrock, the bottom depth, and the blow count at each measured depth. Thus a simple database table is created with columns (fields) matching these entries, and is populated by field staff on a laptop using a simple secure web-enabled form:



This field form has some built-in quality control on data entry with some simple logic. Users select a borehole from a pre-populated list (i.e., populated during the project initiation) to ensure that the spelling of a given borehole name is consistent across the system. Additionally, the elevation and depth columns restrict data entry to positive numerical values and entries into the bottom depth column are required to be greater than the entries other depth columns. Finally, the digital form automatically records the date/time and username when a given entry is entered or modified.

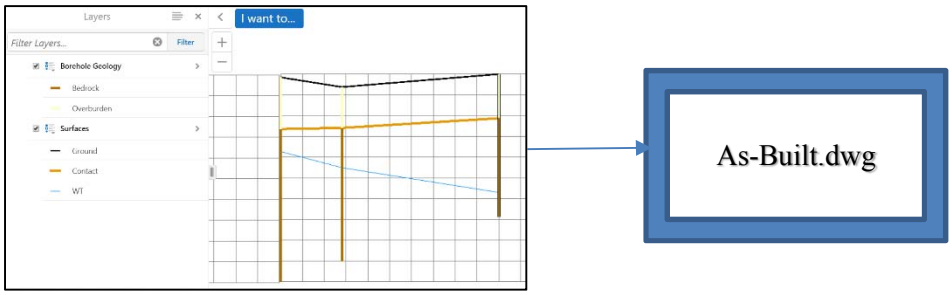
In this small project, a paper log is sufficient to meet the contractor's needs so no digital log (e.g., gINT format) is required. However, if a digital log were to be created, the PDF of the log would be uploaded to the FTP site as in Step 1. Furthermore, the data from the logging software would be exported to a text file (or linked directly to the database), replacing the digital data described here.

3. Visualization of geology



The data entered into the digital form can quickly be visualized in a profile view using Geographical Information Systems (GIS) technology, or another technology that converts values in a database into spatial or graphical images. In this example, a basic web-based viewer was deployed and linked to the database such that as soon as data are entered into the form the viewer is updated to show the latest entered (or edited data). The database contains a spatial view that uses the ground surface and depths (as well as the coordinates or station/offset of the boreholes) to "connect the dots", creating lines representing borehole components and a simple linear interpolation to represent the ground and water table surfaces. The viewer connects to that spatial view and applies symbology (color-coding) based on table values to instantly show the geology in one or more profile views (depending on the geometry of the borehole array) to quickly assess the shape of the water table and top of bedrock surface. Users can also click on a given borehole to "pop" open the scanned borehole log from Step 1, given the use of the file naming convention.

4. Automatic Generation of As-Built Drawings

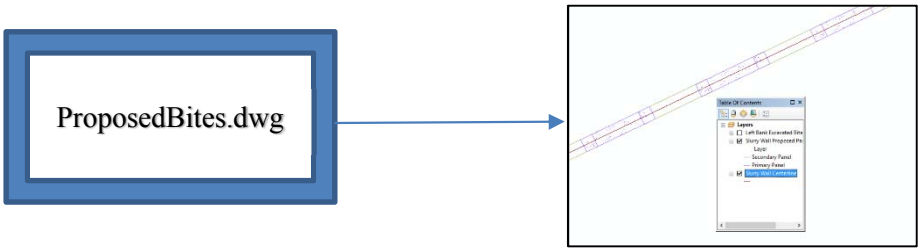


Once a database and GIS are available, at any time (or on an automated schedule), the viewer can export a file that shows the profile geology within a Contractor border box. This can be exported as a "flat" image (paper or PDF), or to a CAD or MicroStation file depending on the Contractor preference.

Short Slurry Wall

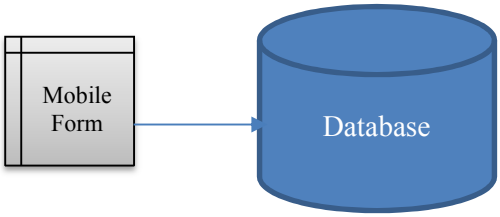
In this example (based on a 120 foot long, 62 foot deep slurry wall), data management principles are applied to compilation and visualization of data collected during the slurry wall installation, with the intent of quickly communicating the installation status to owners.

1. CAD-GIS Conversion of Design Drawing



In this scenario, the design of the slurry bites was drafted in AutoCAD, resulting in a simple CAD file containing polygons representing the footprint of each proposed bite. This file was converted to a GIS feature class (for later linkage to the database) with the bite name assigned as an attribute.

2. Electronic Field Data Collection



A simple electronic field form was deployed using the free ArcGIS "Survey123" application (ESRI©; usable on all modern mobile device platforms) to facilitate quick and high-quality collection of key information during the bite excavation. Field QC personnel used this application to select the current bite and enter the as-built depth, equipment, completion dates, and weather. Any data input into this application were instantly uploaded (or stored and uploaded later where a cellular internet connection was not available on site) to a cloud-based database.

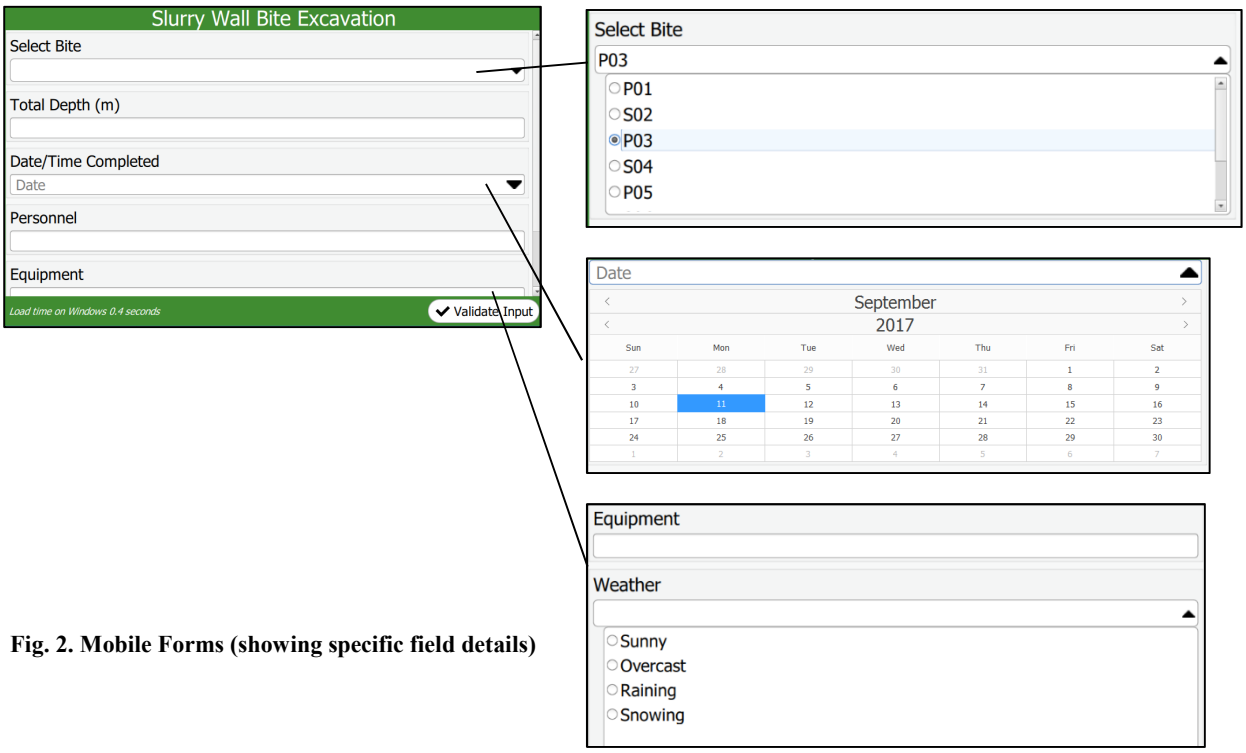
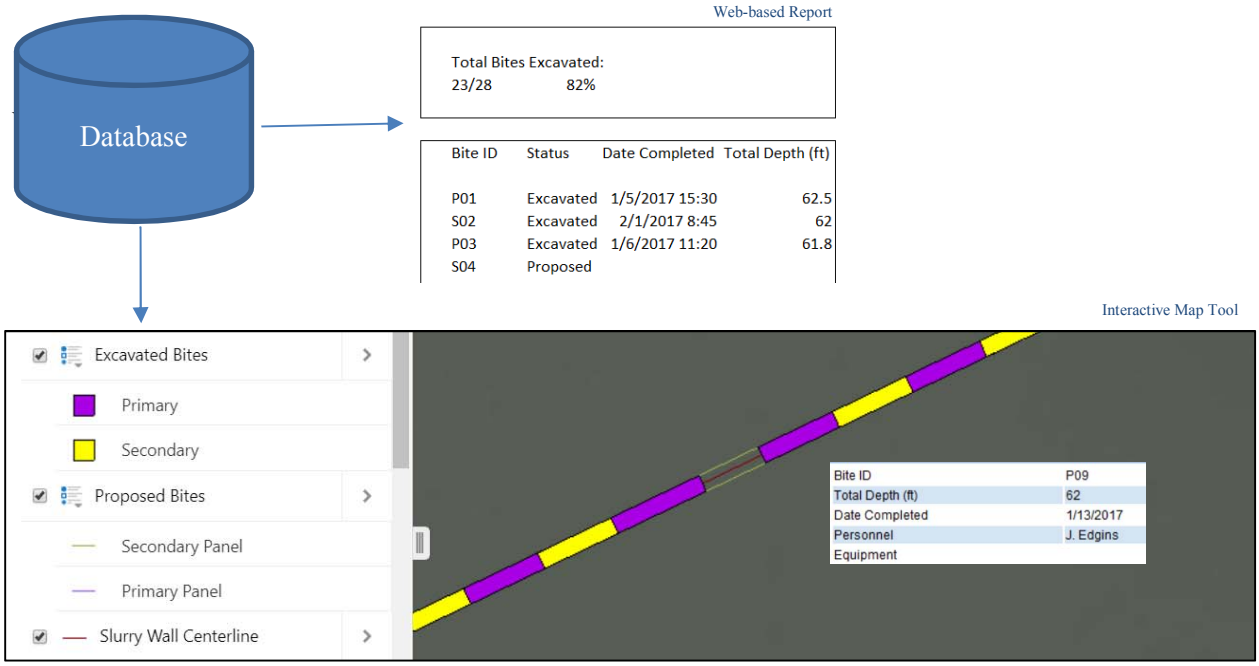


Fig. 2. Mobile Forms (showing specific field details)

3. Web-Based Reporting

By linking the database (populated directly with the electronic field form) to the GIS feature class, users were able to view the data in a simple web-based interactive map and report (each of which can be exported to CAD or PDF format for use as as-built drawings):

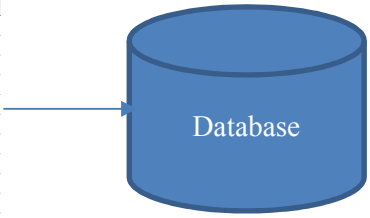


Small Grout Curtain

In this example (based on a 1,200 foot long grout curtain), data management principles are applied to compilation and visualization of grout take data read off of a grout monitoring device. For larger projects or when the technology is available, data from grout monitoring devices are generally streamed directly into a database for reporting, however for this example this task is reduced to some simple data entry.

1. Electronic Data Entry of Drilling Details

PointID	HoleDepth	Boring Type	Elevation	Plunge	Bearing	Station	Offset	North	East
S210U	70.7		985.21	-60		212.96		359,940.823	2,264,525.08
S230D	70.8		985.33	-60		226.93		359,947.892	2,264,509.46
S230U	70.6		985.1	-60		232.95		359,936.896	2,264,505.479
S250D	68.4		984.33	-60		248.14		359,943.706	2,264,488.636
S250U	67.4		982.47	-60		251.38		359,933.275	2,264,487.42
S270D	66.7		981.85	-60		268.99		359,939.639	2,264,468.223
S270U	66.6		981.68	-60		270.95		359,929.45	2,264,468.225
S290D	66.3		981.58	-60		289.2		359,935.675	2,264,448.391
S290U	65.9		981.22	-60		290.61		359,925.595	2,264,448.947
S301F20U	59.3		979.85	-70		300.88		359,923.089	2,264,438.965
S301F-20U	59.4		980.03	-70		301.05		359,924.028	2,264,438.618
S301F-40D	73.6		980.87	-50		300.69		359,932.939	2,264,437.218

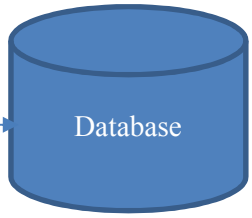


Similar to the "Electronic Logging of Major Details" component of the first example above, in this stage users populate a simple web-based form with data sufficient to define the geometry of grouting boreholes in a profile dimension. These details generally consist of the borehole name, location coordinates or station/offset, surface elevation, direction and batter of hole (for inclined holes, common in grout curtains), and total depth.

2. Electronic Data Entry of Grout Takes by Stage

Following the grouting of each borehole stage, the field personnel populate a similar web-based form by selecting the borehole (i.e., from the list linked from the above table), entering the top and bottom depth, and inputting the total grout take for that stage (as well as the associated grout mix design, date/time of grouting, and any other applicable details):

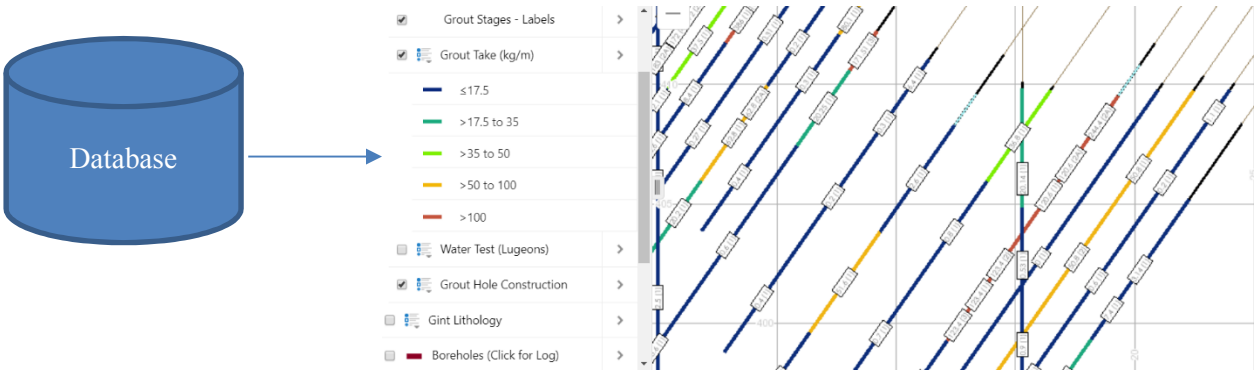
BoreholeID	Top_depth_ft	Bottom_depth_ft	Injected_Volume_gal
P000D	15.8	34.3	1.07
P000D	34.3	64.4	1,078.72
P000U	12.5	23.3	2,021.11
P020D	15.5	32.8	429.82
P020D	15.5	37.7	1.25
P020D	23	35.9	0
P020D	32.8	46	1,654.3
P020D	37.7	67.7	33.36
P020U	13.8	30	2,180.1



As with other examples of web-based forms discussed above, any data entered into these forms are immediately sent to a database which, in turn, immediately serves the data to the GIS and reports described below.

3. Visualization of Grout Takes in Profile View

Given the geometry calculated from the first table and the grout takes by stage entered into the second, the above information is sufficient to immediately visualize grout takes in profile view (a common way of assessing a grout curtain). A web-based interactive GIS, or simply GIS-produced PDFs sent to an owner, can be used for this visualization:

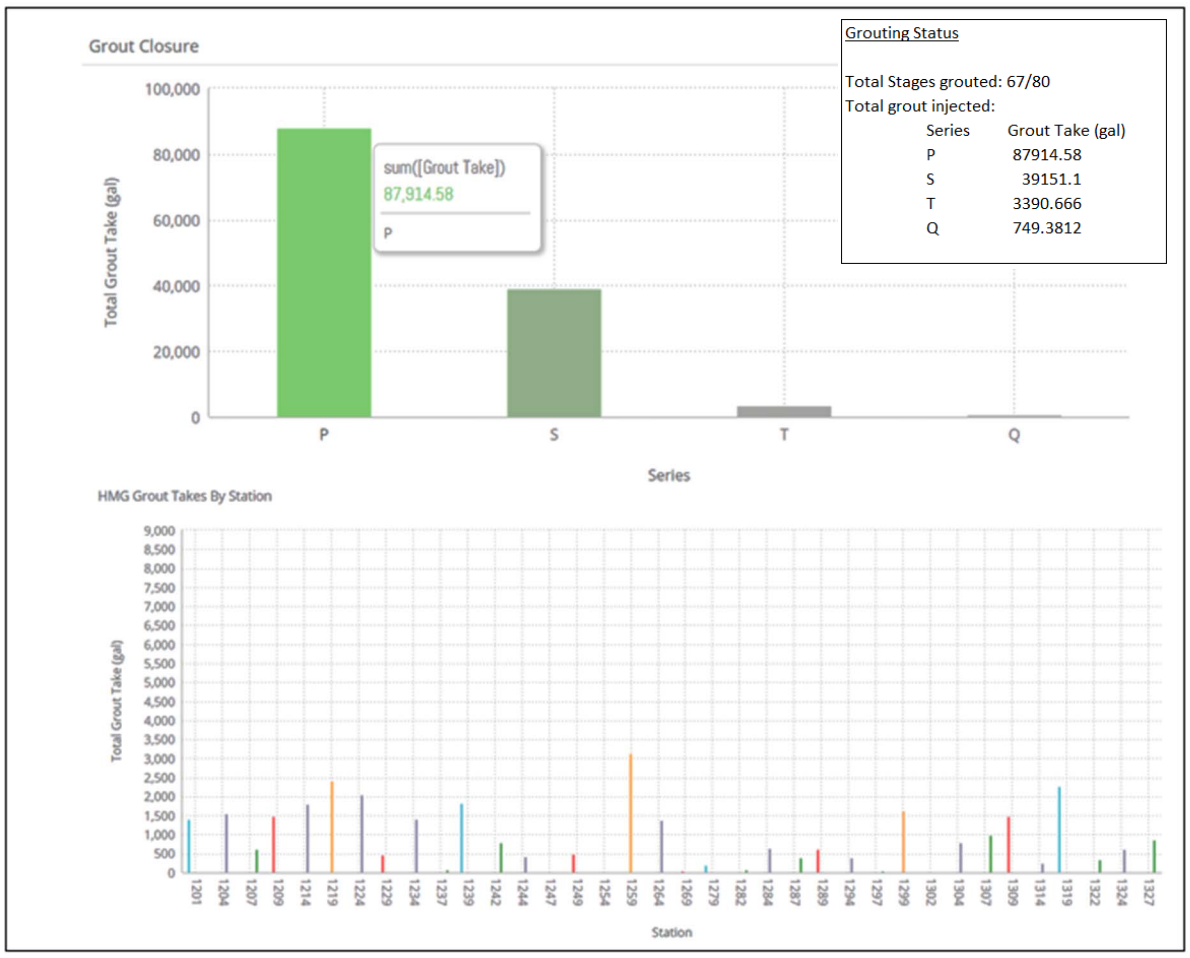


4. Automatic Generation of Grouting As-Built

Once in the GIS, these data (i.e., the grout stage geometry and grout take values) can be automatically and routinely printed to paper/PDF or exported to CAD (or MicroStation) format for submission as As-Built or Progress Drawings.

5. Reporting of Grout Closure and Pay Items

Frequently grout curtain data are reported in terms of "grout closure" (total grout take by hole series); progress (number of stages grouted as a function of the total proposed) and total grout placed. These (and any other metrics calculable from the entered data) are generally available as a database report on a website and/or electronically transmitted on a routine basis to the contractor and owner:



CONCLUSIONS

Good data management principles apply to data at any scale, including small or inexpensive foundation work. The web, database, and geospatial technologies described in this paper have matured to the point that they can be cost-effectively applied to small projects. With good data management tools and templates borrowed from larger projects, these smaller projects can benefit from the same efficiency and quality improvements required by owners at the larger scale.

DEEP FOUNDATION JOB SITES OF THE FUTURE: DIGITIZATION AND NETWORKING AS MAJOR STRATEGIC FACTORS FOR INFORMATION MANAGEMENT SYSTEMS

Halbeisen Arno MA, MA, Product Management IT Solutions, Liebherr-Werk Nenzing, Nenzing, Austria, +43 690 500 44906, arno.halbeisen@liebherr.com

ABSTRACT

The progress in computer development and data processing influences industries in different ways. Digitization and connectivity as key elements of this "digital transition" encompass a multitude of supportive and directive possibilities throughout the complete life span of a deep foundation job site. Information management systems (IMS) are characteristics of the changing environment and are comprehensive, multilevel, interdisciplinary tools that assist in the decision-making and planning of job sites.

The significance of the information and data, which form the foundation of these systems, will become more important in the future to fulfill the ever-changing legal, qualitative, and executing factors in the geotechnical construction sector. The success factor, and at the same time, the major challenge of IMS lies in the availability of clearly structured information. In addition to the planning aspect (based on empirical data, experience, algorithms and calculated models), it will be necessary to increasingly focus on the acquisition of actual job site data. Recorded information from various sources on the job site is interconnected, evaluated, and made available to the IMS.

Actual data are the result of continuous data flows, which facilitate the qualitative verification and evaluation of planning data for geotechnical projects on the job site. Added value is generated over the complete life span of the job site through close data networking on the planning, execution, and evaluation and/or documentation levels. Innovative digitization solutions are deployable, as a standard, for a large variety of deep foundation projects regardless of their complexity or dimension. Hereby, the emphasis lies on the benefit of actual data within IMS and their contribution to the success of geotechnical construction projects.

Keywords: digitization, networking, information management system, IMS, PMIS, BIM, data, information

INTRODUCTION

The development and modernization of a variety of economic processes is inevitably progressing at all levels of the economic chain. New technologies and innovations have become part of our daily work and private life. The introduction and more frequent use of communication and information technologies is a huge milestone with all its facets and possibilities. Many new catchwords are associated with this progress. To name but a few: Internet of things, Big Data, Industry 4.0 and above all Construction 4.0. These synonyms are linked to a variety of devices, specific practices, tools, and systems.

The digital world is changing our lives and our patterns of thinking in a major way. In many cases, digital systems are not only supportive applications and tools but also change the way in which business is transacted. The advancement of technical development in digital management industries will have an impact on all industries and will help to overthrow conventional industrial and economic approaches (Zukunftsinstitut, 2017).

There is a widespread belief that the megatrend of digitization will bring many new possibilities and opportunities. The expectation in the economy is primarily due to the potential for cost reduction and improvement of efficiency (Oesterreich and Teuteberg, 2016). However, many do not clearly understand how to benefit from digital changes.

© 2018 Deep Foundations Institute

Digitization will also have a significant impact on the construction industry, which is a spearhead of innovation in many areas. In particular, keywords were created to name this digital transformation, such as: IMS, Building Information Modeling (BIM) and Construction 4.0. How these are interpreted and how the needs of the construction industry can be fulfilled with these digital approaches, however, is rarely mentioned, leaving the interpretation to each individual. Terminology without substantive concretization and solutions is practical in its names, but quite often brings confusion rather than benefits. Only by the implementation of precise digitized possibilities, practical examples and approaches can they generate synergies and advantages.

In this publication specific processes and solutions for the construction industry will be pointed out, focusing in particular on the future needs of deep foundation job sites. The target is to answer the questions of how digitization and networking of technologies can be applied to deep foundation construction sites and how technologies can be used as a foundation for the implementation and operation of IMS. As digital change influences all levels of a construction site, the focus here will be to describe the value added for all participants involved in the process.

First, the definition and understanding of IMS, as well as digitization and networking within the framework of information and communication technology, will be discussed. As mentioned in the title, these two forms of technological change in the construction industry that form the foundation for IMS, intelligent machine control systems, IT tools and assistance systems. An approach of data consolidation and allocation on the construction site and its integration with the IMS is described in detail. Further aspects discuss how digitization and networking affect the known processes in the field of deep foundation construction, the challenges to be mastered and how future visions are already being implemented today.

INFORMATION MANAGEMENT SYSTEMS (IMS)

Within the context of the paper, IMS is determined as the overall expression for the concept of information utilization and handling. Depending on the organizational nature and structure of the applied IMS, the functions and possibilities are adapted to meet the different needs of the users. Hereby, the most common IMS applied for construction sites are Project Management Information Systems (PMIS) and information systems, allocated to the BIM methodology. Both approaches as well as their general understanding concerning the utilization of construction data are described in the following paragraphs.

Project management information systems focus on construction processes from a project and work package perspective. Referring to the definition of project management by the Project Management Institute, a project is of temporary nature with a clearly defined start and end point (PMI, 2017).

The PMIS is based on manual and electronic information from communication technologies consolidating data from various sources through a wide range of tools, software and methods. The main goal of the PMIS is to plan, calculate and manage tasks between stakeholders as well as document, report and execute work within the defined time period. The information and data are mainly needed and utilized during the existence of the project.

BIM identifies a cooperative working method. Based on a digital model of the construction site, all relevant information and data are recorded, administrated and exchanged through a multi-faced transparent communication layer between the involved parties (Mondino, D., 2017).

Data sets are used to calculate and visualize desired aspects, ensuring a flawless construction process. BIM methodology considers the entire construction life cycle beginning with planning and realization and ending with the maintenance of a building and construction site. In comparison to the PMIS, the BIM relies more on digital data provided from various sources and the data are used over a longer time period. Therefore the applications behind the BIM methodology function best when linked to automatic data streams.

IMS, PMIS and the BIM methodology are characteristics of the changing technical environment and are comprehensive, multilevel, interdisciplinary tools that assist in the decision-making and planning of job sites. To be competitive in the ever-changing market, to meet today's legal requirements and to cover all aspects necessary for providing safe working processes, construction managers have to be able to execute tasks flexibly and make decisions quickly based on reliable information.

The most important factor for speeding up the decision process and for preventing extra work and incorrect decisions is having accurate, proper, and well-timed information. The main tasks of an IMS within both approaches includes collecting, processing, and refining raw project data at the construction site and create a basic consolidated database for management (Yeganegi and Safaeian, 2012).

Although the two approaches differ in their perspective of a construction site and the utilization of information, the core remains the same. The core element of information systems is to collect data from all kind of sources related to the construction site. Data are gathered, consolidated, processed and transformed with the main objective to produce useful information and to distribute it to the persons whose work depends on it. The target-oriented allocation of up-to-the-minute information to the individual as well as the entire construction organization can be seen as the ultimate goal of the IMS database.

The database once established can be applied on the construction site for documentation, proof of quality, cost calculation, risk prevention, and as a basis for management decisions. The success factor and at the same time the major challenge of PMIS and BIM, lies in the availability of clearly structured information, which is appropriately prepared and specifically assigned to the relevant tasks of the parties involved. To go one step further, the structured information in these systems bares most advantages, depending on the stage of the construction life cycle, if it is based on actual data consolidated from various sources on the job site. The emphasis lies on the benefit of actual data within IMS and their contribution to the success of geotechnical construction projects.

DIGITIZATION AND NETWORKING

Digitization has its starting point in the increasing computerization after the turn of the century. Successively it became possible to convert analog values into electronic information. The processing and storage of digital data and the resulting endless possibilities, as well as the variety of possible applications represent the core element of digitization (Drenth, 2001).

The increasing use of new technologies and intelligent machine control systems in a variety of workspaces makes it possible to generate an all-encompassing data-driven information flow. Data are continuously generated and further processed, converted, and stored temporarily within the control system. Most of the data are stored automatically in the background or recording is initiated manually.

Construction machinery are a key element and play a major role in the construction process. The machine operator controls the movement of the construction machine and these physical analog pulses are converted into electronic data. In this context, the control systems of intelligent machines compile and combine data from a wide range of sources, thereby generating a continuous stream of data.

These data are on the one hand, relevant for the control of the machine, but on the other hand identifies a multitude of options and potential for further utilization. If it is extracted and edited in the right form the resulting machine data pool is a rich source of knowledge and information, which can make the construction processes transparent and comprehensible.

Digital data is the framework for the digitization of the entire value added chain that will be the basis of all construction processes. The intelligent interconnection of these digital data represents the second core element of digital transformation and is to be understood as a series of electronically supported processes, applications, devices, and machines as well as data sources.



Fig. 1. Deep foundation equipment is the key element for data generation on a construction site

The various base data flows are integrated, channeled, and combined. The complexity of the data streams is simplified, knowledge becomes clear and visible and access for authorized persons is considerably straightforward and can be separated locally as well as asynchronously.

In the project highlighted in figure 1, under the perspective of digitalization, deep foundation tasks were one part of a superior BIM process. The requirements for the deep foundation contractor were based on providing reliable and tamper-proof data to ensure the accuracy of the piling and drilling tasks. Additionally the awarding authority requested a continuous status report of the process in their office and the automatically upload of the information in the database of the planning system to compare the actual situation with the plan.

A digital workflow was created around the piling and drilling machinery, which is the central element for data handling on a job site. A data recording system was installed and connected to a DGNSS-positioning system and the machine control unit. A mobile concrete pump was connected to the control system of the drilling and piling machine, which was also equipped with its own comprehensive telematics system.

The digital, inter-connected and modularly structured IT-solutions allowed for the constant flow of concrete-, process- and machine data. The position accuracy, and depth of each pile was recorded as well as the concrete volume. The telematics system was used to transmit the data with a high data rate to a cloud system enabling a constant monitoring of the information outside the construction site. A separate software running on a tablet was used for displaying the information graphically. In the background, a specifically created data interface uploaded the same information to the IMS allowing the comparison between the actual and planned data. This information was further used for the quality assurance documentation.

Digitization is the driving force, which intensifies the networking of processes. The use and merger of technologies create positive effects that can be used in a targeted manner within the construction industry;

for example, data created from these technologies can be imported into IMS and further applied in various ways.

CHALLENGES FOR DIGITIZATION AND NETWORKING ON DEEP FOUNDATION JOB SITES

Different aspects must be considered when providing IMS with data from construction sites; for example, safety issues, technical, and ergonomic matters. Challenges in digitization and networking in the construction industry concern data security, the meaningful use of data in the background of data consolidation as well as the generation of acceptance among the users of new technologies (Oesterreich and Teuteberg, 2016).

In designing the solutions, the aspect of data security is of utmost importance. In this respect it is vital to ensure that the three important safety mechanisms (Holtgrewe et al., 2015) are respected.

1. **Functional safety of the machine and equipment:** Construction equipment manufacturers must make sure that the digital applications and solutions designed around the machine do not pose a risk for the construction site workers or their working environment. On the job site, this responsibility is taken over by the operator. Assistance systems and semi-automatic systems are checked in detail for potential hazards. Applications and devices must be intuitive and for safety reasons may not be a physical obstruction.

2. **Data security:** This safety mechanism ensures that the connectivity, reliability, integrity, accuracy as well as confidentiality of all the recorded data are secured. Digitally interconnected systems require secure authentication, authorization, and communication between the digital solutions has to be encrypted.

3. **Data protection:** The protection of corporate data as well as exclusive access rights have to be clearly defined.

The selection of data is of major importance within the framework of data consolidation. This is especially true for digital systems with the key function to select existing data within a data pool. Therefore, the design of these applications, especially in data recording and data evaluation solutions, focuses on easy handling, user-friendliness, clarity, and data uniformity. The generated data have to be processed in the background in such a way that they can easily be applied to the applications linked to the IMS and that the information is clearly visible and understandable.

Digitization and networking have a strong influence on the understanding of the different disciplines and the cooperation of the various participants. Therefore, the replacement of analog information and manual recording by digital, transparent, and comprehensible processes is not a purely technical topic, but its success depends in particular on the acceptance and openness of the persons involved. The daily contact with digital systems in the workplace makes it much easier to manage and implement such systems. When it comes to designing new technologies and applications, it is of particular importance that the operating patterns correspond to the devices in the private environment, so as to avoid any initial concerns.

Whether the implementation of an IMS is successful or not strongly depends on how the above mentioned challenges are met through respective measures and conditions. Only a secure and well thought-out system, the creation of valuable data out of an information pool, and ergonomically designed applications that generate the rough data ensure that IMS offer advantages for construction projects.

DATA CONSOLIDATION AND ALLOCATION TROUGH IT SOLUTIONS ON THE CONSTRUCTION SITE

Construction projects figure among the most complex work processes due to their extremely differentiated value added chains. They are unique and strongly based on the division of labor. Furthermore, the environmental factors are constantly changing. Implementation takes place within a limited timeframe and in a specific environment (Oesterreich and Teuteberg, 2016). Construction projects are subject to legal frameworks and requirements which are often include record-keeping and verifiability. Deep foundation work, as a branch of the construction industry, requires specific knowledge both in geotechnics and measurement technology. Many processes require a high degree of verifiability with regard to quality and function and are therefore associated with high competencies of the companies in planning and execution. Due to amendments to European standards, for example, the execution of construction projects becomes even more difficult and complex.

With all its factors, circumstances and complexity, deep foundation construction work offers considerable potential for intelligent machine control systems, IT tools, and assistance systems. Digital solutions can lead to rationalization and optimization of the processes, transparency and traceability as well as qualitative assessment. The possibilities arise from the generation of data from various IT solutions, the transmission of pre-consolidated and transformed data from the job site to a central database and finally the data import into an application which is part of an IMS.

The advantages of digitization in deep foundation projects are linked to the synergy effects achieved through high-tech drilling, trenching, and piling equipment in combination with a wide range of attachments, geotechnical measurement, construction logistic, and concrete mixing techniques. Deep foundation machinery, as a constant in changing construction projects, is already able to store a large amount of digital data from a wide variety of construction process sources and to use them in a targeted manner. In doing so, value is placed upon connecting data from internal sources and external systems in order to generate the best possible added value for the operator of the machine at that time and especially for the IMS user later on.

Cross-linked solutions offer a multitude of different advantages and added value for companies, persons and corporations involved in the construction process, such as:

- a uniform data recording system allowing consistent data collection and verification. An existing data pool on the machine linked to the machine control system is the basis for the use of other digital solutions.

- digital operator assistance systems such as control systems for machine tool positioning and vertical measurement, as well as process monitoring systems, using data on a constant basis and producing valuable information. They also enable easier operational use of the machine, contribute to safety on the construction site, and increase efficiency. Work processes can be sped up and costs saved.

- data transmission solutions networking the different systems together, thereby enabling access to authorized persons and allowing to make use of data independent of location and time. At the same time, the main focus is on a seamless transmission of data while adhering to the safety mechanisms.

- data evaluation solutions and fleet management systems as part of the IMS are fed with actual data, thus increasing transparency of the work process, allowing for the identification of possible improvement potential and measurement of the value added process. Data records can be used as proof of quality and serve to trace the work carried out.

In the following paragraphs a practical approved modularly structured approach and workflow is presented on how the structure of data generation and data transmission on a deep foundation site can be designed under the aspects of the above mentioned challenges. Furthermore, it will be described how the data can be utilized in applications as part of an IMS to create added value.

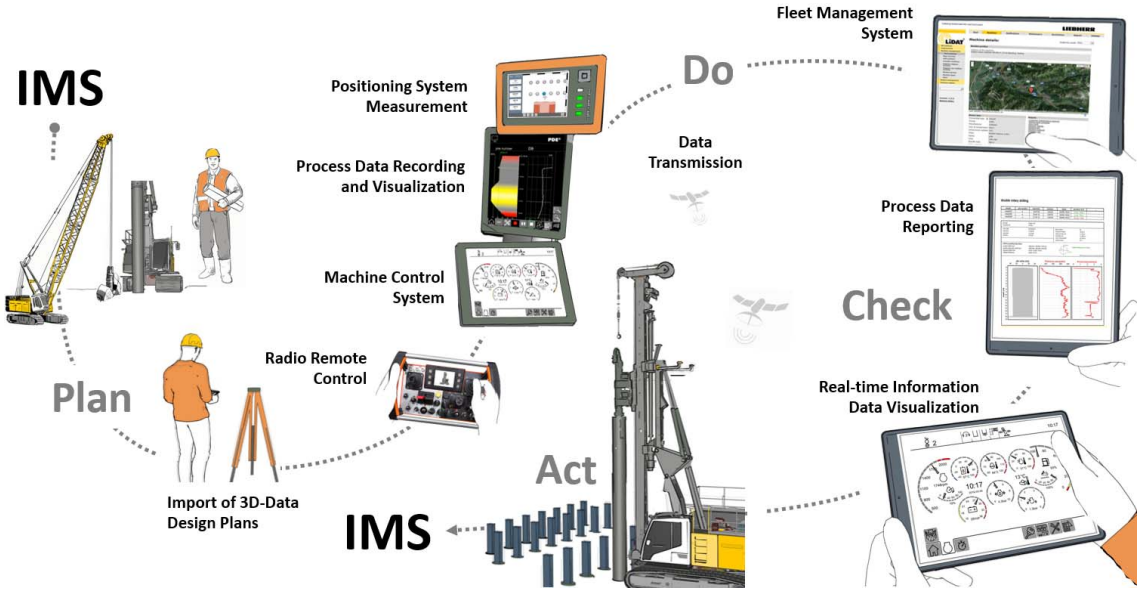


Fig. 2. Digital, inter-connected and modularly structured IT-solutions for deep foundation construction sites

Figure 2 shows that the different IT-solutions available for a deep foundation construction site are connected to an IMS from the beginning and to the end of the workflow. The workflow acts like a bridge, not only between the planning and execution of the piling and drilling tasks but to further construction site tasks as well. The workflow shows a wide range of solutions, closely inter-connected and modularly structured.

As an example presented in Figure 2, Liebherr deep foundation machinery and its built-in electronic control systems represent a central element on the construction site. Standardized protocols, data interfaces and transmission networks enable the gathering and storage of tamper-proof data from various sources. This includes data from embedded and integrated control systems for machine positioning and vertical location as well as machine-produced data, operational data, and many more. Big Data analysis of the various sources is done in real-time on the machine during operational use. This allows for a complete, transparent and traceable workflow.

Digital solutions, which are linked to the constant data flow include piling and drilling design planning software for the surveyor and planner, remote radio control, machine positioning control, verticality quality measurement, wireless data transmission solutions and a process data recording and visualization system for the operator. For the construction supervisor an IMS tool set is available including a fleet management system, a teleservice solution and a reporting, documentation and evaluation software. This tool set is again connected to a superior IMS.

The key elements for data handling within the deep foundation machinery are, on the one hand, the machine software and the built-in electronic control system. On the other hand, there is a process data recording and storage system, physically linked and integrated on a data level with the machine control system. Such a system allows the storage of digital parameters of various origins and data types: logistic data, machine data, control data, process data, sensor data, measurement data, position data and transfer data. Data consolidation of the various data sources is done in real-time on the machine during operational use.

Standardized protocols and data interfaces available on the built-in recording system enable the gathering and storage of data from external systems and their further integration into the machine control

system. This allows for real-time combination of information, an enhancement of possibilities for data utilization and extended data recording in the process.

Machine tool positioning and vertical measurement control systems are embedded into the process data recording system. As a result, the data pool is fed and differentiated with valuable information. The use of a Differential Global Navigation Satellite System (DGNSS) machine control system for positioning facilitates the digital bridge between the planning side and the operational side of a job site. A digital design plan is created as part of the IMS and uploaded onto the machine. The operator positions and navigates the machine tool according to the predefined geotechnical requirements.

Vertical measurement systems are used to measure the quality of the operation underground. The integration of both systems enable a uniform, consistent flow and recording of position and measurement data. The resulting data are tamper-proof and represents a multifaceted and combined documentation of the actual process that is carried out. The recording of data includes potential for semi-automated processes and functions. Certain process functions can be automated based on the collected data pool whereby the machine control system's safety mechanisms are taken into account. Radio remote control connected to the machine control unit data pool allows for a wireless navigation of the machine and set up of the different machine attachments. Automated digital recognition of the attachment creates data which enables a continuous virtual overview of the piling or drilling process.

With the help of the data recording solution, the machine operator is assisted during the working processes with displayed process-relevant parameters; this makes it possible to adjust the currently ongoing process. Data visualization acts as an assistance system for the operator and allows to monitor the process. Furthermore, selective functions in the visualization can be presented as a guideline. Technology-based process supervision enables active operational corrections and error prevention. Supervision based on data recording allows the mirroring of the entire process later within an IMS and comparison to the requirements set in advance.

The collected data pool is exported wirelessly from the machine using a networked internal telematics system with the aid of mobile radio technology. For the data transmission, a special network is designed to meet the requirements of data security, functional security, and data protection. In this context, special emphasis has to be placed upon the design performance as well as the security mechanisms such as confidentiality, data integrity, authentication, and authorization.

Data transmission solutions are the interface between the construction site and the database of the IMS, preferably as a cloud solution. Thus, the data are made available to other users for the optimization of the working processes. Mobile and remote access for authorized and defined persons is possible at any time. Within a comprehensive IMS, applications in which the data creates specific values are data reporting and evaluation solutions as well as fleet management systems. These applications are either part of an IMS, a stand-alone software linked via a database, or integrated into the IMS.

Using a database function in the IMS, the data packages can be directly imported from the machine, managed and used in a flexible user-friendly way. Functions within the scope of an IMS combine the different networked data sets and create corresponding individual or standardized protocols. A diversity of parameters are displayed graphically and enable optimized planning and site-independent monitoring. Access to the information is available via intelligent license management. Data can be used regardless of a person's location or time zone. Real-time recording and transmission solutions enable tele-maintenance functions in the IMS to help the machine operators independent of their actual location and time zone during maintenance and fault finding.

The above mentioned digital solutions are networked and allow for a comprehensive, transparent and traceable workflow. The intelligent networking of the different digital applications encompasses the entire value added chain of the deep foundation construction work and enables a uniform, consistent flow of data. The persons involved can use different data purposefully and access for authorized persons is available regardless of their location and time.

CONSTRUCTION SITE REPORT

A deep foundation construction project in May 2016 for the construction of a multifunctional lifting bridge in Hamburg played a leading role in the application of innovative, networked, and digital solutions.

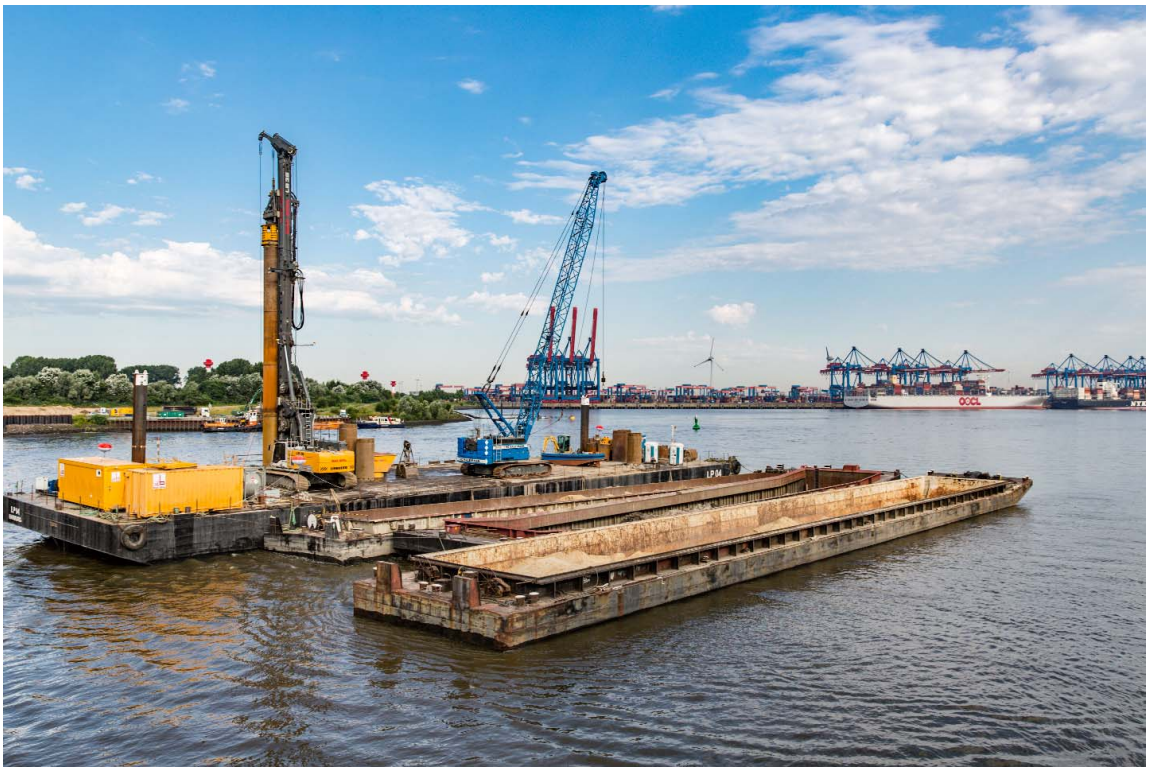


Fig. 3. Deep foundation project in Hamburg, Germany

For the construction of the bridge foundations, complex underwater foundations were necessary. The circumstances and conditions of this project normally require a considerable amount of surveying work, as conventional work processes used on land are not applicable. A drilling rig equipped with a machine control system for tool positioning was installed on a floating pontoon. The drilling rig was operated in Kelly drilling mode to remove the sediment and soil underwater. After which, sand was filled into the casing one meter above seabed level that was later used for piling of the bridge fundament.

Process data was directly integrated from the machine control system for drilling and pile driving equipment into the process data recording and reporting system. State-of-the-art DGNSS technology provided precise and efficient positioning of the rotary drilling machine and Kelly attachment on the pontoon.

The analog plans for the foundation construction were used as basis for the positioning of the riverbed exchange. The plans were digitized by a special software as part of an IMS and uploaded to the machines control system located in its cabin. The interconnection between digitized drilling plans, actual DGNSS and machine data assisted the operator in the precise positioning of the machine tool and allowed for pin-point accuracy of the drilling in the seabed. Figure 3 shows the machine navigation on the barge with the DGNSS position system.

The integration of data from the machine control system for positioning of the tool allowed a comprehensive and uniform recording of the position data, process data, logistics data and machine data. Data transmission solutions allowed the automatic transmission of data via Global System for Mobile

Communications (GSM) and General Packet Radio Service (GPRS) from the machine to the data cloud in the information management software used in the construction site office located nearby on land.

The construction progress could be continuously monitored on a tablet and compared with the requirements stipulated in the design plan. The IMS created standardized reports based on the recorded tamper-proof data. The reports were used as quality assurance and the data was stored in the IMS for validation purposes. Through digitized data, the soil exchange workflow became traceable and transparent.

SUMMARY AND CONCLUSION

Digitization and networking on the construction site represents significant strategic factors for implementation and operation of IMS. To illustrate this, the paper defined digital and networking solutions, IMS as well as major challenges concerning IT solutions on construction sites. Based on the definitions an approach for data consolidation and allocation was presented and substantiated through a job site report.

The job site report from Hamburg showed that data generation, consolidation and transmission to a database, and especially the target-oriented utilization in a multifaceted IMS is no longer a vision, but already exists as a promising base today. By establishing a consistent data framework, actual data from a deep foundation site input in an IMS identifies potential for validation, traceability, proof of quality, and monitoring. The construction workflow becomes even more transparent through the emphasis placed upon the appliance of digital solutions on deep foundation sites thereby extending the amount of data recorded and possibilities for utilization.

ACKNOWLEDGEMENTS

First of all, I would like to thank Liebherr-Werk Nenzing and their representatives for the support and assistance during the development of this paper. Special thanks to Marcel Flir, Wolfgang Pfister, Sascha Bechter, Martin Amann, Sebastian Vallaster, Chris Tammadge, and Eva-Maria Pirchner.

REFERENCES

Drenth, P. J. D., 2001. Die digitale Revolution in den Wissenschaften: ein „mixed blessing“. Festvortrag. https://web.archive.org/web/20121114112415/http://www.uni-heidelberg.de/presse/news/2112drent.html. Accessed 17-09-26.

Holtgrewe, U., Tiresenecker-Caba T. and Flecker J., 2015. Industrie 4.0 – Eine arbeitssoziologische Einschätzung. Forschungs- und Beratungsstelle Arbeitswelt FORBA, pp. 14-16.

Mondino, D., 2017. Architektur – Planung. Planen Bauen 4.0, http://planen-bauen40.de/handlungsfelder/architektur-planung/. Accessed 17-09-26.

Oesterreich, T. D. and Teuteberg, F., 2016. Chancen und Risiken der Digitalisierung in der Bauindustrie im Kontext von Industrie 4.0 – Situationsanalyse im Zuge einer Technikfolgenabschätzung. Proceedings zur INFORMATIK 2016, 46. Jahrestagung der Gesellschaft für Informatik e.V. (GI), Lecture Notes in Informatics (LNI), pp. 1429-1443.

PMI, 2017. What is Project Management?, https://www.pmi.org/about/learn-about-pmi/what-is-project-management. Accessed 17-09-26.

Yeganegi, K. and Safaeian S., 2012. Design of Project Management Information System. Proceedings of the 2012 International Conference on Industrial Engineering and Operations Management Istanbul, Turkey, 2012 July 3-6, pp. 2545-2551.

Zukunftsinstitut, 2017. Reiseführer Digitalisierung. Verlag Wirtschaftskammer Österreich, 4 p.

ELECTRONIC SUPPORT IN INSTALLATION OF SPECIAL FOUNDATION PRODUCTS - ENSURING SAFE PRODUCTION AND INCREASING QUALITY CONTROL

Franz-Werner Gerressen, Bauer Maschinen GmbH, Germany, franz-werner.gerressen@bauer.de

ABSTRACT

New developments are required day by day. On the one hand site to improve the actual situation, on the other hand to create the future and to ensure that future demands can be fulfilled. This requires for instance the development of technical support systems, which enable a more constant and quality ensured installation of special foundation products like piles. For instance, assistance systems relieve the machine operator by automating monotonous or repetitive operations. As part of the quality control, real time installation control of the production process, data transfer and reporting systems become more and more important ensuring the five dimensions of a jobsite. That means not only the three dimensions are covered, but also the dimension of time and money. Therefore, the paper will describe some of these new approaches and activities required for these new developments. It will describe also the main equipment which will be needed to execute these works.

Keywords: Electronic, Assistant Systems, CFA, 5d bim, Piling, Piling data, Rig instrumentation

INTRODUCTION

New developments are required day by day. Either to improve the actual situation, or to create the future and to ensure that future demands can be fulfilled. Therefore, there is an increasing demand for the development of Assistance systems. Assistance systems are for example technical support systems, which enable a more constant and quality ensured installation of special foundation products like piles, for example an assistance system like the later explained “drilling” assistant. As part of the quality control, real time installation control of the production process, data transfer and reporting systems become more and more important ensuring the five dimensions of a jobsite. That means not only the three dimensions are covered, but also the dimension of time and money. For instance the use of assistance systems leads to cost saving opportunities like reduced concrete overconsumption or reduced wear and tear.

THE MACHINE UNDER CONTROL

General

The actual used electronic systems like e.g. the B-Tronic enables you to efficiently operate, maintain, and administer individual machines as well as entire fleets. The highly efficient systems are based on dozens of small sensors, such as heat, pressure and level sensors, placed at all critical locations on the machines, which continuously collect data. These data are logged centrally and processed. High-resolution touch-screens with a range of different display modes inform the machine operator instantly and comprehensively about the current status of his machine and provide him with valuable information for the optimal use of the machine. It helps you to securely monitor and precisely evaluate your projects and work processes. Data transmission systems, such as W-LAN, USB and DTR (a BAUER specific communications unit), facilitate the transmission of machine operating and production data both locally as well as globally.

© 2018 Deep Foundations Institute

In addition to these basic operational data, general machine operating parameters (e.g. engine data) can be also acquired and monitored. The display of current machine operating states and error messages is a valuable aid for targeted and effective fault finding by service personnel on site, but also by specialists based at the offices, as data can be transferred real time via internet connection. This does not only allow the control of equipment and installation process including relevant reporting, it also allows comparing "virtual reality" and "reality", hence planned and actual execution, which enables the project manager to control not only the schedule, but also the use of budget.

Assistance Systems

In a growing global market for the specialist foundation industry it will become more and more difficult to find experienced operators or to get new operators educated to the level which is required to fulfil the demands of quality ensured installation of the product, as well as high productivity and cost saving. Therefore, it becomes more and more important to equip the machines with a kind of "intelligence" to assist the operator in optimized use as well as to avoid operating errors. For instance, the definition of drilling parameters for an optimized drilling process in the complex interaction of ground condition, machine regulation and operator intuition is not easy.

As experience counts, therefore, a special focus was given in the recent past to the development of practice-oriented and process-specific support systems which aid the machine operator in the execution of his routine tasks, such as crowd and torque control during drilling with the Drilling Assistant, or volume and pressure control during concreting with the Extraction Assistant - both hands free operations. These systems relieve the operator by automating repetitive operations with a system like the B-Tronic system. They help to prevent faulty operation of the machine and therefore protect both man and machine. Automatic, fast control processes increase the drilling performance and reduce wear of both, equipment and tools. Assistance systems thereby ensure a consistently high production quality. Actually more than 20 different assistant systems are available for various applications. All assistant systems are integrated into the general electronic monitoring and control system. They ensure for instance that piles are installed to a high and consistent quality standard. All relevant data is displayed on the operator's monitor (Fig. 1).



Fig. 1: Exemplary B-Tronic display during the concreting process in automatic extraction mode

Some of these assistant systems will be discussed in the following.

Satellite-based Navigation System for Positioning and Documentation

With the Assistant Positioning System, the machine operator can utilize the advantages of a satellite based navigation system for positioning the drilling rig. The system guides the rig operator simply, quickly and accurately to the next pile position (Figure 2).

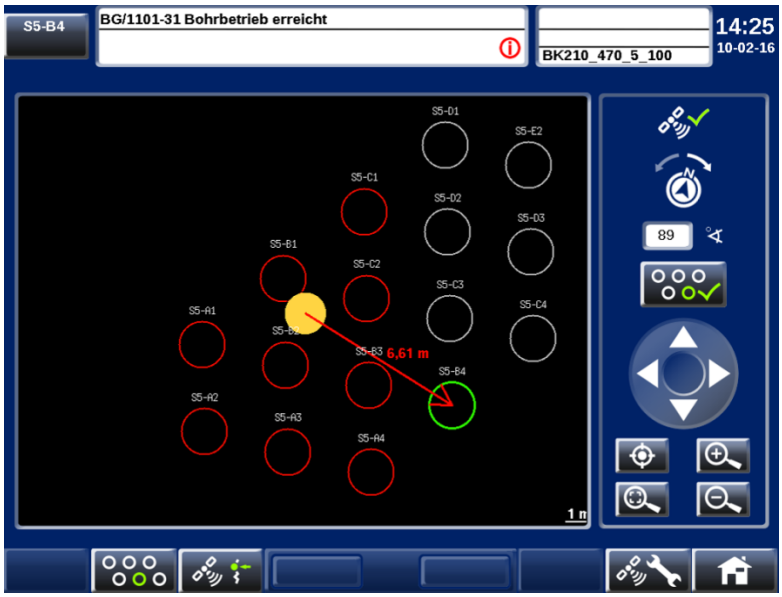


Fig. 2: Operating screen for satellite based positioning

Nominal and actual coordinates of each pile are logged after completion and can be used to verify that all piles have been drilled with the specified accuracy. In addition to the benefit of quality control, time and cost saving for single, manual setting-out of pick-up points can be achieved.

Controlling the installation process, e.g. by using a "Drilling" and "Concreting Assistant"

Most rigs can be equipped with electronic software for use with the so called "Drilling Assistant", which modulates the optimum rate of penetration and crowd force during the drilling process for an optimal speed of rotation of the drilling tool, especially working in single pass methods like Continuous Flight Auger (CFA), Full Displacement Piles (FDP) and Cased CFA. The desired initial parameters can be input by the rig operator with the help of simple onscreen menus.

The drilling assistant therefore not only relieves the operator from duties which requires full concentration over a long time, but also increases the drilling performance compared to manual working.

In addition, the system avoids for a system like CFA-Drilling two unwished situations. The one is the well-known over-rotated and excessive soil removal, known as "over-flighting" (Figure 3). That means penetration speed is to low compared with rotation speed. This leads to a situation, where the surrounding soil get loosened and the load capacity of the pile might be reduced. In addition, beside the increased amount of spoil, also significant overconsumption of concrete can be observed. Both leads to increased cost for pile installation. Moreover, as a worst case scenario, this can cause ground around the tool to become unstable and ground settlement induced.

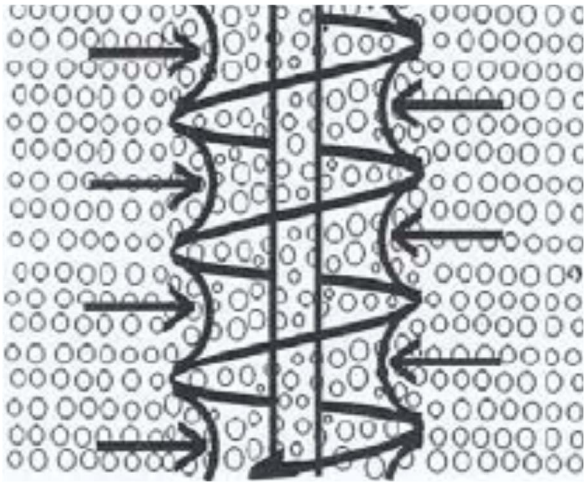


Fig. 3: principle of “over-flighting” [3]

The second situation to be avoided is the so called “corkscrew effect”. Here the situation is the other way around. Penetration speed is too fast and rotation speed is too low in relation. In this case the tool can get stuck in the ground and removal can cause damages either to the tool or to the machine.

Both scenarios can be avoided by using the “Drilling Assistant”.

While the focus of the “Drilling Assistant” is more about performance, the “Concreting Assistant”, especially for the single pass methods, focusses on the pile quality.

By using the "Concreting Assistant", the speed of extraction and volume of concrete can be adjusted. This involves measuring the volume of concrete continuously throughout the concreting process and automatically regulating the speed of extraction based on the concrete flow rate. Of course, also the concrete pressure is monitored and controlled during the concreting process. As control of all relevant parameters takes place, concrete overconsumption can be reduced and blockages can be avoided.

Advancements for CFA drilling

Even though the assistant systems are quite helpful; there is still demand for improvement. As the European Standard states, that “During continuing placement, the concrete at the tip of the auger shall be kept under a pressure exceeding the external pressure, so that the volume vacated by the auger’s extraction is concurrent and completely filled”, the measurement of the concrete pressure is of high importance. However, as the concrete pressure is usually measured at the top of the tool, the real concrete pressure at the bottom of the pile is significantly higher than measured and therefore also higher than required.

A possibility of measuring the concrete pressure at the bottom of the auger would be highly appreciated to have a more exact quality control as well as an additional cost saving potential in concrete overconsumption. This requires not only special sensors which can be integrated in the drill string, but also a feasible and reliable data transfer through the drill string to the data monitoring system. In the past several trials have been made using standard wire inside the drill string. This solution was not well accepted as it was uncomfortable in handling on site while assembling, maintaining or disassembling the drill string and unreliable as wires broke too fast.

An improvement can be seen already with a system provided by Jean Lutz (Figure 4), where the sensor measures the data during the installation process, stores it and transfer it wireless as soon as the drill string reaches the ground surface.

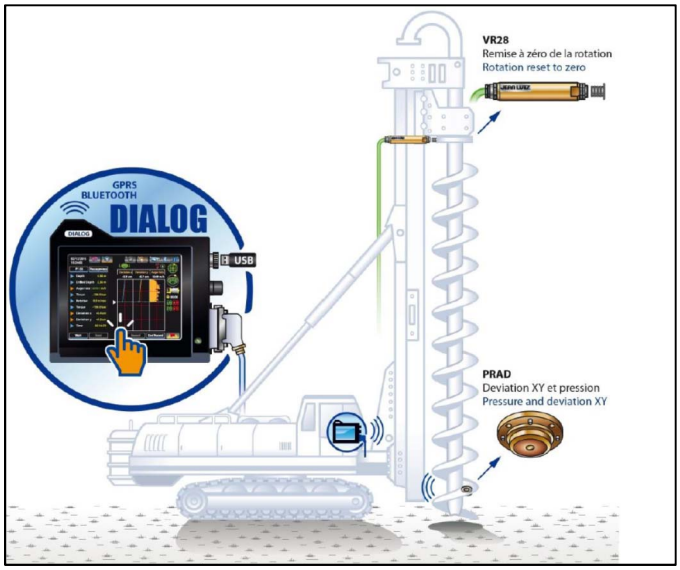


Fig. 4: Jean Lutz concrete pressure measurement system [5]

This development provides concrete pressure information of the bottom for documentation, but unfortunately not in real time for the operator to react in case it's needed.

Another approach is the development of the so called iCFA system.

iCFA

The iCFA system is a development to fulfil the growing demands in quality assurance for the installation of CFA piles. As mentioned before, the monitoring of a higher concrete pressure than earth pressure is required. As usually the concrete pressure is measured at the top of the drill string, the real pressures in the ground are much higher than required and can cause unnecessary concrete overconsumption and in a worst case scenario blockages of the concrete line. The iCFA system is now equipped with a pressure sensor at the bottom of the drill string which allows a more accurate pressure measurement and therefore provides potential cost savings in concrete overconsumption. In addition, the iCFA drilling rod measures as well the inclination of the pile at the bottom of the drilling string.

As measurement at the bottom is quite complicate, a special drill string was developed. A specific feature is that the data transmission is not done by wire, but by inductive data transmission through the auger joints, which were somehow eponym for the "i" in the name. Figure 5 shows the general configuration and highlighted details of such a drill string.

Obviously, this specific drill string is more expensive than a standard drill string, mainly due to the couplers and of course due to the additional sensors. This investment will be paid off over a reasonable time by the potential savings.

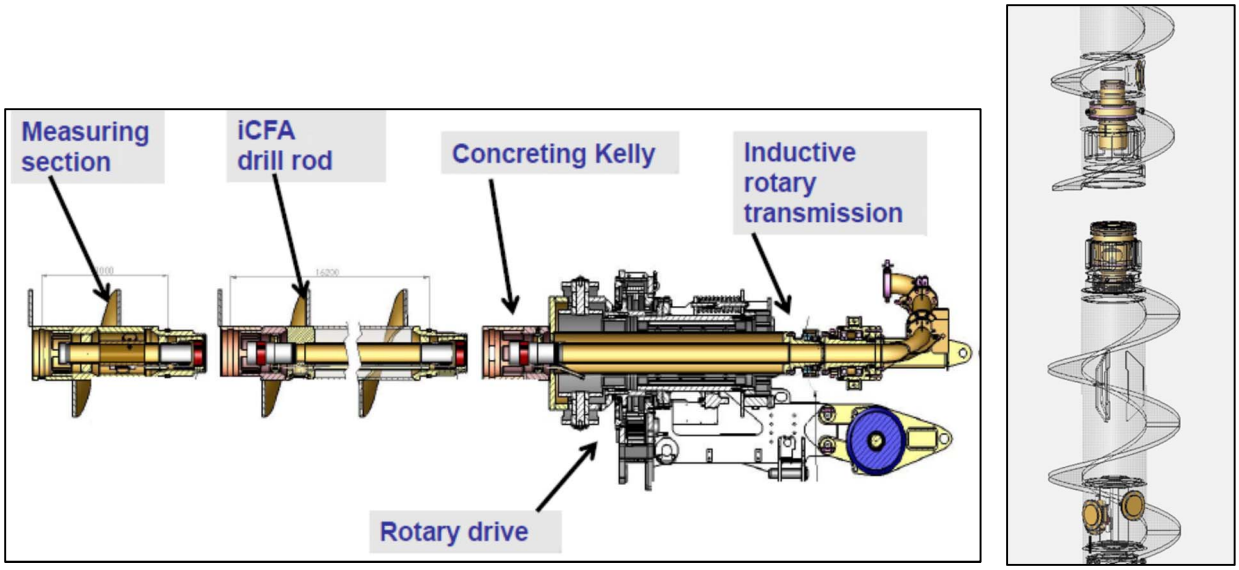


Fig. 5: Configuration of the iCFA, relevant parts of I-System are highlighted in the drill string (right detail)

The system has been proved on a couple of sites, where the concrete pressure has been measured parallel at the top as well as at the bottom (Figure 6)

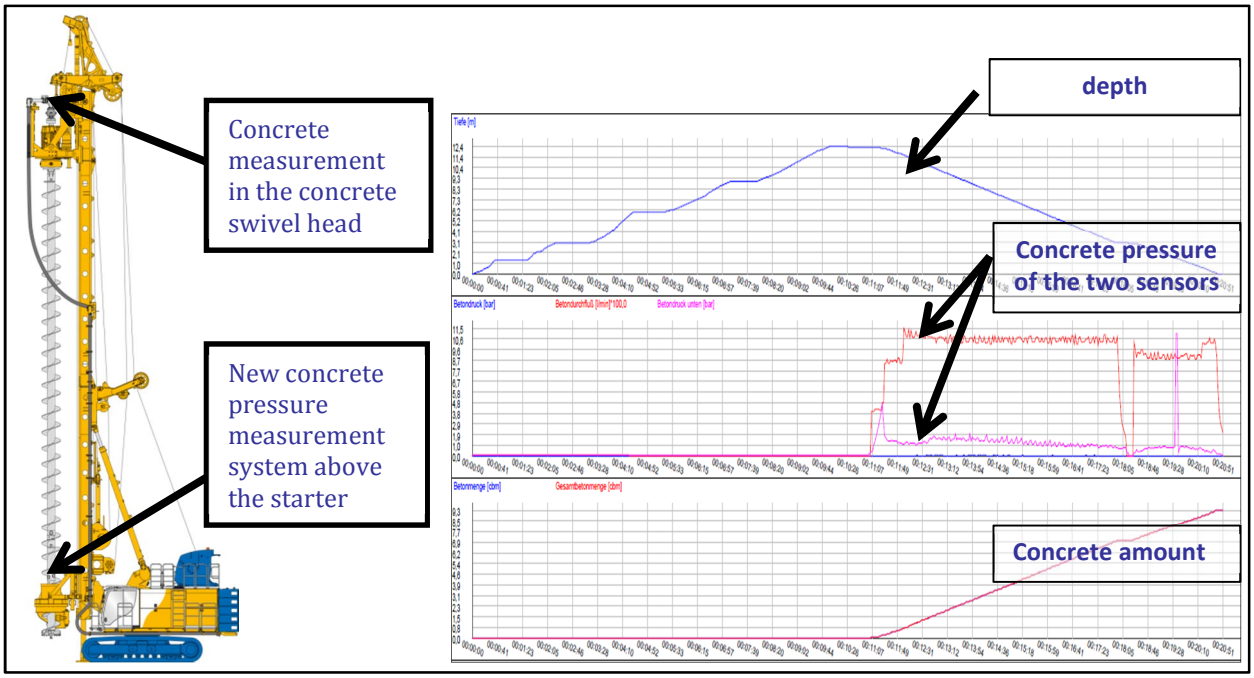


Fig. 6: positions of pressure sensors (left), pile report with both pressure measurements (right)

The graph shows the difference between two pressure measurements. It can be seen that the concrete sensor at the bottom shows a significant difference to the sensor on top.

As both values are provided real time to the operator (Figure 7), the operator can immediately react as required.

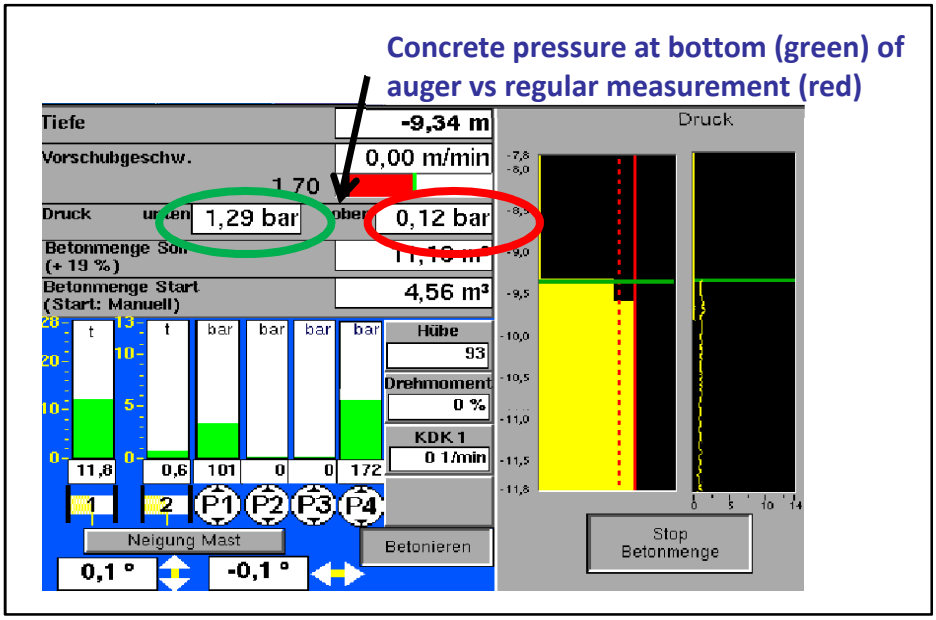


Fig. 6: B-Tronic screen with both concrete pressures in real time

Reference projects for iCFA

Several projects have been carried out using the iCFA system. Exemplarily two projects in the south of Germany can be named.

For the first project, the main demand was to control the concrete pressure. Due to cavities in the weathered lime stone, the concrete pressure was restricted to protect nearby water wells.



Fig. 7: Installation of CFA piles using the iCFA auger

The use of the iCFA auger was the key to get the job as no real alternative existed. Figure 7 shows the installation. 3.200 m of CFA piles were installed successfully.

Another project required a high demand of verticality control. The installation of a secant pile wall with CFA can cause huge problems if the verticality is not given. Usually you see the result when doing the excavation. As this might be too late, it is not really recommended to go for CFA piles when installing a secant pile wall. With the use of iCFA now the verticality can be controlled during the installation process and the operator has the chance to react early enough if required. This leads to a reduced risk for leakage

due to failed installation of CFA piles for secant pile walls. A positive result can be seen in figure 8, showing a partly excavated secant pile wall.



Fig. 8: Partly excavated secant pile wall using the iCFA

AN EYE ON PROJECTS AND COSTS

Verification of the production output and quality is an essential component for rounding-off a professional realization of construction projects. While today's installed control systems record all relevant measured data from both the machine and the production process, the recorded data are accessible from practically any location.

Anytime, anywhere you can have access via internet to the current status of your equipment or the production process via live online display of the operator's screen (Figure 9).



Fig. 9: live online display in the communication network of today's electronic support systems

As all data are accessible practically anywhere, necessary evaluations can be performed locally at the site office as well as at the company's headquarters.

For instance, the user can individually select data and map the entire work process with using adequate reporting tools like B-Report. All machine and production data are documented to illustrate the progress for subsequent verification. The data can be processed into texts, charts, or 3D presentations and the reports can be customized to your design requirements, corporate identity standards, and logos and so on.

The online analysis of the machine status outputs warning messages and trouble reports from machines being operated in different locations. Downtimes and problems are immediately detected, thus significantly reducing reaction times. Via the online connection to the operator's screen, experienced staff members can provide remote support.

The analysis is based both on the automatically recorded machine and production data and on the data input by the machine operator. This aids overall construction site planning and process optimization and facilitates the timely supply of wear parts. A target-performance comparison of current data provides a more accurate basis for predictions on future projects.

SUMMARY

Real time installation control, data transfer and reporting systems become more and more important and will serve also future demand ensuring the five dimensions of a jobsite.

The assistant systems will relieve the operator and will help to ensure constant quality. Of course, operator need’s to get trained on these systems, but the effort to train these additional features is low as these are just small add-ons to the general required training to operate such equipment.

In addition they will provide cost saving potentials as well for wear and tear as for materials like concrete. These will, after a reasonable time, cover the investment cost which are obviously going along with the implementation of these features.

Beside the assistant systems, developments like iCFA open chances for additional quality assurance and cost savings. References show the success of its use.

More developments will come soon, as the demand for quality control, documentation and cost saving will constantly increase. The shown examples are just a few first steps into the future.

REFERENCES

[1] Sebastian Bauer, Elektronik auf Baugeräten, BauPortal 7/2015

[2] BAUER Maschinen GmbH, BAUER B-Tronic System, 03/2017

[3] Fleming, W. G. K. (1995), The understanding of continuous flight auger piling, its monitoring and control. Proceedings of the Institution of Civil Engineers - Geotechnical Engineering: 157 - 165..

[4] DIN EN 1536, Execution of special geotechnical work –Bored piles

[5] Mark Lutz, Jean Lutz’s Latest Revolutionization of Instrumentation and Improvement of the Management of Advanced Works for the various piling and soil improvement works, Piling Technical Seminar “Advances and latest technologies in piles Construction”, Singapore, 08/2017

EVALUATION OF SPATIAL VARIABILITY FOR SITE CHARACTERIZATION BASED ON STANDARD PENETRATION TEST RESULTS

Salwa Yassin, MICE, CENG, Ph.D, Geotechnical Consultant and Senior Geotechnical Engineer, Dar Company, Cairo, Egypt, Salwa.Yassin@dar.com

ABSTRACT

Site characterization based on adequate investigation and accounting for site variability is a prime requirement for different design codes in Geotechnical engineering. Site variability is commonly evaluated through the determination of the first and the second-moment statistics (Statistical Variable Parameters), then evaluating the spatial variability of the considered parameter or variable using a relevant geostatistical method or tool. In this paper, the considered parameter or variable is the Standard Penetration Test blow count and the applied geostatistical tool is called variogram. The Standard Penetration Test (SPT), despite the inherent variability and measurement error, is still one of the most commonly used in-situ tests, and sometimes is the only available test, for site characterization. Even more, some geotechnical design methods are based directly on SPT measurement, or indirectly on a relevant correlation. Variogram is a simple geostatistical tool that is normally used to investigate the distance or the domain over which parameters are auto-correlated and the value of unmeasured point could be predicted. The purpose of the analyses carried out in this paper is to study the suitability of the variogram to investigate the spatial variability and the auto-correlated domain of a site using SPT blow counts.

Keywords: site characterization, spatial variability, geospatial method, variogram

INTRODUCTION

Most of the current reliability-based design codes emphasized that site characterization should be based on an adequate site investigation. However, they have made an allowance for the inevitable site variability and the uncertainties associated with the geotechnical parameters, (Uzielli et al. 2007 and Cherubini et al. 2007). As per Lacasse and Nadim (1996), all geotechnical parameters show different levels of variability in vertical and lateral directions due to measurement error, environmental impact, geological factors or spatial proximity.

According to many researchers (Lumb 1974; Rethati 1988; Phoon and Kulhawy 1999a and 1999b; Duncan 2000; Uzielli et al 2007; Ang and Tang 2007; DNV 2007; Fenton and Griffiths 2008; Goovaerts 1997 and Deutsch 2002), Site variability is commonly investigated through the following statistics procedure:

(1) For a considered soil parameter or variable, define the relevant Statistical Variability Parameters (SVP), which are (among others), mean, standard deviation and coefficient of variability. Then,
(2) Investigate the spatial variability of that soil parameter or variable by using a geostatistical method, or tool specialized in analyzing and interpreting geographically referenced data. This method is called a Variogram

Geostatistical methods have been used successfully for predicting the spatial variability of some soil parameters (Trangmar et al. 1985, Gaston et al. 1990, Cambardella et al. 1994, Saldana et al. 1998, Zebarth et al. 2002, Lark, 2002), and normally applied through the Variogram which is considered as the basic tool in identifying the extent over which the considered soil parameter could be correlated (auto-correlated domain) to each other and illustrates the rate at which mutual interactions between parameters decreases with distance (Matheron 1963; and Journel and Huijbregts 1978; Olea 1994; Cressie 1993; Sarma 2009, and Cellmer 2014).

In this paper, spatial variability for a construction site was investigated using SPT blow counts. According to the above-mentioned procedure, SVP (i.e. Mean, variance, standard deviation, and coefficient of variability)

© 2018 Deep Foundations Institute

for the recorded SPT values were determined, then those values were used in the Variogram to investigate the spatial variability.

RELEVANT GEOSTATISTICS DEFINITIONS

The Variogram comprises two different forms which are related to each other and named experimental and model, refer to Fig. 1. The experimental variogram is calculated first using the actual site measured parameter or variable. Then, model variogram is produced by fitting the experimental variogram using any of the common models, such as linear, spherical, exponential… etc.., (Isaaks and Srivastava 1989; Goovaerts, 1997).

The experimental variogram is expressed by equation (1),

$$2\gamma(h) \quad = \frac{1}{n}\sum_{i=1}^{n}\left[z(\overrightarrow{u_i}) - z\left(\overrightarrow{u_i}+\vec{h}\right)\right]^2 \qquad [1]$$

Where z = analyzed variable or parameter, $2\gamma(h)$ = value of the variogram at a separation distance h (or lag), z(u) = value of the variable (parameter) at location u, and z (u + h) = value of the variable at a distance h from z (u) between pairs of points (n).

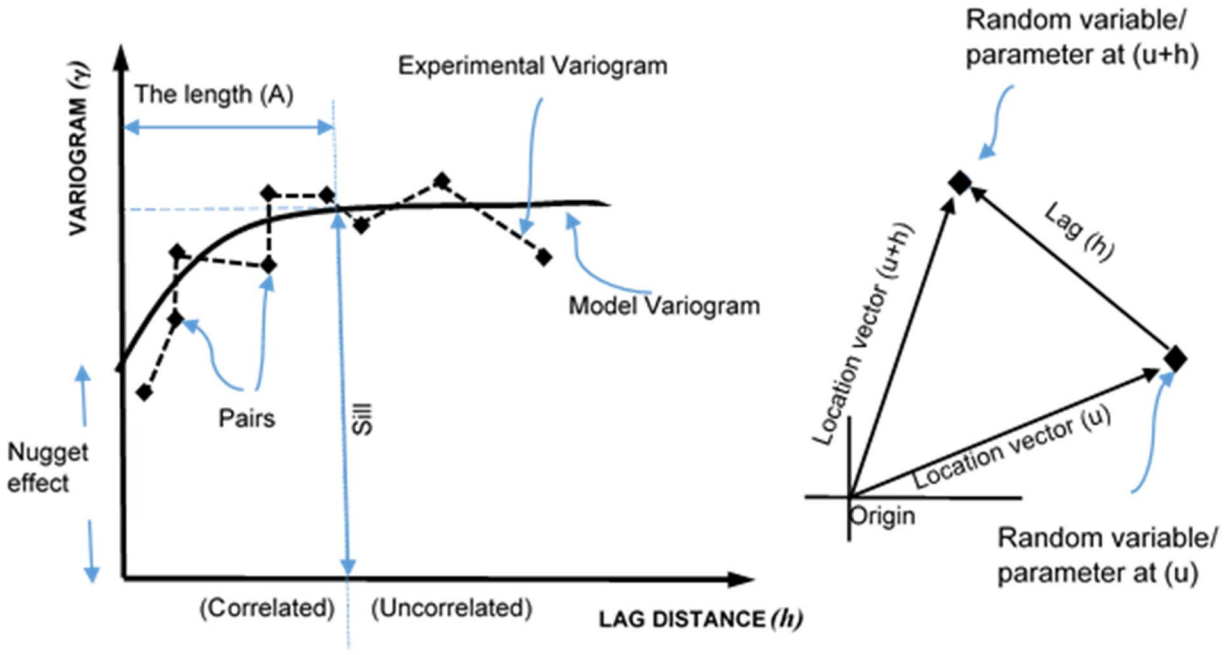


Fig. 1. Experimental and model variogram

The variogram, Fig. 1, measures the change or dissimilarity (between pairs of variables or parameters) with distance until reaching a constant value which is called the sill. The distance over which the variogram reaches the sill is called the length (A), which defines the auto-correlated domain of a variable or parameter (Bohling 2005).

If the variogram shows a discontinuity and intersects the ordinate, the value of $2\gamma(h)$ at the intersection is called a nugget effect. The nugget effect represents the apparent discontinuity in the variogram function (Armstrong

1998), and could be defined as a measure of a direct repeatability of the data, measurement error, diversity of samples and sparse data (Bohling 2005; Phoon, and Kulhawy 1999 a).

FACTORS FOR OPTIMAL VARIOGRAM

There are several factors that affect the accuracy and reliability of the variogram calculations and results. If these factors have not been considered or fulfilled before calculation the variogram, they will represent an additional source of errors in the calculations and translated into a higher nugget effect on the variogram. Most of these factors could be summarized as follows:

Number of the analyzed variables or data:

Some authors emphasized that all the analyzed data or variables should be of sufficient number for more reliable statistics and minimal errors (Phoon and Kulhawy 1999 a). As a rule of thumb, parameters used in computing variogram should not be less than 10 point pairs as suggested by Kelkar and Perez (2002), or 30 point pairs in computing the experimental variogram (Cellmer 2014; Journel and Huijbregts 1978). According to Webster and Oliver (2001), a minimum of 50 observations is required for a reasonably reliable variogram. Generally, the form of the variogram can be very difficult to identify when limited data is available, (Kokesz 2010), and the differences between experimental and model variograms can be expected to decrease with an increase in the number of observations or data.

Spatial Distribution:

The spatial distribution of variables or data points is also an important factor. If data points do not reliably represent the analyzed area or represent only its central part, the resulting model will be burdened by significant errors, (DeWijs 1951). Generally, Spatial-correlation analyses are difficult to perform when data are sparse, therefore, variables or data points should also be distributed evenly and, if possible, they should represent areas proximate to the boundaries (Cellmer 2014).

Continuous, normally distributed and stationary variables or data:

Geostatistical methods, including the variogram are used based on a general assumption that the analyzed data are continuous, normally distributed and stationary, (Site et al. 2011; Cellmer 2014; and Bohling 2005). Continuous variable implies that the value of the variable can be measured or read at any point of the analyzed area, and changes gradually with distance, demonstrating no gaps on the representative variogram, whereas discrete data can only take certain values, with gaps. Accordingly, soil parameters such as permeability or mobilized skin resistance (as in pile load test results) present problems with variogram calculations (Manchuk et al. 2009; Rocha and Yamamoto 2000).

A normal distribution is an arrangement of a data set in which most values cluster in the middle of the range and the rest taper off symmetrically toward either extreme. Stationary data means they have no trend, however, if analyzed data turned to be nonstationary, then they should be transformed into stationary data prior use (Jaksa 1997).

Therefore, for spatial variability analyses, it is crucial to commence the analyses by looking at a histogram or similar plot to check for normality and significant trends (Jaksa 1997; and Bohling, 2005).

Correlated length and lag distance:

An initial estimate of the correlation length could perhaps be based on a prior geological study of the site or similar sites, in such case, the maximum lags should not exceed two to three times the correlated length.

However, if there is no estimate of the correlation length, as a rule of thumb, the maximum lag distance should be equal to the "diameter" of the area or the site containing the data. Identifying the best lag interval sometimes is frustrating, but generally is an iterative process (Isaaks and Srivastava 1989; Chambers et al. 2000; Olea, 1994; and Hohn, 1999). For an efficient experimental variogram, Kelkar and Perez (2002) suggest a maximum lag of half the maximum possible distance.

ANALYZED DATA AND DISCUSSION

The considered SPT values for the current study belong to an approximately flat site with a homogeneous geological formation of loose to medium dense cohesion-less material for the top 3 m, followed by a competent over-consolidated cohesion-less material till the end of drilling. The latter was adopted as a foundation layer due to the high recorded SPT values. Foundation design for that site was based on a direct correlation with SPT values (AASHTO 2010). Accordingly, it was essential to investigate the distribution and variation of the SPT values both vertically and horizontally. Site dimensions and location of 75 boreholes considered for this study are shown in Fig. 2.

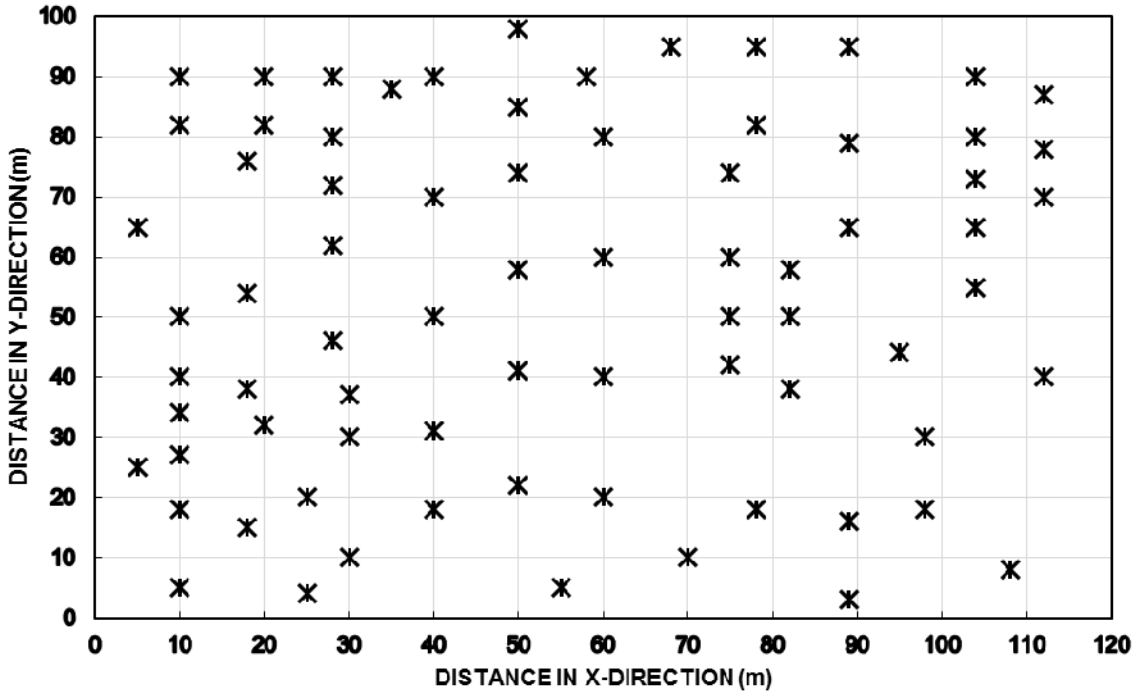


Fig. 2. Layout and distribution of standard penetration test locations

For each borehole across the site, a characteristic SPT value was evaluated for the competent layer. The Statistical Variability Parameters (SVP) for the characteristic SPT values were determined in the form of mean, standard deviation and coefficient of variability. Table 1 shows the SVP, where **the characteristic SPT ranged between 50 and 100, with a** mean value of 92.6 and low coefficient of variability (COV) of 12%. The **characteristic SPT values will be referred to as the variable or data throughout the coming sections.**

Table 1. Statistical Variability Parameters (SVP) for SPT values

Factor	SPT (Univariate)
Minimum	50
Maximum	100
Mean	92.6
Standard Deviation	11.76
Coefficient of variation	12%

According to FHWA (2010), the published range of COV inherent variability for SPT could be up 45%. Consequently, and with reference to the COV for the current data, it is obvious that the analyzed SPT values are on the low side of inherent and measurement errors. Accordingly, it is anticipated such error (inherent and measurement error) most likely have insignificant impact on the variogram results and, hence, spatial variability analyses

The final step to assess the spatial variation was to calculate the experimental variogram then the model variogram using the following steps:

(1) To simplify the calculation, the depth effect on the SPT values within the competent layer was considered as zero, especially it has the same effect on all values. Accordingly, the characteristic SPT values considered in the analyses were considered at the ground level.
(2) The location of each SPT measuring point (i.e. borehole locations) was identified by measuring distance (x, y) from point (0, 0) as shown in Fig. 2.
(3) The trend of the SPT values was investigated in both directions of the site (i.e. Y and X directions), Fig. 3 and 4 respectively, showing a low coefficient of correlation (R^2). Hence, with the absence of any deterministic trend, the SPT data can be considered as stationary and no data transformation will be required for variogram calculation.

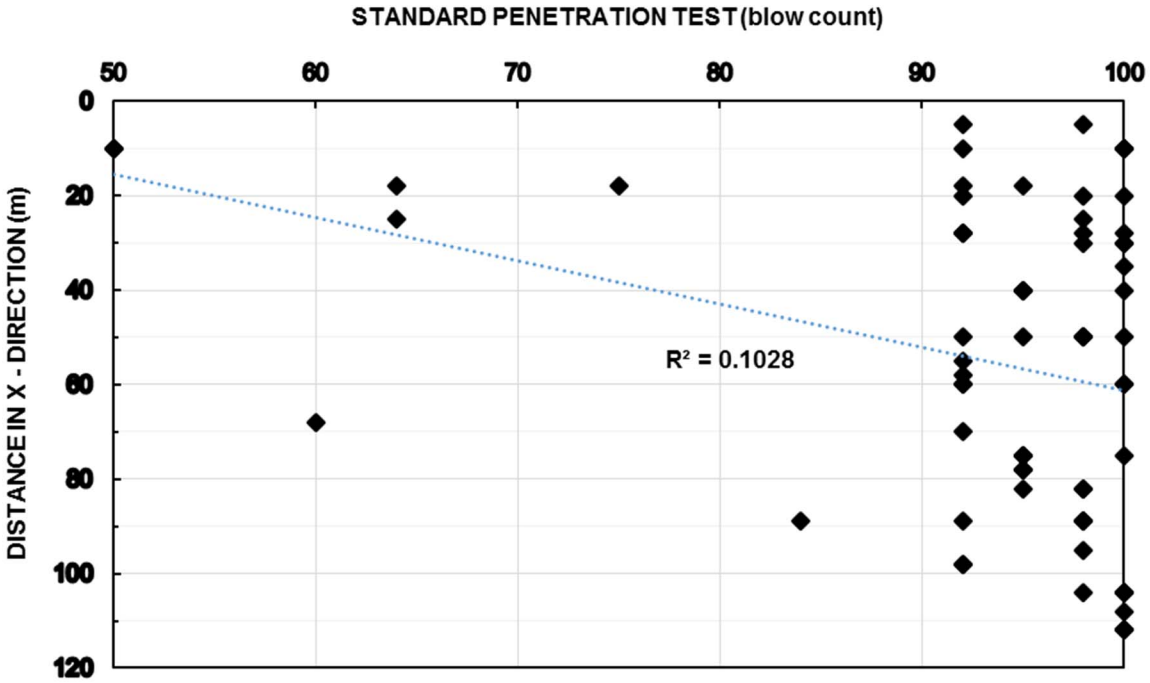


Fig. 3. Distribution of standard penetration test blow count in x-direction

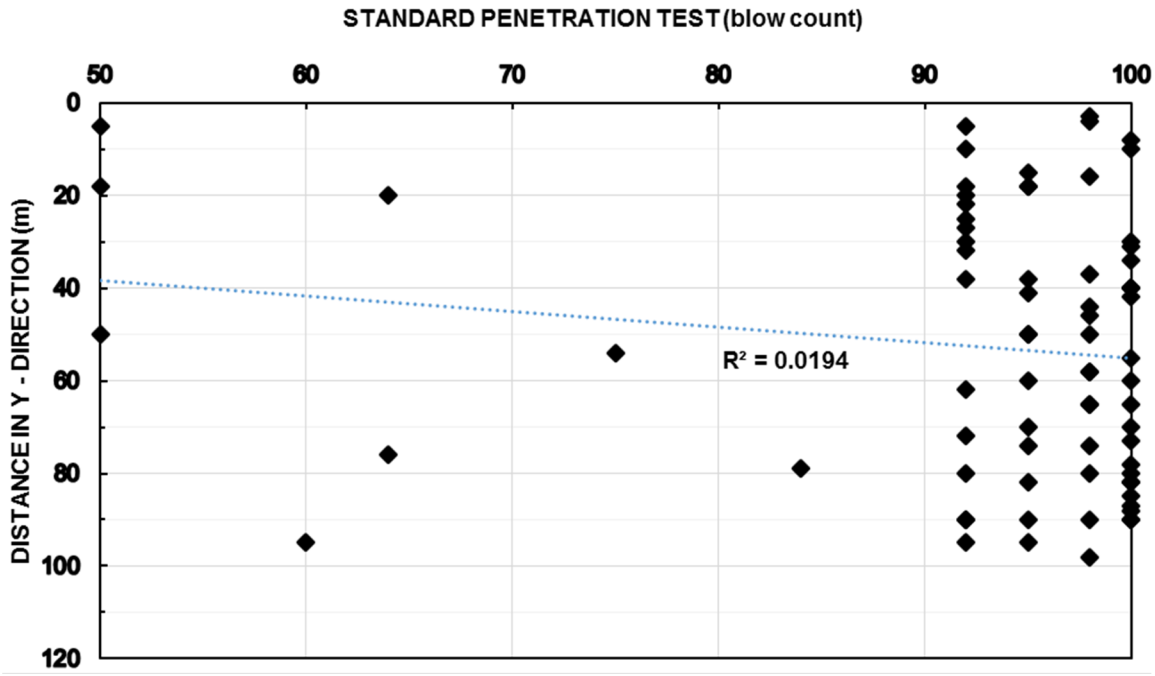


Fig. 4. Distribution of standard penetration test blow count in y-direction

(4) A histogram was calculated as shown in Fig. 5, to check the SPT frequency across the site, and as shown in Fig. 5, the data are not normally distributed. In addition, due to the nature of the SPT results as a blow count, the data can't be considered continuous, i.e. it is a discrete data.

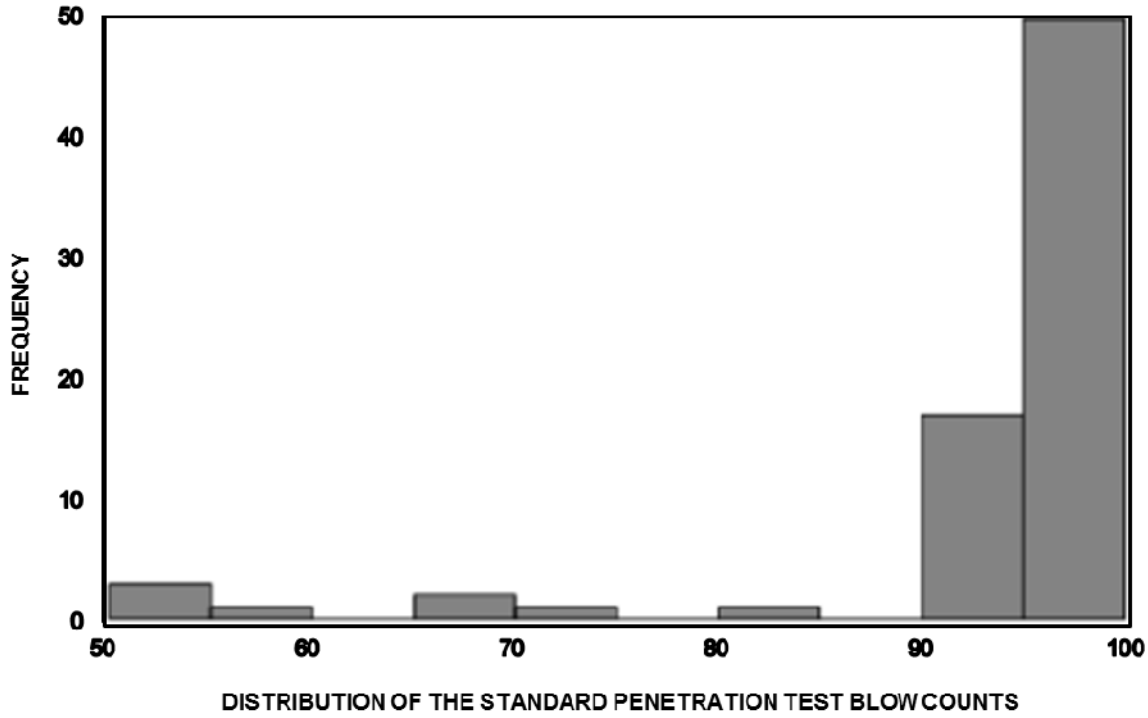


Fig. 5. Histogram for the distribution of the standard penetration test blow counts across the site

(5) The final step was calculating the experimental and model variogram using a commercial software Surfer, version 11, by entering each SPT value with the corresponding (x, y) coordinates. During calculation, using the software, different directions and grouping of the SPT data were investigated to confirm isotropy, and almost the same results were obtained in all directions. The lag or the distance over which the variogram was calculated had been chosen based on trials as advised by several researchers (Journel and Huijbregts 1978; Trangmar et al., 1985; Webster and Oliver, 1990), and the adopted distance was equal to a diameter equivalent to the site area. The calculated experimental and model variograms are shown in Fig. 6.

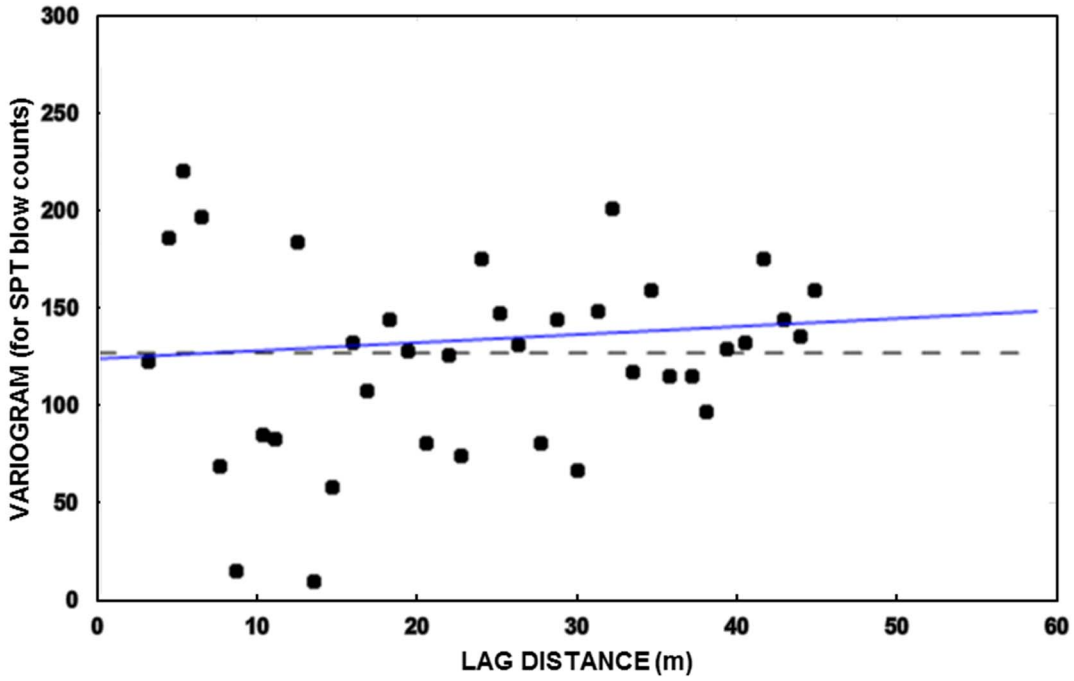


Fig. 6. Variogram for the standard penetration test blow counts

The variogram results in Fig. 6, shows almost a pure nugget effect which is an indication of a considerable spatial variability and uncorrelated data across the whole site, which means a prediction of any SPT value between the measured points will be doubtful or false (Journel and Huijbregts, 1978). As per geotechnical design perspectives, and based on the number of the carried out boreholes across the site and the range of the SPT values, it should be anticipated that whole site is auto-correlated and SPT value at any point between the boreholes could be predicted or assumed with a high level of confidence.

However, it's worth remembering, all the analyzed SPT values were stationary, with an adequate number and low coefficient of variability which are adequate for reliable variogram analyze and results. These results could be justified, as the analyzed data were missing one of the basic assumptions of the geostatistical method, which is continuity. As mentioned previously, geostatistical method (variogram) is based on the assumption that all the analyzed data should have a continuous character and can be measured (or read) in any point of the analyzed area and changes gradually with distance.

CONCLUSION

The purpose of this paper is to study the suitability of a common geostatistical tool (Variogram) to investigate site spatial variability using SPT blow counts. The main function of the Variogram, as a geostatistical tool, is to evaluate the distance over which data are auto-correlated and prediction of the value of unmeasured points could be carried out.

The adopted site for this study was deliberately chosen to have homogenous formation (geologically) with a high SPT blow counts and regarded as a competent and reliable foundation layer from geotechnical perspective. The analyses carried out for the SPT values comprised:

(1) Adopting 75 of SPT values (data) which is adequate for variogram calculations as recommended by several researchers, as presented in the paper.
(2) Evaluating the common Statistical Variable Parameters (mean, Standard Deviation and coefficient of variability).
(3) Identifying the trend of the investigated data, i.e. SPT values and a normality and distribution by calculating a histogram. The investigated data were stationary data with no deterministic trend, but not normally distributed.
(4) Then, calculating the experimental and model variogram using Surfer software.

However, despite the low coefficient of variability and the narrow range of the investigated SPT values, the experimental and model variogram confirmed, almost, a pure nugget effect which is an indication of a high level of spatial variability across the site. Whereas, for the investigated data with the small difference between the observation points, a common average process could be adopted for the geotechnical design across the whole site with a high level of confidence. Accordingly, a conclusion could be drawn that, using the variogram to evaluate site spatial variability based on SPT data will be misleading and falsely indicate a high level of spatial variability as per the case presented here.

REFERENCES

Ang, A. and Tang, W. H., 2007. Probability Concepts in Engineering. Hoboken, NJ: Wiley.

Armstrong, M., 1989. Geostatistics, vol. 1 and 2, Kluwer Academic Publishers, pp 1027.

Bohling, G., 2005. Introduction to geostatistics and variogram analysis. C & PE 940, Kansas Geological Survey (online). Available: http://people.ku.edu/~gbohling/cpe940

Cambardella, C. A., Moorman, T. B., Novak J. M., Parkin T. B., Parkin, D. L., Karlen, Turco, R. F., and Konopka , A. E., 1994. Field-Scale Variability of Soil Properties in Central Iowa Soils. Soil Sci. Soc. Am. J. 58:1501-1511.

Cellmer, R., 2014. The possibilities and limitations of geostatistical methods in real estate market analyses. Real Estate Management and Valuation, vol. 22, no. 3, s. 54-62.

Chambers, R.L., Yarus J.M., and Hird, K.B., 2000. Petroleum Geostatistics for the Non- geostatistician," — Part 1. The Leading Edge.

Cherubini, C., Vessia , G., and Pula, W., 2007. Statistical Soil Characterization of Italian Site for Reliability Analyses, in Characterization and Engineering Properties of Natural Soils, T. S. Tan, K. K. Phoon, D. W. Hight, and S. Leroueil (eds.). London: Taylor and Francis.

Cressie N., 1993. Statistics for Spatial Data, revised edition, John Willey & Sons, New York.

Deutsch, C.V., 2002. Geostatistical Reservoir Modeling, Oxford University Press.

Deutsch, C.V. and Journel, A.G., 1998. GSLIB: Geostatistical Software Library and User's Guide, Second Edition, Oxford University Press

De Wijs, H.J. 1951. Statistics of Ore Distribution. Part 1: Frequency Distribution of Assay Values. Geologie en Mijnbouw 13: 365.

Duncan, M. J., 2000. Factors of Safety and Reliability in Geotechnical Engineering. Journal of Geotechnical and Geoenvironmental Engineering (ASCE), Vol. 126, No. 4, pp. 307-317.

Fenton, G. A., and Griffiths, D. V., 2008. Risk Assessment in Geotechnical Engineering. Hoboken, NJ: Wiley.

FHWA-NHI-10-016, FHWA GEC 010, 2010. Drilled Shafts: Construction Procedures and LRFD Design Methods"

Gaston, L., Nkedi-Kizza, P., Sawka, G., and Rao, P. S. C., 1990. Spatial variability of morphological at a Florida Flatwoods site. Soil Science Society American Journal, 54: 527-533.

Goovaerts, P., 1997. Geostatistics for Natural Resources Evaluation, Oxford University Press,

Hohn, M.E. 1999. Geostatistics and Petroleum Geology, second edition. Amsterdam, The Netherlands: Kluwer Academic Publishers.

Isaaks, E. H. and R. M. Srivastava, 1989. An Introduction to Applied Geostatistics. Oxford University Press, Inc. New York, 561 pp.

Journel, A.G., and Huijbregts, C.J., 1978. Mining Geostatistics. London, England: Academic Press.

Jaksa, M. B., Brooker, P. I. and Kaggwa, W. S. 1997. Inaccuracies Associated with Estimating Random Measurement Errors. Journal of Geotechnical and Geoenvironmental Engineering (ASCE), Vol. 123, No. 5, pp. 393-401.

Kelkar, M., and Perez, G. 2002. Applied Geostatistics for Reservoir Characterization. Richardson, Texas: Society for Petroleum Engineers.

Kokesz, Z., 2010. Uwarunkowania stosowania krigingu zwyczajnego do sporządzania map izoliniowych, Biuletyn Państwowego (Conditions of the use of ordinary kriging for isolinear mapping) Instytutu Geologicznego, nr 439, pp. 403-408.

Lacasse, S., and Nadim, F., 1996. Uncertainties in Characterizing Soil Properties. In Uncertainty in the Geological Environment: From Theory to Practice, C. D. Shackleford, P. P. Nelson, and M. J. S. Roth (eds.), Geotechnical Special Publication No. 58, pp 49 - 75. New York: ASCE.

Lark, R.M., 2002. Optimized spatial sampling of soil for Estimation of the variogram by maximum likelihood. Geoderma, 105: 49-80.

Lumb, P.,1974. Application of statistics in soil mechanics in Soil Mechanics – New Horizons, I. K. Lee, ed., New York: Elsevier

Matheron, G., 1963. Principles of Geostatistics, Economic Geology, no 58 pp. 1246-1266.

Matheron, G., 1971. The Theory of Regionalized Variables and its Applications, Les Cahiers du Centre de Morphologie Mathematique de Fontainbleau nr 5, Ecole Nationale Superieure des Mines de Paris.

Manchuk, J.G., Leuangthong, O., and Deutsch, C..V., 2009. The proportional effect; Mathematical Geosciences, October 2009, Vol. 41, Issue 7, pp 799-816.

Olea, R.A., 1994. Fundamentals of Semivariogram Estimation, Modeling, and Usage. Stochastic Modeling and Geostatistics, 3, 27-35, ed. J.M. Yarus and R.L. Chambers. Tulsa, Oklahoma: AAPG Computer Applications in Geology, AAPG.

Phoon, K.K., and Kulhawy, F.H., 1999a. Characterization of Geotechnical Variability. Canadian Geotechnical Journal, 36: 612-624.

Phoon, K.K., and Kulhawy, F.H., 1999b. Evaluation of Geotechnical Property Variability. Canadian Geotechnical Journal, 36: 625-639.

Rethati, L.,1988. Probabilistic Solutions in Geotechnics. Amsterdam: Elsevier

Rocha, M.M., Yamamoto, J.K., 2000. Comparison between kriging variance and interpolation variance as uncertainty measurements in the Capanema Iron Mine, state of Minas Gerais—Brazil. Nat Resour Res 9(3):223–235

Saldana, A., Stein, A. and Zinck , J.A., 1998. Spatial variability of soil properties at different scales within three terraces of the Henares River (Spain). Catena, 33: 139-153

Sarma, D.D., 2009. Geostatistics with Applications in Earth Sciences, Springer.

Site, O., Xin, K., Louis, G., and Richard, S., 2011. Variability Analysis of Undrained Shear Strength for Reliability-Based Design, Geo-Frontiers 2011, ASCE 2011

Trangmar, B.B., Yost, R.S. and Uehara, G., 1985. Application of geostatistics to spatial studies of soil properties. Advanced Agronomy, 38: 45-94.

Uzielli, M., Lacasse, S., Nadim, F. and Phoon, K.K., 2007. Soil Variability Analysis for Geotechnical Practice. In Characterization and Engineering Properties of Natural Soils, T. S. Tan, K. K. Phoon, D. W. Hight, and S. Leroueil (eds.). London: Taylor and Francis.

Webster, R., oliver, M., 2001. Geostatistics for Environmental Scientists Statistics in Practice, Wiley, Chichester.

Webster, R. and Oliver, M.A., 1990. Statistical Methods in Soil and Land Resource Survey. Oxford University Press, 316 pp.

Zebarth, B.J., Rees ,H., Walsh, J., Chow ,L., and Pennock , D. J., 2002. Soil variation within hummocky podzolic landscape under intensive potato production. Geoderma,110: 19-33.

MOSUL DAM - BUILDING 2D & 3D PROJECT INFORMATION SYSTEMS FOR CONSTRUCTION MONITORING AND RISK ASSESSMENTS

Bateman, Vanessa C., US Army Corps of Engineers, Nashville District 615-736-7906
Worsham, Baron M., US Army Corps of Engineers, Nashville District 615-736-5750
Blackman, Laurel E., US Army Corps of Engineers, Nashville District 615-736-7987
Williams, Nathan D., US Army Corps of Engineers, Nashville District 615-736-5972
Sells, Bobby S., US Army Corps of Engineers, Nashville District 615-736-5632

ABSTRACT

One of the more challenging aspects of a modern grouting program is managing and assessing the large quantity of data generated by the project. Grouting information needs to be quickly accessible by the whole construction team and put into context with the surface data, subsurface details, optical televiewer logs, drilling records, QA observations, photographs, flow measurements, artesian pressures as well as with instrumentation and other key features. Understanding the effects of grouting in a large project such as Mosul Dam where there have been repeated grouting programs over an extended period adds another layer of complexity to the problem. Automated grout monitoring provides a wealth of information about each hole, but as with all grouting projects it is the details of the subsurface and previous programs that are needed to gain a full understanding. The USACE (US Army Corps of Engineers) SIMDAMS (Site Information Modeling and Data Management Solutions) tools and methods are being used on the Mosul Dam project to support both the current construction grouting efforts and the ongoing risk assessments and dam safety modification study of the project. The method develops GIS (Geographic Information System) based 2D models in plan, profile and section views along with a 3D model. Features are hyperlinked to a document library allowing the models to act as a visual index to project information. The 2D and 3D GIS models have been developed to aid in the quick display of data allowing both the construction staff to see current grouting data and risk assessment/dam safety modification study personnel to understand the details of the subsurface, of previous work and the impacts of current grouting. Models are delivered over the web to the Government of Iraq, to the on-site construction team and to the "reach back" team in the United States. These easy to use web based models allow users with no previous GIS experience to fully engage with the information that has been gathered to date. It allows the dam safety community access to a BIM-like (Building Information Management) model of an earthen embankment dam along with its foundation that is continually updated as progress continues on the project.

Keywords: Mosul Dam, PIMS, BIM, dam safety, grouting, automated monitoring

INTRODUCTION

Mosul Dam, located in the northern part of Iraq along the Tigris River is the largest dam in Iraq and the 4th largest in the Middle East. With a storage capacity of 11.1 billion cubic meters, it provides hydropower, irrigation, water supply and flood control benefits for Iraq. This 113m high, 3.4km long zoned embankment dam includes a 5 gate service spillway, a hydropower facility rated to 750 MW and features a bottom outlet structure with two gates and an emergency spillway (Figure 1). Built on a karst foundation that features gypsum, anhydrite, marls and limestones, this dam contains a unique grouting gallery located at the contact with the foundation and at the base of the embankment dam (Figure 2). The gallery was specifically designed to deal with the considerable challenges posed by the karst foundation and to allow repeated grouting efforts to continue over the lifetime of the dam. As per the design, the original contractors

© 2018 Deep Foundations Institute



Figure 1. Location and Main Features of Mosul Dam

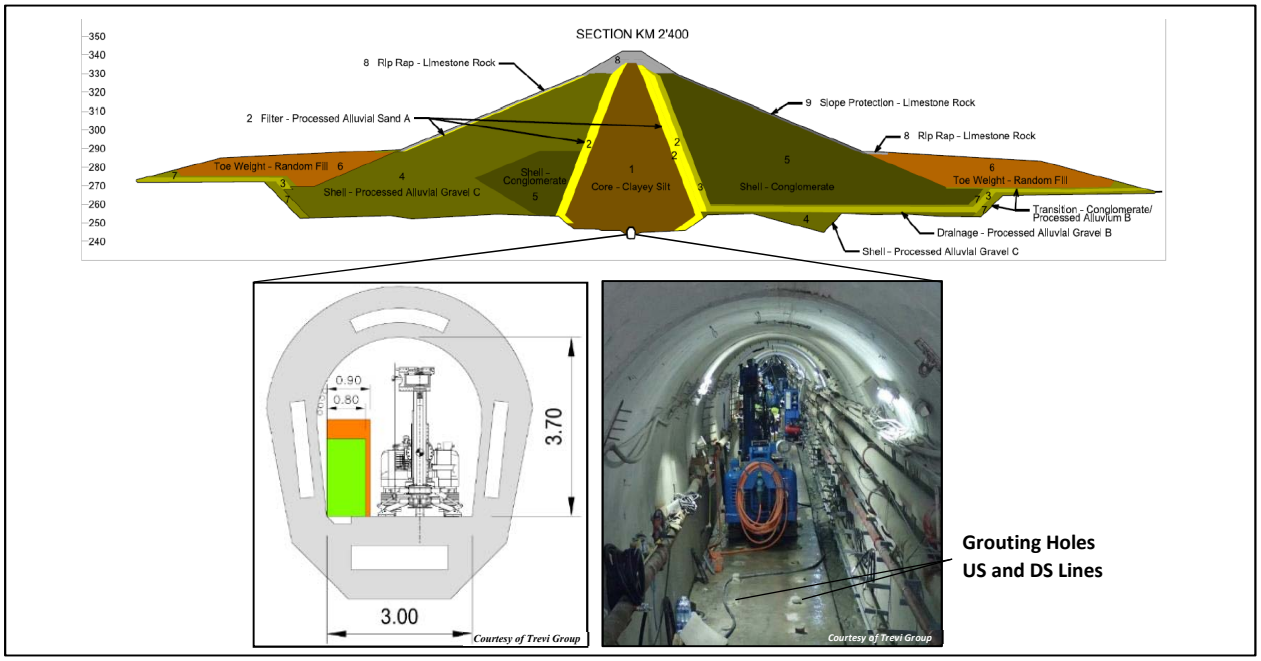


Figure 2. Typical Cross Section of Embankment with Grouting Gallery Dimensions and Photograph

initiated an aggressive grouting program starting in 1987 and the Ministry of Water Resources (MoWR) in Iraq has continued grouting ever since the dam was completed in 1985. In 2016 the MoWR issued a contract to Trevi Group, an Italian foundation company, to conduct grouting operations with updated equipment and methods and requested that the US Army Corps of Engineers (USACE) serve as the Engineer for these efforts. USACE staffed the construction office with a combination of deployed USACE personnel and with staff provided by AECOM under contract to USACE. AECOM built and maintains the QA database of on-

site observations. Site production began in November 2016 and is ongoing. This new effort brought a number of new methodologies to the site such as automated grout monitoring (Trevi Group), optical televiewer borehole analysis, tablet data entry of QA data (AECOM), automated instrumentation monitoring (AECOM and USACE) and the development of an information management system for the project developed on the USACE SIMDAMS platform.

THE CHALLENGE

What makes this project so challenging from a data point of view is the volume of data that needed to be quickly integrated in order to analyze not only the current grouting operations but to accurately assess the risks to the dam both before and after the most recent grouting. When USACE first engaged in the process, few boring logs were available and most of the information was the "Mosul Data Library" (Washington International/Black and Veatch, 2004) which was compiled in 2004. This library contained multi-generation photocopies of as-built drawings and narrative reports that did not present the data in a readily usable spatial manner. These data existed either in paper form, or the digital equivalent of paper as scanned images. While this can be very useful when all the information that is needed is contained on only a few locations, the data format did not allow the data to be readily searched or queried for relevant information. In other words, while the files were digital, the data they contained were in a form that had to be manually searched to extract relevant information. This means the data were difficult to use effectively as there was 30 years of grouting and instrumentation data, as builts and current grouting data that needed to be integrated into one comprehensive picture. This is especially true when the information is fragmentary and incomplete.

Adding to the challenge is the need to update the understanding of the foundation geology and its' implications to the safety of the dam. At the beginning of the project, only a geologic map underneath the grouting gallery from original construction was available. However, it quickly became apparent during the risk assessment project, that numerous cross sections and a 3D model of the geology were needed in order to accurately assess potential failure modes and to calculate risk. As-built drawings needed to be compared with geological details and old grouting records needed to be found, entered, verified and understood in order to be of use.

A large volume of construction data was also being generated at the same time the baseline model was being built. As of October 2017, over 15,000 tonnes of grout solids have been injected into the foundation in nearly 20,000 grout stages. All of these stages have drilling records, grouting trend plots, issue table records, QA/QC related records and other data. The project has maintained 12 rigs drilling and grouting in the gallery and on the surface with 24/6 operation and will complete 1950 grouting holes in the first year in addition to exploration drilling and instrumentation upgrades. In order to be effective, an information management system of this type must be able to integrate data very quickly and make it rapidly accessible on site, to reach back assets, to the engineers analyzing the data and to the Owner. Especially when conditions are changing rapidly, and the team is located not only on-site but across several countries, information needs to be disseminated quickly and accurately.

SIMDAMS FOR MOSUL DAM

In order to meet the challenges to provide construction support, continued analyses and risk assessments, USACE implemented the SIMDAMS tools and methods to the Mosul Dam project. SIMDAMS (Site Information Modeling and Data Management Solution) was developed by USACE to provide a BIM-like environment for dams and levees that can be used both for risk assessments and for continuous construction monitoring. It has been implemented by USACE on more than 50 dam and levee safety projects. SIMDAMS had its genesis in the collaboration between USACE and the data management sub-contractor

(Geosyntec) during the construction of the Wolf Creek Barrier Wall in 2011 when an RFP to develop a data management system for the project was sent to the barrier wall contractor joint-venture Treviicos and Soletanche. The original system was developed solely for Wolf Creek Dam and was specific to the data at that project. This implementation, called WCIMS (Wolf Creek Information Management System) proved the value of comprehensive data management and using a BIM-like environment to monitor and assess subsurface construction (Rosen & Bateman, 2015). USACE then proceeded to develop through pilot projects a standard schema, baseline geodatabases (an industry standard database for storing, relating and documenting spatial data) and tools to rapidly turn data into geospatial features which could be served out over the web for dam and levee safety projects (Bateman, et al., 2015; Hlepas & Bateman, 2017).

SIMDAMS is a set of tools and methodology, rather than a software product. It incorporates data management principles to rapidly visualize, integrate and combine data into a complete model that can be accessed on the web through a browser. This allows the end-user the ability to use the system without needing to be proficient in databases, GIS or CAD. Builders and data managers must know how to use the development tools and methods, but on any dam safety assessment or dam safety modification project there are many people who need access to the data who may to be proficient in high level GIS or BIM software. Taking the project out to the web makes the whole model easy to use and share.

Information generated by a project is stored in a geodatabase along with an organized file library of documents that are hyperlinked to different features on a central server. Data are generated on site by contractor and QA staff. These are compiled into databases which are then compiled in a central geodatabase at USACE. The SIMDAMS tools and methods are used to process the data for spatial representation (Figure 3). Due to the type of data that are generated on this project and the specific project needs additional tools have been built for the Mosul project to make processing of grouting and drilling data faster, allowing for minimal time between data generation and inclusion into the system. This allows reachback personnel to create features in a variety of visualizations such as plan view, profile views, section views and 3D views that are available to the onsite and reachback staff on a 24/7 basis.

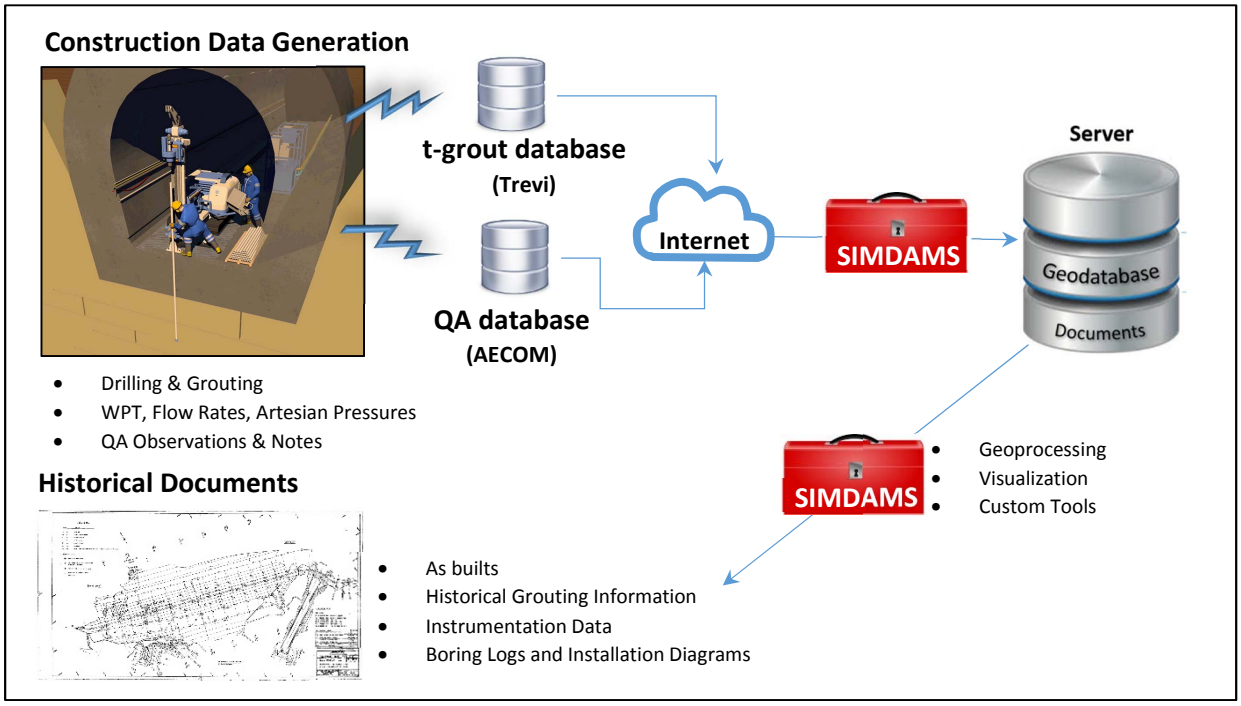


Figure 3. Typical Data Flow into the USACE SIMDAMS Server

Once data are incorporated into the SIMDAMS framework located on secure servers within the USACE firewall, they can be served to users through a Web Interface, which means the end-user does not have to be a GIS professional to make good use of the project data. The web interface is custom programmed with map printing/exporting tools, drawing tools that can be used to transmit annotations to other users, and search and highlight tools that allow onsite personnel to visualize grouting activities within a narrow time window. These maps are used on-site, by reachback, and are also used by personnel from the Government of Iraq to monitor the progress of current grouting efforts.

Users who require more customizable control can access the model data through the commercially available ArcGIS desktop applications which permit additional analysis, data processing, and visualization using custom (SIMDAMS) and other built-in geoprocessing tools. These data are provided back to the whole team on an as-needed basis and are regularly updated with new information and features as new data sources become available (Figure 4). Using these data and the models, the reachback team also provides a wide variety of figures, drawings, maps, graphs and analyses of the data to support the project.

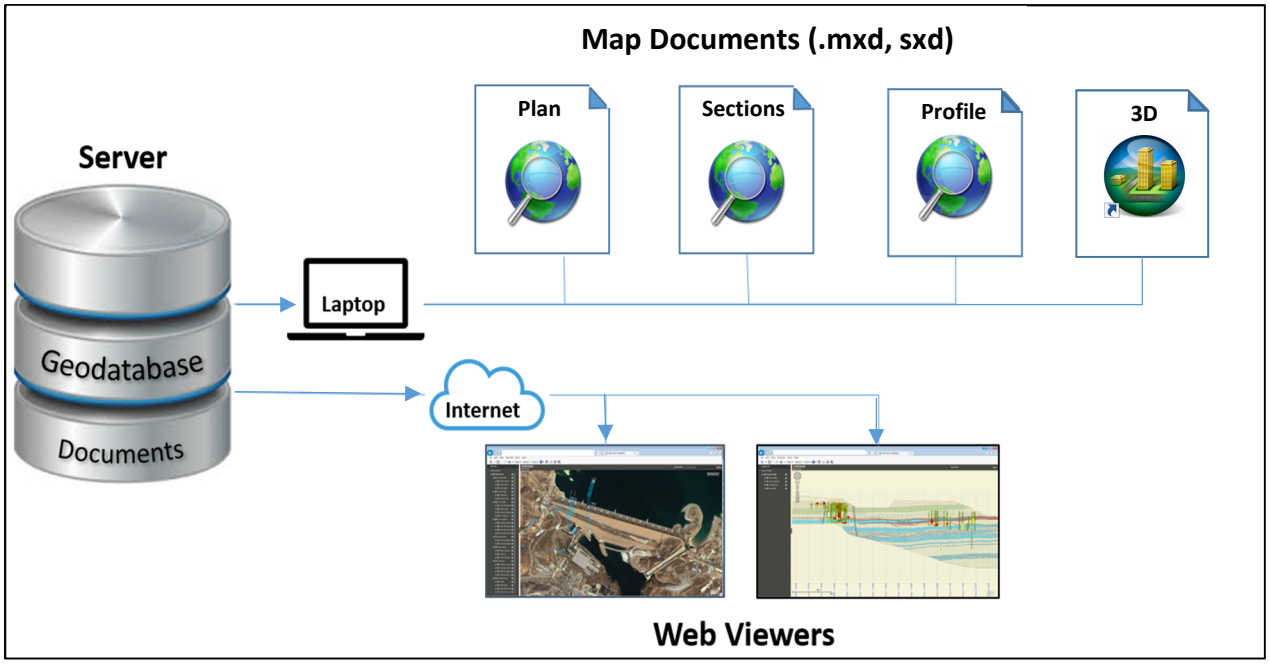


Figure 4. Typical Data Flow from USACE Server to User Access Points

MODEL SERVES AS VISUAL LIBRARY FOR PROJECT INFORMATION

There are a number of benefits to compiling a central model of a dam safety modification project such as the grouting operations at Mosul Dam. The first is that the viewer provides all members of the team with ready access to a wide variety of up-to-date information about the project in an easy to use interface. As-built and other documents such as photographs, drawings, design reports, condition reports, instrumentation installation details and geological mapping are hyperlinked to the corresponding spatially located features. In practice, this means the easiest way to find a great deal of information on the project is to use the model as a spatial library navigating to the area of interest and following the hyperlinks that work in both the web and the full scale GIS environment. To build this, the documents are located on a central server and organized for ready access. Given the 30 year grouting history there are a wide variety of files in a wide variety of formats that has been compiled for the project and the current documentation directory contains more than 290 GB of data. A simple example of how this is used can be illustrated with photographs that

have been taken of a wide variety of features over time. These have been added into the model and oriented with the correct viewing angle. By a few simple mouse clicks, these are easily accessed (Figure 5). The web viewers have a legend (Table of Contents) which show all the data that may be selected at the site and includes search, measuring, annotation and printing tools

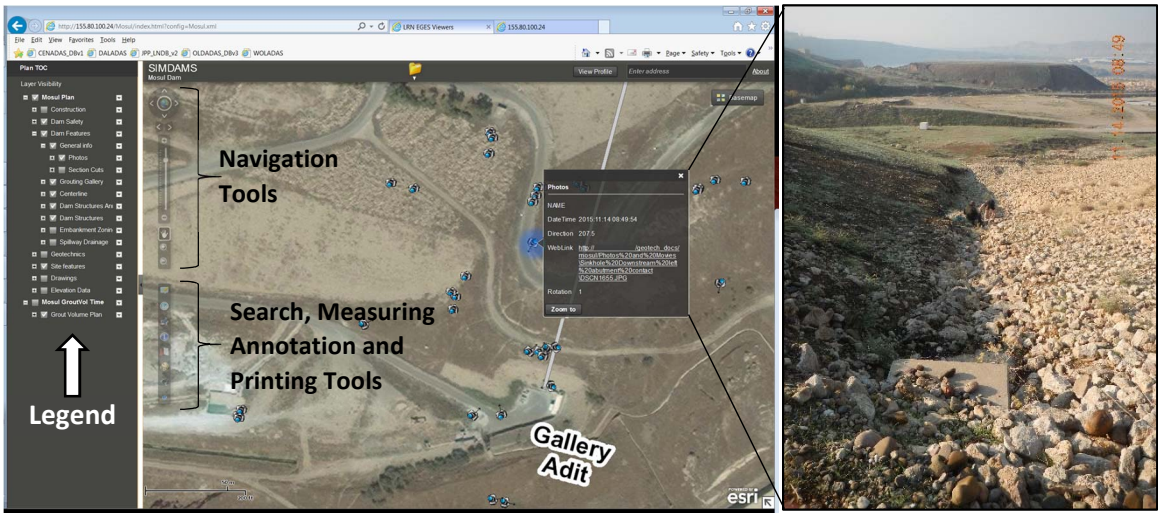


Figure 5. Photographic Library within Mosul SIMDAMS Model

However, the value of this goes well beyond locations of photographs at the site. As data are generated for the grouting stages, these are continually updated in the model and the data are hyperlinked to the appropriate grouting stage. Thus the model provides a continually updated as-built for the site documenting the work and providing access to trend plots, QA observations and other important data (**Figure 6**). Various layers of data can be turned on an off from the legend, like the drilling observations at the site, comparisons with historical grouting data, geological models and previous as-built information.



Figure 6. Grouting Data Accessible through Mosul SIMDAMS Model

ANALYSIS OF DATA SUPPORTED BY THE MODEL

The second primary benefit of building a BIM type of model for Mosul Dam and other dam safety projects is that it makes analysis of data being generated both faster and easier than other methods. Data from different sources, such as historical and current grouting can easily and quickly be compared. As soon as the grouting data are received from the site it is geoprocessed and updated in the model, making it more readily available both on site and in reach back. We can then cross correlate much of the data in one coherent model which can be viewed in 2D plan, 2D profile or 3D views. This gives the data much better context and makes it easier to highlight areas of interest and to compare current observations with instrumentation monitoring on the site (**Figure 7**). Cylinders in the figure are sized based on grout take with the largest takes shown in red, and smaller but still significant takes shown in yellow.

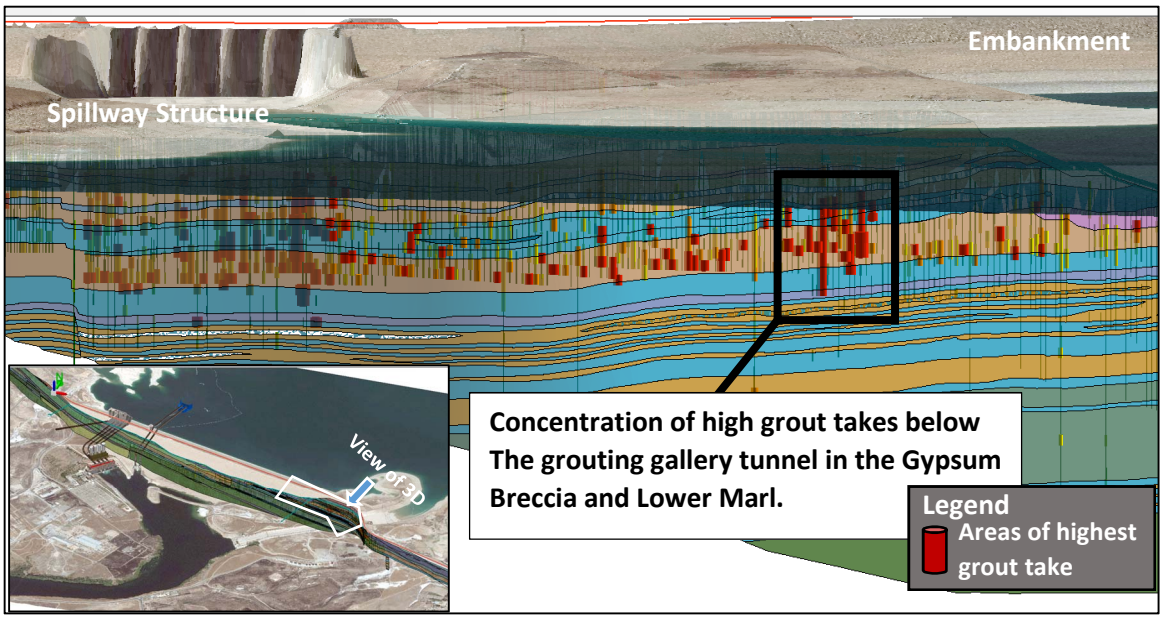


Figure 7. Grouting Data in 3D view below Mosul Dam

Geoanalysis tools also become easily available and statistical analysis of grout takes, for example, can be performed with respect to the geological layers, identifying "Hot Spots" of significant grout takes and "Cold Spots" of lesser takes across the project. For example the grout concentration shown in Figure 7 can also be discerned in the analysis shown in **Figure 8** as it shows up as a statistically significant area.

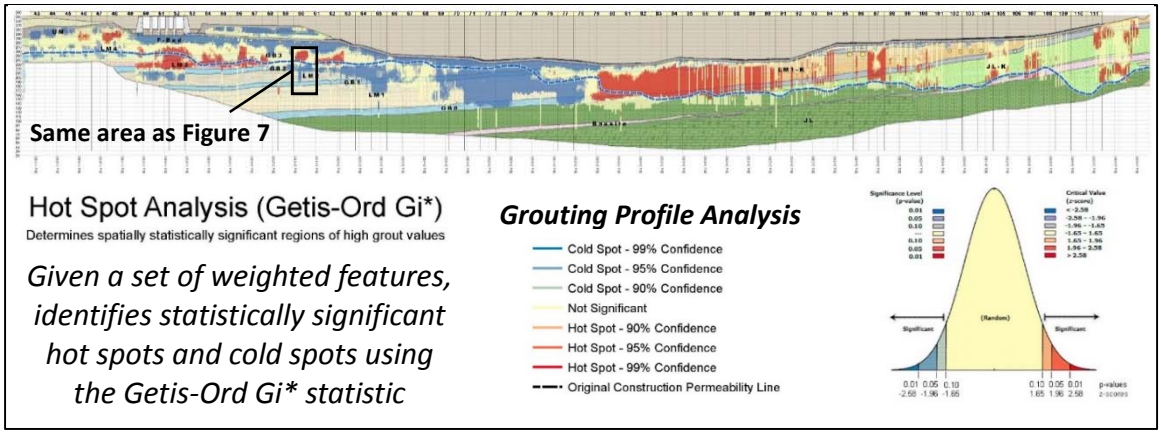


Figure 8. Grouting Data in Profile with Hot Spot Analysis

These products are also continually updated as the project proceeds. These types of analyses make it easier to plan future grouting operations as well as to facilitate dam safety risk analyses when comparing the effectiveness of a particular grouting program.

Additionally, standard split space closure graphs, often called PSTQ analysis for the order of split space grouting holes, can be automatically updated as the new data are added. Tools can be used both in GIS and with analysis programs such as excel with data links to the central database. These plots and graphs are automatically updated as soon as the user tells the tool to refresh the data link. This gives the personnel charged with monitoring and analyzing the grouting many additional tools that provide rapid data analysis (**Figure 9**). It prevents wasted time creating and re-creating graphs and plots that the computer can more rapidly update from standard tools and templates created for the site. This would not be possible without organized data stored on a central server due to the volume of data and the rate at which it is generated.

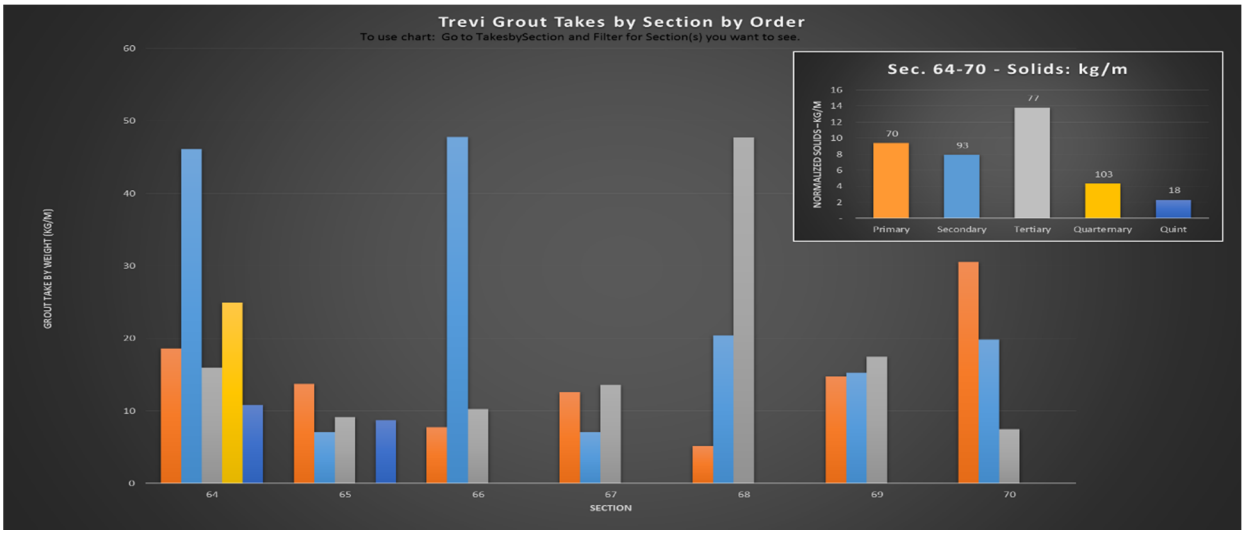


Figure 9. Snapshot PSTQ Graph for Grouting Sections at Mosul Dam – Current Program

However, the Mosul project has more than the current construction data. In order to perform a risk analysis and complete a dam safety modification study to recommend next actions at the project, it is necessary to compare all the current grouting data with the original construction and other historical grouting data. One such analysis that has been performed for the project is an assessment of the blanket grouting and foundation treatments completed during original construction underneath the core. Original as-built records were digitized and incorporated into the GIS, which have been used to generate maps and graphs for the entire dataset as well as specific, geographically-defined subsets of interest (**Figure 10**).

Now rather than looking at 24 separate as built drawings, the data can be presented and analyzed in its entirety. We can see from this map both the locations of every vertical blanket grouting hole as well as the grout takes for the holes. As the blanket grouting was split spaced during original construction, we can also construct graphs that show how much of the grout take for the whole area, or on a section by section basis, went into each type of hole. On this graph in Figure 10 we see the expected pattern that the Primary grouting holes took the largest quantities of grout with decreasing grout takes in the Secondary, Tertiary and Quaternary holes.

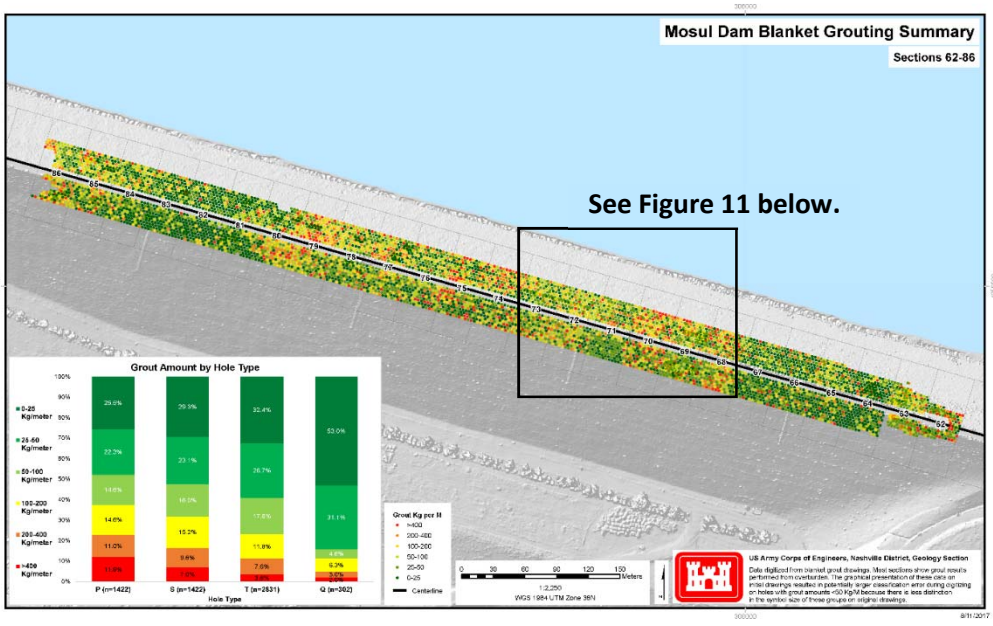


Figure 10. Original Blanket Grouting Vertical Holes – Sections 62-86

These data can then be compared with the inclined check holes that were installed after the initial blanket grouting was completed. When assessing the effectiveness of the blanket grouting in protecting the core from the foundation, the benefits of this approach become obvious. For example, the outlined area in **Figure** 10 can be seen in **Figure 11** below. Here the vertical blanket grouting holes are shown with increased transparency along with inclined check holes installed 2-3 years later. This data presentation de-emphasizes the vertical holes while still showing the spatial relationship with the later check holes.

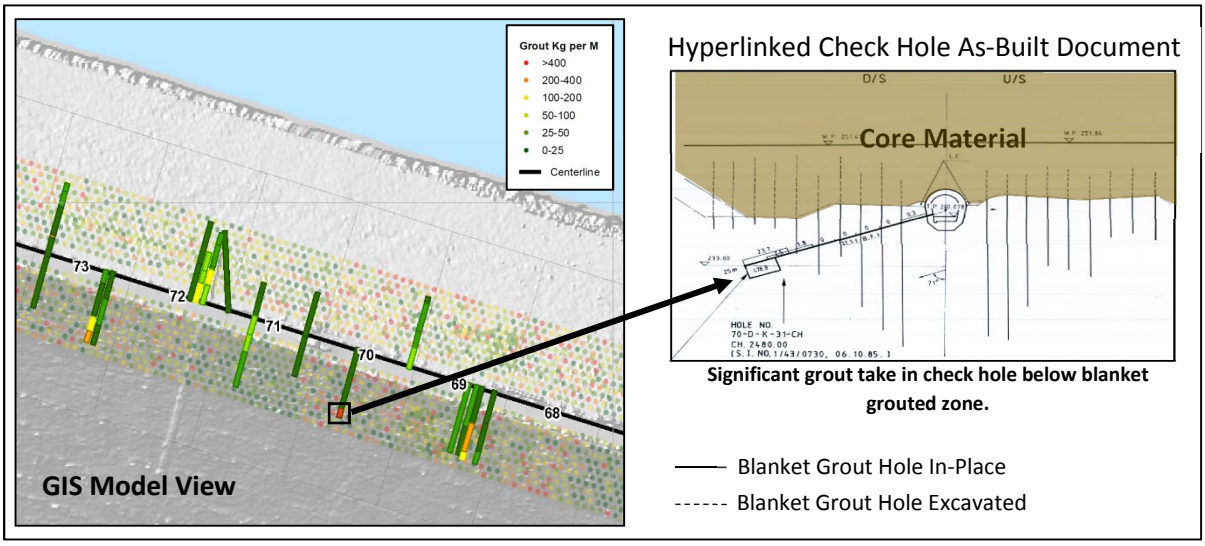


Figure 11. Original Blanket Grouting Compared to Inclined Check Holes

In this particular example the check hole, while it was installed in an area of higher takes during the blanket grouting, does have significant take, but it is below the original blanket grouting zone. Here most of the rock that received blanket grouting on the outer four downstream rows was removed by excavation. Thus

in this area the blanket grouting may be considered somewhat ineffective on the downstream size for this limited area. While this analysis may not comment on the current grouting efforts, work of this type is critical to understanding potential failure modes at the project, which speaks directly to any dam safety assessment being performed at the site. As before all these documents again hyperlinked to the feature class to make quick evaluation and access to these details rapid and simple.

CONCLUSIONS

Analysis of all the data at the project continues and at the writing of this paper, a second year of grouting has been proposed to the Government of Iraq. Further improvements and refinements to the system continue to be made as new data, or old data not yet located are made available. Expected updates to the system include further tool development to facilitate the rapid generation of custom map products, further use of 3D integrated with an exploratory program to provide more rapid generation of cross sections, training of Ministry of Water Resource (MoWR) staff on how to use and build an information management system such as the Mosul SIMDAMS model, and application of this data to future recommended dam safety modifications on the site.

There are, as discussed above, many different uses and applications of the SIMDAMS models to construction and dam safety assessments. Only some of the benefits directly related to the Mosul Project have been elucidated here. The model serves as a data library for the project, providing rapid access to information for a team on-site and that spans many parts of the world. Hyperlinks of documentation to spatial features makes it easier to find critical data when it is needed. The model serves as a living as-built of the grouting data as the grouting program continues making the data available to USACE, our engineering partners and to the Government of Iraq. Integration of the data sources provided by Trevi and by AECOM working for USACE have made the system much more effective and ensures the entire reachback team can remain up to date on current progress. The addition of new data sources made available by the Government of Iraq has added significant benefit to the model and as as-builts are uncovered and scanned, they are added into the system to aid in the refinement of a risk assessment of the project and to provide input for a Dam Safety Modification Study. However, current usage of the model has aptly demonstrated the value of a BIM-like environment for dam safety on both this and other projects.

References

Bateman, V. C., Kelly, C. J., Worsham, B. M., Walker, W. G., Wygonik, M. M., & Wiles, S. G. (2015). The SIMDAMS Project: Bringing Dam Safety into the Information Age. *Association of Environmental and Engineering Geology Annual Meeting.* Pittsburgh, PA.

Hlepas, G., & Bateman, V. C. (2017). Lessons Learned from USACE Seepage Barrier Construction: Wolf Creek to Present. *Environmental and Engineering Geoscience*.

Rosen, J., & Bateman, V. C. (2015). Barrier Wall Installation at Wolf Creek Dam and Center Hill Dam - Data Management, Ana;ysis, Visualization and Sharing. *SC/SA Joint Engineer Training Symposium (JETS), Nashville TN*.

Washington International/Black and Veatch. (2004). *Mosul Dam Library of Documents, Thirteen volumes of data and information on Mosul Dam 1984-2004.* Washington, DC: Unpublished.

RECENT ADVANCES IN BIM IN GEOTECHNICS

Jim De Waele. Keller Limited, Ryton-on-Dunsmore, Coventry, United Kingdom, 4424 7651 1266, jdw@keller.co.uk

ABSTRACT

The use of Building Information Modelling (BIM) is becoming more widespread throughout the various sectors and professions of the UK construction industry, however, in its "*National BIM Report 2016*", the National Building Specification (NBS) concluded that BIM was still a) "*Far from embracing all parts of the supply chain*" and b) "*Not reaching the O&M phase of the building*".

Of course a positive step was taken when in April 2016 the UK Government departments were mandated to use collaborative 3D Level 2 BIM. However we still need more clients and the operators of constructed assets to follow the initiative, if we are going to improve upon the NBS's findings.

This paper examines two recent advances in BIM in the field of geotechnics. The first case study relates to the sharing of site generated data, that is gathered electronically on site, processed and then uploaded to the BIM model, all automatically. In this way, the stakeholders are seeing the object attributes updated in the integrated model in real time - as the work is done. The advantages of this process include the obvious savings in time and effort, avoiding mistakes, self-certification and the manifest openness that supports collaboration.

The second case study relates to how monitoring data can be accessed from the BIM model. Whilst strictly not an "object" in BIM terminology, this information is important to the construction team during the building of the asset and surely to the operator and maintainer too. The monitoring database provides a way of all parties being able to interrogate the same data, both in real time and historically. This information truly spans between design, construction and the O&M phase, and has the potential to bridge some of the traditional gaps.

Both advances support the wider uptake of BIM and its continuing development. More importantly, in the author's view, both give further impetus to the changing landscape of construction procurement and the way that the industry works.

If we are to continue to improve the efficiency and effectiveness of the construction industry we must learn to collaborate and digitalise. The author believes that BIM has the power to deliver this, almost by default, encouraging and cajoling the parties to act in this way.

Keywords: Building Information Modelling, BIM, collaboration, geotechnics

INTRODUCTION

There are many of us involved in the construction industry that want it to change and modernise. Much has been said and written on the necessity to collaborate and use digital tools far more than we currently do [Ref: PAS1192 series]; but the reality is that progress is painfully slow and largely because of poor returns, commitment towards research and development is scant. However, some are seeing that by adopting BIM, those professionals working in the sector might be pushed or incentivised into a better way of working. The implementation of BIM requires a change in traditional processes and relationships. The very fragmented nature of our industry makes this collaborative method of working a challenge, but one that the author hopes BIM will make inevitable. Viewed in this way the adoption of BIM should be seen as an enabler. Used properly, contractually [Ref: CIC (2013)] and collaboratively it is a tool that should:

- Enable better information flows through improved technology.
- Enable better decision making during design and construction.

© 2018 Deep Foundations Institute

- Enable the full construction team to participate effectively in the process and;
- Enable the end user to better understand and manage their asset.

BRIEF INTRODUCTION TO KELLER

Keller is the world's largest geotechnical specialist. It has operations in over 40 countries and employs 10,000 people. It's UK operation makes up one of the leading companies in the market and offers a full range of foundation and ground improvement solutions. Most of the work that Keller does is design and build and normally through a subcontract with the Principal Contractor (as a tier two supplier to the ultimate client). Keller works in all sectors of the construction industry from housing, commercial, infrastructure and utilities. Because of the nature of what it does, the company often has involvement with architects, design consultants, cost consultants, housebuilders, clients and contractors. In many-ways its position as a design-build tier two has required the business to collaborate across the industry for many years. This means that Keller, and companies like it, have a unique perspective when it comes to the adoption of BIM.

So, it is in this context that two case studies are presented that are leading, or at least interesting in their own right, but have benefits beyond their technical merits.

The first case study relates to getting data directly from the on-board rig computers to the BIM model; a "data-drop" exercise, whilst the second exemplar details a way that a user of a BIM model can access data held on another server that is useful for the stakeholders of a project, in other words, using BIM as a gateway to other information.

FIRST CASE STUDY - DATA DROP PROJECT

The subsurface realm is complex and heterogeneous. The performance of soils is self-evidently highly variable and difficult to predict with precision. Natural and man-made obstacles add to the ground-related risks.

Currently, relevant geotechnical information is limited, if it is included at all, in commonly used BIM models, and ground conditions, the foundation system applied, and the execution of geotechnical works have minimal or no impact on the entire planning, construction and investment process. This is a clear contrast to the lessons learned since ground problems are one of the major causes of project delay, and when they occur they are normally difficult to handle and expensive to rectify. Therefore geo-related data, such as geological, hydrogeological and geotechnical objects and properties, should be considered as a vital and integral part of an extended and future-looking BIM model.

From the geotechnical engineer's perspective, an un-federated BIM model, even separate from the overall Project BIM model (let's call it a GeoBIM model) would improve the understanding of how any geotechnical solutions "fits" the ground. Not just through a 3D representation of what is being installed, but how the foundation relates to the geographical strata that is either known about or postulated. Resistances, or pressures, or torques that have been used during the installation of the foundation are also important parameters to have captured in the objects within a GeoBIM model to aid understanding of the underlying conditions and to validate the design assumptions that have had to be made.

With all of that in mind, Keller decided in March 2016 to move towards an environment where first it could use a GeoBIM model for its own purposes to validate and check its own work, but hopefully also move towards a way of linking or federating this with the overall Project BIM Model.

It is already possible to plot ground information such as boreholes into a GeoBIM model, particularly if the "AGS" electronic data format is used [Ref: ICE (2016)]. However, obtaining and then manually entering the as-built data, is a time consuming and frankly boring process. Engineers become overly involved in the administration and cease doing what they have trained and are paid to do; engineer.

Thus, Keller decided that both to improve its internal processes and to encourage the uptake of BIM, that this dataflow needed to be automated, meaning that site construction data would flow into both the GeoBIM model and ultimately into the Project BIM model directly. In the future this will be common place, but presently a lot of manual site records are distilled and entered into the model by manual keying in.

Process

Many of the rigs and items of equipment used in the geotechnical sector already have on-board computers controlling the process and recording installation data [Ref: (ICE 2016)]. The data-drop project essentially takes this source data, collected during construction, and pushes it into the Autodesk Revit Project BIM Model for all the other project stakeholders to view.



Fig 1.1. Typical on-board rig computer

The philosophy has been to meet the requirements of BIM Level 2 using Keller's existing systems as far as possible. K2 software fulfils this requirement perfectly as it is tailored to link databanks that would otherwise operate independently.

The process requires the use of an application to application interface program (API) to take the data from the site computer, into a SharePoint environment and then beyond into Revit [See Fig 1.2].

The process executes on a schedule and moves data from the site (via mobile links) into the Keller repository first, then either into the GeoBIM (un-federated) model or better still directly into the Project BIM. Selected data and specifically any object attributes that are required are moved into the model, but all the source information is permanently maintained (and archived) in the Keller server.

The Keller database provides a secure electronic data input into the system drawing from several different types of instrumentation and sources. This repository hosts the master input data. This is a rich data environment and so can be easily portioned as necessary, by client or by project for example.

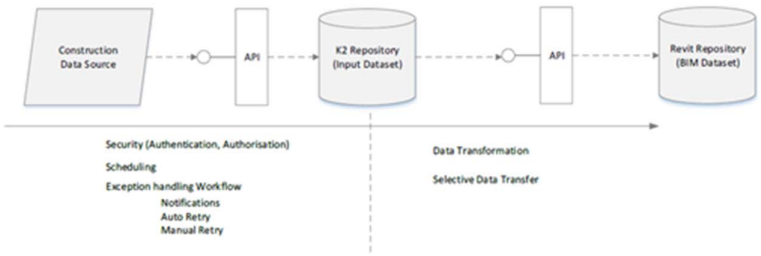


Fig 1.2. API Logic

A simple search within the SharePoint site allows the user to interrogate the rig instrumentation database retrieving construction information for a specific project, product, rig and/or shift. This is cross-checked against the design intent and any discrepancies between the as-built record and the original design are flagged within the system as requiring a further check by an engineer.

The next step is that selected data is sourced from the repository and published to the BIM model. The data that is chosen could be selected by the client or other stakeholders. The application provides data transformation and translation services to ensure that it is mapped correctly to the objects and the attributes are then assigned into the Revit model.

The overall system processes are orchestrated using K2, removing human intervention and bureaucracy. This also allows automatic scheduling, provides notification to the users and allows system-human task creation. An example of a BIM model automatically populated with such site data is included in figure 1.3.

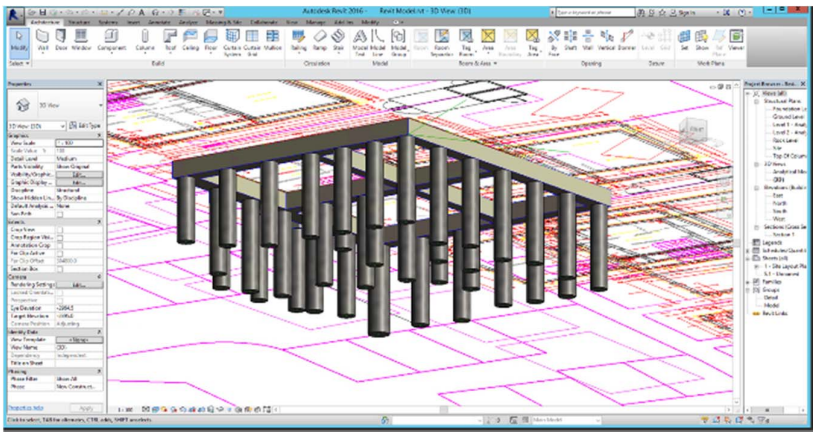


Fig 1.3. The Populated Revit Model

In addition to populating the model, using the construction data, the application also automatically populates the more traditional daily report sheets often used by the Principal Contractor as a record. In time, we would hope that this paperwork becomes obsolete as the BIM model becomes the one true record, available to all stakeholders.

SECOND CASE STUDY - BIM AS A GATEWAY TO MONITORING DATA

The second advance is in the use of monitoring data. Monitoring and the instrumentation of either existing infrastructure that might be affected by construction, or the monitoring of the new works, or the collection of data relating to the environment is now common place and increasing in popularity.

The traditional linear approach of procurement is being challenged by BIM and situations are being created where all parties have to share from a common information pool. But, breaking through the barriers of the parties protecting their own interests, or not freeing up the data into the model, remains a challenge and this is where Keller has made some important headway.

It is not unheard of that, in some traditional arrangements, monitoring is carried out (procured) separately by the client, by the Principal Contractor and possibly some of the sub-contractors too. Data is not typically shared freely and when it is, it can be conflicting, unsurprisingly.

In a collaborative way of working, this monitoring service would only be procured once, for the project; for everyone, but access to the information has to be open and transparent with all parties having the same unfettered access. The BIM model provides a perfect way of achieving this.

However, monitoring data can be difficult to handle. Firstly, it often needs processing, and there are various ways that the data can be presented; graphical representation is an obvious way, but more innovative techniques such as heat mapping can be more easily read. Secondly, the amount of data is problematic. Monitoring could on some jobs last decades and if, as is the case with some instruments, data is being read and logged every minute, then the database soon swells. If this were all to be stored directly within the BIM model then it would be quickly become unwieldy.

So the solution that Getec (a Keller subsidiary) has arrived at is to write a plug-in to the Revit standard menu that allows the user to access the I&M database through interaction with the model.

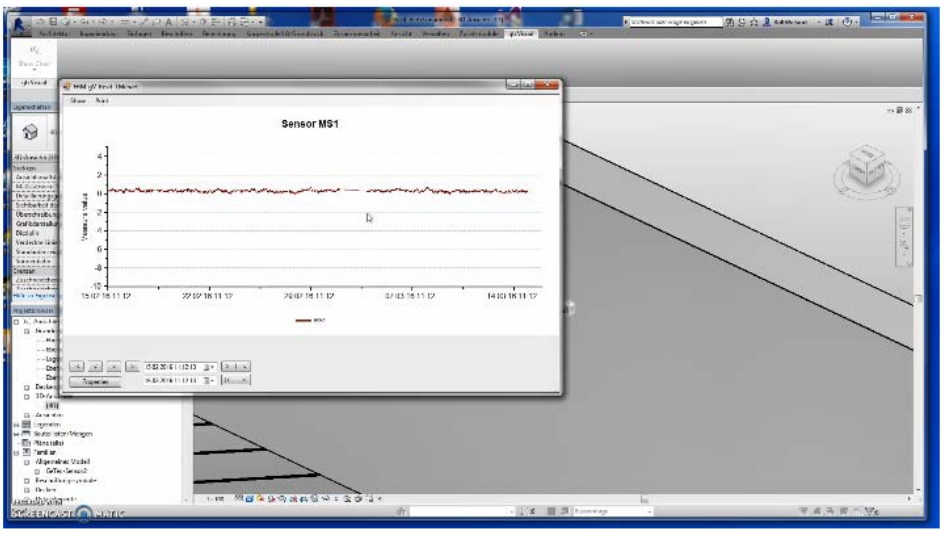


Fig 2.1 I&M through Revit

The user can navigate through the model in the usual way. Sensors and instruments are drawn into the model like any other piece of hardware and each of them is an object in the 3D model with useful attributes that can be used throughout the construction and the O&M phase.

When the user wants to see the monitoring information, one or more of the sensors is selected and

access to the monitoring database is activated. This allows the I&M information to be presented with the full functionality of the I&M software running behind the BIM model.

If access to this data is to be restricted, then this is easy to arrange. The sensors and instruments would be visible in the model, but the link to the I&M software would be only available to those that are authorised.

One issue to address is, who owns the data? Permissions can be allocated, but one could argue that ultimately the client pays for the data whether or not he sees or uses it. Surely, any client would want the benefit of monitoring data pre, during and post construction? This opens up the opportunity for the BIM model to be truly used as envisaged, from concept, through design, into construction and finally in the O&M phase.

Perhaps the offer of I&M data that can be used for many years after the building is commissioned could move some clients to also embrace the benefits of BIM after construction. In this scenario, the model could not only be used for the fabric of the building or piece of infrastructure, but the monitoring data could be extended to cover heating and lighting performance, air conditioning systems, or for maintenance, condition based monitoring tools. Whilst these are recognised virtues of other asset management systems the potential for overlap is obvious.

This approach of providing a "live" BIM model rather than just a record of what has been built at handover, supports the UK Government's Soft Landings philosophy [Ref: BSRIA (2009)] and is perhaps the holy grail for BIM in the future.

CONCLUSIONS

Most commentators concur that wide adoption of BIM in the construction industry is inevitable. It is not a question of if; but when. In addition to the obvious digital progress, the author also hopes that BIM will be the enabler, or the catalyst, for change towards a more collaborative industry too.

The value of data is underestimated. The cost of collecting and collating data is often expensive and time consuming. With the data drop solution, real time and accurate data, direct from the construction site, can now be sent directly to the BIM model without any human processing.

Our industry is terribly fragmented. The UK Department for Business, Innovation & Skills in 2013 identified that on a typical medium sized project (with a spend of circa £20M) up to seventy sub-contractors can be involved. Managing this number of parties to a project is complex and problematic, as anyone in the industry will confirm. We need to find ways where we can work in partnership, both on a live project, but also between organisations where relationships can span several or many projects. Whilst far from the complete solution, BIM does present an opportunity to assemble a supply chain that can get involved earlier in the asset life cycle, and stay around for longer too. The use of BIM requires tier-two contractors working within the project team to coordinate the way in which the information contained and associated with the model is created and managed.

Keller's commitment to BIM and in particular its focus on transparent solutions is a good example of how the tier-two contractors are responding. Contrary to some findings, many subcontractors are ready and are wanting to fully engage with BIM. But for this to happen it needs the commitment from the clients and also the tier-one or general contractors.

Keller would like to think that with the I&M data so obviously being relevant to all the stakeholders and the phases of a construction project, then this might present a further impetus for clients to think again about deploying BIM on their scheme.

Our industry is still in search of the cultural shift that will see us working in collaboration. We should collectively take the opportunity now to make BIM the catalyst to that change.

ACKNOWLEDGEMENTS

The author acknowledges Keller Limited for its investment so far in BIM and Arno Van Rooyen and Velocity IT, the business that has written much of the code for the data-drop project.

REFERENCES

BSI (2007) BS1192 Part 1. *Collaborative production of architectural, engineering and construction information code of practice,* British Standards Institute, London.

BSI (2013) PAS1192-2 *Specification for information management for the capital/delivery phase of construction projects using building information modelling,* British Standards Institute, London.

BSI (2014) PAS1192-3 *Specification for information management for the operational phase of assets using building information modelling,* British Standards Institute, London.

BSI (2014) BS1192 Part 4 *Collaborative production of information: fulfilling employer's information exchange requirements using COBie – code of practice,* British Standards Institute, London.

BSRIA BG4 (2009) *The soft landings framework,* Building Services Research and Information Associations, Bracknell,

CIC (2013) *BIM Protocol,* Construction Industry Council, London.
Institution of Civil Engineers [2016]. "*ICE Specification for piling and embedded retaining walls*". Thomas Telford, London.

NBS [2016]. "*National BIM Report 2016*". NBS is a trading name of RIBA Enterprises Ltd, Newcastle.

THE SOCHI CASE: THE FIRST REAL COMPARISON BETWEEN NATM AND A.DE.CO-RS

G. Lunardi, CEO Rocksoil S.p.A., p.zza S. Marco 1, Milan, Italy, giuseppe.lunardi@rocksoil.com
G. Cassani, Technical Director, Rocksoil S.p.A., p.zza S. Marco 1, Milan, Italy, giovanna.cassani@rocksoil.com
A. Bellocchio, Technical manager, Rocksoil S.p.A., p.zza S. Marco 1, Milan, Italy, andrea.bellocchio@rocksoil.com

ABSTRACT

The main feature of the A.DE.CO-RS approach is that the design Engineer focuses primarily on the deformation response of the ground to the action of excavation. This deformation response is first analysed and predicted using a variety of instruments (full scale and laboratory tests, mathematical models), then it is controlled by using appropriate stabilisation measures. The A.DE.CO-RS approach investigates the deformation response very thoroughly, right from its onset where it starts ahead of the face, as opposed to traditional approaches, that only consider deformation behind the face. The approach controls the deformation response acting first and foremost ahead of the face, using preconfinement action, and not just ordinary confinement action as in traditional approaches. In this way the A.DE.CO-RS approach is able to successfully tackle any type of ground and stress-strain conditions, especially in the most difficult ones. The A.DE.CO-RS Approach has been applied in Italy, for the first time, in 1988 to Tasso Tunnel and then to San Vitale and Vasto tunnels. The first application outside of Italy was in 1997 with the Tartaiguille tunnel (high speed rail line between Marseille and Lyon in France). In this paper the authors describe the real case by which it is possible to start to make a direct comparison between A.DE.CO-RS and NATM. The Sochi Case reports the main differences observed in terms of production and of safety between the two different approaches used during excavation the Dubler Kurortnogo Prospekta tunnels.

Keyword: Conventional Excavation Method, N.A.T.M, A.DE.CO-RS, Design Method, Full Face Excavation

INTRODUCTION

Between the end of ‘800 and the beginning of ‘900 no established method wasa vailable for the design and excavation of tunnels in difficult ground conditions. It must be recognized however that, in order to meet the needs posed by the new transportation means and the increasing mobility requests, spectacular tunnels were excavated and completed, such as Frejus and Simplon railway tunnels through the Alps and “La Grande Galleria dell'Appennino” through the Apennines between Bologna and Firenze. This was achieved although a number of workers lost their lives for the sake of reaching the objective. In the absence of established methods, different ways of tunnelling were applied such as the Belgian, Austrian and Italian methods, etc. It was only between 1920 and 1960 that landmark contributions in tunnelling took place by Terzaghi (the “rock load” due to the weight of the broken ground resulting from the excavation of the tunnel), Kastner and Fenner (the development of a “plastic zone” in the rock mass surrounding the tunnel), and Rabcewicz (the New Austrian Tunnelling Method), to mention a few.
It has to be un underlined the great merit of Rabcewicz who pointed out: (1) the importance of conserving and mobilizing the inherent strength of the ground surrounding the tunnel, (2) the need to minimize ground loosening and excessive deformations by means of a primary support system, flexible rather than rigid, and placed to remain in physical contact with the ground and deform with it, (3) the installation of instrumentation to monitor tunnel deformation and build-up of load in the support, for gaining information on tunnel stability and optimizing the load bearing rock mass ring. Naturally, the tools available to Rabcewicz were those of the time when his “approach or philosophy” was developed, by integrating the principles of rock mass behaviour and the monitoring of this behaviour. Use was still made of ground classes (Lauffer-Pacher,Bieniawski and so on) and the analyses to understand the ground behaviour were performed in two-dimensional conditions and limited to the tunnel cross section. No sophisticated and advanced three dimensional computational tools were available at that time as presently adopted. To control tunnel stability during face advance, the only option was to adopt sequential excavation. Rabcewicz was well aware of the need to improve the way of thinking of the time, when he pointed out that “Tunnels should be driven full face whenever possible, although (today) this cannot always be done...” (Rabcewicz, 1964). It is indeed in this context that in the mid ‘80s Lunardi (2008) pointed out the importance of the stability of the “core-face” and conceived the A.DE.CO-RS approach. He suggested that understanding and controlling the behaviour of the ‘‘core’’ ahead of the

advancing tunnel face is the secret to successful tunnelling in difficult ground conditions (Lunardi P. et al 2015).

HYSTORICAL OVERVIEW

After several years of researches and studies it has been formalized the A.DE.CO.RS Approach (Analysis of controlled deformations in rock and soil) which shared the concepts of Rabcewicz by applying them to the "extreme":

- the ground considered as a construction material
- the importance of the ground deformational response during excavation
- the advantage of driving the tunnel always full-face in every stress-strain situation
- the importance of the invert in difficult ground conditions (to "close the ring")
- the relevance and value of stress-strain monitoring during face advance.

It is important to highlight how the above concepts are the fundamental components of A.DE.CO-RS. These were agreed upon and further developed. The "inherent" weaknesses associated with NATM, mainly due to the limited knowledge, at the time of development, on the control of the ground response during excavation were "corrected". The Deformation Response of the ground and rock-mass, subject to excavation action, in terms of "Analysis and Control" should be carefully studied (theoretical forecasting in the design phase and experimental verification during the actual excavation). Deformation response is complex and involves not just the tunnel cavity, but also the volume of ground that lies ahead of the face, virtually cylindrical in shape, with dimensions quite similar to that of the diameter of the tunnel to be excavated. This region, called the "advance core", is affected by a primary component of the deformation response: "extrusion", which manifests on the surface of the face along the longitudinal axis of the tunnel (bellying or rotation of the face), and "pre-convergence" of the cavity, i.e. the convergence of the theoretical profile of the tunnel ahead of the face (Fig.1). These primary components depend on the relationship between the strength and deformation properties of the advance core and its original stress state (Lunardi, 1997). The A.DE.CO-RS Approach has been applied in Italy for the first time to Tasso Tunnel (1988) and then to San Vitale (1990) and Vasto tunnels (1991). Starting from its very beginning the A.DE.CO-RS approach has aroused considerable interest and rapidly established itself as an advantageous alternative to those employed to date. The first application outside of Italy was in 1997 the Tartaiguille tunnel (high speed rail line between Marseille and Lyon) in France.

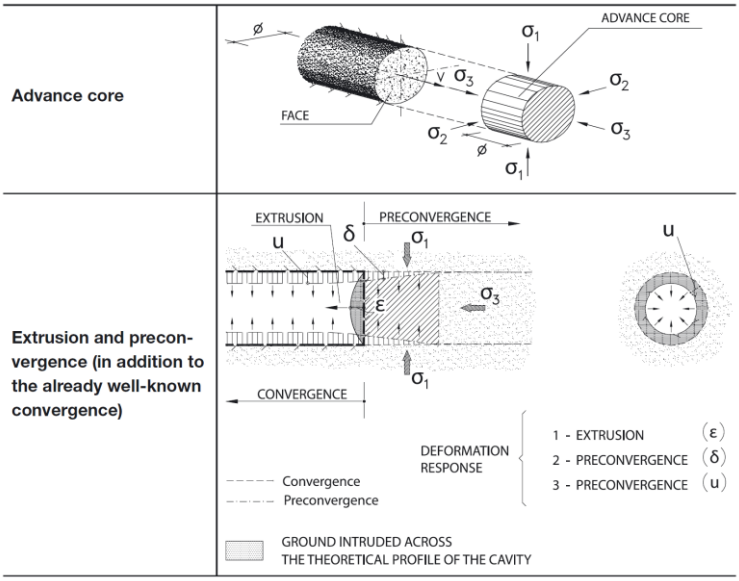


Fig. 1. The influence of advance core (Lunardi, 2008)

The Tasso Tunnel (Italy, 1988)

The "Tasso" tunnel is one of a series of tunnels excavated towards the end of the 1980's for the new "High Speed" Rome to Florence railway line. The original design involved half face advance, stabilising

the walls with arches and shotcrete. The arches were anchored at the feet with sub-horizontal tie bars and given a foundation of micropiles or columns of ground improved by jet-grouting. Initially excavation proceeded with no appreciable deformation phenomena either at the face or in the tunnel. As the overburden increased, and therefore also the stress state of the medium, and given also the poor geomechanical characteristics of the ground, conditions of face stability rapidly changed to those of an unstable face. Following the failure of the face despite half-face advance, approximately 30-40 m of already excavated tunnel also collapsed during the course of one single night with convergence in the order of 3-4 m (see Fig.2.a-b).The deformation of the advance core of a tunnel was the true cause of the whole deformation process in all its components (extrusion, pre-convergence and convergence) and then, as a consequence, the rigidity of the core played a determining role in the stability of a tunnel both in the long and short term. The rigidity of advanced core can be regulated by different technologies: fibre glass elements (GFRP), horizontal jet grouting, chemical and cement injections. In case of Tasso Tunnel, after the collapse, has been decided to reinforcing the advance core using fibre glass (Fig.2.c).

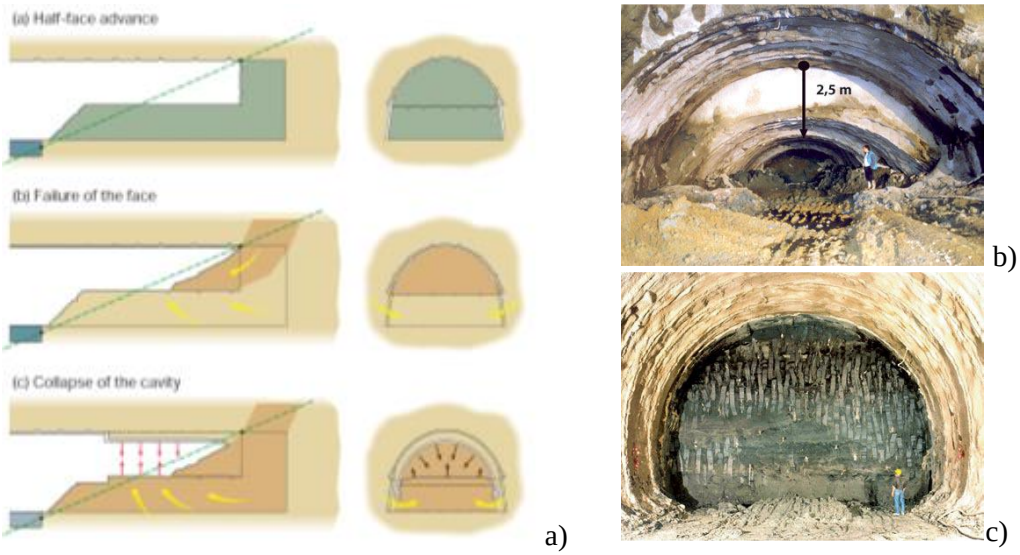


Fig. 2. Rome to Florence railway line – Tasso Tunnel: a) Chronology of observed deformation in a collapse during half-face advance; b) collapse during half face advance (NATM); c) full face advance after reinforcing the advance core with fibre glass tubes

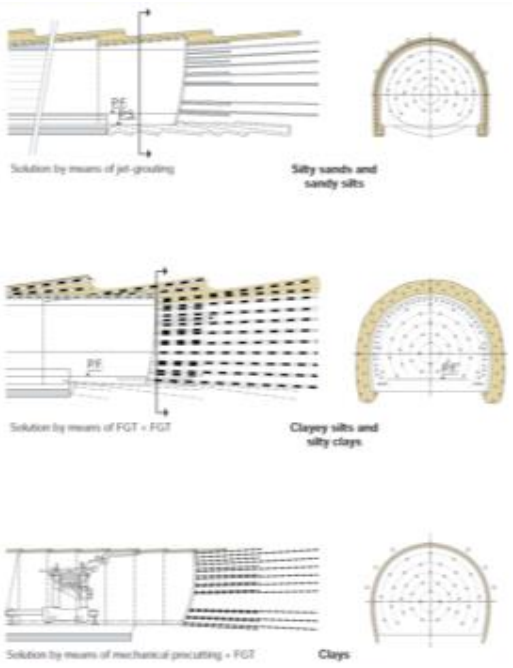
The Vasto Tunnel (Italy, 1990)

The "Vasto" tunnel is located along the railway line Ancona-Bari. The works began in 1984 at the North portal and continued slowly between repeated and serious incidents until April 1990. The original design involved half face excavation, immediately protected with a temporary lining of shotcrete, steel arches and welded steel mesh reinforcement. The final lining made by reinforced concrete characterized by a thickness of 1,0 m was cast straight behind the face and still in the presence of the core. The side walls of the tunnel were cast subsequently for underpinning and the casting of the tunnel invert completed the work. After the first serious incident of tunnel deformation, an attempt was made to resume tunnel advance employing several methods, which all, however proved to be completely inadequate. Finally a disastrous cave-in occurred at chainage Km. 38+075 under an overburden of 38 m., which involved the face (Fig.3) and then a section of approximately 40 m behind it. It produced deformation of enormous size (greater than one meter) in the final lining and it was impossible to continue working (Lunardi, 2008). Three alternative tunnel section types (Fig.4) have been designed to be adopted according to the homogeneity and consistency of the ground encountered during tunnel advance. The only difference between the three types was the type of treatment (preconfinement) to be applied ahead of the face around the future cavity, while the method of ground reinforcement performed in the advance core was the same for all three. The choice of technique to be applied around the core was strictly dependent on the nature and the acquired consistency of the ground to be tunnelled. In granular ground or where cohesion was poor, characterised by weak shear strength, horizontal jet-grouting was specified. The

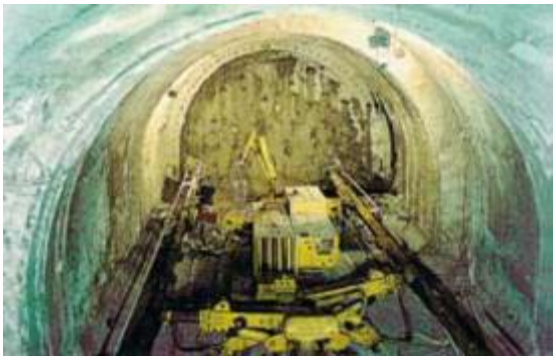
most appropriate technology to create strong shells ahead of the face in cohesive, compact and homogeneous ground, able to guarantee the mobilisation of an "arch effect" is mechanical precutting.



Fig. 3. Vasto Tunnel (Italy, Ancona to Bari Rail Line, ground: silty clay, overburden: 135 m, tunnel diameter: 12.20 m.). The extrusion of the ground through the face during heading and bench excavation (according to NATM principles)



a)



b)

Fig. 4. Vasto Tunnel: a) Full face excavation section types; b) reinforcing of the advance core with fibre-glass tubes during full face excavation (according to A.DE.CO.-RS principles)

New high speed rail line between Marseille and Lyon: the Tartaiguille Tunnel (France 1997)

Excavation of the Tartaiguille tunnel (180 m^2 in section), for the new railway line "TGV Méditerranée" Lyon – Marseille, began for both entrances (North and South) in February 1996. The initial approach consisted of advancing in partitioned face, excavating the heading and the bench about 200 m back. At the end of September 1996, while excavating the Aptien marls, convergence at the southern face raised well-above the expected values. This caused fissuring and cracking in the shotcrete pre-lining. Soon, excavation needed to face the worst stretch on both sides: 900 m through the feared "Lower Stampien" formation, which alternated strata of marls, clays and silts, with a high percentage (75%) of montmorillonites which were highly sensitive to air humidity and at risk of swelling (c' = 0.05 Mpa, φ' = 18°). Those in charge were quite worried and had therefore conducted an integrative geognostic campaign. The revision of the initial project proved that the excavation systems used previously were inadequate for the Stampien clays. These systems required partitioning of the excavation face which would have caused in that case unacceptable deformation phenomena. In order to solve the problem, in 1997 the SNCF (Societè National du Chemin de Fer), formed a study group ("Comité de pilotage") with

the technicians of the French Railways themselves, the G.I.E. TARTAIGUILLE consortium, the Coyne et Bellier consultants, the Terrasol-Simecsol consortium geotechnicians and the CETU. Said group started consulting the greatest European tunnelling experts and invited them to present a design solution capable of facing the clayey stretch both in safety and in line with the contracted timetable. In March 1997 a solution which adopted A.DE.CO-RS approach has been proposed with a detailed design of the 860 m of tunnel which needed to be constructed. The new design solution radically changed the traditional design criteria: full-face advancement (with control of deformation phenomena by means of the reinforcement of the core-face used as a stabilisation instrument), casting of the final invert at the face and final lining within 20 ÷ 40 m. (see Fig.5). G.I.E. TARTAIGUILLE recommenced advance works on the tunnel in July 1997, under strict supervision of the designer, who kept a trusted engineer on the site for the full duration of the work. The new advance system respected the contractual timetable of the works with an industrialised production of 1.7 m/day, which was even above the design phase prediction of 1.4 m/day. The tunnel was completed after just a year after recommencing with the full-face system, about 1 month and a half ahead of schedule (Lunardi et al, 2016).

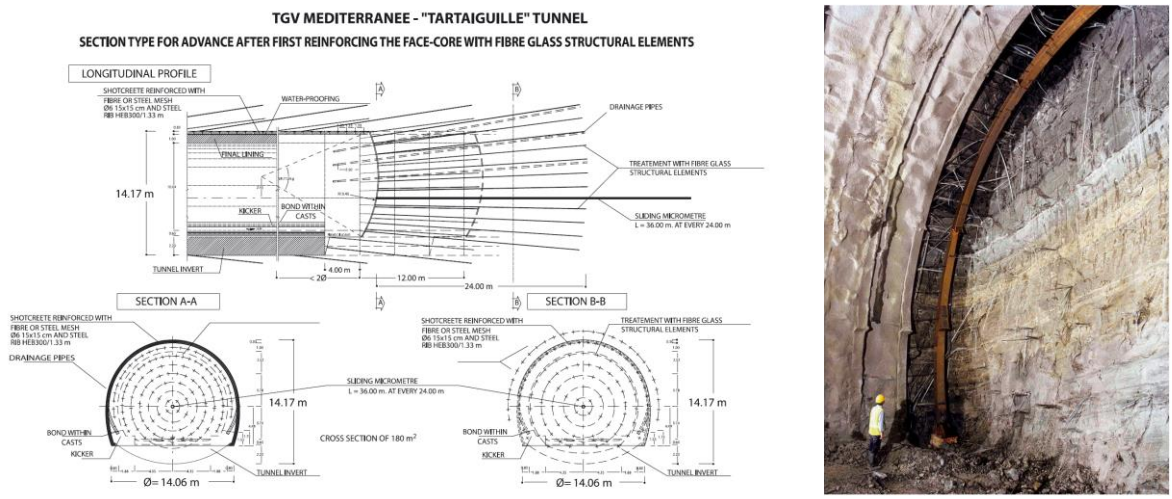


Fig. 5. Section types and cavity preconfinement after reinforcement of the core-face with fibre glass reinforcement: detail of the reinforced face (TGV Méditerranée, Lyon-Marseilles railway line, Tartaiguille tunnel, 1997, ground: clay, max. overburden: ~ 110 m)

THE SOCHI CASE

During the preparation for the XXII Winter Olympic Games in Sochi (Russia) from 7 to 23 February 2014, the Russian Federation allocated important investments in fixing the city's lack of infrastructure and in strengthening its transportation web. One of these projects is the new Sochi by-pass motorway, also known as "the alternative to the Kurortnyi road", which runs parallel to the black sea and makes it possible to reach the Olympic sites and the Adler airport without having to cross the city.
Construction of the new artery, which remained of decisive and strategic importance, presented many obstacles, especially regarding the short time slot available. Indeed, the project required the construction of eight double-bore natural tunnels, as well as open-cut sections, embankments and bridges for a total length of 16 kilometres (Fig.6). In searching for a solution, the Russian Federation heard about the exceptional success of the A.DE.CO-RS approach, used in Italy to build more than 100 km of tunnel – between line tunnels, access tunnels and safety tunnels – for the high-speed railway between Bologna and Florence (within the territory of the Tuscan-Emilian Apennines, which presents similar grounds to those of Sochi). The Federation therefore decided to minimize risks and to adopt the same approach for the design and for the construction of the 8 and 8A tunnels (these two being the longest and most complex of the motorway) after verifying the reliability of the approach by sending Russian technicians to investigate the major Italian A.DE.CO-RS tunnel sites. Following this decision, Rocksoil S.p.A. in Milan was appointed the detailed design in 2010, followed by the working design of the two tunnels as well as the necessary technical assistance during construction.

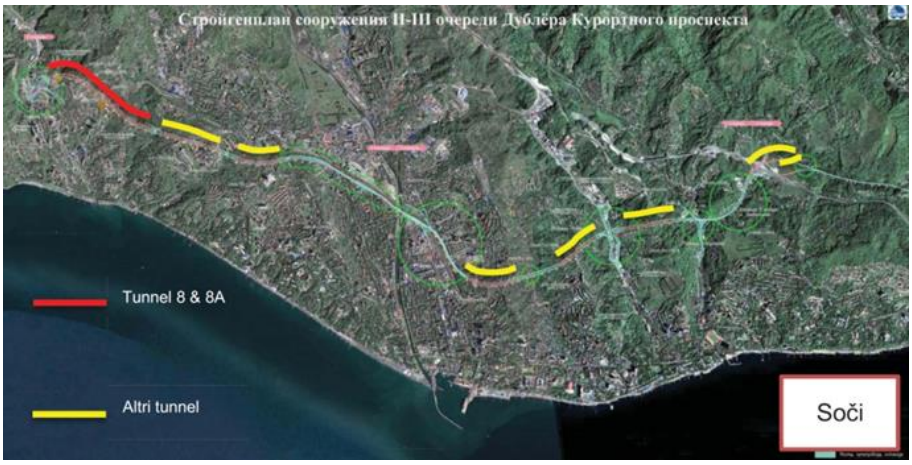


Fig. 6. The "alternative to the Kurortnyi road"

The project

The new Sochi by-pass motorway presents two separate carriageways, each with 2 lanes per direction, adjusted for a design speed of 120 km/h. Construction required the excavation of a series of tunnels. Of these, the T8 and T8A were the most difficult due to the geological context faced as well as – considering the reduced times available to design, construct and open the works – due to the Tunnel 8 & 8A length of the underground layout (1,550 m for the T8 tunnel and 1,523 for the T8A tunnel) and due also to size of the excavation faces, which could vary from 120 m^2 up to 220 m^2. (see Figg.7, 8). The project required the construction of 3 lay-bys in the tunnel and the implementation of widened face sections, so as to guarantee necessary visibility on bends. Furthermore, at the exit from the northern portal, the tunnels needed to welcome 3 lanes for the presence of an important junction connecting the new road with the existing one. Added to this was the low average coverage of the crown, in a heavily anthropized context.

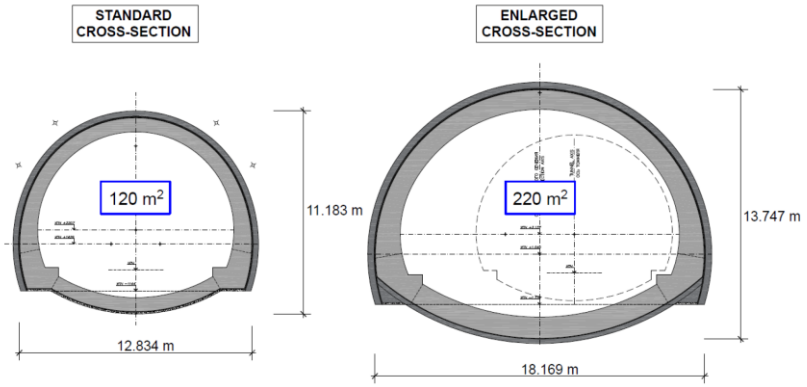


Fig. 7. Road outlines - 2 lanes / 3 lanes



Fig. 8. Standard and widened outline

Geology and Geotechnics of the T8 and T8A tunnels

Sochi is located at the western slope of the Caucasus Mountains, a chain which stretches for around 1,100 – 1,200 km between the Black sea and the Caspian Sea. Like the Italian Alps, the mountain system formed during the Cenozoic era, around 25 million years ago, following the collision between the Arabian plate and Eurasian plate.
The Caucasus mountain chain is actually made up of two separate chains: the Greater Caucasus and the Lesser Caucasus, these run parallel to each other, separated by the valleys of the Kura and the Rioni rivers, and finally meeting again at the Surami pass (949 m a.s.l.). The Greater Caucasus stretches between the cities of Sochi and Baku, and is today the political frontier between Russia in the north and Georgia and Azerbaijan in the south. On the other hand, the Lesser Caucasus passes through the states of Georgia, Azerbaijan and Armenia. Many of the peaks are higher than 5000 m, such as Mount Elbrus (5642 m), the Dykh Tau (5205 m), the Shkhara (5200 m), the Koshtan Tau (5144 m), the Janga (5051 m) and the Kazbek (5047 m).
The project layout (Fig.9) of the T8 and T8A regards a coastal hill belt, with softened morphology and mostly made up of low elevations with a rich vegetation. This coastal path is part of the southern slope of the Greater Caucasus and is crossed by many rivers and canyons. The distinctive trait of this hill landscape is the high geomorphological dynamicity – the result of many factors interacting with each other: the current rise of the area, the following exogenous processes of disaggregation and - not least of all the typical climate of this coastal area (Lunardi et al, 2013).

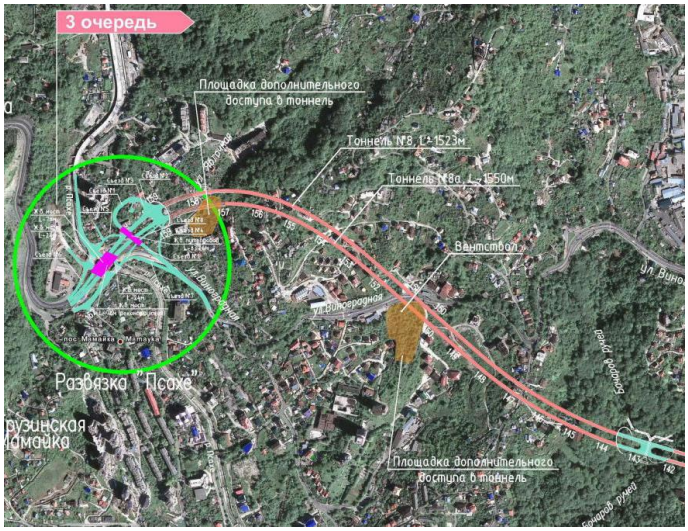


Fig. 9. Aerial survey of the area

The area presents two main geological formations: the “Sochi formation” and the “Mamai formation”. Each of these are flyschoid units on the southern margin of the main Greater Caucasus chain.
The Sochi formation follows most of the layout for the T8 and T8A tunnels, from the southern portal to the middle area (highlighted in green in Fig.10). This area is for the most part made up of dark grey shale and clay siltite; these rocks are poorly lithoidal, brittle, and with rare or low levels of sandstone. The shale is frequently laminate, rapidly alterable and sensitive to contact with water.

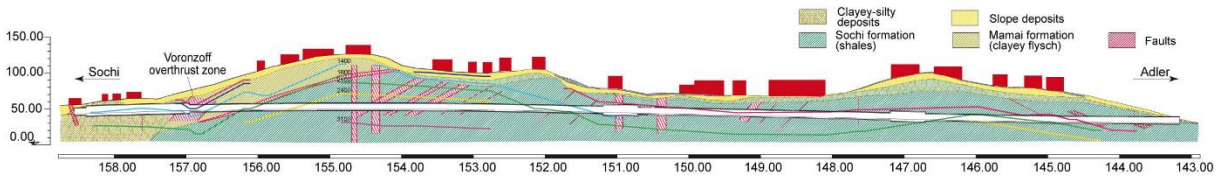


Fig. 10. Geological profile in axis with the T8 tunnel (fault areas in red)

The Manai formation is present in only a few areas at the northern part of the tunnels (highlighted in brown in Fig.10) and alternates siltite, marl and grey/green-grey fine sandstones; and local levels of scale-structured shale of a blue and grey colour. From a tectonic point of view, the project area belongs

to the Greater Caucasus seismogenic structure, which includes a long belt of mostly constant faults, sub-parallel to the Black Sea's coast (NW-SE) and characterized by an extension towards NNE-SSW (red lines in Fig.10).
In general, the external geological processes (mudslides, landslides, etc.) and the internal ones (seismicity) heavily affect the area of the region; analysis of the seismic and tectonic context, as well as the development of these dangerous geological processes required care during the design stage. Many faults were found along the tunnel's length, generally characterized by intensely fractured and narrow strips. The plicative tectonics were equally evident, with wide folds which locally determined verticalization in the Sochi formation. An important tectonic contact is present towards E-W, causing the Mamai formation to pass over the Sochi formation, and affects the tunnel track for around 250 m near the north portal (Fig.10).
Both formations are largely covered by eluvium-colluvial coverings of varying thickness: from a few metres near the south portal, up to 10-15 m in the central section and near the north portal. These coverings directly affect excavation in the portal areas and in those segments with reduced covering, they are characterized by reshaped rubble portions of silty clay and have been set in place by gravity and by the alteration of the ground mass below, furthermore their geotechnical traits are quite poor.
There are a few extents affected by active landslide movements in the area of excavation and in particular near the north portal, these extents affect significant volumes of ground and portions of the underground rock mass. Intense rainfall, which often affects the territory (especially in autumn) favours the saturation of the ground and the complex distribution of interstitial pressure between the numerous lithologies. Each of these is poorly water resistant and can easily give way to the triggering or reactivating of landslide phenomena.

The portals and the midway access to the tunnel

Lacking the necessary eminent domain at the north and south portals, due to an underestimation of the need on the behalf of the authorities, the works were delayed for about a year. For this reason, in accordance with the client, it was decided to insert a midway access with connection to the tunnels located under the overhead Federal Road. Since this was the only technology available at the moment in Russia, the portals were built using large-diameter pile bulkheads in reinforced concrete, fittingly contrasted by means of bracing and strutting (Fig.11).



Fig. 11. North portal almost finished

The applied section types

From the diagnostic study of the T8 and T8a tunnels, developed according to the A.DE.CO.RS approach, it was clear that the excavation would need to take place in either unstable or short-term stable (stress-strain behaviour categories "C" and "B") core-face stability conditions for the entire length of the underground layout. It was therefore designed during the therapy phase to advance in full face for the

entire length, in order to achieve this, it would be necessary to use correctly scaled section types alongside necessary protection and/or reinforcement measures of the core face and to implement the casting of the kickers and of the invert near the excavation face. In particular, at the landsliding north portal, the C2W section type with an invert strut was designed in order to limit deformation to the highest level. Figure 12 reports the main designed section types; as regards the C section type, alongside reinforcement of the core-face by means of fibre-glass structures, the figure highlights the treatment along its outline which was carried out by operating injections through fibreglass structures equipped with manchette valves. Figure 13 shows the face of the T8A tunnel, close to the North portal in the landslide area. For those few tunnel sections that didn't require systematic treatment of the core face, due to significant horizontal mass pressure, the decision was made to bring the systematic casting of the second-phase lining in proximity to the excavation face.

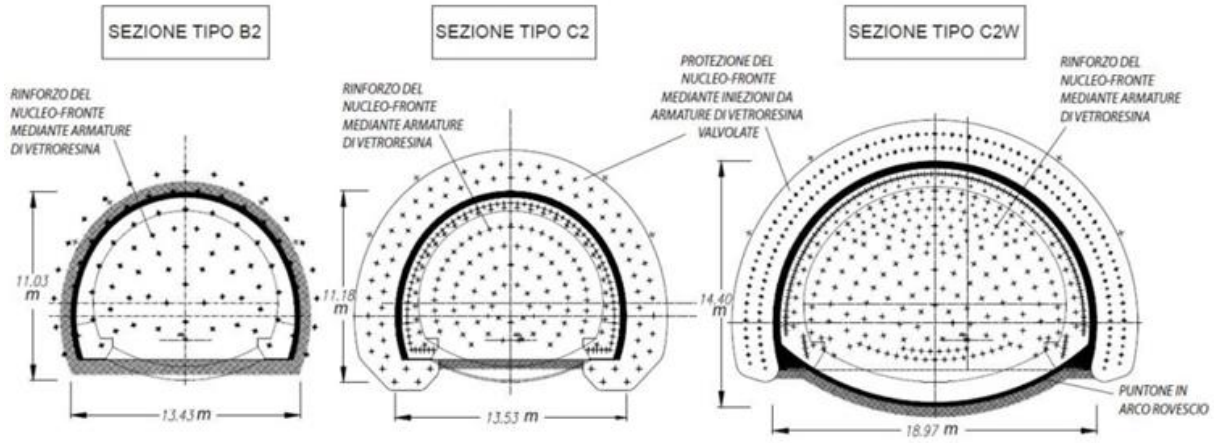


Fig. 12. Applied Section Type

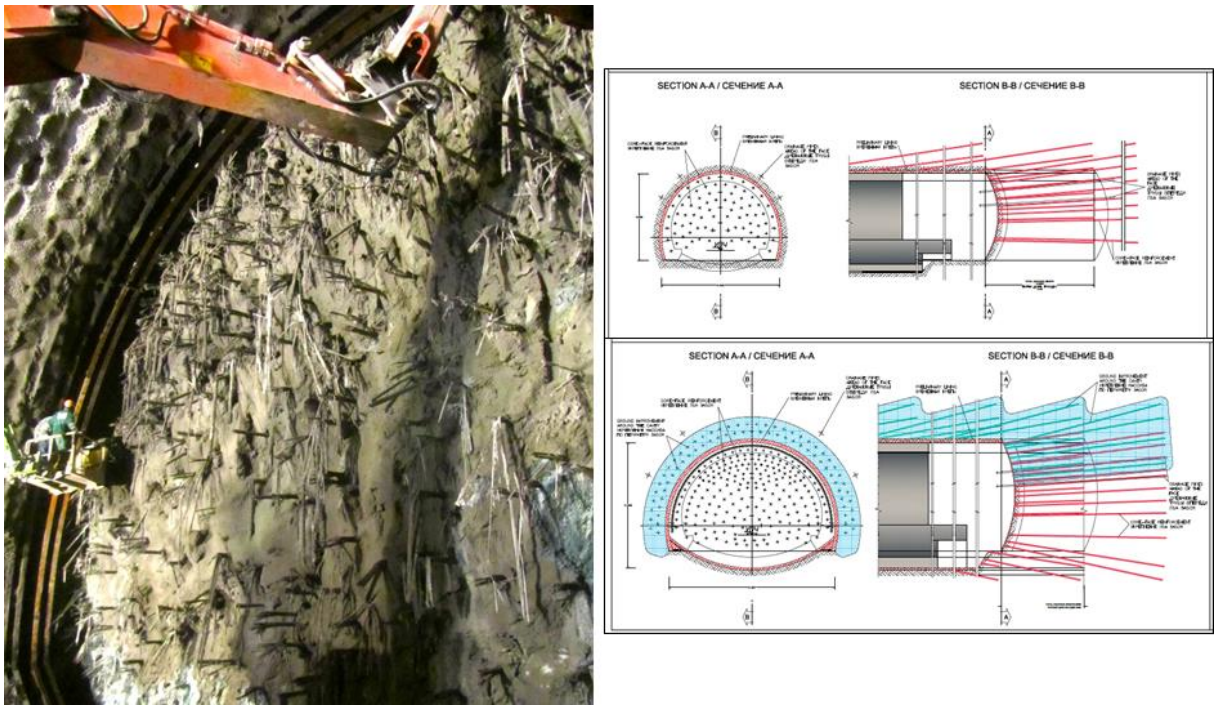


Fig. 13. Face of the T8A tunnel – North portal in the landslide area – slope deposits

Tunnel 8 - 8A: Production

During the detailed design phase, the construction times were defined according to:

- Past experience in similar contexts.
- Start up times for the acquisition of necessary machinery.

- Necessary time to acquire the required know how and resulting reduced production for at least 6 months.
- Logistical difficulties due to transportation of construction material, machinery and necessary spare parts to the site.
- Socio-cultural context.

Some of these are difficult to evaluate in that they are linked to factors that can be difficult to quantify. For example, the enormous investments allocated towards construction in Sochi lead to an incredibly high request and concentration of raw material. The transportation and rail systems weren't initially capable of supporting such a massive movement of material; furthermore, the winter weather conditions made it difficult for ships to dock, thus invalidating sea delivery as well. Despite the fact that authorities progressively provided all raw necessities, this still created significant difficulties towards the efficient application of a highly industrial system such as the A.DE.CO-RS.

Overall, the project forecast the following times and stages: 18 months for the excavation of the T8 tunnel (1,550 m), 22 months for the excavation of the T8A tunnel (1,523 m). Indeed, the two tunnels differ in the length of the three lane carriageway (furthermore located in a landslide area): this section is 85 metres long for the T8 tunnel, while it's 170 m long for the T8A. Production levels varied according to the diverse geological conditions, the size of the sections of excavation and the applied type of pre-containment and lining used. Excavation productivity also increased over time thanks to the Transtoy Company's growing familiarity with the A.DE.CO-RS approach. When advancing in extreme depth under landslide conditions and using exceptionally large sections of excavation (up to 200 m^2) production averaged between 12 and 13 metres/month of completed tunnel (already lined), up to values between 57 and 88 metres/month of standard sections of excavation (120 m^2) and geological conditions that didn't require particularly heavy stabilizing operations (Fig.14).

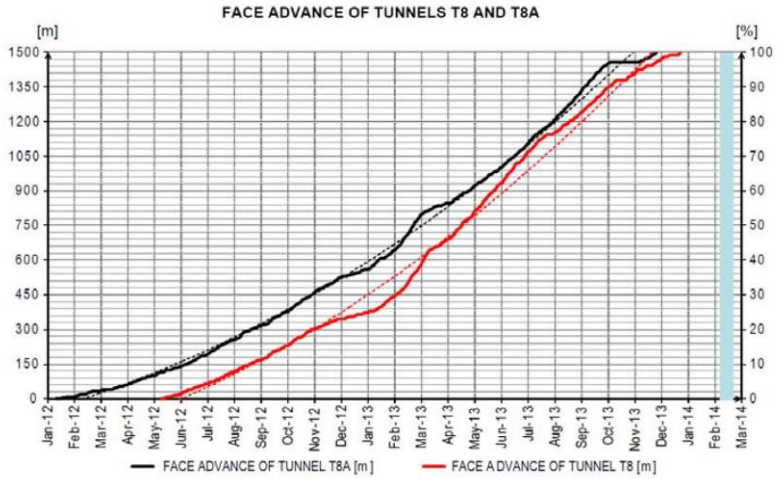


Fig. 14. Production levels while excavating the T8 e T8a tunnels

"Dubler Kurortnogo Prospekta" tunnels productions

The "Dubler Kurortnogo Prospekta" tunnel, as illustrated in the introduction, is made up of 6 double bore tunnels for a total of: 10 tunnels bored using the NATM approach (New Austrian Tunnelling Method) and 2 tunnels using the A.DE.CO-RS approach (Tunnels 8 and 8a). It was the first time that these two approaches were directly and reliably compared to each other, in relatively similar conditions (despite the difficulty regarding those tunnels constructed using the A.DE.CO-RS). Illustrated below, the two approaches are compared both in terms of average production and in terms of "bored volume/month" and in terms of "metres of tunnel finished/month".

The geological conditions affecting the 8-8a tunnel excavation were clearly worse than those of the other tunnels, and the excavation sizes were also greater. Indeed, the 8-8a tunnels occupy a harsh geological context and measure excavation sizes between 120 m^2 and 220 m^2, while the tunnels bored using the NATM passed through better contexts with excavation sizes just equal to 113-115 m^2.

Despite this, the comparison between the two approaches clearly exhibits extreme efficiency of the A.DE.CO-RS system over the NATM: in terms of volume of excavation/month for single face the A.DE.CO-RS approach produced results 2.4 times higher than the NATM; in terms of linear metres of completed tunnel, productivity was 40% greater than the NATM approach (Figg.15, 16).

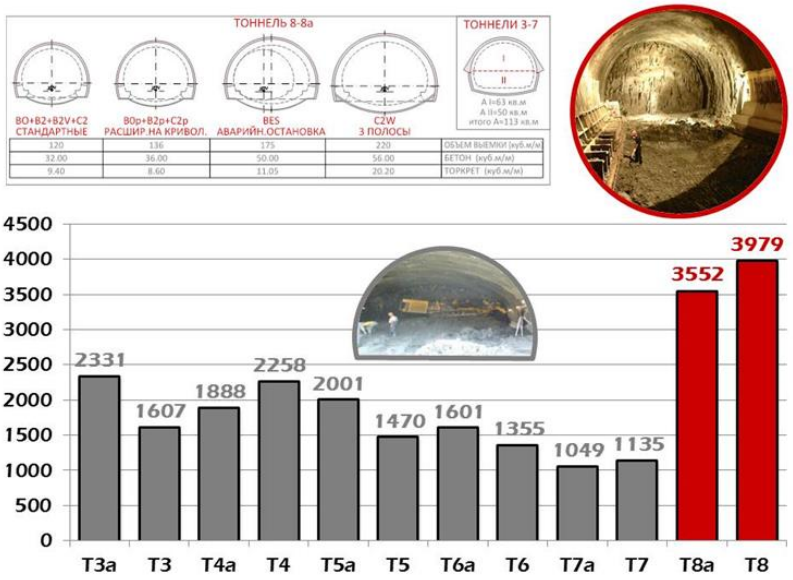


Fig. 15. Cubic metres bored/month for single excavation face: comparison between NATM and A.DE.CO-RS

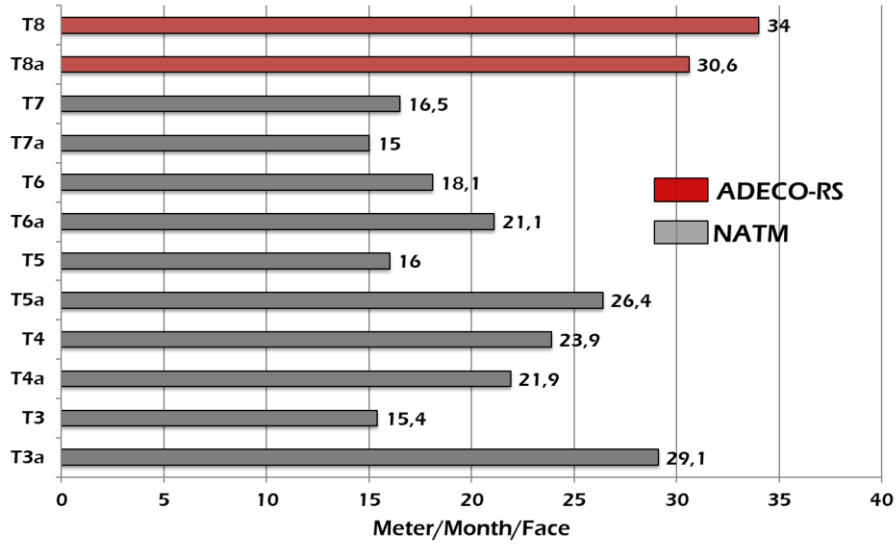


Fig. 16. Average production of finished tunnel: metres month/excavation face

Equally interesting is the comparison of time passing from the breakthrough of the excavation face and the completion of final lining casting, which corresponds to the completion of all the tunnel's safety measures.

The A.DE.CO-RS approach is naturally fast in closing the lining (Fig.17), in the case of Sochi this was completed under 3 weeks. Instead, the NATM approach showed much greater times: from a minimum of 10 weeks to a maximum of 43; such a time frame has clear repercussions on safety. From this point of view, the A.DE.CO-RS method can complete all necessary safety measures for the tunnel in a short time frame, thus greatly limiting the deformation phenomena linked to excavation.

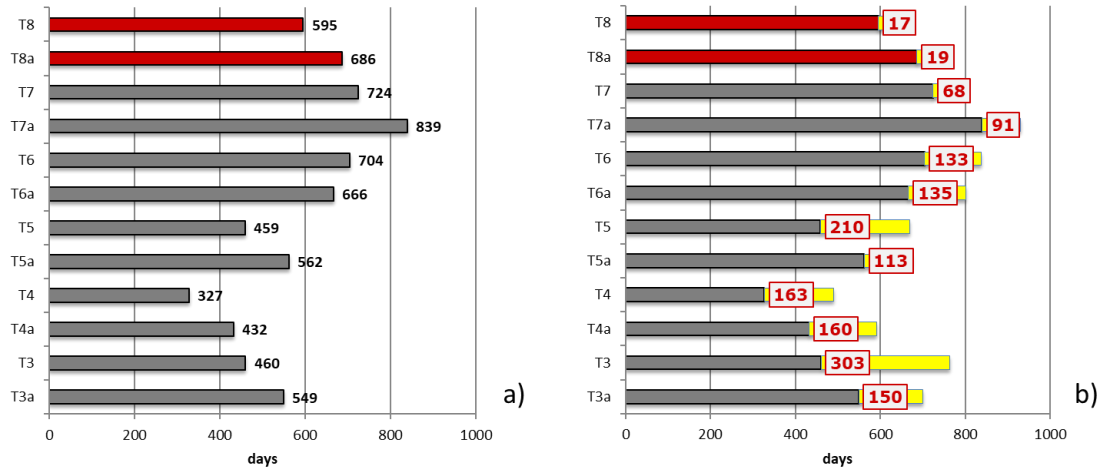


Fig.17. a) Time for breakthrough; b) Time interval between breakthrough and tunnel cast

CONCLUSION

The A.DE.CO-RS Approach has been applied in Italy, for the first time, in 1988 to Tasso Tunnel and then to San Vitale and Vasto tunnels. After these successful experiences the method easily spread out and was rapidly adopted in Italy by all the Clients and introduced in their design specifications. The first application outside Italy was in 1997 with the Tartaiguille tunnel (high speed rail line between Marseille and Lyon in France). The benefit highlighted from the method, in reference e.i. to the reinforcement of the advanced core, has been largely adopted in the last 15 years also from the NATM method.
The first implementation of the A.DE.CO-RS approach in Russia has been positive, both in terms of production and in tunnelling safety.
Introducing the A.DE.CO-RS approach in Russia will certainly take more time and will necessarily pass through a series of phases which required many years in Italy. The article reports the main differences observed in terms of production and of safety between the two different approaches used when excavation the Dubler Kurortnogo Prospekta tunnel (A.DE.CO-RS and NATM). A direct and reliable comparison was finally possible due to the similar conditions they faced (despite the fact that it was certainly more difficult for the tunnels bored using the A.DE.CO-RS method).
Russia has a strongly-rooted tradition towards the NATM system, but the Federal Administrations have of late been following a philosophy of deep technological innovation towards industry and production. The A.DE.CO-RS approach enters perfectly in said new attitude and is of special interest to administrations and construction companies for its capability in tunnel construction within definite times and costs.

REFERENCES

Lunardi P., 2008. Design and construction of tunnels, analysis of controlled deformations in rock and soils (A.DE.CO-RS), Springer-Verlag Berlin Heidelberg.

Lunardi, G., Cassani, G., Bellocchio A., 20013. La realizzazione delle gallerie T8 e T8A nell'ambito del "Dubler Kurortnogo prospekta" a Sochi (Russia). Primi risultati dell'approccio A.DE.CO-RS nella Federazione Russa. Atti del Congresso Internazionale su "Gallerie e spazio sotterraneo nello sviluppo dell'Europa", Bologna, 17-19 ottobre 2013.

Lunardi P., G. Cassani, M. Gatti, C.L. Zenti, 2016. The A.DE.CO-RS approach and the recent European application experiences. Proceedings 13th International Conference Underground Construction Prague 2016, 3rd Eastern European Tunnelling Conference (EETC 2016), Prague, 23rd – 25th May, 2016, JPM, ISBN 978-80-906452-0-2.

Rabcewicz L., 1964. "The New Austrian Tunnelling Method", Part one, Water Power.